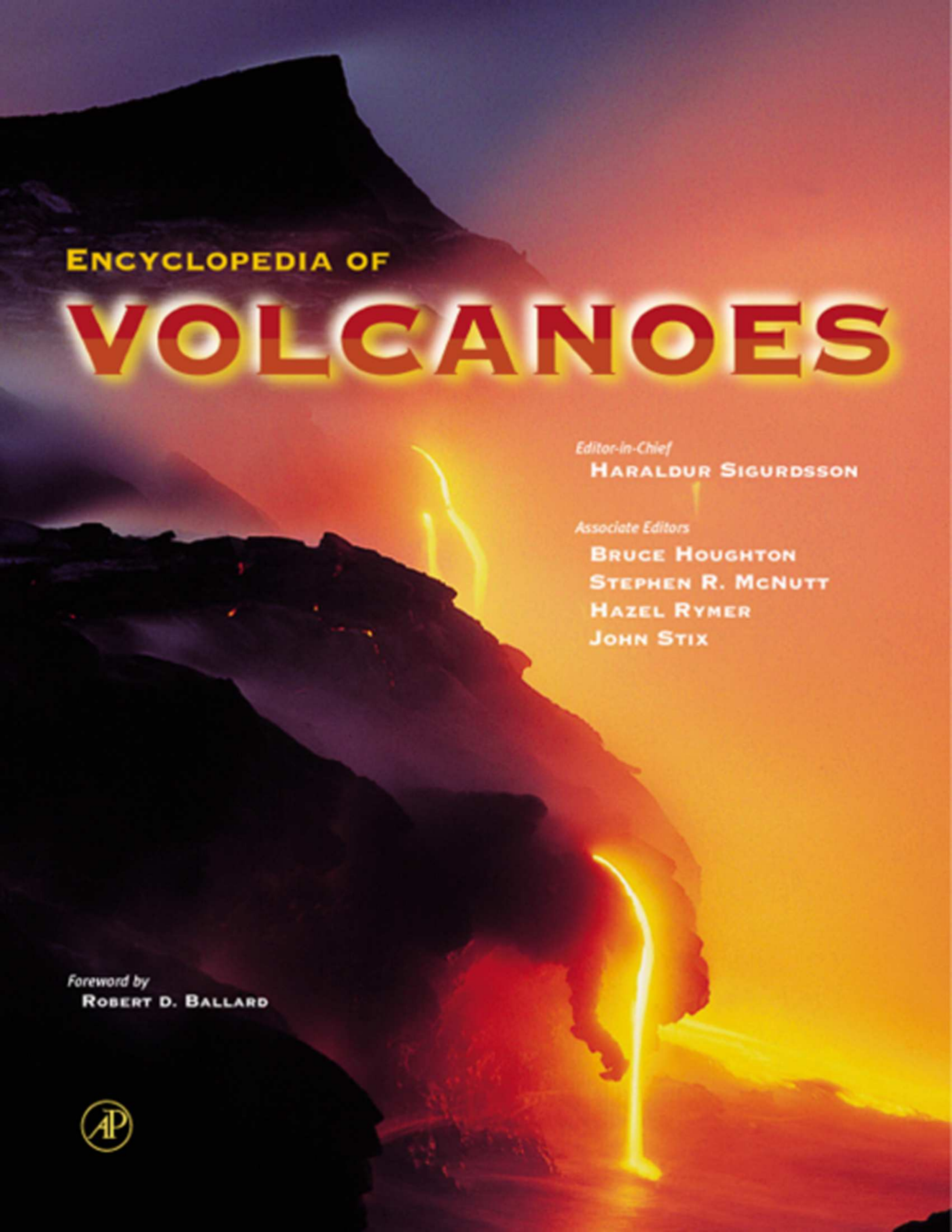

ENCYCLOPEDIA OF VOLCANOES

Editor-in-Chief
HARALDUR SIGURDSSON

Associate Editors
BRUCE HOUGHTON
STEPHEN R. MCNUTT
HAZEL RYMER
JOHN STIX

Foreword by
ROBERT D. BALLARD

ENCYCLOPEDIA OF

VOLCANOES

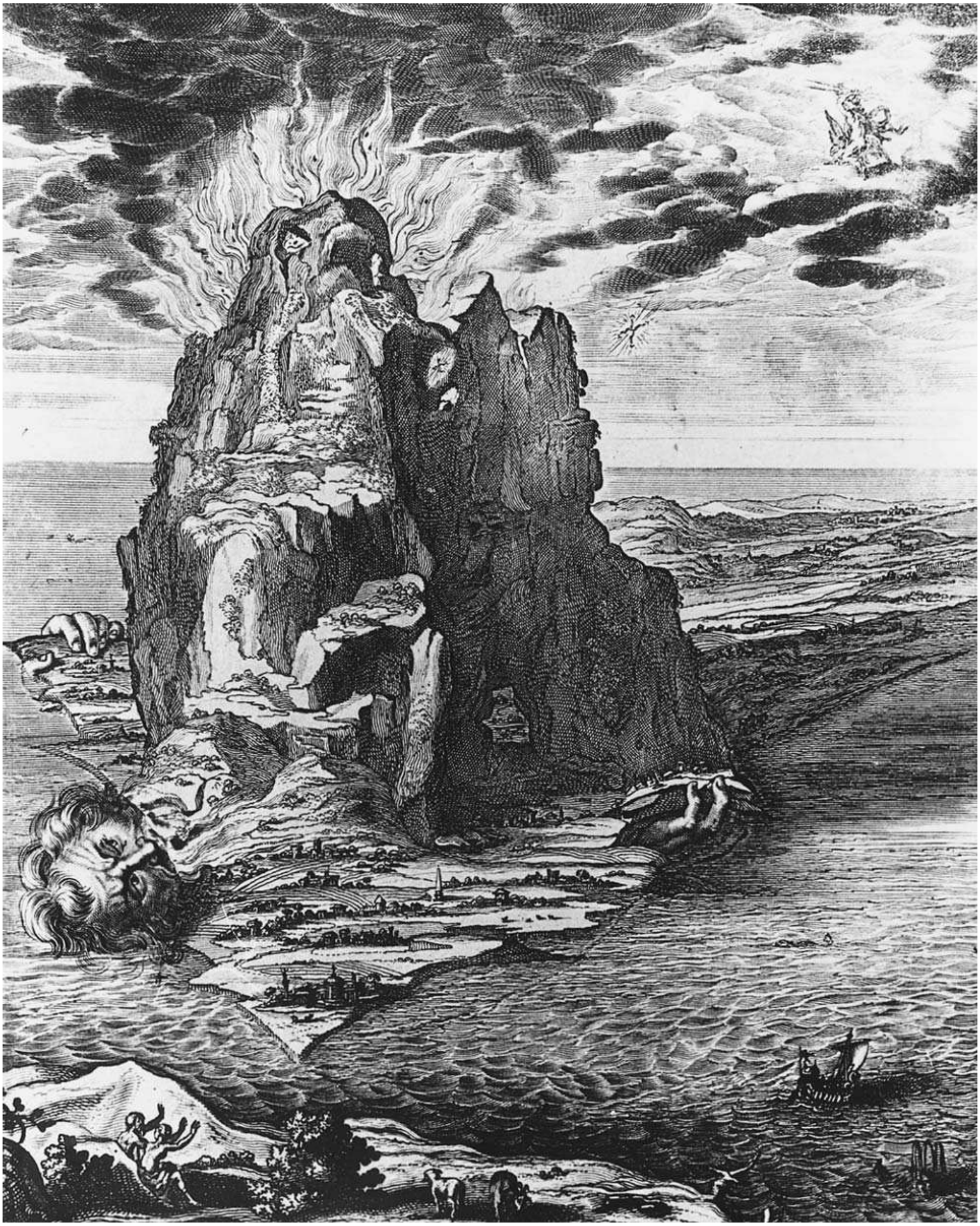

According to Greek Mythology, the giant Typhon is buried under Etna volcano. Whenever the giant stirs, the volcano erupts violently. Eighteenth century print. (See The History of Volcanology, p. 15.)

ENCYCLOPEDIA OF VOLCANOES

Editor-in-Chief

HARALDUR SIGURDSSON
University of Rhode Island, U.S.A.

Associate Editors

BRUCE F. HOUGHTON
Institute of Geology and Nuclear Science, New Zealand

STEPHEN R. MCNUTT
Alaska Volcano Observatory and University of Alaska Fairbanks, U.S.A.

HAZEL RYMER
Open University, United Kingdom

JOHN STIX
McGill University, Canada

Foreword by

ROBERT D. BALLARD

ACADEMIC PRESS

A Harcourt Science and Technology Company
San Diego San Francisco New York Boston London Sydney Toronto

Academic Press to Supply Copyright Page

CONTENTS

ARTICLE INDEX xi

CONTRIBUTORS xiii

FOREWORD xix
Robert D. Ballard

PREFACE xxi
The Editors

GUIDE TO THE ENCYCLOPEDIA xxiii

INTRODUCTION 1
Haraldur Sigurdsson

THE HISTORY OF VOLCANOLOGY 15
Haraldur Sigurdsson

PART I
ORIGIN AND TRANSPORT OF MAGMA

MANTLE OF THE EARTH 41
Raymond Jeanloz

MELTING THE MANTLE 55
Paul D. Asimow

MIGRATION OF MELT 69
Martha J. Daines

PLATE TECTONICS AND VOLCANISM 89
Michael R. Perfit and Jon P. Davidson

COMPOSITION OF MAGMAS 115
Nick Rogers and Chris Hawkesworth

ORIGIN OF MAGMAS 133
Timothy L. Grove

VOLATILES IN MAGMAS 149
Paul Wallace and Alfred T. Anderson, Jr.

PHYSICAL PROPERTIES OF MAGMAS 171
Frank J. Spera

MAGMA CHAMBERS 191
Bruce D. Marsh

RATES OF MAGMA ASCENT 207
Malcolm J. Rutherford and James E. Gardner

PLUMBING SYSTEMS 219
Charles R. Carrigan

MAGMA ASCENT AT SHALLOW LEVELS 237
Claude Jaupart

PART II
ERUPTION

EARTH'S VOLCANOES AND ERUPTIONS: AN OVERVIEW 249
Tom Simkin and Lee Siebert

SIZES OF VOLCANIC ERUPTIONS 263
David M. Pyle

VOLCANIC EPISODES AND RATES OF VOLCANISM 271
Haraldur Sigurdsson

PART III
EFFUSIVE VOLCANISM

BASALTIC VOLCANOES AND VOLCANIC SYSTEMS 283
George P. L. Walker

LAVA FLOWS AND FLOW FIELDS 291
Christopher R. J. Kilburn

LAVA DOMES AND COULEES 307
Jonathan H. Fink and Steven W. Anderson

LAVA FOUNTAINS AND THEIR PRODUCTS 321
John A. Wolff and Janet M. Sumner

BASALTIC VOLCANIC FIELDS 331
Charles B. Connor and F. Michael Conway

FLOOD BASALT PROVINCES 345
Peter R. Hooper

SUBMARINE LAVAS AND HYALOCLASTITE 361
Rodey Batiza and James D. L. White

SEAMOUNTS AND ISLAND BUILDING 383
Ralf Schmidt and Hans-Ulrich Schmincke

SUBGLACIAL ERUPTIONS 403
John L. Smellie

PART IV
EXPLOSIVE VOLCANISM

MAGMATIC FRAGMENTATION 421
K. V. Cashman, B. Sturtevant, P. Papale, and O. Navon

PHREATOMAGMATIC FRAGMENTATION 431
Meghan Morrissey, Bernd Zimanowski, Kenneth Wohletz, and Ralf Buettner

HAWAIIAN AND STROMBOLIAN ERUPTIONS 447
S. Vergniolle and M. Mangan

VULCANIAN ERUPTIONS 463
Meghan M. Morrissey and Larry G. Mastin

PLINIAN AND SUBPLINIAN ERUPTIONS 477
Raffaello Cioni, Paola Marianelli, Roberto Santacroce and Alessandro Sbrana

SURTSEYAN AND RELATED PHREATOMAGMATIC ERUPTIONS 495
James D. L. White and Bruce Houghton

PHREATOPLINIAN ERUPTIONS 513
B. F. Houghton, C. J. N. Wilson, R. T. Smith, and J. S. Gilbert

VOLCANIC PLUMES 527
Steven Carey and Marcus Bursik

PYROCLAST TRANSPORT AND DEPOSITION 545
Colin J. N. Wilson and Bruce F. Houghton

PYROCLASTIC FALL DEPOSITS 555
B. F. Houghton, C. J. N. Wilson, and D. M. Pyle

PYROCLASTIC SURGES AND BLASTS 571
Greg A. Valentine and Richard V. Fisher

IGNIMBRITES AND BLOCK-AND-ASH FLOW DEPOSITS 581
A. Freundt, C. J. N. Wilson, and S. N. Carey

LAHARS 601
James W. Vallance

DEBRIS AVALANCHES 617
Tadahide Ui, Shinji Takarada, and Mitsuhiro Yoshimoto

VOLCANICLASTIC SEDIMENTATION AROUND ISLAND ARCS 627
Steven Carey

CALDERAS 643
Peter W. Lipman

COMPOSITE VOLCANOES 663
Jon Davidson and Shan De Silva

SCORIA CONES AND TUFF RINGS 683
Dirk Vespermann and Hans-Ulrich Schmincke

PART V

EXTRATERRESTRIAL VOLCANISM

VOLCANISM ON THE MOON 697
Paul D. Spudis

VOLCANISM ON IO 709
Rosaly Lopes-Gautier

VOLCANISM ON VENUS 727
L. S. Crumpler and Jayne C. Aubele

VOLCANISM ON MARS 771
James R. Zimbelman

CRYOVOLCANISM IN THE OUTER SOLAR SYSTEM 785
Paul Geissler

PART VI

VOLCANIC INTERACTIONS

VOLCANIC GASES 803
Pierre Delmelle and John Stix

GEOTHERMAL SYSTEMS 817
Fraser Goff and Cathy J. Janik

SURFACE MANIFESTATIONS OF GEOTHERMAL SYSTEMS WITH VOLCANIC HEAT SOURCES 835
Manfred P. Hochstein and Patrick R. L. Browne

DEEP OCEAN HYDROTHERMAL VENTS 857
David A. Butterfield

VOLCANIC LAKES 877
Pierre Delmelle and Alain Bernard

MINERAL DEPOSITS ASSOCIATED WITH VOLCANISM 897
Noel C. White and Richard J. Herrington

PART VII

VOLCANIC HAZARDS

VOLCANIC ASH HAZARDS TO AVIATION 915
T. P. Miller and T. J. Casadevall

Volcanic Aerosol and Global Atmospheric Effects 931
Michael J. Mills

Hazards from Pyroclastic Flows and Surges 945
Setsuya Nakada

Lava Flow Hazards 957
Donald W. Peterson and Robert I. Tilling

The Hazard from Lahars and Jökulhlaups 973
Kelvin S. Rodolfo

Hazards of Volcanic Gases 997
Glyn Williams-Jones and Hazel Rymer

Volcanic Tsunamis 1005
James E. Begét

Volcanic Seismicity 1015
Stephen R. McNutt

Impacts of Eruptions on Human Health 1035
Peter J. Baxter

Volcanic Contributions to the Carbon and Sulfur Geochemical Cycles and Global Change 1045
Michael A. Arthur

The Ecology of Volcanoes: Recovery and Reassembly of Living Communities 1057
Ian W. B. Thornton

Volcanism and Biotic Extinctions 1083
Michael R. Rampino and Stephen Self

PART VIII

ERUPTION RESPONSE AND MITIGATION

Seismic Monitoring 1095
Stephen R. McNutt

Ground Deformation, Gravity, and Magnetics 1121
John B. Murray, Hazel Rymer, and Corinne A. Locke

Gas, Plume, and Thermal Monitoring 1141
John Stix and Hélène Gaonac'h

Synthesis of Volcano Monitoring 1165
Stephen R. McNutt, Hazel Rymer, and John Stix

Volcano Warnings 1185
Christopher G. Newhall

Volcanic Crises Management 1199
Servando De La Crùz-Reyna, Roberto Meli P., and Roberto Quaas W.

Volcanic Hazards and Risk Management 1215
Russell Blong

Risk Education and Intervention 1229
David Johnston and Kevin Ronan

PART IX

ECONOMIC BENEFITS AND CULTURAL ASPECTS OF VOLCANISM

Exploitation of Geothermal Resources 1243
Stefán Arnórsson

Volcanic Soils 1259
Chien-Lu Ping

Volcanic Materials in Commerce and Industry 1271
Jonathan Dehn and Stephen R. McNutt

Volcanoes and Tourism 1283
Haraldur Sigurdsson and Rosaly Lopes-Gautier

ARCHAEOLOGY AND VOLCANISM 1301
Stephen L. Harris

VOLCANOES IN ART 1315
Haraldur Sigurdsson

VOLCANOES IN LITERATURE AND FILM 1339
Haraldur Sigurdsson and Rosaly Lopes-Gautier

APPENDIX 1: COMMON UNITS AND CONVERSION FACTORS 1361

APPENDIX 2: CATALOG OF HISTORICALLY ACTIVE VOLCANOES ON EARTH 1365
Tom Simkin and Lee Siebert

ACKNOWLEDGMENTS 1385

INDEX 1389

This Page Intentionally Left Blank

ARTICLE INDEX

ARCHAEOLOGY AND VOLCANISM 1301

BASALTIC VOLCANIC FIELDS 331

BASALTIC VOLCANOES AND VOLCANIC SYSTEMS 283

CALDERAS 643

COMPOSITE VOLCANOES 663

COMPOSITION OF MAGMAS 115

CRYOVOLCANISM IN THE OUTER SOLAR SYSTEM 785

DEBRIS AVALANCHES 617

DEEP OCEAN HYDROTHERMAL VENTS 857

EARTH'S VOLCANOES AND ERUPTIONS: AN OVERVIEW 249

ECOLOGY OF VOLCANOES: RECOVERY AND REASSEMBLY OF LIVING COMMUNITIES 1057

EXPLOITATION OF GEOTHERMAL RESOURCES 1243

FLOOD BASALT PROVINCES 345

GAS, PLUME, AND THERMAL MONITORING 1141

GEOTHERMAL SYSTEMS 817

GROUND DEFORMATION, GRAVITY, AND MAGNETICS 1121

HAWAIIAN AND STROMBOLIAN ERUPTIONS 447

HAZARD FROM LAHARS AND JÖKULHLAUPS 973

HAZARDS FROM PYROCLASTIC FLOWS AND SURGES 945

HAZARDS OF VOLCANIC GASES 997

HISTORY OF VOLCANOLOGY 15

IGNIMBRITES AND BLOCK-AND-ASH FLOW DEPOSITS 581

IMPACTS OF ERUPTIONS ON HUMAN HEALTH 1035

INTRODUCTION 1

LAHARS 601

LAVA DOMES AND COULEES 307

LAVA FLOW HAZARDS 957

LAVA FLOWS AND FLOW FIELDS 291

LAVA FOUNTAINS AND THEIR PRODUCTS 321

MAGMA ASCENT AT SHALLOW LEVELS 237

MAGMA CHAMBERS 191
MAGMATIC FRAGMENTATION 421
MANTLE OF THE EARTH 41
MELTING THE MANTLE 55
MIGRATION OF MELT 69
MINERAL DEPOSITS ASSOCIATED WITH VOLCANISM 897
ORIGIN OF MAGMAS 133
PHREATOMAGMATIC FRAGMENTATION 431
PHREATOPLINIAN ERUPTIONS 513
PHYSICAL PROPERTIES OF MAGMAS 171
PLATE TECTONICS AND VOLCANISM 89
PLINIAN AND SUBPLINIAN ERUPTIONS 477
PLUMBING SYSTEMS 219
PYROCLAST TRANSPORT AND DEPOSITION 545
PYROCLASTIC FALL DEPOSITS 555
PYROCLASTIC SURGES AND BLASTS 571
RATES OF MAGMA ASCENT 207
RISK EDUCATION AND INTERVENTION 1229
SCORIA CONES AND TUFF RINGS 683
SEAMOUNTS AND ISLAND BUILDING 383
SEISMIC MONITORING 1095
SIZES OF VOLCANIC ERUPTIONS 263
SUBGLACIAL ERUPTIONS 403
SUBMARINE LAVAS AND HYALOCLASTITE 361
SURFACE MANIFESTATIONS OF GEOTHERMAL SYSTEMS WITH VOLCANIC HEAT SOURCES 835
SURTSEYAN AND RELATED PHREATOMAGMATIC ERUPTIONS 495
SYNTHESIS OF VOLCANO MONITORING 1165
VOLATILES IN MAGMAS 149
VOLCANIC AEROSOL AND GLOBAL ATMOSPHERIC EFFECTS 931
VOLCANIC ASH HAZARDS TO AVIATION 915
VOLCANIC CONTRIBUTIONS TO THE CARBON AND SULFUR GEOCHEMICAL CYCLES AND GLOBAL CHANGE 1045
VOLCANIC CRISES MANAGEMENT 1199
VOLCANIC EPISODES AND RATES OF VOLCANISM 271
VOLCANIC GASES 803
VOLCANIC HAZARDS AND RISK MANAGEMENT 1215
VOLCANIC LAKES 877
VOLCANIC MATERIALS IN COMMERCE AND INDUSTRY 1271
VOLCANIC PLUMES 527
VOLCANIC SEISMICITY 1015
VOLCANIC SOILS 1259
VOLCANIC TSUNAMIS 1005
VOLCANICLASTIC SEDIMENTATION AROUND ISLAND ARCS 627
VOLCANISM AND BIOTIC EXTINCTIONS 1083
VOLCANISM ON IO 709
VOLCANISM ON MARS 771
VOLCANISM ON THE MOON 697
VOLCANISM ON VENUS 727
VOLCANO WARNINGS 1185
VOLCANOES AND TOURISM 1283
VOLCANOES IN ART 1315
VOLCANOES IN LITERATURE AND FILM 1339
VULCANIAN ERUPTIONS 463

CONTRIBUTORS

Alfred T. Anderson, Jr.
University of Chicago
Chicago, Illinois, USA
Volatiles in Magmas

Steven W. Anderson
University of Arizona
Tucson, Arizona, USA
Lava Domes and Coulees

Stefán Arnórsson
University of Iceland
Reykjavik, Iceland
Exploitation of Geothermal Resources

Michael A. Arthur
Pennsylvania State University
University Park, Pennsylvania, USA
Volcanic Contributions to the Carbon and Sulfur Geochemical Cycles and Global Change

Paul D. Asimow
Lamont-Doherty Earth Observatory
Palisades, New York, USA
Melting the Mantle

Jayne Aubele
New Mexico Museum of Natural History and Science
Albuquerque, New Mexico, USA
Volcanism on Venus

Rodey Batiza
University of Hawaii
Honolulu, Hawaii, USA
Submarine Lavas and Hyaloclastite

Peter J. Baxter
Cambridge University
Cambridge, England, UK
Impacts of Eruptions on Human Health

James E. Begét
University of Alaska
Fairbanks, Alaska, USA
Volcanic Tsunamis

Alain Bernard
Universite Libre de Bruxelles
Brussels, Belgium
Volcanic Lakes

Russell Blong
Macquarie University
North Ryde, New South Wales, Australia
Volcanic Hazards and Risk Management

Patrick R. L. Browne
University of Auckland
Auckland, New Zealand
Surface Manifestations of Geothermal Systems with Volcanic Heat Sources

Ralf Buettner
Universität Würzburg
Würzburg, Germany
Phreatomagmatic Fragmentation

Marcus I. Bursik
State University of New York, Buffalo
Buffalo, New York, USA
Volcanic Plumes

David A. Butterfield
University of Washington
Seattle, Washington, USA
Deep Ocean Hydrothermal Vents

Steven N. Carey
University of Rhode Island
Narragansett, Rhode Island, USA
Ignimbrites and Block-and-Ash Flow Deposits
Volcaniclastic Sedimention Around Island Arcs
Volcanic Plumes

Charles R. Carrigan
Lawrence Livermore National Laboratory
Livermore, California, USA
Plumbing Systems

Thomas J. Casadevall
U.S. Geological Survey
Reston, Virginia, USA
Volcanic Ash Hazards to Aviation

Katharine V. Cashman
University of Oregon
Eugene, Oregon, USA
Magmatic Fragmentation

Raffaello Cioni
Universita di Pisa
Pisa, Italy
Plinian and Subplinian Eruptions

Charles B. Connor
Southwest Research Institute
San Antonio, Texas, USA
Basaltic Volcanic Fields

F. Michael Conway
Arizona Western College
Yuma, Arizona, USA
Basaltic Volcanic Fields

Larry S. Crumpler
New Mexico Museum of Natural History and Science
Albuquerque, New Mexico, USA
Volcanism on Venus

Servando De La Cruz-Reyna
Instituto de Geofísica UNAM, C University
Mexico City, Mexico
Volcanic Crises Management

Martha J. Daines
University of Minnesota
Minneapolis, Minnesota, USA
Migration of Melt

Jon P. Davidson
University of California, Los Angeles
Los Angeles, California, USA
Composite Volcanoes
Plate Tectonics and Volcanism

Jonathan Dehn
Alaska Volcano Observatory
University of Alaska
Fairbanks, Alaska, USA
Volcanic Materials in Commerce and Industry

Pierre Delmelle
Université de Montréal
Montreal, Quebec, Canada
Volcanic Gases
Volcanic Lakes

Jonathan H. Fink
Arizona State University
Tempe, Arizona, USA
Lava Domes and Coulees

Richard V. Fisher
University of California, Santa Barbara
Santa Barbara, California, USA
Pyroclastic Surges and Blasts

Armin Freundt
GEOMAR Research Center
Kiel, Germany
Ignimbrites and Block-and-Ash Flow Deposits

Hélène Gaonac'h
Université de Quebec, Montréal
Montréal, Quebec, Canada
Gas, Plume, and Thermal Monitoring

James E. Gardner
University of Alaska
Fairbanks, Alaska, USA
Rates of Magma Ascent

Paul Geissler
University of Arizona
Tucson, Arizona, USA
Cryovolcanism in the Outer Solar System

JENNIE S. GILBERT
Lancaster University
Lancaster, England, UK
Phreatoplinian Eruptions

FRASER GOFF
Los Alamos National Laboratory
Los Alamos, New Mexico, USA
Geothermal Systems

TIMOTHY L. GROVE
Massachusetts Institute of Technology
Cambridge, Massachusetts, USA
Origin of Magmas

STEPHEN L. HARRIS
California State University, Sacramento
Sacramento, California, USA
Archaeology and Volcanism

CHRIS J. HAWKESWORTH
Open University
Milton Keynes, England, UK
Composition of Magmas

RICHARD J. HERRINGTON
Natural History Museum
London, England, UK
Mineral Deposits Associated with Volcanism

MANFRED P. HOCHSTEIN
University of Auckland
Auckland, New Zealand
Surface Manifestations of Geothermal Systems with Volcanic Heat Sources

PETER R. HOOPER
Washington State University
Pullman, Washington, USA
Flood Basalt Provinces

BRUCE F. HOUGHTON
Institute of Geological and Nuclear Sciences
Wairakei Research Center, New Zealand
Phreatoplinian Eruptions
Pyroclastic Fall Deposits
Pyroclast Transport and Deposition
Surtseyan and Related Phreatomagmatic Eruptions

CATHY J. JANIK
U.S. Geological Survey
Menlo Park, California, USA
Geothermal Systems

CLAUDE JAUPART
Institut de Physique du Globe
Paris, France
Magma Ascent at Shallow Levels

RAYMOND JEANLOZ
University of California, Berkeley
Berkeley, California, USA
Mantle of the Earth

DAVID JOHNSTON
Institute of Geological and Nuclear Sciences
Wairakei Research Center, New Zealand
Risk Education and Intervention

CHRISTOPHER R. J. KILBURN
University College
London, England, UK
Lava Flows and Flow Fields

PAUL KIMBERLY
U.S. National Museum of Natural History
Smithsonian Institution
Washington, DC, USA
End Paper Map

PETER W. LIPMAN
Volcanic Hazards Team
U.S. Geological Survey
Menlo Park, California, USA
Calderas

CORINNE A. LOCKE
University of Auckland
Auckland, New Zealand
Ground Deformation, Gravity, and Magnetics

ROSALY LOPES-GAUTIER
Jet Propulsion Laboratory
Pasadena, California, USA
Volcanism on Io
Volcanoes and Tourism
Volcanoes in Literature and Film

MARGARET MANGAN
Hawaiian Volcano Observatory
U.S. Geological Survey
Hawaii National Park, USA
Hawaiian and Strombolian Eruptions

PAOLO MARIANELLI
Universita di Pisa
Pisa, Italy
Plinian and Subplinian Eruptions

BRUCE D. MARSH
Johns Hopkins University
Baltimore, Maryland, USA
Magma Chambers

LARRY G. MASTIN
Cascades Volcano Observatory
U.S. Geological Survey
Vancouver, Washington, USA
Vulcanian Eruptions

STEPHEN R. MCNUTT
Alaska Volcano Observatory
University of Alaska
Fairbanks, Alaska, USA
Seismic Monitoring
Synthesis of Volcano Monitoring
Volcanic Materials in Commerce and Industry
Volcanic Seismicity

ROBERTO MELI P.
Instituto de Geofísica UNAM, C University
Mexico City, Mexico
Volcanic Crises Management

THOMAS P. MILLER
Alaska Volcano Observatory
U.S. Geological Survey
Anchorage, Alaska, USA
Volcanic Ash Hazards to Aviation

MICHAEL J. MILLS
University of Colorado
Boulder, Colorado, USA
Volcanic Aerosol and Global Atmospheric Effects

MEGHAN M. MORRISSEY
Colorado School of Mines
Golden, Colorado, USA
Phreatomagmatic Fragmentation
Vulcanian Eruptions

JOHN B. MURRAY
Open University
Milton Keynes, England, UK
Ground Deformation, Gravity, and Magnetics

SETSUYA NAKADA
Earthquake Research Institute
University of Tokyo
Tokyo, Japan
Hazards from Pyroclastic Flows and Surges

ODED NAVON
Hebrew University
Jerusalem, Israel
Magmatic Fragmentation

CHRISTOPHER G. NEWHALL
University of Washington
U.S. Geological Service
Seattle, Washington, USA
Volcano Warnings

PAOLO PAPALE
Universita di Pisa
Pisa, Italy
Magmatic Fragmentation

MICHAEL R. PERFIT
University of Florida
Gainesville, Florida, USA
Plate Tectonics and Volcanism

DONALD W. PETERSON
U.S. Geological Survey
Albuquerque, New Mexico, USA
Lava Flow Hazards

CHIEN-LU PING
University of Alaska, Fairbanks
Fairbanks, Alaska, USA
Volcanic Soils

DAVID M. PYLE
University of Cambridge
Cambridge, England, UK
Pyroclastic Fall Deposits
Sizes of Volcanic Eruptions

ROBERTO QUAAS W.
Instituto de Ingeniería UNAM, C University
Mexico City, Mexico
Volcanic Crises Management

MICHAEL R. RAMPINO
New York University
New York, NY, USA
Volcanism and Biotic Extinctions

KELVIN S. RODOLFO
University of Illinois at Chicago
Chicago, Illinois, USA
Hazard from Lahars and Jökulhlaups

NICHOLAS W. ROGERS
Open University
Milton Keynes, England, UK
Composition of Magmas

KEVIN RONAN
Massey University
Palmerston North, New Zealand
Risk Education and Intervention

MALCOLM J. RUTHERFORD
Brown University
Providence, Rhode Island, USA
Rates of Magma Ascent

HAZEL RYMER
Open University
Milton Keynes, England, UK
Ground Deformation, Gravity, and Magnetics
Hazards of Volcanic Gases
Synthesis of Volcano Monitoring

ROBERTO SANTACROCE
Universita di Pisa
Pisa, Italy
Plinian and Subplinian Eruptions

ALESSANDRO SBRANA
Universita di Pisa
Pisa, Italy
Plinian and Subplinian Eruptions

RALF SCHMIDT
GEOMAR Research Center
Kiel, Germany
Seamounts and Island Building

HANS-ULRICH SCHMINCKE
GEOMAR Research Center
Kiel, Germany
Scoria Cones and Tuff Rings
Seamounts and Island Building

STEPHEN SELF
University of Hawaii at Manoa
Honolulu, Hawaii, USA
Volcanism and Biotic Extinctions

LEE SIEBERT
U.S. National Museum of Natural History
Smithsonian Institution
Washington, DC, USA
Earth's Volcanoes and Eruptions: An Overview

HARALDUR SIGURDSSON
University of Rhode Island
Narragansett, Rhode Island, USA
Introduction
History of Volcanology
Volcanic Episodes and Rates of Volcanism
Volcanoes and Tourism
Volcanoes in Art
Volcanoes in Literature and Film

SHAN DE SILVA
Indiana State University
Terre Haute, Indiana, USA
Composite Volcanoes

TOM SIMKIN
U.S. National Museum of Natural History
Smithsonian Institution
Washington, DC, USA
Earth's Volcanoes and Eruptions: An Overview

JOHN L. SMELLIE
British Antarctic Survey
Cambridge, England, UK
Subglacial Eruptions

RICHARD T. SMITH
University of Waikato
Hamilton, New Zealand
Phreatoplinian Eruptions

FRANK J. SPERA
Institute for Crustal Studies
University of California, Santa Barbara
Santa Barbara, California, USA
Physical Properties of Magmas

PAUL D. SPUDIS
Lunar and Planetary Institute, NASA
Houston, Texas, USA
Volcanism on the Moon

JOHN STIX
McGill University
Montréal, Quebec, Canada
Gas, Plume, and Thermal Monitoring
Synthesis of Volcano Monitoring
Volcanic Gases

BRAD STURTEVANT
California Institute of Technology
Pasadena, California, USA
Magmatic Fragmentation

JANET M. SUMNER
University of Liverpool
Liverpool, England, UK
Lava Fountains and Their Products

SHINJI TAKARADA
Geological Survey of Japan
Sapporo, Japan
Debris Avalanches

IAN THORNTON
La Trobe University
Bundoora, Victoria, Australia
The Ecology of Volcanoes

ROBERT I. TILLING
U.S. Geological Survey
Menlo Park, California, USA
Lava Flow Hazards

TADAHIDE UI
Hokkaido University
Sapporo, Japan
Debris Avalanches

GREG A. VALENTINE
Los Alamos National Laboratory
Los Alamos, New Mexico, USA
Pyroclastic Surges and Blasts

James W. Vallance
McGill University
Montréal, Quebec, Canada
Lahars

Sylvie Vergniolle
Institut de Physique du Globe
Paris, France
Hawaiian and Strombolian Eruptions

Dirk Vespermann
GEOMAR Research Center
Kiel, Germany
Scoria Cones and Tuff Rings

George P. L. Walker
University of Bristol
Gloucester, England, UK
Basaltic Volcanoes and Volcanic Systems

Paul J. Wallace
Texas A&M University
College Station, Texas, USA
Volatiles in Magmas

James D. L. White
University of Otago
Dunedin, New Zealand
Submarine Lavas and Hyaloclastite
Surtseyan and Related Phreatomagmatic Eruptions

Noel C. White
BHP Minerals Exploration
London, England, UK
Mineral Deposits Associated with Volcanism

Glyn Williams-Jones
Open University
Milton Keynes, England, UK
Hazards of Volcanic Gases

Colin J. N. Wilson
Institute of Geological and Nuclear Sciences
Wairakei Research Center, New Zealand
Ignimbrites and Block-and-Ash Flow Deposits
Phreatoplinian Eruptions
Pyroclastic Fall Deposits
Pyroclast Transport and Deposition

Kenneth Wohletz
Los Alamos National Laboratory
Los Alamos, New Mexico, USA
Phreatomagmatic Fragmentation

John A. Wolff
Washington State University
Pullman, Washington, USA
Lava Fountains and Their Products

Mitsuhiro Yoshimoto
Hokkaido University
Sapporo, Japan
Debris Avalanches

Bernd Zimanowski
Universität Würzburg
Würzburg, Germany
Phreatomagmatic Fragmentation

James R. Zimbelman
National Air and Space Museum
Smithsonian Institution
Washington, DC, USA
Volcanism on Mars

FOREWORD

If one could drain the world's oceans and remove their sediment cover, one would quickly realize that the majority of the Earth's surface is covered with lava flows. Although the human race has lived in close contact with volcanic activity since our early origins in the African Rift Valley, only recently have we begun to comprehend how volcanically active our planet really is. Even more recently, exploration of our solar system shows us that volcanism has played and continues to play an important role in the early genesis and subsequent evolution of both the planets and the moons within our solar system and beyond.

Given our growing awareness of the importance of volcanism to the past, present, and future history of Earth and its celestial partners, the publication of the *Encyclopedia of Volcanoes* is clearly needed and appropriate at this time. Thanks to the efforts of Editor-in-Chief Dr. Haraldur Sigurdsson and his highly qualified Associate Editors and contributing authors, the *Encyclopedia of Volcanoes* is drawn from a vast and enlarging data base.

I was first introduced to volcanoes by Dr. Sigurdsson in the early 1970s. At the time, I was preparing for the first manned exploration of the Mid-Ocean Ridge during Project FAMOUS. This was a critical time in the earth sciences when our community sought to better understand this mighty undersea mountain range and the important role its volcanic and tectonic processes played in the then newly evolving concept of plate tectonics and seafloor spreading.

I vividly remember traveling with Haraldur to his native country of Iceland, which sits astride the Ridge. There we scaled one volcano after another, including Surtsey, Eldfell, and Krafla. That introduction to terrestrial volcanism prepared me for the many years I would spend investigating undersea volcanic processes.

Those efforts eventually led to the discovery of hydrothermal vents in 1977 and the exotic life forms that live on the internal energy of the Earth through a process we now know as chemosynthesis. That effort was followed in 1979 with our discovery of high-temperature "black smokers" and a clearer understanding of the chemistry of the world's oceans.

Since that time the study of volcanism has expanded rapidly, branching out to embrace many fields of research. As a result, the study of volcanism is no longer an isolated field of research but one closely linked to other disciplines and areas of research including the chemistry of the world's oceans and atmosphere, the creation of important mineral assemblages, the role volcanism has played in the origin of life as well as its negative impact upon biological evolution, and most recently its impact upon mankind itself.

The *Encyclopedia of Volcanoes* has been an immense undertaking involving the collective efforts of over 100 international experts on the subject, resulting in a 1000-page volume broken down into 82 chapters.

Clearly, this volume is the most comprehensive presentation on this subject, a work important to those in the field as well as to others seeking a broader understanding of this subject.

DR. ROBERT D. BALLARD
PRESIDENT, INSTITUTE FOR EXPLORATION
AND EMERITUS OF THE WOODS HOLE
OCEANOGRAPHIC INSTITUTION

PREFACE

The *Encyclopedia of Volcanoes* is a complete reference guide, providing a comprehensive view of volcanism on the Earth and on the other planets of the Solar System that have exhibited volcanic activity. It is the first attempt to gather in one place such a vast store of knowledge on volcanic phenomena.

The volume addresses all aspects of volcanism, ranging from the generation of magma, its transport and migration, eruption, and formation of volcanic deposits. It also addresses volcanic hazards, their mitigation, the monitoring of volcanic activity, and economic aspects and, for the first time, analyzes several specific cultural aspects of volcanic activity, including the impact of volcanic activity on archaeology, literature, art, and film. To compose a single volume that is a complete reference for such a far-ranging phenomenon is indeed a daunting task.

ARRANGEMENT OF CONTENT

When the editors began to develop the fundamental structure of this Encyclopedia, we were faced with two choices: either constructing a dictionary-like volume composed of defined terms, arranged in alphabetical order, or following a thematic approach, where the multitude of volcanic processes are defined, described, and elaborated in a series of chapters. We have adopted the latter approach in this volume.

To provide our readers with the best possible treatment of volcanic processes, we have adopted the time-honored custom of Denis Diderot and Jean D'Alembert of recruiting the leading experts in each branch of volcanology and related fields to author the chapters that lie outside the expertise of the editors. When Diderot and D'Alembert began to compile information for their monumental 21-volume *Encyclopédie* (1751-1765), they went to the carpenters, the masons, the embroiderers, and the other experts for help with the specific terms and concepts, in order to get all the technical details right. Thus they secured an article for the *Encyclopédie*, penned by the pioneer field volcanologist Nicholas Desmarest (1725-1815), on the volcanic origin of columnar basalt. Similarly, the editors of the *Encyclopedia of Volcanoes* have recruited the recognized authorities in each field or speciality of volcanology to contribute chapters to this volume. Thus this volume is the product of over 100 volcanologists, petrologists, and other scientists who have specialized knowledge about volcanoes and related processes.

SECTIONAL PLAN

In this volume, the principal aspects of volcanic activity are dealt with in 82 chapters, divided between nine major parts. An introduction to each part written by the editors is provided to give a general perspective of the topics and processes contained in that part. Each chapter covers one fundamental volcanic process in depth and stands alone as a comprehensive overview of the phenomenon in question. Nevertheless, the sequence of major parts and their chapters is intended to be directional and evolutionary, as far as possible, following magma from its place of deep origin to the surface of the Earth.

Thus in the first part, the volume commences with 12 chapters on the principal source regions of magmas, the mantle of the Earth, melting processes, magma generation, and transport and geochemical evolution of magmas, as they rise into the Earth's crust. The second part addresses the fundamental aspects of distribution of volcanism in space and time and the range in the scale of volcanic eruptions, in terms of magnitude and intensity. In the three subsequent parts, chapters address the various styles of eruption of magmas, namely, effusive (lavas) versus explosive, and the multitude of types of volcanic deposits that result.

Part V provides comprehensive overviews of volcanic activity on other members of the Solar System, namely, on the Moon, Io, Mars, and Venus and the unusual cryovolcanism on the Galilean satellites of Jupiter. Extraterrestrial volcanology is probably the area of volcanologic research that will experience the greatest growth in the future, as space exploration continues to provide new discoveries in other worlds. In Part VI the interactions of volcanism with hydrosphere and atmosphere are discussed, as well as formation of those mineral deposits that owe their origin to volcanic processes. The impact of volcanoes on society is explored in Part VII, where the various types of volcanic hazards are discussed. Volcano monitoring is treated in Part VIII, along with the mitigating measures that have been developed to counteract volcanic disasters. In the final section of the Encyclopedia, a variety of economic benefits accruing from volcanism are described, and the volume closes with four chapters on the cultural aspects of volcanism and its impact on archaeology, art, literature, and film.

CONVENTIONS OF STYLE

In this volume, we have adopted the convention of using lowercase in the spelling of those adjectives that describe volcanic processes, such as surtseyan and plinian.

As this volume is intended for the general reader, such distracting paraphernalia as references or footnotes have been dispensed with as much as possible. Instead, a section of Further Readings, containing a list of half a dozen or more major texts on the subject matter, is provided at the end of each chapter for those interested in the chief sources.

APPENDIXES

Two appendixes are included in the volume. Appendix 1 consists of a series of tables that give common scientific and mathematical units and conversion factors. It also provides a variety of numerical data on the Earth.

Appendix 2 is a table of active volcanoes on Earth, as compiled by Tom Simkin and Lee Siebert of the Smithsonian Institution. A listing containing all the volcanoes on Earth, with data on their eruptions, is beyond the feasibility of this work, as this list alone would equal this volume in length. The editors have therefore opted to list only historically active volcanoes, i.e., the volcanoes whose eruptions have been witnessed and documented, totaling 550 in number. The oldest eruption in this list is therefore the plinian eruption of Vesuvius in Italy on 24 August in 79 A.D. This selection of the historical period is admittedly somewhat arbitrary, as the "historical period" varies greatly in length from place to place on Earth. In Europe and Japan the historical record of volcanism extends back over one thousand years, whereas in New Zealand and North and South America, for example, it is merely a matter of a few centuries, because written records in these regions begin generally with European settlement.

In Appendix 2 the historically active volcanoes are listed in alphabetical order, and their locations are given in terms of longitude and latitude. The tabulation also includes all of their historic eruptions.

ACKNOWLEDGMENTS

The number of people who have assisted the authors and editors in the creation of this volume is literally in the hundreds. A list of those we especially thank is given in the Acknowledgments section at the end of the volume.

We single out here, however, the following staff members at Academic Press for their outstanding work: the project's sponsoring editor, Frank Cynar, who bears the responsibility for recruiting the editors of this volume; the project manager, Cathleen Ryan; and the production editor, Jacqueline Garrett.

THE EDITORS

GUIDE TO THE ENCYCLOPEDIA

The *Encyclopedia of Volcanoes* is a complete reference guide to this subject, including studies of the origin and transport of magma, of eruptions, and of effusive volcanism and explosive volcanism. Other sections of the work discuss extraterrestrial volcanism, volcano interactions, volcanic hazards, eruption response and mitigation, and economic and cultural aspects of volcanism. Each article in the Encyclopedia provides a scholarly overview of the selected topic to inform a broad spectrum of readers, from researchers to the interested general public.

In order that you, the reader, will derive the maximum benefit from the *Encyclopedia of Volcanoes*, we have provided this Guide. It explains how the book is organized and how information can be located.

ORGANIZATION

The *Encyclopedia of Volcanoes* consists of 82 individual articles arranged in a thematic manner; that is, the placement of a given article is based on its content and not on its alphabetical wording. Articles on related topics are placed together in sequence.

Each article is a full-length treatment of the subject at hand. Thus the Encyclopedia's format will allow its readers to choose their own method for referring to the work. Those who wish specific information on limited topics can consult the A-to-Z Article Index (see p. xi) and then proceed to the desired topic from there. On the other hand, readers who wish to obtain a full overview of a larger subject can read the entire series of articles on this subject from beginning to end; e.g., Eruptions. In fact, one can even read the entire Encyclopedia in sequence, in the manner of a textbook (or a novel), to obtain the ideal view of the complete subject of volcanoes.

ARTICLE FORMAT

Each article in the *Encyclopedia of Volcanoes* begins at the top of a right-hand page, so that it may be quickly located. The author's name and affiliation are displayed at the beginning of the article. The text of the article is organized according to a standard format, as follows:

- Outline
- Glossary
- Defining Statement
- Body of the Article
- Cross-References
- Bibliography

OUTLINE

Each article in the Encyclopedia begins with an outline that indicates the general content of the article. This outline serves two functions. First, it provides a brief preview of the text, so that the reader can get a sense of what is contained there without having to leaf through all the pages. Second, it serves to highlight important subtopics that will be discussed in the article. For example, the article "Volcanic Plumes" begins with the subtopic "Generation of Volcanic Plumes."

The outline is intended as an overview and thus it lists only the major headings of the article. In addition, extensive second-level and third-level headings will be found within the article.

GLOSSARY

The Glossary contains vocabulary terms that are important to an understanding of the article and that may be unfamiliar to the reader. Each term is defined in the context of the particular article in which it is used. Thus the same term may appear as a Glossary entry in two or more articles, with the details of the definition varying slightly from one article to another. The Encyclopedia includes approximately 500 glossary entries.

The following examples are glossary entries that appear with the article "Flood Basalt Provinces."

hotspot An area in the Earth's upper mantle that is hotter than the ambient temperature.

picrite A volcanic rock with a large proportion of the magnesium-rich mineral olivine.

DEFINING STATEMENT

The text of each article in the Encyclopedia begins with a single introductory paragraph that defines the topic under discussion and summarizes the content of the article. It thus serves the purpose of a brief abstract of the article. For example, the article "Pyroclastic Surges and Blasts" begins with the following defining statement:

> The recognition that volcanic explosions could produce density-driven currents that flow rapidly away from the vent, devastating the landscape and leaving thin pyroclastic deposits and ash dunes, was an important step towards our current understanding of volcanic systems. Deposits left by these pyroclastic surges are a key in interpreting the eruptive history of a volcano and in predicting the hazards a volcano might pose for the future.

CROSS-REFERENCES

Articles in the Encyclopedia contain references to other articles. These cross-references appear at the end of the text for the article. They indicate related articles that can be consulted for further information on the same topic, or for information on a related topic. For example, the article "History of Volcanology" has cross-references to "Archaeology and Volcanism," "Earth's Volcanoes and Eruptions: An Overview," "Mantle of the Earth," "Origin of Magmas," "Plate Tectonics and Volcanism," "Volcanoes in Art," and "Volcanoes in Literature and Film."

FURTHER READING

The Further Reading section appears as the last element in each article. This section lists other sources outside the Encyclopedia that will aid the reader in locating more information on the topic at hand.

The entries in this section are for the benefit of the reader, to provide references for further research or browsing on the given topic. Thus they consist of a limited number of entries. They are not intended to represent a complete listing of all the materials consulted by the author or authors in preparing the article. The Further Reading section is in effect an extension of the article itself, and it represents the author's choice as to the best sources available for additional information.

INDEX

The Subject Index for the *Encyclopedia of Volcanoes* contains more than 3800 entries, arranged alphabetically. Reference to the general coverage of a topic appears as a marginal entry, such as an entire section of an article devoted to the topic. References to more specific aspects of the topic then appear below this in an indented list.

ENCYCLOPEDIA WEBSITE

The *Encyclopedia of Volcanoes* maintains its own editorial Website on the Internet at:

http://www.apnet.com/volcano/

This site provides complete information about the contents of the Encyclopedia. For information about other current Academic Press reference works, such as the *Encyclopedia of the Solar System*, go to:

http://www.apnet.com/reference/

INTRODUCTION

HARALDUR SIGURDSSON
University of Rhode Island

I. The Melt of the Earth
II. Volcanism and Plate Tectonics
III. The Midocean Ridge
IV. The Subduction Factory
V. Volcanoes on Hot Spots
VI. Volcanism on Other Worlds
VII. Volcanic Processes
VIII. The Impact of Volcanism

GLOSSARY

convection The process by which the Earth's mantle loses heat, producing currents of solid but deformable rock that rise toward the surface and contribute to plate motion.

eclogite A rock type common in the Earth's mantle, with the same chemical composition as basalt, but with a mineral assemblage that is stable at high pressure.

intensity The rate of flow of magma out of a volcano during eruption, expressed as mass eruption rate (MER) in kilograms per second (kg/s).

magnitude The size of a volcanic eruption, expressed as the volume of material erupted, usually in cubic kilometers (km^3).

peridotite The principal rock that forms the Earth's upper mantle, consisting mainly of the mineral olivine, with lesser amounts of pyroxene, garnet, and/or spinel. It is the source of basaltic magmas, which are formed from peridotite by partial melting.

photodissociation Chemical reactions that occur in the atmosphere, due to ultraviolet radiation.

proterozoic eon The period in Earth's history that began 2.5 billion years ago and ended 0.57 billion years ago.

pyroclasts Fragmentary material ejected during a volcanic eruption, including pumice, ash, and rock fragments.

radionuclides Chemical elements that undergo spontaneous and time-dependent decay, resulting in the formation of other elements and the release of radioactive energy in the form of heat.

stromatolites The earliest calcium carbonate-secreting organisms on Earth, first appearing during the Proterozoic. Their activity contributed to drawing down carbon dioxide from the atmosphere and fixing it in limestone and other sedimentary rocks, contributing to changing atmospheric chemistry and climate.

subduction The process of sinking of crustal plates into the Earth's mantle. Subduction causes magma generation and results in buildup of island arcs above subduction zones.

volatiles Those chemical compounds or elements contained in magmas that are generally released as gases to the atmosphere during a volcanic eruption. They include water, carbon dioxide, and sulfur dioxide. They are generally dissolved in the magma prior to eruption or when the magma is under high pressure, but exsolve during ascent of the magma to the surface.

Copyright © 2000 by Academic Press
All rights of reproduction in any form reserved.

volcanic aerosol Tiny particles of sulfuric acid droplets, formed by reactions between volcanic sulfur dioxide gas and water vapor in the stratosphere. The resulting aerosol dust veil has important effects on backscattering and absorption of solar radiation and leads to a net surface cooling on the Earth, with possible climate change.

I. THE MELT OF THE EARTH

Volcanic eruptions are the most awesome and powerful display of nature's force. The idea that terra firma may explode under our feet and bombard us with glowing hot ejecta seems almost incomprehensible. Every year about 50 volcanoes throughout the world are active above sea level, threatening the lives and property of millions of people. A single eruption can claim thousands of lives in an instant. For example, in the 1902 eruption of Mont Pelée on the Caribbean island of Martinique, a flow of hot ash and gases overwhelmed the city of St. Pierre, killing all but one of its 28,000 inhabitants. More recently, a mudflow triggered by the 1985 eruption of the volcano Nevado del Ruiz in Colombia killed nearly all of the 25,000 inhabitants of the town of Armero.

The relationship between people and volcanoes is as old as the human race. Our earliest ancestors evolved in the volcanic region of the East African Rift, where their activities and remains are preserved by volcanic deposits, such as the stunning 3.7-million-year-old *Australopithecus* hominid footprints crisscrossing a volcanic ash deposit at Laetoli. In fact, the wealth of information we now have on early hominid evolution has only been made possible because of the rapid burial and excellent preservation of their remains in volcanic deposits. Is it a mere sport of nature that humans evolved in a volcanic region, or was this African volcanic environment especially favorable to human evolution? Was it the abundant game and fertility of the volcanic plains, with their rich soils? We shall probably never know the answer, but humans quickly learned to make use of volcanic rocks in toolmaking and captured fire from volcanoes, to open up the realms of the dark and the cold for further expansion of the race.

When humans first sought explanations for volcanic phenomena, they linked these violent processes to mythology and religion. But with the rise of Western philosophy and learning, Greek scholars in the third century before Christ began the search for the actual physical causes of volcanism, as outlined in Chapter 2. The Greeks speculated that eruptions were the result of the escape of highly compressed air and gases inside the Earth, but later the Romans proposed that volcanoes were natural furnaces in which combustion of sulfur, bitumen, and coal took place. This search for the actual causes of volcanism on Earth and other planets has continued to our day, but we now have many of the answers.

Volcanology is the study of the origin and ascent of magma through the planet's mantle and crust and its eruption at the surface. Volcanology deals with the physical and chemical evolution of magmas, their transport and eruption, and the formation of volcanic deposits at the planetary surface. Some volcanic processes constitute a major natural hazard, whereas others are highly beneficial to society. Thus, the study of volcanism has far-ranging significance for society. For most people, volcanology conjures up a picture of an erupting volcano. Volcanoes and their eruptions, however, are merely the surface manifestation of the magmatic processes operating at depth in the Earth, and thus the study of the volcanism is inevitably highly interdisciplinary, most closely linked to geophysics, petrology, and geochemistry.

In this volume, we examine volcanology in the widest sense, covering not only the traditional aspects of the generation of magmas (traditionally the domain of petrology and geochemistry) and their transport and eruption (the field of traditional volcanology), but also the multitude of effects that volcanism has on the environment and on our society and culture. Volcanism is the best way to probe the interior of Earth. Adopting an anthropomorphic view, we could regard magma as the sweat of the Earth, resulting from the labors of moving the great crustal plates around on the planet's surface and maintaining the Earth's mantle well stirred. The analogy is not that far fetched, because magma and volcanism in general are also a means of heat loss for the Earth. For the Earth scientist, these fluids emerging from the Earth carry valuable clues about the internal constitution of our planet. Just as the medical doctor analyzes the various fluids of the human body, the geochemist samples and analyzes the magmatic liquids that issue from Earth's volcanoes.

For the human race, the Earth is a blessed planet, because of its position in the solar system and because of its physical dimensions and vigorous dynamic internal processes, among which volcanism plays a fundamental role. Our Earth is just sufficiently far away from the Sun to benefit from its heat, but not so close as to lose its crucial oceans by rapid evaporation or its precious water by photodissociation at the top of the atmosphere and subsequent escape to space. The Earth is cool enough that liquid water stays on its surface—but not so cool that all water freezes. Earth's gravity is sufficiently high to exceed the escape velocity of water and carbon dioxide molecules, allowing it to retain a unique atmospheric composition, with enough carbon dioxide to create a comfortable greenhouse and to provide the building blocks for life, as well as to shield us against harmful solar ultraviolet radiation. Earth's internal heat reservoir is not so hot that it makes life unbearable because of continuous volcanic eruptions, but is sufficient to drive mantle convection and plate tectonics. The volcanism resulting from plate tectonics continuously recycles volatile elements such as water, carbon dioxide, and sulfur between the inner Earth and its surface reservoirs: the oceans and atmosphere. It is a very ancient cycle. In the distant history of the primitive Earth, the original atmosphere and oceans probably resulted from the early degassing of the interior of the globe, largely through volcanic activity.

Volcanism is flux of energy and matter. It is an expression of the storehouse of Earth's inner energy, derived in part from cooling of an originally hot planet and in part from heat resulting from the radioactive decay of naturally occurring uranium, potassium, thorium, and other radionuclides present deep in the Earth. Thus, volcanic eruptions are the surface expression of these deep Earth processes. When viewed on a geologic timescale, the motions of the inner Earth are veritable storms raging within the planet, with thunderheads rising up through the mantle to form plumes that break the surface as great volcanic hot spots. Other internal storms also lead to convective rollover of the mantle, pulling and pushing along the great crustal plates at the surface, resulting in volcanic activity where plates converge or are pulled apart. When we compare Earth to the other planets in the solar system, we may wonder why our home planet is so prone to volcanic eruptions. The logical question is, however, why does the Earth have such vigorous plate tectonics, the driving force of volcanism?

II. VOLCANISM AND PLATE TECTONICS

Earth may be unique among the planets in the solar system in that its outer rigid skin—the crust and lithosphere—is continuously being destroyed and regenerated. It has active plate tectonics, where the heat and smoke of volcanism rise from the two main battlefields between the plates: the rifts or ocean ridges and the subduction zones. The most important consequence of plate tectonics, discussed in Chapter 6, is geologic recycling of materials, turning the Earth into an immense chemical factory where volcanism plays a crucial role. As great crustal plates are pulled apart in the ocean basins, the solid but mobile Earth's mantle below the rift responds to the decrease in overburden and rises upward to fill in the rift. When the rising peridotite mantle experiences a decrease in pressure, it spontaneously undergoes melting, without addition of heat. The reader who does not have a background in petrology or volcanology should pause at this point and ponder the last sentence, for here lies the key to an understanding of the vast majority of volcanic processes: decompression melting, as described further in Chapter 4. It may be difficult at first to comprehend that rock may melt, without addition of heat, simply because the pressure acting on it decreases, but this is the most common melting process in the Earth. The idea that melting could occur simply as a result of the decrease of pressure (decompression melting) dates back to the beginning of the 19th century, but it was not generally accepted by geologists until the latter part of the 20th century. Early volcanologists knew that the Earth's interior was hot but solid, and from the basic principles of thermodynamics that were developed in the 1830s, they could theorize that melting would occur if pressure decreased, that is, if the mantle rock were brought upward to a region of shallower depth in the Earth. It was only with the advent of the theory of plate tectonics that a mechanism for vertical motion leading to decompression was discovered.

The interstitial melt that forms during decompression, behaving rather like the water that seeps between the sand grains on the beach, forms no more than a few percent of the rising mantle during melting. But the new basaltic magma is less dense and rises faster than the mantle. It collects into pockets that form magma reservoirs, eventually pushing its way upward into the rift in the midocean ridge, to erupt as lava from fissures on the ocean floor. Thus, volcanism is continuously adding new mantle-derived volcanic crust to the plate margins, temporarily welding together the rifted plates, until they break again in another eruption (Fig. 1).

But why are the plates moving apart? Are they being pushed or are they sliding "downhill" because of the elevated position of the midocean ridge? Are they being dragged along by the convection of the underlying mantle? Or are they pulled along by the subduction of the old, cold, and therefore dense leading edge of the plate into the mantle? To comprehend the fundamental underlying causes of volcanism in island arcs and midocean ridges, we need to answer this important question. Empirical evidence shows that the plates today are moving primarily because of the force we call *slab pull.* The plates that are moving fastest are all attached to long and very active subduction zones. Once the cold leading edge of the plate enters the mantle, its fate is sealed: It will subduct. Solid-state phase transitions occur in the minerals making up the plate, converting low-pressure minerals into a much more dense high-pressure assemblage, thus increasing the bulk density of the plate to a point where it exceeds the density of the upper mantle and spontaneously sinks, dragging along with it the attached plate at the surface.

How was this cycle of plate tectonics started, or has it always operated on Earth? We do not yet know the answer, but its operation goes back at least to the Proterozoic eon (0.57–2.5 billion years ago). One fascinating idea is that subduction was literally initiated by biological processes on Earth. When the stromatolites, the first calcium carbonate-secreting organisms, began to flourish in the Earth's oceans, they mined the abundant CO_2 from the planet's atmosphere and fixed it into dense rock: limestone. In the process, they and other carbonate-fixing organisms gave off the oxygen that created for us an atmosphere that is fit to breathe. When the great masses of dense limestone rock first accumulated around the continental margins late in the Proterozoic, they may have downwarped the underlying oceanic crust to such an extent that the high pressure resulted in conversion of low-pressure basaltic crust to its high-pressure form of eclogite. With a density greater than that of the upper mantle, the eclogite crust would sink into the mantle and pull along with it the attached crustal plate, initiating subduction and setting in motion the first plate tectonic cycle (Fig. 2).

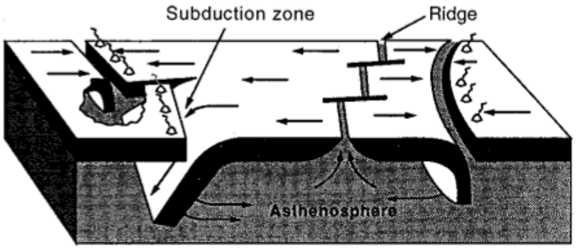

FIGURE 1 Most of Earth's volcanism occurs at the junctions of the dozen or so plates that make up the exterior shell of the Earth. Midocean ridge volcanism occurs at the boundaries where plates are pulling apart. Arc volcanism occurs where plates are converging, above the subduction zones. Below the plates resides the asthenosphere, the part of the Earth's mantle from which most magmas originate. (After Allegre, 1992.)

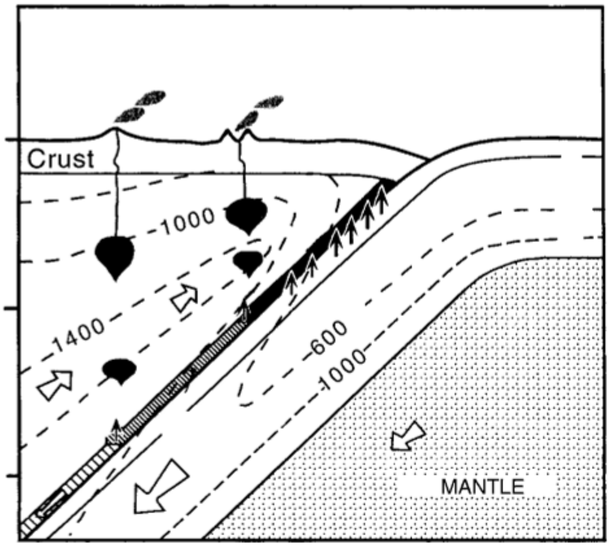

FIGURE 2 Arc volcanism above a subduction zone. The descent of the cold subducting plate causes upwelling of hotter mantle below the volcanic arc. Furthermore, volatile components, such as water, are released from the subducting plate to the overlying mantle wedge, promoting melting of the mantle and formation of magmas that feed the arc volcanoes above. The dashed lines are isotherms of temperature distribution in the mantle and subducting plate (in degrees centigrade).

III. THE MIDOCEAN RIDGE

A remarkable discovery made only 35 years ago was that the vast majority of volcanism on Earth—perhaps more than 80%—occurs at depths beneath the ocean waves. Although we had an inkling of the importance of the global midocean ridge system, its importance was only revealed in the 1960s with the exploration of the ocean floor and establishment of a global seismic network. We cannot generally witness this type of volcanic activity on the ocean floor, but in certain regions, such as Iceland, the midocean ridge literally grows out of the ocean or is exposed on land. In November 1963, as I tossed about in the frigid and turbulent waters south of Iceland, I had the privilege of witnessing the result of the rifting of the Mid-Atlantic Ridge and the growth of the volcanic island of Surtsey.

Normally, the basaltic eruptions on the ridge are effusive and create pillow lava flows on the ocean floor. At these depths in the ocean the pressure is so high that seawater does not boil explosively even in contact with the red-hot lava. On the other hand, when the underwater volcano grows and reaches shallow levels, the style of activity changes dramatically, as we observed when Surtsey emerged. Violent explosions sent showers of black ash, lapilli, and muddy steam over our boat, as the hot magma flashed the seawater to superheated steam in shallow water. The steam explosions literally tore apart the molten lava and generated a type of eruption that we now know as *surtseyan*.

Hydrothermal activity is an important consequence of volcanic activity at the midocean ridge, and this process has made its imprint on the chemical composition of the oceans. The injectin of magma into the fractured volcanic crust at the midocean ridge sets in motion a vigorous hydrothermal system. In a way, this system is rather like the radiator on the front of the great magma engine. It circulates cold seawater from the ocean down through the fractured crust, where it encounters hot volcanic or intrusive rocks at depth, in proximity to young dikes or even close to the magma reservoir. Here the water is heated. It exchanges chemicals with the rocks, leaving some chemicals from seawater behind and picking up others from the rock that is hydrothermally altered in the process. The heated seawater transports metal-rich solutions toward the surface.

Volcanism on the midocean ridge has a profound impact on the chemistry of the oceans. The hydrothermal circulation process is so forceful at the midocean ridges that the entire mass of the world's ocean is recycled through the hot volcanic crust at a rate of about 1.5×10^{14} kg/year. This rate is sufficient to cycle the entire ocean through the midocean ridge about once in 5 million years. This huge flux of seawater through the oceanic crust has greatly influenced the chemical composition of the oceans through time, resulting in addition and removal of certain chemicals from seawater. This process leads, for example, to the addition of calcium, potassium, and lithium to seawater, from magmas and rocks at the ocean ridges, and the removal of, for example, magnesium from seawater into the oceanic crust. The discovery of midocean ridge hydrothermal activity has explained several puzzles regarding the "sources" and "sinks" of several chemical components in the ocean geochemical cycle. Thus, the midocean ridges are major sinks for magnesium and sulfate and an important source of calcium and manganese.

Hydrothermal fluids also transport metals in solution toward the surface. Upon emerging onto the ocean floor, the solutions cool and precipitate metals, leading to the formation of iron-manganese-rich sediments at the midocean ridge. Locally, the hydrothermal solutions emerge through vents on the ocean floor at very high temperature (350°C). These solutions carry high concentrations of metals and precipitate sulfides, sulfates, and oxides around the vent, to form chimneys up to 10 m high that belch out hot solutions. The solutions precipitate various minerals as they emerge into the ocean, forming black smokers. These solutions are very rich in silica, hydrogen sulfide, manganese, carbon dioxide, hydrogen, and methane, as well as potassium, calcium, lithium, rubidium, and barium. Minerals precipitated on the ocean floor by this process include pyrite (FeS_2), chalcopyrite ($CuFeS_2$), and sphalerite (ZnS). The high concentrations of hydrogen sulfide in these vents support a unique biological assemblage, including sulfide-oxidizing bacteria, which form the basis of a food chain.

IV. The Subduction Factory

The vast majority of land or island volcanoes on Earth are in volcanic arcs above subduction zones. Although they represent only about 10–20% of the volcanism on Earth, the arc volcanoes are most important in terms of their impact on our society. Because they are subaerial and vent directly into the atmosphere, their eruptions can affect our atmosphere. Furthermore, the regions around arc volcanoes are often densely populated and thus may be regions of high risk.

Whatever mechanism may have initiated it, subduction is a dominant component in the great geologic machine that processes and recycles the Earth's oceanic crust and upper mantle. Although the 100-km-thick subducting plate is composed primarily of oceanic crust and upper mantle rocks, it also contains a sliver of sediment at its upper surface and water, carbon dioxide, and other volatile elements bound in clays and other hydrous minerals. In this fashion, the volatile elements are returned to the Earth's mantle from whence they came originally, when they were emitted as volcanic gases in eruptions during the degassing of the early Earth.

Water may also facilitate plate motion, lower mantle strength and viscosity, and play a crucial role in lubricating the subduction zone, because the presence of water in the subduction zone environment promotes the formation of structurally weak hydrous silicate minerals that results in rocks of low strength (Fig. 3). Similarly, water, even in trace amounts, promotes partial melting by lowering the beginning of melting of mantle rocks.

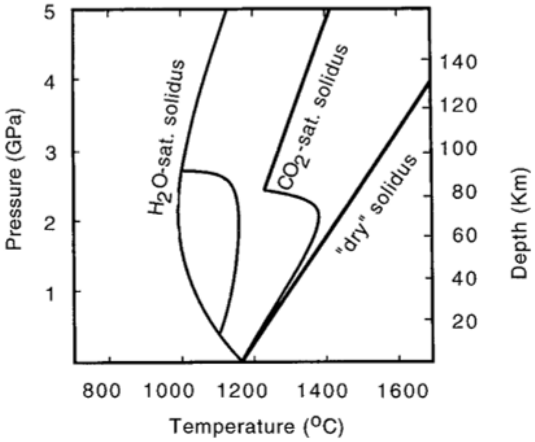

FIGURE 3 The solidus defines the location of the beginning of melting in the Earth's mantle. The figure shows the effects of pressure and volatiles (water and carbon dioxide) on the configuration of the solidus of peridotite, the dominant rock type in the upper mantle. Right-hand vertical scale is depth below the surface; left-hand scale is in units of pressure (GPa). The four solidi shown are the "dry" solidus (neither H_2O nor CO_2 present), the CO_2-saturated solidus, the H_2O-saturated solidus, and (intermediate and unlabeled) the H_2O-undersaturated solidus (water is present, but only in sufficient amount to form hydrous minerals). The presence of either H_2O or CO_2 has a dramatic effect of lowering the beginning of melting of the mantle. Under most Earth conditions, melting is likely to begin in the depth range of several tens of kilometers.

When this occurs in the upper mantle at the base of the lithosphere (the low-velocity layer), plate motion is facilitated. Further, subducted water decreases mantle density in the wedge below the volcanic arc, promoting melting and buoyant upwelling of partially molten mantle material and thus promoting volcanism at the surface.

The presence of water in the magma further sets the chemical evolution of the magma on an entirely different course from "dry" magmas, leading to the silica enrichment typical of magmas in volcanic arcs above subduction zones, as discussed in Chapters 7 and 8. Without the subduction of water, the majority of volcanism on Earth would be submarine, of the type we observe on the midocean ridge: eruption of basaltic magmas of relatively narrow compositional range, releasing dominantly carbon dioxide and sulfur dioxide gases to the ocean, but without emission to the atmosphere. In this subduction-free world, only a small fraction of volcanism would release volcanic gases directly to the atmosphere, that is, the hot spot volcanism of the type we see in Iceland and Hawaii today.

One of the interesting paradoxes of the Earth is that subduction occurs because the leading edge of the plate is cold and dense enough to sink, yet in this apparently frigid environment, volcanism is a characteristic feature. How is it that magma generation occurs in the subduction zone, in response to the descent of the cold plate? The explanation for this paradox is twofold. On one hand, the water introduced into the mantle wedge above the subduction zone lowers the melting point of mantle rock (peridotite), facilitating magma generation and volcanism at the surface (Fig. 3). In addition, the descent of the plate stirs up the mantle, bringing upward a current of warmer mantle material from the depth, again facilitating melting by decompression and resulting in magma generation.

It has been suggested that the island arcs above subduction zones are the "kitchen" where continental crust is made. The process of magmatic differentiation or geochemical evolution of magmas beneath the volcanic arcs results in the formation of relatively high-silica andesitic or rhyolitic magmas that solidify as low-density rocks, as described in Chapter 8. In the "kitchen," the high-silica magmas may be regarded as the cream that evolves from the primary basaltic magma and rises to the top. The high-silica rocks are too light to subduct, and they accumulate in the arc environment, typically at continental margins. The process by which arc volcanics and associated intrusive rocks accumulate is referred to as *continental accretion* and may be the principal mechanism for continental growth. In this manner, the subduction zone acts as a giant still, melting the mantle and separating the continent-forming material out of the melts, adding it to the continents and leaving behind a depleted upper mantle. Thus, the great subduction zone still treats chemical elements in two ways. Some are continuously recycled, namely, the volatile components, such as water and carbon dioxide, whereas others are largely retained in the arc crust.

To what extent is the water, which drives explosive volcanism in arcs, derived from the subduction of the oceans? If the recycling is working, then we should find geochemical evidence of subducted material in the magmas erupted from island arc volcanoes. One of the spectacular success stories of geochemistry is its role in providing proof of the recycling of certain trace chemical components. The discovery came with the detection of the isotope Be^{10} in arc volcanics. This relatively short-lived isotope (half-life about 1.5 million years) is derived solely from reactions in the atmosphere, and it accumulates in marine sediments that may be subducted. The fact that Be^{10} is present in some arc magmas in measurable amounts is proof that relatively young oceanic sediments or fluids must have been subducted and become incorporated in the magma sources underneath the volcanic arcs. Although it is likely that oceanic sediments and related fluids contribute only 1–2% of the magma (the rest is mantle contribution), their chemical imprint is clear and the consequences are evident in the explosive character of these water-rich magmas.

V. VOLCANOES ON HOT SPOTS

The plate tectonic revolution of the 1960s did not explain the origin of a number of the better known volcanoes on Earth, particularly the volcanic islands like Hawaii, the Galapagos, and Iceland. In many cases they show no direct relation to plate boundaries and thus do not fit into the paradigm of plate tectonics. They are volcanic, however, and have a high eruption rate, which has earned them the name *hot spots*. Perhaps the most insidious hot spot is the Yellowstone volcanic field in the United States, a hot spot located in the center of a continental plate. Its prehistoric giant explosive eruptions include some of the largest known on Earth, but because of the long dormant periods, it is a potential continent-wide or even global volcanic threat that we often overlook.

Unusual geochemical signatures in the basaltic hot spot lavas, described in Chapters 7 and 8, suggest a magma source deeper in the mantle than the midocean ridge source or a source that has not been tapped before by earlier magma extraction. This has led to the idea that hot spot volcanoes are supplied by deep mantle plumes, focused mushroom-like currents of solid but hot rock, rising from either the lower mantle or even from the boundary layer between the mantle and the core of the Earth. This is a radical idea, but if correct, it could mean that volcanoes such as Kilauea in Hawaii bring a signature to the surface from rocks that originally were near the core of the Earth, some 2900 km below the volcanoes.

An alternative model for the origin of hot spot magmas brings us back to subduction. It is likely that great masses of ancient subducted masses of lithosphere reside within the deep mantle. Here the subducted slab of cold lithosphere eventually warms up and its density becomes equal to or even less dense than the surrounding mantle, causing its rise toward the surface as a plume of rock. Nearing the surface, the hot material undergoes decompression melting and magma generation. Again, geochemical evidence from volcanics in some hot spots supports the idea that subducted slabs may be the fuel for mantle plumes and at least some hot spot magmas.

VI. VOLCANISM ON OTHER WORLDS

Those who expected that volcanism on other planets of the solar system would be similar to that on Earth were in for a series of big surprises when exploration of the planets began in earnest. Early ideas on extraterrestrial volcanism were largely directed toward the Moon, where craters were seen to be abundant. In 1665 Robert Hooke first proposed the presence of volcanoes on the Moon, but he had observed the lunar craters telescopically. In the 18th century, Pierre Laplace proposed that meteorites were volcanic material ejected from the Moon. Volcanism on the Moon did not seem such a bad idea at the time, considering its cratered and pockmarked visage. In 1785, however, Immanuel Kant pointed out that most lunar craters were much larger than any volcanic features known on Earth, and Kant proved to be correct in his assessment that the lunar craters are not of volcanic origin; we now know that most are the products of meteorite bombardment. Exploration of the lunar surface during the Apollo program revealed vast areas or "oceans" of volcanic rocks, known as Maria, but they turned out to be extremely old, mostly on the order of 3.7 billion years (Chapter 45).

One of the major surprises—and a disappointment to volcanologists—has been that most of the planets are volcanically "dead." That disappointment was, however, compensated by the discovery of spectacular volcanism on Io, where sulfur-rich magma fountains are ejected to heights of hundreds of kilometers (Chapter 46). But Io has more surprises. Its volcanism is most likely not the result of internal thermal energy, as on Earth, but rather due to the tidal energy transferred from the gravitational pull of the giant parent planet Jupiter, causing the interior of Io to heat up. We will no doubt have many similar volcanic surprises awaiting us when we explore other strange worlds in the future.

VII. VOLCANIC PROCESSES

A bewildering variety of volcanic processes occur at the surface during an eruption, and the list of the volcanic rock types and types of volcanic deposits is seemingly endless. Fortunately, as volcanology has progressed in the latter half of the 20th century from a descriptive endeavor to a truly interdisciplinary science, we have discovered the major factors that control eruption processes and account for the diversity of the products, as described in parts II, III, and IV of this volume. Although each eruption is unique, and each volcano seems to have its distinct "personality," several fundamental parameters dictate the style of eruption (Table I).

By far the most important parameter is the mass eruption rate (eruption intensity), which depends on the rate of supply of magma during eruption. The observed range in mass eruption rates on Earth is huge, more than at least three orders of magnitude, and extending beyond 10^9 kg/s. It is beyond our comprehension to visualize 1 million tons of red-hot molten rock jetting out of the crater of a volcano every second—not for a few seconds, but for hours or days, such as occurs during large ignimbrite-forming eruptions. We are accustomed to referring to such events as "explosions," but that is somewhat of a misnomer, because they are not instantaneous bursts, but rather sustained emissions of magma and gases; only the onset is really explosive. The mass eruption rate is truly a measure of eruption intensity, because it controls the height of the eruption column in explosive events and the length of lava flows in effusive eruptions.

As shown in Fig. 4, eruption intensity shows a good correlation with the total mass or volume of magma erupted (magnitude). Although we may intuitively expect that the largest magma bodies within the Earth result in the highest magnitude (largest volume) eruptions, but why they should also be the highest intensity events is not immediately obvious. The flow rate is, of course, a function of the magma pressure and the diameter of the conduit. The explanation may lie in the time it takes for the volcano to widen its conduit by erosion during eruption and allow more magma to pass to the surface. In most major explosive eruptions, the intensity increases with time during the event, and it is most logical to assume that this is simply due to gradual widening of the conduit as it is eroded by the passage of hot magma and the explosive blast of rock, ash, and pumice fragments.

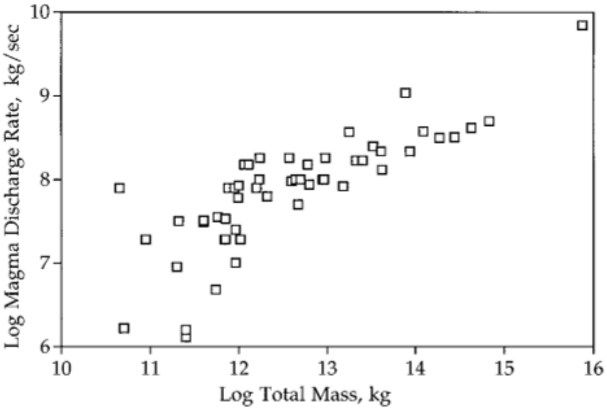

FIGURE 4 The figure shows the range in volcanic intensity and magnitude for a number or eruptions on Earth, shown as log units. The magma discharge rate (intensity) during a volcanic eruption can range from 10^6 to 10^{10} kg/s in the most violent events. The total erupted mass (magnitude) can range to more than 10^{15} kg, equivalent to a magma volume of several thousand cubic kilometers.

During an explosive eruption, as mass eruption rate increases, so does the height of the eruption column, attaining more than 40 km in the Earth's atmosphere for the largest eruptions. Although this correlation is in part related to increase in the height of the jet of magma and pyroclasts emerging from the vent, it is really more influenced by the thermal energy from the eruption,

TABLE I Some Factors That Influence Volcanic Processes

Factor	*Typical range*	*Comments*
Magma temperature	800–1250°C	Influences magma viscosity and affects energy available for eruption plume rise.
Magmatic water	0.1–6 wt% H_2O	Controls magma fragmentation through the vesiculation process.
Magma viscosity	10^2–10^{10} poise	Determines flow properties of magmas, vesiculation, bubble growth; controls the rise and escape of bubbles out of magmas.
Mass eruption rate	10^6–$>10^9$ kg/s	The rate of flow of magma out of the vent is single most important factor.
External water	0.01–0.5 vol. fract.	The fraction of external water that mixes with magma in the conduit or vent.
Crystal content	0–50%	Affects bulk viscosity and thus rheology of magma.

available to drive a convective plume. In fact, most of the eruption column above a volcano is a thermal plume, where heat is transferred from the hot pyroclasts to the surrounding air, which in turn convects vigorously, mixes with the ash and other pyroclasts, and drives the plume sky-high.

Paradoxically, however, when the mass eruption rate reaches a critical value, the eruption column ceases to rise; in fact, the column begins to collapse. The process of column collapse generates the most destructive phase of volcanic eruptions and produces pyroclastic flows and surges: hot ground-hugging cloudlike density currents of ash, pumice, volcanic gases, and heated entrained air.

It seems at first paradoxical that the column should collapse with increasing mass eruption rate, but the explanation lies in the efficiency of mixing of air with the mixture of pyroclasts erupting from the vent. Under conditions of moderate mass eruption rate, the erupting mixture entrains and mixes with a large volume of air, which is heated, becomes buoyant, and contributes to the rapid rise of the eruption column. As the mass eruption rate increases, however, pyroclasts in the interior of the column become isolated from the atmosphere and have less opportunity to mix with air. Consequently, the entraining of air is no longer contributing to the bouyancy of the column; it becomes denser and collapses as a fountain of hot ash, gases, and pumice, to generate a density current.

The second factor that influences volcanic processes, listed in Table I, is the concentration of magmatic water. Water is almost absent in the basaltic magmas erupted on the midocean ridge, but occurs in concentrations of up to 6% in the high-silica magmas of island arcs (Chapter 9). The role of water is twofold, both as the agent that causes vesiculation and fragmentation of magmas and as an important component in accelerating the magma and pyroclasts out of the vent. It is the presence or amount of water in the magma that primarily determines the division between effusive and explosive eruptions, but only a little water goes a long way. With a few percent of water dissolved under high pressure at depth, the magma begins to grow steam bubbles as it rises to the surface. The solubility of water decreases rapidly with decreasing pressure, and the volume fraction of the exsolving steam grows fast. If the bubbles are unable to rise and escape from the magmatic liquid, they will continue to expand until they burst and tear apart the magma into pyroclasts of ash and pumice. As the exsolution and volume expansion of water occur in the conduit of the volcano, this will result in a great volume increase of the erupting magma mixture, propelling it out of the vent.

Magma viscosity is another important factor affecting flow properties of magmas and determining the ability of steam bubbles to rise and escape out of the magma. Viscosity is influenced by temperature, magma composition, and crystal content. In high-temperature and low-silica basaltic magmas, the viscosity is so low that gas bubbles can generally rise in the magma, whereas in high-silica low-temperature magmas, the high viscosity inhibits bubble rise; they move passively with the magma in the conduit, up toward the vent (Chapter 14).

All of the factors just mentioned are internal to magma or the volcanic system, but a number of external parameters can also influence the volcanic process. The most important of these factors is external water. Magmas rising through the crust and to the Earth's surface have a high probability of encountering water, either in the form of oceans, lakes, glaciers, or as water-rich rock formations. We saw earlier, in connection with the 1963 Surtsey eruption, that the interaction of external water and magma is relatively passive when it occurs in regions of high hydrostatic pressure, such as in the deep ocean, but violent explosions will, on the other hand, occur in shallow water. Similarly, magma rising through highly porous and water-logged rocks at shallow levels in the crust can result in explosive eruption because of the conversion of water to steam in contact with the magma. Thus even "dry" basaltic magmas, virtually devoid of magmatic water, can erupt with explosive violence if external water is at hand.

VIII. The Impact of Volcanism

As emphasized earlier, volcanism is the surface manifestation of deep Earth processes, and eruptions are merely the smoke rising from the "subduction factory" or the midocean ridge "kitchen." In the greater scheme of things, volcanic activity is thus a part of a geodynamic system that is essential for maintaining a balanced environment for life on Earth. On a local scale, however, both hazards and benefits are associated with volcanoes, as discussed in Chapters 56 to 67 and 76 to 82, respectively.

Despite their awe-inspiring, spectacular, and even deadly fireworks, volcanic eruptions have not been nature's most deadly hazard in living memory. The principal volcanic disasters since 1700 have taken a total of 260,000 lives, which pales in comparison with the death toll from earthquakes and tropical storms. The deadliest disaster known was probably the 1556 Huahsien earthquake in China, which killed more than 820,000 people. In 1976 the magnitude 7.8 Tangshan earthquake, also in China, killed more than 240,000 people. The worst hurricane in history occurred in 1970 in the Ganges Delta in Bangladesh, with a loss of 500,000 lives. Yet living with a dormant or active volcano, looming large above village or town, is a visible and permanent threat and qualitatively different from the transient threat of a hurricane or a sudden earthquake.

When we view volcanic hazards, however, we must take the long view and keep in mind that the historical period is too short to display the full range of the magnitude and intensity of volcanic eruptions that the Earth can muster. Even in the 6000-year life span of our civilization, we have been spared a mega-eruption of the type that can occur. We are all familiar with the concept of the storm of the century—an event so large that it occurs only very rarely—but the probability of its recurrence increase with time. Similarly, high-magnitude and high-intensity volcanic eruptions are low-probability events, but they will recur in the future. In our limited human experience, we have the eruption of the type that occurs once in 100 years, such as Krakatau in 1883, or the eruption that occurs once in 1000 years, which must be regarded as the Tambora eruption of 1815. What about the 10,000 or 100,000 or every million years eruption? The Toba eruption on Sumatra, about 75,000 years ago, is probably at the upper limit of eruptions that can occur on the Earth, emitting 2000 km^3 of magma. That there is an upper limit on the magnitude of eruptions is itself an interesting concept, but most likely any larger magma chamber cannot be contained in the Earth's crust and will spontaneously erupt. Because the Toba event occurred in the far distant past, our information of its environmental impact is still blurred, but a cataclysmic event of this type would have a catastrophic impact on global society today, as discussed in Chapter 67. When we take the geologic perspective of time and volcanism, we are therefore reminded of the the chilling words of the American historian Will Durant: "Civilization exists by geologic consent, subject to change without notice." The Tambora eruption on the island of Sumbawa in Indonesia in 1815 gives an inkling of what may happen in such a volcanic event.

The regional impact of the 1815 Tambora eruption in the East Indies has been dimmed by the passage of time, and only incomplete counts exist, but they indicate a natural disaster of enormous gravity for the Indonesian people. The disaster struck both on the island of Sumbawa, where Tambora is located, and on the neighboring islands of Lombok, Flores, South Sulawesi, and Bali. Even Java was not spared. During the climax of the explosive eruption on April 10, 1815, hot pyroclastic flows swept down all flanks of the volcano and wiped out the feudal kingdoms of Tambora on the north side and Sanggar on the east side of the mountain. In the Kingdom of Tambora, the loss of life was so complete that it extinguished the Tambora language, probably the easternmost Austro-Asiatic language at the time, with more than 10,000 people killed outright in the pyroclastic flows. The blanket of ash fallout on Sumbawa also destroyed all the crops, resulting in a famine immediately after the eruption. It was accompanied by a variety of diseases, and clean water was not to be had anywhere. For some reason, the island's climate changed, becoming so hot and dry that crops would not grow—probably because of the destruction of the vegetation and higher runoff. An additional 38,000 people died of starvation and disease, having lost 75% of their livestock, and 36,000 fled the island. It took the island at least one century to recover from this ecological and human disaster.

The effects of the Tambora eruption were not, however, restricted to Sumbawa. The ash fall was principally to the west. In Lombok and Bali, the ash was so thick that many people were killed immediately as the roofs of their homes collapsed under the weight of huge quantities of ash. Even on these distant islands the toll from famine and disease brought about by the eruption was severe. On Lombok, estimates of the death toll ranged between 44,000 and 100,000 and on Bali at least 25,000. The depth of famine and disease was so great that it even claimed lives among the Balinese royalty. A conservative number of dead in the East Indies from the Tambora 1815 eruption is at least 117,000.

News of this distant eruption in Indonesia did not reach the Western world for some time, but unusual atmospheric phenomena and climate deterioration set in during 1816—"the year without summer." As detailed in Chapter 57, Tambora-size (ca. 100 km^3 of magma) explosive volcanic eruptions emit large quantities of sulfur dioxide gas into the stratosphere, where it is converted into a sulfuric acid aerosol dust veil that encircles the Earth. The aerosol has the effect of reducing solar heat reaching the surface of the planet, leading to global cooling. Strange atmospheric phenomena had been observed in Europe before the summer of 1816. In May 1815 the sunsets in England were exceptionally colorful, and by September the sky seemed to be on fire every evening. But the spectacular skies brought bad weather the following year, and the year 1816 is the worst on record in Europe, with the mean temperature about 3°C below average across the entire continent from Britain in the north to Tunisia in the south. In England the summer was miserable, with the mean temperature for June the lowest on record, or 12.9°C. In France it was so cold that the wine harvest was later than at any time since record keeping began—delayed until November in those districts where the grapes were not already frozen on the vine. In Germany crops failed, a situation exacerbated by the war with Napoleon, and famine and price inflation were widespread. Conditions in Germany became so intolerable that people in many districts rioted and set off in search of better living conditions, starting the great migration from northern Europe east to Russia and west to America. The severe weather in fact led to crop failure of all the major crops in Europe and a doubling of the price of wheat from 1815 to 1817. When we consider that in the early part of the 19th century agriculture was the mainstay of society, it is clear that the climate change had a strong impact on the economy of the Western world.

In North America the year 1816 was also unusually cold and dry, especially in New England and, as mentioned, is known in annals as "the year without summer." In early May, most farmers had planted their corn, the main crop at that time. But by mid-May the weather deteriorated, with severe frost that froze the fields as far south as New Jersey. As late as mid-June frosts also plagued New England, New Jersey, and New York. Then a great drought began, stunting or destroying the few remaining crops. In early July frost again swept over New England, from Maine to Connecticut, and again in late August in Maine, Vermont, and south to Massachussetts. By the end of September a final frost destroyed the few crops that had survived the frigid summer. These crop failures, in both Europe and North America, have rightfully been called "the last great subsistence crisis of the Western world." The growing season, of course, was much shorter than normal. In New England the average growing season is about 120 to 160 days, but in 1816 it was only 70 days in Maine, 75 in New Hampshire, and 80 in Massachussetts—a reduction of 40–50% (Fig. 5). Many farmers suffered such heavy losses that they abandoned their farms and migrated to the western territories.

The abnormal climate conditions in 1816 have frequently been proposed as an important factor in the first worldwide cholera epidemic. The bad weather also caused a series of crop failures in India, and as a consequence a cholera epidemic broke out in Bengal. It was spread further afield by British soldiers, to Afghanistan, Nepal, and Indonesia in 1820. A second epidemic broke out in India in 1826 and spread to Europe in 1831 and North America in 1832. It is likely that the severe climate conditions (abnormal weather, crop failures, subsequent famine, and reduced resistance to disease) brought about by Tambora may have played a role in the origin of a new and aggressive form of cholera that first did its deadly work in Bengal in 1817.

The global climate impact of large eruptions is a major reason that an understanding of volcanic phenomena is important for society today. A Tambora-size eruption in the 21st century will have much more profound effects on humans living on an overcrowded Earth, where natural resources are strained to the limit. The effects of a Toba-size eruption (ca. 2000 km^3) in the future are incalculable, but it will occur—we hope not in our lifetime.

For the most part, humans not only have learned to live with the slumbering volcanic giant, but have managed to extract a variety of economic benefits from the material and energy resources that lie at the roots of volcanoes. The precious diamond is merely carbon that has been crystallized under the high pressure (equivalent to the weight of the Eiffel tower resting on a 10-cm plate) and the high temperature in the Earth's mantle. Diamonds are brought up to the surface in volcanic pipes, such as the famous diamond pipes of Kimberley in South Africa. Even the carbon in precious diamond may be of mundane origin, reminding us of the steady recycling of material in Earth's kitchen. Thus isotopic analyses show that the carbon in at least some diamonds is probably derived from marine sediments that were subducted into the mantle early in Earth's history. As described in Chapter 55, a wealth of mineral deposits is also associated with the roots of volcanoes, where hydrothermal activity has led to concentration of metals.

One of the more promising benefits from volcanic activity is the harnessing of geothermal energy. The Earth's crust and lithosphere are in reality a boundary layer between the hot mantle and the hydrosphere and atmosphere. In volcanic regions the heat flux across this boundary layer is very large, and it can be tapped effectively by drilling. For example, about 85% of all homes in Iceland are heated with geothermal water, making Icelanders the largest users of geothermal energy per capita in the world (24,000 kWh per capita). It is estimated that the use of geothermal energy alone is saving imported oil costs of about $560 per year per person (Chapter 76). With the modern technology of deep drilling, the exploitation of this cheap and clean energy resource from the interior of the Earth does not

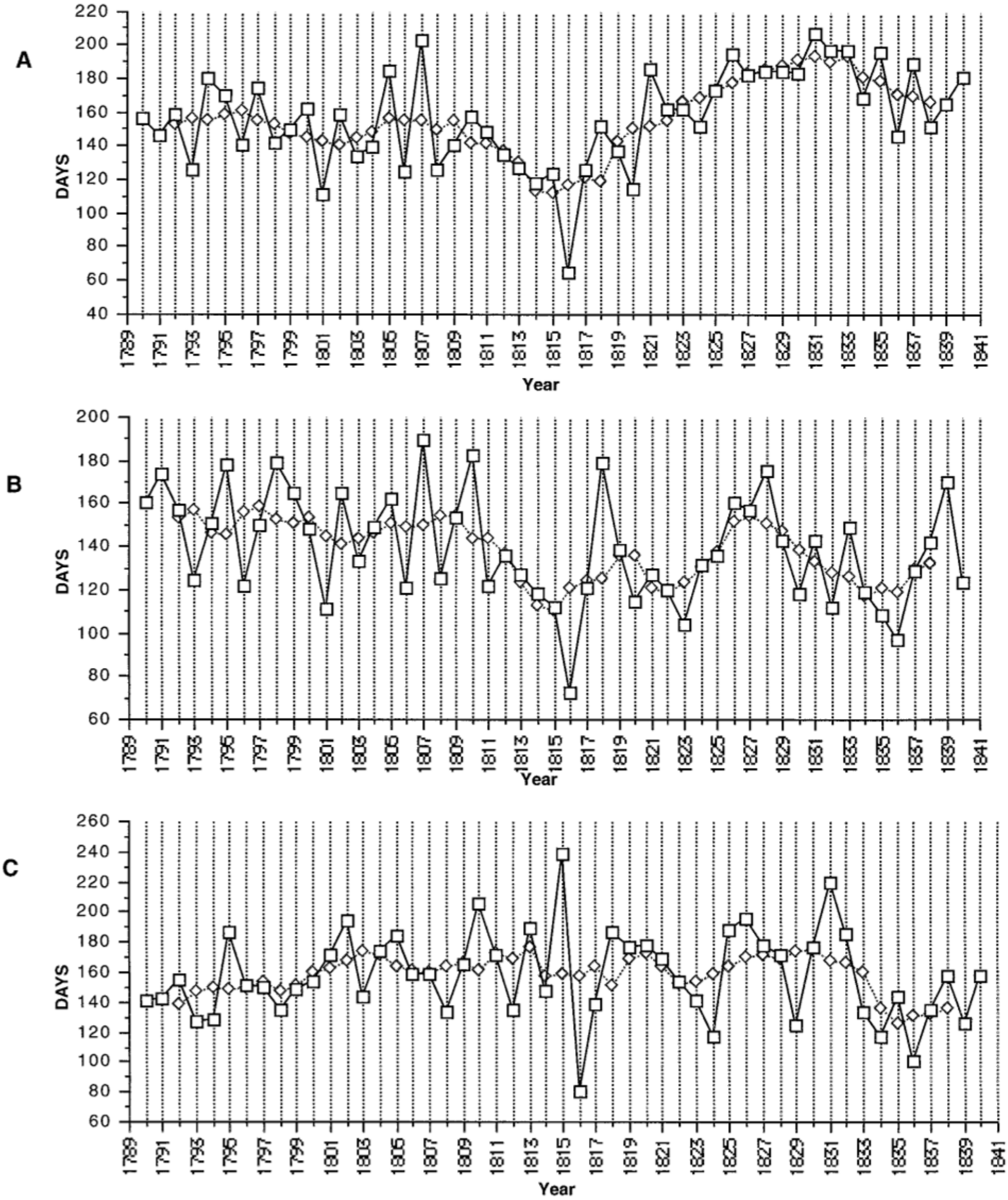

FIGURE 5 Volcanic eruptions can change the climate. The great Tambora volcanic eruption in Indonesia in 1815 led to a short-term global climate change that dramatically shortened the growing season in New England the following year. The sulfur dioxide gas emitted by the volcano produced a veil of sulfuric acid aerosol in the stratosphere worldwide, decreasing the amount of solar radiation reaching the Earth's surface, causing global cooling. The figure shows the length of the growing season on an annual basis (dots) from 1789 to 1841 and the 5-year running average (solid line). Growing season in the states of (A) Maine, (B) New Hampshire, and (C) Massachussetts. The shortest growing season on record was in the year following the Tambora eruption. (Reproduced from *The Year Without a Summer? World Climate in 1816,* published by the Canada Museum of Nature, Ottawa, 1992.)

have to be restricted to active volcanic regions such as Iceland, Italy, and New Zealand, but may be one of the major global sources of energy of the future.

SEE ALSO THE FOLLOWING ARTICLES

History of Volcanology

FURTHER READING

Allegre, C. (1988). "The Behavior of the Earth." Harvard University Press, Cambridge, MA.

Allegre, C. (1992). "From Stone to Star." Harvard University Press, Cambridge, MA.

Hawkesworth, C. J., Gallagher, K., Hergt, J. M., and McDermott, F. (1993). *Mantle and slab contributions in arc magmas. Ann. Rev. Earth Planet. Sci.* **21,** 175–204.

This Page Intentionally Left Blank

THE HISTORY OF VOLCANOLOGY

HARALDUR SIGURDSSON
University of Rhode Island

I. Introduction
II. The Beginnings
III. The Legends and Hell
IV. Wind in the Earth
V. Internal Combustion
VI. Exothermic Chemical Reactions
VII. The Cooling Star
VIII. Plutonists Victorious over the Neptunists
IX. The First Field Volcanologists
X. Experiments of the Plutonists
XI. A Solid Earth
XII. Decompression Melting
XIII. Stirring the Pot: Convection
XIV. Birth of Petrology
XV. The Source
XVI. The Role of Water

GLOSSARY

decompression melting The melting that occurs when some portion of the Earth's mantle undergoes a decrease in pressure, such as due to convective rise or upwelling of mantle peridotite beneath midocean ridges and volcanic arcs. The upwelling results in melting, because the melting point (beginning of melting) of peridotite occurs at a lower temperature with decreasing pressure.

eclogite An igneous rock with a mineralogy characterized by high-pressure minerals, but whose chemical composition corresponds to that of basalt.

exothermic reaction A chemical reaction that produces heat. The early chemists proposed that exothermic chemical reactions deep within the Earth, such as reactions between sulfur and iron, or oxidation of the alkali metals could be the cause of heat and volcanic activity.

neptunists The group of 18th-century geologists who believed that basalt and similar rocks were not of volcanic origin, but had formed by precipitation from a primordial ocean.

obsidian High-silica volcanic glass, generally black or dark gray in color, with the chemical composition of rhyolite.

palagonite A claylike mineral produced by the hydration of basaltic volcanic glass.

peridotite An ultramafic (high-magnesia, low-silica) igneous rock, whose mineralogy is dominated by olivine and pyroxene. Peridotite is the principal rock type of the Earth's upper mantle and the most likely source rock for basalt by partial melting.

plutonists The group of 18th-century geologists who believed that basalt and related rocks were produced by solidification from magma or silicate melt.

sideromelan Basaltic volcanic glass, which produces palagonite upon hydration.

xenoliths Rock fragments originating in the deep Earth (primarily the mantle), brought to the surface by volcanic eruptions.

Copyright © 2000 by Academic Press
All rights of reproduction in any form reserved.

I. INTRODUCTION

This chapter is on the history of ideas about the generation of magma within the Earth—the root cause of all volcanic phenomena. It is a process that results in the transport of material and heat from depth to the surface of our planet. It would seem logical that the history of ideas on melting in the earth would be synonymous with the history of "classical" volcanology. This is not the case, however, because up to the mid-1970s volcanology was essentially a descriptive endeavor, devoted primarily to the geomorphology of volcanic landforms, geography of volcanic regions, and the chronology of eruptions. Until recently, volcanologists have shown little insight as to the physical processes of volcanic action and often ignored the causes of the melting processes that lead to the formation of magma. Volcanology thus became a descriptive field, lacking rigor, and on the fringes of science. It is now timely to redefine modern volcanology as the science that deals with the generation of magma, its transport, and the shallow-level or surface processes that result from its intrusion and eruption. Modern volcanology is, however, highly interdisciplinary and draws widely from diverse geoscience subspecialities.

The processes that bring about melting in the Earth had been discovered by physicists in the mid-19th century, but due to the bifurcation of scientific fields, volcanologists were on the whole ignorant of these findings of the early natural philosophers or geophysicists and continued to pursue a descriptive approach to surface features without acquiring an understanding of the fundamental processes at work deep in the Earth. Table I lists some of the principal historical advances made in the study of volcanism up to the 20th century.

II. THE BEGINNINGS

In prehistoric times, opportunities to "discover" fire and to observe heat abounded in the natural world. Lightning strikes ignited fires in the primeval forest or on arid, grassy plains. Volcanic eruptions and lava flows threw forth showers of glowing sparks and incandescent heat. Most likely these were the sources our early ancestors borrowed from, carefully nurturing the fires they kindled, for their sources were only fickle and local. With fire at their command, humans could venture into new realms of cold and dark—into polar terrain and mountain caves.

Our knowledge of human precursors and early humans is intimately linked with volcanic eruptions (see Chapter 80). It is because of the excellent preservation of fossils in volcanic deposits that paleoanthropologists have begun to unravel the mystery of human origins. Most of the oldest remains of early man come from volcanic regions in Africa and Indonesia, and the association of volcanic activity with these fossils is no mere coincidence. The most logical explanation for their relative abundance and good preservation in such environments is that the bones were rapidly covered by volcanic deposits. Just as the Roman cities of Pompeii and Herculaneum were instantly buried by the eruption of Vesuvius in 79 A.D. and preserved virtually intact to our day, so have earlier volcanic deposits sealed in the remains and fragile artifacts of our more distant ancestors, preserving them for millions of years. The stunning discovery of 3.7-million-year-old *Australopithecus* hominid footprints crisscrossing a volcanic ash deposit at Laetoli in the East African Rift is a graphic testament of the power of preservation by volcanic ash fall. Volcanic deposits also contain minerals that can conveniently be dated by measuring the decay of radioactive isotopes of potassium and argon, a method that has enabled the dating of fossil remains of the oldest human, *Homo habilis*, at Olduvai as 1.75 million years old. A similar setting in the African rift at Hadar in Ethiopia has yielded fossils of the possible human precursor, *Australopithecus afarensis*, permitting its dating at 3.5 million years. Volcanic stone is the earliest known material used in the creation of tools by genus *Homo*. The earliest stone artifacts are about 2.5 million years old, implements made from lava, found on the shore of Lake Turkana in east Africa. Following their humble beginnings as toolmakers with the fashioning of these crude "cores," early humans gradually improved the techniques of working stone into flakes, choppers, hand axes, cleavers, and, finally, delicate obsidian stone blades in the upper Paleolithic.

More mundane materials such as pumice and volcanic ash have been used for nearly 3000 years in making cement. A mixture of volcanic ash and lime produces a very durable and water-resistant hydraulic cement. Volcanoes were also a principal source of sulfur. Early on people realized that sulfur burns with a strange and sputtering flame, giving off an evil-smelling and choking vapor. Probably the first uses for sulfur were to kill insects and to bleach wool, feathers, and fur. Homer knew of its fumigation property, and praised the "pest-averting sulfur" and Ulysses called out: "Quickly, bring fire that I may burn sulfur, the cure of all ills." Over the centuries the burning of a sulfur candle was a house-

TABLE 1 The Evolution of Ideas about Volcanic Activity

Scientist	*Year*	*Discovery or hypothesis*
Anaxagoras	5th cent. B.C.	Eruptions caused by great winds inside the Earth
Seneca	65 A.D.	Combustion as a source of heat in Earth
Pliny the Elder	79 A.D.	First scientific expedition to study an eruption
Pliny the Younger	79 A.D.	First volcanic eyewitness account, Vesuvius eruption
Snorri Godi	1000 A.D.	Basaltic rock in Iceland recognized as of lava flow origin
Liberti Fromondi	1627	Explosive eruptions compared to combustion of gunpowder
Edward Jorden	1632	"Fermentation" chemical reactions of sulfur generate terrestrial heat
René Descartes	1650	Incandescent Earth core as source of volcanic heat
Athanasius Kircher	1665	First global map of the distribution of volcanoes on Earth
Francesco d'Arezzo	1670	First experiments with molten rocks; melts Etna lava
J.-E. Guettard	1751	Identifies rocks at Volvic in Auvergne, France, as lava
Pierre Grignon	1761	Extracts crystals from glass slags; products of glass furnaces compared to products of volcanoes
Nicholas Desmarest	1763	Prismatic basalt columns in Clermont of volcanic origin
William Hamilton	1776	Pioneer in field volcanology; recognizes dikes and magmatic veins
Ben Franklin	1783	Volcanic eruptions have atmospheric effects and can cool Earth
James Hutton	1785	Recognizes intrusions of magma into the crust of the Earth
James Hall	1790	Melting and crystallization experiments on basalt
D. Dolomieu	1790	Some sediments are stratified and consolidated volcanic ash
Leopold von Buch	1799	Minerals in lavas formed by crystallization from magma
Lazzaro Spallanzani	1794	Earliest chemical analysis of volcanic rocks Water vapor is the dominant magmatic gas; causes explosions
John Playfair	1802	Speculates that change in pressure affects melting of rocks
Robert Kennedy	1805	First complete chemical analysis of basalts
Humphry Davy	1808	Exothermic reactions of alkalis provide volcanic heat
Pierre Cordier	1815	Identifies and analyzes the mineral components of lavas
A. von Humboldt	1822	Linear arrangement of volcanes related to deep-seated tectonics
George P. Scrope	1825	Decompression melting can produce magma in Earth's interior Chemical differentiation produces variety of magma types
Charles Darwin	1835	Crystal settling is the agent of magmatic differentiation
S.-D. Poisson	1835	Recognizes that the high pressure in the deep Earth would lead to solidification of rock at higher temperature
Gustav Bischof	1837	Demonstrates experimentally that the transformation from solid rock to magma results in increase in volume
William Hopkins	1839	Decompression melting as a process in generation of magmas
Robert Bunsen	1851	Magma mixing produces intermediate magma types; recognizes that magmas are solutions
S. Waltershausen	1853	Water vapor expansion causes magma fragmentation and pyroclastic; recognizes importance of submarine volcanic rock formations
Robert Mallet	1858	Map of global distribution of earthquakes and volcanoes
Osmond Fisher	1881	Proposes convection currents within the Earth
John Judd	1881	Volcanic recycling of water from volcanoes to atmosphere, to oceans, and back to magma through solid Earth
Carl Barus	1893	First to determine the melting curve of basalt as a function of pressure
Alfred Lacroix	1902	Documentation of the eruption of Montagne Pelée
Frank Perret	1906	Pioneer in application of technology to study of volcanic phenomena
Alfred Wegener	1912	Theory of continental drift
Arthur Holmes	1915	Calculates a temperature profile for the Earth based on radioactive generation of heat
Arthur Holmes	1916	Basaltic magma generated by partial melting of periodotite
Arthur Holmes	1928	Decompression melting and magma generation by mantle convection
Norman L. Bowen	1928	Fractional crystallization theory developed to explain magma range

cleaning ritual following a case of contagious disease in the home. Sulfur features in Egyptian prescriptions of the 16th-century B.C., and Pliny the Elder describes its medicinal, industrial, and artisan uses in his *Historia Naturalis* (77 A.D.). The Romans also found a new application in warfare for the sulfur they mined in Sicily. By mixing it with tar, rosin, and bitumen, they produced the first incendiary weapon.

III. THE LEGENDS AND HELL

Volcanic eruptions (Table II), the most spectacular and awe-inspiring of natural phenomena, have throughout history inspired religious worship and led to the creation of myths (Chapter 80). Even in the 20th century, these responses can be observed when a volcano erupts. James Hutton, regarded by many as the father of geology, was in 1788 the first to attempt to explode the myth associated with volcanic eruptions. In Hutton's view,

> *[A] volcano is not made on purpose to frighten superstitious people into fits of piety and devotion; nor to overwhelm devoted cities with destruction; a volcano should be considered as a spiracle to the subterranean furnace, in order to prevent the unnecessary elevation of land, and fatal effects of earthquakes; and we may rest assured that they, in general, wisely answer the end of their intention, without being in themselves an end, for which nature has exerted such amazing power and excellent contrivance.*

Primitive people the world over have long believed that volcanoes were inhabited by deities or demons that were highly temperamental, dangerous, and unpredictable. To appease the capricious gods, humans have for centuries made the ultimate sacrifice. Thus the Mayans, Aztecs, and Incas offered humans to their volcanoes. Nicaraguans long believed that their dangerous volcano Coseguina would stay quiet only if a child were thrown into the crater every 25 years. Similarly, young women were thrown into the crater of Masaya volcano in Nicaragua to appease the fire. Until recently, people on Java

TABLE II Historic Eruptions

Eruption	*Significance*
Thera (Santorini), 1650 B.C.	One of the largest explosive eruptions on Earth; may have contributed to the decline of Minoan civilization
Vesuvius, A.D. 79	First major historical eruption to occur within range of major cities; first eruption to be documented by an eyewitness
Etna, 1669	Major lava flow event with widespread destruction in Catania from lavas
Lakagigar, 1783	Largest lava flow eruption on Earth; catastrophic impact on Iceland population from haze produced by volcanic gas emission
Asama, 1783	Local devastation from pyroclastic flows; country-wide impact in Japan from climate effects
Tambora, 1815	Largest historic volcanic eruption on Earth; highest eruption column (43 km); global sulfuric acid aerosol causes global climate change; largest known death toll of over 92,000 people
Krakatau, 1883	First large eruption of the modern age; severe impact and death toll from tidal waves (tsunami)
Mount Pelée, 1902	The classic example of a small eruption causing severe loss of life; the beginning of the study of pyroclastic flow and surge processes
Paricutin, 1943	The birth and growth of a new volcano observed
Bezymianny, 1956	One of the highest known eruption columns in a historic event (42 km)
Surtsey, 1963	Best evidence of magma–water interaction during explosive eruption
Mount St. Helens, 1980	First major eruption to be monitored intensively with modern technology
El Chichon, 1982	Most widespread pyroclastic surges from a historic explosive event
Nevado del Ruiz, 1985	Another example of a small eruption causing severe loss of life; tragic example of lack of hazard mitigation measures
Pinatubo, 1991	Largest eruption of the 20th century; major societal impact in Philippines; important global atmospheric effects

sacrificed humans on Bromo volcano, and still throw live chickens into the crater once a year. People living near the feared volcanoes of Nyamuragira and Nyaragongo in central Africa annually sacrificed 10 of their finest warriors to the cruel volcano god Nyudadagora. To those who were skeptical of such rites and pointed out that earlier sacrifices had failed to prevent or stop an eruption, the believers have countered with the argument that things would have been much worse without the sacrifice.

The Aztec people named the volcanoes surrounding the Valley of Mexico after their gods. Popocatepetl and Iztaccihuatl, lying to the east of the valley, were worshiped as deities, linked to a beautiful love story. When Popocatepetl ("Smoking Mountain") returned victorious from war to claim his beloved, his enemies sent word ahead that he had been killed, and princess Iztacchiuatl ("Sleeping Woman") died of grief. Popocatepetl then built two great mountains. On one he placed the body of Iztaccihuatl; on the other he stands eternally, holding her funeral torch.

Volcanic eruptions featured high in Greek mythology, which abounds with allusions to volcanoes, associating them with such gods as Pluto, Persephone, Vulcan, and the fearsome Typhon. The idea that volcanic activity represents the stirrings of the Titans, giants imprisoned in the Earth, goes back to the classical time of the Greeks. The mythical association of volcanic eruptions with battles between the Olympian gods and the Titans is very likely to date back to Preclassical antiquity. The Greeks saw the Titans as huge man-creatures, born of the Earth to attack the gods. Confined under various volcanic regions, their appearance on the land or in the air seemed the logical precursor to a volcanic eruption. The most awe-inspiring of all the Greek monsters was Typhon. The firstborn of Gaia (Mother Earth) and Zeus, he was the largest monster that ever lived. His arms, when spread out, reached a hundred leagues, fire flashed from his eyes, and flaming rocks hurtled from his mouth. Even the gods of Olympus fled in terror at his sight. Typhon rebelled against the gods and even opposed Zeus, who then hurled Mount Etna at him, trapping the frightful creature under the mountain. When Typhon was thus imprisoned under Etna, a hundred dragon's heads sprang from his shoulders, with eyes that erupted flames, a black tongue and a terrible voice. Each time Typhon stirs or rolls over in his prison, Etna growls, and the Earth quakes, with eruptions and veils of smoke covering the sky (Fig. 1).

The Hades of the Greeks and Romans made an easy transformation into the Hell of the early Christians, described in the Bible as a place with an eternal fire that shall never be quenched. St. Augustine spoke of Hell as containing a lake of fire and brimstone. By the Middle Ages, Hell had taken on great importance, with most scholars convinced that it was a real and fiery place. One place most often cited as the gateway to Hell was Mount Etna volcano in Sicily, and "sailing to Sicily" became a euphemism for going to Hell.

IV. WIND IN THE EARTH

The earliest known ideas on the cause of volcanic eruptions date to the Greek natural philosophers of the fifth-century B.C. Anaxagoras proposed that eruptions were caused by great winds stored inside the Earth. When these winds were forced through narrow passages or emerged from openings in the Earth's crust, the friction between the compressed air and the surrounding rocks generated great heat, leading to melting of the rocks and the formation of magma. To anyone who has observed an explosive volcanic eruption, this is a perfectly logical idea, one that in fact was taken up by Aristotle and passed on by scholars until the Middle Ages.

Aristotle (384–322 B.C.) discussed the origin of earthquakes, attributing the same or similar origin for volcanic eruptions. "The Earth," he wrote in the *Meteorologica*, possesses "its own internal fire," which generates wind inside the Earth by acting on trapped air and moisture, leading to earthquakes and volcanic eruptions. He even makes a comparison with human anatomy in discussing the effect of the "internal wind": "For we must suppose that the wind in the earth has effects similar to those of the wind in our bodies whose force when it is pent up inside us can cause tremors and throbbings." Aristotle thought that the heat associated with volcanic eruptions was generated by friction produced when the wind moved rapidly through restrictions within the Earth. "The fire within the Earth can only be due to the air becoming inflamed by the shock, when it is violently separated into the minutest fragments. What takes place in the Lipari Isles affords an additional proof that the winds circulate underneath the Earth."

The identification of volcanic activity with "wind and fire" by the early Greeks follows logically from actual observations of a volcanic eruption. The most striking phenomena are first the explosive uprush of hot gases or "wind" from the Earth through the crater; then the incandescent red-hot glow of molten rock, giving the appearance of fire. It was on the basis of these phenom-

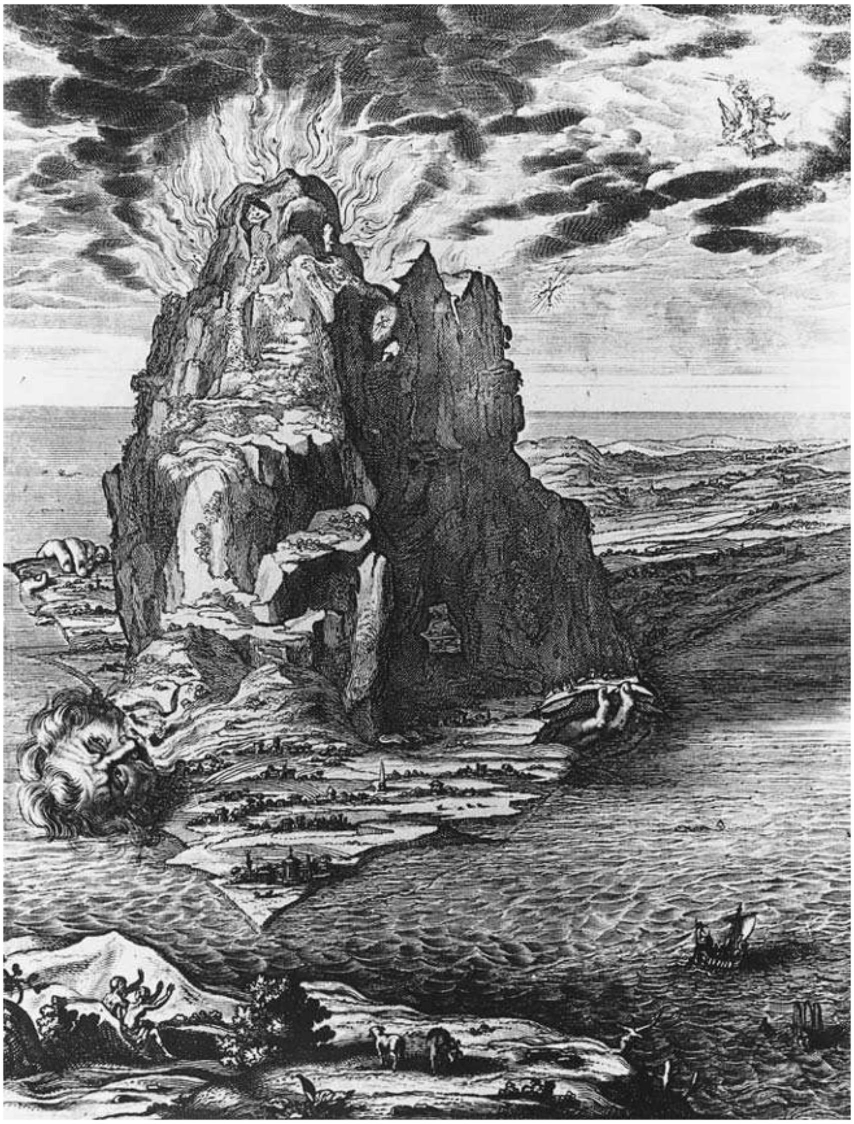

FIGURE 1 According to Greek mythology, the giant Typhon is buried under Etna volcano, and whenever the giant stirs, the volcano erupts violently. (Eighteenth-century print.)

ena that Aristotle postulated a vast store of pent-up wind within the Earth, which generated friction and high heat and found its escape in volcanoes. After all, the Platonic view was that heat is a kind of motion. Aristotle's concept of volcanism is thus firmly rooted in his ideas about the capacity of motion to generate heat as stated in his *Meteorologica*: "We see that motion can rarefy and inflame air, so that, for example, objects in motion are often found to melt." This theory, which dates in fact to his predecessors, Anaxagoras, Plato, and Democritus, was remarkably long lived and had adherents well into the 16th century.

V. INTERNAL COMBUSTION

Initially the Roman philosophers adopted the Greek view of the causes of volcanic eruptions, but eventually they proposed another explanation, one more in keeping with the practical Roman mind. Lucius Annaeus Seneca (2 B.C.–A.D. 65) wrote on volcanism in his work on natural philosophy, *Questiones Naturales*. He attributed volcanic eruptions in part to the movement of winds within the Earth, struggling to break out to the surface, thus in part following Aristotle. But his most notable and truly original contribution to theories of volcanism is his proposal that the heat liberated from volcanoes is derived from the combustion of sulfur and other flammable substances within the Earth—an idea that was to have many adherents into and even beyond the Middle Ages. His claim was that there were great stores of sulfur and other combustible substances in cavities within the Earth, and that when the great subterranean wind rushed through these regions, frictional heating would set these fuels on fire. It is in his discussion of hot springs and thermal waters that Seneca first makes reference to sulfur and other combustible materials as a potential heat source, proposing that "water contracts heat by issuing from or passing through ground charged with sulfur." He then extends this process to explain the blasts from a volcanic eruption in his work *Questiones Naturales*:

> *We must recognise, therefore, that from these subterranean clouds blasts of wind are raised in the dark, what time they have gathered strength sufficient to remove the obstacles presented by the earth, or can seize upon some open path for their exit, and from this cavernous retreat can escape toward the abodes of men. Now it is obvious that underground there are large quantities of sulfur and other substances no less inflammable. When the air in search of path of escape works its tortuous way through ground of this nature, it necessarily kindles fire by the mere friction. By and by, as the flames spread more widely, any sluggish air there may be is also rarefied and set in motion; a way of escape is sought with a great roaring of violence.*

Seneca's ideas were long lived and formed the basis of the interpretation of the causes of volcanic eruptions throughout the Middle Ages and even well into the 18th century.

Other significant writing on volcanism in the Roman world is found in poetry. The Latin poem *Aetna*, written between A.D 63 and 79, is of considerable importance in the history of volcanological thought; its likely author is Lucilius Junior. The poet maintained that the Earth is not solid, but has numerous caverns and passages. Heat, he argues, is more intense and powerful when in action in a confined space within the Earth, with the bellows-like action of winds in subterranean furnaces giving rise to volcanoes. In his view, the flames of Etna were fueled by a combustible substance, such as liquid sulfur, oily bitumen, or alum.

Philostratus the Elder (ca. A.D. 190) also discusses subterranean passages in the Earth, with fires breaking out through volcanoes: "If one wishes to speculate about such matters, the island of Sicily provides natural bitumen and sulfur, and when these are mixed by the sea, the island is fanned into flame by many winds, drawing from the sea that which sets the fuel aflame."

The eruption of Vesuvius in 79 A.D. marks a watershed in the study of volcanism. When he observed the eruption from Misenum, at a distance of 30km, Pliny the Elder set out on the first expedition devoted to the study of a volcanic process; he died in the attempt. His nephew Pliny the Younger stayed at home, where he had a spectacular view of the eruption, and wrote the first eyewitness account of the phenomenon, a classic description in the volcanological literature (Fig. 2).

VI. EXOTHERMIC CHEMICAL REACTIONS

Study of the Earth, like many scholarly activities, suffered a setback with the growth of the new Christian religion; and the only role of volcanoes in this new world order was to serve as a reminder of the hellfires burning below. This irrational attitude toward science continued well beyond the Middle Ages. Even by the 18th century, most writers on the philosophy of nature still considered that God created the Earth as a habitat for humans, that it had undergone certain stages of evolution since, and that it would ultimately be transformed or destroyed by Him. This was still manifest in the writings of John Wesley (1703–1791), the founder of Methodism, who taught that before sin entered the world, there were no earthquakes or volcanoes. These convulsions of the Earth were simply the "effect of that curse which was brought upon the earth by the original transgression."

The Early Middle Ages of Western Europe coincided with a remarkable growth of learning in Asiatic countries, which were in their prime from A.D. 800 to 1100. Contrary to the Christian philosophy, the Koran encouraged the Islamic scholar to practice the mastery of *taffakur*, or the study of nature. Unlike most learned Europeans, who saw nature as a vivid illustration of the moral purposes of God, the Arabs sought knowledge that would give them power over nature. They were the first alchemists; and one element that figured prominently in their studies was sulfur, which was in part mined from volcanoes. Their discovery that sulfur could also give off heat in chemical reactions was to generate the idea that volcanic action was also fueled by sulfur in the Earth.

The early chemists dealt a death blow to the theory of internal combustion as the source of subterranean fires. In his work on *Discourse of Naturall Bathes and*

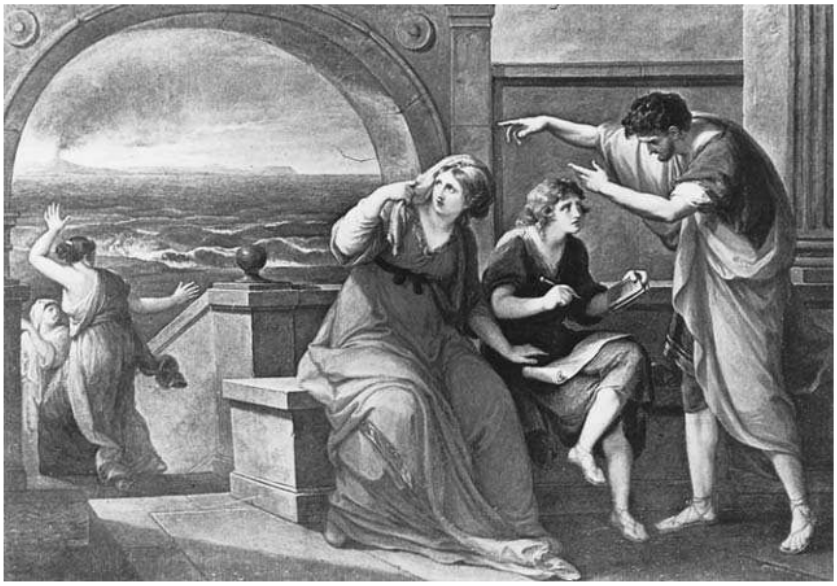

FIGURE 2 During the A.D. 79 eruption, Pliny the Younger remained at home in Misenum to do his homework, while his uncle set out on a research and rescue mission toward the volcano, where he perished. (From a painting by Angelica Kauffmann, 1785. Oil on canvas, The Art Museum, Princeton University.)

Minerall Waters (1632), Edward Jorden (1632) rejected the notion that the Earth is a hollow and fiery furnace with a universal fire fueled by combustible coal, bitumen, or sulfur. He pointed out the fundamental problem regarding the internal fire: It would require a tremendous amount of air to keep it buring. Any flame that is confined without access of abundant air would soon be put out, because "fuliginous vapours … choake it if there were not vent for them into the ayre." Such abundance of air could not reach the deeper portions of the Earth to fan the central fire. Instead, Jorden proposed that volcanic regions are underlain at only a shallow depth by "fermenting" material. As a source of the heat, he sought an explanation in the process of chemical reactions as a basis for a new system of the Earth. "Fermentation" or chemical reaction could take place in the presence of water, which was clearly abundant deep in the Earth's crust, whereas combustion could not proceed in the presence of water. Although his reasoning logically should have ended the hypothesis of combustion as the heat source in the Earth, the idea persisted well into the late 18th century.

Another pioneer chemist was Robert Hooke (1635–1703), who began his career as Robert Boyle's laboratory assistant in Oxford. Hooke was one of the first to make a clear distinction between heat, fire, and flame, and, together with Boyle, to study the various phenomena of heat. He developed a "nitro-aerial" theory of combustion, in which thunder and lightning were likened to the flashing and explosion of gunpowder, during the combustion of sulfur and nitre. These ideas are reminiscent of the work of Liberti Fromondi in the *Metteorologicorum* (1627), in which the explosive power of earthquakes and volcanic eruptions was compared to the effect of gunpowder. Volcanic activity Hooke attributed to "the general congregation of sulfurous, subterraneous vapors." In his work on *Lectures and Discourses of Earthquakes and Subterraneous Eruptions* (1668), Hooke also claimed that geologic activity was on the wane, and that subterranean fuel had been more plentiful in the past history of the Earth, when eruptions and earthquakes were apparently more severe: "That the subterraneous fuels do also waste and decay, is as evident from the extinction and ceasing of several vulcans that have heretofore raged." This concept of a finite supply of "subterranean fuels" was widely accepted and was endorsed by Lord Kelvin in 1889.

Isaac Newton (1642–1727) concerned himself with the process of volcanism, but his ideas on the causes of this phenomenon were derived from his contemporary alchemists and early chemists. His ideas on the causes of "burning mountains" are clearly a direct outcome of his secret work on alchemy. In Newton's chemical experiments, he had observed the evolution of heat, or exothermic reactions, when certain substances were mixed together, such as "when *aqua fortis*, or spirit of vitriol, poured upon filings of iron dissolves the filings with great heat and ebullition." With some other sulfurous mixtures "the liquors grew so very hot on mixing as presently to send up a burning flame," and "the *pulvis fulminans*, composed of sulphur, niter, and salt of tartar, goes off with a more sudden and violent explosion than gunpowder." By 1692 Newton had formulated opinions about the origin of heat in the Earth and its intensity, and compared it to the irradiance received by the Earth from the sun: "I consider that our earth is much more heated in its bowels below the upper crust by subterraneous fermentations of mineral bodies than by the sun." In an experiment described in his work *Opticks*, Newton tested his fermentation hypothesis and drew his conclusion on the causes of volcanism:

> *And even the gross body of sulphur powdered, and with an equal weight of iron filings and a little water made into a paste, acts upon the iron, and in five or six hours grows too hot to be touched and emits a flame. And by these experiments compared with the great quantity of sulphur with which the earth abounds, and the warmth of the interior parts of the earth and hot springs and burning mountains, and with damps, mineral coruscations, earthquakes, hot suffocating exhalations, hurricanes, and spouts, we may learn that sulphureous steams abound in the bowels of the earth and ferment with minerals, and sometimes take fire with a sudden coruscation and explosion, and if pent up in subterraneous caverns burst the caverns with a great shaking of the earth as in springing of a mine.*

A new and influential hypothesis on exothermic chemical reactions as a driving force of volcanism was developed with the discovery of the alkali metals by Humphry Davy. The new chemical theory did not call for a fluid interior, a vast storehouse of sulfur, or an internal fire in the Earth, and was consistent with the prevailing idea that volcanic activity in the Earth was progressively decreasing. Davy had a great interest in geology, eventually founding in 1807 the Geological Society of London. That year he was able to isolate by electrolysis for the first time the metals of the alkaline earths—potassium and sodium and later calcium, strontium, magnesium and barium. The high heat liberated upon the oxidation or "burning" of these metals upon reacting with water, with spectacular flames and explosions, so impressed Davy that it led him to propose a new hypothesis for volcanism in 1808. After his famous chemical discoveries, Davy was convinced that the heat given off during oxidation of the alkalies and the alkaline earths was the source of heat for volcanic action, supposing the existence of large quantities of the metallic alkaline earths within the Earth under volcanic regions.

One of the fiercest critics of Davy's theory about volcanic heat was Gustav Bischof in Germany. The arrangement of volcanoes in great continent-wide lines on the Earth's surface was taken by Bischof as a clear indication of a deep-seated origin of volcanic action, ruling out any superficial source within the crust. Davy had maintained that air could circulate through the Earth via volcanic craters and thus participate in heat-giving oxidation reactions. But the French chemist L. J. Gay-Lussac had shown by logic that it was impossible for atmospheric air to enter deep into volcanoes, because the pressure of the high-density magmatic liquid is acting outward. Air could not possibly flow into the volcanic system and fuel the oxidizing reactions against such a steep pressure gradient.

Charles Lyell in the *Principles of Geology* (1830) considered the possible role of oxidation of the alkalis and alkaline earths as a chemical heat source, following Davy's ideas closely:

> *Instead of an original central heat, we may, perhaps, refer the heat of the interior to chemical changes constantly going on in the earth's crust; for the general effect of chemical combination is, the evolution of heat and electricity, which, in their turn, become sources of new chemical changes. It has been suggested, that the metals of the earths and alkalis may exist in an unoxidized state in the subterranean regions, and that the occasional contact of water with these metals must produce intense heat. The hydrogen, evolved during the process of saturation, may, on coming afterwards in contact with the heated metallic oxides, reduce them again to metals; and this circle of action may be one of the principal means by which internal heat, and the stability of the volcanic energy, are preserved.*

Even near the end of the 19th century the chemical theory was still alive.

Despite the many objections, the chemical theory of volcanism was surprisingly long lived and continued to be entertained by prominent scientists well into the middle of the 20th century. Arthur L. Day was the last of the proponents of the chemical theory, when he proposed in 1925 that chemical reaction between gases plays a leading part in generating volcanic heat. In his view, various gases from different sources in the Earth meet within the crust, and their reactions lead to local fusion and generation of magma. This idea was particularly appealing to Harold Jeffreys, a leading geophysicist in the early 20th century. He considered vulcanism as "local and occasional, not perpetual and world-wide." In accounting for the "local and occasional" eruptions, Jeffreys appealed to Day's chemical theory of heat generation and melting in the Earth.

VII. THE COOLING STAR

During the latter part of the 17th century, several philosophers adopted the view that volcanism was due to original or primordial heat in the Earth. The first of these was the French mathematician René Descartes (1596–1650), whose works were to have a profound influence on thinking about the origin of the Earth. The solar system originated, he proposed, as a series of "vortices," with the Earth first appearing as a star, "differing from the sun only in being smaller," and collecting dense and dark matter by gravitational attraction and losing energy as matter falls into place by gaseous condensation. He divided the Earth into three regions: a core consisting of incandescent matter, like that of the Sun; a middle region of opaque solid material (formerly liquid but now cooled); and an outermost region, the solid crust. All of these layers had been arranged in this concentric fashion by virtue of their density. In this scheme, he maintained, there was enough primordial heat remaining to supply any volcano. Descartes's ideas influenced Baron von Leibniz (1646–1716), a German mathematician who proposed that the Earth must have existed originally in a state of fusion, and had thus acquired its spherical form and concentric shell structure, with denser metals concentrated in the center. Lacking an independent source of heat, the planet had cooled by simple conduction over geologic time, forming a stony and irregular crust. The hypothesis of Descartes that the Earth contained a vast store of primordial internal heat was of fundamental significance in evolution of geophysics and volcanology.

VIII. PLUTONISTS VICTORIOUS OVER THE NEPTUNISTS

Some rocks, which were later found to be of volcanic origin, were thought by the medieval philosophers to have originated by precipitation from water. Thus the Swiss philosopher Konrad Gesner (1516–1565) was convinced that the perfectly symmetrical and hexagonal basalt columns of many lava flows had precipitated as giant crystals from a primordial ocean (Fig. 3). Two centuries later, Richard Pococke still claimed that the columns of the Giant's Causeway, those huge six-sided pillars of basalt that rise from the sea in Northern Ireland, were formed by precipitation from an aqueous medium. The concept of a crystallization form for these highly ordered rock structures is not surprising, considering their regular shape: The pillars of the Giant's Causeway resemble in many respects giant crystals that might have precipitated out of ocean waters. The debate on volcanic versus aqueous origin of basalt was to become one of the fiercest controversies in the history of Earth science.

The idea of precipitation of rocks from a great ocean had strong theological origins in the legend of the Great Deluge. The leading figure of the Neptunist school was Abraham Gottlob Werner (1749–1817). Among his students were the most famous geologists of his day, including Alexander von Humboldt, Leopold von Buch, Georges Cuvier, Johann Wolfgang Goethe, Jean François d'Aubuisson, and Robert Jameson. Werner considered volcanoes of minor importance, as accidental and relatively recent or postaqueous phenomena on the Earth. They owed their existence, he claimed, to the action of fire (much as the medieval philosophers had proposed), activated by the ignition of coal deposits or other flammable materials in the Earth: "Most if not all volcanoes arise from the combustion of underground seams of coal." To support this notion, he proposed

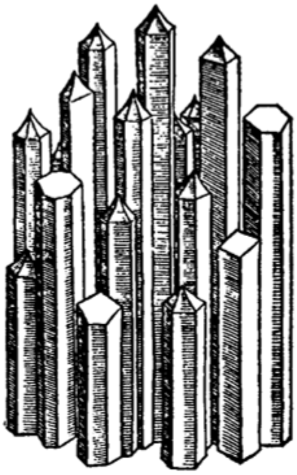

FIGURE 3 In the late 16th century, Konrad Gesner drew hexagonal basalt columns of lava flows with terminations as crystals, because he believed that they had precipitated as giant crystals from a primordial ocean—in keeping with the Neptunist view of the aqueous origin of basalt.

that deposits of coal or other combustible materials were invariably present in the vicinity of volcanoes.

By the first half of the 18th century, chemists were familiar with the formation of crystals in the laboratory as a product of precipitation from an aqueous solution. Because Werner and his followers had recognized that basalt was a crystalline rock, it was perhaps not unnatural that they also deduced its origin as a precipitate from an aqueous solution. It was not until after the middle of the 18th century that the idea slowly began to spread that crystallization could also occur as a result of the removal of heat from a silicate melt. In 1761 Pierre Clement Grignon complained that chemists overemphasized aqueous systems, pointing out, after he managed to extract crystals from glass slags, that the products of glass furnaces compared to the products of volcanoes. The idea that magma was a solution that could produce crystals was beginning to emerge, and a group of geologists embraced the view that basalt owes its origin to solidification of magma. The adherents of this theory became known as the Plutonists. A profound difference between the Neptunist and Plutonist theories related to the quantity and role of heat in the planet's interior. The Neptunists saw a negligible role for heat as a geologic agent and considered volcanoes to be a minor phenomena related to shallow-level processes. The Plutonists, on the other hand, saw heat as the fundamental driving force, pointing out the abundance of volcanoes, basalts, and granite as evidence of melting of rocks at high temperature within the Earth. By the early 19th century, the Neptunist theory had become severely weakened and was encountering increasing opposition, especially when it was shown that the silicate minerals that compose crystalline rocks such as basalt and granite are insoluble in aqueous solutions at normal temperature.

IX. THE FIRST FIELD VOLCANOLOGISTS

Most of the early ideas about heat in the Earth were based on "armchair geology," speculation based on little or no field observation. In the 18th century, the approach to the study of the origin of the Earth gradually evolved from pure speculation to a search for answers in rock formations exposed at the surface and in mine shafts. It was the labors of certain men, including those connected with the great mining industry in southern Germany, that brought about the revolution in the study of the Earth and the invention of field geology. A great leap in volcanology was made when geologists were able to identify ancient rocks as of volcanic origin, in regions far removed from active volcanism. This breakthrough occurred in the middle of the 18th century in France.

In 1751 Jean-Etienne Guettard (1715–1786) and his friend de Malesherbes made a journey through the Auvergne region, where they noticed some very unusual, black, and porous stones in mile posts, and Guettard immediately suspected that they were lava rock. They then visited Volvic, where Guettard noted dipping layers of the rock with scoriaceous upper and lower surfaces and other unmistakable signs of volcanic activity. He concluded that the stones were indeed from a large lava flow. When they came to the area of Puy de Dome, Guettard recognized that basaltic rock of the hardened lava had flowed from an ancient crater in the cone-shaped hill above (Fig. 4).

The geologist who first demonstrated the volcanic origin of basalt was Nicholas Desmarest (1725–1815). In 1763 he found prismatic basalt forming hexagonal columns in southwest Clermont. Tracing the rocks to their source, he found similar columns standing vertically in the cliff above, grading upward into the scoriaceous top of the lava flow. His simple observation of the association of columnar basalt as a component of a lava flow stands as a major advance in science (Fig. 5). Although Desmarest had demonstrated unequivocally the volcanic origin of basalt, the debate between the Vulcanists and Neptunists continued to rage into the 19th century. His theory of basalt as lava was bitterly opposed by many.

Among the pioneers in field volcanology was William Hamilton, who resided in Naples for several decades and had ample opportunity to study Vesuvius. Among his many observations were precise drawings he made of the changing outline of the volcano during the eruption of 1767 (Fig. 6). Hamilton was also fortunate to be resident in Naples when the early discoveries and excavations were being made in Herculaneum and Pompeii, findings that brought to light the destructive power of the A.D. 79 Vesuvius eruption (Fig. 7).

X. EXPERIMENTS OF THE PLUTONISTS

The undisputed leader of the Plutonists was the Scottish geologist James Hutton (1726–1797). He demonstrated the phenomenon of intrusion of magma into layered

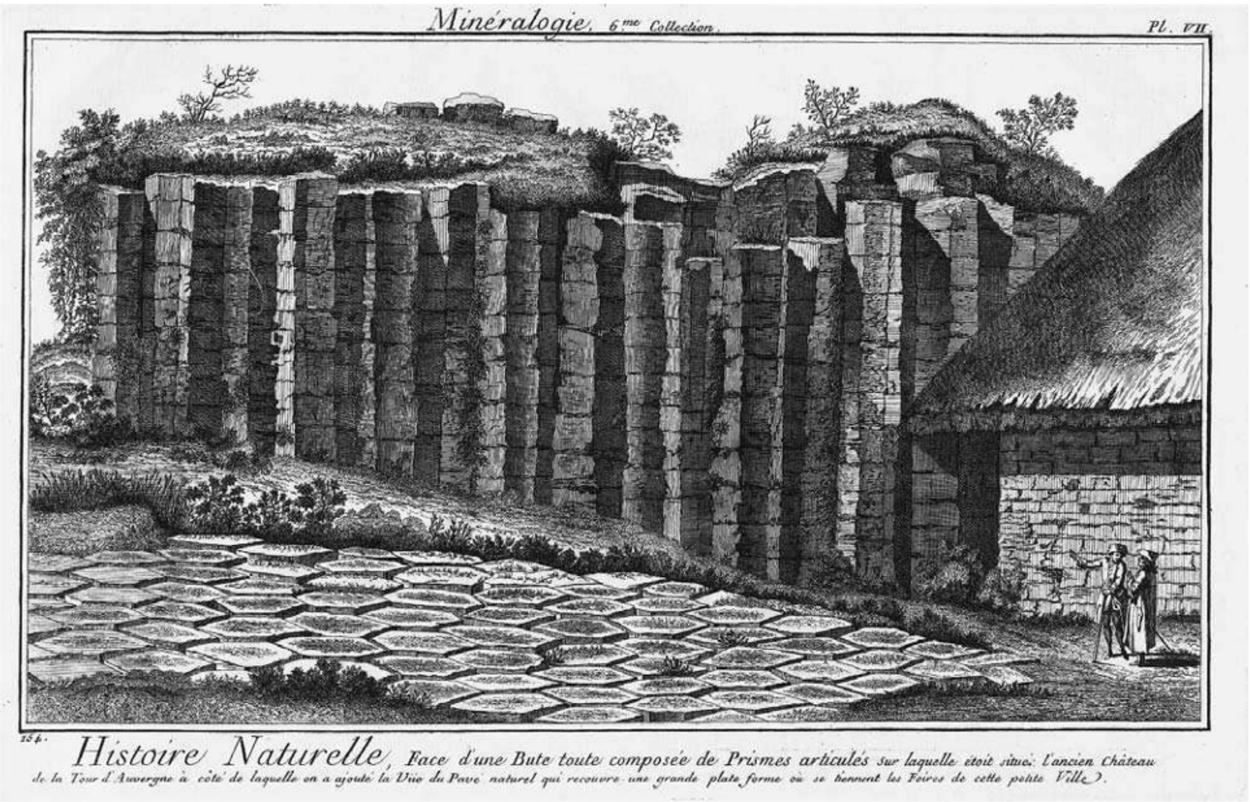
Minéralogie, 6me Collection.
Pl. VII.
154.
Histoire Naturelle, Face d'une Bute toute composée de Prismes articulés sur laquelle étoit situé l'ancien Château de la Tour d'Auvergne à côté de laquelle on a ajouté la Vüe du Pavé naturel qui recouvre une grande plate forme où se tiennent les Foires de cette petite Ville.

FIGURE 4 The pioneer geologists Nicholas Desmarest and Jean-Etienne Guettard identified ancient rocks in central France as volcanic in origin, although they were far removed from active volcanoes. This 17th-century print shows hexagonal columnar basalts in the Auvergne region, where Desmarest demonstrated their volcanic origin.

strata, and proposed that this molten rock originated in the highly heated interior of the deep Earth. Hutton devoted much energy to field work, examining geologic strata in Scotland, England, and France.

Hutton was an intensely religious man and argued that the Earth's processes followed a divine plan. Thus, volcanoes existed both as safety valves for the release of excess heat from within the Earth, and as a global force, because their expansive and uplifting power was needed to raise the surface of the Earth and contribute to the soils, so that plants and animals might flourish. Hutton thus saw volcanism as a means towards the realization of a higher purpose in the natural order of things.

Hutton and his followers had observed layers in the Earth's crust that, while they resembled basalt in mineralogical and other properties, were sandwiched between layers of sedimentary rock. They recognized that these rocks, which they referred to by the common mining term *whinstone*, were not volcanic but of igneous origin, and had been forcefully intruded between the sedimentary layers. Furthermore, they concluded that these rocks had solidified from magma.

Many of Hutton's opponents had maintained that the melting and solidification of crystalline rocks, such as granite or gabbro, would only yield an amorphous, glassy mass upon cooling, as observed in glass-making furnaces, and therefore the process could not produce basalt, whinstone, or other volcanic rocks. This objection to the Huttonian theory was tackled experimentally by the Scottish geologist and chemist Sir James Hall (1761–1832). To test Hutton's claim that rocks such as whinstone or basalt were derived from magma, Hall set out to do experiments on melting and cooling of basalts. First Hall melted the lava and basalt specimens, and then he converted the melted rock to glass by quenching. Next Hall remelted the crystal-free glass and allowed the melts to cool slowly. In so doing he produced crystalline or partly crystalline rocks, rough and stony in texture, which resembled the original rock samples. These

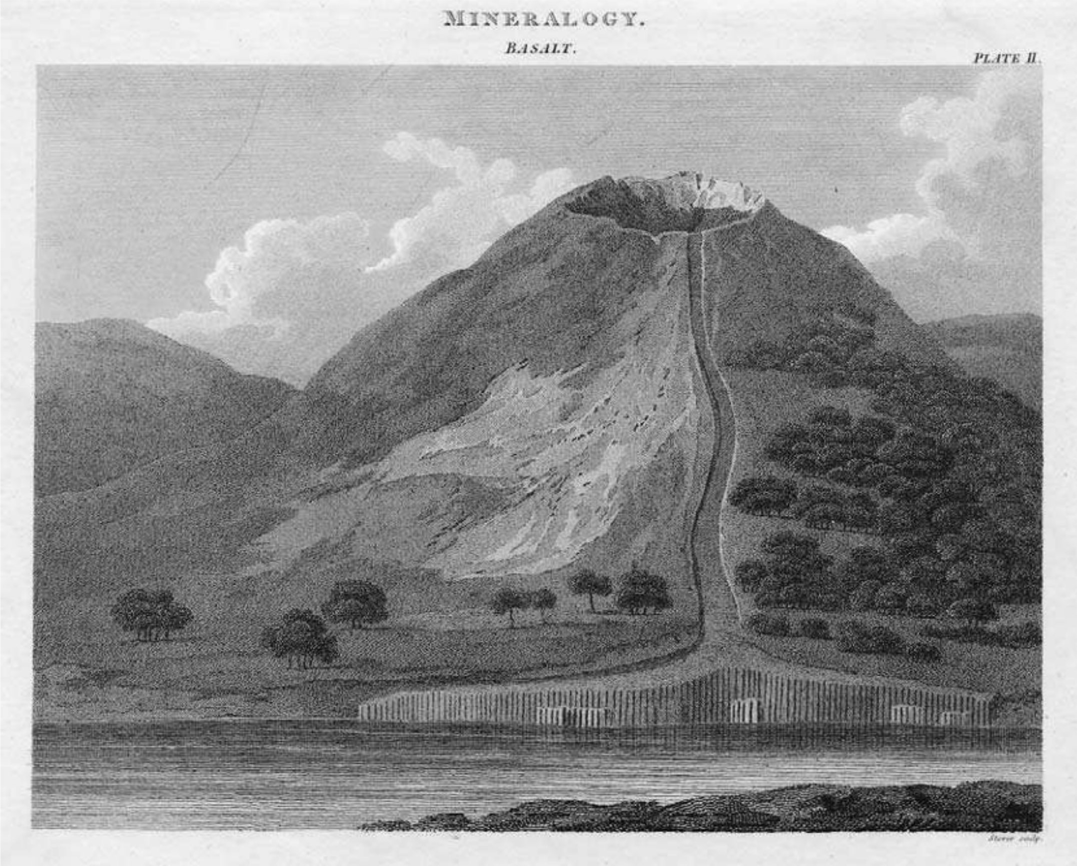

FIGURE 5 When the volcanic origin of columnar basalt was accepted, the early volcanologists quickly showed that it occurred as lava flows, and was connected to volcanic vents, as shown in this 18th-century engraving.

rocks, he showed, had melting and crystallization features exactly the same as those of basalts.

Demonstrating that melts of basaltic rocks precipitate silicate crystals upon cooling was of fundamental importance in establishing the volcanic theory on the origin of basalt. But if basalt rock was merely a product of solidification from a high-temperature silicate melt, then the experimental fusion and recrystallization of the rock should not affect its chemical composition. To test this, Hall submitted specimens of the products of his melting experiments to Robert Kennedy for chemical analysis in 1805, who found that their composition was essentially the same as the original rocks. Hall's demonstration, which was of fundamental importance in establishing the volcanic theory for the origin of basalt, dealt a final blow to the Neptunist theory of an aqueous origin for basalt, granite, and other rocks of igneous origin. Although Hall was a pioneer in experimental work on high-temperature and high-pressure experimental petrology, he was not the first to conduct experiments with molten rocks. The first melting experiments on basalts were done by the Italian scholar Francesco d'Arezzo in 1670, who fused Etna's lavas.

XI. A SOLID EARTH

Most geologists studying volcanic activity in the early and mid-19th century continued to envisage a planet with a solid crust and a largely molten interior, influenced by the ideas of Descartes. Heat within the Earth was considered a residue of the central, primitive heat held by the Earth at the time of its formation, a supply that had been diminishing over geologic time. The idea of a central, primitive heat was developed primarily from the observation of increasing temperature with depth

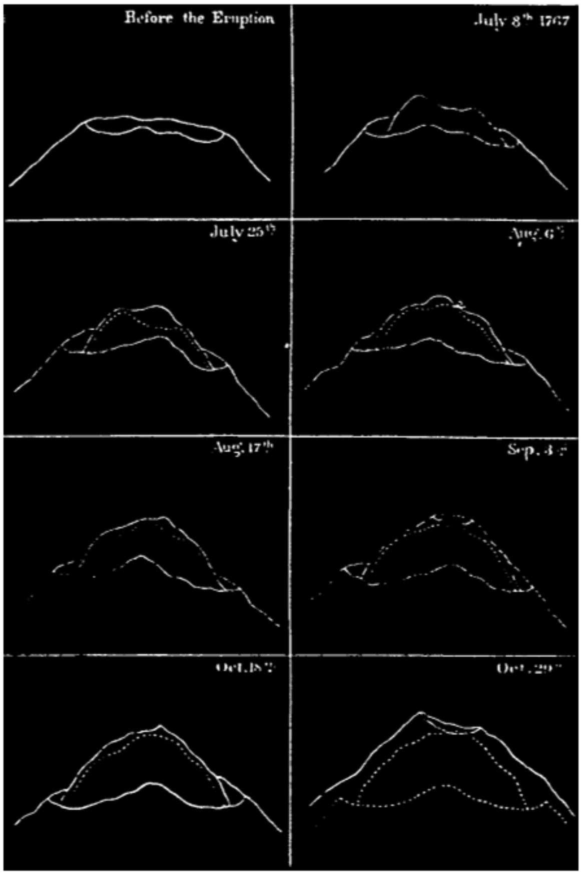

FIGURE 6 William Hamilton made some of the first quantitative measurements of volcanic morphology, when he carefully traced the changing outline of the summit of Vesuvius during the 1767 eruption.

in the Earth, based on measurements in mines and drill holes. Such observations led to the theory that the Earth began as a molten sphere, and has been cooling ever since. But if the interior of the globe were molten, it should yield to the gravitational attraction of the Sun and the Moon, and there would be little or no relative movement of the Earth's surface and the ocean's, that is, no sea tide. The response of the Earth to tidal forces, then, became a critical test for the molten Earth hypothesis. The French physicist Andre-Marie Ampere (1833) was the first to point out that observations of tidal action did not support the hypothesis of a fluid interior.

From 1839 to 1842 William Hopkins analyzed the effects of the Moon and the Sun on the rotation axis of the Earth. He concluded that the outer rigid crust must be at least 1500 km in thickness: "We are necessarily led, therefore, to the conclusion that the fluid matter of actual volcanoes exists in subterranean reservoirs of limited extent, forming subterranean *lakes*, and not a subterranean ocean." Hopkins's studies were continued by his student, William Thomson (Lord Kelvin), who showed, on the basis of the effects on the Earth of gravitational attraction of the Sun and the Moon, that the Earth was essentially rigid and that the ideas of James Dwight Dana of "an undercrust fire-sea" were untenable. Geologists were now in a great quandry: There was no evidence for a large body of magma within the Earth, yet there was a requirement for supplying magma to countless volcanoes throughout the history of the planet. How can you derive magma from the interior of a solid planet?

The Earth's structure at the turn of the century was regarded as a series of concentric, solid shells or layers, with an outermost 30- to 40-km-thick, low-density layer of granitic crust (sial) making up the continents. This was underlain by a very thick layer (sima or the mantle) of high-density, ultrabasic rock with the composition of perioditite, and finally by the central core. Those who were searching for a molten region in the Earth as a source of magmas were now faced with a geophysical picture of a largely solid interior. A magma source in the molten core seemed impossible, at a depth of more than 2900 km below the surface.

XII. DECOMPRESSION MELTING

The discovery that the Earth beneath the crust was essentially solid completely eliminated the "undercrust fire-sea" that Dana and others had proposed as a source of the magmas that feed Earth's volcanoes. Scholars, now faced with the task of showing how hot magma could be derived from within a solid Earth, found in the science of thermodynamics a partial solution to the problem. In the early years of the 18th century, it had been appreciated that pressure influences the temperature at which substances will undergo a change of phase—such as from a liquid to a gas, or from a solid to a liquid. The possible effects of pressure on melting of rocks in the Earth had been qualitatively appreciated very early on in the development of geologic thought. Perhaps the earliest recognition of this fundamental effect was made in 1802 by John Playfair. He pointed out that just as a change in pressure affects the boiling point of water, so would melting in the Earth be influenced by the great pressure exerted by the overlying rocks.

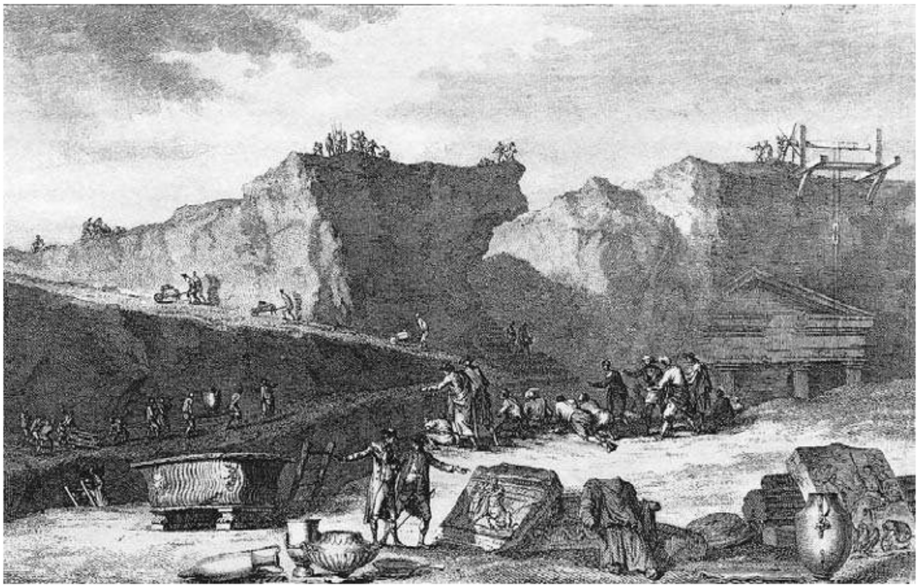

FIGURE 7 An 18th-century engraving showing the excavations of the Roman city of Herculaneum, burried by the A.D. 79 eruption of Vesuvius. Although the impact of the excavations was primarily on archaeology and art history, it was also a forceful reminder of the total destructive force of a volcanic eruption for visiting scholars like Johann Wolfgang Goethe and William Hamilton.

The next to address the importance of pressure in volcanic systems was George Poulett Scrope. By 1825 in his work *Considerations on Volcanos*, Scrope had realized the effect of pressure on the solubility of water in magmas, and was one of the first to point out that decrease of pressure on a water-rich magma could explain volcanic explosions due to the release of dissolved water. He also argued that a change of pressure could either lead to melting or crystallization of magma, without change in temperature:

> *Having thus far considered the effect of an increase of temperature, or a diminution of pressure, on a mass of lava under such circumstances, let us examine what will follow from the reverse; namely, an increase of pressure, or a diminution of temperature. Upon the solid lava, it is clear, no corresponding change will be produced; but every diminution of temperature, or increase of pressure, on a mass, or a part of the mass, liquified in the manner stated above, must occasion the condensation of a part of the vapour which produces its liquidity, and so far tend to effect its reconsolidation.*

Simeon-Denis Poisson had proposed in 1835 that the excessively high pressure in the deep interior of the Earth would lead to solidification of rock material at much higher temperatures than at the low pressures near the surface.

While Playfair and Scrope were struggling with a qualitative approach to the question of the effect of pressure on melting, a more elegant and quantitative approach was being developed in France and Germany, marking the birth of thermodynamics. From the work of Sadi Carnot, Rudolph Clausius, and Benoit-Pierre-Emile Clapeyron came the Clausius-Clapeyron equation, which quantifies the relationship between temperature, volume and pressure of a substance:

$$\frac{dT}{dP} = \frac{T\Delta V}{\Delta H}.$$

Consider two phases of the same chemical substance, for example, a liquid and solid (magma and rock), in equilibrium with one another at temperature T and pressure P. By supplying heat slowly to the system, one phase changes reversibly into another to bring about melting, with the system remaining at equilibrium. In the equation, the fraction dT/dP represents the rate of variation of the melting point T with change in pressure P. The value ΔV represents the volume change on melting and is generally positive (i.e., the specific volume of the solid is smaller than the volume of the corresponding liquid), while the value ΔH is the entropy change. The equation expresses the variation of pressure and temperature for a system in equilibrium. The magnitude and sign of the slope of the melting curve, dT/dP reflects the magnitude and sign of the volume change, ΔV, of the substance in question upon solidification or freezing.

It was shown early in the 18th century, in melting and crystallization experiments, that the specific volume of a volcanic rock such as basalt is lower than that of the corresponding magma. Many of the geologists who studied columnar basalt correctly interpreted its structure as evidence of contraction of magma upon cooling and solidifying to rock. During cooling and solidification, the material shrunk in volume, forming roughly hexagonal columns separated by a pattern of contraction joints. Thus it was clear that the term ΔV in the Clausius-Clapeyron equation was positive, and consequently, the equation predicts that the pressure–temperature melting curve (dT/dP) of the source rock of basaltic magma has a positive slope in the Earth, that is, the temperature of melting increases with pressure. This interpretation of columnar basalt was consistent with the experimental results of the German chemist Gustav Bischof in 1837, who carried out one of the first measurements on the volume change of basalt and other volcanic rocks upon fusion and showed that rocks contract upon solidification from magma. He concluded that a melt of granite rock contracted about 25% upon solidification, trachyte about 18%, and a basaltic melt 11%.

Another German chemist, Robert Wilhelm Eberhard Bunsen, was one of the first to experiment on the relation between pressure and melting point of substances. The laboratory facilities available in Bunsen's time (1850) permitted only modest pressures to be achieved, roughly the equivalent of the pressure at a depth of 1 mile in the ocean. He therefore performed his experiments on materials with a relatively low melting point, such as ambergris and paraffin, and extrapolated these results to the high pressures and temperatures prevailing deep in the Earth. His work showed that a pressure increase of only 100 atm increased the melting point of these substances by several degrees centigrade. At about the same time (1851), William Hopkins began to experiment with James Joule, Lord Kelvin, and William Fairbairn, on the effects of pressure on the solidification of the Earth's interior. A large lever apparatus generated pressure up to 5400 atm, equivalent to the pressure at approximately 15-km depth in the Earth. Initially the experiments were on substances with low melting point, such as beeswax and spermaceti, and they essentially confirmed the work of Bunsen.

These pioneers had established that a solid hot substance such as rock at depth in the Earth could spontaneously begin to melt if the presure is decreased, without the addition of heat. They had finally found the secret of the generation of magmas in a solid Earth: decompression melting. But the solution of one problem led to the creation of another, even more daunting problem: What is the mechanism that brings about decompression? Some ingenious proposals were put forth to solve this problem. Thus in 1878 the American geologist Clarence King, realizing that local relief of pressure leads to melting in the Earth, suggested that the pressure release could occur with the erosion and removal of overlying crustal rocks: "So that the isolated lakes of fused matter which seem to be necessary to fulfill the known geological conditions may be the direct result of erosion." This seemed perfectly logical at the time, but if true, the rate of erosion of a given area must occur at a higher rate than that of heat conduction from the rising hot rock. Geologic evidence did not support this theory on two counts. First, many mountainous regions, where erosion is highest, show no signs of volcanism; and second, the rate of pressure relief due to erosion is so slow that heat lost through conduction would prevent melting at depth.

As director of the U.S. Geological Survey, King fostered the fundamental experiments of Carl Barus on rocks at high pressure. Barus determined the volume change and latent heat of basalt upon melting. He concluded that the term dT/dp in the Clausius-Clapeyron equation was equivalent to 0.025 for basalt, that is, the melting point increases at a rate of 2.5°C for every 100-atm increase in pressure. In 1893 Carl Barus was also the first to determine the melting curve of basalt as a function of pressure, which enabled King to propose a geothermal gradient for the Earth (Fig. 8).

In 1909 the British geologist Alfred Harker summed up his opinion on magma generation in *The Natural History of Igneous Rocks*: "We must seek the immediate cause of igneous action, not in the generation of heat, but chiefly in *relief of pressure* in certain deep-seated parts of the crust where solid and molten rock are approximately in thermal equilibrium. We are thus led by an independent line of reasoning to the principle already enunciated, which connects igneous action primarily with crustal stresses, and so secondarily with crust-movements." Furthermore, "at a sufficient depth, such conditions of temperature prevail that solid and liquid rock are in approximate thermal equilibrium. Any local relief of pressure within that region, connected with a redistribution of stress in the crust, must then give rise to melting." These statements were an incisive expression of the fundamental principle of melting, but what was still lacking was the mechanism that brought about the relief of pressure.

Not all geologists were ready to embrace this as a solution to the origin of magma, because a viable geo-

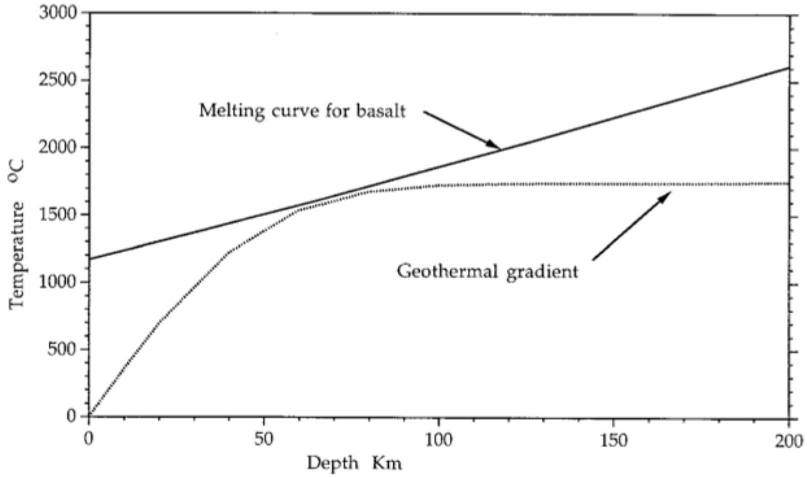

FIGURE 8 At the end of the 19th century, a geotherm had been calculated for the earth by Clarence King and others. The temperature of melting of basalt as a function of pressure had also been determined experimentally by Carl Barus. It was assumed that melting of the Earth's mantle occurred in the depth range where the geothermal gradient approached the basalt melting curve, that is, in the depth range of about 60–80 km below the surface.

logic process that could bring about a pressure decrease was not known. The American geologist Reginald Aldworth Daly stated (1933): "Local relief of pressure is hopelessly inadequate and need not be further discussed." Similarly, according to S. James Shand (1949), this pressure effect on melting of silicates was "a quantity scarcely large enough to have any important petrological consequences."

The progress made in understanding melting and the internal constitution of the Earth by the first part of the 20th century was truly profound, but it had created a paradox. All the evidence was in favor of a solid interior or an exceedingly thick crust at any rate, yet there was a need to account for the magmas erupted from volcanoes. Experimentalists and geophysicists had discovered a process by which melting could occur simply by decompression, but the geologists were unable to find an acceptable decompression mechanism to produce this melting.

XIII. STIRRING THE POT: CONVECTION

The discovery of radioactivity caused a great stir among scientists, who quickly applied it to an understanding of the Earth. When Pierre Curie discovered in 1903 that radioactive materials emit heat, the Irish physicist John Joly was the first to point out that the abundance and distribution of radium and other radioactive elements may determine the terrestrial heat. In 1910 the British geologist Arthur Holmes (1890–1965) began a study of the natural radioactivity of rocks, and thus began a career that would make a major contribution to both understanding of heat distribution and melting of the Earth by convective flow of solid rocks toward the surface. By 1915, Holmes had calculated a temperature profile for the Earth based on radioactive generation of heat.

After radioactivity was discovered as an internal heat source, it became even more important to establish the principal means of heat loss from the planet. How is this great flux of heat transferred from the deep Earth toward the surface? Holmes proposed that convection was the most effective mechanism to transport heat from depth to the surface. It was an idea that dates back to Osmond Fisher (1881), who proposed, in the days of an Earth with a totally molten interior, that there were convection currents rising under the ocean and descending beneath the continents. In 1928 Holmes proposed that the excess heat is discharged from the Earth by circulation of material in the solid *substratum*, or the Earth's mantle, forming thermal convection currents. Convection, and in turn continental drift, was seen as a mechanism to rid the Earth of the great heat generated by the radioactive natural reactor. He considered this substratum to be a solid peridotite rock, which could flow like a fluid at a rate plausible for a deep Earth process—about 5 cm/year. Holmes's scheme included downward currents below geosynclines, the great sedimentary troughs that today we recognize as subduction zones, and ascending currents below midoceanic "swells," where "a discharge of a great deal of heat" occurs due to upwelling of peridotite mantle, decompression, and melting. Holmes's views in 1928 were amazingly modern and laid the foundations for the concept of plate tectonics, although this has not been generally recognized by Earth scientists.

The concept of plate tectonics had a long gestation period, and it began with the realization in the 17th century that volcanoes and earthquakes are distributed in great linear belts over the Earth. This systematic trend of volcanoes and earthquake zones, and the arrangement of the continents, eventually led to the theory known as continental drift in the early 20th century. The earliest map showing the global distribution of volcanoes was drawn by Athanasius Kircher in 1665. With the spread of geographic knowledge, a more refined picture gradually emerged, one of the systematic, linear or curvilinear arrangement of volcanoes on the surface of the globe. Ideas on the relationship between volcanic activity and major structures and tectonics date to Alexander von Humboldt (1822), who pointed out that the linear arrangement of volcanoes on the Earth was proof that the mechanism that generates volcanism was a deep-seated feature. Robert Mallet (1858) compiled the first map showing the global distribution of both earthquakes and volcanic eruptions in a "vast loop or band round the Pacific," indicating a strong coincidence in their geographic distribution. He also recognized that most of the Earth, especially the interior of the continents, is seemingly free of earthquakes and volcanic activity. He divided the Earth into a series of basins, separated by "girdling ridges," which are present even on the ocean floor: "It is along these girdling ridges, whether mountain-ranges or mere continuous swelling elevations of the solid, which divide these basins beneath the ocean surface one from the other, that all the volcanoes known to exist upon the earth's surface are found, dotted along these ridges or crests in an unequal and uncertain manner." He regarded these ridges as "suboceanic linear volcanic ranges" which mark "the great lines of fracture of the earth's crust." Mallet's recognition of the distribution of these geological structures, which are now basic to the theory of plate tectonics, was probably the earliest.

The recognition of the linearity of volcanoes and earthquake zones coincided with a mobilistic view of the Earth toward the end of the century, a view based both on geophysical reasoning and geologic evidence. Osmond Fisher had argued in 1881 that cooling of the Earth could not be brought about solely by the process of conduction, as had been proposed by Kelvin, but was in part brought about by convection currents in a plastic substratum. In Fisher's view, these convection currents led to lateral movement of the overlying crust, accounting for much of the character of the Earth's surface, including linear arrangement of volcanoes, earthquakes, and mountain chains. The ideas of a mobile Earth were first crystallized into a coherent theory of continental drift in 1912 by Alfred Wegener. One of those who sided with Wegener was Arthur Holmes, who greatly strengthened the theory by proposing in 1928 a more plausible thermal convection mechanism for crustal movement than Wegener had put forward. Holmes's mechanism involved the flow or upwelling of the Earth's mantle, providing a process whereby decompression of the hot mantle would occur, leading to melting and volcanism. Continental drift was an inevitable consequence of this circulation, but the process was much wider in scope: It involved the lateral motion of the oceanic crust as well. By 1931 Holmes had constructed a complete theory of continental drift, sea-floor spreading and subduction, based on this mechanism.

Holmes differentiated between a largely granitic crust in the continents and a basaltic crust in the oceans. He considered the mantle beneath the oceanic crust as most likely of peridotite composition, and argued that although it was probably crystalline and thus highly rigid, it had some of the properties of a fluid in the context of its large-scale dimensions. He proposed that the convection cells have dimensions at the scale of the mantle, some 2900 km in depth, and that their ascending limbs rise beneath the oceans, where they generate oceanic "swells" analogous to our modern concept of midoceanic ridges. Ascending currents he proposed were accompanied by decompression and partial melting of peridotite, to form basaltic magma, giving rise to volcanism. Descending currents were caused in the mantle by sinking of high-density rocks. The process he outlined was essentially the same as the modern concept of subduction: The convergence of crustal plates on the Earth leads to underthrusting of one plate and its descent deep into the mantle. Holmes estimated that the velocities of the convection current were on the order of 5 cm/year, which, as was discovered in the 1960s, is perfectly within the range of typical sea-floor spreading rates. Although widely accepted in Great Britain, Holmes's ideas on mantle convection and a mobile Earth were generally not embraced elsewhere for some time. When the idea of sea-floor spreading was finally accepted by a majority of Earth scientists in the 1960s Holmes's fundamental contribution was frequently ignored. One is reminded of the chilling words of Sir William Osler: "In science the credit goes to the man who convinces the world, not to the man to whom the idea first came."

Is it more important in science to convince than to discover?

The discovery of plate tectonics has now provided the long-sought mechanism for decompression in the Earth's mantle—the most important process that brings about melting and generation of magmas. It is clearly the mechanism that generates magmas below the midocean ridges of the Earth and is thus responsible for most of our planet's volcanism.

XIV. Birth of Petrology

Among the earliest observations on the mineral content or petrography of volcanic rocks were Leopold von Buch's studies in 1799 on volcanic rocks near Rome. Von Buch concluded that the crystals of leucite had formed while the lava was still fluid, and discounted any hypothesis to the effect that they had been precipitated from an aqueous solution and later incorporated in the magma. Basalts and other volcanic rocks, however, are composed of exceedingly small crystals, which are invisible with the naked eye or even through a magnifying glass. The pioneer geologists were therefore unable to investigate the internal structure of these rocks and identify their tiny crystal components. The microscopic study of volcanic rocks was first carried out by Pierre Louis Cordier in 1815, who crushed basalts and other volcanic rocks to a fine powder, separated the various particles by a flotation process, and examined them by microscopic and chemical tests. He concluded that ancient basalts were very much like modern volcanic rocks in texture, mineralogy, and other characteristics—an important step in solving the Neptunist versus Plutonist controversy over the origin of basalts.

The art of making thin sections began with the sectioning of fossil wood, but the method was soon applied to rocks. They could be sliced so thin as to be transparent, and their minerals could be identified and their textures studied in detail. By 1829 the polarizing microscope had been invented by William Nicol and was used widely for the study of crystals. Henry Clifton Sorby (1826–1908) was the first geologist to make thin sections of volcanic and other igneous rocks for microscopic study.

Another crucial step in the study of volcanic rocks was the development of chemical analysis. Studies of the chemical composition of volcanic rocks date back to the work of Abbé Lazzaro Spallanzani (1794), who reported on the chemical composition of volcanic rocks in Italy in terms of weight percent of the five major oxides of silica, alumina, lime, magnesia, and iron. In 1805 the Scottish chemist Robert Kennedy reported chemical analyses of *whinstone* or basaltic rocks. He was able to dissolve basalt by melting the rock powder with caustic potash at high temperature in a silver crucible. He then showed that it contained 48 wt% silica, 16% alumina, 9% lime, 16% iron oxide. Water and other volatile components accounted for about 5%. About 6%, then, was not accounted for. Kennedy suspected this was in part "a saline substance," and, after an elaborate analytical routine, showed that it was about 4% soda. He thus accounted for 99% of the chemical constituents of the rock—a great feat at the time.

When the early geologists began to accumulate data on volcanic rocks, they discovered that the chemical composition of the rocks, even those from the same volcano, varied greatly. Confronted with the problem of how to account for this diversity, George Poulett Scrope proposed in 1825 that all types of igneous rocks were formed from a single parent magma, which gave rise to a variety of types through a process of *differentiation* before crystallization. It was Charles Darwin, however, who laid the foundation for the process of "magmatic differentiation," through his discovery of crystal settling due to density differences between crystals and the magmatic liquid. During his exploration of the volcanic Galapagos archipelago in 1835, Darwin studied a basaltic lava flow on James Island (now San Salvador). He noted that the crystals of feldspar were much more abundant in the base of the lava than in the upper part, and deduced "that the crystals sink from their weight." Von Buch had earlier (1818) noted a similar concentration of crystals in the lower part of obsidian lava flows on Tenerife in the Atlantic, interpreting this as the settling of crystals in the lava during and after flow. In his *Geological Observations on The Volcanic Islands*, Darwin considered this observation as "throwing light on the separation of the high silica versus low silica series of rocks." He realized that once early formed crystals sink, the remaining magma would be chemically different from the initial liquid.

Another process was developed by Robert Bunsen in 1851 to account for the chemical range of volcanic rocks, after his discovery of two magmas in Iceland, with radically different chemical composition. Bunsen was struck by the abundance of two volcanic rock types: yellow and multicolored, silica-rich volcanic rocks (rhyolite), and the dark-colored basaltic rocks. A few volcanic rocks were of intermediate composition, and he proposed that they were the result of mixing of the silcic and basic magmas. Bunsen's contribution was to put forward the first viable hypothesis that could account for the diversity of the chemical composition of volcanic rocks by the mixing of two primary magma: basalt and rhyolite. Traveling with Bunsen in Iceland was Sartorius von Waltershausen. He was the first to discuss the distribution and occurrence of the trace elements, as well as the major oxides in volcanic rocks, and listed 23 trace elements.

In the 18th century the volcanic fluid had become known as *magma*, derived from the Greek word which refers to a plastic mass, such as a paste of a solid or liquid matter. The term magma was used early on in pharmacy as in "magnesia magma," or milk of magnesia, and the word passed from pharmacy into chemistry to represent a pasty or semifluid mixture. From chemistry it passed into petrology to replace "subterraneous lava." What was the nature of this fluid inside the Earth? Bunsen, in *Uber die Bildung der Granites*, stressed that magmas are nothing more than a high-temperature solution of different silicates: "No chemist would think of assuming that a solution ceases to be a solution when it is heated to 200, 300 or 400 degrees, or when it reaches a temperature at which it begins to glow, or to be a molten fluid." This was a fundamental breakthrough in thinking about crystallization from magmas. Bunsen further recognized that minerals crystallized from magmas at a much lower temperature than the melting point of the pure minerals. If magmas are true solutions, then they should be able to mix, as indeed Bunsen had proposed on the basis of his Iceland work.

During the latter part of the 19th century the chemical analysis of volcanic rocks became commonplace. Leading petrologists considered that most igneous rocks were derived from basaltic magma by a process of differentiation, but no one researcher contributed more to the understanding of the processes that account for the chemical diversity of igneous rocks than the American petrologist Norman L. Bowen. From high-temperature experiments, Bowen discovered that magma could greatly change in composition as it cooled, if the early formed crystals were effectively separated from the liquid, thus providing proof for the fractional crystallization process first proposed by Darwin. Bowen was a strong advocate for fractional crystallization as the primary process responsible for differentiation, and considered that basaltic magma was the primary or parent magma of all volcanic rocks. The new understanding of magmatic differentiation was made possible by Bunsen's recognition that magmas were true solutions, Darwin's concept that settling of crystals resulted in a change in the composition of the liquid, and Bowen's systematic experiments on crystallization of a primary basaltic liquid. But how, then, was this primary basaltic liquid formed?

XV. THE SOURCE

Throughout the first half of the 20th century, two principal hypotheses existed on the nature of the source of magmas. Because the principal type of magma erupted was basalt, it appeared logical to some that the source region was also basaltic in composition, and possibly the high-pressure form of basalt known as *eclogite*. The basaltic magma would then be derived by wholesale melting of the source. The other view was that the magma was derived by partial melting of peridotite. It had long been noted that xenoliths of both peridotite and eclogite were ejected from some volcanoes. Because they were brought up in the magma, it seemed logical that these rock types might be an indication of the source region. As early as 1879 it was suggested that peridotite was the source of basaltic magmas, and by 1916 Arthur Holmes proposed that magma was generated by melting of peridotite at a depth of several hundred kilometers.

At the beginning of the 20th century, geophysical measurements were giving results in favor of a peridotite source. This was done by measuring in the laboratory the physical properties of a number of rock types under high pressure and temperature. By comparing these results with the speed of earthquake waves traveling through the deep Earth, it was shown that properties of the Earth's interior are comparable to those of peridotite and other ultrabasic rocks under great pressure in the laboratory. Geophysicists therefore generally adopted a peridotite composition for the mantle.

Bowen (1928) also proposed that the only rock type that could give rise to basaltic magma by partial melting is peridotite, and suggested that this occurs at depths of 75–100 km. Bowen then addressed the question of whether the partial melting occurred as a result of reheating or due to pressure release. Arthur Holmes's ideas on convective flow in the mantle were published in the same year as Bowen's classic work, but Bowen seemed unaware of them. Having no plausible mechanism to bring about a pressure release, he stated: "It seems necessary to leave open the question whether selective fusion takes place as a result of release of pressure or as a result of reheating." He therefore had considerable difficulty in developing a scenario of pressure-release melting in the peridotite mantle. Only with the development of geodynamics and acceptance of Holmes's theory of mantle convection could it be shown that a peridotite mantle can rise to regions of lower pressure, thus bringing about melting without the addition of heat.

The theory of partial melting of peridotite was still debated and considered on a weak foundation by many in the first half of the 20th century. Another group of geologists adopted a totally different view, and maintained that basaltic magma was derived from a deep melted layer or from the complete melting of a basaltic layer at depth in the Earth. This view persisted with some until the 1960s. In an influential book on volcanoes, Alfred Rittmann proposed in 1936 that all volcanic rocks were ultimately derived from a global layer of basaltic magma. Rittmann's views were adopted by the petrologist Tom F. W. Barth in 1951: "The fact that wherever the crust is deeply rifted, be it in continents, oceans, or geosynclines, basaltic magma is available and capable of invasion is a proof of the existence of a subcrustal basaltic magma stratum." He was fully aware of the objections of geophysicists, that such a layer could not transmit some seismic waves, contrary to observations, and proposed that the basaltic magma behaved like glass at the high pressures beneath the Earth's crust and was thus able to transmit these waves. In his 1962 work on *Theoretical Petrology* Barth stated: "It is necessary, therefore, that the basaltic substratum is in a molten (noncrystalline) state at its subterranean locale. Otherwise it would not reach the surface with a homogeneous composition as we actually observe."

The American geologists Francis J. Turner and John Verhoogen accepted the seismic evidence for a solid character of the Earth's mantle in 1951, and considered it composed either of peridotite or of eclogite. From this it followed that primary basaltic magma had to be derived from a largely solid mantle, whose composition was other than basalt. The observed temperature increase with depth and heat generation by radioactive decay within the Earth could produce the required heat source. In their classic textbook on *Igneous and Metamorphic Petrology*, Turner and Verhoogen stated: "The problem of the origin of basaltic magma is thus not so much that of finding adequate heat sources as that of explaining how relatively small amounts of heat may become locally concentrated to produce relatively small pockets of liquid in an otherwise crystalline mantle." In what seemed like a fleeting moment, Turner and Verhoogen considered the hypothesis that basaltic magma could be produced by melting of a peridotite mantle due to pressure release, but then quickly rejected it: "This hypothesis of magma generation is possibly the most popular one, although it is unacceptable to the present writers. It is difficult indeed to see how pressure can effectively be reduced at such depths." They realized of course, that melting could occur if convective transport of mantle material occurred to shallower levels, as originally proposed by Arthur Holmes. This was clearly a viable mechanism as long as the deep mantle temperature was greater than the melting point of the mantle at shallower depth. Yet they were not ready to accept the existence of convection in the solid Earth, which led them to conclude: "Whether convection does occur in the mantle is not definitely known, nor is it known whether it could be effective in the upper part of the mantle where magmas are generated. Thus, although convection might lead to melting, it cannot be shown that it does, and the problem of the generation of magma remains as baffling as ever."

This statement is a good reflection of the state of affairs regarding theories of magma generation at the middle of the 20th century. While great strides had been made in understanding the chemistry and mineralogy of volcanic rocks, the Earth scientists were at a loss to explain melting. This was due almost entirely to the static view taken of the Earth's interior at the time—it seemed inconceivable to most that the rigid and solid mantle could convect. However, the discoveries made on the ocean floor in the 1960s and development of geodynamics were to change all that. Although melting was poorly understood at the time, knowledge of the mantle source region was advancing through studies of xenoliths. A great number of xenoliths are of peridotite composition, giving further credence to the idea that the source region of basalt magma, the Earth's mantle, is dominantly composed of peridotite.

XVI. THE ROLE OF WATER

Great clouds of gases and steam emitted by volcanoes were long considered to be derived from groundwater, surface waters, such as nearby lakes or streams, or seawater. This was evident, according to many scholars, from the location of volcanoes near the ocean or on islands. The role of water was thought to be crucial in generating explosive eruptions and to have an important effect on the viscosity of magmas. In 1794 Spallanzani recognized that several gases are important in lavas and volcanic regions, including "hydrogenous gas, sulfurated hydrogenous gas, carbonic acid gas, sulfurous acid gas, azotic gas." But another, more powerful agent, he noted, was "water, principally that of the sea," which communicates by passages with the roots of volcanoes. On reaching the subterranean fires it suddenly turns to vapor, and the elastic gas expands rapidly, causing volcanic explosions. Supporting his hypothesis, on a more practical level, Spallanzani cited accidents in glass-making factories, in which molten glass was poured into molds not completely dry or free of water, causing dreadful steam explosions.

Scrope (1825) attributed the fluidity of magmas to water: "There can be little doubt that the main agent . . . consists in the expansive force of elastic fluids struggling to effect their escape from the interior of a subterranean mass of *lava*, or earths in a state of liquification at an intense heat." These "elastic fluids" Scrope considered to be mainly steam and other volcanic gases. It was the expansion of gas in the magma that led to its rise in the Earth's crust, and led to violent and explosive eruption upon reaching the surface.

Scrope discussed in some detail the evolution of steam in magmas at depth, and was perhaps the first to point out that under great pressure, water would be dissolved in the melt, but upon decrease in pressure or increase in temperature the water would be vaporized, leading to explosive eruption. From the increase of temperature with depth in mines, Scrope concluded that at great depth, the Earth was at an intense heat, and that this great accumulation of *caloric* in the deep Earth led to continued flow of caloric toward the surface, in order for the heat to attempt to attain equilibrium. Thus Scrope considered the formation of magma as due to the passage of caloric by conduction from depth to upper levels in the Earth, where the caloric led to melting of rocks. Scrope proposed that the caloric in molten rocks was in large measure due to water: "There is every reason to believe this fluid to be no other than the vapour of water, intimately combined with the mineral constituents of the lava, and volatilized by the intense temperature to which it is exposed when circumstances occur which permit its expansion." The water of the oceans, he theorized, was derived from the interior of the Earth due to degassing through volcanoes. Large quantities of water "remain entangled interstitially in the condensed matter" in the deep-seated rocks, and the escape of steam during volcanic eruptions carries off an immense amount of caloric, leading to rapid cooling and consolidation of magmas at the surface.

By 1865 the French geologist M. Fourque had measured the amount of water in the volcanic products of Etna and estimated the amount of steam discharged from the vent. In the latter part of the 19th century geologists began to develop more sophisticated models, proposing that the steam emitted by volcanic eruptions was primordial or of deep-seated origin, rather than just recycled surface waters. Among them was Osmond Fisher (1881), who regarded volcanic gases as original constituents of magma. The potential role of escape of water from volcanoes in the formation of the oceans began to surface as an important hypothesis. The German geologist Eduard Suess proposed that all water in the oceans and atmosphere came from the outgassing of the interior of the Earth. The concept of volcanic recycling of water from the ocean to the atmosphere and back again to the deep Earth was proposed by John Judd (1881), who pointed out that volcanoes are generally located near the ocean, and speculated that fissures may transport seawater from the ocean to the magma at depth. "Volcanic outbursts" could be due to water finding its way down to a highly heated rock mass, lowering the melting temperature and causing melting. Judd considered high temperature and the presence of water and gas as the key factors of volcanic action and argued that magmas can absorb or dissolve large quantities of water, which escapes violently during explosive volcanic eruption, as Spallanzani had first pointed out. The magmas could absorb water or gases either initially, as primordial gases during formation of the globe, or at any stage in geologic history, due to infiltration of water into the Earth's crust.

With the widespread recognition of water in magmas, it was logical to consider its role in explosive eruptions. In the age of steam during the Industrial Revolution of the 19th century, John Judd pointed out that "a volcano is a kind of great natural steam-engine." Bonney (1899) also compared volcanoes to a boiler, emphasizing that the steam in magma is the main explosive force in an eruption. He noted that the volume of steam is nearly 1700 times that occupied in the form of water, an enormous expansive force, adequate to account for volcanic explosions. The origin of volcanic water, according to Bonney, is related to the proximity of volcanoes to the ocean and the percolation of rainwater into the magma. He stressed the importance of addition of water to lower the melting point of rocks, and followed Osmond Fisher and others in attributing eruption to the presence of water. When water is depleted or withdrawn from the system, the eruption ceases.

In the latter part of the 18th century, Dolomieu had determined that many deposits in Italy and on Sicily, which at first sight looked like normal stratified sediments, were in fact consolidated volcanic ash deposits, the products of fallout from explosive eruptions. The disruption of magma as it is blown into the air leads to fragmentation and the formation of volcanic ash, tephra, scoria, and other forms of pyroclastic material. We now know that the primary agent of this disruption is the explosive expansion of steam. Sartorius von Waltershausen (1853), a true pioneer in the study of pyroclastic rocks, was the first to attribute their formation to the effects of water on the magma. He proposed that magma rises and erupts due to pressure of water vapor escaping from the magma and that the volume increase of water vapor was also responsible for the fragmenting process—the formation and ejection of pyroclasts such as pumice and ash. He also recognized that peculiar volcanic rock deposits can result when magma enters the ocean or is erupted under water. It was during travels in Sicily in 1835 that he first came across a brown tuff, a homogenous rock, composed largely of a single mineral. He named the rock *palagonite* after the nearby town of Palagonia, and by chemical analysis determined it as one unusually rich in water and iron, with about 12–23 wt% water. He became curious as to the rock's origin, and noting that it was often associated with marine deposits, proposed that it was a volcanic product that forms thick layers in many submarine volcanic formations. In 1846 he and Robert Bunsen studied palagonite mountains in Iceland, and noted that a zone of palagonite tuffs stretches across Iceland. Often in association with palagonite he noted, was a black, water-free and glass-like material, similar to obsidian, which he gave the name *sideromelan.* He was able to show that palagonite is basically sideromelane or basaltic glass that has taken up water, and from its geologic setting, that palagonite is a product of shallow subaqueous or submarine basaltic eruptions. Von Waltershausen was correct in this deduction; we now know that the Icelandic palagonite rocks are formed by volcanic eruptions below the thick ice cap that covered Iceland during the last ice age, and that the Italian palagonites were erupted in the ocean.

Bunsen, on the other hand, disagreed with von Waltershausen, considering the palagonite tuffs as the products of basaltic rocks metamorphosed in the presence of much water and carbonate. He showed by chemical analysis that the tuffs were virtually identical to basalt lava after the high water content had been subtracted. His study was not restricted to Icelandic rocks, because Charles Darwin had given him samples of palagonite from the Cape Verde islands.

Another volcanic rock of basaltic composition is lava-like but composed of rounded or pillow-like forms. The origin of this rock does not have a bearing on water in magmas, but rather on magma in the water. The identification of *pillow lava* dates back at least to the 1870s. Later it was proposed on the basis of observations in Italy that it forms due to submarine eruption. The British geologist Tempest Anderson observed an eruption in Samoa, noting that when the basaltic lava was flowing into the sea, the submarine component of the lava formed bulbous masses and lobes with the shape of pillows. By 1914 a subaqueous origin for pillow lavas had been established. They were already known to be present in the geologic record in association with marine sediments in Scotland, and also as products of subglacial eruptions, such as in Iceland. Oceanographers discovered only in the 1960s that basaltic pillow lava forms the floor of most of the world's oceans and is thus the Earth's most abundant volcanic rock but also the most remote for study.

When high-pressure melting experiments were first carried out at the beginning of the 20th century, it became evident that magmas residing deep in the Earth can contain much more water in solution, and that this water must be liberated when they are erupted at the surface. In 1903 C. Doelter was one of the first to propose that magmas at great pressure in the Earth's crust may dissolve water and that the magmas may become explosive when they reach the surface of the Earth. In support of this theory, the French geologist Armand Gautier carried out laboratory experiments on volcanic activity in 1906, suggesting that magma rises in the crust as a result of gas expansion, and attributed the violence of volcanic eruptions to the explosive liberation of water from the magmas. By the early 20th century the fundamental ideas about the causes of explosive volcanism and the importance of water had thus been firmly established.

SEE ALSO THE FOLLOWING ARTICLES

Archaeology and Volcanism • Earth's Volcanoes and Eruptions: An Overview • Mantle of the Earth • Origin of Magmas • Plate Tectonics and Volcanism • Volcanoes in Art • Volcanoes in Literature and Film

FURTHER READING

Brush, S. G. (1979). "Nineteenth-century debates about the inside of the earth: Solid, liquid or gas?" *Ann. Sci.* **36,** 225–254.

Kushner, D. S. (1990). The emergence of geophysics in nineteenth century Britain. Ph.D. thesis, Princeton University, Princeton, NJ.

Laudan, R. (1987). "From Mineralogy to Geology. The Foundations of a Science 1650–1830." University of Chicago Press, 278 pp.

Sigurdsson, H. (1999). Melting the Earth; The Evolution of Ideas about Volcanic Eruptions. Oxford University Press, New York, 250 pp.

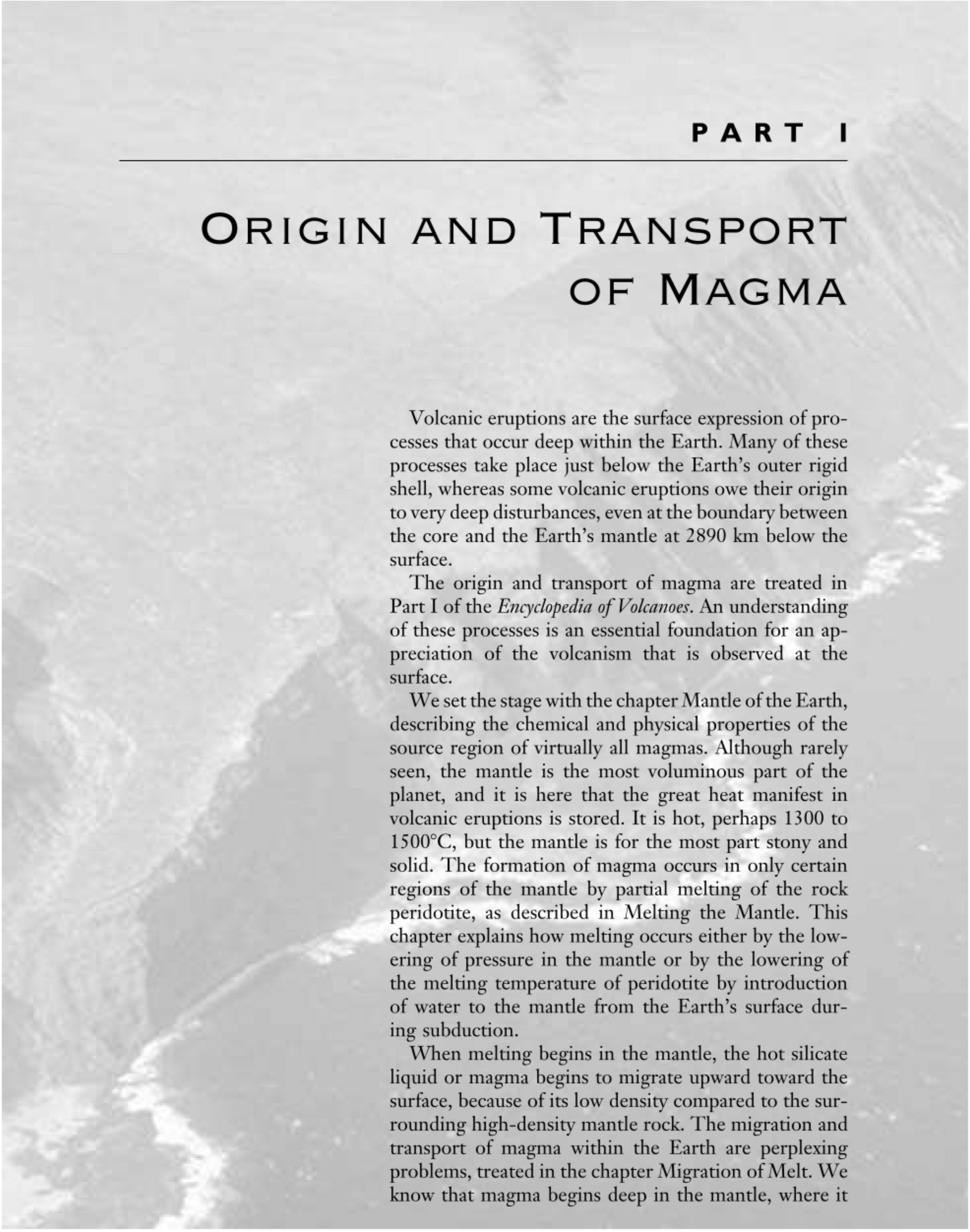

PART I

ORIGIN AND TRANSPORT OF MAGMA

Volcanic eruptions are the surface expression of processes that occur deep within the Earth. Many of these processes take place just below the Earth's outer rigid shell, whereas some volcanic eruptions owe their origin to very deep disturbances, even at the boundary between the core and the Earth's mantle at 2890 km below the surface.

The origin and transport of magma are treated in Part I of the *Encyclopedia of Volcanoes*. An understanding of these processes is an essential foundation for an appreciation of the volcanism that is observed at the surface.

We set the stage with the chapter Mantle of the Earth, describing the chemical and physical properties of the source region of virtually all magmas. Although rarely seen, the mantle is the most voluminous part of the planet, and it is here that the great heat manifest in volcanic eruptions is stored. It is hot, perhaps 1300 to 1500°C, but the mantle is for the most part stony and solid. The formation of magma occurs in only certain regions of the mantle by partial melting of the rock peridotite, as described in Melting the Mantle. This chapter explains how melting occurs either by the lowering of pressure in the mantle or by the lowering of the melting temperature of peridotite by introduction of water to the mantle from the Earth's surface during subduction.

When melting begins in the mantle, the hot silicate liquid or magma begins to migrate upward toward the surface, because of its low density compared to the surrounding high-density mantle rock. The migration and transport of magma within the Earth are perplexing problems, treated in the chapter Migration of Melt. We know that magma begins deep in the mantle, where it forms a small part of the peridotite rock, like water in a sponge, and we know that eventually it pools into large liquid bodies near the surface. The intermediate stage in magma transport, between the source and the shallow reservoir, is one of the major problems in the study of magma evolution, as discussed here.

How does the magma percolate upward toward the surface? Does it migrate upward through the action of dikes?

Melting in the mantle determines the location of volcanoes on Earth, but the location of melting is largely determined by plate tectonics, the theory that describes the motion of the great crustal plates that make the rigid exterior shell of the Earth. As described in the chapter Plate Tectonics and Volcanism, melting occurs beneath plate boundaries where plates are either moving apart, such as below the mid-ocean ridges, or below converging plates in subduction zones. In the former case, melting is due entirely to decompression, as the mantle rises up to fill the void between the diverging plates. In the latter case, however, decompression melting is further aided by the introduction of water and lowering of the solidus. However, a significant fraction of Earth's volcanism occurs totally independent of plate motion, creating hot spots. It is hypothesized—although not yet proven—by many geologists that hot spots are the result of great mantle plumes, which may originate from a region near the boundary of the mantle and the core.

Our most important clues about the formation and origin of magmas come from studies of the chemical and mineralogical composition of volcanic rocks, as described in the chapter Composition of Magmas. These silicate liquids, drawn from deep inside the Earth, have much to tell about their peridotite source rock as well as about the history and formation of the planet. The chemical diversity of magmas or volcanic rocks seems at first bewildering, with a plethora of names used by geologists to describe all of these rock types. The reason for this great diversity is explored in the chapter Origin of Magmas, which explains the great variety of physical and chemical processes leading to the differentiation of magmas.

Virtually all of the known chemical elements occur in magmas, although most are present only in trace amounts. Many chemical compounds in magmas, including water, carbon dioxide, and sulfur dioxide, are normally dissolved in the magma at high temperatures and pressures, but come out of solution when the magma nears the surface and erupts. These are the volatiles in magmas, whose properties and evolution are dealt with in the chapter Volatiles in Magmas. The concentration and behavior of the volatiles are particularly important, as their abundance in the magma largely determines the explosive nature of volcanic eruptions. The distinction between the quiet effusion of lava flows and the explosive ejection of volcanic ash and pumice is primarily a reflection of the original water content in the magma. However, the rheological behavior of magmas is also dictated by their physical properties, such as viscosity and temperature, as discussed in the chapter Physical Properties of Magmas. The importance of the bulk viscosity is, for example, demonstrated by the fact that volatiles can rise and escape freely to the surface as gas bubbles from a low-viscosity basaltic magma, whereas the viscosity of andesitic or rhyolitic magmas is so high that the bubbles cannot rise but are carried with the magma to the surface, with explosive results.

Magmas rising from the mantle may often gather in reservoirs at the base of the crust or within the Earth's crust. Reservoirs may be tens of kilometers in dimension and thus represent huge reserves of magma. The chapter Magma Chambers explains the behavior of these magma chambers, the geological and geophysical evidence for their size and dimensions, and the processes that occur within them. The chapter Rates of Magma Ascent describes how petrologic studies and geochemical research on short-lived isotopes in magma are providing information on the rates of magma ascent.

Most of the magma is transported in dikes from the deep reservoir to the surface, as described in the the chapter Plumbing Systems. During dike flow the magma experiences extreme gradients in temperature and pressure as it moves through the cold and rigid upper crust of the Earth. It seems at first amazing that magma may flow for several kilometers in a 1-m-wide dike without solidifying, but as explained in this chapter, the magma may retain most of its heat during dike flow and arrive at the surface in a fiery eruption.

During its ascent in a dike or a conduit, magma experiences a very important change, as the volatiles—mainly water, carbon dioxide, and sulfur dioxide—exsolve from the magma to form a separate gas phase. Exsolution occurs when the pressure decreases below the solubility limit of these volatiles in the magma, as described in the chapter Magma Ascent at Shallow Levels. In the crust above this level, the magma in the dike or conduit behaves as a two-phase flow, consisting of a silicate melt and a gas phase that continues up the ally, expanding as pressure decreases. This is the most dynamic region of magma evolution, and rates of motion are on the order of meters per second, whereas rates of deeper magma flow are centimeters per second. The exsolving gas appears as growing bubbles that expand until they burst, tearing apart the magma in the conduit and expelling it to the surface.

Haraldur Sigurdsson
University of Rhode Island

This Page Intentionally Left Blank

MANTLE OF THE EARTH

RAYMOND JEANLOZ
University of California, Berkeley

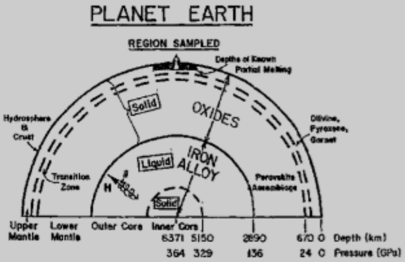

I. Introduction
II. Structure and Physical Properties
III. Mineralogy and Composition
IV. Dynamics

GLOSSARY

basalt A lava (or solidified, glassy equivalent) having the bulk composition of a gabbro.

chondritic Refers to a rocky meteorite, typically consisting of an ultramafic silicate assemblage plus lesser amounts of metal. The most primitive (unheated, undeformed) are the CI class, and are considered to be samples of the material left over from planet formation.

D″ region Region at the base of the mantle that is characterized by strong lateral heterogeneity in seismic wave velocities.

gabbro A rock consisting primarily of pyroxene and feldspar; it may contain olivine.

kimberlite An explosively emplaced volcanic rock that is originally a fluid-rich ultramafic in overall composition and typically contains many xenoliths.

liquidus Temperature below which a molten compound begins to crystallize.

lithosphere Crust and uppermost mantle behaving in a quasi-rigid fashion over geological timescales, it corresponds to the tectonic plates at the Earth's surface and is typically no more than ~100–150 km thick.

low-velocity zone An intermittent zone exhibiting slightly reduced seismic-wave velocities and enhanced wave attenuation at depths of ~50–150 km in the mantle.

magma Molten rock inside the earth. Lavas are magmas that have erupted at the Earth's surface.

moho A discontinuous increase with depth of seismic-wave velocities, from ~7 to 8 km/s for compressional waves. Named after A. Mohorovicic, the Croatian seismologist who discovered it, the discontinuity defines the interface between the crust and mantle.

ophiolite A piece of oceanic crust and topmost mantle that has been uplifted and exposed at the earth's surface.

peridotite An ultramafic rock consisting predominantly of olivine, coexisting with other minerals rich in Mg and Fe, such as pyroxene.

pyrolite A ~3 : 1 mixture of peridotite and basalt that is intended to simulate undepleted ("fertile") periodotite of the upper mantle.

refractory Refers to an element or compound having a high condensation (or evaporation) temperature and, correspondingly, a high melting (or freezing) temperature.

silicate A compound containing silicon and oxygen. Most common minerals are silicates or oxides (oxygen-containing compounds), such as SiO_2 quartz or Mg_2SiO_4 olivine.

solidus Temperature above which a crystalline compound begins to melt.

ultramafic Rich in Mg and Fe, or in Mg- and Fe-rich minerals such as $(Mg, Fe)_2SiO_4$ olivine.

ULVZ Ultra-low-velocity zone; a thin zone just above certain regions of the core–mantle boundary that is charac-

Copyright © 2000 by Academic Press
All rights of reproduction in any form reserved.

terized by very low seismic-wave velocities (e.g., 20% decrease in shear-wave velocity from the overlying mantle).

volatile Refers to an element or compound having a low condensation (or evaporation) temperature and, correspondingly, a low melting (or freezing) temperature.

xenolith A rock fragment brought up from depth within a different rock or magma.

I. INTRODUCTION

The mantle is the ~2850-km-thick shell of rock surrounding the metallic core of the earth (Fig. 1). Because it contains the bulk of the planet's rocky material, the mantle is the ultimate source of the silicate magmas that cause volcanic eruptions, even though the mantle itself is predominantly crystalline, not molten. In particular, partial melting of a few percent of the outermost mantle is the source of magma for midocean ridges, the planet's most active chain of volcanoes. Even magmas that are produced in the crust can ultimately be attributed to the mantle, in that the material making up the crust was initially derived from the mantle; also, it is the mantle that provides much of the heat and tectonic activity causing melting in the crust. This chapter reviews the physical and chemical properties of the Earth's mantle, and the dynamic processes that lead to the melting of the mantle.

II. STRUCTURE AND PHYSICAL PROPERTIES

A. Overall Structure

The structure of the Earth's interior, and hence the dimensions and properties of the mantle, are primarily determined from seismological observations. Recordings of both compressional and shear waves generated by earthquakes or large explosions, as well as oscillations of the entire planet caused by large earthquakes, make it possible to derive the elastic-wave velocities and density as a function of depth (Fig. 2). That the wave veloci-

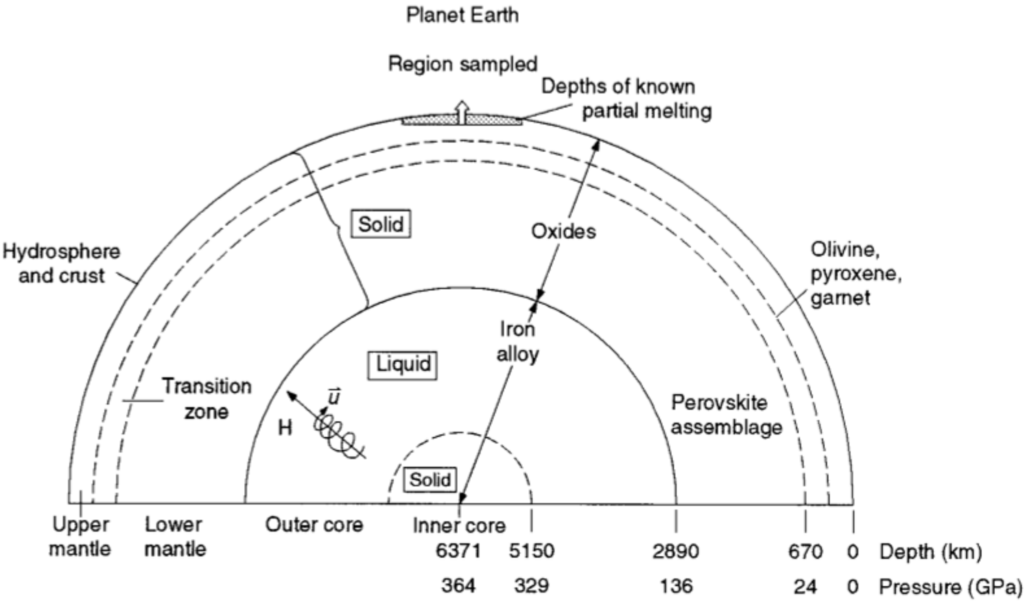
Planet Earth
Region sampled
Depths of known partial melting
Solid
Oxides
Hydrosphere and crust
Olivine, pyroxene, garnet
Iron alloy
Liquid
Transition zone
$\vec{u}$
H
Perovskite assemblage
Solid
Upper mantle
Lower mantle
Outer core
Inner core
6371 5150 2890 670 0 Depth (km)
364 329 136 24 0 Pressure (GPa)

FIGURE 1 Schematic cross section through the Earth, summarizing the seismologically determined structure as a function of depth and corresponding pressure (100 GPa = 1 Mbar). The mantle and overlying crust consist almost entirely of oxides that are not melted ("solid"). Volcanic processes bring rock fragments up to the surface from as deep as ~200 km into the mantle (and possibly deeper), thereby showing that the uppermost mantle consists of peridotite, a rock made up of olivine, pyroxene, and garnet minerals. Laboratory experiments demonstrate that peridotite transforms at conditions of the lower mantle to a rock consisting predominantly of the high-pressure perovskite phase. Cyclonic motions (*u*) in the molten iron alloy of the outer core create the geomagnetic field (**H**) via a dynamo process. [From Jeanloz, R. (1990). *Annu. Rev. Earth Planet. Sci.* **18,** 357–386.]

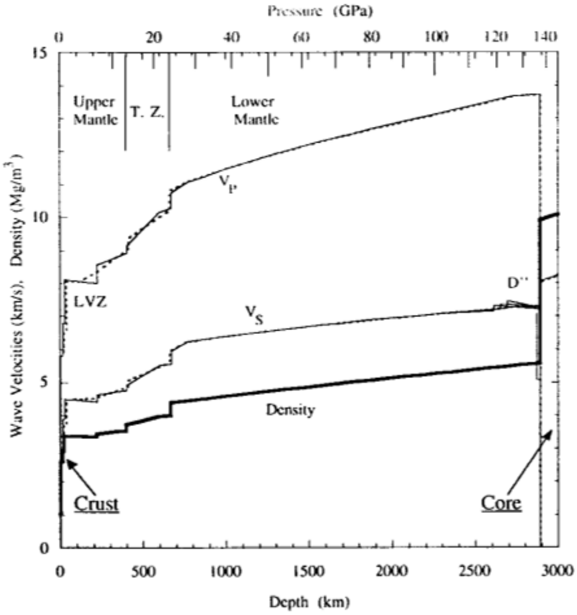

FIGURE 2 Seismologically observed properties of the mantle, from the surface to the core. Compressional- and shear-wave velocities (V_P and V_S; thin curves) and density (bold curve) as a function of depth (bottom) and pressure (top) through the upper mantle, transition zone (T. Z.) and lower mantle according to the preliminary reference earth model (PREM; solid curves) and iasp91 (dotted curves). The low-velocity zone (LVZ) is indicated in the upper mantle, and several illustrative V_S profiles are shown for the D″ region at the base of the mantle. The pressure is very nearly hydrostatic through the interior, so is determined directly from the density profile. [Data from Dziewonski, A. M., and Anderson, D. L. (1981). *Phys. Earth Planet. Int.* **25,** 297–356; Kennett, B. L. N., and Engdahl, E. R. (1991). *Geophys. J. Int.* **105,** 429–465; and Wysession, M. E., *et al.* (1998). *In* "The Core–Mantle Boundary Region." American Geophysical, Union, Washington, DC].

ties and density generally increase with depth throughout the mantle can be attributed to the effects of increasing pressure. Although temperature also increases with depth, the effect of pressure dominates everywhere except in the low-velocity zones described below.

The top of the mantle is identified by the depth at which the velocity of compressional waves jumps discontinuously from values typically less than 7 km/s to greater than 8 km/s (the Mohorovicic discontinuity, or Moho). The thickness of the overlying crust is approximately 25 km on average, but ranges from ∼6 km in oceanic regions up to ∼70 km beneath the Himalayas. The base of the mantle, at a depth of 2890 km, is defined by the disappearance of rigidity. Unlike the mantle, the outer core is liquid; also, it is far denser than the overlying rock. Indeed, the core–mantle boundary is the most significant structure of the Earth in that the contrast in observed properties is even greater than that between the atmosphere and crust.

Two smaller but still significant discontinuities in seismic-wave velocities define the primary subdivision of the mantle, into the upper mantle, transition zone, and lower mantle (Fig. 2). These velocity jumps appear to be globally present at about 410- and 650-km depths, although the exact depths can vary by a few tens of kilometers from one location to another. In addition, both discontinuities appear to be quite sharp, taking place within a depth interval of a few kilometers (i.e., a fraction of the ∼10-km minimum wavelengths of seismic waves that are used to probe its thickness).

B. Low-Velocity Zone and D″

At a more subtle level, there are at least two additional structures that are pervasive, if not globally present, and are considered important: the low-velocity zone in the upper mantle, and the D″ region at the base of the mantle (Fig. 2). The low-velocity zone is a region exhibiting a velocity decrease, typically of no more than ∼1–2%, at depths as great as ∼100–200 km. The magnitude of the velocity decrease and its depth are highly variable from one location to another (and apparently not present in some locations), but it is observed often enough to be considered a common feature of the uppermost mantle. It is especially evident beneath tectonically young areas, such as oceanic crust, or the Basin and Range region of the western United States.

Because increasing temperature is known from laboratory experiments to cause the seismic-wave velocities in rock to decrease (increasing pressure has the opposite effect), the low-velocity zone is considered to be a depth at which high temperatures are reached. For example, average temperatures are thought to approach the melting point (solidus) of the mantle rock at these depths. Studies of anelasticity, the degree to which seismic waves are attenuated as they propagate, show that the low-velocity zone can be highly attenuating, and this observed "mushiness" also supports the view that it is a region of high temperatures. In fact, it may locally be partially melted, and therefore be a zone where magma is commonly present at depth.

The D″ region ("D double prime," a historical name) is a zone in the lowermost mantle that is characterized by significant heterogeneity in seismic-wave velocities.

The detailed velocity profiles vary considerably from one region to another (e.g., beneath the central Pacific versus underneath India or the Caribbean), with both increases and decreases in velocity having been documented over the bottom 200–300 km of the mantle. The region is also characterized by enhanced scattering of seismic waves, further documenting a lateral heterogeneity in velocities. This heterogeneity extends to 500 km or more above the core–mantle boundary, in some areas; in other areas, the D″ region appears to be less than 10 km thick or perhaps missing altogether. Most notable is recent evidence for extreme velocity decreases, of up to 10 and 30% for compressional and shear waves, extending over a zone less than 20–40 km thick at the base of the mantle. Such ultra-low-velocity zones (ULVZs) have been interpreted as demonstrating that magma is present at the base of the mantle.

III. MINERALOGY AND COMPOSITION

A. Samples

The mineralogy and bulk composition of the uppermost mantle can essentially be determined from direct sampling, most notably from ophiolites and xenoliths. In combination with (1) geophysical observations on the deeper mantle, (2) laboratory measurements of mineral and rock properties, and (3) general arguments from geochemistry, it is then possible to deduce the nature of most of the mantle. Before proceeding to the evidence, the result is that the upper mantle consists of peridotite, a rock made up of about 50% olivine [$(Mg, Fe)_2SiO_4$], 40% pyroxene [$(Mg, Fe, Ca)SiO_3$], and 10% garnet [$(Mg, Fe, Ca)_3Al_2Si_3O_{12}$] (Table I). Mineral names and properties are summarized in Table II.

Ophiolites are sections of oceanic lithosphere (crust plus uppermost mantle) that have been uplifted, and even emplaced onto continental crust, by tectonic processes. They classically exhibit a stratigraphic sequence of marine sediments, lying over a basaltic layer (pillow basalts—basalts that were erupted under water—above basaltic dikes and gabbros) that, in turn, is above ultramafic rocks representing the topmost mantle. This sequence of rock types corresponds well with the velocity structure obtained from seismic refraction studies in ocean basins, for example, of sediments above a ~6-km-thick layer of basalt comprising the oceanic crust. In particular, the velocities of the ultramafic rocks sampled from ophiolites can be measured in the laboratory, and are found to match those observed seismologically in the topmost mantle, just below the Moho.

TABLE I Composition of the Upper Mantle Estimated from Natural Samples[a]

Oxide component	*Weight fraction (%)*[b]	*Element*	*Atomic Fraction (%)*
SiO_2	45.0 (±1.4)	O	58.3
TiO_2	0.18 (±0.05)	Mg	20.1 (±1.0)
Al_2O_3	4.5 (±1.5)	Si	15.8 (±0.5)
Cr_2O_3	0.4 (±0.1)		
FeO[c]	7.6 (±1.7)	Fe	2.2 (±0.5)
MnO	0.11 (±0.05)	Al	1.9 (±0.6)
NiO	0.23 (±0.05)	Ca	1.2 (±0.4)
MgO	38.4 (±2.0)		
CaO	3.3 (±1.0)	Na	0.27 (±0.14)
Na_2O	0.4 (±0.2)	Cr	0.11 (±0.03)
K_2O	0.01 (±0.1)		
		Ni	0.06 (±0.01)
Total	100.1	Ti	0.05 (± 0.01)
		Mn	0.03(±0.01)
		K	0.004 (±0.04)

Atomic or Molar Proportions[d]

$X_{Mg} = Mg/(Fe + Mg) = 0.90\ (\pm 0.05)$

$Ol/(Ol + Px) = [Mg + Fe + Ca - Si]/(Si - Ca) = 0.54\ (\pm 0.08)$

[a] *Sources:* Aoki, K. (1984). Pages 415–444 *in* "Materials Science of the Earth's Interior," (I. Sunagawa, ed.). Terra Scientific, Tokyo; Basaltic Volcanism Studies Project. (1981). "Basaltic Volcanism on the Terrestrial Planets." Pergamon, New York; Green, D. H., Hibberson, W. O., and Jacques, A. L. (1979). Pages 265–299 *in* "The Earth: Its Origin, Structure and Evolution" (M. W. McElhinny, ed.). Academic Press, San Diego; Ringwood, A. E. (1975). "Composition and Petrology of the Earth's Mantle." McGraw-Hill, New York; Yoder, H. S. (1976) "Generation of Basaltic Magma." National Academy of Sciences Washington, DC.

[b] Average values and uncertainties are representative of the range of published estimates.

[c] All iron listed as Fe^{2+}.

[d] Magnesium number and olivine : pyroxene (Ol : Px) ratio, respectively.

Ophiolites have the advantage of giving a large-scale geological cross section through the oceanic crust and uppermost mantle, so it is possible to reconstruct thicknesses and geometric relations among the different rock layers. The disadvantage, however, is that ophiolites are typically highly faulted (presumably as a part of the uplift and emplacement process), such that it can be difficult to make sense of how the different rock types are interrelated. Also, the rocks are often heavily weathered, usually

TABLE II Mineral Phases of the Mantle and their Properties[a,b]

Mineral phase	*Chemical formula*	*Density ρ (Mg/m^3)*	*Bulk modulus K_S (GPa)*	*Shear modulus μ (GPa)*
Olivine	$(Mg, Fe)_2SiO_4$	3.22	129	81
Pyroxene[c]	$(Mg, Fe, Ca)SiO_3$	3.21	108	76
Garnet	$(Mg, Fe, Ca)_3Al_2Si_3O_{12}$	3.56	174	89
Majorite	$(Mg, Fe)_4Si_4O_{12}$	3.51	175	90
β-Phase	$(Mg, Fe)_2SiO_4$	3.47	174	114
γ-Spinel	$(Mg, Fe)_2SiO_4$	3.55	184	119
Orthorhombic perovskite	$(Mg, Fe)SiO_3$	4.10	262	155
Cubic perovskite	$CaSiO_3$	4.25	281	—
Magnesiowüstite	$(Mg, Fe)O$	3.58	163	131

[a] *Sources:* Ahrens, T. J., ed. (1995). "Mineral Physics & Crystallography, A Handbook of Physical Constants." American Geophysical Union, Washington, DC.

[b] Experimentally determined values for Mg end members (and $CaSiO_3$) at zero pressure and room temperature.

[c] Two forms are typically present, clinopyroxene and orthopyroxene.

(at least in part) due to hydrothermal circulation of ocean water, so that what is observed is a hydrated version of the primary rock types (for example, serpentine occurs instead of olivine).

Xenoliths are rock fragments brought up to the surface from depth, usually by volcanic processes. Ultramafic fragments thought to come from the mantle are most commonly found in basaltic lavas, but it is the rarer ones found in kimberlite deposits that are probably the most significant (Fig. 3; also see color insert). This

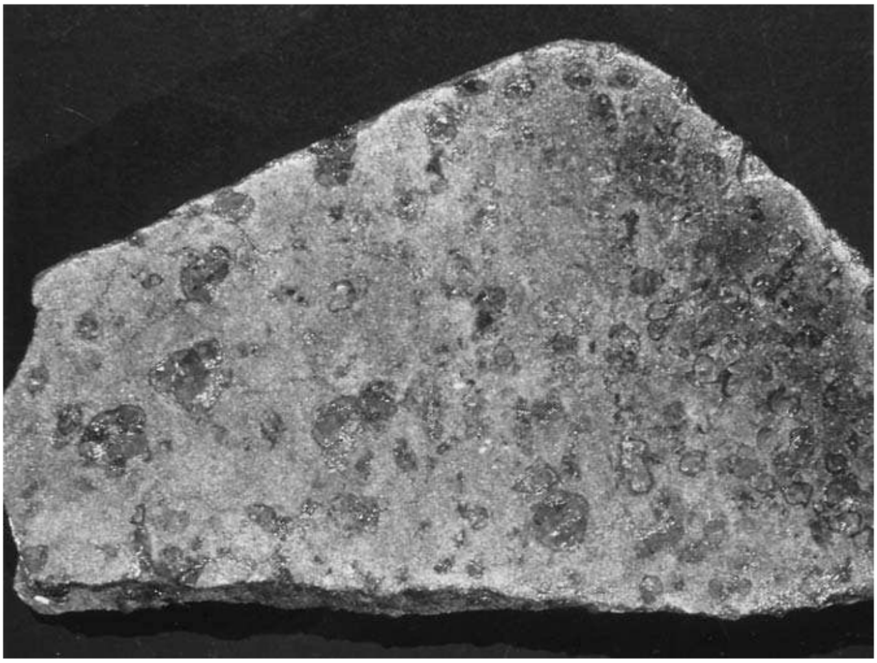

FIGURE 3 Garnet peridotite is the principal rock type in the earth's upper mantle, the source region of magmas. This colorful rock is composed of olivine (olive), orthopyroxene (gray), clinopyroxene (bright green), and garnet (burgundy). The width of this polished slab of mantle rock is 4 cm. [see Yoder, H. S., Jr. (1976). "Generation of Basaltic Magma." National Academy Press, Plate 1, p. 44a]. (Also see color insert.)

is because kimberlites are explosive eruptions that extract the xenoliths very rapidly, and can be shown at least in some cases to originate from great depths. In particular, the presence of diamond in some kimberlites indicates a source at pressures of at least 4–5 GPa (40,000–50,000 atm), the pressure above which diamond is stable relative to graphite at mantle temperatures; this corresponds to depths in excess of 100–150 km. Moreover, laboratory studies show that the detailed compositions of the pyroxenes (e.g., abundances of Ca and trace amounts of Al) vary systematically with temperature and pressure at which the rock is formed. This effect has been calibrated such that it is possible to infer the temperatures and depths of origin of natural peridotite xenoliths from the compositions of their pyroxene minerals (analyses referred to as *geothermometry* and *geobarometry*). The result is that many peridotite xenoliths from kimberlites are found to originate from depths of 100–200 km or possibly deeper. Because the mineral compositions reflect the last conditions under which thermodynamic equilibrium was established, it is possible that a given xenolith was previously at a higher pressure and temperature, therefore greater depth, than is last recorded by the pyroxene compositions.

The seismic-wave velocities and density of peridotite (or its constituent minerals, averaged in the appropriate proportions) have been measured in the laboratory as a function of pressure and temperature, and do match the seismological observations on the upper mantle. Therefore, because peridotite is the rock that is brought up from the mantle by geological processes, and because its properties match those observed geophysically for the upper mantle, there is strong evidence that this is indeed the primary material making up the outer mantle of the Earth.

In addition, it is found that partial melting of peridotite produces basaltic liquids, comparable to those erupted in abundance at midocean ridges. Indeed, detailed seismological studies show that patches of reduced velocities and enhanced attenuation can be found within the top ~40 km of the mantle beneath midocean ridges, implying the presence of partial melt. Taking the melting conditions that have been determined experimentally for peridotite, one finds that enough basaltic melt of appropriate composition can be made to produce the 6-km-thick oceanic crust with about 15% (=6/40) overall melting of the upper mantle rock (the amount of melt present at any one time may be far less, however). This compatibility between laboratory studies and geophysical observations is in good accord with the conclusion that peridotite is the predominant rock of the upper mantle.

There needs to be a bit of care in describing the chemical compositions of natural peridotites, in that basaltic liquid is very mobile and therefore tends to separate quickly from its peridotite source in the upper mantle. The extraction of basalt changes the composition of the initial peridotite slightly; for example, iron, aluminum, and silicon tend to preferentially go into the liquid, leaving the residual crystalline phases slightly depleted in these elements. Most peridotite samples exhibit small but varying degrees of depletion of these key elements, so the tendency is to identify an end member composition that (as far as one can tell) has not suffered any basalt extraction and consider this to represent pristine, "fertile" peridotite. That is, the rock is fertile in the sense that it readily produces basalt upon partial melting, whereas depleted peridotite has had much of the basalt extracted from it. (Pyrolite, a synthetic model for the fertile peridotite comprising the upper mantle, consists of partially depleted peridotite plus basalt in approximately a 3 : 1 ratio.)

B. Experiments

One test of the hypothesis that peridotite is the predominant rock of the outer mantle is to consider what happens to it, and its constituent minerals, as a function of depth (Fig. 4). Numerous laboratory experiments demonstrate that with increasing pressure, the olivine transforms to new phases having spinelloid and then spinel crystal structures (β-phase or wadsleyite, and γ-spinel or ringwoodite, respectively). In parallel, the pyroxenes dissolve into the garnet structure, which then transforms to an ilmenite-structured phase (Table II). All of these transformations are complete at pressures below that of the 650-km discontinuity. In fact, most take place at the conditions of the transition zone (pressures of ~12–20 GPa), whereupon both the olivine and the garnet-pyroxene phases transform to an assemblage of silicate perovskite [$(Mg, Fe)SiO_3$ + $CaSiO_3$ in orthorhombic and cubic perovskite structures] plus magnesiowüstite [$(Mg, Fe)O$ in the rocksalt structure]. The elastic properties of all of these mineral phases have been measured experimentally, often as a function of temperature and pressure, and complementary theoretical calculations (including, first-principles quantum mechanical calculations) help verify and expand on the existing measurements.

The striking fact is that the peridotite minerals undergo their primary transformations at the pressures corresponding to the 410- and 650-km discontinuities.

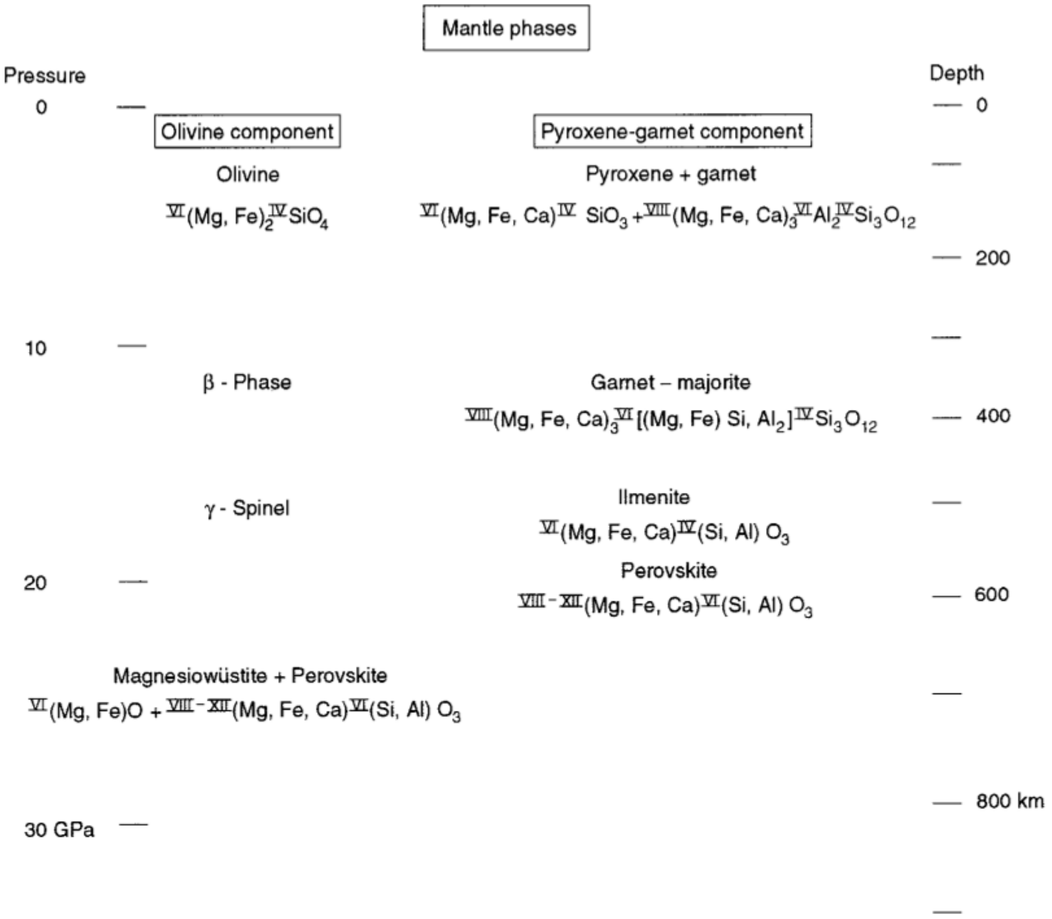
Mantle phases
Pressure
Depth
0
10
20
30 GPa
0
200
400
600
800 km
Olivine component
Pyroxene-garnet component
Olivine
$^{VI}(Mg, Fe)_2^{IV}SiO_4$
Pyroxene + garnet
$^{VI}(Mg, Fe, Ca)^{IV} SiO_3 + ^{VIII}(Mg, Fe, Ca)_3^{VI}Al_2^{IV}Si_3O_{12}$
β - Phase
Garnet – majorite
$^{VIII}(Mg, Fe, Ca)_3^{VI}[(Mg, Fe) Si, Al_2]^{IV}Si_3O_{12}$
γ - Spinel
Ilmenite
$^{VI}(Mg, Fe, Ca)^{IV}(Si, Al) O_3$
Perovskite
$^{VIII-XII}(Mg, Fe, Ca)^{VI}(Si, Al) O_3$
Magnesiowüstite + Perovskite
$^{VI}(Mg, Fe)O + ^{VIII-XII}(Mg, Fe, Ca)^{VI}(Si, Al) O_3$

FIGURE 4 Summary of mineral transformations that take place in a rock of garnet-peridotite bulk composition as a function of pressure (equivalently, depth) in the mantle. Roman superscripts give the coordination number (number of nearest-neighbor oxygen ions) for each cation. The minerals making up peridotite can be separated into two groups, (1) olivine and (2) a combination of pyroxenes and garnet. As a function of increasing pressure through the upper mantle and transition zone, olivine transforms to the spinelloid (β-phase) and spinel (γ) structures, whereas pyroxene dissolves into the garnet structure (ultimately forming majorite, a mineral phase having the composition of pyroxene and the crystal structure of garnet), which then transforms to the ilmenite structure. Orthorhombic and cubic perovskites become stable, along with magnesiowüstite, at lower mantle conditions. [From Jeanloz, R., and Thompson, A. B. (1983). *Rev. Geophys. Space Phys.* **21,** 51–74.]

Indeed, if one uses laboratory measurements to estimate the wave velocities and density for the transforming peridotite with increasing pressure and temperature as a function of depth, very nearly the same values and jumps are obtained as are observed seismologically. The uncertainties in such a comparison are significant, in that wave-velocity measurements are still not possible at the simultaneously high temperatures and pressures of the transition zone (i.e., it is necessary to extrapolate from lower pressures and temperatures at which measurements have been made), but the basic conclusion that a peridotite-like bulk composition reproduces the average seismological properties of the upper mantle, transition zone, and lower mantle does seem to be robust in broad terms.

The changes in mineral properties with increasing depth in the mantle are relatively well understood, due to numerous experimental measurements and theoretical studies that have been carried out during the past few decades. Specifically, the elastic moduli (bulk modulus or incompressibility, and shear modulus or rigidity) of minerals tend to increase rapidly as the crystal structures are compressed under pressure. The overall packing of the atoms increases with depth in the mantle, both due to simple compression of the crystal structures and as a result of the phase transformations. These processes yield the observed increases in both density and wave velocities through the transition zone region. For example, the olivine structure is made up of sheets of oxygen ions that are closely packed in two dimensions but loosely packed in the third (a loose stacking of hexagonal close-packed sheets); the cations are situated in octahedral (for Mg and Fe) and tetrahedral (for Si) pockets in between the oxygens. The effect of the transformation to the spinel or spinelloid structure is to cause the packing of the oxygen ions to become dense in all three dimensions (a nearly ideal cubic-close packing), with the remaining cations still in octahedral (six nearest-neighbor oxygens) and tetrahedral (four nearest-neighbor oxygens) sites.

Perhaps the most profound change in atomic packing is that the tetrahedral (fourfold) coordination of silicon by oxygen that is typical of crustal and upper-mantle minerals transforms to an octahedral (sixfold) coordination of silicon by oxygen at lower-mantle conditions. For example, olivine and pyroxene contain, respectively, isolated units and chains of SiO_4 tetrahedra, whereas the ilmenite and perovskite phases of $(Mg, Fe)SiO_3$ contain SiO_6 octahedra.

The perovskite phase is notable for its ultradense packing of ions, with the Mg and O ions together forming a cubic close-packed array. Also, it is the high-pressure product (along with coexisting oxide) of all the primary upper mantle minerals, and it appears to be stable at all pressures existing throughout the lower mantle. Thus, Mg-silicate perovskite is expected to be the predominant mineral of the lower mantle, and its properties are found to match closely the observed density and wave-velocity values of the lower mantle. Consequently, although it is only stable above 20 GPa, silicate perovskite is considered to be the single most abundant mineral of the planet.

C. Cosmochemistry

In addition to the evidence provided by xenolith and ophiolite samples, the composition of any terrestrial (rocky, Earth-like) mantle is expected to be broadly peridotite-like based on general cosmochemical arguments. Because the Sun contains the bulk of the mass of the solar system, its composition provides a good estimate of the composition of the solar nebula from which the planets formed (the composition of the Sun, in turn, is understood based on the properties of atomic nuclei and theories of stellar evolution). During or shortly after their formation, high temperatures caused the terrestrial planets to lose most of their volatile (nonrefractory) elements, particularly the lightest ones such as hydrogen and helium; in fact, the Earth is still losing hydrogen to space. The more refractory elements, however, are thought to be largely retained in their original abundances. This is empirically found to be the case, in that the primitive chondritic meteorites, silicate-plus-metal assemblages representing fragments of the material left over from planet formation, do exhibit relative abundances of nonvolatile elements that are generally in close agreement with the spectroscopically observed distribution of abundances for the Sun (Fig. 5). Although there are discrepancies in detail (most of which are well understood), the agreement over many orders of magnitude of abundance is significant.

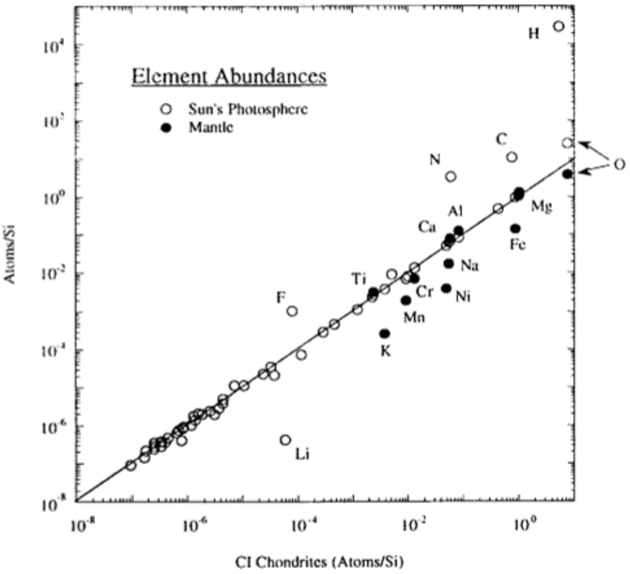

FIGURE 5 Comparison of element abundances, expressed as number of atoms per Si atom, shown for the Sun's photosphere (open symbols; H, O, C, N, F, and Li are labeled) and the Earth's upper mantle (filled symbols: data from Table I, all elements are labeled) relative to the Orgueil meteorite, which is a typical primitive chondritic composition (CI chondrite). Chondrites are depleted in the volatile elements H, O, C, N, and F, relative to the Sun, and the upper mantle is further depleted in O, Na, and K (presumably due to volatility) as well as Fe and Ni (perhaps due to inclusion in the core). Not visible at this scale is the significantly higher Mg/Si ratio for the upper mantle (1.27) relative to chondrites (1.03) and the Sun (1.07). [Data from Anders, E., and Ebihara, M. (1982). *Geochim. Cosmochim. Acta* **46,** 2363–2380; Anders, E., and Grevesse, N. (1989). *Geochim. Cosmochim. Acta* **53,** 197–214.]

Similarly, estimates of the Earth's upper mantle composition based primarily on xenolith samples (Table I), are in general agreement with the solar system ("cosmic") abundances of refractory elements (Fig. 5). This is not surprising, in that chondritic meteorites generally consist of ultramafic assemblages (~80% olvine + pyroxene together, plus ~20% iron alloy). During accretion of the Earth, the metal presumably sank to form the core, with the remaining silicates building up the mantle to yield a peridotite-like assemblage of minerals that is just like the silicate portion of meteorites. The agreement is imperfect in detail, in that the predominant element of the mantle (oxygen) is apparently volatile enough to have been partially depleted (relative to Si) during Earth formation. Also, the ratio of the next most abundant elements, Si/Mg, is found to be systematically (~20%) higher for chondritic than Earth-mantle compositions (the olivine:pyroxene ratio observed for meteorites is lower than that observed for samples from the upper mantle; Table I). Against the backdrop of broad agreement between mantle and chondritic abundances for nonvolatile elements, the significance of these smaller deviations remains unclear.

IV. DYNAMICS

A. Heat Transfer and Mantle Temperatures

The distribution of temperature with depth in the mantle is determined from a combination of measurements (Fig. 6): (1) the observed temperature and its depth dependence in the crust, (2) geothermometry and geobarometry on mantle xenoliths, and (3) comparison of laboratory experiments giving the pressure at which olivine transforms to the β-phase at various temperatures, with the pressure at which the transformation is observed (as the 410-km seismic discontinuity) in the Earth. The last of these provides a determination of 1400° (±200) C at the top of the transition zone, with the geotherm rising to temperatures above 2000°C in the lower mantle.

To understand the temperature distribution throughout the mantle and, hence, the conditions under which magmas are formed at depth, it is necessary to characterize how heat is transported through the planet. The observation of plate-tectonic motions clearly documents that the uppermost mantle convects in a fluidlike manner over geologic time periods (Fig. 7): The ~1–10 cm/yr rates of plate motion are now measured nearly in real time using GPS (global positioning system) and related technologies. Indeed, it has long been recognized that the "solid" Earth behaves as though it is a fluid body, in that it has the flattened-spheroidal shape of a rotating fluid. The early assumption was that the Earth's interior is molten; however, this became problematic about 100 years ago, when seismological observations began to show definitively that the crust and mantle are solid, in the sense of transmitting shear waves (i.e., supporting

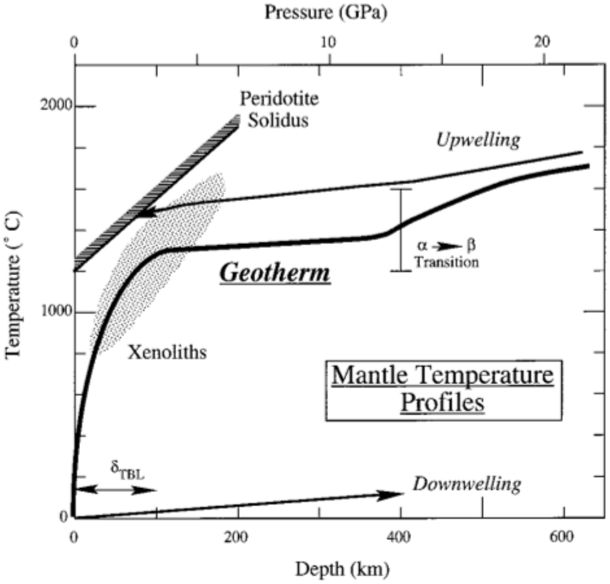

FIGURE 6 Average temperature profile through the upper mantle (geotherm: bold curve), as determined by mineral compositions in xenoliths (stippled) and comparisons of the seismologically observed depth (equivalently, pressure) of the 410-km seismological discontinuity with laboratory measurements of the effect of temperature on the pressure for the transformation of olivine to the spinelloid β-phase (uncertainty indicated by error bar). The thermal boundary layer, the region across which vertical heat transfer occurs primarily by conduction, is characterized by a steep temperature gradient and a thickness δ_{TBL}. Temperature profiles for upwellings (e.g., hottest temperatures beneath midocean ridges) and downwellings (e.g., coldest temperatures beneath subduction zones) are shown for comparison: Both are characterized by adiabatic temperature gradients (~0.2–0.5°C/km), as is the geotherm below the thermal boundary layer. For comparison, typical solidus temperatures for peridotite are indicated as a function of pressure (shaded line). Geothermometry on xenoliths only represents the geotherm (average) temperature to the degree that the rocks are fragments that have been fortuitously sampled by a rapidly moving flow originating at greater depths; to the degree that the xenoliths are samples of the upwelling portion of the mantle (ultimately bringing the rocks to the surface), the geothermometry should reflect higher than average temperatures.

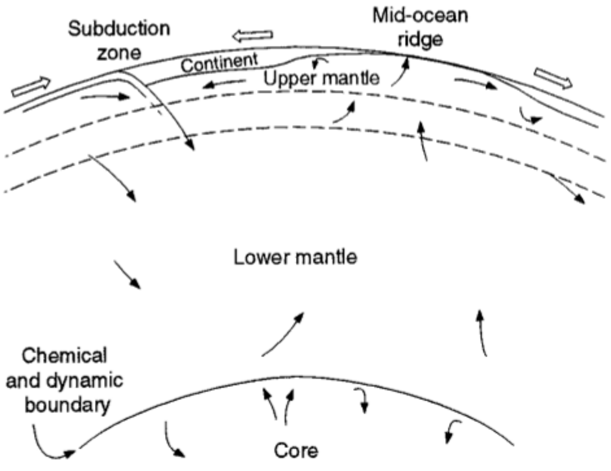

FIGURE 7 Schematic illustration of the possible flow pattern in the convecting mantle, and the consequent motions of lithospheric plates observed at the surface. New lithosphere is formed at midocean ridges, moves horizontally along the surface (large arrows), and sinks into the mantle at subduction zones. In this figure, the mantle is assumed to be of uniform composition and to be thoroughly stirred by convection. The underlying core is liquid, and convects at a rate $\sim 10^6$ times faster than the mantle. [After Jeanloz, R. (1981). *In* "Proceedings of the American Chemical Society 17th State-of-the-Art Symposium." American Chemical Society, Washington, DC, p. 74.]

shear stresses). The apparent conflict between the evidence in favor of a solid versus a fluid interior has now been resolved by the recognition that *both* views are correct; although the crust and mantle are predominantly crystalline, not molten, they can undergo sufficient plastic deformation to behave in a fluidlike manner over periods of millions of years or longer.

Geodetic observations of how the Earth's surface is uplifting since the melting of the last major ice sheets, starting about 2×10^4 yr ago, yield values for the mantle's effective viscosity in the range of $\eta \sim 0.5\text{–}10 \times 10^{20}$ Pa s. Analysis of the resulting force balances leads to the modern conclusion that the mantle undergoes vigorous, probably chaotic convection. The pattern of convection is not well understood at present, and is likely to be time dependent over Earth history. Nevertheless, it is possible to reach general conclusions about the temperature distribution at depth based simply on the knowledge that the vertical transfer of heat across the bulk of the mantle is by convection. In contrast, conduction of heat through rock is so poor that it does not contribute significantly to cooling the interior on a global scale: With a typical thermal diffusivity of $\kappa \sim 10^{-6}$ m^2/s for rock, heat is only transported a distance of $\sim[(10^{-6}\ \text{m}^2/\text{s})\ (4.5 \times 10^9\ \text{yr})(3.2 \times 10^7\ \text{s/yr})]^{1/2} \sim 380$ km by conduction over Earth history.

Midocean ridges are the surface manifestation of hot upwellings of (predominantly) crystalline rock rising through the mantle (Fig. 7). Because of the low thermal conductivity of rock there is relatively little heat lost from the upwelling, and its temperature therefore decreases adiabatically upon rising through the mantle. The hottest region in the upwelling becomes partially molten near the surface, releasing basalt that forms the oceanic crust. The crust and underlying mantle comprising the lithosphere must then move sideways in order to make room for more rock coming up from depth. Because it is moving laterally, the only way that the lithosphere (or tectonic plate) can transfer heat vertically is by conduction. Thus, as the lithospheric plate moves the $\sim 10^3$-km distance across an ocean basin, it cools from above by conduction.

The depth to which cooling extends over the $\sim 10^8$-yr life of the oceanic plate is $\delta_{\text{TBL}} \sim 10^2$ km, and defines the thickness of the thermal boundary layer (Fig. 6). The theory of thermal boundary layers, which evaluates the vertical heat loss by conduction from the laterally moving plate, can be used to determine the bathymetry and the heat flow for oceanic crust as a function of age (or, for a given plate velocity, distance from the midocean ridge); the success in fitting observed values provided one of the first quantitative verifications of plate tectonics. Furthermore, because the effective viscosity of rock increases exponentially with decreasing temperature, the cool region of the thermal boundary is very stiff, giving it the platelike characteristics that define the lithosphere. There is thus a close connection between the thermal boundary layer at the top of the mantle (defined by thermal characteristics) and the lithosphere (defined by mechanical properties).

As with most materials, rock expands on heating and contracts on cooling. Therefore, the oceanic lithosphere becomes denser as it cools, so much so that it ultimately sinks into the mantle. At a subduction zone, where oceanic lithosphere plunges back downward, there is effectively a cold and dense sheet of material being inserted into the mantle (Fig. 7). The temperature of the downwelling rock increases adiabatically with depth (Fig. 6). Ultimately, part or all of this subducted material becomes slowly reheated, either by the hot outer core that underlies the mantle or by heat sources within the mantle, and therefore becomes buoyant again.

The result of the convective motions is that temperatures vary at any given depth by an amount comparable (to within a factor of ~ 2 after removing the adiabat) to the temperature difference between the bottom and top of the mantle. The geotherm merely describes the average temperature at each depth, whereas it is the temperature difference at each depth that causes buoyancy differences—with hot rock rising and cold rock sinking—driving mantle convection. The temperature distribution is thus both a cause and a consequence of mantle dynamics.

The buoyancy driving convection is given by the density difference of the upwelling relative to the downwelling regions of the mantle. It is a remarkable fact that because the thermal expansion coefficient of rock is of the order of percent per 1000°C ($\alpha \sim 10^{-5}$ K^{-1}), mantle convection and the resulting plate tectonics are driven by density variations of only a few percent (temperature variations of order 10^{3}°C). The stresses driving convection are similarly minuscule. These equal the viscosity times the strain rate, the latter being given roughly by plate velocities divided by the thickness of the mantle: $\varepsilon_t \sim (10^{-2}\ \text{m/yr})/[(3 \times 10^{6}\ \text{m})\ (3 \times 10^{7}\ \text{s/yr})] \sim 10^{-16}$ s^{-1}. Therefore, the magnitude of stresses driving the thermal and tectonic evolution of the mantle is of the order $\eta\varepsilon_t \sim (10^{20}\ \text{Pa s})(10^{-16}\ \text{s}^{-1}) \sim 10^{4}$ Pa, which is less than atmospheric pressure at sea level and far less than the pressures reached in the mantle. (This is why pressures throughout the mantle can be taken to be very nearly hydrostatic.)

B. Heat Sources

The energy sources that ultimately heat the Earth's interior, hence cause mantle convection and volcanism, are a combination of heat left over from the accumulation of the planet (accretionary or "primordial" heat) and heat that has been produced by naturally occurring radioactive elements present in rock. It is difficult to estimate how much the planet was heated on accretion because the gravitational energy that is released (basically, the heating produced on impact as material is swept together to form the planet) is enormous, and would amount to a temperature rise for the mantle of ~ 3–4×10^{4}°C except that most of this heat is reradiated to space. Moreover, the last stages of the Earth's accumulation were no doubt characterized by giant impacts, of which one is thought to have involved a glancing blow from a Mars-sized object that effectively splashed the Moon out of the Earth. Modeling studies show that such giant impacts cause temperatures of the mantle rock to reach values as high as $\sim 10^{5}$°C. Although the amount of this heat that is retained within the planet is not well determined, it is clear that temperatures of ~ 1–5×10^{3}°C could well have been reached throughout most of the interior. In fact, current theories suggest that part or all of the mantle was molten 4.5×10^{9} yr ago, forming a "magma ocean" right after the Earth had formed. If so, much of the Earth's currently high internal temperature could be a remnant of the accretion process: volcanism at the surface is, at least to some degree, caused by 4.5-billion-year-old heat that is only now emerging from the deep interior.

Chemical analyses of meteorites and terrestrial rocks (samples of both mantle and crust) show that the decay of K, Th, and U isotopes produce most of the planet's natural radioactive heating, amounting to an estimated ~ 25–30 TW ($\sim 1.5 \times 10^{-4}$ J kg^{-1} yr^{-1}) for the present Earth. Accounting for the decay of the isotopes over time, the radioactive heat production was at least four to five times higher at the time the Earth was formed. Therefore, naturally occurring radioactivity has also contributed to the planet's internal heat.

To put these values into perspective, the current heat flow out of the Earth's surface is about 44 TW [average flux of 87 (± 2.0) mW m^{-2}], and was no doubt higher early in Earth history. This is significantly higher than the rate at which heat is being produced by radioactivity, but only by a factor of 50–80%. Part of this difference can be ascribed to the contribution of primordial heating. According to the estimates given here, roughly one-third to one-half (~ 15–20 TW) of the heat currently lost from the interior is left over from the Earth's accretion. However, there is also the fact that the Earth is cooling, and probably has been cooling since its formation, hence that more heat is being lost than is being produced. Indeed, convection of the "solid" mantle is the mechanism by which the deep interior is being cooled. Modeling studies suggest that the heat lost from the surface is only a small amount larger than the magnitude of all internal sources (both accretionary and radioactive), such that the interior has only cooled by several hundred degrees during the past 4 billion years.

In addition to the physical origin of the Earth's internal heat, the distribution of heat sources within the planet is also of importance. In particular, estimates of the temperature in the core indicate that this region is hotter than the overlying mantle, perhaps by as much as 1000°C or more, which implies that the mantle is to some degree heated from below. Most current models suggest that only about 20–50% of the heat driving mantle convection comes from the underlying core, with the remainder (50–80%) originating internally. Such values are uncertain but seem reasonable: Given that the mantle makes up 84% and the core 15% of the planet on an atomic basis, the bulk of the Earth's internal heat probably comes from the rocky portion rather than the metallic core.

C. Causes of Melting

The measurements of naturally occurring radioactivity in rocks demonstrate that, although radioactive decay has contributed to heating the planet over its geologic history, it probably plays only a minor role in directly heating rock to the melting point and producing any magmas at depth. For example, the specific heat ($C_P \sim 10^3$ J K^{-1} kg^{-1}) can be used to convert radioactive heat production to a corresponding temperature rise: $\Delta T \sim (1.5 \times 10^{-4}\ \mathrm{J\ kg^{-1}\ yr^{-1}})/(10^3\ \mathrm{J\ K^{-1}\ kg^{-1}}) \sim 10^{-7}$ K/yr, using the present-day value of average heat production given earlier. Even taking into account the increase in radioactive heat production as one goes back in geologic time, most of the Earth's 4.5-billion-year history is required to achieve a temperature increase of $1–2 \times 10^{3}$°C by radioactive decay. Thus, a sizable fraction of the Earth's ~2000°C internal temperature is likely due to radioactive heating, but the $\sim 10^2–10^3$°C heating required to bring rocks to the melting point can only be accomplished over time periods of hundreds of millions of years.

Over a time period of 10^8 yr, upwelling mantle rock rises $\sim 10^3$ km (using plate-tectonic velocities of $\sim 10^{-2}$ m/yr) and a piece of the deep mantle reaches the surface before radioactivity can produce very significant heating. Instead of the upwelling rock being heated to its melting temperature, it is because the adiabatic temperature drop on rising is sufficiently small that the temperature of the upwelling crosses the melting point of the mantle rock (Fig. 6). In general, melting on adiabatic decompression of initially hot rock being brought up from depth is considered one of the most common causes of melting in the mantle and crust. Thus, it is not so much by direct heating but primarily by way of the convective motions they induce throughout the mantle that both primordial and radioactive heat sources eventually lead to the formation of magmas in the Earth.

From this point of view, one would expect melting of the mantle to be exclusively associated with upwellings, such as the regions beneath midocean ridges. It is a fact that most of the Earth's volcanism occurs at midocean ridges, and it is no coincidence that most of the heat flow from the interior is also concentrated along the ridges. It might therefore appear surprising that a considerable amount of volcanic activity, and the predominant volcanism associated with continents, occurs at subduction zones—exactly where the coldest lithosphere is sinking into the mantle.

The basic reason that magmas are formed at subduction zones is that water is drawn into the mantle, along with the sinking slab of cold lithosphere. The water is present as a fluid phase, within pore spaces of sediments and along grain boundaries of crustal rocks being subducted. It is also dissolved within crystal structures (as OH^- hydroxyl molecules) of hydrated minerals that have been formed by weathering of the crust and uppermost mantle rocks of the oceanic lithosphere (exactly the weathering and hydration referred to in describing ophiolites).

The effect of water is to lower dramatically the solidus temperature of most rocks, so that it effectively acts as a flux at subduction zones. As the sinking lithosphere heats up, water is released and can migrate upward toward hotter rock within the wedge of mantle material and the deep crust lying above the subducted slab. Because the effective melting temperatures of the mantle and crustal rocks are reduced by hundreds of degrees, simply due to the presence of water, the result is that magmas are formed as water-rich fluid percolates upward from the slab of subducting lithosphere.

The magmas formed by water-fluxing in the mantle tend to be more silica-rich than the basalts formed at midocean ridges, and have nearly the average composition of continental crust. In truth, it is thought that most continental crust is produced by water-induced lowering of the melting temperature above subduction zones. It is for this reason that water is thought to be necessary for the formation of the continental crust, such that Earth-like continental rocks would not be expected on terrestrial planets devoid of water.

In summary, the formation of magmas within the Earth is predominantly due to two events: (1) adiabatic decompression of upwelling rock and (2) lowering of the solidus by water (and other volatile components) brought into the mantle by subduction. Once a melt is formed at depth, it can move relatively quickly (meters to kilometers per year; near the surface, velocities up to kilometers per day are recorded), thereby separating the liquid from its source rock. Because melts typically differ in bulk composition from their source rocks, the combination of melt formation and (relatively) rapid migration is the essential process of geochemical differentiation: the separation of large-scale portions of the planet into chemically distinct regions.

D. Plumes and the Core–Mantle Boundary

Although plate tectonics and the thermal-boundary layer model describe much of the global pattern of volcanism at the Earth's surface, a notable exception is provided by hot spots. Each hot spot is characterized by a chain of volcanoes exhibiting a systematic age dependence along the length of the chain, making it appear that the volcanism is the result of a stationary source of heat in the mantle underlying the moving tectonic plate. The Hawaiian-Emperor chain of volcanic islands and seamounts is the clearest example, and also corresponds to the largest hot spot in terms of flux of heat or lava volume.

One of the most remarkable features of the few dozen hot spots that have been identified is that they appear to be nearly stationary with respect to each other, moving at less than $\frac{1}{10}$ the rate at which tectonic plates move. This has led to the idea that each hot spot represents the tip of a plume, an axially symmetric jet of hot rock (in contrast to the sheetlike upwellings beneath midocean ridges, or downwellings at subduction zones) emanating from the great depth—perhaps even the lowermost mantle—in order to explain the apparent lack of any influence from the plate-tectonic motions at the Earth's surface.

The evidence for where plumes originate is, like any discussion of large-scale motions across the depth of the mantle, not well resolved at present. Some of the most direct evidence comes from recent advances in seismic tomography, which involves the determination of horizontal variations in wave velocity at each depth as determined by an analysis of seismic records from cross-cutting ray paths. That is, by comparing the arrival times and amplitudes of seismic waves traveling between many combinations of sources (earthquakes or explosions) and receivers (primarily, modern digital seismometers), it is possible to reconstruct the three-dimensional velocity structure of the mantle.

Because seismic-wave velocities are influenced by temperature, with propagation through hotter rock being slower than through colder rock, one can roughly ascribe low and high velocities at a given depth with, respectively, higher and lower temperatures (hence, more and less buoyant rock) at that depth. The correspondence with temperature is confounded somewhat by the fact that changes in rock type (differences in bulk composition or constituent minerals) also influence the wave velocities and densities. However, there is clear evidence of slabs of fast seismic-wave velocities observed in the upper mantle beneath subduction zones and, in several notable examples (e.g., around the Pacific basin), these appear to depths of 1500 km or more. There appears to be, therefore, a strong indication that many if not all slabs of subducted material penetrate well into the lower mantle (some slabs appear to become deflected at, and perhaps stopped by, the transition zone at depths of ~400–700 km).

Although regions of faster seismic velocity are systematically easier to image than regions of slower wave velocities, recent studies have revealed a few clear examples of plumes exhibiting a slow ("hot") seismic signature to depths well into if not through the transition zone, for example beneath Hawaii and Iceland. Such observations support the idea that plumes may originate from the lower mantle.

More remarkably, there are indications of very strong seismological anomalies at the core–mantle boundary beneath some plumes. For example, there appears to be a distinct ultra-low-velocity zone (ULVZ) directly under Iceland, and Hawaii is situated above (or nearly above) another ULVZ. The connection between ULVZ and plume is circumstantial and perhaps even speculative at present, but does suggest the possibility that hot spots represent the surface markings of heat emanating from the Earth's core. In this sense, volcanism at hot spots may provide a relatively direct link between the core and the Earth's surface.

More generally, the preponderance of volcanic activity—at midocean ridges and subduction zones, as well as at hot spots—is a manifestation of large-scale mantle convection and hence the mechanism by which the bulk of the planet has evolved geologically over its 4.5-billion-year history.

SEE ALSO THE FOLLOWING ARTICLES

Composition of Magmas • Melting the Mantle • Physical Properties of Magmas • Plate Tectonics and Volcanism • Volcanic Plumes

FURTHER READING

Ahrens, T. J., ed. (1995). "Global Earth Physics, A Handbook of Physical Constants." American Geophysical Union, Washington, DC.

Ahrens, T. J., ed. (1995). "Mineral Physics & Crystallography, A Handbook of Physical Constants." American Geophysical Union, Washington, DC.

Anderson, D. L. (1989). "Theory of the Earth." Blackwell Scientific Publications, Boston.

Bott, M. H. P. (1982). "The Interior of the Earth: Its Structure, Constitution and Evolution." Elsevier, New York.

Brown, G. C., and Mussett, A. E. (1981). "The Inaccessible Earth." Allen & Unwin, London.

Decker, R., and Decker, B. (1982). "Volcanoes and the Earth's Interior." Freeman, San Francisco.

Hemley, R. J., ed. (1998). "Ultrahigh-Pressure Mineralogy: Physics and Chemistry of the Earth's Deep Interior." Mineralogical Society of America, Washington, DC.

Lewis, J. S. (1995). "Physics and Chemistry of the Solar System." Academic Press, San Diego, CA.

Ozima, M. (1981). "The Earth: Its Birth and Growth." Cambridge University Press, New York.

Taylor, S. R. (1992). "Solar System Evolution, A New Perspective." Cambridge University Press, New York.

Turcotte, D. L., and Schubert, G. (1982). "Geodynamics." Wiley, New York.

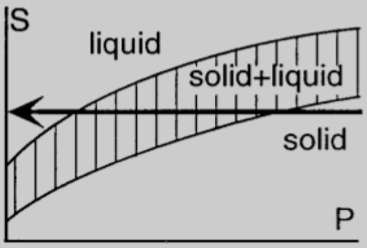

MELTING THE MANTLE

PAUL D. ASIMOW
Lamont-Doherty Earth Observatory

I. Introduction
II. How to Melt a Rock
III. Decompression Melting
IV. Melting by Changing Composition
V. Melting by Temperature Increase
VI. The Mantle Adiabat
VII. Summary

GLOSSARY

adiabatic A thermodynamic process during which heat flow by conduction is negligible.

batch melting Melting process in a closed system in which liquid and solid remain in equilibrium.

component A chemical formula. The number of components in a system is the minimum needed to describe all possible chemical variations in the system, so a pure system with no chemical variation has one component.

equilibrium A state in which all natural processes have gone to conclusion and no further change is observed in any macroscopic variable.

fractional melting A melting and distillation process in which liquid is continuously and instantaneously removed from the system as it forms.

isentropic A thermodynamic process occurring at constant entropy; equivalent to *adiabatic* and *reversible.*

liquidus The temperature at which a liquid of given composition begins to crystallize at a given pressure.

phase A compositionally and structurally homogeneous material such as a mineral, liquid, or vapor.

productivity The increase in extent of partial melting per unit decrease in pressure, expressed in percent per gigapascal and usually a positive number.

reversible An idealized path that proceeds through a sequence of equilibrium states with no spontaneous processes occurring.

solidus The temperature at which a solid assemblage of given composition begins to melt at a given pressure.

I. INTRODUCTION

The stony part of the Earth is solid under normal conditions at the present day. Volcanism is the eruption of molten or partially molten rock, that is, magma. The first stage of any volcanic process therefore must be melting: We have to produce a liquid by partial melting before it can migrate from the source region (see Migration of Melt chapter) and subsequently erupt (Part II). The locations of volcanoes on Earth are controlled primarily by where melting takes place. The volume, frequency, and style of eruptions are dependent on many factors but the first considerations are how much magma is supplied by melting, at what depth melting takes place,

Copyright © 2000 by Academic Press
All rights of reproduction in any form reserved.

and the distribution of melt production in the source region in space and time.

Before roughly 1960, igneous petrology was mostly concerned with the evolution and differentiation of magma after it left its source region. In the following two decades, attention shifted to the pressure (P) and temperature (T) at which primary melts were extracted from the mantle, without detailed understanding of how the melts were produced. In the last 20 years, however, the application of ideas from thermodynamics, experimental petrology, and fluid dynamics has provided a strong basis for understanding the basic physical processes underlying the melting of Earth's mantle. This chapter explores *how* and *why* the crust and mantle of the Earth melt, which together with information about tectonic processes and chemical composition (discussed in other chapters in this part) determines *where* and *when* melting takes place.

II. HOW TO MELT A ROCK

There are three ways to melt a rock. The most obvious way is *to raise the temperature* (T). In the Earth, however, the other two methods are dominant: melting by *lowering the pressure* (P) and by changing the chemical composition of the system to *lower its solidus temperature* below the current temperature. The *solidus* is the temperature at which a system of given composition begins to melt at a given pressure, whereas the *liquidus* is the temperature at which the system becomes completely liquid. Rocks melt over a range of temperatures so it is imprecise to speak of the melting point as we would for a pure substance. Melting by decompression and melting by addition of a flux (i.e., a component that lowers the solidus) dominate in the mantle because in the asthenosphere mass transport is much faster than heat transport and because internal heat generation by radioactivity is minor at the present era. In the lithosphere, which includes the crust, mass transport is slower and ambient temperatures are low enough that a temperature increase, whether by conductive heat flow or local heat generation, is required. For the earth as a whole, however, asthenospheric melting generates a much larger volume of magma every year than lithospheric melting.

Why three ways? The answer derives, like most of our reasoning about the physical and chemical behavior of rock systems, from thermodynamics and from the assumption of chemical *equilibrium*. Situations certainly occur, such as explosive eruptions, in which equilibrium is a poor assumption, but at the source of melting temperatures are quite high and the processes considered are fairly slow. Long times and high temperatures favor the achievement of equilibrium, so while we know that equilibrium reasoning is an approximation, we consider it a rather accurate one at least for the early stages of magma production. For a system in chemical equilibrium, we must specify its chemical composition and two additional parameters (such as P and T) to define uniquely the state of the system. Therefore, to cause a change of state such as melting, we see that we can group all the ways we can act on the system into changes in T, changes in P, and changes in composition. It is, as far as we know, universally true that high T favors the liquid state over the solid state, so that *raising the temperature* or *lowering the solidus temperature* (by changing composition) can lead to melting. On the other hand, while it is more common for low P to favor the liquid state over the solid state so that *lowering the pressure* can lead to melting, this is by no means universal (water is a well-known exception, and mantle rocks may experience the opposite behavior at very high pressures as well).

We can define the state of a system by specifying parameters other than P and T and in many cases it is quite convenient to do so because other parameters may be conserved or controlled (i.e., independent) during the physical process we are considering. Likewise, P or T may be dependent parameters, in which case we learn little by trying to specify them or by using them as axes on our diagrams. In an isochoric system such as an inclusion in a rigid mineral host, volume (or density) is held constant and P changes in a dependent manner as we approach equilibrium. For mantle melting, we are concerned with an approximately *adiabatic* system, that is, one in which heat flow by conduction is negligible. This is a reasonable approximation because the source regions of magmas in the mantle are large, thermal gradients are low, and the timescale for material to be transported across the source region by advection is shorter than the time for temperatures to equilibrate across the source region by thermal diffusion. If an adiabatic process is also *reversible*, then the independent variable is not T but entropy, S (see Table I). This follows directly from the second law of thermodynamics,

$$dS = \frac{dq}{T} + d\sigma, \tag{1}$$

which states that the change in entropy for any process is equal to the ratio of heat flow dq to temperature plus the irreversible entropy production $d\sigma$. If a process is adiabatic ($dq = 0$) and reversible ($d\sigma = 0$), then $dS =$

TABLE 1 Symbols Used

Symbol	*Name*	*Units*
T	Temperature	°C, K
P	Pressure	GPa
S	Specific entropy	J/K/kg
q	Heat	J/kg
σ	Irreversible entropy production	J/K/kg
H	Specific enthalpy	J/kg
F	Extent of melting by mass	
s	Solid phase	
l	Liquid phase	
ΔS_{fus}	Entropy of fusion (one-component system)	J/K/kg
ΔV_{fus}	Volume of fusion (one-component system)	J/GPa/kg
α	Coefficient of thermal expansion, $\frac{1}{V}\left(\frac{\partial V}{\partial T}\right)_P$	K^{-1}
ρ	Density	kg m^{-3}
C_P	Specific heat capacity at constant pressure	J/K/kg
$\left(\frac{\partial T}{\partial P}\right)_S$	Slope of an isentrope in *P-T* space	K/GPa
$\left(\frac{\partial T}{\partial P}\right)_{\text{solidus}}$	Slope of the solidus curve in *P-T* space	K/GPa
$-\left(\frac{\partial F}{\partial P}\right)_S$	Isentropic productivity	%/GPa
$\left(\frac{\partial T}{\partial P}\right)_F$	Slope of a constant *F* contour in *P-T* space	K/GPa
$\left(\frac{\partial F}{\partial T}\right)_P$	Isobaric productivity	%K
$\left(\frac{\partial S}{\partial F}\right)_P^{\text{rxn}}$	Isobaric entropy of melt reaction	J/K/kg
$\left(\frac{\partial S_X}{\partial P}\right)_F$	Entropy change due to compositional effects per unit change in *P* at constant *F*	J/K/GPa/kg
$\left(\frac{\partial S_X}{\partial F}\right)_P$	Entropy change due to compositional effects per unit increase in *F* at constant *P*	J/K/kg
G	Gravitational constant (6.67×10^{-11})	m^3 kg^{-1} s^{-2}
$M_\oplus$	Mass of the Earth (6×10^{24})	kg
$R_\oplus$	Radius of the Earth (6371)	km
X_Y^{bulk}	Mole fraction of component *Y* in bulk system	
X_Y^l	Mole fraction of component *Y* in liquid phase	
D_Y	Partition coefficient for component *Y*: (X_Y^s/X_Y^l)	

0, which is to say S is constant and we call the process *isentropic*. For our purposes, this property defines entropy. We can also imagine an adiabatic but irreversible process such as the Joule-Thomson experiment of forced flow through a nozzle in which enthalpy H is conserved. Some authors have suggested that adiabatic upwelling is an isenthalpic process (using a definition of enthalpy corrected for the presence of gravity), but although mantle melting is not strictly reversible, it is not clear why it should be isenthalpic. We find it easier to begin with the isentropic case and add known sources of entropy production (gravity and viscosity) to arrive at an accurate description of the natural process. In the section on decompression melting, we shall see why it is instructive to use the conserved quantity S in our thinking and on our diagrams rather than the dependent parameter T.

In the following sections, we review the essentials of decompression melting, flux melting, and melting by direct heating. Our principal focus is on decompression melting, since at least for the present-day terrestrial mantle, that is the dominant mechanism.

III. DECOMPRESSION MELTING

Decompression melting is the best understood mechanism of melt production. It occurs at midocean ridges and ocean islands such as Hawaii and Iceland. The melting process underlying convergent margin volcanism is different and is discussed in a later section. The main points of this section are that from simple considerations we can show why the mantle melts when decompressed and how much melt we should expect to be produced during decompression.

A. One-Component System

We begin by considering a pure substance or one-component system (a *component* is a chemical formula, and the number of components in a system is the minimum needed to describe all possible chemical variations in the system, so a pure system with no chemical variation has one component). The mantle is a multicomponent system, but we can learn a great deal from the very simplest system that can then be generalized to systems that are more complex. First, let us imagine that this substance can only form two phases, a solid s and a liquid l (a *phase* is a compositionally and structurally homogeneous material). Let our system be well behaved so that liquid is favored by high temperature and low pressure, so if we map the stable assemblage in P-T space we will find a *phase diagram* like that shown in Fig. 1a. A phase diagram divides a plane or space according to what phases are stable at each point. There are three elements to the phase plane in Fig. 1a: a one-phase region where solid s is stable, a one-phase region where liquid l is stable, and a two-phase curve where s and l coexist. In this space, this two-phase curve is both solidus and liquidus. Thus if we take P and T as our independent variables, for example, along an isothermal decompression path, our one-component system in passing from one equilibrium state to another as we reversibly lower P would melt completely at a single point along the path.

Pressure and temperature have the special property that they are equal among all phases coexisting at equilibrium (except for surface tension effects), which is why the two phases s and l coexist along a curve in the P-T plane. Entropy (as well as enthalpy and volume), on the other hand, differs between coexisting phases. If, therefore, we draw the phase diagram for our one-component system in the P-S plane, we obtain something like Fig. 1b. This plot still has one-phase regions where s and l are stable alone, but now we see a two-phase region $s + l$ crossed by vertical tie-lines showing s and l coexisting at the same pressure but different entropies (the length of the tie-line at each pressure is ΔS_{fus}, the entropy of fusion). Now we recognize the boundary between the s and $s + l$ regions as the solidus and the boundary between regions $s + l$ and l as the liquidus. By taking entropy S as an independent variable, we have opened the two-phase curve up into a region and we see that in this case we no longer expect the system to melt or freeze completely at a single pressure. Instead, even in this one-component system, isentropic decompression leads to *partial melting*. An isentropic decompression path is shown in Figs. 1c and 1d. In the P-S plane (Fig. 1d), this is a straight line, and it is obvious that the melting begins at the pressure where the solidus crosses the prescribed entropy and ends at the pressure where the liquidus crosses the prescribed entropy. On the other hand, in the more conventional P-T plane (Fig. 1c), the isentropic decompression path kinks to follow the two-phase boundary for what seems an arbitrary interval: There is no simple way to predict the behavior of the system at fixed S by looking at a diagram that considers T independent.

During isentropic decompression melting, it is clear from Fig. 1c that the temperature actually decreases as the system melts, contrary to intuition. At constant

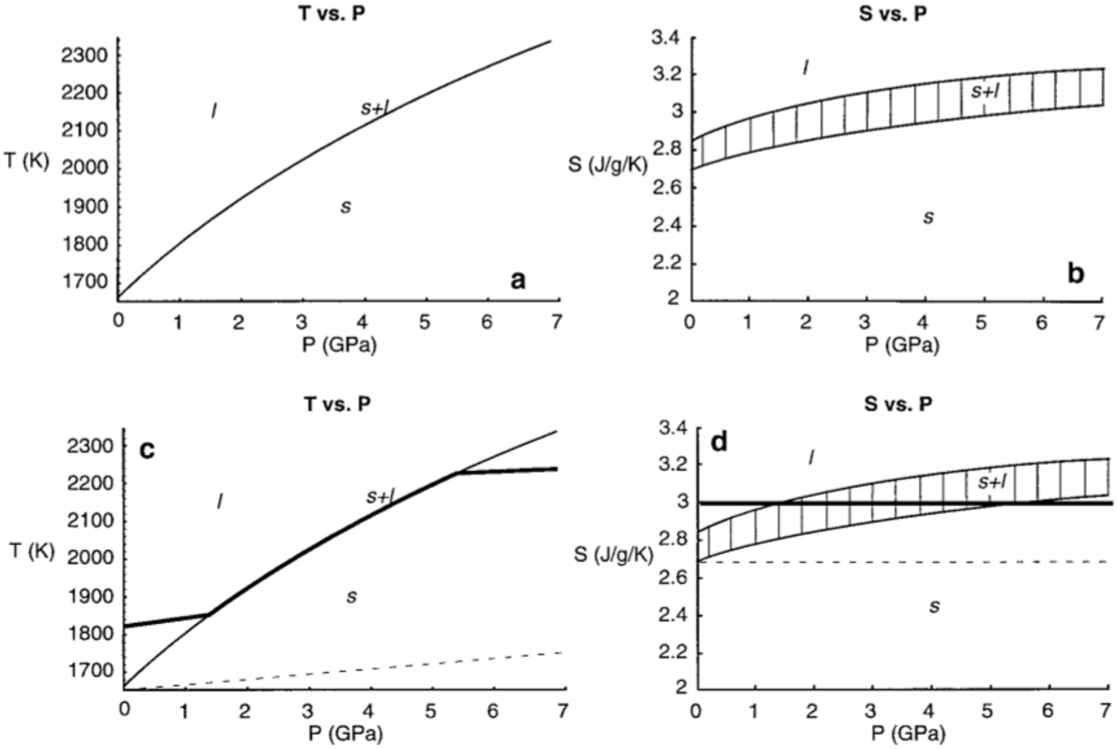

FIGURE 1 Phase relations and isentropic decompression melting of a one-component system. (a) A phase diagram in the pressure (*P*) versus temperature (*T*) plane is divided into a region where solid phase *s* is stable, a region where liquid phase *l* is stable, and a curved boundary *s* + *l* where the two phases coexist at equilibrium. (b) The same system plotted in the *P* versus entropy (*S*) plane; here the two phases coexist over a region *s* + *l* bounded by the solidus and liquidus curves (which coincide in part a). The vertical tie-lines in the *s* + *l* field indicate that solids coexist with liquids at higher entropy but the same pressure. (c) The *P-T* diagram with two isentropic decompressions path indicated; the slope of isentropes in the one-phase regions is about 10 K/GPa. The bold path shows a typical partial melting path. The light dashed path shows an adiabat so cold that melting would not occur even if adiabatic upwelling continued to the surface. During partial melting, the *P-T* path in a one-component system is restricted to the coexistence curve *s* + *l*, but there is no way to read from this diagram how much melt is present at any point or how long the melting interval is. (d) The bold constant-entropy line superposed on the *P-S* diagram shows that the size of the isentropic melting interval as well as the melt fraction at any point can be read directly from this diagram using the lever rule (see Fig. 2). Again, the light dashed line shows an isentrope cold enough to avoid melting.

total entropy, this behavior results because the entropy of fusion required to transform solid to liquid can only be obtained by decreasing the temperature of the system.

B. Beginning of Melting

Isentropically lowering the pressure on a solid will generally cause it to intersect the solidus and begin partial melting. This is clear immediately on the *P-S* diagram, where the isentrope is horizontal and the solidus has a positive slope, so that only isentropes with less entropy than the intersection of the solidus with atmospheric pressure can avoid decompression melting altogether. On the *P-T* diagram, this is not quite as obvious, but we can assign approximate numerical values to the slopes of the adiabat and the solidus in *P-T* space and hence make the same argument. The slope of the subsolidus isentrope, that is, the change in temperature per unit change in pressure at constant entropy, is written in partial derivative notation $(\partial T/\partial P)_S$ and is given by the formula

$$\left(\frac{\partial T}{\partial P}\right)_S = \frac{T\alpha}{\rho C_P}, \tag{2}$$

where α is the coefficient of thermal expansion, ρ the density, and C_P the isobaric heat capacity of the solid phase. For mantle minerals, this slope is approximately 10 K/GPa. In the one-component system, the slope of the solidus is given by the Clausius-Clapeyron equation:

$$\left(\frac{\partial T}{\partial P}\right)_{\text{solidus}} = \left(\frac{\Delta V_{\text{fus}}}{\Delta S_{\text{fus}}}\right), \tag{3}$$

where ΔV_{fus} is the difference in specific volume and ΔS_{fus} the difference in specific entropy between liquid and solid. This slope is approximately 130 K/GPa for mantle minerals at low pressure. This value is much larger than the slope of the adiabat such that once again the adiabat will intersect the solidus on decompression unless the temperature of the adiabat at atmospheric pressure is less than the solidus at atmospheric pressure (see Fig. 1c). For mantle minerals, this "no melting" adiabat is much colder than today's mantle adiabat; anywhere the adiabatic geotherm extends to near the surface will be a region of melting. Conversely, the bulk of the shallow parts of the earth are subsolidus only because the lithosphere cools conductively to the surface and does not lie on the mantle adiabat.

C. Progress of Melting

To describe fully a system undergoing partial melting, we need to keep track of the composition of liquid and residue as well as the quantity of melt produced. The compositions of liquids produced by mantle melting are dealt with in later chapters. Here, we focus on the amount of melt generated. To track the amount of melt during progressive upwelling the quantity we most need to know is the *productivity*, $-(\partial F/\partial P)_S$, the increase in extent of partial melting F per unit decrease in pressure (expressed in percent per gigapascal and usually a positive number) and how the productivity evolves during progressive upwelling and melting. This variable is particularly hard to obtain by direct experimental measurement or from P-T phase diagrams, but many authors have estimated that productivity should be about 10%GPa for adiabatic mantle melting, which is an adequate average value.

For many purposes, the average estimate of 10%/GPa is sufficient. Going beyond this average, we may ask whether we should expect any systematic behavior in the variations of productivity during the progress of melting. Different authors have argued, variously, for increasing, constant, and decreasing productivity. We can demonstrate, however, simple reasons why we should in fact expect productivity to increase from the beginning of adiabatic melting until the exhaustion of a phase (usually clinopyroxene) from the residue. We can see some of the variables that cause increasing productivity on the P-S diagram for a one-component system. Geometrically, on the P-S diagram and in any two-phase region of any phase diagram, we apply the *lever rule* (Fig. 2) to calculate relative proportions of the phases. At any point (P, S) in the two-phase region the extent of melting F is given by the ratio of the distance from the entropy of the system, S, to the entropy at the solidus, $S_s(P)$, divided by the length of the tie-line between the entropy of the liquidus, $S_l(P)$, and $S_s(P)$:

$$F = \frac{[S - S_s(P)]}{[S_l(P) - S_s(P)]} = \frac{1}{\Delta S_{\text{fus}}}[S - S_s(P)]. \tag{4}$$

If we take the partial derivative of Eq. (4) with respect to P at constant S and rearrange a little, we obtain an expression for the productivity, which is simplest in the case that ΔS_{fus} is constant:

$$-\left(\frac{\partial F}{\partial P}\right)_S = \frac{1}{\Delta S_{\text{fus}}}\left(\frac{\partial S_s}{\partial P}\right)_{\text{solidus}}, \tag{5}$$

that is, productivity is given by the slope of the solidus divided by the entropy of fusion ΔS_{fus}. To relate this

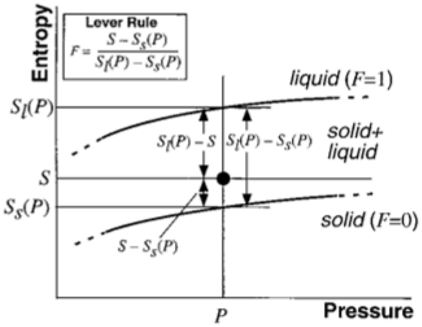

FIGURE 2 Graphical illustration of the lever rule. The lever rule is just a statement of conservation of an intensive property in a two-phase system. On the (P, S) plane, if the system has total specific entropy S then at equilibrium and at pressure P, the system will be totally solid ($F = 0$) if $S < S_s(P)$, the specific entropy of the solid phase at the solidus. The system will be totally molten ($F = 1$) at $S > S_l(P)$, the specific entropy of the liquid phase at the liquidus. If $S_s(P) < S < S_l(P)$, however, the system will be partially molten and the mass fraction of liquid F will be given by the lever rule as shown.

expression to known or measurable quantities requires some thermodynamic identities, but the result is

$$
\begin{aligned}
-\left(\frac{\partial F}{\partial P}\right)_S &= \frac{1}{\Delta S_{\text{fus}}}\left[\frac{C_P}{T}\left(\frac{\partial T}{\partial P}\right)_{\text{solidus}} - \frac{\alpha}{\rho}\right] \\
&= \frac{1}{\Delta S_{\text{fus}}}\left[\frac{C_P}{T}\left(\frac{\Delta V_{\text{fus}}}{\Delta S_{\text{fus}}}\right) - \frac{\alpha}{\rho}\right],
\end{aligned}
\qquad (6)
$$

where C_p is the heat capacity of the system $[C_P = (1-F)C_P^s + FC_P^l]$, α is its coefficient of thermal expansion, and ρ is its density. Equation (6) is correct even in the case that ΔS_{fus} is not constant because it is written in terms of the heat capacity, thermal expansivity, and density of the partially molten system rather than the solid phase; the assumption of constant ΔS_{fus} is equivalent to the statements $C_P^s = C_P^l$ and $(\alpha^l/\rho^l) = (\alpha^s/\rho^s)$. How then does productivity evolve during progressive decompression melting of a one-component system? In general, ΔS_{fus} and C_P are effectively constant while α/ρ is a very small number. Hence, changes in productivity in this system are dominated by T, which decreases as we move down the solidus from high pressure to low pressure (the solidus has a positive slope), and ΔV_{fus}, which increases with decreasing pressure because liquids are typically much more compressible than solids (hence the solidus has negative curvature, i.e., $(\partial T/\partial P)_{\text{solidus}}$ increases with decreasing pressure). Both of these effects contribute to *increasing productivity* with decreasing pressure or progressive decompression melting from a given intersection with the solidus. For melting of pure diopside ($CaMgSi_2O_6$) beginning at 7 GPa, productivity increases from 6%/GPa at 7 GPa to 35%/GPa when it reaches the surface at $F = 0.9$.

D. Multicomponent Systems

Earth's mantle, of course, is not a pure substance. It contains at least 10 different oxide components in amounts greater than 0.1 wt%. Here we attempt to generalize the simple insights apparent in the one-component example to systems more like the mantle. In systems of more than one component, two or more phases that differ in composition can often coexist anywhere in a region of the P-T plane, so that the solidus and the liquidus can be distinct in P-T space and partial melting is to be expected even when temperature is the independent variable. In other words, the isobaric productivity $(\partial F/\partial T)_P$, which is infinite for one-component systems, generally has a finite value. The derivation of a productivity equation for multicomponent systems is more complicated than the one-component example above since it involves conservation of mass as well as conservation of entropy, but the general form of Eq. (6) turns out to be:

$$
-\left(\frac{\partial F}{\partial P}\right)_S = \left[\frac{\dfrac{C_P}{T}\left(\dfrac{\partial T}{\partial P}\right)_F - \dfrac{\alpha}{\rho} + \left(\dfrac{\partial S_X}{\partial P}\right)_F}{\dfrac{C_P}{T\left(\dfrac{\partial F}{\partial T}\right)_P} + \left(\dfrac{\partial S}{\partial F}\right)_P^{\text{rxn}}}\right], \qquad (7)
$$

which requires a little explanation: C_P, α and ρ are, as before, the heat capacity, thermal expansivity, and density of the partially molten system, respectively; they depend on the composition of the phases as well as P, T, and F. Instead of the P-T slope of the solidus, we have the analogous quantity $(\partial T/\partial P)_F$, which is the slope of the constant F contour calculated locally; away from the solidus, the slope of the solidus itself is not relevant. The isobaric productivity $(\partial F/\partial T)_P$ appears in the denominator; when this quantity goes to infinity [which implies $(\partial T/\partial P)_F$ is the same for all F between 0 and 1 and is therefore equal to $(\partial T/\partial P)_{\text{solidus}}$], we recover the one-component version, Eq. (6). Instead of the entropy of fusion (which is ill-defined for multicomponent systems) we use $(\partial S/\partial F)_P^{\text{rxn}} = S^l - S^S + (\partial S_X/\partial F)_P$, which we call the *isobaric entropy of melt reaction*. The terms $(\partial S_X/\partial P)_F$ and $(\partial S_X/\partial F)_P$ involve a subtle point in the entropy budget, but for multicomponent systems they must be included both to obtain an accurate productivity equation and to define precisely the quantity that acts like the entropy of fusion. In a closed system where the coexisting phases differ in composition (e.g., basalt and residual peridotite), moving an increment of mass from solid to liquid necessarily involves changes in the composition of at least one (and generally all) of the phases. Similarly, changing pressure at constant melt fraction involves changes in the equilibrium composition of various phases because phase equilibria and partition coefficients depend on pressure and temperature. In turn, the specific entropies of the phases depend on their composition and the specific entropy of the system depends on which phases the components reside in. Therefore an equation such as Eq. (7) that expresses conservation of mass and conservation of entropy needs to include sums over all components and phases of the partial specific entropy of each component in each phase times the changes in mass fractions of the components and phases per increment of melting at constant pressure, $(\partial S_X/\partial F)_P$, and per increment of pressure change at constant melt fraction, $(\partial S_X/\partial P)_F$.

With Eq. (7) in hand, we can discuss the variables that determine productivity and how it changes during melting of various simple and natural multicomponent systems. We need to know all the variables in Eq. (7) to calculate the actual value of productivity, but here we focus on variations in productivity during progressive upwelling. As in the one-component case, C_P, α, and ρ are not important sources of variation. It also turns out that $(\partial S_X/\partial P)_F$ is small and that, although according to some models $(\partial S/\partial F)_P^{\mathrm{rxn}}$ may vary by nearly a factor of 2 during melting of fertile peridotite, the first term in the denominator is larger in magnitude and dominates the variations in productivity. Also, T varies systematically, but we find that its influence is generally swamped by the variations in $(\partial T/\partial P)_F$ and especially $(\partial F/\partial T)_P$. To a reasonable approximation then, we can understand the behavior of productivity during isentropic upwelling of multicomponent systems just by considering the behavior of $(\partial T/\partial P)_F$ and $(\partial F/\partial T)_P$. We can state with considerable certainty that except in the vicinity of changes in the solid phase assemblage $(\partial T/\partial P)_F$ increases with decreasing pressure like the slope of the solidus in the one-component system, simply because silicate liquids are more compressible than minerals. This contributes to increasing productivity with decreasing pressure, just as in the one-component system.

The behavior of $(\partial F/\partial T)_P$ has been the subject of considerable disagreement among researchers. We present here a simple argument that leads us to expect that $(\partial F/\partial T)_P$ increases with F away from the solidus in natural peridotites, but experimental data are equally consistent with nearly constant $(\partial F/\partial T)_P$ and many authors have constructed models in which $(\partial F/\partial T)_P$ decreases with F. Indeed isobaric productivity is sometimes taken as infinite up to some F, which is the case for univariant melting as in the one-component system; this behavior is sometimes misleadingly called *eutectic*. The idea that melting of peridotite is invariant descends from the behavior simple systems such as CaO-MgO-Al_2O_3-SiO_2, which are thought to be suitable analogues of the mantle because these oxides constitute roughly 90% of the mass of mantle rocks. It turns out, however, that minor components and solid solutions dominate the melting behavior at low melt fractions. The simplest model system that captures the effect of a minor component such as Na_2O on productivity is a binary system with one major component Z that forms a nearly pure solid phase and one minor component Y that partitions preferentially into the liquid phase [that is, its partition coefficient $D_Y \equiv (X_Y^s/X_Y^l)$ is less than one, where X_Y^s and X_Y^l are the mole fractions of component Y in the solid and liquid phases, respectively]. At low concentrations of Y, the liquidus temperature of such a system is described approximately by the cryoscopic or freezing point depression relation

$$X_Y^l = k(T_Z^{\mathrm{fus}} - T), \tag{8}$$

where T_Z^{fus} is the melting point of pure solid Z and k is a constant that depends only on the properties of Z. To solve for the behavior of F and $(\partial F/\partial T)_P$, we only need the standard equations for the concentration of a trace element in the liquid as a function of F during batch and fractional melting (*batch melting* is a closed system in which liquid and solid remain in equilibrium; *fractional melting* is a distillation process in which liquid is continuously and instantaneously removed from the system as it forms):

$$X_Y^l = \frac{X_Y^{\mathrm{bulk}}}{F + (1 - F)D_Y}\ (\text{batch}) \tag{9}$$

$$X_Y^l = \frac{X_Y^{\mathrm{bulk}}}{D_Y}(1 - F)^{(1/D_Y - 1)}\ (\text{fractional}). \tag{10}$$

The phase diagram and isobaric melting relations of this system are shown in Fig. 3. For any given bulk composition, the productivity $(\partial F/\partial T)_P$ is lowest at the solidus, where the concentration of the incompatible element in the liquid and hence the temperature [these are linearly related per Eq. (8)] is changing most quickly per unit change in F. At the solidus the productivities of batch and fractional melting are equal, but the productivity of batch melting increases more quickly at low F. At higher F, where the concentration of Y in the liquid during fractional melting becomes nearly constant at zero, the productivity of fractional melting becomes larger than that for batch melting. Furthermore, at equal F, $(\partial F/\partial T)_P$ is *lower* in instances of this system with higher bulk concentrations of the incompatible component Y, although the opposite is true at equal T.

The productivity behavior of the systems described by Eq. (8) through (10) is much like that of systems like forsterite-fayalite or diopside-hedenbergite, that is, a nearly ideal solid solution in equilibrium with a liquid solution. Using the solidus and thermodynamic properties of the minerals diopside and hedenbergite, the isentropic melting behavior of such a system can be calculated using Eq. (7) and is compared with the isentropic melting behavior of the diopside-anorthite eutectic binary and with the results of a thermodynamic model of natural peridotite melting in Fig. 4. The eutectic and peridotite systems all show a prominent drop in productivity at the exhaustion of clinopyroxene from the residue, but as long as the residual phase assemblage remains the same, all of these systems show very similar behavior, namely, monotonically increasing productivity as a function of increasing F or decreasing P. Figures 4e and

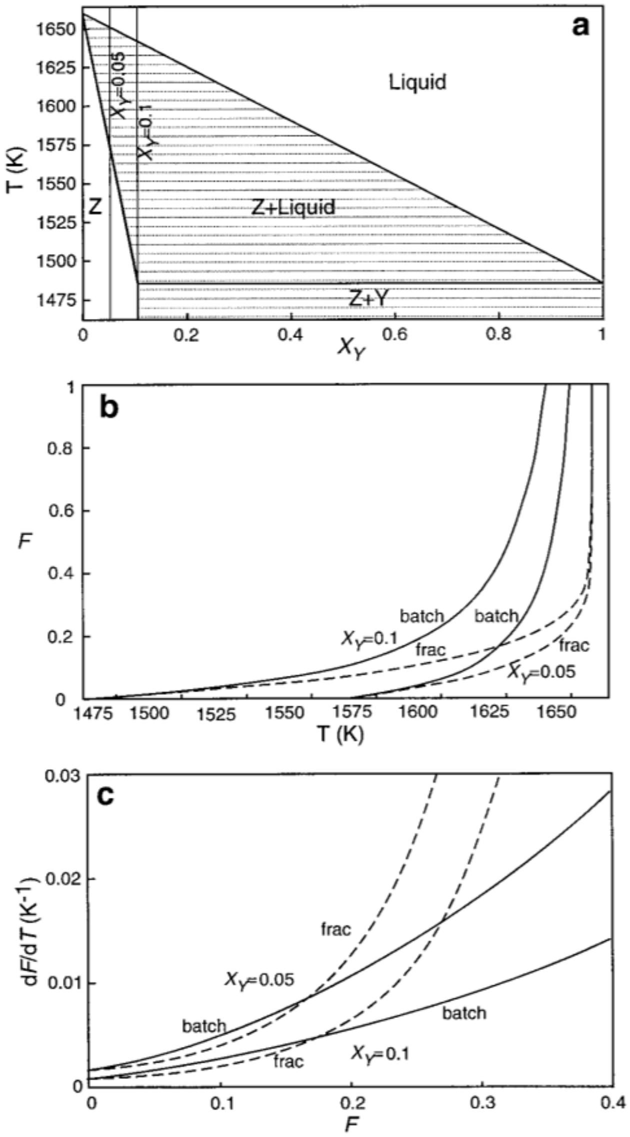

FIGURE 3 Isobaric melting behavior of a simple binary system containing a solid phase *Z* in which the component *Y* is incompatible. The partition coefficient D_Y has the constant value 0.1 in this example. (a) A phase diagram in the $T - X_Y$ plane is divided into a one-phase region where solid *Z* exists alone, a one-phase region where liquid solution exists alone, a two-phase region where *Z* coexists with liquid 10 times richer in *Y*, and a two-phase region where *Z* coexists with pure solid *Y*. Two bulk compositions are marked by vertical lines. For any bulk composition X_Y and temperature *T* in the two-phase $Z +$ liquid region, the equilibrium melt fraction *F* can be read from this diagram using the lever rule. (b) The isobaric melting behavior of the two bulk compositions marked in part (a), plotted as melt fraction *F* versus *T*. (c) Isobaric productivity $(\partial F/\partial T)_P$ versus *F* along the melting paths plotted in part (b).

4f show that, for natural peridotite, a calculation of productivity that holds all variables constant except $(\partial T/\partial P)_F$ and $(\partial F/\partial T)_P$ provides an adequate approximation to the results of the full thermodynamic calculation of all the variables in Eq. (7).

The results of all of these considerations are that adiabatically upwelling mantle will produce melt with an average productivity of about 10%/GPa, but this average probably conceals variations from as little as 2%/GPa to as much as 30%/GPa. Melting proceeds from the intersection of the adiabat and the solidus up to the base of the lithosphere. Specifically, melting is stopped either by the mechanical lithosphere (which arrests upwelling) or the thermal lithosphere (where conduction cools the system), whichever is thicker. A thick lithosphere, such as we expect at oceanic islands like Hawaii, stops melting without regard to considerations of productivity. Where lithosphere is thin, for example, at a fast-spreading midocean ridge, the large productivity approaching exhaustion of clinopyroxene and the decreased productivity thereafter imply that over a fairly wide range of mantle temperatures, the peak extent of melting will be near that required to exhaust clinopyroxene from the source. This corresponds to observations of many oceanic peridotite samples and to the typical melt fractions inferred from normal midocean ridge basalt. Under most circumstances, the low productivity "tail" at the beginning of melting contributes a small volume of high-pressure melts, often with distinctive chemistry, to the aggregate liquid.

IV. MELTING BY CHANGING COMPOSITION

After decompression melting, melting induced by changes in composition is the next most important melting process in the earth. It is mostly responsible for island-arc volcanism, whose often explosive manifestations dominate the rest of this encyclopedia. The origins of arc volcanism are only imperfectly understood; tracing contributions from the subducting slab, subducted sediment, mantle wedge, and overriding plate represents a major area of contemporary research. Still, the basic phenomenon of subduction puts a cold slab into the mantle, generating low temperatures and downward flow. We know from midocean ridges and hot spots that decompression melting requires upward flow and generates more magma given higher temperature. The only reasonable process to induce melting in such a setting is the addition of components such as water that

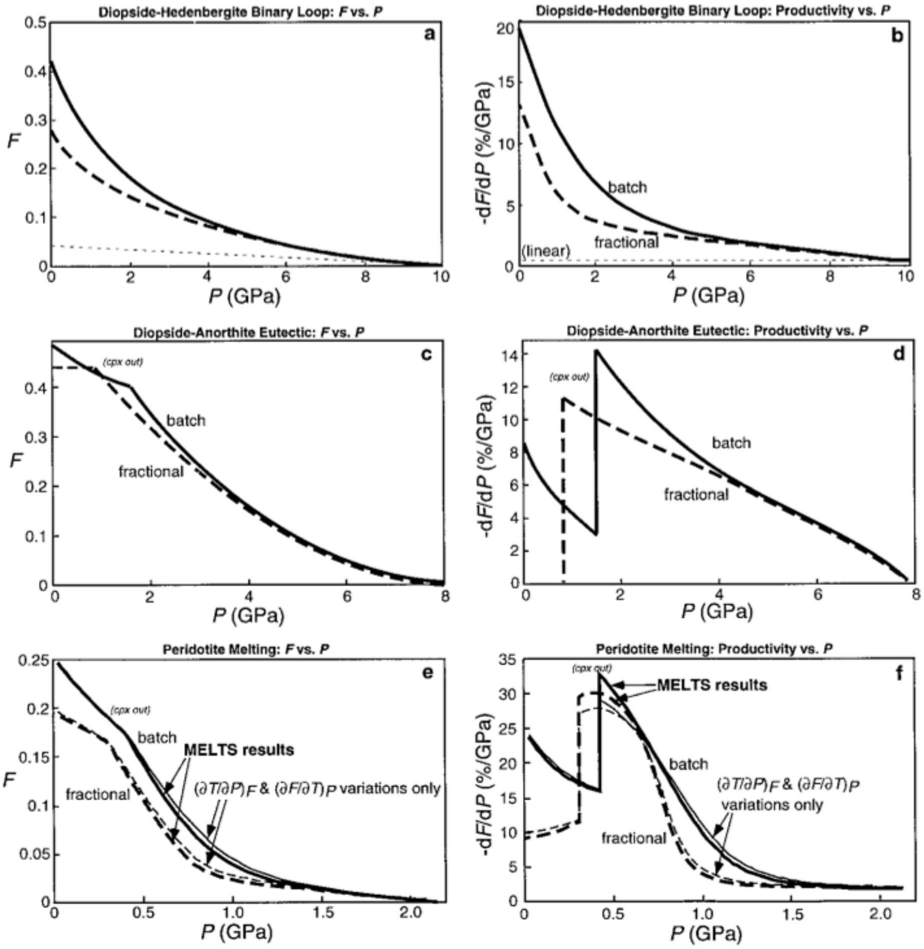

FIGURE 4 Isentropic, polybaric melting behavior of three multicomponent systems; bold solid lines are batch melting paths, bold dashed lines are fractional melting paths. (a) and (b) show F and productivity $-(\partial F/\partial P)_S$ against P for a binary system with complete solid-solution (diopside-hedenbergite), plotted for a bulk composition close to the high-temperature endmember diopside (10% hedenbergite, 90% diopside) along an isentrope that intersects the solidus at 10 GPa. The light dotted lines show a hypothetical constant-productivity melting path for comparison. (c) and (d) show the behavior of a binary system with no solid solution and a eutectic point, diopside-anorthite. The particular case shown has a starting composition of 75% anorthite, 25% diopside; while both phases and liquid are present, the system is restricted to the eutectic curve and behaves much like the one-component system. When diopside is exhausted from the residue, there is a large drop in productivity of batch melting and a total cessation of fractional melting. (e) and (f) show a thermodynamic model of natural peridotite melting that combines aspects of the behavior of both of the preceding systems. Within regions where the residual phase assemblage does not change, productivity increases during progressive melting. The thin curves show an approximate calculation in which all variables are held constant except $(\partial T/\partial P)_F$ and $(\partial F/\partial T)_P$ (see text); this approximation captures most of the productivity variations in this system. As in the binary case, there is a large drop at the exhaustion of clinopyroxene from the residue, but it does not stop melting altogether, even for the fractional case.

drastically lower the solidus temperature of peridotite. That the magmas produced and erupted at arc volcanoes contain abundant water is evident from their explosive behavior.

We can use the binary system illustrated in Fig. 3, with some caution, to discuss the effect of addition of water to peridotite. Like any component that preferentially partitions into silicate melts rather than solids, it expands the stability field of liquid and lowers the solidus temperature. Hence, a water-bearing system can be partially molten at temperatures where the dry system would be entirely solid. The amount of melt produced is a function of the amount of water added as well as temperature. At temperatures below the dry solidus, the amount of melt is small and is limited by the amount of water present and ultimately by the solubility of water in the melt under appropriate conditions. The binary system of Fig. 3 approximates this behavior at temperatures well below the dry solidus, but it is quite misleading as we approach the dry solidus temperature, since it implies that even for a small amount of water the melt fraction increases to unity at the dry solidus temperature. This results from using a one-component system where liquidus and solidus are equal for the water-free part of the model system. For peridotite plus a small amount of water, it is evident that the melt fraction does not approach 1 until nearly the dry *liquidus* temperature, since with a large quantity of melt present the concentration of water in the melt becomes quite dilute and the liquidus depression correspondingly small.

The fundamental problem for models of melting at arc volcanoes is the large volume of magmas produced. It is not clear that the water flux from the subducted slab is sufficient to explain the flux of melt from the mantle wedge by simple water-induced melting at temperatures well below the dry solidus. An alternative is that addition of water induces a small amount of melting and a large drop in viscosity that allows buoyancy-driven diapirism to begin. Rising blobs will undergo additional melting due to decompression as described earlier. In this way, a small amount of water may nucleate processes that lead to a large amount of melting.

V. MELTING BY TEMPERATURE INCREASE

Several distinct mechanisms can directly incrase the temperature of a rock mass so as to induce melting. None is volumetrically significant on today's Earth, but each may have been important at some time in Earth's history or on other planets.

A. Impact Melting

Impacts of extraterrestrial objects large enough to induce substantial amounts of melting are rare at present. When earth was forming, however, it was constantly being bombarded by large objects, including possibly a few impacts large enough to melt the entire mantle and induce a magma ocean. We can easily calculate the amount of energy carried by the impact of an object of given mass and hence to place some bounds on the amount of melting that may occur. In detail, though, large impacts are complex and only imperfectly understood and the efficiency of melt production is difficult to calculate with any precision.

For concreteness, let us consider impacts on Earth after the time when it had essentially achieved its modern mass ($M_{\oplus} = 6 \times 10^{24}$ kg) and radius ($R_{\oplus} = 6371$ km). The minimum kinetic energy per unit mass of an incoming object is equal to the gravitational potential at the Earth's surface relative to infinite separation, $GM_{\oplus}/2R_{\oplus} = 3.14 \times 10^{4}$ kJ/kg, corresponding to a minimum velocity $\sqrt{2GM_{\oplus}/R_{\oplus}} = 11.2$ km/s. The enthalpy of fusion of the Earth's mantle is about 750 kJ/kg. Hence if all the kinetic energy of the impact went into melting (requiring the target to start at the melting point, and totally unphysical compression behavior) an impactor can melt at most itself plus 40 times its own mass of the target planet. The impact of a Mars-sized planetesimal with ~10% the mass of the Earth (such as the event which is thought to have created the Moon) seems likely to result in complete melting of the mantle.

In practice, hypersonic collisions heat and compress the target material along an irreversible thermodynamic path and accelerate much of the target material out of the crater. Thus, much of the impact energy goes into dissipation and kinetic energy. For large cratering events, the work against gravity involved in excavating the crater and lofting the ejecta consumes more of the impact energy. Also the target is generally well below the melting point and so much of the energy goes into heating without inducing melting. Furthermore, the energy of impact ends up very unevenly distributed in the target. Closest to the impact, materials will receive so much energy as to be vaporized, which consumes a great deal of energy and leaves less available to melt rocks that see lower shock pressures.

When large craters on Earth are examined, there typically is a thin (a few meters) sheet of impact melt lining the crater and underlying the ballistic ejecta blanket. Likewise, roughly 1% of the lunar soil consists of glass droplets that presumably originated as molten ejecta from nearby craters. These observations demonstrate that impacts do produce some melt, but at the same time support the argument that impact is an inefficient process for generating magma. On Venus, radar observations taken by the *Magellan* spacecraft reveal evidently fluid outpourings from large impacts, but it is not at all clear whether these flows consist of impact melt or fluidized debris. Finally, although the largest impact basins on the Moon are filled with voluminous floods of Mare basalt, this volcanism was not a direct product of the impact but a later process that preferentially filled the topographic depressions of the impact basins with basaltic magma denser than the lunar crust.

B. Radioactive Heat Generation

Natural radioactive heat sources are too weak at the present day to bring any rock mass to its melting point or power its melting. Furthermore, the Earth almost certainly began very hot, not because of radioactivity, but rather from the release of gravitational potential energy involved in assembling a planet (unless it accreted so slowly that radiation to space maintained a cool starting Earth, but this scenario is not favored by dynamic models or radiometric studies of accretion). Nevertheless, radioactivity bears mention as a source of heat for melting for two reasons. First, it has certainly contributed to keeping the Earth hot and volcanically active for longer than would have been possible with only the heat of accretion. Second, in the very early solar system it was the principal source of heat for the melting of small planetesimals that formed the igneous meteorites.

The principal heat-producing isotopes at present are ^{40}K, ^{235}U, ^{238}U, and ^{232}Th. In material of bulk-Earth composition these presently contribute a total of $\sim 1.5 \times 10^{-4}$ J/kg/year in radiogenic heat. These elements are all strongly partitioned into liquids during melting, however, and so are highly concentrated in the continental crust. Average continental crust generates about 100 times more radiogenic heat than bulk-Earth material. While the excess heat flow from the continental crust is clearly measurable, it is still insufficient to heat crust of normal thickness to its melting point or provide the latent heat of fusion on reasonable timescales. Only in the very early solar system, when the heat flux from K, U, and Th was ~5 times higher but more importantly short-lived radionuclides such as ^{26}Al and ^{129}I were active, could radioactivity by itself heat an asteroid-sized body enough to cause differentiation (melting and core formation).

C. Heating by Conduction

In continental regions, away from plate boundaries and hot spots, volcanoes do occur that require a mechanism other than decompression melting. Their source materials are embedded in the lithosphere, which, aside from rapid and large-scale tectonic extension, prevents drops in pressure fast enough to overwhelm thermal conduction. Conduction therefore is the most likely mechanism for bringing these sources into their melting range by direct heating. This begs the question of why conduction should deliver more heat in one place than another, and the answer generally goes back to decompression melting in the underlying mantle. Geochemical and geophysical evidence typically shows that, although the principal source of intraplate volcanism lies within the crust, there is often a mantle component. Ponding of basaltic magma and subsequent underplating of basaltic rocks at the base of the crust is the most efficient way to focus a large heat flow into a specific region of the crust. Because basalts crystallize at temperatures above 1000°C and the rocks of the continental crust can begin melting (in the presence of water) near 700°C, it is clear that crustal melting is a likely consequence of the arrival of a large mass of basalt at the base of the crust.

D. Frictional Heating and Viscous Dissipation

Neither of these mechanisms is likely to generate a sufficient mass of magma to migrate to the surface and form a volcano. Exhumed fault zones do sometimes contain a narrow zone of glassy rock called pseudotachylyte that appears to represent melt produced by frictional heating, and this process has recently been invoked to explain the faulting mechanism of some very large deep-focus earthquakes. Furthermore, exposed low-angle normal faults and metamorphic core complexes are spatially associated with syntectonic plutonism and some volcanism, but the mechanisms more likely include decompression by isostatic rebound of the footwall and melting of the hanging wall by direct juxtaposition against a hot footwall.

VI. THE MANTLE ADIABAT

In the preceding discussion of decompression melting, we noted that decompression is likely to cause mantle rocks to intersect their solidus and begin melting. Very cold mantle, however, could reach atmospheric pressure without intersecting its solidus, and very hot mantle might be partially molten all the way to the core–mantle boundary. The Earth's mantle happens to be in between these two states such that its typical adiabat intersects the solidus in the range of 50 to at most a few hundred kilometers (Fig. 5). This depth range corresponds to a temperature range (measured at equal depth below the solidus) of 200–300°C sampled along midocean ridges, ranging from the deepest, thinnest crust ridge segments up to ridge-centered hot spots such as Iceland. Away from ridges, it is more difficult to map the temperature variation in the mantle because the depth of melting is not generally available as a probe. Instead, we rely on models of thermal convection and on other indirect

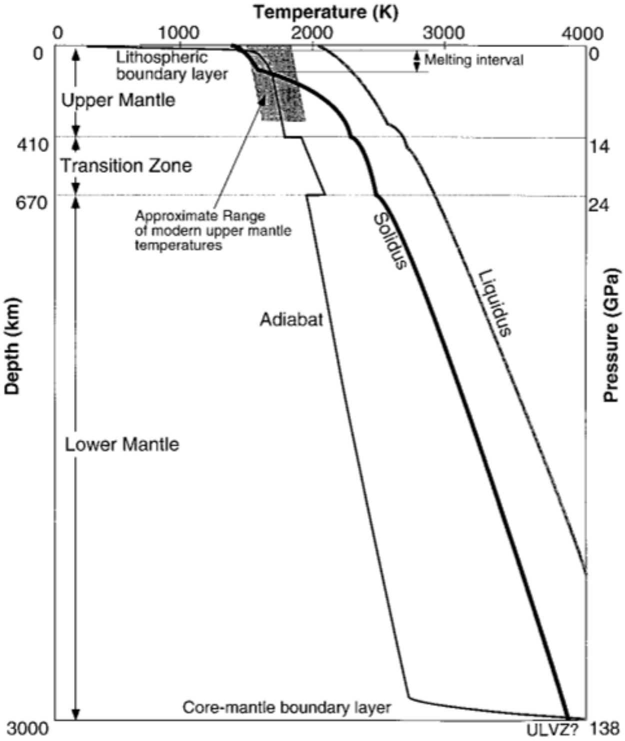

FIGURE 5 Schematic illustration of the temperature structure of the Earth's mantle at the present era. The mantle is conventionally divided into upper mantle, transition zone, and lower mantle, with the boundaries set at the 410- and 670-km seismic discontinuities. The solidus (heavy black curve) and liquidus (heavy shaded curve) are inferred from melting experiments on probable mantle compositions; these curves bracket the range where partial melting can occur. A probable typical temperature structure of the mantle is shown assuming whole-mantle convection with a cold upper boundary layer (the lithosphere) and a hot lower boundary layer where heat is conducted out of the core. In between these boundary layers the temperature profile is adiabatic (see text and glossary). The shaded band shows the likely global range of temperatures of oceanic upper mantle; anywhere the adiabatic part of any of these geotherms extends to shallow pressure, melting will occur. Except possibly for the recently discovered ultra-low-velocity zone (ULVZ) at the core–mantle boundary, melting is restricted to the upper 100 or 200 km of the mantle.

indicators of temperature such as seismic velocity, seafloor depth, and gravity. All of these lines of evidence are broadly consistent with a mantle that contains a very cold upper thermal boundary layer that is subducted into the interior at trenches as well as hot thermal plumes rising from a lower boundary layer that transport ~10% of total heat flow through the upper mantle. The magnitude and origin of temperature variations away from slabs and plumes remain controversial.

Considering that the mantle is 2900 km deep, the depths at which mantle adiabats intersect the solidus are remarkably close to the surface. It is legitimate to inquire whether this is a coincidence or the result of some regulating mechanism, and hence whether this depth range is particular to the present era and steadily declining or else maintained at a quasi-steady value over long periods of geologic history. Because the viscosity of rocks is exponentially dependent on inverse temperature, it is clear that the temperature of a convecting system such as the mantle does regulate itself so that it can flow fast enough to deliver to the surface all the heat that enters the bottom and is produced internally. There is, however, no necessary relationship between the temperature that provides sufficiently low viscosity for mantle convection and the temperature at which melting occurs. Standard plate tectonic theory assigns no particular role to basaltic volcanism in the heat engine of convection; the mantle cools itself primarily by forming and subducting oceanic lithosphere (not crust). One may speculate, however, that the mantle adiabat dwells in the range where basaltic volcanism occurs because basaltic volcanism is somehow a necessary part of the plate tectonic cycle. Perhaps the formation of basalt, which converts to the very dense rock eclogite when subducted, is necessary to sustain subduction. If so, it seems likely that the mantle temperature will remain high enough to support ocean ridge volcanism until its heat flow is low enough to be transported by a qualitatively different and less efficient mechanism than plate tectonics. This remains a question for future work.

VII. SUMMARY

Decompression melting occurs anywhere that upward flow of mantle reaches shallow depths. Such upward flow occurs at midocean ridges due to plate spreading and at hot spots due to thermal plumes in the mantle. Melting begins at the intersection of the adiabat with the solidus curve of the mantle source composition. Melting proceeds at an increasing productivity with an average value near 10%/GPa until the base of the lithosphere stops upwelling or cools the system off the adiabat. The addition of components such as water that substantially lower the solidus temperature of mantle rocks induces melting above subducting slabs in spite of low temperatures and downward flow. Occasional small volumes of magma may be produced by other means such as conductive heating by underlying magma intrusions, but decompression and fluxing are the dominant sources of the magmatic liquids that supply the world's volcanoes.

SEE ALSO THE FOLLOWING ARTICLES

Geothermal Systems • Mantle of the Earth • Migration of Melt • Physical Properties of Magmas • Volcanism on the Moon • Volcanism on Venus

FURTHER READING

Asimow, P. D., Hirschmann, M. M., and Stolper, E. M.(1997). An analysis of variations in isentropic melt productivity. *Phil. Trans. R. Soc. Lond. A* **355,** 255–281.

Elliott, T., Plank, T., Zindler, A., White, W., and Bourdon, B. (1997). Element transport from slab to volcanic front at the Mariana arc. *J. Geophys. Res.* **102,** 14,991–15,109.

Kushiro, I. (1990). Partial melting of mantle wedge and evolution of island arc crust. *J. Geophys. Res.* **95,** 15,929–15,939.

Langmuir, C. H., Klein, E. M., and Plank, T. (1992). Petrological systematics of mid-ocean ridge basalts: Constraints on melt generation beneath ocean ridges. Pages 183–280 *in* "Mantle Flow and Melt Generation at Mid-Ocean Ridges," Geophysical Monograph 71, (J. Phipps Morgan, D.K. Blackman and J.M. Sinton, eds.), American Geophysical Union, Washington, DC.

McKenzie, D. (1984). The generation and compaction of partially molten rock. *J. Petrol.* **25,** 713–765.

McKenzie, D., and Bickle, M. J. (1988). The volume and composition of melt generated by extension of the lithosphere. *J. Petrol.* **29,** 625–679.

Stolper, E. M., and Newman, S. (1994). The role of water in the petrogenesis of Mariana trough magmas. *Earth Planet. Sci. Lett.* **121,** 293–325.

Turner, S., and Hawkesworth, C. J. (1995). The nature of the sub-continental mantle: Constraints from the major-element composition of continental flood basalts. *Chem. Geol.* **120,** 295–314.

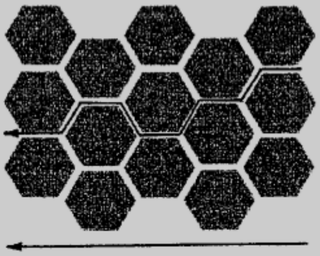

MIGRATION OF MELT

MARTHA J. DAINES
University of Minnesota

I. Porous Flow Model of Melt Migration
II. Melt Viscosity
III. Permeability
IV. Mechanical Properties of the Matrix
V. Melt Localization and Flow Focusing
VI. Future Directions

GLOSSARY

compaction A process in which the solid matrix deforms to expel intergranular melt. Compaction processes could include granular flow or rearrangement of matrix grains without any distortion of individual grains, or changes in grain shape as a result of intracrystalline plasticity or diffusive transfer processes.

compaction length The distance over which the compaction rate in a column of partially molten rock decreases by a factor of *e*. The compaction length, δ_c, is the characteristic length scale in gravity-driven compaction models of melt migration. This distance is a function of the viscosity and permeability of the matrix and the viscosity of the melt migrating through the matrix.

dihedral angle Measured at triple junctions where two grains and melt meet; it is the angle at which the two grains intersect. The value of the dihedral angle is a function of the ratio of the solid–solid interfacial energy to the solid–melt interfacial energy. Dihedral angles lower than 60° imply an interconnected melt network is present at all melt fractions.

permeability A measure of how easily fluid flows through a porous medium. Ease of flow is a function of the size, shape, and connectivity of the porosity network.

viscosity A measure of the resistance of a material to flow in response to stress.

MAGMA ERUPTED ON the Earth's surface is generated by partial melting of rocks at depth. How does this melt separate from the residual solid and migrate to its eruption location? Recent models of physical processes, combined with constraints imposed by the chemical and isotopic compositions of erupted lavas and magmas, suggest that melt migration in the Earth's interior occurs by porous flow along grain-size channels and by flow through larger conduits.

I. POROUS FLOW MODEL OF MELT MIGRATION

Because melting of rocks results in a distribution of melt throughout the rock, the separation of melt from the

Copyright © 2000 by Academic Press
All rights of reproduction in any form reserved.

residual solid requires that melt flow for at least some distance through a connected network of grain-size channels. This type of flow is referred to as *two-phase* or *porous flow;* the partially molten region is regarded as a porous medium. As such, the flow of melt can be described by Darcy's law:

$$v = K/\mu \; dP/dx, \tag{1}$$

where v is the flux of melt (i.e., the volume of melt per unit time passing a unit cross-sectional area perpendicular to the flow direction), K is the permeability, μ is the viscosity of the fluid, and dP/dx is the pressure gradient that drives melt flow. The driving force for melt migration can be chemical and/or physical in nature. Chemical driving forces can be related to differences in interfacial energies; physical forces can be related to the buoyancy of melt relative to residual solids or to applied nonhydrostatic stress. All three of these types of driving forces have been exploited in laboratory studies of melt migration.

The permeability K is a measure of how easily melt flows through the partially molten rock. Ease of flow, as measured by permeability, is a function of the size, shape, and connectivity of the network of porosity or melt channels. Because the permeability of partially molten rocks is difficult to measure directly, permeability is usually calculated using an expression such as:

$$K = a^2 \varphi^n / b, \tag{2}$$

where a is the grain size, φ is the melt fraction, n is usually assumed to be 2 or 3, and b is a geometric constant of the order 1000. Basically, as grain size and melt fraction increase, permeability increases because the size of melt channels becomes larger. The larger the melt channel, the easier it is for melt to flow. Channel shape and connectivity can also affect permeability; these characteristics are taken into account in the geometric constant b as well as the melt fraction dependence n.

Darcy's law is applicable as long as the total amount of melt in the system remains constant. If the amount of melt entering the system is different from the amount leaving the system, then Darcy's law must be modified to take this fact into account. Gains in melt volume, perhaps due to increases in melting rate relative to melt extraction rate, result in either increases in rock volume or increases in the melt pressure. Ramifications of high melt or pore pressure will be discussed in a later section. Reduction of the total amount of melt, perhaps due to rapid melt extraction relative to the melt production rate, implies that the solid matrix must deform to accommodate the change in fluid volume. The reduction in pore volume requires that the matrix compact. Compaction processes could include granular flow or rearrangement of matrix grains without any distortion of individual grains, or changes in grain shape as a result of intracrystalline plasticity or diffusive transfer processes. Compaction means that the mechanical properties of the matrix must be considered when determining the melt flux.

Gravity-driven compaction models of melt migration have dominated theoretical work on the problem of melt extraction for the last 20 years. In these models a column of partially molten rock with an underlying impermeable base compacts due to density differences between melt and solid. Figure 1 shows the stages of this compaction process. At the base of the column, melt volume decreases as the matrix compacts. Above this compacting layer, the upward flux of melt from the compaction zone maintains the melt volume. At the top of the column, melt accumulates, forming a melt-rich layer. Essentially, the extraction of melt due to buoyancy is resisted by the strength of the matrix and the viscosity of the melt.

The thickness of the compacting zone depends on the properties of both the matrix and melt; the matrix can compact only if melt is removed and melt will be expelled only if the matrix compacts. Compaction occurs most rapidly at the base of the column; the rate of compaction decreases exponentially with distance from the base. The distance over which the compaction rate decreases by a factor of e is the characteristic length scale

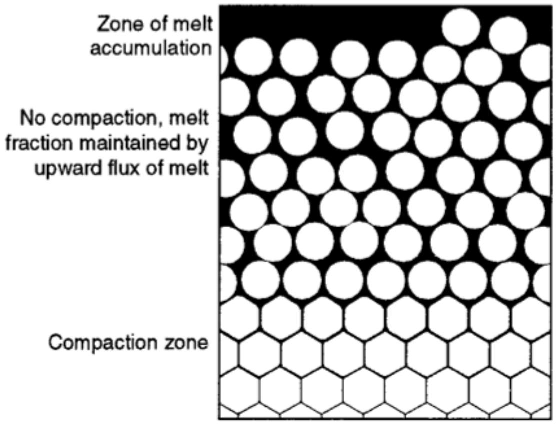
Zone of melt accumulation
No compaction, melt fraction maintained by upward flux of melt
Compaction zone

FIGURE 1 Illustration showing the stages of compaction that result from gravity-driven melt migration. At the base of the column, melt volume decreases as the matrix compacts. Above the compacting zone is a layer in which melt fraction does not change. At the top of the column, melt accumulates.

of the compaction process. Known as the compaction length, δ_c, this length scale is:

$$\delta_c = [K(\lambda + 4\eta/3)/\mu]^{1/2}, \tag{3}$$

where λ and η are the effective bulk and shear viscosities, respectively, of the partially molten rock. The expression within the parentheses ($\lambda + 4\eta/3$) describes how the partially molten rock deforms in response to the applied pressure gradient. In this model both the melt and the matrix are assumed to be linearly viscous. That is, the flow of matrix and melt depends linearly on the applied stress. A characteristic timescale for this process is given by τ_0, which is the time required to reduce the melt fraction by a factor *e* at the base of the compacting layer:

$$\tau_0 = \delta_c/[w_0(1 - \varphi)]. \tag{4}$$

In this equation, w_0 is the relative velocity between the melt and matrix in the interior layer where no compaction is occurring. If melt migration is driven by density contrasts only, then:

$$w_0 = K(1 - \varphi)(\rho_s - \rho_f)g/\mu\varphi, \tag{5}$$

where $(\rho_s - \rho_f)$ is the density contrast between solid and melt.

Another way to compare characteristic extraction times is to calculate the time, t_h, to reduce the porosity of a layer of thickness *h*, by a factor of *e:*

$$t_h = \tau_0(h/\delta_c + \delta_c/h). \tag{6}$$

If the thickness of the layer *h* is much greater than the compaction length, then:

$$t_h = \tau_0 h/\delta_c = h/[w_0(1 - \varphi)]. \tag{7}$$

In essence, this means that if the total thickness of the partially molten region is much greater than the compaction length, the time to reduce the melt volume by a factor of *e* is independent of the viscosity of the matrix.

These equations suggest that the important physical parameters in the two-phase flow model of melt migration are melt viscosity, μ, permeability, K, and, depending on ratio of compaction length to layer thickness, the mechanical properties of the matrix, ($\lambda + 4\eta/3$). Substituting the values of the physical parameters into these equations allows one to calculate characteristic times and distances over which melt migration via porous flow occurs, allowing one to evaluate the likelihood of sufficiently rapid or volumetrically significant melt extraction occurring in a particular geologic environment by this process.

The next three sections of this chapter focus on our current understanding of the physical factors (i.e., melt viscosity, permeability, and matrix mechanical properties) that affect rates of melt migration in both the crust and mantle. Although it is likely that the behavior of a layer containing an initially constant melt fraction is much simpler than that of any real geologic problem, examining the effects of physical parameters using this one-dimensional model can provide a great deal of insight into the melt extraction process. The solutions to more complicated models show that various instabilities can develop during melt migration by porous flow. These instabilities may allow melt to be extracted into melt channels that are larger than those present along individual grains, allowing for much more rapid melt migration. These and other flow focusing mechanisms of melt extraction are discussed in the later portion of this chapter.

II. MELT VISCOSITY

The rate of melt migration depends on the viscosity of the melt that is percolating through the rock. Melt viscosity can vary by more than a factor of 10^{14} depending on the composition of the melt. For example, a dry rhyolitic melt at 700°C has a calculated viscosity on the order of 5×10^{11} Pa s, whereas a carbonatite melt has a viscosity of less than 5×10^{-3} Pa s. These differences translate into large variations in compaction length, separation velocity, and compaction time. These characteristic length, velocity, and timescales were calculated using Eqs (3)–(7) and are listed in Table I for melts with different viscosities. These values were calculated assuming the same melt fraction (0.1), grain size (1 mm), matrix viscosity (10^{18} Pa s), permeability ($K = 1 \times 10^{-12}$ m^2), and driving force ($\rho_s - \rho_f = 0.5 \times 10^3$ kg m^{-3}). Hence, the differences listed in Table I are only the result of variations in melt viscosity.

Mantle melts of basaltic or picritic composition have viscosities of ~1 Pa s. These melts separate rather easily from the residual solid matrix. If the average melt fraction produced beneath a midocean ridge is 0.1, then the compaction length is ~1 km, assuming that the average grain size of mantle rocks is 1 mm. If the partially molten region extends vertically for roughly 50 km, h/δ_c is ~50. From Table I, τ_0 is ~800 yr, implying that t_h, or the time to reduce the melt fraction by a factor of *e*, is ~40,000 yr. Since this time is about 1000 times less than the cooling time for a lithospheric plate, melt extraction

TABLE I Characteristic Compaction Length, Separation Velocity, and Compaction Time for Melts with Different Viscosities

Melt composition	*Melt viscosity (Pa s)*	*Compaction length σ_c*	*Separation velocity (m/yr)*	*Compaction time τ_0 (yr)*
Dry rhyolite	5×10^{11}	1.4 mm	2.8×10^{-12}	5.5×10^{8}
Wet granite	5×10^{4}	4.5 m	2.8×10^{-5}	1.8×10^{5}
Basalt	1	1 km	1.42	8×10^{2}
Carbonatite	5×10^{-3}	14 km	280	56

beneath the ridge should be rapid enough to keep the melt fraction well below 0.1 at any given time. Geophysical data support this conclusion. Although shear wave velocities beneath midocean ridges are anomalously slow, a melt fraction of less than 0.03 can account for these anomalies as long as the melt is present as an interconnected network. Reducing the thickness of the partially molten layer to 100 m, however, changes the efficacy of melt extraction as h/δ_c is reduced to 0.1. The time for significant melt extraction t_b then becomes $\sim$8000 yr; comparison of this time with the time required for cooling a 100-m-thick partially molten region suggests that not much compaction or melt segregation would occur before the melt crystallized due to cooling.

Crustal melts with characteristically high viscosities take much longer to separate from their solid residuum than more fluid mantle-type melts. Consider a 1-km-thick layer of partially molten crustal rocks with a grain size of 1 mm. If 10% of the layer is melted to form a dry rhyolitic melt, how long will it take for most of the melt to separate by gravity driven grain-scale flow? From Table I, the compaction length is $\sim$1 mm, so h/δ_c is $\sim 1 \times 10^6$. The value of τ_0 is $\sim 10^8$ yr, implying that t_b, or the time to reduce the melt fraction by a factor of e, is $\sim 10^{14}$ yr. In other words, insignificant volumes of melt would segregate over the whole of geologic time.

Reducing the viscosity of the melt by adding water, however, does make gravity-driven segregation in crustal environments somewhat more feasible. If the same 1-km-thick layer of partially molten crust now contains 10% of wet granitic melt, the compaction length is increased to about 5 m with h/δ_c decreased to $\sim 10^2$; τ_0 is also reduced to $\sim 10^5$ yr, implying that t_h, or the time to reduce the melt fraction by a factor of e, is $\sim 10^7$ yr.

Even this timescale is problematic for efficient segregation of melt in crustal environments by gravity-driven compaction alone. Separation of melt will be more rapid than that described here if the permeability of the residual solid is higher than that assumed above; increasing the grain size of the matrix by a factor of 10 to 1 cm would increase the permeability by a factor of 100. This change would decrease the time required for significant melt extraction by a factor of 10. Separation of high-silica melts may also require that the driving force for melt extraction be related to pressure gradients in excess of those induced by density contrasts between melt and solid. Nonhydrostatic stress resulting from tectonic activity or due to contrasts in matrix strength with composition are discussed in a later section.

III. PERMEABILITY

Permeability is a measure of how easily fluid flows through a porous media. From Darcy's law it is clear that melt flux scales directly with permeability. So, if permeability increases by a factor of 10, melt flux will increase by a factor of 10. Table II shows the values of the characteristic length, velocity, and compaction time as a function of permeability. These values were calculated using Eqs. (3)–(7), assuming the same melt fraction (0.1), matrix viscosity (10^{18} Pa s), melt viscosity (1 Pa s), and driving force ($\rho_s - \rho_f = 0.5 \times 10^3$ kg m^{-3}). Hence, the differences listed in Table II are only the result of variations in permeability. Clearly, the permeability of the partially molten rock can have a huge effect on the rates of melt extraction.

At the Earth's surface the permeability of rocks to the flow of water and other low-temperature fluids can be directly measured. At depth or in rocks at their melting temperature, these direct measurements are difficult to impossible to make. As a result, the permeability of partially molten rocks is constrained using observations about the geometry of melt networks present in the rock or through laboratory experiments.

TABLE II Characteristic Compaction Length, Separation Velocity, and Compaction Times for Different Matrix Permeabilities

Permeability K (m^2)	*Compaction length* δ_c*(m)*	*Separation velocity* w_0 *(m/yr)*	*Compaction time* τ_0 *(yr)*	*Time for significant melt extraction in a 50-km-thick layer* t_h *(yr)*
10^{-10}	10^4	6	2×10^3	10^4
10^{-12}	10^3	6×10^{-2}	2×10^4	10^6
10^{-14}	10^2	6×10^{-4}	2×10^5	10^8
10^{-16}	10	6×10^{-6}	2×10^6	10^{10}
10^{-18}	1	6×10^{-8}	2×10^7	10^{12}

Textural observations of melt networks can be made on both rock analogues synthesized in a laboratory or on natural rocks. Observations made on natural samples are often difficult to interpret because the original geometry of the melt phase may be obscured by the effects of crystallization or other subsequent processes. Estimates of permeability using textural observations are also complicated by the fact that most observations are made on planar sections; this means that determining permeability first requires one to put two-dimensional features together into a three-dimensional network geometry, then deduce what that complicated three-dimensional topology means about the permeability of the rock. Uncertainties can creep in at either stage of this process. Laboratory measurements of permeability are hampered by experimental difficulties and by uncertainties related to interpretation of the results.

A. Models of Permeability

Permeability models can be used to estimate the permeability of partially molten rock. In these models, melt flow is generally assumed to be steady and nonturbulent, with a parabolic velocity structure across the melt channel. This assumption of Poiseuille flow means that simple relationships can be derived between permeability and melt fraction or porosity if the melt channel geometry is not very complex. For example, the permeability relationships used in most two-phase flow models assume that melt flows either through parallel cracks ($K \propto \varphi^3$) or through cylindrical tubules ($K \propto \varphi^2$). Although these relationships can be useful as first-order approximations and have been used very extensively, observations of partially molten rocks indicate that melt networks are more complex than these simple relationships suggest.

More accurate approximations of permeability are derived using one of two approaches. In the first approach, the rock is approximated by an equivalent porous medium or an idealized representation of the melt network in order to derive analytic solutions for permeability as a function of measurable physical characteristics of the rock. Examples of these measurable characteristics include melt fraction, pore shape and size, and the tortuosity of the melt network. Tortuosity is the ratio of the length of the actual path to the length of the apparent path (Fig. 2). Essentially, the partially molten rock is presumed to be equivalent to a channel with a highly complex cross section of constant area. Permeability in these models is often defined by the Kozeny-Carman equation:

$$K = \varphi^3/[bt^2S^2(1 - \varphi)^2], \tag{8}$$

where b is a constant, T is the tortuosity, and S is the surface area of pores per unit volume of solid. Although this approach has been applied with some success to the

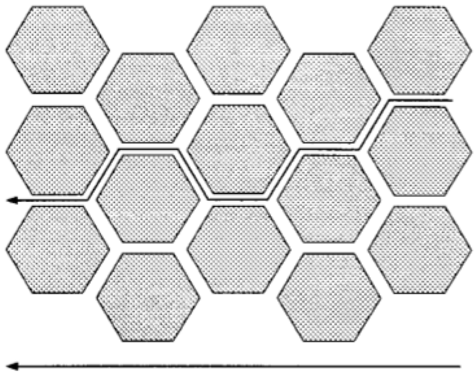

FIGURE 2 Tortuosity is the ratio of the actual flow path (the zigzag line) to the shortest flow distance (straight line). Very complex flow paths have high tortuosity.

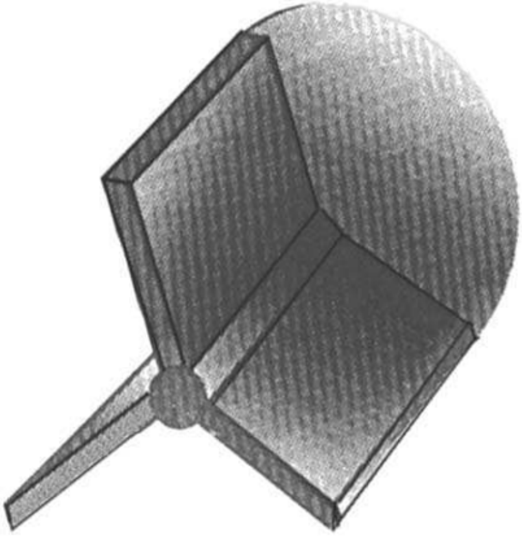

FIGURE 3 A typical model of a melt network used in permeability models. Spherical pores are connected to one another through tubes and sheetlike channels.

flow of low-temperature fluids in sandstone, it has at least two drawbacks. First, both *S*, the melt–solid interfacial area, and *T*, the tortuosity, are difficult to measure accurately in partially molten rocks. This difficulty is partly due to the fact that both require detailed knowledge of the three-dimensional structure of the melt network, knowledge that has been difficult to obtain using conventional microscopy of planar sections. Three-dimensional reconstructions of the melt network using such techniques as serial polishing or confocal microscopy combined with image analysis could result in more accurate measurements of these properties. Second, the model assumes that the flow network is homogeneous, implying that the network has no dead-ends or preferred flow paths. Because melt channels in partially molten rocks are typically quite heterogeneous in terms of shape and size, the equivalent channel or medium approach may not accurately predict permeability.

A second approach to estimating or measuring permeability uses numerical simulations of flow in networks that approximate those found in natural materials. The melt network in some of these models consists of a collection of tubes, penny-shaped or sheetlike channels, and spherical pores of different sizes (Fig. 3). These individual porosity elements are distributed on a grid; equant pores are connected by tubes or sheetlike channels. The permeability is controlled by the size and connectivity of the channels; the pores contribute to the storage capacity of network. By changing the relative proportion, distribution, and connectivity of these elements, the permeability of different melt networks and melt fractions can be determined. For example, a melt network that has spherical pores connected by penny-shaped or sheetlike channels will have lower permeability than a network with the same pores connected by cylindrical tubes.

B. Geometry of Melt Networks in Partially Molten Rocks

Application of these permeability models to partially molten rocks requires a detailed knowledge of the melt network geometry. The initial melting of a rock occurs at the junctions of grains taking part in the reaction. Once melt is present, the melt–rock system adjusts to minimize its total energy. The energy of the system is reduced by minimizing the area of high-energy interfaces and by changing the shapes of interfaces to reduce chemical potential gradients. This energy reduction results in the redistribution of melt, with melt wetting grains if melt–crystal interfaces are of lower energy than crystal–crystal boundaries or melt pooling if the opposite is true. This equilibrium grain-scale distribution of melt in partially molten rock can be characterized by the dihedral angle. The dihedral angle is measured at triple junctions where two grains and the melt meet; it is the angle at which the two grains intersect (Fig. 4). In an ideal rock, composed of identical grains with no variation of surface energies with crystal orientation, dihedral angles less than 60° imply that the melt network is composed of completely connected triangular-shaped tubules along three-grain junctions, whereas dihedral angles greater than 60° imply that at low melt fractions melt is isolated in more spherically shaped pockets at four-grain corners (Fig. 5). In rocks with dihedral angles

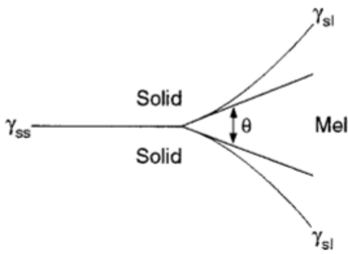

FIGURE 4 The dihedral angle is the angle at which the two grains intersect with melt. The value of the dihedral angle is a function of the ratio of the solid–solid interfacial energy (γ_{ss}) to the solid–melt interfacial energy (γ_{sl}).

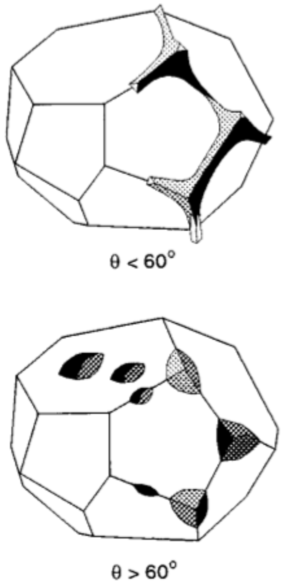

FIGURE 5 Idealized melt networks in partially molten rocks with dihedral angles. (A) <60° and (B) >60°. For dihedral angles <60° melt forms an interconnected network along three- and four-grain junctions. For dihedral angles >60°, melt is isolated at four-grain junctions or along some grain boundaries. (Adapted from Wark and Watson, 1998, with permission from Elsevier Science).

in the range of 1–40°, permeability should follow the relationship for flow in tubes, that is, $K \propto \varphi^2$. In this ideal rock, boundaries between two grains are free of melt unless the dihedral angle is zero or the melt fraction exceeds a critical value.

Most rocks contain more than one mineral. Because surface energies vary among minerals, these additional phases will alter the connectivity of the melt network. The addition of a mineral with a high dihedral angle will decrease the connectivity of the melt network; the reduction in connectivity and change in shape of melt channels will depend on the concentration and distribution of additional minerals.

Dihedral angles in a wide range of rock types have been measured and interpreted using this ideal model. Almost all measured angles for melt in contact with crystals are ≤60°. As a first-order approximation of melt network geometry, these measurements suggest that partially molten rocks in both the crust and mantle will have an interconnected melt network at all melt fractions. Recent work on the melt distribution in olivine-rich mantle rocks, however, points to a more complicated melt geometry in these and other rock types due to the effects of crystalline anisotropy with respect to surface energy. Olivine has been demonstrated experimentally to be anisotropic with respect to surface energy; the contact angle between basaltic melt and (100) olivine crystal surfaces are a factor of 3 to 10 greater than between other surfaces. Flat crystal–melt interfaces, rather than the smoothly curved boundaries predicted for isotropic minerals, are prevalent and preferentially developed perpendicular to *b* axes, parallel to (010) (Fig. 6). Quantitatively, more melt is present in these planar channels between two grains than is found in tubules as would be predicted from simply examining the characteristic dihedral angle. As melt fraction increases, this effect is amplified, because more penny-shaped channels develop as two-grain junctions become melt filled. Increasing the melt fraction in these rocks essentially causes the growth of penny-shaped or sheetlike channels rather than simply increasing the size of tubular channels. These penny-shaped channels contribute very little to the overall melt flow until they reach a critical thickness. Hence permeability may increase slowly with increasing melt fraction until a critical melt fraction is attained.

Because all rock-forming minerals show some degree of anisotropy with respect to surface energy, the dihedral angle-based tubule model in Fig. 5 may not be the best melt network geometry to assume when estimating permeability. This conclusion may be especially applicable to rocks containing minerals such as amphibole, feldspar, and biotite, which are highly anisotropic with re-

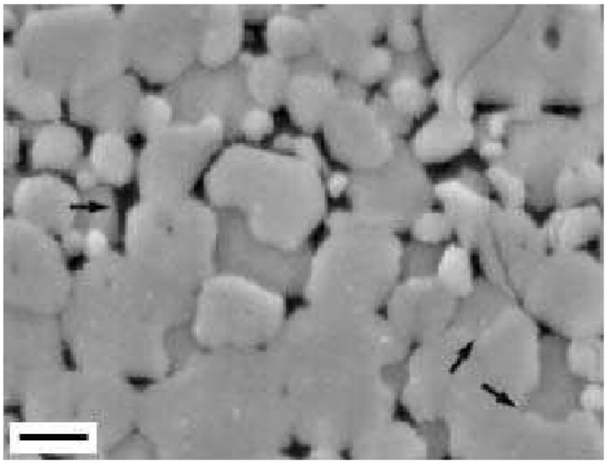

FIGURE 6 Reflected light image of an undeformed lherzolite. Olivine is light gray, pyroxene is medium gray, and quenched melt is darkest gray. Arrows point to planar melt–mineral interfaces and melt-free triple junctions, both features which indicate that crystalline anisotropy with respect to interfacial energy is an important determinant of melt distribution. Scale bar is 10 μm.

spect to surface energy. Biotite, for example, because of its layered structure and high degree of anisotropy, develops very prevalent planar rational crystal faces in contact with melt. Although the range of dihedral angles measured in rocks exhibiting such clear evidence of anisotropy may give one some qualitative idea about the permeability of the rock to melt, any attempt to evaluate quantitatively the permeability using these measurements would be suspect. As a result, recent textural observations of melt geometries tend to focus on using image analysis techniques to more quantitatively measure the size, shape, and other important characteristics of melt channels.

Melt distribution is also complicated by nonhydrostatic stress and deformation. The ideal model is derived assuming hydrostatic stress conditions and, thus, no inelastic deformation of the rock. The distribution of melt in rocks that have been deformed while partially molten, however, can be significantly different from that predicted by the isotropic model depending on the mechanism of deformation (Fig. 7). At low differential stresses, the melt geometry appears unaffected and is indistinguishable from that present in undeformed rocks. As differential stress increases, however, the melt geometry is modified. In partially molten peridotites deformed at differential stresses up to 40 MPa, the majority of grain boundaries exhibit melt along all or part of their length, regardless of orientation with respect to the compression axis. This result, attributed to rapid grain boundary migration during dynamic recrystallization, is in contrast to the primarily melt-free grain boundaries of partially molten peridotites and olivine-silicate melt aggregates annealed under hydrostatic conditions but is similar to microstructures present in some mantle xenoliths. This stress-induced wetting results in more thin sheet-like channels and so could cause a reduction in the permeability of the rock.

In partially molten lherzolite deformed at higher differential stresses, melt forms a network of channels along recrystallized grain boundaries preferentially oriented at angles of 20–30° to the compression axis, but is not found on other grain boundaries (Fig. 7). In this case, differential stress applied to a partially molten rock leads to variations in the stress field associated with the melt network. Depending on the orientation of melt pockets or segments of the network, local pressures may be high or low. These pressure gradients lead to the growth of melt pockets as melt migrates into those pockets preferentially oriented at some angle to the compression axis. This melt redistribution could lead to high permeability in the direction in which melt is preferentially oriented relative to the permeability in the direction perpendicular to the preferred orientation. In fact, permeability parallel to the melt preferred orientation could be enhanced by as much as a factor of 50, greatly increasing the ease of melt migration in that direction.

A similar melt distribution has also been observed in deformed partially molten granitic rocks, where after deformation melt occupies grain boundary segments and transgranular cracks parallel to compression leaving grain boundaries normal to compression essentially melt free. This melt preferred orientation, however, is attributed to melt redistribution in response to cracking of the rock. This cracking or brittle failure of the rock occurs if local pressure gradients near a melt pocket or inclusion are high enough to exceed the strength of the rock. Cracks are melt-filled and oriented with respect to the applied stress; cracks initially open at orientations similar to those described earlier for partially molten peridotites, but eventually grow or extend parallel to the axis of maximum compression (Fig. 8).

Deformation to high strains with subsequent annealing under hydrostatic stress conditions also affects melt network geometries due to the development of a preferred crystallographic orientation of the minerals in the rock. Preferred orientation of crystals typically develop during dislocation creep. For example, in olivine deformed in the dislocation creep regime during uniaxial compression, the *b* axes (010) are preferentially aligned parallel to the compression axis. This preferred orientation of olivine leads to an anisotropic melt distribution with melt preferentially oriented perpendicular to the axis of compression as (010) crystal faces are preferentially wetted by the melt. This preferred orientation of melt again leads to an anisotropy in permeability. This permeability anisotropy would be much stronger in rocks containing minerals with anisotropies in interfacial energy stronger than those of olivine. For example, biotite-rich layers that develop a high frequency of flat crystal faces and tend to have crystals aligned could act as a barrier to melt migration across the layers while enhancing melt flow parallel to the layers. The anisotropy in permeability and its effects on melt migration in biotite-rich layers is enhanced by the development of a shape fabric or foliation defined by the flattening and elongation of grains with respect to the compression axes. Elongation of grains results in elongation of the melt channels perpendicular to the compression axis because melt channels occur along the edges of grains, that is, along triple junctions.

Clearly, the network of melt channels present in partially molten rocks is much more complicated than the simple relationship $K \propto \varphi^n$ would imply. Estimates of permeability based on geometry abound, but most are still

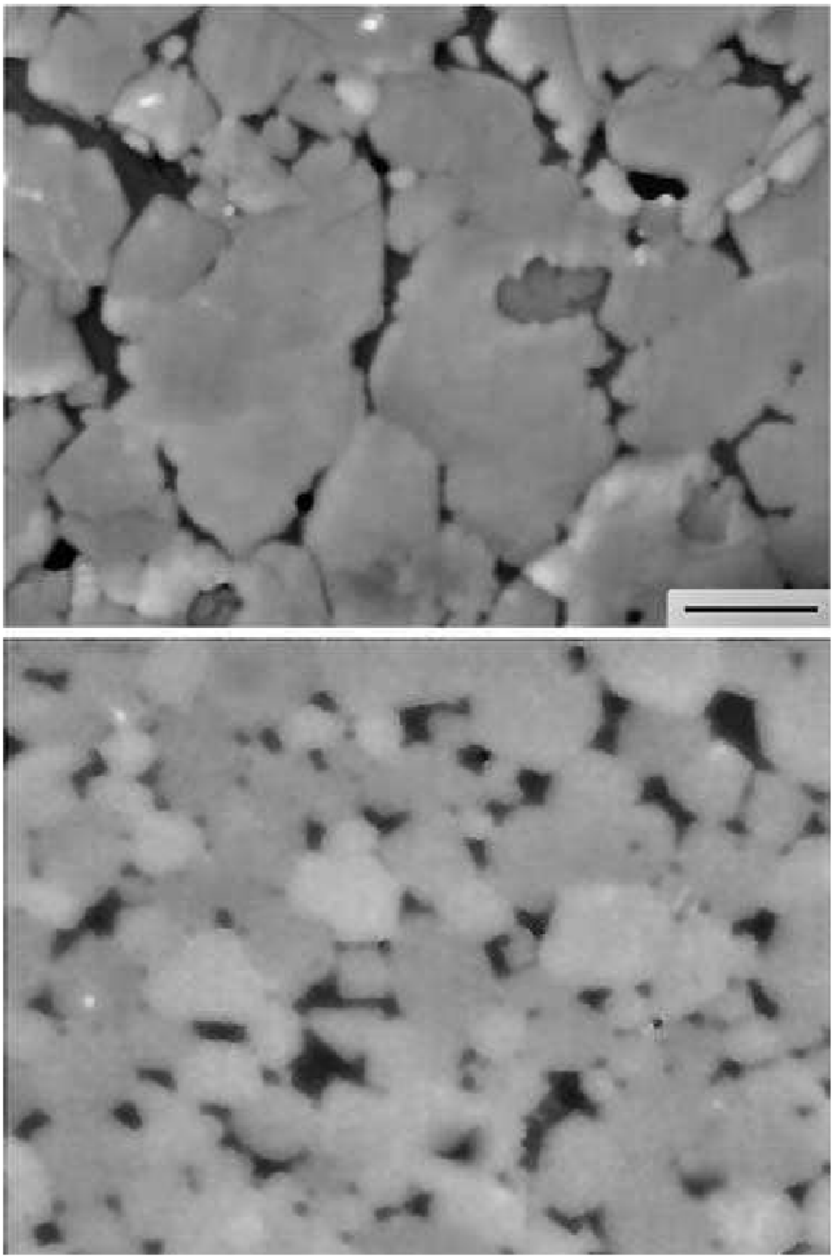

FIGURE 7 Reflected light images of olivine-basalt aggregates deformed at differential stresses of (A) 152 MPa and (B) 42 MPa. Olivine is light gray, quenched melt is dark gray, pores are black and circular. The orientation of the maximum compressive stress (σ_1) is vertical. Melt pockets in part (A) show a distinct preferred orientation relative to σ_1. This preferred orientation is not present in part (B). Scale bar is 20 μm for (A), but 10 μm for (B). (From Daines and Kohlstedt, 1997.)

based on highly simplified versions of the melt network. The focus has also been primarily on establishing the relationship between permeability and porosity. Investigations of the relationship between grain size, melt geometry, and permeability have only begun.

C. Laboratory Measurements of Permeability

Attempts to determine experimentally the permeability of partially molten rocks as well as the relationship be-

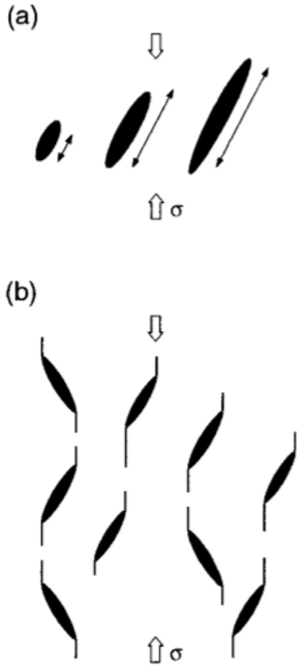

FIGURE 8 Anisotropic permeability structures can develop in deforming partially molten rocks either by (a) extension of melt pockets favorably oriented relative to the maximum compressive stress (σ_1) or by (b) microcracking. Propagation and coalesence of cracks results in the development of veins parallel to σ_1, whereas extension of the melt pockets results in the development of veins oriented at an angle of ~30° to σ_1.

tween permeability and melt fraction have led to somewhat ambiguous results. Experiments using aggregates of glass spheres as analogs of partially molten systems indicate that $K \propto \varphi^2$ holds true in the range of $0.005 < \varphi < 0.25$. These experiments suffer from the fact that the glass spheres used were the same size and did not interact with the fluid phase in the same manner that grains in a partially molten rocks interact with the melt.

A variety of experiments using more realistic materials have led to other conclusions. For example, experiments designed to look at migration rates of basalt in olivine-rich rocks indicate that $K \propto \varphi$, a relationship not predicted by any theoretical considerations of flow in any shaped network. Melt migration in these experiments was driven by differences in initial melt content; capillary forces resulting from interfacial energy considerations led to the movement of melt from a melt-rich disk to a melt-poor disk. In some experiments the melt-poor disk initially contained no melt, whereas in other experiments the melt-poor disk initially contained a melt fraction of ~0.01. For both starting conditions, permeability in these experiments was determined through comparison of numerical simulations of two-phase flow with the actual melt migration profiles of the experiment. From these comparisons permeability was found to range from $5.2 \times 10^{-15}\ \varphi\ \mathrm{m}^2$ to $1 \times 10^{-18}\ \varphi\ \mathrm{m}^2$, depending on the initial quantity of melt in the melt-poor disk and on the composition of the melt. Only in experiments in which the melt-poor disk was melt free was permeability found to be linearly dependent on melt fraction; in other experiments it was impossible to resolve the relationship between melt fraction and permeability. The unexpected linear dependence of permeability on melt fraction yields relatively high permeabilities at low melt fractions, implying that melt extraction by porous flow through grain size channels is efficient enough to keep melt fractions beneath midocean ridges below 0.001.

In contrast, direct permeability measurements on monomineralic aggregates of quartz and calcite synthesized at high pressure and temperature in the presence of water suggest that, for melt–fluid fractions greater than 0.01, the functional dependence of permeability on melt or fluid fraction is cubic ($K \propto \varphi^3$), the same as that predicted by some theoretical models. In these experiments, the annealed sample contains a network of pores filled with a water-rich fluid during the synthesis process. To measure the permeability of this now empty network, a pressurized air reservoir is placed against one end of the sample. As air moves through the pore network in rock, the decrease in the pressure of the air reservoir is recorded. From the decay in pressure, permeability is calculated. For melt–fluid fractions above about 0.01, permeability in quartz aggregates is

$$K = d^2\varphi^3/[1800(1-\varphi)^2]\mathrm{m}^2. \tag{9}$$

At melt–fluid fractions below 0.01, however, permeability levels off or increases if the dihedral angle is <60°. This permeability relationship should apply to other natural fluid- or melt-bearing rocks provided no major differences exist in the degree of crystalline anisotropy or the extent of development of flat faces.

IV. MECHANICAL PROPERTIES OF THE MATRIX

Partially molten material will deform if subjected to stress. In gravity-driven compaction models, the stress arises from the density differences between the solid and the interstitial melt; stress can also arise from tectonic activity. In any case, the deformation or compaction of the matrix results in melt pressure gradients; melt flows in response to these gradients. The importance of matrix deformation during melt migration by porous flow depends on the relative values of the compaction length and the height of the partially molten column. Table III shows the values of the characteristic length, velocity, and compaction time as a function of the mechanical properties of the matrix. These values were calculated from Eqs. (3)–(7), assuming the same melt fraction (0.1), melt viscosity (1 Pa s), and driving force ($\rho_s - \rho_f = 0.5 \times 10^3$ kg m^{-3}). Hence, the differences listed in Table III are only the result of variations in matrix viscosity. The times for significant extraction of melt from two layers of different thickness (50 km and 50 m) are also listed. Clearly, compaction of the matrix has little effect on melt migration rates unless the thickness of the partially molten region is less than or about the same as the compaction length. When the matrix viscosity is relatively high, the compaction length is relatively large, so that the deformation of the matrix is more likely to control the rate of melt expulsion.

Calculation of the compaction length requires that one know the values of λ, the bulk viscosity, and η, the shear viscosity of the matrix. These values are difficult to determine independently from typical deformation experiments. Deformation experiments can determine flow laws that govern the partially molten rock's response to stress. These laws can be used to calculate an effective viscosity (η_{pm}) that can be substituted into the equation for compaction length. For example:

$$\eta_{pm} = \sigma/\varepsilon = A\sigma^{1-n}a^{-p}\exp(Q/RT), \qquad (10)$$

where σ is differential stress, ε is the axial strain rate, a is grain size, n is the stress exponent, A is a materials parameter, Q is the activation energy for creep, R is the ideal gas constant, and T is absolute temperature. With sufficient data, the effective viscosity can be calculated. Unfortunately, data are not currently available for all rock types.

The effective viscosity of a partially molten rock is dependent on the amount of melt present in the rock. Increasing the melt fraction decreases the viscosity of the rock. The degree to which melt affects the rheology of the rock depends on the mechanism by which the rock is deforming. A range of deformation mechanisms has been observed in partially molten rocks exposed to stress. These mechanisms are dependent, in part, on the amount of melt in the rock. One of several deformation mechanisms may be dominant: diffusion creep, dislocation creep, or granular flow with or without fracturing.

At relatively low melt fractions, diffusion and dislocation creep mechanisms may dominate. In diffusion creep-dominated deformation, deformation may be limited by the rate of diffusion through the matrix grains or grain boundaries or by the rate of interface reaction. The presence of melt along grain boundaries can accelerate creep by providing high diffusivity paths and by enhancing the stress concentration at melt-free boundaries. For a melt fraction of about 0.03 and a dihedral angle of 35°, the presence of melt enhances the rate of diffusion creep by a factor of 2. Because higher melt fractions lead to more two-grain boundaries containing melt, this enhancement factor also increases as melt fraction increases. In partially molten fine-grained olivine-rich aggregates deformed in the laboratory, a marked change in diffusion creep rate or effective viscos-

TABLE III Characteristic Compaction Length, Separation Velocity, and Compaction Times Calculated Assuming Different Matrix Viscosities

Matrix viscosity (Pa s)	*Compaction length δ_c (m)*	*Separation velocity w_0 (m/yr)*	*Compaction time τ_0 (yr)*	*Time for significant melt extraction in a 50-m-thick layer t_h (yr)*	*Time for significant melt extraction in a 50-km-thick layer t_h (yr)*
10^{14}	10	1.5	7.4	38.6	3.7×10^4
10^{16}	10^2	1.5	7.4×10	1.9×10^2	3.7×10^4
10^{18}	10^3	1.5	7.4×10^2	1.5×10^4	3.7×10^4
10^{20}	10^4	1.5	7.4×10^3	1.5×10^6	3.85×10^4
10^{22}	10^5	1.5	7.4×10^4	1.5×10^8	1.85×10^5

$K = 1 \times 10^{-12}$; $\mu = 1$ Pa s; $\phi = 0.1$, $\rho = 0.5 \times 10^3$.

ity occurs at melt fractions above about 5%, the melt fraction at which high percentages of grain boundaries contain melt. However, based on model results and geophysical evidence described earlier, this melt fraction is not likely to be present, at least in midocean ridge environments, because melt extraction processes are efficient enough to maintain melt fractions below this value.

An enhancement of deformation rates with increasing melt fraction has also been observed in partially molten fine-grained mantle rocks deformed in the dislocation creep regime. Theoretically, this enhancement should be limited to that associated with the increased concentration of stress at melt-free grain boundaries, and so should be quite small, depending on the geometry of the melt network. Models based on the dihedral angle melt network geometry predict a creep rate enhancement of less than 15% for a melt fraction of 0.03. Measured enhancements in mantle rocks, however, can be much greater. For example, the presence of melt fractions of 0.03 and 0.1 increased the creep rate by factors of 1.5 and 25, respectively, in olivine-rich rocks deformed in the dislocation creep regime. This increased enhancement probably results from unexpected but significant contributions of grain boundary deformation mechanisms to the creep process. These processes include grain boundary sliding as well as grain boundary diffusion. The involvement of grain boundary processes implies that this increased creep rate enhancement in the dislocation creep regime is in part a grain-size dependent phenomenon; estimating its applicability in partially molten regions of the mantle requires grain size constraints.

The diffusion and dislocation creep data for the viscosity of partially molten mantle rocks can be fit by the following relationship:

$$\eta_{pm} = \eta_s \exp(-45\varphi), \tag{11}$$

where η_{pm} and η_s are the viscosity of the solid with and without melt, respectively. This relationship is plotted in Fig. 9, assuming that η_s is 10^{18} Pa s. Use of this effective viscosity when calculating compaction length decreases the compaction length by factors of 1.5 and ~10 if melt fractions are 0.01 and 0.1, respectively. Again, the impact of this reduction on melt extraction will depend on the total thickness of the partially molten layer of interest.

In crustal rocks, because of low dihedral angles and crystalline anisotropy, the penetration of melt into grain boundaries may be even more prevalent than in mantle lithologies, suggesting that enhancements of diffusion or dislocation creep rates could be even greater in these rocks. Unfortunately, partially molten granites rarely show evidence of diffusion or dislocation creep processes when deformed in the laboratory. Instead, these materials deform by a combination of cataclastic deformation of grains and granular flow. As a result, quantitative determination of the matrix viscosity as a function of melt fraction during creep has not yet been accomplished. The minimal experimental data that do exist, however, suggest that, at the low strain rates and stresses at which partially molten granites deform in nature, melt-enhanced diffusion creep will be important.

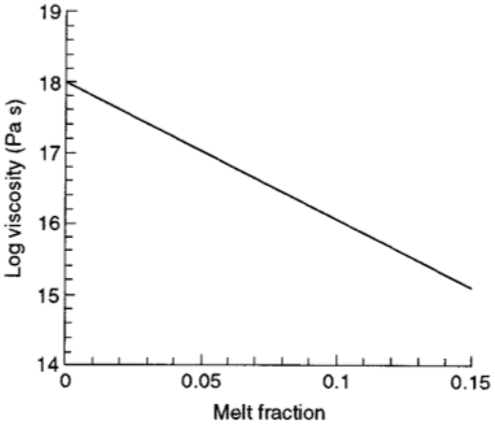

FIGURE 9 The viscosity of mantle rocks decreases with increasing melt fraction calculated using Eq. (11). A melt-free viscosity of 10^{18} Pa s was assumed in the calculation. Equation (11) is based on data from Hirth and Kohlstedt (1996).

Despite the fact that flow mechanisms may be dissimilar to that in natural rocks, results of deformation experiments on partially molten granites and other crustal compositions have been used to estimate the strength and viscosity of crustal materials. Based on these experiments the strengths of these partially molten rocks as a function of melt fraction can be approximated by:

$$\log(\sigma) = 9.15 - 5.1\varphi, \tag{12}$$

where σ is the differential stress in Pa. This relationship is plotted in Fig. 10. The effect of melt fraction on matrix viscosity is evident. These and other data indicate that partially molten crustal materials likely have effective viscosities between 10^{17} Pa s for low melt fractions to 10^{14} Pa s at moderate melt fractions.

The data shown in Fig. 10 call into question the notion of a rheologically critical melt fraction at least for the dry granitic material on which these experiments were performed. The rheologically critical melt fraction

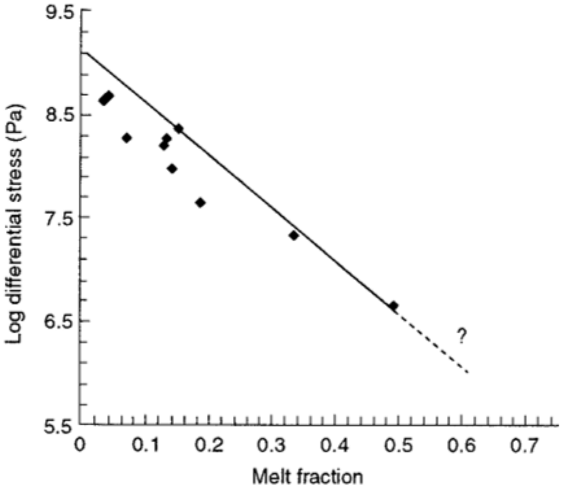

FIGURE 10 The strength of granitic rocks decreases smoothly with increasing melt fraction. The heavy line is calculated using Eq. (12), which was taken from Bagdassarov and Dorfman (1998). Diamonds are experimental data from Rutter and Neumann (1995).

is the melt fraction at which partially molten rocks cease to be frameworks of interlocking solid grains and begin to behave as dense suspensions with effective fluid properties. Estimates of the critical melt fraction in crustal materials range from 0.2 to 0.4; the change in the effective viscosity associated with this transition has been proposed to be as much as 14 orders of magnitude. The data plotted in Fig. 10, however, do not show this abrupt change in viscosity associated with the rheologically critical melt fraction; it may be that the conditions of the experiment or the composition of the materials increased the aggregates' resistance to grain boundary sliding, damping out an abrupt transition. The concept of a critical melt fraction has not been applied to a great extent to mantle materials, primarily because melt migration rates are rapid enough to keep melt fractions well below this theoretical critical limit.

V. MELT LOCALIZATION AND FLOW FOCUSING

Although the initial segregation of melt from the solid residuum must occur by the two-phase model for percolation described earlier, calculation of melt migration rates and length scales, combined with field evidence and geochemical constraints, suggests that at some stage in the extraction process melt must be focused into larger conduits for more rapid melt extraction.

In mantle rocks this conclusion is based in part on chemical and isotopic signatures of both melt and residuum. Abyssal peridotites, assumed to be the residues of partial melting that formed midocean ridge basalts (MORB), are strongly depleted in light rare Earth elements and so are not in trace element equilibrium with MORB. MORB is also not saturated in orthopyroxene, one of the major constituents of these residual peridotites. This disequilibrium requires the efficient extraction of very small amounts of melt (<0.01) throughout the melting region, and little or no reequilibration between melt and solid as melt is transported from depth to the surface. Essentially, the melt extraction is efficient enough to generate near-fractional melting. Pervasive two-phase flow of large volumes of melt through grain scale channels would result in extensive chemical interaction, wiping out these disequilibrium features. ^{238}U-^{230}Th-^{226}Ra abundances in MORB and other tholeites also indicate a fractional mode of melting. Field relationships in ophiolites also indicate that melt flow is focused into larger conduits at some stage of melt extraction. Elongate dunite bodies and ductile shear zones in ophiolites and ocean floor drill core have both been interpreted as former channels for focused melt flow in the shallow mantle.

In the crust, calculations of compaction times and segregation velocities indicate that gravity-driven flow alone can not efficiently segregate significant volumes of melt over geologic time scales unless melt viscosity is less than $\sim 10^4$ Pa s. Partially molten crustal regions must be subjected to an applied stress if significant melt segregation is to occur in most of these rocks. Or high-viscosity crustal melts must collect and migrate through a network of veins and dikes, minimizing the distance over which melt must migrate through intragranular channels. Field evidence abounds, both for the inefficiency of gravity-driven compaction and for the focusing of flow into veins and larger conduits. For example, layers, pods, or veins of granitic material (leucosomes) found in plastically deformed metamorphic rocks could represent melt crystallized in a drainage network in the end stages of melt extraction or melt crystallized before any appreciable melt migration has even occurred. Shear zones, however, undoubtedly represent relatively high permeability channels for melt extraction.

The next sections examine several mechanisms for localizing melt and focusing melt flow into larger conduits. These larger conduits serve to increase the permeability of the partially molten region and to chemically isolate the melt from the residual solid as the melt moves to the surface.

A. Effects of Deformation

1. *Role of Strength or Viscosity Contrasts*

Most rocks are not homogeneous on some scale. Heterogeneities can lead to strength or viscosity contrasts. In a partially molten region that is deforming at a comparable rate throughout, weaker regions will develop slightly lower melt pressures than strong regions. These lower pressures are contingent on the assumption that the strain rate is the same in all areas. Because melt pressure correlates with stress and weak regions deform at lower stresses than strong regions, melt pressures in weak regions are lower than in strong regions, provided they are deforming at the same rate. As a result of these pressure gradients, melt will flow into weaker regions from surrounding stronger regions. For this mechanism to operate effectively, the pressure gradients due to differing strength must be greater than the pressure gradient produced by interfacial energy forces, which are generally trying to redistribute melt homogeneously. Estimates of pressure gradients produced by differing strength suggest that pressure differences could be on the order of hundreds of bars if strength differs by a factor of 10. Interfacial energy forces, assuming appropriate grain sizes and melt fraction contrasts, generally lead to pressure gradients of less than 1 bar/m.

Rheological contrasts can develop as a result of differences in mineralogical composition, grain size, and/or melt content. Mineralogical variations on a variety of scales are present in both crustal and mantle rocks. Source rocks for crustal melts are frequently compositionally layered. Strength contrast due to compositional differences may be further amplified when melting occurs, because melt fraction is negatively correlated with the strength of the partially molten rock. The degree of amplification of the strength contrast may depend on where melting occurs. For example, if an already weak layer also produces more melt than a nearby strong layer at the same temperature and pressure conditions, the relative strengths of the two layers will become even more disparate due to the dependence of viscosity on melt fraction. In essence, the original rheologic contrast results in a dynamic instability with respect to melt distribution, leading to concentrations of melt or melt veinlets. With continued growth, these veinlets could become interconnected, providing a higher permeability path for melt extraction.

2. *Development of Anisotropic Permeability*

Deformation of a partially molten rock can result in the development of an anisotropic permeability structure that may focus melt flow. Two different types of deformation-related anisotropic melt distributions were discussed in Section III—those due to stress and those due to strain.

Stress-induced anisotropic melt distributions are defined by an increase in the size, length, and melt content of melt pockets oriented relative to the axis of maximum compressive stress (σ_1). In fine-grained (<40-μm) partially molten peridotites deformed both in compression and in shear, a large fraction of the total melt present is in those segments of the melt network oriented at 20–30° to σ_1 (Fig. 7). This preferred orientation develops due to the concentration of stress that develops at the edges or ends of melt pockets. If the melt network is treated as an interconnected network of elliptical melt inclusions, then in a compressive stress field, melt inclusions inclined at an angle γ to σ_1 will yield the greatest tensile stress concentration. The value of γ is given by:

$$\cos 2\gamma = 0.5(\sigma'_1 - \sigma'_1 + \sigma'_3), \qquad (13)$$

where σ'_3 is the least compressive stress. The primes in this equation indicate effective stress components, meaning that each has been reduced by a value equal to the melt pressure (i.e., $\sigma'_{ij} = \sigma_{ij} - \alpha\delta_{ij}P_m$ where σ_{ij} is the applied stress, δ_{ij} is the Kronecker delta, P_m is the melt pressure, and $\alpha = 1$). In this formulation, the melt inclusions act as defects in the rock; these defects produce local stress concentrations and gradients in mean pressure, which depend on the orientation of the defect in the stress field. In response to these gradients, melt flows into regions of the melt network that have the lowest mean pressure, essentially extending the melt inclusions in the most favorable orientation with respect to stress (Fig. 8A). This extension results in an anisotropy in permeability. In the case of partially molten mantle rocks deformed in the laboratory, substituting appropriate experimental conditions into Equation 13 gives $20° < \gamma < 30°$. These values are in excellent agreement with the preferred orientation of melt measured in these experiments.

For this mechanism to operate effectively in the mantle, the pressure gradients due to stress in the mantle must be greater than the pressure gradient produced by surface tension, which are generally trying to redistribute melt homogeneously. The driving force for melt redistribution due to applied stress scales approximately with the square root of the grain size (*a*); the driving force for melt redistribution due to surface tension, based on the relationship between pressure and radius of curvature ($P \propto 1/r$), scales approximately with the reciprocal of grain size. Comparison of these relationships between grain size and driving force indicates that as grain size increases the driving force for development of a stress-induced melt distribution will increase by a factor of $a^{1.5}$ relative to the driving force for melt redistribution due to surface tension forces. This observation, combined with laboratory results, suggests that the stress-induced melt distribution should be observed at differential stresses of a few kilopascals for rocks with grain sizes of ~1 mm. These stresses are considerably lower than those expected in the upper mantle, implying that stress-induced anisotropic melt distributions will dominate in deforming regions of the mantle. An important point to note is that, because of limitations of experiments (i.e., total strain, duration, stress resolution), the full extent of stress-induced melt redistribution has not been investigated. Some important questions remain unanswered. For example, with continued deformation will the melt network simply be reduced to long parallel channels as virtually all melt moves into network segments with favorable orientations and these segments link? If so, this stress-induced melt redistribution could lead to the focusing of melt flow into larger conduits. In any case, the permeability anisotropy that results from stress-induced melt redistribution in partially molten rocks is significant and, when combined with appropriate models for mantle flow beneath midocean ridges, is one possible mechanism for focusing of melt toward ridge axes, even if the melt flow occurs in grain scale channels.

Anisotropic melt distributions are also present in partially molten crustal rocks deformed in the laboratory. In these rocks, however, melt is not preferentially oriented at 20–30° to σ_1, but rather is parallel to σ_1. This difference in orientation indicates that the mechanism for melt redistribution in crustal rocks might be different than for mantle rocks. This mechanism is discussed in the next section.

Strain-induced anisotropic melt distributions can also be defined by an increase in the size, length, and melt content of melt pockets oriented relative to the axis of maximum compressive stress (σ_1). In this case, however, the melt redistribution is not associated with the stress, but rather with the changes that occur in the shape and orientation of minerals in the rock in response to the stress. Shape fabrics, defined by the elongation and alignment of grains, could enhance flow in parallel to the developed foliation. This enhancement results from the reduced tortuosity of the melt path parallel to the foliation relative to that perpendicular (Fig. 11). If this shape fabric is combined with a crystallographic preferred orientation of crystals and anisotropy in interfacial energies corresponding to elongation of grains, the effect could be amplified, resulting in high permeability parallel to the foliation.

As described in Section III, strain-induced melt redistribution accounts for the preferred orientation of melt observed in fine-grained partially molten mantle rocks deformed to high strain and annealed. This effect may also dominate in partially molten crustal rocks in which the original source rock initially was foliated. For example, a major component of crustal rocks is biotite, a mineral that has a high anisotropy in interfacial energy, commonly displays a strong crystallographic preferred orientation, and is often found in layers. In a partially molten crustal rock, biotite-rich layers could effectively inhibit melt transport perpendicular to the layering while enhancing layer parallel flow, depending on the orientation of these layers relative to the driving force for melt migration. If layers are perpendicular to the flow direction favored by the driving force, melt might accumulate, unable to migrate through the bordering impermeable layer. This melt accumulation or localization could lead to the development of melt veins.

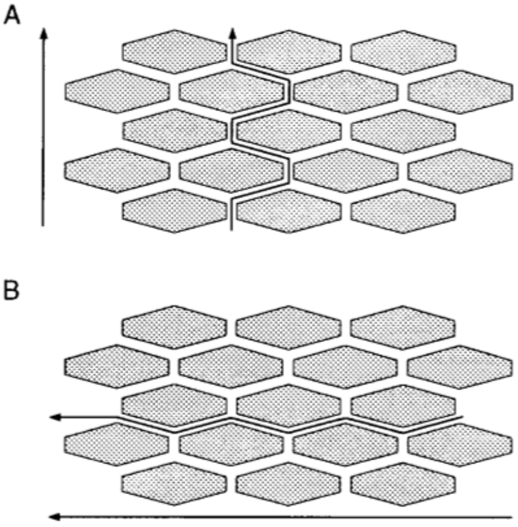

FIGURE 11 The development of a shape fabric during deformation can result in an anisotropic permeability structure as tortousity increases perpendicular to the direction of grain elongation (A) and decreases parallel to that direction (B).

3. Brittle Failure

Perhaps the most attractive mechanism for melt localization and focusing of melt flow has been brittle failure or magma fracturing. On the laboratory scale this process may begin with microcracking along grain boundaries and through grains. In partially molten rocks these cracks are filled with melt. With continued deformation, these cracks link, eventually forming networks of veins and dikes at scales larger than the grain size. Failure can be distributed throughout the partially molten region or localized in shear zones.

In a rock containing melt, the melt pressure acts to reduce the effective stresses. If the effective confining pressure is low enough and the differential stress is high enough, microcracking will occur. As stated earlier, the effective stresses that govern failure in rocks containing melt or fluid are

$$\sigma'_{ij} = \sigma_{ij} - \sigma\delta_{ij}P_{\mathrm{m}}. \tag{14}$$

If melt does not flow easily out of the partially molten rock so that deformation occurs at constant volume, the conditions are described as *undrained*. Most deformation experiments are carried out under undrained conditions. The melt pressure when volume is constant is

$$\sigma_3 \leq P_{\mathrm{m}} \leq (\sigma_1 + 2\sigma_3)/3, \tag{15}$$

where σ_3 is the confining pressure and the quantity on the right-hand side is the mean pressure. In rocks in which the fluid can move freely in response to stress, the pore pressure equals the confining pressure, whereas in rocks in which the fluid cannot move freely the pore pressure is more likely to equal the mean pressure.

If the melt network is again treated as an interconnected network of elliptical melt inclusions, then in a compressive stress field, then same analysis used earlier for stress-induced melt distribution holds true. That is, melt inclusions inclined at an angle γ to σ_1 will yield the greatest tensile stress concentration. Melt migrates into those most favorable oriented cracks as above, but in this case, the maximum local tensile stress around the melt inclusion exceeds the tensile strength of the rock and cracking of the solid matrix occurs. The stress condition for failure is

$$\sigma_3 - P_{\mathrm{m}} = T, \tag{16}$$

where T is the tensile strength of the rock. Cracks will be oriented initially at the same angle to σ_1 as described for stress-induced melt redistribution, but will propagate more nearly parallel to σ_1 (Fig. 8B). On failure, melt pressure decreases within the crack; this decrease results in additional pressure gradients that drive melt into the crack. If melt is distributed throughout the rock, these cracks will develop throughout the rock. As cataclastic failure continues, these cracks grow and coalesce, leading to the formation of a network of veins and fractures in the rock. Under certain conditions (e.g., low temperature and pressure), cracks may coalesce to form localized shear zones. The melt distribution observed in many partially molten granites deformed in the laboratory is due primarily to this process.

The development of fractures or veins depends on the ability to generate melt pressures that exceed the tensile strength of the solid matrix as well as on the temperature, pressure, and stress conditions.

Conditions in the crust are generally favorable for the formation of veins and fractures due to the relatively low pressures and temperatures at which deformation occurs. High melt pressures can also develop in partially molten crustal rocks as a consequence of the high viscosity of the melt and positive volume changes associated with melting. As described in Section II, high melt viscosity considerably reduces the ability of melt to migrate in grain scale size channels. If melt cannot migrate quickly enough to keep up with the imposed rate of deformation, melt pressure will increase locally, possibly leading to failure. If slow melt migration within grain scale channels is combined with melting in which a positive change in volume occurs, this effect is exacerbated. A positive change in volume occurs on melting in relatively dry granitic systems. Not only is melt pressure increased by the positive volume change on melting, but also by the step-wise manner in which melt is produced in these systems. Laboratory experiments of melting in dry crustal rocks indicate that melt fraction increases rapidly over very small temperature intervals due to the breakdown of hydrous minerals such as biotite, muscovite, or hornblende. These rapid increases in melt fraction combined with the positive volume changes associated with melting favors the development of high melt pressures, cataclastic failure, and the development of vein or fracture networks.

In the mantle, brittle failure seems unlikely, primarily because, at typical pressure and temperatures, mantle rocks can deform viscously at differential stresses much lower than the tensile strength of the rocks. However, as discussed earlier, brittle failure can occur if melt pressure is high enough to exceed the confining pressure and the tensile strength of the rock [Eq. (16)]. The mechanisms described for inducing high melt pressures in crustal rocks generally do not apply to mantle rocks, primarily because melt movement in response to deformation and imposed pressure gradients is relatively rapid. The maximum possible difference between the melt pressure and the confining pressure that can be generated due to melt buoyancy in the compacting mantle is

$$\sigma_3 - P_m = (\rho_s - \rho_f)g\delta_c. \qquad (17)$$

Fracture will occur if the right-hand side of this equation is $\geq T$, the tensile strength of the rock. Estimates of T, based on laboratory experiments, suggest that T is at least ~50 MPa. This minimum estimate means that, for appropriate density contrasts, the compaction length δ_c must be greater than 10^4 for fracture to occur. In contrast, most estimates of compaction length in the mantle beneath midocean ridges are less than 10^3. In fact, many theoretical models of melt migration beneath midocean ridges assume that the compaction length is of order 0. In other mantle environments, it may be possible that δ_c is $\sim 10^4$, but only if mantle viscosities are high or if melt is already focused into high-porosity channels with coarse grain sizes. Focusing melt into coarse-grained channels increases the permeability; since $\delta_c \propto K^{1/2}$, δ_c also increases. Brittle failure in the mantle, then, may only occur after melt has been localized to form veins and may not be an effective mechanism for vein formation.

B. Effect of Reaction

Melt–rock reactions in the mantle not only may account for the compositions of erupted magmas and rocks through which melt has moved, but also may provide a mechanism for the focusing of melt flow into larger conduits. Geochemical data suggest that many dunites found in ophiolites and other mantle sections are replacive features formed by reaction between ascending basaltic melt and mantle peridotite. These dunites occur in a variety of shapes and sizes and have sharp boundaries in which pyroxene content changes <2% to >15% over distances of millimeters. In many mantle peridotites, these replacive dunites form an interconnected network of anastomosing channels. These dunite channels represent former conduits for focused melt flow through the mantle. Focusing of flow into dunite channels essentially isolates the melt from further interaction with the surrounding mantle, leading to the geochemical signatures for near fractional melting described above.

These dunite channels develop because mineral solubilities are dependent on pressure. For example, melt produced at depth in the mantle may become saturated in olivine, but undersaturated in pyroxene as it ascends through the overlying rock. At some critical depth or degree of under saturation, melt will begin to dissolve the pyroxene in the rock through which it is moving. This reaction increases the melt fraction, which in turn enhances the permeability of the rock. The increased melt flow that results in turn enhances the rate of reaction, so that a positive feedback loop exists between reaction and melt flow. Although initially the reaction occurs throughout the rock, small differences in pyroxene content may cause an instability to develop. For example, an area with an initially larger proportion of pyroxene will have a higher melt fraction after all the pyroxene is dissolved. This higher melt fraction implies greater permeability; this effect focuses melt into the region. With continued reaction and focusing of flow, olivine-rich channels containing high melt fractions form and grow.

Numerical and laboratory experiments both indicate that this reaction instability could operate in the mantle. Figure 12 shows a typical channel developed during laboratory experiments in which melt undersaturated in pyroxene migrated into a fine-grained rock containing equal amounts of pyroxene and olivine. The initial melt migration-reaction front was planar; after several hours at high temperatures and pressures, several channel features developed. These channels had sharp boundaries defined by changes in melt and pyroxene content. Within the channel no pyroxene remained; outside the channel the initial pyroxene content was unchanged. Experiments in which water flowed through a mixture of glass balls and salt show very similar results.

Although these reaction channels seem likely to develop in the mantle, questions still remain about the time and length scales for this channeling process. For example, channels that develop by reaction during melt migration may have only a limited ability to focus flow in the mantle if the length of channel that develops is limited or if extensive branching of channels occurs. However, even with limited development, this process could provide a starting point for the melt focusing effects of deformation described earlier. For example, the high melt fractions developed in the reaction zones will cause these regions to be significantly weaker than the surrounding region. As discussed earlier, strength contrasts can cause melt to flow from strong to weak areas during deformation. Deformation would then draw more melt into the existing channels, increasing the length of these features beyond that obtained by reaction alone. If the channels become long enough, fracturing could occur as melt pressure at the top of the column of melt exceeds the rocks strength.

Although the relationship between aqueous fluid flow and reaction in crustal rocks has been examined, the

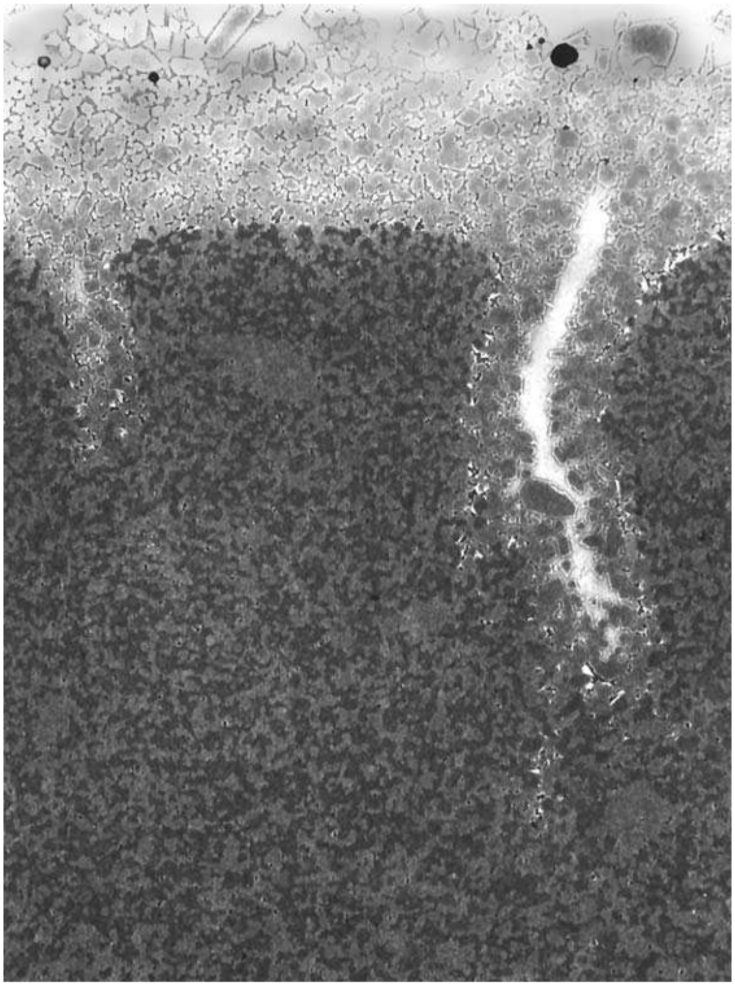

FIGURE 12 Backscatter electron micrographs of melt migration experiments in which the infiltrating melt was saturated in olivine, but undersaturated in Ca-poor pyroxene. Light gray mineral is olivine; medium gray mineral is pyroxene. The glass in these images is light gray to white to dark gray depending on location and degree of undersaturation in pyroxene. A distinct reaction zone is apparent at the top of the image. Within the reaction zone, all of the pyroxene has dissolved, the olivine grains are larger, and the glass is light gray to white. The instability of the reaction front during melt migration is indicated by the finger-like projections of the reaction front. These channel features indicate that melt is being focused due to reaction during melt migration. Field of view is ~600 μm.

effect of reaction on the focusing of melt flow in crustal rocks has not been considered in any detail.

VI. FUTURE DIRECTIONS

Melt migration in both the crust and mantle is a complicated process that requires an understanding of microscopic and macroscopic properties of partially molten rocks. Considerable progress has been made in the theoretical understanding of the extraction of melt, particularly when this separation is driven by density differences between melt and solid. Numerous models of large-scale melt migration have been developed based on gravity-driven compaction; many of these apply to melt migration beneath midocean ridges. Examination of these models, however, suggests that our understanding is still limited by our incomplete knowledge of the basic physical properties of partially molten systems. In particular, we need to know more about the permeability and viscosity of both mantle and crustal rocks.

Despite considerable work on the distribution of melt in partially molten rocks, permeability estimates remain qualitative at best. Recent experiments that directly measure permeability hold a great deal of promise, but so far are limited to aqueous fluids rather than silica melts. Techniques to measure permeability at high pressures and temperatures need to be developed.

Most permeability models to date are based on two-dimensional analyses of melt networks; three-dimensional imaging techniques hold great promise for determining more accurate relationships among permeability, melt fraction, and grain size. In the past, three-dimensional imaging techniques were difficult due to lack of computational power for processing and storing images, poor resolution at which images could be attained, or time requirements for attaining images. Volumetric image data sets are extremely large and have been difficult to use effectively in the past. With recent advances, such as laser scanning confocal microscopy or high-resolution microtomography, three-dimensional images of melt networks should be obtainable. Images combined with flow simulations using Lattice-Boltzmann methods, for example, should resolve the relationship between melt network geometry and permeability in both undeformed and deformed rocks.

In the last 20 years, numerous laboratory studies have examined the mechanical properties of deforming partially molten rocks. In peridotites and other mantle analogues, detailed flow laws obtained through these experiments provide very good constraints on the effective viscosities of these rocks during melt migration. Despite the development of these flow laws, a fundamental understanding of the ongoing microscopic processes that result in these flow behaviors eludes us. This lack of understanding is compounded by recent discoveries of very thin melt films on grain boundaries in mantle samples. The effect these thin melt films have on macroscopic properties of the mantle and their relationship to melt migration processes is unclear. Future work on mantle rocks will undoubtedly focus on these issues.

Much work remains to be completed to constrain mechanical properties of partially molten crustal rocks. Experiments need to be performed at lower stresses and strain rates to examine deformation in the diffusion and dislocation creep regimes; current quantitative results apply only to deformation by cataclastic flow. Technological advances that allow for resolution of lower stresses and strain rates make these experiments possible. Not only will these experiments provide data to develop flow laws, but also they will provide insight into the role of deformation in the localization of melt and the focusing of melt flow in crustal rocks.

SEE ALSO THE FOLLOWING ARTICLES

Composition of Magmas • Melting the Mantle • Physical Properties of Magmas • Plumbing Systems

FURTHER READING

Bagdassarov, N., and Dorfman, A. (1998). Granite rheology: Magma flow and melt migration. *J. Geol. Soc. Lond.* **155,** 863–872.

Brown, M., and Rushmer, T. (1997). The role of deformation in the movement of granitic melt: Views from the laboratory and the field. *In* "Deformation-Enhanced Fluid Transport in the Earth's Crust and Mantle" (M. B. Holness, ed.). Chapman and Hall, London.

Daines, M. J., and Kohlstedt, D. (1997). Influence of deformation on melt topology in peridotites. *J. Geophys. Res.* **102,** 10,257–10,271.

Hirth, G., and Kohlstedt, D. (1996). Water in the oceanic mantle: Implications for rheology, melt extraction and evolution of the lithosphere. *Earth Planet. Sci. Lett.* **144,** 93–108.

Keleman, P. B., Hirth, G., Shiumzu, N., Spiegelman, M., and Dick, H. J. B. (1997). A review of melt migration processes in the adiabatically upwelling mantle beneath oceanic spreading ridges. *Phil. Trans. Roy. Soc. Lond. A* **355,** 283–318.

Keleman, P. B., Shiumzu, N., and Salters, V. J. M. (1995). Extraction of mid-ocean-ridge basalt from the upwelling mantle by focused flow of melt in dunite channels, *Nature* **375,** 747–753.

Kohlstedt, D. L., (1992). Structure, rheology, and permeability of partially molten rocks at low melt fractions. Pages 103–121 *in* "Mantle Flow and Melt Generation at Mid-Ocean Ridges" (J. P. Morgan, ed.). American Geophysical Union, Washington, DC.

LaPorte, D., and Watson, E. B. (1995). Experimental and theoretical constraints on melt distribution in crustal sources: The effect of crystalline anisotropy on melt interconnectivity. *Chem. Geol.* **124,** 161–184.

McKenzie, D. (1984). The generation and compaction of partially molten rock. *J. Petrol.* **25,** 713–765.

Nicolas, A. (1986). A melt extraction model based on structural studies in mantle peridotites, *J. Petrol.* **27,** 999–1022.

Riley, G. N., Jr., and Kohlstedt, D. L. (1991). Kinetics of melt migration in upper mantle-type rocks, *Earth Planet. Sci. Lett.* **105,** 500–521.

Rutter, E. H., and Neumann, D. (1995). Experimental deformation of partially molten Westerly granite under fluid-absent conditions, with implications for the extraction of granitic magmas. *J. Geophys. Res.* **100,** 15,697–15,715.

Sleep, N. H., (1988). Tapping of melt by veins and dykes. *J. Geophys. Res.* **93,** 10,255–10,272.

Spiegelman, M. (1993). Physics of melt extraction: Theory, implications and applications. *In* "Melting and Melt Movement in the Earth" (K. G. Cox, D. McKenzie, and R. S. White, eds.). Oxford University Press, Oxford, England.

Stevenson, D. (1989). Spontaneous small-scale melt segregation in partial melts undergoing deformation. *Geophys. Res. Lett.* **9,** 1067–1070.

Wark, D. A., and Watson, E. B. (1998). Grain-scale permeabilities of texturally-equilibrated, monomineralite rocks. *Earth Planet. Sci. Lett.* **164,** 591–605.

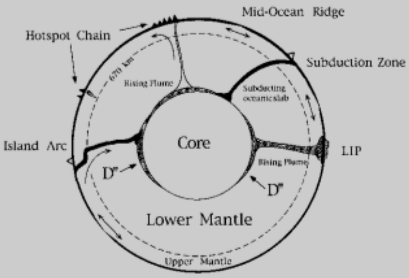

PLATE TECTONICS AND VOLCANISM

MICHAEL R. PERFIT
University of Florida

JON P. DAVIDSON
University of California, Los Angeles

I. Introduction
II. Distribution of Volcanism
III. Volcanism at Divergent Plate Boundaries
IV. Volcanism at Convergent Plate Boundaries
V. Intraplate Volcanism
VI. Geochemical and Petrographic Associations

GLOSSARY

arc A curved chain of volcanic islands or volcanic mountains located near the margins of continents that are formed as a consequence of magmatism related to subduction.

asthenosphere The plastic layer of the Earth's mantle below the lithosphere where most magmas are generated and in which seismic-wave velocities are attenuated and relatively low.

axial graben A linear, down-dropped section of a midocean ridge bounded by normal faults.

crust The outermost layer of the Earth above the mantle primarily comprised of basaltic igneous rocks in the oceans and a wide variety of more felsic igneous rocks, sedimentary rocks, and metamorphic rocks in the continents.

flood basalts Voluminous and thick sequences of mafic lavas erupted from fissures over relatively short periods of time; also known as *plateau basalts*.

hot spot A large volcanic center created by partial melting of the mantle due to the rise of deep, hot mantle material.

incompatible trace element An element with low concentration (<1000 ppm) that does not substitute for major elements in crystal lattices of minerals and instead is concentrated in the melt during the processes of melting or crystallization.

isostasy Mechanism whereby the crust (or lithosphere) rises or falls until its mass is buoyantly supported by the mantle (or asthenosphere) that lies below. Essentially, the less dense crust "floats" at a certain equilibrium level on the more dense, underlying mantle.

lithosphere The brittle 100-km-thick outer layer of the solid Earth overlying the asthenosphere, which consists of the crust and solid uppermost mantle.

neovolcanic zone Narrow region of focused magmatism and hydrothermal activity on midocean ridges

petrogenesis The study of the histories and origins of rocks.

picritic basalt A primitive, magnesium-rich lava, with abundant olivine phenocrysts, that may represent a primary mantle melt.

plume An elliptical or tail-down, drop-shaped mass of the mantle that ascends within the Earth's interior due to its relatively lower density and higher heat content compared to the surrounding mantle; associated with intraplate volcanism and rifting.

primary magma A melt generated by the direct partial melting of its source that is unmodified by crystallization or contamination before it erupts.

Copyright © 2000 by Academic Press
All rights of reproduction in any form reserved.

slab The subducted portion of oceanic lithosphere that undergoes dehydration and/or partial melting beneath arcs.

subduction zone Elongate region on the edges of an active continental margin or island arc where oceanic lithosphere sinks into the mantle; generally characterized by a deep-sea trench and landward dipping seismic belt.

volatiles Elements and compounds that are gases under normal atmospheric conditions or that readily vaporize when heated. During crystallization or eruption of magma, many of these elements come out of solution to form bubbles and escape.

PLATE TECTONICS IS the fundamental paradigm of the Earth sciences, enabling us to understand an overwhelming number of previously puzzling natural phenomena, including the origin and distribution of mountain belts, continents, earthquakes, and volcanoes. As far as we can tell, the Earth is unique among the planets of the solar system in having plate tectonics. Our planet is also unique in having abundant liquid water at the surface. Both of these factors strongly influence the formation of magma, the compositions of magmas, and the locations and behaviors of volcanoes. This in turn controls related aspects such as potential volcanic hazards and economic benefits, discussed later in this volume.

I. INTRODUCTION

Plate tectonics is a simple consequence of the planet's loss of heat. The Earth's internal heat results from original or primordial heat that was accumulated during the processes of accretion and formation some 4.5 billion years ago, together with heat generated by natural radioactivity, as isotopes of elements such as K, U, and Th decay through time. The Earth was much hotter in the past, and has been cooling at a decreasing rate for most of its history. The consequences of an early hotter Earth, in terms of the vigor of convection, the intensity of volcanism, and whether liquid water could exist at the surface, are interesting aspects of Earth's history about which we continue to speculate. Certainly it is arguable whether plate tectonics as we know it today operated in Earth's early history.

The principal mechanism for transferring heat from the deep interior to the surface is by convection. As material heats up at the base of the mantle, as much as 2900 km below the surface, it buoyantly rises because it expands slightly and becomes less dense than its immediate surroundings. At the top of the mantle, approximately 7–35 km below the surface, this material cools and becomes more dense, sinking back down in a return flow. This convection is similar to that observed in a pan of soup on a stove, although the mantle is a much more viscous fluid, and moves at rates of only millimeters to centimeters per year. As a result, over short timescales it behaves more like a plastic material than a liquid. This simple model is complicated by the existence of a rigid, brittle layer called the *lithosphere* that covers the surface of the Earth beneath the atmosphere and hydrosphere. The lithosphere, which includes the crust, is typically 70–120 km thick and is broken into a several large fragments called *lithospheric* or *tectonic plates*. The plates move relative to each other and relative to the underlying convecting mantle. The base of the lithosphere slides over a weak zone of upper mantle called the *asthenosphere*. The weakness of the asthenosphere is due to it being at, or near, the temperature at which it begins to melt. Consequently, some regions of the asthenosphere are partially molten although for the most part it is solid. This leads to an apparent paradox—the mantle flows (by convection) even though it is largely solid. The paradox is resolved only when it is realized that the behavior "fluid" versus "solid" is dependent on the timescales under consideration. For geophysical purposes the solid mantle can be considered a high viscosity fluid.

Note that the lithosphere is different from the crust. The lithosphere comprises both the crust and brittle uppermost part of the mantle. The crust is often erroneously referred to as a synonym for plates, but it is a physically and chemically distinct layer that forms just the uppermost part of the lithosphere. The crust is mainly formed by magmatic differentiation processes and is the underlying factor controlling the difference between continents and oceans. Continents are composed of a thicker (ca. 35-km), lower density crust with average ages of typically 1–2 billion years. In contrast, oceanic crust is thin (ca. 7 km), more dense, and with ages no greater than 200 million years old. The surface of the continents is largely above sea level because the thicker, less dense crust tends to "float" higher in the underlying mantle than the oceanic crust. The equilibrium level at which crust resides due to its density is controlled by a principle known as *isostasy*.

The lithosphere is a continuous layer at the surface to the Earth. The separate plates that comprise the lithosphere are always in contact with each other, but

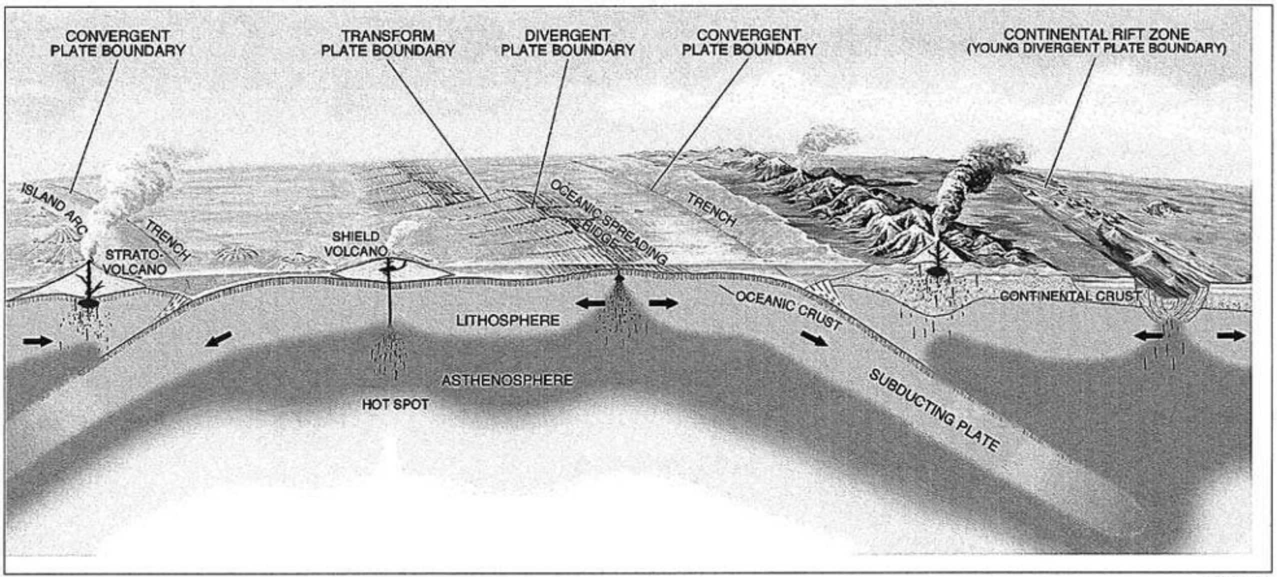
CONVERGENT PLATE BOUNDARY
TRANSFORM PLATE BOUNDARY
DIVERGENT PLATE BOUNDARY
CONVERGENT PLATE BOUNDARY
CONTINENTAL RIFT ZONE (YOUNG DIVERGENT PLATE BOUNDARY)
ISLAND ARC
TRENCH
STRATO-VOLCANO
SHIELD VOLCANO
OCEANIC SPREADING RIDGE
TRENCH
OCEANIC CRUST
CONTINENTAL CRUST
LITHOSPHERE
ASTHENOSPHERE
HOT SPOT
SUBDUCTING PLATE

José F. Vigil

FIGURE 1 Schematic cross section depicting the main plate boundaries and their relation to volcanism. [Courtesy of USGS.]

meet in different configurations leading to three fundamentally different types of plate boundaries or margins (Fig. 1):

1. *Divergent (or constructive); plates move away from each other*. New lithosphere is formed by magmatic processes along the boundary. The feature formed by this is termed a *spreading center* or *rift zone*. Mid-ocean ridges characterize these plate boundaries.
2. *Convergent (or destructive); plates move toward each other and one sinks beneath the other*. The feature so formed is called a *subduction zone*. Subduction zones are characterized by deep oceanic trenches and chains of volcanoes on the overriding plate that parallel the trench. The amount of lithosphere cycled back into the mantle balances the amount created at divergent plate boundaries, keeping the surface area of the lithosphere constant.
3. *Transform (or conservative); plates slide horizontally against each other*. Transform boundaries are a geometrical requirement for a continuous system of moving plates on a globe, and typically link pairs of divergent and/or convergent plate boundaries. This type of boundary is defined by a transform fault, which is usually characterized by a linear fault(s) or fracture zone(s).

This system of plate boundaries is dynamic and evolving, so that a particular boundary may change location or orientation through time, thus causing it to change morphology. They can also change from one boundary type to another or cease to function as a plate boundary while new ones appear elsewhere.

II. DISTRIBUTION OF VOLCANISM

A. Relationship of Volcanism to Plate Boundaries

A glance at Fig. 2 provides compelling support for the association of volcanism with plate tectonics. The distribution of most volcanoes and the locations of plate boundaries correspond very strongly. Rather than a random distribution, most volcanoes are arranged in narrow belts. Many of these exist along the edges of ocean basins—most notably the well-known circum-Pacific "Ring of Fire," which runs around the Pacific Ocean from New Zealand to the Philippines, Japan, Kamchatka, the Aleutians, the Cascades, central America, and southward along the great chain of the Andes Mountains in South America. The association between volcanoes and the oceans was noted several hundred years ago, and volcanoes were thought to result from seawater getting into subterranean caverns. We now have a much

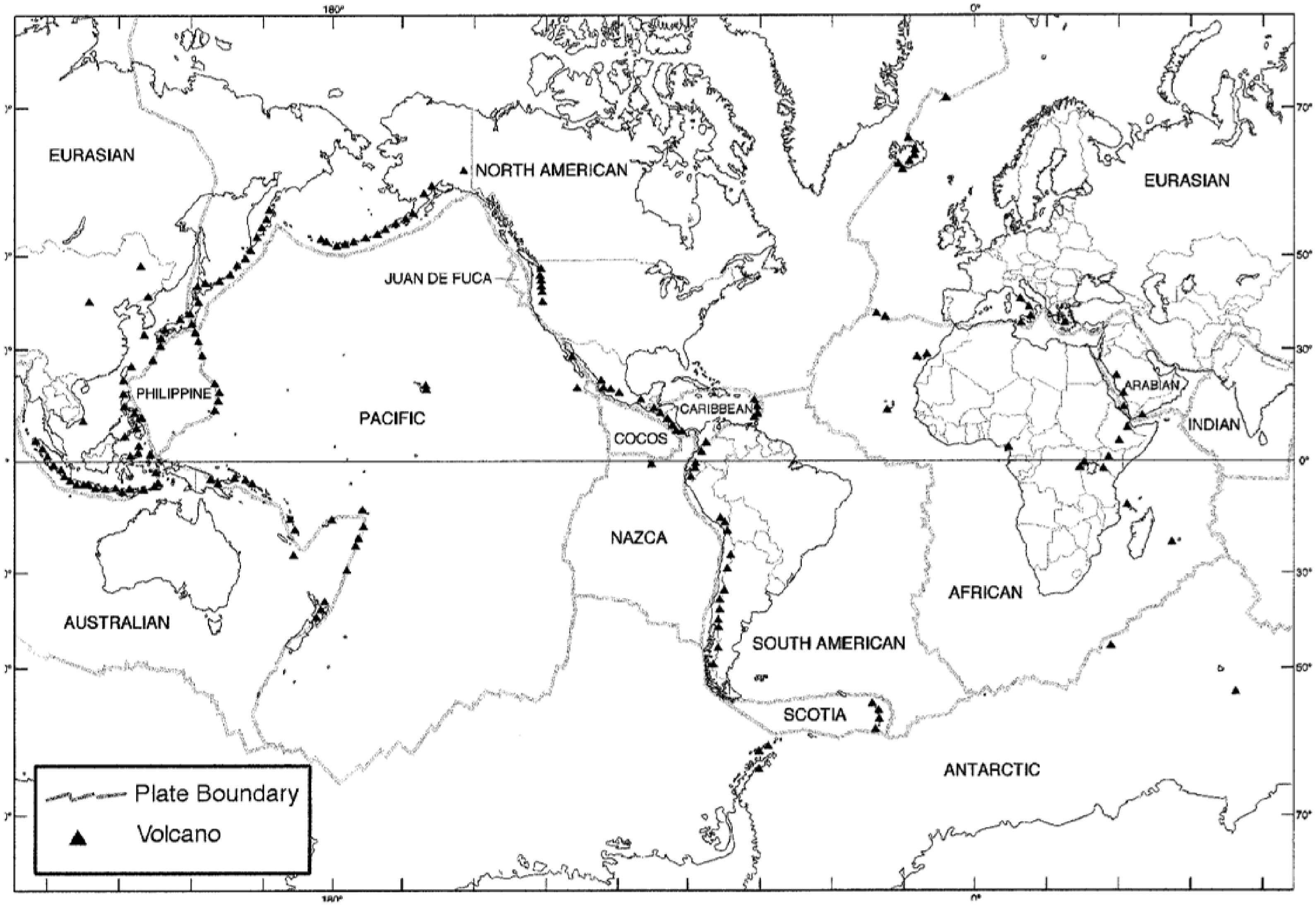
180°
0°
70°
50°
30°
0°
30°
50°
70°
EURASIAN
NORTH AMERICAN
EURASIAN
JUAN DE FUCA
PHILIPPINE
PACIFIC
CARIBBEAN
COCOS
ARABIAN
INDIAN
NAZCA
AFRICAN
AUSTRALIAN
SOUTH AMERICAN
SCOTIA
ANTARCTIC
Plate Boundary
Volcano
180°
0°

FIGURE 2 World map indicating locations of major active volcanoes and plate boundaries. [Courtesy of USGS.]

better understanding of the Ring of Fire, although interestingly, water does turn out to play an important role in the generation of magma. These volcanic chains are related to convergent plate boundaries.

Volcanism also occurs along divergent plate boundaries. This may not be as evident on Fig. 2 because (1) much of the volcanism occurs periodically along cracks or fissures and does not build volcanoes in the classical sense, and (2) most of the divergent plate margins are hidden from view, deep under the oceans. Although we have observed the effects of recent magmatic activity (young lavas, hot springs, hydrothermal vents) along divergent margins using manned submersibles and remotely operated vehicles (ROVs), we rarely actually record eruptions occurring.

The occurrence of volcanism along divergent and convergent plate boundaries or margins argues strongly for a causative mechanism. In contrast, volcanic activity rarely occurs along transform plate boundaries. There are exceptions to the association of volcanic chains with plate boundaries. Some volcanoes or small volcano groups are scattered, apparently randomly, far from plate margins. These are therefore referred to as *intraplate* or *hot spot volcanoes*. Even though they are not directly related to plate boundaries, they owe their origin to hot mantle plumes, which are related to the driving force behind plate tectonics.

B. Influence of Plate Tectonics on Magma Generation

Magma is formed in two principal ways in the mantle (Fig. 3). The first involves simple decompression of hot, solid mantle material (from m to a on Figure 3), whereas the second involves lowering the melting temperature (solidus) of the mantle material by the addition of volatiles (especially H_2O). The connection between plate tectonics and volcanism is in the ways in which plate tectonics can provide these melting mechanisms.

Mantle decompression is effected at mantle plumes and at divergent plate boundaries. In the case of plumes they are an integral part of the mantle convection system and are thought to originate near one of two major physical boundaries in the mantle; the 670-km discontinuity (boundary between the upper and lower mantle) and the core–mantle boundary (around 2900 km). Mantle plumes comprise buoyant mantle material that is solid until the pressure–temperature ascent path, which is typically thought to be adiabatic, crosses the solidus curve for mantle material of the composition represented by the plume. This typically occurs at relatively shallow depths (<200 km), and leads to the production of some melt (magma) in the rising solid mantle. The mechanism and rapidity with which the melt segregates from the solid matrix is still hotly debated and very important because it is critical in determining the composition of the magma that leaves the mantle.

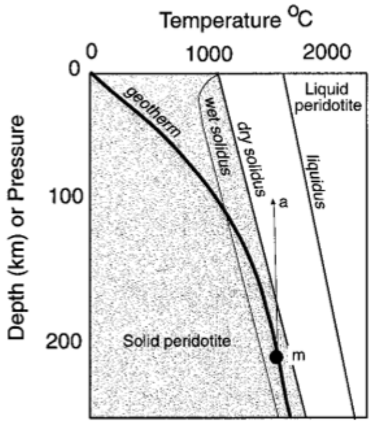

FIGURE 3 Melting mechanisms associated with the three major plate tectonic/magmatic environments. Intraplate and spreading center magmatism is represented by decompression melting, the former associated with deep-origin plumes, the latter with passive upwelling caused by lithospheric extension. Subduction zone magmatism is caused by fluid fluxing of the mantle in the wedge above the subducted slab, which lowers the melting point below the local geotherm temperature.

At divergent plate margins, mantle moves upward, in part, due to convection in the mantle but possibly more in response to the removal of the lithospheric lid above it, which is spreading laterally. The upwelling mantle partially melts in response to this process, exactly the same way as for plumes. Differences exist, however, in the compositions of the melts so formed. Such differences reflect differences in the segregation process, and in the composition of the mantle material that melts, which comes from deep within the mantle in the case of plumes, and from relatively shallow mantle depths at divergent plate margins.

The difference between plume and divergent margin magmatism is that the former is active upwelling while the latter is passive. The former is the fundamental upwelling that represents the heat advection driving plate tectonics. In principle, the location of plumes is not determined by the lithospheric geometry of the outer layer of the Earth. Divergent plate boundaries therefore may represent passive mantle upwelling—here it is the lithospheric geometry, specifically the locations of spreading centers, that are thought to largely control magmatism. Nevertheless, the distinction is not quite so clear-cut in space and time. Certainly a more careful examination of Fig. 2 might belie such a claim, particularly in the Atlantic where several hot spot volcanoes, believed to be related to plumes, are located close to the Mid-Atlantic Ridge. In fact, as explained later, it is the action of mantle plumes that, in many cases, leads to rifting of the lithosphere, making one plate into two and generating a spreading ridge as a consequence. Thus the association of plume-related volcanism with divergent plate margins is an artifact of the process of lithospheric rifting.

Melting due to lowering of the solidus (the temperature at which a solid begins to melt) is the principal cause of magmatism at convergent plate boundaries. Subduction of cold oceanic lithosphere would intuitively be expected to have a cooling effect on the mantle into which it sinks, so the occurrence of magmatism at subduction zones may be surprising. But the subducted lithosphere is not simply cold, but also water rich at its surface. The lithosphere has at its upper surface both a layer of waterlogged sediment and a layer of oceanic crust that has become hydrated as a result of seafloor alteration and hydrothermal processes that occur near spreading centers. As the oceanic lithospheric slab sinks to greater pressures and temperatures it undergoes metamorphism, which drives off the fluids into the overlying mantle wedge. The actual process of subduction may have an extra dynamic effect too. Subduction of the slab causes counterconvection in the wedge-shaped region between the slab and the upper plate, which draws hotter mantle into the region above the slab into which the volatiles are released. The overall effect is to cause melting, generating water-rich magmas, which ultimately predisposes them to become more explosive upon eruption than those erupted at other tectonic localities.

C. Relative Volumes of Magma Fluxes

The flux of magma from the mantle to crust is concentrated along plate boundaries (Fig. 4). This magmatism is broadly correlated with heat flow. Sixty-two percent by volume of Earth's magma flux, amounting to ca. 21 km^3 per year, currently is found along divergent plate margins, and 26% along convergent plate margins; the remainder primarily occurs in intraplate settings. The flux is partitioned between extrusive (erupted at the surface) and intrusive, in a ratio of typically 1 : 9, although this varies with environment. In particular, the ratio of intrusive to extrusive material is greater for the continents, where the thicker, lower density crust acts as a more efficient filter.

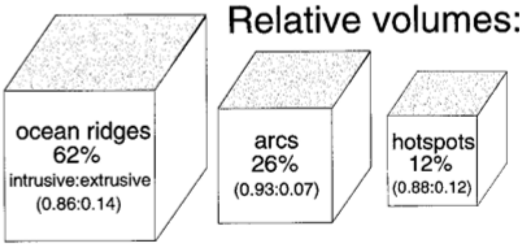

FIGURE 4 Relative volumes of magma produced at different environments. [Data from Fisher and Schmincke, 1984.]

Although these averages may represent the current state of affairs, there is no reason to suppose that this is a constant steady state. The flux of plume-related volcanism in particular is highly variable over timescales of tens of millions of years. There have been specific periods in Earth history known as flood basalt events, when enormous volumes of intraplate basalts were erupted, believed to be a consequence of a large mantle plume head impinging on the base of the lithosphere. During such periods the flux of intraplate magmatism may actually dominate the overall flux, certainly exceeding the 4 km^3 currently erupted annually at intraplate locations.

III. VOLCANISM AT DIVERGENT PLATE BOUNDARIES

A. Structure and Tectonics at Midocean Ridges

Approximately 60% of the surface of the Earth can be considered "oceanic." Most of the oceanic crust has been formed by magmatic processes that occur at midocean ridges (MORs), which form along divergent plate boundaries. These volcanic mountain ranges (which are not always in the middle of oceans) represent the largest, most continuous volcanic system on Earth. Although the ridge system is a globe encircling feature, it is broken up into segments that vary from long, first-order segments (~400–600 km) bounded by major transform faults, to short, fourth-order segments (~10 km) defined by bends or offsets in the linearity of the ridge crest (Figs. 1, 2, and 5). Ridge axis discontinuities that occur

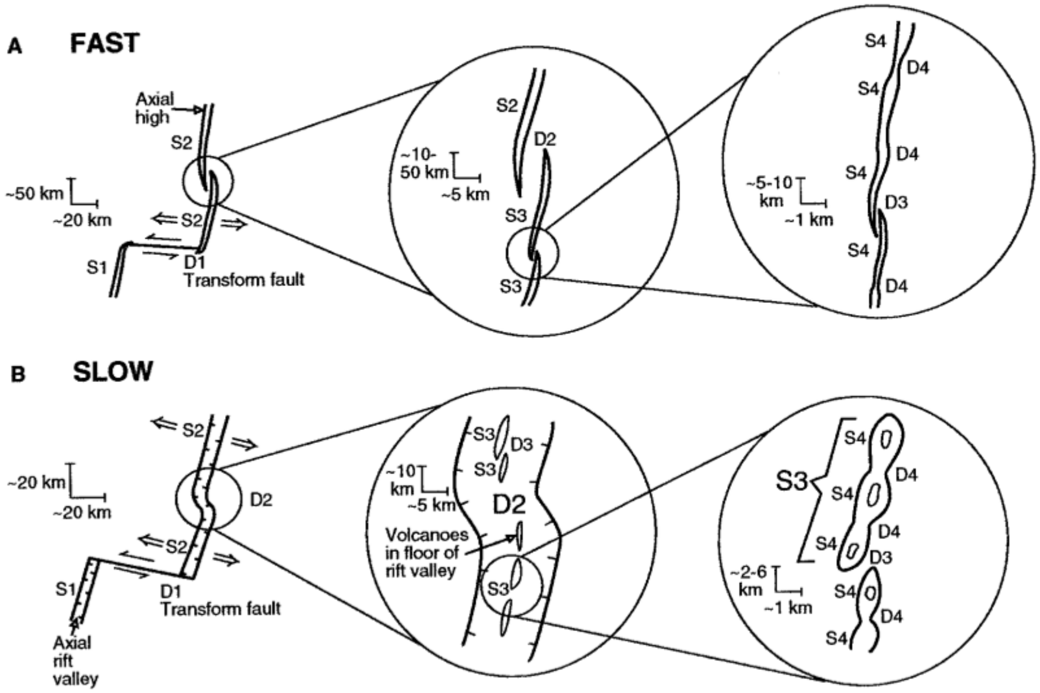

FIGURE 5 Diagrammatic representation of the hierarchy of MOR segmentation for (A) fast- and (B) slow-spreading ridges. S1–S4 are ridge segments of order 1–4 and D1–D4 are first- to fourth-order ridge axis discontinuities. The hierarchy of segmentation is likely a continuum and each order may develop into either higher or lower order segments with time. [From Macdonald, 1998.]

at local depth maxima along ridges can be long-lived, substantial tectonic features such as transform faults (first order), smaller (0.5–30 km) overlapping spreading centers (second and third order), or subtle (<1-km), short-lived and mobile deviations from axial linearity (Devals, fourth order). These discontinuities reflect breaks in the volcanic plumbing systems that feed the axial zone of magmatism. Recent hypotheses suggest that the shallowest and widest portions of ridge segments correspond to robust areas of magmatism, whereas deep, narrow zones are relatively magma starved. The unusually elevated segments of some MORs (e.g., south of Iceland, central portion of the Galapagos Rift, Mid-Atlantic Ridge near the Azores) are directly related to the influence of a nearby mantle plume.

Major differences in the morphology, structure, and temporal and spatial scales of magmatism along divergent boundaries vary with the rate of spreading (Figs. 6 and 7). Slowly diverging plate boundaries, which have low volcanic output, are dominated by faulting and tectonism whereas fast-spreading boundaries are controlled more by volcanism. Many of the morphologic differences observed along ridges can be explained in terms of the competing interaction between volcanic and tectonic processes. While the balance between intrusion and extrusion at MOR axes, in general, has been difficult to constrain volumetrically, it appears that a significant amount of crustal construction occurs by intrusion at all spreading rates. The volumetric ratio of extrusive rock to intrusive rock in the oceanic crust is approximately 1 : 7.

The region along the plate boundary within which volcanic eruptions and high-temperature hydrothermal activity are concentrated is called the *neovolcanic zone*. It is the region where magmatism is focused at the ridge crest. The part of the ridge crest that encompasses the neovolcanic zone has variously been described as the axial valley, rift valley, inner valley floor, median valley, elongate summit depression, axial summit graben, and axial summit caldera. Differences in description are largely a result of the various morphologic expressions of the axis of the ridge crest (Fig. 6). The continuous spectrum of axial morphologies that are observed is a function of two competing processes that vary in time and space: volcanic activity, which results in the construction of relatively smooth features on the seafloor, and faulting/rifting, which results in the creation of

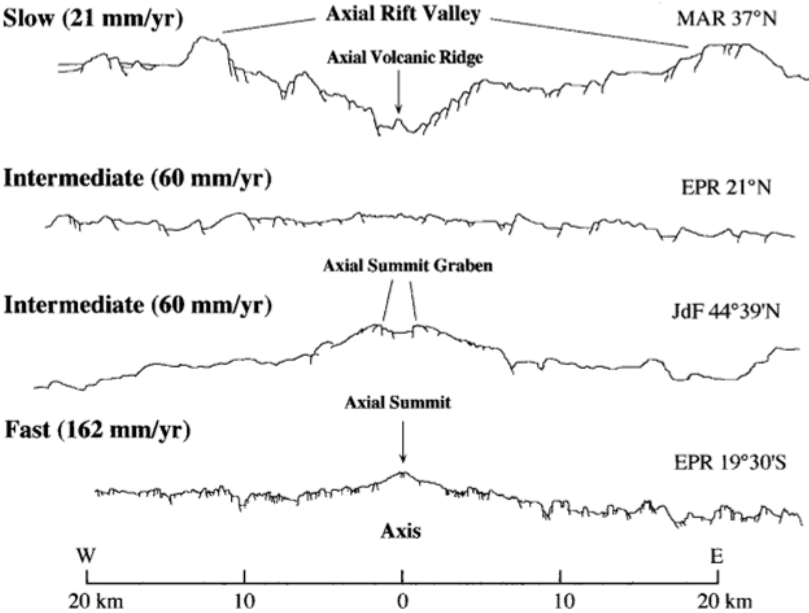

FIGURE 6 Cross-axis bathymetric profiles of selected MORs with different spreading rates. Profiles across fast-spreading (southern East Pacific Rise) and slow-spreading (northern Mid-Atlantic Ridge) ridges show the morphologic contrast between an axial high and a rift valley, whereas intermediate spreading rate ridges (Juan de Fuca Ridge) have transitional features.

rough, linear features at many scales. The width of the neovolcanic zone, its structure, and the style of volcanism within it vary considerably with spreading rate. In all cases, the neovolcanic zone on MORs is roughly linear, similar to rift zones in some subaerial volcanoes, but different than the circular craters and calderas associated with typical intraplate and convergent margin volcanoes. Not all MOR volcanism occurs along the neovolcanic zone. Relatively small, near-axis seamounts are common within a few tens of kilometers of fast and intermediate spreading ridges. Recent evidence also suggests that significant amounts of volcanism may occur up to 4 km from the axis off-axis mounds and ridges or associated with the formation of abyssal hills.

1. *Slow-Spreading Ridges*

Slow-spreading ridges (10–40 mm/yr), like the Mid-Atlantic Ridge, have large axial valleys (8–20 km wide and 1–2 km deep), and the neovolcanic zone can extend across the entire axial valley floor (5–12 km wide). The neovolcanic zone is more difficult to define because magmatism there is relatively unfocused, both across and along axis, and recent volcanic events are extremely rare. Commonly, a discontinuous axial volcanic ridge that can be up to 1–5 km wide, several hundred meters high, and tens of kilometers wide lies at the center of the inner valley floor. Among slow-spreading ridges various axial morphologies are seen, probably related to differences in magma supply. Within single segments on slow-spreading ridges, the axial depth can vary by 1–2 km between the shallow axial highs at the center of the segments and the deeper segment ends (Fig. 7). Lava morphology on slow ridges is dominantly pillow lava, which tends to construct hummocks (<50 m high, <500 m diameter), hummocky ridges (1–2 km long), or small circular seamounts (tens to hundreds of meters high and hundreds to thousands of meters in diameter) that often coalesce to form axial volcanic ridges along the inner valley floor. The prevalence of small seamounts in the neovolcanic zone of slow-spreading ridges is in marked contrast with fast-spreading ridges where virtually no seamounts or large constructional edifices are found in the neovolcanic zone and at intermediate ridges where seamounts are only rarely associated with the neovolcanic zone.

Near-bottom observations on the Mid-Atlantic Ridge show that the inner valley floor is more faulted and fissured and large earthquakes (indicating major faulting events) are much more common than on faster spreading ridges. A high density of faults and fissures, larger earthquakes, and large axial valleys reflect the dominance of tectonism over volcanism at slow ridges. In fact, the nature and scale of ridge segmentation on slow ridges may be primarily due to deformation processes rather than magmatic processes, which control segmentation on fast-spreading ridges. Lower magma supply, thicker crust, and deeper extent of hydrothermal cooling at slow ridges all lead to volcanic events being relatively infrequent.

2. *Fast-Spreading Ridges*

There is no axial valley on fast-spreading ridges (80–160 mm/yr full rate), but along most of an axial crest, there is a narrow, linear depression or trough, which is typically 5–40 m deep, and 40–250 m wide that marks the locus of the neovolcanic zone (Fig. 6). The most striking characteristic of the neovolcanic zone at fast-spreading ridges is that it is very narrow (generally <2 km), indicating that most intrusions are focused beneath the ridge in a linear fashion (Fig. 8). This focusing of magmatism along the axial summit trough is apparently the direct consequence of the fast rate of plate spreading, greater magma supply, a shallower and more steady-state magma reservoir, and more frequent intrusive events than at slow-spreading centers. Lavas erupted within the trough are dominantly fluid sheet flows that vary

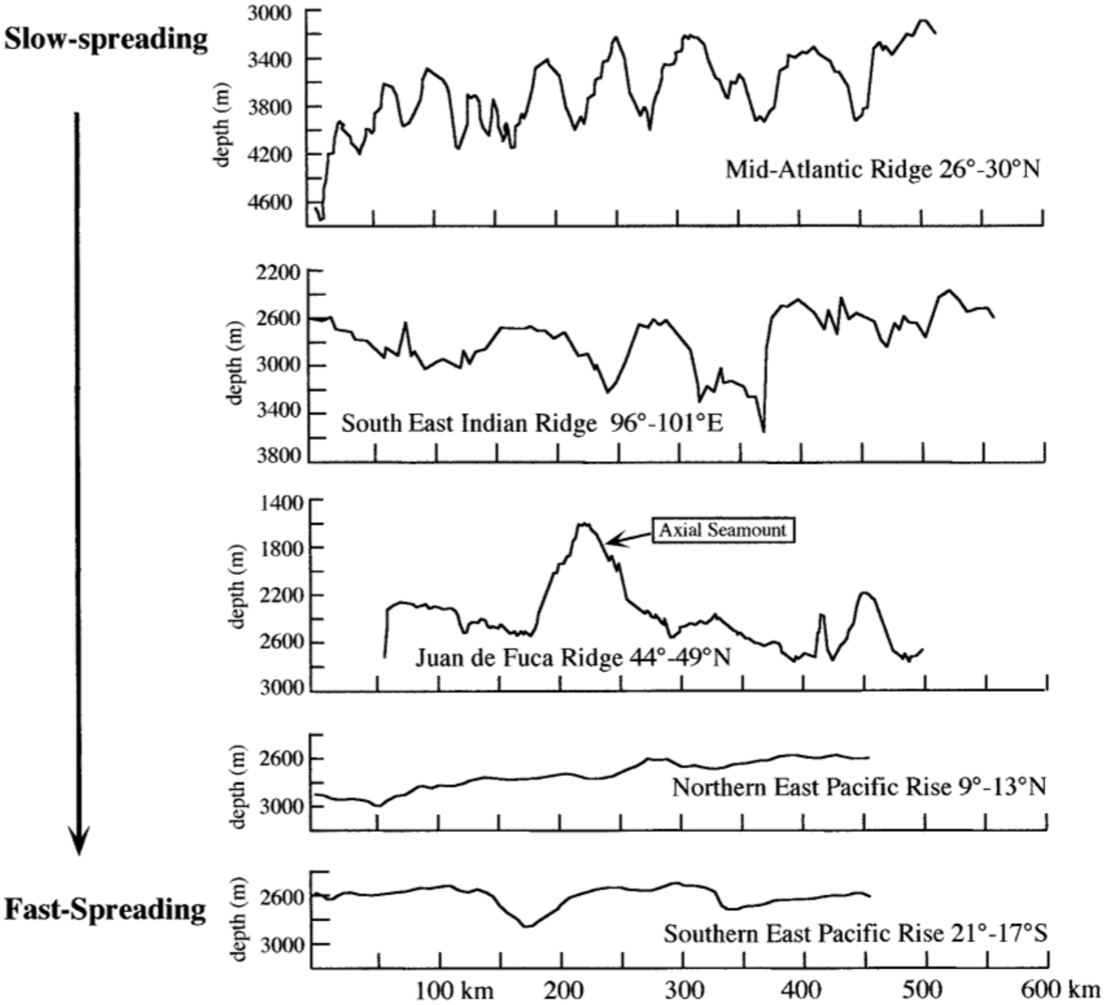

FIGURE 7 Along-axis, minimum depth bathymetric profiles of MORs with different spreading rates. The magnitude and wavelength of depth variations as well as the absolute depths change systematically with spreading rate. Note that the depth ranges differ for each ridge and the large excursion in the center of the Juan de Fuca Ridge profile is Axial Seamount, a hot spot volcano on the ridge axis. [From Perfit and Chadwick, 1998, and references therein.] Depth profile along the Southeast Indian Ridge illustrates the range of axial morphologies observed along this intermediate spreading ridge.

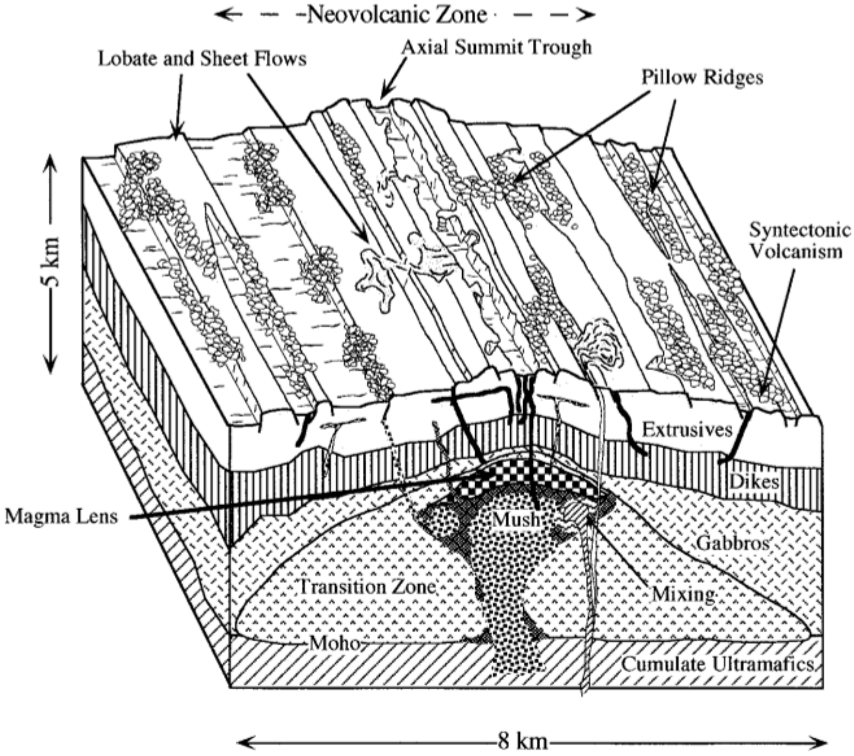

FIGURE 8 Diagrammatic three-dimensional representation of oceanic crust formed along the northern East Pacific Rise [from Perfit and Chadwick, 1998] based in part on the composite magma chamber model of Sinton and Detrick (1992). It can explain many of the chemical systematics observed in MOR basalt suites. The model proposes that there are melt-rich zones (magma lens) separate from crystal-rich zones (mush) that are variably affected by fractional crystallization, magma mixing, and crustal assimilation. Slow-spreading ridges, which do not have steady-state magma bodies, are dominated by mixing and processes such as *in situ* crystallization that occur in the mush zone, whereas magmatically robust fast-spreading ridges are most heavily influenced by fractional crystallization. The model explains why MOR basalts may vary with tectonomagmatic evolution at individual ridge segments, particularly at intermediate rates where magma lenses may be small and intermittent.

from remarkably flat and thin (<4 cm) to ropy and jumbled varieties with chaotically folded and deformed surfaces that can be tens of centimeters thick. These are in stark contrast to the bulbous, pillowed lavas that dominate slow-spreading ridges.

3. Intermediate-Spreading Ridges

The neovolcanic zone at intermediate rate spreading ridges (40–80 mm/yr) has morphologic characteristics that are transitional between those at fast and slow ridges (Fig. 6). However, individual ridge segments on an intermediate ridge can be significantly different in character from one another; some closer to one end member or the other. The morphology of intermediate ridges is variable, but generally consists of a small axial valley, 1–5 km wide, with bounding faults 50–1000 m high. The neovolcanic zone is located within the floor of that valley. Well-studied intermediate ridges include the Juan de Fuca and Gorda Ridges, the Galapagos Ridge, the East Pacific Rise at 21°N, and the Southeast Indian Ridge.

The zone of focused accretion on intermediate rate ridges tends to be wider than at fast ridges but narrower than at slow ridges. There is evidence for episodic and spatially discontinuous magma supply to intermediate ridges, which helps explain the hydrothermal activity observed along intermediate ridges and the wide diversity of morphology (Fig. 6). The frequency of events is moderate, but probably variable and cyclic, more frequent during a magmatically robust phase and less frequent between such phases. The extrusive products of accretion events are also varied; both sheet flow and pillow lava eruptions are common.

Although the data are somewhat limited, calculated volumes of individual flow units that have been documented on MOR show an inverse exponential relationship to spreading rate, contrary to what might be expected. The largest eruptive units are cones in the axis of the northern Mid-Atlantic Ridge, whereas the smallest units are sheet/lobate flows on the East Pacific Rise. The data suggest that fast-spreading ridges erupt on yearly to decadal time scales; intermediate on 10- to 100-yr intervals; and slow-spreading ridges on 1000-yr to 10-ka intervals. This means that within a 10-ka time interval there may be thousands of small flows that build the crust out to ~500 m from the axes of fast-spreading ridges but only a few (<10) large flows near the axis of slow-spreading ridges. Morphologic, petrologic, and structural studies of many ridge segments suggest they evolve through cycles of accretion related to magmatic output followed by amagmatic periods dominated by faulting and extension.

B. Types of Magmas at Divergent Boundaries

Volcanic rocks that comprise the oceanic crust primarily are low-K_2O, tholeiitic basalts with very low abundances of incompatible trace elements such as Cs, Ba, Rb, U, Th, volatile elements, and the light rare Earth elements—all of which are considered to be incompatible in typical mantle mineral assemblages (see Composition of Magmas chapter). These incompatible element-depleted basalts are termed ocean floor tholeiites or, more commonly, normal midocean ridge basalts (N-MORBs). Some ridge basalts contain slightly greater concentrations of incompatible elements and are therefore termed enriched or E-MORBs. Although tholeiitic lavas occur in other tectonic localities (e.g., hot spots, island arcs), MORBs are distinctly more depleted in incompatible elements and have some of the least radiogenic isotope compositions of any terrestrial rock type. Very low abundances of volatile elements such as H_2O and CO_2 in MORB magmas, coupled with the great hydrostatic pressures that exist on the seafloor, explain why explosive eruptions (and hence any pyroclastic rocks) on MOR are extremely rare.

Although MORB form a relatively homogeneous population of rock types when compared to lavas erupted at other tectonic localities, there are subtle, yet significant, chemical differences due to variability in source composition, extents of melting and mixing, and processes that modify primary magmas in the shallow lithosphere (see Origin of Magmas chapter). Densely sampled sections of ridges show that quite a diversity of lava compositions can exist along individual ridge segments. Petrologic data suggest that magma is supplied from several centers of injection along axes that may correspond to second-, third-, and fourth-order ridge axis discontinuities. The melts from these magmatic focal points may coalesce to form continuous but incompletely mixed magma bodies over significant ridge lengths. Mixing of melts from depleted and enriched mantle sources in subaxial magma chambers (Fig. 8) is partly responsible for the spectrum of MORB compositions observed.

MORBs from normal, robust ridge segments typically exhibit only minor compositional variation due to relatively frequent magma recharge and mixing. However, in environments proximal to transforms, propagating rift tips and overlapping spreading centers highly differentiated FeTi basalts (basalts that are particularly enriched in iron and titanium) are common and iron-rich andesites and rhyodacites are often found. This is due to extensive fractional crystallization in crustal magma chambers as a consequence of the relatively cooler thermal regimes and the magmatic processes associated with rift propagation. In general, the paucity of primitive MORBs and the variety of evolved lava types primarily results from shallow-level fractional crystallization although deeper crystallization, magma mixing, and crustal assimilation can also play important roles. Greater estimated depths of crystallization at slower spreading ridges are consistent with observations of increased depths of magma lens or fault rupture depth with decreasing spreading rate.

MORB chemistry of individual ridge segments is, in general, controlled by the relative balance between tectonic and magmatic activity, which in turn may determine whether a steady-state magma chamber exists and for how long. Ultimately, the tectonomagmatic evolution is controlled by temporal variations in input of melt from the mantle. Global correlation of abyssal peridotite and MORB geochemical data suggest that the extent of mantle melting beneath normal ridge segments increases with increasing spreading rate and that both ridge morphology and composition are related to spreading rate.

The depths at which primary MORB melts form and equilibrate with surrounding mantle remain controversial, as does the mechanism(s) of flow of magma and solid mantle beneath divergent plate boundaries. The debate is critical for understanding the dynamics of plate spreading and is focused on whether flow is "passive" plate-driven flow or "active" buoyantly driven solid convection. At present, geologic and geophysical observations support passive flow, which causes melts from a broad region of upwelling and melting to converge in a narrow zone (neovolcanic?) at ridge crests.

C. Faulting Associated with Volcanism

It is clear in many places on MORs that volcanism is related to faulting and fissuring of the crust (hence the concept of a "rift zone"). Graben (extensional rift valleys) often form above intruding dikes in volcanic rift zones because a dike creates two zones of maximum tensional strain at the surface, parallel to the dike axis but offset to either side. In the tectonic environment of a spreading ridge, a dike intrusion releases horizontal tensional stress that has built up by divergent plate motion since the last rifting (intrusion or faulting) event. When a dike-induced graben forms above a dike, the faulting occurs before the dike reaches the surface and once an eruption begins, lava may then fill or partially bury the graben.

Distinct graben, 10–100 m wide and 5–15 m deep, are associated with recent eruptive sites on the Juan de Fuca Ridge. These graben are interpreted to have formed directly over the dike that fed the eruptions as it was intruding. Similar, but wider, graben formation has been documented during dike intrusions in Iceland. Along fast-spreading ridges, dike-induced graben subsidence is questionable because there is little direct evidence for structural control of the axial summit trough which appears more related to volcanic drainout.

The narrow dike-induced graben observed on intermediate and fast-spreading ridges imply that a relatively low level of ambient horizontal tensional stress exists perpendicular to the ridges, whereas the wide graben that characterize slow-spreading centers suggest high levels of horizontal tensional stress. The differences in tensional regimes may be a consequence of more frequent eruptions at fast-spreading ridges (magmatically robust) compared to the infrequent eruptions at slow-spreading ridges (tectonically dominated). Horizontal extension without magmatism has led to the exposure of mafic plutonic rocks and peridotites that must come from the deep oceanic crust, and the development of strong geologic and structural asymmetry in the axes at some slow-spreading ridges. During amagmatic periods, tectonic stretching creates numerous normal faults and low-angle, listric, or detatchment faults that extend down to the brittle–ductile transition zone in the oceanic lithosphere. The associated large-scale stretching and thinning of the lithosphere results in the formation of *megamullions*—similar to core complexes in highly extended continental rift zones where deep-level crustal rocks are exposed.

D. Off-Axis Volcanism

Although most of the magma delivered to a MOR is focused within the neovolcanic zone, off-axis volcanism and near-axis seamount formation add significant volumes of material to the oceanic crust formed along ridge crests. Detailed sampling and U-series dating of lavas from the crestal region of fast- and intermediate-spreading rate MORs have shown that some lavas have been erupted up to 4 km outside the axial summit trough on the crestal plateau (Fig. 8). This recent off-axis volcanism is expressed as young-looking lava fields and prominent pillow ridges up to 20 m high that have a larger and more complex range of compositions than the lavas on-axis and show significant chemical variations over small spatial scales. Observational and chemical data suggest that these off-axis eruptions may be fed from different magma plumbing systems than the ones at the axis or from the distal edges of subaxial magma bodies.

In some portions of fast-spreading MORs, off-axis eruptions are related to the syntectonic volcanism and the formation of abyssal hills (Fig. 9). Volcanic growth faults form in a flanking tectonic province 2–6 km from the ridge axis, and are repeatedly covered by lava flows associated with ridge parallel faults. The lavas are interpreted to have been erupted either from the ridge axis itself or from a zone 2–3 km off-axis, consistent with the geochemical studies discussed earlier. This model for abyssal hills is specific to fast-spreading ridges, and other processes may be important at intermediate and slow ridges. On segments of slow- and intermediate-spreading MORs that are magma-starved, abyssal hill faults may rarely get covered with lava.

Some models for volcanism on MORs suggest that there is a bimodal distribution of lava flows: frequent short flows confined to the axis and occasional voluminous flows that spill out of the axial trough and flow for considerable distances. Only a few examples of extremely large (10–200 km^2) lava flows or lava fields have been found on or near some sections of the MOR in the northeast Pacific and the southern East Pacific Rise. These types of flows represent tremendous volumes of lava, but it is unknown how often these kinds of events

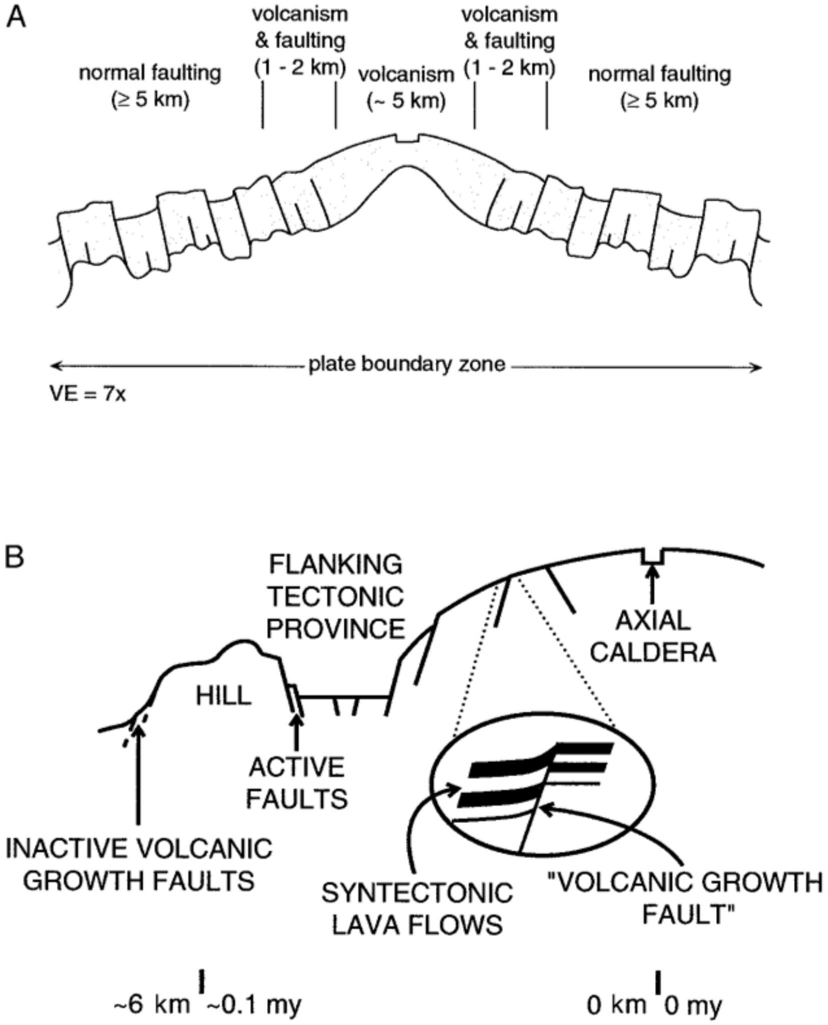
A
volcanism & faulting (1 - 2 km)
volcanism (~ 5 km)
volcanism & faulting (1 - 2 km)
normal faulting (≥ 5 km)
normal faulting (≥ 5 km)
plate boundary zone
VE = 7x
B
FLANKING TECTONIC PROVINCE
AXIAL CALDERA
HILL
ACTIVE FAULTS
INACTIVE VOLCANIC GROWTH FAULTS
SYNTECTONIC LAVA FLOWS
"VOLCANIC GROWTH FAULT"
~6 km ~0.1 my
0 km 0 my

FIGURE 9 (A) Diagrammatic crustal cross section showing the various tectonic and volcanic zones associated with a fast-spreading ridge. The volcanic layer develops in the first 5 km and then normal faults begin to develop. These faults may be partially buried by the off-axis eruptions shown below. Abyssal hills are formed by large-scale faulting beyond the neovolcanic zone. (B) Depiction of the development of growth faults and their association with syntectonic volcanism on fast-spreading ridges. These are common off-axis features and have been proposed to explain the morphology and origin of most abyssal hills on fast-spreading centers. The cross section below shows the tectonic and volcanic zones that develop near the axis of fast-spreading ridges. [From Macdonald, 1998.]

occur, if they are the result of single or multiple eruptions, and what combination of regional tectonic and/or magmatic processes provokes such large-scale outpourings of lava near spreading axes.

1. *Off-Axis Seamounts*

Another aspect of infrequent but volumetrically significant off-axis volcanism is the formation of near-axis seamounts. These consist of small (typically <500-m-high), singular circular volcanoes, or slightly larger (<1-km-high) cones in chains, that appear to have developed above point sources near, but off of the ridge axis. (Here we are not considering the few cases where a hot spot is centered on a ridge axis.) Off-axis volcanism is best documented on intermediate and fast-spreading ridges where the neovolcanic zone is relatively narrow. On fast-spreading ridges, seamounts do not form on the ridge crest at all, but apparently form within a zone 5–15 km from the axis. There are greater numbers of near-axis seamounts adjacent to parts of the MOR that have a larger cross-sectional area, suggesting that more magma is available for off-axis volcanism where the axial supply is larger. On intermediate- and slow-spreading ridges, increasing numbers of seamounts are found in the neovolcanic zone with decreasing spreading rate. This dependence on spreading rate as to whether or not seamounts are excluded from the neovolcanic zone is related to the relative continuity of magma supply and the focusing of melt beneath the ridge axis. At fast-spreading ridges, seamounts do not form on axis because most of the eruptable melt generated in the mantle directly beneath the ridge is focused upward into a thin magma lens and associated crystal mush zone directly beneath the axis. Consequently, these near-axis seamounts can only form by melt diapirs that occasionally segregate from the mantle and rise outside this zone of focused upwelling. As spreading rates decrease, the zone of upwelling beneath the ridge axis is less focused and the lateral continuity of the subaxial magma lens breaks down, allowing the possibility of individual melt diapirs to rise directly beneath the ridge to form seamounts on axis. Abundant small seamounts observed on the axial valley floor of the Mid-Atlantic Ridge may result from more focused eruptions from many individual magma bodies that reside in the crust.

Craters or calderas in some chains tend to be offset from the center of the seamount in the direction toward the ridge axis. This is consistent with a model of formation in which early, rapid, voluminous extrusion is followed by a long waning stage of growth, culminating in magma withdrawal and collapse. The duration of seamount growth is a few tens of ka—long enough for plate motion to move the seamount off its relatively stationary subplate source before collapse. Many off-axis seamounts form relatively short, linear chains that are subparallel to absolute plate motions, suggesting that melting is somehow fixed in the mantle. It is not clear what deep-seated processes are involved in generating these chains of volcanoes and why they erupt from point sources over long periods of time to form distinct voluminous cones. Geometrical and geochemical arguments suggest that small thermal anomalies cause episodic melting of depleted but heterogeneous mantle sources up to 50 km away from ridge axes and rapid transport of melt via dikes to central vents. Both enriched and depleted basalts have erupted at some near-ridge seamounts in the eastern equatorial Pacific, suggesting derivation from heterogeneous mantle sources consisting of a very depleted component and one that is more enriched in incompatible elements than average ocean island basalts.

2. *Transform Fault Volcanism*

Although transform faults are supposed to be plate boundaries where no crust is created or destroyed, recent evidence suggests that volcanism occurs in some transform domains that offset first-order segments of fast-spreading MORs. Volcanism occurs in these locales either at small intratransform spreading centers where seafloor spreading takes place or at localized eruptive centers within the shear zones or relay zones between spreading centers. Spreading has been documented in three transform faults in the eastern Pacific: Blanco (Juan de Fuca Ridge), Siqueiros (northern East Pacific Rise) and Garrett (southern East Pacific Rise). Unlike their adjacent ridge segments, they contain a variety of basalt types that range from very depleted picritic types to highly fractionated ferrobasalts and some enriched MORBs. The diversity of magma types may simply reflect a lack of steady-state magma chambers in these magma-starved regions, which allows distinct melts to erupt without being homogenized in crustal magma chambers.

Many features on the MOR that vary with spreading rate—the width of the neovolcanic zone, the overall morphology of the ridge crest, the size and frequency of eruptions, the morphology of lava flows—appear to be fundamentally related to whether or not a steady-state magma reservoir can be sustained at a given spreading rate. This single factor has tremendous control over the volcanic output over time. Where a steady-state magma reservoir exists, volcanism can keep pace with or dominate over tectonism; where magma reservoirs are intermittent, tectonism tends to dominate. This variation in the degree of magma input also has a profound influence on the resulting structure of the upper oceanic crust, both in terms of the character of volcanic constructs and the degree of subsequent structural reorganization. The critical spreading rate, above which a steady-state magma reservoir can form and below which one cannot, appears to be about 50 mm/yr.

IV. VOLCANISM AT CONVERGENT PLATE BOUNDARIES

A. Architecture of Convergent Margins: Island Arcs, and Continental Margin Arcs

Magmatism at a convergent plate margin is most obviously manifest as a linear or curved chain of volcanoes called a *volcanic arc*. The chain is broadly parallel to the trench—the deep topographic feature on the seafloor that reflects the surface trace of the plate boundary (Fig. 1). The arc can be constructed on oceanic or continental lithosphere. In the former case, since the oceanic lithosphere lies underwater, the volcanic cones are required to build up a considerable volume before the tops of the edifices rise above the surface to form islands. The chain of volcanoes so formed is accordingly referred to as an *island arc*. Several classic island arcs of this type are found around the western Pacific Ocean Basin (the Aleutians, Kuriles, Izu-Bonins, Marianas, New Hebrides, and Tonga-Kermadec arcs). These regions, known as supra-subduction zone (SSZ) settings, are very active tectonic environments where mantle-derived magmas erupt in the forearc, arc, and backarc; sediments are metamorphosed and accreted to the arc; and fragments of oceanic-like crust (ophiolites) are thrust upon the arc crust. Given a sufficiently large accumulation of magmatic material and sediment deposition and metamorphism over time, island arcs can amalgamate to form extensive land areas underlain by young arc crust, intermediate between true island arcs built directly on the oceanic lithosphere, and continental margin arcs built on old continental lithospheric basement. Examples of such intermediate character arcs include New Zealand, Japan, Kamchatka, the Cascades (northwestern United States) and Java. Volcanoes constructed on "true" (old) continental lithosphere, to form a continental margin arc, are typically wholly subaerial. The volcanic chain of the Andes Mountains along the western edge of South America is probably the best developed example of a continental margin arc today.

Although arcs are characterized principally by a chain of volcanoes subparallel to the trench, this chain may be broken in places (segmented) and may have superimposed cross-arc volcano chains. Segmentation may reflect structures in the subducted plate, such as transform faults, or may be largely controlled by structures in the upper plate. Careful structural analysis can commonly relate the distribution of volcanoes and their orientations to features in the lithosphere immediately underlying the arc, suggesting that local stress distribution dictates the capacity for ascending magma to reach the surface. In places, subduction may not produce volcanism on the overriding plate. The Andes, for example, exhibits a major segmentation into three currently active zones of volcanism (with second-order segmentation imposed on them) separated by nonvolcanic zones, despite continuous subduction along the entire western margin of South America. Absence of magmatism appears to accompany particularly shallow slab dips, and changes in magmatic behavior through time at specific arcs can commonly be traced through plate tectonic reconstructions to variations in slab dip.

Subduction is a transient condition. The subducted lithosphere is always oceanic—continental lithosphere is thicker and more buoyant, and cannot be effectively subducted. Consequently, if subduction results in the convergence of two fragments of continental (or intermediate) lithosphere, the interaction between them produces deformation, and uplift—in its most dramatic manifestation producing mountain ranges such as the Himalayas, which resulted from the collision of India with Asia, following subduction of the oceanic part of the Indian Plate. Such collisions terminate subduction at that location—although new subduction zones may be initiated in response to the new plate organization and changes in stress.

B. Types of Magmas and Volcanoes at Convergent Plate Boundaries

The mechanism of mantle melting, as alluded to earlier, is generally thought to be due to hydration of the mantle by volatiles released from the subducted slab into the mantle wedge (the corner of mantle material between the subducted slab and the upper plate) with consequent lowering of the mantle solidus (Fig. 3). This is consistent with thermal models of subduction zones, which conclude that in most cases the subducted slab is below its solidus at depths corresponding to those beneath the volcanic arc (100–150 km). There is a remarkably consistent relationship between the location of the volcanic arc front (the trench-ward limit of volcanism, along which most volcanoes are concentrated in a given subduction system) and the depth to the Wadati-Benioff zone (the inclined zone of seismicity, which corresponds roughly to the top of the slab). This depth of 100–150 km implies that the trigger for magmatism is pressure sensitive. Pressure-dependent breakdown of a hydrous phase (such as amphibole or mica) is commonly invoked as a way to release volatiles into the overlying mantle wedge. Detailed tomographic investigations of mantle structure, such as in Japan are consistent with this model (Fig. 10). It is of interest to note that where the subducted slab is present beneath an arc (or portions of one) but moving in a lateral sense rather than deeper within the mantle (e.g., Greater Antillies, western Aleutian Islands), the arc is not volcanically active. This presumably reflects the lack of continued dehydration that is required to instigate melting in the mantle. By the

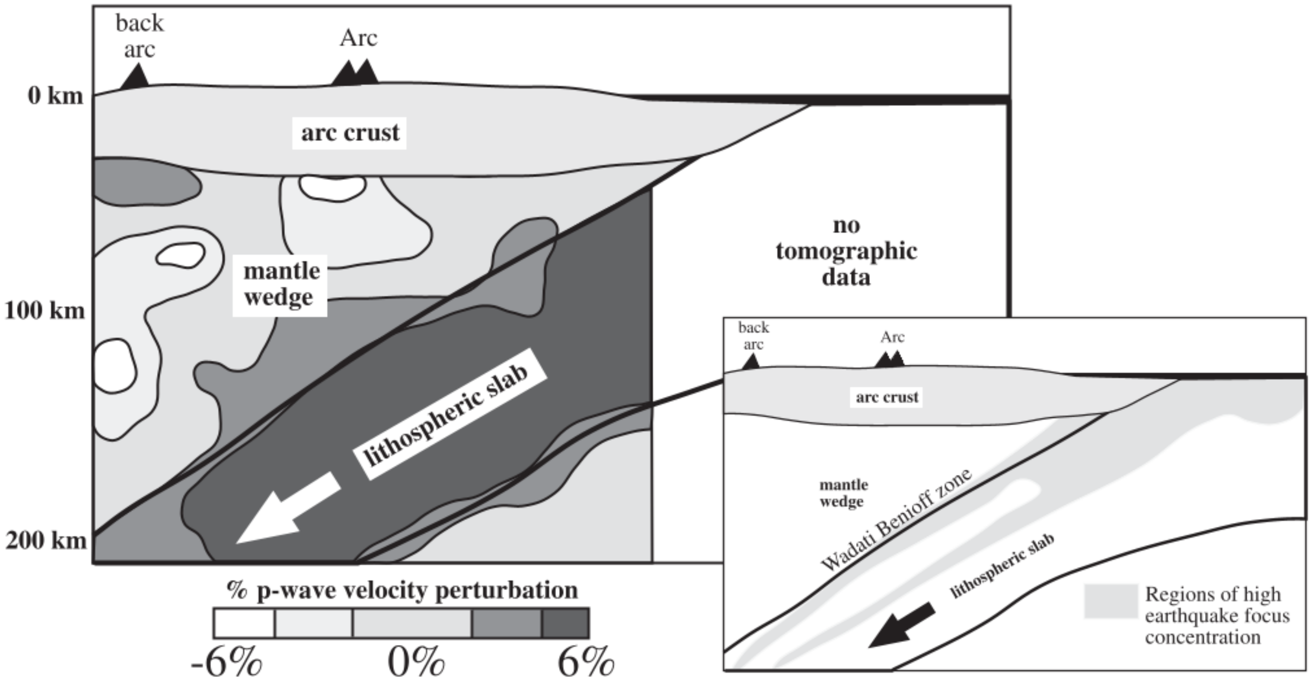

FIGURE 10 Seismic tomography of the mantle beneath Japan, from Hasegawa *et al.,* (1991; figure courtesy of Academic Press). Fast velocities are characteristic of the slab, whereas slow velocities, which may indicate hot and/or partially molten mantle, are found in the mantle wedge above the slab.

same token, the correlation between shallow slab dips and absence of magmatism alluded to earlier probably also reflects an impediment to melting via hydration. In this case, the fluids derived by slab dehydration are introduced into the cooler, shallower lithospheric mantle—which, unlike the convecting asthenospheric wedge, is unable to melt.

The general geochemical characteristics of subduction-related magmas are discussed later. However, it is worth noting here that there are compositional variations in magmas through both time and space. Early magmatism at oceanic arcs is typically basaltic and tholeiitic in composition, while later magmatism tends to be more calcalkaline in composition with a greater predominance of more differentiated andesitic magmas. Indeed the common occurrence of andesites (so named after the Andes Mountains) at convergent plate margins led to early suggestions that this was a primary magma composition. This broad, general (and not inviolate) trend may simply reflect the thickening maturation of the arc crust through time, leading to an increasing depth and extent of differentiation for the magmas. In the early stages of magmatism at some arcs, and toward the trench (at depths $\leqslant$100 km above the Wadati-Benioff zone), unusual types of magmas called *boninites* are formed. These comprise high-magnesium, high-silica lavas with very low concentrations of all but the most fluid mobile incompatible trace elements. Overall, there is commonly a trend (again general and not ubiquitous) of increasing incompatible element concentrations at volcanic centers across the strike of an arc. This is expressed as the "K-*h* relationship," which claims that potassium concentrations at a given degree of differentiation increase with depth (*h*) to the Wadati-Benioff zone. In some well-established arcs with magmatism significantly behind the arc front (large depths to the slab), K-rich and alkaline magmas (shoshonites) are erupted. This is particularly true at continental arcs (such as the Andes) although the effects of crustal contamination increasing incompatible element contents may complicate the issue here. The K-*h* relationship may be largely a reflection of the decreasing degree of partial melting with distance behind the volcanic front/depth to the top of the slab. The degree of partial melting may, in turn, be controlled by the flux of volatiles (principally H_2O) from the subducted slab, which is high beneath the arc front—leading to high degrees of melting—but decreases as depth increases.

There are a few subduction zones in which the subducted slab appears to attain unusually high temperatures and actually melt. The slabs in these cases typically comprise very young oceanic lithosphere, which is consequently anomalously warm as it enters the trench (see Ridge Subduction section later). The compositions of magmas produced in such systems are distinct from those at "normal" arcs (high SiO_2, low K), and resemble in many ways the compositions of ancient continental crust, leading to the suggestion that early crust was actually formed by high-pressure melting of basaltic crust—either deep under the continents or subducted much like today's convergent plate boundaries. These unusual subduction-related magma compositions are referred to as *adakites*.

Volcanoes at convergent margins are diverse in their types and in their distribution. The principal type of volcano is the composite cone (see Composite Volcanoes chapter), composed of blocky lavas and pyroclastics, although most other volcano types can also be found, ranging from shieldlike volcanoes through many varieties of smaller, commonly monogenetic types such as cinder cones, lava domes, and maars. Explosive volcanism is more typical than the effusive basaltic outpourings that characterize both intraplate and divergent margin volcanism. This produces a wide range of pyroclastic deposits accompanying lava flows that are basalt through rhyolite in composition. The tendency toward more explosive eruptions is primarily a function of higher water contents in the primary magmas at arcs. The relatively protracted differentiation of primary magmas to produce andesites through rhyolites that are erupted at arc volcanoes exacerbates the explosivity by concentrating the volatiles into progressively more viscous magma.

C. Extensional versus Compressional Arcs

Perhaps because of our perspective of living on the "horizontal" surface of the Earth, there is a tendency to imagine subduction zones as regions of compression where one plate is thrust beneath another. Indeed this prejudice is underscored by using terms like *plate collision*. In fact, subduction may be driven by the simple negative buoyancy of dense cold oceanic lithosphere, which can sink back into the mantle under its own weight. Having said this, the actual origination of subduction zones is still an area of debate and beyond the scope of this chapter.

The state of stress across the arc is actually controlled by the relative motion of both the subducting plate and the upper plate. Sinking of oceanic lithosphere is driven by the magnitude of the density difference between it and the underlying mantle. Density of the lithosphere is, in turn, largely a function of age. When formed at a spreading center, oceanic lithosphere is hot, thin, and therefore buoyant. As it ages and moves farther away from the spreading center, it progressively cools, thickens, and becomes denser. In cases where the slab sinks rapidly, it will sweep back through the mantle like a paddle, subsiding at a steeper angle and causing the hinge line to migrate away from the arc in a process known as *slab rollback*. Despite their relative movement the two plates are in continuous contact with each other and cannot part company and leave a gap. The upper plate is, therefore, pulled along in the direction of rollback and may be extended in the process leading to backarc spreading (Figs. 11 and 12).

The age (and therefore density) of the lithosphere entering the trench may not be constant though. If the slab entering the trench becomes progressively younger, for instance as a ridge moves toward the subduction zone, it will become more buoyant. The effect will be to impede subduction. The angle of subduction will decrease, leading to a greater area of contact between

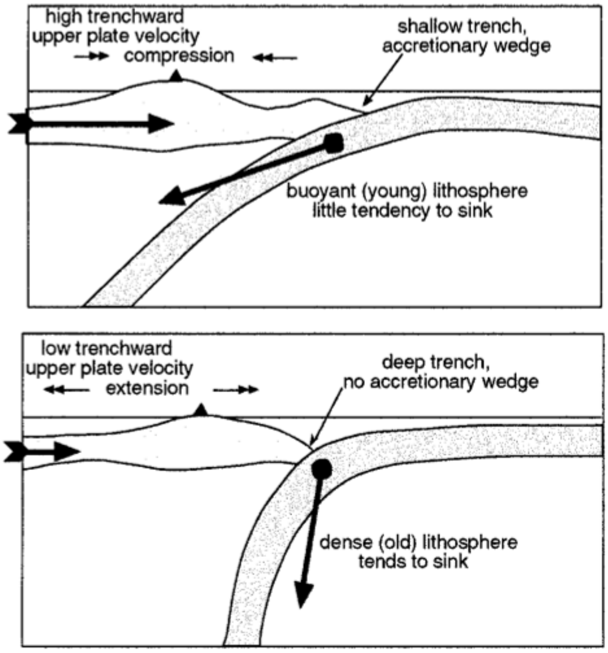

FIGURE 11 Variations in the state of stress in the arc crust as a function of relative plate velocities. If the upper plate moves rapidly trenchward the angle of subduction shallows and compression occurs. If the slab sinks rapidly and rolls back away from the trench it extends the upper plate.

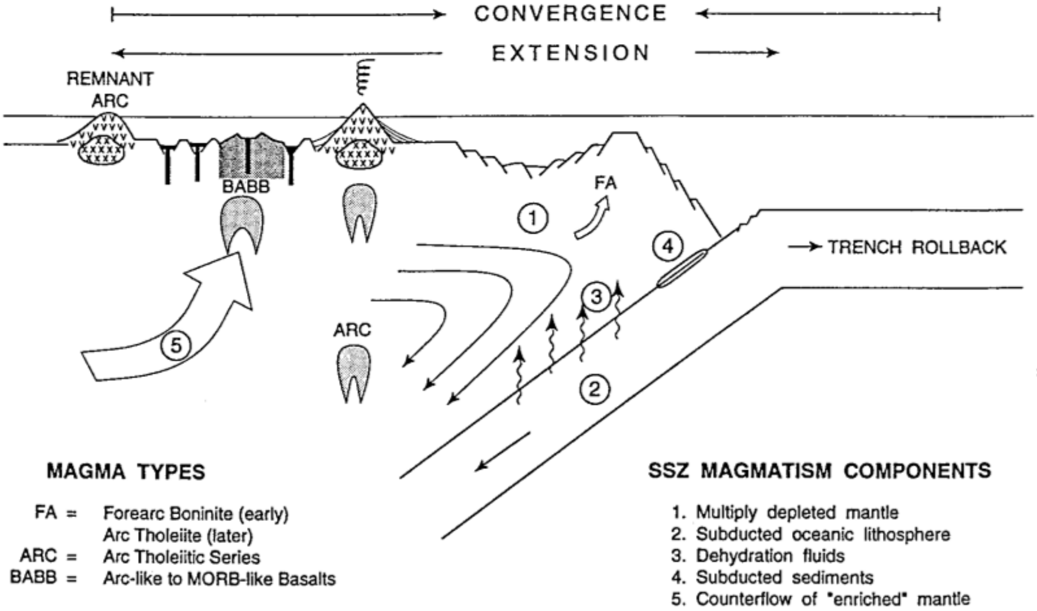
CONVERGENCE
EXTENSION
REMNANT ARC
BABB
FA
①
④
→ TRENCH ROLLBACK
③
⑤
ARC
②
MAGMA TYPES
FA = Forearc Boninite (early)
Arc Tholeiite (later)
ARC = Arc Tholeiitic Series
BABB = Arc-like to MORB-like Basalts
SSZ MAGMATISM COMPONENTS
1. Multiply depleted mantle
2. Subducted oceanic lithosphere
3. Dehydration fluids
4. Subducted sediments
5. Counterflow of "enriched" mantle

FIGURE 12 Diagrammatic cross section of an intraoceanic convergent margin showing the salient tectonic and volcanic features. The arrows and shaded areas represent sites of magma formation in different tectonic environments beneath the forearc, active arc, and backarc basin. Potential components that contribute to SSZ magmatism are numbered 1–5. [From Hawkins, 1995].

the two plates along higher viscosity lithosphere. This will cause compressional stresses to be transmitted into the upper plate and may lead to deformation such as folding and thrust faulting in the crust. It can be appreciated that the relative velocity of the upper plate is important in controlling the stress field—if the plate moves rapidly toward the trench it may lead to a shallowing of subduction and more compressive stresses (Fig. 11). The velocity of the upper plate, while controlled in part by interaction at the subduction zone, will also be affected by forces acting on any other plate boundaries surrounding it.

Volcanism is more prevalent along convergent plate margins undergoing extension than those suffering compression. Extensional stresses tend to promote magma ascent through the crust, commonly providing conduits. Compression inhibits ascent, and any additional obliquity in convergence may also lead to arc-parallel strike-slip deformation. Furthermore, the shallow angles of subduction, which are typically associated with compressional stresses in the upper plate, may actually prevent the production of magma. For example, it is fairly certain that melting at subduction zones is the result of releasing fluids from the subducted slab into the hot overlying mantle. If the slab dip is shallow, fluids are likely to be released into cooler, overlying mantle of either the lithosphere, or asthenosphere, which is impeded from convecting by the restricted geometry of the narrow mantle wedge. Evidence for this control has been seen along the Andes today, where there are zones along which recent volcanism is absent despite ongoing subduction. These zones correspond to unusually shallow slab dips compared with the regions of active volcanism along the arc.

The different geodynamic architectures of subduction zones led to the definition of end member types—a Mariana type and a Chilean type. The former, typical of the western Pacific, involves extension and the development of backarc basins, associated with steep subduction of old lithospheric slabs. The Chilean-type margins involve shallower subduction, on occasion accompanied by compression, but in any case, generally lacking backarc extension.

D. Backarc Basins

The ultimate consequence of extension in arc environments is that the upper plate rifts apart. When this happens, rifting will occur along the line of greatest weakness, which typically corresponds to the volcanic arc where the crust has been heated by magmatism. The first stages of extension may be amagmatic but continued rifting has the effect of inducing passive upwelling in the subjacent lithosphere, which leads to magmatism and the generation of new lithosphere—effectively producing a spreading center in the SSZ setting, which is geodynamically analogous to a divergent plate boundary. The relatively deep sea that contains this spreading center is known as a *backarc basin*. As new lithosphere forms, the spreading center migrates away from the trench and the arc may be able to reestablish itself at the subduction zone. A diagrammatic representation of some of the magmatic and tectonic aspects of arc and backarc volcanism are shown in Fig. 12. Western Pacific arcs are commonly characterized by backarc basins, an observation that likely reflects the very old age of the Pacific seafloor in this region, and the consequent tendency for this dense lithosphere to sink easily.

Lavas erupted in backarc basins (backarc basin basalts, BABBs) range in composition from island arc tholeiites to MORB-like basalts that have some arclike traits (e.g., depletions in high field strength elements and slight enrichments in large ion lithophile elements and volatiles). These common transitional characteristics are a consequence of melting a multiply depleted MORB-source mantle that has been enriched by subduction-derived fluids/melts. Lesser amounts of FeTi basalts and low-K andesites recovered from backarc spreading centers are related to BABB by fractional crystallization and crustal assimilation. In some cases, these fractionated suites are associated with rift propagation in the backarc.

E. Ridge Subduction

A consequence of plate tectonics is that ridges (and associated transforms) will, on occasion, intersect subduction zones in a configuration know as a ridge-trench *triple junction* and when this happens, divergent ridges may be consumed along the convergent margin. Theoretically, volcanism in the overlying arc may be related to (1) the subduction of "normal," but hotter oceanic lithosphere, (2) segments where the oceanic lithosphere is missing and consequently so would any slab-derived fluids/melt, or (3) the subduction of transform faults that may allow the lithosphere to "tear" as it descends beneath the arc. There are many cases in the geologic record where triple junction migration is known to have occurred (e.g., Kula-Faralon spreading center beneath the Aleutian Islands; Kula-Pacific Ridge beneath Japan) and others that are occurring at the present time (e.g., Mendocino Triple Junction, northwest United States; Woodlark Basin, Solomon Islands; Chile Triple Junction; Rivera Triple Junction, Mexico).

As a triple junction migrates along a convergent margin, the subducted young oceanic lithosphere is relatively hot and the divergent plate boundary may create a gap or "slab window" beneath the overlying arc (Fig. 13). A diverse group of geological effects has been ascribed to the effects of a slab window and the increased thermal input associated with it, but little consensus identifying the distinctive structural and petrologic characteristics directly related to ridge subduction. Some of the magmatic and tectonic manifestations of triple junction interactions along a convergent plate boundary include anomalous forearc volcanism, cessation of volcanism, increased volcanism, accretion of oceanic crustal sections (ophiolites) in the forearc, rapid uplift of the forearc, and intrusion of near-trench granitic rocks. Small degrees of melting of the hot, subducted oceanic slab prior to the opening of a slab window may produce adakite magmas.

The compositional variety of volcanic rocks associated with ridge subduction appears to be great—dominated

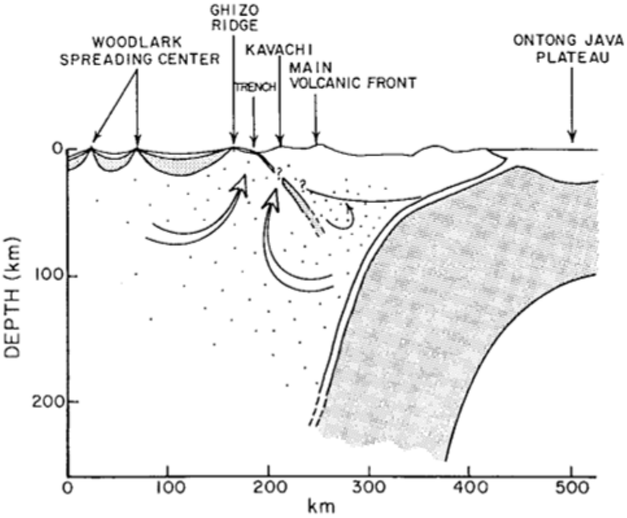

FIGURE 13 Diagrammatic cross section across the Woodlark Basin, Solomon Islands, and Ontong Java Plateau that shows the possible relationships between thickened Pacific lithosphere that is no longer subducting and young, thin lithosphere formed at the active Woodlark spreading center that is currently being subducted beneath the arc. Openings in the Woodlark lithosphere represent asthenospheric windows. Arrows represent regions where mantle sources or magmas may mix. Kavachi is an active tholeiitic volcano and Ghizo Ridge (in the Woodlark Basin) is comprised of both MORB-like and arclike lavas. Basalts erupted from the Woodlark spreading center primarily are normal MORB. [From Perfit *et al.,* 1987.]

by arc tholeiitic and calcalkaline assemblages but also including rare boninites and sodium- and titanium-enriched basalts (NaTi basalts). The tholeiitic and calcalkaline rock types vary from picritic basalts to quite fractionated dacites. In at least two locations (Woodlark spreading center and Chile Rise), submarine volcanic rocks with oceanic, arc, or transitional chemical characteristics have been erupted along the divergent zone on the oceanic side of the plate boundary. Because of the many possible plate configurations at triple junctions, it has been difficult to make generalized statements regarding how volcanism is related to tectonics in these complex regions.

V. INTRAPLATE VOLCANISM

A. Plumes and Their Distribution

While the distribution of magmatism by and large coincides with the locations of plate boundaries (divergent and convergent), examination of Fig. 2 shows that there are important exceptions. The Hawaiian islands, for instance, one of the most familiar regions of volcanism, lie thousands of kilometers from the nearest plate boundary in the midst of the Pacific Plate. And there are numerous other examples of intraplate volcanoes—most of the islands in the Atlantic are not located at plate boundaries. They may be close to the Mid-Atlantic Ridge, such as the Azores and Ascension Islands, or may be at the edges of the ocean such as the Canary and Cape Verde Islands. Intraplate magmatism is scattered throughout the continents too, represented, for instance, by the Snake River Plain (Idaho, USA) and Yellowstone (Montana, USA) or the many volcanic centers on the African continent. Recent investigations indicate there may be many hundred currently active intraplate volcanoes.

The foci of intraplate magmatism are commonly referred to as *hot spots*—an obvious reference to the high heat flow advected to the surface with the magmas. Recent geodetic surveys have correlated the locations of many hot spots with geoid highs—a rise in the gravitational potential surface—which in turn are believed to reflect the buoyancy of warmed lithosphere. Tomographic analyses of the mantle also commonly correlate the surface location of hot spots with decreases in seismic-wave velocity in the subjacent mantle. The interpretation is again that the lower velocity mantle is warmer, perhaps incorporating a small fraction of molten material (although the observation of decreased velocities might also be explained by alternative mechanisms such as a greater content of H_2O or CO_2).

These observations, taken together, suggest that hot, low-density material is advected from depth in the mantle toward the surface. Melting occurs as the rising material undergoes decompression which takes the *P-T* trajectory across the peridotite solidus (Fig. 3). The rising material is generally referred to as a *plume*, and is considered an integral part of the Earth's mantle convection system—the principal mechanism by which heat is lost from the interior. In fact, spherical convection models representing a simple core–mantle system develop a radial convection system in which plumes (narrow axisymmetric upflow domains) rise from the lower thermal boundary layer and spread out near the upper thermal boundary layer (Fig. 14). The head of the plume displaces denser, normal asthenosphere and heats the base of the lithosphere, which leads to regional uplift, lithospheric thinning, and magmatism. Complementary zones of downflow comprise sheets or curtains of material, which to a first order seem to resemble subducted slabs, although the more sophisticated models currently under development incorporate an upper mechanical boundary layer to more realistically represent the lithosphere.

The initiation of plume ascent occurs episodically—although apparently not regularly through time. The plume begins as an instability at a deep thermal (and possibly compositional) boundary layer known as seismic layer D″, which is typically taken to be the core–mantle boundary (Fig. 14). Similar arguments have also been made for plumes initially forming at the upper/lower mantle boundary at 670 km. Fluid dynamic experiments that attempt to reproduce appropriate viscosity contrasts suggest that a plume is characterized by a voluminous plume head, which is able to entrain the ambient mantle through which it rises, followed by a thin plume tail. If plumes in the Earth are similar, we would predict that the temporal pattern of magmatism would be characterized by a voluminous outpouring as the large volume plume head reaches the depth at which it crosses the solidus, followed by a prolonged period of less voluminous but sustained magmatism. The record for much intraplate volcanism, where preserved, is consistent with this prediction.

The period of sustained magmatism produces a mass flux at the surface. Since the location of the plume is independent of preexisting plate boundaries, a hot spot trail will form on the crust as a lithospheric plate moves over the locus of the plume. The track of the hot spot is represented by a series of volcanoes aligned in the direction of plate motion that become progressively younger toward the presumed present-day location of

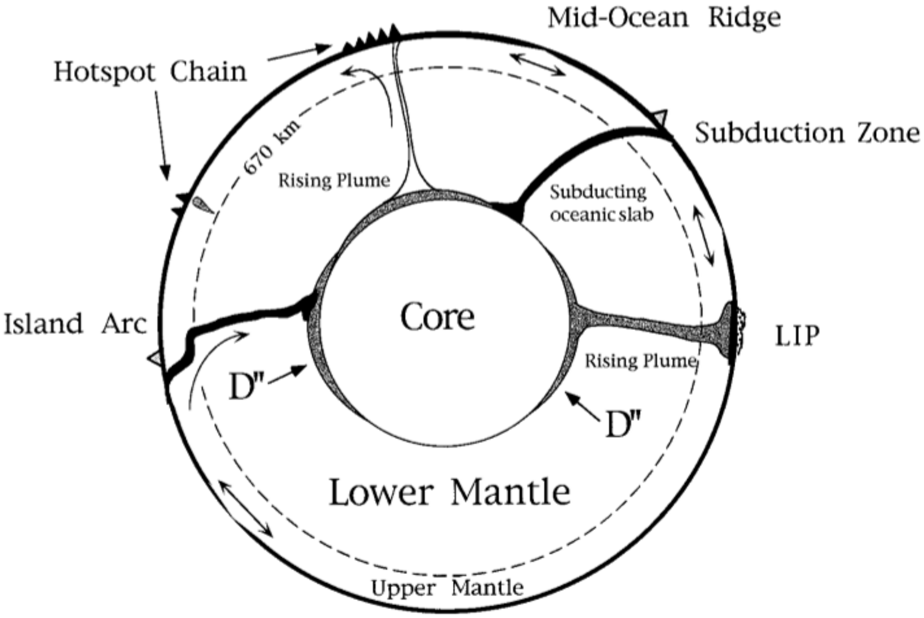

FIGURE 14 Schematic cartoon showing hypothesized recycling of oceanic lithosphere into the mantle and the origin of mantle plumes from the D″ seismic layer at the core–mantle boundary. This model is based on tomographic images of the interior of the Earth based on seismic studies. Features shown and depths are not to scale. The thickness of the D″ layer is greatly exaggerated for illustrative purposes. Large igneous provinces (LIP) may form by voluminous volcanism associated with the impingement of the head of a rising plume on the base of the lithosphere. Hot spot chains may result from either shallow plumes from the 670-km discontinuity or continued upwelling of the tail of deep mantle plumes.

the plume (Fig. 14). The Hawaiian Islands are commonly cited as the classic example of such a hot spot trail. Other island chains or groups, such as the Galapagos Islands and Canary Islands, do not conform to a simple linear pattern but seem to reflect interaction of the plume head with structural features in the lithosphere. The complex distribution and timing of voluminous Cenozoic volcanism in east and central Africa may also reflect the effects of a single large plume ponding and flowing in preexisting zones of lithospheric thinning.

B. Flood Basalts and Continental Rifting

While the distribution of lithospheric plates may have no influence on the distribution of plumes, the reverse may not be true. The burst of magmatism accompanying the ascent of a substantial-sized plume head to shallow depths may have a profound effect on the superjacent lithosphere. The specific effects depend on whether the lithosphere is continental or oceanic. If the lithosphere is continental, it may be uplifted and domed and eventually rift apart (e.g., East African Rift Valley). Voluminous outpouring of magma forms a flood basalt province or large igneous province (LIP)—of the order of 100,000 km^3 or more of basalt may be erupted within a few million years. Less voluminous, more steady-state volcanism may follow as the plume tail rises to the surface. If rifting of the continental lithosphere continues to completion, new oceanic lithosphere is formed and a new divergent plate boundary is initiated. At this stage the plume and divergent plate boundary are coincident and will remain so until the plate boundary migrates in response to lithospheric processes. Many hot spots in the Atlantic are found close to the midocean ridge, reflecting their earlier role in the rifting apart of continental landmasses now located either side of the basin. The island of Iceland is actually located on the divergent plate boundary marked by the Mid-Atlantic Ridge, and chemical tracers in Icelandic lavas confirm that the magmatism is related to a deep-seated plume, believed to be the same plume responsible for initiating rifting in the north Atlantic region 60 Ma ago. Thousands of meters of flood basalts in east Greenland reflect the earliest stages of plume-related magmatism in the North Atlantic. Flood basalt records of rift initiation are commonly preserved along the margins of the ocean basin, which are now passive continental. The Parana and Etendeka basalts, now located in South America and southern Africa, respectively, formed 130 Ma ago during the rifting event that formed the South Atlantic Ocean. Paired aseismic ridges like the Rio Grande Rise and Walvis Ridge in the south Atlantic represent traces of the plume as oceanic lithosphere was created after the continents rifted apart.

If, on the other hand, the lithosphere above the plume head is oceanic, the result is an oceanic LIP—an oceanic plateau. Plateaus such as the Ontong Java and Manihiki, in the western Pacific Ocean, represent some of the largest outpourings of basalt in the geological record (the Ontong Java Plateau is estimated to have a volume on the order of 15–18 million km^3). In such cases the oceanic lithosphere, which apparently is stronger than its continental counterpart, does not rift apart. The magmas formed from decompression melting of the plume head are simply transferred into (as intrusions) or onto the surface of (as eruptions) the oceanic crust causing it to become anomalously thick (20 km thick in comparison to 7 km). The consequence of such lithospheric thickening is that it is isostatically compensated—even after the additional thermal buoyancy has waned as the plume's influence diminishes—such that its surface stands much higher than the surrounding seafloor. In this way the characteristic extensive submarine plateaus are formed. The plateaus may be topographically connected, via a hot spot chain to active plume-related regions of volcanism. The plateaus also, by virtue of their thickness and consequent buoyancy, are resistant to subduction. Upon encountering a convergent plate boundary the plateau will typically collide with material of the upper plate, whether it be continental or oceanic arc, and will terminate the subduction process at that location (e.g., Solomon Islands, Fig. 13). In this fashion, oceanic plateaus may be permanent residua of oceanic magmatism and, like arcs, may be accreted laterally to the continents. Some terranes along the northwest margin of North America and much of the Caribbean Sea, for instance, are interpreted to be oceanic plateaus that have been rafted in from their sites of origin in the Pacific Ocean Basin.

From the preceding discussion it is clear that plumes may initiate and drive rifting of the continental lithosphere. Nevertheless, not all continental rifts are convincingly associated with plumes. In some cases it appears that the magmatism is a response to lithospheric extension that is driven by plate interactions. The interior of a plate may fail if subjected to pulls from plate edge forces, such as subduction. As the lithosphere is attenuated, hot underlying asthenosphere must inevitably move up into the region beneath the rift. This decompression may then lead to melting (Fig. 3). The relative roles of active upwelling of deep mantle plumes versus passive upwelling of shallow asthenosphere and thinned lithosphere in producing continental rift zones and their associated magmatism vary significantly. In instances such as the East African Rift the signatures of a deep mantle plume are clear—uplift and magmatism occur early in rifting and, among the volcanic rocks, the chemical characteristics associated with the deep mantle are unmistakable. The origin of rifts such as Baikal in Russia are, however, less well constrained. The paucity of magmatism here may reflect a modest passive response to rifting driven by lateral forces.

VI. GEOCHEMICAL AND PETROGRAPHIC ASSOCIATIONS

A. Processes Related to Plate Tectonics

It will become clear, as the reader progresses through this volume, that volcanoes from different plate tectonic environments are distinct in terms of their behavior, the morphology of landforms associated with volcanism, the compositions of magmas and associated volatiles, and the characteristics (textures, mineralogy, composition) of related volcanic deposits. It is the purpose of subsequent chapters to examine the petrography (mineral types, compositions, and textures) and geochemistry of volcanic rocks. By means of introduction, though, it is important to point out that these characteristics are closely related to tectonic environment since ultimately the chemistry of magmas is related to plate tectonic processes.

The two diagrams (selected from many) of Fig. 15 show compositional distinctions between rocks from different plate tectonic environments. The geochemical principles needed to understand the differences are explored more fully in the chapter titled Composition of Magma. Suffice to say that plate tectonic control is clear. Most magmas generated at spreading centers are depleted in elements considered incompatible in mantle peridotite. In particular, large ion lithophile elements such as Cs, Ba, Rb, and K have very low concentrations in MORBs (Fig. 15). This incompatible element depletion is likely a consequence of the suboceanic mantle having been previously melted to form the continental crust during the history of the Earth. In addition, most of the subridge mantle—in particular away from hot spots—has not been reenriched in these elements by secondary processes.

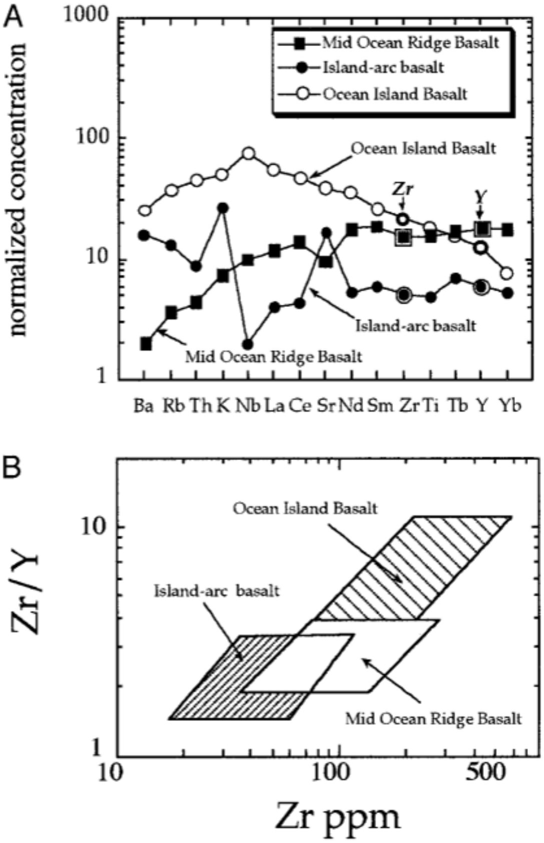

FIGURE 15 Diagrams illustrating the control that plate tectonic association has on magma composition. (A) Distribution of incompatible trace elements (incompatibility increases to the left). (B) Zr/Y versus Zr ppm discriminant diagram. [After Pearce and Cann, 1973.] The elements Zr and Y are highlighted in Part (A) to illustrate how the slope of the "spidergram" pattern relates to ratio, and to emphasize how specific ratios may be selected to provide a suitable means of discrimination among tectonic environments. Note the relatively low normalized abundances of the most incompatible elements in MORBs; hence it is believed to have been derived from a "depleted" source.

Perhaps the most distinct characteristic of the convergent margin magmas is their low abundance of a group of elements known as high-field strength elements, which includes Nb, Ta, Ti, Zr and Hf. These elements are notable in that they are highly insoluble in H_2O-dominated fluids. The mechanism of magma generation at subduction zones, by addition of fluid from the slab to the mantle, is consistent with this observation—the fluid causes a relative enrichment in most of the trace elements (including the large ion lithophiles) but not the fluid insoluble ones. The differences between divergent margin magmas and intraplate magmas are less obvious, but the latter clearly have much higher concentrations of the most incompatible trace elements. This is consistent with derivation of intraplate magmas from a different source (mantle that has been carried from deeper levels within a plume or enriched continental mantle lithosphere), perhaps coupled with differences in the process of melt generation and the extent of partial melting—lower amounts of melting lead to more enriched magmas. The principal differences in the distribution of trace elements among magmas from different tectonic environments are emphasized in the representative patterns of Fig. 15A. Diagrams such as this, comparing the incompatible trace element concentrations (normalized to some nominal reference composition—typically an estimated composition for the primitive mantle) are colloquially referred to as "spidergrams," emphasizing the irregular trace of the pattern—as if a spider has tracked ink over the paper! These diagrams can serve to highlight differences in behavior between specific elements or element pairs, but are limited in the number of actual samples that can be plotted before they become messy and indecipherable. Diagrams such as Fig. 15B make use of only those elements that are most distinctive in comparison—for our purposes we have selected Zr and Y. Because each sample only plots as a point, large numbers of analyses can be compiled on these types of plots.

Despite these clear distinctions there are spectra of magma compositions between the end member compositions illustrated. To a large extent this reflects concurrent variations in plate tectonic environment. Despite the clear-cut instances of magma generation introduced earlier (mantle plume, divergent plate boundary, convergent plate boundary) there are actually intermediate cases. For instance, backarc basins share properties in common with subduction zones and spreading centers—and backarc lavas are typically geochemically intermediate between MORB and arc lavas. Similarly, where mantle plumes and spreading centers are roughly coincident, such as at Iceland, the magmas are chemically intermediate between those of hot spots and those of spreading centers. The connections are illustrated in Fig. 16.

The link between magma chemistry and plate tectonic environment is sufficiently strong that it can be applied as an investigative tool for ancient rocks. In instances where the original environment in which a suite of magmatic rocks formed is unclear, as is commonly the case in deformed, ancient rock series, plotting their compositions onto discriminant diagrams, for which plate tectonic fields have been empirically defined on the basis of modern data (such as Fig. 15B), can serve to indicate the tectonic environment in which the ancient rocks most likely formed. These observations together with

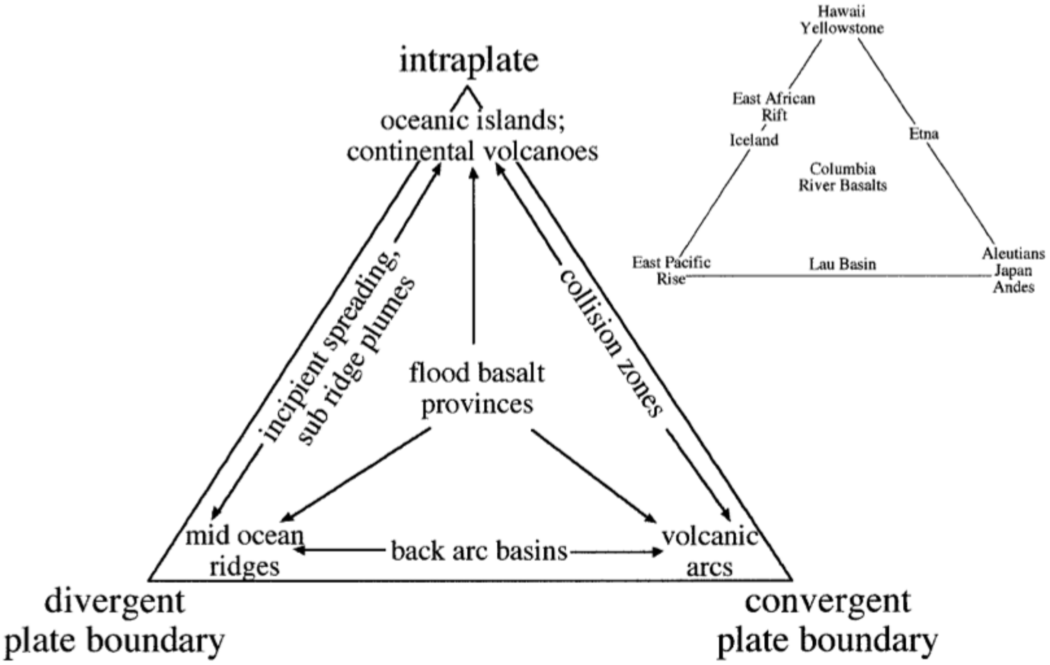
intraplate
oceanic islands; continental volcanoes
incipient spreading, sub ridge plumes
collision zones
flood basalt provinces
mid ocean ridges
back arc basins
volcanic arcs
divergent plate boundary
convergent plate boundary
Hawaii
Yellowstone
East African Rift
Iceland
Etna
Columbia River Basalts
East Pacific Rise
Lau Basin
Aleutians
Japan
Andes

FIGURE 16 Diagram illustrating the variations that occur between the three main magma associations, which are reflected in variations in the chemistry of lavas from different tectonic environments [Figure modified after Pearce, 1996.] Some specific examples are shown in inset.

careful field mapping and integration with observations from associated rock types can enable geologists to unravel the geological history of a region.

B. Effects of the Lithosphere on Volcanism

It was suggested earlier that the lithosphere is a fundamental product of the plate tectonic process. The crust, the chemically distinct upper layer of the lithosphere, is the product of plate tectonic-related processes in the shallow Earth, the most important of which is magmatism. The lithosphere plays an important role in modulating the character of volcanism. It acts as a filter, modifying the compositions of magmas from the time that they are generated (mostly in the asthenosphere) to eruption at the surface. The thicker and lower density the filter, the greater its effect at impeding the ascent of mantle-derived magmas, which are largely basaltic. These basaltic magmas can pond in the lower continental crust in some instances due to their greater density. As a consequence, this leads to fractional crystallization coupled with assimilation of country rock to produce less dense, more evolved and crustally contaminated magmas that erupt on the surface. In addition, heat added to the lower continental crust may be great enough to partially melt large volumes of crust to form viscous and volatile-rich rhyolitic melts that may crystallize to form granites at depth or rise to the surface to violently erupt. This type of volcanism creates large intracontinental caldera complexes like Long Valley Caldera in California, and Valles Caldera in New Mexico, which are associated with voluminous outpourings of rhyolitic pyroclastics. In many continental regions, rhyolitic volcanics are temporally and spatially related to voluminous basaltic lavas—an association known as *bimodal volcanism*. The bimodal distribution of compositions is a consequence of both mantle-derived basalts and the rhyolites they create by partially melting the lower crust, erupting during the same volcanic episode. In some cases, the basaltic volcanism is plume related (e.g., Snake River Plain–Yellowstone) while in others (e.g., Rio Grande Rift–Jemez Volcanic Field, New Mexico) it may be due to rift-related decompression melting of the upper mantle.

It is important not to overlook the connection between magma composition and many of the volcanological and hazard-related aspects of volcanoes that will be discussed at length later in this volume. As magmas evolve to more silica-rich compositions and concentrate water, they have an increased propensity to erupt explosively and produce pyroclastic deposits rather than effusive lavas. The evolution to silica-rich magmas is typically promoted by residence in (and partial melting of) crust. Volatile concentration occurs inevitably during evolution, but is further controlled by the original water content, which is a function of source and plate tectonic environment. Subduction-related magmas typically have higher water contents than those from other environments. It is, therefore, hardly surprising that some of the more infamous violent eruptions are associated with subduction-related volcanoes built on continental or intermediate lithosphere (Katmai, 1910; Taupo, 1800 years before present; Crater Lake 6850 years before present)

The processes of magma ponding, fractional crystallization, crustal assimilation and melting, and magma mixing in the lithosphere result in a great variety of volcanic rocks being generated. They also explain why the proportion of basalts, relative to more evolved rock types, is greater in the ocean basins than on the continents. Thus, the character of the lithosphere together with the plate tectonic environment determine many of the important characteristics of a given volcano.

SEE ALSO THE FOLLOWING ARTICLES

Calderas • Composition of Magmas • Magma Chambers • Melting the Mantle • Physical Properties of Magmas • Seamounts and Island Building • Volatiles in Magmas • Volcanic Plumes

FURTHER READING

Bebout, G. E., Scholl, D. W., Kirby, S. H., and Platt, J. P., eds. (1996). "Subduction Top to Bottom," Geophysical Monograph 96, American Geophysical Union, Washington, DC.

Crisp, J. A. (1984). Rates of magma emplacement and volcanic output. *J. Volcanol. Geotherm. Res.* **20,** 177–211.

Davidson, J. P. (1991). Continental and island arcs. *In* "Encyclopedia of Earth Systems Science." Academic Press, San Diego.

Fisher, R. V., and Schmincke, H.-U. (1984). "Pyroclastic Rocks." Springer Verlag, Berlin.

Gill, J. G. (1981). "Orogenic Andesites and Plate Tectonics." Springer Verlag, Berlin.

Hamilton, W. B. (1988). Plate tectonics and island arcs. *Geol. Soc. Am. Bull.* **100,** 1503–1527.

Hawkins, J. (1995). Evolution of the Lau Basin—insights from ODP Leg 135. *In* "Active Margins and Marginal Basins of the Western Pacific." Geophysical Monograph 88. American Geophysical Union, Washington DC.

Kearey, P., and Vine, F. J. (1990). "Global Tectonics." Blackwell Scientific Press, Oxford.

Langmuir, C. H., Klein, E. M., and Plank, T. (1992). Petrological systematics of mid-ocean ridge basalts: Constraints on melt generation beneath ocean ridges. *In* "Mantle Flow and Melt Generation at Mid-Ocean Ridges," Geophysical Monograph 71. American Geophysical Union, Washington, DC.

Macdonald, K. C. (1998). Linkages between faulting, volcanism, hydrothermal activity and segmentation on fast spreading centers. *In* "Faulting and Magmatism at Mid-Ocean Ridges," Geophysical Monograph 106. American Geophysical Union, Washington, DC.

Nicolas, A. (1990). "The Mid-Ocean Ridges." Springer Verlag, Berlin.

Pearce, J. A. (1996). A user's guide to basalt discrimination diagrams. *In* "Trace element geochemistry of volcanic rocks: Applications for massive sulphide exploration." Geol. Assoc. Canada Short Course Notes *12*, 79–113.

Perfit, M. R., and Chadwick, W. W. (1998). Magmatism at mid-ocean ridges: Constrainsts from volcanological and geochemical investigations. *In* "Faulting and Magmatism at Mid-Ocean Ridges," Geophysical Monograph 106. American Geophysical Union, Washington, DC.

Sinton, J. M., and Detrick, R. S. (1992). Mid-ocean ridge magma chambers. *J. Geophys. Res.* **97,** 197–216.

Sleep, N. H. (1992). Hotspot volcanism and mantle plumes. *Ann. Rev. Earth. Planet. Sci.* **20,** 19–43.

Taylor, B., and Natland, J., eds. (1995). "Active Margins and Marginal Basins of the Western Pacific," Geophysical Monograph 88. American Geophysical Union, Washington, DC.

Thorpe, R. S., ed. (1982). "Andesites." John Wiley and Sons, New York.

This Page Intentionally Left Blank

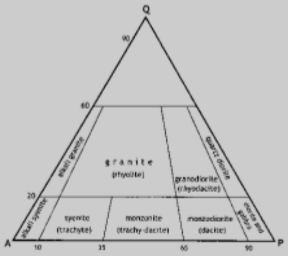

COMPOSITION OF MAGMAS

NICK ROGERS
CHRIS HAWKESWORTH
The Open University

I. Introduction
II. Rock Names and Compositions
III. Basaltic Magmas
IV. Silicic Magmas: Granites and Rhyolites
V. Igneous Rocks and Radiogenic Isotopes
VI. Crustal Evolution

GLOSSARY

accessory mineral Accessory minerals are not an essential component of a rock and are often rich in a trace element. For example, sphene, a calcium titanate, is found in many granites and diorites but is not ubiquitous and is not an essential component of all granites and diorites. Other common accessory minerals include zircon (Zr), monazite (Th), rutile (Ti), allanite (REE), apatite (P), and garnet. They are usually present in small quantities ($<1\%$).

CFB Continental flood basalt provinces are large volumes of dominantly tholeiitic basalt, in the form of sheet flows with few intervening sedimentary or other beds. They are thought to have been erupted in geologically short periods of time at high extrusion rates.

compatible element A compatible element has a high partition coefficient (*D*-value) between a mineral and a coexisting melt.

felsic Felsic rocks have high proportions of quartz, feldspars, and feldspathoid minerals. Granite is a felsic rock.

geotherm The geotherm is defined by the variation of temperature with depth within the earth.

HFSE High field strength elements are those with a high ionic charge (+3, +4, +5) and a small ionic radius. Examples include Y and the heavy REE, Yb and Lu (+3); Zr, Hf, Ti, Th (+4); Nb, Ta (+5).

incompatible element An incompatible element has a low partition coefficient (*D*-value) between a mineral and a coexisting melt.

LILE Large ion lithophile elements are those trace elements with low ionic charge (+1, +2) and relatively large ionic radii. Examples include the alkali elements K, Rb, Cs (+1), and the alkaline earth elements, Sr, Ba (+2).

mafic Mafic rocks have high proportions of minerals rich in MgO, FeO, and CaO, that is, olivine, pyroxene, amphibole and mica. Basalt is a mafic rock. Mafic is the opposite of felsic.

metaluminous Metaluminous rocks are poor in aluminium (Al_2O_3) relative to the total of calcium, sodium, and potassium ($Al_2O_3 < CaO+Na_2O+K_2O$ expressed as molecular %). They are also rich in feldspars and aluminous mafic minerals such as biotite, hornblende, and melilite.

MORB Midocean ridge basalts are produced at a midocean ridge and are tholeiitic.

OIB Ocean island basalts are generated away from plate boundaries and are commonly alkaline but also tholeiitic. Generally produced from a mantle plume.

Copyright © 2000 by Academic Press
All rights of reproduction in any form reserved.

partition coefficient (*D*-value) This is the ratio of the concentration of a trace element in a mineral to its concentration in a coexisting liquid or melt.

pegmatite Pegmatites are coarse-grained, mineralogically complex veins, commonly associated with granitic rocks, containing unusual minerals of often economic significance. They are often dominated by unusual minerals, enriched in elements that are only present in trace quantities in the associated granites.

peralkaline Peralkaline rocks are depleted in aluminum (Al_2O_3) relative to the alkali elements Na_2O and K_2O ($Al_2O_3 < Na_2O+K_2O$, expressed as molecular %). Peralkaline rocks are rich in feldspars and feldspathoids (if SiO_2 is also low) and contain Na-rich pyroxenes and amphiboles such as aegerine, riebeckite, and richterite.

peraluminous Peraluminous rocks are rich in aluminum (Al_2O_3) relative to the total of calcium, sodium, and potassium ($Al_2O_3 > CaO+Na_2O+K_2O$ expressed as molecular %). They are rich in feldspars and the excess aluminum is accommodated by minerals such as muscovite, topaz, tourmaline, garnet, and corundum.

petrogenesis Petrogenesis is the collective noun used to describe all those processes that contribute to the production of an igneous rock, including melt production, segregation and transport, fractional crystallization, magma mixing and contamination, degassing, and eruption or emplacement.

radiogenic isotope A radiogenic isotope is a stable isotope produced by the radioactive decay of an isotope of another element. For example, in the decay scheme ^{87}Rb to ^{87}Sr, ^{87}Sr is the radiogenic isotope produced by the beta decay of ^{87}Rb.

REE The rare earth elements are the 15 4f series elements between La (atomic number 57) and Lu (atomic number 71). They generally have +3 ionic charge and their ionic radii decrease systematically from La–Lu.

solidus The solidus is the melting temperature of a rock and it varies with pressure and volatile content.

I. INTRODUCTION

The generation of melts, and the movement and crystallization of those melts, is the primary mechanism whereby planet Earth has evolved into a core, its mantle, and the continental and oceanic crust. At the present time melting is limited to the outer 200 km of the Earth, within the crust and the uppermost layers of the mantle. Because melts are generally less dense than the source regions from which they are derived, they tend to rise toward the surface and while some may crystallize at depth, many reach the surface at active volcanoes. Thus, volcanoes are located above zones of partial melting within the earth, but the compositions of the volcanic products depend on the causes of melting, the nature of the source material, and the processes that have affected the melt en route from its source to the surface.

Molten rocks are very rarely erupted on the surface as pure liquids. Rather they are complex mixtures of silicate liquid and crystals that may have either crystallized from the same liquid or been picked up by the melts as they moved toward the Earth's surface. *Magma* is the term given to these mobile, largely molten mixtures of liquid and solid material generated in the Earth and, probably, other planets. On Earth the liquids are generally of complex silicates complete with a range of dissolved gases including water, carbon dioxide, and other more exotic compounds. When it approaches the surface, magma generates volcanic activity during which mobile silicate lava may be erupted and solidify to form volcanic rocks. Alternatively, magma may be trapped at depth and cool more slowly to form plutonic igneous rocks that may eventually be revealed by erosion. Thus it is tempting to equate the composition of magmas with the composition of igneous rocks. However, because the processes of eruption and solidification allow volatiles to be released to the atmosphere, often explosively, and crystals to separate from the liquid, igneous rocks typically have different compositions from the magmas generated within the Earth. Despite this, great progress has been made in our understanding of the processes that lead to the compositional diversity of magmas through the study of igneous rocks, and that is the subject of this chapter.

II. ROCK NAMES AND COMPOSITIONS

Igneous rock compositions are conventionally expressed in terms of major, minor, and trace elements. Major and minor elements are expressed as oxides: SiO_2, Al_2O_3, FeO, Fe_2O_3 CaO, MgO, and Na_2O (major elements) and K_2O, TiO_2, MnO, and P_2O_5 (minor elements). Major elements are, by definition, those with oxide abundances above 1 wt%, whereas minor elements are those between 0.1 and 1 wt%. Some elements, such as potassium and titanium, are present in minor element abundances in some rocks but attain major element proportions in others. Below 0.1 wt% we enter the realm of trace elements, the concentrations of which are conventionally expressed in terms of ppm (parts per million, or μg g^{-1}) of the element alone. Thus conventional chemical analyses of igneous rocks appear as in Table I, which lists the compositions of a variety of igneous rocks from selected geological environments. Volatile elements and oxides are less frequently reported but can be added to the list as H_2O CO_2, SO_2 F, Cl, etc.

Two points are clear from Table I. First, igneous rock compositions vary considerably, from those with, for example, very low SiO_2 to others dominated by SiO_2 almost to the exclusion of other elements. The second point is that it is very difficult to assimilate such geochemical information from a list of numbers alone and igneous petrologists have devised a number of graphical methods for summarizing such data that render them more easily understood. Indeed the so-called "variation diagram" is a standard tool of modern igneous petrology, and one of the most commonly used in the definition of igneous rocks is a plot of SiO_2 abundance against the total alkali content, ($Na_2O + K_2O$). An example of this plot is shown in Fig. 1, in which a large number of analyses of volcanic rocks are plotted and a grid superimposed to demonstrate how chemical composition can be used to define rock names.

Rock names also depend on mineralogy and grain size and, to a lesser extent, on the presence or absence of specific minerals, resulting in an even greater variety of names than those given in Fig. 1. In Fig. 2 the mineralogical variations of some of the more common rock types are illustrated graphically as a function of bulk composition. Thus, basalt is the name given to a volcanic rock with low Si, Na, and K; high Mg, Fe, and Ca; and a mineralogy of pyroxene, olivine, and plagioclase. However if a basaltic magma cooled slowly beneath the surface, a coarse-grained rock called gabbro would be formed. Similarly rhyolite is a volcanic rock with high Si, Na, and K; low Ca, Mg, and Fe; and is dominated by quartz and feldspar with small amounts of mica or amphibole. Its coarse-grained equivalent is granite.

The origins of the names of the commonest rock types, such as basalt and granite, are diverse and rather obscure. Others rock types recognized more recently are named after the locality where they were first identified; hence, icelandite, hawaiite, and andesite. Others record the presence or dominance of a specific mineral; for example, nephelinite (nepheline), leucitite (leucite), and carbonatite (carbonate), all of which add to the complexity of igneous taxonomy. Despite this plethora of specific names, igneous rocks are dominated by two compositional types: basalts and granites. Rocks of basaltic composition dominate the crust beneath the world's oceans, whereas granitic rocks and their volcanic equivalents (rhyolite) are the most abundant igneous rock types of the continents. Indeed, the higher silica and lower iron content of granitic rocks makes them less dense than basalt and this difference is the reason why the continents are on average 5 km higher in elevation than the ocean basins. In the following two sections these two dominant magma types are described in relation to the places where they are found.

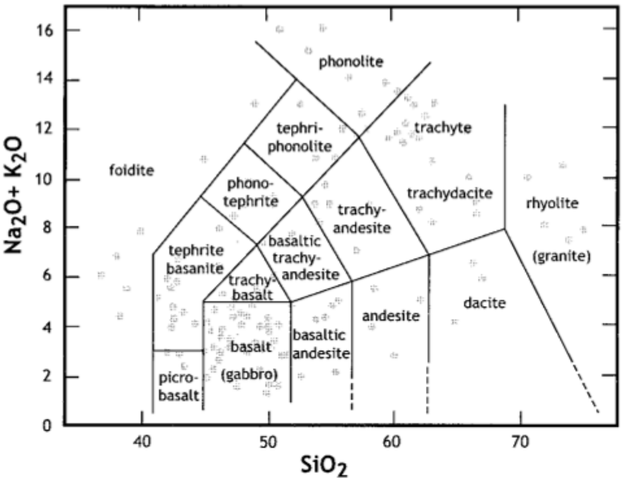

FIGURE 1 Total alkalis versus silica diagram with ~100 volcanic rock analyses illustrating the enormous variation in rock compositions. Superimposed are the boundaries that delineate different rock types with examples of extrusive (volcanic) and intrusive (plutonic) names superimposed. (Plutonic rock names are given in parentheses.)

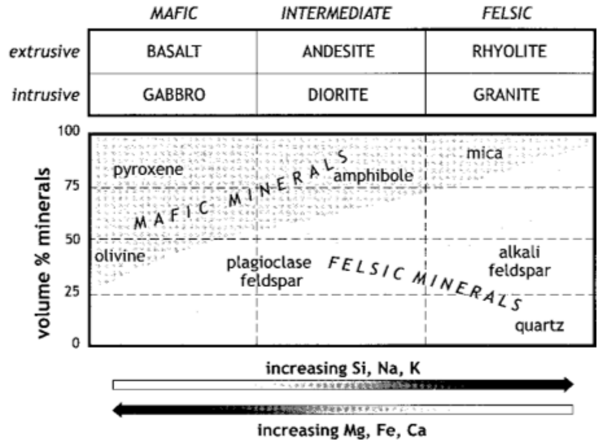

FIGURE 2 This chart summarizes the mineralogy and the general compositional characteristics of the most common igneous rock types.

TABLE I Major and Trace Element Analyses of Selected Igneous Rocks

	Peridotite	*Tholeiitic basalt MORB*	*Alkali basalt OIB*	*Andesite*	*Metaluminous Granite*	*Peraluminous Granite*	*Peralkaline granite*
Major and minor elements (wt%)							
SiO_2	44.20	48.77	47.52	59.89	67.89	69.08	70.87
TiO_2	0.13	1.15	3.29	0.95	0.45	0.55	0.1
Al_2O_3	2.05	15.90	15.95	17.07	14.49	14.30	14.78
Fe_2O_3	0.75	1.33	3.16	3.31	1.27	0.73	2.64
FeO	7.54	8.62	8.91	3.00	2.57	3.23	
MnO	0.13	0.17	0.19	0.12	0.08	0.06	0.06
MgO	42.21	9.67	5.18	3.25	1.75	1.82	0.1
CaO	1.92	11.16	8.96	5.67	3.78	2.49	0.34
Na_2O	0.27	2.43	3.56	3.95	2.95	2.20	6.47
K_2O	0.06	0.08	1.29	2.47	3.05	3.63	4.19
P_2O_5	0.03	0.09	0.64	0.31	0.11	0.13	0.02
H_2O+		0.30	1.16				0.33
F (ppm)		210	1150				
Total	99.29	99.67	99.81	99.99	98.39	98.22	99.90
Trace elements (ppm)							
V	70	262	350	125	74	72	9
Cr	3200	528	421	484	27	46	5
Ni	2300	214	153	38.6	9	17	3
Rb	0.64	0.56	31	75.4	132	180	148
Sr	21	90	660	886	253	139	1.8
Y	5	28	29	12	27	32	188
Zr	11	74	280	240	143	170	772
Nb	0.7	2.3	48	15	9	11	100
Ba	7	6.3	350	886	520	480	
La	0.7	2.5	37	38	29	31	59.6
Ce	1.8	7.5	80	67	62.9	69	152
Nd	1.4	7.3	39	32	23.4	25	93.7
Sm	0.44	2.63	10	5.82	4.25	4.89	25.4
Eu	0.17	1.02	3	1.57	2.23	1.74	1.99
Gd	0.6	3.68	7.62	4.73	4.16	4.35	27.8
Tb	0.11	0.67	1.05	0.66	0.59	0.64	4.80
Yb	0.49	3.05	2.16	1.64	1.81	2.25	16.3
Lu	0.07	0.46	0.3	0.25	0.27	0.34	2.46
Ta	0.04	0.13	2.7	0.88	0.42	0.56	6.68
Hf	0.31	2.05	7.8	5	4.1	5.5	26.3
Th	0.08	0.12	4	6.5	16	19	17.8
U	0.02	0.05	1.02	1.89	3	3	4.59

Key: MORB, midocean ridge basalt; OIB, ocean island basalt.

III. BASALTIC MAGMAS

A. Major Elements and Formation

1. *Ocean Floor Basalts*

Basalts dominate the floor of the oceans, forming the oceanic crust, which is generated at constructive plate margins at midocean ridges. Magma is produced in response to the separation of two plates, which allows the underlying mantle to rise up and melt as a result of decompression. Decompression melting is one of the major mechanisms of melt generation within the Earth and occurs when hot mantle material (peridotite) rises from depth (high pressure) to shallower levels (lower pressures) as a result of thinning of the overlying crust and lithosphere. This process is illustrated schematically in Fig. 3. As pressure is reduced, the temperature of the mantle decreases slightly (adiabatically). This decrease in temperature is less than the decrease in the melting point of the mantle (which also decreases with decreasing pressure) so that eventually the rising mantle moves from conditions of pressure and temperature in which it is solid to *P-T* conditions that produce a melt.

A key feature of melting in the Earth is that rocks melt over a range of temperatures, even while the pressure is kept constant. One consequence is that the composition of a partial melt is different from that of the initial source rock, because the different minerals within the source rock melt at different rates. In the case of the Earth's mantle, the common rock is peridotite, which is composed of four minerals: olivine, orthopyroxene, clinopyroxene, and an aluminous phase (plagioclase, spinel, or garnet). (On Fig. 2 peridotite falls to the left of basalt, having even lower Si, Na, and K and higher Mg.) These four minerals contribute to the melt in different proportions, and it is clinopyroxene and the aluminous phase that melt first—hence, the melts have higher Al_2O_3 and CaO contents than peridotite, and also higher SiO_2 and lower MgO contents. Such melts of peridotite are called *basalts* (Fig. 1).

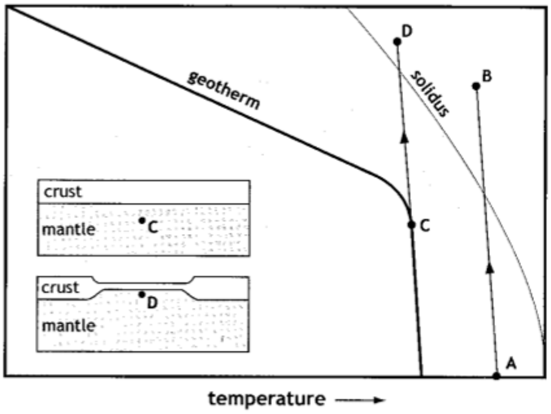

FIGURE 3 Illustration of the principles of decompression melting. A parcel of mantle lies on the geotherm at point C. If the overlying crust is rifted or extended, then that parcel of mantle rises to point D at a lower pressure but with a minimal drop in temperature. Point D is above the solidus and so the mantle melts. The vector *A–B* shows the trajectory of a similar parcel of mantle with a higher temperature, for example, as in a rising mantle plume. Decompression of this parcel induces melting at a greater depth and a higher degree of melting overall.

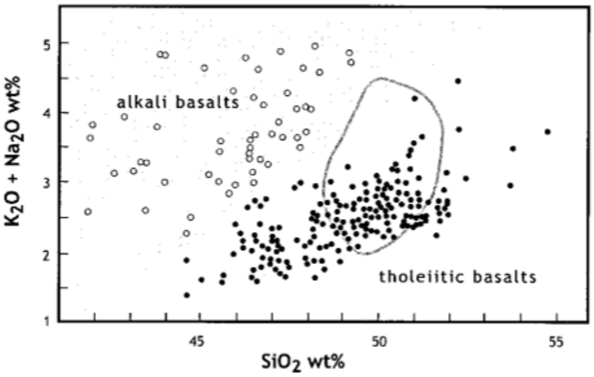

FIGURE 4 A diagram showing the variation in total alkalis and silica in basalts from Hawaii and the compositional differences between alkali and tholeiitic basalts. The outlined field represents the region in which most midocean ridge basalts plot.

Melting beneath ocean ridges occurs over a range of depths depending on the ambient temperature of the mantle (Fig. 3), and the melt that is emplaced in the crust or erupted on the ocean floor is called *tholeiitic basalt* (after the type locality in Germany). This type of basalt is poor in sodium and potassium and contains about 50% SiO_2 (Fig. 4). Once emplaced within the crust, the basalt cools and starts to crystallize. However, just as melts differ in composition from their parent rocks, the material that crystallizes first has a different composition from the basaltic liquid—it is the MgO-rich mineral olivine. Olivine is denser than the basalt melt and the two are physically separated by, for example, crystal settling due to gravity. This separation leaves the basaltic melt poorer in MgO but richer in those elements not included in olivine (e.g., CaO, Al_2O_3, alkali elements), and so changes the composition of the liquid. As this process continues, the liquid becomes depleted in MgO and enriched in CaO, Na_2O, and Al_2O_3 and, eventually, a second mineral phase crystallizes which is rich in these elements. This mineral is plagioclase feldspar, and it too separates from the melt, depleting the latter in CaO and Al_2O_3. This process is called *fractional crystallization*, and it is one of the most important magmatic processes, after partial melting, for generating the wide range in the compositions of magmas and igneous rocks (Fig. 5).

The effects of fractional crystallization on lavas erupted on the ocean floor are illustrated in the variation diagram in Fig. 6. The diagram shows how the Na_2O contents vary in basaltic lavas dredged from three different regions of the midocean ridge system that encircles the earth. The diagrams show how Na_2O increases as MgO decreases in each of the three examples, consistent with the removal of MgO-rich and Na_2O-poor phases such as olivine, clinopyroxene, and calcic plagioclase. In fact, the samples shown in Fig. 6 are all tholeiitic basalts and the inflection in, for example, the trend labeled AAd at ~8 wt% MgO is caused by the crystallization of calcic plagioclase in addition to olivine, which is the only phase crystallizing at MgO contents above 8 wt%.

A second important feature emerges from this diagram, and that is that the basalts from the three different ridge regions lie along separate trends that do not converge on a single Na_2O content at high MgO abundances. This discrepancy suggests that there is a range of different parental magma compositions with different Na_2O contents for midocean ridge basalts (MORB), and debate continues as to the underlying causes of these differences. In the case of Na_2O, which is an incompatible element in the mantle (see later discussion), its abundance is probably related to the amount of melting in the mantle. Thus for the parent of the AAd trend, melt fractions in the mantle would be small and their Na_2O contents would be high, whereas for the parent of the Kolbeinsey trend they would be higher.

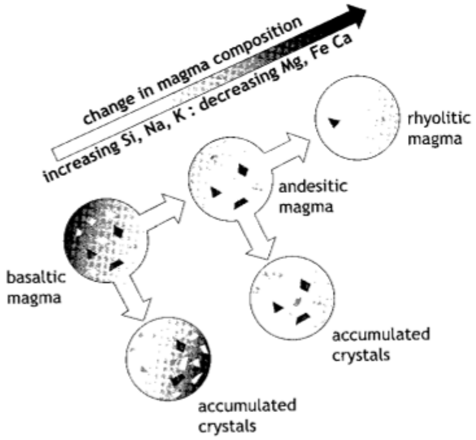

FIGURE 5 Illustration of the evolution of progressively more silica-rich magma as a result of repeated fractional crystallization. The process may be continuous or occur in a number of stages.

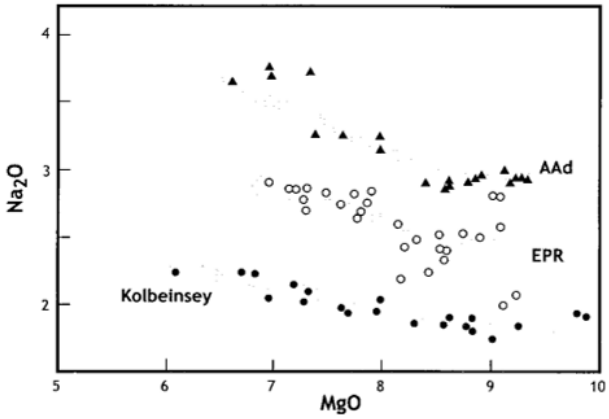

FIGURE 6 The variation of sodium with magnesium (both expressed as wt% oxides) in basalts from three segments of the midocean ridge system. The Kolbeinsey Ridge is the extension of the Mid-Atlantic Ridge, north of Iceland, the EPR is the East Pacific Rise, and the AAd lavas are from a segment of ocean ridge south of Australia (the Australia Antarctic discordance). Each region shows an increase in sodium as magnesium decreases, but the trends start at different sodium concentrations at high magnesium abundances.

2. *Ocean Island Basalts*

A second important location where basalts are found is in ocean islands, such as Hawaii, Tahiti, Easter, Reunion, the Azores, and the Canary Islands, to name but a few. These active basaltic volcanoes are located away from the midocean ridges in an intraplate or withinplate setting. In these locations there is no crustal or lithospheric extension and melting is induced by the active upwelling of hot mantle, popularly known as *mantle plumes*, beneath the moving oceanic plates.

Mantle plumes can occur beneath continents as well as oceans and are an integral part of the convective overturn of the Earth's mantle. They have their origin at great depth, in some cases possibly at the boundary between the core and the lower mantle, and because the mantle within a plume is intrinsically hotter than the mantle through which it is rising, it can start melting as a consequence of decompression at a greater depth than occurs beneath the ocean ridges (Fig. 3). However, unlike the ocean ridge setting, the top of the melting regime is limited by the thickness of the overlying plate or lithosphere. Thus the average depth from which ocean island basalts are derived is greater than that for MORB, and the amount of melt that is produced from a given parcel of mantle is less. As a result, ocean island basalts (OIB) tend to be richer in alkalis and iron and poorer in silica than MORB. Despite this change in the melting regime, larger ocean islands above large mantle plumes (e.g., Hawaii) and mantle plumes that upwell beneath constructive plate margins (e.g., Iceland) both produce tholeiites. By contrast, islands situated above smaller plumes and/or located on old and thick ocean lithosphere are characterized by a variety of basalt that has lower SiO_2 but higher Na_2O and K_2O contents than tholeiites. Such basalts are termed *alkaline olivine basalts* or *alkali basalts.* Both varieties occur on Hawaii and the total alkalis versus silica diagram can be used to discriminate between them (Fig. 4).

The mineralogical variety of alkali basalts is considerable and is a result of both a reduction in SiO_2 and an increase in the alkali elements, particularly Na_2O, and other minor and trace elements. This trend toward increasing alkalinity also produces magma compositions outside the field of alkali basalts, which are generally known as *basanites* and *foidites* (Fig. 1). These tend to be the result of yet smaller degrees of partial melting than are responsible for alkali basalts and in extreme cases, also reflect the effects of CO_2 on mantle melting at great depths. Rock types produced in this way include basanites, nephelinites, leucitites, and melilitites and are frequently found on smaller ocean islands, or in the final stages of volcanic activity on larger islands, such as Hawaii.

3. Island Arc Basalts

The third oceanic location where basalts are generated is above subduction zones where old, cold oceanic lithosphere descends back into the mantle. Subduction zones are consequently regions of generally low heat flow and at first glance it is surprising that melt should be produced in regions where the mantle is cold. However, the subducting lithosphere carries water back into the mantle temporarily trapped in sediments and in seafloor basalts that were hydrothermally altered at midocean ridges. This water is released as the subducting plate warms up and it is the fluxing of the mantle wedge overlying the subduction zone by this water that induces melting by lowering the solidus of peridotite by 2–300°C. The basalts produced in this environment tend to be tholeiitic and have a crystal fractionation assemblage similar to that of MORB.

In regions where subduction takes place beneath continents, such as beneath the Andes, the basaltic magma may be trapped within the thick, low-density continental crust. Basaltic magma is denser than the continental crust and can only rise to a level of neutral buoyancy, often at the junction between layers of contrasting density such as the boundary between the crust and mantle (the Moho), or at boundaries within the crust. In addition the magma is richer in water, derived from the subducting lithosphere, than either ocean ridge or ocean island basalts. These differences in composition and the higher pressure of crystal fractionation have a profound effect on the composition of the crystallizing minerals and as a result basaltic magma crystallizes along a different path, producing magmas with lower iron contents (Fig. 7). Such trends are termed calcalkaline and lead to the production of an intermediate rock known as *andesite.* This rock type is named after the Andes where it is one of the dominant volcanic rock types. Calcalkaline fractionation trends and andesites result from a number of different processes, such as mixing between basalts and granitic melts, fractional crystallization of Fe-rich minerals, and complex reactions between crystallizing phases and coexisting liquid.

Further fractional crystallization of andesitic magma, possibly combined with the assimilation of crustal material, leads to the production of even more silica-rich compositions such as dacites and rhyolites. As fractionation proceeds, the concentration of water builds up in the magma because the crystallizing minerals are essentially anhydrous. The end product is a silica-rich magma charged with water, and the explosive release of water when such magma reaches the surface produces the violent volcanic eruptions that can prove so hazardous to

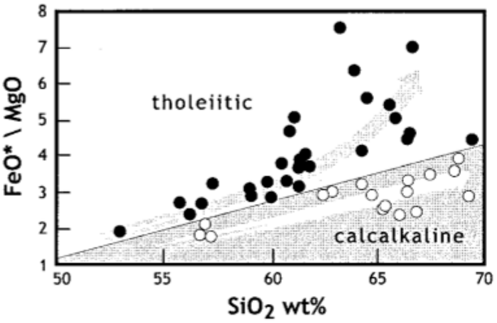

FIGURE 7 Contrasting FeO/MgO ratios in calcalkaline and tholeiitic rocks from Aso, a Japanese volcano. Fractionation of olivine and plagioclase in the tholeiitic suite produces iron enrichment and hence high FeO/MgO ratios for a given increase in SiO_2, whereas early fractionation of clinopyroxene and olivine in the calcalkaline trend produces less iron enrichment and a more rapid increase in SiO_2.

property and life close to destructive plate margins (e.g., Mount St. Helens, Pinatubo, Montserrat).

4. Continental Basalts

As in the oceans, both tholeiitic basalts and alkaline basalts erupt on the continents. Rift zones, such as the East African Rift system, the Baikal Rift in Siberia, the Rhine Graben and the Rio Grande Rift in the United States are dominated by alkali basalts, basanites, and nephelinites. These are regions where the crust and lithosphere are under extension, leading to fracture and the development of rift valleys. However, the amounts of crustal and lithospheric extension are small, and so mantle melting is restricted to depths similar to that beneath ocean islands, albeit in the presence of a lithosphere that may be thicker than that in the oceans (Fig. 8). Consequently, the basalts and associated lavas from such regions broadly resemble those from the ocean islands and are dominated by alkaline compositions and their evolved derivatives, such as trachytes and phonolites (Fig. 1).

By contrast, continental flood basalt (CFB) provinces contain large volumes of tholeiitic basalts (perhaps $>10^6$ km^3) that may have been erupted in geologically short periods of time (1–2 My). They represent vast catastrophic events, and in a number of cases it is speculated that they were linked with major mass extinctions in the fossil record, such as the eruption of the Deccan CFB, 65 Ma ago, broadly coincident with the extinction of the dinosaurs. Such flood basalt provinces are often, but not exclusively, associated with continental breakup and the development of a new ocean. Moreover, many CFB occur at the end of hot spot traces on the adjacent ocean floor, and so they are linked in some way to the presence of a mantle plume. In general, the large volumes require the presence of anomalously high mantle temperatures, as in a plume, and an association between CFB provinces and the initiation of a mantle plume is often invoked.

As more data become available it appears that there are differences in major and trace element compositions (see later discussion), and also perhaps in the average eruption rates of different CFB. These differences may in turn reflect differences in the source regions, and in the causes of partial melting in the different CFB provinces, and an alternative view to the plume initiation theories relates CFB to the conductive heating and melting of source regions within the mantle section of the continental lithosphere.

The mantle lithosphere is the cool and relatively rigid part of the mantle immediately below the continental crust that extends to depths in excess of 100 km, and beneath the oldest continental nuclei, perhaps to 200 km. As in the oceans the mantle lithosphere beneath the continents is widely regarded as being the residue after partial melting and therefore incapable of generating further magmas. However, if it contains a small percentage of water locked up in the form of hydrous mineral phases, such as amphibole or mica, then these phases reduce the mantle solidus so that melt can be generated if the lithosphere is heated. A mantle plume impinging on the base of the lithosphere could supply the necessary heat by conduction while the release of volatiles, particularly water, would ensure the generation of a tholeiitic magma. Thus flood basalts may be produced both by a process of conductive heating prior to extension and continental breakup, by adiabatic melting within mantle plumes where they coincide with areas of extension and hence thinner lithosphere, or by melt-

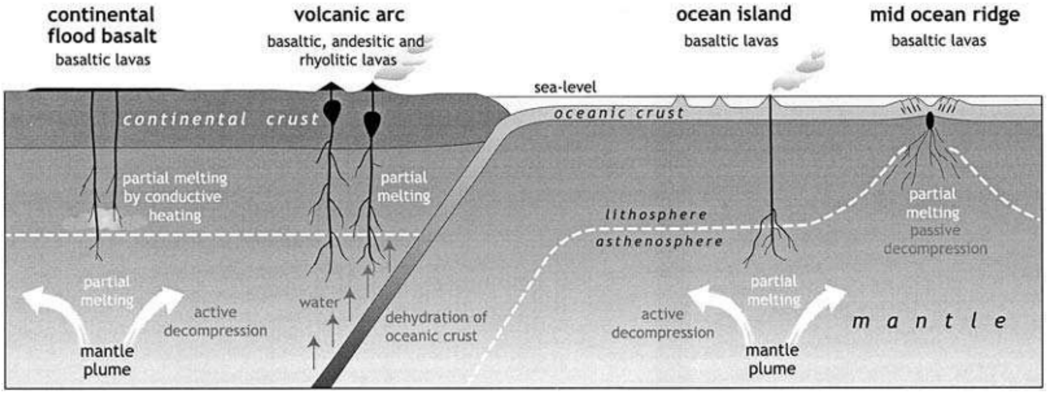
continental flood basalt
basaltic lavas
volcanic arc
basaltic, andesitic and rhyolitic lavas
ocean island
basaltic lavas
mid ocean ridge
basaltic lavas
sea-level
continental crust
oceanic crust
partial melting by conductive heating
partial melting
lithosphere
asthenosphere
partial melting
passive decompression
partial melting
active decompression
water
dehydration of oceanic crust
active decompression
partial melting
mantle
mantle plume
mantle plume

FIGURE 8 A diagrammatic section through the continent and ocean showing crust and mantle lithosphere and melting mechanisms for MORB, OIB, island arcs, and continental flood basalts.

ing of the anomalously hot regions of mantle associated with the initiation of new mantle plumes.

5. Summary

Basaltic magmas are generated by partial melting of the peridotite mantle by adiabatic decompression beneath midocean ridges (tholeiitic MORB), by adiabatic decompression in mantle plumes (alkalic and locally tholeiitic OIB), and by depression of the melting point by the addition of volatiles in subduction zones (tholeiitic and calcalkaline basalts). In continental regions, basalts are also produced by adiabatic melting within mantle plumes in regions of extension although they may also be generated in response to conductive heating of lithospheric mantle that contains a small amount of volatile elements. These different mechanisms for generating melting within the mantle are summarized in Fig. 8.

B. Trace Elements

By definition the major elements dominate the bulk composition of an igneous rock, and their relative abundances reflect the depths at which melting took place, and the amount of differentiation which has subsequently taken place. However, minor and trace elements are widely used in the study of volcanic rocks to understand the processes that produce igneous rocks because they are very much more sensitive to the amounts of melting, the residual minerals present during melting, and the element abundances in the original source rock. As an example, the major element composition of a melt changes only gradually with increases in the degree of melting, while the same residual minerals are present, and yet the abundances of some trace elements in the melt may change by two orders of magnitude between 0.05 and 5% melting. Similarly, the minor and trace element abundances of mantle peridotites vary much more than their major elements. Consequently, trace element variations in basaltic rocks are critical in assessing the origins and the scale of chemical variations in the Earth's mantle and whether different suites of igneous rocks might have been derived from similar source regions.

The distribution of trace elements in a melting or crystallizing magmatic system is often described in terms of partition coefficients, which are defined as the concentration of the element in the mineral or solid divided by its concentration in the coexisting liquid. Partition coefficients vary enormously and depend on the size and charge of the trace element cation and the size of the crystallographic site in the coexisting mineral into which the element substitutes. In general those elements with D-values of <1 are described as incompatible elements, whereas those with values of >1 are described as compatible. Examples of elements that are compatible during mantle melting include Ni in olivine, Cr in pyroxene, and Yb (one of the rare earth elements) in garnet. Others, such as Zr, Nb, and the light rare earth elements, are incompatible because they do not easily fit into the structure of any common mantle mineral. Other elements become compatible within the crust. Sr and Eu, for example, fit easily into plagioclase and alkali feldspar, which are common minerals within the crust, but they are generally incompatible elements in the mantle. The relative abundances of such trace elements can therefore be used to identify the minerals that were present, either during melting or fractional crystallization. Moreover, because certain minerals are stable over particular pressure ranges, critical trace element ratios can in turn be used to infer the depths at which melting or fractional crystallization took place.

A convenient way for comparing trace element abundances in basaltic rocks is via the use of mantle or chondrite (meteorite) normalized abundance diagrams, such as those illustrated in Fig. 9. The elements are ordered in their approximate sequence of compatibility in the mantle, with the most incompatible element at the left. The elements conventionally illustrated this way include the incompatible trace elements and the minor elements, K, P and Ti. These three minor elements generally behave incompatibly in the mantle, and only rarely form discrete silicate phases during mantle melting. It is only their intrinsically high natural abundances that allowed them to be recognized traditionally as minor elements.

The analyses shown in Fig. 9 include an average MORB and an average OIB. A striking feature of such diagrams is that for rocks which represent more than a few percent of partial melting, the shape of the pattern of incompatible elements in the basalts will be similar to that in their source—albeit at different abundances. Note, therefore, how the abundance pattern for the MORB has a convex upward curve, and that the more incompatible elements have lower concentrations than the less incompatible. This pattern is characteristic of MORB worldwide and reflects the broad pattern of the trace elements in their mantle source regions. The fact that there are relatively low concentrations of the more incompatible elements indicates that those elements have been preferentially removed in a previous partial melting event. In most models this depletion of the most incompatible elements in the source of MORB is attributed to a previous melting episode(s) including the

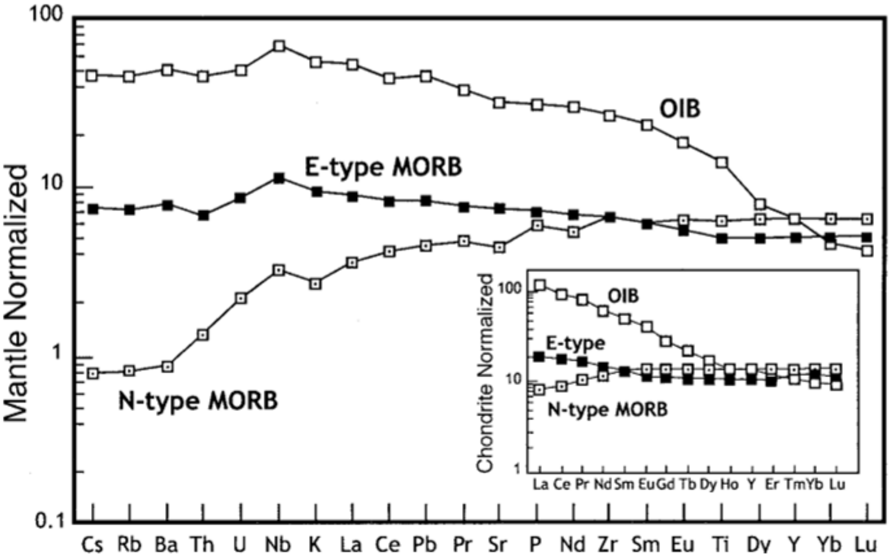

FIGURE 9 The variation of incompatible trace elements in a typical MORB and OIB. Trace elements are normalized to their concentrations in the upper mantle and arranged in order of their incompatibility, the most incompatible elements to the left of the diagram. The inset shows the rare earth elements (REE) normalized to their abundances in chondritic meteorites. Note the depletion of the most incompatible elements in N-MORBs and the low abundances of the most compatible in OIB. E-type MORBs are found in areas of the midocean ridge system close to ocean islands and imply interaction between an actively upwelling mantle plume and the MORB source; hence, their intermediate abundances of trace elements.

progressive extraction of the continental crust throughout Earth history.

In comparison to MORB, OIB have higher abundances of the more incompatible elements and slightly lower abundances of the less incompatible elements such as Y, Yb, and Lu. This difference reflects two aspects of the generation of OIB. The higher abundances of the incompatible elements are due to the smaller overall melt fraction in the generation of OIB compared with MORB, since highly incompatible elements are concentrated in the first small amount of melt to form, and simply diluted as the degree of melting increases. The lower abundances of Y, Yb, and Lu reflect their compatibility in the mineral garnet. Garnet is the stable aluminous phase in peridotite at pressures >25–30 Kb, and so this evidence for the presence of residual garnet during the generation of OIB indicates that they were generated at relatively high pressures. A final point is that the trace element patterns for both MORB and OIB are relatively smooth on Fig. 9. Since the order of the elements plotted is that of increasing compatibility in common mantle minerals from left to right, the smooth patterns are indicative of partial melting of a peridotite source which itself had a relatively smooth pattern. Other basaltic rocks do not have smooth patterns (see later discussion) and show the development of minor and trace element anomalies, which are highly diagnostic of the processes involved in their formation.

Figure 10 illustrates four analyses of basalts from the Marianas island arc on a diagram normalized to abundances in N-MORB. The differences between these

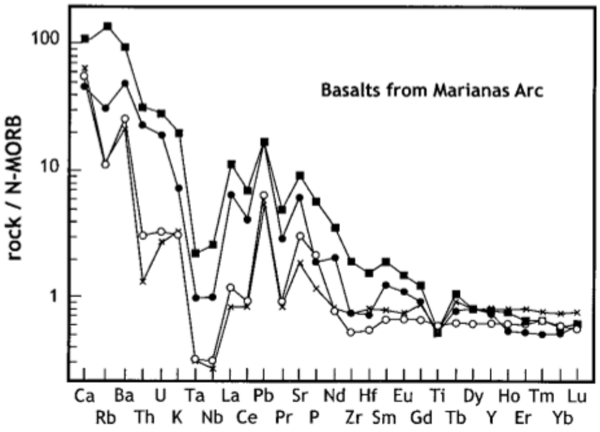

FIGURE 10 Incompatible trace element abundances of basalts from the Mariana arc, western Pacific, normalized to abundances in N-MORB (cf. Fig. 9). Note the low abundances of Nb and Ta and the high abundances of elements such as Cs, Ba, K, Pb, and Sr.

profiles and the profiles for MORB and OIB in Fig. 9 are very clear, in that the island arc basalts have high abundances of elements such as K, Rb, Ba, and Sr (large ion lithophile elements, LILE) relative to the rare Earth elements (REE), and low abundances of Nb and Ta. These latter elements, along with Zr, Hf, and Ti are referred to as the high field strength elements (HFSE), having high ionic charges but small ionic radii, and their depletion is frequently referred to as the *niobium* (or *tantalum*) *anomaly.* It may be expressed as high values of trace element ratios such as Ba/Nb, Ba/Ta, La/Nb, or La/Ta, and high values of these ratios have long been regarded as distinctive characteristics of subduction-related igneous rocks.

In detail, basalts from different arcs show a wide variety of trace element abundances with varying amounts of enrichment of the light REE and the large ion lithophile elements (LILE) and varying depletions of Nb and Ta, and sometimes Ti. What is unique about island arc rocks is that they are thought to be derived by melting of peridotite triggered by the introduction of water-rich fluids from the subducted oceanic crust. Thus, some models invoke the effect of residual Ti-rich minerals, stabilized during hydrous melting, as the cause of the Nb anomaly, while others relate element abundances in arc rocks to the differing mobilities of elements in fluids and melts derived from the material within the subducted oceanic crust. Hydrous fluids will preferentially contain the more mobile LILE, and if the slab is heated sufficiently for sediments to melt they will contribute a full range of elements, but with relative abundances distinct from those generated during anhydrous melting of peridotite. Consequently, most island arc rocks are modeled as some mixture of MORB-like melts of the mantle above the subduction zone, and both hydrous fluids and melts of sediment from the subducted crust.

In addition to subduction-related basalts, some continental basalts also have incompatible element profiles with positive and negative anomalies. Figure 11 illustrates the trace element abundances in some lavas from the Parana continental flood basalt province. Some have smooth trace element profiles similar to those from Hawaii (cf. Fig. 9, OIB), suggesting that they too were probably derived from partial melting within an upwelling mantle plume. By contrast, others show uneven trace element patterns and anomalies strikingly different from the smooth patterns seen in MORB and OIB. These CFB would therefore appear to have been derived from source regions different from those commonly present in the convecting upper mantle, and one model is that they were derived not from the convecting upper mantle, but from the mantle part of the continental lithosphere. A second feature is that the uneven patterns of these anomalous CFB are similar to those seen in subduction-related basalts.

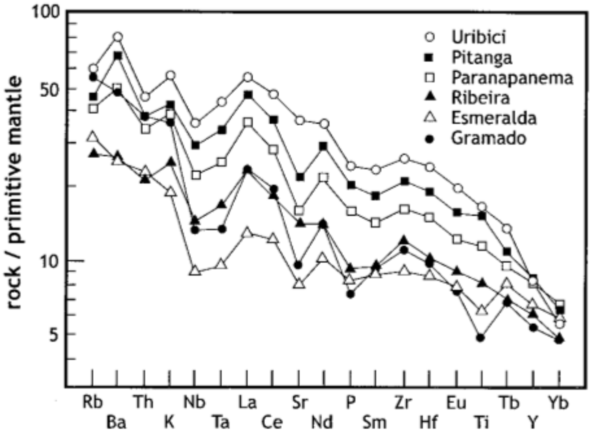

FIGURE 11 Mantle normalized trace element diagram of basalts from the Parana continental flood basalt province. Note the negative Nb, Ta, and, in some cases, Ti anomalies and the high abundances of the LILEs, Rb, Sr, and Ba.

Much of the continental crust is thought to have been generated along destructive plate margins, and it certainly preserves a lengthy record of repeated subduction-related magmatic and tectonic events. Thus it may be that aspects of continental flood basalts reflect interaction with the continental crust. Alternatively, it is likely that during crust generation segments of the underlying mantle become isolated from the convecting interior and become incorporated into the lithosphere, which may then preserve geochemical features similar to those of island arc magmas. These enriched zones of mantle lithosphere can subsequently be melted if heated when a mantle plume impinges on the base of a continental plate, provided they contain small amounts of volatiles to lower the peridotite solidus, and would impart these characteristics to the magmas so generated.

IV. SILICIC MAGMAS: GRANITES AND RHYOLITES

Silicic magmas have a more restricted major element compositional range than basalts, a feature that results from the processes that lead to their production, namely, partial melting of crustal rocks and fractional crystallization of silicate melts. As their name implies, silicic magmas have high SiO_2 and total alkalis and low MgO and

FeO contents (Fig. 1 and 2) and their compositions lie close to the lowest melting fraction of crustal silicate systems. If, for example, a basalt is melted, then the first melt that forms has a silica-rich composition. Likewise, during fractional crystallization of a basalt, the progressive loss of minerals such as olivine, pyroxenes, and calcic-plagioclase feldspar enriches the liquid phase in silica, sodic palgioclase, and alkali feldspar. Thus two possible routes to silicic magmas exist, one by extensive fractional crystallization of basaltic magma, the other by partial melting of pre-existing crustal rocks.

As with basaltic magmas, silicic magmas can crystallize at depth to form coarse-grained intrusive rocks known as *granites* and this is the most common fate of silicic magmas. Sometimes, however, they erupt at the surface to form fine-grained or glassy volcanic rocks known as *dacites* and *rhyolite*. When this happens, the magma rapidly releases its dissolved volatiles (mainly water), resulting in a violently explosive eruption. Such events capture the public imagination because of their destructive power. Indeed, the largest and most violent volcanic eruptions in both historic and prehistoric times are related to the eruption of silicic magmas [e.g., Mt. St. Helens, Crater Lake, Yellowstone, Long Valley (United States), Santorini (Greece), Toba, Krakatoa, Tambora (Indonesia), Taupo (New Zealand)]. In the following text, for convenience silicic magmas are referred to as granites, but it should be remembered that rhyolites and dacites are chemically equivalent although their fine-grained or glassy texture often renders mineralogical classification difficult or impossible.

All granites contain alkali feldspar, plagioclase feldspar, and at least 20% quartz, and classification schemes for granitic rocks depend on a combination of mineralogy and bulk composition. The detailed nomenclature of plutonic rocks, summarized in Fig. 12, is based on the relative proportions of alkali feldspar to plagioclase. Of these different rocks types, granites and granodiorites are the most abundant in the continents, closely followed by diorites and gabbros, whereas gabbros dominate the deeper sections of the oceanic crust. Syenites and monzonites are somewhat less abundant and generally restricted to the continents.

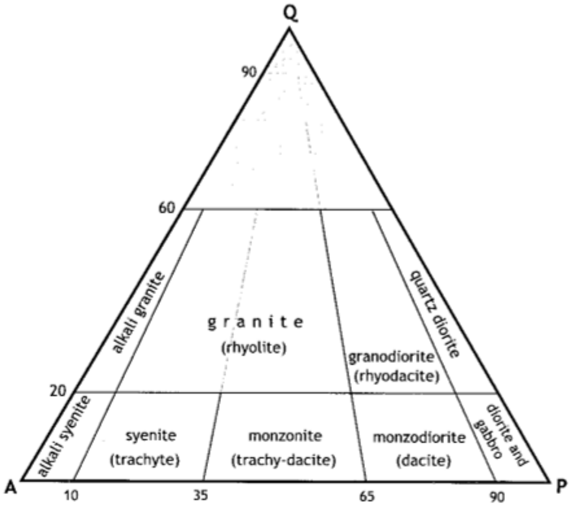

FIGURE 12 The mineralogical classification of plutonic rocks. Q refers to the amount of quartz in the rock, P the amount of plagioclase, and A alkali feldspar. Granites (*sensu lato*) include all those rock types with more than 20% quartz, whereas those rocks with less than 20% quartz are classified as intermediate. Note that on this diagram basaltic and andesitic rocks are restricted to a small region close to the P apex because they are dominated by plagioclase feldspar, pyroxenes, and olivine.

Chemical classifications add further complexity to this system but reveal important differences, possibly related to the processes of magma formation. The primary classification depends on the molecular ratio $Al_2O_3/(Na_2O + K_2O + CaO)$. If this is less than 1, then the granite is defined as metaluminous; whereas if it is greater than 1, it is peraluminous. Metaluminous granites tend to be rich in sodium and are often associated with a broad range of other igneous rocks. Peraluminous granites have lower sodium contents, but are richer in potassium and tend to be restricted in their association to high-silica magmas. An alternative classification divides granites at value of the $Al_2O_3/(Na_2O + K_2O + CaO)$ ratio of 1.1. Above this ratio (i.e., highly peraluminous) granites are classed as "S-type," while below a value of 1.1 they are "I-type." It is generally thought that I-type granites are derived, either by fractionation or partial melting, from igneous precursors, whereas S-type granites are derived from melting of pre-existing sedimentary rocks. The value of such classifications based on petrogenetic theories remains debatable.

A subcategory of I-type granites is the peralkaline or A-type granites, in which the critical compositional parameter is the molecular ratio $Na_2O + K_2O/Al_2O_3 > 1$. Such granites tend to be associated with alkaline basalts in within-plate or continental rift environments and they are often rich in volatiles such as F_2 and CO_2.

The trace element contents of granites are considerably more variable than those in basalts, largely because of the effect of small amounts of accessory minerals such as zircon, monazite, allanite, and titanite that can accommodate high concentrations of many trace elements. However, the abundances of critical trace ele-

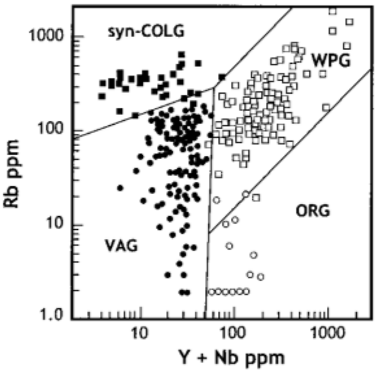

FIGURE 13 Trace element discriminant diagram for granites from contrasting geological environments. VAG, granites from volcanic island arcs (I-type); ORG, granites from ocean ridges; WPG, granites from within-plate environments (A-type); syn-COLG, granites produced in continental collision zones (S-type).

ments can be used to discriminate between granites formed in different geological environments, in the same way that characteristic interelement ratios in basalts can be used to indicate different geological regimes. One example is shown in Fig. 13, which illustrates that granites from oceanic environments have particularly low Rb contents but high Nb+Y, whereas those from volcanic arcs have low values of both. Peralkaline granites from within-plate environments have moderate to high Rb and Nb+Y, whereas granites in continental collision zones have high Rb and generally low Nb+Y.

These differences in trace element contents mirror those of basalts in the same environments, such that within-plate basalts are enriched in Nb and Y, whereas these elements are less abundant in arc or midocean ridge environments. To a greater or lesser extent, these similarities are the result of the processes that are unique to different geologic settings and the controlling effect of critical phases during basalt and granite melt generation.

Volatiles, particularly water, play an important role in crustal melting. Water decreases the melting temperature of crustal rocks, in much the same way it does in the mantle, and it is the dehydration of water-bearing minerals, such as biotite, muscovite, and amphibole, that allows the production of large volumes of granitic melt at moderate temperatures within the crust. Furthermore, magmas rich in SiO_2 are very viscous because the Si–O bonds link to form chains and complex three-dimensional structures within the melts. In general the higher the silica content of a magma, the more highly structured the magma is and the higher its viscosity. Volatiles, particularly water, break the Si–O bonds and so reduce the viscosity, enabling the melt to move through the crust more readily. Thus water has a dual role in granite formation, first by reducing the melting temperature of crustal rocks and, second, by reducing the viscosity and enabling the magma to rise to shallower levels in the crust.

As a final emphasis on the importance of water in the evolution of silicic magmas, it is instructive to explore the effect water has on the melting point of granite (Fig. 14). The ability of a granite to dissolve water increases as pressure increases, thereby reducing its melting point considerably. However, hydrous minerals are stable within the crust to higher temperatures than the water-saturated granite solidus, and if the temperature is increased and the hydrous mineral breaks down, the ensuing release of water will induce melting. The water-bearing granitic magma produced by this reaction can then rise to a shallower depth (lower pressure) within the crust, as shown by the downward pointing arrow on Fig. 14. However, it can only rise as far as the water-saturated liquidus curve because at pressures below this, even silicic magmas saturated with water solidify. This is the primary reason why most silicic magmas stall at depth and solidify as granites rather than reaching the surface to erupt as rhyolite.

During solidification of granite magma, the volatiles are released from the magma in the form of a high-temperature fluid. This fluid is highly reactive and mobile and transports elements that do not easily fit into the feldspar-rich granite in the rocks surrounding the

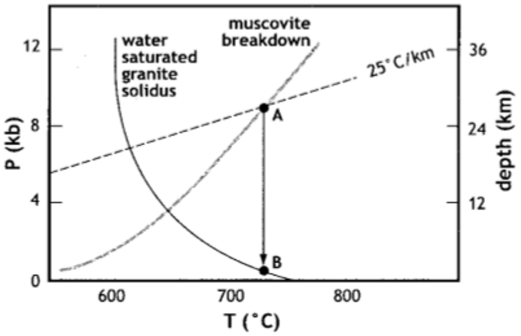

FIGURE 14 A graph of pressure against temperature showing the water-saturated solidus of granite, that is, the temperature at which granite melts in the presence of excess water. Water released by the breakdown of a water-bearing mineral, such as mica or amphibole, induces melting at point A. This melt rises along the line A–B until it intersects the water-saturated solidus at B, at which point the granite solidifies and moves no further.

granite. Thus granites are commonly associated with economic deposits of metal-rich minerals and the differences in the volatile phases associated with different types of granites leads to variations in the style of mineralization and their economic importance. For example, metaluminous granites, such as those in the Andes, are often characterized by Cu-Mo mineralization in the well-known "copper porphyry" association. Peraluminous granites, as for example in the Cornubian batholith of southwest England, have a range of mineralization that includes Sn and W-greisens, tourmaline (boron) mineralization, and veins of Pb and Zn sulfides. This variety in part reflects the heterogeneous crustal source regions of peraluminous granites. Finally, peralkaline granites often include rare metal pegmatites, rich in Nb, Ta, P, Cs, the rare Earth elements, and Y.

In summary, silicic magmas are produced by partial melting in the crust and the details of their compositions are controlled by the nature of their source regions (i.e., igneous or sedimentary). Their production, mobility, and final crystallization are controlled by volatiles, particularly water, and on those occasions when they do reach the surface they produce the most violent volcanic eruptions. If, however, they freeze at depth they are responsible for many of our important economic mineral deposits.

V. IGNEOUS ROCKS AND RADIOGENIC ISOTOPES

One of the major goals of terrestrial geochemistry is to determine how and when the Earth differentiated into the core, the mantle, and the crust. Such problems require information on the age of the crust and the complementary residual portions in the upper mantle, and the continuing fluxes of elements between the different reservoirs in the crust and the mantle. To determine *when* chemical changes took place, it is necessary to use *radiogenic isotopes*, that is, those produced by the decay of long-lived radioactive parent isotopes. Their increasingly routine application since the 1960s has revolutionized many areas of the Earth sciences. They are also widely used as tracers for the different materials that may have contributed to the generation of different magmas, and their application has revealed the hybrid nature of many of the igneous rock types that occur at the Earth's surface.

Isotope abundances are extremely difficult to measure, and so radiogenic isotopes are presented normalized to a stable isotope the abundance of which is not changed by the processes of radioactive decay. The most widely used isotopes are those of strontium, among which ^{87}Sr is generated by radioactive decay from ^{87}Rb with a half-life of 4.88×10^{10} yr. A measured ^{87}Sr/^{86}Sr ratio then depends on the ^{87}Rb/^{86}Sr ratio (and hence the Rb/Sr ratio) of the sample, the time since the ^{87}Rb/^{86}Sr ratio was last changed and the ^{87}Sr/^{86}Sr ratio at the time of that change. The ages that are determined by such systems are the time since the last change in ratio of the parent to the daughter element, in this case Rb/Sr, and so it is important to have established independently just what geologic processes were responsible for element fractionation. Similarly the isotope ratio of Nd, ^{143}Nd/^{144}Nd, depends on the Sm/Nd (parent/daughter) ratio of the rock. However, because in general Sm is less incompatible during melting than Nd, but Rb is more incompatible than Sr, rocks with low ^{87}Sr /^{86}Sr tend to have high ^{143}Nd/^{144}Nd and vice versa.

Figure 15 summarizes variations in ^{87}Sr/^{86}Sr and ^{143}Nd/^{144}Nd ratios in MORB and OIB and reveals the differences between these two types of basaltic magma. The lines at ^{87}Sr/^{86}Sr = 0.705 and ^{143}Nd/^{144}Nd = 0.51264 represent estimates of the composition of the

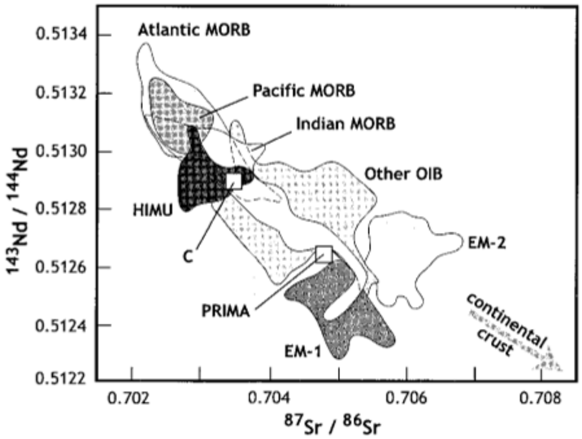

FIGURE 15 Nd-Sr isotope diagram, showing fields for MORB and different groups of OIB. PRIMA, an abbreviation for primitive mantle, and C are different estimates of the composition of the deep mantle. PRIMA is based on the composition of meteorites, whereas C is derived from the inferred composition of mantle plumes. Abbreviations HIMU, EM1, EM2 denote those OIB with particular isotopic characteristics. They are thought to represent distinct components within the mantle and there is much heated debate concerning their origins.

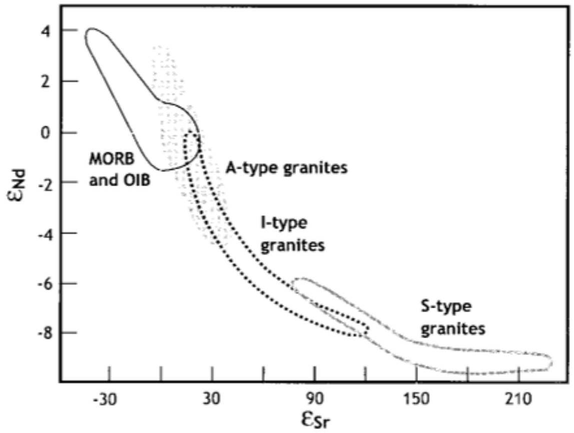

FIGURE 16 Nd-Sr isotope diagram for I-, S-, and A-type granites from southeastern Australia. Isotope ratios are expressed as ε units, the difference between the isotope ratio of the granite and that for the bulk Earth composition at the time of granite formation, in parts per 10,000.

bulk Earth. In Fig. 16 similar isotope data for granites from southern Australia fall in a different part of the diagram that is complementary to MORB and bulk Earth and many granites from other continents have isotopic compositions similar to those shown here. The isotope ratios are corrected to the time of emplacement and are expressed as differences from the bulk Earth value in parts per 10,000 (ε unit). Thus they are a reflection of the composition of the source region of the parent magma. The differences in isotope ratio suggest that the mantle source of MORB has high ^{143}Nd/^{144}Nd and low ^{87}Sr/^{86}Sr ratios, which reflect the high Sm/Nd and low Rb/Sr ratios of their source regions relative to these ratios in the bulk Earth. By contrast, the crustal source regions of S-type granites have complementary isotopic and, hence, trace element characteristics to the mantle source of MORB and OIB that is, higher Rb/Sr and lower Sm/Nd ratios than the bulk earth. Such observations have led to models of crust generation and evolution as a result of the progressive depletion of the convecting upper mantle by the extraction of basaltic magmas throughout geologic time.

Radiogenic isotope data from OIB generally lie between MORB and bulk Earth (sometimes denoted by the acronym PRIMA) and have been classified into a number of groups (labeled EM1, EM2, HIMU etc., on Fig. 15). The origins of these different isotope signatures remain speculative although models involving recycling of sediments and oceanic crust via subduction are popular, linking mantle composition with the plate tectonic cycle and current models of mantle convection. However, the generation and migration of mafic melts within the mantle can lead to the fractionation of parent/daughter trace element ratios, which, with time, can produce anomalous isotope ratios. The possibility remains that isotope heterogeneity may be generated entirely within the mantle as a result of magmatic processes.

Notable exceptions to the general rules on the trace element and isotope compositions of basalts and granites are basalts from some CFB provinces and continental subduction zones. Many continental flood basalts that have incompatible element abundances and ratios similar to OIB have Nd and Sr isotope ratios that are also similar to those found in OIB and other mantle plume-related basalts. However, those CFB with anomalous incompatible element abundances and ratios, as discussed earlier, also have high ^{87}Sr/^{86}Sr and low ^{143}Nd/^{144}Nd, plotting in the same region of the isotope diagram as granites and the continental crust. These deviations from the composition of the convecting mantle have been attributed to the effects of crustal contamination, but in many cases mass balance calculations show that addition of crustal material to a typical plume basalt cannot reproduce critical aspects of the CFB composition. The alternative proposal is that the compositions of these basalts in part reflect that of their mantle source regions, which may be located within the mantle lithosphere.

The other location in which basalts may take on the isotopic characteristics of crustal rocks is above subduction zones. Once again the lithosphere (either crust or mantle) may play a role where a plate is being subducted beneath a continent (e.g., the Andes). Elsewhere, where the overlying crust is more youthful, such as in the Philippines, or even oceanic, high ^{87}Sr/^{86}Sr and low ^{143}Nd/^{144}Nd ratios cannot be derived from the mantle. Rather they indicate a contribution from subducted sedimentary material, itself derived from ancient continents. Such a situation is apparent in parts of the Lesser Antilles where sediment derived from the South American crust, an area dominated by ancient rocks, is being recycled into the mantle by the subducting Atlantic plate (Fig. 17). In this case, isotope ratios can be used to constrain the amount of sediment in the mantle source region of the erupted basalts and hence the amount of sediment being recycled back into the mantle. In general, the amount of sediment required to give arc basalts their distinctive characteristics is very small ($<5\%$), implying that much of the material being subducted is recycled back into the mantle.

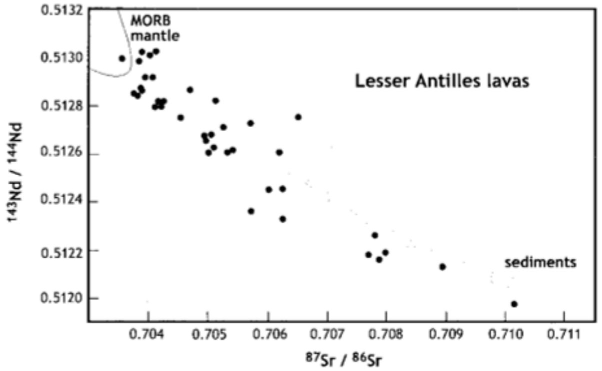

FIGURE 17 Nd-Sr isotope diagram for basalts and andesites from the Lesser Antilles island arc in the Caribbean. Many of the analyses plot close to those of MORB (see Fig. 15), whereas others define a trend toward lower ^{143}Nd/^{144}Nd and higher ^{87}Sr/^{86}Sr. This is a particularly good example of mixing subducted crust into the source of arc magmas, displacing their Nd and Sr isotope composition toward that of sediment derived from the continents.

In Fig. 16, the isotope ratios of granites appear to vary systematically with granite type. Thus peraluminous, S-type granites have low εNd values and high ^{87}Sr/^{86}Sr ratios, reflecting their crustal source regions as discussed earlier. Peralkaline granites tend to plot closer to mantle-derived rocks, supporting the notion that they are derived from mafic material in the deep crust, whereas the intermediate position of metaluminous, I-type granites reflects the complex interplay between mantle and crustal source regions in their evolution.

VI. CRUSTAL EVOLUTION

The continental crust is dominated by igneous rocks and their metamorphic equivalents and it is clear that magmatism has played an important role in the evolution of the crust over the 4.6-Ga history of the Earth. The bulk composition of the present-day continental crust is andesitic (dioritic), and its low density makes it difficult to recycle it back into the mantle via subduction. Thus the continents survive on the surface of the Earth and record the effects of geologic processes that have affected them over the past 3.9 Ga. The generation of the continental crust is therefore considered to be the result of melting in the mantle and a largely irreversible process. Such a notion is supported by the complementary nature of radiogenic isotopes in the crust and the convecting mantle and the overall abundances of trace elements in the continental crust (Fig. 18). These are, with a few exceptions, similar to those in OIB, which are, in essence, small melt fractions of the upper mantle.

One of the exceptions is the element Nb and the continental crust is thought to be characterized by a negative Nb anomaly, very similar to those seen in island arc magmas. Thus a popular model for the evolution of the continental crust is as a result of subduction-related magmatism throughout Earth history. However, while the estimated composition of the continental crust is andesitic, melts of the mantle are generally basaltic and the present-day flux of material from the mantle to the crust, whether at destructive plate margins or in intraplate settings, is basaltic. Moreover, basalt has been the dominant mantle-derived magma throughout much of the history of the Earth. Andesitic (dioritic) magma can only be produced by fractionational crystallization of basaltic magma (or possibly partial melting of basalts) within the crust, but because any crystals separated during fractional crystallisation would remain in the crust, the latter would retain a bulk composition similar to basalt. We are therefore left with the apparent contradiction that while the crust has the trace element characteristics of a melt derived from the mantle, its bulk composition is that of a magma that has experienced fractional crystallization. This contradiction remains as

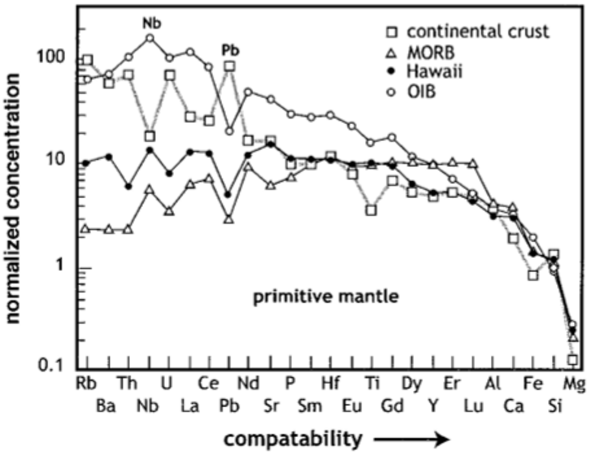

FIGURE 18 Mantle-normalized trace and selected major element abundances in MORB, OIB (Hawaii and Tristan da Cunha), and the average continental crust. Note the overall similarity between the element abundances of OIB and the continental crust and the anomalous behavior of elements such as Nb, Ti (depleted in the crust), and Pb (enriched in the crust).

yet unresolved. It may be that our estimates of the composition of the bulk crust are incorrect and that it is closer to basalt than andesite. Alternatively, crustal generation may not be a one-way process and may involve transport of mafic material from the crust back into the mantle.

In summary, the outer portions of the Earth differentiated into the continental crust, the oceanic crust, and enriched and depleted portions of the mantle primarily by the processes of melt generation, melt extraction, and the movement of those melts. The mantle source regions for MORB are depleted in incompatible elements relative to estimates for the bulk Earth, and the compositions of the MORB-type mantle and the continental crust are thought to be complementary such that the depletion of the MORB-type mantle is attributed to the formation of the continental crust throughout the history of the earth. The bulk composition of the continental crust represents, on average, just a few percent of partial melting of the upper mantle, but the details of the processes by which the continental crust was formed and their timing remain the subject of lively debate.

SEE ALSO THE FOLLOWING ARTICLES

Melting the Magma • Origin of Magmas • Physical Properties of Magmas • Seamounts and Island Building • Volcaniclastic Sedimentation around Island Arcs

FURTHER READING

Wilson, M. (1989). "Igneous petrogenesis," Chapman Hall.

Clarke, D. B. (1992) "Granitoid Rocks," Topics in Earth Sciences, Vol. 7. Chapman Hall, London.

Cox, K. G., Bell, J. D., and Pankhurst, R. J. (1989). "The Interpretation of Igneous Rocks." Allen & Unwin.

Hofmann, A. W. (1997). Mantle geochemistry: The message from oceanic volcanism (review article). *Nature* **385,** 219–229.

McBirney, A. R. (1992). "Igneous Petrology." Jones and Bartlett.

Rollinson, H. R., "Geochemical Data: Evaluation, Presentation, Interpretation." Longman.

This Page Intentionally Left Blank

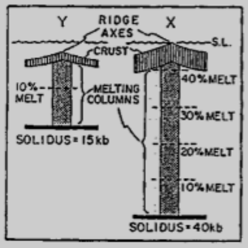

ORIGIN OF MAGMAS

TIMOTHY L. GROVE
Massachusetts Institute of Technology

I. Introduction
II. Magmatic Processes as Controls on the Composition of the Crust and Deep Interior
III. Compositional Variations in Magmas
IV. Magma Generation Processes beneath Midocean Ridges
V. Fractionation, Assimilation, and Mixing in Oceanic Environments
VI. Magma Generation Processes in Subduction Zones
VII. Fractionation, Assimilation, and Mixing in Subduction Zone Environments

GLOSSARY

adiabatic The thermodynamic process of expanding or compressing a substance without allowing it to exchange heat with its surroundings.

amphibole Rock-forming silicate mineral that contains Fe, Mg, Al, Ca, Na, Al, Ti, and ~1.5 wt% H_2O.

assimilation The incorporation of material originally present in surrounding wallrock into a magma. If the wallrock is incorporated into the liquid, thermal energy is required to heat and melt the solid rock.

asthenosphere The part of the upper mantle beneath the lithosphere that deforms by plastic flow as a result of high temperatures at depth in the Earth.

clinopyroxene (cpx) Rock-forming silicate mineral with the general formula $Ca(Mg,Fe)Si_2O_6$. In mantle peridotite most of the Na_2O, TiO_2, and Al_2O_3 in the rock is contained in this mineral.

crust The part of the Earth lying above the Mohorovicic discontinuity. Continental crust varies from 30 to 80 km in thickness and oceanic crust ranges from 6 to 20 km in thickness.

fractional crystallization Crystallization of minerals from a silicate liquid (magma) during cooling causes the liquid to change composition. The possible compositional variations that can occur through this process are governed by thermodynamic state functions for the crystals and melt.

latent heat of melting or latent heat of crystallization Heat of reaction required to accomplish the phase change from solid to liquid form.

liquidus Temperature above which a magma is completely liquid, or the temperature below which a melt begins to crystallize.

liquidus volume The range of composition for a liquid solution over which a particular solid is the liquidus phase.

lithosphere The portion of the earth's crust and upper mantle above the asthenosphere that is rigid and deforms by brittle fracture as a result of lower temperature.

magma Molten rock that consists of up to three components: liquid silicate melt, suspended crystalline solids, and gas bubbles. Lavas are magmas that solidify at the surface to crystalline or glassy igneous rocks that are referred to as volcanic rocks. When magma cools in the interior of the earth, the resulting igneous rocks are referred to as intrusive or plutonic rocks.

Copyright © 2000 by Academic Press
All rights of reproduction in any form reserved.

magma mixing The mixing of two magmas to form a hybrid. Such a process presents the immediate problems of how the two magmas were produced and what caused them to remain separate and then mix.

mantle Portion of the Earth's interior lying below the Mohorovicic discontinuity and above the outer core. Divided into an upper mantle that extends to a depth of ~400 km, a transition zone that extends to ~670 km, and a lower mantle that extends to the core mantle boundary at ~2900 km.

melt reaction coefficient The proportion of a crystalline phase that is reacted during melting. Positive reaction coefficients indicate that the solid is consumed during melting. Negative reaction coefficients indicate that the solid is produced along with the melt phase.

olivine (ol) Rock-forming silicate mineral in the crust and mantle with the composition $(Mg,Fe)_2SiO_4$.

orthopyroxene (opx) Rock-forming silicate mineral in the crust and mantle with the general composition $(Mg,Fe)SiO_3$.

peridotite A crystalline rock consisting dominantly of olivine and pyroxenes. The principal rock type present in the Earth's upper mantle.

plagioclase Rock-forming silicate of crust with the composition $(Ca_{1-x},Na_x)Al_{2-x}Si_{2+x}O_8$.

primary magma A liquid produced by partial melting of a source region and unmodified by any postsegregation process.

solidus Temperature below which a magma is completely crystallized, or temperature at which a solid begins to melt.

spinel Rock-forming oxide mineral. In the mantle the composition is $(Mg,Fe)(Al,Cr)_2O_4$. In the crust the composition is $Fe_2TiO_4 - Fe_3O_4$.

I. INTRODUCTION

The chapter describes the processes that lead to the compositional diversity in magmas in active volcanic regions. The chapter focuses on midocean ridge and subduction zone volcanoes—the two dominant melt production regimes operating on the modern Earth (see chapter on Plate Tectonics and Volcanism). The chapter introduces the methods that are used to determine the conditions of and controls on compositional diversity in magmas. The influence of partial melting on magma generation is discussed for active midocean ridge spreading centers. The next section describes the processes that control compositional diversity after a melt has migrated from its source region into the oceanic lithosphere. For each of these processes, the physical and chemical controls are described. A similar approach is used to discuss magma generation and magma modification processes in subduction zone environments.

II. MAGMATIC PROCESSES AS CONTROLS ON THE COMPOSITION OF THE CRUST AND DEEP INTERIOR

A. Magmatic Processes throughout Geologic Time

The Earth is a dynamic and active planet. It formed from crystalline solids that had condensed from the solar nebula 4.5 billion years ago. These solids were swept up by gravitational attraction to form the Earth and the inner terrestrial planets. During this process magmas were created by impacting planetesimals. Some of the impactors may have been as large as Mars, and their collision with the early Earth supplied enormous amounts of energy. These early giant impacts led to heating and melting on a large scale. Giant magma oceans covered the surface of the early Earth, and the early Earth may have melted entirely. The most obvious consequence of these early processes is the presence of a metal-rich core. Evidence of the nature, timing, and extent of the early magma ocean phase has been largely erased from the solid silicate portion of the Earth's interior by continued magmatic activity on Earth. There exists little direct evidence of when this phase of Earth history came to an end. The magmatic processes that occur today have been operating for a significant part of the Earth's history. The oldest rocks found on Earth, the 4.0-billion-year-old Acasta gneisses in the Northwest Territories in Canada, record magmatic processes much like the ones that take place in subduction zone and convergent margins today.

The most active sites of melt generation on the Earth occur at midocean ridges, and the products of this volcanism form oceanic crust. Oceanic crust, overlying sediments, and other volcanic rocks that occur in the oceans are recycled back into the mantle on time scale of 0.1 billion years or less and are blended back into the solid interior. However, ancient ocean floor crust is sometimes preserved in the Earth's continental crust, and these rock associations are called *ophiolites.* Examples are found in Cyprus and Oman. Thus, the geologic record contains evidence that the processes that are occurring in active volcanic centers today have been taking place for a large portion of Earth history.

B. Tectonic Controls on Magma Generation

Magma generation and tectonic setting are closely linked and this topic is discussed in the Plate Tectonics and Volcanism chapter. The current global annual rate of magma production of volcanic and plutonic igneous rocks is about 30 km^3/yr (Crisp, 1984). Magma generation at midocean ridges (divergent margins) accounts for 75% of the volume, and 20% occurs in subduction zone environments (convergent margins). The remaining 5% occurs as intraplate magmatic activity within either oceanic or continental plates (intraplate volcanism). Magma generation in these environments probably occurs through the same mechanism that leads to midocean ridge magmatism. The following discussion focuses on the midocean ridge and subduction zone environments because they dominate the global magma production rate. Melting processes in these two environments lead to a broad spectrum of compositional variation in magmatic products.

At midocean ridges the production of magma is dominated by passive convective upwelling of mantle asthenosphere. As the solid mantle ascends, its temperature follows that of an adiabat, and the mantle peridotite will begin to melt at a depth where the peridotite encounters its solidus (see chapter titled Melting the Mantle). The magmas produced by this melting process are basaltic in composition (see chapter titled Composition of Magmas). The primary controls on melt generation are the temperature of the upwelling mantle and mantle composition. The control of temperature on melting is illustrated in Fig. 1 for two different adiabatic paths. Magma is produced by cooling the solid mantle after it crosses its solidus, and using the heat derived from cooling to melt solid rock. Melting continues until the cold, shallow oceanic lithosphere is encountered. At this depth magmas may cool below their liquidus and undergo fractional crystallization.

In subduction zones (convergent margins), magma generation is controlled by a process that involves the interaction of fluid released by the subducted slab with overlying mantle. Fluid that has been transported into the mantle by the subducted slab is released when hydrous minerals decompose and release their H_2O. This H_2O dissolves some of the silicate components in the subducted slab and the resulting fluid ascends into hotter overlying mantle (Fig. 2). Mantle melting occurs when H_2O-rich fluid reaches a depth that exceeds the peridotite + H_2O solidus. As shown in Fig. 3, the addition of H_2O has a dramatic temperature-lowering effect on the mantle solidus. Magma production is controlled by the temperature distribution with depth above the subducted slab and by the flux of H_2O. Magmas produced through this process are hydrous (water bearing). The amount of water that is incorporated into the melt depends on pressure and temperature. The solubility of H_2O in magma is negligible at surface pressures, but increases dramatically with increasing pressure. At a pressure of 3.0 GPa (1 GPa = 10 kbar) or a depth of 90 km in the mantle about 20 wt% of the magma is H_2O. Also present in the subduction environment are magmas produced by adiabatic decompression. Deep

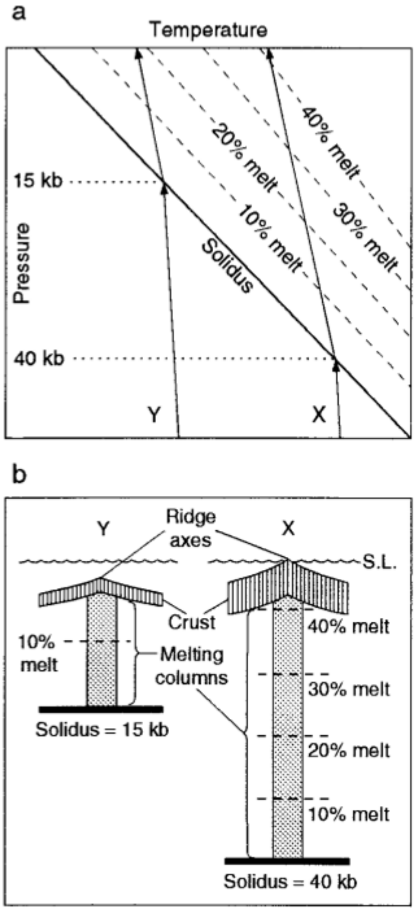

FIGURE 1 (A) Schematic pressure–temperature diagram for melting of mantle peridotite. Path X represents a hotter convective upwelling that crosses the solidus at greater depth and higher temperature and undergoes a greater extent of melting. Path Y crosses the solidus at a lower pressure and temperature and undergoes a lesser extent of melting. (B) Cross section of the oceanic crust and mantle corresponding to melting histories shown by paths X and Y. Path X is similar to the melting model shown as squares in Fig. 5, but differs in starting at a greater depth. Path Y is similar to the melting model shown as triangles. [Klein, E. M. and Langmuir, C. H. (1989) Local versus global variations in ocean ridge basalt composition. *J. Geophys. Res.* **94,** 4241–4252.]

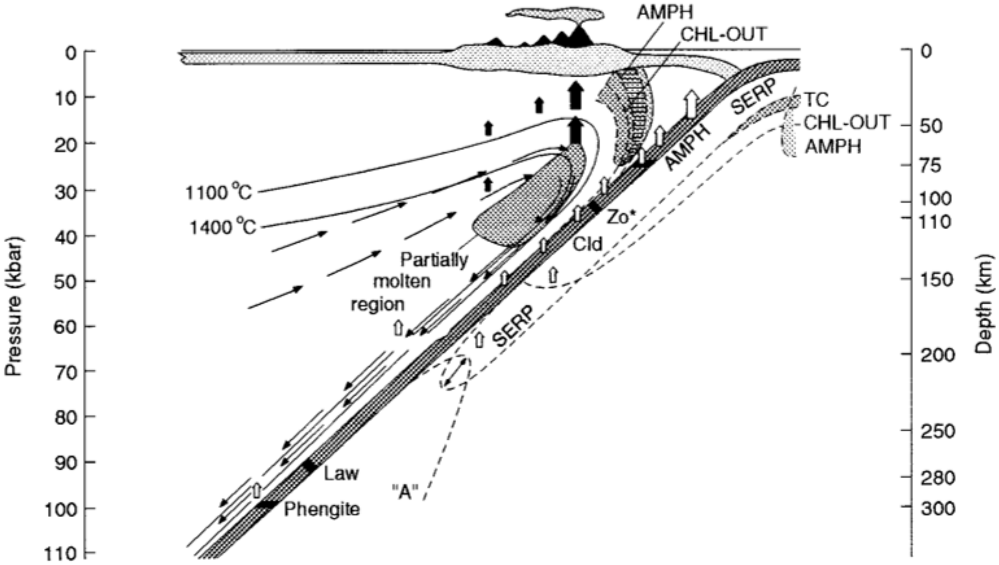

FIGURE 2 Model cross section of a convergent margin showing some of the processes that lead to the generation of subduction zone magmas. Dehydration of minerals in the subducted peridotite and ocean crust provide H_2O to the overlying mantle wedge over a broad range of depths (indicated by open arrows). Isotherms show the temperature distribution in the wedge overlying the slab, and the inferred partly molten region. Hydrous minerals are indicated by abbreviations: AMPH, amphibole; SERP, serpentine; TC, talc; CHL, chlorite; Cld, chloritoid; zo = zoisite; law, lawsonite; "A," phase A. Dashed lines show limits of stability in the descending slab. [Reprinted from Schmidt, M. X. and Poli, S. (1998) Experimentally based water budgets for dehydrating slabs and consequences for arc magma generation. *Earth Planetary Sci. Lett.* **163,** 361–379, with permission from Elsevier Science.]

mantle ascends as it approaches the slab-wedge corner and melts during its ascent to produce anhydrous magmas similar to those found in ocean floor environments. Both the hydrous and decompression-produced magmas ascend into the overlying oceanic or continental crust, where they cool and undergo fractional crystallization. The magmas heat, melt, and interact chemically with shallow crust. These processes give rise to a large variation in the chemical composition of convergent margin magmas. The resulting magmas range from basaltic to andesitic to rhyolitic in composition (see Composition of Magmas chapter).

III. COMPOSITIONAL VARIATIONS IN MAGMAS

A. Representing Magma Compositional Variation

The emphasis of this chapter is on the origin of variations in major element composition of magmas. Magmas show a wide range in major element composition, which reflects the conditions under which the magma was generated in the source and/or modified after melt generation. A common way of illustrating compositional variations is to plot covariations of the oxides of two elements (see Fig. 5 in the Composition of Magmas chapter). Lavas that are spatially and or temporally associated are often chosen. The assumption is made that the variations in composition represent a process (or processes) that affected the chosen lavas and that each was erupted at a different stage of the process. This may or may not be a valid assumption and the examples shown later in this chapter illustrate ways in which spatially associated lavas can be used to infer the operations of magmatic processes.

Magmas produced by melting of a mantle peridotite source will have chemical characteristics that allow their identification. A very useful chemical index is the Mg# of the magma. This value is the molar proportion of MgO relative to FeO in the magma:

$$\text{Mg\#} = (\text{wt\% MgO}/40.311)/[(\text{wt\% MgO}/40.311) + (\text{wt\% FeO}/71.846)].$$

The melt of mantle peridotite will be in equilibrium with the minerals in the source region. Exchange reactions govern the partitioning of FeO and MgO between the crystals in the source and the melt. For olivine (ol), the exchange equilibrium is:

$$\text{FeSi}_{0.5}\text{O}_2^{\text{ol}} + \text{MgO}^{\text{melt}} = \text{MgSi}_{0.5}\text{O}_2^{\text{ol}} + \text{FeO}^{\text{melt}}. \quad (1)$$

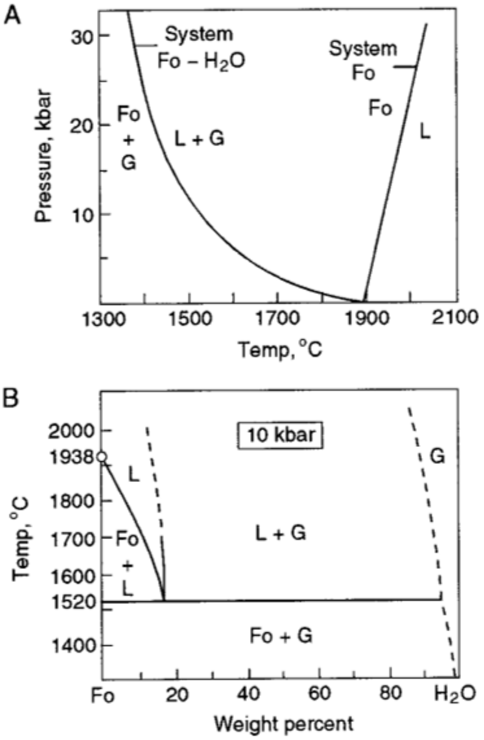

FIGURE 3 (A) Pressure–temperature diagram showing the melting of forsterite (Mg_2SiO_4) dry and with H_2O present. (B) Temperature composition diagram at 10 kbar showing the melting relations in the system forsterite–H_2O. Melting of pure forsterite in the absence of H_2O occurs at 1938°C at this pressure. G = gas, L = liquid and Fo = forsterite. [Morse, S. A. (1980) Basalts and Phase Diagrams: An introduction to the quantitative use of phase diagrams in igneous petrology. Figs. 19.1 and 19.2, p. 493. Copyright notice of Springer-Verlag.]

The equilibrium constant for this reaction is called $K_D^{\text{Fe-Mg}}$ and is given by the expression:

$$K_D^{\text{Fe-Mg}} = [(1 - \text{Mg\#}^{\text{ol}})^*(\text{Mg\#}^{\text{melt}})]/[(\text{Mg\#}^{\text{ol}})^*(1 - \text{Mg\#}^{\text{melt}})]$$

and

$$\begin{aligned} \text{Mg\#}^{\text{melt}} &= K_D^{\text{Fe-Mg}}/\{K_D^{\text{Fe-Mg}} + [(1 - \text{Mg\#}^{\text{ol}})/\text{Mg\#}^{\text{ol}})]\} \\ \ln K_D &= -\Delta G_{\text{reaction}}/\text{RT}. \end{aligned} \tag{2}$$

Over the temperature range for magma generation in the Earth's upper mantle the value of $\Delta G_{\text{reaction}}/RT$ is nearly constant and as a result the value of $K_D^{\text{Fe-Mg}}$ for olivine and coexisting melt is 0.30. A representative value for the Mg# of olivine in mantle peridotite is 0.90. Equation (2) predicts that the Mg# of a melt in equilibrium with that of olivine is 0.73. Magmas produced by melting a mantle mineral assemblage are called *primary magmas*, and the Mg# test is one way of identifying such magmas. A lower value of Mg# indicates that the magma has undergone modification by processes of fractional crystallization, assimilation, or magma mixing. If crystals are present in the magma and gather together and concentrate preferentially in one part, the Mg# can be increased above the correct value for the magma. Magmas with the highest Mg# are sought because they are likely to contain information on melt generation processes.

B. Methods for Determining the Controls on Magma Composition

Earth scientists have developed several techniques for understanding and interpreting the compositional variation observed in magmas. The most common approach is to reproduce the conditions of pressure and temperature relevant to the melting process and to determine directly the chemical reactions between crystals and liquids. Materials with chemical composition similar to natural magmas and the rocks that melt to produce them have been subjected to laboratory-controlled conditions of melting for time periods sufficient to achieve chemical equilibrium. These experimental efforts began in the 1900s and continue in the present. The exchange between olivine and melt [reaction (1) given earlier] and a similar exchange reaction for plagioclase-liquid NaSi-CaAl exchange are examples of chemical reactions that have been investigated through experiments. Research on the influence of pressure and on the influence of volatiles (like CO_2 and H_2O) has provided a framework for determining the conditions of magma generation and modification.

Experimental data sets on natural magmas have been used to develop several approaches to determine the melting and crystallization behavior of magmas. The method used by Roeder and Emslie (1970) was to obtain analytical expressions for temperature and melt chemical composition that allowed the description of liquidus volumes for olivine and plagioclase. Ghiorso and Sack (1995) provide a model of chemical mass transfer from liquid to solids by predicting the lowest free-energy state and the compositions of the phases for a given chemical system under a set of temperature and pressure conditions. Longhi (1991) presented a graphical approach that allows one to calculate the melting and crystallization paths followed by magmas. The discussion that follows will draw on a number of these approaches. The interested reader should consult the references cited in this paragraph for discussions of the application of these approaches to prediction of melt composition.

IV. MAGMA GENERATION PROCESSES BENEATH MIDOCEAN RIDGES

Melting in the upper mantle occurs as the result of convective upwelling of mantle asthenosphere that accompanies crustal extension at midocean ridge spreading centers. This melting process is known as *adiabatic decompression melting*. When the mantle ascends beneath a spreading center, it cools slightly as its temperature follows the adiabatic gradient (0.3°/km). At a depth that depends on the temperature of the upwelling mantle (Fig. 1), the solidus of the mantle material is encountered and melting begins. Melting in the mantle involves four crystalline phases: olivine (~50–60 wt% of mantle peridotite), orthopyroxene (opx, ~20–30 wt% of mantle peridotite), clinopyroxene (cpx, ~10–15 wt% of mantle peridotite), and an aluminous phase (garnet or spinel, ~5% of mantle peridotite). Melting occurs in response to the thermal energy that is obtained from the difference between the temperature that would be achieved in the mantle material if it rose along an adiabat and no melting occurred versus the temperature that is achieved if it stays on the solidus of the mantle material. This thermal energy can be imagined to be released when the mantle cools and remains on the solid–melt phase transition. The heat obtained from cooling the mantle is used to supply the latent heat of fusion, and melting continues until a depth is reached at which the temperature of the parcel of mantle is lower than the solidus temperature for the mantle. The latent heat of fusion for mantle peridotite (~130 cal/g), the heat capacity (0.3 cal/g°C), the ambient mantle temperature, and the pressure and compositional dependence of the mantle solidus control the rate of melt production. Thus, if the mantle could rise 100°C above the solid–melt phase boundary, cooling it to that boundary would supply 33 cal/g of thermal energy that could be used to melt the mantle by 25%.

If the melt stays with its solid residue during ascent and is only extracted at the shallowest depth, the melting process is called *batch melting*. If the melt is constantly extracted from the residue and rises without reacting with the rock that it passes through, the melting is referred to as *fractional melting*. If the melt ascends through the solid mantle and constantly reacts with its surroundings, the melting mechanism is called *equilibrium porous flow*. Whether or not the melt remains with its solid residue as the mantle rises through the melting regime influences the volume and composition of the melts and the residues of the melting process. If the melt stays with the solid as the solid rises and separates at the top of the melting regime, then the bulk composition of the melting system (residue + melt) is constant, and the pressure signature of the melt produced will be equivalent to the pressure of segregation (the pressure at the top of the melting regime). As we will show in Section VI, this may be the case for melting in subduction zones. In the batch melting case, bulk system composition and pressure of melting are effectively constant for the melting process. The volume and composition of magma produced will be a function of the starting composition of the mantle, the pressure of segregation, and the extent of melting achieved, which is a function of temperature.

If melts segregate from the rising mantle in small fractions, as they are produced, then the bulk composition of the melting system changes continuously as melting proceeds. Moreover, as long as the fractions of melt do not equilibrate with the overlying mantle as they rise, the pressure signature associated with the magma formed by aggregating these small fractions of melt at some depth shallower than the melting regime will reflect the range of pressures over which each of the small melt fractions was produced. This melting process is called *polybaric near-fractional melting*. The volume and composition of the aggregate magma composition that results from this process will depend on temperature, the range of pressures over which the melting occurred, and the changing mantle residue composition. This process is thought to be the mechanism by which melts are produced beneath midocean ridges.

In this view, the magma emplaced into the spreading center is regarded as an aggregate of melts collected from a range of extents and depths of melting and segregation. Thus, this magma consists of a blend of magmas, each produced by relatively small extents of melting (0.1–5%) and segregated from a range of pressures, referred to as an *aggregate primary magma*.

A. Crystal–Melt Reactions That Control Mantle Melting

The compositions of both the residual solids and the liquid respond to the effects of variations in pressure and temperature according to their thermodynamic state functions, which dictate the compositions that are stable at a given set of pressure and temperature conditions for a given bulk composition. In the case of natural peridotite melting processes, a relatively complete characterization exists for the changes in melt and solid compositions over the pressure (depth) range of melting that generates midocean ridge basalts. Most of the melting occurs in the upper part of the upper mantle at depths less than 75 km. The information on solid and melt compositional variations can be combined and shown as the mantle melt reaction. Figure 4 shows the variations in melt reaction coefficients for the major minerals of mantle peridotite. At the pressure of Fig. 4, the stable aluminous phase in peridotite is spinel.

The melt-producing reaction is incongruent, which means that one or more crystalline phases is produced along with melt as melting proceeds. Minerals with positive reaction coefficients in Fig. 4 are consumed by melting, and minerals with negative reaction coefficients are produced along with melt. As pressure increases, the melting reaction changes continuously in response to changes in the bulk composition of the liquid and solids. Above a pressure of about 16 kbar (1.6 GPa), opx appears on the product (melt) side of the reaction. Thus, a near-fractional melting process at pressures greater than 16 kbar will enrich the residue in opx while depleting it in the constituents that are in the phases that are on the reactant side of the equation (cpx, olivine, and spinel).

When examining melt reactions like the one shown in Fig. 4, recall that the bulk compositions of the reactants and products are continuously changing in response to variations in pressure and temperature. It is this systematic change that leads to a change in the melting reaction coefficients.

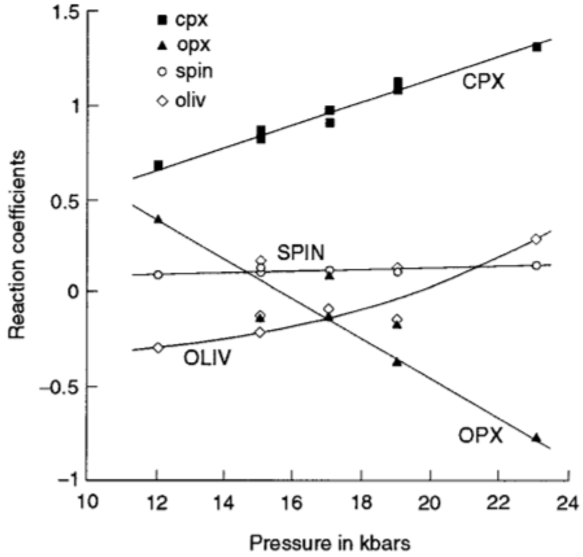

FIGURE 4 Variation in the reaction coefficients for mantle peridotite melting over the pressure range of 12–24 kbar (1.2–2.4 GPa). A reaction coefficient is positive, indicating that the mineral is consumed to produce melt. A negative reaction coefficient indicates that the mineral is produced along with melt. [Kinzler, R. J. and Grove, T. L. (1999) Origin of depleted cratonic harzburgite by deep fractional melt extraction and shallow olivine cumulate infusion. Proc. 7th Intl. Kimberlite Conf. (in press).]

An idealized melting column model of the sort illustrated in Fig. 1 can be used to conceptualize the melting process and explore the effects of melting that begins at different depths and temperatures. Melt is produced in small increments (1%), and then 90% of the melt produced is removed at each step. This variant of near-fractional melting is calculated over a range of pressures to simulate polybaric near-fractional melting. The increment of melting that occurs in mantle peridotite per kilobar of adiabatic rise above the depth of mantle solidus intersection is estimated to be 1%. At some initial pressure, during the adiabatic ascent of mantle peridotite, its temperature reaches that of the mantle solidus, and melting begins. The depleted parcel of mantle, retaining a small amount of melt, rises another kilobar and melts another 1%. Ninety percent of this batch is removed and accumulated with the previous batch, etc. Melts are accumulated and mixed to become an aggregate of primary melts sampled from a range of pressures. Between each step of melt production, the composition and mineral mode of the residual mantle parcel are recalculated using the melt reaction illustrated in Fig. 4. The amount of melt generated at any pressure within the melting column is always the same, and the average pressure of melting is the mean pressure of the melting column.

Compositions of melt increments (solid symbols) are shown for two models on Na_2O versus FeO and Na_2O versus SiO_2 diagrams (Fig. 5). One model corresponds to a hot mantle adiabat where melting begins deeper (25 kbar or 75 km) and at higher temperature and the second represents melting on a cooler adiabat (15 kbar or 45 km). The curvature of each of the arrays of melt increments (Fig. 5) arises from the combined effects of decreasing pressure and increasing depleted character of the mantle source. The Na_2O variation is a function solely of extent of depletion of the source peridotite. As a parcel of peridotite rises in the mantle and melt increments are produced and stripped away, the residual solid becomes increasingly depleted in Na_2O. The FeO variation, however, is a function of both the increased extent of depletion and the associated decrease in pressure during the polybaric, near-fractional melting process.

The aggregate primary magma from one melting path or column (open symbols, Fig. 5) is the average composition of the individual increments and represents an equal sampling and complete mixing of all the increments

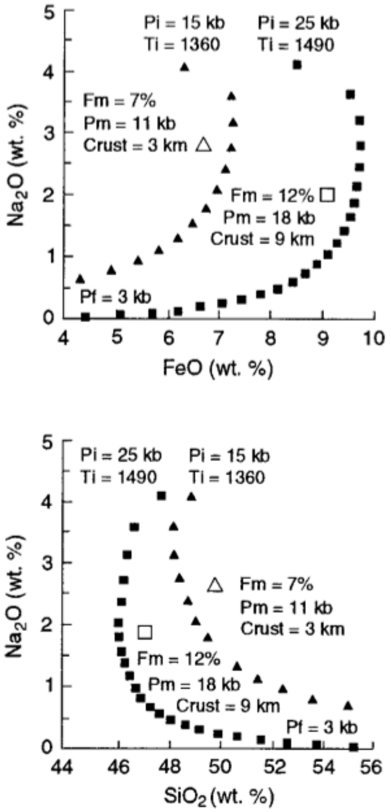

FIGURE 5 Plots of wt% (A) Na_2O versus FeO and (B) Na_2O versus SiO_2 for near-fractional melt increments (solid symbols) and aggregate melts (open symbols). Triangles represent a model where the mantle begins to melt at a shallower depth and cooler temperatures. Squares represent a model where the mantle begins to melt at higher pressures and higher temperatures, and melting extends over a larger depth interval. P_i and T_i indicate pressure and temperature of initial melting and P_f = final pressure of melting. F_m = amount of melting in wt%, and P_m = mean pressure of melting. Crust = thickness of midocean ridge basalt produced from the melting process. (From Kinzler, 1997.)

from that path. In the case where melting begins at a greater depth and extends over a greater depth interval (open square, Fig. 5) the FeO is higher and the Na_2O content is lower. In the example where melting begins at shallower depths (open triangle, Fig. 5) FeO is lower and Na_2O is higher. For both examples in Fig. 5, melting terminates at the same depth due to the intersection of the rising mantle with an assumed lithospheric boundary, above which it is too cool to melt. Because melting is initiated at different depths, however, the total extent of melting achieved from the melting column in each example varies from ~12% in the 25–3 kbar example to ~7% in the 15–3 kbar example. These differences in melting extent lead to differences in the amount of lava that is generated at a spreading center. In the examples shown in Fig. 5, crust varies between 3 and 9 km thick. The observed average thickness of young oceanic crust is ~6 km and the range is from 3 to 8 km.

When the compositions of all midocean ridge basalts are examined (Fig. 6), a negative correlation of FeO and Na_2O is observed. The covariation of these elements in the global data set results from the coupling of increased extent of melting (which decreases Na_2O in primary magmas) and increased pressure of melting (which increases FeO in primary magmas). The low-Na_2O, high-FeO end of the aggregate primary magma array (Fig. 6) is thus from the deepest, hottest melting column, in which the mantle is melted the most. The high-Na_2O, low-FeO end of the array is from the shallowest, coolest melting column, in which the mantle is melted the least. The mantle solidus temperature implied by the one-dimensional melting models (Fig. 1) varies from ~1475°C in the 12% aggregate melt to ~1315°C in the 7% aggregate melt and indicates that there are temperature differences of at least 150°C in the mantle that ascends beneath ocean ridges.

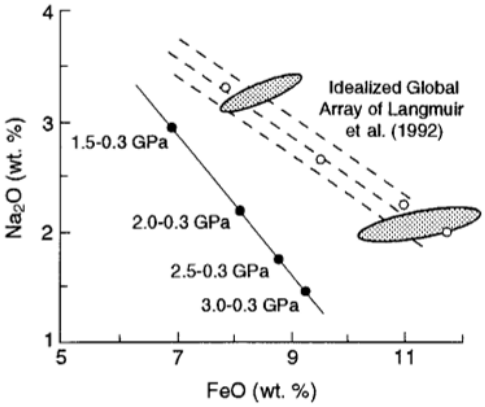

FIGURE 6 Plot of wt% Na_2O versus FeO for a suite of aggregate magmas produced from variable mantle temperature models (solid circles). Pressure range gives the beginning and end of melting for each model. These primary melts have been fractionated down temperature until the melt contains 8 wt% MgO (open circles) and ellipses. Superimposed is a region encompassed by the global data set of Langmuir *et al.* (1992) of regionally averaged ocean ridge basalt compositions (three dashed lines). This global data set has also been corrected to 8 wt% MgO and shows a well-defined inverse correlation between Na_2O and FeO. 10 kbar = 1 GPa. (From Kinzler, 1997.)

V. Fractionation, Assimilation, and Mixing in Oceanic Environments

Very few sampled ocean ridge basalts have compositions that are similar to those of primary magmas. The Mg# [see Eq. (1)] of a midocean ridge basalt (MORB) that would be in equilibrium with the olivine in mantle peridotite would be >0.73. Most ocean floor lavas have Mg# lower than 0.71 and thus are not primary magmas. Therefore, most MORBs exhibit evolved compositions. To use the chemical compositions of sampled MORBs to infer the melting processes beneath midocean ridge spreading centers, the effects of postsegregation magmatic processes must be removed. Postmelt generation processes include any or all of the following: (1) low-pressure crystallization and mixing processes that occur within the oceanic crust, (2) crystallization of primary magmas in the upper mantle, en route to emplacement into the spreading center, and (3) assimilation of mantle or crust by primary magmas.

Earth scientists traditionally view the process of magma modification as one in which a lava composition (or some subset of lava compositions) may be identified as a parent magma. The parent magma is one that has been least affected by melt modification processes and may be closest to a primary magma. Crystallization induced by cooler surroundings modifies the composition of this parent magma to produce derivative magmas. If the derivative magmas are sampled sequentially during a fractional crystallization process by a series of eruptions from the magma reservoir, the resulting suite of compositions records the modification process. If fractional crystallization is the only modification process that operates on a parent magma, the compositional variation of the derivative suite provides a record of the conditions.

As a midocean ridge primary magma encounters cooler overlying mantle lithosphere and crust, it begins to crystallize. As the magma cools olivine and spinel are the first minerals to crystallize. Continued cooling and crystallization involves olivine, plagioclase, and cpx; the crystallization assemblage depends on the pressure (depth) at which cooling occurs. The paths followed by magmas as they experience fractional crystallization provide a signature of the depth of crystallization, because changes in pressure modify the compositions of the phases that crystallize, the temperature of appearance, and the proportions of the minerals in the crystallizing assemblage. Several techniques are available that provide a quantitative description of the crystallization paths for ocean floor basaltic compositions, and these were described earlier in Section II. In the case of ocean floor basalts the composition of the magma is adjusted for the effects of crystallization to a reference value. In Fig. 6, for example, the effects of crystallization have been evaluated for FeO and Na_2O for ocean floor magmas and their compositions have been adjusted to 8 wt% MgO. The two shaded ellipses shown in Fig. 6 are the polybaric, near-fractional aggregate primary magmas from Fig. 5 corrected for fractional crystallization to 8.0 wt% MgO. There is a correspondence between the primary magmas evolved to 8.0 wt% MgO and the global array of ocean floor magmas. The low-FeO, high-Na_2O end corresponds to shallow melting regimes in which the mantle is depleted to a lesser extent, and the high-FeO, low-Na_2O end of the trend corresponds to a deeper melting regime in which the mantle is depleted to a greater extent. The high-FeO, low-Na_2O portion of the global array can be produced by melting at a mean pressure of 15 kbar, to a total extent of ~18 wt%. The low-FeO, high-Na_2O portion of the global array can be produced by melting at a mean pressure of ~8 kbar to a total extent of melting of ~6 wt%.

In addition, there is also a strong correlation between Na_2O and FeO and the water depth above an ocean floor spreading center (Fig. 7). The water depth variations are a response to variations in mantle temperature beneath the ocean ridge depth. Hotter mantle that has undergone a higher extent of melting correlates with the shallow water depths and cooler mantle that has begun melting at lower pressures and temperatures is represented by deep water depth above the spreading center.

Relationships between MgO, FeO, and Na_2O also yield information about the fractional crystallization history of MORBs that can be used to infer the depth of crystallization. The influence of pressure on crystallization is best illustrated using a specific example. Consider a primary magma that is emplaced at shallow levels beneath the spreading center. This primary magma first crystallizes olivine + spinel, followed by olivine + plagioclase. After a total of 33% crystallization at 0.001 kbar the differentiated magma contains 2.71 wt% Na_2O, 8.77 wt% FeO, and 52.4 wt% SiO_2 at 8.0 wt% MgO. Upon emplacement of the same aggregate primary magma at a depth in the upper oceanic mantle equivalent to 4 kbar pressure, it crystallizes olivine + spinel (2%), followed by olivine + plagioclase (16%), followed by olivine + plagioclase + cpx (20%). After a total of 38% crystallization at 4 kbar the differentiated magma contains 2.85 wt% Na_2O, 9.59 wt% FeO, and 51.8 wt% SiO_2 at 8.0 wt% MgO. The higher Na_2O and FeO and lower SiO_2 abundances in the magma fractionated at the higher pressure result from the appearance of cpx in the higher pressure fractionation path. Both Na_2O and FeO are incompatible in the assemblages olivine + plagioclase and olivine + plagioclase + cpx. The crystallization of either assemblage therefore enriches the liquid in Na_2O and FeO. However, the crystallization of olivine + plagioclase + cpx takes out less MgO as compared to the crystallization of olivine + spinel or olivine + plagioclase (for a given mass of the assemblage crystallized). The elliptical shaded areas in Fig. 6 also illustrate the influence of variable pressure of fractional crystallization. The high-Na_2O, high-FeO end of the ellipse corresponds to fractional crystallization at elevated pressure and the low-Na_2O, low-FeO end of the ellipse corresponds to low-pressure fractional crystallization.

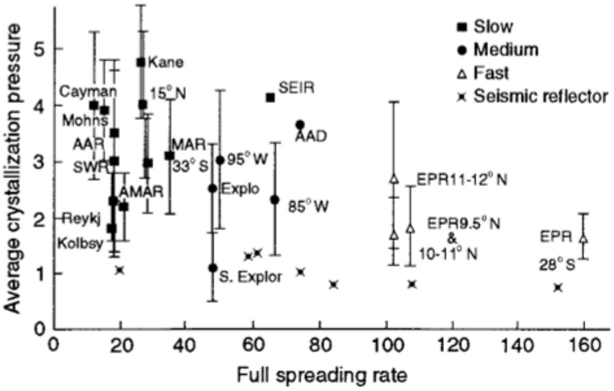

FIGURE 8 Average crystallization pressure (in kbars) for MDRBs versus spreading rate (in mm/yr). Bars show one standard deviation about mean pressure. Crosses show seismic reflectors interpreted to represent the tops of magma reservoirs beneath the indicated ridge. Crystallization depth is estimated using magma compositional parameters (see Michael and Cornell, 1998).

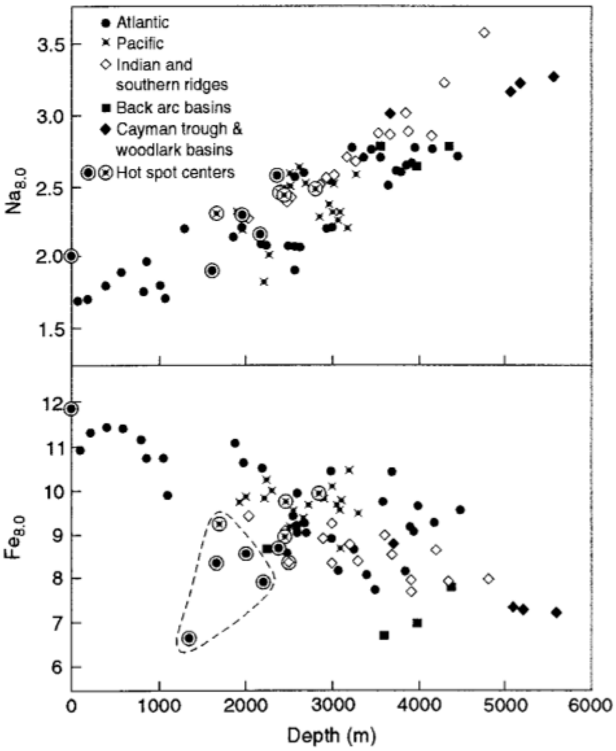

FIGURE 7 Regional averages of ocean ridge basalts showing the relationship between element compositional parameters and axial depth (depth below sea level to the active spreading ridge). The depth to the spreading center reflects mantle temperature. Hotter adiabat = shallower water depth = higher extent of melting. Cooler adiabat = deeper water depth = lower extent of melting. [Klein, E. M. and Langmuir, C. H. (1987) Global correlations of ocean basalt chemistry with axial depth and crustal thickness. *J. Geophys. Res.* **92,** 8089–8115.]

The temperature of the oceanic lithosphere influences the depth of fractional crystallization. In Fig. 8, the average pressure of crystallization has been calculated for suites of ocean floor basalts. There is a correlation between ridge spreading rate and crystallization depth. At fast spreading ridges, magmas ascend into the shallow mantle before encountering cool and rigid lithosphere. In contrast, magmas generated at slow-spreading ridges encounter rigid and cold lithosphere at greater depths, which impedes the ascent of magma to the site of eruption at the ridge. Instead, the magma stalls in deep magma chambers, cools, and crystallizes.

In addition to crystallization at variable pressures, two other postsegregation processes may generate compositional variations. The first involves mixing of a range of evolved magma compositions that achieved their compositions by varying amounts of fractional crystallization from the same primary magma in a crustal level magma chamber. The second involves assimilation of mantle material that may occur and that may modify the melt composition. Assimilation may occur as melts percolate through the mantle, or it may occur within the region where the increments of melts are collected or "aggregated." Both of these processes are discussed in the following section on subduction zone magmas.

VI. MAGMA GENERATION PROCESSES IN SUBDUCTION ZONES

Magma generation in subduction zones is generally thought to be a consequence of the presence of H_2O in the source region of magmas. Subduction zone settings are distinguished by the presence of H_2O as a component in the magma, but there are also other dynamic processes that lead to melt generation. The influence of H_2O on mantle melting processes is shown in Fig. 3. Figure 3 shows pressure–temperature (*P-T*) and temperature–composition (*T-X*) relationships for a mantle analog consisting of pure forsterite olivine (Fo, Mg_2SiO_4). Shown on Fig. 3A are the melting relations for pure Fo and the melting behavior for the system Fo + H_2O. The solubility of H_2O in the melt phase is pressure dependent and increases from ~0.1 wt% at surface pressure to 27 wt% at 30 kbar. The effect of increased H_2O solubility with pressure is to stabilize the melt phase to much lower temperatures than in the H_2O-free system. At 30 kbar, Fo melts in the presence of H_2O at a temperature ~600°C lower than its dry melting point. The *T-X* diagram for 10 kbar shows the melting behavior when H_2O is present. The first melt of the olivine + vapor assemblage contains nearly 20 wt% H_2O.

In a subduction zone H_2O is supplied to the mantle by dehydration of H_2O-bearing minerals as they are carried to depth in the downgoing subducted lithosphere. Figure 2 shows a schematic cross section through a subduction zone. In the subducted lithosphere the maximum stability limits for H_2O-bearing minerals are shown by dashed curves. The subducted lithosphere consists of layers of sediment, hydrated basaltic crust, and hydrated mantle peridotite. The volumetrically dominant reservoirs for H_2O are minerals in the lithospheric mantle that are produced during seafloor alteration by circulating fluids when the mantle is altered at the active ridge spreading center. They include the minerals serpentine and chlorite, which contain 8–10 wt% H_2O. In the ocean crust the dominant minerals are lawsonite, chloritoid, and amphibole. Lawsonite and chloritoid can contain up to 10 wt% H_2O and amphibole contains about 1.5 wt% H_2O. As the slab descends the increase in pressure and temperature puts these minerals outside of their stability field and they decompose to anhydrous products and release H_2O. An H_2O-rich fluid ascends into the overlying mantle, where it encounters progressively higher temperatures as it ascends. At depths between 110 and 75 km the mantle + fluid melts to an H_2O-rich melt. This melt is very buoyant, because it contains a large amount of dissolved H_2O. (The molar volume of H_2O in silicate melt under these conditions is ~17 cm^3/mol, about one-third that of anhydrous silicate melt.) The hydrous melt ascends into hotter overlying mantle, where it is heated by the shallow mantle. At these higher temperatures and shallower depths, melt is no longer in equilibrium with its surrounding mantle and it reacts with the solids, forming more melt and diluting the H_2O content of the melt. This process continues until the melt ascends into the hottest part of the wedge, where the maximum amount of melting occurs. Upon further ascent into cooler, shallower mantle, the melt will presumably cool and crystallize.

If this melt is sampled as a magma, it should record the conditions under which it equilibrated with the mantle. These magmas are found in subduction zones globally, though they are rare. These primary magmas have been sampled, brought into the laboratory and subjected to elevated pressure–temperature conditions to determine their liquidus phase relations. Figure 9 shows the effect of adding variable amounts of H_2O to basaltic andesite sample 85-44 from the south Cascades (United States) subduction zone with Mg# = 0.71. At 6 wt% H_2O, the near-liquidus phases for this melt consist of olivine and orthopyroxene, which are the dominant minerals in the mantle. The temperature of this solid–melt equilibrium is about 150°C cooler than the temperature at which the mantle would melt beneath an ocean spreading center. Thus, the magma records a cool temperature because of the influence of H_2O on melting. The melt extraction depth inferred from the experiments corresponds to ~30 km, which is near the Mohorovicic discontinuity in the south Cascades. This melt records the depth in the shallow mantle. If it started to melt as a result of the presence of H_2O, the shallow last pressure of equilibration with the mantle may indicate that the magma is a batch melt that equilibrated with its mantle source up to the final shallow depth at which it was extracted.

Figure 10 shows a basalt (sample 79-35g) from the Cascades with an Mg# = 0.71. The liquidus phase relations also show saturation with shallow mantle peridotite

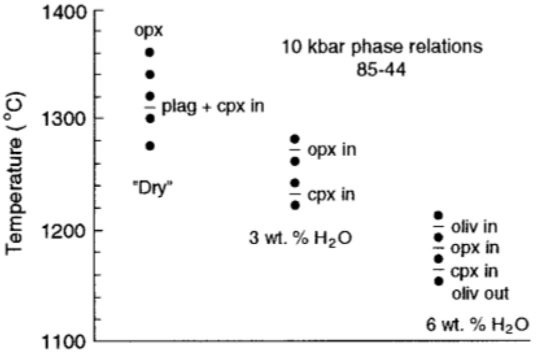

FIGURE 9 Near-liquids melting relations for basaltic andesite 85-44 from the south Cascades, United States, for anhydrous conditions and as a function of increasing water content. Each point shows the conditions of a laboratory experiment. [Baker, M. B., Grove, T. L. and Price, R. (1994) Primitive andasite from the Mt. Shasta region, N. California: Products of varying melt fraction and water content. *Contrib. Mineral Petrol.* **118,** 111–129.]

source under anhydrous conditions. For this magma the melting temperature is near that characteristic of ocean spreading centers. The pressure of multiple-phase saturation is similar for both magmas and corresponds to a depth near the top of the mantle at the crust–mantle boundary. The implications of their phase relations are that the subduction process beneath the Cascades leads to magmatism that involves H_2O and magmatism that is H_2O free (anhydrous). In fact, this variation in H_2O content and temperature of magmas is observed in other subduction zones. Figure 11 is a compilation of pre-eruptive magmatic H_2O contents and shows variation in the H_2O in magmas from the Aleutians, Central America, and Japan that are similar in magnitude to those observed in the Cascades.

In subduction zones, it is possible that there is a combination of mechanisms for melt generation. One melting process may be triggered by the rise of H_2O into the overlying mantle wedge. The second may be the result of mantle convection that occurs near the corner of the wedge. The subduction zone cross section (Fig. 2) shows vectors for mantle flow. Hot mantle ascends from depth and moves toward the slab-wedge corner, before it turns the corner and descends above the slab. Adiabatic decompression melting may occur in the shallow part of the mantle flow regime above the part of the mantle that is being flux melted by H_2O. This shallow melting leads to the production of anhydrous magmas.

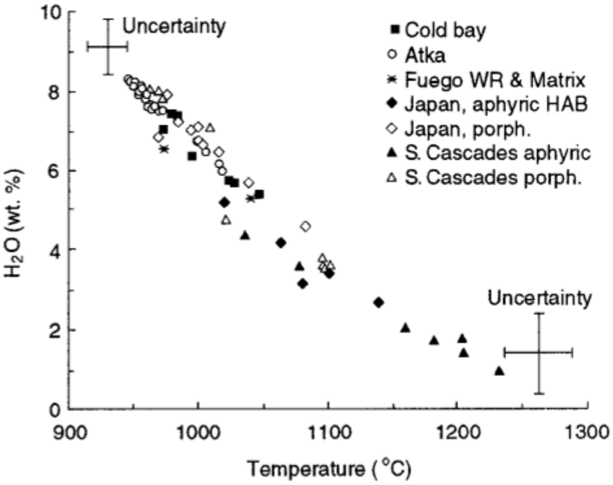

FIGURE 11 Temperature and pre-eruptive H_2O contents for representative basalts and andesites from subduction zone environments. See Sisson and Grove (1993) Temperatures and water contents of low-MgO high-alumina basalts. *Contrib. Mineral Petrol.* **113,** 167–184 for method of estimation.

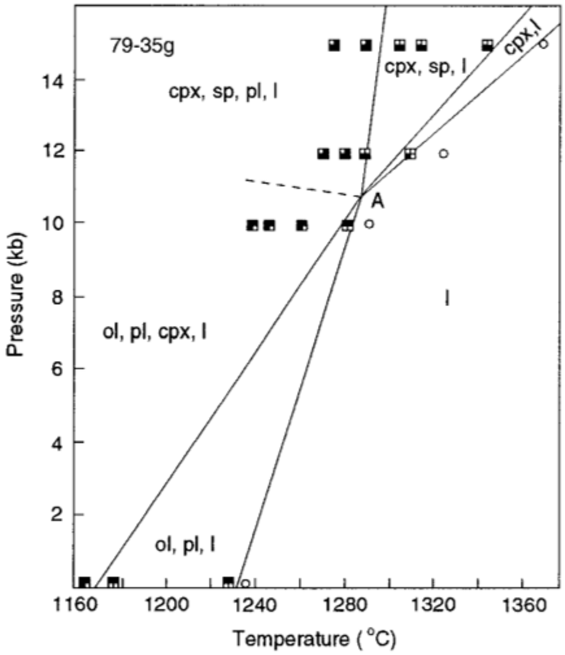

FIGURE 10 Pressure–temperature diagram showing the near-liquids melting behavior of basalt magma from the south Cascades, United States, under dry conditions. At about 11 kbar pressure and 1300°C at point A, the lava is saturated with a mantle peridotite mineral assemblage of olivine + pyroxene. Each square shows the conditions of a laboratory experiment. [Bartels, K. S., Kinzler, R. J. and Grove, T. L. (1991) High pressure phase relations of primitive high-alumina basalts from Medicine Lake volcano, northern California. *Contrib. Mineral Petrol.* **108,** 253–270.]

VII. FRACTIONATION, ASSIMILATION, AND MIXING IN SUBDUCTION ZONE ENVIRONMENTS

A. Fractional Crystallization in Subduction Zones

The presence of magmatic H_2O also has a large effect on the composition of magmas that undergo fractional crystallization. H_2O changes the relative sizes of the olivine, high-Ca pyroxene, and plagioclase primary liquidus volumes with the result that hydrous basalt and basaltic andesite magmas saturated with these minerals have high Al_2O_3 and higher proportions of olivine and high-Ca pyroxene than similarly saturated dry magmas. These differences, which are observed between subduction zone and ocean floor magma series, suggest that the fractional crystallization controls on the two magma suites result from high- and low-H_2O contents, respec-

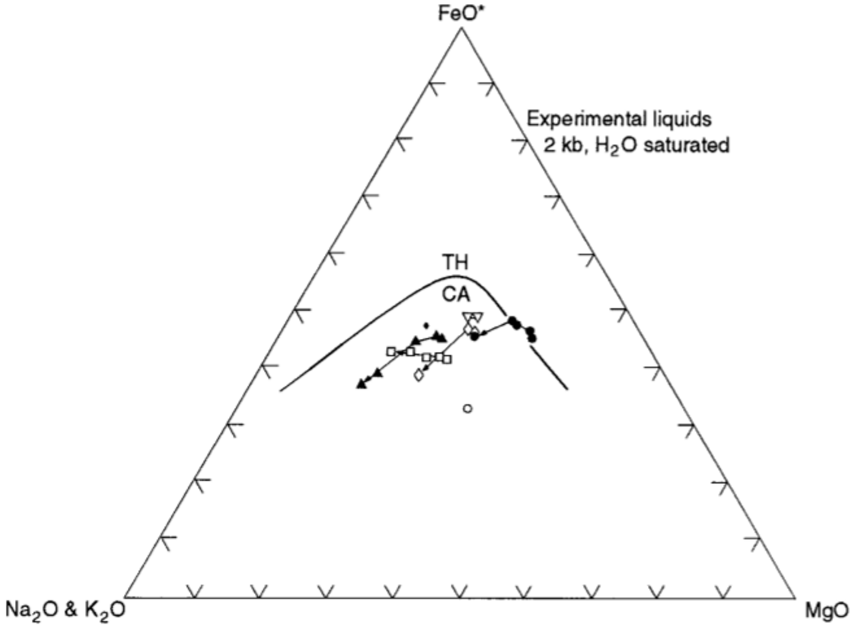

FIGURE 12 The AFM triangular discrimination diagram is used to distinguish fractional crystallization trends that are found in subduction zone environments. Trends that follow paths above the curve labeled TH are characteristic of anhydrous crystallization. Paths that follow trends below the curve in the CA field are characteristic of hydrous fractional crystallization. Symbols show experiments on basalts that were performed at 2 kbar with 6 wt% H_2O dissolved in the melt. These experimental crystallization paths follow a trend that parallels that of many subduction zone magmas (Sisson and Grove, 1993).

tively. H_2O also lowers the temperature where silicate minerals crystallize (Fig. 9), but has lesser effect on spinel. Thus, an Fe-rich spinel phase can appear near or at the liquidus of a hydrous basaltic melt. As a consequence, H_2O-bearing basalts and basaltic andesites can produce derivative liquids by fractional crystallization that are depleted in FeO and enriched in SiO_2 when compared to differentiated ocean floor basalts. The plagioclase that forms from high-H_2O basaltic melts is CaO- and Al_2O_3-rich and alkali- and SiO_2-poor plagioclase. Crystallization of this phase further promotes the alkali and silica enrichment that is characteristic of the subduction zone magmatic suites and is consistent with the calcic-plagioclase found in many arc magmas. Amphibole stability is sensitive to melt compositional features in addition to H_2O content. Amphibole will only appear in a subduction zone magma if the melt is Na_2O rich and at low temperature.

Subduction-related magmas have been long recognized to show distinctive variations in composition. This variation in composition has been called the *calcalkaline differentiation trend* and it is characterized by early iron depletion and silica enrichment. Iron depletion has been illustrated in two ways. One form of iron depletion is an overall decrease in FeO in the liquid. This is exhibited in Fig. 12 as an enrichment of Na_2O and K_2O relative to FeO. The other form is one of enrichment of SiO_2 with only a modest increase in FeO/MgO (Fig. 13). Also shown in Figs. 12 and 13 are the results of laboratory crystallization experiments of H_2O-saturated basalts at upper crustal pressures. The crystallization paths de-

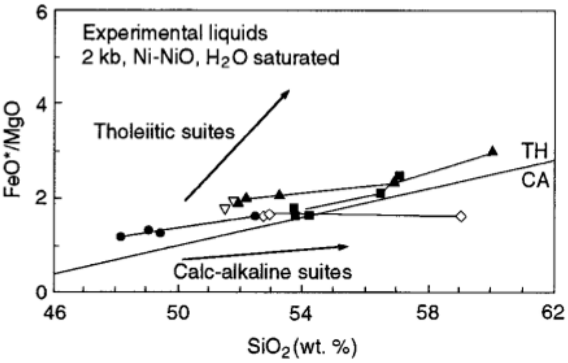

FIGURE 13 FeO*/MgO versus SiO_2 diagram that is used to discriminate fractional crystallization paths. Gray arrows show the trends followed by anhydrous fractional crystallization (tholeiitic suites) and hydrous fractional crystallization (calcalkaline suites). Experimentally produced hydrous crystallization paths for basalts are shown as symbols. Symbols are the same as in Fig. 12 (Sisson and Grove, 1993).

fined by these experiments follow the trend of a modest increase in FeO/MgO. The other trend shown in Figs. 12 and 13 has been called the *tholeiitic trend* and it parallels the trend followed by ocean floor magmas during fractional crystallization (discussed earlier in Section IV). The crystal-liquid controls on the tholeiitic trend are crystallization dominantly of plagioclase, reduced proportions of Fe-Mg silicates, and appearance of oxides only at late stages and low temperatures. Plagioclase is enriched in Na_2O and SiO_2, and alkali enrichment is suppressed. Fe-Mg silicates crystallize in diminished proportions, and the residual liquid becomes FeO enriched.

B. Magma Mixing and Assimilation in Subduction Zone Environments

Magmas in subduction zones often contain evidence that processes other than fractional crystallization have operated to modify their compositions. A careful examination of the minerals in a lava often reveals that the crystals are not in equilibrium with their enclosing magma. A test using Mg# (2) often reveals the presence of disequilibrium magma–mineral assemblages, and indicates mixing of several distinct magmatic components. In continental settings the underlying crust is often compositionally distinct from the andesite and basalt that is erupting through it. The basalt can heat the surrounding crust, melt it, and incorporate melted crust into the magma. This process of assimilation can be quite dramatic in its compositional influence.

Volcanic systems are often episodic, and it is the periodic and repeated injection of magma through the same plumbing system that allows significant assimilation to occur. The processes that lead to mixing and assimilation are illustrated in Fig. 14. In this model, an initial input of basaltic magma is emplaced at shallow levels in the crust. This magma cools, crystallizes, and undergoes fractional crystallization to produce a derivative andesite. The crystallization releases a latent heat of solidification that is supplied to heat and melt the surrounding country rock. Another cycle of magmatic activity brings a fresh, undifferentiated batch of basalt into the magma reservoir. This undifferentiated basalt mixes with the differentiated andesite and the melted crust. In panel 1 (Fig. 14A) the geometry is shown for a dike swarm that has intruded into granite crust. The heat from crystallization of the dikes melts the crust at the dike–wallrock boundary (panel 2). A new pulse of undifferentiated basalt intrudes and mixes with the melted granite and differentiated andesite (panel 3). In (Fig. 14B) the process is depicted for a magma reservoir where the differences in density between the magma can now play a role. The parent basalt magma intrudes (panel 1). The magma crystallizes and the dense crystals accumulate at the base of the magma chamber (panel 2). A fractionated

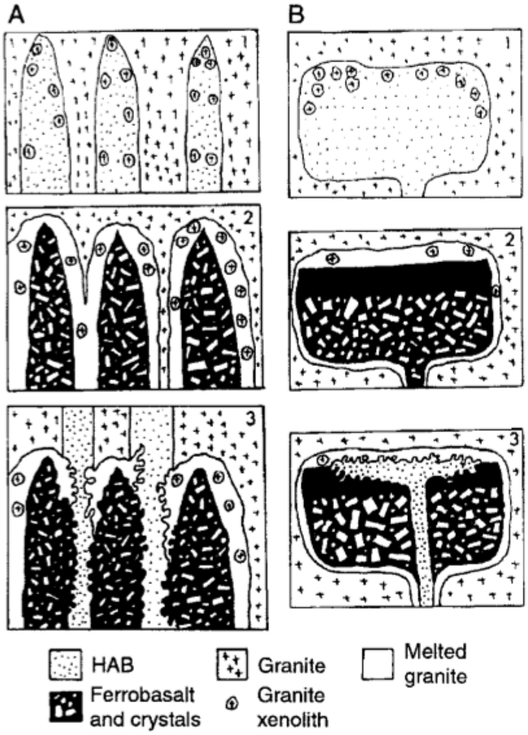

FIGURE 14 Schematic cross sections showing the processes that lead to assimilation of crust by magmas. Panel A shows a dike swarm system that intrudes into granitic crust (panel 1), crystallizes and supplies heat that melts the wallrock (panel 2). The replenishment of the system by fresh undifferentiated magma mixes the fresh input of magma with differentiated liquid and melted crust. Panel B shows the same process for a hypothetical magma chamber. Magma intrudes in panel 1. In panel 2 magma crystallizes and forms a dense cumulate pile and overlying less dense differentiated melt. Heat of crystallization melts wallrock. In panel 3 a fresh batch of undifferentiated magma replenishes the system and rises to a level of neutral buoyancy between the underlying cumulates and derivative liquid and overlying less-dense melted crust. Mixing occurs at the interface from induced convection. HAB = magma produced by mantle melting. Ferrobasalt = magma that has experienced fractional crystallization. [Grove, T. L., Kinzler, R. J., Baker, M. B., Donnelly-Nolan, J. M. and Leshar, C. E. (1989) Assimilation of granite by basaltic magma at Burnt Lava Flow, Medicine Lake volcano northern California: Decoupling of heat and mass transfer. *Contrib. Mineral Petrol.* **99,** 320–343.]

liquid segregates from the crystals and concentrates at the top of the magma reservoir. Heat from the solidification of the basalt is transferred through the top of the magma chamber and it melts the surrounding wallrock (panel 3). The cap of melted granite crust is significantly less dense than the differentiated basalt (density of the melted silicic cap, $\sim$2.2 g/cm^3; density of differentiated basalt, $\sim$2.7 g/cm$_3$). A new pulse of undifferentiated magma is supplied to the chamber (density, $\sim$2.65 g/cm^3), and it rises through the accumulated crystals and the dense fractionated andesite into the interface between the differentiated melt and the silicic cap. The hot, low-viscosity undifferentiated magma undergoes turbulent convection when it encounters the cooler melts in the chamber and mixing occurs. Thus, replenishment of a magma reservoir by undifferentiated basalt is one plausible mechanism that leads to mixing of magmas.

SEE ALSO THE FOLLOWING ARTICLES

Composition of Magmas • Melting and Mantle • Physical Properties of Magmas • Plate Tectonics and Volcanism

FURTHER READING

Coleman, R. G. (1977). "Ophiolites." Springer Verlag, Berlin.

Crisp, J. A. (1984). Rates of magma emplacement and volcanic output. *J. Volcanol. Geotherm. Res.* **20,** 177–211.

Ghiorso, M. L., and Sack, R. O. (1995). Chemical mass transfer in magmatic processes IV. A revised and internally consistent thermodynamic model for the interpolation and extrapolation of liquid–solid equilibria in magmatic systems at elevated temperatures and pressures. *Contrib. Mineral. Petrol.* **119,** 197–212.

Gill, J. (1981). "Orogenic Andesites and Plate Tectonics." Springer Verlag, Berlin.

Holloway, J. R., and Wood, B. J. (1988). "Simulating the Earth: Experimental Geochemistry." Unwin Hyman, Boston.

Kushiro, I., and Yoder, H. S., Jr. (1969). Melting of forsterite and enstatite at high pressures under hydrous conditions. *Carnegie Inst. Wash. Yrbk.* **67,** 153–158.

Kinzler, R. J. (1997). Melting of mantle peridotite at pressures approaching the spinel to garnet transition: Application to mid-ocean ridge basalt petrogenesis. *J. Geophys. Res.* **102,** 853–874.

Langmuir, C. H., Klein, E. M., and Plank, T. (1992). Petrologic systematics of mid-ocean ridge basalts: Constraints on melt generation beneath ocean ridges. Pages 183–280 *in* "Mantle Flow and Melt Migration at Mid-Ocean Ridges," Geophysical Monograph 71 (J. P. Morgan, D. K. Blackman, and J. M. Sinton, eds.). American Geophysical Union, Washington, DC.

Longhi, J. (1991). Comparative liquidus equilibria of hypersthene-normative basalts at low pressure. *Am. Mineral.* **76,** 785–800.

Michael, P. J., and Cornell, W. C. (1998). Influence of spreading rate and magma supply on crystallization and assimilation beneath mid-ocean ridges: Evidence from chlorine and major element chemistry of mid-ocean ridge basalts. *J. Geophys. Res.* **103,** 18,235–18,356.

Roeder, P. L. (1975). Thermodynamics of element distribution in experimental mafic silicate–melt systems. *Fortsch. Mineral.* **52,** 61–73.

Roeder, P. L., and Emslie, R. F. (1970). Olivine–liquid equilibrium. *Contrib. Mineral. Petrol.* **29,** 275–289.

Sisson, T. W., and Grove, T. L. (1993). Experimental investigations of the role of water in calc-alkaline differentiation and subduction zone magmatism. *Contrib. Mineral. Petrol.* **113,** 143–166.

This Page Intentionally Left Blank

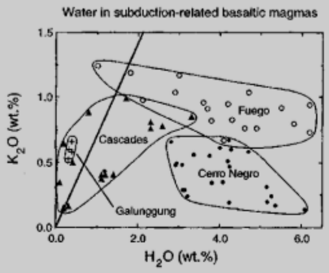

VOLATILES IN MAGMAS

PAUL WALLACE
Texas A&M University

ALFRED T. ANDERSON, JR.
University of Chicago

I. Definition and Significance of Magmatic Volatiles
II. Solubility of Volatiles in Silicate Melts
III. Measuring Magmatic Volatile Contents
IV. Analytical Techniques for Measuring Volatile Abundances in Silicate Glasses
V. Volatile Abundances in Basaltic Magmas
VI. Volatile Abundances in Silicic Magmas
VII. Importance of Volatiles in Volcanic Eruptions
VIII. Effects of Volatiles on Physical Properties of Silicate Melts
IX. Origin of Volatiles, Earth Degassing, and Volatile Recycling via Subduction
X. Future Directions

GLOSSARY

exsolved gas Gas that has been released from solution in a magma. Gas exsolution occurs when pressure is decreased, such as when magma moves toward Earth's surface.

fugacity A gas is considered to be perfect if its behavior can be described by the ideal gas law: $PV = nRT$, where P is pressure, V is volume, n is number of moles, R is the ideal gas constant, and T is temperature. Most gases are not perfect, especially at high pressures or low temperatures. The fugacity is a kind of equivalent pressure that accounts for the deviation of a real gas from ideal gas behavior.

glass If a liquid is cooled very rapidly, it may harden to a glass and not crystallize. Magma contains silicate liquid that, if cooled rapidly enough, forms glass.

immiscible Some types of liquids such as molten iron sulfide will not fully mix with or dissolve into a silicate melt to form a homogeneous solution. Such coexisting liquids are described as immiscible.

magma Natural silicate melt with or without suspended crystals and bubbles.

melt (glass) inclusion During crystallization of magma, many crystals grow imperfectly, trapping small blebs of silicate melt inside the crystals. If the magma is erupted and cooled rapidly, then these trapped inclusions of silicate melt become glass.

saturation A melt can be saturated with respect to certain chemical elements in three ways: It may contain bubbles of a pure gas like H_2O, it may contain crystals rich in the element, such as anhydrite ($CaSO_4$, rich in S), or it may contain droplets of immiscible liquid rich in the element, such as drops of sulfide melt (rich in S). In this review we use the word saturation to refer to saturation with respect to a gas (bubbles of an impure gas are present) and to refer to saturation with respect to a crystal or immiscible melt.

solubility The maximum amount of a volatile species or component that can be dissolved in a silicate melt under a given set of conditions such as pressure, temperature, and melt composition.

viscosity All fluids will flow in response to an applied shear stress, but some fluids flow more slowly than others.

Copyright © 2000 by Academic Press
All rights of reproduction in any form reserved.

Viscosity can be thought of as the resistance of a fluid to flow. A high-viscosity fluid flows very slowly.

volatile An element or compound such as H_2O or CO_2 that forms a gas at relatively low pressure and magmatic temperature. Volatiles can be dissolved in silicate melts, can occur as bubbles of exsolved gas, and can crystallize in minerals such as biotite and amphibole.

I. DEFINITION AND SIGNIFICANCE OF MAGMATIC VOLATILES

> The observatory worker who has lived a quarter of a century with Hawaiian lavas frothing in action, cannot fail to realize that gas chemistry is the heart of the volcano magma problem.
>
> —*T. A. Jaggar, 1940*

The quote from T. A. Jaggar, founder of the Hawaiian Volcano Observatory and an influential volcanologist in the first half of the 20th century, attests to the importance of gases in governing volcanic eruptive phenomena. As early as the middle of the 19th century, it was recognized that gas plays a fundamental role in forcing magma to the Earth's surface and generating explosive eruptions. Many different species of gas can dissolve in a molten silicate liquid in the same way that carbon dioxide can dissolve in water. Such gas species are referred to as *volatile components* or *magmatic volatiles* because of their tendency to form gas bubbles at relatively low pressure. The amount of a volatile component that can dissolve in silicate melt increases with pressure. As magma ascends toward the Earth's surface, pressure decreases, thereby decreasing the solubility of volatiles and causing them to come out of solution to form bubbles. In addition, the bubbles expand with further decrease in pressure. At 1 atm pressure and typical magma temperatures, an amount of exsolved H_2O equivalent to one one-thousandth of total magma mass is sufficient to produce a magmatic foam that has more than 90% bubbles by volume! Truly tremendous expansion occurs near the surface as a result of such volatile exsolution, and this provides the driving force for volcanic eruptions, similar to the fountaining of champagne from an uncorked bottle.

Water and carbon dioxide are the most important volatile components in natural magmas. At higher pressures, deeper within the Earth, most of the water and carbon dioxide are dissolved in the silicate melt portion of the magma, and they have important effects on magma crystallization, temperature, density, and viscosity. In the upper mantle, where basaltic magmas are generated by partial melting, volatiles affect the composition of melts and their physical segregation from the residual mantle minerals. After H_2O and CO_2, the most abundant volatiles are sulfur, chlorine, and flourine; sulfur is particularly important for understanding the composition and fluxes of volcanic gas, and all can be significant in the formation of ore deposits. Many other volatiles, such as He, Ar, and B, can dissolve in natural silicate melts (magmas), but they are generally much less abundant. The noble gases, for example, are usually present at concentration levels of <1 part per million (ppm, 0.0001% by weight) in natural magmas. Despite such low concentrations, the isotopic compositions of noble gases have been studied extensively because of their value in understanding large-scale degassing of the Earth and the formation of the atmosphere.

In this chapter, we focus on the abundant volatiles: H_2O, CO_2, and S. We review (1) experimental data on the solubility of volatiles in natural silicate melts, (2) analytical and sampling techniques used for measuring the abundances of volatiles in magmas, (3) volatile abundances in basaltic and silicic magmas typical of various tectonic environments, and (4) Earth degassing and volatile recycling by subduction. We also discuss the evidence for volatile gradients in magmas and pre-eruptive vapor saturation, because both of these are important for understanding explosive eruptive behavior of volcanoes, fluxes of volcanic gases, and the formation of ore deposits. Solubilities and abundances of Cl and F are also mentioned, and we present several references at the end of the chapter that treat Cl and F in more detail.

II. SOLUBILITY OF VOLATILES IN SILICATE MELTS

A. Water and Carbon Dioxide

Solubility refers to the maximum amount of a volatile species or component that can be dissolved under a given set of conditions, such as pressure, temperature, and melt composition. Laboratory measurements of the solubilities of H_2O, CO_2, S, and many other volatile components have been made for a number of different melt compositions. In such laboratory experiments, it is possible to control the parameters that affect solubility. As an example, a silicate melt can be equilibrated with water vapor at high temperature and a variety of

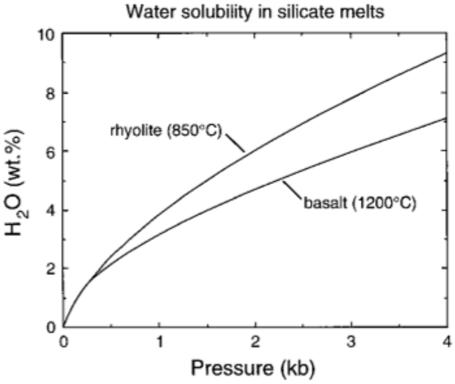

FIGURE 1 Experimental determinations of water solubility in basaltic and rhyolitic melts at typical magmatic temperatures. The solubility of water is greater in rhyolitic melt than in basaltic melt at pressures greater than 0.5 kb. (See Carroll and Holloway, 1994, for reviews of experimental solubility data.)

pressures in order to determine the solubility of water (Fig. 1). Such melt is described as *water saturated* because in the experiment, the melt coexists with water vapor. As seen in the experimental data, the solubility of H_2O in silicate melts is strongly dependent on pressure. This pattern, in which the solubility increases with increasing pressure, is observed for many volatile components, and occurs because the gaseous form of a volatile component has a larger molar volume than does the same component when it is dissolved in a silicate melt. The solubility of H_2O in silicate melts is also dependent on temperature and melt composition, such that H_2O solubility is greater in silica-rich melts (rhyolite) than in silica-poor ones (basalt) at comparable pressures (Fig. 1).

Early studies on the solubility of water in silicate melts recognized that there is a linear relationship between the partial pressure (or fugacity) of H_2O and the square of the mole fraction of dissolved water in the melt. Such a relationship is consistent with a solution mechanism in which water dissolves by forming OH^- groups that are structurally bound to the aluminosilicate network of the melt. More recent studies using infrared spectroscopy have shown that dissolved water in silicate melts occurs as two different species: OH^- groups and H_2O molecules. The relative proportions of the two species vary systematically with total water concentration. At low total dissolved water concentrations, virtually all of the water is present as OH^- groups. As total dissolved water concentration increases, the relative proportion of molecular H_2O increases as well. In rhyolitic melts, the proportions of OH^- groups and H_2O molecules are equal at about 3 wt% total dissolved water, whereas in basaltic melt, the proportions of the two species are equal at about 3.5 wt% total water.

As with H_2O, the solubility of CO_2 in silicate melts is strongly dependent on pressure (Fig. 2). However, CO_2 solubilities are much lower than for H_2O. The amount of CO_2 that dissolves into both basaltic and rhyolitic melts is 50–100 times less, by weight, than the solubility of H_2O at comparable pressure and temperature. Carbon dioxide dissolves in silicate melts in two different species, but in contrast to water, the speciation is controlled by the bulk silicate melt composition. Thus in silica-poor glasses (basalts, basanites, nephelinites), CO_2 is present as structurally bound carbonate (CO_3^{2-}), whereas in high-silica (rhyolitic) melts it occurs as CO_2 molecules. Glasses with intermediate silica contents (andesitic) contain both species. Experimental studies have demonstrated that the solubility of CO_2 is strongly dependent on melt composition, and this compositional dependence reflects, in part, the differences in speciation. For example, carbon dioxide is more soluble in rhyolitic melt (as molecular CO_2) than in basaltic melt (as CO_3^{2-}) (Fig. 2). However, in silica-poor melts, the solubility of CO_2 as carbonate increases with decreasing silica content. Thus the solubility of CO_2 in basanitic

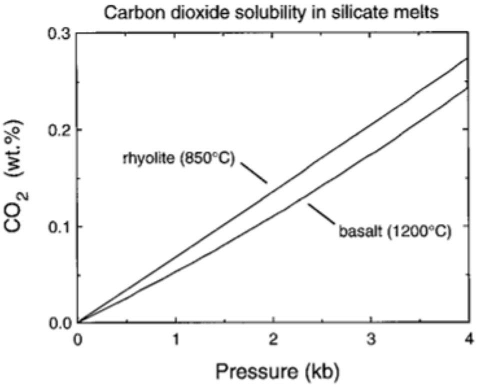

FIGURE 2 Carbon dioxide solubility in basaltic and rhyolitic melts at typical magmatic temperatures as determined by experimental studies and thermodynamic models. As with water, the solubility of carbon dioxide is greater in rhyolitic melt than in basaltic melt. Carbon dioxide dissolves in rhyolitic melts as molecular (CO_2), whereas in basaltic melt it is present as a dissolved carbonate ion (CO_3^{2-}). The slight curvature of the solubility curve for basaltic melt relative to rhyolitic melt results from two factors: (1) small differences in the pressure dependence of solubility for the different melt compositions and (2) greater nonideal behavior for CO_2 gas at the lower temperature of the rhyolitic melt. (See Carroll and Holloway, 1994, for reviews of experimental solubility data.)

melt is similar to that in rhyolitic melt and greater than that in the basaltic melt shown in Fig. 2.

In discussing solubility, it is important to distinguish between saturation and undersaturation with a particular volatile component. *Solubility* refers to the maximum amount of a volatile species or component that can be dissolved in silicate melt at a given set of conditions. In both natural and experimental silicate melts, however, the melt can have a concentration of a dissolved volatile component that is less than the maximum possible. Such a melt is described as *undersaturated* with respect to the volatile component of interest. As an example, laboratory experiments show that a rhyolitic melt can contain about 6% dissolved H_2O at 2 kbar, but this does not mean that all natural rhyolitic melts that are at 2-kbar pressure in the Earth's crust contain this much water. Instead, they could have any amount from 0 to 6 wt%. A rhyolitic melt containing less than the dissolved H_2O needed to saturate the melt at a given temperature and pressure is thus *water undersaturated*.

It is possible in laboratory solubility experiments, as described earlier, to equilibrate a melt with a single gas component such as H_2O. However, in magmas, many volatile components are present together. It is therefore important to distinguish between the dissolved concentrations of individual volatile components and their concentrations in the separate exsolved gas phase. If the sum of the partial pressures of all dissolved volatile components in a magma is equal to the local confining pressure, then the magma is saturated with bubbles of a multicomponent gas containing H_2O, CO_2, S, and other minor gases like Cl, F, and noble gases. Because the volatile species have different solubilities, their relative abundances dissolved in the melt will differ from their relative abundances in the gas phase.

For vapor-saturated silicate melts, the solubilities of individual volatile components are dependent in part on the abundances of other volatiles that are present in the system. This is because the amount of a given component that is dissolved in the melt is proportional to the partial pressure of the volatile component in the coexisting equilibrium vapor. As a example, consider a silicate melt that is saturated with vapor consisting only of H_2O and CO_2. The sum of the partial pressures (P_{H_2O} and P_{CO_2}) of these components in the vapor phase must equal the total pressure in a vapor-saturated melt. Thus at constant total pressure an increase in P_{H_2O}, and hence dissolved H_2O in the melt, must result in a decrease in P_{CO_2} and dissolved CO_2. On a diagram of dissolved H_2O versus dissolved CO_2 in silicate melts, vapor saturation isobars, which show the maximum dissolved H_2O and CO_2 at a given total pressure, have negative slopes (Fig. 3). In many common igneous systems, the partial pressures of other volatile components (e.g., Cl, F, S) are probably relatively small compared with those of H_2O and CO_2. Knowledge of the pre-eruptive concentrations of H_2O and CO_2 in a magma can thus potentially constrain the pressure at which the magma was stored before eruption.

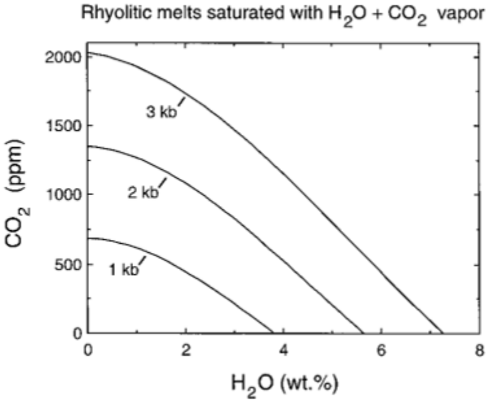

FIGURE 3 H_2O and CO_2 solubility in vapor-saturated rhyolitic melts at 850°C and 1- to 3-kb pressure based on experimental data and thermodynamic models. The curvature of the saturation curve for a given pressure results from the nonlinear dependence of H_2O solubility on pressure (see Fig. 1). (See Carroll and Holloway, 1994, for reviews of experimental solubility data and thermodynamic models.)

B. Sulfur

The behavior of S in silicate melts is complex because the solubility of S is controlled by the stabilities of sulfide and sulfate-bearing phases and because dissolved S can occur in multiple valence (oxidation) states. The speciation of dissolved S in silicate melts is related to the relative magmatic oxygen fugacity (Fig. 4). At relatively low oxygen fugacities, S is present in solution mainly in the reduced form sulfide (S^{2-}), whereas under more oxidizing conditions, sulfate (S^{6+}) appears to be the dominant species. For the range of oxygen fugacities from slightly lower than the nickel-nickel oxide (NNO) buffer to almost 2 $\log_{10}$ units above NNO, both dissolved sulfide and sulfate are present in significant quantities (Fig. 4). The maximum S that can be dissolved in silicate melt is controlled by saturation of the melt with an S-bearing phase. At relatively low oxygen fugacities, this phase is either an immiscible iron-rich sulfide liquid (with as much as 10% oxygen), which occurs in high-temperature basaltic melts, or crystalline pyrrhotite ($Fe_{1-x}S$) in intermediate (andesitic) and silicic (rhyolitic) melts. A Cu-Fe sulfide mineral known as *intermediate solid solution*

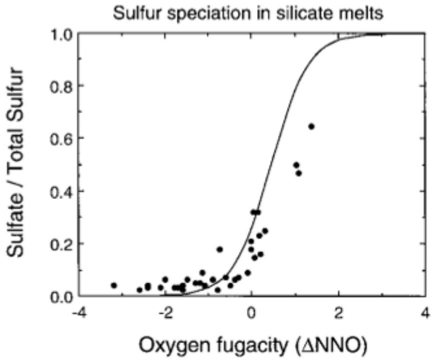

FIGURE 4 Percent of total sulfur that is present as sulfate (sulfate/total sulfur) as a function of oxygen fugacity, relative to the nickel-nickel oxide buffer (ΔNNO). The curve shows the experimental relationship for hydrous andesitic to dacitic melts. Filled circles are data for natural submarine glasses ranging from basalt to andesite in composition. (See Carroll and Holloway, 1994, for reviews of sulfur speciation data.)

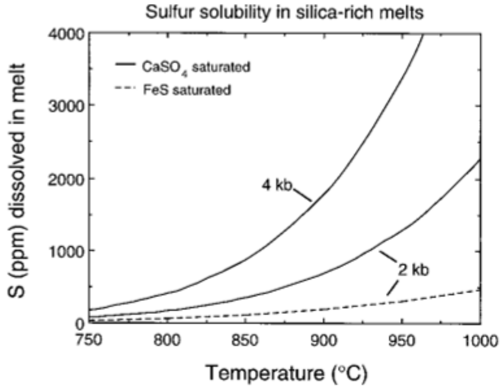

FIGURE 5 Experimental determinations of sulfur solubility versus temperature for hydrous silica-rich melts at different pressures and oxygen fugacities. Curves are shown for both sulfide-saturated melts (oxygen fugacity at the NNO buffer) and sulfate-saturated melts (oxygen fugacity at the MnO-Mn$_3$O$_4$ [MNO] buffer). At 2-kbar pressure, S is more soluble under oxidizing conditions (MNO) than under reducing conditions (NNO). The solubility curve for sulfate-saturated melts (MNO buffer) at 4 kbar shows that sulfate solubility increases with increasing pressure. (See Carroll and Holloway, 1994, for reviews of experimental solubility data.)

may also crystallize from andesitic to rhyolitic melts. At higher oxygen fugacities, the sulfate mineral anhydrite ($CaSO_4$) crystallizes from a wide range of melt compositions. Silicate melts at intermediate oxygen fugacities can crystallize both pyrrhotite and anhydrite, an assemblage that was found, for example, in trachyandesite tephra from the 1982 eruption of El Chichón in Mexico. Experimental solubility studies show that S is more soluble at high oxygen fugacities, under which conditions the dissolved S is present as sulfate, and anhydrite is the stable S-bearing mineral (Fig. 5). The solubility of reduced S (S^{2-}) increases with the Fe concentration in the silicate melt (Fig. 6), which indicates that S^{2-} dissolves largely by complexing with Fe^{2+}. Sulfur solubility under both oxidizing and reducing conditions increases with temperature (Fig. 5).

C. Halogens (Cl and F)

As with S, the solubility of Cl is complex because silicate melt can be saturated with an immiscible alkali chloride melt (molten salt). If water is present, as it invariably is in natural melts, then the immiscible alkali chloride melt will also contain dissolved water and is referred to as a hydrosaline melt. Chlorine solubility in silicate melts is strongly dependent on silicate melt composition, and the solubility generally increases as the ratio (Na + K)/Al in the silicate melt increases. A silicate melt saturated with molten salt has the maximum dissolved Cl. The saturation concentration of Cl varies with pressure, temperature, dissolved water concentration, and silicate melt composition. For silicate melts that are saturated with an H_2O and CO_2-rich vapor phase, maximum Cl solubilities range from several thousand parts per million to ~2 wt%. Thus, Cl solubility in silicate melts is somewhat intermediate between that of H_2O and that

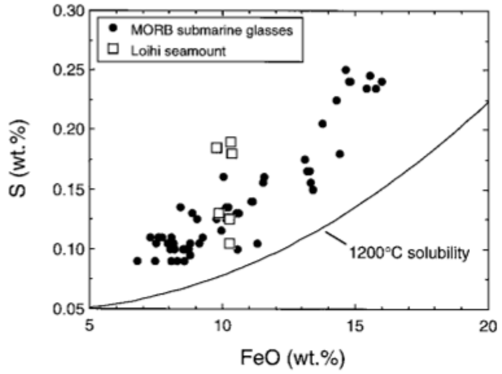

FIGURE 6 Covariation of sulfur and FeO in submarine mid-ocean ridge basalt (MORB) glasses and submarine basaltic glasses from an oceanic island volcano (Loihi seamount). Experimental solubility curve for S in basaltic melts at 1200°C is shown for comparison. Both natural and experimental data are for total S. The natural glasses form an array parallel to the experimental solubility data but offset to higher S contents. This is due to the lower oxygen fugacities of the experimental data compared with natural basaltic magmas. (Data from Wallace and Carmichael, 1992.)

of CO_2. In addition, it is possible for a silicate melt to be saturated with both hydrosaline melt and an H_2O and CO_2-rich vapor phase.

A natural silicate melt may contain less dissolved Cl than the amount needed to saturate the melt with either molten salt or hydrosaline melt. Many common magma types do not contain Cl-rich mineral phases or evidence of hydrosaline melt. By comparison with experimental Cl solubility studies, most magmas probably have insufficient dissolved Cl to be saturated with hydrosaline melt. In some Cl-rich magmas, however, formation and separation of a hydrosaline melt phase or alkali-chloride-rich vapor may play an important role in the formation of magmatic-hydrothermal ore deposits. For magmas that are saturated with an H_2O and CO_2-rich vapor phase, Cl partitions strongly into the vapor. Experimental studies suggest that the concentration, by mass, of Cl in the vapor phase can be 5–20 times or more greater than the mass concentration dissolved in the melt.

The solubility and speciation of dissolved F in silicate melts is complex and still not well understood, but available data clearly show that solubility is strongly dependent on silicate melt composition. In general, F is highly soluble in silicate melts, similar to H_2O. In granitic composition melts, as much as 10 wt% F can be dissolved. Natural melts generally have much lower dissolved F. Rare melts, such as those in tin and topaz-bearing rhyolitic magmas, may contain as much as 5 wt% F, and ultrapotassic mantle-derived magmas can contain as much as 2 wt% F.

III. Measuring Magmatic Volatile Contents

All terrestrial magmas contain dissolved volatiles, the most abundant being H_2O, CO_2, S, Cl, and F. If the dissolved concentrations of volatiles are sufficiently high, a magma may be vapor saturated such that the magma also contains an exsolved vapor (gas) phase. Assessing the total volatile content of magma requires that both dissolved and exsolved volatile abundances be known. Because the solubility of most volatile components is strongly pressure dependent, magmas exsolve gas during ascent to the surface. To understand the crystallization and physical properties of magma, as well as to understand eruptive behavior, it is important to know the total volatile content of magma during its pre-eruptive storage within the Earth's crust. Dissolved volatiles may be estimated in many ways, but exsolved volatiles are difficult to assess. The following discussion focuses primarily on dissolved volatiles; we discuss exsolved volatiles in a subsequent section.

A. Experimental Phase Equilibria

One of the most valuable methods for estimating dissolved volatile concentrations in magmas, particularly H_2O and CO_2, is through the use of phase equilibrium experiments. The assemblage of minerals that crystallizes from a melt of a given bulk composition and the sequence and temperature of appearance of those minerals during cooling, varies depending on pressure and dissolved H_2O concentration (Fig. 7). By equilibrating a given rock composition at various temperatures, pressures, and H_2O concentrations, it is frequently possible to find a relatively narrow range of conditions under which the observed phenocryst assemblage in the rock is in stable equilibrium. This technique is particularly suited to constraining the dissolved concentrations of H_2O during pre-eruptive crystallization and storage of magma within the Earth's crust. Experimental studies

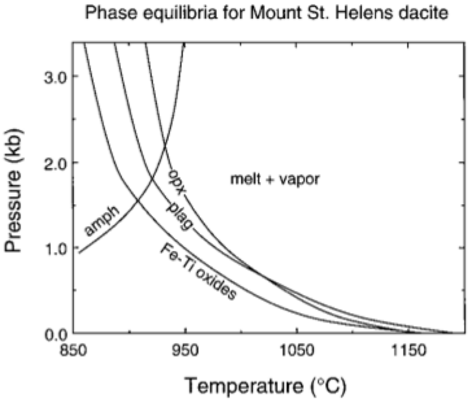

FIGURE 7 Experimental phase equilibria for 1980 Mount St. Helens dacite as a function of temperature and pressure for water-saturated melts. Because dissolved H_2O increases with pressure (Fig. 1), the water contents of the experimental melts increase along the vertical axis of the diagram. With increasing pressure (and dissolved H_2O), the temperatures at which anhydrous minerals (pyroxene, plagioclase, Fe-Ti oxides) begin to crystallize are significantly diminished. In contrast, increasing pressure and dissolved H_2O increase the stability of amphibole, which therefore crystallizes at higher temperatures as pressure increases. Comparison with the actual observed mineral assemblage in the 1980 Mount St. Helens dacite indicates pre-eruptive temperature and pressure of 920°C and ~2.2 kbar. (Modified from Rutherford *et al.,* 1985.)

have been applied with great success to a number of recent volcanic eruptions, most notably, the eruptions of Parícutin (1943–1951), Mount St. Helens (1980), El Chichón (1982), Mt. Pinatubo (1991), and Montserrat (1996–1998).

In addition to its effect on phase stability, dissolved H_2O also affects the composition of minerals that crystallize from silicate melts. The most useful effect related to magmatic H_2O concentrations is the change in plagioclase composition that occurs with variations in dissolved H_2O. As the dissolved H_2O concentration in a melt is increased, the equilibrium plagioclase composition becomes more calcic (anorthite-rich). As discussed later, anorthite-rich plagioclase phenocrysts are common in subduction-related basaltic magmas, providing evidence of relatively high concentrations of H_2O compared to basaltic magmas from other tectonic environments.

B. Analysis of Quenched Glass (Submarine Glasses, Melt Inclusions, Matrix Glass)

Subaerially cooled volcanic rocks and tephra have lost nearly all of their original magmatic volatiles because of the low pressures of Earth's atmosphere. In contrast, during deep submarine eruptions, the confining pressure exerted by the overlying water may prevent exsolution and loss of many volatile species. Such pressures can be as great as 500–600 bar. Submarine-erupted magmas typically form glassy skins where hot magma is rapidly quenched against cold seawater. Volatiles may be retained dissolved within such glassy basalt, which can be analyzed for volatiles directly. H_2O is relatively soluble in basaltic melt and as much as 2 wt% may be retained in deep sea basalt glass without eruptive loss. In contrast, for relatively insoluble CO_2, the pressures on the seafloor are commonly insufficient to prevent exsolution. This results in small vesicles in quenched submarine glasses, usually less than 1% by volume. The small size of these vesicles and their relatively low volumetric abundance result in isolated (noninterconnected) bubbles trapped in the quenched glass. Bulk analyses of these glassy rocks can therefore be used to assess total volatile concentration in the erupted magma, but the magma may have gained or lost bubbles before eruption. Bulk analyses of low-solubility volatiles like CO_2 in samples of glass with trapped bubbles commonly give greater concentrations than do direct microanalyses of the glass.

Another important source of information on the dissolved volatile concentrations of magmas is through the analysis of glass inclusions trapped inside of crystals. When melts crystallize, the crystals grow imperfectly, causing small amounts of melt to be trapped inside of the crystals. If the magma erupts and cools rapidly, then these trapped melt inclusions quench to glass (Fig. 8). Because the crystalline host for the inclusions is relatively rigid, they act as tiny pressure vessels and keep the trapped melt at high pressure, even though the bulk magma decompresses to surface pressure during eruption. For this reason, trapped melt (glass) inclusions commonly retain their original dissolved volatiles. However, melt inclusions may in many instances leak volatiles during explosive eruption due to cracks in the host mineral. This is especially problematic for inclusions in minerals with relatively good cleavages, such as hornblende and plagioclase. Melt inclusions in phenocrysts are trapped during crystal growth and thus sample the liquid from which the crystals grew at the time of entrapment. Inclusions that are trapped at different times during crystallization may preserve a record of changing magma compositions due to processes such as crystal fractionation and magma mixing. Glassy reentrants and hourglass inclusions (Fig. 8C) reveal the composition of melt just before eruption. Pressure-dependent concentrations of volatiles in melt inclusions, hourglass inclusions, and reentrants can reveal crystal settling and decompressive ascent of magma.

Quenched glassy scoria or pumice that formed during subaerial eruptions can also be analyzed for volatiles. Generally such material has extensively degassed during eruption and quenching, so measured volatile contents do not reflect those before eruptive decompression. Analyses of scoria glass or pumice can, nevertheless, be useful for interpreting degassing and eruptive processes.

C. Thermodynamic Calculation Based on Mineral Compositions

One method that has commonly been used to estimate volatile concentrations in magmas is the application of thermodynamic calculations. For example, reactions involving hydrous minerals and their anhydrous breakdown products can be used along with thermodynamic properties of the phases to estimate water concentrations. One exemplary reaction is:

$$\begin{array}{llllll} KFe_3AlSi_3O_{10}(OH)_2 & + & 1/2O_2 & & & \\ \text{biotite} & + & \text{gas} & & & \\ & = & KAlSi_3O_8 & + \; H_2O & + & Fe_3O_4 \\ & = & \text{feldspar} & + \; \text{gas} & + & \text{magnetite} \end{array}$$

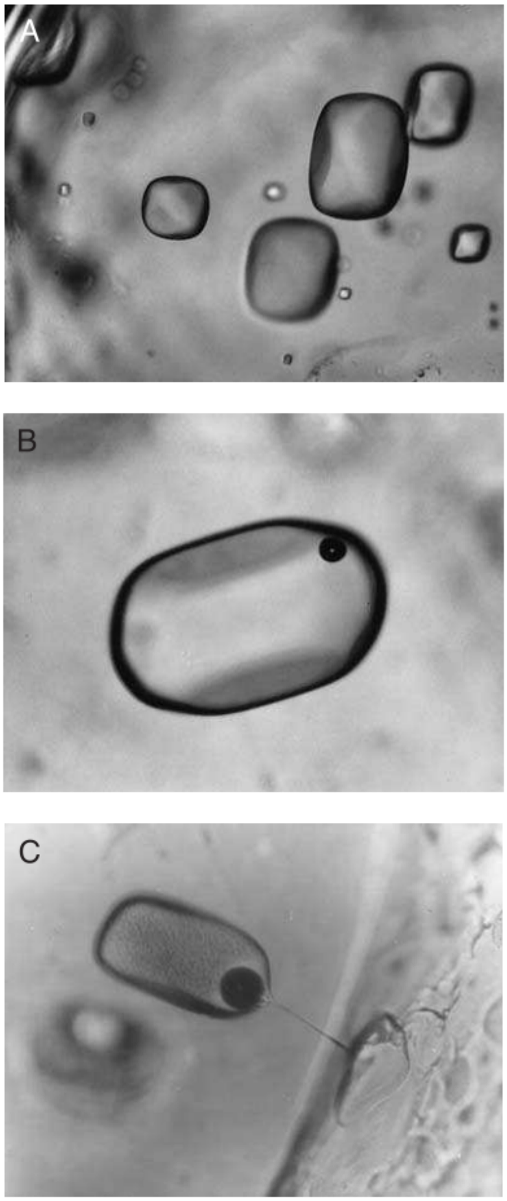

FIGURE 8 Glass (melt) inclusions in crystals from volcanic rocks. (A) A fragment of an ~3-mm quartz phenocryst from the rhyolitic Bishop Tuff containing inclusions of glass up to about 100 μm in diameter. (B) Close-up of a melt inclusion containing a small vapor bubble. The inclusion is about 80 μm long and is partly faceted. Bubbles that are small relative to the inclusion size form during cooling after the inclusion is trapped because the melt in the inclusion contracts more on cooling than does the surrounding quartz host crystal. (C) An hourglass inclusion in a late Bishop quartz. The neck of the hourglass is about 3 μm in diameter and it connects the inclusion to a small depression or dimple on the exterior surface of the quartz phenocryst. The main body of the hourglass is partly faceted, partially finely devitrified, and it contains a ~5 vol% bubble near the neck. The bubble grew as melt moved outward from the inclusion through the neck to the ascending (decompressing) melt outside of the crystal. Study of hourglass inclusions provides a way to estimate the rate of magma rise and the duration of eruption.

This equation can be used to calculate the water fugacity at the time of crystallization for any volcanic rock containing biotite, feldspar, and magnetite, provided the oxygen fugacity can also be estimated. Then a thermodynamic solubility model calibrated on experimental data can be used to convert the H_2O fugacity to dissolved H_2O concentration. Comparison of this technique with estimates of dissolved H_2O from phase equilibrium and melt inclusion studies shows variable agreement. In general, this approach does not offer the precision or accuracy of modern techniques used to analyze directly volatile concentrations in glasses, but it can be very useful if other types of data are unavailable.

Another way in which thermodyamic equations are commonly used to infer volatile concentrations is through the use of pyrrhotite composition to estimate fugacities of S species. Pyrrhotite ($Fe_{1-x}S$) has variable Fe (and other minor element) concentrations. Experimental data on pyrrhotite combined with thermodynamic calculations make it possible to use pyrrhotite composition to estimate S_2 fugacity. Provided the oxygen and water fugacities are independently known, one can calculate the fugacities of both H_2S and SO_2. It is not possible, however, to convert the fugacities of the various S species into concentrations of dissolved S, as is done with H_2O, because experimentally calibrated solution models for pyrrhotite-saturated melts are not available.

D. Fluid Inclusions

The presence of primary fluid inclusions in minerals from volcanic or plutonic rocks provides evidence that crystallizing melts were vapor and/or brine saturated. However, it can be difficult to distinguish between primary fluid inclusions, trapped during igneous crystallization, and secondary inclusions formed by lower temperature hydrothermal processes. Many volcanic phenocrysts from basaltic rocks contain dense CO_2-rich, primary fluid inclusions, indicating that the basaltic magma was CO_2 saturated during crystallization. Such inclusions can be used to estimate the pressure of inclusion entrapment. Knowledge of this, coupled with experimentally determined CO_2 solubilities in basaltic melt, can be used to estimate the dissolved CO_2 concentration of the basaltic magma at depth. Phenocrysts in more evolved volcanic rocks (dacites, rhyolites) may contain inclusions containing one or more of the following: fluid, vapor, hydrosaline melt, daughter crystals. The presence of these inclusions also can be taken as evidence for vapor saturation during crystallization, but the multicomponent nature of such inclusions (H_2O–CO_2–NaCl) makes it difficult to infer the original dissolved volatile concentrations in the coexisting silicate melt.

E. Saturation with Volatile-Rich Minerals and Immiscible Liquids

The most common volatile-rich minerals and immiscible liquids that occur in magmas are sulfide and sulfate minerals and immiscible sulfide (Fe-S-O) liquid. The presence of one or more of these phases in a quenched volcanic rock indicates pre-eruptive saturation with a S-rich phase. By comparison with experimental solubility data, this makes it possible to infer a pre-eruptive dissolved S concentration. For basaltic melts at low oxygen fugacities, thermodynamic solution models similar to those for H_2O and CO_2 are available, allowing precise estimates of dissolved S for sulfide-saturated melts. Under oxidizing conditions and for more silica-rich magmas, no such solution models are available, but there is an excellent experimental database covering a wide range of melt compositions and oxygen fugacities that can be used to make estimates of dissolved S concentration.

For volatile species whose solubility in a melt is controlled by the presence of a volatile-rich mineral or melt, such as a sulfide phase, complex changes in solubility can occur during magma cooling and differentiation. As an example, it has been observed in quenched glassy submarine pillow rinds from midocean ridge basalts (MORB) that only a small amount ($<1.5\%$ by mass) of the total S in the magma is present as quenched sulfide globules. This observation may seem somewhat surprising when one considers that the strong temperature dependence of S solubility should cause considerable precipitation of immiscible sulfide liquid during cooling. However, the observed low quenched sulfide globule abundance is consistent with thermodynamic and experimental assessment of the effects of differentiation on S solubility. During the cooling and crystallization of MORB magmas, residual liquids become increasingly Fe enriched due to fractional crystallization of silicate phases. The increase in Fe content increases the S solubility in the melt by an amount that is greater than the decrease in S solubility brought about by cooling. This results in differentiated Fe-Ti basalts that have higher dissolved S than the parental (unfractionated) magmas. This effect, combined with the increase in residual melt S brought about by crystallization, keeps MORB magmas finely balanced just at the S saturation point, causing the total mass of S in immiscible sulfide liquid to be small throughout the course of differentiation. In contrast, Kilauean tholeiitic magmas do not show an Fe-enrichment trend because crystallizing and fractionating olivine contains approximately the same weight percent FeO as the liquid from which it precipitates. In the absence of Fe enrichment, if the melt is saturated with immiscible sulfide liquid, then the solubility of S will decrease significantly as temperature decreases.

IV. ANALYTICAL TECHNIQUES FOR MEASURING VOLATILE ABUNDANCES IN SILICATE GLASSES

A large number of analytical techniques have been used to measure volatile concentrations in silicate glasses. These techniques fall into two main categories—bulk extraction techniques, in which a bulk rock or glass sample is crushed and analyzed, and microanalytical techniques, in which a tiny portion of glass is analyzed. Bulk extraction techniques can make it difficult to distinguish between the volatiles that are actually dissolved in quenched magmatic liquid (e.g., glassy submarine pillow rinds) and the volatiles that may be present in unopened vesicles. Furthermore, it is critical to select material for analysis that is free of alteration. Microanalytical techniques offer high spatial resolution, making it possible to analyze a tiny portion of alteration-free glass. The variety of analytical techniques available for volatile analysis makes a thorough review beyond the scope of this chapter. References to detailed reviews of analytical techniques are given at the end of the chapter.

V. VOLATILE ABUNDANCES IN BASALTIC MAGMAS

As an introduction to discussing volatiles in basaltic magmas, we first briefly review the abundance and storage of volatiles in Earth's mantle, from which basaltic magmas are generated by partial melting. Volatiles in the Earth's mantle can reside in a number of potential minerals. Recent infrared spectroscopic studies have demonstrated that significant quantities of water can be present as structurally bound OH^- in the nominally anhydrous minerals olivine, pyroxene, and garnet. Water and other volatiles, such as Cl and F, could also be stored in hydrous minerals such as amphibole, phlogopite, and apatite. Carbon may be stored in magnesian carbonate minerals or as diamond, graphite, or amorphous carbon along grain boundaries of other minerals. Sulfur is bound in sulfide minerals. Estimates of the water content of the depleted upper mantle that is the source region for normal midocean ridge basalts (N-MORB) are on the order of 100–200 ppm H_2O, based on studies of water in MORB glasses. If the depleted mantle extends to the 670-km discontinuity, then an amount of water equivalent to ~10% of the mass of water in the present-day ocean could be contained in the upper mantle. The mantle source regions for enriched midocean ridge basalts (E-MORB) probably contain 300–500 ppm H_2O.

During partial melting, water and other volatiles generally behave as incompatible elements—elements that are enriched in the melt phase—because they are not stoichiometric constituents of the major mantle silicates. Even S, which is contained in sulfides, behaves as an incompatible element because of the low modal abundance of sulfide. Thus basaltic magmas act as agents for outgassing the Earth's mantle by carrying volatiles to the surface.

In the following sections, we discuss the volatile concentrations of basaltic magmas from various tectonic settings. We focus particularly on H_2O because it is the most abundant volatile and exerts the strongest influence on magma physical properties, crystallization and differentiation, and eruptive style. Because of its relatively high solubility, little or no water is degassed from basaltic magmas that are quenched on the seafloor or basaltic melt inclusions trapped inside of growing phenocrysts at crustal pressures. In contrast, less soluble volatiles like CO_2 and the noble gases are strongly concentrated into a coexisting CO_2-rich vapor phase because of their low solubility. Thus quenched basaltic glasses and melt (glass) inclusions do not generally have dissolved CO_2 concentrations that reflect their deep mantle (original) values. Instead, their CO_2 contents are an indication of the pressure at which the glass was quenched on the seafloor or was trapped inside a phenocryst. Other volatiles such as S, Cl, and F remain largely dissolved in melt like H_2O. They are useful in basaltic magmas as indicators of crystallization, degassing, and, in the case of Cl, pre-eruptive contamination of basaltic magma by seawater.

A. Midocean Ridge Basalts

N-MORB magmas have relatively low H_2O contents, typically less than 0.4 wt%, but frequently as low as 0.1–0.2 wt% (Fig. 9). E-MORB magmas, which form a volumetrically minor component of the oceanic crust, have systematically higher concentrations, as great as 1.5 wt%. Water concentrations from comagmatic suites of MORB glasses typically show positive covariation with K_2O. Because K_2O is a non-volatile, incompatible trace element, these correlations indicate that H_2O behaves as an incompatible element during partial melting of the mantle and that significant H_2O is neither lost by degassing nor gained by assimilation in magma reservoirs.

Dissolved CO_2 concentrations in quenched MORB glasses vary from 50 ppm to nearly 400 ppm. Most MORB glasses contain small vapor-filled bubbles as well, indicating vapor saturation of the melt at the time of eruption and quenching. Equilibrium thermodynamic calculations, using measured H_2O and CO_2 contents and experimental solubility data, suggest that the coexisting vapor phase would be 93–100 mol% CO_2. Actual measurements of the vapor composition in MORB vesicles are limited, but most have more than 90 mol% CO_2. Because MORB magmas are saturated with a nearly pure CO_2 vapor, the dissolved CO_2 mea-

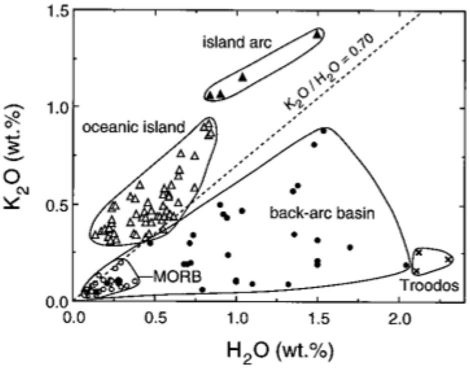

FIGURE 9 Variations in H_2O and K_2O in submarine basaltic glasses from different tectonic environments. Data are shown for midocean ridge basalt (MORB), backarc basin basalt (BAB), ocean island basalt (OIB), island arcs, and for unaltered vesicular glasses from the Troodos ophiolite. (Modified from Muenow *et al.,* 1990.)

surements can be used to estimate a pressure of quenching. Such calculations indicate that many MORB melts were supersaturated with CO_2; that is, they contain more CO_2 than should be dissolved given the pressure equivalent to their depth of eruption on the seafloor. This supersaturation is probably caused by slow diffusion of CO_2 in the basaltic melt during ascent, eruption, and quenching.

Sulfur concentrations in MORB glasses are typically between about 800 and 1400 ppm, but may reach as high as 2500 ppm in Fe-Ti rich basalts. Sulfur contents show strong positive correlation with the FeO content of the melt, consistent with isothermal experimental solubility relations (Fig. 6). Most MORB glasses contain small amounts of quenched immiscible Fe-S-O liquid, indicating that the melts were S saturated at the time of eruption. The most primitive MORB magmas contain 20–50 ppm Cl. In contrast, highly differentiated Fe-Ti-rich basalts contain as much as 1100 ppm Cl, an amount that greatly exceeds what would be expected during closed-system crystallization of basaltic magma. These high concentrations likely reflect assimilation of wallrocks that have been hydrothermally altered by seawater. Fluorine contents of MORB glasses are very low, generally about 0.01–0.06 wt%. Fluorine contents in suites of comagmatic glasses show F increasing with increasing fractionation, in accordance with enrichment in residual liquids during closed-system fractionation.

B. Ocean Island Basalts

Dissolved H_2O in submarine basaltic glasses from ocean island volcanoes ranges from about 0.2 to nearly 1 wt%, significantly higher than N-MORB glass (see Fig. 9). Sulfur concentrations are commonly similar to those in MORB, suggesting that ocean island basaltic magmas, like their midocean ridge counterparts, are saturated with immiscible Fe-S-O liquid before eruption (Fig. 9). Some ocean island basaltic magmas contain as much as 3000 ppm dissolved S but are not highly enriched in FeO, in contrast to S-rich MORB magmas, which are FeO rich. This contrast is consistent with higher oxygen fugacities for these S-rich ocean island basaltic magmas. The higher oxygen fugacities decrease the stability of immiscible Fe-S-O liquid, and a higher dissolved S concentration is required before the basaltic melt is saturated with immiscible Fe-S-O liquid. Thus some ocean island basaltic melts contain more dissolved S than MORB at comparable melt FeO (Fig. 9). Chlorine and F concentrations in ocean island basaltic magmas are relatively low and are comparable to those found in MORB glasses.

An unusual and voluminous series of deep submarine sheet flows composed of highly silica-undersaturated lavas (alkali basalts, basanites, nephelinites) was recently discovered in the North Arch volcanic field, located north of the Hawaiian island of Oahu. Dissolved H_2O in glass samples dredged from these sheet flows are variable and in part high, 0.7–1.4 wt%. Dissolved CO_2 varies from 260 to 800 ppm. These magmas have compositional similarities to the posterosional alkalic volcanics that are erupted on many of the Hawaiian islands after the shield-building stage has ended. Thus the North Arch volcanics provide important information on the volatile contents of alkalic magmatism on oceanic islands.

The best understood oceanic island volcano, and probably the most thoroughly studied volcano on Earth, is Kilauea on the island of Hawaii. The dissolved H_2O concentrations in a variety of basaltic melt inclusions and submarine glasses from Kilauea are shown in Fig. 10. MgO-rich (picritic) glasses from the submarine east rift zone contain mostly 0.37–0.56 wt% dissolved H_2O. In contrast to this rather narrow range, the H_2O contents of basaltic glasses (6.2 ± 0.4 wt% MgO) from the submarine east rift zone vary from 0.10 to 0.85 wt%,

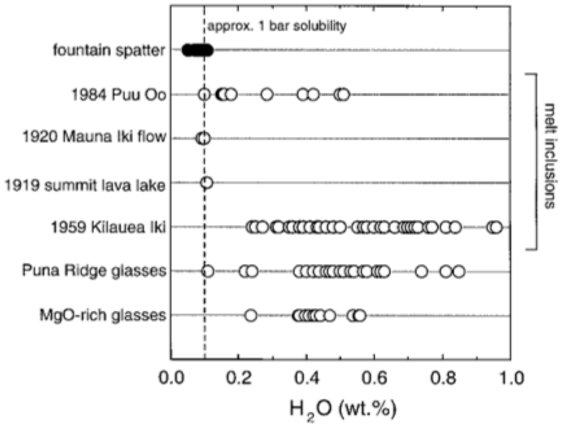

FIGURE 10 Dissolved H_2O concentrations of submarine basaltic glasses (open circles), melt inclusions in olivine phenocrysts (shaded circles), and glassy tephra from lava fountains (solid circles) from Kilauea volcano. Data are shown for MgO-rich glasses, which occur as sand grains in turbidites (Clague *et al.*, 1995) and basaltic glasses (Dixon *et al.*, 1991) from the Puna Ridge, the submarine extension of Kilauea's east rift zone. Data for melt inclusions from the Kilauea Iki eruption of 1959 are from Anderson and Brown (1993). The approximate solubility of H_2O in basaltic melt at 1-bar pressure is shown by the vertical dashed line. (Modified from Wallace and Anderson, 1998.)

and basaltic melt inclusions from olivines in the 1959 Kilauea Iki picrite contain 0.24–0.96 wt%. Melt inclusions from episode 16 of the Puu Oo eruption (1984) contain 0.10–0.51 wt% H_2O. Other melt inclusions from glassy fountain spatter erupted in the summit region and on the southwest rift zone (Mauna Iki) contain about 0.10 wt% dissolved H_2O, which is approximately the 1-bar solubility of water in basaltic melt. Glass from fountain spatter from Kilauea Iki, the 1919 summit lava lake, and Puu Oo all have ≤ 0.10 wt% H_2O.

Degassing at Kilauea is inferred from gas monitoring studies to occur mainly in two stages that are related to subsurface storage and transport of magma. New batches of mantle-derived magma that enter Kilauea from below are probably saturated with a gas rich in CO_2. The solubility of CO_2 at the pressures within the summit magma reservoir is low, and the first stage of degassing occurs as most of the CO_2 is lost through noneruptive degassing. The amount of H_2O that is lost with the CO_2 in the first stage depends on the amount of CO_2 and the pressure, but is generally small, because H_2O is highly soluble in melt. The second stage of degassing occurs when CO_2-depleted magma from the summit reservoir moves along one of the two rift systems through dikes several kilometers below the surface, and then erupts, releasing H_2O-rich gas.

Recognizing primary magmatic volatile contents and undersanding eruptive degassing can be complicated by drainback of magma. Drainback was well documented for the 1959 Kilauea Iki eruption: Magma that degassed during eruption collected into a surface lava lake and then drained back into the vent. Drainback magma can mix with unerupted magma stored at depth to yield partially degassed hybrid magmas. Degassed hybrid magmas, with variable and in part low concentrations of H_2O (0.1–0.85 wt%) and S (0.02–0.15 wt%), have been erupted on the deep submarine flanks of Kilauea. Although the submarine basalts erupted and were collected from depths at which hydrostatic pressure would have prevented significant coeruptive loss of H_2O, the low concentrations of H_2O have been interpreted as reflecting low-pressure degassing prior to repressurized submarine eruption. Such degassing could have occurred by (1) eruption and drainback in the summit region prior to magma being transported down the rift, (2) existence of open fractures connecting magma storage zones to the surface such that pressures were much less than lithostatic, or (3) noneruptive degassing by magma convection in a conduit. The wide range in both submarine glass and melt inclusion H_2O contents and, in particular, some very low values that occur (Fig. 10), presumably reflect degassing at pressures substantially less than those in Kilauea's summit magma storage reservoir.

C. Island Arc and Continental Margin (Subduction-Related) Basalts

It was first suggested in the early 1960s, before the advent of the modern concept of plate tectonics, that subduction of altered oceanic rocks beneath the Aleutian arc was responsible for recycling water into the mantle source region of arc magmas. Early measurements of the H_2O content of submarine basaltic glasses from the Marianas arc (0.8–1.5 wt% H_2O) and in melt inclusions from the 1974 eruption of Fuego, Guatemala, led to a view that water played a relatively minor role in the generation of arc basalts. More recent experimental studies on plagioclase-melt equilibria in low-MgO, high-alumina basalts, which are common in arcs worldwide, suggested H_2O concentrations of 4–6 wt%. Recent measurements of melt inclusions from arc basalts by ion microprobe and IR spectroscopy have yielded H_2O concentrations as high as 6 wt% (Fig. 11).

High H_2O concentrations in arc basaltic melts support the view that water is recycled into the mantle by subduction, where it fluxes significant partial melting and formation of hydrous basaltic magma. However, there are other possible sources for some of the water in arc basaltic magmas apart from a recycled oceanic crustal component, especially in arcs built on continental crust, in which significant assimilation of lower crustal material

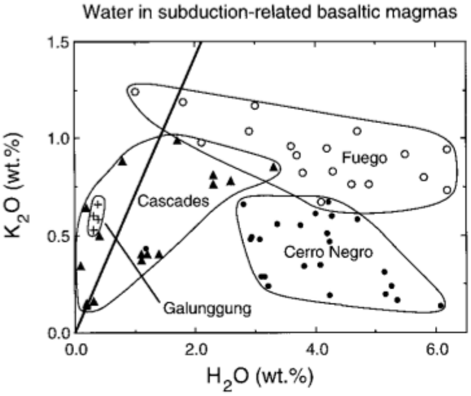

FIGURE 11 Variations in H_2O and K_2O in subduction-related basalt and basaltic andesite melt inclusions from Cerro Negro (Nicaragua), Galunggung (Indonesia), Fuego (Guatemala), and the southern Cascades, western United States. Data are from studies by Roggensack *et al* (1997), Sisson and Layne (1993), and Sisson and Bronto (1998). Heavy line shows a K_2O/H_2O ratio of 0.7 (c.f. Fig. 9).

may occur. On a global scale, it is now recognized that arc basaltic magmas may vary considerably in H_2O content, both within and between arcs. Some arc basaltic magmas also contain significant dissolved carbonate, with reported concentrations as high as 1000 ppm in melt inclusions in olivine phenocrysts from Central America and Indonesia. The carbonate may, in part, have ultimately been derived from subduction of carbonate-rich marine sediments. Indeed, the isotopic composition of carbon in CO_2 from gases at some arc volcanoes provides evidence for such recycling of carbon by subduction processes. The complex relationship between recycling of volatiles by subduction to the mantle beneath arcs and the generation of basaltic magmas is still poorly understood.

D. Backarc Basin Basalts

Basaltic magmas from backarc basins show wide variations in H_2O concentration, ranging from values as low as those in the most H_2O-poor N-MORBs (0.1–0.2 wt%) to values as high as 2 wt% (Fig. 9). Such variations reflect the range of bulk chemical composition of backarc basin basalts, which can vary from MORB-like to showing many similarities to island arc volcanics. Dissolved CO_2 in submarine basaltic glass samples from the Marianas Trough are between 100 and 200 ppm. Negative covariation between H_2O and CO_2 in these glasses and pressure estimates based on experimental solubility data suggest that the samples were vapor saturated at their depth of eruption and quenching, consistent with the presence of vesicles in the glassy pillow rims. Therefore, the bulk magmatic concentrations of H_2O and CO_2 may be significantly greather than the dissolved concentrations. Chlorine concentrations vary from 100 to 800 ppm and show positive correlation with H_2O in some comagmatic suites of glasses.

Some H_2O-rich basaltic magmas erupted in backarc basins or the submarine portions of island arcs have high enough water concentration that they vesiculate and degas dissolved H_2O even during eruption in very deep water. These glasses are distinguished by their relatively high vesicularities (as much as 50% vesicles by volume). As expected, they also have anomalously low concentrations of volatile components, such as S, that exsolve from magma together with H_2O.

Vesicular fresh glasses from pillow margins in the Troodos ophiolite (Cyprus) have volatile contents that are similar to backarc basin basaltic glasses (Fig. 9). These similarities support the interpretation that this ophiolite originated in a backarc basin tectonic setting.

E. Flood Basalts and Large Igneous Provinces

Huge outpourings of basaltic lava to form continental flood basalts and oceanic plateaus (or large igneous provinces; e.g., Kerguelen plateau, Ontong Java plateau) have various ages and tectonic settings. Large igneous provinces were common during the Cretaceous and may reflect a mode of heat loss (and consequent outgassing) from the interior of the planet that is fundamentally different than in currently active plate tectonics. Few data are available on pre-eruptive magmatic volatile abundances in these types of magmas. Such data would be of considerable importance because these very large volume units could have released sufficient volatiles to Earth's atmosphere in a short time to significantly perturb global climate. For example, flood basalts of the Deccan traps erupted near the Cretaceous–Tertiary boundary, leading to the idea that their associated ashes and sulfuric acid aerosols cooled the planet enough to cause the mass extinction. This idea does not have wide acceptance now that a large impact structure has been identified as dating from the Cretaceous–Tertiary boundary. However, the rates of formation of provinces of flood basalts and large igneous provinces, and thus their effects on climates and oceans, are poorly constrained.

VI. VOLATILE ABUNDANCES IN SILICIC MAGMAS

A. Andesites

Andesitic magmas typify convergent plate margins and their volatiles play major roles in planetary degassing and differentiation. However, volatile abundances have been less well studied in andesitic magmas than in either basaltic or silicic magmas. Several reasons for this are that (1) deep submarine-erupted andesitic glasses are rare, and typical subaerial andesites have 30 wt% or more of phenocrysts set in a more siliceous matrix or glass; (2) andesitic magmas do not normally contain either olivine or quartz, the minerals that commonly have large melt inclusions and are the best containers for melt inclusions to prevent posteruptive volatile leakage; and (3) experimental studies of H_2O-rich andesitic compositions have been hampered both by technical problems as well as by problematic application to natural disequilibrium mineral assemblages. Probably the most important result of phase equilibrium studies on andesitic magmas is that a minimum of ~3 wt% dissolved H_2O is necessary to stabilize hornblende, a common phenocryst mineral in andesites. However, hornblende stability is also strongly affected by other factors, such as the Na_2O content of the coexisting silicate melt. Thermodynamic analysis of plagioclase-liquid equilibria in andesitic magmas from the western Mexican volcanic belt suggests about 2.5–4 wt% H_2O in hornblende-bearing andesites and about 1 wt% in andesites that lack hornblende. Analyzed melt inclusions from andesitic magmas in other subduction-related volcanic arcs vary from about 1–4 wt% H_2O. We should reemphasize, however, that these analyses are from phenocryst-rich andesitic magmas in which the interstitial melt portion of the magma, as well as trapped melt inclusions, are relatively silica rich (69–74 wt% SiO_2).

Sulfur concentrations measured in andesitic melt inclusions from subduction zone magmas are normally $\leq$1000 ppm, with typical values of 200–400 ppm. Sulfur generally shows a positive correlation with the FeO content of the melt. There is a significant difference in the origin of this correlation and the one observed for MORB magmas, though both are related to the effect of melt FeO content on S solubility. During cooling, crystallization, and differentiation of MORB magmas, there is an increase in melt FeO in residual liquids that increases S solubility. In contrast, during crystal fractionation of andesitic magmas, residual liquids have decreasing FeO contents, such that the S solubility in andesitic melts decreases during cooling and crystallization. A further complexity of interpreting S variations in andesitic magmas is related to oxygen fugacity. The range of oxygen fugacity for typical andesitic magmas varies from slightly below the NNO buffer reaction to about 2 log units more oxidized than NNO. Over this range, sulfur speciation changes from dominantly sulfide to dominantly sulfate (see Fig. 4). Thus solubility limits for S in andesitic magmas and their variations during crystallization differentiation are potentially complex. In a few cases, S in andesitic melt inclusions is as great as 3000 ppm; this probably reflects a relatively high magmatic oxygen fugacity because sulfate is much more soluble than sulfide.

Limited data on halogen abundances in andesitic melt inclusions indicate ~1500 ppm Cl and ~500 ppm F.

B. Dacites and Rhyolites

Water and many other volatiles are relatively abundant in silicic magmas both as dissolved species and in exsolved gas. High concentrations of H_2O, in particular, provide the energy for the powerful explosive eruptions that typify silicic magmas. Glassy dacitic and rhyolitic melt inclusions are common in rapidly quenched phenocrysts from explosive eruptions, and analyses of the inclusions commonly reveal 3–7 wt% H_2O. Experimental phase equilibrium studies reveal temperatures and depths of equilibration, and dissolved H_2O concentrations. Analytical (melt inclusion) and experimental results are broadly consistent for dissolved volatiles. Experimental phase equilibria studies cannot be used, however, to determine whether a magma was vapor saturated before eruptive decompression. For cases where independent data suggest pre-eruptive vapor saturation, phase equilibria can constrain the composition of the vapor.

Water-rich rhyolitic melt inclusions are typical of low-temperature (700–800°C) melts containing hydrous phenocrysts of biotite and amphibole. Less H_2O is found in rhyolitic glasses that cooled from higher temperatures (900–1000°C) and contain pyroxene but no hydrous phenocrysts. Wide variations in dissolved CO_2 are found in rhyolitic melt inclusions, varying from 10 to about 1200 ppm. Based on the pressure-dependent solubilities of H_2O and CO_2 in rhyolitic melts, the melt inclusion data can be used to compute the pressure at which the melt would be saturated with a vapor phase (the vapor-saturation pressure) and thereby constrain pressures of crystallization (inclusion formation). For vapor-saturated magmas the indicated vapor-saturation pressure equals the pressure of crystallization. For magmas lacking vapor (vapor undersaturated), the actual pressure of crystallization is greater than the vapor-saturation pressure. Vapor-saturation pressures based on melt inclusion H_2O and CO_2 concentrations vary from about 1 to 4 kbar, implying a range of upper crustal depths through which silicic volcanic magmas differentiate and reside before eruption.

Detailed experimental phase equilibrium studies have been performed on the 1980 Mount St. Helens dacite (Fig. 7) and the 1991 Mt. Pinatubo dacite. The results for both indicate crystallization pressures of ~2.2 kbar and temperatures of 920 and 780°C, respectively, as well as significant dissolved H_2O. For the Mount St. Helens dacite, the experimentally synthesized mineral assemblage and mineral compositions match the natural assemblage when there is about 4.6 wt% H_2O dissolved in the melt. If the magma was vapor saturated before eruption, then the experimental data can be used to infer a vapor phase composition of 50–70 mol% H_2O and 30–50 mol% CO_2. In contrast, the experimental data for Mt. Pinatubo dacite indicate a higher H_2O concentration of ~6 wt%, consistent with analyses of melt inclusions trapped in quartz phenocrysts. These pre-eruptive dacitic magmas appear to have contained a vapor phase during crystallization, because the vapor-saturation pressures and pressures based on phase equilibria are equal.

One of the best studied rhyolitic eruptions in terms of magmatic volatile abundances is the 0.76-Ma explosive, caldera-forming eruption that formed the 500-km^3 Bishop Tuff. Melt inclusions in Bishop quartz phenocrysts reveal systematic, pre-eruptive gradients in dissolved H_2O and CO_2 during crystallization (Fig. 12). Melt inclusions from early erupted pumice fall deposits contain 5.3 ± 0.4 wt% H_2O and 60 ± 40 ppm CO_2, whereas those from the middle of the eruption contain higher H_2O (5.7 ± 0.2 wt%) and CO_2 (120 ± 60 ppm). Thus early erupted magma contained less dissolved H_2O and CO_2 than magma from the middle of the eruption. Compared with melt inclusions from early and middle Bishop Tuff samples, inclusions from late erupted magma have much lower H_2O (4.1 ± 0.3 wt%), and higher and variable CO_2 (150–1100 ppm). The estimated pressures of crystallization (vapor-saturation pressures) are lower for inclusions from the earliest erupted samples than in samples from the middle of the eruption. This pattern is consistent with sequential tapping of a large zoned body of gas-saturated magma, because the first material erupted would likely come from the shallowest (lowest pressure) portion of the magma body.

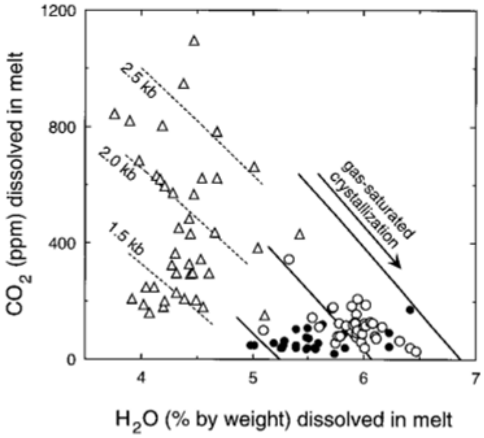

FIGURE 12 Dissolved H_2O and CO_2 in rhyolitic melt inclusions in quartz phenocrysts from the 0.76-Ma Bishop Tuff. Data are shown for samples from the early (solid circles), middle (open circles), and late (open triangles) parts of the eruption. Diagonal lines show the H_2O and CO_2 contents of rhyolitic melt saturated with H_2O-CO_2 gas at pressures from 1.5 to 2.5 kbar and temperatures of 725°C (solid lines) and 790°C (dashed lines), which correspond to the pre-eruptive temperatures for the early and late erupted magmas, respectively. The arrow indicates the trend of H_2O and CO_2 contents in successive residual liquids formed by isobaric, gas-saturated crystallization. (Modified from Wallace *et al.,* 1995, *Nature.*)

Dissolved S concentrations in silicic magmas tend to be relatively low (≤200 ppm), and are frequently below the minimum detection limit of common analytical techniques. These low concentrations occur despite the fact that most silicic magmas are saturated with a sulfide (pyrrhotite) and/or sulfate phase (anhydrite). The low S solubility is caused by a combination of low melt FeO content and the low temperature of silicic magmas. The former is an important factor at relatively low magmatic oxygen fugacity where dissolved S is dominantly sulfide, whereas decreasing temperature significantly decreases both sulfide and sulfate solubilities (see Fig. 5).

Fluorine and chlorine abundances are relatively low in metaluminous dacites and rhyolites (F, 200–1500 ppm; Cl, 600–2700 ppm). In the Bishop Tuff melt inclusions, F varies from 160 to 460 ppm and Cl varies from 550 to ~800 ppm. Both elements are more abundant in the most highly differentiated, early erupted Bishop Tuff whereas lower concentrations occur in the least differentiated magma that erupted later. Melt inclusions from the 1991 Mt. Pinatubo dacite contain ~1000 ppm Cl. In contrast to halogen abundances in metaluminous magmas, peralkaline rhyolites (pantellerites) contain as much as 1.3 wt% Cl and 1.5 wt% F. These high concentrations reflect the highly differentiated nature of these magmas, which causes Cl and F to increase like other incompatible trace elements, and to the effects of alkalies in increasing Cl and F solubilities in silicate melts. Peraluminous tin and topaz rhyolites of the western Unites States and central Mexico also contain high halogen concentrations, with Cl reaching 0.5 wt% and F as great as 5 wt%.

C. Gradients in Volatile Abundances and Vapor Saturation in Magmas

Gradients in dissolved volatiles, especially H_2O, within individual silicic magma bodies have been inferred from (1) variations in phenocryst assemblages and compositions; (2) variations in whole-rock abundances of F and Cl; and (3) the observation that many volcanic eruptions evolve with time from high-energy Plinian columns to pyroclastic flows, or culminate with quiescent dome extrusion. Gradients in dissolved H_2O in silicic magma bodies have more recently been confirmed using ion probe and infrared spectroscopic techniques on melt inclusions in phenocrysts. However, changes in eruptive style from Plinian column to pyroclastic flow often do not appear to be related to differences in pre-eruptive dissolved water, insofar as this is recorded by melt inclusions in phenocrysts. Even effusive (nonexplosive) eruptions of silicic magma appear to involve magma with initially high dissolved H_2O concentrations. That such magmas are erupted nonexplosively requires that water be lost prior to extrusion. This probably occurs when magma decompression induces sufficient vesicularity to form a magmatic foam that is highly permeable to gas loss.

It has commonly been thought that magmas of intermediate to silicic composition only become gas-saturated during shallow ascent and emplacement, during eruptive decompression, or during advanced (pegmatitic) stages of plutonic crystallization. However, studies of eruptive dynamics, CO_2 and SO_2 emissions, and melt compositional features all suggest that many magmas in subvolcanic reservoirs are saturated with a multicomponent vapor. Volcanoes could be viewed primarily as gas vents. In particular, the small but finite solubility of CO_2 in silicic magmas at crustal pressures could result in saturation with H_2O-CO_2 vapor during partial melting as well as during ascent, emplacement, and crystallization. High-temperature fluid inclusions in phenocrysts from some silicic volcanic rocks provide direct evidence of pre-eruptive vapor saturation. Gradients in alkali and trace element abundances might result in part from upward flux of exsolved gas in a large magma body.

Correlations between CO_2 and trace elements in melt inclusions from the Bishop Tuff indicate that the magma was gas saturated during pre-eruptive crystallization. Quantitative models of gas exsolution during crystallization of the Bishop magma are consistent with exsolved gas contents varying from about 1 wt% in the deeper regions of the magma body to nearly 6 wt% near the top (Fig. 13). Thus the data and models suggest that there was a gradient in exsolved gas, with mass fractions of gas increasing upward toward the roof of the magma body. Because the exsolved gas phase would be H_2O rich, such large exsolved gas contents imply that the early erupted Bishop magma had a bulk (dissolved + exsolved) H_2O content of ~10 wt%. However, these interpretations assume that gas traveled with and remained in the magma during most of its evolution. The presence of significant mass fractions of exsolved gas in Bishop magma is consistent with H_2O and CO_2 dissolved in minimally degassed rhyolitic obsidians at Mono Craters, California. Similar mass fractions of pre-eruptive exsolved gas have been inferred for the magma bodies of the 1982 El Chichón and 1991 Mount Pinatubo eruptions by assuming that all SO_2 released (measured by remote sensing techniques) was stored in the erupted volume of magma.

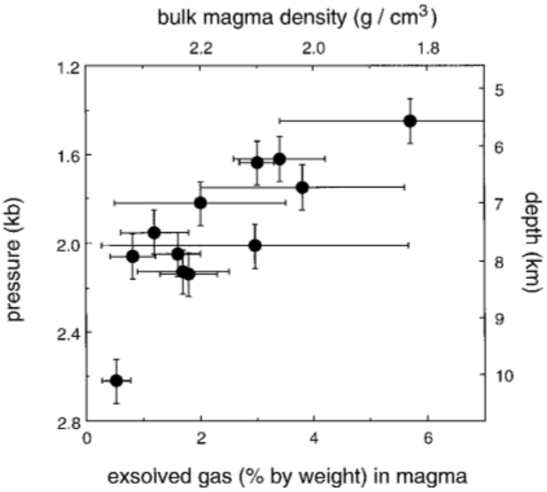

FIGURE 13 Exsolved gas content in the crystallizing Bishop rhyolitic magma as inferred from volatile and trace element analyses of melt inclusions. The bulk magma (melt + crystals + gas) density is given along the top of the diagram. (Modified from Wallace *et al.,* 1995, *Nature.*)

D. Volcanic Gases, SO_2 Emissions, and Pre-Eruptive Vapor Saturation in Magmas

One of the most important constraints on bulk (dissolved + exsolved) magmatic volatile contents comes from studies of the fluxes of SO_2 from erupting volcanoes. During the last several decades, scientists have discovered that SO_2 gas injected into the stratosphere by explosive eruptions is converted in a matter of days into aerosols rich in H_2SO_4 (sulfuric acid) that can affect both climate and atmospheric chemistry. Measurements of the amounts and fluxes of SO_2 emitted from erupting volcanoes can be made with remote sensing techniques, including both ground- and air-based use of the ultraviolet correlation spectrometer (COSPEC) and the satellite-based total ozone mapping spectrometer (TOMS). Comparison of SO_2 emissions with petrologic estimates of dissolved S in volcanic magmas has led to a conundrum, known as the "excess" sulfur problem. Inclusions of melt in erupted phenocrysts indicate dissolved sulfur contents that are far too low (by a factor of 10–100) for the melt to exsolve the total mass of SO_2 erupted. Excess eruptive S is observed in most eruptions for which remote sensing and melt inclusion data are available. Exceptions to this general pattern are eruptions of basaltic magma from the Hawaiian volcanoes, Kilauea and Mauna Loa. Most SO_2 emission estimates that are based on melt inclusions in volcanic phenocrysts assume that the only source of sulfur released during an eruption is that which was originally dissolved in the silicate liquid (melt) portion of the magma shortly before eruption. However, there is a large body of evidence, based on petrologic, remote sensing, and volcanic gas data, that nearly all of the SO_2 released during many explosive eruptions was actually contained in pre-eruptive exsolved gas. As a result, eruptions of exsolved-gas-rich silicic magmas can release large amounts of SO_2 derived from pre-eruptive exsolved gas, notwithstanding very low concentrations of dissolved S.

VII. IMPORTANCE OF VOLATILES IN VOLCANIC ERUPTIONS

A main goal of volcanology is to understand volcanic eruptions. Decompression of volatile-rich, viscous magmas can result in explosive eruptions because of the thousand-fold volumetric expansion of gas with decompression from 1000 to 1 bar. Gas that occupied 1 vol% of the magma at 1000 bars occupies 91 vol% at 1 bar, and the latter corresponds to a dilute spray of particles in a gas jet. Importantly, gas exsolution generally begins at depth with small amounts of relatively CO_2-rich gas followed by increasing proportions and amounts of H_2O-rich gas nearer the surface. Some stiff (high viscosity) magmas may have internal pressures approaching 100 bars only a few meters below the surface, because gas has been slow to escape from the magma. Theoretical modeling reveals that magmatic volatile contents largely govern the explosivity of eruptions. Conversely, plume height and tephra dispersal can be used to infer pre-eruptive volatile contents. Modeled and observed volatile concentrations have been partly at odds, and this has led to critical reassesments and model improvements. In some cases, reconciliation has tended to increase the amount of volatiles needed for specific effects, implicating the presence of significant exsolved pre-eruptive gas.

Modeling of explosive silicic eruptions shows that the velocity of erupting material is strongly dependent on the amount of exsolved gas. Eruption velocities at the vent, estimated from the maximum size of blocks deposited near the vent, are as much as 400–600 m/s for the most powerful Plinian eruptions. Such velocities are estimated to require 3–6 wt% exsolved H_2O, an amount that is consistent with dissolved concentrations indicated by experimental work and measured in melt inclusions. In many eruptions, there is an observed or inferred transition from a Plinian eruption column to a collapsing column, resulting in a transition from pumice-fall to ash-flow deposition. Lower magmatic H_2O concentrations, or increased mass flux of erupting magma with the same H_2O concentration due to widening of the vent can, theoretically, cause the Plinian column to become unstable and collapse to form pyroclastic flows. Interpretations of the Bishop eruption based on tephra characteristics, however, suggest synchronous eruption of one or more sustained jets that fed both a buoyant (Plinian) column, from which pumice-fall material was deposited, and collapsing clouds, which deposited ash-flows. As the eruption continued, the proportion of ash-flow material increased, the amount of H_2O in melt inclusions increased slightly (Fig. 12), and the amount of pre-eruptive exsolved gas decreased (Fig. 13). Thus the amount of pre-eruptive exsolved gas may be especially important in regulating eruptive style.

The height of basaltic lava fountains is also controlled largely by the amount of exsolved gas in the erupting magma. The initial (pre-eruption) amounts of H_2O that are necessary to propel lava fountains to 200- and 800-m heights are about 0.3 and 0.6 wt%, respectively. These estimates have been revised upward in light of the fact that much of the magma in typical Hawaiian-style fountains falls back into a bowl-shaped crater surrounding the vent, forming a pond of relatively dense, degassed magma. Newly vesiculating magma from depth loses some of its kinetic energy as it fountains through this degassed magma pond. After accounting for this effect, the resulting estimates of H_2O concentration based on observed fountain heights are consistent with both dissolved H_2O contents determined from analyses of melt inclusions trapped in olivine phenocrysts and with estimates based on the composition and fluxes of volcanic gases. Modeling also suggests that the transition from lava fountaining to intermittent Strombolian explosions is not likely to be related to a decrease in volatile content but rather is caused by a reduction in the ascent velocity of magma, which results in more time for bubble coalescence to occur. In contrast, a decrease in magmatic volatile content is predicted to result in a transition to passive effusion of vesicular basaltic lava.

VIII. EFFECTS OF VOLATILES ON PHYSICAL PROPERTIES OF SILICATE MELTS

Small amounts of dissolved volatiles have important effects on the density, viscosity, and crystallization of melts and magmas, and these can influence magma ascent, eruption, and differentiation. Experimental data are available concerning the effects of H_2O, CO_2, and F on melt density and viscosity, but comparable data for Cl and S do not exist.

A. Density

The partial molar volume of H_2O dissolved in melt of albite composition ($NaAlSi_3O_8$) has been directly measured by experiment as 14–20 cm^3/mol over the temperature range from 750 to 950°C. Partial molar volumes of dissolved H_2O in rhyolitic and basaltic melts estimated indirectly from solubility data are generally similar to the low end of the range for albite melt. In detail, however, determinations from solubility data can be complex because of the concentration-dependent speciation of dissolved H_2O into both OH^- groups and molecular H_2O. Given the molecular weight of H_2O (18 g/mol) and a partial molar volume of ~14 cm^3/mol, addition of dissolved H_2O to a melt represents a component with a density slightly greater than 1 g/cm^3 compared with densities for anhydrous basaltic and rhyolitic melts of ~2.7 and ~2.3 g/cm^3, respectively. Thus addition of dissolved water to a melt decreases the melt density. The effect of adding 6 wt% dissolved H_2O to a rhyolitic melt is to decrease the density by about 5%, whereas addition of 2 wt% H_2O to a typical basaltic melt decreases its density by 2–3% relative to anhydrous values.

The best estimates for the partial molar volume of dissolved molecular CO_2 (rhyolitic melt) and carbonate (basaltic melt) derived from solubility data are between 21 and 28 cm^3/mol. The low solubility of CO_2 results in relatively low concentrations in magmas at crustal depths, such that CO_2 is not expected to have a strong effect on the densities of magmas stored in the Earth's crust. At mantle depths, especially in silica poor magmas in which CO_2 solubility (dissolved as carbonate) is relatively high, CO_2 can have significant effects on melt densities. The molecular weight of CO_2 (44 g/mol) and the range of partial molar volumes given earlier indicate that dissolved carbonate represents a component with a density of ~2 g/cm^3. The effect of adding 3 wt% CO_2 to an alkali basaltic melt is to decrease the melt density by ~3%. For comparison, addition of 3 wt% dissolved H_2O to the same melt decreases melt density by ~5%.

Determining the effects of dissolved F on silicate liquid density is complex, but available data clearly indicate that addition of F decreases melt density.

B. Viscosity

Experimental studies of viscosity demonstrate three important features of the viscosities of silicate melts. The first is that silicate melts exhibit Newtonian behavior, defined as a liquid in which the rate of shear in the liquid is linearly proportional to the magnitude of the applied shear stress. The second important feature is that silicate melt viscosity increases rapidly with decreasing temperature. Thirdly, silicate liquid viscosities are also strongly dependent on melt composition, the most important component being SiO_2. With increasing SiO_2 content in a melt, viscosity also increases. The combination of the inverse dependence of viscosity on temperature and the positive covariation with SiO_2 content results in low-temperature rhyolitic melts having a viscosity that is as much as 8 orders of magnitude (10^8 times) greater than that of a high-temperature basaltic melt.

Addition of dissolved H_2O to a melt decreases the viscosity, probably because H_2O weakens or breaks apart the aluminosilicate framework of the melt, which makes it flow more readily. Experimental studies have shown a nonlinear effect of H_2O in decreasing viscosity (Fig. 14). Over the range from 0 to 3 wt% H_2O, water has

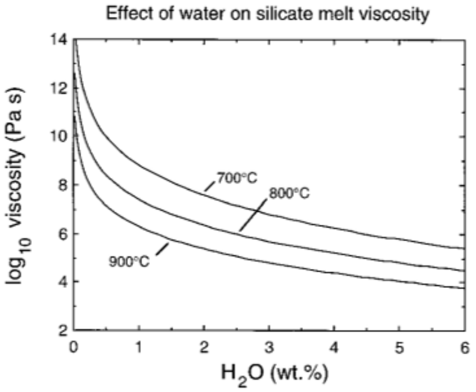

FIGURE 14 Effect of dissolved water on the isothermal viscosity of a granitic (rhyolitic) melt. Note that at low water concentrations, the 700 and 800°C curves are for supercooled melt, because the temperatures are below the solidus temperature for melting of dry granite (900°C for H_2O-free granite). Calculated from Hess and Dingwell (1996).

a very strong effect in reducing viscosity. In the case of siliceous melts, addition of 3 wt% H_2O to a dry melt may reduce the viscosity by as much as 5 orders of magnitude. For dissolved H_2O greater than 3 wt%, addition of more water has a much smaller effect on the viscosity. The reason for the change in the effect of H_2O is plausibly related to the speciation of dissolved water. From 0 to 3 wt% H_2O, water is dissolved predominantly as OH^- groups bound to the aluminosilicate framework—thus in this concentration range, dissolved water has a relatively large effect on viscosity. Above 3 wt% H_2O, the amount of water that is present as OH^- reaches a maximum value, and additional dissolved water is mostly present as H_2O molecules that do not cause weakening or breaking of aluminosilicate bonds. Thus at higher concentrations water has a smaller effect on silicate melt viscosity.

Determining the effects of dissolved CO_2 on melt viscosity is difficult. Available experimental data suggest that dissolved CO_2 reduces the viscosity of silicate melts, but the effect is much smaller than for H_2O. Experimental studies show that F has a relatively large effect in reducing the viscosity of SiO_2-rich melts. Although the concentration of F in most natural magmas is low enough to preclude it having a significant effect, F-rich topaz rhyolites have sufficient F to reduce magma viscosity by as much as 3 orders of magnitude. A manifestation of this effect is the eruption of topaz rhyolites to form unusually long lava flows with little associated explosive tephra.

IX. ORIGIN OF VOLATILES, EARTH DEGASSING, AND VOLATILE RECYCLING VIA SUBDUCTION

Studies of both inert and reactive volatile elements help scientists evaluate the origin and evolution of the Earth. This chapter has as its primary focus the reactive volatiles that mostly become chemically bound into either minerals or molecules in air, water, oil, and ice. In this section, we give an elementary overview of some of the inert volatile elements (usually termed *noble gases*): helium, neon, argon, krypton, xenon, and radon. Studies of inert gases, particularly helium and argon, help constrain ideas about Earth's origin and evolution. The noble gases readily enter the Earth's atmosphere, and they comprise both radiogenic and nonradiogenic isotopes. Thus certain isotopic ratios change in time and may reflect ratios of radioactive parent nuclides and nonradiogenic inert gas in compositionally distinct and physically separate parts of the Earth. Helium and argon are especially interesting in this regard. Helium has two isotopes: ^{3}He and ^{4}He. Radioactive decay of uranium and thorium yield ^{4}He, whereas radiogenic production of ^{3}He is negligible in virtually all Earth environments. Furthermore, helium escapes from the atmosphere because in the upper stratosphere, the pressure is low, atoms are far apart, and the average speed of low mass atoms may exceed the threshold value at which Earth's gravitational field can slow outward-moving atoms and return them to the Earth. The more helium there is in the air, the greater the outgoing escaping flux (number of atoms of helium escaping per year, for example). At some point the amount of helium in air is just right for the escaping flux to be balanced by the rate of supply from the interior of the Earth.

Geological processes such as ocean circulation, seafloor spreading, and continental erosion affect the fluxes of helium from various storage reservoirs within the earth. As a result, the ratio of nonradiogenic ^{3}He to radiogenic ^{4}He in different rocks and water bodies characterizes various sources of He: Helium in air is relatively poor in ^{3}He compared to helium in oceanic ridge basalts and basalts associated with hot spots such as Hawaii. Thus it is likely that most of the helium in air comes from continental rocks, which are rich in uranium and thorium, and have therefore produced significant ^{4}He from radioactive decay. Such rocks have evolved near the Earth's surface for geologically long periods of time and probably their original ^{3}He was lost from the Earth's atmosphere long ago. Only deeply buried sources plausibly retain ^{3}He that was initially present in the Earth when it formed from objects in the solar nebula. Thus comparatively high ^{3}He/^{4}He ratios of basalts from Hawaii suggest that Hawaiian basalts are derived, at least in part, from deep within the mantle, possibly from an undegassed remnant of lower mantle material left over from early in Earth's history.

Similarly, investigations of radiogenic ^{40}Ar (produced from the radioactive decay of ^{40}K) compared with nonradiogenic ^{36}Ar in both terrestrial and meteoritic rocks support the view that the mantle consists of at least two parts. One part has largely lost its argon and presumably most of its other volatiles, including reactive ones such as H_2O, which readily dissolve in silicate melts and are carried toward the surface in magmas. A second part seems to still have much of its nonradiogenic argon (^{36}Ar) and evidently is relatively primordial. An atom of argon is 10 times more massive than one of helium and nearly all argon is retained in the atmosphere by Earth's gravitational field. Nearly all argon in air is ^{40}Ar, but there is less ^{40}Ar than the amount expected based on the ^{40}K content of the Earth, which is independently reasonably well known. Thus there must be a significant part of the Earth that contains much of the ^{40}Ar that has been produced by decay of ^{40}K during the history of the Earth and which has not yet reached the atmosphere. If an incompletely degassed mantle reservoir contains the missing radiogenic ^{40}Ar, then this reservoir would likely also contain a significant amount of reactive volatiles such as H_2O and CO_2.

Studies of inert gases are consistent with the theory that early in its history, the Earth was covered by a deep magma ocean, caused by conversion into heat of some of the gravitational potential energy of accreting material. Inert volatiles would have become predominantly degassed and concentrated in the atmosphere during the Earth's formation. Such an early atmosphere could have been largely lost from the Earth as a result of solar activity or violent impacts. Significant amounts of reactive volatiles such as H_2O could have dissolved in the magma ocean. Subsequent crystallization of the magma ocean and formation of minerals poor in H_2O would promote degassing by concentrating the reactive volatiles in a diminishing residue of liquid, thereby leading to the formation, rise, and escape of bubbles of gas.

It is conceptually important that present degassing rates of primordial, nonradiogenic inert gas from ocean ridge magmatism (based on the ^{3}He rate and ratios of other inert gases to ^{3}He), when multiplied by the age of the Earth, yield much less total nonradiogenic neon and argon than is presently in Earth's atmosphere. Thus it is inferred that the rate of degassing from the Earth either was much greater in the past, or that significant inert gas has been separately added to the outermost Earth by meteoritic infall. The present-day isotopic composition of nonradiogenic inert gases being degassed from the Earth is noticeably different from that in air, and intermediate between that of inert gases from the Sun and from meteorites. The discrepancy can therefore be reconciled with either a mixture of sources for the Earth's inert gases or preferential loss from Earth's atmosphere of less massive isotopes.

Subduction provides a mechanism by which sediments and altered oceanic crust are recycled back into the mantle. The sediments and altered crust are relatively rich in the two major reactive volatiles: carbon dioxide stored as carbonates, and water, both as pore water and as water bound in hydrous minerals such as clays. Most of the hydrous minerals break down to anhydrous minerals and release water vapor as the subducting rock heats up. The pore water and the water released from hydrous minerals are buoyant, and increasing pressure from the weight of overlying rocks collapses pores and forces water out of deeply buried rocks. Some deep storage of water is possible, however, in view of experimental studies which show that some dense hydrous magnesian silicates are stable to very high pressures and temperatures. Also, small concentrations of water occur as structurally bound OH^- in nominally water-free minerals such as olivine and pyroxene. Subduction-related basaltic magmas are notably more water-rich than midocean ridge and ocean island basaltic magmas, and such magmas may return most or all of the subducted water to the surface. A small fraction of the subducted water may be cycled into the deeper mantle, but this is unconstrained.

The isotopic composition of water is unaffected by radioactive decay (except for bomb tritium) and has probably been negligibly affected by preferential escape from Earth of hydrogen compared to more massive deuterium. Ratios of hydrogen to deuterium in various water reservoirs mainly reflect the geologic processes that partition water into these reservoirs. Water initially released from magmas at igneous temperatures is eventually redistributed by formation of new low-temperature minerals in the reservoirs of altered rocks, seawater, freshwater, and ice. Isotopic fractionation during this redistribution causes the oxygen and hydrogen isotopic composition of seawater to differ from that dissolved in parental basaltic magmas; the balance is made up mainly by the isotopically light water bound in altered rocks. There is no isotopic evidence for a significant source of surface water beyond that which degasses from basaltic magmas. Nor is there evidence for preferential subduction and hidden storage of water that is isotopically distinct from that which is in parental basaltic magmas.

The isotopic composition of carbon in parental basaltic magmas and various terrestrial reservoirs is not certain. There may be a significant isotopic shift upon degassing and this makes it difficult to assess the isotopic composition of carbon in parental basaltic magmas. The predominant recognized reservoir of terrestrial carbon is in sedimentary limestones and dolomites and it differs significantly from that which degasses from basaltic magmas at igneous temperatures. Photosynthesis yields reduced carbon in biological tissues that is relatively poor in ^{13}C and this affects the isotopic composition of carbon in surficial reservoirs. Existing knowledge permits the amount and isotopic composition of buried organic matter (mainly reduced C in shales and coals) to balance the amount and isotopic composition of carbon in carbonate rocks, yielding a sedimentary average that is consistent with igneous gas. However, significant additions of isotopically distinctive carbon to Earth's early atmosphere during the final stages of accretion as well as storage of carbon in Earth's core are possible. Furthermore, it is possible that the isotopic composition of carbon now released from magmas reflects a recycling steady state, and it may have differed in the remote past, reflecting a smaller proportion of recycled carbon.

Carbonate rocks, if mixed with quartzose rocks will undergo decarbonation reactions during subduction into the deep crust and shallow upper mantle, and carbon dioxide-bearing gas will form and return to the surface. This may be a source of some carbon dioxide in gas reservoirs and hot springs, but most carbon dioxide in such environments is derived from superficial sources like heated groundwater. Carbonate rocks alone or with silica-poor minerals are refractory and may remain stable to great depths in the mantle. Thus subduction of limestones can potentially introduce carbon dioxide as carbonate rocks into the deep mantle where it may persist. Subduction of carbonate rocks plausibly increased during the past 180 million years owing to biological evolution of pelagic foraminifera and formation of abundant, subductable deep oceanic carbonates, possibly reversing the net flux of carbon dioxide back into the mantle from the crust. The flux of carbon dioxide associated with subduction zone volcanism is poorly known, and this topic could benefit greatly from further study.

The downgoing view of carbon dioxide is illuminated by the fact that at fairly shallow mantle depths the carbonate mineral dolomite becomes stable in a typical assemblage of mantle silicates. Thus a deep residence of mineralogically bound carbon dioxide is feasible. Under the conditions of pressure and temperature where dolomite is stable in the mantle, carbon dioxide is quite soluble in silicate melts and can flux partial melting at comparatively low temperatures. The upgoing view of ascending carbonate-rich magmas is marked by the expected release of carbon dioxide gas at shallow upper mantle pressures. Plausibly this pressure-sensitive effervescence of carbon dioxide gas is partially responsible for the explosive nature of rare magmas, bringing diamonds and fragments of the mantle to the upper crust.

Yearly amounts of reactive volatiles H_2O and Cl that are subducted are in the range of rough estimates of what is returned surfaceward by arc magmatism. If there were no surfaceward return of subducted H_2O and Cl, then the formation, alteration, and subduction of oceanic crust would comprise a net drain on the water and salt in the oceans. The geologic record and understanding of tectonism reveal that continental crust and ocean water have existed for most of Earth's history; subduction has not caused the oceans to dry up. Thus water lost to altered oceanic crust is probably largely returned to the oceans via dewatering of subducted crust and subduction-related magmatism.

X. FUTURE DIRECTIONS

The study of magmatic volatiles lies at the interface of igneous petrology and volcanology. Much of our present state of knowledge has been derived relatively recently due to major advances in techniques of microanalysis. Improvements that are under way will soon make it possible to measure the isotopic composition of volatile and nonvolatile species in silicate melt inclusions, as well as the determination of some volatile trace metals in trapped fluid or vapor + melt inclusions in volcanic phenocrysts. Combined analyses of volatile species, trace elements, and isotope ratios (e.g., H, O, S, C, He, Sr) will contribute to a better understanding of volatile recycling in the Earth, melting processes, magmatic differentiation, and magma degassing.

The pressure-dependent solubilities of the major volatiles H_2O and CO_2 in silicate melts make it possible to use melt inclusions as geobarometers. Combined with major, trace, and isotopic data, and detailed knowledge of time–volume–compositional variations in eruptive deposits, melt inclusions can be used to place constraints on magma chamber configurations, and magmatic and eruption processes. In this context, petrologic techniques for estimating the bulk (dissolved + exsolved) volatiles in magma bodies need to be further developed and refined in order to better understand volcanic gas fluxes, low-pressure degassing, and the relationship between volatiles and eruption dynamics. Although the interpretation of melt inclusion data is frequently complex due to effects of magma mixing, crystallization, and volatile leakage, the ability to sample melt inclusions from different stratigraphic levels of an eruptive deposit makes it possible to get an unprecedented look at the workings of magma bodies.

It is increasingly being recognized that magmatic volatiles, including volatile trace metals, make important contributions to magmatic-hydrothermal ore deposits. Future analytical developments that make it possible to measure the stable and radiogenic isotope ratios of melt inclusions will significantly add to our knowledge of magmatic inputs to ore-forming systems. Another important area of future research will be the relationship between volatile abundances in volcanic rocks and their plutonic equivalents. The goal of such work will be to gain a better understanding of the relationship between plutonic and volcanic rocks and, in particular, whether volcanic eruptions tap the volatile-enriched upper portions of larger crustal magma reservoirs, leaving behind less volatile-rich, uneruptable material that eventually solidifies as a pluton.

SEE ALSO THE FOLLOWING ARTICLES

Basaltic Volcanoes and Volcanic Systems • Earth's Volcanoes and Eruptions: An Overview • Flood Basalt Provinces • Lava Fountains and Their Products • Magma Ascent at Shallow Levels • Physical Properties of Magmas • Rates of Magma Ascent

---

FURTHER READING

Anderson, Jr., A. T., and Brown, G. G. (1993). CO_2 and formation pressures of some Kilauean melt inclusions. *Am. Mineral.* **78,** 794–803.

Carroll, M. R., and Holloway, J. R., eds. (1994). Volatiles in magma. *Mineral. Soc. Am. Rev. Mineral.*, **30**.

Clague, D. A., Moore, J. G., Dixon, J. E., and Friesen, W. B. (1995). Petrology of submarine lavas from Kilauea's Puna Ridge, Hawaii. *J. Petrol.* **36,** 299–349.

Dixon, J. E., Clague, D. A., and Stolper, E. M. (1991). Degassing history of water, sulfur, and carbon in submarine lavas from Kilauea volcano, Hawaii. *J. Geol.* **99,** 371–394.

Hess, K.-U., and Dingwell, D. B. (1996). Viscosities of hydrous leucogranitic melts: A non-Arrhenian model. *Am. Mineral.* **81,** 1297–1300.

Jackson, I., ed. (1998). "The Earth's Mantle: Composition, Structure, and Evolution." Cambridge University Press, Cambridge, UK.

Jaggar, T. A. (1940). Magmatic gases. *Am. J. Sci.* **238,** 313–353.

Muenow, D. W., Garcia, M. O., Aggrey, K. E., Bednarz, U., and Schmincke, H.-U. (1990). Volatiles in submarine glasses as a discriminant of tectonic origin: Application to the Troodos ophiolite. *Nature* **343,** 159–161.

Roggensack, K. R., Hervig, R. L., McKnight, S. B., and Williams, S. N. (1997). Explosive basaltic volcanism from Cerro Negro Volcano: Influence of volatiles on eruptive style. *Science* **277,** 1639–1642.

Rutherford, M. J., Sigurdsson, H., Carey, S., and Davis, A. (1985). The May 18, 1980, eruption of Mount St. Helens: melt composition and experimental phase equilibria. *J. Geophys. Res.* **90,** 2929–2947.

Sisson, T. W., and Bronto, S, 1998. Evidence for pressure-release melting beneath magmatic arcs from basalt at Galunggung, Indonesia. *Nature* **391,** 883–886.

Sisson, T. W., and Layne, G. D. (1993). H_2O in basalt and basaltic andesite glass inclusions from four subduction-related volcanoes. *Earth Planet. Sci. Lett.* **117,** 619–635.

Thompson, J. F. H., ed. (1995). Magmas, fluids, and ore deposits. *Mineral. Assoc. Canada Short Course,* **23**.

Valley, J. W., Taylor, Jr., H. P., O'Neill, J. R., eds. (1986). Stable isotopes in high temperature geological processes. *Mineral. Soc. Am. Rev. Mineral.* **16**.

Wallace, P., and Anderson, Jr., A. T. (1998). Effects of eruption and lava drainback on the H_2O contents of basaltic magmas at Kilauea. *Bull. Volcanol.* **59,** 327–344.

Wallace, P., and Carmichael, I. S. E. (1992). Sulfur in basaltic magmas. *Geochim. Cosmochim. Acta* **56,** 1863–1874.

Wallace, P. J., Anderson, Jr., A. T., and Davis, A. M. (1995). Quantification of pre-eruptive exsolved gas contents in silicic magmas. *Nature* **377,** 612–616.

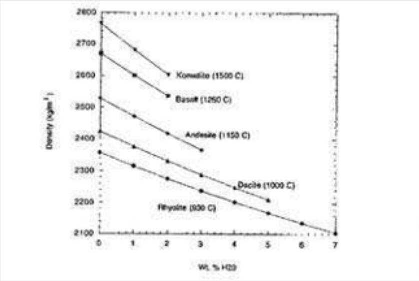

PHYSICAL PROPERTIES OF MAGMA

FRANK J. SPERA
University of California–Santa Barbara

> Still, however, the highest value is set on glass that is nearly colorless or transparent, as nearly as possible resembling crystal. For drinking vessels glass has quite superseded the use of silver and gold
> —*Pliny the Elder (c. AD 23-79)*

I. Introduction
II. Magmatic Systems: Timescales and Length Scales
III. Magma Thermodynamic Properties
IV. Magma Transport Properties
V. Conclusions

GLOSSARY

basaltic magma Most typical type of magma erupted on Earth and other terrestrial planets. Basaltic magma is erupted at temperatures of 1000–1300°C, and is made up mainly of SiO_2 (50 wt%), Al_2O_3 (15%), CaO (12%), and roughly equal amounts of FeO and MgO (10%). The alkalis (Na_2O+K_2O) make up most of the difference although trace amounts of every naturally occurring element are invariably present. About 25 km^3 of basaltic magma are generated and erupted or emplaced each year on Earth, primarily along the 75,000 km of diverging plate boundaries. The density, specific heat, viscosity, and thermal conductivity of a typical basaltic magma at 1200°C at low pressure is 2600 kg/m^3, 1450 J/kg K, 100 Pa s, and 0.6 W/m K, respectively. The heat needed to completely fuse (melt) gabbro, the plutonic (crystalline) equivalent of basaltic magma, is about 400 kJ/kg. Small amounts (0.2–2 wt%) of volatile compounds (mainly H_2O and CO_2) mainly in the dissolved state are commonly found in magmas. These volatile constituents are liberated as gases at low pressure upon eruption and decompression of magma.

magma High-temperature multiphase mixture of solids (crystals and lithic fragments), silicate or carbonatitic liquid and H-O-C-S-Cl-rich gas or supercritical fluid formed by partial or total melting of parental source material.

magma rheology The science of deformation and flow of magma. The rheological properties of magma depend on temperature, bulk composition, pressure, phase mixture, and shear rate in a complex and intertwined manner. Knowledge regarding the rheology of magma comes from both field observations and laboratory studies.

magma transport phenomena The dynamic processes responsible for the generation, ascent, and eruption or emplacement of magma and its subsequent quenching or solidification and interaction in hydrothermal-magmatic systems. These processes involve simultaneous consideration of heat, mass, and momentum transport between various magmatic subsystems. Rates of momentum, heat, and mass transfer are widely varied ranging from creeping (percolative) flow of small degree partial melts

Copyright © 2000 by Academic Press
All rights of reproduction in any form reserved.

through an otherwise solid parental source rock in response to pressure, buoyancy, and viscous forces to the rapid (several hundred meters per second) eruption of low-density highly expanded magmatic mixtures characteristic of high-silica, volatile-rich rhyolitic magma. The flow of magma in fractures, buoyant rise of magma diapirs, and evolution of magma within crustal magma bodies that undergo simultaneous assimilation of wall rock, recharge of fresh parental magma, and fractional crystallization and convective mixing (or unmixing) are all examples of magma transport phenomena.

metasomatism Metasomatism refers to the process whereby a preexisting igneous, sedimentary, or metamorphic rock undergoes compositional and mineralogical transformations associated with chemical reactions triggered by the reaction of fluids (called metasomatic fluids) that invade the protolith. A large-scale example is provided in subduction environments. Dehydration of hydrothermally altered oceanic crust and attached upper mantle generates fluids that migrate upward and metasomatize the ultramafic mantle wedge lying above the subducting slab. Because the peridotite solidus temperature is lowered by the presence of water, metasomatism of the mantle wedge can trigger partial melting there. A smaller scale environment in which metasomatism is important occurs in contact metamorphic aureoles surrounding granitic plutons when emplaced into cooler preexisting crust. The magma body acts as a heat engine and drives hydrothermal circulation in the surrounding country rock. Economically important mineral deposits often form in contact metamorphic environments.

relative viscosity Relative viscosity is the ratio of the viscosity of a multiphase mixture (solids + melt + vapor) to the viscosity of the melt. The relative viscosity of crystal–liquid suspensions invariably exceeds unity, whereas for magmatic emulsions (melt + vapor), the relative viscosity depends on shear rate. At very low shear rate, magmatic froths can exhibit a yield strength. At higher rates of shear, spherical bubbles become highly deformed and relative viscosities decrease dramatically.

rhyolitic magma Rhyolitic magma is erupted at temperatures of 750–1000°C, and is made up mainly of SiO_2 (75 wt%), Al_2O_3 (13%), and the alkalis Na_2O and K_2O in roughly equal amounts (3–5%). Only a small fraction of a cubic kilometer of rhyolitic magma is erupted each year mainly in continental environments although a significant fraction of rhyolitic and intermediate composition magmas may stagnate at depth within the crust, crystallizing there to form granitic plutons. Granitic batholiths are generally associated with subduction zone magmatism and can extend for hundreds to thousands of kilometers roughly parallel to the strike of oceanic trenches and along active continental margins. The density, specific heat, viscosity, and thermal conductivity of typical rhyolitic magma bearing 2 wt% dissolved H_2O at 900°C at low pressure is 2260 kg/m^3, 1450 J/kg K, 500,000 Pa s, and 1 W/m K, respectively. The heat needed to completely fuse (melt) granite, the plutonic (crystalline) equivalent of rhyolitic magma, is 250 kJ/kg. A water-free rhyolitic melt of otherwise identical composition has a density and viscosity of 2350 kg/m^3 and 1.2×10^{10} Pa s, respectively. Pristine volatile contents of typical rhyolitic magmas lie in the range of 1–6 wt% and are mainly H_2O.

thermodynamic properties Magma thermodynamic properties may be separated into two families: thermal functions and the equation of state (EOS). Thermal functions relate the temperature of a substance to its internal energy. These properties include the enthalpy, entropy, and heat capacity. The EOS relates the density of a substance to its composition, pressure, and temperature. The reactivity of a material depends on its chemical potential, which involves both thermal functions and EOS data.

transport properties In typical dynamic (nonequilibrium) magmatic systems, gradients in pressure, stress or velocity, temperature, and chemical potential give rise to transport of momentum, heat, and material, respectively. Momentum, heat, and mass or species can be transported by advective or diffusive flow. The transport properties that govern diffusive flow of momentum, heat, and matter are the viscosity, thermal conductivity, and species diffusivity, respectively.

I. INTRODUCTION

A central goal of studies in igneous petrology and volcanology is to understand the factors that lead to the compositional diversity of magmatic rocks. This understanding is most powerful when framed in terms of petrogenesis—the origin of magma and the rocks formed from cooling and solidification of magma—within the context of the coupling between the thermal evolution and chemical differentiation of the Earth. The growth of oceanic and continental crust throughout the 4560 million years of Earth history, the extent of recycling of crust and lithosphere by subduction, the relationship of mantle plumes to the compositional differentiation of Earth, and the role of subduction in island arc magmatism are problems on which studies of magmas and magmatic processes shed light. In addition, a close connection exists between magmatic diversity and practical problems, such as volcano forecasting and the mitigation of volcanic hazards. The thermodynamic and transport properties of magma are central to all of these considerations; in this chapter an attempt is made to overview this subject. There has been a sustained and accelerating effort to measure the properties of magma in the last century. It is no exaggeration to claim that without these foundational measurements petrology could not have evolved far beyond its early descriptive stage.

The composition of lava emitted from a volcanic center reflects both the composition of its source as well as myriad dynamic phenomena operative during its generation, segregation, ascent, and eruption. For the purposes of this chapter, magma is defined as a high-temperature (generally >900 K), multiphase mixture of crystals, liquid, and vapor. The vapor can be either a gas or a supercritical fluid. The term *liquid* is used interchangeably with the term *melt* in this chapter. The solid fraction of magma is primarily made up of oxide and silicate crystals, the relative abundance of which depends strongly on composition, temperature, pressure, and additional nonequilibrium or kinetic factors, such as cooling rate, rate of decompression, and rates of mass transfer by molecular diffusion, mechanical dispersion, and advective transport. Bits of local wall rock (lithic inclusions), cognate crystal cumulates, or exotic xenoliths are also commonly found in plutonic and volcanic rocks and provide key clues to understanding magma genesis and dynamics as well as the bulk composition of the source. The liquid or melt portion of magma is generally a multicomponent (O-Si-Al-Ca-Mg-Fe-K-Na) silicate liquid; crustal melts (silicic or rhyolitic to intermediate or andesitic) are rich in O-Si-Al-Na-K-H, whereas melts generated within the Earth's mantle are richer in O-Si-Al-Ca-Mg-Fe (mafic or basaltic). Carbonatitic melts containing >50 wt% carbonate are also generated within the mantle. Although the volumetric rate of eruption of carbonatitic magma is very small compared to the circa 25 km^3/yr of midocean ridge basaltic (MORB) magma produced, rare carbonatitic magmas may be important players in the process of mantle metasomatism. Carbonatites also have an affinity with economically important diamond-bearing kimberlitic magmas, which are rapidly erupted from depths of several hundred kilometers.

Common magmas vary nearly continuously in composition from rhyolitic (75 wt% SiO_2) through basaltic (50 wt% SiO_2). These magmas usually contain small amounts (on the order of a few weight percent) of dissolved H_2O, CO_2, and other volatile species. H_2O dissolved in melts occurs in two forms: molecular H_2O as well as the hydroxyl group OH^-. When sufficient total volatiles are present, a melt becomes supersaturated and a discrete vapor or supercritical fluid forms. This fluid has a small viscosity and density compared to common melts and is particularly rich in the components O-H-C-S-N-Cl-F. At crustal pressures and temperatures, supercritical fluids are quite corrosive and can dissolve a few percent or more by mass of various oxide components. At very high pressure and temperature even larger quantities of solid may dissolve in these fluids; silicate melt and hydrous fluids may even become completely miscible under some conditions. The concentration of dissolved volatiles in a melt strongly depends on pressure since the partial molar volume of a volatile species in the dissolved state is much smaller than its molar volume in the gaseous or supercritical fluid state. The huge expansion of a magmatic mixture that accompanies exsolution of volatiles is one of the primary causes of explosive volcanism as pressure–volume expansion work is converted to magma kinetic energy. Other factors, such as magma viscosity and the rate of volatile diffusion, are also important in assessing the dynamics of explosive volcanism.

Volcanic rocks in particular play a unique role in efforts to understand magmatic transport phenomena because, unlike plutonic rocks, they are quenched relatively rapidly and provide more or less direct information regarding the composition of natural melts. To understand the significance of the chemical composition of volcanic rocks, the dynamic and physical aspects of its parental magma evolution must first be unraveled. This is not an easy task. The range of transport phenomena of potential relevance to petrogenesis is quite varied and covers a large span of scales in time and space. Although the dynamics can be complex, it is clear that the thermodynamic and transport properties of magma are absolutely pivotal to the success of any quantitative dynamic theory of magma genesis and transport. If 20th-century research in petrology can be summarized in a few words, it is not too hyperbolic to claim this has been the century of quantification of the physical properties of magma. Although far more needs to be learned, it is reasonable to claim that geologists now have a first-order understanding of the basic properties of the common magma types and are beginning to understand how such properties relate to petrogenesis. In this chapter the most critical properties are briefly reviewed in the context of petrogenesis. Many data are presented in the tables and figures of this chapter. It is generally not possible to tabulate adequate descriptions of all the materials summarized here; particular research applications may require a return to the sources for additional details.

Table I includes most if not all of the symbols used in the text.

TABLE I Nomenclature

T	Temperature	K
P	Pressure	Pa
ρ	Density	kg/m^3
C_p	Molar isobaric heat capacity	J/mol K
c_p	Specific isobaric heat capacity	J/kg K
$\overline{C}_p$	Partial molar isobaric heat capacity	J/mol K
S	Entropy	J/K mol
H	Enthalpy	J/mol
σ	Interfacial surface energy	N/m
β_T	Isothermal compressibility, $+(\partial \ln \rho/\partial P)_T$	K^{-1}
α_P	Isobaric expansivity, $-(\partial \ln \rho/\partial T)_P$	Pa^{-1}
X_i	Mole fraction of ith component	
V_i	Partial molar volume of ith component	m^3/mol
K_T	Isothermal bulk modulus	Pa
K'	Pressure-derivative of bulk modulus	
η	Viscosity	kg/m s
E_a	Activation energy for viscous flow	J/mol
V_a	Activation volume for viscous flow	m^3/mol
η_r	Relative viscosity, ratio of mixture viscosity to melt viscosity	
ϕ	Volume fraction dispersed phase (solid or vapor)	
K_R	Radiative (photon) conductivity	J/m K s
k	Thermal conductivity	J/m K s
κ	Thermal diffusivity, $k/\rho c_p$	m^2/s
E_A	Activation energy for diffusion	J/mol
V_A	Activation volume for diffusion	m^3/mol
D	Tracer, self, or chemical diffusivity	m^2/s
Subscripts:		
fus	Fusion	
form	Formation	
conf	Configuration	
mix	Mixing	
r	Relative	

II. MAGMATIC SYSTEMS: TIMESCALES AND LENGTH SCALES

Lifetimes of magmatic systems and processes vary widely—from the rapid radiative quenching of a pyroclast during its high-speed ejection from a vent (several seconds), to the slow cooling of a single lava flow (weeks or months), to the 10^5- to 10^6-yr lifetime of a large, slowly cooled pluton. Individual magmatic-hydrothermal systems, such as at Yellowstone National Park in the United States, can be active for a few millions of years. In terms of dynamic process, creeping percolative flow in a partial melt region is of the order of several meters per year and may be contrasted with the explosive eruption of a volatile-rich magma at several hundred meters per second. Although rates of heat, mass, and momentum transfer are wildly different in these systems or subsystems, knowledge regarding the thermodynamic and transport properties of magma is critical in order to meaningfully analyze and ultimately predict the relevant dynamics regardless of the particular scale.

Length scales relevant to magma transport and genesis also vary over many orders of magnitude. At the smallest scale, on the order of millimeters or less, the diffusion of a constituent near the interface of a growing crystal or vapor bubble is relevant to the nucleation and growth of that crystal or bubble from its surrounding melt. At larger scale, individual lava flows and continental dike swarms can extend over many hundreds to thousands of square kilometers and individual plutons emplaced in batholithic terrains can extend for hundreds of square kilometers. In the early part of Earth history it is possible that a globe-encircling magma ocean hundreds of kilometers deep existed. Modeling this sort of system accurately demands knowledge of the properties of magma and phase equilibria for temperatures in the range of 1000–5000 K and pressures from 10^{-4} GPa (1 bar or 10^5 Pa) to the core mantle boundary at 135 GPa. Knowledge of the physical, thermodynamic, and transport properties of magmas is therefore essential to virtually all facets of magmatism at a wide variety of scales in both space and time, extending throughout Earth history and includes the very real environmental problems posed by volcanic hazards. Because the terrestrial planets and minor bodies (asteroids) of the solar system have a similar origin, study of magmatism is also a key element in understanding solar system origin and early evolution.

III. MAGMA THERMODYNAMIC PROPERTIES

Magma properties can be separated into two groups: equilibrium thermodynamic quantities and transport properties. Important equilibrium thermodynamic quantities include density (ρ); heat capacity (C_p); third law and configurational entropies (S); enthalpies of formation (ΔH_{form}), fusion (ΔH_{fus}), and mixing (H_{mix}); and interfacial surface energy (σ). Application of equilibrium thermodynamic data are most useful in addressing the influence of source bulk composition, pressure, and temperature on the composition and amount of melt generated during partial fusion as well as the composition of solids and residual melts during solidification of magma. Although chemical and thermal equilibrium are not perfectly attained in nature, the concept of local equilibrium is useful because equilibrium is often closely approximated at some scale and because it represents a sort of reference state from which deviations from equilibrium can be assessed. When chemical equilibrium is assumed, all the classical theory of chemical thermodynamics can be applied and many times this greatly simplifies a problem and allows one to test and discriminate between competing hypotheses. For example, at constant temperature and pressure, minimization of the Gibbs free energy for a fixed bulk composition allows one to compute the composition and abundance of each phase in the equilibrium assemblage. To compute the energetics of melting, heat capacities and enthalpies of fusion of appropriate phases are essential. Although not strictly an equilibrium process, calculation of magma heat transport requires heat capacity and fusion enthalpy data. The variation of melt density with temperature, pressure, and composition is needed for analysis of momentum transport since buoyancy is a significant factor driving the segregation, ascent, and eruption of magma. The differentiation of an emplaced magma body by gravity-driven crystal fractionation critically depends on the density difference between melt and newly formed crystals. Like an iceberg in the ocean, there are conditions in temperature and pressure space where crystals grown in a melt float rather than sink. The final solidified state of such a system is obviously quite dependent on the equation of state (EOS)—the relationship between density, temperature, and pressure—for all relevant phases. The compressibility of magma, defined according to $\beta_T = (\partial \ln \rho / \partial P)_T$, is a thermodynamic property related to the explosive eruption of magma at or near the Earth's surface. Volatile-rich magma is sometimes erupted at the sonic condition where magma eruption velocity is equal to the speed of sound in the magmatic mixture. The sonic velocity in a mixture is a function of its compressibility. The compressibility informs one regarding the variation of magma density with pressure and is therefore also important in understanding the segregation of melt from its source protolith in the creeping flow regime as well.

These examples show that there is a deep connection between the equilibrium thermodynamic properties of magma and its petrogenetic transport history. Without fundamental property data, it is impossible to breathe life into the equations governing conservation of energy, mass, species, and momentum and thus to solve quantitatively magma transport problems. The equilibrium chemical thermodynamic model provides a logical starting point for the analysis of magma production. Natural silicate melts contain SiO_2, Al_2O_3, MgO, CaO, iron oxides, the alkalis (Na_2O and K_2O), P_2O_5, transition metals and rare earth elements, and minor but important amounts of volatile compounds made up of H-O-C-S-Cl-F-N. A complete thermodynamic description of such a complex multicomponent system over the relevant range in temperature–pressure–composition space is beyond the scope of this chapter, if indeed it is possible at all. Many excellent reviews include quantitative information on the thermodynamic properties of silicate liquids. Only an outline of the salient features drawing on published work in an illustrative rather than exhaustive manner is given here.

A. Density and Equation of State

The density of a silicate melt may be determined by evaluation of the quotient:

$$\rho = \Sigma X_i M_i / \Sigma X_i \overline{V}_i, \tag{1}$$

where X_i is the mole fraction, M_i is the molar mass, and $\overline{V}_i$ is the partial molar volume of the ith oxide component in the melt. Although $\overline{V}_i$ depends weakly on composition, to a good approximation, it may be taken independent of composition and only as a function of temperature and pressure for most petrological calculations. Partial molar isothermal compressibilities for the major oxide components have been determined from ultrasonic sound speed laboratory experiments. These parameters can be used to compute melt density as a function of temperature, composition, and pressure up to several gigapascals using a simple empirical EOS:

$$\begin{aligned} V(T, P, X) = \Sigma X_i [\overline{V}_{i,T_r} + (\partial \overline{V}_i / \partial T)_P (T - T_r) \\ + (\partial \overline{V}_i / \partial P)_T (P - P_r)], \end{aligned} \tag{2}$$

where T_r and P_r are constant reference conditions [generally 1400°C and 10^{-4} GPa (1 bar), respectively] and $\overline{V}_i$ is the partial molar volume of the ith component. Information for computing melt density as a function of pressure (up to several gigapascals) and temperature is presented in Table II. Densities of some common natural melts at their respective approximate liquidi

TABLE II Partial Molar Volumes, Thermal Expansions, and Compressibilities of Oxide Components[a]

$$V_{\mathrm{liq}}(T,P,X)=\sum X_i[\overline{V}_{i,1673\mathrm{K}}+(\partial\overline{V}_i/\partial T)_{\mathrm{p}}(T-1673\ \mathrm{K})+(\partial\overline{V}_i/\partial P)_{\mathrm{T}}P]$$

	$\overline{V}_{i,1673\mathrm{K}}$ (10^{-6} m^3/mol)	$(\partial\overline{V}_i/\partial T)_{\mathrm{P}}$ (10^{-9} m^3/mol·K)	$(\partial\overline{V}_i/\partial P)$ (10^{-6} m^3/mol·GPa)
SiO_2	26.86 ± 0.3	0.0	−1.89 ± .02
TiO_2	23.16 ± .26	7.24 ± 0.46	−2.31 ± .06
Al_2O_3	37.42 ± .09	0.0	−2.26 ± .09
Fe_2O_3	42.13 ± .28	9.09 ± 3.49	−2.53 ± .09
FeO	13.65 ± .15	2.92 ± 1.62	−0.45 ± .03
MgO	11.69 ± .08	3.27 ± 0.17	0.27 ± .07
CaO	16.53 ± .06	3.74 ± 0.12	0.34 ± .05
Na_2O	28.88 ± .06	7.68 ± 0.10	−2.40 ± .05
K_2O	45.07 ± .09	12.08 ± 0.20	−6.75 ± .14
Li_2O	16.85 ± .15	5.25 ± 0.81	−1.02 ± .06
H_2O	26.27 ± 0.5	9.46 ± 0.83	−3.15 ± 0.61
CO_2	33.0 ± 1.0	0.0	0.0

[a] Note that $(\partial V_i/\partial P)_{\mathrm{T}} \equiv -\beta_{\mathrm{T}}V_i$ where β_{T} is the isothermal partial molar compressibility of the ith component and $(\partial V_i/\partial T)_{\mathrm{p}} \equiv \alpha_{\mathrm{P}}V_i$ where α_{P} is the isobaric expansivity. Modified after Lange and Carmichael (1990), Lange (1997), and Ochs and Lange (1997). Uncertainties are 1σ.

TABLE IV Density and Viscosity of Molten Carbonate and Supercritical H_2O[a]

Composition	Pressure (GPa)	Temperature (°C)	Density (kg/m^3)	Viscosity (Pa s)
$K_2Ca(CO_3)_2$	10^{-4}	975	2014	—
	2.5	950	2750	0.032
	2.5	1150	2580	0.018
	4.0	1050	2800	0.023
K_2CO_3	4	1500	3100	0.023
$K_8Ca_3Mg(CO_3)_8$	2	1250	—	0.065
$K_2Mg(CO_3)_2$	3	800	—	0.036
	3	900	—	0.022
	5.5	1200	—	0.006
H_2O	0.3	500	—	10^{-4}
		800	—	7×10^{-5}

[a] Consult references for sources.

temperatures are given in Tables III and IV and are portrayed graphically as a function of temperature, pressure, and volatile content in Figs. 1 and 2. As a rule of thumb, adding FeO, Fe_2O_3, MgO, TiO_2, and CaO to a melt increases its density, whereas adding alkalis (Li_2O, Na_2O, and K_2O) and volatiles (H_2O, CO_2) has the opposite effect. The temperature derivative of the partial molar volumes of SiO_2 and Al_2O_3 are both effectively zero. As a consequence, the density of a melt rich in silica and alumina is insensitive to temperature. Densities of melts vary from 2500 to 2900 kg/m^3 at magmatic temperatures (∼1100°C) for silicic through intermediate to mafic and ultramafic compositions at low pressure. Density increases as pressure rises, although increasing the concentration of the alkaline earth metals, Ca and Mg, serves to decrease the pressure dependence of melt

TABLE III Estimated Properties of Common Natural Melts at 10^{-4} GPa and Respective Liquidus Temperature[a]

Composition	Liquidus temperature (°C)	Specific heat of fusion (kJ/kg) Δh_{fus}	Density (kg/m^3) ρ	Specific isobaric heat capacity (J/kg K) c_{p}	Melt viscosity (Pa s) η
Granite (dry)	900	220	2349	1375	1.2×10^{10}
Granite (2 wt% H_2O)	900	250	2262	1604	5×10^5
Granodiorite	1100	354	2344	1388	1.3×10^6
Gabbro	1200	396	2591	1484	30.0
Eclogite	1200	570	2591	1484	—
Komatiite	1500	540	2748	1658	0.15
Peridotite	1600	580	2689	1793	0.25

[a] All compositions anhydrous except where indicated.

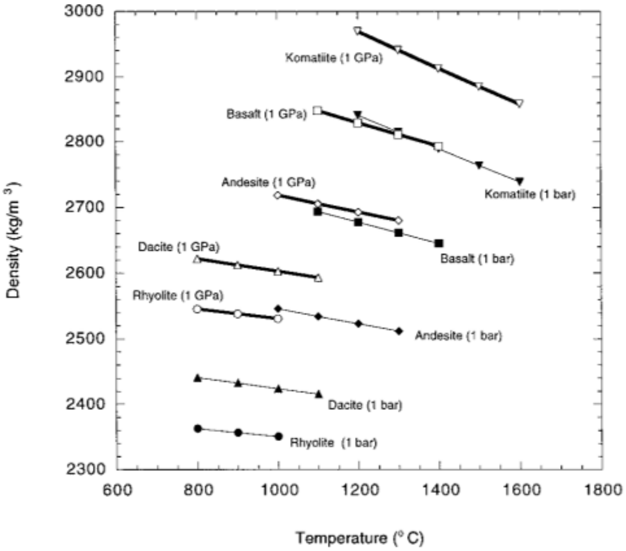

FIGURE 1 Melt density as a function of temperature for natural melts spanning the compositional range rhyolite to komatiite at 1 bar (10^{-4}GPa) and 1 GPa pressure. All compositions are volatile-free.

density. The alkali metals and water are relatively compressible and contribute significantly to the pressure dependence of density. It is important to note that small differences in composition can compensate for relatively large differences in temperature because of the strong dependence of melt density on composition. Whereas a typical value for the isobaric expansivity is $\alpha_p \approx 5 \times 10^{-5}\,K^{-1}$, the analogous quantity describing the variation of density with composition is of order 0.1–3 depending on component. The volatile components H_2O and CO_2 have an especially large effect on melt density. The partial specific densities ($M_i/\overline{V}_i$) for CO_2 and H_2O in natural melts are ~1400 and 900 kg/m^3, respectively, for typical crustal magmas. For comparison, M_i/V_i for K_2O, MgO, FeO, and SiO_2 are ~2000, 3500, 5300, and 2200 kg/m^3, respectively. Small amounts of dissolved water dramatically lower melt density and significantly affect other properties such as viscosity and isobaric heat capacity as well.

The change in volume of a crystalline silicate upon fusion is important because it influences the slope of the melting curve in pressure–temperature space and therefore the generation of magma by partial fusion. Additionally, melt density influences the separation rate of melt from its source. In Table V, volume changes accompanying melting of some silicates are given. Typically, the molar volume of a crystalline phase increases by about 10% upon fusion although silica (like ice) may shrink (i.e., become more dense) when fused at low pressure. Less is known regarding density–temperature–pressure relations or EOS for natural carbonatite melts. Some data pertaining to the density and viscosity of simple carbonate liquids as well as supercritical H_2O are given in Table IV. Relative to common silicate melts, carbonatite liquids are both less dense (by about 30%) and less viscous by several orders of magnitude compared to mafic melts and up to 10 orders of magnitude compared to silicic ones.

At pressures corresponding to depths greater than about 100 km (>3 GPa), the density of melt is most reliably determined from shock wave and static high-pressure experimental data. A useful relationship is the Birch-Murnaghan EOS, which relates the density of a melt to pressure and temperature according to:

$$P = 3/2\, K_T \{(\rho/\rho_{T,0})^{7/3} - (\rho/\rho_{T,0})^{5/3}\} [1 - 3/4(4 - K')((\rho/\rho_{T,0})^{2/3} - 1)], \qquad (3)$$

where $\rho_{T,0}$ is the density of melt at 10^{-4} GPa and temperature T, K_T is the isothermal bulk modulus ($K_T = 1/\beta_T$) at 1 bar (10^{-4} GPa), K' is the derivative of K_T with respect to pressure, and ρ is the melt density at pressure P and temperature T. Some compressibility data from shock wave studies are collected in Table VI. For detailed calculations the original references should be consulted. Density–pressure relations for a model basalt

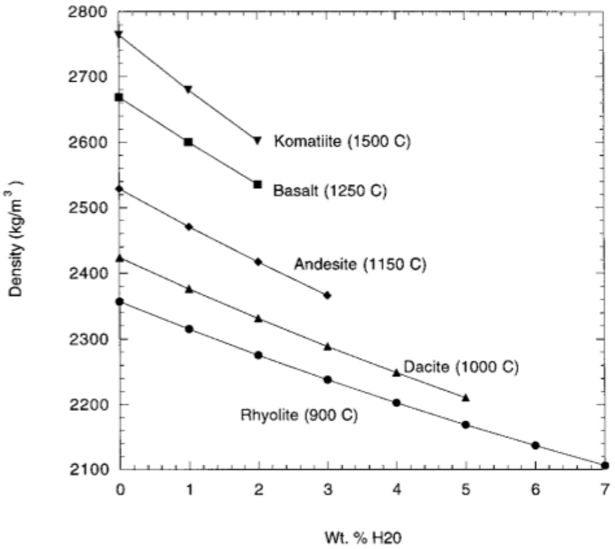

FIGURE 2 Melt density as a function of dissolved water content for natural melts spanning the range rhyolite to komatiite. Temperatures for each composition are characteristic eruption temperatures. Densities are calculated at a pressure of 1 bar (10^{-4} GPa).

TABLE V Molar Volume of Typical Silicate Crystals and Melts at High Temperature and 10^{-4} GPa[a]

Mineral	*Melting temperature (K)*	V_{melt} *(10^{-6} m³/mol)*	V_{crystal} *(10^{-6} m³/mol)*	V_m/V_c	ΔV_{fusion} *(10^{-6} m³/mol)*
SiO_2 (cristobalite)	1999	26.91	27.44	0.98	−0.53
$NaAlSi_3O_8$	1393	112.83	104.13	1.08	8.64
$KAlSi_3O_8$	1473	121.24	111.72	1.09	9.75
$CaAl_2Si_2O_8$	1830	108.41	103.42	1.05	5.48
$CaSiO_3$	1817	43.89	41.87	1.05	2.31
$MgSiO_3$	1830	38.85	33.07	1.18	5.99
$CaMgSi_2O_6$	1665	81.80	69.74	1.18	12.62
$Ca_2MgSi_2O_7$	1727	99.70	97.10	1.03	2.60
$Ca_3MgSi_2O_8$	1848	118.09	105.92	1.12	13.07
Fe_2SiO_4	1490	53.15	48.29	1.11	5.49
Mg_2SiO_4	2174	52.37	47.41	1.12	5.53
$CaTiSiO_5$	1670	67.61	57.57	1.17	10.04
H_2O (ice)	273	18.01	19.64	0.92	1.63

[a] Depolymerized compositions typically decrease in density 10–20% upon fusion. The volume change is less for tetrahedral fluids like SiO_2. Modified from Lange and Carmichael (1990). Molar volumes at 1400°C except for H_2O at 273 K.

melt are shown in Fig. 3 at temperatures corresponding to the upper mantle of the Earth. An interesting application of high-pressure EOS studies is that MgO-rich komatiitic melts, probably the most common magma type erupted in the first billion or so years of Earth history, become denser than olivine crystals at pressure corresponding to depths of roughly 250–400 km. This may have important implications for differentiation of the silicate part of Earth including internal mineralogical layering as well as possible chemical stratification.

B. Enthalpy, Entropy, and Heat Capacity

In addition to volumetric or EOS data, the calorimetric properties of high-temperature and molten silicates are needed to analyze magma transport problems. These properties inform us regarding the internal energy of melts and crystals and how internal energy and other closely related thermodynamic functions change with temperature. These properties include the enthalpy, entropy, and heat capacity and are inextricably bound to the thermal evolution of magma and relevant to processes such as partial melting, solidification, and the advective transport of heat. In Table VII, melting temperatures, enthalpies of fusion, entropies of fusion, and specific heats of fusion are listed for some common phases. The specific enthalpy of fusion is the heat per unit mass needed at constant pressure to transform a crystal or crystalline assemblage to the liquid state. There is a wide variation in the specific enthalpy of fusion from 100 to 300 kJ/kg for silica, albite, and sani-

TABLE VI Approximate Values of the Isothermal Bulk Modulus (K_T) and Its Pressure Derivative ($K' = dK_T/dP$) for Use in the Birch-Murnaghan Equation of State for Some Silicate Liquids[a]

Composition	K_T *(GPa)*	K'	dK_T/dT
$Mg_3Al_2Si_3O_{12}$	11.3	25.2	-4.3×10^{-7}
$CaMgSi_2O_6$	22.4	6.9	—
$CaAl_2Si_2O_8$	17.9	5.3	—
$MgSiO_3$	21.8	11	-3.9×10^{-8}
$FeSiO_3$	28.1	~8	—
Mg_2SiO_4	52.4	4.4	-8.2×10^{-3}
Fe_2SiO_4	54.9	2.82	-8.6×10^{-3}
SiO_2	27.5	28.7	—
$An_{36}Di_{64}$ (basalt)	24.2	4.8	—
$Fo_{70}Di_{20}An_{10}$ (komatiite)	32.1	~9	—

[a] Consult references for sources.

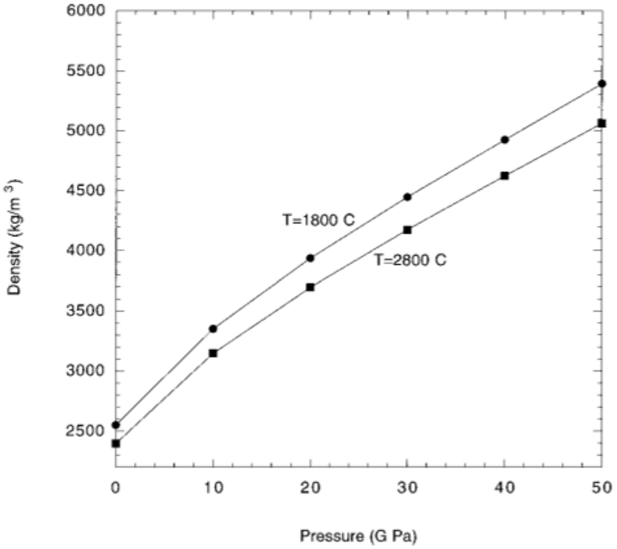

FIGURE 3 Density as a function of pressure in model basalt melt for 1800 and 2800°C. Density is computed using the Birch-Murnaghan EOS and parameters from Table VI. (See Rigden *et al.,* 1984, for details.)

dine, all important components of crustal-derived melts, to ~1000 kJ/kg for refractory phases, such as forsterite, enstatite, and rutile relevant to mafic and ultramafic compositions. Estimates of fusion enthalpies for common magmas computed using data in Table VII and typical modal abundances are listed in Table III. There is a factor of 3 difference in the specific heat of fusion for a model granite (~200 kJ/kg) compared to an ultramafic composition (~600 kJ/kg). The more refractory nature of the ultramafic composition is due to the higher fusion enthalpy of olivine and the pyroxenes relative to quartz, alkali feldspar, and plagioclase. Garnet also has a high specific fusion enthalpy. Fusion of an eclogite (pyroxene plus garnet) at high pressure requires more heat (570 kJ/kg) than a corresponding low-pressure plagioclase-pyroxene gabbro (~400 kJ/kg). The relatively low fusion enthalpy for phases making up continental crust implies that anatexis of crust by heat exchange between mafic magma and its crustal host is thermally efficient. It is worth noting that the heat required to completely melt the Earth's mantle, $\sim 3 \times 10^{30}$ J, is less than 10% of the kinetic energy delivered to the Earth by impact of a Mars-sized body (15% mass of Earth) with an impact velocity equal to the Earth's escape velocity of 11.2 km/s. If in fact the Earth did possess a magma ocean in the Hadean, then its lifetime would have been controlled by the rate at which $\sim 10^{30}$ J of heat could be dissipated by conduction, radiation, and convection.

In addition to heat effects associated with solid to liquid phase change, it is important to consider sensible heat effects or the variation of melt enthalpy with temperature. This is measured by the molar isobaric heat capacity, C_p. For most aluminosilicate glasses and melts of petrologic significance, C_p can be approximated as an additive function of oxide component partial molar isobaric heat capacities. As temperature increases for glasses, an increased number of vibrational modes become excited and so C_p increases. In Table VIII, parameters are given for the common oxide components to estimate the isobaric heat capacity of a glass as a function of composition and temperature at low pressure. At the glass transition temperature (T_g), there is generally a discontinuous jump in isobaric heat capacity. The magnitude of this jump depends on the atomic structure of the liquid with highly polymerized melts—so-called strong liquids—exhibiting little or no discontinuity in heat capacity at T_g. For petrologic purposes, it is sufficient to note that the jump in C_p at the glass transition temperature is small for silica-rich liquids (e.g., rhyolitic melts) and it becomes larger as more and more of the oxygen becomes bonded to a single Si or Al atom rather than two Si or Al atoms as in fully polymerized melts.

For silicate melts (unlike silicate glasses), the temperature dependence of C_p can generally be neglected unless great accuracy is needed. Parameters for the estimation of C_p for melts as a function of composition at magmatic temperatures are presented in Table IX. Of the common oxide components, H_2O appears to have the highest partial molar isobaric heat capacity. Glassy silica containing 1200 ppm OH has a heat capacity 30% greater than silica that is essentially anhydrous. Illustrative values for C_p of common melts at their liquidus temperatures are provided in Table III. Silicic anhydrous melts have specific isobaric heat capacities around 1300–1400 J/kg K whereas melts with higher MgO concentrations have specific heats around 1600–1700 J/kg K. For comparison, note that the specific isobaric heat capacity of tap water is about 4184 J/kg K. Because the advective transport of heat is directly proportional to C_p, mafic and ultramafic magmas are good transporters of magmatic heat. Addition of 2 wt% H_2O to an otherwise anhydrous granitic melt increases C_p by 15%.

IV. MAGMA TRANSPORT PROPERTIES

Transport properties of magma play a crucial role in development of petrogenetic theory. Simple consideration of the various stages of magma transport from source to surface makes this abundantly clear. Some

TABLE VII Melting Temperature, Molar and Specific Enthalpy of Fusion and Entropy of Fusion at 10^{-4} GPa for Some Silicate and Oxide Phases[a]

Formula	*Melting temperature (K)*	ΔH_{fus} *(kJ/mol)*	ΔS_{fus} *(J/mol K)*	Δh_{fus} *(kJ/kg)*
H_2O	273	7.401	27.11	116
NH_3	195	5.657	29.01	333
CH_4	90.6	0.937	10.34	58
ZrO_2 (baddeleyite)	3123	87.03	27.87 ± 0.20	706
$Fe_{0.947}O$	1652	31.3 ± 0.2	19.0 ± 0.1	454
$FeTiO_3$	1640	21.7 ± 0.1	13.2 ± 0.1	143
TiO_2 (rutile)	1870	67.0 ± 0.1	35.8 ± 0.1	838
Fe_2O_3 (hematite)	1895	114.5 ± 0.2	60.4 ± 0.2	717
PbO (Massicot)	1170	25.52 ± 0.01	21.81	114
Fe_3O_4 (Magnetite)	1870	138.07 ± .05	73.83	596
$LiAlO_2$	1883	87.9 ± 0.3	46.7 ± 0.5	1333
$MgAlO_2$	2408	107 ± 11	44 ± 4	752
$Ca_2Fe_2O_5$	1750	151 ± 0.5	86.3 ± 0.1	556
Al_2O_3	2323	107.5 ± 54	46.3 ± 23	1054
SiO_2 (quartz)[b]	1700	9.40 ± 1.0	5.53 ± 0.56	157
SiO_2 (cristobalite)	1999	8.92 ± 1.0	4.46 ± 0.50	149
$MgSiO_3$[b]	1834	73.2 ± 6.0	39.9 ± 3.3	729
$CaSiO_3$ (wollastonite)[b]	1770	61.7 ± 4.0	34.9 ± 2.3	531
$CaSiO_3$ (pseudowoll)	1817	57.3 ± 2.9	31.5 ± 1.6	493
$CaMgSi_2O_6$	1665[c]	137.7 ± 2.4	82.7 ± 1.4	636
$Ca_2MgSi_2O_7$	1727	123.9 ± 3.2	71.7 ± 1.9	454
$Ca_3MgSi_3O_8$[c]	1848	125 ± 15	67.5 ± 8.1	350
Fe_2SiO_4	1490[b]	89.3 ± 1.1	59.9 ± 0.7	438
Mn_2SiO_4	1620	89 ± 0.5	55.2 ± 0.3	633
Mg_2SiO_4	2174	142 ± 14	65.3 ± 6	1010
$CaTiSiO_5$	1670	123.8 ± 0.4	74.1 ± 0.2	755
$NaAlSi_3O_8$	1393	64.5 ± 3.0	46.3 ± 2.2	246
$NaAlSi_2O_6$[b]	1100	59.3 ± 3.0	53.9 ± 2.7	293
$NaAlSiO_4$[b]	1750	49.0 ± 2.1	28.0 ± 1.2	345
$Na_2Si_2O_5$	1147	35.6 ± 4.1	31.0 ± 3.6	196
$KAlSi_3O_8$[b]	1473	57.7 ± 4.2	39.2 ± 2.8	207
$CaAl_2SiO_8$	1830	133.0 ± 4.0	72.7 ± 2.2	478
$Mg_3Al_2Si_3O_{12}$[b]	1500	243 ± 8	162 ± 5	603
$Mg_2Al_4Si_5O_{18}$[b]	1740	346 ± 10	199 ± 6	591
$KMg_3AlSi_3O_{10}F_2$	1670	308.8 ± 1.3	185 ± 1	733

[a] Consult references for sources.

[b] Metastable congruent melting.

[c] Incongruent melting.

TABLE VIII Coefficients for Estimating the Isobaric Heat Capacity of Silicate Glasses Valid for Temperatures in the Range 400 K $< T <$ 1000 K at 10^{-4} GPa[a]

$C_p(T) = \sum a_i X_i + \sum b_i X_i T + \sum c_i X_i T^{-2}$ ($\mathrm{J\,K^{-1}\,gfw^{-1}}$)

	a_i	$b_i \times 10^2$	$c_i \times 10^{-5}$
SiO_2	66.354	0.7797	−28.003
TiO_2	33.851	6.4572	4.470
Al_2O_3	91.404	4.4940	−21.465
Fe_2O_3	58.714	11.3841	19.915
FeO	40.949	2.9349	−7.6986
MgO	32.244	2.7288	1.7549
CaO	46.677	0.3565	−1.9322
Na_2O	69.067	1.8603	2.9101
K_2O	107.194	−3.2194	−28.929

[a] X_i is the mole fraction of the *i*th oxide component. The gfw is defined according to gfw $= \sum X_i M_i$ where M_i is the molar mass of the *i*th component. Modified after Stebbins et al. (1984).

examples include the generation of magma by partial melting, melt segregation by porous or channel flow, and magma ascent by viscous flow in magma-filled propagating cracks. Other examples include differentiation of magma by crystal fractionation and the processes of magma mixing and crustal anatexis. In all of these phenomena significant amounts of momentum, heat, and chemical component transport occur. Transport of momentum, heat, and species by magmas involves the material properties of viscosity, thermal conductivity, and mass diffusivity, respectively. Although data and models for the composition and temperature dependence of melt viscosity are available, relatively little is known regarding the rheological properties of magmatic mixtures. There are relatively few experimental data bearing on the thermal conductivity of melts at high temperatures; this is perhaps the most uncertain of all magma transport properties but one with enormous significance with respect to the thermal history of the Earth. Some chemical and tracer diffusivity data exist and correlations have been developed for estimation of tracer diffusivities as a function of species charge and size for melts of various temperature and composition. The pressure dependence of tracer diffusivity follows roughly the pressure dependence of melt viscosity since the mechanism of oxygen self-diffusion is closely related to that for viscous flow. A brief review of these properties is presented next. The original references should be consulted for more detail.

A. Melt Viscosity

The viscosity of magma modulates momentum transport. Critical issues include the effects of composition, pressure, and temperature on the viscosity of melts as well as the rheological properties of magmatic suspensions. Although to a good approximation silicate melts behave as Newtonian fluids (that is, they show a linear relationship between shear rate and shear stress), this is not the case for magmatic multiphase suspensions nor natural glasses although for different reasons.

The temperature dependence of melt viscosity can be described by several models. The simplest one is the Arrhenian model described by the relation:

$$\eta = \eta_0 \exp[(E_a + pV_a)/RT]. \tag{4}$$

In Eq. (4), η_0 is the asymptotic viscosity at infinite temperature, E_a is the activation energy for viscous flow (a

TABLE IX Partial Molar Isobaric Heat Capacity for Molten Oxide Components Applicable to Silicate Melts at 10^{-4} GPa[a]

$C_p = \sum \bar{C}_{p_i} X_i$ ($\mathrm{J\,K^{-1}\,gfw^{-1}}$)

	Molar $\bar{C}_{pi}$ (J/gfw K)	Specific $\bar{c}_{pi}$ (J/kg K)
SiO_2	80.0 ± 0.9	1331
TiO_2	111.8 ± 5.1	1392
Al_2O_3	157.6 ± 3.4	1545
Fe_2O_3	229.0 ± 18.4	1434
FeO	78.9 ± 4.9	1100
MgO	99.7 ± 7.3	2424
CaO	99.9 ± 7.2	1781
SrO[b]	88.7 ± 8	855
BaO	83.4 ± 6.0	544
H_2O[b]	107.0 ± 5.0	5940
Li_2O	104.8 ± 3.2	3507
Na_2O	102.3 ± 1.9	1651
K_2O	97.0 ± 5.1	1030
Rb_2O	97.9 ± 3.6	524

[a] C_p is approximately independent of temperature at $T \geq 1400$ K. Modified from Stebbins *et al.* (1984).

[b] Estimated by author.

constant for an Arrhenian fluid), V_a is the activation volume for viscous flow, and R is the universal gas constant. Activation energies vary systematically with composition from values around 200 kJ/mol for mafic and ultramafic melts to 400 kJ/mol for more silicic compositions. Increasing the concentration of non-framework components such as the alkalis, the alkaline earths, and especially H_2O results in creation of oxygens bridged to only a single Si or Al. The presence of nonbridging oxygen (NBO) destroys the network structure of the melt created by the formation of tetrahedral rings at intermediate atomic scales of order 0.5 to 1 nm. For the ideal network tetrahedral melt, each oxygen is bound to two Si, two Al, or one Si and one Al simultaneously. The archetypal example is molten silica in which each oxygen has two nearest neighbors of silicon and each silicon is surrounded by four nearest neighbors of oxygen. The increase in the concentration of NBO serves to lower both η_0 and E_a and, in fact, makes the temperature derivative of viscosity a function of temperature itself. Small (several percent by mass) concentrations of water have a dramatic effect in lowering the viscosity of melts because water is 8/9 oxygen by mass, unlike any other common oxide component. This is illustrated in Table IV for the granitic composition where addition of 2 wt% H_2O to a granitic melt lowers its viscosity by a factor of 10^5. H_2O also tends to lower the viscosity of more mafic compositions, although the effect is considerably subdued, because fewer bridging oxygens exist in anhydrous mafic melts.

The activation volume, a measure of the pressure dependence of viscosity, is usually a small fraction of the molar or specific volume of the melt and changes sign, from negative to positive, as the fraction of NBO increases. Fully polymerized network melts, for which essentially all the oxygen is bridging oxygen (BO), typically possess intermediate-range order defined by the formation of n-membered rings ($n = 4$ to 10) of tetrahedra. As pressure increases, the ring structure collapses and the "anomalous" effect of viscosity decrease with increasing pressure disappears. Specifically, as pressure increases, the concentration of pentahedral (fivefold) and octahedral (sixfold) Si and Al increases, driving the oxygen into a higher number coordination with both Si and Al as well as with itself. Consequently, the proclivity to form rings decreases significantly. A typical value for V_a for a network tetrahedral melt such as $NaAlSi_3O_8$ is around -6×10^{-6} m^3/mol, whereas in a more depolymerized melt V_a is around 3×10^{-6} m^3/mol. Melts with a negative value of V_a show a decrease in viscosity as pressure increases; the opposite is true for melts with positive V_a. There is a close connection between the V_a for viscous flow and the activation volume for oxygen self-diffusion. For rough estimates, the former may be equated to the latter.

Unfortunately, not all silicate melts follow the Arrhenian temperature–viscosity relationship. This is especially true for so-called fragile melts or melts that have a significant fraction of NBO. A good example of a fragile natural melt is a water-rich peralkaline rhyolite. An empirical rule for predicting the temperature dependence of viscosity data in fragile non-Arrhenian melts is the so-called Tammann-Vogel-Fulcher (TVF) expression:

$$\eta = \eta_0 \exp[B/(T - T_k)], \tag{5}$$

where B is a function of composition but not temperature and T_k is closely related to the so-called Kauzmann catastrophe temperature. At $T < T_k$, the entropy of supercooled liquid is smaller than that of its corresponding crystal. At $T = T_k$ viscosity diverges according to Eq. (5). The relationship between the TVF and the Arrhenian model is noted by examining the temperature derivative of the viscosity. In the Arrhenian model, $[\partial \ln \eta_A/\partial(1/T)] = E_a/R$ whereas for a TVF fluid $[\partial \ln \eta_{TVF}/\partial(1/T)] = BT^2/(T-T_k)^2$. In the limit $T_k \to 0$, the TVF and the Arrhenian models are identical with $B \equiv E_a/R$. In general, T_k is close to but usually somewhat less than T_g, the glass transition temperature; typically $T_g \approx 1000$ K for silicate compositions of geochemical importance. The T_g for pure silica is somewhat higher (1400 K). The TVF model therefore shows that the variation of melt viscosity with temperature decreases as temperature increases and is not a constant (E_a) as in the Arrhenian model.

Perhaps the conceptually best model for predicting the viscosity of simple silicate liquids is the Adams-Gibbs-Di Marzio (AGD) configurational entropy theory. In this model, viscosity depends on temperature according to

$$\eta = \eta_0 \exp(B/T\,S_{conf}), \tag{6}$$

where S_{conf} is the configurational entropy of the melt and includes a contribution computed from liquid and glass isobaric heat capacity data, as well as the residual entropy of glass (frozen liquid) at the glass transition temperature, T_g. The parameter B is temperature independent but varies with composition. An important aspect of the AGD theory is that it connects melt thermodynamic and transport properties. It is based on a theory of cooperative behavior relevant to the dynamic rearrangement of atomic configurations characteristic of the liquid state. The AGD theory can be extended to provide a basis for predicting the pressure and, perhaps, compositional dependence of magma viscosity. Unfortunately, the TVF and AGD theories have not yet been fully developed for application to multicomponent natural melts. There is no comprehensive model to predict η_0, E_a, V_a, and B for a given magma composition as a function of temperature and pressure, although there are good prospects that such an extension is possible within the framework of the AGD theory.

For petrologic purposes, it is usually necessary to employ the simpler Arrhenian model. Values for the viscosity of common melts at their 10^{-4} GPa liquidus temperatures are presented in Table III and portrayed graphically in Fig. 4. Melt viscosity can span over 10 orders of magnitude given the variation in composition and temperature in natural systems. Dissolved water has a dramatic effect on lowering melt viscosity; this has important implications for the transport and eruption of silicic and intermediate composition magmas. The effects of dissolved water on the viscosity of common melts at typical eruptive temperatures are shown in Fig. 5.

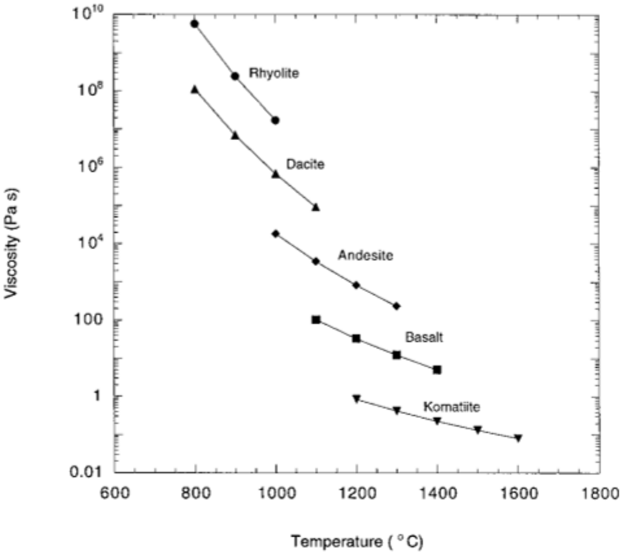

FIGURE 4 Viscosity as a function of temperature at 1 bar (10^{-4} GPa) for natural melts spanning the compositional range rhyolite to komatiite. All compositions are volatile free. The temperature range is illustrative of typical eruption temperatures for each composition.

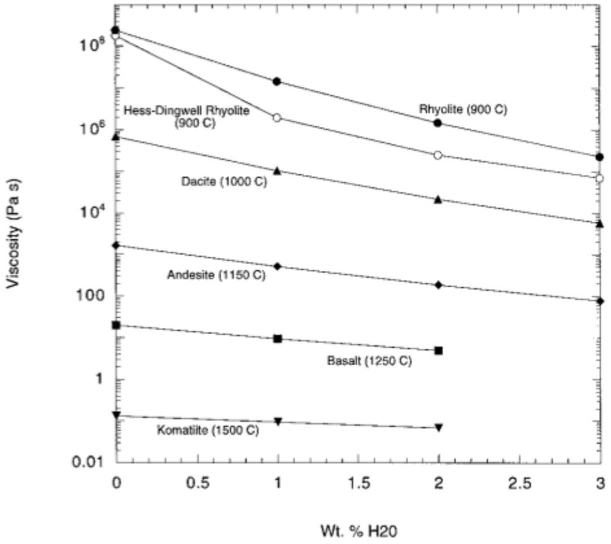

FIGURE 5 Melt viscosity as a function of dissolved water content for natural melts spanning the range rhyolite to komatiite. Temperatures for each composition are characteristic eruption temperatures. Viscosities are calculated for pressure equal to 1 bar (10^{-4} GPa). For the rhyolite composition, two different models are shown. Note the very dramatic effect of dissolved water on the viscosity of natural melts. Viscosity models are from Shaw (1972) and Hess and Dingwell (1996).

B. Magma Viscosity

Far fewer data exist on the rheological properties of magmatic suspensions compared to silicate melts. Magma, a mixture of suspended crystals and vapor bubbles in a melt matrix, may be expected to exhibit complex rheological behavior especially when significant amounts of suspended crystals and bubbles are present. There have been few experiments exploring the rheological properties of magma containing significant amounts of crystals and vapor bubbles. Fortunately, there has been some study of two-phase mixtures (both crystal–melt suspensions and melt–vapor emulsions). Silicate foams, defined as concentrated emulsions with porosity greater than about 60 vol% ($\phi > 0.6$) are found in small quantities at virtually all volcanic centers because magma typically contains some volatiles (0.1–10 wt%) and the common volatiles (H_2O and CO_2) are practically insoluble in melts at low pressure.

Many attempts have been made to model the variation of magma viscosity with volume fraction of a unimodal size distribution of spherical solids. To first order, the effect of increasing the volume fraction of crystals, ϕ, in a melt is to increase the relative viscosity, η_r, according to:

$$\eta_r = \eta_{\text{mix}} / \eta_{\text{melt}} = (1 - \phi/\phi_0)^{-5/2} \qquad (7)$$

where η_{mix} is the viscosity of the crystal-laden suspension, η_{melt} is the viscosity of melt, and the constant ϕ_0 is the maximum packing fraction of the solid. Relation (7) shows that the loading level of crystals is limited by ϕ_0, the geometric limit for contact of solids in the most efficient packing condition. For rhombohedral packing of spherical particles, $\phi_0 = 0.74$, whereas in simple cubic packing and body-centered cubic packing $\phi_0 = 0.52$ and 0.60, respectively. In practice, random packing of spheres generally gives ϕ_0 in the range 0.60–0.65. Equation (7) clearly shows that the volume fraction as well as the maximum packing fraction ϕ_0 of solids are the two important parameters governing the viscous response of magma. Polydispersity, the presence of a nonunimodal distribution of particles, tends to reduce the viscosity of a magma at a fixed value of ϕ because smaller particles can fit between the larger ones. The viscosity of a unimodal crystal-bearing magma with $\phi = 0.3$ is about 10 times higher than its value for the melt phase alone based on Eq. (7). In more detail, it is both the size and shape variation of individual crystals, as well as the overall structure of the mixture, that controls the rheological properties of multiphase magmatic mixtures. An extension of the model that takes into account melt entrapped between solid particles and hence not available for shear is given by:

$$\eta_r = \eta_{mix}/\eta_{melt} = (1 - \phi/\psi_M)^{-q}, \tag{8}$$

where Ψ_M depends on ϕ according to:

$$\psi_M = 1 - \phi[1 - \phi_0]/\phi_0, \tag{9}$$

and q is a positive number in the range 2–3. The parametric variations of Ψ_M and q are a direct consequence of the shape, size distribution, and prevailing structure of the solid network within the suspending melt. For magmatic mixtures, it is recommended that Eqs. (8) and (9) be used with $0.5 < \phi_0 < 0.75$ and $q \approx 2.5$. For $\phi = 0.35$, Eqs. (8) and (9) give $\eta_r = 2.9$ for $\phi_0 = 0.70$ and $q = -2$ and $\eta_r = 10.2$ for $\phi_0 = 0.50$ and $q = -3$, respectively. Some typical suspension viscosity values as a function of volume fraction of solids for various q and ϕ_0 are shown in Fig. 6. More experimental work is needed to better constrain the rheometric parameters q and ϕ_0 and especially the shear rate dependence of suspension viscosity. Because the rate at which a suspension is sheared can profoundly alter the distribution of suspended solids, suspension viscosity is likely to depend on shear rate as well as the fraction of solids.

In bubble-melt mixtures, η can be either an increasing or decreasing function of ϕ depending on the rate at which the mixture is sheared. At low rates of shear ($\dot{\gamma}$), bubbles act as nondeformable inclusions and η increases with increasing ϕ as when solids (e.g., crystals) are added to a melt. In distinction, at high shear rate, bubbles readily deform and the mixture viscosity decreases with increasing bubble fraction. A dimensionless parameter termed the capillary number (Ca) is useful in determining the appropriate rheodynamic regime. The capillary number is defined as $\mathrm{Ca} = \eta\gamma r_b/\sigma$ where η, γ, r_b and σ represent the melt viscosity, shear or deformation rate, bubble radius, and melt–vapor interfacial tension, respectively. The capillary number can be thought of as the ratio of viscous tractions acting on the boundaries of a bubble that distort it from a spherical shape relative to interfacial surface tension that tends to preserve a spherical shape. Small values of Ca correspond to conditions with dominant surface tension for which bubbles retain their spherical shapes. This is favored in finely dispersed (small bubble size), low-viscosity emulsions subjected to low rates of deformation. One expects a relative viscosity relation of the form $\eta_r = f(\phi, \mathrm{Ca})$ such that for small capillary number (roughly $\mathrm{Ca} < 1$), η_r is an *increasing* function of ϕ. In contrast, for regimes where Ca is large ($\mathrm{Ca} >$ unity), the relative viscosity *decreases* with increasing bubble content. Natural systems span the range from $\mathrm{Ca} < 1$ to $\mathrm{Ca} \geqslant 1$ so it is important to consider the dynamic regime when considering the effect of bubbles on the viscosity of magma. Relative viscosity can drop by a factor of 10 as the bubble content increases from 0 to ~50 vol% in the high Ca regime.

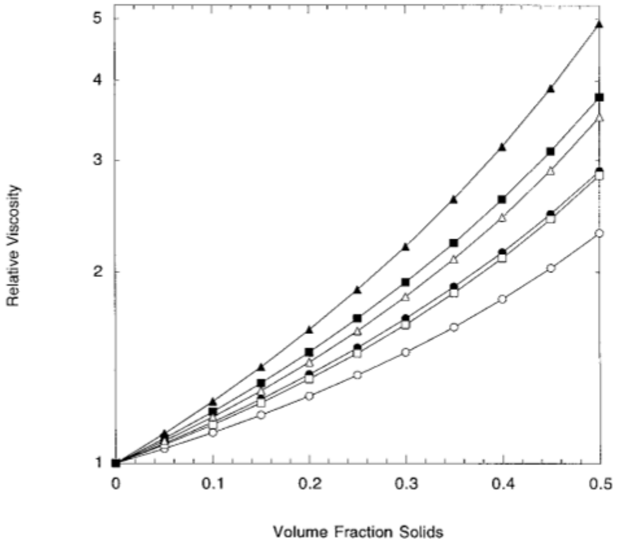

FIGURE 6 Relative viscosity of magmatic suspensions containing solids as a function of volume fraction of solids. The power-law parameter q equals 2, 2.5, and 3 for circles, squares, and triangles, respectively. Open symbols correspond to ϕ_m equal to 0.52; closed symbols correspond to ϕ_m equal to 0.70.

It is likely that magmatic suspensions of solids and bubbles become significantly nonlinear (non-Newtonian) at high loading and at high rates of shear. That is, the mixture viscosity depends not only on the fraction of the dispersed phase (bubbles or solids) and the capillary number but also on the shear rate. Self-organization of dispersed particles (solids or bubbles) to form structured mixtures giving rise to large spontaneous changes in magma viscosity during flow itself may also be important. These issues have not been adequately studied to date despite the relevance for pyroclastic and lava flows and the mobility of debris avalanches and other particulate flows of petrologic and volcanologic importance. Many volcanic hazards involve the flow of such highly non-Newtonian mixtures. Future experimental work is needed to address these questions and apply them in a meaningful way to various volcanologic and petrologic problems.

C. Thermal Conductivity

Transport of magmatic heat occurs by several mechanisms including convection (heat transported by bulk flow), phonon conduction (heat transported by atomic vibration), and radiation (an electromagnetic phenomenon involving photon transfer). Radiation travels through a vacuum at the speed of light; most gases are transparent to radiation. Radiative transport of heat may be important in transition metal poor melts due to their relative transparency. Because most gases are transparent, radiative heat transfer may also be important across bubbles in magmatic emulsions and foams. In contrast, radiative heat transport can generally be ignored in mafic melts containing significant amounts of transition metals (e.g., Fe, Ti, Ni) because such melts are relatively opaque to thermal radiation. In these nontransparent magmas, the mean free photon path is short of order several millimeters. The photon (radiative) conductivity (K_R) can sometimes be approximated as:

$$K_R = 16/3\ \sigma n^2 T^3 \ell_R \tag{10}$$

where σ is the Stefan-Boltzmann constant (5.67×10^{-8} J/m^2 K^4 s), n is the index of refraction, and ℓ_R is the mean free path for photons. The thermal transfer by photons depends in a critical way on ℓ_R as well as the emissivities of the surfaces across which heat is being transferred. When $\ell_R \sim 0$ (as in an opaque melt) or when one is concerned with transport of heat across distances much larger than ℓ_R, radiative transfer is negligible. It is only when ℓ_R is relatively large, as in transparent high-silica melts or in transparent vapor–melt emulsions, that photon conduction may become appreciable. Because geometric factors are often relevant, the importance of radiative heat transfer in geological processes (as opposed to laboratory small-scale experiments) always needs to be carefully considered.

The thermal conductivity (k) provides a quantitative measure of the importance of phonon heat conduction in solids and melts. The thermal diffusivity (κ) defined as $\kappa = k/\rho C_p$ is often used in the analysis of magmatic heat transport and involves a combination of thermodynamic properties and the phononic thermal conductivity. Quantized thermal waves called *phonons* carry heat in silicate crystals and melts. Thermal resistivity (W), which is inversely proportional to thermal conductivity (i.e., $k \propto W^{-1}$), arises due to both phonon–phonon interaction and structural disorder. Because disorder is an outstanding characteristic of the glassy and molten state, one might expect the mean free path for the dominant thermal phonons to approximately equal the scale of structural disorder, roughly 5–10 Å in a typical glass or melt. The thermal conductivity of a solid may be estimated according to the relation:

$$k \infty \lambda\, C_p c^2/3\alpha_P^2 T, \tag{11}$$

where λ is an interatomic length scale (~0.5 nm), c is the sonic velocity (several kilometers per second), and $\alpha_p \equiv 1/V(\partial V/\partial T)p$ (see Table II). In general, k decreases as temperature increases. Unfortunately, there are relatively few measurements of the thermal conductivity of molten silicates and even fewer for petrologically important compositions. Because radiative transfer tends to dominate at high temperatures in the laboratory, it can be difficult to accurately separate the effects of phonon conduction from photon radiative energy propagation and hence to determine the intrinsic phonon thermal conductivity. Based on existing measurements of k for melts (Table X), the dependence of thermal conductivity on temperature and composition in molten silicates may be considerable, although very few reliable measurements have been made. Data on the pressure dependence of k for melts is even more limited; theory suggests that the pressure derivative of k scales with β_T, where β_T is the isothermal compressibility. It is estimated that $(\partial \ln k/\partial P)_T$ lies in the range 0.05–0.5 GPa^{-1} for silicate melts. Values of k for some crystals, glasses, and melts at various temperatures and low pressure are listed in Table X. There is a clear need for more measurements of specific compositions across a large temperature interval (subsolidus to superliquidus) where the effects of radiation are carefully separated from phonon conduction.

TABLE X Thermal Conductivity for Some Solids and Melts[a]

Composition	*Temperature (°C)*	*Thermal conductivity (W/m K)*
$CaNa_4Si_3O_9$ (melt)	1244	0.22
	1300	0.12
	1400	0.09
Na_2SiO_3 (melt)	1190	0.48
	1290	0.31
	1400	0.09
$CaMgSi_2O_6$ (melt)	1400	0.31
	1600	0.04
SiO_2 (glass)	0	1.12
	500	1.92
	900	2.57
Obsidian (natural glass)	0	1.34
	300	1.67
	500	1.89
Basaltic (glass)	0	1.15
	300	1.48
Olivine (Fo_{90})	800	2.69
	1400	2.18
Forsterite	400	2.47
	800	1.84
	1400	1.59
Orthopyroxene (bronzite)	0	4.62
	300	3.05
Diopside	20	4.27
Diabase	300	2.09

[a] Sources given in references.

D. Diffusion

Mass is transported in magmatic systems by bulk flow and by molecular diffusion, the latter of which is defined as the relative motion of different constituents or species in a melt. Diffusive transport of species is characterized by the diffusion coefficient or diffusivity (D) of a species and is a function of melt temperature, pressure, and composition including oxidation state. Several types of diffusive transport can be distinguished. Self- or tracer diffusion refers to the mobility of a constituent or species in a homogeneous melt free of any chemical or thermal gradient; there is no net flux of species in tracer or self-diffusion. Self-diffusion refers to the mobility of a constituent that is present in significant concentration. An example is self-diffusion of oxygen in a melt of natural composition. Tracer diffusion is essentially the same as self-diffusion except that the concentration of the species of interest is low at the parts per million by mass level (ppm). In contrast, chemical diffusion is driven by gradients in chemical potential or activity and results in a net flux of species. Chemical diffusion, unlike tracer or self-diffusion, is complex because coupling exists between the flux of one component and the gradients of all other independent components in the system. That is, for an n-component system, the flux of the ith component depends on the chemical potential gradient of any independent set of $n-1$ components and not simply the ith component. Because the chemical diffusion rate of the ith component depends on $n-1$ chemical potential gradients, whereas isotopic equilibration of the ith component depends on the tracer or self-diffusivity of that species, decoupling between elemental and isotopic concentrations can and does occur in both natural and laboratory systems.

There is an extensive body of information pertaining to diffusion in melts and glasses as a function of temperature, composition, and, to a lesser extent, pressure. This is due in large measure to myriad industrial and materials processing applications of diffusion as well as the importance of diffusion in petrologic processes such as crystal nucleation and growth, the growth of vapor bubbles, the homogenization of melt inclusions, the resetting of geochronological clocks, and the mixing of magmas. Because of the complexity of dealing with multicomponent systems, chemical diffusion is less studied than self- or tracer diffusion in molten silicates. There is a deep connection between the atomic structure of a melt or glass and the mobility of its constituents. The self-diffusion of oxygen, the most abundant constituent of natural melts and glasses, is intimately related to melt viscosity, a macroscopic property. Hence study of the systematics of diffusion bridges the gap between the microscopic and macroscopic realms relevant to magma transport phenomena. There are many excellent reviews of diffusion for both industrial and geologic materials and these primary references should be consulted for details. In this section, a brief summary along with some typical values of self-, tracer and chemical diffusivities are given to indicate the main trends and illustrate the orders of magnitude.

E. Self-, Tracer, and Chemical Diffusion

The dependence of tracer, self-, and chemical diffusivity of a constituent as a function of pressure and temperature is given by:

$$D = D_0 \exp[-(E_A + pV_A)/RT], \qquad (12)$$

where D_0 is constant for a fixed composition and E_A and V_A represent the activation energy and activation volume for diffusive transport, respectively. Very roughly, E_A and V_A for oxygen self-diffusion in a melt are equivalent to E_a and V_a for viscous flow because viscous flow in a silicate melt is ultimately related to the mobility of oxygen, the predominant constituent. This relationship, in general, does not hold for other species. E_A is of order 300–400 kJ/mol for network-forming atoms like Si and Al and is in the range 250–180 kJ/mol for transition metals and the alkaline earth metals. Alkali metals have activation energies in the range 120–220 kJ/mol. Far less is known regarding V_A. Molecular dynamics simulations suggest values around -10 cm^3/mol for network-forming atoms, whereas network modifiers have values in the range -2 to $+5$ cm^3/mol. These relations apply approximately to melts across the compositional range basalt to rhyolite. In contrast, the pre-exponential term (D_0) depends strongly on melt composition and the size and charge of the species. Network-modifying ions of high charge and large size have smaller diffusivities than small cations of low charge, other factors remaining the same. At fixed temperature, D_0 is larger in basaltic melt compared to rhyolitic by a factor of 5–500 depending on the species. In a basaltic melt at 1300°C, oxygen and the network atoms Si and Al have $D \sim 3 \times 10^{-12}$ m^2/s. This compares with transition metals (e.g., Fe, Ti) and alkaline earths (e.g., Mg, Ca, Sr) for which $D \sim 1 \times 10^{-11}$ m^2/s and $\sim 2 \times 10^{-11}$ m^2/s, respectively. The alkalis are more mobile with $D \sim 3 \times 10^{-10}$ m^2/s; there is a strong dependence of D with ionic radius for the alkalis such that $D_{Li} \gg D_{Na} > D_K > D_{Rb} > D_{Cs}$. The diffusivity of the carbonate group (CO_3) is $D \sim 1.2 \times 10^{-10}$ m^2/s, whereas for H_2O, $D \sim 1 \times 10^{-9}$ m^2/s and depends on the concentration of dissolved water. The diffusive length during the 10^5-yr solidification time of a 10^3-km^3 gabbroic pluton (characteristic length ~10 km) is ~3 m for O and Si, whereas for Li and H_2O it is ~60 m. Diffusive length scales in a granitic magma body are smaller, by factors of 2–20 at 1300°C and factors of 10–1000 at 1100°C compared to a gabbroic body. Self- and tracer diffusivity coefficients, including estimates of activation energy for some species in basaltic and rhyolitic melts, are presented in Tables XI and XII.

TABLE XI Self- and Tracer Diffusivity for Some Species in Basaltic Melts at 10^{-4} GPa

Species	*T* (*°C*)	*D* (*m²/s*)	*E_a* (*kJ/mol*)
O	1260	1.7×10^{-10}	216
	1450	2.5×10^{-11}	325
Si	1450	2.5×10^{-11}	325
	1300	0.3×10^{-11}	—
Li	1300	100.0×10^{-11}	117
Na	1300	28×10^{-11}	167
K	1300	4.2×10^{-11}	—
Rb	1300	2×10^{-11}	—
Cs	—	1×10^{-11}	272
Mg	1400	7.8×10^{-11}	180
Ca	1400	6.9×10^{-11}	—
	1300	1.7×10^{-11}	123
Sr	1300	2.3×10^{-11}	218
Ba	1400	3.5×10^{-11}	172
Fe	1300	1.2×10^{-11}	210
Ti	1400	1.8×10^{-11}	—
Zr	1400	1.2×10^{-11}	—
Th	1400	1.3×10^{-11}	214
Nd	1400	2.2×10^{-11}	210
Eu	1400	2.2×10^{-11}	196
Carbonate (CO_3 group)	1300	12×10^{-11}	—

Chemical diffusion is more complicated than self- or tracer diffusion because the mass flux of the ith component depends on the chemical potential gradients of all $n-1$ independent species, where n is the number of chemical components in the system. Multicomponent chemical diffusion is described by an $(n-1)$ by $(n-1)$ diffusion matrix with elements D_{ij}. In a multicomponent system it is possible to have concentration gradients of more than one component at some location and time. Consequently, simultaneous fluxes of components will occur. Consideration of local charge balance and total mass conservation together with hydrodynamic factors (e.g., a species chooses the path of least viscous resistance) leads to curious phenomena such as uphill diffusion whereby a species moves up its own concentration gradient. In the last few years, there have been several studies of chemical diffusion in three- and four-component systems. There also has been some progress in building models to predict chemical diffusion coefficients, including off-diagonal terms, from appropriate tracer and self-diffusivities and to correlate chemical diffusivities with other transport properties such as viscosity. The systems studied in detail to date are mainly for $n \leq 4$ (e.g., CaO-MgO-Al_2O_3-SiO_2). Absolute values of chemical D_{ij} are about the same as tracer and self values and their pressure and temperature dependencies are probably approximately the same. The on-diagonal D_{ii} are usually larger in absolute value than off-diagonal

TABLE XII Self- and Tracer Diffusivity for Some Species in Rhyolitic Melts at 10^{-4} GPa

Species	T (°C)	D (m^2/s)
Na	800	1.0×10^{-10}
K	800	5.0×10^{-12}
Rb	800	2.5×10^{-13}
Cs	800	1.4×10^{-16}
	1140	5.2×10^{-14}
Mg	1140	8.3×10^{-15}
	1400	1.5×10^{-13}
Ca	1140	1.9×10^{-14}
	1400	3.5×10^{-13}
Sr	1300	1.9×10^{-13}
	1140	6.6×10^{-14}
	800	2.5×10^{-14}
Ba	800	7×10^{-15}
	1140	9×10^{-14}
Y	1140	2.8×10^{-16}
	1300	4.0×10^{-14}
	1500	3.8×10^{-12}
Zr	1140	5.6×10^{-17}
	1300	5.6×10^{-14}
	1500	2.4×10^{-12}
Nb	1140	4.5×10^{-16}
	1300	7.8×10^{-14}
	1500	1.7×10^{-12}
B	1140	1.9×10^{-16}
	1300	0.6×10^{-14}

terms although in natural systems with $n \approx 8$ this may not always be the case. Off-diagonal terms are commonly negative and this can sometimes lead to the observed effects of uphill diffusion seen in some natural examples. Biotite-rich rinds often surround mafic enclaves, intruded in the molten state into a host of granitic or granodioritic magma. Enrichment in K_2O along the granite/gabbro interface may be a natural example of uphill diffusion. The main point regarding chemical diffusion is that mixing is not generally describable by linear mixing of two compositions.

V. CONCLUSIONS

The important thermodynamic and transport properties of magma have been briefly reviewed in this chapter. The complete description of multicomponent and multiphase magma at temperatures from 800 to 5000 K and pressures from 10^{-4} (surface) to 135 GPa (base of mantle) is an ambitious program that will take many years to accomplish. Although an enormous task, there are reasons to be optimistic. Within the last quarter century knowledge of the thermodynamic properties of high-temperature crystalline, molten, and glassy silicates including melts of natural composition has grown dramatically. Although still far from complete, thermodynamic properties for many crystalline phases relevant to magmatic systems are known at the high-temperature and -pressure conditions equivalent to the base of the lithosphere around 3–4 GPa.

An approximate model for the Gibbs free energy of natural silicate liquids has also been developed in the past 15 years and is undergoing continuous revision and expansion and can only improve efforts to describe and predict equilibrium phase relations involved in the melting and solidification of magma. Similarly, studies of the temperature, pressure, and composition dependence of melt viscosity, the rheology of magmatic (solid-melt-vapor) mixtures, chemical, tracer, and self-diffusion and thermal conductivity have been made for a variety of natural and synthetic melts and glasses. Correlations have been developed for some properties valid in specific regions of temperature–pressure–composition space that enable one to obtain order of magnitude or better estimates of many critical properties.

Development of models based on condensed matter theory has come to supercede earlier purely empirical models and hence are far better suited to rational interpolation. These models, though only approximate, provide a foundation for careful extrapolation as well. In the computational realm, molecular dynamics simulations are increasingly being applied to investigate the structure and properties of molten silicates at very high temperatures and pressures. This method, which involves use of a potential energy expression describing the electrostatic interactions between the various atoms in a fluid or melt, enables one to compute thermodynamic, spectroscopic, and transport properties under a variety of conditions. Although properties so computed are estimates, they do provide a means for understanding, at the atomic level, the effect of temperature, pressure, and composition on physical properties and for identifying critical laboratory experiments.

Study of the properties of molten, glassy, and high-temperature crystalline silicates and oxides of geological relevance has burgeoned in the past quarter century due to the contributions made by an international cast of researchers. The rate of acquisition of new information is accelerating as new techniques are applied to old problems. There are hundreds of volcanic eruptions each year and many of these present dangers involving the loss of life and property. The first step in taming magma is to understand its nature from a fundamental and broad perspective. At the same time a deeper understanding of the evolution of planet Earth and, by analogy, other terrestrial planets both within our solar system and beyond depends on knowledge regarding the physical properties of magma.

SEE ALSO THE FOLLOWING ARTICLES

Composition of Magmas • Lava Flows and Flow Fields • Migration of Melt • Mineral Deposits Associated with Volcanism • Volatiles in Magmas • Volcanic Gases

FURTHER READING

Baker, D. R. (1990). Chemical interdiffusion of dacite and rhyolite: Anhydrous measurements at 1 atm and 10 kbar, application of transition state theory, and diffusion in zoned magma chambers. *Contrib. Mineral. Petrol.* **104,** 407–423.

Baker, D. R. (1995). Diffusion of silicon and gallium (as an analogue for aluminum) network-forming cations and their relationship to viscosity in albite melt. *Geochim. et Cosmo. Acta* **59** (17), 3561–3571.

Behrens, H., and Nowak, M. (1997). The mechanisms of water diffusion in polymerized silicate melts. *Contrib. Mineral. Petrol.* **126,** 377–385.

Bottinga, Y. (1991). Thermodynamic properties of silicate liquids at high pressure and their bearing on igneous petrology. *Adv. Chem.* **9,** 213–232.

Bottinga, Y., Richet, P., and Sipp, A. (1995). Viscosity regimes of homogeneous silicate melts. *Am. Miner.* **80,** 305–318.

Chakraborty, 8. (1995). Diffusion in silicate melts. *Rev. Mineral.* **32,** 411–497.

Dingwell, D. B., and Webb, S. L. (1989). Structural relaxation in silicate melts and non-Newtonian melt rheology in geologic processes. *Phys. Chem. Min.* **16,** 508–516.

Dobson, D. P., Jones, A. P., Rabe, R., Sekine, T., Kurita, K., Taniguchi, T., Kondo, T., Kato, T., Shimomura, O., and Urakawa, U. (1996). In-situ measurement of viscosity and density of carbonate melts at high pressure. *Earth Planet. Sci. Lett.* **143,** 207–215.

Gier, E. J., and Carmichael, L. S. E. (1996). Thermal conductivity of molten Na,SiO, and CaNa,Si,O. *Geochim. et Cosmo. Acta* **60**(2), 355–357.

Goto, A., Oshima, H., and Nishida, Y. (1997). Empirical method of calculating the viscosity of peraluminous silicate melts at high temperatures. *J. Volcan. Geothermal Res.* **76,** 319–327.

Haar, L., Gallagher, J. S., and Kell, G. S. (1983). "Steam Tables: Thermodynamics and Transport Properties and Computer Programs for Vapor and Liquid States of Water in SI Units." National Bureau of Standards and National Standard Reference Data Systems, Washington, DC.

Henderson, P., Nolan, J., Cunningham, G. C., and Lowry, R. K. (1985). Structural controls and mechanisms of diffusion in natural silicate melts. *Contrib. Mineral. Petrol.* **89,** 263–272.

Hess, K. U., and Dingwell, D. B. (1996). Viscosities of hydrous leucogranitic melts—a non-Arrhenian model. *Am. Mineral.* **81** (9–10), 1297–1300.

Jambon, A., and Shelby, J. E. (1980). Helium diffusion and solubility in obsidians and basaltic glass in the range 200–300°C. *Earth Planet. Sci. Lett.* **51,** 206–214.

Lange, R. A. (1997). A revised model for the density and thermal expansivity of K_2O-Na_2O-CaO-MgO-Al_2O_3-SiO_2 liquids from 700 to 1900 K: Extension to crustal magmatic temperatures. *Contrib. Mineral. Petrol.* **130,** 1–11.

Lange, R. A., and Carmichael, I. S. E. (1990). Thermodynamic properties of silicate liquids with emphasis on density, thermal expansion and compressibility. *Rev. Mineral.* **24,** 25–59.

LaTourrette, T., and Wasserburg, G. J. (1997). Self diffusion of europium, neodymium, thorium, and uranium in haplobasaltic melt: The effect of oxygen fugacity and the relationship to melt structure. *Geochim. et Cosmo. Acta* **61**(4), 775–764.

Navrotsky, A. (1995). Energetics of silicate melts. *Rev. Mineral.* **32,** 121–149.

Nevins, D., and Spera, F. J. (1998). Molecular dynamics simulations of molten $CaAl_2Si_2O_8$: Dependence of structure and properties on pressure. *Am. Mineral* **83,** 1220–1230.

Ochs III, F. A., and Lange, R. A. (1997). The partial molar volume, thermal expansivity, and compressibility of H_2O in $AnAlSi_3O_8$ liquid: New measurements and an internally consistent model. *Contrib. Mineral. Petrol.* **129,** 155–165.

Richet, P. (1983). Viscosity and configurational entropy of silicate melts. *Geochim. et Cosmo. Acta*, **48,** 471–483.

Richet, P., and Bottinga, Y. (1995). Rheology and configurational entropy of silicate melts. *Rev. Mineral.* **32,** 67–89.

Rigden, S. M., Ahrens, T. J., and Stolper, E. M. (1988). Shock compression of molten silicate: Results for a model basaltic composition. *J. Geophys. Res.* **93**(B1), 367–382.

Rivers, M. L., and Carmichael, I. S. E. (1987). Ultrasonic studies of silicate melts. *J. Geophys. Res,* **92**(B9), 9247–9270.

Ross, R. G., Andersson, P., Sundqvist, B., and Backstrom, G.

(1984). Thermal conductivity of solids and liquids under pressure. *Rep. Prog. Phys.*, **47,** 1347–1402.

Scarfe, C. M., Mysen, B. O., and Virgo, D. (1987). Pressure dependence of the viscosity of silicate melts. Pages 59–67 *in* “Magmatic Processes: Pysiochemical Principles” (B. O. Mysen, ed.), Geochim. Soc., Special Publication No. 1.

Shaw, H. R. (1972). Viscosities of magmatic silicate liquids: An empirical method of prediction. *Am. J. Sci.* **272,** 870–893.

Snyder, D., Gier, E., and Carmichael, I. (1994). Experimental determination of the thermal conductivity of molten CaMgSi,O, and the transport of heat through magmas. *J. Geophys. Res*, **99**(B8), 15503–15516.

Stein, D. J., and Spera, F. J. (1993). Experimental rheometry of melts and supercooled liquids in the system $NaAlSiO_4$-SiO_2: Implications for structure and dynamics. *Am. Mineral.* **78,** 710–723.

Stolper, E. (1983). The speciation of water in silicate melts. *Geochim. et Cosmo. Acta* **46**(12), 2609–2620.

Trial, A. F., and Spera, F. J. (1994). Measuring the multicomponent diffusion matrix: Experimental design and data analysis for silicate melts. *Geochim. et Cosmo. Acta* **58**(18), 3769–3783.

Urbain, G., Bottinga, Y., and Richet, P. (1982). Viscosity of liquid silica, silicates and alumino-silicates. *Geochim. et Cosmo. Acta* **46,** 1061–1072.

Watson, E. B., Sneeringer, M. A., and Ross, A. (1982). Diffusion of dissolved carbonate in magmas: Experimental results and applications. *Earth Planet. Sci. Lett.* **61,** 346–358.

Zarzycki, J. Page 505 *in* “Glasses and the Vitreous State” R. W. Chan, ed.). Cambridge University Press, Cambridge, UK.

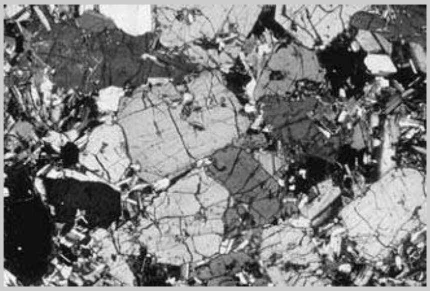

MAGMA CHAMBERS

BRUCE D. MARSH
Johns Hopkins University

I. Introduction
II. Magma Bodies: Types and Sizes
III. Magma Crystallization and Solidification Fronts
IV. Phenocrysts and Solidification Fronts
V. Differentiation Processes in Chambers
VI. Chamber Processes Revealed in the Pluton Rock Record
VII. Chamber Evolution and Pluton Formation
VIII. Magmatic Systems as Mush Columns

GLOSSARY

batholith A vast collection of solidified magmatic bodies (plutons) commonly forming a mountain range like the Sierra Nevada or Andes.

capture front The position in a solidification front denoting a region inward of which crystals are able to move freely relative to one another and outward of which crystals move in concert with their neighbors.

critical crystallinity The point in a solidification front where the packing of crystals is close enough to allow formation of a crystalline network.

dike A discordant sheetlike body of magma, commonly near vertical, cutting the country rock.

dilatancy The tendency of an assemblage of particles to expand or dilate during shear deformation.

mush zone The region in a solidification front where crystals and solids tend to move altogether even though the solids are not all physically connected.

neck A stalklike magmatic feeder connecting a volcano to a deeper supply of magma.

plug The solidified lump or mass of magmatic rock filling a volcanic vent or crater.

pluton An isolated solidified parcel of magma found in Earth's crust and thought to represent an extinct magma chamber.

Rayleigh number A pure, dimension-free number the magnitude of which indicates the tendency of a layer to undergo sustained thermal convection. The larger this number the more vigorous is convection.

rigid crust The region marking the trailing half of a solidification front where all the crystals are interconnected to form a matrix possessing strength.

sill A sheetlike concordant magmatic body usually emplaced horizontal in Earth's upper crust.

solidification front The marginal zone encompassing all active magmatic and volcanic bodies within which most crystallization takes place.

stock Any cylindrical subterranean solidified magmatic body with no clear connection to a volcanic vent.

suspension zone The inward leading region of the solidification front in which small, newly formed crystals are able to move with ease relative to one another.

Copyright © 2000 by Academic Press
All rights of reproduction in any form reserved.

I. INTRODUCTION

Planet Earth owes its gross structure and great diversity of its surface igneous rocks to physical and chemical processes occurring during the crystallization and transport of magma. Although we know broadly what has happened, what exactly goes on in magma to produce these end results is not yet entirely clear. As early as the voyage of the Beagle (1828–1833), Charles Darwin noted in examining Galapagos lavas that magma can evolve chemically simply through the sinking of crystals. Because crystals are always of a different composition than their parent magma, sorting of crystals from melt chemically distills or fractionates magma. The ensuing trail of chemical compositions defines a differentiation sequence. The classical home of the physical and chemical processes of differentiation is the *magma chamber*.

Undoubtedly the largest magma chamber in the solar system is Earth's outer core. Consisting of mainly molten iron, the outer core contains about 30% of Earth's mass. The slow crystallization of the outer core produces crystals that sink to form the inner core, which rotates slightly faster than Earth itself. Even buried at the great depth of about 3000 km, the general spherical shape and size (~2500 km thick) of this magma chamber is well known from seismology. Oddly enough, although the physical nature of this active magma chamber is known in detail, its chemical composition is not nearly as well known. This is quite the reverse of magma chambers associated with volcanism where chemical composition is known in excruciating detail, but the shapes, sizes, and cooling rates of the active reservoirs are not well known.

II. MAGMA BODIES: TYPES AND SIZES

Magma itself, as also defined by Darwin, is any molten mass of Earth material containing any combination of crystals, liquid, and gas. Postmortem studies of old, now solid, magma reservoirs or chambers (generally called *plutons*) exhumed by erosion are commonplace. This is where the most direct information comes from on the nature of near surface chambers. The message from these studies is clear. Magma bodies can be of almost any imaginable shape and size, but some types are much more common than others.

A. Sills and Dikes

Planar sheets, which parallel local rock strata, are called *sills* and *dikes* when they cut the strata and are by far the most common igneous bodies. In general, dikes transport magma and sills store magma. They each can be of almost any size from a few centimeters to more than a kilometer thick and with aspect ratios from 10 to well over 1000. The Basement sill in the Dry Valleys region of Antarctica, for example, is generally 300–400 m thick and can be traced for 100 km. Single dikes a few meters thick and traceable over tens of kilometers are commonplace in many terranes. Their sheetlike form reflects the fact that these are propagating elastic cracks filled with buoyant magma, and the overall shapes of these bodies are spreading disks and pods with very thin edges. Over a distance of 10 km the Basement sill, for example, thickens from 1 cm at its edge to more than 700 m near the center.

B. Necks, Plugs, and Stocks

Other once-molten magmas were clearly not sheets, but vertical cylindrical intrusions. Called *necks*, *plugs*, *pipes*, and *stocks*, these were conduits linking deeper reservoirs to volcanoes. Eroded remnants of these feeders, such as Devil's Tower in Wyoming and the Hopi Buttes diatremes—necks that apparently penetrated upward almost as locomotives—in northern Arizona, are particularly distinctive. Although these forms could occur at depth, they are probably only common near the surface where the original crustal rock can be punched out or excavated to the surface by the rising magma. The diamond-bearing pipes of South Africa, for example, connect downward over several kilometers into more dikelike features. The diameter of most necks is in the range of 100 m to 1.5 km.

C. Plutons

Plutons are bulbous masses that commonly develop beneath strings of volcanoes associated with plate subduction. *Batholiths* may contain vast nests of hundreds of plutons intimately crowded against or penetrating one another. The Sierra Nevada range of California and the Andes literally define the notion of batholiths. Yet the individual plutons within these batholiths are horizontally flattened and, to some degree, sheetlike, although with much smaller aspect ratios (2–20) than sills and dikes. Rather than being injected like sills and dikes, plutons rise diapirically in the fashion of a sluggish thunderhead, eventually losing buoyancy at the leading edge, slowing, and spreading as the lower reaches continue to ascend. The body inflates in place just as do other bodies that begin as necks and locally balloon into a pluton. Although the area of plutons can be enormous (hundreds of square kilometers), many plutons are equivalent to spheres having diameters of 2–10 km.

D. Volumes

To put these numbers in perspective, the volumes of composite and stratocone volcanoes are well represented by a cone of a height equal to its radius, which is equivalent to a sphere of diameter 1.25 times that of the volcano's height. With volcano relief commonly in the range of 1–2 km, although the largest are 3–4 km, magma sphere diameters are in the range of 1–9 km. And considering that most stratocones are made principally of pyroclastic materials, which is of high porosity, this range should be reduced to 0.5–5 km. This result should not be construed to mean that volcanoes are simply the outpouring of a pluton of magma, but that volumes of magma of this magnitude (i.e., 0.1–60 km^3) are not unusual to Earth. The Dufek (Antarctica) and Bushveld (South Africa) intrusions, each on the order of 10^5 km^3, are the largest known basaltic plutons; both are also strongly sheetlike. Close behind in volume (~30,000 km^3) is the 1.85-Ga-old Sudbury impact feature, which was originally a multiringed crater perhaps 200 km wide and several kilometers deep filled with extremely high temperature (~1900°C) melt. Single lava flows, either basaltic or silicic ash flows, reach volumes of 2000–3000 km^3, and these are often part of much larger complexes of either flood basalts or silicic calderas. Some cogenetic igneous complexes, such as oceanic plateaus and rift-related diabase terranes, attain volumes of more than 10^6 km^3, but these are clearly often the result of volcanism over millions years. For even the largest plutons it is not clear how much of the system was simultaneously molten and dynamically connected. The dynamics of molten systems are determined by the behavior of solidification fronts, which link the smallest scale processes of crystal nucleation and growth to the largest scale dynamics and also determine the nature of the final rock record.

III. MAGMA CRYSTALLIZATION AND SOLIDIFICATION FRONTS

A central key to understanding the dynamic evolution of magma is understanding the crystallization of silicate melts. Magma crystallizes over a wide range of temperature (~200°C) and unlike aqueous solutions and molten metals, silicate melts generally do not form large dendritic crystals (Fig. 1). Moreover, regardless of the size of the magmatic body, crystal sizes commonly range from 1 to 50 mm. This tiny length scale is crucial to the chemical and physical evolution of the magma as a whole. Silicates in magma generally grow in tiny, essentially symbiotic clusters. Individual crystals grow by diffusion of chemical components through the melt at similar rates. The effective rates are similar because coupled multicomponent diffusion depends critically on the slowest diffusing component. Because diffusion is so slow (e.g., ~100 yr/cm), components rejected by one mineral locally build up and the melt saturates in a new mineral; eventually enough minerals appear to use all the local melt.

This is in contrast to dendritic crystallization where large crystals, large buoyant boundary layers of rejected melt, and low residual melt viscosity (<~1 poise) allow continual circulation of melt among the growing crystals. The much larger viscosity of silicate melts, the tiny crystal size, and crystal clustering inhibit melt motion and, instead, favor local equilibration with stagnant melt.

In most common magmas several minerals appear after relatively little cooling (~25°C) and these minerals dominate the chemical evolution of the melt over most of the cooling history. Other minerals appear as needed to use up melt components rejected by the existing minerals. The crystallizing assemblage forms a dynamic, growing feature of all magmas: the *solidification front* (SF).

A. Solidification Fronts

The spatial relation between the liquidus (all melt) and solidus (all solid) defines a solidification front about any magmatic body (see Fig. 1). Across this front magma goes from fully liquid at the leading or innermost edge to fully solid at the outer or trailing edge. This bundle of isotherms envelops the body and propagates inward, meeting in the interior at the point of final solidification. Although thin and sharp just after emplacement, with

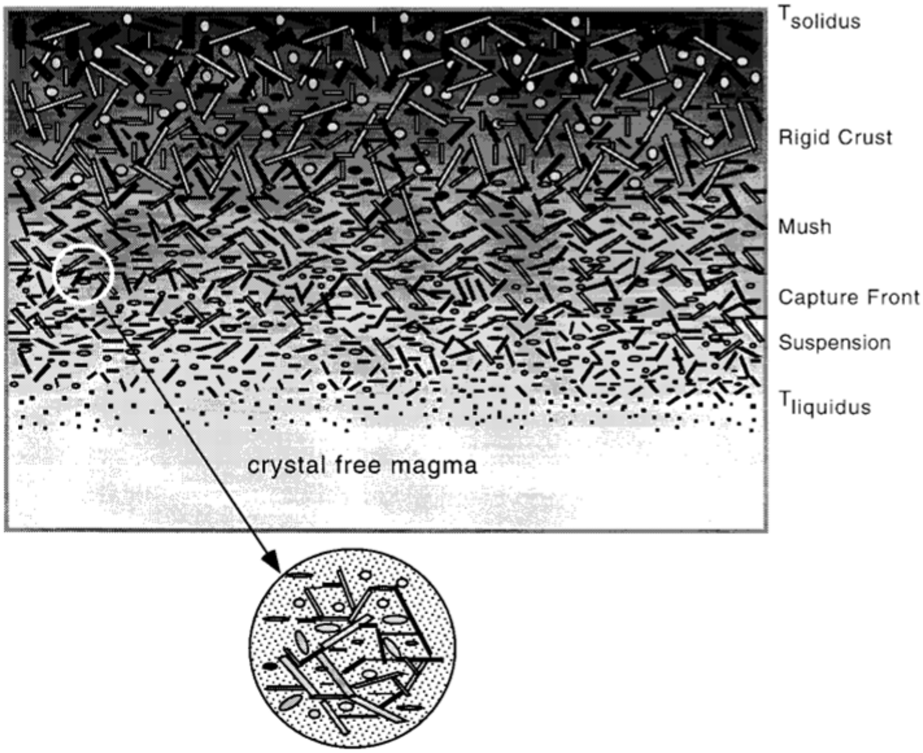

FIGURE 1 Upper solidification front. The base (top here) of the front is defined by the solidus and the leading upper edge is the liquidus. The overall thickness of the front depends on the thermal regime and especially the age of the front and the temperature of the roofrock. The inset depicts the framework-like structure of the crystals at about 30% crystals.

time the SF thickens in proportion to the square root of time, as is well known from the drilling of Hawaiian lava lakes.

Within any SF at least four dynamic and rheological divisions can be identified (see Fig. 1):

1. *Suspension zone:* Beginning at the leading edge or liquidus, the percentage of crystals, N, equals 0; nucleation commences and crystals grow to an overall concentration of about $N = 25\%$ at the trailing edge. The small, sparse crystals can move freely relative to one another and perhaps even escape downward from the front itself.
2. *Capture front:* The boundary marking the trailing edge of the suspension zone ($N = 25\%$) where the bulk viscosity has increased by a factor of 10 over that at the liquidus and behind which settling crystals are unlikely ever to escape the advancing solidification front.
3. *Mush zone:* Bounded by the capture front ($N = 25\%$) at the leading edge and the point of critical crystallinity at the maximum packing of the solids at the trailing edge where $N = 50\text{–}55\%$; individual crystal migration is difficult due to mutual hindrance.
4. *Rigid crust:* Outward of and adjacent to the mush zone and bounded by the solidus ($N = 100\%$) and the point of critical crystallinity ($N = 50\text{–}55\%$). This is the drillable portion of the solidification front commonly referred to as the "crust" in studies of Hawaiian lava lakes.

Two aspects of this subdivided solidification front are important to emphasize. First, these are generalized definitions and are closely tied to the specific phase equilibria of the magma under study; the defining crystallinities will naturally vary somewhat with magma type. In plagioclase-rich basalts, for example, an interlocking network of significant strength may form at crystallinities as low as about 30%. Second, the entire solidification front, which is always present, is a dynamic feature of solidification; it propagates inward at an ever-decreasing rate and thickens with time. All physical and chemical processes occurring as a result of crystallization do so within the solidification front, and the rates and duration of these processes are limited by the rate of motion of the front itself. Thus the entire evolution of the magma, whether being transported or held in a chamber, is reflected by the dynamic behavior of the solidification front, even when the chamber experiences additional injections.

In an ideal magma emplaced free of crystals, nucleation and growth begin at the inwardly advancing liquidus; the viscosity there is essentially that of the crystal-free magma and only when the crystallinity increases to about 25% does the viscosity increase by a factor of about 10 at the capture front. At the other extreme at the trailing edge of the solidification front, near the solidus, the viscosity is enormous, as the rock is nearly solid. Inward from this point crystallinity decreases, but the crystals form a strong interlocking network and viscosity remains enormous until the crystallinity decreases to about 50–55%. Here the viscosity decreases dramatically as the magma makes the transition from a partially molten solid to a mushy liquid. This is the point of *critical crystallinity*, marking the region of maximum packing of the solids where at all higher crystallinities the crystals form an interlocking network of great strength. Moreover, beyond this point the magma is a dilatant solid, where under shear it expands and chokes any conduit. Thus it is uneruptible. High-alumina basalts in some island arcs erupt carrying 40–50% large crystals, and because they are so near to *dilatancy*, they can erupt explosively. At lower crystallinities the network of crystals is not fully interlocking and the material behaves as a crystal-laden fluid possessing a large effective viscosity. The crystals are, nevertheless, unable to move freely relative to one another and the region behaves as a mush. This mushlike behavior continues inward with decreasing crystallinity (i.e., increasing temperature) until reaching the suspension zone, which connects to the crystal-free deep interior of the body.

IV. Phenocrysts and Solidification Fronts

Magmas can be put into two convenient categories: (1) those that carry phenocrysts upon emplacement and (2) those that do not. Phenocrysts, being relatively large cognate crystals, are easily recognized in lavas, but much less so in plutons where they can be mistaken for crystals grown after emplacement. Unusually large crystals in the chilled margins of the body are one indication of initial phenocryst presence. Another is the internal distribution of phenocrysts. Because SFs initially grow exceedingly fast upon emplacement, they capture all phenocrysts in the magma near the contacts. But as the SFs move inward they advance ever more slowly and, at some point, all but the smallest phenocrysts can escape capture and settle to the floor, which is formed by an upward-moving SF. The net result is a loss of phenocrysts in the upper half of the body and an accumulation of phenocrysts in the lower half. The final distribution of phenocrysts from top to bottom is S-shaped (Fig. 2). The efficiency of this process depends on phenocryst size and density and also on magma viscosity; however, many basaltic bodies show this distribution. Shonkin Sag loccolith and Kilauea Iki lava lake are good examples.

A cumulate layer of phenocrysts within a sheetlike body is also an indication of phenocryst emplacement. Many large diabase sills have orthopyroxene or, more rarely, olivine cumulate layers in the central or lower half of the sill, but these phenocrysts are not found elsewhere in the sill. Phenocrysts are most commonly cognate and thus represent an earlier (i.e., prior to em-

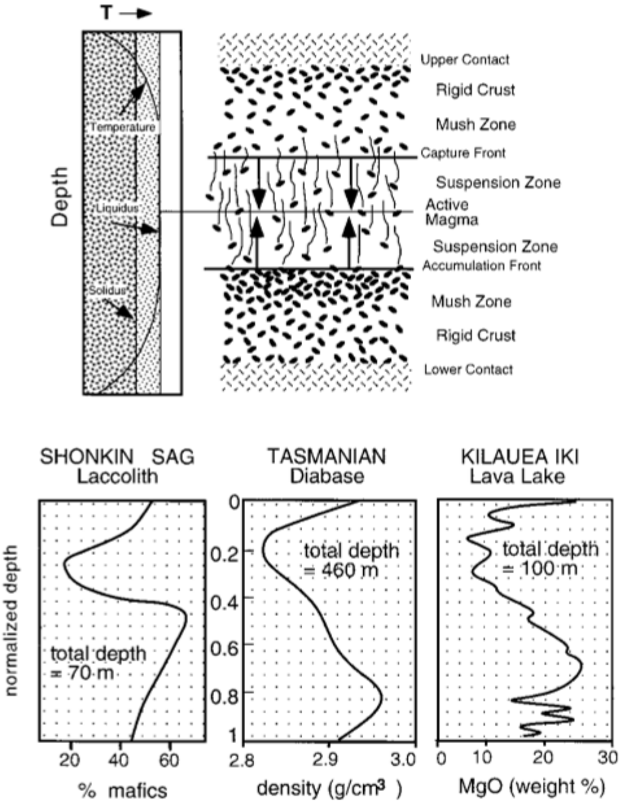

FIGURE 2 The settling and capture of phenocrysts during solidification of a sheet of magma.

placement) crystallization event. This distribution reflects not only the emplacement of the phenocryst-rich magma late in the injection sequence, but also that the magma was *flow differentiated.* That is, the phenocrysts were segregated in the ascending magma into a tonguelike central concentration trailing the leading, phenocryst-free magma (Fig. 3). The leading magma, which forms the margins of the body, therefore, is fractionated, and the central tongue rock is more primitive. Neither rock is a true measure of the original magma composition. Bodies with more evolved compositions at the margins are formed by flow-differentiated magma, and the spectrum of compositions is not something produced *in situ.*

Magma emplaced free of phenocrysts is, of course, also dominated by SFs, but the crystals are formed after

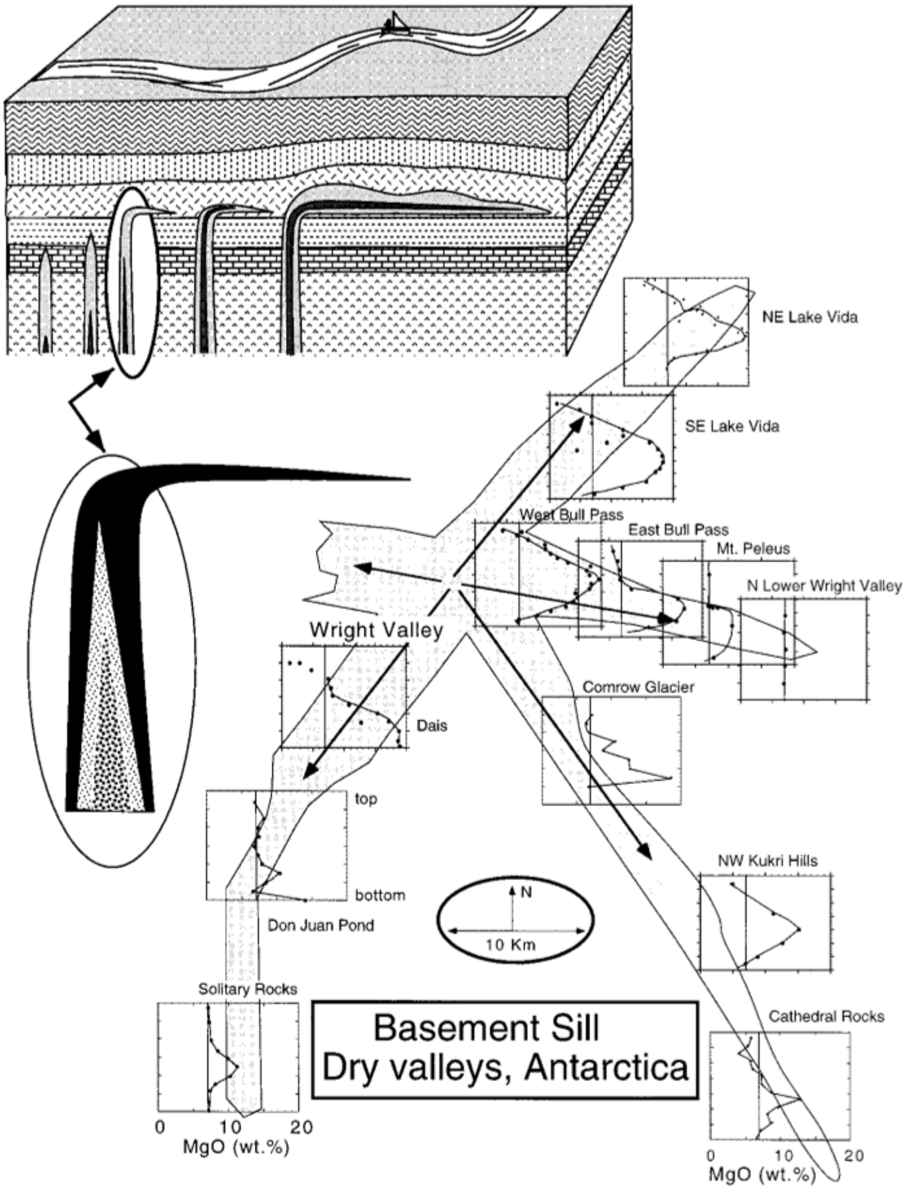
NE Lake Vida
SE Lake Vida
West Bull Pass
East Bull Pass
Mt. Peleus
N Lower Wright Valley
Wright Valley
Dais
Comrow Glacier
top
bottom
Don Juan Pond
N
10 Km
NW Kukri Hills
Solitary Rocks
Basement Sill
Dry valleys, Antarctica
Cathedral Rocks
0 10 20
MgO (wt.%)
0 10 20
MgO (wt.%)

FIGURE 3 Schematic sorting of phenocrysts during transport and emplacement of a sheet of magma (upper left). Actual distribution of orthopyroxene phenocrysts, as measured by bulk MgO content, from top to bottom in the Basement sill. Each chemical plot is run from 0 to 20 wt% MgO.

emplacement—few magmas are probably ever free of nuclei and very small crystals. As the SFs move inward, crystals are nucleated and the ensemble grows to a solid by the time the solidus isotherm arrives. So crystallization can be viewed as the passage of a packet of isotherms through a particular local volume of melt. The rate of cooling determines the rate of SF advancement and the melt becomes solid regardless of the time given for solidification. The melt does this through a combination of crystal nucleation and growth. Because growth is diffusion controlled, it is slow and insensitive to changes in cooling rate. Nucleation, on the other hand, is sensitive to cooling rate. A balance between growth and nucleation thus sustains solidification. Fine-grained chilled margins and coarse interiors reflect this balance.

Differentiation by crystal fractionation is difficult in phenocryst-free magmas because the crystals are confined to the SFs from which they must escape to fractionate. Once the magma reaches a crystallinity of about 25 vol% it is within the capture front, and escape of individual crystals is unlikely. At lower crystallinities, in the suspension zone at the leading edge of the upper SF, plumes of slightly cooled magma containing small crystals may drop from the SF, traverse the core of the body, and, if the intrusion is not too thick, reach the leading edge of the lower, upward-advancing SF. But since there is no net separation of crystals from the initial melt, chemical differentiation is negligible. Moreover, if the body is sufficiently thick, the plumes will become heated and lose negative buoyancy before reaching the floor, destroying the crystals, and becoming incorporated into the interior melt. This is why phenocryst-free bodies, especially sheetlike intrusions, are frequently uniform in composition from top to bottom.

The 350-m-thick Peneplain sill of the Dry Valleys region of Antarctica is a good example of a phenocryst-free intrusion (Fig. 4). Except for the horizon of silicic segregations near the roof, which will presently be considered, the composition is essentially uniform from top to bottom. Although it might be imagined that this could only occur in relatively small bodies like sills, on a grander scale the Sudbury igneous complex, which is about 3 km thick, shows the same feature. Sudbury is an exceptional example in this respect because it was produced in a matter of minutes by a meteorite impact. Because the initial melt was heated to at least 1900°C, it was initially free of phenocrysts. In more detail, Sudbury consists of an ~2-km layer of granitic rock overlying ~1 km of dioritic. The granitic layer is much too thick to have been produced from differentiation of the diorite and is clearly the result of impact melting of granitic continental crust. The diorite may simply be melted lower crustal rock; the transient cavity reached depths of 25–30 km. But what is interesting in the present context is that both layers, granitic and basaltic, are essentially uniform in composition. From these and similar bodies, it is becoming clear that differentiation is critically dependent on the presence of crystals in the initial magma. How, then, is the wide range of diversity of igneous rocks produced?

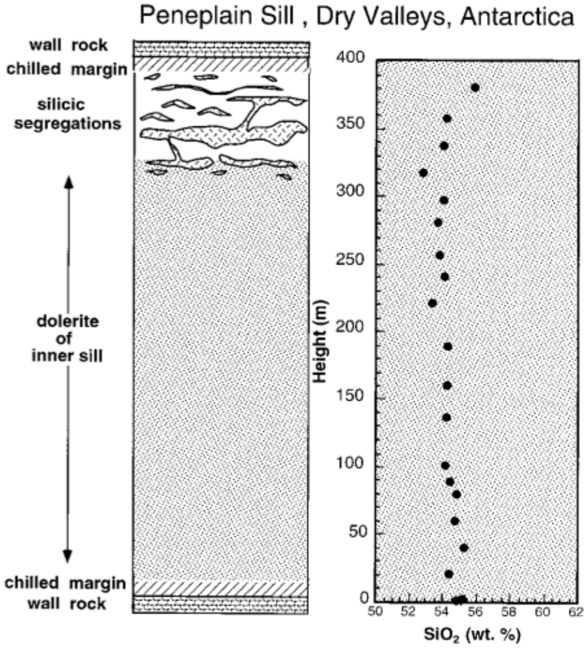

FIGURE 4 The petrologic and chemical variations through the Peneplain sill of Antarctica. This sill was emplaced without phenocrysts and it is nearly homogeneous except for the silicic segregations near the roof.

V. DIFFERENTIATION PROCESSES IN CHAMBERS

There is no doubt whatsoever that chemical differentiation in igneous systems results from the physical separation of crystals and melt. Crystal compositions are always distinct from any natural melt, and progressive crystallization produces residual melts that match the observed compositions of naturally occurring rocks. Thus it would seem simple to produce compositional diversity by removing crystals (by sinking or floating) from the melt. This process of differentiation by crystal fractionation was elucidated in great detail by N. L. Bowen (1887–1955) in the first half of this century.

Numerous mass balance calculations involving reasonable solid phases and derived melts show the great feasibility of crystal fractionation as a means of efficient chemical differentiation. But as reasonable as this process is chemically, the details of the physical process of extensive crystal removal have remained obscure. Many massive basaltic magmatic systems, like Hawaii, produce no silicic magmas whereas other small (~1-km^3) island arc volcanoes erupt lavas of a wide range of compositions. With the recognition of the central role of SFs in crystallization, the controls on the processes of separating crystals and melt have become clear. Refined or fractionated melt is buried deep within the solidification front, and this makes the separation of crystals from melt difficult. Over the first 50% of crystallization, there is relatively little chemical evolution of the melt. It is over the last 50% of crystallization that the melt becomes highly fractionated. Where the melt is hardly fractionated, the melt and crystals are easiest to separate (i.e., at low crystal contents). Where the fractionation is strong, the melt is held in a rigid network and virtually impossible to separate from the crystals. Unless this interstitial melt can be collected into an eruptible mass, the system will show little diversity. The SF must somehow be physically disrupted in order to be purged of the interstitial melt. There are three fundamental ways to do this, as discussed next.

A. Solidification Front Instability and Silicic Segregations

Because SFs are relatively cool and are partially solid, they are denser than the underlying uncrystallized melt. Once a SF becomes sufficiently thick, it becomes gravitationally unstable. The internal strength is locally overcome by the weight of the leading half of the front and tears begin to develop. As the tears open, local interstitial melt is drawn into them, producing silicic pods and lenses. Interdigitating lenses of silicic rock, 2–3 m thick and 40–50 m long, are common in the upper parts of tholeiitic sills regardless of the initial phenocryst content. Plagiogranite segregations of the oceanic crust are undoubtedly products of solidification front instability (SFI). The silica contents of silicic segregations are in the range of 60–70 wt% and the bulk composition of the sill is near 50%. The more siliceous the sill, the more siliceous are the segregations. Mass balance calculations show that the segregations are produced from local melt and that the tears open when the local crystallinity is about 65%. This is spatially just behind the point of critical crystallinity when the mush becomes locked into a rigid, but still somewhat weak, network.

If the intrusion is thick enough, the instability may mature to the extent that a large portion of the front detaches and sinks into the core of the chamber. This frees the silicic segregations to collect into eruptible masses of magma; repeated buildup and failure of the SF may thus produce sizable volumes of silicic magma. Overall, however, a characteristic of suites produced by SFI is that they are distinctly bimodal. There are basaltic and silicic compositions, but nothing intermediate. This is a characteristic of many volcanic and plutonic suites, especially in oceanic islands like Rapa Nui (Easter Island), Galapagos, and Iceland, which are considered shortly.

B. Mush Flow Fractionation

When the center of a magmatic body reaches an advanced stage of crystallization, it is ripe for differentiation by flow fractionation. This occurs when new magma invades the system and forces its way through the established crystalline meshwork, pushing out the fractionated interstitial melt. The original body is thus purged of fractionated melt by replacing it with new magma. Not only is fractionated melt freed to erupt, but also the new magma is contaminated by older crystals of the meshwork, which are thermally and chemically out of equilibrium. The SF meshwork will be partly dissolved, perhaps even disrupted, and the escaping fractionated melt may also carry small telltale pieces of the original SF in the form of clots or clusters of crystals.

The ideal location for this process is in reactivated fissures associated with flank eruptive systems of large active volcanoes. During periods of repose, magma remaining in the dominant fissures can solidify to the point of critical crystallinity (~55%). New activity displaces the residual melt, yielding an eruption of fractionated melt on the flanks of the volcano. This is seen at Hawaii, where the only fractionated lava issues from fissures on the far flanks; and this melt carries small clots of the SF. Deep in these same fissures thick accumulations of phenocrysts form (at Hawaii these are olivine cumulates) and may also be re-entrained and similarly purged by the invading magma, yielding unusually primitive (i.e., olivine-rich) basalt compositions.

The amount of melt available for purging is proportional to the size of the existing SFs. Because magma will always follow the path of least resistance, it will not normally invade an existing SF unless that is the only course available. Moreover, as the residual melt in the SF becomes enriched in silica its viscosity rises dramatically, making displacement increasingly difficult. It is thus unlikely that highly silicic melt could be freed in this fashion unless enough volatiles build up in the SF to offset the effect of silica on viscosity. In extensive, geometrically diverse, and long-lived magmatic systems, such as mush columns (see later discussion), this form of melt fractionation is most effective.

C. Reprocessing

The formation of silicic segregations is a normal consequence of solidification. Some alkalic basalts become siliceous only at the latest stages of crystallization when the SF is too strong to be torn, and some bodies are too small to undergo SFI. But in general most basaltic bodies will produce silicic segregations, and once formed they remain as silicic noise in otherwise basaltic systems. Even if the entire body was remelted, these silicic pods are so much more viscous than basalt that they are physically (but not chemically) immiscible in basaltic magmas. Stirring is ineffective in reblending these silicic blobs. Wholesale remelting of basaltic crust frees swarms of segregations to collect into eruptible volumes of rhyolitic magmas. This is very likely the means of producing both rhyolite and basalt in Iceland.

About 15% of the surface rocks of Iceland are rhyolitic. There is a preponderance of basalts, but a paucity of lavas of intermediate composition. The suite is strikingly bimodal. Iceland is a prime location for reprocessing of the basaltic crust because it straddles the Mid-Atlantic Ridge. And within Iceland the ridge jumps periodically, refocusing magmatism at a new location in older crust. Prolonged use of new fissure swarms steadily heats the crust, forming outward-propagating, progressive—instead of regressive—solidification (i.e., melting) fronts. These fronts systematically break down and reprocess the crust, freeing silicic segregations to collect as rhyolitic magma (Fig. 5). The ensuing rhyolities, such as those at the large Torfajokull silicic center, are nearly crystal free, but carry ubiquitous, diagnostic crystalline debris from the original SF, including pieces of granophyric rock in various stages of melting. The massive 1875 pumice eruption of Askja volcano in northern Iceland, for example, was laced with chunks of silicic segregations quenched in all degrees of fusion. The oxygen isotopes of the rhyolites show the effects of extensive prior hydothermal alteration when the silicic segregations were a part of the crust. This is also even true for comagmatic basalts. Thus the Iceland crust undergoes wholesale differentiation through remelting.

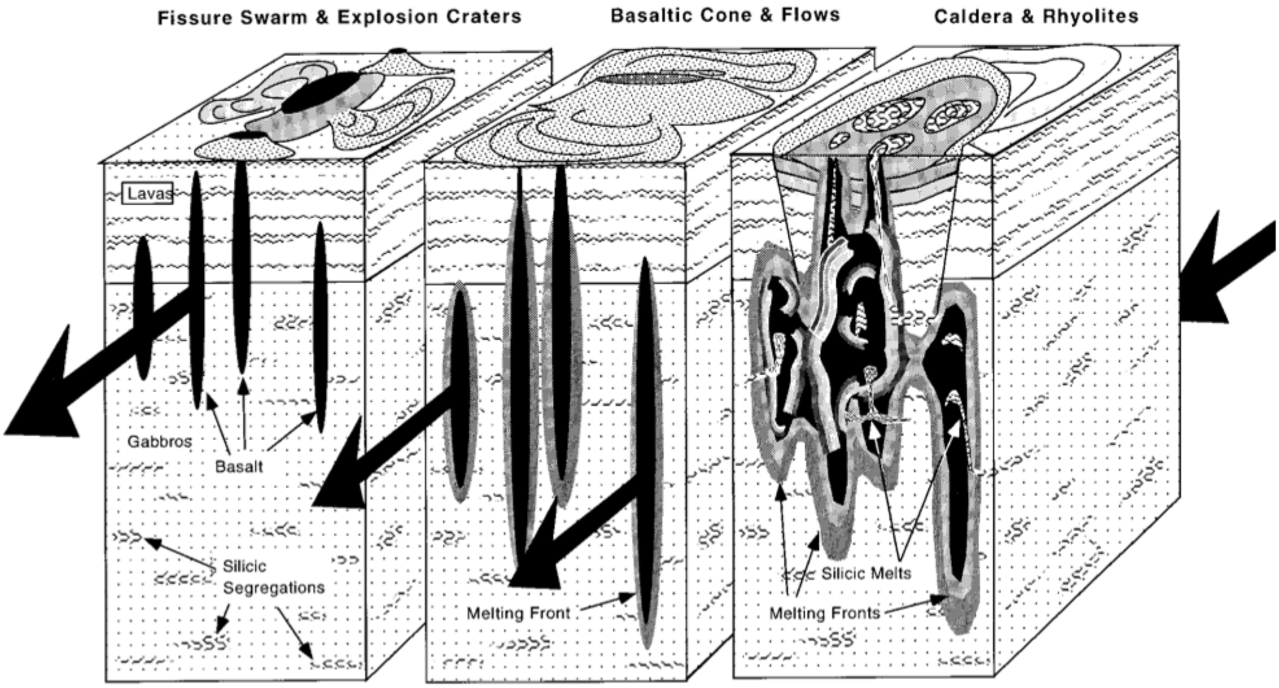

FIGURE 5 Generation of rhyolitic magma in Iceland through reprocessing of older crust.

D. Compaction

Solidification fronts growing upward on the floors of magma chambers can become so thick or distended that their weight is enough to deform the crystalline matrix and squeeze out the interstitial melt. This is a slow process that can only occur when the growth of the front itself is slow, which occurs either at advanced stages of crystallization in large bodies or deeper in the crust where the wallrock/floor rock is suitably hot, making inward propagation of the solidus sluggish. Depending on the melt density, the evicted melt may accumulate within the upper reaches of the front or continue upward through the core of the body and lodge within the upper solidification front. In thick sheetlike chambers the changeover from solidification control to compaction may be sudden enough to produce a distinct compositional horizon higher in the system, and these segregations may also be collected during reprocessing.

E. Chemical Fractionation Effects

The chemical aftermath of SF fractionation is virtually indistinguishable from massive crystal fractionation. Both processes involve the separation of an ensemble of slowly grown indigenous solids. There are, strictly speaking, small chemical differences between pulling a melt from an equilibrium assemblage of solids fairly late in the crystallization sequence and separating crystal by crystal from the melt as they appear. But there is no physical process that can systematically cleanse a melt of tiny crystals over a wide crystallization interval. Moreover, it is doubtful whether the resulting rocks contain enough discriminatory evidence to reveal the details of the fractionation process. Nevertheless, certain constraints due to mass balance considerations are generally consistent with solidification front processes. It is the physical evidence, coupled with the chemistry, that reveals process. This is also evident in the deciphering of the dynamics of large magmatic systems.

VI. CHAMBER PROCESSES REVEALED IN THE PLUTON ROCK RECORD

Exotically layered and compositionally varied plutons would seem to hold the key to understanding magmatic processes. The stratigraphic record left on the floors of Skaergaard, Stillwater, Rum, Bushveld, the Great Dike, and Dufek, among others, have been carefully studied with the hope of discovering the fundamental dynamics, chemical and physical, of magma chambers. All other bodies would then simply be subsets of these more dynamically rich systems. An easy reading of this rock record has proven difficult. It has become clear, however, that the chemistry of the rock record is not enough, in and of itself, to reconstruct the solidification history.

Unlayered plutons have been viewed as containing definitive evidence of processes distinct from those of layered plutons. And lavas and ash flows, lacking any information on pre-eruption stratigraphy, have been examined strictly in terms of chemistry. Thus three separate sets of principles exist that have been garnered from the study of layered, unlayered, and erupted bodies, and they fail to produce a consistent dynamic depiction of magma chambers.

A. Layered Plutons and Initial Conditions

The historical approach to interpreting layered plutons has been to assume an instantaneous emplacement of a more or less homogeneous magma at or near its liquidus temperature. All subsequent layering and differentiation come from processes occurring in the chamber. Progressive crystallization throughout the magma either rains crystals to the floor, producing more or less homogeneous gabbroic cumulates, which evolve upward into more fractionated compositions, or periodic overturns of crystal-laden melt makes sedimentary layers on the floor. Some crystallization at the roof is unavoidable and an upper border group also develops, but it is much thinner than the floor sequence. A sandwich horizon occurs where the floor and roof sequence meet, and this is where the most evolved rocks should lie.

These irrefutable facts came from the earliest field observations at Shonkin Sag laccolith by L. V. Pirsson (1860–1919) in 1905. Floor sequences, where present, are normally much thicker than roof sequences. This has been interpreted to reflect strong cooling from the roof, promoting strong crystallization and convective circulation throughout the interior and major deposition of crystals on the floor. The inversion of this rock record would seem to be straightforward. But other than the usual sporadic silicic or granophyric segregations, significant volumes of silicic rock are rarely found at the inferred sandwich horizon. They could have been erupted away, but perhaps there were none there in the first place.

Even stranger has been the realization that thick floor sequences are not seen in phenocryst-free diabase sills, no matter how thick the sill itself may be. A precise determination of the true sandwich horizon is also possible in many sills and lava lakes from the mismatch in roof and floor joints, which are shrinkage or cooling cracks that track the inward propagation of the upper and lower solidification fronts. They always meet approximately in the middle. Cooling would seem to be equal from top and bottom. Thermal modeling, both with and without convection, bears this out. Thus the absence of silicic sandwich horizons points to a fundamental problem with the historical concept of magma solidification in chambers. The field evidence has another interpretation.

Thick accumulations of crystals on the floors of bodies such as Shonkin Sag laccolith are from the deposition of crystals (phenocrysts) carried in by the initial magma. They are essentially snowfalls of crystals; this is sudden and massive cumulate formation. Phenocryst-bearing magmas injected into chambers of any sort—sills, dikes, plutons—form cumulates; it is unavoidable as long as the body is not so small as to cool instantaneously.

Initially crystal-free magma, such as the Sudbury igneous complex, crystallizes to almost featureless rock. The instantaneous emplacement of such magma of any significant size is a rare occurrence. Yet it does happen. Individual eruptions of continental flood basalt reaching volumes of 1000–2000 km^3 often contain very few phenocrysts (2–5%) and are chemically homogeneous. And 100-m-thick ponds of these basalts solidify into featureless rock with some silicic segregations. Were these magmas to cool, instead, in sheetlike chambers at depth, as some must, they would be homogeneous gabbros with signs of SFI.

The central problem in interpreting plutonic rock sequences is that the initial conditions of the system are unknown. Was the body formed of one massive injection? Or did it form by many periodic emplacements, as in long-term volcanic eruptions at Hawaii? What was the phenocryst content of these inputs? Although general impressions are sometimes attainable from nearby dikes and sills, more generally the answers to these and many similar questions have been inaccessible. Some answers may come from layered sequences.

B. Layering

Phenocryst-charged magma cannot solidify without crystal sorting into layers, however cryptic or well formed; it is unavoidable. The separation of solids from fluids is a vast subject rich in process and dynamics. Almost any conceivable final sequence of solids of arbitrary shape, size, and density is attainable through reasonable sedimentation scenarios. Moreover, the ensemble of scenarios increases greatly if the shape of the magmatic container is also varied. In a relatively narrow chamber with outward-slanting walls, for example, the well-known Boycott effect controls sedimentation by greatly enhancing the rate of deposition. Crystals near the walls settle quickly and avalanche *en masse,* sorting crystals according to size and density in a delicate fashion (Fig. 6). Moreover, repeated injections of varying intensity supply inputs to the chamber of varying phenocryst concentration and size. The net effect of crystal sorting, chamber form, and input history is to establish a vast dynamic regime that can give rise to intricate layered sequences.

Knowing the dynamic regimes of layering it would seem straightforward to read the history of the injection process, but annealing clouds this inversion, making it nonunique. That is, once any mechanical segregation of crystals takes place, local thermodynamic equilibrium controls further maturation of the texture. Certain minerals may be unstable and dissolve to refine cryptic layering into nearly monomineralic layers. This form of annealing or textural ripening is known from metallurgy and ceramics. Annealing can only be avoided by rapid cooling, which itself is possible only in small bodies.

Large bodies, then, commonly show good layering for two principal reasons. They were formed by many injections; hence the probability is high that phenocryst-laden magma was present. Also, unusually long cooling times provide maximum opportunity for textural ripen-

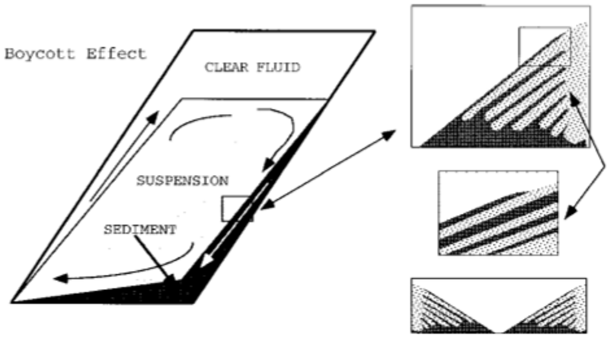

FIGURE 6 The enhanced sedimentation due to an inclined wall. Once on the wall, the sediment avalanches downward along the wall, inducing an upward return flow beneath the hanging wall. Avalanching promotes layering because small and large particles have different angles of repose. The result of two slanting walls is also depicted.

ing. In addition, large bodies may form extensive mush regions, extending at some point through the entire body. This allows interstitial melt to flow and supply nutrients to layer-forming crystals and to destabilize other crystals. This late-stage flow through the porous mush blurs the final chemical spatial state of the system, making inversion to an active magma chamber nonlinear and difficult.

C. Thermal Convection

If magma did not crystallize and form solidification fronts, the convective regime in chambers could be easily predicted from the shape, thickness, temperature, and viscosity of the magma. From these and a few other physical properties, the magnitude of a pure number (i.e., free of dimensions) called the *Rayleigh number* (Ra) can be determined. Everything dynamic about noncrystallizing fluid can be learned from Ra; the temperature distribution, rate of convection, and rate of cooling are each set by Ra. The enormous literature on thermal convection in fluids of almost every kind tells this in great detail, but it tells relatively little about fluids undergoing solidification. Although the general concepts still hold, the details of the dynamic regime cannot be safely predicted from the conventional consideration of Ra. It is particularly unclear exactly how to estimate the temperature difference driving convection.

The main reason for this is that the cool, denser magma along the roof, which would normally form descending plumes to be replaced by ascending hotter, lighter magma, is mainly locked in solidification fronts. This minimizes the amount of cool fluid available to drive convection. The SFs also propagate inward with a velocity that tends to override incipient plumes forming at the leading edge of the SF, trapping them forever within the SF. And the onset of nucleation throughout the interior may produce enough heat from latent heat of crystallization to offset the heat potentially transferable by convection. Although the detailed physics is only now emerging, it is clear from a growing set of experiments that solidifying fluids do not convect much, if at all, once they are below their liquidus temperature. If the fluid is superheated (i.e., above the point of initial nucleation), however, vigorous convection occurs in the conventional sense. The absence of erupting superliquidus magma may well reflect the efficiency of convection in dispatching superheat. The absence of superheat indicates a diminished role for thermal convection as a dominant process in chambers, but this does not mean that chambered magma is motionless. Along the walls in tall chambers, for example, crystal-laden flows may cascade down and sweep across the floor, possibly forming troughs in the basal front and at the same time depositing crystals.

D. Convection in Sedimentation

Swarms of crystals in freshly injected magma can never be uniformly distributed and so the uneven density along horizontal (i.e., equipotential) surfaces will spawn convection. The motion can take on many forms, but descending plumes is the most common. If the crystals are small ($<\sim 0.1$ mm), have a low-density contrast, and their concentration is low ($<\sim 5\%$), the crystals form a dusty suspension that may slowly circulate in cells as the dust is deposited on the floor. The flow will be relatively gentle, as it is for highly concentrated ($>\sim 40\%$) mushes, which are too viscous and sluggish to move vigorously.

Between these extremes there is a wide range of dynamic behavior where crystal sedimentation can strongly stir the magma. The more basic the magma, the lower its viscosity and the more pronounced the effects of sedimentation. The aftermath is a sequence of layering clearly due to convection, but not thermal convection. Considering the large size of magmatic systems, the physics of crystallization, and the possible shapes of chambers, some motion, however small, is probably always present.

VII. CHAMBER EVOLUTION AND PLUTON FORMATION

The age-old dilemma in interpreting plutonic rocks is whether to read the sequences as due to purely *in situ* processes or as a result of a series of injection events. This issue, which historically is almost a philosophical matter in petrology, still plagues interpretations; for it is always easy to interpret a complex rock sequence as due to a specific string of injection events, which moves the problem to another venue. Given the geochemical tools and physical insight now available on crystallizing systems, however, this question can be approached with far more objectivity and certainty than ever before. Thick continuous sequences of cumulates on the floor reflect a chamber formed of phenocryst-laden magma (e.g., Shonkin Sag). Thick expanses of uniform texture gabbro or diabase reflect crystallization of mainly phenocryst-free magma (e.g., Sudbury). These are perhaps end members (Fig. 7) and the larger the body the higher the probability that it was formed over a significant period of time (say, hundreds to 10^5 years) involving many injections of magma with varying amounts of phenocrysts. The net result can be exotically layered sequences sandwiched within monotonous nonlayered sequences, or even a thick, coarsely layered sequence followed by a finely layered sequence, marking perhaps two distinct injection episodes, much as seen in volcanism itself. The detailed isotopic record through such sequences generally shows the number of injections to increase with the size of the body. Bodies as large as Stillwater, Rum, and Dufek, for example, which are each more than 5 km thick, may have experienced thousands of injections during formation. In spite of this, the thickness of highly fluid magma at any time may have been only a few hundred meters or less, as has been recognized at Rum in piles of pieces of the lower front dislodged by the injections. The lower solidification front, including any cumulates, was locally disrupted time and again by these injections. Crystals were reworked and redeposited and crystal growth was interrupted many times. Individual crystals may carry zoning telling of a long and dynamic history.

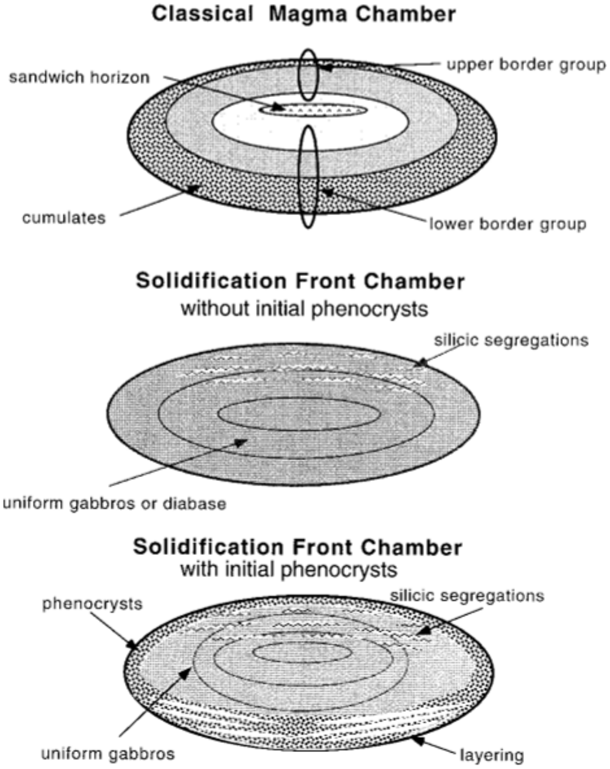

FIGURE 7 Magma chamber final rock sequences with and without initial phenocrysts (lower two sketches) in comparison to the historical interpretation of rock sequences (top). If multiple injections of crystal-laden magmas are added, almost any sequence can be achieved.

Further variations on this basic theme come from the geometry of the wallrock container holding the magma. Injection of phenocryst-laden magma along steeply inclined walls, as mentioned already, promotes rapid sedimentation, avalanching, and sorting, leaving a telling sequence reflecting an intricate dynamic record that continues to evolve via diffusion until dropping temperature finally freezes in the record.

The net result is a pluton whose size, container geometry, and overall composition greatly influence the rocks it is composed of. The larger the body, the more injections necessary to build it; the more injections, the higher the probability of injecting a wide variety of phenocryst concentrations and sizes. The wider the variety of phenocryst assemblages, the greater the crystal sorting and layering. Inclined walls enhance this variety, but increasing silica content stifles sorting and variety.

Small, single-injection sills and dikes are most often unremarkable in variety because they are small and of simple geometry. Yet, their story is still important. They tell what systems become when they are not steadily reinjected and cool quickly. At another extreme are lavas. Volcanic sequences are clearly the result of long periods of subareal reinjection or eruption, but the small size of individual injections (i.e., flow thickness) promotes rapid cooling without crystal sorting and annealing. At yet another extreme is large, long-lived, and heavily reinjected chambers.

The lesson learned is that the three dynamic regimes of magma, characterized by large chambers, sills, and lava flows, each show different aspects of the same spectrum of physical and chemical processes common to magma. Magma chambers are thus integrated systems behaving in response to system size, nature of holding regime, and state of crystallinity of the magma itself. An integrated magmatic system is more aptly characterized as a mush column.

VIII. MAGMATIC SYSTEMS AS MUSH COLUMNS

Mush columns are vertically extensive active magmatic systems in the crust and lithosphere (Fig. 8). At depth they are a blend of sills, stocks, and original wallrock,

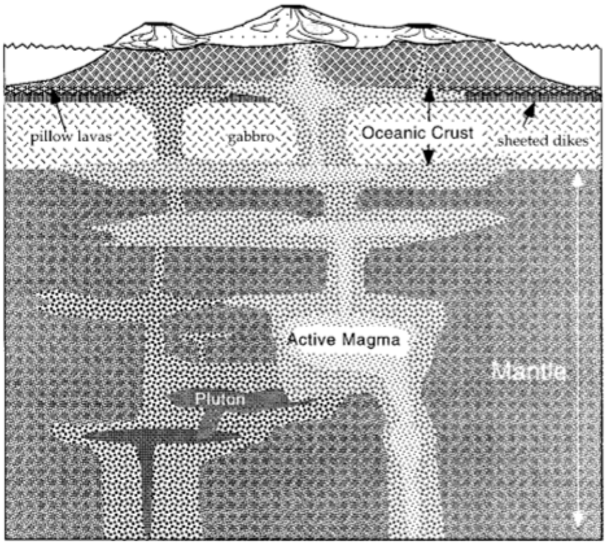

FIGURE 8 A schematic depiction of a mush column magmatic system as might exist beneath Hawaii, Easter Island (Rapa Nui), or other isolated oceanic volcanic centers.

where with time all boundaries, both physical and chemical, become blurred. Thick expansive sills cool slowly and, on average, always contain a core of magma containing few crystals. Narrow interconnecting passages, on the other hand, cool much faster and are choked with crystals in a relatively short time. Yet as long as the magnitude and frequency of magmatism sustain supersolidus temperatures, a distinct, however tortuous, core region is always available to transport magma upward. In the narrow, mushy necks, crystals are entrained and flushed away. The local mush state thus depends on the local magmatic flux or the magnitude and frequency of magma transmission.

A. Geophysical Detection

Direct evidence of this kind of system comes from studies of deeply eroded subvolcanic terranes combined with geophysical inferences (e.g., earthquake distributions) on large active systems like Hawaii and the ocean ridges.

Beneath volcanoes, contrary to petrologic expectations, seismic studies find little sign of large magma-filled caverns or chambers. Teleseismic studies generally do find a general slowing of seismic waves (i.e., travel time residuals) around large calderas, like at Yellowstone and Long Valley, but more detailed local surveys do not find anything easily ascribable to a large concentration of highly fluid magma. Near source studies at Katmai on the Alaska Peninsula showed strong S-wave shadowing presumably due to magma, and the distribution of earthquakes both prior to and after eruption at Mt. Pinatubo (Philippines) as well as at Kilauea (Hawaii) shows a diffuse magmatic region, but nowhere is the picture very clear on *in situ* magmas beneath volcanoes.

Recognizing the dominant role of SFs in magmatic systems, these results are not surprising. Mature solidification fronts, as already mentioned, are made mostly of an interconnected network of crystals that give the SF elastic strength and the ability to transmit seismic waves at velocities not much slower than the solid rock itself. Moreover, large active magmatic systems are generally mature (i.e., size is age) and possess extensive mush regions and relatively small volumes of low crystallinity magma. And individual bodies themselves are small relative to the wavelengths of seismic waves (3–5 km), making detection difficult. Magmatic regions may thus appear seismically solid, and were it not for the manifestations such as surface inflation and eruption itself, the presence of the magma would not be suspected. Detailed seismic reflection studies at ocean ridges find a thin (50- to 150-m) lens or sill of magma residing just below the sheeted dike complex and perched at the top of an extensive mush column (see later discussion). At fast-spreading ridges like the East Pacific Rise the lens is clear and near the surface, but at slow ridges like the Mid-Atlantic Ridge the lens presence is unclear, perhaps ephemeral, and possibly deeper due to the more subdued thermal regime associated with slower plate spreading.

Gravity and magnetic surveys also do not reveal any simple magma chamber system. Near-surface magmas being almost neutrally buoyant have small density contrasts, so resulting gravity anomalies are subtle to detect among background anomalies. The high temperature of magmas makes them nonmagnetic and in magnetic contrast to most country rock. But volcanic areas are often magnetically noisy, again making detection difficult.

The arrival of magma into the near-surface swells the reservoir and inflates the surface, which is directly measured through leveling. This is commonly seen at large shield volcanoes like Kilauea in Hawaii and Krafla in Iceland. Modeling of this inflation gives some idea of the general position and size of the local reservoir, and this inference is also consistent with mush column systems (see Fig. 8). In island arc-style magmatic systems, characterized by small volume central vent eruptions as at Mount St. Helens, inflation is much more localized to the immediate area of the volcano itself.

The associated mush column is similar in basic features, but is weaker, cooler, and much more spatially restricted.

Thus the theory of large swimming pools of magma immediately beneath volcanoes and ocean ridges, a model held for nearly a century, has not proven out. Instead the magmatic system is more like a vertically distended mush column. And it is the individual dynamic and chemical characteristics of mush columns that are responsible for the distinctive petrologic character of these systems.

B. Igneous Diversity and Bimodality

It may seem odd that neither petrologic diversity nor bimodality (i.e., a preponderance of basaltic and rhyolitic rocks with a paucity of rocks of intermediate composition) is proportional to system size. This is a direct reflection of mush column dynamics.

In relatively small, sluggish, and tectonically immobile magmatic systems, the magnitudes and frequencies of eruption are small, and magma repeatedly traverses similar pathways and encounters earlier intrusions at various stages of crystallization. Tectonic immobility of the magmatic center along with intermittent eruption over a 1- to 5-million-year period, for example, allows most intrusions within the underlying magmatic column, regardless of size, to become highly mushy or even locally to solidify and yet remain in place to be reprocessed through reheating by later magmas. Immobility is central to reprocessing, and reprocessing is central to bimodality. This is the primary difference between Hawaii and Iceland. Hawaii is highly mobile relative to its deep-seated source and escapes reprocessing, whereas Iceland straddles the Mid-Atlantic Ridge, which periodically relocates and extensively reprocesses the crust of Iceland. Bimodality is well developed only at Iceland. The silicic lavas contain pervasive restitic debris, and mingled lavas are not uncommon. Both features reflect reprocessing.

If the mush column is relatively cool and sluggish, only fairly evolved or fractionated basalts reach the surface, which is the rule at small, intermittent magmatic centers like Rapa Nui (Easter Island) and perhaps many island arc centers. The basalts will not form a chemically cohesive group easily related to one another through simple fractionation, instead the compositions of each eruptive batch, in detail, will each be distinct, and the suite as a whole will show a characteristic scatter. Reactivating a cool, weak mush column may also force earlier stagnated magmas to ascend and sequentially invade one another as new magma climbs toward the surface. Stagnated magma has the highest probability of having compositionally evolved through any number of processes. The erupting magma may thus be a haphazard mix of less and more evolved magma. Reheating by fresh magma also locally remobilizes mushy sills, freeing solidification front-bound silicic segregations to collect and eventually erupt as silicic magma.

If, on the other hand, a resumed flux of magma through the mush column is strong, recently formed cumulate beds can be disrupted and the crystals entrained, partially resorbed, and redeposited higher in the column. They can also be carried in part to the surface. In this fashion a strong vigorous system can erupt primitive, olivine-laden picritic lavas. At Hawaii, for example, both olivine abundance and size are proportional to the eruptive flux of Kilauea. The compositions of these Hawaiian lavas are characterized by strong olivine control, and olivine fractionation produces a basalt with $<\sim 7$ wt% MgO and multiply saturated, at low pressure, in olivine, clinopyroxene, and plagioclase. The compositions of successive lavas are easily related to one another through simple crystal fractionation, and the suite as a whole will show a certain chemical cohesiveness reflective of this process.

The net chemical result of the mush column, thus, depends on the magmatic strength of the system. Weak, sluggish columns produce a series of disjoint magma compositions due to a series of distinct local differentiation histories, each related to the others through the basic chemistry of the ultimate source of the entire magmatic event itself. Strong systems, especially if immobile, show good chemical cohesiveness due to continual crystal entrainment, transport, and deposition. A general feeling for the evolution of the entire system can be gained by considering the system as a whole, tied together by crystal fractionation in a virtual magma chamber, which at some level must always be true. It is the details of the rock chemistry, petrography, and temporal occurrence that record the details of the local magmatic processes. It is these processes that define magma chambers.

SEE ALSO THE FOLLOWING ARTICLES

Basaltic Volcanoes and Volcanic Systems • Calderas • Composition of Magmas • Lava Flows and Flow Fields

FURTHER READING

Cawthorn, R. G., ed. (1996). "Layered Intrusions." Elsevier, The Netherlands.

Gunnarsson, B., Marsh, B. D., and Taylor, Jr., H. P. (1998). Generation of Icelandic rhyolites: Silicic lavas from the Torfajokull central volcano. *J. Volcanol. Geotherm. Res.* **83,** 1–45.

Irvine, T. N., Andersen, J. C. O., and Brooks, C. K. (1998). Included blocks (and blocks within blocks) in the Skaergaard intrusion: Geologic relations and the origins of rhythmic modally graded layers. *Geol. Soc. Am. Bull.* **110,** 1398–1447.

Mahoney, J. J., and Coffin, M. F., eds. (1997). "Large Igneous Provinces: Continental, Oceanic, and Planetary Flood Volcanism," Geophysical Monograph 100. American Geophysical Union, Washington, DC.

Marsh, B. D. (1996). Solidification fronts and magmatic evolution. *Mineral. Magazine* **60,** 5–40.

McBirney, A. R. (1993). "Igneous Petrology," 2nd ed. Jones and Bartlett, Boston, MA.

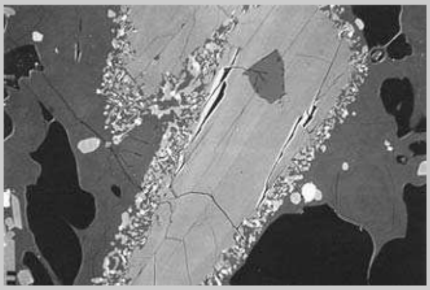

RATES OF MAGMA ASCENT

MALCOLM J. RUTHERFORD
Brown University

JAMES E. GARDNER
University of Alaska

I. Introduction
II. Magma Source and Magma Reservoirs
III. Bubble Formation and Evolution during Magma Ascent
IV. Groundmass Crystallization during Magma Ascent
V. Phenocryst-Melt Reactions during Magma Ascent
VI. Magma Ascent Rates Calculated from Mass Eruption Rates
VII. Seismic Evidence for Magma Movements
VIII. Xenolith Transport and Magma Ascent Rates
IX. Magma Ascent Rates Based on Xenolith–Magma Reactions
X. U-Th Disequilibrium Dating Constraints on Magma Ascent Rate
XI. Summary of Magma Ascent Rate Estimates

GLOSSARY

hypocenter The point of initiation of an earthquake in the Earth; also called the *earthquake focus.*

kimberlite A very low silica igneous rock rich in volatiles that erupts explosively from sources in the upper mantle. Commonly contains mantle xenoliths; occasionally contains diamonds.

Newtonian fluid A simple fluid in which the velocity gradient is directly proportional to the applied stress; the constant of proportionality is the viscosity.

reaction rim Outer rim on a crystal of different composition, or different minerals, which has formed by a chemical reaction of the crystal with the surrounding magma.

subduction zone volcanoes Volcanoes that occur along the Earth's plate boundaries where one is being subducted or taken down into the Earth's interior. The magmas erupted are typically rich in volatiles and the eruptions often explosive.

xenolith A foreign rock fragment in an igenous rock or a magma.

pumice A light-colored, cellular, and glassy rock, typically less dense than water because of the large fraction of bubbles (vesicles) in the glass.

I. INTRODUCTION

Volcanoes can erupt explosively, generating high columns of ash and occasional pyroclastic flows, or they can erupt slowly forming lava flows and domes. Mass eruption rates are controlled by the rates of magma ascent through the volcanic conduit and the conduit size. The magma ascent rate itself is a function of the pressure in the magma storage region, the physical properties of the magma, such as its density and viscosity, the conduit diameter, and the resistance to flow in the conduit that connects the magma storage zone to the surface. A number of important characteristics of volcanic eruptions are affected or controlled by the rate at

Copyright © 2000 by Academic Press
All rights of reproduction in any form reserved.

which magma ascends from depth. For example, the bubble content (i.e., vesicularity) and the degree of crystallization that develop in the melt can be significantly different in rapidly versus slowly ascended material. In fact, the inability of rapidly ascending magma to effectively lose exsolved gas may cause an eruption to change from effusive to explosive, as occurred during the 1997 Soufrière Hills eruption on Montserrat in the West Indies. To better understand the mechanisms of volcanic eruptions, it is therefore important to quantify the rates at which magmas rise to the surface.

The rate of magma ascent strongly influences a number of chemical and mineralogical reactions that occur in volatile-rich magmas, and this relationship provides a number of ways to study ascent rates. One reaction that is a direct result of magma ascent is the exsolution of volatiles from the melt to form gas bubbles. Water is the most abundant bubble-forming gas in many magmas, but CO_2, SO_2, and Cl are also important in some magma types. These gases diffuse out of the melt at different rates as pressure exerted on an ascending magma decreases during ascent. It is therefore possible to use the extent of degassing of each of these different species as an indicator of the time involved in magma ascent from depth.

Degassing during ascent also causes the melt portion of the magma to crystallize. The rate and extent of this crystallization have been determined for some magma types and can be used to estimate magma ascent rates. Similarly, some crystals formed in magmas at depth can contain volatile species such as OH, CO_2, and S in their structure, for example, biotite, hornblende, and Fe-sulfide, and these phenocrysts tend to become unstable and react with the surrounding melt during magma ascent. These reactions occur because the decrease in pressure during ascent causes a decrease in the volatile species dissolved in the melt, which destabilizes the phenocryst. The amount of reaction between phenocryst and melt is controlled by the ascent rate and the kinetics of the mineral breakdown. These degassing-related reactions are particularly important in studying volatile-rich, subduction zone volcanoes such as Mount St. Helens. They are less useful in studies of basaltic volcanic centers because of the generally lower volatile contents in these magmas. Magma ascent rates can also be estimated using the rate of movement of seismic activity toward the surface or theoretical analyses of conduit flow together with measurements of the mass eruption rate for a given event.

Other methods of assessing magma ascent rates involve study of xenolith transport from depth by the magma, the extent of chemical reaction between these xenoliths and their host liquid in the magma, and evidence of U-Th-Ra isotopic disequilibrium in a magma. The latter approach involves the identification of isotopic disequilibrium of the short-lived isotopes in the U and Th decay series; the disequilibrium indicates a maximum time of magma existence (4–5 half-lives for the decay involved, i.e., ~8000 yr for ^{230}Th-^{226}Ra and 30 yr for ^{232}Th-^{228}Ra) since the disequilibrium was generated. The ability of magma to physically transport xenoliths to the surface depends on the ascent velocity and the rheology of the magma as well as the xenolith size and density. Reactions between xenoliths and magma may occur where a xenolith crystal and magma are in contact but not in equilibrium; the crystal undergoes a time-dependent diffusional exchange of atoms with the melt, allowing an assessment of the time involved in magma ascent. The following sections describe some of the more interesting results on magma ascent rate determinations using these different approaches, but first we consider the problems of the magma source and where ascent begins.

II. MAGMA SOURCE AND MAGMA RESERVOIRS

One of the significant problems that has to be addressed when attempting to determine magma ascent rates is the question of where ascent was initiated. For many volcanoes there is good evidence for a magma storage region in the crust, a magma reservoir from which the final ascent began. Crustal storage zones have been identified seismically for almost all well-studied volcanoes in subduction-zone environments, including Mount St. Helens, Mount Pinatubo in the Philippines, Soufrière Hills on Montserrat, and Unzen in Japan, and the presence of these near-surface (5- to 15-km depths) reservoirs is confirmed by petrological data (Fig. 1a). Density contrasts between magma and surrounding rocks also indicate that there should be both deep and shallow magma reservoirs beneath many calcalkaline volcanoes, and recent data indicate that two such reservoirs did exist at 3–5 and >8 km under Mount Rainier at the time of its most recent (2200 yr ago) explosive eruption. Using the methods outlined earlier, estimates of magma ascent rates for such volcanoes will generally refer to the transport from the higher, crustal-level storage chamber to the surface. Large-scale eruptions, such as those that occurred at Long Valley and Yellowstone in

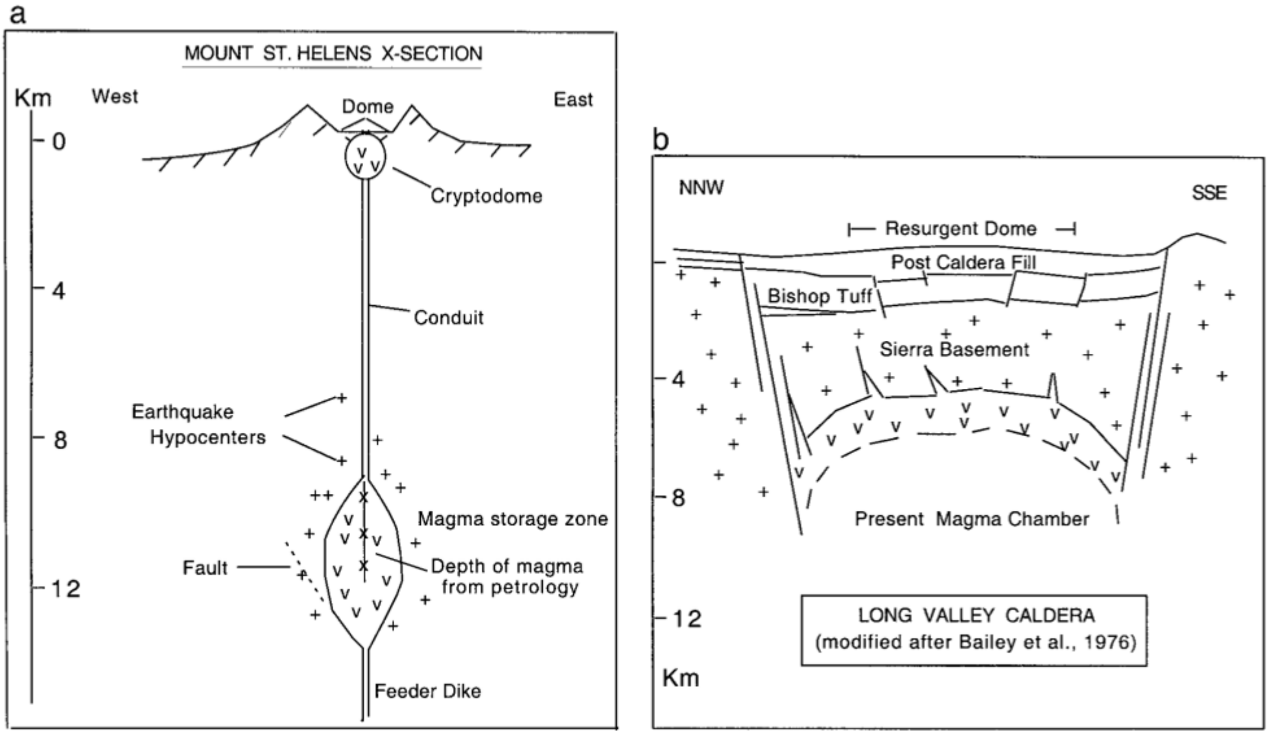
a
MOUNT ST. HELENS X-SECTION
Km
West
Dome
East
0
4
8
12
Cryptodome
Conduit
Earthquake Hypocenters
Magma storage zone
Fault
Depth of magma from petrology
Feeder Dike
b
NNW
SSE
Resurgent Dome
Post Caldera Fill
Bishop Tuff
Sierra Basement
4
8
12
Km
Present Magma Chamber
LONG VALLEY CALDERA
(modified after Bailey et al., 1976)

FIGURE 1 (a) A vertical cross section through Mount St. Helens showing the magma storage zone delineated by surrounding seismic activity and determined to be at this depth by the phenocryst-melt phase equilibria. [Modified from Rutherford and Hill, 1993.] (b) Vertical cross section through Long Valley, California, caldera showing the collapse and fill resulting from the eruption of the Bishop Tuff about 700,000 yr ago. The magma chamber depth is indicated by studies that pinpoint the source of resurgent doming, by seismic activity generated around it, and by petrological study of post-Bishop Tuff eruptions. [Modified from Bailey *et al.,* 1976.]

the United States, also originated from well-established crustal reservoirs as indicated by the calderas (Fig. 1b) produced during these eruptions.

Eruption from a crustal reservoir has also generally been the case for basaltic volcanoes such as in Hawaii, Iceland, Etna, and the Canary Islands. For eruptions of basaltic magma at midocean ridges, a magma storage region near the crust–mantle boundary is generally indicated by available seismic evidence. However, it is also proposed that some magmas, specifically kimberlites, and more mafic magmas erupting in midplate oceanic islands and in some island arcs, ascended directly from the mantle without encountering a crustal storage region. In such cases, the magma ascent rate would refer to the time between separation of magma from its source in the Earth's mantle and its arrival at the surface. However, most of the magma ascent rate estimates are for volcanic centers where there is strong evidence of a crustal-level magma storage zone, and the ascent rate is for magma transport from this reservoir to the surface.

III. BUBBLE FORMATION AND EVOLUTION DURING MAGMA ASCENT

When magma rises from its storage zone, volatiles dissolved in the melt will tend to exsolve and form bubbles because of their lower solubilities in melt at lower pressures. What is the rate of this process, and can measurements of the amount of exsolution be used to estimate the rates of magma ascent? Analyses of volcanic glasses in both explosively erupted and extrusively erupted samples illustrate that most of the water originally in the melt at depth has been lost to the gas phase during ascent. In other words, even for the relatively rapid ascent involved in explosive eruptions of a volatile-rich magma, there appears to have been sufficient time during ascent for most H_2O to escape from the melt. Other volatile species that have an affinity for the gas phase include CO_2, SO_2, and Cl, based on their common occurrence in volcanic gas emissions. The available diffusion data for silicate melts suggest that these species diffuse at somewhat slower rates than water. Thus, analytical data on the abundance of the different volatile species lost from the melt to the gas phase during an eruption may record the rate of magma ascent, although the rapid diffusion of H_2O may mean that it is nearly all transferred to the gas phase in most eruptions. Experiments indicate that the loss of water from melt into gas bubbles during decompression (ascent) of a rhyolitic melt is very rapid. At pressure drops of 0.025 MPa/s (1 bar per 4 seconds) water is able to diffuse out of the melt and into the bubbles rapidly enough to maintain equilibrium. At faster decompression rates of 0.25 and 1.0 MPa/s, water diffused too slowly to maintain equilibrium and the melts became supersaturated with water. These experiments indicate that a transition occurs between 0.025 and 0.25 MPa/s decompression rates, beyond which gas bubble-melt equilibria cannot be maintained. Given typical magma densities, these decompression rates equal ascent velocities of 0.7 and 5 m/s, rates much faster than are typically inferred for effusive lava and dome eruptions.

In the high-silica rhyolite (77 wt% SiO_2) decompression experiments, the 825°C temperature results in a magma that is relatively viscous, so water diffusion is relatively slow. In less viscous basaltic magmas, water diffusion will be faster because of the lower SiO_2 contents and the higher temperatures (typically 1100–1200°C). Numerical modeling of bubble growth in basaltic magmas suggests that for reasonable ascent rates, water diffusion and bubble growth are rapid enough to always maintain equilibrium between bubbles and melt. This includes ascent rates up to 100 m/s.

The earlier discussion focused on degassing of water, which is probably the fastest diffusing volatile species in melts. In contrast, the diffusivity of S and Cl in rhyolitic melts is tens to hundreds of times slower than water at a given temperature. If magma ascends during explosive eruptions at rates controlled by water exsolution (the maximum at which water and melt can maintain equilibrium), then it would be expected that slower diffusing gas species would not maintain equilibrium. Indeed, this appears to be the case, because matrix glasses in volcanic pumices typically contain much if not all of the pre-erupted contents of S and Cl. For example, the pre-eruptive concentrations of H_2O and Cl in the Pinatubo magma are about 6.4 wt% and 1200 ppm, respectively, whereas their final concentrations dissolved in matrix glasses are about 0.4 wt% and 880 ppm. Degassing of Cl and S is complicated, however, because the partitioning of Cl and S between the melt and a water-rich gas phase varies strongly as a function of water content, pressure, melt composition, and temperature. This is a research area where additional study may be very productive in understanding magma ascent during volcanic eruptions.

An important implication of the findings is that water is able to diffuse out of silicate melts very rapidly during magma ascent. This is important because several of the processes described later are driven by water degassing during ascent. Hence, the rates at which those reactions occur are not constrained by the exsolution of water from the melt, but by their own reaction kinetics.

IV. GROUNDMASS CRYSTALLIZATION DURING MAGMA ASCENT

The degassing of the melt in ascending magma discussed in the previous section causes gas bubbles to form, but also transforms the melt into a variably crystallized groundmass. Groundmass crystals are readily identified by their small grain size relative to large (mm to cm) phenocrysts; they replace the bubble-rich glass that makes up the groundmass in more rapidly erupted magma. Although driven by the loss of volatiles from the melt, the crystallization of the groundmass melt does not necessarily occur at the same rate. For example, while the exsolution of water from a decompressing melt follows equilibrium solubility for decompression rates of <0.25 MPa/s (magma ascent rates less than 5 m/s), a rhyolitic glass crystallizes much more slowly. The rate of crystallization will also differ for different melt compositions, being slower for more silica-rich melts at a given water concentration.

A study of groundmass glass crystallization in the eruption products of the 1980–1986 Mount St. Helens eruption products illustrates what can be done using the extent of groundmass crystallization to estimate magma ascent rates. Earlier work established that all of the erupted magmas came from a storage region at 8- to 11-km depth, and also established that the depth, temperature, and water content of the magma in that storage zone did not change over the time of these eruptions. In addition, the similarity of phenocryst and groundmass mineral compositions (Fe-Ti oxides) in these samples indicates that there was essentially no change in the temperature of any of these magmas during ascent. It can be concluded that differences observed in the groundmass crystallinity of these samples are the result of different ascent rates.

Data on the extent of groundmass crystallization in natural samples can be compared with the results of

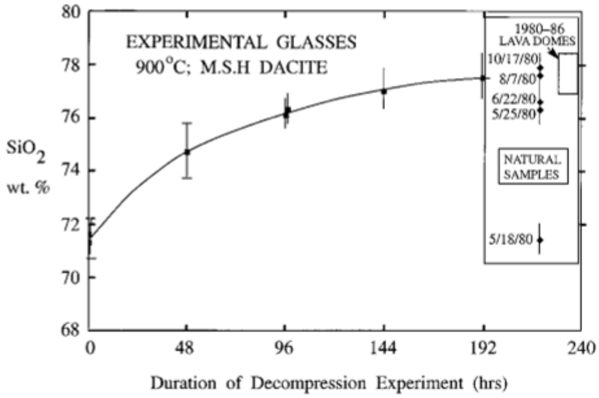

FIGURE 2 Evolution of matrix glass in Mount St. Helens dacite as a function of the duration of the decompression from 220 to 2 MPa compared to natural glasses in different 1980–1986 natural dacites. Crystallization caused by the water loss during decompression produces the melt composition change [From Geschwind and Rutherford, 1995.]

experiments carried out at different decompression rates. The experiments performed on the Mount St. Helens dacitic magma demonstrate that nucleation and growth of microlites in the melt phase is detectable after a 1-day decompression from 220 to 2 MPa, and is essentially complete in a decompression taking 8 days, as measured by the change in melt (glass) composition (Fig. 2). Using the composition of the remaining matrix glass in the experimental and natural samples as an indicator of approach to complete crystallization, average magma ascent rates have been obtained that range from >0.2 m/s for the 1980 explosive plinian event to 0.01–0.02 m/s for the different dome-forming eruptions of 1980–1986 (Fig. 2). Nucleation is unlikely to have been a factor affecting groundmass crystal development in either the natural system or the experiments because the Mount St. Helens magma was crystal rich prior to ascent. A similar study of a crystal-poor magma might show that growth of microlites from the groundmass melt takes much longer when phenocrysts are not present to serve as nucleation sites.

V. Phenocryst-Melt Reactions during Magma Ascent

Another reaction driven by the loss of volatiles from the melt as magma rises toward the surface is the decomposition of volatile-bearing phenocrysts, such as hornblende and biotite. Sulfur is also lost from the melt during magma ascent, and thus anhydrite, which occurs in some volcanic rocks, would also tend to similarly break down. Most of these reactions are controlled by the kinetics of the reaction between the phenocrysts and melts involved. These rates have generally not been determined because they are complex functions of many variables, including mineral and glass compositions, melt viscosity, and temperature. However, there are data on the rates of reaction between hornblende phenocrysts and the coexisting rhyolitic melt in the magma recently erupted at Mount St. Helens.

The 1980–1986 eruption of Mount St. Helens began with an edifice collapse that triggered both a lateral blast and a vertical, plinian-style eruption. They produced the blast dacite and dacitic pumice deposits, respectively. Several smaller, vertically directed explosions during the next several months produced less voluminous pumice deposits, but in October 1980 magma began to extrude as a dome-forming lava in the newly formed crater, and this dome continued to grow until 1986. The bulk composition of the magma did not change throughout the entire series of eruptions. Sample studies show no detectable reaction between the hornblende phenocrysts and the groundmass glass (melt) in the May 18, 1980, pumice samples, even though the melt clearly lost all but about 0.3 wt% of the ~4.6 wt% dissolved water it contained before erupting. In all subsequently erupted samples, however, the hornblende phenocrysts have reaction rims at the contact of the crystal with the groundmass melt (Fig. 3). Each post–May 18 sample had a main population of hornblende phenocrysts (30–100 vol% of the crystals present) with uniform thickness (0- to 50-μm range) reaction rims, and a second group with rims ranging to greater thicknesses. These are interpreted to represent, respectively, a main batch of magma that ascended directly from the storage region at 8–11 km beneath the surface, and magma left behind in the conduit from previous eruptions.

Constant-decompression-rate experiments carried out at magmatic temperatures with water contents equal to those in the magma serve to calibrate the time necessary to form the reaction rims observed. Experiments that simulated ascent from 8-km depth to the surface in less than 4 days showed no reaction rims on hornblende crystals, 2-μm-wide rims were produced in 7-day ascents, and 32-μm rims formed in 20 days. Using this calibration (Fig. 4), the magma ascent rates during the lava dome phase of the Mount St. Helens eruption varied from as low as 0.004 m/s up to 0.015 m/s. This is in contrast with the 2–3 m/s at which the magma ascended during the May 18, 1980, plinian phase of the eruption.

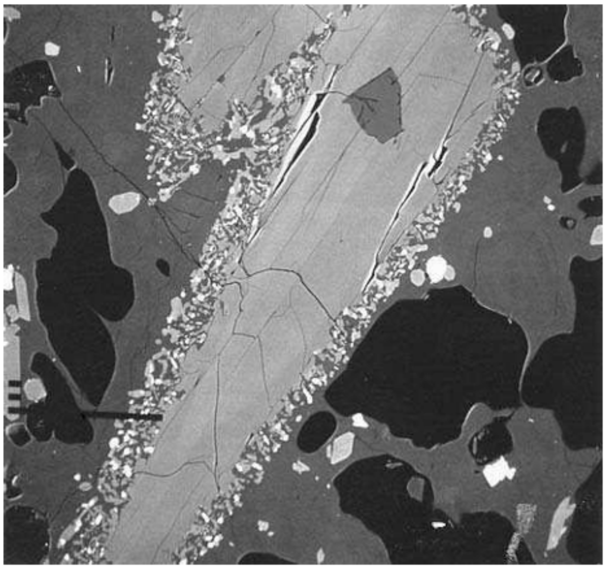

FIGURE 3 Backscatter electron photomicrograph of a hornblende phenocryst in a Mount St. Helens 1981 lava dome sample showing a 20-μm-thick reaction rim at the phenocryst-melt contact. [Courtesy of the American Geophysical Union.]

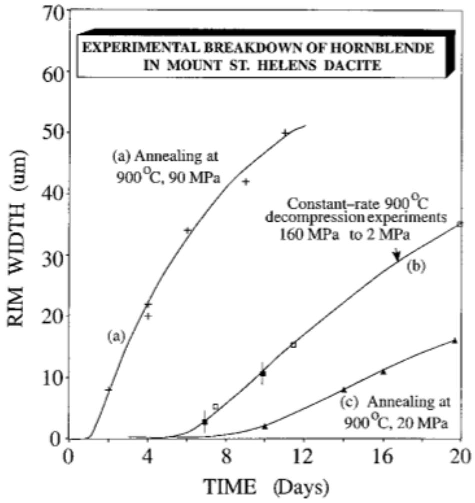

FIGURE 4 (a) Experimental determination of hornblende reaction-rim width as a function of time in a water-rich magma. [After Rutherford and Hill, 1993.] (b) Constant-rate decompression from 160 to 2 MPa. (c) Decompression from 220 to 2 MPa. Curves (a) and (c) are for a constant *P* and *T* anneal at 900°C and 90 and 20 MPa, respectively.

An application of hornblende reaction rim data can also be made to the hornblende-bearing magmas recently erupted at Soufrière Hills on the island of Montserrat in the Lesser Antilles. Magma first reached the surface in October 1995, following several months of steam eruptions and elevated seismic activity. A lava dome gradually grew at the site, slowly filling an old crater. This dome-forming lava appears to have come from a magma storage region at 5- to 6-km depth (130 MPa). The temperature of the pre-eruption magma was 830°C, although the magma was clearly heated to ~850–900°C prior to erupting. More importantly, however, reaction rims on hornblende crystals adjacent to groundmass melt show significant changes in samples collected during the next 2 years. These changes are not the result of changes in the magma storage region; they formed during magma ascent. The first magma erupted contains hornblendes with 120-μm-thick rims. The magma that erupted 2 months later, in February 1996, has only 18-μm-thick rims, and the rims were only 10 μm wide in an April 1996 eruption. Most hornblendes in magma erupted in July through September 1996 contain no reaction rims.

Using the previously mentioned experimental calibration of rim width versus time, absolute ascent rates and ascent rate changes can be calculated for the Montserrat eruption (Fig. 5). The magma ascent rate increased from 0.001 to 0.012 m/s during the first 300 days of this eruption. Interestingly, the mass extrusion rate increased over this same time period (Fig. 5). The ascent rate data show that this increase in extrusion rate was not produced simply by an increase in the size of the conduit. The other important observation is the association of numerous explosive eruptions from the summit of the dome with periods of high magma ascent rate.

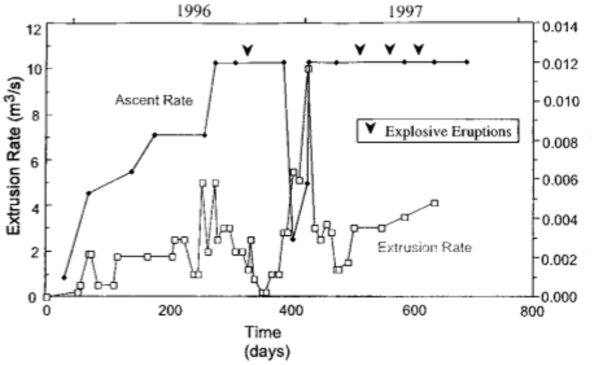

FIGURE 5 Magma ascent rate from hornblende reaction rim thickness and experimental calibration as a function of time for the 1996–1997 eruption at Soufrière Hills on Montserrat. Also shown are the changes in the magma extrusion rate. [From Rutherford *et al.*, 1998.]

These explosions indicate times of less efficient separation of gas and magma, a logical consequence of higher magma ascent rates.

VI. MAGMA ASCENT RATES CALCULATED FROM MASS ERUPTION RATES

Measurements of the mass eruption rate of magma can be used to calculate conduit diameter and ascent velocity if certain assumptions are made about an eruption. This technique is illustrated by an application to the May 18, 1980, plinian eruption of Mount St. Helens. Magma flowing through a conduit below the depth where it is saturated with a gas phase can be described as a one-phase, laminar flow of an essentially Newtonian fluid. In this case, magma ascent in the conduit can be modeled by the Hagen-Poiseuille law

$$M = (\Delta P/\Delta L)^{*}(\pi \rho_F r^4)/8\eta,$$

where M is mass flux (in kg/s), $\Delta P/\Delta L$ is the pressure gradient driving the flow, ρ_F is the fluid (magma) density, η is fluid viscosity, and r is conduit radius. Exsolution of a vapor phase changes the bulk density and viscosity of the magma and thus affects flow conditions, but exsolution is slow at first and does not significantly affect the flow until the magma is within a kilometer of the surface. We make a calculation for depths greater than 1 km, assuming that the driving force for flow is due to the density difference between the surrounding rocks and the magma. For quantitative applications of the Hagen-Poiseuille law, numerical values for the magma mass flux, density, and viscosity of Mount St. Helens magmas are needed. Using recently revised data for these parameters, and assuming the conduit radius remains constant at depth, the conduit radius during the explosive 1980 eruption of Mount St. Helens is calculated to be 33 m. For the late 1980 and subsequent eruptions, the calculated radius decreases to 7 m and remains essentially constant.

Ascent velocities for the Mount St. Helens eruptions can be calculated from the relationship expressing conservation of mass, $M = \Pi r^2 \rho_F u$, where u is the velocity. Given the conduit radii calculated earlier, conservation of mass requires ascent velocity to have decreased from 2 to 3 m/s on May 18, 1980, to 0.08 m/s (290 m/hour) in October 1980. The latter velocity leads to an ascent time of 30 hours from a depth of 8.5 km, which is less than the approximately 4 days indicated by the petrological methods above for the dome-forming eruptions. Exsolution of a vapor phase and crystallization of microlites lead to increases in magma viscosity as the eruption progresses, however, which decreases the magma velocity in the upper parts of the conduit. This may explain the differences between the calculated velocity and the velocity derived from hornblende breakdown. A near-surface decrease in ascent velocity is consistent with modeling of surface deformation, which indicates a velocity of only 0.014–0.028 m/s for magma ascent near the surface during the dome eruptions of 1981 and 1982.

VII. SEISMIC EVIDENCE FOR MAGMA MOVEMENTS

Earthquakes are commonly associated with volcanic eruptions and volcano unrest and have been effectively used for monitoring and forecasting eruptions. Volcanic earthquakes generally occur in four main types: high- and low-frequency earthquakes, explosion earthquakes, and tremor. The direct association of earthquakes with magma migration can be ambiguous, however, because earthquake generation requires stressed and brittle rock, and so aseismic regions may be unstressed and unfractured or hot and ductile. On the other hand, pressured magma may generate earthquakes in brittle rock adjacent to magma conduits. Hence, magma zones may be either seismic or aseismic.

One case of an unambiguous association of earthquakes and magma movement occurred during the September 1977 deflation of Krafla Volcano in Iceland. Earthquakes began under the central volcano, at the same time that the volcano began to deflate, and then migrated along the adjacent rift zone. When the hypocenters of this migrating tremor passed a geothermal bore hole, fresh basaltic pumice erupted from the hole. The tremor hypocenters migrated along the rift system at a rate of about 0.5 m/s.

Migration of tremor hypocenters like that at Krafla Volcano has also been observed in the East and Southwest Rift Zones of Kilauea Volcano, Hawaii. These swarms also define the motions of magma in the rift systems, as many of them are related to the eruption of basaltic magma. The rates of down-rift swarm movement span a range of about 0.005–8.5 m/s, and are similar regardless of whether magma simply intruded into the rift or eventually erupted. In a few cases, upward movement of earthquake swarms in the rift is also identified, with rates on the order of 0.03–1.7 m/s. Interestingly, this upward migration tends to slow as the magma approaches the surface.

Although it is expected that earthquake hypocenters should migrate as magma migrates beneath volcanoes, as in the earlier-described cases of Krafla and Hawaii, there are surprisingly few documented cases of such trends. A magma ascent velocity of 0.6–0.7 m/s is estimated for the explosive May 18, 1980, eruption of Mount St. Helens based on the arrival time of new magma at the surface as detected initially by a change in the seismic signals adjacent to the 8- to 11-km-deep storage zone. For a time later in the Mount St. Helens eruption, seismic signals at depth and the following onset of an eruption at the surface indicate an ascent velocity of 0.007–0.01 m/s, essentially identical to estimates from hornblende reaction rims. Preceding the 1991 eruption of Unzen Volcano, Japan, earthquakes migrated from a depth of 10 km to about 3 km beneath the volcano, possibly indicating magma movement toward the surface. Magma ascent during the final kilometer is estimated to have been at 0.007–0.3 m/s.

VIII. XENOLITH TRANSPORT AND MAGMA ASCENT RATES

Some basaltic magmas are extruded on the Earth's surface carrying pieces of the mantle, called *mantle xenoliths.* These xenoliths make it possible to estimate how rapidly these magmas ascended from depth to the surface, because the upward flow of magma must exceed the settling velocity of the xenoliths. Two magma types, alkali basalt and kimberlite, commonly carry such mantle xenoliths. Both originate by small degrees of partial melting in the upper mantle near the base of the lithosphere. Interestingly, tholeiitic basalt magma, which originates by higher degrees of partial melting in the upper mantle, almost never carries mantle xenoliths. One possible explanation is that tholeiitic basalt eruptions are commonly staged from magma reservoirs within or at the base of the crust, and any mantle xenoliths may settle out in these reservoirs. Such magma reservoirs have been documented for tholeiitic eruptions on Iceland, Hawaii, and at most midocean ridge sites studied in detail.

The common occurrence of dense mantle xenoliths in tephra and lava flow eruptions of alkali basalt indicates that this magma carried them from depth. An average settling rate for xenoliths of different sizes can be calculated by balancing the different forces on the xenoliths during ascent, and by making certain assumptions about the rheologic properties of the magma. Figure 6 shows the results of settling calculations for spherical xenoliths, a density difference of 500 kg/m^3 between the xenoliths and the melt (melt density = 2800 kg/m^3), and an assumption of Bingham plastic rheology for the xenolith-laden magma.

As a Bingham fluid, the magma has a yield strength that correlates well with the apparent viscosity. A yield strength of 100 N/m^2 corresponds to a phenocryst content of ~25 vol% in a basalt. The calculation (Fig. 6) indicates that a 20-cm-wide xenolith will settle at a rate of 0.1 m/s. Obviously, the magma ascent rate would have to be greater in order to carry the xenolith to the surface; the xenolith settling velocity gives a minimum estimate of magma ascent rate. Published minimum estimates for alkali basalt ascent rates range from 2 to 10 m/s.

Two factors that have not been considered in this calculation are the effect of nearby xenoliths and the effect of bubbles in the magma. If significant, both of these would decrease the settling rate of xenoliths, and therefore reduce the minimum ascent rate required to carry a xenolith of a given size to the surface. Based on the relative abundance of vesicles and xenoliths in alkali basalt, however, it is possible that neither has a significant effect on calculated ascent rates.

Kimberlites, the other mantle xenolith-bearing magma, are known to be very gas-rich and also com-

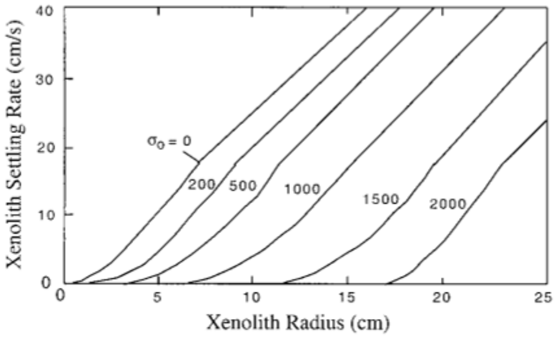

FIGURE 6 Calculated xenolith settling velocity as a function of xenolith radius for different magma yield strengths. A density difference of 500 kg/m^3 is assumed between the xenolith and the melt; the melt density is 2800 kg/m^3, and a Bingham rheology (viscosity 350 poise) is assumed. Units of yield strength are N/m^2, and yield strength of 1000 N/m^2 is approximately equal to a crystallinity of 25%. [From Spera, 1984.]

monly have high phenocryst and/or xenolith contents. Thus, the magma ascent rates estimated for kimberlitic volcanism from xenolith settling velocities (10–100 m/s at 1-km depth) may be somewhat high; estimates from phenocryst-melt reactions range from 10 to 30 m/s for kimberlites.

IX. MAGMA ASCENT RATES BASED ON XENOLITH–MAGMA REACTIONS

Some magmas erupt at the surface carrying inclusions of rock or a second, variably crystallized, magma with clear textural and compositional evidence to indicate that the inclusion is not in equilibrium with the host magma. The extent of reaction that takes place at the magma-inclusion contact can be used, along with available kinetic data, to estimate the rate of magma ascent. To make this estimate, the depth at which the inclusion was incorporated into the magma must be determined, and the ascent must have been essentially isothermal. This section describes an eruption where these determinations can be made.

Alkali basalt laden with inclusions of peridotite has erupted both historically (six eruptions in the past 500 yr) and prehistorically on La Palma in the Canary Islands. The inclusions are spinel-bearing peridotites, ranging up to 15 cm in diameter, and they are almost always encased by a crystalline selvage zone (<1 mm thick) of titanium-rich augite, hornblende, and magnetite. The selvage minerals are fine grained at the inclusion contact, and coarsen toward the host magma. Fluid inclusions in recrystallized grains and in the selvage minerals are essentially pure CO_2, and their densities indicate that the selvage minerals and recrystallized grains in the peridotite grew at pressures of 200–400 MPa, which is equivalent to a depth of 7–15 km.

Olivine crystals in the peridotite adjacent to the selvege zone have developed diffusion zones that are 0.9–2.6 mm wide as a result of reaction with the magma (Fig. 7). This diffusion zone is interpreted to have developed in olivine at the xenolith margins while the magma was stored in a deep (7–15 km) crustal reservoir. Using recent diffusion data for Fe and Mg in olivine for a magma temperature of 1200°C, the measured diffusion zone thicknesses yield development times of 8–110 yr. These times are interpreted as indicating the length of time the inclusions spent in the crustal magma storage zone.

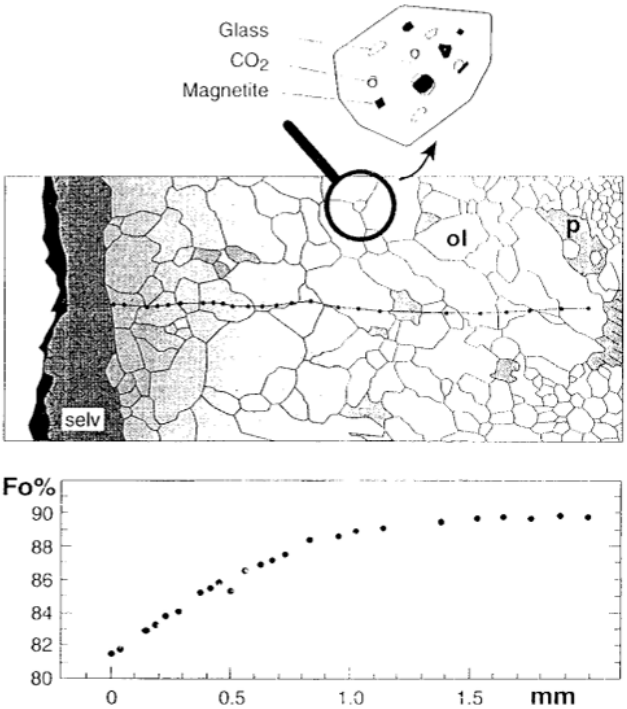

FIGURE 7 Drawing of a contact between an olivine-rich xenolith and basalt with a thin selvage zone at the boundary typical of such occurrences in the La Palma lavas (Canary Islands). Lower panel shows the zoning profile (Fo% is equal to the mole % Mg) in the Fe-Mg olivine. Time to create this type of zonation is calculated to be 8–100 yr for profiles ranging from 0.9 to 2.2 mm long. [After Klugel, 1998.]

Interestingly, some of the fractures and surfaces in the xenoliths in the Canary Island samples have no selvage zones. The diffusion zones in olivine adjacent to the melt along these surfaces are 0–0.02 mm wide. The fractures with no selvage zone are interpreted to have formed by a fracturing event at the time of the final eruption. The times calculated for development of the thin diffusion zones range from 0 to 4 days. If it is correct to assume the surfaces formed when the magma began to ascend, then average ascent rates of greater than 0.06 m/s are calculated for the movement of this alkali basalt from 11 km to the surface. This is in the same general range as the >0.2 m/s magma ascent rates calculated to carry the xenoliths to the surface in this magma. The lack of diffusion rims of intermediate thickness on olivine in the xenoliths is interpreted to mean that the xenolith-bearing magma was stored in the lower crust and was not affected by a fracture-producing event in the 8- to 110-yr period before the eruption began.

X. U-TH DISEQUILIBRIUM DATING CONSTRAINTS ON MAGMA ASCENT RATE

The study of magma dynamics and magma ascent in volcanic systems is theoretically possible using U and Th isotopic series disequilibrium. The possibility is best illustrated by an example where magma leaves the source region at depth, and there is a fractionation of U and Th in the melting process. Equilibrium is generally assumed for the short-lived isotopes of the decay series in the source region. Such isotopes would include ^{226}Ra, ^{210}Pb, ^{228}Ra, and ^{228}Th with half-lives of 1600, 22, 5.77, and 1.9 yr, respectively. With melt separation following U-Th fractionation during melt formation, the (^{230}Th-^{226}Ra) and (^{232}Th-^{228}Ra) ratios will reach equilibrium after about 8000 and 30 yr ($\sim$5 half-lives), respectively. If magma reaches the surface with a $^{226}\mathrm{Ra}/^{230}\mathrm{Th} = 1.0$ and a ($^{228}\mathrm{Ra}/^{232}\mathrm{Th}$) other than 1.0, it can be concluded that the fractionation took place between 8000 and 30 years before erupting. If both ratios are out of equilibrium, it means that the fractionation occurred $<$30 yr earlier.

To make use of disequilibrium dating in estimating magma ascent rates, some knowledge of U-Th fractionation is required. Where and when did it occur, and were there secondary perturbations? Obviously, if a fractionation occurred during magma genesis in the upper mantle and the magma produced moved to a mid-crustal storage region for some period of time before eruption, the time evolved according to the disequilibrium detected includes more than just the time of ascent.

Data for the Mount St. Helens 1980 eruption products illustrate the nature of the problem as well as the potential of the disequilibrium dating method. All samples analyzed contain an excess of ^{226}Ra over ^{230}Th, but none contains an excess of ^{228}Ra. This implies a magma formation event more than 30 and less than 10,000 yr before the eruption. Indications of an excess of ^{210}Pb over ^{226}Ra indicate that magma formed between 30 and 150 yr before the eruption. Obviously, the magma was not continuously ascending during this entire period because, as mentioned earlier, there is good evidence that the 1980–1986 eruption initiated from a magma storage zone at 8- to 11-km depth. In such a situation, the ascent rate derived from the disequilibrium data is a minimum rate unless there is reason to believe the U-Th fractionation occurred in the crustal magma chamber, which in this case there is not.

To make better use of disequilibrium dating in estimating magma ascent rates, the focus needs to be on elemental fractionations that occur in the magma storage region or as magma begins to ascend; that is, a fractionation initiated by crystallization or degassing. It does appear possible to use disequilibrium dating to make estimates of the time evolved from mantle separation to eruption for midocean ridge basalts. Again, however, the interpretation of these data is complicated by uncertainties as to when and where the magma actually separated from the residual mantle, and by possible mixing processes and storage time which might have occurred during magma ascent.

XI. SUMMARY OF MAGMA ASCENT RATE ESTIMATES

The estimates of average magma ascent rates for silicic to intermediate composition lava extrusions are fairly well constrained in the range of 0.001 m/s for very slowly ascending magmas, to 0.015 m/s for more rapidly ascending extrusive magmas (Table I). These estimates come from a variety of observations made at different volcanoes, and it is important to remember that they are average rates. Ascent surely must vary over the vertical extent of the conduit carrying the magma, because the density and viscosity of the magma vary considerably over this length, particularly in water-rich magmas. One topic for future study is the nature of changes in flow within volcanic conduits. It is rather interesting that observations made for basaltic composition magma extrusions give essentially the same range of average ascent rates as those obtained for more silica-rich magmas.

The assessment of magma ascent rates during explosive eruptions is more complex because there is almost certainly a much greater variation in the ascent rate from the base of the conduit to the surface. The magma leaves the top of the conduit at essentially sonic velocities for truly explosive eruptions. This high rate of ascent is achieved as a result of the low density and rapid expansion of the gas phase in these gas-rich magmas. Deep in the conduit, little of the gas is exsolved, the magma is more dense, and depending on the size and shape of the conduit, flow rates are much lower.

In our view, some of the more profitable areas for study of magma ascent lie with investigations of the behavior of the various magmatic volatiles, the rates of

TABLE 1 Magma Ascent Rate Estimates from Different Observations[a]

Volcano	*Observation*	*Explosive ascent rate (m/s)*	*Extrusive ascent rate (m/s)*
Mount St. Helens	Groundmass crystallization (IV)	$\geqslant$0.2	0.01–0.02
Mount St. Helens	Hornblende rims (V)	>0.18	0.04–0.15
Mount St. Helens	Calculation from mass eruption rate (VI)	1–2	0.01–0.1
Mount St. Helens	Seismicity Movement	0.6	0.007–0.01
Soufrière Hills	Hornblende rims (V)	>0.2	0.001–0.012
Mount Unzen	Magnetite zonation	Not present	0.002
Hualali, Hawaii	Xenolith transport (VIII)	Not present	>0.01
La Palma, Canary Is.	Olivine zonation (IX)	Not present	>0.06

[a] Observations are numbered according to section of paper in which they are discussed.

their diffusion in melts, the properties of the different composition gases, and the processes by which gas is lost from magmas during ascent.

See Also the Following Articles

Calderas • Magma Ascent at Shallow Levels • Magma Chambers • Plate Tectonics and Volcanism • Seismic Monitoring • Volatiles in Magmas • Volcanic Gases

Further Reading

Carey, S., and Sigurdsson, H. (1985). The May 18, 1980, eruption of Mount St. Helens, 2: Modeling of dynamics of the Plinian phase. *J. Geophys Res.* **90,** 2948–2958.

Clague, D. A. (1987). Hawaiian xenolith populations, magma supply rates, and the development of magma chambers. *Bull. Volcanol.* **49,** 557–587.

Condomines, M., Hemond, Ch., and Allegre, C. J. (19xx). U-Th-Ra radioactive disequilibria and magmatic processes. *E.P.S.L.* **90,** 243–262.

Geschwind, C. H., and Rutherford, M. J. (1995). Crystallization of microlites during magma ascent: The fluid mechanics of 1980–86 eruptions at Mount St. Helens. *Bull. Volcanol.* **57,** 356–370.

Hurwitz, S., and Navon, O. (1994). Bubble nucleation in rhyolitic melts: Experiments at high pressure, temperature and water content. *Earth Planet. Sci. Lett.* **122,** 267–280.

Jaupart, C., and Allegre, C. J. (1991). Gas content, eruption rate and instabilities of eruption regime in silicic volcanoes. *Earth Planet. Sci. Lett.* **102,** 413–429.

Klein, F. W., Koyanagi, R. Y., Nakata, J. S., and Tanigawa, W. R. (1987). The seismicity of Kilauea's magma system. U.S.G.S. Professional paper 1350, pp. 1019–1185.

Klugel, A. (1998). Reactions between mantle xenoliths and host magma beneath La Palma (Canary Islands): Constraints on magma ascent rates and crustal reservoirs. *Contrib. Mineral. Petrol.* **131,** 237–257.

McNutt, S. R. (1996). Seismic monitoring and eruption forecasting of volcanoes: A review of the state-of-the-art and case histories. Pages 99–146 *in* "Monitoring and Mitigation of Volcano Hazards" (Scarpa and R. F. Tilling, eds.). Springer Verlag, Berlin.

Nakamura, M. (1995). Continuous mixing of crystal mush and replenished magma in the ongoing Unzen eruption. *Geology* **23,** 807–810.

Rutherford, M. J., and Devine, J. D. (1988). The May 18, 1980, eruption of Mount St. Helens; 3 Stability and chemistry of amphibole in the magma chamber. *J. Geophys. Res.* **93,** 11949–11959.

Rutherford, M. J., and Hill, P. M. (1993). Magma ascent rates from amphibole breakdown: Experiments and the 1980–1986 Mount St. Helens eruptions. *J. Geophys. Res.* **98,** 19,667–19,685.

Rutherford, M. J., Devine, J. D., and Barclay, J. (1998). Changing magma conditions and ascent rates during the Soufrière Hills eruption on Montserrat. *GSA Today* **8** (3), 1–7.

Spera, F. J. (1984). Carbon dioxide in petrogenesis III: Role of volatiles in the ascent of alkaline magma with special reference to xenolith-bearing magmas. *Contrib. Mineral. Petrol.* **88,** 217–232.

This Page Intentionally Left Blank

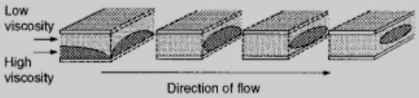

PLUMBING SYSTEMS

CHARLES R. CARRIGAN
Lawrence Livermore National Laboratory

I. Thermal and Dynamic Aspects of Dike Formation in the Cool Crust
II. Physical Model of Magma Flow in a Dike
III. Computerized Magma Transport
IV. Pressure Gradients Required for Magmatic Flows
V. The Eruption of the Inyo Chain of Volcanic Domes
VI. Conclusions and Implications for Volcanism

GLOSSARY

andesite Volcanic rock with 53–63% silica content (SiO_2) having a viscosity when molten that is typically intermediate to that of basalt and rhyolite.

basalt Volcanic rock with 44–50% silica content that in conjunction with typically higher flow temperatures results in relatively fluid magmas.

Brinkman number A dimensionless ratio giving the relative importance of the rate of heat production produced by viscous heating to the rate of heat loss by conduction of heat to cooler boundaries.

caldera Crater or surface depression resulting from collapse of an underlying magma chamber roof during withdrawal of magma.

coextrusion Process of simultaneously forcing two or more distinct magmas to flow in magmatic plumbing.

conduit A pipelike pathway for the transport of magma that evolves by preferential channeling (process involving both melting and solidification) of flow within a dike.

contact Boundary or surface separating hot magma from cooler host rock.

dike A vertically oriented, sheetlike magmatic pathway formed by injection of magma into a thin fracture that fills and propagates within the brittle crust of the Earth.

exsolution The transition of a volatile component (e.g., CO_2, H_2O) from solution in a magma to a gas phase. The formation of a gas phase results in significant driving forces for magmatic transport.

lava Molten rock expelled at the Earth's surface by volcanic processes.

lithostatic Change in static pressure with depth or pressure gradient associated with the overburden of crustal rock. Lithostatic pressures for a given thickness of crustal rock are approximately 2.5–3 times greater than pressures encountered in a layer of water having the same thickness.

magma A mantle- or crust-derived, physically and chemically complex mixture of molten rock, solids (e.g., crystalline or refractory fragments), and gases (e.g., CO_2 or H_2O).

magmastatic Change in static pressure with depth change in a fracture or reservoir filled with magma. Because magma densities are similar to crustal rock densities, lithostatic and magmastatic densities are also comparable.

phenocryst One of the larger, more distinct crystals in a rock with an otherwise fine-grained texture.

Copyright 2000 by Academic Press
All rights of reproduction in any form reserved.

Reynolds number A dimensionless quantity characterizing the relative importance of inertial or momentum related forces to viscous forces in fluid flow. In magmas viscous forces usually dominate, resulting in a Reynolds number that is much less than 1.

rheology The study of the deformation and flow of fluids.

rhyolite Volcanic rock with more than 68% silica having exceptionally sluggish flow characteristics owing to its high silica content and typically lower emplacement temperatures.

seismicity The detectable seismic activity that is associated here with the transport of magma.

silicic Having or being characterized by a high silica content.

subliquidus State of magma in which crystalline solids exist in an otherwise liquid regime. This state is associated with higher viscosities than magmas that are purely liquid (liquidus).

thermal diffusivity A quantity characterizing the ability of a material to allow heat to be transported by conduction (thermal diffusion) alone. The diffusivity is the ratio of the thermal conductivity to the product of the material density and the specific heat.

viscosity The resistance of a fluid to flowing in response to applied pressure forces. The higher the viscosity, the more resistant a fluid is to flowing.

volatiles A compound such as CO_2 and H_2O that can exist as a gas at magmatic temperatures and pressures characteristic of the shallow crust. The exsolution of volatiles results in the existence of a gas phase that is important for driving the transport of magma.

xenolith A piece of mantle or crustal rock picked up by flowing magma.

THE ERUPTION OF a volcano signals the rather rare and successful arrival of very hot magma, which is prone to solidification as it traverses the comparatively cool crust of the Earth. Besides the negative impact of lower crustal temperatures on the probability of reaching the surface, magmas may not be transported by the most direct route. A magma may start its journey by being squeezed from a zone of melt as a result of the formation of pressure imbalances caused by density differences between the melt and surrounding crust. At this early stage of the magmatic journey, flow is likely to be by plastic deformation of the mantle or deeper crust to make way for the invading magma. However, at shallower levels, the cooler crust makes a transition from plastic deformation to fracturing in response to the intrusion of magma. Such a transition varies with depth at different locations on the Earth. Magma-induced fracturing permits magma to flow between different crustal locations (e.g., between a magma chamber and a sill or dike), and occasionally these pathways intersect the Earth's surface, causing eruption of lava in a spectacular event. In this chapter we consider those physical processes that permit this remarkable phenomenon involving the transport of viscous, molten rock across many kilometers of much cooler crust in thin fractures that promote solidification.

I. THERMAL AND DYNAMIC ASPECTS OF DIKE FORMATION IN THE COOL CRUST

Volcanic dikes or sheetlike intrusions result when pressurized magma is forced into and along a crack, causing the propagation of a fracture. Dikes may be propagated more effectively if hot gases from the magma fill the advancing crack tip. It is possible that a pressurized gas pocket at the top of a magma chamber might prevent magma from flowing into a long crack that is being propagated upward by the gas (Fig. 1). Because of the low viscosity and low density of the vapor or gas, any gas or vapor propagated fracturing that results would not be subject to pressure losses associated with either the high viscosity of magma or the weight of the high-density magma column. This latter effect involving the weight of magma in a fracture decreases the pressure that can be transmitted to a crack tip by about 280 atm for every kilometer of fracture height. Of course, for gas pressure to be adequate to drive fracturing, the lid of the magma reservoir must not allow gas to bleed off faster than it can be produced in or channeled to the reservoir from greater depth. We know that some shallow reservoirs may be quite permeable to gas flow as indicated by losses of several hundred metric tons of sulfur dioxide (SO_2) per day from the central pit crater, Halemaumau, which lies directly over the magma reservoir of Kilauea volcano on the island of Hawaii. Gas or vapor propagated fracturing can still be significant in such a leaky system whenever gas is produced faster than it is lost. This may occur when a fresh, volatile-rich supply of magma arrives at a chamber and pressure and temperature conditions are appropriate for exsolution of a separate gas phase.

Thin sheetlike fractures serve only as temporary pathways for magma as it traverses the cooler crust. This is because flow in dikes will become localized into channels

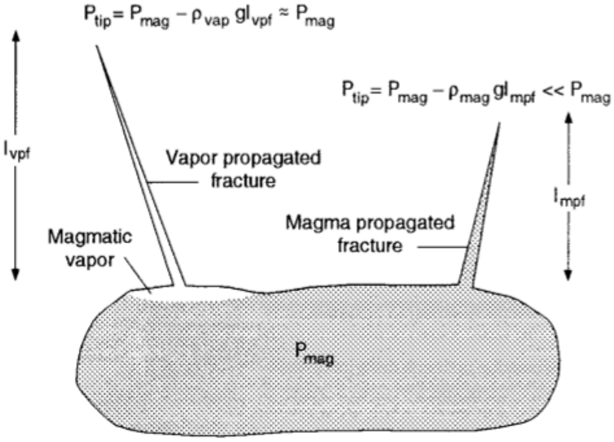
$P_{tip} = P_{mag} - \rho_{vap} g l_{vpf} \approx P_{mag}$
$P_{tip} = P_{mag} - \rho_{mag} g l_{mpf} << P_{mag}$
l_{vpf}
Vapor propagated fracture
l_{mpf}
Magmatic vapor
Magma propagated fracture
P_{mag}

FIGURE 1 Sketch of fracture propagation by vapor and by magma. Presence of a vapor layer at the top of a magma chamber prevents flow of magma in a propagating fracture. Only vapor or gas can flow into the fracture in this case. Low viscosity of vapor permits it to more effectively penetrate the crack tip and process zone. Small vapor density, ρ_{vap}, minimizes pressure losses owing to the weight of vertical column of vapor. Thus, the pressure at the crack tip, P_{tip}, is almost equal to the magmatic pressure P_{mag} in the chamber even if vertical distance of fracture l_{vpf} approaches several kilometers. By comparison, the weight of more dense magma $\rho_{mag} g l_{mpf}$ in magma propagated fracture will substantially reduce pressure that can be applied to the crack tip. [Reprinted from Carrigan *et al.*, 1992, by permission of the American Geophysical Union.]

and cease within a few hours owing to solidification unless further breakup or melting and removal of crustal wallrock occurs to produce centralized vents or conduits with enhanced rates of flow. In some cases a *critical initial width* may determine whether a portion of a dike is blocked eventually by the freezing of magma or enlarges to become a centralized conduit. In portions narrower than the critical width, solidification or blocking will occur while the melting of dike walls to produce more thermally robust conduit-like structures will occur in portions of the dike that are wider than the critical width.

It is not just the rate of heat loss into the wallrock of a dike that determines whether a magma can survive its journey to the surface. The distribution of the heat that remains in the magma as it moves through the dike is an issue of equal importance. To see this, consider magma flowing at an average velocity of 1 m/s in a dike 2 m thick. A simple energy balance argument shows that the bulk or average, across-dike, magma temperature falls less than 20°C over a distance of 10 km, assuming a 5 kW/m^2 rate of heat loss to the host rock, a rate of cooling that is appropriate just after the initiation of a dike in the cold host regime. If the average temperature was the only consideration, it could be readily concluded that the magma would not solidify. However, for simple laminar flow with no mixing to eliminate temperature differences arising in the magma between the center of the dike and its edge, the wall temperature can fall sufficiently low at the contact between the magma and wallrock that solidification occurs. Determination of the wall temperature is considerably more complicated than the estimation of the bulk temperature by the overall energy balance; it requires the solution of a coupled flow and temperature problem. This coupling involves the temperature dependence of the magma viscosity and the production of heat in the magma by the conversion of flow energy as a result of the high viscosity of magma. This latter effect is usually called *viscous dissipation*.

The simplest models of magma transport deal with only laminar flow in plane parallel dikes. However, idealized plane parallel flows are unlikely to occur in nature and might be thought to represent only singular examples of magmatic transport. To better appreciate the effect of small deviations from plane parallel flow in the extreme geometry of a dike (length/width $> 10^3$), one need only consider that the highest temperature region of the flow is at most a few meters from the boundary of the dike where heat loss occurs. Magma flowing at an average velocity of 1 m/s in a 2-m-wide, 2-km-long dike has a residence time in the dike of 2000 s. If the flow also has a transverse (cross-stream) component of only 0.0005 m/s, just 1/2000 of the longitudinal (along-dike) velocity component, the hottest magma will move from the centerline to the wall during its residence in the dike. Alternatively, the role of a transverse flow can be estimated in terms of the cross-stream flow required to transport the same amount of heat as conduction. The quantity $\rho c_p u d$ represents an effective thermal conductivity, where u and d are the characteristic cross-stream velocity and cross-stream transport distance, c_p is the specific heat at constant pressure, and ρ is the magma density. One finds that a transverse velocity of only 10^{-4} to 10^{-3} m/s is required to transport an amount of heat equal to that carried from the center to the edge of the dike by conduction alone.

Numerous possibilities exist for producing small, but significant transverse flows in a dike. These include boundary roughness, the rise of small, centimeter-scale vapor or gas bubbles in the magma as well as the occasional large ones, flow-induced sorting of solids (e.g., crystals) in the magma, and turbulence. Small deviations from a parallel wall geometry, such as the gradual necking down of a dike toward the outlet, will also produce transverse motions, tending to raise boundary temperatures and delay or prevent solidification at the wall.

Realistic laboratory experiments involving magma are difficult to carry out because of the very high temperatures, pressures, and large scales that are usually involved. However, computer models of magmatic processes have become increasingly common and much of the following discussion is based on simulations of magmatic transport that involve numerically solving equations describing the heat and mass transport in flowing magmas. Before we can quantify the transport processes mentioned, we must first more carefully define the magmatic plumbing that is characteristic of crustal volcanism. We will tend to be conservative in our descriptions in the sense that we exclude from consideration those "easy" models that allow magma to get to the surface readily but are also atypical.

II. PHYSICAL MODEL OF MAGMA FLOW IN A DIKE

A. Dimensions

What are the physical dimensions of the dikes that play a role in magma transport? The geometric parameters defining a dike are its characteristic vertical length and width. A dike's vertical length is not well constrained by observations. Presumably, the length of a dike is determined by the depth to significant concentrations of magma. The disappearance of seismicity as a result of crustal weakening associated with large volumes of magma and inferences made from surface bulges caused by the intrusion of magma at depth place the magma storage zone supplying Kilauea volcano at a depth of 2–6 km beneath the surface. A comparable depth for magma under Mauna Loa volcano, which is also on Hawaii, can be inferred from the surface tilt resulting from the accumulation of magma in a crustal reservoir. Similar depths to magmas in the more viscous, siliceous systems such as under the Long Valley Caldera are predicted by seismic studies. In the models presented here, we assume reasonable dike lengths of 2–4 km.

The characteristic width of dikes is a parameter that is easier to determine, at least at the surface. The average widths of dikes in a swarm in Iceland are about 3.5 m. In Mull, Scotland, the average width was found to be 1.5 m, with the maximum width exceeding 50 m. Dikes comprising the Independence swarm in California average 1 m in width while feeder widths for the Columbia River flood basalts average 6 m and exceed 23 m. The average width of silicic dikes is greater than that of basaltic dikes. A silica-rich, rhyolite dike intersected by drilling at 400–600 m beneath the volcanic Inyo Domes in California was found to vary from 6 to 33 m in width. It is possible that dikes may widen near the surface owing partially to the explosive release of volatiles from the rising magma. For the following discussion, the assumption of meter-thick dikes at depth is reasonable for basalts and may be a little conservative for the more viscous silicic magmas such as andesites. The processes that we describe here are particularly important for aiding magma to reach the surface in dikes of this thickness.

B. Magma Rheology

Another important physical property strongly influencing flow in a dike is the viscosity of magma and its dependence on temperature. At the surface, it is observed that the relatively low viscosity of basalts is conducive to at least moderate flow velocities (1 m/s) and to the production of transverse flow by the effects mentioned earlier. The novel lava lake experiments of Herbert Shaw and his colleagues at the U.S. Geological Survey give us some information about subliquidus viscosities of Hawaiian basalts near atmospheric pressure. For basalts flowing in dikes, the dynamic viscosity can be predicted from

$$\mu\,(\text{Pa s}) = 1.0 \times 10^{-6} \exp[26{,}170/(T + 273)], \quad (1)$$

where T is the magma temperature in degrees centigrade. At 1200°C, a reasonable temperature for a Hawaiian basalt flowing in the crust, the viscosity, μ, is predicted by Eq. (1) to be about 52 Pascal-seconds (Pa s), which is roughly equal to the viscosity of glycerin kept in a freezer. Over the temperature range of interest, Eq. (1) tends to yield greater viscosities than some more recent laboratory measurements. Lava lake measurements represent upper limits on the viscosity of a Hawaiian basalt at any given temperature since it has lost most of its water content during its flow to and residence on the surface. High-pressure experiments involving a basaltic melt with a reconstituted water content of 2.7 wt% do show a substantial decrease in estimated viscosity (~3 Pa s at 1200°C). However, Hawaiian basalts tend to be "dry" with dissolved water contents of about 0.3 wt% so the viscosities of basalts flowing in dikes are between 3 and 52 Pa s at 1200°C. Again, we will be conservative by using Eq. (1), which predicts basaltic viscosities that are higher than average for Hawaiian magmas.

For more viscous magmas, an empirical viscosity–temperature relationship has been obtained by Tom Murase of the University of Tokyo and Alexander McBirney from the University of Oregon for medium-silica-content, andesitic lavas from Washington's Mt. Hood volcano. It is approximated by

$$\mu\,(\text{Pa s}) = 8.47 \times 10^{-8} \exp[35{,}000/(T + 273)], \qquad (2)$$

with temperature, T, given in degrees Celsius. For an andesite, the viscosity at 1100°C is estimated to be about 200 times greater than for the Hawaiian basalt. Again, this value of the viscosity may be an upper limit since the presence of water in the melt can substantially lower the viscosity of an andesite, which often contains more water than a basalt. The temperature dependence of the viscosity assumed in Eqs. (1) and (2) is most appropriate above the liquidus temperature where no crystals exist as well as just below, say, 50 degrees, where few crystals are present.

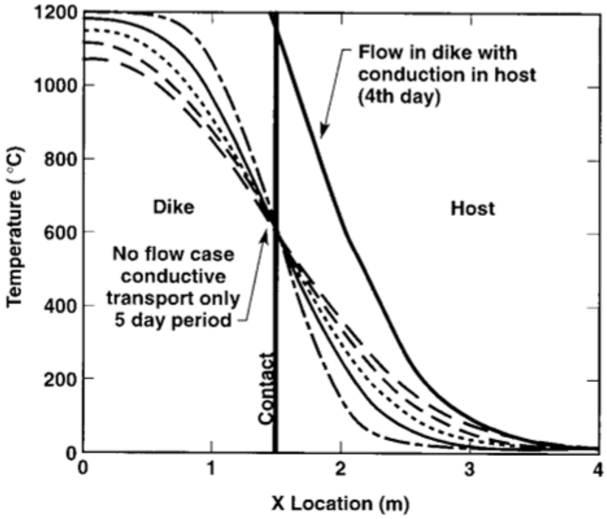

FIGURE 2 Comparison of temperature profiles in magma and in adjacent host rock for cases in which magma is stagnant in a 3-m-thick dike and when it is flowing. Stagnant magma loses heat to the host rock by conduction only. Group of curves intersecting the dike/host contact at 600°C (average of 1200°C dike and 0°C host temperatures at time of emplacement) illustrates thermally diffusive (conductive) temperature profiles during the first 5 days of cooling. The symmetry of this conduction solution about the contact is destroyed if magma is flowing. The thermal boundary layer in the magma is much thinner after 4 days than the thermally conductive layer in the host. This asymmetry results in much higher temperatures at the contact. [Reprinted from Carrigan *et al.,* 1992, by permission of the American Geophysical Union.]

C. Magmatic Heat Loss and Flow Rates

Initially, hot magma flowing along a propagating crack comes into contact with host rock at the ambient or native temperature. Just seconds after emplacement, the temperature at the magma–wallrock contact is the average of the magmatic and ambient temperatures. If heat movement is by conduction only in both the host rock and dike, that is, magma stops flowing in the dike, this boundary temperature would exist until the temperature of the magma at the center of the dike falls below its initial value (Fig. 2). But if magma is flowing, a thermal boundary layer will rapidly develop in the magma at the boundary. This boundary layer is simply a region in the flow where heat moves to the boundary mainly by conduction and is characterized by a gradual change in temperature between the magma and wallrock. The purely conductive (diffusive), time-dependent temperature distribution that develops in the host rock, which is characterized by thermal diffusivity κ, will not match the thermal boundary layer that is established in the flow. At a fixed location along the dike, the boundary layer conductive length scale, that is, the thermal boundary layer thickness, will tend to approach a constant value in time while the host regime conduction length scale given by $\sqrt{\pi\kappa t}$ grows indefinitely with time t. Figure 2 shows this difference after 4 days between the thickness (about 0.05 m) of the flow-induced boundary layer and the conduction length scale in the host rock (about 1.5 m). Because of this difference in thermal conduction length scales, heat is supplied to the boundary more effectively than it can be removed. After emplacement, the boundary temperature will rapidly increase above the average of the host regime and bulk magmatic temperatures and approach some value near the initial magmatic temperature.

A large difference in thickness between the magma thermal boundary layer and the host rock thermal conduction layer causes the host rock to act like a large thermal resistor in series with a small one (the dike boundary layer) and determines the heat flow out of the dike. Now the host rock behaves like the dominating thermal resistance controlling the heat flow from the dike. A typical rate of heat loss is 1 kW/m^2, which is appropriate about 8 days after emplacement of the dike into cold host rock (Fig. 3). On the other hand, 3 kW/m^2 is more appropriate for a day-old dike in cold host rock (Fig. 3). These values of heat loss to the host rock may actually be somewhat high for established volcanic regions. The continuous flow of hot magmatic gases through the crust overlying a magma reservoir, as in the case of Kilauea, can substantially increase the temperature of the host rock above ambient values and significantly reduce the heat loss rate from the magma to the host regime. In addition, preheating of the crust by injections of magma that do not reach the surface may produce a "thermal highway" for later injections of magma that do flow to the surface without solidifying.

The typical average flow speeds of basaltic magma in dikes vary from <1 m/s to >3 m/s. These values are consistent with the range of mass fluxes deduced from eruptions and also typify the range of magma ascent rates required to offset the setting velocity of dense ultramafic xenoliths or host rock fragments that have been transported to the surface in basaltic magmas. Less is known about flow velocities in andesitic dikes, but large-scale eruptions probably require flow velocities exceeding several tenths-of-a-meter-per-second.

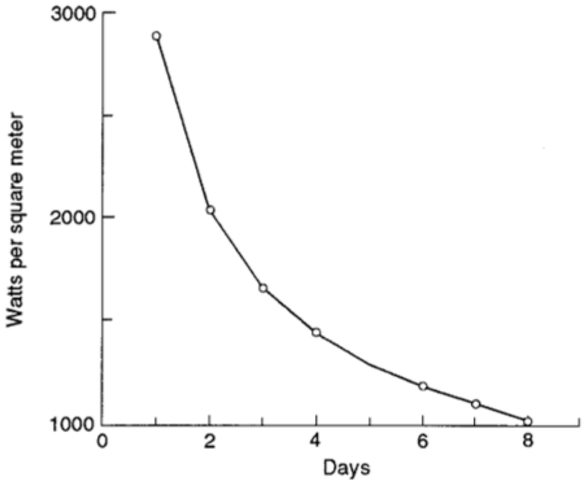

FIGURE 3 Rate of heat loss at the dike wall versus time. As the host rock is gradually heated by magmatic flow, the rate of heat loss decreases. This estimate of the rate of heat loss is given by $Q = k(dT/dx) = k(\Delta T/\sqrt{\pi \kappa t})$. The thermal conductivity $k =$ 1.26 W/m K is appropriate for wallrock at elevated temperatures, while the thermal diffusivity κ is assumed to be 7×10^{-7} m^2/s. The initial temperature contrast between the magma and country rock ΔT is taken to be 1000°C, which is likely to be too large for a volcanic region already subjected to some preheating. Thus we would expect our estimates of the rate of heat loss to bound those values characteristic of volcanic regions. [Reprinted from Carrigan *et al.,* 1992 by permission of the American Geophysical Union.]

III. COMPUTERIZED MAGMA TRANSPORT

As mentioned, it is very difficult to carry out meaningful laboratory experiments simulating the transport of magma in the Earth's crust. In principle, the important aspects of magma trasport can be scaled down to a laboratory model. In practice, the likelihood of finding the right combination of materials having the correctly scaled thermal and fluid mechanical properties at temperatures and pressures readily achievable in the laboratory is remote. The occasional lab experiments that are done never simulate the full behavior of a magmatic plumbing system. Computer models of magma transport do not necessarily share this drawback. As computers have become increasingly powerful, more and more studies of magma storage and transport have been carried out as numerical simulations. Such models have gradually become more realistic as computer programs have become more sophisticated in treating the dynamics of temperature-dependent magmatic flow.

A. Flow of Basaltic (Lower Viscosity) Magma in Dikes

The simplest dike is one with parallel boundaries. A 2-km-long by 1-m-thick dike containing basaltic magma flowing at a maximum speed of 1 m/s suffers a decreasing boundary temperature with distance downstream as illustrated by Fig. 4 (lower curve) assuming that heat is lost at a rate of 1 kW/m^2. Here the temperature at the boundary falls approximately 70°C in just the first kilometer of flow. At this rate, solidification at the boundary of the dike will occur. Curiously, the "mixing cup" temperature of the magma at each downstream location remains nearly constant over the first few kilometers as show in the figure. The mixing cup temperature, which is close to the bulk temperature, is the temperature that would be measured by a hypothetical extraction of all the magma flowing across a given horizontal plane and then mixing it up. A lot of flow energy can be converted to heat as a result of the high viscosity of magma in a high-shear environment. This fluid-dynamic viscous heating effect is analogous to the me-

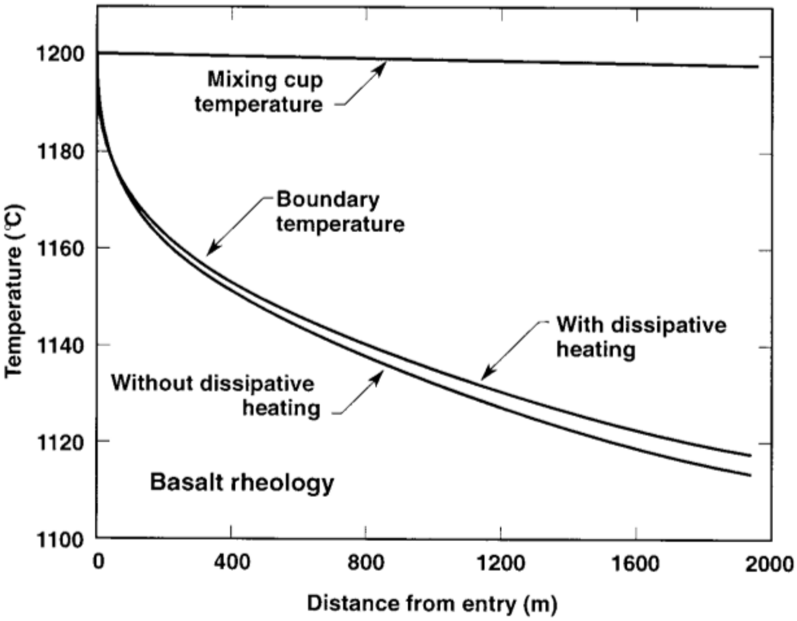

FIGURE 4 Boundary and mixing cup temperatures for a Hawaiian basalt flowing at an average velocity of 0.67 m/s (constant flux inlet condition) in a dike with 1 kW/m^2 cooling at the walls. The mixing cup temperature decreases by only a few degrees over a distance of 2 km as indicated by the nearly horizontal line. However, the boundary temperature decreases by about 70°C even with viscous dissipative heating. [Reprinted from Carrigan *et al.,* 1992, by permission of the American Geophysical Union.]

chanical effect of rubbing two sanding blocks together to generate heat. The upper curve shows the variation of temperature with distance downstream from the inlet when viscous heating is included. With this additional heating effect taken into account, the boundary temperature is slightly higher at each location downstream compared to dike flow without viscous dissipation.

B. Potential Role of Viscous Dissipation

A dimensionless ratio of dike parameters called the Brinkman number,

$$\mathrm{Br} = \mu v^2/k\,\Delta T, \tag{3}$$

is an indication of when viscous dissipation becomes significant compared to the rate of heat loss by conduction. The parameter ΔT is the temperature difference between the magma–wallrock contact and centerline of the dike, k is the thermal conductivity of the magma, v is its velocity, and μ is the dynamic viscosity of the magma. The Brinkman number represents a measure of the rate of heat production by viscous dissipation relative to the amount of heat conducted to the boundary of the dike. In more or less constant viscosity flows, Br must exceed a value of about 2 for viscous heating to affect significantly the shape of the cross-stream temperature distribution. For basalt losing heat at a rate of 1 kW/m^2, this value of Br requires an average flow velocity of a few meters per second. For an average velocity of 2 m/s, the mixing cup temperature actually remains equal to the inlet temperature with increasing distance along the dike. If the rate of heat loss is increased to 2 kW/m^2, the mixing cup temperature is maintained at the inlet value for an average flow velocity of 2.7 m/s, that is, the heat loss is entirely offset by viscous dissipation. However, the boundary temperature still falls as the thermal boundary layer grows with distance along the dike. Thus, even in basaltic dikes where the volume of magma is actually getting hotter owing to viscous dissipation, solidification along the boundaries can still occur in the absence of transverse flow. While viscous dissipation can produce more heat than is lost through the boundaries, cross-stream conduction alone is not adequate to carry enough heat to the boundaries to keep them from cooling.

For basalts, we have seen that the problem of cooling at the boundaries of a dike is not a lack of heat in the magma. Rather it is the distribution of heat or temperature that develops as the loss of heat progresses during flow downstream. It is necessary to look to natural mechanisms for stirring the magma as a means of redistributing this heat in the cross section of the dike.

C. Effect of Rising Gas Bubbles

Because of the release of gas trapped in magma chambers and exsolution of volatiles in rising magma undergoing decompression, the flow of magma may become at least a two-phase problem. (In some cases, the presence of phenocrysts or entrained wallrock fragments could require the treatment of three phases, that is, we must sometimes consider magma as a mixture of solids, liquids, and gases.) For the vertical flow of gas and basaltic magma, the transition from single-phase to two-phase behavior occurs when gas bubble sizes are of the order of 0.01 m. While the separated flow of larger bubbles prevents them from being wholly preserved in lavas at the surface, with 0.02–0.03 m being the observed maximum, the sizes of volcanic bombs or eruptive fragments of lava suggest the common occurrence of bubbles greater than 0.10 m, and 1-m-diameter bubbles may be occasionally observed. In some cases, gas expelled from the magma chamber can create a rapidly rising gas bubble with dimensions comparable to the dike thickness (Fig. 5a). This is called the *slug-flow regime.* Such voids may also be produced by the coalescence of smaller bubbles consisting of volatiles that come out of solution in the rising magma. The buoyancy of a large bubble causes it to rise relative to the surrounding magma. Some of the flow lines in the magma must thus be diverted from the center of the dike toward the boundaries (Fig. 5a). For bubble-rise rates approaching tens of centimeters per second, the resulting cross-stream flow will easily increase dike boundary temperatures to mixing cup values.

The effects of centimeter-size bubbles rising relative to the bulk flow (Fig. 5b) can be determined from computer models by using an eddy thermal diffusivity that allows for the "drift" motion of the fluid caused by the passage of gas bubbles in the flow. For magmas, a bubble-eddy diffusivity κ_b of the form

$$\kappa_b = k_b \alpha \frac{d_b}{2} V_b \tag{4}$$

can be applied where k_b, α, d_b, and V_b are, respectively, an empirical constant having a value of about 1.2, the bubble void fraction, the mean bubble diameter, and the relative bubble rise rate. A crude estimate of the relative rise rate of a bubble appearing in Eq. (4) is given by the Stokes' velocity:

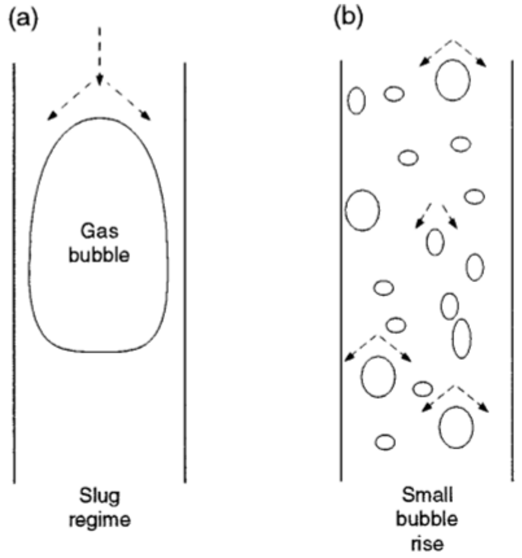

FIGURE 5 In actual dikes and conduits, lateral mixing can be effectively accomplished by the presence of rising gas bubbles produced from accumulated gas in chambers or exsolving volatiles. Both (a) large and (b) small bubbles induce cross-stream velocities in magma as they rise relative to the magma. An effective thermal conductivity given by Eq. (6) can be used to simulate the effect of the rise of small bubbles on heat transport to the walls of the dike. [Reprinted from Carrigan *et al.,* 1992, by permission of the American Geophysical Union.]

$$V_b = \left(\frac{1}{18}\right) \frac{d_b^2 g}{\mu_{\text{magma}}} (\rho_b - \rho_{\text{magma}}), \tag{5}$$

in which g is the gravitational acceleration. An effective thermal conductivity k_{eff} that takes into account bubble-induced transverse or cross-dike motions can then be written as

$$k_{\text{eff}} = (1 - \alpha) k_{\text{magma}} + (1 - \alpha) \rho_{\text{magma}} c_{\text{magma}} \kappa_b, \tag{6}$$

where c_{magma} is the specific heat of the melt taken to be 1.05 kJ/kg K (0.25 cal/g °C). This effective thermal conductivity replaces the magma thermal conductivity in magma transport simulations. Note that k_{eff} is temperature dependent. We take into account that near the boundary, where the temperature is lower, the higher magma viscosity decreases the Stokes' rise rate V_b. As a result, κ_b also is less at the boundary, which means that the eddy thermal conductivity is less effective at the boundary than at the middle of the dike for transporting heat.

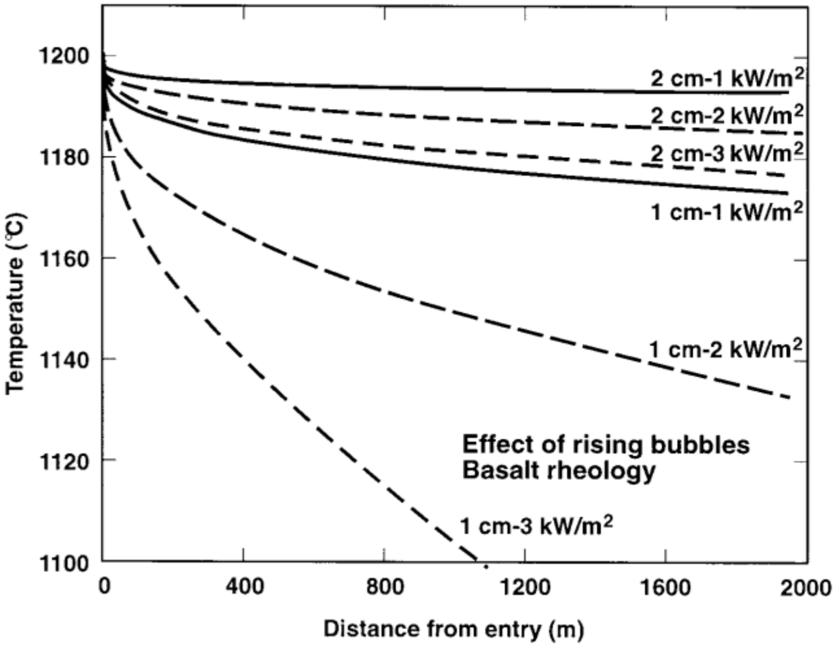

FIGURE 6 Rising bubbles in basalt strongly affect boundary temperatures of the dike. If gas bubbles occupy a 10% volumetric fraction of the dike and have a mean diameter of 2 cm, they substantially increase the effective thermal conductivity as a result of the transverse motion that they induce so that the temperature drop is only 22°C at the boundary after 2 km of flow in a dike with a large 3 kW/m^2 rate of heat loss. For a 1 kW/m^2 rate of heat loss, the temperature drop on the boundary after 2 km is a mere 7°C. Boundary temperature is rather sensitive to bubble size. Reducing mean bubble size from 2 to 1 cm in the 3 kW/m^2 case produces a much larger temperature drop as illustrated by the bottom dashed curve. [Reprinted from Carrigan *et al.,* 1992, by permission of the American Geophysical Union.]

Figure 6 shows the variation of boundary temperature along a basaltic dike for different rates of heat loss and bubble size. For a void fraction of only 10% and mean bubble diameters between 1 and 2 cm, there is a large increase in boundary temperature at any given downstream location compared with cases that do not include bubble rise. There is also a significant dependence of the boundary temperature on the mean bubble diameter d_b. For a dike with an average flow velocity of 0.67 m/s (1 m/s maximum flow rate), losing heat at the rate of 1 kW/m^2, the boundary temperature drops only 7°C over 2 km compared to 80°C for the case without bubbles shown in Fig. 6. Even with a heat loss rate of 3 kW/m^2, the boundary temperature drop is just 22°C after 2 km. This suggests that basaltic magma could flow about 10 km before the onset of solidification at the boundaries. For a bubble diameter of just 1 cm, the figure shows that a temperature drop of almost 100°C occurs after only 1 km in the 3 kW/m^2 cooling case. When bubbles are not important, other mechanisms for inducing cross-dike motions in the magma flow are boundary surface roughness, which breaks up the thin thermal boundary layer, and the occasional onset of turbulence in less viscous flows that results in higher boundary temperatures and reduced pressure gradients.

D. Effect of High Viscosity on Magma Transport

What about higher viscosity andesitic flows in a 1-m-wide dike with viscous heating and bubble flow? Figure 7 gives boundary temperatures versus distance along the dike for a number of different cases. For a maximum flow velocity of 0.5 m/s (average flow velocity of 0.33 m/s) and a heat loss of 1 kW/m^2, the boundary temperature increases downstream owing to viscous heating even in the absence of rising bubbles. Assuming bubbles make up 10% of the dike volume, rising boundary temperatures occur for a heat loss rate of even 2 kW/m^2. Without bubbles, the boundary temperature oscillates with distance along the dike if a heat loss rate of 2 kW/m^2 is used for the 0.5 m/s maximum velocity

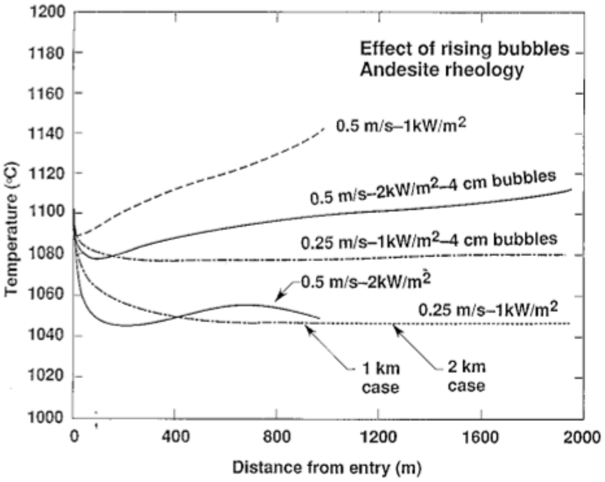

FIGURE 7 The effect of bubbles and viscous heating is shown for a 1-m-wide andesitic dike assuming a variety of magma flow velocities and heat loss rates. Due to viscous heating, boundary temperature rises along the dike for a maximum flow velocity of 0.5 m/s (average velocity = 0.33 m/s) and 1 kW/m^2 rate of heat loss (top dashed curve) and for 2 kW/m^2 rate of heat loss (upper solid curve) if 10 vol% content of bubbles having a mean diameter of 4 cm is present. Neglecting bubbles with 2 kW/m^2 heat loss and 0.5 m/s maximum flow velocity results in the bottom oscillatory solid curve. Halving both the flow velocity and rate of heat loss assumed in the previous case with bubbles (upper solid curve) produces the nearly constant temperature boundary given by the curve at 1080°C (dot-dash). If the effect of rising bubbles is not included in the latter case, the boundary temperature drops to a more or less constant value of 1040°C (bottom dot-dash and dotted curves). [Reprinted from Carrigan *et al.*, 1992, by permission of the American Geophysical Union.]

case. This may be a result of interplay between viscous dissipation and the temperature-dependent viscosity. The effect of bubbles on the thermal regime reduces the pressure gradient required to drive the flow at an average velocity of 0.33 m/s from 36.6 to 31.5 MPa/km (about 366–315 atm/km). At the lower 1 kW/m^2 loss rate, more or less constant boundary temperatures can be achieved if the maximum flow velocity is 0.25 m/s (average flow velocity of 0.17 m/s). However, even at this lower flow rate, the pressure gradient required to push andesite through the dike exceeds 20 MPa/km (about 200 atm/km) for a 1-m-wide dike. Generally, long andesitic dikes are observed to be much wider than 1 m and, for a given mass flux, the required driving pressure gradient is extremely sensitive to the dike width, being proportional to 1/width^3. Thus, we expect that larger dikes will require a substantially lower driving pressure gradient for a given mass flow.

However, during the initial period of flow in a dike, we expect that magma must be forced through fractures that have widths of somewhat less than 1 m. It is difficult to imagine an andesitic magma propagating at any significant rate along a very thin dike because of the large pressure gradients required. In a 0.2-m-wide dike with an average flow velocity of 0.1 m/s, the magma can only flow about 500 m before the bulk temperature falls 100°C, assuming a heat loss rate of 5 kW/m^2. This is a reasonable heat loss rate for a fracture in cool host rock. The required pressure gradient for this flow exceeds 30 MPa/km. For andesitic magma to travel without solidification in a dike several kilometers long would require an even larger pressure gradient. Nevertheless, andesites and even more silicic and viscous rhyolitic magmas propagate significant distances. A two-magma lubrication process, to be discussed later, involves the simultaneous transport of magmas of differing viscosity. It reduces the pressure gradient needed to transport the most viscous magma to the surface and may explain how some rhyolitic magmas are able to reach the surface.

IV. PRESSURE GRADIENTS REQUIRED FOR MAGMATIC FLOWS

A. Lower Viscosity Basaltic Magmas

The pressure gradient required to drive a 0.67 m/s average flow corresponding to a 1 m/s maximum flow rate in a 1-m-wide dike with a heat loss of 2 kW/m^2 is less than 0.5 MPa/km (about 5 atm/km). To maintain the same flow rate in a dike decreasing from a 1- to 0.5-m thickness over a distance of 2 km requires a pressure gradient of about 1.7 MPa/km. These driving pressure gradients are not particularly large. The lithostatic (i.e., the vertical pressure distribution of overlying crustal rocks) load in the crust increases with depth by about 25 MPa/km. For the sake of discussion, let us assume that a pressure condition on the inlet of the chamber applies and has a value equal to the depth times the lithostatic pressure gradient. For a 4-km depth, p_{in} = 100 MPa and at the surface p_{out} = 0. For the magma column in the dike, we assume that the density is roughly comparable to that of the surrounding rock so that the load pressure is about the same as the lithostatic value at any level. Figure 8a shows this situation in which the lithostatic column balances the magmastatic column (i.e., the vertical pressure distribution in magma). There is no excess pressure gradient to drive the flow and hence

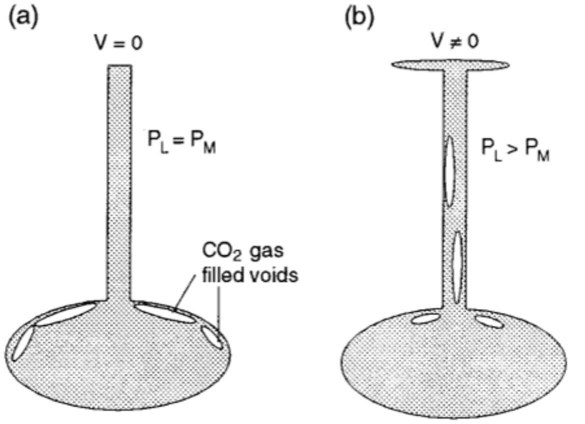

FIGURE 8 Chamber gas entering a dike or conduit can upset the balance between the lithostatic pressure p_L and the magmastatic pressure p_M and drive magmatic flow. (a) Initially, gas accumulates in the magma chamber. Because the lithostatic pressure field (pressure regime in host rock) is approximately balanced by the magmastatic pressure field (pressure regime in dike or conduit) the pressure gradient for driving magma through the dike is small to vanishing and no flow occurs. (b) If, however, gas enters the dike from the chamber, the average density of the magma in the dike falls and p_M becomes less than p_L at every level in the dike. A pressure difference then exists for forcing magma in the dike to the surface. Thus chamber gas (and exsolution of volatiles at shallow levels within the dike) can play a critical role in initiating and maintaining an eruption. [Reprinted from Carrigan *et al.,* 1992, by permission of the American Geophysical Union.]

no flow. Now, suppose that chamber gas is leaked into the dike and rises upward toward the surface (Fig. 8b). If the gas bubbles displace only 10% of the volume of the dike, the pressure at the bottom of the magmastatic column suddenly falls 10 MPa below the lithostatic value. This means that only a 10% void space caused by the presence of gas bubbles in the dike gives rise to a 2.5 MPa/km driving pressure gradient that exceeds the driving requirements of our computer simulations. Our calculations suggest that the average flow velocity would exceed 3 m/s in a 1-m dike and would produce enough viscous heating to more than offset a 2 kW/m^2 rate of heat loss.

The modest 10 vol% bubbles that drive the system in this example will not be distributed uniformly in the magma column. In water-rich systems, the bubble content increases rapidly during the last 1000 m of ascent due both to rapid decrease of water solubility in melt and vapor expansion. In CO$_2$-rich systems, expansion of the gas phase is the main contributor to the upward increase in the bubble fraction, because CO$_2$ is relatively insoluble in melt at crustal pressures. In the general case, when both components are present, the chamber gas will be enriched in CO$_2$ and the gas evolved during dike formation will be rich in H$_2$O. Depending on water content, the expansion of the rising magma by vapor exsolution and expansion can become so great that the melt phase disintegrates near the Earth's surface, that is, the magma fragments to a dusty gas of ash in vapor. These are the conditions that promote explosive eruptions. Thus, once overpressuring of a magma chamber has induced dike propagation to the near surface and the onset of explosive activity, the drastic reduction in density in the upper part of the column of magma will make flow in the dike self-sustaining. Furthermore, the volume fraction of bubbles in the dike and not the bubble size determines dike flow velocity. Thus small bubbles can be as effective as large ones in inducing magma to flow in the dike. The presence of separated gas and liquid phases in a dike will also facilitate its propagation by increasing the available driving pressure gradient (through lowering the average density of the column) and decreasing viscous drag by replacing magma in the narrowing tip of the dike where fracturing is occurring.

B. Magmatic Coextrusion and Transport of More Viscous Magmas

Compared to basaltic flows, andesitic and rhyolitic flows in a dike need extremely high driving pressure gradients. It has been mentioned that a thin (0.2-m) andesitic dike may require a driving pressure gradient that is greater than 30 MPa/km. This value exceeds the lithostatic gradient, which in some cases represents a maximum value for the available driving pressure gradient. However, under certain circumstances, the driving pressure gradient can be substantially reduced for mixtures of magmas. If even a small amount of a lower viscosity magma plates the walls of a dike, it can contribute to decoupling the flow of a higher viscosity component from the walls. Because most of the shear and energy dissipation take place near the walls, where the low-viscosity magma is now located, the pressure gradient required to drive the high-viscosity component through the dike is substantially decreased. In effect, the lower viscosity magma lubricates the passage of the higher viscosity magma. Consider a 10-m-wide dike with a higher viscosity crystal-rich rhyolitic core region rising in the center of the dike. Further, assume all the shear occurs in 1-m-wide layers of lower viscosity, crystal-poor rhyolitic magma adjacent to the boundaries. In 1990, the author and Professor J. C. Eichelberger at the University of Alaska used geologic and drilling studies to show that volcanic domes in the Inyo volcanic system in California were formed by such a core/wall layer arrangement of magmas flowing simultaneously in a dike about 600 yr ago. The dynamic viscosities of the flowing core and wall layer magmas are 3.6×10^6 and 1.6×10^4 Pa s, respectively. The total pressure drop in the core/wall layer flow at an average velocity of 0.05 m/s over 1 km can be shown to be only 0.18 MPa (1.8 atm). If just the more viscous, crystal-rich, rhyolitic magma flowed in the same dike, the required pressure drop for driving the flow rises to about 21 MPa. This is about the largest value that could be produced in a very low density magmatic foam by the lithostatic pressure gradient.

The lubrication of the dike walls by lower viscosity magma is not something that happens by chance when two magmas of differing viscosity flow together. In fact, two-component flows will always tend to be self-lubricating in this manner. As the two layers flow along the channel, the lower viscosity layer will gradually flow around the higher viscosity component encapsulating it (Fig. 9). This encapsulation of the higher viscosity component results in self-lubrication of the flow since the lower viscosity component now occupies all zones of strong shear near the walls, while the higher viscosity component is relegated to a zone of weaker to vanishing shear in the center of the flow. This encapsulation/self-lubrication process is robust and is used in industry for transporting viscous oil in pipelines by injecting water as well as for the formation of composite plastic extrusions.

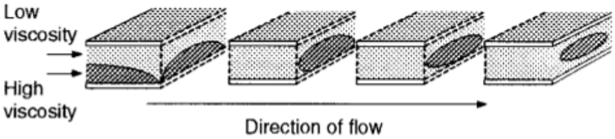

FIGURE 9 A channel sectioned at different locations along the direction of flow of two liquid layers with different viscosities that are injected side by side illustrates the progressive nature of the encapsulation or self-lubrication process. After entering the channel, the initially flat interface between the layers begins to be distorted. The interface between the two liquids increasingly bends back on itself at each successive station downstream as the lower viscosity component (light shading) of the flow encroaches on the contact between the wall and the higher viscosity component (dark shading). Eventually, the higher viscosity component is completely isolated from the high shear, wall region by the lower viscosity liquid. [Reprinted from Carrigan, 1994, by permission of Academic Press.]

Why encapsulation occurs has often been explained in terms of the minimization of the energy dissipated by viscosity in the process of pumping a given mass flux of two different liquids in a channel or pipe. A higher viscosity core and a lower viscosity annular (near wall) zone produces lower dissipation for a given mass flux than the opposite arrangement of higher viscosity at the wall and lower viscosity in the core. This core–annular distribution is also superior, with respect to the driving pressure gradient, to the side-by-side arrangement in which two different viscosity layers are fed together (one on top of or on the side of the other) into a pipe or channel. However, there is some evidence that if the zone of lower viscosity at the wall of the tube gets too thick (>30% of the tube radius), the core–annular flow regime can break down.

Of all the laboratory encapsulation experiments, coextrusion experiments involving molten polymers have dynamics that are probably most like those characterizing the transport of magmas. The dynamics of magma transport are dominated by magma viscosity. Depending on parameters such as temperature, volatile content, and crystal content, the rheology of magma is typically found to vary from purely Newtonian (vanishing dependence of viscosity on shear rate) to a shear thinning power law behavior (viscosity depends mathematically on shear rate raised to some power). The flow of molten polymers in capillary extrusion dies is also dominated by viscosity. As in the case of magmas, polymers can also exhibit both Newtonian and power law behavior. In both polymeric and magma mixtures, surface tension can be neglected relative to viscous effects.

Another feature of polymer coextrusion experiments that is common to magma flow in a dike or conduit is that any inertial forces in the flow can be neglected compared to viscous forces. Thus, the Reynolds number which represents the ratio of inertial (momemtum-related) to viscous forces is much less than unity for both the coextrusive magmatic and polymeric flows of interest. The similarities in the physical properties of the molten materials and in the dynamics of the flow systems strongly suggest an excellent correspondence between the coextrusion experiments and the simultaneous flow of two magmas in a dike.

The results of a coextrusion experiment (Fig. 10) performed by Professor C. D. Han of the Polytechnic Institute of New York illustrate the effects of viscosity differences on the side-by-side flow of two polymers having different viscosities. Using cylindrical dies of different aspect ratios, it was found that the lower viscosity component (low-density polyethylene) gradually flowed around the higher viscosity component (polystyrene) to

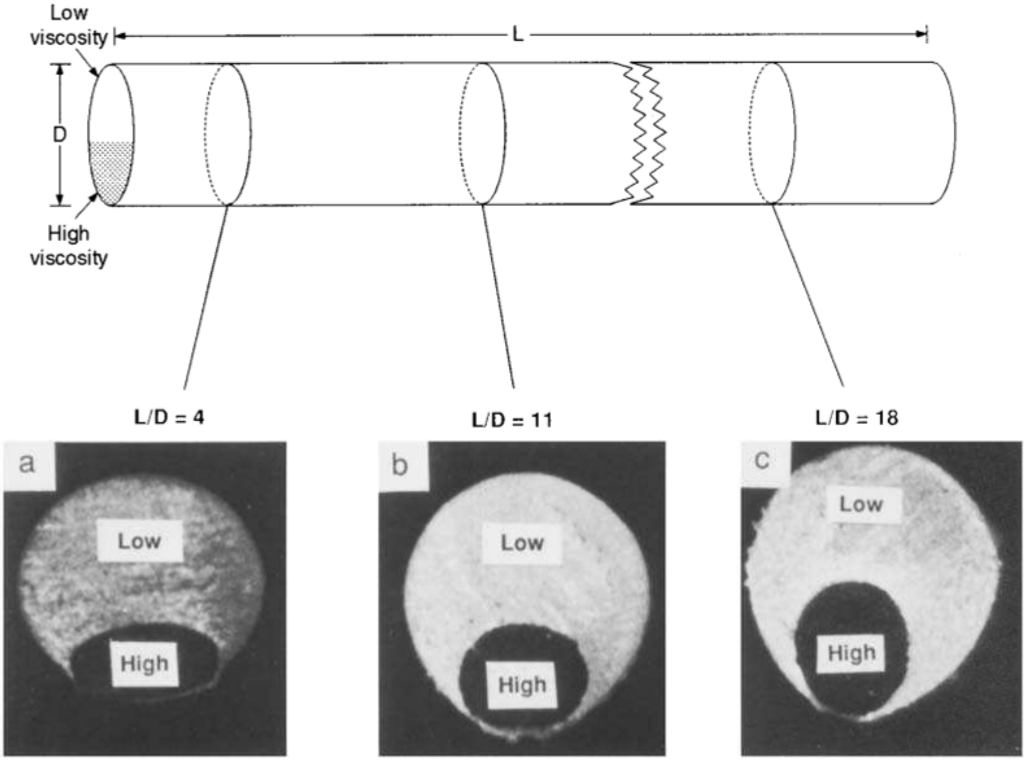

FIGURE 10 A coextrusion experiment involving two molten polymer layers injected side by side into tubular capillary dies having different length to diameter (L/D) ratios illustrates the encapsulation of the higher viscosity component. The ratio of the viscosities indicated for the two layers varies from 0.14 to 0.34 over the range of extrusion rates studied. Careful examination of the extrusion at L/D = 4 shows that the lower viscosity component has already almost completely flowed around the higher viscosity component. With greater distances downstream the higher viscosity component migrates away from the wall toward the center of the flow. [Adapted from C. D. Han, *J. Appl. Polym. Sci.* **17,** 1289. Copyright © 1973 with permission of John Wiley & Sons, Inc. Reprinted from Carrigan, 1994.]

completely encapsulate it. While the higher viscosity component never became centered in the lower viscosity encapsulant for dies with length-to-diameter (L/D) ratios of up to 18, it was fully encapsulated (separated from the die wall) within only 4 diameters of the die inlet. In polymer experiments the exact details of the encapsulation/self-lubrication process, such as the interface shape, may vary in a way that depends on the rheology of a particular melt system.

Another set of experiments by Minagawa and White (1975) at the University of Akron produced similar results for side-by-side extrusion both in a tubular (conduit-like) die and in a rectangular (dike-like) die. The coextrusion experiment using tubular geometry (Fig. 11a) illustrates the gradual bending around of the interface between the melts as the higher viscosity (dark) component is encapsulated by the lower viscosity component with increasing distance down the tube. As a result of the high shear, the contact area between the higher viscosity component and the tube wall gradually decreases with distance down the tube. Encapsulation would eventually isolate the higher viscosity layer from the wall, as in the case of Han's experiment, if a longer tubular die had been used. The rectangular slot experiments (Fig. 11b) varied both the viscosity ratio of the layers and their initial orientation at the inlet of the slot. When both components have the same viscosity (viscosity ratio equal to one), no encapsulation occurred so that the interfaces remained essentially flat at the outlet for both the horizontal and the vertical initial orientations. When both layers had different viscosities (viscosity ratio different from 1), the interface between higher and lower viscosity components curved around so as to isolate the higher viscosity melt from the wall of the slot.

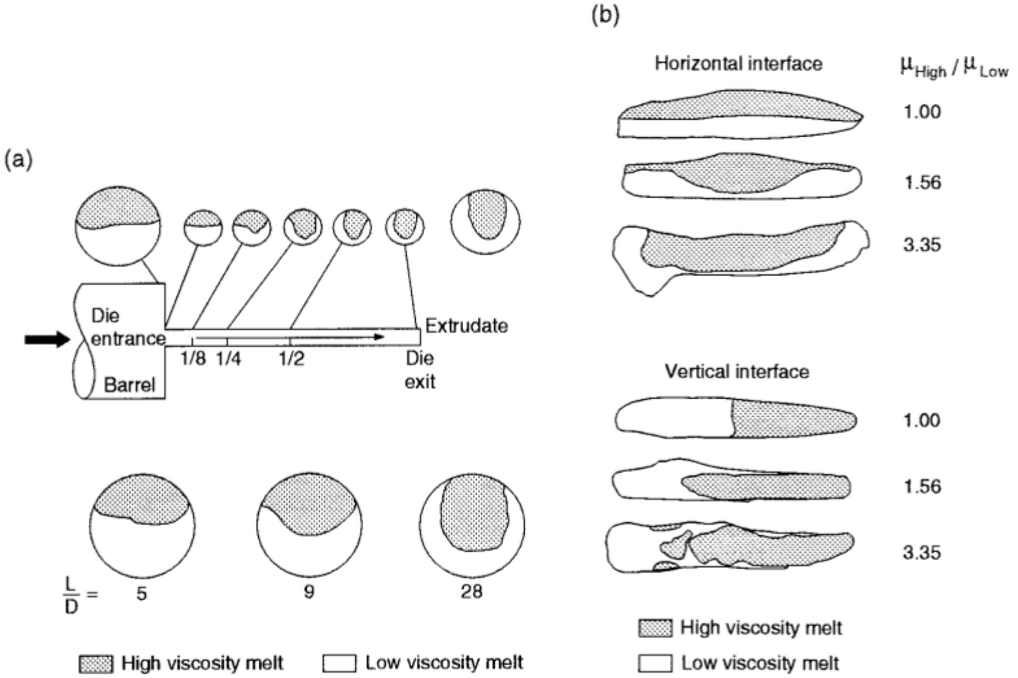

FIGURE 11 (a) Another coextrusion experiment with side-by-side initial conditions illustrates the bending of the interface and the gradual isolation of the higher viscosity component from the wall with increasing distance downstream (normalized by the pipe diameter *D*). The viscosity ratio is 1.56. (b) In a rectangular, dikelike channel, side-by-side injection is studied for two different orientations of the interface between the two layers and for different viscosity ratios. The aspect ratio (downstream length : thickness) is 15. For viscosity ratios of unity, significant interfacial distortion does not occur. The maximum encapsulation for given length of the channel takes place when the interface is parallel to the shortest dimension (thickness) of the channel. This is the anticipated orientation that will give rise to encapsulation in the inyo chain model for magma withdrawal through a dike. [Adapted from Minagawa and White, 1975, Figs. 6–9, with the permission of the Society of Plastics Engineers. Reprinted from Carrigan, 1994.]

V. THE ERUPTION OF THE INYO CHAIN OF VOLCANIC DOMES

In an effort to understand the subsurface processes leading to the formation of a chain of young volcanoes in California's Long Valley Caldera, J. C. Eichelberger, who was at Sandia National Laboratories at the time, and his colleagues embarked on a scientific drilling program in the 1980s. A major goal of their work was to understand the origin of the volcanoes or domes and the feeder dike that connected them. Obsidian Dome is one of the three composite volcanoes that is thought to have erupted more or less contemporaneously about 600 yr ago along a north-trending line that crosses the northwestern boundary of the caldera (Fig. 12). The hypothesis that a common dike connects all three domes was partially validated by the intersection of a shallow, rhyolitic dike between Obsidian Dome and Glass Creek Dome. It was found that at least three physically distinct magmas have contributed to the formation of the composite domes.

Deadman Dome, the southern-most flow in the chain, consists of a coarse, crystal-rich rhyolite (70–74% SiO_2) that overlies a rhyolite of lower crystal content, which also tends to have a slightly lower silica content (71.5%). The middle flow in the chain, Glass Creek Dome, lies on the rim of the caldera. Like Deadman Dome, it consists of a coarse, crystal-rich rhyolite overlying a finer rhyolite with lower crystal content. Obsidian Dome lies beyond the rim of the caldera and consists of a fine, low crystal content rhyolite overlying a fine, low crystal and low silica rhyolite or rhyodacite. Since any increase in crystal content or silica (SiO_2) content means higher viscosity, lower crystal and silica content rhyolite magmas are expected to encapsulate higher crystal and silica rhyolites, and such layering sequences are observed in the domes.

Figure 13 illustrates how the progressive breaching of the sloping roof of a zoned chamber could produce the observed gross compositional variations during a

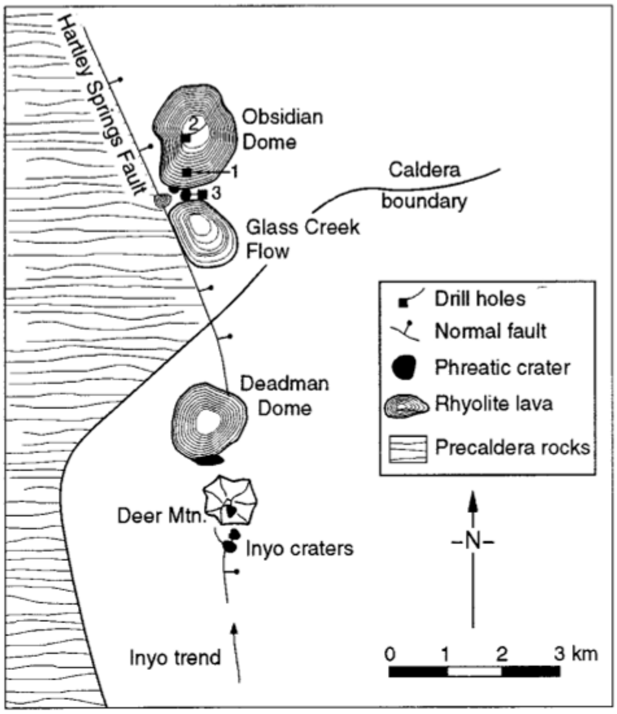
Hartley Springs Fault
Obsidian Dome
2
1
3
Caldera boundary
Glass Creek Flow
Drill holes
Normal fault
Phreatic crater
Rhyolite lava
Precaldera rocks
Deadman Dome
Deer Mtn.
Inyo craters
-N-
Inyo trend
0 1 2 3 km

FIGURE 12 Map view of Inyo domes with associated volcanic and geologic features. The numbered squares on and by Obsidian Dome indicate the locations of scientific drill holes. [Figure adapted from Eichelberger *et al., J. Geophys. Res.* **93,** 13,208, 1988, with the permission of the American Geophysical Union. Reprinted from Carrigan, 1994.]

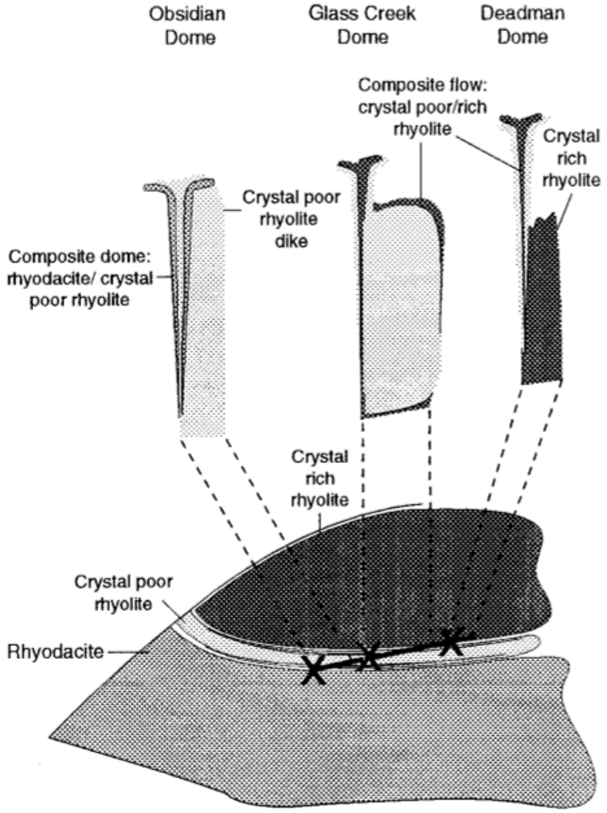
Obsidian Dome
Glass Creek Dome
Deadman Dome
Composite flow: crystal poor/rich rhyolite
Crystal rich rhyolite
Crystal poor rhyolite dike
Composite dome: rhyodacite/ crystal poor rhyolite
Crystal rich rhyolite
Crystal poor rhyolite
Rhyodacite

FIGURE 13 Using an encapsulation model for two-component magma transport, a multicomponent transport model is described for the contemporaneous formation of three 600-yr-old composite lava flows in the Inyo volcanic chain. If a breach in the magma chamber roof is initiated over the crystal-rich rhyolite, the high viscosity would tend to prevent this magma from reaching the surface. As the breach progresses down slope, it crosses into a zone of lower viscosity, crystal-poor rhyolite. This magma lubricates the rise of the higher viscosity, crystal-rich component and results in the composite Deadman Dome lava flow (X's indicate points over which lava flows have formed). The continued breaching of the roof causes the composite dike to finally "bud" a conduit that reaches the surface to form the Glass Creek Dome having a similar composition to Deadman Dome. The breach continues its descent across the crystal-poor rhyolite zone and produces a rhyolite dike that does not reach the surface. A rhyodacitic layer is finally sampled by the dike as it crosses a compositional boundary and provides lubrication for the rhyolite to erupt to the surface to form Obsidian Dome as the magma chamber pressure wanes. [Reprinted from Carrigan, 1994.]

sustained period of increased pressure in the chamber. The formation of a common dike may have started by a breach in that portion of the roof in contact with a layer of coarse, crystal-rich, high-silica rhyolite. Owing to its very high viscosity, the magma does not allow a dike to reach the surface. At the same time, the dike also propagates horizontally, breaching the chamber roof along the line indicated in Fig. 13. This horizontal breaching continues until the lower silica and crystal content rhyolitic layer begins to be withdrawn in addition. Because of its lower viscosity, this magma encapsulates the crystal-rich rhyolite, successfully lubricating its rise to the surface to form the composite Deadman Dome lava flow by the simultaneous venting of both crystal-rich and crystal-poor lavas. Elevated pressures in the magma chamber continue to cause breaching of the chamber roof along the line. Because of the nearness of the dike to both the crystal-poor and crystal-rich rhyolite magma layers, both magmas are withdrawn simultaneously and encapsulate to form a composite dike that once again reaches the surface to form the composite Glass Creek Dome consisting of the same types of magmas as Deadman Dome. Continuation of the breach moves it into the zone of crystal-poor rhyolite away from the zone of crystal-rich rhyolite so that the dike now consists of a uniformly crystal-poor rhyolite. This is in agreement with the cores obtained from drilling the dike near Obsidian Dome. Finally, the breach in the roof approaches and begins to draw the contents from the less viscous rhyodacitic zone. Lubrication of the crystal-poor rhyolite by the rhyodacite results in the budding of a conduit to form the Obsidian Dome flow.

VI. CONCLUSIONS AND IMPLICATIONS FOR VOLCANISM

We find that basaltic models of dike flow that include deviation from laminar or unmixed flow produce higher temperatures at the dike walls than laminar models and support the notion that dikes of meter thickness or less can remain viable pathways over lengths of kilometers and do not need to solidify. If magma flow in a 1-m-thick dike is constrained to be laminar, our models suggest that solidification should begin on the sidewalls within several kilometers of the inlet. We also find that the heating of basaltic magma by viscous dissipation could offset the total rate of heat loss from the dike, but boundary temperatures would still continue to fall, leading to solidification along the walls.

Even though the Reynolds number may be too small for turbulence to occur in many cases, laminarity is likely to represent an unlikely state for magmatic flow since several mechanisms encourage both mixing and cross-stream heat transfer in dikes. From our models, we found gas-bubble-augmented flow to be very effective in producing a near isothermal regime in basalts. While still significant, it is less effective in causing cross-stream flow in andesitic magmas owing to the high melt-phase viscosity. Gases present in magma are also likely to be important for fracture propagation during the initial emplacement of the dike. Computer simulations show that the thermal boundary layers are sufficiently thin (typically 0.1 m) that disruption and local mixing should be expected as a result of boundary roughness.

An understanding of how more viscous, silicic magmas propagate distances of kilometers presents a challenge. Viscous heating can offset heat loss for bulk magma velocities in the range of 0.2–0.3 m/s. Boundary temperatures level out and become more or less constant whether or not lateral mixing occurs. Viscous heating near the wall is evidently sufficient to offset heat losses without requiring heat to be transported from the core flow. However, driving pressure gradients for these flows exceed lithostatic values. Increasing the dike width does have a strong effect on decreasing the pressure gradient required to drive a given mass flux. But, how do silicic dikes propagate significant distances before their width has achieved its maximum value? The required pressure gradients seem too high for the amount of crustal penetration achieved. A crystal-rich rhyolitic magma flowing in a 10-m-wide dike requires a very large driving pressure gradient of 21 MPa/km. If encapsulation of crystal-rich rhyolite occurs by a crystal-poor rhyolite, as evidently happened in the feeder of the Deadman volcanic dome, the driving pressure gradient can be reduced to a mere 0.18 MPa/km. It is possible that extraordinarily viscous magmas often reach Earth's surface successfully only because of lubrication by a lower viscosity component, which substantially decreases the required driving pressure gradient.

SEE ALSO THE FOLLOWING ARTICLES

Geothermal Systems • Lava Domes and Coulees • Magma Ascent at Shallow Levels • Magma Chambers • Rates of Magma Ascent • Volcano Warnings

FURTHER READING

Carrigan, C. R., and Eichelberger, J. C. (1990). Zoning of magmas by viscosity in volcanic conduits. *Nature* **343,** 248–251.

Eichelberger, J. C., Carrigan, C. R., Westrich, H. R., and Price, R. H. (1986). Non-explosive silicic volcanism. *Nature* **323,** 598–602.

Fujii, N., and Uyeda, S. (1974). Thermal instabilities during flow of magma in volcanic conduits. *J. Geophys. Res.* **79,** 3367–3370.

Minagawa, N., and White, J. L. (1975). Co-extrusion of unfilled and TiO_2-filled polyethylene: Influence of viscosity and die cross-section on interface shape. *Polymer Eng. Sci.* **15,** 825–830.

Murase, T., and McBirney, A. R. (1973). Properties of some common igneous rocks and their melts at high temperatures. *Geol. Soc. Am. Bull.* **84,** 3536–3592.

Ryan, M. P., Koyanagi, R. Y., and Fiske, R. S. (1981). Modeling the three dimensional structure of macroscopic magma transport systems: Application to Kilauea Volcano, Hawaii. *J. Geophys. Res.* **86,** 7111–7129.

Sharp, A. D. L., Davis, P. M., and Gray, F. (1980). A low velocity zone beneath Mt. Etna and magma storage. *Nature* **287,** 587–591.

Shaw, H. R. (1980). The fracture mechanisms from the mantle to the surface. Pages 201–264 *in* "Physics of Magmatic Processes" (R. B. Hargraves, ed.). Princeton University Press, Princeton, NJ.

Shaw, H. R., Peck, D. L. Wright, T. L., and Okamura, R. (1968). The viscosity of basaltic magma: An analysis of field measurements in Makaopuhi lava lake, Hawaii. *Am. J. Sci.* **266,** 225–264.

Stockman, H. W., Stockman, C. T., and Carrigan, C. R. (1990). Modelling viscous segregation in immiscible fluids using lattice-gas automata. *Nature* **348,** 523–525.

Yoder, H. S. (1976). "Generation of Basaltic Magma." National Academy of Sciences, Washington, DC.

This Page Intentionally Left Blank

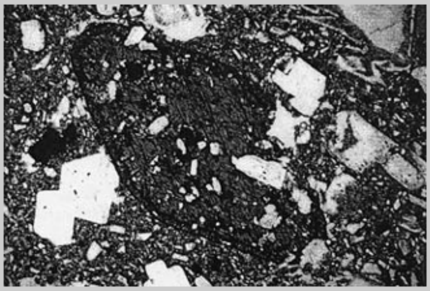

MAGMA ASCENT AT SHALLOW LEVELS

Claude Jaupart
Institut de Physique du Globe

I. Introduction
II. Magma Ascent and Decompression
III. Flow Dynamics
IV. Mass Discharge Rate and Ascent Velocity
V. Conclusions

GLOSSARY

annular flow One of four two-phase flow regimes, in which magma lines the conduit walls and gas flows in a central jet.

bubbly flow One of four two-phase flow regimes, in which the gas phase appears as bubbles suspended in a continuous magma phase.

degassing The process by which magma loses its dissolved volatile species as pressure decreases.

dispersed flow One of four two-phase flow regimes, in which magma takes the form of fragments in a continuous gas phase.

fragmentation Process by which bubbly magma breaks up, generating magma fragments and a continuous gas phase.

laminar flow Flow regime where viscous effects dominate and flow trajectories are parallel to the conduit walls.

Reynolds number Dimensionless parameter that defines the relative importances of viscous and inertial forces during flow.

slug flow One of four two-phase flow regimes, in which large gas pockets, which are almost as large as the eruption conduit, rise through magma.

turbulent flow Flow regime where inertial effects dominate, such that the flow is well mixed by small-scale eddies.

volatiles Chemical species or compounds that are dissolved in natural magmas at high pressure and that appear as low-density gas at low pressures. The most common ones are water and carbon dioxide.

I. INTRODUCTION

Magma spends time in the Earth's crust before erupting at the surface. In this chapter, we investigate how it evolves during ascent, what determines its flow conditions, and what sets the state and physical properties of the erupted mixture. We emphasize that the fate of an eruption is very sensitive to the last stages of ascent, at shallow levels in the Earth's crust. Our knowledge of eruptions is based primarily on surface observations and our ultimate goal is to relate eruption characteristics to processes that occur in the volcanic conduit at depth. Many different parameters must be known to predict accurately the fate of surface and atmospheric volcanic

Copyright © 2000 by Academic Press
All rights of reproduction in any form reserved.

flows. For example, eruptions may last for long periods and may alternate between different regimes or types of behavior. In a common sequence, an eruption may start as a Plinian event, such that the erupted material rises to great height above the vent and is dispersed by high-altitude winds, but the eruption then switches to a pyroclastic flow phase, such that the eruption column collapses and generates dense flows cascading down the volcano's slopes. Specifying which behavior prevails requires knowledge of the eruption velocity, the mass fraction of gas at the vent, the vent dimensions, and the size of magma fragments. Another example is that an explosive eruption expels huge amounts of ash, pumice, and gases into the atmosphere with dangerous consequences to the environment and to the climate. To follow the dispersal of such products, one must know their size and this is determined in part by processes acting in the volcanic conduit.

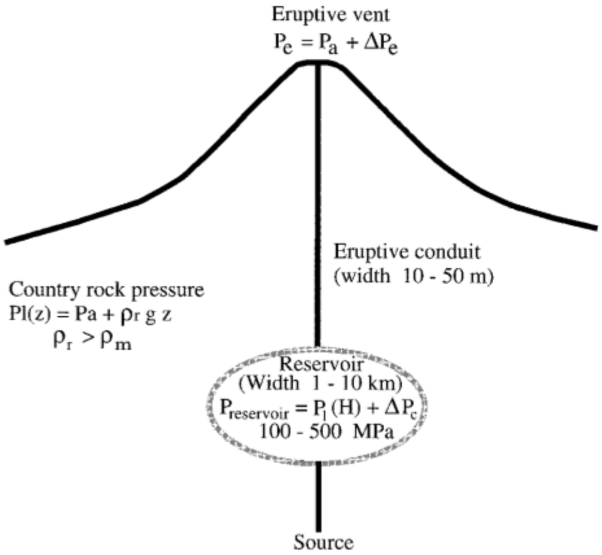

FIGURE 1 Schematic diagram showing the major components of a volcanic plumbing system. A magma at depth *H* in the Earth's crust reservoir empties into a thin eruption conduit. The reservoir pressure, $P_{reservoir}$, is equal to the "equilibrium" pressure due to the weight of country rock, $P_l(H)$, which is $\rho_r g H$, plus an overpressure ΔP_c, which varies with time as a function of the input/output magma budget. The volcanic plumbing system feeds an eruption with an exit pressure that may not be equal to the atmospheric value. Parameter ρ_r is the crustal rock density, ρ_m is the magma density, P_a is the atmospheric pressure, P_e is the vent pressure, and ΔP_e is excess vent pressure.

II. MAGMA ASCENT AND DECOMPRESSION

We start our journey in a reservoir or magma chamber, which is typically located several kilometers below the Earth's surface (Fig. 1). This depth may be greater than 15 km in a few cases, but usually does not exceed 10 km. As magma rises from depth, it undergoes a large pressure decrease. At a 10-km depth, for example, pressures are about 300 megapascals (MPa), or 3000 times the atmospheric pressure. Such a large pressure change has many consequences for the physical properties and flow of magma.

A. Magma Composition and Volatile Content

At high pressure, magma contains volatile species in solution, the most abundant being water (H_2O) and carbon dioxide (CO_2). Magma is generated from a deep source, usually located below Earth's crust. The source material is an assemblage of different mineral phases that may contain various amounts of volatiles and is only partially molten. The primitive magma composition is thus a function of source composition and of the degree of partial melting. As this magma rises and collects into a shallow reservoir, it may melt country rock and may mix with other magmas stored in the plumbing system. Further, in a reservoir, it cools and crystallizes, which induces further chemical modifications. The final magma that becomes involved in an eruption is therefore the end result of a long sequence of events. Its composition and volatile content cannot be predicted from first principles and must be determined in each case.

Solubility dictates how much of a given chemical species can be dissolved in a liquid under given conditions. For each volatile species, solubility is a function of magma composition, temperature, and pressure. Temperature and composition are linked in nature as most magmas are near their liquidus (the point at which they start to crystallize), and hence it is simpler to think of solubility as a function of composition and pressure only. For a given composition, therefore, one may think in terms of pressure only. Under most circumstances, magmas are undersaturated in volatiles as they begin their ascent toward Earth's surface. During their rise, they reach the saturation threshold, such that the initial volatile content is equal to the solubility limit. As pressure decreases below this threshold, magma becomes supersaturated, volatile species can no longer stay in solution, and they start forming a separate phase as bubbles. As pressure decreases further, an increasing mass fraction of volatiles exsolves and the gas phase expands. The solubility of volatile species can be given by the so-called Henry's law, which expresses concentration as a function of pressure. This simple form of the solubility law is not valid at large pressures but is a good approximation at pressures less than 200 MPa. For water in rhyolite magma, one has (Fig. 2):

$$C_g(P_g) = K_H \sqrt{P_g},$$

where C_g is the concentration of water in the magma, P_g is the pressure, and K_H is a constant. We can see from Fig. 2 that more than 5 wt% water can be dissolved in silicic magmas at typical crustal depths. One important fact is that, for this form of the solubility law, the exsolution rate is largest at small pressures and, hence, at shallow levels.

As pressure decreases, the magma loses its volatile constituents, which acts to increase its liquidus temperature. The effect is far from negligible and may in some cases amount to as much as 100 K for every percent of water. This has far-reaching consequences for magma. As a magma parcel degasses, it finds itself undercooled by significant amounts, which promotes crystallization. Under such conditions, the nucleation rate is large but the crystals have little time to grow. This results in a large density of very small crystals, referred to as *microlites* or *nanolites*. They act to change the magma properties and, in particular, may increase the viscosity significantly.

How gas pressure evolves during magma ascent dictates further volatile exsolution and phase relationships in the melt. At any level in the conduit, gas pressure is in general equal to neither the flow pressure (or bulk pressure) nor the surrounding rock pressure. Three different pressures are therefore involved. Gas bubbles grow in size because they contain an increasing mass of volatiles by diffusion from the melt and because gas expands as pressure decreases. Such a volume change is achieved by deforming the liquid around the bubble and is driven by a pressure difference between gas and liquid. In other words, gas is overpressured with respect to the liquid. At the Earth's surface, this overpressure may be responsible for catastrophic expansion of lava, that is, an explosive event. The flow pressure is in general not equal to the country rock pressure, because it is determined by the starting pressure (the chamber pressure) and the head loss due to flow. A typical circumstance is that the flow is overpressured with respect to country rock, and this may lead to fracturing of country rock. In the field, researchers often see dykes, or thin magma-filled fractures, radiating outward from a central conduit. The opposite situation can also occur, and the conduit may "cave in," with dramatic consequences to the eruption.

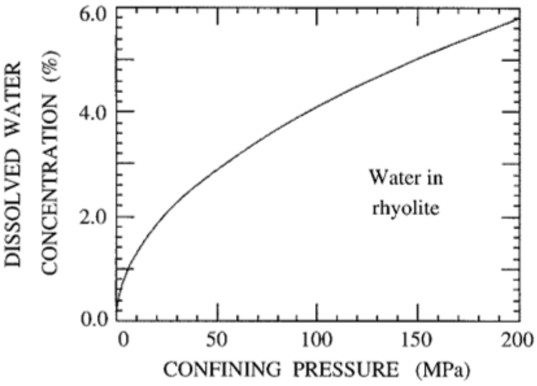

FIGURE 2 Solubility of water in a rhyolitic magma as a function of pressure.

B. Gas Budget of an Eruption

For a given amount of magma, we can estimate the amount of gas that erupts simultaneously using solubility laws, initial volatile content, and assuming closed-system conditions, that is, that the gas and melt phases do not separate. This procedure may not give the correct answer because of three different effects. One is that equilibrium thermodynamics may not apply for large decompression rates: Exsolution and gas expansion are sensitive to the kinetics of bubble growth. Another factor is that the gas may have a significant velocity with respect to the liquid phase. A third factor is that gas may be added to or subtracted from magma. We have just seen that pressures in the flow and in country rock may not be equal to one another. If the flow pressure is larger than the country rock pressure, gas may be driven out of the conduit. Thus, an initially volatile-rich magma may end up as gas-poor lava at the surface. If pressures are smaller in the flow than in the surroundings, groundwater may be siphoned out of country rock into the rising magma.

C. Decompression and Degassing

With falling pressure, gas starts to exsolve and collect into individual bubbles. Two independent processes are involved: bubble nucleation and growth. Studies of these processes have progressed rapidly in recent years and it has been shown that, in most circumstances, degassing may be approximated by conditions of local thermodynamic equilibrium between the gas phase and the bulk liquid. Departures from such local equilibrium conditions are achieved at large eruption velocities. For our present purposes, it is sufficient to consider equilibrium relations. At any pressure P_g smaller than the saturation threshold, the local concentration of volatiles in the magma is equal to C_g, which is less than the initial concentration C_i. In a closed system, the difference between the two concentrations is taken up by the gas phase. The mass fraction of gas in the mixture, x_g, is approximately equal to

$$x_g = \frac{m_g}{m_T} \approx C_i - C_g,$$

where m_g is the mass of gas in a parcel of total mass m_T. This approximation is only valid if volatile concentrations are much smaller than 1, which is also required for Henry's law. If the system is not closed, but open to gas escape, the mass fraction of gas is smaller than this value. In a limit case, the mixture may lose all of its gas, and the mass fraction of gas is kept at zero throughout ascent. The density of the magma/gas mixture, ρ, is calculated as follows:

$$\frac{1}{\rho} = \frac{x_g}{\rho_g} + \frac{1 - x_g}{\rho_m}$$

where ρ_g and ρ_m are the densities of the gas and magma, respectively. At crustal pressures, a reasonable approximation for the equation of state of water is the ideal gas law:

$$\rho_g = \frac{M P_g}{GT}$$

where M is the molar mass, G the perfect gas constant, and T temperature. The volcanic mixture expands rapidly, such that gas eventually becomes the dominant phase by volume. Figure 3 shows how the gas volume fraction evolves for two different, but rather small, initial water concentrations. Even in those cases, gas takes up more than 80% of the mixture by the time it leaves the vent. Many magmas have higher volatile contents, and hence lead to erupted mixtures with as much as 98% gas by volume.

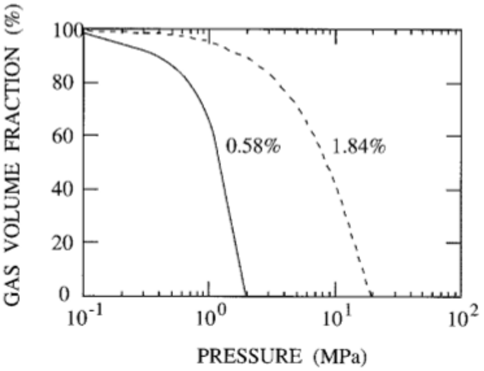

FIGURE 3 Volume fraction of gas for a magma parcel with given initial water concentration, as a function of pressure. Two different initial water concentrations are shown: 0.58%, corresponding to a saturation pressure of 2 MPa, and 1.84%, corresponding to a saturation pressure of 20 MPa. Note that in both cases the gas phase dominates over the melt phase in terms of volume.

III. FLOW DYNAMICS

How magma deforms is critical for understanding which flow velocities are reached for given pressure conditions in the plumbing system. At high temperatures, magma behaves as a Newtonian fluid, with the shear rate (the gradient of velocity) being directly proportional to the applied stress. Flow behavior is described by a single parameter, viscosity, noted as μ. However, the magma that rises in the conduit is more complicated because it is made of melt, gas, and possibly some suspended crystals. Crystals act to increase viscosity and, if they take up a sufficiently large fraction, change the flow behavior. At very large values of velocity, magma is deformed rapidly, so rapidly in fact that it may not respond viscously. In this case, magma behaves as brittle material and breaks into pieces. The viscosities of natural magmas vary within a very large range. The most fluid magmas are probably carbonatites, with viscosities of about 0.5 pascal seconds (Pa s; 500 times the viscosity of water). This general end of the viscosity range also encompasses one of the most common magma types: basalts. At the other end of the viscosity range, we find dry high-silica rhyolites, whose viscosities may exceed 10^{12} Pa s. Such an extraordinary variation of physical properties has fundamental consequences for the movement and eruption of magma. Silicic lavas such as rhyolites and dacites are much more viscous than basalts. One important feature of magmas is that their viscosity varies dramatically with decreasing dissolved water concentration (Fig. 4). The rate of change of magma viscosity with falling pressure is largest at small water contents and, hence, at shallow levels.

A. Two-Phase Flow Regimes

Close to the Earth's surface, the ascending magma is a mixture of gas and liquid. How such a mixture flows

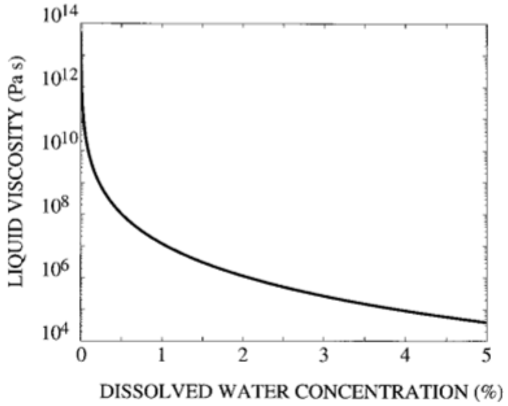

FIGURE 4 Viscosity of silicic melt as a function of dissolved water concentration. [Adapted from Hess and Dingwell, 1996.]

depends on the relations between the gas and liquid phases (Fig. 5). At small values of gas volume fraction, gas is contained in individual bubbles carried by the liquid, which corresponds to the *bubbly flow* regime. In this regime, the bulk behavior of the magma/bubble mixture depends on whether or not bubbles deform. At small velocity (small shear rate), surface tension keeps gas bubbles spherical. This impedes flow because shear gets focused in thin liquid regions between neighboring bubbles. At larger velocity (large shear rate), bubbles are elongated, which acts to lubricate the flow.

At larger values of gas volume fraction, individual bubbles may coalesce and generate large gas pockets, and the flow is in the *slug* or *intermittent* regime (Fig. 5). At still larger values of the gas volume fraction, the gas pockets extend over most of the conduit and the flow is best described as a central gas core with a thick film of liquid lining the conduit walls. In the fourth regime, called *dispersed*, magma is in the form of small fragments carried within a continuous phase. This regime may be achieved in two different manners, depending on magma viscosity. In viscous silicic melts such as rhyolites or dacites, bubbles cannot move through magma and the *slug* and *annular* regimes are not possible. With decompression, a magmatic foam develops and becomes unstable near the surface. At this stage, bubbles burst, pulverizing magma into droplets. This has been called *fragmentation* and may involve several mechanisms, which are outside the scope of this chapter. For our present purposes, what matters is that the magma/gas mixture changes from a continuous liquid phase into a continuous gas phase. In low-viscosity basaltic melts, bubbles can migrate within magma and the flow is expected to go through the slug and annular flow regimes. With increasing decompression, the central gas jet becomes increasingly more powerful and eventually blows the film of magma lining the conduit walls. The end result is the same dispersed regime.

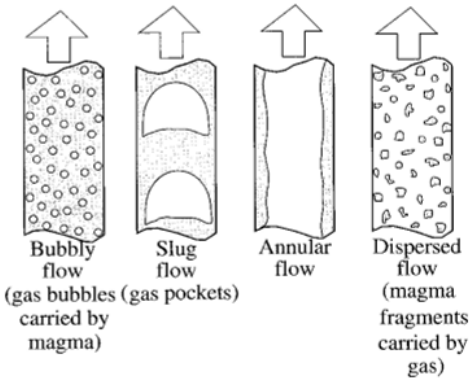
Bubbly flow (gas bubbles carried by magma)
Slug flow (gas pockets)
Annular flow
Dispersed flow (magma fragments carried by gas)

FIGURE 5 The four major types of flow regimes predicted for a mixture of gas and liquid. These four types of behavior can be observed in natural eruptions.

We can recognize the four different regimes in natural eruptions. Vesicular lava oozing out of a vent in an effusive eruption gives an example of the bubbly flow regime. This regime may be observed in all settings, regardless of magma composition and viscosity. "Strombolian" activity is characterized by the bursting of large gas pockets at the top of a magma-filled conduit and corresponds to the intermittent regime. Annular flow seems much less common and may be associated with fire fountaining, where "curtains of lava" are ejected out of basaltic vents. Strombolian activity and fire fountaining are restricted to low-viscosity magmas such as basalts. The dispersed regime is very common and corresponds to the Plinian and pyroclastic flow eruptions. These two eruption types are most common in silicic volcanoes but have also been achieved in basaltic ones. Fire fountaining may also be an example of this behavior.

C. Bulk Flow Conditions

It is convenient to think of flow in terms of a balance between different forces. In most cases of volcanological interest, we can neglect the motion of gas bubbles and it is sufficient to treat the ascending mixture as a material whose physical properties depend solely on gas content. For a given driving pressure, flow develops against the weight of the magma/gas mixture and the inertial and viscous stresses. If viscous forces dominate, flow is in a laminar regime, with flow trajectories parallel to the conduit walls. If, on the other hand, inertial forces are more important, flow is in a turbulent regime, such that it is well mixed by energetic eddies. These two regimes differ strongly in their dynamics and velocity profiles and can be defined using a single dimensionless number called the Reynolds number:

$$\mathrm{Re} = \frac{\rho W R}{\mu},$$

where W is a typical value for the velocity, R the conduit radius, ρ is the flow density, and μ the mixture viscosity. Below a threshold value of about 100, flow is laminar and the radial velocity profile is parabolic with a maximum at the conduit axis (noted W_M). The mass discharge rate is calculated to be

$$Q = \frac{\pi}{2}\rho W_M R^2.$$

In steady state, mass flux Q must remain constant and independent of height in the conduit. Thus, if the conduit radius does not vary by large amounts, quantity (ρW_M) is constant. Volatile exsolution and gas expansion lead to a large reduction of density and hence to a very large increase of velocity (up to 100-fold). Thus, for magma rising through a conduit, density and velocity change by significant amounts due to volatile exsolution and gas expansion, but such changes counterbalance one another and the Reynolds number only varies as a function of viscosity. In general, mass discharge rates seldom exceed 10^8 kg s^{-1} and conduit radii are typically in a range of 10–100 m. For typical silicic magma viscosities (larger than 10^6 Pa s), the Reynolds number is less than 10. This reasoning is only valid insofar as the relevant viscosity is that of magma. This is true for the bubbly flow regime, but not for the other regimes. In the dispersed regime, the mixture is made of gas and fragments. In this case, the relevant viscosity drops to very small values, less than 10^{-3} Pa s, and the Reynolds number jumps to very large values. We must therefore envision a volcanic conduit as being separated in two sections where the flow dynamics are totally different: a lower part where flow is laminar and an upper part with turbulent conditions (Fig. 6). For magma parcels rising through the conduit, the consequences are important. In the lower part, parcels that rise through the conduit center are subjected to large decompression rates, whereas parcels rising near the walls experience very small decompression rates. Degassing kinetics may therefore be markedly different. In the upper and turbulent part of the flow, however, we can treat the rising mixture as well mixed.

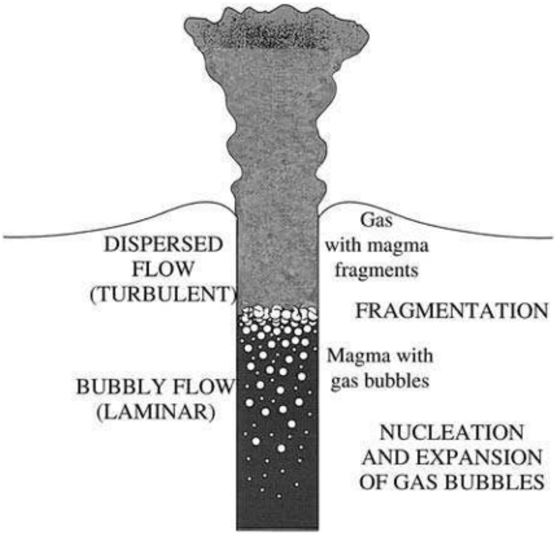

FIGURE 6 Diagram showing the main phases of magma ascent at shallow levels, such that the magmatic gas phase plays a key role.

IV. MASS DISCHARGE RATE AND ASCENT VELOCITY

We have so far treated a flow with prescribed characteristics. The next step is to predict those characteristics using fluid mechanical models. Many such models have been used by volcanologists to investigate different eruption types, but they can only be considered exercises because they require many inputs that remain poorly known. We can regard a volcanic system as a conduit with specified pressures at the two ends. The two critical inputs are the conduit dimensions and mixture rheology. To solve for the flow conditions, we use classical equations for the conservation of mass, momentum, and energy. In an eruption, the mass discharge rate rarely stays constant and we might frequently observe a sequence of increasing mass discharge rate followed by a waning phase, which eventually leads to the cessation of activity. We might also witness fluctuations of mass discharge rate. Such changes may be due to changes of driving pressure, magma composition, or conduit size.

A. Driving Pressure

The driving pressure difference can be calculated simply for a volatile-free magma, such that the magma density, ρ_m, remains constant over the whole conduit height.

Consider a magma column extending from a reservoir located at depth H to the vent. At the vent, the exit pressure may not be equal to the atmospheric pressure P_a, either because the flow has reached sonic velocities (see later discussion) or because a lava flow has built up over the vent. The pressure difference between the top and bottom of the magma column is

$$\Delta P_1 = \rho_m g H + \Delta P_e,$$

where ΔP_e is the vent overpressure (Fig. 1). For a lava flow, the vent overpressure is due to the weight of overlying lava, and is $\Delta P_e = \rho_m g h$ for lava thickness h. The pressure difference across the magma column is then

$$\Delta P_1 = \rho_m g (H + h).$$

This can be compared to the pressure difference between the surface and the top of the magma reservoir:

$$\Delta P_2 = \rho_r g H + \Delta P_c.$$

This pressure is equal to the lithostatic pressure, that is, due to the weight of the overburden, plus a pressure differential ΔP_c due to the fact that country rock may deform. The driving pressure is $\Delta P = \Delta P_2 - \Delta P_1$. If it is zero, the magma column is in static equilibrium and there is no flow. In the lava flow case,

$$\Delta P = (\rho_r - \rho_m) g H + \Delta P_c - \rho_m g h.$$

This shows three terms. The first represents magma buoyancy, showing that magma is driven upward if it is less dense than country rock. The two other terms may vary with time and hence may be held responsible for variations of mass discharge rate. The chamber overpressure, ΔP_c, changes as a function of input of magma from depth and output into the eruptive conduit. If the output exceeds the input, the overpressure diminishes, and the mass discharge rate decreases. In the opposite case, the chamber may become increasingly overpressured. The last term on the right-hand side is the weight of lava over the vent, which depends on the dynamics of lava flow at the surface. If a thick lava flow develops, this term may become significant and may even lead to the cessation of activity. One striking example is that of Montagne Pelée in 1902, which grew a tall spine exceeding 300 m in height after its climatic eruption.

B. Conduit Geometry

The conduit is a critical component that, for obvious reasons, is difficult to observe over the whole distance between reservoir and vent. Its walls are not straight and smooth and its shape is poorly known. The conduit may not remain the same during a single eruption. For example, if the flow is very energetic, it may be enlarged by erosion or reduced by foundering of the walls. In a slow eruption, it may be choked by the chilling of magma against the walls. It is therefore difficult to predict *a priori* the value of mass discharge rate. Basaltic eruptions may occur out of fissures, several hundred meters long and a few meters wide. For silicic magmas, direct observations during an ongoing eruption are seldom possible but we might observe fossil conduits in a variety of geologic settings with widths of 10–100 m. At Mount St. Helens, following an explosive event that left the vent free of lava, it was possible to measure a conduit radius of about 30 m. Toward the surface, volcanic conduits seem to flare upward. Observations of fossil conduit walls show that they are fractured and have highly irregular outlines. The fractures may contain ash and pyroclasts, showing that the ascending material has leaked into the country rock. Gas escaping from the conduit feeds the ubiquitous fumaroles found on volcanic slopes and craters.

C. Flow Rate

In laminar flow conditions, the horizontal profile of ascent velocity is parabolic (the “Poiseuille” profile) starting from zero at the walls and reaching a maximum at the conduit axis. Assuming that the conduit has a circular cross section with radius R, the mass flux at some arbitrary height z in the conduit is

$$Q = \frac{\pi R^4}{8\mu}\left[-\frac{dP}{dz} - \rho g\right]$$

where $dP;dz$ is the vertical pressure gradient. Assuming that the mixture viscosity and density are constant over the whole conduit, and equal to the values for pure magma, we obtain

$$Q = \rho_m \frac{\pi R^4}{8\mu}\frac{\Delta P}{H} = \rho_m \frac{\pi R^4}{8\mu}\left[(\rho_r - \rho_m) g + \frac{\Delta P_c - \rho_m g h}{H}\right]$$

where we find the driving pressure ΔP calculated earlier. This shows that the mass flux is highly sensitive to the conduit radius. It also shows that, for given pressure conditions and conduit dimensions, the mass flux is inversely proportional to magma viscosity. This explains why basaltic lavas are in general erupted at higher velocities than silicic lavas. This equation also shows how pressure conditions affect the flow rate, but is in general inadequate because of viscosity and density changes. In this case, the “local” equation at height z still holds,

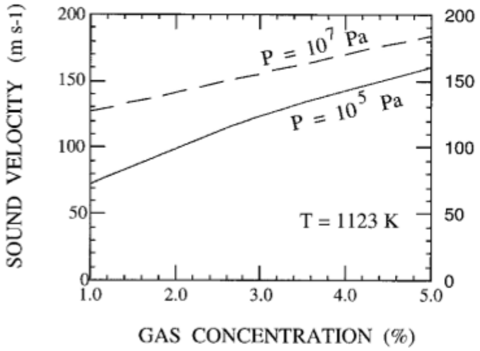

FIGURE 7 Sound velocity in a mixture of gaseous water and magma, as a function of water content. Two curves are shown for two different values of pressure.

however, and may be rewritten as an equation for the pressure gradient:

$$-\frac{dP}{dz} = Q\,\frac{8\mu}{\pi\,\rho\,R^4} + \rho\,g$$

This shows that the pressure gradient is the sum of the head loss due to viscous stresses and the weight of the magma. This also shows that an increase of viscosity implies an increase of pressure gradient. Conversely, an increase of radius implies a decrease of pressure gradient.

At large Reynolds number, the dynamics are different and the ascent velocity is almost constant in a horizontal cross section. The eruption velocity tends toward that of sound waves propagating through the mixture:

$$W_S = \left[\frac{d\rho}{dP}\right]^{-1/2}$$

The values of this threshold velocity are given in Fig. 7. In a straight conduit, this is the maximum velocity that can be achieved, which corresponds to *choking*, a self-explanatory term. Many volcanic eruptions contain sufficient amounts of gas to be in such conditions, with two important consequences. One is that the exit velocity is independent of magma viscosity and, for all practical purposes, independent of magma composition and conduit dimensions. The second consequence is that the flow does not exit the vent at atmospheric pressure and expands dramatically above it. In this regime, the mass discharge rate is given by

$$Q = \pi\,R^2\,\rho\,W_S,$$

which differs from the laminar flow equation given earlier in two important ways. One is that the mass discharge rate is much less sensitive to the conduit dimensions than in laminar conditions and the other is that it is independent of magma viscosity. Thus, the mass discharge rate varies within a restricted range.

D. Model of Magma Ascent with Degassing

We can solve the equations of motion from the reservoir to the surface including the effects of a major rheological change at fragmentation, when the rising mixture changes from a bubbly liquid to a gas carrying suspended magma fragments. In this calculation, the *closed-system* approximation is used, such that the exsolved gas does not escape to the country rock, and the viscosity of the magmatic phase varies as a function of dissolved water content as illustrated in Fig. 4. Here, for the sake of example, fragmentation is taken to occur at some threshold value of the gas volume fraction (70%). The evolution of flow pressure in the conduit is characterized by three distinct regions (Fig. 8). From the base of the conduit to the saturation pressure, when exsolution begins, the flow pressure decreases linearly due to both the weight of the magma and viscous shear. Between the exsolution and fragmentation levels, pressure decreases rapidly, due to the large increase of magma viscosity. Above the fragmentation level, friction is much smaller than before because the ascending mixture is basically a gas, implying that pressure decreases at a reduced rate. Figure 8 illustrates that magma ascent involves marked changes of physical properties and flow regime. It also indicates that flow pressures are in general not equal to pressures in the surroundings. Toward the surface, the flow pressures are predicted to be significantly smaller than those in country rock. This is due to two factors. One is that the density of the gas/magma mixture is very small, which implies a small head loss. The other

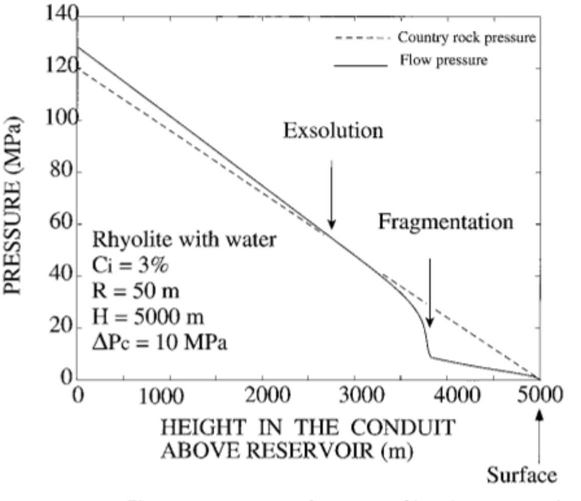

FIGURE 8 Flow pressure as a function of height in a conduit for rhyolitic melt. The dashed curve shows the pressure distribution in the country rock. [Adapted from Massol and Jaupart, 1999.]

is that fragmentation has occurred, implying a reduced wall friction. If we allow for extensive gas escape toward country rock, we might obtain a completely different solution. In a limiting case, the magma loses all of its gas to the surroundings and therefore flows almost as a pure liquid in laminar conditions. The end result is a flow pressure that remains above country rock pressures.

E. Postfragmentation Events

After fragmentation, the rising mixture is made of a continuous gas phase carrying magma fragments. At this stage, flow velocities are very large and magma fragments spend little time in the conduit before ejection into the atmosphere. However, several processes modify the structure of the flow prior to eruption at the surface. Magma fragments expand and probably burst, generating smaller fragments. Additionally, the fragments collide against one another and may break up. Thus, the size of fragments keeps on evolving. Fragment collisions and fragmentation are also held responsible for electrical charging effects and for the spectacular lightning effects commonly observed in volcanic atmospheric plumes. As the volcanic mixture rises toward the surface, it may lose some gas to fractured and permeable country rock. This key process is difficult to understand in detail because it involves many different ingredients: a continuous gas phase through the magma, gas wetting the conduit walls, permeable country rock, and horizontal pressure gradients. Such a variety makes it difficult to assess in each and every case. One key aspect is that its importance depends on the balance between ascent velocity and horizontal "leakage" velocity: A fast eruption leaves no time for large amounts of gas to escape.

V. CONCLUSIONS

As magma rises in a conduit, the gas and flow pressures are not equal to pressures in the surrounding rocks and must be calculated with a dynamic flow model. Such models are required to understand how volcanic eruptions may occur in different regimes, and how they may switch from one regime to the other. They also enable us to use surface observations to obtain constraints on the characteristics of the deep plumbing system. Finally, they help us unravel the various changes brought on magma near the surface. The models emphasize that the key phases of magma evolution occur at shallow levels: gas becomes very abundant at small pressures, implying large velocity changes. Gas leakage is also most significant near the surface because it is there that country rock fractures are numerous and open to flow. Although the models are based on sound physical principles, they suffer from two basic deficiencies. One is that the dimensions of the plumbing system are not known at depth, and the other is that the fragmentation process remains ill understood. Thus, present research is being oriented in two directions. One is to study fragmentation, which may be done in the laboratory and by comparing field data with theoretical predictions. Another direction is to use natural tracers to follow directly the ascent process. Pumice and ash samples, which are quenched fragments of vesicular magma, provide a record of degassing and expansion conditions that can be deciphered using dynamic models.

SEE ALSO THE FOLLOWING ARTICLES

Composition of Magmas • Hawaiian and Strombolian Eruptions • Magma Chambers • Magmatic Fragmentation • Plinian and Subplinian Eruptions • Pyroclastic Surges and Blasts • Rates of Magma Ascent • Volcanic Gases

FURTHER READING

Gilbert, J. S., and Sparks, R. S. J., eds. (1998). "The Physics of Explosive Volcanic Eruptions." Geological Society Special Publication No. 145, London.

Hess, K.-U., and Dingwell, D. B. (1996). Viscosities of hydrous leucogranitic melts: A non-Arrhenian model. *Am. Mineral.* **80,** 1297–1300.

Massol, H., and Jaupart, C. (1999). The generation of gas overpressure in volcanic eruptions. *Earth Planet. Sci. Lett.* **166,** 57–70.

Sparks, R. S. J., Bursik, M. I., Carey, S. N., Gilbert, J. S., Glaze, L. S., Sigurdsson, H., and Woods, A. W. (1997). "Volcanic Plumes." Wiley and Sons, New York.

Wilson, L., Sparks, R. S. J., and Walker, G. P. L. (1980). Explosive volcanic eruptions—IV. The control of magma properties and conduit geometry on eruption column behaviour. *Geophys. J. Roy. Astronom. Soc.* **63,** 117–148.

Woods, A. W. (1995). The dynamics of explosive volcanic eruptions. *Rev. Geophys.* **33,** 495–530.

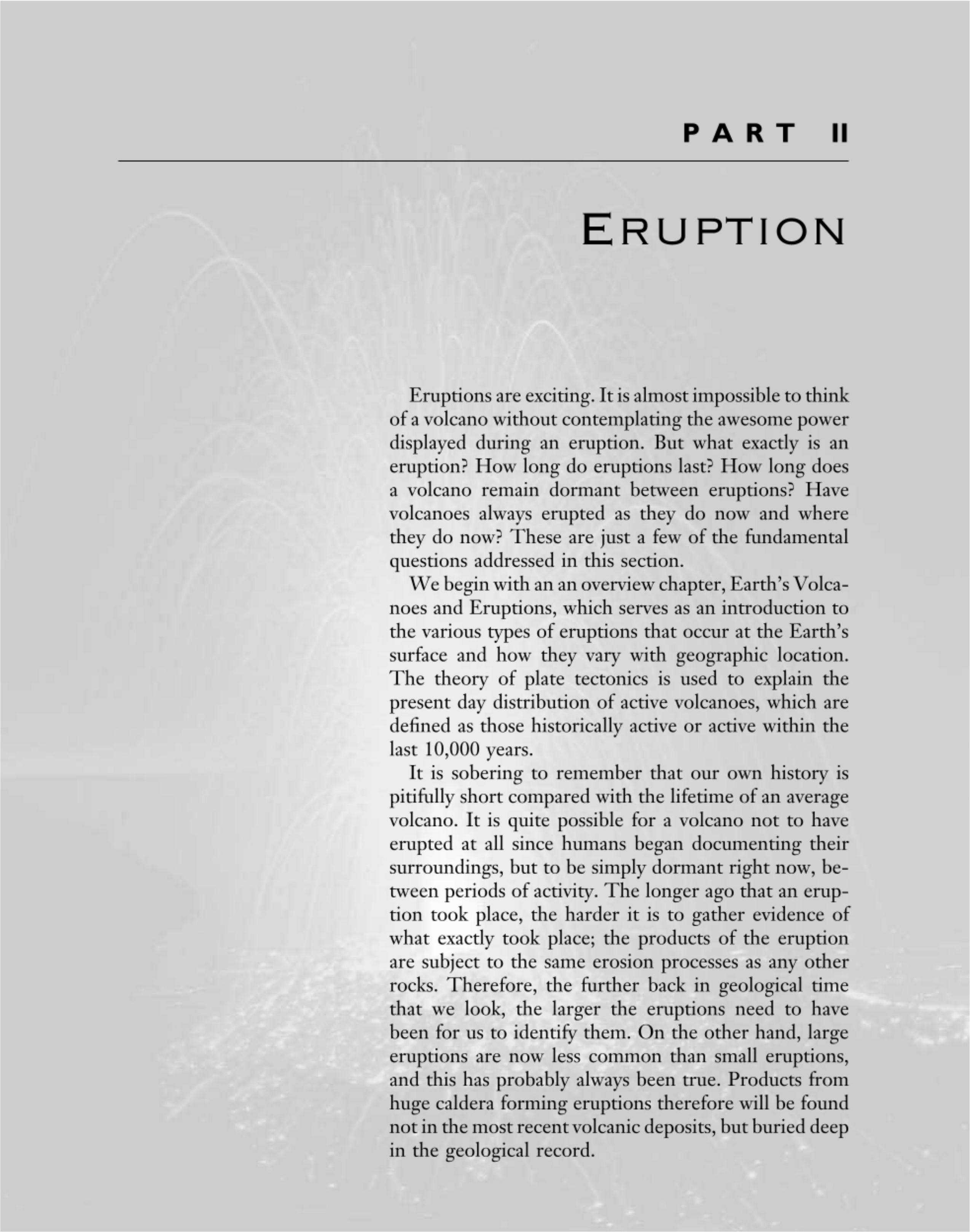

PART II

ERUPTION

Eruptions are exciting. It is almost impossible to think of a volcano without contemplating the awesome power displayed during an eruption. But what exactly is an eruption? How long do eruptions last? How long does a volcano remain dormant between eruptions? Have volcanoes always erupted as they do now and where they do now? These are just a few of the fundamental questions addressed in this section.

We begin with an an overview chapter, Earth's Volcanoes and Eruptions, which serves as an introduction to the various types of eruptions that occur at the Earth's surface and how they vary with geographic location. The theory of plate tectonics is used to explain the present day distribution of active volcanoes, which are defined as those historically active or active within the last 10,000 years.

It is sobering to remember that our own history is pitifully short compared with the lifetime of an average volcano. It is quite possible for a volcano not to have erupted at all since humans began documenting their surroundings, but to be simply dormant right now, between periods of activity. The longer ago that an eruption took place, the harder it is to gather evidence of what exactly took place; the products of the eruption are subject to the same erosion processes as any other rocks. Therefore, the further back in geological time that we look, the larger the eruptions need to have been for us to identify them. On the other hand, large eruptions are now less common than small eruptions, and this has probably always been true. Products from huge caldera forming eruptions therefore will be found not in the most recent volcanic deposits, but buried deep in the geological record.

Detailed analysis of all the available evidence from the last 10,000 years has led the authors to deduce the approximate frequency at which we can expect eruptions of various sizes. For example, small eruptions, such as that at Nevada del Ruiz in Colombia in 1985 killing 23,000 people, occur typically several times a year, although fortunately usually without such tragic consequences. The Mount St. Helens event of 1980 occurs on average once each decade. It is unclear, however, how frequent much larger eruptions are.

Almost as important as predicting the onset of volcanic activity, and certainly more difficult, is predicting when an eruption will cease. With a few notable exceptions, such as Stromboli in the Aeolian Sea offshore Italy, which has been erupting steadily for at least 2500 years, the average eruption duration is about 7 weeks. Some last for only a day and the longer the dormant period, the larger the final eruption.

Just as earthquakes can be defined using scales of magnitude and intensity, so can volcanic eruptions. Estimates of the magnitude and intensity of eruptions can be made for very large events millions of years ago using a comparison of the distribution and volume of erupted products (ash and lava) with those of smaller, recent events. In the chapter Sizes of Volcanic Eruptions, David Pyle defines eruption magnitude and intensity and illustrates the use of these properties for understanding the mechanisms driving the colossal eruptions of the past.

Finally in this section, Haraldur Sigurdsson addresses how the rate of volcanism has varied through geological time. Because there have been no really large caldera forming eruptions since humans have been on Earth, it might be inferred that such things will not occur in the future. However, we know that large eruptions occur less frequently than smaller eruptions. In the chapter Volcanic Episodes and Rates of Volcanism, Sigurdsson considers the last 65 million years of Earth history and puts into geological and geographical perspective the fluctuations in the magnitude and intensity of volcanism over this time. Evidence shows that there have been several episodes of increased volcanism worldwide in the past and a possible link with climate change. Whether climate change is a cause or an effect of variations in the rate of volcanism remains an intriguing question.

Hazel Rymer
The Open University

This Page Intentionally Left Blank

EARTH'S VOLCANOES AND ERUPTIONS: AN OVERVIEW

TOM SIMKIN
LEE SIEBERT
Smithsonian Institution

I. Introduction
II. Volcanoes
III. Eruptions

I. INTRODUCTION

Most volcanoes are slumbering, deceptive agents of change. They may offer benefits such as scenic beauty and geothermal energy, but they may also turn swiftly violent, causing tragic destruction and fatal consequences. Volcano lifetimes are long compared to ours, and most of those lifetimes are spent in repose. However, because our memories (and histories) tend to be short, volcanic violence too often takes us by surprise. In recent decades, though, we have seen major advances in understanding how volcanoes work. These have been spurred in part by dramatic natural events, such as the 1980 eruption and debris avalanche at Mount St. Helens, or the climatic impact of eruptions like Mexico's El Chichón (1982). But these advances also result from improvements in global communication, remote sensing, and interdisciplinary cooperation. In light of these advances, this chapter attempts to answer these questions: Where are the world's volcanoes? What do they do? How often do they do it?

Understanding the impact and hazards posed by volcanic activity requires information on the frequency, duration, magnitude, and rates of volcanism in both space and time. We will review what we have learned, with primary emphasis on the past few thousand years. This record is short, by geologic standards, but it is a rich and important source of information on all but the largest eruptions affecting our planet. It provides our best numerical basis for extrapolating the observations and measurements of contemporary eruptions to better understand those of both the past and the future. Our review draws on two Smithsonian resources: (a) our reporting of current volcanic activity around the world and (b) our computerized, retrospective database of historical and other dated volcanism during the past 10,000 years (Holocene time). The first began in 1968 as the Center for Short-Lived Phenomena, but was moved, reorganized, and renamed as the Scientific Event Alert Network (SEAN) in 1975. Further concentration on volcanology led to its being renamed the Global Volcanism Network (GVN) in 1990, and it continues today with a monthly *GVN Bulletin* and other outlets. The database began in 1971 and has grown steadily, through careful compilation of information from a multitude of sources, to cover more than 1500 volcanoes of the world and 8000 dated eruptions.

II. VOLCANOES

Most volcanoes are not majestic, symmetrically conical, snow-capped giants. They in fact range widely from small cinder cones to huge piles of lava, standing 10 km above the ocean floor. Some, like Yellowstone in the United States or New Zealand's Lake Taupo, do not even identify themselves by rising above the surrounding landscape. Volcanoes reflect the varied processes that shaped them, and with a wide range of plumbing systems, supply rates, magma types, and eruption styles, it is not surprising that a wide range of features results. Furthermore, volcanic processes include many that destroy and modify earlier constructions, adding to the variety of forms that fall under the name *volcano.*

A. Types

Volcanoes are born when subsurface magma, normally less dense than surrounding rock, rises buoyantly toward

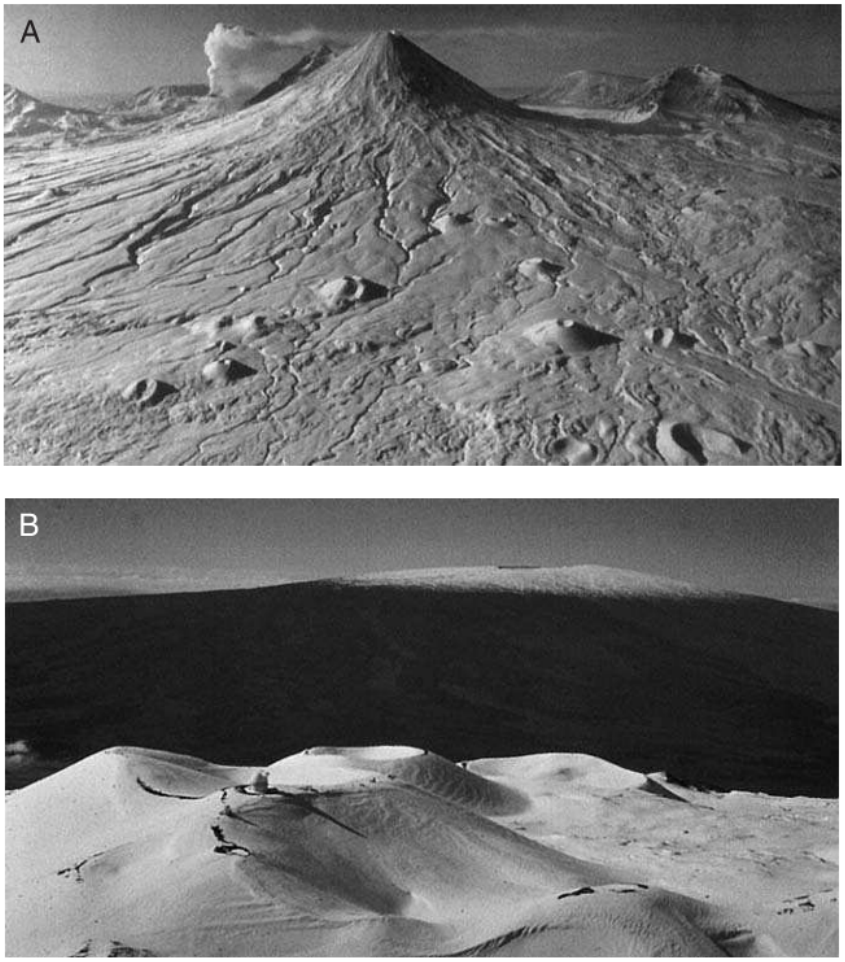

FIGURE 1 Volcano shapes reflect the wide range of variations in lava chemistry, vent orientation, gas content and eruptive style. (A) Stratovolcanoes include towering symmetrical cones like Kamchatka's Kliuchevskoi (center) and irregular compound volcanoes like Ushkovsky (right). Kliuchevskoi's frequent eruptions originate both from the central vent and from radial fissures that produced the flank cinder cones in the foreground. (Photograph by V. A. Podtabachny; courtesy of Anatolii Khrenov, Institute of Volcanology, Petropavlovsk; also see color insert.) (B) Shield volcanoes grow through the repeated effusion of thin lava flows to form Earth's largest volcanic edifices. Their volumes can exceed those of stratovolcanoes by several orders of magnitude. Here the low-angle slopes of Hawaii's broad Mauna Loa volcano, rising 9 km above the seafloor, forms the horizon. In the foreground, a cluster of cinder cones, among Earth's smallest volcanic features, caps the summit of an older shield volcano, Mauna Kea. (Photograph by Don Swanson; U.S. Geological Survey.)

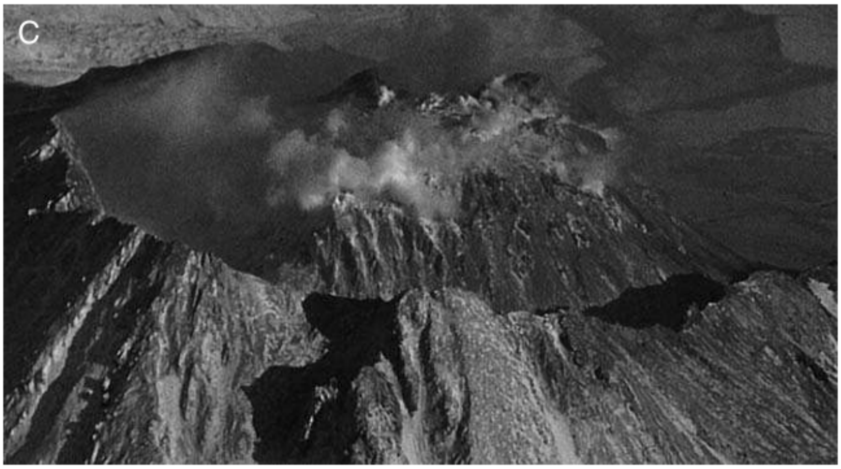

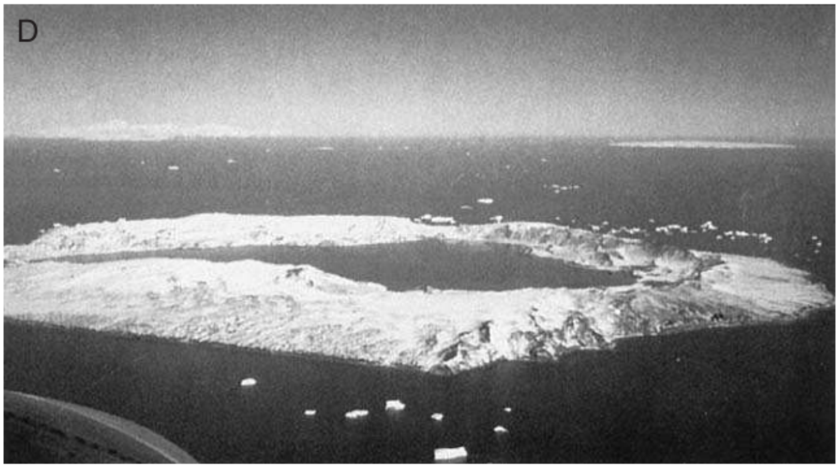

FIGURE 1 (*continued*) (C) A steaming lava dome has grown incrementally through the extrusion of viscous lava inside the breached crater of Kamchatka's Bezymianny volcano. The horseshoe-shaped crater formed as a result of a massive volcanic landslide during a 1956 eruption remarkably similar to that at Mount St. Helens in 1980. (Photograph by Yuri Doubik; Institute of Volcanology, Petropavlovsk; also see color insert.) (D) Large volcanic calderas, formed by inward collapse following the eruption of large volumes of magma, are among Earth's most dramatic volcanic features. A 7-km-wide caldera flooded by the iceberg-laden waters of Antarctica's Bransfield Strait truncates the summit of ring-shaped Deception Island. (Photograph by Juan Bastias; courtesy of Oscar Gonzalez-Ferran, University of Chile.)

the surface. In its path upward, magma understandably exploits local fracture systems and, where long, linear fractures are present, a "curtain of fire" fissure eruption may result. Alternatively, magma may follow the line of weakness formed where two vertical fracture planes intersect, resulting in a pipelike vertical conduit building a symmetrical cone (Fig. 1A). Many gradations and complexities exist, even changing during the course of a single eruption. The supply of magma to the surface is commonly irregular, even sporadic, and if the supply ceases for too long the next batch will be forced to find another route to the surface because the old conduit will have been blocked with cooled, solidified magma. Thus fields of numerous small cones are formed or (again depending on supply rate and plumbing systems) large mountains dotted by smaller cones.

Perhaps the most influential factor in shaping volcano landforms, though, is the manner in which gas exits the magma. As magma nears the surface, the attendant decrease in pressure permits exsolution of dissolved gases, which then drive the eruption vertically (the only direction in which it is free to expand). Both gas content and viscosity vary widely in magmas, and the more gas-rich, viscous, and lower temperature compositions common to continental margin magmas tend to explode violently, fragmenting the liquid into countless small particles that cool swiftly as volcanic tephra. This process can form small cones of ash, layer upon layer, or (depending on the violence and longevity of the explosions) thin, widely dispersed ash layers. In contrast, gas separates more easily from the less viscous, hotter, and less gas-rich magmas of both spreading centers and oceanic islands, where lava flows passively from vents to form gentle slopes as on Hawaii (Fig. 1B). All gradations of products exist—from gentle flows, through near-vent spatter, to scoria, cinder, ash, and pumice—with resulting volcanic shapes depending on the gas content, magma chemistry, and eruptive style. Often the most violent explosive eruptions are followed by slow, "toothpaste tube"-like extrusions of viscous, degassed magma to form steep-sided domes in the vent (Fig. 1C).

The wide variety of initial constructional shapes is further expanded by additional processes during a volcano's lifetime. For example, a lateral shift in the plumbing system of a simple stratovolcano turns it into an asymmetric compound volcano. Destructional processes such as major slope failure (as at Mount St. Helens in 1980) or caldera collapse (as at Crater Lake, 6800 yr ago) may dramatically change a volcano's shape, and erosion is a relentless modifier in most parts of the world. Such varied processes lead inevitably to the enormous diversity of volcanic forms on the planet.

B. Distribution

Volcanoes are not randomly distributed on Earth's surface. The global volcano map (inside back cover) shows the distribution of about 1500 terrestrial volcanoes with probable activity in the last 10,000 years. This broader time interval provides more uniform coverage of active volcanism than the regionally variable historical record, and includes most volcanoes likely to erupt again. Tectonic setting, discussed in more detail later, clearly plays a major role in volcano distribution. Although some volcanoes are scattered, most are concentrated in linear belts, and these belts have accounted for >94% of known historical eruptions. The belts total 32,000 km in length and (assuming a generous 100-km belt width) cover less than 0.6% of the Earth's surface. Most are adjacent to deep oceanic trenches, and it is clear that subduction of one plate beneath another (where oceanic crust is being consumed at converging plate margins) causes most of the volcanism that we see. The complementary tectonic process of rifting (the creation of new crust at diverging plate margins) takes place largely on the deep ocean floor, unwitnessed by humans. The left half of Fig. 2 shows the small proportion of the world's historically documented eruptions that have taken place in the ocean rift environment (and in the intraplate environment, where hot spots deep in Earth's mantle feed molten rock to the surface through any plate passing overhead). It is possible, however, to use relative plate motions to calculate the budget of new lava reaching the Earth's surface each year and these estimates are shown in the right half of Fig. 2. Oceanic ridge volcanism overwhelmingly dominates the planet and, although most of it poses no threat to humans, this dominance must be remembered in a global perspective.

The geometry of Earth's tectonic plates means that the distribution of volcanoes by nations is also quite uneven. This national aspect has gained significance as attention to volcanic hazards—with attendant governmental expenditures for monitoring and other studies—has grown. Fully 80% of the world's population lives in, and presumably pays taxes to, nations with responsibility for at least one Holocene volcano. For some these volcanoes are in a distant overseas protectorate, while for others they loom over the nation's most populous city. Figure 3 shows the distribution of volcanoes by nation in terms of activity during several intervals: the past 10,000 years, variable lengths of historical documentation, and the 20th century. Indonesia leads the world in the number of historically active volcanoes, but many citizens would be surprised by the prominent position of the United States (including the Marianas and American Samoa, as well as Alaska, Hawaii, and the Cascades). The resources for dealing with volcanic hazards are also unevenly distributed, with more than

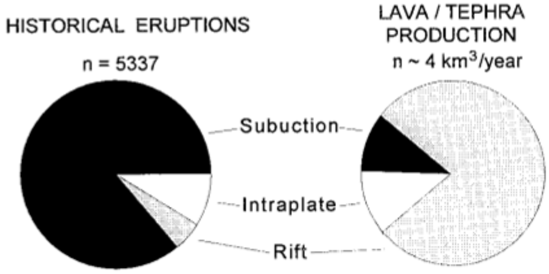

FIGURE 2 Volcanism distributed by tectonic setting (see text and inside back cover map of the world). Pie diagram on left shows proportion of documented historical eruptions from subduction zones (black), midocean ridges (stipple), and hot spot settings (white). Pie diagram on right shows proportion of annual magma budget in the same settings (with same symbols) to emphasize the dramatic contrast between the volcanism that we see and that we don't. Data for right diagram from Crisp (1984) and left from Smithsonian.

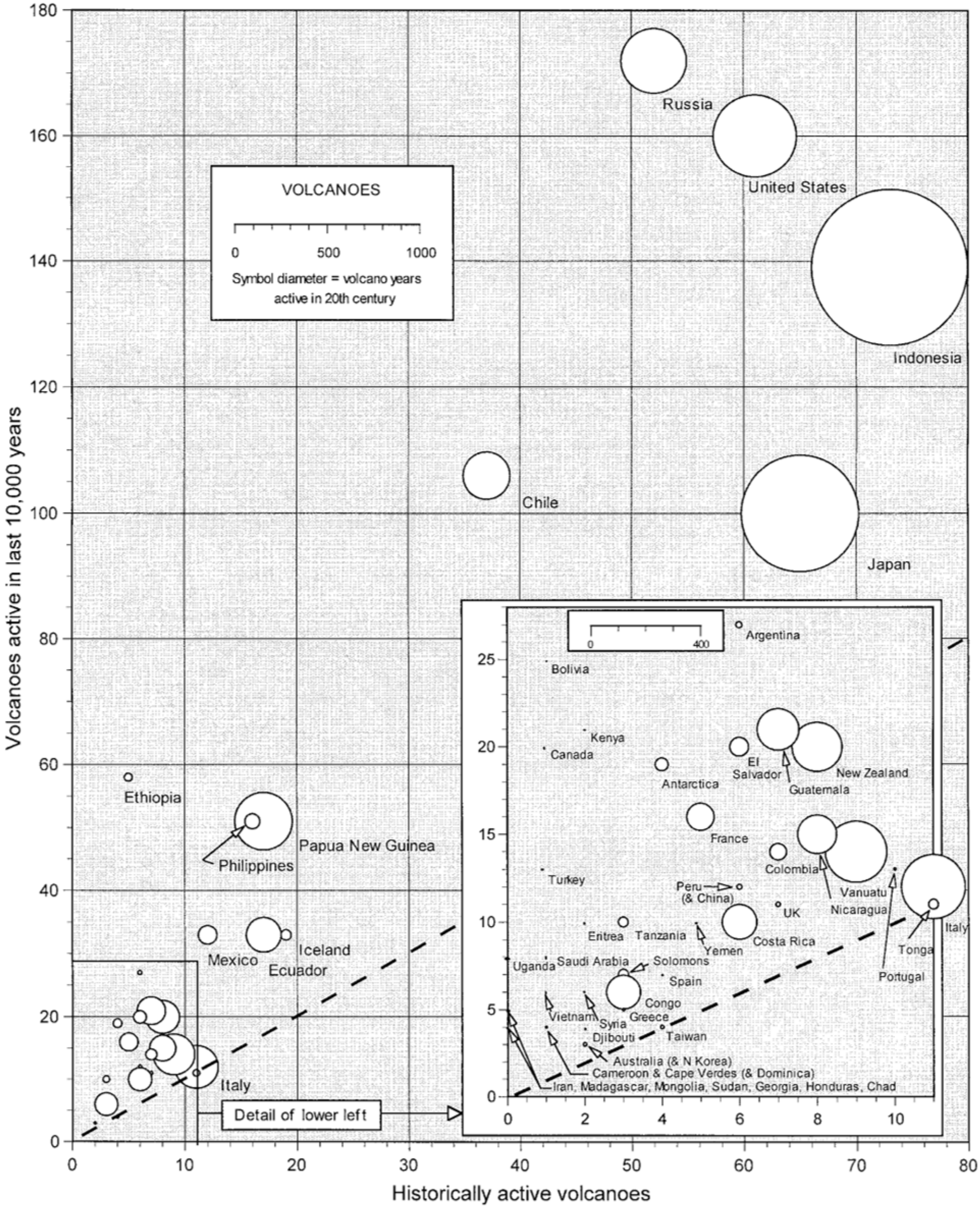

FIGURE 3 Volcano distribution by nation. The 56 nations shown here contain 98% of the world's historically active volcanoes and another 25 contain at least one volcano active in the last 10,000 years. Distance from the dashed line may indicate a short historical record, relatively thorough study of young-but-not-historical volcanoes, or a combination of the two. Circle diameter shows the wide range in volcanism within this century, a measure of the public awareness of volcanism evident in living memories. For this measure, we count all 20th-century years in which each volcano has erupted, and sum the counts for each nation.

half of the world's volcanoes located in nations with a per capita GDP (gross domestic product) of less than one-fifth that of the United States. But volcanoes disrespect national boundaries. Ashfall can be devastating to a downwind nation (e.g., Argentina during the 1991 eruption of Chile's Cerro Hudson); many airlines are threatened by ashclouds from major explosive eruptions along well-traveled flight paths (e.g., great circle routes to Japan over Alaska); and climatic effects of unusually large eruptions can be serious on the opposite side of the globe (e.g., June snowfalls—and crop failures—in New England following the 1815 eruption of Indonesia's Tambora). Clearly volcanic hazards are an international problem, calling for cooperation and resource sharing between nations.

C. Number

How many active volcanoes are there in the world? The answer to this common question depends on use of the word *active*. At least 20 volcanoes will probably be erupting as you read these words (Italy's Stromboli, for example, has been erupting for thousands of years); roughly 60 erupted each year through the 1990s; 165 in the full decade 1980–1989; 550 have had historically documented eruptions; at least 1300 have erupted in the Holocene (past 10,000 years); and some estimates of young seafloor volcanoes exceed a million. Because dormant intervals between major eruptions at a single volcano may last hundreds to thousands of years, dwarfing the relatively short historical record in many regions, it is misleading to restrict usage of *active volcano* to recorded human memories: We prefer to add another identifying phrase (e.g., *historically active* or *Holocene volcano*).

The definition of *volcano* is as important in answering the number question as the definition of *active*. Usage has varied widely, with the term *volcano* being applied to individual vents, measured in meters, through volcanic edifices measured in tens of kilometers, to volcanic fields measured in hundreds of kilometers. We have tended toward the broader definition in our compilations, allowing the record of a single large plumbing system to be viewed as a whole, but this approach often requires careful work in field and laboratory to establish the integrity of a group's common magmatic link. The problem is particularly difficult in Iceland, where eruptions separated by many tens of kilometers along a single rift may share the same magmatic system. A "volcanic field," such as Mexico's Michoacan-Guanajuato field (comprising nearly 1000 cinder cones, derived from a single magmatic system, dotting a 200- by 200-km area) may be counted the same as a single volcanic edifice. Perhaps the most honest answer to the number question is that we do not really have an accurate count of the world's volcanoes, but that there are at least 1000 identified magma systems—on land alone—likely to erupt in the future.

D. Tectonic Setting

Although differences between broad volcano groups were recognized by early volcanologists, the conceptual development of plate tectonics in recent decades has provided a framework for such studies. Much attention has been devoted to understanding the features common to specific tectonic settings and how they relate to processes of magma origin, modification, transport, and eruption.

1. Subduction

The most common eruptions observed by humans, and by far the most dangerous to human populations, are those from volcanoes overlying the world's subduction zones. Because of their explosive nature, these are also the eruptions most likely to affect our climate.

As an oceanic plate descends into the hotter, higher pressure interior, it is dehydrated and fluids from it rise into the overlying mantle wedge. In this complex region of shear and melting, new magma is born and rises in buoyant diapirs, but this rise is not steady. There may be many stops in subsurface chambers along the way, with early crystallizing minerals separating from the magma, and melting of surrounding rocks further changing its composition by contamination. This slow, complex, and varied route to the surface results, not surprisingly, in the eruption of complexly varied materials at different times and places.

In addition to compositional diversity and varied supply rates, a wide variation in the characteristics of subduction further contributes to the broad range of subduction zone volcanism observed. Segmentation of volcanic chains into discrete linear belts 100–300 km long, commonly offset by zones of more intense seismicity, has been recognized in Central America, the Cascades, the Aleutians, and the Andes. The geometry of subduction greatly influences the resulting volcanism. In the Andes, for example, volcanism is weak or absent above downgoing slabs that are inclined at only a gentle angle to the horizontal. We have found that relatively weak volcanism also correlates with thin overriding plates, with young downgoing slabs, with decreased angle between the direction of the downgoing slab and the bearing of the arc itself, and with low aseismic slip rates (where great earthquakes indicate strong coupling between converging plates).

2. *Oceanic Ridge*

Although the majority of Earth's eruptions occur in this setting, these are the eruptions that we normally do not see. Balancing the downgoing material in subduction zones, new magma is added to the planet's surface along the 70,000-km oceanic rift systems. This magma is relatively homogeneous basalt, originating in the uppermost mantle and arriving at the surface in relatively primitive condition. Its extrusion is generally below 1–4 km of water, both shielding it from view and, with substantial pressure, inhibiting volatile release. The result is gentle, effusive eruption from a narrow zone (often only 1–2 km wide). There volcanoes range, with decreasing spreading rate, from flat fissure eruptions, through elongate shields, to discontinuous chains of central volcanoes constructed of fresh pillow lavas. Symmetrical central volcanoes are also found outside the rift itself, particularly near large offsets in the ridge system and near topographic highs of the faster spreading ridges; they outnumber subduction zone and hot spot volcanoes by several orders of magnitude. Hints of the behavior of ocean rift volcanoes can be found in Iceland, one of the few places where the world's rift system emerges above sea level. Here the historical record suggests that, although crustal spreading is probably steady, the rift zone's response to it is episodic: rift eruptions (and intrusions) lasting several years cause a few meters of separation every 100 years or so, rather than a constant few centimeters of separation every year.

3. *Hot Spot and Flood Basalts*

Hot spot volcanoes are believed to be formed by long-lived, relatively stationary plumes, anchored deep in the mantle and feeding magma to the surface through the overlying plate. As an area moves over a hot spot, magma production fuels active volcanism at the surface, but this declines and dies as the plate moves beyond, and a new volcano begins to form above the hot spot. Hawaii is the best known example of hot spot volcanism, and the variable volumes of the progressively older volcanoes to the northwest testify to the correspondingly variable magma supply as they have been carried in that direction by the Pacific plate during the last 70 million years. Steady feeding of relatively consistent basaltic magma to shallow chambers often yields a delicately balanced system ready to erupt over long time periods and therefore vulnerable to triggering influences such as earthquakes and fortnightly tides. Careful study of historical eruptions on Hawaii shows them to be largely random phenomena, temporally, although large-volume eruptions tend to be followed by longer reposes. Distinctive stages in the long-term development of Hawaiian volcanoes have been recognized, the last of which takes place several million years after the volcano has been separated by plate motion from the feeding plume.

Stages in the development of the plume itself are believed by many to begin with the first batch of magma rising buoyantly through the mantle to reach the surface as a giant outpouring of flood basalts. Flood basalt provinces, such as India's Deccan plateau (60–65 Ma) and the Columbia plateau in the northwestern United States (around 15 Ma), have produced hundreds of thousands of cubic kilometers of lava and individual flows that covered thousands of square kilometers in just a few months or even days. Such catastrophic episodes are fortunately rare in the planet's history.

4. *Intracontinental*

This setting has much in common with the two tectonic environments described earlier in that some intracontinental volcanoes result from rifting and others from hot spots. Because of the complexities of the thick, siliceous continental crust that is inevitably involved in these eruptions, they are the most violent and least well understood forms of volcanism on the planet. Such eruptions can produce huge volumes of ash distributed over thousands of kilometers, such as the Cenozoic volcanoes of Colorado's San Juans, or the Pleistocene eruptions of Yellowstone. Studies of nonsubduction volcanism in the western United States emphasize the relatively long life of these centers (perhaps 5 million years, or 10 times the active life of many subduction zone volcanoes). Pulses of plate motion are thought to trigger magma formation and rise into the complex, extensional environment of the western United States, where 60 loci are identified by R. L. Smith as potential eruption sites in the future. Another regional review of intraplate volcanism covers eastern Australia and New Zealand, where the overall eruption rate has been slow but apparently continuous throughout the past 95 million years.

III. ERUPTIONS

Looking at the distribution of volcanism through time again raises questions of definition: Is an individual explosion an *eruption* or should the word be used (as we tend to) for clearly linked events that may be separated by hours, days, or even months of surface quiet? Arrival of volcanic products at the Earth's surface is normally termed an *eruption*, but the historical record is often unclear. Steam venting is commonly only a by-product of subsurface heat, and is rarely dignified by the word *eruption*, but steam may be all that was seen by a sea captain reporting an "erupting" volcano 200 years ago. Volcanic heat is also the prime source of *phreatic* (or *steam-blast*) explosions in which heat and water combine to fragment preexisting volcanic materials and hurl the resulting tephra into the sky. These events can be quite violent, however, and are rightfully called *eruptions*, even without the direct involvement of new magma.

Gas is an unequivocal volcanic product, but the gentle, continuous emission of fumarolic gases—common to most volcanoes—is not considered an "eruption." Occasionally, though, large quantities of gas are suddenly vented—as in the fatal eruption of the Dieng volcano complex on Java in 1979. In 1984 and 1986, the African nation of Cameroon suffered catastrophic expulsions of CO_2 resulting in many fatalities by suffocation. The origin of the African events is controversial, but the evidence suggests that they resulted not from an eruption, but from the sudden overturn of crater lake water, with catastrophic exsolution of volcanic gas that had gradually accumulated in the bottom waters over the course of many years.

The great range of eruption types has already been mentioned. Among the various measures of eruption "bigness," volume of products has been the most widely used by volcanologists. Eruptions of equal volume, however, may release quite different amounts of gas, with comparably different effects on climate. The larger eruptions inevitably receive the greatest share of scientific (and media) attention, but the steady pulse of smaller events adds up to significant contributions. In assessments of annual volcanic SO_2 production, for example, the steady, unspectacular contributions of the world's fumaroles and small, ongoing eruptions are found to outweigh those of the less frequent larger eruptions. In any case, the range of eruption types is large, and there are many that, in the words of G. P. Scrope 135 years ago, "exhibit an infinite variety of phases intermediate between the extremes of vivacity and sluggishness."

A. Durations and Culminations

Clearly some eruptions last for a very long time, like Stromboli's 2500+-yr continuing pyrotechnic show. At the time of this writing (early 1999) the following 16 volcanoes have been erupting more or less continuously through the last 24 years (the reporting span of SEAN/GVN) and are likely to remain active for some time: Stromboli and Etna (Italy); Erta Ale (Ethiopia); Manam, Langila, and Bagana (Papua New Guinea); Yasur (Vanuatu); Semeru and Dukono (Indonesia); Suwanose-jima and Sakura-jima (Japan); Santa Maria and Pacaya (Guatemala); Arenal (Costa Rica); Sangay (Ecuador); and Erebus (Antarctica). However, other eruptions end swiftly: 10% of those for which we have accurate durations lasted no longer than a single day (Fig. 4a), most end in less than 3 months, and few last longer than 3 yr. The median duration is about 7 weeks.

Of particular importance to volcanic hazard mitigation is the time interval between an eruption's start and its culminating, paroxysmal phase. Several famous eruptions (e.g., Krakatau, 1883; Mount St. Helens, 1980; Pinatubo, 1991) have culminated months after the start of low-level eruptive activity, prompting the suggestion that volcanoes provide their own warning and that observatory monitoring of dangerous volcanoes is therefore unnecessary. To show the folly of this suggestion, we have looked at this time interval for the most explosive eruptions for which we have adequate data. These 252 eruptions (Fig. 4b) emphasize the sobering fact that many catastrophic explosions provide little advance warning. More than two-fifths of the eruptions reached their climax within the eruption's first day (42%) and more than half (52%) within the first week. Where data are available, half of the first-day paroxysms (including Tarawera, 1886; Bandai-san, 1888; Hekla, 1947; and Shiveluch, 1964) came within only an hour of the eruption's start.

The range of eruptive behavior is wide, however, and history's largest explosive eruption, Tambora in 1815, provides sobering lessons about eruption duration. Mild eruptive activity over 3 full years was followed by a dramatic eruption, with cloud height estimated at 33 km, but even that was not its climax. After a lull of 5 days, the culminating eruptive cloud reached heights estimated at 44 km and caused 3 days of total darkness 500 km from the volcano. More than 60,000 people died as a result of this eruption. It is understandably difficult to sustain public awareness of hazards during long-term, low-level eruptive activity, but it is dangerous to assume that the worst is over after the initial explosive phase. Predicting an eruption's end is even more difficult than predicting its beginning.

B. Patterns through Historical Time

Has global volcanism changed through time? A look at the number of volcanoes active per year, during the last

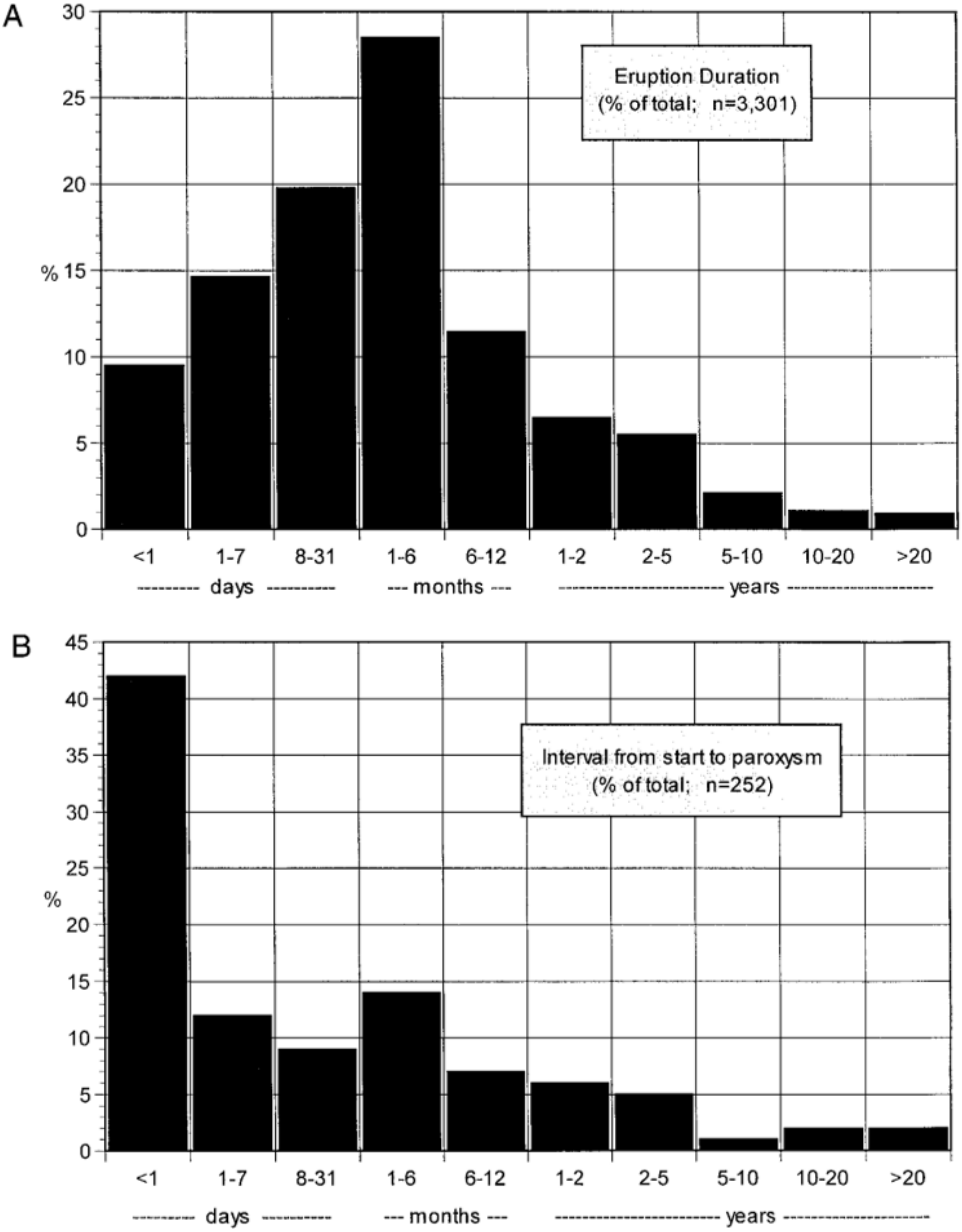

FIGURE 4 Eruption duration and development. (A) 3301 eruptions for which stop (and start) dates are known. (B) Interval between the eruption's start and its climactic phase for 252 highly explosive, well-documented, historical eruptions. These have a volcanic explosivity index (VEI) of 3 or above, indicating more than 10^7 m^3 of tephra or, in the absence of volume estimates, described as "severe" or "violent."

500 yr, shows a dramatic increase, but one that is closely related to increases in the world's human population and communication. We believe that this represents an increased reporting of eruptions, rather than increased frequency of global volcanism: more observers, in wider geographic distribution, with better communication, and broader publication. The past 200 yr (Fig. 5) show this generally increasing trend along with some major "peaks and valleys," which suggest global pulsations. A closer look at the two largest valleys, however, shows

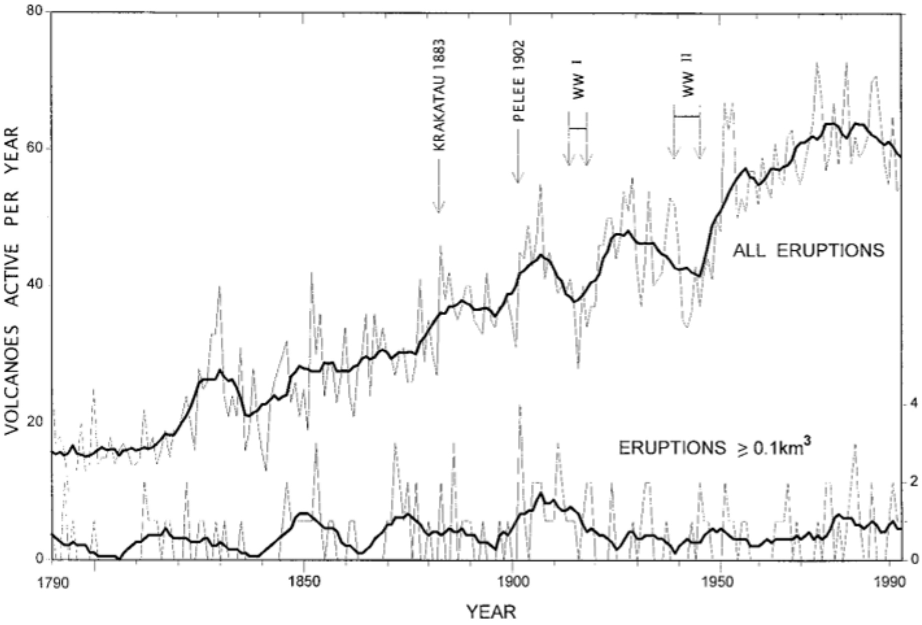

FIGURE 5 Eruption reporting since A.D. 1790. Total number of volcanoes erupting per year (thin upper line) and 10-yr running mean of same data (thick upper line). Lower lines show only the annual number of volcanoes producing large eruptions (≥0.1 km^3 of tephra or magma) and scale is enlarged (on right axis). Thick lower line again shows 10-yr running mean.

that they coincide with the two world wars, when people (including editors) were preoccupied with other things. Many more eruptions were probably witnessed during those times, but reports do not survive in the scientific literature.

If these apparent drops in global volcanism are caused by decreased human attention to volcanoes, then it is reasonable to expect that increased attention after major, newsworthy eruptions should result in higher-than-average numbers of volcanoes being reported in the historical literature. The 1902 disasters at Mont Pelee, St. Vincent, and Santa Maria (Fig. 5) were highly newsworthy events. They represent a genuine pulse in Caribbean volcanism, but we believe that the higher numbers in following years (and following Krakatau in 1883) result from increased human interest in volcanism. People reported events that they might not otherwise have reported and editors were more likely to print those reports. We felt confident enough of this interpretation to predict, in the first (1981) edition of our book, a similar increased reporting of volcanism after the 1980 eruption of Mount St. Helens. This did not happen, but we would like to think, by way of partial explanation, that reasonably comprehensive reporting of global volcanism is finally at hand. Note (in Fig. 5) that the number of erupting volcanoes has leveled off to between 50 and 70 per year during the past three decades.

Further evidence that the historical increase in global volcanism is more apparent than real comes from the lower plot of Fig. 5. Here only the larger eruptions (generating at least 0.1 km^3 of tephra, the fragmental products of explosive eruptions) are plotted. The effects of these larger events are often regional, and therefore less likely to escape documentation even in remote areas. The frequency of these events has remained impressively constant for more than a century, and contrasts strongly with the apparent increase of smaller eruptions with time.

C. Magnitude and Frequency (Global)

How much do eruptions vary in size? Like earthquakes, the frequency of eruptions decreases with increasing size: There are a lot of small ones, fewer medium-sized ones, and not so many large ones. We have borrowed from the seismologists' magnitude–frequency plots, using as our best measure of magnitude the volcanic explosivity index (VEI, see Sizes of Volcanic Eruptions chapter). This closely parallels the volume of erupted tephra, which increases by an order of magnitude with each larger VEI integer. In Fig. 6, the number of eruptions at and above each VEI increment is shown for

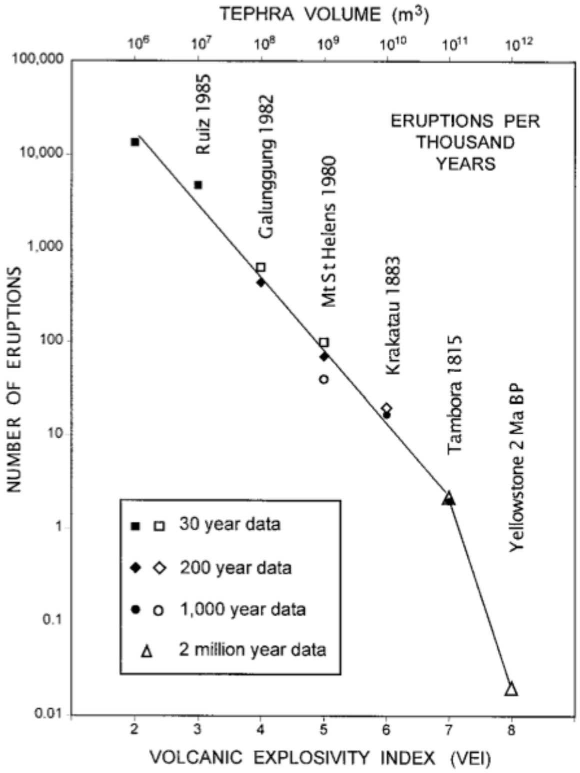

FIGURE 6 Magnitude and frequency of Holocene eruptions. Cumulative number of eruptions during various intervals (going back in time from 1 January 1994) for each VEI class and normalized to "per 1000 years." Eruptions of low explosivity (VEI 0 and 1) are not shown, and a logarithmic scale is used to allow resolution of the lower frequencies found with the larger eruptions. The best fit line is determined by an exponential regression model for VEI 2–7 using data points that are filled. Data points from Decker (1990) for VEI 7 and 8 are shown by open triangles. Well-known eruptions are labeled to illustrate each VEI class.

various time intervals in the recent past: 30, 200, 1000, and 2 million years. We have used longer time intervals for data from successively larger VEI groups because the smaller events have been adequately reported only in recent decades, whereas the larger events, being rarer, need a longer time interval for representative counts. This is a somewhat subjective process, but the intervals are chosen in the hope that they are long enough to be representative yet short enough to have reasonably accurate reporting. As discussed with Fig. 5, larger eruptions are more likely to have been accurately reported over longer periods, on a global basis, than smaller eruptions.

Another way of interpreting this plot is that subaerial eruptions producing at least 10^6 m^3 of tephra (VEI $\geq$ 2) take place at an average rate of once every few weeks somewhere on Earth. Those producing $>10^7$ m^3, like the VEI 3 Ruiz event in Colombia that generated such fatal mudflows in 1985, take place several times a year. Eruptions the size of Mount St. Helens 1980 (10^9 m^3, or 1 km^3 and VEI 5) occur perhaps once a decade, and those like Krakatau in 1883 (>10 km^3) on the order of once a century. The historical record, however, fails to prepare us for the much larger eruptions of the past. The Toba eruption, only 74,000 years ago in Indonesia, produced nearly 10,000 times more magma (2800 km^3) than the Mount St. Helens eruption. Even larger eruptions are known from the older geologic record.

Simple extrapolation of the Holocene record in Fig. 6 is not warranted above VEI 7, however, and that value, we must remember, is based on a single data point. The shape of the magnitude–frequency relationship at this end is unclear, but Decker (1990) has attempted to improve it by plotting data from Newhall and Dzurisin's compilation (1988) of caldera unrest during the past 2 million years. The caldera data set is incomplete, as the authors themselves are quick to acknowledge, and large assumptions are made in extending the historical data, but that extension is probably closer to the truth than extrapolation of the historical data. An eruption the size of Yellowstone's about 2 million years ago, producing 2500 km^3 of magma, is believed to take place every 100,000 years. Volcanic ash from this eruption was distributed over much of the western United States (including Los Angeles, Tucson, El Paso, and Des Moines) with compacted thicknesses of 0.2 m at distances of 1500 km from the source. Its impact was surely profound.

D. Interval and Magnitude (Individual)

While Fig. 6 illustrates the frequency of eruptions on a global basis, most people are more interested in how much longer a particular volcano will remain quiet and what kind of eruption will break that quiet. Such information can come only from detailed study and monitoring, as described elsewhere in this volume, but the volcanological record provides some guidance that is both useful and sobering. One of the certain contributors to large volcanic death tolls is the fact that the repose interval between eruptions is very much longer than the historical records in many parts of the world. Figure 7 shows the relationship between eruption interval and the proportion of historical eruptions in each VEI class. Most eruptions of low explosivity follow repose intervals of only 1–10 yr, but with increasing time intervals the

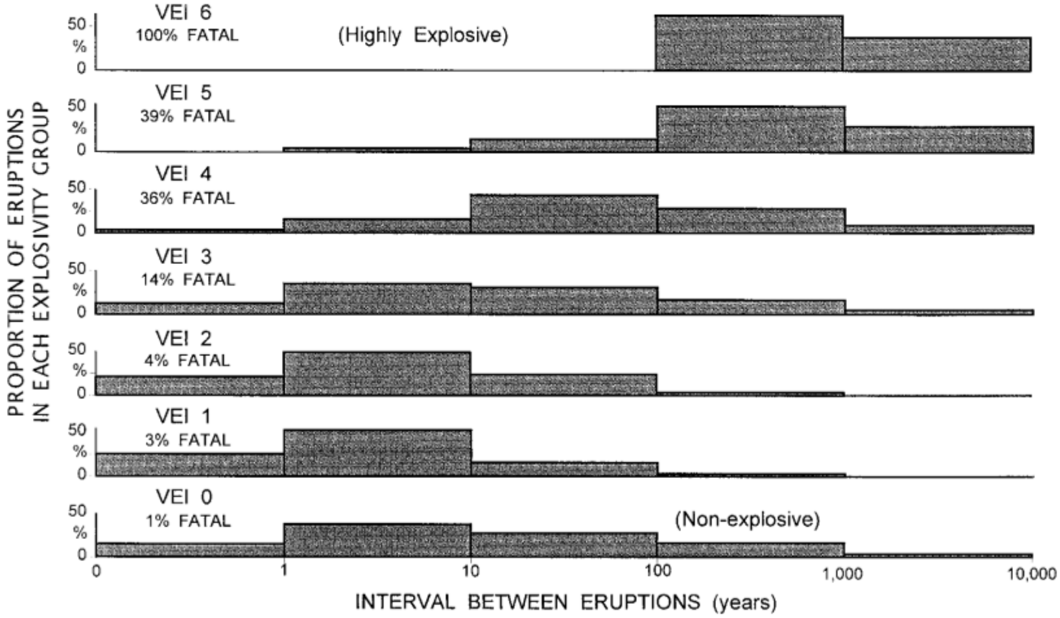

FIGURE 7 Explosivity and time intervals between eruptions. For each VEI unit, eruptions are grouped by time interval from start of previous eruption. The number of eruptions in VEI groups 0 to 6 are, respectively, 446, 677, 2991, 692, 230, 48, 16. For each group, the percentage of historical eruptions that have been fatal is also shown to emphasize the danger of large explosive eruptions from volcanoes that have appeared to be quiet for hundreds to thousands of years.

explosivity increases significantly. Long repose periods precede large eruptions, and in regions with short historical records the human population is commonly unprepared. The results are often tragic.

Humans have not been successful in controlling volcanoes in a substantive way and are not likely to be so in the future. We can, however, develop a more successful coexistence with volcanoes, neither fatalistically accepting their actions nor relying on last-minute attempts at control. To do this, we must emphasize understanding as the first element of prediction, and improve our human response to eruptions when they do occur. This requires understanding of the huge eruptions of the geologic past as well as the more frequent and more familiar events of our own lifetimes. With limited resources, volcanology should concentrate efforts on a limited number of dangerous volcanoes, but it would be a mistake to overemphasize the historical record in selecting them. For at least two centuries we have had an average of one or two eruptions per year from volcanoes with no previous historical activity. Other volcanoes have erupted after hundreds of years of quiet. Because their danger was not widely recognized, and because unusually violent eruptions are known to follow unusually long periods of quiet, these events included some of history's worst natural disasters. Table I lists

TABLE I Largest Explosive Eruptions of the 19th and 20th Centuries[a]

Year	*Volcano*	*First historical?*	*Deaths*
1991	Cerro Hudson (Chile)	No	0
1991	Pinatubo (Philippines)	Yes	>740
1982	El Chichón (Mexico)	Yes	>2,000
1980	Mount St. Helens (USA)	No	57
1956	Bezymianny (Kamachatka)	Yes	0
1932	Cerro Azul/Quizapu (Chile)	No	0
1912	Novarupta/Katmai (Alaska)	Yes	2
1907	Ksudach (Kamchatka)	Yes	0
1902	Santa Maria (Guatemala)	Yes	>5,000
1886	Tarawera (New Zealand)	Yes	153
1883	Krakatau (Indonesia)	No	36,417
1875	Askja (Iceland)	Yes	0
1854	Shiveluch (Kamchatka)	Yes	0
1835	Cosiguina (Nicaragua)	No	5–10
1822	Galunggung (Indonesia)	Yes	4,011
1815	Tambora (Indonesia)	Yes	60,000

[a] VEI ≥ 5, or tephra volume $\geq \text{km}^3$. All but five were the first historical eruptions known from the volcano, and the high death tolls (in heavily populated regions) reflect that fact.

the most violent eruptions of the last two centuries—those with a VEI $\geq$ 5 (or $\geq$1 km^3 of tephra). Notice that 11 of 16 were the first historical eruptions at that volcano (and for others, like Krakatau, earlier activity was not widely known). The study of volcanology tends to concentrate on volcanoes made famous by eruptions that were either destructively large or photogenically long lasting, but we must not neglect the nonfamous, thickly vegetated volcanoes that have had no historical activity. Like Lamington in Papua New Guinea and Pinatubo in the Philippines, they may be the most dangerous of all.

See Also the Following Articles

History of Volcanology • Plate Tectonics and Volcanism • Plumbing Systems • Synthesis of Volcano Monitoring • Volcanic Crises Management • Volcanic Episodes and Rates of Volcanism • Volcanic Hazards and Risk Management

Further Reading

Boyd, F. R., ed. (1984). "Explosive Volcanism: Inception, Evolution, and Hazards," National Academy Press, Washington, DC (several papers, particularly Smith and Luedke's on volcanism in the western U.S.).

"Catalog of Active Volcanoes of the World" (1994) v 1ÿ2D22 International Association of Volcanology and Chemistry of Earth's Interior, Rome.

Crisp, J. (1984). Rates of magma emplacement and volcanic output. *J. Volcanol. Geotherm. Res.* **20,** 177–211.

Decker, R. W. (1990). How often does a Minoan eruption occur? Pages 444–452 *in* "Thera and the Aegean World III" (D. A. Hardy, ed.), vol. 2. Thera Foundation, London.

Harington, C. R., ed. (1992). "The Year Without a Summer: World Climate in 1816." Canadian Museum of Nature, Ottawa.

Izett, G. A., and Wilcox, R. E. (1982). Map showing localities and inferred distributions of the Huckleberry Ridge, Mesa Falls, and Lava Creek ash beds (Pearlette family ash beds) of Pliocene and Pleistocene age in the western United States and southern Canada. U.S. Geological Survey Misc. Invest. Ser. Map I-1325.

Johnson, R. W., ed. (1989). "Intraplate Volcanism in Eastern Australia and New Zealand." Cambridge University Press, Cambridge, UK.

Klein, F. W. (1982). Patterns of historical eruptions at Hawaiian volcanoes. *J. Volcanol. Geotherm. Res.* **12,** 1–35.

Macdonald, K. C. (1982). Mid-ocean ridges: Fine scale tectonic, volcanic and hydrothermal processes within the plate boundary zone. *Ann. Rev. Earth Planet. Sci.* **10,** 155–190.

Machida, H. (1990). Frequency and magnitude of catastrophic explosive volcanism in the Japan region during the past 130 ka: Implications for human occupance of volcanic regions. *Geol. Soc. Australia Symp. Proc.* **1,** 27–36.

Newhall, C. G., and Dzurisin, D. (1988). "Historical Unrest at Large Calderas of the World." U.S. Geological Survey Bull. 1855.

Newhall, C. G., and Punongbayan, R. S., eds. (1996). "Fire and mud: Eruptions and lahars of Mount Pinatubo, Philippines." Philippine Institute of Volcanology and Seismology, Quezon City, and University of Washington Press, Seattle.

Pike, R. J. (1978). Volcanoes on the inner planets: Some preliminary comparisons of gross topography. *Proc. 9th Lunar Planet. Sci Conf.*, pp. 3239–3273.

Scrope, G. P. (1862). "Volcanoes: The character of their phenomena, their share in the structure and composition of the surface of the globe and their relation to its internal forces." 2nd ed. London: Longman, Green, Longmans, and Roberts, 490 p.

Simkin, T., and Siebert, L. (1994). "Volcanoes of the World." Geoscience Press, Tucson, AZ.

Simkin, T., Ungar, J. D., Vogt, P. R., Tilling, R. I., and Spall, H. (1994). "This Dynamic Planet—World Map of Volcanoes, Earthquakes, Impact Craters, and Plate Tectonics," 2nd ed. U.S. Geological Survey Map, Washington, DC.

Sleep, N. H. (1992). Hotspot volcanism and mantle plumes. *Annu. Rev. Earth Planet. Sci.* **20,** 19–43.

Smith, R. L. (1979). Ash–flow magmatism. *Geological Soc. America Special Paper* 180, pp. 5–27.

Solomon, S. C., and Toomey, D. R. (1992). The structure of mid-ocean ridges. *Annu. Rev. Earth Planet. Sci.* **20,** 329–364.

This Page Intentionally Left Blank

SIZES OF VOLCANIC ERUPTIONS

DAVID M. PYLE
University of Cambridge

I. Scales of Eruption Size
II. Mass and Volume of Volcanic Deposits
III. Magnitudes of Volcanic Eruptions
IV. Intensities of Volcanic Eruptions
V. The Relationship between the Intensity and Magnitude of a Volcanic Eruption
VI. Energy of Volcanic Eruptions
VII. Other Measures of Eruption Size

GLOSSARY

destructiveness index The logarithm of the area covered by lava, pyroclastic flows, and surges, or buried under more than 100 kg/m^2 of tephra during an eruption.

intensity The mass eruption rate (kg/s). The **intensity scale** is based on the logarithm of the mass eruption rate.

magnitude The mass of material ejected during a volcanic eruption (kg). The **magnitude scale** is based on the logarithm of the erupted mass.

volcanic explosivity index (VEI) A widely used classification scheme to describe the size of explosive eruptions. This is based principally on the erupted mass or volume of a deposit.

VOLCANIC ERUPTIONS SPAN a huge range of volumes, eruption rates, and styles and vary widely in their violence and destructiveness. Consequently, eruption size can be measured in a number of different ways. The two principal quantities that define the scale of an eruption are *magnitude*, the mass of material erupted, and *intensity*, the mass eruption rate. These two quantities can be determined more or less precisely for both modern and ancient eruptions, and for both effusive and explosive events. Studies of the sizes of past and present volcanic eruptions allow volcanologists to compare recent "smaller" eruptions, with the rare, but colossal, eruptions of past millennia. By so doing, we may learn more about the processes that control eruptions of all scales.

I. SCALES OF ERUPTION SIZE

Because erupted masses and rates of eruption both vary by many orders of magnitude, a logarithmic scale is needed to categorise the sizes of volcanic eruptions, in much the same way as the Richter magnitude scale is used for earthquakes. The first attempts to devise such a scale used a single number (analogous to the Richter magnitude) to describe the size of an eruption. This scale placed an eruption into a magnitude class (I to IX) based on the logarithm of its bulk pyroclastic volume.

A revised scale, called the *volcanic explosivity index* (VEI), developed this concept. The volcanic explosivity

Copyright © 2000 by Academic Press
All rights of reproduction in any form reserved.

TABLE I. The Volcanic Explosivity Index[a]

VEI index	*0*	*1*	*2*	*3*	*4*	*5*	*6*	*7*	*8*
General description	Nonexplosive	Small	Moderate	Moderate–large	Large	Very large			
Qualitative description	Gentle	Effusive	⟵ Explosive ⟶		⟵ Cataclysmic, paroxysmal ⟶				
Maximum erupted volume of tephra (m^3)	10^4	10^6	10^7	10^8	10^9	10^{10}	10^{11}	10^{12}	10^{13}
Eruption cloud column height (km)	<0.1	0.1–1	1–5	3–15	10–25	>25			

[a] Adapted from Newhall and Self, 1982.

index (Table I) uses an integer scale from 0 to 8 to describe both the volume and plume height of any given eruption. This index is based on both magnitude (erupted volume) and intensity (eruption column height) information. For example, a VEI 4 eruption is defined to have a bulk volume of 0.1–1 km^3 of tephra, and a column height of between 10 and 25 km. The volcanic explosivity index can be applied both to modern and ancient explosive eruptions. In practical use, the VEI value given to an eruption is based mainly on the volume of ancient deposits, and mainly on the *explosivity*, or column height, of observed eruptions. This index has been adopted by the Smithsonian Institution in their compilations of past volcanic eruptions and is widely used. This scale is not useful for eruptions of lava, which are primarily nonexplosive and therefore receive a default classification of 0 or 1 (Table I).

The underlying assumption of the volcanic explosivity index is that the magnitude and intensity of eruptions are related in some way, so that a single number can fully describe the different aspects of the size of an eruption. Subsequent work has shown that there is not a simple relationship between magnitude and intensity for many eruptions. Instead, two independent logarithmic scales are needed, one for magnitude and the other for intensity. By undoing the assumed link between erupted mass and eruption rate it becomes possible to describe and compare both explosive and effusive eruptions.

The magnitude scale is based on a logarithmic index of magnitude that is defined as follows:

$$\text{magnitude} = \log_{10}(\text{erupted mass, kg}) - 7.$$

For most eruptions, magnitudes defined in this way will be similar to their VEI. According to this scale, a "large" eruption, like Pinatubo, is of magnitude 6.0 or higher.

Similarly an intensity scale based on a logarithmic index of intensity is defined by:

$$\text{intensity} = \log_{10}(\text{mass eruption rate, kg/s}) + 3.$$

On this scale, an extremely vigorous eruption will have an intensity of 10–12, whereas a very gentle eruption might have an intensity of 4 or 5. One very useful property of these scales is that they can be used to describe both recent and ancient eruptions.

II. MASS AND VOLUME OF VOLCANIC DEPOSITS

Determining the mass of a volcanic deposit is not a trivial matter. Lava flows can have highly variable thicknesses and a complex distribution pattern. Poorly consolidated tephra deposits have a low preservation potential, and can rarely be reconstructed in full without detailed work and some good fortune. Finally, both lava and tephra deposits have variable densities, but this needs to be known before the mapped volume can be converted to an equivalent mass. If all magmas and all pyroclastic deposits had the same physical properties, there would be no problem. However this is not the case. Molten rock that is free of gas bubbles typically has a density of between 2300 and 2700 kg/m^3, depending on its composition. Tephra can have bulk densities between 600–800 kg/m^3, in the case of ash fall deposits, and 1600–2000 kg/m^3 for block and ash flow deposits. Consequently, there is no single, simple correction factor that can be universally applied to convert from volume and mass. The same is true for lavas, which can erupt with vesicle contents as high as 20 or 30%, and bulk densities as low as 1800–2000 kg/m^3.

To make comparisons between different deposits, deposit volumes are often converted to a *dense rock equivalent* volume. This is an estimate of the volume of dense, unvesiculated magma that erupted to form the pyroclastic deposit. The common usage of both bulk and dense rock equivalent volume scales is a source of confusion, because it is not always clear which "volume" is being referred to. Dense rock volumes are also of little value unless the assumptions about the densities of both the bulk and dense deposit are stated. There is no such confusion with erupted mass, which is the reason why mass should be used as the basis for magnitude scales.

III. MAGNITUDES OF VOLCANIC ERUPTIONS

The mass of ejecta thrown out during explosive eruptions spans at least 9 orders of magnitude (Table II). The smallest explosive events are rarely documented, and their deposits are even more rarely preserved. Discrete ash-venting episodes during an eruption, such as those at the Soufrière Hills, Montserrat, between 1995 and 1998, lasted a few tens of minutes and released just a few million kilograms of ash. Small ash-cloud events during the 1986 eruptions of Augustine, Alaska, similarly released a few tens of millions of kilograms of ash during discrete pulses of activity. The smallest of these events have a magnitude of less than 0. At the other end of the scale, caldera-forming events like Tambora (A.D. 1815) or Toba (75 ka B.P.) have magnitudes of 7–9, and erupt 10^{14}–10^{16} kg of magma.

Eruptions of lava similarly span at least 8 orders of magnitude (Table III). At the smallest end, individual carbonatite flows at Oldoinyo Lengai volcano in East Africa range up from just a few cubic meters, or tens of thousands of kilograms. In contrast, 15 km^3, or over 10^{13} kg, of lava was erupted during the largest effusive eruption of the last 300 years at Laki, Iceland, in 1783–1784. Some eruptions of lava attain a large mass simply because the eruption lasts for a long time. The eruption of the Soufrière Hills volcano on Montserrat erupted over 6×10^{11} kg (a magnitude of 4.8) of andesite lava as a series of domes between November 1995 and March 1998. The even longer lasting eruption at Santiaguito, Guatemala, has squeezed out over 2×10^{12} kg of lava since 1922.

Examples from the geologic record extend to even more colossal scales. The 14.7-million-year-old Roza flow of the Columbia River basalts had a mass of at least 3×10^{15} kg (magnitude 8.5) and was a part of a flood-basalt flow field 100 times larger. Flows of a similar scale can be found in many of the other flood basalt provinces of the world.

TABLE II Magnitude, Intensity, and Power Output from Some Explosive Eruptions

Eruption	*Total magnitude (kg)*	*Thermal energy release (J)*	*Total seismic energy release (J)*	*Peak eruption plume height (km)*	*Peak eruption rate, plume-forming phase (kg/s)*	*Power output (W)*	*Magnitude*	*Intensity*
Toba, ca. 75 ka B.P.	7×10^{15}	7×10^{21}	—	—	—	—	8.8	—
Tambora, Indonesia, A.D. 1815	2×10^{14}	2×10^{20}	—	43	2.8×10^{8}	4×10^{14}	7.3	11.4
Taupo, New Zealand, ca. A.D. 180	8×10^{13}	8×10^{19}	—	51	1.1×10^{9}	10^{15}	6.9	12.0
Novarupta, Alaska, 1912	3×10^{13}	3×10^{19}	1.6×10^{16}	25	1×10^{8}	10^{14}	6.5	11.0
Krakatau, Indonesia, 1883	3×10^{13}	3×10^{19}	—	25	ca. 5×10^{7}	ca. 5×10^{13}	6.5	10.7
Santa Maria, Guatemala, 1902	2×10^{13}	2×10^{19}	—	34	1.7×10^{8}	2×10^{14}	6.3	11.2
Pinatubo, Philippines, 1991	1.1×10^{13}	10^{19}	6.3×10^{13}	35	4×10^{8}	4×10^{14}	6.0	11.6
Vesuvius, Italy, A.D. 79	6×10^{12}	6×10^{18}	—	32	1.5×10^{8}	2×10^{14}	5.8	11.2
Bezymianny, Russia, 1956	10^{12}	10^{18}	—	36	2.2×10^{8}	2.8×10^{14}	5.3	11.3
Mount St. Helens, USA, 1980	1.3×10^{12}	10^{18}	2×10^{13}	19	2×10^{7}	2×10^{13}	4.8	10.3
Augustine, Alaska, 31 March 1986	6×10^{10}	8×10^{16}	—	12	7×10^{6}	9×10^{12}	3.8	9.8
Augustine, 27 March 1986	1×10^{10}	1.5×10^{16}	—	8	1×10^{6}	1.5×10^{12}	3	9
Augustine, 30 March 1986	4×10^{8}	5×10^{14}	—	4	7×10^{4}	9×10^{10}	1.6	7.8
Augustine, 27 March 1986	3×10^{7}	4×10^{13}	—	1.8	3600	5×10^{9}	0.5	6.6
Augustine, 6 April 1986	1×10^{7}	1.5×10^{13}	—	0.8	130	1.5×10^{8}	0	5.1

TABLE III Magnitude and Peak Intensity of Some Effusive Eruptions

Eruption	*Total erupted mass (kg)*	*Thermal energy release (J)*	*Seismic energy release (J)*	*Peak eruption rate (kg s^{-1})*	*Mean eruption rate (kg s^{-1})*	*Magnitude*	*Peak intensity*
Laki, Iceland, 1783	3×10^{13}	5×10^{20}	—	2.4×10^{7}	1.4×10^{6}	6.5	10.4
Mauna Loa, Hawaii, June 1950	10^{12}	2×10^{18}	—	7×10^{6}	5×10^{5}	5	9.8
Sakurajima, Japan, 1914, West flank	5×10^{11}	7×10^{17}	—	5×10^{6}	1.5×10^{5}	4.7	9.7
Lonquimay, Chile, 1988–1990	5×10^{11}	7×10^{17}	10^{13}	1.4×10^{5}	1.4×10^{4}	4.7	8.1
Etna, Italy, 1991–1993	5×10^{11}	7×10^{17}	—	6×10^{4}	10^{4}	4.7	7.8
Hekla, Iceland, 1991	3×10^{11}	5×10^{17}	—	4×10^{6}	7×10^{5}	4.5	9.6
Etna, Italy, 1792	2×10^{11}	3×10^{17}	—	3×10^{5}	6000	4.3	8.5
Nyiragongo, Zaire, 1977	4×10^{10}	6×10^{16}	—	—	10^{7}	3.6	>10
Kilauea, Hawaii, March 1965	3×10^{10}	5×10^{16}	—	10^{6}	4×10^{4}	3.5	9
Kupaianaha, Kilauea, Hawaii, 1991	8×10^{9}	1×10^{16}	—	6000	3400	2.9	6.8
Centre 5, Oldoinyo Lengai, Tanzania, 1988	2×10^{5}	1.5×10^{11}		20	4	−1.7	4.3

IV. Intensities of Volcanic Eruptions

The intensity of an explosive eruption, or the rate at which the ejecta leave the vent, is the main factor that controls the height of an eruptive plume. For a sustained eruption, the height reached by the eruption column is proportional to the fourth root of the intensity: $H \propto I^{1/4}$. The plume height in turn controls the dispersal of the volcanic clasts, so it is possible to infer the intensities of ancient eruptions from studies of the deposits. For recent eruptions, direct visual and satellite observations of the heights reached by eruption columns mean that the intensities of a wide range of eruptions can be determined. The intensities of selected explosive eruptions are summarized in Table II. The most powerful Plinian eruptions have intensities of between 11 and 12, corresponding to mass eruption rates of 10^8–10^9 kg/s, and send plumes to between 25 and 55 km above the Earth's surface. The intensities of small ash eruptions can be as low as 5 or 6, with mass fluxes of just 10^2–10^3 kg/s supporting weak plumes.

Explosive eruptions that undergo a transition from a plinian phase to an ignimbrite-forming phase may do so as a result of the increasing intensity of the eruption. In many cases these changes in intensity are linked to the increasing size of the eruptive vent, or the opening of new vents as ring fractures open up above the magma chamber. The intensity of many ignimbrite-forming eruptions may have been as much as 1 or 2 orders of magnitude larger than the plinian phase (i.e., 10^9–10^{11} kg/s). Increasingly good quantitative models are available that allow geologists to infer the paleointensity of ancient ignimbrite-forming eruptions. However, because not all explosive eruptions produce flows of any description, it is probably unwise to base an intensity scale on anything other than the peak intensity of the plume-forming phase.

The intensities of lava eruptions are rather more difficult to constrain than those of explosive eruptions, unless they are actually observed. Many effusive eruptions also show dramatic changes in intensity as the eruption progresses. The fissure-fed eruptions of Laki in 1783 and Hekla in 1991 both started with fire fountains sustained by a total flux of millions to tens of millions of kilograms of lava per second. As the eruptions progressed over subsequent days and weeks, the flux declined by 2 to 3 orders of magnitude. In these cases, the changes in intensity can be linked to changes in the pressure of the magma chamber at depth, or to transitions in the rheology of the erupting mixture. In contrast, during the 1995–1998 dome-forming eruption of the Soufrière Hills volcano, Montserrat, the rate of eruption of lava increased by about an order of magnitude as the eruption progressed, before coming to an abrupt halt in March 1998.

Instantaneous rates of eruption of lava measured at active volcanoes range from less than 2 kg/s (an intensity of 3.3) during the eruption of small pahoehoe flows at

TABLE IV Long-Term Eruption Rates of Lava: Lakes and Domes

Volcano	*Period*	*Eruption type*	*Mean eruption rate (kg s^{-1})*
Soufrière Hills, Montserrat, West Indies	1995–1998	Lava dome	8000
Unzen, Kyushu, Japan	1991–1995	Lava dome	4000
Santiaguito, Guatemala	1922–1925	Lava dome	4500
Santiaguito, Guatemala	1925–1984	Lava dome	800
Mount St. Helens, USA	1980–1986	Lava dome	700
Merapi, Indonesia	1890–1992	Lava dome	80
Nyiragongo, Zaire	1901–1977	Lava lake	1000
Halemaumau, Hawaii	1823–1923	Lava lake	300
Erta 'Ale, Eritrea	1968–1974	Lava lake	160
Stromboli, Italy	Historical times	Lava pond	0.3

the Tanzanian volcano Oldoinyo Lengai in 1988, to more than 10^7 kg/s during the hour-long eruption of Nyiragongo in central Africa in January 1977. Some of the lowest intensities are recorded from eruptions that continue for years, or even longer (Table IV). Typically, dome-forming eruptions continue with an intensity of less than 5 (100 kg/s) to 8. The eruption of Stromboli, Italy, has an average intensity of less than 3.

Flood-basalt-forming eruptions, such as those that formed the Columbia River basalts in the northwestern United States, are thought to be the products of high-intensity eruptions. However, there is some disagreement over precisely how intense they may have been. There are two alternative reconstructions of the eruption that produced the 1300-km^3 Roza flow. An early reconstruction suggested an eruption duration of about 1 week, assuming that the flows were fully turbulent and erupted with an intensity of 12.5–12.8 ($3–6 \times 10^9$ kg/s). A later model suggested the eruption might have lasted for 10 years, assuming an intensity of 10 (10^7 kg/s), similar to that at Laki in 1783. These intensities are of a similar order of magnitude to those encountered during many violent explosive eruptions. However, an important difference between effusive and explosive eruption intensities is that eruptions of lava may take place along fissure systems tens or hundreds of kilometers long, while explosive eruptions tend to originate from vents only tens or hundreds of meters in size. Thus the rate of eruption per unit area of the vent is considerably lower for effusive than for explosive eruptions.

V. THE RELATIONSHIP BETWEEN THE INTENSITY AND MAGNITUDE OF A VOLCANIC ERUPTION

The magnitudes and intensities of a range of different eruptions are summarized in Fig. 1. The scatter of the data shows that there is some decoupling of eruption rate and erupted mass, particularly for nonexplosive eruptions. In other words, eruption duration varies independently of either magnitude or intensity. For short-lived plinian eruptions, there is a fair correlation between the intensity of the plume-forming phase and the magnitude of the whole eruption. Although there is some overlap between the sizes of the most vigorous eruptions of lava and explosive eruptions, in general a given mass of lava will erupt at a lower intensity, over a longer period of time, than the same mass of tephra.

VI. ENERGY OF VOLCANIC ERUPTIONS

Most volcanic energy is dissipated as heat. The thermal energy release will depend on both the temperature and composition of the material erupted, and ranges from approximately 1 MJ/kg for rhyolite erupted at 800°C to ca. 1.5 MJ/kg for basalt erupted at 1150°C. Rates of

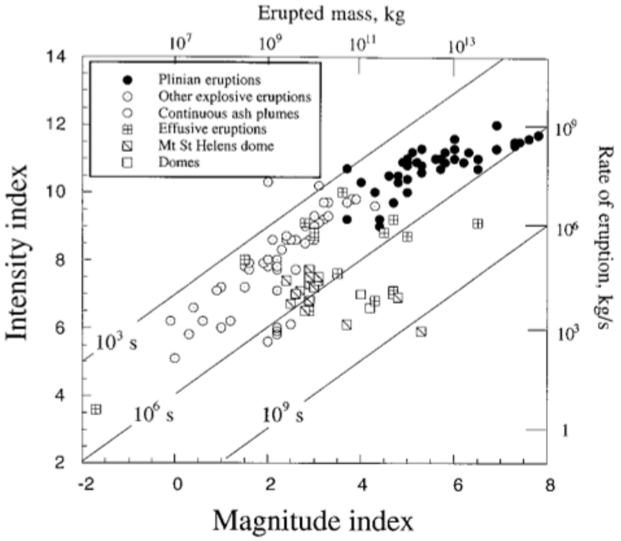

FIGURE 1 Plot of the magnitudes and intensities of selected recent and historical eruptions. Data from explosive eruptions are plotted as circles. Many Plinian eruptions include episodes of pyroclastic flow emplacement. The peak eruption rate during the flow-forming phases might be as much as 1 or 2 orders of magnitude higher than during the Plinian phase, but because this peak intensity is hard to infer, the intensity refers instead to the mass eruption rate during the plume-forming phase. Data from effusive eruptions are plotted as squares. For these eruptions the intensity is defined as the mean mass eruption rate; the peak intensity can be 1 or 2 orders of magnitude higher at the start of fissure-fed eruptions (Table III). The three labeled diagonal lines show the duration (in seconds) of an eruption of a given magnitude and constant intensity. In the case of Plinian eruptions associated with high-intensity pyroclastic flows, this duration is not the true duration of the eruption.

power output range from 10^{13} to 10^{15} W for typical Plinian eruptions and 10^{10} to 10^{12} W for large basaltic eruptions, with a total thermal energy release of 10^{18}–10^{21} J for eruptions of magnitude 5 to 7 (Tables II and III). For comparison, the total energy released by a shallow earthquake with a body magnitude of 7.5 is about 10^{17} J, released at a rate of 10^{15}–10^{16} W.

The kinetic energy of the particles ejected from a volcanic vent rarely exceeds a fraction of a percent of the thermal energy release. Even for a violent eruption where the ejecta leave the vent at the local speed of sound, the kinetic energy release is only of the order of 50 kJ/kg. Seismic energy can be an important component of energy release. Many eruptions are accompanied by a total seismic energy release larger than 10^{13} J (Tables II and III) but this is still several orders of magnitude smaller than the accompanying thermal energy release. Other forms of energy release that have been quantified, but are negligible, include the energy expended as atmospheric pressure waves, the potential energy required to raise the magma up the conduit, and the energy stored in the elastic deformation of the edifice.

VII. OTHER MEASURES OF ERUPTION SIZE

Another parameter that gauges the size of an eruption is the *destructive potential.* If this is defined as the area within which human structures would expect to be com-

TABLE V The "Destructiveness" of Selected Volcanic Eruptions[a]

		Area (km²) covered by:				
Eruption	*Lava flows*	*Tephra fall (>100 kg/m²)*	*Pyroclastic flows, surges*	*Lahars*	*Total area (km²)*	*Destructiveness index*
Millbrig, Ordovician bentonite, USA	—	>10⁶	—	—	>10⁶	6
Kidnappers flow, New Zealand	—	—	45,000	—	45,000	4.7
Taupo, ca. A.D. 180	—	12,000	20,000	—	32,000	4.5
Novarupta, 1912	—	30,000	150	—	30,150	4.5
Pinatubo, 1991	—	1700	400	>400	>2500	3.4
Laki, 1783–1784	599	10	—	—	609	2.8
Mount St. Helens, 1980	—	10	600	100	710	2.9
Hekla, 1991	23	<1	—	—	23	1.4
Etna, 1991–1993	7.2	—	—	—	7.2	0.9

[a] Destructiveness index = $\log_{10}$(total area affected by lava, pyroclastic flows and surges, lahars and tephra accumulations exceeding 100 kg/m²).

pletely destroyed as a result of an eruption, this allows us to compare eruptions of different style and involving different materials. Accumulations of dry tephra that exceed 100 kg/m^2 (a dry, uncompacted thickness of 10–20 cm) can cause roofs and other structures to collapse. Areas covered by lava flows and lahars, or hit by pyroclastic flows and surges — of whatever thickness — will also effectively be devastated by an eruption. If the *destructiveness index* of an eruption is defined as the logarithm of the total area affected by lava, lahar, pyroclastic flows and surges, and tephra fall accumulations of more than 100 kg/m^2, then it is straightforward to compare the relative impacts of different eruptions (Table V). Extremely destructive events, with a destructiveness index of >4, that lay waste to an area of more than 10,000 km^2, are very rare. The Taupo eruption of ca. A.D. 180 probably rates as the most destructive of the past 2000 years. Examples from the geologic record are unlikely to exceed the scale of the 1000- to 2000-km^3 ash-fall deposits that can be found now as Middle Ordovician bentonites. The largest of these has a destructiveness index of 6 (Table V). Moderately to highly destructive events, with a destructiveness index >3, include eruptions of the scale of Novarupta in 1912 and Pinatubo in 1991. Of course, the human and economic impacts of individual eruptions depend on local factors, but the destructiveness index is a useful way of comparing such otherwise dissimilar eruptions as those at Laki in 1783 and Mount St. Helens in 1980.

ACKNOWLEDGMENT

Data on individual eruptions are the products of work by many people, most of which can be found in either of the two principal journals of volcanology. A full list of references can be obtained from the author.

SEE ALSO THE FOLLOWING ARTICLES

Earth's Volcanoes and Eruptions: An Overview • Flood Basalt Provinces • Lahars • Lava Flows and Flow Fields • Plinian and Subplinian Eruptions • Pyroclastic Surges and Blasts

FURTHER READING

Carey, S. N., and Sigurdsson, H. (1989). The intensity of plinian eruptions. *Bull. Volcanol.* **51,** 28–40.

Newhall, C. G., and Self, S. (1982). The volcanic explosivity index (VEI): An estimate of explosive magnitude for historical volcanism. *J. Geophys. Res.* **87,** 1231–1238.

Walker, G. P. L. (1980). The Taupo Pumice: Product of the most powerful known (ultraplinian) eruption? *J. Volcanol. Geotherm. Res.* **8,** 69–94.

This Page Intentionally Left Blank

NAVP
COLR
PIGA
HAWA
DECO
EMAR
NAUR
ONTO
MANI
BROK
KERG
ELAN
60°
30°
0°
30°
60°
0°
180°
90°E

VOLCANIC EPISODES AND RATES OF VOLCANISM

HARALDUR SIGURDSSON
University of Rhode Island

I. Introduction
II. Ocean Ridges
III. Large Igneous Provinces
IV. Mantle Plume Melt Production Rates
V. Volcanic Arcs

GLOSSARY

catastrophists A group of early geologists who maintained that the steady progression of geologic time was periodically disrupted by brief cataclysms.

decompression melting The generation of magma in the Earth's mantle that results from upwelling of solid mantle rock, leading to a decrease in pressure acting on the rock and spontaneous partial melting without the addition of heat. Melting as a result of decrease in pressure occurs because the melting point of mantle rock (peridotite) decreases with decreasing pressure.

directionalism The 19th-century concept that Earth's processes were gradually slowing down, due to progressive heat loss from the interior of the Earth.

flood basalts Vast outpourings of basaltic magmas, resulting in rapid buildup of extensive basaltic plateaus.

hot spots Regions of anomalously high rates of volcanism on the Earth, generally associated with great outpourings of basaltic magmas. Hot spots may originate from deep mantle plumes.

ignimbrites Pyroclastic deposits primarily formed by volcanic ash and pumice, resulting from great explosive eruptions that generate pyroclastic flows.

LIPs Acronym for large igneous provinces, which are massive outpourings and intrusions of basaltic magmas. They are typically localized and transient phenomena, normally lasting for only a few million years.

mantle plume The upwelling of a large region of anomalous mantle material through the Earth's mantle, made buoyant because of either a thermal or chemical anomaly. Mantle plumes may be the source of magmas for LIPs and for the currently active hot spots.

subduction zones Regions of plate convergence, where lithosphere is thrust back into the Earth's mantle. Processes within the subduction zone bring about melt generation in the mantle wedge and cause buildup of the overlying volcanic arc.

tephra layers Layers of volcanic ash particles, generally a few centimeters thick, consisting primarily of glass shards. They are extremely widespread, covering thousands of kilometers on land and in the ocean basins. Tephra (Greek for *ash*) is formed by fragmentation of primarily silicic magma during explosive volcanic eruptions, ejected to the atmosphere in high eruption columns and dispersed widely.

uniformitarians The group of geologists who believed that the rates of geologic processes in the past had been roughly comparable to those observed today.

volcanic arcs Long, arcuate belts of volcanic chains that are created above subduction zones. While most volcanic

Copyright © 2000 by Academic Press
All rights of reproduction in any form reserved.

arcs are island arcs, they are also important on convergent continental margins.

I. INTRODUCTION

In the 18th and 19th centuries, during the early days of the study of the Earth, geologists clashed over two fundamental views of the rates of geologic processes. On one side were the Uniformitarians, whose talismanic principle was "the present is the key to the past"; that is, the rates of volcanism and other convulsions in the Earth were steady state and had not varied greatly in their intensity during geologic time. On the other hand were the Catastrophists, who maintained that the steady progression of geologic time was punctuated by brief cataclysms or periodic catastrophes, when volcanism, mountain building, and major upheavals occurred, often resulting in species extinctions. In the late 18th and early 19th centuries, the Cartesian belief that the Earth was a gradually cooling body gained support, and this gave rise to the concept of *directionalism:* that Earth processes such as volcanism had been much more vigorous in the past and that our planet was eventually destined to lose its internal reservoir of heat, with the slowing down of geologic processes such as volcanic activity. As a result of the wide-ranging exploration of the Earth and its geologic history in the 20th century, we are now in a position to address the issue of the rates of volcanism and episodicity.

Recognizing that the current state of the Earth is not necessarily typical of all tectonic regimes in the past, it is important to study the long-term geochemical and tectonic evolution of the Earth system. This chapter examines the geologic record for evidence of episodes in volcanism. It focuses primarily on the Cenozoic, that is, the past 65 million years, where the geologic record of the rates of volcanism is most complete. Three categories of terrestrial volcanism are considered: (1) ocean ridge volcanism, where the magma production rates have been largely determined by geophysical techniques, primarily by paleomagnetic methods; (2) hot spot volcanism, producing oceanic plateaus (e.g., Iceland) or volcanic island chains (e.g., the Hawaiian-Emperor chain); and (3) explosive volcanic activity in volcanic arcs above subduction zones, where the rate of volcanism is primarily recorded by tephra layers in sediment cores from the ocean basins.

The results of extensive drilling of the sedimentary succession of the ocean basins near volcanic arcs, and of geophysical studies of ocean ridges and oceanic plateaus, show that Earth's volcanism is decidedly episodic, although the causes and processes behind this episodicity of volcanism remain poorly understood.

II. OCEAN RIDGES

The crust that lines the ocean basins represents about 70% of the Earth's surface, and constitutes the most important product of volcanism on the planet. The formation of ocean basins is a consequence of plate motion, where the divergence of plates leads to upwelling of the underlying mantle and formation and segregation of basaltic melt (magma) from the rising mantle due to decompression melting, resulting in the volcanism that builds up submarine ocean ridges. The oceanic crust and lithosphere combined (ca. 80 km thick) form a boundary layer between the mantle of the Earth and the overlying hydrosphere. This boundary layer has probably been forming throughout most of the 4.5-billion-year history of the Earth, but most of the older oceanic crust has been returned into the mantle and destroyed due to the process of subduction. The rate of volcanic or magmatic activity in the ocean ridges is measured by the rate of plate generation, which in turn is calculated from the plate tectonic framework.

Rates of growth of a given plate depend on the length of the adjacent ridge and spreading rate. For example, the Antarctic plate is growing at the highest rate of 0.561 km^2/yr, being totally surrounded by spreading ridges. The worldwide aggregate length of spreading ridges is 5.92×10^4 km, and they generate oceanic crust at the rate of 3 km^2/yr, with a mean half-spreading rate of 2.5 cm/yr. Because of the large range in spreading rate from ridge to ridge, and variable ridge length, the rate of ocean ridge volcanism varies from region to region on the Earth. However, as discussed later, the aggregate global rate has not varied greatly in the Cenozoic.

The currently exposed ocean floor formed by spreading has an area of 297×10^6 km^2 and is up to 180 million years old, that is, the oldest oceanic crust is of Jurassic age. The oldest remnants of oceanic crust are found in the western Pacific and along the east and west margins of the Atlantic Ocean. We do not know the history of oceanic plates prior to 180 Ma, because all of the older crust has been subducted, but if we assume that plate generation and subduction has been a steady-state process, then the currently preserved ocean floor represents only 5% of the ocean floor created during Earth history.

In such a steady-state scenario, 5.94×10^9 km^2 would have been subducted throughout Earth's history; taking 80 km as a lithosphere thickness, this is equal to 4.75×10^{11} km^3 return mass flow into the mantle, or corresponding to about 48% of the volume of the mantle. Thus about half the mantle has been recycled once through the ocean ridge and the subduction zone systems during the history of the Earth, if the rates have remained constant.

The 3 km^2 of oceanic crust formed per year on ocean ridges is produced by the solidification of magmas, in part as volcanic rocks (basalts), and in part as plutonic rocks (gabbros, ultramafic rocks). With an average thickness of the order 6 km for the oceanic crust, the flux of basaltic magma from the mantle to the surface crustal layer at ocean ridges is about 18 km^3/yr (approx. 5×10^{13} kg/yr). The amount erupted as lava on the ocean floor is between 2 and 4×10^{13} kg/yr, or about 1 order of magnitude greater than the rate of volcanism in island arcs and hot spots, as discussed later.

The rates of ocean crust generation just given refer to current steady-state production, and studies of magnetic anomaly patterns on the ocean floor have shown that production rate during the Tertiary has varied between about 17 and 23×10^6 km^3/million years. The rate of global ocean crust production has, however, fluctuated much more significantly in the last 150 Ma (Fig. 1), with a notable maximum in the mid-Cretaceous. During this time, global ocean crust production (ocean ridge plus oceanic plateaus) was of the order 50–75% greater than current rates, largely due to high production of Pacific ridges in the period from 80 to 120 Ma. The mid-Cretaceous volcanic episode produced oceanic crust at a rate up to 32×10^6 km^3/million years and represents the largest magmatic episode known on Earth.

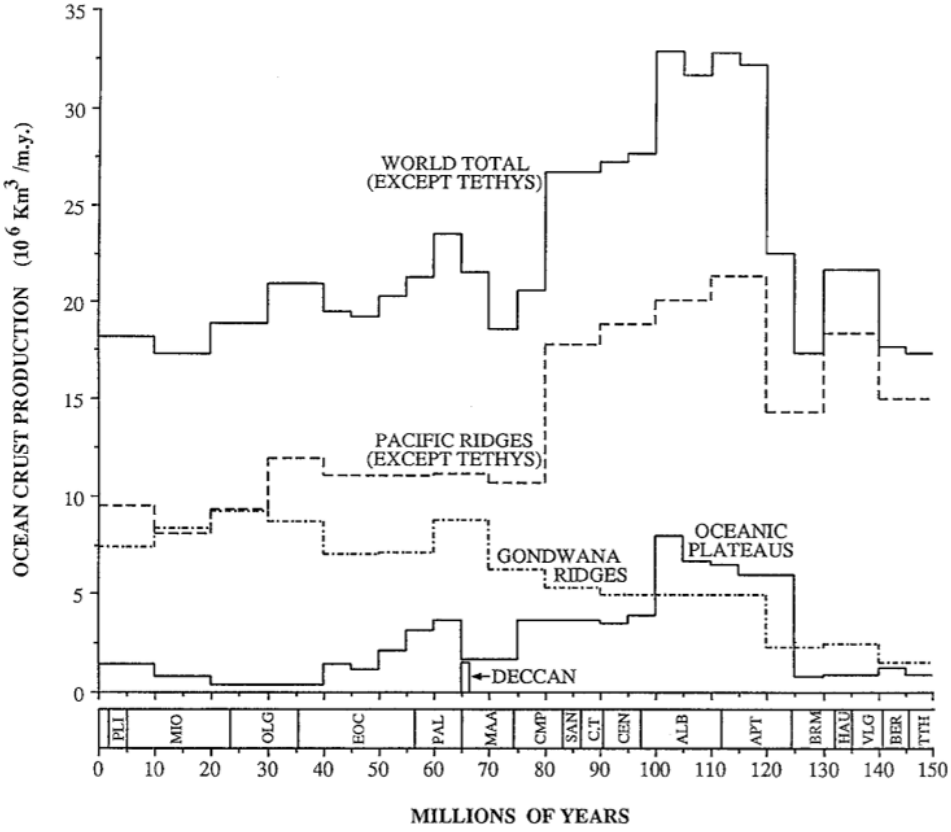

FIGURE 1 The rates of basaltic magma production and volcanism in the ocean basins of the Earth are measured by the rate of ocean crust formation. During the past 150 Ma the global rate has fluctuated mainly around 15 to 25 × 10^6 km^3/million years, but during the mid-Cretaceous the oceanic crustal budget increased dramatically, with rates between 50% and 75% higher than present (Larson, 1991).

III. LARGE IGNEOUS PROVINCES

Large igneous provinces (LIPs) are thick and extensive crustal regions, composed of mafic volcanic and intrusive rocks, that have formed by processes other than normal seafloor spreading. They occur in a variety of structural settings, as oceanic plateaus, submarine ridges, volcanic passive margins, seamount groups, continental flood basalts, and ocean basin flood basalts. They are often attributed to mantle plumes or hot spots, and they represent of the order 5–10% of the mantle output of magma today. However, in terms of magma production, they are episodic in nature, unlike the relatively steady-state activity of the ocean ridges. The volcanic components of LIPs are principally subaerial basaltic (tholeiitic) lava flows, but felsic and intermediate volcanic rocks also occur.

The largest LIPs are oceanic plateaus, forming broad, flat-topped volcanic regions that rise about 2 km above the surrounding seafloor (Fig. 2). Greatest of these is the Ontong Java plateau in the Pacific, covering an area of about 5 million km^2. This great province is of mid-Cretaceous age, but it was erupted in a relatively short time span, from about 118 to 124 Ma, implying emplacement rates of tens of km^3/yr. The Kerguelen plateau in the southern Indian Ocean is somewhat smaller but also a very impressive igneous province, some 2.3 million km^2 in area, emplaced about 110–114 Ma. The North Atlantic volcanic province, which is derived from a hot spot now centered beneath Iceland, has an area of more than 1.3 million km^2, and was mostly emplaced between 55 and 58 Ma. Also notable are the Deccan traps in India (1 million km^2), emplaced between 64 and 69 Ma and the Columbia River basalts of the western United States, erupted between 15 and 17 Ma. Thus they all have in common a relatively brief period of emplacement, and LIPs can be considered as transient magmatic episodes that significantly increase global magma production rates for a brief period (Fig. 3). In terms of Earth history, such events are truly catastrophic, and this raises the question of whether the emplacement and eruption of a large LIP will have far-ranging or perhaps global environmental consequences and affect biotic evolution, and many mechanisms have been proposed. The release of large amounts of carbon dioxide might raise significantly the global CO_2 levels in the Earth's atmosphere, which could potentially induce an enhanced greenhouse effect and global warming. Conversely, if the LIP volcanism is subaerial, then the emission of sulfur dioxide gas to the atmosphere could lead to stratospheric aerosol formation and global cooling events. While the nature and sign of the climate effects resulting from LIP emplacement remain controversial, we can state with confidence that their rapid eruption on the ocean floor will result in displacement of seawater and in turn a modification of global sea level. Thus it is estimated that the creation of the Ontong Java Plateau would have elevated sea level at least 10 meters.

LIPs occur in both oceanic and continental settings, intraplate and on plate boundaries, and their distribution is worldwide. The most prevalent hypothesis to account for LIP magmatism links them to mantle plumes or plume tails. This is supported by the fact that most but

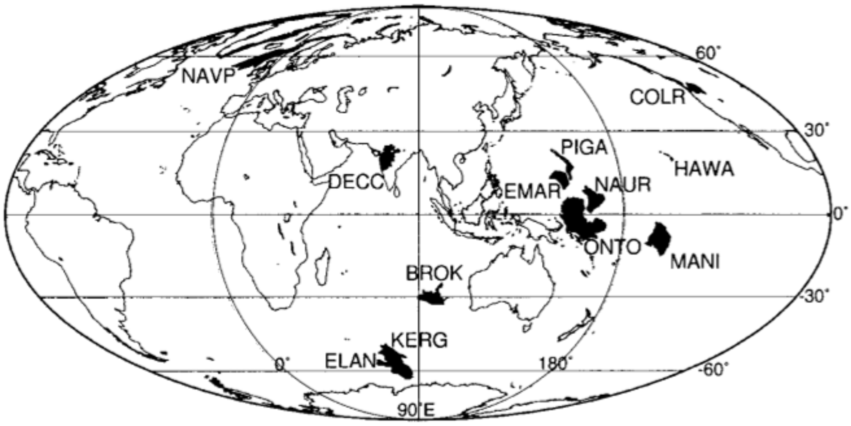

FIGURE 2 The location of some of the largest and best known LIPs on the Earth: Broken Ridge (BROK), Columbia River basalts (COLR), Deccan traps (DECC), East Mariana Basin flood basalts (EMAR), Elan Bank (ELAN), Hawaiian Islands (HAWA), Kerguelen Plateau (KERG), Manihiki Plateau (MANI), Nauru Basin (NAUR), North Atlantic volcanic province (NAVP), Ontong Java Plateau (ONTO), and Pigafetta Basin flood basalts (PIGA). (After Coffin and Eldholm, 1994.)

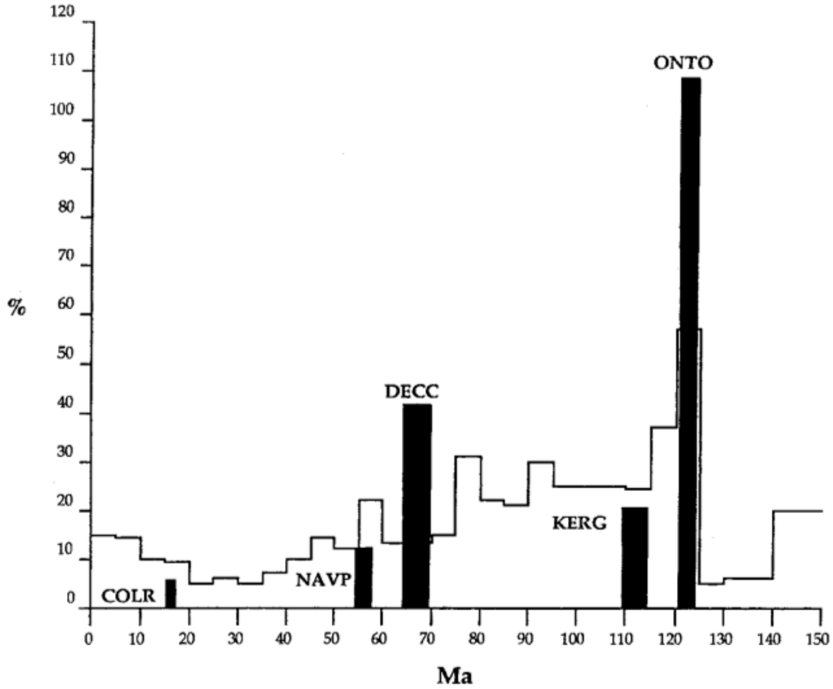

FIGURE 3 The crustal production rates of LIPs, as a percentage of midocean ridge crustal production rate versus time. The LIPs shown are Columbia River basalts (COLR), North Atlantic volcanic province (NAVP), Deccan traps (DECC), Kerguelen Plateau (KERG), and the Ontong Java Plateau (ONTO). Thin line is the global ocean crust production rate. (Adapted from Coffin and Eldholm, 1994.)

not all of the LIPs can be linked to hot spots, such as the link between the North Atlantic volcanic province and the Iceland hot spot, Deccan traps and the Reunion hot spot, and Kerguelen Plateau and the Kerguelen hot spot.

IV. MANTLE PLUME MELT PRODUCTION RATES

If LIPs are produced by mantle plumes, then the huge emplacement of oceanic crust, such as that of the Ontong Java at rates up to 12 km^3/yr, must be viewed in the context of the dynamics of mantle plume activity. Comparisons with the currently active plumes are instructive, although they are all dwarfed by the huge LIP events in the early Ceonozoic and mid-Cretaceous. The melt production rate of the Hawaiian plume in the Pacific Ocean has increased steadily in the last 35 million years to a value of about 0.18 km^3/yr today (Fig. 4). In contrast, the Reunion mantle plume in the Indian Ocean exhibits the opposite trend in melt production (Fig. 5). In its early stages (ca. 66 Ma), the Reunion plume production was at its peak, with a rate up to 5 km^3/yr, resulting in the formation of the Deccan traps in India. Melt production has steadily declined to the current rate of only about 0.04 km^3/yr in Reunion today. During the past 55 million years, the Iceland plume has pro-

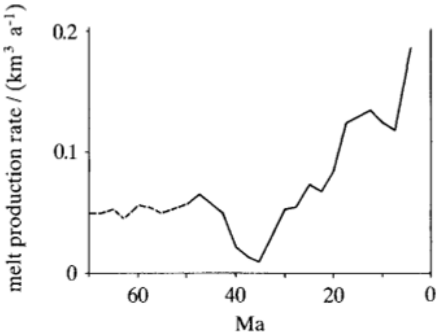

FIGURE 4 Basaltic melt production rate of the Hawaiian mantle plume has increased steadily in the last 35 million years, to a value of about 0.18 km^3/yr today. The rate is calculated from the volumes of individual seamounts and shield volcanoes above the mean seafloor level, and underplated material. (After White, 1993.)

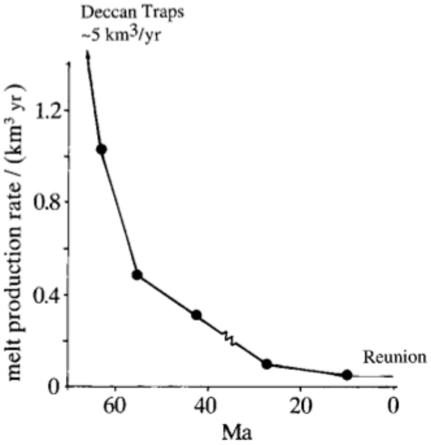

FIGURE 5 Variation in melt production rate with age along the trail of the Reunion mantle plume in the Indian Ocean. The rate was at peak of 5 km^3/yr about 66 million years ago, resulting in the extrusion of the Deccan traps on the Indian continent, but its production has steadily declined since, to the current rate of only about 0.04 km^3/yr on Reunion island today. (After White, 1993.)

duced the Iceland-Faeroes-Greenland ridge and extensive basaltic crustal formations on the rifted margins of the northern North Atlantic. A magma production rate of this plume has been estimated as 0.24 km^3/yr. It is clear from the above earlier discussion that melt production rates in currently active hot spots are at least an order of magnitude lower than those that occurred during peak production of the LIPs discussed earlier. When we consider together the evidence from LIPs and currently active mantle plumes, it appears that the peak magma production rate of a plume lasts only a few (2–5) million years, during which most of the magma is emplaced, and that rates build up and fall off exponentially with time.

The variations in melt production rates in mantle plumes are likely to be controlled by two factors. One is the intrinsic properties of the mantle plume (e.g., its potential temperature, magma flux, and dimensions); the other factor is the thickness of the lithosphere overlying the plume. As the plume rises within the mantle, melting will occur as a result of decompression, and the extent of melting is controlled in part by the thickness of overlying lithosphere. If the lithosphere is thick, decompression is insufficient to bring about extensive melting, and rise of the plume head is checked at great depth beneath the thick lithosphere. Where the lithosphere is thin, however, such as beneath a rifting continental lithosphere or beneath young oceanic lithosphere, large quantities of melt may be produced in response to decompression of the mantle as it ascends to regions of lower pressure.

It is clear from studies of currently active hot spots and from the emplacement of LIPs that this type of volcanism is highly episodic on the Earth, and the inception of such episodes is most likely related to the arrival of the heads of large mantle plumes at the base of the lithosphere. The origin of the mantle plumes remains in the realm of speculation, but they may originate from thermal or mechanical instabilities in the seismically anomalous and heterogeneous D″ layer at the boundary between the Earth's core and the mantle, at a depth of about 2900 km (see Mantle of the Earth chapter).

V. VOLCANIC ARCS

Explosive volcanism above subduction zones plays a fundamental role in the exchange of mass and energy between the solid Earth and the oceans and atmosphere. Just as variations in ocean ridge and plume activity discussed earlier have become the focus of intense study, there is a compelling need to examine long-term variations in volcanism associated with subduction zones, especially when we consider that such events have the potential for profound societal impact. In terms of environmental effects, episodes in volcanic arcs are likely to have a greater immediate impact than any variations in the rates of ocean ridge volcanism, because the former are dominantly subaerial, with discharge of potentially climate-modifying volatiles directly into the Earth's atmosphere. Large-scale siliceous eruptions that generate voluminous pyroclastic flows (ignimbrite deposits) represent the largest type of volcanic event known on Earth, and individual eruptions may discharge up to several thousand cubic kilometers of magma during a single event. Large ignimbrite eruptions occur relatively infrequently (one event every 20,000 years erupts a volume >1000 km^3), but significant uncertainties exist regarding variations in the rate of this type of volcanism on Earth or in a given volcanic province. Such events are of great interest, however, because of their potential for global environmental change.

Unlike the rates of seafloor spreading and oceanic crustal formation, the rates of island arc magma generation and volcanism are difficult to determine in a quantitative manner. The products of subduction zone magmatism contribute to the construction of the volcanic edifice of the arc, but a large fraction of the erupted material is deposited in adjacent ocean basins (see chapter on Volcaniclastic Sedimentation around Island Arcs). Unraveling the land-based record of arc volcanism in a major ignimbrite province is hampered by the paucity and poor precision of many radiometric age dates, lack of mappable stratigraphic levels, and poor preservation of deposits. The evidence of major explosive volcanic eruptions is, however, well preserved in the marine environment adjacent to subduction zones as volcanic ash, or tephra layers, interbedded with deep-sea sediments. The marine tephra record is condensed in thickness compared with the terrestrial one, but it is more likely to be complete and easily dated by biostratigraphic methods and radiometric dating of phenocrysts found in the tephra layers. Thus the relative variations in the rates of explosive volcanism in arcs can be well determined from marine tephra layers, whereas the absolute values of magma production rate are poorly determined.

Estimates of Holocene rates of magma production and eruption in volcanic arcs are from 1 to 5 × 10^{12} kg^{-1} yr^{-1}. Most are probably underestimates, because they rarely take into account the large mass fraction of volcaniclastics deposited in adjacent sedimentary basins. Intuitively, one would expect that the volcanic production rate in an arc correlates with the rate of plate convergence; however, these rates do not appear to be simply related. If we examine the current estimates of extrusion rates (expressed as the volume rate per kilometer of arc length) and rates of plate convergence for the Aleutians, the Lesser Antilles, Japan, and the Cascades province, the extrusion rate varies by about a factor of 2 (from about 4 to 9 km^3 my^{-1} arc km^{-1}), while the plate subduction rate varies by almost an order of magnitude (2 to 9 cm^{-1} yr^{-1}) and there is no simple correlation observed between these two parameters.

A. Volcanic Episodes in Arcs

Explosive volcanism in island arcs is recorded as tephra layers in the ocean basins, and this record forms an important archive of the temporal and regional variations in arc volcanism. The tephra layers are centimeters to tens of centimeters in thickness, and represent the fallout of airborne volcanic ash hundreds or even thousands of kilometers from the source. Their thickness indicates that they are derived from individual explosive eruptions involving hundreds to thousands of cubic kilometers of magma, of the type that occur only about once in 10,000 yr in the Holocene.

Global compilations of the distribution of thousands of tephra layers in deep-sea cores from drilling of the ocean basins during the Deep Sea Drilling Project and the Ocean Drilling Program shows that their occurrence is remarkably episodic in geologic time (Fig. 6). The

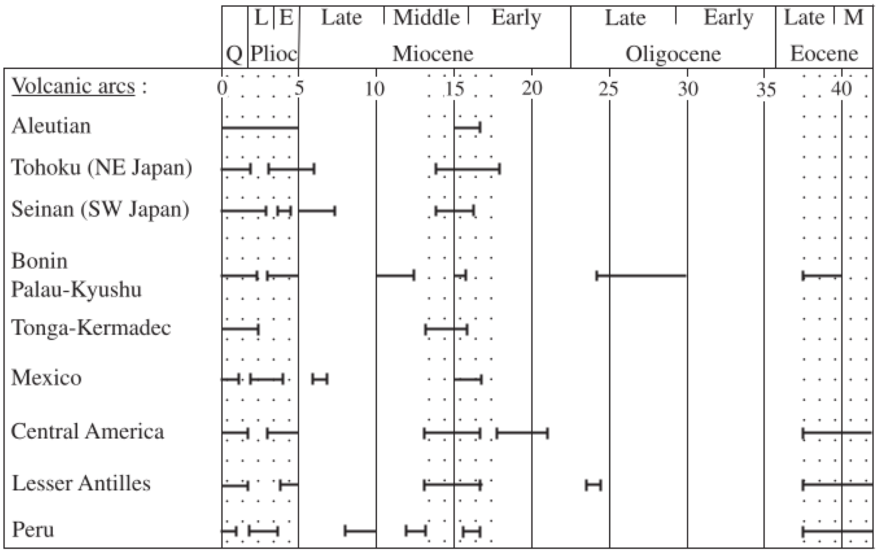

FIGURE 6 The occurrence of volcanic ash layers in deep-sea sediments near volcanic arcs is highly episodic. The horizontal bars show the periods of major tephra deposition for a number of circumpacific and Caribbean arcs, defining three principal global volcanic episodes (dotted regions) in the Pliocene to Quaternary (0–5 Ma), Miocene (13–17 Ma), and Eocene (37–42 Ma). (After Cambray and Cadet, 1996.)

frequency of volcanic ash layers shows a pronounced peak at all circumpacific sites in the Quaternary (0–5 Ma) and in the middle Miocene (ca. 13–17 Ma), and in addition, there is evidence for a volcanic episode in the Eocene (ca. 37–42 Ma). The results of recent drilling on ODP Leg 165 in the Caribbean region have reinforced the concept of volcanic episodes in island arcs, providing a more detailed record of volcanism throughout the Cenozoic with the recovery of more than 2000 tephra layers. The Caribbean tephra record, principally resulting from explosive ignimbrite-forming eruptions in the Central American arc, is compared in Fig. 7 with the global volcanic ash layer record. There is good agreement between the two in terms of a late Eocene to earliest Oligocene episode and the middle Miocene episode, whereas the Quaternary episode is poorly represented in the Caribbean record. While these marine tephra layers faithfully record the larger and typically silicic explosive eruptions, this archive does not normally contain a record of the andesitic and basaltic volcanism that typically forms an important component of arc evolution.

The global volcanic ash record shows an interesting relationship to the foraminiferal oxygen isotope record of the Cenozoic ocean, as also shown in Fig. 7. The ∂^{18}O curve shows three abrupt steps, with major increase in ∂^{18}O coinciding with the volcanic episodes. These oxygen isotope events represent the major global climate cooling stages during the Cenozoic; their relationship to the volcanic episodes is a tantalizing idea, but a cause-and-effect relation remains speculative. One could hypothesize that during a single volcanic episode, the flux of sulfur dioxide gas from explosive eruptions to the atmosphere results in the buildup of a sustained sulfuric acid aerosol in the stratosphere, resulting in global cooling.

Regionally, such as in the Caribbean and Central America, the marine tephra record shows clear evidence of volcanic episodes. Such episodes could be attributed

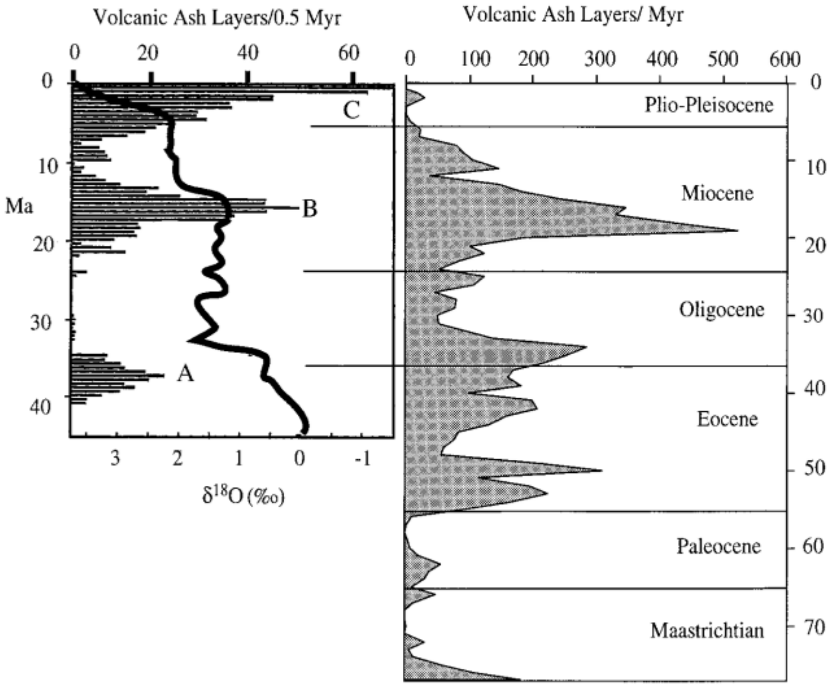

FIGURE 7 Comparison of global and Caribbean volcanic episodes, based on deep-sea tephra layer occurrence. The global compilation of marine tephra layers on the left (Herve Cambray, personal communication, 1999) shows three episodes: (A) in late Eocene to earliest Oligocene, (B) middle Miocene, and (C) Plio-Pleistocene. The right-hand panel show the tephra layer distribution in Caribbean sediments (ODP Leg 165). The early Eocene Caribbean episode is local, related to activity of the Cayman arc, while the late Eocene and middle Miocene episodes correspond to those of the global record. Also shown as a curve superimposed on the left-hand panel is the ∂^{18}O of benthic foraminifera in Atlantic sediments. Major steps in the oxygen isotope trend (increase) coincide with the volcanic episodes, and they mark the principal cooling steps in the climate history of the Cenozoic.

in turn to regional tectonic evolution of the subduction zone. Various ideas have been put forward to explain variations in the rate of volcanism. An accelerated rate of plate subduction could conceivably increase mantle upwelling in the mantle wedge below arcs, and enhance partial melting. Similarly, increased subduction of sediment may increase the flux of water and other volatiles that act as fluxing agents and lower the temperature of beginning of melting in the mantle and arc lithosphere. It is important to recognize, however, that the observed volcanic rate variations are almost entirely measured by the eruptions of high-silica magmas, whereas most of the plate tectonic and petrogenetic parameters relate to generation of primary basaltic melts.

While local or regional variations in rates may be accounted for, the indication of global episodes in explosive volcanism in arcs poses a major and unresolved problem for geologists. The concept of global synchroneity of explosive volcanism is particularly difficult to reconcile with the paradigm of plate tectonics. At any one time, the various subduction zones on Earth experience a spectrum of the parameters that may affect the rates of subduction zone volcanism, such as the rates and direction of plate motion and the age and composition of the subducting slab. No unifying mechanism is obvious that could lead to a simultaneous increase in global eruption rates. A possible exception to this may be the rate of sediment subduction. The high global rates of explosive volcanism in the Quaternary could possibly be related to increased availability of sediment for subduction, when the rate of sedimentation increased globally in response to accelerated continental erosion. In this scenario, the increased availability of sediment could result in greater rate of subduction of sediment and water, accelerating magma generation. Such a hypothesis does not account, however, for the Miocene and Eocene explosive volcanic episodes. Variations in the rate of volcanism may conversely be a response to climate-driven crustal dynamics, such as changes in sea level and glacier loading brought about by climate change.

SEE ALSO THE FOLLOWING ARTICLES

Earth's Volcanoes and Eruptions: An Overview • History of Volcanology • Mantle of the Earth • Melting the Mantle • Volcaniclastic Sedimentation around Island Arcs • Volcanic Plumes

FURTHER READING

Albritton, C. C. (1989). "Catastrophic Episodes in Earth History." Chapman and Hall, London.

Cambray, H., and Cadet, J.-P. (1996). Synchronisme de l'activite volcanique d'arc: Mythe ou realite? *C.R. Acad. Sci. Paris* **322,** series IIa, 237–244.

Chesner, C. A., Rose, W. I., Deino, A., Drake, R., and Westgate, J. A. (1991). Eruptive history of Earth's largest Quaternary caldera (Toba, Indonesia) clarified. *Geology* **19,** 200–203.

Coffin, M. F., and Eldholm, O. (1994). Large igneous provinces: Crustal structure, dimensions and external consequences. *Rev. Geophys.* **32,** 1–36.

Crisp, J. A. (1984). Rates of magma emplacement and volcanic output. *J. Volcanol. Geotherm. Res.* **20,** 177–211.

Crowley, T. J., Christie, T. A., and Smith, N. R. (1993). Reassessment of Crete (Greenland) ice core acidity/volcanism link to climate change. *Geophys. Res. Lett.* **20,** 209–212.

Gill, J. (1981). "Orogenic Andesites and Plate Tectonics." Springer Verlag, Berlin.

Hallam, A. (1983). "Great Geological Controversies." Oxford University Press, London.

Larson, R. (1991). Latest pulse of the Earth: Evidence for a mid-Cretaceous superplume. *Geology* **19,** 547–550.

Parsons, B. (1981). The rates of plate creation and consumption. *Geophys. J. Roy. Astr. Soc.* **67,** 437–448.

White, R. S. (1993). Melt production rate in mantle plumes. *Phil. Trans. Roy. Soc. Lond.* **342,** 137–153.

PART III

EFFUSIVE VOLCANISM

The term effusive volcanism refers to the nonexplosive extrusion of magma at the surface, and thus includes all eruptions of lava flows, coulees, and domes. Effusive volcanism exhibits a remarkable variety of eruptive styles, environments, and deposits. Ranging from subaerial eruptions to those occurring at great depths in the sea or under vast glaciers, effusive eruptions are ubiquitous on the Earth's surface, as well as on some of the terrestrial planets. Although effusive volcanism is by definition nonexplosive, it is clearly related to explosive activity in many instances.

The chapter Basaltic Volcanoes and Volcanic Systems introduces the different types of basaltic volcanoes whose eruptions produce mainly lava flows. These volcanoes should be more properly thought of as volcanic or magmatic systems, since beneath each volcano is a complex system of magma generation, transport, and storage. Monogenetic volcanoes erupt only once, whereas polygenetic volcanoes erupt repeatedly. Lava shields are low-angle volcanoes built by rapid effusions of basaltic lava and intrusions of magma at shallow depths. Stratovolcanoes are steeper edifices constructed of pyroclastic material as well as lavas; these volcanoes are normally associated with subduction zones, with magmas that tend to be rich in gas. Flood basalts are vast lava flow fields that are erupted rapidly from fissure systems located in areas of broad crustal extension. Central volcanoes comprise an outer zone, in part basaltic composition, and an inner zone with more silica-rich compositions; these volcanoes may have central calderas.

The different types of lava flows are treated in the chapter Lava Flows and Flow Fields. Interestingly, lava is the single most common feature on the surface of the terrestrial planets. Three main types of lava crusts are observed on Earth: pahoehoe, aa, and blocky. Pahoehoe is a smooth, continuous basaltic lava crust; aa is also basaltic but broken and irregular; and blocky lava is fragmental but less irregular and more silica-rich than aa. Most lava flows do not travel very fast, but some are extremely rapid. The development of a lava flow depends on the effusion rate at its source, its physical properties, and its environment, such as the local topography, subaerial, submarine, and so forth. The potential lengths of lava flows depend on several factors, chief among which is the effusion rate.

When magmas become more silica-rich than basalt, lava domes may form instead of lava flows. The chapter Lava Domes and Coulees examines different types of lava domes and why they form. Sometimes a lava dome is transitional to a lava flow, in which case it is called a coulee. Since the outer skin of a lava dome may cool and form a crust, buildup of pressure may occur within the dome's interior, leading to explosive activity such as vulcanian eruptions, pyroclastic flows, and pyroclastic surges. Indeed, cyclic dome growth and destruction have been observed at various volcanoes. If a dome grows rapidly, it has an increased tendency to collapse, frequently resulting in pyroclastic flows.

Fire fountains and spatter-fed lavas are discussed in the next chapter, Lava Fountains and Their Products. Fire fountaining is generally characteristic of basaltic magma, which is both fluid and rich in dissolved gas; the reader will no doubt have a good image of the spectacular curtains of fragmental material thrown into the air by fire fountaining to many tens or even hundreds of meters. The fountains can occur along eruptive fissures or from central vents. The combination of rapid magma ascent and decompressive degassing and vesiculation forms the fountains. As the fragments fall to the ground, they may cool and remain in place, perhaps adhering to each other if they are still sufficiently hot and fluid. If the accumulation rate of particles is rapid, then the fragments may actually coalesce and flow as lava. This flow may not show any evidence of its initially fragmental origin.

The following chapter is Basaltic Volcanic Fields. Such fields are favored when the magma production rate is comparatively low and the crustal extension rate is high. The fields comprise a diverse variety of volcanic centers such as cones, maars, tuff rings, small shield volcanoes, and lava domes. The centers are frequently monogenetic, a good example being Parícutin in Mexico, which erupted in the 1940s. The various volcanic centers may show structural control such as linear alignments, suggesting control along fault systems and the presence of dikes beneath the vents. The volcanic centers also may show clustering; they are found frequently on the flanks of larger volcanoes, as well as inside and outside the margins of calderas.

The following chapter is Flood Basalt Provinces. In contrast to basaltic fields where the magma production rate is low, flood basalt provinces are characterized by huge volumes of lava erupted rapidly over only one to two million years. Due to the high extrusion rates, basalt plateaus are formed instead of conical volcanic edifices. The magmas appear to come from great depths and are clearly associated with mantle plumes (hot spots), thinned lithosphere, and the breakup and separation of tectonic plates. Individual lava flows can be enormous in terms of their volume, area, and length, and the flows may be turbulent.

Submarine lava flows are the most abundant igneous rock type on the Earth's surface; the chapter Submarine Lavas and Hyaloclastite details the remarkable deposits found in this environment. At great depths in the ocean, exsolution of volatiles is hindered by the weight of the ocean mass, favoring lava flows at the expense of pyroclastic rocks. At shallower levels where the hydrostatic pressure is diminished, explosions are more feasible. The lavas are characterized by rapid cooling by seawater, resulting in pillow lavas, lobate lavas, and sheet flows, in order of increasing effusion rate. The rapid cooling also can thermally shock the lava, causing fragmentation and forming glassy fragments called hyaloclastite.

As submarine volcanoes evolve, they may progress to build seamounts or oceanic islands, the focus of the chapter Seamounts and Island Building. Seamounts may occur in clusters or chains, with the chains exhibiting a systematic age progression from one end to the other. The sizes of seamounts vary considerably; seamounts found in intraplate settings are generally much larger than those situated on or near mid-ocean ridges. Seamounts record a constructional stage that depends on the water depth, magma composition, eruption rate, and surrounding topography. As a seamount approaches the surface of the ocean, the observed proportion of fragmental rocks to lavas increases because explosive activity is facilitated at shallower depths. Seamounts also record valuable information on mantle upwelling, lithospheric subsidence, and sea level changes.

Subglacial Eruptions closes this section on effusive volcanism by looking at eruptions that occur beneath glaciers. The chapter provides a useful bridge to the next section on explosive volcanism, because subglacial eruptions can be both effusive and explosive in nature. Large volumes of water are generated rapidly by melting of ice by the eruption; these volumes are sometimes drained catastrophically, resulting in huge floods called jökulhlaups. The large volumes of water also result in magma–water interactions that influence eruptive activity, such as hydrovolcanic eruptions.

John Stix
McGill University

This Page Intentionally Left Blank

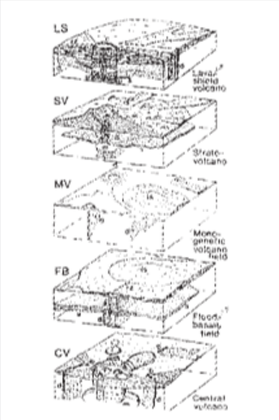

BASALTIC VOLCANOES AND VOLCANIC SYSTEMS

GEORGE P. L. WALKER
University of Bristol

I. Introduction
II. Lava Shield Volcanoes
III. Stratovolcanoes
IV. Monogenetic Volcano Fields
V. Flood Basalt Fields
VI. Central Volcanoes

GLOSSARY

central volcano A volcano that erupts magmas of various compositions, for example, basalt and rhyolite. These volcanoes frequently have calderas in their central parts.

decollement A detachment structure resulting in differential movement of rock above and below.

lava shield volcano A low-angle volcano constructed principally of basalt lava flows.

monogenetic volcano A volcano that erupts only once.

polygenetic volcano A volcano that erupts repeatedly, often in an episodic manner.

stratovolcano A volcano constructed of alternating layers of lava flows and pyroclastic rocks. Stratovolcanoes are steeper than shield volcanoes.

I. INTRODUCTION

More than half of all volcanoes consist wholly or largely of basalt. Basaltic volcanoes are found in all tectonic settings. They follow both convergent (volcanic arc) and divergent (oceanic rift) plate boundaries, occur at hot spots and areas where crustal extension is taking place, and are developed on a vast scale on the ocean floors. This chapter describes their occurrences on land.

A basic relationship is that some volcanoes (called *polygenetic*) erupt repeatedly, whereas other volcanoes (called *monogenetic*) are born, erupt once only, and then die. Polygenetic volcanoes have a sufficiently large and persistent magma supply rate that an ascending magma batch will preferentially follow the still-hot pathway of the preceding batch. Conversely, a volcano is monogenetic if the magma supply is so small or episodic that any pathways have cooled down and are no longer favored routes for the next magma batch.

Polygenetic volcanoes are generally considered to possess a magma storage chamber at a neutral buoyancy level. Magma ascends into this chamber mainly because of its positive buoyancy (but sometimes aided by tectonic forces). Processes in the chamber, such as the exsolution of gases, modulate the output.

Copyright © 2000 by Academic Press
All rights of reproduction in any form reserved.

When describing volcanoes it is of great merit to recognize the existence of a larger entity, namely, the volcanic (or magmatic) system. A system may embrace the melting anomaly at the magma source, the conduits through which magma rises toward the surface, the magma chambers, intrusions, and geothermal zones, and the volcano itself.

A volcanic system may be crudely compared with a civilization system (a city), with the extensive infrastructure of transportation, water and power supply, waste disposal, and communications on which a city depends. Both systems are sustained by an input of energy (as hot magma and gases, or in the city system as fossil fuels, electric power, and food). Very roughly, a city of 1 million people requires about the same annual power input as an average-sized volcanic system having an annual magma input of 1 million cubic meters.

In this chapter a fivefold grouping of basaltic volcano systems is presented (Fig. 1). The two main parameters that control volcano type are the time-averaged magma supply rate and the frequency of incoming magma batches, as shown by Fig. 2.

II. LAVA SHIELD VOLCANOES

Examples of lava shield volcanoes are Mauna Loa and Kilauea in Hawaii. They consist largely of thin lava flows, with minor pyroclastic layers. Their subaerial slopes are mostly 4–8 degrees (less on coastal lava deltas). They have steep-walled summit calderas (Fig. 1a) and also pit craters that are similar to calderas in form but smaller. Mauna Loa, at 40,000 km^3 the largest volcano on Earth, stands 4169 m above sea level and 8 km above the ocean floor, plus an additional 4 km where the base of the volcano has sagged because of its huge mass. Mauna Loa and Kilauca are the most productive volcanoes on Earth, having a combined lava output of about 8 km^3 per century.

The low-angle shield form results from the low lava viscosity, the commonly high effusion rates that drive lavas fast and far, the high proportion of lava that issues from flank vents and not from the summit, and the spreading (widening) and subsidence of the volcano that occurs in the summit area and rifts.

A point of confusion is that lava shields occur on two scales. The name is applied to mainly large polygenetic structures, but also to mainly small monogenetic structures. The latter may be termed shields of scutulum

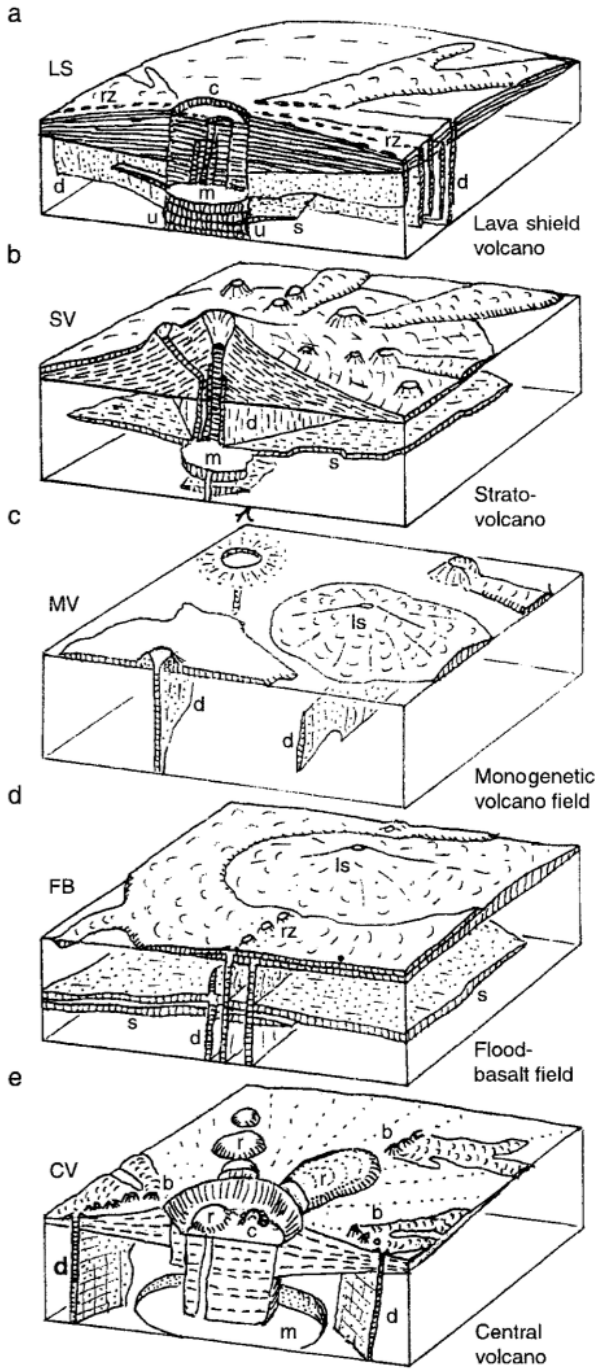

FIGURE 1 The five types of basaltic volcano systems illustated schematically by block diagrams. *Key:* b, basaltic vents; c, caldera; d, dike; is, lava shield of scutulum type; m, magma chamber; rz, rift zone; r, rhyolitic lava dome; s, sill or intrusive sheet; u, plutonic, gabbroic, or ultramafic rocks. (1993, Geological Society of London.)

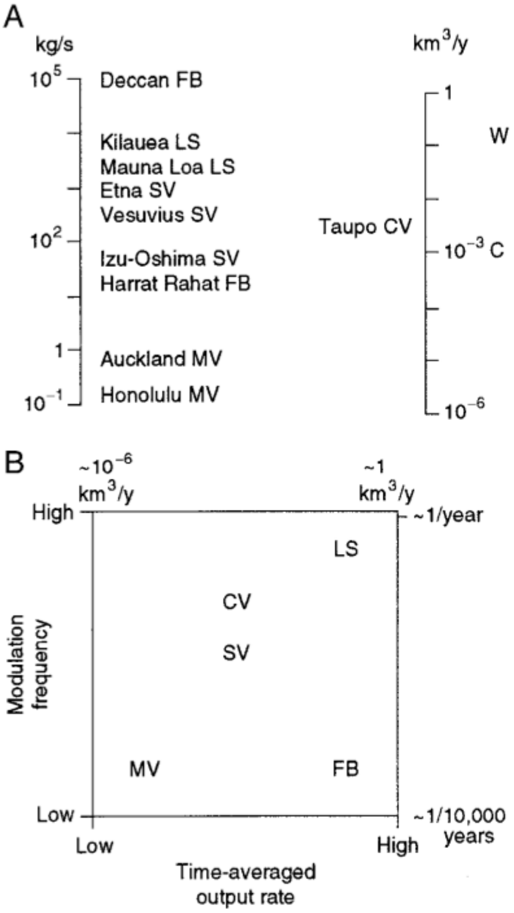

FIGURE 2 (A) Time-averaged output rates of selected volcanic systems in kilograms per second and in cubic kilometers per year. Note that the greatest outputs are by flood basalt and lava shield systems, and the smallest by monogenetic volcano systems. *Key:* W, equivalent world energy consumption by mankind, excluding food; C, equivalent energy consumption, including food, by city having a population of 1 million. (B) Plot of the time-averaged output rate against modulation frequency (i.e., eruption frequency), the two main inferred controls on volcanic system types, showing the approximate average positions occupied by the five kinds of basaltic volcano systems. Semiquantitative scales are shown along the top and right-hand side. (1993, Geological Society of London.)

type (from Latin *scutulus*, the diminutive of *scutus*, meaning "shield").

Each large Hawaiian shield volcano has two narrow and well-defined colinear rift zones extending to as far as 250 km from the summit. Some volcanoes also have a third and less well defined rift. Eruptions are concentrated at the active rift zones. Vent edifices range from low ramparts consisting of highly expanded scoria and spatter formed when magma viscosity was least, to cinder cones up to 200 m high when viscosity was appreciably higher. Spheroidal and spindle bombs are common at cinder cones.

Two main morphologic types of lava flows occur. One, called *pahoehoe*, is smooth surfaced. The other, called *aa*, has a thick upper zone of loose clinkery or rubbly debris. Pahoehoe results when the volumetric flow rate of lava is low, and aa forms when it is high. Viscosity is indirectly involved, because aa still flows strongly after significant cooling, to the point where lava viscosity is too high for breaks in the surface crust to be healed.

Volcanic eruptions are mostly from fissures, and intense complexes of intrusive dikes (the subsurface manifestation of eruptive fissures) underlie the caldera and rift zones. A traverse across the Koolau volcano (Oahu, Hawaii) contains an estimated 7400 dikes, totaling in aggregate 4.5 km wide. It is inferred that coarse plutonic (gabbroic) rocks may underlie the dike complex.

Shouldering aside of the preexisting volcanic edifice by dikes is largely responsible for the seaward movement, by decimeters per year, of the southern flank of Kilauea. Movement is thought to occur on a decollement—a low-angle fracture zone on which lateral movement occurs—in slippery subvolcanic marine sediments. Major prehistoric volcano collapses, some involving as much as 1000 km^3 of rock, have occurred repeatedly in the history of some volcanoes. They include catastrophic rock avalanches that carried debris 200 km over the ocean floor. A surface limestone breccia reaching to 326 m above sea level on Lanai (Hawaii) is widely thought to be the deposit of a tsunami generated by a catastropic collapse event.

Shield volcanoes elsewhere may deviate somewhat from the Hawaiian model. Some in the Galapagos Islands of Ecuador have radial dike swarms; also their shield culminates in a steep dome and deep summit caldera; a circumferential (annular) rift zone occurs around the caldera rim. Piton des Neiges (Reunion Island, Indian Ocean) is cut by swarms of flat-lying intrusive sheets in lieu of dikes. Maderia and Tahiti are dissected by profound erosional canyons.

A few shield volcanoes have persistent active lava lakes in their summit caldera. The most famous lava lake was that in Halemaumau pit crater (Kilauea), which persisted for more than a century until it drained into fissures in 1924. Drainout was accompanied by violent groundwater explosions. Others are found in Erta Ale (Afar, Ethiopia), Mount Erebus (Antarctica), and Nyiragongo (Congo). Lakes are sustained by strong magma convection in the conduit that joins them to their magma chamber.

The escape of a flood of highly fluid lava from Nyiragongo lava lake in 1977 gave rise to remarkably fast-moving (ca. 60 km/hour) lava flows that killed many people. Elephants were also overcome, and in a bizarre twist their carcasses were coated by a thin layer of lava.

Hawaiian lava shields at the peak of their activity erupt tholeiitic lava derived by a high degree of partial melting from mantle peridotite source rock. With declining activity, alkali basalts are erupted from scatters of flank vents as the summit magma chambers solidify and rift zones are no longer preferred pathways. Later, highly alkalic (e.g., nephelinite) lava derived by a low degree of partial melting may erupt in a "rejuvenation stage" of volcanism that builds small fields of monogenetic volcanoes.

III. STRATOVOLCANOES

Stratovolcanoes consist of explosively erupted cinders and ash interbedded with lava flows. They tend to a steeply conical form (Fig. 1b), and in their upper part stand at the repose angle of loose rock (about 35 degrees measured from the horizontal). Among the largest are Huzi (Fuji) in Japan and Klyuchevskoy in Kamchatka, which rise 3700 and 3000 m, respectively, above their surroundings and have estimated volumes exceeding 1000 km^3.

The birth and growth of two stratovolcanoes has been observed. One, Izalco in El Salvador, was born in 1769 or 1770 and was almost continually active until 1966 by which time it had built to 650 m high. The other, Cerro Negra in Nicaragua, was born in 1850 and in the 17 eruptions since then grew to a similar height. Both began as cones of cinders and ash and became buttressed by lava flows.

A few volcanoes, notably Etna and Stromboli in Italy, display very persistent activity, and molten lava resides in their summit crater for decades or longer. Stromboli has many small explosions daily that throw up incandescent lava clots, and evidently it behaved similarly to at least as far back as ancient Roman times when it was referred to as the "Lighthouse of the Mediterranean."

Some stratovolcanoes such as Oshima in Japan erupt at fairly regular intervals (their activity is time predictable), or the volumes of erupted lava are proportional to the lengths of the preceding repose periods (their activity is volume predictable). From a broader perspective, such volcanoes exhibit steady-state conditions, consistent with the notion that magma feeds steadily into the magma chamber, but enough must be stored there before it can erupt.

Basalts in arc settings are tholeiitic or calcalkaline and merge with increasing silica content to andesites. The prevalence of rather violent explosive activity, the occasional generation of pyroclastic flows as were observed on Lopevi (Vanuato) in 1960 and Ulawun (Papua New Guinea) in 1978, and the prevalence of rough rubbly and blocky lava surfaces point to magma viscosities generally higher than those of shield tholeiites.

Many of the volcanic rocks of stratovolcanoes are porphyritic, that is, they contain macroscopic crystals (called phenocrysts) that grow in the cooling magma, likely in the magma chamber or conduit. Phenocryst minerals include plagioclase olivine and pyroxenes. Phenocrysts in the highly fluid shield tholeiites have commonly settled through the lava to produce striking local (decimeter-scale) concentrations. In contrast, the phenocrysts in stratovolcanoes are suspended in the lava and tend to be uniformly distributed through each lava flow. The phenocrysts are, thus, useful indicators of lava viscosity.

Many stratovolcanoes have cinder cones and craters of parasitic (adventive) vents on their flanks. Hundreds occur, for example, on Etna. Alignments of vents mark eruptive fissures. In some volcanoes these linear features have a radial distribution. In others they tend toward a parallel arrangement and delineate rift zones. Rift zones in arc volcanoes tend to be aligned parallel with the tectonic plate-convergence trajectory.

Many stratovolcano cones have been truncated by caldera collapse. Vesuvius in Italy is an example. The caldera in this case is asymmetric and is horseshoe-shaped in plan. The rim is called Monte Somma. Many stratovolcanoes have a lake in their crater. On the more active volcanoes the lake is steaming hot and muddy. It is also strongly acidic, due to the influx of hot acidic gases (SO_2, HCl) from the magma chamber. When hydrothermal and phreatic explosions occur they eject mud and strongly weathered rocks. In the less active lakes the water often has brilliant blue or green colors, attributed to minute particles of sulfur in the water.

IV. MONOGENETIC VOLCANO FIELDS

These are clusters or scatterings of small monogenetic volcanoes, each of which erupts once only. Many of the volcanoes comprise a cinder cone, commonly with associated lava flows (Figs. 1c and 3). Some are small lava shields. Others are tuff rings or maars cored out by phreatomagmatic explosions (where lava exploded in contact with water) at vents on low-lying ground or under water. The shields are of the scutulum type, for example, Rangitoto Island in the Auckland field (New Zealand), which is 5.5 km in diameter, 140 m high, and 1.0 km^3 of it occurs above sea level.

A typical monogenetic field may contain 10–100 volcanoes of aggregate volume about 10 km^3, and may span 50 ka to 5 Ma. The Michoacan-Guanajuato field in Mexico is much larger than average; it contains more than 1000 volcanoes, but merges into and partly consists of flood basalts. It had two historic eruptions. One saw the birth of El Jorullo in 1759–1774, a line of four or five cones along 3.4 km of fissure, and a lava field covering 12 km^2. The main cone rises about 330 m above its base. The other eruption, that of Paricutin in 1943–1952, was andesitic.

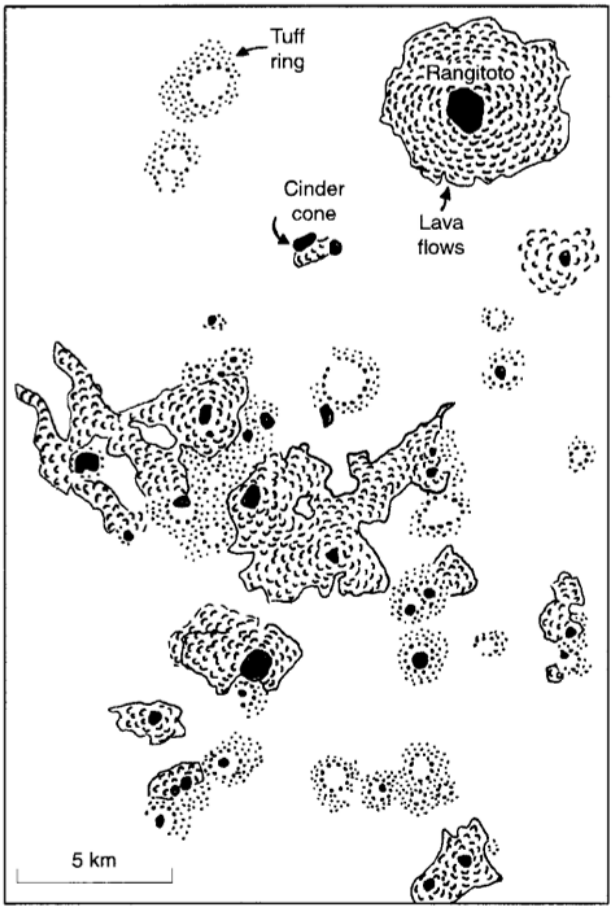

FIGURE 3 Sketch map of the Auckland, New Zealand, monogenetic field, simplified by deleting the coastline. (1993, Geological Society of London.)

Deeply eroded monogenetic fields are known in many places, for example, in East Fife (Scotland) where about 100 volcanic vents, the roots of monogenetic volcanoes, occur over an area 25 km across. Some vents are plugs of basalt. Others are diatremes, which are vertical pipes filled with explosively fragmented volcanic tuff and other debris. Dikes occur in other fields.

Monogenetic fields occur in volcanic arcs, where the basalt is associated with andesites, and they also occur in hot spot settings where the basalt is alkalic. A feature of the latter is that the basalt contains included fragments of mantle-derived ultramafic rock, often loosely referred to as olivine nodules. The presence of these inclusions indicates that the magma rose without pause from the mantle: if the magma had paused, the inclusions would have dropped out.

Rarely, the pipes in monogenetic fields contain diamonds. Diamonds form under very high pressures, equivalent to depths of 200 km or more. Their survival depends on being transported very rapidly from the mantle to the surface, otherwise they oxidize and are destroyed.

V. FLOOD BASALT FIELDS

These consist of voluminous and extensive spreads of lava flows erupted from scattered monogenetic fissure vents. They tend to flood the landscape and generate a new landscape of subdued relief (Figs. 1d and 4). They occur at hot spots where significant crustal spreading has occurred, for example, the Snake River Plain (Idaho), Iceland, and the fields in Arabia and Syria that parallel the Red Sea/Dead Sea rift system. Individual fields cover 3×10^3 to 5×10^5 km^2. Outpourings of particularly large "giant" fields such as the Deccan in India have punctuated Earth's history, and are approximately coincident with mass bioextinction events.

Many individual lava flows have volumes exceeding 10 km^3. Youthful examples include the 1783 Laki lava in Iceland, which covers 565 km^2 and has a volume of 10–15 km^3; and the Toomba flow in Queensland, Australia, which flowed 120 km down an average gradient of only 0.2 degrees. Giant fields such as the Columbia River Plateau in Washington state (USA) contain flows exceeding 1000 km^3 in individual volume. Vents are marked by crater rows of spatter, agglutinate, and cinders. Commonly, fissure vents evolved to point

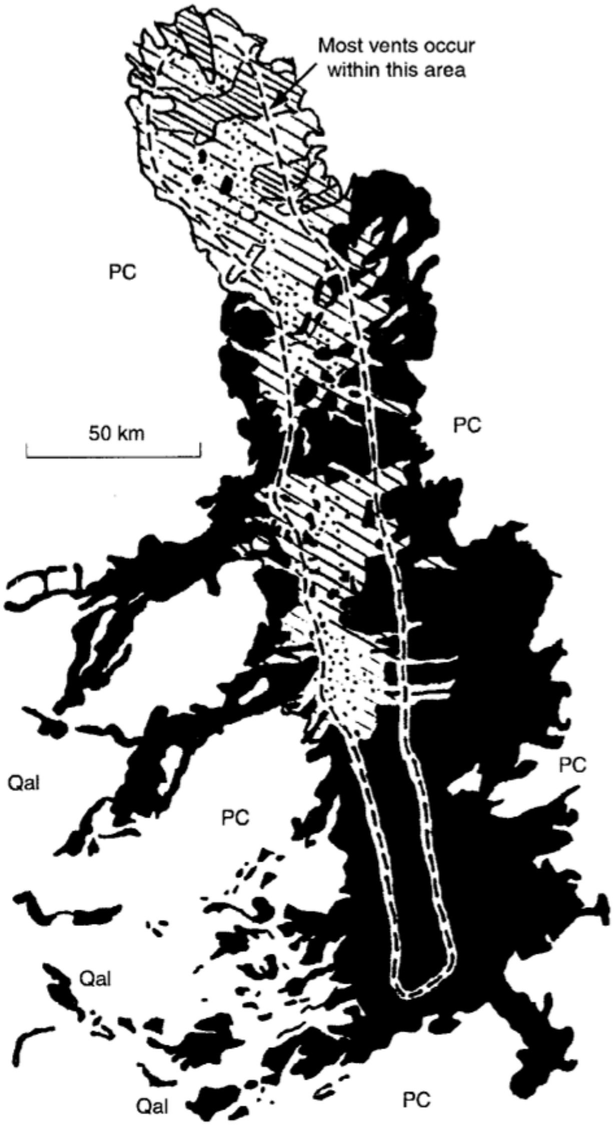

FIGURE 4 Sketch map of a moderate-sized flood basalt field: Harrat Rahat in Arabia. Solid black, lava 10–1.7 Ma; open diagonal shading, 1.7–0.6 Ma; dots, vents; closed diagonal shading, lavas under 0.6 Ma including those of historic eruptions in A.D. 641 and 1256; dashed line, approximate limit of vents; PC, Precambrian basement rocks; Qal, Quaternary sediments near Red Sea coast. (1993, Geological Society of London.)

sources where vent widening by localized wallrock erosion was concentrated.

Many lava flows are compound, meaning that they are divided into flow units, each unit having chilled margins against its neighbors. Great accumulations of pahoehoe flow units form shields of the scutulum type typically sloping at 1–7 degrees. A fine example from Iceland is Skjaldbreid, 8 km in diameter and rising about 500 m above its base. Flood basalt fields in Iceland consist of many overlapping low-angle shields. Many of the compound lavas exhibit structures caused by endogenous growth as freshly erupted lava injected under and lifted up the surface crust, and lava tubes formed where lava drained out from under the crust.

Flow units are thickest where erupted on shallow slopes. They then commonly exceed 10 m thick. They exhibit distinctive pipe vesicles (elongate gas bubbles) and segregation bodies (vesicle cylinders and segregation veins). Lavas ponded in depressions may rest on lignite coal deposits (the fossilized contents of former marshes) and lake sediments. They show columnar jointing.

Eroded flood basalt fields are normally seen to have inwardly directed dips due to subsidence that are greatest where the lava pile is deepest. They are cut by linear dike swarms that locally comprise 5–20% of total rock. Good examples occur in the Hebridean Volcanic Province in Scotland. A typical swarm is 20 km wide by more than 100 km long, and in cross traverses dikes typically number hundreds and may aggregate up to 2 km wide. Dikes are narrowest and the swarm most intense where, locally, a flood basalt field is capped by a central volcano.

VI. CENTRAL VOLCANOES

Central volcanoes are volcanoes that erupt silicic as well as mafic (basaltic) magmas. Commonly, the composition is bimodal, and silicic and mafic rocks may each be more voluminous than intermediate rocks. The broad central part of the volcano is mainly or exclusively made of rhyolitic rocks, and flanks consist of flood basalt. Newberry Volcano in Oregon, for example, has basaltic lower flanks 20 km wide, sloping at 1–3 degrees outward, and scattered with 400 cinder cones (Fig. 1e). The main cone and caldera occur in a central zone 12 km wide and consist mainly of rhyolitic rocks including pumice, ash, and obsidian flows. Some pumice and ash layers extend onto the flanks.

Typically, multiple rhyolitic vents occur. They tend to be monogenetic because intervals between rhyolitic eruptions are long (1–1000 ka). The zone in which they occur is crudely circular and typically about 10 km in diameter, embracing the caldera and caldera rim. This zone reflects the width of the inferred underlying silicic magma chamber from which the rhyolitic eruptions stem.

This central area is a shadow zone from which basaltic vents are excluded. This is because of the general inability of basaltic magma to pass up through a chamber that is at least partially molten and is less dense than basaltic magma.

It is envisaged that basaltic magma ascending beneath the shadow zone, being denser than silicic magma, is trapped at the base of the silicic chamber; being hotter it heats silicic magma and by reducing its viscosity and promoting gas exsolution, it mobilizes silicic magma and may trigger eruptive activity.

The coexistence of rhyolitic and basaltic magmas in central volcanoes is manifest as composite dikes (having basaltic rims and rhyolitic center), streaky mixed pumice, mixed lavas (having fluidal-shaped inclusions of basalt in rhyolite), and hybrid rocks.

Central volcanoes generally have one or more calderas, where subsidence of the magma chamber roof occurred as large silicic eruptions, caused partial evacuation of the chamber. Occasionally, rhyolitic vents occur along arcuate lines, for example, around Valles caldera in New Mexico.

Eroded central volcanoes commonly display granitic plutons (inferred to be solidified magma chambers). Ring intrusions and ring faults delineate cauldrons wherein piston-like subsidences of chamber roof occurred. These occurrences are called *ring complexes.* The type examples are found among the roots of a 400-Ma volcanic field in Scotland.

Many central volcanoes host ore deposits (of Ag, Au, Cu, Mo, Sn, W), including many of the porphyry copper type. The ore metals were transported and deposited by hot volcanic fluids. An unusual gold deposit occurs in the hot caldera floor of Lihir volcano, (Papua New Guinea). Ore deposits in central volcanoes are more closely associated with the silicic than with the mafic volcanism, and likewise the spectacular geothermal manifestations (geysers, hot springs, and geothermal power plants) as seen in the Taupo Zone of New Zealand, the Yellowstone Park (Montana), and Iceland.

SEE ALSO THE FOLLOWING ARTICLES

Basaltic Volcanic Fields • Calderas • Flood Basalt Provinces • Lava Flows and Flow Fields • Magma Chambers

FURTHER READING

Chester, D. (1993). "Volcanoes and Society." Edward Arnold, London.

Fisher, R. V., Heiken, G., and Hulen, J. B. (1997). "Volcanoes, Crucibles of Change." Princeton University Press, Princeton, NJ.

Francis, P. W. (1993). "Volcanoes, A Planetary Perspective." Clarendon Press, Oxford.

Kilburn, C. R. J., and Luongo, G., eds. (1993). "Active Lavas: Monitoring and Modelling." University College London Press, London.

Prichard, H. M., Alabaster, T., Harris, N. B. W., and Neary, C. R., eds. (1993). Magmatic processes and plate tectonics, Special Publication 76. Geological Society of London, London.

Scarth, A. (1994). "Volcanoes—An Introduction." University College London Press, London.

Weisel, D., and Heliker, C. (1990). Kilauea, the newest land on Earth, Special Publication 92. Bishop Museum Press, Honolulu, HI.

This Page Intentionally Left Blank

LAVA FLOWS AND FLOW FIELDS

CHRISTOPHER R. J. KILBURN
University College London

I. What Are Lava Flows?
II. Evolutionary Sequences among Lava Flows
III. Field Classification of Lava Flows
IV. The Lava Spectrum
V. Lava Dynamics and Internal Solidification
VI. Shapes of Lava Flow Margins
VII. Forecasting the Behavior of Aa Flows
VIII. Forecasting the Behavior of Pahoehoe and Blocky Flows
IX. Turbulent Lava Flows
X. Lava Flows and Planetary Development
XI. Summary

GLOSSARY

aa lava Lava flows with extremely irregular surfaces, usually covered by fragments of broken crust that are typically decimeters thick. The thickness of the surface crust is controlled by cooling (compare blocky lavas).

blocky lava Lava flows with fractured surfaces, usually covered by debris up to meters across. The size of surface fragments is controlled by the rheology of the lava interior, rather than by the thinner surface crust (compare aa lavas).

crust The outer part of a lava flow that has solidified after losing heat to the exterior.

flow A discrete body of lava emplaced as a dynamically continuous unit.

flow field A collection of lava flows produced by the same effusion.

lava Molten or partially molten rock erupted at a planet's surface.

pahoehoe lava Lava flows with smooth, continuous surfaces.

LAVA FLOWS are the most common volcanic feature on Earth. They provide fine construction materials and are also an essential source of nutrients for future agricultural soils. They nevertheless remain a persistent threat to human activity. After describing the primary features of lava flows, this chapter will focus on how such features can be used to improve forecasts of how a lava will behave.

On Saturday, March 18, 1944, San Sebastiano was an unassuming Italian village in the foothills of Mount Vesuvius. On Tuesday, March 21, it ceased to exist. In less than 48 hours, lava streams from a new eruption had descended the volcano's flanks and crept through the village, slowly and inexorably eating their way from one building to the next. Today, five decades later, San Sebastiano is flourishing again as a popular residential area 10 km east of Naples. Yet the 1944 flows were the third set to have overwhelmed the settlement in less than 100 years. After both previous eruptions, in 1855 and 1872, the village and its neighboring villages were rebuilt around the very lavas that had caused their de-

Copyright © 2000 by Academic Press
All rights of reproduction in any form reserved.

struction. Not even the menace from Vesuvius could break the lure of the familiar.

The resilience, or perhaps stubborness, that keeps populations returning to hazardous districts is the chief reason why lava flows are a common threat to human settlements, even though they are produced by one of the least powerful styles of eruption. Between 1973 and 1998, lava effusions worldwide caused property losses of hundreds of millions of U.S. dollars (equivalent 1998 prices). Although these losses are small compared to those due to major explosive eruptions, they have long-lasting repercussions on local economies and are a key force driving investigations into how lavas behave and how defensive techniques can be improved.

A second motive for studying lavas is that they are the single most common feature on the surfaces of the terrestrial planets. They cover 90% of Venus, 50% of Mars, at least 20% of the Moon, and some 70% of the Earth, where they are mostly hidden from view on the ocean floor. Understanding how lavas are emplaced is thus crucial to reconstructing the surface evolution of the inner planets and to investigating the conditions below the surface that favor effusive eruptions.

The main factors controlling how lava flows develop are the rate at which lava is effused from the ground, the lava's physical properties, and the local environment (such as ground slope, topography, and whether the eruption occurs on land or below water or ice). Each of these factors can vary greatly among eruptions, as well as during a single effusion, and it might be expected that lavas should show a wide range of behavior. In fact, the contrary holds and common lava types evolve along only a few, clearly defined trends, which link the morphology of lava surfaces to styles and rates of flow advance. Only by understanding why these natural evolutionary sequences occur will it be possible to improve strategies for mitigating lava hazard.

I. WHAT ARE LAVA FLOWS?

Lava flows are outpourings of molten rock, or magma. On Earth, the overwhelming majority have silicate compositions, for which common melting temperatures are in the range 800–1200°C; lavas of sulphur (e.g., Siretoko-Iosan volcano in Japan, and Lastarria volcano in Chile) and of carbonate compositions (e.g., Ol Doinyo Lengai volcano in Tanzania) also occur at lower temperatures (about 150°C for sulphur and 600°C for carbonatite), but these are extremely rare and are not important as far as general hazard studies are concerned. First applied at Vesuvius, the word "lava" is derived from the italian *lavare* (to wash), which is ironic since the washing normally meant cleaning away the fruits of human labor.

Flows are distinguished from lava domes by their extreme elongation downslope. Historically, the volumes produced by single effusions of lava range from minor dribbles to outpourings of a few cubic kilometers (e.g., Etna, Sicily, 1614–1624; Lanzarote, Canary Islands, 1730–1736; Lakagigar, Iceland, 1783–1785). The resulting flow fields can extend tens of kilometers, spread kilometers across, and reach thicknesses of hundreds of meters, although most are more modest in size (Table I). The durations of single eruptions also cover a large range and, while some may reach decades, the majority lie between days and months. Rates of flow lengthening thus rarely exceed a brisk walking pace, so that it is usually possible for people to escape immediate danger. Exceptions occur during the start of effusions, when lavas can sometimes advance as fast as a galloping horse. In the saddest example, on Nyiragongo (Congo) at 10:15 in the morning of January 10, 1977, a fluid lava swept downslope at least 5 km in 20 minutes (15 km/hour), catching a small village unawares and roasting 70 people alive.

The Nyiragongo tragedy ghoulishly illustrates the need to prepare against lava invasion even before an eruption begins. To identify the most vulnerable districts, it is necessary to recognize probable locations of future eruptions and to forecast the likely travel distance of at least the initial lava flow. The first task is achieved by applying statistical analyses to the known distributions of vents at a volcano. The second requires a model that can link probable flow length to factors that can be measured before the next eruption begins, and it is here that the evolutionary sequences of lava flows assume a fundamental importance.

II. EVOLUTIONARY SEQUENCES AMONG LAVA FLOWS

Most lavas are crystallizing on eruption, owing to chemical imbalances induced in magma as it approaches the surface from below. They continue to solidify during effusion, aided by loss of heat to the ground and to the atmosphere. As a result, flows begin to form channels or tubes (Fig. 1 and 2), which concentrate motion along only a small number of paths, so that subsequent lava

TABLE 1 Major Historic Lava Flows

Composition	*Typical length (km)*	*Mean thickness (m)*	*Mean discharge rate (m^3s^{-1})*	*Flow (& flow field) volume (km^3)*
$SiO_2 < 55$ wt% (basalts, basaltic andesites)				
	<10	3–20	10–100	0.01–0.1
	(basalts to 50)		(basalts to 1000)	(<1–2)
For example, Kilauea & Mauna Loa, Hawaii; Etna & Vesuvius, Italy; Iceland; Piton de la Fournaise, Réunion Is; Lanzarote & Tenerife, Canary Is.; Arenal, Costa Rica; Parícutin, México.				
$SiO_2 > 55$ wt% (andesites, dacites, trachytes)				
	<5	20–300	1–10	0.01–1.0
	(some to 15)		(andesites to 100)	(<10–20)
For example, Lonquimay, Chile; Nea Kameni, Santorini, Greece; Hibok-Hibok, Philippines; Trident, Alaska.				

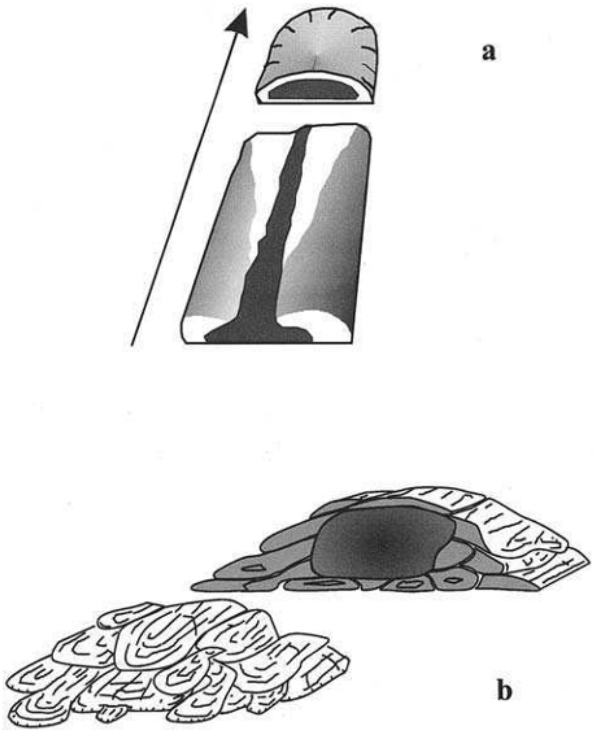

FIGURE 1 Major flow structures. (a) In aa and blocky flows, open channels (*below*) typically feed lava to simple fronts (*above*). Motion, in direction of arrow, is concentrated in the black zones. For major flows, the fronts are commonly ~100 m wide and tens of meters thick. In long-lived eruptions, the channels may evolve into tubes. [After Lipman and Banks, 1987.] (b) The fronts of pahoehoe flows are normally a complex of intermingling tongues and toes (up to meters across and tens of meters long) fed by lava from a tube system.

can be transported more efficiently from the vent to the front.

A flow initially forms a tube or a channel according to whether or not the lava surface can develop a continuous crust. When exposed to the atmosphere, a fresh lava surface chills to a strong, solid crust within minutes. At the same time, the new crust is pulled forward by more mobile lava. If the forward pull is large enough, the crust continually breaks into fragments and so, being unable to form a stable roof, the flow develops an open channel for containing the lava. If the forward pull is too small, a continuous crust can develop across the whole flow and this, anchored to the flow margins, gives birth to a tube.

A similar battle between crustal growth and disruption occurs at flow fronts. When disruption dominates, the front moves forward as a single unit, controlled by the properties of the frontal interior. When crust formation dominates, the front advances by oozing small tongues of lava through localized punctures in the crust. Whatever their style of motion, lava fronts are the slowest part of an advancing flow, in part because of crystallization, and in part because their areas of cross section are larger than the active areas along feeding channels or tubes.

From observation alone, it is clear that crustal structure can be linked directly to the early formation of lava channels and tubes, and to the style with which a flow front moves forward. The link with crustal structure is convenient since only the outer parts of an active flow are normally accessible to investigate, either by direct observation on the ground or by remote monitoring

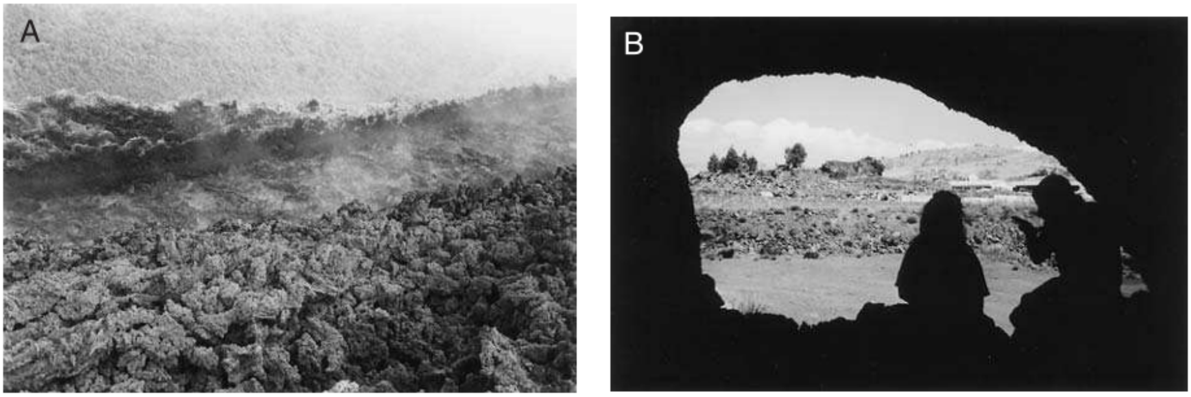

FIGURE 2 (A) A well-developed channel between static banks of aa lava. This example is a few meters wide, but channel widths may reach tens of meters in aa and hundreds of meters in blocky flows. Note the haze due to hot gases (mostly steam) escaping from the lava, moving from left to right [Photograph by C. R. J. Kilburn.] (B) Extensive lava tubes are essential features of pahoehoe flows and may also form in aa flow fields during long-lived eruptions. [Photograph by H. Pinkerton.]

using aircraft or satellites. Difficulties in studying the rest of a flow arise because lavas are hot and viscous. To measure the temperatures, velocities, and fluidities of flow *interiors*, it is necessary to stand close to poorly crusted lava, where it is easiest to insert monitoring equipment. The most active parts of flows have mean surface temperatures commonly between 475°C (when their color is a very dull red) and 1100°C (when they are golden yellow), a range sufficient for radiant heat to cause serious burns even meters away. Protective clothing, although cumbersome, can normally overcome this difficulty. However, even at the start of eruption, the most fluid lavas are frequently a million times more viscous than water (Table II) and it is extremely difficult both to force a measuring device into a flow and, if successful, to retrieve it again.

TABLE II Physical Properties of Lava Flows

Composition	*Eruption temperatures (°C)*	*Density at eruption temperatures (kg m^{-3}) (without vesicles)*	*Viscosities at eruption temperatures (Pa s)*[a]
Basalt	1050–1200	ca. 2600–2800	10^2–10^3
Andesite	950–1170	ca. 2450	10^4–10^7
Rhyolite	700–900	ca. 2200	10^9–10^{13}
Komatiite	>1600?	ca. 2800	<1?
Water at Earth's surface	20	ca. 1000	10^{-3}

	Temperature [°C (K)]	*Color of lava surface*
	1150 (>1423)	White
	1090 (1363)	Golden yellow
	900 (1173)	Orange
	700 (973)	Bright cherry red
	600 (873)	Dull red
	475 (748)	Lowest visible red

[a] Newtonian approximation at low shear rate.

As a result, virtually no data are available from direct measurements of active lava interiors. Investigations must instead rely on theoretical studies or on indirect evidence from solidified lava interiors (exposed by natural collapse or by artificial excavations, such as road cuttings or quarries). In the first case, no theoretical model has yet been completely verified, precisely because the necessary field data are unavailable. In the second, the features preserved by solidified lava interiors (such as crystal size distributions, which depend on a lava's cooling history) may not reflect conditions that prevailed while the flow was still active, because these features (1) may have been dominated by changes (e.g., further crystallization) that occurred after the flow had come to rest, or (2) may have formed at different times during flow advance, and so cannot simply be related to the state of the active flow at any particular moment. Thus, until more reliable data are available for active flow interiors, the links between crustal structure and flow dynamics offer the best prospect for quantifying flow behavior.

III. FIELD CLASSIFICATION OF LAVA FLOWS

Crustal appearance provides the basis for classifying lava flows on land into three major categories: *pahoehoe*, *aa*, and *blocky*. Pahoehoe and aa are Hawaiian terms introduced in the late 19th century to describe the common lava types found on Mauna Loa and Kilauea, but they apply equally to other lavas with silica contents less than about 50–55 wt% (basalts and some basaltic andesites), as well as to the rare flows of sulphur and carbonatite. Blocky flows are common among lavas with silica contents greater than 55 wt% (basaltic andesites to rhyolites).

Diagnostic features are most evident when viewing a crust over distances of decimeters and meters (Table III and Fig. 3). At these distances, pahoehoe surfaces are smooth and, though occasionally broken, are normally continuous, whereas aa surfaces are extremely irregular, frequently fractured, and usually covered by rough, contorted fragments with typical dimensions of centimeters and decimeters. Blocky lavas, like aa, also have fractured surfaces and a covering of debris; they differ from aa flows in that their fragments are smooth and angular with common dimensions from decimeters to meters. From a distance, indeed, both aa and blocky surfaces look as exciting as piles of rubble on a building site.

A. Aa and Blocky Flows

Aa and blocky flows show simple evolutionary trends. As might be anticipated from their broken surfaces, their fronts tend to advance as single units, and it is rare for one part of a front to move far ahead of neighboring sections. Blocky fronts crumble to produce a snout of

TABLE III Common Features of Flow Surfaces

Feature	*Description*
1. Aa lava	Surface is covered by a jumble of irregular crustal fragments.
Cauliflower	Crust twists upward as cauliflower-like protrusions. These break to give fragments up to decimeters across. Surfaces are gray-black, often glassy, and rough and spinose at the millimeter scale.
Rubbly	Crust fractures downward to yield rounded rubble up to meters across, often with an ochre-black granular surface, millimeters deep.
2. Blocky lava	Surface is covered by broken lava, containing fragments up to meters across with smooth, planar, and angular surfaces.
3. Pahoehoe lava	Surface is smooth and continuous, often with a millimeter-scale texture of interweaved lava threads or filaments.
Entrail	Dribbles of lava yield convoluted surfaces reminiscent of entrails.
Ropy (or corded)	Flexible crusts ruck into tight folds before chilling. Surface resembles segment of coiled rope. Each "rope" can be centimeters thick.
Shelly	Highly vesicular, fragile crusts. Often associated with skins, centimeters thick, over hollow lava blisters. The skins break underfoot, giving the impression of walking on egg shells.
Slabby (sometimes slab aa)	Slabs of broken crust, up to meters across and centimeters thick.
4. Toothpaste lava	Protrusions of viscous lava squeezed through gaps in flow crust. They may be tens of meters long and their cross sections often mimic the shape of the source gap, like toothpaste emerging from its container.

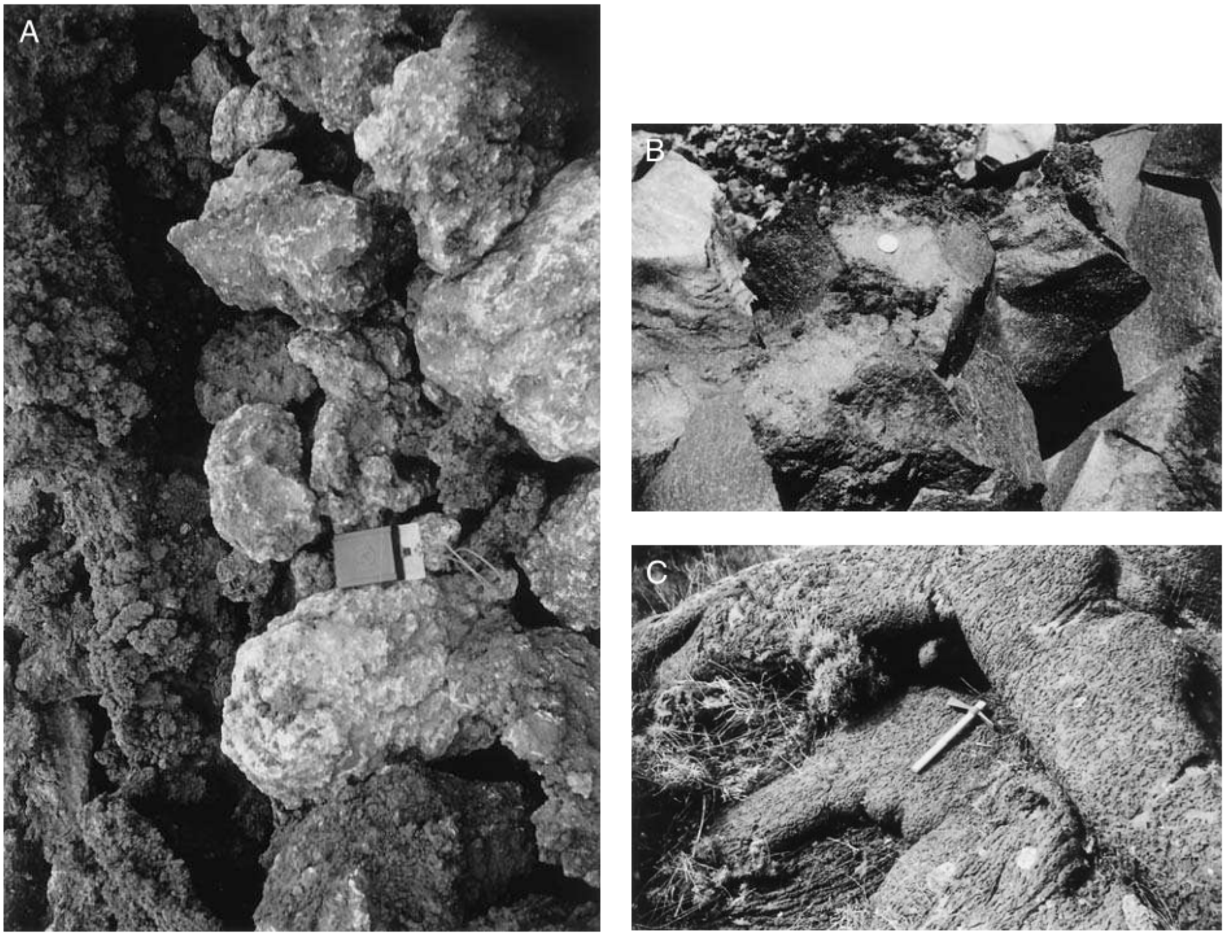

FIGURE 3 The surfaces of aa and blocky flows are covered by broken surface fragments. (A) Aa fragments (Mt. Etna, Sicily) are contorted and initially appear black and spinose (*left*) but, during later stages of advance, the surface breaks to yield rounded and abraded rubble (*right*). (B) Blocky fragments (Nea Kameni, Santorini, Greece) are angular and have planar faces. (C) Pahoehoe surfaces (Vesuvius, Italy) are smooth and often billowy over distances of meters. [Photographs A and B by C. R. J. Kilburn; photograph C by S. Black.]

debris from the early stages of emplacement. Aa fronts show a greater range of behavior, often starting as fluid sheets, but finishing as near-solid masses that fragment throughout their thickness to maintain advance; between these limits, they move by various combinations of fracture and flow.

Fronts thicken while advancing, often growing to more than 10 times their initial thickness. Final thicknesses are typically about 20 m or less for aa fronts, but several tens of meters for blocky flows; their maximum lengths are measured in tens of kilometers and in kilometers, respectively. Major flows can achieve volumes of 1–100 million cubic meters, and tend to be emplaced within days when they are aa but within months when they are blocky.

Both flow types initially develop channels to feed lava to their fronts. Channels form when a flow stops widening and concentrates motion downhill. The fronts themselves grow during advance because they decelerate as they solidify and allow faster lava to accumulate from upstream. For example, during the opening stage of emplacement (when they are fastest), major aa fronts may advance a few kilometers a day (occasionally 10–30 km in the first 24 hours), although the velocity of lava near the vent may be at least 10 times greater.

At one extreme, advance and thickening continue until a flow stops being fed by new lava, whereupon the front slows to a halt as remaining lava drains from the feeding channel. At the other extreme, effusion continues into the flow even though the front has come to rest. Lava begins to pile up within the channel, starting at the front and working its way backward. As it thickens, the channel lava exerts an increasing pressure on its margins, and these may eventually breach to form an outlet through which the channel lava can escape. If the breach is too small, it may be able to heal itself through cooling or by being plugged with crustal debris. Otherwise, the breach may become a permanent outlet from which a major new flow can develop. The new flow, in turn, may halt and thicken until the cycle is repeated. In such a way, a *flow field*, the final product of one effusive eruption, may evolve with time from a single flow to a collection of interconnected flows (Fig. 4).

Breaching is more common among aa than blocky lavas. Apart from high channel pressures, the propagation of new flows by breaching requires channel lava that is much more fluid than its lateral margins. Only in this case can the channel lava easily escape through a breach; if, instead, the channel lava is almost as solid as the margins, breaching simply allows channel lava to spread into the breach and heal it. By virtue of its chemical composition, channel lava in aa flows tends to be more fluid than its blocky equivalent, so that conditions are more favorable in aa lavas for the propagation of new flows.

Although breaching may occur anywhere along a flow, it most commonly occurs somewhere along the upstream half of a flow's length. Newly propagated flows may extend downslope beyond an earlier stream, but rarely do they increase the length of a whole flow field by more than half the length of the initial flow. A result of such behavior is that the propagation of flows tends to widen, rather than to lengthen, the area covered by new lava (Figs. 4 and 5). It also means that, when addressing the hazard from aa and blocky flows, the first goal is to estimate the probable maximum length of the *initial* flow.

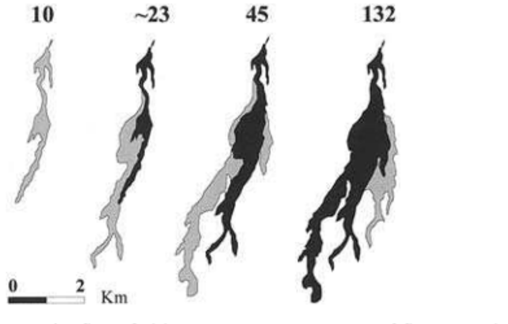

FIGURE 4 Aa flow fields grow as a sequence of flows, with new flows (shaded area) propagating from the sides of earlier streams (black). This example shows the evolution of Etna's 1983 flow field at 10, 23, 45, and 132 days after the start of effusion. Note how the final length of the flow field on day 132 is only about 30% greater than the length of the initial flow on day 10. [Data from Frazzetta and Romano, 1984.]

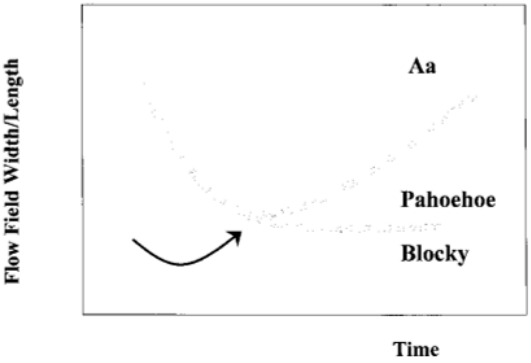

FIGURE 5 All flows initially lengthen so that their ratio of width to length decreases with time. This trend normally continues throughout eruption for pahoehoe and blocky flows. After the first flow is emplaced (*arrow*), aa flow fields tend instead to become wider. The initial aa flows rarely lengthen for more than 10–15 days. For all lava types, major flow fields are normally emplaced within months to years, although some historical effusions (especially of pahoehoe lava) have continued intermittently for a decade or more (e.g., Etna, 1614–1624; Pu'u O'o, Kilauea, continuing since 1983).

As well as promoting flow breaching, flow thickening can trigger the overflow of fluid channel lava across its lateral margins. The margins can thus build themselves up as a series of superposed overflows that, under favourable conditions, develop an inward overhang across the channel surface. As the exposed channel surface narrows, it becomes easier for adjacent segments of crust to congeal and to form a continuous roof over the flow. In this way, a lava channel can evolve with time into a tube, better insulating the lava beneath and allowing it to travel further before solidification sets in.

Tubes form in aa and blocky flows only after a channel has become well established, and may require several weeks to develop. When they occur, therefore, tubes are found along those parts of flows that remained active for long periods, typically behaving as feeders to sites of breaching downstream. As a result, tubes normally form after most major flows have been emplaced, and so rarely contribute in a significant way to extending a flow field (in complete contrast with pahoehoe flows, discussed later). As with the propagation of flows by breaching, the growth of lava tubes is favored by a large contrast between the fluidity of internal lava and its external margins. Accordingly, tubes are more common in aa than in blocky flows. Should lava drain from a tube toward the end of effusion, it may leave behind a tunnel perhaps kilometers long that is large enough at least to crawl through. Among aa lavas, excellent examples can be found on Sicily's Mt. Etna, including the 1971 and 1991–1993 flow fields.

B. Pahoehoe Flows

Pahoehoe flows have dimensions similar to aa flows, but normally advance at least 10 times more slowly. Because they spread slowly, their cooling surfaces resist extensive tearing and, though feeding channels can develop, it is not unusual for continuous crusts to form across a whole flow from the start of emplacement (unlike the weeks necessary in the case of aa lavas). The crust remains continuous around flow margins and fronts, whose initial thicknesses are usually only a few decimeters. Because early flows are thin, they are easily retarded by the crust and spreading occurs by a combination of lava leaking out as small tongues through breaks in the crust, and by allowing new lava from upstream to burrow beneath the tongues and to slowly lift the front upward. The front thus appears as a collection of intermingling tongues, each much narrower (by 10–1000 times) than the width of the whole flow (Fig. 1).

Pahoehoe tongues may extend by some 100 m, and even start to develop, feeding channels, before crusting over and extruding small lava toes, typically a few meters or less in length (analogous to the lava pillows among submarine flows). As a result, pahoehoe fronts and margins soon develop as a complex of budding tongues and toes, all of which are gently uplifted by newly arriving lava. The surfaces of pahoehoe flows thus evolve a curious hummocky form, involving swells that extend distances from decimeters to hundreds of meters. The largest of these seem almost flat to the casual gaze; the smallest appear curiously grotesque and intestinal (Table III).

Lava from the vent continually raises the surface and, within weeks, a flow field may have thickened to several meters, while thin lava tongues continue to emerge from around its edges and from occasional surface ruptures. Although many tongues and toes stagnate after halting, others remain connected beneath the crust to form a network of distributary tubes, casually resembling an underground river system. Compared with the open channels in aa and blocky flows, lava tubes reduce the rate of lava cooling, especially when they are partly drained so that hot gases can collect beneath the tube roof and keep the flowing lava surface at temperatures close to its initial value. Thus, although pahoehoe flows advance more slowly than their aa counterparts, their interiors remain fluid for much longer periods. The greater lengthening time often dominates the slower velocity, so that pahoehoe flow fields can achieve lengths greater than aa flow fields of similar volume.

Historical pahoehoe flow fields have extended several tens of kilometers, the best examples being found on the Big Island of Hawaii. Some prehistoric flow fields, however, have been traced for more than 100 km, notably those in Queensland, Australia. Recently, it has been proposed that ancient flood basalts (such as the Columbia River Basalts in the United States), which have lengths of several hundreds of kilometers, are in fact enormous pahoehoe lavas, and not extreme aa flow fields as previously thought. The drained tube systems in such flows are truly impressive, reaching tens of meters across, up to 10–20 m high, and extending for several kilometers at least (the prehistoric Australian flow fields contain a tube system about 100 km long).

IV. THE LAVA SPECTRUM

In the simplest of cases, a flow maintains the same type of surface morphology throughout emplacement. Frequently, though, a flow surface evolves through more than one type with distance downstream. Among basaltic lavas, downstream transitions occur from pahoehoe to aa morphologies, while the change from aa to blocky is found among some basaltic andesites; both transitions are unidirectional, so that blocky surfaces do not become aa, and aa surfaces do not become pahoehoe (although, as discussed later, special field conditions may give the false impression that reverse transitions can occur). The pahoehoe, aa, and blocky morphologies are thus not independent entities, but parts of a continuous spectrum of lava types. The association of the two transitions with different lava chemistry shows that composition is one underlying control. However, because each transition occurs between lavas of similar composition, other nonchemical factors must also be involved.

Both pahoehoe and aa surfaces are created during the formation of surface crust. At the start of eruption, the lavas are often too fluid to break before cooling, so that the degree of rupture must be controlled by the solidifying surface layers. To break a surface before it has chilled to its maximum strength, the rate of energy supplied predominantly by gravity to a unit volume of crust must be greater than a critical value. The critical value depends on how quickly a crack can be healed by chilling the newly exposed lava beneath. If the critical value is exceeded, a flow breaks its crust more quickly than existing cracks can be healed and so evolves a fragmented aa surface; otherwise, a flow cannot tear its crust quickly enough and develops a continuous pahoehoe surface.

The rate of energy supply is measured by the product of the stress applied to the crust and the rate at which the crust deforms (Fig. 6). Two consequences are that the larger the pull, or applied stress, the smaller the deformation rate at which critical conditions are reached; and to cross the pahoehoe–aa transition, the rate of energy supplied (per unit volume) to the crust must also increase. The change from pahoehoe to aa occurs because, as lava advances downstream, a greater proportion of the gravitational energy flux for moving the whole flow is used in deforming a thickening crust. Eventually, the energy flux exceeds the critical value, after which the surface must break persistently as aa if the flow is to advance.

Blocky surfaces are associated with stronger and more viscous lavas that break before cooling is significant. In this regard, they can be considered magmatic glaciers, slowly moving sheets that flow near their bases but break at their surfaces. The aa–blocky transition thus occurs when the lava interior becomes too crystalline to move forward only by flowing, so that surface fracturing is no longer controlled by crustal cooling. Indeed, the same reasoning explains why pahoehoe and blocky lavas have different surface morphologies, even though both advance much more slowly than aa flows: Blocky flows are slow because of their high viscosity and break because of their large associated strength; pahoehoe flows are slow because they advance as thin sheets or tongues whose fluid interiors are easily restrained by surface crust.

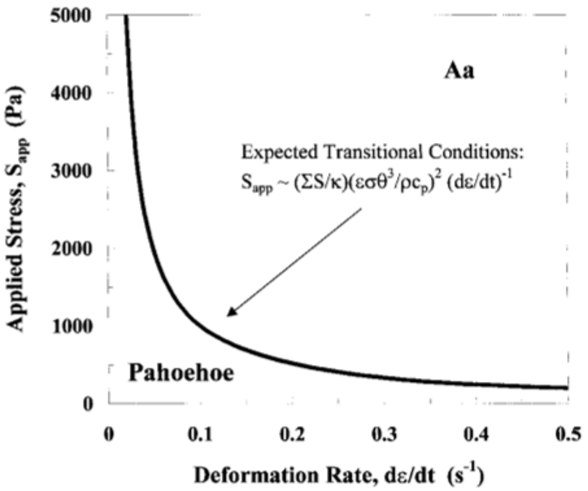

FIGURE 6 The evolution of pahoehoe and aa surfaces depends on the rate at which energy is supplied to deform cooling crust. The rate of energy supply per unit volume is given by the product of applied stress and deformation rate ($S_{app}\, d\varepsilon/dt$). Below a critical energy flux (~ 100 J m^{-3}) controlled by the cooling and strengthening of lava exposed between cracks, the surface chills as a continuous crust to form pahoehoe. When this flux is exceeded, the surface breaks persistently to form aa. Blocky lavas are not shown on this diagram, because they are strong before eruption and, as if magmatic glaciers, they must break their surfaces to advance, independent of cooling effects.

The transitions between surface morphologies are irreversible; highly fragmented surfaces cannot recombine to form continuous crust (hence aa surfaces do not evolve into pahoehoe), while subcrustal lava does not become less solid with time (hence, blocky surfaces do not evolve into aa). On occasion, however, it might *appear* that a reverse transition has taken place, especially between pahoehoe and aa types. The deception occurs under two main sets of conditions. The first corresponds to changing conditions of effusion from the vent. As an eruption decays to its close, so also decreases the rate of effusion. While early, fast lava may produce an aa surface, later lava may emerge slowly enough to form a continuous pahoehoe crust (good examples can be found on Mauna Loa, Hawaii). This change, though, does not represent a transition from aa to pahoehoe, because the later pahoehoe crust formed across an independent flow and did not evolve from lava already erupted with an aa surface. The second condition involves the escape from aa channels of hot internal lava, the result either of a channel overflow or of a margin being breached. In this case, the escaping lava may be less crystallized and, if advancing much more slowly than the parent flow, may form a pahoehoe crust. Once again, such a situation does not correspond to an evolution of the crust from aa to pahoehoe, because the escaping lava comes from deep within the parent flow and has had a crystallization history independent from that of the near-surface lava layers that formed the earlier crust.

V. LAVA DYNAMICS AND INTERNAL SOLIDIFICATION

Because of its high viscosity, lava can rapidly reduce accelerations in a flow. As a result, flows tend to settle into a steady dynamic state. A simple example is shown by the preference of flow fronts to advance at nearly constant velocities for extended periods of time (Fig. 7). Because inertia is not important, flow growth is controlled by how a lava's rheological resistance is overcome by gravity (pulling lava downslope) and by pressure differences due to local variations in flow thickness (notably at the flow periphery).

Another consequence of low inertia is that lava strives to maintain laminar flow, whereby adjacent packets of lava tend to flow past each other, rather than intermingling, as would occur if motion were turbulent (although turbulence may be important in some exotic lavas, discussed later). Without intermingling, a lava interior can diffuse heat only by conduction (i.e., interactions between neighbouring molecules), so that cooling effects tend to migrate inward from the flow exterior, itself maintained at a low temperature by radiation to the atmosphere, by cooling wind, and by precipitation. Lava, however, is a very poor conductor. The time needed for cooling to penetrate a depth D into a flow is given approximately by $D^2/4\kappa$, where the thermal diffusivity (κ) of lava is between 10^{-7} and 10^{-6} $m^2\ s^{-1}$. Thus it takes minutes to chill a layer centimeters deep, but weeks for this layer to thicken to meters.

To give an example of a lava flow 10 km long, the time for lava to travel from the vent to the front may be only hours for pahoehoe and aa flows, and days for blocky flows. (Recall that this travel time is less than the interval since effusion began: The former is given by [flow length]/[mean velocity *along a flow*]; the latter is [flow length]/[mean velocity *of the flow front*].) The corresponding mean flow thicknesses will be measured in meters or tens of meters, implying conductive cooling times of weeks or longer. It might thus be expected that the interiors of pahoehoe and aa flow fronts will contain lava almost as fluid as it was near the vent. This condition is typical among pahoehoe flows, but not so for aa flows, which can develop solidified fronts within days.

Precisely why the interiors of aa flows can solidify so quickly is still not fully understood. One possibility is that, compared with other lava types, aa lavas are initially richer in volatiles. All magmas contain some volatiles, mostly water, that remain dissolved at depth, where the high pressure from surrounding rock prevents them from forming bubbles. As the magma ascends, the imposed pressure decreases and, eventually, bubbles can develop, just as they appear in a bottle of soda water when pressure is released as the bottle is opened. The loss of volatiles upsets the chemical balance in the liquid and can trigger crystallization at a rate that increases with the proportion of gases originally dissolved in the magma, but decreases with increases in liquid viscosity. Thus, compared with aa lavas, pahoehoe interiors may crystallize more slowly due to smaller amounts of initial gas, while crystallization in blocky interiors is retarded by high lava viscosity.

Another explanation appeals to crustal entrainment. Pieces of cold crust are dragged back into the lava interior, accelerating solidification by forcing internal lava to intermingle. Importantly, the intermingling in aa is a result of crustal entrainment and not of natural turbulence; when possible, the flow again seeks a simple laminar motion. This mechanism is less common in pa-

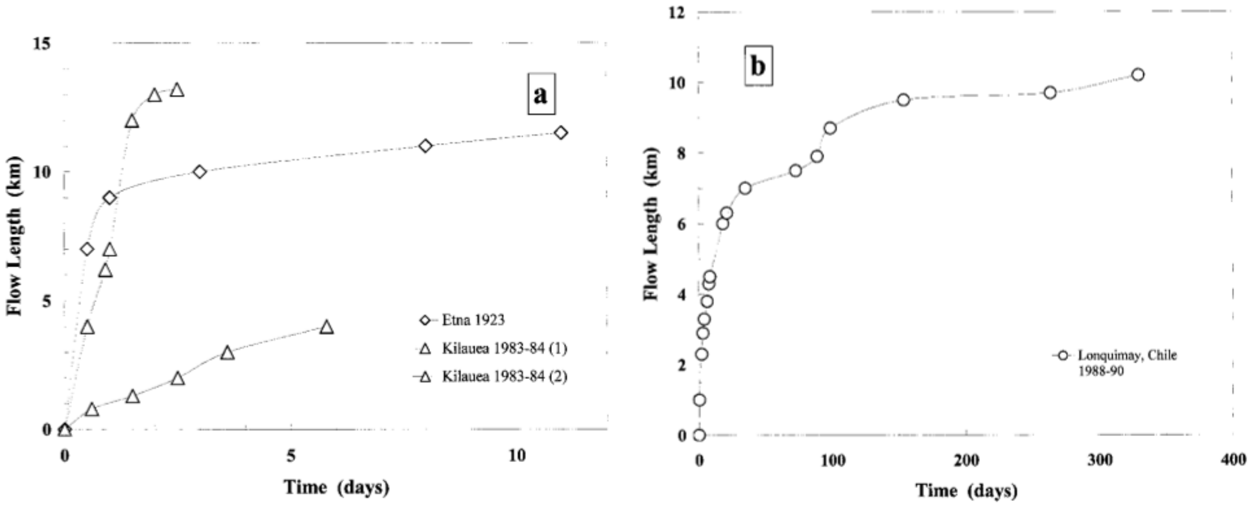

FIGURE 7 Most flow lengthening occurs during the early stages of effusion and at nearly constant rates of advance. This may be followed by a rapid drop in advance rate that, though continuing for a long time, does not extend a flow significantly. [Data for part (a) Ponte, 1923, and Wolfe *et al.,* 1984; for part (b) Naranjo *et al.,* 1992.]

hoehoe flows, since they form continuous crusts, and also in blocky flows, because their very large viscosity impedes incorporation of surface debris.

VI. SHAPES OF LAVA FLOW MARGINS

As they negotiate topographic irregularities and adjust to local variations in physical condition, lava flows are rarely able to spread evenly over the ground and so usually develop margins with irregular outlines. The degree of margin irregularity varies with flow type and, because all types can evolve over similar topography, such variation must reflect differences in style of advance and, hence, also in the governing force balance.

Spreading as collections of tongues and toes, pahoehoe flows develop lobate margins having a degree of unevenness (measuring fluctuations about a smoothed, average outline) that happens to be similar for averaged outlines at least 1–100 m in length. Such a scale-independent (fractal) unevenness suggests that pahoehoe spreading is governed by the *ratio* (scale independent by definition) of imposed forces, and that these forces are of the same type at each scale. Because crustal restraint is essential to the pahoehoe style of advance, the obvious inference is that, whatever their size, tongues and toes propagate when, given sufficiently fluid internal lava, the forces driving lava spreading exceed crustal resistance by only a critical amount; otherwise spreading would cease (driving forces too small) or the crust would fragment and have no significant resistance (driving forces too large).

In contrast, aa and blocky flows spread mostly under conditions for which the driving forces are far greater than crustal resistance. Thus, although locally influenced by crustal debris, the bulk shape of their margins is more dependent on the rheological resistance of internal lava. As a result, the margins appear highly irregular over distances covering a few crustal fragments (notionally 10 m or less), but tend to show only subdued undulations over 100 m or more. Hence the shape of the flow outline is not scale independent, but becomes less uneven as the measuring distance becomes larger, coinciding with a change in the chief shape-controlling factor from the geometry of crustal fragments to bulk lava rheology.

The connection between flow type and margin geometry opens the possibility of using geometric measurements to infer styles of lava emplacement, especially important for investigating inaccessible volcanoes with aerial and spaceborne techniques. However, apart from initial measurements on predominantly basaltic lavas, few data are available on the fractal dimensions (degrees of unevenness) of lava flow margins, and so the full promise of this approach must await future studies.

VII. FORECASTING THE BEHAVIOR OF AA FLOWS

The three main types of lava surface are associated with distinct styles of flow growth. Because lava surfaces are easily monitored in the field, it would be convenient if the conditions for producing a specific surface type could also provide limits on the likely distance and velocity a given flow might travel. Such a state of affairs does exist for aa flows, a happy circumstance since aa flows are the lava type that has most frequently threatened human activity, and they are also intermediate between pahoehoe and blocky flows. Understanding the limits to aa behavior thus provides clues to the limiting behavior of the other flow types.

The aa surface criterion can be used to estimate the advance velocity needed to keep breaking lava crust. The time for which a lava flow can continue to advance is controlled either by the duration of eruption (for short-lived aa flows) or, during long eruptions, by the time needed for the flow to acquire a solid front. Combining the requirement for a lava front to solidify (which gives the longest time for advance) with the aa surface criterion, it is possible to link the *maximum* potential length (L_m) of an aa flow to lava properties, mean underlying slope (angle β), and mean rate of discharge (Q). These expressions are:

$$L_m \approx [(1.5\,\varepsilon S/\rho g)^2\,(\Sigma\sigma\Theta^3)/(\kappa\rho c_p)]/\sin^2\beta \qquad (1)$$

$$\approx [3\varepsilon S/\rho g\kappa]^{1/2} Q^{1/2}, \qquad (2)$$

where the remaining symbols are defined in Table IV.

In both expressions, the terms in square brackets describe the physical properties of the lava crust and are approximately constant for a given lava composition. Thus the maximum potential length is expected to increase as the mean underlying slope decreases [Eq. (1)] and as the discharge rate increases [Eq. (2)], two trends that agree well with observation (Fig. 8).

The length–slope trend is counterintuitive. Other factors being equal, it might be supposed that steeper slopes would favor longer flows. The inverse trend arises because, to keep breaking their surfaces, aa flows must

TABLE IV Parameters in Flow Equations

Symbol	*Meaning*	*Units*	*Nominal value for basalt*
β	Slope angle	°	
c_p	Specific heat capacity	J kg^{-1} K^{-1}	1150 (during crystallization)
D	Thickness	m	
ε	Extension before failure	—	Min. 10^{-3} (for chilled crust)
εS	Energy per unit volume for failure	J m^{-3} (or Pa)	2×10^4 (during crystallization)
g	Gravitational acceleration	m s^{-2}	9.81
κ	Thermal diffusivity	m^2 s^{-1}	4.2×10^{-7}
L_m	Maximum potential length of flow	m	
Q	Mean discharge rate along flow	m^3 s^{-1}	
Θ	Eruption temperature (absolute)	K	1350–1400
ρ	Density of lava crust (not whole flow)	kg m^{-3}	2200 (~20% vol. vesicles)
S	Tensile strength	Pa	Max. 10^7 (for chilled crust)
Σ	Surface emissivity	—	1
σ	Stefan-Boltzmann constant	J m^{-2} s^{-1} K^{-4}	5.67×10^{-8}
t	Time	s	

maintain greater thicknesses on shallower slopes. Thicker flows need longer times for their fronts to solidify. As a result, the maximum *potential* length increases with decreasing slope. In practice (Fig. 8), such lengths are usually not achieved (especially on slopes with angles smaller than 6 degrees) because the eruption finishes or breaching occurs in the meantime. Nevertheless, the length–slope trend is important for hazard analyses because it provides realistic estimates of potential flow length when only the mean slope is known. Accordingly, it is well suited for preparing hazard maps before an eruption occurs.

The length–discharge rate trend may also have predictive value in some special circumstances. At several mature effusive volcanoes, the mean rate of lava effusion generally decreases with increasing altitude of the vent. Equation (2) can therefore be modified to link maximum potential flow length to vent altitude, shorter maxima being associated with higher elevations. Pre-eruptive maps of lava hazard can thus be prepared on the basis of vent elevation, and these provide a useful check on evaluations determined from mean slopes.

Equation (2) may also be used for short-term forecasts while an eruption is in progress. During the 1991–1993 effusion on Etna, for example, secondary aa flows began to overtop an artificial barrier and descend toward Zafferana, a town almost 3 km further downslope. Initial observations suggested that it was unlikely for the mean discharge rate to exceed 1 m^{3}s^{-1} along any flow. From Eq. (2), a maximum flow length of about 2 km was anticipated, indicating that the immediate threat to Zafferana was small. A forecast was issued to that effect and, in the event, the longest secondary flow traveled only 1.8 km beyond the barrier.

The success of Eqs. (1) and (2) is remarkable not only for the simplicity of their underlying assumptions, but also because they use mean values of slope and discharge rate to determine length. In reality, surface slopes are uneven, while discharge rate changes with time and position along a flow. The agreement between theory and observation thus suggests that local variations normally have a secondary effect on maximum potential flow length, so that mean values are sufficient for most purposes. Extreme variations, such as flow over a cliff or through a very narrow ravine, may induce significant changes from the model results and, until more sophisticated analyses are available, these rare cases must be evaluated individually.

The expressions for maximum length assume that an aa flow travels until its front has solidified. The maximum time t required is

$$t \approx [(\varepsilon S/\rho g)(\rho c_p/\Sigma\sigma\Theta^3)]/\sin\beta. \qquad (3)$$

As before, the combination of physical properties (Table IV) in the square brackets is roughly constant for a particular lava composition and, for typical angles of

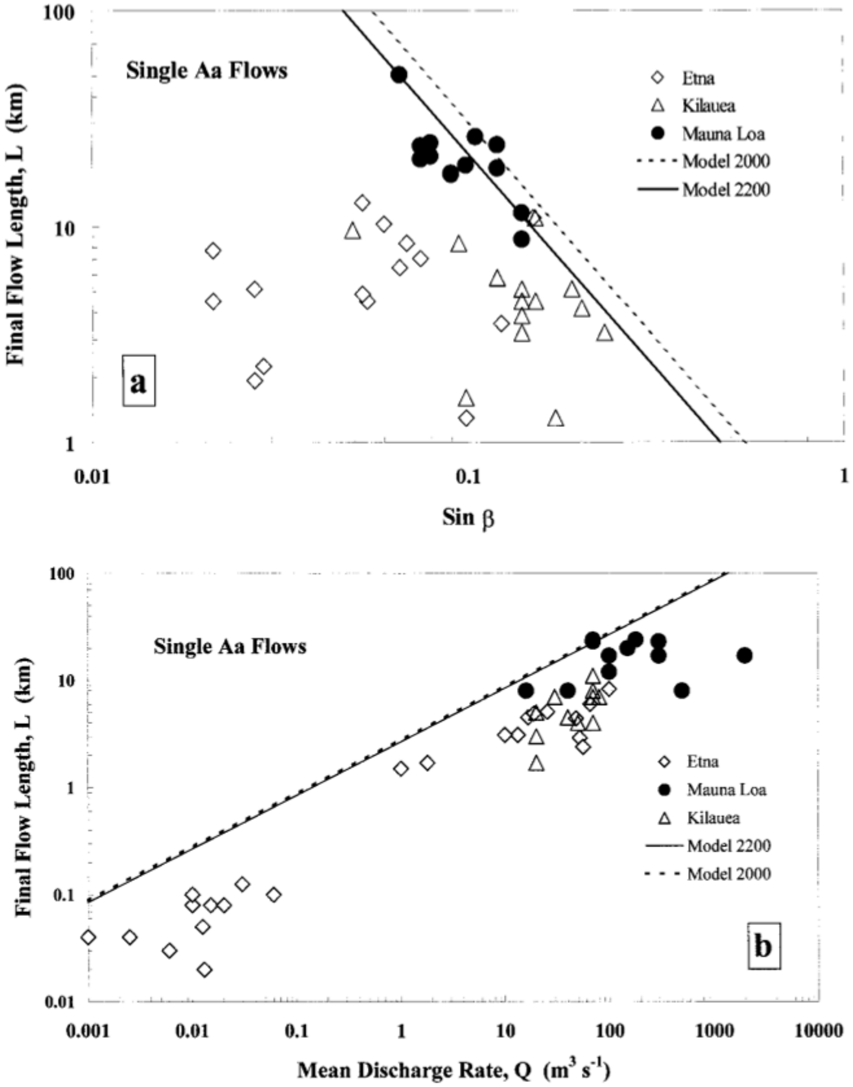

FIGURE 8 The conditions that (1) aa surfaces must break before they cool to their maximum strength and (2) flow fronts advance until solidified yield criteria for relating the maximum potential length of a single aa flow to (a) underlying slope (sinβ) and (b) rate of discharge (Q). These criteria [Eqs. (1) and (2)], shown by the solid and dashed trends, agree well with observations from Etna and Hawaii. The solid and dashed lines refer to respective mean crustal densities of 2200 and 2000 kg m^{-3}.

2–10 degrees for the slopes of basaltic volcanoes, yields lengthening times of about 1–10 days (the longer times corresponding to smaller slopes). During a long-lived eruption, therefore, major breaching and the propagation of new flows is most likely to commence within days following the start of effusion. Because new flows rarely extend a flow field by more than half the length of the first major flow, another forecasting problem is to assess the final width of a flow field, which may stretch to several kilometers.

An aa flow field can widen until halted by topography or by the end of effusion. The topographic control depends on local conditions and must be assessed on a case-by-case basis. The likely duration of an effusion can be estimated by comparison with previous eruptions, but even on well-studied volcanoes, such as Etna, Kilauea, and Mauna Loa, such estimates are rarely better than inspired guesswork. Improvements will follow when it becomes possible either to estimate (probably by geophysical monitoring) the quantity of magma below ground that is available for eruption or to forecast the long-term decay in rate of effusion as an eruption proceeds.

VIII. FORECASTING THE BEHAVIOR OF PAHOEHOE AND BLOCKY FLOWS

It is possible before an eruption to estimate the maximum length of an aa flow because the surface criterion provides a velocity and the solidification control yields a time. Such a combination is not available either to pahoehoe or to blocky flows and so forecasts of their growth are inherently more difficult.

For pahoehoe flows, the requirement to form a continuous crust can be used to constrain maximum rates of advance to about 1 km/day on slopes typical of basaltic volcanoes. Unfortunately, the burrowing mechanism, by which new lava intrudes into the front after traveling through insulated tubes, has so far defied realistic estimates of maximum cooling times. As it happens, observed pahoehoe flows (mostly from Hawaii) have frequently lengthened for the whole of an eruption, even when this has continued for several months (Fig. 5). In practice, therefore, pahoehoe emplacement is often limited by the available supply of magma, and so forecasting flow behavior is subject to the same problems encountered when estimating the final width of an aa flow field.

Among blocky lavas, surface fracturing appears to be controlled by the strength of lava beneath the chilled crust. As a result, fracturing is not required to be faster than the rate of surface chilling, and so no surface criterion is available for forecasting mean rates of advance. Velocity forecasts must therefore rely on knowing the rheologic state of a lava and the rate at which it is effused, factors that can be estimated by analogy with previous effusions from the same volcano.

Because the lava is viscous and slow moving, a blocky front is expected to solidify at a rate controlled by conductive heat transfer to the breaking surface. From standard conduction theory, a crude estimate of the solidification time for common final thicknesses of 10–30 m is from 6 months to more than 4 years, lengths of time that are greater than the usual durations for eruptions of blocky lava. Once again, the volume of magma available appears crucial for determining how far a lava can travel, and estimating this volume remains a fundamental obstacle to improving pre-eruptive forecasts of blocky flow growth.

IX. TURBULENT LAVA FLOWS

Lava flows witnessed in historical time have had physical characteristics that favor laminar motion, and so it is this motion that has been assumed in developing quantitative models of lava behavior. However, some ancient lavas on Earth, erupted for the most part more than 2500 million years ago, may have been sufficiently fluid upon eruption for turbulent advance. Turbulent flow involves the spontaneous intermingling of neighboring packets of lava, so that internal lava cools and solidifies more quickly than would have been the case for simple laminar flow. The net result may well have been the persistent surface disruption of a lava undergoing wholesale internal solidification, analogous to conditions for aa lava flow emplacement (for which, as discussed earlier, internal solidification is induced by factors other than spontaneous turbulence).

Notable candidates for ancient turbulent flows are komatiite lavas (Table II), which, named after their discovery near the River Komati in South Africa, are found dotted across the world's oldest continents (Africa, Australia, and North and South America) and are often associated with economically important nickel deposits. Essentially basalts with unusually large amounts of magnesium, iron, and aluminum, these lavas since their eruption have been buried by younger material and grossly deformed by major changes at the Earth's surface. As a result, it has not been possible to investigate directly the influence of turbulent motion on lava flow morphology. This is unfortunate, because interest has been generated by speculation that komatiites could be among the types of lava flow observed on other planets. Only when direct chemical analyses are available for extraterrestrial flows will it be possible to gauge the potential significance of turbulent flow on volcanoes beyond Earth.

X. LAVA FLOWS AND PLANETARY DEVELOPMENT

Lava flow fields are among the commonest surface features of the terrestrial planets. Quite apart from hazard analyses, therefore, an understanding of flow emplacement is essential for investigating the evolution of planetary surfaces. By virtue of their remote location, most information on extraterrestrial flows concerns their dimensions and geometry. Especially impressive is the fact that flows stretching hundreds of kilometers are commonplace on the Moon, Mars, and Venus, with some exceeding the size of ancient flood basalts on Earth. Primary goals of planetary studies are to use flow shape and size to deduce chemical composition and to infer conditions in the magmatic feeding systems, thereby probing also into the states of planetary crusts and mantles.

Despite their large size, the shapes of planetary flow fields resemble those of their smaller cousins on Earth. Because flow shape depends on the ratios of controlling factors, geometrical similarity suggests that these factors remain within the same range of proportions to each other as they occur on Earth. It is thus realistic to assume that, unless extraterrestrial lava flows have been emplaced exclusively under turbulent conditions, the range of controlling ratios (e.g., among the forces driving and resisting motion) found on Earth can be applied to the neighboring planets and, hence, that extraterrestrial flows will also belong to the pahoehoe–aa–blocky spectrum.

XI. SUMMARY

Lava flows on land evolve along a small number of trends, each of which links surface structure to styles of advance and to modes of flow field growth. These trends correspond to particular combinations of the forces driving and resisting flow motion. Fortunately, one combination (corresponding to aa lavas) provides the possibility for forecasting flow growth before an eruption has started. Unfortunately, emplacement of the remaining flow types, pahoehoe and blocky, appears to need prior knowledge of the amount of lava available, a quantity that it is not yet possible to assess before an eruption has finished. Remedies are expected as geophysical methods for investigating the insides of volcanoes become more sophisticated, so that a complete forecasting potential may be available beyond the millennium.

SEE ALSO THE FOLLOWING ARTICLES

Lava Domes and Coulees • Volcanic Hazards and Risk Management • Volcanism on Mars • Volcanism on the Moon • Volcanism on Venus • Volcano Warnings

FURTHER READING

Fink, J. H., ed. (1990). "Lava Flows and Domes: Emplacement Mechanisms and Hazard Implications." Springer Verlag, Berlin.

Francis, P. (1993). "Volcanoes, A Planetary Perspective," Clarendon Press, Oxford.

Frazzetta, G., and Romano, R. (1984). The 1983 Etna eruption: Event chronology and morphological evolution of the lava flow. *Bull. Volcanol.* **47,** 1079–1096.

Kilburn, C. R. J., and Luongo, G., eds. (1993). "Active Lavas: Monitoring and Modelling." UCL Press, London.

Lipman, P. W., and Banks, N. G. (1987). Aa flow dynamics, Mauna Loa 1984. Pages 1527–1567 *in* "Volcanism in Hawaii" (R. W. Decker, T. L. Wright, and P. H. Stauffer, eds.). U.S. Geological Survey Prof. Paper 1350.

Macdonald, G. A. (1972). "Volcanoes." Prentice-Hall, Englewood Cliffs, NJ.

Naranjo, J. A., Sparks, R. S. J., Stasiuk, M. V., Moreno, H., and Ablay, G. J. (1993). Morphological, structural and textural variations in the 1988–1990 andesite lava of Lonquimay Volcano, Chile. *Geol. Mag.* **129,** 657–678.

Ponte, G. (1923). The recent eruption of Etna. *Nature* **112,** 546–548.

Scarpa, R., and Tilling, R. I., eds. (1996). "Monitoring and Mitigation of Volcano Hazards." Springer Verlag, Berlin.

Williams, H., and McBirney, A. R. (1979). "Volcanology." Freeman, Cooper, San Francisco.

Wolfe, E. W., Neal, C. A., Banks, N. G., and Duggan, T. J. (1988). Geologic observations and chronology of eruptive events. Pages 1–97 *in* "The Puu Oo eruption of Kilauea Volcano, Hawaii: Episodes 1 through 20, January 3, 1983, through June 8, 1984" (E. W. Wolfe, ed.). U.S. Geological Survey Prof. Paper 1463.

This Page Intentionally Left Blank

LAVA DOMES AND COULEES

JONATHAN H. FINK
Arizona State University

STEVEN W. ANDERSON
University of Arizona and Black Hills State University

I. Definition of Lava Dome
II. Why Study Lava Domes?
III. Ways to Study Lava Domes
IV. Major Hazards Associated with Lava Domes
V. Types of Lava Domes
VI. Lava Dome Surface Textures and Structures
VII. Internal Structure of Lava Domes: Flow Bands and Joints
VIII. Transitions between Explosive and Effusive Behavior
IX. Lava Degassing Mechanisms
X. Geophysical and Geodetic Studies of Lava Domes
XI. Domes as Indicators of Tectonic Stress Orientations
XII. Summary

GLOSSARY

coulee An extrusion of lava that has aspects of both a lava dome and a lava flow. A lava dome that has experienced some flow away from the vent.

cryptodome An accumulation of molten material just beneath the surface. This material typically lifts the overlying rock and soil, forming a visible mound on the Earth's surface as the molten rock beneath gradually cools and hardens.

endogenic dome growth The enlargement of a lava dome as its exterior expands to accommodate an influx of new lava.

endogenic explosions Forceful ejection of volcanic material originating from the interior of an advancing lava flow or dome.

exogenic dome growth The enlargement of a lava dome as successive, discrete lobes of lava pile on one another.

exogenic explosions Forceful ejection of material from beneath a volcano through a vent on its surface.

lava dome Mounds of volcanic rock that form as lava flows onto the surface and amasses over a vent.

vesicular Texture of a volcanic rock characterized by an abundance of void spaces.

rheology The study of flowing materials.

I. DEFINITION OF LAVA DOME

Lava domes are mounds of rock extruded from a volcanic vent (Fig. 1). They form as viscous magma cools relatively quickly after emerging onto a planetary surface. Although dome compositions may cover the full spectrum of silica contents, the majority have relatively high

Copyright © 2000 by Academic Press
All rights of reproduction in any form reserved.

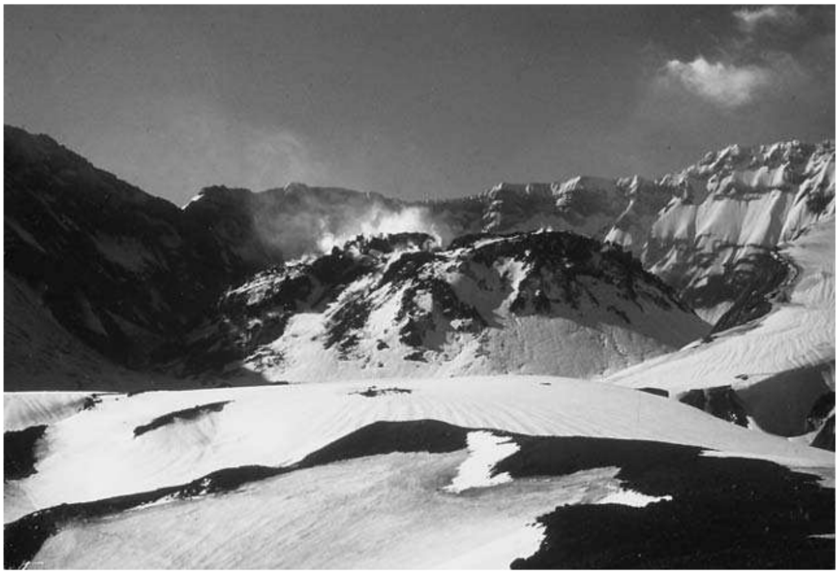

FIGURE 1 The Mount St. Helens composite lava dome in 1985. This dome formed as distinct lobes of lava extruded onto the surface between 1980 and 1986. The dome, which is approximately 1 km in diameter and 300 m high, enlarged primarily through endogenous growth during the late stages of formation.

silica contents. Dome diameters vary from a few meters to several kilometers, and their height varies from a few meters to greater than 1 km. They may be steep sided or tabular in cross section, circular, elliptical, or irregular in outline, and uniform or varied in color and texture. Some occur in isolation, whereas others form linear or arcuate chains up to 20 km long on Earth and more than 150 km long on Venus. They may have steady or episodic growth, with emplacement times ranging from a few hours to many decades. Effusion rates vary from less than 1 m^3/s to more than 100 m^3/s. Some of the larger lava domes exhibit some flow of lava away from the main vent, and are referred to as *coulees*. Generally, lava domes advance too slowly to threaten nearby populations with burial, or to make colorful footage for news broadcasts. Yet in recent years, lava dome emplacement has been among the most deadly types of volcanic eruptions with more than 100 fatalities recorded at active lava domes this decade, including 44 deaths at Mount Unzen (Japan) in 1991 and 66 at Mount Merapi (Indonesia) in 1994 (Table I).

The danger associated with lava domes comes less from their growth than from their collapse. Volcanologists have devoted much attention to understanding why some domes suddenly transform from passively expanding mounds of lava to violently explosive clouds of scalding rock and ash fragments. In this article, we consider the character of lava domes, the different ways geologists try to decipher their growth and hazards, and the significance of their interior and exterior textures and structures.

II. WHY STUDY LAVA DOMES?

Domes are of interest to geologists for several reasons: (1) Although some may grow unaccompanied by significant hazard, they more typically form part of an eruptive cycle that includes dangerous explosive phases. Understanding why eruptive violence waxes and wanes

TABLE I Partial List of Fatalities Associated with Dome Emplacement, Collapse, and Destruction this Century

Volcano	*Date*	*Fatalities*
Mt. Pelée (Martinique)	1902	29,025
Soufrière (St. Vincent)	1902	~1,600
Santiaguito (Guatemala)	1929	~1,000
Merapi (Indonesia)	1954	64
	1976	28
	1994	66
Mt. Unzen (Japan)	1991	44
Soufriere Hills (Montserrat)	1997	19

is one of the main goals of volcanology, because it is necessary for issuing accurate volcanic hazards. (2) In contrast to more widely dispersed explosive eruption products, many domes are well preserved in the geologic record because their mass is confined to the near-vent regions of the volcano. Consequently, their shapes and locations are indicators of conduit geometry, which in turn reflects the prevailing state of stress at the time of eruption. (3) Similarly, mixing or stratification that takes place hidden from view in the magma chamber may cause chemical variations observed in dome rocks. These geochemical signatures can provide volcanologists with evidence of processes occurring beneath the volcano. (4) Water and other volatile phases dissolved in viscous silicic lavas have difficulty escaping, so that the surface of a dome may preserve an assortment of vesicular textures that offer clues about the role of volatiles in eruptive processes. (5) The spreading of active lava domes can be mathematically modeled and simulated in the laboratory, providing rare insights into the rheologic behavior of real magma containing bubbles, crystals, and large temperature gradients. (6) Dome-like features are recognized on the surfaces of the Moon, Mars, Venus, and on some of the icy satellite of Jupiter. Establishing the conditions needed for dome formation on Earth allows for more accurate interpretation of the evolution of these extraterrestrial bodies.

III. WAYS TO STUDY LAVA DOMES

Geologists use an arsenal of tools to learn about lava domes, depending on the questions they are trying to answer. Observations of dome morphology, structure, and texture come from remote sensing, surveying, and other field techniques. Repeated aerial photography or other remotely sensed data record changes in diameter, height, volume, and structure of active domes. Thermal infrared measurements are sensitive to the vesicularity and mineralogy of older dome surfaces, or temperature variations within active domes. Magnetic studies of active domes provide insights regarding cooling rates. Radar studies may describe the blockiness of a dome surface, or the grain-size distribution in pyroclastic deposits formed when lava domes collapse. Carefully constrained surface sampling combined with research drilling is necessary to unravel the geochemical character and degassing behavior of domes. Laboratory simulations help relate the surface structure of a dome to its eruption rate, cooling rate, and lava composition, and the spreading dynamics to magma rheology.

IV. MAJOR HAZARDS ASSOCIATED WITH LAVA DOMES

Most hazards associated with domes originate when a part of a lava flow front collapses, giving rise to an avalanche of hot, fragmented material called a *pyroclastic flow* or *surge*. Pyroclastic phenomena formed from material previously erupted from a volcano are called *endogenic* explosive eruptions. They may occur with little warning and up to several months after a particular lobe began its growth (Figs. 2 and 3; see also color inserts). The cooled outer carapace of a dome can contribute to a buildup of pressure in the flow's interior, releasing a violent explosion when the dome front collapses. The destructive potential is roughly proportional to the volume and volatile content of the collapsing lava. Studies at Mount Unzen and Soufrière Hills (Montserrat) suggest that variations in dome extrusion rate also may correlate with the frequency of pyroclastic flow generation by gravitational collapse. The pyroclastic currents emitted from domes may travel tens of kilometers at very high speed. In the 1990s, such events killed more than 100 people at Unzen, Soufrière Hills, and Merapi. Similar activity at the Santiaguito dome complex on Santa Maria Volcano (Guatemala) produced pyroclastic flows that killed more than a thousand people in 1929.

In contrast to the endogenic pyroclastic events generated by dome collapse, the size and violence of *exogenic* explosive eruptions, those that eject new material from the volcanic conduit or magma chamber beneath a dome, may show little apparent relationship to the lava resting on the surface. These eruptions, which may partially or totally destroy an existing dome, can be easier to predict because they tend to be accompanied by precursory seismicity, deformation, or gas emissions that can be monitored remotely. A small dome preceded the major plinian eruption of Mount Pinatubo (Philippines) in June 1991. The devastating pyroclastic surge that destroyed the city of St. Pierre on the island of Martinique in 1902 is thought to have emerged from the base of a dome that had been visible on the distant skyline of Mount Pelée for several days. In the 5 months that followed the cataclysmic plinian eruption of Mount St. Helens (USA) in May 1980, a series of domes appeared and were then destroyed by explosive eruptions from the conduit. Similarly, the extrusion of 13 separate domes at Mount Redoubt in Alaska in 1991 alternated with explosions that pulverized them.

Because of their position high on a volcanic edifice, many domes pose dangers to the surrounding area even after they have fully cooled and solidified. For instance,

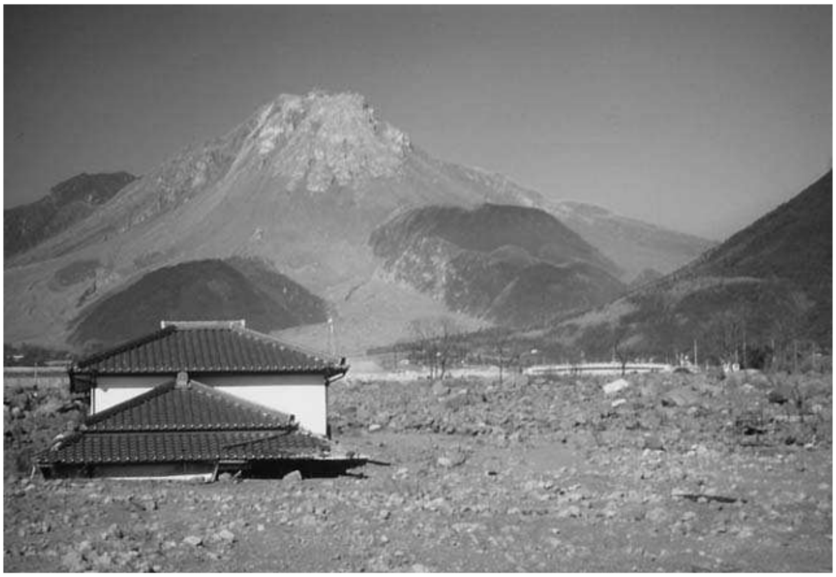

FIGURE 2 Pyroclastic material from the Mount Unzen lava dome (background) has caused extensive property damage in Shimabara, Japan. The eruption on June 3, 1991, was responsible for 44 fatalities. (See also color insert.)

one of the Chaos Crags dacite domes on the shoulder of Mount Lassen (USA) collapsed several hundred years after its extrusion, possibly in response to an earthquake, forming the Chaos Jumbles rockfall avalanche that traveled more than 5 km away from its source. Parts of the dome at Mount Unzen are today perched precariously a few kilometers away from the city of Shimabara, and large-scale failures near the E1 Brujo vent of the Santiaguito dome occurred in 1992, nearly 15 years after extrusion ceased at this vent. Domes in wet climates are subject to hydrothermal alteration, which promotes increased rates of erosion, resulting in voluminous slurries of water, ash, and eroded volcanic rocks that can cause deadly flooding. Such events represent major ongoing hazards at both Santiaguito and Merapi.

V. TYPES OF LAVA DOMES

Volcanic features referred to as *lava domes* share many attributes; they are made of viscous lava, they tend to pile up over their vents, and their surfaces are generally blocky. However, a global inventory suggests that domes may be subdivided into different categories on the basis of morphology, surface texture, and eruptive style. The steepest sided, named Pelean or spiny domes, are circular in plan view and have relatively smooth upper surfaces punctuated by tall vertical spines. Examples include domes at Mount Pelée (both 1902 and 1932–1933) and Santiaguito (1922–present). Somewhat less steep domes are typically composed of a series of distinct lobes that emerge sequentially from a vent. These domes have some portions covered with small blocks and others displaying very smooth surfaces, smaller cross-sectional profiles, and more irregular plan forms (Fig. 4; see also color insert). They include domes that followed major plinian explosive eruptions at Mount St. Helens, Katmai, and Pinatubo, as well as the 13 domes that formed at Redoubt volcano in 1991. A third type, called *platy* or *endogenous domes*, has an even lower profile, blockier carapace, fewer and shallower fractures, and more numerous transverse surface ridges. Examples include the domes at Mount Merapi and Soufrière of St. Vincent (Fig. 5). Domes of the final type have nearly level upper surfaces, highly irregular plan outlines, and surfaces covered with variously colored small blocks and linearly extensive surface corrugations. These are referred to as *axisymmetric domes* because of their tendency to have shapes constrained by local topography. Holocene age axisymmetric rhyolite domes include Little Glass Mountain on Medicine Lake volcano in northern California and Big Obsidian Flow at Newberry volcano in Oregon.

The progression of dome categories just described—spiny, lobate, platy, and axisymmetric—corresponds to conditions of increasing eruption rates and decreasing cooling rates and yield strengths. Carefully scaled laboratory simulations using analog materials allow the quantification of relationships between these dome types and eruption conditions. Slurries of polyethylene glycol wax mixed with kaolin powder can reproduce many of the most common attributes of these four dome types. Comparison with eight well-documented eruptions and their estimated effusion rates allowed the calculation of effective yield strenghts of the active domes. Using a complementary approach, eruption rates of prehistoric and extraterrestrial domes were estimated, values that cannot be determined in any other way.

Cryptodomes are another variety of lava dome, and differ from the previous examples in that lava never reaches the surface of a volcano. Thus, it is an accumulation of molten material just beneath the surface. This material typically lifts the overlying rock and soil, forming a visible mound on the Earth's surface as the molten rock beneath gradually cools and hardens. Usu volcano in Japan produced a cryptodome in 1910, called Meiiji Sin-zan. In 1943, new lava intruded through Meiiji Sin-zan and reached the surface, forming the spiny Showa Sin-zan lava dome.

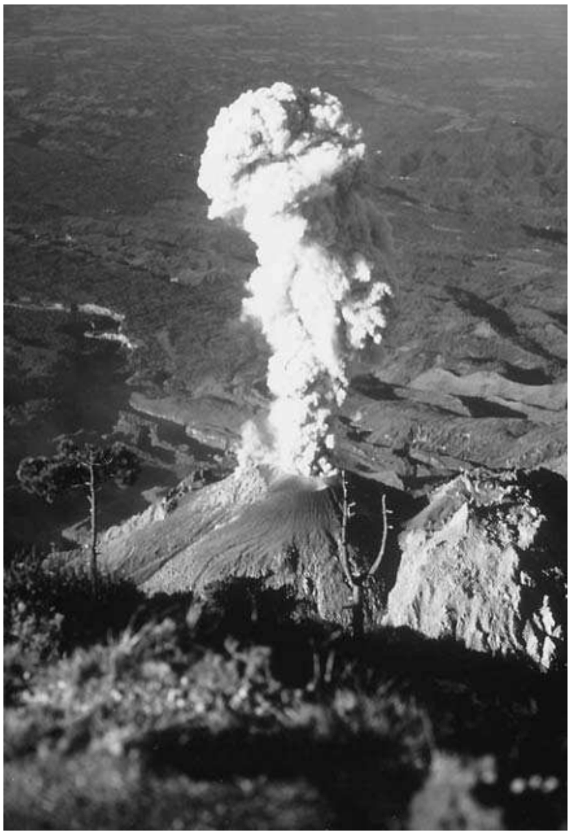

FIGURE 3 An explosion at the Santiaguito lava dome in 1988. These small explosions pose few hazards for local residents, although larger ones could destroy larger sections of the dome. (See also color insert.)

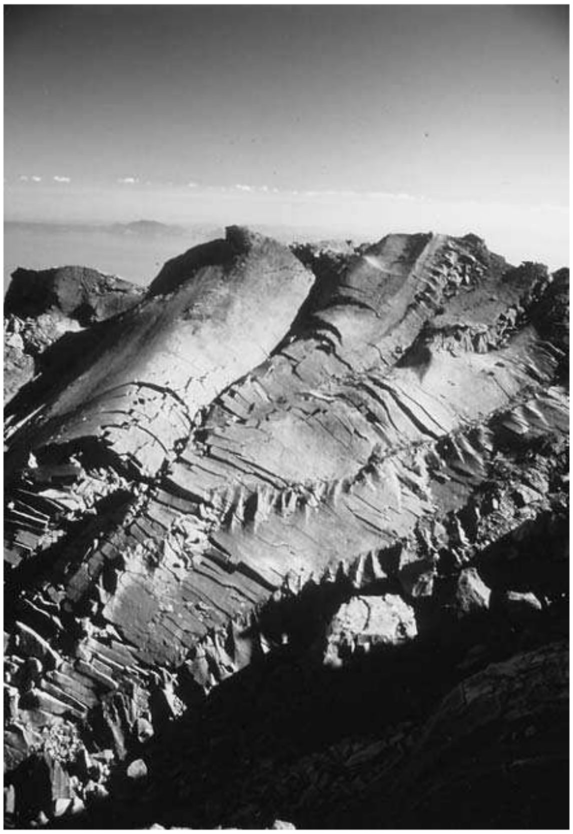

FIGURE 4 Smooth area of the Mount Unzen dacite lava dome in 1995. The width of the field of view is approximately 75 m. (See also color insert.)

Cryptodomes may have significant implications for volcanic hazards. The deformation of the north flank of Mount St. Helens in 1980 was triggered by the formation of a cryptodome. The injection of lava beneath the surface of Mount St. Helens fractured and destabilized the preexisting rocks, eventually leading to the cataclysmic debris avalanche and explosion of the cryptodome on May 18, 1980.

VI. LAVA DOME SURFACE TEXTURES AND STRUCTURES

Walking across a lava dome is not a particularly pleasant experience. In fact, terrestrial lava domes have some of the roughest of geologic surfaces when measured at decimeter to meter scales. Haphazard piles of loose,

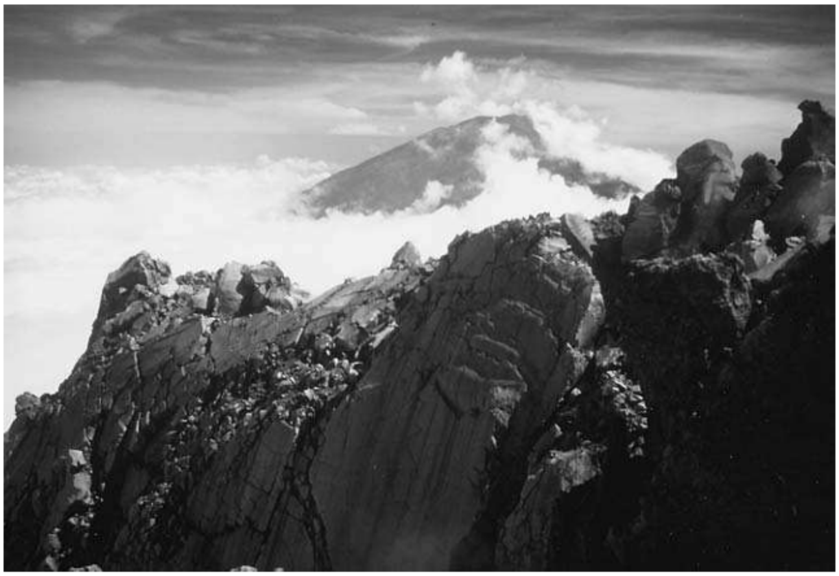

FIGURE 5 Blocky, spiny surface of the Mount Merapi lava dome (foreground) in 1995, with Mt. Merbaru in the background.

sharp blocks separated by deep cracks and hollows conspire against easy walking. Only anomalously smooth areas, most commonly near vents, provide any respite. Aerial photographs reveal that on many domes, the seemingly chaotic mounds and depressions align into regularly spaced ridges and troughs that may extend continuously for hundreds of meters. The same photos show that smooth areas commonly occur in pairs, symmetrically distributed about a central fracture called a *crease structure*. In addition, explosion pits dot the surfaces of some of the larger rhyolitic extrusions. Hand samples collected from dome surfaces reveal a variety of glassy and vesicular textures, and detailed mapping can record their spatial distribution. During the past two decades, volcanologists have found that studies of block size distributions, lava textures, and surface structures each can provide unique information about the emplacement of silicic magmas. These lava textures and structures typically result from brittle deformation, at a variety of scales, of a cooled, rigid flow exterior during emplacement. This is in contrast to basalt lava flows, whose surface morphology is controlled largely by ductile deformation prior to solidification.

A. Blocks

The most basic structural element on a lava dome surface is the block. Blocks on a particular portion of a dome can vary greatly in size, ranging from more than 5 m in diameter to others small enough to sift through gaps between larger blocks to the flow interior. Although the placement of blocks on a lava dome may appear random, block size distributions actually reflect eruption dynamics. Average block sizes generally decrease outward from a vent area to the flow front (Fig. 6). Observations at the active Mount St. Helens and Mount Unzen lava domes showed that high extrusion rates lead to rapid fracturing of the flow surface and the production of small primary blocks. Low extrusion rates cause less intense fragmentation and the formation of large slabs in the vent area. This relationship has been confirmed in laboratory simulations using kaolin/wax slurries; lower eruption rates produce more extensive smooth surfaces.

Although most blocks initially form in the vent region, new ones may be generated downslope through fracturing associated with compressional folding, crease structure formation, and as rootless explosions toss blocks onto the flow surface. These primary blocks may fracture further through mechanical and thermal processes as they are carried downflow. Most silicic lava flows reach a "steady-state" in which the average block size at the surface remains in the 20- to 30-cm range despite increasing distance from the vent. Finer grained material (blocks <12 cm) does not typically accumulate on the flow surface because it falls into the interior. Therefore, long silicic lava flows are not expected to be covered by a blanket of fines along their entire lengths, an important consideration for remote evaluation of extraterrestrial lava flow compositions.

B. Vesicular Lava Textures

Besides varying in size, the blocks that cover lava dome surfaces also display a spectrum of glassy and vesicular textures that develop at different flow depths. Surface and flow-front mapping as well as drilling studies reveal a complex stratigraphy of these textures within many silicic lava domes. Rhyolitic extrusions typically consist of a surface layer of finely vesicular pumice (FVP) underlain by a zone of obsidian (OBS). Beneath this upper obsidian, a layer of coarsely vesicular pumic (CVP) forms where volatiles from the flow interior accumulate beneath the crust of obsidian and FVP. This CVP layer has a lower density than the overlying material and may rise to the surface as regularly spaced diapirs (Fig. 7). These features may then deform into folds and crease structures as the advancing flow surface compresses and stretches. Beneath the CVP zone, the lowermost portion of the flow consists of a combination of more obsidian and a central layer of partially crystallized rhyolite.

Two contrasting models have been proposed to explain the textures in rhyolitic lava domes. According to the first, most of the lava emerges from the vent as dense obsidian that then degasses and inflates during advance to form surficial (FVP) and interior (CVP) vesicular zones. An alternative view, sometimes referred to as the *permeable foam model*, suggests that the entire flow is erupted as a highly inflated magmatic foam that compresses under its own weight to form obsidian zones. Both models assume that most of the originally high magmatic gas content (commonly greater than 5 wt %) is lost into the wallrocks and through the open vent as the magma works its way to the surface. The controversy concerns the texture of the magma as it comes out from the vent.

Dacitic lava domes, such as those at Mount St. Helens and Mount Unzen, exhibit simpler, though similar, textural stratigraphy as compared to the rhyolitic domes. Many of the flow lobes extruded at Mount St. Helens from 1980 to 1983 display a vesicular carapace underlain by a dense interior, analogous to the FVP and OBS layers in rhyolites. Observations of active dacite lobes show that the frothy carapace forms through vesiculation of originally dense lava during surface flow, and chemical analyses demonstrate that a significant amount of water may be liberated from the lava during this process. In contrast, most Mount St. Helens flow lobes formed between 1983 and 1986 have little or no vesicular material on their surfaces, suggesting that more substantial degassing occurred prior to emergence of this magma. One possible interpretation of this relationship is that later in its history, the taller dome with a thicker cooled crust more effectively inhibited magma extru-

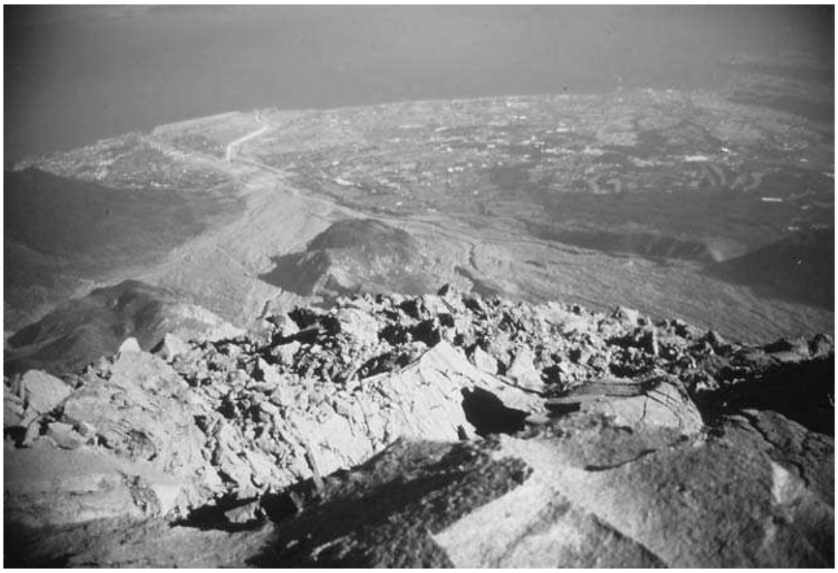

FIGURE 6 Summit of the Mount Unzen dacite dome towering above Shimabara, Japan. Note the large blocks in the foreground with smaller blocks dominating the distal surfaces.

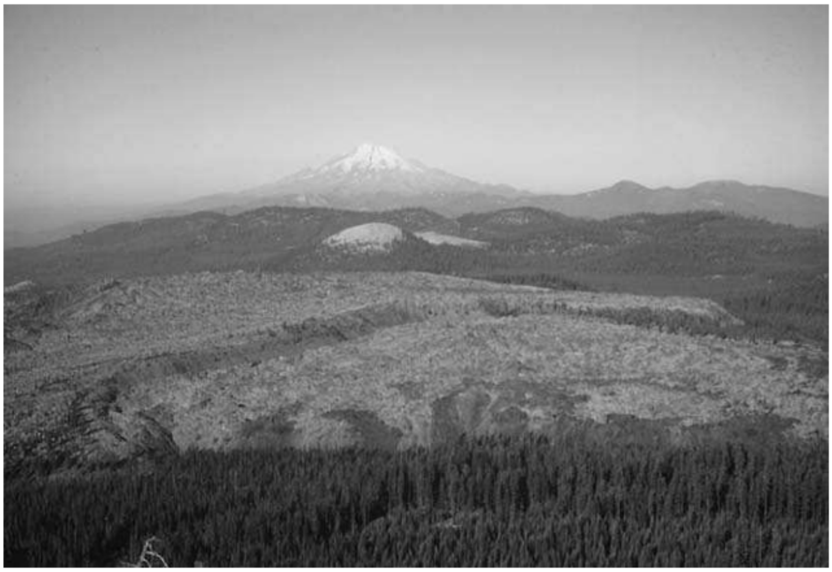

FIGURE 7 The Little Glass Mountain rhyolite flow in northern California with Mount Shasta in the background. The dark, irregularly shaped surfaces in the foreground are outcrops of coarsely vesicular pumice that form as volatiles accumulate beneath a cooled flow surface. The CVP then rises diapirically to the surface.

sion, allowing more substantial degassing to take place beneath the surface.

C. Explosion Pits

On some of the larger rhyolitic lava domes in the western United States, 10- to 15-m deep explosion pits disrupt the flow surface. These craters typically occur in the distal regions of a flow, far from the primary vent. They penetrate the upper FVP and OBS layers, suggesting that they originate in the interior CVP region. Analyses of the CVP zone show that it can have two to three times the water content of the OBS and FVP zones. These anomalously high water contents may develop when gases released by crystallization of the flow interior migrate upward through cracks to accumulate beneath the cooler and less permeable upper obsidian layer. These additional volatiles could provide the energy necessary to drive the explosions that disrupt dome surfaces and increase their hazard potential.

D. Compressional Ridges

Surface ridges form in response to compression parallel to flow during advance of some silicic lavas. Folding theory has been used widely to interpret regularly spaced tectonic structures, and also can be applied to corrugations on lava flows. The geometry of lava folds offers a means of estimating the bulk rheological properties of the magma. These estimates may differ significantly from those determined by laboratory measurements. Experimental procedures use relatively small, homogeneous samples, while natural lavas contain bubbles, crystals, and compositional and thermal gradients that are difficult to replicate in the laboratory. These viscosity estimates can be used to calculate flow velocities, which in turn are needed for hazard assessments.

The growth of surface folds on a viscous fluid requires a particular combination of stress and rheologic conditions. The upper surface of the flow must have a viscosity that is greater than that of the interior, and compression must be sufficiently high to overcome the tendency of gravity to minimize any large-scale topographic irregularities. If the viscosity contrast is too high, the top of the flow will not deform in a ductile manner but instead will fracture. If the contrast is too low, compression will cause the upper part of the flow to thicken rather than fold. Fold wavelengths are roughly proportional to the thickness of the flow's cooled upper carapace. The ratio of wavelength to carapace thickness depends on the flow composition, with more silicic compositions having larger wavelength-to-thickness ratios than more mafic compositions. In some cases, the surface of a flow may undergo more than one folding episode. On photographs of the resulting "refolded" surface, the ratio of first- to second-generation wavelengths can be determined. This ratio, which ranges between 2 and 5, has also been shown to have composition dependence, since flows with more silicic chemistry have smaller ratios. This approach was used to determine that several lava flows on Mars had andesitic compositions.

E. Crease Structures

Probably the best documented emplacement of a lava dome was that of Mount St. Helens between December 1980 and December 1986. The dome consisted of an assemblage of lobes that each required a few days to a few months to grow, separated by repose periods of a few weeks to a year. For many of these lobes, the first and last lava to appear at the surface emerged from a prominent crack on the flow surface called a crease structure. This fracturing process is cyclic, with small increments of crack growth alternating with brief periods of cooling. The result is a pair of fracture surfaces cut by striations that parallel the crack axis and form as the crack tip temporarily stops during inward propagation (Fig. 8). Similar striae are found on the surfaces of cyclically fractured columnar joints.

Detailed studies of crease structure morphology and formation on active and recent silicic flows show that these features develop where lava is allowed to spread laterally, either as the flow advances across a relatively flat area, or along the crests of surface ridges perpendicular to the direction of maximum compression. Crease structures vary greatly in size, with their long axes measuring from less than 3 to more than 250 m. In fact, the entire surface of some lava domes, such as many along the Devils Hill chain on South Sister volcano (Oregon), consists of a single crease structure. Observations of several Mount St. Helens dome lobes that were emplaced as single, large creases provided estimates of strain rate during formation and allowed for modeling of the thermal and mechanical evolution of these structures. Estimated formation times generated from a one-dimensional conductive cooling model were used to calculate extrusion rates for several older rhyolitic domes emplaced as single crease structures. These emplacement rates varied from less than 1.0 m^3/s for domes in the Devils Hill chain, to more than 100 m^3/s at the Glass Creek dome in the Inyo Dome chain (California). These values compare favorably with those determined independently through analysis of overall dome morphology.

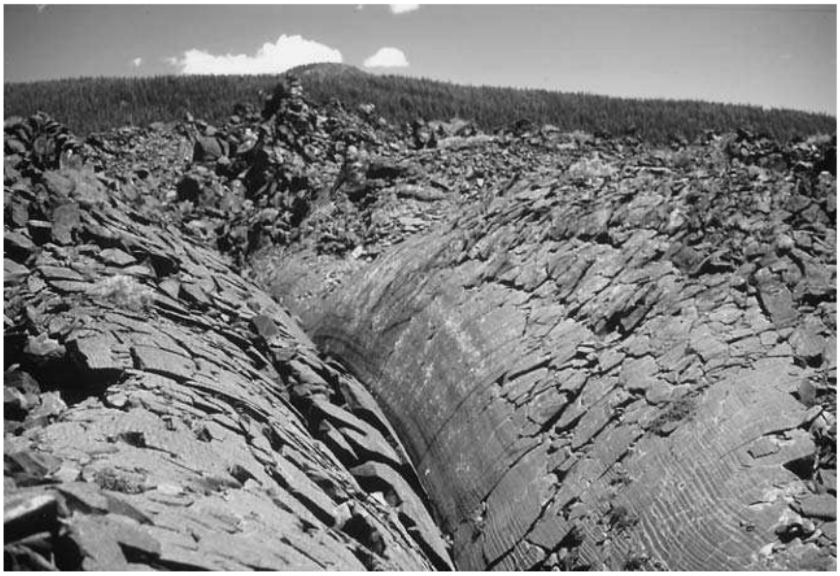

FIGURE 8 Crease structure on the Medicine Lake dacite flow in northern California. The parallel banding evident in the lower right side of the photograph results from a cyclic fracture process. The width of the crease structure visible in the lower part of the figure is approximately 5 m.

VII. INTERNAL STRUCTURE OF LAVA DOMES: FLOW BANDS AND JOINTS

In addition to their textural stratigraphy, many lava domes display two types of internal structure, flow bands and joints, that provide clues about the state of stress in the flow interior. Flow bands are subparallel, planar concentrations of small crystals or bubbles that develop in response to friction along the conduit walls during magma ascent, and deform in response to velocity changes during flow advance. Some domes display a concentric "onion-skin" foliation pattern in which the earliest extruded magma forms the outermost layer, and later magma inflates this rind like a balloon. Other domes have a more fanlike pattern originating when lava emplaced vertically above the vent slowly spreads laterally, accompanied by continual fracturing at the flow's upper surface. Domes with a complex emplacement history may produce flow banding that has no easily discernible pattern, although careful measurements of these foliations may uncover the direction in which the flow moved and the sequence in which different lobes were emplaced.

Older, dissected lava domes also may display a range of columnar, polygonal, or sheetlike joint patterns in their interiors that reflect stresses associated with flow advance and cooling. Columnar joints form in response to thermal stresses accumulated during cooling of a dome, and their diameters are proportional to the cooling rate. Because these joints propagate away from a cooling surface, their orientations can help locate original flow margins. Such relationships have been used in a number of Cascade Range domes to identify where the lava may have been in contact with glaciers that are no longer present. Subparallel, platy joints commonly occur in the interior portions of domes where basal shear dominates the state of stress.

VIII. TRANSITIONS BETWEEN EXPLOSIVE AND EFFUSIVE BEHAVIOR

Lava domes typically extrude as part of an eruption sequence that may involve both effusive and explosive phases. Understanding the processes that favor a particular style of volcanism is essential for assessing hazards. For example, the extrusion of a silicic lava dome at Mount Pinatubo on June 8, 1991, prior to the cataclysmic caldera-forming eruption on June 15 provided volcanologists with a glimpse of the magma composition of the volcano and hinted that a relatively clear conduit was available for any subsequent eruptions. This information allowed for timely and accurate warnings that minimized casualties.

Transitions between early explosive activity and late effusive behavior were originally ascribed to volatile stratification in a magma chamber; the volatile-rich upper part of the chamber first erupts explosively and then the volatile-poor lower portions erupt effusively. However, mineralogic studies later showed that the "dry" magma that forms domes and the "wet" magma that forms pyroclasts both had similarly high water contents prior to eruption. This realization led to the suggestion that variations in eruptive style are caused by differing ability of the ascending magma to lose gas, rather than by differences in the primary volatile content. This gas loss in turn is controlled by the permeability of the conduit walls and the magma ascent rate.

Although this model did a good job of explaining transitions from pyroclastic to effusive eruptions, it was less able to account for detailed textural relations in silicic domes and lava flows. Its proponents argued that all domes emerge from a vent as uniformly frothy magma that then compresses to dense lava during surface flow. However, field mapping and observations of active domes showed that in many cases the opposite is true: dense lava first appears at the vent and then vesiculates to form different textural zones during advance. The two views can be reconciled through a three-part hybrid model. (1) Most gas loss occurs into the wallrocks and out the top of a conduit during magma ascent. (2) Foam collapse takes place in the vent prior to the emergence of lava at the surface. (3) The surface of the advancing dense lava flow can vesiculate, and small amounts of volatiles within the flow interior can become redistributed by migrating through small transient cracks. Resulting zones of unusually high water content are most likely to be the sources of explosive phenomena if exposed suddenly by flow-front collapse.

IX. LAVA DEGASSING MECHANISMS

As indicated in the previous sections, the rate of volatile escape as magma moves from the chamber toward the surface is a major factor determining eruptive style. Stable isotope characterization of the small amounts of water remaining in dome lavas allows discrimination of different degassing processes. *Closed-system degassing* is an equilibrium process that takes place in the chamber, where exsolved gases remain in contact with the magma. *Open-system degassing* occurs in the conduit, where gases released from the magma can escape to the atmosphere or into the host rocks, causing more rapid changes in isotopic signature. *Kinetic degassing* is only observed in extruded lavas whose low water content and high viscosities inhibit isotopic exchange between exsolved and residual gases within bubbles.

At Obsidian Dome (California) glassy rhyolite samples were collected both from the lava flow and from an underlying pyroclastic deposit whose emplacement immediately preceded dome extrusion. Obsidian from the pyroclastic layer had higher water and deuterium contents than obsidian from the dome surface. The data suggested that most of the gas loss accompanying formation of the dome obsidian had been an open-system process, presumably in the conduit. In contrast, the isotopic signatures of lava samples from the Mount St. Helens dacite dome could best be explained by a combination of closed-system, open-system, and kinetic degassing, requiring a more complicated interpretation of the timing of gas loss during the 6-year, episodic extrusion of the dome.

X. GEOPHYSICAL AND GEODETIC STUDIES OF LAVA DOMES

The Mount St. Helens eruption gave volcanologists an unprecedented opportunity to monitor geophysically the growth of an active dome. Seismic, magnetic, geodetic, tilt, and other data were collected during the dome's 6-year emplacement. The cyclic nature of dome growth combined with its proximity to a major urban area and adequate funding provided ideal conditions for acquiring repeated measurements throughout the entire growth sequence. For example, repeated magnetic surveys across the dome's surface before, during, and after several episodes of lobe extrusion showed that the dome contained a hot, nonmagnetized core surrounded by a cool, magnetized carapace and talus apron. The magnetized carapace thickened at an average rate of 0.03–0.01 m/day from 1984 to 1986. Snowmelt, rainfall, and large-scale fracturing all enhanced the rate of cooling. This work enabled volcanologists to predict that the dome would completely solidify within 18–36 yr of the last eruption (1986). Detailed seismic studies gave a view of the plumbing system that fed the dome. These data showed that the conduit was less than 50 m wide, only 2–3% of the final dome diameter. They also suggested that the rising magma passed through two reservoirs at depths of 3 and 6 km beneath the summit.

The repeated data acquired by the U.S. Geological Survey at Mount St. Helens also provided the framework for a number of new models of dome emplacement. Geodetic studies showed that dome growth events were volume predictable; the volume of lava erupted during a single episode was proportional to the preceding period of repose. These extrusions can be explained if overpressurization in the magma chamber occurs at a constant rate. The 1980–1986 eruption also provided the first complete series of detailed topographic data collected during growth of a lava dome. After each of the nearly 20 lobes was extruded, the U.S. Geological Survey took high-resolution aerial photographs of the entire dome and then made digital topographic maps with 2-m contours. These data allowed volcanologists to study the detailed intrusive and extrusive growth patterns of a lava dome.

The overall patterns and rates of dome deformation suggested that the size, shape, and behavior of a lava dome are primarily controlled by the interplay between the strength of the cooled carapace and the magnitude of pressurization in the dome's interior. Furthermore, as a dome grows larger, it can accommodate a greater volume of endogenous (intrusive) growth before the brittle carapace ruptures. This idea explains the progressive increase in endogenous growth that is observed with each successive episode of dome extrusion.

XI. DOMES AS INDICATORS OF TECTONIC STRESS ORIENTATIONS

Dikes feed many silicic domes. These domes tend to occur in groups that are arranged either in linear or en echelon arrays. Many of the individual domes are asymmetrical and elongate parallel to the overall trend of the dome group. Near-vent fractures on the dome surfaces also are aligned preferentially to the orientation of the group of domes. Paired ground cracks, which form above and parallel to a rising dike, are commonly found near domes. Where inferred dike trends pass under topographic highs, the spacings of these pairs of fractures tend to increase, suggesting that the distance between the ground surface and the dike top is increasing. These types of structural evidence have been mapped in the vicinity of several Holocene dome groups, allowing the orientation of the feeding dikes to be inferred. These dike trends can then be related to stress directions determined by other means to evaluate the relative influence of magmatic and tectonic forces. For instance, structures mapped along the trend of the Inyo domes near Long Valley Caldera, California, suggest that the domes were fed by a dike that rose obliquely to the north from an area beneath Mammoth Mountain. Domes on the southeastern slope of South Sister volcano reflect an echelon series of dikes or dike segments that rotated slightly as they approached the surface. Rhyolite domes in the Coso Range of eastern California trace paths that suggest the underlying dikes have predominantly north–south orientations (consistent with tectonic influences) but bend inward to a more radial attitude as they approach an inferred central magma body.

XII. SUMMARY

The hazards associated with the recent, deadly eruptions at Mt. Unzen, Soufriere Hills, and Merapi demonstrate the need to better understand the formation and behavior of lava domes. Past studies of the Mount St. Helens dome form the foundation for current investigations of these more recent extrusive events, and enable volcanologists to better mitigate the hazards associated with these underappreciated volcanic features.

SEE ALSO THE FOLLOWING ARTICLES

Composition of Magmas • Lava Flows • Magma Chambers • Plinian and Subplinian Eruptions • Plumbing Systems • Pyroclastic Surges and Blasts • Volcanic Hazards and Risk Management

FURTHER READING

Anderson, S. W., and Fink, J. H. (1989). Hydrogen isotope evidence for extrusion mechanisms of the Mount St. Helens dome. *Nature* **341,** 521–523.

Anderson, S. W., and Fink, J. H. (1992). Crease structures as indicators of emplacement rates and surface stress regimes of lava flows. *Geol. Soc. Am. Bull.* **104,** 615–626.

Anderson, S. W., Stofan, E. R., Plaut, J. J., and Crown, D. A. (1998). Block size distributions on silicic lava flow surfaces: Implications for emplacement conditions. *Geol. Soc. Am. Bull.* **110,** 1258–1267.

Dzurisin, D., Denlinger, R. P., and Rosenbaum, J. G. (1990). Cooling rate and thermal structure determined from progressive magnetization of the dacite dome at Mount St. Helens, Washington. *J. Geophys. Res.* **95,** 2763–2780.

Eichelberger, J. C., Carrigan, H. R., Westrich, H. R., and Price, R. H. (1986). Non-explosive silicic volcanism. *Nature* **323,** 598–602.

Fink, J. H., and Manley, C. M. (1987). Origin of pumiceous and glassy textures in rhyolite domes and lava flows. Pages 77–88 *in* "The Emplacement of Silicic Domes and Lava Flows" (J. H. Fink, ed.). Geological Society of America Special Paper 212.

Fink, J. H., Anderson, S. W., and Manley, C. R. (1992). Textural constraints on effusive silicic volcanism: Beyond the permeable foam model. *J. Geophys. Res.* **97,** 9073–9083.

Fink, J. H., Malin, M. C., and Anderson, S. W. (1990). Intrusive and extrusive growth of the Mount St. Helens dome. *Nature* **348,** 435–437.

Griffiths, R. W., and Fink, J. H. (1993). Effect of surface cooling on the spreading of lava flows and domes. *J. Fluid Mechanics* **252,** 667–702.

Loney, R. A. (1968). Flow structure and composition of the Southern Coulee, Mono Craters, California—A pumiceous rhyolite flow. Pages 415–440 *in* "Studies in Volcanology" (R. R. Coats, R. L. Hay, and C. Anderson, eds.). Geological Society of America Memoir 116.

Nakada, S., Miyake, Y., Sato, H., Oshima, O., and Fujinawa, A. (1995). Endogenous growth of dacite dome at Unzen volcano (Japan), 1993–94. *Geology* **23,** 157–160.

Reches, Z., and Fink, J. H. (1988). The mechanism of intrusion of the Inyo Dikes, Long Valley Caldera, California. *J. Geophys. Res.* **93,** 4321–4334.

Rose, W. I. (1987). Volcanic activity at Santiaguito volcano, 1976–1984. Pages 17–28 *in* "The Emplacement of Silicic Domes and Lava Flows" (J. H. Fink, ed.). Geological Society of America Special Paper 212.

Sparks, R. S. J., Young, S. R., Barclay, J., Calder, E. S., Cole, P., Darroux, B., Davies, M. A., Druitt, T. H., Harford, C., Herd, R., James, M., Lejeune, A. M., Loughlin, S., Norton, G., Skerrit, G., Stasiuk, M. V., Stevens, N. S., Toothill, T., Wadge, G., and Watts, R. (1998). Magma production and growth of the lava dome of the Soufriere Hills Volcano, Montserrat, West Indies: November 1995 to December 1997. *Geophys. Res. Lett.* **25,** 3421–3424.

Swanson, D. A., and Holcomb, R. T. (1989). Regularities in growth of the Mount St. Helens dacite dome: 1980–1986. Pages 3–24 *in* "Lava Flows and Domes: Emplacement Mechanisms and Hazard Implications: IAVCEI Proceedings in Volcanology (J. H. Fink, ed.). Vol. 2. Springer-Verlag, Heidelberg.

Swanson, D. A., Dzurisin, D. Holcomb, R. T., Iwatsubo, E. Y., Chadwick, W. W., Casadevall, T. J., Ewert, J. W., and Heliker, C. C. (1987). Growth of the lava dome at Mount St. Helens, Washington (USA), 1981–83. Pages 1–16 *in* "The Emplacement of Silicic Domes and Lava Flows" (J. H. Fink, ed.). Geological Society of America Special Paper 212.

This Page Intentionally Left Blank

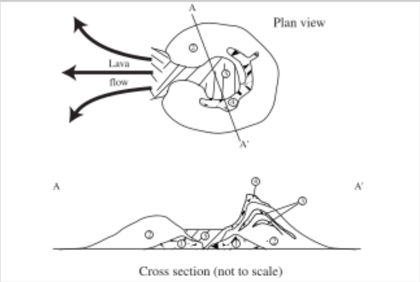

LAVA FOUNTAINS AND THEIR PRODUCTS

JOHN A. WOLFF
Washington State University

JANET M. SUMNER
University of Liverpool

I. Introduction
II. Fountain Production
III. Fountain-Fed Lavas and Associated Eruption Products
IV. Agglutination in Other Compositions and Eruptive Styles
V. Recent Developments
VI. Summary

GLOSSARY

agglutination Instantaneous flattening of hot, soft pyroclasts upon landing. The resultant deposit is an agglutinate or spatter pile; particle outline is in part retained.

ash Pyroclasts smaller than 2 mm in diameter.

basaltic Magma composition with high iron and magnesium content, but low silica content, having highest temperatures and lowest viscosities of common magmas.

bombs Pyroclasts larger than 64 mm in diameter.

clastogenic lava A lava flow formed by the rheomorphic flow of coalesced and agglutinated hot pyroclasts, typically fed by a lava fountain. Lava may contain obvious spatter fragments.

coalescence The process by which hot fluidal pyroclasts form a homogeneous liquid in which the particle outlines are obliterated.

explosive eruption Any eruption in which the magma is torn into fragments by gas pressure as it leaves the vent.

fissure A linear volcanic vent.

Hawaiian A relatively gentle type of explosive eruption involving lava fountains and minor ash and scoria production.

lapilli Pyroclasts between 2 and 64 mm in diameter.

lava fountain An uprushing jet of incandescent pyroclasts that falls to the ground near the vent.

pyroclast A fragment of magma.

scoria A pyroclast containing bubbles that are typically several millimeters in diameter.

spatter Synonymous with agglutinate.

strombolian Slightly more violent than hawaiian activity, strombolian eruptions produce copious amounts of scoria and ash, piled up around the vent to form a cone. The eruption plume typically pulsates with a period of several seconds.

welding Postdepositional compaction of a hot pyroclastic deposit under its own weight. Note that agglutination, coalescence, and postdepositional welding are part of a process continuum.

yield stress A mechanical property of many substances; the stress that must be exceeded for the substance to flow. True (Newtonian) liquids have zero yield stress. Also known as *yield strength*.

I. INTRODUCTION

Explosive volcanic eruptions occur when magma in an open conduit or vent is torn apart by expanding gas,

Copyright © 2000 by Academic Press
All rights of reproduction in any form reserved.

and the fragments are ejected into the atmosphere. If the fragments are still hot, fluid blobs when they fall to the ground, they may agglutinate or coalesce. This process—lava fountaining and fallback—commonly feeds basaltic lava flows in Hawaii, Iceland, Reunion, Japan, and other active volcanic areas. Lava fountains probably fed most of the ancient basaltic lavas that are so common in the geologic record. Many basaltic lavas are thus pyroclastic in origin, although, due to complete clast coalescence, the final lava may yield few clues to a fragmental origin unless one has had the luck to observe the eruption.

Because the hot fragments must be able to coalesce to form a lava after their flight, specific conditions must be met if a fountain-fed lava is to form. These are low magma viscosity and low gas content. The effect of low viscosity is easy to see; the effect of gas content—explored later in the chapter—is complex. Low viscosity is favored by low magmatic silica content and high temperature. These conditions are commonly met by basaltic magmas and occasionally by other compositions, even (rarely) silica-rich compositions such as rhyolite. Where they are not fully met, the process is incomplete, and piles of spatter, or agglutinated, partly coalesced and flattened fragments that did not collapse to form a lava, are preserved around the vent. These spatter piles are very valuable for exploration and to research geologists working in extinct volcanic terranes, because they mark the site of volcanic vents that may otherwise be extremely difficult to identify.

II. FOUNTAIN PRODUCTION

A. Magmatic Volatile Contents, Vapor Saturation, and Degassing

A *magmatic volatile* is any chemical substance, soluble in magma under pressure, that is gaseous at magmatic temperature and atmospheric pressure. Dissolved volatiles come out of solution to form bubbles that expand by decompression as magma approaches the surface, and provide the driving force for pyroclastic eruptions. The final stages are explosive, and tear the magma into blobs that are entrained into the expanding gas and ejected from the vent. Blob velocity is largely a function of initial gas content; too much magmatic gas results in adiabatic cooling and, much more importantly, a high ejecta velocity and consequent long flight path during which the clast loses heat to the atmosphere, and lands as a rigid fragment that cannot agglutinate to form spatter or feed a lava. Too low a gas content and the magma may not be fragmented at all.

The most important magmatic volatiles in terrestrial magmas are H_2O, CO_2, and sulfur species, with relatively minor amounts of others such as HCl and HF. The initial volatile content of magmas is hard to quantify, because these species are partially lost before one can sample and analyze the material. Rough estimates can be obtained from experimental petrology and thermodynamic modeling aimed at finding combinations of temperature, total pressure, and volatile fugacities that result in a duplication of the phase assemblages and compositions found in natural samples. However, the most reliable estimates come from direct analysis of samples that escaped degassing. Samples are of two types: (1) glass inclusions trapped in phenocrysts, representing tiny volumes of pre-eruptive melt, and (2) submarine lavas. Application of inclusion data to bulk magmatic volatile contents assumes that the enclosing phenocryst has acted as a perfectly sealed “bottle” since entrapment, and that the inclusions are fully representative of the liquid enclosing the phenocrysts. Submarine lavas retain volatiles if the water depth is great enough to prevent vapor saturation on eruption, or if vesicular magma is quenched prior to loss of bubbles from the lavas.

Available data for oceanic tholeiitic basalts indicate typical total dissolved volatile contents of 1–2%, with either subequal amounts of H_2O and CO_2 or dominant CO_2. Alkalic basalts may be much richer in volatiles, with up to 7% $H_2O + CO_2$ in the case of lavas of the 4-km-deep submarine North Arch volcanic field near Hawaii. This probably covers the range of volatile contents for subaerial oceanic basalts and continental flood basalts. It is unclear, however, whether basalts with such a high volatile content as the North Arch lavas ever erupt from subaerial volcanoes; CO_2 especially is prone to open-system degassing between source and surface (see later discussion). Subduction-related mafic magmas also have high, but variable, H_2O contents, perhaps as high as 6% in some cases. H_2O contents of intermediate and felsic magmas achieve similar values. In these magmas, CO_2 is probably subordinate.

Because different volatile species have different solubilities, it is necessary to consider all of them simultaneously in order to understand the mechanics of magma degassing. This has been done for H_2O–CO_2 mixtures. Due to its low solubility, the effect of even a small amount of CO_2 on the degassing behavior of hydrous magmas is profound: 500 ppm CO_2 raises the volatile saturation pressure of a magma with 0.5 wt% water from a few megapascals to more than 100 Mpa, with almost all of the CO_2 partitioning into the vapor phase. The practical result of the partitioning behavior in H_2O–CO_2 mixtures is a strong contrast between open- and closed-system degassing. In open-system degassing, where vapor is instantaneously removed after each degassing increment (essentially Rayleigh fractionation), CO_2 is rapidly preferentially removed and the system can be closely described by the pure water vapor case regardless of initial CO_2 content.

During closed-system degassing, however, a substantial fraction of original CO_2 remains in the melt. Because the timescale for bubble flotation in fluid basaltic magma is short (hours to days), vapor-saturated magma stored in a shallow subvolcanic chamber over a significantly longer period will experience something close to open-system degassing, while vesiculation occurring during uprise of magma into a vent system during eruption, which occurs over seconds to minutes, will, prior to the moment of magma disruption, closely approach the closed-system case. Pre-eruptive shallow storage occurs in Hawaii, Iceland, and many other basaltic volcanic areas where lava fountains are common eruption mechanisms, and in these cases we can expect that the exsolving gas has little CO_2. In contrast, magmas that rise steadily to the vent from great depth may feed CO_2-rich eruptions.

Two other factors should be mentioned. First, volatile solubility depends on magma composition, particularly for CO_2, which is several times more soluble in nephelinitic than in olivine basaltic liquids. Second, nonequilibrium degassing, such as could occur during rapid exsolution at low pressures, would tend to enhance concentrations of water in the vapor over CO_2, due to its higher diffusivity.

In summary, the volatile content of erupting magma is largely determined by its prior history of crustal transport and degassing. In eruptions fed from shallow chambers, water is the dominant species in the exsolved vapor and may account for up to 2% by mass of the eruption mixture. Eruptions of deep-seated magma, especially of silica-poor compositions, may be CO_2 rich.

B. Bubble Growth and Magma Fragmentation

Theoretical modeling of the ascent of vesiculating magma, mainly carried out by Lionel Wilson and coworkers, has given us a first-order understanding of the generation of lava fountains. As magma approaches the Earth's surface, volatile exsolution results in bubble growth. For the typical volatile contents noted earlier, most of this growth takes place within a few hundred meters of the surface. Nucleation of new bubbles requires that the magma be sufficiently supersaturated to overcome surface tension pressure of incipient bubbles. Little is known about the surface tension of magma–vapor interfaces under the conditions of interest, but it is likely that nucleation is enhanced by the presence of phenocrysts and by shearing of the liquid. Once formed, bubbles are fed by diffusive transport of volatiles through the liquid and grow as spheres until they begin to crowd each other. Left to itself, a magmatic foam might evolve to become locally permeable and form a network of glassy filaments outlining the edges of polyhedral bubbles with open faces. Excellent examples of a rock called *reticulite*, with porosities up to 99%, are a minor product of hawaiian eruptions and seem to represent such a foam frozen to rock. Usually, however, because the magma is rising toward the surface, individual bubbles become overpressured and explode before bulk permeability develops. Overpressures are a function of conduit-vent geometry and mass fraction of exsolved gas, and are typically of the order of a few bars to tens of bars. Theoretical models for exploding magma have assumed that explosive disruption occurs when the fraction of bubbles reaches 75%, although in reality it probably occurs over a range of porosities centered on this value. The explosively decompressing mixture of gas and magma blobs forms a spreading jet as it emerges from the vent; this is the rising part of the lava fountain. The vertical height reached is chiefly a function of exsolved gas content. In radially symmetrical, vertical fountains, fallback from the top of the spreading jet forms a skirt of descending fragments around the jet. More often, the jet is slightly angled from the vertical, or the falling skirt is affected by wind, causing preferential deposition on one side of the vent.

Lava fountaining is closely associated with strombolian activity, in which individual closely spaced explosions feed the rising jet. The degree of magma disruption is usually greater than in a lava fountain, producing finer ejecta that cool more readily to form scoria and spatter. Lava fountain eruptions usually include at least some strombolian-style activity. The two eruption styles may be closely linked: Observations of strombolian vents have revealed that the individual pulses are related to the explosion of giant bubbles at the magma surface, and they typically have lower mass eruption rates than hawaiian-style fountains. Basaltic magma is fluid enough that bubbles can rise through the magma column as it ascends. If the net bubble velocity is a significant fraction of the upward magma velocity, bubbles will tend to collect toward the upper surface of the magma in the conduit. Large bubbles will collide and coalesce with smaller ones, producing still larger bubbles with greater upward velocities. A snowball effect may result, in which very large bubbles occupy a significant fraction of the conduit width and intermittently arrive at the magma surface. Thus, the difference between hawaiian-style fountaining and strombolian cone-building activity can be explained simply by different magma rise velocities. For basaltic magmas, the critical rise speed may be about 0.5–1 m s^{-1}; much less than this and bubbles segregate (strombolian); much more and a lava fountain results.

C. Fountain Structure

Although hawaiian-style eruptions often initiate along fissures to produce an early "curtain of fire," continued flow of magma usually becomes localized at points along the fissure to produce a series of central vents, such as was observed during the 1973 Eldfell eruption at Heimay, Iceland. This discussion will refer to central vents only; the qualitative structure of fountains is the same in both cases.

The structure of lava fountains, and the deposits that result from them, depends mainly on two parameters: magma gas content and effusion rate. High gas content produces a high, spreading fountain and smaller clasts (magma blobs). High mass effusion rates favor collimated fountains and high accumulation rates of fragments on the ground around the vent. Models predict that the gas contents noted above for subaerial oceanic and continental flood basalts should easily allow fountains of 1 km high to develop. In fact, this is greater than typical observed heights for terrestrial eruptions perhaps because magmas partly degas at very shallow levels prior to eruption. In Hawaii and Iceland, sustained fountains are rarely higher than 500 m. An exception is the 1986 eruption of Izu-Oshima, described in more detail below, in which the fountain height reached 1,600 m. Lava fountaining from a single vent site is commonly most vigorous at the start of an eruption and wanes thereafter although lava production continues unabated. This pattern of activity (which may be modified where the eruption migrates along a fissure, opening new vents) may be caused by the establishment of a degassing lava pond in the vent, so that newly arriving magma mixes with the partly degassed pond liquid, resulting in a lower effective magma gas content and reduced fountain height.

Observations, especially of the long-lived Pu'u O'o eruption on Hawaii, allow fountains to be divided into an inner, hot, yellow to orange incandescent portion and an outer, dull red to brown or nonincandescent portion (Fig. 1). Wind may strip, and rapidly chill, fine particles from the outer portion of the fountain. High mass eruption rates produce fountains in which most of the ejected mass is in the hottest, inner portion, while high gas content favors the cooler, outer part. Hot, inner fountain material has little opportunity for cooling and may fall so close to the fountain base that it is recycled into the vent system, leading to a steady increase in the mass of fluid lava in the vent, forming a pond or, if it can move away from the vent, feeding a flow. Outer fountain clasts may be too cool to completely recoalesce and build up a cone around the vent, while dispersed fines form a downwind ash deposit. We now turn to a consideration of processes occurring when clasts of different temperatures and, hence, rheologies are deposited.

D. Agglutination and Welding

Welding is the process by which a pyroclastic deposit becomes compacted into a coherent rock through load-pressure deformation of hot, plastic magmatic fragments. Because it occurs after deposition (although it may begin before the entire thickness has been deposited), it helps to visualize welding as being distinct from syndepositional agglutination (see later discussion), although in reality the two processes form a continuum. One of the main parameters influencing welding is clast accumulation rate; it is favored if a clast at the surface of the accumulating deposit is buried before it can cool significantly, and if the number density of falling hot clasts above the surface is great enough that radiative heat loss, both from the surface and the falling clasts, is minimized. Agglutination refers to the adhesion and deformation of clasts on deposition. It differs from welding in that it is almost instantaneous, and that the energy required for deformation is the kinetic energy of the falling clast. Both welding and agglutination involve porosity loss, although equal-volume spreading or splashing (cow-dung effect) is additionally involved in agglutination. Agglutination requires lower magmatic viscosities than simple welding. Hence, for clasts of identical composition, agglutination requires higher temperatures than welding.

Modeling of the agglutination process indicates that 1-cm or larger clasts with viscosities of 1000 Pa s or less

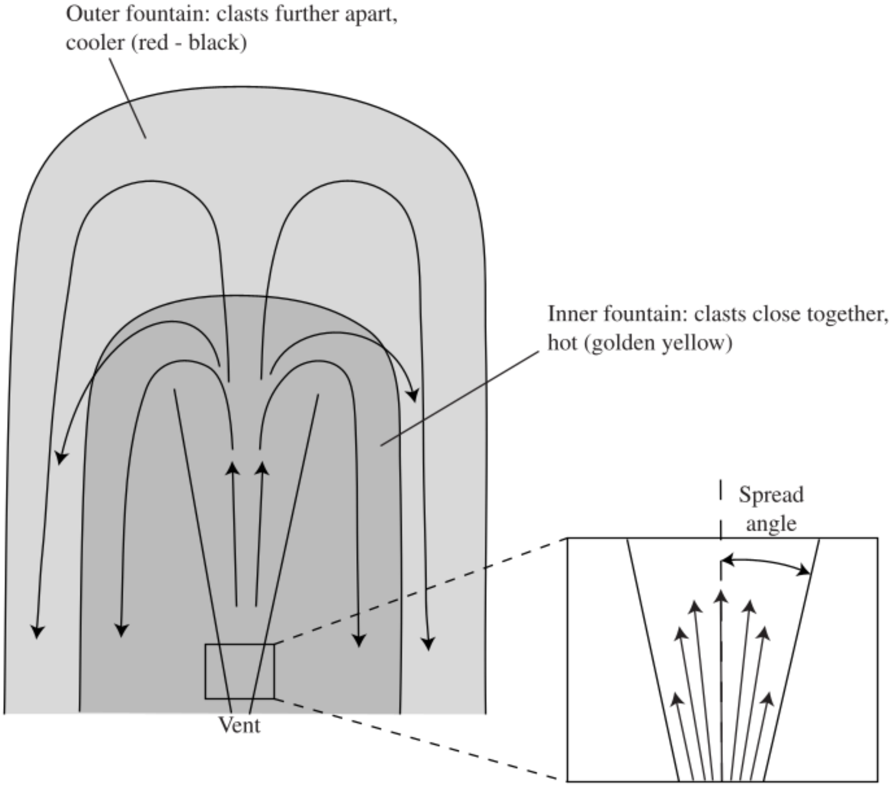
Outer fountain: clasts further apart, cooler (red - black)
Inner fountain: clasts close together, hot (golden yellow)
Spread angle
Vent

FIGURE 1 Sketch of the basic elements of lava fountain dynamic structure. The fountain actually consists of many thousands of clasts following the general paths indicated by arrows. Relative widths of inner and outer fountains may vary. Lengths of arrows in inset indicate velocity profile. Note that fountain asymmetry may result in more inner fountain material being deposited on one side, leading to deposit relationships like those sketched in Fig. 5. Based on the observations of Head and Wilson (1989).

will agglutinate (Fig. 2). This is a good description of most of the mass in the inner part of a fountain for basaltic magma compositions. As clast viscosity increases with falling temperature, only large fragments experience deformation upon landing, although smaller clasts may still compact during postdepositional welding. At up to 10,000 Pa s, complete welding is accomplished in a matter of seconds. Also, large clasts with chilled rinds may burst on landing and their fluid cores can still coalesce. At these viscosities, the agglutinated and welded mass begins to flow immediately, forming a clastogenic lava. A more important measure of the rheology of cooling basaltic magma may be the development of yield stress due to progressive groundmass crystallization. Yield strength is necessary for the preservation of agglutinate piles (Fig. 3) that do not collapse to form lava flows; the common occurrence of small drips, liquid segregations, and postflattening gas inflation structures in spatter piles indicates that the material did not immediately solidify upon landing, contained low-viscosity

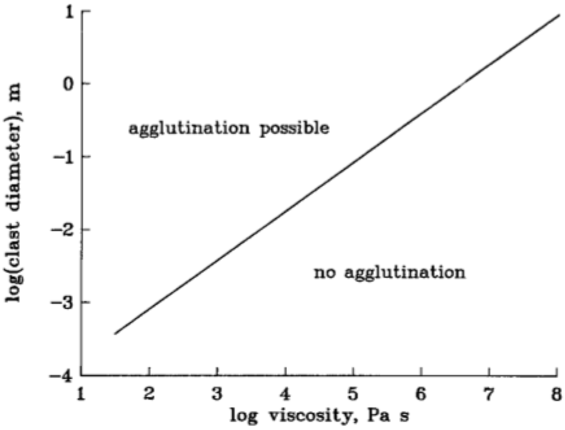

FIGURE 2 Plot of $\log_{10}$(clast viscosity) versus $\log_{10}$(clast diameter) to show limits of conditions under which syndepostional agglutination of falling tephra, exclusive of later welding, is possible. Model assumes that clasts reach terminal velocity before landing, hence, the boundary of the "no agglutination" field is conservative.

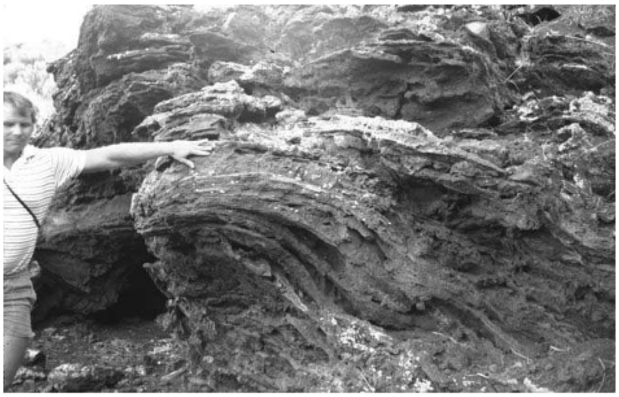

FIGURE 3 Spatter (agglutinate) pile at the Sproul vent, San Francisco volcanic field, Arizona. Each layer is an individual flattened spatter bomb. Note bombs draping a small intraformational high in center of photograph.

residual liquid, yet did not flow en masse. A lava may still form if the combination of thickness and ground slope causes the yield strength of the spatter pile to be exceeded at the base, which occurs for most cases where the yield strength is 10^4 Pa or less. Yield strengths 2 to 3 orders of magnitude greater are required to completely resist agglutination, hence there is a range of values around 10^5 Pa favoring the formation and preservation of spatter piles. Preservation is most likely for thin agglutinate layers.

III. FOUNTAIN-FED LAVAS AND ASSOCIATED ERUPTION PRODUCTS

We are now in a position to link fountain structure to final products (Fig. 4), although these processes have yet to be quantitatively modeled in detail. The inner part of the fountain experiences little heat loss and essentially remains at magmatic temperatures, with viscosities around 1000 Pa s and negligible yield strength. If the accumulation rate (chiefly a function of magma production rate) is high enough, a lava flow will be fed from the point where the magma fragments land. It is worth noting that, at the start of an eruption at a new vent, the environment is cold and cooling rates may be sufficient to form an early spatter pile. The outer parts of the fountain will yield clasts that experience sufficient in-flight cooling to develop either a yield strength due to groundmass crystallization and/or a viscoelastic skin. Small clasts may be completely cooled to a brittle glass.

Because of the annular fountain structure, the pile that results from outerfountain deposition forms a collar, growing to a cone, around the vent, and its contents are quite sensitive to changes in accumulation rate, fountain width, and wind speed. Low accumulation rates will favor spatter layers and brittle scoria, which are very commonly seen to be interbedded in old, eroded vent cones. The extreme sensitivity of spatter preservation to eruption conditions is shown by thin, vertical walls of spatter such as are seen around vents for the prehistoric Devil's Garden flow, Oregon. Agglutinate accumulations on the cone may collapse to form small, spatter-fed lava flows down the cone flanks. The growing cone acts as a funnel to confine the inner fountain-fed lava to a vent pool, which may breach or overtop the cone. Alternatively, if lava has been flowing from the start of the eruption, the cone will be open on one side as falling scoria fragments are carried away by the lava. Coherent pieces of spatter or welded scoria from the cone may be carried away on the surface of the lava, especially

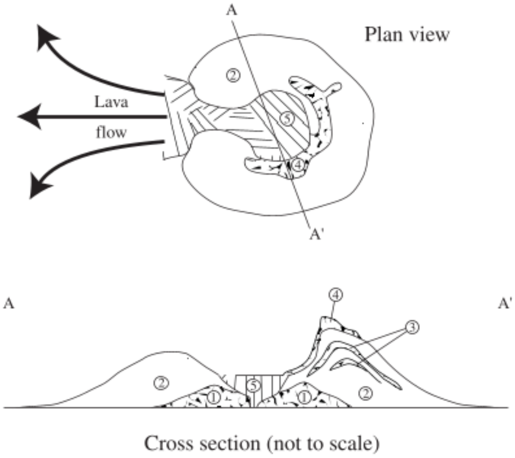

FIGURE 4 Plan view and cross-section sketches of the deposits resulting from an asymmetric lava fountain. Deposition rate is higher on the righthand side of the cross section than on the left. The fountain itself has been omitted for clarity, but compare this diagram with the fountain dynamic structure in Fig. 1. Key: 1, early-formed spatter ring; 2, scoria cone; 3, layers of spatter and small clastogenic lavas, formed by agglutination, interbedded within the scoria cone; 4, actively forming spatter layer, depicted as slumping down the crater wall to form a small clastogenic lava that is feeding the central lava pond; 5, central lava pond, fed mainly by direct fallback from inner fountain, and also from layer 4. In the plan view, the central lava pond is shown breaching the left-hand side of the cone to feed the main lava flow. The sketches are based on the observations of Head and Wilson (1989).

during a breaching episode, when large sectors of the vent cone may be rafted out on the flowing lava.

Vents may undergo morphologic evolution to complex structures that outwardly bear little resemblance to this simple picture, and eventually cease lava fountaining altogether. Cones may be modified by repeated breaching and healing; shifts in vent location or simultaneous activity at nearby vents on a fissure may produce overlapping cones; the lava may roof over to emerge as an incandescent stream some distance away, spatter walls may develop to form overhangs and restrict central vents; and temporary cessation may allow the vent lava pool to roof over and suffer subsequent partial drainage.

IV. AGGLUTINATION IN OTHER COMPOSITIONS AND ERUPTIVE STYLES

Agglutination and coalescence of fluid tephra, sometimes to the degree of nonparticulate secondary flow as a reconstituted coherent lava, are not restricted to hawaiian-style eruptions of basaltic magma. The deposits from violent plinian and ignimbrite eruptions may include agglutinated material, and a fountain-fed origin has been deduced for some prehistoric rhyolitic lavas. In nearly all cases, the magma compositions and/or temperatures are such that ejecta viscosities are significantly less than those of typical rhyolites ("typical," or calcalkaline, rhyolites are the most viscous magmas known, with depositional viscosities frequently greater than 10^8 Pa s).

Agglutinated andesitic pyroclastic flow deposits occur in arc settings such as Santorini and the New Hebrides, and alkali-rich ignimbrites (pantellerites and phonolites) in the Canary Islands and Italy. The distinctive feature of these "spatter flows" or "high-grade" ignimbrites is an imbricated texture consisting of large flattened clasts that were sheared by flow during deposition and consequently have a consistent upflow dip. This structure may be preserved at the base of the sheet, or where the fine matrix is nonwelded. In some cases, clast coalescence has continued until most of the thickness of the sheet is reconstituted and undergoes nonparticulate or lava-like flow. Extended nonparticulate flow may largely destroy evidence for a particulate origin.

Spatter-fed alkaline felsic lavas have been described for Mayor Island (New Zealand), the Canary Islands, and Italy. The inferred formation mechanism is similar to that of typical Hawaiian lava fountains. None of these eruptions was observed, and the interpretations are based in part on preserved spatter-like structures in the final rocks. Caution is necessary here, because similar structures occur in true lavas, where marginal rubble becomes partly recoalesced.

V. RECENT DEVELOPMENTS

Mechanisms of agglutination, clast deformation, coalescence, and the transition to clastogenic lava have received relatively little attention from volcanologists. In fact, unusual occurrences such as those noted in the previous section have been studied in greater detail than the common process of lava generation from Hawaiian lava fountains. In part, this is because the slightly higher viscosities (and probably yield strengths) of intermediate and alkaline felsic ejecta favor preservation of agglutinate piles, whereas almost all of the agglutinating mass in a Hawaiian eruption rapidly coalesces to lava. Nonetheless there is a clear need for more field data on the near-vent products of fountain activity.

A recent, well documented and observed mafic to intermediate composition fissure eruption generating fountain-fed lavas, spatter deposits, and a scoria cone occurred in November 1986 at Izu-Oshima volcano in eastern Japan. The B phase of the eruption lasted for about 8 hours on November 21, producing unusually high fountains reaching a maximum of 1600 m. Examination of eruption products in the light of eyewitness reports of the timing of lava flows (both syn- and postdepositional) has shown that lavas were generated by three distinct mechanisms. The first was reconstitution of fountain-generated spatter around the vent by syndepositional agglutination, commonly assumed to be the only mechanism involved in lava production from fountains. The second mechanism was syneruptive collapse of a rapidly built scoria spatter cone by a slumplike process of rotational slip and extensional sliding (Fig. 5A), consequent on failure of the cone along a completely coalesced basal spatter layer, which thus acted as a lubricating layer. The third mechanism involved generation of a similar basal coalesced layer, which then extruded through the side of the cone to form a lava without wholesale cone collapse (Fig. 5B). Within each lava there is a range of textures from nonwelded through welded scoria and agglutinate to homogeneous, holocrystalline lava. Future studies should indicate whether the latter two mechanisms, and perhaps others not hitherto recognized, are common.

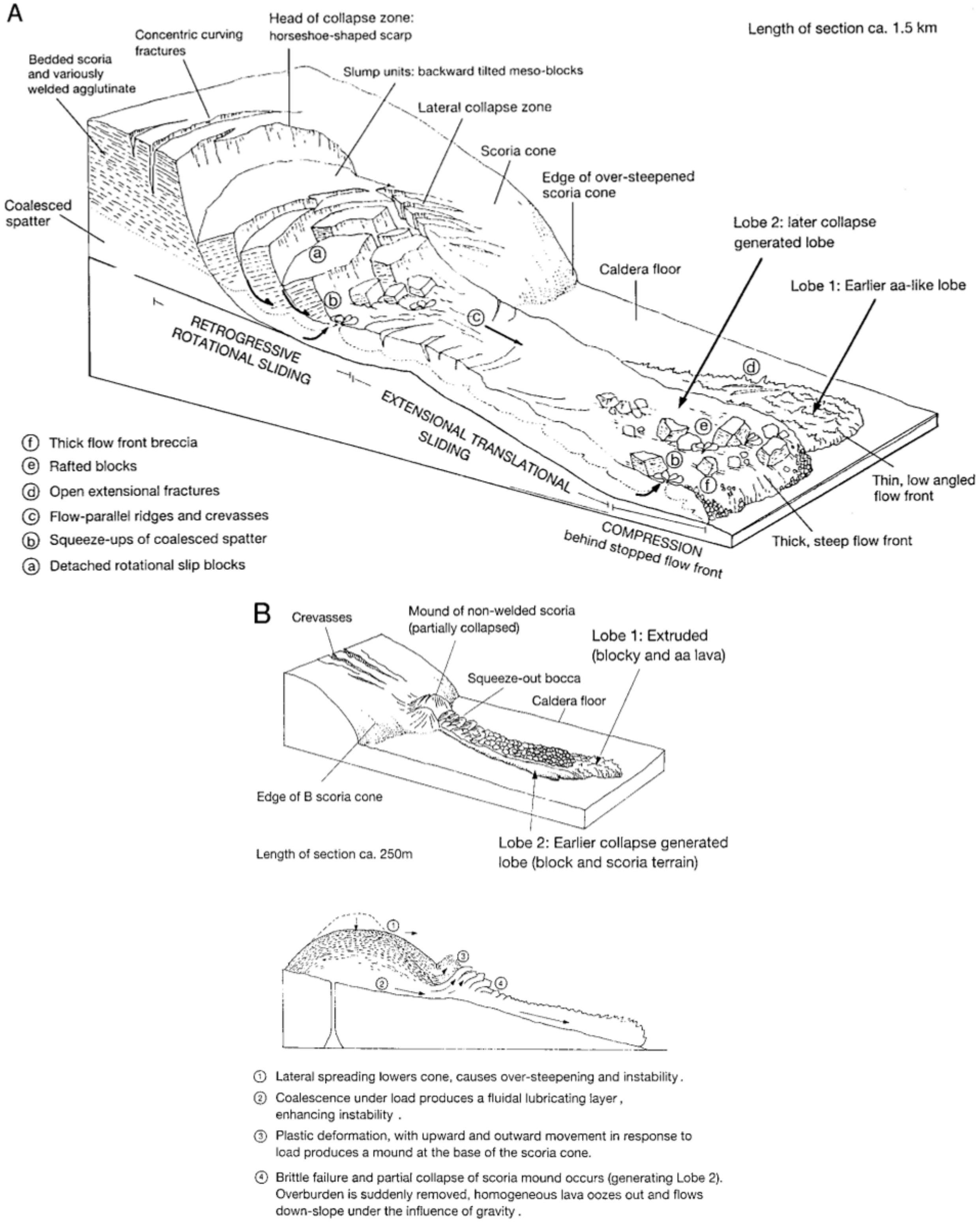
A
Length of section ca. 1.5 km
Head of collapse zone: horseshoe-shaped scarp
Concentric curving fractures
Bedded scoria and variously welded agglutinate
Slump units: backward tilted meso-blocks
Lateral collapse zone
Scoria cone
Edge of over-steepened scoria cone
Coalesced spatter
Lobe 2: later collapse generated lobe
Caldera floor
Lobe 1: Earlier aa-like lobe
a
b
c
d
e
b
f
RETROGRESSIVE ROTATIONAL SLIDING
EXTENSIONAL TRANSLATIONAL SLIDING
COMPRESSION behind stopped flow front
Thin, low angled flow front
Thick, steep flow front
ⓕ Thick flow front breccia
ⓔ Rafted blocks
ⓓ Open extensional fractures
ⓒ Flow-parallel ridges and crevasses
ⓑ Squeeze-ups of coalesced spatter
ⓐ Detached rotational slip blocks
B
Crevasses
Mound of non-welded scoria (partially collapsed)
Lobe 1: Extruded (blocky and aa lava)
Squeeze-out bocca
Caldera floor
Edge of B scoria cone
Length of section ca. 250m
Lobe 2: Earlier collapse generated lobe (block and scoria terrain)
①
②
③
④
① Lateral spreading lowers cone, causes over-steepening and instability.
② Coalescence under load produces a fluidal lubricating layer, enhancing instability.
③ Plastic deformation, with upward and outward movement in response to load produces a mound at the base of the scoria cone.
④ Brittle failure and partial collapse of scoria mound occurs (generating Lobe 2). Overburden is suddenly removed, homogeneous lava oozes out and flows down-slope under the influence of gravity.

FIGURE 5 Lava generation mechanisms during the 1986 Izu-Oshima eruption, Japan. (From Sumner, © 1988 Springer-Verlag.) (A) Block diagram showing the main features and processes involved in lava production by syneruptive, slumplike collapse of rapidly built scoria cone. An aa-like lobe, formed by earlier nonparticulate flow of vent agglutinated spatter, is shown for comparison. (B) Diagrams showing the production of lava through basal coalescence and lateral extrusion from scoria cone. Upper panel: summary diagram showing main morphological features; lower panel: interpreted sequence of events.

VI. SUMMARY

1. The character of explosive eruptions is largely a function of magma volatile content, which for mafic magmas is in turn controlled by crustal residence history.
2. Sustained lava fountains develop where the magma rise speed is sufficient to prevent bubble accumulation near the surface of the erupting magma; otherwise pulsing strombolian activity, less likely to produce lava, results.
3. Sustained fountains consist of a hot inner and a cooler outer portion. Deposits from the inner part rapidly coalesce to feed lava flows and/or vent pools, whereas deposits of the outer zone may produce spatter and scoria that builds up to form a collar around the vent.
4. Processes of clast agglutination, coalescence, welding, and lava generation depend critically on the rheologic properties of the ejecta during, and up to hours after, deposition. Preservation of spatter piles that do not collapse into lava requires a finite yield strength.
5. Andesitic eruptions, and other compositions of similar rheology such as phonolites and pantellerites, may produce a wide range of deposits, including ignimbrites, that undergo agglutination during deposition.
6. A range of mechanisms may be involved in the transformation of agglutinating ejecta to lava, but the subject has, as yet, received little attention.

SEE ALSO THE FOLLOWING ARTICLES

Basaltic Volcanoes and Volcanic Systems • Hawaiian and Strombolian Eruptions • Magmatic Fragmentation • Physical Properties of Magmas • Pyroclastic Fall Deposits • Scoria Cones and Tuff Rings • Volatiles in Magmas

FURTHER READING

Branney, M. J., and Kokelaar, P. (1992). A reappraisal of ignimbrite emplacement: Progressive aggradation and changes from particulate to non-particulate flow during emplacement of high-grade ignimbrite. *Bull. Volcanol.* **54,** 504–520.

Cas, R. A. F. and Wright, J. V. (1987). "Volcanic Successions: Modern and Ancient" Allen and Unwin, London.

Dixon, J. E., Clague, D. A., Wallace, P. and Poreda, R. (1997). Volatiles in alkalic basalts from the North Arch volcanic field, Hawaii: Extensive degassing of deep submarine-erupted alkalic series lavas. *J. Petrol.* **38,** 911–939.

Head, J. W., III, and Wilson, L. (1989). Basaltic pyroclastic erutions: Influence of gas-release patterns and volume fluxes on fountain structure, and the formation of cinder cones, spatter cones, rootless flows, lava ponds and lava flows. *J. Volcanol. Geotherm. Res.* **37,** 261–271.

Mellors, R. A., and Sparks, R. S. J. (1991). Spatter-rich pyroclastic flow deposits on Santorini, Greece. *Bull. Volcanol.* **53,** 327–342.

Stevenson, R. J., Briggs, R. M., and Hodder, A. P. W. (1993). Emplacement history of a low-viscosity, fountain-fed pantelleritic lava flow. *J. Volcanol. Geotherm Res.* **57,** 39–56.

Sumner, J. M. (1998). Formation of clastogenic lava flows during fissure eruption and scoria cone collapse: The 1986 eruption of Izu-Oshima volcano, eastern Japan. *Bull. Volcanol.* **60,** 195–212.

Turbeville, B. N. (1992). Tephra fountaining, rheomorphism, and spatter flow during emplacement of the Pitigliano Tuffs, Latera caldera, Italy. *J. Volcanol. Geotherm. Res.* **53,** 309–327.

Wilson, L. and Head, J. W., III (1981). Ascent and eruption of basaltic magma on the Earth and Moon. *J. Geophys. Res.* **86,** 2971–3001.

This Page Intentionally Left Blank

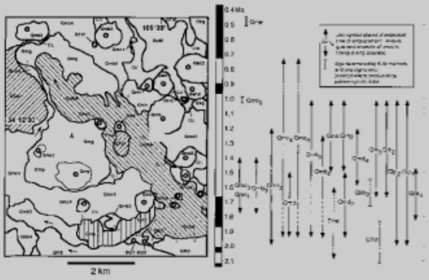

BASALTIC VOLCANIC FIELDS

CHARLES B. CONNOR
Southwest Research Institute

F. MICHAEL CONWAY
Arizona Western College

I. Introduction
II. Physical Characteristics of Volcanic Fields
III. Geologic Structure of Volcanic Fields
IV. Petrogenesis of Basalt Volcanic Fields
V. Origins of Volcanic Fields
VI. Summary

I. INTRODUCTION

Often, volcanic activity results in the formation of volcanic fields rather than single large volcanic edifices. Volcanic fields comprise small volcanoes (usually with volumes less than 1 km^3), such as cinder cones, maars, tuff cones, tuff rings, small shield volcanoes, and lava domes. These volcanoes are dominantly basaltic in composition and each is produced by a single episode of volcanic activity that can last from several days to a few years or, in rare cases, decades. Volcanoes formed during single episodes of volcanic activity, without subsequent eruptions, are referred to as *monogenetic.* Monogenetic volcanoes are commonly clustered within volcanic fields or may constitute linear chains that follow tectonic structures, such as faults. Volcanic fields also form on the flanks of composite or large shield volcanoes and within calderas, where they are often distributed along rift zones. Over periods of hundreds of thousands to millions of years, monogenetic volcanic activity can result in areally extensive volcanic fields consisting of hundreds to thousands of individual volcanoes and cumulative volumes approaching those of individual composite volcanoes.

Studies of volcanic fields are among the earliest works in volcanology. Desmarest mapped the cinder cones of Auvergne, France, around 1766, in the process making one of the first geographically accurate geologic maps and employing what Lyell (1830, p. 59) referred to as "minute accuracy and admirable graphic power." One of Desmarest's major contributions was the relative dating of cinder cones in Auvergne using the geomorphology of the cinder cones and superposition of lava flows that he carefully correlated to vents where possible. Desmarest's techniques have subsequently been emulated by virtually all volcanologists mapping in volcanic fields. The 1759–1774 eruption of Jorullo volcano, Mexico, in the Michoacán-Guanajuato volcanic field focused additional attention on volcanic fields. Geologists such as von Humboldt, Scrope, and Lyell noted the tremendous number of cones around Jorullo and realized that these cones formed during episodes of activity evinced by the Jorullo eruption. The 1943–1952 eruptions of Parícutin volcano, also in the Michoacán-Guanajuato volcanic field, led to more systematic mapping in this area. In his seminal work on volcanoes of the Parícutin region, Williams (1950) conducted petrologic investiga-

Copyright © 2000 by Academic Press
All rights of reproduction in any form reserved.

tions, mapping, and relative dating of volcanoes in this region, resulting in the first comprehensive, modern treatment of basaltic volcanic fields.

Recent studies of volcanic fields have employed advancing geochronological, geophysical, and geochemical techniques to describe the rates of activity, longevity, and tectonic settings of volcanic fields. Many of these studies have focused on the distribution and timing of volcanism to better understand the processes that govern magma supply and magma ascent. Numerous studies have considered the development of volcanic fields in terms of their regional neotectonic setting, and the influence of geologic structures, such as faults, on vent distribution. Others have focused on the petrologic evolution of volcanic fields through time, attempting to relate changes in petrogenesis to changes in patterns and rates in eruptive activity. Cumulatively, these studies provide substantial insight into the volcanology of basaltic volcanic fields. Increasingly, these insights are used to evaluate the long-term hazards associated with volcanic fields located near cities or sensitive facilities such as nuclear power plants and port facilities. Such long-term hazard issues drive the need to improve models of the timing and distribution of eruptions within basaltic volcanic fields.

TABLE I Physical Characteristics of Selected Basaltic Volcanic Fields

Volcanic field	*Basaltic vents*	*Silicic vents and vent complexes*	*Area (km^2)*	*Age range (Ma)*	λ_t *(vents/yr)*	*Data sources*
Eifel Volcanic Field, Germany	323	7 phonolite centers	1,000	0.7–0.01	5×10^{-4}	Schminke *et al.,* 1983
Camargo, Mexico	308	0	2,500	4.5–1.6	1×10^{-4}	Luhr *et al.,* 1997, *Eos. Trans. Am. Geophys. Un.* **78,** F843.
Trans-Mexican Volcanic Belt, Mexico	1096	120 shields and stratovolcanoes	40,000	3.5–0	3×10^{-4}	Hasenaka and Carmichael, 1987; Connor, 1990, *J. Geophys. Res.* **95,** 19,395–19,405
Klyuchevskoy Group, Russia	300	12 composite volcanoes	2,500	Quaternary	2×10^{-4}	Fedotov *et al.,* 1991, Pages 275–279 *in* "Active Volcanoes of Kamchatka," (S. A. Fedotov and Yu. P. Masurenkow, eds.). Nauka Press
Springerville, AZ, USA (Fig. 1)	409	0	3,000	2.1–0.3	2×10^{-4}	Condit and Connor, 1996
San Francisco, AZ, USA (Fig. 8)	606	8 large dome complexes	5,000	5.6–0	1×10^{-4}	Tanaka *et al.,* 1986; Conway *et al.,* 1998
Coso, CA, USA	54	38 small domes	1,200	2.0–0	3×10^{-5}	Duffield *et al.,* 1980; Bacon, 1982
Pancake, NV, USA (Fig. 6)	75	0	2,500	6–0.3	1×10^{-5}	Foland and Bergman, 1992, Pages 2366–2371 *in* "Third Int. Conf. High-Level Radioactive Waste Management." Am. Nucl. Soc., La Grange Park, IL; Scott and Trask, 1971, *U.S. Geol. Sur. Prof. Pap.* 599-I
Big Pine, CA, USA (Fig. 7)	24	1 small dome	500	1.2–0.1	2×10^{-5}	Ormerod *et al.,* 1991; Turrin and Gillespe, 1986, *Geol. Soc. Am., Abs. Prog.* **18**(6), 414
Cima, CA, USA (Fig. 3)	70	0	150	4.5–0.01	8×10^{-5}	Dohrenwend *et al.,* 1986; Turrin *et al.,* 1985, *Isochron/West* **44,** 9–16
Yucca Mountain, NV, USA (Fig. 2)	30	0	1,200	3.4–0.1	1×10^{-5}	Connor and Hill, 1995

II. PHYSICAL CHARACTERISTICS OF VOLCANIC FIELDS

Fundamental physical characteristics of basaltic volcanic fields include the number of individual vents, the timing and recurrence rates of volcanic eruptions, the distribution of vents, and their relationship to tectonic features, such as basins, faults, and rift zones. Table I summarizes the number of vents in some basaltic volcanic fields, their areas, and the age ranges of activity. It is evident that basaltic volcanic fields encompass a wide range of areas, volumes, and longevities. Small basaltic volcanic fields typically contain <50 vents distributed over <1000 km^2. Large volcanic fields contain >100 vents distributed over >1000 km^2. No apparent correlation exists between the number of vents in a volcanic field and its longevity (Table I). For example, the Springerville volcanic field (Fig. 1) contains approximately 400 vents formed within 2 million years (Ma). In contrast, the Yucca Mountain volcanic field (Fig. 2) has approximately 30 vents formed over 4 Ma. In these two volcanic fields, as in many others, Plio-Quaternary volcanic activity followed earlier episodes of volcanism in the Miocene and Early Pliocene. Rates of volcanism typically wax and wane over long time periods (>1 Ma) in basaltic volcanic fields.

A. Temporal Recurrence Rates

Determination of the timing of volcanism has been a central issue in the study of volcanic fields. Age determinations for individual volcanic vents are used to estimate temporal recurrence rates of volcanism, sometimes referred to as the intensity of volcanic activity, and to correlate rates of volcanic activity with other factors, such as plate motion, rates of crustal extension, and changes in petrology. Age dating techniques applied to basaltic volcanic fields include relative dating of lava

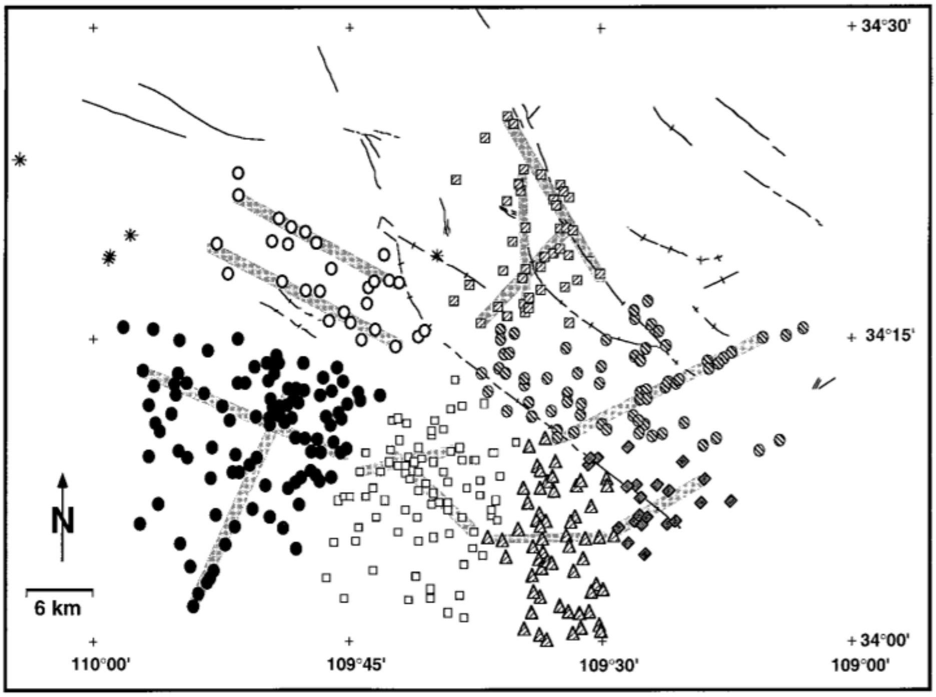

FIGURE 1 With over 400 vents, the Springerville volcanic field in Arizona is a typical large volcanic field located on the margins of the Colorado Plateau in the western United States. Most of the mapped vents formed between 2.1 and 0.3 Ma during volumetrically steady-state volcanism. Coupled studies of vent distribution and timing of volcanism have shown that rates of activity varied from cluster to cluster, suggesting that individual source regions for magma were localized and short lived compared to the entire volcanic field; this idea is supported by geochemical trends. Vents indicated by symbols correspond to clusters; thick shading shows vent alignments; thin lines show faults.

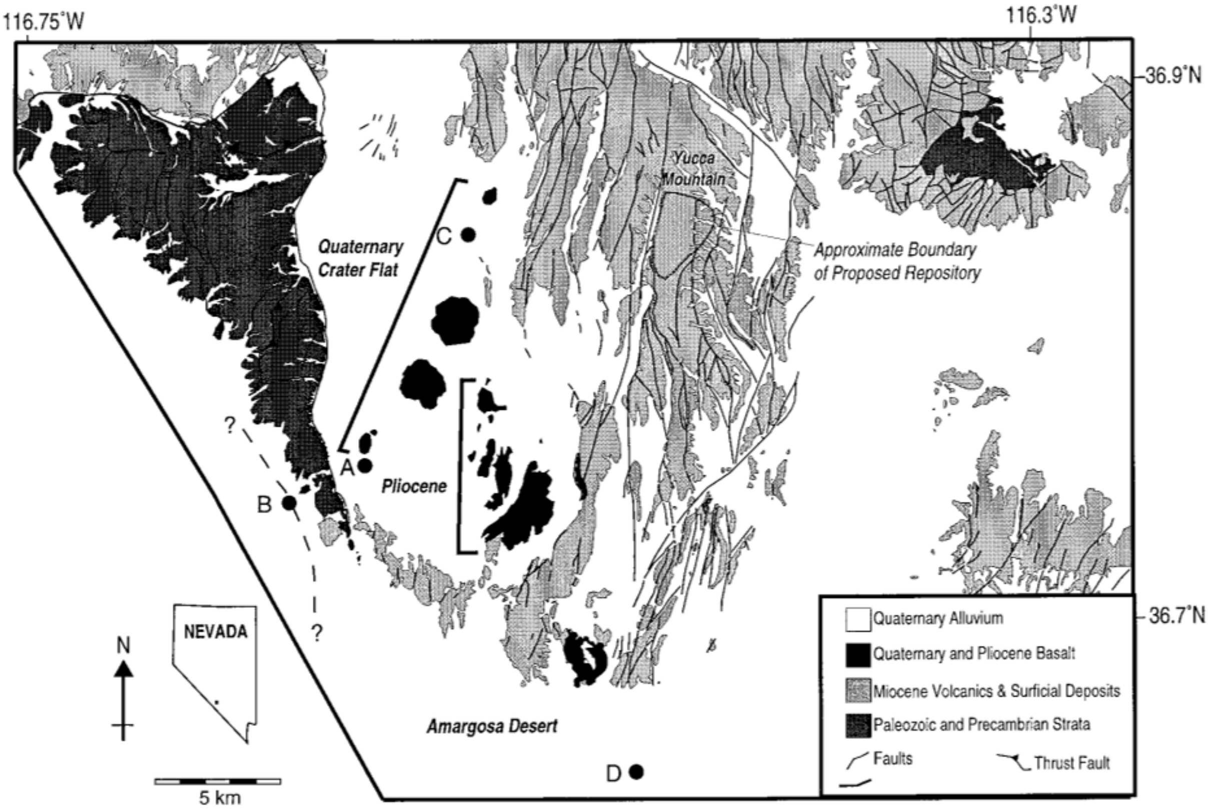
116.75°W
116.3°W
36.9°N
36.7°N
Yucca Mountain
Approximate Boundary of Proposed Repository
Quaternary Crater Flat
Pliocene
A
B
C
D
?
?
NEVADA
N
5 km
Amargosa Desert
Quaternary Alluvium
Quaternary and Pliocene Basalt
Miocene Volcanics & Surficial Deposits
Paleozoic and Precambrian Strata
Faults
Thrust Fault

FIGURE 2 The Yucca Mountain volcanic field in Nevada is a small volcanic field active since large-volume, caldera-forming silicic eruptions ceased about 8 Ma. As in larger volcanic fields, Plio-Quaternary volcanism occurs in spatial clusters. Thus the volcanic eruptions leading to the formation of the northeast-trending Quaternary Crater Flat alignment (Northern Cone—Little Cones) were preceded by volcanism at nearby Pliocene vents. Magnetic anomalies (A–D) are buried volcanoes in this area, which has high sedimentation rates. Delineating the volcanic history of this region and the relationship between volcanism, faulting, and episodes of extension is a key element of geologic hazards investigations for the proposed high-level radioactive waste repository at Yucca Mountain.

flows using stratigraphy, paleomagnetic age dating, cinder cone geomorphology, and detailed radiometric age determinations of individual vents (Fig. 3). Often a variety of dating techniques need to be implemented and linked to geologic mapping in order to delineate the chronology of eruptions within a basaltic volcanic field (Fig. 4).

Even where excellent age determinations are available, confusion can arise over the definition of the volcanic events used to estimate recurrence rates. Ideally, volcanic events would correspond to volcanic eruptions. However, subsequent volcanic eruptions often obliterate or obscure evidence of previous activity. A more easily implemented definition is based on morphology: An individual cinder cone, maar, or similar edifice represents a volcanic event. Alternatively, volcanic events can be defined as mappable eruptive units, each unit being an assemblage of volcanic products indicating a cogenetic origin from a common vent. This definition can become complicated by the formation of multiple vents during a single episode of activity. For example, three closely spaced vents formed during 1975 eruptions in the Klyuchevskoy Group, Kamchatka, forming the New Tolbachik cinder cones. This alignment of three cinder cones might be considered to represent a single volcanic event. These cones extended an alignment formed by three older Holocene cones, creating an alignment that is about 5 km long. In the geologic record, it would be quite difficult to determine if these cones represent one, two, or six volcanic events. Similar alignments are found in many basaltic volcanic fields.

In older, eroded volcanic systems, evidence for the occurrence of vents such as vent buds and breccia zones may constitute volcanic events. In these eroded systems it is clear that the number of dikes reaching the shallow crust can far exceed the number of vents formed at the surface. For example, in the San Rafael volcanic field in Utah more than 1700 dike segments are mapped in an area with approximately 60 breccia pipes and buds that are interpreted as vents. Even where detailed mapping is available, grouping dikes and vents in such areas into volcanic events or episodes is problematic.

A straightforward method of estimating average recurrence rates of volcanic activity is given by:

$$\lambda_t = \frac{N - 1}{t_o - t_y},$$

where N is the total number of volcanic eruptions or vents, t_o is the age of the oldest event, and t_y is the age of the youngest event. Long-term average recurrence rates in volcanic fields are typically on the order of 10^{-4}–10^{-5} volcanic events per year (v/yr) (Table I). These average rates are very low compared to the frequencies of eruptions at individual composite cones. Long-term averages smooth out significant variation in recurrence rates that may span comparatively short periods of time (<100 kyr). For example, in the Michoacán-Guanajuato volcanic field in Mexico, average recurrence rates since 40 ka are on the order of 2×10^{-3} v/yr, higher than the long-term average. In the Springerville, Arizona, volcanic field, recurrence rates reached a maximum of $3–4 \times 10^{-4}$ v/yr during peak activity in the field about 1 Ma. In contrast, average recurrence rates of vent formation in the Yucca Mountain, Nevada, volcanic field are on the order of 8×10^{-6} v/yr during the last 1 Ma. Episodic behavior can produce orders-of-

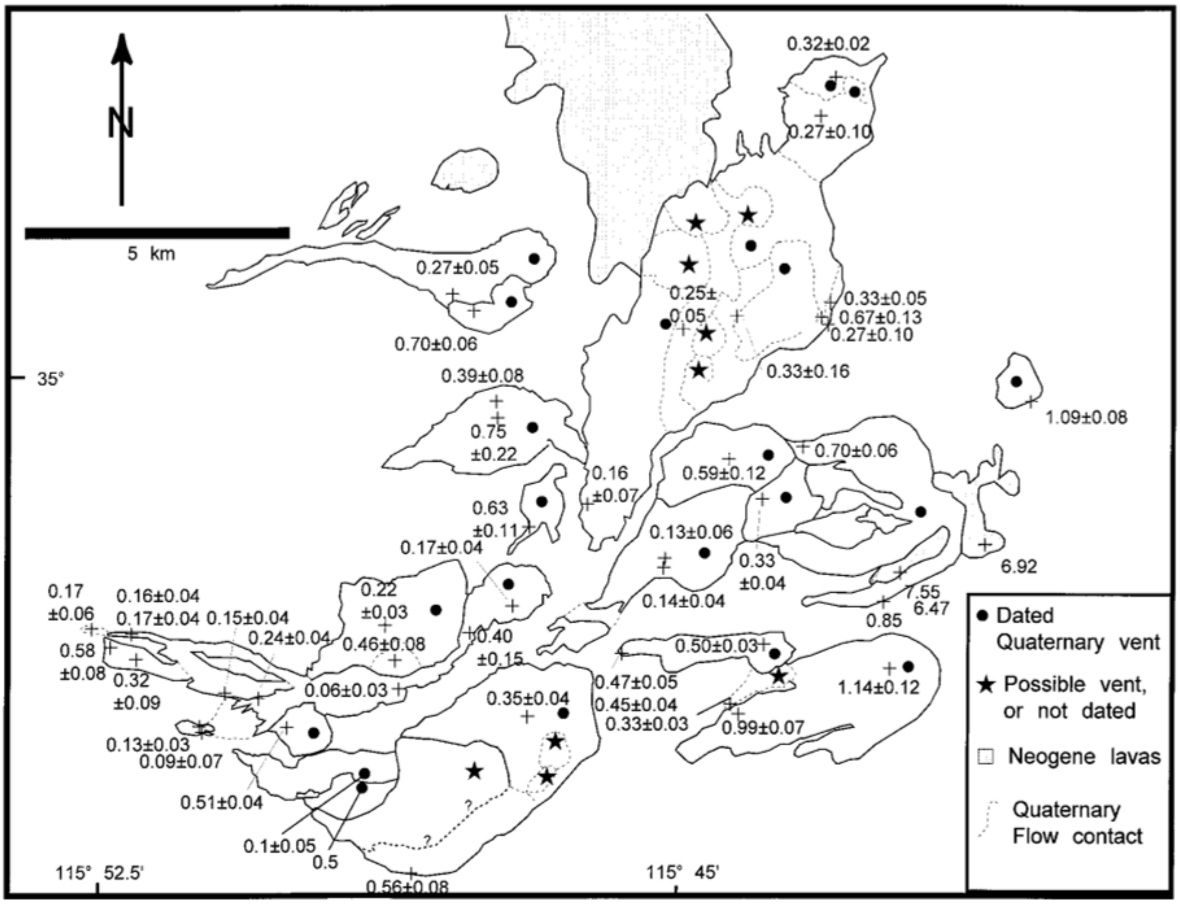
N
5 km
35°
115° 52.5'
115° 45'
0.32±0.02
0.27±0.10
0.27±0.05
0.70±0.06
0.25±
0.05
0.33±0.05
0.67±0.13
0.27±0.10
0.33±0.16
0.39±0.08
0.75
±0.22
1.09±0.08
0.16
±0.07
0.59±0.12
0.70±0.06
0.63
±0.11
0.13±0.06
0.17±0.04
0.33
±0.04
6.92
0.17
±0.06
0.16±0.04
0.17±0.04
0.15±0.04
0.22
±0.03
0.14±0.04
7.55
6.47
0.85
0.24±0.04
0.46±0.08
0.40
±0.15
0.58
±0.08
0.32
±0.09
0.50±0.03
0.06±0.03
0.47±0.05
0.45±0.04
0.33±0.03
1.14±0.12
0.35±0.04
0.99±0.07
0.13±0.03
0.09±0.07
0.51±0.04
?
?
0.1±0.05
0.5
0.56±0.08
● Dated Quaternary vent
★ Possible vent, or not dated
☐ Neogene lavas
Quaternary Flow contact

FIGURE 3 The southern part of the Cima volcanic field in California provides an excellent example of how detailed mapping and age determinations are essential for understanding the evolution of volcanic fields. This cluster of approximately 30 vents formed largely during the last 0.7 Ma. This pulse of activity accompanied a significant shift in the locus of volcanic activity in the field—older vents are located north of this cluster.

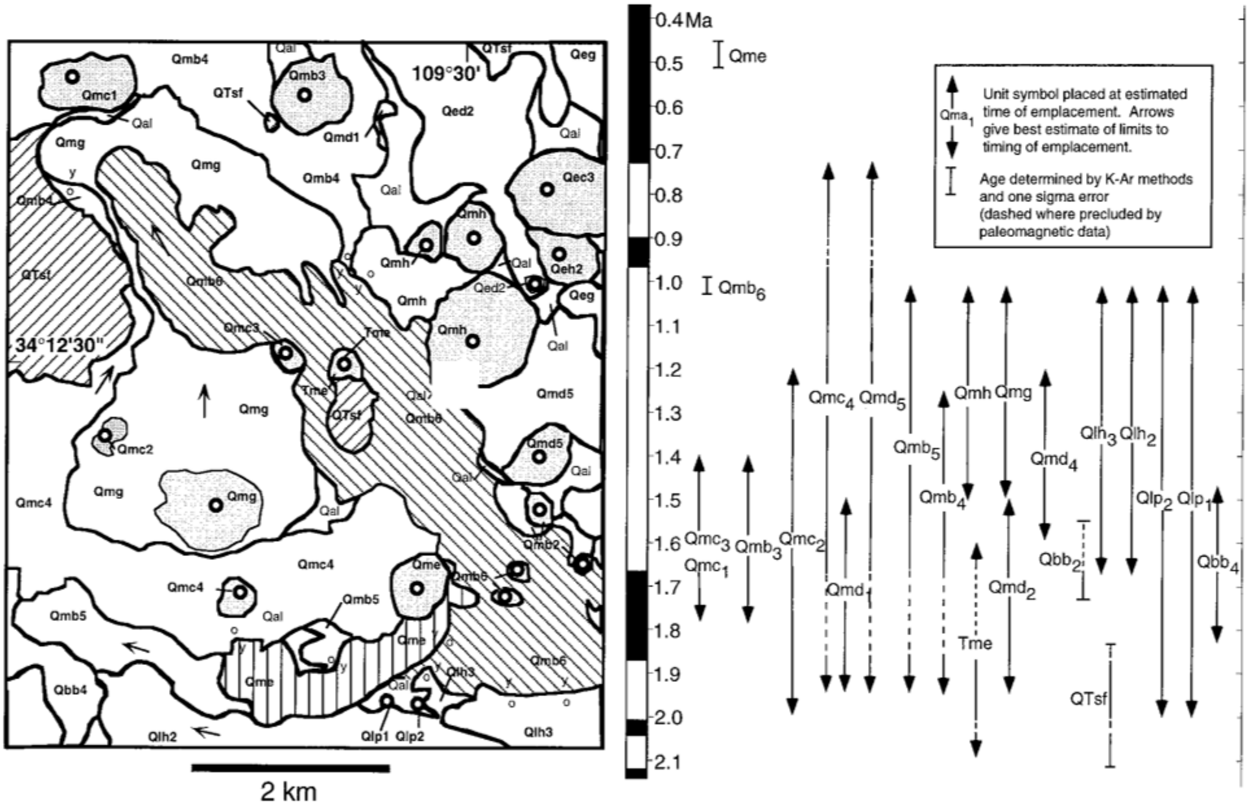

109°30'
34°12'30"
2 km
0.4 Ma
0.5
0.6
0.7
0.8
0.9
1.0
1.1
1.2
1.3
1.4
1.5
1.6
1.7
1.8
1.9
2.0
2.1
Qme
Qmb6
Unit symbol placed at estimated time of emplacement. Arrows give best estimate of limits to timing of emplacement.
Qma1
Age determined by K-Ar methods and one sigma error (dashed where precluded by paleomagnetic data)
Qmc4 Qmd5
Qmh Qmg
Qmb5
Qmb4
Qmd4
Qlh3 Qlh2
Qlp2 Qlp1
Qmc3 Qmb3 Qmc2
Qmc1
Qmd1
Qmd2
Qbb2
Qbb4
Tme
QTsf
Qmb4
Qmb3
Qmc1
Qal
Qmg
Qed2
Qmd1
Qeg
Qec3
Qeh2
Qmh
Qmb6
Qmc3
Tme
Qmd5
Qmc2
Qmc4
Qmb5
Qbb4
Qlh2
Qlp1
Qlp2
Qlh3
Qmb2

FIGURE 4 A combination of stratigraphic relationships, radiometric age determinations, and paleomagnetic dating is used to delineate the volcanic history of the Springerville, Arizona, volcanic field (see Fig. 1). Here, a geologic map of a small part of the volcanic field illustrates how stratigraphic relationships are used to constrain the age of each eruptive unit. The age range chart illustrates the uncertainty in each age estimate. Stippled pattern shows near-vent facies, lined pattern shows radiometrically dated lavas, arrows indicate lava flow directions, o and y indicate older and younger units where relative ages of adjacent units can be determined.

magnitude variation in eruption recurrence rates compared to long-term averages. Currently, a significant challenge is to better delineate the timescales of such episodes.

Average recurrence rates of volcanic events are a simple measure of the relative activity in volcanic fields, but more detailed analyses have revealed time trends relating eruption volumes and rates of activity. For example, the cumulative erupted volumes of both basalts and rhyolites in the Coso volcanic field of California are remarkably linear in time. Hence, successive eruptions occur at time intervals that depend on the volumes of the previous eruptions. This linear relationship has been used to forecast the timing of future eruptions. A similar pattern of activity has been identified in the Springerville volcanic field, where the areas of individual lava flows rather than volumes were used to estimate magma output rates, primarily because the highly variable thickness of lava flows makes the volume estimates difficult. In the Springerville volcanic field, the rates of volcanic eruptions waxed, then waned during the last 2 Ma but the cumulative area impacted by eruptions remained constant during much of the time prior to 0.3 Ma, despite major changes in the geochemistry of the basalts (Fig. 5).

B. Spatial Patterns

The episodic character of small-volume basaltic volcanism is further revealed by spatial patterns in vent distributions common to nearly all basaltic volcanic fields. Studies of spatial patterns of vent distribution in volcanic

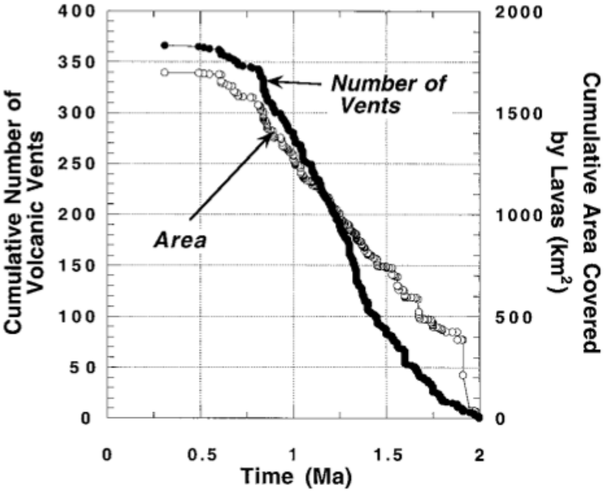

FIGURE 5 Temporal trends in volcanic activity can be represented by the cumulative number of volcanic vents and cumulative volume of volcanic events through time. Here, volume is represented as area covered by lava flows, which is more easily and accurately determined from maps than lava flow volumes. The cumulative area covered by lavas was remarkably steady in the Springerville volcanic field (see Fig. 1) between 1.75 and 0.75 Ma. Such steady-state volume–time relationships have been observed in several volcanic fields. In contrast, the recurrence rate of volcanic events waxes then wanes during this period.

fields have revealed the following: (1) Shifts in the locus of cinder cone volcanism are a common phenomenon in volcanic fields; (2) cinder cones cluster within these fields, often on several scales; and (3) vent alignments are ubiquitous, including short local alignments of several vents and more regional alignments that are usually more than 20 km in length and consist of numerous vents. These spatial patterns exist because recurrence rate is often not uniform across a volcanic field even if volumetric output in the field as a whole is steady state. Various density estimation techniques are used to delineate and characterize spatial patterns in basaltic volcanic fields.

Large-scale shifts in the locus of volcanism have been observed in numerous volcanic fields. For example, Plio-Quaternary volcanism in the Pancake, Nevada, volcanic field (Fig. 6) has shifted from southwest to northeast through time, creating an elongate volcanic field that parallels many local Basin and Range structures. This trend in the Pancake field extends Miocene–Early Pliocene volcanic activity in the Reveille Range southwest of Pancake, now preserved as dikes and eroded vents. Similar shifts in activity through time have been observed in the San Francisco, Springerville, Coso, Cima, and Camargo volcanic fields. In some of these volcanic fields, shifts can be related to regional tectonic processes such as plate motion. In other areas, however, shifts in the locus of volcanism seem independent of regional tectonic processes.

Vent clustering is a widely recognized phenomenon in volcanic fields. Vent clusters occur on several scales. In the Michoacán-Guanajuato and the Springerville volcanic fields (Fig. 1), vent clusters consist of 10–100 individual vents and have diameters up to 50 km. In smaller volcanic fields, statistical methods can delineate clusters of 1–10 vents. In some volcanic fields, volcanic activity within clusters waxes and wanes on short timescales compared to the volcanic field as a whole. In other areas, recurrent volcanism occurs within individual clusters over most of the history of the volcanic field.

A simple explanation for vent clustering is that magma supply varies across volcanic fields. Mantle rocks beneath vent clusters are close to their solidus and produce melts more readily in response to small changes in the thermophysical or geochemical state of the mantle. Magma in these areas can be generated repeatedly in response to episodic extension or heating as long as the fraction of partial melting is sufficiently small that the source region of the magma is not depleted substantially as a result of repeated melt generation. The scale and longevity of vent clusters, therefore, may reflect the scale of geochemical, temperature, and pressure variations in the mantle source region. An alternative explanation is that crustal structures are somehow responsible for the development of clusters. However, the distribution of clusters in most volcanic fields does not directly correlate with the distribution of faults or other features that may ease magma transport through the crust. Although vent alignments and individual vents within clusters often occur near or on faults, fault densities are rarely high within vent clusters compared to nearby areas.

C. Probability of Future Eruptions

Spatial patterns and temporal recurrence rates may be combined to estimate probabilities of future volcanic activity within volcanic fields. The probability of future volcanic eruptions within some small area within a volcanic field, Δx, Δy, during some time interval, ΔT, can be estimated as follows:

$$P[\text{volcanic eruptions within } \Delta x, \Delta y, \Delta T] = 1 - \exp[-\lambda_r \lambda_t \Delta T \Delta x \Delta y],$$

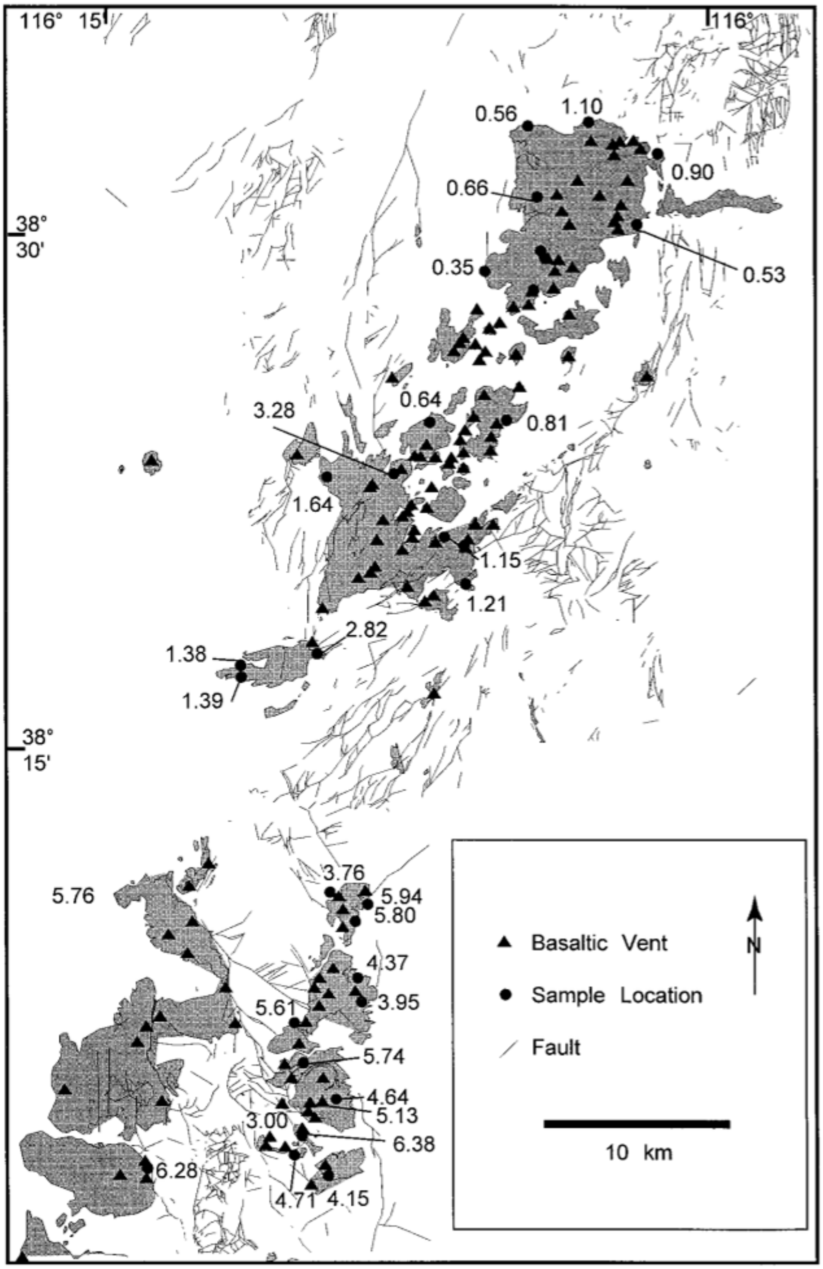
116° 15'
116°
38° 30'
38° 15'
0.56
1.10
0.90
0.66
0.53
0.35
0.64
3.28
0.81
1.64
1.15
1.21
2.82
1.38
1.39
5.76
3.76
5.94
5.80
4.37
3.95
5.61
5.74
4.64
5.13
3.00
6.38
6.28
4.71
4.15
▲ Basaltic Vent
● Sample Location
Fault
N
10 km

FIGURE 6 Vent distribution in the Pancake–Reveille range, Nevada, shows a clear northeast shift in volcanic activity through time, creating an elongate volcanic field that parallels local faults and regional neotectonic patterns.

where λ_t is the temporal recurrence rate and λ_r is a spatial weighting factor. Both λ_t and λ_r are usually estimated from past patterns of volcanic activity. This equation can be integrated over some larger area than Δx, Δy to estimate the probabilities of volcanic eruptions within all or part of the volcanic field while still capturing smaller scale variations in recurrence rate, or integrated over some long period of time. Alternatively, probability of volcanic eruptions may be contoured across the volcanic field.

III. GEOLOGIC STRUCTURE OF VOLCANIC FIELDS

Alignments of basaltic vents are common in volcanic fields, on shield volcanoes, and in calderas. These alignments and their related structures are used to infer the presence and orientation of subsurface dikes and dike sets, as indicators of crustal stress orientation, and to infer mechanisms of shallow dike injection in active volcanic areas (Fig. 7). In active Holocene volcanic fields, such as Craters of the Moon, Idaho, the Laki fissures, Iceland, and the south flank of Tolbachik, Kamchatka, a strong correlation has been recognized between structural trends (faults and fractures) and volcanic alignments consisting of contemporaneous cinder cones associated with single episodes of dike injection. Development of volcano alignments has also been increasingly important in the assessment of long-term volcanic hazards because of the comparatively large map extent of these features.

Distinguishing alignments in basaltic volcanic fields comprising hundreds of vents is problematic, however,

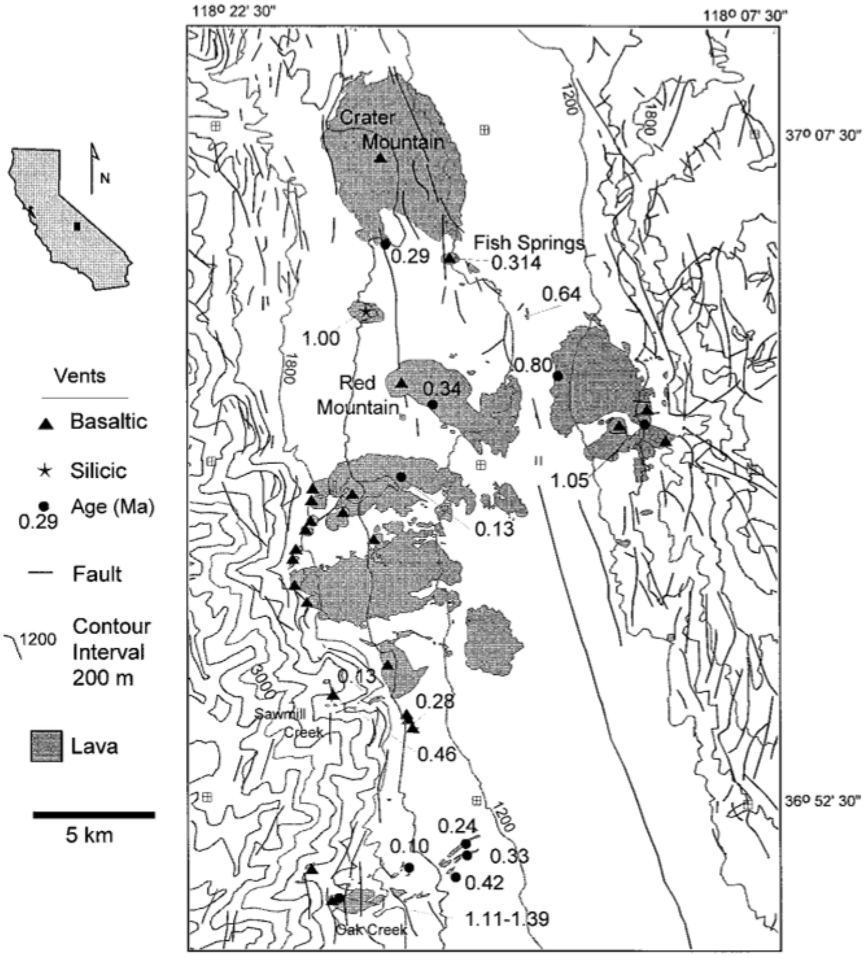
118° 22' 30"
118° 07' 30"
37° 07' 30"
36° 52' 30"
N
Crater Mountain
Fish Springs
0.29
0.314
0.64
1.00
1800
1200
Red Mountain
0.34
0.80
1.05
0.13
3000
0.13
0.28
0.46
Sawmill Creek
0.24
0.10
0.33
0.42
1.11-1.39
Oak Creek
Vents
▲ Basaltic
★ Silicic
● 0.29 Age (Ma)
— Fault
1200 Contour Interval 200 m
▨ Lava
5 km

FIGURE 7 The Big Pine volcanic field in California illustrates the relationship between regional faults and vents in basaltic volcanic fields. Three young vents and their lava flows (Crater Mountain, Fish Springs, and Red Mountain) are cut by fault splays of the Owen's Valley fault. A vent alignment on the west side of the valley appears to have formed during a single episode of activity and is fault controlled. Near Fish Springs and Oak Creek, some Quaternary basalt lavas cannot be traced back to vents, an indication of the high rates with which volcanoes are covered by alluvium and displaced by faulting in this rapidly subsiding basin. Water wells reveal that much of the subsurface in this area consists of intercalated basalt flows and alluvium.

because aligned vents are often interspersed among a greater number of unaligned cones. Recently, statistical methods have been used to identify vent alignments and improve the ability to discriminate these features objectively (Fig. 1). Vent alignments delineated by statistical methods typically parallel regional and local structures, which suggests that vent alignments can form because ascending magmas exploit preexisting structures repeatedly during separate episodes of activity (Fig. 6–8).

One explanation for the occurrence of volcanic vents along faults is that during ascent a dike may abandon its course perpendicular to the least principal stress in favor of a more energy-efficient path along a preexisting joint or fault. This effect can be modeled in two dimensions, treating the country rock as a uniform, linear-elastic, brittle rock that fractures at some tensile stress level, σ_o. The stress needed to create an open vertical fracture in the undeformed rock is

$$\sigma_v = \sigma_o + \sigma_3 + \sigma_d,$$

where σ_3 is the least principal *in situ* stress and σ_d is the additional stress needed to deform the fractured host rock to create an aperture. Where a preexisting fracture exists, dipping at angle θ, the stress required to dilate this preexisting fracture is

$$\sigma_f = \sigma_3 \sin^2 \theta + \sigma_1 \cos^2 \theta + \sigma_d,$$

where σ_1 is the greatest *in situ* principal stress. A dike will exploit the preexisting fracture when $\sigma_f < \sigma_v$. Using a range of appropriate bounding values, the minimum fracture dip a dike is likely to follow at a depth of 10 km is between 75° and 86°. The minimum exploitable dip decreases at shallower depths. Stress effects near the Earth surface may cause a dike to break out of a fault zone at shallow depths. Such near-surface effects become important at a depth of about 500 times the dike width.

In three dimensions, the orientation of a fault relative to σ_3 plays an essential role in determining whether a fault zone is likely to dilate in response to dike injection. Faults oriented roughly perpendicular to σ_3 are termed *high-dilation tendency faults* and are more likely to provide low-energy pathways to the surface than faults of other orientations. Considering these factors together, vent alignments may form in response to a variety of fault geometries (Fig. 9).

Faults and dikes are further interrelated because faulting and dike injection play a similar role in accommodating crustal stress, by slip in the case of faults and increased total crustal volume in the case of dikes. In some areas, topography related to faults is suppressed near volcanic fields and individual vent alignments because stress is accommodated by dilation of the crust during dike injection rather than by fault slip. This relationship can explain much of the variation in structure of volcanic fields. For example, cinder cone alignments are common in low-volume, low-density volcanic fields (e.g., Fig. 2 and 7). In larger volume basaltic volcanic fields, like the Springerville volcanic field (Fig. 1), mapped faults are rare and cinder cone alignments, though present, are less pervasive. In the former case, rates of dike injection are not sufficient to fully accommodate crustal stress. As a result, fault systems continue to experience slip and dikes tend to parallel or inject into these fault systems. In the latter case, rates of dike injection are sufficient to completely accommodate regional tectonic stresses within the volcanic field. This equalizes, or nearly equalizes, the magnitudes of principal horizontal stresses, and their orientations may vary substantially across the volcanic field and over time. Thus, vent alignments are less common in volcanic fields with comparatively high rates of volcanic activity.

The linear or nearly linear behavior of total eruptive volume through time (e.g., Fig. 5) has suggested a link between crustal strain rate and volcanic activity. If crustal strain rates are relatively uniform over a long

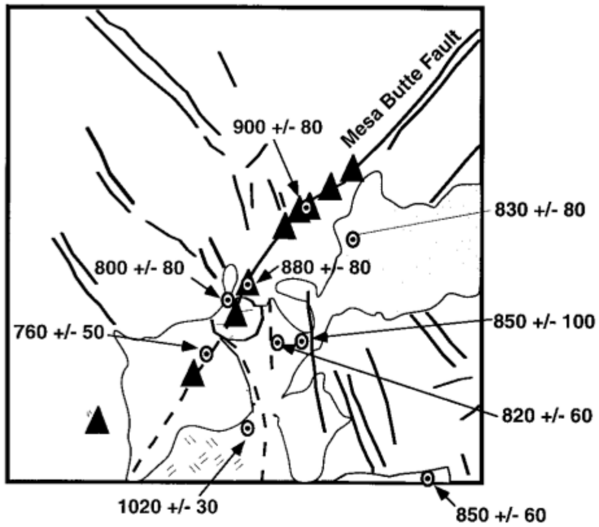

FIGURE 8 Cinder cone alignments can form as a result of several episodes of volcanic activity when ascending magmas are captured by faults. Such an alignment is shown on a geologic map of the Mesa Butte fault zone in the northcentral part of the San Francisco volcanic field in Arizona.

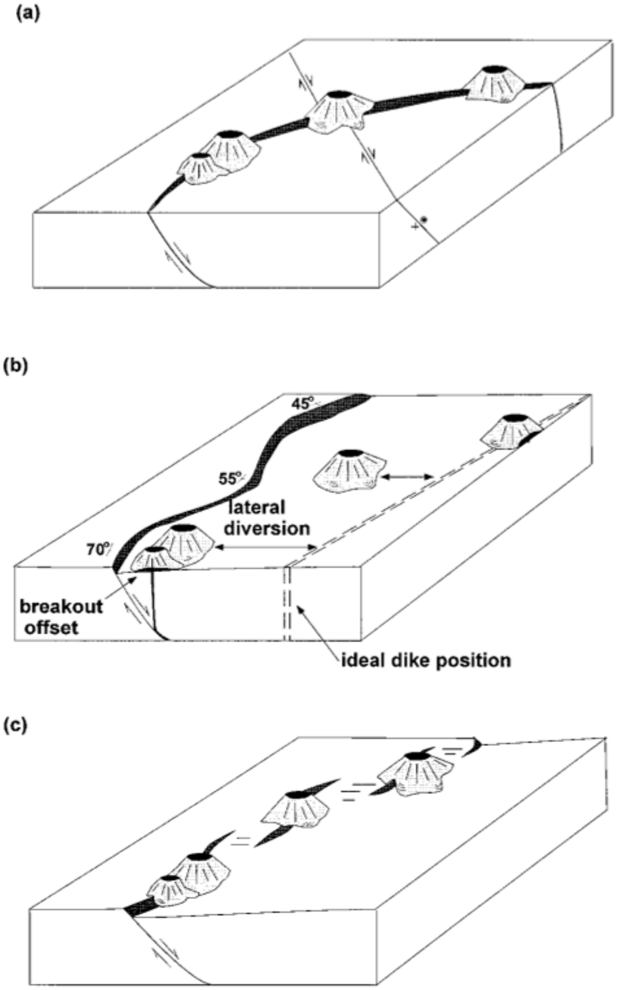

FIGURE 9 Cinder cone alignments can form along faults in a variety of geometries. (a) Cones can be aligned along the fault trace or at the intersections of two faults. (b) Cones can be offset laterally from the fault as a function of fault dip, which controls the distance from the fault trace at which the ascending dike will break out of the fault zone. (c) Cones can form an en echelon array along the fault trace.

period of time and melts are produced by decompression in response to extension, then a direct relationship between crustal strain rate and volume eruption rate should exist. Conversely, changes in the strain rate may result in changes in the rate of volcanic activity. If such a relationship between crustal strain and volcanism recurrence rates proves correct, estimates of volcanic hazards associated with basaltic volcanic fields might be substantially improved by accurate measurements of variation in crustal strain.

IV. PETROGENESIS OF BASALT VOLCANIC FIELDS

Basaltic volcanic fields are volumetrically dominated by basaltic ($\leq$52 wt% silica) and basaltic andesite lavas (52–56 wt%). The importance (i.e., volume) of more evolved andesitic to rhyolitic lavas varies considerably from field to field. For example, the San Francisco volcanic field has erupted substantial volumes of evolved lavas that crop out in seven large silicic domes (dacite through rhyolite composition) and the voluminous ($\approx$100 km^3), andesitic San Francisco Peaks composite volcano. In sharp contrast, the Springerville volcanic field, which lies just south of the San Francisco field, erupted few intermediate lavas.

Basaltic lavas in volcanic fields display a broad range of petrographic features, with every possible gradation from vesicular to nonvesicular, aphyric to porphyritic, and wholly crystalline to glass-rich lavas. In most cases, phenocryst phases of mafic lavas comprise, in widely variable proportions, olivine, plagioclase, clinopyroxene, and less commonly orthopyroxene and magnetite. The groundmass of most basalts is typically dominated by the same phases accompanied by titaniferous magnetite, apatite, sparse ilmenite and spinel, and frequently basaltic glass.

Basalt magmas originate from partial melting of a lithospheric mantle or asthenospheric source material; the most frequently named parent materials are peridotite and eclogite. Regardless of the source composition, basaltic magmas erupted onto continents are required to rise through substantial thickness (approximately 20–45 km) of continental crust before erupting. The compositional variability in basaltic volcanic fields can be explained by some combination of the following:

1. Variable degrees of partial melting of various garnet-bearing upper mantle sources
2. Mixing of at least two components in the source region of the mantle
3. Fractional crystallization in the deep crust
4. Assimilation of crustal material with concomitant fractional crystallization

Geochemical analyses confirm that the short-lived, monogenetic nature of cinder cones precludes the involvement of long-lived shallow basaltic magma reservoirs beneath basaltic volcanic fields.

The variety of mafic rocks erupted in basaltic volcanic fields is exemplified by the San Francisco volcanic field. This field comprises a broad spectrum of mafic lavas, including basanite, alkali olivine and tholeiitic basalts, and basaltic andesites. Chemically, lavas range from strongly nepheline-normative to quartz-normative basalts. While the locus of basaltic volcanism in the San Francisco volcanic field migrated, broadly, from east to west, extensive sampling and geochemical analyses (including 1000 major and 200+ trace element analyses) do not show any evidence of a corresponding systematic spatial or temporal change in basalt lava composition. Remarkably, a single cinder cone cluster, SP cluster which comprises just 60 Early Pleistocene through Holocene basaltic vents, shows a breadth of mafic geochemistry comparable to that of the entire field.

Overall, field-wide geochemical trends have been indentified in some volcanic fields (e.g., Eifel, Big Pine, Springerville) that can be related to changing source conditions. Elsewhere (e.g., Michoacán-Guanajuato and Cima volcanic fields) temporal and spatial trends in geochemistry are indistinct. Rather, the geochemistry of basalts from these fields appears to reflect the natural variability in steady-state, low-volume, basaltic magmatic systems.

V. ORIGINS OF VOLCANIC FIELDS

Early ideas on the formation of volcanic fields often involved widespread partial melting with ascending magmas relying on structures to serve as low-energy pathways to the surface. In such a model, rates of volcanic activity would be governed directly by crustal processes, rather than rates of melt generation. The origin of this idea is easy to understand—in many volcanic fields the crust appears to have leaked basalt from every conceivable fault and fracture. However, this idea is not consistent with the petrogenesis of basaltic volcanic fields, which almost always involves low rates of partial melting and melt production from a variety of levels in the lithosphere, asthenosphere, or both. These melts do not have long residence times in the crust or upper mantle, waiting for tectonic processes to ease their ascent and ultimate eruption. Instead, current evidence indicates that distributed basaltic volcanism is a natural consequence of ongoing low rates of magma production. Nonetheless, rates of extension or subduction are involved, because these rates can play a critical role in rates of partial melting.

A thermophysical model has been developed for distributed clustered volcanic fields based on observations in the Klyuchevskoy Group. Central volcanoes such as composite cones develop when magma supply is sufficient to maintain a thermal anomaly about a central conduit. This conduit provides a low-energy pathway to the surface as long as the thermal anomaly persists. In volcanic fields, magma supply rates are so low that such a conduit is not maintained between volcanic eruptions; new ascending magma batches find their own path to the surface, with no opportunity to accumulate in shallow crustal magma chambers. Thus, low rates of heat transfer due to low rates of magma production lead to distributed volcanic fields. This model has been augmented by suggesting that rates of extension also play a role. Numerical and physical analog experiments indicate that crack and dike coalescence is more likely within lithosphere that is experiencing low rates of extension compared to lithosphere experiencing high rates of extension. Therefore, distributed volcanoes are more likely to occur in areas of high strain rate due to the decreased opportunity for dike interaction and coalescence of magmas in crustal magma chambers. Thus, bimodal volcanism can develop in volcanic fields in response to changes in rates of magma production, extension, or both. Cumulatively, this work provides a mechanistic basis for the observation that low rates of magma production and high rates of extension result in formation of volcanic fields rather than central volcanoes.

VI. SUMMARY

Basaltic volcanic fields vary in size, total volume, longevity, and rates of eruptive activity. Commonality among volcanic fields in found in their low rates of magma production, clustered vent distributions, and petrogenesis dominated by mantle, rather than crustal, processes. Delineation of the timing of volcanism, petrologic evolution, and neotectonic setting of volcanic fields involves detailed investigation, a formidable undertaking given the large number of vents in most basaltic volcanic fields. The interplay between magma production and the neotectonics of the brittle crust exerts a strong control on development of volcanic fields, indicating that such comprehensive study is necessary. Although volcanic fields are characterized by low average rates of magma production, current data indicate that most volcanic fields experience dramatic changes in rates of vent formation and vent distribution over periods of 100 ka or less. As geophysical and geochronological techniques develop, it should become possible to delineate episodes of activity in volcanic fields with greater resolution and to relate such episodes to regional tectonics. This degree of resolution will enable volcanologists to move toward a more deterministic understanding of the processes governing the evolution of volcanic fields.

SEE ALSO THE FOLLOWING ARTICLES

Basaltic Volcanoes and Volcanic Systems • Flood Basalt Provinces • History of Volcanology • Melting the Mantle • Origin of Magmas

---

FURTHER READING

Arculus, R. J., and Gust, D. A. (1995). Regional petrology of the San Francisco volcanic field, Arizona, USA. *J. Petrol.* **36,** 827–861.

Bacon, C. R. (1982). Time-predictable bimodal volcanism in the Coso Range, California. *Geology* **10,** 65–69.

Condit, C. D., and Connor, C. B. (1996). Recurrence rates of volcanism in basaltic volcanic fields: An example from the Springerville volcanic field, Arizona. *Geol. Soc. Am. Bull.* **108,** 1225–1241.

Connor, C. B., and Hill, B. E. (1995). Three nonhomogeneous Poisson models for the probability of basaltic volcanism: Application to the Yucca Mountain region, Nevada, U.S.A. *J. Geophys. Res.* **100** (B6), 10,107–10,125.

Conway, F. M., Connor, C. B., Hill, B. E., Condit, C. D., Mullaney, K., and Hall, C. M. (1998). Recurrence rates of basaltic volcanism in SP Cluster, San Francisco volcanic field, Arizona. *Geology* **26,** 655–658.

Dohrenwend, J. C., Wells, S. G., and Turrin, B. D. (1986). Degradation of Quaternary cinder cones in the Cima volcanic field, Mojave Desert, California. *Geol. Soc. Am. Bull.* **97,** 421–427.

Duffield, W. A., Bacon, C. R., and Dalrymple, G. B. (1980). Late Cenozoic volcanism, geochronology, and structure of the Coso Range, Inyo County, California. *J. Geophys. Res.* **85,** 2381–2404.

Fedotov, S. A. (1981). Magma rates in feeding conduits of different volcanic centers. *J. Volcanol. Geotherm. Res.* **9,** 379–394.

Hasenaka, T., and Carmichael, I. S. E. (1987). The cinder cones of Michoacan-Guanajuato, central Mexico: Petrology and chemistry. *J. Petrol.* **28,** 241–269.

Ho, C.-H., Smith, E. I., Feuerbach, D. L., and Naumann, T. R. (1991). Eruptive probability calculation of the Yucca Mountain site, USA: Statistical estimation of recurrence rates. *Bull. Volcanol.* **54,** 50–56.

Lyell, C. (1830). "Principles of Geology," Vol. 1, reprinted 1990 by University of Chicago Press, Chicago.

Mertes, I., and Schmincke, H.-U. (1985). Mafic potassic lavas of the Quaternary West Eifel volcanic field. *Contrib. Mineral. Petrol.* **89,** 330–345.

Ormerod, D. S., Rogers, N. W., and Hawesworth, C. J. (1991). Melting of the lithosphere mantle: Inverse modeling of alkali-olivine basalts from the Big Pine volcanic field, California. *Contrib. Mineral. Petrol.* **108,** 305–317.

Schmincke, H.-U., Lorenz, V., and Seck, H. A. (1983). The Quaternary Eifel volcanic fields. Pages 139–150 "Plateau Uplift" (K. Fuchs, ed.). Springer-Verlag, Berlin.

Takada, A. (1994). The influence of regional stress and magmatic input on styles of monogenetic and polygenetic volcanism. *J. Geophys. Res.* **99,** 13,563–13,574.

Tanaka, K. L., Shoemaker, E. M., Ulrich, G. E., and Wolfe, E. W. (1986). Migration of volcanism in the San Francisco volcanic field, Arizona. *Geol. Soc. Am. Bull.* **97,** 129–141.

Williams, H. (1950). Volcanoes of the Parícutin Region. *U.S. Geol. Survey Bull.* **965B,** 165–279.

This Page Intentionally Left Blank

FLOOD BASALT PROVINCES

PETER R. HOOPER
Washington State University

I. Introduction
II. Diversity of Flood Basalt Provinces
III. Physical Parameters
IV. Chemical and Isotopic Parameters
V. Source of Flood Basalts
VI. Oceanic Flood Basalts
VII. Tectonic Implications and Genetic Models
VIII. Environmental Effects
IX. Summary

GLOSSARY

asthenosphere The relatively plastic low (seismic) velocity zone in the Earth's upper mantle that underlies the more rigid lithosphere that forms tectonic plates.

basalt A volcanic rock with high iron and magnesium and low silica content and composed mainly of small crystals of the minerals plagioclase and clinopyroxene, with Ti-Fe-Mg oxides and often olivine or orthopyroxene.

eclogite A rock of basalt chemical composition, but composed primarily of the minerals clinopyroxene and garnet, which are stable under mantle conditions of temperature and pressure.

hot spot An area in the Earth's upper mantle that is hotter than the ambient temperature.

lithosphere The brittle outer layer of the Earth, made up of the crust and uppermost part of the mantle, that "floats" on the asthenosphere and constitutes the tectonic plates.

magma Mobile rock, created by the partial melting of rocks at high temperature.

mantle The largest part of the planet Earth, between the core and thin outer skin or crust.

mantle plume The hypothetical cause of a hot spot, originating in the deep mantle, with a large plume head and a much narrower plume tail.

MORB Midocean ridge basalts, formed by the decompressional melting of mantle peridotite previously depleted by partial melting. MORB forms new oceanic crust.

nephelenite Strongly alkalic volcanic rock with low silica content.

picrite A volcanic rock with a large proportion of the magnesium-rich mineral olivine.

syenite An alkalic intrusive rock.

tholeiite A relatively siliceous and iron-rich basalt.

I. INTRODUCTION

Flood basalt provinces are products of the largest volcanic events known on Earth. They are characterized by their prodigious volumes of homogeneous tholeiitic basalt erupted in a very short time span. These provinces form extensive plateaus on all continents and on all ocean floors (Fig. 1). The plateau surfaces result from

Copyright © 2000 by Academic Press
All rights of reproduction in any form reserved.

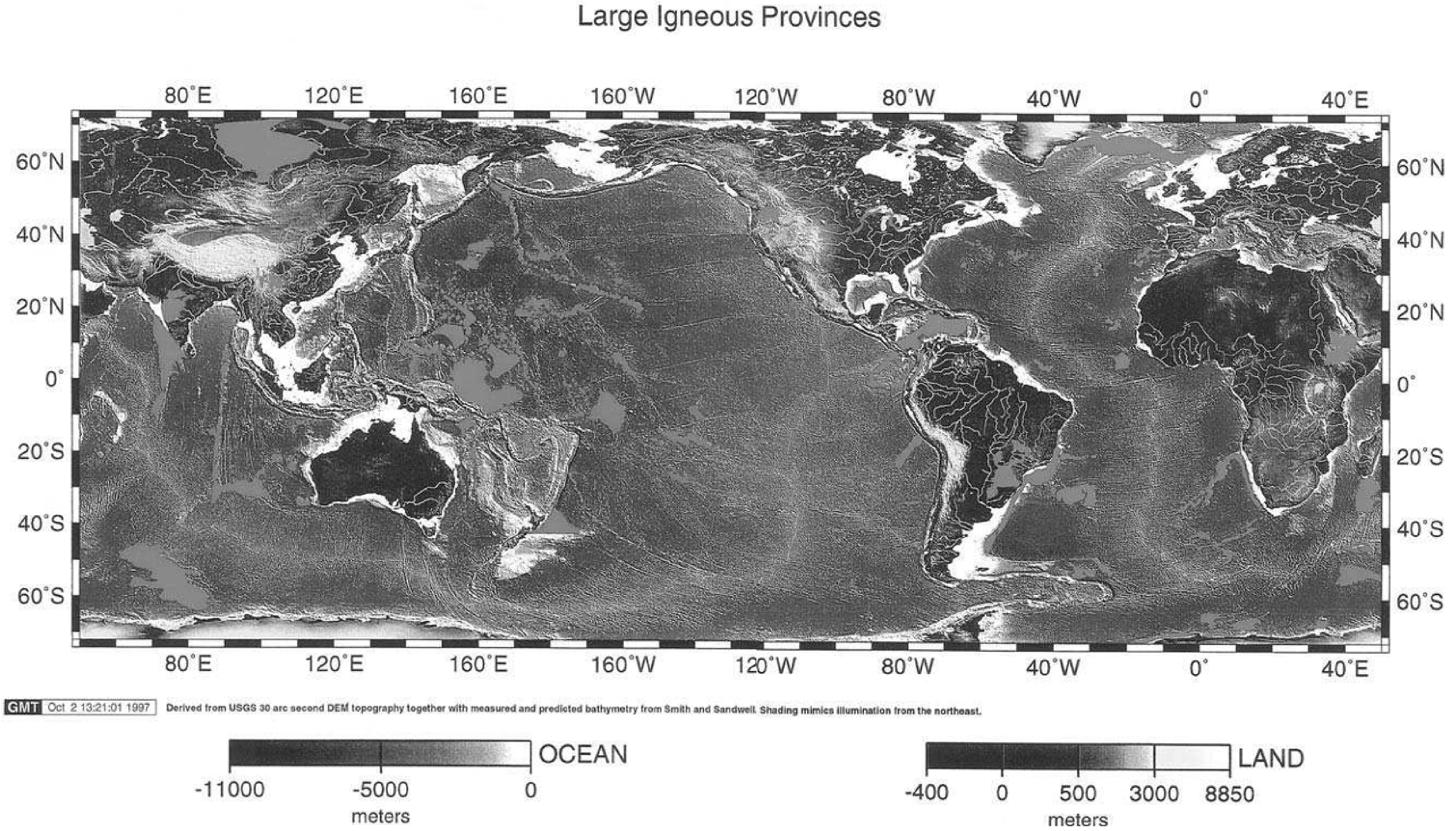
Large Igneous Provinces
80°E
120°E
160°E
160°W
120°W
80°W
40°W
0°
40°E
60°N
40°N
20°N
0°
20°S
40°S
60°S
GMT Oct 2 13:21:01 1997
OCEAN
-11000
-5000
0
meters
LAND
-400
0
500
3000
8850
meters

Derived from USGS 30 arc second DEM topography together with measured and predicted bathymetry from Smith and Sandwell. Shading mimics illumination from the northeast.

FIGURE 1 Map showing global distribution of flood basalt provinces. These large basalt provinces are not connected with ocean floor spreading or subduction. [From Mahoney and Coffin, 1987.]

the very large volumes of basaltic magma erupted rapidly from fissures in the Earth's crust to form sheet flows, typically tens of meters thick and covering tens of thousands of square kilometers, instead of the central volcanic cones characteristic of smaller, more normal, eruptions (Figs. 2 and 3). Flood basalt provinces formed episodically throughout the Mesozoic and Cenozoic periods, and remnants of older examples are known from the Proterozoic.

Plate tectonic theory postulates that most new crust is formed at the margins of tectonic plates from magmas produced by partial melting of underlying mantle. At divergent plate margins along midocean ridges, upwelling mantle rock is partially melted by decompression to form new ocean crust from the resulting midocean ridge basalts (MORBs). At convergent plate margins old ocean crust is partly consumed as one plate sinks beneath the other in the subduction process. As the subducted slab sinks, temperatures rise and dehydration occurs. The hydrous fluids driven off act as a flux in the overlying mantle wedge, which partially melts, the new magma rising to crystallize as new crust in the form of oceanic and continental arcs above the subduction zone. New crust is formed more or less continuously around the plate boundaries by these two processes.

Flood basalt eruptions, in contrast, are not confined to plate boundaries. They are associated with hot spots or mantle plumes and are both more sporadic and more dramatic. A mantle hot spot is anchored in the more mobile asthenosphere underlying the rigid tectonic plates of the lithosphere where its higher than ambient mantle temperature creates a partial melt that rises to the surface. As the plate moves over the hot spot, a chain of volcanic islands is formed across the ocean floor, such as the Emperor Ridge running northwest from the current hot spot beneath Hawaii. Most large basaltic igneous provinces, which include continental flood basalts, their submerged offshore equivalents known as seaward-dipping reflector sequences, and oceanic basalt plateaus, are closely associated with hot spots. Hotspots

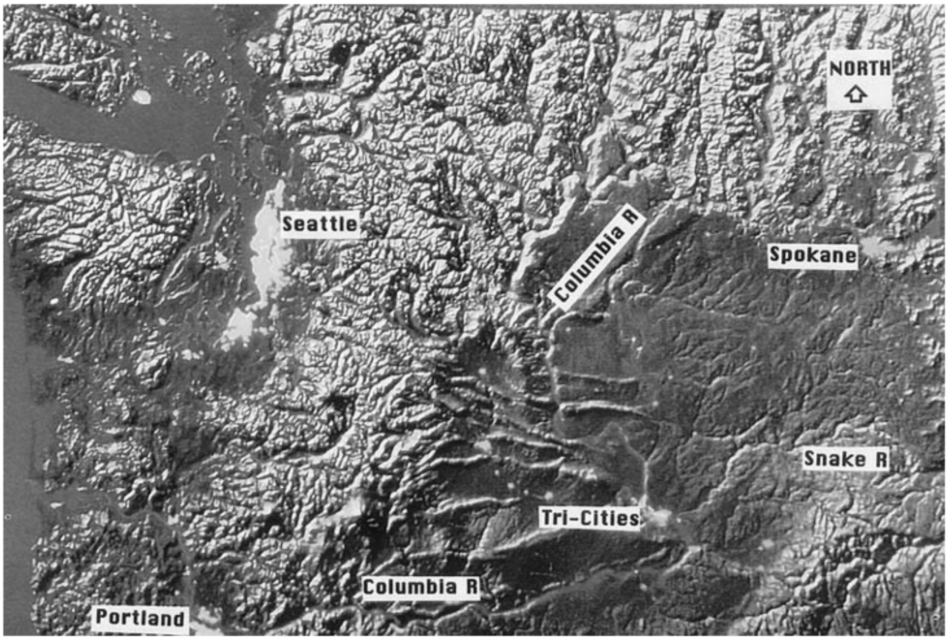

FIGURE 2 Satellite image of the northwestern United States showing the Columbia Plateau, east of the Cascade Range. The plateau is formed of huge flat-lying basalt flows that cover a large part of southeast Washington State and northern Oregon. Ninety-seven percent of the 174,000 km^3 of basalt in this province was erupted in just over 1 million years. Some individual eruptions produced more than 700 km^3 of tholeiitic magma from NNW–SSE fissures on the eastern edge of this image, as exemplified by the Pomona flow. The Pomona lava flowed down the Snake River, filled the Pasco Basin where the Snake and Columbia Rivers join in the center of the plateau, then continued down the ancestral Columbia River, across the rising Cascade Arc to plunge beneath (invade) the wet sediments along the Pacific Ocean coast line on the extreme west of this image. Over the 600 km that the Pomona flow can be traced, the concentrations of all 27 elements analyzed remain the same, implying minimal loss of heat and little crystallization.

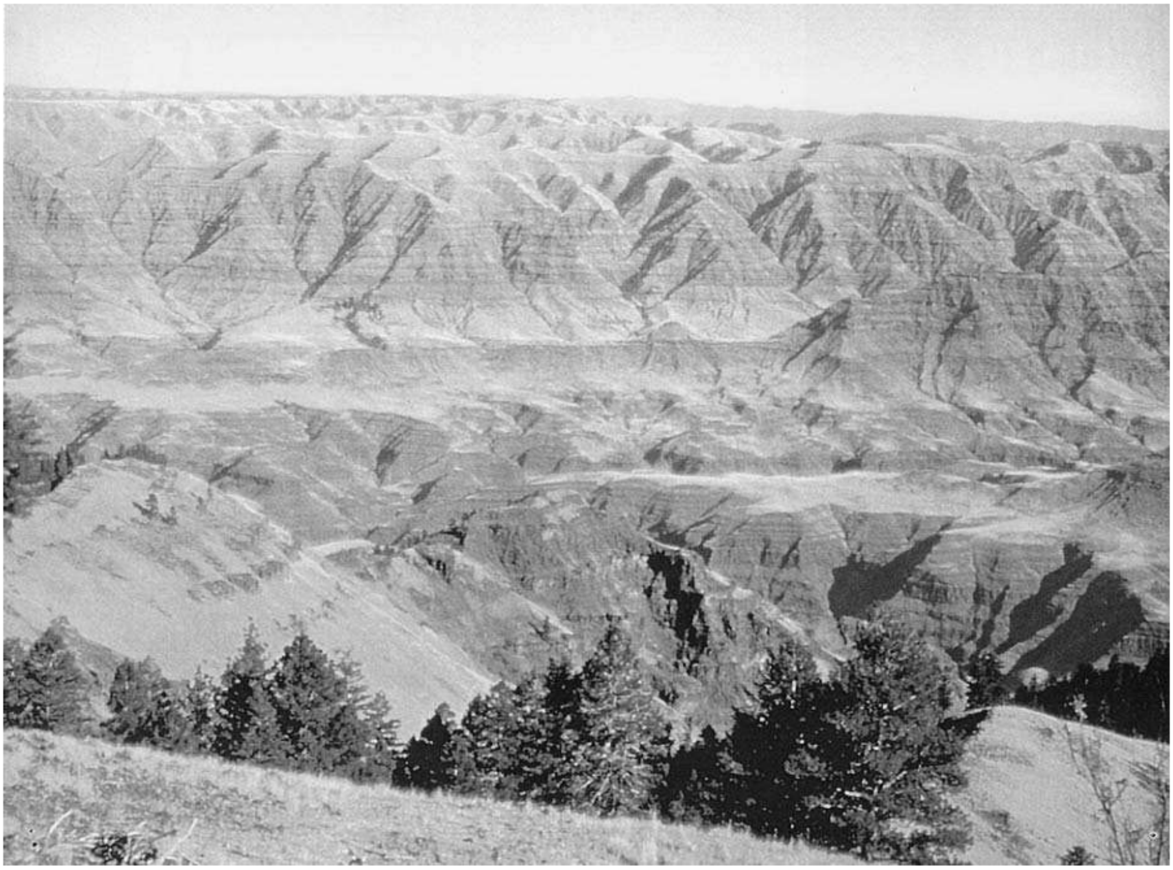

FIGURE 3 View of the Western Ghats, which form the western escarpment of the Deccan Plateau, India. The view shows flows of the upper part (Wai subgroup) of the main tholeiitic eruption (65.5 ± 1 Ma). The Deccan flood basalt province had an original estimated volume of $1–2 \times 10^6$ km^3 and all but a few percent of that volume was erupted within 1 million years. (See also color insert.)

are probably formed by plumes of hot material rising from the deep mantle; while they are not the principal means of creating new crust, because their eruptions are too intermittent, their contribution to this process is not trivial. The Ontong Java Basalt Plateau beneath the southwestern Pacific, one of the largest flood basalt provinces, covers almost 1% of the Earth's surface and has an estimated volume of 10^7 km^3.

We know from recent events such as the eruption of Mount Pinatubo in 1991 that major volcanic eruptions have profound effects on the Earth's climate. The large prehistoric eruptions of flood basalts must have had much more severe climatic effects. Indeed, the relatively tiny fissure eruption of Laki in Iceland in 1783, the only fissure eruption of historic times, caused a devastating famine across northern Europe. It is not surprising, therefore, that the dates of two of the largest continental flood basalt eruptions, the Siberian Traps (248 Ma) and the Deccan Traps (65.5 Ma), coincide as closely as current radiometric dating permits (±1 Myr) with dates of the two most dramatic mass extinction events in the Earth's history, at the Permian–Triassic and the Cretaceous–Tertiary boundaries. Less convincing correlations have been made between extinction events and some other flood basalt eruptions.

In addition to their roles in the formation of the Earth's crust and on the evolution of life on our planet, we know that continental flood basalts and their associated mantle plumes are intimately associated with the breakup and separation of tectonic plates. The nature of these associations remains controversial, but it is clear that knowledge of the origin of flood basalts is a critical factor in our understanding of mantle dynamics and plate motions.

II. Diversity of Flood Basalt Provinces

"Flood basalt" is a broad and somewhat ill-defined term. The classic continental flood basalts are relatively well studied in that an outline of a flow-by-flow stratigraphy is available and adequately dated radiometrically. But knowledge of ocean basalt plateaus and seaward-dipping reflector sequences is rudimentary. Other large basaltic igneous provinces have flood basalt affinities but are less well exposed, less well studied, and may possess many atypical features. Discussion of current knowledge of flood basalt provinces must therefore be uneven, concentrating on the younger and better exposed continental flood basalts, with less reference to both the older and sometimes more controversial continental provinces and the larger but relatively unstudied oceanic provinces. For ease of description the large basaltic provinces are arbitrarily divided into four categories:

1. Classical flood basalt provinces include the Siberian Traps, the Karoo province of South Africa, the Parana-Etendeka province of South America and South Africa, the Deccan Traps of India, and the Columbia River province of the American Northwest (Table I);
2. Less well studied or less typical provinces include the Rajmahal Traps of India, the basalts of Madagascar, the small province of Ethiopia-Afar-Yemen, and the huge province of the North Atlantic with its well-recognized seaward-dipping reflector sequences separating the exposed flood basalts from true MORB. These last two provinces, unlike all the classic continental flood basalt provinces, are still centered above their respective mantle plumes.
3. The apparent remnants of pre-Mesozoic flood basalt provinces include the Proterozoic Keweenawan of north-central United States and the Proterozoic Coppermine River basalt with its associated McKenzie dike swarm of northern Canada (Fig. 1).

TABLE I Estimated Physical Dimensions of the Various Types of Large Basalt Provinces, Including Continental and Oceanic Flood Basalts

		Age (Ma)	*Area (km^2)*	*Present volume (km^3)*	*Original volume (km^3)*	*Plume*
1. Classic Continental Flood Basalts (CFBs)						
Columbia River		16	1.6×10^5	1.8×10^5	1.8×10^5	Yellowstone
Deccan, India		66	5×10^5	5.2×10^5	$1–2 \times 10^6$	Reunion
Parana, S. America		132	1.2×10^6	8×10^5	1.5×10^6	Tristan
Karoo, S. Africa		183	3×10^6	n/d[a]	$1–2 \times 10^6$	? Bouvet
Siberian Traps		248	3.4×10^5	3.4×10^5	$>2 \times 10^6$	? Jan Mayen
2. Basaltic Provinces with Flood Basalt Affinities						
North Atlantic	PhI	62	1.3×10^6	6.6×10^6	6.6×10^6	Iceland
	PhII	54				
Ethiopia-Afar-Yemen		25 (40–0 My)	6×10^5	3.5×10^5	n/d	Afar
Madagascar		88	1×10^6	n/d	n/d	Marion
Rajmahal		116	2×10^5	n/d	n/d	? Kerguelen
3. Precambrian CFBs and Major Dike Swarms (Selected)						
Keweenawan, USA		1100	n/d	1.5×10^6	$>2.0 \times 10^6$	Lake Superior
Coppermine River		1267	n/d	n/d	n/d	?
4. Oceanic Plateaus (Selected)						
Ontong-Java	I	122	n/d	1.5×10^6	$>5.7 \times 10^7$	Ontong-Java
	II	90				
Kerguelen		112	n/d	n/d	10^7	Kerguelen
Wrangellia		230	n/d	n/d	n/d	?
Caribbean-Colombian		88	n/d	6×10^5	n/d	Galapagos

[a] n/d, not determined.

4. Oceanic plateaus include Ontong Java in the southwest Pacific, Kerguelen in the southern Indian Ocean, Wrangellia wedged on to the northwestern margin of North America, and the Caribbean-Colombian ocean flood basalt (Fig. 1).

III. PHYSICAL PARAMETERS

Continental flood basalts form exceptionally large plateaus of flat-lying flows with a uniform tholeiitic basalt composition (Fig. 3). Table I lists the estimated area, volume, and age of the better known provinces and the mantle plume with which each province is associated. The typical continental flood basalt province erupted between 1.0 and 2.0×10^6 km^3 of basalt, but the most comprehensively studied Columbia River province is smaller by one order of magnitude. Lack of sedimentary interbeds and absence of erosion or even significant weathering between flows, particularly at the base of these lava piles, imply that eruption followed eruption without substantial time gaps, although a slowing of the eruption rate and frequency is indicated by more frequent thin sedimentary horizons and boles toward the top in many cases (e.g., the Columbia River and Deccan). In each province most of the huge volume of magma erupted within a time span of 1–2 million years, often during a shorter period than can be recognized by current radiometric dating techniques. More than 96% of the 175,000 km^3 of Columbia River basalt erupted in 1–2 million years, while all but the very earliest and latest eruptions of the much larger Deccan and Karoo flood basalt eruptions appear to have occurred within a similar time span. This implies an average eruptive rate in the larger provinces of 1–2 km^3/yr, a rate 20–50 times greater than rates measured at a typical hot spot such as Hawaii, but less than that reported for the only historic single fissure eruption, that of Laki, Iceland, in 1783–1784.

Individual flows are huge. On the Columbia Plateau, for instance, some sheet flows with volumes of at least 700 km^3, derived from a single eruptive event, can be traced for 600 km (Fig. 2). Volumes of 2000–3000 km^3 have been plausibly suggested for some Columbia River flows, but not yet proven. The magma for these eruptions was supplied through fissure systems, now dikes (Fig. 4; see also color insert), some of which are more than 100 km long. Shield structures are rare. Small cones, including spatter cones, are occasionally preserved and appear to represent the dying phase of an

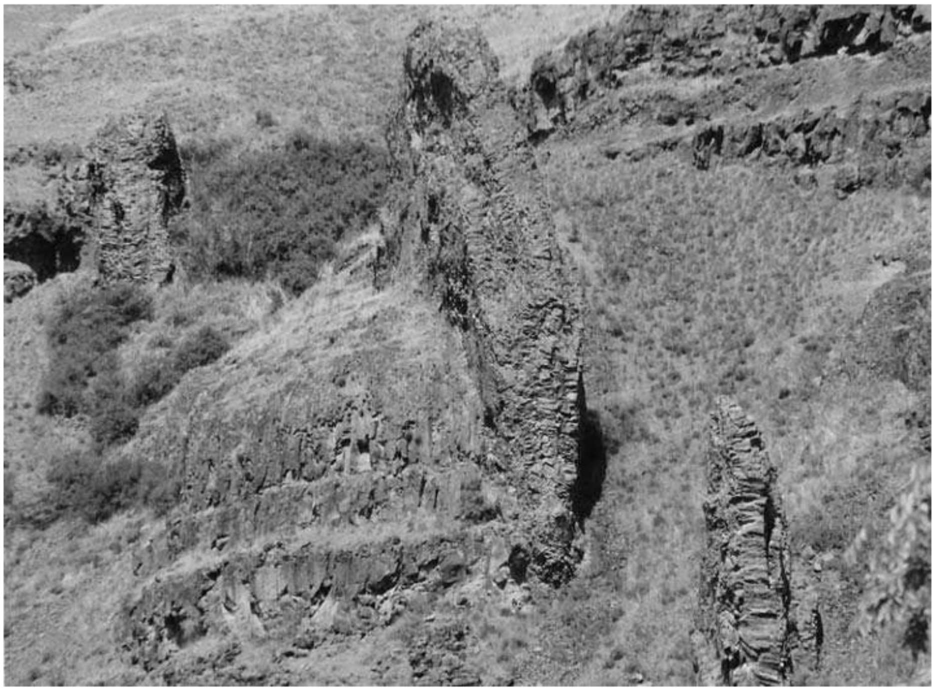

FIGURE 4 NNW–SSE-oriented feeder dikes in the southeast corner of the Columbia Plateau. Many of the dikes in this swarm can be connected to individual basalt flows by their spatial position and chemical composition. (See also color insert.)

eruption, confined to restricted parts of the fissures as the magma supply dwindled.

Although the distances traveled by individual basalt flows across the Earth's surface are demonstrably huge, flood basalt magmas may be able to flow even greater horizontal distances in dike systems within the crust below the surface. The great McKenzie dike swarm of northern Canada covers an area of 2.7 × 10^6 km^2 and extends for 2600 km from its focal point where the Muskox layered intrusion and the Coppermine River lavas occur. The entire suite is interpreted as the remnants of a large Proterozoic flood basalt province. The dikes have been dated to 1267 ± 2 Ma. Similar ages for the Muskox intrusion and Coppermine River flows, together with their very similar tholeiitic compositions, imply that all were derived from the same source. Study of the magnetic fabrics within the dikes indicates steep to vertical flow of magma in dikes close to the focus of the swarm and increasingly horizontal flow at their distal ends.

In the Karoo and Deccan provinces extensive lateral flow within the crust, rather than surface flow, may account for the huge areas covered by basalt flows of almost exactly the same age and composition. Karoo flows in central Namibia are of the same age and composition as flows 1500 km away in Lesotho. An intense complex of dikes and sills of similar age and composition occurs in the intervening area, cutting the older Karoo sediments. Similarly, on the Deccan, flow sequences more than 900 km apart display similar changes in chemical composition with time, but may be fed by separate, local, feeder-dike systems. In some cases such flow-dike systems with indistinguishable chemical compositions have distinctive isotopic signatures. This has led to the suggestion that such magmas are derived from the same mantle source but have followed different paths through the crust, the isotopic differences being ascribed to contamination by the different types of crust encountered during their extensive horizontal flow along dike systems. Lateral flow along fissures within the crust for thousands of kilometers may also provide an explanation for the atypical elongation of the Antarctic flood basalt province. This province forms a narrow extension from the Karoo province of Africa into Queen Maud Land and across Antarctica along the length of the Transantarctic Mountains to Tasmania, possibly following an old and weakened structural zone.

The rate of magma eruption onto the earth's surface in flood basalt provinces is critical to an understanding not only of the origin and evolution of these provinces but of their effect on the environment and world climate. But measuring the rate of magma eruption and the velocity of magma flow in flood basalt eruptions has proved controversial. Only on the relatively small province of the Columbia River (Table I) has enough detailed work been done to gain some insight into the eruptive processes. Individual sheet flows on the Columbia Plateau (Fig. 2) show virtually no change in chemical composition and a very small drop in temperature from point of eruption to flow termination (0.05° C/km). This consistency has been used to imply very rapid rates of extrusion and led to an early model of a fast-moving turbulent lava flow in which large volumes of magma erupted from 100-km-long fissures, with lava fronts many meters high advancing across the plateau at fast walking speed, covering the plateau in days or weeks. More recent studies suggest that the flows were formed by repeated internal injection and laminar flow, a mechanism similar to that observed in the growth of smaller flows through lava tubes on Hawaii. This second model interprets the simple structures of the typical Columbia River basalt sheet flow, a colonnade of thick vertical columns at the base supporting an entablature of smaller irregular columns of finer-grained basalt, topped by a glassy vesicular zone, as interlocking sequences of very large, flattened, lava tubes. The chemically homogeneous individual eruptions are interpreted as large flow fields of compound flows growing by inflation of pahoehoe lava. Both the turbulent and laminar flow models require the rapid and sustained emission of very large volumes of magma. In the second model the mass eruption rate is calculated to be 5 or more million kilograms per second with rates of lava flow from fissure to flow termination of the order of 1–2 km/hour so a whole flow field might take 10 or more years to be emplaced, rather than the few days or weeks envisioned in the earlier turbulent flow model.

Many of the Columbia River basalt flows carried phenocrysts on eruption and the longer the emplacement process continued the greater the degree of fractionation to be expected as the crystals separated from the remaining liquid. Chemical analyses of the flows using high-precision x-ray fluorescence techniques have indicated very consistent compositions, which allow subtle differences between flows to be traced across the province. In the absence of turbulent flow, such remarkable chemical homogeneity provides a potential constraint on the time between eruption and final crystallization.

The rapid eruption of huge volumes of homogeneous magma in short periods requires large reservoirs of well-mixed magma. Yet surface collapse structures, typical of the eruption of large volumes of silicic magma, are not observed. From this it is concluded that the magma reservoirs formed deep in the crust. The most obvious place for these magma reservoirs to develop is at the crust–mantle boundary where the contrast between the dense mantle-derived basaltic magma and the less dense crust would tend to prevent farther upward migration of the magma through the crust until it had fractionated enough at the crust–mantle boundary to decrease the magma density to that of the crust above. Modeling the observed chemical differences between flows supports this conclusion. Either these magmas were derived from an unusually iron-rich mantle or the original mantle melts underwent significant crystal fractionation under deep crustal conditions.

IV. CHEMICAL AND ISOTOPIC PARAMETERS

One of the most unusual aspects of flood basalts is the consistent chemical composition of huge volumes of basalt. Examples are the Lesotho Basalt of the Karoo, the Ferrar of the Antarctic province and the Grand Ronde Basalt of the Columbia River. But significant chemical differences do occur both within and between provinces, and these differences have led to distinct petrogenetic models.

Most provinces show greater compositional variation at the beginning and at the end of the main tholeiitic eruption. In the larger classic continental flood basalt provinces, relatively small volumes of alkalic and picritic magmas signaled the first signs of magmatic activity, whereas silicic magmas tend to be concentrated in the later phases of the eruption. Although normally small in volume, compared to the huge volumes of tholeiitic basalt, these more exotic magma types provide clues to the origin and evolution of the province as a whole.

Each of the five classic continental flood basalt provinces (Table I) has been subdivided into formations or chemical types on the basis of changes in major and trace element concentrations (Fig. 5). These changes may be reflected in mineralogical differences recognizable in the field and are typically accompanied by changes in isotopic ratios. Variation between flows within a formation is usually confined to subtle but remarkably consistent differences in minor and trace element abundances. This is best illustrated on the Columbia Plateau (Fig. 6), where chemical fingerprinting has been used to map individual flows across the province. Similar, if less detailed, chemical distinctions have been made in the other classic continental flood basalt provinces.

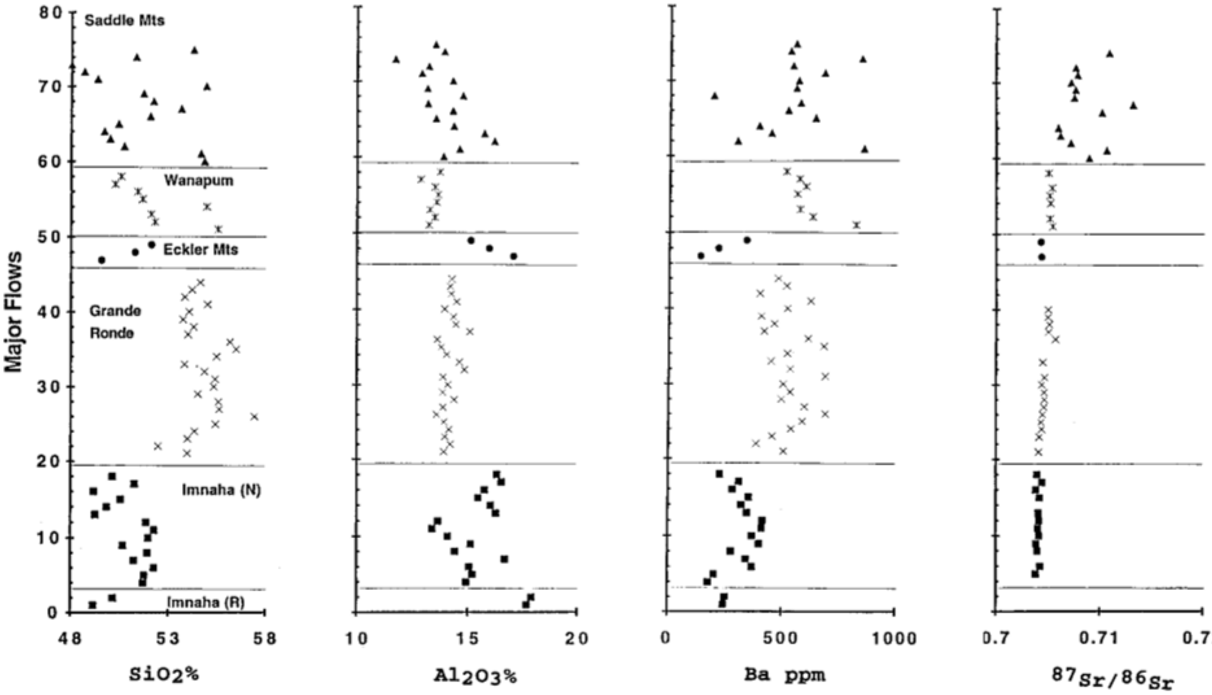

FIGURE 5 Division of the Columbia River Basalt Group into formations by variation in major and trace elements and in isotopic ratios. Other classical flood basalt provinces have been similarly divided.

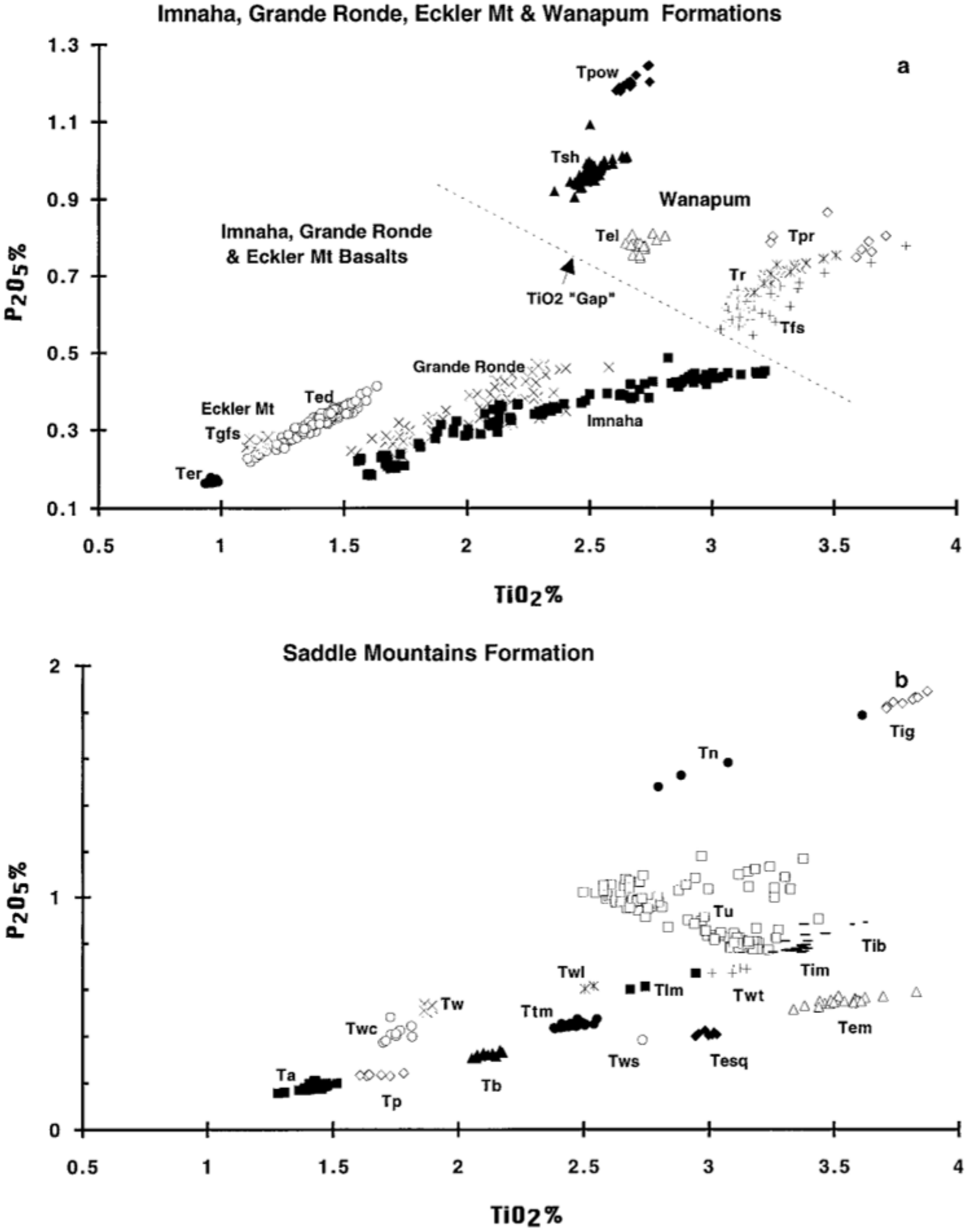

FIGURE 6 Identification of individual flows of the Columbia River Basalt Group on element oxide plots. (a) Phosphorous oxide (P_2O_5) versus titanium oxide (TiO_2) for Imnaha, Grande Ronde, and Eckler Mountain flows. (b) P_2O_5 versus TiO_2 for the Saddle Mountain flows. Each symbol represents a single eruption or flow, except that the Umatilla member (Tu) represents two similar but separate magmas erupted from the same vent, which mixed immediately before or during eruption. This chemical fingerprinting has allowed many individual eruptions to be mapped for hundreds of kilometers across the Columbia Plateau.

The Columbia River lacks early alkalic or picritic magmatism or late eruptions of rhyolitic magma. The Karoo, Parana-Etendeka, and Deccan provinces all include early alkalic magmatism and later silicic magmatism. In the Siberian Traps alkalic and pyroclastic silicic magmatism appear to be dispersed throughout the main tholeiitic event. In the Karoo the earliest magmatic events included the intrusion of syenites and extrusion of nephelinites (approximately 192 Ma), followed by a thick sequence of alkalic picrites in the northern part of the province (Nuanetsi) where their eruption coincides with ancient structural zones of weakness. This was followed by the huge volume of tholeiite that was extruded over most of southern Africa and extended into and across Antarctica (182 Ma). The final Karoo eruptions were dominated by silicic material (Jozini Rhyolites; 178 Ma), again confined to the northern part of the province along the Lebombo monocline, a structure that was probably developed by thinning of the lithosphere as the Antarctic and African plates separated, following the main eruptive event.

A similar sequence is found on the Deccan. Early syenite intrusions and flows of alkalic picrite (68.5 Ma) occur along the Narmada-Son-Tapti zone in the north, an ancient structural zone dating back to the Precambrian. This volumetrically insignificant activity was followed 2 or more million years later by the huge volume of tholeiite that forms Kalsubai Mountain and the Western Ghats (65.5 Ma; Fig. 3), which was erupted from north to south in less than 1 million years as the Indian plate moved rapidly north over the Reunion hot spot. Subsequent to this enormous outburst of tholeiitic magmatism, the western edge of the new basalt plateau was disrupted as east–west extension thinned the lithosphere and the Seychelles plate began to separate from the Indian plate, leading to normal NNW–SSE faulting and to the Panvel monoclinal flexure parallel to the coast. This extension brought the uppermost tholeiitic flows on the top of the adjacent part of the western Ghats down to sea level along the Bombay coast and created a series of horsts and grabens in the much thinner basaltic sequence offshore. A strongly oriented dike swarm parallel to and clearly associated with these NNW–SSE structures is made up of a mixed assemblage of compositions, from rhyolites through trachytes and lamprophyres to more normal tholeiites, some of which appear to have acted as feeders to the rhyolites, trachytes, and tholeiites of the small volume volcanic sequence that forms Bombay Island (61–64 Ma) and probably correlate with later alkalic intrusions farther north in the Cambray Basin dated at 53–64 Ma.

In South America, around the east edge of the Parana province, large alkalic intrusions such as the Jacupuranga complex predate or are contemporaneous with the earliest tholeiitic magmatism. On the Etendeka (African) side of this province, large syenitic complexes are contemporaneous with the later basalt eruptions and continued after the basalt eruptions had ceased. These large intrusive complexes, apparently oriented along ancient structural zones, are believed to have acted as the eruptive centers for the large volumes of silicic lava extruded in the latter part of the Etendeka basalt sequence and which cap the tholeiites on both sides of the South Atlantic. They vented immediately prior to the separation of the African and South American plates. In the Keweenawan province alkalic complexes are concordant with the earliest picritic eruptions, while large volume silicic eruptions, up to 600 km^3, occur later in the sequence.

In all flood basalt provinces, the dominant tholeiites have a simple mineralogy of plagioclase, clinopyroxene (augite and often pigeonite), and Fe-Ti oxides, often with olivine and more rarely orthopyroxene. They may be porphyritic or aphyric, with plagioclase by far the dominant phenocryst phase, followed by olivine, which is frequently replaced by iddingsite and other secondary products. But significant differences occur between provinces. The Grande Ronde Basalt formation of the Columbia River, for example, which forms 85% by volume of the Columbia River Basalt Group, is a very homogeneous aphyric basaltic andesite to andesite with SiO_2 content varying from 53 to 57%. This is significantly more silicic than tholeiites from other provinces with the possible exception of the Ferrar Basalt from the Antarctic. These and the more typical tholeiites of continental flood basalt provinces have the relatively high incompatible element abundances, high iron-to-magnesium ratios, and iron-rich olivine compositions that indicate these magmas could not have been in equilibrium with normal peridotite mantle mineralogy. Either they have undergone considerable crystal fractionation in the crust or they are derived from an unusually iron-rich mantle source. Furthermore, with the exception of some formations like the Ambenali Formation of the Deccan, major and trace element abundances and the isotopic ratios of these tholeiites imply that a component from a lithospheric source has contributed to their origin. Reconciling the chemical and isotopic evidence that indicates a lithospheric source with the large melt fractions that require a hot mantle plume source remains a fundamental problem in modeling the origin of flood basalt provinces.

V. SOURCE OF FLOOD BASALTS

The large volumes of basaltic magma erupted in such short intervals of time can only be formed if temperatures in the mantle source are higher than normal; that is, a mantle hot spot source. The most widely accepted model of a hot spot is a plume with a large head and a much narrower tail rising from the core–mantle boundary or from the lower–upper mantle boundary at about 670-km depth. Modeling of the impingement of a plume on the underside of the lithosphere shows that the large plume head spreads out to form a thermal dome with the potential to form basaltic eruptions by decompressional melting over an area that may be as much as 2000 km in diameter. The unusually large melt fractions formed in the mantle by this process cause the high extrusion rates that typify flood basalt provinces. As lithospheric plates move across a plume, the plume head disperses, leaving only the plume tail erupting basaltic magma at a lower rate. Such plume tails create chains of volcanic islands that terminate in active volcanoes marking the current position of the plume such as Hawaii or Reunion.

Mantle hot spots, like Hawaii, have characteristic chemical and isotopic compositions, including enriched helium isotopic ratios, which are probably derived from the deep mantle. Some flows in flood basalt provinces also contain these deep mantle signatures, but most flows in continental flood basalt provinces are chemically and isotopically distinct from the ocean island basalts of typical ocean hot spots. Continental flood basalts are typically more silicic than ocean island basalts. Most continental flood basalts also have enriched isotopic ratios with decoupled light ion lithophile (LIL) and high field strength (HFS) incompatible trace element concentrations, a decoupling that cannot be explained by partial melting or crystal fractionation processes but may be explained by the variable solubilities of the LIL and HFS incompatible elements in the hydrous fluids emitted by the dehydration of a subducting slab as it sinks. These chemical signatures are typical of rocks formed above subduction zones and of the lithosphere in general and their presence in continental flood basalts is evidence of a lithospheric source component. The isotopic enrichment also requires the incorporation into the magma of older lithosphere, either an enriched lithospheric mantle or older crustal rocks.

The large ocean basalt plateaus appear to have compositions intermediate between the plume-related basalts of the ocean islands and the MORB of the normal oceanic crust. Thus, flood basalt provinces on both continents and oceans appear to be formed from a plume component mixed with a lithospheric component.

The Deccan Plateau provides the most persuasive evidence to date of the origin and evolution of a classic continental flood basalt. The earliest alkalic and picritic units in the Deccan have helium and radiogenic isotopic values that suggest small degree partial melts of two original mantle sources. The first is equivalent to the Reunion hot spot (ocean island basalt) source; the second is similar to Indian MORB. The great majority of the Deccan flows can be modeled, chemically and isotopically, as mixtures of large degree melts of these two mantle source components to which different lithospheric source components have been subsequently added. The first lithospheric component was added early and could be an enriched lithospheric mantle component or a deep crustal component, characterized by high $^{87}Sr/^{86}Sr$ and low $^{143}Nd/^{144}Nd$ isotopic ratios. A later lithospheric component is more variable, characterized by low $^{206}Pb/^{204}Pb$ ratios, and is almost certainly of crustal, probably of upper crustal, origin. On the Deccan Plateau both field and petrographic evidence for crustal contamination may be evident in partially digested sedimentary and other silicic inclusions and in reaction rims around phenocrysts. In addition to the complex mixing patterns between the products of these various sources, which have been defined largely from their isotopic arrays, these magmas appear to have undergone extensive crystal fractionation within the crust.

There is equally strong evidence of crustal contamination in the North Atlantic province. Detailed studies in northwest Scotland have been able to identify the specific crustal components involved. In the Siberian Traps crustal contamination of mantle magmas is seen to cause the segregation of large volumes of sulfide, which host giant deposits of nickel, copper, and platinum group metals in associated intrusions. In contrast, detailed chemical and isotopic work on the Karoo has persuaded most petrologists that the main lithospheric component in the basalts is derived from an enriched mantle, not from the crust. Only in the earliest basalts in Lesotho is there evidence of significant crustal contamination. The high-titanium group of Parana basalts in the north of that province contains little evidence of crustal assimilation (little variation in isotopic ratios), but those in the south show an isotopic and chemical spread that may be due in large part to crustal assimilation accompanying crystal fractionation. But, again, the differences between the main magma types of the Parana province appear to require different mantle melting regimes and/or multiple sources.

In the large Proterozoic Keweenawan province early picritic eruptions are interpreted as small degree melts of a plume head at great depths (>75 km) and were followed by larger degree melts from the same source at lesser depths mixed with melts from an enriched lithospheric mantle to form the huge volumes of the tholeiitic magma that dominate the province. Strong evidence of crustal assimilation is found in silicic magmas erupted after a hiatus in magmatic activity, perhaps because of reduced extension and consequent ponding of the mantle-derived magmas in crustal reservoirs. This process appears to have created very large volumes of rhyolite (>600 km^3) by direct melting of the crust. On the Columbia Plateau both crustal and mantle lithospheric sources have contributed, but opinion is divided as to their relative importance.

Detailed studies of the early Karoo picrites point convincingly to these being asthenospheric melts mixed with enriched lithospheric mantle. On the Deccan, the early picritic rocks may represent small degree partial melts, able to work their way to the surface only along the older fracture systems. The youngest Deccan eruptions, the small volumes of chemically diverse flows (alkalic, silicic, and basaltic) and highly oriented (NNW–SSE) dikes around Bombay, are spatially and temporally related to extensional structures. They have similar isotopic signatures to the main tholeiites and may have been formed by the decompression melting of the earlier tholeiites at the base of the crust as the lithosphere was thinned by extension. A similar crustal melting of the earlier basalts is proposed as the origin of the Jozini Rhyolites in the extension-related Lebombo monocline of the Karoo.

In summary, it is clear that continental flood basalts carry the chemical and isotopic signatures of a hot spot or mantle plume, especially in their earliest eruptions, but that these signatures are effectively masked in the majority of flood basalts by a dominant lithospheric component that imposes its own signature on the most voluminous tholeiites. Opinion on the origin of the lithospheric component remains divided. For the Deccan and the North Atlantic provinces, workers are generally agreed that crustal contamination is dominant, but in the Parana and Karoo researchers are equally convinced that the main lithospheric component in the basalts is derived from an enriched lithospheric mantle. On the Columbia Plateau and in the Keweenawan provinces, participation of both crust and mantle lithosphere can be convincingly demonstrated. But the source of the lithospheric component, apparent in all continental flood basalt provinces, remains ambiguous in many examples and has yet to be resolved.

VI. OCEANIC FLOOD BASALTS

Many oceanic flood basalt provinces are an order of magnitude larger than the classic continental flood basalt provinces. They form broad, flat-topped plateaus, typically remote from continents, lying approximately 2000 m above the surrounding ocean floor. They are dominated by tholeiitic basalt and, although data are still very scarce, they appear to have been erupted in only a few million years and to be younger than the surrounding ocean floor. Chemically and isotopically, ocean basalt plateaus have values intermediate between MORB and ocean island basalt, suggesting that magmas were created by decompressional melting of a plume head (ocean island basalt source) derived from the deep mantle, which was then mixed with a component derived from the depleted upper mantle, the source for MORB.

The two largest oceanic plateaus are the Ontong Java and the Kerguelen (both $>10^7$ km^3) of Cretaceous age in the southern Pacific and southern Indian oceans, respectively. Wrangellia, of Permian age and accreted to the northwest coast of North America, is also believed to have formed as an ocean plateau on top of island arc crust, which was subsequently obducted, or thrust over, the continental coast of western North America. The age of the Ontong Java plateau is about 125 Ma, similar to that of adjacent basalt plateaus in the south Pacific. If all of these adjacent plateaus are part of a single province, as their similar ages suggest, the area of ocean floor covered by this basalt plateau is approximately 5×10^6 km^2, or 1% of the Earth's surface.

Such huge volumes of basalt and their apparent high eruption rates require a source area in the mantle above ambient mantle temperature, like those of their continental counterparts. As yet there is no clear evidence that oceanic flood basalts are associated with lithospheric extension. As for their continental counterparts, the most obvious explanation for their formation is the initial impingement of a mantle plume head on the base of the oceanic lithosphere. The even larger volume of oceanic, as compared to continental, flood basalts can be ascribed to the relative thinness of the oceanic as compared to the continental crust, which would permit a larger melt volume to form at the same temperature. However, the connection between oceanic plateaus and currently active hot spots is less obvious. If the Hawaiian–Emperor volcanic chain represents the end of such a sequence, then the original basalt plateau has already been subducted. The only probable connection between an oceanic plateau and a current hot spot yet proposed is the Caribbean oceanic flood basalt province, which may represent the initial pulse of the plume that now lies beneath the Galapagos Islands.

VII. TECTONIC IMPLICATIONS AND GENETIC MODELS

Once plate tectonic theory was well established during the early 1970s, it became apparent that the onset of major plate separation, such as the opening of the South and North Atlantic Oceans, the separation of Antarctica from South Africa, or the separation of the Seychelles platform from the Indian plate, was associated both with hot spots or mantle plumes and with the formation of a continental flood basalt province. Clearly these three apparently diverse phenomena are somehow related, although the associations are more obvious for some provinces (Afar, North Atlantic, Parana, and the Deccan) than for others (Siberian Traps and the Columbia River). What is not well understood is how these different phenomena affect each other.

Of the three temporally and spatially associated phenomena—plate separation, flood basalt eruption, and mantle plume—a mantle plume originating deep within the mantle would have much the longest history; it would take millions of years for a plume to ascend through the mantle to the surface. So suggestions that some surface event, even as dramatic as a meteorite impact or an extension-related breakup of a lithospheric plate, could trigger the plume is not plausible. If the hot spot is due to a mantle plume and if these three phenomena are associated temporally and spatially, then it is reasonable to conclude that the mantle plume is a primary driving force in the origin of large flood basalt provinces and of plate separation.

It is widely accepted that some additional factor beyond the 200–300°C higher than ambient temperatures of a mantle plume is required to produce the exceptionally large melt volumes of flood basalt provinces. Suggested additional factors include an extending and thinner than normal lithosphere, a hydrous-enriched lithospheric mantle, or an eclogite component in the plume. These three factors are not mutually exclusive.

In one model for the origin of flood basalt provinces the presence of one or perhaps a line of mantle plumes is assumed to weaken the lithosphere enough to focus the point of breakup of a plate already under lateral tension due to the horizontal pull of the subduction process. It has been suggested, for example, that a line of hot spots beneath Gondwanaland created not only the Parana-Etendeka flood basalt province but also a zone of weakness in the lithosphere, which permitted South America and South Africa to pull apart in the early Cretaceous. In this model extension is a consequence and not a cause of the flood basalt eruption, but either an enriched mantle source or an eclogitic component in the plume may be necessary.

An alternative model suggests that hot spots may incubate for long periods beneath continental plates and only create flood basalt eruptions when the continental lithosphere is thinned enough by extension to allow significant decompressional melting. This model contends that previous lithospheric extension and thinning is a necessary prerequisite for the formation of the large volumes of melt that flood basalts represent. It cannot be disputed that flood basalts and extension are intimately associated and it seems probable that lithospheric thickness plays an important role in controlling the much larger volumes of oceanic flood basalt provinces than their continental equivalents. There is also circumstantial evidence that the precise positions where flood basalt eruptions began is controlled by local "thin spots" in the lithosphere caused by earlier extension or simply deep fault zones. Yet the field evidence in those provinces studied most intensely, the Karoo, Deccan, Keweenawan and Columbia River, demonstrates that early extension is directly associated with the rise of the plume and that the major extension leading to plate separation always postdates the main tholeiitic eruptions. This implies that the extension is a consequence not a cause of flood basalt eruptions.

Plume heads would be larger and hotter than the tails that now form ocean island basalts. The large volume differences between flood basalt provinces and ocean island basalts formed above current hot spots (Hawaii, Reunion, Galapagos) strongly suggest that flood basalts are caused by the initial impact of plume heads on the lithosphere and that oceanic island magmatism represents the plume tails.

Recent geophysical evidence has supported the sinking of a subducted slab all the way to the core–mantle boundary. The chemical disturbance caused by this material at this depth could initiate the formation of a plume. If so, the resulting plume is likely to carry a substantial eclogite (basalt) component derived from the recycled subducted crust. This component in the plume may be the origin of an unusually iron-rich mantle source capable of providing the large melt fractions observed in flood basalts. Recent experimental evidence has confirmed that the Grande Ronde Basalt of the Columbia River could be derived from such a source, thus decreasing the need for a lithosphere previously thinned by extension. An eclogite component in the plume would also explain the relatively evolved composition of continental flood basalts without the extensive crystal fractionation within the crust which is otherwise needed but for which the evidence of intermediate compositions is embarrassingly rare. With its significant garnet component such a source might also melt at somewhat lower pressures and still retain a residual garnet signature in its trace element pattern.

No single genetic model can account for all flood basalt provinces. The impingement of a mantle plume, with temperatures 200–300°C above normal, on the base of the lithosphere is probably the driving force in all cases. But the extent to which lithospheric extension is required or the extent to which an enriched lithospheric mantle or an eclogite component in the plume contributes to the unusually large volumes of evolved basaltic magma available in these provinces remains controversial. The very significant physical, chemical, and isotopic differences between provinces may well result from the variable contributions of lithospheric thickness, availability and composition of an enriched lithospheric mantle, and the proportion of an eclogite component in the mantle plume.

VIII. ENVIRONMENTAL EFFECTS

That these large basaltic eruptions had a profound effect on the world climate appears inevitable. Basalts have greater potential than most lavas to emit large volumes of sulfur dioxide (SO_2) or hydrogen sulfide (H_2S). In the only historic fissure eruption known, the relatively tiny 1783–1784 Laki eruption in Iceland, it is estimated that 1.7 megatons of SO_2 was erupted per day in the first few weeks of the 8-month-long eruption. This is more SO_2 in a month than was emitted by the entire 1991 Mount Pinatubo eruption, the second largest volcanic eruption of this century. Very large volumes of hydrochloric acid and hydrofluoric acid were also erupted from Laki. The aerosols created a thick haze that persisted over Europe and into Asia for 3–4 months.

In comparison, a single flow of the Columbia River flood basalt province is estimated to have produced more than 12,000 megatons of SO_2 over a 10-yr period—and this is but one of the 200–300 large flows that erupted across the Columbia Plateau in 1–2 million years. The effect on the world climate of the eruption of the even larger flood basalt provinces, the Deccan, Parana, Karoo, Siberian Trap, and Keweenawan provinces which are at least an order of magnitude larger than the Columbia River province, must have been devastating. The climatic effect appears to be confirmed by the coincidental timing of the largest mass extinctions with the formation of flood basalt provinces, of which the Deccan, at 65.5 Ma, and the Siberian Traps, at 248 Ma, are the most dramatic.

The extinction of the dinosaurs and many other fauna and flora at 65.5 Ma has caught the public imagination. The story is enhanced by evidence that this mass extinction event was caused by the impact of a meteorite from space as shown by a striking increase in the iridium content at the time of the most massive extinctions. Although the evidence for a meteorite impact at about 65 Ma is now very strong, paleontologists have long made it clear that the extinction of dinosaurs, and other fossil groups, actually took place over a protracted period starting well before the 65-Ma impact. In attempts to explain evidence for meteorite impacts and major flood basalt eruptions both coinciding with some but not all of the most dramatic mass extinctions in the Earth's history, it has recently been suggested that the world climate may first have been severely stressed by a flood basalt eruption causing significant disruption to the flora and fauna, which was then further augmented by the impact of a major meteorite. In this model the spectacular extinction event at about 65 Ma resulted from a major meteorite impact during the large Deccan flood basalt eruption. Recent evidence from the Deccan places an iridium anomaly, which implies a meteorite impact, between flows of the Deccan flood basalt eruption. But regardless of whether one believes that flood basalts participated in the mass extinction events of the past, it is quite certain that even a modest flood basalt eruption today would dramatically affect the world climate and put the future of mankind in some jeopardy.

IX. SUMMARY

1. Continental and oceanic flood basalt provinces are characterized by very large volumes of relatively evolved tholeiitic basaltic magma erupted over a short period of time.
2. The fundamental cause of a flood basalt province is probably the impingement of a mantle plume head on the base of the lithosphere.
3. Lithospheric extension and plate separation are thought to be the result and not the cause of continental flood basalt eruptions, although this remains controversial.
4. Lithospheric thickness may control the volume of basalt erupted and may explain the greater volumes of ocean as compared to continental flood basalts, while local thin spots may control the exact location of the eruptions.
5. Isotopic and chemical data on continental flood basalts and probably ocean flood basalts require a mixture of mantle plume and lithospheric source components.
6. The lithospheric component in continental flood

basalt provinces is derived from both an enriched subcontinental mantle and from older continental crust. Which of these is dominant remains controversial.

7. An eclogite component within the plume has become increasingly plausible. This would increase the melt volume of the plume head and reduce the necessity for contemporaneous extension. It would also answer some awkward problems such as that relating to the apparent presence of garnet in the source, implying melting at considerable depth if an eclogite component is absent, and decrease the need for the large degree of fractionation in the crust for which adequate evidence of intermediate fractionation stages is absent.
8. The many differences between continental flood basalt provinces may result from the varying influences or availability of suitably enriched lithospheric mantle, an eclogite component, and lithospheric thickness.
9. Finally, the coincidence of the largest mass extinctions with some of the largest eruptions of flood basalt strongly support the suggestion that these extraordinary eruptions, together with meteorite impacts, have played a major role in the biological evolution of our planet. Flood basalt eruptions may have degraded the Earth's climate over periods of a few million years, and caused progressive extinctions so that a major meteoric impact, occurring within this period, would have had catastrophic effects on climate, fauna, and flora.

SEE ALSO THE FOLLOWING ARTICLES

Basaltic Volcanic Fields • Basaltic Volcanoes and Volcanic Systems • Lava Flows and Flow Fields • Magma Chambers • Melting the Mantle • Plate Tectonics and Volcanism • Volcanic Gases • Volcanic Plumes

FURTHER READING

Mahoney, J. J., and Coffin, M. F., eds. (1997). "Large Igneous Provinces: Continental, Oceanic, and Planetary Flood Volcanism," Geophysical Monograph 100. American Geophysical Union, Washington, DC.

Richards, M. A., Duncan, R. A., and Courtillot, V. E. (1989). Flood basalts and hotspot tracks: Plume heads and tails. *Science* **246,** 103–107.

Self, S., Keszthelyi, L., and Thordarson, Th. (1998). The importance of pahoehoe. *Ann. Rev. Earth Planet. Sci.* **26,** 81–110.

White, R. S., and McKenzie, D. P. (1995). Mantle plumes and flood basalts. *J. Geophys. Res.* **100,** 17,543–17,586.

This Page Intentionally Left Blank

SUBMARINE LAVAS AND HYALOCLASTITE

RODEY BATIZA
University of Hawaii

JAMES D. L. WHITE
University of Otago

I. Introduction
II. Submarine Lava Flows
III. Pillow Lava
IV. Lobate Lava Flows
V. Sheet Flows
VI. Welded Spatter
VII. Silicic Lava Flows
VIII. Hyaloclastites and Associated Rocks
IX. Hyaloclastites from the Present Seafloor
X. Ancient Hyaloclastites
XI. Rhyolitic Hyaloclastites
XII. Hypabyssal Intrusive Complexes: Intrasediment Extrusion
XIII. Ancient Hypabyssal Complexes
XIV. Summary

GLOSSARY

hyaloclastite A deposit consisting of fragments of volcanic glass formed by nonexplosive shattering (sometimes used broadly to include explosively formed fragments as well).

hydroclastic rocks A general term applied to volcanic rocks formed by fragmentation of magma in the presence of water.

hypabyssal intrusive complex Formed by intrusion of magma at shallow levels into unconsolidated sediment. ("Hypabyssal" is derived from old terms referring to injection of deep-seated magma to shallow levels.)

limu fragments Parts of glass bubbles, or balloons, formed by expansion of vapor through the surface of fluid lava.

lobate lava Submarine lava type consisting of elongated, flattish lobes with smooth outer glassy skins.

peperite Genetic term for a rock formed by essentially in-place disintegration and active mixing of molten lava or magma and poorly consolidated, typically wet sediment

pillow breccia A mixture containing coarse, typically glassy, broken to whole pieces of pillow lava together with smaller fragments formed by shattering of pillow lava crusts.

pillow lava Submarine lava type consisting of rounded and tubular shapes with striated outer glassy surfaces.

pillow volcano Small conical or ridgelike edifices of pillow lava found on the seafloor and in on-land ophiolites.

quenching The process of cooling magma rapidly to form a glass. It is accompanied by a volume decrease that can lead to fragmentation of the glass (cooling–contraction granulation).

sheet flows Submarine lava type with smooth, lineated, folded, or jumbled surface textures resembling subaerial pahoehoe.

spall fragments Formed by shattering of the brittle, quenched, crust of a lava by a combination of thermal contraction and flexure at the margins of a still-flowing lava.

Copyright © 2000 by Academic Press
All rights of reproduction in any form reserved.

spatter Fluidally shaped vesicular fragments that are deposited hot, typically deformed, and sometimes welded together.

I. INTRODUCTION

Submarine lava flows are important because they are the most widespread and abundant surficial igenous rock type on earth. They are erupted at a variety of ocean water depths, display a wide spectrum of sizes, shapes, and compositions, and comprise up to a 1- to 2-km thickness of the upper parts of the ocean crust created at midocean ridges or spreading centers (see chapter on Plate Tectonics and Volcanism). Ocean crust is also created in small seas called *backarc basins* (e.g., the Japan and Caribbean seas), lying between continental land masses and offshore chains of island-arc volcanoes resulting from subduction of oceanic crust into the deep mantle. Active volcanoes of the island arcs themselves begin as small submarine volcanoes in deep water consisting of submarine lavas, *hyaloclastite*, and intrusive rocks. In young spreading centers adjacent to landmasses, and where new volcanoes are initiated along island arcs, erupting magma commonly encounters thick successions of water-saturated, unconsolidated sediments. In this situation, much of the rising magma may fail to reach the seafloor to produce lava flows, and instead spreads laterally into the soft sediments to form complex hypabyssal intrusive complexes. Eruptions in the Gulf of California, formed by recent spreading at the tip of the East Pacific Rise system, are known from drillcore studies to have produced a hypabyssal complex, but such complexes are not easily observed in modern settings. They are, however, increasingly recognized as an important component of ancient island-arc and young spreading ridge settings.

After oceanic crust is formed, either at midocean ridges or in backarc basins, newer volcanoes, called *seamounts* may be built on it, and these also are made largely of submarine lava flows. Hot spots can build huge volcanic plateaus like the submarine Ontong Java plateau or long chains of seamounts and volcanic islands like the Hawaii–Emperor chain. Interestingly, rocks from midocean ridges, backarc basins, and seamounts can be preserved in the on-land geologic record of continents as a result of plate collisions. In this chapter we compare modern seafloor deposits with ancient examples preserved on land, considering only lava flows and associated deposits that erupted under water, and in most cases, fairly deep water. We start with modern and ancient submarine lava flows, then discuss hyaloclastites and their associated lava flows and breccias, finally addressing hypabyssal complexes.

A. What Controls Eruption Style?

Volcanic eruptions can in general be divided into those that produce lava flows or hypabyssal intrusive complexes (effusive activity) and those which produce explosive eruptions. One fundamental control on this behavior is the chemistry of the magma that erupts: Basaltic magma with about 50% SiO_2 is hot and very fluid (low viscosity) so it commonly erupts as a spray of droplets (fire fountains) or quietly as lava flows. In contrast, magmas that are richer in SiO_2, such as andesite (55–60% SiO_2), dacite, and rhyolite ($>$70% SiO_2) generally erupt at lower temperatures, higher viscosities, and with more dissolved volatile components that can form gas bubbles, all of which tend to produce more explosive eruptions.

Most submarine eruptions in deep water are basaltic in composition and so are generally not explosive. The basalt magma does contain some volatiles, but the high ambient pressure keeps most of them in solution. Those that come out of solution form bubbles, or vesicles; as expected, vesicles become progressively less abundant as eruption depth increases.

Explosive eruptions can be caused also by rapid transfer of heat from magma to water. At low pressures, boiling of water results in a ca. 1000× volume expansion, and rapid interaction of magma and water is highly explosive. Under greater pressure, however, expansion is much reduced and explosions far less feasible. At pressures greater than the critical pressure of water (at about 3-km water depths), steam explosions are not possible, at least under equilibrium conditions.

The nature of the eruptive site, particularly whether covered with thick loose sediment or formed of rigid rock, provides a final control on eruptive behavior. Magma approaches the surface in dikes that advance by crack propagation. Unconsolidated sediment is insufficiently rigid to crack, and the dike tip "stalls." Simultaneously, the heat of the magma boils water in the sediment, the expansion pushing grains apart and allowing the mixture to behave as a soft plastic or viscous fluid. These effects combine to allow the magma to spread laterally into the sediment at shallow levels, commonly resulting in complex mixtures of magma and sediment termed *peperite*.

B. Modern versus Ancient Examples

We discuss submarine lava flows and associated rocks (hyaloclastites, various types of breccias, and hypabyssal complexes) from presently active deep-sea midocean ridges, backarc basins, and seamounts and their ancient equivalents on land. Modern and ancient deposits are each useful in improving our overall understanding of submarine volcanism and are complementary in the sense that modern seafloor rocks can provide information that cannot be obtained from ancient rocks—and vice versa.

For example, volcanic rocks from modern deep-sea settings are fresh and chemically unaltered, in contrast to ancient examples that are usually chemically altered by burial at moderately high temperatures for long periods of geologic time. Moreover, on the modern seafloor it is possible to map the areal distribution and surface features of lavas and related rocks over large areas, sometimes many tens of square kilometers, which is not possible in ancient successions. Also, modern seafloor deposits have the advantage that their eruption depth is known. In the case of ancient deposits, the depth of eruption must be estimated, and this is difficult to do with accuracy.

On the other hand, modern ocean basins are much more poorly explored than the continents, and are geologically young (less than about 200 million years) compared to the age of the Earth (about 4.5 billion years); modern ocean basins are not representative of the full diversity of submarine volcanic products erupted over Earth's long history. Ancient succession also provide stratigraphic exposure, which allows investigation of the succession of events through time at a single site. In contrast, our view of modern seafloor deposits from bottom cameras, manned submersibles, and remotely operated vehicles (ROVs) is restricted to largely two-dimensional surface exposures, providing a snapshot of the present. Drilling into the deep seafloor by the Deep Sea Drilling Project (DSDP), the International Program for Ocean Drilling (IPOD), and the Ocean Drilling Program (ODP) has provided invaluable information about site histories, but drill holes cannot substitute for good three-dimensional exposure. Geologic work on the seafloor is also inherently more difficult (and more expensive) than comparable work on land, particularly at the outcrop (50- to 100-m) scale.

Another advantage of ancient deposits is that some important rock types, such as peperites, may produce no visible signs at the surface and are thus difficult to find, much less study, in modern deep-sea environments. Ancient and modern deposits provide complementary pieces of the puzzle, together providing a better understanding of submarine eruptions.

II. SUBMARINE LAVA FLOWS

Actively advancing submarine lava flows have been observed at shallow depths by scuba divers, but no deep-water eruptions have ever been witnessed. In the absence of direct observations of how deep-water lava flows behave, volcanologists use laboratory models and study active lava flows on land to better understand modern and ancient submarine flows. In general, the overall shape and small-scale features of lava flows are the result of a balance between cooling, which results in the formation of a solid crust over the lava, and the forces generated by flowing lava to deform and fracture this outer crust and produce a variety of surface textures (Fig. 1). In the case of submarine lava, flows erupting into cold water (about +2° to −4°C for the deep sea), the outer surface of the magma quickly chills to a glass; the rate of crust formation is much faster than for on-land flows. Lava flows erupting under glacial ice experience comparably rapid cooling rates, and subglacial eruptions are good analogs to deep-sea eruptions, not only because of the rapid chilling, but also because of the elevated pressure caused by great thicknesses of glacial ice or meltwater. Surface eruptions on Venus also occur under elevated pressure because of Venus's atmosphere.

Laboratory experiments and theoretical models of flowing lava also provide important clues about lava flows in general and submarine flows in particular. For example, laboratory "eruptions" of polyethylene glycol wax in tanks of cold sucrose solution produce flows very similar in shape and surface texture to several common types of submarine lava flows, including *pillow lava*, *lobate lava flows*, and various types of *sheet flows*. The experiments show that pillows form at the lowest effusion rates and gentlest slopes; gradually increasing the effusion rate or surface slope results in a progression to lobate flows, then lineated, folded, and jumbled sheet flows. By quantifying the cooling rates and physical properties of the wax and with appropriate scaling, it is now possible to estimate the effusion rates and emplacement times of various types of submarine lava flows.

Next we describe various types of known submarine lava flows.

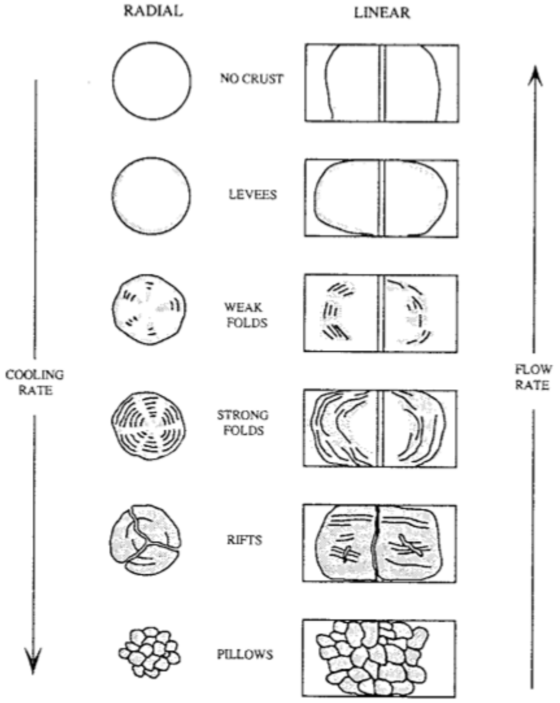

FIGURE 1 Schematic diagram showing the competing effects of cooling rate and volumetric eruption rate on the shapes and textures of lava flows coming from both point sources and line sources. Rapid cooling leads to the formation of crust (shown shaded), whereas large volumetric eruption rates and slow cooling inhibit crust formation. [Reproduced by permission of Elsevier from Fink, J. H., and Griffiths, R. W. (1992). A laboratory analog study of the surface morphology of lava flows extruded from point and line sources. *J. Volcanol. Geotherm. Res.* **54,** 19–32.]

III. PILLOW LAVA

One of the most common types of submarine lava is called *pillow lava* because it consists of roughly spherical or rounded pillow-shaped forms. Pillow lava forms not only in the deep sea, but also when on-land lava flows into the sea, rivers, or lakes. Pillow lava has been observed forming in shallow water off the coast of Hawaii, where lava from Kilauea volcano enters the sea and continues to flow underwater.

The glassy surfaces of pillows are not smooth but have cracks, corrugations, and linear grooves, many of which intersect at right angles (Fig. 2). The outer crust of pillows forms adjacent to spreading cracks, which act like tiny versions of midocean ridges. Corrugations form at right angles to the spreading cracks, and together, the corrugations and spreading cracks define a cross-hatched pattern on the pillow surface. The spreading cracks form when the outer pillow crust fractures (Fig. 3).

Lava pillows are found in a wide variety of shapes including near-spherical bulbous pillows, flattened pillows, elongate and tubular pillows, and trapdoor pillows. In three-dimensional exposures on land, pillows commonly consist of interconnected tubes. A great variety of pillow shapes is shown in deep-sea photographic atlases listed at the end of the chapter and in many journal articles. They vary in diameter from several tens of centimeters to several meters, with typical sizes of 0.5–1 m. In many places, leakage of lava from cracks in pillows leads to the formation of small (5- to 15-cm) ellipsoid or ovoid pillow buds. These are commonly found on the undersides of pillows and, if abundant, appear to form a nest. In other cases, buds may decorate most of the pillow surface, and knobby pillows may be covered with elongate and knobby buds and elongate networks of pillow fingers. Buds differ from their parent pillows in that their outer surfaces are smooth, probably indicating such rapid growth that surface tension can reshape the still-liquid magma and destroy extrusion markings (Fig. 4).

The interiors of pillows cool more slowly than the quenched glass rind, and so are more crystalline. Progressive crystallization at slower cooling rates toward

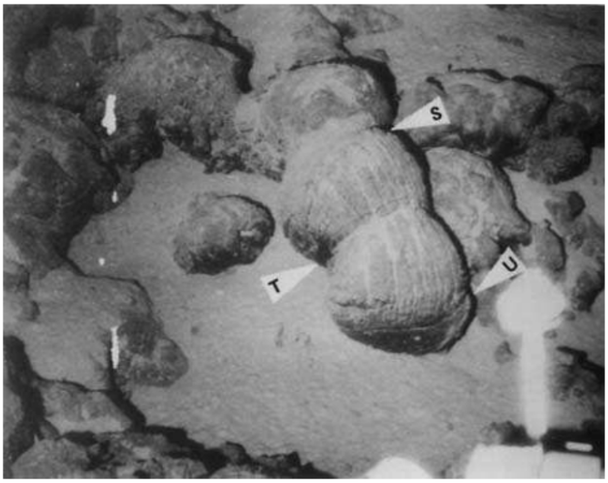

FIGURE 2 Submersible photo of a pillow on the Mid-Atlantic Ridge. The T points to a spreading crack from which the mirror-image pillow lobes grew. Prior to this growth, points S and U were adjacent. Note the cross-hatched pattern of tension cracks and perpendicular corrugations. [From Ballard, R. D., and Moore, J. G. (1977). "Photographic Atlas of the Mid-Atlantic Ridge Rift Valley." Springer-Verlag, Berlin.]

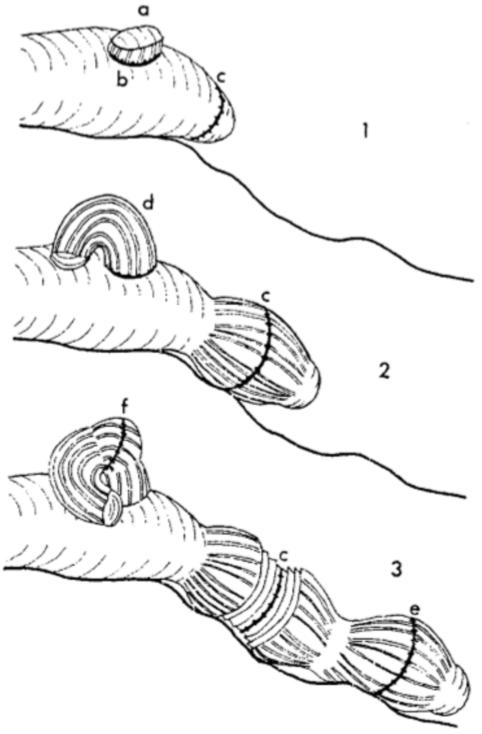

FIGURE 3 Schematic diagram to show growth of pillow lava. Growth from a circular crack (b) produces a trap door pillow (a), which eventually grows to a toothpaste pillow (d) with a spreading crack (f) producing another lobe. Spreading at tension crack (c) produces corrugated pillow lobes, then slows down and stops, after which a new crack develops at (e). [Reproduced with permission from Ballard, R. D., and Moore, J. G. (1977). "Photographic Atlas of the Mid-Atlantic Ridge Rift Valley." Springer-Verlag, Berlin.]

the interior produces a variety of rock textures, and the interiors of large pillows may be almost entirely crystalline. Vesicles are common and are usually concentrated in concentric layers parallel to the outer surface. In on-land pillows, radial pipe vesicles are common. Many pillows are completely solid, although it is common for pillows to have central cavities ranging from small tubular channels in a mostly solid pillow to pillows that are entirely hollow. These cavities form when lava drains back out of a newly formed pillow (Fig. 5), or when lava pushes aside a portion of the outer pillow crust and drains out through the hole to form a spilled pool outside the broken pillow. On locally overhanging slopes, these pillow outflows can form thin strings or ropes of lava several meters long resembling thin stalactites. Drainage can also produce thin tabular lava shelves (Fig. 6) formed during discrete events. The shelves usually have glassy upper surfaces that may be decorated with stringers of lava that dribbled onto the shelf from above, and lower surfaces have frozen lava drips but little or no glass, probably because of their closer proximity to magma (not seawater or steam) during episodic draining.

Pillow lava is a common eruptive product at midocean ridges and its abundance is related to spreading rate. Slow spreading ridges tend to have more pillow lava than fast spreading ridges. Fast spreading ridges with broad cross-sectional shapes and inferred high magma budgets have fewer pillows in the immediate vicinity of the axis, although fresh pillows become more abundant a few kilometers from the axis, suggesting that they represent small-volume, low-magma-supply eruptions slightly off-axis. Pillow eruptions are also common on seamounts. Seamounts near fast spreading ridges have arcuate summit benches composed of pillow lava, and

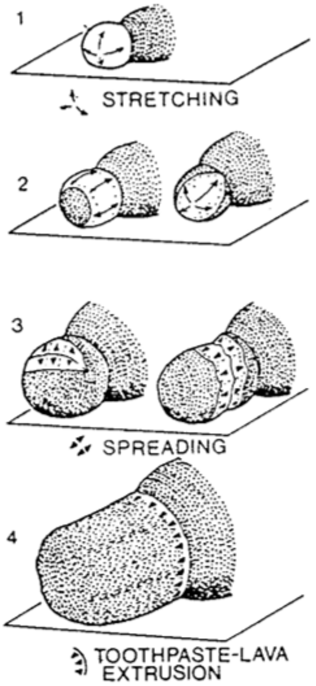

FIGURE 4 Schematic showing four possible modes of pillow growth. Stippling represents crust and lack of stippling indicates incandescent lava. (1) Uniform stretching leads to smooth outer surface, as in pillow buds and lobate pillows, (2) localized stretching, (3) symmetrical spreading, as in Fig. 2 above, and (4) toothpaste-like extrusion, as in Fig. 3 above. [Reproduced with the permission of Springer-Verlag from Walker, G. P. L. (1992). Morphometric study of pillow-size spectrum among pillow lavas. *Bull. Volcanol.* **54,** 459–474.]

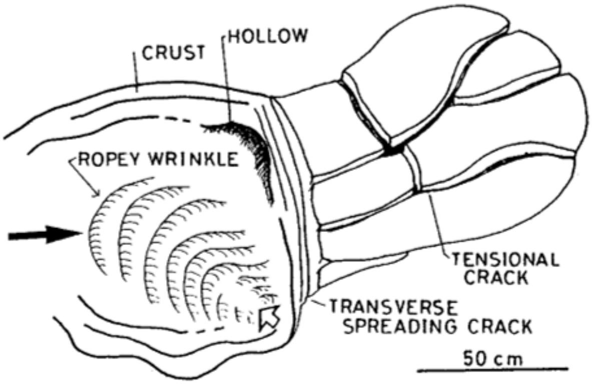

FIGURE 5 Drawing of a pillow lobe with a hollow interior and ropey-textured lava at the bottom of the hollow. Note that the top of the pillow is not shown. Solid arrow shows growth direction of pillow and the hollow arrow shows drain back direction that produced the ropey texture. [Reproduced by permission of Elsevier Science. From Yamagishi, H. (1991). "Morphological and sedimentological characteristics of the Neogene submarine coherent lavas and hyaloclastites in Southwest Hokkaido, Japan. *Sed. Geol.* **74,** 5–23.]

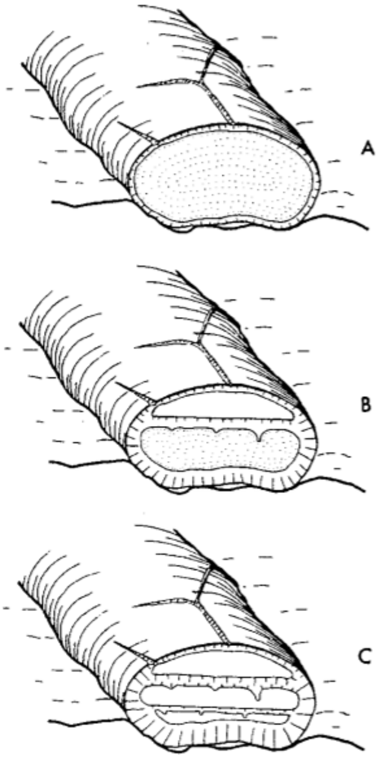

FIGURE 6 Sketch showing the development of drain back ledges in pillow or lobate lava. The dotted pattern indicates fluid lava, glass is shown by hatching, and water-filled regions are blank. [Reproduced with permission from Ballard, R. D., and Moore, J. G. (1977). "Photographic Atlas of the Mid-Atlantic Ridge Rift Valley." Springer-Verlag, Berlin.]

their steep flanks are composed almost entirely of tubular pillows oriented downslope.

Seafloor that is covered with pillow lava is topographically irregular, with relief of 1–5 m defined by networks of intertwined pillows piled irregularly over one another. Usually pillow flows build either conical piles 5–20 m high (Fig. 7) called haystacks, or linear steep-sided pillow ridges. At midocean ridges and the linear rift zones of large island volcanoes and seamounts, haystacks and pillow ridges tend to form discontinuous linear arrays, which may be fed by relatively narrow feeder dikes. In ancient seafloor preserved on land (ophiolites), larger piles 100–200 m high, called *pillow volcanoes*, are commonly recognized, and these are similar in size to modern pillow volcanoes at the axis of the Mid-Atlantic Ridge.

Pillow volcanoes identified in the Troodos ophiolite of Cyprus consist of megapillows, which grade upward into the main mass of normal pillows and tubes, and finally to upper parts consisting of minipillows and breccia. Megapillows are large (up to 6 m and larger) volcanic masses in the core of the pillow volcano and are interpreted as feeder systems for the pile (Fig. 8). It is possible that the cores of modern seafloor pillow volcanoes and haystacks also have megapillows or their equivalents in their interiors. Similar to the Cyprus pillow volcanoes, pillow lavas of the Archean Abitibi greenstone belt in Quebec, Canada, are parts of larger units that grade from nonpillowed lava at the base, to pillow lava, and finally to *pillow breccia* and stratified hyaloclastite at the top. As with the Cyprus deposits, megapillows are found just beneath normal pillows, and the pillow lava is believed to have formed at lower flow rate than the nonpillowed lava, consistent with wax experiments and other data indicating that pillows form at low extrusion rates. A nearly universal feature of well-studied pillow lava

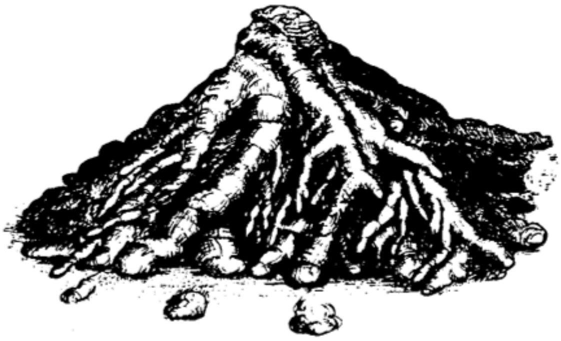

FIGURE 7 Sketch of a 5–10-m-high haystack of the Mid-Atlantic Ridge. [Reproduced with permission from Basaltic Volcanism Study Project (1981). "Basaltic Volcanism on the Terrestrial Planets." Pergamon Press, New York.]

sequences, including those from present ocean basins, Cyprus, Canada, Cedros Island, and the seamount series of La Palma Island, is the decrease of pillow size toward the tops of individual pillow units.

Finally, in addition to conical and linear piles, pillows occur as important components of steep-sided prograding sequences that include flow-foot breccias (Fig. 9). Deposits of this type form in shallow water lava deltas and deep water lava prisms prograding outward from active volcanoes, and consist dominantly of breccia and hyaloclastite. On a small scale, steeply dipping pillow tubes and breccia are components of most deep-sea deposits of seamounts and ridge crests. Breccia and hyaloclastite are important components of flow-foot breccias and are inferred to form by three processes: thermal-shock granulation, *spall fragmentation* (the outer, solidified margins of lava break apart as the interior of the lava deforms and flows), and impact shattering, which occurs as lava pillows become detached from the flow on steep slopes and move as rockfall down to the foot of the flow prism. Modern seafloor pillows are relatively fragile because of the abundance of cooling cracks, whose radial distribution explains why pillows tend to break into tetrahedral pie- or wedge-shaped pieces.

Pillows in the deep sea and on land are generally basaltic to andesitic in composition although rare pillows of dacitic or rhyolitic composition are found on land. Some pillows of Archean age are ultramafic in composition (called komatiites), unlike any modern ocean floor deposits. These pillows, much richer in MgO than basalt, erupted at much higher temperatures and were much more fluid than ordinary basalts; their unusual composition provides evidence that Earth's mantle may have been hotter early in its history.

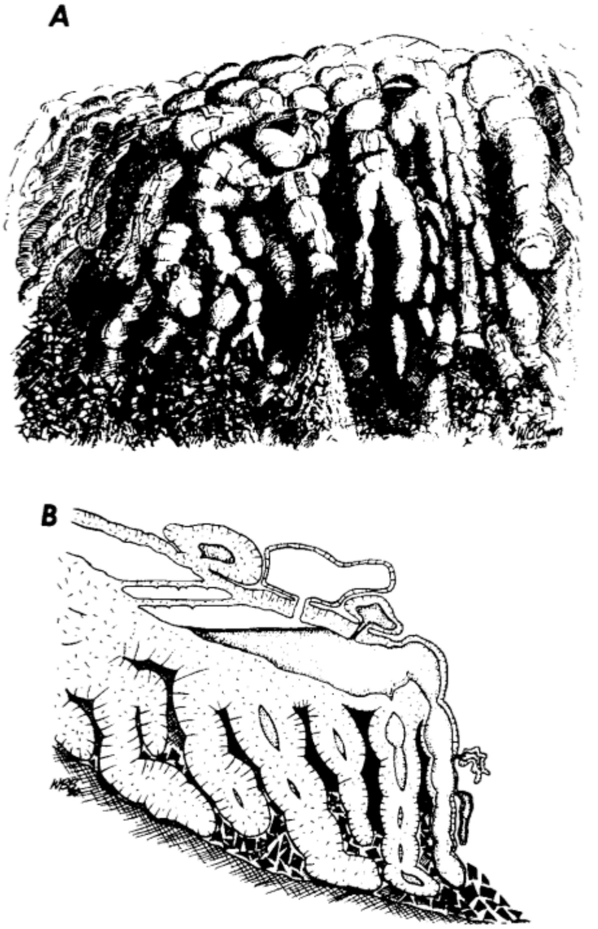

FIGURE 9 Drawing, by W. B. Bryan, of (A) pillow tubes flowing down a steep flow front and (B) a schematic cross section showing prograding of pillow tubes and flow-foot breccia. [Reproduced with permission from Basaltic Volcanism Study Project (1981). "Basaltic Volcanism on the Terrestrial Planets." Pergamon Press, New York.]

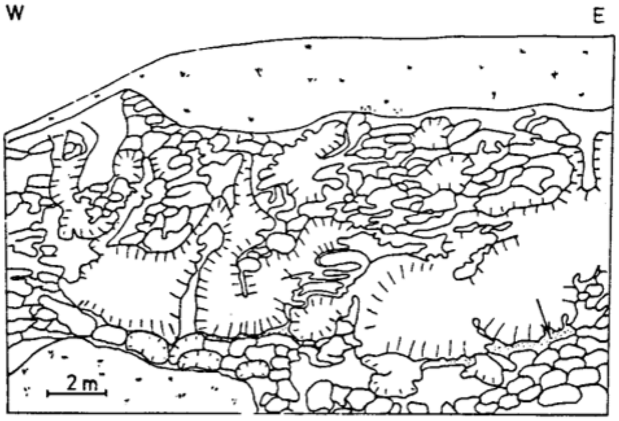

FIGURE 8 Sketch of megapillows at the base of a pillow volcano in the Troodos ophiolite, Cyprus. [Reproduced with permission from Schmincke, H.-U., and Bednarz, U. (1990). Pillow, sheet flow and breccia flow volcanoes and volcano-tectonic hydrothermal cycles in the Extrusive Series of the northeastern Troodos ophiolite (Cyprus). [*In* "Ophiolites: Oceanic Crustal Analogs, Proc. Symp. Troodos 1987." (J. Malpas, E. M. Moores, A. Panayiotou, and C. Xenophontos, eds.). The Geological Survey Department, Republic of Cyprus.]

IV. LOBATE LAVA FLOWS

Superficially, lobate lava flows resemble pillow lava in having tubular and subspherical shapes (Fig. 10). However, lobate lava is more flattened, and, most importantly, the outside surface is not striated but rather is smooth or has a tortoise shell texture of contraction-fractured glass. Probably, individual lobes of lobate lava grow by early formation of a flexible crust that is carried along without further stretching atop an advancing liquid flow (Fig. 4, panel 1). In places where eruptions produce densely packed lobes, the lobes coalesce below the surface crust, as might be expected for lava flowing quickly and carrying its semirigid top crust with it as it advances. At fast spreading midocean ridges with domed or flat cross-sectional shapes, lobate lava comprises a large part of the surface lava (Fig. 11). Commonly, lobate lava flows have abundant drain back shelves or are entirely hollow, and in this they resemble shelly pahoehoe flows. In terms of internal structure, lobate lava closely resembles pillow lava, although lobate lava is more commonly hollow.

At fast spreading ridges, lobate lava appears to form at the surface of filled lava pools, which can subsequently drain away leaving collapsed rubble of lobate flows. At the margins of drained lava pools, lobate flows mark the lava level prior to drainage. A common feature of drained lava ponds is lava pillars (Fig. 11). These pillars may be tens of meters in height, have hollow centers lined with glass, and ragged exterior surfaces of truncated lava shelves that appear to record episodic drainage of the pool around the pillar. It is thought that lava pillars represent pathways for seawater escape at the time that the lava pool first filled with magma, presumably very rapidly. Alternatively, lava pools may "fill" slowly, essentially by inflation of lobate flows. In this case, the lava pillars would form slowly, as the magma level of the pool gradually rises. Because of the strong association of lobate flows with filled and drained lava pools, it is thought that lobate flows are generally tube fed or represent "spillover" from lava ponds that overflow. In some places, lobate flows appear to form at the edges of sheet flows (Fig. 10), possibly as the result of lateral breakouts.

Because lobate lava resembles pillow lava in shape and internal structure, it is possible that some of the flattened tubular "pillow" lava described from ancient submarine volcanic deposits, such as in the Abitibi, is actually lobate lava instead. This is understandable, because lobate lava has only recently been identified on the seafloor, postdating the descriptions of many ancient deposits of "pillow" lava. Moreover, the distinction between pillow and lobate lava can only be made if the exposure and preservation are such that it is possible to differentiate between lineated and striated outer crust (pillows) and smooth crust (lobate lava), which is often difficult in ancient deposits.

In some ancient deposits containing pillow lava and fragmental rock, there occur very thin sheet flows and flattened, somewhat ragged pillows, termed *para-pillow*

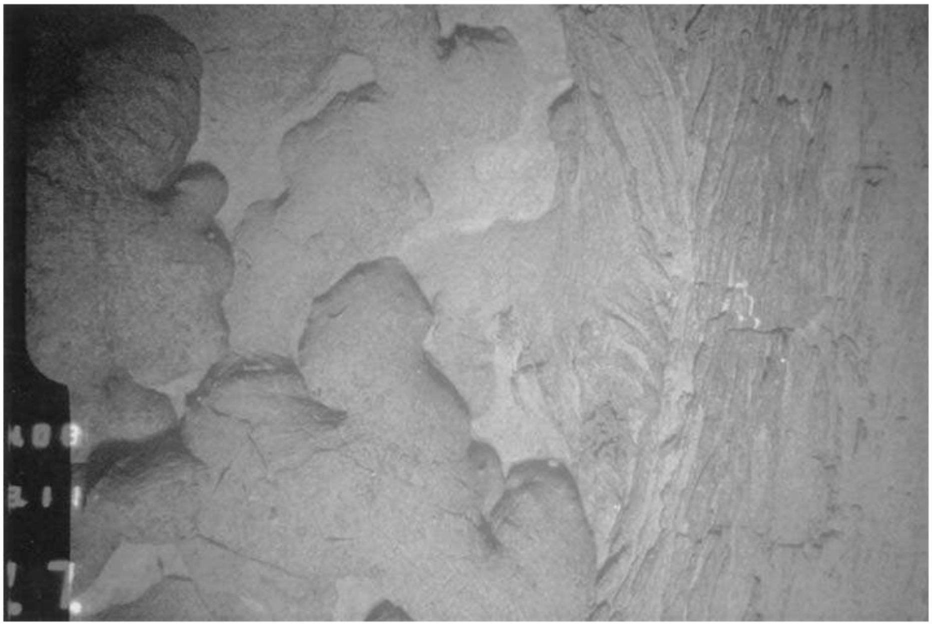

FIGURE 10 Bottom camera photo of a lobate flow on the summit of a small seamount near the East Pacific Rise. In this case, the lobate flows seem to emanate from edges of the lineated and folded sheet flow at the right.

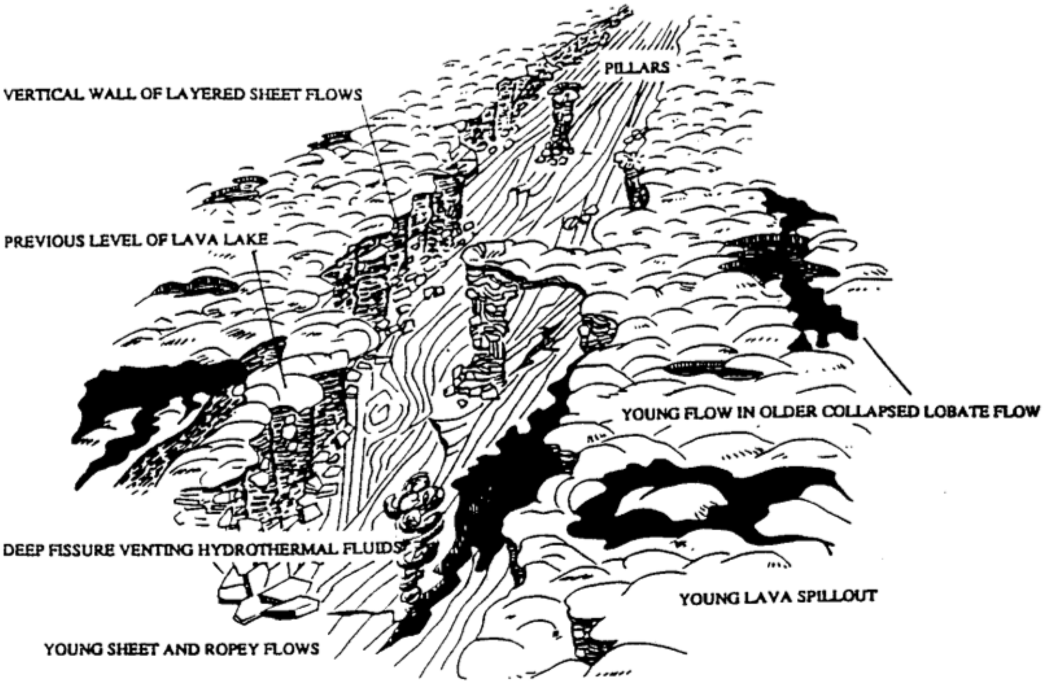
PILLARS
VERTICAL WALL OF LAYERED SHEET FLOWS
PREVIOUS LEVEL OF LAVA LAKE
YOUNG FLOW IN OLDER COLLAPSED LOBATE FLOW
DEEP FISSURE VENTING HYDROTHERMAL FLUIDS
YOUNG LAVA SPILLOUT
YOUNG SHEET AND ROPEY FLOWS

FIGURE 11 Composite sketch of the summit of the East Pacific Rise showing some of the characteristic lava flow morphologies. Most of the lava outside the collapsed region is lobate lava. Dark lava is relatively young. Not shown are young pillow eruptions that occur a kilometer or more away from the axis. [Reproduced with permission from Perfit, M. R., and Chadwick, W. W. J. (1998). Magmatism at mid-ocean ridges: Constraints from volcanological and geochemical investigations. Pages 59–115 *in* "Faulting and Magmatism at Mid-Ocean Ridges," Geophysical Monograph 106. American Geophysical Union, Washington, DC.]

lava and interpreted as pillow lava that failed to inflate because of an unfavorable balance between cooling rate, flow velocity, and magma supply rate. Para-pillows may form on steep slopes, especially if the magma supply needed to inflate a pillow is unsteady; scuba divers have observed para-pillows forming on the active lava delta of Kilauea volcano. Lobate lava and para-pillow lava may be related in the sense that they both represent significant variants of pillow lava: higher volumetric extrusion rate in the case of lobate flows, and steeper slopes in the case of para-pillows.

V. SHEET FLOWS

Sheet flows are found most commonly at fast spreading centers, but also occur at slow spreading centers and seamounts. Sheet flows have a variety of surface features resembling those of subaerial pahoehoe flows including smooth surfaces, lineations, ropes, swirls, coils, folds, and jumbled surfaces produced by deformation of the lava crust. Sheet flows may be primarily fed by lava tubes, and in a well-documented example from the caldera floor of Axial volcano on the Juan de Fuca Ridge, sheet flows with tumuli and other features indicate thickening of sheet flows by lava inflation. It is well known that there are no systematic differences in the chemical composition of pillows, lobates, and sheet flows in modern submarine settings; thus, these differences in flow morphology are produced by differences in the magma supply rate, underlying topography, and conditions of flow, as discussed previously. Sheet flows are common in ophiolites and other ancient deposits of submarine volcanic rocks. They typically are massive flows and in many places have columnar jointing and vesicles distributed in a variety of different patterns. In the Cyprus ophiolite, edifices consisting mostly of sheet flows, with only small amounts of pillows, have been identified.

A rare type of submarine lava that in some ways resembles sheet flow lava consists of thin (1–3 cm or less) very complexly folded tabular sheets or septa lacking glassy outer crusts. These intricately folded masses have abundant thin lava septa and curved, even subspherical folds. Informally, such lava has been called "cow-heart" lava and is known mostly from dredges of the East Pacific Rise and near-ridge seamounts. In some places this lava type has abundant tiny fragments of nonglassy basalt weakly welded to its surface, much like how salt crystals are "welded" to pretzels. The absence of glass suggests that the lava was erupted in hot surroundings, then cooled relatively slowly. This may take place within "ceiling spaces" of partly drained flows in which cold seawater is absent. In shape, cow-heart lava resembles the lava making up submarine hornitos on Teahitia seamount in the Society Islands.

VI. WELDED SPATTER

While fire fountaining activity in deep water is probably a rare phenomenon because the high-pressure greatly inhibits the volatile exsolution needed for fountaining, there are, nevertheless, some deep water *spatter* deposits that appear to be the products of such activity. For example, a deposit about 1 million years old, 135 m thick, and apparently consisting of vesicular basaltic welded clasts was sampled by drilling in the Sumisu rift, a backarc basin behind the Bonin arc. Eruption is inferred to have occurred in water more than 1800 m deep. A somewhat similar deposit of welded spatter, in this case overlying hyaloclastite, was described from Cyprus. Some material in this deposit appears to have flowed for some distance as a rootless flow, and the deposit overall is interpreted as the result of a greatly suppressed submarine fire fountain, with the spatter possibly created within a fissure vent before being weakly expelled onto the seafloor. Products of Archean subaqueous rhyolitic fire fountaining have also been identified and require low-viscosity melt, inferred to have resulted from both high eruption temperatures and some retention of dissolved volatiles (relative to explosive onland eruptions) at the high ambient pressure of the subwave-base eruption site.

VII. SILICIC LAVA FLOWS

Rhyolitic eruptions are rare on the modern seafloor, perhaps because modern sea level is relatively low and most rhyolite is erupted subaerially on the thick crust of well-established arc systems. At various times in the past, sea levels were higher, and island arc sequences in which subaqueous eruption of rhyolite was relatively common formed along young subduction systems lacking thick crust. Pillow lava of dacitic or rhyolitic composition has not yet been found in modern deep-sea environments, but ancient pillows of rhyodacite composition have been described from several localities including the Ordovician of Wales, where a 40-m-thick lava flow grades upward from massive lava into pillows and pillow tubes and then into pillow breccia. Other types of silicic lava flows are quite rare at midocean ridges but appear to be more common in backarc basins. Such flows have been described from the Sumisu Rift, the Mariana Trough, the Lau Basin, and others. In the Lau Basin, silicic rocks occur near propagating ridge tips, as at many other locations along the midocean ridge. In backarc basins, these rocks occur mostly as dome-shaped masses of 1 to several kilometers in diameter, consisting of massive and blocky lava with abundant obsidian. Blocky flows of dacitic lava are found on the Kasuga seamounts in the Mariana backarc basin. Vesicularity of silicic rocks varies greatly and it seems likely that most have undergone some degassing because most are not pumicious, whereas inplace pumice has been dredged from the top of a rhyolite lava dome at 3600-m depth on the west flank of the Mariana Trough.

Many submarine silicic flows preserved in the geologic record are laterally extensive (up to 10 km), dome-shaped, or stubby, tabular masses that are massive near the feeder conduits and grade outward to more fragmental distal facies. Commonly, the units have large lava pods, lobes, and tongues with borders of obsidian in a matrix of silicic breccia, hyaloclastite, and lava fragments. Such units have been described from the Archean of Canada, the Miocene of Japan, and other localities; the breccia flow volcanoes of the Troodos ophiolite are similar. The inferred mode of growth of these large domal complexes (Fig. 12) is thought to be similar to that of silicic domes on land. Given the similarity in size and shape between modern and ancient silicic flows, it seems likely that the modern examples have internal structures and facies development similar to that of the better exposed ancient examples. Much more extensive subaqueous rhyolitic flows, with single flow units only tens to a few hundred meters thick yet extending over 2000 km^2, have been described from the Paleozoic of Australia, but no modern analogs have been recognized.

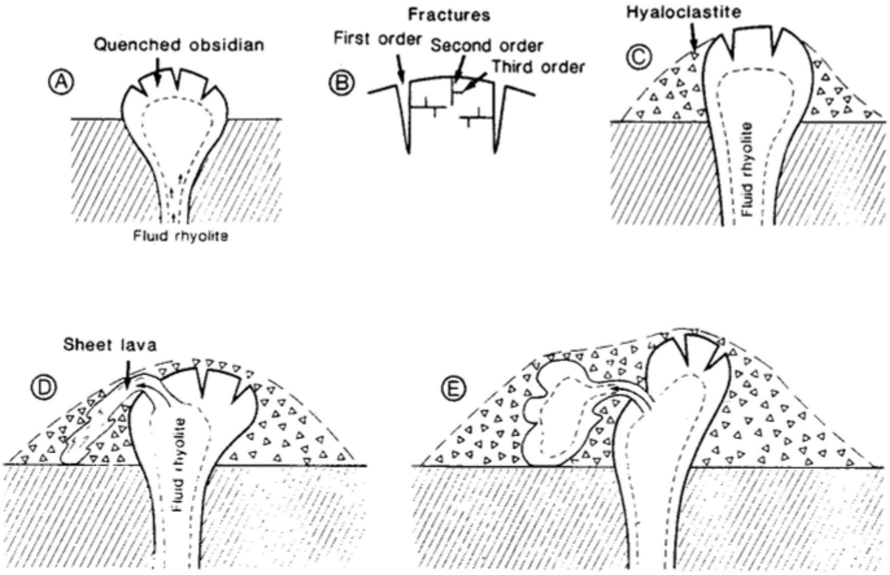

FIGURE 12 Inferred mode of growth of ancient silicic domes and stubby flows from Japan and the Archean of Canada. The hyaloclastite is produced by fragmentation of the rhyolite lava. [Reproduced with permission from Yamagishi, H., and Dimroth, E. (1985). A comparison of Miocene and Archean rhyolite hyaloclastites: Evidence for a hot and fluid rhyolite lava. *J. Volcanol. Geotherm. Res.* **23,** 337–355, Elsevier Science.]

VIII. HYALOCLASTITES AND ASSOCIATED ROCKS

The term *hyaloclastite* means glass-fragment rock. Broadly used, *hyaloclastite* includes all glassy fragmental debris formed by eruptions in which water is involved. Another common usage of the term, adopted here, limits hyaloclastite to glassy debris formed by essentially nonexplosive processes related to rapid aqueous cooling of magma. In this sense, *hyaloclastite* is a subset of *hydroclastic rocks*, which include all clastic rocks resulting from fragmentation of magma involving water. Hyaloclastites with a large variety of characteristics are produced from magma erupted at sites that range from subaerial volcanoes to those of the abyssal deep sea. They occur on many types of volcanoes, and virtually all magmatic compositions are represented. Hyaloclastites and other hydroclastic rocks are known to form during subglacial eruptions, by phreatomagmatic fragmentation, under shallow submarine conditions at emergent islands, and in the deep-sea in island arcs, midocean ridges, and seamounts. In ancient submarine volcanic deposits preserved on land, submarine lava flows are almost invariably associated closely with hyaloclastites and a variety of other fragmental breccia deposits. Submarine stratigraphic associations, when studied in detail, can provide important clues about the nature, causes, and detailed behavior of deep water eruptions. These common associations in ancient rocks probably occur in modern deep-sea environments, but since we are restricted to observing only the surface of the youngest deposits the associations may not always be obvious.

Hyaloclastite forms under a range of conditions, and interpreting the conditions of formation requires detailed study at regional, outcrop, and microscopic scales. On land, ancient hyaloclastites may be exposed in three dimensions and mapped over large areas, and study of the hyaloclastite features and stratigraphy can give a temporal perspective on eruption progress and lateral facies changes (Fig. 13). In contrast, for deep-sea deposits it is very rare to have stratigraphic information. This makes comparisons between ancient and modern hyaloclastite sequences difficult.

IX. HYALOCLASTITES FROM THE PRESENT SEAFLOOR

Hyaloclastite is rare at midocean ridges, but more common at deep water (>1500– to 2000-m) seamounts. Hyaloclastites from deep-water seamounts near the East

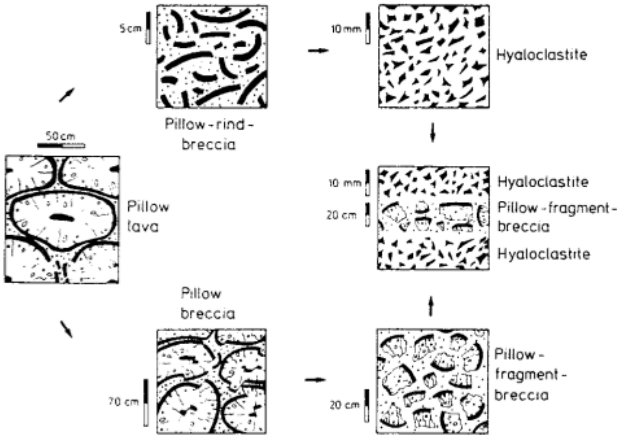

FIGURE 13 Schematic diagram showing relationships among various types of breccia units that may be produced from lava flows. It is important to note that pillow lava is not the only type of submarine flow that can produce breccia units and, further, that in some cases, moderate volumes of fine-grained hyaloclastite may be produced directly from flows without an intervening breccia stage. [Reproduced with permission from Schmincke, H.-U., and Bednarz, U. (1990). Pillow, sheet flow and breccia flow volcanoes and volcano-tectonic hydrothermal cycles in the Extrusive Series of the northeastern Troodos ophiolite (Cyprus). *In* "Ophiolites: Oceanic Crustal Analogs, Proc. Symp. Troodos 1987," (J. Malpas, E. M. Moores, A. Panayiotou, and C. Xenophontos, eds.). The Geological Survey Department, Republic of Cyprus.]

Pacific Rise were studied in the late 1980s and an additional submersible study of the deposits on Seamount 6 took place in 1995. It is now apparent that these thin (<1-m-thick) hyaloclastites are the result of thermal shock granulation and spalling of thin lava flows, because the chemical composition of most of the glass fragments in hyaloclastite is identical to that of underlying glassy lava flows. In addition, samples of flow-hyaloclastite couplets show that the flows have very irregular tops, with thin lava tendrils breaking up to shed contorted and shattered glass fragments into the overlying blocky, polyhedral glass grains of contemporaneous hyaloclastite. A small proportion of thin, fluidal particles occurs in the hyaloclastite and resembles "limu of Pele" produced when lava from Kiluaea volcano enters the sea and interacts with seawater. Probably all *limu* are produced by the fragmentation of magma bubbles inflated by seawater steam when thin, very fluid, basalt flows trap small volumes of seawater. In many cases, limu from Seamount 6 are intricately folded and the folds welded together, indicating that the magma was still hot when the bubbles burst. Limu are found also at the underwater summit of Loihi volcano, south of the big island of Hawaii. The summit of Loihi is ~1000 m below sea level and portions of the summit are covered with loose glass fragments. While the origin of limu-bearing hyaloclastite is still being studied, it appears that local mixing of magma with seawater and production of steam-filled magma bubbles have played a significant role.

Hyaloclastites from Seamount 6 near the East Pacific Rise are thin and in part finely laminated deposits with normal grading and imbrication of platy fragments, consistent with deposition from some sort of suspension density flow. Gravitational potential energy is needed for density flows, but obvious upslope sources are lacking and the glass fragments may have been lofted above the seafloor as they formed. A previous hypothesis was that lofting was accomplished by submarine lava fountaining. While this notion cannot yet be ruled out, several lines of evidence argue against it: (1) vents from fire fountains containing spatter and other vesicular clasts have not been found despite very thorough searches using submersible and bottom cameras; (2) alleged cow-dung bombs identified in the late 1980s are actually thin lava tendrils from the underlying lava flow incompletely covered by hyaloclastite and very thickly covered with manganese; and (3) theoretical models of gas exsolution at high pressures underwater, and low volatile abundances in the Seamount 6 glass, argue strongly against sufficient gas pressure at depths of about 2000 m to produce fountaining.

Alternative hypotheses for a lofting mechanism include gas storage at depth to produce strombolian activity, magma–water interaction to produce steam explosions, and "squirting" of magma at high velocity. The latter notion has been invoked to explain the observation that pillows commonly grade upward into breccia and hyaloclastite. It is proposed that upward growth leads to narrowing of branching magma conduits such that the same volumetric eruption rate and magma pressure that produces pillows from wide conduits would produce breccia and eventually hyaloclastite as the conduits constrict. In this case, production of glass fragments would be by thermal shock granulation.

Hyaloclastites have not been reported from the fast spreading East Pacific Rise, despite fairly intensive study of the ridge axis at many locations. It thus seems likely that hyaloclastite is extremely rare, or perhaps even nonexistent at fast spreading ridges. At the medium spreading Juan de Fuca Ridge, hyaloclastite has been recovered in several dredge hauls at the Blanco escarpment. Along the slow spreading Mid-Atlantic Ridge, hyaloclastite has been found south of the Azores at depths from 1700 to 500 m. The amount of hyaloclastite increases greatly as

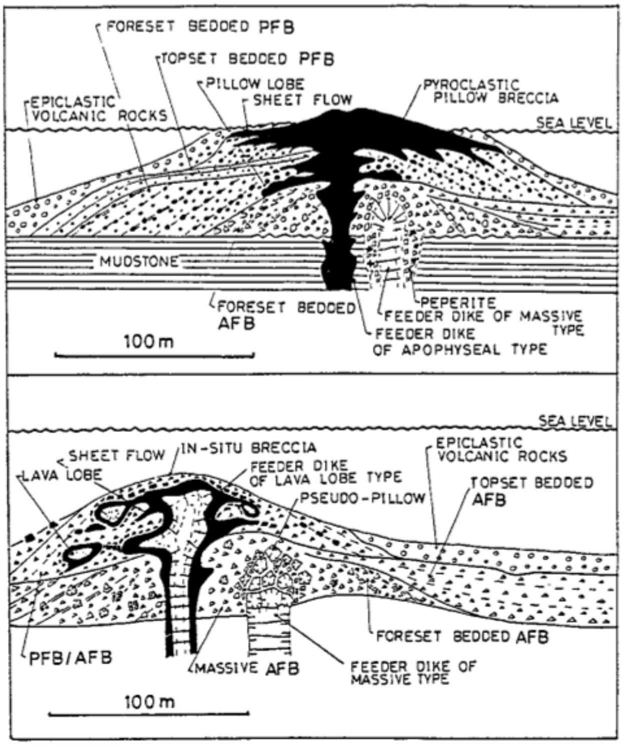
FORESET BEDDED PFB
TOPSET BEDDED PFB
PILLOW LOBE
SHEET FLOW
EPICLASTIC VOLCANIC ROCKS
PYROCLASTIC PILLOW BRECCIA
SEA LEVEL
MUDSTONE
FORESET BEDDED AFB
PEPERITE
FEEDER DIKE OF MASSIVE TYPE
FEEDER DIKE OF APOPHYSEAL TYPE
100 m
SEA LEVEL
SHEET FLOW
IN-SITU BRECCIA
EPICLASTIC VOLCANIC ROCKS
LAVA LOBE
FEEDER DIKE OF LAVA LOBE TYPE
PSEUDO-PILLOW
TOPSET BEDDED AFB
FORESET BEDDED AFB
PFB/AFB
MASSIVE AFB
FEEDER DIKE OF MASSIVE TYPE
100 m

FIGURE 14 Shallow submarine volcanoes illustrating arrangement of lavas, intrusions, and hyaloclastite. Upper frame illustrates mafic to intermediate volcano, with intermediate to felsic products shown in lower frame. *Pyroclastic pillow breccia* is another name for *isolated pillow breccia* Pseudo pillows are concentrically fractured coherent lava. [Reproduced by permission of Elsevier Science. From Yamagishi, H. (1991). Morphological and sedimentological characteristics of the Neogene submarine coherent lavas and hyaloclastites in Southwest Hokkaido, Japan. *Sed. Geol.* **74,** 5–23.]

water depth decreases, and many of the glass fragments, especially from shallow water depths, are highly vesicular. Thus, it is possible that these deposits are partly the result of magmatic explosive activity. In contrast, most hyaloclastite fragments from east Pacific seamounts have no vesicles.

Additional hyaloclastites, probably produced at the Mid-Atlantic Ridge, were drilled by the Deep Sea Drilling Project, Leg 46, at site 396B. Drilling into 13-million-year-old ocean crust penetrated 170 m of pillow basalt and then encountered a 90-m-thick unit consisting mostly of unconsolidated, sand-size, fresh basalt glass fragments. Although this deposit apparently does not contain limu and is very thick, its good layering, sheetlike distribution and sand-size grains strongly resemble those of the hyaloclastites found on East Pacific Rise seamounts. Study of this deposit indicates that fragmentation to produce glass fragments was roughly synchronous with eruption, and granulation of thin glassy lavas by thermal shock is a good possibility.

The absence of hyaloclastite from fast spreading ridges and its occurrence at slow spreading ridges and

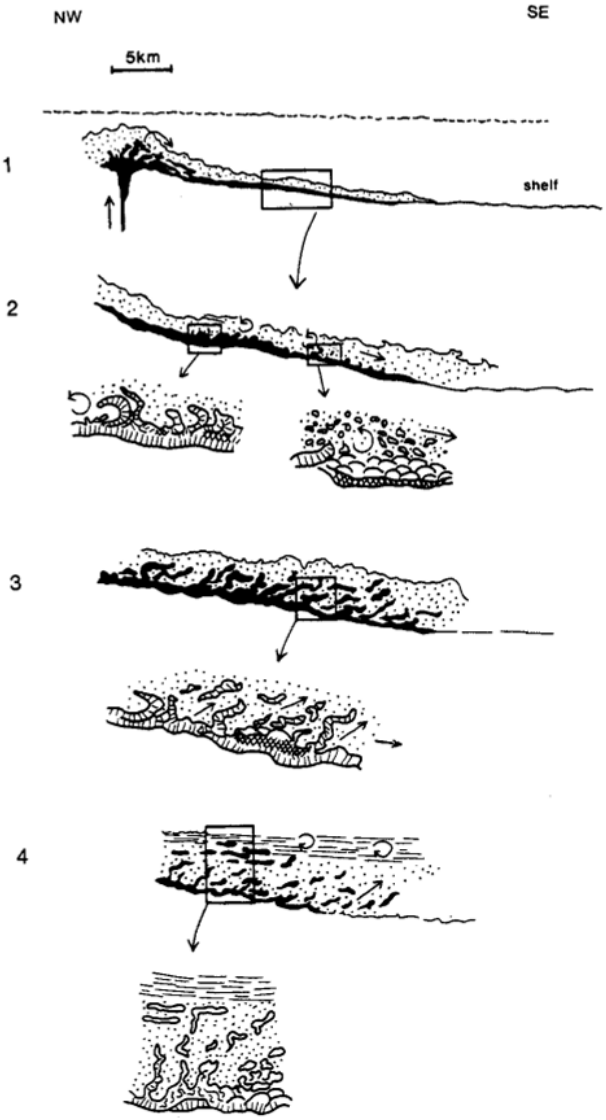
NW
SE
5km
1
shelf
2
3
4

FIGURE 15 Inferred mode of emplacement for lava-hyaloclastite depositional unit from a single subaqueous eruption on the Iceland shelf. Where lava penetrates upward into its clastic carapace, "self-peperitic" mixtures typically result. [Reproduced by permission of Springer-Verlag. From Bergh, S. G., and Gudmunder, E. S. (1991). Pleistocene mass-flow deposits of basaltic hyaloclastite on a shallow submarine shelf, South Iceland. *Bull. Volcanol.* **53,** 597–611.]

Pacific near-axis seamounts suggest another possible explanation for the genesis of hyaloclastites and the nature of hyaloclastite eruptions. It is particularly surprising that hyaloclastite has not been found along the East Pacific Rise, because there seems to be general agreement that thermal shock granulation is favored by high-volume eruption rates. If so, and given that the flow types at the axis of the East Pacific Rise indicate very high eruption rates, why is there no hyaloclastite? One possibility is that pelagic sediment plays a key role in the production of hyaloclastite; the axis of the East Pacific Rise has virtually no sediment, whereas the axial valleys of medium and slow spreading ridges typically do have pelagic sediment. Likewise, the flat summits and small flank basins of seamounts are known to have abundant pelagic sediment.

Evidence in favor of a role for pelagic sediment is the observation that the thin contemporaneous flows underlying hyaloclastite on Seamount 6 commonly have large (up to 10 cm across) roughly cylindrical vugs produced by folding, and these vugs are partly to completely filled with pelagic ooze. In addition, the hyaloclastite contains abundant pelagic fossils in the matrix. Fossils could be added by erosion of sediment by a turbidity current or initially during mixing of magma with pelagic sediment. If a submarine lava flow advances over water-saturated, low-density pelagic ooze, there may be opportunity for mixing needed for thermal shock granulation, as well as for ingestion of water-laden sediment to expand and form limu bubbles.

X. ANCIENT HYALOCLASTITES

Despite the apparently limited occurrence of hyaloclastite on the modern seafloor, bodies of hyaloclastite

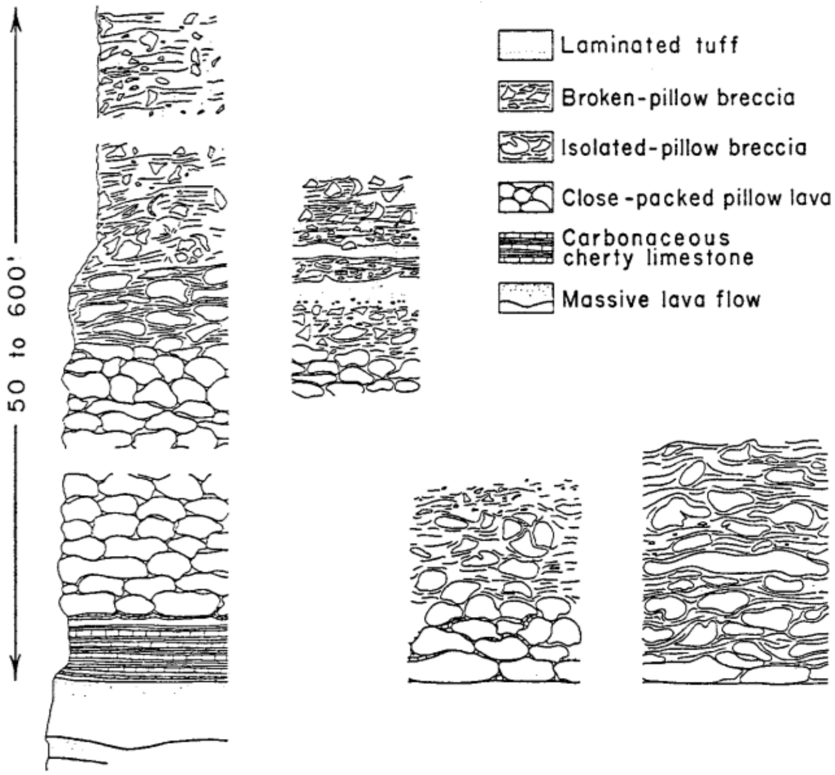

FIGURE 16 Pillow lava and related breccias typical of the ancient submarine plateau forming the Wrangellia terrane. Pillow breccia consists of whole and broken pillows with or without a finer-grained matrix of polyhedral glass fragments. It forms when pillows break loose and avalanche downslope during extrusion, breaking apart as they travel. Isolated pillow breccia contains a large hyaloclastite component that may include vesicular clasts. [Reproduced with permission from Carlisle, H. (1963). Pillow breccias and their aquagene tuffs, Quadra Island, B. C. *J. Geol.* **71,** 48–71, University of Chicago Press.]

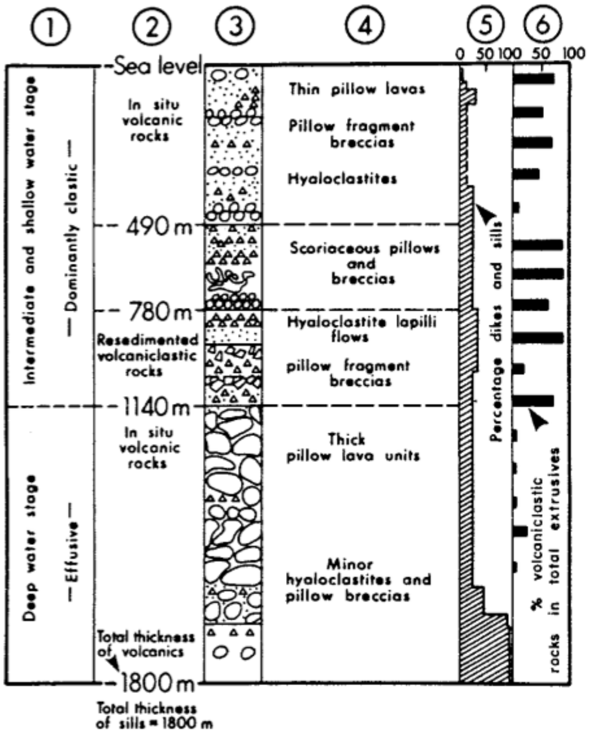

FIGURE 17 A gradual change from pillow lava to hyaloclastite in the uplifted seamount of La Palma is inferred to reflect decreasing depths of eruption. Scoriaceous pillows and breccias have abundant vesicles (cf. isolated pillow breccia, pyroclastic pillow breccia.) [Reproduced with permission from Staudigel, H., and Schmincke, H.-U. (1984). The Pliocene seamount series of La Palma/Canary Island. *J. Geophys. Res.* **89,** 11,195–11,215.]

and related breccias are very commonly associated with subaqueous lavas in ancient seafloor successions. For seafloor formed in open-ocean spreading systems there is only minor hyaloclastite, and it typically occurs as infillings between lava pillows or flows. Study of this material is usually hindered by poor preservation, because the glassy fragments are more easily altered than coherent lava. The zones or layers of fragments also tend to be mechanically weak and thus more strongly affected by tectonic strain that accompanies the incorporation of seafloor into thick crust and its uplift above sea level. No good examples of hyaloclastite similar to the modern ones represented by those at Seamount 6 have yet been recognized in ancient successions.

In contrast, hyaloclastite and related breccias may make up the bulk of deposits formed by eruptions at relatively shallow depths and/or on the steep slopes of seamounts, flanks of island volcanoes, and volcanic plateaus (Fig. 14). Near the source vent, deposits tend to have rags or irregular tubes of coherent lava surrounded by glassy, ragged to blocky polyhedral and locally fluidal clasts. The most common deposits consist of unsorted breccias comprising blocky polyhedral glass fragments and whole or partial pillows in thick, structureless beds with poorly defined boundaries. The breccias appear to originate largely by spalling of stiff, quenched flow margins (essentially an enhanced-chill version of the subaerial "autobrecciation" process that forms the ragged, clinkery surface of aa flows). Thermal

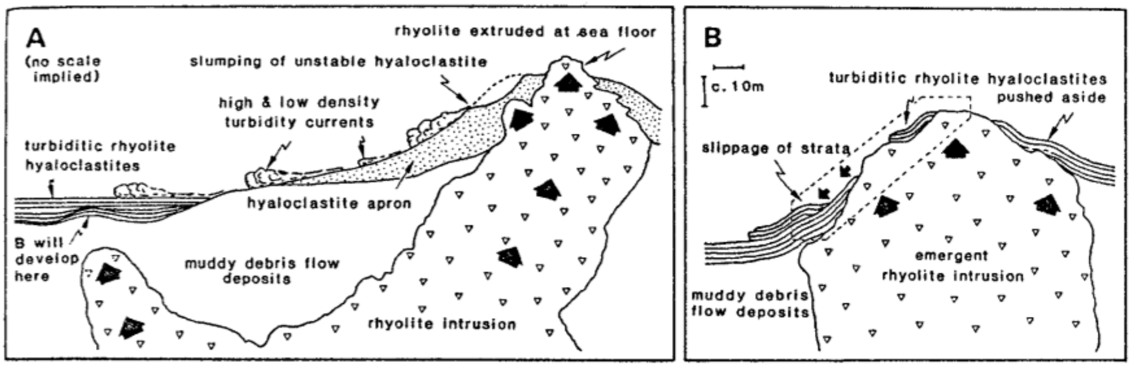
A
(no scale implied)
rhyolite extruded at sea floor
slumping of unstable hyaloclastite
high & low density turbidity currents
turbiditic rhyolite hyaloclastites
hyaloclastite apron
B will develop here
muddy debris flow deposits
rhyolite intrusion
B
c. 10m
turbiditic rhyolite hyaloclastites pushed aside
slippage of strata
emergent rhyolite intrusion
muddy debris flow deposits

FIGURE 18 Diagram showing rhyolitic hyaloclastite formed as a partly intrusive rhyolite breached the surface and developed a carapace of in-place hyaloclastite. Some of this hyaloclastite was redistributed by debris flow and turbidity currents whose deposits were subsequently intruded by the growing rhyolite. [Reproduced with permission from Kokelaar, B. P., Bevins, R. E., and Roach, R. A. (1985). Submarine silicic volcanism and associated sedimentary and tectonic processes, Ramsey Island, SW Wales. *J. Geol. Soc. London* **142,** 591–613.]

shock granulation probably produced the less voluminous component of finer grains, further augmented by shattering of the margins of larger clasts when they jostle against one another during growth of the lava-breccia flows. Pillows develop by budding from the margins of the fluid lava within the flow, often intruding into the breccia carapace, formed from the same flow. Occasional avalanches disrupt parts of the flow and carry the debris downslope to form the poorly bedded deposits.

Some deposits consist almost entirely of concentric "pillows" which are small (ca. 10–50 cm in diameter) subspherical clasts of basalt containing scattered vesicles that have glassy margins with quench crystallites and concentric joints. Hyaloclastite from thermal shattering fills the interstices of the deposits, which grade downward to pillow breccias, the overall sequence being ascribed to decreasing eruption rate. Angular-fragment breccias consist of polyhedral fragments, some having jigsaw-fit textures indicating in-place fragmentation, with varying amounts of matrix consisting of quench granulated hyaloclastite. Work in Iceland indicates that many such complex mixtures of hyaloclastite, hydroclastic breccia, and coherent to dismembered lava can be generated in a short time by ongoing fragmentation and remobilization of fragments during emplacement of a lava (Fig. 15). Dikes with highly irregular to peperitic margins wind through the sequences.

Pillow breccia forms an important part of a vast ancient submarine basaltic lava plateau now exposed as the Wrangellia terrane along the northwestern coast of North America (Fig. 16). An early and influential study of these rocks also identified tiny spheres or globules of glass as an additional minor but significant component of some deposits, and inferred that they formed from submarine lava fountaining of a very fluid lava. Individual layers of pillow breccias are up to 200-meters thick where they were studied. Similar thicknesses of pillow breccia and hyaloclastite are widespread in ancient island arc sequences uplifted and exposed in Japan, Baja California, and tectonically accreted island arc terranes in eastern Oregon.

The succession of eruptive products formed as a volcano grows upward from deep water is represented by the well-studied submarine series of La Palma in the Canary Islands, which exposes an almost 2-kilometer-thick succession of volcanic rocks erupted in water depths ranging from about 1800 m to sea level (Fig. 17). An upward increase in the proportion of fragmental debris is characteristic of such successions, and develops

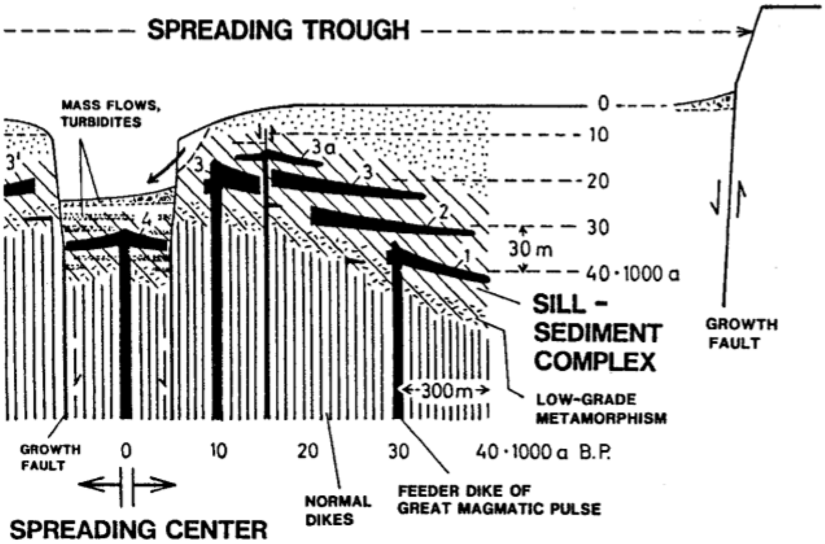

FIGURE 19 Hypabyssal sill–sediment complex developed within seafloor sediments of the Gulf of California. Dikes do not propagate through weak, water-saturated sediment, and the low density of the sediment allows magma to spread laterally into it, aided by fluidization of sediment where steam is formed at the contact between magma and interstitial water in the sediment. [Reproduced with permission from Einsele, G. (1986). Interaction between sediments and basaltic injections in young Gulf of California-type spreading centers. *Geol. Rundsch.* **75,** 197–208.]

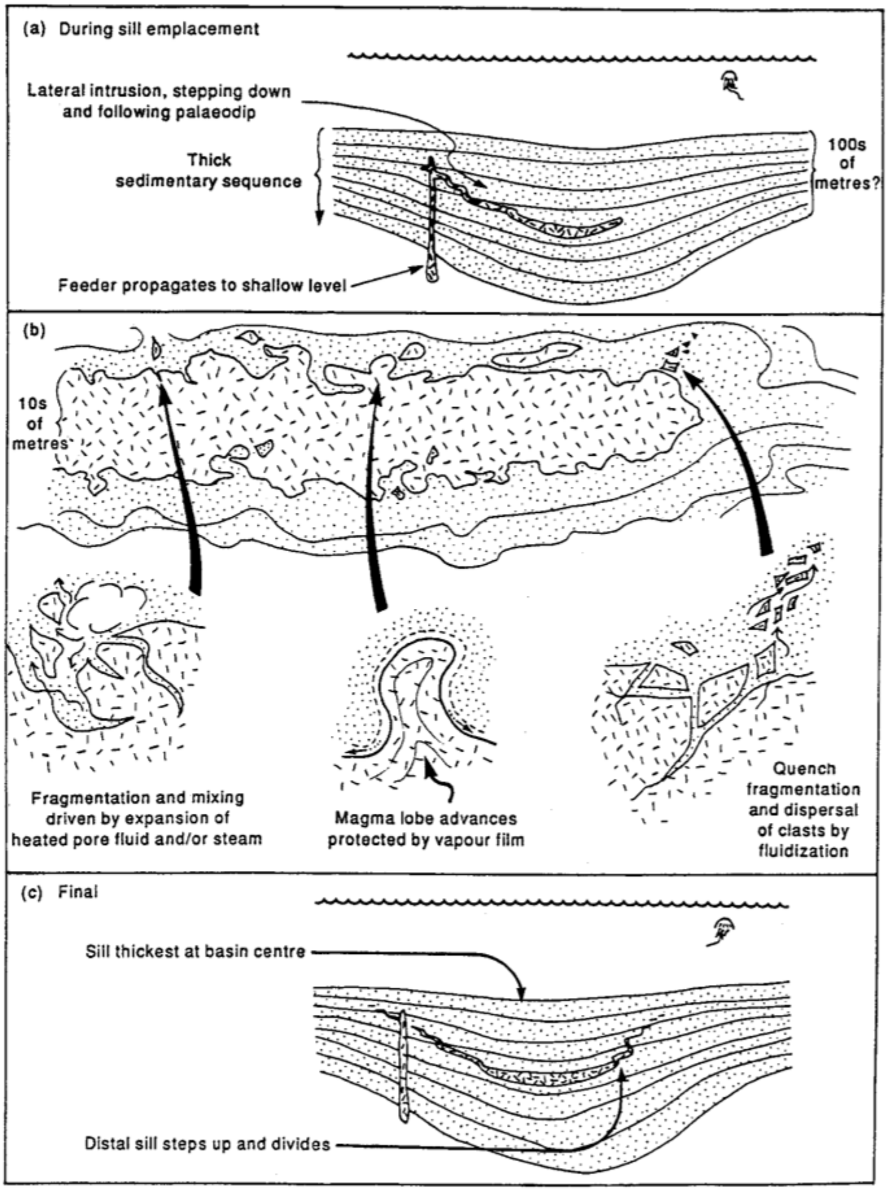
(a) During sill emplacement
Lateral intrusion, stepping down and following palaeodip
Thick sedimentary sequence
100s of metres?
Feeder propagates to shallow level
(b)
10s of metres
Fragmentation and mixing driven by expansion of heated pore fluid and/or steam
Magma lobe advances protected by vapour film
Quench fragmentation and dispersal of clasts by fluidization
(c) Final
Sill thickest at basin centre
Distal sill steps up and divides

FIGURE 20 Model for emplacement of an extensive hypabyssal silicic intrusion with peperite margins. The lateral scale of parts (A) and (C) is tens of kilometers, and the thin, irregularly tabular geometry is quite different from that of rhyolite domes and stubby flows, and indicates fluidal behavior of the magma where emplaced beneath substantial sediment at sub-wave-base depths. [Reproduced with permission from McPhie, J. (1993). The Tennant Creek porphyry revisited: A synsedimentary sill with peperite margins. Early Proterozoic, Northern Territory. *Austral. J. Earth Sci.* **40,** 545–558, Blackwell Science.]

because both magmatic and steam explosivity are more effective in fragmenting the erupting magma at decreased hydrostatic pressure. Pillow breccias of unusual amoeboid and scoriaceous pillows and hyaloclastite were apparently produced in-place at La Palma by eruptions at depths of about 800 m and shallower, with pillow lava and minor hyaloclastite produced at deeper depths. Active seamounts whose summits are in water shallower than about 1000 m probably have similar shoaling successions.

XI. RHYOLITIC HYALOCLASTITES

Like silicic lava flows, silicic hyaloclastites have been far more commonly identified in ancient rock successions than on the modern seafloor. Subaqueous eruption of rhyolite typically occurs in rift settings, which commonly accumulate thick layers of seafloor sediment. Though much erupting magma in such settings is "captured" within seafloor sediments (see ancient hypabyssal complexes below), growing rhyolite domes can breach the seafloor and form thick carapaces of rhyolite hyaloclastite. These hyaloclastites consist of relatively coarse, glassy fragments of nonvesicular to even pumiceous rhyolite and blocky, finer-grained hyaloclastite. Debris flows typically redistribute hyaloclastite breccia from the carapace onto the surrounding seafloor, and finer material winnowed from the flows can form widespread turbidite beds of hyaloclastite ash. Such "emergence" of an intruding rhyolite forms a single rhyolite dome surrounded by in-place hyaloclastite, associated hyaloclastite debris-flow deposits and turbidites, and traceable downward into a hypabyssal intrusion (Fig. 18). Similar sequences have been described from both the Miocene of Japan (Fig. 12) and the Archean, and other examples of various ages are known from Australia.

XII. HYPABYSSAL INTRUSIVE COMPLEXES: INTRASEDIMENT EXTRUSION

The occurrence of hypabyssal complexes, rather than seafloor lava flows, where subaqueous eruptions occur in the presence of thick unconsolidated sediment was predicted in the early 1960s on the grounds that the density of rising basaltic magma is greater than that of wet sediment. This prediction was confirmed in a modern setting when the Deep Sea Drilling Program discovered thick hypabyssal complexes in the Gulf of California in 1979. Here seafloor spreading has recently separated peninsular California from mainland Mexico, and the spreading center is flooded with sediment derived from the adjacent landmasses (Fig. 19). Magma erupting from the spreading center encounters these uncompacted, waterlogged sediments and cannot rise upward through them, instead spreading laterally within the sediments to form *sill–sediment complexes.* The margins of such sills would be expected to display peperite or intrusive pillows, but unfortunately the drillcore recovery was insufficiently complete to evaluate the nature of the sill–sediment contacts; to learn more, we must examine ancient examples.

XIII. ANCIENT HYPABYSSAL COMPLEXES

Hypabyssal complexes are now recognized as a very common component of ancient island-arc volcanic sequences, and are closely associated with a variety of hydrothermal metal deposits. In one example, peperite (a mixture of magmatic fragments and sediment) has been identified along the margins of a Proterozoic rhyolitic body that is tens to a few hundreds of meters thick and forms an approximately 100-km-long outcrop belt hosting gold-bismuth-copper hydrothermal deposits. It is inferred that the body represents a single, rather large

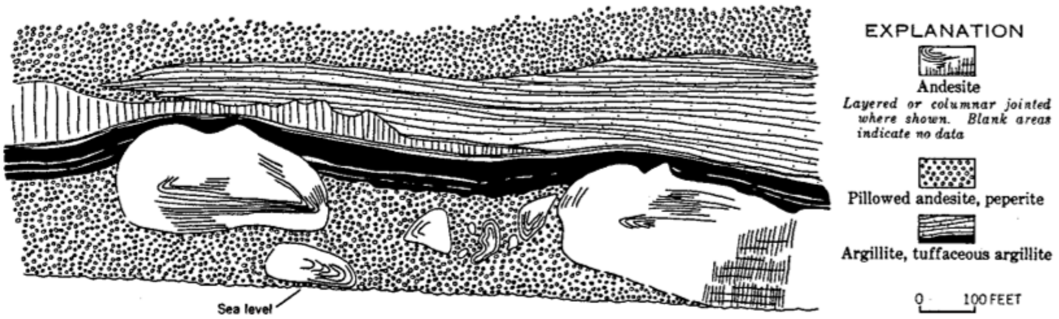
EXPLANATION
Andesite
Layered or columnar jointed where shown. Blank areas indicate no data
Pillowed andesite, peperite
Argillite, tuffaceous argillite
0 100 FEET
Sea level

FIGURE 21 Large tabular to tubular andesite bodies and an abundance of co-erupted peperite and intrusive pillows form a hypabyssal complex intruded into host argillite sediments at Unalaska Island. The entire sequence illustrated, >100 m thick and nearly 1 km across, is intrusive except for the argillites. [Reproduced with permission from Snyder, G. L., and Fraser, G. D. (1963). Pillowed lavas, I: Intrusive layered lava pods and pillowed lavas, Unalaska Island, Alaska. *U. S. Geol. Surv. Prof. Paper* 454B, pp. 1–23.]

INFERRED SEQUENCE OF DEVELOPMENT FOR WISP-BEARING TUFF BRECCIA

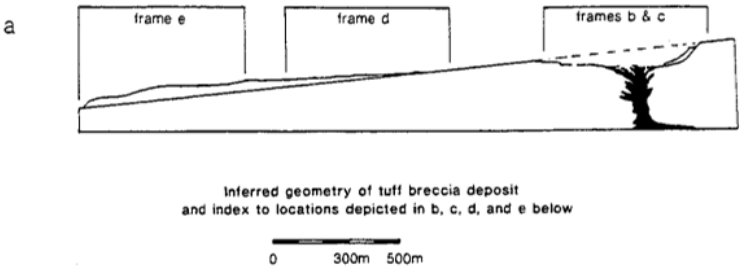

Inferred geometry of tuff breccia deposit
and index to locations depicted in b, c, d, and e below

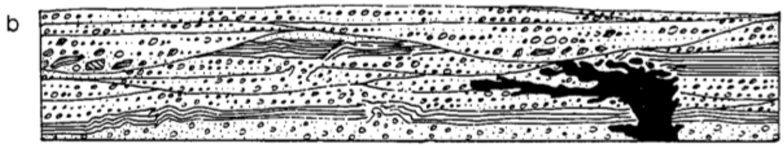

Basaltic magma intrudes volcaniclastic apron deposits

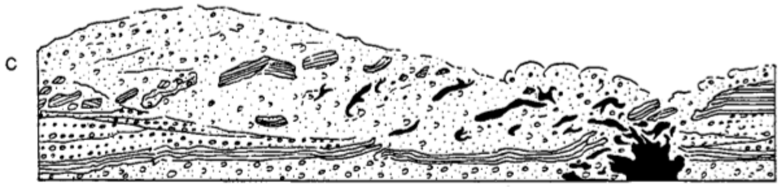

Intruded section fails

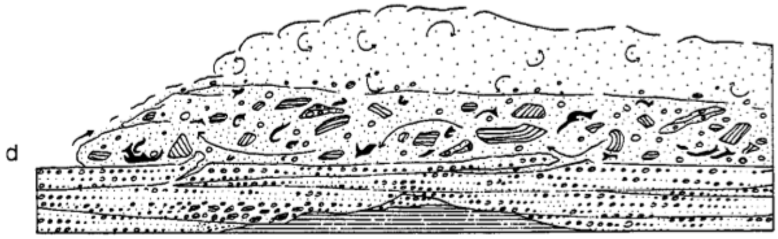

Slump evolves into slightly turbulent debris flow
Relatively dilute, more turbulent flow develops above

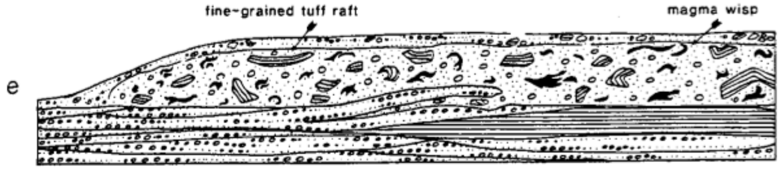

Debris flow deposit overlain by better sorted, weakly bedded deposits

FIGURE 22 Delivery of magma into marine arc-flank environments can result in failure of the flank sediment and incorporation and tearing apart of the magma as the mass flow moves downslope. The degree of magma disruption ranges from simple folding to complete disaggregation and mixing as shown here. [Reproduced with permission from White, J. D. L., and Busby-Spera, C. J. (1987). Deep marine arc apron deposits and syndepositional magmatism in the Alisitos Group at Punta Cono, Baja California, Mexico. *Sedimentol.* **34,** 911–928, Blackwell Science.]

volume (ca. 10-km^3) hypabyssal intrusion emplaced into unlithified sediment at shallow levels beneath the seafloor of a marginal basin (Fig. 20). Under substantial hydrostatic pressure, even rhyolitic melts can have low viscosities because abundant volatiles remain dissolved in the melts. Hypabyssal rhyolite pillows and thin, contorted intrusive tubes of rhyolite encased in seafloor sediment can form from these fluidal rhyolite melts. These are associated with both "emergent intrusions" (Fig. 18) and with extensive peperite development in hypabyssal complexes that can occur over tens or hundreds of kilometers along the axis of extending arcs or young spreading basins, for example, in the Jurassic rocks of southern Chile. Such large-scale hypabyssal complexes have been termed "large-scale peperites" because of the abundance of lava–sediment mixtures along the intrusions, and have been formed by eruptions ranging from basalt to rhyolite in composition. In southern Chile, these vast hypabyssal intrusive complexes of rhyolite are believed to be the subaqueous equivalent of caldera and ignimbrite forming eruptions that occurred further north along the magmatic line under subaerial conditions. Here we focus on subaqueous examples of these complexes, but they also form in sediment-filled basins flooded with groundwater, where the same factors (insufficient rigidity for dike cracking, lower density than magma, and flowage of sediment due to boiling of interstitial water) come into play.

Spectacular exposures of uplifted andesitic hypabyssal complex rocks forming Unalaska Island, Alaska, demonstrate a range of peperites and complicated geometric shapes of intrusive lava (Fig. 21). Peperite forms by mixing of wet sediment and magma, and is typically facilitated by boiling of interstitial water in the sediment to form a steam matrix allowing the sediment to behave fluidally. The resulting deposits range from what are essentially hyaloclastite fragments floating in, and injected by, sediment, to unusual "globular peperite." The latter consists of fluidally shaped lava in droplets, tubes, and globules enclosed and surrounded by sediment; it forms when magma and liquefied sediment mingle as two immiscible fluids. Intrusive pillows, which have the same features as normal pillows (see earlier discussion), and pillowed margins of hypabyssal sills can also form as a result of the fluidal behavior of fluidized or liquefied sediment. In many hypabyssal complexes, intrusive pillow lavas form very thick sequences that may be difficult to distinguish from purely subaqueous pillow piles.

The flanks of marine volcanoes are dominated by volcaniclastic deposits produced by high- and low-concentration turbidity currents. Under the same controls that result in larger hypabyssal complexes, dikes entering such aprons stall before reaching the seafloor. The magma moves laterally into the flank sediments and can initiate mass flows that "unroof" the magma, taking the upper portion along in the flow and tearing the lava into small "rags" by churning flow (Fig. 22).

XIV. SUMMARY

In closing we emphasize that submarine lavas account for the bulk of lavas on Earth. Submarine lavas form with a variety of flow morphologies, controlled largely by the volume extrusion rate and slope angle and their effects on the balance between the rate of crust formation and the deformation of this crust. Deep water lavas are accompanied by little or no hyaloclastite at sediment-free fast-spreading ridges, and by limited amounts of hyaloclastite on slower spreading ridges and seamounts where sediment is also present. Hyaloclastite becomes more abundant at shallower eruption depths. Where sediment on the seafloor is thick, erupting magma is captured within the sedimentary pile to form hypabyssal complexes of peperite, intrusive hyaloclastite and breccia, and intrusive lava in pillows or other forms.

ACKNOWLEDGMENTS

We would like to thank the following people for discussions: John Sinton, Patty Fryer, Mike Garcia, Ken Rubin, Jill Karsten, Keith Crook, Ray Cas, Steve Self, Nathan Becker, RV Fisher, Jocelyn McPhie, David Elliott, Chuck Landis, Ian Skilling, Peter Kokelaar, and many others who over the years have shared their knowledge and ideas about subaqueous eruptions and their products. Useful reviews by W. Mueller, L. Ayres, Tracy Gregg, and Ralf Schmidt helped strengthen the chapter.

SEE ALSO THE FOLLOWING ARTICLES

Composition of Magmas • Flood Basalt Provinces • Hawaiian and Strombolian Eruptions • Lava Domes and Coulees • Lava Flows and Flow Fields • Plate Tectonics and Volcanism • Seamounts and Island Building • Subglacial Eruptions • Volcanism on Venus

FURTHER READING

Submarine Lava Flows

Applegate, B., and Embley, R. W. (1992). Submarine tumuli and inflated tube-fed lava flows on Axial volcano, Juan de Fuca Ridge. *Bull. Volcanol.* **54,** 447–458.

Binard, N., Hekinian, R., Cheminee, J. L., and Stoffers, P. (1992). Styles of eruptive activity on intraplate volcanoes in the Society and Austral Hot spot regions: Bathymetry, petrology and submersible observations. *J. Geophys. Res.* **97,** 13,999–14,016.

Dimroth, E., Consineau, P., Leduc, M., and Sanschagrin, Y. (1978). Structure and organization of Archean subaqueous basalt flows, Rouyn-Noranda area, Quebec, Canada. *Can. J. Earth Sci.* **15,** 902–918.

Fryer, P., Gill, J. B., and Jackson, M. C. (1997). Volcanic and tectonic evolution of the Kasuga seamounts, northern Mariana trough: Alvin submersible investigations. *J. Volcanol. Geotherm. Res.* **79,** 277–311.

Gregg, T. K. P., and Fink, J. H. (1995). Quantification of submarine lava flow morphology through analog experiments. *Geology* **23,** 73–76.

Head, J. W., Wilson, L., and Smith, D. K. (1996). Mid-ocean ridge eruptive vent morphology and substructure: Evidence for dike widths, eruption rates, and evolution of eruptions and axial volcanic ridges. *J. Geophys. Res.* **101,** 28, 265–28, 280.

Perfit, M. R., and Chadwick, Jr., W. W. (1998). Magmatism at mid-ocean ridges: Constraints from volcanological and geochemical investigations. *in* Pages 59–115 "Faulting and Magmatism at Mid-Ocean Ridges," Geophysical Monograph 106. American Geophysical Union, Washington, DC.

Tribble, G. W., (1991). Underwater observations of active lava flows from Kilauea volcano, Hawaii. *Geology* **19,** 633–636.

Hyaloclastites and Related Rocks

de Rosen-Spence, A. F., Provost, G., Dimroth, E., Gochnauer, K., and Owen, V. (1980). Archean subaqueous felsic flows, Rouyn-Noranda, Quebec, Canada, and their Quaternary equivalents. *Precamb. Res.* **12,** 43–77.

Honnorez, J., and Kirst, P. (1975). Submarine basaltic volcanism: Morphometric parameters for discriminating hyaloclastites from hyalotuffs. *Bull. Volcanol* **393,** 1–25.

McPhie, J., Doyle, M., and Allen, R. (1993). "Volcanic Textures: A guide to the Interpretation of Textures in Volcanic Rocks." University of Tasmania.

Schmincke, H.-U., Robinson, P. T., Ohnmacht, W., and Flower, M. F. J. (1978). Basaltic hyaloclastites from holes 396B, DSDP Leg 46. Init. Rep. Deep Sea Drill. Proj. 46, pp. 341–355.

Smith, T. L., and Batiza, R. (1989). New field and laboratory evidence for the origin of hyaloclastite flows on seamount summits. *Bull. Volcanol.* **51,** 96–114.

Hypabyssal Complexes

Hanson, R. E. (1991). Quenching and hydroclastic disruption of andesitic to rhyolitic intrusions in a submarine island-arc sequence, northern Sierra Nevada, California. *Geol. Soc. Am. Bull.* **103,** 804–816.

Kokelaar, B. P. (1982). Fluidisation of wet sediments during the emplacement and cooling of various igneous bodies. *J. Geol. Soc. Lond on* **139,** 21–33.

McBirney, A. R. (1963). Factors governing the nature of submarine volcanism. *Bull. Volcanol.* **26,** 455–469.

This Page Intentionally Left Blank

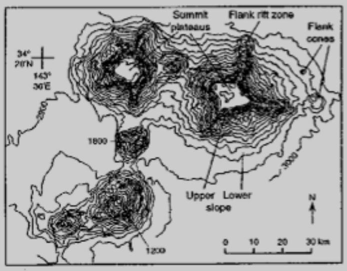

SEAMOUNTS AND ISLAND BUILDING

RALF SCHMIDT
HANS-ULRICH SCHMINCKE
GEOMAR Research Center

I. Introduction
II. Definitions
III. Types of Seamounts
IV. Size and Morphology
V. Areal Distribution
VI. Growth Stages of Seamounts and Island Building
VII. Historical Observations of Emergent Seamounts
VIII. Guyots and Atolls
IX. Chemical Composition
X. Hydrothermal Activity
XI. Significance of Seamounts
XII. Summary

GLOSSARY

abyssal hill A nonvolcanic low-relief feature of the ocean floor. Abyssal hills range up to several hundred meters in height and several kilometers in diameter. They may originate from tectonic uplift. If located near seamounts or oceanic islands, they may represent remnants of mass wasting deposits such as debris avalanches or slides. Recently, the term has evolved to have a very specific meaning used for linear fault blocks that form the ridge-parallel horst/graben topography on ridge flanks.

atoll A truncated, commonly volcanic island capped by a roughly circular to horseshoe-shaped coral reef composed of closely spaced small coral islets that encircle a shallow lagoon. The complex is surrounded by deep water. Atoll formation is restricted to equatorial regions.

endemic An organism or a group of organisms restricted to a particular region or environment.

feeder dike The conduit through which magma passes from a magma chamber to the Earth's surface.

fissure eruption An eruption that takes place from an elongate fissure, rather than from a central vent.

hot spot (mantle plume) An area of copious volcanic activity, usually in intraplate tectonic settings, persistent for millions of years, that is thought to be the surface expression of a more or less persistent rising plume of hot mantle material from which magma is released during decompression.

hyaloclastite A deposit formed by the flowing or intrusion of lava or magma into water, ice, or water-saturated sediment, and its consequent granulation or shattering into small angular glass fragments.

juvenile clast Volcanic particle (pyroclast or hydroclast) derived directly from magma reaching the surface.

peperite A breccia-like mixture of extrusive or intrusive lava with wet sediment.

pillow lava Interconnected, elongated lava tubes formed in a subaqueous environment. Cross sections of tubes resemble pillows that commonly show a convex upper

Copyright © 2000 by Academic Press
All rights of reproduction in any form reserved.

and flat or concave lower surface, and radial fractures. Pillow tubes are surrounded by a chilled glassy margin.

pit crater A small crater formed by subsidence of the surface.

seamount asperity Roughness of subducted oceanic lithosphere due to seamounts, volcanic ridges, and oceanic plateaus.

sideromelane Fresh isotropic basaltic glass.

I. INTRODUCTION

We discuss the types, morphology, areal distribution, growth stages—including island formation, chemical composition, hydrothermal activity, and significance of seamounts. Volcanic edifices with elevations of more than 50–100 m above the surrounding seafloor are called seamounts. Their total number exceeds 1 million (Table I). Volcanic ocean islands, which are highly productive seamounts that have grown above sea level, number only a few thousands, including small islets like atolls.

Seamounts of volcanic origin are the most abundant—but most poorly studied—volcanoes on the Earth's surface. The study of seamounts provides basic insights into processes concerning the evolution of the oceanic lithosphere:

1. The composition of seamount lavas reflects fundamental mantle and crustal processes not affected by contamination due to passage through thick continental crust.
2. Seamounts, including submerged oceanic islands (guyots, atolls), record vertical movements that reflect upwelling mantle material, thermal subsidence of aging lithosphere, and sea level fluctuations.
3. The age progression of large seamount chains is a fundamental parameter in determining past and present plate vectors.
4. The study of abundance, areal distribution, and composition of seamounts helps to understand accretion processes of oceanic crust.
5. Information about the shape of seamounts and orientation of dikes within the edifices is useful to reconstruct the regional tectonic stress and fracture patterns of the surrounding lithosphere.
6. The morphology of the edifices, flow types, volcaniclastic facies, and clast shapes are the result of submarine volcanic processes including fragmentation and emplacement mechanisms.
7. Active submarine volcanoes may be sites of hydrothermal activity.
8. Last but not least, continuous upward growth may lead to the formation of oceanic islands, most attractive places to spend one's holidays.

The aim of this review is to present a summary of the global importance of seamount volcanism, which is second only in intensity to midocean ridge (MOR) volcanism on the Earth's surface.

II. DEFINITIONS

Seamounts are discrete, morphologically distinct elevations on the seafloor. Most seamounts are of volcanic origin while only few are nonvolcanic. They may be isolated or arranged in clusters or linear chains. The restriction to a minimum height of 1000 m in most current definitions of seamounts seems to be based primarily on practical criteria since elevations of less than 1000 m on the seafloor may enclose morphologic features of diverse origins such as fault blocks or blocks within debris avalanche deposits. These morphologic highs are also called *abyssal hills.* There is little scientific justification, however, for not calling submarine volcanoes less than 1000 m high *seamounts.* Isolated submarine volcanoes, like all volcanoes, start small. In detailed studies on seamounts, the size limit is closer to 50–100 m above seafloor (asf), a usage adapted in this summary.

III. TYPES OF SEAMOUNTS

Volcanic seamounts include (1) submarine peaked volcanoes and (2) flat-topped submerged and eroded oceanic islands (guyots, atolls). The term *fossil seamount* has also been applied to uplifted fragments of oceanic volcanoes, for example, La Palma (Canary Islands, East Atlantic), Porto Santo (Madeira Archipelago, East Atlantic), Tok Islands (Korea), Takashibiyama Formation (Shimane Peninsula, Southwest Japan), and Ba Volcanic Group/ Viti Levu (Fiji Islands). Nonvolcanic seamounts are submarine peaks restricted to forearc systems and to the landward slope of trenches. They include serpentinite diapirs and horst blocks consisting of altered and metamorphosed mafic and ultramafic rocks.

IV. SIZE AND MORPHOLOGY

Seamounts on the ocean floor are mapped by conventional bathymetric methods including single-beam echo sounder (2-D), multibeam swath echo sounder (3-D), and high-resolution side-scan sonar systems (3-D) such as SeaMARC, GLORIA, and TOBI. The morphology of volcanic seamounts is highly variable. Their shapes are mainly controlled by (1) the size, geometry, and temporal migration of magmatic conduits; (2) eruption rate and magma viscosity; (3) the development of craters and calderas; (4) preexisting topography; and (5) regional and gravitational edifice stresses. During and after growth, the constructional shape is commonly modified by erosion, mass wasting, and tectonic disruption as well as by tilting due to variable subsidence.

Two morphologic end members have been distinguished from each other depending on the geometry of magmatic conduits: (1) extrusion of magma from a single feeder tube system (point source) may build an isolated lava pile whereas (2) fissure eruptions (linear source) produce ridgelike features. Combinations of both are common. Eruption rate, magma viscosity, and preexisting topography account for the morphologic and structural variability of eruptive products such as sheet flows, pillow lava, ponded flows, lobate tubes, and hyaloclastites and thus determine the small-scale morphology of a seamount. Detailed bathymetric studies in the axial zone of the Reykjanes Ridge (south of Iceland) and further south in the inner valley floor of the Mid-Atlantic Ridge (MAR) revealed smooth-shaped seamounts, consisting of numerous sheet flows and "hummocky" seamounts composed of pillow lava.

Summit craters are common, especially on small seamounts. They vary in size from tiny pits, a few tens to hundreds of meters in diameter, to large and complex calderas up to a few kilometers in diameter frequently bordered by stepped crater walls. Small cones are common on the crater floors.

A. Intraplate and MOR-Related Seamounts

In plan view, circular to elliptical to irregular polygonal and ridgelike shapes are typical. Profile shapes of isolated seamounts vary from shields (resembling Hawaiian volcanoes), to overturned soup-bowl shapes (resembling Galapagos volcanoes), to dome shapes and more complex forms. Many of the larger seamounts display truncated cones with more or less flat summit regions, in some cases the result of postcaldera lava filling from circumferential feeder dikes. The morphology of seamounts is commonly modified by satellite cones and flank rift zones. In general, small volcanoes are more irregular in shape than their larger counterparts. Many large and small edifices display large-scale asymmetries due to tectonic activity and/or flank collapses.

Conical seamounts often show slightly concave flanks steepening toward the top. Moreover, there seems to be a relationship between slope angle and summit height. In the eastern and southern Pacific, seamounts less than 1800 m high show an average slope angle of 18° ± 6° with individual values ranging from 5° to 36°, while taller seamounts (>2600 m high) exhibit more uniform values and lower mean gradients, averaging 15°. Similar results were obtained from Nazca plate-seamounts near the Easter Islands (Southeast Pacific). Two seamount populations were distinguished from each other: one composed of small seamounts (<1200 m high) characterized by slope angles from 5° to 32°, whereas a second group, consisting of larger edifices (>1200 m high), displays more gentle slope angles from 5° to 15°. Thus, seamount slopes are much steeper compared to slopes of subaerial shield volcanoes, which average about 4° to 9°.

Quantitative studies of seamount morphology have been carried out using single-line wide-beam echo-sounding profiles of well-surveyed regions in the Pacific. Based on the analysis of shape parameters (basal width, summit width, maximum height, slope angle, height-to-basal-radius ratio and flatness), obtained from a wide height range of seamounts (140–3800 m), summit height seems to be generally about one-fifth the basal radius. Moreover, the mean flatness decreases with increasing summit height, resulting in isolated conical shapes for large seamounts.

Depending on the magma production rate, seamounts range in volume and height from huge submarine intraplate volcanoes such as Hawaii more than 4000 m high above sea level and volumes exceeding 50,000 km^3, to small MOR-related volcanic cones that only reach 50 m in height. Basal diameters range from a few tens of meters up to more than 100 km. On average, intraplate seamounts are much larger than seamounts formed along the axis or on the flanks of MORs.

B. Island-Arc Seamounts

The morphology of seamounts in island-arc settings in many aspects resembles seamounts in intraplate settings and at MORs, as described earlier. The main difference is the abundance of submarine caldera volcanoes (e.g., northern Izu-Ogasawara arc, Japan), reflecting explosive volcanic activity along island arcs. The global average rate of island-arc caldera volcanoes is about 20%, whereas in the northern submarine portion of the Izu-Ogasawara arc the rate reaches 60%.

The seamounts are conical or elongate in shape, but this morphology can be modified by abundant summit calderas (4–9 km in diameter), some with satellite cones and postcaldera dome complexes inside (e.g., Myojinsho area, Izu-Ogasawara arc, Japan). The height of caldera volcanoes composed of felsic ejecta (dacitic to rhyolitic pumice) is significantly lower than that of more mafic cones. A remarkable symmetric submarine cone, the so-called Myojinsho cone (Izu-Ogasawara arc, Japan) located on a caldera wall, has slopes of almost precisely 21°, interpreted to be the result of angle-of-repose deposition of volcaniclastic gravity flows.

C. Nonvolcanic Seamounts

Two morphologic types of nonvolcanic seamounts occur at convergent margins between the trench axis and the active volcanic front (forearc). Tectonically uplifted blocks are bordered by faults and thus show angular outlines in plan view, whereas diapir-driven serpentinite seamounts (e.g., Conical seamount, Mariana forearc, Japan) are characterized by crescentic and conical shapes. They reach up to 30 km in diameter and are as much as 2–3 km high.

V. AREAL DISTRIBUTION

Seamounts occur in different tectonic settings such as (1) intraplate terrains including passive oceanic margins, (2) MORs, and (3) island arcs above subduction zones. Larger seamounts are commonly grouped into (1) volcanic ridges (e.g., Cocos Ridge in the Pacific, Ninetyeast Ridge in the Indian Ocean, Walvis and Rio Grande Ridges in the South Atlantic) composed of closely spaced volcanoes, (2) large seamount/island chains (e.g., Hawaiian–Emperor chain, Pacific), and (3) patchy clusters (e.g., Canary Islands and associated seamounts, East Atlantic) as well as isolated seamounts (e.g., Shimada seamount, East Pacific; Vesteris seamount, North Atlantic), including guyots (e.g., Great Meteor seamount, East Atlantic) and atolls (e.g., Muroroa Atoll, Tuamotu Archipelago, French Polynesia, Southwest Pacific), which, of course, may also be part of seamount chains.

A. Intraplate Setting

Intraplate seamounts are commonly located far from plate boundaries. Their origin is interpreted to be the surface expression from roughly stationary mantle plumes (hot spots). In fast spreading ocean basins (60–90 mm/yr), such as the Pacific Plate, they are commonly arranged in large linear seamount/island chains or volcanic ridges. As the volcano is carried away from the center of the hot spot, the magma supply is cut off and the volcanic activity ceases, creating a trail of extinct, progressively older volcanoes parallel to the direction of seafloor spreading. This scenario is best illustrated by the Hawaiian–Emperor chain. Most chains show a more complex age progression (e.g., seamount chains in the Gulf of Alaska), the result of a combination of intraplate seamounts and seamounts associated with spreading ridges, variable degrees of magma storage, and interaction with lithospheric fractures. The Hawaiian–Emperor chain shows a sharp bend that separates the younger westward-trending Hawaiian islands from the older northward-trending Emperor seamounts (Fig. 1A). This bend is commonly interpreted to reflect a dramatic change in Pacific Plate motion about 43 Ma ago. Recently, paleomagnetic studies of some Emperor seamounts have shown that the Hawaiian hot spot may not be fixed, but may have moved in late Cretaceous to early Tertiary times (81–43 Ma) at rates similar to those of lithospheric plates (>30 mm/yr). Nevertheless, bends of seamount/island chains in the South Pacific (e.g., Gambier-Tuamotu Line, Austral-Cook, and Gilbert-Marshall) occur roughly at the same time (40–50 Ma), favoring the interpretation of synchronous changes in plate motion direction across a large part of the Pacific Plate.

Aseismic ridges of volcanic origin lacking earthquakes are linear volcanic structures not restricted to fast spreading ocean basins. They are composed of coalesced seamounts rising 2000–4000 m above the surrounding seafloor and may reach a few hundred kilometers in width and a few thousand kilometers in length. Most are attached to continental margins and may continue to active spreading centers. Aseismic ridges are assumed to have formed during the early history of opening of ocean basins due to initial hot spot activity. If the hot spot is located on the active spreading center, paired aseismic (volcanic) ridges may originate on both sides of the MOR (e.g., Walvis and Rio Grande Ridges, South Atlantic). Numerous isolated or clustered seamounts and seamount/island chains occur on volcanic oceanic plateaus. These areas (e.g., French Polynesian Superswell, Southwest Pacific; Ontong Java Plateau, West Pacific) are several hundred kilometers in diameter, may be elevated more than 1000 m above the surrounding seafloor, and are characterized by thickened oceanic crust. They are interpreted to originate mainly from hot spots. Along passive oceanic margins far from MORs (e.g., East Atlantic), seamounts tend to occur in isolation or in clusters (Fig. 1B).

Some solitary seamounts in intraplate settings are associated with fractures caused by extensional stress fields. Such seamounts are assumed to be of nonplume origin (e.g., Vesteris seamount, Greenland Basin, North Atlantic).

B. MOR Setting

Statistical studies of seamount distribution are based on counting isolated peaks on bathymetric charts and on single-line wide-beam echo-sounding data in order to estimate the regional and global seamount abundance. All sizes of seamounts can be taken into consideration depending on the resolution of bathymetric systems used. In contrast to satellite altimetry, data acquisition of smaller MOR-related seamounts is based on single ship tracks covering a very limited area of ocean basins. Hence, the distribution of small seamounts has to be estimated using statistical methods.

The regional abundance of seamounts (Table I) focuses on truncated or elliptical edifices with aspect ratios (ratio of maximum to minimum basal diameter) of less than 2. Estimated seamount abundances are, therefore, minimum values. These studies show that seamount populations generally follow an exponential size–frequency distribution over a large range of summit heights, inasmuch as most small seamounts form very close to the spreading axis, while only few larger volcanoes are added off-axis. The mean seamount abundance estimates are calculated using an exponential model (Table I).

Statistical studies of seamount distribution have been carried out mainly along fast and slow spreading MORs including ridge sections both affected and unaffected by hot spots.

1. *Fast Spreading Ridges*

Small cones on the flanks and in the vicinity of fast spreading MORs are the most common type of seamount in the Pacific Ocean basin, whereas seamounts are absent within the axial zone. The site of seamount formation along the East Pacific Rise (EPR) is restricted to a remarkably narrow band 5–15 km (0.1–0.3 Ma) from the ridge axis, with less significant growth out to ~50 km (~1 Ma) from the ridge crest. The distribution of near-axis seamounts is not random but follows zones of apparent lithospheric weakness including (1) ridge normal, (2) ridge parallel, and (3) oblique directions about 40°–50° to ridge lineation, resulting in clusters and small seamount chains. Short seamount chains are usually oriented either parallel to the relative plate motion (spreading direction) or to the direction of absolute plate motion while others are not. They may originate from moving melting anomalies (i.e., discrete areas of elevated temperatures and partial melt in the upper mantle) possibly associated with large overlapping spreading centers or with major transform offsets in the ridge axis. On the other hand, short seamount chains oriented parallel to the direction of plate motion relative to the upper mantle may originate from stationary melting heterogeneities beneath migrating ridges. Calculated seamount abundances per unit area in the Pacific range from 2 to 13 × 10^{-3} km^{-2} (Table I).

The abundance of seamounts (number of seamounts per unit area) in the Pacific increases monotonically with age from the ridge crest out to seafloor of Eocene age due to off-axis addition of seamounts to the crust over time. This seamount production rate is inversely proportional to the square root of lithospheric age. In other words, seamount production rate decreases with increasing age and thickness of the underlying crust. Young and thin lithosphere is dominated by abundant small seamounts, whereas old lithosphere contains more larger edifices due to increasing load capacity and burial of smaller features by sediments.

2. *Slow Spreading Ridges*

In slow spreading environments such as the Mid-Atlantic Ridge, seamount production is almost restricted to the median valley floor. Isolated volcanoes pile up and coalesce to form the characteristic neovolcanic axial ridges (Fig. 2). Calculated seamount abundance per unit area in the northern MAR axial valley (195×10^{-3} km^{-2}) is more than an order of magnitude higher than along the MOR in the Pacific (2 to 13 × 10^{-3} km^{-2}) and South Atlantic (7×10^{-3} km^{-2}) and further increases to $310 \pm 20 \times 10^{-3}$ km^{-2} at the Reykjanes Ridge due to the influence of the Iceland hot spot (Table I). The estimate of seamount abundance for the North Atlantic Basin of 85 million (Table I) is surprisingly high be-

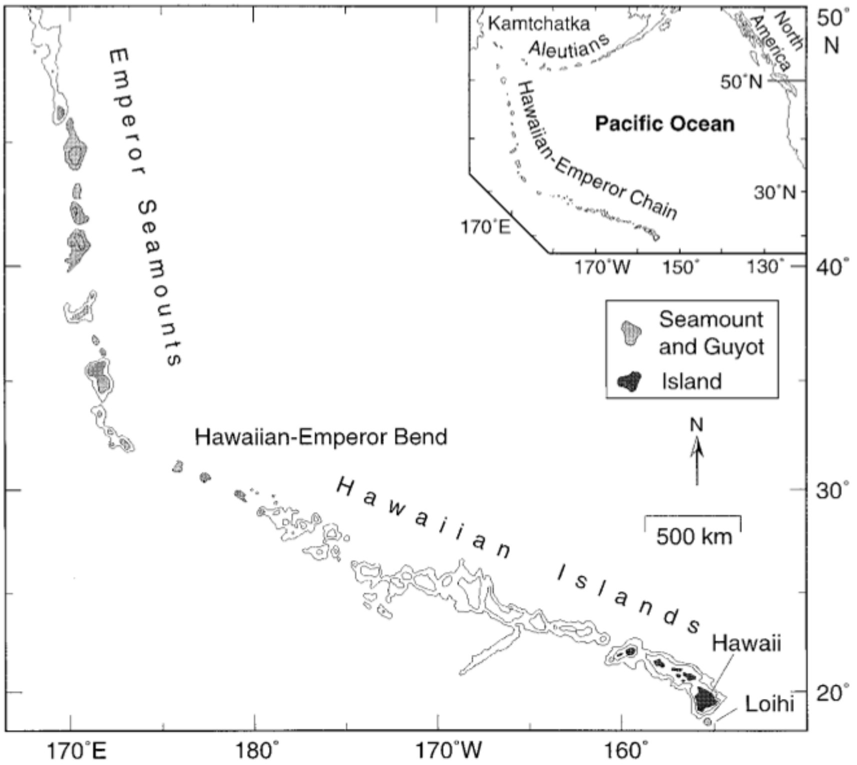

Kamtchatka
Aleutians
North America
50°N
Pacific Ocean
Hawaiian-Emperor Chain
30°N
170°E
170°W
150°
130°
Seamount and Guyot
Island
Emperor Seamounts
Hawaiian-Emperor Bend
Hawaiian Islands
N
500 km
Hawaii
Loihi
50° N
40°
30°
20°
170°E
180°
170°W
160°

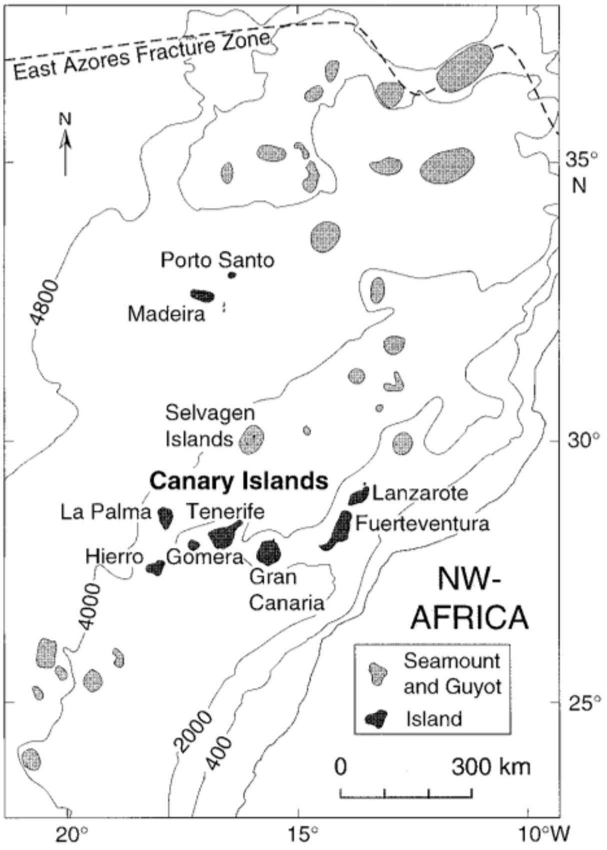

East Azores Fracture Zone
N
35° N
Porto Santo
Madeira
4800
Selvagen Islands
30°
Canary Islands
Lanzarote
La Palma
Tenerife
Fuerteventura
Hierro
Gomera
Gran Canaria
NW-AFRICA
4000
Seamount and Guyot
Island
25°
2000
400
0
300 km
20°
15°
10°W

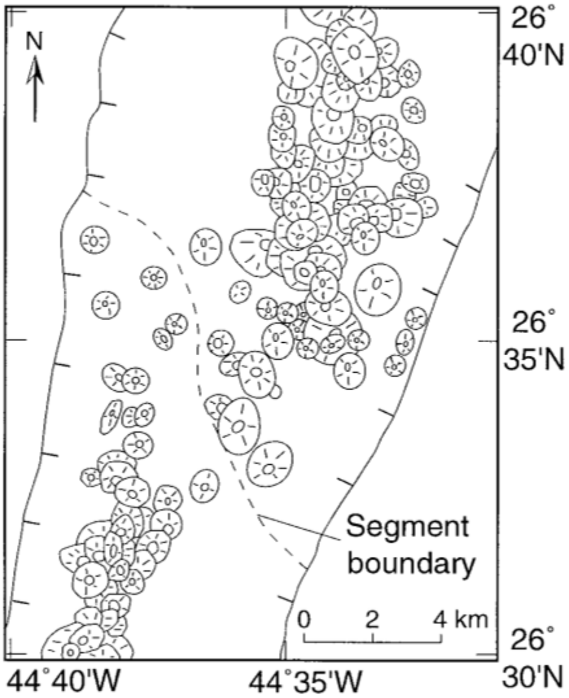

FIGURE 2 Distribution of small seamounts (50–600 m high) in the median valley floor of the slow spreading Mid-Atlantic Ridge north of the Kane fracture zone. The two outer solid lines mark the first major faults that begin the steps up the inner valley wall. The volcanic ridge consists of piled-up and coalesced seamounts marking sites of major crustal construction. The segment boundary marks the offset of the volcanic ridge. [Adapted from Smith, D. K., and Cann, J. R. (1990). Hundreds of small volcanoes on the median valley floor of the Mid-Altantic Ridge at 24–30°. *Nature* **348,** 152–155. Copyright © 1990 Macmillan Magazines Limited, with permission from *Nature* and D. K. Smith.]

cause seamounts formed along the spreading axis cannot be traced out to the ocean basins, due to tectonic disruption along the high-relief ridge crest of the MAR. Ridge flank seamount construction along the MAR in the North Atlantic is restricted to hot-spot-influenced regions, while seamounts along ridge flanks are common in the South Atlantic. Consequently, seamount volcanism in the South Atlantic appears to resemble that in the Pacific, regardless of the differences in spreading rates, including its seamount chains.

In conclusion, the spreading rate seems to have an important control on seamount formation along MORs. Along slow spreading ridges, numerous small seamounts form along the ridge axis, whereas along fast spreading ridges few larger seamounts form off-axis. For further discussion see Section XI,C.

C. Island Arcs

The distribution of seamounts and islands along the volcanic front of island arcs shows an almost linear or slightly curved arrangement parallel to the trench (Fig. 1A, Aleutian seamounts/islands in the index map). Discontinuities from the linear to curved geometry are mainly caused by tectonic segmentation of the volcanic front. Both observations suggest a strong fault control on the distribution of volcanism. The oblique orientation of the Kasuga seamount chain (northern Mariana Trough, Japan), however, is oriented obliquely to the volcanic front interpreted to be the result of interaction between preexisting cross-arc structures, magmatic activity at the volcanic front and in the backarc, and the tectonic activity in the island-arc complex. Large seamounts and islands tend to be regularly spaced at 50–70 km, whereas smaller seamounts are more closely spaced.

D. Pacific Plate

The distribution of seamounts of the Pacific Plate has also been mapped by satellite altimetry. Each bathymetric high on the seafloor produces a positive gravity anomaly reflected by a rise in the sea surface above the feature. The sea surface bulge has to reach a significant value on the order of a few meters spread over an area of a few hundred kilometers to be measured accurately. This method thus takes into account only large sea-

---

FIGURE 1 (A) Linear distribution of seamounts and volcanic islands of the Hawaiian–Emperor chain. Contour intervals are at 2000 and 4000 m. Inset shows the location of the chain in the central North Pacific. The Aleutians display a curved arrangement of seamounts and islands typical for island-arc settings. Inset contour interval at 2000 m. (B) Distribution of seamounts and volcanic islands along the passive continental margin off northwest Africa. Note the irregular, patchy arrangement of seamounts and oceanic islands. The simplified outlines of the seamounts mark the slope break to the surrounding seafloor. [Adapted from Schmincke, H.-U., and Sumita, M. (1998). Volcanic evolution of Gran Canaria reconstructed from apron sediments: Synthesis of VICAP project drilling. Pages 443–459 *in* "Proc. ODP, Sci. Results" P. P. E. Weaver, H.-U. Schmincke, J. V. Firth, and W. Duffield, eds.). Copyright © 1998 Ocean Drilling Program Texas A&M University, with permission from Ocean Drilling Program Texas A&M University.]

TABLE 1 Seamount Abundance of MORs and Intraplate Terrains (Selected Data From the Literature)

Author	*Method*	*Area*	*Lithospheric age (Ma)*	*Height range (m)*	*Dimension of study area*	*Calculated seamounts per 10^3 km^2*	*Global estimates*
Jordan *et al.*, 1983	Wide-beam profiles	Pacific	0–65	200–4000	44,020 km	3.96 ± 1.12	—
Wessel and Lyons, 1997	Satellite altimetry	Pacific Plate[a]	0–169	>1500	Pacific Plate	8882[b]	~70,000 > 1 km entire Pacific
Batiza, 1982	Map counts	N. Pacific	0–157	>200	59.86 × 10^6 km^2	0.117	55,000 entire Pacific; 100,000 worldwide
Smith and Jordan, 1988	Wide-beam profiles	East + South Pacific	0–110	400–2500	156,720 km	5.4 ± 0.65	Close to 1 × 10^6 Pacific basin seamounts
Abers *et al.*, 1988	Sea-beam profiles	Parallel EPR[c] 7°–22°S	0.5–2 5–10 30–40	100–1000	45,667 km^2	12.66 ± 0.76	—
Scheirer *et al.*, 1996	Side-scan systems	SEPR[d] 15°–19°S	0–~6.5	200–1200	200,300 km^2	4.8 ± 0.3	—
Fornari *et al.*, 1987	Sea-beam profiles	Near EPR 0°–24°N	<10	>50	18,400 km^2	~9	>1.5 × 10^6 seamounts for the Pacific
Scheirer and MacDonald, 1995	Sea-beam and side-scan	NEPR[d] 8°–17°N	0–~2	200–800	200,400 km^2	1.9 ± 0.2	—
Rappaport *et al.*, 1997	Sea-beam and side scan	ESC[e] 25°–29°S 113°–104°W	No specification	200–1000	243,400 km^2	2.7 ± 1.5	—
Batiza *et al.*, 1989	Sea-beam profiles	MAR[f] ~26°S	0–7	50–600	16,500 km^2	~7	—
Smith and Cann, 1990	Sea-beam	Median valley of MAR 24°–30°N	No specification	50–210	6,000 km^2	195 ± 9	85 × 10^6 seamounts in the N. Atlantic basin
Magde and Smith, 1995	Multi-beam profiles	Reykjanes ridge 57°–62°N	0–0.7	50–200	2,895 km^2	310 ± 20	—

Seamount abundance from MORs and intraplate terrains (selected data from the literature). Data from Abers, G. A., Parsons, B., and Weissel, K. (1988). Seamount abundances and distributions in the Southeast Pacific. *Earth Planet. Sci. Lett.* **87,** 137–151; Batiza, R. (1982). Abundances, distribution and sizes of volcanoes in the Pacific Ocean and implications for the origin of non-hot spot volcanoes. *Earth Planet. Sci. Lett.* **60,** 195–206; Batiza, R., Fox, P. J., Vogt, P. R., Cande, S. C., Grindlay, N. R., Melson, W. H., and O'Hearn, T. (1989). Morphology, abundance, and chemistry of near-ridge seamounts in the vicinity of the Mid-Atlantic Ridge ~26°S. *J. Geol.* **97,** 209–220; Fornari, D. J., Batiza, R., and Luckman, M. A. (1987). Seamount abundances and distribution near the East Pacific Rise 0°-24°N based on seabeam data. Pages 13–21 *in* "Seamounts, Islands, and Atolls" (B. H. Keating, P. Freyer, R. Batiza, and G. W. Boehlert, eds.), Geophysical Monograph 43. American Geophysical Union, Washington, DC; Jordan, T. H., Menard, H. W., and Smith, D. K. (1983). Density and size distribution of seamounts in the Eastern Pacific inferred from wide-beam sounding data. *J. Geophys. Res.* **88**(B12), 10,508–10,518; Magde, L. S., and Smith, D. K. (1995). Seamount volcanism at the Reykjanes Ridge: Relationship to the Iceland hot spot. *J. Geophys. Res.* **100**(B5), 8449–8468; Rappaport, Y., Naar, D. F., Barton, C. C., Liu, Z. J., and Hey, R. N. (1997). Morphology and distribution of seamounts surrounding Easter Island. *J. Geophys. Res.* **102**(B11), 24,713–24,728; Scheirer, D. S., and MacDonald, K. C., (1995). Near-axis seamounts on the flanks of the East Pacific Rise, 8°N to 17°N. *J. Geophys. Res.* **100**(B2), 2239–2259; Scheirer, D. S., MacDonald, K. C., Forsyth, D. W., and Shen, Y. (1996). Abundant seamounts of the Rano Fahi seamount field near the southern East Pacific Rise, 15°S to 19°S. *Mar. Geophys. Res.* **18,** 13–52; Smith, D. K., and Jordan, T. H. (1988). Seamount statistics in the Pacific Ocean. *J. Geophys. Res.* **93**(B4), 2899–2918; Smith, D. K., and Cann, J. R. (1990). Hundreds of small volcanoes on the median valley floor of the Mid-Atlantic Ridge at 24–30°. *Nature* **348,** 152–155; Wessel, P., and Lyons, S. (1997). Distribution of large Pacific seamounts from Geosat/ERS-1: Implications for the history of intraplate volcanism. *J. Geophys. Res.* **102**(B10), 22,459–22,475.

[a] Intraplate, fracture zones excluded.

[b] Detected seamounts.

[c] East Pacific Rise, hot spot areas excluded.

[d] Southern/Northern East Pacific Rise.

[e] Easter Seamount Chain, EPR and hot spot influenced.

[f] Mid-Atlantic Ridge.

mounts with heights exceeding 1.5 km but their total number and distribution is measured very precisely because entire ocean basins are mapped. A total of 8882 large seamounts were detected (Table I) having the highest density (number of seamounts per area) in the central Pacific and French Polynesia. These areas are interpreted to result from numerous closely spaced hot spot trails. The tallest seamounts (guyots) are found in the western Pacific on the oldest oceanic crust. They are of Cretaceous age and perhaps coincide with the time of formation of large igneous provinces (volcanic oceanic plateaus) in the Pacific Ocean.

VI. GROWTH STAGES OF SEAMOUNTS AND ISLAND BUILDING

Seamounts have been studied mainly with bathymetric methods, rarely by submersibles, and exceptionally through drilling. Our knowledge of their internal structure is thus very limited. Three-dimensional correlations of volcanic facies can only be obtained from cross sections in subaerially exposed fossil seamount sequences such as the Crescent volcanic rocks (Olympic Mountains, Washington), Snow Mountain volcanic complex (California), La Palma (Canary Islands, East Atlantic), Porto Santo (Madeira Archipelago, East Atlantic), Ba Volcanic Group (Viti Levu, Fiji), Takashibiyama Formation (Shimane Peninsula, southwest Japan), Masirah Island ophiolite (Oman), and Troodos ophiolite (Cyprus).

The type of submarine volcanic activity, and thus the emplacement and fragmentation processes, are controlled by (1) hydrostatic pressure (water depth) at which eruptions take place, (2) chemical composition of magma (volatile content, viscosity), (3) topography of the extrusive environment, (4) eruptive rate, and (5) the dynamics of lava–water interactions. Seamounts pass through several growth stages during upward growth characterized by (1) increasing vesicularity of lava flows and clastic particles, (2) increasing proportion of volcaniclastics, and (3) increasing percentage of heterolithologic breccias and mass-wasting deposits. Based on these criteria, a deep-water stage, intermediate water/shoaling stage, and emergent/island stage have been distinguished from each other in some seamount sequences. The uplifted seamount series of the basement complex of La Palma, tectonically undeformed and well exposed, reflects the growth stages particularly well (Fig. 3).

A. Deep-Water Stage

Most seamounts form on oceanic crust or marine sediments, generally starting in deep water (1000–5000 m). They grow by intrusive and extrusive activity in roughly equal portions (Fig. 3A). Initially, dike and sill intrusions into the marine sediments lead to complex intrusive complexes including nonexplosive peperites formed by interaction of magma intruding wet sediments. Repeated intrusions cause doming of the overlying sediment blanket, resulting in redepositional processes (Fig. 3A). During the deep-water stage, continuous but variable magma production rates under high hydrostatic pressure contribute to nonexplosive extrusive activity resulting in pillow and sheet flow volcanoes. Individual pillow sequences are up to 200 m thick and commonly start with massive pillow flows and/or megapillows at the very base displaying significantly decreasing diameter toward the top. Minor amounts of hyaloclastites, locally accumulating in hyaloclastite flows on seamount summits, are intercalated with the pillows and sheet flows and pelagic ooze. The hyaloclastites consist of nonvesicular sideromelane slivers, which form by spalling of the glassy crust of submarine lavas due to cooling contraction. As the seamount grows, the slopes increase and steep fault scarps evolve, causing redepositional processes. This flank facies is dominated by clastic products consisting of monolithological pillow and pillow fragment breccias caused by fragmentation and breakup of lava flows descending the slopes (Fig. 3B). They are commonly deposited by debris flows on the flanks and in the more distant aprons. The basal extrusive portion of the La Palma seamount consists of 76% pillow lavas and 5% sheet flows, representing the core facies and 19% clastic rocks abundant in the summit region and in the flank and apron facies of the seamount. The extrusives are intruded by (1) a massive sheeted "sill swarm," making up roughly 50% of the seamount series, and (2) feeder dikes. The deep-water stage is dominated by quiet effusive activity but there is also some evidence for explosive activity at abyssal depths. Summit regions of deep-water seamounts may show calderas, craters, and pit craters, while many seamount flanks are modified by satellite cones and volcanic ridges.

B. Intermediate Water/Shoaling Stage

The intermediate water/shoaling stage (Fig. 3C) is defined by the onset of (1) increasing vesicularity of pillows and hyaloclastites and (2) hydroclastic and/or pyroclastic explosive activity. The critical depth for explosive volcanism is a function of volatile content of the magma. Explosive activity of volatile-rich alkali basaltic lavas from La Palma starts at water depths of more than 1000 m as shown by recent dredging, while volatile-poor tholeiitic lavas (~0.1 wt% H_2O) start to fragment explosively at shallow depths less than 100–200 m. For more evolved magmas and H_2O-rich basaltic magmas in subduction zone settings, explosive fragmentation depth may exceed 1500 m.

The intermediate water/shoaling stage of the La Palma seamount consists of 69% clastic rocks, 30% pillow lavas, and less than 1% massive flows. The shallow

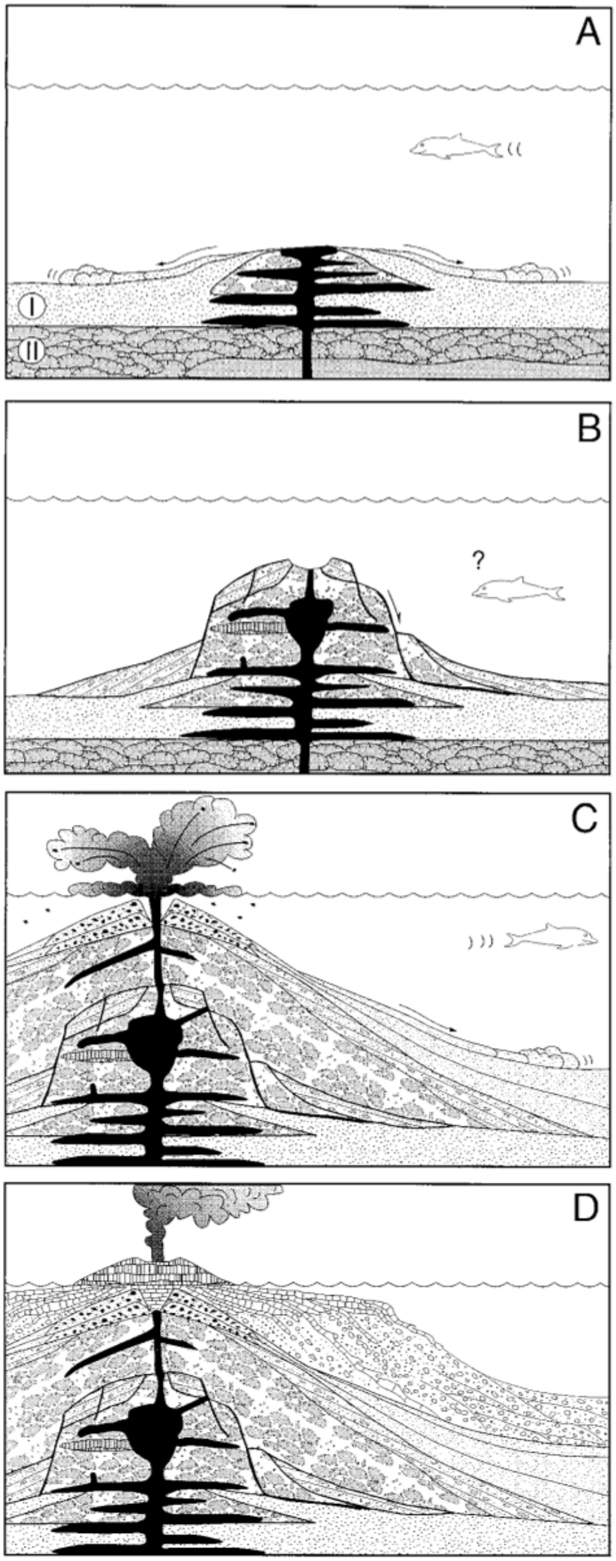

FIGURE 3 Growth stages of seamounts, based on the evolution of the uplifted La Palma seamount, Canary Islands (East Atlantic). I: Layer 1 of the oceanic crust (sediments), II: layer 2 of the oceanic crust mainly consisting of pillow lava and sheet flow lava. Fish not to scale. (A) Most seamounts on oceanic crust are formed in deep water, on top of marine sediments. Volcanic activity commonly starts with intrusion of feeder dikes and numerous sills into pelagic sediments. Intrusion-related uplift of unconsolidated sediments may cause redeposition processes. Interaction of intruding magma with water-saturated sediments may produce nonexplosive peperites and pillows. (B) In the deep-water stage, the bulk of the seamount deposits consists of extrusives (pillows, sheet flows) and intrusives (sills) roughly in same proportion representing the core facies. Continuous constructional activity produces commonly cratered, steep-sided edifices with abundant faults leading to mass-wasting processes. Mostly nonvesicular pillow breccias and pillow fragment breccias are deposited by debris flows on the flanks and in the aprons. The deep-water stage ends with the beginning of explosive eruptions during the intermediate water/shallow water stage (C). Core and flank facies may be similar to those of the deep-water stage but the deposits are generally more vesicular. During the final subaqueous stage, explosive surtseyan activity produces submarine tuff cones consisting of dominantly coarse-grained deposits in the vent area while more distal grain size decreases. Most of the loose clastic material generated during this stage is redeposited by debris flows on the flanks and in the aprons of the seamount. The upward growth of tuff cones above sea level marks the transition to the emergent stage (D). If the vent area becomes isolated from the sea, lava flows are produced, forming lava deltas when entering the sea. The lava delta sequences consist of coarse-grained, foreset-bedded hyaloclastite breccias, pillows, and sheet flows overlain by subaerial lava flows. The boundary between quench fragmented hyaloclastite breccia and subaerial lava flows marks the sea level at the time of formation. [Adapted from Staudigel, H., and Schmincke, H.-U. (1984). The Pliocene seamount series of La Palma/Canary Islands. *J. Geophys. Res.* **89**(B13), 11,195–11,215. Copyright © 1984 American Geophysical Union, with permission of H.-U. Schmincke.]

water succession can be subdivided into a core and a flank facies, but, compared with the deep-water stage, the deposits are generally more vesicular. The core facies is dominated by scoriaceous, amoeboid pillows and associated scoriaceous lapilli breccias. Accumulation of large tephra volumes, combined with continuous intrusive activity, leads to the instability of the loose tephra pile and generates debris flow breccias deposited on the flanks and in the aprons.

On large seamounts, complex shelves can develop distant from vent areas. These shelves consist of thin units of pillow lava and associated pillow breccias and hyaloclastites with abundant fossil debris and small patch reefs.

During the final subaqueous stage of seamounts (Fig. 3C), surtseyan eruptions generate submarine to subaerial tuff cones. Clast formation is mainly governed by (1) disruption of magma due to explosive release of magmatic volatiles (pyroclastic fragmentation); (2) cooling contraction granulation (quench fragmentation), and (3) steam explosions due to magma–water interactions. The juvenile glassy clasts of variable vesicularity are characterized by blocky shapes and are mixed with accidental clasts. The dominantly coarse-grained deposits are massive to crudely bedded. The occurrence of rounded and oxidized fragments, and aerodynamically formed bombs indicate very shallow water conditions with significant impact of wave action and subaerial volcanic activity.

C. Emergent Stage to Island Stage

The emergent stage (Fig. 3D) is characterized by the upward growth of tuff cones above sea level. Associated pyroclastic deposits consist of stratified and cross-stratified fine-grained lapilli and ash with abundant bomb sags, originating from base surges and fallout. Accretionary lapilli and armored lapilli are common. Hydrovolcanic cones consist mainly of loose tephra and are therefore easily eroded by wave action. Phreatomagmatic explosions cease only when the vent area becomes isolated from the sea, and quiet effusions start building a resistant lava cap leading to the stabilization of an island (island stage). Lava flows entering the sea (1) may generate littoral cones and/or (2) may quench fragment and produce coarse-grained hyaloclastite deltas and flow-foot breccias, also termed lava deltas. The stable island stage is established once the unstable tephra pile is covered with voluminous subaerial lava flows forming massive shield volcanoes such as at Kilauea (Hawaii).

D. Erosional Stage

Seamounts that reach the island stage will get truncated in time due to wave erosion and thermal subsidence of aging lithosphere and thus submerge and reestablish as a seamount. Throughout the evolution of volcanoes (seamount stage, island stage, drowned island stage), constructional shapes are frequently modified by destructive processes such as landslides. The most reasonable mechanism providing the impetus for such mass wasting events is earthquakes triggered by magma injections along rift zones. The enormous dimensions of large-scale submarine mass wasting were first recognized along the Hawaiian ridge where landslides cover about one-half of its submarine flanks. Based on morphology and degree of dislocation, landslides can be grouped into (1) slumps and (2) debris avalanches. Slumps are slow rotary movements of largely undeformed masses along discrete shear planes. The slump deposits commonly display transverse ridges with incorporated blocks up to several kilometers in diameter. In contrast, debris avalanches are fast long-runout mass movements (debris slides) up to several tens of kilometers in length in which fragmentation has reduced the landslide mass to individual blocks during sudden slope failures. Debris avalanche deposits form aprons of distinctively hummocky terrain and are generally thinner (0.05–2 km) than slump deposits (<10 km). The largest submarine landslides off Hawaii may reach volumes of up to 5000 km^3, and appear to occur late in the period of active shield growth (island stage) when the volcanoes are close to their maximum size and unstable. In the Canary Islands (East Atlantic) and on Reunion (Indian Ocean), large landslides also have occurred during subaerial volcanic phases (post-shield building). The source areas of landslides are marked by subaerial and submarine scars, embayments, and amphitheaters commonly in strike with submarine canyons.

E. Drilling Results

Similar emplacement and fragmentation processes and corresponding rock types of a shoaling seamount can be deduced from drilling the volcaniclastic apron of ocean islands. The lowermost cores of a systematic study of a volcanic apron (Ocean Drilling Program, Leg 157) extending seaward off Gran Canaria (Canary Islands, East Atlantic) consist of fine-grained hyaloclastite debris flow deposits rich in nonvesicular sideromelane shards formed during eruptions in moderate water depth (>500

m). Vesicularity increases upward, culminating in extremely vesicular ash and lapilli thought to have been produced during very shallow-water explosive activity. The change from shallow submarine to emergent volcanism is represented by coarse-grained lithic-rich breccias and hyaloclastite debris-flow deposits interpreted to originate from collapsed lava deltas at the island–shore interface. The deposits of the island stage consist predominantly of sand-sized epiclastic turbidites. The thin turbidite beds (1–40 cm) are composed dominantly of tachylitic and lesser amounts of altered vesicular sideromelane shards, rounded basalt fragments chiefly derived from erosionally fragmented scoria and lava flows, and minor thick-walled biogenic debris from the littoral environment.

VII. HISTORICAL OBSERVATIONS OF EMERGENT SEAMOUNTS

Why are there huge numbers of seamounts on the seafloor and only a very small number of volcanic islands? First, and probably the main reason, constructional volcanic activity of most seamounts ceases before the edifices reach the water surface because of insufficient magma production rates. Second, as mentioned earlier, the very small number of seamounts that grow large enough to become islands are stabilized only once hydrovolcanic activity changes to continuous strombolian/hawaiian eruptions including lava flows, which begin to weld the island into a more solid structure. But most emerging seamounts never develop beyond the point of hydrovolcanic activity and disappear quickly due to wave erosion.

A. Graham Island (Mediterranean)

A famous example of a shallow submarine to emergent hydrovolcanic eruption took place in the Mediterranean in 1831, located between Sicily and Libya, resulting in an ephemeral island (Graham Island). On June 28, earthquakes were followed by discolored and spouting water, and vigorous steam jets were observed by English seamen on July 10. By July 18, a small cratered islet with a breach to the southwest appeared, rising only a few meters above sea level. Its maximum dimensions of almost half a kilometer in diameter and about 60 m high were reached by the middle of August. During early August, when the eruption was nearing its climax, written comments and sketches of naval officers indicate continuous white steam plumes with intermittent explosively ejected masses of dark cinder and ash resembling cypress trees or cock's tails, a typical scenario characteristic for shallow water to emergent hydrovolcanic, or surtseyan, explosive activity. A painting of a late-stage eruption of Graham Island illustrates a steep-sided edifice resembling tuff cone morphology. Inside the central crater, an active scoria cone ejecting ash and incandescent lava lumps provided evidence for insulation of magma from seawater and thus transition from surtseyan to strombolian activity. By the end of August, the constructional activity had ceased. Since the island consisted of abundant tephra and was lacking in resistant lava flows, the edifice was rapidly eroded by wave action. By the end of October, after only 3 months, the island was more or less leveled to sea surface and by the end of December it had almost disappeared.

B. Metis Shoal (Tonga Islands, Southwest Pacific)

Metis Shoal is one of the most active volcanoes of the Tonga-Kermadec volcanic arc. Throughout historic times, the normally submerged volcano has been reported to be the site of numerous submarine eruptions, five of which produced ephemeral islands. The island-forming eruptions in 1967–1968 and 1979 generated tuff cones consisting mainly of dacitic pumice and lithic clasts, but no lava flows. The loose tephra piles were soon washed away by wave action and ocean currents, leaving a shoal. In contrast, the most recent eruption of Metis volcano in June 1995 generated a voluminous lava dome accompanied by discolored water and minor explosions that were producing ash-laden eruption columns but no pumice. The maximum dimensions of the island were reported to be 200–500 m across and 50–80 m in height. In contrast to the tuff cones, the 1995 lava dome is more resistant to erosion and may persist for some time.

C. Myojinsho Area [Izu-Ogasawara (Bonin) Arc, Japan]

The Myojinsho area, located close to the Bayonnaisse Rocks about 420 km south of Tokyo, is reported to have erupted more than ten times since 1952. The island-forming eruptions in 1952–1953—one of the best documented shallow submarine silicic eruption periods in historic time—included hundreds of phreatomagmatic explosions characterized by episodic dome extrusions, explosions, and associated dome collapses punctuating intervals of relative quiescence. The deposits are mainly composed of dacitic nonvesiculated lithic clasts derived from dome collapses forming a symmetric cone. Moreover, significant amounts of pumice were produced during large pyroclastic eruptions, some of which took place subaerially while others were submarine. On three occasions, dacite domes protruded above sea level forming ephemeral islands as much as 300 m long and up to 100 m high (September 1952 to August 1953). Dome growth was accompanied by discolored water and intermittent phreatomagmatic eruption columns rising up to 2000 m above the sea surface.

The danger of such shallow submarine explosive eruptions is illustrated by the tragedy that befell Japanese research vessel No. 5, *Kaiyo-maru.* When approaching the temporarily quiescent Myojinsho area on September 24, 1952, a vigorous phreatomagmatic eruption destroyed the ship, killing all 31 people aboard.

Many emergent seamounts were reported in historical time in addition to the three examples just described. The most famous example, the island-forming eruptions of Surtsey from 1963–1967, is excluded here because it is treated in the chapter on Surtseyan and Related Phreatomagmatic Eruptions.

VIII. GUYOTS AND ATOLLS

Volcanic islands become submerged after volcanic activity ceases because of thermal subsidence of the underlying oceanic lithosphere, the load of the edifice, and erosion. Charles Darwin first identified drowned ancient volcanic islands, later termed *guyots.* Guyots are characterized by flat to hummocky summit regions covered with beach pebbles, cobbles, and boulders of volcanic rocks.

Guyots may have complex flattish summits (Fig. 4). The irregular topography of the summit regions results from simultaneous shoreline erosion and thermal subsidence of oceanic lithosphere leading to plateau relief ranging from several hundred meters for smaller guyots to more than 1 km for large ones. Ideally, truncation leads to conical summit forms, whose apex represents the last speck of the island to disappear into the surf. Small-scale topographic irregularities result from differences in erosional resistance of different rock types. The flattish tops are located between 200 m and more than 5000 m below sea level. Summit plateau areas range from 14 km^2 (Thomas Washington, Geisha guyot chain, Northwest Pacific) up to 5328 km^2 (Seiko guyot, Mid-Emperor chain, Central Pacific). The height of guyots varies from 5500 to 1000 m when buried by sediments. Guyots of the northeastern Pacific are remarkably small compared to those in the western Pacific probably because most of the guyots in the western Pacific are of Cretaceous age, a period of unusually intense midplate volcanism. Some guyot chains represent hot spot tracks; others occur in clusters and subclusters.

Most guyots are circular to oval in plan but many have star-shaped outlines due to fissure eruptions along radial flank rift zones (Fig. 4). Guyots and atolls are characterized by thick clastic aprons developed during the shoaling to emergent stages, where abundant loose tephra is produced, and during the island stage (erosion, debris avalanches). Consequently, guyots are characterized by apron-related lower slopes averaging 2°–8°, whereas upper slope angles steepen as much as 24°. In general, upper slope angles decrease with increasing edifice volume and plateau area, probably due to higher effusion rates and more voluminous lava flows.

Volcanic islands located at equatorial latitudes may develop fringing reefs, and may be converted into ring-shaped atolls due to continuous upward growth of the coral reefs as the island subsides (Fig. 5). Atolls are constructional features displaying an outer rim consisting of corals while the inner lagoon consists mainly of fine-grained carbonate sediments burying the volcanic basement topography. Atolls also can originate from subaerial erosion of carbonate platforms. Sea level lowstands may lead to the emergence of carbonate platforms modified into hummocky karst landscapes including caves, channels, pinnacles, and sinkholes during subsequent subaerial weathering and dissolution of carbonate sediments. The resulting erosional landscapes include central basins surrounded by perimeter rims resembling atoll-like morphology. Thus, many atolls inherit their form from subaerial landscapes.

IX. CHEMICAL COMPOSITION

The wide range in chemical composition of seamount lavas largely depends on the tectonic setting.

A. Intraplate Setting

Magmas erupted in intraplate seamounts far from spreading ridges are interpreted to originate from rising mantle plumes. Volcanic rocks chemically resemble

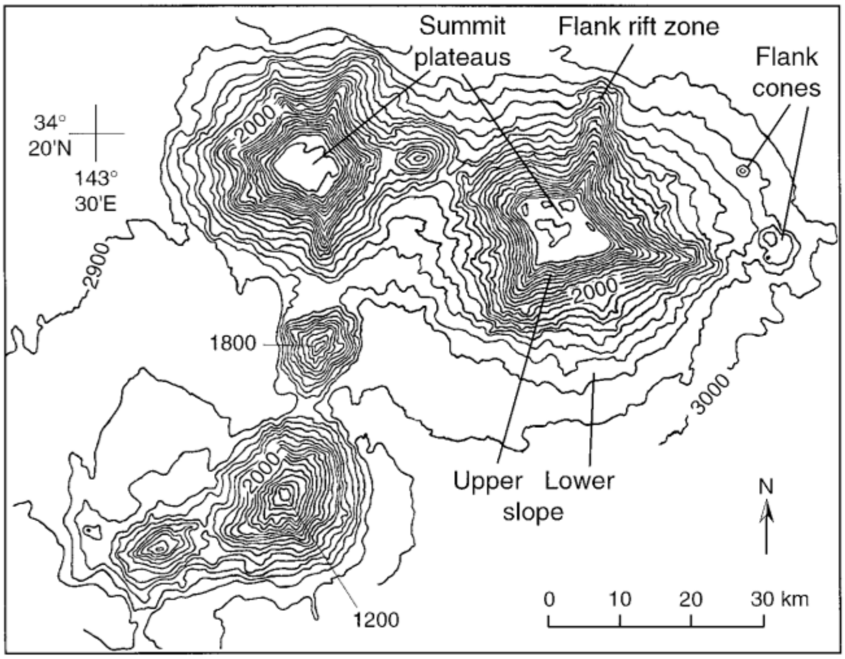
Summit
plateaus
Flank rift zone
Flank
cones
34°
20'N
143°
30'E
2000
2900
1800
2000
3000
2000
Upper Lower
slope
N
1200
0 10 20 30 km

FIGURE 4 Bathymetric chart of the Seiko seamount/guyot cluster illustrating major morphologic features of the Geisha seamount chain (northwest Pacific). The two major edifices in the upper part of the figure show flattish summit regions located 800 m below sea level, steep upper and gentle lower slopes (volcanic apron), and star-shaped outlines characteristic for guyots. The three single-peaked edifices in the lower left display uniform slope angles typical for seamounts. [Adapted from Vogt, P. R., and Smoot, N. C. (1984). The Geisha guyots: Multibeam bathymetry and morphometric interpretation. *J. Geophys. Res.* **89**(B13), 11,085–11,107. Copyright © 1984 American Geophysical Union, with permission of P. Vogt.]

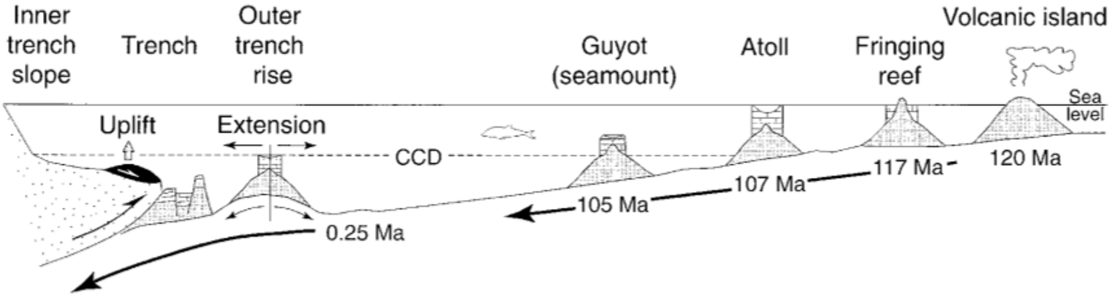
Inner
trench
slope
Trench
Outer
trench
rise
Guyot
(seamount)
Atoll
Fringing
reef
Volcanic island
Sea
level
Uplift
Extension
CCD
120 Ma
117 Ma
107 Ma
105 Ma
0.25 Ma

FIGURE 5 Evolution of volcanic island to guyot stage, ending with subduction of the edifice: the Daiichi Kashima seamount (Japan trench) illustrated. The Barremian to early Aptian midplate volcano originated on 20-Ma-old oceanic crust in equatorial regions of the Pacific. Combinations of plate motion, thermal subsidence of the lithosphere, load of the edifice, erosion, and sea level fluctuations led to the truncation of the island, formation of a fringing reef, and an atoll in early Albian time. After more than 100 Ma of drift, the guyot approached the outer trench rise (bulge) and subsequently became fractured by a trench-parallel normal fault system due to extensional stresses. The sediments of the lower inner trench slope were uplifited by the colliding guyot and subsequently redeposited. Note the existence of the reef complex below the carbonate compensation depth (CCD) due to thermal subsidence outpacing carbonate dissolution. [Adapted from Konishi, K. (1989). Limestone of the Daiichi Kashima seamount and the fate of a subducting guyot: Fact and speculation from the Kaiko "Nautile" dives. *Tectonophys.* **160,** 249–265. Copyright © 1989 Elsevier, with permission from Elsevier.]

ocean island basalts (OIB) and are characterized by an enrichment in incompatible trace elements. They range widely in chemical and isotopic composition depending on the depth and degree of partial melting and the composition and mineralogy of the mantle source. Loihi, which is the youngest volcano of the Hawaiian–Emperor chain, features a complex range of basalts including older alkali basalts and basanites, and younger tholeiites and transitional basalts. Seamount lavas of the Society hot spot region (South Pacific) consist of ankaramites, picrites, alkali basalts, basanites, tephrites, and trachytes and thus show a wide compositional range in their LILE (large ion lithophile elements, e.g., K, Nb, Zr, and Ba) and compatible element variations. Lavas recovered from seamounts and guyots in the Gulf of Alaska and from an uplifted seamount (Porto Santo, Madeira Archipelago, East Atlantic) include alkali basalt, hawaiite, mugearite, benmoreite, and trachyte, reflecting a temporal evolution of alkali-rich magmas that is typical for intraplate volcanoes.

The chemical evolution of intraplate seamounts may resemble the four eruptive stages of Hawaiian volcanoes (e.g., some seamounts northwest of Samoa Islands, West Pacific). Initial volcanic activity (preshield stage) is dominated by alkalic and transitional basalts as well as basanites. During the shield stage, when more than 95 vol% of the edifices are built, tholeiitic basalts are erupted. The post-shield stage consists of alkalic/transitional basalts to trachytes. Finally, SiO_2-undersaturated lavas such as nephelinites and melilite nephelinites with minor alkalic basalts and basanites are produced resembling the rejuvenated or posterosional stage in the Hawaiian cycle.

B. MOR Setting

The lavas of most small cones built at the axis of MORs or in their vicinity are chemically identical to depleted midocean ridge basalts (N-MORB) in terms of major and incompatible trace elements. Both low-relief seamounts formed in the axial valley of the MAR (50–600 m high) and very close to the ridge crest of the EPR (50–300 m high) are interpreted to originate from spreading center magmas. However, many larger edifices (300–>1000 m high) in the vicinity of the EPR show a more complex chemical evolution. Basal parts consist of tholeiitic MORBs, whereas the upper parts contain transitional and locally more enriched alkalic lavas comprising a continuous mixing line.

Despite the fact that most off-axis seamount lavas compositionally resemble MORB they are generally more primitive (higher MgO content) and chemically and isotopically more diverse than axial MORB. Major element concentrations and isotopic variability indicate that near-ridge seamounts are produced by smaller extents of partial melting at slightly higher pressure than axial lavas, preserving evidence of small-scale heterogeneities in the mantle source region. Seamounts formed at progressively greater distances from active spreading ridges may exhibit a shift from depleted to enriched mantle sources and thus mark the transition from ridge- to hot spot-related magma sources.

C. Island-Arc Setting

Island-arc seamount lava compositions range from basaltic to rhyolitic and are dominated by andesitic lavas while tholeiite basaltic and shoshonitic (very alkalic) lavas are rare. Chemical and isotopic compositions vary widely suggesting that (1) a mantle source with affinities to MORB is contaminated by variable degrees of crustal components such as sediments and/or fluids derived from the subducted slab, (2) subducted oceanic crust is hydrothermally altered, and (3) primary heterogeneities of the mantle wedge underlying the volcanic arc may exist. Generally, arc lavas are characterized by selective enrichment in incompatible trace elements of low ionic potential (Sr, K, Rb, Ba) which become easily mobilized from the subducted slab. Lavas of the Kermadec arc (Southwest Pacific) both from seamounts and islands contain more radiogenic Pb and have higher heavy rare earth element (e.g., Tm, Yb, Lu) concentrations than lavas of the southward extending Tonga arc interpreted to be the result of variable amounts of sediment being subducted beneath the arc. Along the Kermadec trench, oceanic crust is covered with a 1000-m-thick layer of sediments compared with approximately 200 m in the southern extension along the Tonga trench. In contrast, the strongly calcalkaline series (andesites to rhyodacites) of Piip seamount (western Aleutian arc, North Pacific) is not enriched in radiogenic Pb probably because the sediment cover has been scraped off by the long, oblique subduction path beneath the forearc. Sediments were accreted rather than subducted and thus do not affect melt composition.

In the uplifted Tok Islands (Korea), for example, the submarine sequence is made of potassic trachytic lavas and related trachytic breccias, whereas the underlying rocks are basaltic in composition.

The lavas of the submarine volcanoes of the Northern Seamount Province (NSP) in the northern Mariana arc (Japan) belong to low-K to very high-K (shoshonitic) series. They include tholeiitic basalts, andesites, dacites, and rhyolites significantly enriched in LILE and light rare earth elements (LREE, e.g., La, Ce, Pr, Nd). The alkalinity increases along-strike toward the north. Moreover, the shoaling to emergent dome of Myojinsho and the ejecta of the caldera-forming submarine pyroclastic eruption at Myojin Knoll and others, also part of the NSP, are more silicic including dacite and low-K rhyolite.

The lavas of the Kasuga backarc basin seamounts (northern Mariana Trough, Japan) vary widely from basaltic to dacitic including low-K calcalkaline basalts to high-K shoshonites.

X. HYDROTHERMAL ACTIVITY

Hydrothermal exhalations at seamounts, discovered in the early 1980s, are important as (1) sources of mantle-derived fluids and gases and as locations of (2) Earth's heat release, (3) polymetallic sulfide deposits, and (4) geochemical exchange between oceanic crust and seawater. The toxic environment generates unique biological ecosystems with abundant bacteria supporting a community of exotic and specialized macrofauna.

A. Hot Spot Seamounts on Active Spreading Centers

Hydrothermal activity of Axial Seamount, an active ridge axis volcano at the intersection of the Juan de Fuca Ridge and the southeastern end of the Cobb-Eickelberg seamount chain (East Pacific), is influenced by both hot spot volcanism and seafloor spreading.

Hydrothermal vents are concentrated within the Axial Seamount Hydrothermal Emissions Study (ASHES)-vent field (200 × 1200 m) located adjacent to the southwest wall of the summit caldera. Low-temperature exhalations (19°–35°C) are dominantly diffuse while focused venting is rare and commonly fracture-controlled or associated with cracks in nearly cooled lava flows. Typical deposits are orange, Fe-rich, amorphous silicates, rarely forming chimneys up to 1 m high.

High-temperature vents (136°–330°C) are restricted to an area of 80 × 80 m within the fracture-controlled ASHES-vent field. They emanate directly from young lava flows. High-temperature vents predominantly form irregularly shaped massive sulfide chimneys, <2 m in basal diameter and about 1–5 (10) m high, while anhydrite edifices are subordinate. The sulfide chimneys are composed of primary Zn-rich and Cu-poor mineral precipitates contrasting with other Juan de Fuca Ridge hydrothermal sulfide deposits in having higher concentrations in Ra, Au, and Ag. High-temperature hydrothermal fluids are commonly acidic (pH $\sim$3–4) and range in composition from gas-enriched (CO_2)/low-chlorinity (66% depleted relative to seawater) fluid to gas-depleted (CO_2)/high-chlorinity (16% enriched relative to seawater) fluid. The large compositional variability is interpreted to result from phase separation (liquid and vapor) of a single fluid rising through the oceanic crust. High- and normal chlorinity vent fluids compositionally resemble vent fluids found at other MOR hydrothermal areas while low-chlorinity, metal-depleted fluids have no counterparts in the literature on MORs. The sites of active low- and high-temperature venting are colonized by specialized, endemic fauna representing unique ecosystems. Typical communities are composed of vestimentiferan tube worms, clams (*Calyptogena* sp.) hosting sulfide-oxidizing endosymbiotic bacteria and bacterial mats.

B. Intraplate Hot Spot Seamounts

Only a few intraplate hot spot seamounts of alkalic composition are known to be hydrothermally active, for example, Loihi seamount south of Hawaii (Central Pacific), Teahitia and Moua Pihaa seamounts, and Macdonald seamount (Southwest Pacific). Low-temperature (<30°C) vent fields from the summit region of Loihi seamount, recently destroyed by younger volcanic activity, were associated with brecciated pillow lava cones. Acidic vent fluids (pH $\sim$5.4) are enriched in, for example, CO_2 Fe, and ^{3}He and depleted in Mg, SO_4, and Cl relative to ambient water. Their composition is very similar to low-temperature hydrothermal fluids of MORs but differs in having a very high concentration of dissolved CO_2 more than 10 times the highest reported values for MORs. Combined with high ^{3}He concentrations, the enrichment of these volatiles is interpreted to originate from degassing of an alkalic, volatile-rich magma body into seawater-derived hydrothermal fluids. Venting is characterized by diffuse flow regimes resulting in nontronite, iron-rich smectite, iron-rich oxide, and silica deposits with abundant bacterial mats. High-temperature hydrothermal mineral assemblages were discovered subsequently after formation of a pit crater in 1996. Acidic vent fluids (pH ~5.6) are significantly enriched in Fe, Mn, CH_4, H_2, and CO_2 with respect to ambient seawater. Sulfide and sulfate minerals such as pyrite, pyrrhotite, wurtzite, and barite are abundant near fractures and fissures associated with the pit crater. The sulfide mineral assemblage indicates fluid temperatures of approximately 250°C.

Although Loihi hydrothermal fluids resemble MOR fluids, fluid chemistry, presence of alkalic lavas, and the absence of benthic macrofauna communities suggest that vents at intraplate hot spot seamounts may differ from those found at MORs. Even though bacterial populations are present, which are the base of the food chain at hydrothermal vents, the expected macrofauna is lacking, probably the result of spatial isolation and the young age of Loihi volcano.

C. Seamounts in Island-Arc Settings

Observations of active venting related to island-arc seamount volcanism are rare. Low-temperature (~39°C), gas-rich vent fluids from Kasuga seamounts are unusually enriched in Mg (+27%) and in SO_4 (+17%), and depleted in Ca (−64%) relative to ambient seawater, contrasting with Loihi and MOR low-temperature hydrothermal fluids, which show the opposite enrichment/depletion pattern.

Volcanic seamounts in the Papua region (New Guinea, West Pacific) located in extensional forearc settings (e.g., Conical seamount, south of Lihir Island) and in the extensional Woodlark Basin (Franklin seamount) are characterized by Au and Ag mineralizations.

In conclusion, the chemistry of hydrothermal fluids and associated deposits shows small-scale variations. Within a given hydrothermal field (e.g., ASHES vent field) fluid composition, temperature, and deposits may vary significantly due to the (1) location of active vents, (2) cooling history of erupted material, and (3) fracture patterns of the crust. Studies of hydrothermal vents around the world have shown that the chemical composition of hydrothermal fluids correlates particularly well with the composition of the surrounding crust. Thus, the chemistry of the substrate seems to control fluid composition and mineral precipitates reflecting the tectonic setting.

XI. SIGNIFICANCE OF SEAMOUNTS

A. Plate Tectonics

Some volcanic island and seamount chains within ocean basins (e.g., Hawaiian–Emperor chain) show a progressive decrease in age toward the active spreading ridge and thus help to reconstruct velocities and directions of tectonic plates in time and space. Moreover, the thermal subsidence of the oceanic crust during aging is represented by drowned oceanic islands and subsiding atolls (Fig. 5). Both observations have contributed fundamentally to the acceptance of both "hot spot" theory (mantle plumes) and global plate tectonics.

B. Thermomechanical Properties of the Oceanic Crust

Seamounts and their volcaniclastic aprons are significant loads on the oceanic lithosphere. The response of the lithosphere to these loads, commonly a downward flexure, is used to infer its thermomechanical properties such as elastic thickness, density, and age-dependent static equilibrium. Thermal rejuvenation of the lithosphere due to reheating caused by thermal anomalies in the mantle and subsequent dynamic uplift as well as underplating processes counteract subsidence.

C. Formation of Oceanic Crust

The study of seamount morphology and abundance along MORs in the Pacific and Atlantic provides basic insights into the construction of the oceanic crust reflecting the magma plumbing systems in different thermal regimes. Abundant coalescing seamounts and associated fissure-fed lava flows along the axial zone of slow spreading MARs are building central volcanic ridges and thus are primary sites of crustal construction (Fig. 2) in a cool thermal regime with low magma supply. These small cones are probably fed by single feeder tubes associated with temporary intermediate-sized magma chambers, which solidify to gabbros forming the lower crust. Consequently, the structure of the oceanic crust at slow spreading ridges differs fundamentally from fast spreading Pacific crust (hotter thermal regime with higher magma supply) where the main crust-forming volcanism along the axial zone is dominated by fissure eruptions leading to sheeted dike complexes and lava sequences with abundant sheet flows.

D. Composition of the Upper Mantle

The areal distribution and wide compositional range of basalts combined with enriched MgO content of near-ridge Pacific seamounts suggest that they are not fed by the ridge-axis magma chamber. They may originate from numerous, isolated batches of magma generated in a heterogeneous mantle rising through the crust without prolonged storage in magma chambers. Consequently, near-ridge seamount magmas are not affected by crustal-level fractionation processes and thus may characterize the chemical composition of the upper mantle in more detail than ridge-axis magmas that have undergone mixing in subaxial magma chambers and mush zones resulting in compositionally more uniform magma.

E. Seamount Asperities

Obduction processes lead to incorporation of volcanic seamounts in accretionary prisms at convergent margins. Seamounts display significant asperities of oceanic lithosphere when subducted. Small seamounts (<40 km in diameter) approaching trenches are fractured by trench-parallel extensional faults at the outer trench rise (Fig. 5) similar to, or to a greater degree, than surrounding seafloor, whereas larger seamounts (40–100 km in diameter) show less evidence of fracturing prior to subduction. Large seamounts may interrupt normal subduction, which may be responsible for gaps in Beni-

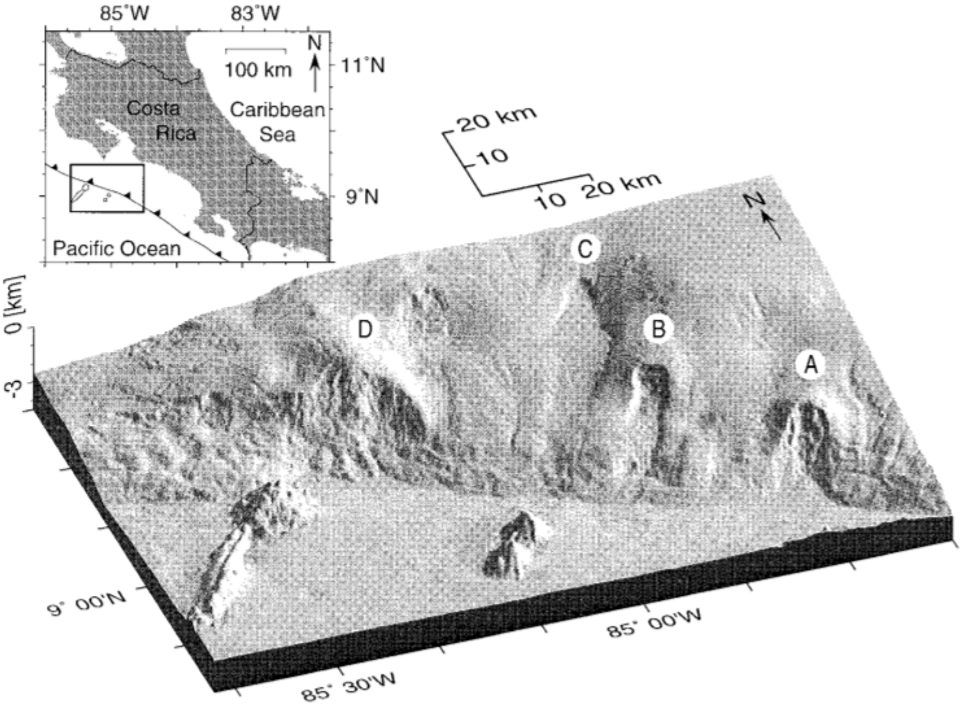

FIGURE 6 Seamount traces at the Pacific continental margin of Costa Rica. The right half of the figure shows three stages of furrows systematically increasing in age from A to C, produced by seamount impact on the continental margin. The youngest and shortest furrow (A) displays a V-shaped embayment, sediment uplift along the sides, and a low landward mound. Subsequent collapse of oversteepened slopes is sending slump blocks from the sides into the center. Point B shows a furrow where the breached lower slope has been reconstructed along the trench axis. Point C is the longest furrow (55 km) illustrating a subdued topography and a low slump scar at its head compared with those from A and B. Note that furrow C is on strike with the two seamounts in the foreground, evidence for subduction of a seamount chain. Impact of more complex feautres than single seamounts (e.g., volcanic ridges) (D), may produce highly irregular features at the continental margin. [From von Huene, R., Ranero, C. R., and Weinrebe, W., in prep., Subduction of Cocos plate segmentation and convergent margin tectonics of Costa Rica. Preprinted with permission of R. v. Huene.]

off-zone seismicity. At convergent margins where seamounts are subducted, the continental slope is marked by a highly irregular topography lacking at margins where subducted oceanic crust is smooth.

Remarkable features are straight furrows trending parallel to the direction of relative plate convergence (Fig. 6). They are on strike with seamount chains and thus are interpreted to represent traces of seamounts that were thrust beneath the continental margin during subduction. Furrows originate when seamounts initially impact the seaward side of the continental margin and thus thin accretionary prisms. Slope sediments must flow around the subducting seamounts leaving V-shaped embayments and depressions behind. In front, the slope material is ponded, folded, and uplifted during underthrusting of seamounts producing oversteepened swells, a condition that produces slides. Most furrows show sharp boundaries, whereas others are more obscured by later sedimentation (Fig. 6).

F. Faunal Communities on Seamounts

Isolated seamounts and isolated volcanic islands are characterized by a highly endemic marine fauna. Species types and population density on seamounts are governed by the occurrence of hard substrate and the local current regime. High current velocities, commonly found above seamounts, lead to a dominance of suspension feeders such as sponges, horny corals (gorgonians), black corals (antipatharians), ahermatypic (non-reef-building) scleractinian corals, anemones, tunicates, brisingid seastars, and crinoids. Based on faunistic studies of more than 100 seamounts at depths of 29–3000 m, endemism is estimated at approximately 15% among invertebrates (mainly suspension feeders) and 11% among fishes. On seamounts shallower than 1000 m below sea level, provincial species make up ~50% of the entire population, whereas on deeper seamounts (>1000 m below sea level) cosmopolitan/widespread species dominate. The increasing amount of specialized species on shallow seamounts is mainly caused by the onset of explosive volcanic activity, producing highly unstable tephra piles and thus increasing the stress on the inhabitants.

The high degree of endemism cannot be sufficiently explained by the geographic isolation alone. In addition, active seamounts are (1) highly unstable environments because constructional volcanic activity and mass wasting processes may lead to drastic and temporal changes in seamount topography through time, modifying the local current regime which controls sedimentation patterns (substratum) and thus the colonization of flora and fauna on deep hard-bottom seamounts; (2) shallow intrusions and volcanic eruptions locally heat the bottom water generating complex and chaotic convective currents; and (3) volcanic earthquakes, tectonic uplift, or submergence strongly affect the habitat of both benthic and nektonic (actively free-swimming) fauna.

This instability in time, the specific environmental conditions, and the geographic isolation generating a high-stress habitat lead to the evolution of an unusual or even unique biological community with a high degree of endemic species differing qualitatively and quantitatively from those found at continental shelves at the same latitude and at similar water depths.

XII. SUMMARY

The theories of global plate tectonics and "hot spots" were established based on areal distribution and age evolution of large intraplate seamount/island chains. The global distribution and abundance of seamounts is still highly speculative because large areas of the ocean basins have not been mapped bathymetrically, and satellite altimetry underestimates small seamounts. The size and morphology of seamounts are highly variable. In general, intraplate seamounts are much larger than seamounts in MOR settings.

The morphology of seamounts depends mainly on magma composition, eruption rate and depth, and geometry of magmatic conduits. The constructional morphology of seamounts is commonly modified by mass wasting processes that occur throughout the evolution of seamounts. Small MOR-related seamounts in fast (EPR) and slow (northern MAR) spreading settings reflect different processes in crustal accretion depending mainly on the spreading rate. Along the northern MAR, numerous tiny seamounts form in the axial zone while along the EPR larger but less abundant seamounts form off-axis. Seamounts start small, passing through several growth stages dominated by quiet effusive activity in deep water while explosive eruptions dominate the shallow water succession. If magma supply is high, upward growth may lead to the formation of ocean islands that subsequently become truncated due to wave erosion after volcanic activity has ceased. Guyots are truncated islands that have subsided due to contraction of the lithosphere—the result of cooling away from hot spots. These now inactive seamounts are passively carried on top of the moving plate, eventually ending in subduction zones. Geochemical studies of seamount lava characterize the mantle source in different tectonic settings (MOR, intraplate, subduction zones) particularly well.

SEE ALSO THE FOLLOWING ARTICLES

Debris Avalanches • Deep Ocean Hydrothermal Vents • Flood Basalt Provinces • Hawaiian and Strombolian Eruptions • Magmatic Fragmentation • Mineral Deposits Associated with Volcanism • Plumbing Systems • Submarine Lavas and Hyaloclastite • Surtseyan and Related Phreatomagmatic Eruptions • Volcaniclastic Sedimentation around Island Arcs

FURTHER READING

Batiza, R. (1989). Seamounts and seamount chains of the eastern Pacific. Pages 289–306 *in* "The Eastern Pacific Ocean and Hawaii" (E. L. Winterer, D. M. Hussong, and R. W. Decker, eds.). The Geology of North America, Vol. N. Geological Society of America, Boulder, CO.

Fisher, R. V., and Schmincke, H.-U. (1984). "Pyroclastic Rocks." Springer-Verlag, Berlin.

Floyd, P. A. (1991). "Oceanic Basalts." Blackie, New York.

Fornari, D. J., Perfit, M. R., Allan, J. F., and Batiza, R. (1988). Small-scale heterogeneities in depleted mantle source: Near-ridge seamount lava geochemistry and implications for mid-ocean-ridge magmatic processes. *Nature* **331,** 511–513.

Hekinian, R., Bideau, D., Stoffers, P., Cheminee, J. L., Muhe, R., Puteanus, D., and Binard, N. (1991). Submarine intraplate volcanism in the South Pacific: Geological setting and petrology of the Society and the Austral region. *J. Geophys. Res.* **96**(B2), 2109–2138.

Johnson, H. P., and Embley, R. W., eds. (1990). Axial seamount: An active ridge axis volcano on the central Juan de Fuca Ridge. Special section in *J. Geophys. Res.* **95**(B8), 12,689–12,966.

Keating, B. H., Fryer, P., Batiza, R., and Boehlert, W., eds. (1987). "Seamounts, Islands, and Atolls." Geophysical Monograph 43. American Geophysical Union, Washington, DC.

Nunn, P. N. (1994). "Oceanic Islands." Blackwell, Oxford. UK.

Smith, D. K., and Cann, J. R. (1992). The role of seamount volcanism in crustal construction at the Mid-Atlantic Ridge (24°–30°N). *J. Geophys. Res.* **97**(B2), 1645–1658.

The origin and evolution of seamounts (1984). Special section in *J. Geophys. Res.* **89**(B13), 11,066–11,292.

Wessel, P., and Lyons, S. (1997). Distribution of large Pacific seamounts from Geosat/ERS-1: Implications for the history of intraplate volcanism. *J. Geophys. Res.* **102**(B10), 22,459–22,475.

Zindler, A., Staudigel, H., and Batiza, R. (1984). Isotope and trace element geochemistry of young Pacific seamounts: Implications for the scale of upper mantle heterogeneity. *Earth Planet. Sci. Lett.* **70,** 175–195.

SUBGLACIAL ERUPTIONS

JOHN L. SMELLIE
British Antarctic Survey

I. Introduction
II. When Fire Meets Ice—An Account of a Recent Subglacial Eruption
III. In the Geologic Record, How Do We Know That Eruptions Occurred Beneath Ice?
IV. Properties of Glaciers That Affect Subglacial Eruptions
V. Basaltic Subglacial Eruptions
VI. Felsic Subglacial Eruptions
VII. Large Subglacial Volcanoes—An Untapped Source of Paleoenvironmental Information
VIII. Subglacial Volcanism—The Way Forward

GLOSSARY

breadcrust texture Texture of a volcanic bomb whose surface has cracked open due to vesiculation and expansion of the bomb interior after chilling of its surface.

continuous uprush A style of explosive eruption in shoaling volcanoes like Surtsey. Caused by a high frequency of explosions, which combine into a continuous uprush and are characterized by a tall nonspreading eruption column.

cowpat bomb Type of volcanic bomb resembling cow dung, whose flattened shape is due to its impact while still viscous.

eskers Long, low, narrow steep-sided sand and gravel ridges formed within ice tunnels by retreating glaciers.

hyaloclastite breccia Coarse volcanic rock composed of angular glassy fragments formed by quenching of magma by water.

jökulhlaup Glacier outburst flood often, but not always, related to eruptions.

palagonite Conspicuous yellowish alteration product of hydrated basaltic glass, mainly composed of clay minerals.

passage zone Subhorizontal junction between flat-lying lavas and steep-dipping hyaloclastite breccia in a lava delta, representing the water level coeval with eruption.

pillow lava Lava, usually basaltic, with close-fitting discontinuous pillow-shaped masses usually <1 m in diameter, formed as a result of subaqueous extrusion.

tephra finger jets Parcels of bombs, wet tephra, and gas that follow spreading parabolic trajectories and are ejected by discrete, relatively low frequency shallow explosions.

tindar Ridge- and cone-shaped successions of tephra (tuff and lapilli tuff) from subglacial eruptions, deposited in a water-filled vault or lake thawed in a glacier by volcanic heat.

tillite Glacial deposit (also known as boulder clay) consisting of clasts up to boulder size dispersed in sandy-muddy matrix.

trachyte Fine-grained lava with an alkaline composition, typically with prominent large alkali feldspar crystals.

Copyright © 2000 by Academic Press
All rights of reproduction in any form reserved.

turbidite Sediment or rock deposited from a gravity-driven flow of suspended sediment in water (turbidity current), characterized by well-developed sedimentary structures arranged in a regular sequence.

tuya Flat-topped, steep-sided volcano (also known as a table mountain) that erupted into a lake thawed in a glacier by volcanic heat.

I. INTRODUCTION

Subglacial eruptions are those that occur from a vent situated beneath a valley glacier or ice sheet. They may be explosive or nonexplosive and typically involve substantial volumes of water generated by melting the overlying ice. Construction of the volcano takes place within the ice sheet (i.e., englacially). Because of the intimate association with meltwater, subglacial volcanoes are sometimes indistinguishable from other volcanoes constructed in nonglacial aqueous settings (e.g., volcanoes in lakes or beneath the sea). However, eruptions beneath ice can result in diagnostic structural features in the volcanic sequences. Ice is widely distributed on Earth. It is mainly found in temperate and polar regions, but also occurs in mountainous terranes at lower latitudes and even within the tropics. The largest areas of continuous ice sheets are confined to the polar regions and Greenland, places where human populations are sparse or absent. Conversely, dense populations are commonly present adjacent to active volcanoes with glaciers and ice sheets in mountain ranges at virtually all other latitudes. The potential for devastation during subglacial eruptions may be significant and regions most at risk include parts of the west coasts of North and South America, Japan, and Iceland. Subglacially erupted volcanoes have even been postulated on Mars, where ice sheets may have been formerly much more extensive.

II. WHEN FIRE MEETS ICE—AN ACCOUNT OF A RECENT SUBGLACIAL ERUPTION

During midmorning on September 29, 1996, an earthquake of magnitude 5.4 (Richter) shook the Vatnajökull ice cap in Iceland. The ice cap is Europe's largest, with an area of 8300 km^2. It covers part of the Icelandic eastern neovolcanic zone and has been the locus of numerous subglacial eruptions during the last 1000 yr, occurring about every 10 yr during this century. An intense earthquake swarm occurred after the initial event. Activity continued at an enhanced level, culminating in continuous low-amplitude volcanic tremor. The eruption probably commenced some time between 2200 and 2300 hours on September 30. The new site, called Gjálp, was located about midway between the Grímsvötn and Bároarbunga subglacial volcanic centers in the northwestern part of Vatnajökull. It last erupted 60 yr previously. An overflight on October 1 revealed a heavily crevassed depression on the surface of the ice (Fig. 1). The depression enlarged to about 2 km in diameter and 200–300 m deep and other aligned depressions appeared, indicating an eruption along a 4- to 5-km subglacial fissure. Simultaneously, water from the eruption site poured into the subglacial cauldron at Grímsvötn at a rate of about 5000 m^3 s^{-1}, raising the 200- to 250-m-thick floating ice shelf.

At about 0500 hours on October 2, the eruption broke through the 400- to 600-m-thick ice over the fissure, forming a hole several hundred meters wide in the ice by the afternoon. Observers noted that the initial white steam column changed to a dark gray column of ash rising vertically to 0.5 km and characterized by rhythmic explosions scattering volcanic bombs. Above that, buoyant steam rose to 3 km and was deflected by a southerly wind although ash fall was minor. Later that day, the eruption column peaked at about 9 km and was associated with spectacular lightning. A large depression formed on the ice surface at another eruptive site on the fissure some 3 km north of the earlier sites. The sites were linked by a shallow linear trough in the ice surface caused by overflow and melting in a subglacial pathway.

Activity continued during the next week. The eruptions were described as pulsating, with periods of quiet alternating with explosive activity. Water was observed about 200 m below the original ice surface at the active vent site and the erupting fissure extended to 9 km. On October 4, explosive eruptions seemed to be occurring through a water column at least 50 m deep. Volcanic tremors ceased on October 13 and there was no explosive activity thereafter. By then, the eruptive fissure was marked by two large ice cauldrons, with the formerly most active crater represented by a low moundlike island of dark steaming ash in the southern cauldron (Fig. 2). A prominent canyon up to 500 m wide with vertical ice walls 150 m high extended south from the island mound. Water flowed rapidly from north to south within the canyon, and disappeared into a large tunnel entrance. Much of the Vatanjökull ice cap was covered by a thin ash layer.

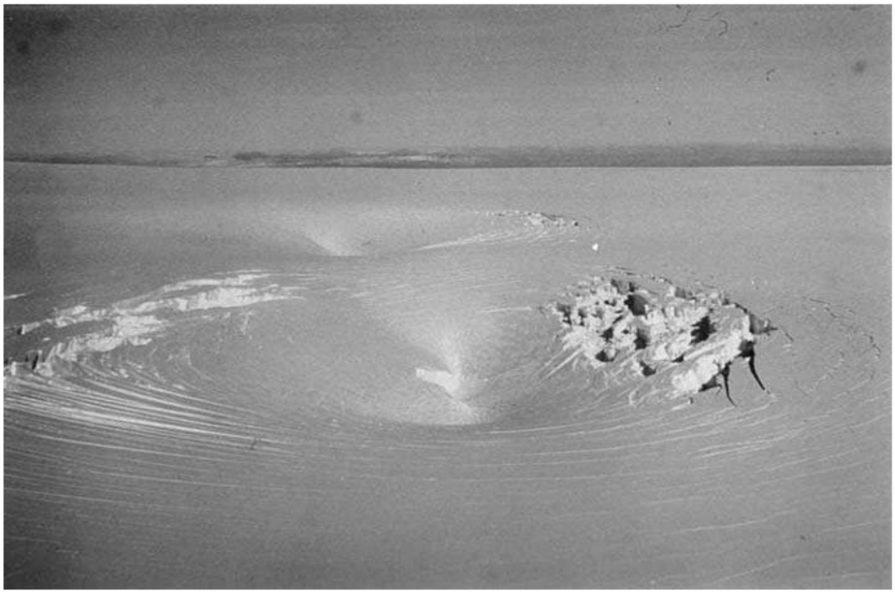

FIGURE 1 Depressions in the surface of the Vatnajökull (Iceland) ice sheet formed by subglacial melting, 15 hours after the start of the October 1996 eruption. The foreground depression is about 100 m deep and both are about 2 km wide. [Photograph by M. T. Gudmundsson.]

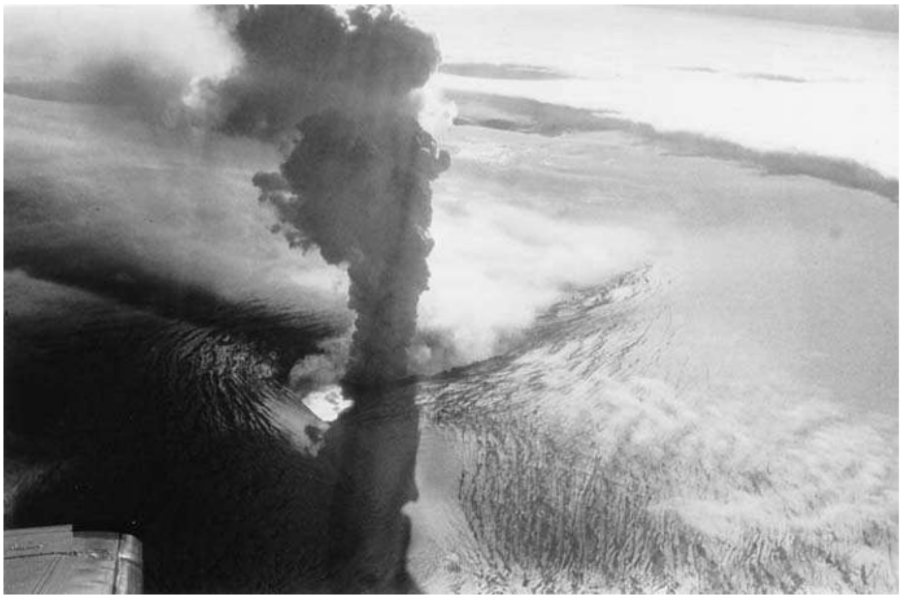

FIGURE 2 Eruption column above a pyroclastic cone (obscured by gases) surrounded by glacially confined meltwater derived by melting of the ice. The meltwater overflowed the glacier southward (away from the observer) within a deep ice canyon. [Photograph by M. T. Gudmundsson.]

During the eruption, Icelandic scientists anxiously monitored the depth of water in the Grímsvötn caldera. Jökulhlaups (glacier outburst floods) occur every 4–6 yr from the subglacial caldera and the hydrologic characteristics of the system were thought to be quite well known. Past experience suggested that flooding would occur when the lake level reached 1455 m above sea level. That level was reached by October 3 and an imminent jökulhlaup was predicted. By October 4, water levels were higher than at any previous time this century, although a comparatively low flood surge was anticipated. By October 7, with no flooding yet evident, the local experts stopped forecasting. About 3 km^3 of meltwater was stored in the Grímsvötn cauldron, increasing at a rate of about 400–500 m^3s^{-1} even after explosive eruptions ceased. The rate diminished to about half by October 25 and the water rose to a final elevation of 1510 m. The jökulhlaup finally began early on November 5, reaching a rate of 6000 m^3s^{-1} within the first 2 hours and rising to 25,000 m^3s^{-1} late in the afternoon. The flood waters, carrying icebergs the size of houses and weighing up to 1000 tons, destroyed or severely damaged bridges across the Sœluhúsakvísl and Skeiðará rivers (Fig. 3). The flood waters peaked late on November 5, when about 45,000 m^3s^{-1} streamed out of the Skeioarárjökull outlet glacier and south across the alluvial floodplain, briefly making it the second largest river on Earth. The jökulhlaup ceased on November 7. A volume of 0.7–0.75 km^3 of volcanic products formed a new subglacial ridge 6–7 km long. About 4 km^3 of ice was melted above the fissure. Floods affected an area of 750 km^2, locally extending the coastline by 800 m and creating about 7 km^2 of new land. The eruption and flood were the fourth largest such events to occur in Iceland this century.

III. IN THE GEOLOGIC RECORD, HOW DO WE KNOW THAT ERUPTIONS OCCURRED BENEATH ICE?

Although parts of the Antarctic ice sheet may be half a million years old, and there is also a (disputed) record of 8-million-year-old ice preserved in Antarctic sediments, ice is normally a comparatively short-lived substance not generally preserved in sedimentary and volcanic sequences. Instead we must look at the proxy record of preserved deposits in order to interpret the eruptive environment. Criteria that have been used are listed in Table I and illustrated in Figs. 4 and 5, but it should be understood that unambiguous evidence for the former existence of ice coeval with eruptions is sometimes im-

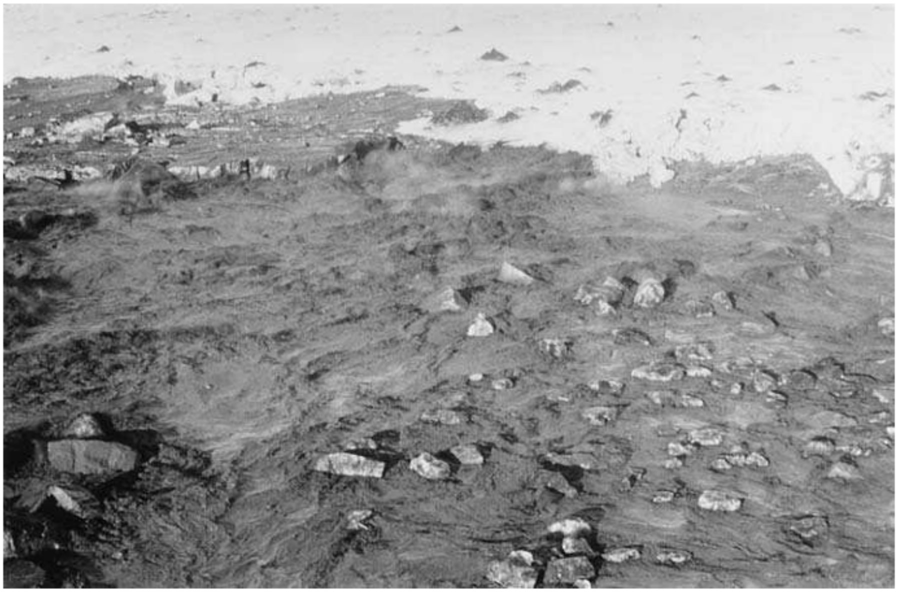

FIGURE 3 Glacier outburst flood (jökulhlaup) in Skeiðará caused by the October 1996 subglacial eruption in Iceland. The flood has entrained numerous large ice blocks, some the size of houses and individually weighing up to 1000 tons, which were ripped from the glacier margin seen at the top of the photograph. [Photograph by M. T. Gudmundsson.]

TABLE 1 Criteria Used to Determine If a Volcanic Sequence Was Erupted beneath Ice

Criteria	*Interpretation*
History of glaciation	A known history of glaciation(s), documented from other research, can at least raise the possibility that volcanic sequences were erupted in association with ice.
Paleotopography	In very young sequences (<10–15 Myr) it is often possible to assess whether the paleotopography could have been able to form lakes. Where appropriate topography was absent, ice may have been a barrier able to pond water.
Fossils	Even rapidly constructed submarine volcanoes at high latitudes are colonized by marine plants and animals soon after eruption. A lack of fossils indicates either nonmarine or severe, possibly glacial conditions.
Sedimentary structures and rock characteristics	Sedimentary structures caused by flowing or agitated water, and presence of well-rounded clasts are characteristic of shallow water or river settings. Their absence indicates a very protected environmental (possibly lake or englacial vault). The presence of these features does not exclude some subglacial environments. Association with nonvolcanic glacial deposits, such as tillites (glacial boulder clay deposits), containing dropstones or striated and facetted clasts, and sediment structures such as sediment-filled ice wedges, ice-melt collapse pits and cone or ring-shaped mounds of ice-rafted debris indicate coeval glaciation. These features are uncommonly preserved or are hard to recognize.
Structural features of the volcanic sequence	The presence of subaerially erupted and emplaced lavas and tephra, draping subaqueous deposits from the same eruption, indicates that contemporaneous water levels dropped unusually rapidly. Similarly, evidence for water level rising and/or falling between closely spaced eruptions, sometimes by up to a few hundred meters (Fig. 4), indicates a change too rapid to be caused by a (globally) changing sea level and it is more likely caused by a sudden drainage of a glacial lake by collapse of an ice barrier or time-related fluctuations of the surface elevation of an enclosing ice sheet. Outcrop-wide erosional surfaces cut by wave action are absent because of protected englacial (lake/vault) environment. Presence of striated, molded, or ice-polished surfaces within the sequence indicate coeval ice. Bedding back-tilted toward a source vent reflects the proximity of retaining ice walls, later removed by melting, against which the sediments were banked (Fig. 5).

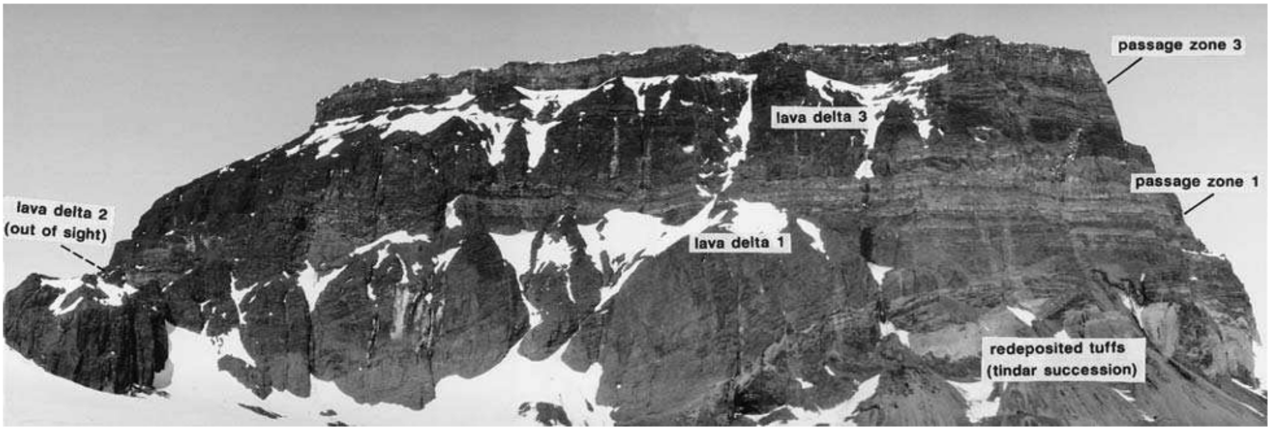
passage zone 3
lava delta 3
passage zone 1
lava delta 2 (out of sight)
lava delta 1
redeposited tuffs (tindar succession)

FIGURE 4 Nunatak constructed of three superimposed lava deltas formed beteen 6.20 and 6.50 Ma, recording very different water levels contemporaneous with each eruption. The approximate elevations of the former water levels, indicated by passage zones, are shown. Passage zone 2 is obscured in this view, but is *lower* than passage zone 1. The section is about 200 m high. Hedin Nunatak, Antarctica.

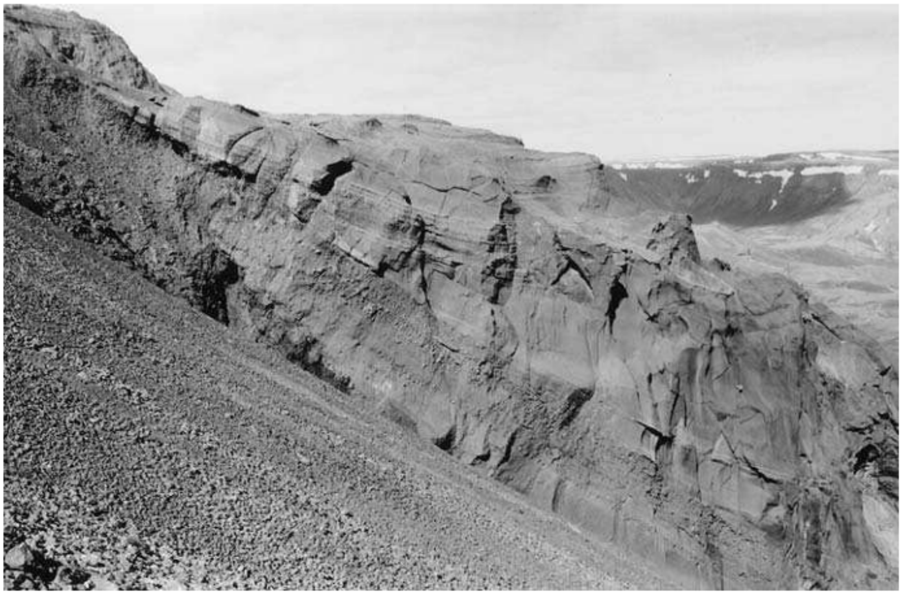

FIGURE 5 Subaqueously emplaced pillow lava (upper left side of section) and breccias and tuffs high on the flank of a subglacially constructed volcano. Bedding in the higher part of the section flattens out rapidly to the right (away from the vent) and is locally back-tilted (to the left), probably because of the proximity of former confining ice walls of a water-filled englacial chamber, against which the sediments were banked. The section is about 35 m high. Kalfstindar, Iceland.

possible to obtain. However, arguments based on several internally consistent observations are often sufficient to identify a subglacial eruptive setting.

IV. PROPERTIES OF GLACIERS THAT AFFECT SUBGLACIAL ERUPTIONS

The temperature distribution, structure, and hydrology of glaciers exert a fundamental control on subglacial eruptions. A common simple classification of glaciers is based on temperature distribution. *Temperate* glaciers are at the pressure melting temperature throughout their thickness (except in a thin surface layer), whereas *polar* glaciers are well below freezing and they are frozen to their bed. Because movement of polar glaciers takes place by internal deformation of the ice, only temperate (wet-based) glaciers are able to modify significantly their bedrock substrate. Although simplistic, the distinction into two glacier types is important, because unlike polar glaciers, water can migrate in temperate glaciers. This has very important consequences for the course of events in many subglacial eruptions. The influence of polar ice on subglacial eruptions has not been critically examined and only temperate glaciers are considered in this chapter.

The movement of water in glaciers (glacier hydraulics) is fundamentally affected by glacier structure, in particular the distribution of permeable layers whose presence is predominantly a consequence of the conversion of snow to ice. Snow is a loose aggregation of ice crystals and grains that are essentially unchanged since they were deposited. Compressing snow results in the progressive elimination of trapped air. In ice, the interconnecting air passages between the ice crystals and grains have been sealed off. Snow that is in an intermediate stage of densification (i.e., not yet ice) is called *firn.* Snow and firn are permeable, whereas unfractured ice is essentially impermeable. Fractured (e.g., crevassed) ice is also permeable. Most fractures pinch out at a depth of 30 m due to internal deformation and flow of the ice. Many glaciers thus have a crude layered structure, comprising an uppermost permeable layer (snow, firn, and fractured ice) overlying impermeable unfractured ice. Layer boundaries are gradational.

The direction of meltwater flow in a glacier is determined by the hydraulic gradient, which is itself largely controlled by the slope of the glacier *surface*. The glacier bed is largely ineffective in determining water flow except in cases where its gradient is about 11 times that of the glacier surface. During eruptions, the ice surface becomes depressed as ice is melted over the erupting vent. This distorts the local hydraulic gradient, causing meltwater to flow in toward the vent, and the site becomes sealed by an encircling ice barrier. A water-filled vault forms, which may become an englacial lake when melting penetrates right through to the surface. When the water becomes deep enough, the encircling ice barrier floats and the vault drains. This results in a jökulhlaup, as occurred spectacularly toward the end of the 1996 eruption in Iceland.

V. BASALTIC SUBGLACIAL ERUPTIONS

Recent research into basaltic subglacial volcanism has identified distinctive sequence "types" whose principal characteristics are controlled by the thickness and structure of the overlying glacier (Fig. 6). Distinction is based on the types and relative proportions of the volcanic, volcaniclastic, and sedimentary lithologies present and their organization into distinctive bundles of rock types separated usually by unconformities. The prominent, mainly erosional surfaces are an expression of the natural internal geometry of the volcanoes and they hold important clues to volcano construction. The sequence types are interpreted to correspond to eruptions beneath "thin" (≤100–150 m) and "thick" (mainly ≫150 m) temperate glaciers. Further subdivision of eruptions beneath thick glaciers is also made depending on glacier structure (see later discussion).

A. Eruptions beneath Thin Glaciers

Thin glaciers, either valley-confined ("Alpine") glaciers or the thinned margins of more extensive thicker ice sheets or ice caps, are defined as those formed almost entirely of snow, firn, and/or fractured ice. Measured depths to the firn ice transition range up 115 m, yielding an approximate limiting thickeness of 100–150 m for thin glaciers as defined here. However, thicknesses of just a few tens of meters are typical for most temperate glaciers. Because the glacier is permeable, meltwater is able to migrate according to local hydraulic gradients. An eruption will cause extensive melting of the ice and create a cavity or vault but pillow lava effusion is unlikely because meltwater will not pond over the vent. A depres-

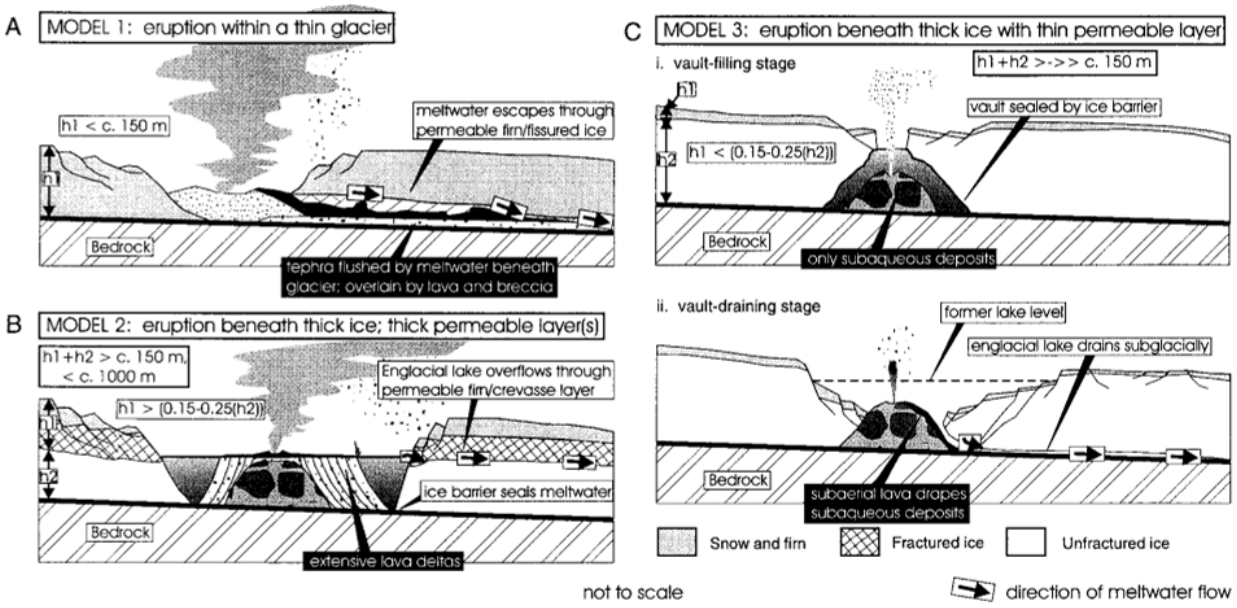
A
MODEL 1: eruption within a thin glacier
h1 < c. 150 m
h1
meltwater escapes through permeable firn/fissured ice
Bedrock
tephra flushed by meltwater beneath glacier; overlain by lava and breccia
B
MODEL 2: eruption beneath thick ice; thick permeable layer(s)
h1+h2 > c. 150 m, < c. 1000 m
h1 > (0.15-0.25(h2))
Englacial lake overflows through permeable firn/crevasse layer
h1
h2
ice barrier seals meltwater
Bedrock
extensive lava deltas
C
MODEL 3: eruption beneath thick ice with thin permeable layer
i. vault-filling stage
h1+h2 >->> c. 150 m
h1
h1 < (0.15-0.25(h2))
h2
vault sealed by ice barrier
Bedrock
only subaqueous deposits
ii. vault-draining stage
former lake level
englacial lake drains subglacially
Bedrock
subaerial lava drapes subaqueous deposits
Snow and firn
Fractured ice
Unfractured ice
not to scale
direction of meltwater flow

FIGURE 6 Cartoons showing three empirical models for subglacial eruptions beneath glaciers of different thickness. The hydrodynamic conditions are different in each case, resulting in significantly different sequences of rocks and volcano construction.

sion or hole will rapidly form in the glacier surface and meltwater will drain away continuously as a sheet or within thermally eroded channels. The eruption is likely to be explosive (hydrovolcanic) initially, forming a pyroclastic cone. As the vent becomes isolated from meltwater, the eruption will change to relatively nonviolent strombolian or hawaiian explosions or effusion of degassed lava.

The author knows of only one published example of volcanoes formed under conditions broadly similar to these—those formed during a subglacial eruption on Deception Island (Antarctica) in 1969. Examination of two of the eruptive centers by the author showed them to be pyroclastic cones formed of unstratified, loose, highly vesicular gray scoria and fluidal textured bombs overlying brick-red, weakly bound coarse lapilli and abundant flattened (cowpat) bombs. Chilled breadcrust textures are common and lapilli are cube shaped (i.e., bounded by fractured surfaces). In most respects the tephra resemble those formed in Strombolian ("dry") eruptions, but the abundance of fractured clasts and breadcrusted textures suggests an additional minor influence of water during the eruption.

By contrast, the record of these eruptions deposited off the flanks of the volcano can be very distinctive, particularly if lava effusion has occurred. Although published examples are uncommon, there are well-documented sequences in Iceland and Antarctica. They are typically only a few tens of meters thick although multiple effusive eruptions can build up more substantial thicknesses far exceeding the thickness of the coeval glacier. This reflects the ability of ice to reform or "heal" over an eruptive site. It contrasts with eruptions associated with seawater or lakes, in which the water always remains at a regional base level. A knife-sharp basal unconformity usually separates the sequences associated with each effusive phase. It commonly shows signs of ice-molding, polishing, and striations due to glacial erosion. The overlying succession typically comprises unbedded tillite overlain by, or interbedded with, gravelly sandstone and conglomerate (Fig. 7). The sedimentary deposits are largely formed of resedimented glassy fragments flushed by meltwater down thermally eroded tunnels at the glacier bed. They are prominently stratified, including small-scale channel structures and cross stratification and are the volcanic equivalent of glacial eskers.

Although lava may override or bank against adjacent ice, observations suggest that it will also thermally erode glaciers. Pillow lava bases to some flows are ascribed to limited involvement with surface snow. Interaction with a subglacial tunnel will also cause chilling, granulation, and formation of hyaloclastite breccia on the flow surface, which will be carried to the flow front and overridden. Further breccia is likely to be formed by steam explosions where lava crosses water-rich unconsolidated sediments and pockets of trapped water in bedrock surface irregularities. Meltwater draining over and through the lava may rework and redeposit any hyaloclastite breccia. Molten lava can be insulated by a protective carapace of breccia, with fresh lava capable of traveling long distances to the flow front and/or injected up into overlying breccia.

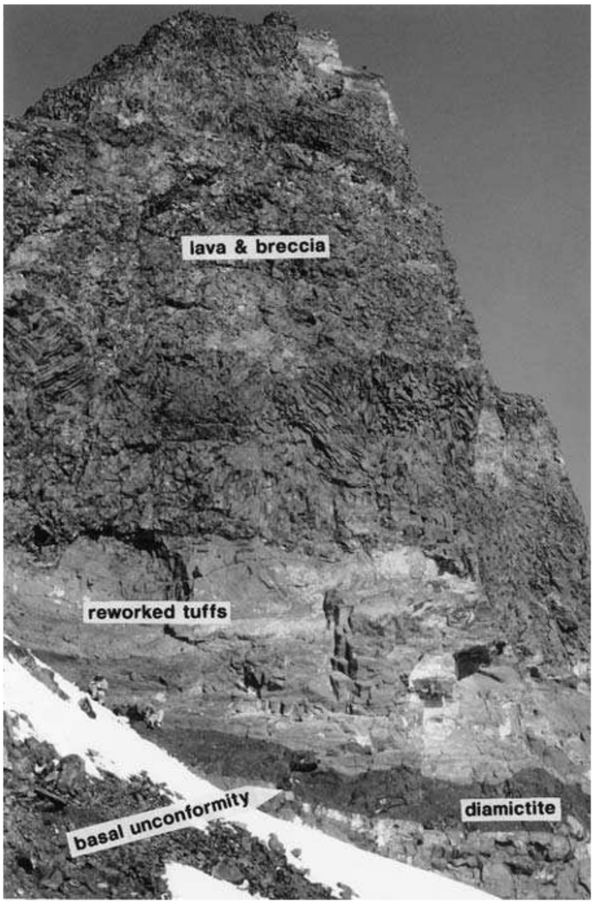

FIGURE 7 Sequence of massive glacial tillite overlain erosively by paler-colored tuffs deposited from flowing water and succeeded by intermixed hyaloclastite breccia and lava with widely varying columnar joint orientations. The sequence is about 30 m thick and rests on a sharply defined glacial unconformity. It probably formed beneath a relatively thin permeable cover composed mainly of snow and firn. Mount Murphy, Antarctica.

Thus, a single effusive eruption beneath a thin glacier should lead to an idealized sequence comprising glacial (tillite) and volcaniclastic lithofacies overlain by lava and hyaloclastite breccia sandwiched between sharply defined glacial unconformities (Fig. 7). An important feature is the evidence for flowing water preserved in the sedimentary lithofacies, which contrasts with the ponded water conditions characteristic of eruptions beneath thicker glaciers (see later discussion).

B. Eruptions beneath Thick Glaciers

Thick glaciers, corresponding to ice sheets or ice caps, are defined as those formed largely of impermeable ice. They are typically $\gg 150$ m thick. Under these circumstances, meltwater can be sealed in vaults following distortion of the local hydraulic gradient surrounding the erupting vents. Because ice is less dense than water, the volume change caused by melting at the base of a glacier will rapidly cause a depression to form in the glacier surface. Observed examples suggest that the rate of heat transfer from erupting magma to ice is extremely rapid and several hundred meters of ice may be melted through completely in only a few hours. Simple calculations indicate that the volume of meltwater generated in a perfectly sealed vault must be much greater (possibly by a factor of 10) than the volume of magma emplaced, simply in order to create space for the mass of magma. In reality, however, subglacial leakage is predicted during the first few moments of melting and may create subglacial channels. Depending on rates of thermal erosion, the channels may maintain hydraulic continuity with the rest of the glacier. The water level in the vault depends on a balance between rates of meltwater generation and basal leakage. The few observed examples suggest that vaults fill rapidly and overflow. This may cause widespread sheet flooding, as occurred at an early stage in the 1969 Deception Island eruption (beneath a thin glacier composed mostly of ice), or else more focused overspill and confinement in supraglacial channels, as occurred during a late stage of the Deception Island eruption and exemplified by the 1996 eruption in Iceland.

The structure of the glacier determines the precise course of events during these eruptions. In eruptions beneath thick glaciers with a relatively thick *permeable upper layer*, meltwater will accumulate in a vault until it encounters a layer of snow, firn, or fractured ice, through which it will drain by overflowing. If the thickness of the permeable layer is greater than about 10–25% of that of the underlying impermeable ice, water in the vault can never reach a depth sufficient to float the surrounding ice. The water level will stablilize at the elevation of the lowest exit point, diminishing slowly as thermal erosion occurs at the exit.

Eruptions involving subaerial lava effusion into a water-filled overflowing englacial lake yield table mountain volcanoes (known as *stapi* in Iceland or *tuyas* in British Columbia). Eruptions that cease before subaerial emergence form steep-sided ridges predominantly composed of palagonitized (clay-altered) tuff and breccia that are sometimes called *tindars.* Table mountains are distinctive landforms consisting of relatively small, isolated, roughly circular or more commonly subrectangular plateaux. Icelandic table mountains are characteristically <10 km wide and a few hundred meters high (up to 1000 m in some compound edifices), with abrupt edges and steep flanks. These dimensions and morphologies are similar to supposedly comparable table mountains on Mars.

The flat or gently convex top of a table mountain is composed of lavas that may construct a small shield volcano with a summit crater or cinder cone(s). It is formed by a combination of subaerial lava effusion and generation of hyaloclastite breccia in lava deltas. The subhorizontal boundary between the flat-lying lavas and steep-dipping breccia foresets is called a *passage zone* and its recognition in a volcanic sequence of this type can be used to identify unambiguously contemporaneous water levels and, by inference, the approximate elevation of the coeval encircling glacier surface (Fig. 8). However, the passage zone elevation will only crudely correspond to the surrounding ice sheet surface. Although probably within a few tens of meters of temperate glacier surfaces, it may be more than 100 m lower than some polar glacier surfaces.

The lava-delta capping sequence overlies a pedestal-like foundation of palagonitized glassy tuff, breccia, and pillow lava. The lithofacies present are identical to those forming tindars. Tindars can be regarded as incompletely formed table mountains. It is thus convenient to refer to an entirely subaqueous *tindar stage* in the evolution of a table mountain. This stage may commence in effusion of pillow lava and hyaloclastite breccia and is analogous to the pillow volcano stage that is well documented in submarine volcanoes. It may also contain sheet flows, and tabular and lensoid intrusions that drive hydrothermal alteration in overlying units.

Effusion of pillow lava is nonexplosive partly because of the suppression of magmatic volatiles by the confining pressure of overlying ice and/or water in the vault, although many factors influence explosivity. For example, observations of submarine eruptions indicate that explosivity can be suppressed by water depths of only a few tens of meters, whereas other explosive eruptions

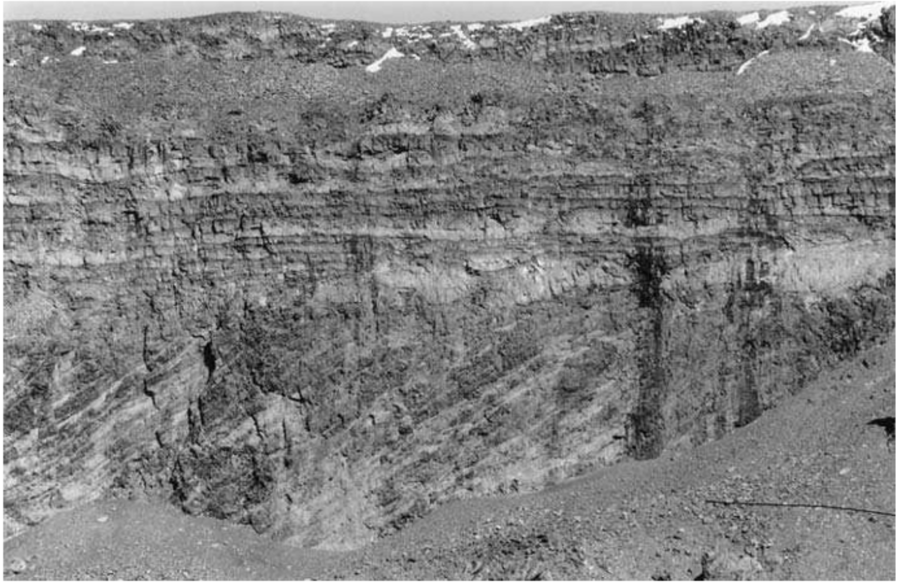

FIGURE 8 Subaerial pahoehoe lava flow and coeval steep-dipping subaqueous hyaloclastite breccias, which together form a lava delta. The subhorizontal junction between the lava and breccias (known as a *passage zone*) marks the position of a former water level, in this case, meltwater in an englacial lake. The section is about 75 m high. James Ross Island, Antarctica. [Photograph by I. P. Skilling.]

can take place beneath several hundred meters of water. However, most eruptions become explosive as the lava pile grows upward, probably by a combination of explosive bubble growth in the magma and simultaneous interaction with meltwater and water-soaked tephra slurry in the vent (an eruptive style known as *surtseyan*). Much of the vertical aggradation of the edifice takes place during *continuous uprush* periods of high magma discharge, resulting in the construction of a subaqueous tuff cone. Less efficient thermal to mechanical energy conversion, more rapid deceleration of a subaqueous column, turbulent mixing with water, and difficulty in breaching the water : air interface combine to produce a lower, denser eruption column. Tephra dispersal is mainly by fallout close to the vent.

A continuously collapsing tephra-charged column, dumping wet tephra around the vent, will construct an unstable oversteepened cone. The coarse tephra is rapidly distributed down the submerged flanks mainly by a variety of sediment gravity flows. Their presence indicates ponded water rather than the flowing water conditions characteristic of eruptions beneath thin glaciers. The resulting deposits are formed of sandy–gravelly glassy pyroclasts, which occur mainly in continuous even beds with gradational surfaces that are typically structureless or crudely graded. They form thick unbroken sequences individually a few meters to tens of meters thick. Each sequence is envisaged linked to a single continuous uprush episode in which the tephra was dumped and more or less instantly transformed into high-density turbidity currents. In some of the sequences, the beds become thinner, finer, and more palagonite altered upward (Fig. 9). These features probably indicate diminishing energy and tephra input, possibly reflecting more pulsed magma discharge in the later stages of the continuous uprush episode. The greater surface area provided by the finer grains caused the enhanced alteration.

At lower discharge rates, discrete pulses of magma initiate spectacular activity known as *tephra finger jetting* in which shallow explosions eject bombs and parcels of wet tephra and gas that follow spreading parabolic trajectories. The tephra-laden jets probably have the potential to transform into sedimentary gravity flows as they pass into water, resulting in gravelly sandstone beds similar to classical turbidites and occurring in thinner sequences with well-defined bedding surfaces (Fig. 10). Thinly bedded graded-laminated fine sandstone and mudstone units, generally just a few decimeters thick, are a minor part of these sequences and probably formed from sandy low-density turbidity currents during short periods of quiescence.

An important feature of the subaqueous successions, and one that is useful in distinguishing products of submarine and subglacial eruptions, is bedding orientation. In both eruptive settings, bedding dips radially away

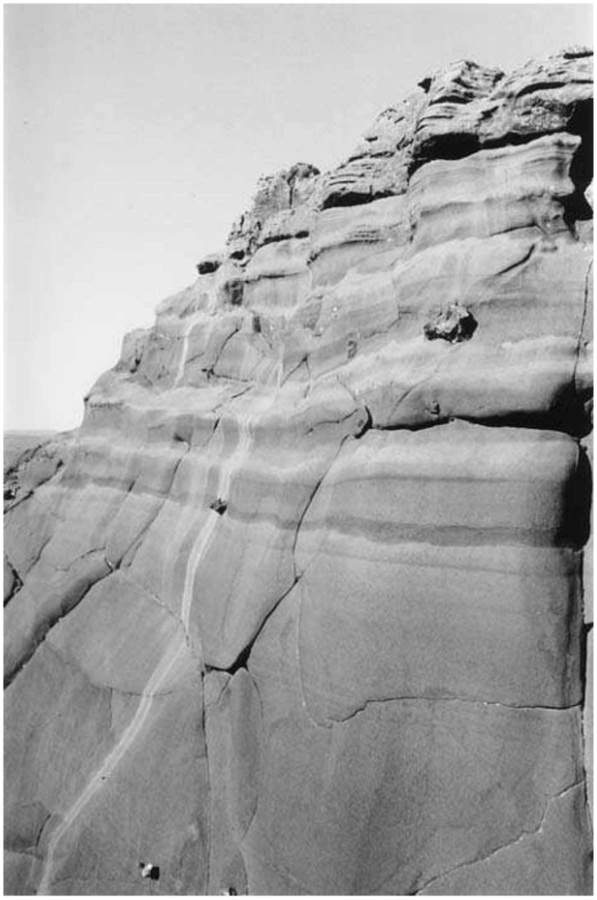

FIGURE 9 Normal graded and ungraded beds of redeposited tuff at Kalfstindar, Iceland. The well-developed upward-thining, fining, and better stratification are attributed to waning explosive activity during a continuous-uprush episode. Note the very poor stratification characteristics of the lower thicker part of the sequence. A total thickness of 6 m is shown.

from the vents. However, in some subglacial volcanoes, the bedding flattens out rapidly away from vents by banking against former confining ice walls (cf. Fig. 5). The ice walls move away because of melting, thus removing support from the volcano flanks and precipitating slope failure. Evidence for collapse is widespread and conspicuous in the preserved successions, and includes slump scars on a range of scales up to many tens of meters, deformed sediment packages, and synsedimentary faults. Many coarser breccia beds present are likely to be a result of these slope failures. Like uncorking a bottle, the sudden pressure release from removing overlying sediments can also cause focused discharge of overpressured pore fluids. This is preserved as cross-cutting slurry-like deposits that terminate at slump scar surfaces.

It is possible for subaerial lava to overlie directly coeval subaqueously deposited tephra or pillow lava sequences, an important relationship that is diagnostic of a subglacial setting. It implies drainage of the vault during eruption and requires special circumstances. The rate of meltwater generation and overflow must be exceeded by basal leakage either through early formed channels or expansion of the vault over an appropriate bedrock topography. Note that the surrounding ice "barrier" is not floated. It is a "leaky" barrier.

By contrast, in glaciers formed mainly of *impermeable ice* (i.e., an upper permeable layer less than about 10–25% of the thickness of impermeable ice), meltwater accumulates in the vault and ultimately floats the surrounding ice barrier. This releases the meltwater as a sudden flood whose volume reflects that of the englacial vault. Eruptions that take place within the ice-filled caldera of Grimsvötn volcano in Iceland are apparently of this type. Our knowledge of the internal structure of these volcanoes is minimal. However, it is possible to predict the kinds of structures, principal rock types, and history of construction based on interpretation of the hydraulic history. Meltwater is unable to overflow because the surrounding ice barrier is floated before the water level in the vault reaches the glacier surface or any permeable upper layer. Because the volume of meltwater accumulates at a much faster rate than the magma, the volcano cannot become emergent until after the ice barrier floats and the vault drains. Lava deltas cannot form and there will be no table mountain landform. The volcanoes will be dominated by subaqueous lithofacies, probably mainly pillow lava and hyaloclastite breccia. If eruptions persist after the vault has drained, the subaqueous pile will be unconformably draped by subaerial lava and/or pyroclastic cone(s). Although this juxtaposition is diagnostic of subglacial volcanoes, it has a different hydraulic origin from that found in some table mountains. A failure to interpret correctly the subglacial conditions responsible could lead to meaningless interpretations of the tectonic, volcanic, and paleoenvironmental histories of a region.

Once the meltwater has commenced draining from the vault, the conditions that led to floating of the ice barrier are no longer sustained and the surrounding ice will collapse back into place, thus bringing the flood to a close. However, early leakage of meltwater in subglacial tunnels and enlargement of the tunnel system by enhanced thermal erosion during the massive discharge from the vault will prevent a sudden shutdown. The flood will diminish as the tunnels are constricted by

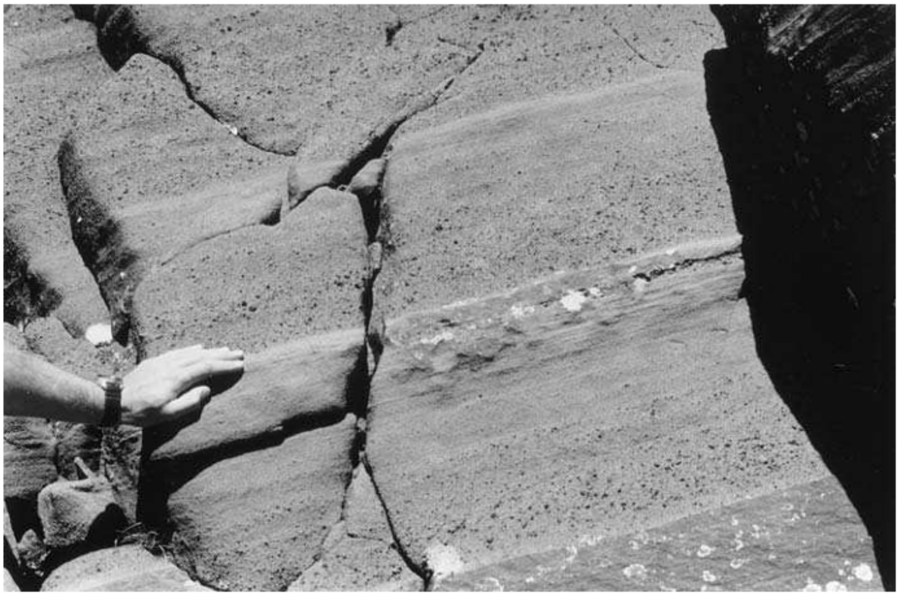

FIGURE 10 Well-defined normally graded-stratified beds (turbidites) formed of redeposited tephra possibly formed from discrete tephra jets during intermittent jetting activity. Kalfstindar, Iceland.

ice deformation concurrent with the falling hydrostatic pressure. Conditions are reestablished in which the vault may refill with meltwater and the eruption can become subaqueous once more. The resulting association of repeated subaqueous and subaerial lithofacies could be very complicated in a prolonged eruptive episode. As far as the author is aware there are no published descriptions of a volcanic succession of this type.

VI. FELSIC SUBGLACIAL ERUPTIONS

There are very few published descriptions of subglacial eruptions of felsic magmas (andesite/dacite/rhyolite compositions). There has been no modern volcanological study of these sequences and they were last investigated in the 1970s. Two different types of occurrence are described.

In southwest Iceland, felsic centers are up to 2 km in diameter and 500 m thick. They consist of lava lobes, hyaloclastite, and pumice breccia erupted beneath glaciers <400 m thick. The lithofacies form prominent interlayered sequences comprising alternating pumice breccia and lobe complexes, the latter formed of lobes of lava intimately associated with cogenetic hyaloclastite breccia. The pumice breccia consists of angular and ragged gray pumice mixed with minor angular fragments of obsidian glass, in featureless to poorly bedded units up to 40 m thick. A wide range of grain sizes is present, including submillimeter-sized fine clasts. By contrast, the hyaloclastite breccia is formed of angular fragments of obsidian, flow-banded pumiceous glass and crystalline rhyolite. Clasts are coarse (millimeters to 40 cm) and they form unbedded deposits 20–40 m thick that grade laterally into ellipsoidal and irregular rhyolitic lava lobes and interconnected lobe complexes (Fig. 11). Some lobes are greatly elongated vertically and apparently intrude overlying and adjacent breccia. Lobe size varies considerably; they are commonly 2 to 70 m in diameter, but exceptionally range from 40 cm to 900 m. The lobes are mineralogically and chemically similar to the pumice and obsidian clasts in the adjacent breccias and they normally display alternating textural zones of black obsidian, flow-banded pumiceous glassy rhyolite, and slightly to completely crystalline vesicular rhyolite with well-developed curving columnar joints.

The field relationships clearly indicate that the hyaloclastite breccia formed by the progressive mechanical disintegration of massive flow lobes. The brecciation must have occurred during emplacement and concurrent chilling of the lobes by meltwater, perhaps during effusion beneath ice and/or intrusion into water-saturated pumice breccia. Conversely, the pumiceous deposits were interpreted as products of highly explosive mag-

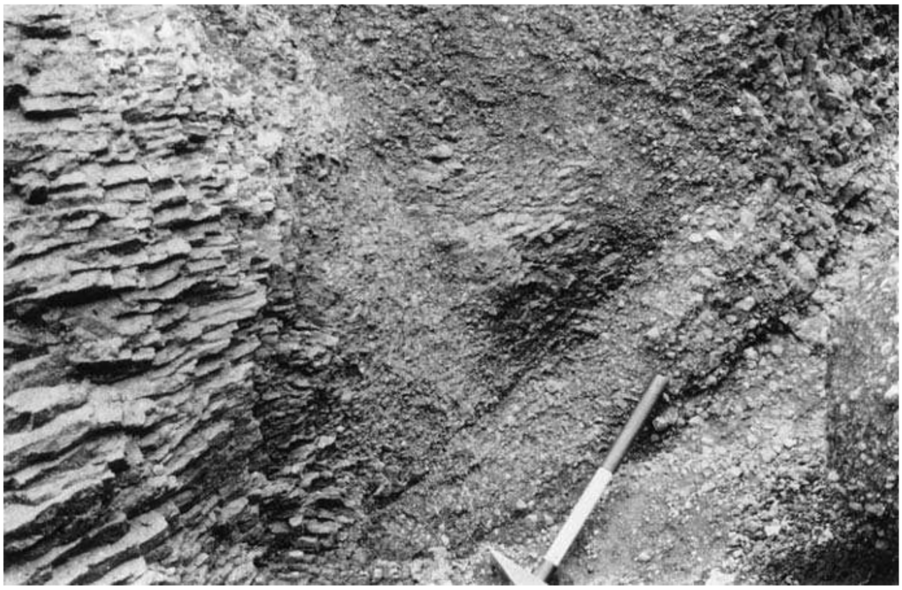

FIGURE 11 Closely jointed margin of a rhyolite lobe changing laterally into glassy and crystalline breccia caused by chilling, quenching, and disintegration when the lobe came into contact with water melted from an adjacent glacier. Blahnukur, Iceland.

matic eruptions. The presence of fines and fracture-bounded clasts was attributed to minor water interaction. Comparisons were made with subglacial table mountains and explosive surtseyan eruptions, although this author notes that there are also surprising similarities in scale and lithofacies characteristics to sequences formed by subglacial basaltic eruptions beneath thin glaciers.

An unusual subglacial volcano constructed entirely of andesite lavas within a former ice sheet at least 500 m thick has been described from a locality in British Columbia known as The Table. The volcano forms a pillar-like mass with sheer cliffs 300 m high, rising to a nearly flat summit measuring 300 m long and 225 m wide. It is constructed of horizontal lavas 30–75 m thick in its central part and subvertical lavas on some sides. The lavas show spectacular columnar joints with styles characteristic of rapid cooling, and one of the steep-dipping flows overlies a deposit of glacial boulder clay at the foot of the cliff. The outcrop was interpreted as an original structure little modified by erosion and, with no trace of a preexisting rock mass or ash cone in the vicinity, effusion within a confining cylindrical ice vault drained of meltwater was postulated. The lavas were envisaged spreading laterally until they came in contact with ice walls, which they solidified against. Later lavas poured into the steep gap thawed around the cooling lava pile. Contemporaneous ice flow would have caused the vault to deform and extend downstream of the (protective and warm) vent and lava masses. Thus, the outcrop elongation, parallel to the local paleo-ice flow direction, was interpreted as an original constructional feature.

VII. LARGE SUBGLACIAL VOLCANOES—AN UNTAPPED SOURCE OF PALEOENVIRONMENTAL INFORMATION

Volcanoes can be very sensitive indicators of climatic variations. With their potential for precise isotopic dating, the analysis of long-lived large volcanoes in glaciated regions may permit the reconstruction of temporal and spatial variations of former ice sheets. Thus, the research can contribute to our knowledge of climatic fluctuations. There are very few published descriptions of large subglacially erupted volcanoes. They are common in Antarctica and Iceland but most of the investigations are rather dated now and lack the input from modern volcanological studies. On the basis of geomorphological evidence interpreted from photographs, Olympus Mons, the largest volcano on Mars and far larger than any volcano on Earth, may also have erupted through an ice sheet in times past.

Mount Murphy is a basalt to trachyte shield volcano about 25 km in diameter with a postulated small ice-covered caldera. It was constructed relatively quickly between 8 and 9 Ma on a prominent basement massif that rises to more than 2000 m above sea level. Younger satellite centers (7–4.5 Ma) on the west side are the remains of several small dissected surtseyan volcanoes with predominantly basaltic compositions; they were probably erupted beneath a gently north-sloping ice sheet whose elevation fluctuated through 200 m during their eruptive period. Interpretations of the Miocene glacial history based on the Mount Murphy shield succession are complicated by the coastal position of the volcano [marginal to the West Antarctic Ice Sheet (WAIS)] and possible influence of the basement topography on the local elevation of the WAIS. Striations and molded surfaces on the basement surface suggest the presence of a thin mountain ice cap prior to activity in the shield.

More than 2000 m of section is exposed at Mount Murphy. The lower half is dominated by subglacially emplaced basaltic pillow lava and hyaloclastite breccia, and is succeeded by subaerial basalt and trachyte lavas. The basal hydrovolcanic section consists of several sequences of water-reworked gravelly sandstone and breccia intercalated with columnar lava lobes and pillow lava–hyaloclastite breccia (Fig. 7). The individual volcanic and volcaniclastic sequences are each a few tens of meters thick. Some contain intercalated tillite formed entirely of locally derived volcanic debris and they are separated by striated and polished glacial unconformities. Striations on the unconformities indicate radial ice flow from the shield summit. There is a remarkable similarity in thickness and lithofacies to sequences of small basaltic volcanoes erupted beneath thin valley-confined glaciers but the Mount Murphy succession differs in the generally much more widespread sequences and presence of subordinate subaerially erupted and emplaced units. The latter include strongly welded strombolian bomb and lapilli fall deposits, which have been interpreted as an indication of reduced ice cover. This could have occurred in the short periods immediately following eruptions when the ice was removed from parts of the volcano flanks. The presence of a capping subaerial lava sequence suggests that the ice cap was very thin or absent once the volcano summit grew above a critical elevation, possibly like some volcanoes in the region today (e.g., Mount Erebus).

The Mount Murphy volcano also underwent postvolcanic overriding by a continental ice sheet. This is indicated by striated surfaces strewn with basement-derived erratics up to 1800 m above sea level on the present-day flanks of the volcano, which show ice transport directions obliquely traversing the volcanic topography. Recycled microfossils suggest a minimum early Pliocene (<3.5 Ma) age for the overriding period. The surface of the present-day WAIS south of the volcano lies about 1000 m below the fossiliferous deposit. Thus, a complicated glacial history is preserved at Mount Murphy, recording an early ice cap and later ice sheet(s). Any ice sheet present at 9 Ma must have been below 400 m above sea level, but, between 7 and 4.5 Ma, the western satellite centers record an ice sheet with a surface elevation fluctating between about 400–600 m above sea level. The ice sheet surface rose above 1800 m in post–Early Pliocene times, before reducing to its present elevation.

VIII. SUBGLACIAL VOLCANISM—THE WAY FORWARD

Despite sometimes spectacular recent eruptions (e.g., Iceland 1996) and associated major flooding, research into subglacial eruptions has, until recently, been neglected. We are still largely ignorant about many aspects. The thermodynamics of the eruptions are particularly poorly understood and none of the published studies appears capable of explaining the way in which melting at the base of a glacier is so rapid that several hundred meters of overlying glacier ice can be melted through completely in only a few hours. The magma is often treated as if always emplaced as pillows, although observations of many real sequences suggest that this may not be typical. Each basalt mass contains enough energy to melt at least 10 times its mass of ice, if the basalt is able to cool from 1200° to 0°C. Thus, there is abundant total heat in the magmatic system to melt the ice and create space for the magma. However, it is unlikely that each basalt mass will cool to 0°C before the next extrusion, and the solidification time of basalt pillows is much too slow (by at least an order of magnitude) to account for the observed energy flux per unit area. Observations of real eruptions suggest that magma is apparently emplaced at a much faster rate than space can be created by melting, a presently unsolved enigma. Studies of the rate of meltwater generation, the timing of floods, and effects of water on eruptive events will also strongly influence our assessment of the volcanic risks associated with subglacial volcanoes and in the formulation of plans for risk mitigation.

Long-lived, large subglacially erupted volcanoes are very poorly described so far. Yet, they could be a prime source of information on paleoenvironments and environmental variations with time. In particular, recent developments in our understanding of the hydraulic controls on subglacial eruptions have yielded the clear potential to map the important characteristics of ice sheets associated with eruptions, including their thickness, thermal state, structure, and age. Concurrent investigations of the pore-filling and coeval glass alteration minerals are also yielding chemical criteria for identifying whether eruptions were into freshwater (therefore possibly glacial) or were submarine and they provide critical additional support for interpreting eruptive palaeoenvironments. Studies of the large subglacial volcanoes in Antarctica, which are associated with a globally important ice sheet, are likely to be particularly significant. With concurrent studies of other large volcanoes associated with lower latitude glaciers (e.g., Andes), the potential exists for investigating the geographical synchroneity (or otherwise) of glaciations.

The fluid dynamic processes of subglacial eruptions are only relatively well known for small-scale basaltic eruptions beneath wet-based or temperate glaciers. We know that hydraulic conditions in temperate glaciers are largely responsible for determining the sequence of events during subglacial eruptions. By contrast, polar or dry-based glaciers are frozen to their bed. Meltwater flow beneath polar ice may be impossible and any subglacial vault will only be able to drain by overflowing, but there is no published modeling of the processes involved. We also lack much information on subglacial felsic eruptions, and it is unclear how they differ from eruptions of basaltic magmas. With the very different magma properties involved, there could be significant differences in styles of eruption and volcano construction.

It has been suggested that there are elevated ground temperatures associated with active subglacial volcanoes beneath the WAIS. The thermal flux regulates the supply of meltwater ultimately responsible for ice streaming, thus forming a control on the dynamics of the ice sheet independent of global climate. Ice streams stabilize the slowly moving inland ice sheet by protecting it from oceanic degradation. Increased basal melting may lubricate the basal sediment layer, thereby increasing ice streaming and leading to rapid ice sheet drawdown. If the WAIS were to melt completely, sea level would rise by about 6 m globally. However, observations of the effects of modern eruptions on basal ice conditions are conflicting. Over the eruptive fissure during the 1996 Icelandic eruption, the glacier showed no obvious tendency to rapid basal sliding, whereas the section between Grimsvötn and the glacier terminus apparently underwent a partial collapse, although the extent of sliding was unclear.

Distinctive bedforms and sequence types in subglacial volcanoes have been linked tentatively to the style of explosive eruption. This work is still in its infancy, but a logical extension would be to conduct detailed studies of grain size populations, clast composition, and morphology in the different bed types. These could provide critical information specific to eruptions from flooded vents, in particular the nature of the postulated vent-filling slurries and extent of the influence of steam cupolas that may partially insulate hot pyroclasts from cold ambient water.

SEE ALSO THE FOLLOWING ARTICLES

Lahar and Jökulhlaup Hazards • Submarine Lavas and Hyaloclastite • Volcanism on Mars

FURTHER READING

Allen, C. C. (1979). Volcano–ice interaction on Mars. *J. Geophys. Res.* **84,** 8048–8059.

Björnsson, K. (1988). Hydrology of ice caps in volcanic regions. *Vísindafélag Íslendinga, Societas Scientarium Islandica* **45.**

Blankenship, D. D., Bell, R. E., Hodge, S. M., Brozena, J. M., Behrendt, J. C., and Finn, C. A. (1993). Active volcanism beneath the West Antarctic ice sheet and implications for ice-sheet stability. *Nature* **361,** 526–529.

Furnes, H., Fridleifsson, L. B., and Atkins, F. B. (1980). Subglacial volcanics—on the formation of acid hyaloclastites. *J. Volcanol. Geotherm. Res.* **8,** 95–110.

Gudmundsson, M. T., Sigmudsson, F., and Björnsson, K. (1997). Ice–volcano interaction of the 1996 Gjálp subglacial eruption, Vatnajökull, Iceland. *Nature* **389,** 954–957.

Höskuldsson, A., and Sparks, R. S. J. (1997). Thermodynamics and fluid dynamics of effusive subglacial eruptions. *Bull. Volcanol.* **59,** 219–230.

Jones, J. G. (1969). Intraglacial volcanoes of the Laugarvatn region, south-west Iceland—I. *Q. J. Geol. Soc. London* **124,** 197–211.

Mathews, W. H. (1947). "Tuyas": Flat topped volcanoes in northern British Columbia. *Am. J. Sci.* **245,** 560–570.

Skilling, I. P. (1994). Evolution of an englacial volcano: Brown Bluff, Antarctica. *Bull. Volcanol.* **56,** 573–591.

Smellie, J. L., Hole, M. J., and Nell, P. A. R. (1993). Late Miocene valley-confined subglacial volcanism in northern Alexander Island, Antarctic Peninsula. *Bull. Volcanol.* **55,** 273–288.

Smellie, J. L. (In press). Lithofacies architecture and construction of volcanoes erupted in englacial lakes: Icefall Nunatak, Mount Murphy, eastern Marie Byrd Land, Antarctica. *In* "Lacustrine Volcaniclastic Sedimentation," (J. D. L. White and N. Riggs, eds.). Special Publication. International Association of Sedimentologists.

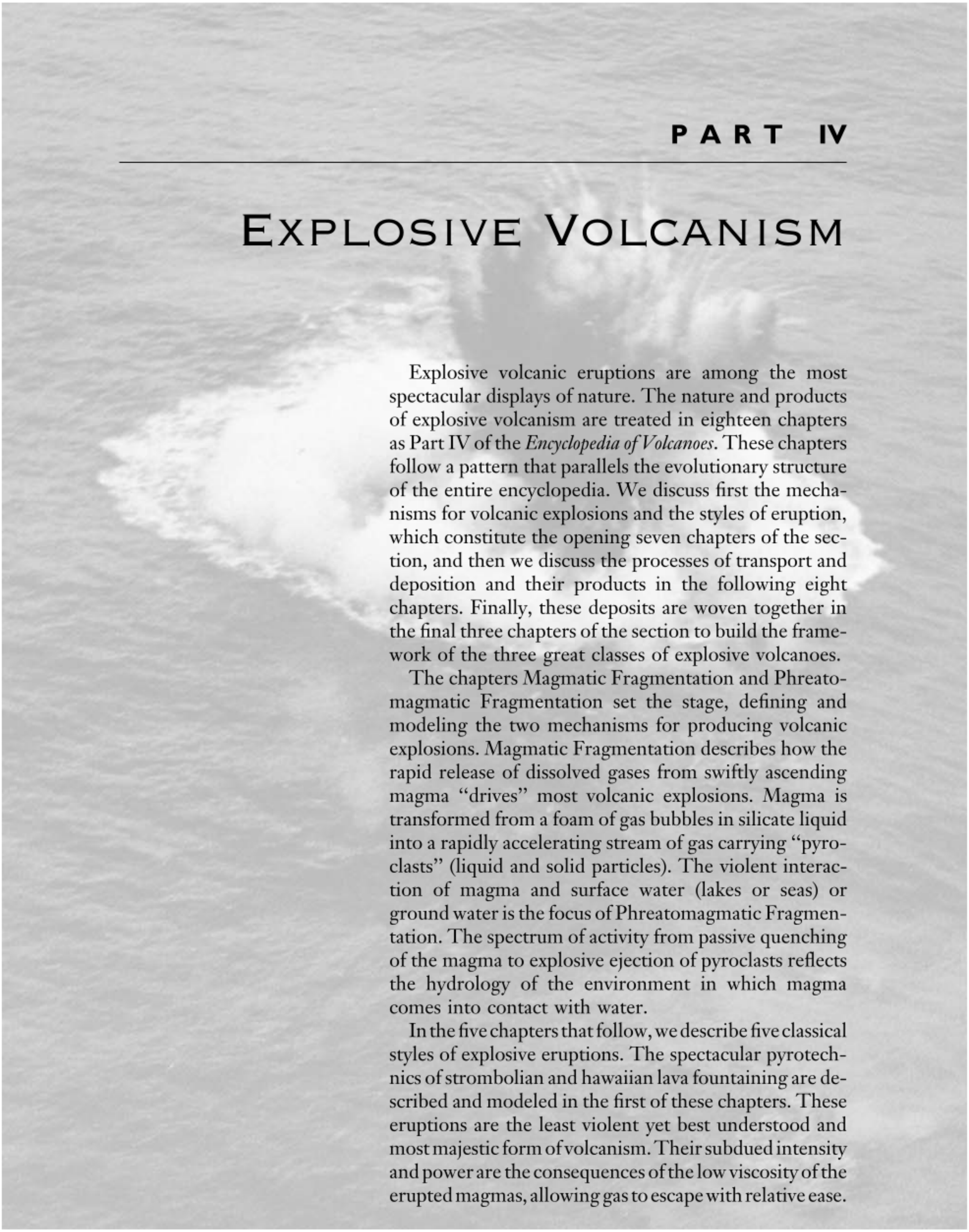

PART IV

EXPLOSIVE VOLCANISM

Explosive volcanic eruptions are among the most spectacular displays of nature. The nature and products of explosive volcanism are treated in eighteen chapters as Part IV of the *Encyclopedia of Volcanoes*. These chapters follow a pattern that parallels the evolutionary structure of the entire encyclopedia. We discuss first the mechanisms for volcanic explosions and the styles of eruption, which constitute the opening seven chapters of the section, and then we discuss the processes of transport and deposition and their products in the following eight chapters. Finally, these deposits are woven together in the final three chapters of the section to build the framework of the three great classes of explosive volcanoes.

The chapters Magmatic Fragmentation and Phreatomagmatic Fragmentation set the stage, defining and modeling the two mechanisms for producing volcanic explosions. Magmatic Fragmentation describes how the rapid release of dissolved gases from swiftly ascending magma "drives" most volcanic explosions. Magma is transformed from a foam of gas bubbles in silicate liquid into a rapidly accelerating stream of gas carrying "pyroclasts" (liquid and solid particles). The violent interaction of magma and surface water (lakes or seas) or ground water is the focus of Phreatomagmatic Fragmentation. The spectrum of activity from passive quenching of the magma to explosive ejection of pyroclasts reflects the hydrology of the environment in which magma comes into contact with water.

In the five chapters that follow, we describe five classical styles of explosive eruptions. The spectacular pyrotechnics of strombolian and hawaiian lava fountaining are described and modeled in the first of these chapters. These eruptions are the least violent yet best understood and most majestic form of volcanism. Their subdued intensity and power are the consequences of the low viscosity of the erupted magmas, allowing gas to escape with relative ease.

Next is Vulcanian Eruptions, which describes short (seconds to minutes) discrete explosions, capable of ejecting incandescent lava bombs and blocks of fragmented rock to distances greater than 5 km. During the past two decades, understanding of the causes and timing of vulcanian eruptions has improved dramatically.

Following this chapter is Plinian and Subplinian Eruptions, which describes eruptions characterized by the formation of high eruption plumes resulting in atmospheric ash and particle injection and dispersal by winds over huge areas. The name for these eruptions is taken from the 79 A.D. eruption of Vesuvius that provoked the death of Pliny the Elder. The dynamics of these awesome events are modeled in this chapter, drawing from the classical eruptions of Vesuvius and plinian events at Mount St. Helens in 1980 and El Chichon in 1982.

The classical eruption of the Icelandic volcano Surtsey in 1963 gave rise to the term surtseyan volcanism. The chapter Surtseyan and Related Phreatomagmatic Eruptions examines this event and other examples of fluid basaltic magma mingling with external water.

In phreatoplinian eruptions, silicic magma interacts violently with abundant water often residing in caldera lakes. This chapter reexamines the deposits of classical eruptions of this type in Iceland and New Zealand and the role of the water in the formation of clusters and aggregates of ash particles in the eruption plumes.

A volcanic explosion produces a jet of gas and pyroclasts, which may entrain air and atmospheric moisture and continue to rise as a billowing, buoyant eruption plume. Large volcanic plumes that penetrate the tropopause may trigger global environmental effects and produce short-term regional changes of climate. Elegant models for eruption plumes are presented in the chapter Volcanic Plumes.

The authors of Pyroclast Transport and Deposition use four parameters (particle trajectory, particle concentration, the extent to which the concentration fluctuates with time, and presence or absence of cohesion during deposition) to explain the characteristics of the great proportion of subaerial pyroclastic deposits.

Important clues about eruption processes come from a study of the textures and fabrics of pyroclastic fall deposits, as described in the next chapter. These deposits, produced by the rain-out of clasts through the atmosphere, are the simplest of pyroclastic products, and their value is in the ease with which their properties can be used to infer eruption parameters.

The perception of pyroclastic density currents as a highly dangerous and devastating type of explosive volcanic activity was brought about dramatically by the 1902 eruptions of Mount Pelée, Martinique, which killed 30,000 people. Since then, several destructive pyroclastic-flow eruptions have occurred every decade. Pyroclastic surges and blasts, described in the next chapter, are a class of pyroclastic density currents that have low particle concentrations, are turbulent and often pulsating, and produce deceptively thin, bedded, and cross-bedded massive deposits. Depositing flows of high particle concentration (tens of volume %) produce ignimbrites and block-and-ash flow deposits. The architecture and characteristics of these units are described in the following chapter.

The next chapter, Lahars, covers what occurs when large masses of volcanic sediment, and water, sweep down and off volcano slopes incorporating additional sediment. This chapter describes how both liquid and solid interactions determine the unique behavior of lahars and distinguish them from debris avalanches and floods. The rock fragments carried by the flows make them especially destructive.

The next chapter describes the architecture and internal fabric of debris avalanche deposits and the models used to describe their emplacement. A debris avalanche is the product of a large-scale collapse of a sector of a volcanic edifice often triggered either by intrusion of new magma or by a phreatic explosion or an earthquake. The 1792 debris avalanche at Unzen volcano killed 15,190 people.

Calderas are described next as large volcanic craters, more or less circular, with diameters many times greater than those of the volcanic vents they enclose. Formation of calderas by roof collapse over an underlying shallow magma reservoir is now recognized as accompanying most eruptions that involve magmatic volumes greater than a few cubic kilometers. Caldera-forming explosive eruptions probably are the most catastrophic geologic events that affect the earth's surface, other than rare large meteorite impacts.

Ask a small child to draw a volcano and chances are that he or she will draw a composite cone. Human populations are attracted to these magnificent landforms by the fertile soils generated on the cones and yet are threatened by the hazards associated with their frequent eruptions. The chapter Composite Volcanoes builds an elegant model for the life spans, geometry, and internal structure of these volcanoes.

Small basaltic volcanoes, scoria cones, tuff rings, tuff cones, and maars are the most common volcano types, on land, yet each center is tiny compared to calderas or composite cones. Scoria Cones and Tuff Rings explains the behavior of these systems in terms of the eruption of small batches of hot fluid magma.

Bruce Houghton
Institute of Geological and Nuclear Sciences, New Zealand

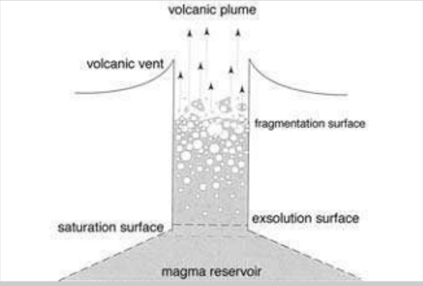

MAGMATIC FRAGMENTATION

K. V. CASHMAN
University of Oregon

B. STURTEVANT
California Institute of Technology

P. PAPALE
Gruppo Nazionale per la Vulcanologia

O. NAVON
The Hebrew University

I. Introduction
II. Bubble Formation — The Exsolution Surface
III. Conduit Processes — Exsolution to Fragmentation
IV. Fragmentation
V. Summary

GLOSSARY

bubble A pocket of gas in a melt.

fragmentation The transition from a continuous melt with a dispersed gas phase to disconnected parcels of bubbly melt within a continuous gas phase.

magma Silicate melt with dissolved gases (volatiles); may also contain crystals and/or bubbles.

pyroclasts All solid fragments ejected from volcanoes (from Greek meaning "fire broken").

pumice Solidifed fragments of quenched vesicular silicic melt (vesicularity $>\sim 60\%$).

scoria Basaltic pumice.

tephra All pyroclasts that fall to the ground from eruption columns (from Greek meaning "ashes").

vesicle A hole (bubble remnant) preserved in a solidified pyroclast.

vesicularity The volume percent of bubbles in a melt or the volume percent of vesicles in pumice.

vesiculation Nucleation and growth of gas bubbles in a magma.

I. INTRODUCTION

Explosive eruptions are the most powerful and destructive type of volcanic activity. Explosive eruptions produce large quantities of fragmental (pyroclastic) material that are carried upward in convecting columns or transported laterally in energetic pyroclastic flows. Recent eruptions of volcanoes such as Mount St. Helens (United States) and Mount Pinatubo (Phillipines) serve as vivid reminders that this pyroclastic material can have devastating effects on human populations. Tephra falling from convecting columns disrupts daily life in downwind communities and may completely devastate areas close to a volcano. Fine ash and aerosols injected into

Copyright © 2000 by Academic Press
All rights of reproduction in any form reserved.

the stratosphere during very large eruptions may modify global climate for years after the eruption.

Two different mechanisms can generate explosive eruptions. Magmatic, or "dry," eruptions are driven solely by gases originally dissolved in the magma, while phreatomagmatic, or "wet," eruptions result when magma is mixed with external water (see Phreatomagmatic Fragmentation). In this chapter we focus on magmatic eruptions and specifically on the explosive process itself — the process of *fragmentation* — as this process is central to our understanding of how volcanoes work. Fragmentation transforms a magma from a liquid with dispersed gas bubbles to a gas with dispersed liquid drops (± bubbles and solids) or isolated solid particles. The explosive force of magmatic eruptions is generated during fragmentation, where the potential energy of an expanding magma (melt + bubbles) is converted to the kinetic energy of individual fragments and then thermally expanded in volcanic plumes. Magmatic fragmentation occurs when magma ascends rapidly, as in plinian eruptions (see Plinian and Subplinian Eruptions), after rapid decompression caused by volcanic edifices or lava dome collapse, or when hot solid lava blocks fragment on impact during dome collapse (see Domes and Coulees). These different processes can occur individually or sequentially as a single eruption changes style during its initiation and quasi-steady phases.

Direct observations of magmatic fragmentation are not possible, thus models of fragmentation are derived from studies of volcanic deposits, theoretical analysis, and analog experiments. Early models of fragmentation include magma disruption by (1) bubble coalescence, (2) expansion waves traveling through the magma at sound speed, and (3) excess pressure within bubbles in a coherent magma. The latter model has been the most widely accepted, with magma fragmentation viewed as bursting of bubbles at a free surface (the fragmentation surface; Fig. 1) as a consequence of the pressure difference across the interface. In this model, the location of the fragmentation surface within the conduit is controlled by the point at which the vesicularity of the rising and expanding magma reaches ~70–80% (representing closest packing of spherical bubbles). Recent years have seen the emergence of several new perspectives on the fragmentation process, perspectives that combine contributions from (1) experimental studies of volatile exsolution and vesiculation, (2) numerical models of magma ascent in volcanic conduits, (3) fragmentation simulations, and (4) studies of pyroclasts. Below we use this new work to describe magma ascent from its source to the point of fragmentation (see Fig. 1) and to review current models of the fragmentation process itself.

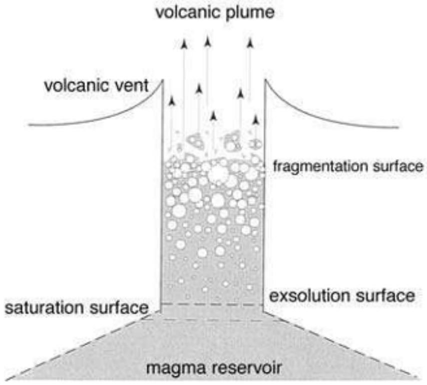

FIGURE 1 Schematic illustration of processes that occur in volcanic conduits. Magma is saturated in volatiles at the top of the reservoir (the saturation surface). Bubbles nucleate at a slightly higher level (the exsolution surface), as magma rises and experiences a decrease in pressure. Between the exsolution and fragmentation surfaces, the magma is a two-phase mixture of silicate melt and gas bubbles. Fragmentation occurs when gas occupies 70–80% of the available volume. At this point, the magma transforms from a liquid with suspended bubbles to a gas with suspended clots of liquid. The abrupt density decrease (expansion) that accompanies this transformation results in acceleration of the gas mixture out of the vent, in the form of a volcanic plume. [Modified from Sparks, 1978.]

II. BUBBLE FORMATION — THE EXSOLUTION SURFACE

Explosive magmatic eruptions occur when volatile exsolution (primarily H_2O) from magma is rapid. What triggers rapid H_2O vesiculation? To answer this question, we must first determine the volatile saturation of magma prior to an eruption plus the ease with which the magma can respond to that saturation by nucleating bubbles. Together, these two processes (volatile saturation and bubble nucleation) will determine the location of the exsolution surface (Fig. 1).

A. Magma Storage Regions

Recent data suggest that the upper parts of many silicic magma chambers are not only volatile-saturated prior to an eruption, but that magma in these reservoirs contains at least a small volume fraction of gas bubbles. Thus the presence of bubbles is not sufficient, by itself, to cause an explosive eruption. This conclusion is supported by abundant evidence for noneruptive gas emissions from volcanoes, emissions that indicate the "leakiness" of many reservoirs to magmatic gases. However, accumulation of even a small volume fraction of bubbles at the roof of a magma reservoir can increase the pressure exerted by the magma on the surrounding rocks. It is thus possible that vesiculation in magma storage regions could generate sufficient overpressure to cause the rock fracture required for magma ascent and eruption. Other eruptions may require external triggers, such as the injection of a new batch of magma into an existing reservoir. In all cases, however, the rapid vesiculation required for explosive eruptions probably initiates somewhere above the level of magma storage, accompanying magma ascent to the surface.

B. Bubble Nucleation

Vesiculation (the formation of a separate gas phase) occurs when a magma becomes supersaturated in a volatile phase and starts with bubble nucleation. According to classical homogeneous nucleation theory, there will be a critical size (R_{crit}) above which nuclei are stable and additional growth can occur. Bubble nucleation may thus be described as the initial formation of the smallest possible stable bubble. This critical bubble size is described mathematically as the size at which the energy decrease resulting from creation of a gas phase more than offsets the energy increase required to maintain the gas–liquid interface (Fig. 2a). This theory suggests that homogeneous nucleation of bubbles in a silicate melt should require extremely high supersaturations, and thus that magma would have to rise far above the volatile saturation surface before bubbles could form. However, nucleation may also be heterogeneous. In heterogeneous nucleation, existing impurities provide sites for bubble nucleation, nucleation can proceed at much smaller supersaturations, and vesiculation will not be limited by the kinetics of bubble formation.

On the basis of nucleation behavior alone, two end member models have been used to describe vesiculation in volcanic conduits. At one extreme, bubble nucleation is homogeneous, supersaturations required for bubble nucleation are large, and vesiculation is delayed until the magma is high in the conduit (Fig. 2b). In this case, delayed nucleation results in rapid magma expansion and fragmentation, as seen in many analog (shock-tube) experiments (see below). At the other extreme, nucleation is heterogeneous, the kinetics of nucleation do not hinder volatile exsolution, and volatiles exsolve during magma ascent according to equilibrium models (Fig. 2c). Such an equilibrium model is commonly assumed in numerical descriptions of magma ascent. Is there evidence to support one model over the other? Evidence for supersaturation conditions in volcanic conduits may lie in the vesicles preserved in pumice and scoria. When supersaturations are large, nucleation dominates and the resulting bubble number density (number per volume)

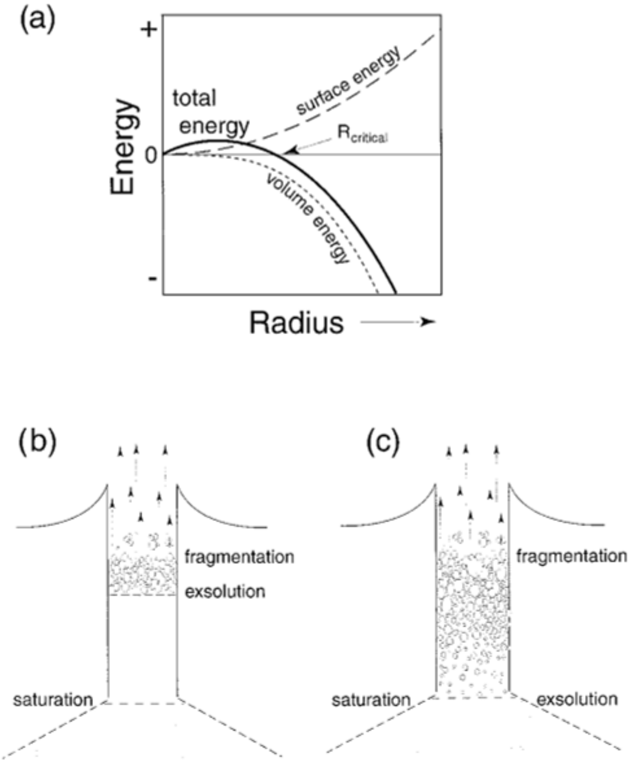

FIGURE 2 Bubble nucleation. (a) Energy balance important in generation of stable bubble nuclei. Nucleus formation results in a negative energy contribution from phase formation (volume energy) and a positive energy contribution from interface formation (surface energy). When the nucleus size is larger than R_{crit}, the energy decrease from the formation of the gas phase exceeds the positive energy of the interface, and bubble growth can occur. (b) Schematic illustration of the expected locations of the saturation and exsolution surfaces when bubble nucleation is homogeneous (nucleation is delayed). (c) Schematic illustration of the equivalence of the saturation and exsolution surfaces when bubble nucleation is heterogeneous (there is no kinetic barrier to nucleation). Explosive eruptions are expected to be more violent in the scenario shown in (b) than in that shown in (c).

is high. High vesicle number densities typical of silicic pumice ($\sim 10^{14}$–$10^{16}/m^3$) may thus indicate nucleation at very high supersaturations, although heterogeneous nucleation of bubbles on submicroscopic crystals cannot be ruled out. In contrast, vesicle number densities preserved in basaltic scoria are substantially lower ($\sim 10^{10}/m^3$), a possible reflection of nucleation at much lower supersaturations than in silicic systems. However, even in basaltic magmas equilibrium concentrations of volatiles are not completely maintained, so that the actual exsolution history of any particular magma probably lies somewhere between the two end member models for nucleation.

III. CONDUIT PROCESSES — EXSOLUTION TO FRAGMENTATION

Once nucleated, bubbles can grow. Magma expansion resulting from bubble growth accelerates magma up volcanic conduits. If bubbles grow faster than they can rise or escape laterally through conduit walls, the magma ascends rapidly to the fragmentation surface, and erupts explosively. If bubbles can rise through the ascending magma, or if bubble networks are sufficiently interconnected to allow permeable gas escape, the magma may reach the surface without fragmenting (it will erupt effusively; see Effusive Volcanism). Thus the relative rates of bubble growth, magma transport, and gas loss will control the style of eruptive behavior (explosive vs effusive).

A. Bubble Growth

Bubble growth is controlled by both diffusion of water molecules toward the bubble–melt interface and expansion against the surrounding viscous melt. Growth of a single bubble at constant pressure occurs in two stages: exponential (viscosity-limited) growth and parabolic (diffusion-limited) growth. *Exponential* growth dominates immediately after nucleation, when diffusion is rapid and the bubble radius increases at a rate limited by the melt viscosity (Fig. 3, segment A). As the bubble grows, equilibrium saturation pressure in the bubble cannot be maintained by diffusive flux of water through the interface, and growth is *parabolic* (Fig. 3, segment B), although more rapid growth is possible if the liquid undergoes high strains. The combined growth history of a bubble for these idealized conditions (a single bubble in a stationary liquid at a constant pressure) will be determined by both melt viscosity and volatile abundance. For example, bubble growth in a water-rich (low viscosity) rhyolite would be limited by diffusion after less than 1 s, while bubble growth in a water-poor (high viscosity) rhyolite may be exponential for hours to days.

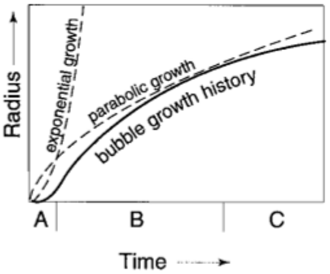

FIGURE 3 Time-dependent changes in the form of bubble growth. The bubble growth history curve is divided into three segments, as follows. Growth is initially exponential (viscosity-limited) when the bubble is very small (segment A). Growth becomes parabolic when limited by diffusion of volatiles into the bubble (segment B). In real systems at long times, bubble growth will be limited by proximity of neighboring bubbles and will thus drop below the parabolic curve (segment C). Shown for reference are anticipated growth histories for exponential and diffusional growth (dashed lines). [Modified from Navon and Lyakhovsky (1998), in Gilbert and Sparks (1998).]

In real systems, bubbles do not grow singly, nor do they grow at constant pressure; thus bubble growth will be limited by both the proximity of neighboring bubbles and the rate of magma decompression. Bubble proximity is determined by the initial separation distance of bubble nuclei (bubble number density; Section IIB). Separation distance determines the length scale of volatile diffusion and, as a result, the timescale required to achieve equilibrium bubble growth during magma ascent. In hydrous silicic melts, the time to achieve equilibrium is about 30 s for moderate ascent velocities (~ 1 m/s) and bubble separations of 10 μm (bubble number densities of $\sim 10^{14}/m^3$; see above). Larger bubble separation distances increase the time required to achieve equilibrium. The rate of magma decompression affects the relative rates of diffusion-controlled and expansion-controlled bubble growth. Deep in the conduit, bubble growth is limited by the rate of volatile diffusion. High in the conduit expansion becomes more important, the magma accelerates, and bubble growth may by limited by the viscous resistance of the surrounding magma (Fig. 3, segment C). The result of rapid expansion is the development of excess internal bubble pressures at shallow conduit depths, excess pressures that may lead to fragmentation. Such a departure from equilibrium will be enhanced by rapid decompression and by large increases in melt viscosity that may accompany decompression (anticipated as H_2O contents drop below 1 wt%, particularly if volatile loss is accompanied by crystallization).

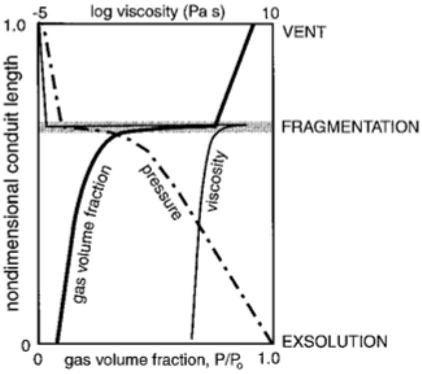

FIGURE 4 Calculated distribution of gas volume fraction and nondimensional pressure (pressure divided by magma chamber pressure; scale shown along the bottom axis) and mixture viscosity (scale shown on the top axis) along a conduit (from exsolution level to the vent). Simulation is shown for a rhyolite magma with 6.5 wt% total water content, conduit length of 7000 m, conduit diameter of 127 m, magma temperature of 827°C, and magma chamber pressure of 192 MPa. Note that all parameters change abruptly just below the level of fragmentation and then again at the point of fragmentation. [Modified from Papale *et al.,* 1998.]

B. Magma Ascent Dynamics

Flow models of magma ascent through volcanic conduits provide estimates of pressure and velocity changes with transport and allow important constraints to be placed on processes that lead to magma fragmentation. Current models are for steady-state flow in one dimension and simple magma rheologies. The steady state assumption is justified by the steady discharge of fragmented magma (over a period of hours) that characterizes explosive plinian eruptions. The need for models of flows in two dimensions and models that include non-Newtonian rheologies appropriate for bubble-bearing melts provides clear directions for future research in this area.

Early models of magma flow through conduits calculated the velocity of a homogeneous fluid moving steadily up a cylindrical pipe. Velocities were calculated using volatile exsolution and expansion as dictated by solubility models, combined with frictional energy losses dictated by wall shear stresses. Fragmentation was assumed to occur when bubbles occupied 70 to 80 vol% of the erupting mixture. More recent nonhomogeneous models allow thermal and mechanical disequilibrium between the gas and the liquid phases. In these models, the conduit region below the level of fragmentation has large gradients in both flow variables and magma properties (conduit variations in gas volume fraction, magma viscosity, and normalized pressure are shown in Fig. 4 for ascent of a volatile-rich rhyolite). An abrupt drop in viscosity marks the fragmentation surface itself, as the erupting mixture changes from liquid- to gas-dominated. These simulations emphasize the importance of both volatile (H_2O and CO_2) content and anhydrous magma composition on the depth of volatile saturation and magma fragmentation. The newest models also allow dynamic controls on fragmentation, with magma disruption occurring not at a set bubble volume fraction, but instead at a strain rate sufficient for liquid rupture (see below).

Further improvements to models of conduit flow will require improved understanding of the effects of crystals and bubbles on magma rheology, evaluation of the strength and stability of magmatic foam flowing in conduits, and incorporation of non-Newtonian rheologies into flow models. It is well known that subliquidus (crystal-bearing) magmas have viscosities that are a function of crystal content and that magmas have non-Newtonian rheologies at crystallinities $>\sim25–30\%$, when individual crystals start to interact. Crystallinities $>60\%$ probably cause flow to cease entirely. Bubbles deform in a shear flow, as illustrated by highly elongated vesicles found in some silicic pumice. Both experimental and numerical results suggest that transient effects related to bubble deformation may decrease the viscosity of bubbly melt below that of the bubble-free melt. Such transient effects may have importance consequences for magma flow in conduits. For example, under these conditions, flow gradients prior to fragmentation may not show the abrupt changes illustrated in Fig. 4. Non-Newtonian magma rheologies may also cause the flowing foam to decouple from conduit walls and thus move unimpeded in a slug flow prior to fragmenting.

C. Volatile Loss from Volcanic Conduits

The models for bubble growth and magma ascent described above assume that magma acts as a closed system with respect to the gas phase until the point of fragmentation. However, there is abundant evidence that magmatic gas can be lost from volcanic systems during magma ascent, evidence that includes long-period seismicity that accompanies volatile loss, the eruption of dense (vesicle-poor) yet degassed magma, and the syn-ascent breakdown of hydrous phases (see Rates of Magma Ascent). As substantial syn-ascent gas loss may prevent explosive eruptions, conditions of volatile loss during magma ascent must be addressed.

Volatile loss from volcanic conduits requires either two-phase flow (relative motion between bubbles and the enclosing melt) or the development of a permeable bubble network within the magma. Relative motion is important in strombolian eruptions (see Hawaiian and Strombolian Eruptions), where magma viscosities and ascent rates are sufficiently low that individual bubbles can rise and coalesce within the conduit. Lateral bubble migration during slow ascent of more viscous melts may allow volatile escape via permeable wall rocks and consequent lava dome effusion. When magma ascent rates are similar to those of bubble rise, bubbles move with the magma and gas loss must be through permeable networks in the magma itself. Conditions required for such permeable foam formation are not well constrained. The porosity at which magmas become permeable, the extent to which interaction with surrounding hydrothermal systems affects eruptive activity, the conduit conditions that permit the entrance of groundwater (see Phreatomagmatic Fragmentation) and the limiting rates of gas escape necessary to prevent fragmentation all remain as questions.

IV. FRAGMENTATION

Prior to an eruption, magma at depth is held at high pressure by the strength of the surrounding rock. The pressure difference that drives an eruption acts when the magma source is connected to a region of lower pressure, such as the atmosphere, across the fragmentation surface. By Newton's laws, the force imbalance, or thrust, causes the magma to accelerate. Two processes have been proposed to drive the expansion that powers explosive eruptions. In the first, vesiculation and bubble growth provide the driving force for expansion, with fragmentation occurring by the *disintegration* of the resulting foam. Fragmentation may result from instabilities in the fluid or by brittle fracture as the tensile strength of the melt is exceeded, but in either case the fragmentation results from high strain rates in the expanding two-phase mixture. In the second, fragmentation is accomplished in an already-vesiculated magma, which may or may not be moving in a conduit, by the failure of suddenly loaded bubbles in a *fragmentation wave* similar to that which causes rockburst in mines. This fragmentation wave model is applicable to the failure of volcanic domes, and may also be applicable to the explosive disruption of more viscous melts during plinian and subplinian events. Below we discuss these mechanisms in more detail and then use textural analysis of eruptive products to speculate on fragmentation mechanisms operative during different types of explosive eruptions.

A. Fragmentation Resulting from Rapid Acceleration

Recent laboratory experiments on low viscosity fluids have examined the fragmentation of rapidly flowing vesiculating liquids in conduits. High-speed photography has shown that vesiculation can power large accelerations of the bubbly mixture to high velocities, with fragmentation occurring after acceleration. As bubbles grow, they merge and form a foam moving at high velocity. Eventually the bubble walls get so thin that the foam becomes unstable and breaks up to form relatively large-scale finely vesicular clots. The breakup is associated with violent motions, such as impingement of the flow on conduit walls. Violent motions accompanying fragmentation may induce further breakup via the fragmentation wave mechanism (see below) if vesicles contain pressurized gas when large relative motions lead to impact. The experiments produce a finely dispersed droplet aerosol, and appear directly applicable to fragmentation in basaltic (hawaiian) fire fountains, where pyroclasts are variably vesicular and commonly show fusiform shapes (see Hawaiian and Strombolian Eruptions). These results are also suggestive of processes in a high-velocity heterogeneous multiphase flow that can simultaneously produce pumice and volcanic ash. Large accelerations may lead to fragmentation in high-viscosity silicic liquids, although fragmentation is likely to be brittle as a consequence of rate-limited crossing of the glass transition. Magma flow modeling shows that elongational strain rates may exceed the strength of silicic melts at gas volume fractions of 0.6–0.85 and that magma vesicularity and mixture viscosity are inversely related at the point of fragmentation.

B. Fragmentation by Rapid Decompression

Rockburst models have been applied to the flow generated by a volcanic blast after rapid decompression by edifice collapse. The rapid decompression model is a quantitative treatment of the concept illustrated in Fig. 1, by which one or several rows of bubbles at the edge of a body fail by fluid rupture or solid fracture when exposed to low ambient pressure. This rupture exposes adjacent rows of bubbles in the magma interior to low pressure, and, consequently, a sequential inward progression of the fragmentation process. The theory is incomplete, in that it does not treat the conservation of momentum. Instead, an empirical constitutive relation substituted in its place yields fragmentation waves that propagate at several tens of meters per second, and generate dusty-gas flows of 100–200 m/s.

The rapid decompression model was designed to describe volcanic blasts, where the depressurization front is predicted to move downward at speeds from a few to several tens of meters per second. Such conditions may occur when a conduit is sealed by emplacement of a lava dome or conduit plug, and gas pressure beneath the plug increases with time by either anhydrous crystallization or upward volatile migration through permeable networks. However, a rapid decompression model could equally well apply to other types of fragmentation. Small scale comminution of brittle foams during dome collapse and disruption of vanguard magma to initiate eruptions may both involve fragmentation by rapid decompression. Additionally, some component of fragmentation by rapid decompression may be important during plinian eruptions, where the steady character of such eruptions suggests that the depressurization wave is fixed in space over time.

C. Products of Fragmentation

Any model of fragmentation must explain the textural characteristics and the size distribution of particles produced. Clast sizes and shapes, preserved vesicle sizes and shapes, and the relative abundance of different clast size populations, in turn, all provide important insight into the fragmentation process. Most attention has been focused on the interpretation of textures characteristic of pumice from plinian eruptions. Plinian pumice typically has a narrow range in vesicularity [70–85%; Figs. 5a and 5b]; to what extent does this vesicularity preserve information about the fragmentation surface? One view is that pyroclasts are quenched soon after fragmentation and that pumice textures can be used directly to understand fragmentation. In this model, pumice vesicularities of 70–85% and permeabilities $\sim 10^{-12}$ m^2 represent conditions necessary for pumice preservation during the process of fragmentation. An alternative interpretation is that fragmentation occurs at lower vesicularities (~60%), and that final clast vesicularities result from extensive postfragmentation expansion.

Additional insight into fragmentation may be gained by examination of pyroclasts with anomalously high (>90%) or low (<60%) vesicularities. Generation of extremely high vesicularities requires reorganization of bubbles into elongated cylinders ("long-tube" pumice) or polyhedral cells ("reticulite") and probably requires fragmentation by rapid acceleration. In contrast, low clast vesicularities (<60%) may result from fragmentation by rapid decompression. *Long-tube pumice* (Fig. 5c) is a minor to moderate component of most silicic pyroclastic deposits. The extreme bubble elongation preserved in these clasts is commonly interpreted to result from high elongational strains near conduit margins (thus providing support for some component of strain-induced fragmentation) and requires rapid quenching after fragmentation. *Reticulite* (Fig. 5d), in contrast, results from unconstrained postfragmentation expansion of vesicular liquid clots. Reticulite is unique to high basaltic fire fountains, and forms where clasts initially formed by strain-induced fragmentation of the liquid continue to expand in the thermal core of the fountains. *High density* (low vesicularity) *juvenile clasts* are common in vulcanian and subplinian eruptions. High clast densities may result when high microlite crystallinities inhibit bubble expansion (Fig. 5e) or when vesicular magma experiences varying degrees of bubble collapse during ascent (Fig. 5f), perhaps along conduit margins. Strain-induced fragmentation of low vesicularity clasts seems unlikely; thus dense clast formation is best explained by interaction of ascending, partially vesiculated magma with a downward-propagating decompressional wave.

Finally, what can the characteristics of pyroclastic deposits tell us about fragmentation? While data are scarce, it appears that the size distribution of pyroclasts may vary with fragmentation style (Fig. 6). The unimodal size distributions typical of vulcanian eruptions may result from fragmentation by rapid decompression of a lava plug. Clast size distributions from these eruptions are similar to those resulting from comminution of sol-

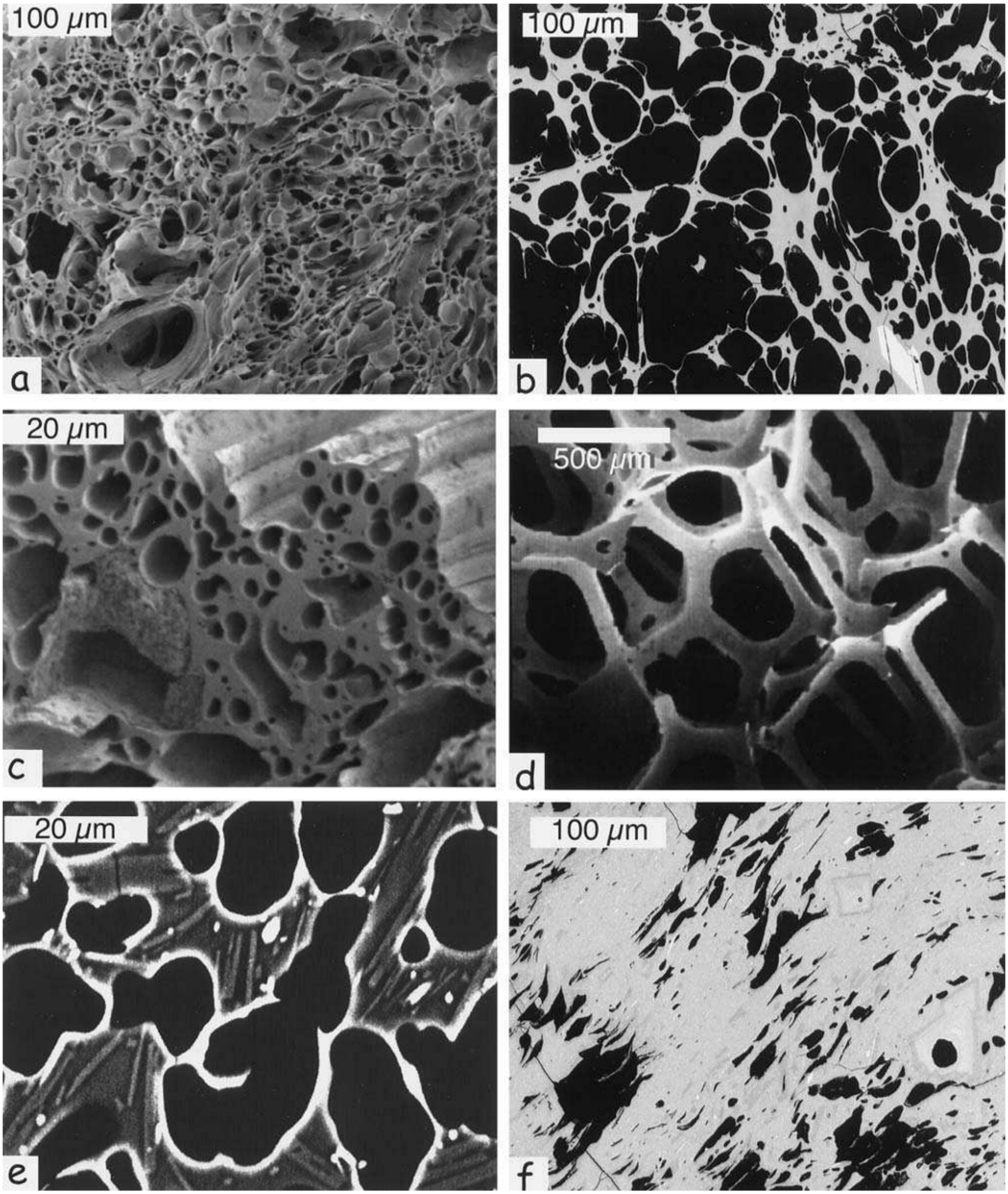
100 μm
a
100 μm
b
20 μm
c
500 μm
d
20 μm
e
100 μm
f

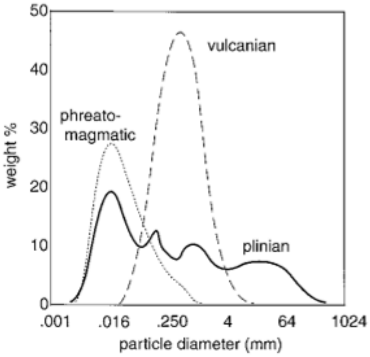

FIGURE 6 Schematic illustration of whole deposit grain size distributions from plinian and vulcanian eruptions. The vulcanian peak is unimodal and is likely a consequence of the fragmentation wave mechanism acting on a partially solidified plug within the volcanic conduit. The plinian peak is polymodal and suggests that fragmentation in plinian eruptions is complex and possibly the result of more than one fragmentation mechanism. Relative proportion of fine ash (<63 μm) increases with the increasing intensity of eruption and may provide a measure of fragmentation efficiency. Distribution from a phreatomagmatic eruption shown for comparison (see Phreatomagmatic Fragmentation).

ids. In contrast, the polymodality of plinian deposits may reflect a complex fragmentation history, with both fragmentation mechanisms (rapid acceleration and rapid decompression) acting simultaneously. Pumice may form through magma disruption during rapid acceleration facilitated by inhomogeneous distribution of elongational strain (particularly along conduit margins), with preservation of large clasts allowed where high permeabilities permit adequate volatile loss. Silicic fine ash (fractured remnants of bubble walls and interstices) may form by rupture of individual bubble walls through interaction of a decompression wave with the bulk of the finely vesicular (low permeability) conduit interior. If so, then the proportion of fine ash in a plinian deposit should correlate with eruption intensity, and could provide a quantitative measure of fragmentation efficiency.

V. SUMMARY

Magmatic fragmentation occurs in a variety of eruptive settings, and the actual process of fragmentation is probably different in magmas of different rheologies. Two end member types of fragmentation are identified. In the first, vesiculation and bubble growth provide the driving force for expansion and acceleration of the two-phase (bubble + melt) flow. Fragmentation results from high strain rates in the expanding mixture, either from instabilities in the fluid or by brittle fracture, as the tensile strength of the melt is exceeded. Fluid instabilities are the likely fragmentation mechanism in low viscosity magmas, such as hawaiian fire fountains and strombolian bubble bursts, and brittle fracture may be important in plinian eruptions. In the second, fragmentation of an already-vesiculated magma occurs by sudden decompression and bubble rupture. This fragmentation model applies to the failure of volcanic domes, and may also describe explosive disruption of viscous melts during vulcanian eruptions. The mechanism(s) of fragmentation in silicic plinian eruptions remains a question, although we speculate that both fragmentation mechanisms (rapid acceleration and rapid decompression) may be acting simultaneously. In this scenario, pumice lapilli may be interpreted as magma disrupted but not fully disintegrated during rapid acceleration, perhaps as a consequence of some limiting permeability. Fine ash formation, in contrast, appears best explained by rupture of individual bubble walls through passage of a decompression wave. The relative proportions of fine ash and pumice record the relative importance of the two fragmentation mechanisms.

As vesiculation is the dominant process responsible

FIGURE 5 Scanning electron microscope (SEM) and backscattered electron (BSE) images of volcanic pyroclasts. (a) SEM (three-dimensional) image of “normal” plinian pumice (80% vesicles), showing the narrow range in vesicle size and generally spherical shape of the vesicles. (b) BSE (two-dimensional) image of plinian pumice (70% vesicles), showing that vesicles in pumice, in detail, show a range of sizes, shapes, and extent of coalescence (vesicles are black and glass is gray in this image). (c) SEM image of long-tube pumice (88% vesicles); note that vesicles are small (<10 μm diameter) but extremely elongate (>20 : 1). (d) SEM image of basaltic reticulite (98% vesicles) showing the polyhedral cell network developed when expansion of the gas–melt mixture is not constrained by conduit walls. (e) BSE image of microlite-rich pumice clast (55% vesicles) illustrating ways in which microlites (light gray, elongate crystals in dark gray glass; vesicles are black) may inhibit bubble expansion. (f) BSE image of collapsed vesicles (black) in a dense pyroclast (<40% vesicles); bubbles in this clast were severely compressed prior to clast quenching. Images a, b, c, and f are of pumice clasts from Crater Lake, OR; image d is of a pyroclast from Kilauea volcano, Hawaii; image e is of a gray pumice clast from Mount St. Helens, WA.

for magma acceleration up volcanic conduits, improved modeling of conduit processes requires a better understanding of vesiculation (particularly bubble nucleation) and the rheology of bubbly melts. For example, large numbers of very small vesicles in silicic pumice may indicate either nucleation at very high supersaturations or heterogeneous nucleation on submicroscopic impurities. Distinguishing between these alternatives is critical for understanding conditions of vesiculation in silicic magmas. Also critical are better descriptions of the changes in material properties that a magma experiences as bubbles grow, deform, and collapse on conduit walls. As changes in rheology will feed back into the dynamics of magma ascent, such changes may ultimately dictate the point at which fragmentation occurs. All of these topics represent fertile areas of research, and improvements in all of these areas will certainly increase our understanding of explosive magmatic eruptions in the future.

SEE ALSO THE FOLLOWING ARTICLES

Hawaiian and Strombolian Eruptions • Lava Domes and Coulees • Magma Chambers • Phreatomagmatic Fragmentation • Plinian and Subplinian Eruptions • Rates of Magma Ascent • Volatiles in Magmas

FURTHER READING

Alidibirov, M. (1994). A model for viscous magma fragmentation during volcanic blasts. *Bull. Volcanol.* **56,** 459–465.

Carroll, M. R., and Holloway, J. R. (1994). Volatiles in magmas. *Rev. Mineral.* **30,** 517.

Freundt, A., and Rosi, M. (1998). "From Magma to Tephra: Modelling Physical Processes of Explosive Volcanic Eruptions," Elsevier, Amsterdam.

Gilbert, J. S., and Sparks, R. S. J. (1998). The physics of explosive volcanic eruptions. *Geol. Soc. London. Spec. Publ.* **145.**

Klug, C., and Cashman, K. V. (1996). Permeability development in vesiculating magmas: Implications for fragmentation. *Bull. Volcanol.* **58,** 87–100.

Mader, H. M., Brodsky, E. E., Howard, D., and Sturtevant, B. (1997). Laboratory simulations of sustained volcanic eruptions. *Nature* **388,** 462–464.

Mangan, M. T., and Cashman, K. V. (1996). The structure of basaltic scoria and reticulite and inferences for vesiculation, foam formation, and fragmentation in lava fountains. *J. Volcanol. Geotherm. Res.* **73,** 1–18

Papale, P., Neri, A., and Macedonio, G. (1998). The role of magma composition and water content in explosive eruptions I. Conduit ascent dynamics. *J. Volcanol. Geotherm. Res.* **87,** 75–93.

Sparks, R. S. J. (1978). The dynamics of bubble formation and growth in magmas: A review and analysis. *J. Volcanol. Geotherm. Res.* **3,** 1–37.

PHREATOMAGMATIC FRAGMENTATION

MEGHAN MORRISSEY
Colorado School of Mines

BERND ZIMANOWSKI
University of Wuerzburg

KENNETH WOHLETZ
Los Alamos National Laboratory

RALF BUETTNER
University of Wuerzburg

I. Characteristics
II. Theoretical and Experimental Results
III. Fragmentation Mechanisms
IV. Field Observations
V. Summary and Future Research

GLOSSARY

phreatomagmatism Volcanic activity resulting from the interaction between magma/lava and groundwater or surface water including seawater, meteoric water, hydrothermal water, or lake water.

FCI An abbreviation for fuel–coolant interaction, referring to an industrial analog to phreatomagmatic explosion involving a fuel such as molten iron and a coolant such as water. The interaction of the fuel and coolant has resulted in vapor explosions in industrial environments and are a potential hazard associated with nuclear core meltdown.

superheated liquid A metastable thermodynamic state of a liquid resulting from rapid heating to a temperature well above the boiling point.

Kelvin–Helmholtz and Rayleigh–Taylor instabilities Interfacial fluid instabilities caused by relative motion of two immiscible fluids. Kelvin–Helmholtz instabilities are induced by shear stresses along the interface, whereas Rayleigh–Taylor instabilities develop during acceleration of a denser fluid by a less dense fluid. In both cases fragmentation occurs when surface tension forces are exceeded.

vapor film A layer of vapor formed at the interface of water and a hot liquid or solid body (temperature ≫ boiling point).

wet/dry eruptions At standard conditions (25°C and 0.1 MPa), water is a two-phase (liquid and vapor) fluid. Depending on the quantity of available heat energy, when water comes into contact with magma it may become a liquid-rich fluid or a vapor-rich fluid, resulting in a dry eruption or a wet eruption, respectively.

> *IT WAS FASCINATING to watch the lava crater and glowing rivers and rivulets flowing down the slopes of the lava dome. Still more exciting, however, was the relentless struggle between the advancing lava and the sea. From the very beginning of the lava eruption it was noteworthy how much of the lava became fragmented when it came into contact with the sea.*
>
> —*S. Thorarinsson, 1966*

Copyright © 2000 by Academic Press
All rights of reproduction in any form reserved.

The above quote was made by Thorarinsson as he observed the eruption of Surtur volcano and the formation of a new island (Surtsey) off the south central coast of Iceland in 1964. His observations of this eruption led to a new classification of volcanism known as phreatomagmatism and the awareness of fragmentation processes associated with the interaction between magma and nonmagmatic water.

I. CHARACTERISTICS

A. Global Occurrence

Phreatomagmatic activity involves the physical interaction of magma or lava with an external source of water either within the Earth or on its surface. A spectrum of activity results when magma contacts water as illustrated by the following examples. (1) Since 1990, lava has been pouring into the sea along the shores near Kalapana, Hawaii, producing a range of activity from the explosive ejection of fragmented lava to a continuous emission of steam and passive quenching of lava (Fig. 1a). (2) The subglacial eruption at Grimsvotn volcano (Iceland) in 1996 caused extensive flooding in south central Iceland and produced explosive jets of ash (Fig. 1b). (3) At Mount Ruapehu (New Zealand) in 1995, a vigorous uprush of water, vapor, and scoria bombs was observed through the crater lake, producing cock's tail explosive jets of ash. (4) In 1977, the two Ukinrek Maars (Alaska) formed by several hundred periodic blasts which were accompanied by a pervasive production of steam when rising magma surfaced into a shallow lake.

The array of eruption styles associated with phreatomagmatic activity reflects the many environments in which magma or lava may encounter water. Specific environments include deep or shallow submarine, littoral, lacustrine, phreatic, and subglacial. Phreatomagmatism is not restricted to magma type or vent type (monogenetic or polygenetic) and reflects the pervasive occurrence of water in the crust. Volcanoes that build up from repeated eruptions (polygenetic) such as stratovolcanoes and shield volcanoes, often have a phreatomagmatic phase or phases (i.e., vulcanian, phreatoplinian, or surtseyan) during an eruption period. The distinguishing features of a phreatomagmatic eruption phase are that plumes tend to be more steam or water rich and the grain size of the eruptive products tend to be finer than those from the associated magmatic eruptive phases. Explosive phreatomagmatic activity is also characterized by intensive fragmentation and ejection of the wall rocks in the vicinity of the explosion site, which results in the formation of large craters. Volcanoes that build up from a single phreatomagmatic eruption (monogenetic) form either a tuff ring, tuff cone, or a maar volcano when rising magma contacts water. The deposits of such volcanoes may consist of some 10 to more than 1000 single layers and result dominantly from

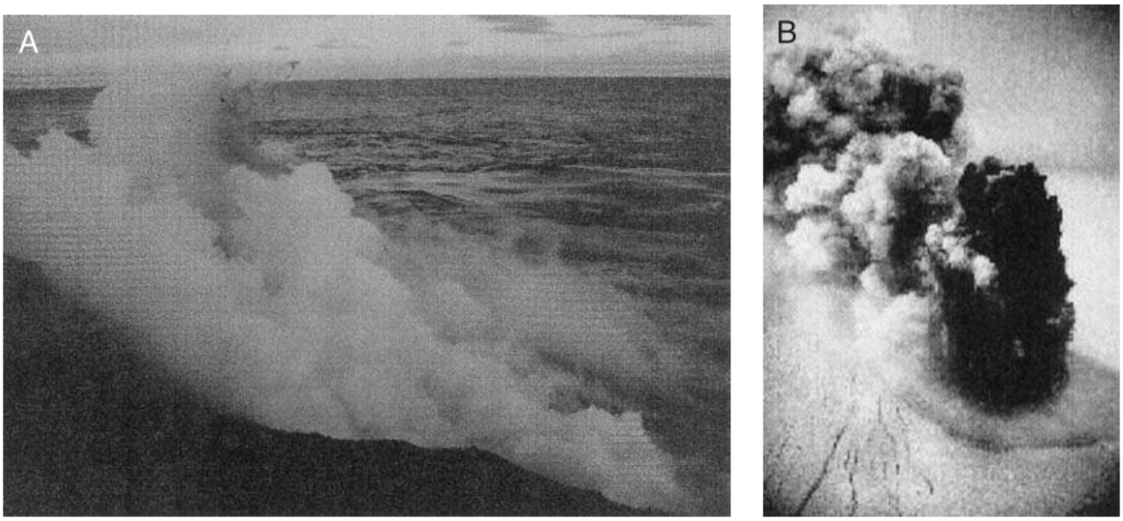

FIGURE 1 (A) Photo of the lava from Kilauea volcano entering the coast near Kalapana in 1992 (taken by Thorvaldur Thordarson). (B) Photo of the October 2, 1996, eruption column after it broke through the ice at Grimsvotn volcano (Courtesy of Freysteinn Sigmundsson, Nordic Volcanological Institute).

transport and deposition by pyroclastic surges. These types of volcanoes are found all around the world and include Craters of the Moon, United States; Deception Island, Antarctica; Eifel volcanic field, Germany; Iwo Jima, Japan.

B. Eruption Styles

A phreatomagmatic eruption is driven primarily by the volumetric expansion of external water after it has been rapidly heated by contact with magma. Exsolving magmatic volatiles may also contribute to expansion and fragmentation during a phreatomagmatic event. When water comes into contact with magma, it will either transform to steam (vapor) or a two-phase (liquid and vapor) fluid depending on the relative masses of water and magma interacting. It may also become superheated to a metastable liquid state which will flash to steam when acted on by an external force. In general, the more water available during the interaction, the wetter (liquid-rich fluid) the eruption will be. There is a wide variety of eruption styles that results from magma/water interaction. The style of activity ranges from passive quenching and granulation of magma or lava to large scale thermohydraulic explosions, representing the most energetic result of magma/water interaction.

The most commonly recognized phreatomagmatic eruption style is that characterized by cypressoidal (cock's tail) explosive jets of ash accompanied by billowing clouds of steam. This style of activity was well described during the emergence of Surtsey volcano off the coast of Iceland in 1964 and appropriately named surtseyan. Ejecta are directed vertically and laterally with the laterally directed ejecta producing a base surge. Similar activity has been observed at Capelinhos (Azores), Taal (Philippines), St. Augustine (Alaska), Ruapehu (New Zealand), and Vulcano (Italy) where magma has come into contact with either seawater or lake water filling a crater. Deposits related to this style of activity have been described as wet deposits, indicating that not all of the water was converted to steam during eruption and deposition.

Other phreatomagmatic eruption styles include vulcanian and phreatoplinian. Vulcanian eruptions are discrete, explosive events that last seconds to minutes. These eruptions are thought to be caused by highly pressurized gases derived from the magma or from a phreatomagmatic interaction. Phreatoplinian eruptions are similar in style to plinian eruptions except that deposits are finer-grained. Deposits related to these two styles of activity are dry relative to surtseyan deposits in that most of the water was converted to steam during eruption and deposition.

C. Tephra Characteristics

The products from a phreatomagmatic eruption are predominantly a mixture of glass, crystals, and foreign or wall rock lithics (fragmented material from the conduit and vent). In many cases, the lithic fragments represent by far the dominant part of the ejecta with grains ranging in size from fine ash to blocks. Their shapes may indicate fragmentation by fracturing (i.e., angular edges) and not by abrasion (i.e., rounded edges). In terms of grain size, phreatomagmatic tephra generally are finer grained than magmatic tephra (Fig. 2a), particularly for high water/magma ratios.

Under optical and electron microscopes, the juvenile (glass) component of phreatomagmatic tephra contains distinct grain shapes. These shapes include blocky, fusiform, mosslike, platey, and spherical or droplike as shown in Fig. 2b. Other distinguishing textural features are particles adhering to glass surfaces, grooves or scratches, chipped edges, and rounded edges. Also, the glass constituents may be more hydrothermally altered than magmatic tephras of equivalent age, especially in samples from wet tephra deposits in which hot water was captured. Basaltic glasses alter to palagonite, whereas rhyolitic glasses alter to a fine-grained mosaic of quartz, potassium feldspar, and clays.

D. Phenomonology

The physical dynamics of phreatomagmatic fragmentation parallel a well-studied process called fuel–coolant interaction (FCI). FCI refers to a heat transfer process which can occur in any environment, converting thermal energy into kinetic energy on a short time scale (<1 ms) during the interaction of a cold volatile fluid (coolant) and a hot fluid (fuel) with a solidus temperature well above the homogeneous nucleation temperature of the coolant. In volcanological terms, the fuel is the magma and the coolant is water. Water at atmospheric conditions has a homogeneous nucleation temperature exceeding 300°C. Magmas have temperatures well above this temperature, therefore, in principle, phreatomagmatic explosive eruptions can occur in any volcanic environment.

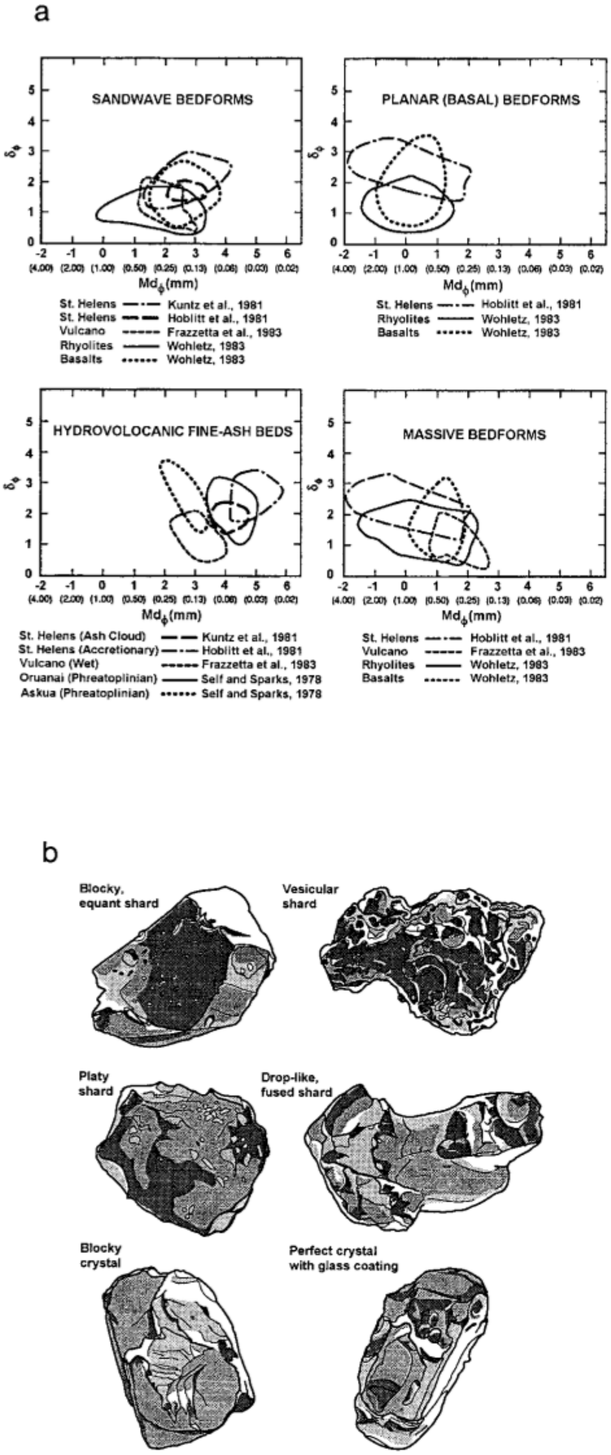

FIGURE 2 (a) Grain size distributions for phreatomagmatic tephra. (b) Clasts shapes characteristic of phreatomagmatic fragmentation.

FCI may be explosive or nonexplosive depending on the rate of heat transfer between the fuel and coolant and the subsequent pressurization rate of the coolant. The rate of heat transfer is a function of the surface area of the fuel which, in an explosive FCI, increases by a cascading fragmentation process. The fragmentation process is enhanced by thermal expansion of the coolant that creates new contact surfaces.

The physical dynamics of an explosive FCI are represented by the following stages:

1. Initial contact and coarse mixing of fuel and coolant under stable vapor film boiling conditions (Leidenfrost phenomenon).
2. Complete vapor film collapse caused either by the passage of a pressure pulse which may be of external origin (e.g., seismicity) or by a local implosion (i.e., water hammer) due to rapid condensation of coolant vapor. Once the coolant vapor is completely condensed, the fuel and coolant are thermally and mechanically coupled.
3. Episodic increase of heat transfer from fuel to coolant and fine fragmentation leading to superheated and pressurized water. As the coolant is heated, it expands at a rate of <1 ms, leading to rapid increase in load stress on the melt. Relaxation of load stress in the brittle mode (elastic rebound) causes the explosive release of seismic energy. Up to 90% of the total kinetic explosion energy is released in this phase.
4. Volumetric expansion of the fuel–coolant mixture from the transformation of the superheated water to superheated steam. At this stage, the fuel and coolant are thermally and mechanically decoupled.

All FCIs, explosive or nonexplosive, are initiated by Stage 1. A nonexplosive FCI terminates at Stage 1 or Stage 2. The wetness of an explosive FCI reflects the degree of fragmentation and the rate of heat transfer (or the efficiency of the feedback mechanism) during Stages 2 and 3.

II. THEORETICAL AND EXPERIMENTAL RESULTS

A. History

Theoretical and experimental studies at Sandia National Laboratory (New Mexico) in the 1970s and 1980s provided a strong basis for understanding FCIs and a framework for the study of phreatomagmatic activity. These experiments were designed to investigate the occurrence of steam explosions during core meltdown at nuclear reactors and others industrial environments such as metal smelters. The primary goal of the experiments was to constrain models for the conditions for a steam explosion when a coolant comes into contact with a fuel. Fuel (melt) used in the experiments ranged from molten salts to thermite-generated melts. Results from these studies include the four steps describing the physical dynamics of a FCI.

Phreatomagmatic explosions are complex interactions of four phases which are often internally heterogeneous (magma, magmatic volatiles, external water, and wall rock). Experimental studies of simple systems offer powerful tools for understanding the eruption dynamics.

B. Thermite: Water Experiments

Experiments conducted at Los Alamos National Laboratory were designed to simulate phreatomagmatic activity using an Fe–Al thermitic melt and water. The objectives were to monitor dynamic events and to determine what controls the rapid conversion of the melt's thermal energy into mechanical energy when it interacts with water. The melt, simulating basaltic magma, resulted from an exothermic reaction of fine-grained aluminum (~24 wt%) with magnetite (~76 wt%). In general, this thermite composition yields about 1130 kJ excess heat per mole of iron oxide at 1800 K. The physical and thermal properties of Fe–Al thermite melt are compared with those of a typical tholeiitic basaltic melt in Table I.

Four designs, shown and described in Figs. 3a–3d, were employed to evaluate the effects of contact geometry, the mass ratio of water to melt, and the confining strength (or pressure) on the explosivity of the experimental phreatomagmatic eruption. High speed cameras were used in all experiments and samples of ejected thermite were collected from some of the experiments.

TABLE I Physical and Thermal Properties of Fe–Al Thermite and Basaltic Melt

Properties	*Fe–Al melt*	*Basaltic melt*
Liquidus T	1000–2000 K	1370–1520 K
Enthalpy	3700 kJ/kg	1150 kJ/kg
Viscosity	10^2 Pa s	10^2–10^3 Pa s
Density	3.0–4.0 Mg/m^3	2.5–2.7 Mg/m^3
Surface tension	0.5 N/m	0.35 N/m
Thermal conductivity	2.4 J/(m s K)	2.1 J/(m s K)

More than one style of melt ejection, each resembling a type of natural volcanic activity, resulted from these experiments:

1. Continuous fountaining of centimeter-sized liquid fragments of thermitic melt, which resembled a hawaiian eruption
2. Pulsating ballistic ejections of partially quenched and vesicular (scoriaceous) fragments, which resembled a strombolian eruption
3. Dry vapor-rich explosions ejecting micrometer-sized fragments in expanding jets of superheated steam, which resembled a surtseyan eruption
4. Wet vapor explosions ejecting millimeter-sized fragments in ballistic plumes of condensing steam
5. Passive chilling of the thermitic melt into centimeter-sized fragments with quenched surfaces, which was analogous to the formation of pillow lavas or peperites

A fifth experiment was designed to resemble a propulsion rocket (Fig. 3e) in order to quantify the water-to-melt mass ratio and confining pressure controls on the mechanical energy of an interaction. In this design, ejection of high pressure steam and fragmented thermite passing through the vent caused the vessel to lift off the ground. Measurements of the internal pressure history and ejecta characteristics were recorded, as was the maximum height reached by the vessel. Three confining pressures were used, 6.8, 16.3, and 35.7 MPa; the last exceeds the critical pressure of water (22.0 MPa). The water-to-melt mass ratio investigated ranged from 0.38 (1.82 kg of water and 4.73 kg of melt) to 2.00 (4.00 kg of water and 2.00 kg of melt).

The results from these experiments include three distinct pressurization histories or groups which were found to correspond to three specific ranges of lift-off heights (LOH) and produced clasts with distinct morphologies. The three pressurization histories are characterized by (1) exponential pressure–time curves; (2) an initial linear pressure rise and after approximately 0.3 to 0.8 s, a parabolic pressure increase to a value near the confining pressure; and (3) an initial linear pressure increase followed by an event that pressurized the chamber to a maximum value within 5 to 20 s.

Although the number of experimental samples is limited, an interesting correlation was observed between the six distinct grain shapes (Fig. 4a) identified in recovered samples and the three pressure groups: Group 1 experiments produced predominantly mosslike grains; Group 2 produced mainly spherical or droplike and aggregate grains; Group 3 experiments produced mainly blocky and irregularly shaped grains. Platelike grains were found in the fine-grain fraction of most samples. The correlation between grain shapes and the three pressure groups suggests that the grains are a consequence of the dynamic behavior of water as it is being heated by the melt during preburst interaction. Although sampling did not adequately represent the fraction of the sample finer than 62 mm (4 ϕ), the distributions shown in Fig. 4b are very similar to some phreatomagmatic tephra size distributions (Fig. 2a).

In order to facilitate the use of these experiments as analogs of hydrovolcanic eruptions of much larger scale, the explosive energy is expressed as the ratio of the measured and calculated mechanical energy to the initial internal (thermal) energy of the melt. This ratio is called the conversion ratio (MCR) and was calculated from the conservation of momentum.

As shown in Fig. 5, a positive correlation was found between MCR and the water-to-melt mass ratio (R_m) within the three pressure groups. This plot shows that the observed pressurization mode is strongly linked to the resulting conversion ratio for each experiment. The pressure–time histories associated with each pressure group reflects the degree to which the water–thermite melt interaction approached thermal equilibrium. Thus,

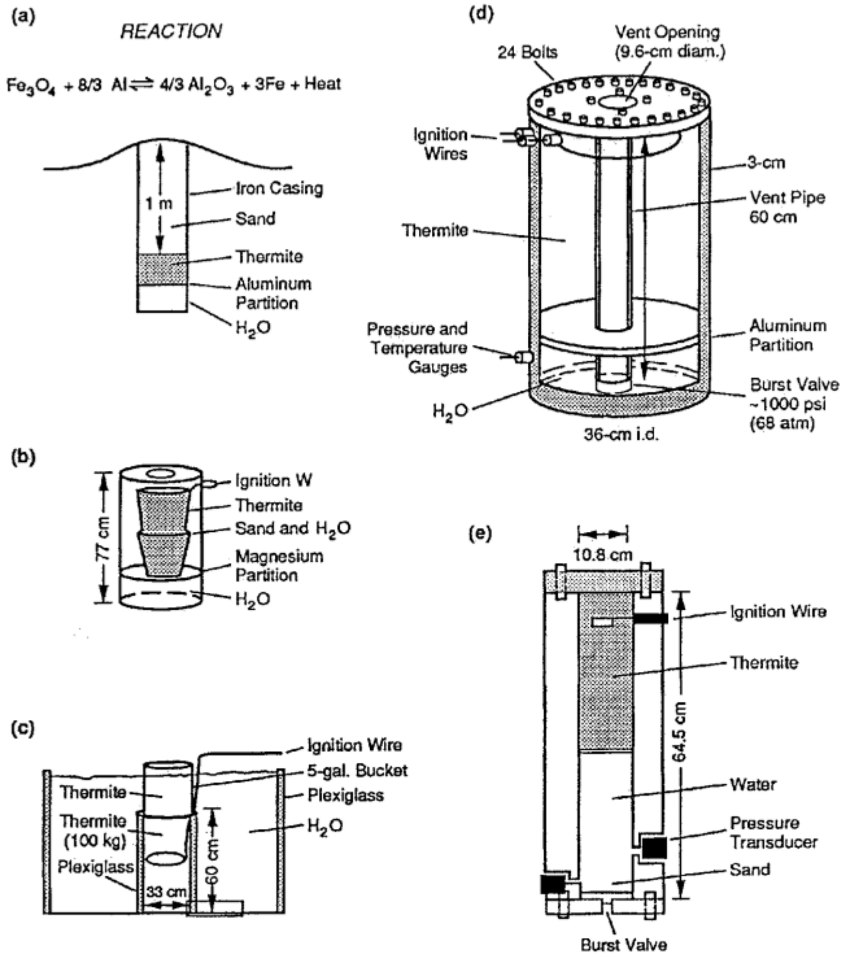
(a)
REACTION
$Fe_3O_4 + 8/3\ Al \rightleftharpoons 4/3\ Al_2O_3 + 3Fe + Heat$
1 m
Iron Casing
Sand
Thermite
Aluminum Partition
H_2O
(b)
77 cm
Ignition W
Thermite
Sand and H_2O
Magnesium Partition
H_2O
(c)
Ignition Wire
5-gal. Bucket
Plexiglass
H_2O
Thermite
Thermite (100 kg)
Plexiglass
33 cm
60 cm
(d)
24 Bolts
Vent Opening (9.6-cm diam.)
Ignition Wires
3-cm
Vent Pipe 60 cm
Thermite
Pressure and Temperature Gauges
Aluminum Partition
Burst Valve ~1000 psi (68 atm)
H_2O
36-cm i.d.
(e)
10.8 cm
Ignition Wire
Thermite
64.5 cm
Water
Pressure Transducer
Sand
Burst Valve

FIGURE 3 Schematic drawings of the five thermite–water interaction experiments conducted at Los Alamos National Laboratory. (a) Emplacement of 10 kg of thermite in an iron pipe above a second pipe filled with water; (b) immersion of a Plexiglas tube in a large Plexiglas box filled with >1 cubic meter of water; (c) emplacement of 90 kg of thermite held above water by an aluminum disk in a sealed steel cylinder with a vent at the top that burst open when the internal pressure exceeded 7 MPa; and (d) same as design (c) except the vent pipe extended down through the thermite into the water compartment. (e) The lift-off experiment designed similarly to (d) except the burst valve is located at the base of the vessel.

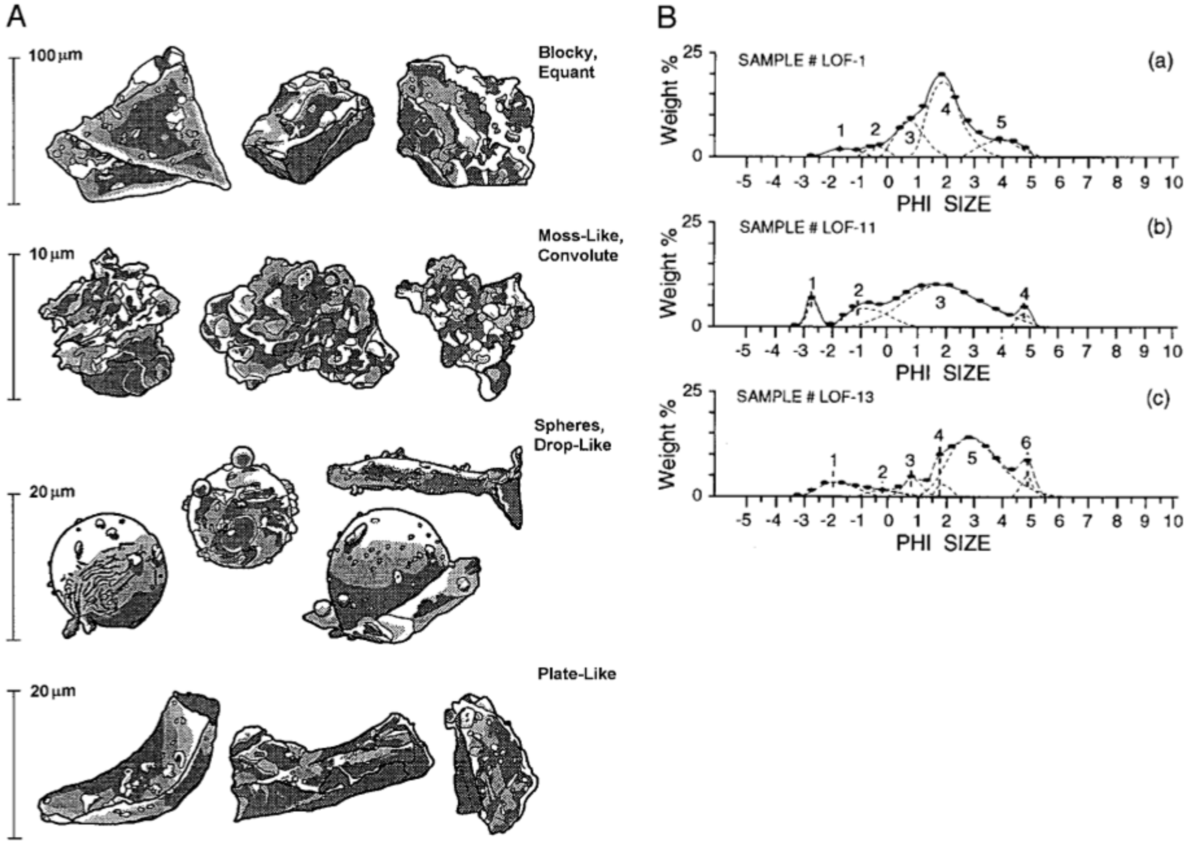

FIGURE 4 (A) Sketches of the four grain shapes observed in samples collected from the LANL experiments: (1) blocky; (2) mosslike convoluted surfaces; (3) spherical and droplike; and (4) curvey, plate-like. (B) Results of sieve analysis of three samples of experimental debris. Sample characterization where $\phi = -\log_2$ (diameter in mm) includes: (a) LOF-1 with mean $\phi = 1.74$ and standard deviation $(\sigma) = 1.45$; (b) LOF-11 with mean $\phi = 1.25$ and $\sigma = 1.99$; and (c) LOF-13 with mean $\phi = 2.19$ and $\sigma = 1.90$.

water–melt interactions involved with Group 1 experiments were the most efficient and explosive, and came closest to thermal equilibrium. These equate to "dry" phreatomagmatic events. Water–melt interactions involved with Group 3 experiments were the least efficient and explosive and did not approach thermal equilibrium. These experiments were considered analogs to submarine phreatomagmatic events. Group 2 experiments fell between Groups 1 and 3 and were considered analogs to "wet" phreatomagmatic events.

C. Experiments Utilizing Rock Samples

A series of thermal explosion experiments (TEE) at University of Wuerzburg were designed to study phreatomagmatic fragmentation using remelted volcanic rock samples with compositions ranging from ultrabasic to andesitic. The experiments evaluated the effect of the mode of contact between water and melt, the mixing conditions, the fragmentation processes during an explosive FCI which is also termed a thermohydraulic explosion, and the expansion phase of an explosive FCI. All experiments involved high resolution measurements of physical processes and properties associated with an explosive FCI and the evaluation of fragmented melt.

These experiments included two configurations: (1) water entrapment achieved by injection of a water volume into a melt volume and (2) melt entrapment achieved by the stratification of water and melt on an experimental scale of 5–20 cm (Fig. 6). The latter produced only very weak FCI with low reproducibility and thus were not useful analogs to phreatomagmatic explosions. The former were useful as these produced energetic explosions very effectively. For timing purposes, an explosion in each experiment was initiated by a projectile

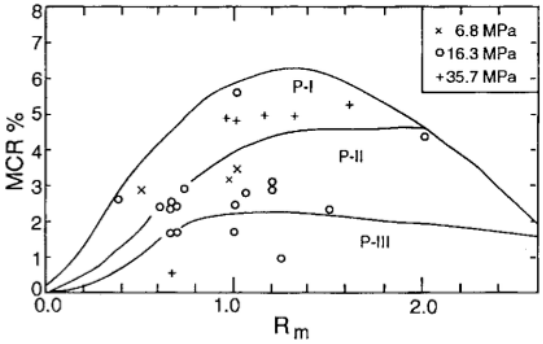

FIGURE 5 Trend of mechanical conversion ratio (MCR) with the water/melt mass ratio (R_m) for experiments with different p_{conf}. The delineated field shows the range of data for the experiments exhibiting pressure records of a given group. P-I experiments showed MCR values greater than those of P-II, and P-III experiments showed the lowest MCR values. This relationship strongly indicates that the mode of pressurization is linked to the mechanism of fragmentation and heat exchange for these experiments.

that was fired at the melt surfaces to breakdown insulating vapor films.

A third experiment was designed to identify and quantify fragment populations generated by processes associated with the expansion of superheated steam (Stage 4 of a FCI). These experiments involved a sudden release of a compressed inert gas (argon) in the melt filled crucible (Fig. 6).

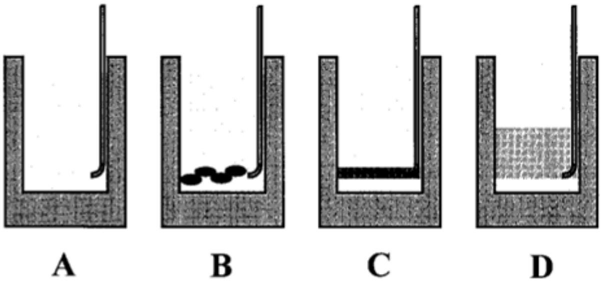

FIGURE 6 Entrapment of water in melt. Schematic cross sections of crucible used in the experiments: (A) A thin walled steel tube is inserted into the melt to the desired depth. (B) Water is injected into the melt; thus a local water/melt premix is produced. (C) After triggering, the escalating process of thermohydraulic explosion takes place in this premixed zone, during which water is superheated. Once the superheat reaches a critical value the phase transition to superheated steam is enforced, resulting in very rapid volume expansion. (D) The superheated steam finally expands to ambient pressure in an adiabatic way, thus accelerating the overlying melt strata out of the crucible.

Results from the first two experimental designs suggested that heat loss from the melt during the initial contact and premixing phase is critical for the generation of an explosion. Two contact modes were investigated, hot melt surrounded by excess water or water surrounded by excess melt. When the melt was dispersed in excess water, the heat transfer, even under stable vapor film boiling conditions, was very effective such that melt particles with diameters <1 cm completely solidified or a thick crust formed around larger melt particles within <1 s. In this case explosive FCI did not occur. In the case of water entrapment by excess melt, an explosive FCI was found to be highly probable. Here, the intensity of a resulting thermohydraulic explosion is proportional to the initial contact areas.

The mixing phase was found to be the primary control on the intensity of an explosive FCI. The available interfacial area between the two liquids is governed by (a) the differential flow speed (hydrodynamic energy) between the two fluids and (b) by the material properties of the fluids. Efficient mixing (i.e., creation of a large interfacial area in a short time), was achieved when the flow speed is high, and the densities and viscosities of the liquids are similar and low. Silicate magmas have densities between 2500 and 3000 kg m^{-3} and viscosities ranging from few Pa s to $>10^6$ Pa s. In contrast, water has a density near 1000 kg m^{-3} and a viscosity of 10^{-3} Pa s. In Figs. 7 and 8, the optimum mixing conditions for low viscosity, ultrabasic melts are the maximum values for the water-to-melt volume ratios and the differential flow speeds which correspond to 11 vol% water and

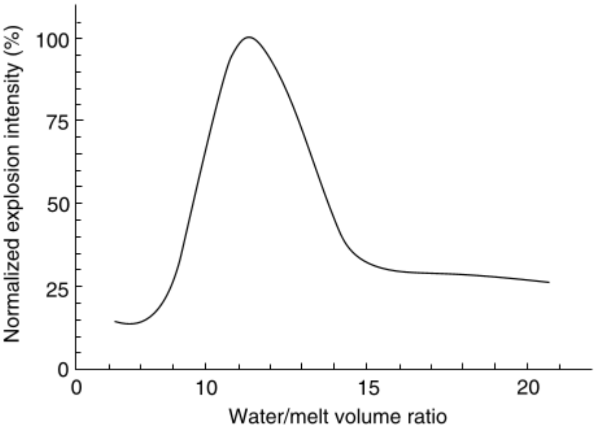

FIGURE 7 Water/melt volume ratios of mixing in entrapment configuration. The melt used in this experiments was a remelted olivine–melilitite at 1350°C and a viscosity of about 1 Pa s.

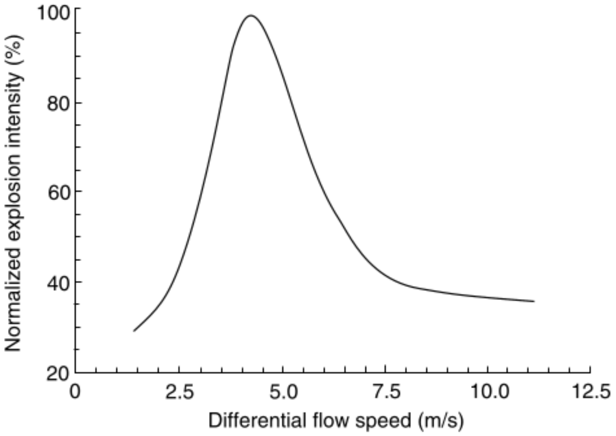

FIGURE 8 Differential flow speeds of mixing at a water/melt volume ratio of 11% in entrapment configuration. The melt also was remelted olivine–melilitite at 1350°C and a viscosity of about 1 Pa s.

~4.5 m/s, respectively. These values are thought to be valid for all basic magmas for cases in which water intrudes on the magma. Although these maxima are well defined, explosions occurred in a wide hydrodynamic mixing range.

Three fragmentation regimes were distinguished:

1. Fragmentation of the melt inside the crucible without measurable expansion of the mixture during fine-fragmentation and heat transfer (Stage 3 of a FCI)
2. Fragmentation of melt strata during acceleration of the melt by expansion of superheated steam inside the crucible
3. Fragmentation of the melt during high speed ballistic trajectory outside the crucible

Particles produced by the fine-fragmentation, regime 1, resembled the ash-sized particles generated by the LANL experiments. The fine-fragmentation phase was found to be the crucial phase for an explosive FCI, during which the maximum kinetic energy (explosion energy) is released. This phase produced angular shaped particles with diameters between 30 and 130 μm. Fragmentation during melt acceleration in a confined geometry produced spherical fragments with diameters between 90 and 180 μm. Fragmentation during decelerated movement of melt on ballistic trajectories in free air produced elongated shapes to hairlike shapes similar to Pelè's hair, depending on the ejection velocity.

An experimental explosive FCI is a highly energetic, short-time process occurring on a timescale of <1 ms. Within this time frame, new surfaces were created by a brittle type of fine fragmentation. The particles exclusively produced during this event were identified and quantified. The total of new surface area was found to correlate linearly with the respective explosion intensity.

III. FRAGMENTATION MECHANISMS

A. Types of Fragmentation

A fragmentation mechanism associated with each phreatomagmatic grain type (i.e., blocky, fusiform, moss-like, platey, and spherical or drop-like) can be inferred from results of the phreatomagmatic analog experiments and FCI theory. The blocky grains found in tephra deposits and produced in lab experiments resemble shattered glass or glass that has been partially twisted and deformed while still plastic. These fragments form when stress waves propagate through a melt and produce deformation rates that exceed its bulk modulus (Fig. 9). Also it is envisioned that the local temperature of the melt is near solidus and brittle fractures develop in response to thermal contraction or tensional stress waves produced by vapor film collapse. Because stress waves typically propagate faster than thermal waves, it is likely that thermal contraction affects only melt surfaces while

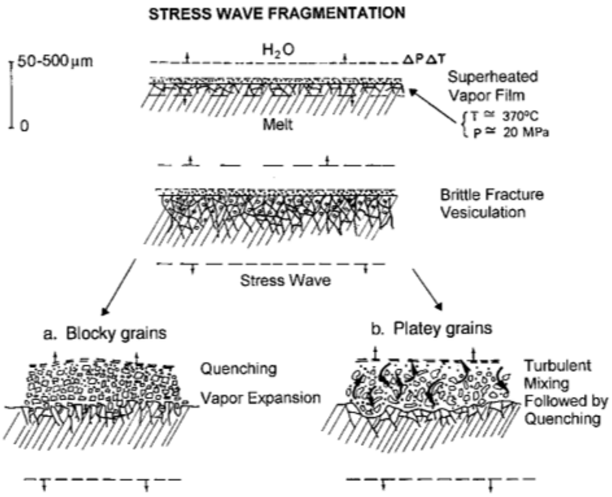

FIGURE 9 The collapse of a superheated vapor film or the explosive expansion of the film will produce stress waves in the melt. If these exceed the bulk modulus of the melt and it fractures in a brittle fashion, (a) blocky Type 1 or (b) Type 2 pyroclasts will form. [Reprinted with permission from Wohletz, 1983.]

the bulk of the melt is rapidly subjected to mechanical stresses.

In quenched portions of the melt, fractures tend to propagate at angles less than 45° to the melt surface, forming block-shaped clasts with planar to curviplanar surfaces. Vapor film oscillation may produce turbulence that tends to spall quenched melt fragments from the surface of the molten body and expose unquenched surfaces (Fig. 9). For portions of the melt that fragment prior to quenching, vapor turbulence can cause deformation of unquenched shards with melt surface tension promoting formation of fluidal surface textures.

Moss-like grains develop by viscous deformation under tensional stress conditions created during rapid vapor formation. These conditions are predicted by the development of Rayleigh–Taylor and Kelvin–Helmholtz instabilities. These instabilities are caused by the relative motion of the vapor along the melt surface (Fig. 10). They perturb the melt surface and introduce additional morphological characteristics. Tiny plumes of melt rise from the surface when surface tension forces are exceeded by Rayleigh–Taylor instabilities (Fig. 11). Kelvin–Helmholtz instabilities are induced by shear stresses that further stretch and disperse the melt surface. Because these instabilities form with a range of wavelengths and orientations, melt surfaces can become very convoluted, resulting in tortuous, high surface area fragments.

Spherical or droplike grains develop from the effect of surface tension when magma is still hot enough to behave like a fluid. As with moss-shaped grains, melt surface instabilities both grow and detach to form spherical or elongated ribbon-like structures in response to the force of locally collapsing vapor films (Fig. 12). The most rapid mechanism contributing to production of these grains occurs when compression waves associated with vapor film collapse become large enough to shatter the surface undulations produced by instabilities; this results in the production of a multitude of fine-grained fragments. When axisymmetric collapse of vapor films produces accelerations sufficient to overcome surface tension forces of fluid melt, water jets can penetrate into the melt and become partially or completely entrapped beneath the surface. The trapped water becomes superheated and expands, thus causing additional fragmentation of melt.

Platey grains have been interpreted as pieces of quenched crust stripped off the surface of the magma (Fig. 9b). The stripping process can be attributed to the turbulence of vapor film oscillation, vaporization wave

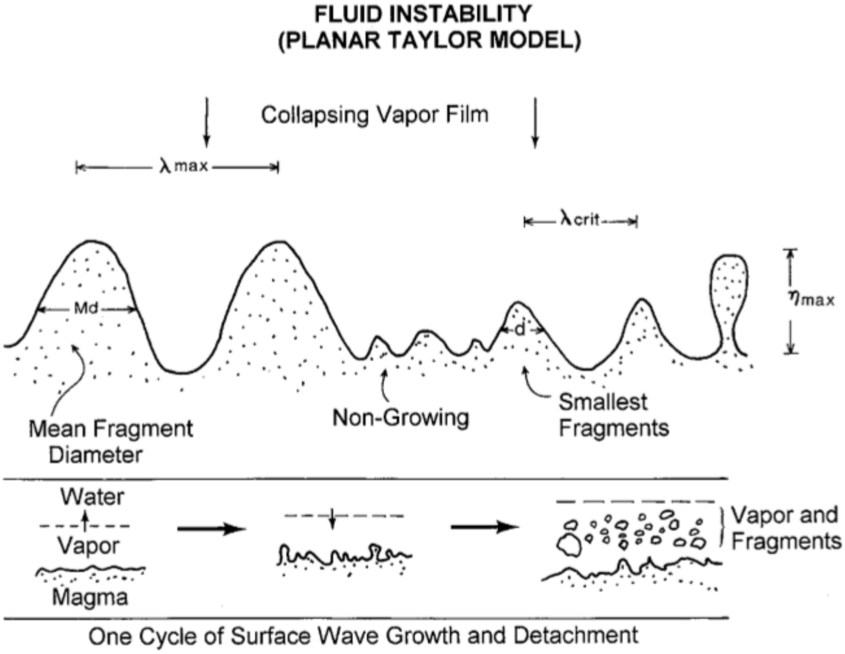

FIGURE 10 (Top) Sketch of a planar Taylor instability at the interface between magma and a collapsing vapor film. (Bottom) Diagram of a complete cycle of instability growth. The oscillation of the vapor film transmits sufficient momentum to the magma surface so that it becomes distorted into waves. [Reprinted with permission from Wohletz, 1986.]

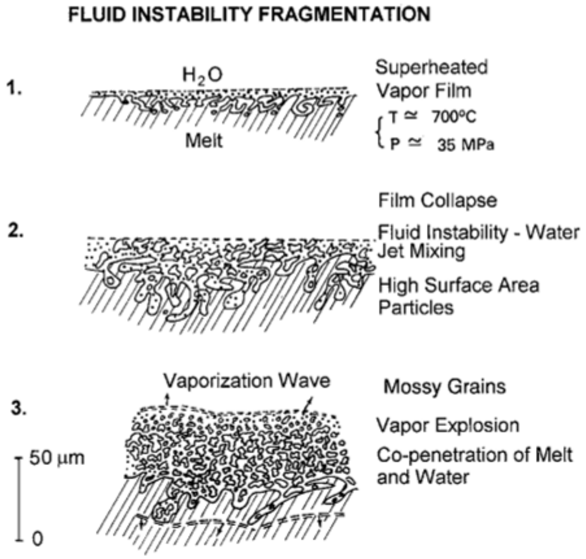
FLUID INSTABILITY FRAGMENTATION
1.
H₂O
Superheated Vapor Film
T ≃ 700°C
P ≃ 35 MPa
Melt
2.
Film Collapse
Fluid Instability - Water Jet Mixing
High Surface Area Particles
3.
Vaporization Wave
Mossy Grains
Vapor Explosion
Co-penetration of Melt and Water
50 μm
0

FIGURE 11 Fluid instabilities can form at the contact of water with melt. These instabilities are of a Rayleigh–Taylor or Kelvin–Helmholtz type, both of which may cause axisymmetric film collapse that causes water jets to penetrate the melt. The result is high surface-area fragmentation, rapid heat exchange, followed by vapor explosion. The explosion then generates new contact areas and/or a shock wave that fragments more melt and acts as a detonation wave. This process requires abundant water to be present. [Reprinted with permission from Wohletz, 1983.]

propagation, or Kelvin–Helmholtz instability. High velocity ejection of liquid melt leads to the formation of rock wool.

B. Growth and Evolution of Fragmentation Events

Phreatomagmatic fragmentation evolves in a number of different manners depending upon the primary controlling parameters of viscosity, temperature, confining pressure, and water/magma contact mode (i.e., mixing conditions and mass ratio). These parameters are largely determined by the environmental setting of the volcano and its magma characteristics, discussed below, and they determine the rate of heat transfer from the melt to water. Fragmentation events follow a complex growth history that includes premixing, pressure growth, triggering, failure, and ejection. These stages are similar to those associated with an FCI.

Premixing is an increased intermingling of water with the melt, which leads to a large increase in surface area, and hence in heat transfer. The intermingling is driven by diffusional and kinetic mechanisms, including hydraulic fracturing, stress corrosion, capillarity, vapor-film collapse and water jetting, molecular diffusion, and Taylor and Helmholtz instability. It is important to note that this intermingling occurs over a wide range of scales from submicrometers to meters, and that it occurs without significant heat transfer to the water, because of vapor-film insulation.

After premixing, thermal energy is transferred to the water over a large effective surface area, and with this transfer, pressure builds, in many cases making the water a supercritical fluid or a metastable superheated fluid. From experiments this phase of pressure growth may show several different temporal patterns, including exponential, parabolic, and cyclic growth with time. For exponential growth pressure increases with surface area during premixing, which requires that premixing produces melt fragments that decrease in size linearly with time. This produces an exponential rise in surface area, hence in heat transfer with time, and an accompanying exponential rise in water pressure. On the other hand, a parabolic pressure rise probably reflects simple thermal diffusion in which heat transfer is initially rapid and slows with time as diffusional distances increase. Cyclic pressure increases best reflect cyclic growth and collapse of vapor films as premixing progresses. Rapid heat transfer at a water–melt interface causes a vapor film to pressurize and rapidly expand past its stable size, leading to overcooling of the film and its immediate condensation and collapse, which may produce water jets that

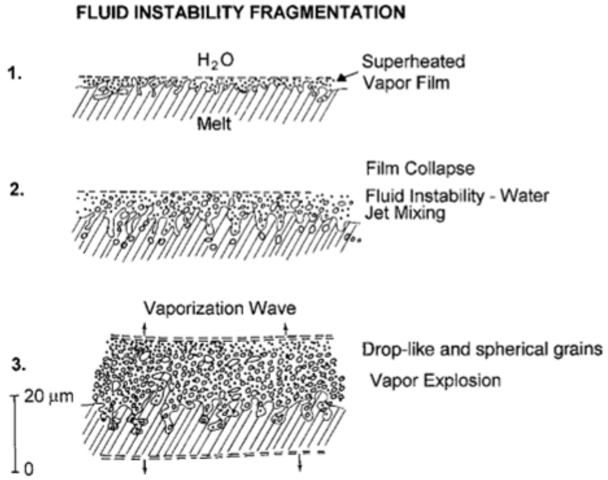
FLUID INSTABILITY FRAGMENTATION
1.
H₂O
Superheated Vapor Film
Melt
2.
Film Collapse
Fluid Instability - Water Jet Mixing
3.
Vaporization Wave
Drop-like and spherical grains
Vapor Explosion
20 μm
0

FIGURE 12 Fluid instabilities will form spherical or drop-like shapes of melt if viscosity is low and surface tension effects are strong. [Reprinted with permission from Wohletz, 1983.]

impinge the surface of the melt. The initial film pressure then becomes the force exerted on the melt surface by the film's collapse, which leads to the eventual breakup of the melt into smaller particles and an increase in heat transfer surface area. As the surface area grows, the pressure of each cycle of film growth also increases.

Premixing and pressure growth may continue or may decline with time, the latter case resulting in a highly metastable situation that can exist only in high confining pressures (>16 MPa). However, for the former case, water will gradually increase in temperature until it spontaneously vaporizes in whole or part. If a small portion of the water reaches this point first, its vaporization produces a pressure pulse that triggers the vaporization of the rest of the water and may cause an explosion.

An explosive vapor expansion drives a shock wave by which the melt is rapidly accelerated. This acceleration produces stresses that can exceed the bulk modulus of the melt, leading to its whole-scale failure and production of fragments; fragments formed during premixing are further comminuted and intact melt is torn apart. The mode of failure is largely determined by the properties of the melt, and it ranges from brittle to ductile in behavior.

The final stage of fragmentation is the ejection phase where fragments are moving at high speeds. If the explosion originates away from a free surface, then as the shock wave emerges through the free surface it will create a rarefaction wave that propagates in the opposite direction. This rarefaction wave allows immediate vapor expansion as it propagates into the conduit. It is at this stage when the wall rock (nonjuvenile lithics) becomes fragmented and incorporated into the erupting mass. With vapor expansion, fragments are accelerated and ejected out of the system. During this ejection, the speed of the fragment is proportional to its size because of inertial effects, such that fragments will move at different speeds and collide with one another, leading to further fragmentation.

Melt fragment shapes and size distributions are controlled by the types of premixing, triggering, failure modes, and ejection. Although growth and evolution cannot be directly observed, the overall pattern of phreatomagmatic fragmentation is portrayed by eruption phenomena. In this light, fragmentation evolution can be classified as: (1) escalating, (2) declining, (3) cyclic, or (4) delayed. Escalating fragmentation during eruption results in larger and larger volumes of tephra produced in each successive burst. Such behavior requires the mass of magma fragmented to increase by an increase in the water flux and/or magma flux. As discussed above, the water/melt mass ratio (R_m) determines in part the energy of fragmentation with higher fragmentation energy leading to more magma fragmentation. Conversely, decreasing fluxes or a change in R_m away from high energy fragmentation leads to a declining fragmentation evolution. Cyclic evolutions are common where fragmentation repeatedly grows and then declines. This situation is most common where water supply is depleted after large fragmentation events, resulting in less energetic ones until the water supply is reestablished. Delayed fragmentation refers to a situation where a fragmentation event occurs after a prolonged period after premixing. Prior to fragmentation, the system is metastable, requiring a trigger. This type of fragmentation, although well-observed in experiments, is difficult to sustain in volcanic situations. Such situations might include a upper-crust magma chamber that interacts with water saturated rocks for a long time prior to eruption.

C. Fragmentation Controls

Through the experiments and theory described above and observations at numerous volcanoes around the world, it has become clear that phreatomagmatic fragmentation is largely controlled by three key parameters: magma viscosity, temperature/pressure, and water/magma contact mode. The third is a function of the supply rate of magma and external water which is determined by the hydrology of and around the vent and conduit.

During phreatomagmatic fragmentation part of the thermal energy of the magma is converted to mechanical energy, including seismic and acoustic energy, fragmentation energy, and kinetic energy of fragment motion. With an increasing *efficiency* or conversion ratio, more mechanical energy is released and fragmentation increases. In field observations at volcanoes, the relative efficiency of phreatomagmatic fragmentation is reflected by fragment size distribution and mode of fragment dispersal.

In general, (1) higher temperature melts have greater thermal energy available for conversion to mechanical energy, (2) viscosity retards the mixing of magma and water in a manner that generally predicts that fragmentation will be greater in lower viscosity magmas, and (3) the amount of water relative to that of magma involved in fragmentation determines the intermediate and final thermodynamic states of water for phreatomagmatic eruptions. Magma and water temperatures prior to interaction influence the heat transfer rates and equilibrium temperature approached during mixing. In a simple way, the higher the equilibrium temperature, the more energy is available for mechanical work, but the rate of heat transfer is complexly linked to water temperature, rising rapidly with temperature until the onset of vapor-film boiling. Thermal equilibrium is probably never reached during fragmentation because instability and vapor expansion occurs before this point is reached. For the instantaneous heating case, the temperature of the interface, T_i, is theoretically constrained by

$$T_i = \frac{T_m(\alpha_m/\sqrt{\kappa_m}) + T_w(\alpha_w/\sqrt{\kappa_w})}{(\alpha_m/\sqrt{\kappa_m}) + (\alpha_w/\sqrt{\kappa_w})},$$

where α and κ are thermal conductivity and diffusivity, respectively, of the respective phases water, w, and melt, m. If T_i is greater than the spontaneous nucleation temperature of water, then a spontaneous superheat vaporization would occur.

The effect of ambient (or confining) pressure is less understood. Pressure is thermodynamically linked to temperature, and, as such, the pressure-volume work of a fragmentation should increase with pressure, but there are some experimental indications that pressure also acts to subdue interaction because it limits vapor-film growth and the amount of premixing. However, the most violent experimental fragmentations have occurred where confining pressure is in excess of the critical pressure of water.

The viscosity of magmas ranges from few Pa s in the case of basaltic composition to millions of Pa s in the case of silicic magmas. Viscosity is additionally coupled to temperature in magmas (higher temperature magmas have generally lower viscosities). While temperature may vary several hundreds of degrees, viscosity varies over many orders of magnitude. Viscosity (and surface tension) is an important parameter for growth and propagation of fluid instabilities at the interface between magma and water. Such instabilities have been cited as likely mechanisms.

The combined effect of viscosity and temperature on the efficiency of fragmentation is markedly less than that of water/magma ratio, which varies over two orders of magnitude. This observation reflects the major control of water expansion during fragmentation, a control determined by intermediate and final thermodynamic states of water. If very little water is available, it can be heated to high temperatures and pressures, but fragments only a relatively small volume of magma. At the other extreme, abundant water may never get enough thermal energy for fragmentation. At intermediate mass ratios, there is enough thermal energy to take all the water to high states of internal energy, thus resulting in rather complete magma fragmentation.

Water involved in the interaction may not always be a pure liquid, it may contain particles (sediment or tephra) or other impurities such as dissolved compounds (seawater or hydrothermal fluids). The effects of these impurities on the fragmentation process are related to the changes in the physical properties of the impure water. Depending on the concentration of impurities in the water, its viscosity may increase up to an order of magnitude, the density may double and the heat capacity may decrease by one-fourth.

IV. FIELD OBSERVATIONS

Hydrologic settings for phreatomagmatic fragmentation vary from deep ocean (marine) to near shore (littoral) to lake (lacustrine) to surface drainages (fluvial) and groundwater (phreatic) settings. The hydrological settings affect the abundance and supply rate of water and the ambient pressure at which interaction occurs. Accordingly, the character of phreatomagmatic fragmentation varies in a systematic manner with setting.

For marine settings, deep water explosive fragmentations are not generally observable. In fact, many researchers propose that for depths where hydrostatic pressure is greater than the critical pressure of water, explosive fragmentation does not occur. These researchers explain deep ocean hydroclasts to have resulted from simple quench fragmentation of extruded lava, because most hydroclasts are blocky shaped and coarse to medium in size. On the other hand, experimental and theoretical evidence shows that the critical pressure of water is not the maximum pressure at which explosive fragmentation may occur. In fact, for most substances that undergo such rapid vaporization (leading to explosive expansion), the phase change may occur well above the critical pressure. Future research involving actual observation of deep water eruption or documentation of explosive effects in deep water tephra deposits may resolve this debate.

Littoral fragmentations have been well documented in Hawaii where lava flows enter the sea. A large variation in fragmentation dynamics is observed from passive steam and quench-fragmentation to violent bursts that form high-speed sprays of fine-grained hydroclasts. One control is thought to be whether or not lava contacts water within the confined space of a lava tube or not. The fragmentation starting in a lava tube is observed to be very violent, suggesting that such confinement allowed buildup of high pressure during the event. Consequently, fragments from littoral fragmentation show a wide range of shapes and sizes from centimeter-sized fluid-shaped clasts to micrometer-sized blocky shards. Cones that form in the littoral zone are similar to tuff cones that grow in lacustrine environments. These eruptions are observed to produce large amounts of saturated steam and are called “wet” eruptions. The associated cones are referred to as littoral cones or rootless craters for those that form where lava has traveled over a marsh or a bog.

Phreatomagmatic fragmentation in fluvial or phreatic hydrogeological environments is governed by a limited supply of water. Such fragmentations, though, can be the most violent because water/magma ratios are in the range of optimal interaction and the contact modes under confined conditions (i.e., in hydraulically active fault systems) are optimal for the generation of thermohydraulic explosion. Tuff rings (e.g., Crater Elegante, Mexico; Panum crater, United States) in these settings show wide-area, high energy dispersal with superheated vapor that does not produce such wet deposits; hence palagonitization is limited. Such fragmentation is called *dry* and in many places occurs with scoria deposits that result from little or no water interaction. Typically the fragments are fine-grained ash, showing a range of shapes from blocky to mossy aggregates to micrometer-sized spheres. Tuff cones (e.g., Cerro Colorado, Mexico; Koko crater, United States) show low energy dispersal with saturated steam that produce palagonitized deposits. Such fragmentation is called *wet* and in many places produce basal surge deposits that result from a progressively water-rich interaction. Typically the fragments are fine- to medium-grained ash, showing a range of shapes from blocky and platey with dust-sized fragments adhering to surfaces, forming accretionary type grains.

The depth of fragmentation is likely determined by the depth of the aquifer. During eruption, an aquifer may be drawn down such that fragmentation level gets deeper while the hydrostatic pressure onto the system is more or less constant. Explosions propagating downward will fragment and erupt wall rock at deeper and deeper levels, thus enlarging the conduit (e.g., a diatreme) to the depth of the aquifer. The amount of lithic ejecta also reflects the stability of the walls. Very little fragmented wall rock is erupted when the walls are stable and the eruption is fairly continuous and weak. If the walls are unstable, then the walls may be eroded during a weak eruption, thus producing a significant amount of fragmented wall rock. The collapse of eroded wall rock can trigger a strong, discrete explosive phreatomagmatic eruption that erupts mostly lithic material.

V. SUMMARY AND FUTURE RESEARCH

1. Phreatomagmatic fragmentation is quite distinct from magmatic fragmentation in both the eruptive phenomena and the driving mechanisms as well as in the types of fragments produced. Phreatomagmatism produces unique juvenile grain populations that reflect the relative amount of water and magma involved in the interaction. The quantity of nonjuvenile (fragmented wall rock) material found in deposits reflect the stability of the conduit walls and the explosivity of the eruption.

2. Phreatomagmatic fragmentation results in a spectrum of eruptive activity ranging from passive quenching of magma/lava to explosive ejections of ash. The style of eruption primarily reflects the hydrologic environment in which magma/lava come into contact with water.

3. Much of our understanding of phreatomagmatic fragmentation stems from laboratory experiments related to fuel–coolant interactions (FCIs) as well as field observations and laboratory analysis of the fragments. It is future experimental studies that may best improve our current knowledge of the controls of phreatomagmatism. For example, experiments have thus far only covered a rather narrow range of melt compositions, including thermitic melts and some remelted volcanic rocks. Detailed experiments may reveal how fragmentation is affected by compositions ranging from mafic to silicic and with different proportions of dissolved volatiles. Similarly, experimental coolants have been pure or nearly pure water, so very little is known about how impurities in the coolant effect the fragmentation process. These areas for future research are just a few that could further the relevance of experimental analogs to phreatomagmatic volcanism.

SEE ALSO THE FOLLOWING ARTICLES

Magmatic Fragmentation • Phreatoplinian Eruptions • Surtseyan and Related Phreatomagmatic Eruptions • Scoria Cones and Tuff Rings • Vulcanian Eruptions

FURTHER READING

Buettner, R., and Zimanowski, B. (1998). Physics of thermohydraulic explosions. *Phys. Rev. E.* **57**(5), 5726–5729.

Colgate, S. A., and Sigurgeirsson, T. (1973). Dynamic mixing of water and lava. *Nature* **244,** 552–555.

Heiken, G., and Wohletz, K. (1985). "Volcanic Ash." University of California Press, Berkeley, CA.

Lorenz, V. (1986). On the growth of maars and diatremes and its relevance to the formation of tuff rings. *Bull. Volcanol.* **48,** 265–274.

Sheridan, M. F., and Wohletz, K. H., (1983). Hydrovolcanism: Basic considerations and review. *J. Volcanol. Geotherm. Res.* **17,** 1–29.

Wohletz, K. H., and Heiken, G. (1991). "*Volcanology and Geothermal Energy*." University of California Press, Berkeley, CA.

Wohletz, K. H., and McQueen, R. G. (1984). *In* "*Studies in Geophysics*" (F. R. Boyd, Jr., eds). National Academy Press, Washington, DC.

Wohletz, K. H. (1983). Mechanisms of hydrovolcanic pyroclast formation: Grain size, scanning electron microscopy, and experimental results. *J. Volcanol. Geotherm. Res.* **17,** 31–63.

Wohletz, K. H. (1986). Explosive magma–water interactions: Thermodynamics, explosion mechanisms, and field studies. *Bull. Volcanol.* **48,** 245–264.

Wohletz, K. H., McQueen, R. G., and Morrissey, M. (1995). Pages 287–317 *In* "*Intense Multiphase Interactions*" (T. G. Theofanous and M. Akiyama, Eds.), Proceedings of US (NSF) Japan (JSPS) Joint Seminar, Santa Barbara, CA, June 8–13, 1995.

Zimanowski, B., Buettner, R., Lorenz, V., and Haefele, H.-G. (1997). Fragmentation of basaltic melt in the course of explosive volcanism. *J. Geophys. Res.* **102,** 803–814.

Zimanowski, B., Buettner, R., and Lorenz, V. (1997). Premixing of magma and water in MFCI experiments. *Bull. Volcanol.* **58,** 491–495.

This Page Intentionally Left Blank

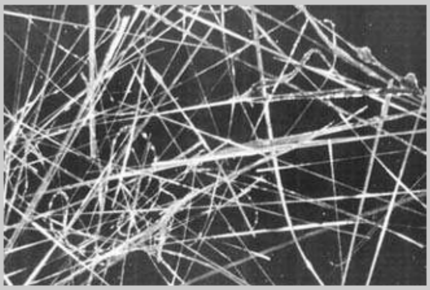

HAWAIIAN AND STROMBOLIAN ERUPTIONS

S. VERGNIOLLE
The Australian National University and
Institut de Physique du Globe de Paris

M. MANGAN
U.S. Geological Survey

I. Defining Characteristics
II. Dynamic Processes
III. Eruption Models
IV. Conclusion

GLOSSARY

annular flow Two-phase flow (gas and liquid) in a tube. Central gas jet surrounded by an annulus of magma. Volcanic equivalent: hawaiian fire fountains.

gas–piston activity A rhythmic rise and fall of the magma level within a volcanic conduit due to ascent and escape of large pockets of magmatic gas.

Hawaiian eruptions Basaltic eruptions with very low viscosity magma (10–100 Pa s). Fire fountains and lava flows. Examples: Kilauea Iki (United States), Piton de la Fournaise (France), Heimaey (1973, Iceland).

lava fountain A pillar-like jet of gas and molten pyroclasts that towers tens to hundreds of meters above a central vent.

lava pond An accumulation of coalesced molten pyroclasts that are trapped at the vent by the walls of a developing spatter or cinder cone.

pyroclast A general term for any fragment of lava ejected during an explosive volcanic eruption.

reticulite A delicate scoria containing 95–99% void space within a honeycomb-like network of thin glass struts.

scoria A porous, glassy pyroclast containing 70–85% void space.

slug flow Two-phase flow (gas and liquid) in a tube. Large gas pocket rising in a liquid and filling up the entire width of the conduit. Characteristic of strombolian explosions and gas–piston events during hawaiian eruptions.

spatter bombs A glassy pyroclast >64 mm across that develops a fluidal shape by the force of ejection.

Strombolian eruptions Basaltic eruptions with a low viscosity magma (100–1000 Pa s). Series of explosions. Examples: Pacaya (Guatemala), Paricutin (Mexico), Sakurajima (Japan), Stromboli (Italy), Tolbachik (Russia), Yasur (Vanuatu).

tremor A continuous vibration of the ground around active volcanoes.

HAWAIIAN AND STROMBOLIAN eruptions are the least violent, and perhaps the most majestic, form of volcanism. Their subdued intensity, magnitude, and dispersive power are the consequence of the low viscosity of the magma erupted, typically basalt or basaltic andesite, which allows gas to segregate and escape with relative ease. During strombolian eruptions,

Copyright © 2000 by Academic Press
All rights of reproduction in any form reserved.

gas is released in discrete, often rhythmic, bursts, each of which disrupts the top of the magma column and ejects a shower of incandescent lava fragments, or pyroclasts (e.g., long-standing eruptions of Stromboli, Aeolian Islands or Mount Etna, Sicily; 1943–1954 Paricutin, Mexico; 1993–1995 Mount Veniaminof, Alaska; 1995–1996 Pacaya, Guatamala; 1996 Rabaul, Papua New Guinea; 1996–1998 Villarrica, Chile). During hawaiian eruptions, gas is also released in discrete rhythmic bursts and each burst in gas flux gives rise to a sustained lava fountain (e.g., 1959, 1969, 1983–1986 Kilauea and 1950, 1975, 1984 Mauna Loa eruptions in Hawaii; 1992, 1998 Piton de la Fournaise, Reunion Island).

In actuality, a continuum exists between the two styles of volcanism, and it is not uncommon for one type of activity to give way to the other (e.g., 1961 Askja and 1973 Heimaey, Iceland; 1975 Tolbachik, Kamchatka; 1987 Izu-Oshima, Japan; 1996 Mount Etna, Sicily; 1996–1997 Pavlof and 1997 Okmok, Aleutian Islands). In this chapter, we first describe the end member characteristics of strombolian and hawaiian eruptions and then integrate these observations with two-phase flow models (e.g., analog gas–liquid systems) to infer the dynamics of hawaiian and strombolian eruptions and the transition between them.

I. DEFINING CHARACTERISTICS

A. Eruptive Style

Hawaiian-style eruptions begin with a swarm of propagating earthquakes and ground fissures. Vents spawn along a fissure as it lengthens, creating a wall of lava, or "curtain of fire," that may extend for kilometers (Fig. 1A; see also color insert). Gradually, over a period of hours to days, differential cooling due to irregularities in the width of the feeder dike causes wall solidification at narrow points. Parts of the fissure seal off, and the original line-source (Fig. 1A) becomes a point-source (Fig. 1B). The curtain of fire collapses back into a single, pillar-like fountain towering above a central vent (Fig. 1B). During a fountaining episode, the vent expels approximately 50–1000 m^3 s^{-1} of lava, which rises to heights h of 100–500 m and occasionally higher. Unusually high fountains reaching upward of 1600 m were observed during the 1986–1987 eruption of Izu-Oshima volcano (Japan).

The structure of the fountain is essentially that of a sustained gas jet carrying a dispersed load of centimeter- to meter-sized, molten clots. Gas emission and lava volume measurements made during the 1983–1986 eruption of Kilauea volcano give average effusion rates of 4.7×10^5 kg s^{-1} lava (dense rock equivalent) and 2.5 10^3 kg s^{-1} gas (0.42 wt% combined H_2O, CO_2, SO_2). The gas to clot ratio averaged for the eruption is 70 : 1 by volume, assuming lava and gas densities of 2700 and 0.2 kg m^{-3}, respectively. The clots exit at near vertical angles at speeds v, determined from the ballistic approximation $v^2 = 2gh$, of $\approx$ 100 m s^{-1}. Eruption temperatures are highest in the center of the fountain, creating an incandescent yellow-white axis that extends almost to the top of the fountain. Eruption temperatures ranging between 1150°C (1986–1987 Izu-Oshima eruption) and 1216°C (1959 Kilauea eruption) have been reported. The hot, thermal core of the fountain passes outward into a fiery orange-red region of slightly cooler temperature and lower clot density, and then to a sparse, black halo of chilled pyroclasts. Although the jetting is continuous, brightly glowing fronts pulse upward through the core of the fountain at 1- to 5-s intervals.

A central vent (i.e., a point source, Fig. 1B) may experience many fountaining episodes. The 4-week-long eruption of Kilauea volcano in 1959, for example, underwent 16 2- to 32-hour fountaining phases after the initial outburst. Typically, the fountaining ends with magma draining to deep levels in conduit amid sporadic bursts of molten ejecta and gas, and then gradually, over periods of several hours to days, it rises in preparation for the next event. As it nears the surface, the level of magma in the conduit may begin to rise and fall rhythmically (gas–piston activity) due to the ascension and release of large gas pockets (e.g., 1969–1971 and 1983–1986 eruptions of Kilauea; Fig. 2). The top of the column begins to churn and a low, commonly dome-shaped, lava fountain spawns as the new episode commences. Usually within several tens of minutes to a few hours the incipient fountain builds to a maximum height, which may hold constant through a significant part of the episode. The end of each episode is often abrupt compared to the period of buildup. In the first 17 fountaining cycles of the 1983–1986 eruption of Kilauea volcano, for example, 100- to 300-m fountains built up over several tens of minutes to 2 hours time, whereas the height usually dropped to zero in 3–10 minutes at the end of the episode.

It is not unusual for a long span of successive fountaining episodes to yield to an era of continuous, quiescent lava effusion before the eruption finally comes to an end (e.g., the 1969–1971 and 1983 to present eruptions of Kilauea). The long-standing eruption of Kilauea vol-

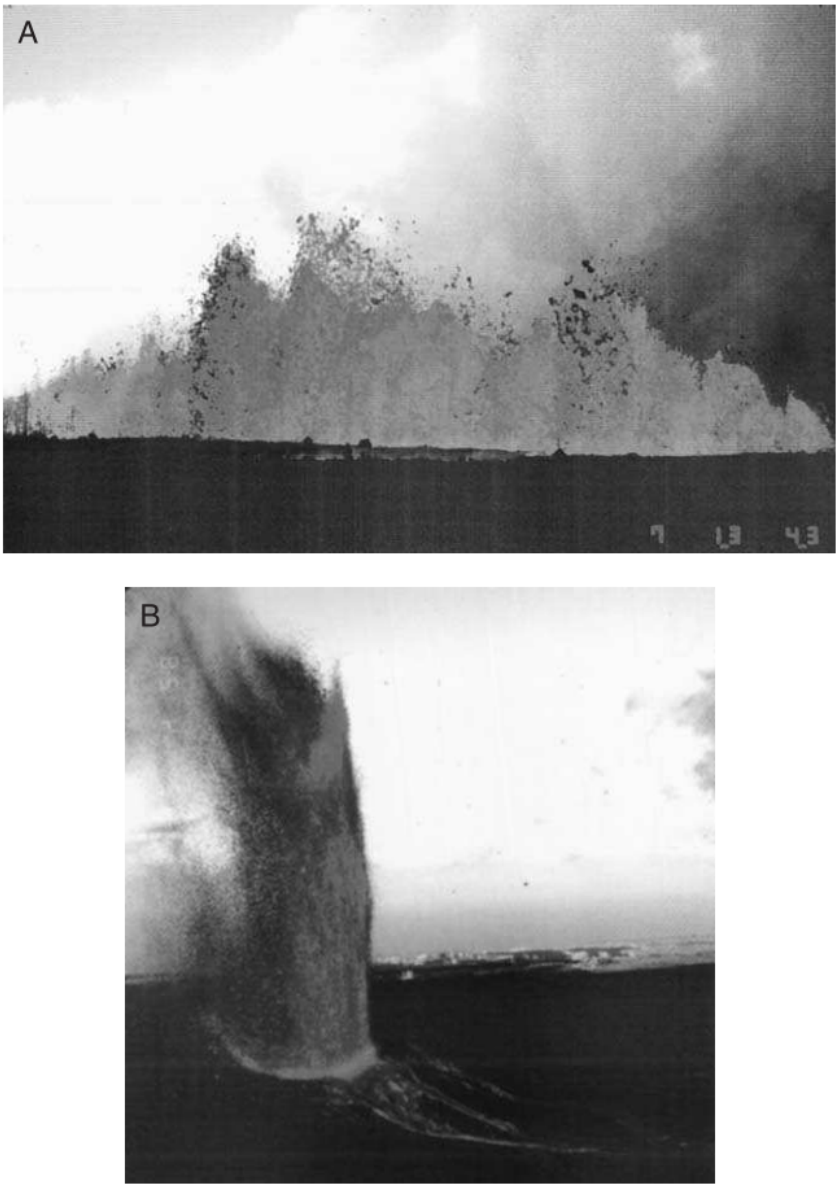

FIGURE 1 (A) A 60- to 100-m-high curtain of fire from the opening stages of the 1983 to present eruption of Kilauea volcano, Hawaii. The photograph shows a 500-m-long segment of an eruptive fissure that extended for 1 km. (Photograph by J. Griggs, U.S. Geological Survey.) (B) A 395-m-high lava fountain from the 1983–1986 fountaining episodes of Kilauea volcano, Hawaii. The photograph was taken 8 minutes before fountaining ceased. (Photograph by G. Ulrich, U.S. Geological Survey.)

cano at the Pu‘u‘O‘o and adjacent Kupaianaha vents, which started in 1983 and continues at the time of this writing, is a prime example of the explosive to effusive transition common to basaltic eruptions. In this instance, the initial fissure opening was followed by 3 years of high lava fountains occurring on a predictable schedule of one fountaining episode every 25 days, on average. These spectacular events gave way in 1986 to near-continuous, low-level lava effusion, which persists after nearly 13 years of activity.

Strombolian eruptions start with a hawaiian-style fissure eruption, or, alternatively, a vent-clearing vulcanian explosion of rock and ash. The magma involved is often of higher viscosity, because of both cooler eruption tem-

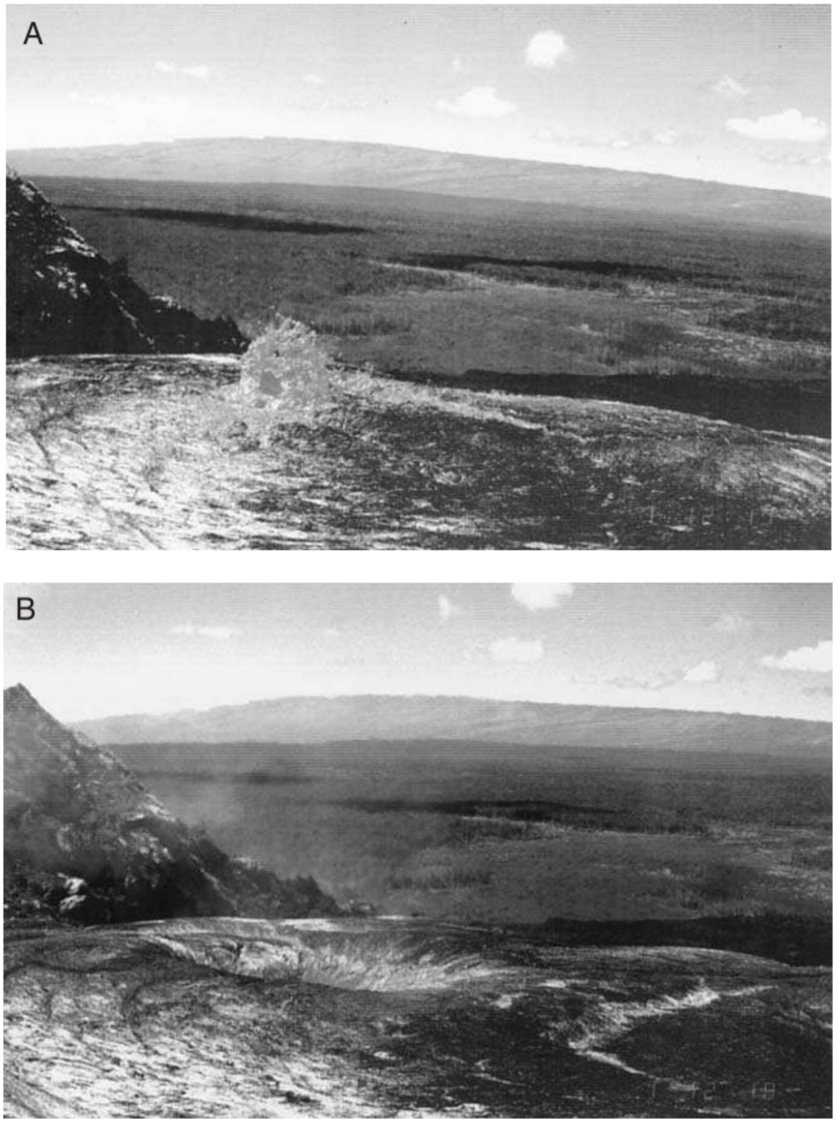

FIGURE 2 (A) Bursting of a large gas bubble in repose-period gas–pistoning during the 1983–1986 fountaining episodes at Kilauea volcano, Hawaii. Note the distention and tearing of the uplifted, pliable lava crust covering the surface of the upwelling lava. (Photograph by G. Ulrich, U.S. Geological Survey.) (B) Drainback of lava into the vent as seen 1 min after the release of the gas pocket in (A). (Photograph by G. Ulrich, U.S. Geological Survey.)

peratures (e.g., 1080°C is common at Mount Etna) and the involvement of slightly more siliceous magmas, typically in the basaltic andesite range. Gas release is episodic, leading to larger overpressures, more intense eruptions, and higher degrees of magma breaking (i.e., smaller ejecta sizes) relative to hawaiian-style activity. Prior to each explosion, gas accumulates in the conduit in a large bubble that rises and lifts the lid of overlying magma to form a gas-filled blister several meters in diameter. The blister swells and eventually explodes with a resounding roar, perhaps $\approx$1–10 s in duration, expelling a spray of gas loaded with centimeter- to meter-sized fragments of the disrupted lid (Fig. 3; see also color insert).

Overall, the flux of gas relative to lava in strombolian eruptions is considerably larger than in hawaiian erup-

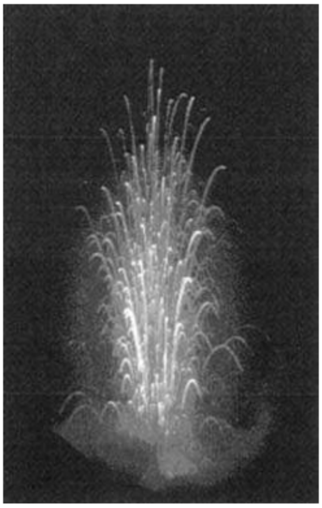

FIGURE 3 April 1992 strombolian explosion at Stromboli volcano, Aeolian Islands. (Reprinted with permission from G. Brandeis, O.M.P., France.) (See also color insert.)

tions (cf. Fig 1 and Fig 3), mainly because the lava column involved in strombolian activity is confined to the volcanic conduit. Ballistic analysis of ejecta and modeling of jet dynamics for eruptions at Stromboli, Etna, Paricutin, and Tolbachik volcanoes suggest typical gas:lava volume ratios of $\approx 10^5:1$, with lava volume between 10^{-3} and 10^2 m^3 per explosion (dense rock equivalent) and gas volume of 10^3 m^3 per explosion. Photoballistic analysis of ejecta trajectories at Stromboli (1971) and Heimaey (1973), show that fragments exit the vent at angles of 45° to over 75° from the horizontal at speeds of 40–100 m s^{-1}, reaching heights greater than 100 m. The tracking of the smallest particles on a series of photographs suggests that gas velocities are roughly double that of most magma fragments. Recent measurements based on the Doppler effect show similar results. The high ratio of gas to lava on ejection allows heat to dissipate relatively rapidly so that most fragments solidify in the air during flight.

Strombolian explosions characteristically occur at quasi-regular intervals. Ongoing activity at Stromboli volcano, for example, averages 3–5 explosions/hour. Violent but rare episodes at Stromboli exhibit cycles of 100 to 1000 explosions/hour.

B. Eruptive Products

During hawaiian fire fountains and strombolian explosions, magma fragments into bubbly, molten clots. Gas bubbles within the melt undergo decompressional expansion in the conduit and in the eruption column, causing the bubbly melt to expand as it rises (see Magmatic Fragmentation). The largest clots and those rising in the core of the fountain remain sufficiently fluid through transport and deposition to coalesce at the vent into rootless lava flows or lava ponds (Fig. 1B). Others cool rapidly as they mix with entrained air, or quench, and are deposited as discrete, glassy clasts. In many instances the deformation that the molten droplet has experienced in response to aerodynamic forces and surface tension is preserved in the clot by quenching. The timing of quenching, the magnitude and rate of decompression during magma ascent, and the temperature, composition, and viscosity of the melt control the crystallinity (volume percent crystals relative to glass) and vesicularity (volume percent gas bubbles relative to crystals plus glass) of the quenched clast. Strombolian eruptions often produce clasts that are of lower vesicularity and marginally higher crystallinity (due to cooling at the top of the magma column) relative to hawaiian eruptions.

Spatter bombs are centimeter- to decimeter-sized clots that undergo limited cooling prior to deposition (Fig. 4A; see also color insert). A thin skin of congealed lava forms on the exterior of the bomb during flight, but the clot as a whole remains sufficiently fluid to flatten upon landing and anneal, or weld, to an existing surface. Slow postdeposition cooling and degassing creates a finely crystalline interior interspersed with irregularly shaped relict gas bubbles, or vesicles.

Pele's tears are small droplets of shiny black glass molded and quenched during flight into spherical, dumbbell, or tadpole shapes (Fig. 5A). These droplets range from a few millimeters to a few centimeters in size and can be quite vesicular (up to 70%), although they are more commonly dense. Pele's hair are long, golden threads of glass that have been drawn out, or spun, from molten droplets flung from the vent (Fig. 5B; also see color insert). The strands are cylindrical, with diameters of 1–500 micrometers and can be up to 1 m in length. The thickest strands (>50 micrometers) contain stretched vesicles parallel to the long axis. These clasts are readily carried by wind and can be found tens of kilometers from the vent.

Scoria are thoroughly quenched, frothy clasts centimeters in size that are sufficiently porous and brittle to break when they hit the ground (Fig. 4A). Vesicularities between 70 and 85% and crystallinities of 2–50% are commonly observed (e.g., Kilauea, Etna, Mount Lassen, Paricutin, Izu-Oshima, Stromboli). Scoria with extremely high vesicularities of 95 to 99% are produced

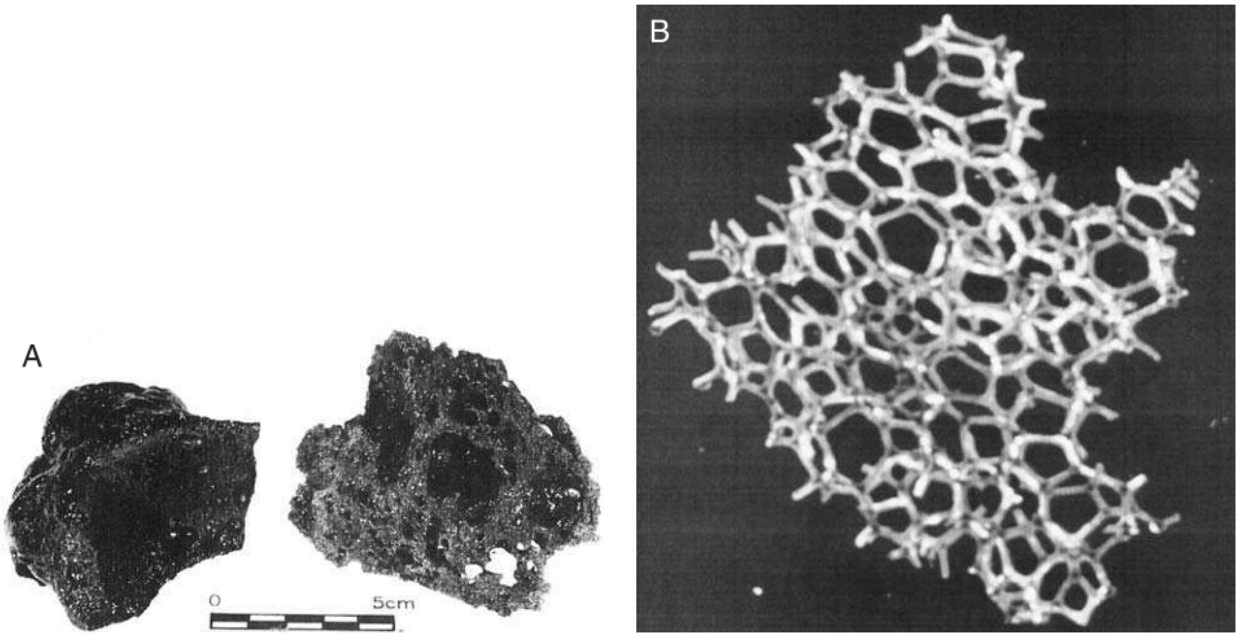

FIGURE 4 (A) Scoria (right) and spatter bomb (left) from the 1983–1986 fountaining events at Kilauea volcano, Hawaii. The frothy scoria clast has a vesicularity of 85% and a bulk density of 400 kg m^{-3}, and the spatter bomb 65% and 900 kg m^{-3}, respectively. (Photograph by J. Griggs, U.S. Geological Survey.) (B) Reticulite from a 1983–1986 fountaining episode at Kilauea volcano. The 1-cm clast has a vesicularity of 98%, and a bulk density of 50 kg m^{-3}. (Photograph by M. Mangan, U.S. Geological Survey.) (See also color inserts.)

in high lava fountains and have been quenched while expanding. These fragile clasts, known as reticulite, have the appearance of a delicate, golden-brown honeycomb (Fig. 4B) in which close packing has deformed bubbles into 12- to 14-sided polygons. Relict bubble walls, ≤ 1 μm thick, are mostly shattered, and virtually no closed space exists in the clast.

C. Deposition Features

The low eruption column and coarseness of the ejecta produced in hawaiian and strombolian eruptions limit their dispersal potential. More than half of the ejecta falls within approximately 500 m of the vent in spatter cones or cinder cones (see Scoria Cones and Tuff Rings). These conical deposits, which may reach heights of 100 m or more, are in stark contrast to the massive sheet-like deposits produced in more explosive types of volcanism (e.g., plinian).

Spatter cones form when partially molten clots fall to the base of a lava fountain and enclose the vent in a ring of welded clasts. Very fluid clots may become trapped and coalesce within the developing ring, creating a molten pond that gradually deepens as the ring grows taller and more cone-like. A cinder cone formed in strombolian eruptions, in contrast, is composed of loose, nonwelded clasts because most of the ejecta are rigid at the time of deposition. Rates of cone building in hawaiian and stromblian eruptions may exceed 5 m $hour^{-1}$.

Typically, a small volume (<1–20%) of millimeter- to centimeter-sized clasts (scoria, reticulite, Pele's tears, and hair) blanket areas surrounding the vent, especially on the downwind side (Fig. 1B). The sheet-like deposit thins abruptly outward from the spatter (or cinder) cone, generally diminishing to 10% of the maximum near-vent thickness over dispersal areas of <10 km^2 (e.g., Kilauea, Hawaii; Serra Gorda, Azores; Teneguia, Canary Islands, Heimaey, Iceland; Mount Etna, Sicily). In plinian deposits a 10% diminution in thickness in likely to occur over an area of >1000 km^2.

Of less importance in terms of ejecta dispersal and deposition is the dilute convective plume of volcanic gas, aerosols, and ash that forms above the eruption column during hawaiian and strombolian events. These plumes contain <0.17% of the total mass fraction of lava erupted and rarely penetrate the tropopause.

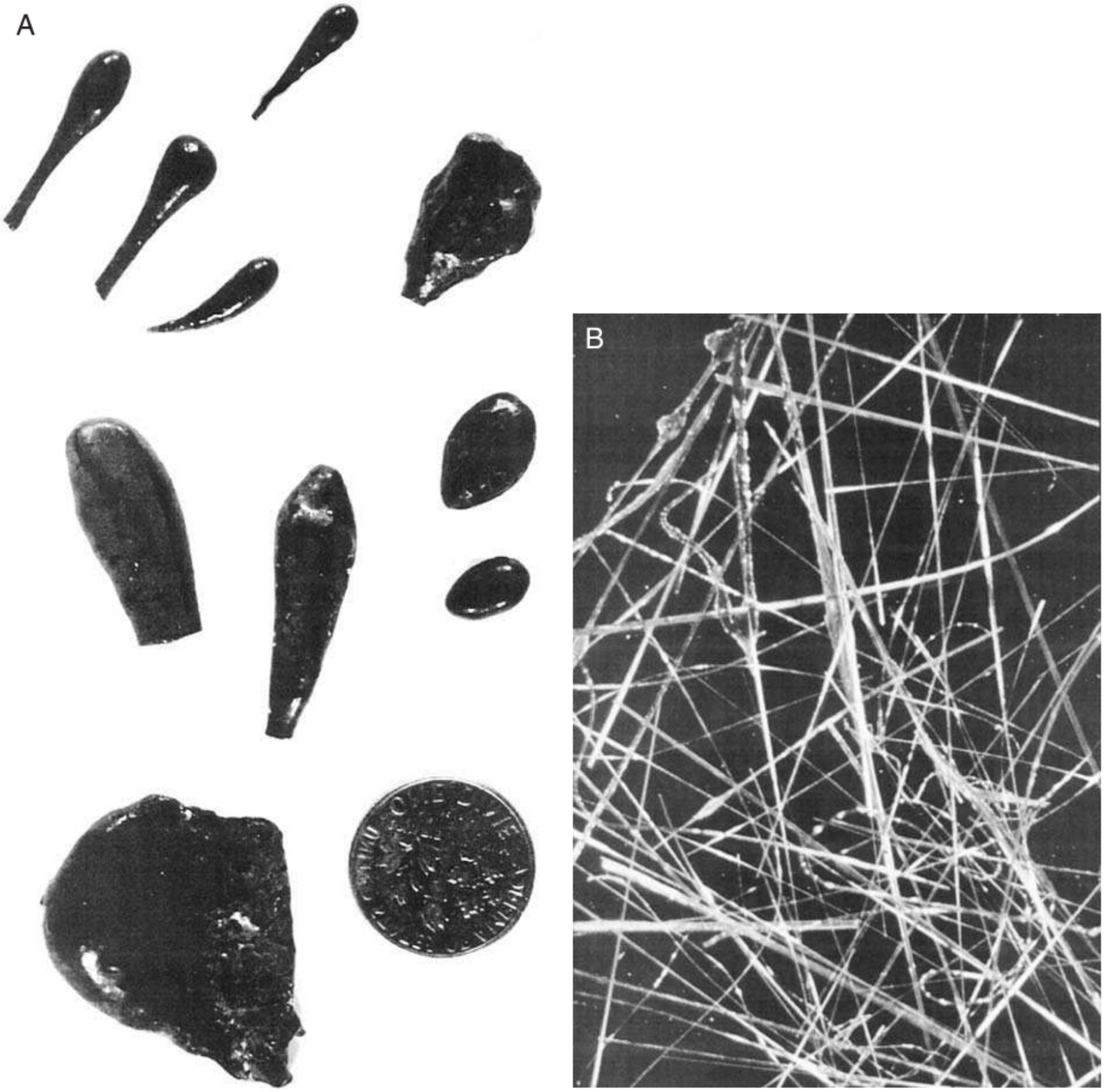

FIGURE 5 (A) Pele's tears: quenched droplets of lava shaped by surface tension and aerodynamic forces upon ejection from the vent. (Photograph by J. Griggs, U.S. Geological Survey). (B) Pele's hair: quenched filaments spun from molten droplets by turbulent air/gas mixing upon ejection from the vent. (Photograph by M. Mangan, U.S. Geological Survey.) (See also color insert.)

II. DYNAMIC PROCESSES

A. Degassing

Basaltic volcanoes display varied and complex behavior due to the existence of a separate and evolving gas phase. Gas emission measurements at Kilauea, Etna, Stromboli, and Pacaya have shown that hawaiian and strombolian eruptions involve the evolution and release of $\approx 10^5$ metric tons/day of H_2O-, CO_2-, and S-rich gas during peak activity. Further, evidence for the importance of the gas phase in eruption processes comes from the fragmentation of magma into discrete, highly vesiculated ejecta, the existence of a volcanic plume above the eruption column, and the deep draw-down of magma at the end of the eruption. Furthermore, Pele's hair, deposited during fire fountaining, is very likely formed by the drag exerted on the magma droplets by a strong gas jet by analogy with methods used in producing glass fibers.

In a broad sense, degassing is a two-stage process. Basaltic magma begins to exsolve CO_2-rich gas when it ascends to within a few tens of kilometers of the surface (e.g., 30 km at Kilauea). The second stage is initiated once the magma is within a few hundred meters of the vent (e.g., 150 m at Kilauea) at which time H_2O and S begin to exsolve in significant amounts.

During both stages, volatile exsolution during ascent leads to the nucleation of bubbles and their growth both by chemical diffusion and decompressional expansion. Bubble growth is initially dominated by diffusion, with decompressional growth becoming increasingly important as the magma approaches the vent. There may be differential movement of melt and gas resulting from the size-dependent buoyancy of individual bubbles relative to the rise velocity of the magma. In general, the larger CO_2-rich bubbles generated at depth are likely to be sufficiently buoyant to rise up through the ascending magma whereas the smaller H_2O-rich bubbles generated near the surface are quasi-stationary in relation to the melt.

B. Two-Phase Flow

A useful way of examining the behavior of a melt-bubble mixture is provided by the separated two-phase flow models developed in chemical engineering applications. In this context, specific regimes are classified on the basis of gas volume fraction, which determines the geometry and partitioning of gas "elements" in the melt rising in the conduit. For a gas content of less than 30%, the melt contains small, discrete bubbles in suspension and is classified as bubbly flow (Fig. 6). Effusive eruptions are the consequence of bubbly flow in the conduit.

At gas contents of about 70%, small bubbles may coalesce, either in the magma reservoir or in the transport system, to produce large gas pockets that fill the entire width of the volcanic conduit (Fig. 6). These gas pockets are separated by smaller regions of bubbly magma and this regime is called slug flow. Strombolian explosions and the gas–piston events observed between some eruptive episodes are the surface expression of slug flow. Both phenomena are due to the bursting of a large slug of gas at the top of the magma column.

Slug flow makes a transition to annular flow at gas volume fractions above 70%. In this regime, gas forms a central jet surrounded by an annular sheet of magma along the conduit walls (Fig. 6). Two types of annular flow exist: at gas volume fractions close to 70%, the melt falls downward under its own weight while the gas phase moves upward in the conduit. At somewhat higher gas fractions, the annulus of melt is driven upward along the conduit walls by the gas jet. If the gas volume fraction is substantially larger than 70%, the regime becomes a dispersed flow in which the magma around the central gas core is fragmented into upward-moving droplets (Fig. 6).

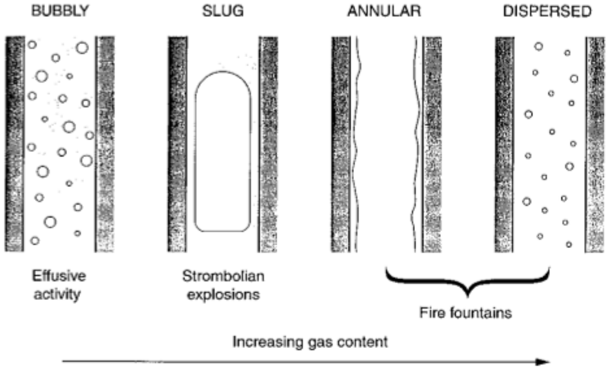

FIGURE 6 Classification of two-phase flow regimes and their volcanic counterparts. Gas fraction increases from the left to the right.

Lava fountains can be described as the surface expression of an annular to dispersed flow regime in the conduit. Although it is often difficult to deduce conditions in the conduit from observations made at the surface, an observation made during the 1959 summit eruption of Kilauea supports the annular flow model. In the most energetic fountaining episode of the eruption (episode 15; maximum height: 570 m), lava was seen draining back into the vent during the final minute of high fountaining (height drop: from 180 m to below the vent). The simultaneous motion of liquid upward in the fountain and downward in the conduit is suggestive of a transition between the two types of annular flow described above.

However, some numerical models suggest that a fire fountain corresponds to a dispersed flow. There are only two primary mechanisms by which a dispersed flow can be produced in the conduit: in the first process, the gas volume fraction is slowly increased from bubbly to slug and annular flows (Fig. 6), whereas in the second one the coalescence of a foam trapped in the shallowest part of the magma conduit causes fragmentation, a mechanism very similar to that involved in the formation of plinian eruption columns. However, the coalescence of a shallow foam produces fragments of magma which are initially disconnected and distributed homogeneously across the jet. Unless an extra, yet unknown, mechanism concentrates the fragments close to the walls into a continuous layer of liquid, characteristic of an annular flow, fire fountains such as that during episode 15 during the Kilauea Iki eruption (involving annular flow, see above) are more likely to be formed either by increasing progressively the gas volume fraction (Fig. 6) in the conduit or directly at the roof of the magma chamber. However, the first mechanism, very standard in chemical engineering, is not favored because measurements of lava vesicularity during effusive activity suggest that there is no significant coalescence of bubbles during rise in the conduit.

C. Magma Reservoirs and Conduits

Volcano-tectonic earthquakes and ground deformation patterns crudely define the magmatic plumbing systems underlying basaltic volcanoes. The general view that emerges is that of a large reservoir at a few kilometers depth that is connected to the surface by a narrow conduit a few tens of meters wide (Fig. 7). At Kilauea, for example, earthquake locations define an aseismic, melt-rich zone 2–6 km below the summit caldera that is approximately 2 km in diameter.

Most basaltic volcanoes display cycles of inflation and deflation that correlate with eruptive events. Before an eruption, the ground surface gradually inflates due to an increase in reservoir pressure by injection of magma from below and/or degassing. As the eruption commences, the volcano deflates abruptly and continues to deflate, often at somewhat lower rates, as the eruption proceeds. The deformation pattern at Kilauea volcano, which has been extensively monitored for the past 30 years, offers a classic example of these patterns (Fig. 8). The center of deformation at Kilauea shifts within the summit region over time, suggesting that the reservoir may actually consist of several, smaller, interconnected chambers. Deformation and seismicity also show steeply dipping tabular bodies of magma along the volcano's two rift zones radiating outward to the southwest and to the east of the summit. A rift zone reservoir is located ≈2.5 km beneath the currently active Pu'u'O'o vent, for example, which is continuously fed magma from Kilauea's summit reservoir more than 15 km away. At the time of its emplacement it was estimated to be 2.5 km high, 11.0–15.0 km long, and 3.5 km wide. Similar deformation patterns have been observed on some strombolian volcanoes.

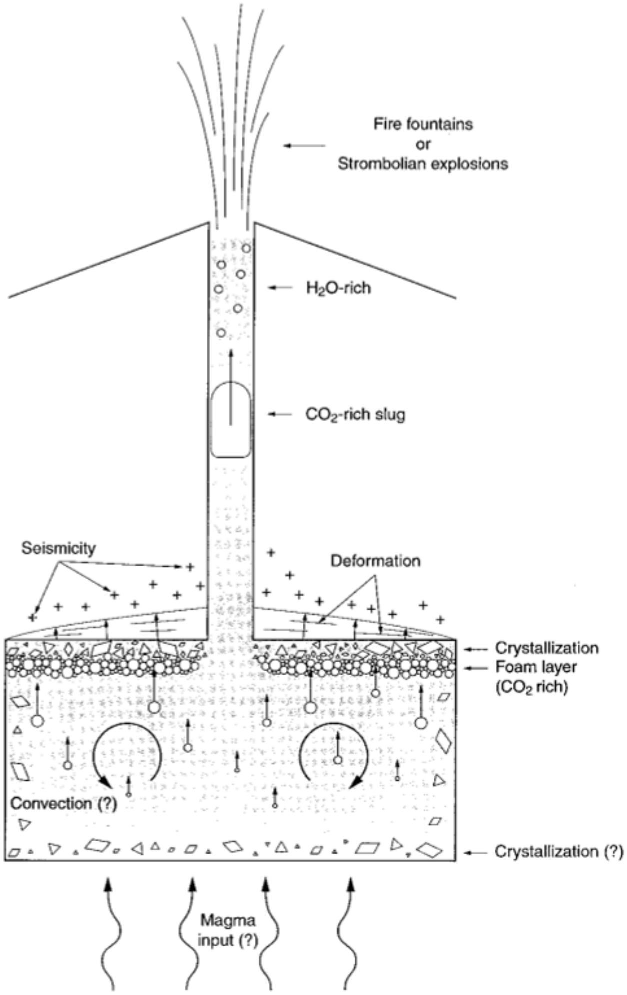

FIGURE 7 Sketch of a basalt volcano and phenomena related to magma storage and eruption.

The large difference between the cross-sectional area of the roof of the magma reservoir, which at Kilauea is ≈30 km^2, and that of the connecting conduit, which is likely to be ≤0.001 km^2, imposes a strong constraint on the velocity of magma ascent. Because mass flux must be conserved between the magma chamber and the vent, the drastic reduction in cross-sectional area requires a very large increase in velocity. For example, a small upward velocity of 10^{-5} m s^{-1} in the magma chamber produces a velocity of 1 m s^{-1} at the vent. In addition, the large difference in density between a slightly bubbly liquid and a gassy lava fountain can lead to a 100-fold increase in the velocity between the bottom and the top of the volcanic conduit.

Eruptions may be triggered by crystallization and ve-

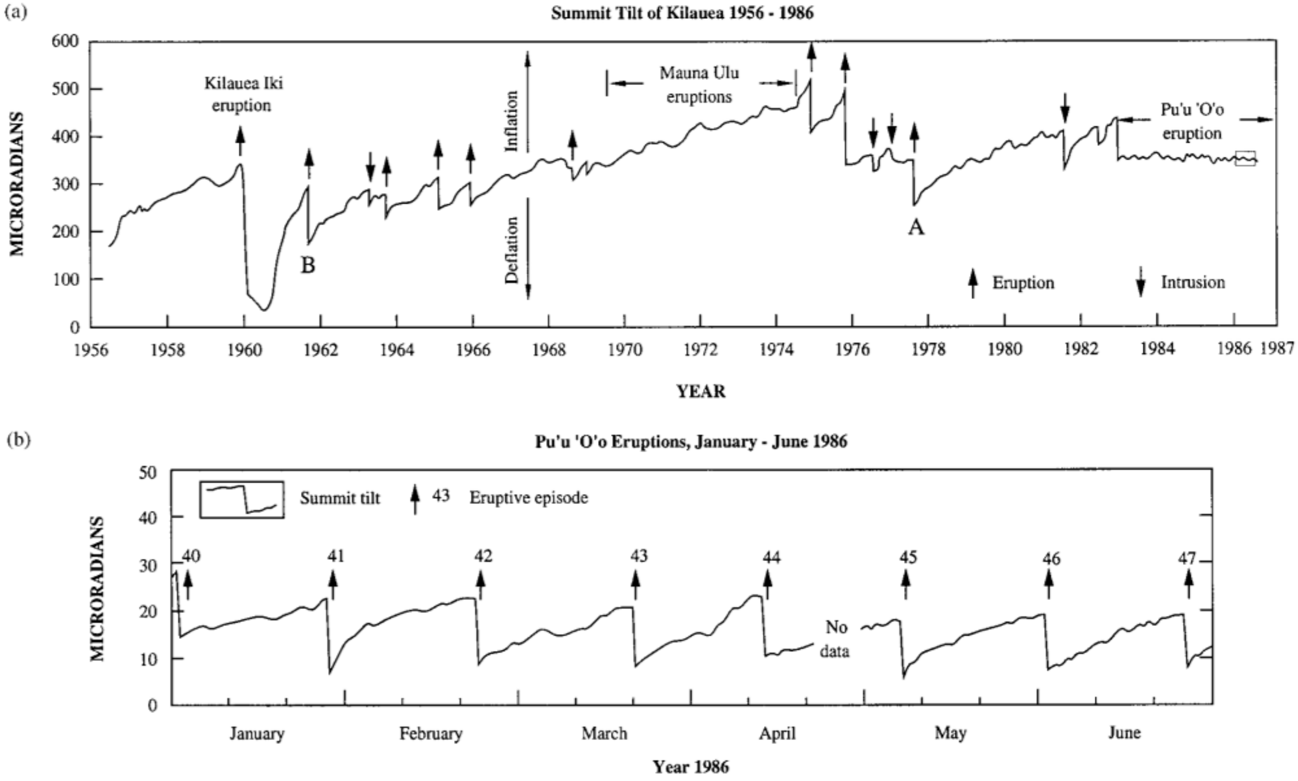

FIGURE 8 Summit tilt deformation (East–West component) at Kilauea volcano, Hawaii (from Tilling *et al.,* 1987; see text): (a) for the past 30 years; (b) during fire fountains.

siculation in the magma chamber. Cooling of reservoirs leads to the formation of crystals, thus enriching the remaining melt in volatiles. When the solubility limit is reached, gas exsolution occurs and the magma chamber increases in both volume and pressure as vesiculation proceeds. Ultimately, the internal pressure may exceed the strength of the surrounding rocks to trigger an eruption. Alternatively, replenishment from a deep magma source may be the triggering mechanism. The input of an additional volume of a bubbly magma combined with the volume increase due to decompressional expansion of tiny bubbles that enter and rise toward the roof of the chamber, may sufficiently pressurize the system to trigger an eruption. The presence of gas bubbles in basaltic magma chambers also has consequences for the development and duration of an eruption as shown at Kilauea Iki (Hawaii), where bubble diameters in the reservoir are ≈0.4 mm.

D. Sources of Vibration

Other constraints on the dynamics of transport emerge from the analysis of volcanic tremor, which is a continuous vibration of the ground around active volcanoes. Volcanic tremor is usually characterized by a sharply peaked spectrum with one dominant and several subdominant peaks (Figs. 9, 10a, and 10b). The tremor recorded during lava fountain episodes at Kilauea has several peaks between 3 and 10 Hz (Fig. 9) and is produced at a depth of <1 km. Tremor recorded during the repose periods, as well as during gas-piston events, shows only two dominant peaks between 2 and 4 Hz. Resonators of various geometries have been called upon to explain volcanic tremor, from the vibration of a crack filled by liquid, to the vibration of a spherical magma chamber. The role of gas as a trigger was suggested at Kilauea because of the similarity between tremor and the seismicity induced by gas–piston events. Gas–pistoning generates a unique signature consisting of a spindle-shape amplitude envelope persisting for a duration of 80 s. Visual observations confirm that each “spindle” correlates with the bursting of large gas bubbles at the top of the magma column.

At Stromboli, the main peak in the tremor is approximately 2 Hz with a secondary peak slightly above 4 Hz. The depth at which the tremor is produced is, for the most part, less than 200 m and results from continuous

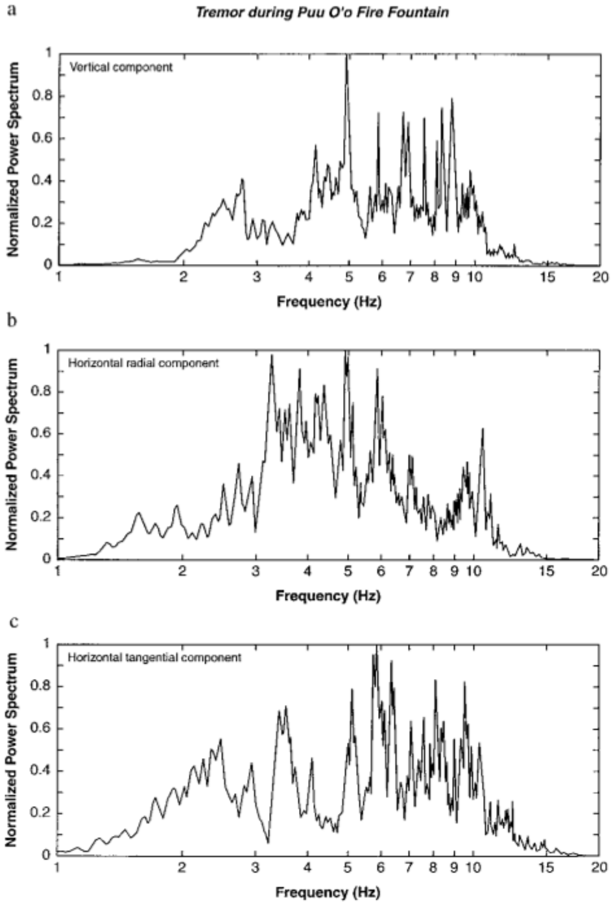

FIGURE 9 Tremor recorded during the Pu'u 'O'o fire fountain, Hawaii (from Koyanagi *et al.*, 1987; see text): (a) vertical component; (b) horizontal radial component; (c) horizontal tangential component.

bursting of small gas bubbles. However, its frequency of ≈2 Hz can also be interpreted as oscillations of a bubble cloud 50 m in length, with 1% gas volume fraction. Both are reasonable values for the height of the shallow magma column and the gas content at Stromboli. With the development of broad band seismometers, more is to be learned in the future from tremor at periods less than 1 s because it offers constraints on pressure fluctuations resulting from unsteady magma transport.

The pressure waves induced by explosions have been measured at Stromboli volcano and provide additional constraints on conduit transport (acoustic measurements). Although the audible sound radiated by an explosion is very striking, most of the acoustic energy is infrasonic, i.e., below 20 Hz (Fig. 10c). The power spectrum of acoustic pressure before an explosion is very similar to the seismic recording (Fig. 10b and 10c) with a powerful peak at ≈2 Hz. However, during explosions the acoustic frequency shifts toward a higher frequency of ≈10 Hz. The strong acoustic pressure recorded during explosions (Fig. 11) has been associated with the breaking of a gas bubble with a radius of a few meters that is still overpressurized (by 0.3 10^5 Pa) at the top of the magma column. Because the vibration of the bubble in air does not have direct interactions with the solid walls of the conduit (part 2; Fig. 11) no seismic waves at ≈10 Hz are produced in the volcanic edifice (Fig. 10b). Sound waves, albeit of very low intensity, can also be generated by oscillations of the magma column induced by a rising bubble (Fig. 11, part 1), or by oscillations of the bubble bottom after the gas pocket breaks

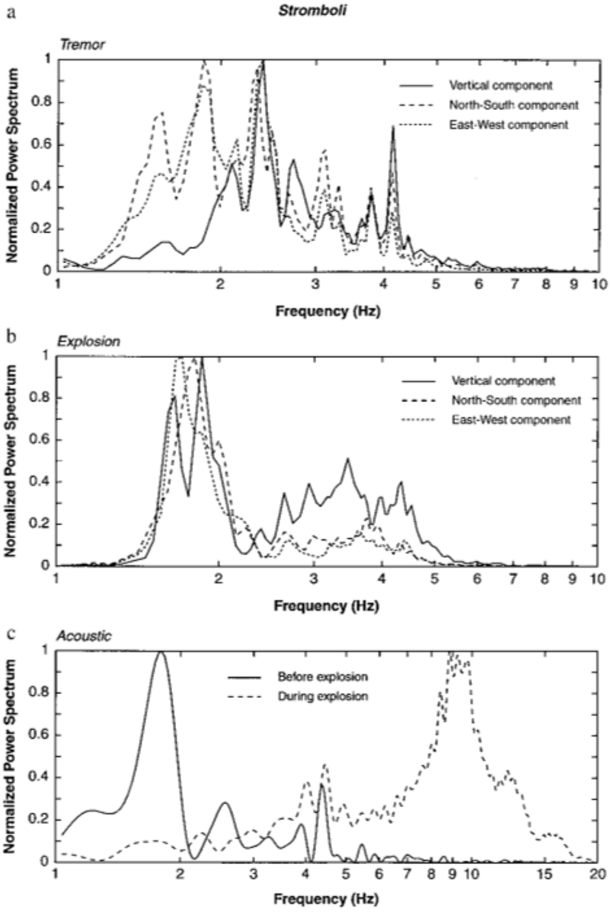

FIGURE 10 Stromboli. (a) Seismicity during tremor (reprinted with permission from Chouet *et al.*, 1997); (b) seismicity during an explosion (reprinted used with permission from Chouet *et al.*, 1997); and (c) acoustic pressure before and during an explosion (reprinted with permission from Vergniolle *et al.*, 1996). Note the similarity in power spectra.

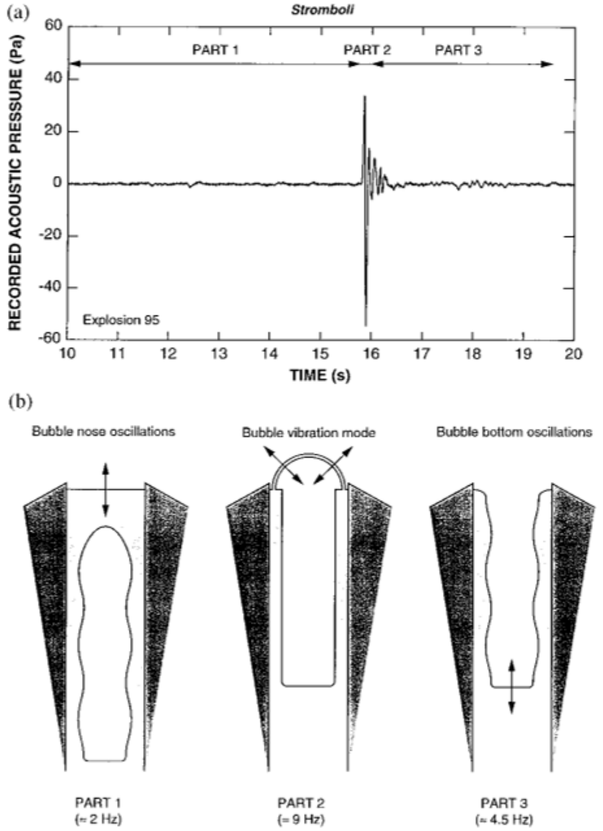

FIGURE 11 (a) Measurements of acoustic pressure at Stromboli. (b) Sketch of the three stages of bubble rise corresponding to the three parts in acoustic pressure. (Reprinted with permission from Vergniolle *et al.,* 1996).

(Fig. 11 part 3). By combining these oscillations, the magma viscosity is estimated at ≈300 Pa s. In very quiet conditions, bubble rise can be followed on acoustic records (the ≈2-Hz mode) in the uppermost 30 m of the magma column. An alternate explanation for the sound waves at Stromboli is that the acoustic sources of the explosions lie at depth and the resonant modes of a magma column can be calculated from them.

III. ERUPTION MODELS

The evolution and release of a separate gas phase induces complex, time-dependent behavior, and two general approaches have been taken to examine and explain these complexities. Both models recognize that variations in eruptive behavior are the consequence of the volume of gas present and how this volume is partitioned in the melt: small gas volumes lead to effusive eruptions and lava flows (bubbly flow), whereas large gas volumes cause either strombolian explosions as large gas pockets reach the surface (slug flow) or continuous gas jetting as in hawaiian lava fountains (annular or dispersed flow). The models differ in how and where gas separates from the melt.

The first of the two models uses numerical methods to investigate the rise and expansion of an initially bubbly mixture in the conduit. The decompression of a bubbly magma during rise leads to nucleation and growth of new gas bubbles as well as continued growth of the original bubbles. The model suggests that it is the extent of bubble coalescence (mechanism by which numerous small bubbles are transformed into a smaller number of larger bubbles) that occurs in the conduit during magma ascent that distinguishes hawaiian from strombolian eruptions. Coalescence, in turn, is controlled by the ascent rate of the magma. Slow magma rise may facilitate coalescence because transit times are long and bubbles have ample opportunity to overtake, collide, and coalesce with one another. An initially homogeneous population of small gas bubbles rising in the conduit could thus form large gas slugs that rise through the melt column and burst at the surface in classic stombolian style.

Higher magma rise rates may limit coalescence because the distance bubbles travel relative to the melt is small and the transit time is short, making bubble collisions less likely. The mixture remains essentially homogeneous until the volume fraction of exsolved gas reaches a critical point where bubbles become so closely packed that they deform and burst (≈75% by volume), causing the magma to fragment. Subsequent rise of the disrupted mixture of gas and clots (dispersed flow) leads to considerable expansion in the conduit, resulting in the formation of lava fountains. The flow conditions in the fountain, such as the emitted mass flux and the exit velocity and pressure, are strongly dependent on the geometry of the conduit and vent. The episodic fountaining pattern exhibited by many hawaiian eruptions is modeled by nonuniform magma cooling that creates a temporary "plug" at narrow sections of the plumbing system of sufficient yield strength to stop the flow of magma between two successive fire fountains.

In the 1990s, two-phase flow concepts and laboratory experiments have been combined and they offer an alternative view. In this model variations in eruptive style are the consequences of the differential motion of bubbles compared to magma inside a large magma reservoir (Fig. 7). A laboratory volcano has been built with a large reservoir filled with viscous oils topped by a narrow conduit. During the experiment, small gas bubbles formed at the bottom of the chamber rise and accumulate in a foam layer at the roof of the chamber (Figs. 12 and 13). Bubbles in the foam deform as the layer builds and eventually collapse on masse. Sudden coalescence of bubbles in the layer creates a large gas pocket that rises in the conduit and bursts at the surface. Foam accumulation then resumes and a new cycle begins.

This pattern of foam buildup and coalescence is very regular for a given melt viscosity, which dictates the volume of gas in the gas pocket and the timing between the creation and ascent of successive gas pockets. Hawaiian-style lava fountains were qualitatively reproduced using a liquid of relatively low viscosity (0.1 Pa s). These experiments generated a foam layer that gave rise to a large, single gas pocket upon collapse. The ensuing "eruption" is that of a central gas vent surrounded by a film of liquid along the walls of the conduit (annular flow; Fig. 12). Minor and frequent coalescence events occurred at the top of the reservoir between successive total collapses, the former being reminiscent of the gas–piston activity often observed between fountaining episodes in hawaiian eruptions. Strombolian activity is reproduced by experiments using more viscous oils (1 Pa s). Here, collapse involves only parts of the foam and a number of intermediate size gas pockets are produced. The pockets rise and burst intermittently at the top of the conduit (slug flow; Fig. 13). This regime corresponds to a quasi-stagnant liquid column (Fig. 13), analogous to most strombolian eruptions in contrast to the previous regime (Fig. 12) in which huge variations in liquid levels exist, similar to the difference in height between a fire fountain and effusive activity.

In all experiments a critical gas flux to the roof is required for the foam to thicken and ultimately collapse.

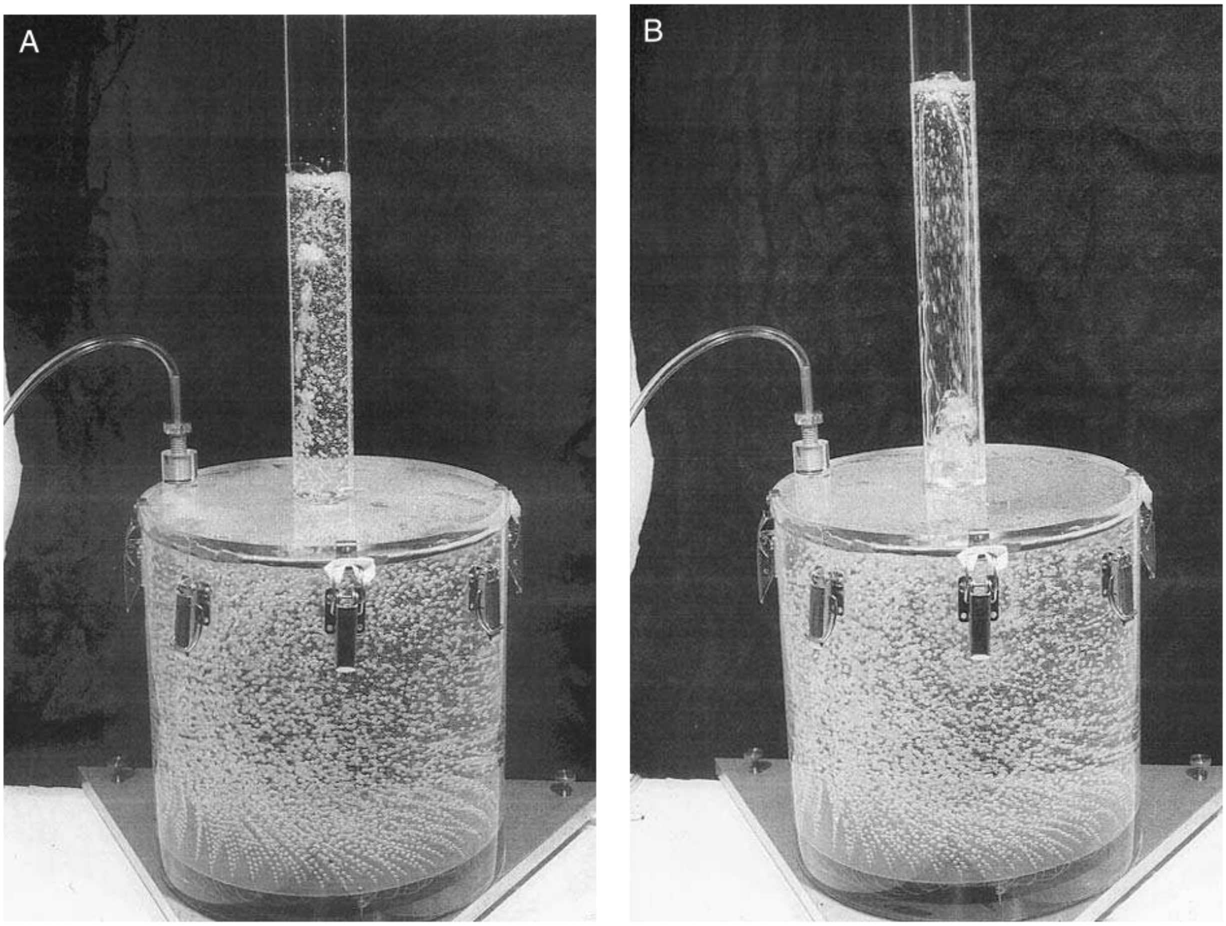

FIGURE 12 Laboratory volcano model using the low viscosity oil (0.1 Pa s), analogous to a hawaiian eruption. (Reprinted with permission from Vergniolle and Jaupart, 1990.) (A) Buildup of the foam at the top of the reservoir. Regime analogous to effusive activity. (B) Foam collapse and gas pocket rise in the conduit. Regime is analogous to fire fountain.

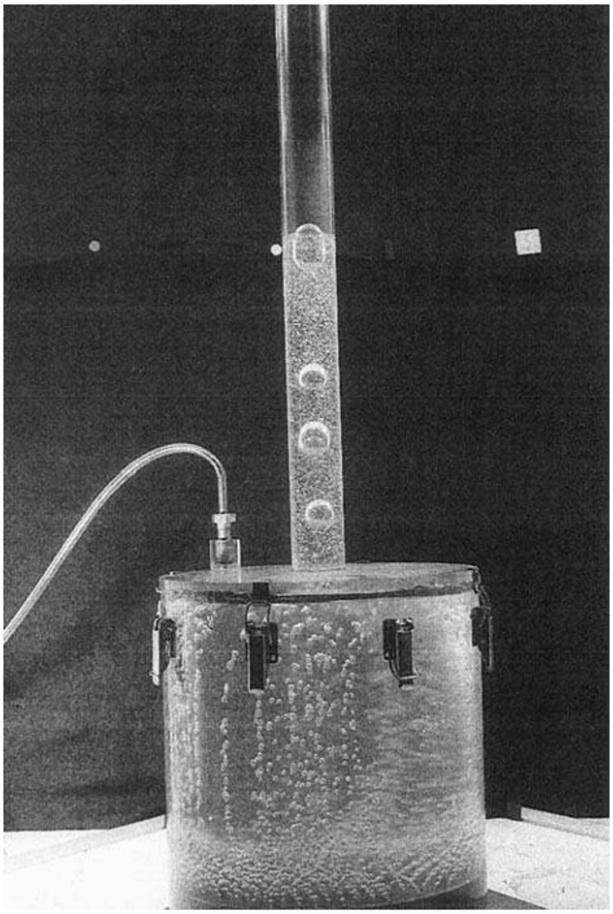

FIGURE 13 Laboratory volcano with a more viscous viscosity oil (1 Pa s), analogous to a strombolian eruption. (Reprinted with permission from Vergniolle and Jaupart, 1990.)

The threshold is dependent on the size and proportion of rising bubbles and the viscosity and surface tension of the melt. At less than critical gas fluxes there is a steady stream of foam rising in the conduit (bubbly flow), and the "eruption" is effusive. The transition between cyclic fountaining episodes to quiescent effusion that is often observed in hawaiian eruptions may thus be a reflection of a waning gas flux to the reservoir roof.

IV. CONCLUSION

Although more quantitative field measurements of variables such as pressure, velocity, and gas content will be useful for constraining models more tightly, a general pattern for basaltic eruptions is starting to emerge, showing, in particular, the importance of the role of the gas phase. Bubbles trigger eruptions and explain many of the features of hawaiian and strombolian eruptions. Lava flows are the consequence of the effusion at the vent of a bubbly flow in the conduit, whereas the most dramatic events in basaltic eruptions are related to very large gas pockets breaking at the vent and ejecting fragments of magma. Furthermore, there are rare situations in which basalts can erupt explosively in plinian basaltic eruptions, typical of a dispersed flow (Fig. 6). The continuum existing between hawaiian and strombolian activity is a direct consequence of the patterns of two-phase flow and the entire spectrum of flow regimes exist in basaltic eruptions.

SEE ALSO THE FOLLOWING ARTICLES

Basaltic Volcanoes and Volcanic Systems • Lava Flows and Flow Fields • Lava Fountains and Their Products • Magma Chambers • Plinian and Subplinian Eruptions • Rates of Magma Ascent • Scoria Cones and Tuff Rings

FURTHER READING

Chester, D. K., Duncan, A., Guest, J., and Kilburn, C. (1985). "Mount Etna, The Anatomy of a Volcano." Chapman and Hall, London.

Chouet, B. (1996). Pages 23–97 *in* "Monitoring and Mitigation of Volcano Hazards" (R. Scarpa and R. Tilling, Eds.). Springer-Verlag, Berlin.

Chouet, B., Saccarotti, G., Martini, M., Dawson, P., De Luca, G., Milana, G., and Scarpa, R. (1997). Source and path effects in the wave fields of tremor and explosions at Stromboli volcano. *J. Geophys. Res.* **102,** 15129–15150.

Gerlach, T. M. (1991). Exsolution of H_2O, CO_2 and S during eruptive episodes at Kilauea volcano, Hawaii. *J. Geophys. Res.* **91,** 12177–12185.

Jaupart, C., and Tait, S. (1990). Dynamics of eruptive phenomena. Rev. Miner. **24,** 213–238.

Koyanagi, R. Y., Chouet, B., and Aki, K. (1987). Origin of volcanic tremor in Hawaii. 1. Data from the Hawaiian volcano observatory 1969–1985. *U.S. Geol. Surv. Prof. Paper* **1350,** 1221–1257.

Mangan, M. T., and Cashman, K. V. (1996). The structure of basaltic scoria and reticulite and inferences for vesiculation, foam formation, and fragmentation in lava fountains. *J. Volcanol. Geotherm. Res.* **73,** 1–18.

Parfitt, E. A., and Wilson, L. (1995). Explosive volcanic eruptions-IX. The transition between Hawaiian-style lava fountaining and Strombolian explosive activity. *Geophys. J. Int.* **121,** 226–232.

Swanson, D. A., Duffield, D. A., Jackson, D. B., and Peterson, D. W. (1979). Chronological narrative of the 1969–1971 Mauna Ulu eruption of Kilauea volcano, Hawaii. *U.S. Geol. Surv. Prof. Paper* **1056,** 1–55.

Tilling, R. I., Heliker, C., and Wright, T. L. (1987). "Eruptions of Hawaiian Volcanoes: Past, Present, Future." Department of the Interior/U.S. Geological Survey.

Tilling, R. I., and Dvorak, J. (1993). Anatomy of a basaltic volcano. *Nature* **363,** 125–133.

Vergniolle, S., and Jaupart, C. (1990). The dynamics of degassing at Kilauea volcano, Hawaii. *J. Geophys. Res.* **95**(B3), 2793–2809.

Vergniolle, S., Brandeis, G., and Mareschal J-C. (1996). Strombolian explosions: Eruption dynamics determined from acoustic measurements. *J. Geophys. Res.* **101**(B9), 20449–20466.

Wallis, G. B. (1969). "One Dimensional Two-Phase Flows." McGraw-Hill, New York.

Wolfe, E. W., Garcia, M. O., Jackson, D. B., Koyanagi, R. Y., Neal, C. A., and Okamura, A. T. (1987). The Pu'u'O'o eruption of Kilauea volcano, episodes 1–20, January 3, 1983 to June 8, 1984, U.S. Geol. Surv. Prof. Paper **1350,** 471–508.

This Page Intentionally Left Blank

VULCANIAN ERUPTIONS

MEGHAN M. MORRISSEY
Colorado School of Mines

LARRY G. MASTIN
US Geological Survey

I. Introduction
II. Field Examples
III. Eruption Processes
IV. Plume Dynamics
V. Eruption Source Models
VI. Concluding Remarks

GLOSSARY

andesite The second most abundant volcanic rock type, containing mainly phenocrysts of zoned plagioclase, pyroxene, or hornblende and a glassy or fine-grained groundmass.

blocks/bombs Blocks and bombs are fragments of solid rock and semimolten lava, respectively, with diameters >64 mm.

explosive earthquakes Isolated, large amplitude earthquakes lasting 10–20 s with peak frequencies between 1 and 5 Hz.

juvenile clasts Fragments of solidified magma involved with the eruption.

lava dome Solified lava, roughly circular in plan view with small surface area that occupies the vent.

shock waves A pressure wave that travels at a velocity greater than the sound speed of the medium through which it propagates.

VULCANIAN ERUPTIONS are small to moderate-sized volcanic outbursts that eject material to heights <20 km and last on the order of seconds to minutes. These eruptions are characterized by discrete, violent explosions, by ballistic ejection of blocks and bombs, by atmospheric shock waves, by emission of tephra and by deposits that range widely in the percentage of juvenile versus nonjuvenile components. The juvenile components are composed of fragmented intermediate magma that ranges in composition from andesitic basalt to dacite. Eruptions described as vulcanian generally occur in the summit craters of stratovolcanoes, in some cases through summit crater lakes or lava domes. They have taken place as precursors to subplinian or plinian eruptions, during the waning stages of such eruptions, or with no accompanying larger magmatic eruptions. Moreover, a vulcanian eruption may be a single discrete event or occur as a pulsatory series of explosive events.

I. INTRODUCTION

In 1907, Mercalli coined the term vulcanian to describe eruptions of the sort that took place on the island of Vulcano (Aeolian Islands) between August 3, 1888, and May 17, 1890. Lacroix later incorporated the term into

Copyright © 2000 by Academic Press
All rights of reproduction in any form reserved.

a classification scheme that ranked eruption types qualitatively in order of increasing explosivity: hawaiian, strombolian, vulcanian, and peléan. Modern textbooks cite not only the eruptions of Vulcano, but more recent ones at Ngauruhoe, New Zealand (1975), Irazu, Costa Rica (1963–1966), and Sakurajima, Japan (since 1955), among others, as examples of the vulcanian eruptive style.

Discrete, violent explosions lasting seconds to minutes in duration are perhaps the most distinctive characteristic of vulcanian activity. During the 1888–1890 eruptions at Vulcano, shock waves from some explosions broke windows in the town of Lipari, 7 km from the vent. Eruptions bearing vulcanian characteristics have produced higher ejection velocities (200–400 m/s) and ejected blocks and bombs to greater distances (<5 km from the vent) than any other eruption type. Blocks ejected in vulcanian eruptions have killed visitors at summit craters several times during recent decades. Vulcanian eruptions through summit crater lakes have also generated lahars that have killed many thousands of people during historical time.

The explosive nature of vulcanian events has been attributed to several mechanisms. One is the brittle failure of a strong, impermeable cap rock beneath which magmatic gas has accumulated. Another mechanism involves interaction of rising magma with external water such as eruptions through crater lakes. The involvement of external water was proposed, in part, based on the similarity between eruptive deposits at Vulcano and at phreatomagmatic maars.

II. FIELD EXAMPLES

A. Vulcano, Aeolian Islands

The island of Vulcano, home of the Roman god Vulcan, has erupted numerous times since the dawn of recorded history. The eruptions of 1888–1890 at Vulcano were among the best-documented eruptions anywhere in the world during the 19th century. They took place at a time when volcanologists were recording and classifying different kinds of eruptions. A commission appointed by the Italian government and led by Prof. O. Silvestri documented the events.

The first explosions at Vulcano, on August 3–5, 1888, expelled purely nonjuvenile ejecta from the upper edifice of the central cone (Fossa Cone). Juvenile phases of the eruption began on August 18, 1888, and continued until March 22, with especially violent events on December 26, 1889, and March 15, 1890. The eruptions were characterized by discrete explosions with repose intervals that varied from minutes to hours or greater. The largest explosions followed the longest repose intervals. They expelled juvenile blocks that were solid enough to resist deformation upon landing, though many vesiculated into breadcrust structures (the term *breadcrust structure* was coined by Johnston–Lavis in 1888 in describing ejecta from this eruption). In 1907, Mercalli described black clouds ("finger jets" in today's terminology) shooting up from the crater at hundreds of meters per second, spiked by lightning and containing, at the head of the cloud, arrow-like projections whose apices contained large ballistic fragments. Tephra plumes emanating from smaller explosions lacked large ballistic fragments and assumed cauliflower or mushroom shapes.

In 1891, Mercalli and others noted that "just as we have the "*plinian*" or "*vesuvian*" eruptions of Vesuvius accompanied by violent outbursts of "ashes" and welling out of lava, and the incessant milder "*strombolian*" type of eruption, so we may distinguish a "*vulcanian*" type. These distinctions in eruptive style became the basis for the eruption classifications proposed by Mercalli in 1907 and modified by Lacroix in 1908.

Contemporary reports surmised that explosions at Vulcano were caused by accumulation of gas below a plug of solidified magma. In 1977, however, Schmincke noted similarities in eruptive and deposit characteristics at Vulcano with those at Surtsey (a volcano that erupted through seawater near Iceland) in 1963–1967. He therefore suggested that the 1888–1890 eruption of Vulcano involved mixing of groundwater with magma. Frazetta and others reached similar conclusions for pre-1888 deposits at Vulcano. Barberi and others, however, argued that evidence for external water interaction in the deposits of 1888–1890 is less clear than that in pre-1888 deposits. The earlier eruptive sequences generally contain wet surge deposits, which are lacking in the 1888–1890 deposits. The 1888–1890 deposits, on the other hand, contain abundant breadcrust bombs and pumice fall, which are not generally present in older layers. To date, no consensus has been reached regarding the involvement of external water in the 1888–1890 eruptions.

B. Ngauruhoe, New Zealand

The 1975 eruption of Ngauruhoe volcano, located on the North Island of New Zealand, was one of the first well-documented vulcanian eruptions. The 11-month-long eruption commenced on February 12 with a series of intermittent ash eruptions from the summit crater. After a 1.5-hour gas-steaming subplinian event on February 19, nine cannon-like explosions occurred from the summit crater. The subplinian phase was accompanied by a volcano-tectonic earthquake that was followed by 2-hours of volcanic tremor. Seismic activity declined once the series of explosive events commenced.

Each cannon-like explosion generated a visible atmospheric shock wave which preceded the ejection of the pyroclastic slug. Figures 1a–1c show a time series of photographs of one of the cannon-like explosions. Each of these photographs was taken by a different observer attempting to photograph the shock front. None were quick enough to capture the shock front, but its passage is manifested by the appearance of a short-lived white condensation cloud (recorded in Fig. 1b). The condensation cloud forms immediately behind the shock front in the trailing rarefaction wave. The eruption cloud developed from a dense mixture of ash, high-pressure gases, and massive blocks of andesite from the magma column cap and conduit walls. These blocks were transported as projectiles and then fell back to the ground as the ash and gas continued to rise to 4–5 km (Fig. 1d). The center of the eruption cloud was observed to collapse, forming a pyroclastic avalanche.

The pyroclastic avalanches followed channels down the flanks of the volcano and formed deposits with lobate fronts and 0.5- to 0.8-m-high levees. The deposits are up to 10 m thick, 1–1.5 × 10^6 m^3 in total volume and are composed of large, rounded blocks in a matrix of pulverized scoria and lithic fragments. Ballistic blocks ~0.8 m in diameter of massive andesite and scoriaceous breadcrust bombs were also found in ash fall deposits up to 2.8 km from the crater. The largest ballistically ejected block was 27 m long, 15 m wide, and weighed roughly 3000 tons. The fall deposits are up to 1 mm thick at 21 km from the crater and are well sorted. Near (<2 km from) the eruptive vent, the deposit is 3–4 cm thick and has a bimodal grain-size distribution. Scoria 20–30 mm in diameter are present within the fine

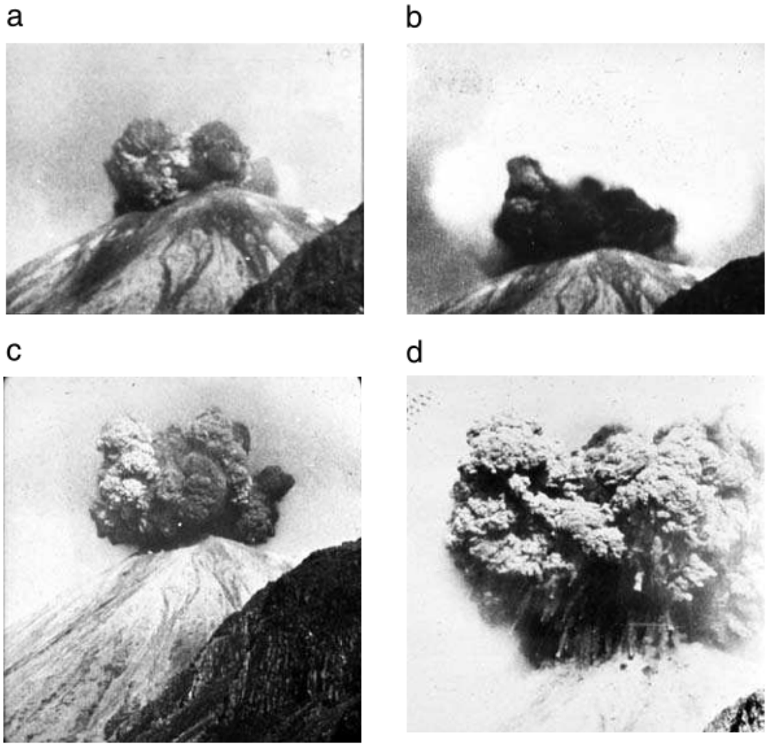

FIGURE 1 Snapshots of a vulcanian eruption at Ngauruhoe in 1975 taken aprroximately (a) 0.5 s, (b) 1 s and (c) 2 s after initiation. Notice the white halo (condensation cloud) above the ash cloud in (b) that forms after the passage of a shock wave. (d) Eruptive event displaying the characteristic ballistic blocks and ash cloud of vulcanian eruption occurring 11 s after (a).

ash layer (1–3 mm median grain diameter). The total volume of the fall deposits is roughly 2.4×10^6 m^3. Ngauruhoe produced similar eruptions in 1954 and 1974 that were not as well documented as the 1975 eruption.

C. Sakurajima, Japan

Sakurajima volcano is one of the most active volcanoes in the world. Its recent eruption phase, which began in 1955, is characterized by an annual eruption rate of up to 400 explosive events per year. This andesitic stratovolcano is situated on the southern rim of Aira caldera which is located in the northern part of Kagoshima Bay on Kyushu, Japan. All recent eruptions have been concentrated at the summit crater (Minamidake crater), with earlier activity occurring predominantly along the flanks. Typical summit eruption clouds reach heights above the crater between 0.8 and >4 km and eject blocks 40–180 cm in diameter to distances of 0.8 to 3.3 km from the crater.

Due to the proximity (<5 km) of the volcano to the city of Kagoshima, activity at Minamidake crater has been monitored with geodetic, seismic, and video equipment since 1964 by the Sakurajima Volcanological Observatory of Kyoto University. Summit eruptions are typically vulcanian (Fig. 2a; see also color insert), yet nonexplosive or effusive eruptions and continuous ash eruptions (e.g., plinian) do occur. Nonexplosive eruptions are usually accompanied by volcano-tectonic earthquakes (a.k.a. A-type earthquakes) and plinian eruptions are accompanied by swarms of microearthquakes or volcanic tremor. Vulcanian eruptions are characterized by precursory or accompanying explosive earthquakes (large amplitude, isolated events lasting 10–20 s), volcanic tremor, and sometimes long-period earthquakes (a.k.a. B-type earthquakes). For example, in Fig. 2b, the ejection of ash and blocks from the vent is defined by the emission of an atmospheric shock wave which is preceded (10 s) by an explosive earthquake.

Explosive and nonexplosive eruptions are also accompanied by two respective patterns of ground deformation based on tilt- and strainmeter recordings made below the summit crater. Prior to nonexplosive eruptions, the ground slowly inflates until the eruption and thereafter gradually deflates. Likewise, gradual ground inflation precedes explosive eruptions, followed abruptly by deflation at the onset of the eruption. The amount of inflation associated with a typical vulcanian eruption is estimated at 10^3 to 10^5 m^3 at a depth between 2 and 6 km. Volume changes associated with deflation at the onset of an explosive eruption are estimated at 10^3 to 10^4 m^3. The mass of ejected material is equal to two-thirds of the magma mass equivalent to the deflation volume.

The source of vulcanian eruptions at Sakurajima has been interpreted from the relationship between seismicity and geodetic data and the onset of an eruption by several researchers. It has been proposed that as the volcano inflates without an eruption, magma is transported to shallower depths (<2–6 km) beneath the Minamidake crater. As magma ascends, volatiles are exsolved and accumulate at the top of the shallow magma body. When a critical pressure is reached which corresponds to the strength of the surrounding rock, the accumulated gas is released into a conduit that is connected to the summit crater. The release of gas is thought to be the source of the precursory explosive earthquakes. At the vent, high pressure gas is released into the atmosphere creating air shock waves that mark the onset of an eruption. The shock waves are immediately followed by the ejection of ash and fragmented magma forming pyroclastic clouds. From photographic analysis, the emitted shock waves travel at speeds of 441–500 m/s from the vent, and block ejecta travel at velocities of 110–160 m/s.

D. Galeras Volcano, Colombia

Galeras is among the most active volcanoes in Colombia and among the most dangerous in South America. Located near Colombia's western border, Galeras lies about 8 km west of the town of Pasto (pop. 350,000). Because of the danger it poses to surrounding communities, its activity has been the subject of intense research and has been monitored continuously since 1989.

Following a 50-year period of quiescence, seismic activity increased at Galeras in June 1988. A series of small, explosive, mostly nonjuvenile eruptions began in February, 1989, which increased in frequency and became semicontinuous from May 4 to May 9 within the secondary crater *El Pinta.* Between May 1989 and the end of 1990, seismicity and SO_2 emissions remained at a relatively high level (1400 long-period earthquakes/month and 2000–5000 tonnes/day, respectively). During the first half of 1991, a series of minor ash emissions was accompanied by long-period earthquakes, tremor, and inflation of the summit area and by a decrease in SO_2 flux to <1000 tons/day. These trends continued until a dome of 400,000 m^3 volume was emplaced in the crater between October and December of that year.

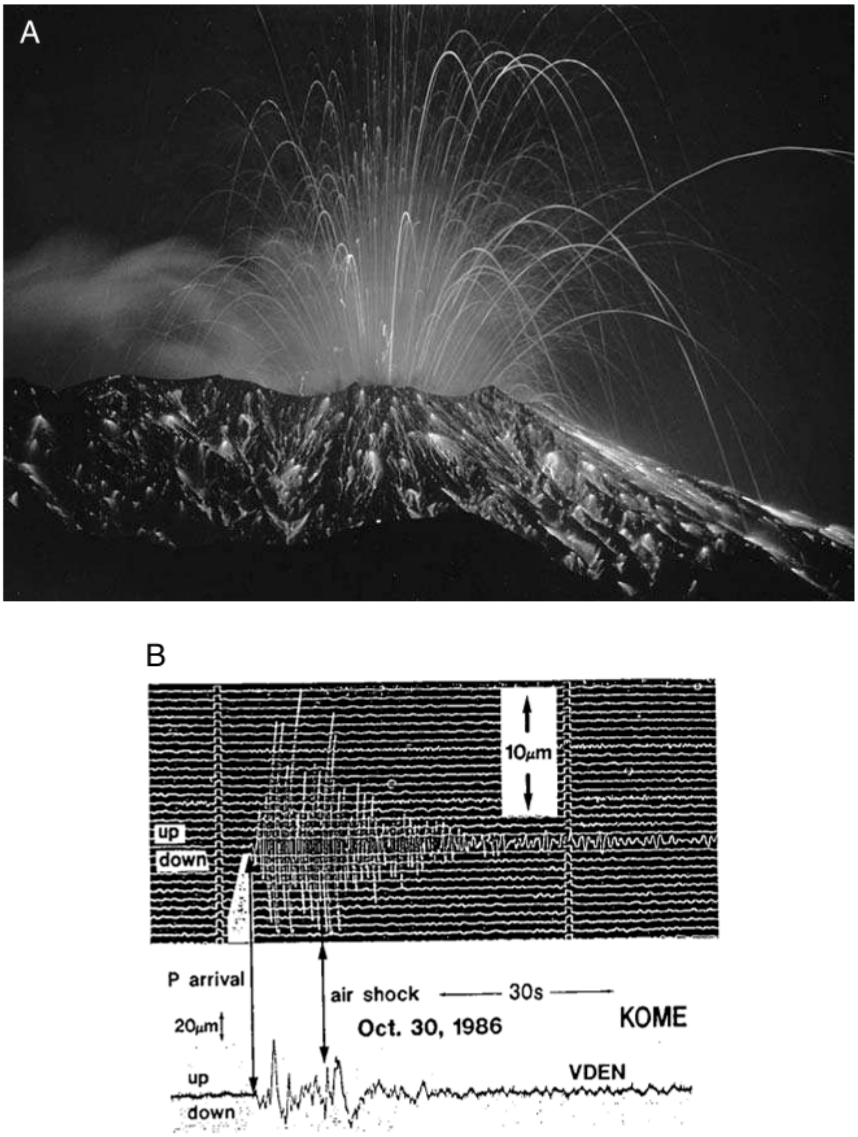

FIGURE 2 (A) Vulcanian eruption that occurred at Sakurajima at 22:53 JST on February 6, 1990. Incandescent arcs define the trajectory paths of ejected blocks. Photo taken at the Sakurajima Volcano Observatory by Tetsuro Takayama with an exposure time of 30 s. (See also color insert.) (B) An example of a short-period (top) and long-period (bottom) seismogram of vertical ground motion. The *P*-wave arrival of an explosion earthquake is followed within 10 s by an air shock which marks the onset of the October 30, 1986, eruption. [Reprinted with permission from Uhira and Takeo, (1994) *J. Geophys. Res.* **99,** 17,775–17,789, American Geophysical Union.]

From July 16, 1992, until June 7, 1993, Galeras produced six small but explosive vulcanian eruptions, followed by small gas emissions in September 1994 and January 1995. The first vulcanian explosion, on July 16, 1992, destroyed 90% of the lava dome, produced a plume about 4 km high, generated shock waves that broke windows 9 km from the volcano, ejected blocks 40 cm in diameter up to 2.3 km from the vent, and produced at least 277,000 m^3 of tephra. The second, on January 13, 1993, killed six volcanologists and three tourists who were at the summit of the volcano. The eruption lasted about 15 minutes, produced ash plumes 2.5–4 km in height, distributed incandescent blocks and lapilli throughout the 1-km-diameter caldera, and was

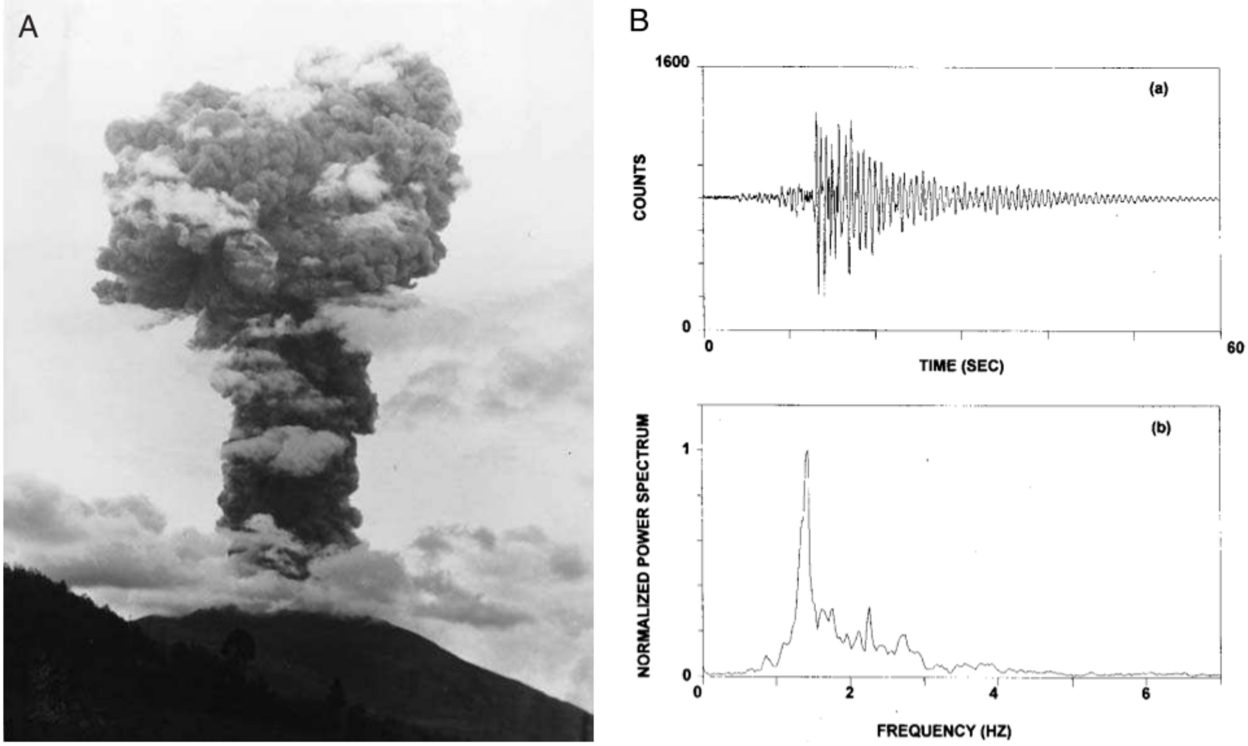

FIGURE 3 (A) Vulcanian eruptive plume from the April 4, 1993, eruption of Galeras. (Photo taken by Luis Esparza of INGEOMINAS, Colombia.) (B) Examples of the vertical ground motion and spectral peaks for a *tornillo* or long-period seismic event at Galeras. [Reprinted from Cruz, G., and Chouet, B. (1977) *J. Volcanol. Geotherm. Res.* **77,** with permission from Elsevier Science.]

followed for several hours by vigorous jetting of gas from the vent. Later eruptions in the sequence (e.g., on April 4, Fig. 3a) were similar in character but decreased progressively in size and increased in frequency through the end of 1993. During the entire 2-year eruptive sequence, SO_2 flux remained low except for dramatic increases for a few days following each vulcanian eruption.

None of the vulcanian explosions was preceded by any significant increase in seismicity, gas flux, or deformation. However, following the deadly January 1993 eruption, seismologists recognized that each event was preceded by small numbers (a few per day) of distinctive, monochromatic long-period seismic events of a few minutes duration with long codas of constantly decreasing amplitude (Fig. 3b). These events were termed *tornillos* (screw, in Spanish) after their screwlike appearance on helicorder records. The number and duration of the *tornillo* signals tended to increase over a period of weeks, then decrease in the days prior to the eruptions. The appearance of *tornillos* in May 1993 allowed seismologists to warn local authorities of an eruption that occurred on June 7. The warning was attributed to the fact that long-period seismic events are thought to be related to a pressurizing fluid flow at shallow depth.

From gas-flux data and considerations of magmatic cooling rates, it has been argued that vulcanian eruptions at Galeras were caused by generation of gas as the magma cooled and crystallized in the shallow conduit. After late 1991, gas escape through the conduit was impeded by the emplacement of magma, causing gas pressures to build up and vent explosively during vulcanian events. The decrease in eruption size and in the time interval between eruptions were inferred to be related to some combination of two factors: (1) a temporal decrease in tensile strength of the magmatic cap, allowing it to breach under progressively smaller loads, and (2) a deepening of the source of gas from each eruption to the next.

This interpretation was supported by analysis of the seismicity that accompanied the emplacement and extrusion of the lava dome in October 1991. The accompanying seismicity was characterized by a mix of repetitive, long-period events and tremor. Waveform analysis of the long-period events (*tornillos*) in October and November showed that the dominant periods range from 0.2 to 1.0 s. These events correlated with observed intermittent emissions of gas venting through a crack in the lava dome. Using a fluid-driven crack model to interpret the seismicity, it was inferred that the sources of the long-period events were two resonating cracks within the lava dome. A crack resonated when a gas slug was released from the magma column and dilated the preexisting crack, allowing the gases to escape to the surface. As the gases moved through the crack, progressive mineralization occurred along the crack walls and eventually sealed the crack. The July 16, 1992, eruption occurred when sufficient pressure built up to cause dome failure.

III. ERUPTION PROCESSES

A. Ballistic Ejection

Among the first features to be studied at vulcanian eruption sites were the trajectories and velocities of erupted blocks. The most energetic vulcanian eruptions have ejected blocks to distances of 5 km (at Arenal volcano, Costa Rica in 1968). Prior to the 1990s, estimates of the velocity required to produce the observed ejection distances have generally assumed that blocks were ejected through still air. Those estimates yielded velocities significantly greater than more recent calculations which consider decreased air drag near the vent. Accordingly, the highest velocities estimated prior to the 1990s, ~600 m/s for the 1968 eruption at Arenal volcano and 400 m/s for the 1975 eruption at Ngauruhoe, have been revised down to roughly 300–400 and 220–260 m/s, respectively. Much higher velocities are likely to be produced within gas jets following the vulcanian outburst, but these velocities have not been successfully measured. The most reliable velocity measurements have been obtained from photographs and videos of explosions, albeit of smaller eruptions than those at Arenal and Ngauruhoe.

B. Estimates of Eruption Velocity and Pressure

The great distance over which large blocks are ejected in some eruptions suggests intuitively that the pressure required to accelerate them was very high. Beginning in the 1940s, investigators attempted to estimate pre-eruption pressure using either relations derived for projectiles within gunbarrels (the "gun barrel equation") or a modified form of the Bernoulli equation (MBE) that did not consider the compressibility of the erupting mixture and inappropriately used the density of the solid phase rather than of the solid–gas mixture. These estimates gave initial pressures more than an order of magnitude too high (hundreds of megapascals) (Figure 4A). Contemporary pressure–velocity relations, introduced in the early 1980s, assume that block masses are accelerated by an adiabatically decompressing volume of gas in the upper conduit. They show that vulcanian-eruption velocities can be produced by a gas–solid mixtures containing several weight-percent gas or less at magmatic temperatures and at pressure usually less than 10 MPa (Figure 4B).

C. Deposit Characteristics

Brief, violent explosions are the hallmark feature of vulcanian eruptions, and consequently the most salient deposits from such eruptions are produced by ballistic block ejection, pyroclastic avalanches, or nuées ardentes and pyroclastic flows. Block fields at volcanoes such as Galeras, Vulcano, Arenal, Asama, and Sakurajima cover areas ranging up to several square kilometers and contain blocks up to several meters in diameter. When masses of ejected blocks and ash fall to the ground with significant horizontal momentum, or land on steep slopes, they develop into moving pyroclastic avalanches or flows. Pyroclastic avalanches cut undersea cables during the 1888–1890 eruptions at Vulcano and were spectacularly photographed on the flanks of Ngauruhoe in 1975. The deposits are composed of lithics and poorly vesiculated pyroclastic flow or block-and-ash flow materials.

Vulcanian eruptions have also produced widely dispersed, fine-grained fall deposits with volumes up to 1 km^3 reflecting whether the eruption was a discrete or a pulsatory event or a discrete event preceding a sustained eruption phase (e.g., plinian eruption). Fine-grained tephra fall deposits develop by at least two mechanisms: (1) upward convection of fine ash clouds following discrete ash explosions (e.g., Ngauruhoe, 1975) and (2) development of a sustained subplinian or plinian column after an initially vulcanian outbreak (e.g., Redoubt, 1989). The second mechanism produces deposit volumes on the order of 10^{-1}–10^{0} km^3, which could only be produced by subplinian or plinian mass flux rates sustained over a period of hours or more. Deposit volumes of $<10^{-1}$ km^3 are produced by discrete and pulsatory events and are more proximal to the crater than those related to the second mechanism.

The components of vulcanian fall deposits are characterized by the proportions of nonjuvenile versus juvenile fragments and vesicularity. Nonjuvenile clasts make up a large fraction of the deposits and are presumed to

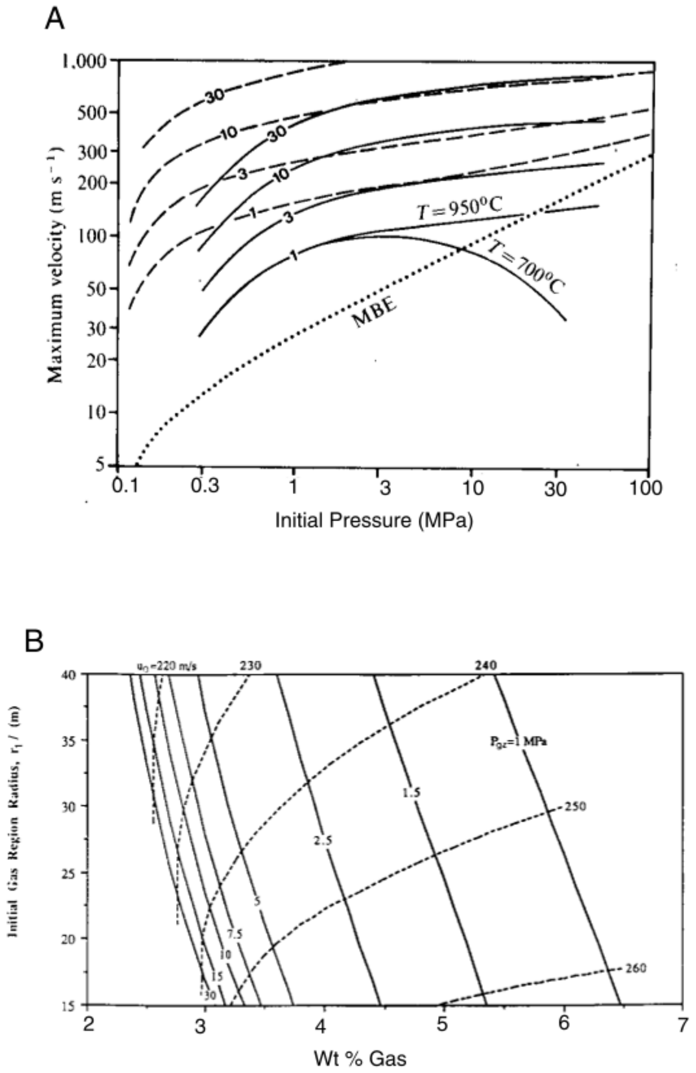

FIGURE 4 (A) Maximum theoretical velocity that can be attained by a mixture of gas and solid particles decompressing from the initial pressure shown on the horizontal axis, and an initial temperature of 950°C. Labels on each line indicate the wt% of gas (assumed H_2O) in the mixture. Dashed lines assume that the ash and gas are in thermal equilibrium, solid lines assume that the gas expands adiabatically. The dotted line shows the theoretical velocities calculated by the modified Bernouilli equation. [Reprinted with permission from Self *et al.,* 1979.] (B) Maximum theoretical velocity as a function of distance from vent, preburst pressure and wt% gas calculated for the 1975 Ngauruhoe eruption. [Reprinted with permission from Fagents and Wilson, 1993.]

result from the clearing of the vent during these short-lived eruptions. The lithology of nonjuvenile clasts, which include lava dome material or country rock from the vent or conduit walls, may constrain the source depth and intensity of the eruption. Juvenile components may be vitric to crystalline, poorly to moderately vesicular, angular, and block- to ash-sized. The lack of well-vesiculated juvenile fragments in these deposits and the short duration of the eruptions suggest that the upper conduit contained mostly gas or heated groundwater as opposed to vesiculating magma.

D. Seismic and Air Wave Characteristics

Vulcanian eruptions are commonly preceded by long-period and tremor events and explosion earthquakes.

Unlike volcano-tectonic earthquakes, which are thought to reflect the brittle response of the volcanic conduit to stresses induced by magma migration, long-period and tremor events are thought to be the manifestations of pressure disturbances in fluids flowing through the edifice. Long-period events are recognized by a high frequency onset followed by a monochromatic wavetrain with a duration of seconds to minutes, whereas tremors may last for hours to days. These types of seismic events have provided vital information about the role of gases in the eruption process, such as the July 16, 1992, eruption at Galeras volcano, as mentioned previously, and the onset of the 1989–1990 eruption at Redoubt volcano, Alaska. In the Redoubt volcano case, a swarm of 1400 long-period events were recorded over an 18-hour period prior to its onset which was marked by a vulcanian eruption. These seismic events were interpreted as reflecting the pressurization of the volcanic edifice due to the accumulation of exsolved magmatic volatiles at the top of the magma column. At several volcanoes in Japan (Asama, Mount Tokachi, and Sakurajima), explosion earthquakes have preceded the surface outbreaks of vulcanian eruptions by several seconds. Such earthquakes are thought to represent rapid pressurization 2–3 km beneath the volcanic crater which induces the upward flow of either gas or magma. At other volcanoes (e.g., Mount St. Helens), explosion earthquakes are not accompanied by surface outbreaks.

Atmospheric shock waves are another characteristic of vulcanian eruptions. Their occurrence indicates that the erupting fluid at the vent is overpressurized with respect to the atmosphere as illustrated in Fig. 5A and 5B. The air shock propagates ahead of the erupting fluid at a velocity exceeding the atmospheric sound speed (340 m/s at 25°C). The shock wave is momentarily visible above the volcano when it passes through clear air or a preceding eruption cloud and condenses water vapor (Fig. 5C). This process produced short-lived condensation clouds surrounding the expanding eruption plume at Ngauruhoe volcano in 1975 and Sakurajima volcano.

Air shocks have been recorded on microbarographs at distances of >50 km from the the active vent and appear as N-shaped signals followed by a long-period coda as shown in Fig. 6A. The N-shape signal is composed of a leading compression wave followed by an expansion wave that raises the pressure behind the shock back to ambient conditions. Results from numerical simulations of vulcanian eruptions shown in Figs. 6B and 6C demonstrate how the peak-to-peak pressure and wavespeed of the signal can be used to estimate the eruption burst pressure and the gas (or steam) concentration in the eruptive ash–gas mixture. For example, the peak-to-peak pressure, P_k, (0.0004 MPa) of the shock wave recorded during the 1975 Ngauruhoe eruption at a distance of 9 km from the vent corresponds to a burst pressure of 5–6 MPa and 50 wt% gas. These values agree well with those calculated by Fagents and Wilson using ejection velocities. Figure 6C can be used to estimate the weight percent steam in the erupting fluid based on the travel speed of the air shock and recording location.

IV. PLUME DYNAMICS

The height, shape, rise velocity, and rise times of vulcanian eruption plumes have been studied by many investigators. Individual vulcanian explosions tend to last only seconds to minutes—not long enough to develop sustained eruption columns unless many follow in close succession. Vulcanian eruption clouds can reach altitudes of several kilometers for individual explosions or <20 km for repeated or pulsatory explosions over periods of hours. Once expelled into the atmosphere, large blocks fall rapidly out of the mass of ejected debris (Fig. 5D).

The remaining cloud of tephra entrains air and generally becomes buoyant, rising as a thermal (Fig. 5E) at velocities of meters to tens of meters per second until its density just equals that of the surrounding atmosphere. The final elevation of the thermal is controlled by the initial diameter and temperature of the plume, the adiabatic lapse rate for air, and the ambient atmospheric temperature gradient with elevation. Plumes with initial diameters of <1 km will generally rise <12 km into the atmosphere and will achieve that height in a few to several minutes. Photographs of discrete thermals were analyzed following individual vulcanian explosions at Fuego volcano.

More commonly, explosions follow closely one after another, producing a semicontinuous plume. Examples of the latter were noted during vulcanian eruptions at Soufrière volcano, St. Vincent, in 1979 and during vulcanian eruptions at Lascar Volcano, Chile, in 1990. These plumes reached heights (15–18 km) significantly greater than one would expect from discrete explosions, apparently due to the accumulated buoyancy of the consolidated thermals. The heights of semicontinuous and continuous eruption columns are controlled primarily by the average magma-flux rate or mass-eruption rate.

Mass-eruption rates for vulcanian eruptions are on

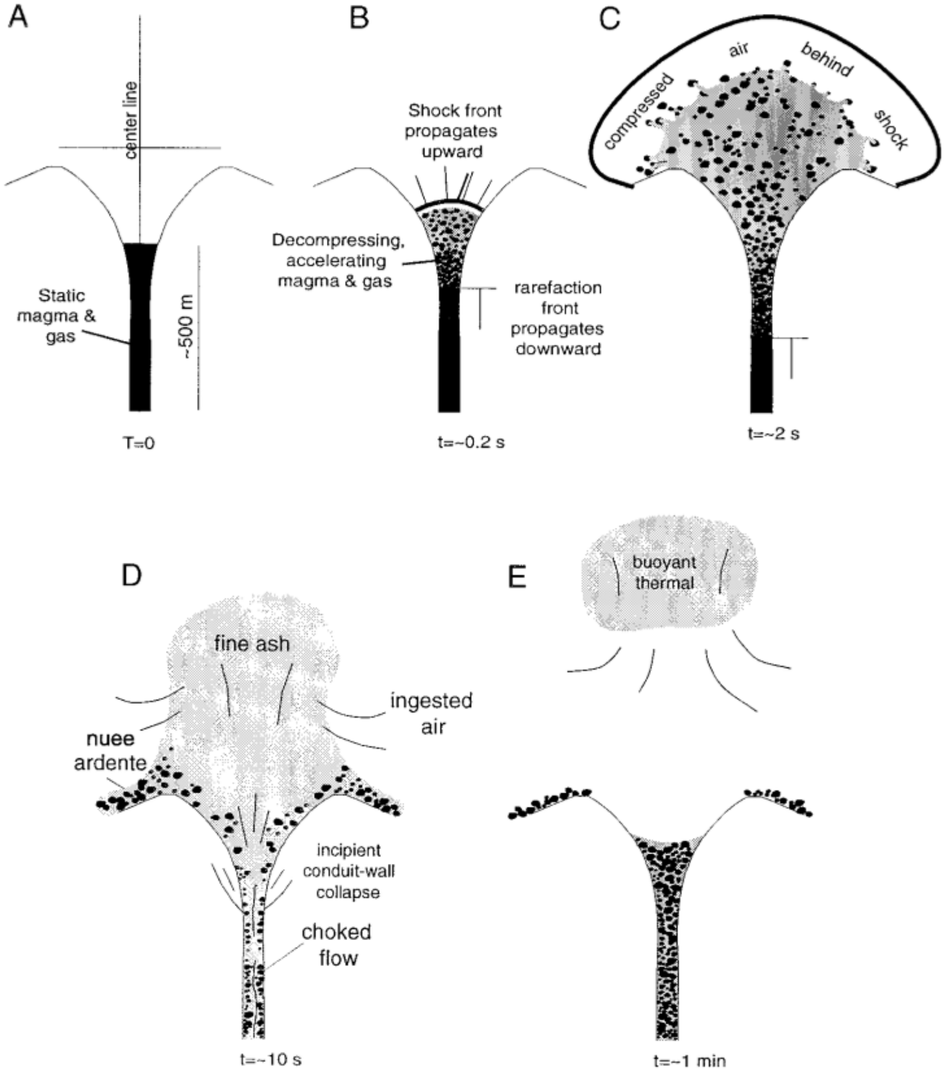
A
center line
Static magma & gas
~500 m
T=0
B
Shock front propagates upward
Decompressing, accelerating magma & gas
rarefaction front propagates downward
t=~0.2 s
C
compressed air behind shock
t=~2 s
D
fine ash
ingested air
nuee ardente
incipient conduit-wall collapse
choked flow
t=~10 s
E
buoyant thermal
t=~1 min

FIGURE 5 Schematic illustration of the development of fluid flow in and above a volcanic conduit during a single vulcanian explosion. (A) Structure of the conduit and crater prior to an explosion. (B) Crater and conduit ~0.2 s after initiation of the eruption. (C) Events about 2 s after initiation; (D) ~10 s after initiation; (E) ~1 minute after initiation.

the order of ~10^4 kg s^{-1} m^{-2} based on the diameter of the vent and the velocity at the vent. A conduit some tens of meters in diameter would produce mass-eruption rates comparable to subplinian or plinian eruptions, though the duration of vulcanian events is far shorter. For a conduit diameter of a few tens of meters and a depth of half a kilometer, a single explosion would produce about 10^5 m^3 of erupted magma (dense-rock equivalent).

Vent velocities are constrained by the sound speed of the erupting fluid. Because gases associated with these eruptions are overpressured with respect to the atmosphere, the flow at the vent is considered choked. This implies a vent velocity at the most constricted part of the vent that is equal to the sound speed of the erupting fluid. The sound speed of the fluid is a function of gas composition, temperature, and volume fraction of solid particulates. A gas at 900°C composed of H_2O will have a sound speed ~800 m/s and one that is more SO_2- or CO_2-rich will have a sound speed near 400–450 m/s. The sound speed will increase with temperature and will decrease as the volume fraction of solids increases.

Volcanic gas–ash mixtures generally have sound speeds of about 50–150 m/s. Above the vent, the flow velocity increases with height in the supersonic (where velocities are greater than the sound speed) region of the jet. Only fine-grained tephra will travel at these velocities. Larger materials separate from the flow within <1 km above the vent. Thus the travel distance reflects the initial velocity of each block at the vent, plus interactions between the block and the surrounding gas and ash in flight.

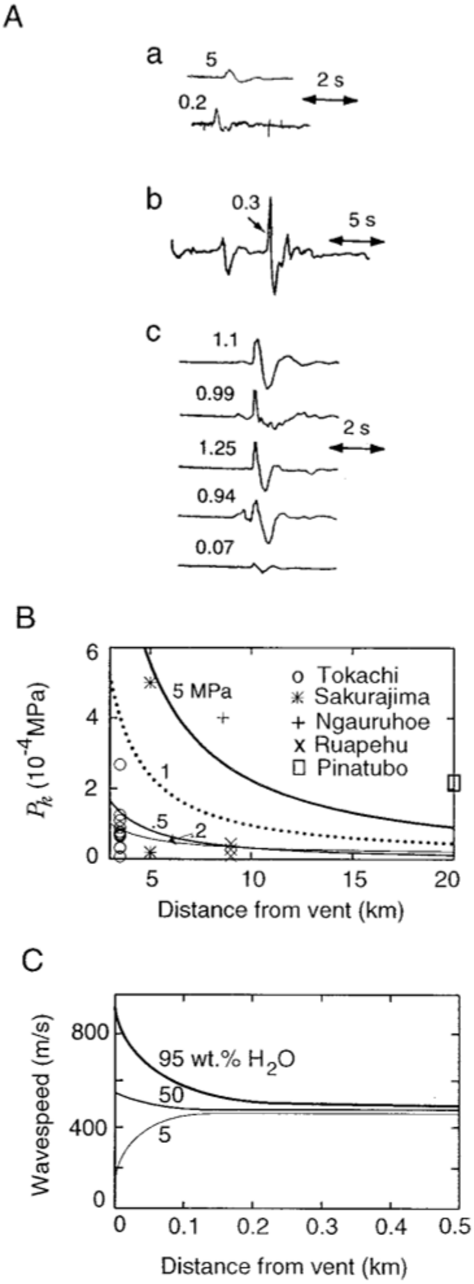

FIGURE 6 (A) Examples of N-shaped air waves recorded on microbarograms from eruptions at (a) Sakurajima volcano in 1989 at 5 km from the vent; (b) Ruapehu volcano in 1995 at 9 km from vent; and (c) Mount Tokachi in 1988 at 3.5 km from the vent. (B) Theoretical decay curves of the magnitude of the difference between the maximum and minimum pressures P_K on the air wave as a function of distance from vent and 50 wt% H_2O. Each curve represents a different eruption burst pressure. Superimposed are P_K values (in MPa) from (A) and other volcanoes. (C) Theoretical wavespeeds for air waves associated with eruptions of different H_2O concentrations. (Reprinted with permission from Morrissey and Chouet, 1997.)

V. ERUPTION SOURCE MODELS

Several hypotheses have been proposed for the source of gases that drive vulcanian eruptions; they relate either to exsolution of magmatic volatiles or superheating of groundwater. One hypothesis involves pressurizing the lava cap or lava dome by exsolution of magmatic volatiles from rapid microlite growth. This scenario was applied to the eruptions at Galeras in 1992–1993, Mount Unzen in 1991, and Soufriere Hills volcano, Montserrat in 1996. Calculations show how microlite crystallization can increase the pressure within a lava dome and upper conduit by tens of MPa which would be sufficient to cause a lava dome to fail. By this process, the rate of pressurization is on the order of days to weeks. Laboratory modeling of microlite growth using an andesitic melt demonstrates how pressurization rates can occur on timescales of minutes to hours by the subsequent formation of a lava plug. These results may explain pulsatory vulcanian eruptions that recur on similar timescales.

Another hypothesis involving the exsolution of magmatic gases is closed system magmatic degassing at depth (>3 km below the vent). This scenario has been applied to recent eruptions at Sakurajima volcano, the onset of the 1989–1990 eruption at Mount Redoubt as mentioned previously, and the 1992–1993 eruptions at Galeras volcano.

A third hypothesis for a source of gases and pressurization involves rapid heating of groundwater by either conductive heating by an underlying magma body or the physical mixing of magma and groundwater. Conductive heating would gradually pressurize groundwater which would eventually lead to failure of the lava cap. Physical mixing is known as a fuel–coolant interaction (FCI) and is described in detail in the chapter on Phreatomagmatic Fragmentation in this volume. FCIs may be explosive or nonexplosive; the former may produce a vulcanian type of eruption. An explosive, volcanic FCI arises when rising magma encounters a water-saturated layer or a surface body of water such as a lake. When magma contacts water, the water may become superheated which rapidly raises the temperature of water past its critical point without changing it to steam. The metastable water will flash to vapor which in turn pressurizes the system at an explosive rate (microseconds) when the superheating condition is exceeded or an external force perturbs the system such as fall-back material or seismic events. Once an explosive FCI occurs, another may follow within 10^{-3}–10^{0} if the surface of the magma becomes fragmented, thus creating new surface areas for heating additional water. This cycle may continue until there is no longer a source of water or the rate of heat transfer between the magma and water is insufficient.

This mechanism does not require the presence of a sealing lava plug/dome but if one does exist, it can easily pressurize the plug/dome above failure conditions. Explosive magma–water interactions (phreatomagmatic) may explain individual vulcanian explosions, or pulsatory vulcanian eruptions on times scales of seconds to minutes. This mechanism was postulated by some investigators for the 1888–1890 and pre-1888 eruptions at Vulcano.

Explosive phreatomagmatic events that appear as discrete finger jets were observed during the 1995–1996 eruption at Mount Ruapehu volcano in New Zealand. The first phase of the eruption involved a crater lake that led volcanologists to consider all these eruptions to be phreatomagmatic. Many of these eruptions were short-duration explosive bursts characteristic of vulcanian eruptions. Similar eruptions occurred during the 1977 eruption of the Ukinrek maars in Alaska. A series of discrete, explosive eruptions occurred over a 10-day period when rising magma encountered a shallow water-saturated sediment layer. Vulcanian eruptions that involve groundwater may be considered a subclassification of phreatomagmatic eruptions.

VI. CONCLUDING REMARKS

The characteristics that make vulcanian eruptions unique from other eruption styles are that they are short (seconds to minutes) discrete explosions, sometimes pulsatory, capable of ejecting incandescent lava bombs and blocks of fragmented rock to distances <5 km. The associated eruption cloud of fine-grained tephra composed of essentially nonjuvenile lithics, can reach altitudes several kilometers high for individual explosions or <20 km for repeated explosions. Shock waves are another feature that are usually recorded or observed during a vulcanian eruption. Some of these features are also characteristic of surtseyan and subplinian eruptions; however, the combination of all listed features separate vulcanian eruption from the other eruption styles.

During the past few decades, our understanding of the causes and timing of vulcanian eruptions has improved dramatically. The improvements have been the consequence of at least four factors: (1) an increase in the number of volcanoes under observation; (2) incremental improvements in monitoring techniques involving seismic and acoustic measurements; (3) improved communication by volcanologists of the characteristics of these eruptions; and (4) more realistic numerical models that consider both subsurface and surface processes.

SEE ALSO THE FOLLOWING ARTICLES

Hawaiian and Strombolian Eruptions • Lahars • Lava Domes and Coulees • Phreatomagmatic Fragmentation • Plinian and Subplinian Eruptions • Pyroclast Fall Deposits • Pyroclastic Surges and Blasts • Volcanic Plumes

FURTHER READING

Fagents, S. A., and Wilson, L. (1993). Explosive volcanic eruptions. VII. The ranges of pyroclasts ejected in transient volcanic explosions. *Geophys. J. Int.* **113,** 359–370.

Fudali, R. F., and Melson, W. G. (1972). Ejecta velocities, magma chamber pressure and kinetic energy associated with the 1968 eruption of Arenal Volcano. *Bull. Volcanol.* **35,** 383–401.

Ishihara, K. (1990). *In* “Magma Storage and Transport” (M. P. Ryan, Ed.). Wiley, New York.

Lacroix, A. (1908). “La Montagne Pelée et ses éruptions, avec observations sur les Éruptions du Vesuve en 79 et en 1906.” Masson, Paris.

Mastin, L. G. (1995). Thermodynamics of gas and steam-blast eruptions. *Bull. Volcanol.* **57,** 85–98.

McBirney, A. R. (1973). Factors governing the intensity of explosive andesitic eruptions. *Bull. Volcanol.* **37,** 443–452.

Mercalli, G. (1907). “I vulcani attivi della terra.” Hoepli, Milan,

Minakami, T. (1950). On explosive activities of andesitic volcanoes and their forerunning phenomena. *Bull. Volcanol.* **10,** 59–87.

Morrissey, M. M., and B. A. Chouet (1997). Burst conditions of explosive volcanic eruptions recorded on microbarographs. *Science* **275,** 1290–1293.

Nairn, I. A. (1976). Atmospheric shock waves and condensation clouds from Ngauruhoe explosive eruption. *Nature* **259,** 190–191.

Schmincke, H-U. (1977). Eifel-Vulkanismus östlich des Gebiets Rieden-Mayen. *Fortschr. Miner.* **55,** 1–31.

Self, S., Wilson, L., and Nairn, I. A. (1979). Vulcanian eruption mechanisms. *Nature* **277,** 440–443.

Sparks, R. S. J. (1997). Causes and consequences of pressurization in lava dome eruptions. *Earth Planetary Science Letters* **150,** 177–189.

Wilson, L. (1980). Relationships between pressure, volatile content and ejecta velocity in three types of volcanic explosion. *J. Volcanol. Geotherm. Res.* **8,** 297–313.

Woods, A. W. (1995). A model of Vulcanian eruptions. *Nucl. Eng. Design* **155,** 345–357.

This Page Intentionally Left Blank

PLINIAN AND SUBPLINIAN ERUPTIONS

RAFFAELLO CIONI
PAOLA MARIANELLI
ROBERTO SANTACROCE
ALESSANDRO SBRANA
Dipartimento di Scienze della Terra, Pisa, Italy

I. Characteristics
II. Direct Observations of Plinian Eruptions
III. The Inverse Problem: From Deposits to the Eruption
IV. Discussion of Eruption Dynamics

GLOSSARY

intensity A measure of the rate at which magma is discharged during an eruption.

magnitude The total mass of material ejected during an eruption.

VEI Volcanic Explosivity Index. A measure of the size of an eruption, mainly based on magnitude, intensity and destructive power of an eruption. VEI has an eight-point scale.

IN PLINIAN AND subplinian eruptions most of the erupted mass is discharged during phases characterized by the formation of high, convective eruption columns resulting in atmospheric ash and particle injection and dispersal by winds over huge areas. The name recalls the 79 A.D. eruption of Vesuvius which provoked the death of Pliny the Elder, which his nephew, Pliny the Younger, narrated in two letters to Tacitus.

I. CHARACTERISTICS

A. Definition, History, and Characteristic Features of Plinian Eruptions

During an eruption, the style of activity and the nature and type of products can change within minutes, hours, days, or months. Changes in eruption style are functions of changes in magma composition and crystallinity, the amount and nature of exsolved volatiles, vent and conduit geometry, and access of external water to the plumbing system. Any period during which a homogeneous style is sustained, however variable in its intensity, can be referred to as a phase of the eruption.

The systematic study of volcanic eruptions suffers from use of an ambiguous nomenclature. Classical names such as plinian, vulcanian, hawaiian, etc., are used both for well defined single phases of an eruption, as well as the entire complex sequence of events that makes up a polyphase eruption. To avoid ambiguity, we prefer to apply these terms only to those eruptions in which the dominant phase represents clearly one of these styles. For example, a plinian eruption can contain phases with different eruption styles (e.g., ignimbrite-producing), but the dominant phase (in terms of volume and/or intensity) is plinian.

The account of Pliny the Younger is the first description of a plinian eruption. Since then, numerous erup-

Copyright © 2000 by Academic Press
All rights of reproduction in any form reserved.

tions of similar intensity have occurred, especially concentrated along convergent margins of the lithospheric plates. The eruption that issued from Lake Taupo (New Zealand) around 181 A.D. is an example of the upper limit of size for this type of eruption. In the last century a dozen plinian to subplinian events have occurred. Among the most famous, is the 1912 eruption of Novarupta (Alaska), whose associated pyroclastic flow deposits formed the Valley of the Ten Thousand Smokes and in more recent times, the eruptions of May 18, 1980, at Mt. St. Helens (United States). March 29–April 4, 1982 at El Chichon (Mexico) and June 15, 1991, at Pinatubo (Philippines). These last three eruptions have provided a clearer definition of the eruptive processes and the dynamic evolution of explosive eruptions, giving new insights for the interpretation of deposits from past eruptions.

During plinian phases, a mixture of gas and particles (juvenile and wallrock) is discharged from a vent(s) at velocities between 100 and 400 m/s. The volume of ejected material ranges typically between 0.1 and 10 km^3 (magnitude = 10^{11}–10^{13} kg) with mass discharge rates (MDR) of 10^6–10^8 kg/s. The duration of these events is therefore limited, from a few minutes to a few hours. It is difficult to separate conceptually plinian from subplinian events. In simple terms, the eruptions in the lower ranges of magnitude (~10^{11} kg) and intensity (~10^6 kg/s) can be classified as subplinian. They are often characterized by important discharge variations that lead to relatively short phases of sustained discharge separated by pauses of variable length or other types of activity. This can result in the frequent generation of pyroclastic density currents (PDC) related to destabilization of the eruption column. Values of the Volcanic Explosivity Index (VEI) of 4–6 characterize plinian and subplinian eruptions. Larger magnitudes and intensities generally induce continuous column collapse and ejection of most of the erupted mass as pyroclastic density currents. These are ignimbrite phases of ultraplinian or ignimbrite eruptions. Table I summarizes the main features of these types of eruption.

The motion in the atmosphere of a plinian plume can be described in terms of three different regions (Fig. 1): (i) a gas thrust region, where the gas–particle mixture rapidly loses its initial momentum by turbulent entrainment of air at its margins; (ii) a convective region, where trapped air is heated and the bulk density is less than the surrounding atmosphere; and (iii) an umbrella region,

TABLE I Main Features of Plinian-Type Eruptions

Type of eruption	*Subplinian*	*Plinian*	*Ultraplinian or ignimbritic*
Magnitude (kg)	$\approx 10^{11}$	10^{11}–10^{13}	$>10^{13}$
Intensity (kg/s)	$\approx 10^6$	10^6–10^8	$>10^8$
Column height (km)	<20	20–35	>35
Thickness half-distance (b_t, km)	0.5–4	2–10	>10
Clast half-distance (b_c, km)	1–3	3–8	8–15
Main phases	Unsteady sustained, convective column	Steady sustained convective column	Sustained fountaining
Associated eruptive styles	Surge generation, dome extrusion	Partial or total column collapse	Convective column with increasing flow rate
Dominant fallout deposits	Thinly stratified	Massive to variously graded	Generally reversely graded
Dominant flow deposits	Surges and small sized pumice and scoria flows	Pumice and ash flows	High and low-grade ignimbrites
Fall/flow vol. ratio	>1	>1	$\ll 1$
Typical magma composition	Mildly evolved (dacitic, phonotephritic)	Highly evolved (rhyolitic, trachytic, phonolitic)	Highly evolved (rhyolitic, trachytic)

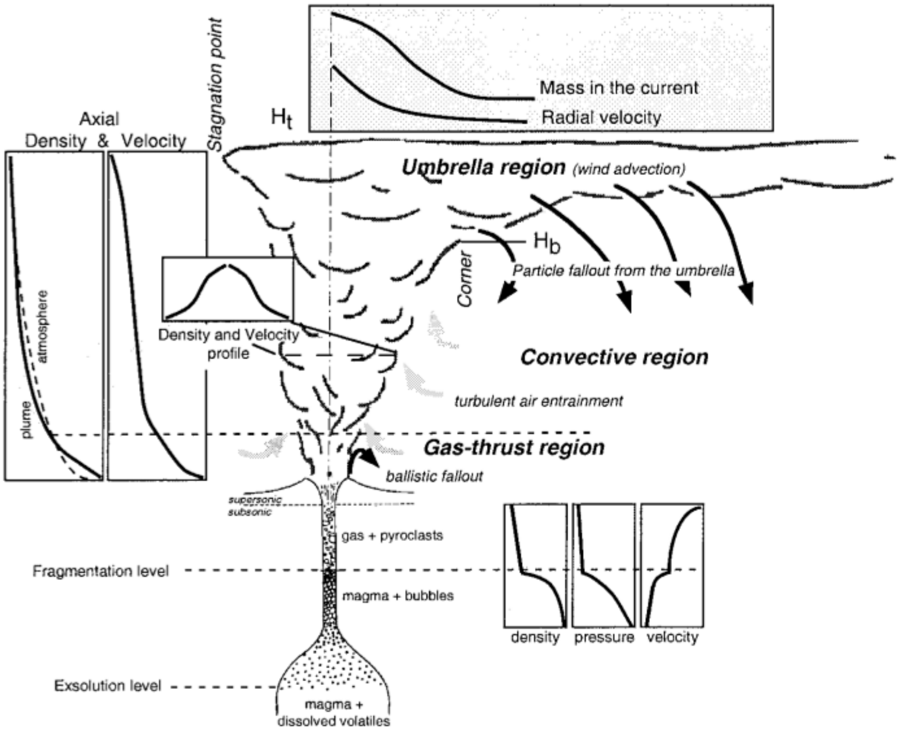
Mass in the current
Radial velocity
Axial
Density & Velocity
Stagnation point
H_t
Umbrella region (wind advection)
H_b
Particle fallout from the umbrella
Corner
atmosphere
plume
Density and Velocity profile
Convective region
turbulent air entrainment
Gas-thrust region
ballistic fallout
supersonic
subsonic
gas + pyroclasts
Fragmentation level
magma + bubbles
density
pressure
velocity
Exsolution level
magma + dissolved volatiles

FIGURE 1 From the magma chamber to the stratosphere. The figure shows the different zones, the variation of the main physical properties (density, pressure, velocity) of the erupting mixture, and the main processes associated with the flow of magma in the conduit and the formation of the convective column.

where the mixture, after having reached the height of neutral buoyancy (H_b), continues to rise due to its momentum to a maximum height (H_t) and expands laterally under the influence of the prevailing winds. The top of the gas thrust region is generally not more than few kilometers above the vent, while the base of the umbrella region can be on the order of tens of kilometers high. The efficiency of air entrainment in the mixture and thermal exchange with pyroclasts is the fundamental key to generating buoyancy needed for the rise of the volcanic plume to great heights in the atmosphere. The thermal energy provided by the magma is a function of its discharge rate. The maximum height reached by the eruptive column, which depends on its momentum at H_b, is scaled to the fourth root of the mass discharge rate of magma and is on the order of 1.3 times H_b.

The dynamics of plinian and subplinian eruptions require volatile-rich, high viscosity magmas. Basaltic compositions are consequently quite rare and unusual in these events, which are generally associated with evolved calcalkaline (high-silica andesite to rhyolite) and alkaline (trachyte to phonolite) magmas. Most magmas erupted during plinian events exhibit clear evidence of being evolved within shallow reservoirs, with rapid emptying frequently generating collapse of summit calderas.

B. Magma Fragmentation

Plinian volcanic eruptions are generally initiated by fracturing of the rocks overlying a crustal reservoir and subsequent magma ascent. The fracturing can be related to overpressure by magma influx from depth, volatile exsolution following crystallization, mixing, assimilation, etc., or to external factors such as tectonic earthquakes. The pressure decrease in rising magma progressively induces oversaturation and release of the dissolved volatile components. Acceleration and the volume increase of exsolved fluids result in fragmentation of magma, which is ejected as a gas dispersion of liquid clots and solid fragments. Prior to fragmentation, the high viscosity of silicic melts does not allow an efficient separation of the liquid from the volatile phase, and the magma rises in a bubbly flow regime, with bubbles having a small relative ascent velocity with respect to the liquid. Very high values of mixture acceleration are reached in the region of fragmentation, with a feedback effect on magma rise velocity related to the rapid decompression of bubbles after reaching volatile supersaturation in the melt (Fig. 1).

Mechanisms of magma fragmentation in plinian eruptions are classically related to a critical concentration of bubbles in the magma (about 75 vol%). At this concentration, decompressional and diffusional growth of the bubbles is inhibited by the viscosity of the residual, volatile-poor liquid, and rupture of the liquid films separating the bubbles can occur. Fragmentation of the magmatic foam is still a matter of debate. Analog experiments have shown that the explosive disintegration of a static foam is an unlikely process, while its acceleration in the conduit could explain the explosive fragmentation. The general evidence is that bubble content is in a relatively narrow range (65–85 vol%), depending on the shape and size distribution of bubbles. The introduction in the volcanological literature of the glass transition concept could help in explaining the fragmentation process. If the timescale for deformation (strain rate) is shorter than the timescale for viscous relaxation of the liquid (the time needed for the liquid to keep pace with an applied strain), the bubble–liquid mixture crosses the glass transition, behaving in a brittle fashion and disintegrating. A process, which may play an important role in the grain-size distribution of pyroclasts generated by fragmentation, is permeability development during vesiculation. Permeability (through bubble coalescence) will favor gas escape and consequent formation of pumice versus ash.

Fragmentation processes acting during subplinian events reflect the unsteady character of many of these eruptions. The alternation of sustained columns with periods of quiescence has been explained in terms of syneruptive degassing and viscosity increase of the magma column during the slow refilling of the conduit. The degassed portion of the magma crystallizes rapidly, causing magma stagnation in the upper portions of the conduit (possibly culminating in dome extrusion), and the progressive buildup of pressure that eventually reopens the system. The discontinuous nature of several subplinian eruptions may result from differences between the rates of magma discharge at the surface (MDR) and the rates of magma supply from the magma chamber (MSR). If MSR<MDR, the fragmentation surface rapidly migrates downward in the conduit, until fragmentation ceases and the eruption stops. MSR is strongly dependent on magma properties and conduit diameter. Conditions which favor a decrease of MSR are viscosity increase of magma during degassing and groundmass crystallization, as well as plating of the walls of the conduit crystallizing magma, thus decreasing its diameter.

C. Deposits

The products of plinian eruptions consist of pumice lapilli and ash forming pyroclastic fall and flow deposits. Lapilli fall deposits form thick (up to several meters) blankets over hundreds of square kilometers, while thinner (several centimeters thick) ash layers can be dispersed over thousands of square kilometers. These are well preserved in the marine sedimentary successions, and frequently provide very important chronostratigraphic markers for the correlation and absolute age determination of these sequences.

Plinian falls form sheet-like deposits generally dispersed by the wind field into elliptical fans. Only a few known eruptions have occurred under no-wind conditions, giving deposits with a subcircular distribution. Pumice fall beds are massively to crudely stratified, the stratification being always related to variations in the grain size of the deposit. Pumice vesicularity is very high and it often shows vertical variations within a deposit.

Subplinian deposits generally reveal a stronger stratification into beds of contrasting grain size and dispersal, which is often asymmetrical. Distribution of subplinian ejecta is more susceptible to external parameters such as vent geometry and low level winds. The juvenile fragments show highly variable density even within the same stratigraphic level.

The thickness of proximal to medial plinian fall deposits follows a general exponential decrease with distance from the vent (Fig. 2), often characterized by an overthickening in the most proximal areas related to the fall of ballistic material and increased sedimentation from the outer margins of the convective plume. Detailed mapping of some recent plinian fall deposits reveals that the thickness decrease with distance is well described as three line segments following at least three different exponential or power laws, valid respectively for the proximal, medial, and distal deposits (Fig. 2), as a result of different settling laws involving fragments with different size. The grain size of the deposits decreases with distance from the vent. This is particularly evident when looking at the maximum dimensions of lithic clasts rather than pumice fragments (Fig. 3). Grain-size polymodality can be related to the different terminal settling velocity of fragments with variable density (e.g., pumice vs foreign lithics), or to an efficient separation of crystals from glass during fragmentation, which results in the generation of an important population of free crystals (Fig. 4). Distal deposits consist of massive fine ash layers. The products of some recent eruptions reveals the presence of a secondary maximum (for thickness of a few millimeters) related to an increased rate of ash deposition due to aggregation and

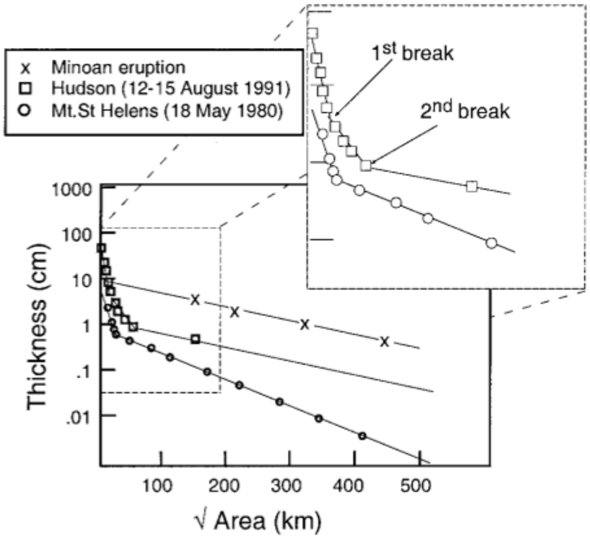

FIGURE 2 Variation of thickness with distance (represented by the square root of the area enclosed in the isopach of corresponding thickness). Each segment represents an exponential decay. The deposits of the August 1991 plinian eruption of Hudson volcano (Chile) clearly show three different segments, related to differences in the settling velocity of particles with distance [data from C. Bonadonna, G. G. J. Ernst, and R. S. J. Sparks (1998). Thickness variation and volume estimates of tephra fall deposits: The importance of particle Reynolds number. *J. Volcanol. Geotherm. Res.* **81,** 173–187].

subsequent increase of mean grain size of the falling particles.

Plinian and subplinian eruptions have been generally classified on the basis of their fall deposits. In the classical Walker classification scheme, the dispersal and fragmentation of the deposits (measured as two indexes D, area of the isopach enclosing the deposit with a thickness higher than 1% of the maximum thickness, and F, percentage by weight of the deposit finer than 1 mm at a distance along the dispersal axis where thickness is 10% of the maximum thickness) are used (Fig. 5). In this scheme, plinian and subplinian eruptions differ in D by two to three orders of magnitude. Recently, a new classification diagram for explosive eruptions was introduced by David Pyle based only on dispersal features of the fall deposits (Fig. 5). The thickness half-distance (b_t, the distance at which thickness decays to half of its maximum value) and clast half-distance (b_c, the distance at which the value of the maximum clast diameter becomes half of its maximum value) appear to have a more stringent physical significance than D and F.

Using stratigraphy, plinian fall deposits can be classified as simple, stratified and multiple. Simple plinian deposits result from a continuous accumulation of pyroclasts from columns, which remain stable for several hours. A massive, generally inversely graded, deposit forms. Stratified plinian deposits result from a single, fluctuating unstable column, sometimes generating pyroclastic flows and surges, which interrupt the fall sequence. In the absence of PDC deposits, the fall sequence contains layers defined by fluctuating grain size that maintain a similar dispersal, testifying to the presence of similar atmospheric conditions during their emplacement. Multiple plinian deposits contain fall beds with different grain size, lithology, and, at times, dispersal. They result from distinct plumes formed at intervals of days or months. Time-breaks are marked by ash partings. The features of the fall layers suggest a brief duration (from several minutes to few hours) of each single eruptive pulse, implying that the feeding system was unable to reach and maintain steady conditions.

In many plinian and subplinian eruptions PDC deposits are frequently interbedded with fall deposits. They result from pyroclastic flows generated by the collapse (partial or total) of the eruptive column. In many cases, a transition from fall, to surge to flow deposits has been recognized; this sequence, however, cannot be generalized, as shown by the following examples (Sections II and III). Asymmetric (or lateral) collapse from the column margins can occur when plume density is very close to atmospheric density. Such a collapse can enhance the buoyancy of the convective part of the column, enabling stronger convection. The deposits related to such partial collapses are interbedded within the fall deposit, with no signs of interruption.

The effect of the sudden release of huge volumes of magma can alter the geometry of the plumbing system, destabilize the shallow reservoir, and induce structural collapse. Such a situation frequently increases the eruption intensity, inducing contact between phreatic fluids and magma, as well as explosive decompression of the hydrothermal system associated with the shallow reservoir. Phreatomagmatic and lithic-rich deposits frequently interbedded in plinian sequences are often generated during these phases.

II. DIRECT OBSERVATIONS OF PLINIAN ERUPTIONS

Plinian eruptions have been observed and described in the last decades. These observations have enormously

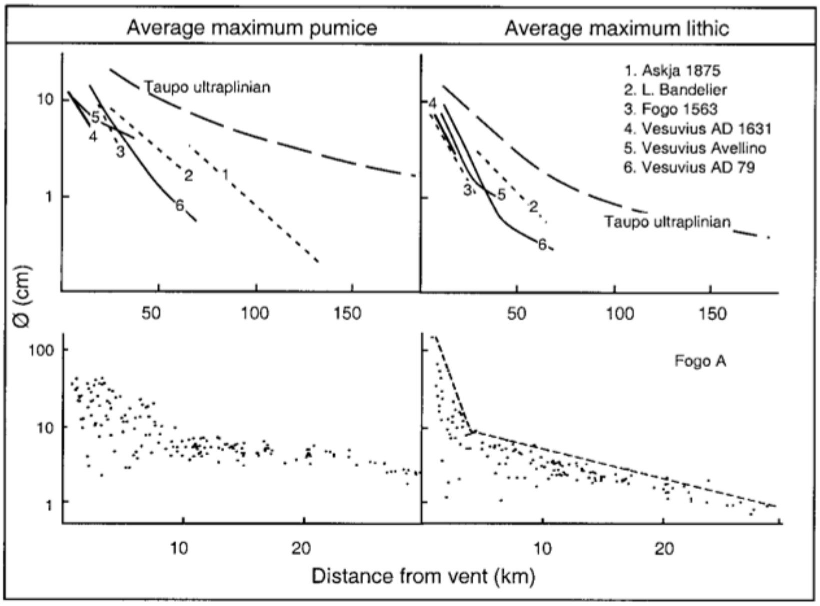

FIGURE 3 Variation with distance of the size of maximum pumice and lithic clasts for different plinian and subplinian eruptions (the ultraplinian eruption of Taupo is reported for comparison). For the Fogo A eruption of Fogo volcano, Azores, the available data show the rather wide variability in this type of data [modified from G. P. L. Walker, and R. Croasdale (1970). Two plinian-type eruptions in the Azores. *J. Geol. Soc. London* **127,** 17–55].

increased and accelerated the knowledge and understanding of eruptive processes. The Mt. St. Helens eruption of May 18, 1980, can be probably considered the trigger of this process. Although it represents a medium- to small-scale event when compared with other historical plinian eruptions it preserves all the major characteristic features of these eruptions.

The other example presented here deals with the eruption crisis of El Chichon volcano (Mexico), in 1982. It can probably be considered as an event transitional between plinian and subplinian eruptions. Its peculiarity lays in the uncommon time evolution, characterized by three major eruptive pulses that occurred over a period of several days, in contrast with the general behavior of the major plinian eruptions, which exhaust their energy in the space of a few hours.

A. May 18, 1980, Eruption of Mount St. Helens

The first plinian eruption entirely observed and described occurred at Mount St. Helens (United States) on May 18, 1980. The main phase of the eruption that was followed for several months by minor subplinian events culminating with dome extrusion phases was preceded by a strong bulging of the north flank of the mountain related to cryptodome intrusion. On May 18, following a magnitude 5+ earthquake, the northern flank of the mountain failed, forming a large debris avalanche. Seconds after the first block slid, a directed blast devastated 600 km^2 and ash rising from the directed blast formed a convective cloud that rose to more than 30 km.

The lateral blast was followed by 9 hours of continuous magma discharge, generating an oscillating plinian column (Fig. 6) in response to flow rate variations. Four main phases have been distinguished in the climactic eruption, which are reflected in the stratigraphy of the fall deposit. The vertical plinian column required around 30 minutes to form and was preceded by a slowly growing cloud, depositing the so-called "preplinian" pumice fall and some pyroclastic flows.

During the first hour-long phase of the plinian eruption the column grew to an altitude of 16 km, forming an umbrella-shaped top near the tropopause that was subsequently dispersed by prevailing westerly winds. Some minor pyroclastic flows were observed spilling over the crater, but they did not interrupt the column.

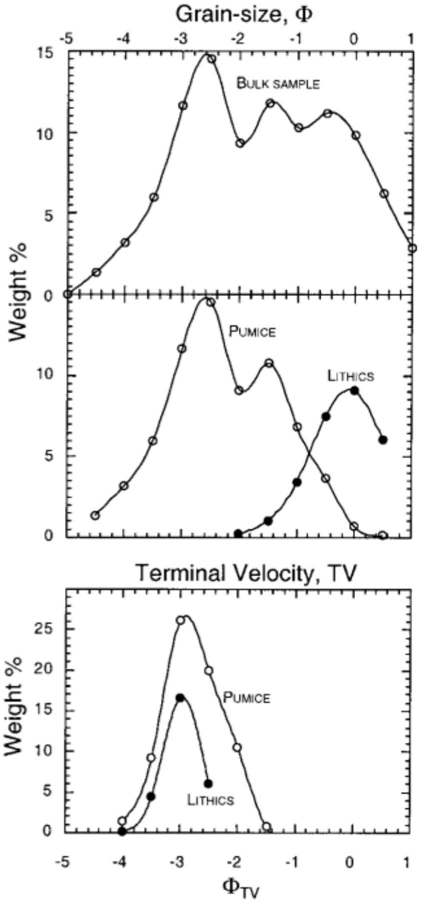

FIGURE 4 Grain-size of plinian deposits is often polymodal (upper). Such polymodality can be related to the presence of fragments with different density (middle), and is reduced by considering settling velocity of the clasts rather than their size (bottom).

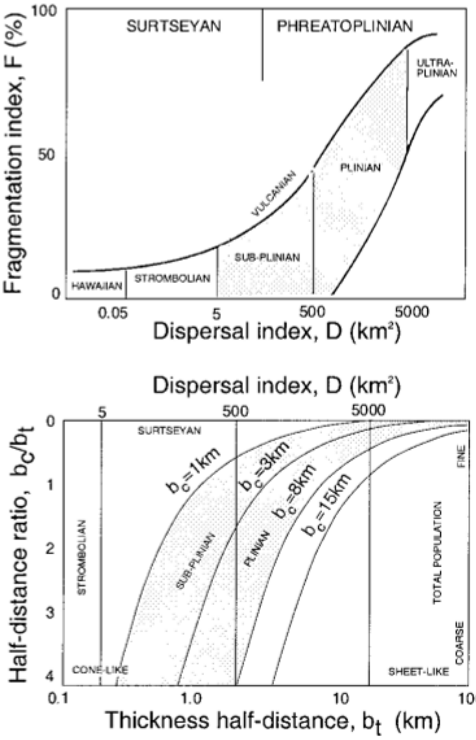

FIGURE 5 The two diagrams commonly used for the classification of explosive eruptions based on characteristics of fall deposits [modified from G. P. L. Walker (1973). Explosive volcanic eruptions—A new classification scheme. *Geol. Rundsch.* **62,** 431–446, and D. M. Pyle (1989)].

During the last 30 minutes of this phase, the column appeared darker, with distinctive feathered lower edges from which large particles fell from the ascending convective cells, indicative of decreased convective power. The resulting proximal deposits consist of a lower, pumice rich, normally graded lapilli layer capped by a thinner, inversely graded lithic ash layer, suggesting that the conduit–crater system was enlarging and the minor pyroclastic flows followed by the darker column were related to lithic loading in the eruptive mixture.

For the next 75 minutes the plinian column contained lighter colored billowing cell structures, increasing its height up to around 18 km. The inversely graded pumice lapilli layer deposited during this phase accounts for the thickest and coarsest portion of the entire fall deposit. The pumice component in tephra from the entire morning almost completely consists of highly vesicular, white, mafic dacitic pumice. Denser, gray clasts of silicic andesite are very rare, scattered in the deposit of the more intense, late phase.

For the next 4 hours the eruption progressed toward the formation of a collapsing fountain, which fed numerous pyroclastic flows. During this period, however, a convective cloud rivaling in height the plinian cloud was continuously present, fed by elutriation of ash from the pyroclastic flows and clast release from the fountain. This convective cloud was responsible for the deposition of two thin ash and lapilli layers in the proximal tephra sequence. Pyroclastic flow generation was interrupted, and a strong central column was reestablished for 90 min, rising up to 19 km. Another lapilli pumice layer corresponds to this phase. It shows a dispersal displaced slightly southward with respect to the underlying tephra. Mafic dacitic white pumice and up to 25 vol% of gray silicic andesitic dense scoria, together with abundant lithic fragments, form the deposit. The column then rapidly decreased its height down to 6 km and for the

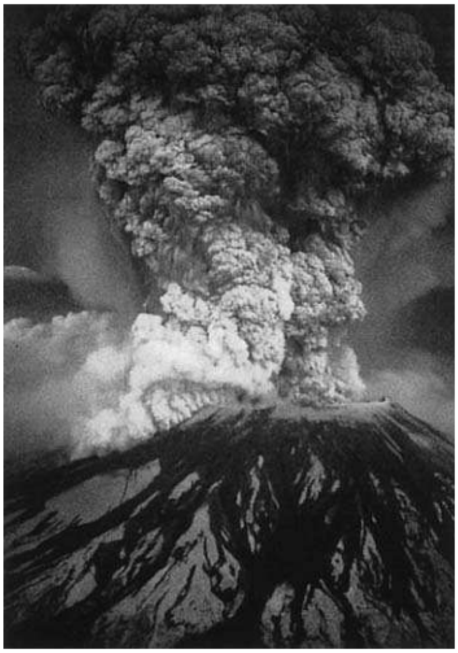

FIGURE 6 View of the plinian plume of the May 18, 1980, at Mt. St. Helens [source USGS/Cascade Volcano Observatory].

final 90 minute phase minor pyroclastic flows were generated with the continuous presence of a low altitude, co-ignimbrite ash cloud.

On the basis of clast size data and volume estimates, the pyroclastic flow phase probably corresponds to the highest peak in MDR, estimated at 4.4 × 10^7 kg/s. This value is an average over 4 hours, corresponding to the entire central phase of the eruption, during which the activity involved mostly pyroclastic flow generation. The phase of maximum flow rate corresponds to a maximum in magma mixing as recorded by the whole composition of pumice, and also in the largest amount of scoria of silicic andesite. This can be interpreted in terms of maximum depth of withdrawal in a vertically stratified reservoir during the phases of maximum MDR, with contemporaneous extraction of magma from different depths in the chamber.

B. The 1982 Eruption of El Chichon, Mexico

El Chichon Volcano (Mexico) suddenly awakened in the spring of 1982 after 550 years dormancy. One month of intense seismic activity preceded the first explosive event and seismic activity shifted from 5 to 2 km depth in the 2 days before the eruption, increasing in frequency from 25 events/day up to 60 events/hour. The eruption lasted from March 29 to April 4, with 10 explosive episodes. Only six episodes had a clear seismic signature and only four of these left major deposits. The seismic activity that followed the eruption lasted until April 16, rapidly decreased in frequency with time, and was very deep, between 12 and 20 km under the volcano.

Of the four main phases that deposited tephra layers, three had a plinian dispersal (March 29, 05.32 UT; April 4, 01.35 UT and 11.22 UT). All of the plinian plumes penetrated the tropopause and were detected by satellite. The duration of each event (respectively 5, 4, and 7 hours) was estimated on this basis. Each event was characterized by a plume dispersal in two main directions, related to opposite stratospheric and tropospheric winds. The resulting isopach and isopleth maps were asymmetrical in shape. Estimation of the column heights from field data gives peak (>25 km) and mean values (respectively 20, 24, and 22 km for the three main phases) in agreement with the satellite observations, corresponding to averaged MDR of 3.5 to 6 × 10^7 kg/s.

The three plinian phases left fall deposits of trachyandesitic pumice whose normal grading suggests that the MDR reached a peak at the onset of the eruption and successively decreased. The deposits are not very thick; the maximum recorded thickness of tephra from the first phase (A1) is 26 cm, while the deposits from the April 4 events (B and C) are always thinner. The A layer thins out very quickly. The estimated volumes of the three events are similar (respectively 0.30, 0.39, and 0.40 km^3 Dense Rock Equivalent). Another episode occurred on April 3, dispersing a thin layer of volcanic coarse and fine ash. It was related to a small eruption generating a plume that reached the tropopause.

Phreatic to phreatomagmatic activity punctuated the eruptive crisis. Repeated small explosions that occurred after the first event of March 29 are interpreted as related to the interaction of external water with hot rocks and/or magma in the vent area. The larger explosion on April 3 involved (newly arrived) magma and marked the transition to the plinian activity of the following day. The 01.35 UT phase of April 4 started with the generation of debris flows, pyroclastic flows, and surge clouds, inducing the complete removal of the remnants of the ancient summit dome. These phenomena were probably related to phreatomagmatic explosions, which cleared the conduit, resulting in a transition to the plinian phase. Tephra from this phase (layer B) was characterized by a high lithic content throughout its duration, indicating a continuous erosion of the crater–conduit system. The last plinian phase, responsible for the deposition of layer

C, was again followed by phreatomagmatic pyroclastic surges.

This eruption is useful in understanding processes governing eruptive style transitions during plinian eruptions. The occurrence of three different sustained plinian columns was in this case probably related to the failure of the system to form a stable conduit–vent system. Water gained access to the plumbing system, resulting in a sequence of phreatomagmatic explosions. The largest eruption, which occurred on April 4, 01.35 UT, was unusual. A transition from fall to surge to flow deposits, generally considered a classical sequence in plinian eruptions, was not seen. The first plinian phase is in fact preceded by phreatomagmatic activity and early emplacement of PDC, while the following plinian phase shows a smooth decrease of MDR after an initial peak. Moreover, final fountaining of the column produced pyroclastic flows and surges unrelated to an MDR increase or to a drastic decrease of magma volatile content, but probably caused by a pressure reduction in the magma chamber.

The El Chichon event was the first eruption of the century with well-documented effects on climate. These effects were significantly stronger than those of the similarly sized Mount St. Helens eruption for two reasons: the column deeply penetrated the tropopause, and the tephra contained up to 2 wt% sulfates. The eruption column injected large quantities of sulfur-rich aerosol, mainly derived from SO_2, into the stratosphere. The cloud rapidly drifted around the world, at an average westerly speed of about 20 m/s, returning to Mexico after 22 days. The total amount of SO_2 released was estimated at 3.3×10^9 kg. The SO_2 was converted into H_2SO_4 within the 3 months following the eruption. The climatic effects were a sudden warming of the equatorial stratosphere of about 4°C, due to the absorption of solar radiation by the H_2SO_4 aerosol, and a small decrease of surface temperature (0.2°C) in the Northern Hemisphere in June 1982.

III. THE INVERSE PROBLEM: FROM DEPOSITS TO THE ERUPTION

A large amount of information about plinian and subplinian eruptions can be derived from the study of the pyroclastic deposits. The recent development of theoretical models on column behavior and clast dispersal enables the reconstruction of the eruption dynamics from the accurate study of the pyroclastic deposits and, where available, from direct observations. In this section, some examples from Somma–Vesuvius will be reported, using field, compositional, and observational data to reconstruct a likely sequence of events for each eruption.

Somma–Vesuvius is a K-alkaline quaternary stratovolcano of southern Italy, with a somma caldera (Mount Somma) and an inner cone (Vesuvius). During the past 18 ka several explosive eruptions of different magnitude, including at least four plinian and six subplinian outbursts, have occurred. All the main eruptions have both plinian phases and important phases dominated by magma–water interaction, which always involves fluids hosted in the deep Mesozoic carbonate formations or in the shallow volcanic sequences. The detailed stratigraphy of Somma–Vesuvius volcanic successions is an example of how to invert volcanological data from the study of the deposits (and, whenever possible, from eyewitnesses accounts) to reconstruct the sequence of events which characterized the main eruptions and to establish links between preeruption compositional gradients in the magma chamber and variations in the eruption dynamics. Three examples of a relatively complete spectrum from plinian to subplinian eruptions from Vesuvius (Fig. 7) will be discussed.

A. Plinian Eruptions

The deposits of the four main plinian eruptions of Vesuvius all reflect a complex sequence of events, with opening phases immediately followed by the generation of high, sustained, columns and their partial or total collapse (plinian phase) and final phreatomagmatic phases, dominated by flow and surge emplacement following caldera collapse. More than 70% of the total volume of products is ejected during the plinian phase of each eruption. The products reflect the tapping of shallow, compositionally stratified, magma chambers. Phreatomagmatic phases that follow caldera collapse, due to the large emptying of the reservoir, are likely related to the entrance of external water into the failing magma chamber rather than to interaction during magma ascent in the conduit. The involvement of hydrothermal fluids from a thermometamorphic halo of the magma chamber is sometimes suggested by the presence of altered lithics and their fluid inclusions.

1. 79 A.D. Pompeii Eruption

On 24th August of 79 A.D. Vesuvius awakened after some hundred years of dormancy, suddenly interrupting the life of flourishing Roman towns such as Pompeii,

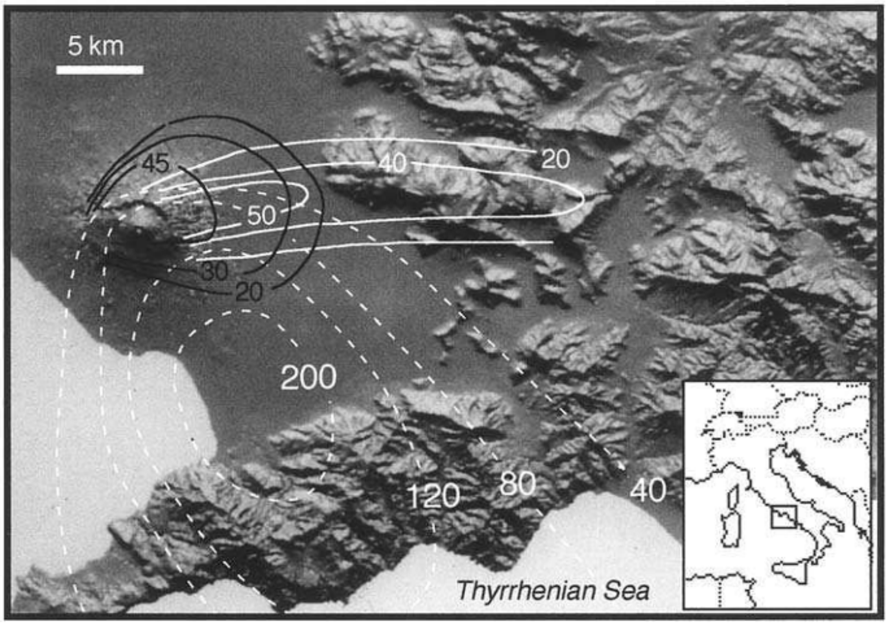

FIGURE 7 Isopachs (in cm) of the Vesuvius eruptions of 79 A.D. (white, dashed line), 1631 A.D. (white, solid line), and AP2 (black line). Note the very different scale of the three deposits [Digital Elevation Model by permission of M. T. Pareschi, CNR-CGSDA, Pisa].

Stabiae, and Herculaneum. The eruption was preceded by only modest seismic activity, except for a strong volcano-tectonic earthquake that had occurred 17 years before. According to the letters of Pliny the Younger, the paroxysmal phase lasted no longer than 20 hours, although there is uncertainty about the duration of the eruption's final stages. The deposits record a complex eruptive sequence (Fig. 8), with a thick blanket of pyroclastic fall and flow products covering the whole volcano and a wide area SSE from it (Fig. 7). Three main phases can be distinguished.

Phreatomagmatic opening phase. The basal bed (EU1) of the 79 A.D. deposits is a whitish-gray, fining upward, pisolitic, ash fall deposit, dispersed eastward by low-level winds, and by surge units whose dispersal is strongly controlled by the preexisting caldera walls. The fall bed can be recognized up to 20 km downwind as a thin blanket with a maximum thickness of only 15 cm. The strong fragmentation of the juvenile fragments, the high foreign lithic content and its wet depositional features suggest this bed records a first, transient phreatomagmatic phase, with an oscillating, low plume.

The plinian column. During this phase two composite eruption units (EU2 and EU3) were deposited (Fig. 9). They are formed by a thick sequence of white and gray pumice fall deposits, interrupted by at least five ash flow units. The white pumice of EU2 forms a SSE dispersal fan, with a maximum thickness of 150 cm at Pompeii. It shows a symmetric, reverse to normal grading (maximum grain size at 2/3 of the bed). In some proximal sites it is topped by a thin ash flow layer marking a partial destabilization of the eruptive column just at the transition between the two different magmas. The gray pumice of EU3 has a SE dispersal, with a slight counterclockwise rotation with respect to the EU2 axis. It forms an inversely graded layer (the lower 1/4 of the sequence) followed by a slow decrease of the grain size with minor oscillations.

In the proximal area the accumulation rate of the fall deposits can be estimated at 10–15 cm/hour. The lithic isopleths can be used to calculate the variation of the height of the column and magma discharge with time and the average wind velocity at the tropopause (around 30 m/s). White pumice shows a progressive increase of MDR (up to 8×10^7 kg/s), resulting in the continuous rise of a convective column up to 26 km, followed by a slight decrease prior to the compositional shift to gray pumice. Following the shift in magma composition, a new, rapid increase of MDR (to 1.5×10^8 kg/s) occurred, with the growth of a column up to 32 km. During the next 9 hours the column declined to about 17 km (MDR of 1×10^7 kg/s).

In the southern proximal sites, the gray pumice fall contains at least four PDC units, resulting from inter-

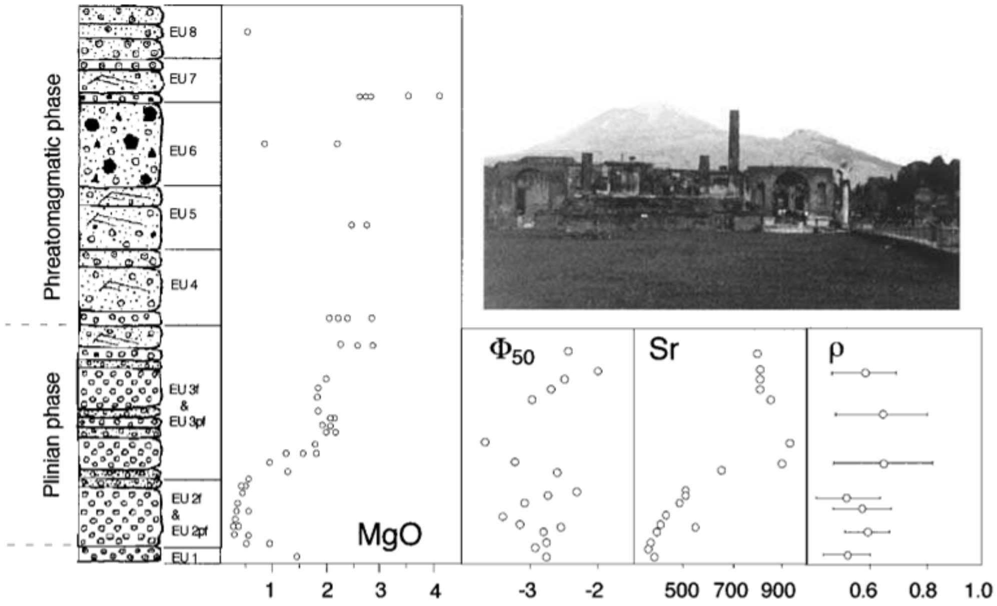

FIGURE 8 Reconstructed stratigraphy of 79 A.D. eruption of Vesuvius (in the photo Vesuvius and Mt. Somma as seen from Pompeii excavations). A nice covariation of compositional parameters (in this example MgO, wt%, and Sr, ppm) with mean grain-size of the fall deposit (Φ_{50}) is observed. A large density contrast (ρ, g/cm^3) occurs between white and gray pumice.

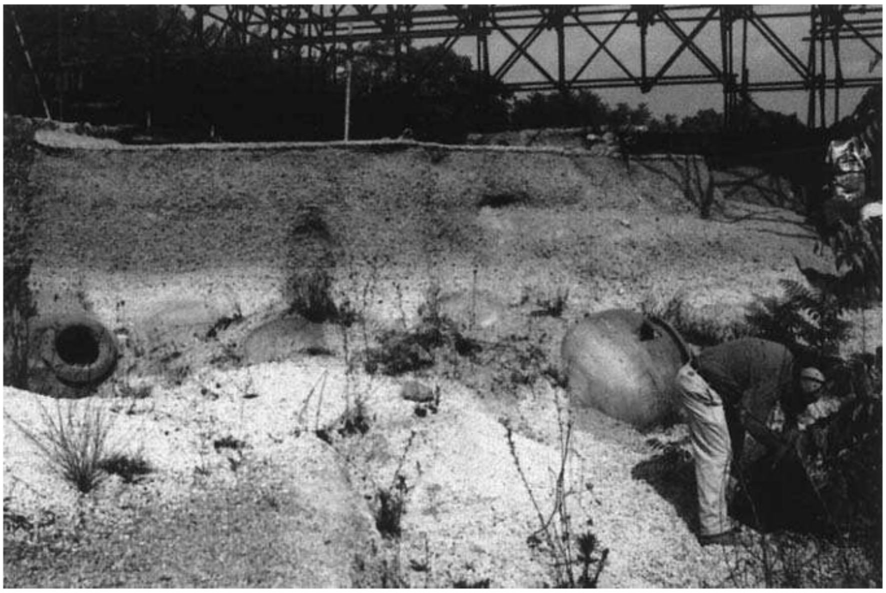

FIGURE 9 The 79 A.D. fall deposit at Pompeii, topped by thin ash flow deposits. The transition between white (EU2) and gray (EU3) pumice is evident over the back of the figure.

mittent, partial collapses of the eruptive column. In the northern and western sectors, not covered by the fall deposits, these units laterally pass to pumice and ash flow deposits that are strongly topographically controlled. The fall sequence is closed by thick ignimbrites, which rapidly thin at a few kilometers from the volcano. They record the final collapse of the sustained column.

Caldera collapse and final phreatomagmatic activity. During this phase several eruption units were emplaced (EU4 to 8) by phreatomagmatic explosions. Such units consist of PDC deposits with rare, thin, lithic-rich, fall interbeds. They are characterized by a high lithic content, with abundant xenoliths from deep-seated rocks. The ubiquitous presence of highly fragmented limestones suggests that magma–water interaction involved the deep, regional aquifer. Marbles and skarns from the external carapace of the magma chamber suggest that the interaction occurred at deep levels after the destabilization of the magma chamber. The lithic content increases upward, where pisolite-bearing ash beds and vesiculated tuffs are prevalent, suggesting that the phreatomagmatic character of the deposits increases from the base to the top of the sequence.

Lithological and sedimentary features of the lithic-rich bed EU4 suggest derivation from the emplacement of a widespread, turbulent PDC, with a radial distribution around the vent, reaching distances of at least 15 km in the southern plain, which was preceded by a short-lived phreatomagmatic convective column. The strong earthquake and the dark cloud witnessed by Pliny the Younger on the morning of 25 August could correspond to this event. This unit represents the starting of a "caldera-forming phase" in the eruption, culminating in the paroxysmal collapse of the feeding system recorded by the deposits of EU6, on the SE slopes of the volcano. Their areal distribution and lithic type and content suggest eruption from the caldera ring fracture. Protracted withdrawal from the magma chamber, favored by magma–water interaction, led to the tapping of the more mafic crystal-rich melt during the emission of EU7 pyroclastic flow deposits. The waning stages of the eruption are represented by wet, phreatomagmatic, ash-rich pyroclastic flows (EU8).

Geochemical features of the products. The plinian phase is represented by a compositionally zoned pumice fall deposit, consisting of white, phonolitic, and gray, tephriphonolitic pumice. EU8 shows a sharp compositional reversal toward the more salic compositions that characterize the initial phase of the eruption (Fig. 8).

The geochemistry of the erupted products has been interpreted in terms of important syneruptive mixing processes. All the products result from admixing of three end members: a salic end member (the white phonolitic pumice), a cumulate end member supplying mafic crystals (mainly diopside and phlogopite), and a phonotephritic mafic end member, never erupted without being mixed. This situation suggests a magma chamber stratigraphy characterized by a lower, homogeneous, convective phonotephritic magma overlain by a stratified, phonolitic liquid.

A nice relationship exists between composition of tephra erupted during the plinian phase and median grain-size of the deposits (a proxy to illustrate MDR variations), suggesting the tapping of different portions of the magma chamber by varying the MDR, with variable proportions of mixing between the different liquids in the reservoir.

During the white pumice fall, the increase in MDR extracted progressively deeper magma, "reversing" the compositional gradient in the upper portion of the chamber. The first destabilization of the column occurred as a consequence of the onset of an extensive mixing between phonolitic and phonotephritic magmas, which produced an important change in the rheological properties of the erupting liquid. By this time the products had drastically changed composition (mixed gray pumice).

During the gray pumice fall a progressive transition from physical mingling to complete chemical hybridization occurred. Most of the mixing occurred inside the magma chamber. The MDR fluctuated, extracting mixed magma from different depths in the chamber. Initially, the amount of white magma physically mixed in the gray pumice decreased with increasing MDR, but, after a few hours, the mixing inside the chamber went to completion and the erupted products consisted of truly hybrid pumices regardless of MDR and depth of withdrawal. As the eruption proceeded caldera collapse occurred. The structural modifications and the massive influx of external fluids, gases, and water into the plumbing system changed the eruption dynamics, and magma extracted during the phreatomagmatic phase was relatively heterogeneous due to the highly variable content of cumulate crystals from the collapsing walls as well as to the extraction of white magma pockets left untapped and not mixed roofward.

B. Subplinian Eruptions

Several eruptions of Vesuvius had magnitudes in the range 0.5–0.05 km^3, and most of the mass was ejected during phases of low intensity (MDR around 10^6 kg/s), sustained column activity. They are therefore referred to as subplinian. The deposits of each eruption show a range of features varying with eruptive magnitude. The largest events show both fall and flow deposits. Fall deposits are variably stratified, ranging from massive beds with minor grain-size oscillations to strongly stratified alternations of lapilli and ash layers, which reveal a recurrent unsteadiness in the magma discharge. Pyroclastic surges and phreatomagmatic, lithic-rich pyroclastic flows occur frequently during these major events. PDC are not common in the minor subplinian eruptions. The phreatomagmatic phases of subplinian eruptions generally occur during the final stages of the sustained column. The phenomenon is a "classical" magma–water interaction in the conduit, triggered by pressure drops in the ascending mixture, in contrast with the catastrophic phases of caldera collapse that provoke magma–water interaction during plinian eruptions.

A clear distinction between plinian and subplinian deposits on the basis of their dispersal and fragmentation indices is not simple at Vesuvius (and probably anywhere). Two events have been selected to show the variability of the dynamics of Vesuvius subplinian eruptions, 1631 A.D. and AP2, which occurred around 3200 years ago. They well represent the end members of this variability.

1. 1631 A.D. Eruption

The biggest explosive eruption of the past 500 years at Vesuvius occurred in 1631 A.D., claiming more than 3000 lives and heavily damaging a large area around the volcano. The eruption started on December 16, with 30 hours of heavily destructive activity. The eruption continued to the end of December with intermittent moderate steam blasts. The depositional sequence consists of five main units. These have been related to distinct phases of the eruption.

Opening phase. Shortly after a strong earthquake, a fracture opened in the WSW sector of the cone with the violent discharge of gas, ash, and incandescent material, forming a progressively rising cloud. The deposits consist of a few-centimeters-thick, inversely graded, crystal-rich, ash to lapilli fall layer. The very low content of fine ash suggests its efficient removal by wind, while the fine-grained, inversely graded deposit indicates settling from a low yet progressively rising plume. The fine grain size and the abundance of loose crystals and lithics suggest the involvement of external water.

Sustained column phase. The vent migrated to the central crater and a sustained eruption column fully developed. It remained stable for 8 hours, causing significant downwind tephra fall. The deposits consist of well-sorted, subangular scoriaceous lapilli, with minor lithics and crystals, forming an elliptical fall blanket. The eastward, strongly elongated shape of the deposit (Fig. 7) indicates strong winds driving the dispersion of the cloud, as well as the relatively weakness of the plume. The subplinian fall layer is marked by a sharp darkening upward of juvenile clasts, reflecting a compositional variation from lighter tephriphonolite to darker phonotephrite. The fall deposit is variably graded, reflecting a slight counterclockwise rotation of the dispersal axis of the dark fall in respect to the light one. The crosswind range of the maximum lithic isopleth expands from light to dark fall, suggesting an increase of the column height, from 13–16 to 19–21 km, respectively. The variations in column height reflect variations in MDR from 1 to 1.5 and 8 to 9 × 10^7 kg/s for the light and dark fall phases, respectively.

Intermediate pulsating "vulcanian" phase. A series of seismic shocks and violent detonations characterized the night between the 16th and the 17th and the morning of 17th, with short resumption of lapilli and ash fall. Heavy rains induced lahars from the northern slopes of Monte Somma. The fall deposits have very limited distribution and small volume. On the Somma rim they consist of poorly sorted block, lapilli, and ash breccia (50 cm thick) very rich in lithic material. The breccia is remarkably indurated, suggesting that ash was deposited as wet or muddy. It has been interpreted as a compound fall layer from several discrete explosions of variable energy, involving partly degassed magma as well as external water.

Phreatomagmatic phase. According to a recent consruction, at 10–11 am of December 17 an enormous mass of ash, gas, and stones was spewed from the central crater and poured down the Vesuvius cone, being confined inside the Somma caldera. At the same time a violent, 5 minute-long, earthquake shook the volcano and was felt as far away as Naples. Descending toward the sea the glowing cloud spread and divided into several lobes (Fig. 10). This activity had possibly 2 hours duration and coincided with the structural collapse of the cone (470 m of lowering). It generated massive, valley filling, lithic-rich, ignimbrite deposits and thin pyroclastic surge deposits draping the upper slopes of the cone as well as part of the Somma rim.

On the afternoon of December 17, light clouds slowly rose from the crater and a muddy, pisolite-bearing, fine ash fall started and continued intermittently for several days. Condensation of water on ash particles produced persistent torrential rainfalls, triggering a series of la-

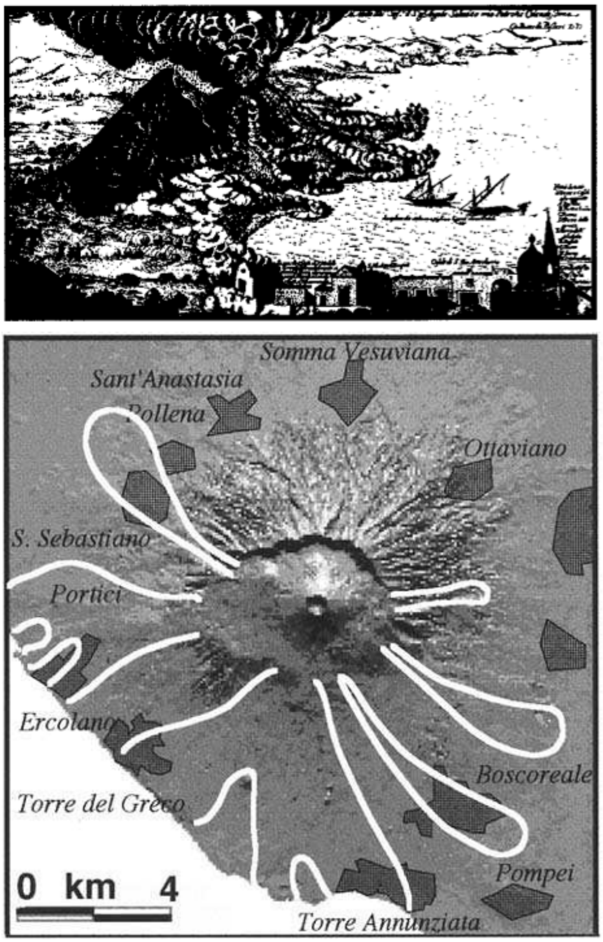

FIGURE 10 The pyroclastic flow deposits of the phreatomagmatic phase of 1631 A.D. eruption of Vesuvius. The distribution of the different flow lobes was strongly controlled by the preexisting caldera wall, as also suggested by a contemporaneous engraving (upper) showing a view of the eruption from Naples [modified from Rosi *et al.* (1993)].

hars, hyperconcentrated flows rushing down the volcano flanks and the mountains ENE of Vesuvius. Extensive flooding occurred.

This reconstruction of the 1631 eruption is not unanimously accepted. The main controversies concern the timing of pyroclastic flow emplacement and their origin from column collapse, and the existence of an effusive phase of the eruption on December 17–18.

2. *AP2 Eruption*

The period between 3500 years BP and 79 A.D. was characterized by several minor events ranging in size from subplinian (AP1, AP2) to strombolian–vulcanian (AP3, AP4, AP5).

The stratigraphic sequence of AP2 deposits is complex (Fig. 11), and the deposits are dispersed in a subcircular, asymmetrical fan, off-axis from the present crater (Fig. 7). A basal fall bed of phonolitic pumice (Unit 1) is followed by fall ash and minor surge deposits (Unit 2) limited to the more proximal areas. Three beds of massive to thinly stratified, tephriphonolitic fall lapilli with several ash interbeds form the upper layer (Unit 3). Sorting of these beds is poor, suggesting deposition from ash-rich eruptive columns and an important unsteadiness in the magma discharge. An increasing importance of magma–water interaction can be inferred by the increasing amount of altered lithics in the topmost portion of the deposits, closed by the pisolite-bearing ashes (Unit 4). The mean density of the juvenile fragments regularly increases toward the top of the sequence (Fig. 11). Vesicle size and shape vary from the strongly elongated, tubular vesicles of pumice from Unit 1, to the more irregular bubbles in scoria from Unit 3, to small, largely spaced, spherical bubbles of shards from Unit 4. All these features, and the ubiquitous presence of alteration on glassy surfaces of juvenile fragments from Units 3 and 4, suggest that fluctuations in the MDR, revealed by the stratigraphy of the deposits, were probably associated with important, conduit related, magma–water interaction processes.

We infer that a highly efficient syneruptive degassing, as suggested by the tubular shape of the bubbles, resulted in a brief, relatively high MDR (10^5–10^6 kg/s) phase, leading to the establishment of a sustained, quasi-steady subplinian column from which Unit 1 deposited. The alternation of lapilli and ash fall beds in Unit 3 is a typical feature of several subplinian deposits, which are generally interpreted as the repetitive rising of short-lived sustained columns, each depositing thin lapilli layers and ash.

The presence of dense and vesicular fragments in the same stratigraphic levels could suggest both enhanced fragmentation by magma–water interaction and a relatively high MDR associated with a low magma supply rate from the chamber, which induces a rapid downward migration of magma fragmentation toward zones with lower vesicularity. Both these processes could concur in determining the fragmentation mechanism. Rapid drawdown of magma could in fact induce a parallel decrease of pressure in the conduit, causing the contact between phreatic water and fragmenting magma. Involvement of water during such low MDR eruptions could have boosted the eruptive column, increasing the dispersal of the ejecta.

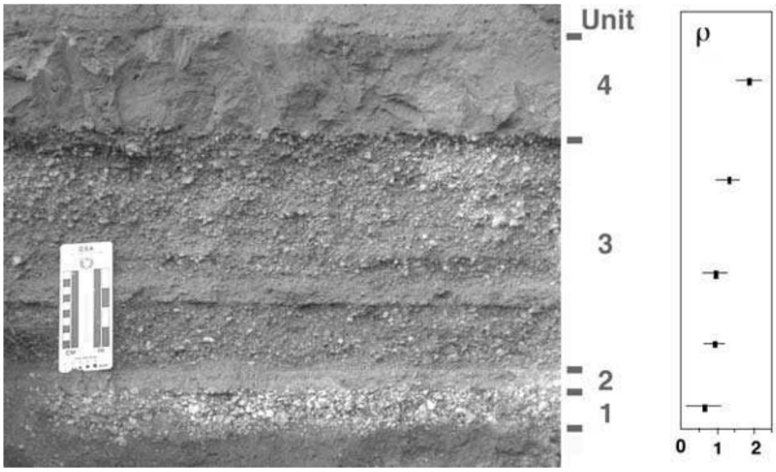

FIGURE 11 The deposits of AP2 eruption, showing the characteristic stratification related to grain-size oscillation. The continuous increase in density (ρ, g/cm^3) of the juvenile material is interpreted as an evidence for an increasing phreatomagmatic character of the eruption.

IV. DISCUSSION OF ERUPTION DYNAMICS

The reconstruction of past eruptions is important if we want to gain insights both into the eruptive process and preeruptive and syneruptive conditions, which determine the onset and progress of a large explosive eruption. All these topics can be tackled by studying the sedimentological, physical, and geochemical features of the products of past eruptions, with the important integration, when possible, of information from direct observations. The examples described above and the analytical data on their deposits offer a database of the different kinds of information we may obtain.

The comparison of plinian and subplinian eruption sequences also allows an understanding of the gradation existing between these two eruption styles. The examples from Vesuvius can help in this goal, because a quite complete gradation between these styles exists in the recent activity of this volcano.

A. Constraints from Physical and Geochemical Analyses of the Products

The sequence of events of an eruption is recorded by the stratigraphy of its deposits. The products related to a plinian eruption very often comprise both fall tephra and PDC deposits. Proximal stratigraphy is a fundamental tool for interpreting and reconstructing the dynamics of the eruption, especially when partial column collapses generate flow deposits which very rapidly thin out from the vent area. Marker beds help in subdividing the deposit in isochronous intervals. Maxima in grain size, lithic enriched layers, and ash interbeds can all represent isochronous markers in the field. The eruption sequence can be reconstructed from the study of the layers sandwiched between these markers.

This approach can trace variations in the dispersal of the fall deposits that are essentially due to column height and wind strength and direction, two factors that can change rapidly during a plinian eruption. Each layer can provide information about the variations of physical parameters such as MDR (from tracing the isopleth of maximum clasts) and exit velocity of the eruptive mixture (from the dispersal of the largest ballistics), the main parameters controlling the stability of the eruption column (Fig. 12). Geochemical and petrologic data of well-constrained eruptive sequences give additional information on eruption processes. Analyses of whole-rocks, melt inclusions, residual glass matrix, and the isotopic composition of separated minerals and matrix allow the reconstruction of the preeruptive condition of the magma chamber and the definition of syneruptive mixing processes and their relationship to eruption dynamics. This is particularly clear in fall deposits, where total grain size and maximum lithic size give insights on the temporal variation of MDR. In general, the compositional gradient observed in the products is not a simple reversal of the gradients in the magma chamber. During

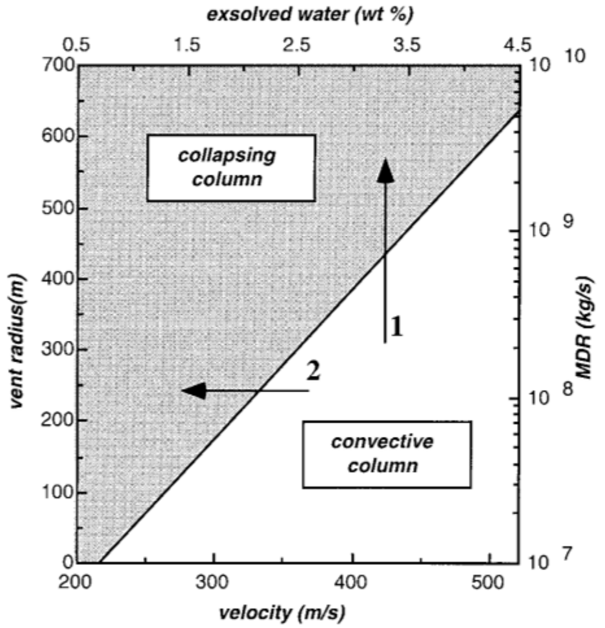

FIGURE 12 Stability of an eruption column (for a rhyolitic magma) as a function of magma discharge rate (MDR), vent radius, exit velocity of the erupting mixture and amount of exsolved water. Starting from convective conditions, column collapse can be achieved through MDR increase (path 1, as generally occurs during ignimbrite-forming eruptions), or by extraction of a magma progressively depleted in volatiles (path 2, generally followed by plinian eruptions fed by small-sized, compositionally zoned, magma chambers) [modified from Wilson *et al.,* (1980)].

an eruption, complex mixing depends on combinations of discharge rate, magma density and viscosity, and the shape of the magma chamber. All these factors affect the dynamics of the eruption column.

In low aspect ratio (height versus width) chambers, the depth of withdrawal is directly correlated to the fourth root of MDR. Larger MDR values correspond to deeper magma tapped in the chamber and, if the magma chamber is zoned, to the extraction of less evolved compositions. Numerical models define, for specific geometric and rheologic factors (size and shape of the magma reservoir, relative dimensions of the reservoir and the conduit system, magma density and viscosity) the evacuation isochrons, representing the "locus of points in two-dimensional space such that magma parcels along a given isochron arrive at the entrance of the volcanic conduit concurrently" (Fig. 13). In these models, magmas from different depths arrive simultaneously at the entrance of the volcanic conduit where the local mixing can be very efficient, due to the turbulent regime of flow. In a layered magma chamber, portions of magma with different composition are tapped simultaneously, causing syneruptive mixing. Depending on thickness and rheology, the extent of mixing is affected by the dynamics of the extraction. Sudden changes in MDR affect the composition of products and can result in compositional gaps even in the case of a gradually zoned reservoir. All these processes can occur within the draw-up cone and the conduit, but efficient syneruptive magma mixing can also occur inside the magma chamber, as demonstrated for the Pompeii eruption. Initially mingling produces banded pumices. Complete hybridization requires more time and is easier if mixing starts inside the magma chamber. Magma vesiculation following decompression of the reservoir determines the increase of instability of the interface separating different layers of a stratified magma chamber, and a sudden large-scale turbulent mixing which involves the entire volume of the magma chamber. These syneruptive processes are not only reflected in compositional variations of the erupted products, but also strongly affect the dynamics of the eruption.

Stratigraphic relationships and the sedimentological features of the flow deposits interbedded in the plinian fall sequence are important to discriminate partial collapses of the eruption column from fountaining phases. Large plinian eruptions often show a progressive shift from phases of sustained convective column to continuous fountaining, generating widespread ignimbrites. This behavior seems to fit a general model of an increasing flow rate achieved by a progressive enlarging of the conduit (Fig. 12). The Campanian Ignimbrite and several eruptions of Vico and Vulsini in central Italy are

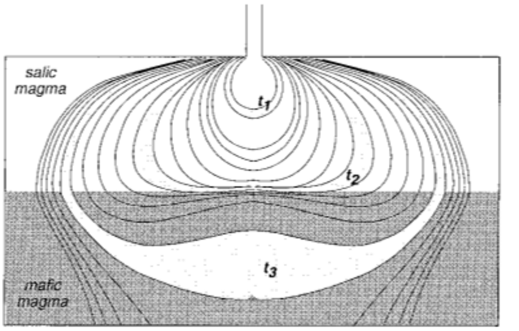

FIGURE 13 Extraction isochrons from a magma chamber as derived from numerical models. During an eruption, deeper portions of the magma chamber are progressively withdrawn; after t_2, an important syn-eruptive mixing occurs, with the involvement of increasing amounts of the lower (mafic) magma.

well known examples of this type of eruption. On the contrary, the extraction of magma from the small-volume, zoned reservoirs which characterize smaller plinian eruptions (for example those at Vesuvius) are characterized by magma progressively poorer in volatiles. This may result in the formation of a collapsing fountain at the end of the eruption, with the emplacement of small volume PDC.

Plinian eruptions of alkaline magmas often show a progression from magmatic to phreatomagmatic phases (good examples are the eruptions of Vesuvius and those at Laacher See, in West Germany). These eruptions largely evacuate magma chambers, leaving more mafic magma residuals. In this case, the collapse of the shallow reservoir provokes external fluid intervention. During these final phases, volatile-poorer mafic magma and pieces of the cumulate and metasomatic shell of the chamber are efficiently propelled out of the vent from the action of the residual magmatic gases and the phreatic fluids. The Vesuvius examples indicate that hydromagmatism involves the contact between water and primarily fragmented magma, suggesting that, in these final phases, magmatic gases also played an important role.

Plinian eruptions of calcalkaline composition generally end with dome emplacement, sometimes followed by dome disruption during minor subplinian or vulcanian activity (as in the case of the 1980 Mount St. Helens eruption). This may reflect the generally higher viscosity of calcalkaline magmas with respect to their alkaline counterparts and their generally lower total volatile content. Furthermore, syneruptive variations in the total volatile content or small differences in magma crystallinity, driven by syneruptive degassing, leave high viscosity residuals, favoring a slow rise of these evolved melts.

B. Gradation between Plinian and Subplinian Activity

Plinian and subplinian eruptions show a continuous gradation in MDR and magnitude. Eruption dynamics are dominated by the rise of convective plumes of varying duration and height (Table I). The variability presented by plinian fall deposits is mirrored in subplinian deposits. The two Vesuvius examples above can be described as simple (1631 A.D.) and multiple-stratified (AP2) fall. The 1631 A.D. represents the upper limit of subplinian events of Vesuvius. It could be also considered a small plinian event, with low MDR and erupted volume, marked by column collapses and phreatomagmatic events. On the contrary, the strongly stratified character of AP2 deposits is more similar to most subplinian deposits (e.g., eruptions of Mono Craters (California), to some eruptions of the Azores and to the 1980–1981 postclimactic eruptions of Mount St. Helens). These are typical of the subplinian events in which pulsatory behavior is the most distinguishing feature.

In subplinian eruptions, columns are weakly or discontinuously sustained, resulting in several eruptive pulses separated by periods of days to months, or in the unsteady but continuous feeding to a convective, oscillating column. Longer pauses between the different pulses characterize those eruptions with calcalkaline compositions. In such cases, each pulse is often associated with dome growth and destruction, revealing an important control of volatile content and rheology of magma. The frequent presence in these deposits of degassed clots of magma, with a high content of groundmass microlites, is generally interpreted as related to low rise velocity of viscous magma which determines conditions of open degassing.

Pulsating subplinian eruptions of Vesuvius are instead characterized by numerous instabilities in the MDR, without long pauses. This could reflect the different response of alkaline magmas to decompression during rise, where lower viscosity inhibits the formation of rigid plugs and domes and favors more rapid changes of the eruption style in response to differences between magma rise and magma discharge. The very different rheological properties of alkaline and calcalkaline magmas must be kept in mind when discussing subplinian eruption mechanisms.

SEE ALSO THE FOLLOWING ARTICLES

Calderas • Magmatic Fragmentation • Phreatomagmatic Fragmentation • Phreatoplinian Eruptions • Plumbing Systems • Pyroclastic Fall Deposits • Pyroclast Transport and Deposition

FURTHER READING

Carey, S. N., and Sigurdsson, H. (1986). The 1982 eruptions of El Chichon volcano, Mexico (2): Observations and numerical modeling of tephra-fall distribution. *Bull. Volcanol.* **48**, 127–141.

Carey, S. N., and Sigurdsson, H. (1987). Temporal variations in column height and magma discharge rate during the 79 A.D. eruption of Vesuvius. *Geol. Soc. Am. Bull.* **99,** 303–314.

Carey, S. N., and Sigurdsson, H. (1989). The intensity of plinian eruptions. *Bull. Volcanol.* **51,** 28–40.

Carey, S. N., Sigurdsson, H., Gardner, J. E., and Criswell, W. (1990). Variations in column height and magma discharge during the May 18, 1980 eruption of Mount St. Helens. *J. Volcanol. Geothermal Res.***43,** 99–112.

Cioni, R., Civetta, L., Marianelli, P., Metrich, N., Santacroce, R., and Sbrana, A. (1995). Compositional layering and syn-eruptive mixing of a periodically refilled shallow magma chamber: The A.D. 79 plinian eruption of Vesuvius. *J. Petrol.* **36,** 739–776.

Pyle, D. M. (1989). The thickness, volume and grainsize of tephra fall deposits. *Bull. Volcanol.* **51,** 1–15.

Rosi, M., Principe, C., and Vecci, R. (1983). The 1631 Vesuvius eruption. A reconstruction based on historical and stratigraphical data. *J. Volcanol. Geothermal Res.* **58,** 151–182.

Walker, G. P. L. (1981). Plinian eruptions and their products. *Bull. Volcanol.* **44,** 223–240.

Wilson, L., Sparks, R. S. J., and Walker, G. P. L. (1980). Explosive volcanic eruptions. IV. The control of magma properties and conduit geometry on eruption column behaviour. Geophys. J. R. Astron. Soc. **63,** 117–148.

SURTSEYAN AND RELATED PHREATOMAGMATIC ERUPTIONS

JAMES D. L. WHITE
University of Otago

BRUCE HOUGHTON
Institute of Geological & Nuclear Sciences

I. Definition
II. The Surtsey Example
III. Observations from Other Eruptions
IV. Summary of Observations
V. The Components of Phreatomagmatism
VI. Classifications and Pigeonholes

GLOSSARY

accretionary lapilli Aggregates of fine ash, commonly having a concentric structure and formed by accretion of damp ash in eruption clouds.

armoured lapilli Lapilli coated with one or more complete or partial layers of accreted fine ash; essentially a variant of accretionary lapilli.

cock's tail jets The common type of tephra jet, with an arching, multifingered form likened to the shape of a rooster's tail.

continuous uprush Sustained phreatomagmatic eruption column that is fed by ongoing or closely spaced explosions.

frittering Erosion of particles from a vent wall by rushing gases.

pseudo-ballistic lapilli Lapilli deposited individually by fall from a plume that form impact sags similar to those from true ballistics transported by momentum.

spall dome Subhemispherical gas-driven shock zone expanding outward from a subaqueous explosion.

tachylite and sideromelane Basaltic glass. Sideromelane is translucent; tachylite is cryptocrystalline and opaque as a result of microlite crystallization and is inferred to result from slightly slower chilling.

tephra jets Discrete ejections containing tephra and steam driven by steam expansion and momentum of large clasts.

vesiculated tuff Tuff containing open, fluid-form spaces among the fragments reflecting entrapment of air in wet fine-grained ash.

THE 1963 ERUPTION of Surtsey brought dramatically to the attention of the volcanological community the explosive influence of water on the eruption style of otherwise effusive or only mildly explosive eruptions. Similar eruptions have occurred both at other emergent volcanoes that have grown through water during eruption and at fully subaerial volcanoes to which water had access via streams or aquifers. This chapter uses information from these observed small-volume phreatomagmatic eruptions to show how the entrance of water into the vent of an erupting volcano affects

Copyright © 2000 by Academic Press
All rights of reproduction in any form reserved.

fragmentation processes and pyroclast populations, ejection and dispersal of tephra, and depositional processes and features. Related chapters discuss mechanisms of phreatomagmatic fragmentation processes (see Phreatomagmatic Fragmentation) and larger scale phreatomagmatism (see Phreatoplinian Eruptions).

I. DEFINITION

George Walker first applied the term *surtseyan* to a group of fine-grained and locally dispersed pyroclasts inferred to be the phreatomagmatic equivalent of hawaiian and strombolian deposits. Since then some authors have expanded the term to encompass virtually all phreatomagmatic deposits, while others have restricted it to only those eruptions that closely resembled Surtsey, introducing additional descriptive terms, such as taalian, for other styles of pheatomagmatism. This chapter is not the place to propose a new or modified nomenclature for eruption styles and its focus is *all* small-scale phreatomagmatism, that is, the weakly energetic interaction of generally small volumes of magma with external water in a range of environments. We start by reviewing the classical 1963–1967 eruption of Surtsey volcano in Iceland, but the discussion that follows extends to many other phreatomagmatic eruptions in a range of settings.

II. THE SURTSEY EXAMPLE

Surtsey's eruption was extensively observed and recorded by geologists, and Sigurdur Thorarinsson brought together many observations, photographs, and an informed interpretation of events in the book *Surtsey: The New Island in the North Atlantic* (1967, Viking, New York), from which all quotations in this section are taken. The eruption lasted a total of about 1300 days during which $>10^9$ m^3 of magma was erupted from five clusters of vents along NE trending fissures. The activity passed through submarine and marginally emergent phases and ended in a period of strombolian and hawaiian activity.

A. Subaqueous Explosions and Emergence from the Sea

Surtsey's eruption began some 100 m below sea level on the seafloor south of Iceland and proceeded unnoticed until the volcano had built to perhaps 10 m below the surface. On 14 November 1963, black eruption columns rose just above the sea's surface. The tephra columns soon reached a height of 200 feet (66 m), rising out of the sea in two or three separate places. The eruption was notably silent. A large circle of whitened water lay around the vent, representing a zone of agitation containing vapor bubbles, and long-wavelength concentric waves traveled away from the vent. By the next morning Surtsey had emerged from the sea and was in fairly constant eruption.

Three sets of satellite vents to Surtsey (Surtla, Syrtlingur, and Jolnir) were also observed as they shoaled. Prior to emergence, broad, low-relief tephra mounds were visible near the surface. The mound surfaces accreted tephra from the varied eruptive activity and were disturbed both by normal sea waves and concentric eruption-generated waves. Initial observations of the Surtla vent took place when the mound had closely approached the surface and eruptive activity began to produce turbulence in the water. Steam was reported rising from the sea the next day and

> *. . . the sea showed considerable signs of unquietness . . . a short way under the surface—our guess was 2 feet (0.66 m)—three small vents were active in about an 820-foot-long fissure (269 m) . . . When we flew very low straight above these new vents quick flashes from fire under the surface could be seen at intervals of half a second, causing abrupt concentric waves all around that made the sea look like quivering jelly. Occasionally steam columns rose above the surface, and in between there were black outbursts of tephra which ejected columns . . . highest reached a height of 160 feet (52 m). (Thorarinsson, 1967, p. 21; Fig. 1 of this chapter).*

The eroded remnant of Surtla, 40 m below sea level, was later found to hold plastically deformed clasts and abundant tachylite grains.

Turbulence in the surface waters at the Surtsey vents probably represented agitation of the water surface by hot, convecting water, whereas steam rising above the water indicated passage of vapor bubbles through the water surface. The whitened circles of water surrounding vents during explosive eruption are interpreted as spall domes intersecting the surface; the circles thus represented the zones within the primary pressure waves (shock waves) generated by the explosions (Fig. 2). Slightly later, subaerial tephra jets joined with the turbulence and steam, fed by subaqueous tephra jetting, the result of explosive phreatomagmatic disruption of magma at shallow depths. Vigorous tephra jets from vents slightly below the surface had sufficient momen-

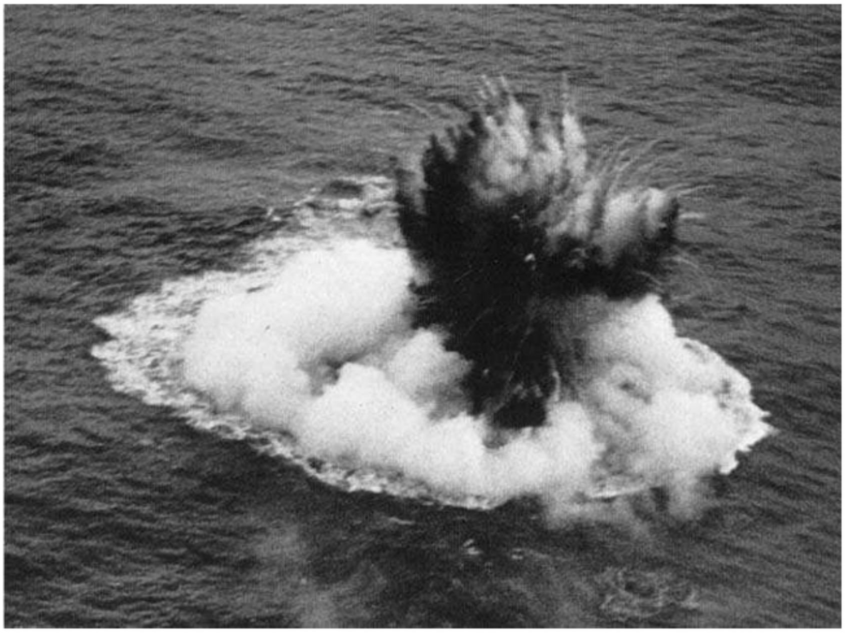

FIGURE 1 Photograph of tephra jets from slightly submerged Surtla vent representing the earliest phase of volcano-building *observed* during the eruption of Surtsey. Note the change from dark base to pale tips of the jets, due to steam condensation, and their spreading form. A base-surge of steam spreads outward above agitated, whitened water resulting from intersection of a spall dome with the water surface. [Reprinted with permission from Thorarinsson, 1967.]

tum to clear the water surface. Less vigorous ones lost momentum before breaching the surface but generated sufficient steam, as the jet collapsed and fragments directly contacted the surrounding water, to feed a vapor column rising through the surface. Hot fragments continued to generate steam even after deposition, as indicated by steam from a subaqueous crater rim. Weaker, intermittent bursts agitated the water and sent heated pockets of water to roil the surface, but the steam generated from the bursts was recondensed in the cold ambient seawater before reaching the surface.

Explosive, phreatomagmatic fragmentation is indicated by the subaqueous incandescent flashes noted at Surtla and the subaqueous explosions at all the vents. The subaqueous flashes are interpreted to have been caused by explosive disruption of large lumps of incandescent magma by phreatomagmatic explosions. Shock waves and outward-traveling concentric surface waves were seen at each vent during shoaling. Explosion-induced shaking likely caused local failure of the growing edifice, displacing variably sized parts of the mound downward along local slips. The main effects of the shocks were to agitate the water, generate vapor bubbles, and initiate concentric surface waves.

Wide craters, as observed at Surtla and perhaps at Jolnir, would have accumulated a tephra slurry by fallback from nonbreaching jets. This *almost emergent* phase of edifice construction, in which emergent eruptive activity is commonplace, lasted for more than 2 weeks at Syrtlingur vent. Including the period during which emergent eruptive activity precedes *lasting* edifice emergence, the time can run to months for single vents (Surtsey itself and the Syrtlingur and Jolnir satellite vents) to decades or longer.

The presence of tachylite grains and plastically deformed clasts suggest that direct magma–water contact was not ubiquitous during the growth of Surtla. These features indicate development of a steam cupola during eruption that shielded much of the erupting tephra from the surrounding water.

B. Emergence from the Sea

Once Surtsey built above the sea, Thorarinsson (1967) noted

> *... two clearly discernible types of activity. When the sea had an easy access to one or more of the vents ... the activity was the typical one for submarine eruptions*

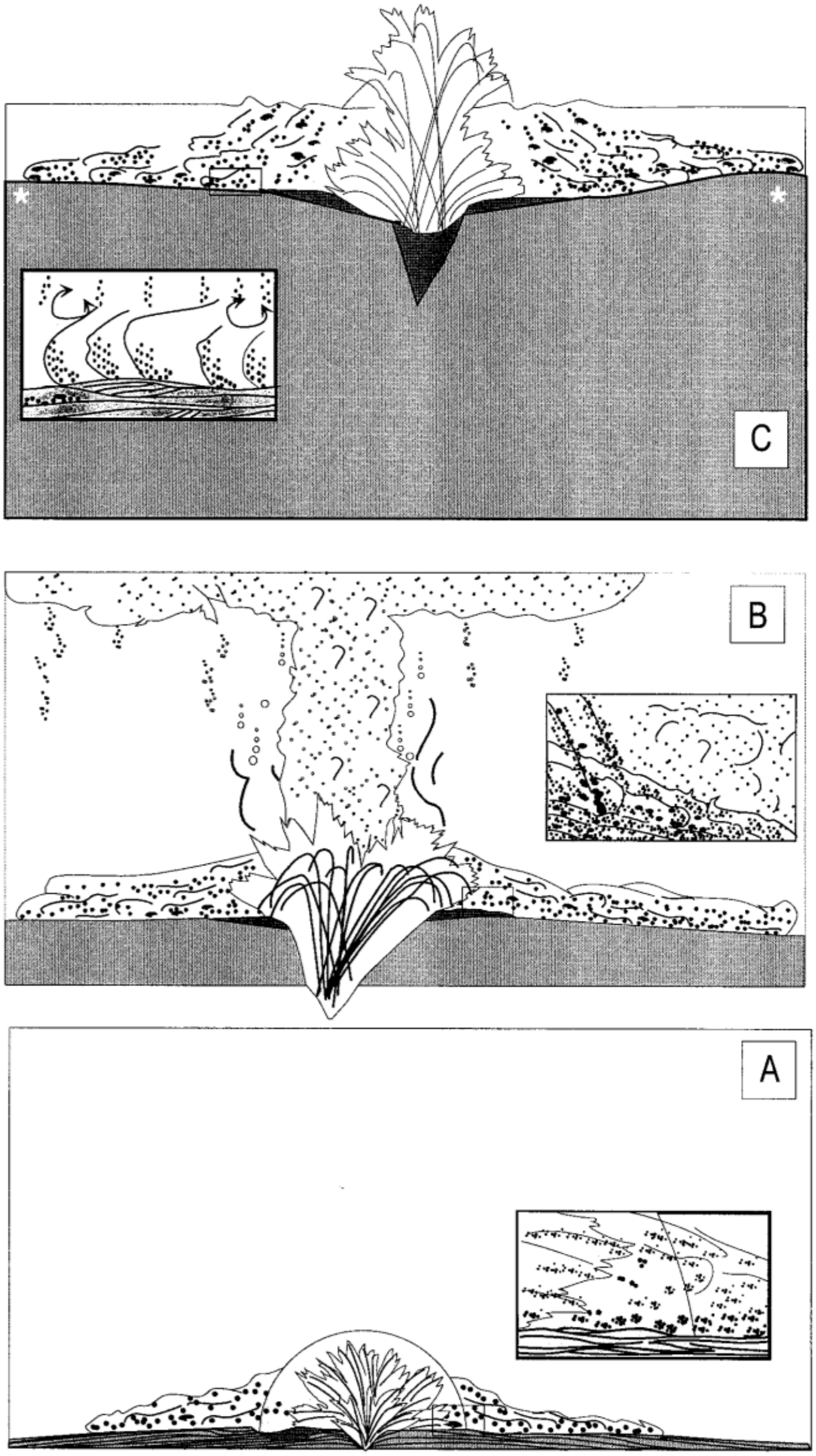
C
B
A

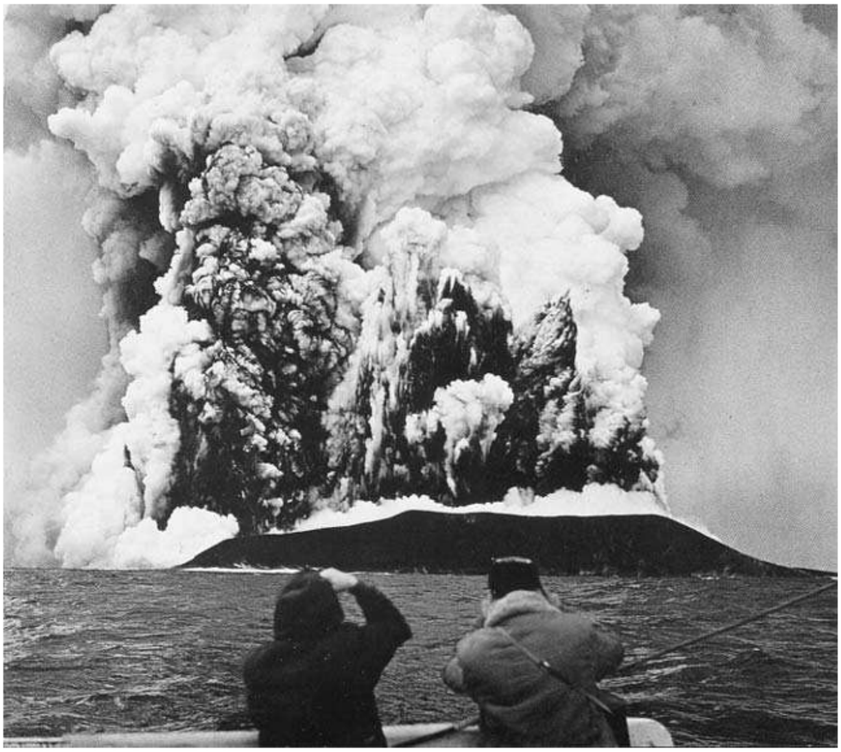

FIGURE 3 Photograph showing differing eruptive activities from adjacent vents at Surtsey. To the left is a maintained plume of the sort formed by continuous uprush activity. Cock's tail tephra jets occur to the right of this plume, lofting black tephra along subballistic trajectories with condensing vapor forming white moisture laden steam at the margins of the jets. Billowing convective steam clouds form a backdrop. [Reprinted with permission from Thorarinsson, 1967.]

> *. . . After each explosion a tephra-laden mass rushes up, and out of it shoot numerous lumps of liquid or plastic lava, called bombs, each with a black tail of tephra. Within a few seconds these black tails turn grayish white and furry as the superheated vapor . . . cools and condenses. (pp. 17–18)*

Such activity from a flooded vent is termed *tephra jetting*, or *cock's tail* plumes (see Fig. 3). In contrast, *continuous uprush* activity was linked with tephra accumulation that blocked seawater from pouring into the vent.

> *Instead of intermittent explosions the uprush of vapor and tephra was then continuous . . . at the base of the eruption column the speed of the uprush was about 400 feet per second. The black columns of tephra frequently reached half a mile in height . . . accompanied by a heavy rumbling noise. The tephra production from such*

FIGURE 2 Diagram illustrating inferred subaqueous development of a surtseyan volcano. The top and bottom of each frame represent the sea surface and the seafloor. (A) Early, fully subaqueous jetting activity. Explosions and collapsing jets produce a turbulent, dilute gravity flow having strong temperature contrasts and moving unsteadily outward from the vent. Deposition takes place largely from traction under unsteady flow conditions, but occasional ejection of the vent slurry or collapse of unusually concentrated tephra jets forms high-concentration dispersions that deposit more massive beds. (B) The tephra pile (stippling) is shallowing. Vigorous, more-sustained activity produces local water-exclusion zones at the vent margin in which clasts are transported in part through steam. This results in deposition of armored lapilli and tachylitic clasts having impact sags. Most ejecta are not deposited at vent margins, but are carried laterally in sediment gravity flows. Fragments of marine sediment may result from quarrying into the seafloor during this activity. (C) The volcano has now grown into shallow water (asterisks denote wavebase), and wave-influenced sedimentary structures begin to form during deposition. Jets are intermittently emergent (e.g., Fig. 1). Gravity flows carrying tephra outward along the volcano's surface interact with oscillatory currents beneath ambient surface waves and longer wavelength concentric waves induced by the eruption. [After White, J. D. L., 1996, Pre-emergent construction of a lacustrine basaltic volcano, Pahvant Butte, Utah (USA). *Bull. Volcanol.* **58,** 249–262.]

> *a continuous uprush was much greater than from the intermittent explosive activity … uprush of this kind might last for a few hours at a time. (Thorarinsson, 1967, pp. 18–19)*

Tephra jets carried tephra and steam along modified ballistic paths outward from the vent. Several jets per minute were commonly produced, but jets also occurred in isolation at widely spaced and irregular intervals, or in increasingly close succession at the onset of continuous uprush episodes. Strong pulsatory vapor plumes commonly rose from the vent while jetting took place and were associated with lightning, whirlwinds, and tephra–hail showers, in which each hailstone was cored by a sand-sized tephra grain. As the inner parts of larger jets at Surtsey descended they formed steam and tephra density currents that rolled down the cone and out over the sea.

Continuous uprush activity formed relatively stable, dark-colored eruption columns up to a couple of kilometers in height carrying uncondensed water vapor and heavily charged with tephra (see Fig. 3). Incandescent clasts were abundant in such columns and fell back onto the cone in spectacular abundance. Tephra dams were observed to prevent flooding of the vent during uprush activity.

Subaerially deposited tephra at Surtsey is mostly poorly sorted and often includes *vesiculated tuff* rich in accretionary lapilli and sideromelane. Deposits contain widely scattered pebbles and local blocks of indurated marine sediments from the preeruption seafloor and pillow basalt. Vesiculated tuff beds on steep cone slopes (>20°) are broken by channels formed by small tephra debris flows (Fig. 4); on very steep slopes (>35°) such tuff beds slipped downslope, breaking into plastic slabs. Quenched bombs with fluidal internal textures and a rugged, glassy exterior are present in beds formed shortly before strombolian activity began; they indicate heterogeneous interaction of water with erupting magma.

III. OBSERVATIONS FROM OTHER ERUPTIONS

The eruption styles described above for Surtsey characterize only a small proportion of weak phreatomagmatic eruptions. We describe below the characteristics of six other well-described historical eruptions chosen to illustrate the range of such phreatomagmatic eruptive styles. The selection includes examples of both short-lived and long-lived eruptions, both silicic and basaltic magmas, magmas that were ascending at the time of fragmentation and others that were stagnant or retreating, interaction with standing water and with groundwater, and eruptions where the conduit walls were strong and coherent and others where unconsolidated loose sediment filled the vent and shallow conduit.

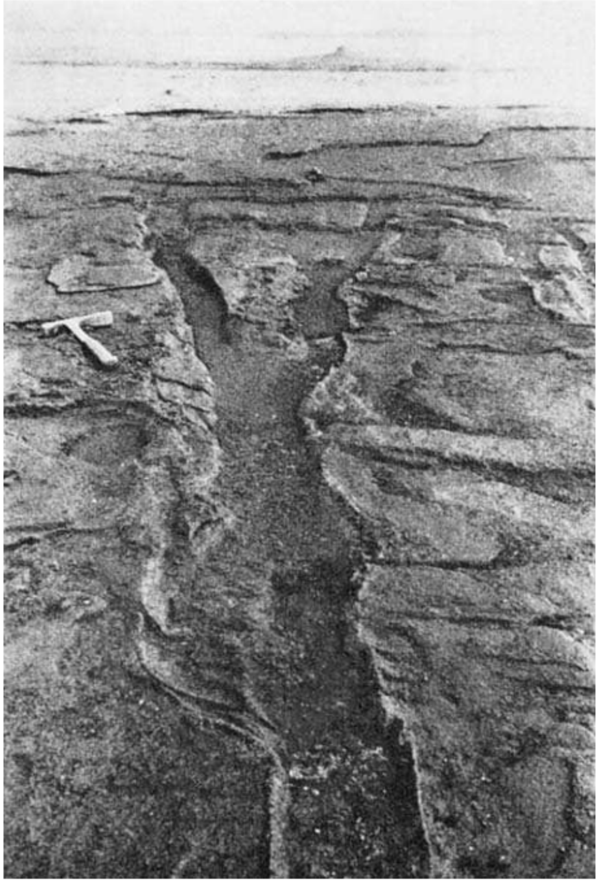

FIGURE 4 Eruption-fed lahars are formed by transformation upon impact of water-rich tephra jets and when seawater, ejected onto the volcano flanks during jetting, entrains tephra from the cone. [Reprinted with permission from Lorenz, 1974.]

A. Myojinsho 1952–1953

The 1952–1953 eruption of Myojinsho involved the intermittent interaction of a growing submarine/emergent silicic lava dome with seawater. The 1952–1953 eruption lasted about 370 days beginning 16 September with submarine explosions and generation of small tsunamis. Myojinsho, also known as Myojin reef, is a subaqueous cone volcano, 2.5–3 km^3 in volume, which extends to within 30 m of sea level. It has erupted at least a dozen times since 1946, though most eruptions produced no more than discolored water at the surface. A blocky hypersthene–augite–dacite lava dome emerged from the sea by 17 September 1953, was destroyed by two explosions on the 23rd, emerged again in early November, was again destroyed in early March 1953, reemerged in April, and was finally beheaded 1 September 1953; a few weeks afterward all activity apparently ceased. Eruptive behavior followed a pattern in which growth of the dome was accompanied by variably powerful explosions, some initiated subaerially and others originating at depths estimated at between 40 and 70 m. Larger subaqueous explosions produced vigorous tephra jets (cf. Fig. 3), surges, and low (<2 km) eruption columns. Explosions at times occurred at rates of three to five per minute, with one or a few larger explosions each day. The larger explosions were accompanied by freshly vesiculated clear white dacite pumice. This pumice, far more vesicular than the dome dacite, suggests that arrival of fresh magma triggered the blasts, probably by fracturing the dome carapace to allow ingestion of water into direct contact with the new magma. Plumes of water discolored by an abundance of volcanic dust rose in the sea virtually throughout the eruption, including between explosive phases. Recent bathymetric surveys show very smooth, 16°–20° upper slopes on the cone, shallowing to 8°–10° on the lower flanks, with shallow downslope-oriented channels, together suggesting deposition from high-concentration sediment-gravity flows fed from the eruption. Floating pumice and fine particles were distributed by plumes in surface water well beyond the limits of the cone.

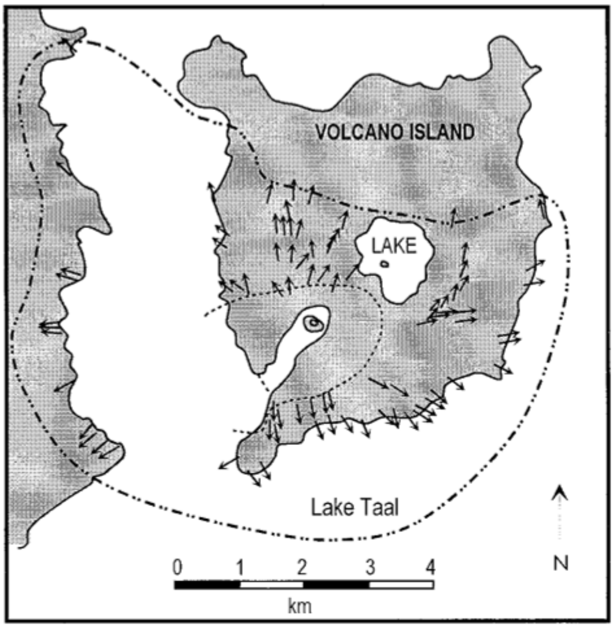

FIGURE 5 Map of Taal volcano showing the elongate eruption crater intersecting the lake. Transport directions of pyroclastic density currents (surges) are indicated by blown down and abraded trees and by surge dunes. [Redrawn after Moore *et al.,* 1966.]

B. Taal 1965

The well-described eruption of Taal volcano in 1965 involved strombolian and phreatomagmatic fissure eruptions as rising basic magma interacted with lake water. It produced about 0.4 10^7 m^3 of ejecta and a crater of 0.24 10^7 m^3 and lasted for 61 hours. Numerous historic small-volume eruptions have occurred from Volcano Island, which lies within Taal caldera surrounded by Lake Taal, with one in 1911 killing over 1000 people. The 1965 eruption began with strong seismicity and vigorous strombolian activity about a kilometer inland from the lake on Volcano Island (Fig. 5). After about an hour, a major explosive phase began and the eruption fissure propagated until it reached the lake. Eruption columns attained heights of 15–20 km, and pyroclastic density currents extended radially from the base of the eruption columns. Explosions occurred irregularly at different vents along the 1.5-km-long fissure, with the strongest and most persistent activity at the NE end where the eruption initiated. Activity waned after 7 hours, initially with numerous explosions generating a much reduced column; then after a couple of days there were only small explosions 5–10 minutes apart, which expelled steam and tephra that mostly fell back into the crater area where a small cone was formed.

Deposits of the major explosive phase at Taal are dominated by nonjuvenile material: lake sediment and fragmented older lava, derived from enlargement of the fissure. Deposition during the main explosive phase occurred by fallout of mud rain and accretionary lapilli to 80 km from the vent and by volumetrically dominant pyroclastic density currents (surges) that flowed over the lake surface to between 3 and 6 km from source, forming crudely bedded, poorly sorted wet ash/block beds. Large ash dunes, a meter high with wavelengths of 3–15 m, formed with crests normal to surge transport directions. The surges knocked down trees near the vent, abraded as much as 15 cm of wood from the vent-facing side of the trees at intermediate distances, and accreted thin, normally graded layers of fine to medium ash to more distant trees. None of the trees were charred. The early and late stage activity produced typical coarse, well-sorted strombolian deposits containing basaltic spatter and ash with some abraded grains.

C. White Island 1976–1982

The 1976–1982 eruption episode at White Island consisted of seven phases of alternating dry (strombolian) and phreatomagmatic explosive volcanism involving basic andesitic magma and a high-temperature geothermal system. The eruption was associated with the rise of a batch of basic andesitic magma to the surface between 1973 and 1977 but the magma was stationary or slowly retreating through much of the eruption. The eruptions ejected a total of 10^7 m^3 of ejecta over 2500 days accompanied by the formation of two coalescing maar craters. Discharge rates were 1–2 orders of magnitude higher during strombolian phases relative to the phreatomagmatic eruptions. Vent position changed repeatedly during the eruption along a line connecting two earlier historical vents. The eruption took place through a long-lived hydrothermal system and the conduit walls consisted of soft unconsolidated hydrothermally altered ash. A key feature was the role of decoupled magmatic volatiles, even in the phreatic phases, ejecting less than 1 wt% juvenile material. The phreatomagmatic phases of the eruption contained two styles of activity:

(1) near-continuous emission of gas and ash, and
(2) discrete larger explosions.

The near-continuous eruptions resulted from the streaming of magmatic volatiles and phreatic steam through open conduit systems, frittering juvenile particles from the quenched margins of the magma and eroding loose particles from the unconsolidated wall rock (Fig. 6A). The deposits were exceedingly complex with pseudo-ballistic lapilli, dry ash particles, damp ash aggregates, and ash-charged water droplets being deposited simultaneously from the eruption column.

The larger discrete explosions produced ballistic block aprons, downwind lobes of fall tephra, and cohesive wet surge deposits. The key features of the larger eruptions were:

(1) shallow depth of fragmentation,
(2) a random frequency and lack of precursors, and
(3) thermal heterogeneity of the ejecta.

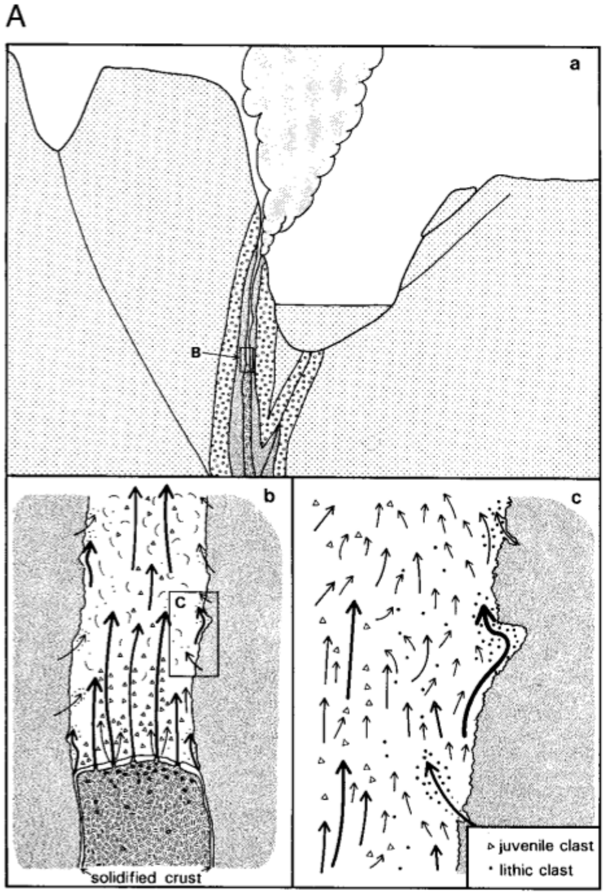

FIGURE 6 (A) Model for near-continuous phreatomagmatic eruptions by frittering. [Reprinted with permission from Houghton and Nairn, 1991.] (*continues*)

These larger explosions (Fig. 6B) appear to have been triggered by sudden contact of the magma with brine-saturated wall rocks after collapses of the weak conduit walls. The components that were mixed in this fashion were highly heterogeneous: magma that was thermally stratified and partially degassed; magmatic gas, decoupled from the magma and containing both steam and noncondensible gases; wall rock that had widely varying preexisting grain size and was at temperatures from ambient to gas-heated incandescence; and a groundwater component that ranged from cold meteoric runoff through heated brine to brine/vapor mixtures.

D. Ukinrek March–April 1977

A 10-day eruption at Ukinrek in Alaska resulted from rising and ponded magma interacting with small

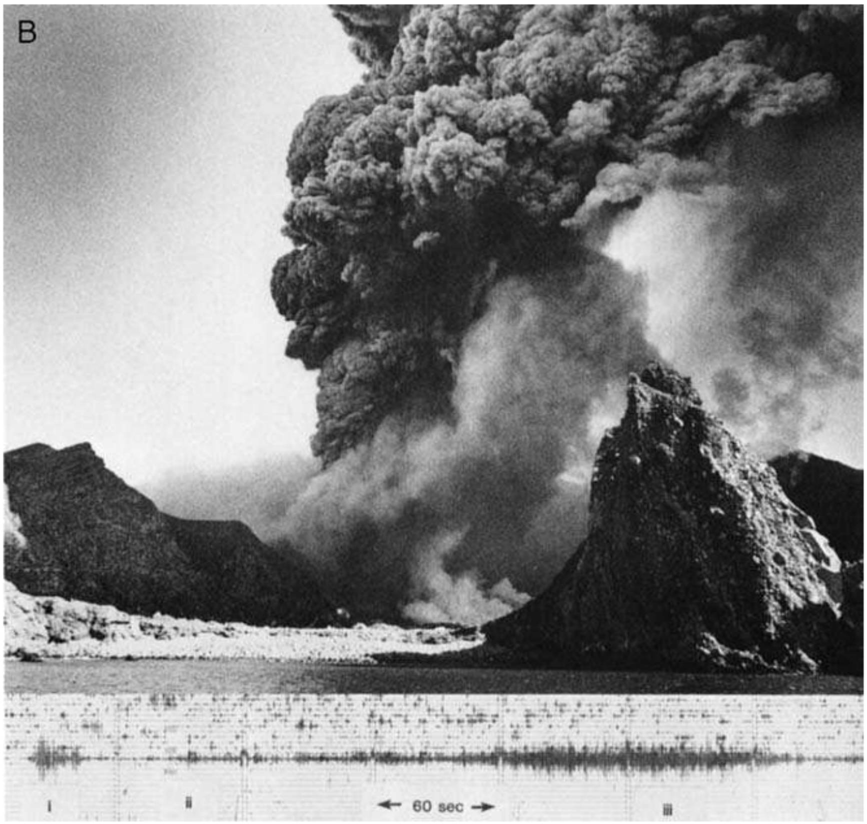

FIGURE 6 (*continued*) (B) A 3-km-high convective plume associated with a discrete explosive eruption from White Island volcano on 7 September 1987. [Reprinted with permission from R. Mead.]

amounts of shallow, perched groundwater in glacial till and underlying silicic pyroclastic deposits. It formed two maar craters (of volume 4×10^6 m^3) and ejected 2×10^7 m^3 of alkali olivine basalt and foreign lithics. The west maar formed over the first 3 days of eruption and was 170 m wide and 35 m deep. The larger east maar formed over the following 7 days and is 300 m wide and 70 m deep. Maar collapse was gradual over the course of the eruption. Magma formed an incandescent pond in the vent and then a dome late in the eruption sequence.

Eruption plumes occasionally reached 6 km in height and distal ash fall was recorded over an area of 20,000 km^2. The eruptions were phreatomagmatic throughout but activity at both vents showed a progressive trend toward drier activity (transitional to strombolian eruptions), marked by a lower content of foreign lithics and an increased abundance of ragged scoria lapilli in the deposits. This change was interpreted as due to depletion of the supply of external water delivered by flow through and collapse of the shallow aquifers. From day 5 contrasting eruptive styles were observed from two vents within the east maar. One vent within the lava pond experienced relatively dry explosions coeval with dark ash-rich plumes from the second vent.

The deposits, which reach a maximum thickness of 26 m on the rim of the east maar, are of four types: (i) lithic-rich ash and lapilli fall deposits, (ii) scoria-rich lapilli fall deposits, (iii) late-stage lithic block aprons extending to only 800 m from the rims of the maars, and (iv) minor pyroclastic surge deposits. The lithic rich lapilli fall deposits contain up to 75 wt% foreign lithics and subordinate rounded dense cauliflower juvenile lapilli yet are well sorted. On grain size criteria alone, the phreatomagmatic units cannot be distinguished from transitional–strombolian ones.

E. Kilauea 1924

An 18-day phreatomagmatic explosive eruption of Halemaumau crater on Kilauea volcano occurred when re-

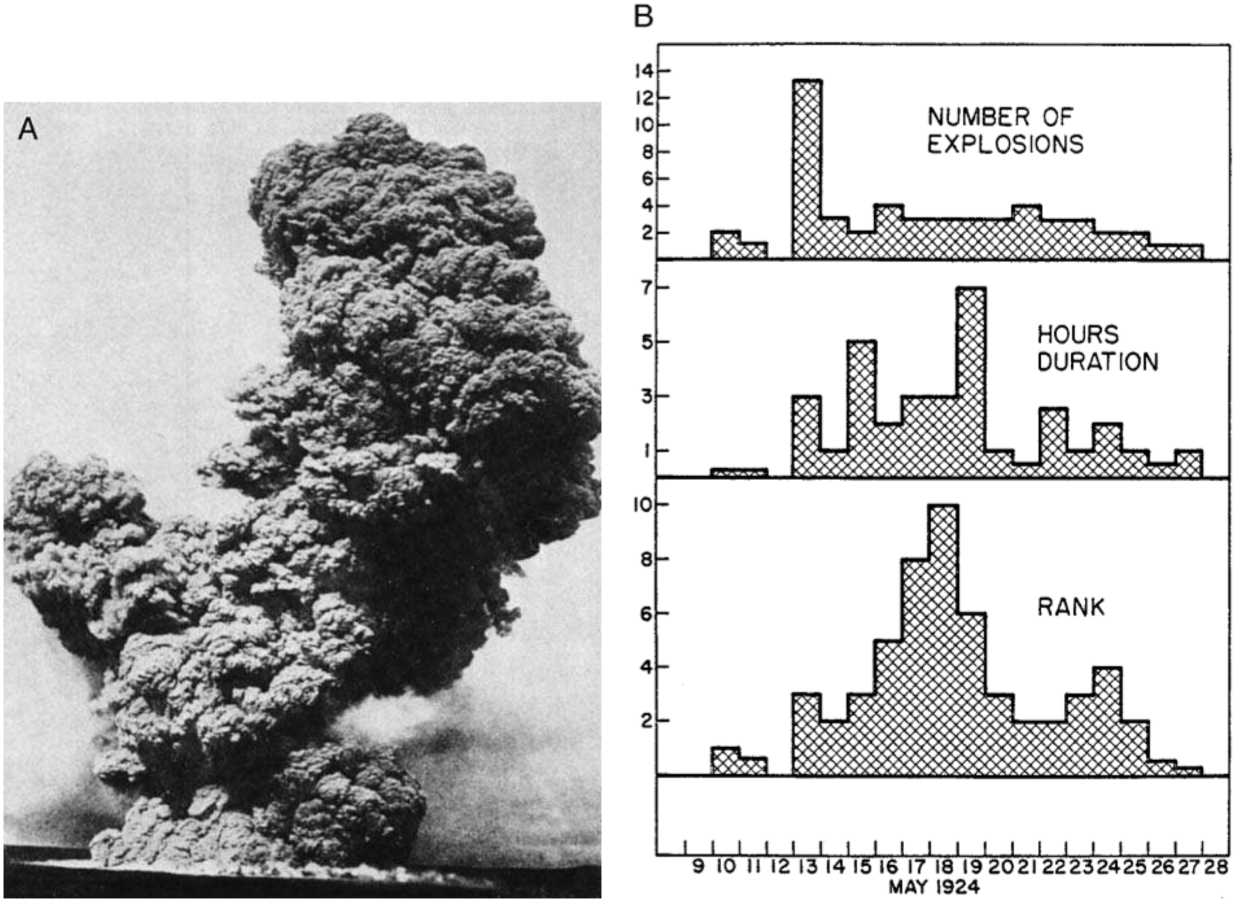

FIGURE 7 (A) Photograph of plume formed by discrete explosion during Kilauea 1924 eruption. (B) Histogram illustrating scale and timing of discrete explosions. [Reprinted with permission from Decker and Christiansen, 1984.]

treat of magma from the lava lake brought hot yet solidified basaltic rock into contact with perched groundwater in the conduit walls, at a depth of approximately 500 m. Up to 13 explosions occurred each day, producing eruption plumes to 2 km in height, depositing ash and accretionary lapilli, and ejecting ballistic blocks to 1 km from the vent (Fig. 7). The blocks ranged greatly in temperature from ambient to approximately 700°C. The total tephra volume was approximately 10^6 m^3 consisting entirely of previously solidified or at least brittle lava. The crater had widened by 430 m during the eruption but the missing material is largely inferred to have collapsed into the crater and the underlying conduit.

F. Teishi Knoll 1989

An eruption of Teishi knoll in Japan in September 1989 intruded approximately 1.4×10^6 m^3 of basaltic magma into shallow marine unconsolidated silicic ash, melting some of the ash and triggering a series of five submarine explosions. Five days of volcanic tremor accompanied injection of magma to shallow levels below the 100-m-deep seafloor. Strong tremor on day 3 accompanied the series of five submarine explosions that produced dome-like bulges of the water surface and tephra jets that ascended to $>$100 m. Material ejected by the eruption consisted of well-vesiculated clear glass pumice enclosed within or coated by basalt scoria with a crystalline groundmass. Comparison of preeruption bathymetric surveys with one during and another after the eruption shows that a small circular knoll 25 m high and 450 m in diameter had formed and then was largely destroyed during excavation of a 200-m-diameter crater. The remnants of the knoll were covered with marine sediment underlain by basaltic lava. Basalt-covered pumice was derived by fusion and vesiculation of the marine sediments as a result of heating by the magma (Fig. 8A). A scenario is that, following intrusion of magma into and

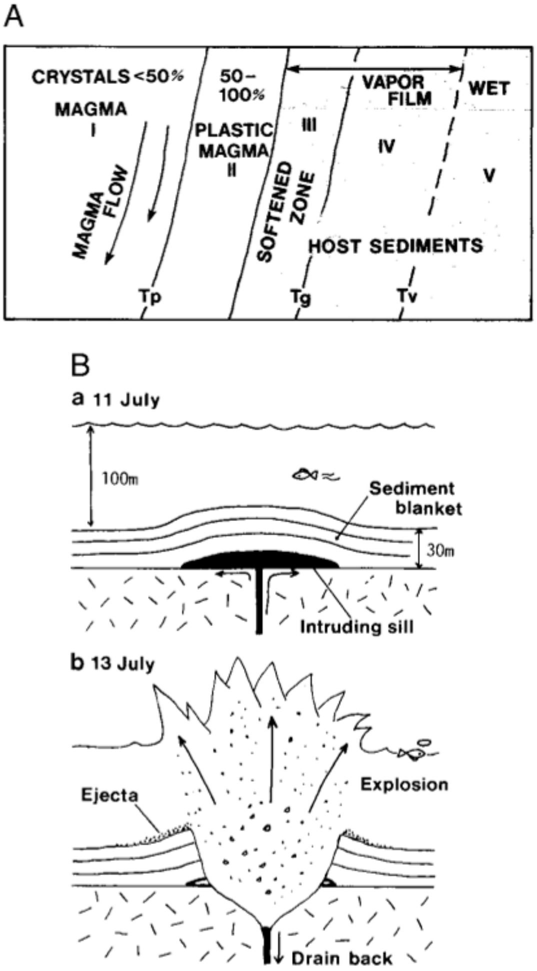

FIGURE 8 (A) Diagram of relationship between intruded basalt magma and marine sediment forming Teishi knoll. (B) Withdrawal of magma and triggering of eruption. [Reprinted with permission from Yamamoto *et al.,* 1991.]

partial melting of the shallow marine sediments, the magma was withdrawn and water gained access to the interior of the basalt intrusion, causing the series of strong explosions (Fig. 8B).

IV. Summary of Observations

A. Diversity of Activity

The eruptions described above show great diversity of magnitude, intensity, and eruptive style. This range is widened if we consider the larger database of recent and well-described events (Table I). The volumes of these deposits range from 10^4 to 10^9 m^3 and the durations of eruptions from as short as 1 hour to as long as 6 years. The eruptions are dominantly basaltic or basic andesitic composition although more silicic compositions occur. If the database is expanded to include prehistoric tuff rings and cones, even rhyolitic compositions occur.

B. Heterogeneity of Material

The unifying characteristics of small-volume phreatomagmatic eruptions are the involvement of external water and heterogeneity of eruptive process and products. Dry magmatic eruptions (strombolian, hawaiian, etc.) involve two phases, the silicate liquid phase and a gas phase, both of which we can often pretend are thermally, compositionally, and physically homogeneous. In wet systems the starting point is magma at high temperature in contact with external water and the material that contains or confines the water at much lower and commonly ambient temperatures. The end product is a mixture of juvenile particles, magmatic gas, steam, wall rock particles, and often liquid water (Fig. 9). Both the starting ingredients and the end products are very heterogeneous. Total mixing is rarely achieved, and a wide temperature range often characterizes the products of a single explosion. It is not uncommon for both liquid water droplets and steam to be present in the eruption column and for cold and incandescent clasts to be ejected simultaneously.

In the next section we explore how the properties of these heterogeneous components influence the style of volcanism.

V. The Components of Phreatomagmatism

The eruption styles described here involve relatively small volumes of variably yet relatively fluid magma interacting with water or an impure fluid consisting of water and particles. We can picture these types of eruptions as involving three complex and interdependent starting materials: magma, external fluid, and the wall rock that surrounds and defines the vent(s) and conduit(s).

TABLE 1 Compilation of the Characteristics of Some Relatively Well-Studied Historical Eruptions

Eruption	*Duration (days)*	*Volume (m^3)*	*Magma type*	*Vent type*	*Magma dynamics*	*Water source*	*Other styles during the eruption*
Surtsey 1963–1964	1300	10^9	Basalt	Four-fissure segments	Advancing	Seawater	Strombolian
Taal 1965	3	10^8	Basalt	Fissure	Advancing	Lake water	Strombolian
White Island 1976–1982	2500	10^7	Basalt, andesite	Multiple-point sources	Varying	Geothermal system	Strombolian
Capelhinos	480	10^8	Basalt	Multiple-point sources	Advancing	Seawater	
Ukinrek 1977	10	10^7	Basalt	Multiple-point sources	Ponded	Groundwater	Strombolian
Myojinsho 1952–1953	370	10^5	Dacite	Single-point source	Ponded	Seawater	Dome building
Kilauea 1924	18	10^6	Basalt	Single-point source	Drain back	Groundwater	Hawaiian
Teishi knoll 1989	1	10^4	Basalt	Single-point source	Drain back	Seawater	Extrusive
Deception Island 1967	4	?	Andesite	Fissure	Advancing	Seawater/groundwater	
Deception Island 1969	<3	?	Andesite	Five-kilometer fissure	Advancing	Groundwater/ice	
Deception Island 1970	2	?	Basalt	Twelve vents over 5 km	Advancing	Seawater/ice/groundwater	
Iwo Jima 1957	.05	10^4	Trachyandesite	Single-point source	Advancing	Groundwater	
Nilahue 1955	100	10^8	Basalt	Two-point sources	?	Groundwater	
Irazu 1963–1965	900	10^8	Andesite	Multiple-point sources	Ponded	Groundwater	Strombolian
Rotomahana 1886	0.25	10^8	Basalt	Fissure	Advancing	Geothermal system	Subplinian/strombolian
La Palma 1949	38	10^5	Basanite/tephrite	Multiple-point sources	Varying	Groundwater	Strombolian/hawaiian
Karymskoye lake 1996	2	10^7	Basalt	Single-point source	Advancing	Lake	
Miyake-jima 1983	1	10^7	Basalt	Fissure	Advancing	Shallow groundwater	Strombolian/hawaiian
Soufriere 1979	14	10^7	Basalt, andesite	Single-point source	Ponded	Crater lake	Dome building
Ruapehu 1945	250	10^7	Andesite	Single-point source	Advancing	Crater lake	Dome building
Ruapehu 1995–1996	100	10^7	Andesite–dacite	Single-point source	Advancing	Crater lake	Subplinian/strombolian

A. Magma

As in all volcanic eruptions, magma is the source of energy for surtseyan and related phreatomagmatic explosions. Most phreatomagmatic events are modifications of eruptions that would occur in the absence of external water. Many of the eruptions considered in this chapter are the phreatomagmatic equivalents of hawaiian and strombolian eruptions. Exceptions are the equivalent of extrusive events, for example, Myojinsho and Teishi knoll 1989, which, in the complete absence of water, would presumably have erupted only dacite domes or lava flows, or Kilauea 1929, which at the time of the explosive eruption was, in the absence of water, an actively receding lava lake. In interpreting the style and products of phreatomagmatic eruptions it is important to consider the influences of both the intrinsic physical properties of the magma phase and the background magmatic processes (the dynamic properties of the magma phase).

1. *Intrinsic Properties of Magma*

Intrinsic properties of the magma include its temperature, viscosity, dissolved volatile content, and crystallinity. During fragmentation, thermal energy is converted to seismic and acoustic energy, fragmentation energy, and kinetic energy. Magma (and water) temperatures prior to interaction influence the heat transfer rates and the temperatures attained during mixing. The absolute amount of heat available is clearly a key factor; hotter magma has more heat available for conversion to mechanical energy. However, more significant is the extent/efficiency with which this heat can be used during fragmentation and transport; this is strongly influenced by a number of processes described below.

The effect of ambient pressure is not well understood. An increase in confining pressure should boost the vigor of fragmentation and yet, by limiting vapor-film development, it may inhibit fragmentation.

Viscosity is strongly dependent on chemical composition, volatile content, and temperature. An increase in viscosity will retard the mixing of magma and water and yet, by slowing the advance of magma, may prolong the opportunity for contact between the two phases. The magmas described in this chapter show a range of viscosity at liquidus temperatures from a few Pa s^{-1} in the case of basalts, to millions of Pa s^{-1} for silicic magmas. A 200°C decrease in temperature will produce a 1 to 2 orders of magnitude increase in viscosity. Viscosity of the magmatic phase at the time of fragmentation may

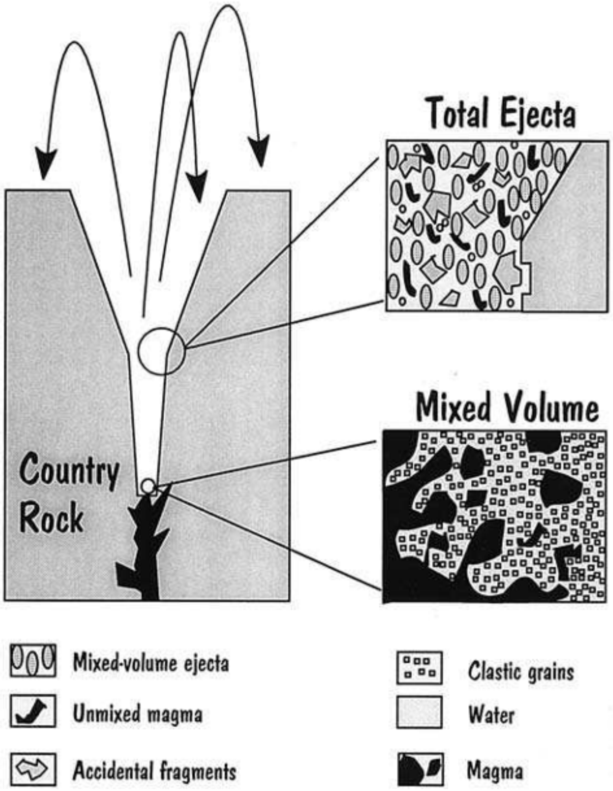

FIGURE 9 Highly schematic representation of a phreatomagmatic vent showing the different populations of particles that can be formed and ejected and their sites of formation/entrainment. All eruption energy is produced by phreatomagmatic explosions in the *mixed volume*. [Reprinted with permission from White, 1996.]

reflect both lower temperatures, as a result of cooling during ascent and interaction with the conduit walls, and processes of degassing and microlite crystallization that accompanied ascent. The nonexplosive degassing of magma during ascent has a pronounced effect on temperature and rheology. Vesiculation also increases surface area while reducing the density of the bulk melt phase and may therefore influence the geometry of mixing. Depending on magma viscosity and ascent rates degassing may be *open* or *closed*, and, in an open system, a decoupled gas phase will form a fourth component during eruption.

Rising magma may also partially crystallize during ascent, affecting both magma temperature and rheology. The growth of crystals and/or addition of wall rock fragments increases viscosity as predicted by Stokes–Einstein derivative functions, again by a factor of about 1 order of magnitude (for approximately 25% particles). Behavior becomes more complex above 40% rigid particles. The presence of numerous millimeter to centimeter sized lithic inclusions in the magma is also a thermal sink, which further increases the viscosity of the magma. Hard to quantify during this process are the effects of the introduction of any external water present in cracks or pores in the conduit walls.

2. *Dynamic Properties of Magma*

Dynamic properties of the magma include its ascent rate, discharge velocity, discharge steadiness, state of vesiculation, and state of fragmentation. The history of magma ascent toward the fragmentation zone has a major influence on the ensuing style of phreatomagmatism. The extent of degassing and microlite crystallization is strongly influenced by the ascent history, and degassing and crystallization in turn influence magma rheology and rise rate at shallow levels. A magma that rises rapidly and continuously to the surface is likely to undergo most of its vesiculation at shallow levels and be relatively fluid, hot, and homogeneous at the point of fragmentation. Relatively simple phreatomagmatic eruption styles result. If magma ascends in staged fashion and/or subsequently ponds in the shallow conduit, then at least some portion of this melt will have undergone quenching, and nonexplosive interaction with material forming the conduit walls, often becoming physically and thermally heterogeneous. Very complex magma:water interaction and phreatomagmatism often results.

If rising magma encounters external water then the fluid magma, often gas-rich and vesiculating, mixes with water or a slurry. Magmatic fragmentation processes (volatile nucleation and expansion) operate simultaneously with explosive and nonexplosive phreatomagmatic fragmentation. Shear along the boundaries of forcefully injected magma inhibits generation of a stable steam film, particularly where magma passes through a slurry (see below). Fragmentation and expansion due to vesiculation similarly create large surface areas that may directly contact water and initiate phreatomagmatic explosions. Shock waves generated by explosive expansion may further fragment the mixture and enhance fluid interpenetration. The frequency with which bursts of decoupled magmatic volatiles are released may determine the tempo of discrete explosions. Sustained phreatomagmatic explosivity is contingent largely upon mixing driven by shear along the margins of continually injected magma (Fig. 10).

Eruptions where magma has ponded or begun to withdraw down the conduit may involve passive frittering of conduit walls by streams of magmatic gas and/

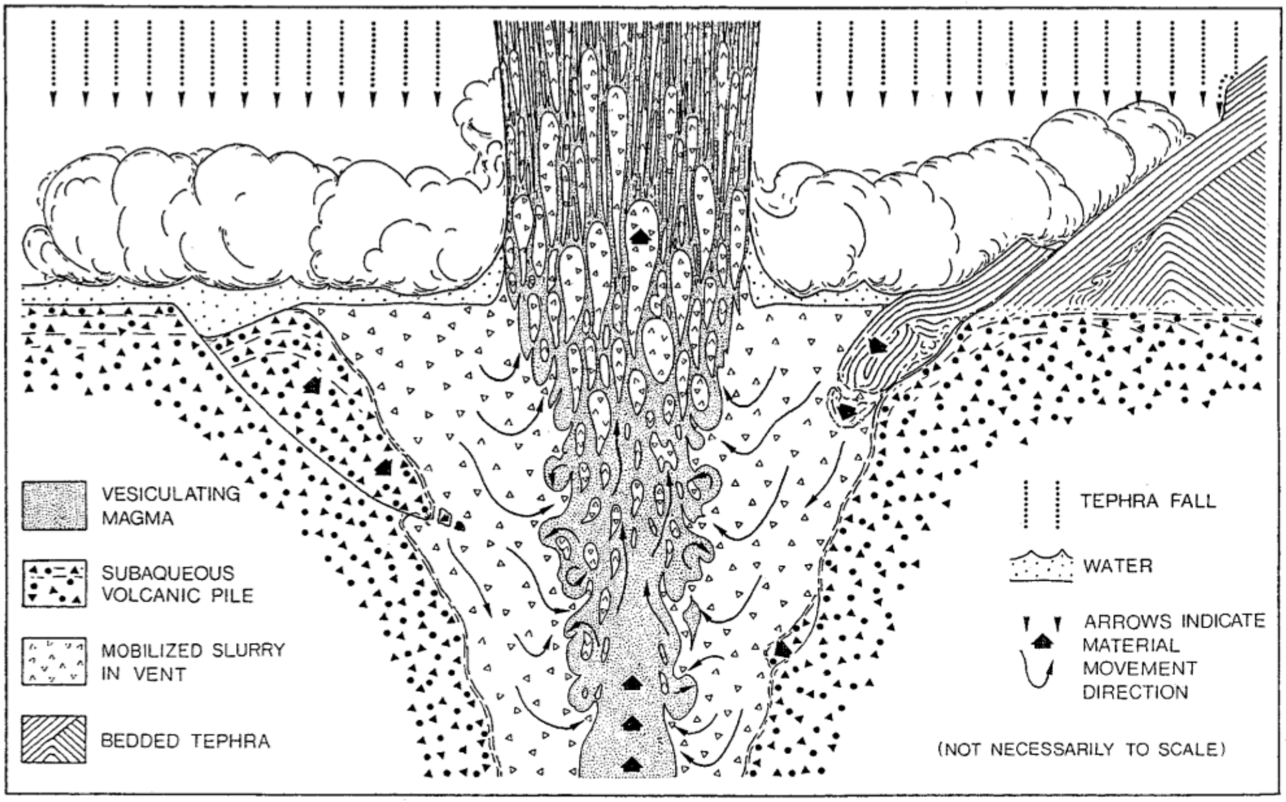

FIGURE 10 Model for processes in the surtseyan vent in which shear-instability entrainment and mixing of a slurry of recycled tephra and water with rising magma drives discrete or continuous uprush activity. [Reprinted with permission from Kokelaar, 1983.]

or collapse of unstable water-laden vent walls triggering discrete phreatomagmatic explosions. Magma withdrawal facilitates interaction in the following manner. Slowly rising or passive magma boils adjacent water, forming a stable steam film in contact with a chilled outer magma surface. Withdrawal of magma buckles the chilled outer surface, which fractures rapidly to allow direct contact of water with magma beneath the chilled surface, which results in a strong explosion. This sort of explosivity is self-driven after triggering and can result in impressive blasts.

B. Water

The availability of water/external fluid has a first-order influence on the style of phreatomagmatism. The amount of water relative to that of magma and the efficiency with which they mix determine the thermodynamic states of water in phreatomagmatic eruptions. If very little water is available, it can be heated to high temperatures and high pressures if confinement is available, but its expansion to vapor can fragment only a relatively small volume of magma. (Most of the work of fragmentation is done during the volume increase from liquid water to steam rather than by subsequent expansion of the steam phase.) At the other extreme, abundant water will receive insufficient heat for full vaporization and hence most effective fragmentation. At intermediate mass ratios, the available heat will take all the water to high states of internal energy, thus resulting in efficient magma fragmentation.

A variety of relatively shallow influences can disturb the supply of external water, and so most wet eruptions are characterized by abrupt changes in the proportions of water and magma. In special cases the rate of supply of water can be controlled by external factors, such as the tide or the frequency of rainstorms.

In most situations the water phase included in magma–water interactions is a liquid initially at ambient temperatures. However the eruptions described here also include examples of magma contacting:

(1) vapor-dominant geothermal fluid at temperatures up to 800°C,
(2) superheated geothermal liquids at temperatures of 200–250°C,
(3) snow or ice,
(4) impure fluids in which sediment particles are suspended in water, and
(5) vent slurries with significant yield strengths.

Where magma intrudes a preexisting hydrothermal system, the water phase prior to interaction may be steam, two-phase steam–water mixtures, or hot water. Steam is a minor contributor to the explosivity because the major volume change is that of vaporization, and subsequent (super)heating causes only a minor volume increase. The state of water most effective in forming phreatomagmatic explosions is superheated liquid water; it will undergo large volume changes upon vaporization, which can be accomplished by small additions of heat from interaction with magma and by subsequent disruption of the hydrothermal system.

Water involved in the interaction may contain suspended particles (sediment or tephra) or dissolved species (such as silica and chlorine in hydrothermal fluids). These impurities change the physical properties of the water phase and introduce nonvaporizable components. Depending on the concentration of impurities in the water, its viscosity may increase up to an order of magnitude, the density may double, and the heat capacity may decrease by 25%.

C. Vent and Conduit Wall Rock

1. *Vent/Conduit Wall Properties*

During phreatomagmatic eruptions the walls of the vent allow, in one or more ways, external water to encounter magma and contribute to initial and/or subsequent fragmentation and expansion. The simplest way in which this happens, exemplified by activity at Surtsey, Ruapehu, and Miyojinsho, is for surface water to occupy or flow directly into the vent during eruption. In such a situation the first phreatomagmatic explosions take place by interaction of magma with some small part of an effectively unlimited supply of clear ocean or lake water, and the ejecta consists of juvenile pyroclasts and H_2O. Under these circumstances the form of the vent and shallow conduit strongly influences the geometry of the interaction.

Terrestrial phreatomagmatic eruptions, such as at Ukinrek, begin under circumstances different than those of submerged volcanoes. In particular, there is no body or sizable domain of clear water with which magma can interact. Instead, magma encounters interstitial water contained within a framework of sedimentary clasts. Two endmember modes of interaction can be described for this situation: (1) water flows through the clast framework or fractures in the wall rock to interact with magma; (2) the clast framework and contained interstitial water are disrupted and together interact with magma as an impure fluid.

In many explosions the yield strength of shallow wall rock is negligible and the primary grain size of the vent-wall material has a strong effect on the grain size of the lithic population of the resulting pyroclastic deposit. In particular, if there is abundant ash-sized wall-rock material, its inclusion (often without any modification to its size distribution by the explosions) will lead to a misleadingly high estimate of the efficiency of fragmentation. Surtsey itself exemplifies another type of wall instability, in that the fragmental deposits formed early in the eruption form the walls of the vent later in the eruption. In this situation the vent is occupied by a slurry (see above) of seawater and tephra sloughed and slipped back into the vent, which strongly affects eruption style (Fig. 10).

2. *Vent Geometry*

The geometry of the vent will change as an eruption proceeds and this may *feed back* to modify the style of the eruption. Cone growth will influence the hydrology of the vent and in general act to restrict ingress of water. Growth of the cone or tuff ring may also permit magma to *pond* in the growing volcano at levels above the water table, bringing an end to *wet* phreatomagmatic fragmentation. Vent wall collapse is more important in phreatomagmatic eruptions than in dry magmatic eruptions. Collapse of the inner walls of the growing tuff cone or tuff ring may promote further magma–water interaction or may temporarily block the vent leading to episodic eruptive activity. Vent widening as a result of shallow collapse may promote a change to wetter explosions if surface water can pond in the crater.

Recycling of clasts is a process strongly influenced by vent geometry. Most pyroclastic deposits contain both first-cycle juvenile clasts, derived from magma at the instant of eruption, and recycled juvenile clasts that were fragmented in earlier explosions but then fell or collapsed back into the vent (e.g., Figs. 9 and 10). The recycled clasts are similar to wall-rock lithics in that they contribute no heat to further magma–water interaction, but they can be difficult to separate from *first-cycle* clasts in outcrop. Textural features, such as a combination of uneven mud coating and a mixture of fluidal and angular faces on many clasts, indicate that they were fragmented at least twice—once while the magma was fluid and subsequently in a brittle state.

VI. CLASSIFICATIONS AND PIGEONHOLES

There are many parameters that could be chosen to classify styles of mild phreatomagmatic activity. A study could use:

(1) the geometry of the products, for example, tuff ring versus tuff cone versus maar;
(2) the inferred setting of the volcano as submarine, emergent, or terrestrial;
(3) the absolute or relative intensity of the eruptions;
(4) the involvement of standing water versus groundwater;
(5) the nature of the external water phase as water, steam, or ice;
(6) the relative abundance of pyroclastic density current and fall deposits;
(7) grain size of the eruption products;
(8) the ratio of juvenile to wall rock clasts.

This range of possibilities reflects the complexity of this class of volcanic eruptions, which are similar only to the extent that they are characterized by abrupt, rapid changes in eruptive style and involve an external aqueous fluid. No existing classification deals adequately with this complexity and we do not attempt to refine these schemes here. Instead, we conclude this chapter with a brief summary of the two principal classes of eruption styles.

A. Discrete Explosions

A discrete phreatomagmatic explosion ejects a mixture of material that may be partitioned among ballistic blocks, tephra jets, pyroclastic density currents, and nonsustained, generally weak discrete eruptive plumes. Ballistic blocks comprise the largest particles ejected by an explosion and may travel through, or independently of, jets, surges, or plumes formed simultaneously with them. Smaller particles are transported by either tephra jets or plumes. In eruptions involving abundant external water much of the ejecta is partitioned into tephra jets and the associated convective plumes are essentially thermal in origin. These plumes carry very little tephra and arise from gravitational partitioning at the conduit mouth of steam from the simultaneously originated inertia-driven jet and ballistic transport and expansion-driven density currents. Higher ash-charged vertical plumes are generally associated with drier eruptions, that is, those in which liquid water is less abundant. Such plumes form elliptical fall sheets roughly symmetrical around the vent(s) and extending kilometers to tens of kilometers from the source. Tephra jets form sectoral fall deposits, generally extending only a few hundred meters to a few kilometers from the vent. Tephra jets are characteristic of eruptions through standing water. Surges arise from discrete explosions as both base surges, which strictly are expansion-driven collars of vapor flowing laterally from the base of a jet or plume, and surges fed by descending tephra from a plume or tephra jet.

B. Continuous Plume

Two types of continuous discharge occur during mild phreatomagmatic eruptions. Persistent and thorough interaction of rising magma with external fluid forms maintained eruption plumes that contain both steam and liquid water and deposit ash-rich fall deposits. Such plumes may be driven by either closely spaced explosions or a sustained discharge. The dynamics of such plumes closely resemble those of better studied endmember dry or magmatic systems. A weaker form of sustained activity occurs where magma is stagnant or receding within a vent, and weak interaction of incoming external fluid with the rigid carapace of the magma and passive degassing produces streaming gas and vapor that fritter ash from the conduit margins as a continuous, but dilute and weak, eruptive column driven by expansion of the gas phases.

SEE ALSO THE FOLLOWING ARTICLES

Hawaiian and Strombolian Eruptions • Magma Ascent at Shallow Levels • Phreatomagmatic Fragmentation • Phreatoplinian Eruptions • Pyroclastic Surges and Blasts • Rates of Magma Ascent • Seamounts and Island Building

FURTHER READING

Fiske, R. S., Cashman, K. V., Shibata, A., and Watanabe, K. (1998). Tephra dispersal from Myojinsho, Japan, during its shallow submarine eruption of 1952–1953. *Bull. Volcanol.* **59,** 262–275.

Houghton, B. F., and Smith, R. T. (1993). Recycling of magmatic clasts during explosive eruptions: Estimating the true juvenile content of phreatomagmatic volcanic deposits. *Bull. Volcanol.* **55,** 414–420.

Kokelaar, B. P. (1986). Magma–water interactions in subaqueous and emergent basaltic volcanism. *Bull. Volcanology* **48,** 275–289.

Schmincke, H.-U. (1977). Phreatomagmatische Phasen in quatären Vulkanen der Osteifel. *Geol. Jahrb.* **39,** 3–45.

Thorarinsson, S. (1967). "Surtsey: The New Island in the North Atlantic," Viking, New York.

Waters, A. C., and Fisher, R. V. (1971). Base surges and their deposits: Capelinhos and Taal volcanoes. *J. Geophys. Res.* **76,** 5596–5614.

White, J. D. L. (1991). Maar-diatreme phreatomagmatism at Hopi Buttes, Navajo Nation (Arizona), USA. *Bull. Volcanol.* **53,** 239–258.

This Page Intentionally Left Blank

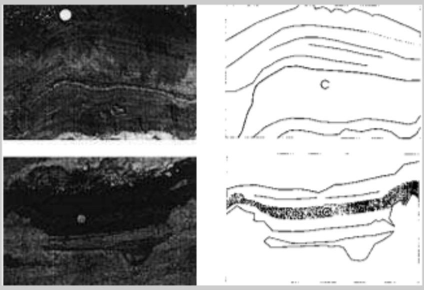

PHREATOPLINIAN ERUPTIONS

B. F. HOUGHTON
C. J. N. WILSON
Institute of Geological & Nuclear Sciences

R. T. SMITH
University of Waikato

J. S. GILBERT
Lancaster University

I. Characteristics
II. Eruption and Transport Processes
III. Deposition Processes
IV. Discussion

GLOSSARY

accretionary lapilli In the strict sense, spherical aggregates of fine ash that form in eruption plumes. In practice used more widely for all ash aggregates including "mud lumps."

ash aggregation Processes leading to the formation of clusters of ash particles during transport in an eruption plume.

dispersal index (*D*) A measure of the area covered by a pyroclastic fall deposit, specifically the area enclosed by an isopach drawn at 1/100 of the maximum thickness of the deposit. Phreatoplinian deposits have D values greater than 50 km^2.

external water Any water phase during explosive volcanism that was not originally dissolved in the magma such as surface and groundwater.

fragmentation index (*F*) A parameter measuring the grain size of a pyroclastic fall deposit, specifically the percentage of ash finer than 1 mm at the point on the dispersal axis corresponding to 1/10 of the maximum thickness of the deposit. Phreatoplinian deposits typically have F values greater than 80%.

mud lump/mud pellet Ash aggregates of irregular shape and with no discernible concentric internal structure.

mud rain Fall-out of ash-bearing droplets of water and dissolved gas species from an eruption plume.

phreatoplinian deposits Widespread phreatomagmatic fall deposits (as defined requiring a dispersal index of 50 km^2 or greater and a fragmentation index of generally greater than 80%).

THE TERM *PHREATOPLINIAN VOLCANISM* has proved an enigma, widely incorporated in theoretical classifications since its introduction in 1978, in practice, it has been applied to only relatively few deposits or eruptions. The term was introduced to describe widely dispersed, fine-grained pyroclastic fall deposits formed when silicic magma interacted with large quantities of surface or groundwater (collectively termed *external water*). Such large *wet* eruptions (see Phreatomagmatic Fragmentation) are a poorly understood style of explosive volcanism, largely because of the lack of observed historic examples. A number of large eruptions in the 1980s and 1990s were probably characterized by

Copyright © 2000 by Academic Press
All rights of reproduction in any form reserved.

limited involvement of external water, but there have been no observed modern examples of large eruptions with the moderate to high water : magma ratios inferred to typify the phreatoplinian style. Unlike the other eruptive styles described in Strombolian and Hawaiian Eruptions, Volcanian Eruptions, Plinian Eruptions, and Surtseyan and Related Phreatomagmatic Eruptions, phreatoplinian volcanism was first proposed to describe a group of mostly *prehistorical* eruptions.

In reexamining phreatoplinian volcanism and the type deposits we will ask the following questions.

- Is high vesicularity of the erupting magma part of the definition for phreatoplinian eruptions?
- Should all vent-derived, fine-grained fall deposits with wide dispersal be called phreatoplinian?
- Must phreatoplinian eruption columns be sustained?
- What dispersal index is an appropriate lower limit for phreatoplinian deposits?
- How useful are grain size parameters in delineating phreatoplinian deposits?
- What range of water to magma ratios should phreatoplinian volcanism be applied to?

I. CHARACTERISTICS

A. Examples

The current definition of phreatoplinian volcanism is based on four type examples. We discuss these below, incorporating information from our more recent studies (Figs. 1 and 2).

1. Askja-C, Iceland, 1875

Phase C of the 1875 eruption of Askja caldera in Iceland remains the only widely recognized historical example of a phreatoplinian eruption. The complete eruption lasted 6.5 hours and consisted of an alternation of subplinian, plinian, and phreatoplinian eruptive styles. Phreatoplinian phase C lasted 1 hour and produced a 0.2-km^3 deposit, consisting of a lower fine-grained, highly stratified unit and an upper, coarser-grained but poorly sorted unit. The Askja-C deposit has a low lithic content similar to that in plinian layer D. Workers envisaged a two-stage fragmentation process for Askja-C, first by vesiculation, with subsequent re-fragmentation of the clast population by magma/water interaction.

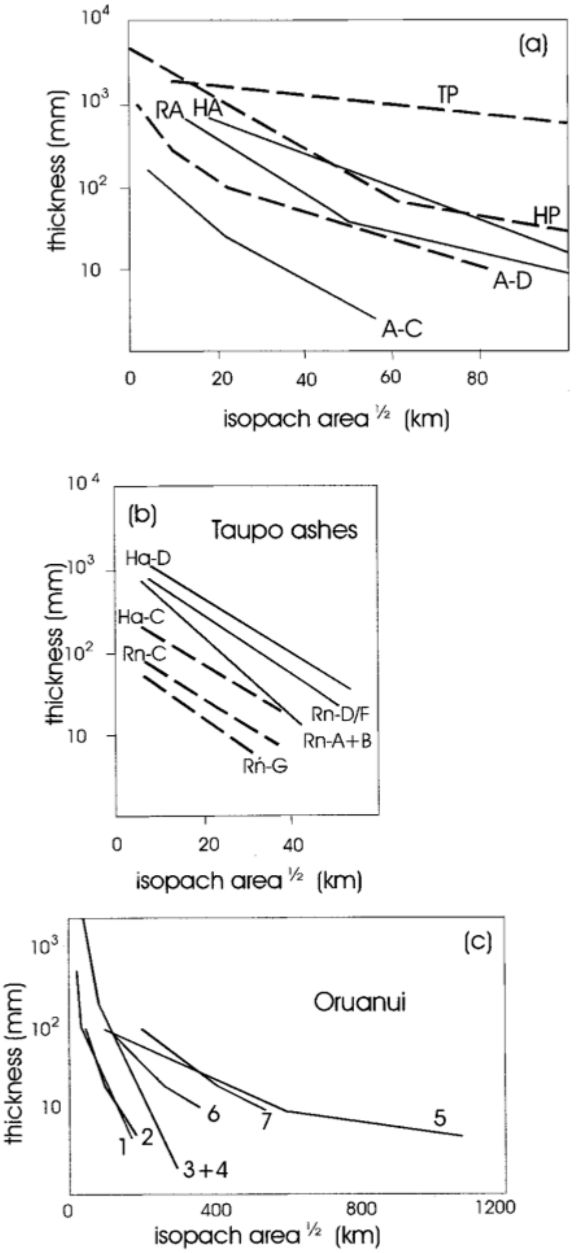

FIGURE 1 Plots of thickness versus square root of isopach area for selected deposits. (a) Contrast between plinian (dashed) and phreatoplinian (solid trace) units from single eruptions. HP and TP are the Hatepe and Taupo plinian deposits that enclose the Hatepe and Rotongaio ashes (HA and RA, respectively). A-C and A-D are the phreatoplinian C and plinian D phases of the 1875 AD Askja eruption. (b) Contrasting ash-rich (solid trace) and lapilli-rich (dashed) phases of the Hatepe and Rotongaio ashes. (c) Subunits of the Oruanui deposit (see Table I).

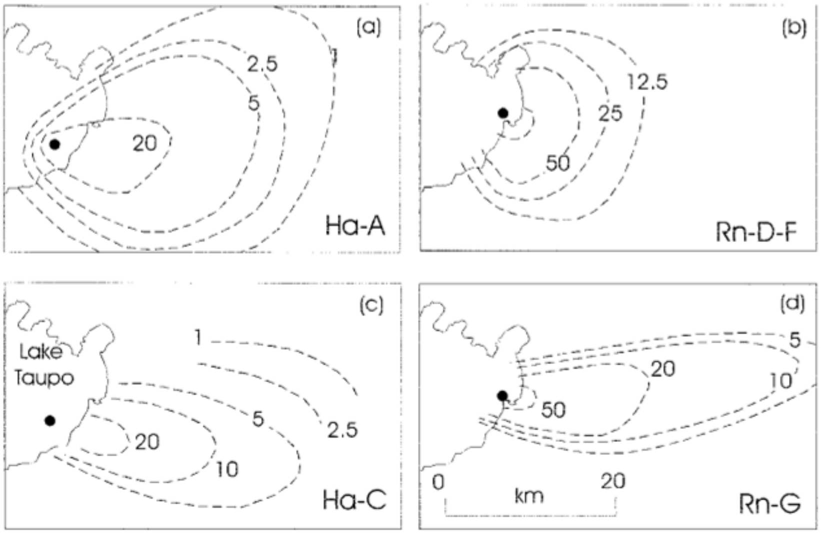

FIGURE 2 Isopach diagrams for selected units of the Hatepe and Rotongaio ashes showing the contrasting patterns of ash-rich (a and b) and lapilli-rich (c and d) beds. Thicknesses in cm (a–c) or mm (d).

2. *Hatepe and Rotongaio, New Zealand*

Two phases of the 181 AD eruption of Taupo caldera, the Hatepe and Rotongaio ashes, are among the type examples of phreatoplinian volcanism. The Hatepe ash is typical of most phreatoplinian deposits; shower bedded and rich in fine ash, it is dominated by highly vesicular pumice. It contains four subunits (Fig. 3). Fine ash and accretionary lapilli dominate two subunits, a third is dominantly lapilli-sized, and the fourth contains a mixture of fine ash and lapilli. Medial and distal exposures are of fall origin; proximal outcrops contain a significant proportion of material inferred to have been laterally emplaced by wet, dilute pyroclastic density currents. The vesicularity mode of pumice in the Hatepe ash is only slightly wider than that for the preceeding and following plinian fall deposits (Fig. 4), and it can be modeled as produced by the interaction of variable but moderate amounts of lake water with highly vesiculated magmatic foam.

The Rotongaio ash has dispersal and whole-deposit grain size characteristics similar to those of the Hatepe ash (Figs. 1 and 2) but is very different in detail. Its key characteristics are very wide dispersal and exceedingly fine grain size, with close to 100 wt% of the deposit finer than 1 mm; a finely laminated character even in the most proximal exposures; and a lack of lateral continuity for distances greater than 10 m of these fine-grained beds. The Rotongaio ash has an extremely low wall rock lithic content and a predominance of dense glassy juvenile clasts (Fig. 4). Many laminae consist of partially flattened, structureless, <1–2 mm in diameter ash pellets. A delicate balance apparently existed between accumulation and erosion during its deposition. Individual beds show a complete range of textures from primary fall through slope-affected material to water-reworked ash. The model for the eruption involves abundant lake water coming into contact with magma well after the peak of degassing, with development of highly unstable, short-lived eruption plumes and wide fluctuations of the water : magma ratio in these plumes.

In both the Hatepe and Rotongaio ashes there is a marked contrast in the dispersal pattern of relatively coarse (lapilli bearing) and relatively fine-grained subunits (Fig. 2). Coarse-grained packages were significantly more affected by crosswinds and hence have more restricted crosswind dispersals similar to the plinian phases of the same eruption; ash-rich subunits have much more symmetrical patterns of dispersal.

3. *Oruanui, New Zealand*

The 22.6 ^{14}C-ka Oruanui eruption of Taupo generated a ca. 500-km^3 fall deposit and a ca. 300-km^3 nonwelded ignimbrite. Evidences for interaction between magma and water (contained within a large lake) are:

(1) the exceptionally fine-grained nature of most fall deposits (F = 97–100%, Table I);
(2) the nonwelded nature of the ignimbrite, even where >200 m thick; and

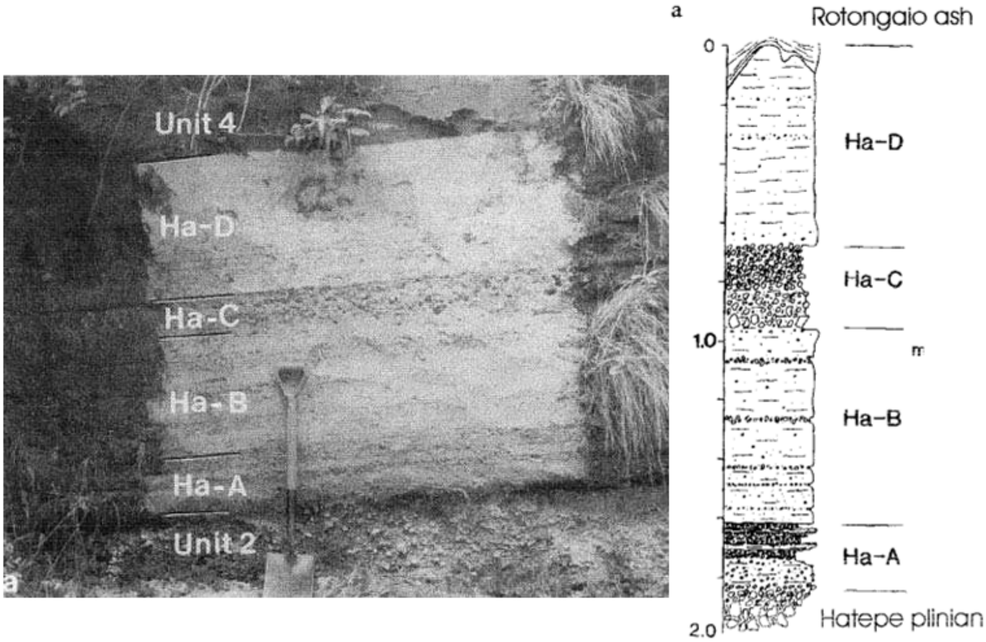

FIGURE 3 Stratigraphic log and photograph of the Hatepe ash, a typical phreatoplinian deposit.

(3) the abundant accretionary lapilli and vesicular cohesive ash textures in many fall units.

The fall deposits are multiple-bedded, mostly on decimeter to millimeter scale, reflecting the episodic nature of much of the eruption on perhaps a 1- to 20-km^3 volume scale. The eruption contained several time breaks, seen by minor erosion and/or fine ash beds in the deposits. The longest break was perhaps on the order of several months; the shortest was only a few hours to days.

Eight clearly demarcated fall units include (1) moderately to well-sorted pumice-fall beds (units 1, 5, and 7) that superficially resemble normal plinian deposits but show exceptionally wide dispersal, (2) similar beds that contain variable amounts of fine grained, water-flushed ash (units 2, 4, and 6), and (3) two units (units 3 and 8) dominated by cohesive fine ash. The latter are similar to the Rotongaio ash. Two overlying fall beds show only indistinct bedding, are more uniformly fine-grained vitric ash, and represent most of the total volume of the fall deposit. The macroscopic juvenile component in all beds is pumiceous, as in the Hatepe ash. All beds show some evidence of water involvement on deposition but, unlike the 181 AD examples at Taupo, there are virtually no signs of syneruptive remobilization of the depositing ash by running water. Water served to promote early deposition of ash by clumping, rain flushing, and formation of accretionary lapilli, which reach diameters up to 3–4 cm and locally make up to 50% of the volume of the deposit.

The associated ignimbrite was formed by numerous pyroclastic currents over most of the lifetime of the eruption and contains many tens to hundreds of flow units. It shows three unusual features:

(1) it increases in grain size upward as well as with proximity to the source, such that both the coarsest and the finest grained deposits are found at exposures close to the source;
(2) it typically contains 10–25 wt% of lithic material in proximal to medial sections, reflecting large-scale (tens of km^3) excavation of country rock during syn-eruptive caldera collapse; and
(3) distribution of the ignimbrite is bilaterally symmetric, with the farthest traveled flows reaching to the NE and SW.

B. General Characteristics

The unifying feature of the phreatoplinian eruptions listed above is that they all involve silicic magma interacting with lake water, yet even in these type examples there is an enormous range of attributes. All have *F*

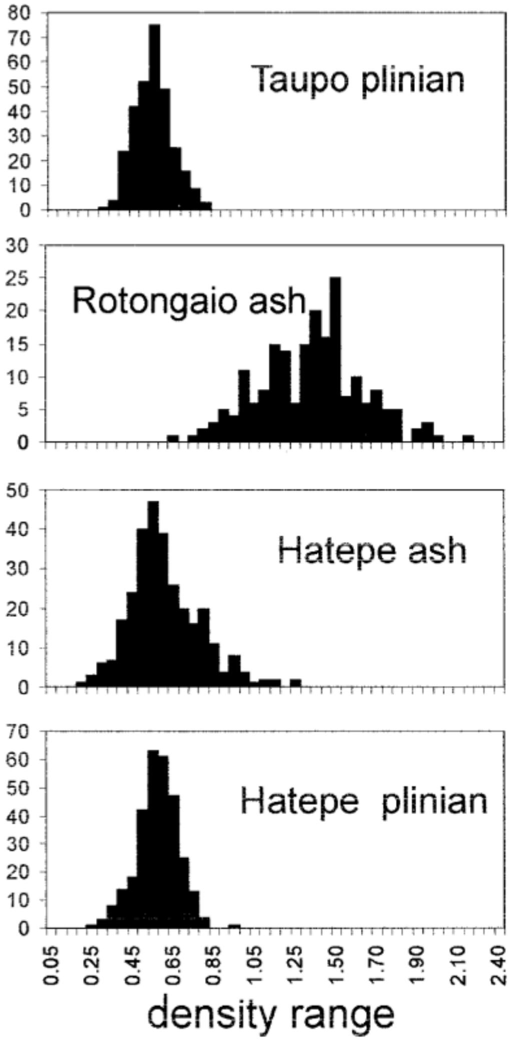

FIGURE 4 Density histograms for phases of the 181 AD Taupo eruption. The Hatepe ash shows density data broadly similar to those of the enclosing Taupo and Hatepe plinian deposits, whereas the Rotongaio ash shows a much wider range of values with no pronounced density mode.

indices of 80% or more, but the volumes of fall deposits vary by >3 orders of magnitude, from 0.1 to 500 km^3 (Table I). They form thin blankets dispersed over areas of 10^3 to $>10^6$ km^2 (B_t values from 3 up to 150 km, D values of 400 to 225,000,000 km^2). The duration of events has been measured (at Askja) to be as short as a few hours and estimated to be as long as weeks to months (in the case of Oruanui). Inferred intensities (discharge rates) thus overlap the ranges of subplinian and plinian eruptions. Some examples involve sustained discharge of magma on a timescale of hours, but others, notably the Rotongaio ash, show conspicuous evidence for repeated episodicity. Most examples are rich in pumiceous ejecta, implying that fragmentation may in (large?) part have been due to exsolution of magmatic volatiles prior to interaction with water. The Rotongaio ash, with its abundance of poorly vesicular clasts, and possibly the Askja-C deposit are clear exceptions. Most phreatoplinian fall deposits have very low wall rock contents (typically less than 5 wt%), with surprisingly little difference between ash-rich and lapilli-rich subunits. This implies that the magma : water interaction occurred at very shallow or surficial levels, consistent with the water sources being in crater or caldera lakes, rather than in aquifers. Exceptions are where fall deposition accompanies caldera collapse and emplacement of voluminous ignimbrites, for example, the Oruanui deposits, which typically contain 3 to 18 wt% wall rock.

The diversity between beds *within* individual phreatoplinian eruptions is also extreme, and some units within the phreatoplinian phases are identical in grain size and componentry to the deposits of plinian phases of the same eruption. This review highlights that even these classical deposits are diverse and internally complex. As discussed later, this diversity reflects the varying roles played by external water during fragmentation, transport, and deposition.

The type phreatoplinian deposits are divided here into three facies, which reflect three broad but very different modes of pyroclast transport and deposition. These are lapilli fall deposits, ash accretion fall deposits, and deposits of pyroclastic density currents.

The lapilli fall facies includes both fines-poor lapilli beds and fines-bearing lapilli beds. Fines-poor, coarse ash-lapilli beds are often indistinguishable from the products of plinian fall activity on the basis of grain size alone. Phreatomagmatic lapilli fall beds also show typical plinian isopach geometries and become progressively finer grained with distance from the vent. These features result from relatively dry processes in which clasts fall dominantly as individual particles, and size-fractionation and density-fractionation are effective during transport. Fines-bearing lapilli beds, in which lapilli are typically coated in very fine ash and set in a sparse matrix of massive ash or ash aggregates, are also common. The lapilli fall facies beds are interpreted as relatively dry fall with minor water-aided ash aggregation often due to either mixing with earlier erupted wet ash or due to regional rain storms.

In many eruption plumes, ash particles accrete to form aggregates that behave as individual particles during continuing transport and deposition. Ash accretion textures in the resulting deposits include *matrix-rich* beds

TABLE I Properties of the Type Phreatoplinian Deposits

Unit	V (km^3)	b_t (km)	b_c (km)	D (km^2)	F (wt%)
Askja 1875 C	0.2	4.5	4.0	400	79
[a]Oruanui fall 1	0.8	18		10000	100
fall 2	0.8	20		49000	100
fall 3 (distal)	4.8	18		45000	99
fall 5 (proximal)		68			
fall 5 (distal)		148			
fall 5 (total)	14		26	1.6×10^6	99
fall 6	5.5	44		260000	100
fall 7	15	58	39	470000	96
All fall deposits	500	>79		2.3×10^6	100
[b]Rotongaio ash G	0.02	4.4		2900	90
F	0.11	3.3		1500	100
E	0.27	4.7		3000	100
D	0.13	4.0		2200	100
C	0.04	5.0	6.5	3700	75
B	0.16	3.8		2000	100
A	0.07	2.9		1100	100
Hatepe ash D	0.80	5.5		4100	95
C	0.14	5.5	4.9	4000	70
B	0.66	5.2		3800	95
A	0.15	4.4		2000	85

[a] C. J. N. Wilson, unpublished data.

[b] R. T. Smith and B. F. Houghton, unpublished data.

Note. Unit 8 of the Oruanui eruption has been excluded because its unusual geometry precludes determination of the dispersal or grain size parameters. Columns are V, eruptive volume; b_t, thickness half-distance (see Fall Deposits); b_c, clast half-distance; D, dispersal index; F, fragmentation index.

containing scattered accretionary lapilli, *matrix-poor* beds of closely packed accretionary lapilli, and *vesicular* ash beds with remnant, partially coalesced accretionary lapilli (Fig. 5). A fourth fine-grained ash facies lacks any evidence for remnant accretionary lapilli but commonly passes gradationally, both laterally and vertically, into the other ash accretion facies. These features reflect a wide range of contents of liquid water during transport and on deposition. Field evidence implies that the development of these textures can vary rapidly in time and (in the Rotongaio and Hatepe examples described above) over distances as short as hundreds to a few thousand meters.

The products of pyroclastic density currents (PDC) in phreatoplinian eruptions are, with few exceptions (notably the Oruanui below), subordinate in volume to the fall deposits and only occur in proximal areas. Because there is so little contrast in grain size characteristics between phreatoplinian fall deposits and PDC deposits, bedforms yielding evidence for lateral emplacement are the most important diagnostic feature. These are seen in the form of pinching and swelling of laminae in the Rotongaio ash, through to the development of cross-bedded megaripples in the Askja 1875 deposits, and spectacular megaripples in the Phase 2 deposits of the Minoan eruption of Santorini. Other proximal PDC facies include massive to poorly bedded ignimbrite units, known from the 22 ^{14}C-ka Aira eruption in Japan (Tsumaya ignimbrite) and phase 3 of the Minoan eruption.

In the Oruanui deposits, two contrasting styles of PDC deposit are seen. The first is relatively normal nonwelded ignimbrite, which extends as far as 90 km from the vent and ranges up to 200–250 m in thickness. The bulk of the ignimbrite was emplaced as nongraded decimeter to meter scale flow units, whose contacts become blurred upward to form a vaguely stratified deposit in proximal areas. This material is interpreted as the product of relatively concentrated currents, that is, pyroclastic flows (s.s.). The second style of deposit forms a small proportion of the main ignimbrite (particularly

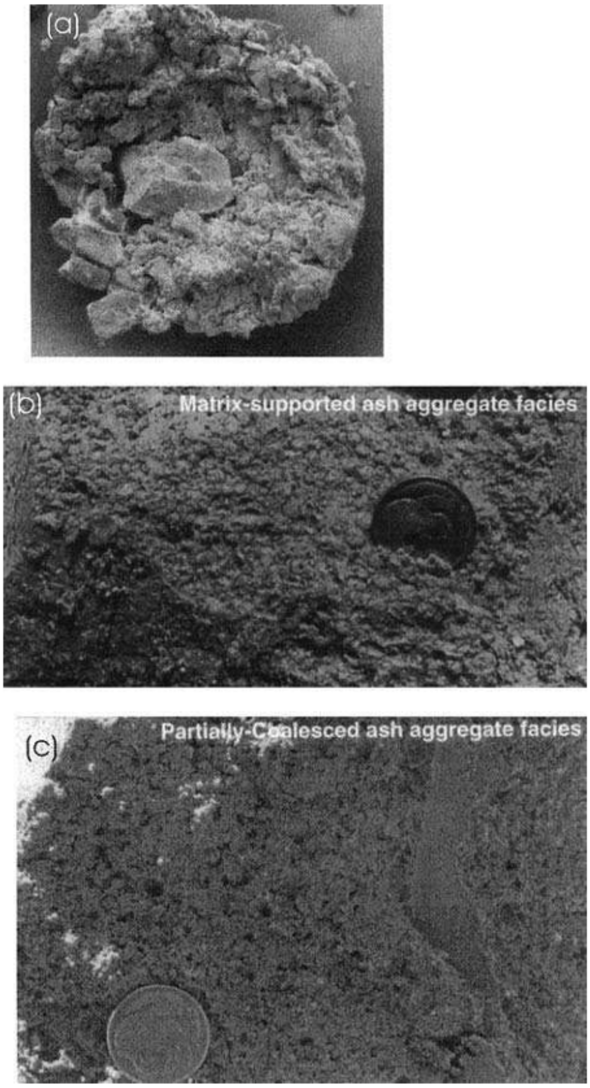
(a)
(b)
Matrix-supported ash aggregate facies
(c)
Partially-Coalesced ash aggregate facies

FIGURE 5 Photographs of ash aggregates: (a) a single accretionary lapillus from Sakurajima. [From *Volcanic Plumes* R. S. J. Sparks *et al.* Copyright John Wiley & Sons Limited. Reproduced with permission.] (b) a mixture of ash aggregates and disaggregated fine ash, and (c) a unit in which ash aggregates have partially coalesced to leave an open *vesicular* structure.

the distal fringes of flow units) and much of the proximal parts of fall unit 3. It consists of beds that are normally graded from coarse-ash bases (with nonerosive to mildly erosive basal contacts) up to fine-ash dominant material that is indistinguishable from the contemporaneous fall material. These units resemble turbidites in their grading and are interpreted as the products of relatively dilute suspension currents that temporarily interrupted fall deposition at any particular locality.

Grain size data from phreatoplinian ignimbrites are limited, but suggest that they are somewhat finer grained than typical ignimbrites, both lacking abundant lapilli- to block-sized material and having a higher proportion of <1/16-mm ash. Both features are attributed to enhanced fragmentation during magma : water interaction.

C. Other Potential Candidates for Phreatoplinian Eruptions?

1. *Vesuvius*

The type plinian and subplinian eruptions of Vesuvius end with phreatomagmatic phases for which there is compelling evidence that the external water phase was groundwater, in an aquifer at kilometer scale depths beneath the volcano. Typically each phreatomagmatic deposit contains two phases: a lower unit characterized by ignimbrite, lapilli fall, and surge deposits (e.g., the 79 AD phreatomagmatic dry phase) and an upper unit rich in fine ash containing surge and fall deposits often rich in accretionary lapilli (e.g., the 79 AD phreatomagmatic wet phase). The upper units are generally limited in their dispersal (i.e., analogous to subplinian) but are otherwise texturally identical to the classical phreatoplinian deposits described above. The lower portions of the phreatomagmatic units are multiple bedded and these beds are coarser grained and better sorted than the type phreatoplinian deposits and, in these regards, more similar to the associated plinian falls. However there are two forms of textural evidence from the pyroclasts that support the notion that magma : water interaction occurred during fragmentation in both types of phreatomagmatic product. First, the juvenile clasts show a wide range of vesicularities and coatings of fine ash particles, the glass phase is commonly altered, and secondary minerals encrust clasts and fill vesicles. Second, these deposits contain a high proportion of deep-derived wall rock lithics that can be matched only to the lithologies encountered in drill holes at the level of the deep aquifer. Whether either or both types of phreatomagmatic deposit at Vesuvius should be termed phreatoplinian is discussed in Section IV, A.

2. *18 May 1980, Mount St. Helens*

The fall deposit associated with the 18 May 1980 eruption of Mount St. Helens is a widespread unit that has generally been regarded as classically plinian and coignimbrite in nature. Accumulation of the distal fall is inferred to have involved significant aggregation of very fine ash, leading to a secondary thickness maximum 325 km from the vent. The 18 May 1980 deposit is one of few fall deposits for which a calculation can be made of the whole deposit grain size. The deposit is strikingly fine-grained, polymodal, and poorly to very poorly sorted at all medial to distal sites, leading to the suggestion, made in the principal study of the ash, that the deposit could be classified as phreatoplinian. The proximal equivalents of the ash fall are principally the accretionary-lapilli-bearing unit A3 (a coignimbrite fall deposit) and the vent-derived lapilli fall units B1, B2, and B4. The latter are lapilli or coarse-ash sized and relatively well sorted.

II. ERUPTION AND TRANSPORT PROCESSES

A. Fragmentation and Eruption Mechanisms

Fragmentation (and explosive eruption) in the majority of the examples described here was brought about by vesicle nucleation and growth as well as by quenching by external water. The high degree of vesiculation of the juvenile clasts has generally been taken to imply that the magma was already a foam and perhaps starting to fragment when it first encountered external water. The precise mechanism for both of these processes is far from well defined (see Magmatic Fragmentation, and Phreatomagmatic Fragmentation). In one significant exception that we are aware of, the Rotongaio ash, fragmentation appears to have taken place after degassing, and explosivity driven by the rapid exsolution of large volumes of magmatic volatiles appears to have been unimportant.

Most of the documented phreatoplinian deposits represent eruptions where the frequency of individual explosions was such that a continuous plume was maintained for periods of hours or more. There are three significant exceptions to this: the Rotongaio ash, the Ikedako ash from Ikeda caldera in Japan, and Unit E of the 260AD Terra Blanca Jovan tephra from Ilopango caldera in El Salvador. Each of these deposits contains numerous sharply defined millimeter- to centimeter-thick beds suggesting that the deposits are the products of numerous powerful but discrete explosions that gave rise to individual short-lived plumes and numerous short-lived episodes of deposition.

B. Accretionary Lapilli and Ash Aggregation

The processes of collision, binding, and breakup of particles in moisture-bearing eruption plumes lead to the formation of aggregates of ash (Fig. 5a) that in turn play an important role in the deposition of ash from phreatoplinian plumes. Ash aggregates fall with greater velocities than their component particles and so the process of aggregation results in the premature flushing of large quantities of fine ash and the simultaneous deposition of a wide range of grain sizes. This creates poorly sorted and fine-grained fall deposits even close to the vent.

The formation of aggregates is governed by factors such as the concentration, shapes, and size distributions of ash, the abundance and physical state of water in the plume, and the temperature and relative humidity of the plume and surrounding atmosphere. Phreatoplinian ash aggregates form a spectrum, which can be related, in the first instance, to the liquid content (water plus dissolved gas species) of the depositing pyroclast assemblage. The spectrum ranges from weak clusters of grains at the dry end to ash-free rainfall at the wet end. In between these two endmembers are accretionary lapilli of various types, sizes, and structures and mud rain. The dry end of the ash aggregation spectrum is represented by weak clusters of grains, which have been observed to fall from dry plinian plumes. With condensation of water in an eruption plume, ash will accrete into denser clumps as accretionary lapilli. Recent experimental work shows that the likely origin of accretionary lapilli is through collision of liquid-coated ash particles in the plume. Ash particles in a water-rich plume act as condensation nucleii for water vapor and clasts and may be continually coated in acidic liquid or ice. When clasts collide, due to different fall velocities and convection in the plume, the potential for binding is enhanced because of the effect of strong, short-range surface tension forces. Electrostatic attraction is also important for attraction of particles and the fine-grained outer layers on many accretionary lapilli probably form this way.

C. Pyroclastic Density Currents and Phreatoplinian Volcanism

In phreatoplinian eruptions, formation of pyroclastic density currents occurs both on a local scale by lateral ejection of material directly from the base of an otherwise stable plume and through partial or complete column collapse, forming flows on a large scale. A wide spectrum of PDC has occurred in phreatoplinian events:

(1) weak dilute currents (e.g., Rotongaio) that leave only subtle evidence for lateral transport,
(2) energetic dilute currents that generate cross-bedded surge deposits (e.g., Minoan phase 2, Hatepe) or normally graded turbidite-like beds (e.g., some Oruanui units), and
(3) concentrated flows of low to high energy that deposit conventional ignimbrite (e.g., most Oruanui units).

Two features are useful in distinguishing phreatoplinian PDC deposits from their dry counterparts: first, the presence of accretionary lapilli and, second, evidence for cohesion (induced by liquid water) on deposition, such as oversteepened beds and plastering of vertical surfaces.

D. Numerical Models for Phreatoplinian Plumes

There are some indications that existing models for eruption columns are inadequate to quantify phreatoplinian systems, due to complexities and uncertainties in the nature of surficial magma: water interaction. Theoretical models suggest that limited amounts of added water (to about 15 wt%) serve to expand the field of stability for buoyant plumes (which produce fall deposits) and have little effect on the height (i.e., dispersal power) of the buoyant plume. Excessive amounts of water (>40–50%) cause column collapse, generating pyroclastic density currents. Field evidence to test against these hypotheses is generally lacking, because there is no linkage in the published literature between estimates of water contents in the depositing material (which is all that can be assessed) and the inferred water contents in the eruptive plumes.

There is, however, sufficient field evidence to suggest that the models for stability fields of phreatoplinian plumes are not adequate at present. The Hatepe and Rotongaio units were deposited with enough water to locally generate contemporaneous streams, yet are dominantly (>95 vol%) composed of fall material. The large amounts of water involved in these eruptions apparently did not cause major fountain collapse, and only local, proximal PDC deposits are known. In contrast, in the Oruanui eruption, the volumes of fall and PDC deposits are similar (and large) but the plume water content was probably much lower. In addition, the extremely powerful dispersal of the Oruanui fall units (both drier and wetter deposited) seems at odds with the suggestion that the height of phreatoplinian plumes is reduced relative to their dry analogs (as theory predicts for such large events). Perhaps either phreatoplinian plume expansion rates are correspondingly more rapid or some unknown mechanism is operating to carry pyroclasts further from the vent prior to their deposition.

III. DEPOSITION PROCESSES

A. Processes of Fall Deposition

Phreatoplinian deposits contain mixtures and alternations of clasts that were deposited as discrete particles and as ash aggregates. Lapilli-rich units contained within the type phreatoplinian deposits share the grain size and dispersal characteristics of plinian falls and were not significantly influenced by processes of particle aggregation. The type examples also contain some beds of relatively well-sorted, fine or medium ash. These are likely to have been products of fallout of loosely bound dry aggregates of grains and weakly cohesive accretionary lapilli that disintegrated on impact.

Ash aggregates are deposited with a wide range of water contents. Direct observations of historical eruptions include very dry clusters that crumbled on impact (Mount St. Helens 1980), aggregates that remained intact (e.g., Sakurajima), those that splashed on impact (Soufrière, St. Vincent 1979), and those that landed intact but defrosted into a mud slurry (Ruapehu 1969).

At the very wet end of the spectrum of ash deposition is mud rain. Where a plume is rich in water vapor and liquid, droplets form up to a few millimeters in diameter and scavenge particles as they fall, leading to rainout of wet mud. Quantitative records of this style of ash fall are rare.

We infer that beds containing accretionary lapilli/mud lumps in a matrix of loose ash of comparable grain size (Fig. 5b) reflect simultaneous deposition of accretionary lapilli/mud lumps that crumbled and were destroyed on impact and aggregates that fell frozen/cemented and intact. Beds of well-sorted accretionary lapilli reflect deposition of intact frozen accretionary lapilli or lapilli cemented by secondary mineral growth during transport. Beds of partially coalesced accretionary lapilli (Fig. 5c) represent deposition of accretionary lapilli that deformed plastically at or soon after deposition and adhered at contact points (note that the contrast with the well-sorted beds of accretionary lapilli may simply reflect the ambient temperature at the Earth's surface at the time of deposition). Massive fine ash beds with relict vesicular textures are more difficult to interpret unequivocally, but may represent the deposition of wet mud lumps, transitional to mud rain. The degree of agglutination of the aggregates probably reflects both liquid–ash ratio and accumulation rate. In either case the process requires liquid–ash ratios higher than those of the other facies types. Thick beds of coalesced aggregates may represent prolonged episodes of wet mud lumps/mud rainfall, whereas thin, irregular intervals may reflect ephemeral changes in accumulation rate.

B. Syneruptive Erosion

The products of secondary processes occur interbedded with primary phreatoplinian products on a centimeter or decimeter scale in some units and, locally, secondary beds can be found juxtaposed with, or transitional into, primary beds at the same stratigraphic level (Fig. 6). Field evidence clearly shows that such secondary processes were *syneruptive* and a complex and intimate relationship existed between primary pyroclastic deposition and secondary reworking. The relative timing of primary depositional events and secondary modification is variable and in many instances secondary modification must have been coincident with primary accumulation, both temporally and spatially.

Throughout deposition of units such as the Rotongaio ash there was always a delicate balance between accumulation, reworking, and erosion. This balance was affected by factors related to vent conditions, plume dynamics, regional scale topography and local relief, hydrological conditions at the point of deposition, external meteorological influences, and the interaction between many of these factors. The extent to which a bed is secondary was, in large part, a function of primary deposition of the ash, controlled by eruptive conditions but influenced by aspects of the local depositional environment.

The products of reworking range from well-sorted ash lenses, produced by sheet washing, to channel-confined, well-sorted, lithic- and crystal-rich fluvial sand. The sheet wash lenses are diffuse, millimeter scale fines-poor partings or wisps that are laterally discontinuous and occur within otherwise primary fall beds. The fluvial beds are typically massive and well-sorted with no evidence for tractional structures. This reflects the scale of the sedimentary processes involved, with typically very short transport distances (i.e., meters rather than kilometers).

A feature of all ash-rich beds of the Rotongaio ash is plastic deformation and thickness variations along out-

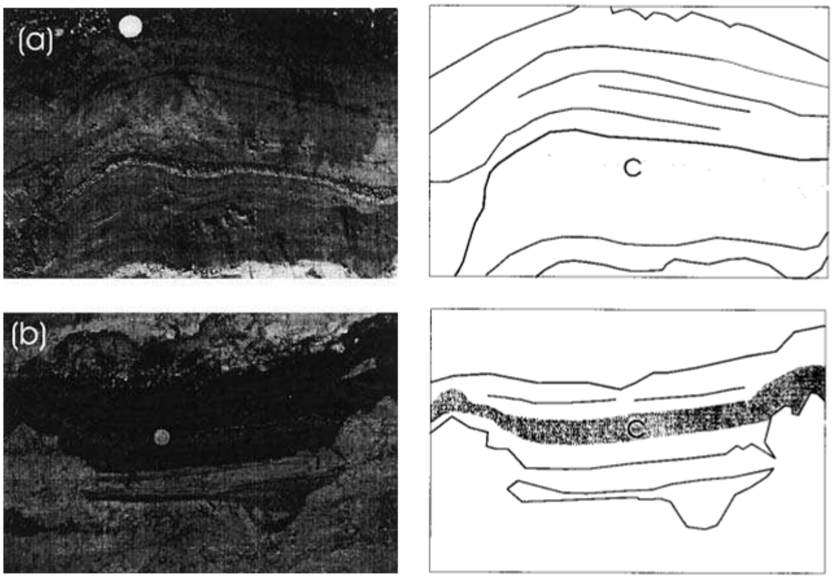

FIGURE 6 Photographs showing syneruptive reworking of the Rotongaio and Hatepe ash. Note the multiple gullies within the Rotongaio ash in (a) and the presence of lenses of reworked Hatepe ash (pale material) within the overlying Rotongaio ash in (b). Subunit Rn-C is labeled C for reference.

crop in response to the local topography. The extent of these variations is a function of the liquid–particle ratio of the deposition system, the extent and form of the micro- and regional topography, and the nature of the underlying bed at the time of deposition. In some cases ash has clearly flowed off high ground as a viscous liquid producing flat-topped gully infills.

IV. DISCUSSION

A. Wet Eruption versus Wet Deposition

One of the major outstanding problems in studies of phreatoplinian volcanism is that there is some degree of independence between processes occurring at the eruptive vent and those influencing deposition. Phreatoplinian volcanism, by definition, implies wet activity at the vent, but the extent to which that is revealed in wet *deposition* is highly variable, as discussed in previous sections. For example, in the Rotongaio ash, liquid : ash ratios during deposition varied significantly on a *local* scale of tens to hundreds of meters, from locations where matrix-free pellets were being deposited to sites where surface erosion and rilling was occurring through runoff of excess water. Thus even where reconstruction of the proportion of water involved on deposition can be carried out, the ash : water ratios thus derived need not reflect relative or absolute values of the magma : water ratio at the vent.

Equally well, explosive eruptions that are dry at the vent can generate deposits that in many respects are indistinguishable *on the outcrop scale* from phreatoplinian deposits, reflecting entrainment of atmospheric moisture or the impact of regional weather systems. Rain-flushed beds within dry plinian fall deposits are attributed, for example, to the chance passing of storms during the eruption. The most extreme example of this occurred during the 15 June 1991 climactic phase of the Pinatubo eruption, when the plume interacted with a tropical cyclone, and much of the proximal to medial fall deposition was as wet, water-saturated material.

In young well-exposed deposits commonly there are additional kinds of evidence, apart from that of wet deposition of ash, to facilitate identification of phreatoplinian volcanism. However, in ancient or poorly exposed deposits the discrimination of phreatoplinian deposits from other fine-grained, poorly sorted deposits is problematic.

B. The Spectrum of Widespread, Phreatomagmatic Fall Deposits

The type phreatoplinian deposits are conspicuously fine grained and were singled out on the basis of the presence of ash-rich beds often containing accretionary lapilli. However within these predominantly fine-grained phases there are coarser grained and better sorted beds (e.g., Oruanui units 1, 2, 5, and 7; Rotongaio ash C; Hatepe ash C; Table I). A key question is, are these units plinian, that is, the products of absolutely dry or magmatic fragmentation, or do they represent phreatomagmatic intervals with a low water : magma ratio?

All these type units, fine-grained or coarse-grained, aggregate-bearing or aggregate-free, are inferred, on the basis of the known hydrology of the vent area, to have resulted from the interaction of magma with surface water. The equally well-studied historical eruptions of Vesuvius contain similar deposits where the evidence is equally compelling that the erupted magma encountered deep groundwater contained within a limestone aquifer. The Vesuvius deposits also contain ash-rich, poorly sorted beds rich in accretionary lapilli and coarse-grained, better sorted lapilli fall deposits. By comparing these two types of youthful well-studied deposits we can observe some differences between the interaction of silicic magma with surface water and with groundwater. In comparison to the former, the latter contain a wider range of vesicularities and morphologies among the juvenile clasts, evidence for coating and alteration of juvenile clasts and a generally (but not exclusively) higher abundance of wall rock lithic clasts linked to stratigraphic units found only at great depths below the volcano. However it is extremely doubtful whether such a distinction between surface water and groundwater sources could be made consistently during study of ancient deposits.

The Vesuvius phreatomagmatic deposits help us with the dilemma over units like Oruanui units 1, 2, 5, and 7; Rotongaio ash C; and Hatepe ash C. The Vesuvius beds show much more convincing evidence that low water : magma ratios have little effect on fragmentation levels and hence the grain size properties of the deposits, yet other indicators, such as clast vesicularity and morphology, lithic clast abundances, and coatings of ash and secondary minerals, show that some external water was involved in the eruption. This is strong circumstantial evidence suggesting that grain size parameters are not the most sensitive indicators of limited magma : water interaction and conversely that moderate-to-high water/magma ratios are required to produce fine-grained, poorly sorted deposits rich in accretionary lapilli.

C. Gradation to Other Eruptive Styles

The distinction between plinian and phreatoplinian styles of explosive eruptions is in the involvement of recognizable quantities of external water in eruption and transport processes; in practice, the distinction between plinian and phreatoplinian deposits is based on grain size parameters. In outcrops of the Askja 1875 and Taupo 181 AD deposits there is a clear distinction between plinian units, which are both coarse-grained and relatively well sorted (Askja-D, Hatepe plinian, Taupo plinian), and phreatoplinian deposits, which are dominantly fine-grained and very poorly sorted (Askja-C, Hatepe ash, Rotongaio ash). However within the fine-grained phreatoplinian units there are beds or packages of beds whose grain size characteristics are indistinguishable from those of plinian deposits.

Some vulcanian eruptions have instantaneous discharge rates equivalent to phreatoplinian and plinian events and produce widely dispersed sheet-like fall deposits. They differ from plinian and most phreatoplinian eruptions in that they are nonsustained and are typically a sequence of discrete explosions. In vulcanian deposits the time breaks are recorded by the presence of sharply defined, centimeter to meter scale bedding.

D. A Practical Definition of Phreatoplinian Volcanism

Plinian and phreatoplinian deposits were first distinguished on the basis of the *fragmentation index*. More recent classifications (see Pyroclastic Fall Deposits) lack a measure of absolute grain size and thus do not distinguish even the type phreatoplinian units from plinian deposits.

The classical examples of phreatoplinian eruptions involved sustained eruption of highly vesiculated silicic magma through a source of abundant lake water. The Rotongaio ash is an exception to this in two ways. First, the eruption was not sustained but formed a sequence of short-lived high plumes, related to discrete explosions, and, second, the juvenile component was largely degassed at the time of fragmentation. A key question is how significant are these differences and how restrictive should the definition of phreatoplinian be? At its broadest this definition could be *Phreatomagmatic eruptions whose products have plinian or subplinian dispersal.* This definition would include the Rotongaio ash and also widespread phreatomagmatic falls associated with magma interacting with groundwater, for example, phreatomagmatic phases of the historical Vesuvius eruptions. We strongly favor adoption of such a broad definition. The most obvious flaw in this definition is that proof of a phreatomagmatic origin becomes more difficult as the water : magma ratio decreases—how different for example are the lapilli falls in the Hatepe ash from dry plinian falls?

In answer to the questions asked at the start of this chapter:

- *Is high vesicularity of the erupting magma part of the definition for phreatoplinian eruptions?* No, the Rotongaio and Askja-C ashes and many of the Vesuvian phreatomagmatic deposits contain dense, relatively poorly vesicular clasts.
- *Should all fine-grained fall deposits with wide dispersal be called phreatoplinian?* Yes *if* one can infer or observe the involvement of external water in the eruption process (thus excluding, for example, equally fine grained layer 3 deposits of ignimbrites).
- *Must phreatoplinian eruption columns be sustained?* No, although, at some stage in the future, it may be practical to separate a class that includes units like the Rotongaio and Ikedako ashes from units like the Hatepe and Askja-C deposits.
- *What dispersal index is an appropriate lower limit for phreatoplinian eruptions?* The current limit seems a better alternative to the introduction of a name such as *phreato-subplinian*.
- *How useful are grain size parameters in delineating phreatoplinian deposits?* Grain size criteria alone can be used to identify deposits corresponding to moderate to high water : magma ratios but not the products of weakly phreatomagmatic eruptions.
- *What range of water : magma ratios should phreatoplinian volcanism be applied to?* Low water : magma ratios often cannot be detected either during eruptions or from deposits. In a philosophical sense a lower limit corresponding to equal amounts of external water and intrinsic dissolved volatiles is appealing but, for a practical classification, it is preferable not to set a rigid hypothetical limit.

SEE ALSO THE FOLLOWING ARTICLES

Magmatic Fragmentation • Phreatomagmatic Fragmentation • Plinian and Subplinian Eruptions •

Pyroclastic Fall Deposits • Surtseyan and Related Phreatomagmatic Eruptions

FURTHER READING

Carey, S. N., and Sigurdsson, H. (1982). Influence of particle aggregation on deposition of distal tephra from the May 18, 1980, eruption of Mount St. Helens. *J. Geophys. Res.* **87,** 7061–7072.

Cioni, R., Sbrana, A., and Vecci, R. (1992). Morphological features of juvenile pyroclasts from magmatic and phreatomagmatic deposits of Vesuvius. *J. Volcanol. Geotherm. Res.* **51,** 61–78.

Koyaguchi, T., and Woods, A. W. (1996). On the formation of eruption columns following explosive mixing of magma and surface water. *J. Geophys. Res.* **101,** 5561–5574.

Self, S. (1983). Large scale silicic phreatomagmatic volcanism: A case study from New Zealand. *J. Volcanol. Geotherm. Res.* **17,** 433–469.

Self, S., and Sparks, R. S. J. (1978). Characteristics of widespread pyroclastic deposits formed by the interaction of silicic magma and water. *Bull. Volcanol.* **41,** 196–212.

Sigvaldason, G. E. (1979). Rifting, magmatic activity, and interaction between acid and basic liquids: The 1875 Askja eruption in Iceland. Nordic Volcanological Institute Science Report 7903, Reykjavik, Iceland.

Sparks, R. S. J., Wilson, L., and Sigurdsson, H. (1981). The pyroclastic deposits of the 1875 eruption of Askja, Iceland. *Philos. Trans. R. Soc. London A* **299,** 241–273.

Walker, G. P. L. (1981). Characteristics of two phreatomagmatic ashes and their water-flushed origins. *J. Volcanol. Geotherm. Res.* **9,** 395–407.

This Page Intentionally Left Blank

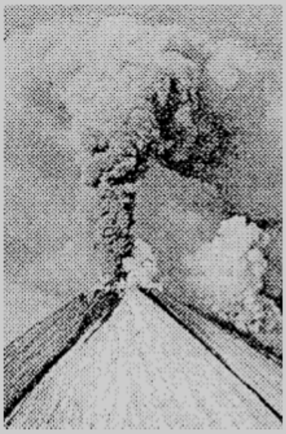

VOLCANIC PLUMES

STEVEN CAREY
University of Rhode Island

MARCUS BURSIK
State University of New York at Buffalo

I. Generation of Volcanic Plumes
II. Structure and Behavior of Volcanic Plumes
III. Atmospheric Effects on Plume Dispersal
IV. Future Research

GLOSSARY

advection Horizontal transport of material.

chaotic advection The stretching of air parcels into complex shapes by wind.

co-ignimbrite plume Plume produced from a pyroclastic flow.

elutriation Loss of small particles by the upward flow of gas through a pyroclastic flow.

entrainment The process of picking up and carrying along.

hemispheric flow The largest scale of the atmospheric flow, generally in distinct latitudinal bands; also called zonal flow.

latent heat of condensation Heat released upon conversion of vapor to liquid.

neutral buoyancy level Height at which the plume density is equal to the surrounding atmosphere.

stratosphere The upper portion of the atmosphere from an altitude of about 10 to 50 km.

thermal A discrete mass of air or particles and gases that rise in the atmosphere by buoyancy.

troposphere The lower portion of the atmosphere from ground level to about 10 km.

tropopause Boundary between the troposphere and stratosphere.

turbulent diffusion Mixing by turbulent flow.

VOLCANIC PLUMES are mixtures of volcanic particles, gases, and air that are produced mainly by explosive eruptions. They are injected into the atmosphere and can disperse ash and gases on a global scale. Buoyancy plays a fundamental role in the motion of plumes and determines how they interact with the atmosphere. Energetic plumes can rise to altitudes as great as 50 km above the Earth's surface. Many different types of eruptions can produce plumes and their behavior is controlled by such factors as the composition of erupted magma, the amount and nature of volatile components, the rate of magma discharge, and the geometry of the source vent. Some plumes are maintained for relatively long periods of time by the continuous discharge of material from a vent. For example, the eruption of Mount St. Helens (United States) on May 18, 1980, produced a volcanic plume for over 9 hours. In other

Copyright © 2000 by Academic Press
All rights of reproduction in any form reserved.

cases, plumes form discrete injections of gases and particles into the atmosphere that may last for only a few minutes.

Plumes are a complex phenomena to model and understand because they are mixtures of gases, solids, and liquids. However, much has been learned about volcanic plumes through the application of basic theories on turbulent convective plumes. In particular, the transition in plume behavior from convective rise to collapse is especially important. Rising plumes are generally able to disperse volcanic particles and gases over large areas by transport and fallout through the atmosphere. This type of activity poses relatively low deadly volcanic risk to the surrounding population. An exception, however, is the hazard to aircraft in flight that inadvertently encounter volcanic plumes. Ingestion of particles and gases can lead to engine failure and the potential for disaster. In contrast, collapsing plumes generate hot mixtures of gases and particles (pyroclastic flows and surges) that move down the slopes of a volcano at high speeds and can result in large numbers of fatalities.

I. GENERATION OF VOLCANIC PLUMES

Volcanic plumes are generated when magma is fragmented into small pieces and discharged from a vent at high velocity. The erupted mixture consists of partially molten or solid particles that represent the magma, gases from the magma or the surrounding environment (which may condense to liquids), and pieces of the volcanic edifice, referred to as wall rock lithics. Rapid acceleration of this material into the atmosphere is largely driven by the expansion of gases due to the decrease in pressure as material is erupted at the surface.

A. Fragmentation by Volatile Degassing

Most magmas contain small amounts of dissolved volatile components such as water, carbon dioxide, and sulfur dioxide prior to eruption when they are stored beneath the Earth's surface. The solubility of these components increases as a function of pressure, or depth. Conversely, as magmas rise to the surface these volatile components begin to come out of solution to form bubbles (Fig. 1). Bubble expansion occurs by a combination of pressure drop and diffusion of the volatile components from the dissolved state in the magma to a gas phase. As the volatile components form bubbles the magma's viscosity increases. As a result of the high viscosity, bubble growth is impeded and high internal pressures develop within the bubbles. The net result is that bubble walls rupture and the magma is transformed into a mixture of broken bubble fragments and gas in the conduit. Above this fragmentation region gas becomes the continuous phase carrying particles suspended in a rapidly accelerating and turbulent mixture (Fig. 1). Discharge of this material out of a vent forms volcanic plumes. Examples of such plumes include the explosive eruptions of Mount St. Helens in 1980 (Fig. 2; see also color insert), the 79 A.D. eruption of Vesuvius, and the great 1815 eruption of Tambora in Indonesia (see Magmatic Fragmentation).

B. Fragmentation by Interaction with External Water

Volcanic eruptions often involve the interaction of hot magma with water at, or near, the Earth's surface. Under certain conditions the transfer of heat from magma to water can result in the explosive conversion of water to steam and fragmentation of magma into small pieces. This type of activity is referred to as phreatomagmatic. The factors that influence whether the magma–water interaction will be explosive or not include the mass ratio of water to magma, the degree to which the interaction is confined, and the rate at which the interaction takes place. The maximum energy release occurs when the ratio of water to magma is about 0.3. Volcanic plumes generated by this mechanism may contain larger quantities of water and be cooler than those produced by degassing of volatiles directly from magma. Spectacular examples of plumes generated by magma–water interaction occurred during the emergence of Surtsey Volcano from the sea south of Iceland in 1963. Instantaneous releases of particles and steam may also occur when magma encounters water under confined conditions. One example would be when rising magma intersects an aquifer during its ascent beneath a volcano (see Phreatomagmatic Fragmentation).

C. Elutriation from Pyroclastic Flows and Surges

In most cases the mixtures of hot gas and particles that are ejected from volcanoes during explosive eruptions have an initial bulk density (gas+particles) that is higher

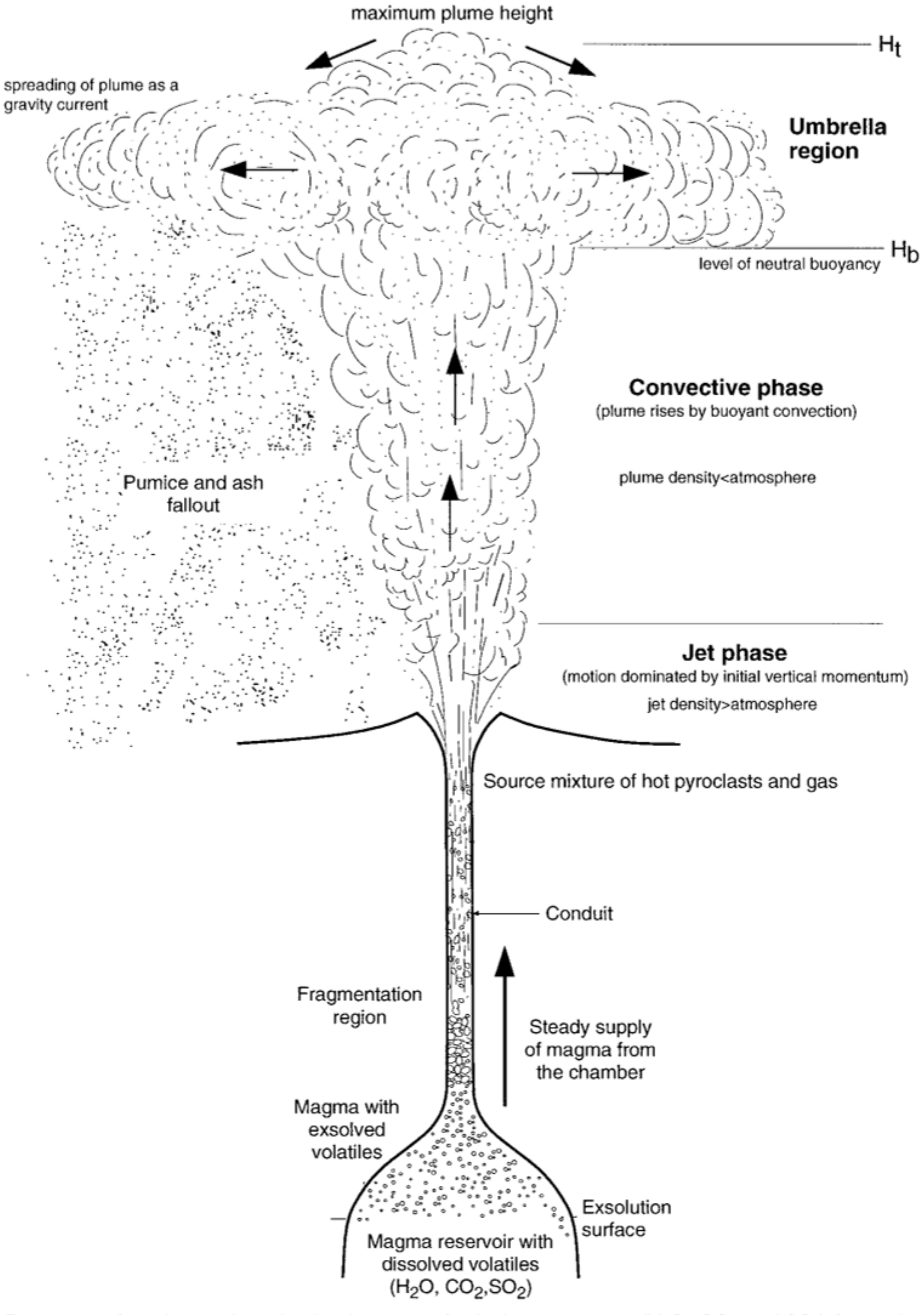
maximum plume height
H_t
spreading of plume as a gravity current
Umbrella region
H_b
level of neutral buoyancy
Convective phase
(plume rises by buoyant convection)
plume density<atmosphere
Pumice and ash fallout
Jet phase
(motion dominated by initial vertical momentum)
jet density>atmosphere
Source mixture of hot pyroclasts and gas
Conduit
Fragmentation region
Steady supply of magma from the chamber
Magma with exsolved volatiles
Exsolution surface
Magma reservoir with dissolved volatiles (H_2O, CO_2,SO_2)

FIGURE 1 Formation of a volcanic plume by the degassing of volatile components (H_2O, CO_2, and SO_2) from a high silica magma. Magma with bubbles (foam) is converted to a highly turbulent mixture of gas and magma fragments within the fragmentation region. Above this level the mixture accelerates and is discharged from the vent at high velocity, forming a jet phase. Entrainment and heating of air causes the plume to rise buoyantly in the convective phase. At high levels in the atmosphere the plume reaches a neutral buoyancy level and spreads out to form an umbrella region. H_t is the maximum height attained by the plume and H_b is the height at which the plume density is equal to that of the surrounding atmosphere.

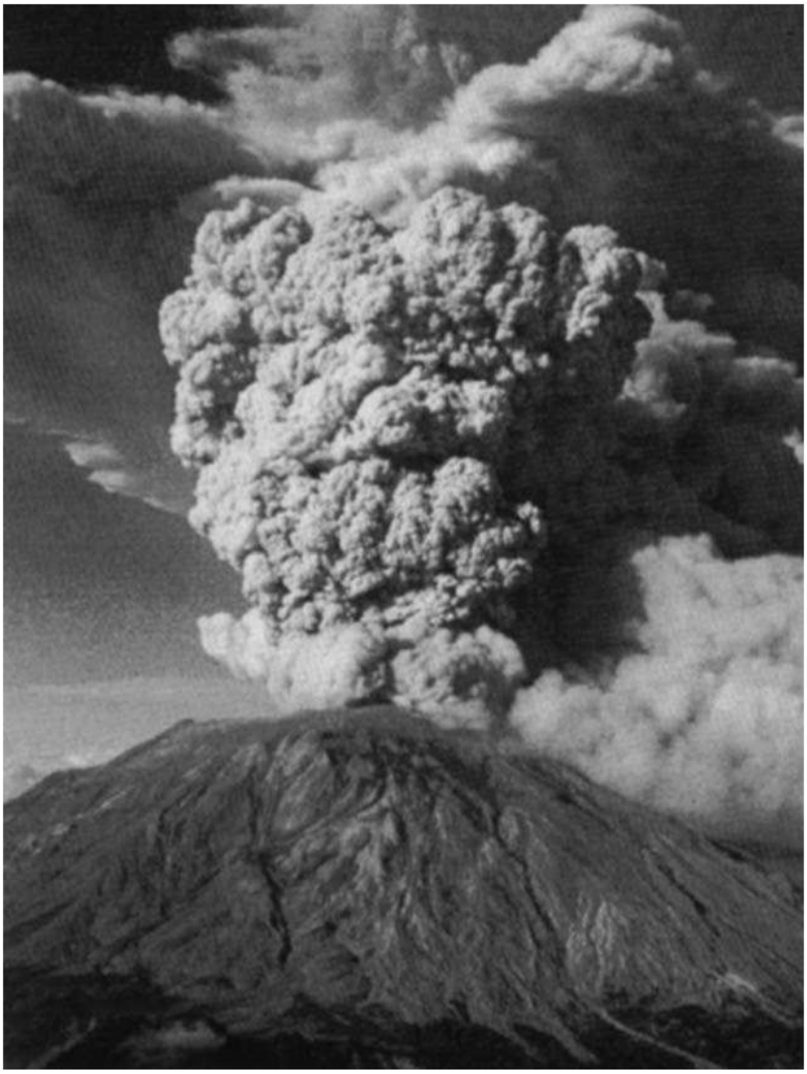

FIGURE 2 Volcanic plume generated by the July 22, 1980, explosive eruption of Mount St. Helens volcano. Magma fragmentation was driven by exsolution of dissolved volatiles in a dacitic magma. [Photo by Michael Doukas, reprinted with permission of the USGS Cascades Volcano Observatory. See also color insert.]

than that of the surrounding atmosphere. Unless they can achieve positive buoyancy they will collapse and flow down the slope of the volcano as pyroclastic flows or surges. As these flows travel away from their sources, sedimentation of particles from their bases and the heating of entrained air leads to a decrease in bulk density. Secondary plumes, or co-ignimbrite plumes, are then generated from the tops of flows by buoyant rise. The source of the plume is thus displaced laterally away from the source vent and may encompass an enormous area. During the initial phase of the Mount St. Helens eruption in 1980 a giant plume was generated from the top of a pyroclastic surge that traveled up to 29 km from the volcano.

D. Heat Transfer During Effusive Eruptions and Fire Fountaining

Particle-poor volcanic plumes may be generated during eruptions that discharge large volumes of basaltic magma. In general, basaltic magmas contain lower amounts of volatile components, such as water and carbon dioxide, compared to more silicic magmas. In addition, their low viscosity allows for the differential movement and coalescence of bubbles to take place during magma ascent. Consequently, the degree of fragmentation is poor and the acceleration of material out of the vent is not as great as during the explosive eruption of viscous magma (see Hawaiian and Strombolian Eruptions). The ejected material commonly forms fire fountains that rise to only a few hundred meters above the vent. The majority of particles follow ballistic trajectories because their large size enables them to decouple from the motion of the gases. Plumes can be generated, however, by heat from the limited amounts of small particles and high temperature gases exsolved from the magma and by heat exchange between entrained air and the large clasts that fall back quickly to the surface.

II. STRUCTURE AND BEHAVIOR OF VOLCANIC PLUMES

A. Sustained Plumes from a Single Vent

Large-scale volcanic plumes are generated during the continuous discharge of fragmented silicic magma and gases from a single vent. A classic example of this was the 79 A.D. eruption of Mount Vesuvius that buried the ancient cities of Pompeii and Herculaneum. This style of volcanism is referred to as plinian, in honor of Pliny the Younger, who provided the first written description of an explosive eruption (see Plinian Eruptions). He described the appearance of the plume over Vesuvius as resembling a giant tree with the main part rising along a trunk but then spreading out at the top like a series of branches.

Plinian plumes are fed at their base by the discharge of hot gas and particles rising at velocities of 100–600 m/s. Production of this mixture is due to fragmentation of magma as dissolved gases are exsolved during ascent. As the material exits the vent its bulk density is usually greater than that of the surrounding atmosphere and rise of the material is due to the momentum gained by gas exsolution. Rapid deceleration occurs from the effects of gravity and by drag from the surrounding atmosphere. This jet phase typically extends up to several kilometers above the vent and is characterized by highly turbulent flow (Fig. 1). Atmospheric air is drawn into the gas thrust region by the development of turbulent eddies along its margins. The air is heated and expansion results in a decrease in plume density with height.

A critical transition occurs when the bulk density of the gas thrust material becomes less than that of the surrounding atmosphere. The forces driving the motion of the plume now become dominated by buoyancy and continued rise occurs like a hot air balloon. This convective phase represents a large part of the plume "trunk" and may extend for tens of kilometers into the atmosphere (Fig. 1). The width of the plume increases progressively with height as entrainment of air continuously adds to the mass flux. Vertical velocities are of the order of 10s to 100 m/s, but their variation is related to the source conditions. Small vent radii promote a rapid transition to a convective regime and the vertical velocity decreases monotonically with height (Fig. 3). However, as vent radius increases the entrainment of air becomes slower and deceleration of the jet phase can lead to a nonlinear variation of velocity where there is an acceleration of the plume above the jet phase (Fig. 3). This condition is referred to as superbuoyancy.

Within the convective phase the vertical velocities are highest along the central axis and decay exponentially toward the plume margin. For plinian eruptions these velocities are sufficient to support centimeter-sized particles to tens of kilometers into the atmosphere. However, some are lost from this region when they migrate towards the margins and encounter lower average vertical velocities. In addition to losing particles, the temperature of the convective part of the plume decreases with height and its density difference with the surrounding

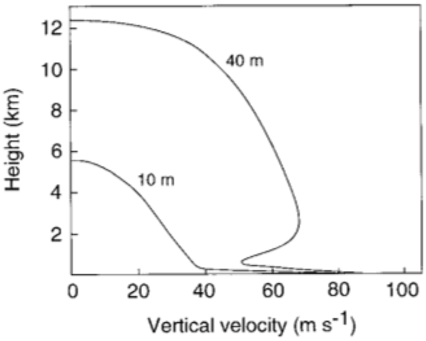

FIGURE 3 Variations in the vertical velocity of volcanic plumes from a central vent with radii of 10 and 40 m based on theoretical modeling. The initial conditions for both were an eruption velocity of 100 m/s, a magma temperature of 1000 K (727°C) and a water content of 3 wt%. Note the acceleration of the 40-m plume between 1 and 2 km height. [Modified from "Volcanic Plumes," Sparks *et al.,* 1997; copyright John Wiley & Sons, Ltd. Reproduced with permission.]

atmosphere decreases as colder surrounding air is drawn into the plume.

The Earth's atmosphere decreases in density with height and eventually the convective part of a volcanic plume will reach a level where densities of the plume and surrounding atmosphere are the same (Fig. 1). At this point buoyancy is no longer a driving force of the plume and material will begin to move laterally at a level of neutral buoyancy, H_b. The ultimate top of the plume, H_t, will, however, be higher than this level because of the excess momentum that the plume has when it reaches the neutral buoyancy level. Between H_t and H_b material spreads out laterally to form a large intrusion into the atmosphere (Fig. 1). This umbrella region forms a distinctive mushroom-shaped cap to plinian plumes and corresponds to the spreading branches described by Pliny the Younger during the 79 A.D. eruption of Vesuvius. The proximal behavior of umbrella regions is similar to the movement of large-scale gravity currents.

The dynamics and dimensions of umbrella regions can be remarkable. Because large amounts of particles and gas enter the umbrella from below, conservation of mass requires that the flux of material be maintained between H_t and H_b. Near the plume axis lateral velocities are of the order of tens of meters per second and symmetrical spreading can occur over a large area. A good example is the umbrella cloud formed during the 1991 eruption of Mount Pinatubo in the Philippines (Fig. 4). Lateral expansion of material produced an umbrella region that had reached a diameter of 400 km after about 5 hours. At least 200 km of horizontal expansion took place against the prevailing northeasterly winds, attesting to high values of mass flux.

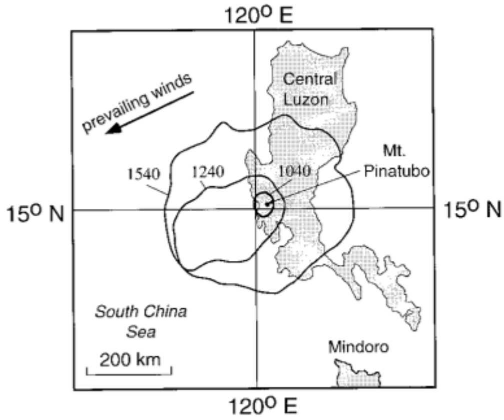

FIGURE 4 Sequential enlargement of the umbrella region during the 1991 eruption of Mount Pinatubo in the Philippines. Traces of the plume margins are shown for the times 1040, 1240, and 1540 local time. The prevailing upper level winds during the eruption were from the northeast. [Modified from "Volcanic Plumes," Sparks *et al.,* 1997, copyright John Wiley & Sons, Ltd. Reproduced with permission.]

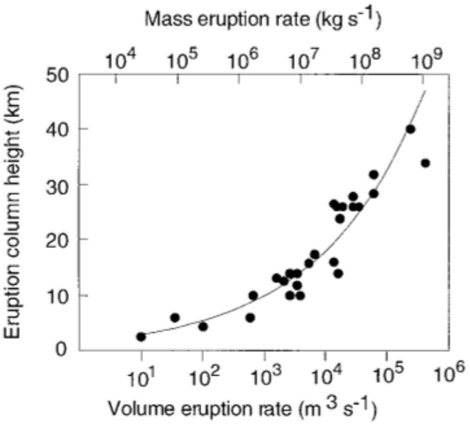

FIGURE 5 Eruption column height versus magma discharge rate for historic eruptions (solid circles). The solid line is the predicted relationship from Eq. (34.1) in the text. [Modified from "Volcanic Plumes," Sparks *et al.,* 1997, copyright John Wiley & Sons, Ltd. Reproduced with permission.]

An important aspect of plumes from maintained sources is the height to which they will rise in the atmosphere. The maximum height, H_t, is a function largely of the thermal flux at the vent, the stratification and moisture content of the atmosphere, and the volatile content of the magma. Thermal flux is the most important factor and is related to the mass discharge rate of magma and its thermal content. A simple approximation for column height can be found from

$$H_t = 1.67Q^{0.259}, \qquad (1)$$

where H_t is the maximum plume height, Q is the volume discharge rate of magma in m^3/s, and 1.67 is a constant related to the stratification of the atmosphere. Observations of historic eruptions are in good agreement with this simple relationship (Fig. 5).

A consequence of magma–water interactions is an increase in the degree of fragmentation and the production of large volumes of fine grained volcanic ash. Phreatomagmatic eruptions that produce high altitude, maintained plumes are called phreatoplinian and often involve viscous high silica magma such as dacite, rhyodacite, or rhyolite (see Phreatoplinian Eruptions).

Plumes produced by phreatoplinian eruptions bear many similarities to those of plinian eruptions with the development of gas thrust, convective, and umbrella regions (Fig. 1). However, the presence of additional water has important effects on plume behavior. One effect is that as liquid water is converted to steam the bulk density of the erupting mixture will decrease and the formation of buoyant plumes is enhanced. However, an offsetting effect is that incorporation of relatively low temperature water results in an overall decrease in the temperature of the erupting mixture and a reduction in the thermal flux. A lower thermal flux tends to reduce the potential buoyancy of the plume and decrease its ultimate height.

The effects of external water on the behavior of an eruption plume are illustrated in Fig. 6, for fixed initial conditions. Under conditions of no external water, buoyant plumes are generated for mass eruption rates of up to 10^8 kg/s. Above this value an eruption will produce a low collapsing fountain that yields pyroclastic flows and surges. With the addition of 10 to 30% external water buoyant plumes can be generated at higher mass eruption rates ($>10^9$ kg/s) because of the higher initial buoyancy flux of the mixture. However, when the amount of external water is 40% or greater, the plume becomes unstable at lower mass eruption rates owing to the lower initial temperature of the mixture and its higher density. Thus, phreatoplinian eruptions that involve large quantities of external water would be expected to produce more pyroclastic flows and surges than plinian eruptions with the same mass eruption rate.

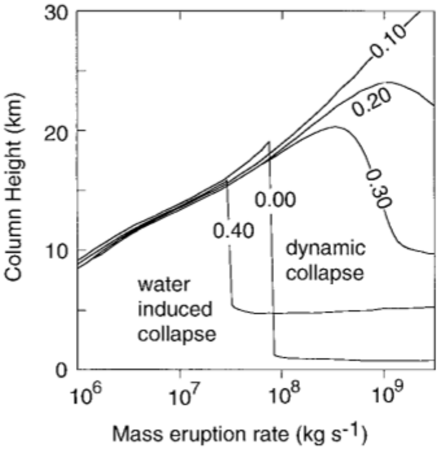

FIGURE 6 Effect of external water on the stability of eruption plumes produced by different magma discharge rates. Values on curves correspond to the weight fraction of water in the erupting mixture. The presence of water initially expands the conditions for a stable rising plume (up to 30%), but higher values (e.g., 40%) cause the plume to collapse at much lower magma discharge rates. [Modified from "Volcanic Plumes," Sparks *et al.*, 1997, copyright John Wiley & Sons, Ltd. Reproduced with permission.]

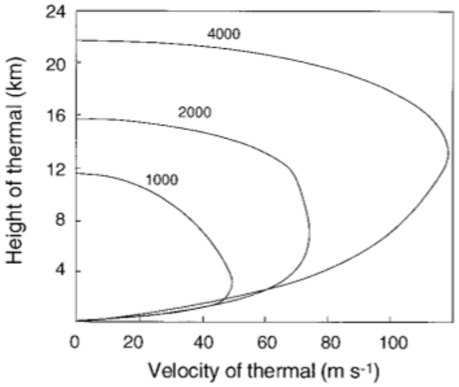

FIGURE 7 Theoretical modeling of the rise speed and maximum height of thermals with initial radii of 1000, 2000, and 4000 m. Thermals with the largest radius rise the highest and have the greatest vertical velocities. [Modified from "Volcanic Plumes," Sparks *et al.*, 1997, copyright John Wiley & Sons, Ltd. Reproduced with permission.]

B. Discrete Plumes from a Single Vent

Vulcanian eruptions differ from plinian events in that the discharge of gases and particles occurs as a series of discrete explosions separated by a few minutes to several hours (see Vulcanian Eruptions). The process of fragmentation may involve the exsolution of juvenile gases and/or interaction of magma with external water at shallow levels of a volcano. A characteristic feature of such eruptions is the discharge of a large amount of lithic material that had previously blocked the path of magma to the surface. The eruptions are thus more analogous to a canon-like discharge of material. In some cases, however, the frequency of eruption may be sufficiently high to generate a near-continuous discharge of material.

Plumes generated by vulcanian eruptions exit the vent at high velocities (up to 400 m/s) and may rise into the atmosphere as discrete pulses or collapse to form small volume pyroclastic flows or surges. If the time between eruptions is greater than the ascent time of the plume, then the plume is considered as a thermal and its behavior will be different than that of a plume generated by a continuous discharge of material. The rise height of a thermal is given by

$$H_t = N^{-0.25} F_t^{0.25}, \tag{2}$$

where F_t is the initial buoyancy and volume of the thermal and N is the ambient stratification of the atmosphere. Modeling of thermals has been carried out assuming that they entrain air in a similar fashion to laboratory thermals and that they possess no initial momentum (Fig. 7). Heating of entrained air causes a thermal to ascend as its density decreases. The rise velocity initially increases but then decreases with height (Fig. 7). Deceleration of the thermal occurs because the density contrast with the surrounding atmosphere begins to diminish as the thermal energy is exhausted. Larger initial thermals (large radius) rise to higher elevations than smaller ones because they are able to entrain less air per mass of erupted material in a given time than thermals with a small radius, and therefore it takes longer for the thermal energy to be exhausted. During vulcanian eruptions the plumes possess an initial vertical momentum controlled by the discharge of material from the vent at high velocities. Thus, model predictions of plume rise are not expected to fit well at low rise heights.

Vigorous steam-rich plumes are often generated when magma is erupted in shallow water. A surtseyan eruption sends steam-rich cock's-tail style plumes along parabolic trajectories. The tephra-laden plumes are produced as a series of discrete events that may take place on a variety of timescales ranging from minutes to hours. The vent area of a Surtseyan eruption is a slurry of hot water and tephra mixed with new magma. Upward migration of the mixture and heat transfer causes the hot water to flash to steam and be rapidly accelerated out of the vent as a jet.

Observations of the 1963 Surtsey eruption in Iceland indicated that during ejection of material as a series of cock's-tail jets there is rapid decoupling and fallout of large poorly fragmented clasts. The remaining steam-rich parts of the plume rise as a series of thermals or, if the frequency of explosions is high, they may coalesce to form a steam-rich convective plume that carries small highly fragmented particles. Such plumes rarely rise to high altitudes because the thermal flux is generally low.

C. Maintained Plumes from Extended Sources

An important mechanism for the generation of volcanic plumes is the buoyant rise of gas and particles from the top of pyroclastic flows and surges. These flows are concentrated mixtures of hot particles with gases and entrained air that form by a variety of mechanisms during explosive volcanism (see Pyroclast Transport and Deposition). Observations of historic flows at volcanoes such as Mount Pelee, Mount St. Helens, Soufriere Hills, and Mount Pinatubo have shown that they are invariably associated with turbulent co-ignimbrite plumes that can rise to great heights in the atmosphere. A dramatic example of this process occurred during the initial phase of the May 18, 1980, eruption of Mount St. Helens Volcano. A hot flow of gas and particles moved to the north of the volcano at speeds up to 100 m/s and covered an area of about 600 km^2. The surge rapidly decelerated at a distance of about 25 km from source and became buoyant, generating an enormous mushroom-shaped plume that rose to an elevation of 25 km (Fig. 8). Volcanic ash from this plume was spread over a large part of Washington and Idaho. Evidence from the geologic record indicates that large volume explosive eruptions have generated enormous co-ignimbrite plumes that are likely to have caused global environmental change. An eruption of the Toba caldera in Indonesia 75,000 years ago spread ash from a co-ignimbrite plume over much of the northern Indian Ocean and may have initiated a switch to an ice age climate.

A basic requirement for the generation of a co-ignimbrite plume is the formation of a mixture of hot particles and gas that is less dense than the surrounding atmosphere. Even though pyroclastic flows begin as mixtures that are denser than the atmosphere, modification of their physical properties occurs during flow that allows for plume development. The lateral movement of pyroclastic flows is driven primarily by gravity, but the support of particles within the moving flow is the result of particle to particle collisions and, most importantly, the velocity of hot gases. Fluxing of gas through the flow results in drag on the solid particles and can fluidize a bed of solid particles and enable it to move downslope at high velocities. Explosive eruptions produce a very large range of particle sizes, and some of the smaller particles are lost from the flow by elutriation with the flux of gases into a more dilute, overlying portion of the pyroclastic flow (Fig. 9). The sources of gas for the fluidization process include exsolution from juvenile clasts, vaporization of vegetation ingested by the flow during its movement downslope, flashing of water to steam as flows move over rivers, lakes, or the sea, and the entrainment of air. Heating of entrained air is a particularly important mechanism in the generation of co-ignimbrite plumes. Air enters a moving flow at its head and along its upper surface where a turbulent mixing zone is established. The entrained air is rapidly heated and its expansion results in enhanced fluidization and elutriation of small particles.

A second process for the reduction of pyroclastic flow density and the generation of buoyancy is sedimentation of particles. As flows move downslope, larger and denser particles move to the base of the flow where they are deposited. Thus, with increasing distance from the source the concentration of particles decreases as a result of both sedimentation and dilution by the entrainment

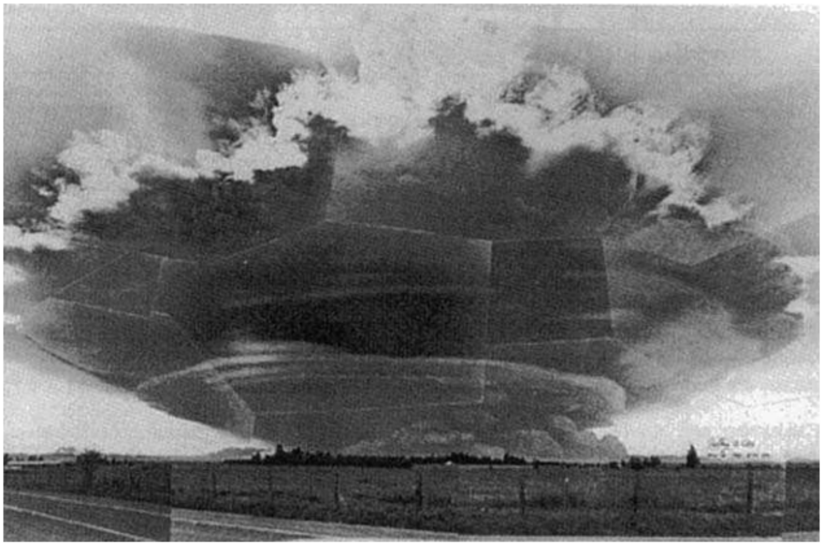

FIGURE 8 Giant plume formed at the beginning of the May 18, 1980, eruption of Mount St. Helens. Generation of the plume was by buoyant uplift of a pyroclastic surge that traveled up to 29 km away from the volcano. [Photograph used with permission from J. G. Moore, USGS.]

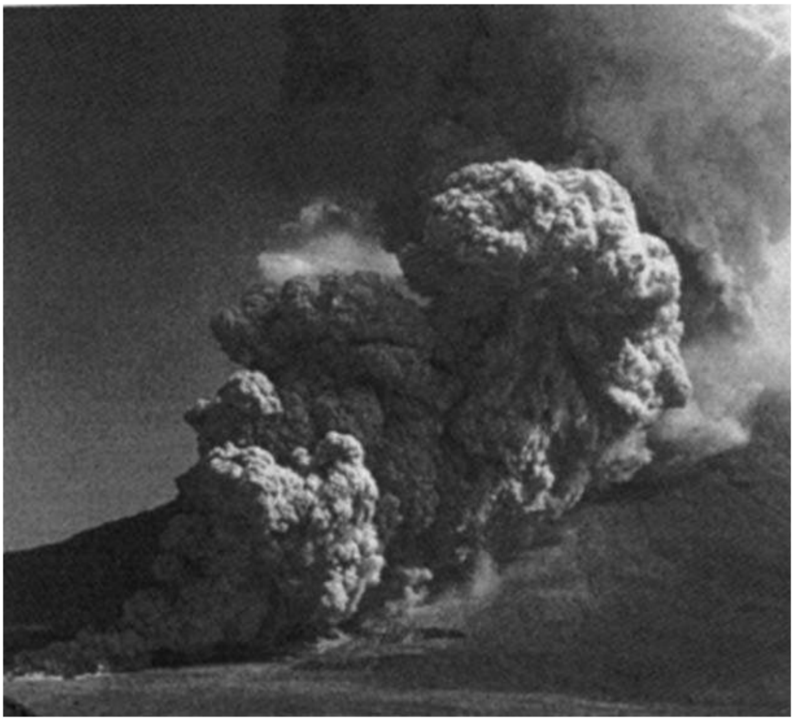

FIGURE 9 Small co-ignimbrite plume rising off the top of a pyroclastic flow descending the slopes of Mount St. Helens volcano. [Photo used with permission from the USGS Cascades Volcano Observatory.]

and heating of air. Eventually the flow will reach a point where the bulk density becomes less than the atmosphere and convective rise of its upper part will occur (Fig. 10). Depending on the initial flow conditions, this buoyant lift-off may occur over an extensive area, as shown by the Mount St. Helens example (Fig. 8). This process can generate plumes from a source area with a width of tens to hundreds of kilometers and is probably the main plume-generating mechanism during large-scale pyroclastic flow-forming eruptions. During such events the discharge of magma can occur for prolonged periods of time, feeding a giant maintained flow source area.

The structure of a maintained co-ignimbrite plume differs substantially from a large-scale convective plume generated from a central vent. First, the co-ignimbrite plume does not have the high velocity jet phase associated with a single vent eruption (Fig. 1). It begins its ascent with very low velocity and little initial momentum. Second, the source area, and thus radius, of the plume base can be very large. Entrainment of air is therefore quite different for a co-ignimbrite plume. The large initial radius means that it entrains a larger fraction of dense lower atmospheric air compared to a central vent plume that starts out with a small initial radius and then expands upwards. Thus, the buoyancy of the co-ignimbrite plume is reduced compared to a single vent eruption having a similar thermal flux.

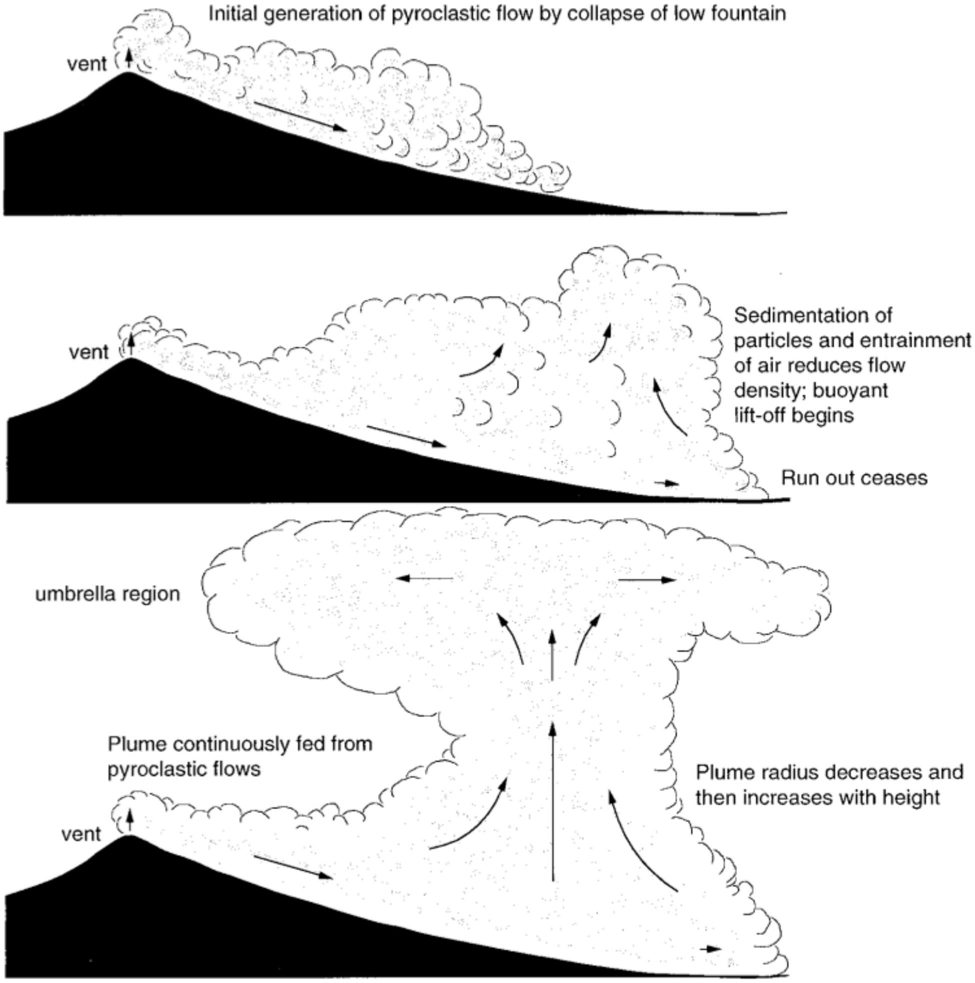
Initial generation of pyroclastic flow by collapse of low fountain
vent
vent
Sedimentation of particles and entrainment of air reduces flow density; buoyant lift-off begins
Run out ceases
umbrella region
Plume continuously fed from pyroclastic flows
Plume radius decreases and then increases with height
vent

FIGURE 10 Development of a co-ignimbrite plume from a pyroclastic flow descending the slopes of a volcano. The initial erupted mixture is denser than the atmosphere and flows down the slope of the volcano under the influence of gravity. During flow, particles are deposited and air is entrained and heated. The bulk density of the flow decreases until the upper part is less dense than the atmosphere and a plume rises off the top.

Modeling of large co-ignimbrite plumes predicts that the radius of the plume initially decreases but then increases again with height (Fig. 11). This predicted behavior has been observed during some historic eruptions and is portrayed in Fig. 11. The velocity of the plume increases with height to a maximum and then decreases to the final height (Fig. 11). As with a plume from a single vent, a co-ignimbrite plume will also form a well-defined umbrella region where the plume density is similar to that of the surrounding atmosphere and lateral advection of material takes place as a large-scale gravity current. The ultimate height of the plume is also primarily related to the magma discharge rate. However, during pyroclastic flow-forming eruptions only a fraction (≈30–40% maximum) of the total thermal energy can be utilized for co-ignimbrite plume generation. The remainder is retained in the hot pyroclastic flow deposits formed from the basal part of the moving flow. Consequently, for a given magma discharge rate a co-ignimbrite plume will not rise as far as a plume from a central vent. However, mass eruption rates are often higher during pyroclastic flow forming stages of explosive eruptions. There is geological evidence to suggest that this is true for very large explosive eruptions associated with caldera formation and discharge of large volumes of magma (>25 km^3).

Many pyroclastic flows are not maintained for long periods of time and may last for only a few minutes. Under these circumstance the release of hot particles and gas occurs on a timescale that is less than the total ascent time of the plume. In this case the plume behavior is best approximated as a thermal that begins with fixed radius and rises as a discrete volume of particles and gas. The behavior of such plumes is similar to that described in Section II.B and shown in Fig. 8.

Another type of co-ignimbrite plume may be developed over the source vent where material is feeding pyroclastic flows. Formation of a plume in this area may be related to either (1) segregation of large clasts or (2) inhomogeneities in the eruption mixture. If rapid segregation of large clasts can occur shortly after the erupting mixture exits the vent, then the bulk density of part of the plume may be reduced sufficiently that it becomes buoyant. Such a process would be expected to occur during eruptions that generate a very large range in particle sizes during fragmentation. Alternatively, variations in volatile content or physical properties of the magma may lead to a range of bulk densities within the erupting mixture. Under these circumstances, low density portions of the erupting mixture would feed a quasi-steady convective plume centered over the vent while the denser portions of the mixture would collapse to form pyroclastic flows.

Large-scale basaltic eruptions often take place from fissures that may extend several to tens of kilometers in length (see Flood Basalt Provinces). Plumes are generated above the fissures if fragmentation can produce a source of sufficient small particles and gas. The generally low fragmentation of basaltic magmas means that only a small fraction of the total thermal energy can be utilized to drive a convective plume above the vent. As with ignimbrites, a large fraction of the heat is retained in the clasts that fall back to the surface near the vent at high temperature. There are three main sources of thermal energy for the production of plumes above a large fissure eruption (Fig. 12). The first are small fragmented particles (millimeters or less in size) that can be carried aloft by the gas. This fraction is generally less than 20% of the total erupted magma. A second source is the hot gas, either water, carbon dioxide, or sulfur

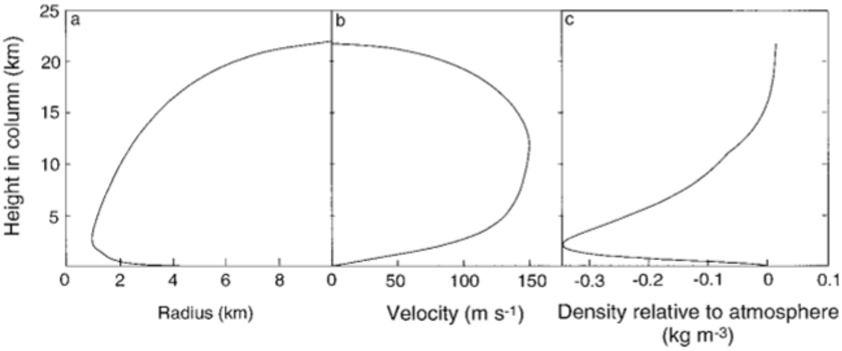

FIGURE 11 Variations in radius, velocity, and density relative to the atmosphere for a co-ignimbrite plume based on theoretical modeling. Note that the radius of the plume initially decreases as it rises but then increases up to the top. Initial assumptions of the model were a magma temperature of 1000 K, starting velocity of 1 m/s, and source radius of 5 km. [Modified from "Volcanic Plumes," Sparks *et al.,* 1997, copyright John Wiley & Sons, Ltd. Reproduced with permission.]

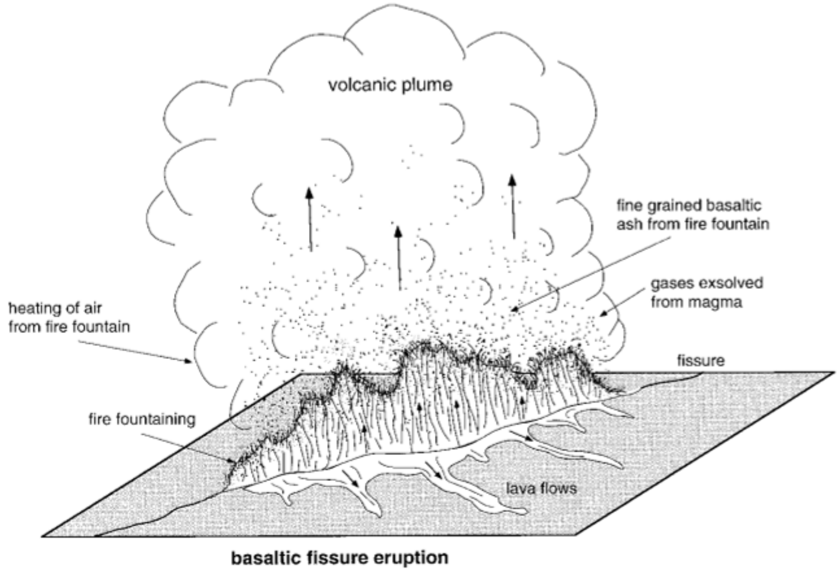
volcanic plume
fine grained basaltic ash from fire fountain
gases exsolved from magma
heating of air from fire fountain
fissure
fire fountaining
lava flows
basaltic fissure eruption

FIGURE 12 Development of a volcanic plume over a basaltic fissure eruption. The plume is fed by thermal energy from fine grained basaltic ash, gases exsolved from the magma, and air heated by the cooling of magma in fire fountains.

dioxide that is decoupled from the magma upon eruption. The amount of gas may vary considerably depending on the original volatile content of the magma and any enrichment or depletion processes that may have affected the distribution of bubbles. The third source is heat exchange between the fountain and the surrounding air. Temperature decreases of a few to tens of degrees have been inferred for the main volume of magma in the fountain. These three sources can contribute to the development of a gas and particle plume that ascends above the top of the fountain by convective rise (Fig. 12).

Plumes developed over large basaltic fissure eruptions are important because of their potential for climatic impact. Basalt carries higher amounts of sulfur per unit mass than more evolved magmas and sulfur is an especially important agent for altering the heat budget of the atmosphere (see Volcanic Aerosol and Global Atmospheric Effect). However, for sulfur injection to be important for climate change it must reach high altitudes (>10–15 km) in the atmosphere. The height to which a basalt plume will rise in the atmosphere is a function of the mass eruption rate of magma, the fraction of ash produced by fragmentation, and the amount of cooling experienced by the eruptive fountain (Fig. 13). For a given magma discharge rate, the eruption of basaltic magma generates lower plumes than eruptions of more evolved magma (Fig. 13). This is mainly because of the inefficient use of thermal energy to drive the buoyant plume. The 1783 basaltic fissure eruption of Laki in Iceland generated a plume that rose to a height of at least 12 km. This height implies an eruption rate of about 1 $m^3/s/m$ of vent length based on theoretical modeling of basaltic plumes (Fig. 13). Although such rates are unusual for historic eruptions, there is evidence in the geologic past for very large fissure eruptions that exceeded discharge rates of 10 $m^3/s/m$. For example, the great Roza basaltic flow in eastern Washington (United States) is inferred to have been fed by a discharge of 10

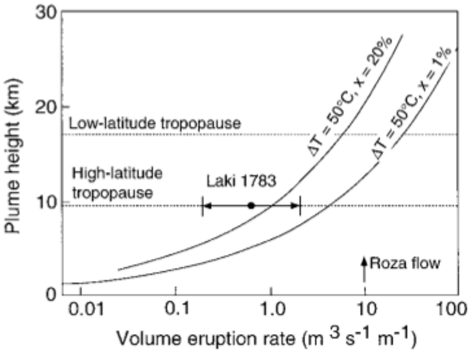

FIGURE 13 Plume height versus magma discharge rate for basaltic eruptions. Solid curves show the predicted heights based on theoretical modeling. Each curve assumes a cooling of the fire fountain by 50°C and utilization of 20 and 1%, respectively, of the energy in fine grained basaltic ash. [Modified from "Volcanic Plumes," Sparks *et al.,* 1997, copyright John Wiley & Sons, Ltd. Reproduced with permission.]

$m^3/s/m$ (Fig. 13). It is likely that major atmospheric plumes are generated during such events, with the potential for significant climatic impact.

III. ATMOSPHERIC EFFECTS ON PLUME DISPERSAL

For several hundreds to thousands of meters above the vent, the motion of a volcanic plume is controlled by the source conditions. Differences in atmospheric conditions play little if any role in determining plume motion in this jet phase. Once plume velocity has slowed, at the top of the jet phase, the plume motion involves the convective entrainment of vast quantities of air, and the driving upward of the plume material relative to an atmosphere in a specific state, in terms of relative humidity, wind speed, and temperature stratification. In the umbrella region, where the column material spreads around the neutral bouyancy level, the gravity-driven outward flow can be modified and even counteracted by the winds. Because of the typical sizes of volcanic plumes, the neutral bouyancy level is often within or near the jetstream. The high wind speeds typical of the jetstream play a profound role in distal plume transport.

A. Crosswinds

All volcanic plumes are eventually distorted by the wind. The largest plumes and those erupted into a still atmosphere are able to form umbrella clouds. In contrast, less vigorous plumes rise buoyantly in a wind field even as they are carried along by it. These plumes do not form umbrella clouds. Once a plume is completely bent over in the wind field, it begins to move with the wind and travels as a downwind plume. In general, downwind plumes seem to be oval in cross section, with their long axis horizontal. In planview, they often consist of downwind-elongated lenses of gas and ash that become detached from the volcano when the eruption ceases. Sometimes, however, smaller plumes can have rather irregular outlines because of their susceptibility to local atmospheric motions (Fig. 14). They can even have several lobes at different heights due to wind shear effects.

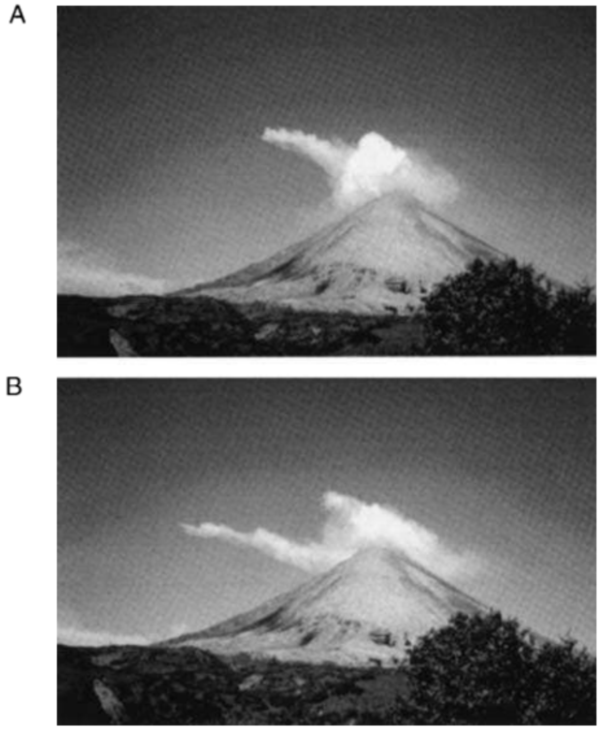

FIGURE 14 Sequence of two photographs (A, B) of small plumes from Karymsky volcano, Kamchatka, Russia, showing effects of wind shear to produce highly irregular plume shapes. Note that different parts of the plume are spreading in different directions. [Photo used with permission from M. Bursik.]

Based on how they are affected by the wind, plumes can be thought of as being of two types: strong and weak. Strong plumes are those that form an umbrella cloud, whereas weak plumes do not. The difference between strong and weak plumes can be expressed in terms of the ratio of the wind speed to the upward plume speed. A weak plume, for which this ratio is large (>1), is much affected by the wind, taking on the characteristic "bent-over" shape (Fig. 15). A strong plume, for which

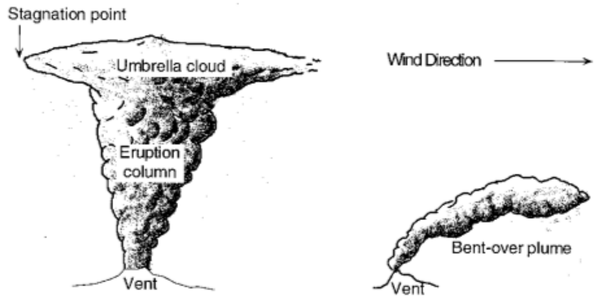

(a) Strong Plume (b) Weak Plume

FIGURE 15 Schematic illustration of eruption plumes generated from a volcanic vent. (a) Eruption of a strong plume; (b) eruption of a weak plume under windy conditions in which the plume is bent over.

the ratio is small, is little affected by the wind as it rises. In general, for plumes with a total rise height greater than 20 km, no typical values of windspeed are able to affect plume rise substantially, and all eruption columns above this height will develop umbrella clouds.

Most tropospheric plumes in weak winds are strong plumes, as are most plumes that reach the stratosphere. These plumes rise relatively unmodified through the atmosphere to form typical umbrella clouds. As the gravity current spreads upwind, it encounters resistance. At the stagnation point, the wind speed and the current speed are equal, and the upwind progress of the current is halted (Fig. 15). For strong plumes the stagnation point can occur at substantial distances upwind of the vent. For example, the umbrella cloud from the May 18, 1980, Mount St. Helens blast plume spread upwind 15 km before it was balanced by stratospheric winds. In the crosswind direction, the plume may continue to spread as a gravity current to hundreds of kilometers from the vent, as was the case with the Pinatubo eruption of June 15, 1991 (Fig. 4). In the downwind direction, the plume is carried along in the windfield. As the plume propagates progressively further downwind, its speed approaches the windspeed as the plume loses pyroclasts and the gravity-driven spreading weakens.

Further downwind from the vent, the wind completely dominates plume motion. Shearing stresses between the upper and the lower interfaces of the downwind plume and the atmosphere and direct atmospheric entrainment result in downwind transport at the windspeed. The plume loses its density contrast with the atmosphere and can be advected as a lens of aerosol and gas with nearly constant width. Only slowly might it thin, spread, and disperse as shearing and small-scale atmospheric turbulence act at its margins and as very fine ash settles out. The elongated shape of such plumes is illustrated by the aerosol band generated during the El Chichon eruptions of 1982. This band maintained nearly constant width and became gradually more dilute due to shearing at its margins as it completely encircled the globe.

In the case of weak plumes, a subvertical eruption column cannot develop. Instead, a bent-over plume whose motion is dominated by the wind rises from the vent. Unlike strong plumes which form umbrella clouds, weak plumes maintain a cloudlike structure as they reach their maximum rise height, since their flow characteristics are not reorganized in the upper atmosphere by gravity current motion. The plume is not only bent over by the wind, but also mixes with the turbulent atmosphere as it is carried along. This enhanced entrainment results in lower total plume heights for a given mass eruption rate as the wind speed increases, because of the more rapid dilution of the plume's thermal energy by the entrained air. The plume–wind interaction in weak plumes can also result in spectacular organized motions under certain conditions. The combination of an upward-directed plume meeting a horizontal wind can create vorticity in the downwind side of the plume. This vorticity has occasionally manifested itself as a line of tornadoes shed from the plume margin, as occurred during the eruption of Surtsey in 1963.

B. Latitudinal Control of Vertical Temperature Profile

Variations in the atmospheric stratification result from vertical temperature variations caused by the differential heating of the solid earth and air. In particular, the height of the tropopause is strongly dependent on surface heating and hence on latitude. In general, the troposphere is only weakly stratified, while the stratosphere is more strongly stratified. In a typical mid-latitude atmosphere, the temperature decreases steadily to the tropopause, which is located at about 11 km. The temperature then remains nearly constant up to a height of about 20 km, where it begins to increase, and the atmosphere becomes strongly stratifed. In the tropical atmosphere, the tropopause is located at about 16–18 km. The temperature increases steeply above this point, producing a very stably stratified atmosphere. In polar latitudes, the tropopause may occur as low as 8 km, and the stratosphere above is much less strongly stratified than it is in the tropics or mid-latitudes.

As a result of such variations in the ambient stratification, the maximum rise height of an eruption column at a fixed eruption rate can vary by a few kilometers. In a given atmosphere, the rate of increase of column height as a function of the mass eruption rate decreases for columns that penetrate the tropopause. This can be seen in Fig. 16 by comparing results for plume rise models in tropical, mid-latitude, and polar conditions. In conjunction with this effect, as the latitude of a hypothetical eruption changes from tropical to polar, a given column will penetrate the tropopause at ever-decreasing heights. Therefore, the plume ascends to a lower height for a given mass eruption rate and eruption temperature in a polar atmosphere (lower tropopause) because the plume propagates through a deeper region in which the temperature increases with height. The modeled rise heights of eruption columns can be compared in polar, mid-latitude, and tropical atmospheres, in which the

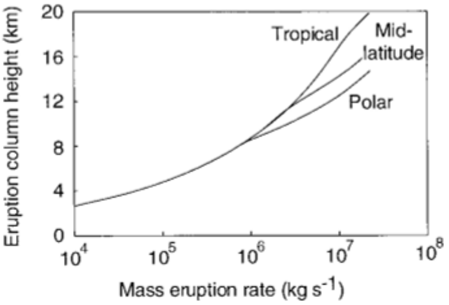

FIGURE 16 Variation in the rise height of an eruption column as a function of latitude. Differences in column height correlate with differences in altitude of the tropopause; thus there are no differences in column height for eruption columns that do not pierce the tropopause. [Modified from "Volcanic Plumes," Sparks *et al.*, 1997, copyright John Wiley & Sons, Ltd. Reproduced with permission.]

tropopauses are located at 8, 11, and 17 km, respectively and the ground temperatures are chosen to be 263, 273, and 293 K, respectively (Fig. 16). In the tropical atmosphere the model plumes rise significantly higher as expected, owing to the deeper troposphere.

C. Atmospheric Moisture

The volatile content of magmas is too low for the exsolved gases to have a major impact on column motion. However, in moist air, a significant mass of water vapor can be entrained and convected upward in the column. This air will be cooled and become saturated. Once saturated, the vapor condenses into liquid water, releasing its latent heat of condensation. The latent heat increases the temperature of the gases in the eruption column, thereby increasing the buoyancy and ultimately the eruption column height. For low mass eruption rates, the entrainment and convection of atmospheric moisture upward in the plume can provide the dominant energy source driving the motion of the eruption column. An analogy is provided by forest and brush fires, which heat the air near the ground. As this heated air rises, the water vapor within it becomes saturated and condenses. The latent heat released provides thermal energy, which enables the hot smoke to continue to rise. Such a fire plume thus ascends higher when the relative humidity is high than it does when the relative humidity is low.

In humid air, the height to which a small volcanic plume rises is likewise considerably greater than it is in dry air (Fig. 17). This is because the thermal energy released by the condensing atmospheric vapor is comparable to or even greater than is the thermal energy associated with the erupted material. For small eruptions in relatively dry air, the column remains unsaturated. In larger eruptions or in moister air, the column becomes saturated and therefore the height of rise of the column increases significantly. However, as the erupted mass flux increases above about 10^6 kg s^{-1}, the erupted thermal energy begins to significantly exceed the energy that can be extracted from condensing water vapor even at 100% relative humidity. This is because the ambient moisture is confined to the lower atmosphere. Only smaller columns can entrain a sufficient mass of water vapor relative to the erupted thermal energy so that the latent heat produced on condensation is comparable to or exceeds the thermal energy erupted in the pyroclasts. Larger columns ascend far above the region in which most of the atmospheric water vapor is found, and so only a small fraction of the entrained air is moist. As a simple criterion, eruption columns whose total ascent heights exceed about 12 km are not significantly affected by atmospheric moisture.

D. Downwind Evolution

As an eruption comes to a close, the accumulated volcanic gas and ash ejected into the atmosphere assumes one of two typical forms. Smaller plumes are often markedly elongated in the downwind direction, with a prominent taper toward the upstream end (Fig. 18; see also color

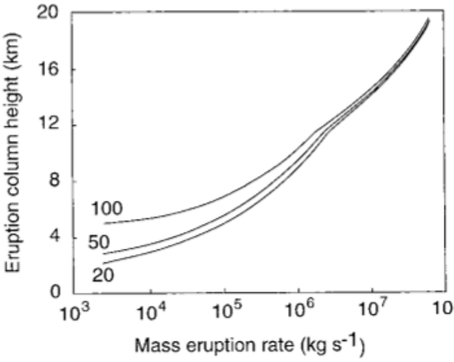

FIGURE 17 Variation in the rise height of eruption columns as a function of atmospheric relative humidity (numbers on the curves). The more humid the air, the more vapor is entrained and carried upward in the column, thus releasing more latent heat and increasing column height. Because most of the vapor is in the lower atmosphere, larger eruption columns are less affected. [Modified from "Volcanic Plumes," Sparks *et al.*, 1997, copyright John Wiley & Sons, Ltd. Reproduced with permission.]

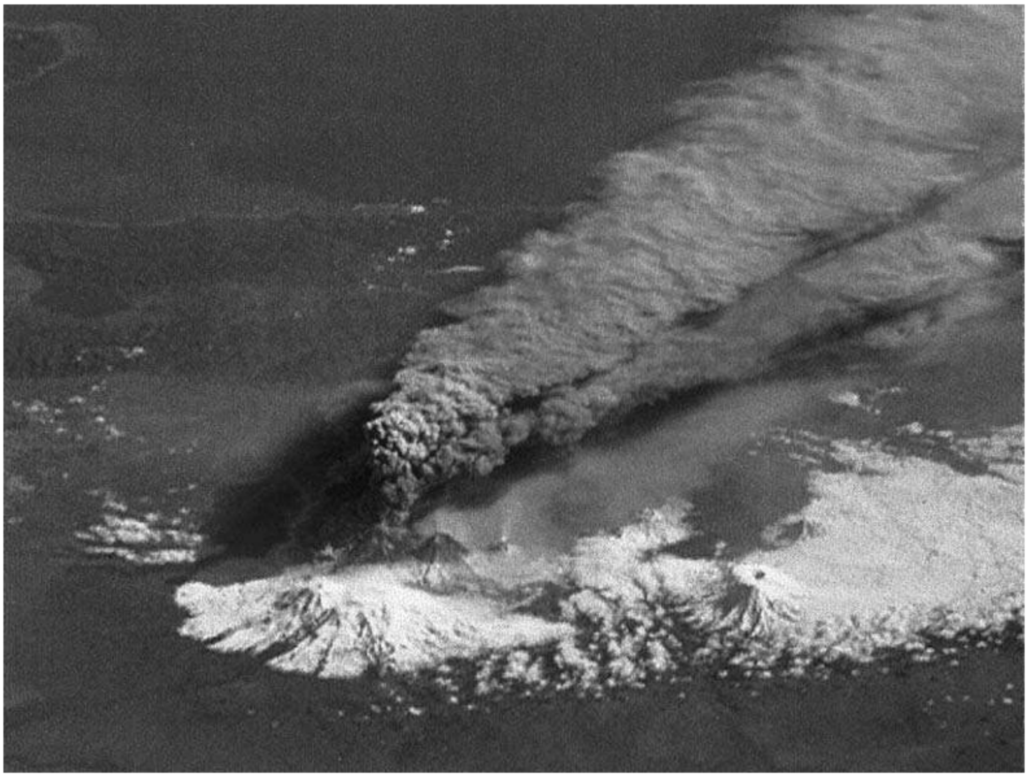

FIGURE 18 Photograph from the Space Shuttle mission STS-068 showing the elongated spreading of the October 1, 1994, plume of Klyuchevskaya near the tropopause. Note also that the plume border becomes smoother with height and distance because of the weakening of the internal turbulence. (See also color insert.)

insert). The taper is the result of either the gravity current spreading or atmospheric turbulent diffusion having affected the downstream end of the plume for a longer time than the upstream end. Lareer umbrella clouds are more often subequant in planview, with an elongation in the downstream direction that makes them occasionally ovoid (Fig. 19). Because they are often the result of a complex sequence of events, larger, developed umbrella clouds may be compounded from several separate clouds. They can therefore display a complex digitate geometry. In addition, the most massive umbrella clouds, such as that from the 1991 eruption of Pinatubo, display another type of digitate margin that indicates they have reached the Rossby radius, the size at which the Earth's rotation begins to affect cloud motion.

When any volcanic plume has persisted for a sufficiently long time, it becomes fully subjected to atmospheric motions. These motions fall into a spectrum of characteristic sizescales, from microscopic molecular agitation to hemispheric flow. To gain an understanding of the effects of the atmosphere on the long-range dispersal of eruption clouds, horizontal and vertical mo-

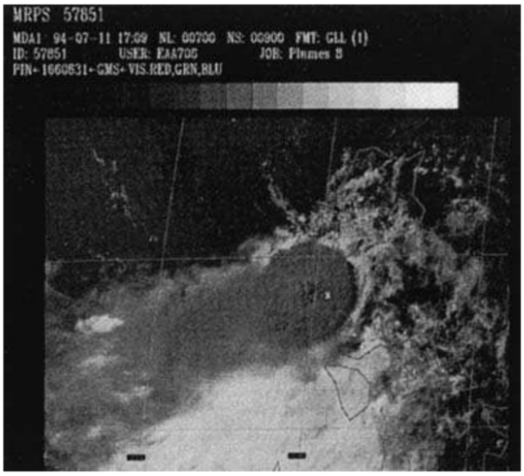
MRPS 57851
MDA1 94-07-11 17:09 NL: 00700 NS: 00900 FMT: GLL (1)
ID: 57851 USER: EAA706 JOB: Plumes 8
PIN+1660631+GMS+VIS.RED,GRN,BLU

FIGURE 19 Satellite image of the giant June 15, 1991, umbrella cloud of Pinatubo, Philippines. Outline of the Philippines and lines of latitude and longitude are shown for scale. Central upwelling of plume (x) is offset from volcano due to geometric image distortion. [Modified from "Volcanic Plumes," Sparks *et al.*, 1997, copyright John Wiley & Sons, Ltd. Reproduced with permission.]

tions can be thought of separately. Horizontal dispersal is controlled by the nearly two-dimensional nature of the largest atmospheric motions that transport ash on regional and global scales. The vertical dispersal of the particles is controlled by the smallest scale turbulence and gravitational settling, which act on much smaller length scales. In addition, aggregation of small ash and aerosol particles in the months and years following an eruption results in the gradual increase of particle size. Eventually particles become sufficiently large that their settling speeds cause the particles to be deposited.

The large-scale, quasi-two-dimensional atmospheric motions responsible for the distal transport of ash clouds can be described by a "turbulence energy spectrum." The effect of the different scales of motion in this spectrum on plumes of different characteristic sizes is vastly different despite the fact that all atmospheric agitation has its origin in the heating of the Earth and air by the Sun. The largest scale motions ($>\sim10^3$ km) primarily draft along virtually all plumes, but cause little growth or turbulent spreading. Observations of plumes distorted in these zonal winds suggest that distortion primarily occurs as simple stretching and very moderate bending of plume outlines. Intermediate scale turbulence structures (10^2–10^3 km) are primarily responsible for complex bending and relative diffusion (spreading and dilution) of small to moderate-sized ash clouds. The complex bending or contortion is known as chaotic advection, as plume–fluid elements are distorted in a chaotic fashion, despite the completely deterministic nature of the velocity field itself. The plume from the Hudson eruption of 1991 exhibited this phenomenon as it drifted at the edge of the polar vortex (Fig. 20). The motion of the largest volcanic ash clouds, such as that generated by the eruption of Pinatubo, seem to show almost exclusively relative diffusion by the intermediate scale motion, with little apparent stretching or bending.

Vertically, a downwind volcanic plume does disperse, but at rates very different from the horizontal dispersion rates discussed above. This vertical dispersion occurs because of the coupled effects of the settling properties of the particles and of the turbulence structure of the stratosphere. The stratosphere consists of alternating layers of 1 to 2 km thickness. Every other layer seems to display turbulent motions with vertical wind speeds between −0.5 and 0.5 m/s. The intervening layers are relatively quiescent. These observations are consistent with the layered temperature structure observed in

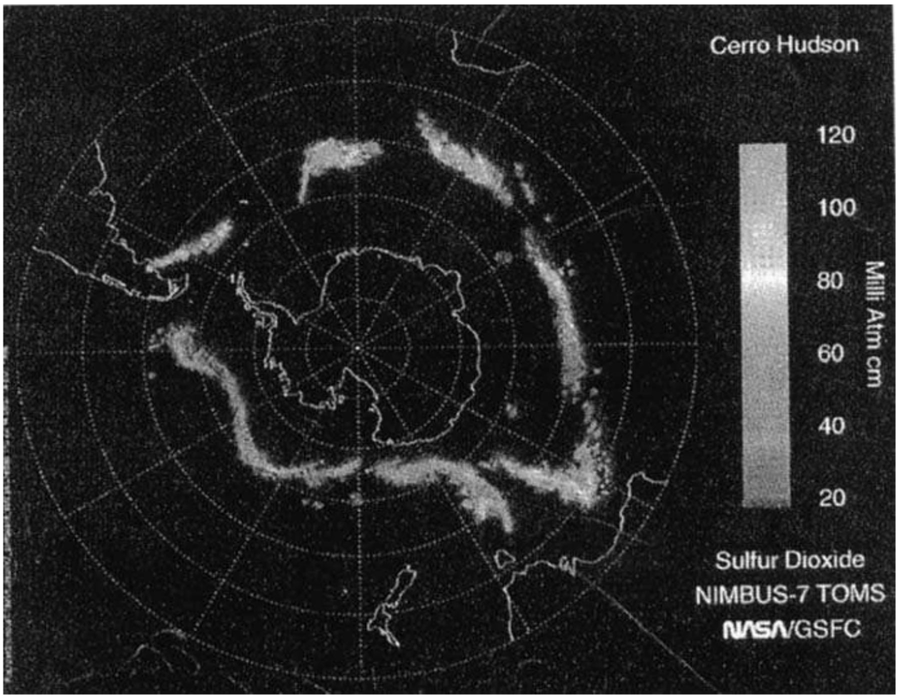

FIGURE 20 Composite satellite image based on sulfur dioxide concentration of the plume from Hudson volcano, Patagonia, Chile, generated on August 15, 1991. Image shows the advection, stretching, and bending of the plume around the southern polar vortex for a period of 8 days (the data for the last two days are overlapping). [Modified from "Volcanic Plumes," Sparks *et al.,* 1997, copyright John Wiley & Sons, Ltd. Reproduced with permission.]

stratospheric soundings. The turbulent layers will be able to retain particles longer than will the quiescent layers because the turbulence will hinder particles from settling from the convecting layer. Particles will fall out relatively rapidly from the quiescent layers which lack a counteracting agitation. Because of this alternating turbulent and quiescent structure in the stratosphere, volcanic ash and aerosol clouds will tend to separate into layers over long time periods, lending to them a distinct banded appearance when viewed from the side. Over a period of months to years, however, virtually all volcanic particles settle completely from the atmosphere.

IV. FUTURE RESEARCH

Volcanic plumes have the potential for affecting human society on both a local and a global scale. Areas close to active volcanoes are subject to tephra fallout and the effects of deadly pyroclastic flows and surges. In more distal areas, volcanic plumes can lead to global environmental change by injecting aerosol-forming gases into the stratosphere. Although much progress has been made toward understanding the nature and behavior of volcanic plumes, several areas need to be emphasized in future research. One area deals with the conditions whereby volcanic plumes change from buoyantly rising conditions to collapse. Understanding the parameters that control this transition is essential because these determine whether an eruption will pose significant threat to local populations by the generation of pyroclastic flows and surges.

A second area is concerned with the dispersal of large-scale plumes in the atmosphere. In particular, how do such plumes evolve with time in terms of their geometry and composition? The hazards of volcanic plumes to commercial and military aviation have been highlighted by several dramatic encounters and are likely to increase in the future as air traffic expands over volcanically active areas. Because the impact of volcanic plumes to aircraft is related to the particle concentration in the atmosphere it is critical to understand how plumes lose particles as they move downwind from source. Prediction of the path and particle composition of volcanic plumes should be a high priority in order to minimize accidental encounters with aircraft and the potential for disastrous results. Furthermore, an understanding of how plumes are dispersed on a global basis is necessary for predicting the potential climatic effects of volcanic aerosols. Sophisticated supercomputer models coupled with analog laboratory experiments are two of the tools that volcanologists can use to better understanding the dynamic processes of volcanic plumes.

SEE ALSO THE FOLLOWING ARTICLES

Flood Basalt Provinces • Hawaiian and Strombolian Eruptions • Magmatic Fragmentation • Phreatoplinian Eruptions • Plinian and Subplinian Eruptions • Pyroclast Transport and Deposition • Surtseyan and Related Phreatomagmatic Eruptions • Volcanic Aerosol and Global Atmospheric Effect • Vulcanian Eruptions

FURTHER READING

Sparks, R. S. J., Bursik, M. I., Carey, S. N., Gilbert, J. G., Glaze, L. S., Sigurdsson, H., and Woods, A. W. (1997). "Volcanic Plumes." Wiley, Chichester.

Francis, P. (1993). Chapters 8–12 *in* "Volcanoes: A Planetary Perspective" Oxford University Press, Oxford.

Decker, R., and Decker, B. (1998). Chapter 16 *in* "Volcanoes." Freeman, New York.

Chester, D. (1993). *In* "Volcanoes and Society." Routledge, Chapman and Hall, New York.

Self, S., and Walker, G. P. L. (1994). Pages 65–74 *in* "Volcanic Ash and Aviation Safety: Proceeding of the First International Symposium on Volcanic Ash and Aviation Safety" (T. J. Casadavall, Ed.). U.S. Geological Survey Bulletin 2047.

Sparks, R. S. J. (1986). The dimensions and dynamics of volcanic eruption columns. *Bull. Volcanol.* **48,** 3–15.

Wilson, L., Sparks, R. S. J., Huang, T. C. and Watkins, N. D. (1978). The control of eruption volcanic eruption column heights by eruption energetics and dynamics. *J. Geophys. Res.* **83,** 1829–1836.

Woods, A. W. (1988). The dynamics and thermodynamics of eruption columns. *Bull. Volcanol.* **50,** 169–191.

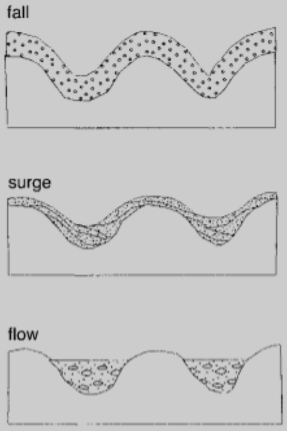

PYROCLAST TRANSPORT AND DEPOSITION

COLIN J. N. WILSON
BRUCE F. HOUGHTON
Institute of Geological & Nuclear Sciences

I. Generation of Pyroclast Assemblages
II. Transport Systems
III. Deposition Systems
IV. Summary

GLOSSARY

deposition system The entity that deposits pyroclasts and forms pyroclastic deposits. This term is used to emphasize the controls on the manner in which particles come to rest.

particle cohesion The sticking together of particles due to either the presence of water (at low temperatures) or to particle plasticity (at high temperatures).

particle trajectory The path taken by a moving particle. Used here to describe the inclination of a pyroclast as it comes to rest.

pyroclastic density current A gravity-controlled, laterally moving mixture of pyroclasts and gas.

pyroclastic fall The rain out of clasts through the atmosphere from an eruption jet or plume during an explosive eruption.

pyroclastic flow A pyroclastic density current where most of the material and momentum is contained in a basal concentrated particulate dispersion.

pyroclastic surge A pyroclastic density current where the material and momentum are widely distributed through a deep, dilute, highly turbulent particulate suspension.

solids concentration The volume concentration of particles in a transporting or depositing medium, ranging from low (discrete particles) to high (dense-packed assemblages of particles).

transport system The entity that carries pyroclasts from vent to the depositional system. This term is used to emphasize processes responsible for the transport of pyroclasts.

THIS CHAPTER GIVES a framework for the main stages by which fragmental materials ejected in explosive eruptions are transported and deposited to form pyroclastic deposits in the subaerial environment. It mentions the behavior of buoyant plumes only in passing (see Volcanic Plumes) and describes only general characteristics of the deposits (see Fall Deposits, Deposits of Surges and Directed Blasts, and Ignimbrites and Deposits of Block-and-Ash Flows). We define and distinguish transport and deposition systems to describe key processes involved during emplacement of fall, surge, and flow deposits. Four principal controls (particle trajectory, solids concentration, the extent to which

Copyright © 2000 by Academic Press
All rights of reproduction in any form reserved.

this concentration fluctuates with time, and the presence or absence of cohesion during deposition) are used to explain the characteristics of the great proportion of subaerial pyroclastic deposits and provide a framework for the spectra of processes and products between the three end-member types of deposit. Further complexities arise, particularly in the proximal environment, out to a maximum of 3–5 km from the vent, but are not volumetrically important in most pyroclastic deposits.

I. GENERATION OF PYROCLAST ASSEMBLAGES

Explosive volcanism involves the transfer of fragmented magma (together with phenocrysts, dissolved volatiles, and country-rock material entrained from the conduit walls or ground surface) from some depth onto the Earth's surface. A widespread convention, which we follow, is to distinguish between a *transport system*, which is responsible for the movement of the assemblage of fragmental material, and a *deposition system*, which controls the manner in which the material comes to rest to form a deposit. Most pyroclastic transport systems (including virtually all explosive eruptions of volume >1 km^3) begin with expulsion of the fragmental material from a conduit as a high-speed jet that interacts with the atmosphere. However, in some cases, the transport system is created via an intermediate process of lava extrusion or cryptodome formation and is initiated by either (i) rupture of overpressured systems especially cryptodomes (e.g., Mount St. Helens 1980, Mont Pelée 1902) or (ii) gravitational collapse of nonoverpressured to partially overpressured lava flows or domes (e.g., Unzen 1990, 1991).

II. TRANSPORT SYSTEMS

A. Introduction

Two major classes of transport systems are identified in explosive eruptions. They are primarily distinguished by the density of the emerging jet with respect to the atmosphere in the first hundreds of meters to kilometers above the vent, that is, buoyant versus nonbuoyant behavior. To a first order, these correspond respectively with

(1) vertical plumes (where the dominant trajectory of motion is upward initially) that generate fall deposits by deposition from wind-driven clouds at elevations of several kilometers to tens of kilometers above the Earth's surface, and
(2) laterally moving systems (where the dominant trajectory of motion is sideways initially) that generate surge and flow deposits from gravity controlled, ground-hugging density currents (Fig. 1).

In reality the situation is more complex, for example, because of the interaction between pyroclastic density currents and the atmosphere which will generate buoyant material that can rise to form second-order vertical plumes. The structure and dynamics of buoyant plumes are dealt with separately in Volcanic Plumes, while the variety of density currents are reviewed briefly here.

An additional complexity arises in the proximal environment where large clasts, which are little affected by interaction with the atmosphere, follow ballistic trajectories that are controlled by their initial velocities and ejection angles. Ballistically emplaced materials form a second category of fall deposit, but are normally a small proportion of the total volume of ejecta. They vary in nature from isolated individual clasts in otherwise conventional plume-deposited fall deposits to the situation (in hawaiian and strombolian activity) where the emerging jet consists mostly of large clasts forming a fountain around the vent. In this instance clasts accumulate to form a spatter or scoria cone or recombine to generate a lava flow (see Scoria Cones and Tuff Rings).

B. Pyroclastic Density Currents

Two end-member types of pyroclastic density current, dilute and concentrated, are recognized from observations of historical eruptions and studies of historic and prehistoric deposits (Figs. 1 and 2). The dilute end-member is commonly referred to as pyroclastic surge and the concentrated end-member as pyroclastic flow. There is considerable ongoing debate about the boundaries between these end-member types, particularly with regard to the nature of the high-velocity density currents (*blasts*) generated in historic eruptions such as Mont Pelée 1902, Bezymianny 1956, and Mount St. Helens 1980.

1. Dilute Currents/Surges

These have been observed to travel at speeds of typically tens of meters per second, but blast-like phenomena,

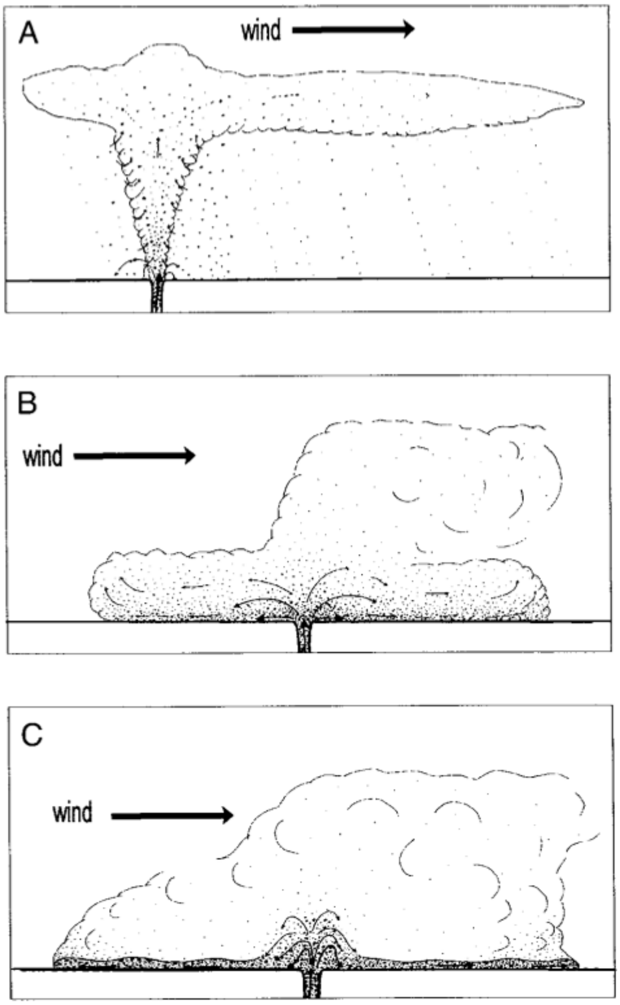

FIGURE 1 Schematic diagram to illustrate the three main end-member transport systems for the emplacement of pyroclastic deposits. (A) Fall: high buoyant plume carrying all except coarsest particles to heights of kilometers to tens of kilometers above the surface; particles sedimented from plume to form deposit; plume dispersal controlled by wind direction and strength. Coarsest clasts (arrows) follow ballistic trajectories and fall within 3–5 km of vent regardless of wind. (B) Surge: ground-hugging relatively dilute density current with gradual (exponential?) downward increase in density; not influenced by wind, but generating a secondary buoyant plume that is wind affected. (C) Flow: ground-hugging, clearly defined, concentrated density current with accompanying dilute overriding cloud; not influenced by wind, but generating a secondary buoyant plume that is wind affected.

which share many characteristics of end-member surges, have propagated at 100–300 m/s. Eyewitness accounts, theoretical modeling, and the products of prehistoric eruptions imply that these transport systems

(1) contain less than 0.1 to 1% by volume of solids even close to the ground surface,
(2) are density stratified with the highest particle concentrations close to the ground surface, and
(3) transport material primarily by turbulent suspension, with a lesser population of coarser clasts moving as a saltating and/or sliding traction carpet.

Surges have been modeled by considering their dynamics to be controlled by the loss of particles by sedimentation into the deposition system (from which the particles eventually come to rest), thus depleting the transport system of mass. Therefore, the surge terminates where it becomes positively buoyant with respect to the ambient atmosphere and lifts off to form a buoyant plume. The density contrast between surges and the ambient atmosphere is relatively low, and surge dynamics can thus be modeled to some degree using relationships derived for aqueous, pure-liquid or sediment-bearing liquid gravity currents.

2. *Concentrated Currents/Flows*

These have been observed to travel at a range of speeds similar to that of surges, i.e., from a few meters to several tens of meters per second. Velocities much greater than this (to 200–300 m/s) have not been observed but are inferred from the heights of obstacles climbed or overcome by some flows. Eyewitness accounts, theoretical modeling, and records of historic eruptions imply that flows

(1) have solids concentrations of the order of tens of volume percent,
(2) have a free surface, above which the solids concentration diminishes sharply, and
(3) transport material by a combination of support mechanisms, including particle–particle contact, fluidization support, matrix support, dispersive pressure and buoyancy (i.e., of large, low-density pumice clasts in the concentrated matrix). Turbulence may or may not be present, but is not dominant as a particle support mechanism, unlike in surges.

Although moving flows and surges look superficially similar from the outside, there is a fundamental contrast between their structures (Fig. 2). In flows, almost all the

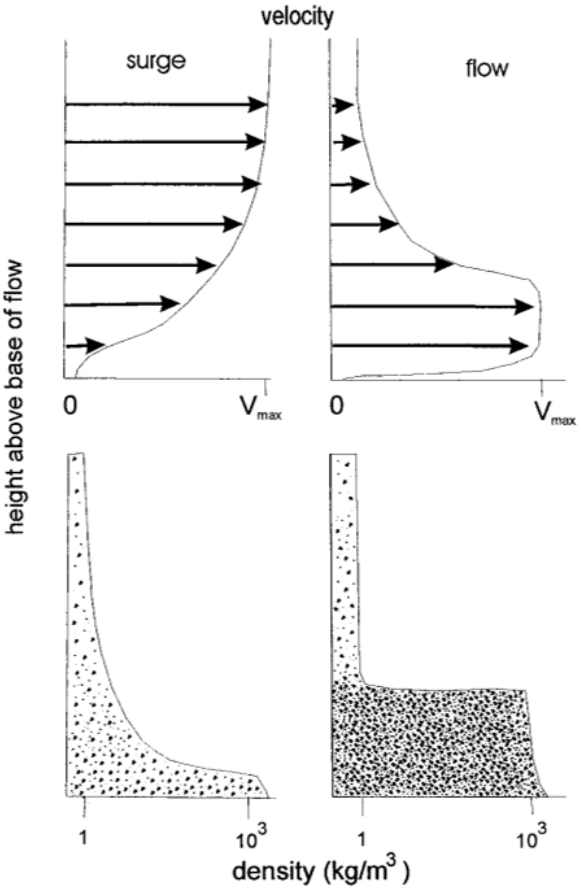

FIGURE 2 Schematic cross-section through end-member dilute (surge) and concentrated (flow) density currents to show the differences in structure. Values of V_{max} can vary from a few meters per second up to ca. 300 m/s in surges and flows; note that the arrows represent time-averaged trajectories and neglect the short-order turbulent fluctuations. Density values shown are indicative only. In their basal few meters to tens of meters, *surges* show a gradual downward increase in density due to sedimentation and a decrease in mean velocity due to ground friction; deposits are generated by sedimentation through this basal zone in a deposition system. Solids concentrations in the moving surge are a few percent or less, and the deposition system controls how material is converted into the final deposit. In contrast, *flows* in their basal few meters to tens of meters are concentrated, with rapid decreases in concentration and mean velocity across an upper interface to the overriding cloud. Flow deposits represent, at one extreme, portions of the flow, slowed by ground friction and left behind, or, at the other extreme, the flow itself which has come to rest; however, differences in particle concentration between the moving flow and the stationary deposit are relatively small.

mass and lateral momentum is concentrated in the basal undercurrent (the flow proper), and the overriding cloud, although visually impressive, is dynamically insignificant and derives its existence and momentum only from the passage of the flow. In surges, the mass and momentum are more evenly distributed in the current; any basal concentration of material is derived by sedimentation from this current and hence is traveling slower than the bulk of the current due to ground friction.

III. DEPOSITION SYSTEMS

A. Introduction

Every clast involved in an explosive eruption has a period of transport, yet ends up as a stationary object in a deposit. The processes whereby this happens are often complex and controversial. The *deposition system* has been proposed as a concept to emphasize that the features of the deposit reflect processes operating only in the latest stages of movement, but the applicability of this is clearly different between fall, surge, and flow deposits. For example, coarse (plinian style, see Fall Deposits) fall deposits are observed to form by the grain-by-grain accumulation of individual clasts, and a separate deposition system as such does not exist. In contrast, clasts supported by turbulent suspension in a dilute current must go through some kind of discrete deposition system as they slow and are deposited. The concept of a separate deposition system is important, because it limits which features can be inferred for the transport system from the deposits themselves, and the nature of explosive eruptions makes direct measurements of transport system properties often difficult or impossible. Here we introduce a simple approach that can be used as a field-based criterion to understand the processes leading to the main features seen in pyroclastic deposits.

B. Simple Controls on Deposition Mechanics

On a broad scale there are four fundamental controls active during the deposition of pyroclastic deposits (Fig. 3):

(1) The *trajectories* of the clasts as they are being deposited, which can vary from vertical to horizontal.

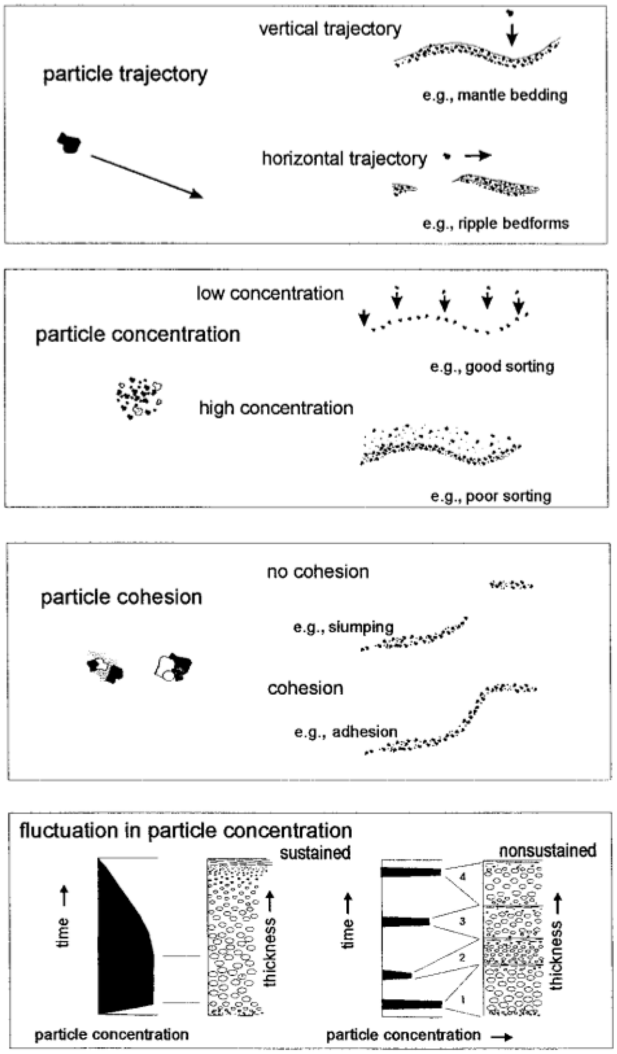
particle trajectory
vertical trajectory
e.g., mantle bedding
horizontal trajectory
e.g., ripple bedforms
particle concentration
low concentration
e.g., good sorting
high concentration
e.g., poor sorting
particle cohesion
no cohesion
e.g., slumping
cohesion
e.g., adhesion
fluctuation in particle concentration
sustained
time
thickness
particle concentration
nonsustained
4
3
2
1
time
thickness
particle concentration

FIGURE 3 Schematic diagram of the four major controls on deposition processes during the formation of pyroclastic deposits: particle trajectory, particle concentration, presence or absence of cohesion, and fluctuations in particle concentration with time.

These trajectories will control the extent to which clasts mantle the ground surface or show evidence for lateral emplacement, for example, unidirectional bedforms.

(2) The *concentration* of particles in the depositing material, ranging from low (discrete particles) to high (dense-packed assemblages of particles). The volume concentration of solids in the depositing material will determine to a large extent the degree of sorting and the scale of the bedforms that can be formed.

(3) The presence or absence of particle *cohesion*. Particle cohesion will cause deposition to tend to be more rapid and irreversible, as well as increasing the maximum slope angle on which deposition can occur.

(4) The presence or absence of *fluctuations* of particle concentration with time, that is, is the deposition system steady or unsteady, sustained or nonsustained. This will determine whether deposition produces a single uniformly graded bed or a succession of beds of contrasting character.

The first two controls are considered by us to be the most important and vary between absolutely definable limits that can be quantified to a greater or lesser extent with present technology and understanding. The third and fourth controls vary more widely, exert a primary control only in a minority of cases, and at present are mostly treated qualitatively.

C. Fields of Pyroclastic Deposition

Setting aside particle cohesion (Section III,E, below) and the effects of fluctuations (Section III,F), we can draw up a diagram that plots particle concentration against particle trajectory (Fig. 4). We can then outline three fields corresponding to the archetypal kinds of pyroclastic deposit:

fall: vertical trajectory, low solids concentration,
surge: horizontal trajectory, low solids concentration,
flow: horizontal trajectory, high solids concentration.

These fields, to a first order, can explain the fundamental characteristics of the great proportion of pyroclastic deposits (Fig. 5).

Archetypal *fall deposits* drape the landscape and lack evidence for lateral emplacement, such as cross-bedding or wave bedforms. In the absence of particle cohesion (Section III,E), they are well sorted and can be bedded on a scale down to millimeters because they are gradually

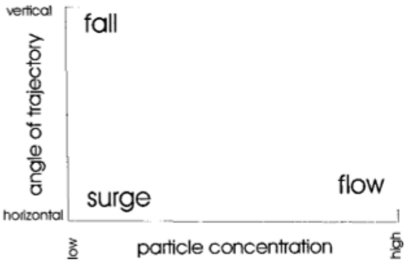
vertical
angle of trajectory
horizontal
fall
surge
flow
low
particle concentration
high

FIGURE 4 Sketch diagram of the particle concentration in the depositing material versus the trajectories of depositing clasts to show the end-member fields of fall, surge, and flow deposition.

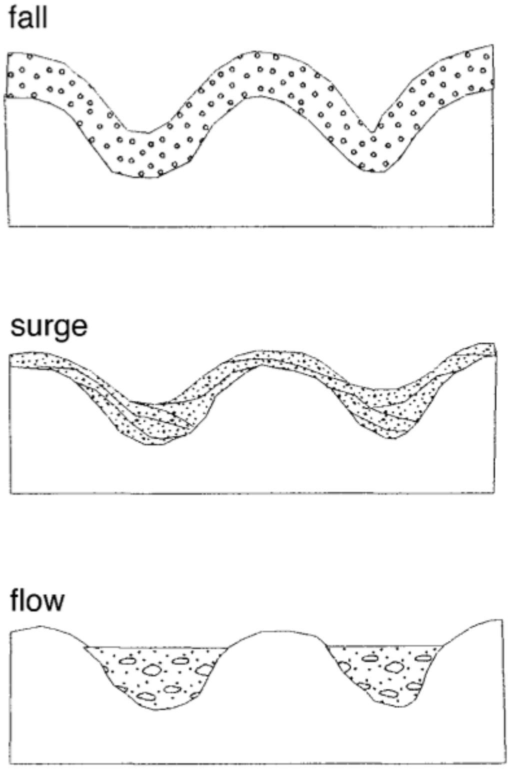

FIGURE 5 Schematic diagram of the archetypal characteristics of the three main pyroclastic deposit types. Fall—mantle bedding, with plane parallel beds and no internal erosion, good sorting (except where water is present; see Section III,E), juvenile clasts with angular to ragged shapes. Surge—nonmantling beds, thickening into low-lying areas, with cross-stratification, pinch-and-swell bedding and scoured contacts, moderate sorting, juvenile clasts with some degree of rounding. Flow—landscape-filling units, generally poorly bedded to nonbedded, poor sorting, rounded juvenile clasts.

deposited at low particle concentrations. Evidence for high temperatures, except for welding in extreme proximal areas, is scarce because of strong cooling of clasts during transport and relatively slow deposition rates.

Archetypal *surge deposits* do not evenly drape the landscape but pinch and swell, reflecting limited control over their travel paths by gravity. They show evidence for lateral transport in the form of basal scouring, unidirectional bedforms such as megaripples, and internal cross-bedding. The deposits vary in their sorting characteristics from good to poor. Evidence for transient high temperatures is common, in the form of burns suffered by victims, or by carbonized vegetation, but sustained temperatures high enough to cause syn- or post-emplacement particle cohesion are rare.

Archetypal *flow deposits* do not drape the landscape, but thicken into or are confined to valleys, reflecting the control of gravity over their travel paths. They show other evidence for lateral transport in the form of basal scouring, but lack internal bedforms, and their sorting is usually poor. Indications of high temperatures during deposition are the norm, ranging from carbonized vegetation and thermal oxidation colors to post- (and less often syn-) eruption welding and cohesion of clasts. The ubiquity of welding in pyroclastic flow deposits has often been taken to indicate a thermally efficient transport mechanism for flows, that is, one that does not involve much mixing with air.

D. Boundaries between Fields of Pyroclastic Deposition

As well as defining the end-member deposit types, it is appropriate to consider the nature of the boundaries between them (Fig. 6).

1. *Fall:Surge*

There are no grounds for supposing there is any clear boundary between these two end-member styles. Consider a fall deposit; if it is being deposited in windless conditions, then there is no mechanism for accumulating the deposit other than vertically, except for slumping or tumbling of grains down steep slopes. However, in the presence of wind, the horizontal component of the particle trajectory due to the wind may be comparable or greater than the vertical component due to gravity,

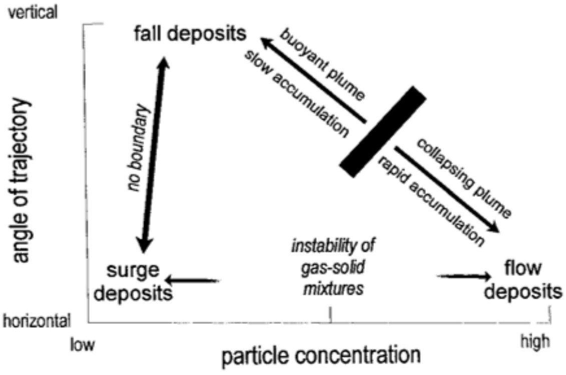

FIGURE 6 Sketch diagram of the particle concentration in the depositing material versus the trajectories of depositing clasts showing the inferred boundaries between the three main depositional regimes that lead to the three main types of pyroclastic deposit. See text for discussion.

especially for finer material (Fig. 7). The particles are thus depositing at an angle, exactly analogous to snow drifting in wind. If the wind velocity is strong enough, material on the ground surface may be picked up, saltated, and redeposited by wind, to produce bedforms that should be, in principle, identical in many respects to deposits laid down by a surge traveling at the same velocity. Examples of wind drifting are very common in reports of modern eruptions, but rare in documented prehistoric deposits. In part this is due to a bias toward study of plinian fall units that are coarse enough to have required unusually strong winds to modify, and in part because the presence of cross-bedding and ripple waveforms is taken automatically to indicate either reworking or surge deposition. The latter distinction is important in delineating the associated hazards (a wind-driven fall may be unpleasant, but a surge is most likely to be fatal) and to understanding and interpreting the dynamics of surge emplacement.

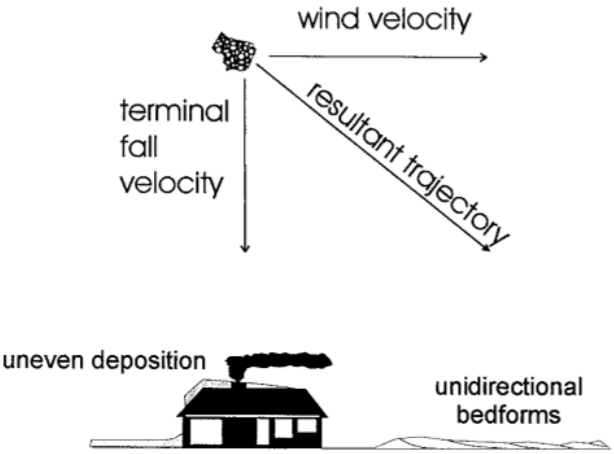

FIGURE 7 Sketch of a single clast being deposited from a buoyant plume in a strong wind; the inclined trajectory is the sum of the wind velocity and the terminal fall velocity vectors. The lower part shows some of the resulting effects on the deposition patterns of fall deposits.

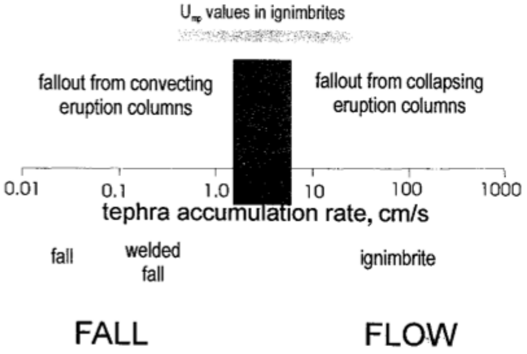
U_mp values in ignimbrites
fallout from convecting eruption columns
fallout from collapsing eruption columns
0.01
0.1
1.0
10
100
1000
tephra accumulation rate, cm/s
fall
welded fall
ignimbrite
FALL
FLOW

FIGURE 8 Graph illustrating a concept of the boundary between flow and fall activity, based on the different depositional regimes of material in the area immediately around the vent. The range of U_{mp} values in ignimbrites represent the maximum velocities (values refer to air at room T, P) at which gas can pass through poorly sorted material representative of the grain-size characteristics of typical pyroclastic flow deposits and inferred to be similar to the composition of the material being delivered to the surface beneath a collapsing eruption plume. With a stable, buoyant plume, the depositing material is generally coarse and well sorted, with U_{mp} values in excess of 100 cm/s; deposition rates are thus too low to initiate mobilization of depositing tephra, because there is enough time for interstitial gas to drain out. With a collapsing plume, accumulation rates are so high that gases cannot escape and the accumulating material is mobile and moves off as a flow.

2. *Fall:Flow*

There are good grounds for thinking there is normally a clearly definable threshold between these styles of deposition (Fig. 8). To generate a pyroclastic flow from material accumulating about a vent requires that material to trap gas. Fall end-members accumulate at rates that are low enough such that interparticle gases can escape easily; consideration of observed or inferred accumulation rates for proximal to medial fall deposits suggests that these will rarely exceed 0.01–0.001 m/s, which are several orders of magnitude too low to trap gases in depositing material of the appropriate grain size characteristics. In contrast, any pyroclastic flow generated by column collapse (as is often the case; see Volcanic Plumes) will involve the sedimentation of material around the vent at rates of >1 m/s. At what threshold of accumulation rate will interstitial gases be trapped? In fluidization experiments, the maximum velocity at which gas can escape through a particulate material evenly (i.e., without channeling or forming bubbles) is, for poorly sorted materials, of the order 0.01–0.1 m/s. Thus in the area beneath a collapsing eruption column, material is accumulating far faster than the interparticle gases can escape, the material will have essentially all of its weight supported by the interstitial gas, and it will flow and deform under stresses like a conventional liquid. Therefore it seems that there is an effective demarcation between fall and flow, largely due to the huge differences in accumulation rates around the vent generated by sedimentation from a high buoyant plume versus a collapsing column. Fall depositional systems that approach the accumulation rates required for particulate flow do occur, but are almost invariably associated with the low fountaining of fluid magmas (i.e., hawaiian style, characterized by a decoupled gas phase) and result in lava flows, not a particulate flow.

3. Surge:Flow

The relationships between archetypal surge and flow modes of transport and deposition are the areas of greatest interest and controversy. Recently the term *pyroclastic density currents* has become popular to refer to all laterally moving currents, regardless of their solids concentration, and *flow* and *surge* are used to refer to concentrated and dilute currents, respectively. There are two divergent schools of thought. One treats flows and surges as the end-members of a completely variable spectrum of currents with all variations of particle concentrations possible in between. The other believes there to be some variation within both flows and surges but that they are fundamentally distinct phenomena, separated by a hiatus that reflects the difference between the mechanics of the transport processes (Section II,B).

In part confusion has arisen in the literature over the terms *flow* and *surge* because of differing opinions over what is the most important characteristic to define each phenomena and explain their patterns of transport and deposition. The two parameters considered most important are solids concentration and the presence or absence of turbulence (or some other kind of unsteadiness). Different groups of workers emphasize one or the other of these as the most important criterion for labeling deposits and inferring their transport mechanics. Here we infer solids concentration to be the key criterion. A second source of debate has been the extent to which subaqueous liquid or liquid/particle gravity currents, the physics and sedimentological consequences of which have been extensively studied, can be used as analogs for gas/particle gravity currents in subaerial settings.

As a contribution to the debate over whether flows and surges form a continuum it should be noted that some kind of phase instability is characteristic of those particulate systems where the interstitial medium is a gas. This instability arises primarily from the high density contrast between the particles and interstitial fluid; it is seen in gas–solid systems (e.g., sand in air), but is very noticeably absent in liquid–solid (e.g., sand in water) systems. This phase instability is seen in fluidized systems, where excess gas, beyond that needed to fluidize the material, passes through the system as bubbles that rise through a concentrated matrix that has not expanded beyond its state when bubbles first appeared. In contrast, the same particles, if fluidized by a liquid will evenly expand to accommodate the extra liquid flow and bubbles are not seen. The phase instability is also seen, for example, in vertical and horizontal pneumatic conveying where the solid particles and the carrier gas travel through pipes. In both cases, increasing the solids loading from the end-member pure gas does not result in a gradually increasing solids concentration, but instead at a certain loading (typically <10 vol%) the system breaks down into separate concentrated and dilute phases. Again, such behavior is not seen in liquid–solid systems. It is tempting to suggest that some similar kind of behavior may apply to the gas–solid particulate systems that in nature form subaerial pyroclastic density currents.

E. Role of Particle Cohesion

Particle cohesion is important in several respects in the deposition (and to a lesser extent transport) systems that generate pyroclastic deposits. Setting aside the effects of electrostatic attraction, which have been observed in historic ash falls (e.g., Mount St. Helens, Sakurajima) but which are poorly documented or undocumented from prehistoric events, the two circumstances where particle cohesion is particularly important occur at two extremes of temperature. These are at low temperatures (≤100°C), where liquid water can cause bridging between particles, and at high temperatures (≥700–800°C), where juvenile clasts can adhere because they are molten and sticky.

At *low temperatures*, cohesion can occur in both the transport system and on deposition, and preferentially affects fine particles. Accretion and clumping of particles due to water in buoyant plumes has been observed in historic eruptions in the form of ash-bearing liquid drops (rain) and moist accreted aggregates (accretionary lapilli) and is inferred to also occur in cool, wet surges. Such accretion is responsible for the premature deposition of finer particles that would otherwise have been carried farther from the vent by the transport system and causes the resulting fall deposits to be more poorly sorted and have more matrix material than their dry counterparts (see Phreatoplinian). Evidence for water-induced accretion on deposition is preserved as vesicular matrix textures and/or rain-splash bedding, indicating that liquid water was present as the deposits were accumulating, and has been reported from numerous fall and surge deposits, but rarely from flow deposits.

The presence of liquid water at low concentrations imparts a cohesive strength to the material that allows fall and surge-emplaced deposits to adhere to surfaces much steeper than the dry angle of repose. However, at higher concentrations, water will allow soft-sediment deformation or syndepositional removal of material as ash-laden slurries. In surge or wind-driven fall deposits, any cohesion will alter the geometry of bedforms by inhibiting the subsequent reentrainment of material back into the transport system, but such effects have not been systematically documented.

At *high temperatures*, cohesion caused by plasticity or fluidity of pyroclasts occurs in two main environments, in both cases preferentially affecting coarser clasts (as these retain heat the longest). First, in extreme proximal areas (i.e., within hundreds of meters of the vent) where clasts have short travel times with limited opportunity for cooling, cohesion of hot clasts is important in building oversteepened pyroclastic structures like spatter cones or ramparts (see Strombolian and Hawaiian Eruptions). Second, in medial to distal areas, high temperature cohesion can only occur in systems where minimal mixing has occurred with the atmosphere, that is, in pyroclastic density currents. In these cases, the role of particle cohesion in influencing transport and deposition conditions is controversial (see Ignimbrites and Deposits of Block-and-Ash Flows), partly because of uncertainties in the relative timescales for cohesion of viscous clasts versus the transport history and partly because of limited data on the viscosity and effective stickiness of clasts.

The most extreme cases involve pyroclastic material that has coalesced on deposition back into a coherent liquid that may retain momentum from the transport system (especially in pyroclastic density currents) but subsequently flows down slope under the influence of gravity. Units formed by this mechanism include fountain-fed lavas (in proximal areas, i.e., within kilometers of vent) and rheomorphic flow deposits (in medial areas, i.e., to distances of tens of kilometers from the vent). Such rheomorphic materials can be difficult to distinguish from conventional lavas, and welded falls may be hard to separate from high-grade ignimbrites; debates over the origin of documented examples are ongoing.

F. Role of Fluctuations in Particle Concentration

All the pyroclastic transport and deposition systems outlined in this chapter show fluctuations, effectively of particle concentration, with time. Such fluctuations are instrumental in generating many of the outcrop-scale features that contribute to the recognition and interpretation of fall, surge, and flow deposits. With fall deposits, fluctuations serve to create a first-order subdivision between the products of accumulation from (i) sustained, relatively steady eruptions and (ii) nonsustained, discrete explosions of fluctuating intensity. This *steady* versus *unsteady* character is reflected in the bedding and grain size properties of fall deposits (see Fall Deposits). In pyroclastic density currents, many authors lay emphasis on the inherently fluctuating nature of transport and deposition in dilute currents (surges), versus a more steady-state mode for transport and deposition in concentrated currents (flows). This contrast is interpreted to reflect both the contrasting momentums of the transporting systems (i.e., for a given velocity, a flow has a higher momentum due to the greater particle concentration) and the length scales over which deposition occurs (e.g., thinner beds or laminae from surges versus thicker beds or individual flow units from flows).

IV. SUMMARY

Pyroclastic deposits are the end product of complex phenomena that are still poorly understood but frequently deadly to observers. The overall morphologies and internal characteristics of pyroclastic deposits reflect phenomena associated with both transport and deposition systems. Many features of pyroclastic deposits can be documented and interpreted within a simple framework of four parameters, namely, the trajectories of the depositing clasts, the concentration of particles in the depositing mixture, the presence or absence of particle cohesion, and the extent and timescale of fluctuations in transport and/or deposition systems.

SEE ALSO THE FOLLOWING ARTICLES

Hawaiian and Strombolian Eruptions • Hazards from Pyroclastic Flows and Surges • Ignimbrites and Block-and-Ash Flow Deposits • Phreatoplinian Eruptions • Pyroclastic Fall Deposits • Pyroclast Surges and Blasts • Scoria Cones and Tuff Rings • Volcanic Plumes

FURTHER READING

Cas, R. A. F., and Wright, J. V. (1987). "Volcanic Successions Modern and Ancient." Allen & Unwin, London, England.

Fisher, R. V., and Schmincke, H.-U. (1984) "Pyroclastic Rocks." Springer, Berlin, Germany.

Freundt, A., and Rosi, M. (Eds.) (1998). "From Magma to Tephra: Modelling Physical Processes of Explosive Volcanic Eruptions." Elsevier, Amsterdam, The Netherlands.

Gilbert, J. S., and Sparks, R. S. J. (Eds.) (1998). "The Physics of Explosive Volcanic Eruptions." Special Publication 145, Geological Society of London, England.

Sparks, R. S. J., Bursik, M. I., Carey, S., Gilbert, J. S., Glaze, L. S., Sigurdsson, H., and Woods, A. W. (1997). "Volcanic Plumes." Wiley & Sons, Chichester, England.

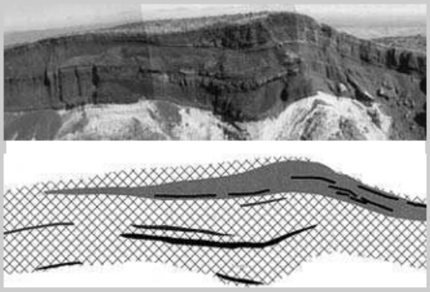

PYROCLASTIC FALL DEPOSITS

B. F. HOUGHTON
C. J. N. WILSON
Institute of Geological & Nuclear Sciences

D. M. PYLE
University of Cambridge

> Fewer than 10% of the explosive eruptions of the present century have been reasonably well documented scientifically, and few volcanologists have the opportunity to observe more than 3 or 4 large explosive eruptions in their lifetime. It is not difficult however for one person in a year to measure the deposits of several large eruptions of the past, and the volume of data forthcoming from such measurements is enormously greater than that forthcoming from observations on current activity.
> —*Walker (1973)*

I. Introduction
II. Large-Scale Properties
III. Medium-Scale Properties
IV. Small-Scale Properties
V. Discussion

GLOSSARY

componentry Study of the abundances of different individual particle types in a pyroclastic deposit

dispersal index (*D*) A measure of the extent of a pyroclastic fall deposit, specifically the area enclosed by an isopach drawn at 1/100 of the maximum extrapolated thickness of the deposit.

external water Any water (e.g. seawater) involved in explosive volcanism that was not originally dissolved in the magma.

fragmentation index (*F*) A parameter measuring the grain size of a pyroclastic fall deposit, specifically the percentage of ash finer than 1 mm at the point on the dispersal axis corresponding to 1/10 of the maximum thickness of the deposit.

grain size half-distance (b_c) The "average" distance over which the maximum clast size in a pyroclastic deposit halves.

isopach Line joining points of equal thickness in a deposit.

isopleth Line joining points where the sizes of the largest clasts (pumice or lithic) are the same.

pyroclastic fall The rain-out of clasts through the atmosphere from an eruption jet or plume during an explosive eruption.

thickness half-distance (b_t) The "average" distance over which the thickness of a pyroclastic deposit halves.

PYROCLASTIC FALL DEPOSITS are produced by the rain-out of clasts through the atmosphere from an eruption jet and/or plume during an explosive eruption. Fall deposits are the simplest of pyroclastic products, and their value within physical volcanology lies in this simplicity and in the ease with which

Copyright © 2000 by Academic Press
All rights of reproduction in any form reserved.

their properties can be used to infer eruption parameters. Fall deposits result from both "dry" magmatic and "wet" phreatomagmatic eruptions, and the "whole deposit" grain size distribution and morphology of the pyroclasts reflect principally the nature of the fragmentation process. Falling pyroclasts are fractionated during their transport through air (and sometimes also through water). Aerodynamic properties of the clasts, the vigor of eruption, and the nature of the transport process impart distinctive thinning and fining characteristics to the beds.

I. INTRODUCTION

We here describe the properties of fall deposits on three scales:

Large scale:	Those properties that may be inferred only from examination of the entire deposit
Medium scale:	Those features that may be observed and used on outcrop scale
Small scale:	The properties of the particles that make up fall deposits

Large-scale features include the rates at which fall deposits thin and fine away from source and the grain size properties of the entire deposit. Bedding and grading, absolute grain size, and sorting and welding are medium-scale properties. The morphology and vesicularity of juvenile clasts and the content and nature of foreign (wallrock) clasts are small-scale features.

II. LARGE-SCALE PROPERTIES

Fall deposits are generated from three mechanically distinct but spatially overlapping regions during an explosive eruption (see the chapter entitled "Volcanic Plumes"):

1. The *jet* or *gas-thrust* region where the material first emerges from the vent at high velocities
2. The *plume* region where the mixture rises buoyantly in the atmosphere to a height determined by the thermal flux
3. The *umbrella-cloud* region where the eruption plume spreads laterally, in response to atmospheric stratification and the wind

Fall deposits form concave-upwards cones of tephra that thin away from a point of maximum thickness that is usually close to or coincident with the eruptive vent (Fig. 1a and 1b). Isopach and isopleth maps of the distribution of tephra thickness and maximum grain size, respectively, are used to quantify the thickness and coarseness of the deposits. The individual isopachs/isopleths usually form more or less regular ellipses (Fig. 1c) that are elongated in the downwind direction; the direction of elongation away from the vent defines the *dispersal axis* of the deposit. Complexities, such as (1) secondary thickening of the deposits due to the aggregation and early fallout of fine particles, (2) elongation of the umbrella cloud in different directions at different levels in the atmosphere, or (3) changing wind directions during the course of an eruption, can be recognized sometimes in isopach and isopleth maps of well-preserved deposits (Fig. 2).

A. Thinning of Fall Deposits

The thickness and maximum grainsize of proximal to medial fall deposits decay exponentially, or nearly so. Exponential decay of thickness can be recognized by a straight-line relationship on a plot of the (natural) logarithm of thickness ($\ln T$) versus the square root of the corresponding isopach area ($\sqrt{A}$). The rate of thinning can be described by a simple parameter, the "half-distance" (b_t), which is the distance over which the thickness halves (Table I), analogous to the half-life in radioactive decay. The extrapolated value of the thickness to $\sqrt{A} = 0$ yields a maximum thickness value, T_0. For any deposit that shows an exponential decay of thickness, the volume of the deposit (V) can then easily be estimated from the empirically derived equation

$$V = 13.08 T_0 b_t^2.$$

In practice, there are departures from simple exponential decay shown by many fall deposits (Fig. 3), which result in deviations from straight-line relationships on diagrams of $\ln T$ versus $\sqrt{A}$. There are three fundamental causes for this, ultimately related to the grain size distribution of the erupting mixture and its influence on eruption column behavior (see the chapter entitled "Volcanic Plumes"):

1. Changes in transport mode between the regions of the eruption column. In those eruption styles dominated by coarse clasts (e.g., strombolian, hawaiian), much of the material is too coarse to be carried up in the buoyant plume region, but instead is distributed in

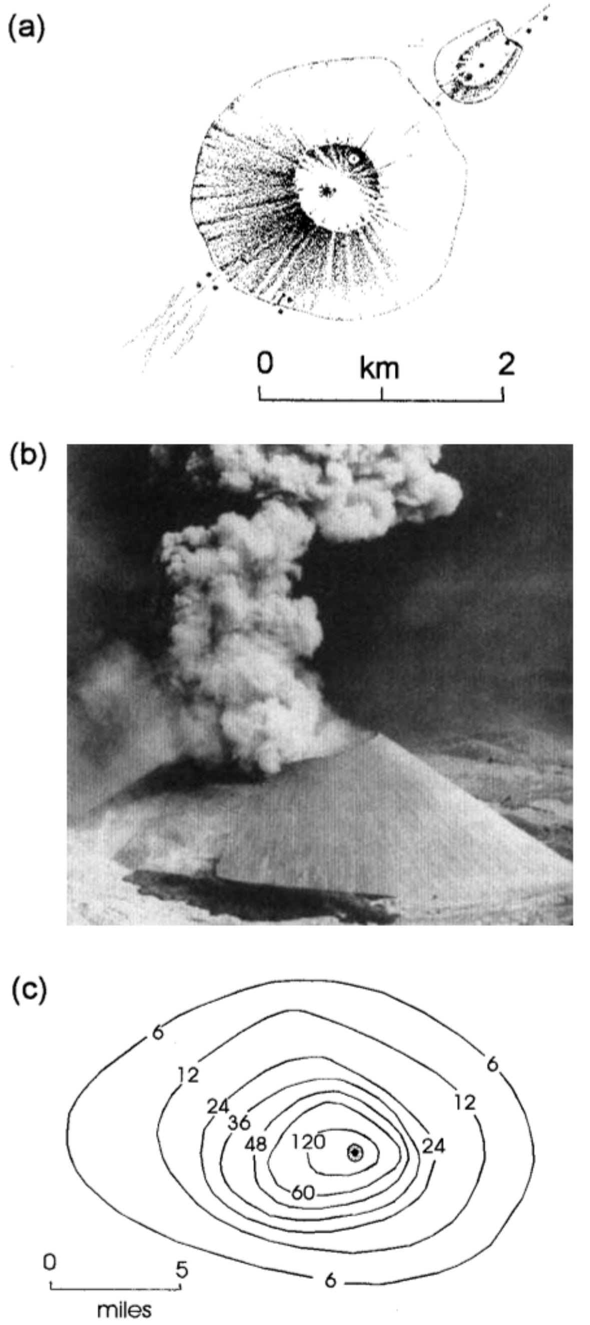

FIGURE 1 Sketch and photograph of Paricutin scoria cone, Mexico and isopach map for the distal fall deposit (reproduced from Krauskopf, K; McWilliams, H. (1946). The activity of Paricutan during its third year. *American Geophysical Union Transactions* **27,** 406–410). The main cone of Paricutin formed between 1943 and 1944 in a series of strombolian and subplinian eruptions.

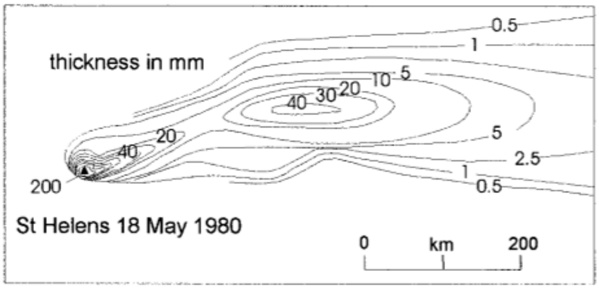

FIGURE 2 Isopach map for the 18 May 1980 Mt. St. Helens fall.

ballistic fashion around the vent. Where the slope of the cone of accumulation exceeds the angle of rest ($\sim 35^\circ$), slumping will generate a cone of uniform slope rather than an exponentially decaying sheet. In the rare cases where the extreme proximal regions of widespread ("plinian") deposits are preserved, there is usually evidence also for accumulation of a thick pile of material around the vent that represents a steep, "ultraproximal" segment on a plot of ln T versus $\sqrt{A}$, with b_t values on the order of tens to a few hundreds of meters. In addition there are many examples known where there is an inflection point in a plot of ln T versus $\sqrt{A}$ a few kilometers to tens of kilometers from the vent (Fig. 3b); this change is attributed to the differing transport regimes in the buoyant plume versus the umbrella cloud region. Typically, b_t ranges between 1 and 10 km for the proximal portion, and can range from 20 to 100 km, or more, over the distal portion.

2. Changes in the fall behavior of clasts with differing grain sizes. The size and density spectra of clasts carried into the umbrella cloud region are equivalent to a wide range of particle fall velocities. Differences in these fall rates (controlled by the particle Reynolds number, N_{Re}) are sufficiently large that the finest fragments (chiefly vitric ash) that settle under Stokes' law conditions at low N_{Re} are carried significantly farther and generate a distal segment on a plot of ln T versus $\sqrt{A}$.

3. Complex sources of pyroclastic material. In eruptions where a buoyant vent-derived plume coexists or is interspersed with buoyant portions of pyroclastic density currents (see the chapter entitled "Volcanic Plumes"), the fall deposits may show complex thinning relationships and mixing of material from different sources. In part this is driven by the dominance of fine ash in the second of these sources, which causes the bulk of the combined fall deposits to be transported farther from the vent, and, in part, it is related to the fact that the "source" of any plume coming from a

TABLE 1 Key to Deposits Used to Construct Fig. 3

	Deposit	*Style*	b_t *(km)*	*Source*
1	Etna 1971	Strombolian	0.04	*Phil. Trans. Roy. Soc.* **274,** 147–151
2	Kilauea Iki 1959	Hawaiian	0.22	*J. Volcanol. Geotherm. Res.* **84,** 197–208
3	Algar do Carvao I	Strombolian	0.41	*J. Geol. Soc. London* **132,** 645–666
4	Galiarte	Strombolian	0.47	*J. Geol. Soc. London* **132,** 645–666
5	Terceira E	Subplinian	1.5	*J. Geol. Soc. London* **132,** 645–666
6	Terceira B	Subplinian	1.4	*J. Geol. Soc. London* **132,** 645–666
7	Paricutin 1944–45	Subplinian	2.4	*Amer. Geophys. Un. Trans.* **27,** 406–410
8	Hekla 1970	subplin./plinian	2 + 7	*Bull. Volcanologique* **36,** 269–288
9	1875 Askja-C	Phreatoplinian	5	*Phil. Trans. Roy. Soc.* **299,** 241–273
10	St Helens 18 5 1980	Plinian	3 + 34	*Bull. Volcanol.* **51,** 28–40
11	1875 Askja-D	Plinian	9	*Phil. Trans. Roy. Soc.* **299,** 241–273
12	Pululagua	Plinian	5	*Bull. Volcanol.* **55,** 523–535
13	Oruanui 1	Phreatoplinian	18	C. J. N. Wilson, unpublished data
14	Oruanui 2	Phreatoplinian	20	C. J. N. Wilson, unpublished data
15	Oruanui 5	Phreatoplinian	68 + 148	C. J. N. Wilson, unpublished data
16	1991 Hudson	Plinian	3 + 9	*Bull. Volcanol.* **56,** 121–132
17	Novarupta B	Plinian	10	*Bull. Volcanol.* **54,** 646–684
18	Novarupta A	Plinian	10	*Bull. Volcanol.* **54,** 646–684
19	Quizapu	Plinian	5 + 62	*Bull. Volcanol.* **54,** 93–125
20	Oruanui 6	Phreatoplinian	44	C. J. N. Wilson, unpublished data
21	Oruanui 7	Phreatoplinian	58	C. J. N. Wilson, unpublished data

pyroclastic density current may be geographically detached from the primary vent, as was observed with the May 18, 1980, Mt. St. Helens eruption.

Many fall deposits, especially those for which data are not available in the most proximal or distal areas, show a single straight-line relationship on a plot of ln T versus $\sqrt{A}$, and the method of volume calculation just given provides a useful minimum volume estimate. The proportion of this volume that is enclosed within the final mapped isopach depends on the ratio of the thickness of the last mapped isopach (T_{last}) to the extrapolated maximum thickness, T_0:

$$V/V_{\text{total}} = 1 - (T_{\text{last}}/T_0)(1 - \ln(T_{\text{last}}/T_0)).$$

So as long as (T_{last}/T_0) is less than 0.05, at least 80% of the calculated volume will be enclosed within the final mapped isopach. Other deposits are known for which there are three or even four straight-line segments; volumes can still be calculated, but these have to be integrated separately for each segment. There is no simple relationship between maximum thickness and dispersal (Fig. 4a).

B. Dispersal Indices of Fall Deposits

The thickness half distance may be used to separate classes of fall deposit with differing dispersal characteristics (e.g., Fig. 3a). An alternative method for quantifying how widespread is a fall deposit is the dispersal index (D), introduced by G. P. L. Walker. This index is defined as the area enclosed within the $0.01T_0$ isopach, and it ranges from <1 km^2 in small, cone-dominated deposits to >2 × 10^6 km^2 in some phreatoplinian fall deposits (see the chapter entitled "Phreatoplinian Eruptions"). Walker later suggested that a more rational index of dispersal might be the area that enclosed half of the volume of the deposit, but this requires the fall deposit volume to be accurately known (see Section II,C). If a fall deposit is a simple exponential cone the dispersal

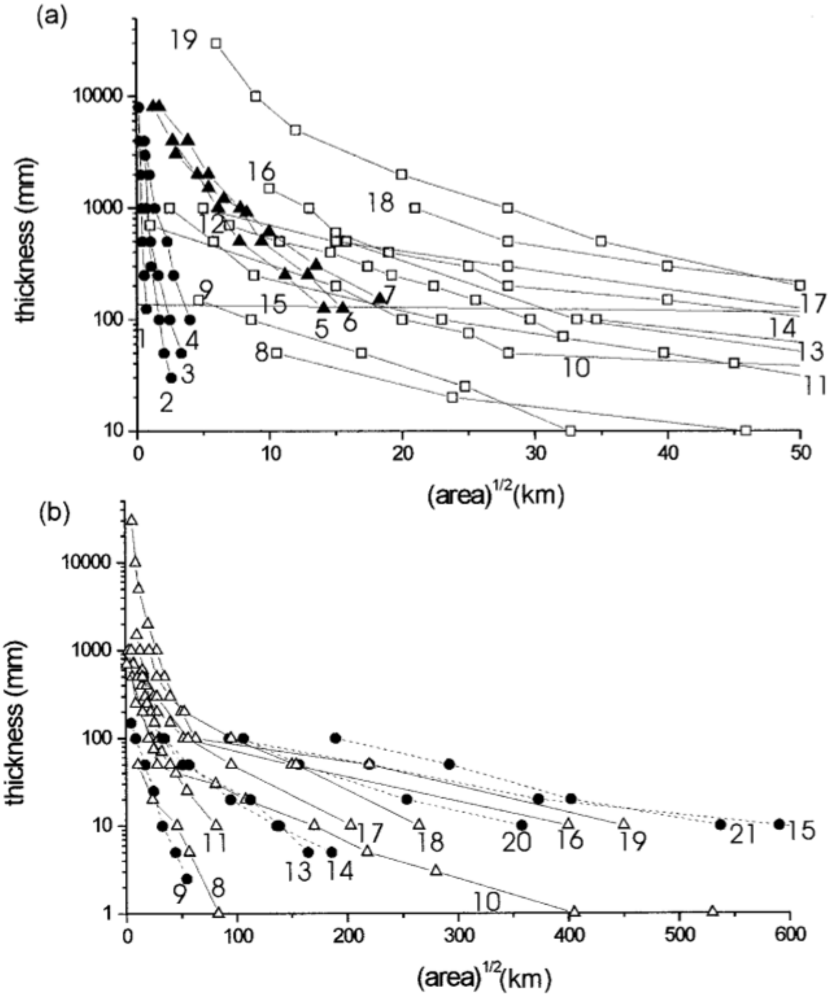

FIGURE 3 Plots of ln T versus $\sqrt{A}$. (a) Plot of proximal thinning relationships for representative hawaiian/strombolian (solid circles), subplinian (solid triangles), and plinian/phreatoplinian (open squares) tephras. (b) Similar plot at expanded scale for the plinian (open triangles; solid line) and phreatoplinian (solid circles; dashed line) units.

index is proportional to b_{t}^2; $D = 138.7b_{\mathrm{t}}^2$, and the area within the $0.01T_0$ isopach encloses 94% of the erupted volume. The area of the same deposit that encloses half of the volume of the deposit is marked by the isopach with $T = 0.186T_0$ and encloses an area of $18.4b_{\mathrm{t}}^2$.

C. Fining of Fall Deposits

All fall deposits show some diminution of grain size between proximal and distal areas. For many purposes (especially modeling of plume dynamics, and comparing the "power" of eruptions), the maximum grain size is the key parameter that is measured. Various workers have used different techniques; for example, averaging lengths of the longest, or all three, axes of the 3, 5, or 10 largest clasts at any exposure, or measuring in similar fashion but only over a defined area (1 m^2, 10 m^2) at any exposure.

The decay of the maximum grain size of fall deposits is also often exponential, or nearly so, and can also be described by a "half-distance," b_{c}, over which the maximum grain size (however measured) diminishes by half. The grain size half distance is principally influenced by the energetics of the column and ranges up to 18 and 40 km, respectively, for the most energetic "dry" (plinian) and "wet" (phreatoplinian) eruptions known.

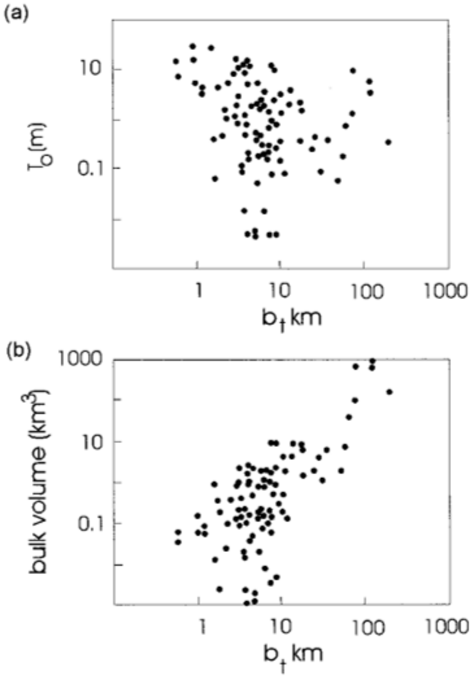

FIGURE 4 Plots of bulk volume and extrapolated maximum thickness against thickness half-distance.

Two parameters, the inferred maximum clast size and the mean grain size, can be used to define a "size half-distance." The latter has not been widely used, and its full significance remains unexplored.

The ratio of thickness and maximum grain size half-distance (b_c/b_t) is principally controlled by the grain size characteristics of the erupting mixture at the vent. There is a wide variation of values, b_c/b_t being lower for deposits dominated by finer-grained clasts, but most deposits have b_c/b_t between 0.5 and 1.5 (Fig. 5).

D. Volume

Two methods are widely used for determining bulk volumes of fall deposits. The first uses the observed (or inferred) exponential decay of thickness with area and integrates under the lines of ln T versus $\sqrt{A}$ to obtain a volume estimate. This method is dependent on accurate measurements (or assumptions) to extrapolate values of $\sqrt{A}$ as T approaches 0. The second method estimates the total mass of magma erupted by comparing the measured mass proportions of loose crystals in the fall deposit with the mass ratio of phenocrysts to glass in pumices from the deposit. It assumes that the crystals have a narrow size distribution and hence that they are all deposited and preserved in proximal to medial areas, then uses the phenocryst : glass mass ratio in pumices to estimate masses (hence volumes) of the "missing" finer-grained vitric ash deposited in inaccessible distal environments. This method is dependent on accurate knowledge of the phenocryst : glass ratios in the pumices and deposit (in an eruption where the magma was zoned with respect to phenocryst content, this may be effectively impossible) and is unusually labor-intensive. Volumes estimated from the former method yield values that are as low as one-third to one-half of volumes for the same deposits estimated using the latter method.

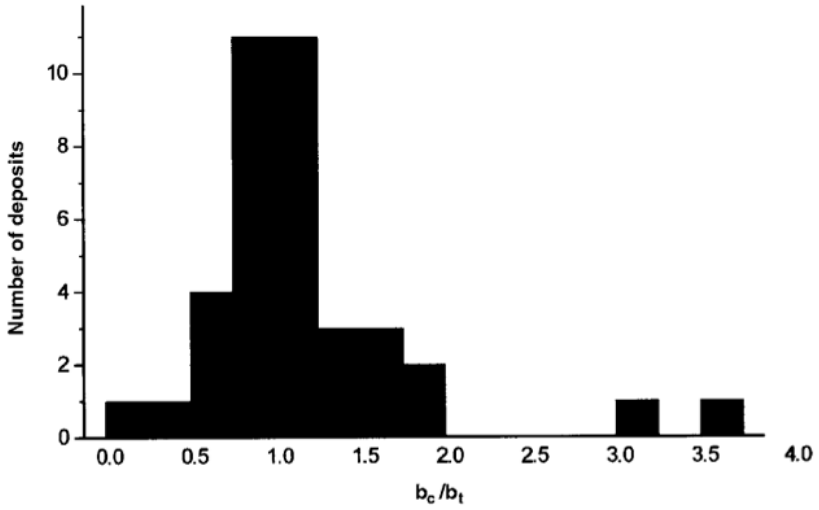

FIGURE 5 Frequency plot for deposits with a given ratio of thickness and grain size half-distances (b_c/b_t).

In large part, conflicts between these methods for estimating fall deposit volumes exist because of uncertainties in estimates of the volume of distal-deposited fine ash fall associated with eruptions, especially those where large-volume pyroclastic density currents are generated. However, another reason for conflict is because theoretical models for deposition from eruption plumes and umbrella clouds predict deposition in terms of mass per unit area, whereas this parameter is largely ignored in field measurements in favor of simple thickness measurements. The two can be compared only if accurate measurements of *in situ* pyroclast mass (or dry bulk density) are available and/or data on pyroclast mass per unit area are collected. With the notable exception of the Mt. St. Helens 1980 fall deposits, both forms of data are sparse, and rectification of this is important for future studies.

The most voluminous fall deposits tend to be those that are the most widely dispersed (Fig. 4b). This relationship is correlated over 3–4 orders of magnitude (eruption rates of $\sim 10^6$ to 10^9 kg/s; deposit masses 10^{11} to 10^{15} kg) and implies that the magma discharge rate is related in some fashion to the size of the magma chamber being tapped.

E. Whole-Deposit Grain Size

The grain size characteristics of entire fall deposits (whole-deposit grain size) reflect only processes of fragmentation and eruption, not transport. As such they hold real potential as a parameter for classification of fall deposits and comprehension of eruption dynamics. Unfortunately, few sets of data exist, and most of these are for relatively small historical eruptions. The difficulty lies in (1) the low potential for preservation of deposits beyond the 1-cm isopach in subaerial environments, and (2) the fact that the distal portions of many fall deposits are deposited offshore. In prehistoric fall deposits, where distal deposits are not preserved, only crude estimates of the whole-deposit grain size can be made in most cases. Techniques applied include one or more of (1) integration of relative abundances for individual size fractions using a plot of ln(mass per unit area) versus $\sqrt{A}$ for each size fraction, (2) using broad constraints on the abundance of fine distal ash fractions (estimated using the crystal measurement method described in the previous section) to control the fine "tail" of the whole deposit, and (3) using grain size populations in syneruptive water-flushed fall or pyroclastic density current deposits where the particles are less widely segregated and dispersed.

III. MEDIUM-SCALE PROPERTIES

A. Stratification and Grading in Fall Deposits

The nature of the stratification and the fluctuations in grain size in fall deposits offer insight into the changing intensity of the parent eruptions, particularly for very proximal sections. Most fall deposits consist of an alternation of coarser and finer grained intervals (Fig. 6). Sharp bedding planes, dividing units of contrasting grain size, imply spasmodic, nonsustained eruption (Figs. 6a, 7); sustained events produce deposits lacking well-defined bedding planes (Figs. 6b, 7). The absolute grain

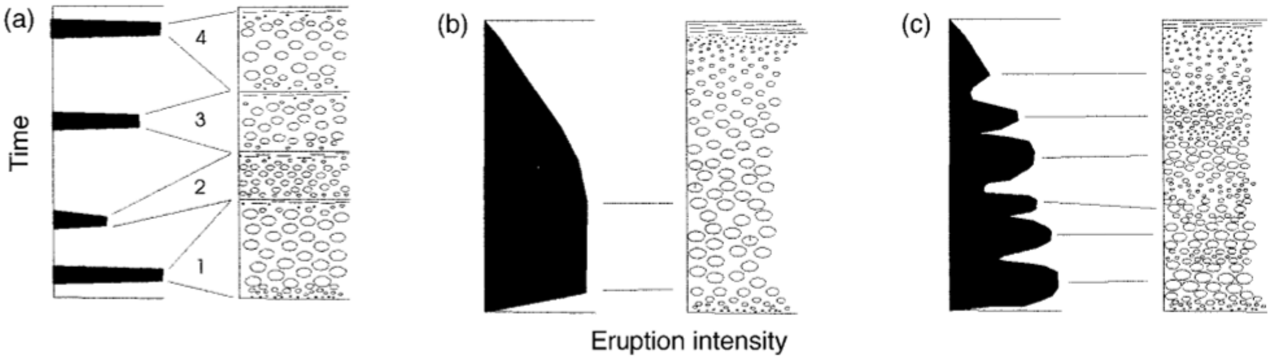

FIGURE 6 Schematic cartoon of the relationships between eruptive intensity, the development of bedding, and the maximum clast size for a given component.

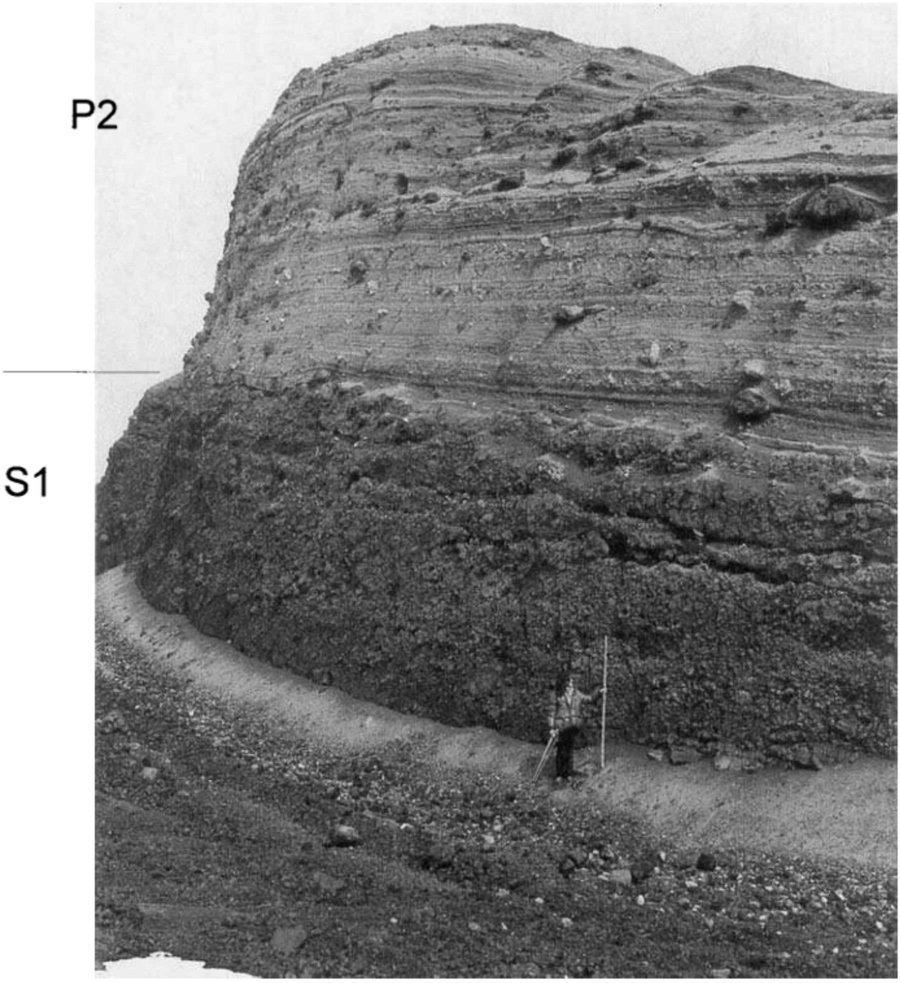

FIGURE 7 Contrasting bedding and grading in sustained Strombolian and episodic phreatomagmatic pyroclastic deposits at Rothenberg scoria cone, Germany. The darker lower Strombolian S1 beds show cryptic fluctuations in grain size (shower bedding) interpreted as due to sustained eruption with fluctuating intensity of the type sketched in Fig. 6c; the upper lighter phreatomagmatic P2 beds were produced by multiple discrete explosions (see Fig. 6a). Note also the greater abundance of lithic blocks (light-colored) in P2. Photograph by Paul van den Bogaard.

size of the finest ash "partings" in a deposit gives some estimate of the duration of pauses in the eruption; for example, 10-μm sized ash can persist in the atmosphere for 2 to 3 days so that beds of this grain size in a sequence imply breaks of at least this duration (provided that flushing of this ash by moisture and/or electrostatic attraction has not occurred). Conversely, small amounts of very fine ash erupted in early phases of a prolonged "dry" eruption may not settle until after the close of the last phases of eruption, as has been proposed for the 1912 A.D. eruption of Novarupta in Alaska. Passing away from vent the definition of partings in a deposit may fade, as the period of plume transport becomes significantly longer than the duration of fluctuations in the intensity of the eruption.

Progressive vertical changes in particle size or composition within a bed are known as *grading*. Density grading is a progressive change in particle density with or without a change in grain size. Density grading is a more common feature of flow deposits, whereas size grading is typical of all pyroclastic deposits (Fig. 6b), but can be expressed in very subtle fashion. Both normal and inverse size grading are common in fall deposits. Grading is most commonly interpreted in terms of fluctuating vigor of the eruption (Figs. 6b and 6c), but can also be produced by wind shifts and/or alteration in the inclination of the eruption column or jet. *Shower bedding* is a term given to gradual fluctuations in grain size within a fall deposit (Fig. 7).

Fall deposits tend to lack the internal unidirectional sedimentary structures that characterize the deposits of vent-fed pyroclastic density currents, although near-surface winds and coeval plume-fed density currents occasionally create cross bedding and pinch-and-swell structures in fall deposits. Mantle bedding (Fig. 8a) is a classical feature of fall deposits—plane-parallel fall units drape and follow preexisting relief on slope angles up to 25° to 30°. On steeper surfaces material may roll, slide, or avalanche down slope and, in extreme cases, form better-sorted lensoid inverse-graded units on or below any steep slope (Figs. 8b, 9b).

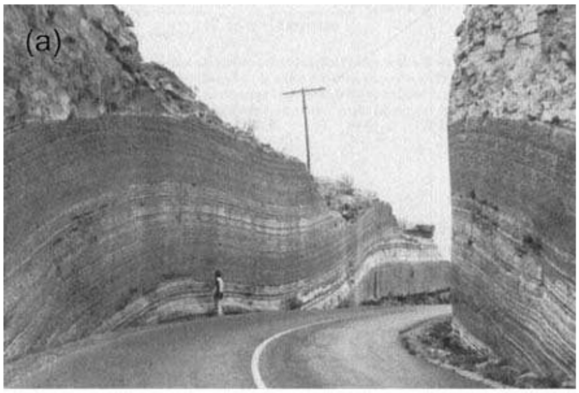

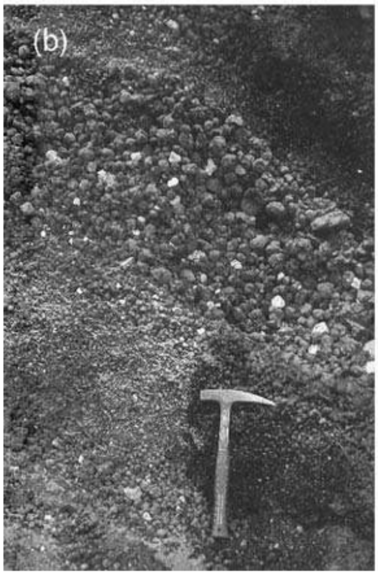

FIGURE 8 The response of fall deposits to preexisting topographic relief. (a) Mantle bedding in Quaternary fall tephras of Tenerife, Canary islands. (Photo reproduced from Fisher, R. V., and Schmincke, H. U. (1984). "Pyroclastic Rocks." Berlin. Copyright © Springer Verlag.) (b) Lensoid slope-affected bedding in a strombolian phase of the Harry Johnson Road basalt deposit, Taupo Volcanic Zone. The slope-affected beds are significantly better sorted (data from these beds defines trend C in Fig. 9c) than the primary strombolian fall deposit.

B. Absolute Grain Size and Sorting

The behavior of particles that form pyroclastic fall deposits is strongly influenced by their terminal fall velocities. The residence time of any clast in an eruption plume is inversely proportional to its fall velocity (V_t), which increases with clast diameter (d) and density (ρ) as

$$V_t \approx (3.1\, g\rho d/\sigma)^{1/2} \qquad \text{for Reynolds numbers} > 500, \text{ or}$$
$$V_t \approx g\rho d^2/18\mu \qquad \text{for Reynolds numbers} < 0.4,$$

where σ is the density of air and μ the dynamic viscosity.

George Walker recognized, at a very early stage, a crude correlation of absolute grain size with eruption style. Fall deposits of very wet eruptions are typically very fine-grained, whereas deposits of dry eruptions are coarse-grained (Fig. 9a). This correlation was originally linked to a greater efficiency of phreatomagmatic explosions. However, the possibility arises that part of the differences between wet and dry fall deposits is due to the effect of liquid water in causing premature flushing of fine ash from the eruption column. Absolute grain size can be described in terms of either maximum clast size (as in the construction of isopleth diagrams) or some measure of average clast size. The two commonly quoted parameters are Md_ϕ ($=\phi_{50}$) and M_Z ($=[\phi_{16} + \phi_{50} + \phi_{84}]/3$), where the numbers refer to percentiles coarser than the phi-size stated and ϕ is the negative log to the base 2 of the grain size in millimeters.

There is considerable overlap between the grain size of dry or "magmatic" fall deposits and that of phreatomagmatic deposits from eruptions with low water/magma ratios (Figs. 9b and 9c). In contrast, many deposits of phreatomagmatic eruptions involving abundant water typically have $\sigma\phi$ values of 2 or higher.

The size of juvenile particles in a deposit is a measure of both the efficiency of the fragmentation processes and the vigor of the eruption. It is important to realize that these factors are not always coupled. For example, hydrothermal explosions (see the chapter entitled "Surface Manifestations of Geothermal Systems"), powered by flashing of superheated water to steam, produce highly fragmented assemblages of clasts, because they utilize the available thermal energy very efficiently (down to ~100°C). However, they are generally rather weak, as the total energy available to eject and transport clasts is constrained by the low preeruptive temperature of the systems (typically only 230–300°C).

There are some tricks in interpreting particle size distribution:

1. The size of lithic clasts is not always a measure of the efficiency of fragmentation, especially in deposits rich in foreign lithics. In the case where such clasts are derived from a preexisting unconsolidated tephra or sediment, their particle size distribution may be effectively inherited from this predecessor, and very large or very small clasts may be absent from the lithic population. Many very fine grained but lithic-rich phreatomagmatic falls should not be interpreted as representing highly efficient fragmentation for this reason. Likewise, recycling of clasts through the vent (see later discussion) can also promote an unusually fine grain size distribution.
2. One process that can complicate interpretation is if apparently juvenile clasts fall back into or close to the source and then are recycled through the vent. The grain size and also morphology of these clasts then has no relationship to the eruptive conditions at the moment when they finally leave the vent. These clasts share a transport history with truly juvenile clasts in the same deposit but may have been fragmented under very different conditions and indeed refragmented several times.
3. Another process leading to an apparent reduction in the grain size of a deposit is the breakup of large clasts in flight or, more commonly, on impact. The latter

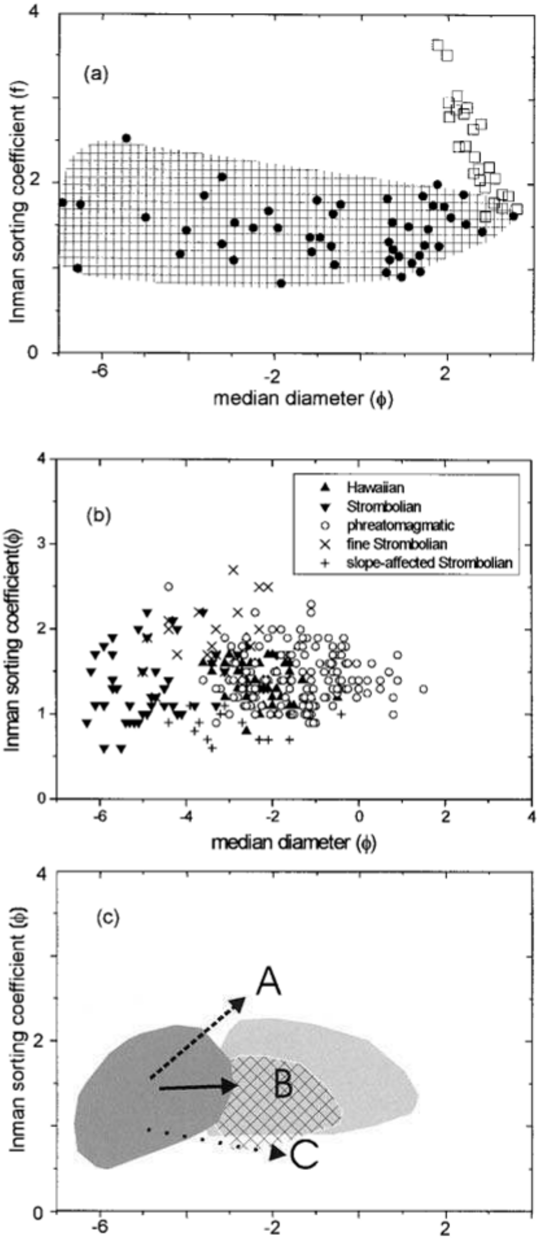

FIGURE 9 Contrasting grain size properties for a variety of pyroclastic fall deposits from eruptions involving widely different water/magma ratios. (a) Dry (plinian) and wet phases of the 1875 A.D. eruption of Askja caldera, Iceland, after Sparks, R. S. J., Wilson, L., and Sigurdsson, H. (1981). The pyroclastic deposits of the 1875 eruption of Askja, Iceland. *Phil. Trans. Roy. Soc. London A* **299;** 241–273. The phreatoplinian phase C at Askja was characterized by relatively high water/magma ratios when silicic magma interacted with abundant external water, and the contrast in deposits to the associated plinian phase D is clear. (b) Dry (strombolian and hawaiian) and wet phases of basaltic volcanism. The phreatomagmatic units were all linked to low water/magma ratios as basaltic magma contacted limited quantities of ground water and thus the contrasts in sorting and absolute grain size are less marked than in (a). Data are from our research on numerous deposits from Taupo Volcanic Zone and the Eifel and Auckland volcanic fields. (c) Summary of data from (b). Hawaiian fall samples (cross-hatched) in particular show a strong overlap with the coarse-grained phreatomagmatic deposits (pale gray). Three processes operating during Strombolian volcanism also produce deposits whose grain size characteristics also mimic the associated phreatomagmatic fall deposits:

A: Partial blockage of the vent by wall collapse or formation of lava ponds, (which produces fine-grained and relatively poorly sorted beds)
B: Size fractionation and fining with distance from vent (distal samples are finer grained but similar to proximal samples with respect to sorting)
C: Rolling, sliding, and avalanching of material down slope (leading to finer grained and better-sorted deposits)

TABLE II Typical Foreign Lithic Contents of Some Basaltic Fall Deposits[a]

Lithics wt%	*Eruptive style*	*Deposit*	*Source*
70–98	'wetter' phreatomagmatic	White Island 1976–1982	*Bull. Volcanol.* **54,** 25–49
60–90	'wetter' phreatomagmatic	Tokachi-dake 1988–1989	*Bull. Volcanol. Soc. Japan* **35,** 131–145
10–50	'drier' phreatomagmatic	Rothenberg scoria cone	*Bull. Volcanol.* **52,** 28–48
5–10	'drier' phreatomagmatic	Ohakune tuff ring	*J. Volcanol. Geotherm. Res.* **21,** 207–231
20	'drier' phreatomagmatic	Herchenberg scoria cone	*Bull. Volcanol.* **52,** 426–444
<1	Hawaiian	Kilauea Iki 1959	*J. Volcanol. Geotherm. Res.* **84,** 197–208
<1	Strombolian	Rothenberg scoria cone	*Bull. Volcanol.* **52,** 28–48
<1	Strombolian	Ohakune scoria cone	*J. Volcanol. Geotherm. Res.* **21,** 207–231
5–15	Strombolian[b]	White Island 1977	*Bull. Volcanol.* **54,** 25–49

[a] Illustrates the general contrast in lithic content between magmatic ("dry") and phreatomagmatic ("wet") fall deposits. "Wetter" phreatomagmatic fall deposits show evidence for abundant liquid water at the time of deposition, such as mud lumps, soft-sediment deformation, and deep bomb sags. "Drier" phreatomagmatic fall deposits are relatively well sorted and do not contain accretionary lapilli or mud lumps.

[b] Represents a Strombolian eruption through soft, hydrothermally altered host rock.

process can often be inferred from the jigsaw fit of adjacent clasts in a bed.

The combination of sorting and grain size parameters was used at an early stage to define fields for "wet" and "dry" fall deposits. Where clasts are deposited from "dry" plumes (see chapters entitled "Plinian and Subplinian Eruptions" and "Volcanic Plumes") there is minimal interaction with neighboring clasts and marked size and density fractionation develops in the plumes; this is reflected in the deposits. The resulting deposits show both a marked decline in clast size with distance from vent and good sorting throughout. Certain components with fixed (or restricted) ranges in size and density will be concentrated at specific distances from the vent; for example, free crystals commonly form girdles of maximum abundance some tens of kilometers from the vent in plinian deposits. A general improvement in the degree of sorting beyond the near-vent region is a common feature of many dry fall deposits.

In contrast, if aggregates of ash form in moist plumes, through collision and binding of particles, then the aggregates will fall with greater velocities than the terminal velocities of their component particles. This process of ash aggregation results in the "premature" removal ("flushing") of ash-sized ejecta from the plume and simultaneous deposition of a wide range of grain sizes. Many such "wet" deposits are poorly sorted and fine-grained even close to the vent (see the chapters entitled "Surtseyan and Related Phreatomagmatic Eruptions" and "Phreatoplinian Eruptions"). Figure 9a shows contrasts in grain size and sorting for alternating wet and dry phases of the 1875 A.D. Askja eruption.

The originally defined fields now seem rather too restrictive, but use of the *Md* versus $\sigma\phi$ diagram in a more subtle way for considering the distinction between different units in one eruptive sequence and particularly trends within a sequence is still extremely valuable. It is possible to use sorting values to distinguish sequences in which contrasts in grain size reflect changing vigor of the explosions or wind shifts, for example (sorting remains constant or improves with decreasing grain size) from those where finer grained beds are the result of weak magma–water interaction or conduit wall collapse (marked decrease in sorting efficiency with decrease in grain size).

Submarine and sublacustrine fall deposits are distinctive in their stratification and in their grading patterns. Settling through water enhances size and, particularly, density fractionation. Pumice lapilli and blocks will only sink once they become partially water-saturated; thus, proximal pumiceous subaqueous fall deposits have concentrations of lithic clasts at their base followed by sharply inverse-graded pumice. Distal water-laid ashes commonly have sharp bases and diffuse tops due to bioturbation and mixing with nonvolcanogenic sediment. In both environments sorting is enhanced relative to subaerial tephra.

C. Thermal Effects

One natural consequence of the mode of formation of fall deposits is that there is substantial interaction between pyroclasts and air that involves transfer of large amounts of thermal energy to the air and cooling of the pyroclasts. Thus, in comparison with many pyroclastic density current deposits (notably ignimbrites; see the chapter entitled "Ignimbrites and Block-and-Ash Flow Deposits"), fall deposits show less abundant thermal features. These features form an overlapping spectrum from thermal coloration through welding to agglutination.

The most common and widespread manifestation of high-temperature thermal effects is in coloration of pyroclasts, principally controlled by the growth or alteration of iron-oxide mineral species, especially as microscopic crystals. In mafic to intermediate deposits where the background color is black, such thermal oxidation results in the characteristic red color frequently seen in scoria cones and other proximal fall deposits. Such coloration tends to be pervasive throughout the deposits. In more evolved compositions, where the unaltered color of pyroclasts is pale gray to white, a wide range of hues from orange through pink, red to purple, or black to brown are reported from proximal deposits. Commonly these colors are preferentially developed in larger clasts (though pervasive coloration of deposits is also known), this being interpreted to reflect greater retention of heat by the larger clasts during flight.

At higher retained temperatures than those causing coloration are the effects caused by viscous deformation and flow of pyroclasts after landing forming an overlapping suite of effects. *Welding* is represented by the slow-scale deformation of individual pyroclasts together with interclast cohesion under the influence of load stresses induced by accumulation of further material. Factors that promote welding are the retention of heat in individual clasts (e.g., coarse clast size, short flight time, and high initial temperature) and high accumulation rates (to cause rapid burial and loading). The role of the load stress caused by overlying deposits is to make clast viscosity less of a factor in initiating welding than it is in causing agglutination (see later discussion). Welded fall deposits are commonest in deposits of peralkaline or intermediate composition, but are also known from highly silicic compositions. *Agglutination* is the process by which individual pyroclasts, which are still sufficiently hot and fluid, deform and flow on impact under their own momentum. The degree of agglutination varies with the clast viscosity and size and the flight time, and hence is an important process in deposition from low, fountaining eruption columns of low-viscosity magmas, such as Hawaiian fire fountains (see the chapter entitled "Hawaiian and Strombolian Eruptions"). Agglutinates are also common in intermediate and peralkaline fall deposits, but rare in silicic compositions (see later discussion).

These thermal phenomena form a series of facies, with a regular increase in thermal intensity toward the vent; this contrasts with thermal effects in ignimbrites that vary more with deposit thickness, which in turn often varies nonsystematically with distance from source. Welding and agglutination in fall deposits are an especially useful indicator of proximity to vent, but some such deposits merge genetically and in time and space with welded ignimbrites and clastogenic lavas. In proximal areas, the distinction between welded deposits of fall versus flow origin is based on the lack of an ash-grade matrix (Fig. 10a) and rapid (decimeter- to meter-scale) vertical variations in welding intensity in the former (Fig. 10b). Clastogenic lavas are abundant at basaltic volcanoes, common in intermediate/peralkaline ones, but scarce among the products of silicic eruptions. This reflects a trend of increasing volatile content (hence explosivity, which controls the clast size population and extent of cooling by interaction with air in the eruption column) and magma viscosity. In the case of highly silicic magmas, clastogenic lavas are either the products of unusually high-temperature melts that were relatively dry or of hydrostatically suppressed eruptions in which retention of volatiles caused low viscosities and limited transport minimized the opportunity for cooling.

IV. SMALL-SCALE PROPERTIES

Many small-scale properties of fall deposits relate to the nature of individual clasts or the abundance of contrasting types of clasts. The study of these properties, componentry, is a technique developed for one purpose but now used more widely for a second. George Walker, who first applied componentry to understand processes of column transport and density fractionation of clasts, used a simple threefold split into pumice, crystals, and lithics (dense clasts). More recently, componentry has been recognized and used as a powerful tool in understanding fragmentation processes. Use for this end requires more subtle division into component classes on the basis of the vesicularity and morphology of juvenile clasts and the lithology of wallrock clasts.

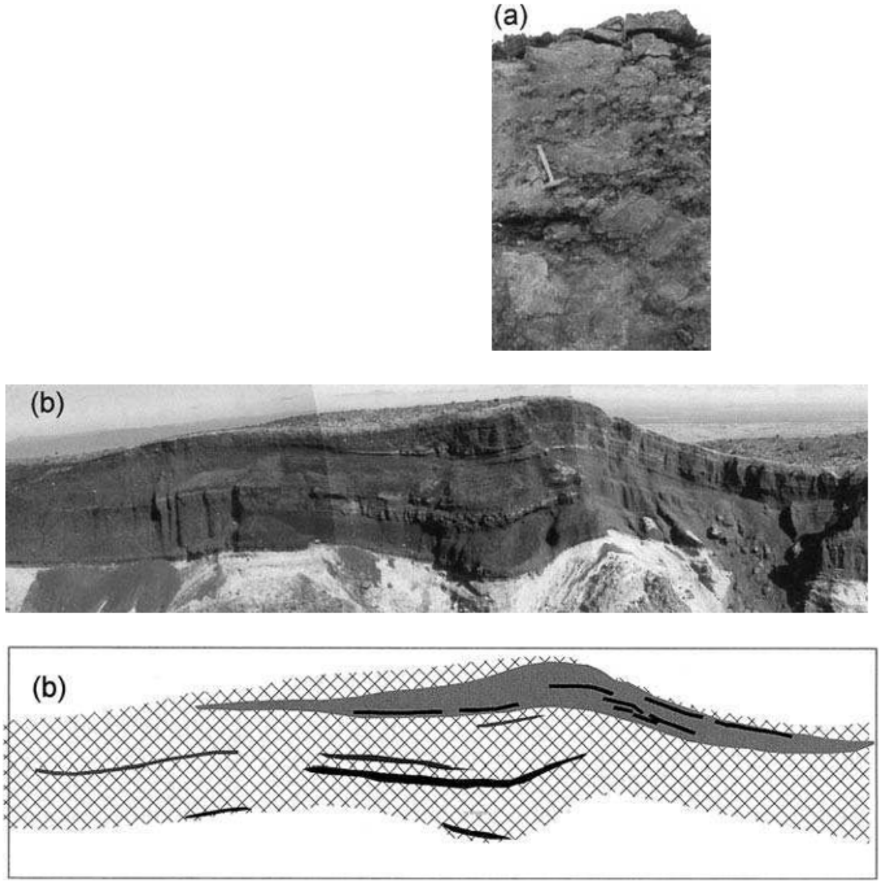

FIGURE 10 Welding textures in pyroclastic fall deposits. (a) Partially welded agglutinate, Ohakune craters, New Zealand showing (i) the presence of "ghost" boundaries between bombs, and (ii) the absence of abundant fine matrix. (b) Lenses of welded scoria of variable intensity within the deposits of the 1886 A.D. eruption of Mount Tarawera, New Zealand. The deposit formed from the mingling of ejecta from numerous point sources along a 17-km fissure and increasing welding intensity (shown as increasingly darker gray tones) is correlated with increased accumulation rate during periods of vigorous fire fountaining from adjacent vents.

A. Juvenile Clast Morphology

Juvenile pyroclasts have shapes that are related to their origin and their transport history. Large clasts can be examined directly; the morphology of fine particles is best studied using a scanning electron microscope.

Magmas that erupt in a hot, fluid condition will fragment to form droplets or spray and hence fluidal clasts. *Achneliths*, *Pelée's tears*, and *spatter* are products of such behavior. In contrast, material fragmented in a brittle state is markedly angular and the resulting clasts have blocky planar and curviplanar surfaces. Brittle fracture is often a result of quenching by contact with external water or very high strain rates during fragmentation. Quenching leads to the production of cooling cracks and "breadcrust" texture, hydrated and/or chilled rinds and adhering coats of ash or sublimates on the surface of clasts and in vesicles.

Transport of pyroclasts may modify the original morphology of particles. Chipped or rounded edges and corners and hackly fracture surfaces are features of transport in a concentrated medium and so may help to distinguish clasts in pyroclastic flow deposits from those of fall deposits.

B. Juvenile Clast Vesicularity and Crystallinity

The vesicularity of the juvenile clasts highlights the role of degassing in explosive fragmentation. Vesicle populations in juvenile clasts from plinian (large dry) eruptions are strikingly uniform, indicating fragmentation of relatively homogeneous foam, a reflection of the high viscosity of plinian magmas. Simple, small, dry eruptions (hawaiian, strombolian) are characterized by a similar clast population, but most small dry eruptions show a wider range of vesicularities corresponding to the decoupling of the more fluid magma and volatiles, and progressive degassing of magma remaining in the vent. Because of the decoupling and streaming of the magmatic volatiles through the silicate liquid, there are progressive changes in the portion of the magma that remains in the vent. There are two end members to this process. The first is where magma at shallow depths is well mixed throughout and the result is a progressive decrease in the vesicularity of juvenile clasts with time. In the second extreme, a discrete degassed crust develops on top of the magma pond, and this crust must be passively disrupted by the explosions in order for explosive volcanism to continue. More silicic magmas that undergo slow ascent may also undergo vesicle collapse and syn- and intraeruptive passive loss of volatiles, often accompanied by microlite nucleation (see later discussion), leading ultimately to a population of predominantly dense juvenile clasts.

Clasts from wet explosive eruptions (see the chapters entitled "Surtseyan and Related Phreatomagmatic Eruptions" and "Phreatoplinian Eruptions") show complex patterns with two extremes represented by fragmentation by magma–water interaction alone and fragmentation by magma–water interaction boosted by rapid vesiculation (Fig. 11).

The phenocryst content of juvenile clasts is related to residence time and conditions in the magma chamber, and glass inclusions within phenocrysts may be used to estimate the preeruptive volatile content of the magma. The microlite content of juvenile clasts is linked to the extent of subsurface cooling and volatile loss from the magma while in the conduit. This, in turn, has a strong influence on eruption dynamics. Quantitative measurements of microlite size and shape can be coupled with vesicularity data, and grain size and bedding information to understand the nature of eruptive pulses in complex eruptions such as Pinatubo in 1991.

C. Wallrock Lithics

The content of wallrock (foreign) lithics is a sensitive indicator of the competence and stability of the rocks forming the conduit walls, as well as the extent of interaction of the rising magma with groundwater in aquifers. The content of foreign lithics also correlates with eruptive intensity; thus, Hawaiian fall deposits have probably the lowest lithic content (<1 wt%) of all types of pyroclastic deposit. Plinian and phreatoplinian deposits where magma interacts with lake or sea water typically have foreign lithic contents of 3 to 20 wt% but many phreatomagmatic deposits associated with aquifer systems have lithic contents of >50 wt%. The contrast is most striking where such deposits are interbedded with strombolian or plinian phases from the same volcano (Fig. 7).

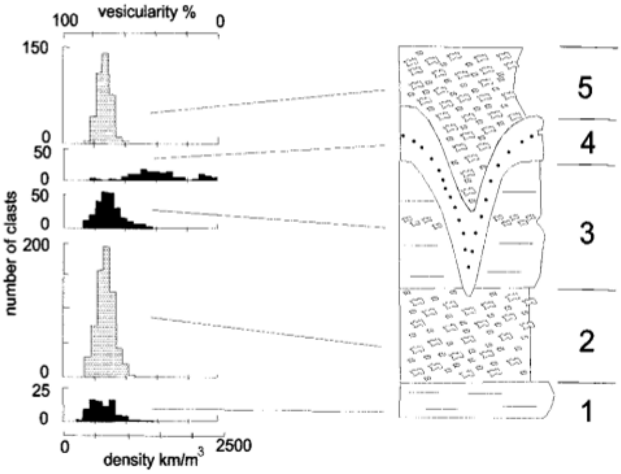

FIGURE 11 Contrasting patterns of density/vesicularity in clasts from "dry" (plinian) and "wet" (phreatoplinian) phases of the 181 A.D. Taupo eruption, New Zealand. Units 1, 3, and 4 show two contrasting patterns of vesicularity. Units 1 and 3 are "wet," yet are dominated by uniform populations of highly vesicular pumice, suggesting that the magmatic phase was a vesiculated foam at the moment of fragmentation. Unit 4 contains a broad mode of much less vesicular juvenile clasts, suggesting that rapid vesiculation was not occurring during fragmentation.

The lithology of wallrock lithic clasts can help both to locate vent position and to constrain the depth over which fragmentation occurs. In wet explosive eruptions, the nature of the wallrock clast can help "fix" the hydrology of the vent region. For example, an abundance of well-rounded wallrock blocks may correlate with a gravel aquifer, or faunal assemblages in blocks of unconsolidated marine sediments may help fix water depth for submarine vents. If the basement geology is well constrained, then changes in the lithic assemblage with time may record either the opening of new vents in areas of contrasting basement lithology or drawdown of the fragmentation region to deeper levels. Extremely detailed studies of historical eruptions at Vesuvius (see the chapter entitled "Plinian and Subplinian Eruptions") enabled a close match to be made between lithic lithology and the basement stratigraphy. Marked increases in wall rock lithic content accompany the transitions from dry to wet behavior at Vesuvius, and the nature of the lithics enabled identification of the aquifer supplying external water to the eruption. Pulses of shallow-derived lithic fragments in the fall deposits accompanied intervals of vent widening.

V. DISCUSSION

A. The Role of External Water and Indicators of Magma/Water Interaction

External water flashing to steam is a very efficient way of utilizing magmatic heat to "fuel" an explosive eruption. The inferred effects of this thermodynamic efficiency on the resulting grain size of the deposits is the basis for suggesting that absolute grain size might be used to infer the water/magma ratio for prehistoric pyroclastic fall deposits. There are at least three important caveats. First, it is clear from historical eruptions that in many phreatomagmatic eruptions the extent of mixing and heat transfer is very incomplete, and there may be portions of the magma ejected in a phreatomagmatic explosion that never contact external water and vice versa. Second, magma–water interaction can occur at any point in the degassing history of a batch of magma. If magma encounters external water at the peak of vesiculation, then both volatile exsolution and flashing of external water may operate simultaneously and combine to boost further the efficiency of the fragmentation. Third, there is some evidence that the critical role of external water in inducing poor sorting and fine grain size in fall deposits is not simply at fragmentation, but also during transport and deposition, where water scavenges fine ash from eruption plumes and promotes the formation of accretionary lapilli and other ash aggregates.

Grain size measures have been used with great success (e.g., Fig. 9a) to separate the products of completely dry or "magmatic" fragmentation (plinian, strombolian etc.) from eruptions involving ample amounts of external water (surtseyan, phreatoplinian). However, there exist classes of other phreatomagmatic fall deposit where there is direct (observational) or indirect (textural) evidence for limited magma–water interaction but whose grain size is identical to that of purely dry fall deposits. In these situations, other quantitative parameters linked to componentry, such as the abundance of foreign lithics or vesicularity of the population of juvenile clasts, are more effective.

In situations where magma has come in contact with groundwater, changes in the foreign lithic content are often much more precise indicators of slight changes in the water/magma ratio than any grain size parameters.

B. Spectra versus Pigeon Holes

Pyroclastic fall deposits naturally form continua rather than "end-member" clusters, and any one parameter or pairing of two parameters will be inadequate to form a comprehensive classification system for pyroclastic fall rocks. The most widely used classification of deposits, pioneered by George Walker (the "*F–D*" plot) separates adequately (1) all deposits on the basis of their dispersal, and (2) products of dry magmatic fragmentation from phreatomagmatic deposits characterized by high water/magma ratios. It does not separate the products of phreatomagmatic eruptions where fragmentation was boosted by release of magmatic volatiles from those that were not, nor does it delineate phreatomagmatic deposits characterized by a low water/magma ratio from strombolian or plinian deposits. For any new classification to be more effective it will need to incorporate new parameters related to deposit componentry while being sufficiently flexible to apply to both modern and ancient fall deposits.

SEE ALSO THE FOLLOWING ARTICLES

Hawaiian and Strombolian Eruptions • Hazards from Pyroclastic Flows and Surges • Ignimbrites and Block-and-Ash Flow Deposits • Phreatoplinian Eruptions • Plinian and Subplinian Eruptions • Pyroclast Transport and Deposition • Surface Manifestations of Geothermal Systems • Surtseyan and Related Phreatomagmatic Eruptions • Volcanic Plumes

FURTHER READING

Bonadonna, C., Ernst, G. G. J., and Sparks, R. S. J. (1998). Thickness variations and volume estimates of tephra fall deposits: the importance of particle Reynolds number. *J. Volcanol. Geotherm. Res.* **81,** 173–187.

Hammer, J. E., Cashman, K. V., Hoblitt, R. P., and Newman, S. (1999). Degassing and microlite crystallization during pre-climactic events of the 1991 eruption of Mt Pinatubo, Philippines. *Bull. Volcanol.* **60,** 355–380.

Heiken, G., and Wohletz, K. (1985). "Volcanic Ash." University of California Press, Berkley.

Pyle, D. M. (1995). Assessment of the minimum volume of tephra fall deposits. *J. Volcanol. Geotherm. Res.* **69,** 379–382.

Walker, G. P. L. (1973). Explosive volcanic eruptions—a new classification scheme. *Geologische Rundschau* **62,** 431–446.

Walker, G. P. L. (1980) The Taupo Pumice: product of the most powerful known (ultraplinian) eruption? *J. Volcanol. Geotherm. Res.* **8,** 69–94.

PYROCLASTIC SURGES AND BLASTS

GREG A. VALENTINE
Los Alamos National Laboratory

RICHARD V. FISHER
University of California—Santa Barbara

I. Introduction
II. Historical Perspectives
III. Deposit Characteristics
IV. Physical Processes
V. Future Research Directions

GLOSSARY

base surge A turbulent density current that flows outward from the base of a partially collapsing vertical eruption column derived from a hydrovolcanic (phreatomagmatic) eruption; a type of pyroclastic surge.

bed form (or bedform) The surface configuration of a bed; also the three-dimensional configuration of groups of strata having geometric shapes that repeatedly occur in nature such as ripples, dunes, and plane beds.

bedset (or bedding set; also bed set) A sequence of beds with distinct internal structures, textures, colors or compositions that sets them apart from other sequences, usually bounded by unconformities, or by fallout layers.

blast A sudden, violent, overpressured explosion projected laterally or vertically. At Mt. St. Helens the blast was directed laterally and produced a high-velocity dilute pyroclastic density current, or pyroclastic surge.

blocking Deflection of the lower, denser parts of a pyroclastic density current (PDC) by a topographic barrier while the low-density upper parts of the PDC continue to travel over the barrier.

flow regime Hydraulic conditions of noncohesive flow of sand and silt that develop ripples, dunes, plane parallel beds, and antidunes. Progressive changes in bed forms occur as flow regime increases. Low-flow regime conditions form small scale ripples that progress to dunes; high flow regime conditions form plane beds and then antidunes.

flow transformation Reversible changes (in sediment gravity flows) between turbulent and steady flow related chiefly to particle concentration, thickness of flow, and flow velocity.

hydrovolcanic All volcanic activity resulting from the interaction between meteoric or connate water and lava, magmatic heat, or gases at or near the earth's surface (also *phreatomagmatic*).

pyroclastic surge Low concentration, turbulent pyroclastic density currents (PDCs). Two kinds of pyroclastic surges are *wet surges*, having temperatures less than 100°C where steam condenses and the surge is a three-phase system with water drops, solid particles, and gas; and *dry surges*, which have mean temperatures greater than 100°C and form by (1) hydrovolcanic eruptions with a low water/magma ratio, or (2) by magmatic eruptions that are driven solely by volatiles. Also see **base surge**.

transport and depositional system The transport system carries particles from source to area of sedimentation. The depositional system deposits particles and includes

Copyright © 2000 by Academic Press
All rights of reproduction in any form reserved.

local movement of particles, such as movement of a mass of particles down a steep slope, after being carried to a particular locality by the transport system.

THE RECOGNITION THAT volcanic explosions could produce density-driven currents that flow rapidly away from the vent, devastating the landscape and leaving thin pyroclastic deposits and ash dunes, was an important step toward our current understanding of volcanic systems. Deposits left by these *pyroclastic surges* are a key in interpreting the eruptive history of a volcano and in predicting the hazards a volcano might pose for the future.

I. INTRODUCTION

Pyroclastic surges are a type of pyroclastic density current (PDC) that produce relatively thin, bedded and cross-bedded to massive deposits. PDCs are laterally moving gas–particle mixtures with density greater than that of the surrounding atmosphere; original energy sources may be from gravitational potential energy or from a laterally directed explosion (blast). Two main factors profoundly influence type of flow and therefore physical features of the deposits. First is the bulk particle concentration; second is steadiness, or variation in time, of the currents.

Rapid fluctuations in velocity and particle concentration can occur during movement of pyroclastic surges, whereas movement of high-concentration PDCs is relatively steadier. Particle concentration greatly affects the transport mechanism of pyroclasts within a PDC. In a pyroclastic surge, low particle concentration allows turbulence to be the dominant transport mechanism. In contrast, high concentration PDCs (also termed pyroclastic flows) support particles mainly by particle collisions.

A precise quantitative criterion to distinguish high-concentration PDCs from low-concentration PDCs is lacking. We believe that a transition occurs over a range of concentration values rather than a single value, resulting especially from effects of grain size distribution and particle shapes. We expect that the switch from one transport mechanism to the other occurs through a range of particle concentrations around 0.1 (by volume), but this should be viewed only as an estimate until experimental and theoretical work further quantifies the transition.

During a single eruptive event there can be a range of PDC-generating processes that produce temporal variations in the initial grain size distributions, mass fluxes, and energy of PDCs. The topography over which a PDC moves can cause transformations from low to high concentration transport (and/or turbulent to non-turbulent) conditions. Even without fluctuations in PDC generation and the presence of a complex terrain, particle concentration varies vertically within a current, and laterally as particles sink in the current. These factors contribute to the possibility for flow transformations to occur, which ultimately may be recorded in the deposits left by the PDC.

Pyroclastic surges are generated by several mechanisms.

- Collapse or fountaining of an eruptive mixture from a vertical eruption column. This is the mechanism for the classic "base surge" that was also observed in the ejecta clouds from large man-made explosions (see later discussion).
- Rapid expansion (decompression), or blast, of an eruptive pyroclastic mixture into the atmosphere. The 18 May 1980 Mt. St. Helens eruption is an excellent example of a directed blast from the side of a volcano. We also expect that vertically directed explosions can produce shock waves strong enough to pull eruptive debris along the ground as they expand away from a vent, as suggested in numerical models.
- Collapse of a steep surface of a growing lava dome can generate pyroclastic surges as the chunks of material from a dome fall, break explosively, and generate dust. The small and large particles together form dilute PDCs as they flow along the ground.
- Interaction of a dense pyroclastic flow with rough substrate or valley margins, producing a turbulent boundary layer.
- Lateral flow of low-particle-concentration (dilute) ash clouds generated from moving pyroclastic flows, and in regions where pyroclastic flows accelerate down steep slopes or where a hydraulic jump occurs at a break in slope.

The distribution of the most commonly observed pyroclastic surge deposits indicates that in most cases surge run-out extends from only a few hundred meters (e.g., at tuff rings and tuff cones) to about 10 km (e.g., from sub-Plinian to Plinian eruptions) from their vents. However, some surge deposits can extend tens of kilometers, even more than 100 km, from their vents. Examples of far-traveled pyroclastic surges, probably generated by blasts, include the 18 May 1980 Mt. St. Helens surge (~35 km), those from the 1883 eruptions of Krakatau (~80 km), and surge deposits associated with the widespread Peach Springs Tuff, California and Arizona, USA (>100 km; we note that interpretations of these deposits are somewhat controversial).

II. HISTORICAL PERSPECTIVES

In July 1946, the United States military establishment conducted a crude experiment to determine the effects of an atom bomb attack on a fleet of ships. They detonated two atom bombs, one 160 m above Bikini Lagoon, and one 30 m beneath the water. The underwater explosion created a short vertical explosion column consisting of an aerosol of gases from the nuclear explosion and water droplets from the lagoon. The water-drenched explosion cloud was too heavy to rise far into the atmosphere. It collapsed and created a turbulent density current cloud that moved away from the base of the explosion column over the surface of the lagoon at about 100 kilometers per hour, drenching the ships with a pervasive radioactive fog. Physicists at Bikini named it a *base surge*.

In 1962, the U.S. government exploded a 100 kiloton atomic bomb at a depth of 194 meters in alluvial deposits at the Nevada Test Site. The explosion excavated a man-made crater 370 meters in diameter and 98 meters deep. The fallback of its explosion column, a mixture of gases from the atomic explosion mixed with dust and sand of the alluvium from the desert floor, produced a base surge with an initial velocity of over 50 meters per second as it spread across the desert floor, leaving a carpet of deposits with an undulating dunelike surface.

In 1965, eruptive activity at Taal Volcano (Philippines) began as a strombolian eruption with an incandescent lava fountain. Were it not for the water mixing with magma, a scoria cone would likely have been constructed. But a crack that opened allowed water from the lake surrounding the volcano to pour into the vent and interact with the magma. This radically changed the behavior of the eruption from strombolian to highly explosive hydrovolcanic. Pyroclastic surges were produced, sweeping out over the landscape like hurricanes, tearing trees from the ground and sandblasting the trunks of those left standing. As the surges moved across the landscape, they left a deposit of cross-bedded, dune-like bed forms. It was recognized that the pyroclastic surges at Taal were the volcanic equivalent of the base surge from nuclear explosions. This link represented a major step in our understanding of the mechanisms and driving forces of pyroclastic surges and the origin of bedded and cross-bedded deposits around volcanic vents (formerly they were thought to be wind-blown dunes).

In the late 1960s it was discovered that maar volcanoes, constructed of tephra produced by hydrovolcanic eruptions typically display low-angle cross beds and dune structures that record currents moving radially away from the vent. This showed that pyroclastic surges as observed at Taal are a common eruption phenomenon at such volcanoes. In the 1970s, comparison of wavy and bedded pyroclastic deposits genetically associated with thick, massive ignimbrite deposits led to the realization that turbulent, hot, dilute pyroclastic surges could form during magmatic explosive eruptions, along with hot, magmatic high-density pyroclastic flows.

III. DEPOSIT CHARACTERISTICS

A. Bedforms

Pyroclastic surge deposits are most easily identified in the field by the occurrence of cross bedding including thinly bedded (centimeter to decimeter), low-angle cross beds (Fig. 1) and slightly wavy bedded structures to relatively large dune forms. They are characteristically associated with planar beds, and in some instances only planar beds are present. Ash-poor planar base surge deposits are granulometrically similar to fall deposits, making them difficult to interpret. Large ballistic fragments deform surge beds by impact to form bedding sags. Large fragments that rest on underlying beds without deforming them can be interpreted as having been emplaced by a laterally driven current rather than ballistic flight.

Different kinds of cross beds in surge deposits may be related to regimes of flow, a concept originally developed for fluvial sands. Flow regimes are defined by bed forms such as ripples, dunes, and antidunes, which are related to hydraulic conditions of flow. Important hydraulic conditions are velocity, shear stress imparted to the underlying bed by the flowing medium, and grain size of the material being carried.

Ripples and small dunes are classified as lower flow regime bed forms. Plane parallel beds, antidunes, and chute-and-pools are upper flow regime bed forms. Preservation of bed forms in pyroclastic surge deposits requires rapid deposition without erosion, because changing conditions of flow regime governed principally by concentration factors erase bed forms that are not in

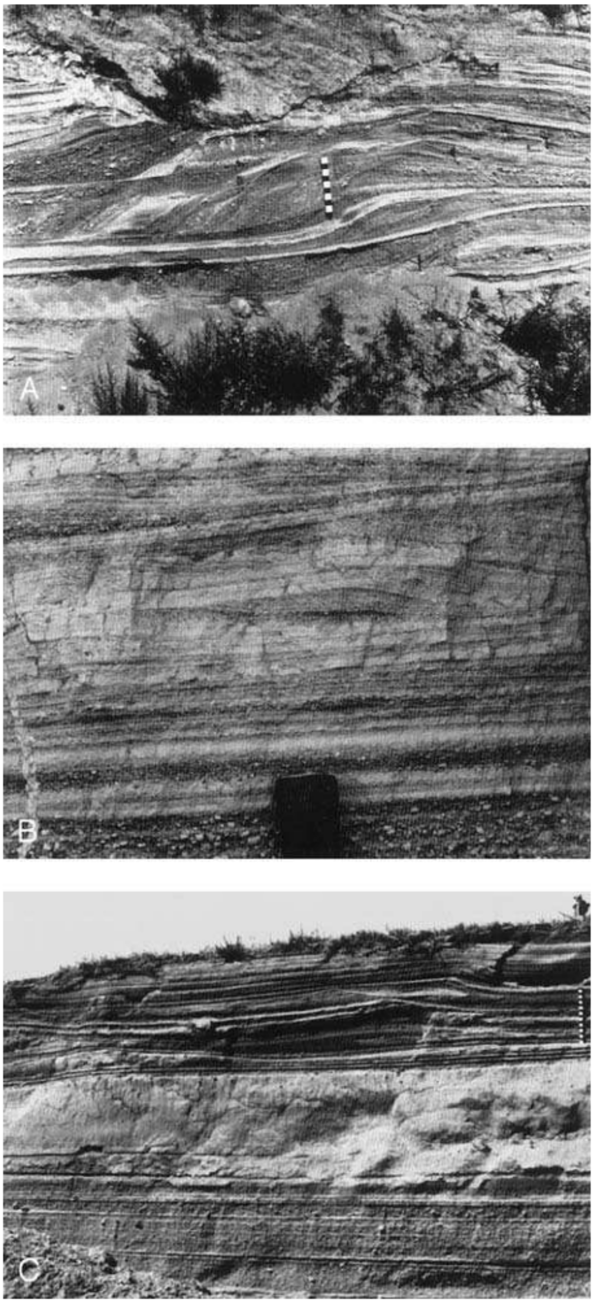

FIGURE 1 Photographs of common bed forms in pyroclastic surge deposits. (A) Chute-and-pool structure in deposits of the Laacher See volcano (Germany). 1-m-long measuring stick for scale, marked in 10-cm increments. (B) Thin-bedded deposits with small-scale cross laminations, Ubehebe Crater (USA). Bottom of rock hammer handle, ~2 cm wide, for scale. (C) Planar, massive, and sandwave bed forms at Laacher See volcano; 2-m-long measuring stick for scale, marked in 10-cm increments. (From Fisher and Schmincke, 1984.)

equilibrium with flow conditions. Within the transition from low to high flow regime, previously formed ripples and dunes are destroyed and the bed becomes flat. If deposition occurs at this stage, internal laminations are parallel and are called plane parallel bed forms, or planar beds, even though subtle cross-bedding features may be internally preserved. Plane parallel beds resemble fallout tephra, but are clearly surge deposits if they grade laterally into cross-bedded layers or if they have very subtle, low-angle cross laminations.

At higher regimes of flow, the planar beds can change to a dune or antidune shape, which is roughly symmetrical in cross section; they may also migrate upstream or downstream, or remain stationary.

B. Granulometry

Granulometric analyses consist of two major kinds of data: (1) sizes of maximum fragment (mainly lithic and pumice) or the average of 3, 5, or 10 such measurements, and (2) statistically generated size distributions.

Plots of maximum average size of three or more measurements are conducted on selected layers and then plotted and contoured over the unit's distribution area. Contoured isopleth maps of average maximum size can be used to estimate eruption energy and carrying capacity of pyroclastic surges, to determine direction toward the source, and to determine wind directions during eruptions or directions of angled eruption columns (e.g., during the 1957–58 Capelinhos eruption, wind directions affected flow directions of some base surges).

Size distribution curves of bulk samples give median and mean size values as well as values of sorting and skewness. These parameters can be used to interpret eruptive energy, height of eruption columns, mechanisms of transport or deposition, and kinds of transport systems and environments of deposition. Care must be taken in sampling surges because many have multiple layers of different grain sizes and sorting parameters.

Median diameters of pyroclastic surges range from -3.0 to $+4.0\phi$, but most occur within the 1.0 to 2.0ϕ range. Inman sorting values range from about 1.0 to 4.0ϕ with most at about 1.5ϕ. Sorting values of surge deposits are intermediate between flows and fallout, but there is wide overlap (Fig. 2). Surge deposits lack the very fine and the coarse size fractions, and therefore typically have a more restricted grain size than pyroclastic flow deposits. Pyroclastic surge deposits are better sorted and contain smaller maximum clast sizes than

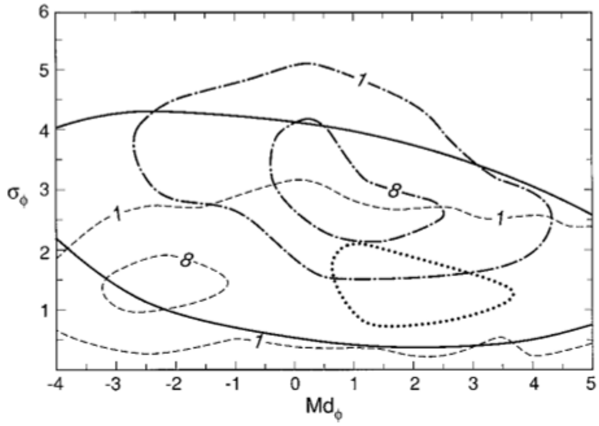

FIGURE 2 Diagram showing Inman sorting values versus median diameter (ϕ units) for surge deposits from around the world. Solid line encloses most surge samples; dotted line encloses examples of cross-bedded deposits from Ubehebe Crater (USA) and Taal Volcano (Philippines). (Modified from Fisher and Schmincke, 1984.)

high concentration pyroclastic flow deposits. Sorting becomes better with distance from source in all pyroclastic surge deposits.

C. Facies Variations

Pyroclastic surge deposits commonly have systematic facies variations laterally and vertically as functions of distance from vent, pre-eruption topography, eruption processes, and condensed water content. A *facies* is defined by a set of shared characteristics of deposits, such as grain size, sedimentary structures, and local deposit geometry.

1. *Proximal to Distal Variations*

In 1979 K. H. Wohletz and M. F. Sheridan published a detailed analysis of proximal-to-distal facies variations at several tuff rings and maars in the southwestern United States and northern Mexico, and in surge deposits associated with the large-volume Bishop Tuff in California (note that the interpretation of the latter deposits has recently become controversial). They determined that these deposits include three main facies. In *sandwave facies* the dominant bed forms are sandwave bed forms (dunes, antidunes, ripples, and cross laminations) and massive beds that have little or no internal structure. *Massive facies* is defined by significant occurrence of three types of beds: massive, sandwave, and planar (the latter have generally planar geometries but may exhibit some cross stratification and pinch and swell features that are transitional to sandwave beds). Finally, in the *planar facies*, the dominant bed forms are massive and planar. In the deposits studied by Wohletz and Sheridan, which, except for the Bishop Tuff example, had lateral extents of ~1 km from their crater rims, there was a consistent pattern of sandwave facies in proximal areas, massive facies in medial exposures, and planar facies in distal reaches of the deposits.

Wohletz and Sheridan attributed this variation to progressive deflation of an initially well-mixed, turbulent, low particle concentration surge near the vent. In these proximal locations particles are transported along the ground by saltation and form dunes and other sandwave features, with transient periods of less turbulent transport and deposition of massive beds. In distal areas particles that are remaining in the surge are carried along the ground in traction carpets to form planar, inversely graded beds. The massive facies, in medial locations, represents a transitional zone between sandwave and planar deposition mechanisms. A likely additional effect is the increasing particle concentration (and thus bulk density) gradient at the bottom of a pyroclastic surge as it moves away from its source. As such a gradient becomes stronger, it will progressively damp turbulence and the formation of related bed forms, which would also favor the facies variations observed by Wohletz and Sheridan.

Y. K. Sohn and S. K. Chough conducted further detailed facies analyses of pyroclastic surge deposits associated with tuff rings on Cheju Island, Korea. As with most of the deposits studied by Wohletz and Sheridan, the surge deposits on Cheju Island have lateral extents on the order of several hundred meters. Particularly in the Suwolbong tuff ring, variations in individual beds or bed sets could be traced laterally from proximal to distal locations. Lateral facies variations in these studies are illustrated in Fig. 3. General trends are for the proximal deposits to be relatively unbedded, massive, and disorganized, grading laterally into ill-defined massive beds, to sandwave beds, and finally to planar or sandwave, thinly bedded/laminated tuffs in the most distal reaches.

Sohn and Chough explained these lateral variations as resulting from high particle concentration, highly turbulent flow near the vents, resulting in a sufficiently high rate of fallout of particles from turbulent suspension that no tractional processes could occur to form bedding structures. With increasing distance, the parent surges became more dilute and the suspended-load fallout rate decreased so that tractional bedding processes became increasingly dominant. Detailed studies of lat-

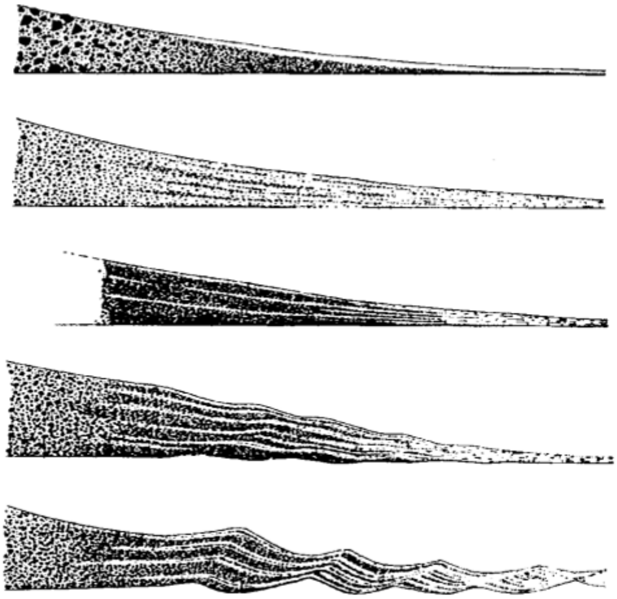

FIGURE 3 Examples of lateral facies variations in pyroclastic surge deposits of the Suwolbong tuff ring (Korea), deduced from facies studies. Lateral distances are at or near crater rim (left side) to several hundred meters from the rim (right side). Dark dots are used to indicate stratification of coarse clasts (lapilli and blocks) relative to ash (white). Wavy forms indicate chief types of bed forms at a given location. (Modified from Sohn and Chough, 1989.)

eral facies variations in deposits of the 18 May 1980 Mt. St. Helens lateral blast by T. H. Druitt indicate that proximal-to-distal variations are dominated by a decrease in particle concentration and sedimentation rate with increasing distance from vent, consistent with the Sohn and Chough interpretations.

Wavelengths of sandwave features in surge deposits commonly decrease with distance from the vent. This, plus the transition from sandwave to planar or laminated beds in all the studies, is consistent with the effects of increasingly strong density stratification near the base of the surges as they traveled away from their vents. At first glance the observations of Sohn and Chough may seem to be at odds with those of Wohletz and Sheridan, but the apparent differences may result from different definitions of bed types, or may simply be differences between the studied deposits, or different initial particle concentration.

2. *Topography-Induced Variations*

Superimposed on proximal-to-distal facies variations are variations due to local topography. When ridges and valleys are roughly parallel to flow, deposits on valley floors tend to be thicker, coarser-grained, and more massive in texture than those on ridges that are thin, relatively finer grained, and exhibit more bedding and cross bedding (e.g., surge deposits at Ubehebe Craters, California). The primary reason for these differences are that the part of a pyroclastic surge that is at or above ridgetop level is inferred to have a lower particle concentration and carries smaller particles than the lower-elevation parts of a surge; this promotes, obviously, finer grain size in deposits, and stronger turbulent fluctuations, giving rise to abundant bedding. Obstacles such as ridges that are oriented at higher angles to flow direction tend to produce similar facies variations, with relatively massive and coarse deposits at the foot of the obstacle and thinner, more bedded and finer grained deposits at the top. The mechanism for this is referred to as "blocking." In a density stratified surge encountering such an obstacle, a parcel of the flowing mixture from low levels in the surge will have to overcome a density gradient in order to rise up into lower-density regions of the surge and pass over an obstacle. The level in the surge below which a mixture cannot rise over the obstacle, in other words is blocked, and above which it can, is called the "dividing streamline" (Fig. 4). Blocked portions of a surge then produce the facies found at the bottom of such an obstacle.

Important for understanding pyroclastic surge deposits is the interpretation that they form by the combined action of a *transport system* and a *depositional system*. This concept was emphasized in R. V. Fisher's studies of the Mt. St. Helens blast surge deposit, where direct observations of the lateral spread of the blast were combined with descriptions of the effects of rugged topogra-

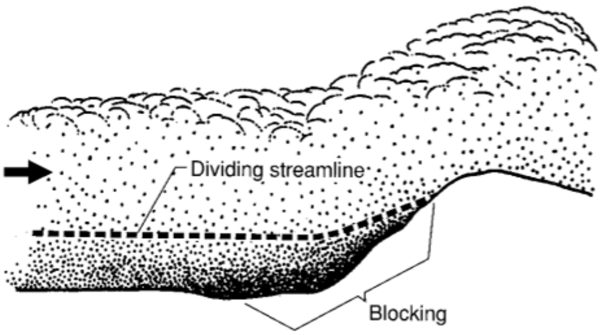

FIGURE 4 Illustration of the effect of blocking in a stratified pyroclastic surge, flowing from the left, encountering a ridge. The dividing streamline represents the level below which material is not able to surmount the ridge. (Modified from Valentine, 1987.)

phy on deposit facies. The transport system, regional in scale, is responsible for general trends such as fining and thinning of deposits away from the vent. The depositional system, at the base of a moving surge, is very local in scale with characteristics determined by the rate of material supplied by the transport system and the influence of local terrain. In some cases at Mt. St. Helens, the local depositional system formed thick (several meters), massive, deposits from high-particle concentration flows in valley bottoms. These deposits were developed directly in the valleys from blockage and diversion by terrain, or from flow off valley walls too steep to retain rapidly depositing debris. In this case the depositional system locally decoupled from the transport system, flowing independently down valleys, regardless of the orientation of the valleys, for perhaps hundreds of meters, while the overriding transport system flowed (mainly) radially away from the vent. On flatter terrain, recent granulometric studies by M. I. Bursik and colleagues have shown that movement of particles in the basal depositional system was limited to distances of ~1–10 m, parallel to the transport system.

3. Vertical Variations

Vertical variations in pyroclastic surge deposits can be quite extreme owing to the rapid fluctuations of surges. Sohn and Chough observed several vertical facies variations at the Suwolbong tuff ring (Fig. 5). Vertical variations differ in detail, but all share a common trend in becoming finer grained and thinner bedded upward, as the surges wane and sedimentation rates decrease with time. A common vertical sequence developed from a blast-driven pyroclastic surge is as follows: A coarse, fines depleted, massive basal layer overlain by a finer grained, massive layer with crossbeds at the top, and an ash fall layer at the very top (e.g., deposits of the Mt. St. Helens blast).

4. Variations due to Condensed Water Content

In addition to proximal-to-distal, topographic, and vertical variations, a fourth factor influencing surge facies is the relative abundance of condensed water in the blast surge. There are several sources of water in surges: water exsolved from the parent magma during its ascent, groundwater that mixes with the rising magma, surface water (e.g., lakes, oceans) through which an eruption occurs, and atmospheric water vapor entrained into the surge. In dry pyroclastic surges with temperatures greater than 100°C, most or all of the water will be in vapor form; therefore, the sand- and silt-size pyroclasts are generally not cohesive. Also, particles depositing from the bottom of a dry surge are capable of moving in traction carpets and by saltation, similar to wind-blown sand and dust. They produce bedforms with relatively low angles that resemble eolian deposits in many ways (although important differences are caused by the poorer sorted nature of surges and by their relatively higher sedimentation rates compared to eolian processes). In wet surges, having temperatures less than 100°C and typically produced by explosive magma/water interaction, ash particles may stick together because of cohesion. In such cases, ash may enter the depositional system as clusters rather than as individual particles, and the aggrading bed tends to behave plastically. Deposits of such wet surges tend to have steep-sided bed forms that may exceed the angle of repose of the dry material, be more poorly sorted than their dry equivalents, commonly contain accretionary lapilli, and behave plastically when impacted by ballistic fragments.

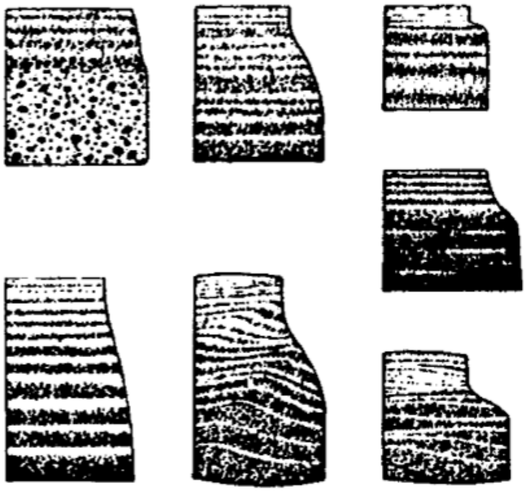

FIGURE 5 Schematic examples of vertical facies variations in surge bed sets of the Suwolbong tuff ring (Korea), deduced from facies studies. Dark dots are used to indicate stratification of coarse clasts (lapilli and blocks) relative to ash (white). Columns represent variations over decimeters to a few meters height in the deposits. Wavy forms indicate chief types of bed forms at a given height. (Modified from Sohn and Chough, 1989.)

There has been debate about the relative importance of cohesive aggradation versus flow regime in determining the migration direction of dune forms in surge beds. Recent studies support the dominating role of flow regime in migration of surge bed forms.

The presence of liquid water in wet basaltic surges and their fresh deposits facilitates alteration of glassy material to palagonite, a combination of hydrous glass, zeolites, and clays. Palagonite commonly appears in the field as a yellow, brown, gray, or greenish waxlike substance. The color and texture of individual beds in wet surges may vary considerably owing to different eruptive conditions of each surge event, resulting in spectacular multicolored outcrops.

D. Association with Other Pyroclastic Deposits

Pyroclastic surges occur alone or in association with both of the other two main types of pyroclastic deposits: fallout and pyroclastic flow. Surge and fall deposits of hydrovolcanic origin are the main "building blocks" of tuff rings and tuff cones. Larger volume eruptions that produce ignimbrites also produce pyroclastic surges that occur at the bases and tops of pyroclastic flow units (or packages of flow units). Pyroclastic surge deposits that underlie pyroclastic flow units are interpreted as forming from unsteady explosive activity during the transition to relatively steady pyroclastic flow eruption and/or the relatively dilute leading edges of pyroclastic flows. Surge deposits on top of flow units record deposition from the dilute ash cloud (ash cloud surge) that develops from an underlying pyroclastic flow. Ash cloud surges may extend considerably farther from the vent than less mobile, parent pyroclastic flows. Ash cloud surges result from differential settling of clasts in a pyroclastic current, from mixing between the top of a pyroclastic flow and the atmosphere, and from interclast abrasion in a pyroclastic flow. A pyroclastic surge deposit on top of a pyroclastic flow unit may also reflect a period of unsteady eruptive activity as well. Pyroclastic surge beds are sometimes interbedded with sub-Plinian to Plinian fallout deposits or vice versa and represent brief periods of column collapse or unsteady explosions. Finally, deposits of blast surges are commonly associated with debris avalanche deposits; this reflects the relationship between collapse of an unstable volcanic edifice and resulting explosive relief of pressure within a volcano.

E. Distinguishing between Surge, Eolian, and Water-Lain Sediments

Cross bedding and dune forms can be developed by surge, wind, or water flow, but there are several features that allow one to distinguish between these mechanisms. This is important for establishing the history of a volcano from its geologic record and for predicting potential future hazards.

One of the most obvious differences is general sorting features. Eolian material is commonly very well sorted sand; wind cannot pick up and carry larger particles in suspension. Ordinary water currents (not in flood stage) carry mainly sand, but can also move larger particles ~2 or 3 cm by traction. Fluvial sands are commonly well sorted, though not as well as wind-blown sand. Pyroclastic surge deposits can carry particles ≥10 cm in proximal localities and remain much more poorly sorted than wind or water sorted materials to distal localities.

Bed forms of pyroclastic surge deposits differ from wind- and water-deposited material in some striking ways. Dune bed forms in dry surge deposits, for example, can show wavelengths of 20 m and wave heights up to 2 m thick—relatively low-angle features compared to eolian and water-lain dune forms. Wet surge deposits can, on the other hand, have relatively steep dune sides compared to eolian and water-lain examples due to cohesion between wet ash particles. Unlike ripples and dunes in water or wind transported materials, the angle of backset beds of surge dunes are commonly steeper than foreset beds. G. A. Smith and D. Katzman show how vertical sequences of dunes produced by pyroclastic surges tend to preserve both lee- and stoss-side layering and often the dune crests as well. This differs from eolian sequences where typically only lee-side structures are well preserved and dune crests are truncated by planar erosional surfaces. Individual strata within dune forms produced by pyroclastic surges are commonly relatively massive and poorly sorted compared to their counterparts in eolian deposits. In addition, pyroclastic bed sets are commonly capped by fine-ash fallout layers, often containing accretionary lapilli.

Another set of criteria for distinguishing between pyroclastic surge, eolian, and water-lain deposits are their overall geometric relationships. For pyroclastic surge deposits, there will be systematic variations in facies, maximum grain size, sorting, thickness, and dune wavelength away from a central location (the vent). Dune migration directions and other flow direction indicators will show radiating patterns from the vent location, although local complications resulting from pre-eruption topography need to be accounted for. The nature of these proximal to distal variations in surge deposits has already been discussed in this chapter. In contrast, the geometry of water-lain deposits will generally be constrained by drainage channels or basins; dunes will show migration directions generally along these channels or basins, and thickness and grain size will also vary in the same direction (accounting for cross-channel variations). Wind-blown deposits will also show dune migration and facies variations in directions that do not radiate from central locations and that are unrelated to any volcanic structures.

Deposits from laterally directed eruptions such as the 18 May 1980 Mt. St. Helens blast may not have such radial variations, although there will be systematic variations from the source vent. However, in the case of such blast surges, the vertical stratigraphy described earlier makes them easily distinguishable from eolian and water-lain deposits.

Pyroclastic surges that travel over vegetated and forested areas commonly incorporate plant fragments. An observation of downed tree casts in a bedded deposit of pyroclastic material is a strong indication of surge origin. In deposits of dry, hot surges it is common to find charred wood and other plant fragments (note that in ancient deposits these may be difficult to recognize).

IV. PHYSICAL PROCESSES

Pyroclastic surges and blasts, like most other explosive volcanic phenomena, have three characteristics that challenge understanding from a theoretical standpoint. First, they are multiphase flows, with particles of a variety of sizes and densities dispersed in a gas. Furthermore, phase changes from steam to liquid water droplets are important multiphase aspects for many pyroclastic surges (e.g., wet surges). Second, they are strongly turbulent; turbulence not only is a major particle transport mechanism, but also results in complicated interactions with the surrounding atmosphere. Finally, velocities of tens to hundreds of meters per second mean that surges are compressible flows; the effects of compressible flow on the final deposits are not known.

A consequence of the multiphase, turbulent nature of pyroclastic surges is that they are density-stratified, meaning that there are vertical variations in the bulk density (gas plus particles) of the current. This arises because particles tend to settle according to their size and density, although this is counteracted by the mixing action of turbulence. There are several important ramifications from density stratification that all arise from the fact that the higher-density mixture from low in the current will be retarded from moving upward because of the density contrast with material higher in the current. One consequence of this is the process of blocking when a surge encounters rough terrain, as described earlier. A second consequence is the role of turbulence near the base of a surge where deposition results in an aggrading bed. If the density gradient becomes strong enough at the base, boundary layer turbulence will be retarded, which in turn affects the nature of the deposits. Since it is likely that the density gradient will become more pronounced with increasing distance from vent, because of downward migration of particles with time, lateral facies variations will in part reflect this stratified flow process. Another consequence of stratified flow is its effects on the Froude number of the base of the flow. The Froude number is the ratio of flow speed to gravity wave speed, the latter of which is determined by the density gradient in the flow. For Froude numbers less than 1, surge bedforms will migrate downstream, while for values greater than 1, upstream-migrating antidunes will form. Finally, the density gradient influences the frequency and wavelength of waves in the flow—steeper gradients will result in shorter wavelengths, which may relate to decreasing dune wavelength with distance from vent that is observed in many deposits.

V. FUTURE RESEARCH DIRECTIONS

Research on pyroclastic surge mechanisms has greatly progressed from Fisher's discussion in the early 1960s of qualitative flow dynamic principles but without recognition of a partitioning of flows and surges, which began with discovery of volcanic base surges in the late 1960s. In the past two decades eruptions of Mt. St. Helens, Mt. Pinatubo, Mt. Unzen, and Montserrat have provided impetus for accelerated research in volcanic hazards, transport and depositional mechanisms, and eruption predictions. Volcanic processes are increasingly being investigated by laboratory experimentation and numerical modeling. Paralleling the research on flow dynamics of pyroclastic flows have been investigations of granular flow by the engineering profession. Within the 1990s, the two approaches have begun to converge.

In our view, the following are key issues deserving focused research over the coming years.

- *Critical particle loading*. An open question that remains to be answered definitively is, What is the particle loading in a PDC that separates the regime of dominantly turbulent transport from that of dominantly particle-collision transport? How broad is that "transition" zone in terms of particle loading? What are the quantitative relationships between the rate at which particles sediment out from the transport system into the depositional systems, and the resulting deposit characteristics?

- *Bed form regimes*. It would be useful to generate, from a combination of experiments and field observations, a "phase diagram" that defines the characteristics of pyroclastic surge bed forms as functions of the eruptive conditions and flow regime of the parent surges. Such diagrams have been developed for fluvial and eolian systems and have proven extremely useful for both predicting behavior and for interpreting the geologic record.
- *Compressible flow effects*. Most of our deposit-based inferences about pyroclastic surges are extensions of our knowledge from incompressible flow systems such as wind-driven and fluvial sediment transport. The effects of shock waves and supersonic flow, such as occur in many pyroclastic surges, on resulting deposits is largely unknown.
- *Risk assessment*. An ultimate goal of volcanologists is to minimize loss of life and property from explosive eruptions. Risk assessment, which accounts for both the probability of an event and its consequences, is an important step in attaining that goal. The ability to recognize pyroclastic surge events in the geologic record of a volcano is key in establishing probabilities of surge events. An area that needs particular focus is constraining the effects, or consequences, of pyroclastic surge events. This will involve predicting the dynamic conditions within surges and the responses of structures and people to those conditions.

SEE ALSO THE FOLLOWING ARTICLES

Hazards from Pyroclastic Flows and Surges • Ignimbrites and Block-and-Ash Flow Deposits • Pyroclast Transport and Deposition • Scoria Cones and Tuff Rings

FURTHER READING

Bursik, M. I., Kurbatov, A. V., Sheridan, M. F., and Woods, A. W. (1998). Transport and deposition in the May 18, 1980, Mount St. Helens blast flow. *Geology* **26,** 155–158.

Chough, S. K., and Sohn, Y. K. (1990). Depositional mechanics and sequences of base surges, Songaksan tuff ring, Cheju Island, Korea. *Sedimentology* **37,** 1115–1135.

Cole, P. D. (1991). Migration direction of sand-wave structures in pyroclastic-surge deposits: implications for depositional processes. *Geology* **19,** 1108–1111.

Druitt, T. H. (1992). Emplacement of the 18 May 1980 lateral blast deposit ENE of Mount St. Helens, Washington. *Bull. Volcanol.* **54,** 554–572.

Fisher, R. V. (1996). Mechanism of deposition from pyroclastic flows. *Am. J. Sci.* **264,** 350–363.

Fisher, R. V. (1990). Transport and deposition of a pyroclastic surge across an area of high relief: the 18 May 1980 eruption of Mount St. Helens, Washington. *Geol. Soc. Am. Bull.* **102,** 1038–1054.

Fisher, R. V., and Waters, A. C. (1970). Base surge bed forms in maar volcanoes. *Am. J. Sci.* **268,** 157–180.

Smith, G. A., and Katzman, D. (1991). Discrimination of eolian and pyroclastic-surge processes in the generation of cross-bedded tuffs, Jemez Mountains volcanic field, New Mexico. *Geology* **19,** 465–468.

Sohn, Y. K., and Chough, S. K. (1989). Depositional processes of the Suwolbong tuff ring, Cheju Island (Korea). *Sedimentology* **36,** 837–855.

Valentine, G. A. (1987). Stratified flow in pyroclastic surges. *Bull. Volcanol.* **49,** 616–630.

Valentine, G. A. (1998). Damage to structures from pyroclastic flows and surges, inferred from nuclear weapons effects. *J. Volcanol. Geotherm. Res.* **87,** 117–140.

Wohletz, K. H., and Sheridan, M. F. (1979). A model of pyroclastic surge. *Geol. Soc. Am. Sp. Pap.* **180,** 177–194.

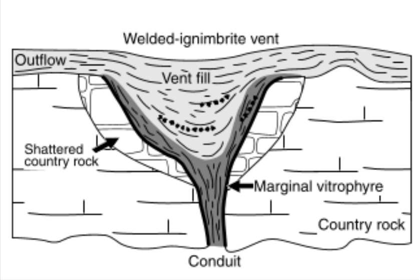

IGNIMBRITES AND BLOCK-AND-ASH FLOW DEPOSITS

A. FREUNDT
GEOMAR Research Center for Marine Geosciences

C. J. N. WILSON
Institute of Geological & Nuclear Sciences

S. N. CAREY
University of Rhode Island

I. General Features of Ignimbrites
II. Welded Ignimbrites
III. Block-and-Ash Flow Deposits
IV. Pyroclastic Flows That Entered the Sea
V. Ignimbrite Source Vents
VI. Products of Secondary Processes
VII. Generation and Transport Processes
VIII. Future Research

GLOSSARY

ash flow/ash-flow deposit or ash-flow tuff Deposit of pyroclastic density current(s) consisting predominantly (>50 wt%) of ash-size material. In practice, *ash-flow tuff* is used for moderate- to large-volume ignimbrites in the U.S. literature.

block-and-ash flow deposit Small-volume pyroclastic flow deposit characterized by a large fraction of dense to moderately vesicular juvenile blocks in a medium to coarse ash matrix of the same composition.

ignimbrite Welded or unwelded, pumiceous, ash-rich deposit of pyroclastic density current(s). This term was formerly used for strongly welded deposits only.

pyroclastic density current A particulate gaseous volcanic flow moving along the ground. This term includes both *pyroclastic flows* and *pyroclastic surges* but has no connotation of particle concentration or flow steadiness.

pyroclastic flow deposit Predominantly massive, poorly sorted, ash-rich deposit laid down by a particulate gaseous flow. This term is mostly used to imply a depositing flow of high particle concentration (tens of volume percent) in contrast to a low particle concentration pyroclastic surge.

pyroclastic surge deposit Strongly bedded (laminated, low-angle cross-bedded) deposits laid down by fast-moving gaseous flows of low particle concentration.

THE PERCEPTION OF pyroclastic flows as a highly dangerous and devastating type of explosive volcanic activity was brought about dramatically by the 1902 *nuee ardente* (glowing cloud) of Mt. Pelée, Martinique, which killed 30,000 people. Studies of recent historic eruptions facilitated the recognition of abundant ignimbrites in the geological record, many of them orders of magnitude larger in volume. It took until the 1960s, however, before large welded ignimbrites with lavalike field characteristics but a clearly fragmental texture became widely accepted as deposits of pyroclastic

Copyright © 2000 by Academic Press
All rights of reproduction in any form reserved.

flows. The deposits of pyroclastic flows are highly variable in bulk volume (<0.1 to >1000 km^3), runout distance (<1 to >100 km), deposit geometry and response to topography (channel confined to radially symmetrical), internal structure (massive through layered; Figs. 1a–c), degree of welding (unwelded to lavalike; Fig. 1d), clast type and size (wall rock lithic- to pumice-dominated, ash- to block-rich; Figs. 1a and 1c; see also color inserts), and chemical composition (mafic through felsic, often compositionally zoned; Fig. 1b). Gradations, rather than sharp boundaries, for all these characteristics occur between different ignimbrites and

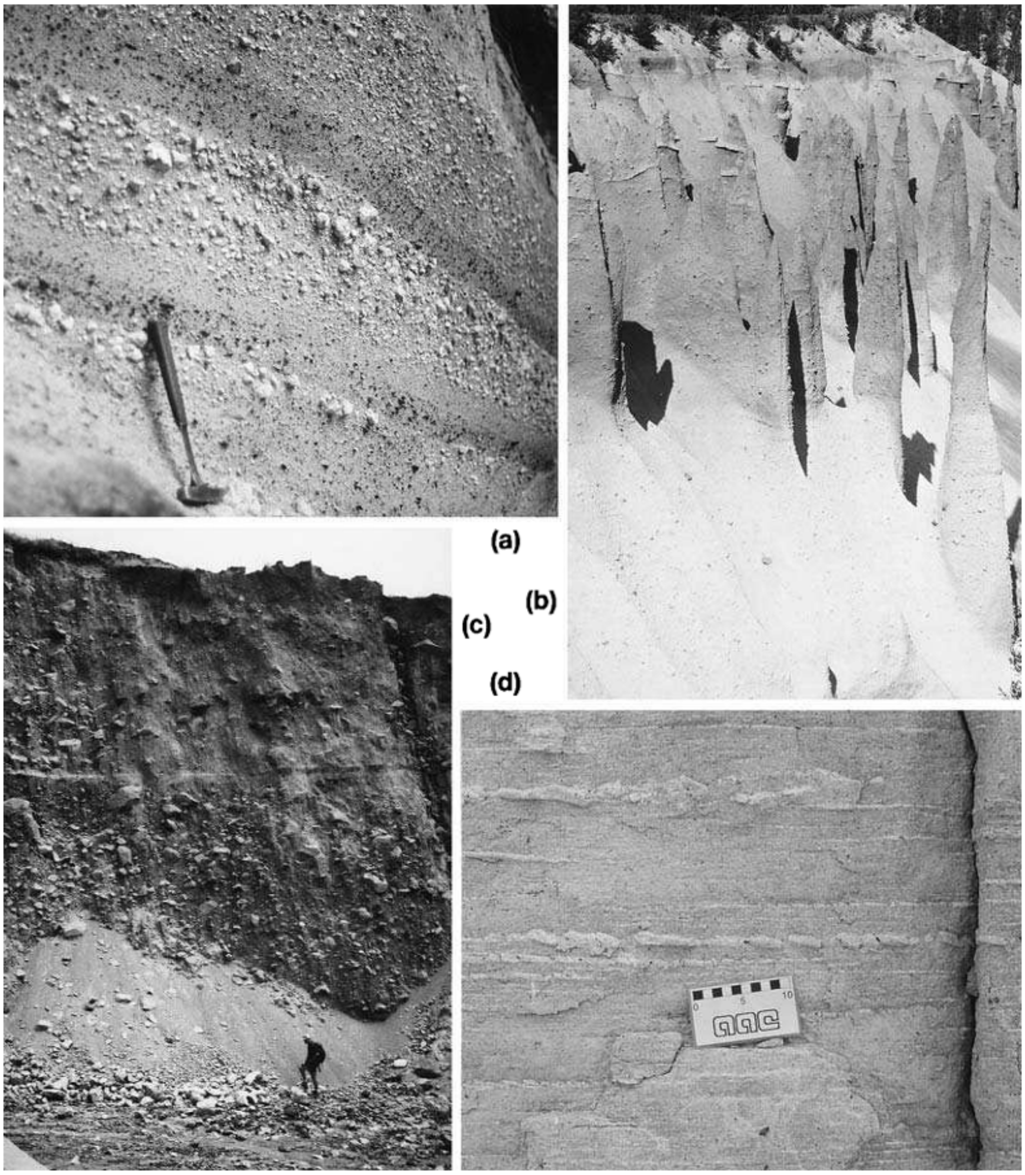

FIGURE 1 (a) Flow units near canyon wall in Laacher See ignimbrite. Sharp boundaries between lower lithic-rich and upper pumice-rich, reversely graded zones reflect local detachment of respective zones in the flows. (See also color insert.) (b) C. 60-m-thick section of ignimbrite at Crater Lake, Oregon, compositionally zoned from lower rhyodacite (white) through upper mafic andesite (gray) with pink oxidation zone near top. Pinnacles are cemented fumaroles that resisted erosion. (c) Two depositional units of block-and-ash flows at Mt. Merapi, Indonesia. Note meter-sized blocks. Person for scale. (See also color insert.) (d) Densely welded ignimbrite from Gran Canaria with highly flattened and sheared fiamme, some pulled apart and rotated.

between different facies within one ignimbrite. Furthermore, there are transitions between pyroclastic flow and pyroclastic surge deposits. Such diversity in the deposits has caused a similar diversity in the inferred transport and emplacement processes. Most authors use the term *pyroclastic flow* to imply a current of high particle concentration as opposed to *pyroclastic surge* of low particle concentration. We use the term *pyroclastic density current* here to avoid specific implications on the nature of the flow other than that it was a gas–pyroclast mixture moving along the ground driven mainly by gravity.

I. GENERAL FEATURES OF IGNIMBRITES

A. Areal Distribution

Moving pyroclastic density currents are gravity-controlled and preferentially follow basins and channels. This topographic control shows in the areal distribution of ignimbrites (Fig. 2a), which typically pond to great thickness in valleys and grade into thin deposits or disappear on topographic highs. Large ignimbrites can, however, form extensive radial sheets that completely bury the pre-eruptive topography (Fig. 2b). Many ignimbrites were emplaced by pyroclastic currents that were able to surmount high topographic barriers at tens of kilometers distance from the vent (Fig. 2c). On the other hand, small pyroclastic flows moving across a plain can confine themselves by forming lateral block levees, similar to lava or debris flows, and terminate in lobes with steep levee fronts (e.g., Mount St. Helens post-May 18 flows; also typical of many block-and-ash flows).

The dimensions of pyroclastic flow deposits vary greatly, and the maxima for any parameter are still being extended. Distances traveled range from a few hundred meters for small block-and-ash flow deposits (Section III) to ca. 200 km for the most widespread ignimbrites. Areas covered are from a few hundred square meters to 45,000 km^2, and volumes from a few thousand cubic meters to about 5000 km^3. The three-dimensional geometry of ignimbrites has been little documented, in part because erosion since deposition has often removed large amounts of material, especially in thinner deposits. A simple quantitative descriptor of the overall shape of a deposit is the aspect ratio, defined as the ratio of the average thickness to the diameter of a circle equal in area to the deposit. Aspect ratios range from $<10^{-5}$ (low-aspect-ratio ignimbrite) to $>10^{-2}$ (high-aspect-ratio ignimbrite). Extreme examples are the high-aspect-ratio VTTS and low-aspect-ratio Taupo ignimbrites (Fig. 2d). Documented deposits have average thicknesses that range over about 2 orders of magnitude and are not simply related to either the volume or the welding state of the deposit. For example, the 30-km^3 Taupo ignimbrite has an average thickness of 1.5 m whereas the 150-km^3 Bishop Tuff is about 100–150 m thick, i.e., having about 5 times the volume yet 100 times the thickness of the Taupo ignimbrite. Thickness of more or less radially distributed ignimbrite sheets diminishes with distance from vent in an approximately exponential fashion (Fig. 2b); the thickness–decay pattern of small channelized pyroclastic flow deposits can be complex, depending on topography.

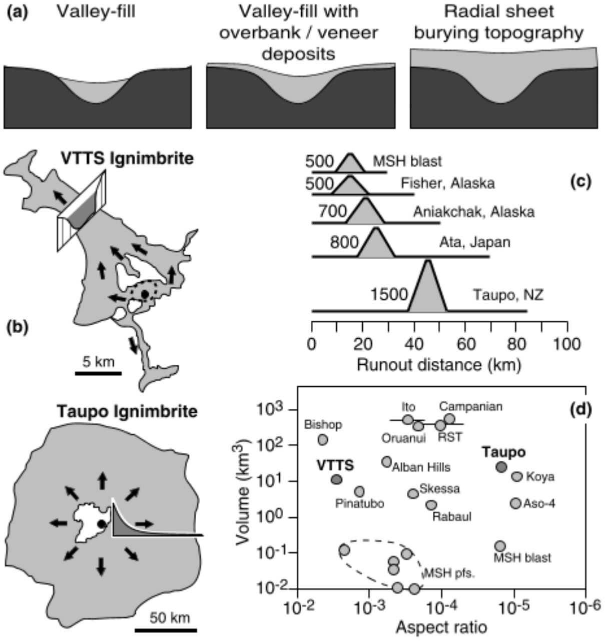

FIGURE 2 (a) Illustration of cross-sectional patterns from strictly valley-confined to topography-burying ignimbrites. (b) Distribution maps of the Valley of Ten Thousand Smokes (VTTS), Alaska, and Taupo, New Zealand, ignimbrites. Arrows indicate flow directions; black dots are vent sites. Schematic cross section shows flat top of ignimbrite in the lower VTTS. Inset diagram illustrates exponential thickness decay of IVD and layer 1 in the Taupo ignimbrite. (c) Illustration of ridge heights surmounted by some pyroclastic currents tens of kilometers from vent. Bold lines show ignimbrite runout length; numbers indicate ridge elevations in meters. Ridge width and steepness not to scale. (d) Plot showing that aspect ratio is not related to volume of ignimbrites. Taupo and VTTS emphasized as low- and high-aspect-ratio examples, respectively.

B. Composition and Componentry

Ignimbrites are composed of juvenile pyroclastic material, represented by pumice or scoria in the block-lapilli fraction and by glass shards and crystals in the ash fraction, and of foreign lithic fragments derived from the conduit walls or picked up from the surface. Juvenile pyroclasts are commonly moderately to highly vesicular but can be poorly vesicular to dense in ignimbrites generated by phreatomagmatic eruptions. The chemical composition of juvenile pyroclasts in small- to intermediate-volume pyroclastic flow deposits ranges across the entire compositional spectrum (basaltic to rhyolitic) of tholeiitic, calcalkaline, and alkaline magmatic series whereas large ignimbrites mostly have highly evolved compositions. Many ignimbrites are vertically zoned or mixed in chemical composition, providing insight into magma chamber structures. Corresponding with composition, ignimbrites occur in all geotectonic settings on land. Ignimbrites generated on land have been emplaced in the sea and some even erupted from calderas in shallow waters of a few hundred meters depth. We are not aware of any ignimbrite generated in deeper seawater (>1 km).

The relative proportions of components vary between grain size fractions as well as with distance from the vent or height within a single ignimbrite, and they vary between ignimbrites as a function of magma composition and mode of pyroclastic flow generation. For example, pyroclastic flow deposits generated during phreatomagmatic eruptions are generally richer in wall rock lithics than those produced by magmatic eruptions. Highly welded ignimbrites are generally poor in lithics probably because lithic fragments incorporated at the vent can drastically cool the pyroclastic mixture and thus inhibit welding. Lithic fragments in ignimbrites may be basement rocks entrained in the magma chamber or conduit or surface rocks entrained during passage of the pyroclastic currents. Wall rock lithics can be useful to constrain magma chamber depth or conduit position, indicate the former presence of a hydrothermal system, or mark major events of vent erosion or caldera subsidence during eruption where they are enriched in particular horizons.

The crystal content of the ignimbrite matrix is often higher than in the juvenile material, implying that some concentration of crystals has occurred during eruption and transport of the currents. The corresponding glass fraction can occur as the distal portions of the same ignimbrite or form co-ignimbrite ash. Rounded pumice clasts, abraded glass rims on crystals, and fine-ash contents increasing with distance from the vent suggest additional vitric-ash formation occurred by abrasion during transport.

Debris from vegetation engulfed by pyroclastic flows is occasionally preserved in deposits emplaced at low temperature; in general, however, finer plant debris is completely destroyed and only thick branches and logs survive transport but become charred. The charred wood can be used to isotopically (^{14}C method) determine the age of eruption.

C. Grain Size, Texture, and Structure

The grain-size frequency distribution of pyroclastic flow deposits is often polymodal and does not follow a single-distribution law (e.g., Gaussian or Rosin–Rammier), although it is common to present distributions on log-normal graphs and employ the Inman descriptive measures that are based on Gaussian distribution (Fig. 3a). The wide range in particle sizes, from micron to meter scale, is reflected in high sorting coefficients (commonly $\sigma_\Phi > 2$) of ignimbrites whereas the predominance of ash-sized particles causes the relatively small median size $Md_\Phi = 0$ to 2 (Figs. 3a and 3b), but local facies can show extremely diverging grain-size characteristics. Some ignimbrite facies have been described as "fines-depleted," by which some authors mean that blocks are enriched relative to ash (case A in Fig. 3c) whereas others imply depletion of ash (case C). We recommend considering the relationships between at least three size fractions (e.g., F_1, F_2, and F_3 in Fig. 3c) in order to be able to identify coarse-enriched (A), coarse-depleted (B), fines-depleted (C), and fines-enriched (D) facies. This approach is necessary to distinguish size fractions that are actively modified by dynamic processes from those that are passively affected by the constant-sum effect.

The polymodality of ignimbrite grain-size distributions has several causes: (1) fragmentation in the vent, which produces different size distributions for each component (e.g., pumice, wall rock lithics, and crystals), (2) segregation of certain components and size fractions during transport and emplacement, and (3) additions to certain component and size fractions either by fragmentation and abrasion during transport or by entrainment of bed material (e.g., surface lithic fragments and older tuff). Interpretation of ignimbrite grain-size distributions thus must consider variations in componentry between grain-size fractions. For example, a mode in the 250- to 500-μm size range might be attributed to a concentration of crystals in this range. Ideally, then, subpopulations characterized by individual modes may

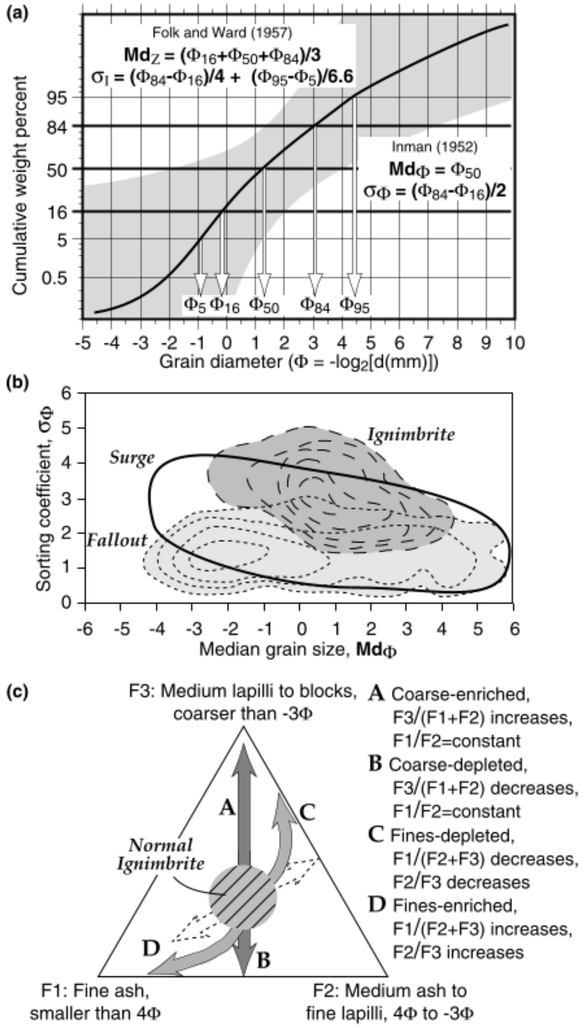

FIGURE 3 (a) Cumulative grain size distribution and definition of the statistical parameters, median size (*Md*) and sorting (σ). Gray field includes most "normal" ignimbrite data. (b) Md–σ diagram illustrating different grain size characteristics of ignimbrites and fallout beds, while surge deposits overlap with both. Dashed lines give probability distribution inside fields. Many ignimbrite facies are now known to have grain size characteristics well outside the ignimbrite field and overlapping with the other fields. This diagram should thus not be used to discriminate deposits based on grain size alone. (c) Illustration of selective enrichment and depletion of certain grain size fractions as discussed in the text.

be identified in the bulk size distribution of each component. These can then be interpreted in terms of fragmentation and transport processes.

In general, with distance from source, median grain size decreases, the content of fine ash increases, and size sorting improves in unwelded ignimbrites. Maximum sizes of vent-derived lithic clasts decrease exponentially with distance from source and may range from meter-sized blocks in proximal outcrops to millimeter-sized lithic particles in distal deposits. Maximum sizes of pumice clasts show more variation in trends with distance from vent; some exponentially decrease outward, others remain high or increase out to an intermediate maximum, and some small-scale historic flows (Komagatake 1929; post-May 18 Mount St. Helens 1980) have carried the largest pumices to the distal tips of the deposits.

The absolute distance from vent up to which clasts of a given size and density (i.e., weight) have been carried is commonly much larger in ignimbrites than in pyroclastic surge deposits (Fig. 4a), suggesting a higher transport capacity of pyroclastic flows compared to surges. On the other hand, the fractional range of clasts, i.e., their absolute distance from vent divided by the runout length of the deposit, is highly variable but generally lower in ignimbrites than in pyroclastic surge deposits (Fig. 4b). This suggests that, with respect to runout distance, pyroclastic flows may lose transport capacity faster than surges.

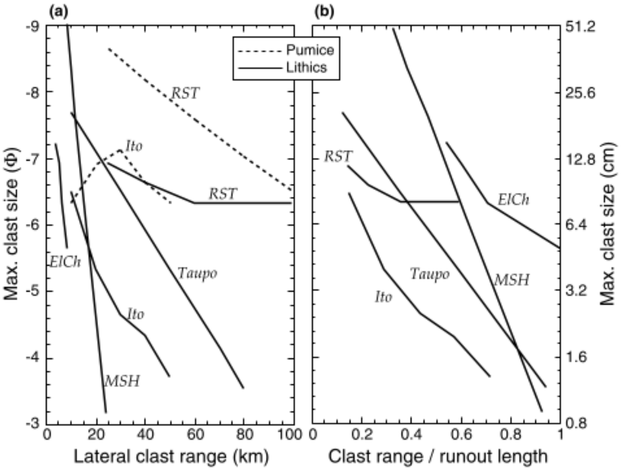

FIGURE 4 (a) Distribution of maximum pumice and lithic clast sizes with distance from vent in selected ignimbrites and surge deposits: Ito pyroclastic flow deposit, Japan; Taupo ignimbrite, New Zealand; Rattlesnake Tuff (RST), Oregon; Mount St. Helens blast deposit (MSH); El Chichon 1982 surge deposits (ElCh), Mexico. Clasts of a given size reach farther from vent in large ignimbrites (Taupo, Ito, and RST) than in small pyroclastic flow or surge deposits (MSH and ElCh). Note pumice size maximum about 30 km from vent in Ito ignimbrite. (b) Data in (a) presented with the maximum lateral range of clasts normalized to runout length. Clasts of a given size reach greater fractional distances in surges than in large ignimbrites.

Platy fragments and tree logs, and fluidal deformation textures in welded ignimbrites, as well as elongate microscopic crystals are often oriented in a systematic fashion that indicates flow direction controlled either by local topography or by radial spreading from the vent. As with local thickness changes, interpretation of local flow directions needs to carefully consider that drainage into valleys may have occurred during or immediately after deposition.

Grading textures commonly allow subdivision of an ignimbrite into depositional units, termed *flow units* (Fig. 1a). The *standard ignimbrite flow unit* comprises three layers (Fig. 5), which are now envisioned to represent different regions within a pyroclastic density current:

Layer 1	Deposit laid down at the flow front during strong interaction with ambient air and ground surface
Layer 2	Deposit of the main body and tail, i.e., the major portion of the flow
Layer 3	Deposit from the overriding dilute ash cloud

The association of all three layers is rarely complete; more often, layer 1 or 3, or both, are not present at all or are at least regionally absent.

1. Layer 1

A great number of specific varieties of layer 1 deposits have been described, suggesting that layer 1 formation is strongly controlled by local environmental conditions. *Ground layers* (also coined layer 1(H) or lithic-rich ground layer) enriched in heavy components (lithics, crystals) appear to be the most common type of layer 1 deposit. They range from meter-thick fines-depleted lithic breccias to centimeter-thin ash beds rich in millimeter-sized lithics and are interpreted as segregation bodies sedimented from within the head of a pyroclastic current, which is postulated to be a highly dynamic region where intense mixing with air occurs. *Ground surges* are fines-poor, laminated and cross-bedded layer 1 deposits thought to be emplaced by surges moving ahead of the pyroclastic current. Ground surges can be either lithic- or pumice-rich (layer 1(H) and 1(P) varieties). *Jetted deposits* rich in fine ash and pumice (major layer 1(P) variety at Taupo, New Zealand) are thought to be deposited from concentrated jets ejected ahead of the current. Common to all layer 1 deposits is their production at or in the head of pyroclastic density currents so that they potentially provide insight into how the currents' fronts interacted with the atmosphere, surface water, roughness and shape of the ground, and vegetation.

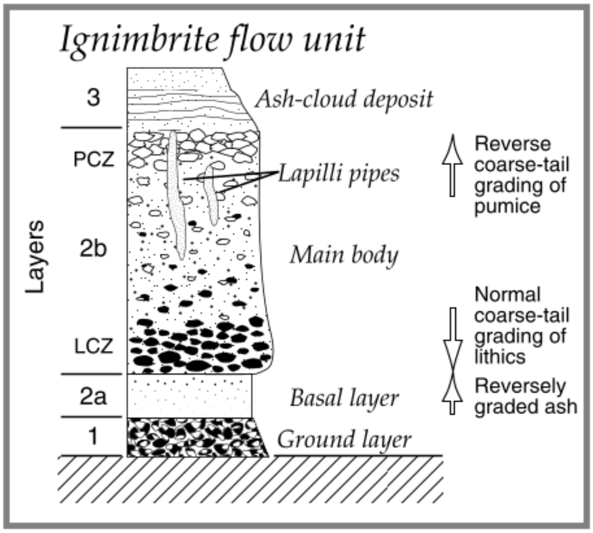

FIGURE 5 Idealized flow unit of ponded ignimbrite. Layer 2 can show a variety of grading structures from no grading to extremely enriched lithic and pumice concentration zones (LCZ and PCZ). Different layer 1 and layer 3 facies are discussed in the text. White particles, pumice; black particles, lithics; dots, ash.

2. Layer 2

Layer 2 is composed of an often reversely graded basal ash *layer 2a* that is variably developed, with sharp contact or gradational transition into overlying *layer 2b*. Layer 2a is thought to form in a lower boundary layer by interaction of the flow with the substratum. The main body of a flow unit, *layer 2b*, is characterized by reverse coarse-tail grading and topward enrichment of pumice clasts and normal coarse-tail grading and baseward enrichment of lithic clasts. The development of grading and segregation structures in ignimbrites varies widely (see Section ID) and is interpreted to reflect vertical motion of clasts according to their density contrast to the current.

Flow units contain *lapilli pipes*, i.e., more or less vertical narrow channels composed of lapilli that are strongly enriched in lithics and crystals but depleted in vitric ash. They form by the localized escape of gas from the compacting deposit that blows out the fine vitric ash. Lapilli pipes preferentially occur in the upper part of layer 2 but also originate from local lithic concentrations or burned logs and can be especially abundant above wet ground. Lapilli pipes are mostly subvertical and formed after emplacement of the flow unit; occasionally, however, lapilli pipes are deformed to sigmoidal shapes by shearing either during flow unit emplacement or during differential compaction. Lapilli pipes may cut through several flow units and in hot pyroclastic flow deposits may form encrustations by vapor-phase mineralization (*fumaroles;* e.g., Bishop Tuff, and Valley of Ten Thousand Smokes).

3. Layer 3

Layer 3 is a deposit of fine vitric ash that is commonly massive with fall characteristics but may also show evidence for lateral transport on the ground, such as miniature flow units, stratification, or even cross-bedding. The ash of layer 3 is believed to have settled from the ash cloud overriding a pyroclastic flow. Layer 3 may not be associated with each flow unit; in fact, layer 3 may only be found on top of the entire ignimbrite if emplacement of the succession of flow units was faster than the settling of fine ash from the overriding ash cloud. Some ignimbrites are associated with very extensive co-ignimbrite ash layers, suggesting that the depositing ash clouds had plinian-like dimensions.

Ignimbrites composed of a single flow unit exist but more often they are composed of flow unit packages. Ideally, a flow unit is envisioned as the deposit of a single pyroclastic current. Flow units have, however, been observed to split into two or more thinner flow units laterally, probably due to splitting into lobes or pulsatory motion of the pyroclastic flow. The number of flow units in an outcrop thus need not be equal to the number of depositing flows. In moderate- to large-volume ignimbrites, and especially in welded ignimbrites, it is often difficult to identify flow units as defined above. This may be due to very thin layers 2a associated with very thick, unstructured layers 2b or to welding compaction and rheomorphic deformation obscuring depositional boundaries. On the other hand, some thick, gradually compositionally zoned ignimbrites do not reveal any clear internal depositional boundaries; this observation provoked the idea that at least some ignimbrites are emplaced by progressive aggradation (grain by grain) from a maintained current rather than layer by layer (flow unit by flow unit) from a number of short-lived flows.

The basal contact of pyroclastic flow deposits is mostly conformable to the preexisting surface but can also be highly unconformable where the pyroclastic currents were able to erode, e.g., close to the vent, on steep slopes, or on soft substrate. Pyroclastic flows of the April 19–20, 1993, eruption of Lascar volcano (Chile) stripped scree and talus from their channels and scratched striations and percussion marks into bedrock; strongest erosion occurred on steep slopes, where flows accelerated through narrow channels and where they already contained abundant lithic blocks. Ash of the strongly welded ignimbrite P1 on Gran Canaria intruded into, completely filled, and welded within (a) void spaces of a canyon boulder bed to several meters depth and (b) tectonic cracks as narrow as a few millimeters and more than a meter deep, indicating great fluidity of the pyroclast–gas mixture.

D. Facies Variations

Within a single ignimbrite, significant changes in facies can occur on a regional scale, including changes with distance from vent and over areas of different topographic character, and on a local scale, where they are commonly controlled by local topographic features.

1. Regional Facies Variations

Many ignimbrites that are massive across intermediate to distal regions contain variably bedded, tractionally formed deposits close to the vent which are associated with erosion and transitional to, or resemble, pyroclastic surge deposits. Such deposits typically show lensoid, wavy, discontinuous bedding, laminations or cross-bedding, with variable grain size and poor to moderate sorting of individual beds, and gradually merge into massive ignimbrite farther from the vent (e.g., Roccamonfina, Italy; Laacher See, Germany; Taupo, New Zealand; Novarupta 1912, Alaska; Pinatubo 1991, Philippines). In addition, cross-bedded pyroclastic flow deposits also occur on steep flow paths, such as at Mount St. Helens, during the 1980 eruptions. The Neapolitan Yellow Tuff (Italy) is an ignimbrite that seems to be characterized by such facies throughout most of its extent. These transitional facies are interpreted to have been emplaced under intermediate-concentration conditions from fast pyroclastic density currents that were evolving from the collapsing eruption column toward higher concentration farther from the vent.

The range of facies developed in ignimbrites is particularly shown by the 30-km^3 Taupo ignimbrite (Fig. 6a), which is interpreted to represent a single short-lived (ca. 400 s) catastrophic outburst of material, i.e., equivalent to a single vent-derived flow unit. These facies are developed in three ways:

First, a spectacular development of layer 1 deposits (as discussed above), which form about 15 vol% of the ignimbrite (Fig. 6b). The exceptional development of layer 1 deposits at Taupo is inferred to reflect the extreme velocities attained by the flow coupled with the abundance of vegetation.

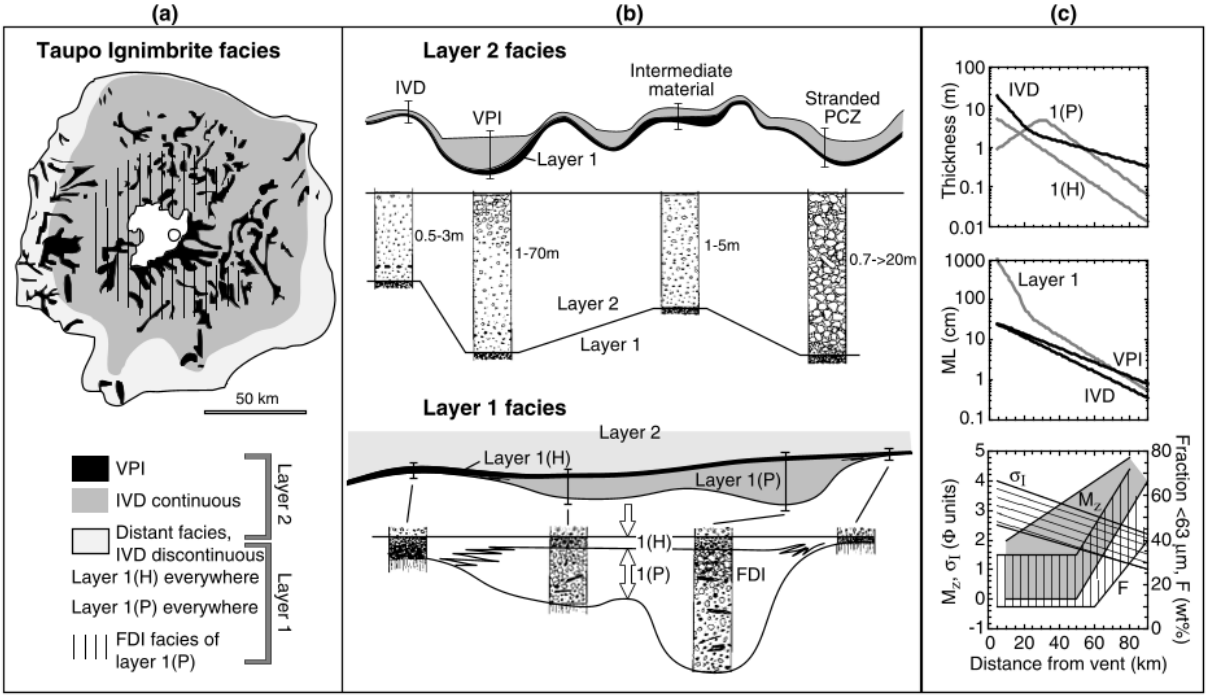
(a)
(b)
(c)
Taupo Ignimbrite facies
50 km
VPI
IVD continuous
Distant facies, IVD discontinuous
Layer 1(H) everywhere
Layer 1(P) everywhere
FDI facies of layer 1(P)
Layer 2
Layer 1
Layer 2 facies
IVD
VPI
Intermediate material
Stranded PCZ
Layer 1
0.5-3m
1-70m
1-5m
0.7->20m
Layer 2
Layer 1
Layer 1 facies
Layer 2
Layer 1(H)
Layer 1(P)
1(H)
1(P)
FDI
Thickness (m)
IVD
1(P)
1(H)
ML (cm)
Layer 1
VPI
IVD
M_Z, σ_I (Φ units)
Fraction <63 µm, F (wt%)
σ_I
M_Z
F
Distance from vent (km)

FIGURE 6 (a) Map of facies distribution in the Taupo ignimbrite. VPI, valley-ponded ignimbrite; IVD, ignimbrite veneer deposit; 1 (H) and 1 (P), lithic- and pumice-rich layer 1; FDI, fines-depleted ignimbrite, a variety of layer 1 (P). (b) Illustration of layer 2 and layer 1 facies changes across topography. (c) Variation with distance from vent of thickness and maximum lithic clast size (ML) in IVD, VPI, and layer 1 deposits, and grain-size characteristics of layer 2 material.

Second, the reaction of the bulk of the ignimbrite (i.e., layer 2) to the landscape over which it was emplaced. In the Taupo ignimbrite, layer 2 comprises a landscape-mantling *ignimbrite veneer deposit* (IVD) and a landscape-modifying *valley-ponded ignimbrite* (VPI; Fig. 6b), the two merging into each other over distances of decimeters to tens of meters. The relationships between the IVD and VPI are seen in many ignimbrites where the current(s) were able to surmount interfluves partly or wholly.

Third, the Taupo ignimbrite shows spectacular variations (up to 2–3 orders of magnitude) in such parameters as mean grain size, contents of lithics and crystals, fine-ash abundances, and largest clast sizes over the 80 ± 10 km from source to distal limits (Fig. 6c). The scale of the lateral variations at Taupo is again in large part driven by the velocity of the parent current, with the concomitant effective segregation and separation of different fractions.

Facies changes from channel-fill to overbank in the much smaller (<1 km^3) multiple-flow-unit ignimbrite at Laacher See, Germany, differ from those in the Taupo ignimbrite. Thick flow units in channels taper out to ash layers on the overbanks that are only a few centimeters thick but flow unit structures, albeit mostly incomplete, persist up to some 300 m out of the channels (Figs. 7a and 7b). Farther out, and with increasing distance from the vent, correlation of gradually thinner overbank ash layers with channel-fill flow units becomes almost impossible. Areal distribution and lateral changes of the overbank facies suggest that the phase segregation into lapilli- and lithic-rich channeled and lapilli- and lithic-poor overbank flow occurred very close to the vent during funneling through passes in the Laacher See basin wall.

2. *Local Facies Variations*

Small-volume pyroclastic flow deposits derived from valley-confined flows terminate marginally against the valley walls. The Valley of Ten Thousand Smokes (VTTS) ignimbrite, with its "high-energy" proximal facies on high ground and perhaps 100-m thickness in upper reaches of the valley, stops dead against a moraine only 15 m high blocking the valley about 15 km from the vent. Apparently, each of the many flows that contributed to the bulk deposit was too sluggish to surmount this small barrier.

At Laacher See, pyroclastic flows funneled through deep, narrow, rough-walled canyons (Fig. 7a) and interacted with canyon walls in a variety of ways, producing marginal flow unit structures that change with travel distance and shape of the valley walls (Fig. 7c). Some flows were not wide enough to touch the canyon walls that are 200–300 m apart. In upstream regions of the canyons, flow units then taper out into thin ash-rich margins, in some places fringed by a carpet of lag-pumice blocks (Fig. 7c, diagram 5), whereas flow units farther down canyon are bounded by steep pumice-block levees (Fig. 7c, diagram 9). Similar marginal structures were also observed at Mount St. Helens. Such rare narrow flows were not accompanied by ash clouds large enough to leave laterally continuous ash layers. In contrast, flows that filled the width of the canyons did have ash clouds depositing on the canyon walls and shoulders but these ash layers were flushed from the steep walls by rain soon after emplacement and are now contained in reworked fine ashes overlying the canyon-fill ignimbrite. The downstream changes (Fig. 7c) from proximal wavy-bedded deposits through flow units containing

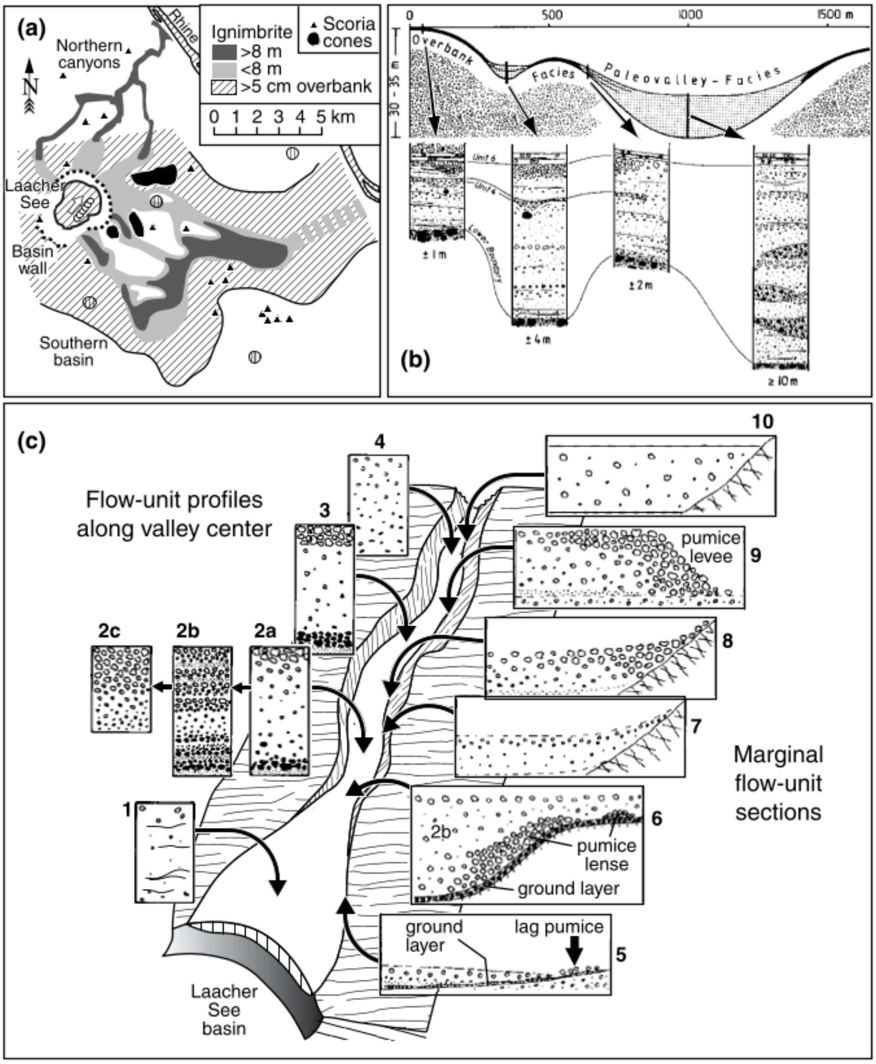
(a)
Northern canyons
Rhine
Ignimbrite
>8 m
<8 m
>5 cm overbank
Scoria cones
0 1 2 3 4 5 km
N
Laacher See
Basin wall
Southern basin
(b)
0
500
1000
1500 m
30 - 35 m
Overbank Facies
Paleovalley-Facies
Unit 6
Unit 4
Lower Boundary
±1m
±4m
±2m
≥10m
(c)
Flow-unit profiles along valley center
1
2a
2b
2c
3
4
5
6
7
8
9
10
pumice levee
2b
pumice lense
ground layer
ground layer
lag pumice
Marginal flow-unit sections
Laacher See basin

FIGURE 7 (a) Map of ignimbrite distribution around Laacher See volcano. Circle with arrow inside lake indicates vent migration during pyroclastic flow production. (b) Transition of thin overbank ash layers into thick flow units in channels on the smooth topography south of Laacher See. (c) Proximal to distal structural and compositional changes in flow unit sections along valley center (left) and along valley margin (right) in the northern canyons in (a). Diagrams 2a–2c show changes from valley center toward the margin.

abundant segregation bodies and complex marginal structures to distally massive flow units without marginal interaction are interpreted to reflect progressive deflation.

3. Lithic Breccias

Heavy lithic clasts are most susceptible to changes in the transport capacity of pyroclastic currents, which diminishes with distance from vent as reflected in the decreasing size of lithics in ignimbrites. Local reductions in transport capacity can be inferred from steps in the lithic size vs distance patterns but are most evidently marked by the occurrence of *lithic lag breccias*. These are commonly clast-supported beds of lithic blocks with an ash matrix that may or not be depleted in fine ash compared to the normal ignimbrite matrix. Lithic blocks are rounded in some breccias, yet others contain large fragments of fragile rock types such as paleosols, lake sediments, or diatomite. Lithic breccias occur in proximal settings, where they are dominated by vent-derived wall rocks, or elsewhere in specific paleotopographic settings, where locally derived lithic fragments may be important.

Near-vent, commonly fines-depleted lithic lag breccias lack evidence of ballistic impact of large blocks but may contain degassing structures such as lapilli pipes. Such breccias are either separated from normal ignimbrite by erosional unconformities or laterally merge into either lithic-rich ground layers (layer 1) or lithic-concentration zones of flow unit layer 2. Proximal lithic lag breccias have been left behind by pyroclastic currents that lost their excess load when dynamically adjusting from column collapse to subhorizontal flow.

The formation of more distal local lithic breccias is controlled by specific topographic conditions. Most commonly, local lithic breccias are found at sudden changes from steep to shallow ground slope, where pyroclastic currents possibly passed through stationary hydraulic jumps. Other local breccias occur inside sharp bends of a valley, where large vortices may have formed or where pyroclastic flows entered large bodies of water. Local lithic breccias can also form immediately downstream of topographic settings that favor erosion and massive entrainment of surface clasts by a pyroclastic current, which subsequently dumps this extra load. Local lithic breccias are mostly not depleted in fine ash and laterally merge into layer 2; they are commonly massive and unbedded although some layering, cross-bedding, or stoss-side stacking beds can be developed close to vent and on steep slopes where the pyroclastic currents had a high velocity.

II. WELDED IGNIMBRITES

A. Introduction

Ignimbrites show textures and structures developed in response to their high postemplacement temperatures and retained volatiles, viz., *welding*, *devitrification*, and *vapor-phase alteration*. The onset of welding in time and space is determined primarily by the magma composition (including retained volatile species that lower glass viscosities), load stresses, and temperature (both the absolute value and the time spent above any given value, i.e., the cooling rate). Typical minimum temperatures for welding are between 500 and 650°C for calcalkaline compositions. Most welded ignimbrites, regardless of temperature, include some material that is nonwelded due to either rapid cooling (e.g., directly overlying a cold substrate) or inadequate load stresses (e.g., the topmost part of a deposit).

B. Small-Scale Features

Welding is the cohesion, deformation, and eventual coalescence of pyroclasts at high temperatures under loading stress. In hand specimen, welding is manifested in turn by (1) cohesion of clasts across point contacts where load stresses are focused ("sintering"), (2) flattening of pyroclasts under the load stress (Fig. 1d), and then, in the most extreme cases, (3) flow as a coherent liquid (the process termed *rheomorphism*).

In young deposits, the contrast between sintered and nonwelded material may be very clear, but in ancient deposits, sintering cannot easily be distinguished from other diagnetic processes causing induration, and clear welding is seen only in the presence of flattened clasts. The higher the emplacement temperature and the lower the clast viscosity, the more intense is the compaction (i.e., elimination of pore space) under a given load and less load is needed to achieve a certain degree of compaction. In extreme cases, vitroclastic textures can be eliminated in densely welded material.

The degree of welding is measured either by the bulk density (Fig. 8a) or by the horizontal to vertical axis ratio (strain ratio) of vitric shards and *fiamme* (Figs. 8b and 1d), i.e., flattened pumice clasts, which can reach values of 100 : 1 in densely welded ignimbrites. The vertical variation of the strain ratio often parallels that of bulk density. Strain ratios larger than 10 : 1 are commonly taken to indicate viscous flow has occurred.

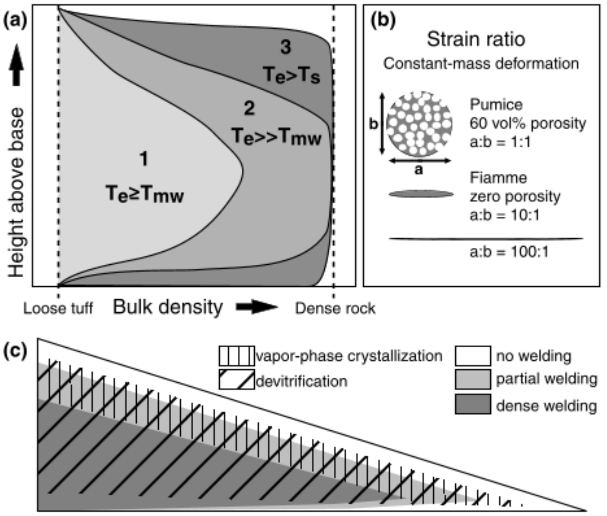

FIGURE 8 (a) Schematic vertical variation in bulk density of welded ignimbrites emplaced at different temperatures T_e above that of minimum welding, T_{mw} (curves 1 and 2). Ignimbrites that are almost entirely densely welded may have been emplaced at above-solidus temperature, T_s (curve 3), especially if they are thin. (b) Illustration of fiamme geometries. Mass remains constant, but volume decreases during compaction as pore space is eliminated. The strain ratio 10 : 1 is achieved by keeping **a** constant and collapsing **b** until pore space is zero. Higher strain ratios involve flowage in addition to simple compaction. (c) Welding and crystallization zones in a schematic, vertically highly exaggerated section through a welded ignimbrite.

Highly stretched fiamme can be cracked, pulled apart, and rotated (Fig. 1d).

Ignimbrites emplaced at temperatures sufficient to weld commonly cool slowly enough for juvenile glass to devitrify. There is a wide spectrum of effects from microscopic crystallization preserving the original pyroclastic texture, though to total overprinting by a coarse granophyric texture. At one extreme, thick, hot ignimbrites (e.g., caldera-fill deposits) can recrystallize to resemble an intrusive rock. However, minor posteruptive devitrification in ancient deposits can be difficult to distinguish from long-term diagenetic devitrification.

Welding and devitrification release most or all of the residual volatiles from the glass, and these volatiles can cause further vapor-phase alteration of the ignimbrite and/or deposition of further mineral species in pore spaces. Common new minerals are alkali feldspar, silica polymorphs, and hydrous minerals, but a wide variety of more exotic mineral species are also known. In addition, movement of vaporized groundwater or rainwater through the still-hot ignimbrite can cause further transport and deposition of mobile elements. Residual volatiles that exsolve during welding can become trapped in densely welded material and accumulate to form subspherical cavities filled by vapor-phase minerals, called *lithophysae*.

C. Large-Scale Features

In a welded ignimbrite, there are often systematic arrangements of the various zones of welding, devitrification, and vapor-phase alteration (Fig. 8c). Ignimbrites deposited rapidly at uniform temperature show vertical variations in density (i.e., welding intensity), with a maximum in the lower part of the ignimbrite, due to downward increasing load pressure and nonsymmetric cooling through the upper and lower boundaries (Fig. 8a). For a given emplacement temperature, the zone of dense welding widens with deposit thickness, whereas for a given deposit thickness, the proportion of the deposit that is densely welded increases with emplacement temperature (Fig. 8a). Overlapping with, but displaced vertically from, the welding zones are zones of devitrification and vapor-phase alteration, the upward displacement being due to the transport direction of heat and released volatiles in the cooling rock body. Welded ignimbrites also typically develop prismatic jointing—the spacing of which is widely interpreted to reflect the cooling time—oriented perpendicular to isotherms in the rock mass.

A welded ignimbrite that accumulated so rapidly that negligible cooling occurred (whether composed of one or many flow units), resulting in a simple arrangement of welding zones (Fig. 8c), is a *simple cooling unit*. *Compound cooling units* show departures from the simple profile, most clearly seen in irregular vertical gradients in bulk density and strain ratio, and are widely interpreted to reflect prolonged emplacement with the opportunity for partial cooling to occur between successive packages of material. It is not clear whether the complex density/welding profiles in compound cooling units represent significant time breaks in deposition (which need not be long if intervening heavy rainfall occurs) or variations in emplacement temperatures of successive flows.

D. Rheomorphism

Ignimbrites on sloping ground may flow rheomorphically as a coherent viscous liquid once dense welding has eliminated intergranular friction. There is a complete spectrum from (1) stretching and boudinage of flattened fiamme to (2) deformation of internal bedding and welding fabrics into flow folds of tens of meters to millimeters amplitude to (3) wholesale flow of the coherent liquid to produce features similar to those of conventional lavas of the same composition. Ramp structures and shear faults then can severely disrupt the initial stratigraphy.

At high temperatures, partially liquid particles may flatten under their own weight (cf. curve 3 in Fig. 8a) and flow downslope as they aggregate on the ground. Welding then is syn-depositional, controlled by viscosity and emplacement dynamics, as opposed to welding after emplacement. Under such conditions viscous flow is a continuation of the particulate pyroclastic current and may follow primary flow directions rather than local slope. Mapping of flow direction indicators and 3-D structural analyses thus provide means to distinguish between syn- and post-depositional welding.

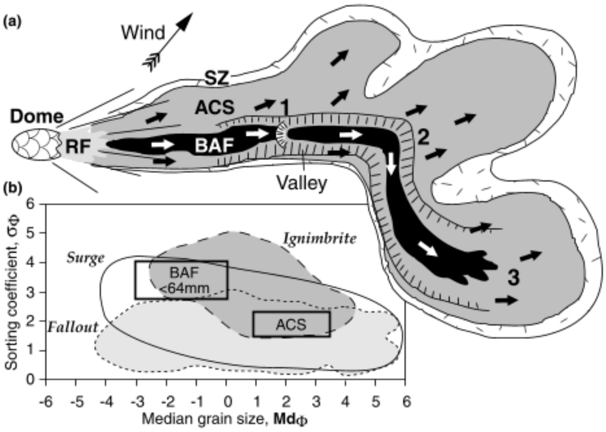

FIGURE 9 (a) Distribution of block-and-ash flow (BAF), ash-cloud surge (ACS; arrows give flow direction), and the seared zone (SZ) below a partially collapsed dome with a rock-fall scree (RF) at its base. Drawn after observations at Unzen and Merapi. Numbers 1–3 indicate enhanced ACS production and detachment where BAF rushes down a waterfall (1), ACS surmounts a bending valley wall that deflects BAF (2), and ACS advances beyond the limit of BAF, coming to rest on lower plain (3). Distribution of ACS deposit can be affected by wind. (b) Range of median size and sorting values for ACS deposits and BAF-matrix material <64 mm; poorly constrained since little data are available.

III. BLOCK-AND-ASH FLOW DEPOSITS

A. Distribution and Facies Associations

Block-and-ash flows can form by collapse of vulcanian eruption columns but most historic examples were generated by partial to total collapse of viscous lava domes as they oversteepen at their fronts during growth. Volcanoes producing lava domes and block-and-ash flows are numerous; among the most recent examples are Mount Unzen, Japan (1991), Mt. Merapi, Indonesia (1984, 1994, 1997–1998), and Montserrat (1995–1996). Dome collapse can be gravitational, explosive, or both. At Unzen, a strong explosion was observed to immediately precede the major block-and-ash flow of June 8, 1991. Video recordings show the formation of abundant ash as soon as the lava front collapsed, and small ash puffs from cracks in the dome can be seen before dome-flank failure, suggesting overpressure in the dome as a major cause of fragmentation, although collapse was probably initiated by gravitational instability.

Block-and-ash flows commonly extend up to 10 km from their source at speeds up to 100 km/h and are accompanied by ash cloud surges, which reach a wider areal distribution compared to the valley-confined block-and-ash flows (Fig. 9a). A seared zone where little or no ash is deposited but vegetation is burned fringes the ash cloud surge deposits. The hot ash-cloud surges can knock down trees and destroy houses. They are the most dangerous aspects of block-and-ash flow activity, most of all because they are less controlled by topography and can detach from their associated channelized block-and-ash flows. The formation of ash-cloud surge is, however, strongly influenced by topography (Fig. 9a). Increased ash-cloud production occurred at Mount Unzen, where the June 3, 1991, block-and-ash flow cascaded down two waterfalls, causing a wider spread of the ash-cloud surge downstream. Farther downstream, a sharp bend in the valley was followed by the block-and-ash flow but not by the ash-cloud surge, which rushed straight on out of the valley and killed 43 people.

B. Structure and Composition

Block-and-ash flows commonly have basaltic–andesite, andesite, or dacite compositions but may also be rhyolitic. The deposits are usually described as monolithologic but it is commonly difficult to distinguish juvenile and older dome fragments, because vesicularity and crystallinity vary across even single domes. Hydrothermal alteration of clasts can be helpful to identify older dome fragments but is ambiguous.

Block-and-ash flow deposits differ from pumiceous ignimbrites by containing little fine ash <1/16 mm (usually <5 wt%) but a large fraction of dense to moderately vesicular, rarely pumiceous, blocks up to several meters in diameter (Fig. 1c) that are derived from the juvenile source dome and possibly from older dome remnants. The deposits are poorly sorted but a complete grain-size distribution (including the block fraction) has not yet been reported (Fig. 9b). Bed structure can be either clast-supported or matrix-supported and generally massive but vague layering may locally occur. Flow unit structures as in ignimbrites are not commonly observed due to the absence of low-density fragments, but a fine-grained (or block-free) basal layer may be present and lapilli pipes are rare. The blocks are either uniformly distributed through the bed or show normal or reverse coarse-tail grading. Large blocks may be carried up to the distal tip of the deposit but the largest block size has been observed to reach a maximum at some intermediate distance, dropping off toward the vent as well as to the flow terminus. Block-and-ash flow deposits are about 1–10 m thick and thin to 1–2 m at their lobate, blunt termini. The detailed variation pattern with distance of both clast size and thickness strongly depends on how the channel gradient evolves. There may be no deposition at all on steep slopes such as immediately below the dome.

Ash cloud surge deposits are typically <1 m thick, consist of sand-sized and finer ash with median grain sizes ranging from 500 to <100 microns, and are relatively well sorted (Fig. 9b). Beds are laminated or consist of discontinuous or wavy layers, dune structures occur, and basal layers can be depleted in fine ash while overall fine-ash content increases toward the top. A topmost fine-ash layer may contain accretionary lapilli. Ash cloud surge deposits are exposed on the margin of the block-and-ash flow deposits but may also cover and/or underlie them.

IV. PYROCLASTIC FLOWS THAT ENTERED THE SEA

A. Flow–Water Interaction

Pyroclastic flows generated at near-shore or ocean-island volcanoes can enter the sea and produce widespread submarine volcaniclastic deposits. There is geologic evidence for a variety of ways in which pyroclastic flows interact with the sea. Scenarios for pyroclastic flows erupted on land or in shallow water include

1. Pyroclastic flows mix with seawater, causing coastal steam explosions or transformation into debris flows or turbidity currents
2. Pyroclastic density currents travel across the water, dropping sediment into the sea
3. Pyroclastic flows remain intact and either push aside shallow water near shore or flow under deeper waters until they come to rest or transform into debris flows

Evidence for submarine pyroclastic-flow-related debris flows and turbidites is abundant, suggesting that mixing of pyroclastic flows with seawater commonly occurs. That such mixing involved phreatic explosions has been implied by increased crystal/lithic ratios or a shift to finer sizes in the crystal population of the submarine deposits compared to those on land, but evidence for coastal explosions is not commonly reported. Welded ignimbrites in ancient near-shore environments probably displaced the seawater without much interaction except for local breccia pipes at the base of the ignimbrite where water in wet sediment was vaporized. Little convincing evidence exists that primary, hot pyroclastic flow deposits were emplaced in deep waters. There is proof, however, that some pyroclastic currents were able to travel large distances across the sea; the Koya flow in Japan, for example, had to cross 30 km over the deep waters of the Japanese sea to be emplaced on Kyushu and neighboring islands.

B. The Krakatau 1883 Example

The 1883 eruption of Krakatau volcano in Indonesia provides an excellent opportunity to examine the effects of pyroclastic flow interaction with the sea. It was a moderate ignimbrite-producing event, which resulted in the formation of a 5-km-diameter caldera that is open to the sea. For 2 days a series of large-volume pyroclastic flows entered the sea around Krakatau. Pyroclastic flow deposits consist of 2- to 4-m-thick flow units and locally have a total accumulated thickness of 60 m. The great thickness of flow deposits directly adjacent to the sea indicates that substantial volumes of flow material must have been discharged into the sea during the eruption.

Outside of the caldera there was significant addition of material to the sea floor as a result of the 1883 eruption (Fig. 10). Coring of the submarine deposits has yielded two distinct facies in water depths less than

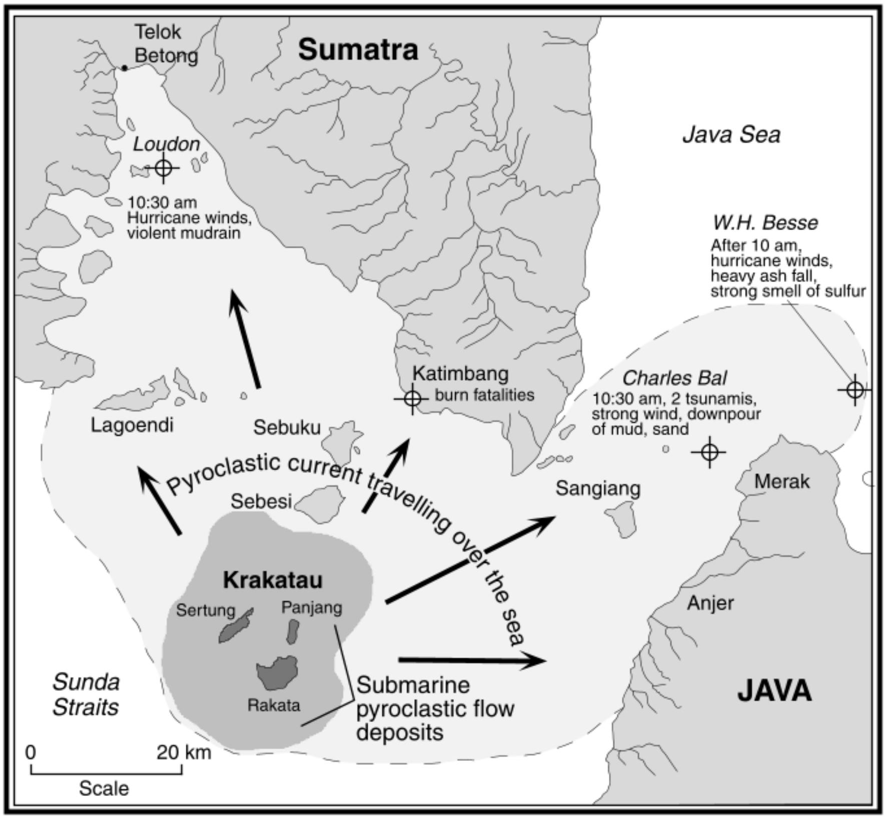
Telok Betong
Sumatra
Java Sea
Loudon
10:30 am
Hurricane winds, violent mudrain
W.H. Besse
After 10 am, hurricane winds, heavy ash fall, strong smell of sulfur
Katimbang
burn fatalities
Charles Bal
10:30 am, 2 tsunamis, strong wind, downpour of mud, sand
Lagoendi
Sebuku
Pyroclastic current travelling over the sea
Sebesi
Sangiang
Merak
Krakatau
Sertung
Panjang
Rakata
Anjer
Sunda Straits
Submarine pyroclastic flow deposits
JAVA
0
20 km
Scale

FIGURE 10 Map of the Sunda Straits area showing Krakatau islands surrounded by submarine pyroclastic flow deposits (gray shading) and extent of the pyroclastic current that traveled over the sea (light gray shading), overran the islands of Sebesi, Sebuku, and Lagoendi, and reached the Sumatra coast, leaving deposits described in the text. Locations of ships that recorded passage of the pyroclastic current (and tsunami waves) are indicated.

20 m. The first, and more abundant, is massive and consists of a poorly sorted mixture of pumice and lapilli in a gray, silty matrix of glass shards, crystals, and lithics. The other facies is marked by better sorting, finer grain size, and the presence of parallel and cross laminations. Thermoremanent magnetization studies of samples from the submarine massive facies indicate deposition at temperatures in excess of 450°C. Because of their high temperature and submarine emplacement, these deposits most likely formed from hot flows that traveled under water.

There is also evidence that a hot gas/particle current traveled over the sea surface during the 1883 eruption of Krakatau. The most compelling observation is a large number of burn fatalities (ca. 2000) that took place 40 km from the vent across the Sunda Straits, along the southeast coast of Sumatra (Fig. 10). Ships 65–80 km away from Krakatau were engulfed by ash clouds. Pyroclastic deposits on islands provide important information about the nature of the ash currents as they traveled to the north and northwest from Krakatau (Fig. 10). The currents overran all of these islands and most of the vegetation was destroyed, with total loss of life. The deposits consist of three major types:

1. Volumetrically most important, poorly sorted massive beds of angular to subangular dacitic pumice and lithic clasts in a matrix of fine ash with small pieces of charcoal
2. Stratified beds containing pumice and lithic clasts that are more rounded
3. Intercalated layers of pumice lapilli with virtually no dense components, which are attributed to tsunami inundation of the islands

Grain-size characteristics of the massive and stratified deposits support deposition from some type of pyroclastic density current. These distal samples form a continuum in grain-size trends defined by the more proximal subaerial and submarine pyroclastic flow deposits. With increasing distance from Krakatau, there is a systematic decrease in the median diameter and sorting coefficients of the deposits. As the currents traveled across the sea surface, they apparently became cooler and more dilute (surgelike). Eventually, the currents became buoyant, producing a large-scale co-ignimbrite plume rich in moisture. From this plume an episode of mudrain deposition affected a large area of the Sunda Straits.

V. IGNIMBRITE SOURCE VENTS

Ignimbrite source vents, especially of large-volume examples, are often hidden by caldera subsidence and caldera fill. Buried vents can be located by mapping regional facies variations in the ignimbrite (thickness, grain size, maximum clast size, degree of welding), by lithic lag breccias, and by the flow-orientation patterns of logs, platy fragments, and crystals. Small- to intermediate-volume ignimbrites are commonly derived from central vents that can be identified by mapping the distribution of associated fall beds. Fall isopachs of Laacher See tephra bracketing the main pyroclastic flow deposits show that these formed during a period of vent migration within the crater basin (Fig. 7a).

Moderate- to large-volume ignimbrites are commonly associated with caldera collapse. Evidence that such ignimbrites erupted through ring fractures rather than central vents has been provided in some cases. In the Bishop ignimbrite, characteristic vent-derived lithic rock types show that earlier fallout and ignimbrite production from a single vent was followed by eruption of middle and upper parts of the ignimbrite from multiple vents along a ring fracture that defined the structural outline of the Long Valley caldera. Sectorial variations in the mixing proportions of rhyolite and trachyte in the composite ignimbrite P1 on Gran Canaria cannot be reconciled with a central vent but require eruption through a ring fissure; there is no associated plinian fall and thus no evidence of previous eruption through a central vent.

During fissure eruptions, activity probably focuses on several sites along the fissure rather than occurring along its whole length. Some ignimbrites have been found not to be associated with any subsidence structure but rather with linear fissures, several to tens of kilometers long, and apparently controlled by regional tectonic fault systems, especially in regions of crustal extension.

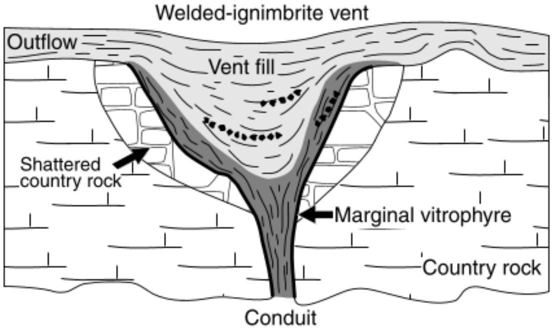

FIGURE 11 Section through a welded-ignimbrite vent showing foliations in marginal vitrophyre and central vent fill and a zone of shattered country rock outside the vent.

Exposed sections through ignimbrite source vents not destroyed by caldera collapse, such as the Gabbs Valley vent in Nevada, are rare but share typical zonation patterns. The vent is roughly funnel-shaped, widening dramatically toward the surface, and is surrounded by a zone of shattered country rock that may be 100 m wide but diminishes with depth (Fig. 11). Inside the vent, a vitrophyric, parataxitic textured zone with foliations (flattened fiamme and flow lineations, local folding) parallel to the wall–rock contact lines the vent walls. The vent interior is filled with welded, devitrified, eutaxitic tuff with more shallowly dipping foliations that may contain zones enriched in lithic lapilli. Deeper into the vent where it narrows, the marginal zones merge to fill the conduit; near the surface, foliation dips decrease and merge with those in the outflow tuff (Fig. 11). Steeply foliated marginal tuff is thought to have agglutinated along the walls during eruption whereas the bowl-shaped interior foliation reflects compaction of vent-filling tuff after eruption.

VI. PRODUCTS OF SECONDARY PROCESSES

A. Compaction and Reworking

The typical concave-up surface of ignimbrite emplaced within valleys or overlying buried pre-eruption valleys is commonly interpreted to result from postdepositional compaction during escape of gas trapped during emplacement and by densification of the grain framework under load and during welding. Such a surface shape, however, may already be present during emplacement when a horizontal velocity gradient across the flow causes marginal portions from an initially deeper flow phase to lag behind and become emplaced next to deposits from a thinner flow tail in the center of the valley. In addition, remobilization and secondary flow down topographic gradients can change the shape of the deposit.

Secondary pyroclastic flows were generated from primary ignimbrite for more than 4 years after the Mount Pinatubo eruption. The secondary pyroclastic flows formed by collapse of primary, largely uncompacted ignimbrite, leaving single or multiple headscarps, and traveled down valleys for up to 10 km in much the same way as did the primary flows. Deposits of secondary pyroclastic flows are up to 10 m thick and almost indistinguishable in structure and composition from the primary deposits, containing basal lithic and topmost pumice segregation layers and lapilli pipes. Discriminating features include moderate fines-depletion and random thermoremanent magnetic polarity of the secondary deposits, which may also overlie epiclastic deposits (e.g., lahars) formed after primary ignimbrite eruption.

Phreatic explosions, which may occur months to years after emplacement, blast craters through pyroclastic flow deposits emplaced on wet ground or trapped water and form laminated to cross-bedded tuff rings on their surface (e.g., at Mount St. Helens).

Heavy rainfall and ice melting on glaciated volcanoes generate floods that easily erode and mix with unconsolidated pyroclastic-flow material to form lahars as, for example, at Mount Redoubt, Alaska. It is often difficult to distinguish primary pyroclastic flow deposits from secondary, reworked material, especially at volcanoes where block-and-ash flow deposits are abundant. Segregation pipes and fragments of charred vegetation are known to occur in secondary, water-reworked deposits, the former due to escape of steam or water and the latter inherited from the primary hot deposit. However, segregation pipes emanating from carbonized vegetation are good evidence for a primary, hot emplacement mechanism, whereas the presence of a vesicular matrix and/or close association with fluvial sediments is indicative of a secondary, wet laharic deposit. In some cases, paleomagnetic techniques (uniformity of magnetization direction, paleotemperature estimates) can also be used to infer a primary or secondary origin.

B. Alteration and Cementation

During slow cooling of pyroclastic flow deposits, precipitation of iron oxides often creates an upper zone of pink color in unwelded deposits, and precipitation of various minerals from vapor phases (predominantly cristobalite, tridymite, and hydrous minerals) can partially to totally fill interstices between particles. Localized degassing channels, or fumaroles, which can be active for many years as vapor formed by interaction between the hot deposit and rain- or groundwater moves up along preferential channels, develop encrustations of vapor-phase sublimates enriched in trace elements.

A common process of alteration and cementation of pyroclastic flow deposits is zeolitization. The assemblage of zeolite minerals (mostly phillipsite, chabasite, and, at a later stage, analcime, but many other zeolites occur), the extent of zeolite cementation, and the distribution of zeolitized zones in the deposit apparently depend on the spatial and temporal variation of water saturation, which, next to external factors, is controlled by the local grain-size distribution (fine-grained, poorly sorted ash is less permeable but, once soaked, retains water longer), although zeolitization zones commonly cross depositional boundaries. Geologic evidence does not support a significant control of emplacement temperature or even magmatic composition on the degree of zeolitization in most pyroclastic flow deposits. Zeolites form from the alkali elements that become mobile during low (i.e., ambient) temperature hydration (Na^+, $K^+ \leftrightarrow H^+$ ion exchange) of volcanic glass by meteoric water.

VII. GENERATION AND TRANSPORT PROCESSES

Having briefly discussed block-and-ash flow formation in Section III, we here focus on the formation of ignimbrites that, based on historic observations, are believed to form by collapse of eruption columns. Eruption modeling provides some insight into physical conditions of pyroclastic flow formation. The high-speed hot pyroclast–gas mixture leaving the vent has a bulk density of the order of 10 kg/m^3 but becomes diluted by entrained air that expands upon heating. Sufficient air entrainment facilitates the formation of a buoyant plinian column of lower than atmospheric density, but eruption conditions such as wider vent diameter limit the efficiency of dilution by entrainment, keeping the mixture denser than air so that it partially or totally collapses back to the surface from the height where initial momentum became exhausted. High mass discharge and wide cross-sectional vent area reduce the collapse height and eventually the pyroclastic mixture may spread sideways shortly above the vent so that the resulting pyroclastic current largely inherits the properties of the mixture at the vent.

However, eruption models are simplified by assuming that the eruption mixture is homogeneous in composition and physical properties across the vent but recent detailed studies of near-vent deposits show that this is not necessarily the case. Column collapse is not irreversible and renewed plinian activity can occur as shown, for example, by multiple flow units intercalated with fallout beds at Laacher See. Furthermore, geologic evidence for simultaneous plinian and ignimbrite-producing activity, such as in the historic 1912 Novarupta and 1991 Pinatubo eruptions and the prehistoric Taupo and Bishop Tuff eruptions, and recent modeling results show that plume buoyancy and collapse are not mutually exclusive. Considering the complexity of natural eruption columns, modeling can only provide a first-order approximation of the initial conditions of pyroclastic currents.

Modeling approaches to pyroclastic density currents employ either a finite-volume, single-pulse release from source or steady-state conditions of maintained material supply during transport. In the first case, the duration of flow generation (or eruption) would be shorter than the duration of lateral transport whereas in the second case, eruption duration would exceed the time needed by the current to reach its runout distance. Eruption durations may range over >3 orders of magnitude from phreatomagmatic discrete explosions through complex collapse patterns of nonsustained eruption columns to more or less continuous long-lived activity and are not simply related to pyroclastic-flow transport times, thus allowing for a wide range of time relationships that must be carefully identified for each deposit and eruption. A pulselike character is attributed to pyroclastic surges derived from instantaneous explosions and to small pyroclastic flows derived from partial column collapse during relatively weak eruptions. At the other extreme, maximum eruption rates of $<10^{10}$ kg/s, limited by viscous magma flow through reasonable conduit dimensions, require eruption durations longer than the transport times of large ($>10^{14}$ kg) ignimbrites reaching about 100 km from source. Some large ignimbrites, however, have been emplaced by a succession of ignimbrite-producing episodes, which may or may not have had a pulselike character, rather than by a single long-lasting eruption.

Much of the present discussion on pyroclastic flow transport relates to whether the presumably low bulk density of the collapsing mixture is maintained for substantial lateral travel distance or the pyroclastic current rapidly deflates to a high concentration mass flow. Generally speaking, deflation will be delayed if the flows are fast and highly turbulent and the grain size is fine. The transport mechanisms of pyroclastic currents are presently being discussed in terms of two extreme models, *dense pyroclastic mass flows* and *dilute pyroclastic suspension currents*, which essentially differ in the factors that control particle support and runout of the flows. None of these models is, as yet, capable of quantitatively predicting both the regional mass distribution and the facies variations of ignimbrites. We will now briefly introduce the physical concepts and then discuss the significance of geologic observations.

The runout of *dense pyroclastic mass flows*, similar to that of avalanches, is controlled by the consumption of initial energy by internal and external friction. A simple (Mohr–Coulomb) model envisions a pyroclastic flow (or avalanche) as a sliding block of some frictional strength that will move on ground slopes $>\theta$ and reach a distance $L = H/\tan\theta$, where H is the height of origin and θ the angle of internal friction of the material. In contrast to cold avalanches, however, H/L ratios calculated for pyroclastic flow deposits (Fig. 12) suffer from poor con-

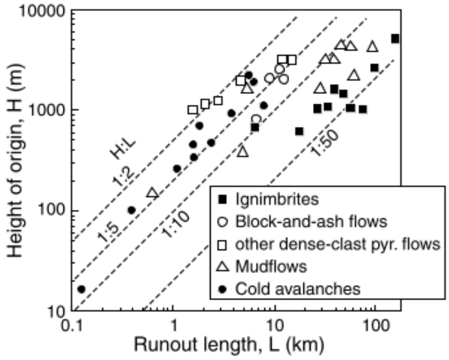

FIGURE 12 Height of origin (*H*) versus runout distance (*L*) of various pyroclastic and other flow deposits. Mudflows have lower *H*/*L* ratios than cold avalanches, and large ignimbrites have lower ratios than small pyroclastic flow deposits, suggesting that both lubrication of the granular material and the mass of flow influence mobility. Note, however, that *H* values for pyroclastic flows derived from column collapse are uncertain.

straints on the value of H; even during observed eruptions, it is almost impossible to determine a specific collapse height as collapse may occur over a height interval. Furthermore, the Mohr–Coulomb model has proved insufficient to reproduce observed pyroclastic flow velocities, and other friction terms, such as turbulent stresses at high speed, need to be included for more successful modeling. The Mohr–Coulomb model also does not consider flow mass, while it is evident that runout length of ignimbrites generally increases with their mass (Fig. 12). Large runout distances require significant reduction of internal friction. The effect of self-lubrication observed in rapid granular flows, where the bulk of material rides on a highly sheared boundary layer, may be applicable to fast pyroclastic flows on steep slopes. Pyroclastic flow mobility may also be enhanced by fluidization, where an upward-moving gas phase partially supports and unlocks particles. The fluidization concept envisions exsolution of magmatic gas from pyroclasts and entrainment of air, preferentially at the flow front, as sources of gas. Hindered settling of grains through trapped interstitial gas may have similar drag-reducing effects. Inertial granular flows should stop dead and be emplaced en masse when shear stresses drop, e.g., upon meeting a flat ground slope. Some block-and-ash flows effectively meet this condition. Effectively viscous, well-fluidized flows with a laminar velocity gradient should smear out their material over the runout length.

The runout of *dilute pyroclastic suspension currents* is controlled by the balance between initial mass flux and pyroclast sedimentation and entrainment of air, which ultimately dilute the current to below atmospheric density, causing it to loft into the air as a co-ignimbrite ash plume. Sedimentation rates depend on grain size and how well pyroclasts are kept in suspension by flow turbulence. Air entrainment depends on the strength of shear at the flow surface and on engulfment at the current's head. It follows from the balance between mass flux, sedimentation, and entrainment that (a) very slow and coarse-grained currents rapidly sediment most of their load near the vent whereas (b) very fast currents quickly dilute by air entrainment and transform into ash plumes carrying a large fraction of the erupted fine pyroclasts, but (c) deep, fine-grained currents at intermediate speed will reach the greatest runout distance. The deposit of a pyroclastic suspension current will of necessity accumulate progressively but, since suspension currents invariably become stratified with higher particle concentration near their base, the depositional process is probably complex and little can as yet be inferred about the resulting bedforms and grain-size characteristics. Studies of the Mount St. Helens May 18, 1980, blast deposit and recent observations during the 1995–1996 eruptions on Montserrat promoted the concept that pyroclastic density currents develop a basal depositional system that controls emplacement conditions and is dynamically distinct from the transport system, which controls overall distribution of the material. Deposit characteristics are then believed to reflect the depositional, but not necessarily the transport, system.

Geologic evidence invoked in favor of one or the other model is mostly ambiguous. For example, how much are massive bedforms with floating pumice, commonly used to imply dense flow, influenced by late-stage motion such as drainage into channels rather than by overall transport conditions? How much dilution is really necessary to produce tractional bedforms, or can dilute currents produce massive poorly sorted beds? Most of what we know about bedform development comes from aqueous systems but it is clear that gaseous systems behave in a very different way because of different viscosity, density, and thermal expansion, so that the value of analogies is fairly limited.

Pumiceous ignimbrite has a bulk density close to that of water and little variation in gas content during flow is required to allow for flow either over or under water. The smaller the density contrast, the more efficient the mixing with water should be and, therefore, dilute currents should travel greater distances across water. These relationships have, however, not been explored quantitatively. Large topographic barriers can be surmounted by dilute pyroclastic currents due to their low density and great depth and by dense pyroclastic flows due to large momentum. Similarly, radial flow patterns little influenced by irregular topography would be compatible with both dilute turbulent or dense high-momentum flows. The suspension-current model predicts that a large mass fraction of erupted material can be emplaced as extensive co-ignimbrite ash. Some co-ignimbrite ash layers subequal in volume to the ignimbrite itself would be difficult to reconcile with elutriation from a dense flow but it has also not yet been shown how these ash layers, except for being time equivalents, physically relate to their associated ignimbrites. Many small channeled pyroclastic flows have clearly been emplaced in an almost en-masse fashion with limited lateral shearing. Other flow units grade laterally into thin widespread ash layers that were clearly emplaced by currents much deeper than the deposits. Thick massive ignimbrites that are continuously compositionally zoned were apparently emplaced by progressive aggradation from sustained currents.

VIII. FUTURE RESEARCH

The deadly and destructive nature of pyroclastic density currents makes their study an important and challenging topic in volcanology. As in the past, most of the relevant information has to be inferred from the resulting deposits. There are still major challenges in the documentation and interpretation of ignimbrites in order to be able to reconstruct the dynamics and timings of their parental currents and eruptions. We suggest that studies of pyroclastic flow deposits should continue to focus on facies transitions in response to topographic and other environmental changes, since these changes are most important in inferring changing transport conditions. In particular, an emphasis on obtaining quantitative data is required, as many of the comparisons, which could be made between deposits, lack a suitable quantitative framework. A number of such studies have been made, but more are needed and should be placed in the context of the general eruption conditions of the volcano investigated. Until quantitative data are available for a variety of examples, modeling scenarios of pyroclastic density currents as a basis for hazard assessment and emergency planning during eruptions are still problematic. In part, this arises from controversies over the different natures and significance of the transport versus depositional processes and the ways in which these are interpreted from deposits. One ultimate goal would be to model these processes as a function of both topography and eruption conditions that can be determined from observations such as magma composition, volatile composition and release patterns, vent configuration(s), and overall eruption dynamics. To advance these approaches, however, a fundamental understanding of the compressible flow dynamics of rapidly moving hot gas–particulate currents is necessary, which requires dedicated experimentation and theoretical approaches.

SEE ALSO THE FOLLOWING ARTICLES

Calderas • Hazards from Pyroclastic Flows and Surges • Lahars • Plinian and Subplinian Eruptions • Pyroclastic Fall Deposits • Pyroclast Transport and Deposition • Volcaniclastic Sedimentation around Island Arcs • Vulcanian Eruptions

FURTHER READING

Carey, S. N. (1991). Transport and deposition of tephra by pyroclastic flows and surges. *In* "Sedimentation in Volcanic Settings," *SEPM Spec. Pub.* **45,** 39–57.

Druitt, T. H. (1998). Pyroclastic density currents. *In* "The Physics of Explosive Volcanic Eruptions" (J. Gilbert and R. S. J. Sparks, eds.), *Geol. Soc. London Spec. Publ.* **145,** 145–182.

Freundt, A. and Bursik, M. I. (1998). Pyroclastic flow transport mechanisms. *In* "From Magma to Tephra: Modeling Physical Processes of Explosive Volcanic Eruptions" (A. Freundt and M. Rosi, eds.), Elsevier, Amsterdam/New York, *Dev. Volcanol.* **4,** 173–245.

Smith, R. L. (1960). Zones and zonal variations in welded ash flows. *U.S. Geol. Surv. Prof. Pap.* **354-F,** 149–159.

Sparks, R. S. J. (1976). Grain size variations in ignimbrites and implications for the transport of pyroclastic flows. *Sedimentology* **23,** 147–188.

Walker, G. P. L. (1983). Ignimbrite types and ignimbrite problems. *In* "Explosive Volcanism" (M. F. Sheridan and F. Barberi, eds.), *J. Volcanol. Geotherm. Res.* **17,** 65–88.

Wilson, C. J. N. (1985). The Taupo eruption, New Zealand, II. The Taupo ignimbrite. *Philos. Trans. R. Soc. London, A* **314,** 229–310.

This Page Intentionally Left Blank

LAHARS

JAMES W. VALLANCE
McGill University

I. Definition and Significance of Lahars
II. Genesis of Lahars
III. Behavior of Lahars: Downstream Processes
IV. Lahar Deposits
V. Physical Modeling

GLOSSARY

bulking The erosion and incorporation of secondary, exotic debris by lahars as they move downstream.

debris avalanche A flowing mixture of debris, rock, and moisture that moves downslope under the influence of gravity. Debris avalanches differ from debris flows in that they are not water saturated and in that the load is entirely supported by particle–particle interactions.

debris flow A water-saturated mixture of debris and water having large sediment concentration that moves downslope under the influence of gravity. Forces related to both solid and fluid phases act together to drive debris flows and determine their distinctive behavior. A fairly uniform mixture of solid and liquid phases in vertical profiles characterizes debris flows and distinguishes them from more water-rich hyperconcentrated flows. The literature suggests a gradational boundary of 50% to as much as 60% sediment by volume separating debris flows and hyperconcentrated flows. Sediment concentration is not definitive because behavior also depends on factors such as sediment-size distribution and degree of agitation.

debulking A process in which the lahar selectively deposits certain particles, owing to their size or density, as it moves downstream. Debulking differs from the general deposition of bulk sediment in preferentially removing particles, usually large or dense ones, from the flow.

granular temperature A measure of degree of particle agitation, usually defined as the ensemble average of the square of the fluctuating components v_s' of instantaneous grain velocities, v_s: $T = \langle v_s'^2 \rangle = \langle (v_s - \overline{v}_s)^2 \rangle$, where $\overline{v}_s$ is the mean velocity component. Granular temperature may be interpreted as twice the fluctuation kinetic energy per unit mass of granular solids.

hyperconcentrated flow A gravitationally driven, nonuniform mixture of debris and water having water content larger than that of debris flow but less than that of muddy streamflow. Some variation with depth of solids fraction characterizes hyperconcentrated flows and distinguishes their behavior from that of debris flows. The literature reports depth-integrated solids concentrations of between 20 and 50–60% for hyperconcentrated flows. Hyperconcentrated flows possess fluvial characteristics, yet carry very high sediment loads.

Copyright © 2000 by Academic Press
All rights of reproduction in any form reserved.

lahar An Indonesian term that most commonly means debris flow, transitional flow, or hyperconcentrated flow originating at a volcano. Though some floods and muddy streamflows are genetically related to lahar events, most are not, and the term lahar is not generally extended to include such flows. Although many workers use lahar for both the process and the deposits that result from it, it is better to restrict the term to the process.

muddy streamflow A flow that essentially transports sediment as normal streams do, with fine-grained sediment in suspension and coarse-grained sediment moving piecemeal along the bed as bedload. Muddy streamflows and floods have smaller sediment concentrations than do hyperconcentrated flows.

phase (of flow) The flow type in a lahar wave at some time and place. Phases associated with lahars include debris flows, hyperconcentrated flows, and muddy streamflows.

stage (of flow) The height above the channel bottom of the flowing lahar. Examples of lahar stages include the initial rising or waxing stage, the peak-inundation stage, and the final long-duration falling or waning stage.

turbulence Chaotic fluid movement [normal to direction of flow], or deviation of flow from laminar. Turbulent flow characterizes streamflows but not debris flows or sediment-rich hyperconcentrated flows.

LAHARS OCCUR DURING volcanic eruptions or, less predictably, through other processes common to steep volcanic terrain when large masses of sediment, and water, sweep down and off volcano slopes incorporating additional sediment. Because lahars are water saturated, both liquid and solid interactions determine their unique behavior and distinguish them from other related phenomena common to volcanoes such as debris avalanches and floods. The rock fragments carried by lahars make them especially destructive; abundant liquid contained in them allows them to flow over gentle gradients and inundate areas far away from their sources. People in such distal areas commonly neither expect the danger nor anticipate the destructive power of lahars.

I. DEFINITION AND SIGNIFICANCE OF LAHARS

A. Historic and Prehistoric Examples of Lahars

Lahars at volcanoes inundate surrounding areas and damage or destroy nearby communities. Torrential rains mobilized loose debris and generated hundreds of lahars after Mount Pinatubo in the Philippines erupted cataclysmically in 1991. Although each of the Pinatubo lahars was relatively small, within 3 years, they cumulatively remobilized nearly 3 of the 10 km^3 of juvenile pyroclastic debris emplaced during the eruption. Filling of downstream channels and overbank flow onto surrounding fields and villages inundated more than 400 km^2 and displaced more than 50,000 people. In contrast, the 1985 pyroclastic eruption of Nevado del Ruiz in Columbia was relatively small (0.01 km^3) but generated much larger lahars (total volume of ~0.1 km^3). The interaction of hot pyroclastic flows or surges and glacial ice and snow at the summit of the volcano caused these lahars. The lahars flowed up to 100 km down four of five drainages that head at the volcano. These were the deadliest lahars worldwide to have occurred during historic time. They destroyed more than 5000 homes and killed more than 23,000 people. In the town of Armero, 73 km downstream of the volcano, virtually all structures in the path of a lahar were obliterated and three-quarters of the inhabitants killed.

Studies of prehistoric lahar deposits indicate the potential for even greater disasters. About 5600 years B.P., the enormous (3.8 km^3) prehistoric Osceola Mudflow from Mount Rainier in Washington state began with a debris avalanche that transformed to a lahar as it deformed [and dilated] because of the enormous volume of water contained in pore spaces and in the volcano's hydrothermal system. It filled valleys from depths of 85 m to as much as 200 m, flowed more than 120 km down valleys, and continued for up to 20 km under the water of Puget Sound while retaining sufficient coherence to transport large gravel and wood fragments. It inundated an area in excess of 350 km^2, which is now populated by hundreds of thousands of people. A large pyroclastic flow that mixed with more than 1 km^3 of glacial ice and snow generated a prehistoric lahar at Cotopaxi in Ecuador that was as voluminous as the Osceola Mudflow. The lahar filled valleys to depths of 80–200 m, flowed more than 300 km to the Pacific Ocean, and covered at least 440 km^2.

B. Purpose

Because the timing of lahar events is unpredictable and working with active flows can be hazardous, much of our present knowledge of flow behavior is inferred from study of lahar deposits. Nonetheless, a few key observational and experimental studies have improved understanding of debris-flow processes. The chief purpose of this article is to summarize what is known about the nature and behavior of lahars on the basis of observations, experiments, and careful examination of deposits and further to describe carefully the nature of deposits derived from such events.

C. Terminology

Lahar is an Indonesian term that most commonly means debris flow, transitional flow, or hyperconcentrated flow originating at a volcano. Muddy streamflows and floods have lower sediment concentrations than do hyperconcentrated flows and essentially transport sediment as normal streams do, with fine-grained sediment in suspension and coarse-grained sediment moving along the bed. Although some floods and muddy streamflows are genetically related to lahar events, most are not, and the term lahar is not generally extended to include such flows. Although many workers use lahar for both the process and the deposits that result from it, it is better to restrict the term to the process.

II. GENESIS OF LAHARS

Lahars may be primary (syneruptive) or secondary (posteruptive or unrelated to eruptions). Lahar genesis requires (1) an adequate water source; (2) abundant unconsolidated debris that typically includes pyroclastic-flow and -fall deposits, glacial drift, colluvium, soil, etc.; (3) steep slopes and substantial relief at the source; and (4) a triggering mechanism. Water sources include pore or hydrothermal water, rapidly melted snow and ice, subglacially trapped water, crater or other lake water, and rainfall runoff.

A. Lahars Induced by Sudden Melting of Snow and Ice, Voluminous Floods, or Torrential Rains

Floods of water moving across the easily erodible loose clastic sediments common on the flanks and aprons of volcanoes easily incorporate that debris and may quickly bulk up to form lahars (Figs. 1A and 1B). Bulking is critical to all lahars that begin with sudden water releases. Lahar formation depends on the right mix of readily available sediment and water discharge. If peak-water discharge is huge, the amount of sediment available for bulking may be inadequate and a flood results instead of a lahar. Similarly, when high-discharge flow continues for many hours or even days to weeks, as it can during lake-breakout floods, there is not enough sediment available along the drainage system to form lahars. Lastly, in catchments where there is little or no easily erodible clastic debris or soil material, bulking is retarded, and lahars do not occur.

At volcanoes, lahars induced by sudden water release can occur by four principal means. (1) Pyroclastic flows and surges mix with and rapidly melt glacial ice and firn. Generally, such pyroclastic flows come to rest or nearly do, forming meltwater that then runs off, coalesces, and erodes the pyroclastic debris to form water-rich lahars. The lahars continue to bulk up with volcaniclastic debris, glacial drift, alluvium, and colluvium as they flow downstream so that within a few kilometers to several tens of kilometers they become debris flows. Lahars of this type are considered primary. (2) Eruptions can displace large volumes of crater-lake water that form lahars downstream. Crater lakes, caldera lakes, and volcanically debris dammed lakes can also break out months to years after eruptions. Such delayed breakouts occur when water levels gradually rise and then overtop and rapidly incise fragile debris dams. (3) Subglacial eruptions can form subglacial lakes that eventually break out when a section of the ice cap becomes buoyant and releases the trapped water. Small-scale outburst floods occur as normal glacial processes during periods of ablation. Although huge eruption-driven outbursts cause sediment-rich, water floods called jökulhlaups, small secondary ones commonly bulk up to form lahars. (4) Lahars owing to intense rainfall often occur after pyroclastic eruptions deposit abundant loose debris in the form of pyroclastic-flow or -fall deposits surrounding vents of volcanoes. Lahars of this type are commonly small but frequent in occurrence during rainy periods. Size and frequency of rain-induced lahars may increase in the months or years following the primary pyroclastic eruption and then slowly decrease as drainage networks and vegetation reestablish themselves (e.g., Mount Pinatubo after its 1991 pyroclastic eruption).

Because clay-rich sediment is both uncommon on the flanks or aprons of active volcanoes and resistant to erosion, lahars induced by sudden water release generally appear to be clay-poor (less than about 5% clay/(sand + silt + clay).

B. Edifice- or Flank-Collapse-Induced Lahars

Although most edifice collapses behave as debris avalanches, those with sufficient, widely dispersed, pore and

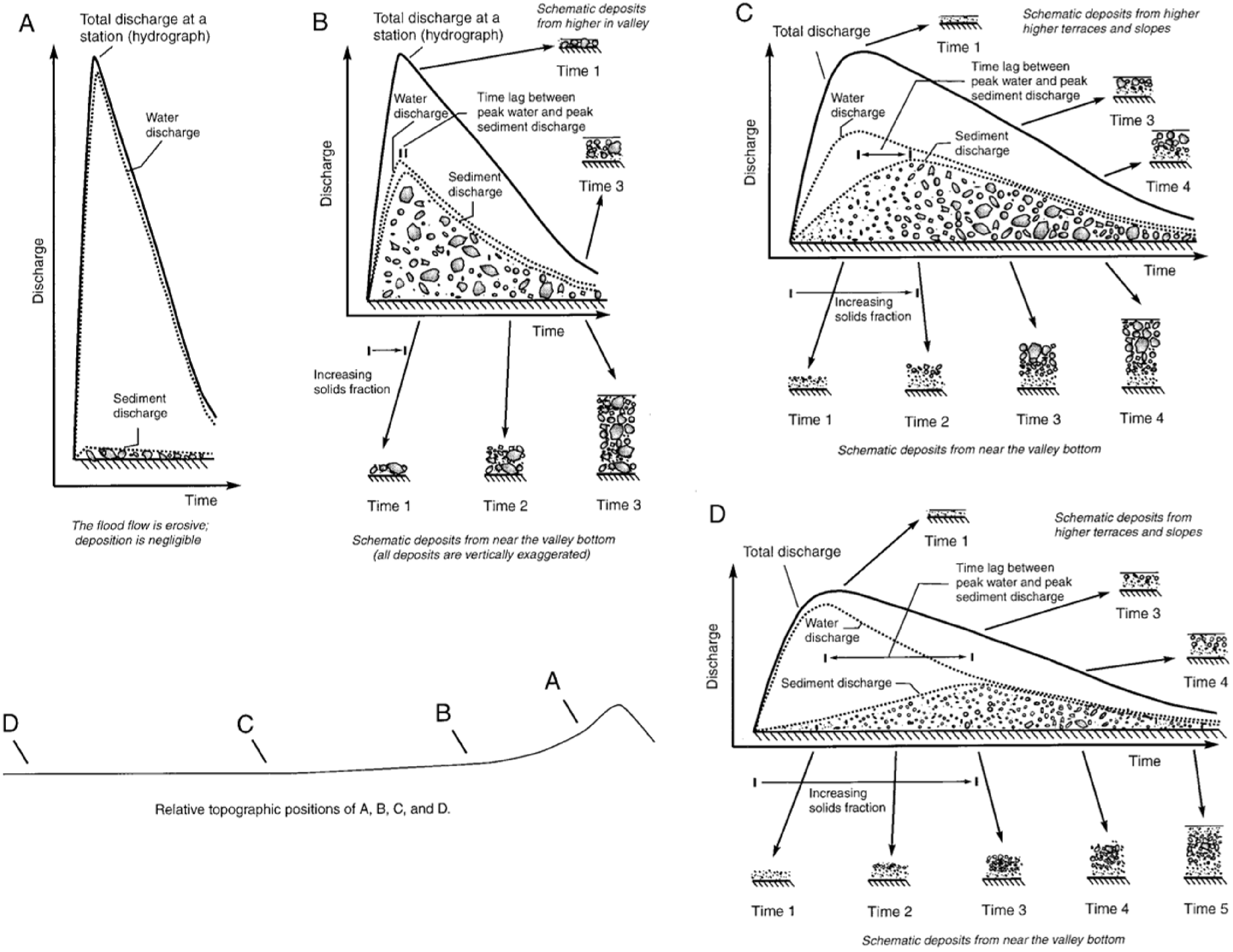
A
Total discharge at a station (hydrograph)
Water discharge
Sediment discharge
Discharge
Time
The flood flow is erosive; deposition is negligible
B
Total discharge at a station (hydrograph)
Schematic deposits from higher in valley
Time 1
Water discharge
Time lag between peak water and peak sediment discharge
Time 3
Sediment discharge
Discharge
Time
Increasing solids fraction
Time 1
Time 2
Time 3
Schematic deposits from near the valley bottom (all deposits are vertically exaggerated)
C
Total discharge
Time 1
Schematic deposits from higher higher terraces and slopes
Time lag between peak water and peak sediment discharge
Time 3
Water discharge
Sediment discharge
Time 4
Discharge
Time
Increasing solids fraction
Time 1
Time 2
Time 3
Time 4
Schematic deposits from near the valley bottom
D
Time 1
Schematic deposits from higher terraces and slopes
Total discharge
Time lag between peak water and peak sediment discharge
Time 3
Water discharge
Time 4
Sediment discharge
Discharge
Time
Increasing solids fraction
Time 1
Time 2
Time 3
Time 4
Time 5
Schematic deposits from near the valley bottom
A
B
C
D
Relative topographic positions of A, B, C, and D.

FIGURE 1 Schematic hydrographs showing how lahars beginning with water floods are initiated and behave when they undergo downstream dilution. Flood phase is shown in A, debris-flow phase is shown in B; and transitional phases are shown in C and D. The diagram also illustrates the progressive-aggradation model of inverse grading in C and D.

hydrothermal water in the precollapse rock liquefy as the material deforms during collapse. The shallow intrusion of magma within an edifice is the likeliest cause of collapse-induced lahars larger than about 0.2 km^3. Smaller collapse-induced lahars may have various triggers, including magmatic or phreatic volcanism and volcanic or tectonic earthquakes.

The process of hydrothermal alteration, especially at glaciated volcanoes, increases the probability of edifice-collapse lahars. Acid-sulfate leaching in hydrothermal systems removes mobile elements, adds sulfate, and breaks down framework silicates to form silica phases, such as cristobalite and opal, and clay minerals, such as kaolinite and smectite. This process weakens the rock so that it more readily disintegrates during deformation after collapse. Thus, huge blocks typical of debris avalanches are less common in lahars of this type even though their origin is the same. Abundant alteration minerals, especially clay minerals, increase porosity and decrease permeability of the rock and thus, in combination with the hydrothermal system, trap a widely dispersed reservoir of water within the precollapse mass. Because of its water content and its tendency to disintegrate, hydrothermally altered rock, unlike fresh rock, easily liquefies as it deforms. Collapse-induced lahars are typically clay-rich, and most are observed to have greater than 5% clay/(sand + silt + clay).

Clay-rich, collapse-induced lahars appear to be more common at ice-clad volcanoes than at volcanoes that are free of ice. Glacial erosion tends to expose deeper, potentially more altered, portions of volcanoes by more effectively incising into an edifice. Further, incised slopes in altered rock are more susceptible to failure not only because the rock is weak but also because it is oversteepened. Lastly, melting glacial ice provides a slow-release source of water that is important to the efficient operation of the acid-sulfate leaching process.

At and near some volcanoes, especially tropical ones, tectonic earthquakes cause multiple slope failures that ultimately coalesce and form collapse-induced lahars. Such lahars are unrelated to volcanism but, owing to characteristics of their deposits (commonly clay-rich, hummocky, and voluminous), can be mistaken for lahars generated by major edifice collapse of hydrothermally altered sectors of volcanoes.

III. BEHAVIOR OF LAHARS: DOWNSTREAM PROCESSES

Lahars can change character downstream. Some floods incorporate enough sediment proximally to become hyperconcentrated flows or debris flows. In medial or distal reaches, debris flows can also transform back to water-rich hyperconcentrated flows or, ultimately, floods. Further, debris avalanches proximal to volcanoes can transform totally to debris flows as they move downstream.

A. Erosion and Bulking

Lahars cause erosion by undercutting steep slopes and terrace scarps and by scouring their beds. Erosion is strongest along steep reaches underlain by loose clastic sediment and weakest either along reaches underlain by highly resistant bedrock or along reaches with very gentle gradients. Along any particular reach, water-rich, hyperconcentrated phases are typically more erosive than sediment-rich debris-flow phases (Fig. 2), but local erosion can occur during any flow phase. The waxing stage of a lahar is likely to coincide with the most widespead and voluminous erosion and bulking. The final waning stages of a lahar are also commonly erosive and ultimately result in the incision of channels in fresh lahar deposits.

Erosion at the base of a lahar occurs by piecemeal dislodgment of particles, by undercutting at upstream migrating knickpoints, and by rip up of sediment owing to root heave of falling trees. The presence of undisturbed, delicate, deposits such as tephra layers at the base of debris-flow deposits suggests that piecemeal erosion of particles occurs chiefly during more water-rich hyperconcentrated phases. Piecemeal erosion is probably not an important process outside of active channels. If channel beds comprise erodible sediment, sequences of upstream migrating knickpoints are common during hyperconcentrated-flow phases. Typically knickpoint steps are a few tens of centimeters to a meter or so high and spaced on the order of tens to hundreds of meters apart. During more sediment-rich flows, knickpoints become higher and more widely spaced. Knickpoints may disappear during debris-flow phases, which, in fact, commonly aggrade rather than erode their beds. Lahars voluminous enough to escape channels knock trees down and incorporate them. Root balls of falling trees drag considerable sediment into the active flow and loosen even more sediment that is then available for erosion. Voluminous lahars that inundate large areas of forested terrain can incorporate considerable quantities of sediment and huge amounts of wood in this way.

Undercutting of steep slopes, fluvial terrace scarps, and active stream banks is probably the most important way in which lahars erode and incorporate sediment.

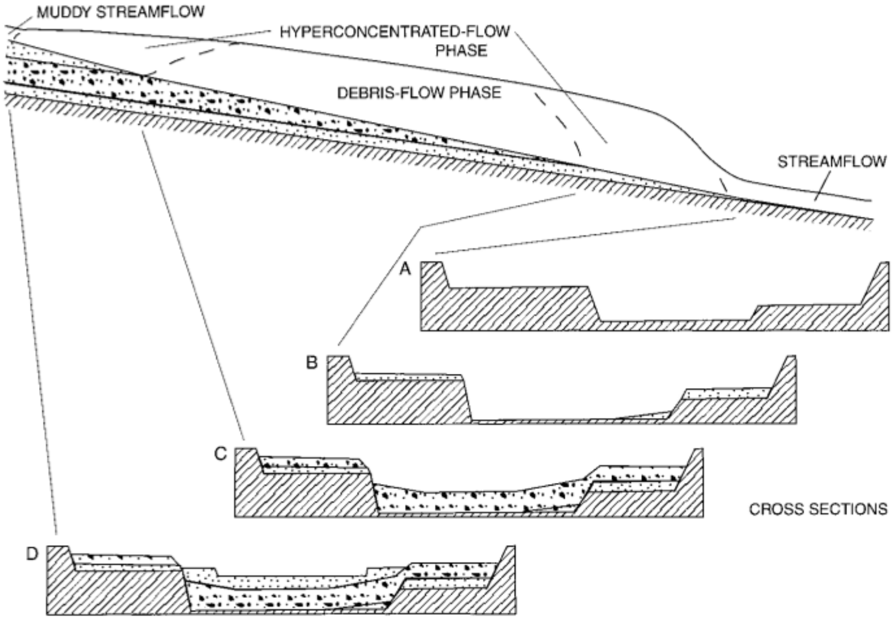

FIGURE 2 Schematic model of a lahar moving down a river undergoing downstream dilution from debris-flow phase to hyperconcentrated-flow phase and deposit facies derived from it [adapted from Fig. 3.31 in Pierson and Scott (1999), "Surficial Hydrological Hazards at Volcanoes," U.S. Geological Survey Open-file Report]. The model shows the expected sequences of hyperconcentrated- and debris-flow deposits in cross section (A–D).

Undercutting is active during both debris-flow and hyperconcentrated-flow phases. Large lahars are capable of incorporating megablocks (>10 m in dimension) of unconsolidated sediment, and sometimes even of bedrock, in this way. Clastic megaclasts may move tens of kilometers downstream before they deform and ultimately break up into individual fragements.

Progressive downstream bulking imposes downstream changes of character on lahars. Bulking transforms flood flows and hyperconcentrated flows to more sediment-rich phases (Fig. 1). If the process continues, both waxing and waning stages of flow ultimately become debris flows. With continued transportation, debris flows become richer in exotic sediment, such as alluvium, colluvium, and glacial drift. Typically, the waxing flow front and following peak stages of the flow are the most erosive and thus most readily incorporate exotic sediment. The sediment-rich falling flow that follows peak flow is less erosive and commonly actively deposits sediment rather than erodes it. The final waning-stage flow is typically more watery, and more erosive, but less voluminous in discharge than the preceding stage. Final waning stages of lahars commonly incise previously deposited laharic sediment.

B. Particle-Size and -Density Segregation Processes

Particles in lahars can effectively segregate by density or size, but the most important segregation processes are mediated by solids fraction, proportion of coarse particles, and fluid density, the latter being determined by the proportion of fine-grained particles in suspension. More dilute flow favors particle settling or buoyant rise because there are fewer particles to hinder these processes. Greater solids fractions hinder these processes and may favor percolation, a process that counteracts preferential settling of large particles. Percolation is a process in which particles, under the influence of gravitational body forces, move downward into gaps that open beneath them. The process occurs chiefly when individual particles influenced by body forces such as gravity rub or collide in vibrating or shearing mixtures.

Particles such as pumice that are less dense than water rise buoyantly. In addition, particles slightly more dense than water rise to the surface of lahars whose fluid phases suspend sufficient fines (generally clay and silt but in some cases fine-grained sand) to increase the effective fluid density. Consequently, low-density particles commonly collect at the surface of lahars and may ultimately form rafts of material that appear to move en masse. Friction at the bed retards lahars and causes vertical profiles in which velocities are smallest at the base and gradually increase upward. Low-density particles will migrate upward toward the surface where velocities are greater than average and will then migrate forward toward flow margins.

Particles that are more dense than the fluid will settle if the solids fraction is not great. In a viscous liquid, large dense particles will have higher terminal velocities and will settle faster than small particles of the same density. Through this process, the largest particles collect in the lowest horizon of the moving flow and progressively smaller particles will collect in horizons above that; thus a normally graded flow develops. If particle concentrations are great enough, particles collide with and rub one another as they settle. Such particle interactions inhibit the settling process.

In shearing or vibrating flows with particles denser than the fluid and with particle concentrations greater than about 40%, percolation predominates rather than settling. In such flows voids periodically open beneath the particles. If the size of a particle is comparable to or smaller than the size of a void, the particle falls down into the void. In a flow with a mixture of grain sizes, the probability is greater that voids of sufficient size will open beneath small particles than will open beneath larger ones. Percolation operates only downward; so in order to preserve vertical mass balance, there must be a process by which particles migrate upward. Force imbalances or particle rotations can push particles from one layer into another. This process, termed squeeze expulsion, can operate either up or down and need not be size preferential. The combination of percolation and squeeze-expulsion processes in shearing or vibrating particle flows is known as kinetic sieving. The net result of kinetic sieving is that small particles migrate downward and displace large ones, and large ones gradually migrate upward. (Readers should note that in granular flows such as lahars, increased dispersive stress corresponds with increased granular temperature or energy dissipation owing to grain collisions and inhibits size segregation rather than promotes it as suggested by Bagnold.) The large particles then migrate forward toward the margins of the flow because velocities are greatest near the surface. The kinetic-sieve process thus not only can cause the inverse vertical grading that is common in moving debris flows but can also cause the accretion of large particles at flow perimeters (Fig. 3).

Waxing flow fronts are commonly the most erosive part of lahars, especially on steep slopes. The debris available to be eroded and incorporated is commonly coarser grained and better sorted (like alluvium, colluvium, or bedrock) than debris in the main body of the lahar and will be preferentially incorporated at the flow front (Fig. 4). This process can enhance or independently form the coarse-grained, better sorted perimeters that are commonly observed in moving debris flows and their deposits.

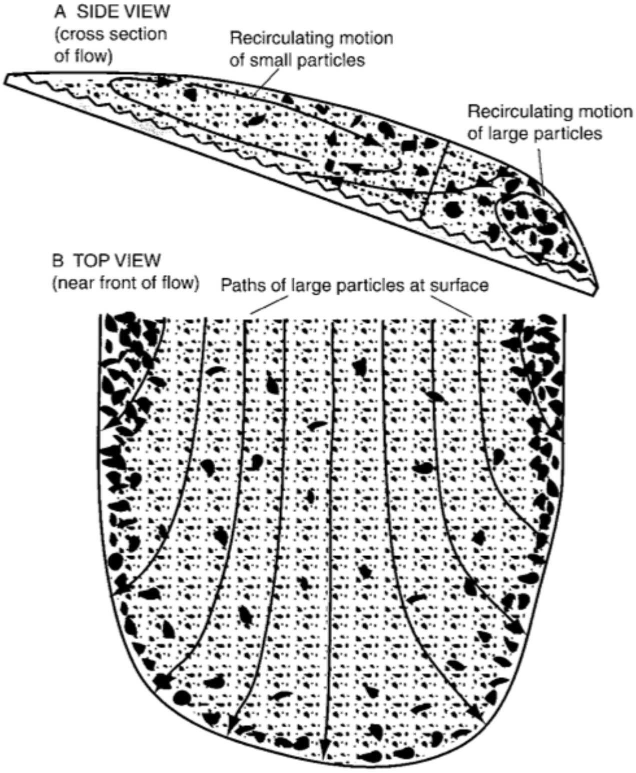
A SIDE VIEW
(cross section of flow)
Recirculating motion of small particles
Recirculating motion of large particles
B TOP VIEW
(near front of flow)
Paths of large particles at surface

FIGURE 3 Schematic diagram illustrating how inverse particle-size segregation results in (A) longitudinally and (B) laterally graded flows.

C. Downstream Dilution and Transformation

The gradual incorporation of water at the front of a lahar flowing down an active stream channel causes progressive loss of carrying capacity and an eventual change in the nature of the flow with distance downstream (Fig. 1). This process is important only in lahars that follow active rivers or other bodies of water. Though dilution of large lahars can occur, the process has little effect on the behavior of lahars so huge that their volumes are

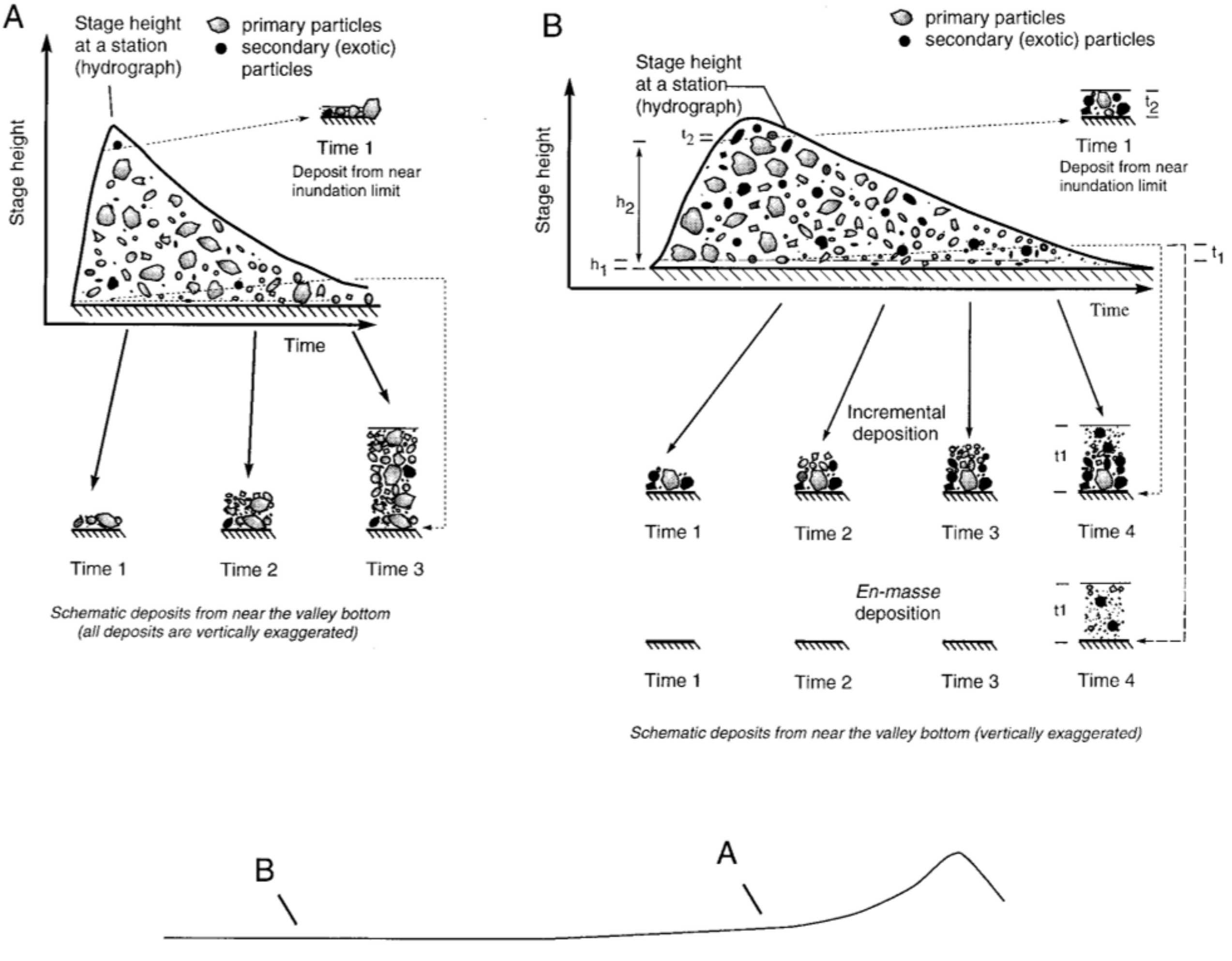
A
Stage height at a station (hydrograph)
primary particles
secondary (exotic) particles
Stage height
Time
Time 1
Deposit from near inundation limit
Time 1
Time 2
Time 3
Schematic deposits from near the valley bottom (all deposits are vertically exaggerated)
B
primary particles
secondary (exotic) particles
Stage height at a station (hydrograph)
Stage height
t_2
h_2
h_1
t_1
Time
Time 1
Deposit from near inundation limit
Incremental deposition
Time 1
Time 2
Time 3
Time 4
t1
En-masse deposition
Time 1
Time 2
Time 3
Time 4
t1
Schematic deposits from near the valley bottom (vertically exaggerated)
B
A

Relative topographic positions of A and B.

FIGURE 4 Schematic hydrographs showing the behavior and downstream changes of lahars that begin as avalanches of water-saturated debris. Note that with distance downstream (A to B), the lahar incorporates secondary exotic particles, especially near its flow front. The diagram (B) also illustrates how an inverse longitudinally graded flow can accrete incrementally to form a normally graded deposit [adapted from Vallance and Scott (1997)]. Exotic particles are most common at the base of normally graded deposits and at inundation limits (B).

significantly greater than that of the water in the river being overrun. The process of downstream dilution occurs more readily in clay-poor lahars than in clay-rich lahars because (i) clay-poor lahars mix more readily with water and (ii) clay-rich lahars are typically much larger.

Once off the flanks of the volcano and confined in river channels, lahars, which typically move faster than normal stream flow, push river water ahead of them and gradually, with distance downstream, begin to mix with that water. As the flow front becomes progressively more watery, it loses its capacity to carry larger gravel particles, and these progressively lag behind the flow front. With time and distance downstream, a dilution front progresses from the front of the lahar to its middle, and eventually the entire lahar becomes more dilute. In lahars that occurred at Mount St. Helens in 1980 and 1982, downstream dilution occurred over the course of tens of kilometers and caused a complete transformation from debris flow to hyperconcentrated flow (Fig. 1D). In medial reaches, the hyperconcentrated-flow phase preceded the debris flow of the lahar because the dilution process began at the flow front and then gradually worked backward toward the tail as the flow migrated downstream (Fig. 1C).

D. Depositional Processes

Emplacement of lahar deposits can occur en masse, by steady incremental accretion, or, most likely, by some intermediate process in which accretion begins and then accelerates, wanes, or does both alternately. Debris-flow deposits are poorly sorted, generally massive, and unstratified. It is common to infer that such massive deposits are emplaced en masse and that they represent a frozen portion of the debris flow itself. In contrast, hyperconcentrated-flow deposits are better sorted, commonly show faint stratification, and hence are assumed to accrete during significant time intervals.

An increasing body of evidence suggests that deposits of both hyperconcentrated flows and debris flows accrete incrementally. Such evidence includes (1) strong alignment of elongate clasts parallel to flow directions or imbrication of such clasts in upstream directions, (2) strong changes in composition of particles with vertical position in outcrops, especially those that are graded, (3) inundation-limit deposits with clast compositions similar to those at the base of thick valley-bottom deposits, (4) marks of peak-flow levels in upland valleys that indicate flow depths 5–10 times greater than deposit thicknesses, (5) abundant evidence of cataclasis (breakage of clasts owing to collisions), and (6) stratification in deposits of transitional or hyperconcentrated flows.

Although rapid deposition of a vertically size-segregated flow can generate normally and inversely graded deposits, incremental accretion of longitudinally size-segregated flow can also be responsible. Because lateral and longitudinal variations in both sizes and compositions of particles commonly occur in moving lahars, accretion from such laterally graded systems during significant time intervals can cause vertically graded deposits. Figure 4B (Times 1 to 5) illustrates schematically how accretion from a debris-flow wave with a concentration of large particles at its front can generate a normally graded deposit. Note that accretion occurs for a short time only near inundation limits where grading does not occur (Time 1–2). The front of a lahar wave that flows down a river becomes progressively more dilute and less capable of carrying larger particles, which lag behind (Figs. 1C and 1D). Therefore, accretion from a dilute debris flow that coarsens from head to tail produces inversely graded deposits (Fig. 1C). Farther downstream, the entire lahar, and especially its flow front, becomes hyperconcentrated so that accretion produces finer grained beds that may be inversely graded or both inversely graded and normally graded (Fig. 1D). Note that deposits in positions higher in the valley may also be graded, but often less obviously so.

Debris flows that do not undergo downstream dilution commonly form cobble–boulder-rich perimeters owing to the size segregation process described above (Fig. 3). The surface of the flow with its concentration of large particles moves faster than the rest of the flow so that cobbles and boulders migrate to the flow front. Once the flow peak has passed at any particular cross section, boulders begin to accrete at flow margins to form coarse levees. Flow fronts, with concentrations of large angular particles, that move onto gentle slopes become progressively drier because water can more easily escape from more permeable coarse-grained flow perimeters than from fines-rich flow interiors. The net result is a dry, frictional, resistant flow perimeter that surrounds a liquefied interior. When flows of this type reach sufficiently gentle slopes, the frictional perimeter slows to a stop and leaves behind a steep-fronted fines-poor margin and a partly liquefied fines-rich interior. Because resistance to flow is greater at the margin than the interior of the flow, bifurcation of the flow into fingers can result as the more mobile fines-rich interior diverts around the more static perimeter.

Avulsion can occur in lowland areas with gentle slopes where sediment-rich portions of lahars accrete and fill the active channel so that its cross-sectional capacity is diminished. When channel capacity is sufficiently diminished, the flow overtops this channel and cuts a new one. In the strict sense, the term applies only to the breaking away and establishment of the new channel, although a precondition for avulsion is accretion during debris-flow phases of lahars.

E. Two Spectra of Downstream Behavior

Edifice-collapse-induced lahars are debris flows that transform directly from avalanching debris that contain enough water to become water saturated upon deformation. Such lahars commonly contain large megaclasts composed of relatively fresh volcanic rock from the edifice. As they migrate downstream, they incorporate exotic debris, especially at their flow fronts (Fig. 4). Because of their size, avalanche-induced lahars [generally] rarely undergo complete transformation to hyperconcentrated flow as they migrate downstream.

Lahars that begin with water floods can bulk up rapidly to form debris flows or hyperconcentrated flows (Figs. 1A and 1B). If they continue down active river channels, they will gradually incorporate water, become progressively dilute, and undergo transformations to hyperconcentrated flow and muddy streamflow (Figs.

1C and 1D). The flow transformation begins at the flow front and migrates back through the lahar wave as it travels downstream. If lahars of this type occur in arid regions without perennial streamflow, they will bulk up to become debris flows, not undergo significant downstream transformation, and remain debris flows to their termini. Such debris flows will typically develop relatively dry bouldery flow fronts that surround more liquefied interiors.

IV. LAHAR DEPOSITS

A. Characteristics of Deposits

Lahar size, origin, and depositional environment all influence the character of deposits and determine the facies that form. Clay-rich lahar deposits at Mount Rainier reflect deposition solely from debris-flow phases. Such deposits are massive, extremely poorly sorted, and commonly normally graded (Fig. 5). The Osceola Mudflow at Mount Rainier, for example, has proximal and medial hummocky facies that are megaclast rich (Fig. 6). Proximal and medial valley-side facies form thin (0.1–1 m) veneers on steep slopes, and proximal, medial, and distal axial facies form thick (2–20 m) fills with common normal grading in valley bottoms and lowlands. Clay-poor lahar deposits at Mount St. Helens have channel facies, floodplain facies, transition facies, and lahar-runout facies (Figs. 7–10). The last three of these facies reflect downstream dilution of the lahar. Changes in grain size, sorting, and grading are shown schematically in Fig. 7.

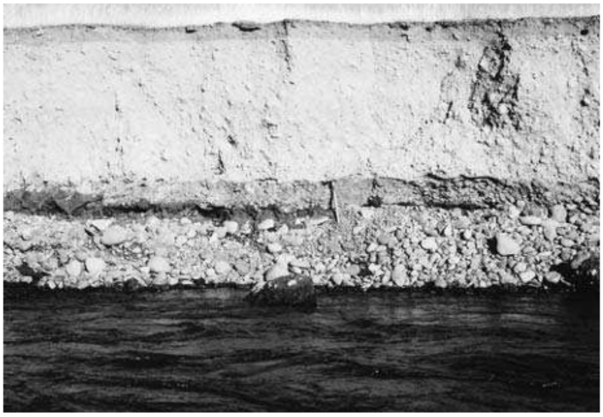

FIGURE 5 Photograph showing normally graded debris-flow deposit. Clay-rich normally graded deposits are common to collapse-induced lahars. A shovel, 60 cm long, is present for scale.

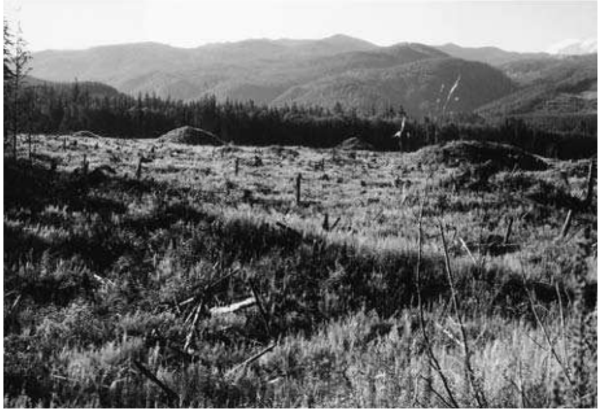

FIGURE 6 Photograph showing hummocks on the surface of an avalanche-induced lahar deposit and, in the upper right, Mount Rainier. Hummocks in foreground are up to 40 m in plan and 10–15 m high. Mount Rainier, 70 km upstream, is the source of the lahar deposit.

In medial reaches, some channel and floodplain facies exhibit unusual basal deposits called sole layers (Fig. 7). Sole-layer deposits are generally fines deficient and contain abundant gravel-size particles that are broken by cataclasis. Unlike other deposits, sole layers apparently accrete during the waxing-flow stages of lahars. Clay-poor lahar deposits not affected by downstream dilution exhibit blunt snouts and prominent lateral levees that contain concentrations of large boulder- and cobble-size clasts (Fig. 11). Deposit interiors are more uniform, massive, poorly sorted, and matrix rich. Deposits left on steep upland slopes typically form thin lags with concentrations of the coarsest, densest particles and a deficiency of matrix.

Generally, lahar deposits may be massive to crudely stratified and graded to ungraded, depending on the proportion of water that the flows contained and the degree of their downstream evolution. Inverse and normal grading, or both in the same outcrop, are common. Sorting is generally extremely poor to poor. Although lahar deposits formed by debris flows, and the hyperconcentrated flows that commonly evolve from them, have some similarities, they have many differences too, and it is necessary to characterize each type of deposit separately.

Debris-flow deposits are massive and very poorly sorted to extremely poorly sorted (greater than 2 Φ units and typically greater than 4 Φ units on the Wentworth scale). Grain-size distributions are commonly bimodal (Fig. 12). They may be normally or inversely graded throughout or, in some cases, can be inversely graded

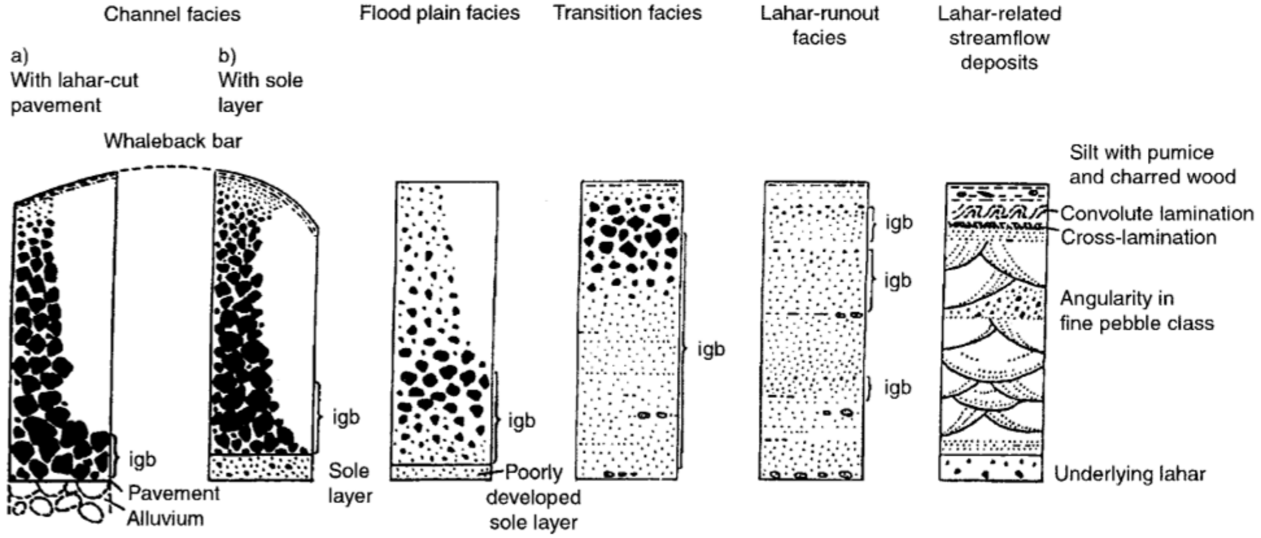
Channel facies
a)
With lahar-cut pavement
b)
With sole layer
Whaleback bar
Flood plain facies
Transition facies
Lahar-runout facies
Lahar-related streamflow deposits
Silt with pumice and charred wood
Convolute lamination
Cross-lamination
Angularity in fine pebble class
igb
igb
igb
igb
igb
igb
igb
Pavement
Alluvium
Sole layer
Poorly developed sole layer
Underlying lahar

FIGURE 7 Schematic portrayal of facies types in lahars (clay-poor type) that undergo downstream dilution and transformation to hyperconcentrated flow [from Scott (1988)].

near their bases and normally graded near their tops. Fabrics generally are weakly developed. Deposits are extremely compact or, in some cases, indurated so that digging in them is difficult. Particles found within lahar deposits can be monolithologic but are more commonly heterolithologic; they can be rounded to angular, but primary particles are usually subangular to angular. Deposits commonly exhibit vesicles in the matrix, which result from entrapment of air bubbles. Other common constituents include wood fragments, casts of wood fragments, and charcoal. Concentrations of coarse particles, especially low-density particles such as pumice, are common at deposit tops.

Thicknesses of debris-flow deposits can vary from tens of centimeters to tens of meters. Thick fill deposits occur in valley bottoms and on lowlands. Deposits on higher terraces and slopes within valleys are thinner

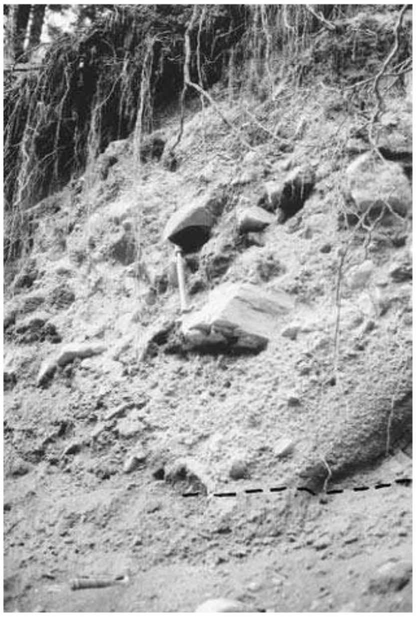

FIGURE 8 Photograph showing clay-poor debris-flow deposit that is inversely graded at its base and both massive and ungraded at its top (dashed line indicates base of deposit). A shovel, 60 cm long, is present for scale.

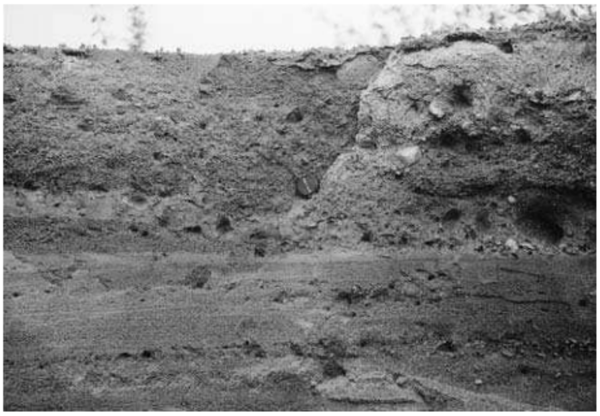

FIGURE 9 Photograph showing faintly stratified hyperconcentrated-flow deposit and overlying transitional debris-flow deposit. A lens cap is present for scale.

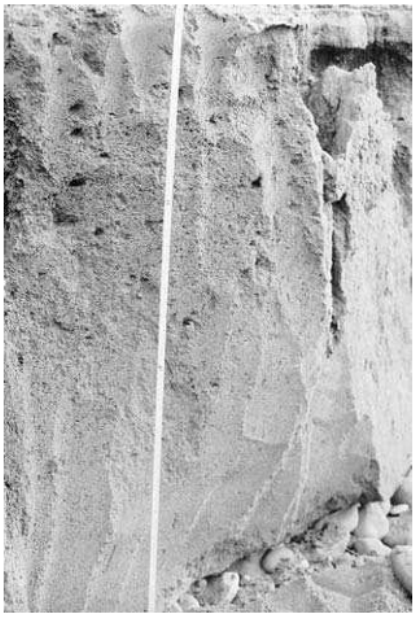

FIGURE 10 Photograph showing hyperconcentrated-flow deposit that is inversely graded in the lowest two-thirds of the outcrop and normally graded in the upper third of the outcrop. Note that the deposit comprises silt, sand, granules, and small pebbles with a single mode of coarse sand and granules. Deposit is about 1 m thick.

than those in valley bottoms, and those on steep slopes will drape underlying topography as thin veneers. Both levees and steep terminal flow fronts are common in the deposits of debris flows relatively unaffected by downstream dilution.

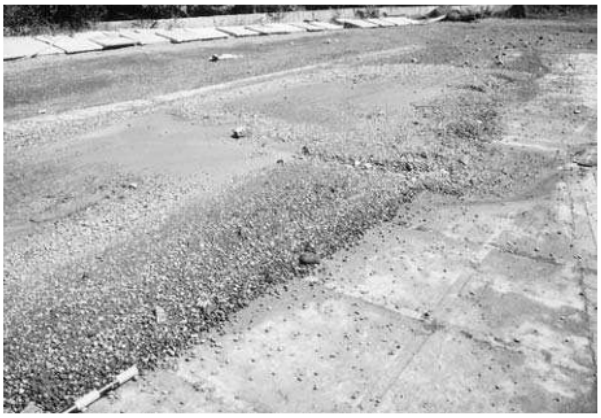

FIGURE 11 Photograph showing coarse-grained lateral levee and terminal snout of an experimental debris-flow deposit. Dimension of grid in foreground is 1 m.

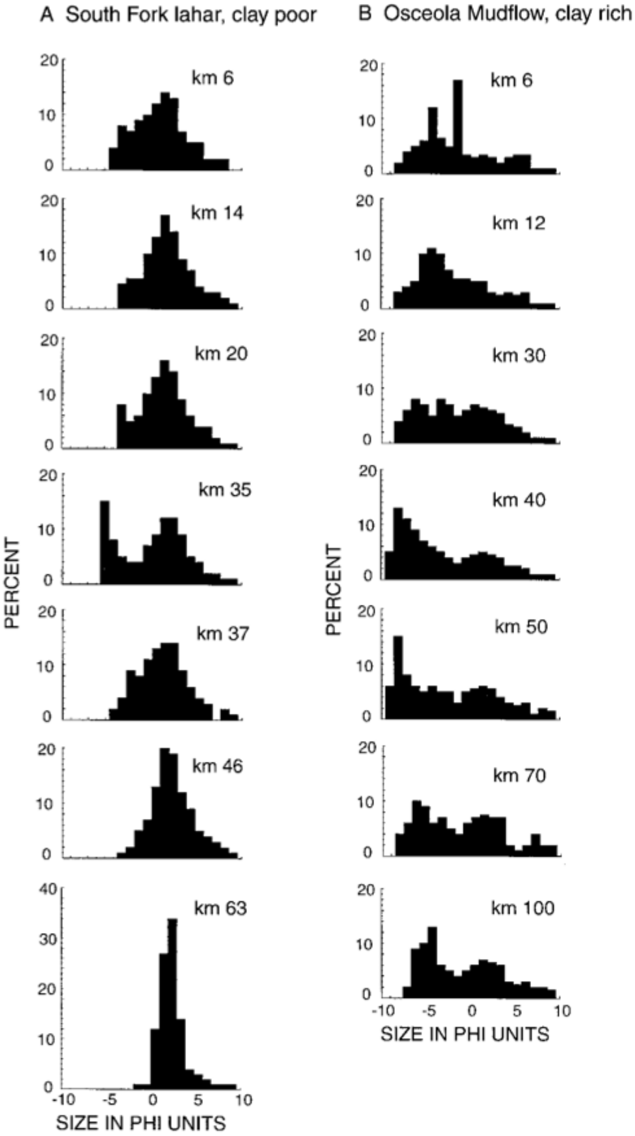

FIGURE 12 Grain-size histograms of (A) clay-poor and (B) clay-rich lahars showing downstream trends [A adapted from Scott (1988); B adapted from Vallance and Scott (1997)].

Hyperconcentrated-flow deposits have characteristics intermediate between debris-flow and alluvial deposits (Figs. 7 and 12). They thus have intermediate sorting coefficients (1–2Φ units) and grain size. They can be massive (Fig. 10) but commonly have weak stratification defined by thin horizontal beds and very low angle cross bed sets composed of fine-grained laminae and thicker coarser grained beds (Fig. 9). Floodplain facies have grain size in the granule, sand, and silt range, with the occasional floating pebble, cobble, or boulder (Fig. 13). If pumice was an important constituent of the flows, zones of nearly 100% pumice are commonly present at the tops of overbank deposits. These pumice concentrations result from pumice rafts stranded during falling-stage hyperconcentrated flow. Channel-facies deposits commonly exhibit strong bimodality and clast support, with huge concentrations of cobbles and boulders surrounding the granule–sand–silt matrix (Fig. 13). Fabrics are moderately strong. Vesicles are sometimes present but less obvious than in debris-flow deposits. Deposits are compact and, except for bouldery channel examples (Fig. 13), have a "chippy" quality when dug with a shovel. Though rare, dewatering features such as dish structures (Fig. 14) and pillar structures are sometimes present.

Hyperconcentrated flow deposits have very flat tops and may vary from a few centimeters to several meters in thickness. Thicker deposits occur in channels or other nearby low areas. Thinner deposits occur on higher ground such as floodplains and valley slopes. Flow tops exhibit scattered pebble and larger particles, especially pumice if present; they also commonly have thin layers of fine sand and silt that form during compaction and dewatering.

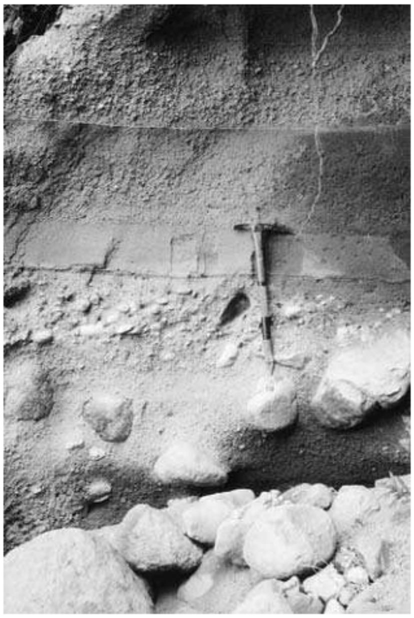

FIGURE 13 Photograph showing transitional debris-flow to hyperconcentrated-flow deposits. The basal unit (at the point of the ice axe) contains floating, rounded cobbles and boulders and probably reflects deposition from a hyperconcentrated flow in a channel.

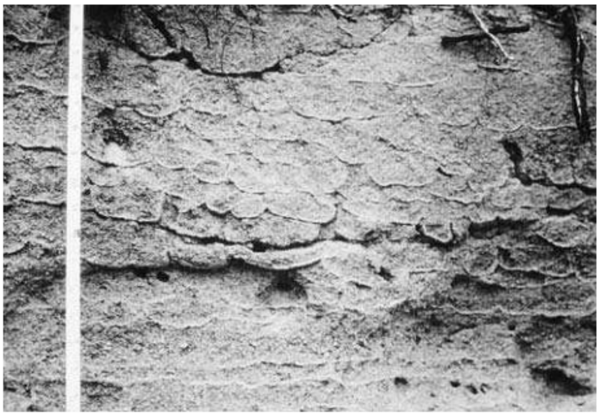

FIGURE 14 Photograph showing dish structure in a hyperconcentrated-flow deposit. The structure evolves during or after deposition owing to dewatering during compaction. Note that the strctures are more strongly inflected toward the top of the unit. Tape measure for scale.

Primary particles in lahar deposits derive from contemporaneous eruptions or, in the case of avalanche-induced lahar deposits, from the original avalanche mass; secondary particles derive from the erosion and incorporation of downstream volcaniclastic debris, alluvium, colluvium glacial drift, bedrock, etc. It is difficult to recognize the provenance of small particles, though it can be done in some instances. Gravel-sized particles can be readily divided into three groups. Angular volcanic rocks derive from the volcano and are generally taken to be primary. Angular secondary clasts derive from exotic colluvium, drift, bedrock, and any other erodible materials along the lahar path. Secondary rounded clasts derive from exotic alluvium, fluvium, or glaciofluvial deposits. Using these criteria (or sometimes unique compositional or textural features of components of the clast population), one can calculate lahar-bulking factors. The lahar-bulking factor for a size fraction (or any other component) is defined as the proportion of secondary particles to secondary + primary particles in that size class. The total bulking factor, which is the bulking factor for all size classes, can be difficult to determine because of the difficulty of measuring lahar-bulking factors for small particles. If there is a size class or another distinctive component that is relatively uniform in proximal deposits and is not present in bulked material, then apparent bulking factors of small particles and total bulking factors can be estimated. The estimated apparent bulking factor is given by the equation

$$\mathrm{ABF} = 1 - (R_f/R_i)(S_i/S_f),$$

where R is the proportion of the reference component (or size class) not affected by bulking, S is the proportion of any other component (or size class) of interest, i indicates proximal (initial) value, and f indicates downstream values. To calculate an ABF total, note that both S_i and S_f have values of 1 and

$$\mathrm{ABF}_{\mathrm{total}} = 1 - (R_f/R_i).$$

Debulking is the selective deposition of a component—generally large or dense particles. If the bulking factor is negative, debulking may be indicated and a debulking factor can be calculated. The debulking factor is defined as the ratio of a component lost through selective deposition to the initial amount of the component. Assessment of debulking factors of large particles is straightforward. For small fractions, a debulking factor can be calculated,

$$\mathrm{ADF} = 1 - (R_i/R_f)(S_f/S_i),$$

where R is the proportion of the reference component not affected by debulking and S is the proportion of any other component (f and i are as before).

B. Distinguishing Lahar Deposits from Other Common Diamictons

No one characteristic serves to distinguish lahar deposits from those of unwelded pyroclastic flows, glaciers, debris avalanches, and local landslides. Unlike lahar deposits, unwelded pyroclastic-flow deposits do not have matrix vesicles, are not indurated, and contain mainly juvenile particles. Carbonized wood and magnetically oriented clasts help to distinguish them from cold lahar deposits (the vast majority) but not necessarily from hot lahar deposits. Unwelded pyroclastic-flow deposits are usually looser and less compact than lahar deposits. Debris-avalanche deposits generally have more irregular surfaces than lahar deposits. Although lahar deposits, especially clay-rich ones, can have hummocks and lateral levees, these features are more prominent in debris-avalanche deposits. Distal and marginal parts of debris-avalanche deposits can be relatively flat and can contain matrix vesicles, but these features are more typical of lahar deposits. Till can be distinguished from lahar deposits if lateral or terminal moraines can be identified. Unlike lahar deposits, till does not contain matrix vesicles, casts of wood fragments, or the wood fragments themselves. Till is also more heterolithologic than most lahar deposits. Landslide deposits generally have more local distribution and more uniform lithology than lahar deposits do. Mapping will distinguish between landslide and lahar deposits.

V. PHYSICAL MODELING

Diverse models have been proposed to explain the behavior of lahars, but there is no convincing evidence that lahars behave according to the assumptions of traditional models. In the absence of evidence to the contrary, it might therefore suffice to model these flows in a unified manner as simple cohesionless grain flows moderated by the influences of diverse grain sizes, sorting processes, varying pore pressure, and varying granular temperature. Any viable model needs to account for significant recent advances in the understanding of granular fluid mixtures. Such advances include recognition that (1) flows of such mixtures are neither steady nor uniform owing to abrupt initiations, flow instabilities, and particle segregation processes; (2) pore pressures in such flows are laterally heterogeneous; (3) the mobility of such flows is often governed by highly fluid interiors with nearly lithostatic pore pressures and resistant coarse-grained perimeters with little or no pore pressure; and (4) there is a gradation from frictional to collisional particle interactions, dictated by the granular temperature.

The Bingham model was developed to describe the behavior of clay slurries and is commonly invoked if a rigid plug is observed or inferred. In its simplest form the model assumes that resistance to flow is the result of viscosity and strength of material:

$$\tau_B = S + \mu \frac{du}{dz},$$

where τ is resisting shear stress, S is the yield strength, μ is viscosity, and u is velocity in the downstream direction. The model assumes a viscous boundary layer and an overriding plug layer but neglects particle interactions such as collisions, frictional rubbing, or segregation. Because cataclasis, rounding, and particle segregation are important in those debris flows with significant gravel fractions (i.e., nearly all debris flows), the Bingham model is incomplete. A simple alternative hypothesis emphasizes particle interactions and explains rigid plugs as the result of particle locking owing to low granular temperature.

A collisional or Bagnold-type model is commonly invoked if inverse grading is observed and if grain collisions are believed important, but Bagnold performed his analysis for a mixture of uniform, neutrally buoyant particles and fluid, and the application of his model to gravity-driven debris flows therefore requires the relaxation of his very restrictive assumptions. Further, high granular temperatures that characterize collisional flow regimes inhibit inverse grading rather than promote it. The resisting stress owing to particle collisions in a shearing granular flow can be simply approximated,

$$\tau_c \sim \nu\rho_s d^2 \left(\frac{du}{dz}\right)^2,$$

where ν is the solids fraction, ρ_s is the solids density, d is the characteristic particle diameter, and $d^2(du/dz)^2$ is proportional to the granular temperature, T. Some authors combine Bingham and collisional (Bagnold type) models to derive a "unified" model. However, the mechanics assumed in the two models are incompatible because collisional models (like that of Bagnold) derive ultimately from particle interactions that the Bingham model does not allow.

A few authors have suggested that lahars, or at least their more dilute phases, can be modeled as gravity or turbidity currents. Models of this type presume very low solids fractions and a consequent lack of particle interactions. Since observations of deposits and eyewitness accounts of lahars refute both of these conditions, gravity–current models are wrongly applied to lahars.

A simple model, in which energy dissipation in the flow includes some combination of Coulomb friction and collisional losses at higher granular temperatures, mediated by viscous pore fluid, appears adequate to explain the behavior of many natural grain flows, including lahars. The resisting stress owing to Coulomb friction can be given in simple form as

$$\tau_f \cong \nu(\rho_s g h - P)\tan(\phi),$$

where g is the gravitational constant, h is the depth from the surface, $\tan(\phi)$ is the friction coefficient, and P, the fluid pressure, is hydrostatic such that $P \sim \rho_f g h$. In large-scale debris-flow experiments, however, $\rho_f g h < P < \rho_s g h$ is common and the flow is thus partly liquefied. (Note that if $P \sim \rho_s g h$, pressure is lithostatic and the flow is completely liquefied such that it will move across even the gentlest gradient.) These experiments further show that P varies with position such that the flow perimeter is commonly not liquefied ($P = \rho_f g h$, or hydrostatic) and the flow interior is approximately 80% liquefied ($P = 0.8\ \rho_s g h$, or close to lithostatic) (Iverson gives a more detailed discussion of this subject).

Variation in P results from the segregation and migration of large particles to flow margins. Concentrations of large particles at flow margins diminish permeability there and thus preclude even short-duration pressures greater than hydrostatic. However, interior parts of flows contain abundant fine-grained particles that greatly decrease permeabilities to such small values that pressures much greater than hydrostatic can be maintained for times greater than the duration of debris flows.

Because lahars are unsteady and nonuniform, owing to particle segregation processes, and, in particular, owing to probable variation in P and other parameters with position in each lahar, no simple mechanical model can be successfully applied to these flows. Numerical analysis can approximate lateral and longitudinal variations that are obviously common in most lahars. A two-dimensional, depth-averaged model can include lateral heterogeneities and gives reasonable predictions of flow shape and runout for a wide variety of conditions. Indeed, such a model can qualitatively explain all observed features of large-scale experimental flows described in Iverson. In the future, modelers may be able to extend models of this type to three dimensions without too many restrictive assumptions or too many troublesome analytical problems.

SEE ALSO THE FOLLOWING ARTICLES

Debris Avalanches • Lahar and Jökulhaup Hazards • Pyroclastic Surges and Blasts • Subglacial Eruptions • Volcanic Lakes

FURTHER READING

Bagnold, R. A. (1954). Experiments on a gravity-free dispersion of large solid spheres in a Newtonian fluid under shear. *Proc. R. Soc. London, Ser. A* **225,** 49–63.

Crandell, D. R. (1971). Postglacial lahars from Mount Rainier volcano, Washington. *U.S. Geol. Surv. Prof. Pap.* **677**.

Iverson, R. M. (1997). The physics of debris flows. *Rev. Geophys.* **35**(3), 245–296.

Pierson, T. P., Janda, R. J., Thouret, J. C., and Borerro, C. A. (1990). Perturbation and melting of snow and ice by the 13 November 1985 eruption of Nevado del Ruiz, Colombia, and consequent mobilization, flow and deposition of lahars. *J. Volcanol. Geotherm. Res.* **41,** 17–66.

Rodolfo, K. S. (1989). Origin and early evolution of lahar channel at Mabinit, Mayon volcano, Philippines. *Geol. Soc. Am. Bull.* **101,** 414–426.

Scott, K. M. (1988). Origins, behavior, and sedimentology of lahars and lahar-runout flows in the Toutle–Cowlitz River system. *U.S. Geol. Surv. Prof. Pap.* **1447-A.**

Smith, G. A., and Fritz, W. J., (1989). Volcanic influences on terrestrial sedimentation. *Geology* **17,** 375–376.

Vallance, J. W., and Scott K. M. (1997). The Osceola mudflow from Mount Rainier: Sedimentology and hazard implications of a huge clay-rich debris flow. *Geol. Soc. Am. Bull.* **109,** 143–163.

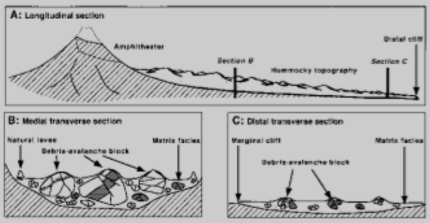

DEBRIS AVALANCHES

Tadahide Ui
Hokkaido University

Shinji Takarada
Geological Survey of Japan

Mitsuhiro Yoshimoto
Hokkaido University

I. Introduction
II. Geomorphic Characteristics
III. Internal Framework
IV. Frequency and Magnitude
V. Eruption Processes
VI. Flow and Emplacement Processes
VII. Examples
VIII. Conclusions

GLOSSARY

amphitheater An arm-chair-shaped landscape formed at the source of a sector collapse. The depth, width, and height of an amphitheater are variable. Amphitheaters associated with a major debris avalanche at composite volcanoes may enclose the summit vent.

debris avalanche The product of a large-scale collapse of a sector of a volcanic edifice under water-undersaturated conditions. The deposit is characterized by two depositional facies, "block" and "matrix." An amphitheater at the source and hummocky topography on the surface of the deposit are characteristic topographic features of a debris avalanche.

debris-avalanche block A fractured and deformed piece of the source volcano included within a debris avalanche deposit. The sizes of single blocks are variable, more than several hundred meters across as a maximum and less than a meter across as a minimum.

debris-avalanche matrix A debris-avalanche matrix is a mixture of small volcanic clasts derived from various parts of the source volcano. This facies is massive, poorly sorted, and made of fragments of volcaniclastic formations and occasionally of fragments of paleosols and plants.

hummocks Characteristic topographic features for debris avalanche deposits. The shape of hummocks is variable and irregular. No overall trend in the alignment of hummocks is found.

jigsaw cracks Jigsaw cracks are characteristic joint patterns within a debris-avalanche block. Jigsaw cracks are typically more irregular than the cooling joints of massive igneous rocks. The joint planes usually remain closed, but many of them open wide due to deformation during the transport of the debris avalanche.

sector collapse A destructive volcanic process during the growth history of a volcano. Debris avalanche deposits are the products of sector collapses.

A SECTOR COLLAPSE of a volcanic edifice produces a debris avalanche. A debris avalanche is triggered typically by intrusion of new magma, a phreatic explosion, or an earthquake. A debris avalanche is generated at water-undersaturated conditions. The

Copyright © 2000 by Academic Press
All rights of reproduction in any form reserved.

deposit is characterized by two depositional facies, the debris-avalanche block and the debris-avalanche matrix facies. The debris-avalanche block facies is composed of large, coherent yet fractured and deformed pieces of the source volcano that formed the debris avalanche deposit. The debris-avalanche matrix facies is a more uniform and fine-grained mixture of volcanic fragments derived from various parts of the source volcano. An amphitheater at the source and hummocky topography on the surface of the deposit are characteristic topographic features produced by a debris avalanche.

I. INTRODUCTION

Debris avalanches are recently recognized volcanic phenomena. One of the recent historical events was when the northern sector of Mount St. Helens collapsed to be emplaced as a debris avalanche deposit in the upper tributary of Toutle River on May 18, 1980. Similar processes were observed and recorded during the 1888 eruption of Bandai in Japan and the 1956 eruption of Bezymianny in Kamchatka. These events were first classified as ultravulcanian eruptions until their true nature was understood. Before the eruption of Mount St. Helens in 1980, most debris avalanche deposits were interpreted as lahar deposits. Some other debris avalanche deposits have been interpreted as pyroclastic flow deposits, lava flows, or moraines, due to the similarities in texture, internal structure, or surface morphology. Scientists from the United States Geological Survey (USGS) analyzed the eruptive processes, flowage, emplacement mechanisms, and depositional structure for the 1980 Mount St. Helens debris avalanche. Other researchers then summarized the general characteristics of debris avalanche deposits. Since this critical eruption, research related to debris avalanches has increased significantly. It is now clear that the formation of debris avalanches is a common phenomenon within the growth history of many composite volcanoes.

II. GEOMORPHIC CHARACTERISTICS

Hummocky topography, natural levees, a marginal cliff, a distal cliff, remnants of temporary river channels, and an amphitheater at the source are characteristic geomorphic features of a debris avalanche deposit (Fig. 1). Hummocky topography is perhaps the most significant geomorphic feature. The shape of individual hummocks is variable and irregular (Fig. 2A). Although parallel alignments of the long axes of hummocks have been described in some deposits, no consistent overall trend has been observed. The volume and height of hummocks are larger in the proximal to medial part of the deposit and decrease toward the distal end. Some glacial terminal moraines show a similar topographic expression. Due to irregularity in form and composition, it is often

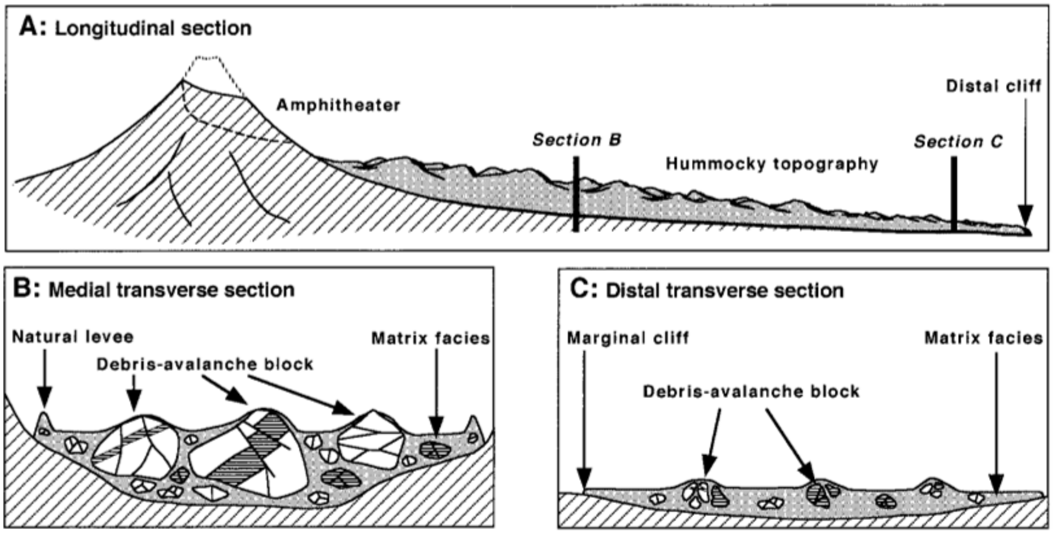

FIGURE 1 Schematic section for a debris avalanche deposit: (A) a longitudinal section stretching from the source amphitheater to the distal end; (B) a transverse section of the medial region; (C) a transverse section for the distal region. Size of hummocks gradually decreases toward the distal area. Debris-avalanche blocks are smaller and scarce at the distal area.

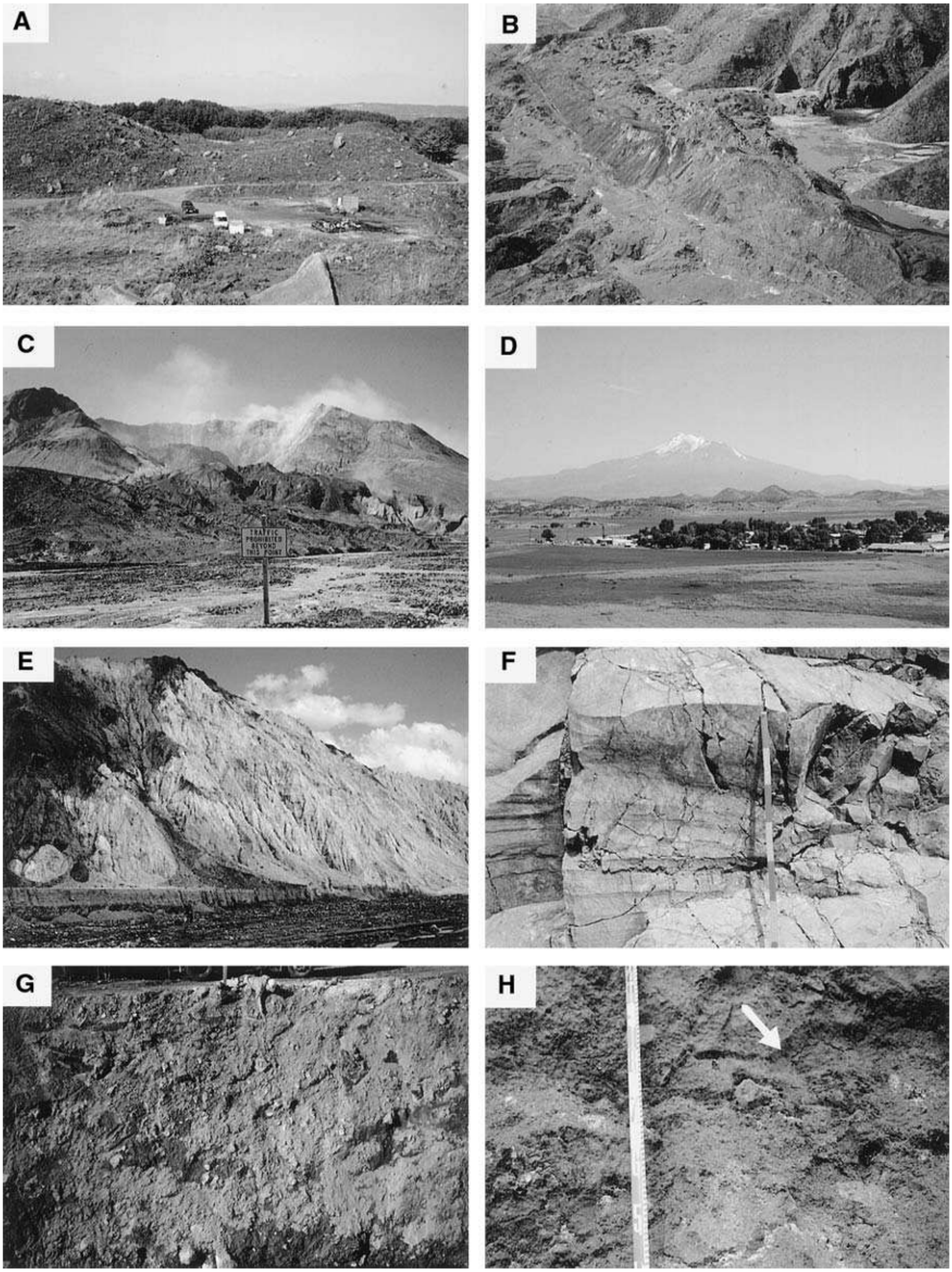

FIGURE 2 Photographs of debris avalanche features: (A) hummocky topography, 466 B.C. Kisakata debris avalanche deposit, Chokai volcano, northern Japan; (B) natural levee in the medial region of the 1980 Mount St. Helens debris avalanche deposit; (C) amphitheater of the 1980 Mount St. Helens debris avalanche; (D) hummocky terrain and a source region already filled with postavalanche volcanic deposits, Mount Shasta; (E) a section of a debris-avalanche block, 1980 Mount St. Helens deposit; (F) a jigsaw crack, Owarabi debris avalanche deposit, Chokai volcano, Japan; (G) a section of debris-avalanche matrix, 466 B.C. Kisakata debris avalanche deposit, Chokai volcano, northern Japan; (H) deformed soft soil fragments (arrow) near the bottom contact of the 1792 debris avalanche deposit, Unzen volcano, Japan.

hard to discriminate debris avalanche deposits based on topography alone. Internal depositional features should be examined to confirm the origin of a deposit. Similar undulating topography is also known in the case of small-scale pyroclastic flow deposits. However, their gentle and regularly undulating pattern differs from the hummocky topography of debris avalanche deposits.

Natural levees (Fig. 2B), a marginal cliff, and a distal cliff are other characteristic topographic features in a well-preserved debris avalanche deposit. Natural levees have been described that rise 40 m above the debris avalanche deposit at Socompa Volcano, in northern Chile. A well-preserved example of a natural levee is the 1792 debris avalanche deposit of Mayuyama lava dome, Unzen volcano, Japan. Marginal cliffs (Fig. 1) occur at both the 1792 Mayuyama debris avalanche deposit and the Zenkoji debris avalanche deposit of Usu volcano, Japan. The height of marginal cliffs is up to 10 m. The cliffs develop at the lower part of a debris avalanche deposit if it is emplaced on a wide plain. Distal cliffs are a continuation of the marginal cliff at the distal end of the deposit. The height of the distal cliff at the nonvolcanic Blackhawk Landslide, California, is about 20 m.

Remnants of temporary river channels are left on the surface of the valley-filling debris avalanche deposits. Typical examples of this are seen at the Kisakata debris avalanche of Chokai volcano and the Nirasaki debris avalanche of Yatsugatake volcano in Japan. Such phenomena form soon after the emplacement of the debris avalanche. In the case of the 1980 Mount St. Helens eruption, stream capture began just after the emplacement of the debris avalanche and the river channel had stabilized within several years after emplacement of the deposit.

The shapes of the source amphitheaters can vary widely. The amphitheater formed during the 1980 Mount St. Helens debris avalanche is a fairly typical example, showing a U-shaped plan view (Fig. 2C). The floor slopes northward toward the opening (Fig. 1). The initially steep wall of the amphitheater has slumped now to form a lower gradient apron. The growth of a central lava dome partially has filled the amphitheater (Fig. 2C). Ultimately, lava flows and dome growth will fill the amphitheater as seen at Mount Taranaki in New Zealand and Mount Shasta (Fig. 2D) and Mount Rainier in the United States. Amphitheaters can also be formed by relatively small-scale debris avalanches on the outer slope of a volcanic edifice, as in the case of the 1792 Mayuyama debris avalanche at Unzen volcano. These amphitheaters show relatively wide angles and shallow depths.

III. INTERNAL FRAMEWORK

The internal framework of debris avalanche deposits comprises debris-avalanche blocks and a debris-avalanche matrix. Debris-avalanche blocks are surrounded by a debris-avalanche matrix. Fracture patterns and fault displacement in debris-avalanche blocks, heterogeneity in the debris-avalanche matrix, and paleomagnetic evidence are clues to the mode of emplacement.

A. Debris-Avalanche Blocks

Most debris-avalanche blocks are fragments derived from the source volcano (Fig. 2E). These blocks are fractured and deformed but preserve many of the primary textures and geologic structures of the source volcano. Some debris-avalanche blocks are fragments eroded from the ground surface during transportation of the avalanche. The size of such debris-avalanche blocks is generally not so big as the blocks derived from the source volcano. The maximum measured diameter for a debris-avalanche block is 280 m in the Mount Shasta debris avalanche deposit. The diameter of smaller debris-avalanche blocks may be less than 1 m. Fracture patterns called jigsaw cracks are commonly observed within debris-avalanche blocks (Fig. 2F). Jigsaw cracks within a debris-avalanche block are typically not as regular as the cooling joints of massive igneous rocks. These joint planes usually remain closed, but some of them open widely, due to deformation during transport of the debris avalanche. Conjugated joint patterns can form in the massive part of debris-avalanche blocks, suggesting the existence of local compressive stresses. Jigsaw cracks are common within debris-avalanche blocks formed from massive lava flows and dikes and are scarce within debris-avalanche blocks made of volcaniclastic materials. The frequency of jigsaw cracks depends on both the rock type and travel distance.

Some debris-avalanche blocks show minor fault displacements (Fig. 1). The paleomagnetic orientations of samples collected from a single debris-avalanche block are often nearly uniform. However, the declination varies between debris-avalanche blocks and differs from that of the source volcano. This implies that initial avalanche material split into many pieces and the rotation of large (>ca. 10 m) debris-avalanche blocks is only about an axis perpendicular to the ground surface. There is little or no rotation parallel to the ground surface.

B. Debris-Avalanche Matrix

The debris-avalanche matrix consists of a mixture of smaller volcanic fragments derived from various parts of the source volcano (Fig. 2G). No jigsaw cracks develop within the debris-avalanche matrix. The paleomagnetic orientation of clasts in the matrix is random. This suggests that the debris-avalanche matrix is formed by the collision and fragmentation of debris-avalanche blocks. Fluvial gravels, soil layers, and basement rocks are eroded and mixed with the primary debris-avalanche matrix material during flowage. The abundance of such exotic material logarithmically increases with distance away from the source. Hummocks are mainly made of huge debris-avalanche blocks and surrounded by the debris-avalanche matrix. Smaller (<ca. 2 m) debris-avalanche blocks float within the debris-avalanche matrix (Fig. 1). The lithology of the debris-avalanche matrix is variable even within a large exposure scale.

The lithology within a few meters of the basal contact of a debris avalanche deposit differs from that of the other parts of the deposit. Fine-grained material is more abundant and large debris-avalanche blocks are not present. Deformed soft sediments are common near the basal contacts (Fig. 2H). This reflects higher shear strains at the base of flows.

"Block facies" and "matrix facies" are terms used to define mappable areas of a debris avalanche deposit. In the block facies many debris-avalanche blocks are assembled to form hummocky terrain. Matrix facies deposits contain a predominance of debris-avalanche matrix and are topographically flat (Fig. 1).

IV. FREQUENCY AND MAGNITUDE

The largest Quaternary debris avalanche deposit known in the world is the 300- to 360-kyr-old Mount Shasta deposit in the United States. The collapse height for the deposit is estimated as 3500 m and the runout distance is at least 45 km. A database for Japanese Quaternary volcanoes includes 71 deposits from 52 volcanoes (Fig. 3) (Table I). The maximum runout distance (*L*) ranges from 1.6 to 32 km, and the maximum collapse height (*H*) ranges from 0.2 to 2.4 km. The ratio *H*/*L* is equivalent to the apparent coefficient of friction during sliding, or the slope of an energy cone for an eruption. *H*/*L* is generally between 0.2 and 0.06. The ratio is generally lower than that of nonvolcanic landslides of similar size. It has been suggested that this greater mobility results either from the presence of fragmented volcaniclastic materials within a volcanic edifice or from phreatic explosions triggered by sudden decrease of the confining pressure at the time of sliding. Another possible cause of lower *H*/*L* is the more common occurrence of weak hydrothermally altered rocks within volcanoes.

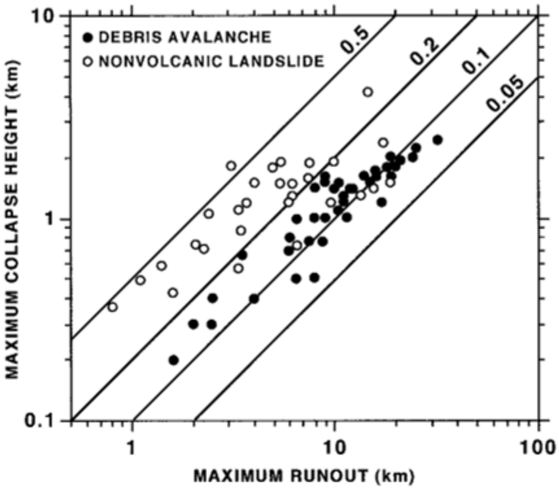

FIGURE 3 Relationship between the collapse height and runout distance for Japanese Quaternary debris avalanche deposits (solid circles) and nonvolcanic landslide deposits (open circles). The ratio of collapse height to runout distance for debris avalanche is generally between 1.2 and 0.06. It is possible to establish hazard zones for future debris avalanches using this ratio.

Some debris avalanches transform during transport to clay-rich lahars and spread more widely than ordinary debris avalanches. The existence of long-runout debris avalanche deposits has been shown at Colima and Citlatépetl volcanoes, Mexico. The source region for the latter is thought to be centered in hydrothermally altered materials in a water-saturated condition. The collapse started in an avalanche manner but transformed to a clay-rich cohesive lahar and moved an unusually long distance, over 120 km away from the source. Collapse height is assumed to be 3–4 km and its *H*/*L* ratio is 0.04. The Osceola Mudflow from Mount Rainier, United States, transformed from a debris avalanche only 2 km away from the source and traveled down to more than 120 km from its origin. The source material included a large volume of pore water and hydrothermally altered rock.

Debris avalanches are common phenomena during the entire growth history of composite volcanoes. The frequency of debris avalanches in the entire Japanese islands is, on average, about once per century. The fre-

TABLE I List of Selected Debris Avalanche Deposits

Volcano	*Deposit*	*Height (km)*	*Length (km)*	*Volume (km^3)*	*Type*	*Source*
Unzen	1792	0.7	6	0.48	U	D
Yatsugatake	Nirasaki	2.4	32	9		S
Tateshina	Otsukigawa	1.4	12.5	0.35		S
Asama	Tsukahara	1.8	20	2		S
Bandai	1888	1.2	11	1.5	Ba	S
Chokai	Kisakata	2.2	25	3.5	Ba?	S
Tashiro-dake	Iwasegawa	0.7	8.8	0.55		S
Komagatake	1640	1.2	15	1.1	Bz	S
Usu	Zenkoji	0.5	6.5	0.3	Ba?	S
Taranaki	Pungarehu	2.6	31	7.5		S
Papandayan	1772	1.5	11	0.14		
Iriga	1628?	1.1	11	1.5		S
Banahao	Lucena and Lucban	1.7	26	5		S
Bezymianny	1956	2.4	18	0.8	Bz	S
Shiveluch	1964	2	12	1.5		S
St. Helens	1980	2.55	24	2.5	Bz	S
Shasta	300–360 kyr B.P.	3.55	50	26		S
Chaos Crags	ca. 1650	0.65	5	0.15		D
Citlaltépetl	Teteltzingo	4	85	1.8	L	S
Colima	Nevado de Colima	4.3	120	22–33	L	S
Socompa	Holocene	3	35	15	Bz	S
Rainier	Osceola	4.7	120	3.8	L	S

Abbreviations: Bz, Benzymianny type; Ba, Bandai type; U, Unzen type; L, long-runout debris avalanche; S, stratovolcano; D, lava dome.

quency of debris avalanches at each composite volcano is less than one per 10 kyr. Older debris avalanche deposits will generally be covered by younger deposits or eroded. Thus the exact frequency of debris avalanche events is often difficult to confirm.

V. ERUPTION PROCESSES

The processes that form debris avalanches are variable. Three types of debris avalanches have been proposed: Bezymianny, Bandai, and Unzen types. Bezymianny-type debris avalanches are associated with magmatic eruptions, as in the case of Mount St. Helens in 1980. The Bandai type is associated with a phreatic eruption, as in the case of Bandai, Japan, in 1888. The duration of precursory phenomena associated with recorded examples is variable. No juvenile material is included within this type of deposit. The Unzen type is not directly related to volcanic activity, but triggered by an earthquake. Another origin for debris avalanches is slumping of a caldera wall during the process of caldera collapse. Major slope failure of oceanic islands also causes submarine debris avalanches.

The collapse process is not always simple as the case of Mount St. Helens in 1980. Two successive collapses creating two separate deposits also occurred during the 1640 debris avalanche of Hokkaido-Komagatake, Japan. In the case of the debris avalanche deposit of Banahao volcano, Philippines, two successive collapses occurred and flowed in different directions in the proximal area but merged into a single flow at the middle to distal area.

A lateral blast accompanied the 1980 Mount St. Helens debris avalanche and the 1956 debris avalanche of Bezymianny volcano. The lateral blasts spread over a much wider area than the debris avalanches and destroyed a large area of forest. A lateral blast did not accompany the 1792 debris avalanche of Unzen volcano.

VI. Flow and Emplacement Processes

More than 20 dynamic emplacement models have been proposed to explain the high mobility of large volcanic and nonvolcanic debris avalanches and many controversies over their emplacement still continue. The air fluidization theory was proposed based on geologic relations of the Saidmarreh, Frank, and Madison debris avalanches as well as on eyewitness accounts of their emplacement. A "hovercraft" mechanism, involving air-layer lubrication, was proposed to explain the long runout and sedimentological and morphological features, for example, preserved intact primary stratigraphy, bulldozed distal ridges, three-dimensional jigsaw-puzzle breccia, distal rims, lateral levees, and transverse ridges and troughs, in the Blackhawk and Sharman debris avalanches, United States. However, the air-layer lubrication mechanism has difficulties in explaining debris avalanches on Mars and the Moon and subaqueous debris avalanches on Earth. A basal gaseous pore pressure model was proposed to explain the rapid velocities and low apparent angle of friction of large coherent debris avalanches using pore fluid vaporization along their bases due to frictional heating during sliding. A basal self-lubrication mechanism is an alternative explanation of the low angle of friction and other characteristic features of the Blackhawk debris avalanche. The Blackhawk debris avalanche bulldozed a distal heap of sandstone ahead of it as it progressed downslope at high speed. The sandstone "breccia" at the front of the flow was "smeared out" beneath the overriding marble breccia, providing a zone of high fluidity beneath the front of the debris lobe (self-lubrication).

A mechanical fluidization model based on the revived idea of grain contact linked with granular flow theory has also been suggested. This assumes the presence of an intergranular fluid and proposes that highly energetic interstitial dust could reduce the effective normal pressure on grains and consequently reduce frictional resistance. For wet debris avalanches, such as the 1970 Huascarán debris avalanche, it is thought that mud could have formed the fluid component between clasts. In the case of large dry debris avalanches, fine dust might act as the interstitial fluid. A combination of mechanical fluidization and sliding on a lubricated substrate model can explain the depositional characteristics of the Sherman Glacier debris avalanche, Alaska. In this case it was thought that the debris avalanche was caused through mechanical fluidization, derived from the vibration and energy of the Great Alaska earthquake. This debris avalanche behaved as a Bingham plastic and its high viscosity prevented turbulence and kept deformation in the avalanche largely confined to shear at the base on glacier ice, so that for the most part, the avalanche slid as a thin flexible sheet.

The acoustic fluidization model has been proposed as a more geologically and energetically acceptable version of fluidization than the dispersive grain flow model. This model suggests that acoustic fluidization is produced indirectly by the released fall energy through the propagation of strong sound waves of just the right frequency through a flowing breccia stream. Acoustic fluidization requires much less energy than mechanical fluidization.

For debris avalanches composed of limestone, notably Films (Switzerland), another lubricated sliding model has been suggested. It is believed that high temperatures developed along a discrete slip surface would continuously dissociate the carbonate rock into a mixture of lime (CaO) and CO_2 gas during travel and the CO_2 gas would provide a lubricant along a basal slip surface.

A mechanical fluidization model in spreading avalanches has been proposed. In this model, the debris avalanche deposits are formed by fluidlike spreading of the debris under the action of gravity, and this spreading occurs due to fluidization of the debris by high basal shear stress as it moves rapidly across the ground. The correlation between volume and the apparent angle of friction is a result of fluidlike spreading of debris avalanches during runout into thin sheets: the larger the volume, the larger the area covered by debris, and the larger the runout length for a given fall height.

A Bingham flow model has been proposed for the Mount St. Helens debris avalanche based on the geomorphology of the Mount St. Helens deposit. The existence of natural levees (Fig. 2B) and marginal and distal cliffs (Fig. 1) suggests non-Newtonian (Bingham) flow behavior. The Bingham flow model has also been used to explain the depositional features and eyewitness of the 1984 debris avalanche, Ontake volcano, Japan. A transport model using initial sliding and later plug (Bingham) flow was proposed after quantitative data were obtained from the Iwasegawa debris avalanche deposit at Tashiro-dake volcano, Japan, and the Kaida debris avalanche deposit at Ontake volcano, Japan.

The granular flow model has also been proposed for the 1980 Mount St. Helens debris avalanche, based on detailed field evidence of the deposit. The granular flow model has also been used for the debris avalanche at Cantal volcano, France, using anisotropy of magnetic susceptibility (AMS) measurements of the matrix fabric. The data suggest transport of the avalanche by liquefied nonturbulent granular flows. Distally, imbricated deposits suggest more turbulent flow. Emplacement of the avalanche results from progressive aggradation of the particles related to a loss of the nonturbulent liquefied stage. The mass of the avalanche becomes a plug flow that exerts strong friction on the basement.

Another model uses basal low-density layers, based on computer simulation of interacting two-dimensional disks. The basal low-density layer is a region where the particles are very active in the sense that they have large random velocity components (high granular temperature). A basal low-density layer supports an overriding high-density, low-mobility debris "plug" during travel. Computer simulations of granular avalanches were performed using from 5000 up to 1,000,000 two-dimensional disks. The model results suggest that the basal friction coefficient varies with shear rate, where higher shear rates give rise to higher friction coefficients. For debris avalanches with a given fall height to particle diameter ratio, debris avalanches with larger volumes have lower internal shear rates, and thus, lower basal friction coefficients.

Another concept is the mass loss model, which suggests the low apparent angle of friction values achieved by debris avalanches occur because they selectively deposit low-velocity material during movement. The ultimate runout length of a debris avalanche traveling by such a mechanism would depend on the rate and timing of the mass loss. In this model, once a debris avalanche reaches a depositional area, material at the trailing end of the moving avalanche begins to deposit, transferring its energy forward to the moving part of the avalanche. The toe of the avalanche continues to move downslope propelled by the input of momentum from decelerating trailing clasts until the stopping wave catches up with the toe.

A seismic energy fluidization model was given for the 1944 Mount Vesuvius block-and-ash avalanches in Italy. In this model the relative importance of seismic tremor to maintaining avalanche mobility is stressed. A basal pressure wave model has also been suggested where a wave propagated along the basal layer at the phase velocity, which is initially greater than the debris avalanche velocity. With increasing avalanche velocity, the avalanche mass catches up with the guided wave. Over a threshold avalanche velocity, a "sonic boom" is generated around the basal layer, and the shock contributes to a loosening of the avalanche mass into a fluidized state.

A biviscous flow model has been used to simulate realistic peak velocities and travel times for the 1974 Mayunmarca debris avalanche, Peru, the 1980 Mount St. Helens debris avalanche, United States, and the 1984 Ontake debris avalanche, Japan. Numerical biviscous modeling indicates that the avalanche at Mayunmarca and avalanche I at Mount St. Helens in 1980 ($H/L \sim 0.2$) were of relatively high strength, with apparent Newtonian viscosities of up to several hundred m^2/s. In contrast, the explosively triggered avalanche II/III flow at Mount St. Helens in 1980 and the Ontake debris avalanche in 1984 ($H/L \sim 0.1$) were of relatively low strength, with apparent Newtonian viscosities 1–2 orders of magnitude lower.

Some combination of these models probably applies in most cases, and each debris avalanche, depending on its composition, cause, volume, and environment, could be simulated by only some of the models listed here.

VII. EXAMPLES

A. 1980 Mount St. Helens (Bezymianny Type)

A swarm of volcanic earthquakes was first detected on March 20, 1980. An initial phreatic explosion occurred on March 27, after 123 years of dormancy. Several phreatic explosions followed and normal faults gradually developed at the summit crater. The north side of the volcanic edifice gradually bulged outward, beginning in early April. Phreatic explosions were repeated and deformation accelerated. A maximum horizontal displacement of 120 m was recorded in the middle of May. Finally, the northern sector of the volcanic edifice collapsed at 8:32 a.m. on May 18. The resulting debris avalanche filled the upper tributary of the Toutle River and traveled up to 28 km away from the source. Its volume was 2.5 km^3. The velocity of the avalanche was about 50–70 m/s, judging from a series of photographs. The collapsing mass was affected by a secondary explosion producing a lateral blast and destroying over 500 km^2 of forest area. The maximum velocity of the blast was assumed to be more than 80 m/s. A plinian eruption followed just after the emplacement of the debris avalanche and a pyroclastic flow of 0.1 km^3 was also emplaced. The climactic eruption was over in the evening of May 18. The total number of fatalities was 57.

Plinian eruptions with pyroclastic flows were produced on several occasions through October 1980 and then a new lava dome began to grow on the floor of the amphitheater. Small-scale explosive eruptions and intrusion of new lobes were repeated until October 1986.

B. 1888 Bandai (Bandai Type)

The first seismic activity began on July 8, 1888. Continuous seismicity occurred almost every day until the morning of July 15. Then a strong earthquake was felt about 7:30 a.m. on July 15. A series of strong earthquakes followed and finally a phreatic explosion occurred at the summit. After a further 15–20 explosions occurred, the northern sector of the volcano collapsed to produce a debris avalanche. The debris avalanche covered an area of 3.5 km^2 and its volume was 1.5 km^3. Small-scale explosions followed 30–40 min after the climactic event. The eruption was over by the evening of the same day. The total number of fatalities was 461.

C. 1792 Unzen (Unzen Type)

A swarm of earthquakes began in November 1791. A magmatic eruption began on February 29, 1792. The volcano produced a dacite lava flow from a vent at the northern slope of Unzen volcano by April 23. Its volume was about 0.03 km^3. A swarm of tectonic earthquakes occurred simultaneously with the discharge of the lava flow. A small-scale collapse of part of a 4000-year-old lava dome, Mayuyama, located 4 km away from the vent of the new lava, occurred on April 9. A second and climactic collapse was triggered by a relatively large tectonic earthquake ($M = 6.4$) on May 21. The avalanche flowed into Ariake Bay and generated a major tsunami. The total volume of the avalanche was 0.48 km^3. The total number of fatalities was 15,190, including 11,000 taken by the tsunami.

VIII. CONCLUSIONS

Debris avalanches constitute an only recently recognized form of volcanic phenomena. Hummocky topography, natural levees, marginal cliffs, and distal cliffs characterize young and well-preserved deposits. An amphitheater at the source is also a characteristic geomorphic feature. The internal framework that characterizes debris avalanche deposits is composed of debris-avalanche blocks and a debris-avalanche matrix. The former comprises large fractured and deformed fragments mostly derived from the source volcano, preserving original internal structures and textures. The latter consists of a mixture of smaller volcanic fragments derived from various parts of the source volcano and mixed with a minor amount of exotic materials.

Three types of link to eruption processes are defined: debris avalanches associated with intrusion of new magma, those associated with phreatic explosions, and those triggered by earthquakes. The ratio of collapse height to runout distance is generally between 0.2 and 0.06. In some cases, clay-rich debris avalanches may transform into lahars and spread over a much wider area.

The eruption and emplacement of debris avalanches are now recognized as common phenomena during the entire growth history of composite volcanoes. However, the transportation process for debris avalanches is not yet fully understood. The frequency of this type of volcanic activity is lower than the other styles of eruption, but the magnitude of single events is generally large and hazardous. Thus, further work, both theoretical modeling and case studies of deposits, is necessary for the mitigation of volcanic risk.

ACKNOWLEDGMENTS

We greatly appreciate valuable comments by Jonathan Dehn, Vincent E. Neall, and James W. Vallance.

SEE ALSO THE FOLLOWING ARTICLES

Composite Volcanoes • Ignimbrites and Block-and-Ash Flow Deposits • Lahars • Plinian and Subplinian Eruptions • Vulcanian Eruptions

FURTHER READING

Campbell, C. S., Cleary, P. W., and Hopkins, M. (1995). Large-scale landslide simulations: Global deformation, velocities and basal friction. *J. Geophys. Res.* **100,** 8267–8283.

Davies, T. R. H. (1982). Spreading of rock avalanche debris by mechanical fluidization. *Rock Mech.* **15,** 9–24.

Goguel, J. (1978). Scale-dependent rockslide mechanisms, with emphasis on the role of pore fluid vaporization. Pages 693–706 *in* "Rockslides and Avalanches 1" (B. Voight, ed.), Elsevier, Amsterdam/New York.

Gorshkov, G. S. (1959). Gigantic eruption of the Volcano Bezymianny. *Bull. Volcanol.* **20,** 77–109.

Shreve, R. L. (1968). The Blackhawk landslide. *Geol. Soc. Am. Spec. Pap.* **108,** 47.

Siebert, L. (1984). Large volcanic debris avalanches: Characteristics of source areas, deposits, and associated eruptions. *J. Volcanol. Geotherm. Res.* **22,** 163–197.

Siebert, L. (1996). Hazards of large volcanic debris avalanches and associated eruptive phenomena. Pages 541–572 *in* "Monitoring and Mitigation of Volcano Hazards" (R. Scarpa and R. I. Tilling, eds.), Springer-Verlag, Berlin/New York.

Siebert, L., Glicken, H., and Ui, T. (1987). Volcanic hazards from Bezymianny- and Bandai-type eruptions. *Bull. Volcanol.* **49,** 435–459.

Takarada, S., Ui, T., and Yamamoto, Y. (1999). Depositional features and transportation mechanism of valley-filling Iwasegawa and Kaida debris avalanches, Japan. *Bull. Volcanol.,* **60,** 508–522.

Ui, T. (1983). Volcanic dry avalanche deposits—Identification and comparison with nonvolcanic debris stream deposits. *J. Volcanol. Geotherm. Res.* **18,** 135–150.

Ui, T. (1989). Discrimination between debris avalanche and other volcaniclastic deposits. *In* "Volcanic Hazards" (J. H. Latter, ed.), *IAVCEI Proc. Volcano.* **1,** 201–209.

Ui, T., Yamamoto, H., and Suzuki-Kamata, K. (1986). Characterization of debris avalanche deposits in Japan. *J. Volcanol. Geotherm. Res.* **29,** 231–243.

Vallance, J. W., and Scott, K. M. (1997). The Osceola Mudflow from Mount Rainier: Sedimentology and hazard implication of huge clay-rich debris flow. *Geol. Soc. Am. Bull.* **109,** 143–163.

Voight, B., Janda, R. J., Glicken, H., and Douglass, P. M. (1983). Nature and mechanics of the Mount St. Helens rockslide-avalanche of 18 May 1980. *Geotechnique* **33,** 243–273.

Site 790
Izu-Bonin island arc
Sumisu Rift
Mariana island arc
Pacific Ocean
West Mariana ridge
Parece Vela basin
Palau-Kyushu ridge
Lau basin
Tofua island arc
30° N
0
30° S
120° E
150°
180°

VOLCANICLASTIC SEDIMENTATION AROUND ISLAND ARCS

Steven Carey
University of Rhode Island

I. Depositional Environments Surrounding Island Arcs
II. Sources and Transport Mechanisms of Volcaniclastic Sediment
III. Depositional Sequences
IV. Volcaniclastic Facies Evolution in Island Arcs
V. Future Research

GLOSSARY

debris flow Dense mixture of particles and water that moves in a laminar fashion downslope under the influence of gravity.

epiclastics Particles formed by the erosion or weathering of preexisting volcanic rocks.

hydroclastics Particles formed by the fragmentation of magma by interaction with external water.

marginal basin Basin located in the backarc area of an island arc that forms by either extension or capture of a piece of oceanic crust.

pyroclastics Particles formed by the explosive fragmentation of magma.

turbidites Deposits produced by sedimentation of particles from a turbidity current.

turbidity current Mixture of particles and water that moves in a turbulent fashion downslope under the influence of gravity.

volcaniclastics Particles formed by the fragmentation of volcanic rocks, irrespective of the method of fragmentation or the nature of the transporting agent.

volcaniclastic apron Wedge-shaped accumulation of volcaniclastic material in the backarc area of an island arc.

ISLAND ARCS ARE arcuate belts of volcanoes linked to subduction of ocean crust into the Earth's mantle. They occur throughout the world's oceans but are especially abundant around the rim of the Pacific Ocean, where they form a nearly continuous belt known as the "Ring of Fire." Volcanic activity at subduction zones produces abundant fragmental material, referred to as volcaniclastics, owing to the explosive nature of the eruptions and the potential for interaction of magma with water. In this article the term volcaniclastic is applied to all clastic material produced by the fragmentation of volcanic rocks, irrespective of the method of fragmentation or the nature of the transporting agent. Pyroclastic is a term applied to particles formed directly from an explosive eruption. Hydroclasts are also particles formed by fragmentation of magma during eruptions but involve the interaction of magma with external

Copyright © 2000 by Academic Press
All rights of reproduction in any form reserved.

water. Finally, epiclasts are particles formed by the erosion or weathering of preexisting volcanic rocks.

The percentage of volcaniclastic material in island arcs is typically in excess of 90% by volume, compared to less than 40% for intraplate oceanic islands, such as Hawaii, and less than 10% for midocean ridges. A majority of the fragmental material produced in island arcs is deposited in the marine environment surrounding the arc as thick sequences of volcaniclastic sediments. The composition, distribution, and facies variations of these deposits are controlled by a complex interplay between the tectonic evolution of island arcs, the rate and type of volcanic activity, and the nature of the transporting processes.

Island arc volcaniclastic sequences are valuable for the reconstruction of the history of volcanic activity associated with plate subduction. Such sequences are often incorporated into continental margins by accretion and constitute an important component of ancient continental crust. In addition, the coarse-grained nature of the deposits and their location in areas of high heat flow make them a potential reservoir for hydrocarbon production if the organic content of the sediments is high enough. Finally, in some arc environments the circulation of high-temperature fluids through these types of deposits provides favorable conditions for the formation of economically important metal ore deposits of copper, lead, zinc, silver, and gold.

Information about the nature of island arc volcaniclastic deposits has come from a wide variety of sources, including drilling in modern arc environments, coring of recent sediments, submersible observations, and the study of ancient uplifted sequences. Deep drilling by the Deep Sea Drilling Project (DSDP) and its successor, the Ocean Drilling Program (ODP), has been especially useful for defining the characteristics, distribution, and facies evolution of arc volcaniclastics in modern and ancient arc environments. This drilling has focused primarily on island arcs of the western Pacific, such as the Marianas, Izu-Bonin, Tonga, and Japan, and provides a wealth of new information concerning these important types of deposits.

I. DEPOSITIONAL ENVIRONMENTS SURROUNDING ISLAND ARCS

A. Structural Elements of Island Arcs

Considerable variability exists among island arcs throughout the world but a generalized model can be adopted for the purposes of defining areas where volcaniclastic sediments accumulate. Subduction of oceanic crust beneath other ocean crust creates a number of distinct depositional environments that trap volcaniclastic sediment derived from various sources in island arcs (Fig. 1). A conspicuous feature of island arcs is a deep sea trench that defines the intersection between the subducting and overriding plates. These trenches can be very deep (up to 11 km), rather narrow, and laterally continuous for hundreds of kilometers. In some cases, trenches are filled with sediment and their bathymetric expression is subdued or obliterated. In others, where sediment supply is low, they contain only minor amounts of sediments and extend to great depths.

Moving toward the volcanic arc, there is a broad fore-

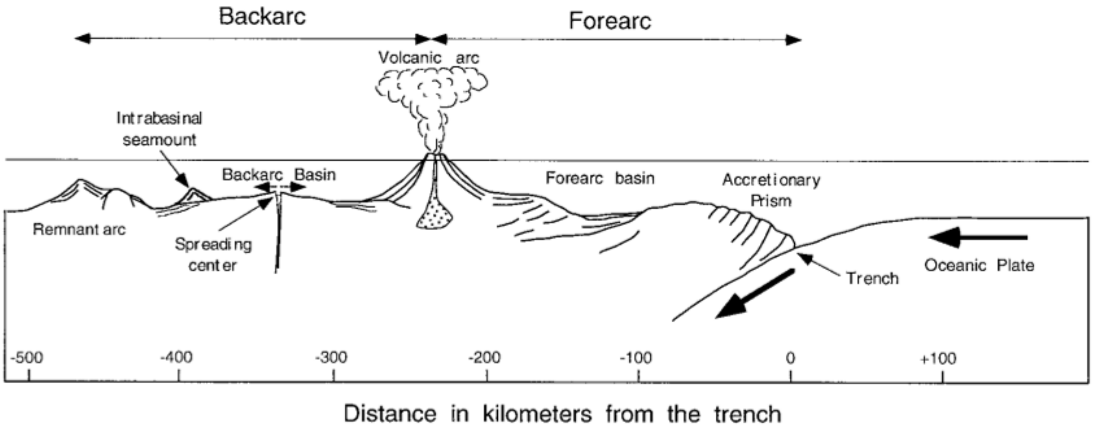

FIGURE 1 Cross section through a typical oceanic island arc showing the major structural components. The arc is subdivided into the backarc and forearc by the active volcanic arc.

arc region that is formed by a combination of the seaward flanks of volcanoes from the volcanic arc and material accreted onto the forearc through the process of subduction (Fig. 1). The accretion of material occurs when the downgoing slab is capped by a sedimentary sequence that can be scraped off as it enters the trench. A decollement typically develops between an upper sequence of sediments that eventually becomes incorporated into the forearc and a lower sequence that continues on beneath the overriding plate. Progressive scraping- off of sediment leads to the development of an accretionary prism, consisting of packages of sediment that are separated from one another by thrust faults (Fig. 1). Each package experiences arcward rotation and uplift. In some cases the uplift is sufficient to raise the sequence above sealevel as a series of nonvolcanic islands in front of the volcanic arc. There are a variety of potential configurations of the forearc area, depending on the supply of sediment to the trench, the extent of scraping off of sediment, and the extent to which the downgoing slab is coupled to the overriding plate. The potential exists to form forearc basins that can trap large quantities of volcaniclastic debris.

The volcanic arc forms the main elevated structural feature of an island arc and consists of an elongate belt of submarine and subaerial volcanic centers where the majority of volcanism takes place (Fig. 1). These centers consist of a core of intrusive/extrusive igneous rocks that record their growth on oceanic crust from deep- to shallow-water conditions and/or emergence as a subaerial edifice. In some arcs small intra-arc basins are developed between volcanic centers and act as traps for coarse-grained volcaniclastic sediment.

A major environment for the deposition of volcaniclastic material in island arcs occurs in the backarc area, where small basins are formed by either (1) backarc spreading (extensional) or (2) trapping of existing segments of ocean crust (nonextensional, Fig. 1). Basins formed by extension show similar characteristics to major ocean basins produced by spreading from midocean ridge systems such as crustal thickness, occurrence of magnetic lineations, basaltic composition, and a layered structure. However, the depths of the backarc basins tend to be deeper compared to typical oceanic basins of similar age.

B. Evolution of Depositional Environments

Island arcs are dynamic systems that evolve tectonically and geomorphically as subduction progresses. Depositional environments change location and size in response to this evolution both in the backarc and in the forearc. In the forearc, the growth of an accretionary prism by accretion of sediments will lead to trenchward extension of the forearc and uplift of forearc basins. Alternatively, tectonic erosion of the overriding plate by the subducting plate may lead to forearc regression and subsidence.

More profound changes occur in the backarc environment of island arcs. Analysis of the history of several western Pacific arcs, such as the Marianas, has revealed that they exhibit a cyclic behavior in the formation of backarc basins (Fig. 2). Initiation of basin formation occurs with rifting of the volcanic arc. Part of the arc becomes inactive and migrates away from the active arc by extension. The inactive segment forms a remnant arc that remains as an elevated, but submerged, ridge. Rifting eventually develops into a spreading center where new crust is generated to feed the growth of the backarc basin. With time, the basin becomes wider and new crust on either side of the spreading center subsides as it cools (Fig. 2). At some point the spreading center migrates far enough away from the active arc that volcanism at the center begins to wane. Rifting then jumps back to the volcanic arc and a new cycle of basin formation begins. The exact cause of the decline is not well understood. Not all arcs exhibit this type of behavior and new rifting can occur either behind or in front of the active volcanic arc. However, the cyclic behavior of backarc basin generation appears to be a common feature of many systems, especially in the western Pacific.

II. SOURCES AND TRANSPORT MECHANISMS OF VOLCANICLASTIC SEDIMENT

A. Subaerial Arc

The principal source of volcaniclastic material to marine basins adjacent to island arcs is the subaerial volcanic arc where the majority of volcanism is focused (Figs. 1 and 3). Explosive fragmentation of magma is a characteristic feature of subduction zone volcanism, with a wide range of compositions being erupted (basalt to rhyolite). Eruption styles vary from small events, such as strombolian, to very energetic eruptions of plinian scale. Large quantities, up to hundreds of thousands of cubic meters, of pyroclastic and/or hydroclastic material can be generated during single eruptions and dispersed over large areas by a variety of transport mechanisms. The main

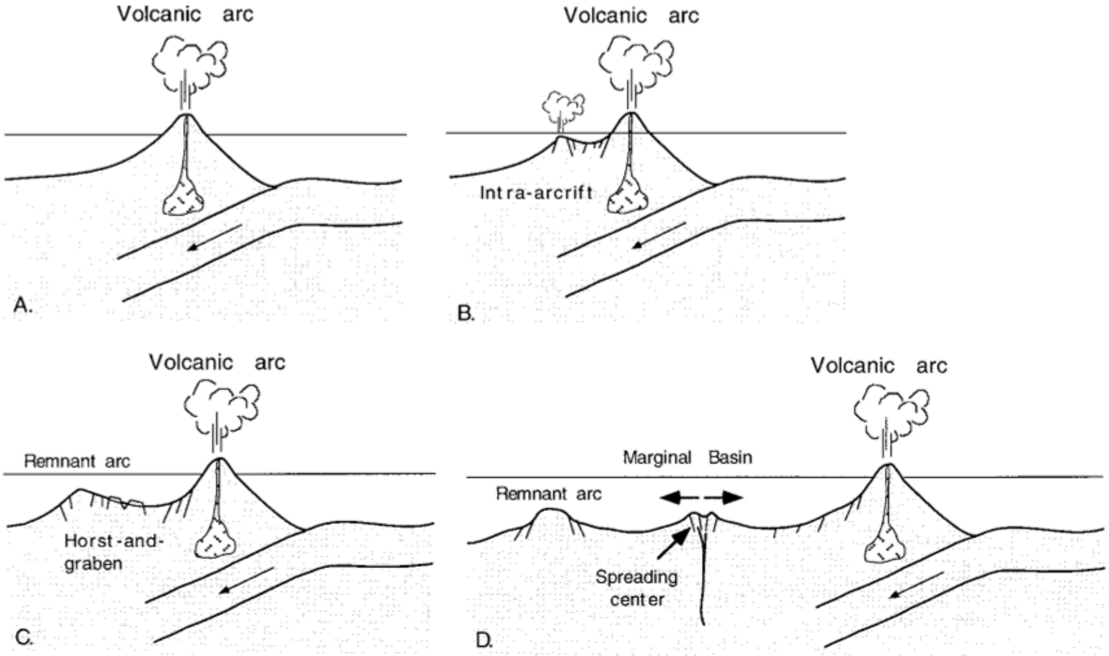

FIGURE 2 Generalized tectonic evolution of an oceanic island arc. A backarc marginal basin is created by rifting of the volcanic arc and the development of a backarc spreading center. The sequence may repeat several times during the history of a single island arc system.

components of this material are (1) pumice and/or scoria (coarse fragments formed by exsolution of dissolved gases from magma), (2) glass shards (fine-grained particles formed by the explosive disruption of magma), (3) crystals (silicate minerals that were growing in the magma prior to eruption), and (4) foreign lithics (pieces of the old volcanic edifice that are ejected during eruption). In general, the compositional variation of material derived from an individual eruption will be restricted and correlation of deposits over a wide area can be accomplished based on geochemical characteristics.

An effective mechanism for dispersal of pyroclastic material into the ocean is by direct fallout from volcanic plumes generated by explosive eruptions. These plumes transport particles and gas high into the atmosphere by thermal convection and are then dispersed over wide areas by the prevailing winds. Fallout of particles from such plumes may extend over thousands of square kilometers and produce a blanket deposit that extends over the entire extent of island arc basins.

Large amounts of pyroclastic material can also be directly discharged into the ocean by different types of pyroclastic density currents generated during explosive eruptions on the volcanic arc (Fig. 3). Pyroclastic flows are hot mixtures of gas and particles that move down the slopes of island volcanoes at high velocity and may discharge directly into the sea. The nature of the interaction between these high-temperature flows (up to 600°C) and seawater is controversial but there is evidence that parts of the flows may continue on underwater and retain high temperatures to form primary submarine pyroclastic flow deposits. In other cases, the flows mix with seawater and are transformed into debris flows or high-concentration turbidity currents. A more dilute form of hot flow, known as pyroclastic surge, can also transport freshly erupted material to the sea. However, the mass transported by surges is usually less than that from pyroclastic flows.

Another important type of flow that can transport large amounts of fresh pyroclastic material to the sea is lahars. These are mixtures of water and pyroclastic material that move as hyperconcentrated flood flow or debris flows. They can be generated during explosive eruptions by rainfall onto freshly deposited pyroclastic deposits on steep volcanic slopes or the ejection of a crater lake by explosive activity. Discharge of lahars along island coasts where river valleys reach the sea produces deltas and turbidity currents that move sediment into deeper water.

It is common for explosive eruptions in island arcs to

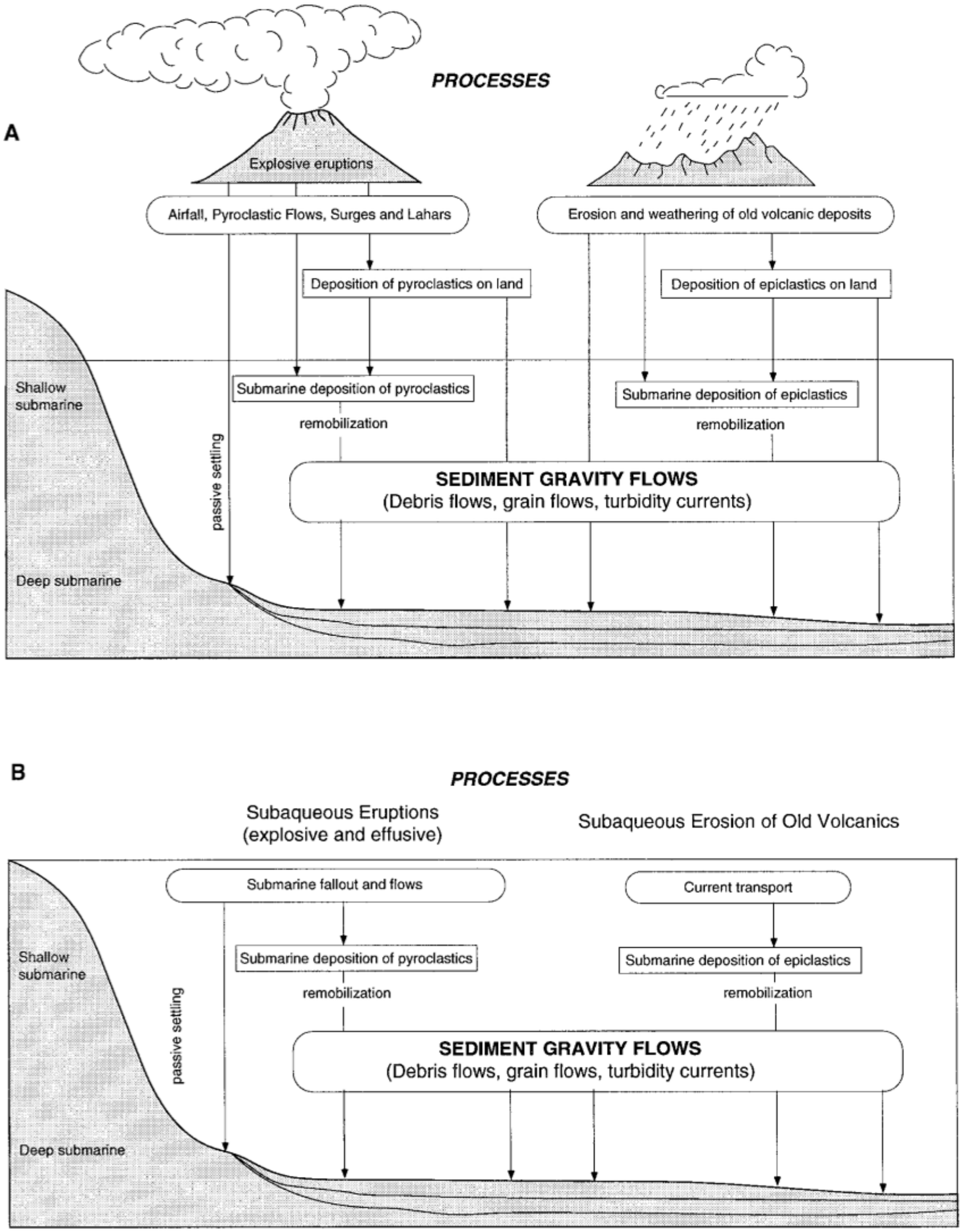
A
PROCESSES
Explosive eruptions
Airfall, Pyroclastic Flows, Surges and Lahars
Erosion and weathering of old volcanic deposits
Deposition of pyroclastics on land
Deposition of epiclastics on land
Shallow submarine
Submarine deposition of pyroclastics
Submarine deposition of epiclastics
remobilization
remobilization
passive settling
SEDIMENT GRAVITY FLOWS
(Debris flows, grain flows, turbidity currents)
Deep submarine
B
PROCESSES
Subaqueous Eruptions (explosive and effusive)
Subaqueous Erosion of Old Volcanics
Submarine fallout and flows
Current transport
Shallow submarine
Submarine deposition of pyroclastics
Submarine deposition of epiclastics
remobilization
remobilization
passive settling
SEDIMENT GRAVITY FLOWS
(Debris flows, grain flows, turbidity currents)
Deep submarine

FIGURE 3 Summary of the sources and transport processes of volcaniclastic sediment in island arcs derived from (A) the subaerial volcanic arc and (B) the submarine volcanic arc.

generate large quantities of low-density pumice. If the density of the clasts is less than the density of seawater, then delivery by fallout or flow can produce thick, extensive rafts of pumice. Eventually all pumice will sink, but some may remain buoyant for several months, allowing for widespread dispersal by ocean currents. The rafts continually lose pumice as they move along, as saturation of smaller pieces takes place and large clasts are broken up by abrasion.

Delivery of freshly erupted pyroclastic material to the ocean occurs episodically during explosive eruptions. Enormous volumes of sediments (100s of km^3) can form during single eruptions in major sedimentation events in adjacent marine basins. The duration of such events can vary widely from a few days to prolonged periods of activity that may span several years. Volcaniclastic material is also supplied to the sea from the subaerial arc on a more continuous basis through the slower erosion of preexisting pyroclastic deposits, lava flows, and other volcanic deposits to form epiclastic particles (Fig. 3). These are delivered by runoff from streams and rivers, aeolian transport by local winds, and slope failure into the sea. The composition of epiclastic material is likely to be more diverse than that of primary pyroclastic material owing to the larger variability of older volcanic deposits that are susceptible to erosion and weathering. Furthermore, deeply dissected volcanic centers may expose plutonic rocks with more diverse compositions, larger crystal sizes, and different mineral assemblages.

B. Submarine Arc

Significant production of volcaniclastic particles also takes place in the submarine environment of a volcanic arc (Fig. 3). Explosive volcanism is limited by the effect of water pressure and studies suggest that it occurs to depths of 200–500 m, and possibly as deep as >1000 m for some gas-rich magmas. Fragmentation by degassing can generate subaqueous eruption columns and submarine pyroclastic density currents consisting of abundant pumiceous material. In addition, the mixing of hot magma with seawater provides an additional mechanism for generating particles by explosive fragmentation. Such phreatomagmatic activity is also limited to water depths of less than a few hundred meters. However, fragmentation of freshly erupted magma can occur even at great water depths as a result of thermal granulation and spallation that takes place during the rapid quenching of magma exposed to cold seawater.

Recent studies of submarine arc volcanoes in the Kermadec arc have led to new insights about volcaniclastic processes operating in these environments. Submarine stratovolcanoes are characterized by fine-scale spatial variability in the distribution of volcaniclastic material, lava flows, and background sediments. Mass movement of material occurs by frequent small-volume debris flows that redistribute material to the lower portions of the edifice. Eruption of submarine lavas is often accompanied by the production of localized pillow breccia. Bottom currents continually rework primary and epiclastic deposits on the submarine slopes of the volcanoes, leaving winnowed and rippled deposits and removing fine-grain material for deposition in deeper water.

C. Backarc Sources

Sources of volcaniclastic sediment in the backarc environment include the remnant arc, the backarc spreading center, and intrabasinal seamounts (Fig. 1). The remnant arc typically represents an inactive protion of an original arc and consequently is not an important source of primary pyroclastic material. However, submarine erosion and weathering of the structure provide a source of epiclastic sediment for adjacent basins. Movement of sediment from the remnant arc occurs primarily by mass wasting, small-scale turbidity currents, and reworking by bottom currents. Downslope movement is likely to be initiated by frequent earthquakes because arcs are seismically very active.

Backarc spreading centers provide a minor source of volcaniclastic sediment by the formation of hyaloclastites associated with the quenching of dominantly basaltic magma. Such deposits of sand-to-silt-sized basaltic glass are usually restricted to the axial spreading zone but can be dispersed to deeper water if strong bottom currents are active. A more important source of volcaniclastic sediment in the backarc is intrabasinal seamounts that form during the early stages of backarc rifting. For example, in the Sumisu rift in the Izu-Bonin arc of the western Pacific, intrabasinal seamounts have been shown to be a source of basic to silicic volcaniclastic sediment for nearby basins. The compositional diversity of magmas from these sources can be large and thus the potential for more explosive types of volcanism is greater.

III. DEPOSITIONAL SEQUENCES

The types of volcaniclastic sequences in island arcs vary greatly depending on their position relative to the arc and the distribution of sediment sources. Deep sea drilling has provided important information about the lithology, thickness, and origin of volcaniclastic deposits within specific arc environments. Furthermore, the drill sites provide a valuable record of the temporal facies changes that occur in different depositional environments. These types of records are critical for building models of sedimentation because the relationships between the depositional sites and their sources are well constrained and facies evolution can be documented. In this section, a series of examples of volcaniclastic sedimentary sequences from each of the major arc environments will be given to illustrate the diversity of these sections and the major processes responsible for their creation.

A. Forearc

Although there are many different potential configurations for a forearc environment, the area east of the Izu-Bonin arc in the western Pacific serves as a good example of the types of deposits that are typical of such areas. ODP Site 792 was drilled in a forearc sedimentary basin about 60 km east of the active volcanic arc in a water depth of 1798 m (Fig. 4). The sedimentary section at this site contains a wide variety of volcaniclastic deposits (Fig. 5). In the upper section (Unit 1) vitric sand and silt layers, usually less than 20 cm thick, are abundant. They consist of fresh glass (mafic and/or silicic) and crystals of orthopyroxene, clinopyroxene, and plagioclase. Some layers show planar laminations and normal

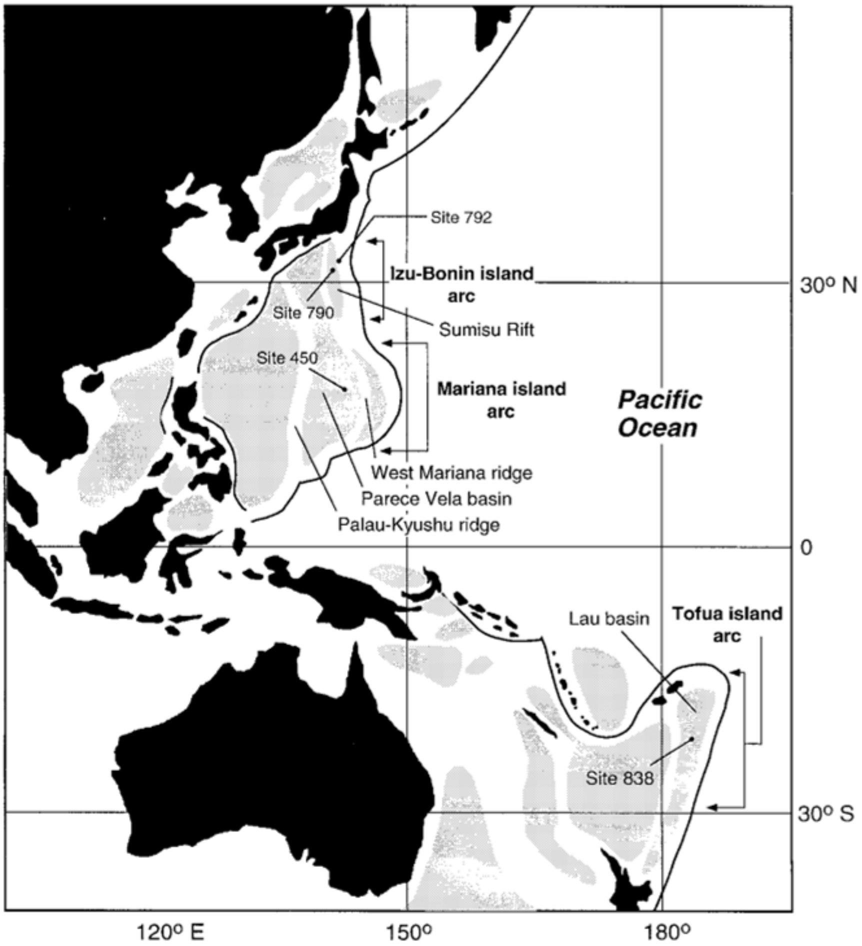
Site 792
Izu-Bonin island arc
30° N
Site 790
Sumisu Rift
Site 450
Mariana island arc
Pacific Ocean
West Mariana ridge
Parece Vela basin
Palau-Kyushu ridge
0
Lau basin
Tofua island arc
Site 838
30° S
120° E
150°
180°

FIGURE 4 Island arc systems of the western Pacific margin. Solid line indicates the trace of the trenches where ocean crust is being subducted. Shaded patterns outline the shape of backarc basins. Drill sites are shown as small solid circles.

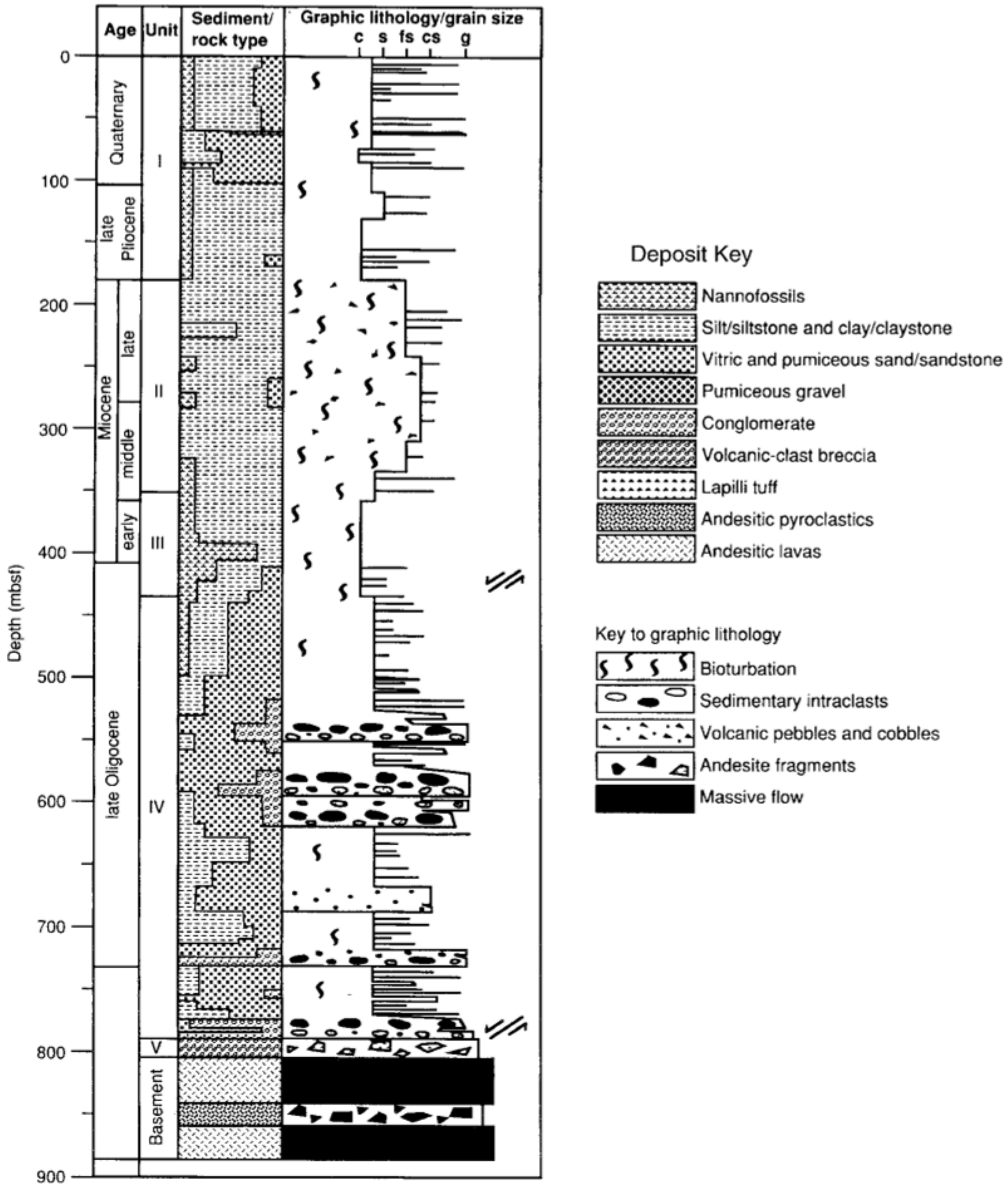
Age
Unit
Sediment/ rock type
Graphic lithology/grain size
c s fs cs g
Depth (mbsf)
0
100
200
300
400
500
600
700
800
900
Quaternary
late Pliocene
Miocene
late
middle
early
late Oligocene
Basement
I
II
III
IV
V
Deposit Key
Nannofossils
Silt/siltstone and clay/claystone
Vitric and pumiceous sand/sandstone
Pumiceous gravel
Conglomerate
Volcanic-clast breccia
Lapilli tuff
Andesitic pyroclastics
Andesitic lavas
Key to graphic lithology
Bioturbation
Sedimentary intraclasts
Volcanic pebbles and cobbles
Andesite fragments
Massive flow

FIGURE 5 Stratigraphic section of ODP Site 792 drilled in the forearc area of the Izu-Bonin island arc (see Fig. 4 for location). In the graphic lithology/grain size, c = clay, s = silt, fs = fine sand, cs = coarse sand, and g = gravel. Mbsf refers to meters drilled below the seafloor.

grading is also a common feature. These deposits are interpreted as fall deposits formed from explosive eruptions that took place on the volcanic arc to the west. Some are also likely to be the result of small turbidites that have reworked relatively fresh pyroclastic material.

Lower in the section the volume of volcaniclastic material increases and thick vitric sandstones and conglomerates are abundant (Unit IV, Fig. 5). Individual vitric sandstones are up to 3 m thick but range down to a few centimeters. The thickest units are typically massive, with some normal grading and rarely with laminated tops. Thinner beds include planar and cross laminations, flute casts, and flame structures. Their composition is dominated by either mafic or felsic components (glass and crystals), but there are rare examples of mixed lithologies. These units are predominantly turbidites and are similar to deposits that are found on the middle and outer parts of submarine fans. There is, however, no strong evidence for the formation of highly structured submarine fan systems in the forearc, and the multiple and episodic source nature of the volcaniclastic material in this area is expected to produce a complex oversupplied depositional system.

Conglomerates form thick, coarse-grained deposits that exhibit both massive and normally graded types. Intraclasts of sedimentary material up to several centimeters in diameter are common and found "floating" within the units. Massive conglomerates likely formed from debris flows whereas the normally graded types are the products of highly concentrated turbidity currents. Some of the conglomerates have a diverse composition, with mixed clasts of andesite, dacite, and other porphyritic rocks. This suggests that they are associated with the erosion of existing deposits and not directly related to eruptive activity.

Figure 6 summarizes the major depositional processes taking place in the forearc environment of the Izu-Bonin island arc. The principal mechanisms of volcaniclastic sediment input include fallout from explosive eruptions, syneruptive turbidity current initiation, redeposition of material by turbidity currents during noneruptive periods, and debris flow generation on the forearc slopes.

B. Early Intra-arc Rift

The evolution of an island arc often involves the repeated formation of backarc basins by rifting and extension (Fig. 2). In the early stages of this cycle, the arc develops isolated basins that serve as important depositional sites for volcaniclastic sediment. The Sumisu rift in the Izu-Bonin arc of the western Pacific is considered to represent the early stages of arc rifting (Fig. 4). It is subdivided into a series of smaller basins by submarine volcanic centers that trend from southwest to northeast. ODP Site 790 was drilled within a small basin (Minami Sumisu) of the Sumisu rift in a water depth of 2222 m (Fig. 4). The upper part of the sedimentary sequence of Site 790 consists of a spectacular sequence of thick pumiceous gravels and sands interbedded with vitric silts and sands (Fig. 7). Pumiceous gravels often grade upward into sands and silts, forming a series of distinct fining-upward sequences that are 15–30 m thick. They typically contain pumice, crystals, and glass of silicic composition. A secondary component of the deposits is

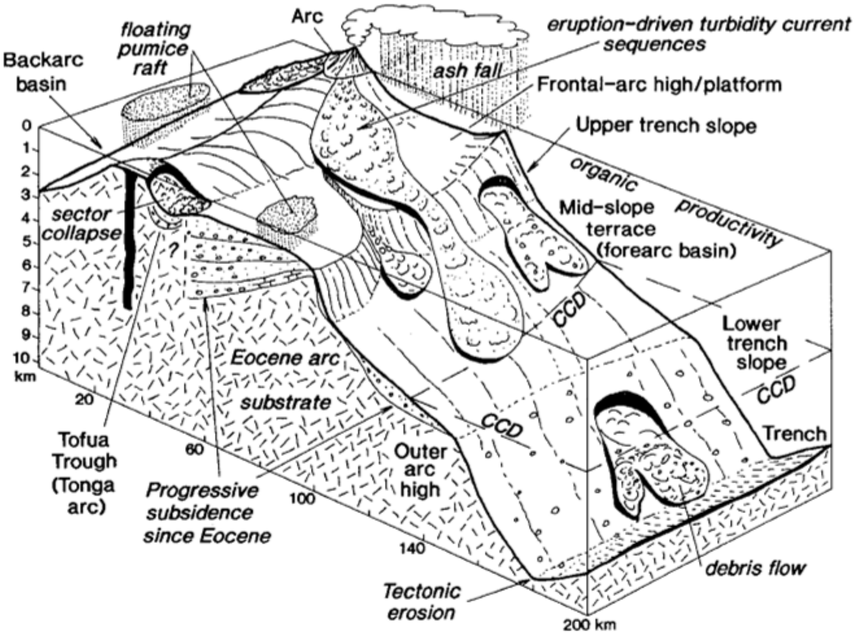
Arc
floating pumice raft
Backarc basin
eruption-driven turbidity current sequences
ash fall
Frontal-arc high/platform
Upper trench slope
organic productivity
Mid-slope terrace (forearc basin)
sector collapse
?
0
1
2
3
4
5
6
7
8
9
10
km
CCD
Lower trench slope
CCD
Eocene arc
substrate
CCD
Trench
20
Tofua Trough (Tonga arc)
60
Progressive subsidence since Eocene
100
Outer arc high
140
debris flow
Tectonic erosion
200 km

FIGURE 6 Summary of volcaniclastic sedimentation processes in the forearc area of an intraoceanic island arc [from Underwood *et al.,* 1995].

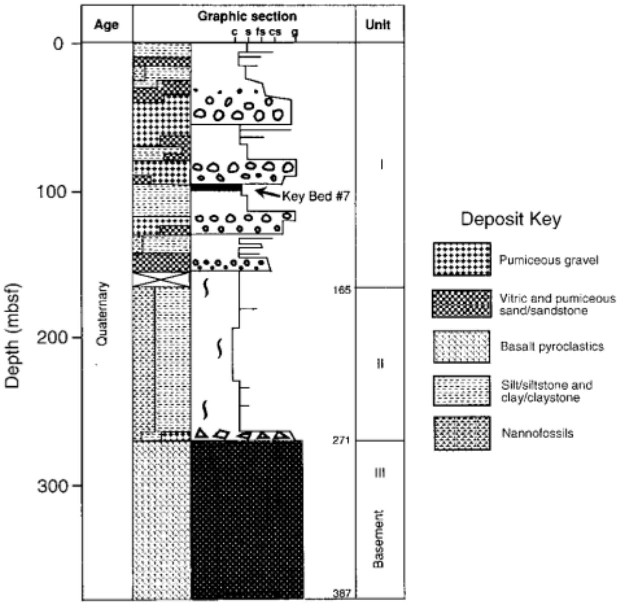

FIGURE 7 Stratigraphic section of ODP Site 790 drilled in the intra-arc rift of the Izu-Bonin island arc (see Fig. 4 for location). In the graphic lithology/grain size, c = clay, s = silt, fs = fine sand, cs = coarse sand, and g = gravel. Mbsf refers to meters drilled below the seafloor.

biogenic grains of molluscs, byrozoans, and foraminifers. Mafic material is restricted to thinner, finer grained intervals separating the coarse units. The gravels are poorly sorted, contain angular to subrounded clasts, and are generally structureless. In contrast, the vitric sands and silts are often normally graded and show parallel lamination. In the lower part of the sequence the thickness and grain size of the volcaniclastic material decrease significantly and only thin ash beds and scattered clasts of pumice and scoria are present (Fig. 7).

The thick silicic pumiceous deposits in the upper part of Site 790 were derived from great submarine explosive eruptions of either the Minami Sumisu or Tori Shima calderas to the east of the Minami Sumisu basin. Emplacement of the units occurred predominantly by sediment gravity flows during the eruptions. These include primary submarine pyroclastic density currents and/or remobilization of submarine fallout as debris flows and highly concentrated turbidity currents. Coarse pumice is also likely to be transported to the basin by floating pumice rafts generated by submarine eruptions that breach the surface. Drifting pumice eventually becomes waterlogged and sinks to the seafloor.

The sequence from Site 790 indicates that young interarc basins are subject to rapid influxes of coarse pumiceous volcaniclastic material that form very thick sequences of gravity flow deposits interbedded with minor amounts of background marine sediment derived from biological and epiclastic inputs. In the Sumisu rift the facies evolution was an overall coarsening upward, suggesting an initially low flux of material at the start of rifting followed by a period of more vigorous explosive eruptions. Because of the proximity of source volcanoes, the sedimentation rates in these environments can be as much as 1000 m/myr.

C. Young Marginal Basin

As backarc extension evolves, the intra-arc rift gives way to a wider basin where spreading centers begin to develop. However, the configuration of such basins can be complex depending on the location of initial rifting. The Lau basin of the Tonga–Kermadec island system is an example of a backarc basin that evolved by the splitting of an island arc in the forearc region (Fig. 4). Consequently, the growth of the basin was accompanied by an eastward migration of arc volcanism until a new arc, the Tofua island arc, was created to the east. The migration of arc volcanism and the development of active spreading centers in the basin created a complicated tectonic structure upon which volcaniclastic sedimentation was superimposed. A principal effect of the migration was to compartmentalize the area into a sequence of small isolated subbasins with horst-and-graben structure. Drilling within these small subbasins revealed sedimentary sequences that were very similar in overall structure yet quite independent of one another. ODP Site 838 was drilled in one of the small subbasins to the west of the Valu Fa ridge in water depth of 2400 m (Fig. 8).

The basal part of Site 838 consists of a thick sequence of polymict vitric gravels, sandstones, and siltstones with minor interbeds of hemipelagic ooze (Fig. 8). The gravels contain fragments of mafic igneous rocks, pumice, and tuffaceous sediment. Their composition consists of a mixture of rhyolite, dacite, and basaltic andesite. Overlying the basal sequence is a thick interval of vitric sands and silts, interbedded with pumiceous gravels. The vitric sands and silts are a few centimeters to 5 m thick. They contain abundant colorless glass shards, pumice fragments, and crystals, together with lesser amounts of brown, more mafic glass shards. Basal contacts are typically erosive and individual units exhibit normal grading and occasional lamination. Pumiceous gravels form thick units (8–15 m), with abundant pumice lapilli.

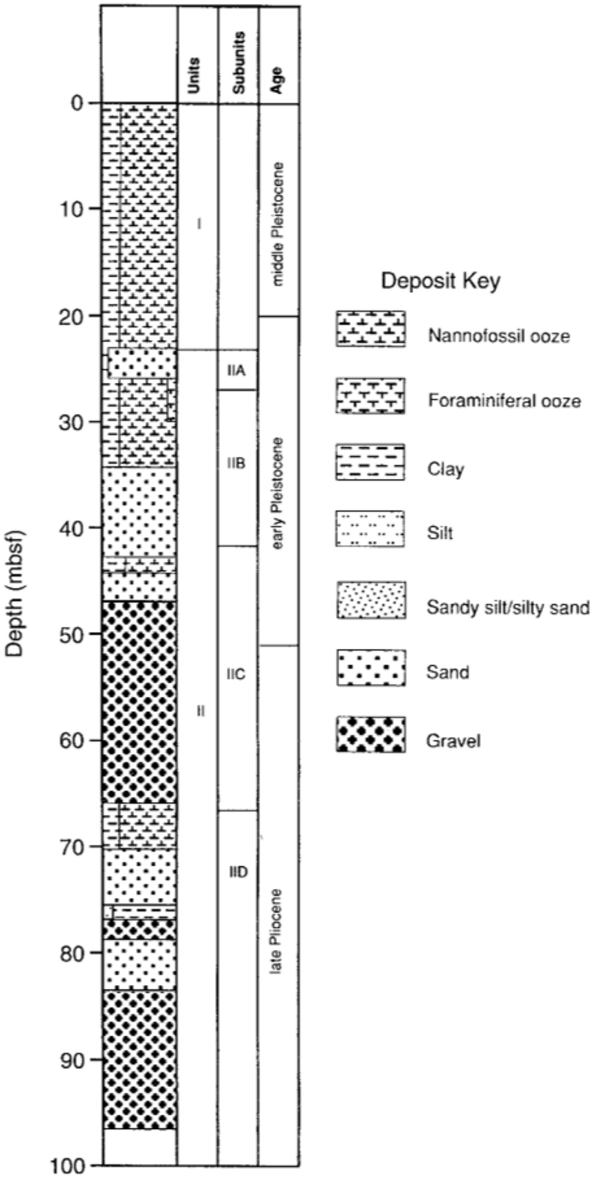

FIGURE 8 Stratigraphic section of ODP Site 838 drilled in the backarc area of the Tofua island arc (see Fig. 4 for location). Mbsf refers to meters drilled below the seafloor.

Pumice diameters are up to 7 cm and the units are poorly sorted. Pumice compositions are dominantly rhyodacitic but hyaloclastites of basaltic andesite composition are also present.

The coarse-grained and mixed-lithology basal conglomerates were produced by mass flows of epiclastic material derived from local sources. Similarly, the overlying coarse-grained pumiceous gravels were deposited from debris flows generated by mobilization of volcaniclastic material near the basin margins. The likely source of this volcaniclastic material is intrabasinal seamounts linked to the migration of arc volcanism to the west. Each small basin was subject to proximal deposition from these centers but then subsequently isolated as the locus of volcanism shifted. The development of horst-and-graben structures eventually led to the isolation of the basins from extensive deposition by mass flow processes. This is seen in the general upward fining of the sequence at Site 838 and other sites located in similar basins. The vitric sands and silts were emplaced by turbidity currents but their source remained proximal to the basin because of the tectonic isolation imposed by the local structure. In the uppermost sediments, corresponding to the most recent times, volcaniclastic input is restricted to the fallout of volcanic ash from subaerial eruption plumes from the active arc to the west and the local redeposition of that material by small turbidity currents.

D. Mature Marginal Basin

Prolonged backarc extension leads to the development of a wide mature basin. Spreading is focused at an axial rift where basaltic volcanism creates new basin crust. The average life span of backarc spreading is usually less than 25 million years. In the Mariana arc system, repeated formation of backarc basins has occurred for at least 30 million years (Fig. 4). The Parece Vela basin represents an inactive mature marginal basin that is flanked on the west by a remnant arc (Palau–Kyushu ridge), contains an old spreading rift (Parece Vela rift), and is bordered on the east by a young remnant arc (West Mariana ridge). DSDP drilling in the Parece Vela basin provides a good example of the types of volcaniclastic sequences developed in mature marginal basins.

Site 450 is located west of the Mariana ridge in 4707 m of water (Fig. 4). At the base of the sequence is a thin sequence of pillow basalts intruded into wet sediments during the earlier stages of basin spreading (Fig. 9). Overlying the pillow basalts is a thick sequence of middle Miocene vitric tuffs and tuffaceous volcaniclastic conglomerates that accumulated at a rate as high as 100 m/myr. The vitric tuffs were produced by fallout from explosive eruptions on the West Mariana ridge and redeposition of pyroclastic and epiclastic material by turbidity currents. Thick tuffaceous conglomerates were the products of concentrated turbidity currents or debris flows. The dominantly epiclastic nature of the conglom-

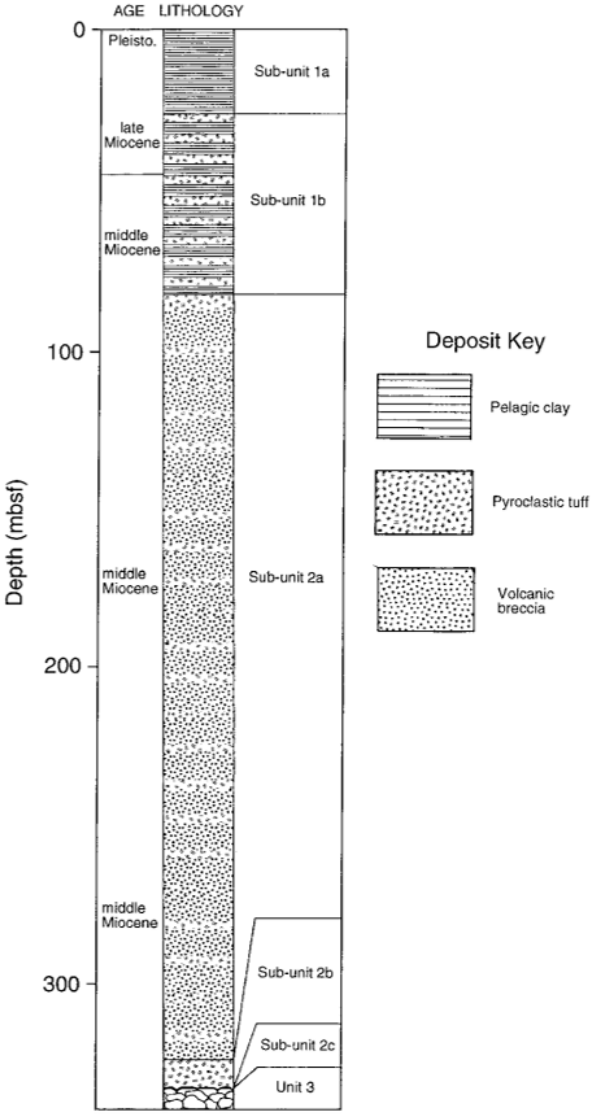

FIGURE 9 Stratigraphic section of DSDP Site 450 drilled in the backarc area of the Mariana island arc (see Fig. 4 for location). In the graphic lithology/grain size, c = clay, s = silt, fs = fine sand, cs = coarse sand, and g = gravel. Mbsf refers to meters drilled below the seafloor.

erates indicates redeposition of material from the erosion and weathering of older volcanic centers. In addition, the lower sequence of tuffs and conglomerates contains a significant amount of hyaloclastites derived from the submarine volcanism. The source of this material was most likely the spreading center of the Parece Vela basin and/or submarine volcanism on the west Mariana ridge. Hyaloclastites disappear upsection, reflecting waning of submarine volcanism in the backarc.

In the upper part of the sequence there are significant decreases in the amount of volcaniclastic sediment and the accumulation rate (Fig. 9). The dominant deposits are thin dark gray and brown vitric layers interbedded with pelagic clay. These were produced mainly by fallout of volcanic ash from explosive eruptions on the west Mariana ridge. However, these layers eventually die out in the most recent sediments, where volcanic ash is mostly found dispersed within pelagic clay. The sequence at Site 450 thus records an initial period of high volcaniclastic influx from the active west Mariana arc and the backarc spreading center to the east. As the basin widened, the supply of material from the backarc spreading center diminished, either because of the increased distance to the site or the waning of volcanism. In addition, the source of volcaniclastic material from the west Mariana ridge decreased as well, eventually becoming inactive in the late Miocene.

IV. VOLCANICLASTIC FACIES EVOLUTION IN ISLAND ARCS

The results of deep sea drilling and sediment core studies can be combined with the tectonic evolution of island arcs to produce a model for temporal and spatial facies changes in volcaniclastic sediments. The following discussion assumes a simple model for the tectonic evolution of an arc (Fig. 2) with the understanding that it will not apply to all oceanic arcs but nevertheless encompasses many of the stages shown by a typical arc. The model considers volcaniclastic and nonvolcanic marine sediments that form an integral part of the sedimentary sequence. In deep water the nonvolcanic sediments include (1) carbonate oozes consisting of microfossils of foraminifers, nannofossils, and pteropods, (2) pelagic clay consisting of windblown dust and dispersed volcanic ash, and (3) hemipelagic clay formed from a combination of microfossils and terrigenous input.

A. Initial Arc Rifting

Initial stages of arc rifting produce a narrow trough that is flanked by volcanoes of the active arc and elevated portions of the arc platform (Fig. 10A). Smaller volcanic centers within the rift subdivide it into a series of subbasins. These small basins receive large amounts of volcaniclastic material from nearby arc volcanoes and, to a

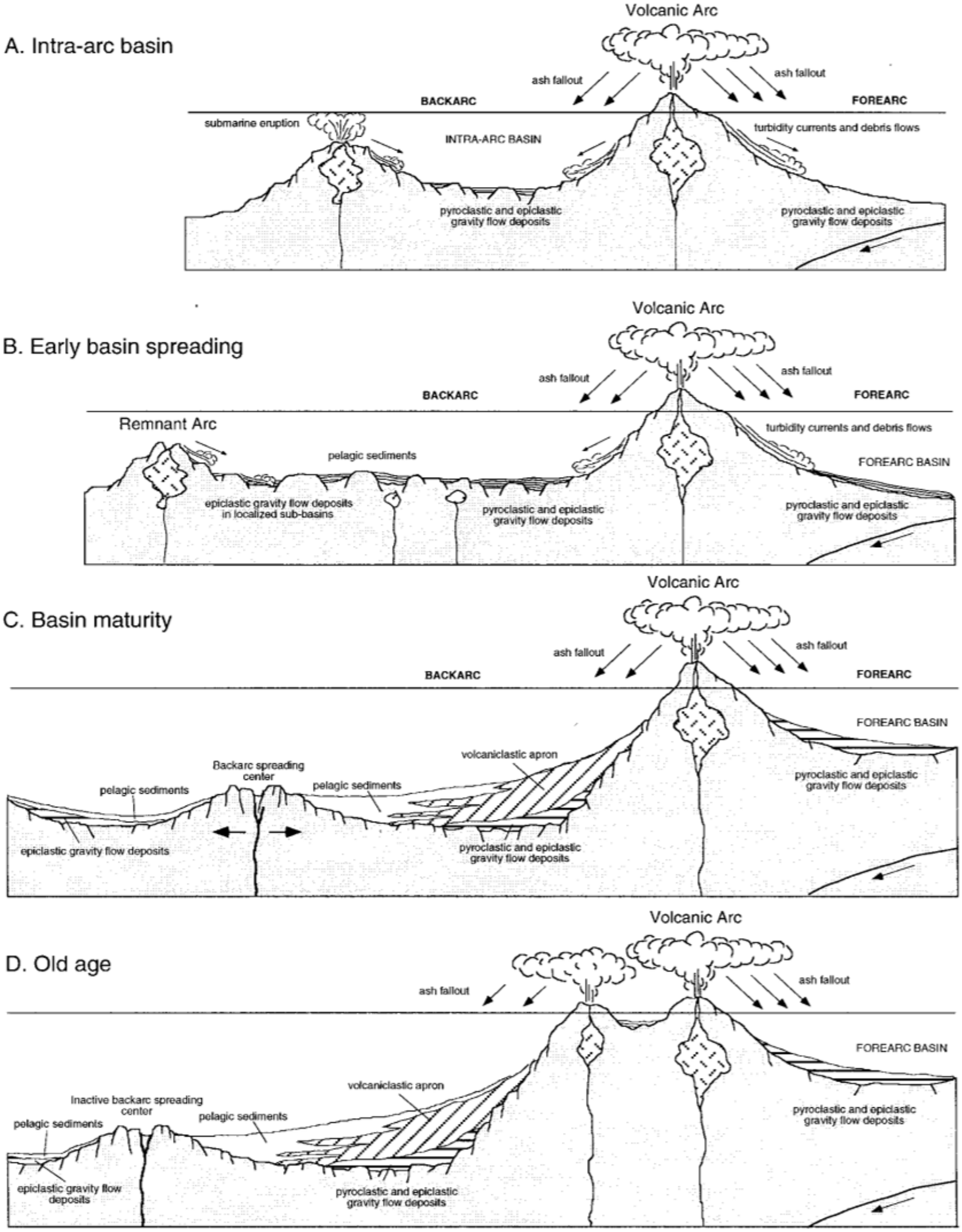
A. Intra-arc basin
Volcanic Arc
ash fallout
ash fallout
BACKARC
FOREARC
submarine eruption
INTRA-ARC BASIN
turbidity currents and debris flows
pyroclastic and epiclastic gravity flow deposits
pyroclastic and epiclastic gravity flow deposits
B. Early basin spreading
Volcanic Arc
ash fallout
ash fallout
BACKARC
FOREARC
Remnant Arc
pelagic sediments
turbidity currents and debris flows
FOREARC BASIN
epiclastic gravity flow deposits in localized sub-basins
pyroclastic and epiclastic gravity flow deposits
pyroclastic and epiclastic gravity flow deposits
C. Basin maturity
Volcanic Arc
ash fallout
ash fallout
BACKARC
FOREARC
FOREARC BASIN
volcaniclastic apron
Backarc spreading center
pelagic sediments
pelagic sediments
pyroclastic and epiclastic gravity flow deposits
epiclastic gravity flow deposits
pyroclastic and epiclastic gravity flow deposits
D. Old age
Volcanic Arc
ash fallout
ash fallout
FOREARC BASIN
volcaniclastic apron
Inactive backarc spreading center
pelagic sediments
pelagic sediments
pyroclastic and epiclastic gravity flow deposits
epiclastic gravity flow deposits
pyroclastic and epiclastic gravity flow deposits

FIGURE 10 Sources and transport processes of volcaniclastic sediments during the tectonic evolution of an oceanic island arc.

lesser extent, the intra-arc submarine volcanic centers. Pyroclastic material is transported by subaerial eruption plumes and by sediment gravity flows triggered by syneruptive activity or posteruptive remobilization of freshly erupted material. Thick, coarse-grained pumiceous deposits are produced by high particle concentration turbidity currents and debris flows. Rifting of the arc also generates epiclastic material, by erosion of faulted terrains, that is similarly transported to the basins by sediment gravity flows. The ratio of pyroclastic to epiclastic material will depend upon the level of volcanic activity in the arc and the extent of tectonic displacement. Accumulation rates of volcaniclastic material in these intra-arc rifts are among the highest of any submarine arc environment, up to 1000 m/myr. Nonvolcanic sediment represents a small percentage of the total sediment because of the large volcaniclastic input.

The early stages of rifting are generally accompanied by active arc volcanism and therefore transport of material will also take place into the forearc area. Deposition of volcaniclastic material will occur by fallout from eruption plumes and the generation of syneruptive sediment gravity flows. In the forearc the material will be distributed over a broader area and consequently the accumulation rates will be less than those of the intra-arc basins. Fallout will produce thin, widespread deposits of vitric ash depending on the strength and direction of the local winds. Influx of pyroclastic and epiclastic material to the forearc by sediment gravity flows builds up significant sequences of turbidites in forearc basins. However, because the number of sediment sources can be large and the influxes highly episodic, the sequences do not resemble submarine fan assemblages that are typically found offshore of areas with significant coarse-grained sediment influx. The volcaniclastic material is interbedded with hemipelagic clay and/or carbonate oozes close to the arc. With increasing depth and distance from the arc, the nonvolcanic sediment will be replaced with pelagic clay due to the dissolution of calcium carbonates in water depths greater than 4500 m. Rates of sediment accumulation in the forearc area can be as high as 300 m/myr.

B. Early Basin Spreading

Enlargement of the backarc basin by rifting produces a complex bathymetry of small subbasins isolated from one another by faults and intrabasin volcanic centers (Fig. 10B). These are depositional centers for volcaniclastic sediment from adjacent bathymetric highs. Coarse pyroclastic material is deposited from submarine eruptions of nearby volcanoes as turbidity currents and debris flows. Volcanic activity may migrate across the area prior to the establishment of a focused spreading center and thus the influx of primary volcaniclastic material to a particular basin may be terminated abruptly. The complex bathymetry of these rifted environments results in the isolation of the small basins from sediment gravity flows generated from more distal sources. Fallout of volcanic ash from eruption plumes remains one of the only ways to supply these basins with additional material. The forearc environment may not experience major structural changes during this time and consequently the sedimentation patterns remain similar to those of the first stage.

C. Basin Maturity

Establishment of active backarc spreading centers leads to the widening of the backarc area by crustal formation (Fig. 10C). Volcanism becomes more focused along the spreading rift and the basin deepens due to crustal aging and subsidence. During this period volcaniclastic sedimentation in the backarc is concentrated in several different areas. The most important is along the margin of the basin flanked by the active volcanic arc. In this area a thick sequence of deposits referred to as the volcaniclastic apron is established. The apron accumulates by primary volcaniclastic influx from subaerial and/or subaqueous arc eruptions, a semicontinuous supply of epiclastic material from erosion of the subaerial and/or subaqueous arc complex, and deposition of nonvolcanic sediment. Influx from multiple sources along the arc produces an apron that is elongate parallel to the trend of the arc and wedge-shaped in profile. The growth of the arc and its lateral extent into the backarc are directly related to the intensity of arc volcanism. During vigorous arc volcanism the apron will prograde into the basin toward areas previously dominated by nonvolcanic sedimentation. Peak accumulation rates of the volcaniclastic apron will be in the range of several hundred meters per million years. As arc volcanism wanes, the extent of the apron will recede and nonvolcanic sedimentation will become more important. Temporal variations in the extent of the apron into the backarc thus provide a record of the history of arc volcanism during basin spreading.

The volcaniclastic apron consists mostly of turbidites and debris flows but like the forearc sequences, does not resemble a typical deep-sea fan. Deep-sea fans are most often found at the base of a single submarine canyon that funnels sediment from a continental shelf or subaerial river source. They show systematic changes in the types of deposits as a function of position on the fan that result from sediment influxes of various strengths through a main distribution channel. In contrast, the volcaniclastic apron receives massive, periodic influxes of coarse-grained volcaniclastic sediment that is delivered from multiple sources and not constrained by a single distribution path. Consequently the apron builds up by the overlapping of many different flow deposits, with significant amounts of transport parallel to the arc. Under these conditions, it is not surprising that systematic facies variations within the apron are rare.

Another area of active volcaniclastic deposition within the backarc area is along the border of the basin with the remnant arc. Erosion of the submerged structure leads to the deposition of epiclastic material in the basin by sediment gravity flows. The composition of the deposits is likely to be heterogeneous as a result of the dissection of the older arc structure. Accumulation of material in this area will be less than in the volcaniclastic apron adjacent to the active arc and is of the order of several tens of meters per million years. With time the influx of epiclastic material from the remnant arc is expected to diminish as it subsides and is continuously modified by erosion. At the base of the remnant arc the sedimentary sequence will become more fine grained upward and nonmarine sediments will constitute an increasingly larger fraction of the deposits.

In the forearc the accumulation rate of volcaniclastic material also responds to the level of volcanic activity in the active arc. Shallower submarine slopes and the partitioning of the area into multiple forearc basins result in a less continuous accumulation of volcaniclastics compared to the wedge-shaped apron formed in the backarc. The evolution of the forearc is difficult to generalize because of the many factors that affect its development. In some cases, the forearc experiences subsidence associated with extension or tectonic erosion by the descending slab. Subsidence will increase the supply of epiclastic material and lead to changes in the type of nonvolcanic sediment. Alternatively, some forearcs experience uplift related to progressive buildup of an accretionary prism by scraping off of sediment. These forearc basins may become isolated from the influx of pyroclastic and epiclastic material by sediment gravity flows or limited to only proximal sources. However, fallout of volcanic ash from eruption columns will continue to supply some volcaniclastic material if explosive eruptions are occurring along the volcanic arc. Nonvolcanic sediment would change its character to reflect the prevailing water depths.

D. Old Age

At the end of a tectonic cycle, a wide marginal basin has developed and the backarc spreading center becomes inactive (Fig. 10D). A new episode of rifting begins in the volcanic arc with extension somewhere in the vicinity of the active arc. In the backarc the extent of the volcaniclastic apron is diminished by the deposition of nonvolcanic sediment. Primary pyroclastic sediment is still dispersed by fallout from eruption plumes but widespread transport by gravity flows has waned. The new arc rifting may supply a fresh influx of epiclastic material to the backarc but its extent may be limited by structural complexity. If arc volcanism remains vigorous during the new rifting stage, volcaniclastics will continue to be supplied to the forearc by fallout and gravity flow processes.

V. FUTURE RESEARCH

Significant progress has been made toward the understanding of volcaniclastic sedimentation around island arcs. Largely through the Ocean Drilling Program, there has now been deep sampling of the stratigraphic sequences in different environments around active arcs. This has provided key information about the general distribution and lithology of volcaniclastic sediments and the evolution of sedimentary sequences in response to changes in volcanism and structural complexity. These results have led to the development of regional-scale models such as shown in Fig. 10. However, much remains to be learned about the finer scale details of sedimentary processes and the architecture of the deposits. At present, the density of sample sites does not allow for the development of detailed sedimentological models similar to those already existing for other types of marine depositional systems. Smaller scale observational experiments that integrate high-density sampling and subbottom imagery are required to improve the spatial resolution of volcaniclastic sediments in island arcs. The potential for economically important mineral deposits, volcanic hazards from transport and depositional processes, and value for hydrocarbon source reservoirs provides important impetus to invest in such studies.

SEE ALSO THE FOLLOWING ARTICLES

Lahars • Magmatic Fragmentation • Phreatomagmatic Fragmentation • Plate Tectonics and Volcanism • Pyroclast Transport and Deposition • Seamounts and Island Building • Volcanic Plumes

FURTHER READING

Carey, S., and Sigurdsson, H. (1984). A model of volcanogenic sedimentation in marginal basins. *In* "Marginal Basin Geology" (B. Kokelaar and M. Howells, eds.), *Geol. Soc. London Spec. Publ.* **16,** 37–58.

Fisher, R. V., and Smith, G., eds. (1991). "Sedimentation in Volcanic Settings," *SEPM Soc. Sediment. Geol. Spec. Publ.* **45**.

Fisher, R. V., and Schmincke, H. U. (1994). Volcaniclastic sediment transport and deposition. Pages 351–384 *in* "Sediment Transport and Depositional Processes" (K. Pye, ed.), Blackwell, Oxford.

Klein, G., de V. (1985). The control of depositional depth, tectonic uplift, and volcanism on sedimentation processes in the backarc basins of the western Pacific. *J. Geol.* **93,** 1–25.

Marsaglia, K., Boggs, S., Clift, P., Seyedolali, A., and Smith, R. (1995). Sedimentation in western Pacific backarc basins: New insights from recent ODP drilling, *in* "Active Margins and Marginal Basins of the Western Pacific" (B. Taylor and J. Natland, eds.), American Geophysical Union Geophysical Monograph **88,** 291–314.

Sigurdsson, H., Sparks, R. S. J., Carey, S., and Huang, T. C. (1980). Volcanogenic sedimentation in the Lesser Antilles arc. *J. Geol.* **88,** 523–540.

Underwood, M., Balance, P., Clift, P., Hiscott, R., Marsaglia, K., Pickering, K., and Ried, P. (1995). Sedimentation in forearc basins, trenches, and collision zones of the western Pacific: A summary of results from the Ocean Drilling Program, *in* "Active Margins and Marginal Basins of the Western Pacific" (B. Taylor and J. Natland, eds.), American Geophysical Union Geophysical Monograph **88,** 315–354.

CALDERAS

Peter W. Lipman
U.S. Geological Survey

I. Introduction: Calderas and Eruptive Processes
II. Caldera-Forming Eruption Cycles
III. Caldera-Subsidence Processes
IV. Societal Implications

GLOSSARY

ash, volcanic Fine pyroclastic material, down to dust size, that is formed by explosive volcanic eruptions.

ash-flow tuff Rock formed by the deposits of pyroclastic flows. Synonymous with ignimbrite; common usage in North American literature.

crater A bowl- or funnel-shaped depression, generally in the top of a volcanic cone, often the major vent for eruptions.

ignimbrite Pyroclastic-flow deposit. Synonymous with ash-flow tuff.

intrusion A subsurface igneous rock body formed when molten igneous rock forces its way into surrounding host rocks and then cools.

magma Molten rock material with dissolved gases that forms igneous rocks on cooling; magma that reaches the surface erupts as lava or pyroclasts.

magma chamber An underground reservoir in the Earth's crust filled with magma, from which volcanic materials are erupted.

pyroclastic flow Laterally transported, fluidized mass of hot dry rock fragments mixed with hot gases. Moves away from a volcano at high speeds.

welded tuff A hard pyroclastic rock compacted by internal heat and the pressure of overlying deposits. Forms the interiors of thick ash-flow (ignimbrite) sheets.

CALDERAS ARE LARGE volcanic depressions, more or less circular in form, the diameter of which is many times greater than that of included vents. Formation of calderas, by some form of roof collapse over an underlying shallow magma reservoir, is now widely recognized as accompanying most eruptions that involve magmatic volumes greater than a few cubic kilometers. Small calderas (<5 km in diameter) associated with lava eruptions are common at crests of basaltic and andesitic volcanoes; calderas as much as 75 km in largest dimension have formed during large ignimbrite (ash flow) eruptions. In general, caldera diameter increases in proportion to volume of the associated eruption. Diverse subsidence geometries and collapse processes for ash-flow calderas are inferred to reflect varying sizes, roof geometries, and depths of the source magma chambers, in combination with preexisting volcanic and regional tectonic influences.

I. INTRODUCTION: CALDERAS AND ERUPTIVE PROCESSES

Calderas have been much studied during the past half century, stimulated by recognition of their association with large ash-flow sheets and by several landmark reviews (see Further Reading), yet the processes of caldera formation remain incompletely understood and controversial. Origin dominantly by subsidence has been overwhelmingly recognized, with only minor proportions of the caldera volume being generated by explosive ejection and removal of older rocks. In their origin by subsidence, even small calderas are thus distinct from large volcanic craters that form by constructional accumulation of cinders and spatter or by explosive ejection of wall rocks adjacent to a volcanic vent. Varied processes have been inferred as important or dominant: piecemeal or chaotic subsidence, plate (piston) subsidence of a relatively coherent floor bounded by ring faults, funnel-shaped subsidence into an areally restricted central vent, and hinged downsag of a central area with little or no boundary faulting. Many calderas are geometrically complex, containing elements of more than a single structural type and subsidence process. Most caldera subsidences have been attributed to collapse accompanying or following large-volume eruptions, but inception of subsidence at some calderas has been attributed to subsurface movement of magma, which in turn may have triggered an eruption. The term caldera, as used here, includes features previously described as "cauldrons," which are considered to represent deeper erosional levels of the same fundamental structures and igneous processes. In many volcanic areas, successive large eruptions and associated overlapping subsidence events have produced caldera clusters that have complex resulting geometries and structures.

In addition to real diversity among caldera structures, the divergent interpretations of dominant subsidence processes reflect ambiguities resulting from the large dimensions of many calderas, gross slumping of caldera walls, incomplete cross-sectional exposures, overprinting by postsubsidence structures, and resulting uncertainties about subsidence geometries. Little-eroded young calderas with well-preserved eruptive morphology generally provide minimal direct information on underlying structures, depth of subsidence, or relation to the source magma reservoir. In contrast, where erosion has proceeded sufficiently to expose subvolcanic structures and granitic rocks of the solidified magma reservoir, the relations of such structures and intrusions to individual eruptions and to surface volcanic morphology commonly have been largely obscured. Complete sections from surface volcanic rocks to deep features of ash-flow calderas are preserved and exposed only rarely—in regions of exceptional topographic relief or sites of rapid tectonic rotation of the upper crust. Geophysical studies and drill-hole information can provide important additional information on caldera geometry and structure, although geophysical models are commonly ambiguous due to uncertain physical properties at depth. Few drill holes penetrate deeply through the fill of large calderas.

On Earth, calderas have been recognized throughout the documented geologic record, back into Archean time, and likely were part of faintly preserved earlier processes of crust formation, as suggested by evidence from other planetary bodies. Calderas of varying sizes are associated with virtually every type of volcanic activity, including summit calderas on basaltic shields of oceanic islands and andesitic stratocones of volcanic arcs. Larger calderas are commonly associated with regions of crustal extension, both within volcanic arcs and in continental rift zones; the largest calderas have formed in regions of thick continental crust. Even larger calderas have been imaged on other planetary bodies, such as Olympus Mons on Mars. Some representative terrestrial calderas, cited in this review, are listed in Table I. Especially informative are many recent studies of the numerous Tertiary calderas in the western United States and in Japan, although only a few of the latter are readily accessible in the international literature.

A. Historical Development of Geologic Concepts

Early 19th century interpretations that large volcanic depressions represent the collapsed crests of structural uplifts ("craters of elevation") or explosive excavation were gradually abandoned later in the century, largely in response to careful observations at La Palma in the Canary Islands (probably the type locality for the term caldera) by Lyell, at Kilauea in Hawaii by Dutton, and at Santorini in the Aegean by Fouqué, and especially by the evidence developed by Verbeek for the great 1883 Krakatau eruption in Indonesia.

Early in the 20th century, arcuate intrusions and ring faults bounding subsided blocks were described as cauldron structures in Scotland by Clough, Bailey, and others; similar structures were recognized in the San Juan Mountains in the United States by Cross and Burbank.

TABLE I Some Well-Documented Caldera Eruptions

Date	*Caldera name*	*Location*	*Edifice; structure*	*Topographic caldera diameter (km)*	*Eruption volume [km^3 (DRE)]*	*Reported collapse geometry*
1991	Pinatubo	Philippines	Stratocone	2.5	4–5	Funnel?
1968	Fernandina	Galapagos	Basaltic shield	5 × 6	0.1	Trapdoor; composite
1912	Katmai	United States	Stratocone	2.5 × 4	12	Funnel?
1883	Krakatau	Indonesia	Clustered stratocones	8	10	Funnel?
1750–1790?	Kilauea	Hawaii	Basaltic shield	3 × 5	??	Plate
1.4 ka	Rabaul	Papau, New Guinea	Volcano cluster	10 × 15	11	Plate
1.8 ka	Taupo	New Zealand	Rift/caldera cluster	35	35	Downsag?[a]; composite
3.6 ka	Santorini	Mediterranean	Volcano cluster	7 × 10	25	Composite
7.7 ka	Crater Lake	United States	Volcano cluster	8 × 10	55	Plate
22 ka	Aira	Japan	Caldera cluster	18 × 22	300	Funnel?[a]
35 ka	Campi Flegrei	Italy	Volcano cluster	13	80	Plate
75 ka	Toba	Indonesia	Dacitic arc; fault zone	30 × 80	1500	Plate (R)[b]
95 ka	La Primavera	Mexico	Volcano cluster	11	20	Plate
600 ka	Yellowstone	United States	Caldera cluster	60	1000–2000	Plate (R)
760	Long Valley	United States	Older volcanoes	15 × 30	600	Plate (R)
1.1 Ma	Valles	United States	Volcano cluster	20 × 22	300	Plate (R)
2.2 Ma	Cerro Galán	Argentina	Volcano cluster	25 × 35	2000	Plate (R)
2.8 Ma	Chegem	Russia	Collision zone	15 × 20	>300	Plate?
5.6–3.8 Ma	Dorobu	Japan	Caldera cluster	6 × 13	??	Piecemeal, composite
25.9 Ma	Lake City	United States	Caldera cluster	15 × 20	200–500	Plate (R)
26.6 Ma	Creede	United States	Caldera cluster	24	>500	Plate (R)
27.6 Ma	Silverton	United States	Caldera cluster	15 × 20	50–100	Trapdoor
27.8 Ma	La Garita	United States	Volcano cluster	35 × 75	5000	Multiple plates? (R)
73 Ma	Tucson	United States	Andean arc	25	>500?	Trapdoor
Ordovician	Scafell	England	Volcanic arc	>15	??	Piecemeal (composite?)

[a] Alternatively interpretable as plate subsidence.
[b] (R), resurgent postcollapse uplift of caldera floor.

By the mid-20th century, the subsidence origin of many volcanic calderas was emphasized by Williams in his study of Crater Lake in Oregon (Fig. 1) and his comprehensive 1941 review "Calderas and Their Origin," by Matumoto's concurrent identification of large clustered calderas in southern Japan, and by later recognition of the Valles resurgent caldera type by Smith and Bailey. More recent studies have built on these concepts to decipher stratigraphy and structure of caldera-related volcanic deposits, constrain timing of eruption and collapse, determine compositional and temporal relations between volcanism and solidification of subcaldera magma chambers, and document unrest and precursors to large caldera-forming events for hazards evaluation. Volcanic studies of calderas have also been applied to societal needs to utilize volcano-generated ore deposits, generate electrical power from geothermal heat, and evaluate potential effects of large caldera eruptions on global climate.

B. Notable Historical Eruptions

Much has been learned about caldera-forming processes from historical eruptions, although none have been on the scale of the largest older caldera-forming eruptions evident in the geologic record. Well-documented historical and near-historical caldera-related eruptions include Pinatubo (1991), Fernandina (1968), Katmai (1912), Krakatau (1883), Kilauea (1750–1790?), Taupo (1.8 ka), and Santorini (3.6 ka). Such young volcanoes

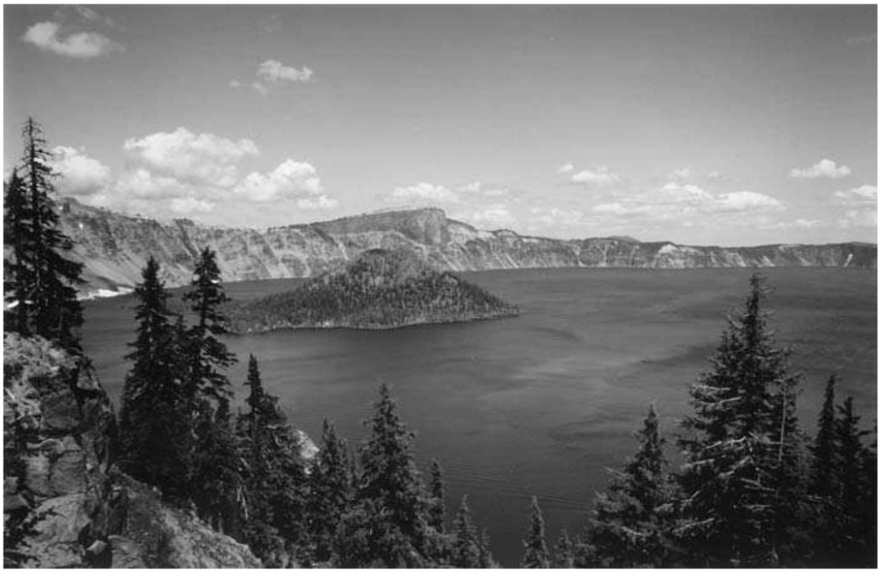

FIGURE 1 Crater Lake caldera, United States, as viewed from its south rim. The caldera formed 7700 years ago by collapse of the volcano known as Mount Mazama. The prominent cliff on the north caldera rim, Llao Rock, is a rhyodacite lava flow erupted within a few hundred years before the caldera-forming eruption. The cinder cones and lava flows of Wizard Island are the top of a 1- to 2-km^3 andesitic cone, erupted soon after caldera collapse. [Photograph by C. R. Bacon, U.S. Geological Survey.]

provide only limited information on the internal structure of magmatic systems, however, in comparison with exposed features of deeply eroded older volcanic edifices. Complementary study of both young and ancient volcanic systems (Table I) are needed to understand caldera-forming processes.

The 1991 eruption of Mount Pinatubo in the Philippines, during which a small caldera (2-km diameter) formed during eruption of 4–5 km^3 (DRE, dense-rock equivalent) of ignimbrite and tephra-fall deposits, has been the best monitored caldera-forming event thus far. This eruption demonstrated that caldera collapse can accompany even relatively small-volume pyroclastic eruptions. The timing of the recurrent subsidence events can be inferred from several peaks in seismic energy release during the eruption.

In 1968, subsidence of 300 m within the summit caldera of the Fernandina basaltic shield in the Galapagos was preceded by a subaerial eruption that was an order of magnitude smaller than the volume of caldera collapse. This event confirmed previous inferences that basaltic calderas can subside recurrently in response to subsurface magma withdrawal, in response to intrusion or perhaps to flank eruptions low on the edifice (underwater at Fernandina?).

The 1912 eruption from the funnel-shaped Novarupta crater in Alaska, the largest eruption of the 20th century (about 12 km^3, DRE), triggered 1200 m of subsidence at the summit of Mount Katmai (at least 5-km^3 subsidence volume), 10 km from the eruptive vent. Katmai thus documents an unusual spatial divergence between eruptive and subsidence processes where the magmatic plumbing system is complex. Stratigraphic relations between dust layers generated by subsidence at Katmai and tephra erupted from Novarupta demonstrate that the caldera subsided incrementally during this eruption.

The 1883 eruption of about 10 km^3 (DRE) of pyroclastic materials from Krakatau in Indonesia played a pivotal role in focusing attention on the relations between highly explosive pyroclastic eruption and formation of large calderas. Some key observations from this eruption include demonstration that erupted lithic debris was inadequate to account for the volume of the caldera (thus disproving prior hypotheses of explosive evacuation of caldera basins), recognition that caldera eruptions could generate destructive tsunamis capable of causing coastal damage far beyond the region directly impacted by eruptive deposits, and the effect of globally distributed volcanic ash dispersed in the atmosphere for several years after the eruption.

The summit caldera of Kilauea volcano in Hawaii, much visited while occupied by a lava lake during much of the later 19th century, was recognized early as having resulted from collapse, probably in connection with eruptions along the long flanking rift zones. The most recent deep subsidence of Kilauea caldera occurred in conjunction with, or just preceding, major explosive activity in 1790; during the 19th century, the caldera was filled to overflow by lavas. Recent work has documented that such large basaltic shields undergo repeated cycles of caldera subsidence and filling throughout their shield-building stage. In addition, short-term inflation–deflation cycles preceding and accompanying eruptions have been documented in great detail by geodetic measurements.

The 1.8-ka Taupo eruption of 35 km^3 (DRE) of magma on the North Island of New Zealand, probably the world's most violent and largest in the past 2000 years, would have been even more renowned than the roughly contemporaneous A.D. 79 eruption of Vesuvius if it had occurred in a populated region where historical records were preserved. The Taupo caldera has been interpreted by Walker to constitute a representative example of subsidence by downsagging, although determination of caldera processes and even caldera size is impeded by poor exposures as a result of location within the extensional trough of the Taupo Volcanic Zone. Recent geophysical studies suggest the subsurface presence of a fault-bounded caldera complex nested within graben structures.

No true historical records exist for the 3.6-ka Bronze Age eruption of Santorini in the Aegean arc (about 25 km^3 DRE), but this eruption is prominent in European archeological and volcanologic studies for its well-preserved caldera and proximal eruptive deposits and also for the Minoan cultural sites preserved beneath proximal deposits. In addition, recent studies by Druitt and associates have documented that the Bronze Age caldera is the youngest of at least four successive caldera cycles involving nearly confocal composite subsidence since 100 ka or earlier.

II. CALDERA-FORMING ERUPTION CYCLES

Many large calderas form at sites of preceding volcanism that record shallow accumulation of caldera-related magma (Fig. 2). Large eruptions (>50–100 km^3 of erupted magma) typically cause caldera collapse concurrently with eruption, as indicated by thick intracaldera ash-flow fill, interleaved collapse slide breccias, and structural features. Postcollapse volcanism may occur from vents within or on the margins of ash-flow calderas; eruptions from the bounding-fault zone are most common in resurgent calderas, reflecting renewed magmatic pressure. In addition to resurgence within single calderas, broader magmatic uplift occurs widely within silicic volcanic fields, reflecting isostatic adjustment to emplacement of associated subvolcanic batholiths. Large intrusions related to resurgence are exposed centrally or along the margins of some deeply eroded calderas.

A. Precollapse Volcanism

Volcanism prior to a major caldera-forming event may provide the only record of the rise to shallow crustal levels and early chemical evolution of the growing magmatic system that culminates in large-volume eruptions and caldera formation. Buoyant rise of the magma body may cause broad uplift and generation of incipient ring and radial fractures. Volcanic "leaks" from the evolving magma body commonly produce clusters of vents over the magma chamber, at times in linear or arcuate patterns controlled by nascent radial and ring faults, at others controlled by regional tectonic structures. Virtually all well-documented young calderas have formed at sites of immediately preceding volcanism, although the volume and composition of such premonitory activity may vary substantially. Many small calderas have formed at the summits of basaltic shield volcanoes (Hawaii, Galapagos) or within single stratovolcanoes, but large ash-flow calderas typically have subsided within clusters of preexisting cones and domes. At many caldera sites, the caldera-forming event has covered or caved away much of the near-source record of precollapse volcanism.

B. Morphologic and Structural Geometry

Major structural and morphologic elements of calderas (Fig. 3) include topographic rim, inner topographic wall, bounding faults (if present), structural caldera floor, intracaldera fill (mainly ponded ignimbrite and landslide debris from caldera walls), and the underlying magma chamber or solidified pluton. Although highly generalized and not intended to accurately depict relations at any actual caldera, such a model provides a basis for discussing caldera structural elements and subsidence processes, computing approximate volumetric proportions between subsidence geometry and caldera-filling deposits, and inferring relations between eruption and subsidence processes.

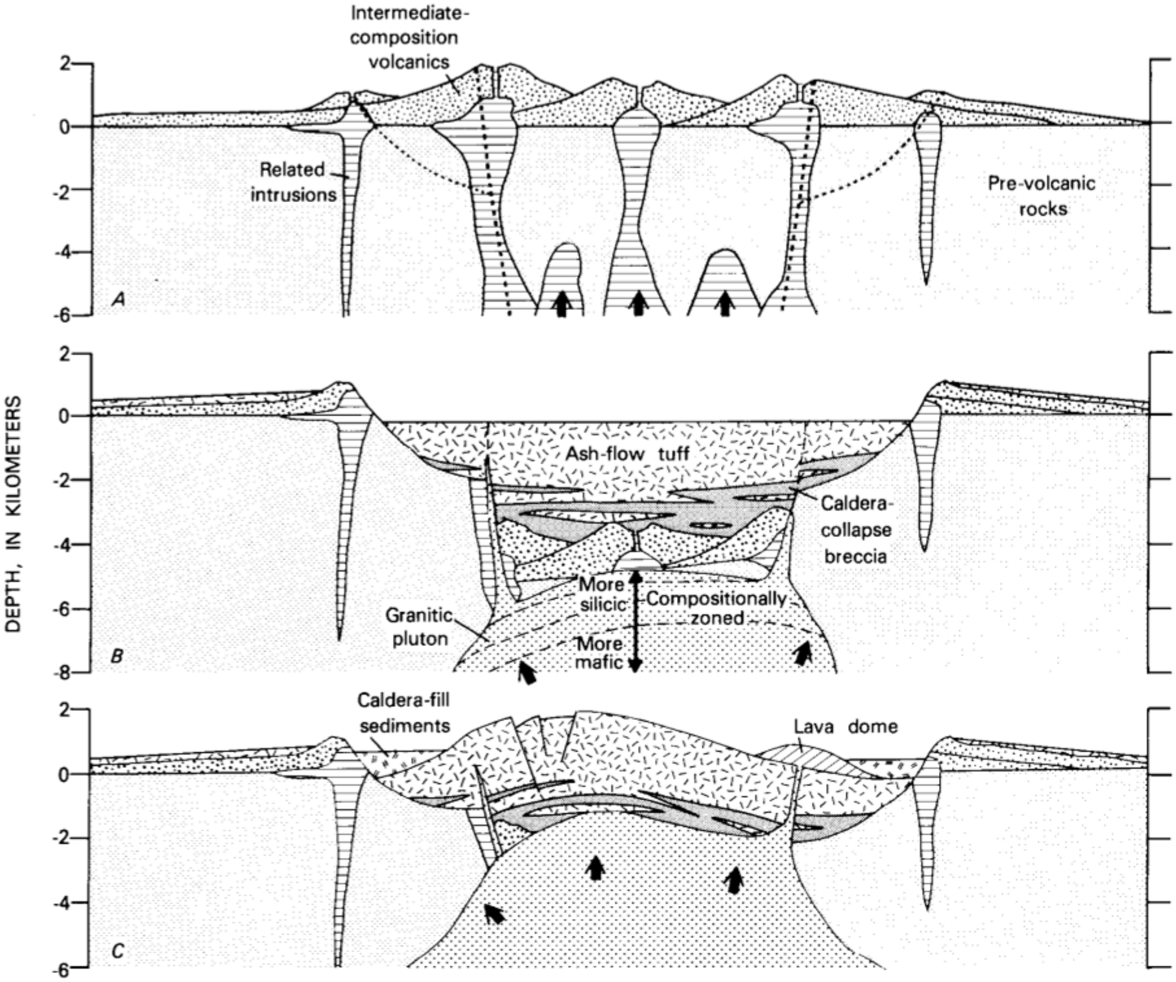
Intermediate-composition volcanics
Related intrusions
Pre-volcanic rocks
A
DEPTH, IN KILOMETERS
2
0
-2
-4
-6
-8
Ash-flow tuff
Caldera-collapse breccia
More silicic
Compositionally zoned
More mafic
Granitic pluton
B
Caldera-fill sediments
Lava dome
C

FIGURE 2 Generalized evolution of ignimbrite calderas (based largely on studies of Cenozoic calderas in the western United States). (A) Precollapse volcanism. Clustered intermediate-composition stratovolcanoes grow over isolated small high-level plutons that mark the beginning of accumulation of batholithic-size silicic magma body that will feed ignimbrite eruptions. Broad uplift related to emplacement of plutons may lead to development of arcuate ring fractures. The site of subsequent caldera collapse is indicated by dotted lines; heavy arrows indicate upward movement of magma. (B) Caldera geometry just after ash-flow eruptions and concurrent caldera collapse. Central area of clustered earlier volcanoes caves into collapsed area. Intracaldera tuff ponds during subsidence and is an order of magnitude thicker than cogenetic outflow ignimbrite sheet. Initial collapse along bounding faults is followed by slumping of oversteepened caldera walls and accumulation of voluminous collapse breccias that interfinger with ignimbrite in the caldera fill. Caldera floor subsides asymmetrically and is tilted to the left side of diagram. Main magma body underlies entire caldera area and is compositionally zoned or layered (or was, prior to eruptions), becoming more mafic downward. (C) Resurgence and postcaldera deposition. Resurgence is asymmetrical, with greatest uplift in area of greatest prior collapse. Extensional graben faults from over crest of dome. Some resurgent uplift is accommodated by movement along ring faults in sense opposite that during caldera subsidence. Magma body has risen into volcanic pile and intruded cogenetic intracaldera ignimbrite. Original caldera floor has been almost entirely obliterated by rise of magma chamber to near level of prevolcanic land surface. Caldera moat is partly filled by lava domes and volcaniclastic sediments. Hydrothermal activity and mineralization are prevalent late in cycle. [From Lipman, 1984].

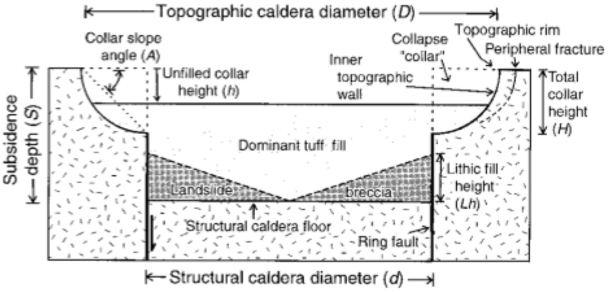

FIGURE 3 Generalized structural model of plate (piston) caldera subsidence, showing simplified geometric relations. Ring faults, which typically dip steeply, are arbitrarily shown as vertical. The landslide breccia is shown schematically at the base of caldera fill, in order to permit geometrically simplified calculation of overall volume relations, rather than the more actualistic complex interfingering that occurs in many calderas. Presence of subcaldera magma chamber, any resurgent structures, and postcollapse volcanic constructs are omitted. [From Lipman, 1997].

1. Topographic Rim

The topographic rim is simply the top of the escarpment that bounds the caldera, beyond which lie largely undisturbed outer volcanic slopes. The rim encloses both the subsided area and also the area of scarp retreat due to rock falls and mass wasting. For young calderas, the topographic rim defines the overall areal extent of subsidence, although outlying circumferential fractures at some calderas (e.g., Kilauea in Hawaii and Chegem in Russia) accompany modest additional sagging toward the main subsided area. For old calderas, erosional mass wasting first tends to enlarge the original topographic rim, but later erosion of outer slopes of the upper caldera edifice can also reduce the apparent topographic diameter.

2. Inner Topographic Wall

The topographic wall is typically steepest in its upper parts, commonly as precipitous cliffs at young calderas, but tends to have a concave profile that flattens downslope. Upper slopes of the inner topographic wall virtually never represent an unmodified subsidence fault scarp; rather, they develop in response to landslide enlargement and rock falls from oversteepened slopes during and after caldera collapse. At the base of the topographically enlarged caldera wall, intracaldera fill may deposit directly against caldera-boundary faults that have been unmodified by gravitational slumping (Glen Coe, Scotland; Lake City, United States; calderas of the Olso graben in Norway). Such contacts are rarely preserved, because continued caldera subsidence causes further faulting.

In plan view, the topographic walls of most large ash-flow calderas are scalloped by scarps of landslides and rock falls. Suggestions that topographic enlargement and scalloped embayments along some caldera walls result from irregular peripheral subsidence of overhangs along satellitic bounding faults may be valid for irregular walls of basaltic pit craters and other small collapse structures (e.g., pit craters of Kilauea's east rift zone) but are inconsistent with the structurally coherent bedrock stratigraphy that has been mapped and documented by drilling along the footwall embayments in many large calderas (Creede, La Garita, Timber Mountain, and Valles in the United States; Aso in Japan; Campi Flegrei in Italy; Chegem in Russia), some projecting 5 km or more back from the main caldera wall. Such shallowly rooted embayments can only have formed by surficial collapse and insliding along oversteepened caldera walls, an inference that is confirmed by the provenance and large volume of slide material in adjacent caldera fill. Large scallops in walls of some multicyclic ash-flow calderas may be related to successive eccentrically overlapping subsidences associated with recurrent eruptions (Toba, Santorini). At other multicyclic calderas, late large eruptions have caused subsidence of the entire prior caldera area, and earlier subsidence structures lie within the late caldera (e.g., Valles and Platoro in the United States and Taupo in New Zealand).

3. Collapse Collar

Material removed by mass wasting and scarp retreat defines a collapse collar (Fig. 3): the volume of rock lying between the topographic caldera wall and the structural caldera boundary. Average overall slopes of inner topographic walls (collar slope angle) are moderate: 25° is typical, and 45° a probable upper limit. Lower slopes along the collapse collar, dipping as gently as 10–15°, are the only parts preserved in many eroded calderas, where the inner wall is expressed as an irregular unconformity between precaldera and caldera-filling rocks. Gentle dips on lower slopes of the collapse collar permit exposure, by erosion or drilling, of precaldera rocks at shallow depths well inboard from the topographic rim. Such geometric relations had been inferred to demonstrate funnel geometry for large calderas such as Aso, Japan, where geophysical and drilling data now document the presence of concealed bounding faults.

4. Bounding Faults

Arcuate bounding faults (ring faults) are exposed at some deeply eroded volcanic areas (mainly 5 km and greater in diameter), unambiguously defining plate (piston) subsidence at calderas, as well as at many volcanic "cauldrons" and plutonic ring complexes in older terranes. The presence of bounding ring faults in some less eroded calderas can be inferred from the distribution of caldera-forming or postcollapse vents and symmetrical resurgent uplift of caldera-filling volcanic rocks. Ring faults can accommodate uplift, as well as subsidence: e.g., domical magmatic resurgence at Lake City caldera, United States, occurred along the same faults as earlier had accommodated caldera collapse, and magma was injected as partial ring dikes. Similarly, trapdoor uplift within the 45-ka Cinque Denti caldera in Pantelleria was accommodated by reversed movement along old ring fractures.

Most observed ring faults are near-vertical or dip steeply inward. Ring faults that dip steeply inward at shallow crustal levels may steepen with depth and dip outward at levels just above the magma chamber into which the caldera subsided. Such a geometry may reflect sequential change, from an early stress field related to magma withdrawal (Fig. 4A) to later stresses related to slumping along caldera walls, as the thickness of precaldera rocks in the subsiding region is reduced by stoping during continued upward rise of magma (Fig. 4C). Because of such complexities and uncertainties, all ring faults are shown arbitrarily as vertical in Figs. 3 and 6. Some sizable young calderas lack clear evidence for the presence of arcuate bounding faults, but limited erosion depths typically preclude unambiguous interpretation. At many calderas, regional tectonic trends have influenced the geometry of collapse to varying degrees, but deeply eroded calderas bounded by strongly polygonal faults appear to be much less common than those with arcuate fault boundaries.

Circumferential extensional fractures peripheral to the topographic rims of young calderas are commonly associated with recurrent gravitational slumping of the free face of the inner caldera wall. Such peripheral fractures at Kilauea caldera have opened and closed repeatedly during major historical earthquakes, independently of caldera eruptive or subsidence events.

5. Intracaldera Fill

Intracaldera fill provides key evidence of caldera processes because most or all large calderas collapsed during the associated eruptions, and ignimbrites and interleaved caldera-wall slide breccias accumulated to multikilometer thickness within the subsided area. Distributions and volumes of slide breccia vs intracaldera tuff provide critical evidence on timing and geometry of subsidence.

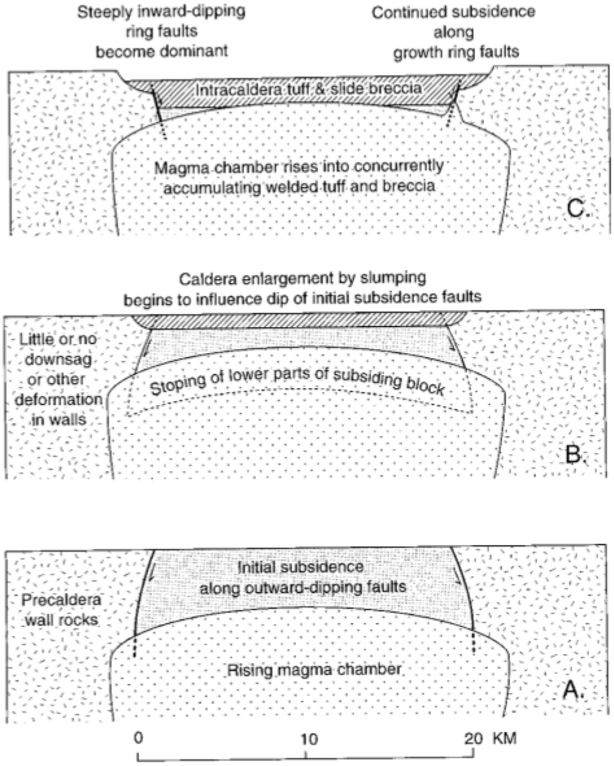
Steeply inward-dipping ring faults become dominant
Continued subsidence along growth ring faults
Intracaldera tuff & slide breccia
Magma chamber rises into concurrently accumulating welded tuff and breccia
C.
Caldera enlargement by slumping begins to influence dip of initial subsidence faults
Little or no downsag or other deformation in walls
Stoping of lower parts of subsiding block
B.
Initial subsidence along outward-dipping faults
Precaldera wall rocks
Rising magma chamber
A.
0
10
20 KM

FIGURE 4 Possible evolution of ring-fault geometry, in which initial outward-dipping ring faults are replaced by inward dips, as progressive subsidence destabilizes the caldera walls and continued upward rise of magma reduces the thickness of the subsiding plate or piston.

In addition to ignimbrites and slide breccia that accumulated synchronously with caldera subsidence, most pre-Holocene calderas are partly to completely filled by younger lavas and tuffs erupted from postcollapse caldera-related vents, sedimentary debris eroded from adjacent volcanic highlands, and volcanic deposits derived from other volcanic centers. Such postcaldera deposits tend to conceal the primary volcanic structures, especially at nonresurgent calderas, impeding interpretation of subsidence processes or even the presence of some large calderas.

6. Caldera Floor

The geometries of caldera floors have been well documented at only a few large ash-flow calderas (e.g., Scafell in England; Tucson, Organ Mountain, Stillwater Range in the United States; Kumano in Japan), and the typical degree of disruption during subsidence remains uncertain. The structural floor is the subsided precaldera land surface, in contrast to the topographic caldera floor exposed at the surface within a young caldera. Few calderas that provide a clear record of volcanic evolution are eroded to depths sufficient to expose their structural floors, and in many, cogenetic magma has risen to such shallow depth that much of the floor has been destroyed. Structures at many deeply eroded calderas are further complicated or obscured by multiple subsidence events associated with successive ignimbrite eruptions or by later regional tectonism.

For some calderas (Chegem, Cerro Galan, Lake City), exposures of structurally coherent fill that accumulated within the caldera concurrently with subsidence provide strong evidence of, at most, limited disruption of the caldera interior. Even where the fill consists of massive ignimbrite, partial cooling breaks, flow-unit partings, compositional boundaries, and interlayered landslide breccia sheets commonly provide stratigraphic markers to evaluate fault disruption within calderas. Most faulting of intracaldera fill that has been documented so far by such stratigraphic features occurred not during subsidence but during later resurgent doming or other uplift of the caldera floor, as indicated by displacement of all caldera-fill units (e.g., Valles, Bachelor, and Campi Flegrei). Intracaldera deposits are less well exposed in most nonresurgent calderas than those on resurgent domes, but erosionally inverted topography at some nonresurgent calderas, such as Chegem in Russia and Superstition in the United States, provides exceptional exposures of widely continuous flow units and cooling breaks within thick exposed intracaldera tuff without significant fault disruption. Complex disruption of caldera floors may accompany overlapping subsidence during successive caldera-forming eruptions, but available evidence suggests that most large calderas subside fairly coherently during individual eruptions.

Growth faults, with upward decreasing displacement, should be present within syncollapse fill if the caldera floor were significantly disrupted during subsidence, but documented examples are rare. Because synsubsidence faulting would disrupt high-temperature ignimbrites as they welded, growth faults should be marked by conspicuous local rheomorphic zones, even where offset of lithologic markers was obscure. Widespread growth faulting has been well documented at the Ordovician Scafell caldera, but these faults variably displace multiple separate eruptive units, and relations to individual collapse events are less clear.

Small calderas (less than a few kilometers in diameter) merge in geometry with diatremes and likely lack a coherent floor. Rather, the inner walls converge downward into the eruptive conduit in a funnel-shaped geometry, as discussed later.

7. *Subcaldera Magma Chamber*

Magma chambers, preserved as solidified plutons or batholiths, are exposed in many deeply eroded ash-flow calderas, as indicated by petrologic and age correlations with erupted volcanics (Chegem in Russia; Lake City, Questa, and Turkey Creek in the United States; Kumano in Japan). Such plutons have commonly been emplaced within a few kilometers of the regional volcanic surface, some roof zones protruding into the syneruptive fill of the associated caldera. Accumulation of low-density silicic magma in a large shallow chamber, which can generate uplift and tensile stresses at the surface, could be important in initiating ring faulting and permitting caldera collapse. Tumescence associated with growth of a subvolcanic magma chamber has been recorded instrumentally during many monitored eruptions and episodes of volcanic unrest, but the magnitude of uplift has typically been too small to generate geologic structures that would be detectable in the prehistoric record.

Shallow depths to incompletely solidified caldera-related magma chambers are documented for a few active calderas by seismic-attenuation studies, magnetic curie-temperature depths, and other geophysical data. Such studies indicate the presence of magma at depths as shallow as 4–7 km at the 0.76-Ma Long Valley caldera in the United States. At the historically active Rabaul caldera in Papua, New Guinea, seismic hypocentral locations define an elliptical area 5 × 10 km, interpreted as bounded by ring faults, that overlies a central region of low seismicity at depths below 2–4 km that is inferred to represent the present-day magma chamber. For some older systems, the petrology of eruptive products also requires shallow depths of magmatic crystallization (e.g., presence of clinopyroxene rather than hornblende phenocrysts in H_2O-rich magma).

Although only small intrusions are exposed at present erosional levels in eroded Tertiary calderas, geophysical data commonly document the subsurface presence of large magma bodies or solidified granitic rocks. For example, the clustered Tertiary calderas of the San Juan volcanic field, United States, lie within a large negative Bouguer gravity anomaly (−50 mgal), characterized by steep marginal gradients, that has been interpreted to delimit a shallow batholith about 75 × 150 km across with its roof at an average depth of about 5 km. Upper crustal accumulation and fractionation of magma in the subvolcanic batholith is interpreted to have been recorded by the regional volcanic succession in the San Juan field, involving eruption of intermediate-composition lavas from scattered volcanoes, followed by large ash-flow eruptions associated with caldera collapse (Fig. 2). Individual calderas of the central cluster, as well as the overall caldera cluster, have only minor gravity expression, indicating that the density of caldera-filling rocks is only a minor component of the overall anomaly.

Detailed inferences about shapes of exposed intrusions and collapse geometry commonly remain ambiguous at eroded calderas, because subvolcanic magma bodies likely continue to evolve in composition, shape, and depth after cessation of the caldera-forming volcanism. Despite such uncertainties, some consistent relations have emerged between collapse geometry and pluton shape. For example, some trapdoor calderas expose high-level plutons along the most subsided side of an asymmetrical caldera (Silverton, Tucson), suggesting that maximum subsidence was influenced by the shallowest portion of the magma chamber. At several calderas, high-resolution dating has documented cooling of subcaldera plutons within brief time intervals after caldera subsidence. For example, at Chegem in Russia the intracaldera tuff and central granitic intrusion yield ^{40}Ar/^{39}Ar ages that are indistinguishable at 2.82 ± 0.02 Ma.

Several recent studies have inferred important roles for sills or shallow domical laccoliths of fine-grained hypabyssal rocks during caldera collapse and resurgence (Turkey Creek and several "laccocalderas" in the United States). Floors of such intrusions are generally not exposed, however, and their overall geometry remains uncertain. Other deeply eroded calderas expose large steep-sided subcaldera plutons containing granitic textures transitional to typical mesozonal batholithic bodies (e.g., Questa, United States). Perhaps resurgent intrusions initially spread as sill-like bodies near the base of the caldera fill, developing into stocklike plutons as continued emplacement of intrusive material gravitationally loads caldera floor rocks and encourages block stoping.

Any large caldera (>20-km diameter) must necessarily have been underlain by a large-scale magma chamber of broadly tabular aspect ratio in order for the intrusion to reside in the middle and upper crust, but to describe such large granitic bodies as laccoliths seems misleading. The concept of a laccolith, as used by most geologists, implies making space by doming the roof rocks; no such evidence exists for most large plutons, including sizable upper crustal bodies with associated volcanism. Few if any large subvolcanic batholiths can be demonstrated to have strongly domed their roofs, and many are composite aggregates of multiple plutons with smaller map dimensions and steep intrusive contacts. Many subcaldera plutons have steep margins, cut across gently dipping wall rocks, and intrude associated volcanic sequences (Glen Coe, Peruvian Andes, Olso Graben). The most feasible mechanism for generating the space needed for a batholith to rise into the upper crust in places like the San Juan Mountains, where regional tectonic faulting is nonexistent, is by large-scale stoping, and caldera formation can be considered a near-surface component of such stoping. Crustal rocks have negligible strength to support regional loads, as long recognized from isostatic adjustments to loading by glaciers or even manmade reservoirs. Much additional space for growing upper crustal batholiths likely results from subsidence of crustal rocks of the magma-chamber floor.

C. Postcollapse Magmatism and Resurgence

Volcanic activity within and around margins of calderas after collapse can include eruptions from vents randomly scattered within the caldera, eruptions localized along regional structural trends, and eruptions along the caldera margins. Such events may begin shortly after initial collapse and continue intermittently for millions of years. Such postcollapse volcanism can closely constrain the timing and nature of differentiation in the subcaldera magma chamber. Thermal modeling of heat flow around young calderas suggests that heat loss by hydrothermal convection is so great that shallow caldera-related magmatic systems cannot survive more than a few hundred thousand years without replenishment by additional magma. Long histories of postcollapse volcanism at many calderas suggest that such replenishment is common.

Renewed rise of magma after collapse has resurgently uplifted many calderas (Fig. 5). Such uplift varies from doming or block uplift of the cores of individual calderas to broad regional uplift of one or more calderas and adjacent portions of the volcanic field. Best known, although relatively uncommon, is symmetrical resurgent doming of the caldera floor, as in the Valles, Creede, Timber Mountain, and Turkey Creek calderas in the United States. Resurgent calderas appear to be more numerous within continental crust, as along the Cordilleran margin of the Americas than in young volcanic arcs within ocean basins. The first identified resurgent caldera was Toba in Sumatra, however, and although only a few of the numerous Tertiary calderas in Japan have been described in the international literature, several are reported to contain resurgently uplifted blocks

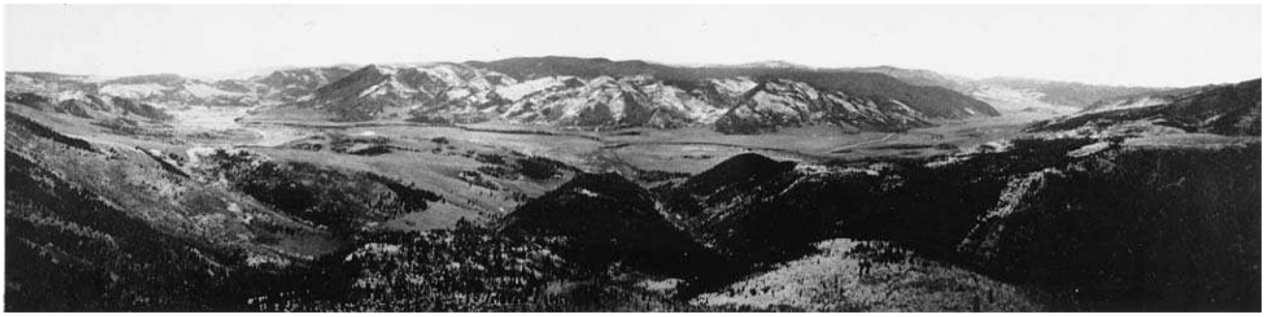

FIGURE 5 The resurgent Creede caldera, Colorado, as viewed from near its northwest topographic rim. Broad rounded hill in middle distance is the postcollapse resurgent dome. Arcuate valley marks topographic moat, now followed by the Rio Grande (see Fig. 7), which is underlain by Oligocene caldera lake sediments. Despite formation at 26.5 Ma, primary volcanic morphology is well preserved due to infilling of the caldera moat by sediments that have only been erosionally excavated in geologically recent time. [Photograph by J. C. Ratté, U.S. Geological Survey.]

or high standing intrusions (e.g., Onikobe, Hiwada, and Okueyama).

In addition to resurgent structures that are specific to individual calderas, some silicic volcanic fields containing clusters of calderas show weak regional uplift centrally within the volcanic field that is interpreted as indicating broad late resurgence over an underlying batholithic magma body larger than any individual caldera. Such broad uplift can be reflected in young volcanic fields by regionally high topography, mild tilting of volcanic strata away from central parts of the field, and extensional structures trending between individual calderas.

D. Hydrothermal Activity and Mineralization

Hydrothermal activity and mineralization can accompany all stages of ash-flow magmatism, becoming dominant late during caldera evolution. Caldera-forming ignimbrite eruptions are probably unlikely to directly produce major ore deposits, because such explosive activity would tend to disperse any concentrations of metals that accumulated in upper parts of precaldera magma chambers, but the resulting caldera structures can be important loci for subsequent magmatic and hydrothermal ore-forming events. Much rich mineralization is millions of years younger than caldera collapse, where the caldera served primarily as a structural control for late intrusions and associated hydrothermal systems. Some calderas show little or no evidence of associated hydrothermal activity.

III. CALDERA-SUBSIDENCE PROCESSES

Prior approaches to subdividing and classifying calderas have tended to distinguish caldera types based on eruption style and magma composition at representative volcanoes: for example, Krakatoan type, Valles type, Katmai type, etc. Size of the eruption and geometry of the cogenetic magma chamber also bear on subsidence processes. For example, stated distinctions between "Krakatoan" and "Valles" caldera types (foundering of the top of a composite volcano versus subsidence independent of preexisting volcanoes) are mainly functions of reservoir area and eruption volume, which influence resulting caldera size without any necessary difference in subsidence processes.

Alternatively, the broad diversity of well-documented ash-flow calderas can be considered in terms of a continuum of features and processes. Many calderas have such varied transitional geometries and structures that subclassification into discrete types seems less useful than relating subsidence geometry and resulting structures to a few geometrically simplified end members (Fig. 6). Many larger calderas dominantly involve *plate (piston) collapse* of a coherent floor, bounded by steeply dipping faults. *Trapdoor subsidence*, bounded by an incomplete arcuate fault and by a hinged segment, reflects early downsagging and incipient plate collapse. Simple *downsag subsidence* seems rare, although many plate-subsidence calderas contain inward-tilted blocks along their margins. A component of *piecemeal-fault disruption* of caldera floors is fairly common, although such structures do not seem to accommodate the bulk of subsidence in

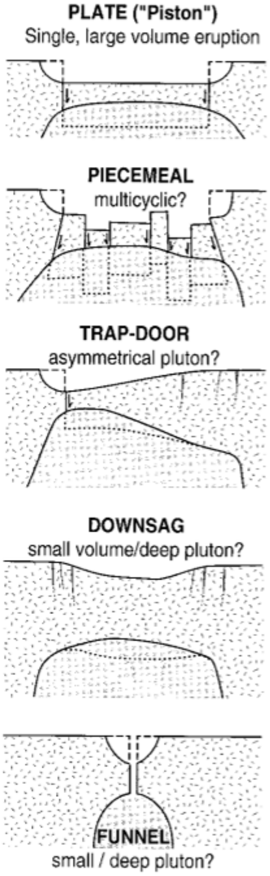

FIGURE 6 Schematic models of alternative subsidence geometries in relation to depth and roof geometry of underlying magma chamber. Dashed lines indicate postsubsidence depths of downdropped caldera floor blocks, which are inferred to have been partly removed by stoping into magma chamber during and immediately after caldera collapse. [From Lipman, 1997].

most large calderas. Pervasively brecciated *chaotic disruption* of subsiding caldera floors is rare, at least at calderas more than a few kilometers across. Small calderas (<3–5 km in diameter) commonly have a *funnel geometry* because of dominant enlargement by slumping into an areally restricted vent.

A. Plate Subsidence

Many large calderas have long been recognized to involve plate (piston) subsidence of a relatively coherent floor, bounded by steeply dipping bounding faults with kilometer-scale displacements ("Valles type"). Ring and arcuate intrusions have long been recognized as deeply eroded analogs of large plate-subsidence calderas. Displacements along the bounding faults of a plate-subsidence structure, by definition, must be much greater than on any faults within the caldera floor, but some calderas contain structures transitional toward a piecemeal-subsidence geometry. At a few calderas that are well exposed and adequately studied (Glen Coe in Scotland; Grizzly Peak, Bachelor, Stillwater Range in the United States), the subsided lid over the source magma chamber was variably faulted (offsets of tens to hundreds of meters) due to differential movement during ash-flow eruptions and postcollapse magmatism, but the scale of internal disruption is typically an order of magnitude less than displacements on bounding faults. At the type Valles caldera, drilling and geophysical data show that the caldera floor was locally disrupted by faulting that occurred largely or entirely during postcollapse domical resurgent uplift. In some places, such as Glen Coe, current interpretations diverge as to whether subsidence was dominantly along the bounding ring faults or by internal disruption. Subsidence by highly chaotic disruption of the floor has not been clearly documented for any large caldera.

Many plate-subsidence calderas, 10 km or more in diameter and bounded by ring faults, have been recognized recently in Japan, as Tertiary volcanic areas have been mapped geologically and explored by drilling (e.g., work by Yamamoto and associates in the Inawashiro and Aizu districts of northern Honshu). Some calderas as small as 4–5 km in topographic diameter appear to have fault-bounded floors, based on evidence for ring faults and structurally coherent caldera fill. Examples in the United States include the 8 × 10 km Crater Lake and 4.5 × 8 km Kulshan calderas in the Cascade Range.

B. Downsag Subsidence

Large-scale downsag subsidence has been inferred by some researchers to be common, based on inward-sloping topography, inward-tilted wall rocks, and apparent absence of large-displacement bounding faults at some major calderas. Many large plate-subsidence calderas involve subordinate downsag, but no deeply subsided calderas appear to have been well documented where downdropping is accommodated dominantly by inward tilting without major bounding faults.

Components of downsag, in conjunction with dominant subsidence along bounding faults, appear to be common and include (1) mild flexuring and fracturing during initial subsidence prior to establishment of a well-defined fault boundary, processes that accompany inception of all faulting of brittle upper crustal rocks; (2)

incomplete ring-fault subsidence, transitional between downsag and plate subsidence, that produces a hinged or trapdoor caldera; (3) subordinate sagging of the structural caldera floor within bounding ring faults; and (4) gravitationally induced inward late tilting and fracturing of oversteepened unstable caldera walls, in conjunction with slumping and landsliding. Monoclinal flexures and extensional fractures probably accompany inception of all bounding faulting, as in regional tectonic faulting of brittle upper crustal rocks. The appearance of downsag on the flanks of multicyclic caldera depressions can also be generated by volcanic units draped over a preexisting caldera or structural basin.

Because most calderas resulting from large ignimbrite eruptions subside several kilometers or more and are topographically enlarged by late slumping, clear evidence for initial flexuring and fracturing is rarely preserved. Subordinate downsagging is common within caldera floors bounded by well-developed ring faults that accommodate the bulk of total subsidence (e.g., Glen Coe in Scotland, Sabaloka in Sudan, Grizzly Peak in the United States). Saucer-like geometry of an otherwise coherent caldera floor may result from inward dips along the bounding faults, inheritance from broader downsagging during initial subsidence prior to full development of the bounding faults, or generally from localized subsidence of the thermally weakened thin lid over a large shallow magma chamber as a result of focused magma drawdown during rapid eruption. Some large coherently rotated inward-dipping blocks along caldera walls are incipient slide blocks, related to second-order enlargement of the topographic caldera wall by landsliding, rather than primary collapse structures bounded by steeply dipping faults or fractures.

Inward-dipping foliations of intracaldera welded tuff that decrease in dip upsection have been cited as evidence of downsag during eruption and subsidence at several calderas (Chegem, Lake City). Alternatively, such geometries can also readily be interpreted as due to differential primary depositional compaction of intracaldera tuff against caldera walls and caldera-margin slide breccias without need for any downsagging. Compaction dips typically are highly varied near caldera walls (locally approaching vertical), and tuff foliations commonly correlate closely with adjacent buried slopes. Older volcanic strata in walls of many calderas dip horizontally or gently outward, and most prevolcanic strata are in continuity with regional structural attitudes—geometries incompatible with downsag as a dominant subsidence process.

Many basaltic lava-flow calderas (Hawaii, Galapagos, Olympus Mons, etc.) that have subsided repeatedly in small increments have an overall inward downstepping geometry that has also been described as downsagged or downwarped. Such a geometry of nested sequential collapses within a single caldera during recurrent lava eruptions or intrusions along rift zones, although differing in scale from catastrophic caldera collapse during individual large explosive eruptions, may involve similar processes and be transitional to the multicyclic collapse histories that characterize many ash-flow calderas. In addition to small-scale incremental caldera collapse at basaltic volcanoes, at least some of these (e.g., Kilauea and Mauna Loa) also preserve evidence of longer term cycles of caldera filling and recurrent collapse. Nested recurrent collapse events, although cumulatively generating an inward-sloping composite subsidence profile, need not involve major downsag during individual eruptions and caldera-subsidence events.

C. Trapdoor Subsidence

Trapdoor subsidence, bounded by a partial ring fault and by a hinged segment, constitutes incomplete or incipient plate collapse, intermediate between plate and downsag subsidence processes. Such partial subsidence may be related to smaller eruptions, an asymmetrical magma chamber, or regional structural influences. Geometrically well-defined examples of trapdoor subsidence in the western United States include Silverton, Organ Mountains, Eagle Mountain, Big John, Whitehorse, and Tucson Mountains calderas. Well-described hinged or trapdoor calderas elsewhere include Snowdon caldera in Wales, Bolsena in central Italy, and Sakugi in southwest Japan.

D. Piecemeal Disruption

Small-displacement piecemeal faulting of subsiding caldera floors is probably common. Fracturing during subsidence has been demonstrated for a few calderas by growth-fault deformation of an intracaldera ignimbrite concurrently with welding. Complex piecemeal subsidence of caldera floors on a coarse scale, involving arrays of arcuate or rectilinear growth faults without large-scale bounding structures, has been interpreted as the dominant subsidence process for a few calderas. Such features could result from interaction with the prevolcanic structural grain or from intricate fracturing of the caldera floor during a single eruption, but without clear evidence of large-scale growth faulting during a single eruption, piecemeal fracturing of a caldera floor can be open to alternative interpretations.

Geometrically complex fracturing should be expected at sites of multiple nested or overlapping collapses that cause incremental subsidence during successive ash-flow eruptions, as is likely present in floors of overlapping caldera complexes that subsided recurrently at intervals of tens to hundreds of thousand years (documented by drilling data for Dorobu caldera in Japan, Bolsena and Latera calderas in Italy, and clustered calderas in the southwest Nevada volcanic field). Other multicyclic calderas, probably comparably geometrically complex but lacking caldera-floor structural data, include Santorini in the Aegean, the Kagoshima Bay area of southern Japan, and the central San Juan caldera complex in the United States). Such complexities in caldera-floor geometry may also be indicated by scattered or transverse distributions of postcaldera postcollapse vents within recurrently subsided calderas, as at Campi Flegrei, Aso, or Santorini. Analogous complexities in subsidence geometry appear likely for the historically active Rabaul caldera in Papua, New Guinea, where geologic relations document successive overlapping caldera subsidences during the past few hundred thousand years, even though present-day seismicity defines a geometrically simple ring structure for the active caldera.

The well-exposed Ordovician Scafell caldera in the English Lake District has been interpreted by Branney as a piecemeal subsidence structure, involving dispersed subsidence along growth faults during a single eruption, but the multiple intracaldera depositional units that have been mapped there appear to record diverse eruption and emplacement processes during accumulation of intracaldera fill. The stratigraphically complex fill at Scafell thus differs from the thick ignimbrite accumulations during single eruptive cycles at many younger calderas and suggests, alternatively, that subsidence could have been incremental during successive eruptions over a sustained time interval.

At the widely known Glen Coe caldera in Scotland, recurrent block faulting, with displacements of tens to a few hundred meters, accompanied successive early eruptions of relatively small-volume pyroclastic deposits. Much deeper subsidence along bounding ring faults at Glen Coe appears to have been associated with more voluminous later ignimbrites. The cauldron block subsided at least 1 km, as recorded by the thickness of preserved volcanic sequence, but this amount is a minimum because correlative volcanic rocks are not preserved outside the subsided block. Despite emphasis of recent work on the role of piecemeal faulting at Glen Coe, its overall structure seems reasonably interpreted as dominated by subsidence along the bounding ring faults, with smaller scale breakup of the floor largely preceding development of the ring-fault subsidence.

E. Chaotic Subsidence

Chaotic subsidence, marked by intense wholesale disruption and brecciation of caldera-floor rocks, has been inferred to be an important caldera-forming process in some reviews, but such processes have not been documented for any well-exposed large ash-flow calderas. Chaotic subsidence has been proposed as a process (1) to generate low-density material within calderas that can account for the observed negative gravity anomalies and (2) to generate lithic breccias by collapse of the roof over a depressurizing magma chamber. However, observed gravity anomalies in calderas can be modeled successfully with alternative assumptions, and voluminous lithic breccias within many calderas are demonstrably formed by gravitational failure and landsliding of oversteepened walls adjacent to bounding faults. Thick megabreccias exposed in deeply eroded calderas typically are interleaved conformably with ash-flow tuff, indicating that such breccias are depositional units of the caldera fill, rather than drastically disrupted floor. Large landslides from the inner caldera walls (collapse collar volume of Fig. 3) are also a potential source of voluminous extracaldera lithic material, in addition to direct vent erosion, that could be entrained in the eruption column and emplaced as lithic lag breccia; chaotic disruption of floor or vent material need not be the sole or even dominant source. The volumes of lithic lag breccia in proximal outflow deposits are typically small in comparison to the slide breccias that accumulate within the subsided area.

F. Funnel Calderas

The term "funnel shaped" is potentially ambiguous for caldera structures. Virtually all calderas are funnel shaped in overall geometry in the sense that their topographic walls flare outward from the structural boundaries due to gravitational slumping (Fig. 3). A funnel-shaped structural boundary could also result from severe downsag or piecemeal subsidence or, probably more commonly, from recurrent subsidence during successive eruptions.

Small calderas (<2–4 km in diameter at topographic rim) commonly have a simple funnel geometry, because enlargement by slumping of the inner wall into an areally restricted vent is the dominant process in establishing the overall size of the subsided area (Fig. 6). Such calderas are associated with explosive eruptions from a central vent, lack a bounding ring fault or a coherent subsided block, and probably overlie relatively small (or deep?) magma chambers. Well-documented funnel calderas, associated with relatively small ash-flow eruptions, include Nigorikawa and Sunagohara calderas in Japan, which are well constrained in three dimensions by geothermal drilling, and Red Hills in the United States. Such funnel calderas appear to merge in geometry and structural type with diatremes associated with explosive eruption of more mafic magma to form tuff rings and maars.

Based mainly on modeling of gravity anomalies, some large young calderas, especially in Japan (Aira, Aso, Kuttyaro), have been inferred to have a funnel structure attributed to broad upward flaring of the primary eruption conduit. Such funnel structures have been inferred to develop in relatively weak crusts of young island arcs, in contrast to ring fault and plate subsidence of calderas in cratonic environments. However, no large funnel structures have been clearly documented for eroded calderas in Japan, even though many ring-fault calderas and plate-subsidence structures have recently been recognized in eroded Tertiary volcanic fields.

A further complexity for large calderas inferred to have funnel geometry is the ambiguity of interpretations based on gravity data. A plate-subsidence structure with lithic debris concentrated near structural margins, as is commonly observed in eroded calderas, could generate a gravity profile indistinguishable from a funnel structure. Geometrically simplistic gravity modeling of some Japanese calderas as funnel shaped (e.g., Aso) is complicated by recurrent eruption of multiple large ash-flow sheets and multistage incremental subsidence. Recent detailed processing of gravity data and results from deep drilling at Aso suggest multiple flat-bottomed gravity lows and an overall "piston–cylinder type structure rather than a funnel-shaped structure." Elsewhere, deep erosional exposure and/or exploration drilling has documented that an overall stepped funnel-like geometry can result at large ash-flow calderas from multistage subsidence along nested ring fractures (e.g., Campi Flegrei, Grizzly Peak, and several San Juan caldera complexes).

G. Ignimbrite "Shields"

While caldera sources have been identified worldwide for most well-preserved large ash-flow sheets, among the late Tertiary volcanoes spectacularly exposed on the altiplano of the central Andes are silicic centers where a large-volume tuff sheet dips gently outward from a central lava dome complex. Initially interpreted mainly from satellite images for this difficult-of-access high-altitude region, these have been described as "ignimbrite shields" that erupted without significant caldera collapse or resurgence. Ignimbrite shields have been proposed as an important but little recognized class of explosive silicic centers that reflect eruption from relatively deep magma chambers.

Because Andean volcanologists have also described many plate-subsidence and resurgent calderas similar to ash-flow centers elsewhere, the apparent absence of comparable ignimbrite shields in North America and elsewhere suggests possible interpretive problems with the Andean ignimbrite "shields" resulting from their lack of dissection, inaccessibility, and resulting limited field study. At least some ignimbrite "shields" seem alternatively interpretable as conventional (structurally bounded) nonresurgent calderas, surrounded by their ignimbrite aprons, that were then filled to overflowing by younger intracaldera lavas and tuffs.

Potentially analogous nonresurgent large calderas that were once completely buried by later lava flows and other volcanic deposits have been variably exposed by erosion in many volcanic areas (Black Mountain and Kane Springs Wash calderas in southwest Nevada and several calderas of the San Juan field in the United States; Cappadocia field in Turkey). Some intracaldera and caldera-margin constructs in the San Juan region were stratovolcanoes originally rising well above the regional terrain; others were clusters of smaller lava domes that interleave with pyroclastic-flow and volcaniclastic sedimentary deposits. The primary pre-erosion morphology of these filled calderas would have looked strikingly like the described "ignimbrite shields" of the Andes. In comparison with the altiplano region, and its superb exposures of near-pristine unvegetated volcanic features, the southern Rocky Mountains provide the advantage of exposing a third dimension in glacial canyons a kilometer or more deep (along with disadvantages such as heavy vegetation).

H. Volcano-Tectonic Depressions

Inferred sources for some large ash-flow eruptions, which have been interpreted during reconnaissance studies as having vented directly from regional graben without developing localized calderas, have been described as volcano-tectonic depressions. While ash-flow eruptions and associated calderas have long been recognized as associated with extensional tectonics, no large pyroclastic eruptions have been shown unambiguously to be accompanied mainly by subsidence along regional fault troughs. Many typical calderas are known within and adjacent to major graben and rift zones. While the margins of subsequant calderas can be influenced by regional structures, some developing polygonal fault boundaries, drastic elongation of individual ash-flow subsidence structures along regional structural trends seems rare. To the contrary, some calderas along regional fault troughs are elongate perpendicular to their graben setting (Long Valley, Questa in the United States).

Association of ash-flow eruptions and caldera formation with regional extension leads to subsidence and burial of calderas along axes of graben, obscuring relations between volcanism and tectonic setting. Increasingly, detailed geologic, geophysical, and deep-drilling data have demonstrated that several regions commonly cited as volcano-tectonic depressions contain clusters of subequant calderas along the graben axis. Examples include the Taupo Volcanic Zone in New Zealand, where at least eight major ignimbrite calderas that have formed since 1.6 Ma are variably concealed beneath volcanic and sedimentary fill; the Toba depression in Indonesia, where four discrete ignimbrite eruptions were accompanied by caldera collapses from varying locations between 1.2 Ma and 75 ka; and Kagoshima Bay in Japan, where at least five calderas have erupted in the past million years. Even where bounding caldera faults consist of linear segments, the surface expression of caldera subsidence typically assumes a more nearly circular geometry as unsupported oversteepened walls slump into the central depression. On a smaller scale, even the strongest linear extensional structures can host circular volcanic subsidences, as exemplified by the development of equant pit craters along rift zones of Hawaiian volcanoes.

I. Discussion

Many well-studied calderas involve subsidence processes intermediate between idealized end members: ring-fault calderas can have complex boundaries involving more than a single arcuate bounding fault, both hinged downsag boundaries and ring faults are involved in trapdoor caldera subsidence, and floors within some ring-fault calderas have sagged or faulted at loci where magma erupted rapidly. Many calderas have such transitional attributes that subclassification can be inherently ambiguous and subjective. For example, the exceptionally exposed Grizzly Peak caldera in the United States, originally described as a nested ring-fault plate-subsidence structure, has impressed others as involving significant downsag and piecemeal subsidence. Interpreting caldera structures in terms of a continuum of subsidence styles, rather than as end-member types, can clarify relations between eruptive and structural processes in comparison to size of the eruption and the location and geometry of the cogenetic magma chamber.

The flaring of inner caldera walls as a result of landsliding during subsidence is a major process in generating caldera morphology and caldera fill. Lithic material, derived from vent enlargement and slumping of caldera walls, is more voluminous in caldera fills than commonly recognized from study of young, little-eroded calderas. In funnel calderas and small ring-fault subsidences, such lithic material is the dominant component of the caldera fill; model calculations suggest that some funnel calderas generate as great a volume of lithic debris as can be contained within the caldera (to the level of the unfilled collar height; Fig. 3). In larger calderas, wall-rock lithics are roughly equal in volume to the juvenile syncollapse volcanic ejecta that accumulate within the caldera. For the largest calderas, the proportion of intracaldera slide debris is lower, and only minor slide material would reach central parts of the caldera fill.

Caldera enlargement by landsliding and changes during postvolcanic erosion complicate comparisons of caldera geometries and structures. Postcollapse erosion of the inner caldera wall first enlarges the area of the topographic caldera basin, but continued erosional dissection down to structural boundaries of calderas will reduce the apparent caldera size. For example, the resurgent Creede caldera in the Oligocene San Juan volcanic field is presently best defined by the unconformity between caldera-filling and caldera-wall rocks (Fig. 7). This boundary is intermediate between the inferred initial topographic rim, parts of which are discontinuously preserved in the modern landscape, and the concealed structural boundary that is approximately defined by arcuate alignment of resurgent structures, postcaldera vents, and hot-spring upwelling loci. The structurally bounded subsided block has only about one-third the area of the original topographic caldera, demonstrating how heavily apparent caldera size is influenced by erosional depth. Despite such uncertainties, calderas associated with explosive eruptive activity worldwide have fairly similar ranges of dimensions, as approximated by plots of maximum diameter (Fig. 8). The largest calderas occur within continental crust, and many of these are composite, are multicyclic, or provide evidence of sequential subsidence into geometrically complex magma chambers.

IV. SOCIETAL IMPLICATIONS

Caldera-forming eruptions, like most volcanic activity, can have both positive and adverse impacts on the envi-

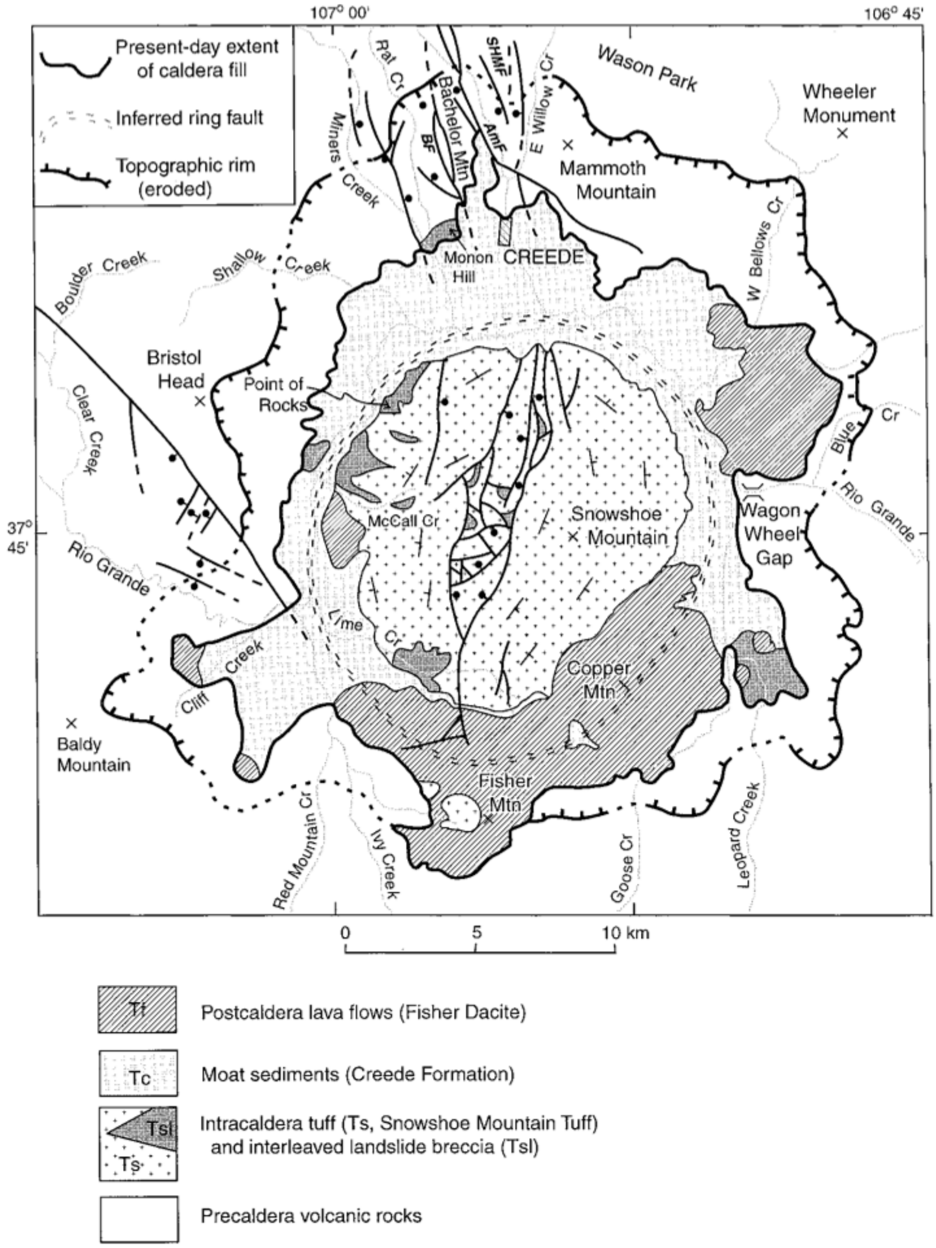
107° 00'
106° 45'
Present-day extent of caldera fill
Inferred ring fault
Topographic rim (eroded)
Rat Cr
SHMF
E Willow Cr
Wason Park
Wheeler Monument
Miners Creek
BF
Bachelor Mtn
AmF
Mammoth Mountain
W Bellows Cr
Monon Hill
CREEDE
Boulder Creek
Shallow Creek
Bristol Head
Point of Rocks
Clear Creek
Blue Cr
Rio Grande
Wagon Wheel Gap
McCall Cr
Snowshoe Mountain
37° 45'
Rio Grande
Lime Cr
Creek
Cliff
Copper Mtn
Baldy Mountain
Fisher Mtn
Red Mountain Cr
Ivy Creek
Goose Cr
Leopard Creek
0
5
10 km
Tf
Postcaldera lava flows (Fisher Dacite)
Tc
Moat sediments (Creede Formation)
Tsl
Ts
Intracaldera tuff (Ts, Snowshoe Mountain Tuff) and interleaved landslide breccia (Tsl)
Precaldera volcanic rocks

FIGURE 7 Generalized geologic map of the Creede caldera, United States, showing approximate location of eroded topographic caldera rim, present-day extent of moat-fill deposits, inferred buried ring fault, and late normal faults formed during resurgent doming and mineralization.

ronment and human society. Large explosive eruptions involve obvious hazards to people and property, while the volcanic ash generated by such events generates some of the world's most fertile soils and agricultural areas (cf. "Volcanic Soils"). Volcanic ash and aerosols generated on vast scales during caldera-forming events can adversely modify global climate. Caldera structures are important loci for valuable metallic ore deposits (cf. "Mineral Deposits Associated with Volcanism") as well as for hydrothermal heat that can become valuable energy resources (cf. "Exploitation of Geothermal Resources").

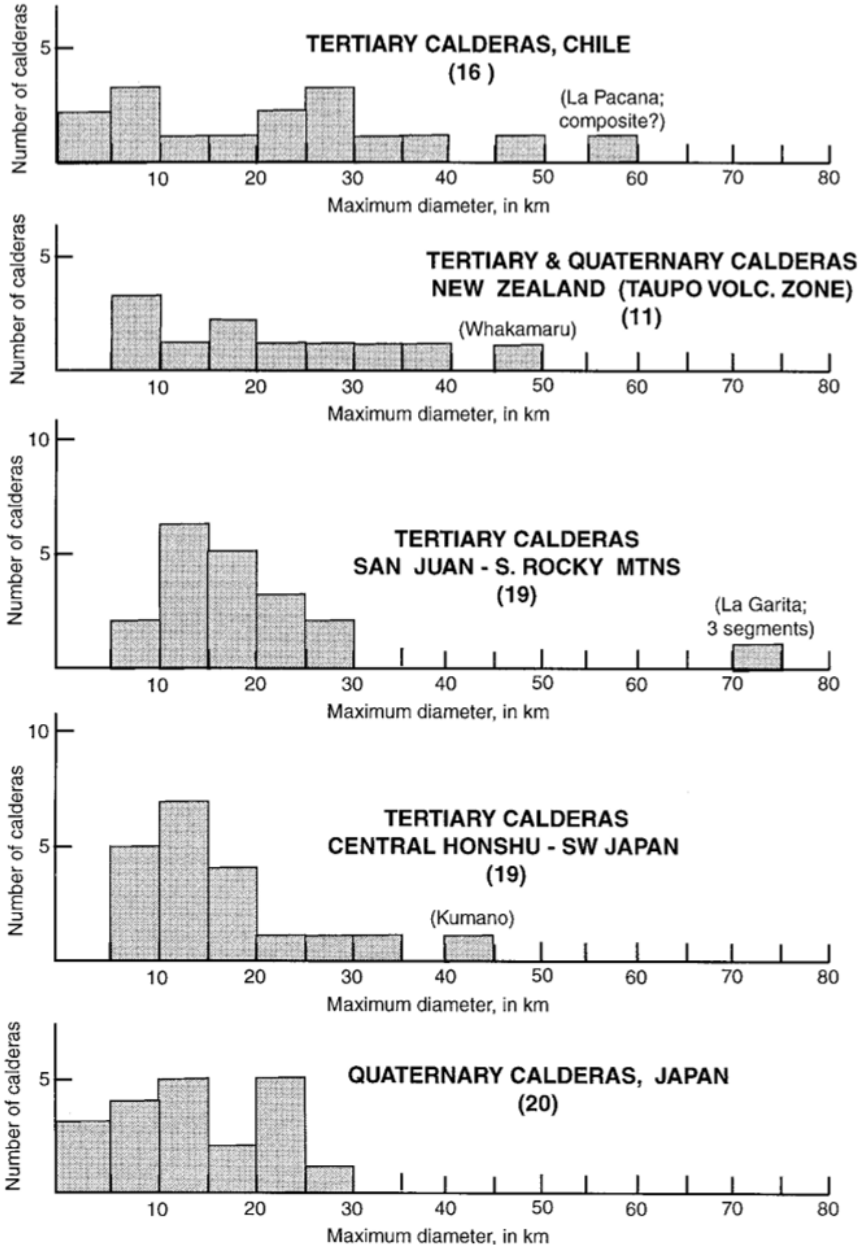

FIGURE 8 Diameters (maximum dimension) of calderas in diverse tectonic settings. Calderas in most regions have similar ranges of diameters. Smaller young calderas, as recorded in the Quaternary of Japan, probably tend to be obscured by erosion and cover by younger volcanic rocks in the older (Tertiary) volcanic fields. The largest calderas tend to be composite (multiple eruptions at La Pacana in Chile) or geometrically complex (successive subsidence of multiple segments during a single eruption at La Garita in the San Juan Mountains).

A. Calderas and Volcanic Hazards

Large caldera-forming explosive eruptions probably represent the most catastrophic geologic events that affect the Earth's surface, other than rare large meteorite impacts. Krakatau in 1883 caused 30,000 deaths, mainly from tsunamis associated with the caldera eruption. The much smaller 1991 Pinatubo eruption in the Philippines could have been comparably deadly because of the high population density on its lower flanks had the onset of this eruption not been accurately forecast and large areas evacuated successfully. The potential societal impact of a future eruption comparable in size to large prehistoric events, should it involve a heavily populated area such as Napoli in Italy or Kagoshima Bay in Japan, are so enormous as to defy comprehension.

In recent years, relatively intense unrest has occurred at Long Valley in the United States (1980 to present), Campi Flegrei in Italy (1983 to present), and Rabaul in Papua, New Guinea (1971–1994). The unrest at Rabaul culminated in 1994, when two volcanoes erupted simultaneously along opposite sides of the ring-fracture system defined by current seismicity, but no large ignimbrite eruptions or caldera-wide subsidence were involved. Both Campi Flegrei and Rabaul have already experienced multiple caldera-subsidence events associated with large eruptions, so additional caldera-forming events are a significant long-term hazard for any existing restless caldera. One of the most important future tasks for volcanologists will be to recognize precursors for potentially devastating caldera-forming eruptions, as contrasted with the more frequent small eruptions at previously active volcanoes. Most future caldera-forming eruptions can be expected to occur at sites of existing calderas, but any cluster of active volcanoes should be evaluated as a potential site of a growing upper crustal magma chamber that could fuel a future caldera eruption. Because calderas form so infrequently, present understanding is woefully inadequate concerning the variety of potential precursors, the proportion of precursor events that lead to major eruptions, and especially the characteristic time intervals between precursors and eruption.

B. Caldera-Forming Eruptions and Global Climate

Large pyroclastic eruptions that generate caldera collapse carry fine-grained ash and sulfur aerosols into the upper atmosphere. Historical caldera-forming eruptions such as Tambora in 1815, Krakatau in 1883, and Pinatubo in 1991, although several orders of magnitude smaller in eruptive volume than the largest prehistoric eruptions, appear to have modified global climate, including visible atmospheric effects such as strange colors and halos on the sun and moon, vivid sunsets and sunrises, and anomalously cold weather. The dominant influence is believed to be injection of sulfur aerosols into the stratosphere, a process whose efficiency varies in relation to magmatic sulfur content and height of the eruption column. As a consequence, some exceptionally large silicic eruptions such as the 0.6-Ma Yellowstone event, characterized by relatively low sulfur contents, may have affected global climate less than smaller eruptions of more mafic sulfur-rich magma. The overall impact of explosive volcanic eruptions on global climate, in comparison to other influences such as polar ice cap volumes and deep ocean currents, remains uncertain.

SEE ALSO THE FOLLOWING ARTICLES

Exploitation of Geothermal Resources • Magma Ascent at Shallow Levels • Magma Chambers • Mineral Deposits Associated with Volcanism • Pyroclast Transport and Deposition • Scoria Cones and Tuff Rings • Volcanic Soils • Volcanic Tsunamis

FURTHER READING

Bacon, C. R. (1983). Eruptive history of Mount Mazama and Crater Lake caldera, Cascade Range, U.S.A. *J. Volcanol. Geotherm. Res.* **18,** 57–115.

Branney, M. J. (1995). Downsag and extension at calderas. New perspectives on collapse geometries from ice-melt, mining, and volcanic subsidence. *Bull. Volcanol.* **57,** 303–318.

Christiansen, R. L. (1984). Yellowstone magmatic evolution: Its bearing on understanding large-volume explosive volcanism, Pages 84–95 *in* "Explosive Volcanism: Inception, Evolution, and Hazards." National Academy Press, Washington, DC.

Druitt, T., and Francaviglia, V. (1992). Caldera formation on Santorini and the physiography of the islands in the late Bronze Age. *Bull. Volcanol.* **54,** 484–493.

Lipman, P. W. (1984). The roots of ash-flow calderas in North America: Windows into the tops of granitic batholiths. *J. Geophys. Res.* **89,** 8801–8841.

Lipman, P. W. (1997). Subsidence of ash-flow calderas: Relation to caldera size and magma-chamber geometry. *Bull. Volcanol.* **59,** 198–218.

Matumoto, T. (1943). The four gigantic caldera volcanoes of Kyushu. *Jpn. J. Geol. Geogr.* **19.**

Newhall, C. G., and Dzurisin, D. (1988). Historical unrest at large calderas of the world. *U.S. Geol. Surv. Bull.* **1855.**

Orsi, G., De Vita, S., and di Vito, M. (1996). The restless resurgent Campi Flegrei nested caldera (Italy): Constraints on its evolution and configuration. *J. Volcanol. Geotherm. Res.* **74,** 179–214.

Simkin, T., and Fiske, R. S. (1983). "Krakatau 1883: The Volcanic Eruption and Its Effects." Smithsonian Institution Press, Washington, DC.

Smith, R. L., and Bailey, R. A. (1968). Resurgent cauldrons. *Geol. Soc. Am. Mem.* **116,** 83–104.

Walker, G. P. L. (1984). Downsag calderas, ring faults, caldera sizes, and incremental caldera growth. *J. Geophys. Res.* **89,** 8407–8416.

Williams, H. (1941). Calderas and their origin. *Univ. Calif. Publ. Depart. Geol. Sci.* **25,** 239–346.

Wilson, C. J. N., Rogan, A. M., Smith, I. E. M., Northey, D. J., Nairn, I. A., and Houghton, B. F. (1984). Caldera volcanoes of the Taupo Volcanic Zone, New Zealand. *J. Geophys. Res.* **89,** 8463–8484.

Yamamoto, T. (1994). Structural development and eruptive history of late Miocene to Pliocene caldera volcanoes in the Inawashiro district, NE Japan. *Bull. Geol. Surv. Jpn.* **45,** 135–155 [in Japanese, with English abstract].

COMPOSITE VOLCANOES

JON DAVIDSON
UCLA

SHAN DE SILVA
Indiana State University

I. Introduction
II. Morphology of Composite Volcanoes
III. Lifetimes of Composite Volcanoes
IV. Characteristics and Distribution of Volcanogenic Products at Composite Volcanoes
V. Concluding Remarks and Future Research Directions

GLOSSARY

composite volcano Relatively large, long-lived constructional volcanic edifice, comprising lava and volcaniclastic products erupted from one or more vents, and their recycled equivalents.

compound volcano Volcanic massif formed from coalesced products of multiple, closely spaced, vents.

debris avalanche Catastrophic landsliding of gravitationally unstable volcano flanks resulting in a widely dispersed deposit at the foot of the edifice, typically characterized by a hummocky surface.

edifice Constructional volcanic mass.

planezes Triangular, flat-faced, facets on volcano flanks formed by the intersection of two master gullies in the upper reaches of a cone.

ring plain Region surrounding a volcano beyond lower topographic flanks, over which tephra and mass-wasting products are radially distributed.

satellite (or flank, or parasitic) vents Small monogenetic volcanic features (domes, cinder cones) distributed over the flanks of a larger composite edifice.

steady-state or equilibrium profile Shape of the edifice (cone) once an active volcano has become well established—follows the initial cone building, precedes long-term erosional degradation, and represents a balance between construction through mass addition (eruption) and degradation through erosion.

topographic inversion Process whereby through time valleys become ridges and vice versa—can occur on volcanoes as volcanogenic products such as lavas are channeled down valleys, focusing subsequent erosion along their edges.

vent Surface opening at which volcanogenic material is erupted.

ASK A SMALL child to draw a volcano. Chances are that child will draw a composite cone. These are the most common types of volcanic edifice, the sites of the most well-known historic eruptions, and the sources of a wide array of volcanic products. Composite volcanoes occur in all regions of volcanic activity across the Earth. Human populations are drawn to composite volcanoes, attracted by the fertile and frequently renewed volcanic soils generated by the volcanoes, while at the same time threatened by the hazards associated with their frequent eruptions.

Copyright © 2000 by Academic Press
All rights of reproduction in any form reserved.

I. INTRODUCTION

A. Definition of Composite Volcanoes

Surprisingly, the definition of a composite volcano is neither straightforward nor uniformly agreed upon. Most volcanoes are constructional features—they build an edifice from erupted material that extends above the original topography in the region of the vent. Exceptions to this are maars and calderas. Among constructional edifices, there are variations in shape and size (Fig. 1). Shape is largely a function of slope angle; at the one extreme are very shallow slopes that characterize shields, and on the other are the steeper slopes that characterize cones and domes. Among the smaller edifices are cinder cones and domes, which are typically monogenetic (formed from a single eruption episode). Shield volcanoes and composite cones are the products of multiple eruptions spanning tens to hundreds of thousand of years, and, as a result, are larger and more diverse in terms of their products (types and compositions). Composite volcanoes are therefore defined as relatively large and long-lived volcanic edifices comprising both lava and volcaniclastic erupted products. Note that our definition is intended to be descriptive and not a rigid classification; composite volcanoes clearly overlap with many other edifice types and may incorporate smaller volcano types (cinder cones and lava domes) in their architecture. Composite cones are commonly taken as synonymous with stratovolcanoes; the latter term is preferred in many introductory texts. We choose to avoid the term stratovolcano, as it conveys an implication (albeit not necessarily intentional, but certainly perpetuated in diagrams from introductory texts) of regularly interlayered pyroclastic deposits and lavas. The term "composite" has been used to describe volcanic cones from the Andes that have a composite growth history, punctuated by one or more episodes of sector collapse, and the term "compound" to denote edifices comprising multiple cones, resulting from limited vent migration over time within a restricted area. Both composite and compound volcanoes in these senses are included under our definition of composite cones.

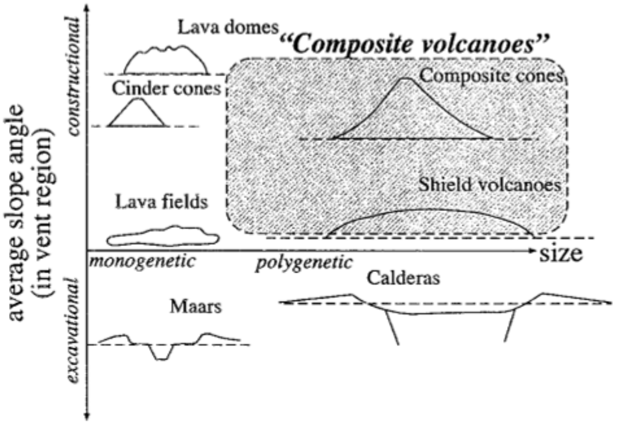

FIGURE 1 Variations in volcanic landforms as a function of size and "steepness." The diagram is intended for illustrative purposes rather than a rigorous classification. The composite volcanoes discussed in this article are constructional features, each with a reasonably protracted history of eruptions. The erupted products typically comprise both lavas and pyroclastic materials, associated with reworked deposits.

B. Distribution of Composite Volcanoes

Composite volcanoes are found globally in nearly all regions of volcanism, although their abundance relative to classic shield volcanoes, lava fields and domes, calderas, and cinder cones varies considerably. At convergent plate margins, composite volcanoes are arguably the type edifices (Fig. 2). Indeed subduction zones are perhaps most dramatically characterized by classic cone-shaped basaltic andesite to andesite volcanoes such as Mount Fuji in Japan. In fact, most well-known historic eruptions have occurred at composite cones located along convergent plate margins (Table I). Although some convergent margin environments where extension occurs in intra-arc grabens or backarc rifts are dominated by cinder cone fields, the magmatic expression of a convergent plate margin is generally a chain of composite volcanoes, subequally spaced, comprising a volcanic arc. The arc is subparallel to the trench and constructed on the upper plate approximately 100–150 km above the upper surface (known as the Wadati–Benioff zone—see "Plate Tectonics and Volcanism") of the subducted slab. The spacing of the volcanoes along the arc is subregular, varying from 30 to 100 km among different arcs, although most arcs may be characterized by an average spacing. The control on volcano spacing is unclear and may reflect the spacing of Rayleigh–Taylor diapiric instabilities in a melt zone above the subducted slab or periodic variations in the stress state of the upper plate lithosphere that impede or allow melt ascent.

Composite volcanoes are not common at divergent plate margins, although examples can be found. Along oceanic divergent margins (midocean ridges) they are effectively absent, although on Iceland, where the midocean ridge lies over a mantle plume, composite cones

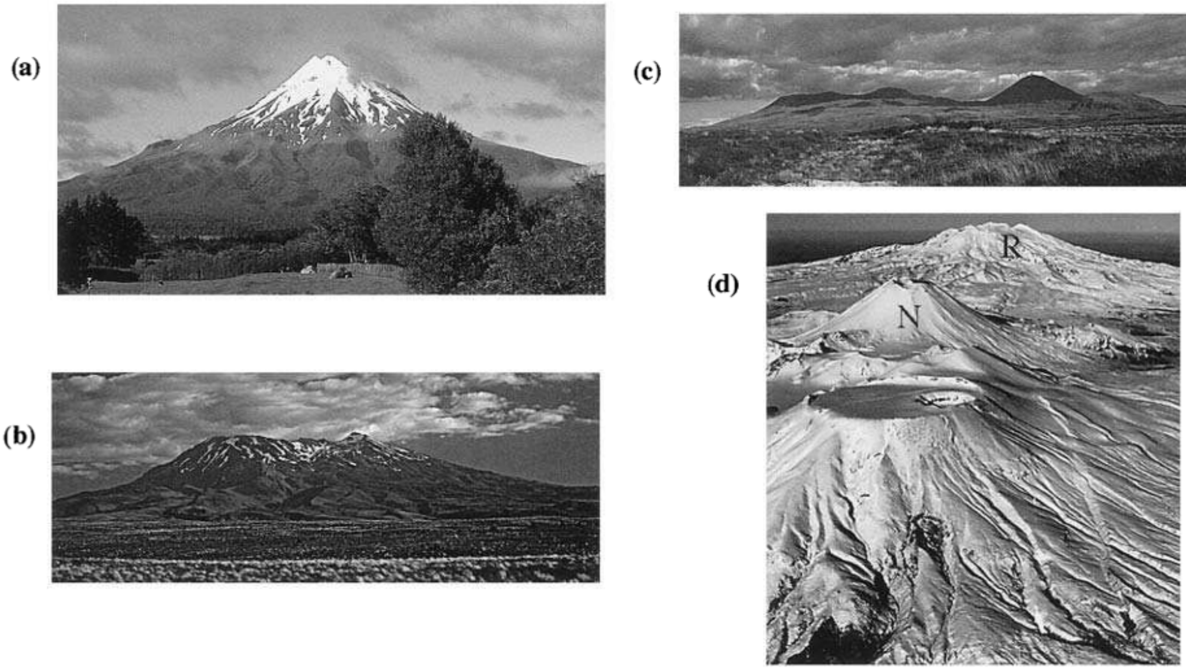

FIGURE 2 Examples of different composite volcano forms from a convergent plate margin setting, the North Island of New Zealand: (a) Mount Taranaki, a "classic" cone shape; (b) Mount Ruapehu, a compound volcano; (c) Tongariro, a compound volcano with numerous Holocene vents (the youngest being the symmetrical cone of Mount Ngauruhoe with a single active vent). Photograph d is an aerial view of Tongariro (N = Ngauruhoe) looking south to Ruapehu (R) in the distance, for comparison. The variation from (a) to (c) reflects an increasing tendency for vent location to migrate over time. Although they are cluster or composite edifices (Table II), Ruapehu and Tongariro might be considered twin volcanoes (to each other) in a broad sense.

are present, such as Hekla and Askja. In the early stages of divergent margin development (continental rifting), composite volcanoes do occur, although they are typically off-axis. Along the East African Rift, for instance, huge composite volcanoes (e.g., Mount Kilimanjaro) are found at the rift shoulders. Intraplate volcanism, perhaps by virtue of the high heat (and therefore magma) flux over a protracted time period, typically gives rise to large composite volcanic edifices. Many, particularly in the ocean basins, are dominated by basaltic effusion and are classic shield volcanoes. Composite intraplate volcanoes may, however, be found in both oceanic and continental environments. They are effectively indistinguishable morphologically from those found at convergent plate margins (Fig. 3), differing only in terms of the rock chemistry and petrography.

What factors determine the surface expression of magmatism, that is, the construction of composite volcanoes rather than other volcano landforms? Two factors at least promote the formation of composite volcanoes: (1) the composition of magma erupted and (2) the style of eruption. Magma compositions at convergent plate margins are largely the result of differentiation and volatile concentration. These factors are, of course, not unconnected, as volatile concentration is typically a consequence of differentiation (cf. "Volatiles in Magmas"). Styles of eruption are controlled more by the physical structure and stress environment of the lithosphere through which magmas ascend (although this also influences the extent of magma differentiation). In order to produce compound volcanoes, eruptions at a given vent are frequent and small to moderate in size.

Differentiation increases SiO_2 content and increases magma viscosity, leading to high aspect ratio lavas and impeding lateral distribution. Thus there is a distinction between shield volcanoes, at which low-viscosity basalts can flow large distances from the vent, and cones, at which lava flows are shorter and construct a steeper sloped edifice around the vent. The combined increase in volatile content and magma viscosity also increases the propensity for explosive eruption and the production of pyroclastic material. Convergent margin magmas are characterized by high H_2O contents, and, at least by the time they reach the surface, they tend to be differentiated (basaltic andesites and andesites). Because magma ascent is fundamentally dictated by the buoyancy con-

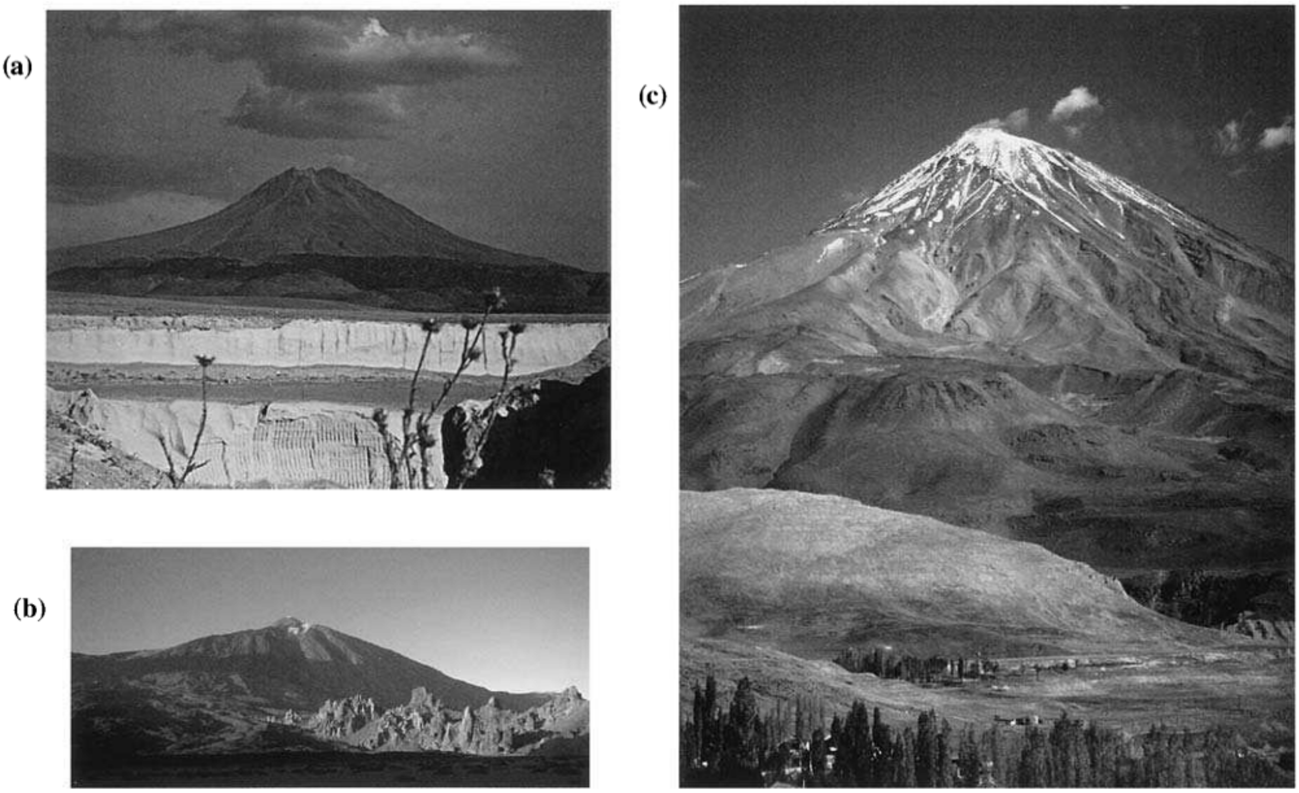

FIGURE 3 Large composite volcanoes from intraplate settings: (a) Hasandag volcano, Cappadocia, Turkey; (b) Teide volcano, Tenerife; (c) Mount Damavand in northern Iran (5671 m) (see also color insert). Both continental (a, c) and oceanic (b) crustal substrates are represented.

trast between magma and the lithosphere, ascent through thick, low-density continental crust will be impeded unless extensive differentiation occurs to reduce the magma density. Protracted differentiation can ultimately produce large volumes of rhyolite in continental regions, which, in turn, may be erupted in caldera-forming events (cf. "Calderas").

The association of calderas with precursor composite volcanoes is common. Smaller, less differentiated caldera systems such as Crater Lake in Oregon may represent the cataclysmic evacuation of a silicic magma chamber from beneath a simple composite cone. Larger caldera-forming eruptions (such as at Long Valley in California and Valles in New Mexico) are typically preceded, albeit by a few million years, by magmatism expressed as clusters of composite volcanoes concentrated in the region of the future caldera. Composite volcanoes and calderas may also be contemporaneous, varying only slightly in location along and across zones of magmatism, such as the Taupo Volcanic Zone of New Zealand. These associations suggest a further complex balance between magma/heat flux and the rheological state of the crust in determining the morphological expression of volcanism.

In summary then, relative to shield volcanoes, composite volcanoes are characterized by the eruption of more differentiated, silica- and volatile-rich magma. Compared with caldera systems, composite volcanoes erupt smaller volumes more frequently and less explosively, which likely inhibits the long-term extreme differentiation, which typifies caldera-forming magmas.

II. MORPHOLOGY OF COMPOSITE VOLCANOES

A. Introduction

Morphology is one of the most fundamental properties of a volcano, and yet surprisingly little work has been

TABLE I Selection of Notable Eruptions from Composite Volcanoes Since A.D. 1500 Involving 1000 or More Fatalities[a]

Volcano	*Country*	*Year*	*Explosive eruption*	*Lava flow*	*Debris flow*	*Tsunami*	*Famine*
Kelut	Indonesia	1586			10,000		
Huaynaputina	Peru	1600	>1,000				
Vesuvius	Italy	1631		18,000			
Etna	Italy	1669		10,000			
Unzen	Japan	1792				15,190	
Mayon	Philippines	1814	1,200				
Tamabora	Indonesia	1815	12,000				80,000
Galunggung	Indonesia	1822	1,500		4,000		
Mayon	Philippines	1825			1,500		
Awu	Indonesia	1826			3,000		
Cotopaxi	Ecuador	1877			1,000		
Krakatau	Indonesia	1883				36,417	
Awu	Indonesia	1892			1,532		
Peleé	Martinique	1902	29,000				
Santa Maria	Guatemala	1902	6,000				
Kelut	Indonesia	1919			5,110		
Merapi	Indonesia	1930	1,300				
Lamington	Papua, New Guinea	1951					
Agung	Indonesia	1963					
El Chichón	Mexico	1982	1,700				
Nevado del Ruiz	Columbia	1985			25,000		

[a] Modified from Report by the Task Group for the International Decade of Natural Disaster Reduction. (1990). *Bull. Volcan. Soc. Jpn. Ser. 2* **35,** 80–95. Numbers refer to fatalities, listed under column for cause of deaths.

done since the seminal work of Cotton in the 1940s. One of the reasons for this may be the general perception that the morphological evolution of a composite volcano is simple; they are positive (constructional) topographic features, with steep flanks and a general conical shape, and they result from local accumulation of erupted products. However, this simple view ignores the fact that while many composite volcanoes are simple cones with a single summit vent and radial symmetry, many are more complex, compound volcanoes with convoluted histories involving cone collapses, rebuilding, and changing vent locations through time (Table II). Nevertheless, they still display a conical profile normal to the length axis, suggesting a consistency to the "normal" conical shape of a single composite cone.

Another fact that is ignored is that the simple conical shape is the result of a complex evolution that is controlled by the interplay of aggradation and degradation. Short-term aggradation by constructive processes of eruption and emplacement of volcanic materials is opposed by degradation as the longer period destructive processes of erosion, punctuated by catastrophic events such as gravity-driven avalanching (cf. "Debris Avalanches") and posteruption mass wasting. The fact that active composite volcanoes maintain a simple conical shape suggests that the average rate of aggradation must exceed the "punctuated equilibrium" of degradation.

B. Evolution of Morphology

Most composite volcanoes around the world have very similar characteristics. These volcanoes are characterized by a concave-upward profile, which should be considered as the equilibrium or steady-state profile of an active composite cone. Classic textbook volcanoes such as Mount Mayon in the Philippines, Mount Fuji in

TABLE II Summary of Morphological Types among Composiite Volcanoes

Morphological type	*Description*	*Examples*
Simple cone	Classic "textbook" radially symmetric shape; tend to be young	Fuji (Japan), Klyuchevskoy (Kamchatka), Mount Mayon (Philippines), Osorno (southern Chile), Shishaldin (Aleutians, United States), Taranaki (New Zealand), Cotopaxi (Ecuador)
Shieldlike	Shallow-sloped flanks, common craters/calderas in summit region, greater diversity of magmas (include evolved types such as dacite/rhyolite)	Newberry (Cascades, United States), Okmok (Aleutians, United States), Gorely (Kamchatka)
Compounds	Limited vent migration—typically resulting in an elongate ridge, more occasionally a large equant massif	Ruapehu (New Zealand), Zhupinovsky (Kamchatka), Lascar and Irruputuncu (northern Chile), Tatara–San Pedro (southern Chile)
Twins	Distinct neighboring volcanoes, considerably closer together than average volcano spacing along an arc; typically there is an age difference between the two edifices (a younger active and an older cone)	Avachinsky–Koryaksky (Kamchatka), Parinacota–Pomerape and San Pedro–San Pablo (northern Chile), Colima (Mexico)
Clusters	Groups of more than two distinct polygenetic edifices	Tongariro (New Zealand), Bromo (Java)
Collapse-scarred	Severe recent modification of morphology by sector collapse, resulting in large summit bowl or amphitheater	Mount St. Helens (Cascades, United States), Bezymianny (Kamchatka), White Island (New Zealand)

Japan, and Mount Taranaki (formerly Egmont, New Zealand) exemplify this (Fig. 4). While this is a useful general observation, it is instructive to note that more youthful or nonequilibrium volcanoes have a more pure conical shape with a more restricted base (Fig. 4b). At most composite volcanoes, it is clear that this shape is produced by early lavas being more voluminous and extensive than later lavas (Fig. 4b, parts iii and iv). Certainly, there is a slight concavity to the flanks, but these volcanoes lack the extensive aprons of talus that accentuate the concavity of the slopes. This suggests that mass transfer through destructive processes modifies the shape of a volcano with time from a cone with simple slopes and a restricted base to one with a more concave-upward profile and a wider base (Fig. 4c). Most active volcanoes are equilibrium or steady state.

C. Factors Controlling Morphology

Notwithstanding the complexities discussed above, the primary shape of a composite volcano is conical. Many of the controls on this shape can be understood by considering the geometry of a cone. The volume v of a simple cone is given by

$$v = \tfrac{1}{3}\pi r^2 h, \tag{1}$$

where r is the radius of the base and h is the height of the cone. For a typical steady-state volcano with the concave-upward profile, a more complex exponential form is needed:

$$r = Be^{Mh}. \tag{2}$$

B and M are constants and the volume has to be found by integration. Below we address the main factors that control the morphology of composite volcanoes.

D. Aggradation

While there is a strong dependency of edifice height on the volume of a composite cone, there also appears to be a limit to the size of composite cones. Edifice heights (base to summit) of composite volcanoes rarely exceed 3000 m and the vast majority of arc-related composite volcanoes are between 2000 and 2500 m. Volumes are similarly restricted; notwithstanding the difficulty in measuring accurate volumes, maximum volumes for arc-related composite volcanoes are around 200 km^3 (e.g., Mount Adams and Mount Shasta in the Cascades of the United States). Intraplate composite cones may attain larger volumes.

One explanation for this is that the conical form exerts a fundamental control on the growth of a volcano. The relationships in Eqs.(1) and (2) suggest that if the conical form is to be maintained, every additional increment in height requires a huge additional increase in volume—the additional volume has to be distributed all over the cone. At some point, this becomes prohibitive to further growth. However, closer examination of volcanoes reveals that the height increment does not necessarily always involve the large volume increment suggested by the relationships described in Eq. (2), because in many cases the increase in height is achieved by adding material to the uppermost parts of the edifice only. In many cases the uppermost parts of composite cones are characterized by small and stubby lava flows or domes reflecting their evolved nature and attendant high viscosity and yield strength (Fig. 4c, part iv). Effusion of these lavas builds up the edifice without much new volume being added and results in the steep slopes that characterize the uppermost slopes.

The consistency of edifice heights and volumes in comparable tectonic settings around the world suggests that some simple geophysical relation must exist to limit the size of composite volcanoes. Several factors can affect the height to which a composite volcano can grow. Among these are the nature of the volcanic products, the duration of magma supply, differentiation of the magmas, and the crustal density profile. Magma supply is certainly an important control because the largest composite volcanoes are intraplate volcanoes such as Mount Ararat, Turkey; Mount Damavand, Iran; and Mount Kilimanjaro, Kenya. Here magma production and supply rates are higher than those associated with arcs and the resulting edifices are much larger. However, even though magma supply rates and other factors are likely to be different between regions or arcs, they may be close to constant for a given region, arc, or portion of an arc. Mature composite volcanoes in comparable tectonic settings are still similar in size the world over.

Most eruptions from composite volcanoes are driven by the hydrostatic "head" or, more appropriately, the overpressure (that in excess of lithostatic (Fig. 5)) in the magma reservoir. Geophysical studies of active volcanoes commonly reveal the presence of shallow (5–10 km) magma storage zones beneath active volcanoes. Petrologic studies confirm shallow reservoir depths as most composite volcanoes are characterized by eruptions of porphyritic magmas dominated by plagioclase. Furthermore, most volcanic products also show evidence of extensive magma mixing—a phenomenon that is best understood in the context of shallow magmatic systems. While it is debatable whether a shallow magma reservoir exists throughout the entire lifetime of the volcano, it is clear that one must exist during the actively erupting stages. Therefore it is reasonable to assume that most eruptions from composite volcanoes occur from shallow magma reservoirs and therefore that the overpressure required to erupt material from the chamber is unlikely to vary much. The consistency of the ballistics of volcanic bombs from composite volcano eruptions supports this contention.

As a volcano grows, two factors may conspire to decrease the eruption rate. First, the growing mass of the volcano increases the lithostatic load on the shallow magma chamber and eventually overcomes the hydrostatic head. Inflation and deflation of volcanic edifices are often modeled as the result of a shallow source of deformation (a Mogi source), suggesting strong feedback between the edifice and the magma reservoir. Second, the distance the magma has to ascend to the surface increases. It should be clear from Fig. 5 that if *h* and the load are increased, there will be a limit (observational evidence suggests this is about 3000 m of edifice height) above which it will be physically unlikely that further lava can be erupted from the summit. Two general observations support this reasoning. First, early lavas tend to be more voluminous and extensive than later lavas. Second, early lavas are commonly less evolved than later lavas. The first directly relates growth to changing effusion rate, and the second implies that the critical overpressure ($P_{ex}>P_{lith}$) can only be maintained if the reservoir magma becomes more evolved and consequently less dense, but more viscous as the volcano grows. Only the higher viscosity of the lower density, evolved lavas permits the condition $P_{ex}>P_{lith}$ to be maintained—the more evolved lavas typically have lower magma densities due to removal of dense crystalline phases and can sustain greater overpressures on vesiculation since the higher viscosities impede volatile outgassing.

This control is well illustrated in Fig. 4b, parts iii and iv. Here, the youthful cone of Licancabur is built from shorter younger flows radially disposed around the vent, overlying older more extensive flows. The true equilibrium profile has not yet developed because there has been insufficient time to significantly degrade the flanks and develop a talus apron. A dramatic decrease in density (with consequent increase in overpressure) can also be achieved by vesiculation of the magma. This condition will depend on magma composition (volatile species, solubility, and content) and on its capacity to achieve supersaturation through depressurization, which is ulti-

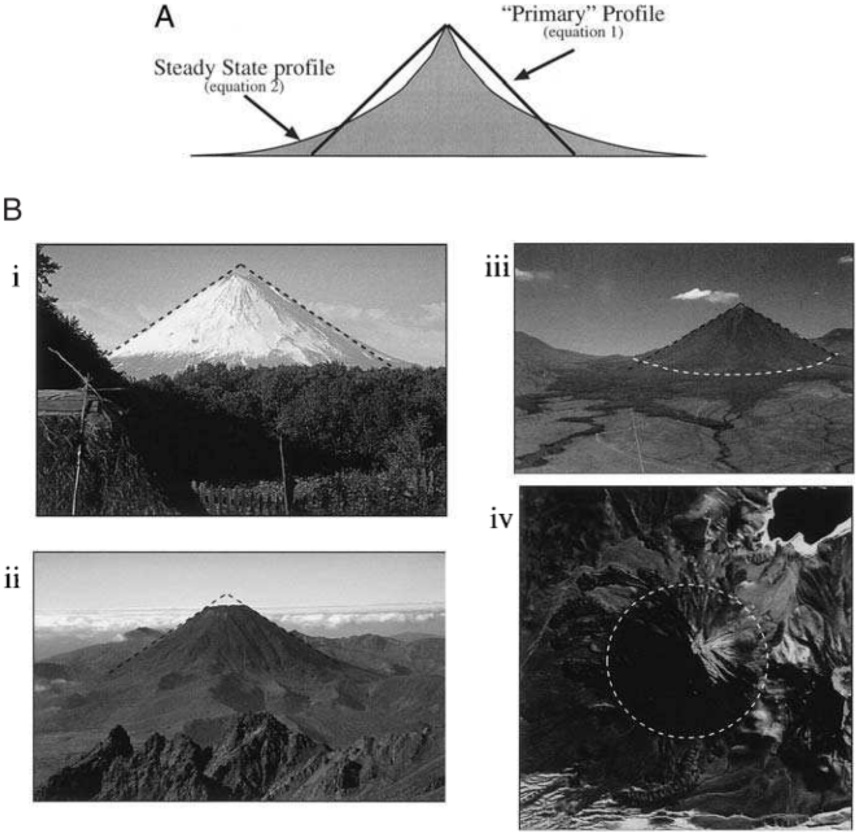

FIGURE 4 (A) Idealized evolution of the shape of a composite volcano. Initially, a pristine volcano will form a pure conical form with constant slopes and a volume given by Eq. (1). Mass wasting results in transfer of mass from the upper parts of the edifice to the lower flanks, building out a talus apron. The edifice evolves to a steady-state profile with concave-upward slopes and a volume given by Eq. (2). Compare with examples of profile evolution given in (B) and (C), respectively. (B) Young nonequilibrium conical profiles: (i) Klyuchevskoy volcano, Kamchatka, one of the world's most active subduction zone volcanoes and <10,000 years old (view from north); (ii) Nguaruhoe cone (ca. 2500 years old), New Zealand (cf. Fig. 2); (iii) Licancabur volcano, view from west together with (iv) Landsat TM image of Licancabur. Photographs iii and iv show the early more extensive lava flows around the base and a more restricted cone formed from later more restricted lavas, outlined in a white dashed line.

mately also controlled by the parameters illustrated in Fig. 5.

E. Degradation

In a heuristic and phenomenological sense, the history of a composite cone can be thought of as the interplay of short-term eruptive phenomena that construct volcanoes periodically and the longer term erosive processes of degradation that conspire to bring them down (Table III). However, while this is a useful working hypothesis, it is important to recognize that the while the averaged rate of degradation on composite volcanoes suggests longer term equilibrium, in reality degradation is highly variable, consisting of a regional "background" rate modulated by more rapid erosion and mass-wasting events. The high degradation rates often accompany and closely follow eruptions and punctuate the equilibrium. For instance, observations after the 1980s eruptions of Mount St. Helens in the USA and the 1991 eruption of Mount Pinatubo in the Philippines showed that peaks of erosion follow closely on peaks of eruption as pyroclastic material is rapidly (months to years) removed from the cone. Catastrophic processes such as landsliding/avalanching further conspire to accelerate degradation.

Long-term erosion depends on climate and the composition of the volcanic edifice. Given comparable rates of production and cone growth, volcanic cones are better

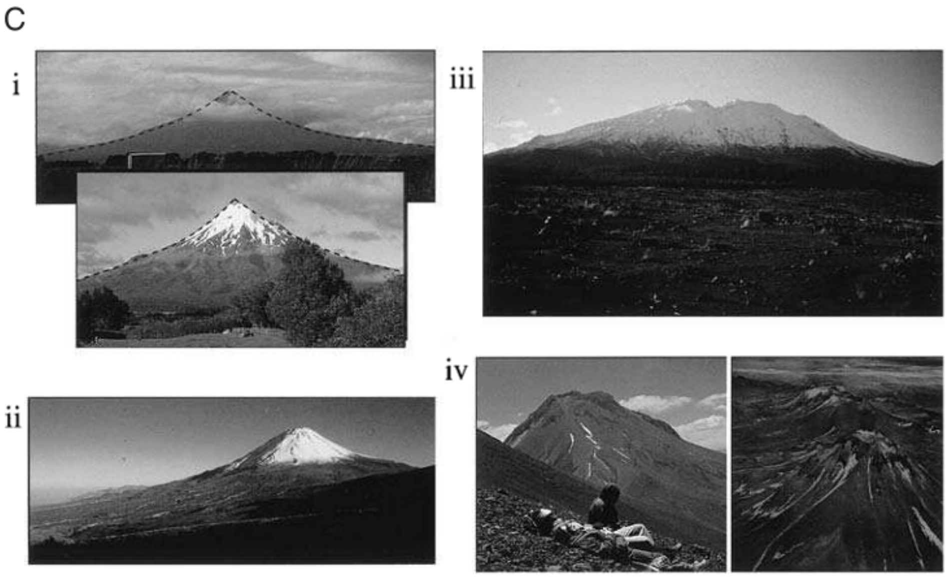

FIGURE 4 (*continued*) (C) Equilibrium profiles: (i) Taranaki volcano, New Zealand (two views from the north emphasizing classic extensive equilibrium profile of concave-up flanks); (ii) Volcan Misti (Peru) from southeast showing extensive ring plain or talus apron and a developing equilibrium profile; (iii) lahar deposits of the ring plain or talus apron (foreground) of Mount St. Helens. Low-angle aprons of this type of material extend out to several kilometers from the base of the cone. View is from the southeast. (iv) Aguas Calientes from Lascar (central Andes), showing the short, stubby lava flows that have built up the steep upper portions of the cone.

preserved in arid/cool climates rather than humid equatorial climates. For instance, climatic differences between the hyperarid central Andes and the tropical northern Andes are highlighted by pristine morphologies of Pleistocene volcanoes in the former and degraded morphologies in the latter. In response to eruptive events that produced large volumes of unconsolidated material and greatly disturbed local topographic equilibria, at Mount St. Helens, 10-m-deep gullies were cut into the pyroclastic deposits within a few months of the

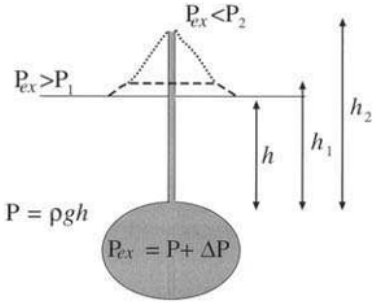

FIGURE 5 Schematic diagram showing the relation between lithostatic pressure P and eruption driving overpressure P_{ex} in the magmatic system of an active volcano. The lithostatic pressure P changes with the mass of the growing volcano and the depth to the magma chamber h. Eruption can take place as long as P_{ex} remains greater than P. At h_2, the edifice has grown to the critical height beyond which P_{ex} is less than lithostatic and therefore eruption from the summit is no longer viable.

TABLE III Stages in the Erosional History of Composite Volcanoes

Stage	*Geomorphic signature*
1	Fresh, young cones, often dark, pristine lava flows and summit crater visible, sharp profile; not glaciated
2	Small gullies on flanks, lavas visible and crater may exist, but degraded; cone still sharp, dark apron gone; moraines present
3	Individual lava flows barely visible, no crater, well-established gullies, constructional surfaces dwindling; planezes initiated
4	No lava flows visible, deeply incised gullies, large planezes, little original cone surface left; considerable relief; major U-shaped glacial valleys in glaciated regions
5	Barely recognizable, low relief; radial symmetry the only clue to volcanic origin

eruption. At Mount Pinatubo, the 1991 pyroclastic flows had similar gullies within a matter of days. On the other hand, pyroclastic deposits at Katmai (Alaska), where the climate is somewhat cooler and drier, are only moderately eroded nearly 100 years after eruption.

The composition of the edifice is an equally important control on degradation styles and rates. Clearly, unconsolidated pyroclastic material will be more readily eroded. Lava is less porous than scoria and will encourage runoff. Porosity and permeability will therefore be important in controlling if runoff or percolation dominates. Since extensive gullying is common on composite volcanoes, we can surmise that runoff dominates. Gullying is the most common indication of degradation of composite cones and occurs in several stages. One of the most significant stages of gullying involves the formation of planezes (Table III). These are the result of two master gullies intersecting in the upper reaches of a cone and isolating a triangular, flat-faced, facet.

The biggest single obstacle to the growth of a volcano is gravity and the hackneyed cliche "what goes up must come down" is nowhere better exemplified than in the catastrophic debris avalanches (cf. "Debris Avalanches") that are now recognized as being part of the normal mode of activity of composite volcanoes. The mass transfer associated with these events is largely responsible for modifying the shapes of volcanoes to the steady-state concave-upward profile as the deposits from these events extend the talus apron of the lower flanks out to several tens of kilometers from the summit.

As a volcano grows, its slopes become steeper and therefore gravitationally unstable. Further, asymmetry resulting from unequal distribution of mass on an edifice adds to the instability. Edifices built on slopes are inherently unstable. Gravitational collapse requires a trigger, and many events of this type probably involve earthquake-triggered flank failures (e.g., Bezymianny, 1956; Mount St. Helens, May 1980). The growing volcanic load may reactivate local basement faults that may penetrate up into the volcanic edifice (e.g., Socomopa, Chile, 7500 a). Finally, inflation of the cone due to a recharge event or degassing may trigger the collapse of an unstable flank (e.g., Tata Sabaya, Bolivia).

The most spectacular examples of gravitational collapse involve the failure of 25–30% of a volcanic cone in a matter of minutes.

The morphologic signatures of collapse are invariably a collapse amphitheater and hummocky topography on the avalanche deposit; the May 18, 1980, eruption of Mount St. Helens (see "Debris Avalanches") provides a typical example. Several other amazing examples have also been recognized around the world, but nowhere more so than in the central Andes. The studies in the central Andes highlight several key features. First, collapsed portions may vary in scale from relatively small (10–15%) portions of the edifice as at Irruputuncu on the Bolivia/Chile border to quite large (30%) portions of the edifice as at Tata Sabaya in Bolivia. Second, regardless of how extensively an edifice is eviscerated, the conical shape is reestablished very rapidly. This may explain why there are currently few clear examples of collapse-scarred volcanoes (Table II). At Parinacota in Chile, reconstruction since a massive collapse 13,000 years ago has virtually rebuilt the entire edifice (Fig. 6e; see also color insert). Only very careful examination of aerial photographs reveals the trace of the amphitheater. At Bezymianny in Kamchatka, a dome growing since the 1956 sector collapse has nearly filled the amphitheater (Fig. 6f). Third, the deposits from these collapses can form a significant portion of the talus apron of volcanoes (e.g., Volcan Misti, Peru).

Gravitational collapse is therefore a significant mechanism of mass transfer on composite volcanoes. The reduction of steep slopes of the upper and middle flanks by collapse and deposition of these materials far from the flanks results in extensive low-angled aprons (commonly referred to as *ring plains*; vide infra) extending to several tens of kilometers out from the edifice. Subsequent "healing" of the cones results in reestablishment of steep middle and upper flanks, perpetuating the steady-state profile.

Also important in determining the volcano morphology resulting from degradation are the effects of hydrothermal alteration. Mature conduits can provide a sufficient heat flux to drive groundwater through a hydrothermal circulation system, with the consequence that the rock volume affected by the system is altered and weakened, making it more vulnerable to erosion by both long-term, slow-mass-wasting, glacial or fluvial processes and catastrophic failure. In volcanoes with well-established hydrothermal systems, the vent region can occupy an enormous bowl of altered volcanic material (such as Mutnovsky volcano, Kamchatka) that may resemble—or on occasion coincide with—a sector collapse amphitheater. The occurrence of hydrothermal activity and the influence of consequent alteration can extend long after magmatic addition to the edifice has effectively ceased and exert considerable control on its morphological degradation.

F. Changes in Vent Locations through Time

The classic conical shape owes its form to the constancy of vent location over a protracted period of time. This

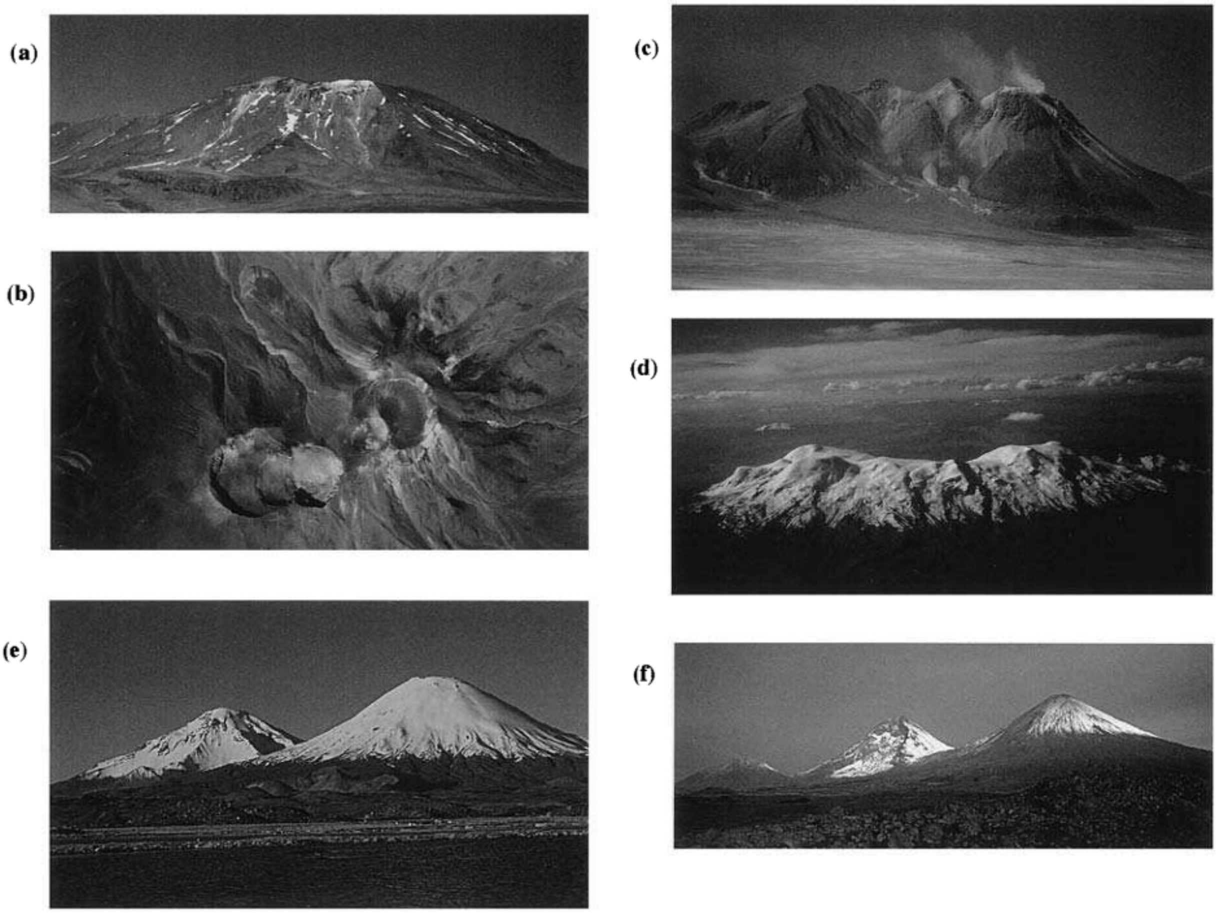

FIGURE 6 More complex or compound composite cones, illustrating effects of local vent migration through time. (a) Lascar from the north, an extensive composite cone that is elongate east to west due to migration of the vent region. (b) Aerial photograph of Lascar clearly showing the nested craters resulting from vent migration (north to top of page). (c) Irruputuncu (Chile/Bolivia), another typical nonconical, ridgelike composite cone (view from the west). The oldest part of the cone is the left. (Photograph courtesy of Gerhard Worner; see also color insert.) (d) Coropuna, Peru, a compound volcano made up of at least five different overlapping cones. (e) Nevados de Payachata, central Andes, comprising twin volcanoes (view from southwest). The older glaciated Pomerape cone is to the north (left), while Parinacota is the young, more symmetrical cone. The hummocky terrane in the foreground is a debris avalanche deposit. (See also color insert.) (f) Klyuchevskoy group volcanoes, Kamchatka, view from the south east. The symmetrical Klyuchevskoy cone in the foreground and the vapor-shrouded Bezymianny volcano (which collapsed in 1956 and now consists of a large active dome in the amphitheater) in the distance are both active, while the central peak (Kamen), which shows the scarp of a collapse event, is inactive.

ensures that volcanic products, and therefore mass, are always added from the summit area and decrease radially away from it. However, many volcanoes show evidence that activity has migrated with time (Table II, Fig. 6). Several interesting questions arise. For instance, it is not clear whether activity migrates in the same direction with time throughout the region, in response to migration of the volcanic front as a whole, or whether it is segment specific or even random.

Some volcanoes are twin systems comprising two quite distinct but neighboring composite volcanoes. Examples include San Pedro–San Pablo and the Nevados de Payachata in the central Andes (Fig. 6e). Typically, twin volcanoes reflect a vent shift such that one of the two is active, leaving its twin extinct. Examples are found, however, such as Bezymianny and Klyuchevskoy volcanoes in Russia (Fig. 6f), where neighboring volcanoes are concurrently active. Others are elongate amalgamated edifices with a migrating summit complex. Examples of these include the following: in the central

Andes, Aucanquilcha, Lascar (Figs. 6a and 6b), Irruputuncu (Fig. 6c), Coropuna (Fig. 6d), and Ojos del Salado, the world's highest active volcano; in New Zealand, Ruapehu (Fig. 2); in Turkey, Ararat; in Kamchatka, Zhupinovsky. Tongariro (Fig. 2) is an extreme example of this as it is a cluster of as many as 30 relatively small edifices. These compound volcanoes offer even greater challenges of interpretation than on "simple" cones. The complex geometries of nested and overlapping cones make determination of individual cone volumes difficult as we commonly do not see basement exposed and the preexisting topography is unknown. Volcanic stratigraphy is similarly problematic to unravel, particularly in light of the close proximity (in both space and time) of potential source vents.

Subsidiary vents, commonly called satellite, parasitic, or flank vents, are common features at many composite volcanoes. The general use of the term parasitic should, however, be discouraged as it implies an often-false dependence on the main volcano. These subsidiary vents are typically in the form of small monogenetic volcanoes like cinder cones or domes (Figs. 1 and 7). Such features are commonly arranged along lineaments and are interpreted as reflecting the influence of faults along which magma can migrate laterally away from the main magma chamber or, more commonly, vertically from a separate magma batch. In some cases, these satellite vents occur as part of an areally extensive field spatially associated with the main volcano as at Mount Adams in Washington state or Payun Matru in Argentina. Geochemically, the erupted products of flank eruptions are commonly found to be significantly different from those of the main vent. Typically, they are more primitive but they can show a wide range in compositions—those of the main vent tend to be more restricted in their range. These observations suggest that in these systems the main vent is supplied by a steady-state magmatic system, whereas flank eruptions might be supplied by separate small magma batches that do not intercept the main magma chamber. In the case of the volcanic fields peripheral to the main cone (e.g., Mount Adams, Washington, U.S.A.; Payun Matru, Argentina; Mount Ararat, Turkey), the more mafic magmas that typically erupt from the satellite vents are probably prevented from ascending beneath the main cone by its subjacent magma storage system.

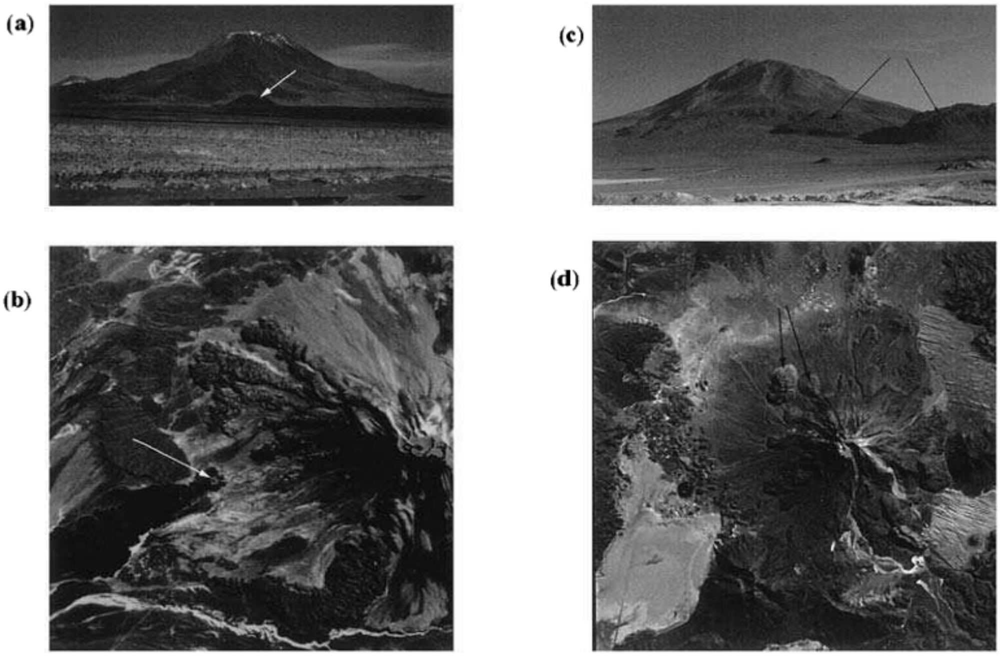

FIGURE 7 Examples of satellite centers and their relation to composite volcanoes: (a) San Pedro composite volcano (central Andes) and La Poruna cinder cone from west (arrowed), together with (b) thematic Mapper image of San Pedro and La Poruna (arrowed). Note the very large lava flow that erupted during the formation of La Poruna. North is to the top, and the image is 15 km × 15 km. (c) Ground view (from the north) of monogenetic dacite flank domes (arrowed) on Ollague volcano and (d) Landsat image of Ollague volcano, central Andes, with dacite flank domes of (c) arrowed.

III. Lifetimes of Composite Volcanoes

It is important at the outset to distinguish the active life of a volcano from its longevity as a topographic entity. A volcano can exist as a topographic entity for a considerable time after its active life—defined as the time span over which volcanic eruptions occur—is over. The time span over which it remains recognizable is largely a function of degradation rate (the "background erosion" of Section IIE), which is a function of climate. In arid regions such as the central Andes, 20-Ma-old volcanoes are well preserved and easily recognizable. In more temperate climates, this time span is considerably shorter. The discussion below focuses on the active lifetime of a composite volcano.

The general impression from the sparse and largely poorly constrained geochronological data on composite volcanoes is that these are long-lived. Observational evidence suggests that during this long lifetime periods of rapid aggradation punctuate the slow background of degradation. Unfortunately, these data do not address more detailed questions that are critical to really addressing the time scales over which volcanoes operate. For instance, does a composite volcano form in one continuous episode or multiple episodes with periods of repose? How long are the eruptive episodes and the repose periods? What are the rates of eruption that characterize periods of aggradation? To answer these questions, one must address issues such as eruption rates during eruptive episodes vs background eruptive rates, episodic cone growth rates vs average long-term cone growth rates, length of repose intervals, eruption recurrence time scales, time–volume–composition relationships, and even the meaning of "active" and "dormant."

The paucity of knowledge exists because addressing these questions requires detailed high-precision geochronology tied to detailed stratigraphy and few studies that have attempted this. The seminal work on the Mount Adams volcanic field in the USA distinguishes itself as a standard, which has recently been complemented by studies of Tatara–San Pedro in central Chile and Tongariro on the North Island of New Zealand. These detailed studies afford a general framework (see Table IV) within which many of the questions above can be addressed. Some of the main observations are

1. *Composite volcanoes grow in spurts*. The main cone of Mount Adams was built in three main episodes between ~520–490, 460–425, and 40–10 ka at eruption rates of 1.6–5 km^3/ka. At Tatara–San Pedro the two youngest

TABLE IV Volume–Time Relationships for Well-Studied Active Composite Volcanoes

	Volume (km^3)	*Inception of activity of the volcanic system (ka)*	*Age of cone-building events (ka)*	*Peak eruption rates (km^3/ka)*	*Background eruption rates (km^3/ka)*
Mount Adams	~200	940	520–490	1.6–5.0	0.05–1.0
			460–425		
			40–10		
Tatara–San Pedro	~55[a]	930	183-83, Pellado	0.2–0.3	0.06[b]
			90-19, Tatara–San Pedro		
Tongariro	~50	250–275	0-2.5, Ngauruhoe	0.88	0.17–0.2
			65-110, Tongariro Trig	0.27 ± 0.11	
			70-115, SW Oturere	0.11 ± 0.05	
			120-190,Pukekaikiore	0.09 ± 0.02	
			200-210, Tama 2	1.00 ± 0.02	
			90-250, NE Oturere	0.37 ± 0.07[c]	
			215-275, Tama 1	0.03 ± 0.02	

[a] Volume of lavas preserved. Original volume assuming 50–95% of material erupted between 930 and 200 ka has been removed by erosion due to glaciation is much higher.

[b] Based on preserved volume. If no erosion is assumed, rate would be 0.2–0.3, which is similar to peak rates.

[c] Applies to main period of cone growth, 110–130 ka.

composite cones of Pellado and Tatara–San Pedro formed between 188–83 and 90–19 ka, respectively. So these two composite cones formed during ~100 ka of eruptive activity at a minimum rate of ~0.2–0.3 km^3/ka. At Tongariro, seven large cones of 2–17 km^3 were built in periods ranging from 2.5–270 ka (or 2.5–70 ky) at rates of 0.09–1 km^3/ka. These data suggest that the length and rate of cone-building episodes are quite variable.

Less comprehensive data from other places confirm this variability. The 250-km^3 Kluchevskoy volcano (Kamchatka) has been built in the past 7000 years at an extremely high rate of 8–35 km^3/ka, whereas the similarly symmetric cone of Mount Fuji (Japan) appears to have been constructed in two phases from 80 to 10 ka and from 5 ka to the present. At Mount St. Helens the 79-km^3 cone has been built in the past 40 ka at a rate of 2 km^3/ka, whereas the 76-km^3 cone of Parinacota (Chile/Bolivia) is thought to have formed in the past 250 ka at peak rates of around 0.6 km^3/ka. Santa Maria and Fuego (Guatemala) are thought to have been constructed entirely in the past 100,000 years.

These reasonably short (generally $<$100 ka) cone-building episodes might be considered the typical timescales to reach "maturity"—an approach to the steady-state equilibrium after which overall size is maintained roughly constant by the opposing effects of construction and erosion discussed earlier and the physical controls outlined in Fig. 5. Increases in the volume of the overall edifice beyond this are typically a function of subsequent vent migration.

2. *Composite volcanoes stay active for periods of up to 500 ka.* Mount Adams in the Cascades dates back to ~520 ka and appears to be typical of other large composite cones in the Cascade arc of North America. Although the data are sparse, Mounts Baker, Rainier, Hood, Jefferson, Mazama, and Shasta are thought to have lasted $>$300 ka. Once a steady-state edifice has been constructed, there appears to be no clear relationship between volume and longevity.

The observations from the Cascades are ratified from other regions. Tongariro (New Zealand) had been active since ~250–275 ka. In the southern volcanic zone of the Andes, composite volcanoes are thought to have been active for periods of up to 300 ka. Volcan Parinacota, in the central Andes, was initiated ~250 ka, after the vent shifted slightly southward from its older twin cone Pomerape (Fig. 6e).

3. *Volcanic systems may remain active between widely spaced pulses of peak activity.* At Mount Adams, the main volcanic field remained continuously active from 940 to 10 ka with an average rate of eruption of 0.05–1 km^3/ka with breaks in activity up to 30 ka. At Tatara–San Pedro, the system was active from ~930 to 19 ka at an overall eruption rate of 0.09–0.12 km^3/yr (adjusted for glaciation associated volume reduction. At Tongariro, the background rate of activity since inception ~250–275 ka is 0.17–0.2 km^3/ka and the background rates of activity are considerably lower than the peak rates of activity discussed earlier (Table IV).

4. *Recurrence time intervals between eruptions at historically active composite volcanoes display a wide range.* Volcanoes such as Sakurajima (Kyushu) and Sangay (Ecuador) have been erupting *persistently*, on an almost daily basis for decades. More typically, composite volcanoes erupt on the *0.1 to 10-year timescale*, as exemplified by Fuego (Guatemala), Klyuchevskoy (Kamchatka), Lascar (Chile), Pavlof (Alaska), and Arenal (Costa Rica). Activity at these volcanoes consists of clusters of minor outbursts, commonly vulcanian, of varying frequency. The next characteristic timescale is the hundred to hundreds of years timescale that characterizes many of our best-known recently active volcanoes such as Mount Pinatubo (Luzon), Mount St. Helens (Cascades), and Mount Fuji (Honshu). Lastly, volcanoes such as Mounts Baker, Hood, Rainier, and Adams that have had few true eruptions in the Holocene may typify a class of composite volcanoes that operate on the timescale of *millennia*.

No doubt our understanding of composite volcano behavior and evolution is biased by the historical record (Table IV), which may be too truncated relative to the timescales of cyclic volcanic activity to be representative.

IV. CHARACTERISTICS AND DISTRIBUTION OF VOLCANOGENIC PRODUCTS AT COMPOSITE VOLCANOES

A. Introduction

Composite volcanoes are characterized by a greater diversity of volcanogenic products than any other volcanic landform (Fig. 8). The controls on the nature and distribution of erupted products are twofold—magmatic differentiation processes and syneruptive modulation by interaction with the surface environment. In the former category are included the melting and differentiation processes discussed earlier in this volume (e.g., "Composition of Magmas," "Origin of Magmas," "Volatiles in Magmas," and "Magma Chambers") that determine

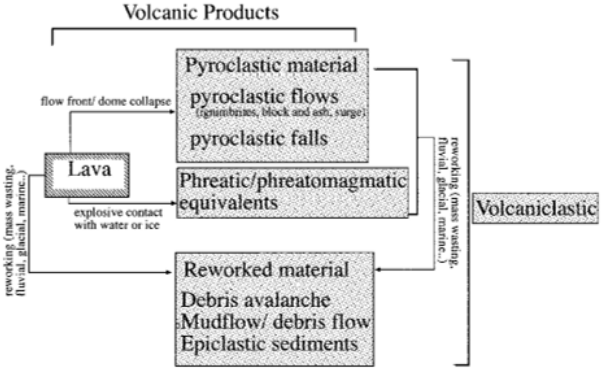
Volcanic Products
Pyroclastic material
pyroclastic flows
(ignimbrites, block and ash, surge)
pyroclastic falls
flow front/ dome collapse
Lava
Phreatic/phreatomagmatic equivalents
explosive contact with water or ice
reworking (mass wasting, fluvial, glacial, marine..)
Reworked material
Debris avalanche
Mudflow/ debris flow
Epiclastic sediments
reworking (mass wasting, fluvial, glacial, marine..)
Volcaniclastic

FIGURE 8 Broad classification of volcanogenic products (lavas vs volcaniclastic rock types, distinguished by shading of boxes) at composite volcanoes.

the physical properties—density and viscosity—of the magma. In this respect, the role of volatiles is critical (“Volatiles in Magmas”). High volatile concentrations increase the propensity for eruption as fragmented magma (pyroclastic) relative to lava, although the influences of effective magma viscosity and ascent rate will ultimately determine the occurrence and extent of explosivity. In the latter category, the surface morphology controls the distribution of lava flows. As gravity-driven phenomena, both pyroclastic and lava flows are typically channeled into valleys, producing a complex interplay of erosion and construction that leads to frequent topographic inversions on volcano flanks.

The morphology of the summit region can have a significant effect in directing volcanogenic flows, particularly if there are distinct crater breaches. Lava domes, a common feature of evolved composition volcanoes, may dominate vent region morphologies over long periods of time—occupying either craters (e.g., Soufrière and Montserrat) or sector-collapse scar amphitheaters (e.g., Mount St. Helens). The domes are commonly active, growing by slow addition of magma to the interior and periodically gravitational collapse—which may or may not be accompanied by explosions. Dome talus landslides or avalanches may on occasion supply more extensive block-and-ash flows. Lava flows in steep summit regions or on upper flanks may also sustain gravitational instability collapse of their flow fronts, producing hot block avalanches. Sustained dome growth can result in a significant fraction of the upper part of a composite cone being formed entirely of one or more domes (e.g., Bezymianny).

Finally, the effects of surface conditions (climate/weather), discussed in the previous section, will have a profound effect on the redistribution of volcanogenic material. In fact, perhaps the single most important element in defining volcano morphology is the balance between construction (a function of magmatic flux to the surface) and erosion/weathering (a function of local climate). The control on the distribution of volcanogenic products is largely a result of this competition and is illustrated schematically in Fig. 9a.

While Fig. 9a usefully summarizes the distribution of volcanogenic products around a composite cone, perhaps the most helpful way to discuss the materials themselves and how they vary in nature and distribution relative to vents and topography is by use of the facies concept traditionally used to describe sedimentary environments. The specific associations that characterize a composite cone can be defined largely on the basis of distance from the vent, which accounts for both the relative predominance of immediate volcanic products near the vent, versus recycled or mixed (with water) volcaniclastic material, and topographic effects with slope steepness typically decreasing away from vents (Fig. 9b). A summary is provided in Table V.

B. Main Vent Association

This association is defined as lithologies related to long-term vents at which volcanic products are erupted to the surface. Typically, for a simple cone this would be a central/summit vent, but in cases where compound cones have been developed, this may be an inaccurate description. The most important defining characteristic is that it is a long-term feature, and for a given volcano, it may change location several times during the history of activity. At the cone surface, the lithofacies found associated with the main vent are of two main types. On the one hand, if the vent takes the form of a crater, it is commonly surrounded by (1) vent-filling breccia comprising disaggregated wall rock material from the vent and (2) coarse primary tephra, commonly welded due to proximity to the vent. The distribution of this material is concentric to the vent, thinning rapidly away from the vent region, where it may simply pinch out (interfingering with proximal cone-building facies association) or grade into well-defined tephra layers or even lava flows of the upper cone. In cases where the vent crater is filled by a crater lake, additional deposits such as lacustrine sediment, intracrater lahars, and phreatic/phreatomagmatic deposits may be an important element of the main vent lithofacies. On the other hand, the vent at the cone surface can be occupied by a lava plug or dome that forms a steep-sided morphological feature

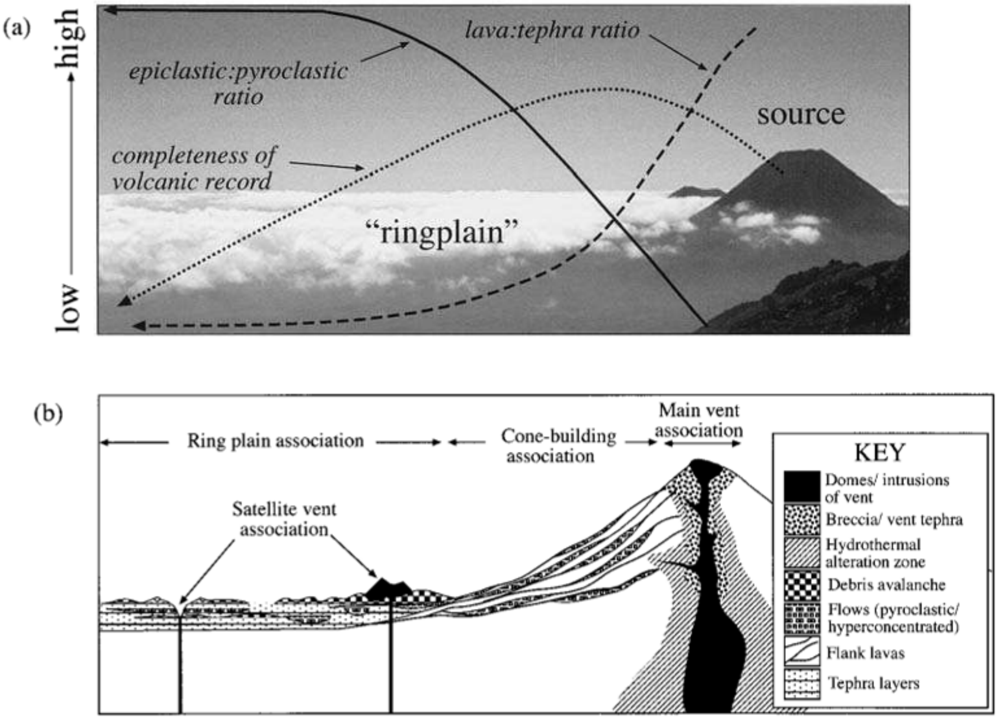
(a)
high
low
epiclastic:pyroclastic ratio
lava:tephra ratio
completeness of volcanic record
source
"ringplain"
(b)
Ring plain association
Cone-building association
Main vent association
Satellite vent association
KEY
Domes/ intrusions of vent
Breccia/ vent tephra
Hydrothermal alteration zone
Debris avalanche
Flows (pyroclastic/ hyperconcentrated)
Flank lavas
Tephra layers

FIGURE 9 (a) Schematic illustration of the distribution of deposits relative to vent for a composite volcano. "Completeness of volcanic record" refers to the number of events recorded in a succession at a given location. The most complete record is preserved in tephra that are deposited over wider areas. However, on the slopes of the volcano, tephra are rapidly reworked and may be washed away. Thus a more complete, albeit condensed, section is typically found in the region immediately surrounding the volcano—the ring plain. (b) Schematic illustration of lithofacies associations for a typical composite cone, showing *types* of deposits-compare with *distribution* of deposits in (a).

occupying or completely overfilling and obscuring a preexisting crater depression. Main vent domes are vulnerable to collapse if they overfill the summit crater [e.g., Mount Unzen (Japan), Soufrière (Montserrat)]. They are also vulnerable to destruction during later eruptions when located over the volcano's main vent. The lava dome itself is commonly surrounded by carapace breccia and breccia aprons—which again may be continuous with upper cone slope facies. In either case, the subsurface vent association is defined by a concentration of brecciated material and by an intensity of hydrothermal alteration. The latter reflects both the intense supply of heat and volcanic gases that define the vent and the permeability of the vent lithologies to vapors and fluids over long periods of time—commonly extending beyond the period of eruptive activity for the cone. Shallow intrusions comprising various geometries, including plugs, dikes, and sills, reflect the focusing of magma into the vent conduit and its movement upward through the edifice. The main vent association at shallow subvent depths (referred to as "hypabyssal") may also host concentrations of metal ores (cf. "Mineral Deposits Associated with Volcanism"), which can be exposed by modest erosion in the deeper portions of the edifice and in the subedifice basement between the surface and the original magma chamber.

C. Cone-Building Association

The lithofacies of this association are those that build and define the edifice itself. They include a diverse array of volcanic products ranging from lava flows to pyroclastic flows to the products of flow transformations or reworking, involving mixing of water with volcaniclastic material. The relative distribution of lithofacies is largely dependent on (1) the style of activity—which we

TABLE V Lithofacies Associations for Typical Composite Volcanoes

Association	*Main lithofacies and architecture*	*Other features*
Main vent	Coarse tephra, commonly welded; breccia Poorly bedded, commonly disturbed/slumped Domes may fill vent at surface	Hydrothermal alteration common Shallow intrusives below vent
Cone building	Lava flows, pyroclastic flows, hyperconcentrated flows Radial from main vent—may grade into vent facies or not be connected Ribbon-like bodies to narrow wedges	Distribution of deposits strongly influenced by erosional topography
Ring plain	Fall tephra, debris fans from lower cone slopes, lahars, debris avalanche deposits Deposits tend to be more continuous and widely dispersed than on cone	Distribution of tephra strongly influenced by wind Preservation of deposits/completeness of record decreases if ring plain is restricted/eliminated by encroachment of surrounding topography
Satellite vent	Cinder cones, with lava flows and tuff ring/maar associations Dome/coulees Distribution may be controlled by basement structures—e.g., aligned along faults	Phreatomagmatic features more likely on lower flanks and ring plain

have seen is determined mainly by the composition of the magma supplied to the volcano—and (2) the balance between the supply of volcanogenic material (eruption frequency) and the rate of erosion. If erosion is able to produce a well-developed drainage pattern between eruptions, then many of the erupted products will be channelized and form ribbon-like bodies radial to the main vent(s). As a result, there may be common stratigraphic inversions—younger flows occupy valley floors while older flows form the canyon walls at higher elevations. Topographic inversions may also occur—if valleys are effectively filled by lava flows that are resistant to erosion, then subsequent incision may take place on former ridges.

If erosion is less effective and the edifice is a relatively smooth-surfaced cone, then, at least for low-viscosity erupted products (basaltic lavas, pyroclastic flows, and hyperconcentrated flows), more widely distributed wedge-shaped veneers will form, again focused at the vent(s) of origination. The distribution of fall tephra is less influenced by the cone topography, but rather will form a veneer with a thickness that is greatest near the vent and strongly influenced by wind directions during eruption.

Lava flows, and their associated autobreccias, originate principally from the main vent, where, in the case of basaltic flows, they are typically the result of quiet effusion from a summit crater (overspill of a lava lake) or rapid accumulation and congelation of fire fountain spatter (clastogenic flows). More silicic andesite and dacite flows form more prominent radial ridges by virtue of their greater viscosities and tend to be topography-formers rather than topography-fillers, as in the case of their more fluid basaltic counterparts. They may be short, stubby coulees, connected to main vent domes, or may be rootless if the steep uppermost portions of the cone cause detachment of the main mass of the flow from its source.

Pyroclastic flows are also dispersed radially from the main vent. Given a well-established topography—that is, deep radial valleys—they will tend to become valley fills; otherwise they may form veneers over quite large angular segments of the flanks. Such flows may originate as column collapse from vulcanian or plinian eruptions or as dome/plug collapses in the vent region. Mixing with stream water in channels or snow and ice on the cone surface may lead to flow transformations, so that the ratio of primary pyroclastic flow deposits to hyperconcentrated flows (lahars and debris flows) typically decreases away from the vent (Fig. 9a). Unmodified pyroclastic flow deposits, as with pyroclastic fall tephra, are also rapidly reworked and removed from the upper parts of the cone to be redeposited low on the cone or on the ring plain.

D. Ring Plain Association

The lithofacies of the ring plain are dominated by fall tephra and by the tephra that has been rapidly reworked from the cone. The ring plain is defined as the area immediately surrounding the volcano, but not including the constructional edifice itself. In cases where the cone is isolated from neighboring volcanoes or other mountainous terrain (e.g., Taranaki and Ruapehu, Fig. 2), the definition is quite obvious. However, in many volcanic terranes, individual edifices merge with their neighbors, including ancestral degraded volcanoes, and the surrounding topography is far from flat so that classic "ring plain" deposits as discussed here will rather be concentrated into drainages, reworked and removed from the system quite rapidly. Furthermore, for many oceanic composite cones such as those of island arcs, the immediate edifice is surrounded by ocean and a true ring plain does not exist—although quite complete records of activity can be recovered from the tephra mantling the nearby ocean floor.

As emphasized in Fig. 9, the ring plain is potentially where the most complete record of explosive activity is preserved. It is sufficiently close to the volcano that the products of volcanism are not too widely dispersed, yet it is beyond the edifice, which, through its topography, has the effect of promoting rapid removal of volcanic products and concentrating them into narrow drainages. Lithofacies include numerous tephra layers—pyroclastic fall material that may be correlative with flow-forming events on the cone but that has been dispersed over much larger areas. The thicknesses of individual tephra layers reflect both the flux and duration of an eruption and the dispersal control by wind. Lateral variations in the thicknesses of individual layers (isopachs) and in the grain sizes of tephra within the layers can be used to accurately reconstruct eruption histories (cf. "Plinian Eruptions" and "Tephra Fall Deposits").

Interbedded with fall tephra are the fluvial and laharic deposits, which may form the distal edges of wedgelike fans of debris from the lower cone slopes or may be concentrated along well-established drainage channels through the ring plain. The distal edges of the most extensive of flows (lava and pyroclastic) from the cone may also reach as far as the ring plain (e.g., Fig. 4b, parts iii and iv).

A typical, albeit occasional, product of composite volcano activity is the debris avalanche—the widely dispersed large-volume product of large-scale gravitational instability, or sector collapse (cf. "Debris Avalanches"). Debris avalanche deposits are a common ring plain lithofacies, distinguished by a hummocky topography, with the size of hummocks decreasing away from the edifice from large toreva blocks at the slope base to the more subtle topography of flow transition lahars and debris flows that drain the deposit far out on the ring plain (e.g., Fig. 6e). The hummocks consist of blocks mobilized from the cone slopes, which have suffered various degrees of disruption. At the base of the deposit, the lithologies are strongly disrupted and smeared, whereas in the interiors of many blocks disruption is minimal and a jigsaw texture is observed among the components reflecting intense fracturing but no turbulent mechanical mixing.

E. Satellite Vent Association

While by no means ubiquitous at composite cones, satellite vents are nevertheless common. As pointed out above, the magma compositions erupted at such vents are commonly distinct from those of the main vent that characterize the bulk of the edifice. The eruptions are also typically monogenetic—a single eruptive episode rather than prolonged and repeated eruptions of the main vent. It should come as no surprise then that there may be distinct lithofacies associations at satellite vents.

Scoria cones are defined by the steep piles of scoria that are accumulated at the angle of repose about the vent crater. A high flux of pyroclast accumulation around the vent can lead to the formation of spatter ramparts or even limited clastogenic lava flows. However, most lava flows associated with scoria cones (and some may be quite extensive; Fig. 7b) breach the cone and may raft large fragments of the cone walls along on the flow.

If a basaltic satellite vent interacts with near-surface water, then maars and tuff rings may form during phreatomagmatic eruptions. The water may occur as shallow groundwater reservoirs or in standing bodies of water such as lakes. In either case interception of shallow water by ascending magma is more likely to occur on the shallow slope lower reaches of the edifice, or on the ring plain, rather than on the cone itself. The common occurrence of accretionary lapilli in such phreatomagmatic deposits is also consistent with the important role for water.

Lava domes may also occur as monogenetic eruptions at satellite vents (e.g., Figs. 7c and 7d). These occurrences, by virtue of their location, have a higher preservation potential than those emplaced at the main vent. Silicic magma batches supplied to flank locations are typically small and degassed, resulting in slow and passive effusion of lava. The earliest phases of emplacement may be volatile-charged, resulting in emplacement within a pumice cone—an effect analogous to effusion of basalt lava from a cinder cone. As with basaltic equivalents, tuff cones of silicic tephra may also be found where silicic magma supplied to flank vents intercepts shallow near-surface water reservoirs.

V. CONCLUDING REMARKS AND FUTURE RESEARCH DIRECTIONS

We are only beginning to understand the complex behavior of composite volcanoes through detailed studies of their histories (erupted products), their subsurface conduits (geophysically imaged), and their occasionally witnessed eruptive activity. In recent years, physical volcanology has made considerable advances enabling the characteristics of individual deposits to be interpreted in terms of eruption styles and magnitudes. At the same time, geochemical techniques examining both rocks and volatiles have enabled us to better understand magma generation and evolution from source to eruption. A major challenge of the next decade is to integrate geological, geochemical, and geophysical approaches in order to decipher the processes occurring in magma chambers, the timescales over which they occur, and the consequences for volcanic eruptions. Such an understanding not only will enable us to address important aspects of magmatism such as mass fluxes between the mantle, lithosphere, and atmosphere but will also have tremendous predictive value, aiding the mitigation of volcanic hazards.

SEE ALSO THE FOLLOWING ARTICLES

Calderas • Debris Avalanches • Plate Tectonics and Volcanism • Pyroclast Transport and Deposition • Volatiles in Magmas • Volcanic Soils

FURTHER READING

Cotton, C. A. (1944). "Volcanoes as Landscape Forms." Whitcombe and Tombs, Christchurch, New Zealand.

de Silva, S., and Francis, P. (1991). "Volcanoes of the Central Andes." Springer-Verlag, Berlin/New York.

Fisher, R. V., and Smith, G. A., eds. (1991). "Sedimentation in Volcanic Settings," SEPM Publication 45.

Francis, P. (1993). "Volcanoes: A Planetary Perspective." Oxford Univ. Press, Oxford.

Hackett, W. R., and Houghton, B. F. (1989). A facies model for a Quaternary andesitic composite volcano: Ruapehu, New Zealand. *Bull. Volcanol.* **51,** 51–68.

Halsor, S. P., and Rose, W. I. (1988). Common characteristics of paired volcanoes in northern Central America. *J. Geophys. Res.* **93,** 4467–4476.

Hildreth, W. E., and Lanphere, M. (1994). Potassium–argon geochronology of a basalt–andesite–dacite arc system: The Mount Adams volcanic field, Cascade Range of southern Washington. *Bull. Geol. Soc. Am.* **106,** 1413–1429.

Hobden, B. J., Houghton, B. F., Davidson, J. P., and Weaver, S. D. (1999). Small and short-lived magma batches at composite volcanoes: time windows at Tongariro volcano, New Zealand. *J. Geol. Soc. Lond.* **156,** 865–867.

Singer, B. S., Thompson, R. A., Dungan, M. A., Feeley, T. C., Nelson, S. T., Pickens, J. C., Brown, L. L., Wulff, A. W., Davidson, J. P., and Metzger, J. (1997). Volcanism and erosion during the past 930 k.y. at the Tatara–San Pedro complex, Chilean Andes. *Bull. Geol. Soc. Am.* **109,** 127–142.

Wright, J. V., Smith, A. L., and Self, S. (1980). A working terminology of pyroclastic deposits. *J. Volcanol. Geotherm. Res.* **8,** 315–336.

This Page Intentionally Left Blank

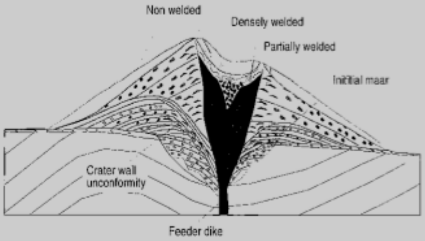

SCORIA CONES AND TUFF RINGS

DIRK VESPERMANN
HANS-ULRICH SCHMINCKE
GEOMAR Research Center

I. Definitions
II. Particle Morphology and Fragmentation Processes
III. Deposits
IV. Morphology and Internal Structure
V. Tectonic Setting and Chemical Composition
VI. Significance
VII. Historic Examples

GLOSSARY

accretionary lapilli Tightly bound, approximately spherical aggregates of ash particles. They form in eruption clouds, by raindrops falling through the eruption cloud or by electrostatic attraction.

achneliths Juvenile ash- to lapilli-sized volcanic particles with smooth, glassy surfaces. They are interpreted to form from chilled lava spray.

armored lapilli Lithic fragments or crystals forming solid nuclei surrounded by fine ash. They form during hydrovolcanic eruptions.

diatremes Funnel-shaped breccia pipes that reach as much as 2500 m in depth. Diatremes are thought to form by hydrovolcanic fragmentation and wall rock collapse. Diatremes may underlie maars and grade at depth into dikes.

fire fountains Fire or lava fountains are highly fluid mixtures of basaltic magma and gas that are common in hawaiian eruptions as in Kilauea volcano.

fuel–coolant interaction (FCI) Intense mixing of hot liquids (fuel) with cooler liquids (coolant) may result in thermal explosions, known as fuel–coolant interactions. Explosive interaction of magma with external water has been interpreted in terms of FCIs.

hydrovolcanic eruptions Hydrovolcanic (hydroclastic, hydromagmatic, phreatomagmatic) eruptions are caused by the mixing of magma with water.

strombolian eruptions Discrete explosions at periodic intervals of a few seconds to minutes or hours, named after Stromboli, a volcano in the Aeolian Islands, Italy. Deposits consist of lava spatter, vesicular bombs, scoriaceous lapilli, and ash.

surtseyan eruptions Hydrovolcanic explosions dominated by jets of wet tephra, as observed at Surtsey (1963), Iceland. They result in tuff cones. The term “surtseyan” is mostly used for volcanoes erupting through seawater.

vesicular tuff Tuffs containing millimeter- to centimeter-sized, irregular to round pores. The cavities are interpreted to form during trapping of air or vapor in wet ash deposits or after deposition of muddy rain.

SCORIA CONES are the most common volcano type on land. Hydrovolcanic tuff rings, tuff cones, and maars are second in abundance to scoria cones.

Copyright © 2000 by Academic Press
All rights of reproduction in any form reserved.

These volcanoes are small compared to shield volcanoes or stratovolcanoes. Here we briefly review the particle morphologies and fragmentation processes, deposits, environments, and eruption style of strombolian/hawaiian scoria cones and hydrovolcanic tuff rings, tuff cones, and maars. Explosive fragmentation results from (a) rapid exsolution and decompression of magmatic volatiles (pyroclastic fragmentation), (b) explosive interaction of magma with external water, or (c) simultaneous interaction of both processes. Pyroclastic eruptions resulting in scoria cones and "wet" hydrovolcanic tuff cones are end members in a wide spectrum of explosive fragmentation.

I. DEFINITIONS

Scoria cones, also called cinder or tephra cones, are relatively small but common volcanoes that form by the eruption of low-viscosity, generally basaltic magma in strombolian or hawaiian eruptions. They commonly occur in groups or fields, some consisting of hundreds of eruptive centers. The volcanoes are truncated, cone-shaped, or horseshoe-shaped. Bowl-shaped craters at the top are filled by debris reworked from the cone rim and younger deposits. Elongate cones are built above fissures with more complex vent systems. Deposits of scoria cones consist of bombs, scoriaceous lapilli, and minor ash whereas spatter cones and scoria–agglutinate cones consist largely of welded lava spatter. Well-known examples include Heimaey (Iceland), Paricutin (Mexico), and Stromboli (Italy). Shallow marine scoria cones constructed by submarine lava fountaining are rare.

Tuff rings, tuff cones, and maars, formed subaerially and/or in shallow water, are second in abundance to scoria cones. They result from phreatomagmatic eruptions due to mixing of ascending magma with groundwater or surface water. Deposits are composed of juvenile (or essential) pyroclasts, derived from the erupting magma, accessory (or cognate) clasts of comagmatic volcanic rocks from earlier eruptions, and accidental clasts, derived from the subvolcanic basement. Magma–water interactions occur in shallow water, beneath ice, or where lava flows or pyroclastic flows enter the sea. The term phreatic eruption is used when explosive eruptions eject exclusively preexisting rocks but no juvenile fragments.

Hydroclastic volcanoes can be subdivided into three different morphological and structural types: (1) tuff rings, (2) tuff cones, and (3) maars. Differences between these volcanoes are mainly controlled by the magma/water ratio, the degree of magma/water mixing, and the depth of fragmentation.

Tuff rings are commonly less than 50 m high. They are defined by craters with small depth to width ratios at or above ground level and low ejecta rims of hydroclastic debris, with beds dipping <25°. The deposits consist of a mixture of juvenile and accidental clasts. Juvenile pyroclasts are the main constituent of the well-stratified deposits.

Tuff cones are characterized by higher profiles than tuff rings and maars and steeper external slopes with bedding dips >25°. Their crater floors are generally above the land surface. Deposits are composed mainly of juvenile clasts and subordinate amounts of accidental clasts. Rim beds are massive and interpreted as having been emplaced laterally by turbulent particle-laden surges, fall, and remobilization processes.

Maars are defined by bowl-shaped craters cutting about 10 m to more than 500 m deep into the preeruption surface. Maars are surrounded by low ramparts of well-bedded ejecta (beds dipping <25°) that decrease rapidly in thickness away from the rim. Maar deposits are distinguished from those of tuff rings/tuff cones by the abundance of nonjuvenile components (country rock). The deposits are mainly emplaced by base surges and fallout.

Hydroclastic volcanoes and scoria cones are commonly termed monogenetic because they may form in a single eruptive episode with nearly constant eruptive conditions during rapid cone growth within a few days, months, or, at most, years. This results in a simple stratigraphy that differs from that of large, long-lived polygenetic shield volcanoes and stratovolcanoes. More detailed studies of scoria cones have revealed complex structures due to alternating magmatic and phreatomagmatic eruptive conditions over long time intervals. Some volcanoes evolve from a maar, tuff ring, or tuff cone phase to a scoria cone phase, followed by lava flows, resulting in a composite volcanic complex.

II. PARTICLE MORPHOLOGY AND FRAGMENTATION PROCESSES

A. Particles Resulting from Dry Magmatic Eruption

Strombolian and hawaiian eruptions producing scoria cones are caused by near-surface expansion and explosive disruption of gas bubbles within fluid, low- to moderate-viscosity magma. During strombolian eruptions, magma becomes fragmented to clasts with moderate to high vesicularity at periodic explosive intervals of a few seconds (e.g., Heimaey, Iceland) to minutes or hours (e.g., Stromboli, Italy; Paricutin, Mexico). Deposits are generally coarse-grained and composed predominantly of lapilli- to bomb-sized particles larger than 2 mm. Common clasts are scoria, vesicular basaltic to andesitic glass less inflated than pumice and mostly composed of tachylite, a nearly opaque basaltic glass. Minor ash-sized particles are more vesicular. Particles with elongate and ragged shapes are common.

Hawaiian lava fountains, in contrast, are produced by nearly homogeneous turbulent mixtures of gas and magma. Hawaiian lava fountains produce spatter, bomb-sized fragments of molten clots, commonly stuck together to form agglutinate deposits or lava flows, glassy achneliths, droplike Pele's tears, and long threads of Pele's hair. Clast shapes are fluidal or ragged.

B. Particles Resulting from Hydroclastic Eruption

In hydrovolcanic explosions, thermal energy is efficiently converted into kinetic energy (Fig. 1). Strong hydrovolcanic explosions generate fine particles by an optimum water to magma mass ratio ranging between 0.2 and 0.3. Larger particles result from explosions with higher or lower mixing ratios. The explosivity of magma–water interactions (analogous to fuel–coolant interactions) is highly controlled by (a) the geometry and location of the vent and contact zone, (b) the depth of interaction, (c) the water/magma mass mixing ratio and premixing mass ratio, (d) the magma ascent rate and the pressure regime between magma and water, (e) the processes by which energy is transferred from magma to water, and (f) the propagation of shock waves through the mixing zone.

The grain size of hydrovolcanic deposits is dominantly in the ash- and lapilli-size range; bombs and blocks are subordinate. Juvenile, glassy particles show fracture-controlled surfaces with blocky-equant shapes. Fine-grained particles with ragged and fluidal surfaces can form during inefficient mixing of magma with water. The vesicularity of hydrovolcanic clasts is strongly influenced by the ascent history of the magma. Clast vesicularity commonly ranges widely from nonvesicular (0–5 vol% vesicles) to highly vesicular (60–80 vol% vesicles), which reflects the relative timing of vesiculation and water-induced fragmentation. Armored and accretionary lapilli, cored ash aggregates, commonly form in wet hydrovolcanic eruptions. Clasts with contrasting vesicularity, clast morphology, and mud coating are interpreted as recycled particles. They may have been generated by fallback or collapse into the crater during an eruption and later reejection.

III. DEPOSITS

A. Scoria Cones

Strombolian deposits are distinguished from deposits of hydroclastic volcanoes by their coarser clast sizes and massive to coarsely bedded structures, the general pau-

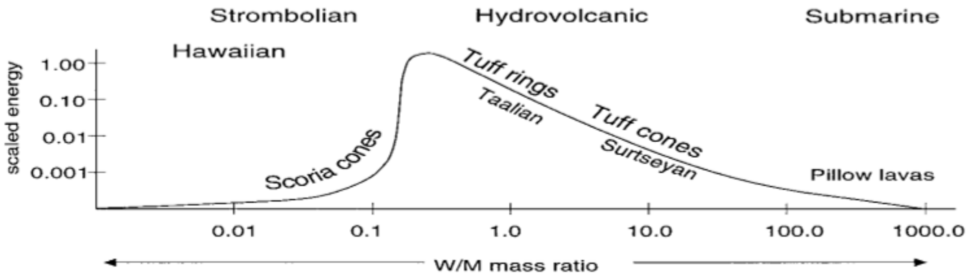

FIGURE 1 Diagram of water/magma ratios. Water/magma (W/M) ratios are an important control on the eruption style and the mode of transport and deposition of ejecta. Scoria cones result from low W/M ratios or dry magmatic eruptions. With increasing W/M ratios, the eruption style changes to hydrovolcanic fragmentation. Tuff rings result from eruptions with relatively low W/M ratios, known as taalian eruptions, and tuff cones from eruptions with relatively high W/M ratios, known as surtseyan eruptions. (Modified from Wohletz, K. H., and Sheridan, M. F. (1983). Hydrovolcanic processes: II. Evolution of basaltic tuff rings and tuff cones. *Am. J. Sci.* **283,** 385–413. Copyright © 1983 Kline Geology Laboratory.)

city of lithic clasts, and higher depositional temperatures. Strombolian deposits are framework supported and mostly well sorted. Bedding may consist of alternating coarser and finer fall beds. Variable sorting may result because of eruptions of fragments with different vesicularities and densities, particle aggradation of ashes, or mixing of clasts transported by flow and fall. Clasts in strombolian deposits have vesicle volumes up to 80 vol%. Angular fracture-bounded clasts with poor to moderate vesicularity (e.g., Rothenberg scoria cone, Germany) in strombolian deposits may have been generated by magma ponding in and around the vent that led to simultaneous eruption of gas-rich magma together with degassed magma.

Massive scoria breccias commonly form as result of submarine lava fountaining in shallow water. Scoria clasts are irregular to amoeboid with up to 60 vol% vesicularity. Intercalations of stratified lapilli tuffs in these scoria cones suggest a change from magmatic to hydrovolcanic fragmentation, caused by significant mixing of water into the fire fountain.

Two main facies can be distinguished from each other in a scoria cone: (a) an inner crater facies and (b) an outer wall facies (Fig. 2). The deposits of the crater facies are more heterogeneous than those of the wall facies. The lower crater facies consists of erupted lava spatter, which was hot on landing and became welded to form an agglutinate. In a transitional area, passing outward toward the crater wall facies, scoria fragments may be welded together but can still be recognized as individual clasts. In the crater interior, lava lakes or lava flows can develop. The upper crater facies characteristically consists of round bombs set in a poorly sorted matrix of lapilli, overlain by well-sorted lapilli layers up to several meters thick. The lapilli layers can extend much farther than the actual scoria cone.

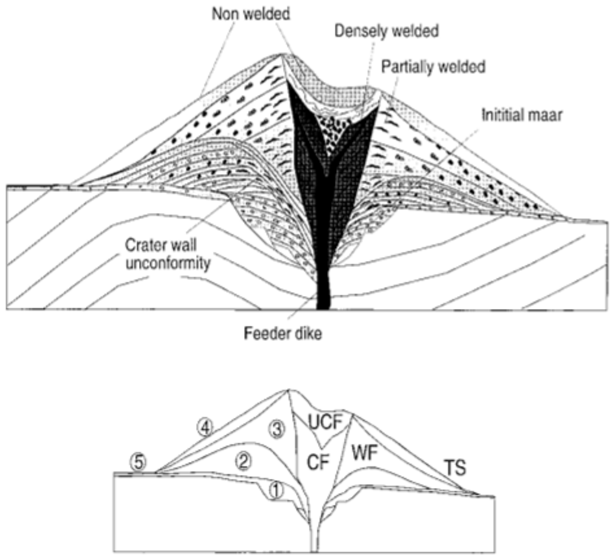

FIGURE 2 Morphology and internal structure of a scoria cone: 1, initial phreatomagmatic eruptions; 2, strombolian eruptions with phreatomagmatic intercalations; 3, strombolian eruptions forming main cone; 4, poststrombolian talus slides; 5, distal fallout; CF (crater facies), agglutinates, feeder dike; UCF (upper crater facies), round bombs set in matrix of lapilli, redeposition and slumping from the walls; WF (wall facies), scoria breccias, partial welded bombs in proximal units and unflattened bombs in distal units; TS (talus slope), redeposition because of slope failure.

The outer wall facies may begin with basal fine ash layers rich in accretionary lapilli overlain by coarse-grained, poorly sorted breccia layers extremely rich in accidental fragments. These deposits result from initial phreatomagmatic explosions during reaming out of the conduit. The inner wall and lower crater facies may contain similar deposits. Coarse-grained scoria bombs and lapilli beds dominate the outer flank facies and may be moderately welded close to the crater rim but become increasingly less welded, uncompacted, and finer grained in the distal facies. Single, denser, in part spindle-shaped bombs are found in wall facies deposits, together with moderately to highly vesicular juvenile lapilli. Wall-rock lithics are sparse. The outer flanks of many scoria cones are covered by fall layers of well-sorted lapilli. Vertical and lateral transitions in scoria cones may reflect common changes in eruptive conditions, distance from the vent, and/or phreatomagmatic influence.

Later redeposition of the products is a major process, especially during the mature stages of scoria cone growth, when the outer slopes become unstable and the clasts slide to the foot of the cone. Redeposition may occur by oversteepening of the cone, where the slope angle is higher than the angle of repose, or when deformation associated with ascending magma leads to cracking and partial collapse. Deposits on steep cones may be mobilized downslope as debris flows, grain flows, or mudflows, commonly resulting in inversely graded beds.

B. Hydroclastic Volcanoes

Typical deposits of hydroclastic volcanoes are rich in accidental lithics. Coarse- to medium-grained fallout deposits may contain up to 90 wt% wall-rock lithics and minor juvenile clasts (e.g., from Ukinrek maar, Alaska), and contain important information on the make-up of the subvolcanic basement and on the depth of the hydroclastic explosions. Most tuff rings, tuff cones, and maars are dominated by surge deposits generated during explosive hydrovolcanic eruptions, as shown by historic eruptions such as Surtsey (Iceland, 1963–1967), Taal (Philippines, 1965), Capelinhos (Azores, 1957–1958), and Miyake-jima (1983), where base surges and cock's tail jets were observed. Fall deposits of better sorted lapilli tuffs, mostly grain-supported openwork and crudely interstratified with fine ash layers, and ballistic fall breccias are common intercalations in hydroclastic deposits. Fine-grained fallout tuffs may be derived from ash clouds accompanying the base surges.

Base surges are gravity-controlled, low-concentration, turbulent pyroclastic density currents with gas (steam) as a continuous phase. Downcurrent flow transformations and variable flow regimes and degrees of wetness result in complex lateral and vertical facies changes (Fig. 3). Base surges may be dry (superheated steam as the fluid phase) or wet (condensing steam as fluid), leading to rapid facies variations. Surges range in transport and emplacement temperatures from cool to 200–300°C. Surge deposits are generally thin bedded, fine grained, and poorly sorted. Bedforms are planar, wavy, or cross-bedded, and bed thickness decreases rapidly in the direction of transport.

Tuff rings and maars are characterized by progressive lateral and vertical facies changes of mostly dry surges. Near-vent deposits may be inversely graded, massive to bedded lapilli tuffs changing with distance from vent into crudely bedded lapilli tuffs, planar-bedded lapilli tuffs, and more distal cross-bedded lapilli tuffs. Outward-dipping deposits may begin with disorganized and scour-filled lapilli tuffs, replaced by stratified lapilli tuffs and dune-bedded lapilli tuffs. Lateral facies sequences for both imply deposition from high-concentration turbulent surges near the vent. Lack of tractional transport leads to unstratified, massive and crudely bedded deposits. Further downcurrent, surges become more diluted through deposition of clasts and mixing with ambient air, forming thinly stratified and laminated deposits. Dilution of surges may also cause cooling and condensation of steam, leading to moistened ash, vesiculated tuffs, and accretionary and armored lapilli.

Lateral facies variations in tuff cones differ from those of tuff rings, because of the higher wetness of the eruption clouds. Ash-coated lapilli in mainly crudely stratified deposits are interpreted as having been deposited by radially propagating dense, wet surges, which do not extend far from the vent. Tuffs containing millimeter- to centimeter-sized, irregular to subspherical pores up to 1 cm around may have developed in wet surges and mudflows on proximal rim beds. The vesicular tuffs are interpreted to form during (a) trapping of air or vapor in wet cohesive fall or surge deposits, (b) sedimentation of viscous mudflows, or (c) gases given off by hot pyro- and hydroclasts. In most examples described, vesiculated tuffs are associated with accretionary lapilli due to steam condensation.

Reworking is commonly a subordinate process in tuff rings and maars because of low slope rims but depends

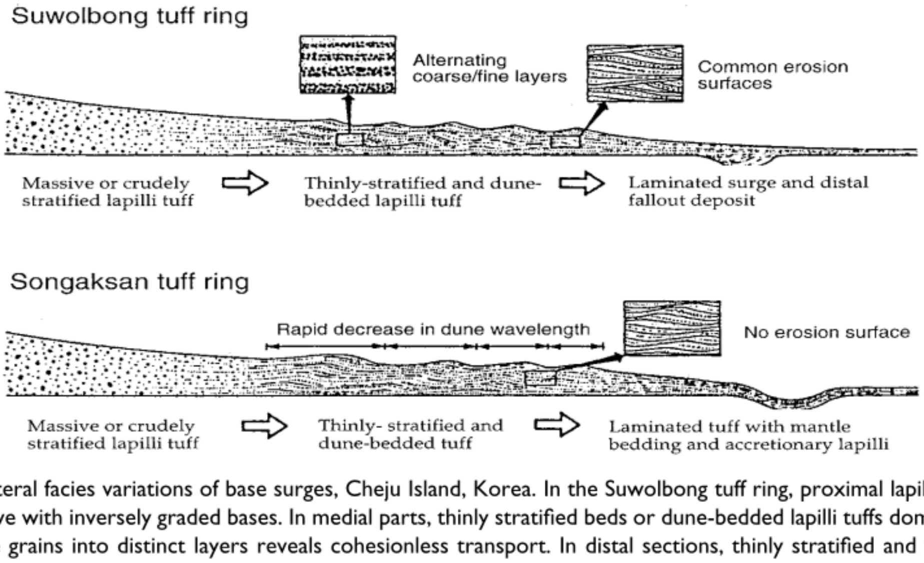
Suwolbong tuff ring
Alternating coarse/fine layers
Common erosion surfaces
Massive or crudely stratified lapilli tuff
Thinly-stratified and dune-bedded lapilli tuff
Laminated surge and distal fallout deposit
Songaksan tuff ring
Rapid decrease in dune wavelength
No erosion surface
Massive or crudely stratified lapilli tuff
Thinly- stratified and dune-bedded tuff
Laminated tuff with mantle bedding and accretionary lapilli

FIGURE 3 Lateral facies variations of base surges, Cheju Island, Korea. In the Suwolbong tuff ring, proximal lapilli tuffs are crudely stratified or massive with inversely graded bases. In medial parts, thinly stratified beds or dune-bedded lapilli tuffs dominate. Segregation of coarse and fine grains into distinct layers reveals cohesionless transport. In distal sections, thinly stratified and wavy-bedded tuffs are present. The Songaksan tuff deposits show similar facies variations, although accretionary lapilli, plastering of deposits on vertical obstacles, and absence of erosion structures suggest wetter surges. (Adapted from Sohn, 1996.)

strongly on the ambient environment. Redeposition is more common in more steeply bedded tuff cones, resulting in lenticular, massive or chaotic bedded lapilli tuffs emplaced by debris flows, grain flows, slides, and/or slumps.

C. Mixed Deposits

Fall and surge deposits of complex magmatic/hydrovolcanic origin are characterized by juvenile clasts with (a) highly variable clast densities, (b) sorting coefficients between strombolian/hawaiian and hydrovolcanic deposits, and (c) angular to blocky clast morphologies with low vesicularities (hydrovolcanic) to ragged (strombolian) and fluidal (hawaiian) with high vesicularities. Mixed deposits may represent mixing of pyroclastic/hydroclastic clasts from simultaneous eruptions of a multiple-vent system.

IV. MORPHOLOGY AND INTERNAL STRUCTURE

A. Scoria Cones

The morphology of scoria cones depends on numerous factors, including (1) total volume of erupted material, (2) range and median ejecta velocity, (3) ejection angles, (4) wind speed and direction, (5) nature and size of particles, (6) occurrence of lava overflows, (7) phreatomagmatic intercalations, and (8) vent geometry.

Scoria cones range from 0.25 to 2.5 km in basal diameter (W_{co}), with a median of 0.8 km (Fig. 4). Cone heights equal $0.18W_{co}$, varying from a few meters and rising to as much as 424 m such as Paricutin volcano, Mexico. Crater diameters equal $0.4W_{co}$ (data from 910 cones). Some spatter cones and scoria–agglutinate cones show basal diameters less than 0.2 km. The crater diameter increases not only by ejection of pyroclastic material but also by slumping into the vent, for example, during seismic shocks. Most cones are initially built during high rates of strombolian or hawaiian activity. The main eruptive center migrates repeatedly during growth of scoria cones and several conduits may be active along a fissure. Late eruptive activity modifies the cone morphology only slightly. Many cones produce lava flows, which mainly extrude after explosive activity has ceased. Lavas may be fed by lava fountaining or are erupted from base-of-cone vents or fissures. Fifty percent of observed scoria cone eruptions lasted less than 30 days, and 95% ended within 1 year. Volumes of cone plus flows range between 10^5 and 10^9 m^3, similar to total volumes of tuff cones and rings. Lava flow volumes are generally higher than associated cone volumes. Coarse pyroclasts (scoriaceous lapilli, bombs) fall near the vent but may move downslope until reaching a position where the slope angle is less than the angle of repose (about 30°) (Fig. 5). Spatter cones and scoria–agglutinate cones can present steeper sided slopes because fragments are welded together. During the last phase of eruptive activity, cones grow only slightly and lava flows dominate over pyroclastic eruptions, resulting in submergence of the base of the cone by its own lava flows. Multiple destruction and rebuilding occurred during the extended growth period of the famous scoria cone Paricutin (Mexico). Well-exposed scoria cones may show several conduits. The spatial arrangement and morphological structure of scoria cones may suggest eruption from a fissure or en-echelon feeder system. Several different eruptive processes can occur simultaneously at different parts of a fissure system, for example, mixed magmatic/phreatomagmatic deposits from Crater Hill (Auckland, New Zealand), or can alternate with each other, leading to the formation of complex volcanic structures (e.g., from Herchenberg and Rothenberg cones, Eifel, Germany).

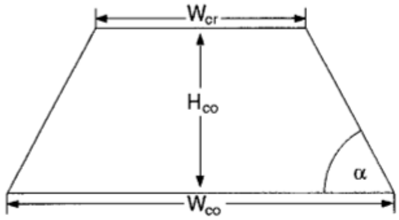

W_{cr} = crater diameter
H_{co} = cone height
W_{co} = basal width of cone
α = slope angle

FIGURE 4 Simple model of cone parameters. Scoria cones range from 0.25 to 2.5 km in basal diameter (W_{co}), with a median of 0.8 km. Cone heights equal 0.18 W_{co}; crater diameters equal $0.4W_{co}$. Slope angle is less than angle of repose and ranges between 25 and 38°, depending on the nature of the ejected material.

Cone height, height/diameter ratio, and slope are reduced systematically by erosion with time. The mode of degradation seems to be similar for all scoria cones but is strongly influenced by rainfall, climate, and cementation rates. Scoria cones in New Guinea showed

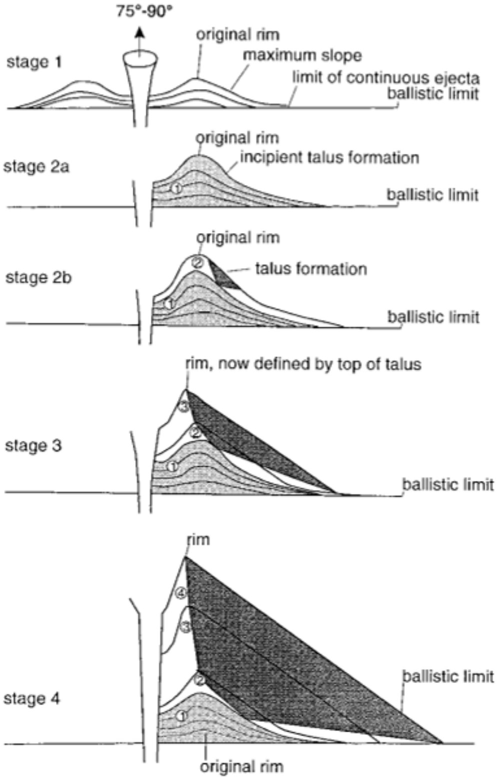

FIGURE 5 Growth stages of scoria cones. Stage 1: Initial phreatomagmatic deposits form a tuff ring with shallow dipping rim beds. Mean ejecta angles range between 75 and 90°. Stage 2: Continuous strombolian eruption activity leads to the growth of a steeper sided cone. Slope instability results in talus formation (Stage 2b); as volume increases, the cone rim migrates outward. Stage 3: Inward migration of the exterior talus pile and destruction of the older rounded rim occur. Collapse of the vent, talus formation of the inner slopes, and destruction by larger eruptions modify the original cone. The cone rim migrates inward. Stage 4: During continuous growth of cone, talus extends beyond ballistic limit of ejecta. (Adapted from McGetchin *et al.,* 1974.)

significant gully erosion 5 years after eruption, in contrast to more arid regions, where erosion is negligible after thousands of years. Cone morphologies and degradation rates are thus useful indicators of ancient climatic regions and changes. The systematic degradation of scoria cones has been used to estimate the approximate ages of undated scoria cones within a single field.

B. Tuff Rings, Tuff Cones, and Maars

The morphology, shape, and size of hydrovolcanic cones and rings are described by the parameters (1) rim diameter, (2) maximum height, (3) height/rim ratio, (4) excavation depth, and (5) maximum bedding dip.

Tuff rings and maars are morphologically similar. In maars, the crater is cut into the pre-eruption surface (Fig. 6). Both have crater diameters averaging 0.7–0.8 km and range from 0.2 to 3.0 km (e.g., Kilbourne Hole, New Mexico). Rim sequences are commonly less than 50 m thick but may reach more than 100 m in height (Joya Honda maar, Mexico; El Cuchillo tuff ring, Lanzarote, Canary Islands). Height/rim diameter ratios range between 0.13 and 0.05. Morphologically asymmetric volcanoes form during strong winds [e.g., Cerro Colorado maar (Pinacate Volcanic Field, Mexico)]. The well-bedded and fine-grained deposits of tuff rings and maars dip gently around 20° near the rim to less than a few degrees outward. They generally lack spatter and agglutinates deposited hot. The maximum diameter of country rock fragments may exceed 3 m. Accidental clasts may reach up to 90 vol% in maar deposits but make up only a minor component in tuff ring deposits. The fragmentation level in tuff rings is generally more shallow than in maars based on the higher abundance of moderately vesicular essential clasts.

Tuff cones vary in rim diameter from <100 m to 1.5 km in length (e.g., Udo tuff cone, Cheju Island, Korea), the height varying between 50 and 330 m (e.g., Koko Crater, Hawaii). The base of tuff cone craters may rise up to 130 m above the surrounding plain (e.g., North Menan tuff cone, United States). Typical height/rim ratios of tuff cones range from about 0.5 to 0.2. Beds of tuff cones dip more steeply (10–30° and up to 45° near the crater rim) compared with tuff rings and maars. Intercalated channels, which may form after slumping of unstable crater walls, commonly dip steeper (between 20 and 50°) than primary bedding. Unstable steep crater walls produce large, funnel-shaped faults (e.g., Surtsey, Iceland; El Golfo, Lanzarote, Canary Islands), with faults dipping about 50–90°, and shear displacements along larger blocks that may subside up to >50 m.

V. TECTONIC SETTING AND CHEMICAL COMPOSITION

Scoria cones and hydrovolcanic cones and rings occur in all tectonic environments such as rift zones, uplifted blocks, subduction zones, and oceanic islands. The volcanoes occur mostly in (a) groups, roughly of the same age, and (b) volcanic complexes, several nested volcanoes of roughly the same age that can be distinguished from

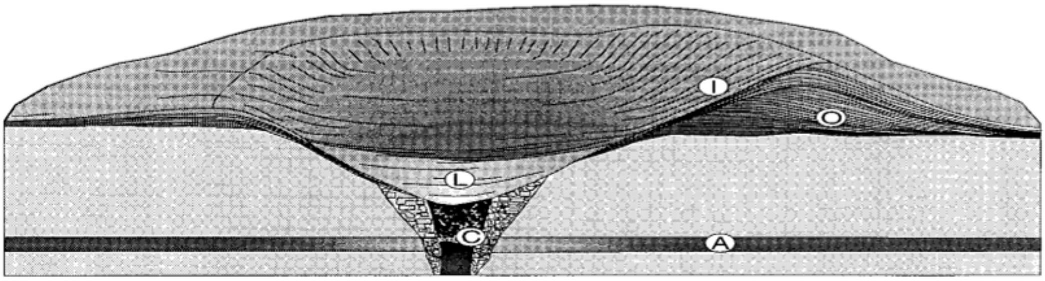

FIGURE 6 Diagram of maar volcano showing different stages of rim evolution controlled by continued excavation of the crater. The rim beds consist of lithic-rich ashes and lapilli deposited by pyroclastic surges and fall. Sectorial distribution of the surges and the influence of wind velocity on the fall deposits produce asymmetric rim beds. O, outward-dipping rim bed; I, inward-dipping rim bed; C, funnel-shaped conduit formed by explosive interaction of magma with groundwater; A, groundwater aquifer; L, crater filling, consisting of fallback tephra, reworked tephra from the rim beds, and lake sediments. [Adapted from "Pyroclastic Rocks," Fisher, R. V., and Schmincke, H.-U., p. 259, 1984, copyright notice of Springer-Verlag.]

each other by structure and types of deposits and contain their own individual vent system.

A. Volcanic Islands

Hydroclastic volcanoes characteristically form during the shoaling to emergent stage of a seamount where hydrostatic pressure is low. A classic example of the growth of a new island is Surtsey, Iceland. Surtsey formed on a shallow insular shelf by phreatomagmatic explosions caused by the interaction of rising magma with seawater. The island is about 1.5 km in diameter and has an area of 2.8 km^2. The deposits are crudely bedded to massive lapilli tuffs consisting of blocky, nearly equant vesicular clasts. Pyroclastic fragmentation followed after sealing of the vent system against external water and growth of the cone above sea level. Alkali basalt flows extended to the south and protected the cone from wave erosion. Surtsey subsided about 1.1 m between 1967 and 1991 because of compaction of the loose hydrovolcanic deposits and/or compaction of the underlying seafloor sediments.

In oceanic islands, scoria cones are commonly restricted to inland areas whereas tuff cones, tuff rings, and maars are mostly distributed along the coastal regions, as on Cheju Island, Korea, where $>$300 scoria cones are distributed in the inland area and about 10 tuff cones, tuff rings, and maars erupted along the shoreline in the transition between submarine and subaerial environments. Tuff cones on Cheju Island formed by direct flooding of seawater into the vent or where subaerial lavas with pervasive joints acted as permeable aquifers, allowing intrusion of coastal seawater or mixed seawater/groundwater. Tuff rings and maars may also form by explosive eruptions in inland areas when aquifers, streams, lakes, or wet sediments are intruded by rising magma (e.g., Bandama and Marteles maars, Gran Canaria, Canary Islands). Historic basalt eruptions on Lanzarote, Canary Islands, in 1730–1736 and in 1824 covered about 20% of the island (Fig. 7). Thirty scoria cones of nephelinite to olivine tholeiite formed during five eruptive phases along a fracture 14 km long. Pleistocene hydrovolcanic tuff cones and tuff rings, distributed along the western coast of Lanzarote and directly controlled by the interaction of seawater or wet lagoonal sediments with ascending magma, were partly buried by lava flows.

B. Rift Areas and Subduction Zones

Scoria cones are the most characteristic subaerial volcanoes in continental rifts. Although scoria cones and tuff cones and rings are numerous, total erupted volumes are small compared to convergent plate boundaries. Extensional stress in the lithosphere is released by rifting or faulting and influences the development of volcanic fields, which are commonly associated with extensional uplifted intraplate plateaus. Continued extension produces graben subsidence, graben shoulder uplift, and thinning of the underlying lithosphere. Single volcanoes and volcanic groups form within the grabens and on the uplifted graben shoulders. Volcanic complexes in intraplate plateaus may consist of hundreds of volcanoes, for example of up to 1000 volcanoes over an area of 60,000 km^2 in the TransMexican Volcanic Belt, often with separate volcano clusters of 20–150 volcanoes within areas of 100–5000 km^2, (see "Basaltic Volcanic Fields"). Well-known examples of Tertiary to Recent

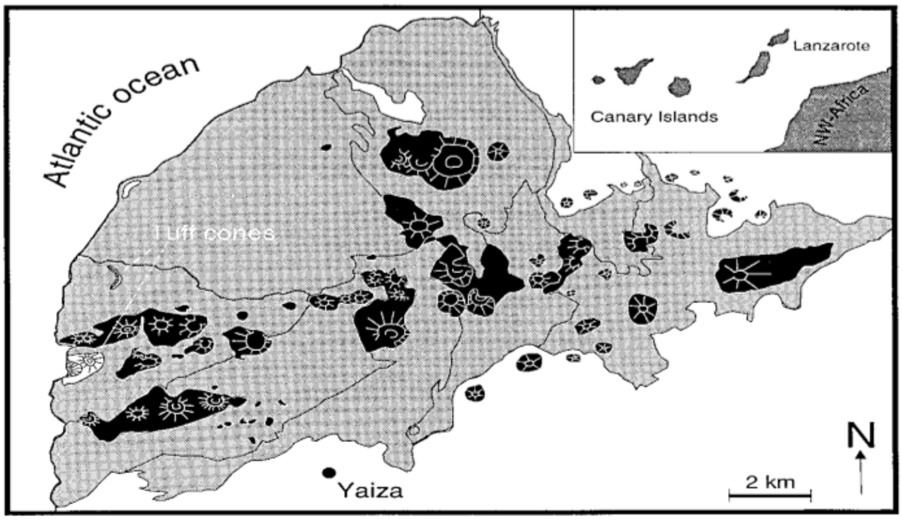

FIGURE 7 Volcanic field, Lanzarote. Map of the 1730–1736 eruptive sites on Lanzarote showing scoria cones (black) and lava flows (gray). Hydrovolcanic cones (white) are Pleistocene in age and are restricted to the former coastline. [Modified from *J. Volcanol. Geotherm. Res.* **53,** Carracedo, J. C., Badiola, E. R., and Soler, V., The 1730–1736 eruption of Lanzarote, Canary Islands: a long, high-magnitude basaltic fissure eruption, 239–250 (1991) with permission from Elsevier Science.]

volcanic fields in uplifted tectonic regions are the Eifel (Germany), Hoggar and the Tibesti Rift system (Algeria), the Rio Grande Rift system, and the Colorado Plateau (United States). Most of the Tertiary to Quaternary volcanic fields in western Europe are restricted to extensional and volcano-tectonic stress fields in grabens (Rhine Graben, Limagne Graben, and Eger Graben) or to associated uplifted graben shoulders (Westerwald, Eifel, and Auvergne). In rifts, cones are commonly alkalic to tholeiitic in composition and grow faster and higher than those erupted on associated rift shoulders. On graben shoulders cones are more alkalic in composition, suggesting a correlation between the rate of extension, the crustal thickness, the depth of the magma reservoirs, and the degree of partial melting of the upwelling mantle. Scoria cone fields may reflect localized mantle upwellings (plumes) beneath the continental lithosphere, for example, the Snake River and Yellowstone Volcanic Fields, United States, believed to be related to a hotspot trace or the Hoggar Volcanic Field, Algeria, which consists of maars and scoria cones. Uplift resulted from the ascending plumes that produced the erupted magmas.

Volcanic fields in compressional tectonic regimes along active continental margins are characteristically related to active fault systems and show cluster alignments (e.g., Wrangell Volcanic Field, Alaska, and TransMexican Volcanic Belt, Mexico). Most clusters of cones show alignments to the regional stress field. In many volcanic fields, scoria cones, tuff rings, and maars, commonly more primitive in composition, are restricted to the vicinity of large, more silicic and evolved andesitic shield volcanoes. In the Tuxtla Volcanic Field, Mexico, of the 250 scoria cones, tuff rings, and maars surrounding a large composite cone, 210 are scoria cones with associated lava flows. The distribution of 40 tuff rings and maars was directly controlled by the groundwater table. Scoria cones are common in many basaltic settings, especially in well-drained areas with deep water tables. They mainly form when the ascending magma fails to intercept a hydrologically important aquifer, if aquifers are empty during dry seasons, or if the permeability of country rocks is limited. Scoria cones also form when the vent is blocked against water entry and the fragmentation depth is above the water table. Tuff cones, tuff rings, and maars predominate in wetter, more basinal fields, where external water is available. Maars and tuff rings often form in basinal lowlands, in playas with shallow ponds, and along ancient streams, where external water is limited such as the Hopi Butte Volcanic Field in New Mexico. Maars were earlier explained by CO_2 explosions, an interpretation still upheld by some workers. Surge and fall derived deposits in maars with juvenile particles showing mostly low to moderate vesicularity and blocky equant particle morphologies generally suggest hydrovolcanic fragmentation. Accretionary lapilli, armored lapilli, and vesiculated tuffs in surge deposits of maars are considered good evidence that the surges were wet. A hydrostatic pressure barrier of about 20–30 bars is assumed to control the maximum depth level of explosive magma–water interaction and the downward migrating fragmentation zone (diatreme structures). Explosive eruptions producing tuff cones are closely restricted to water-rich subaerial environments, both lacustrine and fluviatile, and to hydrogeologic environments with high replenishment rates such as alluvial fans. Sublacustrine tuff cones may be associated with pillow lavas, hyaloclastite deltas, and reworked volcaniclastic deposits.

VI. SIGNIFICANCE

Although tiny with respect to individual erupted magma volume, scoria cones, tuff rings, and maars are much more widely distributed on continents and islands than any other type of volcano. They mainly occur not as isolated cones but in fields whose diameters, mostly around 30–50 km, resemble the basal diameters of large central volcanoes and that of many oceanic islands. Some fields may be hot spots in the sense that they reflect a deep-seated melting anomaly of which only a small part of the magma generated has leaked through the crust to erupt on the surface, commonly interacting with the uppermost crust and surface water or groundwater. The typical composition of scoria cones is alkali basalt generated by lower degrees of partial melting. The search for the depth and shape of the melting anomaly has resulted in the discovery of small plumelike areas as in central France. This aspect is also treated in the earlier article "Basaltic Volcanic Fields."

Most seminal studies on xenoliths of mantle rocks, dominantly peridotite as well as fragments of the lower crust, commonly granulites, are based on the widespread occurrence of such xenoliths in maars and tuff rings worldwide but much less common occurrence in scoria cones. This has led to the model in the older literature that maars are the result of CO_2-rich fluidized systems that start in the mantle and drill their way to the surface. A general consensus has emerged in the past few decades that maars and tuff rings are mainly the result of interaction of rising magma with groundwater.

The reason maars and tuff rings are especially rich in xenoliths is probably that high magma ascent rates and/or the large energy generated by the interaction of magma with groundwater resulted in the ejection of the fragmented magma before the xenoliths had time to sink back in the magma column as they seem to do in the less energetic strombolian phases in scoria cones. This is corroborated by the fact that the roots of scoria cones in many Tertiary areas, for example, in central Germany, where at least 100 m has been eroded since the Oligocene, consist of lava lake and pluglike substructures that are commonly choked with xenoliths.

Scoria cone distributions show common orientations along fault zones and are grouped parallel or en echelon to the strike of the faults. The alignment of scoria cones and the orientation of the long axes of scoria cone fields are major surface features for deducing the current orientation of the stress field of the lithosphere and/or that of older reactivated zones of weakness. In a compressional regime as in the TransMexican Volcanic Belt, scoria cone alignments are induced by faults or fault zones, by which the ascent of magma is enhanced, although local volcanic alignments must not have been affected by fault zones. Scoria cones on the flanks of large central volcanoes have been used to map the stress fields that develop within a large volcanic edifice.

VII. HISTORIC EXAMPLES

A. Capelinhos, Azores

From September 27, 1957, until October 25, 1958, submarine hydrovolcanic and later strombolian/hawaiian eruptions formed a new island named Capelinhos, 800 m off the west coast of Fayal Island (Azores). Earthquakes preceded the eruptive activity. The eruption began at four submarine vents shooting steam and ash-laden eruption columns above the vent. The four vents coalesced during intermittent and continuous-uprush hydrovolcanic explosions, resulting in the formation of a tuff cone. The cone had grown to 80 m above sea level after 6 days and to 140 m in less than 1 month. The cone rim diameter was 300 m, with a 100-m-wide breach on the southwest side. During the horseshoe-shaped cone stage, seawater had direct access to the vent system. Seawater maelstroms flooding down the vent were recorded, which led to wet hydrovolcanic eruptions creating powerful jets and surges after mixing of seawater with hot magma. The eruption started with the spread of white steam clouds from the base of the emerging eruption column crossing the ocean surface, shortly followed by black, particle-laden cock's tail jets up to heights of 1000 m. Finally, the eruption column tumbled back, and a turbulent mixture of particles, gas, and water spread radially in dark surges to distances of up to 3 km from the vent. The eruption clouds were water-rich as shown by the abundance of accretionary lapilli and armored lapilli. Wet mud was plastered onto vertical cliffs and the walls of a lighthouse at a distance of 1.3 km. The deposits are crudely bedded, caused by the wetness and high density of the surges, whereas dune bedding, very characteristic for surges, was rare.

The activity stopped on October 26, 1957, and the island was completely eroded within a few days. Eruptions resumed on November 6, resulting in a new tuff cone connected to the shore of Fayal. After sealing of the vent, activity generated a scoria cone in the center of the tuff cone. Intermittent ("strombolian") explosive activity gave way to hawaiian fire fountains and lava flows late in 1957. The eruption ended on October 25, 1958. The new peninsula Capelinhos had added more than 2.6 km^2 of new land to Fayal Island.

B. Miyake-jima Eruption, Izu Island, Japan

In 1983, a fissure eruption occurred on the oceanic island Miyake-jima, 170 km south of Tokyo. During about 10 h of volcanic activity, 13 scoria cones, 1 tuff cone, and 4 lava flows were produced. This event was documented by aerial photographs and videos, representing a rare opportunity to better understand growth processes of oceanic islands. At 3 pm on October 3, some craters around the western flank of Oyama volcano erupted lava flows and scoria. Hydrovolcanic explosions started about 70 min after the initial fissure eruptions. These explosions are thought to have resulted from the explosive mixing of magma with seawater, lakewater, or groundwater, depending on the location of the vents.

Two eruptive sequences were recorded. During the first sequence, which lasted from 3 pm to 8 pm, strombolian and hawaiian eruptions produced highly vesicular scoria fall, fire fountains, and subsequent lava flows, interrupted by short hydrovolcanic phases. More than 95% of the eruptive products (0.012 km^3) were erupted at this time. After a short interval of decreased activity, the second eruptive sequence began, lasting at least 1 h. Pyroclastic eruptions produced scoria fall, minor bombs, ash, and accidental clasts (0.0006 km^3), while hydrovolcanic eruptions were recorded only from two craters. The eruption ceased in the early morning of October 4. The 13 scoria cones were aligned en echelon along the 4-km-long, north–south trending fissure system. Along the northern part of the fissure, scoria cones consist mainly of black, highly vesicular scoria fall and intercalated lava flows. The scoria cones show only minor phreatomagmatic phases limited by the hydrodynamic regime of the country rocks. Along the southern fissure, hawaiian fire fountaining and strombolian eruptions were periodically replaced by hydrovolcanic explosions. Only one ring-shaped hydroclastic cone with a crater diameter of 150 m was formed during shallow aqueous eruptions at the southern end of the fissure as seawater entered a submarine fissure conduit. The surtseyan cone (see "Surtseyan and Related Phreatomagmatic Eruptions") started with initial explosions rich in breccia, water-chilled bombs, and sideromelane shards. In the second eruptive cycle, thin, stratified sideromelane layers were deposited in the waning stage of the eruption. Ballistic deposits comprising block sags and water-chilled bombs were found only within 300 m of the crater. These ejecta were interpreted as having been emplaced by cock's tail jets, leading to crudely stratified deposits with many bomb sag structures. Common planar bedding and dune bedding in more distal sections suggest emplacement by base surges. The change from the dominance of cock's tail jets in the earlier eruptions to base surges at later stages marked the transition from wetter to drier eruptions.

C. Paricutin Volcano, Mexico

The new volcano Paricutin grew in the Trans Mexican Volcanic Belt, one of the largest scoria cone fields on earth, containing approximately 1000 scoria cones. The birth of Paricutin on February 20, 1943, in a cornfield and its formation by periodic strombolian eruptions until 1952, accompanied by seismic tremors, are well documented. The eruption of Paricutin was characterized by violent strombolian activity. Lava flows rich in granitic xenoliths began to erupt on the second day.

During the initial stage of eruption, the cone grew very rapidly from 5 to 40 m high in 1 day to 167 m within a week. It reached 336 m at the end of the first year. Cone growth rate rapidly increased from 10^4 to 4×10^6 m^3/day and continued for the first 250 days, before slowly decreasing. After eruptions ceased in 1952, the final elevation of Paricutin was 424 m. The basal diameter of the cone was around 1 km. At least 1.3×10^6 m^3 of pyroclastic material and 700×10^6 m^3 of lava were erupted, ranging from early basaltic andesites to late andesites.

Strong strombolian eruptions generated ash plumes several kilometers high. The vent and conduit geometry of Paricutin changed during the eruption from two separate funnel-shaped vents aligned northeast–southwest to one vent during 1949–1951. The southwest vent, 10 m in diameter, erupted ash- and bomb-laden clouds every few hours. Intervals of quiet steady gas emission and periods of explosions followed each other irregularly. Sliding, slumping, and mudflows caused modifications of cone and crater diameters. Ash-mantled slopes started to creep at 32°, which is the angle of repose of the ash. Major erosive unconformities caused by slumps were filled within days or weeks by strong ash-fall eruptions, regenerating the original cone morphology.

SEE ALSO THE FOLLOWING ARTICLES

Basaltic Volcanic Fields • Hawaiian and Strombolian Eruptions • Magmatic Fragmentation • Phreatomagmatic Fragmentation • Pyroclastic Fall Deposits • Pyroclastic Surges and Blasts • Seamounts and Island Building • Surtseyan and Related Phreatomagmatic Eruptions

FURTHER READING

Fisher, R. V., and Schmincke, H. U. (1984). “Pyroclastic Rocks.” Springer-Verlag, Berlin/New York.

Fisher, R. V., Heiken, G., and Hulen, J. B. (1997). “Volcanoes. Crucibles of Change.” Princeton Univ. Press, Princeton, NJ.

Houghton, B. F., and Schmincke, H. U. (1989). Rothenberg scoria cone, East Eifel: A complex strombolian and phreatomagmatic volcano. *Bull. Volcanol.* **52,** 28–48.

Lorenz, V. (1986). On the growth of maars and diatremes and its relevance to the formation of tuff rings. *Bull. Volcanol.* **48,** 265–274.

Luhr, J. F., and Simkin, T. (1993). “Paricutin. The Volcano Born in a Mexican Cornfield”. Geoscience Press, Phoenix.

McGetchin, T. R., Settle, M., and Chouet, B. A. (1974). Cinder cone growth modeled after northeast crater, Mount Etna, Sicily. *J. Geophys. Res.* **79,** 3257–3272.

Self, S., Kienle, J., and Huot, J. P. (1980). Ukinrek maars, Alaska. II. Deposits and formation of the 1977 craters. *J. Volcanol. Geotherm. Res.* **7,** 39–65.

Sohn, Y. K. (1996). Hydrovolcanic processes forming basaltic tuff rings and cones on Cheju Island, Korea. *GSA Bull.* **108,** 1199–1211.

Sparks, R. S. J., Bursik, M. I., Carey, S. N., Gilbert, J. S., Glaze, L. S., Sigurdsson, H., and Woods, A. W. (1997) “Volcanic Plumes.” Wiley, Chichester.

Wohletz, K. H. (1986). Explosive magma–water interactions: Thermodynamics, explosion mechanisms, and field studies. *Bull. Volcanol.* **48,** 245–264.

Wood, C. A. (1980). Morphometric evolution of cinder cones. *J. Volcanol. Geotherm. Res.* **7,** 387–413.

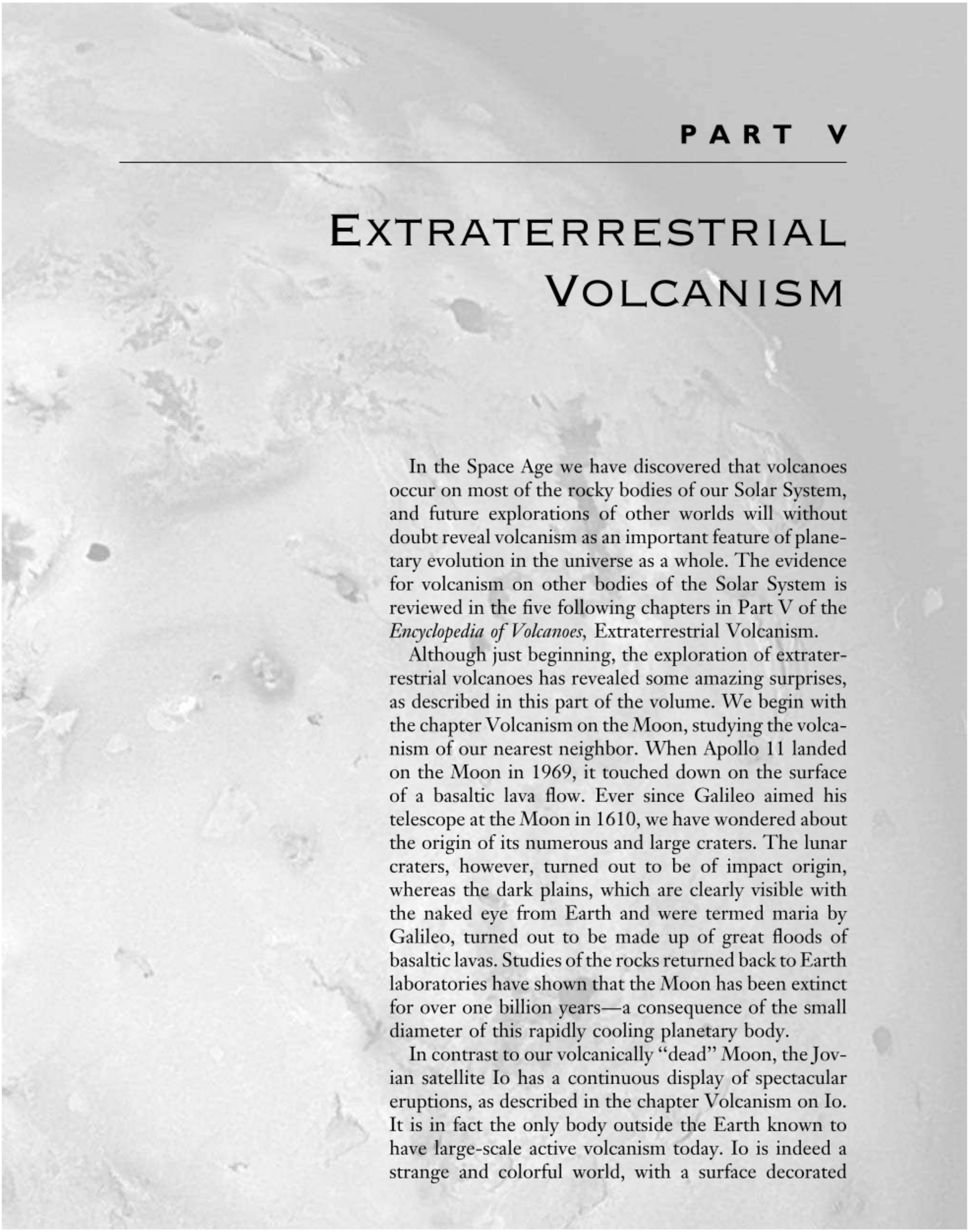

PART V

EXTRATERRESTRIAL VOLCANISM

In the Space Age we have discovered that volcanoes occur on most of the rocky bodies of our Solar System, and future explorations of other worlds will without doubt reveal volcanism as an important feature of planetary evolution in the universe as a whole. The evidence for volcanism on other bodies of the Solar System is reviewed in the five following chapters in Part V of the *Encyclopedia of Volcanoes*, Extraterrestrial Volcanism.

Although just beginning, the exploration of extraterrestrial volcanoes has revealed some amazing surprises, as described in this part of the volume. We begin with the chapter Volcanism on the Moon, studying the volcanism of our nearest neighbor. When Apollo 11 landed on the Moon in 1969, it touched down on the surface of a basaltic lava flow. Ever since Galileo aimed his telescope at the Moon in 1610, we have wondered about the origin of its numerous and large craters. The lunar craters, however, turned out to be of impact origin, whereas the dark plains, which are clearly visible with the naked eye from Earth and were termed maria by Galileo, turned out to be made up of great floods of basaltic lavas. Studies of the rocks returned back to Earth laboratories have shown that the Moon has been extinct for over one billion years—a consequence of the small diameter of this rapidly cooling planetary body.

In contrast to our volcanically "dead" Moon, the Jovian satellite Io has a continuous display of spectacular eruptions, as described in the chapter Volcanism on Io. It is in fact the only body outside the Earth known to have large-scale active volcanism today. Io is indeed a strange and colorful world, with a surface decorated with a wonderful mosaic of yellows, oranges, and reds and sulfurous volcanic plumes that rise over 300 km above its surface. We are accustomed to thinking of volcanic energy as largely derived from primordial heat in the planet, but Io's energy source is different. The intense and continuous volcanism of Io is due to heat from great tidal stresses generated by its giant neighbor Jupiter.

Venus—our nearest planetary neighbor—has volcanic features that are in several respects similar to the activity on Earth, as described in the chapter Volcanism on Venus. While there is no evidence of Earth-style plate tectonics on the Moon, Io, or Mars, there is indication that such global-scale processes may have been operating on Venus, and these may be reflected in its volcanism also. Here both lava flood plains and large central volcanoes occur. But Venus also possesses enigmatic coronae, enormous circular structures that are several hundred kilometers in diameter and found nowhere else in our Solar System.

The chapter Volcanism on Mars answers the question: how did a planet one-half the size of Earth generate volcanoes that are several times larger than the largest volcanoes on Earth? Mars has widespread volcanic plains, like the Moon, but the characteristic Martian volcanic features are huge central volcanoes that dwarf any terrestrial volcanoes. These immense lava shields are the result of hot spot activity, and the largest is Olympus Mons, 25 km high, 600 km diameter. Is the size of these volcanoes a reflection of a much thicker lithosphere and the absence of plate tectonics?

In the farthest reaches of our Solar System, on the moons of Uranus, Saturn, and Jupiter, a unique form of volcanism occurs, in which geyser-like plumes of nitrogen and water-rich "magmas" are ejected from volcano-like structures. The final chapter of this section, Cryovolcanism in the Outer Solar System, discusses this distinctive form of volcanism. Most of the moons around Jupiter, Uranus, and Neptune are made up of water ice and other volatiles. From time to time, heat generated within these satellites churns up a slush of ice and volatiles that are erupted at the surface, forming volcano-like manifestations of "dirty ices" mixed with ammonia, silicates, and other impurities. The discovery of nitrogen-rich and geyser-like plumes on Triton, Neptune's distant moon, by Voyager 2 in 1989 shows that this type of volcanism occurs today.

Haraldur Sigurdsson
University of Rhode Island

VOLCANISM ON THE MOON

PAUL D. SPUDIS
Lunar and Planetary Institute

I. Introduction
II. Mare Volcanism on the Moon
III. Styles of Volcanism and Associated Landforms
IV. Nonmare Volcanism
V. The Beginning and End of Mare Volcanism

GLOSSARY

albedo The reflectivity of an object light and dark are high and low albedo, respectively.

anorthosite A slowly cooled rock made up almost solely of the calcium-rich mineral plagioclase feldspar.

armalcolite An iron titanium oxide mineral, found in lunar mare basalts and named for the crew members of the Apollo 11 mission.

ash Very small fragments of lava, sprayed out at a vent, cooled quickly, and deposited as a blanket of debris.

basalt A dark, fine-grained rock, rich in iron and magnesium, created by solidification of a lava rich in iron and magnesium.

bombardment The collision of a planet with asteroids repeatedly over a long time.

caldera Summit crater of a volcano; collapse depression found over a subsurface magma chamber.

cinder cone Hill produced by the buildup of ash or other pyroclastic (q.v.) fragments around a volcanic vent.

collapse pit Small depression associated with subsurface collapse, as over a shallow chamber after lava has been drained from it.

cone Small volcanic construct, usually having relatively steep sides.

dark mantle deposit Large area of the Moon covered by glassy ash deposits.

dome Bulbous, hill-like volcano.

fire fountain Spray of lava from a vent, producing a dark mantling deposit.

flow front The terminal end of a lava flow.

glass Natural material that possesses no internal order, a liquid of high viscosity.

igneous Of or relating to material formed from a liquid state.

igneous rock Rock crystallized from a liquid (magma).

ilmenite Iron and titanium mineral found in mare basalts.

impact dark halo crater Crater with dark ejecta, caused by the exhumation of buried lava flows in the lunar highlands.

KREEP Acronym for potassium (K), rare-earth elements (REE), and phosphorus (P); a chemical component in lunar rocks, created as the last phase of the magma ocean (q.v.).

lava Liquid magma extruded onto a planetary surface.

lava channel A channel filled with a stream of flowing lava or the landform produced after such a process.

lava tube A lava channel (q.v.) that is partly or completely roofed over to enclose the lava stream; may form a cave after the flow has cooled.

Copyright © 2000 by Academic Press
All rights of reproduction in any form reserved.

mafic Geological property describing an enrichment in iron and magnesium at the expense of silicon and aluminum.

magma Liquid rock within the interior of a planet.

magma ocean State of the early Moon in which the entire globe was covered by a layer of liquid rock hundreds of kilometers thick.

mantle The part of a planet below the crust and above the core. Partial melting of the mantle is the source of magma in most planets.

maria (MAR-ee-ah) Dark areas of the Moon; Latin plural for "seas"; singular is *mare* (MAR-ay).

olivine A magnesium- and iron-rich silicate mineral, common in mafic (q.v.) igneous rocks.

pyroclastic Literally "fire-broken," meaning fragmental rocks produced in explosive volcanic eruptions; includes ash.

pyroxene A magnesium- and iron-rich silicate mineral, an important constituent of mafic (q.v.) igneous rocks, such as basalt (q.v.).

radiometric dating Determining the age of formation of rocks and minerals by measuring their amounts of radiogenic isotopes, which decay at known rates.

rille A linear or sinuous (snakelike) depression on the Moon. Sinuous rilles are lava channels in the maria.

shield volcano A broad, low-relief volcanic construct made up of flows of relatively fluid lava, usually basalt.

sinuous rille A lava channel or tube in the lunar maria.

summit pit Depression occurring at or near the top of a volcano.

terrae (TER-eye) Latin plural for "land," the cratered highlands of the Moon; singular is *terra* (TER-ah).

vent Hole in a planet from which volcanic products (lava, ash) may be erupted.

vesicle Hole (frozen bubble) in a sample of lava rock that results from dissolved gas in magma coming out of solution.

viscosity The property of a fluid that causes it to resist flow or movement. Higher viscosity results in slower rates of flow.

visible maria The dark areas of the Moon, made up of lava flows erupted between 3.8 and about 1 billion years ago. Some mare deposits may not be visible, having been ground up into the cratered terrain of the highlands.

volcanic rock Rock formed by the cooling of liquid rock (lava) extruded onto a planetary surface.

volcanism The process of interior melting of, the movement of liquid rock bodies through, and the eruption of such liquids onto the surface of a planet.

xenolith (ZEE-no-lith) Literally "stranger rock," a fragment of rock from great depth carried to the surface as a clast in a lava flow or pyroclastic deposit.

I. INTRODUCTION

The idea that the Moon is or was volcanically active was prevalent in the years before spaceflight. Astronomers tend to be very fond of volcanoes and the analogy was made between the craters of the Moon and calderas, the large, circular depressions found at the summit of terrestrial volcanoes. Detailed work on lunar craters and terrestrial analogs provided convincing evidence that the abundant craters of the Moon were formed by the collision of solid bodies with the Moon over geological time.

The few who studied the Moon largely ignored the dark maria, the low smooth plains that make up large fractions of the near side of the Moon seen through a telescope (Figs. 1 and 2). Most ideas about the maria related them to ancient sedimentary deposits, either water-laid or mass-wasted material derived from the surrounding highlands. However, in his landmark 1949 book, *The Face of the Moon*, Ralph Baldwin presented convincing evidence that the maria were floods of basalt, a common, dark lava rich in iron that is abundant on the Earth.

Although the debate raged during the 1960s during detailed examination of the Moon in preparation for the Apollo missions, the return of samples of the maria by the Apollo program settled the issue. The maria indeed are made up of floods of lava, but what is most striking from the returned samples is the age of these lavas. The

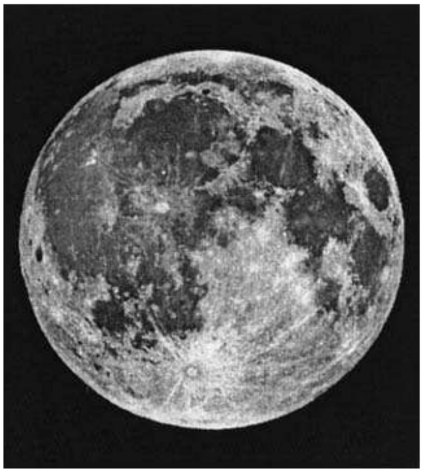

FIGURE 1 Full Moon image showing the two principal terrains of the Moon: the light, rough highlands (or *terrae*) and dark, smooth lowlands (or *maria*). Study has shown that the maria are basaltic lava flows.

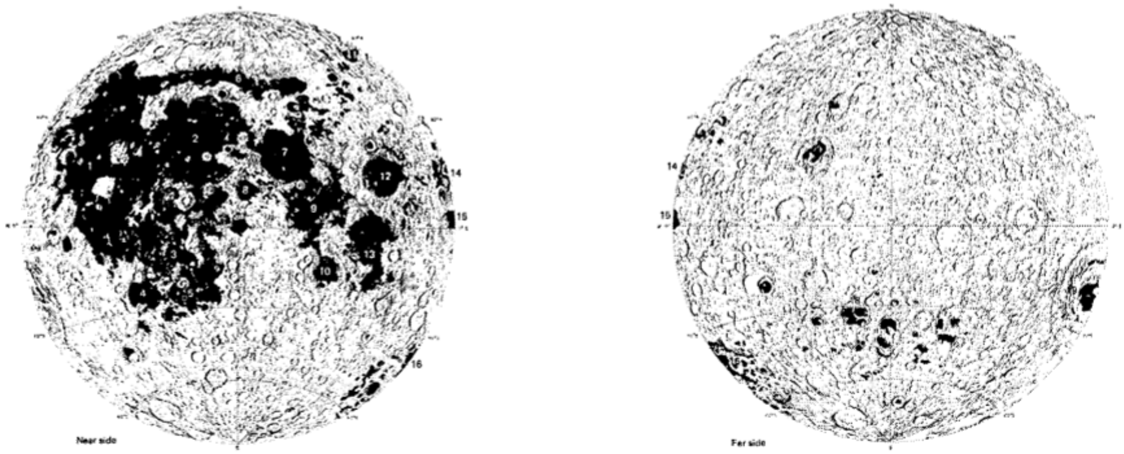

FIGURE 2 Simplified map of the lunar maria. Note extensive mare flooding on near side (left) as opposed to the far side (right). Despite appearances, the maria makes up only 16% of the lunar surface and much less than 1% of the volume of the crust.

basalts returned by Apollo range from 4.3 to 3.1 billion years old, as old as the very oldest rocks on the Earth. The lunar lavas also have some interesting chemical characteristics, including a complete absence of any type of mineral that contains water, minerals that nearly always occur in lavas on the Earth. These properties, determined during the initial examination of the Apollo samples, gave us a first-order understanding of the basic properties of the Moon. We discovered that the Moon has a crust, formed during global melting early in its history (the "magma ocean"). This differentiation produced not only the plagioclase-rich crust but also the mantle source regions for the later mare basalts. Thus, the volcanic rocks of the Moon contain important information about the Moon's deep interior.

II. MARE VOLCANISM ON THE MOON

A. Origin of Mare Basalts

The samples of the maria returned by the Apollo missions are a form of common lava known as *basalt* (Fig. 3). As on Earth, basalt is created by partially melting mantle rocks composed mostly of the iron- and magnesium-rich minerals olivine and pyroxene. From the relatively high density of the mantle and sparse seismic velocity data, we know that the lunar mantle is largely made up of these minerals. Radioactive, heat-producing elements, such as uranium, made the early mantle very hot—in some places, hot enough to partially melt. These blobs of melt coagulate deep in a planet's interior and slowly migrate upward, where they may force their way to the surface and be extruded onto a planetary surface as a lava flow.

Unlike the Earth, we see little evidence for ponding of large amounts of lava at shallow depths in the crust and for its retention in deep, subsurface "holding chambers." Most magmas appear to have migrated upward through the mantle and crust and erupted fairly quickly. The pyroclastic glasses are the most extreme examples of this phenomenon, as they appear to be completely unfractionated, suggesting rapid ascent from the mantle and violent, immediate eruption. Some mare basalts show slight evidence of assimilation of KREEP-like material. Such a process does not imply significant ponding, as KREEP would have a low melting point and could be assimilated easily during brief contact with the basaltic magma.

The chemistry of basaltic magmas tells us approximately where they formed within the Moon (at depths of 150–400 km) and what processes have affected them subsequently. Our study of the mare basalts tells us that many regions of the mantle underwent melting episodes at several depths over a very long period of time, a period at least 700 million years long and more likely over a time span of 1–2 billion years. These melted pockets found their way to the surface through cracks that they themselves propagated or through the fractures induced by the formation of the giant craters and basins of the highlands. However, only a very tiny fraction of the mantle has been melted to make basalt. Although

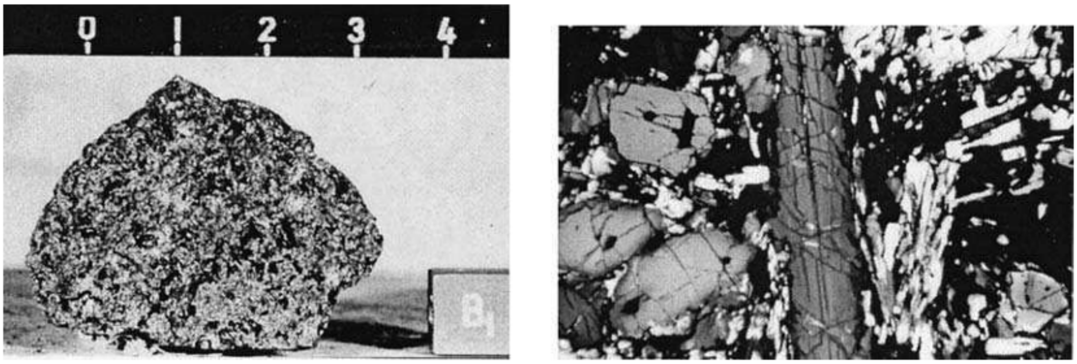

FIGURE 3 Mug shot (left; markings in cm) and thin section (right; FOV ~ 2 mm) of Apollo 17 high-titanium mare basalt. Lunar basalts are made up prodominantly of augite (Ca-rich pyroxene), olivine, plagioclase, and ilmenite. Mare basalts are depleted in volatile elements and show no evidence of any hydrous phases.

the maria appear prominent, the lavas are relatively thin compared with the volume of the crust as a whole. It is estimated that the mare basalts cover about 20% of the Moon by area but probably account for less than about 1% of the total volume of the crust.

B. Apollo Mare Basalts

Like terrestrial basalts, the lunar mare basalts are made of mostly pyroxene and plagioclase and are rich in iron and magnesium. The grain size of basalt is very fine (usually less than 1 mm), a result of its very rapid cooling. Like some terrestrial basalts, some lunar lavas have small, bubble-like holes in them (*vesicles*), indicating that the magmas contained gas during eruption. As are basalts on earth, the lunar mare basalts are all formed by partial melting of the lunar mantle, a mantle made of mostly pyroxene and olivine.

The first basalts returned from the Moon were from the Apollo 11 landing site in Mare Tranquillitatis (Sea of Tranquillity). These rocks are remarkable in several respects. Mare basalts are not only devoid of water or any hydrous phase, they are depleted in all of the volatile elements (those that have very low boiling temperatures), including, for example, sodium, zinc, potassium, and phosphorus. Strangely (and surprisingly), the Apollo 11 basalts have large amounts of titanium, mostly in the form of the mineral ilmenite, an oxide of iron and titanium. The enrichment of the mare basalts in iron and their depletion in aluminum, the exact reverse of the composition of rocks from the lunar highlands, account for the relative darkness (low albedo) of the maria as opposed to the terrae.

Lavas from the Moon were found to contain some minor minerals that are not found in Earth rocks. One of these, another iron–titanium mineral, was given the name armalcolite, named in honor of the Apollo 11 crew (the word coming from the first letters in the names of the crew, *Arm*strong, *Al*drin, and *Col*lins). The compositional properties of the lunar basalts reflect the unique chemical environment that they formed in—a small planet (resulting in low interior pressures), depleted in volatile elements, containing no water, and erupted onto a low-gravity surface in a vacuum.

Additional mare basalts from other Apollo missions largely confirm the initial impressions gathered from these studies, with some surprises and interesting variations. Lavas from the second mission, Apollo 12, are lower in titanium than the Apollo 11 basalts and 600–700 million years younger (Apollo 12 lavas formed about 3.1 billion years ago). Once again, these lavas are low in volatile elements and very rich in iron. The lower titanium and younger ages of the Apollo 12 basalts confirm that the maria were not erupted as a single, massive flood of lava across the surface all at one time but rather that the formation of the maria was an extended process that involved different batches of magma erupted in different places at different times. In short, the samples told us about the complicated volcanic history of a small planet with its own geological evolution.

Mare basalts from the other two mare landing sites extended our picture of mare volcanism, perhaps somewhat misleadingly. Apollo 15, which landed just inside the rim of the basin containing Mare Imbrium, returned low-titanium basalts of slightly older age than those from Apollo 12; these lavas crystallized about 3.3 billion years ago. Apollo 17, landing on the edge of Mare Serenitatis, returned very high titanium basalts (Fig. 3), similar to those from Apollo 11, but of slightly younger ages, about 3.7 billion years old. These results led some to conclude that the Moon had a fairly simple volcanic history, with early eruptions of high-titanium lavas and late eruptions of low-titanium lava. The conclusion was also drawn that the Moon "died" volcanically after the Apollo 12 lavas were erupted at 3.1 billion years, a totally unwarranted conclusion that even today is widely believed and recounted.

In addition to the basalt samples returned from the mare landing sites, little fragments of lava have been found in samples from the highlands as well. These basalts occur in two principal ways: as small rocks in the regolith of highland sites and as fragments of volcanic lava in highland breccias. The former occurrence of mare basalt is likely to result from the deposition of a ray from a crater on the maria, distant from the highland site. Examples are several fragments of mare basalt from the Apollo 16 regolith. Because secondary craters from the large impact crater Theophilus occur near the site, we infer that these rocks were thrown to the site by the formation of this crater and that they represent a sample of the distant Mare Nectaris. Thus we can characterize the rocks of distant maria, if plausible candidate craters can be identified.

In contrast, mare basalt fragments found as clasts in highland breccias offer clues to the variety and ages of the earliest phase of lunar volcanism. These breccias from the highlands were assembled before 3.8 billion years ago; therefore, the lava fragments within them must be older than this. Some of these mare basalts large enough to date were extruded well before 3.9 billion years ago. The oldest mare basalt yet found is about 4.2 billion years old, only slightly younger than the age of the solidification of the crust! Other fragments date from between 4.1 and 3.9 billion years and display a variety of chemical compositions. Curiously, most of the ancient mare basalt fragments tend to have relatively high contents of aluminum compared to the basalts from the "main phase" of mare eruptions, although a few groups of high-aluminum basalt date from this later era as well.

III. STYLES OF VOLCANISM AND ASSOCIATED LANDFORMS

A. Lunar Lava Flows

From pictures taken by telescopes on the Earth, the maria appear smooth and dark. The impression is that these plains fill in the holes and depressions of the Moon, suggesting a fluid emplacement. At close-up scales, small, lobe-shaped scarps can be seen; such scarps are very common in the lava flows basalt found on the Earth. These scarps can even be seen in some of the best telescopic pictures of Mare Imbrium (Fig. 4). Thus, we had direct evidence *before* the exploration of the Moon by spacecraft for emplacement of the maria by fluid flow.

We obtained our first detailed look at the maria from the robotic precursor missions sent to scout the Moon for Apollo. The Ranger 7 spacecraft was the first to return detailed, close-up pictures of the Moon. From these images, we learned that the scale of impact cratering continues downward to the limits of resolution and that the maria is covered by the regolith. Lunar Orbiter took detailed pictures, showing us a wide variety of landforms most easily attributable to volcanism, including a better view of the flow fronts, small domes and cones, snakelike rilles that served as conduits for molten lava (lava channels and tubes), and irregular craters, whose shapes are difficult to explain by impact origins. The Surveyor 1, 3, 5, and 6 craft all performed soft landings in the maria, giving us a close-up view of the surface and telling us about the nature of the mare surface, including the revelation of some dark rocks covered with small holes, a morphology typical of lava samples.

The chemical composition of the mare basalts has an interesting side effect. The *viscosity* of the lava is dependent on the composition and temperature of the magma. The low amounts of aluminum and alkali elements and high amount of iron in the lunar magmas, coupled with their relatively high temperature upon extrusion, result in lavas that have extremely low viscosity. The viscosity of erupted lunar lava was about the same as motor oil at room temperature, about a factor of 10 more fluid than terrestrial lava. Such runny, fluid flows spread out great distances and this property, in addition

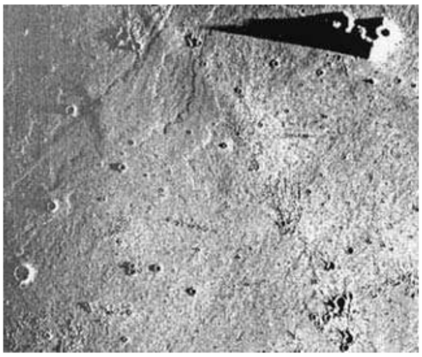

FIGURE 4 Flow fronts in Mare Imbrium (FOV ~ 150 km). Large mountain at top right is Mons La Hire, a pre-mare basin massif. Flows here are up to 800 km long, 20–40 km wide, and 20–60 m thick.

to the low lunar gravity, accounts for the great lengths (up to hundreds of kilometers) that lava flows can reach on the Moon. Such a fluid character to the lava also explains the tendency of mare lavas to form low, broad structures rather than steep-sided volcanoes and to be erupted in lava channels, as are many basalt lava flows on Earth, such as the volcanoes of Hawaii.

Discrete, single flows of mare basalt appear to be rare. Although many units in the maria have a uniform density of impact craters (denoting continuity of age) and single color, they appear to be made up of many thin, small lava flows. High-resolution photographs sometimes reveal scarps or moats occurring around impact craters that may delineate very thin flow lobes (less than a couple of meters thick). The spectacular lava flows within the Imbrium basin (Fig. 4) are often used in textbooks to illustrate the volcanic nature of the maria, but these flows are unique on the Moon and their appearance probably indicates a specialized set of eruption circumstances (e.g., the rapid inflation of the crust and discharge of a large magma body over a short period of time). For the most part, the maria appear to be a smooth, nondescript surface and discrete flows are not visible. It is likely that they consist of a complex series of relatively thin lava flows, in which subsequent regolith production and impact erosion have completely destroyed any original volcanic texture.

Smaller volumes of lava that come out from a narrow, more localized vent (such as a single-pit crater) can produce a variety of other interesting landforms. If the volume of lava erupted cools on timescales similar to the rate of magma supply to the vent, small volcanoes form and may assume a variety of different shapes (Fig. 5). Typically, lunar volcanoes form domes of low relief, a few hundred meters high and a few kilometers across. Such landforms resemble the small basaltic shields found in certain volcanic regions of the Earth, such as Iceland and the Snake River plain of Idaho.

Other domes appear to be slightly larger and steeper. One of the most spectacular areas in the maria is the Marius Hills, a complex area of many small domes in Oceanus Procellarum (Fig. 5). The domes of the Marius Hills appear to be slightly steeper than the basalt shields mentioned above. On the Earth, such differences in shape are caused by differences in the composition of the lava, steeper domes containing more silica and less iron and magnesium than the low, broad shield volcanoes. The causes for steep domes on the Moon are less well understood but appear to be related to styles and rates of extrusion, rather than to lava composition. Eruptions of shorter duration, possibly mixed with minor interludes of ash eruption, would build up a construct with steeper slopes than would the quiet effusion of the very fluid, low-viscosity lavas.

Domes and cones on the Moon seldom are found in isolation but often occur as fields of volcanoes within the maria. The Marius Hills display many domes and cones, which occur on the summit of a broad topographic swell. The complex is several hundred meters high and has a blister-like profile, suggesting that it may be the lunar equivalent of a shield volcano, as are found on the Earth, Venus, and Mars. The Rümker Hills in northern Procellarum is another volcanic complex, similar in appearance to the Marius Hills, but smaller. Small basaltic shields, such as those found near Hortensius, occur in several locations near the margins of Maria Imbrium, Nubium, and Serenitatis. The last type of central vent volcano on the Moon is the cinder cone,

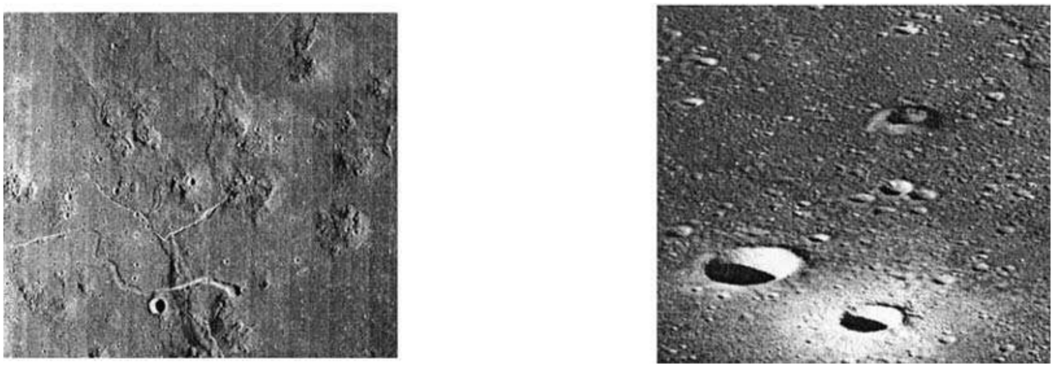

FIGURE 5 Central vent volcanoes on the Moon. Marius Hills (left; FOV ~ 150 km) occurs on a gentle topographic swell and exhibits numerous cones, domes, and rilles. Isolated cone in Mare Serenitis (right; FOV ~ 20 km) is low albedo, steep sided construct. It may be a lunar stratovolcano.

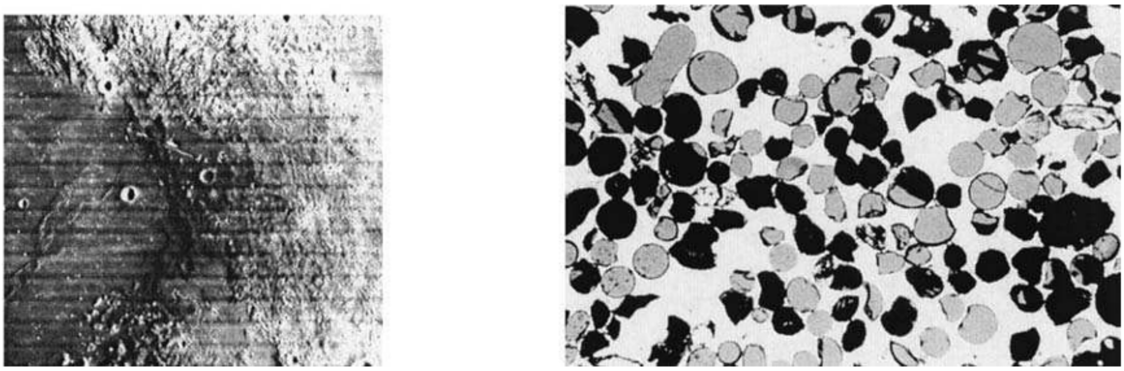

FIGURE 6 Regional view of dark mantling deposits near Rima Bode (left; FOV ~ 180 km), an irregular rille and vent system. Such deposits are made up of basaltic glass of pyroclastic origin, such as the Apollo 17 orange glass (FOV ~ 2 mm).

typified by irregular dark halo craters found along fractures in some crater floors. These features are surrounded by ash deposits (as shown by remote-sensing data) and are often associated with the volcanic modification of large craters that originally formed by impact.

B. Pyroclastics

Both the Apollo 15 and 17 missions returned some unexpected and surprising material. Small glass beads were found in abundance at both sites: clear emerald green glass at the Apollo 15 site and black and orange glass from the Apollo 17 site (Fig. 6). These glass beads are homogeneous, with a basaltic composition, and do not contain the debris of mineral fragments that characterizes the impact-melted glasses from the regolith. The surfaces of these glass beads have small mounds of a variety of volatile elements, including lead, zinc, and halogens such as chlorine. The Apollo 15 green glasses are very rich in magnesium and extremely low in titanium (an unusual composition for a lunar magma), whereas the orange and black Apollo 17 glass is very rich in titanium. Once these glasses were recognized from these two sites where they occur in abundance, small spheres of similar material were recognized from every landing site. More than 20 varieties of this type of glass are known.

These glasses are of volcanic, not impact, origin and they represent the products of a fine spray of low-viscosity lava into space. During some basaltic eruptions on Earth, lava effusion is sometimes accompanied by large sprays of magma from the vent. Such spray eruptions are called fire fountains and result in a deposit of ash around the eruptive vent. The ash from Hawaiian eruptions consists of glass that has basaltic composition and is frequently coated by a layer of volatile elements. On the basis of similar characteristics, the lunar glasses represent the products of fire fountains that existed on the Moon over 3 billion years ago. One difference between the lunar and Hawaiian ash deposits is that so far, no samples of lava with compositions corresponding to the lunar ashes (presumably derived from the same magma) have been recognized.

In addition to their presence in the samples, the glasses are also evident as regional deposits. It was noted during the pre-Apollo systematic mapping that parts of the highlands and maria are blanketed with very dark material (Fig. 6). In the early days of lunar mapping, darkness was often equated with geological youth and these regional dark deposits were thought to represent the ash deposits of young volcanism. In fact, such a concept was responsible in part for the selection of the Apollo 17 landing site near the margin of one of these regional deposits. It was predicted that this material was volcanic ash because it typically occurs in the vicinity of irregular craters of volcanic origin and indiscriminately covers all previous terrain. The principal occurrences of these regional deposits are around the margins of filled mare basins, such as those on the Aristarchus plateau, Sulpicius Gallus, Rima Bode (Fig. 6), and Taurus-Littrow (the Apollo 17 landing site). The Apollo 17 ash is indeed of volcanic origin, but it is old (3.5 billion years), not young.

Several large craters on the Moon have deformed and fractured floors. Along some of these fractures, small (typically a few kilometers in size), irregular craters are found that are surrounded by dark, smooth material. These craters are probably volcanic vents, surrounded by ash deposits. They are the lunar equivalent of *cinder* *cones* found in terrestrial volcanic fields. To create a cinder cone, magma charged with volatiles is squirted out through a very narrow conduit. The release of the low-viscosity lava under high pressure through a small vent causes the lava to spray into a “mist” of liquid rock droplets. The spray of droplets quickly cools in flight and each droplet lands back on the Moon as a small bead, thrown on a ballistic path. Millions of such beads are made during an eruption, building up a deposit of dark ash that surrounds the vent.

Phase chemistry allows us to determine which minerals can coexist at certain temperatures and pressures. Studies of the phase chemistry of volcanic glasses have given us a great deal of insight into the very deep interior. It appears that these glasses were generated by the partial melting of an olivine-rich mantle at depths of about 400 km within the Moon. Moreover, unlike all of the mare basalts, the glasses appear to be largely unmodified from their chemical composition at their point of origin. Such a relation indicates that the magmas from which the glasses formed must have ascended very rapidly up through the Moon from deep in the mantle, with little chemical modification from their point of origin. The glasses then erupted into a violent spray at the surface. As such, lunar volcanic glass is our best sample of the deep interior and is an important material for determining the bulk composition of the Moon.

Both the fountain nature of the eruption and the small coatings of volatile materials on the glass surfaces indicate that pockets of gas and other volatile elements existed deep with the Moon during the main era of mare volcanism over 3 billion years ago. Such an inference is also supported by the presence of the vesicles (holes) that are found in some samples of mare basalt. The composition of this gas phase is something of a mystery. It certainly is not water vapor (which accounts for almost all of the volatile phase in terrestrial volcanoes) because there is a total absence of water-bearing phases and oxidized material in the mare basalts. The reduced chemistry of lunar lavas makes us think that the gas phase might have been carbon monoxide. A detailed search for trapped bubbles of ancient gas within the glass spheres has not been successful to date, but the quest continues.

C. Sinuous Rilles

One common landform of the maria deserves special mention, if only because the Apollo 15 mission (July 1971) was sent specifically to investigate one of them. Sinuous rilles are narrow, winding valleys that occur primarily within the maria (Figs. 7 and 8). Some originate in highlands terrain, but all trend downslope and empty into mare material. Many rilles begin in irregular craters, some of which are surrounded by dark mantling

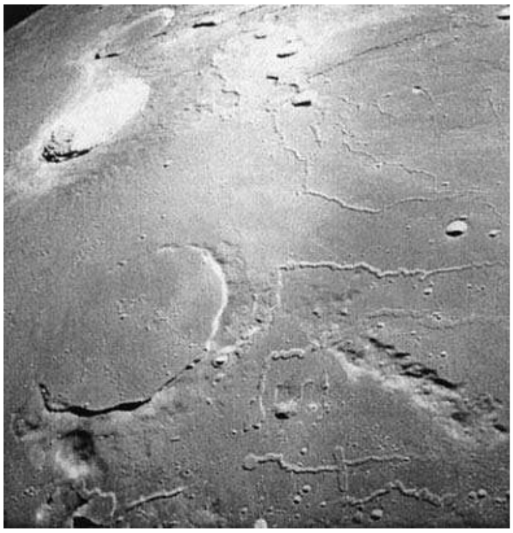

FIGURE 7 Cluster of sinuous rilles around the ancient flooded crater Prinz (D ~ 50 km). Studies have shown the lunar sinuous rilles are lava channels, in some cases roofed over to form lava tubes.

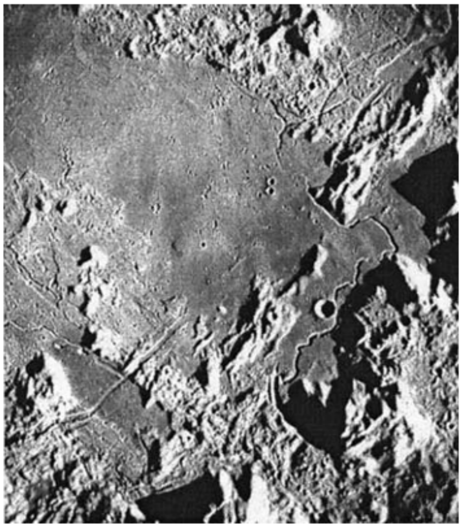

FIGURE 8 Oribital view of the Apollo 15 landing site region (FOV ~ 120 km). Hadley Rille is long sinuous rille, trending NW along base of Apennine scarp. Light plains at left are the Apennine Bench Fm., a rare exposure of pre-mare KREEP volcanism.

material. Many ideas were advanced for the origin of these features before the Apollo missions, including their origin as water-cut stream channels. However, the absence of any water on the Moon, the basaltic nature of the maria, and their irregular shapes all have led to the consensus that these features are lava channels, some of which were partly roofed over to form lava tubes.

The Apollo 15 mission was sent to Hadley Rille, just inside the rim of the Imbrium basin (Fig. 8). Hadley is one of the largest sinuous rilles on the Moon, being over 100 km in length, 1–3 km wide, and up to 1 km deep. The rille begins in an elongate, irregular crater in the Apennine mountains and winds its way through the maria, snaking back and forth through the mare, finally becoming shallow and appearing to merge into a complex set of fractures north of the Apollo 15 site. The rille was examined at its rim near the landing site, where the rille is 1.5 km wide and 300 m deep. Samples of basalt collection on the rille edge are probably the only samples in the Apollo collected that were taken from bedrock. A ledge of bedrock seen in the orbital photographs probably consists of this mare basalt unit. Layers of mare lava are exposed in the walls of Hadley Rille, all confined to the upper 60 m of the rille. Color data from the Clementine mission confirm that the walls of sinuous rilles on the Moon expose mare basalt.

Although all workers agree that sinuous rilles are lava channels and tubes, their exact mode of formation remains contentious. On Earth, lava channels are created when a flow extruded at moderate rates cools from the margins inward; this cooling tends to confine the molten, active part of the flow along a central axis. This axis becomes the channel and in some cases is bridged over to form a lava tube. In this mechanism, lava channels are primarily *constructional* features, where the overflow of lava builds up levees and raises the topographic level of the flow axis. Lava can accumulate laterally on the walls of the channel, narrowing the channel width; in fact, such narrowing away from the vent is a common feature both of lava channels on Earth and of sinuous rilles on the Moon. Another concept that has emerged in the past few years holds that lava channels are primarily *erosional* features. The claim is that the eruption of very high temperature, fluid lava would flow turbulently and would soften, melt, and then remove underlying material, forming a lava channel by erosion. In such a model, the sinuous depression in the maria consists of material removed by the flow of liquid lava and incorporated into the mare deposits.

The occurrence of rille source craters in the highlands that are connected to sinuous rilles by channel segments in terra material indicates that some erosion has occurred. This eroded segment may have been enlarged by collapse, a process common in lava channels. In general, however, geological evidence indicates that sinuous rilles and terrestrial lava tubes and channels are formed dominantly by construction. The large size of sinuous rilles, argued by some as evidence for erosion, can also be a result of the filling in of pre-existing depressions, as clearly shown by Hadley Rille, where the lava channel merges into pre-existing valleys north of the Apollo 15 landing site.

IV. Nonmare Volcanism

During the pre-Apollo mapping of the Moon, many highland landforms, including smooth plains, wormy textured materials, and steep domes, were interpreted to be of volcanic origin. The Apollo 16 mission in 1972 was specifically sent to the Descartes highlands to sample these highland volcanic rocks. The rocks from this mission were all impact breccias, however, and the idea of highland volcanism (specifically, evolved rocks of higher silica and/or lower iron than the mare basalts) was viewed as being discredited by the results of the Apollo 16 mission.

A regional exposure of light plains near the Apollo 15 landing site is the Apennine Bench Formation (Fig. 8). These plains predate the basalts of Mare Imbrium, but postdate the impact that created the basin. As determined by a variety of remote-sensing techniques, these plains have composition identical to small fragments of relatively high-alumina basalts of volcanic origin, the KREEP basalts, so called because they are relatively enriched in potassium (K), the rare-earth elements (REE), and phosphorus (P). In major-element composition, they are fairly aluminous and iron-poor, compared to most mare basalts. Their origin is still debated, but the idea that they may be partial-melting products of an aluminous source (lower crust?) is still viable. This would make the Apennine Bench Formation a major surface manifestation of premare, "highland" (i.e., non-mantle-derived) volcanism.

Numerous domes and color anomalies occur in the highlands that have been suggested to represent different styles of highland volcanism. The blister-shaped Gruithuisen domes are red and occur along the main rim of the Imbrium basin. Spectral data suggest that these features are very low in iron, but otherwise unremarkable. It is still not certain that they are indeed of volcanic origin.

V. THE BEGINNING AND END OF MARE VOLCANISM

The maria were not erupted all at once as a massive flood of lava. The Moon underwent a long and protracted volcanic evolution, characterized by different degrees of interior melting and different types of eruptions of different compositions and places over a long period of time. The production of magma through time is an important basis for reconstructing lunar thermal evolution. Such information allows us to compare the Moon with the other terrestrial planets to understand the many ways that planets lose their heat.

A. Early Phase

The earliest extrusions of lava on the Moon may have been the outpouring of liquid rock onto the still-cooling, crusted-over surface of the early Moon. Indeed, the line between volcanism and crustal formation was probably indistinguishable in early lunar history. The oldest unequivocal volcanism on the Moon is represented by tiny chips of mare basalt from the Apollo 14 highland breccias. These fragments represent pieces of a lava flow extruded onto the surface 4.2 billion years ago, a time so remote that we can only guess at what conditions were like on the Earth. Volcanic eruptions probably were more or less continuous, though sporadic, throughout a period of heavy bombardment between 4.3 and 3.8 billion years ago. Traces of this volcanism can be found in the tiny fragments of lava in the highland breccias but may also be evident as a chemical signature in cratered terrains. Some regions of the highlands appear to contain relatively large amounts of iron. This iron could represent unsampled highland rocks but it is also possible that it represents flows of iron-rich mare basalt that have been ground up into regolith of the highlands by the intense impact bombardment of early lunar history.

During the final phases of the heavy bombardment, 3.9–3.8 billion years ago, several large, well-preserved basins formed. These basins still have recognizable ejecta blankets and the smooth, far edges of their debris layers appear to fill craters and other depressions in several areas. Such deposits have all the compositional properties of highland rocks and Apollo results tell us that the light plains of the highlands are an impact formation, associated with the large multiring basins. However, some of these plains display small (1- to 3-km diameter) impact craters whose ejecta are relatively dark. Dark halo impact craters are found in highlands light plains and cluster in regional groups, such as in the Schiller–Schickard impact basin. Spectral observations of these craters indicate that their low albedo is caused by mare basalt lava making up the crater ejecta—yet this is an area of impact-made plains.

The dark halo impact craters are excavating *buried* deposits of mare basalt. Because the plains that bury the lava flows are themselves 3.8 billion years old, the basalt flows that they cover must be older than this. Thus, a map of the light plains of the Moon that display dark halo impact craters is a map of ancient maria—basaltic lavas that were emplaced before 3.8 billion years ago. This remote-sensing evidence for the regional extent of ancient maria complements the sample evidence of tiny fragments of lava in highlands breccias and indicates that the early Moon was a planet of active volcanism.

B. Main Phase

This stage of mare volcanism began when the very high rates of cratering typical of early lunar history declined to the point where the lava flows were not destroyed and ground up into the megaregolith after they were extruded. This decline of the impact flux was very rapid between 3.9 and 3.8 billion years ago, leveling off after 3.8 billion years. From that time onward, the extruded lava flows were bombarded by impact, but the cratering did not destroy the flows. These flows make up the visible maria. The earliest lavas from this period are the high-titanium basalts of Maria Tranquillitatis and Serenitatis, returned by the Apollo 11 and 17 missions. These flows erupted between 3.8 and 3.6 billion years ago. The complete extent of early high-titanium lavas cannot be determined because they are partly covered by younger flows; they may be extensive over the near side.

A long period of eruption of lower titanium basalt followed, from 3.6 billion years to an undetermined time, certainly as late as 3.1 billion years ago, but perhaps much later. Some of the lavas from this time were of the high-aluminum variety, particularly in the eastern maria Crisium and Fecunditatis, as sampled by the Soviet Luna 16 and 24 sample return missions. These basalts date from 3.6 to 3.4 billion years and have moderate to extremely low titanium contents. Eruption of low-titanium lavas in Mare Imbrium at 3.3 billion years ago (Apollo 15) and Oceanus Procellarum at 3.1 billion years (Apollo 12) followed. The lavas from the Apollo 12 site are the youngest mare basalts in the sample collection.

Eruptions of mare basalt were rare events, even at the height of lunar volcanic activity, between 3.8 and 3.0 billion years ago. Although the maria appear to dominate the Moon (Fig. 2), especially on the near side, the visible mare deposits make up very much less than about 1% of the volume of the crust. The total accumulated thickness of lava in most mare deposits varies widely but is typically less than a few kilometers and large areas of basalt may be thinner than about 100 m. In part, we know this because of the abundance of highlands debris mixed into the mare soils; this fraction may approach 60–70%. Because most of this debris is derived from rocks beneath the local bedrock, the implication is that the stack of mare flows is thin.

There is a tendency to think of the maria as a hotbed of geological activity on the Moon, at least in the past. Certainly there has been activity in the maria, but very long time spans separate times of activity. At the Apollo 11 site, several different lava flows are represented among the samples. The oldest flows are 3.86 billion years old, but samples of flows of similar composition have a variety of ages, some as young as 3.55 billion years. In addition, another group of lavas, of different composition, are also about 3.5 billion years old. Thus, at this one site, we have evidence for at least four (and perhaps more) separate lava flows, emplaced over a period of over 0.3 billion (300 million) years. This geologically "active" area of the Moon has been completely quiet for a period of time longer than vertebrate life has existed on the Earth.

C. Late Phase

The only other source of information on the age of mare lavas is the relative age data provided by geological mapping. This mapping shows that many different kinds of flows spilled out onto the maria between the dated and sampled eruptions, providing for a continuous filling of the basins from 3.8 billion years ago onward. A key piece of information for lunar volcanic history is one we do not have—what is the age of the *youngest* mare basalt eruption on the Moon? This question has an important bearing on the thermal history of the Moon; if we know the age of the last eruption, we know when the Moon "shut down" thermally, at least to the point where no lava could get out of its interior.

Many areas of the maria have been identified that have a lower density of impact craters than the sampled flows of the Apollo 12 site (aged 3.1 billion years). The very young lava flows with well-developed scarps in Mare Imbrium have crater densities about a factor of two to three lower than the lavas of the Apollo 12 site. Thus, these Imbrium flows may be 1.5–2 billion years old; we cannot estimate their absolute age any more precisely than this. Other relatively young flows are found from Oceanus Procellarum in the west to Mare Smythii in the east. One notable example is the Surveyor 1 landing site (the site of the very first American soft landing on the Moon back in 1966) within the lava-filled crater Flamsteed P in Oceanus Procellarum. Crater density suggests that these lavas are some of the youngest flows on the Moon, having an age possibly as low as 1 billion years. Interestingly, television images returned by Surveyor 1 show that this site has the thinnest regolith of any mare site ever visited, estimated to be between 1 and 1.5 m thick. For comparison, the regolith at the Apollo 12 site (which is underlain by the youngest *sampled* mare basalts) is about 4 m thick. As already mentioned, regolith thickness reflects the age of the bedrock upon which it forms. Thus, we have an independent way to estimate the relative age of the Flamsteed basalts from the Surveyor data. These images are consistent with an age for these lavas of about 1 billion years.

The very last gasps of volcanism on the Moon may have occurred about 800 million years ago. Ejecta from the crater Lichtenberg (about 20-km diameter) is covered by a lava flow, which is therefore younger than the crater. Lichtenberg has rays and is a member of the youngest class of craters on the Moon. Estimates of the absolute age of Lichtenberg are uncertain, but craters of this size tend to have their ray systems completely destroyed on timescales of 500–2000 million years. Thus, Lichtenberg, and its overlying lava flow, are probably *younger* than 2 billion years. This mare unit is the youngest lava flow currently recognized on the Moon.

The sum of the evidence suggests that the Moon has been volcanically active for most of its history. Massive extrusions of lava probably began in dim antiquity, during the era when the Moon's crust was being ground to a pulp by very high rates of bombardment. Extrusion of basalt continued throughout the era of basin formation, including the eruption of the massive amounts of lava that now underlie the highland plains deposited by the Orientale basin. As basins ceased to form, large expanses of mare deposits began to be preserved, forming the complex series of overlapping lava flows and ash deposits that make up the visible maria. Slow, prolonged filling of the near-side basins continued for several hundred million years, gradually loading the crust and deforming the filled basins by interior compression and exterior extension. Some impact craters underwent volcanic modification, including interior flooding and the formation of cinder cones on their floors. Large-scale regional deposits of ash were erupted along the margins of some maria. Younger lava deposits tend to be less voluminous than the older deposits, indicating that the intensity of volcanic activity has declined with time. The youngest lava flows are confined to Procellarum and Smythii. Some of these young eruptions may have occurred since 1 billion years ago, a time that seems remotely old, but, in fact, is "only yesterday" in the ancient and silent world of the Moon.

SEE ALSO THE FOLLOWING ARTICLES

Basaltic Volcanoes and Volcanic Systems • Lava Flows and Flow Fields • Volcanism on Io • Volcanism on Mars • Volcanism on Venus

FURTHER READING

Basaltic Volcanism Study Project. (1981). Pages 701–800 *in* "Basaltic Volcanism on the Terrestrial Planets." Pergamon, New York.

Head, J. W. (1976). Lunar volcanism in space and time. *Rev. Geophys. Space Phys.* **14,** 265–300.

Head, J. W., and Wilson, L. (1992). Lunar mare volcanism: Stratigraphy, eruption conditions, and evolution of secondary crust. *Geochim Cosmochim. Acta* **56,** 2155–2175.

Heiken, G. H., Vaniman, D. T., and French, B. M. (1991). "The Lunar Sourcebook." Cambridge Univ. Press, Cambridge, UK.

Papike, J. J., *et al.* (1976). Mare basalts: Crystal chemistry, mineralogy, and petrology. *Rev. Geophys. Space Phys.* **14,** 475–540.

Ryder, G., and Spudis, P. D. (1980). Volcanic rocks in the lunar highlands. *Proc. Conf. Lunar Highlands Crust* 353–375.

Schultz, P. H., and Spudis, P. D. (1983). The beginning and end of lunar mare volcanism. *Nature* **302,** 233–236.

Spudis, P. D. (1996). "The Once and Future Moon." Smithsonian Institution Press, Washington, DC.

Spudis, P. D. (1999). The Moon. Pages 125–140 *in* "The New Solar System," 4th ed. (J. K. Beatty, C. C. Petersen, and A. Chaikin, eds.). Sky Publishing Corp. and Cambridge Univ. Press, Cambridge, UK.

Taylor, S. R. (1982). "Planetary Science: A Lunar Perspective." Lunar and Planetary Institute Press, Houston.

Wilhelms, D. E. (1987). "The Geologic History of the Moon," U.S. Geological Survey Professional Paper **1348,** U.S. Government Printing Office, Washington, DC.

VOLCANISM ON IO

ROSALY LOPES-GAUTIER
Jet Propulsion Laboratory

I. Introduction
II. Interior and Heat Flow
III. Surface Expressions of Volcanism
IV. Surface Changes, Colors, and Composition
V. Hot Spot Temperatures and Composition of Magma
VI. Temporal Variability of Volcanic Activity
VII. Global Distribution of Volcanism
VIII. Volcanic Plumes, Atmosphere, and Torus
IX. Future Studies

GLOSSARY

differentiation The process by which planets and satellites develop layers or zones of different chemical and mineralogical composition.

fly-by Term used to describe the close approach of a spacecraft to a body, without the spacecraft going into orbit around that body.

fountain collapse Term used to describe the collapse of an eruption column, which can lead to the formation of a pyroclastic flow.

Galilean satellites The four largest satellites of Jupiter (Io, Europa, Ganymede, and Callisto), named after their discoverer Galileo Galilei.

heat flow Heat that comes out of a body from its interior and is ultimately radiated to space.

hot spots Regions of enhanced thermal emission on Io, a sign of volcanic activity. The term does not imply a particular eruption mechanism and does not have the same meaning as hot spots on Earth.

IRIS Acronym for Infrared Interferometer Spectrometer, an instrument aboard Voyager.

NIMS Acronym for Near-Infrared Mapping Spectrometer, an instrument aboard Galileo that obtains spectra in the wavelength range 0.7–5.2 μm. The spectra are used to analyze the composition of Io's surface and to measure the temperatures of its volcanic regions.

patera A collective term for a variety of unusual, saucer-shaped, shallow volcanic constructs that often have a central caldera.

pyroclastic materials Fragmented materials ejected during a volcanic eruption, including ash, pumice, and rock fragments.

SSI Acronym for Solid State Imaging system, the CCD camera aboard the Galileo spacecraft.

sulfur allotropes Sulfur cooled rapidly from different temperatures, resulting in different colors.

thermal emission Electromagnetic radiation produced by a body due to its temperature.

volatiles Chemical compounds or elements contained in magmas that are generally released as gases to the atmosphere during a volcanic eruption.

Copyright © 2000 by Academic Press
All rights of reproduction in any form reserved.

I. INTRODUCTION

Io, the innermost of Jupiter's four Galilean satellites, is particularly important to the study of planetary volcanology because it is the only body outside the Earth known to have large-scale active volcanism. The discovery of active volcanism was made by the Voyager 1 spacecraft, which flew close to Io in 1979. Images showed volcanic plumes up to 300 km in height, and a vividly colored surface dominated by large calderas and flowlike features. The study of Io's remarkable volcanism has continued since then using observations by telescopes on Earth, by the Hubble Space Telescope, and, since 1996, by the Galileo spacecraft (Fig. 1). We now know that Io is the most volcanically active object in the Solar System, that its heat flow is much higher than the Earth's, and that several of its volcanoes erupt lavas that are hotter than any erupted on the Earth today.

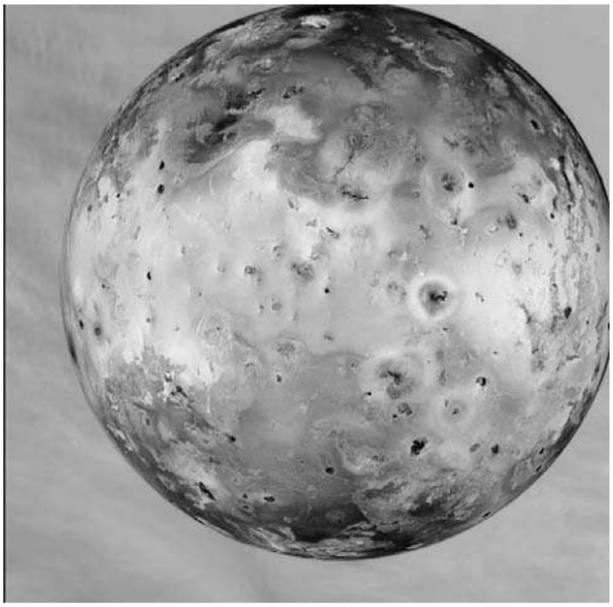

FIGURE 1 Io imaged by Galileo's camera (SSI) on September 7, 1996. Io's surface has a colorful appearance which is the result of its constant volcanic activity, depositing silicate materials and sulfur compounds. (For a color image, see http://photojournal.jpl.nasa.gov/cgi-bin/PIAGenCatalogPage.pl?PIA00494). Red and black deposits are thought to be the most recent volcanic deposits, probably no more than a few decades old. Just to the right of the image center is the Prometheus volcano, one of the most active hot spots on Io. Notice the dark flow snaking its way towards the right and the bright annulus surrounding the volcano, formed by plume deposits. The dark spot on the left edge just below the equator is the volcano Pele, which is surrounded by large red deposits.

TABLE I Facts about Io[a]

Orbital period	1.769 days
Rotational period	Synchronous with orbit
Mean radius	1821.3 km
Bulk density	3530 kg m^{-3}
Mass	$(8.9310 \pm 0.0012) \times 10^{22}$ kg
Gravity	1.80 m s^{-2}
Global average heat flow	>2.5 W m^{-2}
Radius of core	If pure iron, 656 km If iron and iron sulfide mixture, 947 km
Magnetic field	Perhaps
Geometric albedo	0.7
Local topographic relief	Up to 15 km
Active volcanic centers	>70
Hot spot temperatures	Up to at least 1600 K
Active plumes	15 observed
Surface composition	Sulfur dioxide frost mantle's surface Other sulfur compounds and probably silicates
Typical surface temperatures	85 (night) to 140 K (day)
Atmospheric pressure	10^{-9} bar or less, higher at locations of plumes

[a] Sources: McEwen *et al.*, 1999; Matson and Blaney, 1998.

Io's size and bulk density (Table I) are similar to those of the Earth's Moon and suggest a composition predominantly of silicates. We might have expected Io to be a cratered, dead world much like the Moon. However, even before the first close-up images of Io were returned by Voyager in 1979, there were hints that Io was remarkably different from the Moon. Earth-based telescopic observations made in 1974 by W. Wamsteker and colleagues first showed that the overall spectrum of Io closely matched that of sulfur, suggesting that sulfur and sulfur compounds might be abundant on the surface. It was also known that Io's spectrum lacked water ice, unlike those of the other Galilean satellites. Just prior to the Voyager encounters in 1979, two events presaged the discovery of active volcanism. F. Witteborn and colleagues reported a telescopic observation of an intense temporary brightening of Io in the infrared wavelengths from 2 to 5 μm. They explained it, although with some skepticism, as thermal emission caused by part of Io's surface being at a temperature of about

600 K, much hotter than the average expected daytime temperature of about 130 K. A few days before the Voyager encounters, a seminal theoretical paper by Stan Peale and colleagues was published in the periodical *Science*. They had studied the tidal stresses generated within Io as a result of the gravitational fields of Jupiter and Europa. Their calculations showed that the possible heat generated by tidal stresses was on the order of 10^{13} W—much greater than heat that could be released from normal radioactive decay. Their prediction was that Io might have "widespread and recurrent volcanism."

Active volcanoes were not immediately obvious in the first images returned by Voyager 1. The most striking aspect of Io shown in the first images was its colorful surface, with yellows, oranges, reds, and blacks. Scientists on the imaging team nicknamed Io the "pizza moon" and speculated about the presence of large quantities of sulfur on the surface. Another surprising aspect was the absence of impact craters. The obvious conclusion was that Io's surface was very young and the craters must have been obliterated—but how? The answer came soon after, when a navigation engineer at the Jet Propulsion Laboratory, Linda Morabito, noticed a peculiar umbrella-shaped feature emanating from Io's limb in one of the images that was taken to aid navigation of the spacecraft (Fig. 2). The pattern turned out to be an eruption plume rising about 260 km above the surface. A second plume was found on the same image, and more plumes were seen upon close examination of various other images. Additional evidence for active volcanism came from another of Voyager's instruments, the Infrared Interferometer Spectrometer (IRIS), which detected enhanced thermal emission from parts of Io's surface—some areas had temperatures of about 400 K, much higher than the rest of the surface, which has noontime equatorial temperatures of about 107–124 K. When one of the hot areas was found to coincide with one of the plumes, there was no doubt that active volcanism was taking place.

Eighteen weeks after Voyager 1's dramatic discovery, the companion spacecraft, Voyager 2, flew close to Io. Intense activity was still taking place, but significant changes had occurred between the two fly-bys, including the cessation of the largest plume, Pele, and the altered shape of the deposits associated with this plume. An area of about 10,000 km^2 had been filled in, presumably by fresh material falling down from the plume (Fig. 3). It became evident that dramatic changes of Io's surface could occur over short timescales.

Initial analysis of the Voyager data showed nine plumes and nine "hot spots," though not all plumes coincided with hot spots and vice versa. Hot spot is a term used by Io researchers to define a region of enhanced thermal emission, a sign of active volcanism—it does not mean the same as a hot spot on Earth. The Voyager IRIS experiment did not observe all of Io's surface, so it was suspected that other hot spots existed.

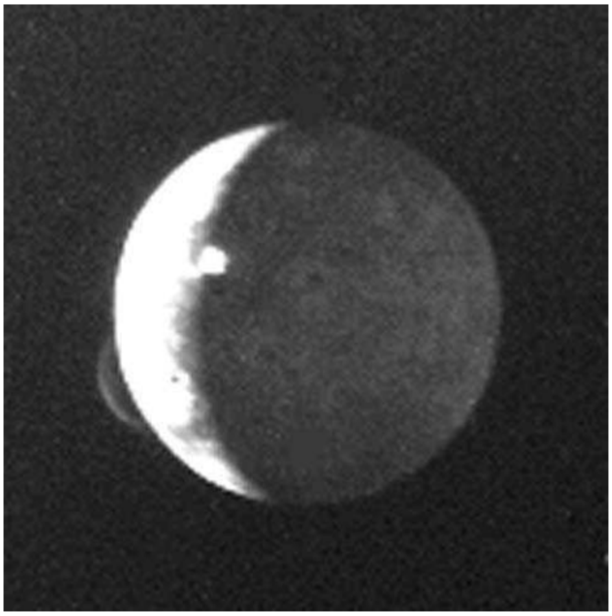

FIGURE 2 Volcanism on Io was first seen on this Voyager 1 image, taken on March 8, 1979. The image shows two plumes. The Pele plume is seen on the edge of the disk against the dark sky and it rises about 260 km above the surface. The other plume, Loki, is seen as a bright spot on the nightside of the terminator (the boundary between day and night). The plume is reaching above the darkness of the disk and catching the rays of the rising sun.

After the two Voyager spacecrafts left the Jupiter system on their way to Saturn and beyond, the study of Io's volcanism was continued from Earth by astronomers using infrared detectors mounted on telescopes. These observations showed that brightenings and fadings of hot spots occur, indicating variations in the level of volcanic activity. Observations by W. Sinton, R. Howell, J. Spencer, and other astronomers have shown that Io's most powerful hot spot, Loki, has brightenings that switch on in one month or less and last several months before fading. Telescopic observations were also used to analyze the reflected light from Io's surface to determine surface composition, confirming that it was dominated by sulfur dioxide (SO_2). Io was also observed by the International Ultraviolet Explorer satellite and more recently it has been observed by the Hubble Space Telescope.

The first spacecraft to orbit Jupiter is Galileo, which has been able to image Io and monitor its volcanic activ-

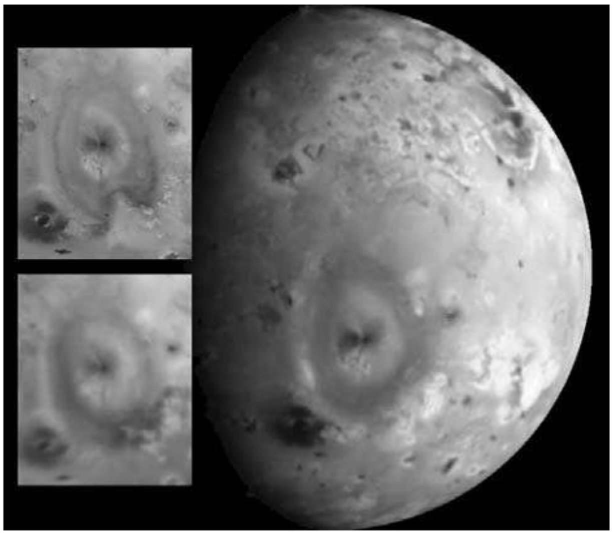

FIGURE 3 Changes in the bright red deposits around the Pele plume. The larger image was taken by the Galileo camera in June 1996 and shows Pele just below the center of Io's disk. The upper inset is an image from Voyager 1 taken in March of 1979, while the lower inset was taken by Voyager 2 in July of 1979. Note the dramatic change in the shape of the annular deposit in the four months between the two Voyager encounters. The differences in the shape of the deposit are thought to reflect the changing shape of the vent from which the plume emerged. For a color image, see http://photojournal.jpl.nasa.gov/cgi-bin/PIAGenCatalogPage.pl?PIA00718.

ity since June of 1996. Galileo was inserted into orbit around Jupiter in December 1995 and flew close to Io at that time. Unfortunately, a problem with the onboard tape recorder prevented any close-up images and other remote-sensing observations to be obtained. However, all was not lost and extremely valuable information was gained using the fields and particles instruments aboard the spacecraft.

Since the radiation environment near Jupiter and Io is extremely hostile to spacecraft and instruments, no other close passes of Io were planned, and Galileo began a series of 11 orbits making close passes to the other satellites (Europa, Ganymede, and Callisto) and observing Io from distances much greater than Voyager had done in 1979. However, Galileo has been unique in that it can monitor Io's volcanoes from Jupiter orbit and thus map their distribution on the surface and detect changes in their activity (Fig. 4). The two major instruments on Galileo that monitor the activity of Io's volcanoes are the camera (Solid State Imaging system, or SSI) and the Near-Infrared Mapping Spectrometer (NIMS). To make up for the loss of data from 1995, three close fly-bys of Io are planned in late 1999 and early 2000. If Galileo and its instruments survive, we should be able to answer many of the questions that have been asked since Io's volcanism was discovered.

II. INTERIOR AND HEAT FLOW

When Galileo approached Io in December 1995, the magnetometer experiment detected a disturbance in Jupiter's magnetic field. A likely explanation for the disturbance is that Io produces its own magnetic field, but this cannot be confirmed until Galileo obtains further measurements from a close pass over the south pole of Io, planned for the end of 1999. Another interesting result was obtained by radiotracking of the spacecraft as it came close to Io. Variations in the spacecraft's motion revealed distortions in Io's gravitational field, which provided evidence that Io is differentiated. Io has a large metallic core with a radius of about half of its total radius, made up of iron or a mixture of iron and iron sulfide. Given Io's intense volcanic activity and high heat flow, it is possible that the metallic core is at least partly molten and may be circulating. This would generate a magnetic field, consistent with the initial indications from the magnetometer experiment. However, if the tidal energy is mostly dissipated within the upper mantle, as recent results from the global distribution of hot spots suggest, then convection in the core might not occur.

Io's heat flow is very large compared with that of the Earth and other planets. The heat flow is measured at infrared wavelengths and the portion due to reflected sunlight is calculated and subtracted, taking into account Io's surface albedo. The difference is the heat flow due to volcanism and originates in Io's interior. The current best measurement of Io's heat flow is 10^{14} W. For comparison, the Earth's total heat flow is 4.42×10^{13} W. Averaged over the whole of Io's surface, the value is about 2 W m^{-2}, high even compared to geothermal and volcanic areas on earth. Io's heat flow is about 200 times what could be expected from heating due to the decay of radioactive elements and illustrates how crucial tidal heating is to drive Io's active volcanism.

III. SURFACE EXPRESSIONS OF VOLCANISM

Compared to other Solar System bodies, Io's colors are truly striking while its global topography is somewhat

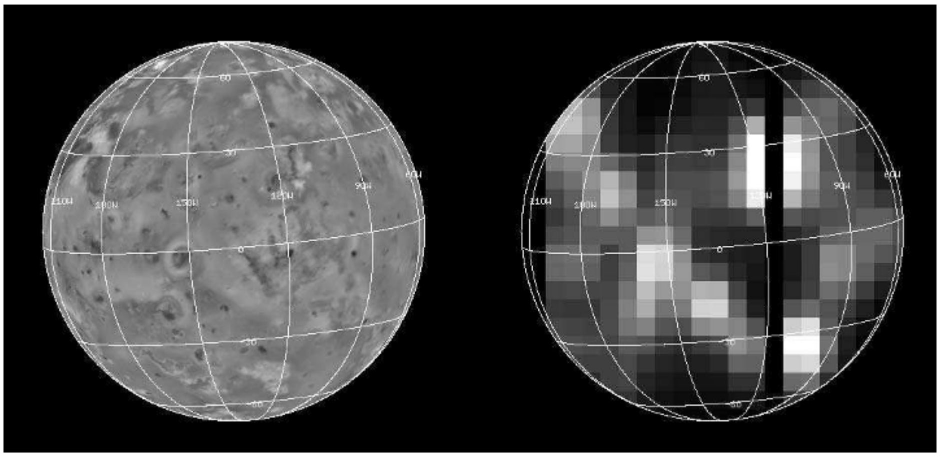

FIGURE 4 Detection of active volcanoes on Io by Galileo's Near-Infrared Mapping Spectrometer (NIMS). The image on the left is a Voyager global mosaic for comparison. The image on the right is a 5-μm map by NIMS. The bright pixels represent hot materials from the active volcanic centers. The dark, roughly circular region on the lower right of the NIMS image is Bosphorus Regio, a cold region surrounded by a ring of hot spots. This NIMS image was obtained on June 29, 1996, and revealed three previously unknown active hot spots. Since then, NIMS has discovered over 20 other hot spots.

subdued. There are relatively few mountains and the surface is dominated by vast expanses of smooth volcanic plains. A major difference between the surface of Io and that of other bodies in the Solar System is that, to date, no impact craters have been found on Io, despite the relatively high flux of comets expected due to Jupiter's gravity and the fact that the surfaces of the other Galilean satellites all show the scars of impacts. The lack of craters on Io implies that the surface must be very young—probably at most a few million years old. Calculations using the expected rate of impacts on Io show that, in order to bury the craters, the resurfacing rate on Io must be at least 1 mm per year. If the resurfacing was uniform, this would mean that all of Io's surface would be buried to a depth of 1 km in only one million years.

Because of Io's high rate of volcanism, it is expected that its surface features must be almost entirely the result of volcanism and related plutonic and tectonic activity. The dominant features on Io's surface are volcanic constructs (such as calderas), mountains, and smooth plains. Plateaus and scarps are seen in some regions. The colors of the surface are mostly yellow, white, red, and black. A few isolated patches of greenish-yellow were recently discovered by P. Geissler from Galileo imaging data. Black materials that spot Io's surface are thought to represent recently erupted lavas. Many of these dark patches lie within and around depressions that appear similar to calderas on Earth (Fig. 5).

The most striking type of feature on Io's surface is volcanic centers. Although the currently available images from Voyager and Galileo do not have enough spatial resolution to show individual volcanic vents, many volcanic centers are seen dotted all over the surface. Over 350 of these have been identified from images, though many of these are not currently active. Their forms include caldera-like depressions, dark circles or ovals, and source areas of flows. About 40% are dark, which is thought to indicate that they were active more recently than the others, which appear as bright or brighter than their surroundings. M. Carr and colleagues have studied the distribution of these volcanic features on the surface and concluded that it appears to be uniform, except that the features are perhaps more sparse at high latitudes. The distribution suggests that volcanic activity has occurred everywhere on Io over the time represented by the present population of vent regions. This may imply that as activity in some areas declines, activity in other areas must be rekindled.

The calderas on Io range in diameter from about 20 to 200 km, are as deep as 2 km, and have steep walls and apparently flat floors. Calderas on Earth form by collapse of the surface above shallow magma chambers after the magma is rapidly withdrawn. It is likely that the calderas on Io are formed by the same process, but on Io they can be much larger in diameter than on Earth, while the Ionian volcanoes they are associated with are in general much more subdued in flank topography than terrestrial volcanoes. Some calderas on Io do not appear to be associated with a volcanic edifice at all and others are seen atop low shield-type volcanoes.

TABLE II Active Volcanic Centers on Io

Volcanic center	*Location*	*Hot spot detected by*	*Plume detected?*
Ruwa Patera	1 N, 3 W	Galileo	No
Nusku Patera (?)	63 S, 7 W	Voyager?	no
Mbali Patera	32 S, 8 W	Voyager	no
Karei Patera (?)	2 N, 16 W	Galileo?, ground	no
Ukko Patera	32 N, 20 W	ground	no
Uta Patera (?)	35 S, 25 W	Voyager?, ground?, HST?	no
Kanehekili	18 S, 37 W	Galileo, ground, HST	Galileo
Unnamed	70 ± 15 N, 35 ± 15 W	ground	no
Janus Patera	3 S, 40 W	Galileo, ground, HST	no
Masubi	44 S, 55 W	Galileo, ground	Voyager
Shamshu	10 S, 63 W	Galileo	no
Unnamed	3 N, 76 W	Galileo	no
Zal Patera	41 N, 76 W	Galileo	no
Hi'iaka Patera	2 S, 79 W	Galileo, ground	no
Gish Bar Patera	17 N, 90 W	Galileo	no
Unnamed	46 N, 92 W	Galileo	no
Sigurd Patera	5 S, 97 W	Galileo	no
Unnamed	16 S, 98 W	Galileo	no
Monan Patera	19 N, 106 W	Galileo	no
Altjirra Patera	35 S, 109 W	Galileo, Voyager?	no
Amirani	25 N, 116 W	Galileo, Voyager	Voyager, Galileo
Maui	20 N, 122 W	Galileo, Voyager?	Voyager
Malik Patera	35 S, 128 W	Galileo, Voyager	no
Unnamed	16 N, 136 W	Galileo	no
Unnamed	65 N, 141 W	Galileo	no
Tupan Patera	18 S, 141 W	Galileo	no
Unnamed	32 N, 147 W	Galileo	no
Shamash Patera	34 S, 153 W	Galileo, Voyager?	no
Prometheus	2 S, 154 W	Galileo	Voyager, Galileo
Culann Patera	19 S, 160 W	Galileo	Galileo?
Zamama	18 N, 173 W	Galileo	Galileo
Volund	23 N, 176 W	Galileo, Voyager	Voyager
Aidne Patera	1 S, 177 W	Galileo	no
Unnamed	20.9 S, 186.7 W	Galileo	no
Fo Patera	40 N, 192 W	Galileo	no
Sethlaus Patera	52 S, 194 W	Galileo	no
Rata Patera	35 S, 199 W	Galileo	no
Lei-Kung Fluctus	36 N, 203 W	Galileo	no
Unnamed	52 S, 203 W	Galileo	no
Isum Patera	29 N, 209 W	Galileo, Voyager, ground?	no
Marduk	27 S, 209 W	Galileo, Voyager	Voyager, Galileo
Kurdalagon Patera	50 S, 218 W	Galileo	no

continues

Continued

Unnamed	2 S, 218 W	Galileo	no
Mulungu Patera	17 N, 218 W	Galileo, ground?	no
Unnamed	22 N, 220 W	Galileo, ground?	no
Unnamed	32 S, 226 W	Galileo	no
Reiden Patera	13 S, 236 W	Galileo	no
Unnamed	22 N, 240 W	Galileo	no
Pillan Patera	12 S, 244 W	Galileo	Galileo, HST
Pyerun Patera (?)	55 S, 252 W	Voyager?	no
Pele	18 S, 256 W	Galileo, Voyager	Voyager, Galileo, HST
Shakura Patera (?)	24 N, 267 W	Voyager?	no
Mithra Patera (?)	59 S, 267 W	Voyager?	no
Svarog Patera	48 S, 268 W	Galileo, Voyager	no
Babbar Patera	39 S, 273 W	Galileo, Voyager	no
Daedalus Patera	19 N, 275 W	Galileo, Voyager	no
Viracocha Patera	62 S, 282 W	Voyager	no
Ulgen Patera	40 S, 288 W	Voyager, Galileo?, ground?, HST?	no
Sengen Patera (?)	32 S, 304 W	ground?, HST?	no
Amaterasu Patera	38 N, 307 W	Galileo, Voyager, ground?	no
Loki Patera	13 N, 309 W	Galileo, Voyager, ground, HST	Voyager
Dazhbog Patera (?)	56 N, 303 W	HST	no
Aten Patera	48 S, 311 W	Voyager, ground?, HST	no
Mazda Catena	8 S, 314 W	Voyager, ground?, HST?	no
Unnamed (?)	49 N, 312 W	HST	no
Nemea	80 S, 320 W	Voyager	no
Ra Patera	8 S, 325 W	no hot spot detected	Galileo
Fuchi Patera	29 N, 328 W	Galileo, ground, HST?	no
Acala Fluctus	11 N, 336 W	Galileo, Voyager, HST, ground?	Galileo
Surt	46 N, 338 W	ground, HST	no
Creidne Patera	53 S, 344 W	Voyager, HST?	no
Tiermes Patera (?)	23 N, 351 W	ground	no
Euboea Fluctus (?)	45 S, 352 W	ground, HST?	no
Fjorgynn Fluctus	12 N, 358 W	ground?, HST	no

[a] Active volcanic centers on Io detected by instruments aboard Galileo, Voyager, the Hubble Space Telescope (HST), instruments mounted on ground-based telescopes. Table modified from Lopes-Gautier *et al.* (1999). Additional data courtesy of A. McEwen, J. Spencer, J. Goguen, C. Dumas, and P. Geissler. Location marked with (?) are tentative identifications of surface features that are the sites of thermal emission. Detection marked with (?) are uncertain.

Given the direct measurements of very high temperature magmas on Io (discussed later), it is possible that the absence of large volcanic edifices could be due to very low viscosity lavas forming lava plains rather than building tall volcanoes.

An obstacle to the detailed study of the morphology of Io's volcanic features is the lack of high-resolution images. The highest resolution images available at the time of writing are at best 500 m per pixel. Lobate features that are interpreted to be lava flows are seen associated with many of the dark markings on Io, but the lack of resolution and topographic information hinders attempts to use their morphology to obtain clues to magma composition, as has often been done using images of flows on other planets such as Mars. It is clear, however, that some of the flows on Io are tens of kilometers long. Comparison of Voyager and Galileo camera images by A. McEwen and colleagues shows that new

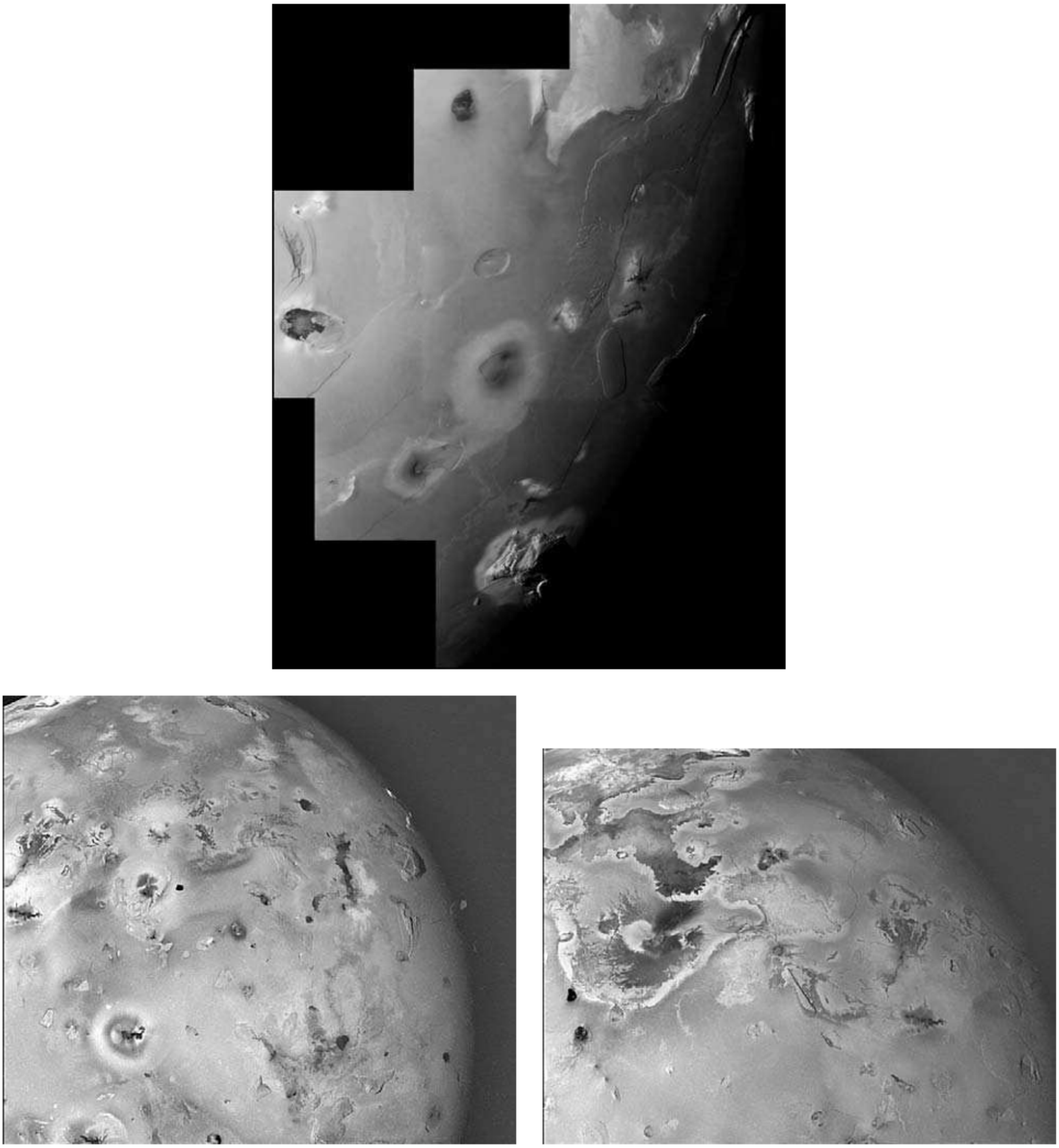

FIGURE 5 Images showing the varied landforms of Io. (a) Voyager 1 image showing the south polar region. Near the bottom of the picture is the 10-km-high Haemus Mons, one of Io's tallest mountains. The partly dark-filled caldera at the far left is Creidne Patera. Elsewhere, eroded volcanic plateaus and other volcanic calderas can be seen dotted on the smooth plains. (b) Topographic mapping image acquired by Galileo's SSI. The Prometheus volcano is prominent on the lower left. Note the bright annulus formed by plume fallout and the dark lava flow. To the right of Prometheus is Bosphorus Regio, a bright, roughly circular area surrounded by active volcanic centers, described as the "ring of fire." Numerous other dark calderas can be seen in this image. (c) Topographic mapping image acquired by Galileo's SSI. The prominent dark flows on the upper left are from the active volcanic centers of Lei-Kung Fluctus and Isum Patera.

flows up to 70 km long were emplaced in the years between these missions.

Mountains (Fig. 5) are also a major type of feature on Io, though they are scarce in comparison with mountains on Earth and do not form long chains and ranges. It is still debatable whether Io's mountains are a direct result of volcanic activity, though it is clear that they do not have the forms of volcanic features such as stratocones or shields. Their distribution on the surface appears uniform, and there is no correlation between their locations and those of hot spots and plumes. Mountains are generally isolated from one another and separated by vast expanses of plains. They can be up to 15 km high and their appearance is rugged, some being multitiered and perhaps disrupted by tectonic forces. The relationship between mountains and plains is still not well understood but, in most places, plains materials appear to be younger than mountains and to lap onto their bases. In one area, Euboea, a landslide of mountain material can be seen overlapping the plains.

Two possible explanations are likely for the origin of mountains. The simplest is that the mountains are indeed volcanic and that the youngest materials were deposited on top of the adjacent plains. The alternative hypothesis is that the mountains are exposures of an old subcrust and that the sides of some of the mountains have failed and the debris flowed over the surrounding plains.

Most of Io's surface is covered by volcanic plains that appear smooth in relief but are striking in their different colors and albedo patterns. The plains are thought to be formed by overlapping flows and deposits from volcanic plumes, such as SO_2 frost and sulfur. Although the flows have mostly sharp edges, other deposits surrounding vents and flows appear diffuse. One of the most intriguing features of the plains is the low, irregular escarpments seen in some areas, which imply that the plains are layered (Fig. 5). Many of the escarpments have a jagged outline, suggesting they may have been formed by erosion. A series of mesas in the south polar regions are particularly striking and appear erosional in nature. These features may have been formed from the explosive eruption of SO_2 from a subterranean reservoir or, alternatively, they may have been carved into the plains by fast-moving, low-viscosity lavas.

No evidence of global-scale tectonism has yet been found on Io. Scarps are seen to cut across the plains, and some of them appear to be tectonic in origin, given their linearity and tendency to occur in parallel groups. However, other scarps are irregular in plan view and appear to be erosional in origin. Alignments of hot spots occur in some areas, but there is no evidence that these are tectonic in origin. Tectonic studies of Io have so far been handicapped by the small number of tectonic-like features that can be seen in the currently available images. It is possible that many previously unseen tectonic features will be revealed when high-resolution images are acquired during Galileo's close fly-bys of Io.

IV. SURFACE CHANGES, COLORS, AND COMPOSITION

Comparison between Voyager and Galileo images taken nearly two decades apart showed many areas of surface changes, but not as many as might have been expected given Io's high rate of volcanism. Surprisingly, hot spots where vigorous activity is known to have occurred, such as Loki, showed little surface change, presumably because the activity is mostly confined to the interior of the caldera. One of the most striking cases of surface change happened on Ra Patera, a region that so far has been identified only as an active plume site and not yet as a hot spot, though this could be due to poor spatial resolution of the thermal data over this region. Voyager images showed Ra to have a dark caldera surrounded by narrow flows. The flows showed a sequence of colors along their lengths that was consistent with the interpretation of Carl Sagan that Io's surface was covered by different sulfur allotropes, with the supposedly cooler materials further away from the vent. However, this interpretation of composition based on color was criticized on a variety of grounds, including the fact that the exact colors of sulfur can be drastically altered by even small amounts of other materials. Ra Patera became even more of a puzzle when observations from the Hubble Space Telescope showed that a significant brightening occurred in this region between 1994 and 1995. When images of Ra were returned after Galileo's first orbit (Fig. 6), they showed that the flows had been covered over by new deposits and that a plume was now erupting from Ra.

The intriguing question of what causes the vivid colors of Io's surface, including the colors of the flows that are now gone, remains unanswered, though Galileo results have brought new insights. The global distribution of the different color deposits gives some clues to their origin. Galileo images show that almost one-third of Io's surface is covered by red and orange materials, particularly at latitudes higher than 30° north and south. At lower latitudes, patches of red materials appear to be associated with hot spots and plumes. Red materials are

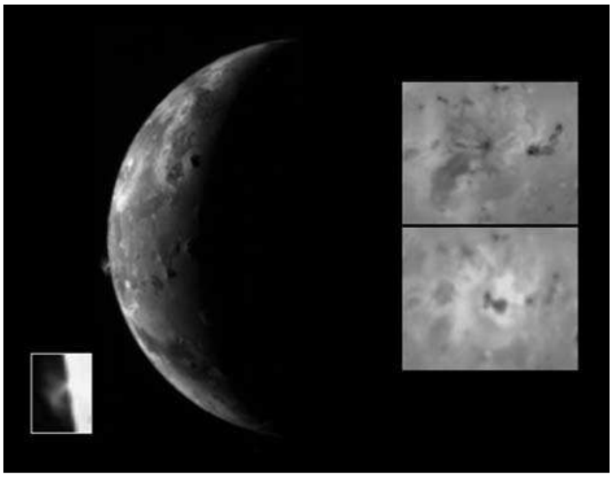

FIGURE 6 The Ra Patera volcano showed dramatic changes in the 18 years between the Voyager and Galileo spacecraft observations of Io. The larger image was taken by the Galileo camera (SSI) on June 28, 1996, and shows a plume about 100 km high over the Ra Patera volcano. The two insets are comparisons of Voyager (top) and Galileo (bottom) views of the volcano. The Voyager image shows a dark caldera near the center of the image surrounded by long, narrow flows. The flows cannot be seen in the lower image, taken by Galileo. They were covered over by a bright deposit that extends over an area of about 40,000 km^2. For a color image, see http://photojournal.jpl.nasa.gov/cgi-bin/PIAGenCatalogPage.pl?PIA00293.

thought to be ephemeral, lasting perhaps a few years, and to be a sign of recent volcanic activity. It is likely that they represent pyroclastic deposits, perhaps fallout from plumes. The origin of the red deposits in the polar regions is probably different, even though the composition may be the same, since there is a clear scarcity of plumes at high latitudes. The red deposits may last longer in the polar regions because of lower surface temperatures.

Very dark deposits also appear to be associated with hot spots. They occur in isolated patches, both as diffuse deposits that are probably pyroclastic in nature and as continuous units confined to caldera interiors. Most dark calderas are found within 60° of the equator. The vast expanses of equatorial plains between individual hot spots are dominated by yellow, white, and gray materials that are generally anticorrelated with the hot spots. The most striking example of the anticorrelation is the "ring of fire" of hot spots (Figs. 4 and 7) surrounding the white, cold region of Bosphorus Regio. (The term is descriptive of the alignment of hot spots and does not imply a tectonic control as is the case for the ring of fire on Earth.)

What are the different compositions of these differently colored materials? Sulfur and sulfur compounds are the most viable compositional candidates for the variegated colors of Io, though silicate materials are thought to be exposed in places. So far, only SO_2 has been definitely identified on Io by its absorption features in the near-infrared. Recent studies by R. Carlson using data from the NIMS experiment on Galileo showed that most of Io's surface is covered by a thin mantle of fine-grained SO_2 frost (probable grain sizes of 30–100 μm in diameter) and that the white and gray materials represent areas covered by moderate to coarse grained SO_2 frost (grain sizes of 250–500 μm in diameter) beneath smaller particles. Because NIMS detects SO_2 in both white and yellow regions, it is possible that the yellow unit may be in places a dilute mixture of sulfur and SO_2, or perhaps a thin veneer of ordinary orthohombic sulfur (S_8) that is colored at visible wavelengths but transparent in the infrared.

The most prominent red deposit on Io is the large ring surrounding the hot spot Pele. The existence of both red and black diffuse materials in the ring suggests that the two could be related in composition and sulfur is the most likely candidate. Red sulfur has considerably higher viscosity than the higher temperature (black) sulfur allotropes. Black is seen nearer the vent of Pele, while red is seen further away in the ring, which would be consistent with more viscous magmas being ejected more energetically, and falling further away, than fluid magmas with similar densities and volatile contents. However, it is possible that the black materials may be pyroclastic silicates rather than sulfur. Some of the very dark materials that are associated with calderas and active hot spots show an apparent spectral absorption feature at 0.9 μm, seen in the Galileo imaging data and interpreted by P. Geissler and colleagues as being due to orthopyroxene. Although further results from Galileo are needed to confirm the presence of this spectral feature and to provide a unique mineral identification, the presence on Io of orthopyroxene, a magnesium-rich silicate mineral common in terrestrial mafic and ultramafic rocks, seems likely.

Perhaps the most intriguing materials on Io's surface are the greenish-yellow deposits seen in a few isolated spots. Unlike other terrains on Io, these areas show a negative near-infrared spectral slope, strongly suggesting that a nonsulfur component is present. These green materials could be made up of sulfur contaminated by iron, as suggested by J. Kargel and colleagues; however, the fact that an active hot spot is seen coinciding with one of these areas supports the alternative explanation of silicates such as olivine or clinopyroxene.

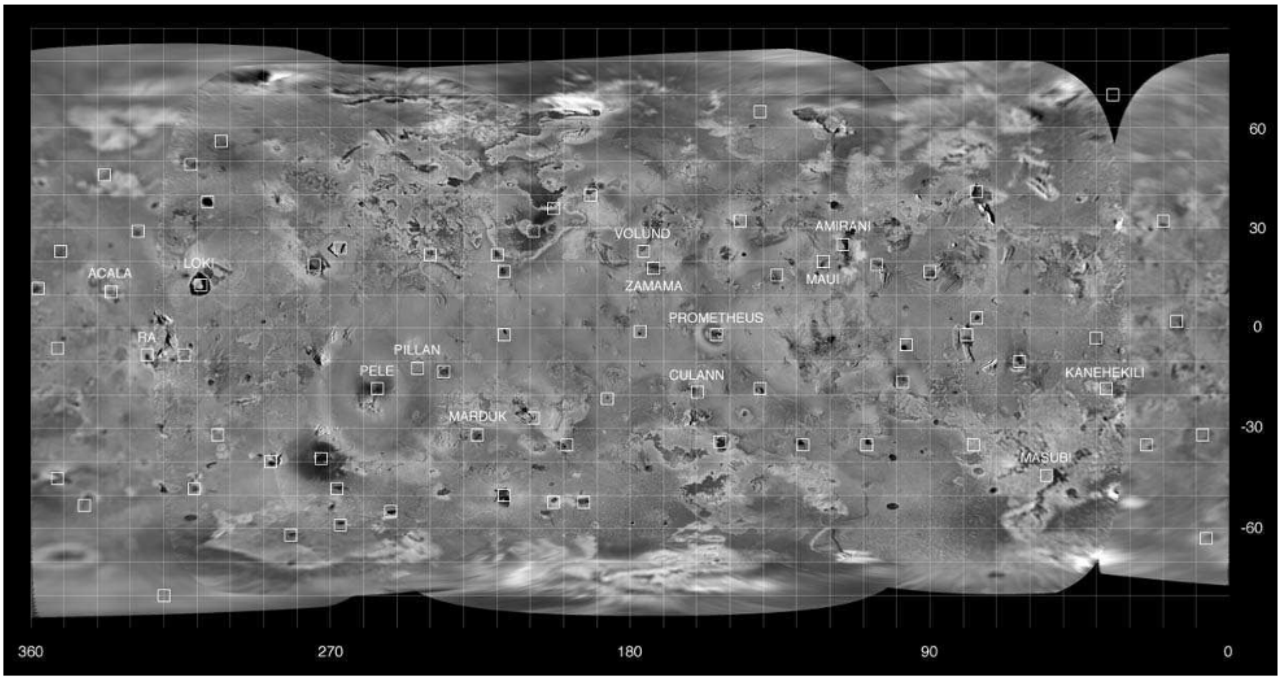

FIGURE 7 Global distribution of active volcanic centers on Io are marked by squares in this Simple Cylindrical global mosaic of Galileo images. The named features are the sites of active plumes. The bright, roughly circular area to the west of Prometheus and Culann and to the south of Amirani/Maui is Bosphorus Regio, which is surrounded by active volcanic centers. (Modified from McEwen *et al.,* 1999.)

The poor spatial resolution of the observations of Io available so far and the thin coating of SO_2 that seems to be prevalent on much of the surface have made it difficult to identify the compositions of the different deposits on Io. One of the most important goals of the close fly-bys of Io by Galileo is to reveal the true nature of Io's differently colored deposits.

V. HOT SPOT TEMPERATURES AND COMPOSITION OF MAGMA

Shortly after the Voyager mission, the major controversy about Io's volcanism concerned the nature of the volcanism: sulfur or silicates? Io's surface colors were initially interpreted as sulfur deposits. The temperatures of the hot spots measured by the Voyager IRIS instrument were relatively low—mostly around 400 K—and could be consistent with either molten sulfur or silicates. IRIS was not capable of detecting small areas at higher temperatures; hence it was "seeing" only the cooler areas, perhaps cooling lava flows. Between the Voyager observations in 1979 and the Galileo observations that started in 1996, several of Io's hot spots were detected by ground-based telescopes. Temperature measurements using infrared detectors mounted on telescopes showed higher temperatures than had been measured by IRIS—such as 900 K reported by T. Johnson and colleagues in 1988 and 1225 and 1500 K reported by G. Veeder and colleagues in 1991. These measurements are consistent with silicate magmas but not with sulfur volcanism. Sulfur boils vigorously on Io's surface at about 500 K and, although sulfur compounds such as sulfur polysulfides could be several hundred degrees hotter, temperatures as high as 1000 K strongly suggest silicate magmas.

Observations by Galileo's instruments have shown that the temperatures are indeed consistent with silicate rather than sulfur volcanism. However, the greatest surprise was the detection of extremely high temperature volcanism on Io. The best studied example is the activity of the hot spot Pillan in 1997. Galileo's NIMS and SSI instruments observed this hot spot within a few minutes of one another and their combined results, reported by A. McEwen and colleagues in 1998, provided unambiguous evidence of temperatures exceeding 1500 K, and

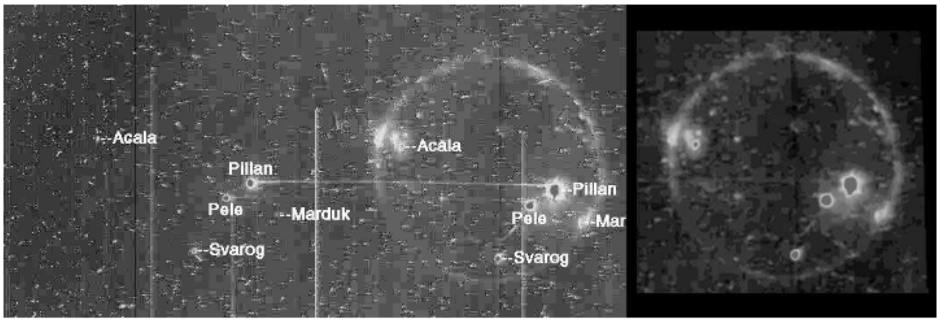

FIGURE 8 Galileo camera (SSI) images showing Io in eclipse. The camera detects thermal emission from active hot spots by imaging Io when the disk is being eclipsed by Jupiter and is in darkness. The major hot spots are marked, including Pillan. The left-hand image was acquired using the camera's 1-μm filter, while the right-hand image is the clear filter exposure. The resolution of the image is 14.6 km/pixel, but the hot spots appear "smeared" over an area about 9 pixels in diameter. Modeling of the data indicates that the areas of the hot spots are smaller than the pixels. The right-hand image shows diffuse glows on Io's limb and the plume over the hot spot Marduk. The glow is due to electronic excitation of gases. The small bright pixels and clusters of pixels seen all over the images are due to noise from radiation, the bright vertical lines are image blemishes, and the horizontal line between the images is due to exposure during motion of the spacecraft's scan platform. For a color image, see http://photojournal.jpl.nasa.gov/cgi-bin/PIAGenCatalogPage.pl?PIA01635.

possibly as high as 2000 K (Figs. 8 and 9). This implies magma liquidus temperatures of at least 1700 K, because lavas are expected to cool rapidly once they reach Io's surface. There is evidence that about 10 other hot spots on Io erupt lavas with temperatures hotter than about 1600 K. These temperatures are higher than any seen on lavas erupting on Earth now and in recent times. It is possible that high-temperature lavas are typical for Io but, given the distant observations of Io by Galileo, these temperatures can only be detected during particularly vigorous episodes, when large quantities of hot magma come up to the surface. The temperatures detected by the low spatial resolution observations of NIMS are mostly in the range of 400–1000 K, although hotter components can be inferred from the spectral data in some cases.

The most likely explanation for the very high temperatures of Io's lavas is that they are ultramafic (magnesium rich) in composition. This explanation is supported by the discovery of the 0.9-μm spectral absorption feature discussed above, which is interpreted as magnesium-rich orthopyroxene. Ultramafic lavas have very rarely been erupted on Earth since the Proterozoic, about 1.8 billion years ago. Therefore, studying Io's current volcanism may lead to a better understanding of the emplacement of ultramafic lavas on the ancient Earth.

It is important to note that although the temperatures of Io's lavas indicate ultramafic compositions, at present there are no direct measurements to confirm this interpretation. The most critical question about Io's volca-

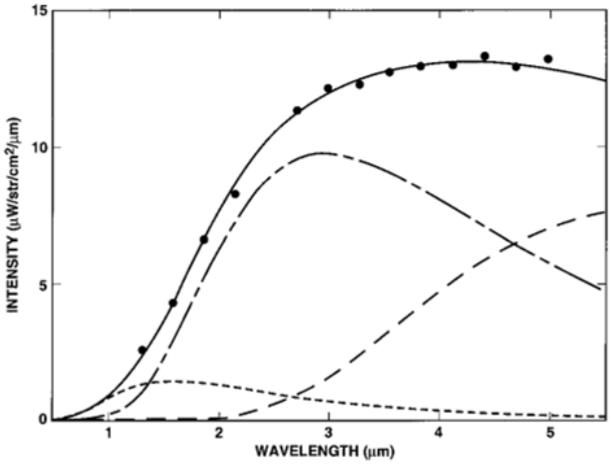

FIGURE 9 Temperature fits to a spectrum of the hot spot Pillan taken by Galileo's Near-Infrared Mapping Spectrometer (NIMS). The spectrum (represented by the solid circles) was taken a few minutes apart from the images in Fig. 7, when Io was in darkness due to an eclipse by Jupiter. All the energy in the spectrum is due to thermal emission, as there is no component due to reflected sunlight. Three blackbody curves were fitted to the spectrum. the long-dash curve represents an area of 544 km^2 at a temperature of 475 K. The long dash–short dash curve represents an area of 17.6 km^2 at a temperature of 975 K, and the short-dash curve represents an area of 0.11 km^2 at a temperature of 1825 K. The smooth solid curve represents the sum of these three temperature–area components and it fits closely the original spectrum. (Modified from McEwen *et al.*, 1998.)

nism—what is the composition of the erupting magma and crust—remains open.

VI. Temporal Variability of Volcanic Activity

Io is a dynamic body—the volcanic plumes turn on and off, the outpourings of magma vary in temperature and extent, and sometimes large-scale changes are seen to occur in a matter of months, completely changing the appearance of a region. Variations in the volcanic activity have been detected since the fly-bys of Voyager 1 and 2, as changes were apparent in the four months between the two spacecraft approaches to Io. However, the most dramatic change so far observed on Io's surface happened sometime between spring and fall of 1997. An image taken by the Galileo SSI camera during Galileo's 10th orbit revealed an enormous "black eye" surrounding the hot spot Pillan (Fig. 10). The diameter of the deposit is about 400 km and it covers an area about as large as the state of Arizona. It is likely that the dark deposit is pyroclastic in nature, and probably consists of silicates.

Pillan is a hot spot discovered by the NIMS instrument during Galileo's second orbit and seen by NIMS to be a persistently bright, active hot spot since that time. Back in 1979, the Voyager cameras had shown Pillan to be a simple caldera located on the edge of the Pele plume fallout deposit. No hot spot or surface changes were found there between the two Voyager fly-bys. Pillan was not apparent as a hot spot in the observation of Io in eclipse taken by Galileo's camera in June 1996 and the caldera appeared unchanged since the Voyager days. In September of 1996, NIMS detected a hot spot at Pillan and camera images showed that the floor of the caldera had become dark—but the floor had become bright again by Galileo's third orbit in November 1996 and in subsequent orbits until April of 1997. The NIMS instrument continued to detect a bright, persistently active hot spot at the caldera. Observations by J. Spencer and colleagues using the Hubble Space Telescope on July 5, 1997, detected an active plume over Pillan, about 150 km high, and around the same time a plume was also detected by Galileo's camera (Fig. 11). When the Galileo camera imaged the Pillan region again in September 1997, it showed the remarkable dark deposit. Also shown in the September image are subtle changes to the Pele plume deposits, which may indicate that the two plumes were active at the same time and interacted with one another.

The surface change observed by the camera coincided with the high-temperature eruption discussed above, which has been so far the most impressive of these eruptions observed on Io. Since then, the eruption at Pillan has continued and it has been observed by both the

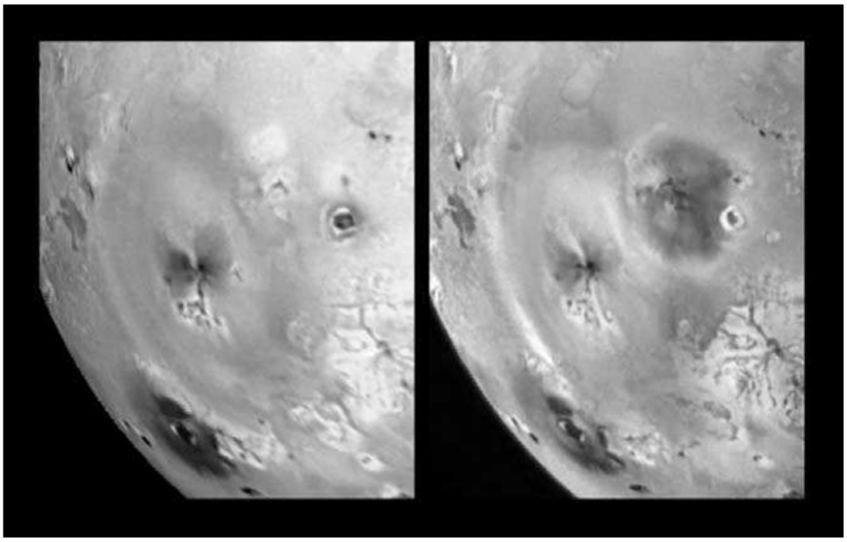

FIGURE 10 Remarkable surface changes on the volcano Pillan Patera observed by Galileo's SSI camera. The image on the left was taken on April 4, 1997, and shows Pillan as a simple caldera on the edge of the red Pele plume fallout deposit. The image on the right, taken on September 19, 1997, shows a circular, dark deposit about 400 km in diameter surrounding the caldera. For a color image, see http://photojournal.jpl.nasa.gov/cgi-bin/PIAGenCatalogPage.pl?PIA00293.

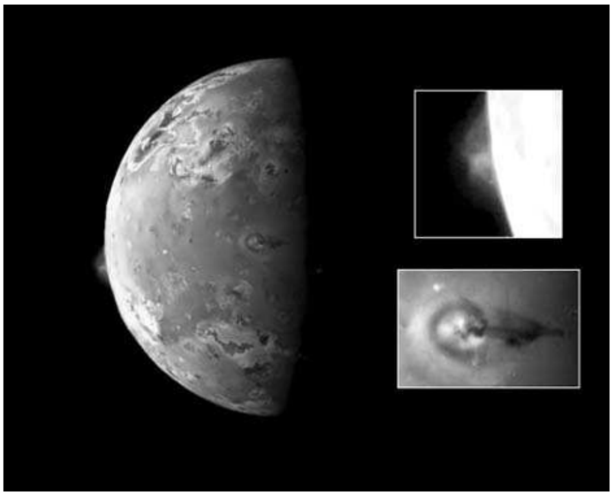

FIGURE 11 Two of Io's volcanic plumes are seen on this image taken by Galileo's camera (SSI) on June 28, 1997. One plume is seen against the bright limb in the larger image and also in the upper inset. This plume rises 120 km above the caldera of Pillan Patera volcano and it was also detected by the Hubble Space Telescope. The second plume in the larger image is seen near the terminator (boundary between day and night) and is being erupted by the Prometheus volcano to a height of about 75 km. The lower inset shows the shadow of this plume extending to the right of the volcano. The vent is near the center of the bright and dark rings. Prometheus was seen by the two Voyager spacecrafts to have an active plume and it is possible that the volcano has been continuously active since 1979. For a color image, see http://photojournal.jpl.nasa.gov/cgi-bin/PIAGenCatalogPage.pl?PIA00703.

camera and NIMS. However, it has decreased in temperature and brightness, implying that activity is declining. Pillan continues to be observed by Galileo's instruments and the waning of its activity may provide clues to the dynamics of all of Io's eruptions.

Impressive as the Pillan eruption was, it is by no means the most energetic that Io can produce. The Loki volcano undergoes major variations in thermal emission, as shown by telescopic observations in the years since Voyager. The most dramatic changes in thermal emission are called "outbursts" and are defined as events having high fluxes and temperatures, and short lifetimes, that cause the total flux from Io at 5 μm to at least double in intensity—one could say that a single outburst "lights up" the whole satellite. Outbursts are relatively rare. J. Spencer and N. Schneider calculated that outbursts occur only about 3% of the time; hence the probability of observing one, either from ground-based telescopes or from a spacecraft, is low.

Outbursts are interpreted as silicate eruptions having a very high eruption rate. The best studied outbursts so far occurred in January 1990 and was observed from a telescope in Hawaii by D. Blaney and colleagues. The outburst is thought to have occurred at the hot spot Loki and it is the only one of these events so far that was observed to significantly cool in a few hours. In the simplest model of the event, Blaney and colleagues assumed that the flux reflected a single temperature and a circular hot spot, which would imply a temperature drop from 1225 to 555 K and a radius increase from 5.4 to 22 km in 2.6 h. This would correspond to a lava flow front speed of a few meters per second.

Io's hot spots commonly vary in brightness in a scale far smaller than that of outbursts. Loki is a common site for brightenings, which typically switch on in less than a month and last for several months before fading. These brightenings have been interpreted as changes in silicate eruption rates, with the fastest rates being considerably greater than those of the Columbia River Basalts. More subtle variations in intensity of hot spots are being studied by the Galileo NIMS instrument. The NIMS monitoring of Io's hot spots has detected variations in hot spot intensity but also shown that, despite variations, the activity of many of the hot spots is extremely persistent, while activity at others appears more sporadic. The combination of Galileo NIMS and SSI data over a period of 2 years showed that 30 of Io's hot spots are active for periods exceeding 1 year. These are classified as "persistent" hot spots, while others, observed active for periods of 3 months or less, are classified as "sporadic," though they might also represent persistent activity at low levels that are rarely detected by Galileo's instruments. Many of the persistent hot spots, such as Loki and Pele, were seen to be active during the Voyager fly-bys and from telescopic observations in the years in between Voyager and Galileo. It is likely that these hot spots remain active for decades and they are likely to represent the major pathways of magma from Io's interior to the surface.

The behavior of persistent-type hot spots can give us a window into the mechanisms involved in the transfer of magma from Io's interior to the surface. It is known that long-lived eruptions on Earth can last for decades. Current examples include the 1983 to present eruption of Pu'u O'o in Hawaii and the 1968 to present eruption of Arenal in Costa Rica. Much longer timescales of activity are known on Earth, up to the 2500 years of nearly continuous activity at Stromboli. "Steady-state" volcanism on Earth occurs when the magma eruption rate is balanced by the magma supply rate and it is likely that this balance is occurring on Io. H. Sigurdsson and R. MacDonald have pointed out that, on Earth, measurements of the magma eruption rate can be used to estimate the minimum magma supply rate. So far, it has been difficult to estimate eruption rates for Io's hot spots because the volume of erupted magma is not known. Observations of Io at close range will give us the opportunity to measure flow sizes and to estimate flow thicknesses, which can then be used to estimate the rate of supply of magma to the surface.

VII. GLOBAL DISTRIBUTION OF VOLCANISM

Detections of hot spots from Voyager, Galileo, and ground-based measurements and observations by J. Goguen and colleagues using the Hubble Space Telescope show that Io's surface is dotted with volcanic activity (Fig. 7). The distribution of hot spots is, to first order, uniform. However, detailed examination of the distribution reveals more significant departures from uniformity. Eclipse images obtained by Galileo's camera showed a field of bright vents near the sub-Jovian point (latitude and longitude 0 on Io) and a glow on the anti-Jovian point (latitude 0, longitude 180) that may be caused by a similar field of bright vents. It is unclear if these are hot spots, because enhanced thermal emission has not been confirmed at these sites and they could be gas vents that, in eclipse, are seen to glow. Another possible departure from uniformity is the hot spot concentration around Bosphorus Regio, as mentioned earlier.

Hot spots are not all the same, as they differ in terms of persistency of activity and energy of thermal emission. Io's most energetic hot spot, Loki, accounts for approximately 25% of Io's heat flow from hot spots. It is significant that the persistent hot spots are concentrated at lower latitudes. Monitoring of Io's active plumes has shown that plumes also occur mainly near the equatorial regions and not at high latitudes. The implication of these findings is that, although volcanic activity occurs all over Io, the bulk of the activity that manifests itself as hot spots and that can be mapped with the currently available instruments is concentrated at lower latitudes rather than nearer the poles. This has important implications for how tidal energy is being dissipated in the interior of Io.

Two basic models have been proposed by M. Segatz and colleagues and M. Ross and colleagues to explain how tidal energy is dissipated in and heats up the interior of Io. Both models assume that convection is the main mode of heat transfer within Io, but differ on where the tidal heating predominantly occurs. If heating occurs mainly in an asthenosphere about 100 km thick, convection should occur globally, with centers of upwelling and downwelling separated by a few hundred kilometers. In the alternative model, tidal heating occurs in the deep mantle and the result is larger scale convection, with a relatively small number of mantle plumes spaced widely apart. The deep mantle model predicts greater heat dissipation toward the poles, while the asthenosphere model predicts greater heat dissipation near the equatorial regions. Although we expect that there are many yet undetected hot spots and "geothermal" regions on Io where heat from the interior is being dissipated and that the hot spots detected so far do not account for all of the heat dissipation, it is also reasonable to assume that the distribution of hot spots detected so far will reflect the dominant form of transfer of heat from the interior to the surface. The fact that the more persistent hot spots, the active plumes, and the most energetic hot spots such as Pele, Pillan, and Loki occur within 30° of the equator supports the asthenosphere tidal dissipation model rather than the deep mantle model. Although the distribution of hot spots cannot prove either model, it provides important observational constraints that any proposed models for Io's internal heating have to address.

VIII. VOLCANIC PLUMES, ATMOSPHERE, AND TORUS

The most spectacular volcanic features on Io are the active plumes that can rise hundreds of kilometers above the surface (Fig. 11). Nine eruption plumes were detected by Voyager 1; eight of these were still active 4 months later when Voyager 2 flew by Io. Galileo has detected 10 active plumes (as of the end of 1998), 4 of which appear to be erupting from the same areas as those detected during Voyager. A total of 15 plumes from different volcanic centers have been observed so far. However, surface changes around other areas known or thought to be active volcanic centers indicate that other plumes may have been active recently. As discussed above, the distribution of active plumes on Io is not uniform, as most plumes are seen within 30° of the equator. All plumes, except for the one observed at Ra Patera, are seen to coincide in location with hot spots. It is possible that there is also a hot spot at Ra, but it has not yet been detected, perhaps because of relatively low temperatures or small spatial extent.

Io's plumes differ in some characteristics. The plumes erupting from the Prometheus and Pele volcanoes are good examples of two different types. The Prometheus plume is lower in height (reaching 50–150 km above the surface) and seems to be very long-lived. It was active during the Voyager encounters and remains active during the Galileo mission; however, the source of the plume migrated about 70 km during the 17 years between spacecraft encounters—or else these are different plumes erupting from the same general region. The Pele plume is significantly fainter than the Prometheus plume at visible wavelengths, reaches higher altitudes—up to 460 km above the surface—and may not be as long-lasting. For example, the plume was not detected 4 months later when Voyager 2 flew by Io.

The fallout deposits from these two types of plumes are also distinct. The Prometheus plume is associated with a bright, white annulus that is probably SO_2 frost, while the deposits from the Pele plume are bright red. Results from Galileo NIMS show that SO_2 is notably absent from the Pele deposits. These differences could imply that sulfur rather than SO_2 is driving the eruptions of the Pele plume, though SO_2 gas has been detected over Pele.

SO_2 not only is common over the surface of Io but also is the major component of Io's tenuous atmosphere. SO_2 and sulfur are probably the volatiles that drive explosive volcanism on Io, as H_2O and CO_2 (the dominant volatiles driving explosive volcanism on Earth) appear to be highly depleted on Io. So far, no definite H_2O or carbonate absorption features have been detected in Io's spectrum, though some results suggest that H_2S may be present on Io.

Early studies of plume emplacement, such as that by R. Strom and N. Schneider, proposed that some of the symmetric "umbrella-like" plume shapes, such as Prometheus, could be explained by models using ballistic trajectories for the particle fallout. Other plumes appeared less simple, perhaps reflecting more complex vent shapes or pressure conditions. Indeed, it is known that the dynamics of Io's plumes are very complex, particularly because models of plume emplacement have to take into account the very low atmospheric pressure on Io (about 10^{-9} bar). S. Kieffer's landmark work in 1982 on the dynamics of Io's plumes discussed possible thermodynamic conditions for the formation of the plumes, which, by comparison with terrestrial conditions, ranged from unusually cold to unusually warm. These conditions correspond to various initial temperatures in the reservoir and to various mixtures of SO_2 and sulfur.

The coldest scenario modeled by Kieffer has liquid SO_2 in a reservoir at temperatures below the liquidus temperature of sulfur (393 K). In this model, the liquid SO_2 in a shallow crustal reservoir begins ascending due to buoyancy and starts "boiling" as it approaches the surface. As it erupts, a plume of vapor and ice condensate forms as the fluid emerges into the cold, low-pressure atmosphere of Io. At slightly higher initial temperatures, the SO_2 boils in the reservoir and also as it ascends toward the surface. Both these scenarios produce a change in the SO_2 from liquid to vapor to ice. In a different scenario, SO_2 vapor coexists with sulfur in a reservoir that has an initial temperature equal to the liquidus temperature of sulfur. In higher temperature scenarios (such as if the reservoir is close to a body of silicate magma), either SO_2 or sulfur exists in a superheated vapor state. The resulting plumes from these "hot" reservoirs consist mostly of gas. Because they may be difficult to detect from images, they have been called "stealth plumes" (discussed below).

Modeling Io's plumes involves not only the thermodynamic considerations, as described above, but also the fluid dynamics of the plume emplacement. Recent work by Kieffer involves numerical simulations varying initial conditions such as temperature, the mass fraction of gas versus particles, and initial pressure. One particularly interesting early result is that pyroclastic flows may form on Io. Previous studies assumed that pyroclastic flows would not form on Io because of the very tenuous atmosphere. However, Kieffer's simulations have shown that plumes that are rich in volatiles can create their own local atmospheric conditions, in which fountain collapse to form pyroclastic flows becomes possible. The activity from Io's plumes feeds its tenuous atmosphere. The low pressure of Io's atmosphere is equivalent to good laboratory vacumms on Earth, although, as Kieffer's work has demonstrated, the local atmosphere near volcanic vents can be higher. The principal constituent of Io's atmosphere is SO_2, but SO has been detected and other species, such as O_2, have been suggested. A major question is, where is the SO_2—and hence the atmosphere—coming from? There are two possible sources for the SO_2 in the atmosphere, and probably both sources are important. The first is from evaporation of the SO_2 frost deposits on Io's surface, but recent studies, including observations of Io at millimeter wavelengths by E. Lellouch and colleagues, show that this mechanism has a minor role. The bulk of the atmospheric SO_2 is thought to be supplied by Io's volcanic activity. Observations in the ultraviolet wavelengths using the Hubble Space Telescope have shown that Io's atmosphere is patchy, very thin, and tenuous over most of the planet but that the density increases at some locations, such as Pele, where SO_2 is being supplied by the volcanoes. Therefore, Io's volcanic activity plays a major role in supplying Io's atmosphere, though some contribution from SO_2 frost deposits is also expected.

The observations of Io's atmosphere at millimeter wavelengths posed a new question about Io: explaining the amount of SO_2 gas detected would require about 30–50 large plumes to be erupting at one time. Since Voyager had only detected nine, the question of "missing plumes" arose. Spacecraft observations detect plumes because sunlight is scattered by the small particles of SO_2 within the plumes. Torrence Johnson and colleagues proposed the existence of stealth plumes, that is, plumes composed almost entirely of gas, which would be hard to detect, but that Kieffer's modeling work suggested to be possible. These plumes are thought to occur when a hot, molten silicate intrusion encounters a reservoir of liquid SO_2 buried at depths of at least 1.5 km. The high temperature and pressure at the subsurface (>1400 K, >40 bars) result in an eruption that is geyser-like, in which particles do not form through condensation. The existence of stealth plumes has been supported by Galileo observations, including those from the camera. The plume over the hot spot Acala is not seen in sunlight, presumably because of lack of particles in the plume, but it can be seen in observations of Io in eclipse, in which the gas appears to glow.

What happens to the gases erupted by the plumes? It turns out that only a relatively minor amount of atmospheric gas is lost to space. The temperatures of the frost deposits on Io's surface are sufficiently low (around 100–110 K) that cold-trapping of SO_2 by condensation is a very important process. However, some material does escape Io, forming a corona and neutral clouds near Io and the Io torus further away. The corona refers to the region within Io's gravitational pull, where bound and escaping atoms and molecules populate a low-density shell. The neutral clouds of sodium, oxygen, and sulfur extend from the corona to distances of many times the radius of Jupiter. The Io torus is a doughnut-shaped trail along Io's orbital path, made up almost exclusively of various charged states of sulfur and oxygen, thought to be derived from the breakup of volcanic SO_2 and S_2. The ionized particles are held within the torus by Jupiter's magnetic field, in a similar way to the mechanism that holds charged particles in the Van Allen radiation belts around the Earth.

The most easily observed of the neutral clouds is the sodium cloud. The cloud is populated by sodium atoms escaping Io at about 2.6 km s^{-1}. The existence of this cloud places an important constraint on the composition of Io: no sodium has yet been detected on Io's surface or atmosphere, but since the atoms are escaping Io, sodium must be present. Neutral clouds of oxygen and sulfur are also seen, but they are faint compared to the sodium cloud and these species have been detected on Io's surface and atmosphere. Where the sodium is coming from remains one of the most puzzling questions about Io.

IX. FUTURE STUDIES

At the time of writing, Galileo is still monitoring Io's volcanoes and the highest resolution observations have not yet been made. The close fly-bys of Io are expected to provide a wealth of totally new information about this intriguing volcanic world. Our current plans are to have three fly-bys, in October 1999, December 1999, and February 2000. These fly-bys will bring Galileo within about 500 km of Io's surface, the first time near the equator, the second over the south pole, and the third over the northern hemisphere. The equatorial pass will provide the opportunity to measure the high magma temperatures of Pele and Pillan from close range. Our goal is to measure temperatures with both the NIMS instrument and the SSI camera, to try to constrain what the maximum lava temperature is. The polar pass will be important to determine if Io has its own self-sustained magnetic field. Galileo images are expected to reveal details of the surface and of the volcanic flows that, together with the spectral data from NIMS, can reveal the composition of Io's lavas, their temperatures, and emplacement mechanisms. Measurements of Io's heat flow by NIMS and by the Photopolarimeter Radiometer (PRR), an instrument that can observe at longer wavelengths and therefore detect lower temperatures than NIMS, will provide tighter measurements on Io's total heat flow. Other areas to be investigated using the close-range observations are the dynamics of plumes, the composition and origin of the mountains, and the composition of the polar volatiles.

If the fly-bys are successful, the observations returned to Earth will not doubt provide the answers to many of the outstanding questions. However, much more could still be learned from future missions, from observations from Earth, and from Earth's orbit. Galileo will only be able to observe a very small part of the surface at high resolution and Io is a dynamic, constantly changing world. Even after Galileo's fly-bys are completed, much will remain for future missions to explore.

SEE ALSO THE FOLLOWING ARTICLES

Calderas • Cryovolcanism in the Outer Solar System • Volcanic Plumes • Volcanism on Mars • Volcanism on the Moon • Volcanism on Venus

FURTHER READING

Carlson, R. W., Smythe, W. D., Lopes-Gautier, R., Davies, A. G., Kamp, L. W., Mosher, J. A., Soderblom, L. A., Leader, F. E., Mehlman, R., Clark, R. N., and Fanale, F. P. (1997). The distribution of sulfur dioxide and other infrared absorbers on the surface of Io in 1997. *Geophys. Res. Lett.* **24,** 2479–2482.

Carr, M. H., McEwen, A. S., Howard, K. A., Chuang, F. C., Thomas, P., Schuster, P., Oberst, J., Neukum, G., Schubert, G., and the Galileo SSI Team. (1998). Mountains and calderas on Io: Possible implications for lithosphere structure and magma generation. *Icarus* **135,** 146–165.

Geissler, P. E., McEwen, A. S., Keszthelyi, L., Lopes-Gautier, R., Granahan, J., Simonelli, D. P. (1999). Global color variations on Io. *Icarus,* **140,** in press.

Johnson, T. V., Matson, D. L., Blaney, D. L., Veeder, G. J., and Davies, A. G. (1995). Stealth plumes on Io. *Geophys. Res. Lett.* **22,** 3293–3296.

Johnson, T. V. (1999). Pages 241–252 *in* Io. "The New Solar System," 4th ed. (J. K. Beatty, C. C. Petersen, and A. Chaikin, eds.).

Kesztheyi, L., and McEwen, A. (1997). Magmatic differentiation of Io. *Icarus* **130,** 437–448.

Kieffer, S. W. (1982). Dynamics and thermodynamics of volcanic eruptions: Implications for the plumes of Io. Pages 647–723 *in* "Satellites of Jupiter" (D. Morrison, ed.). Univ. of Arizona Press, Tucson.

Lellouch, E., Belton, M. J. S., DePater, I., Paubert, G., Gulkis, S., and Encrenaz, T. (1992). The structure, stability, and global distribution of Io's atmosphere. *Icarus* **98,** 271–295.

Lopes-Gautier, R. (1993). Extraterrestrial lava flows. Pages 103–139 *in* "Active Lavas: Monitoring and Control" (C. R. J. Kilburn and G. Luongo, eds.). University College Press, London.

Lopes-Gautier, R., Davies, A. G., Carlson, R., Smythe, W., Kamp, L., Soderblom, L., Leader, F. E., Mehlman, R., and the Galileo NIMS Team. (1997). Hot spots on Io: Initial results from the Galileo Near-Infrared Mapping Spectrometer. *Geophys. Res. Lett.* **24,** 2439–2442.

Lopes-Gautier, R., McEwen, A. S., Smythe, W. D., Geissler, P. E., Kamp, L., Davies, A. G., Spencer, J. R., Keszthelyi, L., Carlson, R., Leader, F. E., Mehlman, R., Soderblom, L., and the Galileo NIMS and SSI Teams. (1999). Active volcanism on Io: Global distribution and variations in activity. *Icarus,* **140,** in press.

Matson, D. L., and Blaney, D. L. (1998). Io. *In* "Encyclopedia of the Solar System" (P. Weissman, L. McFadden, and T. V. Johnson, eds.). Academic Press, San Diego.

McEwen, A. S., *et al.* (1998). Active volcanism as seen by Galileo SSI. *Icarus* **135,** 181–219.

McEwen, A. S., *et al.* (1998). Very high temperature volcanism on Jupiter's moon Io. *Science* **281,** 87–90.

McEwen, A. S., Lopes-Gautier, R., Keszthelyi, L., and Kieffer, S. W. (1999). Extreme volcanism on Jupiter's moon Io. *In* "Environmental Effects on Volcanic Eruptions: From deep oceans to deep space" (J. Zimbelman and T. Gregg, eds.). Plenum, New York, in press.

Nelson, R. M. (1997). Io. Pages 345–351 *in* "Encyclopedia of Planetary Sciences" (J. H. Shirely and R. W. Fairbridge, eds.). Chapman & Hall, London/New York.

Peale, S. J., Cassen, P., and Reynolds, R. T. (1979). Melting of Io by tidal dissipation. *Science* **203,** 892–894.

Ross, M. N., Schubert, G., Spohn, T., and Gaskell, R. W. (1990). Internal structure of Io and the global distribution of its topography. *Icarus* **85,** 309–325.

Spencer, J. R., and Schneider, N. M. (1996). Io on the eve of the Galileo mission. *Annu. Rev. Earth Planet. Sci.* **24,** 125–190.

Spencer, J. R., Stansbery, J. A., Dumas, C., Vakil, D., Pregler, R., and Hicks, M. (1997). A history of high-temperature Io volcanism, February 1995 to May 1997. *Geophys. Res. Lett.* **24,** 2451–2454.

Veeder, G. J., Matson, D. L., Johnson, T. V., Blaney, D. L., and Goguen, J. D. (1994). Io's heat flow from infrared radiometry: 1983–1993. *J. Geophys. Res., Planets* **99,** 17095–17162.

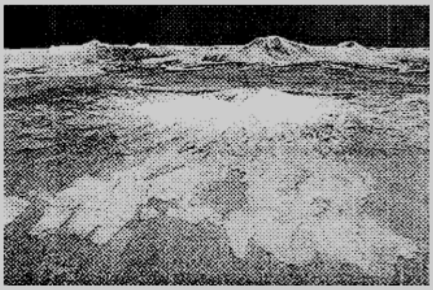

VOLCANISM ON VENUS

L. S. CRUMPLER
JAYNE C. AUBELE
New Mexico Museum of Natural History and Science

> "Venus is a volcanologist's paradise . . .
> and a structural geologist's nightmare."
> —*John Guest, Magellan mission team, 1991*

- I. Definition and Significance of Venus Volcanism
- II. Volcanic Landforms
- III. Factors Influencing Volcanic Eruptions and Volcanic Landforms on Venus
- IV. Future Directions

GLOSSARY

arachnoids Annular structural patterns consisting of concentric or circular pattern of fractures or ridges with radial arrays of fractures or ridges extending outward for several radii and interior flows and small shield volcanoes. The radial fractures frequently merge outward with the linear patterns of the fracture belts on which arachnoids are arranged. The term "arachnoid" derives from this arrangement, like spiders along "webs" of linear fracture belts. The radial patterns are more strongly developed; otherwise arachnoids are similar to coronae.

canali A planetary physiographic term for long sinuous channels, most of which on Venus are thought to be lava channels although the fluid from which they formed is not known.

chasma (pl., chasmata) A planetary physiographic term for a deep, linear valley with steep sides.

colles A planetary physiographic term for a cluster of small hills or volcanoes.

corona (pl., coronae) Dominantly circular or elliptical structures consisting of an annulus of concentric ridges or fractures, an interior that may be topographically positive, a peripheral moat or trough, and, frequently, numerous volcanic centers and tectonic landforms in the interior. Coronae may be associated with mantle plumes or hot spots; related volcanism, in the form of large and small volcanoes, is frequently present within the corona or on its margins.

farrum (pl. farra) A planetary physiographic term for a type of volcano (all of which are less than 100 km in diameter) with a steep perimeter slope and relatively low angle flanks; also referred to as "pancake" domes.

flow field An area covered by numerous individual lava flows, usually digitate, either fan-shaped or uniformly directed patterns down regional slopes and covering large areas.

fluctus (pl. flucti) A planetary physiographic term for a large lava flow field.

fluted dome (also, "modified dome") A type of intermediate size-range volcano characterized by steep margins, flat or broadly concave top or small summit crater, and, usually radiating, ridges or scalloped margins.

intermediate volcano On Venus, centers of volcanic accumulation between 20 and 100 km in diameter are consid-

Copyright © 2000 by Academic Press
All rights of reproduction in any form reserved.

ered "intermediate" compared to small shields and cones (which are <20 km) and the more prominent large volcanoes that are generally several hundred kilometers in diameter. This usage was originally defined from the mapping of the northern one-quarter of Venus by the Russian Venera 15/16 radar-mapping mission.

large volcano On Venus, centers of volcanic accumulation characterized by radially dispersed lava flows and diameters larger than 100 km, frequently associated with concentric or circular central features and radial fracture patterns and centered on a region of positive topography as indicated either by radial lava flows, by topography inferred from radar characteristics of slopes, or by altimetric radar observations.

magmatic center Refers to any center of deformation interpreted to be fundamentally magmatic in origin and in which any eruptive morphologies are subsidiary to larger scale concentrated structural deformation.

patera (pl., paterae) A planetary physiographic term for an irregular depression. The term is frequently applied to calderas but, as used on Venus, may include some arachnoids, coronae, and some large volcanoes.

SAR (synthetic aperture radar) A type of radar that illuminate a surface with radar energy in directions at right angles to the antenna (spacecraft) motion to build up "images" of the surface.

shield fields Localized concentrations of small (less than 20 km), dominantly shield-shaped volcanoes. The individual morphology of each small shield in Magellan data is variable but commonly consists of a low and conical to domelike edifice frequently surmounted by a pit.

small shield Small shield volcano; a characteristic morphology of most of the smaller volcanoes on Venus. Sometimes used loosely to refer to any small volcano on Venus, although many small volcanoes include other morphologies, such as steep-sided domes and steep cones.

small volcano On Venus, any volcano less than 20 km in diameter. Includes shield, cones, and domes.

steep-sided dome A circular, small to intermediate size range volcano on Venus characterized by flat, domical, or distinctly steep margins; broad, flat-topped examples with steep margins are also referred to as "pancake domes."

radial fracture center A magmatic center in which a pattern of fractures radiates from a common center; annular or circular fractures may be present but are subordinate. They are interpreted to be the surface expression of radiating, shallow dikes, possibly analogous to giant radiating dike swarms that are known to occur on Earth.

tessera (pl., tesserae) Complexly fractured, and frequently elevated, terrain characterized by a mosaic-like pattern of pervasive orthogonal fractures, ridges, and troughs. Tesserae are identified as the oldest preserved surfaces on Venus; include most of the large, continent-like elevated areas that constitute ~15% of the surface of Venus; and are frequently embayed or covered by later volcanic plains and individual volcanic centers.

tholus (pl., tholi) A planetary physiographic term usually referring to an upper size range of intermediate volcano in which the flanks appear steep relative to most volcanoes on Venus.

I. DEFINITION AND SIGNIFICANCE OF VENUS VOLCANISM

IN TERMS OF the absolute number of volcanoes on its surface, Venus is second only to Earth. It exceeds Earth and Mars combined in terms of the absolute number of well-preserved and pristine volcanic landforms. This abundance of volcanoes is a reflection of the Earth-like size of Venus. The magnitude and longevity of the geologic activity and volcanism on any planet are related to the planetary size and density, unless there are unusual circumstances. (For example, the strong tidal forces that act on Io, a satellite of Jupiter, maintain active volcanism there even though Io is similar in size to the Moon.) Venus is only ~330 km smaller in diameter than Earth and is similar in density. Venus is therefore the most Earth-like of all the planets in terms of its bulk composition and potential chemistry of its magmas. The geological complexity and young surface ages of both Venus and Earth may be attributed to their more dynamic thermal evolution relative to smaller terrestrial planets, their warmer and more mobile interiors, and corresponding surface deformation (tectonism) and copious production of mantle melts (volcanism) over extended periods of geological time.

The style of volcanism on Venus differs from that on Earth, however. This fact was unknown prior to 1983 when the Russian Venera 15/16 radar-mapping mission mapped the northern quarter of Venus and the early nineties when the U.S. Magellan synthetic aperture radar mission mapped Venus globally at even higher resolutions. Early results from planetary mission data showed that the presence and type of global volcanism on most planets are sensitive to the dominant mode in which internal heat is transferred to the surface. Heat transfer and volcanism on Earth are dominated by plate tectonics in which broad convection, upwelling of mantle at spreading ridges, and sinking of cold plates at subduction zones liberates much of the heat from the interior. In the process, volcanism is generated at the plate boundaries. Other planets appear not to be dominated by plate tectonics, but by a style of volcanism characteristic of the intraplate hot spots on Earth. In this style, referred to as "hot spot tectonics," heat is released in isolated volcanoes distributed over the surface and by normal conduction through the lithosphere rather than large-scale convection and sinking of cold slabs of lithosphere.

The great size and complexity of volcanic and magmatic centers on Venus provides insights into the processes of large magmatic provinces. They are records of the subtle and little appreciated details of the character, magnitude, and timing of deformation arising from regional scales of magma emplacement and the corresponding details of surface eruptions. It is likely that many of the characteristics of large magmatic provinces on Venus also occur on Earth but are not recognized because of the unanticipated large scale of influences on surrounding terrains and because they are not well preserved or easily identifiable. These may not be available for study on Earth because they are continually erased by erosion almost literally as fast as they form.

Another advantage of studying volcanic phenomena on other planets is that it forces volcanologists to consider a range of processes and mechanism not readily apparent on Earth. This results in further insight into volcanic processes and directions of investigation not otherwise anticipated from studies on Earth alone. For example, radial fractures and/or concentric fractures are typical of almost all magmatic and volcanic centers on Venus. Similar deformation may occur on Earth but is generally poorly preserved or erased during the lifetime of the volcanic activity. Given the curatorial preservation of volcanic landforms in the dry, CO_2 atmosphere and the great abundance of examples, Venus offers an opportunity to better understand the details of surface deformation associated with shallow magma bodies. An excellent example of this is the interpretation that radial fracture centers may represent radial dike swarms. On Earth, the only recognized examples of radial dike swarms are deeply eroded; any connection with surface deformation that they may have had is no longer available for study. Even the suggestion that radial fracture patterns may be dike swarms, by terrestrial volcanology standards prior to the Magellan mission, might have been viewed as folly, particularly given that they extend over thousands of kilometers. Yet the case can be made on the basis of Venus data that, in the absence of erosion, shallowly emplaced dikes may have a significant surface expression and that dikes may propagate horizontally over extreme distances from large and shallow magmatic sources.

A. Basic Venus Data

Despite the large-scale similarity to Earth, surface conditions on Venus differ greatly from those on Earth. This has potential influences on the eruption styles and morphology of volcanism as well as fundamental geologic processes. If Venus is a volcanological paradise and a tectonic nightmare, it is also an environmental infernal region that belies the harmony, peace, and beauty that the planet's name implies. The atmospheric surface pressure is nearly 100 times that of Earth (or equivalent to pressures at about 1-km depth in the sea), and surface temperatures are hot enough to melt lead (700 K) and hot enough to potentially increase long-term rates of geological strain in areas of high, mountainous relief. The atmosphere consists mostly of carbon dioxide (~97%), capped with clouds (from 45- to 60-km altitude above the surface) consisting not of water vapor but instead sulfuric acid droplets. These clouds are thick and unbroken and perpetually obscure the surface from Earth or orbital spacecraft observation at optical wavelengths. From the surface one would see not a uniformly blue sky, as on Earth, but a glowing yellowish-white sky. (The Russian scientist Alexander Basilevsky has described being on the surface as probably like "being inside a giant fluorescent light bulb.") It is believed that these non-Earth-like characteristics are a consequence of a "runaway greenhouse effect," a condition first recognized from study of Venus and now frequently used to describe potential environmental problems associated with industrial additions to the atmosphere of Earth.

Venus differs from Earth in several other large-scale characteristics. It is the only major planet that does not have a satellite. Its rotation is retrograde, and a single day is 243.0185 ± 0.0001 Earth-days long. Also unlike Earth, if a magnetic field exists, it is below current detection limits. An extremely weak or nonexistent magnetic field may be a consequence of slow rotation on the circulation necessary to excite a magnetic dynamo in the core, or it could result from fundamental differences in the core composition or size.

Although many of these basic facts were known prior to the Magellan mission, little was actually known about the geological characteristics of the surface or the presence, number, or morphology of its volcanoes. Despite its proximity and overall similarity in dimension to Earth, Venus was the last planet in the inner solar system to be explored geologically. Not only did the dense, opaque atmosphere, extreme pressures, and high surface temperature prevent observation of the surface from a distance, but the extreme surface environment rendered it technologically challenging to design surface landers that could survive long enough to take meaningful measurements with surface instruments. Assessment of the geologic details of volcanism on Venus required the development of Earth-based radar-observing techniques and, later, synthetic aperture radar (SAR) technology on orbiting spacecraft. The latter had to await the funding, construction, transport, and multiyear operation in Venus orbit of a modern spacecraft with radar-imaging capabilities. Ironically, with radar, the surface of Venus is now more completely and uniformly mapped, and at higher resolution, than the seafloor of Earth.

Prior to the availability of high-resolution radar surface images, several lines of evidence suggested that volcanoes might be common on Venus. First, because of the size similarity between Venus and Earth and the overall similarity to Earth in density characteristics and position in the solar system, similar elemental abundances and internal heat sources seemed likely. This implied that the two planets were likely to have had an essentially similar thermal history involving long-lived interior melting, magma production, and surface volcanism. Second, Earth-based radar images of the surface of Venus, and later global altimetric maps, indicated that numerous circular features and symmetric mountains were associated with large-scale valleys bearing tectonic riftlike characteristics of length, width, depth, and distribution. Third, telescopic observation with spectroscopic methods in the late seventies had shown an anomalous short-time scale global change in the sulfur content and related compositions of the atmosphere. The most likely interpretation was that a large volcanic eruption had injected volcanic dust and sulfur-rich gases into the upper atmosphere, as frequently happens with large explosive eruptions on Earth (e.g., the Mount Pinatubo eruption in the Philippines, 1991). Another possibly transient and localized variation in atmospheric composition was detected by one of the atmospheric entry probes of the Pioneer Venus mission in the late seventies and interpreted as being potentially the result of a similar large eruption. Both events require extremely energetic eruptions, which are relatively rare on Earth, but must be particularly rare on Venus given that the high atmospheric pressure is likely to greatly suppress explosive volcanism for all but the most volatile-enriched cases. These early observations of atmosphere-related changes associated with eruptions suggested that not only was currently active volcanism possible, but that the physical products of volcanism were likely to be common on the surface of Venus as well.

Observations from the Magellan radar-mapping mission show that volcanism on Venus is morphologically diverse and appears to represent a wide range of scales and potential rates of magmatic, tectonic, and mantle convective processes. The great range in scales of volcanic centers and associated lava flows on Venus implies that central volcanism and volcanic effusion on Venus are associated with a large range of volume scales of magma transport, storage, and emplacement in the lithosphere. These may be evidence for variable scales of associated mantle convection and melting processes.

B. Previous Observation and Knowledge

In the following we set forth some of the basic observations on which our current understanding of Venus is based. This discussion is not intended to be an exhaustive review, for which there are several volumes listed in the bibliography.

Prior to the first spacecraft fly-bys, passive observations of the thermal microwave emission from Venus using radio telescopes suggested that the surface temperatures were in excess of several hundred kelvin. Later U.S. (including Mariner 2, in 1962, the first interplanetary mission) and Soviet fly-bys, atmospheric entry probes, Soviet Venera and Vega landers, and Vega balloon mission observations confirmed these conditions. However, very little was known about the actual regional surface characteristics of Venus, including the presence or morphology of volcanic centers. Almost nothing was known about the geologic characteristics prior to the early development of interplanetary spacecraft and modern Earth-based radar observations, chiefly from the Goldstone and Arecibo radio telescopes. Radar technology and spacecraft technology paced each other in resolution, with alternately Earth-based and spacecraft-based observations bearing the highest resolution information.

The first global view was obtained at relatively low resolutions (on the order of 100 km) during the Pioneer Venus mission beginning in 1978. The Pioneer Venus mission obtained a global map of altimetry and global thermal emissivity characteristics at low resolution. The Soviet interplanetary space program repeatedly placed landers on Venus (Venera 8, 9, 10, 13, and 14 and Vegas 1 and 2). The missions were able to characterize the surface at lander scales with optical images and chemical analyses, proving that at least those areas observed by landers are fundamentally basaltic surfaces. They also directly measured and confirmed the previous estimates of high surface temperature (700 K), high atmospheric pressures (9 MPa, or 90 atm), and a water-free, dominantly carbon dioxide atmosphere. Optical images taken by the Venera landers are unrevealing as regards the origin of the surface materials. Generally, they showed moderately flat terrain characterized by local soil patches between flat "outcrops" of dark, more consolidated material. The chemical compositions of most of the surface materials are similar tholeiites. One site (Venera 8) suggested the possibility of more evolved, alkali-rich (e.g., trachytic) compositions. Another site (Venera 13) measured compositions essentially similar to alkali basalts. In contrast, Vega 1 identified a much more mafic composition comparable to gabbroic materials and Vega 2 measured a sulfur-enriched surface composition.

Synthetic aperture radar (SAR) images from the Russian Venera 15/16 spacecraft of the northern 25% of the surface of Venus initially demonstrated the morphologic diversity of volcanic centers on Venus, including large volcanoes characterized by patterns of flows radiating for tens to hundreds of kilometers, circular structural patterns up to several hundred kilometers across with associated volcanism (coronae), patterns of lava flow fields, extensive low-lying regions of lava plains, and low-relief domical edifices, many less than several kilometers in diameter that are interpreted to represent globally abundant small shield volcanoes. The division of volcanic centers into "large" (>100 km), "intermediate" (20–100 km), and "small" (<20 km) was based on the Venera 15/16 results and is still in use.

SAR images, radar altimetry, and radiometry data from the Magellan spacecraft were acquired beginning in late 1990 and continued through several global mapping cycles through late 1992. During each cycle Venus rotated once beneath the orbital plane of the spacecraft every 243 days. The spacecraft was in a near-polar orbit, allowing it to image the surface in near-longitudinal strips. Image data were acquired at resolutions of 300 m. For Magellan, each strip was 20 km wide and 17,000 km long. The results of many orbital passes were mosaicked to form broader images, ultimately covering 97% of the surface. Most of the imaged areas are now available on CD-ROM as F-MAPs, that is, full-resolution image mosaics of broad areas of the surface in which the stripes are rarely visible because they have been digitally processed and blended. For a general account of this mission, its results, and our current knowledge about Venus, the reader should refer to the reference works by Bougher *et al.* (1997), Cattermole (1994), Cooper (1993), and the special Magellan issue of the *Journal of Geophysical Research* listed in the bibliography.

In interpreting Magellan images, it is important to note that, because these are not optical images, they have some unique characteristics. SAR is a type of radar that illuminates a surface with radar energy in directions at right angles to the antenna (spacecraft) motion to build up "images" of the surface.

Magellan also acquired altimetric data. These may either be viewed as separate profile tracks across features of interest or combined spatially in map view as color-coded, contoured, or shaded relief maps. There are additional data products, including maps of radar emissivity, radar reflectivity, and radar roughness, but the products described above are the primary ones that are likely to be encountered most frequently.

II. VOLCANIC LANDFORMS

Initial surveys and analysis of Venera 15/16 and Magellan data identified numerous morphologically varied volcanic centers and edifices from small shields less than 1 km in diameter to volcanic edifices greater than 1000 km in diameter and widespread plains-type volcanism with associated lava flows from those less than several kilometers long to vast flow fields, lava floods, and lava channels in excess of 1000 km long. The great abundance of youthful volcanic features and the observed relatively low global crater abundance over the surface imply that global rates of resurfacing due to volcanism on Venus over late solar system history have been high relative to the smaller terrestrial planets.

Several specific types of volcanic center identified from Magellan data include (1) effusive edifices such as small shield volcanoes, low to steep-sided intermediate volcanoes of differing morphology similar to, but much larger than, terrestrial volcanic domes, and large volcanic edifices of low relief and complex structure; (2) centers identified by structural characteristics and relatively minor effusive characteristics; and (3) negative topographic expressions such as calderas and complex topographic annular features such as coronae and arachnoids. Many of these structurally defined annular features are generally thought to represent local formation of large and deep magma reservoirs or diapiric upwellings and evidence for shallow to deep, dikelike magma intrusions such as stellate fracture patterns. The structural and volcanic characteristics of coronae, and related features such as arachnoids, are consistent with origins related to hot spots or underlying mantle plumes, although nothing similar is preserved on Earth.

A. Distribution of Volcanic Centers

We have identified and cataloged 1738 volcanic centers, magmatic centers, coronae, and related features (Table I) larger than 20 km (as well as significant lava flow

TABLE 1. Classification, Location, Dimensions, and Existing Names of All Volcanic Centers on Venus Larger Than 20 km in Diameter

Latitude (deg)	*Longitude (deg)*	*Diameter (km)*	*Name*
		Large volcanoes	
80	260	250	—
76	235	300	Renpet Mons
71.5	256	700	Metis Regio
71	140	100	—
66	323	600	Colette Patera
65.5	279	600 × 300	Feronia Corona
63.5	88	300	—
63	120	300	Melia Mons
60	108	600	Fakohotu Corona
57.5	255	500	Mokosha Mons
53	98	150	Amra Tholus
52.5	267.5	450–500	Atira Mons
51	125	<300	Jael Mons
50	21.5	300	—
48	97	400	Hiei Chu Patera
48	7	>300	—
48	314.5	150	—
47	335.5	160	—
46	212	200	—
46	162	150	—
45	185	150	—
44	240.5	400	Sekmet Mons
40.5	8.5	100	—
40.5	245	400	—
40	206	150	—
40	203	130	—
39	223	450	—
39	208	100	Wurunsemu Tholus(?)
38.5	55	400	Api Mons
38	342	225	Evaki Tholus
37	257	600	—
36.5	308	130	—
36	236	350–400	Furki Tholus
35.5	211.5	400	—
35	277	200	—
35	219.5	500	—
34	246	200	—
33	206.5	150	—
32	244.5	150	—
30	48.5	800 × 600	—
30	45	400 × 300	Tepev Mons
30	265.5	100	—
29.5	355	300	Toci Tholus
29	45.5	600	Otafuku Tholi
28.5	326.5	110	—
28	65	500	Hatshepsut Patera
28	241.5	300	—
26	208	400	—
25.5	198	180	—
25	224.5	150	—
24.5	264	600	—
24	6.5	250	—
24	280.5	1000	Theodora Patera
22	84	400–500	Ereshkigal Corona
22	359	800	Gula Mons
22	352	600	Sif Mons
22	344.5	100	—
21	20	500	—
19.5	344	100	—
19.5	154	900	—
19	80	600	Kunlid Corona
18.5	38	700	—
18.5	303	180	—
18.5	211	500	—
18	303.5	200	—
18	163	200	—
17	194	600	—
16.5	260	400	—
16	69	500	—
14.5	15.5	500	Sappho Patera
14	39	700 × 900	Paulova Corona
14	340	400	—
14	247.5	150	—
14	241	500	—
14	205	500	—
13.5	274.5	250	—
13	211	100 × 80	—
12	226	450	—
11	14.5	600–800	Anala Mons
10	274.5	500	Tuulikki Mons
10	261.5	600	—
10	201	150	—
9.5	348.5	300	Somagalags Corona
9.5	308.5		—
9.5	209.5	300	—
9	29	500	—
9	219.5	150	—
9	188	600	Sapas Mons
9	171.5	500	—
8.5	255.5	200	—
7	208	300	—
7	158	150	—
4.5	207.5	400	—
4	322	400	—
4	199.5	1000	Ozza Mons
3.5	270	400	Xochiquetzal Mons
3	81.5	100–150	Habonda Corona

continues

Continued

Latitude (deg)	*Longitude (deg)*	*Diameter (km)*	*Name*	*Latitude (deg)*	*Longitude (deg)*	*Diameter (km)*	*Name*
3	332	150	—	−33.5	318	300	Nepthys Mons
2.5	45.5	300	—	−34	86	800+	Kokyang Wuti Mons
2.5	314	200–250	—	−34.5	328.5	450	Innini Mons
2.5	301.5	450	—	−35	226	100	—
2	316	800	—	−38	270	500	—
2	198	400	—	−38.5	303	750	Tefnut Mons
1.5	222	600	—	−39	324.5	700	Hathor Mons
1	194.5	500	Maat Mons	−39.5	296.5	600	Rohina Tholus
0	34	>400	—	−42	279	700 × 500	—
0	288	300	—	−43	28	150	Shiwanokia Corona
−1.5	203.5	400	—	−43	258	200	—
−2	256.5	225	—	−43.5	321.5	150	—
−2	194	500	—	−43.5	309	500	—
−2.5	290.5	150	—	−45	274	300 × 225	—
−3	153	350	Seia Corona	−45.5	294	300	Chloris Mons
−6	172.5	100	—	−45.5	287	450	—
−6.5	295.5	300	—	−46.5	215	350	Imdr Regio
−7.5	221	600	—	−52	283.5	250	—
−8	243	500	Pasom Mana Mons	−58.5	351	100+ radius	—
−9	305.5	250	—	−69	90	350	—
−9	224.5	400	—	−70	0	600	—
−9	214	550	—			**Intermediate volcanoes**	
−11	355.5	200	—	57.5	264	40	—
−11	211.5	500	—	47	221	40	—
−11	173	600	—	45.5	329.5	25	—
−12	251	500	—	35.5	317.5	90	—
−12.5	261.5	500	—	29	25.5	50	—
−13.5	305.5	110	Vupar Tholus	33.5	231	20	—
−14	164	600	Miralaidji Corona	33.5	231	20	—
−15.5	215	400	Tsityostinako Mons	33.5	231	20	—
−16.5	255	400	—	32.5	310.5	95	—
−16.5	208	450	—	23.5	255	20	—
−17	214.5	500 × 250	—	20	339	80	—
−17.5	244	600	—	17.5	96.5	25	—
−18	285	500	—	14	133	20	—
−18	259	500	—	13.5	78	80	—
−18.5	292.5	300 × 220	—	10.5	312.5	60	—
−19.5	345	200	Qetesh Corona?	10.5	270	80	—
−20.5	273	200	—	10.5	270	30	—
−20.5	212	250	—	10.5	270	25	—
−21.5	238.5	120	—	10	26	40	—
−22	291	250	—	7.5	311	30	—
−24.5	177	400	—	6.5	328	75	—
−25	323.5	300 × 500	Ushas Mons	5.5	309	40	—
−26	247	250	—	−3	238	20	—
−27.5	262	500	—	−7.5	324.5	25	—
−28	281	500	Uretsete Mons	−9	294	60	—
−28.5	296.5	250	Justitia Tholus	−10	312.5	80	—
−31.5	228	200	—	−10	301	60	—
−32	100	300	—	−13.5	315.5	90	—

continues

Continued

Latitude (deg)	Longitude (deg)	Diameter (km)	Name
−14	286.5	20	—
−14	252.5	30	—
−14.5	286	30	—
−16.5	244.5	35	—
−18	154.5	60	—
−20.5	94.5	20	—
−21	231.5	20	—
−22	202	30	—
−29	249.5	30	—
−29	221.5	30	—
−30	213.5	25	—
−30	213.5	25	—
−32	268.5	20	—
−40.5	226.5	20	—
−44	36	40	—
−44.5	212	20	—
−47	228	25	—
−51	222.5	30	—
−51	222.5	20	—
−57	165	60	—
−58	16	70	—
−59.5	129	25	—
−65.5	114	40	—
−65.5	115	20	—
−70.5	191	30	—
−71.5	54	95	—
−76.5	53	35	—
Intermediate volcanoes (fluted or modified domes)			
78	225	40	—
78	225	10	—
63.5	198	40 × 30	—
55	266	20	—
46	269	25	—
41	305.5	15	—
36.5	329.5	25	—
36	330	25	—
36	330.5	25	—
33.5	312	25	—
32.5	311	25	—
20.5	231.5	25	—
20	230.5	25	—
14	299	20	—
14	218	10	—
12	70.5	20	—
11.5	291.5	15	—
10.5	302	35	—
10.5	301	25	—
10	212.5	30	—
9.5	296.5	20.	—
2.5	169.5	20	—
2	284.5	30	—
1.5	169	20	—
0.5	278	20 × 15	—
0	249	30	—
−0.5	284.5	20	—
−7.5	256	35	—
−9.5	189.5	15 × 7	—
−10	152	8	—
−11.5	207	40	—
−13.5	252	25	—
−17.3	213.5	30	—
−18	5.5	40	—
−18	38	30	—
−20.5	198.5	20 × 10	—
−21.5	201.5	40	—
−22	33	40 × 20	—
−29.5	184	20	—
−30	93.5	15	—
−30	138	25	—
−30	138	20	—
−30	138	15	—
−32	260.5	20	—
−32	260.5	20	—
−32	1	20	—
−33.5	261.5	30	—
−37.5	263	30	—
−40	271	30	—
−41.5	289	20	—
−41.5	274	30	—
−46	287	25	—
−51	291.5	20 × 10	—
−61.5	331	20	—
−62	328.5	60	—
−63.5	327.5	20	—
−63.5	325.5	20	—
Intermediate volcanoes (radial flows)			
44.5	233	30	—
44	233	60	—
39	212.5	30	—
39	212.5	30	—
34.5	273	30	—
22.5	232	20	—
13	201	85	—
1	277.5	40 × 20	—
−7	199.5	80 × 50	—
−8	200.5	60 × 40	—
−8	199.5	60	—
−9	198	40	—
−9.5	201	20	—
−9.5	199	40	—

continues

Continued

Latitude (deg)	Longitude (deg)	Diameter (km)	Name
−13	199	30	—
−13	199.5	40	—
−14	118	20–25	—
−20	253.5	20	—
−29	10	60 × 40	—
−31.5	251	60	—
−34.5	15	80	—
−35	14	30–40	—
−38	13	40	—
−49.5	295	30	—
Intermediate volcanoes (steep-sided domes)			
78.5	230	30	—
74	221	25	—
73	100	20–30	—
73	100	20–30	—
73	100	20–30	—
70.5	97	30	—
66	248	30	Ale Tholus(?)
66	248	30	—
65	203	<20	Semele Tholi
65	203	<20	—
65	203	<20	—
65	203	<20	—
61	83	30	—
61	247	45	Nertus Tholus
60	324.5	25	—
57	85	20	—
51.5	104	25	—
51.5	103.5	40	—
51	102.5	45	—
50	97.5	25	—
48	342	25	—
47	215.5	30	—
46.5	359	35	—
44	284	30	—
44	284	20	—
44	11	30	—
43.5	235	30	—
42.5	79	30	—
41.5	64	20	—
40	4	25	—
39.5	119	20	—
38.5	46	40	—
38	325.5	25	—
37.5	68.5	25	—
37.5	66	30	—
36.5	270.5	20	—
36	236	30	—
36	236	30	—
35.5	21	50	Aegina Farrum
34	311.5	50	—
33.5	312	50	—
33.5	311.5	50	Anqet Farrum
33	305.5	30	—
32.5	304.5	25	—
32.5	304.5	25	—
32.5	304.5	25	—
32.5	304.5	25	—
32	311.5	25	—
31.5	14.5	30	—
31.5	14.5	30	—
31.5	14.5	30	—
30.5	313	20	—
29.5	29.5	30	—
29.5	243	15	—
28.5	320.5	30	—
28	63	30	—
25	314	20	—
24.5	314.5	20	—
18	196	60	—
16.5	41.5	25	—
15.5	281.5	15	—
15.5	117	20	—
15.5	117	20	—
15.5	114.5	20	—
14.5	135	15	—
14	70	15 × 35	—
14	277	10	—
14	277	10	—
12.5	8.5	50	—
12	9	20	—
12	7.5	50–60	Carmenta Farrum
12	299	25	—
11	313.5	10	—
11	301.5	25	—
9	204	15	—
9	204	15	—
7	44	45	—
4	19	40	—
4	19	40	—
4	19	40	—
4	19	40	—
4	19	40	—
3.5	309	60	—
2.5	314	25	—
−1.5	245.5	30	—
−2	226	30	—
−3	151	35	—
−7	30.5	20 ea	—
−9	329	50	—

continues

Continued

Latitude (deg)	*Longitude (deg)*	*Diameter (km)*	*Name*
−2.5	335.5	20	Zorya Tholus
−9.5	324.5	50	—
−9.5	295.5	20	—
−10	249.5	20 × 10	—
−12	43	20	—
−12.5	247	20	—
−13	43	20	—
−13.5	251.5	35	—
−14	218	20	—
−15.5	324	40	—
−16.1	211.8	30	—
−17	292.5	30	—
−16.5	291	35	—
−20	295	10 × 15	—
−20	295	10 × 15	—
−22	223.5	15	—
−22.5	329	30 × 20	—
−23.5	250.5	30	—
−24	353	30	Liban Farra
−24	353	30	—
−24	353	30	—
−24	353	30	—
−24	353	30	—
−26	80	40	—
−26	73	60	Rosna Tholi
−26	73	60	—
−26	73	60	—
−27.5	99.5	30	—
−30	218	20	—
−30	218	20	—
−30	12	25	Seoritsu Farra
−30	12	25	—
−30	12	25	—
−30	12	25	—
−30	12	25	—
−30	12	25	—
−30	12	25	—
−32	301.5	25	—
−32	301.5	25	—
−32	10.5	40–50	—
−34	69.5	25	Padmi Tholi
−35	264	30	—
−35	256.5	20	—
−36.5	41	20	—
−36.5	24	15	—
−42.5	255	25	—
−42.5	255	20	—
−44.5	281.5	40	Meiboia Tholus
−45	273	40	—
−51	305.5	25–50	—
−51	305.5	25–50	—
−51	305.5	25–50	—
−51	305.5	25–50	—
−51	305.5	25–50	—
−52.5	289	80	—
−54.5	292	25	—
−54.5	291.5	25	Gerd Tholus
−54.5	23	15	—
−57.5	162	40	—
−58	162	25	—
−68.5	200	40	—
−69	202.5	25	—
−70	87.5	60	—
−70.5	65	20	—
Fields of small shield volcanoes			
82.5	167	100	—
82	215	150	—
81	190	100	—
80.5	166.5	100	—
79	255	150	—
79	255	150	—
79	216	220 × 150	—
78.5	355	200 × 100	—
78.5	191	100	—
77.5	250	100	—
76.5	264	75	—
76	185	200 × 600	Molpe Colles
75.5	200	130 × 80	—
75	285	50	—
74.5	100	60 × 80	—
74	270	100	—
74	150	225 × 150	—
74	10	250 × 100	—
74	100	150	—
74	0	80	—
73.5	358	100	—
73	105	100	—
72.5	95	60	—
72.5	230	100	—
71.5	210	220 × 150	—
68.5	38	200 × 150	—
68.5	163	200	—
67	227	150	—
67	195	100 × 200	—
66.5	304.5	50	Bremer Patera
66	64	100	—
66	253	130	—
65.5	61	150	—
65	45	100	Pocahontas Patera?
64	228	80	—

continues

Continued

Latitude (deg)	*Longitude (deg)*	*Diameter (km)*	*Name*	*Latitude (deg)*	*Longitude (deg)*	*Diameter (km)*	*Name*
63.5	56	100	—	47	356	300	—
63	75	200	—	47	126	300	—
63	227	<80	—	46	59.5	100	—
62.5	70	150	—	46	196	100	—
62	192	100	—	46	187	70	—
61.5	280	50	—	45.5	323.5	150	—
61.5	279	75	—	45.5	292	150	—
61	33	200 × 150	—	45	81	500 × 300	—
61	110	250 × 200	—	44.5	72	300	—
60	85	1000 × 200	—	44.5	330	130	—
60	225	100	—	44.5	314	50	—
59	302	250	—	44.5	222	100	—
59	250	200	—	44.5	191	150	—
59	165	300	—	44	56.5	50	—
59	155	700	—	44	325	100 × 125	—
58	31.5	150	—	44	25	80	—
58	198	300 × 200	—	44	120	1200 × 300	Akkruva Colles
27.5	268	250	—	43.5	99	120	—
57.5	213	200 × 200	—	43.5	316.5	50	—
57	354	100	—	43	335	150	—
56.5	317	400	—	43	95	300–200	—
56	87	350	—	43	219	75 × 50	—
56	237	225 × 100	—	43	214.5	50	—
56	218	70	Marakie Colles	43	130.5	225 × 80	—
56	196	80	—	42.5	319.5	200 × 300	—
55.5	200.5	50	—	42.5	284	200 × 100	—
55	230	100	—	42.5	229	70	—
55	206	150	—	42.5	163	150	—
54.5	105	350	—	42	6	300	—
53.5	292	100	—	42	315	150	—
53.5	20	100	—	42	308	75	—
53.5	167	150–100	—	42	232	100	—
52.5	209	100	—	41.5	323	300	—
52	351	225 × 150	—	41.5	15.5	75	—
52	163	250	—	41	40	50	—
51.5	324.5	120 × 80	—	41	275	100	—
51.5	119	225	—	41	272	150	—
51	113	300	—	41	237	200	—
50.5	194	80	—	41	177.5	150	—
50	342	250 × 100	—	41	132	180 × 90	—
50	107	150 × 100	—	40.5	128.5	250	—
49.5	229	150	—	40	62.5	100	—
48.5	60	200	—	40	335	600	—
48.5	60	80	—	40	267	100	—
48.5	233.5	80	—	40	189	100	—
48	334	150	—	40	183	100	—
48	216	200	—	39.5	172.5	150	—
47.5	62	200 × 100	—	39	288.5	250	—
47.5	311	50	—	39	269.5	60	—
47.5	225	500 × 225	Nuliayog Colles	39	117	250	—

continues

Continued

Latitude (deg)	*Longitude (deg)*	*Diameter (km)*	*Name*	*Latitude (deg)*	*Longitude (deg)*	*Diameter (km)*	*Name*
38	97	300	—	29	21	150	T'ien Hu Colles(?)
38	241	250	Nahete Colles	29	121	80	—
38	10	200	—	28.5	306	150	—
37.5	96	150	—	28.5	286	100	—
37	276	150	—	28.5	233	60	—
36.5	201	150	—	28.5	228	100	—
36.5	126	300–500	—	28	336	200	—
36.5	120	200	—	28	303	300 × 75	—
36	236.5	150	—	28	139	100	—
36	128	200	—	28	120	250	—
35.5	238.5	100	—	27.5	95	100	—
35	342	350 × 225	—	27.5	129.5	500 × 250	—
35	341	300+	—	27	290	250	—
35	331	140	—	27	136.5	100	—
35	231	150 × 100	—	27	123	150	—
34.5	250	200	—	26.5	78	100	—
34	53	200	—	26	92	150	—
34	346	325	—	26	314.5	130	—
34	203	200	—	26	237.5	400 × 150	—
34	118	200	—	25.5	330	150	—
33.5	91	70–80	—	25.5	246	100	—
33.5	117	150	—	25.5	104	100	—
33	66	300 × 90	—	25	350	300	—
33	349.5	>400	—	25	253	250	—
33	294	200	—	25	13.5	150	—
33	239	300	—	25	117	300	—
33	222	150 × 100	—	24.5	257.5	150	—
33	14	150	—	24	9.5	100 × 180	—
32.5	338	150	—	24	79.5	200 × 100	—
32.5	253	200 × 150	—	24	343	150	—
32	327.5	50	—	24	284	100	—
32	293	300 × 100	—	24	278.5	100	—
32	212	200	—	24	271	150	—
32	198	200	—	23.5	307	120	—
32	123	200	—	23.5	259.5	150	—
31.5	331.5	<100	—	23.5	231	100 × 30	—
31.5	310	100	—	23.5	226.5	100	—
31	280	200	—	23	246.5	100	—
31	131	150	—	23	102	300 × 200	—
30.5	90	220	—	22.5	306.5	80	—
30.5	331	80	—	22	318	600–800	—
30.5	306	40	—	22	15	400+	—
30.5	270	80	—	22	115	300 × 150	—
30.5	215.5	80 × 50	—	21.5	290		—
30.5	128	150	—	21	347	350	—
30	272	150 × 70	—	21	342	500	—
30	227.5	50	—	21	337	300	—
30	210	75	—	21	136	300	—
29.5	233	60	—	21	103	300	—
29.5	192	180 × 90	—	20	290	150	—

continues

Continued

Latitude (deg)	Longitude (deg)	Diameter (km)	Name	Latitude (deg)	Longitude (deg)	Diameter (km)	Name
20	288	200	—	10	267	200	—
20	183	200	—	10	230.5	300	—
20	138	400 × 100	—	10	182	220 × 80	—
19.5	307	100	—	10	147	300 × 225	—
19	187	100	Nokomis Montes	9.5	354	200	—
19	15.5	100+	—	9.5	153	200 × 300	—
18.5	62	250 × 200	—	9	280	400	—
18.5	335	300	—	8.5	74	100	—
18	353	200	Olosa Colles	8.5	296.5	100	—
18	313.5	225	—	8	79	80	—
18	236.5	80	—	8	6.5	150	—
17.5	91.5	100–150	—	8	234	100	—
17	87	150	—	8	212	150 × 100	—
17	77	200	—	7	150	150	—
17	354.5	100	—	6.5	323	400	—
17	279	400 × 300	—	6	7	100	—
17	215	100 × 60	—	6	280	200	—
17	204	100	—	6	156	250	—
17	131	200	—	5.5	231	100	—
16.5	288	150	—	5.5	146	250	—
16	200	150	—	5	262	150	—
16	102	150	—	5	257	200	—
15	57	60	—	5	143	100 × 60	—
15	308	150	—	4.5	295.5	250 × 200	—
15	282	80	—	4.5	217	200	—
15	114	80	—	4.5	199.5	100	—
14.5	94	80 × 40	—	4	349	100	—
14.5	271.5	150	—	4	317	80	—
14.5	268	200	—	4	145	90	—
14.5	263	220	—	3.5	326.5	150 × 100	—
14	300	150	—	3.5	283.5	200 × 150	—
14	131	200	—	3.5	275	150	—
13.5	273.5	200	—	3.5	273.5	250 × 200	—
13.5	118	100	—	3.5	227.5	100	—
13	321	250	—	3.5	190	250 × 100	—
13	314.5	250	—	3	263	200	—
13	280	300	—	3	210	80	—
13	256	80	—	3	12	250	—
12.5	341	80 × 150	—	2.5	245	500	—
12.5	265	150	—	2	315	80	—
12.5	20.5	100	—	2	260	150	—
12	72	50	—	2	163	600	—
12	272	180	—	1.5	277.5	150	—
12	206.5	200	—	1.5	143	150 × 100	—
12	163	600	—	1	335.5	200 × 50	—
12	111	>1000	—	1	318	60	—
11	78	60	—	1	275	150	—
11	287	200	—	1	270.5	60	—
11	136	150	—	1	21.5	250	—
10.5	303.5	150	—	1	168.5	100	—

continues

Continued

Latitude (deg)	*Longitude (deg)*	*Diameter (km)*	*Name*
0.5	320.5	50	—
0.5	173	70	—
0	283	250	—
0	216	200 × 100	—
−1	301	200	—
−1	279	150 × 100	—
−1	239	500 × 350	—
−1.5	173	80	—
−2	307	225	—
−2	286	80	—
−2.5	320	40	—
−3	188	250	—
−3.5	324	150	—
−3.5	246	200	—
−3.5	224	100	—
−4	252	300	—
−4	211.5	70	—
−4	201	100	—
−4.5	331.5	200	—
−4.5	242.5	150	—
−5	344	250	—
−5	292	150	—
−5	251	60	—
−6	5	100	—
−6	309.5	20 × 30	—
−6	305.5	150	—
−6	210	100	—
−6.5	289	100 × 75	—
−7	335	200	—
−7	259.5	80	—
−8	259.5	100	—
−8	236	150	—
−8.5	330	150	—
−8.5	273	150 × 100	—
−9	332.5	200	—
−9	308.5	300+	—
−9.5	300	50 × 60	—
−10	348	300 × 200	—
−10	336	150	Chernava Colles(?)
−10	334	150	—
−10	288	150 × 80	—
−10	32	100	—
−10.5	314	120	—
−10.5	253	70	—
−11	339.5	150	—
−11	281	60	—
−11	246	100	—
−11	230.5	300 × 250	—
−11.5	47	200	—
−11.5	14.5	150 × 100	—
−12	337	100	—
−12.5	69	90	—
−12.5	286	150	—
−12.5	198	200	—
−12.5	17	200	—
−12.5	13	80	—
−13	348	150	—
−13.5	68	150	—
−14.5	317.5	150	—
−15	71	100	—
−15	22	250	—
−15	184	200	—
−15.5	36	200 × 100	—
−15.5	325	250	—
−16	353	100	—
−16	339	70	—
−16	326	175	—
−16.5	300	200	—
−16.5	294	350 × 200	—
−17	70	100	—
−17	338	40	—
−17	298	150	—
−17	159	200	—
−17.5	244.5	150	—
−18	272.5	300 × 150	—
−19	209	150 × 20	—
−19	185	80	—
−19.5	293	150	—
−20	88	100	—
−20	349	200 × 80	—
−20	335	60	—
−20	22	200	—
−20	211	80	—
−20	194	200	—
−20.5	46.5	50	—
−20.5	321.5	150	—
−20.5	296.5	300	—
−20.5	268	100	—
−20.5	232	100	—
−21	255	150	—
−21.5	51	100	—
−21.5	324	120	—
−21.5	224.5	200 × 60	—
−22	326	150	—
−22	305	200	—
−22	258	100 × 50	—
−22.5	209	100	—
−23	331	500 × 300	—
−23	197	150	—
−24	86	200 × 100	—

continues

Continued

Latitude (deg)	Longitude (deg)	Diameter (km)	Name	Latitude (deg)	Longitude (deg)	Diameter (km)	Name
−24	300	150 × 100	—	−31.5	274	150	—
−24	295.5	100	—	−31.5	259	75	—
−24	278	500	—	−32	305	150 × 100	—
−24	236	200	—	−32	25	300	—
−24	234	100	—	−32.5	6	100	—
−24	230.5	100	—	−32.5	316	120	—
−24.5	343	150	—	−32.5	223.5	150	—
−25	92	150	—	−32.5	220	100	—
−25	72.5	100	—	−32.5	137	100	—
−25	303.5	100	—	−33	337	100	—
−25	242	100 × 200	—	−33	298.5	60	—
−26	288.5	75	—	−33.5	296.5	60	—
−26	233	100	—	−33.5	243	150 × 100	—
−26.5	319	250	—	−33.5	234	100	—
−27	237	200 × 100	—	−34	341	100	—
−27	230	100	—	−34	334	80 × 200	—
−27	221.5	100	—	−34	292.5	90 × 50	—
−27	200	250	—	−34	197	200 × 150	—
−27	187	100	—	−35	236.5	80	—
−28	198	120	—	−35	11	100	—
−28.5	256.5	80	—	−35.5	221.5	150 × 250	—
−29	69	200–300	—	−36	256	100 × 70	—
−29	340	60	—	−36.5	6	70	—
−29	327	500 × 500	—	−36.5	284.5	200	—
−29	319.5	150	—	−36.5	246	200	—
−29	305.5	200	—	−36.5	227	80	—
−29	299	100	—	−37	206	80	—
−29.5	322	130	—	−37.5	70.5	150	Indrani Corona
−29.5	315.5	100	—	−37.5	253	>70 × 100	—
−29.5	300.5	100	—	−37.5	253	150	—
−29.5	253.5	100	—	−38	77	200	—
−29.5	245	100	—	−38	235.5	300 × 100	—
−29.5	235	150 × 80	—	−39	54	200	—
−29.5	163.5	200	—	−39	185	100	—
−29.5	157	150	—	−39	182	100	—
−30	85	80 × 100	—	−39	135	200	—
−30	340	100	—	−39.5	316.5	200	—
−30	313	400	—	−40	335	100	—
−30	276.5	100	—	−41	289	150	—
−30	225.5	100	—	−41	266	100	—
−30	221	100 × 80	—	−41	261.5	200	—
−30.5	34.5	100	—	−41	259	200	—
−30.5	289	80 × 50	—	−41	206	100–200	—
−30.5	234	80	—	−41.5	240	80	—
−30.5	19	100	—	−42	66	150 × 100	—
−31	73	400	—	−42	62	200	—
−31	334	60	—	−42	32	200	—
−31	249	150 × 80	—	−42	280	80	—
−31	105	100	—	−42	277.5	80	—
−31.5	315	80	—	−42.5	267	250 × 150	—

continues

Continued

Latitude (deg)	*Longitude (deg)*	*Diameter (km)*	*Name*
−42.5	261	200	—
−43	213	250	—
−44	83	200 × 100	—
−44	345	200 × 300	—
−44	243	150 × 80	—
−44	202	80	—
−44.5	67	200 × 100	—
−44.5	250	150	—
−46	264	300	—
−46	209	150	—
−47	85	100	—
−47	10.5	80	—
−48	36	150	—
−48	274	100	—
−48	22	200	—
−48	211	150	—
−48	159	300	—
−48	12	100	—
−48	115	250	—
−49	343	100	—
−49	300	75	—
−49	197	200 × 150	—
−49.5	59.5	100	—
−50	76	200	—
−50	356	150 × 200	—
−50	33	150	—
−50	297	150	—
−50	286.5	500	—
−50	256	150	—
−50	252	200	—
−50	252	200	—
−50	241	150	—
−50.5	304.5	60	—
−50.5	270	300	—
−51	87	—	—
−51	273	50	—
−51	261	300 × 150	—
−51	160	500	Mena Colles
−51	10	60	—
−52	302.5	150	—
−52.5	317	70	—
−53	164	150	—
−53.5	321.5	50 × 100	—
−53.5	175	400 × 200	—
−53.5	157	150	—
−54	302	50	—
−54	242	100	—
−54.5	339	150	—
−54.5	162	100	—
−55	278	250	—
−55	270	200	—
−55.5	303	150	—
−56.5	238	70	—
−56.5	167	100	—
−57	317	50	—
−57	255	100	—
−59	61	50	—
−59	350	100	—
−59	305	75	—
−59	301	150 × 75	—
−59	300	200 × 100	—
−59	132	50 × 100	—
−60	290	120	—
−60	167	70	—
−60.5	253	70	—
−61	326	150	—
−61	302	100	—
−61	294	80	—
−61.5	55.5	100	—
−62	347	200	—
−62	307	150	—
−62	307	100	—
−62.5	168	200 × 300	Salofa Colles
−63.5	280	70	—
−63.5	109	100	—
−64	317	60	—
−64	156	150	—
−64.5	298	70	—
−65	52	50	—
−65	293	130	—
−65	275	100	—
−65	231.5	200	—
−65.5	65	50	—
−66	27	250	—
−66	179	100	—
−66.5	84	70	—
−66.5	210	150	—
−67	53	150	—
−67	52	100	—
−67	124	200	—
−67	115	80	—
−69	80	70	—
−69	54	100	—
−70	108	100	—
−70.5	79	100	—
−71	50	100	—
−71	48	80	—
−71.5	99	150	—
−71.5	292	100	—
−73	104	150	—

continues

Continued

Latitude (deg)	Longitude (deg)	Diameter (km)	Name
−74	41	100	—
−74	243	100	—
−74.5	140	200	—
−75	195	300	—
−75.5	166	150	—
−76.5	332	150	—
−76.5	150	200	—
−78	117	200	—
−78.5	51	70	—
−78.5	43	150	—
−78.5	40	100	—
−82	73	75	—
		Calderas	
74.5	315	100	—
66.5	60	60	Anning Patera(?)
64.5	335	225 × 150	Sacajawea Patera
61.5	340	70	Siddons Patera
60.5	83	40 × 50	—
57	95	75–80	Boadicea Patera
56.5	242.5	35	—
52.5	96.5	75	—
52.5	200.5	50	—
49.5	334.5	60 × 40	Sachs Patera
48	33	25	Anthony Patera
46	216	20 ea	—
46	216	20 ea	—
45.5	31.5	60	—
45.5	219.5	50	Bakhtadze Patera
44.5	31.5	40	—
39.5	79	100 × 30	Eliot Patera
39.5	203.5	25	—
38.5	205	30	—
32	305	80 × 60	Jaszai Patera
31	218	<20	—
29.5	227.5	80	Mansfield Patera
26.5	234	100	Pchilka Patera
25	212	60	—
20	247	60	Serova Patera
19.5	123	≤75	Nintu Corona
19.5	123	≤75	—
19.5	123	≤75	—
17.5	218.5	30	—
16	311	60	Mehseti Patera
15	135	75	—
14	93	50	—
14	237.5	70	—
12	72	70 × 50	—
10.5	301.5	25	—
9.5	97	40	—
7.5	266	90	—
7	267	40	—
6.5	264.5	60	Shulzhenko Patera
6	227	80	—
4	214	75	—
4	168	50	—
2.5	212	50	—
2	209.5	60	—
1.5	72	50	—
1.5	258	70	—
−1	284	75 × 60	—
−4	154.5	100	Seia Corona?
−5.5	34.5	70	—
−6	308.5	30	—
−6.5	214	100	Jotuni Patera
−7	254.5	60	—
−8.5	256	50	—
−9	255.5	40	—
−9	224.5	100 × 140	Ledoux patera
−9.5	69	50	Kvasha Patera
−10	88	150 × 80	—
−10	70	60 × 40	—
−11.5	194.5	50	—
−12.5	216	40	—
−13	310	40	Panina Patera
−13	238	80 × 90	—
−16	348.5	40	Aitchison Patera?
−17	115	150 × 100	—
−18	253.5	60 × 100	—
−19.5	233.5	40	Beruth Corona
−21.5	266.5	75	—
−21.5	213	50	—
−22	214	100	—
−22	210	100 × 90	Villepreux-Power Pat
−24	226.5	75	Fedchenko Patera
−27	348.5	60	Mikhaylova Patera
−27	195	50 × 60	—
−28	340	30–40	—
−28	123	100	—
−30	288	35 × 20	—
−30.5	224.5	40	—
−31	224	30	—
−31	221	30 × 40	—
−33	69	20 × 40	Mezrina Patera
−33	69	20 × 40	—
−33	196.5	40	—
−35	267.5	35	—
−35	266	150 × 130	Nordenflycht Patera
−35	263	60	Zemaite Patera
−35	253	40	—
−35.5	284.5	80 × 60	Erigone Corona

continues

Continued

Latitude (deg)	*Longitude (deg)*	*Diameter (km)*	*Name*
−36	21.5	120 × 70	Pachamama Corona
−37	264	60	—
−38	310	100 × 60	Vovchok Patera
−39	197	60	Tateoinnan Corona
−47	20	20 × 50	Derceto Corona?
−48	88	100	Cailleach Corona?
−52	14	150	Sarpanitum Corona
−55	63.5	70	—
−73	99	175	Mykh-Imi Corona
−81	183	100	Romi-Kumi Corona?
		Lava channels	
76	330	>150 long	—
68	307	230	—
64	278	80	—
50	167	1400	Baltis Vallis
44	15.5	>300 long	—
33	164	900	Baltis Vallis
32.5	229.5	60	—
12.5	234	300–400	—
5	334	300+ long	—
4	58	60	—
3	82.5	50 long	—
3	82.5	50 long	—
3	82.5	50 long	—
3	335	500+ long	—
1.5	87.5	>225	—
−3.5	201.5	200	—
−11.5	257	70	—
−12	90	>200	—
−12	90	>200	—
−12	90	>200	—
−12	67.5	>300 long	—
−15	142	200	—
−16	182	1–2 × 150	—
−17	10	200–300+	—
−18	14	300	—
−20.5	180	500	—
−24	347	100	—
−26	152	200	—
−27.5	256	60	—
−28.5	252.5	75	—
−29	253.5	100	—
−30	356	50	—
−34	197	>200 × 3	—
−35	251.5	400	—
−40	31	500	—
−40	227	200	—
−42	89	600+	—
−43	197.5	250	—
−45	355	∼600	—
−48	20	600	—
−48	164	400	—
−49	267	600+	—
−49	225	200	—
−49	177	500+	—
−49	151	>350	—
−49.5	273	250+	—
−51.5	25	900	—
−52	0	100	—
−53.5	353	100+	—
−54	171	500	—
−58	195	600–700	—
−58.5	175	500	—
−59	165	1000	—
−59	151	500+	—
−60	268	300+	—
−61	255	300	—
−61	190	300	—
−62	147	900	—
−62.5	163	500	—
−66.5	86	50	—
−66.5	16	>300	—
−75	162	1400	—
−77	128	1400	—
−81	240	600	—
		Lava flow fields	
78	15	200 × 100	—
76	350	500 × 100	—
70.5	204	200	—
66.5	307	230 × 100	Djata Fluctus
61	184	400–500	Mamapacha Fluctus
56	218	300	Turgmam Fluctus
50	347	>600 width	Neago Fluctus
38	29	>400	—
38	250	400	Zipaltonal Fluctus
37	244	500	—
34	229	400 × 300	—
32	230	20	—
29	220	600 × 300	Uzume Fluctus
26	302	250	—
25	48	500	—
24	154	600 × 600+	—
19	268	300	—
12.5	234	300–400	—
12	306	500	Koti Fluctus?
9	97	200 long	—
4	345	20–100	—
4	332	20–40 ea	—
1.5	279	250 × 100	—
0	277	100 × 100	—

continues

Continued

Latitude (deg)	*Longitude (deg)*	*Diameter (km)*	*Name*
−2	336	50	—
−2	314		—
−5	204	300 × 200	Ningyo Fluctus
−6.5	231	200 × 150	—
−8	150	>300	—
−9	299.5	150 × 250	—
−13	313	700	Darago Fluctus
−14	336	50	—
−15	88	>400 km	—
−15	79	300 long	—
−15	197	400 × 400	—
−15	140	600	—
−17	1	300 wide	—
−18	132	150 long	—
−18.5	313	500	—
−19	180	500	Henwen Fluctus?
−21	283	400	—
−21	144	300	—
−21	115	400	—
−22	354	300	—
−25	22	100	—
−26	258	1000	—
−26	152	200	—
−30	264.5	500+	—
−30	250	600 × 300	—
−34	324	400	—
−39	133	100	—
−41	15	200 × 900	—
−43.5	57	600	—
−45	358	300	Kaiwan Fluctus
−47	3	800	—
−47	27	600	Ubastet Fluctus
−49	55	400	—
−50	65		—
−51	354	>300	Mylitlus Fluctus
−59	32	200	—
−71.5	346	600	Cavillaca Fluctus
−72	15	800	—
−76	55	300	—
Unusual lava flows			
71	200	200	—
−6	96	300 × 200	Ovda Fluctus
−37	165	200–250	Mahuea Tholus
Arachnoids (subclass of coronae)			
78	20	75 × 150	—
76.5	26	100 × 150	—
76.5	200	200 × 130	Maslenita Corona(?)
75	220	100	—
74	215	100	Schumann-Heink Coron
69	206	80 × 60	Nzingha Corona
68.5	132	80	—
67	251	100	—
66.5	57	30–40	Anning Patera
65.5	220	100 × 80	—
65.5	207.5	100	Cassatt Corona
65.5	205	150 × 100	Muzamuza Corona
63.5	195	70	—
62.5	79	100	—
62.5	286	150	—
61.5	282.5	150	—
61	246	130 × 80	—
58.5	86	50	—
57	82	80	Malintzin Patera
56	188	150	Aspasia Corona
54.5	326.5	280	—
54	152	70	Mari Corona
50.5	96.5	50	—
50	270.5	40	—
49.5	311	50 × 75	—
48.5	270.5	80 × 60	—
47.5	269	80	Davies Patera
47	11.5	70	
46	321.5	100	—
46	198	200 × 100	Razia Patera
45.5	231	75	—
45.5	213	100 × 75	—
45.5	12	150	Audhumla Corona
45	274.5	75	Keller Patera
45	220	50	—
45	19.5	70	—
45	170	80	—
44	16.5	125	—
44	14	120	—
43	3	100	Vasudhara Corona
43	235.5	100	Mentha Mons(?)
43	218	100	—
42.5	46	100	Stopes Patera
42.5	215	220 × 140	Tituba Patera
42	222	150 × 100	—
41.5	79.5	100	—
41.5	306.5	130	—
41.5	218	170	—
41.5	15.5	175	
41	48	150 × 100	—
41	317	40	—
41	288.5	70	—
41	18.5	150	Trotula Patera
40.5	212.5	150	—
40	307.5	130	—

continues

Continued

Latitude (deg)	*Longitude (deg)*	*Diameter (km)*	*Name*
40	194	80	—
40	13	100	—
39.5	20.5	100 × 70	Yaroslavna Patera
39	319	60	—
38.5	217	150	—
38.5	19	75	—
38	15	65	Cavell Patera
37.5	67.5	100	Olwen Corona
37.5	290.5	150	—
37.5	206	150 × 130	—
37	16.5	100	—
35.5	207	150	—
35	36	50	Hroswithu Patera(?)
35	272	75 × 60	—
35	271	130	—
34	267.5	75 × 50	—
33.5	57	100	Kayanu-Hime Corona
33.5	263	100	—
33	306	100 × 75	—
33	204.5	90	—
32.5	326.5	200 × 150	Renenti Corona
32	38.5	60 × 30	—
31	250	160	—
30.5	245.5	150	—
30	24	75 × 100	—
29	27.5	150	—
29	205.5	80	—
28	312	60	—
28	198.5	≤60	—
28	198.5	≤60	—
28	198.5	≤60	—
28	198.5	≤60	—
28	198.5	≤60	—
25.5	245	90	—
25	313	130	—
25	115	70	—
23.5	218.5	100 × 70	—
23.5	21.5	100 × 80	—
23.5	199.5	70 × 50	—
22.5	240	100	—
22	202	70–80	—
22	114	70	—
21.5	201	20	—
21	56.5	100	—
21	200	35	—
18	341	100	Chiun Corona
18	224	100 × 80	—
17	63.5	80	—
17	56	100ea	—
17	56	100ea	—
16.5	202.5	100	—
16.5	200.5	50	—
16	343	80	Benten Corona
16	132	150	Kubebe Corona
15	221	150 × 80	—
14.5	6.5	100	—
14	6	50	—
14	65	80	—
14	256.5	100 × 75	—
14	255	80	—
14	111	80	Dhisana Corona
13.5	291.5	70	—
13.5	226.5	200 × 150	—
12.5	253	150	—
12	90	100	—
11	6.5	200 × 150	—
10	9	80	—
10	95	100	—
10	251.5	100	—
10	246	150	—
10	205	100	—
9.5	254.5	100	—
9	233.5	150 × 100	—
8.5	92	120	Atse Estsan Corona
8	247.5	100 × 75	—
7	233.5	60 × 40	—
5.5	78	100 × 60	—
5.5	313	60	—
5.5	169	100	—
5	11	70	—
4	169.5	80 × 60	—
3	280	80	—
2.5	280	50	—
2.5	280.5	140	—
2.5	231.5	150	—
2.5	219	100 × 80	—
1.5	296	80	—
1	282	150 × 90	—
0.5	255	150 × 100	—
0	240.5	100	—
0	236.5	100	—
0	125	100–150	Rosemerta Corona
−1	231	100	—
−1	134.5	100 × 60	Blai Corona
−1.5	254.5	90	—
−1.5	242.5	150 × 100	—
−1.5	215	150	—
−2	74	100	—
−2	170	60	—
−2	146	150	Hepat Corona

continues

Continued

Latitude (deg)	*Longitude (deg)*	*Diameter (km)*	*Name*
−3	243	80	—
−3	220.5	150 × 80	—
−3.5	260	130	—
−4	152	150 × 75	Seia Corona?
−4.5	329.5	100	—
−4.5	261.5	150 × 180	Krumine Corona
−4.5	259	75	—
−5	232.5	80	—
−5	175	150	Eigin Corona
−5.5	235.5	80	—
−6	261.5	80	—
−6.5	143	100 × 60	—
−7	145	200 × 100	—
−9	90	150	—
−9	341	50	—
−9	259.5	80	—
−11	338	70	—
−11.5	44	150	—
−11.5	33	100–150	—
−12.5	32	150	—
−14	229	60	—
−14	223.5	100–150	—
−14	223.5	100–150	—
−14	223.5	100–150	—
−15	310	100	—
−15.5	188	150	—
−16	348	150	Iyatik Corona
−16.5	352	80 × 60	Tumas Corona
−16.5	292.5	150	—
−16.5	224	150 × 100	—
−17.5	227.5	75 × 50	—
−18	201	140	—
−18.5	234	150	—
−18.5	234	150	—
−19	232.5	140	Beruth Corona
−19	221.5	200 × 150	—
−19.5	234.5	150	—
−20	343	75 × 100	Qetesh Corona
−20	241	70	—
−20	230	140 × 100	—
−20	230	140 × 100	—
−20.5	220	100	—
−21.5	271	200 × 100	—
−23.5	229.5	100	—
−23.5	229.5	60	—
−24.5	266	80	—
−25	30	20	—
−25	30	20	—
−25	211	100	—
−25.5	195.5	90	—
−26.5	299.5	120 × 80	—
−27	154	150	Mayaeul Corona
−27.5	266.5	150 × 100	—
−27.5	216	100 × 150	—
−28	270	150	Lilwani Corona
−28	165.5	100	—
−28.5	258.5	170	—
−29	282	150	—
−29.5	211	80	—
−30	245.5	130 × 160	—
−30	154	100	—
−30	118	60	—
−31	110	100	—
−32	280.5	150	—
−32.5	219	80	—
−33	268	150 × 100	—
−34	66	90	—
−34	282	150 × 80	—
−34.5	276	100	—
−34.5	199	100 × 70	—
−36.5	247.5	130 × 160	—
−36.5	246	100 × 150	—
−37	49	100	—
−37	36	150 × 100	Inanna Corona
−38	23.5	100	Ninhursag Corona
−38	149	100	Teteoinnan Corona
−39	241	≤150	Hlineu Corona
−39.5	329.5	80	—
−40.5	288	80	Latta Corona(?)
−41	289	80 × 50	—
−41	289.5	70	—
−41.5	265.5	100	—
−42	256	100	—
−42	196	100	—
−42.5	245.5	150	Nungui Corona
−45	324	100	—
−46.5	324.5	100	—
−47	209.5	80	Banba Corona
−47	106	100	—
−48	322.5	60	—
−48.5	297	140 × 100	—
−50	289.5	150	—
−50.5	276	150 × 80	—
−51.5	292	80	—
−51.5	289.5	80	Tureshmat Corona
−53	69	150	Marzyana Corona(?)
−53	69	150	—
−53	69	150	—
−53	41	100 × 180	—
−55.5	167	100 × 150	Utset Corona

continues

Continued

Latitude (deg)	*Longitude (deg)*	*Diameter (km)*	*Name*
−57	131	40	—
−57.5	0	80	—
−58.5	0	60	—
−60.5	166	100	—
−62	87	150	—
−62	42	170 × 200	Toyo-uke Corona
−62	241	100	Seiusi Corona
−64	236	150 × 100	Moombi Corona(?)
−66.5	209.5	150 × 80	Phra Neret Corona
−79	169	140	—
		Coronae	
79.5	300	200 × 300	Pomona Corona
77.5	275	500 × 300	Anahit Corona
75	30	125 × 75	—
70	136	320	Earhart Corona
70	100	150 × 350	Tusholi Corona
69.5	278	300 × 500	Feronia Corona
68	346	230–250	—
68	298	200	Otau Corona
66	254	200	—
66	252	400 × 200	—
63.5	273	220	Coatlicue Corona
63	265	500	Ranuneida Corona
63	130	400 × 500	Nightingale Corona
58.5	29	250 × 400	—
54.5	295	650 × 350	Demeter Corona
53.5	307	180 × 400	—
53.5	155	200	Holde Corona
51	321	250 × 200	Xilonen Corona
49.5	205	250	Neyterkob Corona
49.5	201.5	220	Cerridwen Corona
49	5	300	Onatah Corona
49	29	100 × 150	—
49	247	300	—
48	0	250 × 150	Ba'het Corona
44	223	300 × 150	—
43	227.5	250	Ki Corona
43	219	210	—
41	272	250	Rauni Corona
41	21	150 × 200	—
40.5	102	250	Maa-Ema Corona
38	37	75	—
37	39.5	150 × 100	—
36	49	450 × 250	Nefertiti Corona
35	293	225	Blathmat Corona
34	12	300	—
33	143	250 × 200	Cautcouan Corona
32	240	500 × 300	Mawu Corona
31.5	258	300	Zamin Corona
31.5	255.5	250	—
31	312	200	Zemire Corona
31	306	300 × 200	—
31	306	200	—
29	319	230	Pasu-Ava Corona
29	243	150	—
28	322	220	—
28	205	200	—
28	143	400	—
27	136.5	300 × 225	Boann Corona
26.5	94	225	Eurynome Corona
26	98	220	Metra Corona
26	343.5	200	Purandhi Corona
26	16	400 × 250	Beyla Corona
25.5	355.5	200	Nissaba Corona
25	358	225	Idem-Kuva Corona
24.5	244.5	220	—
23	98	200	Maya Corona
22	224	200	—
20	231.5	300	Pani Corona
19.5	227	250	—
19	47	250	—
19	265.5	250	—
18.5	37.5	300	Didilia Corona
18.5	125.5	250	Abundia Corona
17.5	260.5	250	—
17	299.5	250	—
17	119	220 × 200	Omeciuatl Corona
16.5	252	400	Taranga Corona
16	49.5	350	—
16	293	200 × 150	—
15	98	150–200	Atse Estsan Corona
15	118	200	Bhumiya Corona
15	114	200 × 150	Allatu Corona
14.5	40	400	Pavlova Corona
14	259	80	—
13.5	10	300	Nehalennia Corona
13	356	300	—
13	288	230 × 170	Zhivana Corona
13	24	400	Libera Corona
13	11	200 × 150	Nehalennia Corona
12.5	229	200	—
12	312	100	—
12	308	230	Hulda Corona
12	244	250	—
10.5	300	300 × 250	—
9.5	252	400 × 300	—
9	315.5	220	Madderakka Corona
8	12	200	Sunrta Corona
7.5	313	80	—
6.5	43.5	550	Calakomana Corona

continues

Continued

Latitude (deg)	*Longitude (deg)*	*Diameter (km)*	*Name*
6	273.5	250	—
6	20	300	Belet-Ili Corona
5	311	140	—
4.5	273	200	—
4	21	400	Gaia Corona(?)
3.5	234	225	—
2	354.5	900	Heng-o Corona
2	301	1000 × 600	—
2	285	225	—
2	236.5	225	—
0.5	264.5	150	—
0	74.5	400	—
−1.5	328.5	200	Yanbike Corona
−2.0	146.0	150	Hepat Corona
−3	215	225	—
−3.5	255	225	—
−5	251	400	Javine Corona
−5	10	600	Kuan-Yin Corona
−5.5	65	200	Verdandi Corona
−6	140	220 × 200	—
−7	21.5	250	Cybele Corona
−7	13	200	Thouris Corona
−7.5	221	250	Maram Corona
−7.5	21	500	Cybele Corona
−8	9	400	Atargatis Corona
−8	94	200	—
−8	48	600	Nabuzana Corona
−8	33	250	Thermuthis Corona
−10	324.5	300 × 200	—
−11.5	234.5	250	—
−12	186	450	Zemina Corona
−12.5	328	200	Katieleo Corona
−13	250	300 × 200	—
−13	21	500	—
−13	213.5	200	—
−14	223	200	—
−16	244	350 × 500	Atete Corona
−16	234	225 × 200	Erkir Corona
−16	234	225 × 200	—
−16	151	600 × 500	Ceres Corona
−16.5	18.5	500	Fatua Corona
−17	343	150 × 200	Bhumidevi Corona
−17	236	200	—
−17	128	300	—
−18	120	200	Inari Corona
−19	250.5	150	
−19	238.5	225	Beruth Corona?
−19.5	196	250 × 200	—
−20	309.5	400	Iweridd Corona
−21	119.5	350 × 250	—
−23.5	265	250	—
−23.5	192.5	200	—
−24	251	300 × 500	—
−24	157	300	Bona Corona
−25	72.5	280	Nishtigri Corona
−25	269	225	Hervor Corona
−25	181	210	—
−26	82	320	Aramaiti Corona
−27	85.5	140 × 200	Ohogetsu Corona
−27	31	250	Mama-Allpa Corona
−27	210	150 × 200	—
−27.5	51	350	Umay-ene Corona
−27.5	208.5	250	Epona Corona
−28.5	331	100 × 120	—
−30	276	230	Gertjon Corona
−31	331.5	200 × 250	—
−31	285.5	250	—
−31.5	277	300 × 200	Obiemi Corona
−31.5	260	250	—
−32	359	350	Eve Corona
−32	256	200	Oanuava Corona
−32	202	200	Nott Corona
−32	151	300 × 200	Colijnsplaat Corona
−33.5	50	180	Zemlika Corona
−33.5	304	200	—
−33.5	254.5	150	—
−36.5	6	250	Tamfana Corona
−36.5	298.5	250 × 150	Tamiyo Corona
−37	70	100	Indrani Corona
−37	43	150	—
−37	266.5	200 × 130	Furachoga Corona?
−33	278.5	220	Rigatona Corona
−38.5	291	225	Zywie Corona
−39	42.5	70	—
−39	296.5	300	Ukemochi Corona
−42	7	400	Selu Corona
−42	279.5	400	Shiwanokia Corona
−43	75	300	Copia Corona
−43	327	400	—
−45.5	55.5	250	—
−45.5	278	250 × 200	Nzambi Corona
−46	80	140	Khotun Corona
−47	84	250	Makh Corona
−47	302	500	Bibi-Patma Corona
−47	258	200	Tangba Corona
−47.5	293	200	—
−48	296	150	Navolga Corona
−49	59	200	Mou-nyamy Corona
−50.5	306.5	80	—
−50.5	301	100	—

continues

Continued

Latitude (deg)	*Longitude (deg)*	*Diameter (km)*	*Name*
−52.5	297	350	—
−53	291	250	Obasi-Nsi Corona
−54	95	200 × 300	Triglava Corona
−57	8	500	Eithinoha Corona
−57	32	350	Otygen Corona
−58.5	163	225 × 150	Fotla Corona
−59	350	220	Jord Corona
−60	85	600	Dunne-Musun Corona
−63.5	322	300	Kamui-Huci Corona
−64	123	350	Latmikaik Corona
−65.5	36	150 × 225	—
−66	43	300	—
−67	118	250	Deohako Corona
−68	355	>700	Quetzalpetlatl Coron
−69.5	66	400	Ilyana Corona
−70	40	400	—
−70	306	250	—
−70.5	82	500	—
−78	40	300	—
−83.5	140	400	—

Radial Fracture Centers

Latitude (deg)	*Longitude (deg)*	*Diameter (km)*	*Name*
69	88	100	—
68	282.5	200 × 100	—
66.5	278	150	—
63.5	90	200	—
54	18	250–300	Haumea Corona
53	151	100	Ciaucoatl Corona
34	21.5	150	Lilinau Corona
32	312	70	—
29	348	150	—
27	342	250	Mesca Corona
24	346.5	60	—
22.5	256.5	150	—
20	24	225	—
18.5	37.5	250	—
17.5	252	220	—
17	48	200	—
17	234	220	—
14.5	39	200	—
12.5	49	300 × 200	—
11.5	37	300 × 200	—
11	14.5	200	—
9	68	225	H'Uraru Corona
−5	250.5	150	—
−6.5	251	150	—
−7.5	221	150	—
−8	243	200	—
−8.5	47	250	—
−8.5	106.5	130	—
−9	214	200	—
−9	109	150	—
−10.5	47	100	—
−11	211	200	—
−11	172.5	300	—
−12	251	200	—
−14	164	350	—
−15	215	200	—
−16	57.5	200	—
−16	205.5	100	—
−16.5	162	200	—
−17	203.5	150 × 100	—
−20	335	200	—
−20	102	100–150	—
−20.5	193.5	150	—
−22	271	150	—
−26	238	150	—
−27.5	273	250	—
−28	232	250	—
−30	95	50	—
−32	99.5	200	Tai Shan Corona
−32	95	100	—
−32	276	100	—
−34.5	287.5	150	—
−36	150	200	Annapurna Corona
−37	3	200	Carpo Corona
−37	136.5	150	—
−38	245.5	200	—
−39.5	296.5	150	—
−42	75	200	—
−42	278	200	—
−45.5	303.5	150	—
−47.5	58	200	—
−49	85	150	—
−49	85	100	Makh Corona
−59.5	56	150	—

Notes: This is an abridged version of the complete catalog which also includes detailed comments for most of the features listed, reference MVC number, and other information about relevant C1-MIDRs and F-MIDRs

Feature terminology. The feature designations used here are informal. Some terms imply a geologic origin and other terms are nongenetic. The level of geological detail available from Magellan image data are such that many of the centers may be assigned with reasonable certainty to a broad class of relatively well-known geologic phenomena, such as volcanoes or calderas, and the need for generally nongenetic terminology is diminished.

Several nongenetic terms for many large-scale features originated during the analysis of Venera 15/16 image data because the resolution was such that the geologic origin of many large-scale structures, such as coronae or arachnoids, was indeterminate. Similar informal terms were used early in the Magellan mission for many types of newly identified morphological features. An attempt was made with some preliminary terms used by the Magellan

continues

Continued

team to use Latin derivative terms, as was done successfully with tesserae earlier. Informal usage of Latin in addition to informal and colloquial terms in general impeded this approach and resulted in errors. These and other problems are of the type that are sorted out with usage, but should be noted and avoided. Currently the term "corona" seems to be accepted, "arachnoid" is not favored but may have been in use long enough to continue. We find that "arachnoids" are distinguishable as a class of feature in the broad category under corona. Simple terms that readily characterize a feature are most convenient, and as a rule non-whimsical terms are more appropriate.

For reasons having to do with the direction of detailed research following Magellan, several lists of specific types of volcanic centers were generated by different investigators. Some of these lists include centers smaller than 20 km. Some of these list were focused on a particular type, they are more inclusive, and contain features that we have assigned, on the basis of examining all magmatic centers, to other categories.

1. MVC number. Many features are not formally named; we have assigned a Magellan Volcanic Feature Catalog number to each feature to assist in identification. The MVC number is an abbreviated description of the latitude, longitude, and volcanic feature type for each entry.

2. Locations/catalog accuracy. The data in this catalog were compiled initially by L. Crumpler and J. Aubele, jointly verifying each identification, classification, and numerical entry and acting as a check of the other's observations. In addition to providing a continual check of individual accuracy, the initial tandem survey controlled excessive "drifts" in identification and interpretation criteria that often occur in efforts of this type requiring observations over an extended period by a single individual. The Magellan Volcanic Feature Catalog is assembled with extreme attention to consistency.

Each feature location and classification was subsequently checked and corrected by three people and every effort was thus made during compilation to check and recheck the accuracy of identifications, locations, dimensions, and tabulation. As with any carefully assembled, large geophysical data set of this size and complexity, a certain low percentage (generally ≤5%) of transcription and related "mechanical" errors may occur [for example, see discussion of Pacific intraplate seismicity map in Lay (1991) *EOS*, **72,** 468, or Wysession *et al.*, (1991)]. Users might be alert for the few obvious errors. Errors identified and corrected during the subsequent review process included latitudinal errors resulting from inversion of north or south (e.g., 15° instead of −15°), corresponding misinterpolation from latitudinal scale label points (e.g., −20° misread as 20° and a feature 2° north of that identified as being at 22° instead of −18°), multiplicative longitudinal shifts (e.g., 290° instead of 190°, or 180° instead of 190°), incorrect MVC numbers, and typographical errors in feature descriptions. Remaining instances of these types of errors should be few, but these examples are offered as keys for recovering the data from the most likely occurrences of listing errors.

3. Diameter. Most features are roughly equant in plan shape, but the minimum and maximum dimensions for elongate features are included where appropriate. Dimensions listed for lava channels and flow fields are lengths. The diameters of large volcanoes are measured to the distal edges of the radial lava flows of median length. Diameters of coronae and arachnoids represent the mean diameter of the most prominent concentric ring. The diameter of radial fracture centers or stellate patterns is the diameter defined by using the median fracture length; fractures that are continuations of longer rift or fracture belt trends were not considered in arriving at the value for the median length.

4. Feature names and feature type classification. Names assigned to individual features included in the catalog are those approved by the International Astronomical Union. Great effort has been taken to correlate these names with our list as of the time of this writing. In some cases the coordinates listed in the IAU list for a feature may differ from those judged from Magellan data as representing the center of a particular volcanic feature. The IAU names have been assigned in many cases to terrain features apparent in pre-Magellan data sets and do not always correspond to geologic features visible in the Magellan data. IAU names for which no corresponding volcanic feature is identified have not been included. Where the coordinates of our list and the IAU list differ significantly, the corresponding feature name is listed with a query ("?") symbol. Official IAU physiographic terms such as farrum and fluctus frequently refer to a variety of volcanologically defined features. Many volcanologically defined features have locations close to the IAU feature location, so it is difficult to determine which feature has been named on the basis of coordinates alone. Names and formal terms within the IAU list are constantly evolving and new names have been added subsequent to compilation of the list. Many IAU feature names have been redefined (mons to tholus, corona to patera, etc.) with further study subsequent to initial inclusion in this list. Identification of feature types is here based largely on volcanic criteria and infrequently corresponds to a single IAU physiographic term. For example, "patera" often includes arachnoids, calderas, and large volcanoes. Similarly, some IAU physiographically defined "coronae" are the same as our calderas or even radial fracture centers. A prominent example of this problem is MVC 19/80LV, which is named Kunlid Corona, yet it is a large volcano with a 100-km summit caldera. And many names submitted as a result of this catalog and included tentatively have not been used in IAU nomenclature decisions. The interested student is encouraged to refer to the most recent IAU nomenclature list if there is any question.

Several lists that identified just one individual type of volcanic feature have been generated and these have often been used in constructing IAU lists. Also, due to variations in assumed defining characteristics and differences in interpretation, many individual features may have been assigned to different feature types in other surveys of individual feature types. For example, some lists are concerned with identification of corona give precedence to structural characteristics, whereas in this listing the presence or absence of distinct radial lava flows is used to first identify whether a volcanic center is present. Our list is based on complete examination of all volcanic centers and was thus able to assign individual features to different categories on a the basis of a broad overview of the characteristics of all types. Thus each category in this list tends to be more exclusionary than many lists of individual feature types. Because it includes all categories, this catalog represents a balanced identification of all volcanic centers based on fixed and well-thought-out criteria.

5. Comments. Comments have been kept to the minimum necessary in order to note any salient characteristics or to describe relationships with other features.

Abbreviations. The following abbreviations are used throughout the catalog: *MVC* = Magellan Volcano Catalog; *AR* = Arachnoid; *IV/SSD* = Steep-Sided Dome ("pancake"); *CO* = Corona; *LC* = Lava Channel; *FF* = Festoon Flow (unusual flows); *LF* = Lava Flow, Lava Field; *IV* = Intermediate Volcano; *LV* = Large Volcano; *IV/FD* = Fluted Dome (or modified dome); *RFC* = Radial Fracture Center; *IV/RP* = Radially Pattern volcano; *SF* = small Shield volcano Field

fields and channels) on Venus. Spatial concentrations as well as morphologic groupings are common. The latter include four broad morphologic categories: volcanoes, volcanic fields, magmatic centers (intrusive), and lava fields and plains. Beta–Atla–Themis Regiones, an area of nearly hemispheric concentration of volcanic and magmatic centers several times the global average number density, is a region dominated by relatively higher surface elevation and numerous riftlike patterns of fractures and deep linear chasmata (Fig. 1, see also color insert). Several large volcanic rises consisting of exceptionally large volcanic complexes and many smaller concentrations of volcanic centers appear to be associated with large rifts, rift intersections, and complex global-scale patterns of extension. Because features believed to be representative of mantle upwelling, such as coronae, are common in these clusters, large concentrations of volcanic centers and rifts like these might represent global mantle anomalies resulting from patterns of convection and regional mantle upwelling. In all of these associations, linear arrangements of volcanic centers are not common. The overall distribution of volcanic centers and coronae on Venus is thus more analogous to the distribution of hot spots related to mantle plumes on Earth than volcanism associated with plate boundaries.

Note on the Magellan Volcano Catalog. The following section defines and describes the principal identified volcanic features on Venus and shows some examples of each of the basic types. The text reviews some of their associations, interpreted origins, and remaining questions about their characteristics and origins.

The level of geological details available from Magellan image data is such that many of the centers may be assigned with reasonable certainty to a broad class of relatively well-known geologic phenomena, such as volcanoes or calderas, and the need for generally nongenetic terminology is reduced. Detailed division of feature types is generally more nongenetic. Several nongenetic terms for many large-scale features originated during the analysis of Venera 15/16 image data because the resolution was such that the geologic origin of many large-scale structures, such as coronae or arachnoids, was indeterminate. Similar informal terms were used early in the Magellan mission for many types of newly identified morphological features. An attempt was made with some preliminary terms used by the Magellan team to use Latin derivative terms, as was done successfully with tesserae earlier. Informal usage of Latin in addition to informal and colloquial terms in general impeded this approach and resulted in errors. These

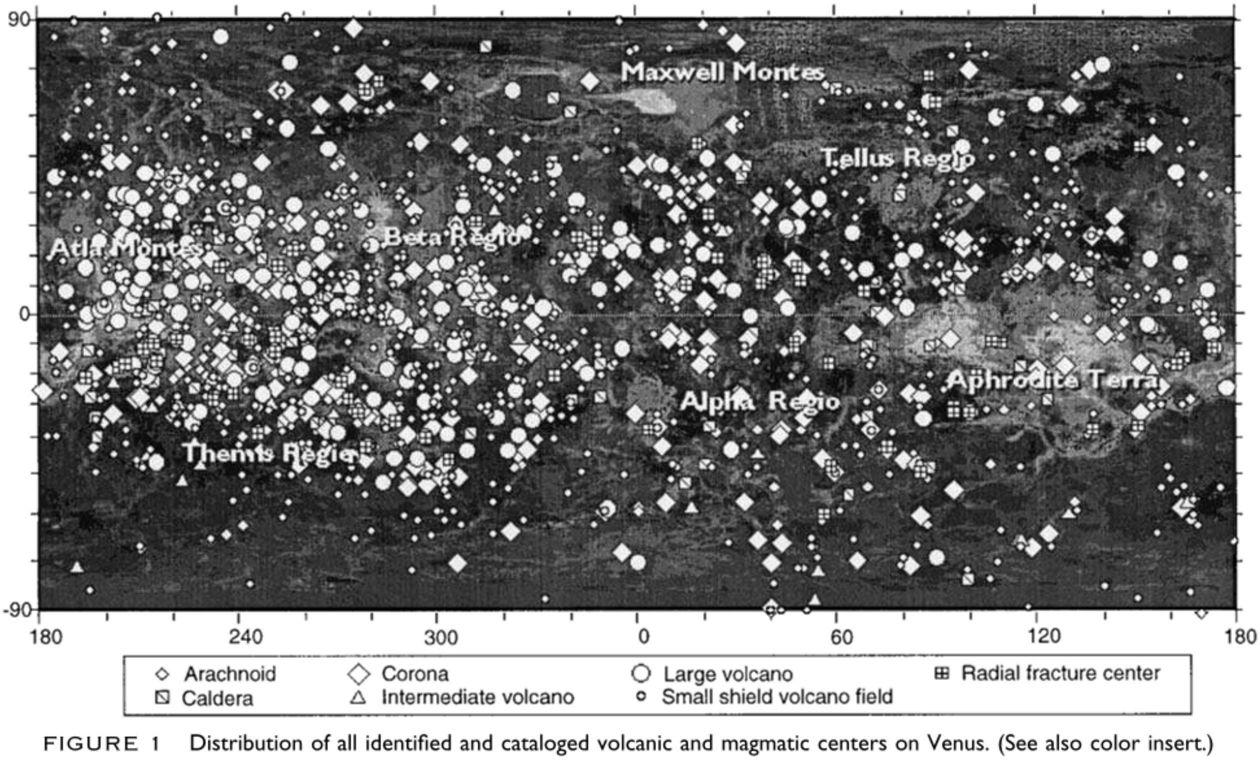

FIGURE 1 Distribution of all identified and cataloged volcanic and magmatic centers on Venus. (See also color insert.)

TABLE II Additional Venus Feature Reference Lists

Feature type	*Reference*
Steep-sided domes	Pavri *et al.*, 1992
Coronae	Stofan *et al.*, 1992
Channels	Baker *et al.*, 1992
Large flow fields	Crumpler *et al.*, 1997
Radial fracture centers	Grofils and Head, 1996
Large volcanoes	Crumpler *et al.*, 1997
Fluted domes	Bulmer and Guest, 1996

Baker, V. R., Komatsu, G., Parker, T. J., Gulick, V. C., Kargel, J. S. and Lewis J. S. (1992). Channels and valleys on Venus: Preliminary analysis of Magellan data, *J. Geophys. Res.* **97,** 13421–13444.

Bulmer, M. H., and Guest, J. E. (1995). Modified volcanic domes and associated debris aprons on Venus. *In* "Proceedings of the Conference on Volcanic Instability on Earth and Other Planets," Geological Society of London Special Publication No. 110.

Crumpler, L. S., Aubele, J. C., Senske, D. A., Keddie, S. W. Magee, K. and Head, H. W. (1997). Volcanoes and centers of volcanism on Venus. *In* "Venus II" (Bougher *et al.*, eds.), Univ. of Arizona Press, Tucson.

Grosfils, E. B., and Head, J. W. (1996). The timing of giant radiating dike swarm emplacement on Venus: Implications for resurfacing of the planet and its subsequent evolution. *J. Geophys. Res.* **101,** 4645–4656.

Pavri, B., *et al.* (1992). Steep-sided domes on Venus; Characteristics, geologic setting, and eruption conditions from Magellan data, *J. Geophys. Res.* **97,** 13445–13478.

Stofan, E. R., Sharpton, V. L., Schubert, G., Baer, G., Bindschadler, D. L., Janes, D. M., and Squyres, S. W. (1992). Global distribution and characteristics of coronae and related features on Venus: Implications for origin and relation to mantle processes. *J. Geophys. Res.* **97,** 13347–13378.

and other problems are of the type that are sorted out with usage, but should be noted and avoided. Currently, the term "corona" seems to be accepted; "arachnoid" is not favored by many researchers but may have been in use long enough to continue. We find that "arachnoids" are distinguishable as a subclass of corona.

For reasons having to do with the direction of detailed research following the completion of the Magellan mission, several lists of specific types of volcanic centers were generated by different investigators (Table II). Some of these lists include centers smaller than 20 km. Others are focused on a particular type, are more inclusive, and contain features that we have assigned, on the basis of examining all volcanic and magmatic centers, to other categories. Many of the thematic papers listed in the bibliography contain additional listings of volcanic features. For these and other reasons discussed below, the reader is referred to these lists for alternative interpretations and dimensional measurements.

B. Volcanoes

The following landforms are classed as volcanoes and are defined as centers of activity dominantly characterized by patterns of radial or circular extruded material extending over 360° from the central vent. This is to distinguish them from the broad class of features referred to as "magmatic centers" in which structural characters are the sole or dominant expression of the center of activity and to distinguish them from areas of extensive volcanism, principally lava flow fields, in which the volcanic materials do not constitute a well-defined edifice.

1. Large Volcanoes

These are volcanic centers (diameters $\geq$100 km) characterized by radially dispersed lava flows, frequently associated with concentric or circular central features and radial fracture patterns and centered on a region of positive topography as indicated either by radial lava flows, by topography inferred from radar characteristics of slopes, or by altimetric radar observations. The lateral dimensions are measured to the average distal end of the associated digitate lava flows that compose the circular part of the edifice; unusual flow fields that run out from a central volcano over great distances in one direction are not specifically included in the dimensional estimate given in Table I. Although large in lateral dimension, most large volcanoes on Venus are actually relatively low in relief, averaging approximately 1.5 km high. Although volcanoes of equivalent diameter occur on Mars, the volumes of large volcanoes on Venus are actually much less because their relief is an order of magnitude lower. Very large volcanoes (exceeding several thousand kilometers in diameter) may be further referred to as "volcanic rises" to allow for the possibility that some or much of the observed topography may be nonconstructional (uplift, "swell," etc.).

A total of 168 large volcanoes have been identified and occur preferentially in intermediate to higher elevations, particularly in broad rises and at the junctions of extensive rifts, chasmata, and belts of fractures. They are morphologically diverse, implying variable levels of volcanological complexity and evolution. Because the radial pattern of lava flows is diagnostic of a volcanic center, in our classification the presence of radially dispersed lava flows is accorded priority over concentric structures. For this reason, some features identified by other researchers as coronae, including those in discussions of Venera 15/16 results, are here considered large volcanoes.

Several fundamental morphological types of large volcano have been identified based on caldera sizes, associated fracture patterns, subsidiary intermediate and small volcanoes on their summits and flanks, and relationships with other identified types of magmatic features. The simplest examples are characterized by a relatively simple radial array of lava flows. An example is Chloris Mons (Fig. 2). Chloris Mons illustrates several of the characteristics typical of the less complex volcanoes. The distal ends of the flows are commonly radar bright and are interpreted to be relatively rough and blockier. Scattered about the summit are small volcanoes, many with steep-sided morphology and central pits, yielding an overall morphology analogous to many terrestrial shield volcanoes such as Etna or Mauna Kea in which subsidiary cones are build around the summits. The summit region is relatively radar dark compared with the lower flanks and topographic summit. Origin of the darker terrains around the summit is unknown; potential causes include lower radar reflectivity due to ash, unusually smoother lava flows, or altitude-dependent chemical phases. The circular shape of the dark area together with faint concentric bands that may be underlying fractures suggests that the dark region may lie within a former caldera-like summit depression, in which case the dark characteristic reflects the accumulation of relatively radar-absorbent dust and ash in low-lying and flat regions near the summit. Superimposed and buried within the pattern of flows and domes are arcuate and radial fractures, suggesting that the volcanic center is in some way associated with radial deformation, either being responsible for the pattern or located on it by virtue of the intersection of preexisting fractures. The occurrence of volcanic centers at loci of global and regional patterns of fractures and rifts is a common characteristic of magmatic centers on Venus.

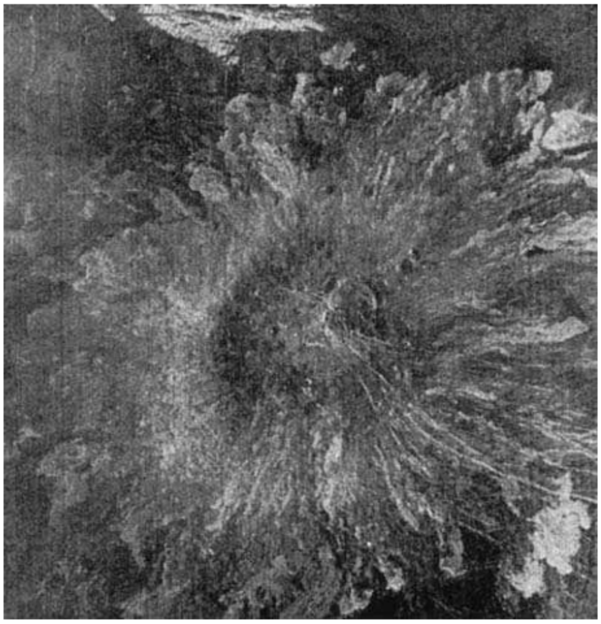

FIGURE 2 Chloris Mons, 300-km-diameter large volcano with numerous digitate bright and dark lava flows, radiating fractures, and several small volcanoes with steep-sided dome morphology near the summit. Like most large volcanoes on Venus, Chloris Mons is a shield volcano. The origin of the concentric bright and dark areas near the summit is unknown. Radar illumination is from the left in both images.

Other large volcanoes may be characterized by complex summit landforms, including strong radial fracture patterns, annular structures similar to coronae, and even multiple and large domical summits. Although the nature of domical volcanoes on Venus is not clear (see discussion of steep-sided intermediate volcanoes below) the presence of such features on the summits of many large volcanoes may be viewed as representing secular evolution of the eruptions during the history of the individual large volcano analogous to late-stage silicic volcanism or late-stage, volatile-rich, pyroclastic-dominated activity in evolved terrestrial volcanoes. Together these characteristics hint at the presence of underlying reservoirs that undergo some type of evolution with time.

2. *Intermediate Volcanoes*

Volcanic centers between 20 and 100 km in diameter are considered "intermediate" between the diameter of small volcanoes and the more prominent large volcanoes that are generally several hundred kilometers in diameter. The term was originally defined from Venera 15/16 radar data.

Several informally named morphologic types of intermediate volcanoes have been identified and include "radially patterned volcanoes," "steep-sided domes," "scalloped domes," "modified domes," or "fluted domes." A total of 289 intermediate volcanoes are recognized. Intermediate volcanoes are notably concentrated in the Beta–Atla–Themis areas. Fluted domes and steep-sided domes frequently occur together and also occur in association with coronae. Otherwise undistinguished volcanoes in this size range are listed here simply as "intermediate volcanoes" and are analogous to simple large simple large shield volcanoes.

"Radially patterned volcanoes" (Fig. 3) are characterized by multiple radial digitate lava flows of strikingly uniform length. The radial lava flows are typically radar

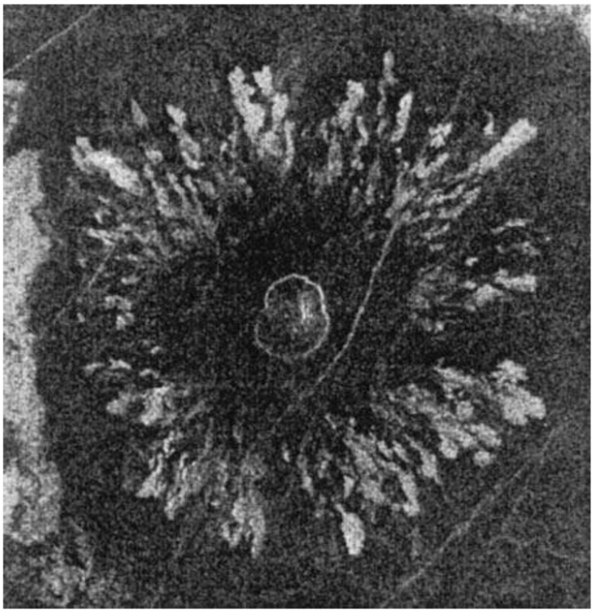

FIGURE 3 A simple intermediate volcano (MVC-9.5/201 IV/RF, courtesy of NASA) 20 km in diameter with radial bright and dark lava flows and a summit caldera. Radar illumination is from the left.

bright at their termini, suggesting increased roughness and blockiness at the distal ends. Also similar to large volcanoes, the summits are frequently relatively dark either as a result of the smoothness of near-vent lava surfaces or due to some radar-dark mantle, such as ash.

"Steep-sided domes" are among the more interesting and enigmatic intermediate volcanoes on Venus. They are also morphologically diverse, including domes that are relatively convex (Fig. 4), domes that are relatively flat on their summits and bounded by steep flanks, or domes that are "pancake-like," broad and flat, very circular, and steep along their perimeter. Others are simple inverted-bowl shapes or shield-shaped edifices. They frequently occur in clusters, or appear to be overlapping. In detail, many steep-sided domes on Venus have small summit pits and complexly patterned fractures on their surfaces. The circular form typical of steep-sided volcanoes appears to be the result of radial growth of a single extrusive mass, analogous to silicic domes on Earth. However, in size (typically 20–40 km and up to 80 km) and in terms of their remarkable circularity, they are unlike the relatively small domes associated with silicic volcanism on Earth.

Several origins have been proposed for steep-sided domes. One possibility is that the domes represent evolved magmas. A flat, pancake-like dome occurs near the Venera 8 landing site, where the surface materials were found to have anomalously high K, U, and Th typical of more alkalic rock compositions such as trachyte. Some steep-sided domes are associated with coronae, particularly along their characteristic ring fractures, implying an origin possibly related to petrologic evolution of large magma bodies responsible for coronae. Others occur on complexly fractured and elevated regions of tessera, suggesting melting or incorporation of preexisting thick crustal rocks into shallow reservoirs and subsequent evolution of more evolved compositions. Another model suggests that the magmas need not be silicic but could be intermediate or even basaltic due to unusual properties of viscosity resulting from excessively high volatile concentration. In the extreme pressures of the atmosphere of Venus, sufficient volatiles could result in a bubble-rich froth but disruption and bursting of bubbles typical of pyroclastic eruptions and ash flows may be impeded. Bubble-rich silicate "foams" occur in isolated instances in lava flows on Earth under certain conditions although not in the cubic kilometers required for formation of the typical steep-sided dome observed on Venus. Large-volume ash-flow eruptions on Earth may be an analogy in terms of volume. The result on

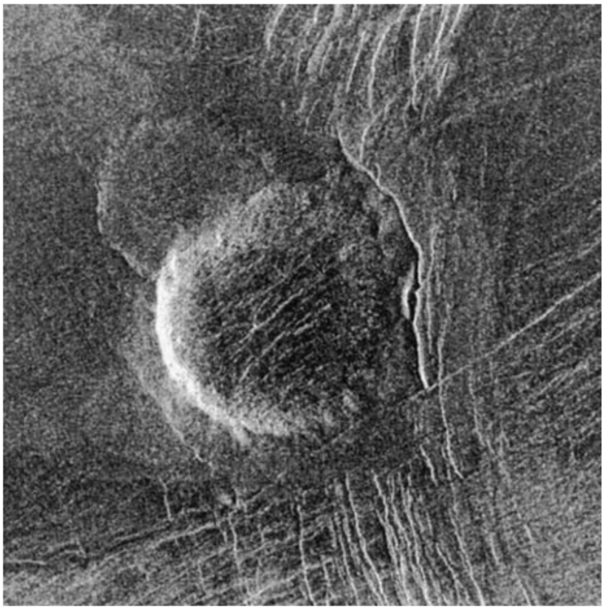

FIGURE 4 A typical steep-sided dome with a convex profile. The particular example (MVC-26/80 IV/SSD, courtesy of NASA) is 40 km in diameter. It is located on a set of annular fractures defining the margins of a corona. The common occurrence of steep-sided domes in association with coronae is further evidence for the presence of shallow magma reservoirs in association with coronae. Radar illumination is from the left.

Venus might be a bubble-charged fluid or voluminous foam. Regardless of the mechanism, the widespread occurrence of steep-sided domes over a large range of scales implies that it is a common process on Venus.

Whereas many steep-sided domes are circular, some have apparently collapsed partially, resulting in a distinctly modified appearance in which deep scallops mar the flanks. In some, the collapsed material has flowed out to form a knobby terrain at the foot of the collapsed flank. Given that the steepest part of the flanks of many steep-sided domes approaches 30°, collapse of the margins in some is understandable. The origin of such gravitational instabilities may not be entirely spontaneous. There are several examples of steep-sided domes that predate nearby impact craters, yet their flanks are relatively undisturbed. The timing of the collapses with respect to the emplacement of the domes cannot be determined, so it is possible that such instabilities are part of the emplacement process rather than a degradation of older domes.

Another common morphology of steep-sided domical edifices on Venus is "fluted domes," characterized by relatively flat upper surfaces, frequently with a central depression or pit, and relatively steep margins with radial buttress-like ridges or flutes. There are tremendous variations in this basic theme: some examples are similar to many steep-sided domes with the exception of their unusually ridged margins (Fig. 5), and others have odd morphologies with deep central depressions, high-standing margins, and regularly arrayed radial ridges.

Considering the similarity of some fluted domes with modified steep-sided domes, one possible interpretation of fluted domes is that they are steep-sided domes in which the outer flanks have collapsed around the entire perimeter, leaving behind distinctly scalloped heads of collapse areas cradled between high-standing chutes. This interpretation is consistent with the "bubble foam" model of steep-sided dome formation in that an edifice built from such materials may be structurally weak. The similarity to some "starfish" seamounts bearing radiating ridgelike rift zones has also been noted. Although they are morphologically similar to some terrestrial tuff rings, their extremely large dimensions (up to 60 km) and close association and morphological similarity with steep-sided domes suggest nonexplosive origins.

3. Small Volcanoes and Fields of Small Shield Volcanoes (Colles)

Small (<20-km diameter) volcanoes are the most abundant volcanoes on Venus and number in the hundreds of thousands, if not millions. Their abundance is so great that they defy identification and tabulation individually. Small volcanoes exhibit almost all of the same characteristics seen in intermediate and large volcanoes, including steep-sided domes, modified and scalloped domes, radial-patterned volcanoes, and, the most abundant morphology, simple low shield volcanoes. Their closest terrestrial analogy in terms of abundance is the small volcanoes that occur on the seafloor of Earth. On Venus, they occur in plains as well as on the flanks of large volcanoes, in rift settings, and within corona and are abundant in the two large regions near Beta Regio and east of Tellus Regio in the Akkruva Colles region.

The most salient characteristic of small volcanoes is their tendency to cluster in fields (Fig. 6). Localized concentrations of small, shield-shaped volcanoes are considered to be "fields" in the sense used in terrestrial volcanology. There are 647 identified fields of small volcanoes, or "shield fields," each consisting of several tens to several hundreds of vents and ranging from several tens to several hundreds of kilometers in diameter, measured across the areal extent of the fields. As with terrestrial volcanic fields, shield fields clearly represent a concentration of numerous small volcanic vents over a localized source supplying magmas at rates insufficient to build a single edifice. The common occurrence of shield fields within the interior of many coronae and

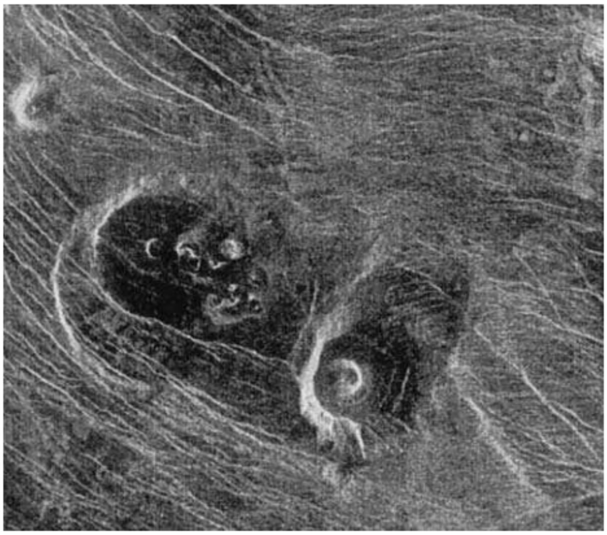

FIGURE 5 MVC-13.5/252 FD (on right) is a 25-km-diameter fluted dome. A deep central crater on the summit has an inverted conical profile. The morphology of the other domes in this image is transitional between typical steep-sided domes and fluted domes. Pancake-like steep-sided dome at left (MVC-13.5/251.5 SSD, courtesy of NASA) is 35 km in diameter. Radar illumination is from the left.

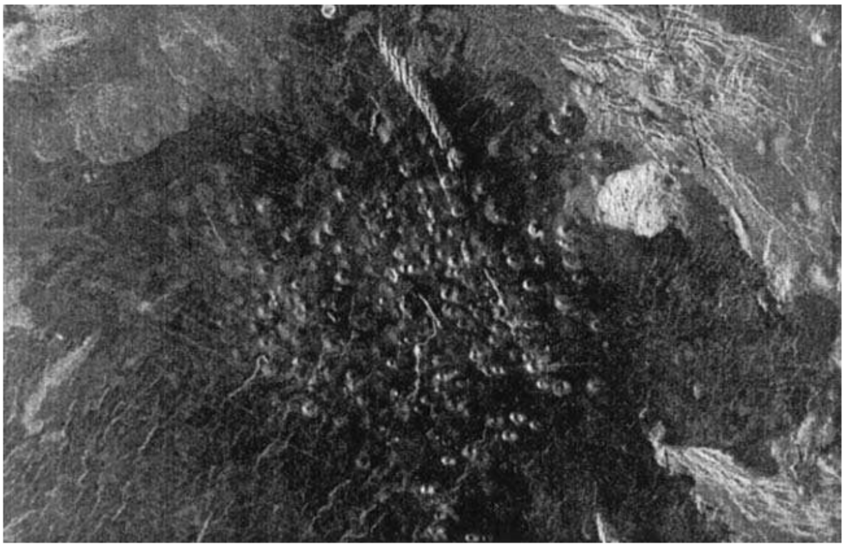

FIGURE 6 A typical small volcano field or "shield field" (MVC-52/302.5 SF, 150 km in diameter, courtesy of NASA) with associated radar dark lava flows that inundate the surrounding plains. Some of the small volcanoes are steep-sided domes, whereas others are shield shaped. Individual volcanoes are several kilometers across. Radar illumination is from the left.

arachnoids is consistent with the interpretation that such large-scale annular structures (see discussion later below) represent relatively localized mantle melting or shallow bodies of magma. It is useful to speculate that annular deformation patterns may characterize fields and large volcanic provinces on Earth but are not as a rule recognized because of the dimensions (several hundred kilometers) and continual erosion that acts to erase any such subtle structural characteristic nearly as fast as it is generated.

In addition to their occurrence as discrete fields, many small shield volcanoes occur with nearly uniform spacing over vast areas, resulting in what are known as "shield plains." There is no terrestrial precedent that may be used as an analog in understanding the origin and emplacement of shield plains except perhaps oceanic seamounts. When examined in detail, shield plains on Venus are found to be among the oldest plains preserved, stratigraphically overlaying (younger than) tessera. Thus they appear to represent small volcano production that occurred over broad regions early in the preserved history of Venus. There is no evidence for structural control on the location or alignment of small volcanoes within shield plains. This implies that their emplacement was remarkably isotropic for a process that was widespread and dependent on lithosphere properties for access to the surface. Considering the abundant evidence for structural control of vent locations in most volcanoes on Venus together with their great age, the emplacement and significance of shield plains are among the more intriguing volcanologic mysteries on Venus.

4. *Calderas (Often, Patera)*

A typical caldera is circular to elongate in shape, surrounded by an annulus of closely spaced fractures along the topographic rim, a floor from 1 to 3 km below the surrounding terrain, and evidence for associated surface volcanism (Fig. 7). Calderas frequently develop at the site of extensive prior eruptions. They are characterized mainly by concentric patterns of enveloping fractures and other geologic characteristics indicative of a depression formed through collapse of the surface. A total of 97 calderas are identified and are most abundant in the size range 60–80 km, with depths up to several kilometers. In many cases the floor is dark and appears to be flooded or partially covered with later flows. Some calderas are the loci of intensely fractured concentric patterns bearing very little evidence of subsequent surface eruptions. This suggests that most of the room for collapse may have been accommodated by lateral intrusions along the typically strong regional patterns of riftlike fractures.

Radial flows may be distinguished in some cases, some of which appear truncated by the central depression. Such examples are identified as calderas in our listing instead of volcanoes in deference to the greater morphologic expression of the collapse feature over any con-

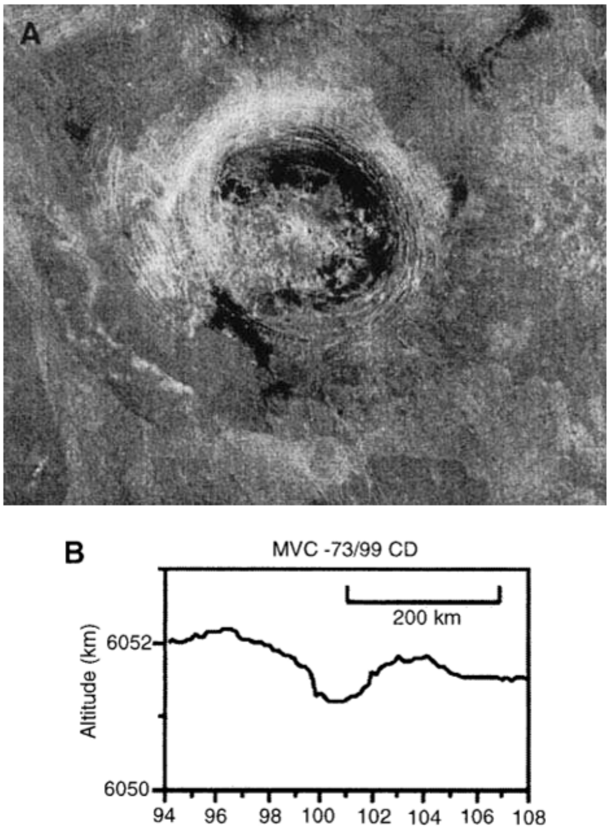

FIGURE 7 (A) A circular caldera (MVC-73/99 CD, 175 km in diameter, courtesy of NASA) encircled with numerous ring fractures. Radar illumination is from the right. A complex array of small volcanoes and radar-bright lava flows contrasts sharply with the radar-dark floor. Note that surrounding plains lavas have partially inundated the ring fractures, suggesting that a slight raised rim occurs where the fractures are preserved. (B) Magellan radar altimetry profile indicates that the floor lies 1 km below the surrounding terrain. This caldera has been identified as a corona (Mykh-Imi Corona) in some other studies, illustrating the confusion in terminology and IAU naming. Shield fields occur to the east (MVC-73/104 SF) and north (MVC-71.5/99 SF).

structional feature. It is useful to note that "caldera" is more interpretive than are the terms "arachnoid" and "corona," which are similar in some respects, including their dimension and some structural characteristics. The use of the term caldera for a volcanic feature on Venus implies that the feature so-named is comparable in apparent geologic mechanism of formation to calderas as defined on Earth and on the other solid terrestrial planets. Calderas on Venus are defined, as they are on Earth, as a large volcanic collapse depression that is circular, or approximately circular, in plan shape, the diameter of which is many times greater than any included vents. There are only a few features recognized as calderas above 100 km in diameter, and the sudden onset of features identified as arachnoids and coronae above that diameter suggests that calderas, arachnoids, and coronae may be related. Annular deformation processes associated with the underlying magma body may be associated with the caldera formation process (or its volcano-tectonic equivalent) at its extreme upper scale. In addition to annular patterns of strain, regional strain patterns associated with emplacement of radiating dikelike bodies could be a component of the overall structure.

C. Lava Flows and Channels

1. *Plains Lavas*

Most of the surface of Venus consists of relatively low elevation, flat, and featureless plains. They are generally radar dark as a result of their smoothness. From the way these plains embay structures and surround local relief features, it is clear that most of the surface is a result of extensive flooding with widespread lava flows. In most of the images reproduced here, the darker areas are examples of these types of flooded surfaces. Many of these were emplaced at or near the same time, early in the observable geologic record of Venus. The hypothesis that Venus was globally and nearly completely resurfaced during a short geologic time interval arises from the pervasiveness and similarity in stratigraphic position of many of these plains (in addition to the low number of recognized impact craters on the plains).

2. *Lava Flow Fields (Fluctii)*

These are distinguished from the lava plains described above by numerous digitate flows notable for their great lengths (10^2–10^3 km long) and unusually large area. Many of these consist of flows thousands of kilometers in uniform directions, indicative of the relatively uniform regional slopes. Several specific informal subtypes of lava flow are noted. Lava floods (also formally, "fluctus") consist of radar-bright and radar-dark lava flow fields, generally digitate in plan and exceeding several hundred kilometers in length, that have flowed in one direction from an apparent source area. The source areas for these floods are often associated with intense bands or belts of linear fractures and riftlike chasma. Some sources have numerous small volcanoes (Fig. 8), and others are the site of calderas. Nearly one-half of all coronae are predated by areally extensive lava flow fields. This asso-

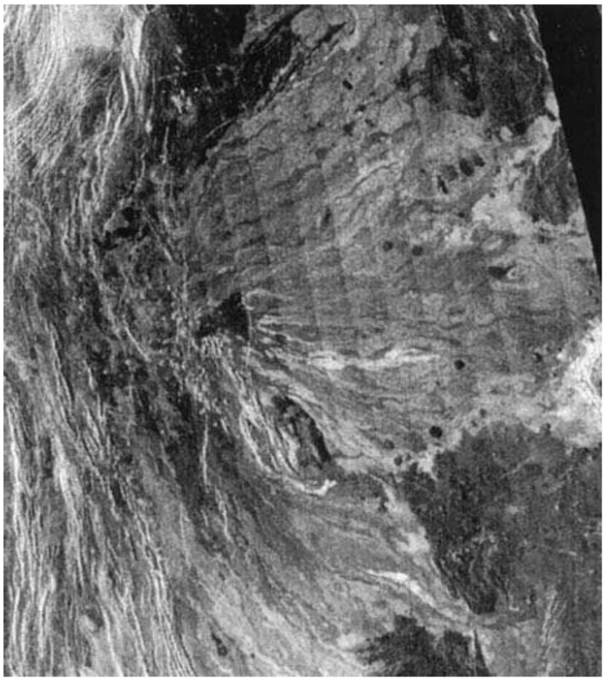

FIGURE 8 Turgman Fluctus (MVC 56/218 LF, courtesy of NASA), a typical large lava flow field consisting of digitate radar-bright and radar-dark flows fanning out from a common point. Many flow fields like this one have sources located on ridge belts. Note the small volcanoes located near the source area. Radar illumination is from the left. Image width, 400 km.

ciation is consistent with the current model for coronae formation as the surface expressions of mantle plumes. Voluminous melting and lava eruption might be anticipated as a result of pressure-release melting as the plume arrives in the shallow mantle.

3. Unusual Lava Flows

Flows with transverse ridges, troughs, and other fluid banding characteristics include radar-bright flows that show organized patterns of internal streamlines analogous to the ridges and flow bands typical of viscous terrestrial lava flow. Several large, lobate, festooned, and thick lava flows occur at isolated points on Venus. The simplest interpretation based on their resemblance to viscous and silicic lavas on Earth is that they are unusually silicic in composition compared to most large flow fields. However, as is the case for steep-sided domes, more mafic composition lavas with unusual viscosity characteristics arising from bubble-rich eruptions are also possible.

4. Lava Channels (Canali)

These are linear to sinuous parallel-sided valleys that are from 0.5 to 1.5 km wide and up to 10 km wide, may extend for 10^2–10^3 km in length, and occur frequently within areas of lava plains or plains associated with larger volcanic centers (Fig. 9A). Several morphologically distinct types of channels have been identified. "Simple" channels are isolated, narrow channels that frequently meander across plains. "Complex" channels may be characterized by multiple channels, frequently with an anastomosing, braided, and even distributary morphology. "Compound" channels exhibit characteristics of both simple and complex channels in combination, and "integrated" channels are analogous to branching valleys such as those associated with sapping processes on Mars and Earth.

The longest channel is over 6800 km long, the record holder for any single channel in the solar system. (The length of the Nile River is 6497 km.) Formation of a lava channel of this length defies our current understanding of likely emplacement processes. The great length and occurrence within extensive plains imply extremely fluid materials with viscosities as low as 0.1 Pa s (comparable to the viscosity of water). Viscosity for basaltic lava flows ranges from 1 to 100 Pa s. Potential lava-forming fluids with a viscosity of 0.1 Pa s include ultramafic compositions such as komatiites, high-Ti lunar-type basalts, carbonatites, and sulfur flows. The great width of most channels, particularly the longer examples, implies that they are not simply collapsed lava tubes. Because our current understanding of Venus excludes the possibility of significant amounts of water now or in the past, the fluid must be related to the emplacement of the volcanic plains lavas. The most likely scenario at present is that the dense atmosphere of Venus resulted in rapid cooling of lavas to form discontinuous, platelike crusts riding on the fluid filling the channels, thus enabling one of the likely silicate compositions to remain molten over great distances with relatively little cooling. Carbonatites and sulfur flows are attractive alternatives, especially due to the abundance of sources for carbon and sulfur on Venus. Current estimates suggest that although these materials have melting points below that of the surface temperature of Venus, thus enabling them to act essentially as water does on Earth, neither material appears to be stable in the surface environment, making them unlikely to survive as fluids long enough to form channels of the observed length.

One final characteristic of channels that makes them of interest beyond their volcanologic significance is that they record changes in elevation subsequent to their

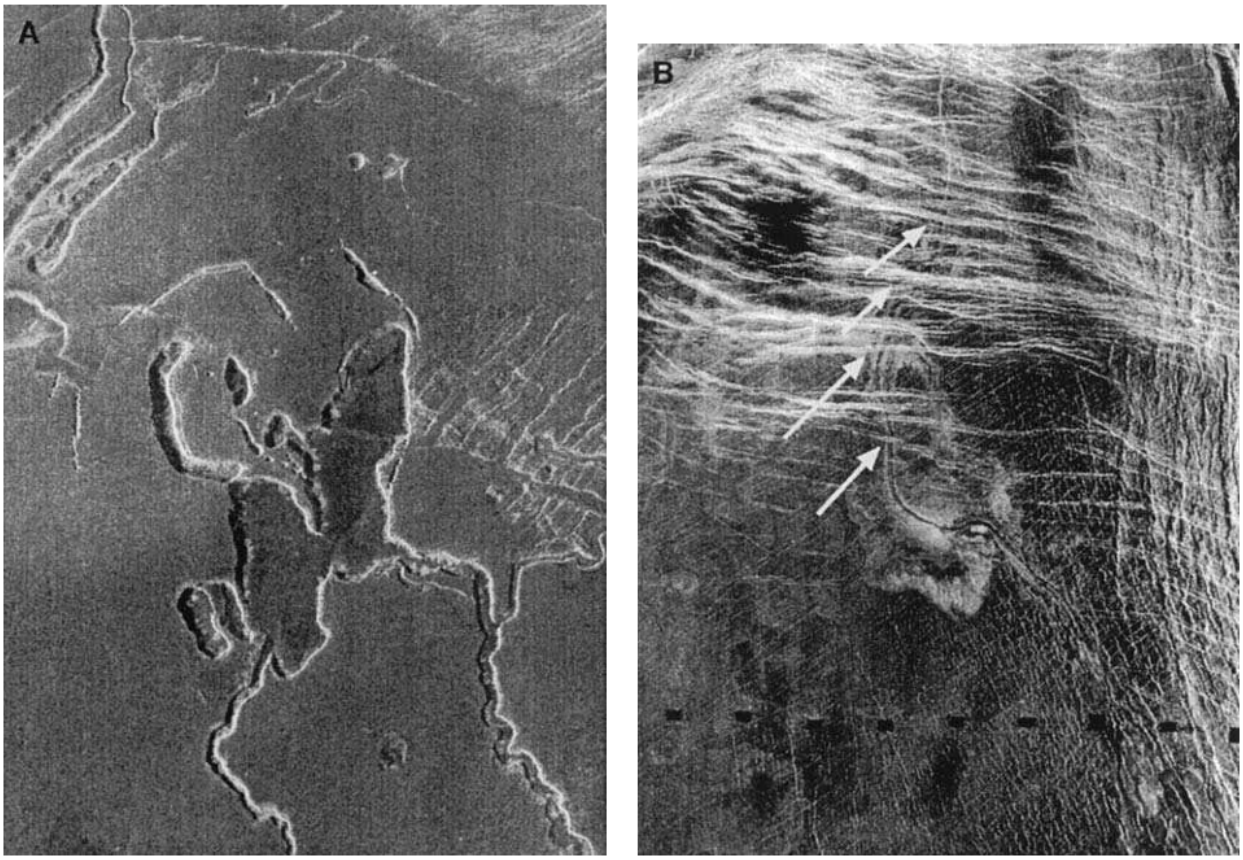

FIGURE 9 (A) Lava channels (MVC-12/90 LC) emerging from an irregular collapsed region. Radar illumination is from the left. Image width, 100 km. (B) Part of an extensive plains lava channel (MVC-35/251.5 LC), this channel has been crossed by subsequent ridges (arrows) during deformation of the plains. Radar illumination is from the left. Image width, 300 km. (Photos courtesy of NASA.)

emplacement. Using Magellan altimetry data, significant undulations in the regional relief can be detected along the length of many channels such that locally the gradient of the channel floors is reversed in places from that which must have existed during their emplacement. These influences are particularly apparent where sinuous ridges that occur throughout the plains areas of Venus, similar to wrinkle ridges on the Moon, intercept channels (Fig. 9B). These changes in elevation imply that, on a geologic timescale, the surface of the plains has swelled and rolled like great seas in slow motion, thus preserving the fundamental motion of a planetary surface in response to mantle convection and tectonic strains over geologic time.

D. Magmatic Structures

Many features on Venus are characterized more by surface deformation associated with subsurface magmatism on a large scale. In these features, volcanic edifices and lava flows may be relatively minor or subsidiary to the structures indicative of deformation. These include the broad class of features known as coronae, including subclass arachnoids, and radial fracture centers. The magmatism may be deep-seated reservoirs, or in the examples that are over several hundreds to 1000 km in diameter, the process of formation may be more allied to dynamic topography associated with regional uplift from upwelling mantle plumes. The close association of surface volcanism in many of these or the apparent evolution to or from large volcanoes and other landforms such as radial fracture centers (Fig. 10) further implies a close association with large magma bodies.

The term cauldron, which is applied to volcanic subsidence-related features on Earth regardless of size, shape, depth of erosion, or association with surface volcanism, may be appropriate for larger caldera-like structures such as arachnoids and coronae, particularly since surface volcanism in those features is frequently limited or

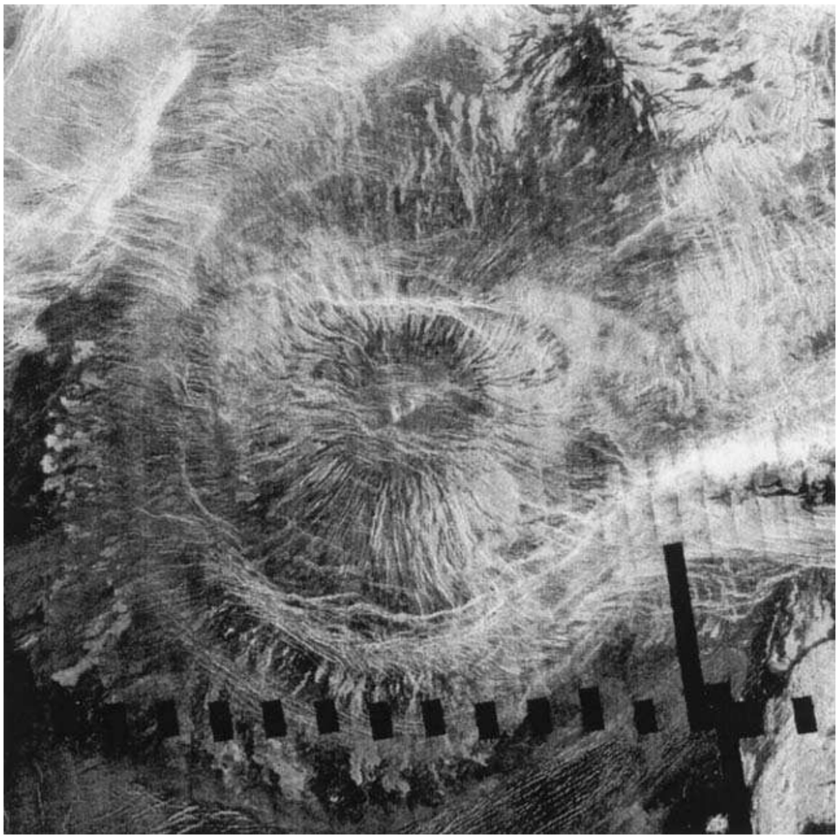

FIGURE 10 Large magmatic centers bearing the characteristics of large volcanoes, coronae, and radial fracture centers such as this example (MVC-14/164 LV; Miralaidji Corona, 600-km diameter, courtesy of NASA) are relatively common on Venus. Note the radial lava flows exterior to the annulus, indicating the original occurrence of a central edifice. Examples such as this imply that all of the large magmatic centers may have fundamentally similar origins, the differences in structure relating to differences in degree of growth, evolution, and modification of the reservoirs. Radar illumination is from the left.

absent. However, since most volcanic terms on Earth are laden with empirical and model-based interpretation, in planetary cases, where the origin of a feature is often not apparent or identifiable with any features on Earth, as is the case with arachnoids and coronae, a distinctive terminology is probably appropriate.

1. *Coronae*

These features, first identified on Venus from Earth-based radar data, are dominantly circular to elongate annular structures consisting of an annulus of ridges or fractures, an interior that is either topographically positive or negative, a peripheral moat or trough, and, frequently, numerous volcanic and tectonic landforms in the interior (Fig. 11). There are 208 coronae identified in the catalog on the basis of the criteria stated here. Coronae decrease in frequency with size from 200 to ~1000 km following an inverse exponential relation and are commonly between 200 and 250 km in diameter.

Topographically, coronae exhibit a variety of forms, including domical profiles, plateaus, plateaus with central depressions, and rimmed depressions. Coronae are included in the volcanological catalog because of the common association of related smaller volcanic centers and the apparent transitional relation of coronae to features of extrusive, constructional, or composite volcanological origin such as large volcanoes and calderas. Because of their great size and associated volcanism, they have been widely interpreted as associated with mantle plumes or hot spots, their topography resulting from a combination of uplift of the surface over mantle plumes and subsequent gravitational relaxation.

Coronae are one of the most extensively studied features of Venus and several models for the origin of coronae have been proposed. Since they are not simple depressions, but consist of annular ridges or concentric

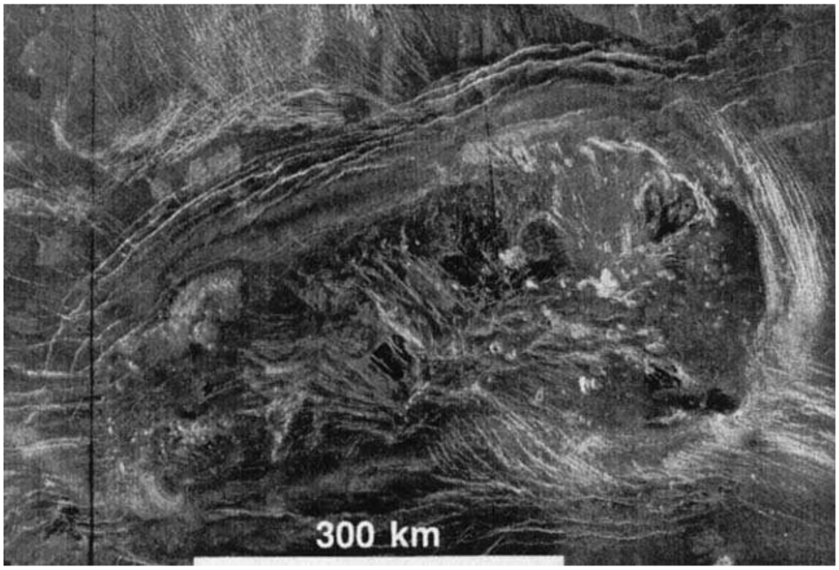

FIGURE 11 Demeter Corona (MVC-54.5/295 CO, 650 × 350 km, courtesy of NASA) is a typical corona and is defined as much by the annular structure as by associated volcanism. The widespread distribution of volcanic vents within the interior implies a locally diffuse, if regionally localized, underlying melt source. Radar illumination is from the left.

fractures with elevated interiors, the process must be related to both uplift and collapse, either concurrently, in sequence, or in cycles. One scenario suggests that coronae start out as radial fracture centers developed during arrival of a mantle "blob" beneath the lithosphere that bulges the surface and induces extensive radial arrays of fractures. Subsequent flattening of the blob against the lithospheric lid and continued uplift result in a plateau-like uplift and continued fracturing and associated volcanism. Subsequent relaxation of the uplift results in annular patterns of strain in the surface characteristic of "mature" coronae.

Because coronae, arachnoids, and large volcanoes may represent localized areas of mantle upwelling, a map of the distribution of coronae and related magmatic features suggests that mantle upwelling has been widespread but particularly concentrated in the hemisphere between. Atla, Beta, and Themis Regiones. Coronae and volcanism in this area tend to occur in association with extensive networks of riftlike chasma, suggesting that, if they are the results of mantle plumes, the concentration of rifting may be closely allied with the processes of an upwelling mantle.

2. *Arachnoids*

These are structures characterized by a combination of radial fracture patterns or ridges extending outward for several radii and a concentric or circular pattern of fractures or ridges. In many cases they include a few interior flows and small shield volcanoes within the interior (Fig. 12A). The radial fractures frequently merge outward with the linear patterns of the fracture belts on which arachnoids are arranged. The term "arachnoid" derives from this arrangement, like spiders along "webs" of linear fracture belts (Fig. 12B). The distinction between arachnoids and coronae is based on the relative abundance of radial versus concentric fractures/ridges, respectively. There also appear to be differences in average size. In general, arachnoid-like circular structures tend to be less than 200 km in diameter.

There are 265 identified arachnoids; thus they are second in abundance after shield fields. The relative dearth of other extrusive volcanic features associated with arachnoids may imply that magmatism associated with arachnoids is largely intrusive and that the radial ridges are compressional features related to subsidence-related deformation. The regional distribution of arachnoids is similar to that of coronae although somewhat more allied with regional rifts and fracture belts. In most other characteristics, arachnoids are similar to coronae and are likely to be a variation on the process of coronae formation in the presence of strong regional tensile stress fields associated with rifts and linear fracture belts. The radial fractures may be similar in origin to the radial fracture patterns described below.

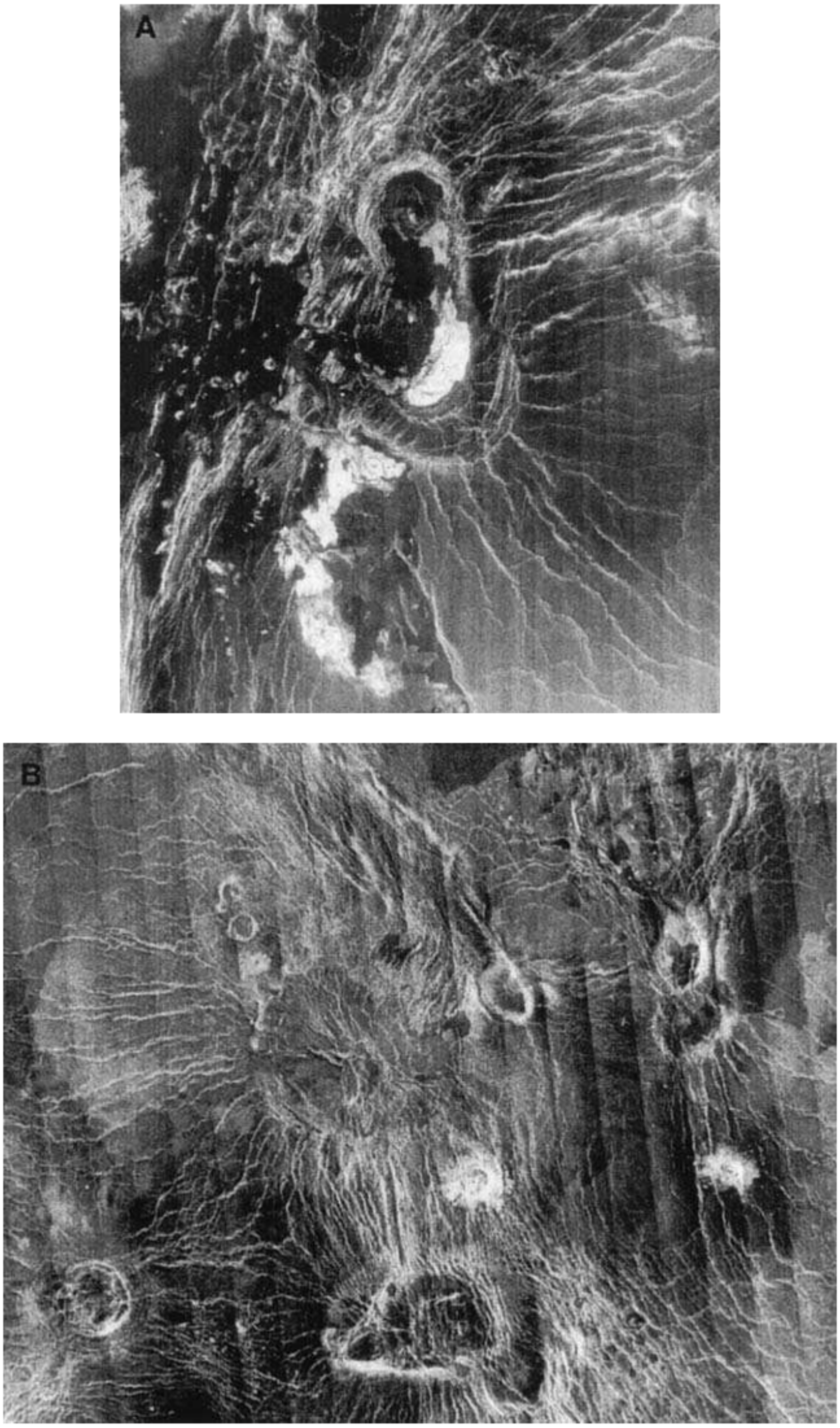

FIGURE 12 (A) Razia Patera (MVC-46/198 AR), a 200 × 100 km diameter arachnoid surrounded by a complex of radiating ridges and whose floor is covered with lava flows. Razia Patera is part of a local concentration of volcanic centers that includes several small shield volcanoes, small calderas, and radar-bright lava flows. Radar illumination is from the left. (B) Regional cluster of arachnoids of various sizes centered about a circular 100-km-diameter arachnoid (MVC-5.5/169 AR). Arachnoids resemble small coronae connected in a web of surrounding fractures. Radar illumination is from the left. (Photos courtesy of NASA.)

3. Radial (or Stellate) Fracture Centers

Prominent radial fracture patterns consist of a plexus of graben radiating from a common point (Fig. 13), resulting in a stellate pattern that frequently crosses preexisting structures and surrounding plains; concentric structure is absent. The stellate pattern is frequently centered on a broad domical topographic high (generally >100 km in diameter), in the center of radial flow patterns, in the interior region of large volcanoes, or within arachnoid-like and corona-like concentric structures. Radial fracture centers occur frequently in association with both large volcanoes and coronae, are clearly superimposed on large volcanoes and coronae in some examples, and predate large volcanoes and coronae in other examples. There are 64 significant radial fracture centers identified ranging from 50 to 300 km in diameter, occurring along the flanks of several rises and situated frequently in chains and at the centers of large volcanoes. As many as 160 radial fracture centers may be identified if those visible on more prominent features, such as coronae, arachnoids, and volcanoes (see Table II), are included.

Two different modes of emplacement have been proposed for radial fracture centers: (1) tensile fracturing associated with domical uplift, probably over shallow magma bodies, and (2) tensile deformation resulting from shallow subsurface dike emplacement. Although both mechanisms are probably influential in the development of radial fracture patterns, domical topography does not characterize all examples of radial fracture centers. Even if the topography has relaxed in such cases, the annular pattern of deformation predicted to occur upon relaxation (see discussion of coronae evolution above) is not present in all cases. In addition, many radial fracture patterns extend for distances much greater than any associated domical rise in the topography. As a result, not all radial fracture centers may be attributed to strain associated with uplift. The recognition that tensile fractures accompany shallow emplacement of dikes on Earth, the similarity to giant radial dike swarms, and the frequent association with clear centers of volcanic activity all suggest that radial fracture centers may be analogous to radial dike swarms. Radial fracture patterns in many cases may be the precursor for more evolved large magmatic centers such as coronae, arachnoids, calderas, and large volcanoes. In this model, they represent the initial events of deformation and magma emplacement upon arrival of upwelling mantle plumes be-

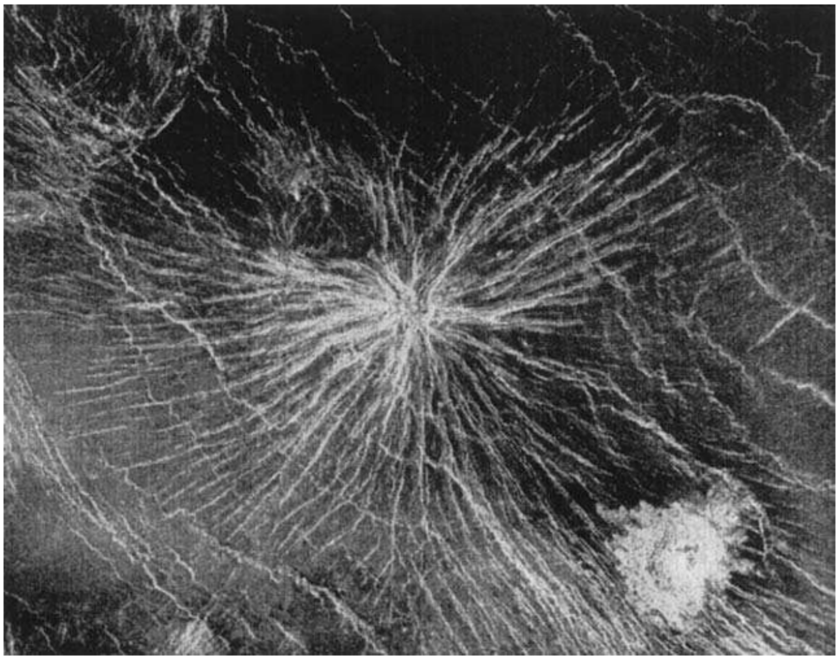

FIGURE 13 A simple radial fracture center (MVC-34/21.5 RFC, courtesy of NASA) located within ridged plains. This example illustrates the confusion between physiographic and volcanic terminology: although it is unlike any corona, it has been identified as a corona by the IAU and named Lilinau Corona. Note impact crater in lower right. Radar illumination is from the left. Image width, 230 km.

neath the lithosphere or initial emplacement of large bodies of magma within the lithosphere, lateral injection of radiating dikes in the shallow subsurface, and corresponding development of graben in the overburden.

III. FACTORS INFLUENCING VOLCANIC ERUPTIONS AND VOLCANIC LANDFORMS ON VENUS

Important questions and goals in the study of Venus include determining how the differences in surface and interior conditions are linked to the observed diversity and complexity of volcanoes. The influence of the extreme temperature and atmospheric pressure and density on magma eruption and emplacement both within the crust and lithosphere and on the surface are likely to be significant.

As yet unaddressed questions associated with the problem of large-scale magma transport and emplacement under the distinctly different conditions of Venus might reveal substantial insights into a variety of basic volcanological phenomena as well as enhance our understanding of the origin of the diverse styles of volcanism on Venus. For example, what governs whether a center of volcanism develops from magma effusions into a single large volcanic shield, a cluster of small shield volcanoes characterized by effusive flows, or a radial fracture center, a corona, or a caldera characterized by very little effusion and a large unerupted magma reservoir? Past study of volcanism and volcanic rocks on the terrestrial planets and recent studies of magma transport-related processes on Earth suggest that the three most important factors in development of individual volcanic centers on Venus are likely to be (1) magma composition, (2) environmental influences, and (3) magma ascent characteristics, specifically emplacement and replenishment rates.

A. Influence of Chemical Composition

Chemical composition is an important influence on the viscosity and volatiles abundances typical of erupted silicate melt. On Venus the question arises as to whether all the observed volcanic landforms are the results of silicate melts. As discussed above, the possibility of exotic compositions such as carbonatites and sulfur flows has been considered in order to account for the apparent extreme fluidity of lava channel-forming materials. The high abundance of sulfur (several percent) in the surface soil analyses of Vega 2 lander implies that sulfur may be important in the surface chemistry. Observed chemical compositions of silicate materials from Venera landers imply whole-rock compositions comparable to tholeiitic basalts, subalkaline basalts, and some evolved compositions with high alkalies.

B. Influence of Extreme Surface Temperature and Pressure

The surface temperature (700 K) and pressure (9.2 MPa) at the mean surface elevation of Venus differ substantially from the environment in which most of the characteristics of volcanism on Earth have been studied and corresponding differences in eruption characteristics and behavior of melts and volatiles on Venus are to be expected. Basically, the influences are thermal effects and pressure effects, although the ways in which these influence volcanism are subtle.

1. Influence of Surface Conditions on Eruptions

The influence of surface conditions on eruptions is primarily a result of the extreme pressure rather than temperature. Although the surface temperature is 700 K, this is far below the solidus of common silicate melts. Given the close chemical similarity between measured Venus surface compositions and terrestrial tholeiitic basalts, melt temperatures similar to those on Earth (1700 K) are likely for most volcanic eruptions. Even melt temperatures for rhyolitic eruptions (1200–1300 K) are far above the surface temperature. Calculations of the rate of cooling of a typical basaltic lava flow erupted onto the surface of Venus show that the temperature at the surface of the flow will be fractionally lower compared to that on Earth soon after eruption. This counterintuitive result merely reflects the enhanced convection in the dense CO_2 atmosphere. The cooling efficiency is such that it may be compared with a subaqueous eruption. In the longer term, the surface temperature of a lava flow will be greater on Venus as it cools to the higher ambient temperature, thus sustaining the length of time slightly over which the flow must cool before complete solidification. A predicted result is that lava crusts will develop more quickly on Venus than Earth, thereby enhancing the early formation of lava tubes.

The atmospheric density is therefore the primary influence. In fact, the pressure on the surface of Venus is equivalent to the pressures at 1 km in Earth's oceans, with many of the same predicted consequences. A significant influence of the high pressure is the suppression of gas exsolution, with important consequences for vesiculation of lava flows and pyroclastic disruption of erupting magmas at volcanic vents. For any magma bearing volatiles in concentration comparable to those on Earth (<2%), pyroclastic eruptions will be unlikely to occur. As a result, large pyroclastic eruptions and corresponding composite volcanoes and ash flows are unlikely to occur unless volatile contents of eruptions on Venus significantly exceed that common on Earth. Early observations of large increases in sulfur content of the upper atmosphere, originally ascribed to a large Plinian-type eruption process, suggest the possibility of significant volatiles. The occurrence of radar-dark areas around the summits of some large volcanoes, attributed to extensive ash deposits, may be an additional clue to the high volatile abundance. Either the erupting magmas may be significantly enhanced in volatiles by some poorly understood process or the interpretation of these phenomena as pyroclastic deposits and eruptions is in error. Similarly, vesiculation of lava flows should be suppressed. However, as discussed in the above section on steep-sided domes, volatile abundances in the normal high range of erupting magma may favor extensive vesiculation, if not disruption, of lavas, leading to extremely frothy basaltic eruptions. One consequence might be that an eruption that on Earth would result in an ash-flow eruption might on Venus result in a massive frothy outpouring. The resulting landform might resemble a giant viscous dome.

2. *Influence of Surface Conditions on Magma Ascent Characteristics*

The high ambient temperature of the lithosphere is likely to influence the thermal efficiency during magma transport so that magma in dikes and plutonic bodies is expected to experience less cooling during ascent. As a result, smaller and slower magma bodies are able to reach the surface than on Earth. This might in part explain the greater variety and distribution of volcanic centers on Venus relative to Earth: special conditions such as lithospheric plate boundaries are not necessary for magmas to make their way to the surface. The greater abundance of shield fields on Venus than that seen on the other terrestrial planets may be another consequence of the thermal efficiency on Venus of ascending magmas. Fields of volcanoes develop from ascent of individual bodies of magma directly from a local melting source instead of from the large, shallow reservoirs that are necessary for development of large magmatic centers. This is consistent with calculations of the magma replenishment rates necessary for shallow reservoirs (discussed further in the next section).

Magma ascent may be governed by the presence of variable magma buoyancy with respect to the country rock, a possible factor contributing to fundamental differences in volcanic style on Venus and on other planets. Here again the extreme atmospheric pressure may be a stronger influence on magma ascent. Because the crust and lithosphere of Venus are probably largely volcanic, the density in the shallow levels will be influenced by the density of erupted rocks. Given the extreme suppression of vesiculation and the greater abundance of lavas over pyroclastic materials, the density of typical crustal rocks will be greater than on Earth. One predicted consequence is the effect that this will exert on the development of neutral buoyancy during magma ascent. On Earth, it is found that magma tends to ascend buoyantly within the lithosphere until the density of the melt approaches the density of the country rocks, at which point the magma stalls. Further arrivals of magma will continue to stall at the same level, resulting in the eventual development of shallow reservoirs from which other effects must take over in order for the magma to continue its ascent. The condition of neutral buoyancy may not occur in many cases on Venus, primarily at the lower elevations where atmospheric pressure is greatest, vesiculation is suppressed, and the corresponding crustal density is high. As a result, in areas of lower elevation, direct ascent and eruption of magmas may occur with very little reservoir development. At higher elevations, where atmospheric pressure is lower, shallow reservoirs might be able to form and large magmatic centers characterized by shallow reservoirs might be more common. Many large centers of volcanism on Venus do occur in intermediate and upper elevations. Currently, the full range of influences on shallow reservoir formation and the fundamental significance of neutral buoyancy as the primary cause of reservoir formation have not been explored sufficiently to enable us to say whether the density structure is the principal cause of this distribution.

C. Influence of Ascent and Emplacement Rates on Eruptions

Differences in volcanologic characteristics of surface features may arise from influences other than variations in chemical composition or direct environmental effects. Part of the diversity of volcanic morphology observed on Venus may reflect the diversity of rates of magma emplacement in contrast to the smaller terrestrial planets. Numerical evaluation of the thermal conditions necessary to establish and maintain an active magma reservoir shows that the two important characteristics necessary for reservoir development under given conditions of magma temperature and ambient crustal rock type are (1) the presence of a level or zone within the crust where the magma is in a state of neutral buoyancy and (2) a rate of magma emplacement great enough that new magma arrives more quickly than the previously emplaced magma solidifies (in other words, the net thermal flux into the magma emplacement zone is positive).

Volcanological studies on Earth over the past decade suggest that many of the salient characteristics and variations in morphology of volcanic centers may depend on the rate of magma production, replenishment, and extrusion within individual magmatic systems and volcanic centers. Although the geochemical character of magmas, surface environment of eruption, and buoyancy considerations may be important in controlling the style of eruptions in individual volcanic centers, the total rate of magma eruption, emplacement, and replenishment (the *magma rate regime*) might exert an equal or greater influence on the presence of shallow magma reservoirs, long-lived volcanic centers, and the overall morphology of the volcanic center as a whole. Reservoirs capable of supplying central volcanic edifices, volcanic complexes, or long-lived centers of intrusive or extrusive activity on Earth frequently occur only for a very narrow range of magma transport rates and storage conditions. These conditions are sensitive to lithospheric structure and thermal gradient. As a result, the presence of magma reservoirs (for example, coronae and calderas) on any planet implies specific magma transfer rates from the mantle and timescales over which magma is stored in the crust. Assessment of these rate-related influences and the rates as recorded in the characteristics of volcanic centers will be one of the few means of determining rates of geologic processes, melt productivity, and heat transfer associated with mantle plumes on Venus. The large-scale effect of tectonic environment (hot spot instead of plate boundary) may also influence the rates of magma emplacement globally and net rates of resurfacing. Volume rates associated with volcanism on Venus are estimated to be similar to or lower than that associated with hot spots on Earth (0.1–1 km^3/a), more than one to two orders of magnitude lower than volume rates of volcanism associated with plate tectonics.

The largest and shallowest magma reservoirs and most voluminous eruptions on Earth are associated frequently with moderate rates of magma emplacement in midcrustal levels, with corresponding development of large magma reservoirs. This rate is approximately equivalent to the rate of magma intrusion and eruption at the Hawaiian hot spot averaged over the past 70 million years. Rates of emplacement lower or higher than this moderate rate tend not to yield well-developed, isolated, long-lived magma reservoirs that evolve chemically and structurally in association with single volcanic edifices. Rates of emplacement lower than this value on Earth frequently result in numerous short-lived volcanic centers and are characteristic of "fields" of small volcanoes. Rates greater than the moderate-rate regime frequently result in massive flow fields, incompletely developed volcanic centers and magma reservoirs, and relatively minor associated amounts of evolved magma compositions. Neutral buoyancy is necessary but is not a sufficient condition for development of complex dike patterns and long-lived magma reservoirs, and variations in reservoir depth appear insufficient to account for all of the disparate morphologies seen in volcanic centers on Venus.

Results of simple calculations of the influence of replenishment rates on Earth are consistent with observed rates of magma replenishment typically associated with reservoir development ($\leq 10^{-3}$ km^3/a). Similar calculations for Venus imply that magma reservoirs are likely to form at volume rates of magma transfer at least a factor of two less than on Earth ($\leq 5 \times 10^{-4}$ km^3/a). This means that magma replenishment rates typical of many fields of small volcanoes on Earth are capable of generating central volcanic centers and magma reservoirs on Venus. Additional details of the process may be significant, including the geometry of the magma emplacement and whether the reservoir is tabular or cylindrical. Rates of magma transport and corresponding style of volcanic centers may also be modulated to a limited extent by magma composition.

IV. FUTURE DIRECTIONS

The list of unanswered questions about volcanism on Venus is as long as the list of volcanoes. No single discussion may cover them all. What follows are just some questions that have been raised during the course of the above discussion.

The great abundance of shield fields over other landforms is a distinctive characteristic of Venus. On Earth, fields of small volcanoes are diagnostic of long-lived magma supply at rates too low to sustain a shallow magma reservoir. If the shield fields on Venus originate by a similar process, the larger abundance of shield fields is understandable given that, in any normally distributed population of magmatic events (magma replenishment rates), the smaller events will be more common than larger ones. For Venus, we estimate that rates $\leq 5 \times 10^{-4}$ km^3/a are necessary to ensure that a shallow magma reservoir does not form. This is about half the rate necessary on Earth. This is a useful hypothesis, and Venus would seem to be an excellent place to test it. But given the near impossibility of determining ages on Venus, how can we test this concept?

It remains to be determined why the large volcanoes of Venus are characterized by extremely low relief. The case can be made that the primary influence on the lateral dimensions of lava flows is volume flux, which, in combination with the extremely low relief of the general surface of Venus, will result in extremely long flows and corresponding shield volcanoes of great width and not much height. If volume flux is a significant influence, why are the lava flows characteristically erupted at high rates from shallow reservoirs on Venus? What characteristics of magma ascent and eruption are likely to be influenced by the lithosphere and tectonic conditions unique to Venus?

In the absence of erosion on Venus, the complete range of processes that operate in the course of evolution of large magmatic provinces are perfectly preserved. Recognizing the existence of some of the large-scale structural phenomena associated with large magmatic provinces based on study of Venus examples, it may be useful to reexamine terrestrial volcanic provinces for similar features. Ultimately, it would be useful to know if large-scale patterns of deformation such as those associated with coronae, arachnoids, and radial fracture centers occur on Earth.

A significant result of early Magellan data analysis was the recognition that much of the surface, particularly vast areas of low-lying plains formed by lava floods, is old (several hundred million years) by Earth standards (although young when compared with the other smaller terrestrial planets). Initial studies, and studies since that time, suggested that a global resurfacing event occurred on Venus. The timing of this event is not known, but based on estimates from the global population of impact craters, it could be either as late as 300 million years ago or up to 1600 million years ago. Geologic mapping and stratigraphic studies imply that most of the volcanic centers have developed since the global resurfacing event. Volcanism appears to have been volumetrically low in the intervening time, accounting for a few tenths of a cubic kilometer per year, or considerably less than the rates for Earth over the same time interval (essentially Phanerozoic). If so, the globally averaged style of volcanism on Venus, particularly the volumetric rate of eruptions, has differed greatly from that associated with plate tectonics on Earth. Current models for how this process might work imply that Venus undergoes a cyclical style in which large outbursts of volcanism occur globally, perhaps every few hundred million years, and that rates of volcanism are relatively low in the times in between these outbursts. It has also been suggested that, whereas plate tectonics does not now characterize the surface, it is possible that during or immediately prior to these global volcanic events, global tectonism is somewhat more akin to plate tectonics. This concept is supported somewhat by the presence of large areas of extremely deformed and elevated terrain know as tessera, which are also among the oldest identified surfaces, somewhat like continents on Earth, although covering less than 15% of the surface. In this model, once the global event runs its course, the planetary style of tectonism reverts back to a simple hot spot style characterized by low rates of volcanism erupted from several large hot spot swells. The process is repeated later when the heat builds up in the interior, large-scale melting takes place, and mobile tectonics and extensive volcanism occur once again. This style is completely unlike any recognized activity of Earth. It remains to be seen what consequences this might have for the fundamental characteristics of its volcanoes.

Although the global tectonic style of Venus currently differs greatly from that of Earth, it is useful to consider the possibility that either Earth-like styles of global tectonic occurred on Venus in the past or Venus-like tectonics have occurred on Earth during some previous phase of its history. The extreme nonuniformitarian style of Venus, characterized by massive outbursts of volcanism and tectonism followed by great periods of relatively low activity, is also a departure from our previous assumptions about the way in which planetary-scale mechanisms of evolution occur. It is therefore of equal benefit to consider ways in which Earth's tectonic cycle may have undergone significant changes in rates. Most of what we consider to be typical Earth geology spans only the Phanerozoic. Similarly, most of what is preserved on Venus spans approximately the same time interval, even though it is of an altogether different character. Both planets could well have presented different volcanic styles prior to 1 billion years ago for the simple reason that the long-term evolution of a planet may depart radically over short intervals of time from that characterizing processes that act over long periods of time. In other words, uniformitarianism may still be an appropriate concept, but may be strongly dependent on the length of time over which one samples the geologic record.

SEE ALSO THE FOLLOWING ARTICLES

Calderas • Lava Flows and Flow Fields • Magma Chambers • Volcanism on Io • Volcanism on Mars • Volcanism on the Moon

FURTHER READING

Barsukov, V. L. (1992). Venusian igneous rocks. Pages 165–176 *in* "Venus Geology, Geochemistry, and Geophysics: Research Results from the Soviet Union" (V. L. Barsukov, A. T. Basilevsky, V. P. Volkov, and V. N. Zharkov, eds.). Univ. of Arizona Press, Tucson.

Barsukov, V. L., Basilevsky, A. T., Burba, G. A., Bobina, N. N., Kryuchkov, V. P., *et al.* (1986). The geology and geomorphology of the Venus surface as revealed by the radar images obtained by Veneras 15 and 16. Proceedings of the 17th Lunar and Planetary Science Conference, Part 2. *J. Geophys. Res.* **91,** D378–D398.

Bougher, S. W., Hunten, D. M., and Phillips, R. J., with 100 collaborating authors. (1997). "Venus II: Geology, Geophysics, Atmosphere, and Solar Wind Environment." Univ. of Arizona Press, Tucson.

Cattermole, P. (1994). "Venus: The Geological Story." Johns Hopkins Press, Baltimore.

Cooper, H. S. F., Jr. (1993). "The Evening Star." Farrar Straus Giroux, New York.

Crumpler, L. S. (1996). Venus. Pages 1129–1135 *in* "Macmillan Encyclopedia of Earth Sciences" (J. Dasch, ed.), Simon & Schuster, New York.

Ford, P. G., Plaut J. J., Weitz, C. M., Farr, T. G., Senske, D. A., Stofan, E. R., Michaels, G., and Parker, T. J. (1993). "Guide to Magellan Image Interpretation," JPL Publication 93–24. Jet Propulsion Laboratory, California Institute of Technology, Pasadena.

Grosfils, E., Aubele J., Crumpler, L., Gregg, T., and Sakimoto, S. (1999). Volcanism on Venus and Earth's seafloor. Chapter 5 *in* "Environmental Effects on Volcanic Eruptions: From the Deep Ocean to Deep Space" (T. Gregg and J. Zimbelman, eds.). Plenum, New York, in press.

Hunten, D. M., Colin, L., Donahue, T. M., and Moroz, V. I., with 69 collaborating authors. (1983). "Venus." Univ. of Arizona Press, Tucson.

International Astronomical Union (IAU). Venus Nomenclature, Maps, and Images: http://wwwflag.wr.usgs.gov/USGSFlag/Space/.

Magellan Science Team and collaborating authors. (1992). Magellan at Venus (in special Magellan results issue). *J. Geophys. Res.* **97,** nos. E8 and E10.

Roth, L. E., and Wall, S. D., eds. (1995). "The Face of Venus: The Magellan Radar-Mapping Mission," NASA Special Publication SP-520, Washington, DC.

Young, C., ed. (1990). "The Magellan Venus Explorer's Guide," JPL Publication 90–24. Jet Propulsion Laboratory, California Institute of Technology, Pasadena.

This Page Intentionally Left Blank

VOLCANISM ON MARS

JAMES R. ZIMBELMAN
Center for Earth and Planetary Studies, Smithsonian Institution

I. Introduction
II. Background
III. Large Central Volcanoes
IV. Paterae and Tholi
V. Highland Paterae
VI. Small Constructs
VII. Volcanic Plains
VIII. Compositional Constraints
IX. Volcanic History of Mars
X. Future Studies

GLOSSARY

Amazonian The youngest of the geologic epochs on Mars identified through geologic mapping of superposition relations, and the areal density of impact craters.

caldera An irregular collapse feature formed over the evacuated magma chamber within a volcano.

central volcano Emplacement of volcanic materials from a centralized source vent rather than along a distributed line of vents.

composite volcano A volcano consisting of intermixed effusive lava flows and pyroclastic materials. Flank slopes are typically >10°, or more than twice as steep as the flanks of a shield volcano.

Fossae Descriptor applied to an aligned series of fractures in a planetary surface.

Hesperian The intermediate geologic epoch on Mars identified through geologic mapping of superposition relations, and the areal density of impact craters.

Icelandite Volcanic rock with silica content comparable to an andesite, but which did not form as a result of subduction or orogenic processes.

Mons Descriptor applied to a large isolated mountain on a planetary surface.

Noachian The oldest of the geologic epochs on Mars identified through geologic mapping of superposition relations, and the areal density of impact craters.

Patera Descriptor applied to an irregular or complex crater with scalloped edges, surrounded by shallow flank slopes.

pseudocrater A "rootless vent" created by the interaction of lava with groundwater or wet sediments beneath the flow.

shield volcano A broad volcanic construct consisting of multitudes of lava flows. Flank slopes are typically ~5°, or less than half as steep as the flanks on a composite volcano.

SNC meteorites A group of meteorites thought to originate on Mars, due to a relatively young age and trapped gases very like the atmosphere of Mars. The acronym is derived from the names of the three meteorites that define the major subdivisions identified within the group: S, Shergotty; N, Nakhla; C, Chassigny.

Copyright © 2000 by Academic Press
All rights of reproduction in any form reserved.

Tholus Descriptor applied to an isolated domical small mountain or hill, usually with slopes much steeper than that of a patera.

volcanic plains Planar mappable units interpreted to consist of volcanic materials, usually with individual flow margins resolvable within the unit.

yardang A rounded erosional landform produced by wind-driven sand. Some yardang fields on Mars are interpreted to be formed in wind-eroded pyroclastic deposits.

I. INTRODUCTION

The advent of spacecraft exploration revealed that Mars possesses some of the most dramatic volcanic features found anywhere in the solar system. How did a planet half the size of the Earth generate volcanoes like Olympus Mons, which is several times larger than the largest volcanoes on Earth? This question is just one example of the issues currently being investigated as part of the relatively recent scientific endeavor called "Comparative Planetology." This article will summarize the basic information presently known about volcanism on Mars. The reader can then compare the Martian volcanoes to the numerous volcanoes studied in great detail here on the Earth as well as to volcanoes observed on other planetary bodies.

Two generalizations can be made before we investigate the Martian volcanoes in greater detail. Volcanoes on Mars appear to be broadly similar in overall morphology (although different in scale) to volcanic features on Earth, so there is no direct evidence for Martian eruptive processes that are somehow significantly different from the volcanic styles and processes known on Earth. This inference strengthens our confidence in using the basic approach of attempting to understand the Martian volcanoes in terms of traditional volcanology. Next, the Martian volcanoes occur on terrains of various relative ages (discussed below), so that volcanism represents a dominant geologic process throughout much of Martian history. This is in contrast to volcanism on the smaller body of Earth's Moon, where volcanic activity was confined to roughly the first third of lunar history (see "Volcanism on the Moon"). Comparative planetology thus supports the concept that volcanism is the primary mechanism for a planetary body getting rid of its internal heat, where smaller bodies tend to lose their internal heat more rapidly than larger bodies (Jupiter's moon Io appears to contradict this trend because this object, the size of Earth's Moon, is the most volcanically active body in the solar system, but this activity is powered by unique gravitational tidal forces within the Jovian system; see "Volcanism on Io"). Next we review some important background information before examining the types of volcanic features present on Mars.

II. BACKGROUND

The first direct evidence of the importance of volcanism on Mars came during the Mariner 9 orbital mission. A massive global dust storm obscured the entire Martian surface when Mariner 9 arrived at Mars on November 14, 1971, but as the weeks passed, the dust slowly began to settle. The first surface features at equatorial latitudes to become visible through the dust pall were four dark "spots" in the region of the planet that telescopic observers called Tharsis. Gradually these spots were revealed to each be topped by a complex crater assemblage, the first clue that four huge volcanoes were present in the Tharsis area. By chance, the three previous fly-by Mariner missions failed to image this area in detail sufficient to show these large volcanoes. Mariner 9 continued to map the entire Martian surface until October 12, 1972, revealing that Tharsis was not alone in containing impressive volcanic constructs. The Mariner 9 view of Mars was updated significantly with the improved resolution of the cameras on the two Viking Orbiter spacecraft that operated at Mars from June 19, 1976, to August 17, 1980. The ~55,000 Viking Orbiter images led to refined interpretations for many Martian features, but they did not significantly alter the first global perspective of Mars revealed by the Mariner 9 images.

The distribution of volcanoes on Mars is not uniform; there are four regions where central volcanoes are concentrated (Fig. 1). Twenty-three volcanic constructs have been given names (Table I) by the International Astronomical Union, the only organization that can officially designate names for planetary features. The largest concentration of Martian volcanoes occurs in the Tharsis region, where the volcanoes are distributed on and around a 4000-km-diameter bulge in the Martian crust, centered on the equator at 110°W longitude. This bulge has lifted the crust to an elevation ~10 km above the Martian datum, twice as high as the highest portions of the cratered highlands that dominate the southern hemisphere of Mars (shaded portion of Fig. 1). The "Tharsis Bulge" is surmounted by three volcanoes collectively called the Tharsis Montes (5, 6, and 16 in Fig. 1), aligned along a N40E trend that includes addi-

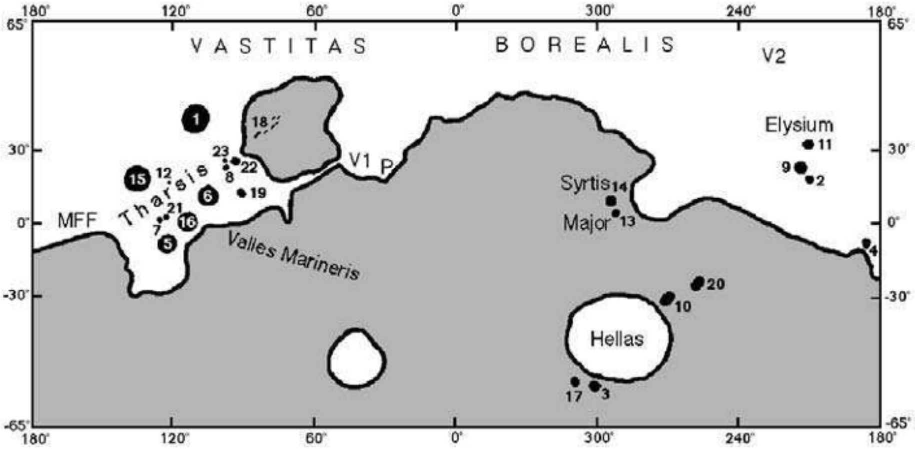

FIGURE 1 Location map for named central volcanoes on Mars. The black areas indicate various volcanic centers, with numbers keyed to Table I. The shaded area represents densely cratered materials typical of the highlands that dominate the southern hemisphere. Letters indicate landing sites (V1, Viking 1; V2, Viking 2, P, Mars Pathfinder) and the Medusae Fossae Formation (MFF). Mercator projection.

tional volcanic centers northeast of the Tharsis Montes. The Tharsis Montes and nearby Olympus Mons (15 in Fig. 1) are the four tallest features on Mars, the summit calderas of which were first imaged by Mariner 9 above the dusty lower atmosphere. Outside of the Tharsis area, Martian central volcanoes are confined to the Elysium, Syrtis Major, and Hellas regions (Fig. 1), all named for broad bright or dark surface markings visible with Earth-based telescopes. In addition to the named central volcanoes, broad expanses of regional plains exist across Mars, many of which include compelling evidence that they were formed by the emplacement of numerous individual volcanic flows.

The Mariner 9 and Viking images showed the physiographic makeup of the entire surface of Mars. Through careful observation of the superposition and cross-cutting relationships of distinctive material units, a global geologic sequence has been developed. The areal density of impact craters present on the various material units allows the relative stratigraphy to be established even where units are not in contact with each other. The convention defined for three major divisions of Martian geologic history are the Noachian (oldest), Hesperian (intermediate age), and Amazonian (youngest) epochs, providing a broad temporal sequence in which we can discuss the various Martian volcanoes. Unfortunately, the absolute age of these Martian epochs is very unconstrained at present; various models of the impact flux on Mars allow the Amazonian period to be from millions to billions of years in age. Most planetary scientists likely would accept that Amazonian materials represent events late in Martian history, but ages for documented samples collected from regionally expansive terrains are needed to constrain the precise time range covered by the cratering record on Mars. In spite of this uncertainty in absolute age, the geologic stratigraphy provides a robust framework in which the relative ages of various materials, including both central volcanoes and regional volcanic plains, can be evaluated.

Remote-sensing data provide information about Martian materials that is complementary to the photogeologic interpretation of spacecraft images. Reflected visual and infrared light provides compositional information by the wavelengths at which some of the light is selectively absorbed. Earth-based telescopic studies can not resolve individual volcanoes but reflectance spectra indicate that bright regions are covered with a dust that includes considerable oxidized iron whereas the dark regions are less dusty and may include pyroxene-bearing material such as mafic volcanic rock like basalt. Thermal infrared measurements by the Viking orbiters indicate that the Martian surface is coated with particulate materials, ranging from micron-sized dust covering practically all of surface in the bright regions to sand-sized particles mixed with larger unresolved blocks in the dark regions. Significantly, the Viking thermal measurements showed no "hot spots" attributable to internally generated heat anywhere on the planet. Radar signals transmitted from Earth and reflected from the Martian surface have shown that some individual volcanoes, such as the Tharsis Montes, display strong scattering behavior. The scattered radar signals indicate

TABLE 1 Named Volcanic Centers on Mars

Number	*Name*	*Center*	*Horizontal scale*[a] *(km)*	*Relief*[b] *(km)*
1	Alba Patera	40°N, 109°W	450	∼4
2	Albor Tholus	19°N, 210°W	160	∼5
3	Amphitrites Patera	59°S, 299°W	130	<1
4	Apollinaris Patera	8°S, 186°W	180	∼5
5	Arsia Mons	9°S, 120°W	350	∼11
6	Ascraeus Mons	11°N, 104°W	350	∼17
7	Biblis Patera	2°N, 124°W	150	∼4
8	Ceraunius Tholus	24°N, 97°W	150 × 100	∼5
9	Elysium Mons	25°N, 214°W	300	∼12
10	Hadriaca Patera	30°S, 266°W	180	<1
11	Hecates Tholus	32°N, 210°W	170	∼6
12	Jovis Tholus	18°N, 117°W	60	∼2
13	Meroe Patera	7°N, 291°W	50	<1
14	Nili Patera	9°N, 293°W	60	<1
15	Olympus Mons	28°N, 133°W	500	∼25
16	Pavonis Mons	0°N, 113°W	350	∼10
17	Peneus Patera	57°S, 307°W	120	<1
18	Tempe Fossae[c]	36°N, 86°W	3 × 1	≪1
19	Tharsis Tholus	13°N, 91°W	170 × 110	∼6
20	Tyrrhena Patera	22°S, 253°W	180	∼1
21	Ulysses Patera	3°N, 122°W	100	∼2
22	Uranius Patera	26°N, 93°W	150	∼1
23	Uranius Tholus	26°N, 98°W	60	∼4

[a] Approximate horizontal dimension (maximum and minimum values for elongate features).
[b] Estimated relief from summit to the surrounding terrain; from U.S.G.S. (1991).
[c] Largest of several small features along Tempe Fossae (Fig. 4).

considerable surface roughness at the 10 cm to meter scale on the surface of the Tharsis Montes, something that may likely also apply to other volcanoes but which are too small to be clearly resolved with Earth-based radar. West of the Tharsis Montes, a region of several million square kilometers returns no radar signal back to Earth; this area has been nicknamed "Stealth" after its very low radar reflectance properties. Stealth could be a deposit sufficiently thick so that the radar signal is fully absorbed, such as through deposition of pyroclastic materials associated with the nearby volcanoes, or Stealth also might have unusual relief that efficiently scatters the radar signals away from the antennas on Earth.

III. LARGE CENTRAL VOLCANOES

Olympus Mons and the three Tharsis Montes each have shapes typical of a basaltic shield volcano on Earth, but at non-Earth-like scales (Fig. 2). The flanks of the four mountains have maximum slopes of ∼5°, with shallower summit and basal slopes, much like the shape of the subaerial portion of the Mauna Loa shield volcano. The great bulk of the Mauna Loa volcano, which with its subaqueous mass comprises the largest mountain on Earth, is still dwarfed by any one of these four mountains, but particularly by Olympus Mons with its 500-km diameter and 25-km vertical relief. The four Tharsis

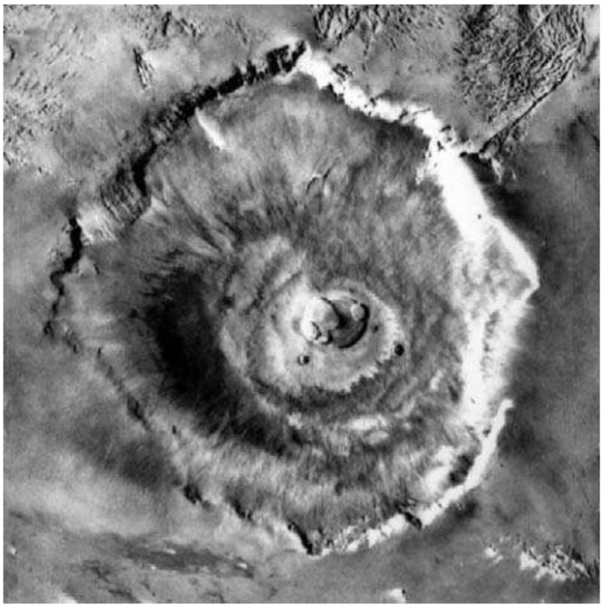

FIGURE 2 Olympus Mons, the largest central volcano on Mars (15 in Fig. 1 and Table I). Olympus Mons has shallow flank slopes typical of a shield volcano. The volcano has 25 km of relief from its summit to the plains surrounding the basal scarp, which is ~600 km in diameter and from 3 to 6 km in height. (Viking Orbiter image 646A28, courtesy of NASA.)

shield volcanoes are so large that their size is not fully appreciated without considering the curvature of the Red planet; an astronaut on the surface anywhere near these mountains could not see their summits because this would be beyond his (or her) local horizon!

The great size and height of the four large Tharsis volcanoes generated considerable discussion about their potential source regions. If bouyancy is assumed to be the sole driving force for a typical basaltic magma on Mars, the summits of the four large Montes volcanoes indicate their sources lie at depths >120 km, potentially implying a thick lithosphere in the Tharsis region. Interestingly, older Martian volcanoes generally display reduced relief (when compared to the Tharsis shields), so lithospheric thickness may have increased throughout Martian history. When combined with the lack of any obvious nearby plate tectonic features such as subduction arcs or transform faults, the great bulk of these mountains may result from mantle sources that released their magma at one location without the lithospheric movement we associate with plate tectonics on Earth. In this light, it is interesting that the volume of Olympus Mons is roughly comparable to the integrated volume of the Hawaiian-Emperor seamounts. The descriptor "Mons" refers to a large isolated mountain, and all four Tharsis shield volcanoes clearly deserve this designation.

The lower flanks of the Tharsis Montes have been buried by plains-forming flows emanating from the volcanoes themselves or vents in between them. Only Olympus Mons is surrounded by an arcuate scarp nearly 600 km in diameter and with 3–6 km of vertical relief (Fig. 2). The origin of the basal scarp at Olympus Mons remains controversial, but several enormous fan-shaped deposits northwest of the volcano have been interpreted to be gravitationally driven landslides, perhaps aided by volatile lubrication along the detachment surface. High-resolution Viking images show multitudes of interwoven lava flows extending down the flanks of Olympus Mons and over the basal scarp, spilling onto the surrounding plains. Many of the individual flows have medial channels similar to channel-fed lava flows on terrestrial volcanoes. Thermal infrared data indicate that all four of the volcanoes are thoroughly coated with fine windblown dust, severely limiting any information about the volcanic rocks that can be learned from most remote-sensing techniques.

As noted earlier, all four shield volcanoes are surmounted by summit calderas. Olympus and Ascraeus Montes have complex calderas revealing multiple episodes of collapse whereas Arsia and Pavonis Montes have only a single collapse rim preserved at present. Geophysical modeling of fractures around the caldera on Olympus Mons verifies that these features are consistent with collapse into evacuated magma reservoirs within the shield construct. By analogy to terrestrial shield volcanoes, these intermediate magma chambers may have been periodically replenished from a larger magma source located beneath the volcanic pile.

A separate volcanic center with its own crustal bulge (but one considerably smaller than the Tharsis Bulge) is present in the Elysium region (11 in Fig. 1). Elysium Mons is the largest construct in the region, and it has some important distinctions from the four Tharsis shield volcanoes. Elysium Mons has considerably steeper flank slopes (up to 12°) than the Tharsis shields, surmounted with one major caldera (although the floor preserves subtle details that suggest repeated collapse prior to the last lava infilling). The shape of Elysium Mons is somewhat reminiscent of conical composite volcanoes typical of subduction margins such as the Andes or the Cascades, but there are no associated features (such as a nearby trench) to indicate that subduction is in any way responsible for this Martian volcano. Following Mariner 9, Elysium Mons was compared to the volcano Tibesti in Africa, where an intracontinental hot spot is a more likely analog than an active plate margin. While there are some vocal supporters of possible subduction on Mars, the consensus impression since Mariner 9 has been the apparent dearth, if not total absence, of any classic plate tectonic features on Mars.

Alba Patera, north of the three Tharsis Montes (1 in Fig. 1), represents another important exception to the broad shield morphology. This volcano is only slightly smaller in horizontal dimension than Olympus Mons, but it lacks the dramatic relief present on the Tharsis shields and Elysium Mons (Table I). Early results from the Mars Orbital Laser Altimeter on the Mars Global Surveyor spacecraft indicate that this volcano has flank slopes ≤1°, much less than the already shallow 5° flanks of the shield volcanoes. Even more unique is a band of dense fractures that makes almost a complete ring around this shallow-sloped construct. Some researchers have compared this tectonic pattern to that which would surround a core of competent rock that is subjected to intense regional stress; such an interpretation would imply that Alba Patera was completely solidified well before the regional stress pattern was imposed. Crater densities indicate that Alba Patera has been exposed to the impacting bombardment longer than either the Tharsis shields or Elysium Mons, but some volcanic effusion may have postdated the stress that produced the distinctive arcuate band. Recently, it was proposed that Alba Patera may be a Martian example of a Venusian corona (see "Volcanism on Venus"); such an interpretation has profound implications for crustal thicknesses on Mars during an epoch when other comparable thin-lithosphere features are not readily apparent. As we shall see next, Alba Patera is not representative of the majority of features that have been given the name "patera."

IV. PATERAE AND THOLI

Alba Patera is the largest member of a class of volcanic construct on Mars that is quite distinct from the Mons-type volcanoes. The descriptor "Patera" refers to an irregular or complex crater with scalloped edges that is surrounded by shallow flank slopes. These features contrast greatly with impact craters or basins of comparable size, and a volcanic caldera is the consensus interpretation. Another distinctive class of volcanic construct, which is consistently smaller than the Mons type, has the descriptor "Tholus" applied to an isolated domical small mountain or hill, usually with slopes much steeper than those of a patera. Both Paterae and Tholi (other than Alba Patera discussed above) are generally smaller than 200 km in diameter (Table II).

Paterae in the Tharsis region (7, 21, and 22 in Fig. 1) tend to have caldera diameters more than half as broad as the overall construct. This observation led some researchers to conclude that such paterae may be the summits of shield volcanoes whose lower flanks have been buried by more recent volcanic plains, which seems quite reasonable for the Tharsis region, where volcanic plains are abundant and likely quite thick. Tholi in the Tharsis region (8, 12, 19, and 23 in Fig. 1) tend to have slopes steeper than those of the shields but usually not as steep as Elysium Mons. Some volcanoes (e.g., Ceraunius Tholus) have sinuous channels carved into their flanks, implying significant effusive (and erosive) flow after the bulk of the construct formed (Fig. 3). A few researchers have interpreted the erosive channels on tholi and paterae flanks to be due to pyroclastic flows. The buried-

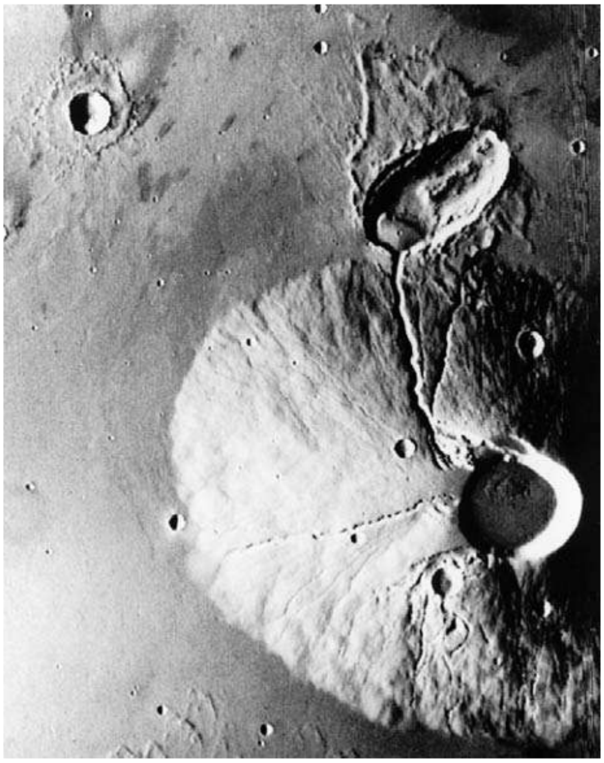

FIGURE 3 Ceraunius Tholus, a volcanic dome with an elongate crater from an oblique impact at its northern base (8 in Fig. 1 and Table I). The volcano is noncircular, with dimensions 150 × 100 km. At least one sinuous channel carved into the volcano was active after the oblique impact since a riverlike "delta" formed in the crater where its rim was breached by the lava channel. (Viking Orbiter image 516A24, courtesy of NASA.)

shield interpretation for paterae has difficulty accounting for the close proximity of both broad patera and steep tholus in the Tharsis region (8, 22, and 23 in Fig. 1), where the tholi volcanoes may indicate either effusive or compositional properties quite different from those of paterae volcanoes.

The Elysium region has paterae and tholi as well, although fewer than in the Tharsis region (2, 4, and 9 in Fig. 1). These volcanoes have both scoured flanks and, on Hecates Tholus, a portion of the summit area where very few impact craters are preserved. Both characteristics have been interpreted to result from pyroclastic activity: erosive pyroclastic flows to generate the flank scours and an inferred ash deposit following a plinian-style eruption at the summit of Hecates Tholus. Neither of these interpretations should be considered proof of pyroclastic activity, but they do suggest an increased possibility for a pyroclastic component associated with paterae- and tholi-style eruptions, as compared to Mons-style volcanoes.

V. HIGHLAND PATERAE

Paterae located in the cratered highlands of Mars deserve special treatment because they appear to have several characteristics distinct from those of the small volcanoes in the Tharsis and Elysium regions. The highland paterae are concentrated in two regions: a linear trend of four volcanoes on the outer rim of the Hellas impact basin in the southern hemisphere (3, 10, 17, and 20 in Fig. 1), and two vents relatively recently identified within the classical dark region of Syrtis Major in the northern hemisphere (13 and 14 in Fig. 1). Both regions include evidence that suggests that pyroclastic materials comprise an important fraction of the products produced by these highland paterae, suggesting that volcanism in the highlands may have involved eruptions fundamentally different from those that produced the broad Mons volcanoes, the shallow paterae, or the steep tholi.

The four paterae on the rim of the Hellas basin are notable in that all possess very shallow flank slopes, likely much less than the shallow 1° flanks of Alba Patera. The Hellas volcanoes are more noteworthy for their intensely eroded appearance than for any obvious construct around the central vent (Fig. 4). The channels cut deeply into the flanks of the Hellas paterae have been interpreted to indicate removal of friable material concentrated around the central vent, possibly through either fluvial or volcanic processes, or both. The logical way to build up a broad low-profile deposit of friable materials around a volcanic vent is through deposition of pyroclastics. Currently, it is not clear if pyroclastic flows or falls are the dominant agent for emplacement of the ash, and both processes appear to be viable candidates. What is apparently rare at these volcanoes is a significant effusive lava flow component. The top of the friable deposit at each volcano appears to be more competent, forming a caprock between channels eroded into the deposit; this resistant zone may be case-hardened or indurated friable materials, or it may involve some effusive lava flows, but this is difficult to resolve with current data. All four Hellas volcanoes represent a substantially different style of eruption and emplacement than the other central volcanoes discussed above, suggestive that the magma involved may have somehow been different (increased volatile content?) from the effusive lavas that dominate the more recent Martian volcanoes.

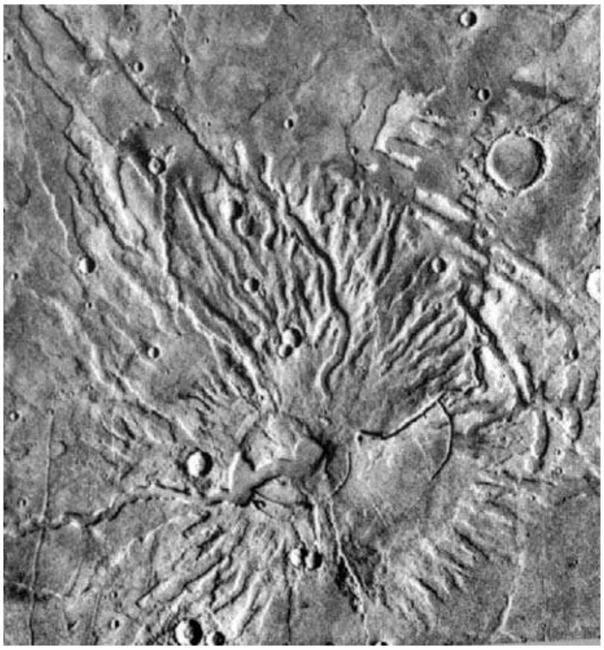

FIGURE 4 Tyrrhena Patera, one of the low-profile paterae in the southern highlands near the rim of the Hellas impact basin (20 in Fig. 1 and Table I). The radiating pattern of channels has eroded into material ~180 km in diameter, interpreted to be ash deposited around the volcanic vent. (Viking Orbiter image 87A14, courtesy of NASA.)

Nili and Meroe Paterae were only recognized as being volcanic vents in the 1980s, long after Mariner 9 and the early Viking images established the presence and types of the other volcanic centers. Both paterae are near the center of the Syrtis Major dark region that has been observed telescopically from Earth for several centuries. Remote-sensing data of the Syrtis Major region indicate the dark materials are significantly less oxidized than the bright dusty portions of the planet, with strong indications of a mafic chemistry that likely includes a pyroxene component. When the volcanic vents were identified, researchers proposed that the dark material in Syrtis Major may in fact be wind-transported mafic volcanic ash. Viking images in Syrtis Major reveal abundant dark dunelike features, supporting the concept that wind action in crucial to the story of this area. The action of the wind on the individual ash particles may help to remove an oxidation coating as the grains bounce into each other.

VI. SMALL CONSTRUCTS

Mars has numerous occurrences of small domes, some of which may have a volcanic origin. Unfortunately, these features are mostly small enough that Viking imaging data are not sufficient to provide definitive evidence for their origin. One of these features that is big enough to show some important physical characteristics is found in the Tempe region, within a zone of fractures called Tempe Fossae (Fig. 5). Here an oblong low mound is present around an elongated summit depression (between the arrows in Fig. 5). The depression follows the trend of the surrounding fractures, so that structural control likely played a role in determining where vented materials could reach the surface. The vast majority of these features are smaller than the Tempe example; typically, the individual domes are <1 km in diameter and at most a few hundred meters in height. A popular interpretation of their origin is that of cinder cones, with the variation that some may be pseudocraters where a lava flow interacted with either a shallow water layer or wet sediments. There are literally thousands of these features in various places throughout the northern lowlands of Vastitas Borealis (Fig. 1), so that either a cinder cone or pseudocrater origin would imply abundant water–lava interaction across the northern plains. An alternative nonvolcanic interpretation is a periglacial feature such as a pingo (an ice-cored mound).

The final category of distinct volcanic landforms on Mars consists of about two dozen deeply dissected conical hills scattered throughout the highlands. These features typically are <30 km in diameter and were only recognized as potentially of volcanic origin through careful study of the extensive Viking database. There are no names given to these features, nor is there any obvious pattern to their occurrence throughout the highlands. The dominant characteristic is deep scours present on all of their flanks, similar to the scoured exteriors of some paterae that are thought to have been subjected to pyroclastic flows. Assuming they are volcanic in origin, they appear to represent yet another distinct style of volcanic deposit confined to the old densely cratered highlands of Mars. The eroded domical hills cannot be dated by crater density due to their small areal extent, but their presence solely within the ancient materials of the cratered highlands leads most researchers to assume an old age for these features.

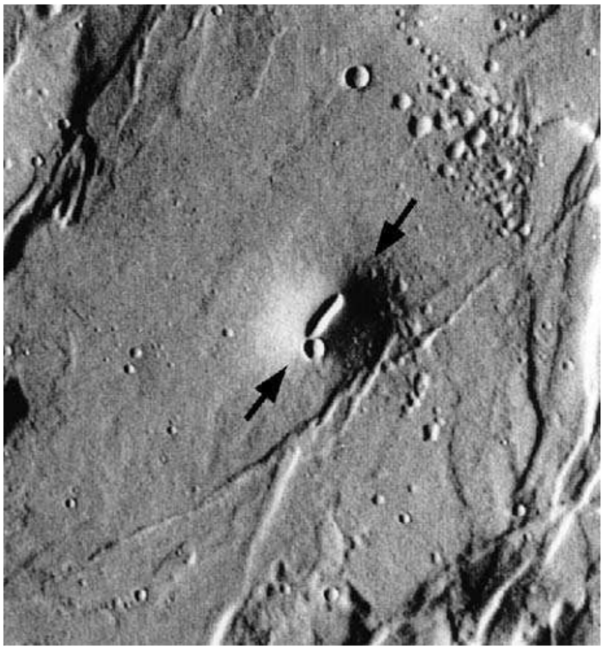

FIGURE 5 Small volcano (between arrows) located along Tempe Fossae (18 in Fig. 1 and Table I). Solar illumination from the left indicates an elongate mound built up around a very elliptical depression, probably analogous to a Strombolian eruption along a linear vent. The feature is ~3 km in length and likely <300 m in vertical relief. (Viking Orbiter image 627A28, courtesy of NASA.)

VII. VOLCANIC PLAINS

Volcanic plains comprise some of the most extensive geologic units on Mars outside of the cratered highlands. The plains tend to be quite featureless at moderate to low resolution, but in high-resolution images, these plains display numerous lobate margins surrounding individual packages of material that appear to have been emplaced through flow of fluid materials (Fig. 6). The lobate margins are sufficiently thick (various measurements indicate lobe thicknesses of tens to hundreds of meters) that the flowing material is widely accepted to be lava rather than something like a water-rich debris flow. Volcanic plains surround both the Tharsis and Elysium volcanic centers, and a stacked sequence of such flows likely accounts for a significant part of the topographic bulges surrounding these centers. Volcanic plains also comprise regionally extensive units in locations that presently do not have visible volcanic constructs. In particular, the plains of the Lunae Planum area east of the Tharsis region and the Hesperia Planum plains northeast of the Hellas basin extend over many thousands of kilometers, and both of these plains have crater densities that indicate a Hesperian age that must be older than the volcanic plains around Tharsis and Elysium. Thus substantial outpourings of plains-forming lava flows, likely from vents that are themselves buried beneath the thick pile of flows, were significant events during both the Hesperian and Amazonian epochs.

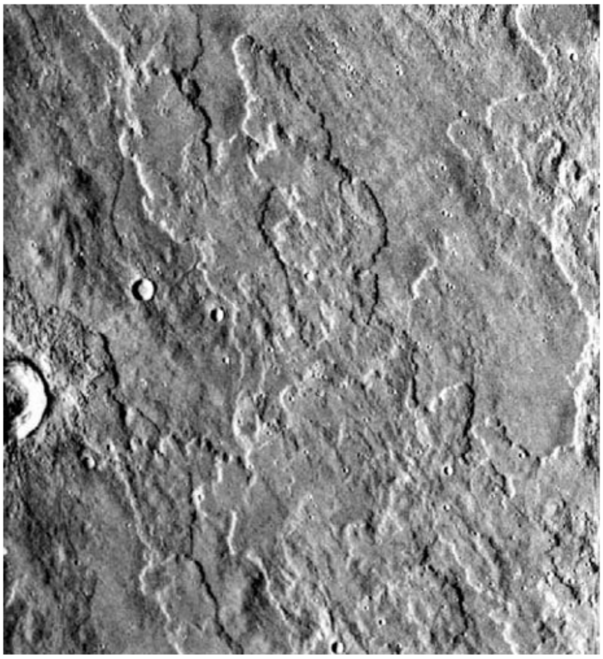

FIGURE 6 Lava flow margins on the Elysium plains near Hecates Tholus. Image width ~54 km, centered on 32.2°N, 213.5°W. (Viking Orbiter image 651A10, courtesy of NASA.)

The volcanic plains of Mars display flow features that can be divided into at least two broad categories: simple and complex. This distinction follows from an extension of George Walker's classification of terrestrial lava flows by the cooling units preserved in the volcanic sequence, with simple flows representing a single cooling unit of great extent (and probable large volume of effusion) and complex flows representing an intermixed sequence of discrete flow lobes that each comprise individual cooling units. Some plains units are nearly featureless in terms of detail visible in even the highest resolution orbital images, and many of these plains units may eventually turn out to be volcanic in origin, even though at present they are not readily placed within the simple or complex designation. Many of the volcanic plains that fill the floors of impact basins (like Hellas) or that lack clearly resolvable individual flows over wide areas are considered to be simple in the sense that the volcanic emplacement most likely was sufficiently rapid or prolonged to allow the plains to be considered as representing one major cooling unit. The younger volcanic plains around Tharsis and Elysium are primarily complex (as in Fig. 6), with numerous finger-like flow lobes traceable in some cases for many hundreds of kilometers. As orbital image resolution improves, as with the Mars Orbiter Camera on the Mars Global Surveyor spacecraft, some of the older volcanic plains likely may turn out to be made up of a series of complex flow lobes like the ones that surround Tharsis and Elysium.

Not surprisingly, some plains units are problematic in origin. These units tend either to be relatively featureless or to have such complicated surface exposures that their origin remains the subject of considerable controversy. The Medusae Fossae Formation southwest of the Tharsis region (MFF in Fig. 1) deserves a brief discussion here because although its origin remains controversial, one of the contending hypotheses is that this material is the result of massive pyroclastic eruptions. The Medusae Fossae Formation consists of several discrete layers of material that is very friable (eroded by the wind into huge fields of yardangs) but locally prominent caprock units help preserve the underlying materials. This observation has been compared to the welded and nonwelded zones present within many ignimbrite deposits on Earth. A significant problem with this hypothesis is that there is no indication of the possible source vent or vents, which is troubling if volcanic eruptions laid down ash that in places is over 2 km thick and that extends over several million square kilometers along the Martian equator, following the boundary between the southern cratered highlands and the northern lowland plains. The prospect of large ash-producing eruptions in this part of the planet is strengthened by recent remote-sensing observations that an area west of Arsia Mons and east of the majority of the Medusae Fossae Formation displays the unique property that Earth-based radar signals are not reflected from this broad area. "Stealth" has been interpreted to be associated with pyroclastic eruptions from vents west of the Arsia Mons volcano, which lends some support to possible major ignimbrite eruptions in the area.

VIII. COMPOSITIONAL CONSTRAINTS

Compositional information for Mars is available from three different sources: remote-sensing data (from either spacecraft instruments or Earth-based telescopes), on-site analyses by instruments on spacecraft that have returned data from three landing sites on Mars, and a special group of meteorites for which there is compelling evidence that these rocks were blasted from the surface of Mars and eventually fell to Earth. Each of these data sources has unique advantages and disadvantages as well as various limitations to the utility of the data. Here we will explore each data type for its implications for volcanic materials on Mars.

Remote-sensing studies of Mars began with telescopic measurements of various properties of the Martian surface and atmosphere, and since the 1960s these data have been augmented with higher spatial resolution data from a host of instruments on spacecraft that either flew by or orbited the planet. Earth-based instruments can achieve very high spectral resolution but only with relatively low spatial resolution on the planet (covering an area that may be hundreds of kilometers across). Spacecraft instruments tend to achieve substantially improved spatial resolution, but often this has come at the expense of spectral resolution. The ubiquitous Martian dust complicates this effort at any spatial resolution, masking significant portions of the surface within the instrument field of view and generally decreasing the contrast of the already subtle spectral features being sought. In spite of this handicap, remote-sensing data have shown that the dark regions of the planet have strong mafic affinities. Unfortunately, only the Syrtis Major volcanoes are present within a dark region, and the spectral information of other volcanic centers is effectively masked (at visual and thermal wavelengths) by the dust. Tens of microns of dust can strongly affect visual reflectance, and only 2 cm of dust can totally obscure even competent bedrock from thermal infrared observations.

The first concrete compositional information obtained for Martian materials came from an X-ray fluorescence instrument that was flown on both the Viking 1 and Viking 2 landers. In spite of the fact that the landers set down over 6000 km apart, the composition of the Martian fines at both sites was remarkably uniform (Table II), which in itself was a strong indication of the homogenizing influence of the regular global dust storms. Although repeated attempts were made to obtain a rock fragment with the Viking sample arm, no Martian rock was analyzed by the Viking instruments (centimeter-sized fragments all turned out to be indurated clods of dust). This situation changed dramatically in July of 1997 when the Mars Pathfinder mission successfully landed near the mouth of the Ares Vallis canyon and deployed the first mobile vehicle on Mars, the Sojourner rover. Sojourner had a spectrometer that the rover was able to place directly on several Martian rocks, as well as on the fine-grained materials between the rocks. The fines at the Pathfinder site were generally quite consistent with the fines observed at the Viking sites (Table II; note the differing sums for columns 2 and 3), but the rocks show distinct chemical differences from the fines ("Yogi" and "Barnacle Bill" in Table II). Images of the rocks at the Pathfinder site give a strong impression of being volcanic in origin, with ubiquitous pits that are likely vesicles. Assuming the rocks are volcanic, the compositions obtained from the Sojourner spectrometer imply they may be basaltic andesite. If the anomalously large sulfur content for the rocks is assumed to be contamination by dust on the rock surface, the measured silica contents become lower limits and at least some of the rocks may turn out to be andesites (e.g., "Barnacle Bill"), although recently the term Icelandite has been applied to these silica-enhanced rocks in an attempt to eliminate the subduction-related processes usually associated with the term andesite. Indeed, there is no evidence in or near the Pathfinder site for orogenic generation of andesite lavas, but fractional crystalization within isolated pockets of basaltic or basaltic andesite magmas could have generated some Icelandite-like rocks. The Pathfinder results are undergoing further refinement in association with the instrument calibration, so these results may be subject to revision at a later date.

The very best chemical information about Martian materials comes from 12 very special meteorites. These meteorites are considered to be from Mars because gases implanted in them during the shock of their ejection from their parent body is essentially identical to the atmosphere of Mars as measured by the Viking landers and unlike gases obtained from any other terrestrial or

TABLE II Chemical Compositions of Selected Martian Materials

Oxide	*Viking 1/Viking 2 fines*[a]	*Pathfinder fines*[b]	*Pathfinder "Yogi"*[c]	*Pathfinder "Barnacle Bill"*[c]	*Shergotty meterorite*[d]
SiO_2	43.3	49.0	55.5	58.6	51.4
Al_2O_3	7.1	8.4	9.1	10.8	7.1
FeO[e]	17.4	16.1	13.1	12.9	19.4
MgO	6.0	7.9	5.9	3.0	9.3
CaO	5.7	6.3	6.6	5.3	10.0
K_2O	0.0	0.2	0.5	0.7	0.2
TiO_2	0.5	1.2	0.9	0.8	0.9
SO_3	7.5	5.4	3.9	2.2	0.1
Na_2O	—	3.0	1.7	3.2	1.3
Cl	0.5	0.5	0.6	0.5	—
Total	88.0	98.0	97.8	98.0	99.7

[a] Average of two samples of fines from Chryse (Viking 1) and four fines samples from Utopia (Viking 2); from Table 6.1 of Frankel (1996).

[b] Average of three fines samples (A2, A4, and A5) from Pathfinder; from Table 1 of Rieder *et al.* (1997). Note that results are reported as normalized to 98.0%.

[c] Results of two rocks (A7, Yogi; A3, Barnacle Bill) from Pathfinder; from Table 1 of Rieder *et al.* (1997). Results normalized to 98.0%.

[d] Martian meteorite Shergotty, a basaltic achondrite; from Table V, p. 605, in Kieffer *et al.* (1992).

[e] Total iron, regardless of oxidation state. Reported as Fe_2O_3 for column 2 and FeO for columns 3–6.

extraterrestrial sample. Eleven are igneous in nature and are only one-third the age (1.3 Ga to 180 Ma) of practically all other meteorites, and the twelfth has an older age more typical of most meteorites. Collectively called SNC meteorites, seven are basalts or lherzolites/harzburgites like the Shergotty (S) meteorite, three are clinopyroxenites or wehrlites like Nakhla (N), Chassigny (C) is the sole dunite, and ALH84001 is a ~4.5-Ga orthopyroxenite with veins of carbonate in which are controversial features that may (or may not) be evidence of primitive life from early in Martian history.

The SNC meteorites have told us a lot about Mars in general, but we unfortunately have no evidence for where on the Martian surface they came from. The abundance of volcanic rocks among the available group is consistent with the extensive coverage of Martian volcanic plains discussed above, but the young crystallization ages cannot be used to calibrate the geologic epochs on Mars without knowledge of what specific unit they came from. Some of the nonbasaltic rocks may have come either from slowly cooled cores of thick lava flows where limited fractionation may have taken place or possibly even from a plutonic body. ALH84001 likely came from somewhere in the cratered highlands of Mars, portions of which must date from practically the formation of the planet. In spite of this wealth of chemical detail, it will require the return of documented samples from known localities on Mars before we can relate the rock histories to regional or local geologic materials.

IX. VOLCANIC HISTORY OF MARS

The information presented in this article can be summarized into a general picture of the volcanic history of Mars. Without constraints on the cratering record for Mars, absolute ages cannot be associated with any of these stages. However, the stratigraphy of geologic units at least gives us a fairly clear picture of how volcanic eruptions developed throughout Martian history.

The oldest terrain on Mars is the Noachian densely cratered highlands, and if ALH84001 is representative of this era, at least some magmatic activity took place during this time of intense cratering. Isolated volcanic centers developed within the cratered highlands, most of which are preserved today only as deeply scoured small hills scattered throughout the southern highlands. The Hesperian epoch witnessed massive eruptions of fluid lava that produced volcanic plains that covered extensive portions of the Martian surface. The composition of these plains-forming materials was likely basaltic in nature, although Pathfinder results suggest that more evolved lavas (such as basaltic andesite) also may have been present. Several volcanic centers developed on the rim of the Hellas impact basin and within what is now the Syrtis Major dark region. These volcanoes involved the generation of considerable amounts of ash, leading to a very low overall profile and intense channelization by either fluvial or magmatic fluids. The unique Alba Patera feature may represent a volcano caught in the transition from the more ash-rich eruptions of the highlands to the more lava-rich eruptions typical of most subsequent eruptions.

The late-Hesperian and Amazonian epochs involved voluminous eruptions that resulted in both broad volcanic plains and numerous central volcanic constructs. Volcanic activity concentrated around the Elysium and Tharsis regions; crater densities suggest that effusive activity was most prolonged in the Tharsis region, where some volcanic surfaces are very sparsely cratered and thus may be quite young. Thousands of small domes in the northern lowland plains may be the result of either localized Strombolian activity (cinder cones) or the interaction of lava with water or wet sediments (pseudocraters). Not all of the volcanic activity in the Amazonian period may have been gentle effusion of lava; significant ash deposits may be present west of the Tharsis Montes, although the true nature of these enigmatic materials remains controversial. Volcanic materials are likely still being redistributed by current winds, such as in the Syrtis Major dark region.

X. FUTURE STUDIES

Several issues about Martian volcanism remain unresolved at present, and hopefully the series of missions NASA has planned for Mars over the coming years will help to address some of these questions. The Pathfinder results have raised the possibility that lavas more evolved than basalt may have been important in Martian history. If this prospect turns out to be true on a global scale, it could have a major effect on our concepts of magmatic evolution on the terrestrial planets. Similarly, the question of the abundance and origin of pyroclastic deposits on Mars remains unclear at present, but this too could have an important influence on issues such as the volatile content of Martian magmas. The absolute age of all Martian terrains, volcanic as well as sedimentary or metamorphic in origin, remains a glaring uncertainty in all studies of the emplacement of volcanic materials on Mars. The return of documented samples from diverse localities on Mars would be the most definitive way to answer these and other outstanding questions about Martian volcanism, and fortunately NASA is actively planning toward that end. The Mars Surveyor program is an ambitious series of landers and orbiters targeted at addressing a host of science questions through repeated visits to Mars, culminating with the return of samples cached by mobile rovers. In preparation for the lander missions, sophisticated remote-sensing data will be collected from new technology sensors in orbit around Mars, as evidenced by the dramatic new data currently being returned by the Mars Global Surveyor spacecraft. All of these new data will undoubtedly add considerable detail to the volcanic history of Mars outlined in this article.

ACKNOWLEDGMENTS

Reviewer comments and the advice of Editor H. Sigurdsson were very helpful in revising the manuscript. This work was supported by NASA Grant NAG5-4164.

SEE ALSO THE FOLLOWING ARTICLES

Basaltic Volcanoes and Volcanic Systems • Calderas • Ignimbrites and Block-and-Ash Flow Deposits • Lava Flows and Flow Fields • Pyroclast Transport and Deposition • Volcanism on Io • Volcanism on the Moon • Volcanism on Venus

FURTHER READING

Carr, M. H. (1975). The volcanoes of Mars. *Sci. Am.* **234,** 32–43.

Carr, M. H. (1981). Pages 87–113 *in* "The Surface of Mars." Yale Univ. Press, New Haven, CT.

Carr, M. H. (1999). Mars: Surface and Interior. Pages 291–308 *in* "Encyclopedia of the Solar System" (P. R. Weissman,

L. A. McFadden, and T. V. Johnson, eds.). Academic Press, San Diego.

Francis, P. (1994). Pages 416–425 *in* "Volcanoes: A Planetary Perspective." Oxford Univ. Press, New York.

Frankel, C. (1996). Pages 100–138 *in* "Volcanoes of the Solar System." Cambridge Univ. Press, New York.

Greeley, R., and Spudis, P. D. (1981). Volcanism on Mars. *Rev. Geophys. Space Phys.* **19,** 13–41.

Kieffer, H. H., Jakosky, B. M., Snyder, C. W., and Matthews, M. S. (1992). Pages 424–452 and 601–611 *in* "*Mars.*" Univ. of Arizona Press, Tucson.

McSween, H. Y., Jr., (1994). What we have learned about Mars from SNC meteorites. *Meteoritics* **29,** 757–779.

Mursky, G. (1996). Pages 219–242 *in* "Introduction to Planetary, Volcanism." Prentice-Hall, New York.

Rieder, R., Economou, T., Wänke, H., Turkevich, A., Crisp, J., Brückner, J., Dreibus, G., and McSween, H. Y., Jr. (1997). The chemical composition of Martian soil and rocks returned by the mobile Alpha Proton X-ray Spectrometer: Preliminary results from the X-ray mode. *Science* **278,** 1771–1776 (Mars Pathfinder special issue).

Scott, D. H., Tananka, K. L., Greeley, R., and Guest, J. E. (1986). Geologic maps of the western equatorial, eastern equatorial and polar regions of Mars. Miscellaneous Investigations Series Maps I-1802-A, B, and C. U.S. Geological Survey, scale 1 : 15,000,000.

U.S. Geological Survey (1991). Topographic maps of the polar, western, and eastern regions of Mars. Miscellaneous Investigations Series Map I-2160. U.S. Geological Survey, scale 1 : 15,000,000.

This Page Intentionally Left Blank

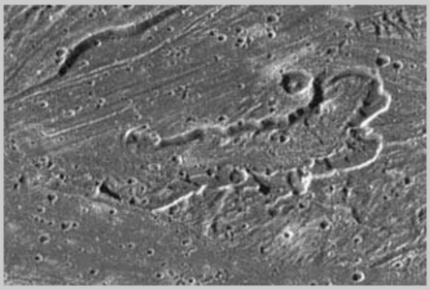

CRYOVOLCANISM IN THE OUTER SOLAR SYSTEM

PAUL GEISSLER
Lunar and Planetary Laboratory, University of Arizona

I. Introduction and Scope
II. Materials and Mechanisms
III. Triton
IV. Moons of Uranus
V. Saturnian Satellites
VI. The Jupiter System
VII. Future Exploration

GLOSSARY

albedo Reflectivity of the surface, ranging from 0 (perfectly absorbing) to 1 (perfectly reflecting), important in determining surface temperature.

clathrates Cage structures formed by H_2O ice having 8 cavities for each 46 water molecules that can trap large "guest" molecules of nonpolar volatile gasses.

cryoclastic eruption Eruption of water or other liquids that is driven by the exsolution of more volatile gasses such as CO or CH_4 and may form frosty "ash" deposits as the liquid condenses and expands.

cryovolcanism Eruption of liquid or vapor phases (with or without entrained solids) of water or other volatiles that would be frozen solid at the normal temperature of an icy satellite's surface.

eccentricity A measure of the ellipticity of an orbit, defined as the ratio of the distance between the two foci of the ellipse to the length of its major axis.

inclination Tilt of a satellite's orbit plane with respect to the plane of the planet's equator, important for determining seasonal variations in insolation.

orbital period Time taken for a satellite to complete one orbit of the planet, usually equal to the satellite's spin period (the length of a "day").

orbital resonance A commensurability between the orbits of two or more satellites, such that their orbital periods are related as the ratio of small integer numbers.

photolysis Dissociation of molecules by absorption of energetic photons.

radiolysis Dissociation of molecules by impact of charged particles.

resurfacing Any internal geologic process such as volcanism or tectonism that eradicates older surface features.

solid-state greenhouse Trapping of solar energy by ices that are transparent to visible light but opaque to longer wavelength thermal radiation.

sputtering Ejection of solid surface materials by the impact of energetic charged particles (an efficient erosion mechanism for satellites and rings located within planetary radiation belts).

I. INTRODUCTION AND SCOPE

Cryovolcanism is the eruption of water and other liquid- or vapor-phase volatiles onto the frigid surfaces of the

Copyright © 2000 by Academic Press
All rights of reproduction in any form reserved.

icy satellites of the giant planets. It is known to occur on only one of these worlds: Triton, a moon of distant Neptune, where geyser-like plumes of nitrogen were discovered during the explorations of Voyager 2. There is indirect evidence that cryovolcanic processes may have taken place elsewhere in the outer solar system and might even be active today. In this article we examine the mechanisms and manifestations of cryovolcanism, beginning with a review of the materials that make up these unusual "magmas" and the means by which they might erupt and concluding with a volcanologist's tour of the farthest reaches of the solar system.

The Voyager spacecraft encountered a bewildering zoo among the natural satellites of Jupiter, Saturn, Uranus, and Neptune (Table I). Several are larger than our own Moon, and two (Ganymede at Jupiter and Titan at Saturn) are bigger than the planet Mercury and would be considered planets in their own right if not for the fact that they are in orbit about larger worlds. Water ice is the most important constituent of the surfaces of most of these moons, with the notable exception of Io, where water either never was abundant or was driven off by eons of sustained geologic activity (see "Volcanism on Io"). Many of the icy satellites are heavily cratered, having surfaces that passively recorded the bombardment of impactors, undisturbed by internal activity. Others appear relatively youthful, with areas "resurfaced" so that part of the cratering record was erased by endogenic processes such as tectonism and volcanism. A focus of scientific study of these satellites is the nature of the processes by which they were resurfaced, and in fairness, it should be pointed out that our knowledge of the materials and mechanisms of this geologic activity is still somewhat rudimentary. Much of the uncertainty concerns whether the resurfacing materials were in the liquid or solid state at the time they were emplaced or deformed. By confining our attention to cryovolcanism, here defined as the extrusion of liquids and vapors of

TABLE I Physical Properties of the Larger Natural Satellites of the Outer Solar System[a]

Planet	*Satellite*	*Radius (km)*	*Density (gm cm^{-3})*	Gravity (m s^{-2})	*Orbit period (days)*	*Orbit eccentricity*	*Orbit inclination (deg)*
Earth	Moon	1738	3.34	1.62	27.32	0.055	5.15
Jupiter	Io	1815	3.57	1.81	1.77	0.004	0.04
	Europa	1569	2.97	1.30	3.55	0.010	0.47
	Ganymede	2631	1.94	1.43	7.16	0.001	0.19
	Callisto	2400	1.86	1.25	16.69	0.007	0.28
Saturn	Mimas	197	1.17	0.07	0.94	0.020	1.53
	Enceladus	251	1.24	0.08	1.37	0.005	0.02
	Tethys	524	1.26	0.18	1.89	0.000	1.09
	Dione	559	1.44	0.22	2.74	0.002	0.02
	Rhea	764	1.33	0.28	4.52	0.001	0.35
	Titan	2575	1.88	1.35	15.95	0.029	0.33
	Iapetus	718	1.21	0.24	79.33	0.028	7.52
Uranus	Miranda	242	1.26	0.08	1.41	0.003	4.22
	Ariel	580	1.65	0.29	2.52	0.003	0.31
	Umbriel	595	1.44	0.22	4.14	0.005	0.36
	Titania	800	1.59	0.36	8.71	0.002	0.14
	Oberon	775	1.50	0.32	13.46	0.001	0.10
Neptune	Triton	1353	2.06	0.78	5.87	~0	156.8
Pluto	—	1142	2.07	0.63			
	Charon	596	2.07	0.21	6.39	~0	94.3

[a] Not listed are moons smaller than about 200 km in diameter, which number at least 40. Pluto and the Earth's Moon are included for reference.

materials that would be frozen solid at the planetary surface temperatures, we deliberately exclude processes such as icy tectonism, diapirism and solid-state convection, and intrusive magmatism, which probably played important roles in resurfacing the icy satellites. This somewhat arbitrary definition calls into question whether rhyolites should be considered "volcanic," given that they have crystal fractions sometimes exceeding 50%, but it admits an example of cryovolcanic activity here on Earth: the so-called "icefoots" on the shores of Lake Superior, where waves generated over open water in winter pump liquid water through cracks in the ice at the lake margins, forming icy mounds around the "vents."

Two conditions must be met for cryovolcanic activity to take place on any icy moon: liquids must be generated in the interior, and the melt must then migrate to the surface of the satellite. These conditions are much more easily met on the larger satellites of the solar system than on smaller objects. A number of heating mechanisms contribute to the generation of fluids in the moons' interiors. The most important energy sources are gravitational (due to accretion and differentiation), radiogenic (through the decay of long-lived radioisotopes), and tidal (frictional heating caused by the daily changes in the shape of the satellite). Solar heating probably drives the nitrogen plumes on Triton, and Io's prodigious heat flow may be fueled in part by electromagnetic induction in addition to the tidal heating known to be important. The planetary factors that determine whether cryovolcanism can occur include size, composition (particularly silicate fraction, which determines radiogenic heating), location in the solar system (related both to composition and surface temperature, which ranges from 38 K at Triton up to more than 165 K in the hottest parts of Callisto), and the history of the moon's orbit from formation through to the present. The orbital history dictates the degree of tidal heating, since the daily tidal distortions are due to noncircular or oblique orbits around the primary planet. Noncircular orbits are commonly induced by gravitational interactions with satellites on neighboring orbits, through orbital resonances that gradually increase the orbital eccentricity (Table I). For example, Jupiter's moon Europa is caught in a tidal "tug-of-war" between Io, which orbits nearer to Jupiter with a period exactly half that of Europa, and Ganymede, which orbits farther than Europa with a period exactly twice as long. The orbital eccentricity forced by this "Laplace resonance" raises tides that may be sufficient to maintain a molten layer of liquid water beneath the satellite's surface. Orbital obliquity (inclination of the satellite orbit with respect to the planet's equator) is generally the result of collision or capture, extremely energetic events that may have contributed to the melting of Triton, for example. Gravity and composition control the manner of magma ascent, as we shall see later. The morphology of lava flows and other volcanic constructs, once erupted, are influenced by magma viscosity and effusion rate in ways familiar from terrestrial experience but also by planetary factors such as gravity, surface temperature, and atmospheric pressure (for example in the case of Saturn's moon Titan, which has an atmosphere denser than Earth's).

II. MATERIALS AND MECHANISMS

A. Composition of Cryomagmas

Several lines of evidence provide us with incomplete and sometimes contradictory information about the composition of the outer solar system satellites. Direct spectroscopic detection is possible only for optically active materials—those with identifiable absorption features in their spectra—and tells us only about what lies on the uppermost surface, generally after processing by solar and charged-particle irradiation, sublimation, and a host of other "space-weathering" processes. Observations of the presumably "raw" icy materials seen in cometary outflows and in distant extrasolar nebulae provide important added constraints. Satellite densities and moments of inertia determined from gravitational measurements allow us to infer their interior structures and place limits on bulk composition and degree of differentiation. Theoretical modeling, constrained by samples of unprocessed protoplanetary materials in the form of primitive meteorites known as carbonaceous chondrites, provides some of the most valuable clues. Fundamental to the understanding of the icy satellites' composition is the idea of equilibrium condensation: the notion that the constituents of the early protoplanetary system, initially present in cosmic relative abundances, condensed and chemically reacted in accordance with the temperatures and pressures found in their local environments, which varied with distance from the early sun and proximity to the still-forming giant gaseous planets. By these calculations a "frost line" is predicted beyond the orbit of Mars, beyond which H_2O ice is expected to have condensed in abundance. Spectroscopic observations confirm that water ice is the dominant constituent of the satellites of Jupiter, Saturn, Uranus, and Pluto. Methane and ammonia should have also been present in the high-pressure nebulae surrounding Jupiter and Saturn, while their oxidized forms (CO, CO_2, and N_2) were favored in the cold outermost solar system, where reactions were too sluggish to proceed to equilibrium. While not predicted by the models, compounds such as methanol (CH_3OH) and formaldehyde (H_2CO) are observed in comets and may be minor components of the most distant satellites. Some properties of these ices are listed in Table II.

As a geologic material, H_2O has a number of unusual properties. Its common hexagonal form (ice Ih) is stable at the low pressures (a few tens of megapascals) attained in the interiors of small satellites such as Enceladus and Miranda, in the thin ice/water crust of Europa, and at depths of up to a few hundred kilometers in the larger satellites. Pressures of hundreds to thousands of megapascals are reached in the interiors of Ganymede, Callisto, and Titan, so that dense high-pressure ice polymorphs should be stable. At the opposite extreme, metastable cubic and amorphous phases of ice can be deposited at the low temperatures (<150 K) and pressures of the icy satellite surfaces. Ice can also form solid cagelike structures known as clathrates which can trap adsorbed gasses such as CH_4, CO, and N_2 which are too volatile to condense otherwise, except in the Neptune and Pluto systems. Unlike silicate minerals and rocks, ice Ih undergoes a volume reduction upon melting so that the liquid is denser than the solid. This presents a profound problem for cryovolcanism, since liquid water magmas should not rise through a pure water ice crust but instead are expected to sink. Water is also an extraordinary solvent, and there is an abundance of highly soluble salts (up to 20% by mass, mostly Mg and Na sulfates and sulfate hydrates) available in the chondritic materials from which the silicate fractions of the icy satellites were formed.

TABLE II Major Ices Detected or Suspected to Be Present on the Outer Solar System Satellites

Name	Formula	Freezing point (K)	Boiling point (K)
Water	H_2O	273.2	373.2
Hydrogen peroxide	H_2O_2	272.7	Decomposes
Sulfur dioxide	SO_2	200.5	263.1
Ammonia	NH_3	195.5	239.8
Carbon dioxide	CO_2	194.7	Sublimes
Hydrogen sulfide	H_2S	190.3	211.4
Formaldehyde	H_2CO	181.2	252.2
Methanol	CH_3OH	175.4	337.8
Methane	CH_4	90.7	111.7
Ozone	O_3	80.7	161.3
Carbon monoxide	CO	68.1	81.6
Nitrogen	N_2	63.3	77.4
Oxygen	O_2	54.8	90.2

[a] H_2O, NH_3, CH_4, and H_2S (the reduced forms of the common elements O, N, C, and S) are expected to make up the bulk of ices condensed from a hydrogen-rich nebula in equilibrium. The other species may have been produced by disequilibrium condensation or by photolysis and radiolysis. The freezing and boiling points listed are for a pressure of 1 bar (0.1 MPa).

Melting of water-rich magmas can be greatly promoted by adding "antifreeze" in the form of salts or particularly ammonia, which should account for up to 15% of the mixture of ices from a fully equilibrated and condensed primordial nebula. Ammonia has not been detected spectroscopically on any satellite surface but is seen in comets and extrasolar nebulae and may be rapidly photolyzed to nitrogen upon exposure to the space environment. The ammonia–water system closely parallels the system $MgO–SiO_2$, with ammonia dihydrate ($NH_3 \cdot 2H_2O$) taking the place of enstatite as the minimum-temperature melt product. Addition of ammonia to H_2O ice lowers the melting point of the mixture to 176 K, conceivably attained in the interiors of even modestly sized satellites. Partial melting in the ammonia–water system slightly ameliorates the density problem of pure water magmas, since the melt is more ammonia-rich (28–34%) than its frozen equivalent, making it marginally positively buoyant with respect to the solid ice mixture. On the other hand, addition of salts to water only slightly depresses the melting point and greatly exacerbates the magma density problem, since the eutectic brines tend to sink with respect to solids of comparable composition. Fractional crystallization of brines results in segregation of salts from the solid, similar to the freezing of terrestrial ocean water, and might produce diapirism of the relatively buoyant solid H_2O phase. (Sulfates rather than chlorides are expected to dominate extraterrestrial brines because of the vastly greater primordial S abundance.) Methane does not significantly lower the melting point of ice, but clathrates of methane can break down to form ice Ih and gas or fluid when the vapor pressure of the contained methane exceeds the confining pressure; at low pressures (<0.03 MPa) this can occur when methane clathrates are warmed to only 176 K by an ammonia-rich water magma. Likewise, methane marginally reduces the melting point of nitrogen on Triton to a chilly 62 K.

The plausible candidate cryomagmas cover a range of viscosities and densities that can be compared with those of silicates (Figs. 1 and 2). Briny solutions at their melting points are many orders of magnitude less viscous than even the most fluid silicate lavas and are unlikely to construct observable topography. Ammonia–water liquids attain viscosities similar to those of silicate magmas and may form solid crusts and partially crystalline slurries that aid their ability to build flow fronts and other constructive features found in terrestrial volcanism. The liquid/solid density contrasts that drive silicate volcanism reach up to 15% (in the case of peridotite), whereas a paltry 1% expansion is achieved in the best case by the melting of ammonia dihydrate. Moreover, the surface layers may be rather porous due to fragmentation by repeated impacts. The ascent of cryomagmas must be assisted by increasing the density of the crust, by pressurizing the liquid lavas, or by even more exotic means.

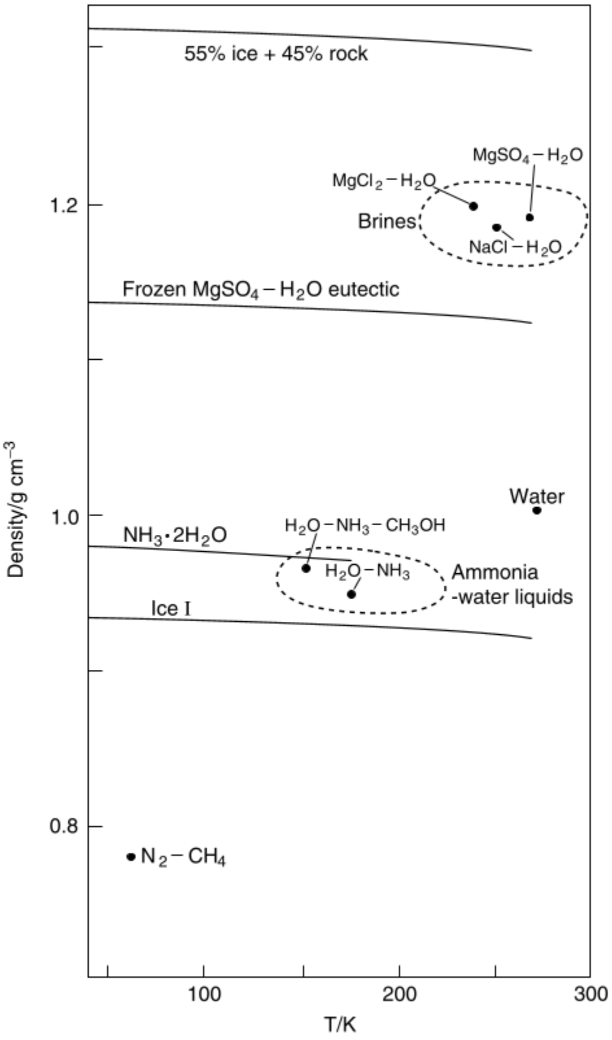

FIGURE 1 Densities of candidate cryomagmas and solids as a function of temperature. (From Kargel, 1990.)

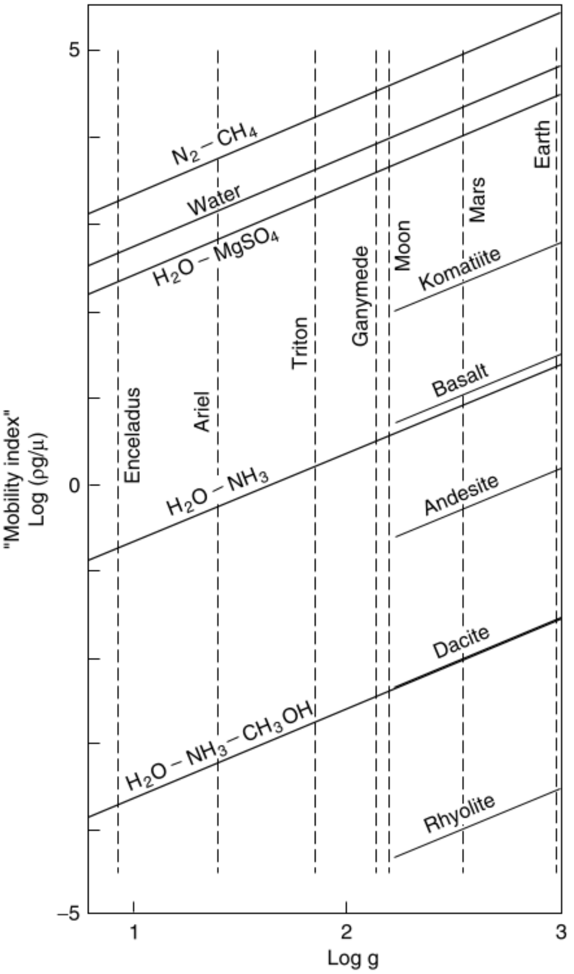

FIGURE 2 Mobilities of crystal-free cryomagmas at their liquidus temperatures compared with those of silicate lavas. (From Kargel, 1990.)

B. Eruptive Processes

Cryovolcanism may have been common early in the histories of the icy satellites, while their primordial surfaces were still rich in rocky material prior to differentiation. Even dense brines would have been positively buoyant with respect to sufficiently silicate-rich crusts. Magmas may have migrated upward along fluid-filled fractures and faults, much the same way as crevasses in terrestrial glaciers allow ponded water to sink downward through the ice, the cracks closing again afterward. In such a situation the effects of gravity control the mechanics of the eruption: the low gravity of the small satellites results in slower ascent speeds and lower effusion rates, but greater eruption volumes, than their counterparts on the larger icy moons (because of the larger crack depths possible on smaller objects). This early volcanism would have been a self-limiting process, shutting itself off after crustal composition and density stratification were achieved.

Other ways to overcome the magma density problem are to overpressurize the liquid or add volatiles to provide effervescence for the eruption. Overpressurization can happen in the late stages of satellite evolution by the cooling and freezing of a subsurface liquid layer. The volume expansion due to freezing of water can then fracture the surface and expel the last melt like an artesian spring. This is an attractive mechanism since much of the tectonism observed on the outer solar system satellites is attributed to global expansion, perhaps in such episodes of freezing. Alternatively, ices can be superheated by volcanism in the underlying silicates or by solar insolation, the latter being the probable explanation for Triton's geysers. The likely incorporation of supervolatiles into solid ice clathrates suggests the possibility of gas-driven cryovolcanism, the icy analog of terrestrial pyroclastic eruptions. The physics of these putative phenomena (dubbed "cryoclastic" eruptions) is similar to explosive volcanism on Earth, with methane and CO taking on the roles of H_2O, CO_2, and SO_2.

Other processes, not yet theoretically explored, have also been suggested to contribute to the widespread resurfacing of the outer solar system satellites described in the next section. Fluids could be derived from pressure-release melting in the course of solid-state convec-

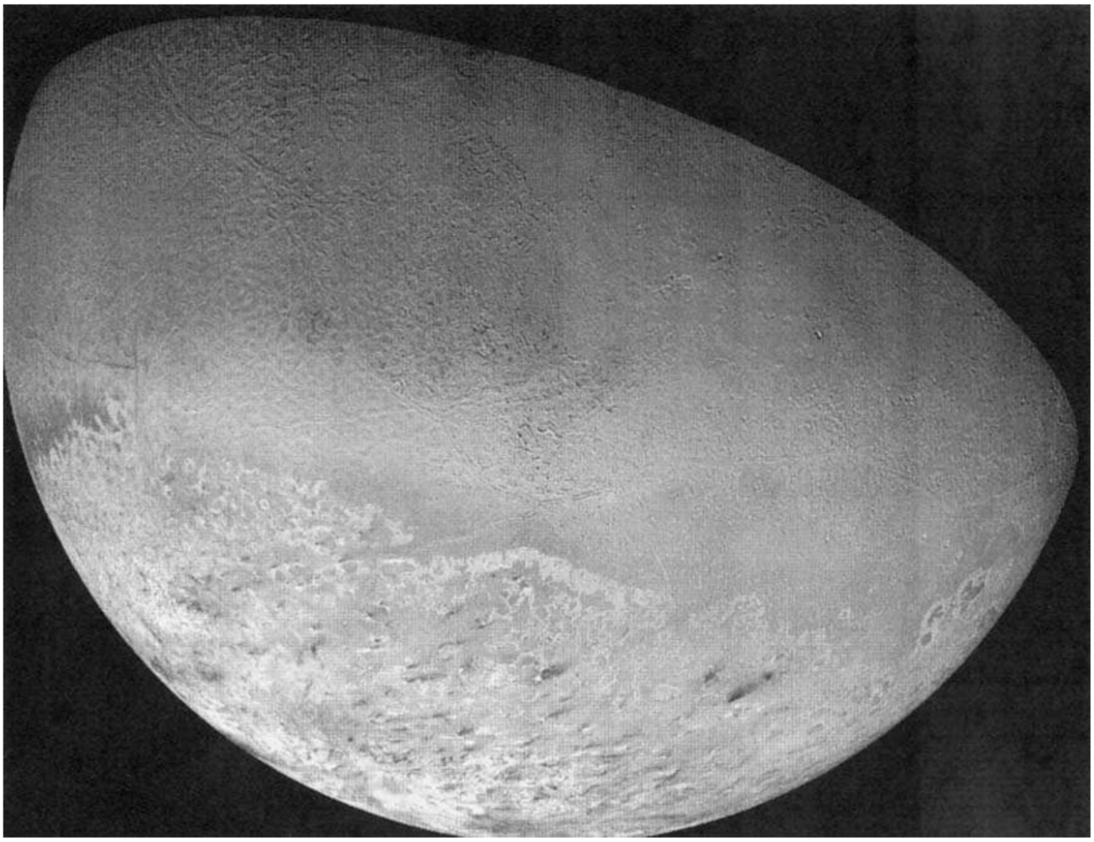

FIGURE 3 Triton. This is a view of the south pole of Neptune's only planet-sized moon. The bright polar cap is made up of relatively mobile N_2 ice, subliming in the summer sunshine. The dark streaks mark the sites of active or recent plumes. (Voyager 2 image mosaic, courtesy of NASA.)

tion, provided that the composition of the convecting material differs from H_2O ice Ih (which has the opposite behavior with respect to pressure). A mechanism of mechanical pumping of wet slurries from the interior has been proposed to account for the curious double ridges of Europa. In all cases, the liquids reaching the surface would be subjected to instantaneous freezing and boiling at the cryogenic temperatures and near-vacuum of the space environment. A solid crust that is meters in thickness would form within hours of such an eruption, but not before the surface surrounding the vent was painted with frost deposits (along with any entrained contaminants) that could be quite extensive under the low gravity of small satellites.

III. TRITON

Active volcanic venting was observed in the last place one would expect to find it. Triton is the coldest and most distant of the moons yet visited by spacecraft, and the last to be imaged before Voyager 2 was hurled out of the solar system on August 25, 1989. In stereo pictures taken as the spacecraft passed under the south pole of the satellite, at least two plumes can be seen jetting from the surface to heights up to 8 km, with trails reaching 150 km downwind. More than 100 dark windblown streaks decorate the polar cap (Fig. 3), testifying to widespread previous plume activity. At lower latitudes, an even more interesting episode earlier in the moon's history is suggested by bizarre "cantaloupe" terrain and flowlike features that may have resulted from volcanic flooding of older surface topography. Triton's north polar region was shrouded in darkness from Voyager's cameras and remains unknown.

At 38 K, Triton's surface temperature is well below the freezing point of nitrogen, the material that makes up the south polar cap. It is near the transition temperature for stability of the cubic and hexagonal forms of nitrogen ice, suggesting that seasonal phase changes are possible. Both N_2 and CH_4 have been spectrally identified on its surface, and CO and CO_2 ices have been detected in minor quantities. H_2O is also expected to be abundant in the crust, but its spectral signature is masked by the more volatile surface constituents. Triton's thin (14 μbar) atmosphere is made up largely of nitrogen vapor with clouds of N_2 ice crystals and traces of CH_4 and CO and is responsible for transporting a couple of meters thickness of nitrogen ice from pole to pole every Triton-year, keeping the surface nearly isothermal.

Triton's "geysers" (Fig. 4) are probably caused by solar sublimation of the polar cap, despite the fact that the satellite is so distant that the Sun would merely appear as a particularly bright star. Triton's year is about 165 Earth-years long, and it was just approaching southern summer solstice at the time of the Voyager flyby. Triton's orbit is oblique with respect to Neptune's equator, and it is retrograde (opposite to the planet's spin direction), indicating that the satellite did not form anywhere in the vicinity of Neptune. Because of its obliquity, the orbit precesses every 688 Earth-years, causing the latitude of the subsolar point (the tropics)

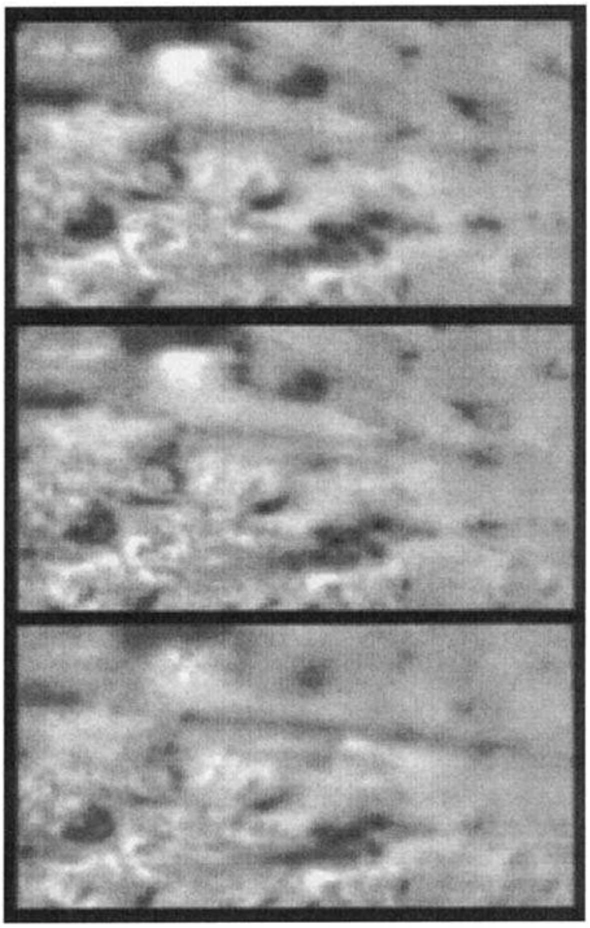

FIGURE 4 Nitrogen geyser on Triton. Two active plumes have been definitively identified in Voyager stereo pictures, and several more are possible. This is Mahilani, located at 49°S, 2°E. In these three separate views, Mahilani (left) can be seen to rise 8 km from the surface, with a dark tail that extends 150 km downwind (toward the right). (Voyager 2 images, courtesy of NASA.)

to vary from year to year, with periodic excursions up to 55° from the equator. It happens that Voyager visited on one of these extreme years, while the Sun beat down on the seldom-illuminated polar reaches of Triton.

All of the active plumes identified on Triton are found between 49°S and 67°S, near the latitude of the subsolar point. One model of their eruption suggests a solar "solid-state greenhouse" in which sunlight penetrates a transparent layer of low-thermal-conductivity nitrogen ice but is absorbed and trapped by dark carbon-rich impurities a few meters beneath the surface. This mild heating is enough to induce explosive venting of the gas, since an increase of only 10 K above the surface temperature is sufficient to raise the vapor pressure of N_2 100-fold. The wind streaks are likely caused by circulation in the tenuous atmosphere, as the flow from the south toward the colder northern hemisphere is deflected by coriolis forces eastward, due to the satellite's retrograde rotation. Photolysis products of methane might make up the carbon-rich absorbers and the dark particulates of the "cryoclastic" wind streaks.

A young, sparsely cratered surface is visible to the north of the polar cap, particularly on the leading hemisphere. About a third of the imaged area is imprinted with regular quasi-circular depressions bounded by ridges, nicknamed "cantaloupe terrain," which may be the surface manifestation of diapirism or solid-state convection in the interior. In other places, older cratered terrain was resurfaced by seemingly liquid or ductile material that flooded craters and other low-lying topography (Fig. 5). The source of the material could be four large depressions up to 200 km across that resemble terrestrial calderas. Steep scarps on the flows suggest that they are made up of relatively refractory H_2O ice, since little topography can be supported by solid nitrogen over geologic timescales, even under Triton's low

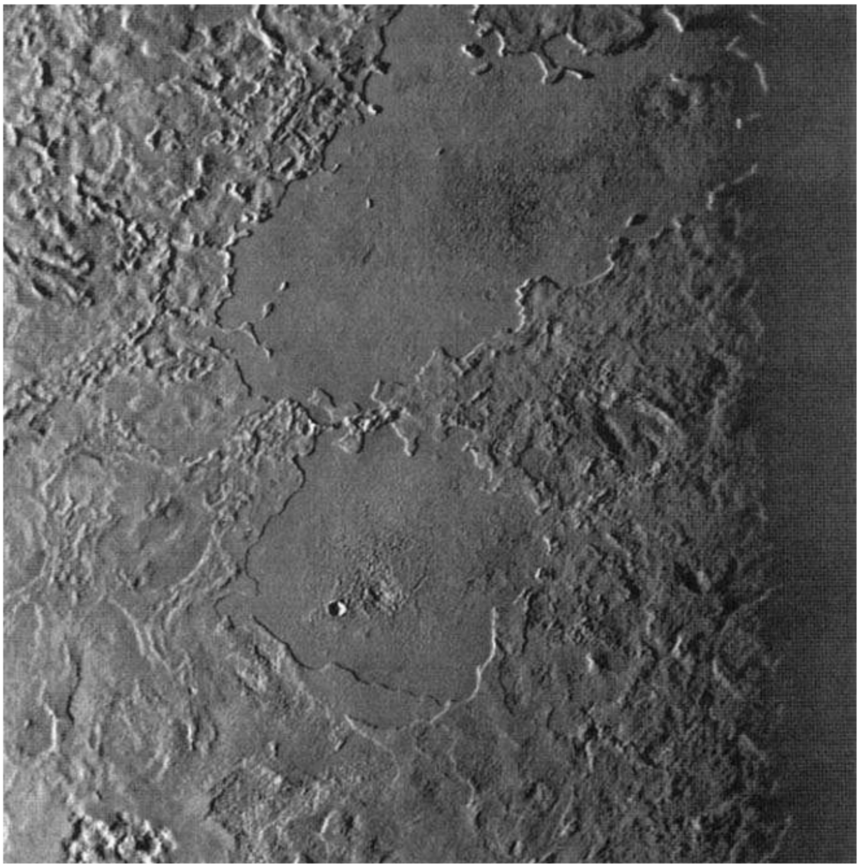

FIGURE 5 Cryovolcanic flows on Triton. The least ambiguous example of cryovolcanism in the solar system, Triton shows evidence of extensive melting, perhaps when the moon was gravitationally captured into orbit about Neptune. This view shows two large caldera-like features near the equator. Rimless pits to the right of the impact crater (in the lower "lake") may be the source of the smooth materials. (Voyager 2 image, courtesy of NASA.)

gravity. If these interpretations are correct, an episode of intense heating must have taken place in the past in order to stir up the icy interior and produce water- or ammonia-rich melts. Enormously energetic heating probably occurred when Triton was captured into Neptune's orbit, perhaps by gas drag in Neptune's extended atmosphere or by collision with another satellite. Most of this energy was dissipated within Triton's first orbit around the planet, but a good deal of heating took place soon afterward as its initially elliptical orbit was circularized by tidal friction. Triton's likely origin is from far beyond Neptune in the Kuiper Belt, the outer solar system counterpart to the asteroid belt, home of the Pluto–Charon system and the likely source of short-period comets. Triton could be compositionally similar to Pluto and its large moon Charon and potentially provides us with an indirect look at these so far unseen worlds.

IV. MOONS OF URANUS

Prior to the Voyager encounter in January 1986, the moons of Uranus were thought too small to have any signs of geologic activity on their surfaces. To explain the extensive resurfacing seen on such small satellites as Miranda, only 242 km in diameter, requires exotic compositions and such violent mechanisms as catastrophic disruption. Titania, the largest uranian moon, is rifted by a system of planet-sized fissures that form 20- to 75-km-wide grabens up to 1500 km long with fault scarps 2–5 km high. Umbriel and Oberon are both heavily cratered and show no indications of internal activity. Only about 35% of Ariel was imaged by Voyager 2, but its surface has the lowest crater density of the uranian satellites. Ariel appears to have been active in the past, with broad grabens similar to those of Titania, suggesting an episode of crustal extension brought about by global expansion, despinning, or relaxation of the satellites' tidal bulges. These grabens appear floored by possible volcanic flows. Smooth deposits within the grabens show flow features such as sinuous medial grooves that appear similar in morphology to familiar lava tubes and channels (Fig. 6). Material spilling out from the ends of the grabens seems to have flooded older cratered terrain, including a 30-km-diameter crater now half buried. The flows show substantial relief, suggesting that the resurfacing material was fairly viscous at the time it was emplaced. Based on the cross sections of the kilometer-thick putative flows, the rheology seems similar to that of terrestrial dacitic to rhyolitic magmas. The flow morphologies would seem to require an ammonia-rich composition, at least partially solidified, perhaps with methanol or some similar material added to thicken the soup.

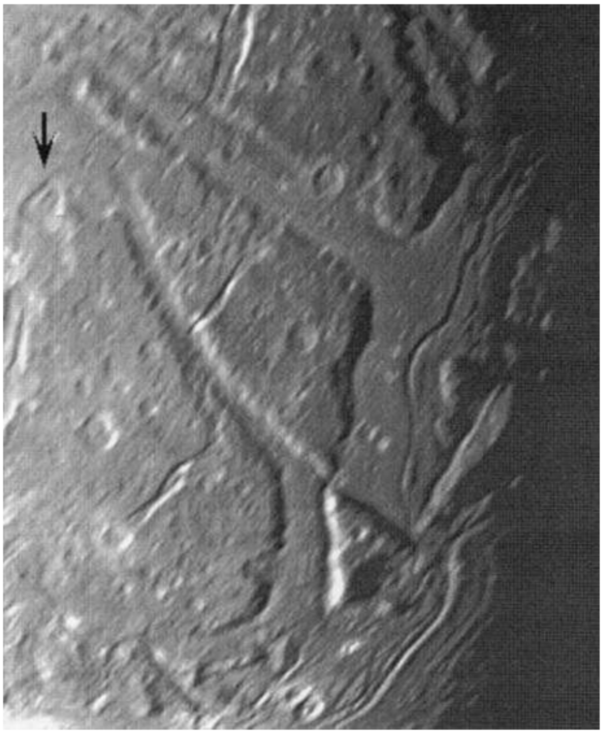

FIGURE 6 Ductile material on Ariel. The central channels (right) resemble collapsed lava tubes. Arrow indicates a 30-km-diameter crater now half buried by viscous flows. (Voyager 2 image, courtesy of NASA.)

Miranda's surface is astonishingly complex for such a tiny moon. Three unique tectonic structures are seen on the hemisphere viewed at close range by Voyager (Fig. 7). These so-called coronae consist of central chaotically deformed regions with patchy albedo markings, ringed by broad belts of concentric parallel faults and ridges. A steep fault scarp 10 km high can be seen near Inverness Corona, the chevron-shaped feature near the middle of the picture. All three coronae are large in comparison to the radius of Miranda and seem to reflect some planetary process not active on other solar system objects. One interesting hypothesis is that Miranda might have been disrupted by a catastrophic collision with another satellite and later reaccreted in a haphazard fashion, leaving dense materials on its surface and trapping lighter ices in the interior. Some time after reassembly, these density differences drove solid-state flow

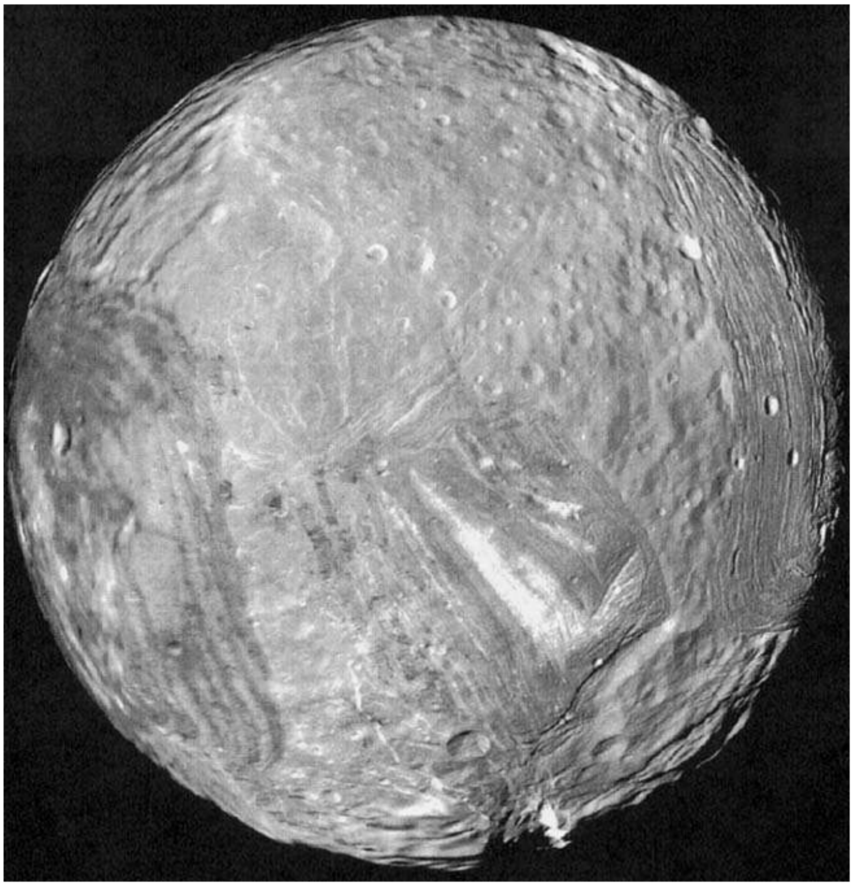

FIGURE 7 Miranda. The tectonic features (from left to right: Arden, Inverness, and Elsinore Coronae) appear to be due to density instabilities, despite the fact that the tiny satellite has little gravity to drive such deformation. (Voyager 2 image mosaic, courtesy A. Tayfun Oner.)

in the ice to produce the observed surface features through diapirism or subsidence as heavy materials sank to the center. Liquids may also have been generated in the process, if two small smooth areas in Elsinore Corona are cryovolcanic flows as has been suggested. Despite the vast difference in size, Miranda resembles giant Ganymede in having ancient heavily cratered terrain that has been partly resurfaced by tectonic deformation on a planetary scale.

V. SATURNIAN SATELLITES

Only slightly larger than Miranda, Saturn's moon Enceladus also shows evidence of extensive resurfacing and, paradoxically, is considered a prime candidate for current activity despite its diminutive size. It has the highest albedo of any solar system satellite (comparable to that of freshly fallen snow) and has a surface composition of nearly pure H_2O frost. These fresh frost deposits are the first clue of recent or active cryovolcanism, since the satellite must be continually bombarded by cometary impactors that contaminate and darken the surface over time. Large areas of the satellite appear smooth and uncratered and have clearly been erased by internal tectonic or volcanic activity (Fig. 8). Narrow fractures cut across the crust, including a prominent strike–slip fault visible in the lower part of the picture. The energy source for all this activity is puzzling—like Miranda, Enceladus is too small for gravitational or radiogenic heating to have been effective. Tidal heating due to its present-day orbital resonance with Mimas is not sufficient to account for the heating, but resonant orbits with other satellites in the past may have been more

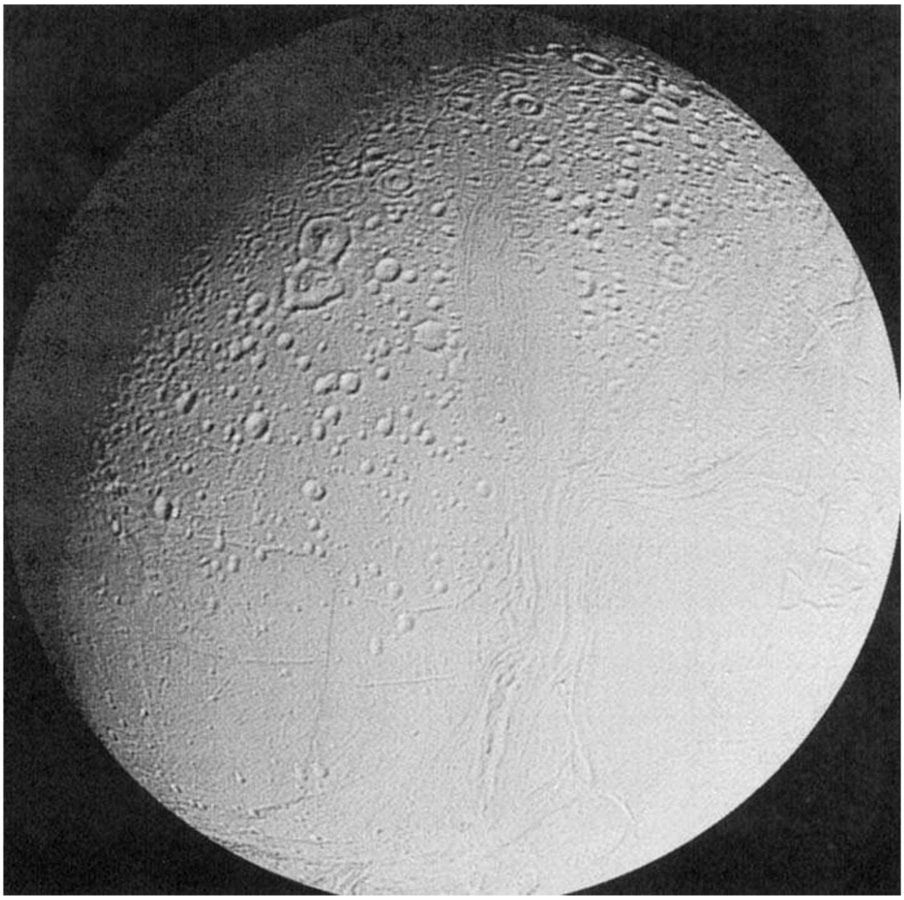

FIGURE 8 Enceladus. Is its snow-white surface the source of the E-ring particles, or the result of them? (Voyager 2 image, courtesy of NASA.)

efficient. Interestingly, Enceladus appears to be the source of the particles that make up the outermost member of Saturn's famous ring system. The faint E ring extends from 3 to 8 Saturn radii from the planet, and the orbit of Enceladus is embedded within the ring's densest part. Ice crystals in the ring are rapidly eroded by charged-particle sputtering and are swept up by Enceladus or gravitationally scattered into unstable orbits and escape the ring. The dynamical lifetime of the E ring is thought to be exceedingly short—on the order of only 10^5 years. If Enceladus is the source of the ring particles, then either a giant impact or perhaps vigorous volcanic venting must have recently taken place. The question for now remains unanswered, since only one side of the satellite was imaged by Voyager. Enceladus will be an important target for scrutiny by the Cassini spacecraft starting in 2004.

Even more mysterious is Titan, Saturn's only planet-sized moon, which is obscured by a dense, hazy atmosphere that made close-up observation impossible during the Voyager encounters. Titan's great mass and density suggest that abundant gravitational and radiogenic energy was available for melting the interior, added to by tidal friction from its eccentric orbit. Its surface is warmed to 97 K by solar greenhouse heating in the atmosphere, which like our own and Triton's atmospheres is mostly made up of N_2. Titan's atmosphere is over four times as dense as Earth's, but because of the low gravity the surface pressure is only 1.5 bar. Methane is present in the atmosphere at the 2–10% level, and traces of organics (photolysis products of methane such as ethane, propane, and acetylene) have been detected as well. HCN, CO, and Ar are probably also present. Titan's atmosphere and its composition have fueled much speculation about geologic processes on Titan and the nature of the satellite's surface. One suggestion is that the atmosphere started out as ammonia erupted from Titan in massive outgassing events and was later converted to nitrogen by ultraviolet photolysis and escape of hydrogen. Methane is also rapidly destroyed by photolysis, and some present-day source of methane at the surface or in the interior of the satellite is needed to replenish the atmospheric supply. Conceivably the gas could come from volcanic venting. At Titan's temperatures, methane behaves much like water on our own planet: liquid lakes of methane and ethane have been proposed for its surface, and methane rain or snow is possible. Volcanic processes on Titan can only be guessed at, but it seems likely that the satellite's dense atmosphere and possible liquid lakes would inhibit vesiculation in icy magmas, instead favoring effusive eruptions and perhaps forming extraterrestrial "pillow lavas."

Two other satellites of Saturn deserve mention as possible sites of cryovolcanic activity. Tethys and Dione are both rifted by large graben similar to the uranian moons, and Dione has the highest density of the Saturn system except for Titan. Bright wispy terrain occurs on Dione's poorly imaged trailing hemisphere (Fig. 9), which may be frost deposited during a cryoclastic eruption. These bright streaks sometimes grade into graben on the better seen Saturn-facing side of the satellite.

VI. THE JUPITER SYSTEM

Our first close-up looks at icy satellite surfaces were provided by the Galileo mission, which began studying the Jupiter system in 1995. Although hampered by a malfunctioning high-gain antenna, Galileo has imaged details on the giant planet's moons as small as a few meters across and revealed a surprising diversity of landforms unsuspected from previous observations. Jupiter's four large "Galilean" satellites exhibit a compositional gradation that mimics that of the solar system, with densities and rock fractions that decrease with distance from the planet. Rocky Io is the innermost of the four moons and due to constant tidal reworking is the most volcanically active body known. Europa is also largely made up of silicates but has a thin outer layer of ice and perhaps liquid water extending to depths of 50 to 150 km below the surface. Ganymede and Callisto both have large ice fractions, but here their similarity ends. Callisto is an only slightly differentiated mixture of ice and rock with an ancient, heavily cratered surface unbroken by internal geologic activity. Ganymede, on the other hand, has a dense core and an exterior that was extensively rifted in a past episode of activity probably associated with differentiation and core formation.

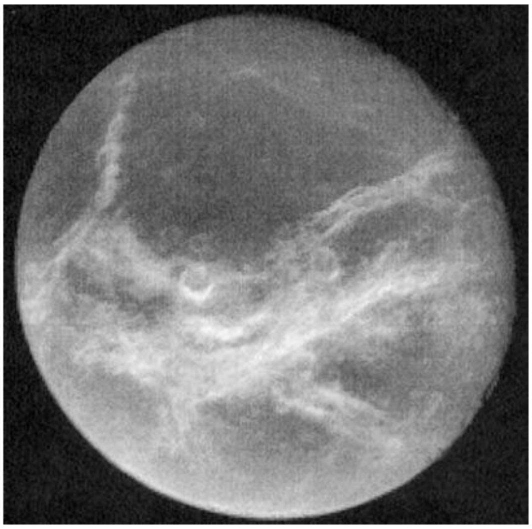

FIGURE 9 Dione. A bright, wispy albedo pattern can be seen on the leading hemisphere, perhaps frost deposited during a cryovolcanic eruption. (Voyager 1 image, courtesy of NASA.)

Prior to Galileo's arrival, much of Ganymede's resurfacing (Fig. 10) was thought to have been volcanic in nature. As high-resolution images began to arrive from Galileo, the evidence for cryovolcanism eroded. The younger grooved terrain, which appeared smooth at the scales visible to Voyager, could be seen to be intensely shattered. Two scales of tectonic deformation can be recognized in the grooved terrain (Fig. 11), both likely caused by crustal extension. Broad topographic undulations probably resulted from ductile necking of the crust, while finely spaced fractures were produced by brittle failure. No fluid flow features can be seen issuing from the fractures, so it appears that most of the resurfacing was achieved by tectonism rather than cryovolcanism. (This example should serve to throw considerable "cold water" on our earlier speculations about the satellites of Saturn and Uranus, which are also based on low-resolution images!) Some evidence of early cryovolcanic activity may be preserved in the form of scalloped depressions found in the older cratered regions of Ganymede (Fig. 12). The origin of these caldera-like features is obscure.

In contrast to its moribund neighbors Ganymede and Callisto, Europa appears to be bristling with signs of recent activity. Europa has long been suspected of harboring a subsurface sea, based in part on its lack of topography: its greatest peaks reach heights of only a few hundred meters, and the largest craters excavate to even shallower depths. Relatively few impact craters scar the satellite, indicating that its surface is comparatively young—by some estimates, as little as 100 million years

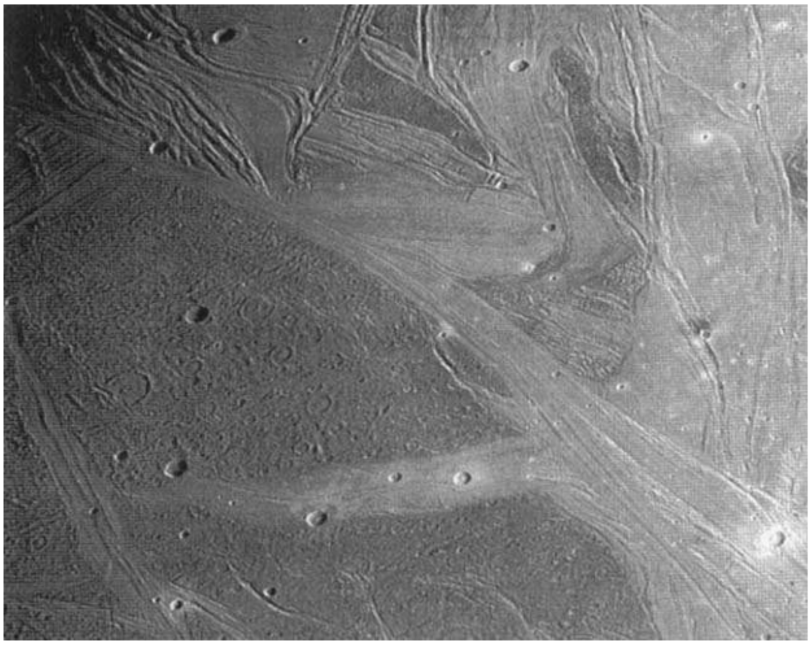

FIGURE 10 Ganymede. Terrains of two distinct ages are seen on the solar system's largest moon. Dark, heavily cratered terrain similar in appearance to Callisto is broken by bright young groove lanes. (Galileo image, courtesy of NASA.)

old. Some of the craters look familiar and seem to have formed in a solid target, but the largest impact structures are exceedingly flat and are ringed by evenly spaced concentric fractures unlike any previously seen. These unique features could have been created when kilometer-sized impactors penetrated the crust to a fluid layer beneath the surface. Two competing processes act to erase Europa's craters. A dense tangle of ridges resurfaces much of the satellite, representing many generations of repeated ridge-building activity over the course

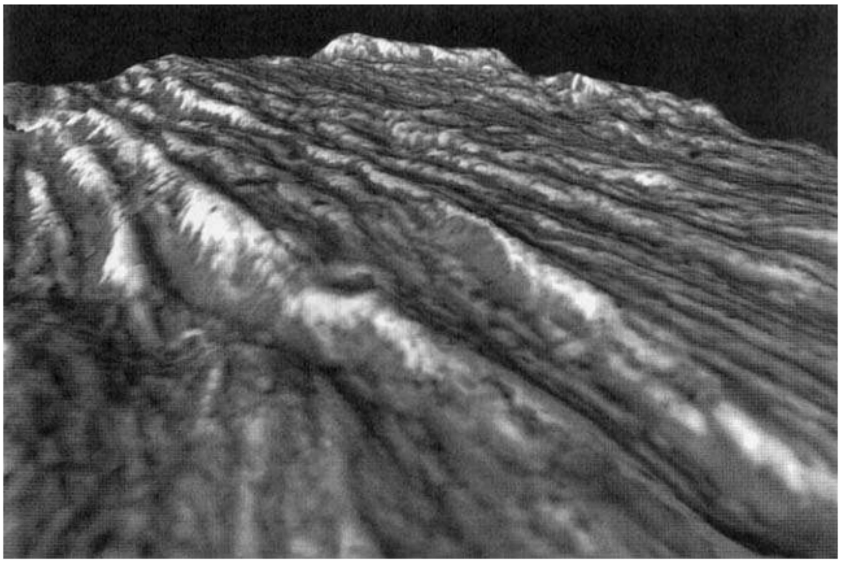

FIGURE 11 Topography in Uruk Sulcus, Ganymede. Stereo pictures have been used to render relief on this high-resolution image of a groove lane, formerly thought to be volcanic. (Galileo image, courtesy of NASA.)

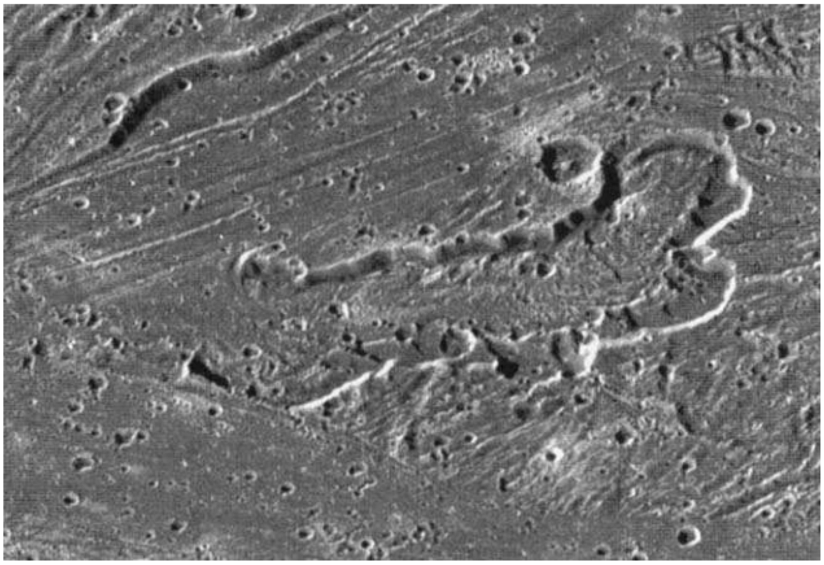

FIGURE 12 Scalloped depression on Ganymede. This feature, found on the older heavily cratered terrain, does not appear to be of impact origin. Perhaps it is evidence of early volcanism. (Galileo image, courtesy of NASA.)

of its short history. In other places, particularly along the equator, the crust has been disrupted by localized heating from below, leaving floe-like fragments that have drifted across the sunken surface (Fig. 13). In fact, the entire ice shell of the satellite may be drifting gradually to the east with respect to the silicate interior, due to tidal torques exerted by Jupiter as Europa circles in its eccentric orbit. If so, it implies that the crust is mechanically decoupled from the interior, as if underlain by ductile ice or floating on a liquid layer.

The origins of Europa's perplexing surface features are still being widely debated. Not far below the surface, the ice could be warm enough to flow like terrestrial glaciers, particularly if it is in thermal contact with liquid water at its melting point. The ridges and thermally disrupted areas might be due to diapirism and convection in the solid ice shell. In these models, the cold ice at the surface is denser than the warmer ice beneath it and tends to sink when disturbed by activity such as solid-state convection taking place in the interior. Buoyant ice from below might also be extruded through fractures in the brittle surface, forming the ubiquitous ridges. Not all of the characteristics of the ridges and disrupted zones are easily explained by solid-state deformation, however. In particular, the last surviving crustal blocks in the areas of thermal disruption are among the largest and presumably heaviest and appear to have floated on a substrate that was even denser. Thus Europa's smooth spots and "maculae," once thought to have been volcanic flows, are probably places where the icy

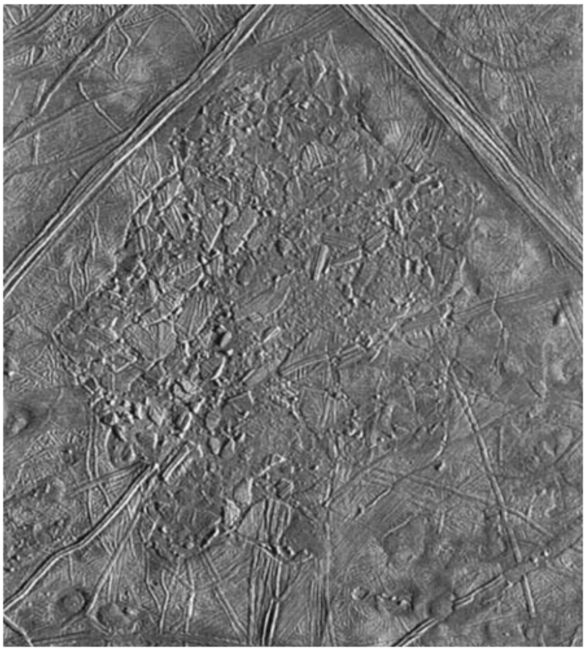

FIGURE 13 Conamara Chaos, Europa. Here the icy crust has been melted through by intense heating from below. A few remaining blocks retain the imprint of the original surface. These "floes" have shifted, rotated, and tilted as if floating on a dense water substrate. (Galileo image mosaic, courtesy of NASA.)

crust was heated to the melting point from below. An unusual example of a possible zone of melt-through is shown in Fig. 14. Even small-scale relief has been erased from this 3-km-diameter "puddle," either by thermal topographic relaxation (implying surface temperatures near the melting point) or by fluid extrusion and flow. The source of such energetic and localized heating is a mystery. Europa receives only one-fifteenth of the tidal heating that churns its violent neighbor Io, but it would not be surprising if some high-temperature silicate volcanism was taking place in the subsurface of Europa as well.

Cryovolcanism may help to explain Europa's peculiar ridges (Fig. 15), which occur in pairs or sets that are symmetric and uniform over distances often comparable to the radius of the satellite. The margins of many ridge sets are darkened and discolored by a non-ice contaminant, perhaps vented from fractures between the ridges. Double ridges are difficult to produce by diapirism and seem to require some cyclic process of extrusion and withdrawal in order to form their central valleys. One possible mechanism is the pumping of fluids along cracks by tidal flexing. If the interior is liquid, tides tens of meters high should be raised each europan "day" (3.5 Earth-days) as the satellite circles Jupiter. Any fractures that penetrate the icy crust are pulled apart for half of each orbit and slammed shut again for the other half. If liquid can seep into the fractures from below, some slush may be squeezed out of the cracks and onto the surface with each daily cycle. Bright plumes or frost deposits should be produced by this process, but so far no such telltale sign of activity has been detected by Galileo.

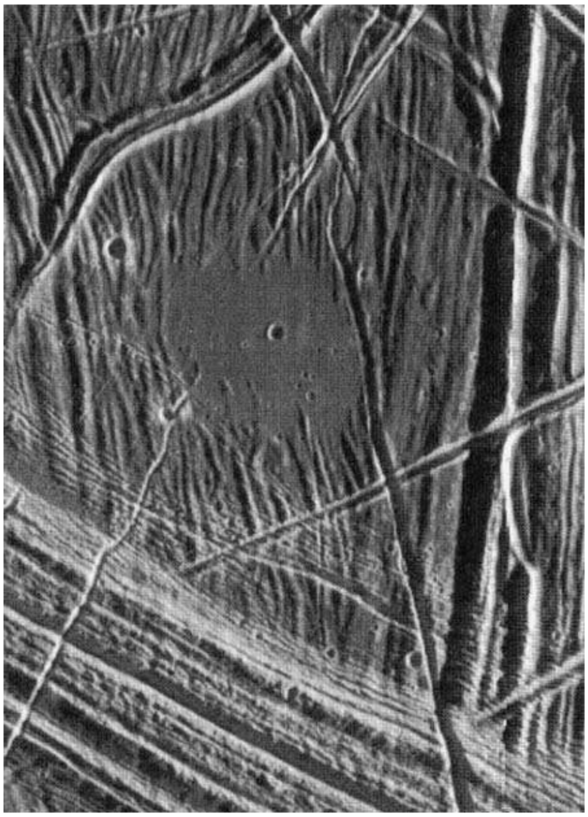

FIGURE 14 The "puddle" on Europa at 11°N, 328°W, imaged at 27 m/pixel. Even small-scale relief has been erased from this 3-km-diameter feature, either by thermal topographic relaxation or by fluid extrusion and flow. (Galileo image, courtesy of NASA.)

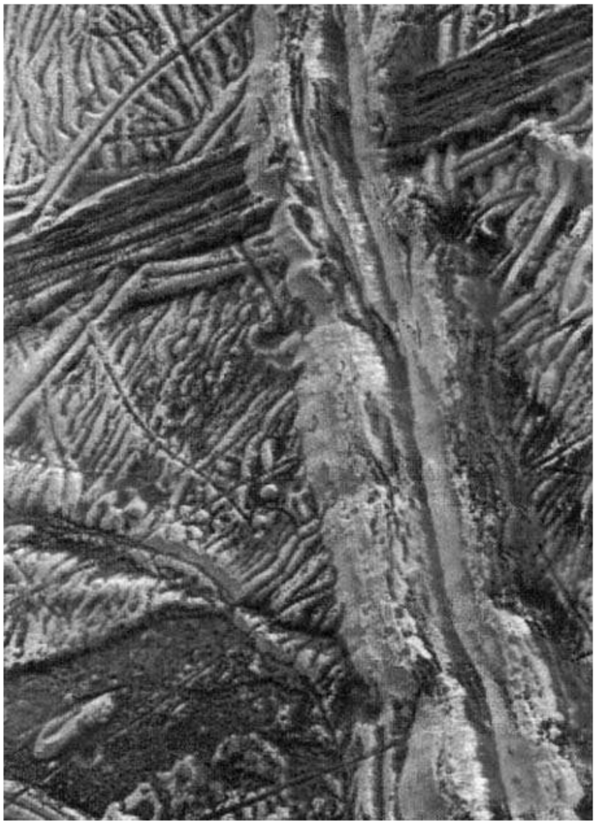

FIGURE 15 Freshly formed doublet ridge on Europa. The origin of these ubiquitous ridge pairs is mysterious. Perhaps they formed when icy slurry was pumped up through fractures by the daily tidal flexing. (Galileo image, courtesy of NASA.)

VII. FUTURE EXPLORATION

The existence of a liquid layer on Europa is by no means proven by the Galileo observations and will be debated for years to come. By looking at the surface of the satellite, we can only make indirect inferences about what is going on down below. However, the possibilities of a subsurface ocean and perhaps seafloor silicate volcanism on Europa cannot be ruled out by the new data and might have profound implications for the likelihood of finding life on the icy world. Soon after the Galileo discoveries, planning began for a follow-up mission designed to directly determine whether a liquid layer lurks beneath the satellite's surface. Europa Orbiter, as the new mission is called, will use gravimetry and altimetry to take the ''pulse'' of the moon by measuring the height of the tides. Only centimeters of flexing should occur each day if the ice is frozen to the bedrock, in contrast to the massive tides expected if the interior is fluid. Europa Orbiter may also employ a radar sounder similar to those used in the Earth's polar regions to penetrate the ice and return reflections from any liquids within a few kilometers of the surface. The spacecraft will also completely map the moon from orbit, a feat that was impossible with the limited downlink from Galileo.

Another ambitious mission is already on its way to Saturn. The Cassini spacecraft will investigate the planet, its rings, and its moons for 4 years beginning in 2004. Cassini will drop an instrumented probe to the surface of mysterious Titan, fitted with an imaging system and designed to float if it is lucky enough to land in an ethane lake. Cassini will also study the satellites from Saturn orbit with optical and radar remote sensing, hopefully shedding light on the manner in which they were resurfaced. Going even farther afield, a project called the Pluto Kuiper Express will launch (also by the year 2004) a spacecraft that will travel nearly a decade before speeding past Pluto and Charon. Gauging by our past experiences, we may well be surprised by the geologic processes that have gone on in this curious binary system in which the moon is fully a tenth as massive as the planet.

SEE ALSO THE FOLLOWING ARTICLES

Migration of Melt • Volcanism on Io

FURTHER READING

Burns, J. A., and Mathews, M. S., eds. (1986). ''Satellites.'' Univ. of Arizona Press, Tucson.

Cruikshank, D. P., ed. (1995). ''Neptune and Triton.'' Univ. of Arizona Press, Tucson.

Kargel, J. S. (1990). Cryomagmatism in the outer solar system. Ph.D. dissertation, University of Arizona, Tucson.

Kargel, J. S. (1995). Cryovolcanism on the icy satellites. Pages 101–113 *in* ''Comparative Planetology with an Earth Perspective'' (M. T. Chahine, M. F. A'Hearn, and J. Rahe, eds.). Kluwer Academic, Dordrecht/Norwell, MA.

Lewis, J. S. (1995). ''Physics and Chemistry of the Solar System.'' Academic Press, San Diego.

Rothery, D. A. (1992). ''Satellites of the Outer Planets.'' Clarendon, Oxford.

Schmitt, B., De Bergh, C., and Festou, M., eds. (1998). ''Solar System Ices.'' Kluwer, Dordrecht.

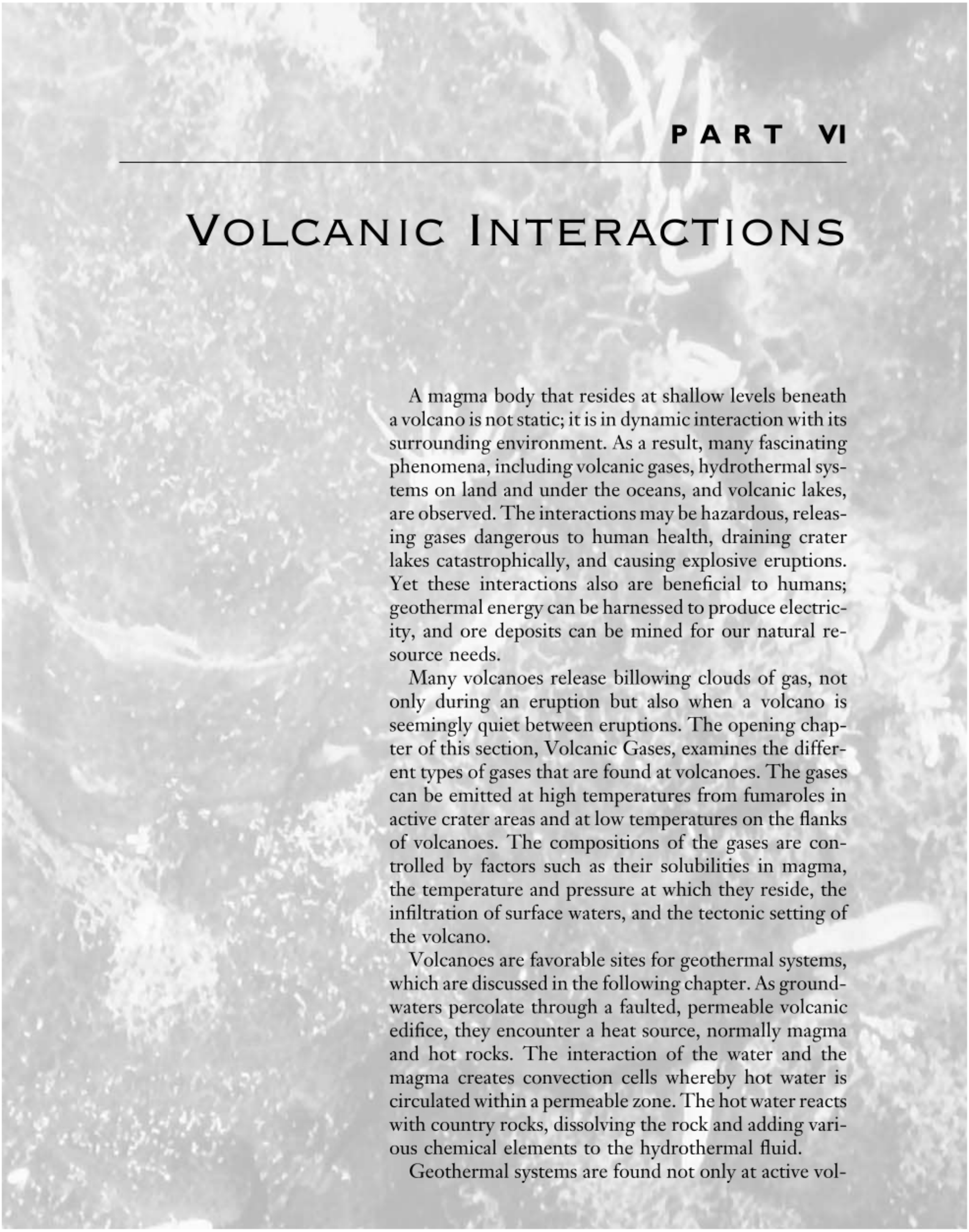

PART VI

VOLCANIC INTERACTIONS

A magma body that resides at shallow levels beneath a volcano is not static; it is in dynamic interaction with its surrounding environment. As a result, many fascinating phenomena, including volcanic gases, hydrothermal systems on land and under the oceans, and volcanic lakes, are observed. The interactions may be hazardous, releasing gases dangerous to human health, draining crater lakes catastrophically, and causing explosive eruptions. Yet these interactions also are beneficial to humans; geothermal energy can be harnessed to produce electricity, and ore deposits can be mined for our natural resource needs.

Many volcanoes release billowing clouds of gas, not only during an eruption but also when a volcano is seemingly quiet between eruptions. The opening chapter of this section, Volcanic Gases, examines the different types of gases that are found at volcanoes. The gases can be emitted at high temperatures from fumaroles in active crater areas and at low temperatures on the flanks of volcanoes. The compositions of the gases are controlled by factors such as their solubilities in magma, the temperature and pressure at which they reside, the infiltration of surface waters, and the tectonic setting of the volcano.

Volcanoes are favorable sites for geothermal systems, which are discussed in the following chapter. As groundwaters percolate through a faulted, permeable volcanic edifice, they encounter a heat source, normally magma and hot rocks. The interaction of the water and the magma creates convection cells whereby hot water is circulated within a permeable zone. The hot water reacts with country rocks, dissolving the rock and adding various chemical elements to the hydrothermal fluid.

Geothermal systems are found not only at active volcanoes but also in other regions of high heat flow, typically along tectonic plate boundaries. Geothermal systems can be exploited commercially for electric production, and this aspect is discussed further in Part IX, in the chapter Exploitation of Geothermal Resources.

Geothermal and hydrothermal systems created by interaction of waters with magma and hot rocks form impressive manifestations at the surface; the chapter Surface Manifestations of Geothermal Systems delves into the details of these manifestations, which may include spectacular fumaroles, acid crater lakes, acidic hot springs, and even acid streams.

High-temperature hydrothermal systems at volcanoes may be dominantly liquid, vapor, or a combination of the two. Lower-temperature systems also are found at volcanic centers; these may be cooling and decaying systems that were once at high temperature. These systems may form certain types of ore deposits (as discussed later in this section in the chapter Mineral Deposits Associated with Volcanism).

Water–magma interaction occurs not only on land but also occurs in the oceans. The chapter Deep Ocean Hydrothermal Vents examines the remarkable hydrothermal systems that are formed in regions of active submarine volcanism. Most of our knowledge regarding these systems is based on discoveries in the past twenty years. As two tectonic plates form and move apart at mid-ocean ridges, the magma that is generated serves as a heat source. Seawater percolates into the fractured oceanic crust and is heated by the magmatic source, setting up hydrothermal convection cells. In fact, submarine hydrothermal circulation is a principal means by which Earth loses its heat. As the heated water circulates, it dissolves rock. The chemically charged water transports metals upward, forming ore deposits when pressure–temperature conditions are reduced. Researchers have even observed and filmed spectacular hydrothermal chimneys, termed "black smokers," venting at the sea floor. In the vicinity of the hydrothermal vent, unique forms of life are nurtured by the hot mineral-rich water.

Back on land, the next chapter, Volcanic Lakes, shows that lakes can form on volcanoes when surface waters are available in large amounts. These lakes typically are situated in craters at the tops of volcanoes and can be hot, containing large amounts of dissolved solids. In some cases, the lakes are actually concentrated mixtures of sulfuric and hydrochloric acid! Some lakes may host molten sulfur bodies, while others have high levels of carbon dioxide dissolved at the bottom. Acidic crater lakes are another surface manifestation of interaction between groundwaters and a degassing magma; they also can be considered the uppermost part of a magmatic-hydrothermal system that may be forming an ore deposit at deeper levels. Volcanic lakes can be hazardous, because they are associated with hydrovolcanic eruptions (see the chapters Phreatomagmatic Fragmentation; Surtseyan and Related Phreatomagmatic Eruptions; Pyroclastic Surges and Blasts), gas bursts of CO_2 (see Hazards of Volcanic Gases), and lahars (see Lahars; The Hazard from Lahars and Jökulhlaups).

We have seen above how volcano interactions potentially can form mineral deposits. These ore deposits are explained in the final chapter of this section, Mineral Deposits Associated with Volcanism. The ores may form directly from the magma, from magmatic fluids when the magma becomes saturated in volatiles, or from hot groundwaters that circulate within a magmatic-hydrothermal system. The type of ore deposit that is formed depends on its tectonic environment. Above mantle plumes, flood basalt and komatiite eruptions host nickel-copper ores and platinum-group deposits. At mid-ocean ridges, black smokers form massive sulfide ore deposits by precipitation of metallic minerals as the hot hydrothermal solution is quickly cooled by seawater. This type of deposit also is formed at oceanic subduction zones. Subduction-related volcanoes on land having hydrothermal systems may host large deposits of gold, copper, and other metals.

John Stix
McGill University

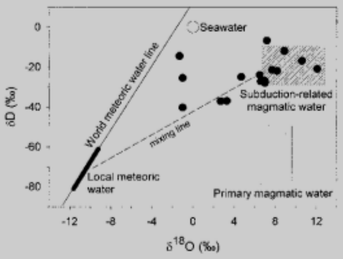

VOLCANIC GASES

PIERRE DELMELLE
Université de Montréal

JOHN STIX
McGill University

I. Introduction
II. Chemical Composition of Fumarolic Gases and Causes of Variability
III. Case Studies
IV. Diffuse Flank Degassing
V. Conclusions

GLOSSARY

connate water Water entrapped in the interstices of pores of a sedimentary rock at the time of its deposition.

convergent plate volcano A volcano located on the boundary between two lithospheric plates that are moving toward each other and being subducted.

divergent plate volcano A volcano located on a boundary between two lithospheric plates that are moving apart, with mantle material and new oceanic crust moving in to fill the gap.

half-life The time required for one half of a given number of radionuclides to decay.

hot spot A volcanic center, 100 to 200 km across and persistent for at least a few tens of millions of years, that is thought to be the surface expression of a persistent influx of hot mantle material. A hot spot may or may not be associated with divergent plate boundaries.

isotope Atoms with the same number of electrons and protons, but a different number of neutrons and therefore different masses. Most chemical elements occur in nature as two or more isotopes. The relative abundances of isotopes of a given chemical element are not constant in all natural materials. Hydrogen, carbon, oxygen, and sulfur, which are prominent elements in volcanic gases, all have stable isotopes. As opposed to radionuclides, stable isotopes do not undergo spontaneous decomposition.

hydrothermal system A groundwater system that has a source (or area) of recharge, a source (or area) of discharge, and a heat source. When a magma supplies the heat source and volatiles, the hydrothermal system qualifies as a magmatic hydrothermal system.

magmatic volatile An element (e.g., sulfur, chlorine, fluorine) or compound (e.g., water, carbon dioxide) dissolved in a magma that forms a gas at relatively low pressure and magmatic temperature.

meteoric water Waters of any age that originate from precipitation: rain, snow, ice, river, lake, and most low-temperature groundwaters. They are derived from ocean water through the atmospheric circulation process.

MORB Abbreviation for mid-ocean ridge basalt, which is erupted at an oceanic divergent plate volcano (sea-floor spreading axis).

redox potential A variable that describes the reduction–oxidation equilibria of chemical reactions that involve transfer of electrons between species having different valence states.

Copyright © 2000 by Academic Press
All rights of reproduction in any form reserved.

subduction The process of one lithospheric plate descending beneath another. Subduction zones are long, narrow belts in which subduction takes place.

I. INTRODUCTION

Volcanic gases are a fundamental part of volcanic activity. Ranging from dramatic emissions of acidic vapors released by highly active volcanoes to invisible emanations of carbon dioxide through soils, volcanic gases play an important, if not dominant, role in influencing the behavior of a volcano. In general, increasing availability of gas within a volcano results in increasingly explosive activity. Thus, the most explosive eruptions are probably the consequence of gas-rich magmas and large pressure buildups within the volcano as the magma releases gas during its ascent to shallow levels. Other volcanoes emit huge quantities of gas passively, i.e., without erupting.

By studying gases, volcanologists can gain insight into a number of phenomena. First, they can assess whether there is magma present at shallow levels in a volcanic edifice. Second, they can determine if a magma is comparatively rich or poor in dissolved gas. Third, they can estimate the various sources of the gas, e.g., from the mantle, from subducted material as a tectonic plate slips beneath another, from sedimentary rocks in the crust, or from fluids at shallow levels in the volcano, such as a hydrothermal system, groundwater, or even rainwater. Fourth, by making repeated measurements over time, scientists can use gas data to help forecast eruptive activity, particularly when this information is integrated with other types of data that are being collected to monitor the state of the volcano, such as seismicity and ground deformation.

Typically, a volcano releases high-temperature acidic gases from its active crater, the gases being released both diffusely and as highly concentrated vapors through fumarolic cracks and vents. Some volcanoes also release low-temperature gases diffusely through their flanks, which are distant from the active crater area. This chapter gives an overview of gases that are released by these two styles of degassing. The chapter is organized in the following fashion. First, we discuss the nature and origin of high-temperature gases and the different factors that control their composition and behavior. Then we present six examples of gas studies that have shed important light on volcanic processes. We then discuss and illustrate diffuse low-temperature gases on volcano flanks, and we conclude by summarizing our state of knowledge concerning volcanic gases: where we stand today and where we are going in the future.

II. CHEMICAL COMPOSITION OF VOLCANIC GASES AND CAUSES OF VARIABILITY

Until the middle of the 19th century, scientists believed that each volcano released one particular type of gas: sulfur dioxide at Etna (Italy); hydrogen chloride at Vesuvius (Italy); and carbon dioxide at Puracé (Colombia). Charles Sainte-Claire Deville, a French mineralogist who pioneered the chemical analysis of volcanic gases in the 1850s, demonstrated that this was not the case; he showed that the same gases occur on each volcano, although in different proportions. Volanic gases indeed exhibit extreme chemical variability, which complicates attempts to read their message.

Over the past 20 years, gas geochemists armed with sophisticated analytical techniques and a good theoretical knowledge have made efforts to understand what dictates the composition of volcanic gases. The controlling factors are the chemical reactions in the gas phase itself, the tectonic and geologic setting, the solubility of gases dissolved in magma (i.e., the magmatic volatiles), and the interaction with a hydrothermal system, groundwater, or rainwater at shallow levels within the volcano.

A. Constituents of Volcanic Gases

Volcanic gases contain a restricted number of chemical elements as various molecular species (Table I). Major elements consist of hydrogen (H), carbon (C), oxygen (O), sulfur (S), nitrogen (N), and halogens including chlorine (Cl), fluorine (F), and bromine (Br). Minor elements include the rare gases helium (He), neon (Ne), argon (Ar), krypton (Kr), and xenon (Xe). Trace amounts of metals (e.g., sodium, vanadium, chrome, bismuth, copper, zinc, gold) occur in high-temperature fumarolic gas discharges. Hydrogen is largely present as water (H_2O), with the other H-bearing species, such as molecular hydrogen (H_2), methane (CH_4), or ammonia (NH_3), occurring in minor or trace amounts. Of the carbon species, carbon dioxide (CO_2) is dominant, while methane (CH_4) and carbon monoxide (CO) occur in lesser amounts. Sulfur dioxide (SO_2) and hydrogen sulfide (H_2S) mainly compose the sulfur species, the remaining

TABLE I Chemical Composition of Some Volcanic Gas Discharges, in Micromoles (10^{-6} mol) per Mole

Volcano	**Kilauea**	**Kilauea**	**Erta'Ale**	**Usu**	**Usu**	**White Island**	**White Island**	**Kudriavy**	**Galeras**	**Nevado del Ruiz**
Location	*Hawaii*	*Hawaii*	*Ethiopia*	*Japan*	*Japan*	*New-Zealand*	*New-Zealand*	*Russia*	*Colombia*	*Colombia*
Tectonic env.[a]	*hot spot*	*hot spot*	*div. pl.*	*conv. pl.*	*conv. pl.*	*conv. pl.*	*conv. pl.*	*conv. pl.*	*conv. pl.*	*conv. pl.*
Activity	*lava lake*	*rift zone*	*lava lake*	*dome*	*dome*	*crater*	*crater*	*crater*	*dome*	*crater*
Date	*25/03/18*	*14/01/83*	*23/01/74*	*08/09/54*	*24/06/85*	*07/02/72*	*13/06/73*	*08/95*	*06/01/90*	*12/86*
Temp. (°C)	1,170	1,010	1,130	800	336	620	135	920	187	85
H_2O	370,900	798,000	794,000	980,000	999,000	911,000	983,000	953,000	943,000	644,000
CO_2	489,000	31,500	104,000	12,000	400	49,480	14,450	16,100	22,230	338,000
SO_2	118,400	149,000	67,800	430	32	18,180	2,008	10,600	—	1,100
H_2S	400	6,220	6,200	4	35	7,190	183	2,100	—	10,400
S_t ($SO_2 + H_2S$)	118,800	155,220	74,000	434	67	25,370	2,191	12,700	23,030	11,500
HCl	800	1,000	4,200	530	170	11,570	131	2,000	7,180	320
HF	—	1,900	—	240	—	410	18	960	—	—
NH_3	—	—	—	1.7	—	17.9	—	—	—	—
He	—	—	—	—	—	—	—	0.13	0.9	—
Ar	—	—	—	0.25	0.25	—	—	0.5	48	7.1
H_2	4,900	9,025	14,900	6,300	390	925	48	5,760	29	1,230
N_2	—	—	1,800	570	14	—	150	220	4,218	2,100
CH_4	—	—	—	17	0.44	—	—	0.03	0.46	1,680
CO	15,100	592	4,600	33	—	—	—	11	<1	<0.4
H_2O/CO_2	0.8	25	8	82	2,498	18	68	59	42	1.9
S_{total}/CO_2	0.24	4.9	0.7	0.04	0.17	0.51	0.15	0.79	1.0	0.03
S_{total}/HCl	149	155	18	0.8	0.4	2.2	17	6.3	3	36

[a] div. pl. and conv. pl. are for divergent plate and convergent plate volcano, respectively. Data compiled from Giggenbach and Sheppard (1989), Giggenbach *et al.* (1990), Symonds *et al.* (1994), Giggenbach (1996), Symonds *et al.* (1996), Fischer *et al.* (1997), and Fischer *et al.* (1998).

gas consisting of molecular sulfur (S_2) and sometimes carbonyl sulfide (COS). Chlorine, F, and Br occur principally as acids, with hydrogen chloride (HCl) predominating over hydrogen fluoride (HF) and hydrogen bromide (HBr). Nitrogen exists almost exclusively as molecular nitrogen (N_2). When present in the gas phase, metals are transported largely as chloride or sulfide salts and, to a minor extent, as elemental volatile species.

As illustrated in Table I, the concentrations of the chemical compounds in fumarolic gas samples vary significantly. However, it is safe to state that H_2O is consistently dominant and normally accounts for more than 60% of the total molar gas content in crater fumaroles. The next most abundant species is CO_2 with typical molar contents between ~10 and ~40%. The highest CO_2 concentration was measured in gas emanations collected during the 1918–1919 summit eruption of Kilauea volcano, Hawaii (Table I). In most fumarolic gas samples, the amount of total sulfur ($S_{total} = SO_2 + H_2S$) is lower than that of CO_2, but usually higher than that of HCl, although the relative abundances of S_{total} and HCl in volcanic gases can vary greatly. Hydrogen and nitrogen gases are typically less than 2% and 1% of the total molar gas content, respectively, but the N_2 concentration is often modified by air contamination during or after sampling. Together, the remaining gas compounds (He, Ar, CO, etc.) generally account for less than 1%. Methane is usually absent in high-temperature fumaroles, although there are cases where it has been detected.

B. Pressure, Temperature, and Redox Potential

Because of various internal reactions, the molecular composition of a gas phase separated from its magma (i.e., the magmatic gases) may change as the gases ascend toward the surface. The reaction

$$SO_2 + 3H_2 \Leftrightarrow H_2S + 2H_2O$$

is important, because it reaches chemical equilibrium rapidly and involves the major gas species H_2O, SO_2, H_2S, and H_2. Thermodynamic modeling indicates that the reaction shifts to the right at high pressures (i.e., the magma degasses at great depths), thus favoring H_2S at the expense of SO_2 as the dominant sulfur species in the gas. Cooling of the rising magmatic gases leads to a similar effect. Conversely, hot gases escaping from a magma body emplaced at shallow levels in the crust will tend to be SO_2-dominated, as frequently observed in the field.

Besides pressure and temperature, the redox potential of the magmatic gas phase also influences its composition. This variable can be conveniently expressed by the H_2/H_2O ratio measured in the volcanic gas sample, but the mechanisms that control this ratio remain controversial. As shown by the work of Terrence Gerlach on Kilauea volcano (Hawaii), the redox potential of magmatic gases seems to be governed by that of the molten rock (i.e., the magma). On the basis of observations made at White Island volcano (New Zealand), Werner Giggenbach suggested that when the hot gases separate from magma and rise rapidly up to the surface, the above process is no longer valid. Instead, the reaction shown earlier exerts the major control on the redox potential. The H_2/H_2O ratios in fumaroles then reflect the relative proportions of SO_2 and H_2S gases. However, at temperatures lower than about 350°C, the H_2/H_2O ratio of fumarolic gas is likely to depart from this high-temperature behavior, because of prolonged interaction of the rising gases with the rocks surrounding the volcanic conduits. Giggenbach's predictions are consistent with many field observations. An alternative view to this scenario was proposed to explain the redox state of the fumarolic gases from the Showa-Shinzan dome, Usu volcano (Japan). In this case, admixture and reequilibration of meteoric water (e.g., rain that permeates through the volcano) with the hot gases moving up toward the surface govern the redox potential of high-temperature fumarole discharges.

C. Tectonic and Geologic Setting

Gases dissolved in magmas can be supplied at depth from various sources, including the mantle, the crust, and subducted material during magma generation and magma ascent. Since these sources have distinct compositions, different types and amounts of volatiles are added to magmas depending on the tectonic and geologic setting of the volcano. The chemical composition of gases released from magma and discharging at the surface as high-temperature fumaroles will vary accordingly. To trace the deep origins of volcanic gases, and thus of magmas, geochemists use both the chemical and isotopic signatures of major and minor gas species.

High-temperature fumarolic gases associated with convergent plate volcanoes have proportionately more H_2O and Cl than gases from divergent plate and hot spot systems. This is a result of addition of significant amounts of seawater to convergent plate magmas during subduction of the oceanic crust and sediments, which both contain hydrated minerals. Several researchers have noted that H_2O in high-temperature fumaroles from convergent plate volcanoes displays high contents of deuterium (D) and oxygen-18 (^{18}O), which are the heavy isotopes of hydrogen and oxygen, respectively (Fig. 1). Until recently, the accepted view was that the isotopic composition of H_2O in fumarolic gases resulted from mixing of a "primary magmatic water" with local meteoric water, the isotopic composition of this primary magmatic water ($\delta D = -65 \pm 15‰$ and $\delta^{18}O = +8 \pm 2‰$) corresponding to that of water extracted from mid-ocean ridge and hot spot rocks. It now seems more likely that the distinct isotopic compositions of H_2O in convergent plate gases point to the existence of a common "subduction-related magmatic water" component, whose source is recycled D- and ^{18}O-rich seawater ($\delta D = 0‰$ and $\delta^{18}O = 0‰$) which was stored initially in hydrated minerals of the subducted oceanic crust and sediments. This "subduction-related magmatic water" may have a very uniform isotopic composition, with

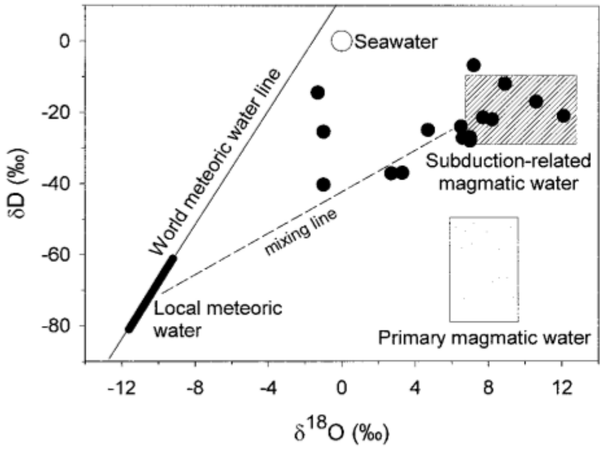

FIGURE 1 Isotopic composition (δD and $\delta^{18}O$) of water from high-temperature fumarolic gases associated with convergent plate volcanoes (black circles) and compositional fields for "subduction-related magmatic water" and "primary magmatic water." The world meteoric water line represents the range of compositions followed by most surface waters. The dashed line connecting "subduction-related magmatic water" to local meteoric water represents the isotopic compositions obtained by mixing these two components in different proportions.

$\delta D = -20 \pm 10‰$ and $\delta^{18}O = +10 \pm 2‰$, and mixes with local meteoric water at shallow levels in the volcanic edifice to produce a characteristic fumarole isotopic composition (Fig. 1). Although rare, there are also examples of island volcanoes whose isotopic and chemical trends suggest shallow contamination of the fumaroles by marine fluids permeating through the volcanic conduit.

Geochemists also use the stable isotopes of carbon and sulfur present in fumarolic gas discharges to infer the deep sources of magmatic volatiles and their respective contributions. This approach is based largely on the assumed isotopic compositions for the Earth's surface reservoirs that contain these chemical elements. The isotopic compositions of CO_2 ($\delta^{13}C_{CO2}$) and SO_2 ($\delta^{34}S_{SO2}$) measured in high-temperature gases emitted by divergent plate (e.g., Erta-Ale, Ethiopia) and hot spot (e.g., Kilauea) volcanoes indicate a mantle origin for carbon and sulfur ($\delta^{13}C = -4.0 \pm 2.5‰$, $\delta^{34}S = 0 \pm 1‰$). By contrast, subduction-related high-temperature gases display more variable $\delta^{13}C$ and $\delta^{34}S$ values ($\delta^{13}C = -12$ to $+2.5‰$, $\delta^{34}S = 0$ to $+12‰$), indicating contamination by crustal and subducted material.

Helium is a good tracer of volcanic gas sources. It has two isotopes: ^3He, which was formed during accretion of the Earth, and ^4He, which is produced by radioactive decay of uranium and thorium in the crust. The helium isotope ratio of gas samples is usually expressed relative to the $^3He/^4He$ ratio of the atmosphere (R_A), which is 1.4×10^{-6}. Basalts erupted from oceanic divergent plate volcanoes, termed MORB, have $^3He/^4He$ ratios eight times higher than atmospheric values (expressed as $8R_A$). However, these ratios are significantly lower than values of about $40R_A$ in the primitive mantle, and so the mantle source for MORB is considered to have been degassed and depleted of ^3He, while ^4He has been added to it over time by uranium and thorium decay. At the same time, the $^3He/^4He$ ratios are significantly higher than atmospheric, so the MORB source has retained some primordial He. The $^3He/^4He$ ratio is thus a useful measure of the degree to which the mantle gases contribute to volcanic gas discharges.

Some hot spots such as Hawaii exhibit very high $^3He/^4He$ ratios reaching up to $30R_A$. These hot spots are considered to tap comparatively pristine, undegassed parts of the mantle. Significant ^3He enrichments have been measured in volcanic gases from Hawaii ($^3He/^4He \approx 15R_A$), in accordance with the inferred mantle origin. The $^3He/^4He$ ratios measured in fumarolic gases at convergent plate volcanoes typically range from 5 to $7R_A$, with some values as high as $8R_A$ and as low as $4R_A$. The He data thus indicate that these gases contain a MORB component which has been variably diluted by crustal material with lower $^3He/^4He$ ratios ($^3He/^4He \approx 0.02R_A$).

Helium also may be used as a reference to estimate various contributions to a volcanic gas. Other important constituents of volcanic gases are CO_2 and N_2, which do not react extensively with rocks inside the volcano. Using the CO_2/He and N_2/He ratios, it readily can be seen that convergent plate volcanoes discharge gases with high CO_2 and N_2 contents. As shown in Fig. 2, these gases typically display CO_2/He ratios of 65,000 to 900,000, which are 3 to 15 times higher than those found in divergent plate and hot spot settings. The H_2O/He and H_2O/CO_2 ratios in gases are also higher in convergent plate volcanoes than in divergent plate and hot spot volcanoes. Similarly, N_2/He ratios for gases from convergent plate settings are considerably higher ($N_2/He > 1{,}500$) than those observed in divergent plate and hot spot environments ($N_2/He < 250$). The most likely source of this excess CO_2, N_2, and H_2O is again the material (sedimentary rocks, altered crust, and organic matter) carried by the subducted slab to the magma generation zone in the mantle. Based on the $\delta^{13}C$ values and $CO_2/^3He$ ratios measured in fumarolic gases from convergent plate volcanoes, up to 80% of the carbon in these environments may be derived from subducted material (carbonate in the crust and limestone sediments) with comparatively small mantle inputs. When the relative contents of N_2, He, and Ar are plotted for subduction-related and non-subduction-related gases (Fig. 3), the two groups exhibit distinct positions. Both types of volcanic gases can be contaminated at shallow

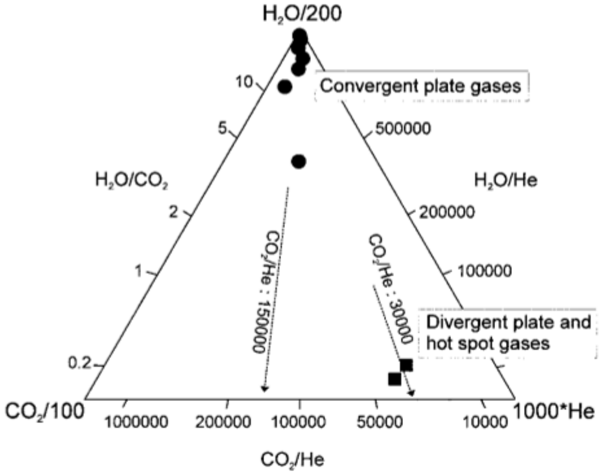

FIGURE 2 Relative H_2O, CO_2, and He contents of fumarolic gases associated with convergent plate, divergent plate, and hot spot volcanoes.

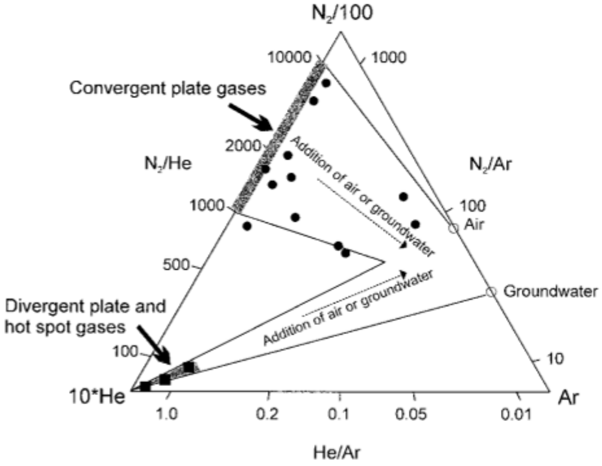

FIGURE 3 Relative Ar, N_2, and He contents of fumarolic gases and inferred compositional fields for volcanic gases associated with convergent plate, divergent plate, and hot spot settings. Also shown are the air and groundwater (air-saturated water) compositions.

levels in the volcanic edifice by air or air-saturated groundwater, leading to a decrease of their N_2/Ar and He/Ar ratios.

D. Magmatic Volatile Solubility

Despite the distinct classes of fumarolic gas compositions associated with the tectonic setting, there is still considerable variability within these groups. Some of these variations may originate from differences in magmatic volatile solubility, and degree of degassing of the magma. Less soluble species such as N_2 and CO_2 are released initially from a magma emplaced at shallow levels in the crust, whereas H_2O and the more soluble sulfur- and halogen-containing compounds remain dissolved in the magma. With time, and if there is no new supply of magma from depth, a high-temperature gas discharge may evolve from a CO_2-rich to a comparatively CO_2-poor composition, with a corresponding decline in the CO_2/S_{total} ratio in the gas. Similarly, the higher solubility of Cl over S in magma can lead to emission of HCl-rich volcanic gases from degassed magma intrusions. Volcanologists have documented these phenomena by monitoring the compositional changes in fumarolic gases over the course of months or years. These observations suggest that the volatile solubility in magmas decreases in the order $HF > HCl \approx H_2O > S_t > CO_2$.

Another complicating factor in the interpretation of volcanic gas compositions is related to the complicated solubility behavior of sulfur and chlorine in magmas as a function of pressure. At Mt. Etna (Italy) variations in the Cl/S ratio of the gas plume were attributed to changes in magma degassing regimes from deep to shallow levels; high Cl/S gas ratios would correspond to volatile escape deep in the magma plumbing system, whereas low ratios would indicate gas release at shallower depths, with most of the sulfur being degassed from the magma. This apparent relationship between depth of gas–magma separation and gas composition may not be straightforward, however, because the solubility of sulfur also depends on other variables such as the redox potential of the magma, temperature, and magma composition.

E. Shallow, Nonmagmatic Processes

Although tectonic setting and magma degassing history control the chemical composition of high-temperature volcanic gases, most temporal and spatial variations appear to be the result of nonmagmatic processes related to the presence of a hydrothermal system or meteoric water in the shallow parts of the volcano. Upon contact with these shallow reservoirs, the hot gases released by a magma react to produce a fumarolic discharge that bears a small remnant of the initial magmatic gas composition.

Water, SO_2, H_2S, and HCl are the gas species that are most readily affected by these secondary processes. Addition of H_2O may occur when the rising gas phase encounters hydrothermal water, groundwater, or rainwater. Conversely, condensation of magmatic water on contact with cooler water reservoirs may decrease the H_2O content in the fumarolic gas. Water in low-temperature gas discharges that is affected by interaction with hydrothermal fluids, groundwater, or rainwater generally will have depleted D and ^{18}O contents compared to high-temperature volcanic gases. Isotopically diluted fumaroles tend to approach the composition of local meteoric water.

Sulfur dioxide gas also may react with liquid water in the hydrothermal system to produce sulfuric acid (H_2SO_4) and H_2S, thus modifying the SO_2/H_2S ratio in the fumarolic gas. In some instances, this reaction yields elemental sulfur, whose deposition decreases the sulfur content of the gas. Formation of elemental sulfur is commonly associated with cooling of the hot rising gas phase. The reverse process, revolatilization of previously deposited elemental sulfur during passage of hot gases, increases the total sulfur content in the fumarole. Finally, the high solubility of HCl vapor in water makes it susceptible to condense in shallow low-temperature zones of the volcanic–hydrothermal system. Interaction of hot magmatic gases with shallow groundwater or a hydrothermal system results in a volcanic gas discharge characterized by relatively high CO_2 and low HCl contents (Fig. 4) and low SO_2/H_2S ratios (e.g., the Nevado del Ruiz gas composition in Table I). In addition, CH_4 commonly appears in low-temperature fumaroles; its origin is thought to be hydrothermal.

III. CASE STUDIES

We now present six case studies of volcanoes where detailed investigations of the fumarolic gas discharges have made major advances to our understanding of both the gases and the volcanoes themselves. The Kudriavy study is an excellent example of determining the ultimate sources of gases. The Mt. St. Helens and Usu cases demonstrate how degassing of magma and progressive contamination by meteoric water alter the fumarolic gas compositions. The White Island, Vulcano, and Galeras examples highlight the nearly ubiquitous interaction of magmatic gases with shallow hydrothermal systems and groundwaters. Importantly, the nature of this interaction can be different from one volcano to the next, depending on factors such as the state of activity and rock permeability.

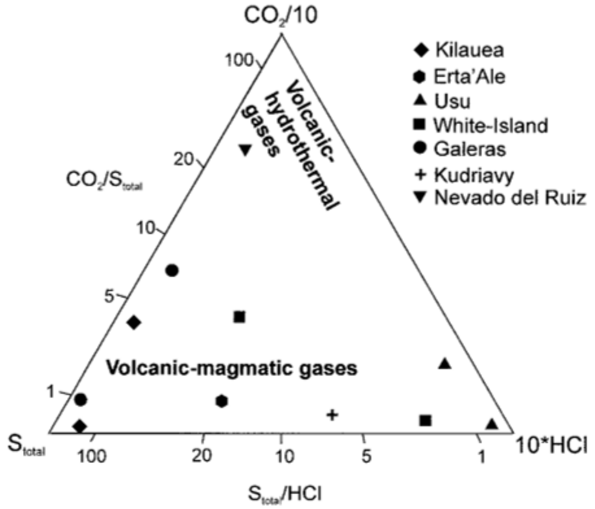

FIGURE 4 Relative CO_2, S_{total}, and HCl of fumarolic gases and inferred compositional fields for magmatic-dominated volcanic gases and hydrothermal-dominated volcanic gases. The gas compositions refer to those in Table I.

A. Sources and Fluxes of He, CO_2, and N_2 at Kudriavy (Kurile Islands, Russia)

Kudriavy volcano is one of the many volcanic edifices of the Kurile convergent plate island arc. Its active summit features several fumarole fields that have been degassing continuously at high temperatures (up to 950°C) for at least 100 years, without eruption. The SO_2 emission rate measured remotely by correlation spectrometer (COSPEC) was 70 ± 25 metric tonnes per day in 1995. The chemical and isotopic compositions of the high-temperature fumaroles (Table I) and the COSPEC measurement allowed scientists to estimate the contributions of the mantle, crustal, and subducted material required to balance the long-term magmatic He, CO_2, N_2, and H_2O output from this subduction-zone volcano. Their study nicely illustrates how an integrated dataset on volcanic gases can be used to derive information on magma sources and the cycling of volatiles through subduction zones from the Earth's mantle to the surface.

Volcanic gas discharges from the Kudriavy high-temperature fumaroles are a good example of magmatic gases in subduction zone volcanoes. The $^3He/^4He$ ratio of these gases range from 6.4 to $6.8R_A$, similar to values observed at other volcanoes in this tectonic setting. The ratio indicates that 84% of the He is of mantle origin, while the rest is from a radiogenic source in the crust. The total output of He from the volcano allowed calculation of the amount of mantle material that is degassing and contributing to the He flux over time. The $CO_2/^3He$ ratios of the magmatic gases indicate that about 12% of the degassing CO_2 is of mantle origin, with the remainder derived from subducted marine carbonates in the oceanic crust and organic sedimentary carbon. Nitrogen degassing from the mantle accounts only for about 2% of the total N_2 discharges from the volcano, with the sediments of the subducted oceanic crust contributing most of the total N_2 flux. The study also supports the view that dehydration of minerals in the subducted oceanic crust is the major source of H_2O degassing from subduction zone volcanoes.

For the case of Kudriavy, it is possible to balance the flux of nonmantle gases with the volatiles supplied to the system by the subduction process, taking into account the rate of subduction, thickness, and composition of the subducted sediments and oceanic crust. The re-

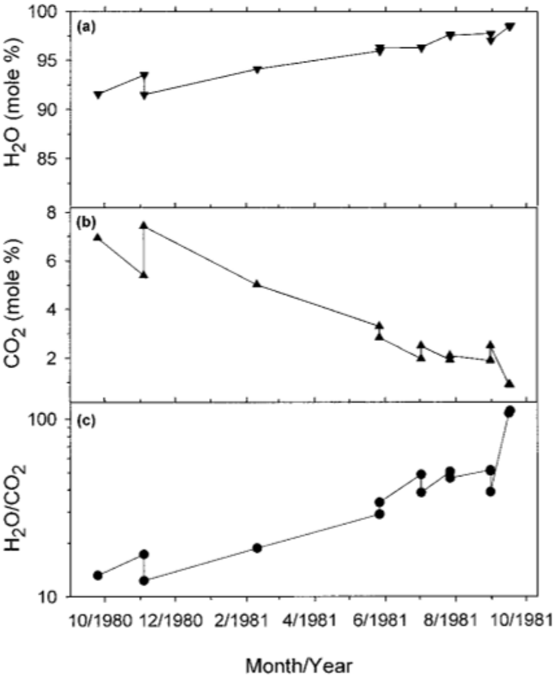

FIGURE 5 Temporal evolution of the (a) H_2O content, (b) CO_2 content, and (c) H_2O/CO_2 ratio in fumarolic gas discharges from Mt. St. Helens, 1980–1981. Data compiled from Gerlach and Casadevall (1986).

sults show how subduction zones not only recycle solid material (rocks) back to the surface of the Earth, which contributes to the formation of continents, but also recycle volatiles through degassing of volcanoes, which contributes to the composition of the Earth's atmosphere.

B. Magma Degassing and Development of a Hydrothermal System at Mt. St. Helens (USA) and Usu (Japan)

Following the catastrophic eruption of 18 May 1980 at Mt. St. Helens, a dome formed within the newly excavated crater. Many fumaroles appeared on the dome and on the crater floor, providing an opportunity to investigate the chemical changes during noneruptive periods of degassing between September 1980 and October 1981. During this time, the H_2O/CO_2 ratio in the gas discharges increased, because of the steady decrease of the CO_2 content and concomitant increase of the H_2O content (Fig. 5). Although showing more scatter, the trend for S_{total} was similar to that for CO_2. These changes were accompanied by a decline in the maximum fumarole temperature from 828 to 600°C. These variations developed in response to progressive dilution of the magmatic gases by hydrothermal steam. The hydrothermal steam component was produced as surface waters started to infiltrate the system and boiled. Admixture of meteoric water accounted for 20–30% of the H_2O content in the fumarolic gases. In addition, decline in the magmatic volatile flux, probably due to a magma that progressively losts its gas, also contributed to the chemical changes in the fumarolic gases (i.e., decrease of CO_2).

A similar scenario was observed at Showa-Shinzan, a dome that grew during the 1943–1945 eruption of Usu volcano (Japan). The gas survey spanned a period of 31 years from 1954 through 1985, during which time the maximum temperature of the high-temperature fumaroles decreased from 800 to 336°C. In parallel, the gas compositions became increasingly H_2O-rich with time because of the progressive infiltration of meteoric water into the dome (Fig. 6). The evolution of the gas chemis-

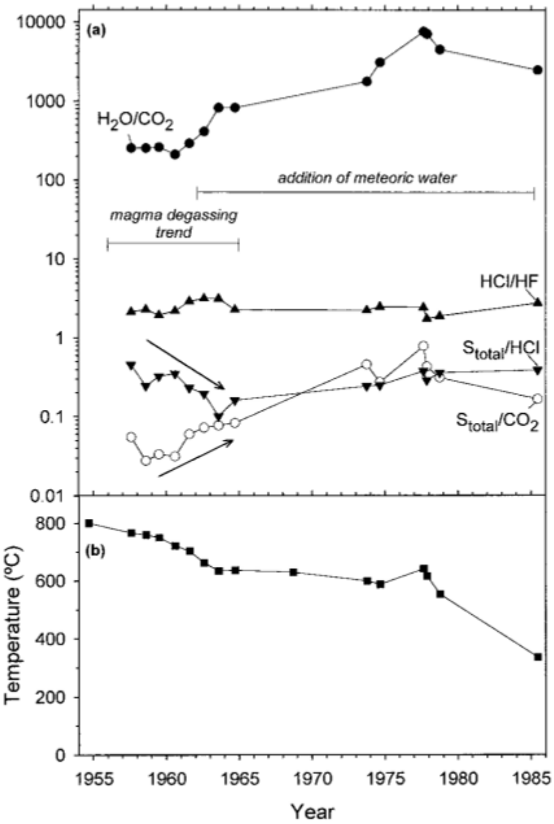

FIGURE 6 Temporal evolution of the (a) H_2O/CO_2, S_{total}/CO_2, S_{total}/HCl, and HCl/HF ratios and (b) maximum temperature in a high-temperature fumarolic gas discharge from Mt. Usu, 1954–1985. Data compiled from Symonds *et al.* (1996).

try between 1954 and 1964 also was controlled by the degassing of the dome. During this period, the S_{total}/CO_2 and S_{total}/HCl ratios of the fumarolic gas increased and decreased dramatically, respectively, while the HCl/HF ratios remained more or less constant (Fig. 6). These trends indicate the early degassing of CO_2 (i.e., the less soluble component), followed by S_{total}, and then HCl and HF from the magma body.

Early escape of CO_2 from magmas is also responsible for the different CO_2 contents of high-temperature volcanic gases vented by Kilauea during summit lava lake and east rift zone eruptions. In the first case, continuous supply of magma from below results in relatively CO_2-rich gases being released at the summit. In the second situation, the rising magma is subsequently transported laterally along the rift zone, resulting in enhanced degassing, depletion of CO_2, and gases with distinctly lower CO_2 contents than at the summit (see the two Kilauea gas compositions in Table I).

C. Temporal Variations in Gas Chemistry at White Island (New Zealand) and Vulcano (Italy)

White Island is an active volcano on an uninhabited island located 50 km offshore at the northeastern end of the Taupo volcanic zone on the North Island of New Zealand. It has been releasing fumarolic gases for more than 150 years and has experienced several periods of eruptive activity. The temperatures of crater fumaroles during this time have ranged from 100 to above 700°C. Regular sampling of White Island fumaroles since 1971 has allowed volcanologists to track the activity of the magma and its associated hydrothermal system. The gas survey results serve to constrain a model for the physical structure of magma–hydrothermal systems. According to this model, a column of high-temperature gases released by a magma body at depth is surrounded by an envelope of highly mineralized hydrothermal water (a brine) and vapor.

As shown in Fig. 7, the high-temperature gases (> 400°C) displayed cyclic changes in temperature and in gas ratios (e.g., H_2O/CO_2, S_{total}/CO_2, and HCl/CO_2) before the start of the 1976–1982 eruptive period. These changes are largely due to variations in the relative contributions from three major components: (1) shallow groundwater; (2) deeper highly acid and hydrothermal brine; and (3) magmatic gases. During periods of low magmatic gas release, the brines invade the main conduit feeding the fumaroles, and interaction of rising hot magmatic gases with the brines leads to drastic reductions in fumarole temperatures and absorption of more water-soluble gases such as HCl, HF, and SO_2. Part of the sulfur content of the gas is removed as elemental sulfur, causing a corresponding decrease in the fumarole S_{total}/CO_2 ratio. Carbon dioxide seems to be less affected by these processes than HCl and SO_2 because of its lower solubility in the brines, and thus is a good "reference" gas to evaluate changes in the more reactive and soluble species. When magmatic gas pressures build up again in the conduit, the process is reversed as reheating evaporates the brines and remobilizes elemental sulfur deposits. As a result, previously absorbed volatiles are quickly released, sometimes producing gas compositions significantly enriched in HCl and S_{total} (i.e., high S_{total}/CO_2 and HCl/CO_2 ratios). Two complete absorption–desorption cycles were observed during the 5 years preceding the 1976–1982 eruption.

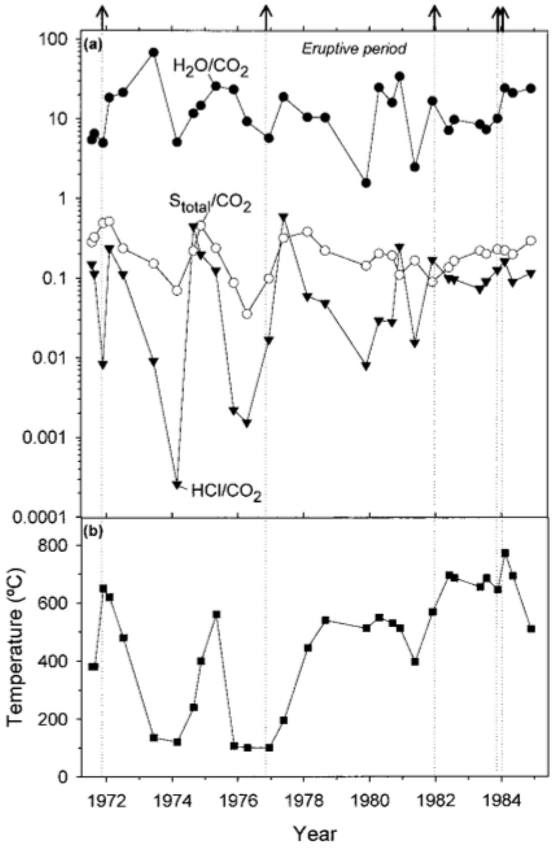

FIGURE 7 Temporal evolution of the (a) H_2O/CO_2, S_{total}/CO_2 and HCl/CO_2 ratios and (b) maximum temperature in high-temperature fumarolic gas discharges from White Island, 1971–1984. Arrows indicate eruptions. Data compiled from Giggenbach and Sheppard (1989).

Vulcano is one of the Aeolian Islands located north of Sicily. The island is renowned for its tourist facilities. Vulcano is a very active volcano, and the last explosive eruption in the Gran Cratere La Fossa occurred in 1888. This eruption was preceded by an increase in the temperature and output rate of the fumarolic gas discharges. A new heating phase of the crater fumaroles, accompanied by significant oscillations in gas chemistry, began in late 1977 and peaked in May 1993 when maximum temperatures reached 690°C. Aware of the potential risk for eruption, Italian volcanologists have conducted numerous studies aimed both at developing a reliable geochemical model of the fumarolic system and at defining a strategy for the geochemical surveillance of the island to help forecast eruptions.

Similar to White Island, deep magmatic gases interact with shallow hydrothermal fluids. However, the hydrothermal component seems to consist mainly of hot steam generated by evaporation of brines entering the high-temperature zone surrounding the conduit of rising magmatic fluids. This hot steam further acquires acid gases (HCl, HF, SO_2, and H_2S) as it reacts with rock minerals and previously deposited salts within the hydrothermal reservoir. Thus, most variations in the acid gas contents of the fumarole gas discharges reflect fluctuations in these reactions, which correlate with changes in subsurface temperature conditions. In parallel, the magmatic component present in the gas discharge also experienced significant short-term increases during periods of high seismic activity beneath the crater. An interesting aspect of Vulcano is that the fumaroles appear to incorporate a marine fluid signature, as inferred from the temporal evolution of its water isotopic compositions (δD and δ^{18}O). The marine contaminant may be seawater that directly enters the magma–hydrothermal system at shallow levels or water trapped in the sedimentary rocks (i.e., connate water) surrounding the magma that is heated and evaporated.

D. Cyclic Sealing of the Magma–Hydrothermal System at Galeras (Colombia)

Galeras is an active 4200-m-high volcano in the Colombian Andes near Ecuador. In 1988, increases in seismicity, gas emission rates, and fumarole temperatures marked the start of a new period of unrest. A lava dome was emplaced in the active cone in October 1991, which was later destroyed by an explosive eruption on July 16, 1992. Five subsequent explosive eruptions occurred in 1993; the 14 January event killed six scientists who were working in the crater. The chemical compositions of volcanic gases collected between 1989 and 1994 showed the effects of long-term magma degassing. During this period, the H_2O/CO_2, S_{total}/CO_2, and HCl/CO_2 ratios increased slightly in the fumarolic gas discharges (Fig. 8). Again, these observations support the idea that CO_2, the least soluble of the major magmatic volatiles, degasses more readily than H_2O, S_{total}, and HCl. In 1995, all the gas ratios had decreased significantly, possibly indicating degassing of a new CO_2-rich magma batch.

In contrast to this long-term trend, variations in the chemical and isotopic compositions of fumaroles both preceded and followed explosive eruptions over the course of days, weeks, or months. Although the SO_2 emission rate measured by COSPEC declined significantly prior to the July 16, 1992 eruption, the gas discharges became more CO_2-rich and the maximum fumarole outlet temperatures dropped. The HCl/CO_2 gas ratio decreased dramatically over the space of 2 weeks prior to July 16, but the S_{total}/CO_2 ratio experienced comparatively minor changes (Fig. 8). At the same time, unusual low-frequency seismic events began to be observed, with the rate of occurrence and duration of individual signals increasing before the eruption. Afterward, the seismicity abruptly disappeared.

These variations show the interaction of high-temperature magmatic gases with a shallow hydrothermal system that selectively absorbed the more water-soluble

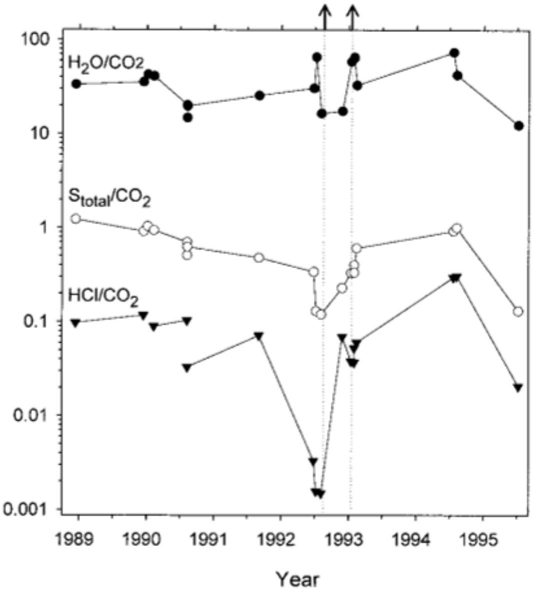

FIGURE 8 Temporal evolution of the H_2O/CO_2, S_{total}/CO_2, and HCl/CO_2 ratios in fumarolic gas discharges from Galeras, 1989–1995. Arrows indicate eruptions. Data compiled from Fischer *et al.* (1997).

gases (SO_2, H_2S, and HCl) into the liquid phase. The failure of hot magmatic gases to escape the volcano appear to be related to the "sealing" of the gas conduits. This sealing process is not well understood but is clearly important, both to the understanding of the shallow magmatic–hydrothermal system and to the development of overpressure within the volcano as gas release was impeded. The low-frequency seismicity that was observed before the Galeras eruptions is a clear indication of the pressure buildup, which eventually resulted in the explosive failure of the seal. The seal may have developed as hydrothermal minerals such as silica were deposited within fractures and openings in the conduit system, clogging the gas pathways to the surface. It is also possible that overpressure was developed in the cooling magma itself that filled the conduit system. Whatever the cause of the sealing and associated pressure buildups, it is clear that magmatic–hydrothermal interaction was important for understanding the explosive 1992–1993 eruptions of Galeras. It is also clear that this type of interaction exists at many volcanoes, and an improved understanding of these processes is a future challenge to permit better forecasting of explosive eruptions.

IV. DIFFUSE FLANK DEGASSING

On a volcano, magmatic gases are clearly channeled through the central conduit or conduits. Magmatic gases also may percolate through a volcano's porous flanks to the surface. Since this type of degassing cannot be seen directly, in contrast to the frequently spectacular crater emissions, diffuse flank degassing tends to be overlooked. Yet this source also may emit significant quantities of gas to the atmosphere. The types of gases that tend to be emitted are nonreactive and do not contain species that are highly acidic (e.g., SO_2, HCl, HF). They also tend to be emitted at low temperatures through the soil and springs. Such gases include CO_2 and He. Radon is also emitted through the flanks, but it is not clear whether it is derived from the magma or from shallow levels within the volcano, even the soil itself.

Although estimates of diffuse CO_2 flank degassing have been made from a number of volcanoes, the numbers vary substantially. There is thus no real consensus at present about the relative importance of flank degassing and how much volcanic gas it contributes to the atmosphere. Nonetheless, as more studies of flank degassing are made, it is becoming increasingly obvious that faults and fractures play an important role in channeling the gases to the surfaces. In fact, the presence or absence of faults having surface expression may be the principal control on whether a volcano is able to degas through its flanks.

A. Diffuse Emissions of Carbon Dioxide

Only several volcanoes have been studied in any detail for their diffuse emissions of CO_2. Chief among these is Mt. Etna, which is a prodigious emitter of volcanic gas. Copious quantities of CO_2, SO_2, and other species are released at the summit crater. In addition, it appears that large amounts of CO_2 may be escaping through the volcano's flanks. The problem is how much; estimates range from 2700 to 35,000 metric tonnes per day! Thus, the exact amount of diffuse degassing remains uncertain, and it probably varies temporally with the activity of the volcano. Yet the various chemical measurements indicate that much if not most of the CO_2 is derived from a deep magmatic source. For example, the isotopic ratio of carbon falls within the magmatic field ($\delta^{13}C \sim -4‰$), and He gas associated with the CO_2 has $^3He/^4He$ values of $5–8R_A$, clearly showing the mantle-derived nature of the gas. At Etna, it is generally recognized that the diffuse gas emissions are concentrated along fractures and faults.

Another interesting example of diffuse CO_2 emissions is Mammoth Mountain, a rhyodacite dome complex located on the southwestern rim of Long Valley caldera (California, USA), which is currently exhibiting restlessness. After a period of elevated seismicity in 1989–1990 in the area, tree kills were observed to develop on the slopes of Mammoth Mountain. These kills were the result of localized emissions of CO_2 passing diffusely through the soil at low temperatures. In places, soil gas concentrations reached nearly 100% in the winter when the CO_2 was retained in the soil by the snow pack. The diffuse flux of CO_2 at Mammoth is 100–500 metric tonnes per day, the fluxes varying with time. Similar to Mt. Etna, carbon isotopic values are magmatic ($\delta^{13}C = -3$ to $-5‰$), as are the mantle-like $^3He/^4He$ ratios ($\sim 5R_A$). Also similar to Mt. Etna, the tree kills appear to be situated on or near mapped faults on Mammoth Mountain. The CO_2 release could be related to dike intrusion, to fracturing of conduits above an older magma body, or to shaking and release of CO_2 bubbles from a magma chamber, triggered by seismicity.

Many interesting questions remain regarding this style of degassing. The carbon isotopic values are suggestive of a magmatic source, but they are not definitive proof. The measured values also can be interpreted as a mixture of mantle and sedimentary carbonate components, or a mixture of mantle and organic components. A third possibility is that the carbon isotopic ratio is fractionated and changes during the degassing process itself. Studies using noble gas isotopes may help to shed light on the sources of the CO_2.

B. Radon, Helium, and Hydrogen

Radon (Rn) is a naturally occurring radioactive gas, with a half-life of 3.82 days, which appears to be a sensitive indicator of permeability within soil or at shallow levels beneath the surface. It can therefore be used to delineate faults and fractures. There is also a clear association between seismicity and Rn concentrations in the soil. However, Rn also is influenced by climatic variations (e.g., dry vs wet seasons) and by soil properties (porosity, humidity, etc.). Its short half-life indicates that on a volcano, much of the Rn measured in the soil is derived from shallow levels and not from the magma or deep faults, unless it is transported rapidly to the surface.

Helium also is present in soil gas and can be indicative of flank degassing. Since its atmospheric concentration is about 5 parts per million (ppm), it is sometimes difficult to observe the magmatic component of He in soils, since concentrations rarely exceed 20 ppm. The isotopic $^3He/^4He$ ratio is a very useful indicator of magmatic gas, as noted earlier. However, measuring this ratio in soil gas can be difficult because of the large atmospheric contamination of the soil gas.

Hydrogen is another gas that can be present in soils, but very little is known of its distribution on volcanoes. In zones of active faulting, however, H_2 is generated by the pulverization and fragmentation of rock during faulting. Thus, high concentrations of H_2 in soil can indicate zones of active faulting, with gas generation at relatively deep levels. Consequently, H_2 is also a potentially useful gas for studying faulting and fracturing on volcanoes.

C. Mechanisms of Diffuse Flank Degassing

The association between faults and fractures on the one hand and diffuse degassing on the other hand seems clear. Yet a general model of diffuse flank degassing on volcanoes does not exist. Are there changes in the relative proportions of crater and flank degassing, whereby changes in permeability in the crater region affect the flank degassing in more distant regions? Are upper slopes of volcanoes, with their cover of recent lavas, relatively impermeable so that they prevent or hinder diffuse degassing, whereas lower slopes which may be more fractured and faulted allow for increased diffuse emissions? Or are the upper slopes of volcanoes a recharge zone where CO_2 is dissolved into groundwater and then transported to lower elevations where it is released? Indeed, cold groundwater appears to transport a small but appreciable fraction of the CO_2. These questions will form the basis for future research on diffuse flank emissions of volcanic gas.

D. Gases Discharging in Hot and Cold Springs

Hot springs and cold springs are a common feature on the flanks of active volcanoes. They contain gases dissolved in their waters, some of which may be of magmatic origin. In addition, cold and hot springs often display gas bubbles discharging from the bottom of the spring to the surface. These gases are predominantly CO_2, but H_2S and other trace gas species (CH_4, N_2, noble gases) may also be present. High $^3He/^4He$ ratios are a good indication of the magmatic sources of these gases. Monitoring of the chemical and isotopic composition of gas discharges from springs can contribute significantly to the monitoring of soil gases and help scientists to understand the activity of a volcano and forecast its time of reactivation.

V. CONCLUSIONS

We have made great advances in our understanding of volcanic gases in the past 30 years, but as is often true in science, many important questions still remain to be solved. We can safely say that the next 30 years will be an exciting time for volcanic gas research. In fact, as the millennium approaches, we may be on the verge of making some fundamental breakthroughs in our understanding of volcanic gases. In this respect, the development of remote sensing techniques that will allow regular measurements of gas plume compositions from a distance marks a new era in the study of volcanic gases.

Our knowledge of how gas is transported and stored within a volcano is rudimentary. We do not have a clear understanding of the complexity of the conduits, fractures, and other pathways that channel gas to the surface. Neither do we have a good model of how diffuse gases are transported through the flanks of a volcano.

We need a reliable geochemical model, based on thermodynamic understanding and gas solubilities, to be able to confidently predict the temporal evolution of individual gas species. We have a reasonable knowledge of the major components of volcanic gas, but we know almost nothing about the many minor and trace species that coexist with the major gases. These low-concentration species (e.g., boron) have great potential for shedding light on deeper processes within a volcano and for improving our eruption forecasting ability.

The behavior of volcanoes that release large amounts of gas on a continuous basis is fundamentally different from that of volcanoes that store gas over long periods. This dichotomy between "open" and "closed" systems is fundamental, yet we do not know why a particular volcano is open or closed, nor is it clear why a volcano's behavior may suddenly change from one style to the other. Some volcanoes emit huge quantities of gas but almost no solid material; this enigmatic behavior is probably the result of a near-continuous magma supply beneath the volcano, but our understanding is primitive. Although the study of volcanic gas is no longer in its infancy, we still have important challenges in front of us.

SEE ALSO THE FOLLOWING ARTICLES

Composition of Magmas • Hazards of Volcanic Gases • Surface Manifestations of Geothermal Systems • Volatiles in Magmas • Volcanic Contributions to the Carbon and Sulfur Geochemical Cycles and Global Change • Volcanic Soils

FURTHER READING

Chiodini, G., Cioni, R., and Marini, L. (1993). Reactions governing the chemistry of crater fumaroles from Vulcano Island, Italy, and implications for volcanic surveillance. *Appl. Geochem.* **8,** 357–371.

Fischer, T. P., Sturchio, N. C., Stix, J., Arehart, G. B., Counce, D., and Williams, S. N. (1997). The chemical and isotopic composition of fumarolic gases and spring discharges from Galeras Volcano, Colombia, *J. Volcanol. Geotherm.* **77,** 229–253.

Fischer, T. P., Giggenbach, W. F., Sano, Y., and Williams, S. N. (1998). Fluxes and sources of volatiles discharged from Kudriavy, a subduction zone volcano, Kurile Islands. *Earth Planet. Sci. Lett.* **160,** 81–96.

Gerlach, T. M. (1993). Oxygen buffering of Kilauea volcanic gases and the oxygen fugacity of Kilauea basalt. *Geochim. Cosmochim. Acta.* **57,** 795–814.

Gerlach, T. M., and Casadevall, T. J. (1986). Evaluation of gas data from high-temperature fumaroles at Mount St. Helens, 1980–1982. *J. Volcanol. Teotherm. Res.* **28,** 107–140.

Giammanco, S., Gurrieri, S., and Valenza, M. (1998). Anomalous soil CO_2 degassing in relation to faults and eruptive fissures on Mount Etna (Sicily, Italy). *Bull. Volcanol.* **60,** 252–259.

Giggenbach, W. F. (1987). Redox processes governing the chemistry of fumarolic gas discharges from White Island, New Zealand. *Appl. Geochem.* **2,** 143–161.

Giggenbach, W. F. (1996). Chemical composition of volcanic gases. Pages 221–256 *in* "Monitoring and Mitigation of Volcano Hazards" (R. W. Scarpa and R. I. Tilling, eds.). Springer-Verlag, Berlin.

Giggenbach, W. F., and Sheppard, D. S. (1989). Variations in the temperature and chemistry of White Island fumarole discharges 1972–85. *N. Z. Geol. Surv. Bull.,* **103,** 119–126.

Giggenbach, W. F., García, P. N., Londoño, C. A., Rodriguez, V. L., Rojas, G. N., and Calvache, V. M. L. (1990). The chemistry of fumarolic vapor and thermal-spring discharges from the Nevado del Ruiz volcanic-magnetic-hydrothermal system, Colombia. *J. Volcanol. Geotherm. Res.* **42,** 13–39.

Kita, I., Nitta, K., Nagao, K., Taguchi, S., and Koga, A. (1993). Difference in N_2/Ar ratio of magmatic gases from northeast and southwest Japan: new evidence for different state of plate subduction. *Geology* **21,** 391–394.

Sano, Y., and Marty, B. (1995). Origin of carbon in fumarolic gas from island arcs. *Chem. Geol.* **119,** 265–274.

Sorey, M. L., Evans, W. C., Kennedy, B. M., Farrar, C. D., Hainsworth, L. J., and Hausback, B. (1998). Carbon dioxide and helium emissions from a reservoir of magmatic gas beneath Mammoth Mountain, California. *J. Geophys. Res.* **103,** 15303–15323.

Stix, J., Zapata, G., J. A., Calvache, V., M., Cortés, J., G. P., Fischer, T. P., Gómez, M., D., Narváez, M., L., Ordoñez, V., M., Ortega, E., A., Torres, C., R., and Williams, S. N. (1993). A model of degassing at Galeras Volcano, Colombia, 1988–1993. *Geology* **21,** 963–967.

Symonds, R. B., Rose, W. I., Bluth, G. J., and Gerlach, T. M. (1994). Volcanic-gas studies: methods, results, and applications. Pages 1–66 *in* "Volatiles in Magmas" (M. R. Carroll and J. R. Holloway, eds.), Vol. 30, *Mineral. Soc. Am. Rev. Mineral.*

Symonds, R. B., Mizutani, Y., and Briggs, P. H. (1996). Long-term geochemical surveillance of fumaroles at Showa-Shinzan dome, Usu volcano, *Japan. J. Volcanol. Geotherm. Res.* **73,** 177–211.

This Page Intentionally Left Blank

GEOTHERMAL SYSTEMS

FRASER GOFF
Los Alamos National Laboratory

CATHY J. JANIK
U.S. Geological Survey

I. Resource Locations and Types
II. Heat Flow in the Earth
III. Heat Content and Heat Flow of Magmatic Intrusions
IV. Conceptual Models of Geothermal Systems
V. Geothermal Fluid Characteristics and Deposits
VI. Geothermal Development
VII. Environmental and Safety Issues
VIII. Summary

GEOTHERMAL SYSTEMS consist of three main elements: (1) permeable reservoir rock, (2) water to carry heat from the reservoir to the earth's surface, and (3) a heat source. Practically any rock type can serve as a host for a geothermal reservoir, and groundwater, usually consisting of ancient to modern precipitation or seawater, circulates to depths of many kilometers virtually everywhere in the crust. Thus, hotter-than-normal rock and water at a relatively shallow depth is the primary characteristic that distinguishes geothermal systems from other groundwater systems.

Geothermal systems commonly produce hot springs and fumaroles as surface expressions of underlying hot reservoirs. Hot and mineral springs have been universally revered for their soothing, therapeutic qualities and cleansing characteristics. Hot spring and fumarole areas were exploited for sulfur and other minerals throughout ancient times. During the Middle Ages the commercial value of Italian hot-spring deposits led to wars among local republics. Electricity was first produced from a steam well at Larderello (Italy) in 1904 and commercial electricity was first marketed in 1913. Since that time, geothermal power has been developed by many countries as an alternative to burning imported or domestic fossil fuels. About 8000 MW of electric power are now produced from geothermal systems worldwide, equivalent to about 80 million barrels of petroleum annually. Although low-temperature resources have been used extensively for many years and are becoming more widely utilized as drilling methods and heat extraction technologies improve, we will focus herein on high-temperature ("high enthalpy") geothermal systems because of their common association with volcanism and tectonic activity, and their ability to produce electric power.

I. RESOURCE LOCATIONS AND TYPES

Geothermal resources are most prevalent in regions of elevated heat flow and vigorous fluid circulation. These regions are commonly located along or near convergent plate margins, near transform plate boundaries, within spreading centers and rifts, and within hot spots. As a result, geothermal resources are not distributed evenly over the globe (Fig. 1) and certain countries or regions are blessed with resources while others are relatively

Copyright © 2000 by Academic Press
All rights of reproduction in any form reserved.

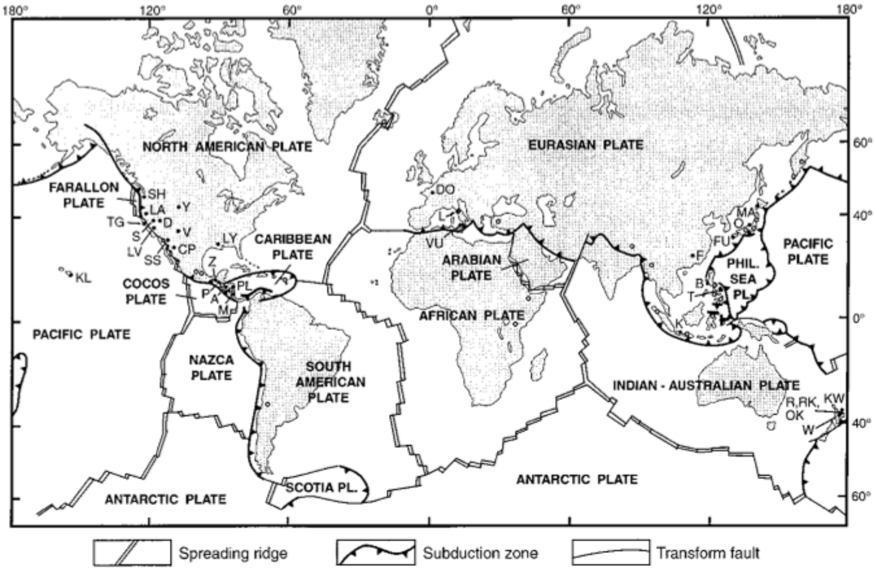
180°
120°
60°
0°
60°
120°
180°
60°
40°
0°
40°
60°
NORTH AMERICAN PLATE
EURASIAN PLATE
FARALLON PLATE
SH
LA
Y
TG
D
S
V
LV
CP
SS
LY
CARIBBEAN PLATE
Z
KL
COCOS PLATE
PL
P
A
M
PACIFIC PLATE
DO
VU
ARABIAN PLATE
AFRICAN PLATE
MA
O
FU
F
B
T
K
PHIL. SEA PL
PACIFIC PLATE
NAZCA PLATE
SOUTH AMERICAN PLATE
INDIAN - AUSTRALIAN PLATE
R,RK
KW
OK
W
SCOTIA PL.
ANTARCTIC PLATE
ANTARCTIC PLATE
Spreading ridge
Subduction zone
Transform fault

FIGURE 1 The global distribution of geothermal resources is highly correlated with lithospheric plate boundaries, although some sites occur at hot spots or within rifts. Locations mentioned in this article are shown by dots: A (Ahuachapán, El Salvador), B (Bulalo, Philippines), CP (Cerro Prieto, Mexico), D (Dixie Valley, USA), DO (Dogger, France), F (Fuzhou, China), FU (Fushime, Japan), K (Kamojang and Darajat, Indonesia), KL (Kilauea, USA), KW (Kawerau, NZ), L (Larderello, Italy), LA (Lassen, USA), LV (Long Valley, USA), LY (Lafayette, USA), M (Miravalles, Costa Rica), MA (Matsukawa, Japan), O (Oku-aizu, Japan), OK (Ohaaki, NZ), P (Pacaya-Amatitlán, Guatemala), PL (Platanares, Honduras), R (Rotorua, NZ), RK (Rotokawa, NZ), S (Steamboat Hills, USA), SH (Mount St. Helens, USA), SS (Salton Sea, USA), T (Tiwi, Philippines), TG (The Geysers, USA), W (Wairakei, NZ), V (Valles caldera, USA), VU (Vulcano, Italy), Y (Yellowstone, USA), Z (Zunil, Guatemala). Locations of other geothermal fields are shown by open circles. Geothermal prospects are not shown. [Modified from "Geothermal Systems: Principles and Case Histories," Rybach and Muffler, 1981, copyright John Wiley & Sons, Ltd. Reproduced with permission.]

barren. Not surprisingly, the 10 leaders in electrical generation occur in regions of active volcanism (Table I). In addition, some countries have been more effective at exploiting either high- or low-temperature resources than others, depending on technology levels, energy requirements, and prevailing economics. Probably the largest and most abundant high-temperature systems on Earth occur along submarine rifts and transform boundaries, yet we know the least about these systems because they are so difficult to explore.

There are five principal types of geothermal systems based on geologic, geophysical, hydrologic, and engineering criteria. The first three exploit natural reservoirs of hot water and are generically called hydrothermal systems. The second two require pumping a fluid, generally water, into the ground and then out again to extract heat. These systems are technically feasible under certain conditions, but commercially impractical with present economics because of the low cost of fossil fuels.

1. *Young igneous systems* are associated with Quaternary volcanism and magmatic intrusions. About 95% of volcanic activity occurs along plate boundaries and within hot spots. Such environments are usually associ-

TABLE I Ten World Leaders in Installed Geothermal Capacity for Electrical Generation and Direct-Use Applications (Late 1998)[a]

Country	*Electrical (MWe)*	*Country*	*Direct-use (MWt)*
United States	2850	United States	2000
Philippines	1780	China	1914
Mexico	743	Iceland	1443
Italy	742	Japan	1159
Indonesia	589	Hungary	750
Japan	530	Italy	314
New Zealand	364	France	309
El Salvador	105	New Zealand	264
Nicaragua	70	Georgia	245
Costa Rica	65	Russian Fed.	210
Total of leaders	7838	Total of leaders	8608
Total worldwide	8029	Total worldwide	9963
Leaders, percent	98	Leaders, percent	86

[a] Energy usage may be less than installed capacity (MWe = megawatts electrical; MWt = megawatts thermal; 1 MWe ≈ 7 MWt).

ated with major tectonic activity and seismicity. Fluids derive their heat from the margins of crystallizing or recently crystallized magma. These geothermal systems are generally the hottest (≤370°C) and reservoir depths are commonly ≤1.5 km, although some are deeper.

2. *Tectonic systems* are those with elevated heat flow but essentially devoid of igneous activity. They occur in backarc environments, regions of crustal extension, collision zones, and along fault zones of any displacement or length. Tectonic systems are usually associated with elevated seismicity due to Quaternary faulting and with elevated heat flow due to thin crust. Deep circulation of fluids into the crust and ascent of these fluids along faults moves heat upwards into favorable geologic structures. Tectonic systems capable of electricity generation usually have reservoir temperatures ≤250°C and occur at depths ≥1.5 km.

3. *Geopressured systems* are found in sedimentary basins where subsidence and deep burial of fluid-bearing strata has formed hot, "overpressured" reservoirs. Wells drilled into geopressured reservoirs exhibit very high artesian pressures. Heat flow and seismicity are comparatively low to normal. Most systems of this type have characteristics resembling oil and gas fields. Energy stored as excess pressure and as dissolved methane is potentially more valuable than the fluid enthalpy. Geopressured systems often require deeper drilling than young igneous and tectonic systems. Typical depths and temperatures are 1.5 to 3 km and 50 to 190°C.

4. *Hot dry rock systems* exploit heat stored in low-porosity, impermeable rocks at varying depths and temperatures. A deep fracture network comprising the "reservoir" is created artificially in such a way that at least two wells intersect permeable structures. Surface water is pumped down an injection well, through the fractures, and out the production well(s), literally mining heat from the rocks. Experimental hot dry rock systems have been developed in several countries (United States, England, France, and Japan) since the mid-1970s, but none are presently capable of commercial production. Drilling and completion costs are high in deep, hot, dense (usually crystalline) rocks. Each system has unique engineering challenges, and most systems have large leak-off rates while water is pumped through the reservoir. Production temperatures and depths have ranged from 120 to 225°C and 2 to 4 km in experimental systems.

5. *Magma tap systems* involve drilling into shallow magma bodies, installing a heat exchanger, and circulating a fluid (probably water) through the exchanger to extract heat. Experiments on this concept have been conducted at a lava lake on Kilauea Volcano, Hawaii, but materials that can withstand the high temperatures and corrosive properties of magma are exceptionally costly. Extending this concept to greater depths adds exploration and drilling challenges that are presently too expensive to overcome. Nevertheless, magma is the purest form of natural heat in the shallow crust (≤1200°C).

II. HEAT FLOW IN THE EARTH

Heat is transferred by conduction, convection, and radiation. However, only the first two mechanisms are important when considering geothermal resources. The basic equation of conductive heat flow, q, is

$$q = k(dT/dz), \tag{1}$$

where k = thermal conductivity of rock, T = temperature, z = depth, and dT/dz = geothermal gradient (°C/km). Units of heat flow are $\mathrm{mWm^{-2}}$ and HFU (heat flow units, where 1 HFU = 41.8 $\mathrm{mWm^{-2}}$). Thermal conductivity of rock is highly variable (typically ≤3.5 W/m) and also depends on temperature. Values of k for crystalline rocks at 250°C are about 20% less than values at 25°C. Crystalline rocks also have virtually no pore spaces and are more conductive than water-rich sedimentary rocks (≤1 W/m). Thermal conductivity is also affected by permeability, fracture density, and hydrothermal alteration.

Most of the heat in the Earth is generated by its gravitational force and eventually flows through the mantle and crust to the surface. Additional heat is generated by decay of radioactive elements, particularly U, Th, and K. Because these elements have differentiated throughout Earth history, they reside mainly in older continental crust. Heat generation factors have been calculated for all rock types. Granitic crystalline rocks, which may be comparatively rich in radioactive elements, typically contribute a Δq of 0.5 to 2.5 $\mathrm{mWm^{-2}}$ per 1 km of crustal thickness, or 5 to 10% of total heat flow in older continental crust. Sedimentary rocks contribute Δq values of 0.2 to 1.0 $\mathrm{mW/m^{-2}}$ depending on water content. By comparison, Mg- and Fe-rich ultramafic rocks such as occur in the mantle contribute Δq of ≤0.01 $\mathrm{mW/m^{-2}}$; thus, heat generation by radioactive decay is only important in some continental environments.

Within the crust as a whole, q varies from high values at or near zones of magmatism, tectonism, and thin crust to low values in most older continental crust (Fig. 2). Within restricted regions, q is more or less constant, but local geology profoundly influences dT/dz, which is rarely the same at all depths in the crust. Consider a

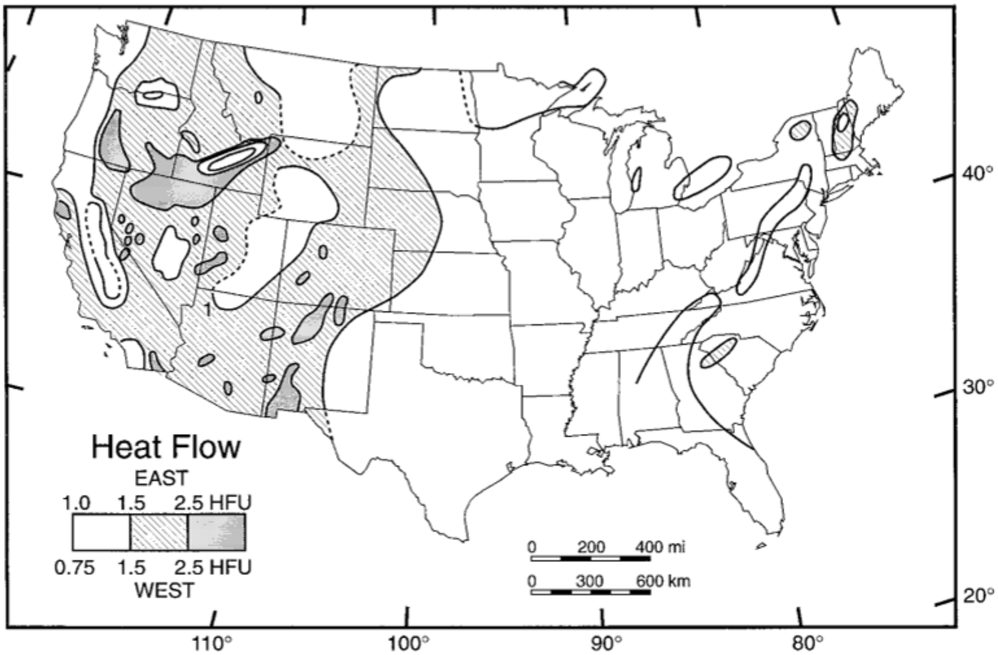

FIGURE 2 Heat flow maps, such as this example for the conterminous United States, show contoured data from wells distributed throughout a given region. Conductive heat flow is relatively low in tectonically stable regions such as the eastern United States, whereas it is relatively high in the volcanically and tectonically active regions such as the western United States.

region where $q = 50$ mWm^{-2} consisting of 2 km of shale ($k = 1.5$ W/m) overlying granite ($k = 3$ W/m). To maintain constant heat flux, the geothermal gradient (dT/dz) in the shale must be 33°C/km, or about twice the value in the granite. Sedimentary basins may have higher near-surface gradients than adjacent terrains because the basin is filled with unconsolidated sediments of low k. As a result, the depth to a given temperature is often less in the basin than around its margins. In effect, low-conductivity sediments act as an insulating blanket over crystalline rocks. Such geologic relations explain why deep sedimentary basins contain fluids at commercially viable temperatures even though q is relatively low.

Upward movement of water or magma transports heat to the Earth's surface more effectively than conduction. Cold waters move downward through favorable pathways in the crust and become heated. Hot water is less dense and relatively buoyant compared to cold water and tends to rise through the crust. Convection cells involving rising hot fluids and descending cooler fluids can occur within a reservoir or can include fluid leakage to the surface. Such convection cells are characteristic features of hydrothermal systems and may produce spectacular surface manifestations such as geysers, fumaroles, and hot springs. The equations describing convective behavior are complex, involving conservation of energy, mass, and momentum. Vapor–liquid separation also must be considered. Information on porosity and permeability of pathways along fractures and strata boundaries is required to determine flow characteristics and storage capacity of the reservoir. Boundaries between flow regimes may be sharp. Hydrothermal systems often contain zones of hot water that overlie formations containing much cooler waters (see Section IV).

III. HEAT CONTENT AND HEAT FLOW OF MAGMATIC INTRUSIONS

Heat content of a magma chamber is dependent mostly on magma volume and temperature. Average silicate magma at 850°C has latent heat of crystallization of 270 J/g, heat capacity of 1.25 J/g/°C, and mean density of 2.5 g/cm^3. The total heat liberated by magma cooling from 850 to 300°C is about 960 J/g. If 1 km^3 of magma has a mass of 2.5×10^{15} g, the heat liberated by 1 km^3 of magma cooling to 300°C is 2.4×10^{18} J. Large intrusions such as those that produce calderas contain immense quantities of heat. For example, the Bandelier pluton that created Valles caldera (USA) is estimated to have contained 3000 km^3 of magma; thus, it would have released roughly 7.2×10^{21} J while cooling from 850 to 300°C.

Heat flow surrounding a magma chamber depends on many variables, especially emplacement temperature, depth, and time. For large magma bodies, surface heat flow q as a function of time, t, after instantaneous intrusion is given by

$$q(t) = T_e k(\pi K t)^{-1/2} \exp(-z^2/4\pi t), \tag{2}$$

where z = depth to top of the magma body (in meters), T_e = intrusion temperature minus ambient temperature, k = thermal conductivity of overlying rocks, and K = thermal diffusivity of magma. The maximum achievable heat flow, $q_{max} \approx 0.5\ T_i k/z$ (where T_i is the emplacement temperature), is reached at time $t = z^2/2K \approx 0.016\, z^2$. As an example approximation, a large intrusion emplaced at 850°C whose top lies at 5 km depth beneath rocks with average k = 1.5 W/m produces a maximum heat flow of about 125 mWm^{-2} roughly 400,000 years after emplacement. This value of q_{max} is about two times the average heat flow of the stable crust in the eastern United States (~55 mWm^{-2}). Shallower emplacement depth raises q_{max} and decreases the time required to achieve the maximum value.

The calculations just described above rely on several assumptions: (1) all heat transfer around the magma body is by conduction; (2) preliminary heating stages of the magma body and the rocks it has consumed or displaced are ignored; (3) replenishment of the magma body by new magma batches, a characteristic of plutons and stocks that form volcanic fields or volcanic complexes, is ignored; (4) removal of heat by circulating groundwater is ignored. These processes have contrasting effects on q and dT/dz within volcanoes.

Convecting hydrothermal fluids can produce geysers, hot springs, fumaroles, and subsurface flows of hot waters that remove heat from a magmatic system much faster than heat loss by conduction alone. The rate of convective heat removal is highly dependent on circulation depth, reservoir temperature, and mass flow of water through the system. For example, deep heat flow (≥3 km) around larger magmatic systems is about 150 to 300 mWm^{-2}, but near-surface heat flow at the largest fumarole areas is commonly ≥5000 mWm^{-2}. Contrasts such as these illustrate the important role of convecting fluid to the dynamics and lifetime of a geothermal system.

IV. CONCEPTUAL MODELS OF GEOTHERMAL SYSTEMS

A. Young Igneous Model

Figure 3 shows a conceptual model for a geothermal system hosted in a potentially active stratovolcano. Emplacement temperatures for andesitic intrusions usually range from 850 to 1050°C. Meteoric waters percolate deep into the ground where they are heated by the intrusive bodies. As the hot water circulates, it becomes richer in Cl, F, Br, B, SO_4, HCO_3, silica, major cations, and soluble metals by reaction with country rocks. Magmatic volatiles such as H_2O, CO_2, sulfur compounds, HCl, HF, Hg, and As may be transferred to the evolving fluid. The fluid generally becomes "neutral-chloride" in character and rises buoyantly through the volcanic edifice because of its decreased density. Alteration minerals and veins form in the reservoir rocks. Frequently, the hot fluids rise through fractures to a level where boiling occurs and a vapor phase containing steam and noncondensible gases forms. These gases feed surface fumaroles. When the steam condenses and mixes with shallow meteoric water, H_2S is oxidized to sulfuric acid, which chemically alters the rock and produces "acid-sulfate" hot springs. Neutral-chloride waters are typically deeper than acid-sulfate waters, and if the two types mix, hybrid acid-sulfate–chloride waters may result. Because of topography and the hydrologic gradient, the fluids tend to flow laterally away from the volcanic center, forming hydrothermal outflow plumes. Springs of neutral-chloride character are often found many kilometers from the heat source and primary reservoir. If the intrusive bodies have largely crystallized because of age or small size, or are very deep, the contribution of magmatic volatiles to the system may be relatively small and undetectable. This general model describes many features of subduction zone systems such as Miravalles (Costa Rica), Pacaya-Amatitlán (Guatemala), Ahuachapán (El Salvador), and Bulalo (Philippines).

Young igneous systems have many other configurations than the idealized model in Fig. 3. The tops of Plio-Pleistocene magmatic complexes at The Geysers and Larderello geothermal systems lie at depths of 2 to 7 km, respectively. Although these intrusions are not associated with significant surface volcanism, they provide widespread heat for geothermal reservoirs that circulate in overlying, structurally deformed, sedimentary and metamorphic rocks. Calderas are circular collapse structures formed when large magma bodies erupt ex-

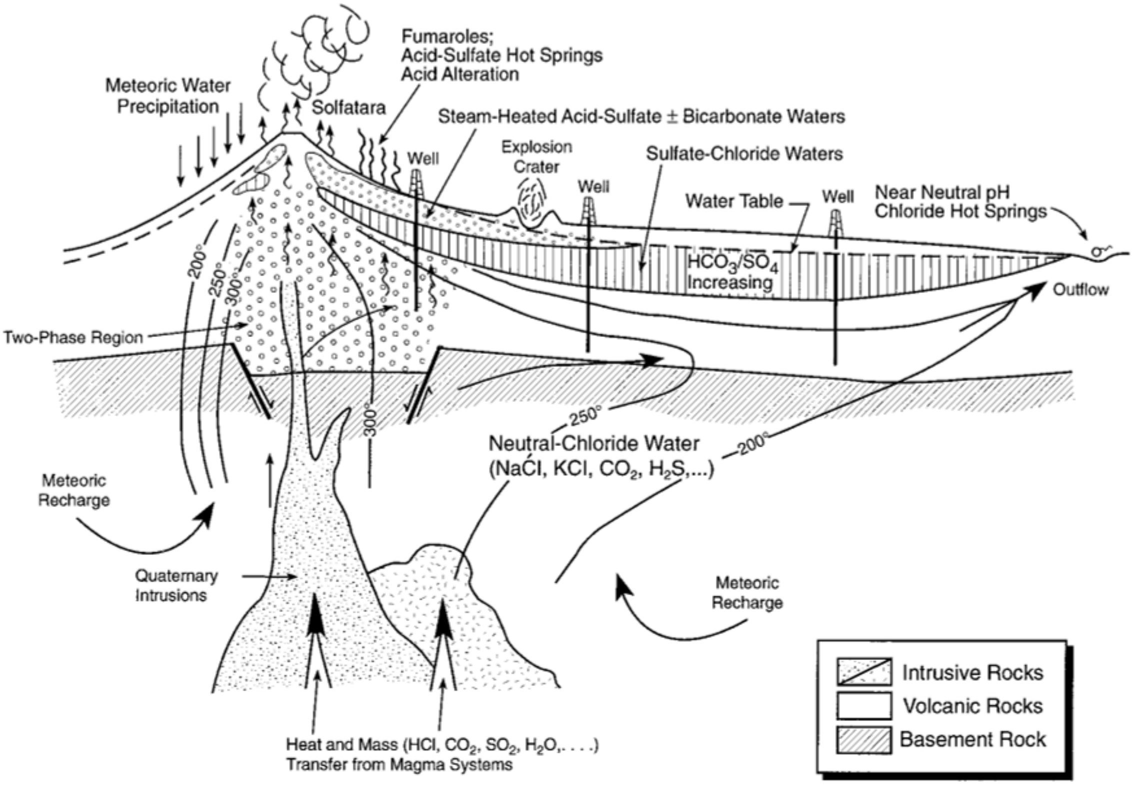
Fumaroles;
Acid-Sulfate Hot Springs
Acid Alteration
Meteoric Water
Precipitation
Solfatara
Steam-Heated Acid-Sulfate ± Bicarbonate Waters
Well
Explosion
Crater
Well
Sulfate-Chloride Waters
Water Table
Well
Near Neutral pH
Chloride Hot Springs
HCO3/SO4
Increasing
Outflow
200°
250°
300°
Two-Phase Region
250°
300°
Neutral-Chloride Water
(NaCl, KCl, CO2, H2S,...)
200°
Meteoric
Recharge
Quaternary
Intrusions
Meteoric
Recharge
Intrusive Rocks
Volcanic Rocks
Basement Rock
Heat and Mass (HCl, CO2, SO2, H2O, . . .)
Transfer from Magma Systems

FIGURE 3 Conceptual model of a young igneous geothermal system hosted in an andesitic stratovolcano. The exploitable reservoir is usually found in horizons ≥200°C. Depth to typical reservoir is ≤1.5 km, whereas depth to intrusions varies from 2 to 10 km. Lateral dimension of reservoir and outflow may exceed 20 km.

plosively. Extensive aprons of tuffaceous rocks are usually deposited around the resulting hole. The faulted and fractured intracaldera rocks trap meteoric waters that are heated by subjacent magmas (usually ≥5 km depth). Because of their great size, calderas such as Yellowstone, Long Valley, and Valles (USA) host larger, longer-lived geothermal systems than those in typical stratovolcanos. Systems in some rifts, transform zones, and hot spots result from injection of dikes that heat waters circulating in grabens or other fault structures (Kilauea, USA).

B. Tectonic Model

A conceptual model of a geothermal system hosted in an extensional tectonic environment is shown in Fig. 4. Where tectonic forces cause stretching and thinning of the crust, very hot mantle material will exist at a relatively shallow depth in the crust. The result is a higher than average thermal gradient and anomalous heat flow,

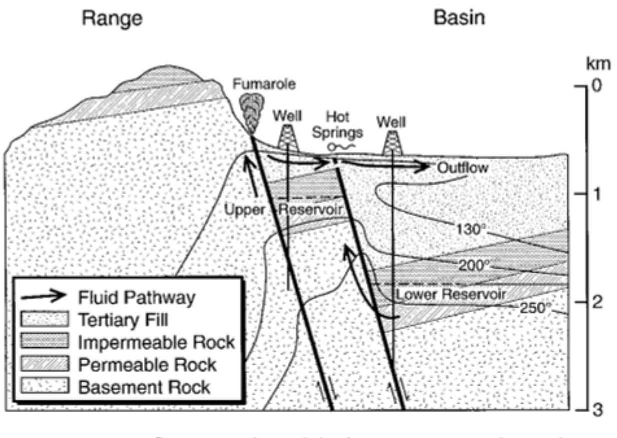
Range
Basin
km
0
1
2
3
Fumarole
Well
Hot
Springs
Well
Outflow
Upper Reservoir
130°
200°
Lower Reservoir
250°
Fluid Pathway
Tertiary Fill
Impermeable Rock
Permeable Rock
Basement Rock

FIGURE 4 Conceptual model of a tectonic geothermal system hosted in an extensional environment. Fault density and displacement vary tremendously from site to site. Fumaroles are absent in lower temperature systems. Temperatures in °C.

usually 1.5 to 3 times greater than normal heat flow. Basins form as a result of crustal extension and fill with low conductivity sedimentary deposits that enhance regional thermal gradients; 50 to 75°C/km is not uncommon. Deeply circulating groundwaters entering the graben form reservoirs at favorable stratigraphic horizons in down-faulted blocks. Fluid chemistry is dictated almost exclusively by rock–water interactions and temperature. Heated fluids rise buoyantly, usually along faults. Fumaroles may form along the fault traces that serve as upflow zones in hotter tectonic systems. Hydrothermal outflow plumes usually form in near-surface permeable sediments or fractured bedrocks. This generalized model describes many features of the Dixie Valley (Basin and Range Province, USA) and Platanares (back-arc environment near triple junction, Honduras) geothermal systems. Major faults with impressive displacements control the location of the preceding examples, but virtually any deep fault may act as a conduit for upwelling thermal waters (Fuzhou, China). Tectonic geothermal systems of varied geologic configuration and temperature occur throughout the world.

C. Vapor-Dominated Systems

A generalized diagram describing conditions within a vapor-dominated geothermal system is shown in Fig. 5a. Relatively impermeable cap rocks locally saturated with shallow groundwater provide a lid over a reservoir in which steam is the continuous phase in open cracks, fractures, and faults. Liquid water fills intergranular pore spaces in the rock, particularly within fine dissolution cavities in veins and veinlets. Surface features consist of fumaroles and acid hot springs. Fluid temperature and pressure (*T* and *P*) increase normally with depth in the impermeable cap. However, within the reservoir *T* and *P* are near the maximum enthalpy of "dry" steam (about 240°C and 3.3 MPa) and remain constant with depth until the bottom of the steam zone is penetrated. During production, boiling of interstitial water provides additional vapor and latent heat that enter the well.

This model implies that recharge by cool groundwaters is blocked by impermeable (hydrothermally altered) rocks on the margins as well as at the top of the reservoir. It also implies that a vapor-dominated system

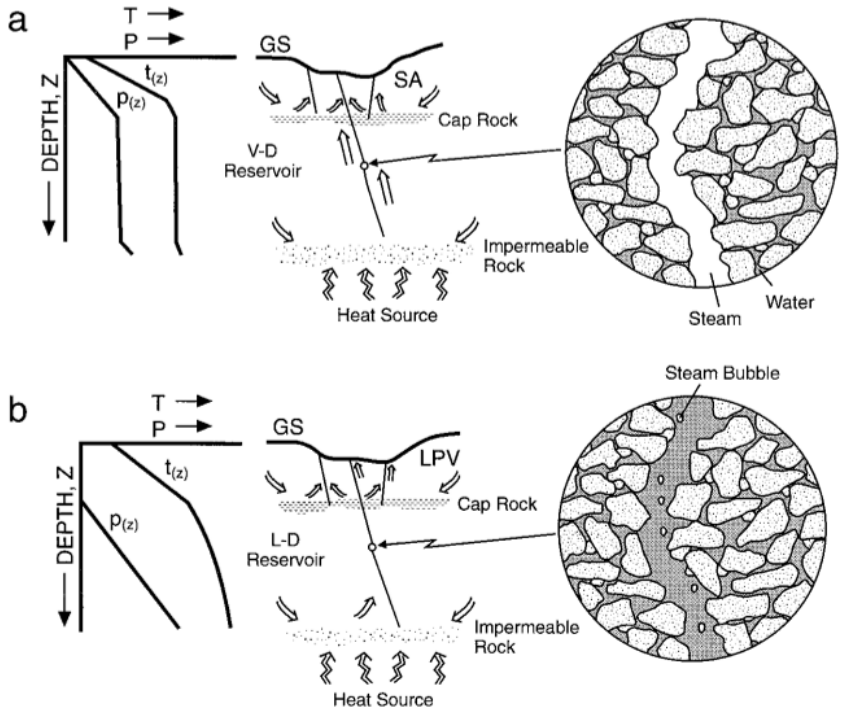

FIGURE 5 (a) Schematic model of conditions in a vapor-dominated system where steam prevails in open fractures but liquid water resides in pore spaces; GS means ground surface, SA means shallow aquifer. (b) Schematic model of conditions in a liquid-dominated geothermal system where liquid water saturates the rock; LPV means low-pressure vapor cap. [Modified from "Geothermal Systems: Principles and Case Histories," Rybach and Muffler, 1981, copyright John Wiley & Sons, Ltd. Reproduced with permission.]

evolves by boiling down of an earlier liquid-dominated reservoir (described later). An alternative mechanism of formation results from descent of the upper surface of the liquid-dominated reservoir as the geohydrology of the system changes by uplift or erosion. Although the "brine" reservoirs that presumably underlie or predate vapor-dominated systems have never been found and sampled, their existence is documented by saline to hypersaline fluid inclusions captured in previously formed vein minerals.

Even though they are not as hot as some systems, vapor-dominated reservoirs are the most prized because, in contrast to liquid-dominated reservoirs, virtually all produced fluid is piped to the power turbines. Only five such systems are known: Larderello (Italy), The Geysers (USA), Matsukawa (Japan), and Kamojang and Darajat (Indonesia). These five fields contain about 35% of the world's geothermal electrical capacity. The Geysers, the world's largest commercial geothermal system, produced a maximum of about 1700 MWe in the mid-1980s but dropped to about 1200 MWe in 1998 because of reservoir depletion.

D. Liquid-Dominated Systems

Most geothermal systems are liquid-dominated. They contain liquid water in all channelways and interstitial pores, although bubbles of steam and gas may be present in the water (Fig. 5b). Groundwater recharge is not as restricted as in the vapor-dominated case, although alteration zones may be extensive. Hot waters from the reservoir commonly leak at the earth's surface. T and P will increase steadily with increasing depth. If the rate of upflow is rapid, boiling springs or geysers will form and temperature changes with depth will closely follow the boiling-point curve.

Many liquid-dominated reservoirs are overlain by a low-pressure vapor zone that may extend hundreds of meters deep (Valles caldera and Lassen, USA). In this case fumaroles and acid hot springs occur at the surface as with true vapor-dominated systems. T rises gradually with depth, however, whereas P remains relatively low. Once the reservoir is encountered, P increases linearly because of the mass of liquid in the reservoir while T remains at or below the boiling point curve.

Liquid-dominated reservoirs have maximum temperatures of ≤370°C and have widely ranging salinities. When fluid is produced by wells, it must be depressurized (flashed) to produce steam for the turbines. This is done under controlled conditions with large steam separators. The basic equation that relates fluid enthalpy, H, to steam fraction, y, is

$$H_r = yH_v + (1 - y)H_l, \tag{3}$$

where H_r is the enthalpy of the reservoir fluid, H_v is the enthalpy of separated steam at separation temperature, and H_l is the enthalpy of separated liquid at separation temperature. Steam tables are used for the calculations. For a well at 250°C supplying fluid to a separator set at 170°C, $y = 0.179$, and 17.9% by mass of the produced fluid becomes steam. A separator receiving 800,000 kg/hour of fluid will produce 143,000 kg/hour of steam at 0.79 MPa absolute, which is piped to the power plant. The remaining 82% of the fluid is liquid water that must be disposed of in some manner, usually by reinjection. A well supplying 350°C fluid to the same separator yields $y = 0.464$ and produces more than double the amount of steam. As steam separates, noncondensible gases such as CO_2, H_2S, and NH_3 partition into the steam phase while the residual brine becomes more concentrated in most chemical species.

V. GEOTHERMAL FLUID CHARACTERISTICS AND DEPOSITS

Geothermal fluids display wide variations in chemical and isotopic composition that reflect their evolution. Fluid composition may dictate the type of power scheme that is eventually designed to utilize a particular resource. Waste fluids generally contain constituents that can have adverse impacts on the environment if not disposed of properly. Some geothermal fluids contain valuable minerals or metals that are sold as by-products of energy utilization. Thus, knowledge of fluid characteristics is important to geothermal development and has applications to understanding volcanic-hosted ore deposits.

A. Gas Chemistry

Geothermal gases form during thermal breakdown of volatile-rich components in reservoir rocks, by reactions of circulating fluids with reservoir rocks, by contributions from degassing magma bodies, and by contributions from air-saturated meteoric water. The fluid produced at the well head from a vapor-dominated system

TABLE II Gas Compositions from Selected Vapor-Dominated and Liquid-Dominated Geothermal Systems Compared with Volcanic Gas Compositions (He, Ar, and O_2, if Present, Are Not Reported)[a]

Site	Larderello[b]	The Geysers[c]	Ahuachapán[d]	Wairakei[e]	Cerro Prieto[f]	Dixie Valley[g]	Platanares[h]	Dogger[i]	Galeras[j]	Satsuma I-J[k]
Country	Italy	USA	El Salvador	NZ	Mexico	USA	Honduras	France	Colombia	Japan
Type[l]	YI	YI	YI	YI	YI(TT)	TT	TT	GP	Volcano	Volcano
Res.	Vap-dom	Vap-dom	Liq-dom	Liq-dom	Liq-dom	Liq-dom	Liq-dom	Liq-dom	Magma	Magma
Rocks[m]	Arg/Carb	Arg/Gw/Fel	Volc	Volc	Arg/Ss	Arg/Gab/Carb	Arg/Ss	Carb/Evap	Andesite	Rhyolite
Temp.	240	240	255	260	$\leq$350	250	165	69	360	885
H_2O	98.0	99.4	99.95	99.94	99.26	99.85	99.3	99.98	89.2	97.5
CO_2	94.1	60.4	86.8	91.7	86.1	96.8	85.3	70.2	75.1	15.1
H_2S	1.5	5.73	12.1	4.4	4.43	0.704	1.37	6.4	5.31	1.16
SO_2	—	—	—	—	—	—	—	—	10.8	38.6
NH_3	0.7	6.96	0.7	0.6	0.707	0.911	3.97	nr	0.077	0.000
CH_4	1.1	5.77	0.03	0.9	2.77	0.497	1.39	11.7	0.000	0.000
N_2	0.6	1.37	0.05	1.5	1.17	1.03	7.84	11.6	2.18	0.708
H_2	2.1	19.9	0.126	0.8	4.66	0.018	0.060	0.16	3.09	19.4
HCl	—	—	—	—	—	—	—	—	2.37	21.6
HF	—	—	—	—	—	—	—	—	0.346	3.16
Total (dry)	100.1	100.1	99.8	99.9	99.84	99.96	99.93	100.1	99.27	99.73
T_{gas}	251	254	235	239	283	192	225	137	(426)	(427)

[a] Reservoir and volcano fumarole temperatures in °C; values in mol-% dry gas except H_2O, which is mol-% steam. Parentheses around T_{gas} value mean calculation violates rules of application.

[b] Average of seven production areas.

[c] Average of 10 production wells; some data from high-temperature zone, $\leq$350°C.

[d] Average from steam separators.

[e] Average well; CH_4 includes all hydrocarbons, and N_2 includes Ar.

[f] Average of 35 production wells.

[g] Average of five from steam separators.

[h] Average of four from steam separators.

[i] Average of 35 production wells; H_2O is mol-% of total flow; HS recalculated as H_2S.

[j] Besolima Fumarole, analysis includes 0.4 mol-% O_2 + CO.

[k] Ohachi Oku Fumarole.

[l] YI = young igneous system, TT = tectonic system, GP = geopressured system.

[m] Arg = argillite, shale, mudstone; Carb = carbonate, marl; Evap = evaporite; Fel = silicic intrusive complex; Gab = mafic intrusive complex; Gw = graywacke; Ss = sandstone, conglomerate; Volc = volcanic flows, tuffs, breccias, and sediments.

contains more noncondensible gases by weight than fluid produced from a typical liquid-dominated system because volatile components are preferentially transported with vapor (steam). However, the gas composition in the two types of systems is more or less similar (Table II). Reservoirs hosted in argillaceous rocks produce gases relatively rich in organic-derived components: H_2S, CH_4, NH_3, and N_2. Reservoirs hosted in carbonates or volcanic rocks tend to be richer in CO_2. The proportions of noncondensible components in gas emitted from fumaroles (Fig. 6A) generally resemble those in underlying reservoirs. In contrast to volcanic gases emitted from magma, geothermal gases usually contain more CO_2, less total sulfur, which is invariably in the reduced form (H_2S), rare acid halides, and higher contents of CH_4, NH_3, and N_2.

B. Water Chemistry

Geothermal waters range widely in composition (Table III). Total dissolved solids in high-temperature reservoir fluids ($\geq$150°C) range from about 1000 to >350,000 ppm (more than 10 times seawater). Liquid-dominated reservoir waters tend to be Na–K–Cl fluids (Fig. 6B; see also color insert), or Na–K–Ca–Cl in the very saline cases. Gas analyses indicate that dissolved CO_2 is usually

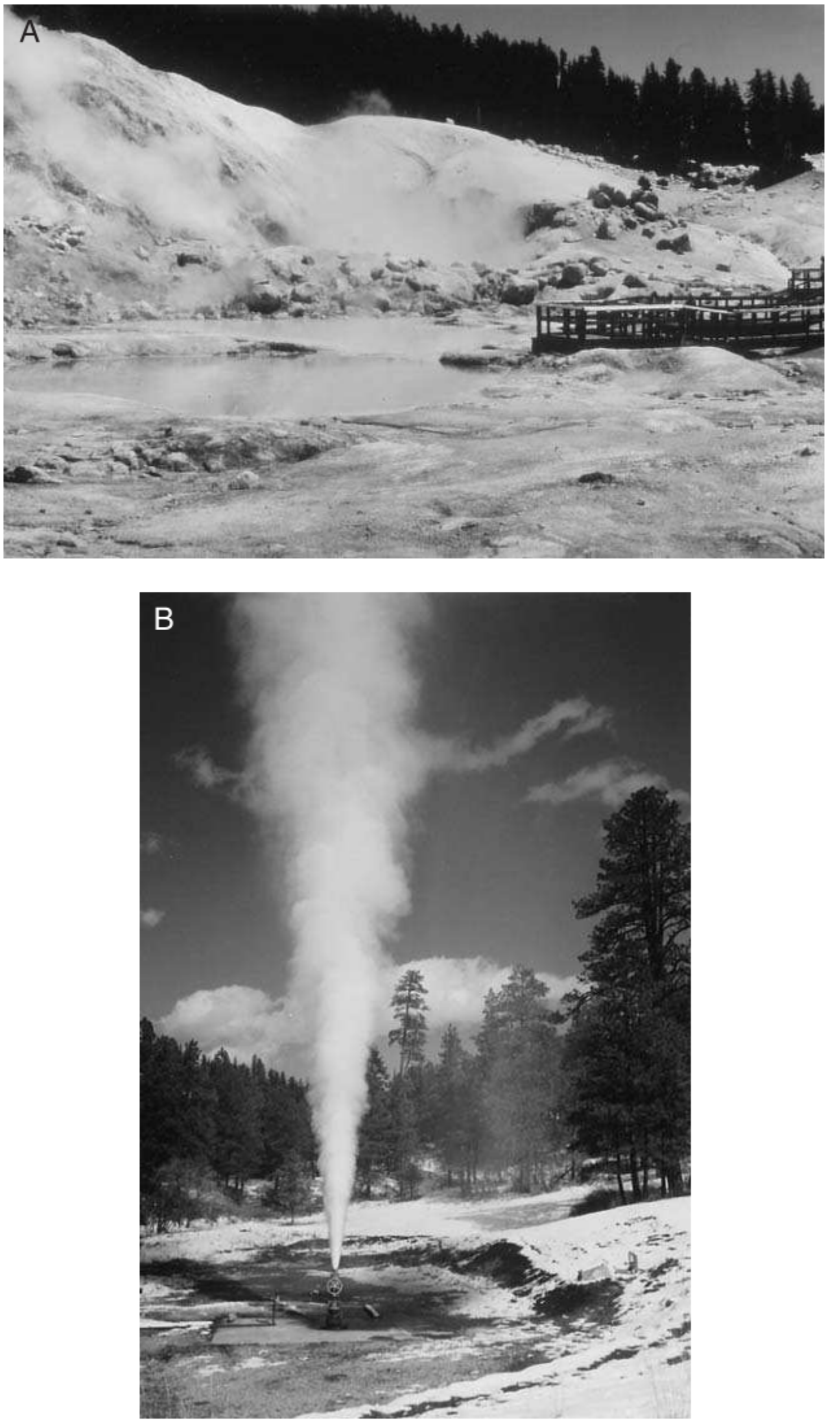

FIGURE 6 (A) Fumaroles, boiling acid-sulfate springs, and acid sublimates create a bleached wasteland at Bumpass Hell, Lassen Volcanic National Park, California. Fumarole temperatures may reach 160°C but are usually near the local boiling point. The pH and sulfate content of some pools are ≤ 1 and $\geq 10{,}000$ ppm, respectively. (B) Neutral-chloride water erupts high in the sky during flow test of well VC-2B, Sulphur Springs, Valles caldera, New Mexico. Average temperature of fluids from production intervals during this test was 225°C, although bottom hole temperature is 295°C at 1762 m. The reservoir pH and chloride content recalculated for steam loss are 6.2 and 3000 ppm, respectively. Wellhead is 2.2 m tall. (See also color insert.)

TABLE III Water Compositions from Liquid-Dominated Geothermal Reservoirs Compared with Acid-Sulfate and Neutral-Chloride Hot Spring Compositions[a]

Site	Ahauchapán[b]	Wairakei[c]	Cerro Prieto[d]	Dixie Valley[e]	Platanares[f]	Lafayette[g]	Dogger[h]	Valles Cal[i]	Y-stone[j]	Dixie Valley[k]
Country	El Salvador	NZ	Mexico	USA	Honduras	USA	France	USA	USA	USA
Type	YI	YI	YI(TT)	TT	TT	GP	GP	YI	YI	TT
Res./Spg	Liq-dom	Liq-dom	Liq-dom	Liq-dom	Liq-dom	Liq-dom	Liq-dom	Acid-sulf	Neu-chl	Neu-chl
Rocks	Volc	Volc	Arg/Ss	Arg/Gab	Arg/Ss	Arg/Ss	Carb/Evap	Volc	Volc	Arg/Gab
Temp	255	260	$\leq$350	250	165	116	64	90	95	82
pH	7.1	8.3	7.5	9.1	8.7	6.7	6.4	1.4	9.1	8.0
SiO_2	537	625	833	599	248	68	34	168	411	105
As	11.3	4.6	1.2	0.49	0.85	—	—	0.04	—	0.004
B	151	28.9	31.3	10.8	13.8	44	11	0.2	4.49	0.96
Na	5690	1310	8740	441	272	44,600	5570	18.9	360	194
K	950	212	2150	66.8	33	410	88.4	72	20.7	4.94
Li	17.5	13.5	20.0	2.15	3.45	9.9	2.2	0.17	5.45	0.42
Ca	443	19	401	8.28	8.0	5240	720	131	0.5	11.0
Mg	0.13	0.01	0.38	0.016	0.23	590	226	50	0.01	0.12
HCO_3	34.2	28.2	45	212	496	780	350	0	190	94
SO_4	34.0	35	4.6	198	201	91	770	6400	25.0	139
F	1.5	7.8	3.3	14.5	10.6	1.0	4.0	5.2	27.5	11.1
Cl	10,430	2205	16,530	481	29.0	80,400	9870	$<$1	425	161
Br	43.9	5.7	46.1	0.38	—	153	56	$<$0.4	—	0.28
TDS	18,340	4995	28,810	2034	1316	132,400	17,700	6845	1470	722
T_{Qtz}	259	274	351[l]	269	195	117	85	(168)	235	140
$T_{Na/K}$	265	262	309	255	234	73	98	(1076)	174	122
$T_{Na\text{-}K\text{-}Ca}$	254	254	298	234	210	113	121	(385)	147	123

[a] Reservoir or spring temperatures in °C; other values in ppm. Reservoir analyses are not reconstructed for steam loss and do not include separated gases. Parentheses around geothermometer calculations mean that rules of application are violated. Abbreviations same as Table II.

[b] Average of nine production wells.

[c] Average of three production wells.

[d] Average of 35 production wells.

[e] Average from two steam separators.

[f] PLTG-3 exploration hole.

[g] Average of 10 production wells.

[h] Average of 21 production wells.

[i] Women's Bathhouse Spring.

[j] Giantess Geyser.

[k] Dixie Hot Spring.

[l] Equation for 0 to 330°C used (in D'Amore, 1991); other calculations based on equations in text.

the next major component. Divalent cation contents, particularly Mg, tend to be low because of inverse solubility of carbonates and sulfates with temperature. Silica levels and contents of trace elements As, B, Br, and Li are relatively high compared to most other groundwaters. The pH generally lies between 6 and 9, although extremely saline fluids may be more acidic. The chemistry of these fluids is dictated by temperature, reactions with reservoir rocks, volume of water relative to rock, residence time of water, and contributions of components from outside sources (cold groundwater, seawater, magma, etc.).

Neutral-chloride spring and geyser waters usually resemble their parent reservoir fluids. These fluids may be modified during flow to the surface by chemical reactions with wall rocks, by dilution with near-surface groundwaters of various types, or by boiling. Such waters are often oversaturated with silica or carbonates at surface conditions and form deposits of sinter or travertine, respectively.

Acid-sulfate springs form where rising steam and volatile compounds condense into near-surface groundwaters, and H_2S that is carried in the steam is oxidized to form sulfuric acid (Fig. 6a). Additional components are added during acid dissolution of near-surface rocks.

Acid-sulfate fluids are comparitively rich in divalent and trivalent cations and low in Na, K, Cl and most trace elements. Sulfur, acid sublimates, and clays are often deposited.

C. Chemical Geothermometers

By the 1960s several researchers had noted the temperature-dependent concentrations of some chemical species in geothermal fluids and were applying these relations to exploration and reservoir development. Chemical geothermometers are of two general types: (1) based on absolute concentrations of a constituent in solution, and (2) based on ratios of two or more constituents in solution. The temperature dependence of some chemical geothermometers has been calibrated by laboratory experiments under ideal conditions, while other geothermometers are based on empirical relations involving many fluids produced from different geothermal fields where reservoir temperatures are known. The solubility of silica polymorphs (quartz, chalcedony, cristobalite, etc.) in pure water as a function of temperature represents the prime example of a laboratory-calibrated geothermometer. Unique equations describe the solubility of each polymorph. In the second type, one or more chemical ratios (usually cation ratios) from production fluids and associated hot spring fluids are plotted against the inverse of reservoir temperature and a linear regression of the data defines the temperature dependence.

Many geothermometers have been developed and refined over the years to meet specific conditions. Four widely used geothermometer equations and their restrictions are as follows.

Quartz conductive:

$$T = \frac{1309}{5.19 - \log \mathrm{SiO_2}} - 273.15$$

$$(T = 150\text{–}250°\mathrm{C}) \tag{4}$$

Na/K:

$$T = \frac{1217}{\log(\mathrm{Na/K}) + 1.483} - 273.15$$

$$(T = >150°\mathrm{C}) \tag{5}$$

Na–K–Ca:

$$T = \frac{1647}{\log(\mathrm{Na/K}) + \frac{1}{3}[\log(\mathrm{Ca^{1/2}/Na}) + 2.06] + 2.47} - 273.15$$

$$(T = >100°\mathrm{C}) \tag{6}$$

Gas:

$$T = \frac{24775}{2\log\alpha - 6\log\beta - 3\log\gamma - 7\log(P_{\mathrm{CO_2}}) + 36.05} - 273.15, \tag{7}$$

$$\text{where } \alpha = \frac{\mathrm{CH_4}}{\mathrm{CO_2}}, \beta = \frac{\mathrm{H_2}}{\mathrm{CO_2}}, \gamma = \frac{\mathrm{H_2S}}{\mathrm{CO_2}}, \text{ and}$$

$$P_{\mathrm{CO_2}} = \begin{array}{l} 0.1, \text{ if } \mathrm{CO_2} < 75 \\ 1.0, \text{ if } \mathrm{CO_2} > 75, \text{ and } \mathrm{CH_4} < 2\mathrm{H_2} \text{ or } \mathrm{H_2S} < 2\mathrm{H_2} \\ 10, \text{ if } \mathrm{CO_2} > 75, \text{ and } \mathrm{CH_4} > 2\mathrm{H_2} \text{ and } \mathrm{H_2S} > 2\mathrm{H_2} \end{array}$$

Concentrations are in ppm except gas compositions (mol-%), and T is °C. Calculated subsurface equilibration temperatures for fluids from selected wells and thermal manifestations are listed beneath the analyses in Tables II and III. The empirical geothermometers yield excellent results for reservoirs in young igneous systems because these hotter reservoirs have provided most of the data for the regressions. The geothermometers are less reliable for tectonic or geopressured systems of lower reservoir temperature, particularly with fluids of high Mg content. The preceding geothermometers are not applicable for volcanic gas condensates, acid-sulfate waters, and many sedimentary basin brines.

Application of geothermometer calculations has many potential pitfalls during exploration, mostly because fluid compositions can change during flow from the reservoir to the surface. Dilution, mixing, boiling, precipitation, and other reactions can modify original fluid chemistry as temperature declines during upflow. Also, many waters (e.g., soda water and fossil seawater) that achieve their initial compositions by reactions at low to moderate temperatures yield spurious calculated higher temperatures. Although several schemes exist to evaluate such processes, independent indicators of high temperature should always be sought. For example, presence of $\mathrm{H_2S}$-rich gases, widespread distribution of boiling Cl-rich springs, and spring deposits of sinter ($\mathrm{SiO_2}$) usually indicate that a reservoir of ≥150°C lies at depth.

D. Water Origins and System Ages

Although the hottest geothermal systems are obviously associated with magmatism, isotopic studies show that the water itself is derived primarily from ancient to modern precipitation (Fig. 7). Other systems contain recycled seawater, fossil seawater and variants, and metamorphic waters (waters released during metamorphism). Positive recognition of magmatic water in geothermal systems was made after studying fluids emitted from active volcanoes. In such systems, the magmatic contri-

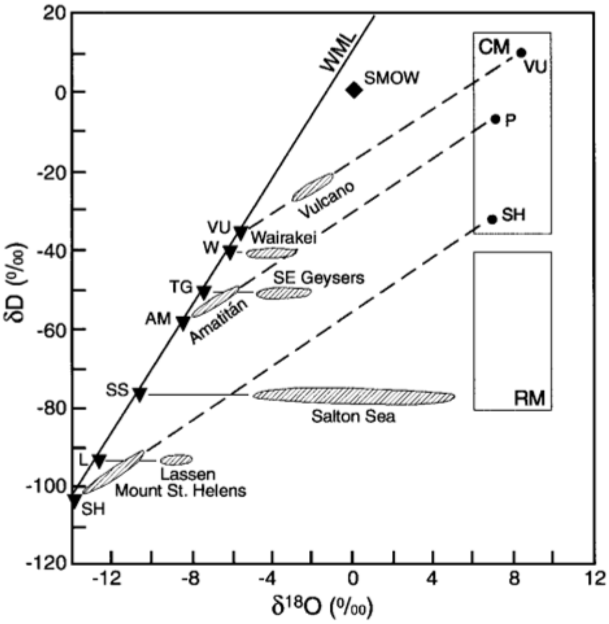

FIGURE 7 Plot of deuterium (δD) versus oxygen-18 (δ^{18}O) for meteoric waters (inverted triangles) and reservoir fluids (clouds) at selected geothermal systems (values in permil relative to Standard Mean Ocean Water, SMOW). Virtually all rocks are isotopically enriched in ^{18}O compared to most waters. Geothermal systems such as Wairakei, The Geysers, Salton Sea, and Lassen contain meteoric waters isotopically enriched in oxygen-18 because of high-temperature rock–water isotopic exchange. Systems such as Vulcano, Amatitlán, and Mount St. Helens contain mixtures of meteoric and magmatic waters (dots). WML is the world meteoric line for precipitation. CM is the box for convergent margin (subduction zone) magmatic waters whereas RM is the box for residual magmatic waters in intrusive bodies. Other labels identified in Fig. 1.

bution is usually <15% of the bulk reservoir fluid, although rare systems may contain as much as 40%.

Tritium, ^{14}C, and ^{36}Cl studies show that geothermal reservoir waters are usually older than 1,000 yr, commonly older than 10,000 yr, and rarely older than 100,000 yr. Hot springs derived from reservoir fluids sometimes contain younger water due to mixing with near-surface groundwaters.

Lifetimes of geothermal systems are dated from studies of alteration minerals and veins, spring deposits, and geologic relations. Systems such as Valles caldera have been continuously active for the last 1 million years even though the present reservoir is not large. Systems found in many arc volcanoes can be no older than the volcanic edifice, often <100,000 yr. Volcanic eruptions can create rapid changes in young igneous systems. For example, the present hydrothermal system at Mount St. Helens (≤175°C) formed after the eruptions of 1980. Lifetimes of most tectonic systems are poorly studied although some are >1 million years based on dated spring deposits. Large geopressured systems are probably ≫1 million years because of slow burial and pressurization of the reservoir strata.

E. Hydrothermal Alteration and Mineral Deposits

Detailed studies of rocks and drill cores from many geothermal systems reveal alteration mineral and vein assemblages, and precious- and base-metal precipitates that resemble those in epithermal ore deposits. Common assemblages in 150 to 350°C reservoirs include quartz, calcite, illite, chlorite, adularia, ± epidote, ± anhydrite, and ± wairakite. Fluids and fluid inclusions in active systems have similar ranges in formation temperatures and salinity as fluid inclusions found in ancient deposits. Most exploited geothermal fluids contain reduced sulfur species and precipitate common sulfide minerals (pyrite, pyrrhotite, galena, sphalerite, chalcopyrite, etc.) found in many ore deposits.

Although the deeper portions of geothermal systems are too hot to mine, near-surface manifestations are accessible. CO_2-rich (soda) waters are bottled for public consumption at many hot and mineral spring areas, and CO_2 gas is compressed for industrial processing. Onyx and travertine deposits ($CaCO_3$) are often mined for decorative stone. SiO_2, CO_2, S, B, and NH_4 compounds were mined at Larderello fumaroles until recently. S is commonly mined from acid-sulfate zones and is recovered as a by-product from several geothermal power plants. Hg was mined from hot spring areas east of The Geysers as recently as the 1950s, and Au and Hg at ppm levels occur in mucks around some alkaline hot springs in nearby mining districts. Sinter deposits and wellbore precipitates at some geothermal systems contain Au, Ag, Hg, Sb, and other metals. Ag-rich deposits from pipelines are recovered and sold at the Salton Sea field (USA). Sulfide precipitates at Oku-aizu field (Japan) contain ≤115 ppm Au, ≤3.5 wt-% Ag and common base metals. Salton Sea brines contain surprisingly high levels of Zn, Pb, and Mn (≤550, ≤110, and ≤1200 ppm, respectively). Similar metals are found in brines from Fushime system (Japan). Sub-ore grade MoS_2 (≤0.5 wt-%) and less abundant base metals are found in a shallow sector of the Valles caldera system. B and Cu as tourmaline and chalcopyrite are locally rich in metamorphosed rocks bordering the intrusive body beneath The Geysers. Borosilicates are also found deep within the Larderello reservoir.

VI. GEOTHERMAL DEVELOPMENT

A. Exploration

The primary objective of exploration is to discover reservoirs of steam or hot water that can sustain commercial development. Statistically, about 70% of geothermal areas with boiling features will host exploitable systems. Thus, regional exploration strategies initially focus on known areas of hot spring and fumarole activity or known areas of hot aquifers. First efforts are to evaluate young volcanic centers, delineate major geologic structures, assess regional heat flow, and calculate subsurface reservoir temperatures from the geochemistry of fluid samples (Tables II and III; see Table IV). Once prospective targets are chosen, exploration involves a more detailed approach to determine the age and structure of the reservoir rocks, a possible depth to the reservoir, fluid characteristics and pathways, and a conceptual model of the system. The model is then tested by drilling, which primarily confirms the presence (or absence) of a reservoir and its temperature.

Exploration drilling usually requires one to five holes that penetrate to depths of ≤1.5 km, depending on budget, knowledge gained and problems encountered during drilling, and the success of the first hole(s). Geophysical logs provide temperature–depth profiles, water levels, formation pressures, production zones, and other information. Cores provide details on stratigraphy, alteration mineralogy and history, fracture patterns, and porosity of the rocks. If high-temperature fluids are encountered, flow tests may be conducted to determine preliminary reservoir parameters. Fluid analyses establish background conditions, assess potential environmental impacts, and evaluate corrosion and precipitation properties. Surface and subsurface studies are then combined to formulate a model of the geothermal system. Model results are used to create an economic field-development strategy, which is used to obtain financing for production drilling and eventual exploitation of the resource. The entire exploration process at a given site should take no more than 1 to 3 years but has been known to take more than 10 years at some prospects because of various technical, economic, and political factors.

TABLE IV Principal Methods Used During Geothermal Exploration

- I. Geology
  - A. Geologic mapping of stratigraphy and structure
  - B. Remote sensing of thermal/geochemical variations
  - C. Photogeology of structure/fractures
  - D. Detailed maps of thermal areas
  - E. Hydrothermal alteration maps
- II. Volcanology
  - A. Age dates and petrology/geochemistry of units
  - B. Analysis of eruptive style, eruptive volumes, eruption temperatures
  - C. Evaluation of magma chamber depth, shape, volume, heat content
  - D. Hazards assessment at active volcanoes
- III. Hydrogeochemistry
  - A. Water and gas chemistry; calculation of chemical geothermometers
  - B. Stable isotope analyses; fluid sources and geohydrology
  - C. Radioisotope analyses for fluid ages
  - D. Gas flux measurements to determine fluid pathways
- IV. Geophysics
  - A. Temperature-gradient and heat-flow studies; define magnitude and extent of prospects
  - B. Gravity studies to locate structures, fault offsets, depth to magma bodies
  - C. Passive seismic studies to define major structure, subsidence, and location of magma
  - D. Active seismic studies to define stratigraphy and structure; location of magma
  - E. Electrical methods to define limits of potential reservoir, subsurface alteration, faults
  - F. Magnetics to define structure and depth to magma bodies
- V. Exploration holes (core or rotary)
  - A. Stratigraphy and fracture analysis
  - B. Temperature and other geophysical logs
  - C. Flow tests; geochemical sampling and analyses; injection tests
  - D. Physical property measurements of core/cuttings
  - E. Alteration and vein studies of core/cuttings

B. Production

Geothermal systems that enter the development stage are called geothermal fields. Governments or private companies acquire ownership or development rights to the land necessary for drilling wells, creating infrastructure, and building power plants. Depending on technical feasibility, financial restrictions, and other factors, the initial development plan determines how much power should be installed in a first phase. Large-diameter (20 to 60 cm) production wells are drilled to intersect fluid-producing fractures or stratigraphic horizons within the zone identified as the reservoir. As each well is completed, it is tested to determine fluid enthalpy, mass-flow rate, pressure declines, permeability thickness, and other parameters. Some wells are discharged simultaneously for an extended period to determine interference characteristics. After the first phase of development generates power, the field may be expanded in blocks (if economically feasible) in which additional wells are drilled to sustain more plants.

Of about 80 drilled geothermal fields, the mean installed capacity is roughly 100 MWe (Table I) and the mean reservoir temperature is 250 ± 40°C. The present cost of a 55 MWe geothermal project including exploration, wells, infrastructure, and plant is about US$110 million or about US$2 million/MWe with an expected lifetime of 25 yr. Some fields have existed for >30 yr. Mean development time after exploration is 6 to 7 yr.

C. Power Generation

Basic plant designs for vapor- and liquid-dominated reservoirs are shown in Fig. 8. As mentioned earlier, vapor-dominated reservoirs are the most desirable because all produced fluid is steam that can be sent to the turbines with minor treatment. In 1998, after 40 yr of exploitation, typical wells in The Geysers field produced steam with enthalpies of 2800 kJ/kg at flow rates (F_v) of about 45,000 kg/hour. Neglecting conversion efficiency, available power, P, is approximately

$$P = F_v \, \Delta H, \tag{8}$$

where ΔH is the enthalpy difference between production steam and ambient steam. Assuming the latter occurs at $T = 25°C$, average power production at The Geysers is about 3 to 4 MW/well gross. Wells at Kamojang produce about 5 MW/well, whereas wells at Darajat produce roughly 15 MW/well. About 20% of the fluid mass is injected back into the reservoir after passing through the condensers. The remaining fluid enters the atmosphere from the condensers.

Liquid-dominated reservoirs above 200°C require steam separation to flash (boil) the fluid at conditions providing the maximum mass of steam at optimum pressure to drive the turbines. Wells cumulatively producing 800,000 kg/hour at 17.9% flash will yield 143,000 kg/hour steam at 170°C and 0.79 MPa at the separator (described above), producing about 10 MW gross. Typical wells produce 5 MW although rare wells will produce more than 30 MW. About 657,000 kg/hour of spent brine must be disposed, preferably by injection. Production and injection fluids are sometimes diluted with sur-

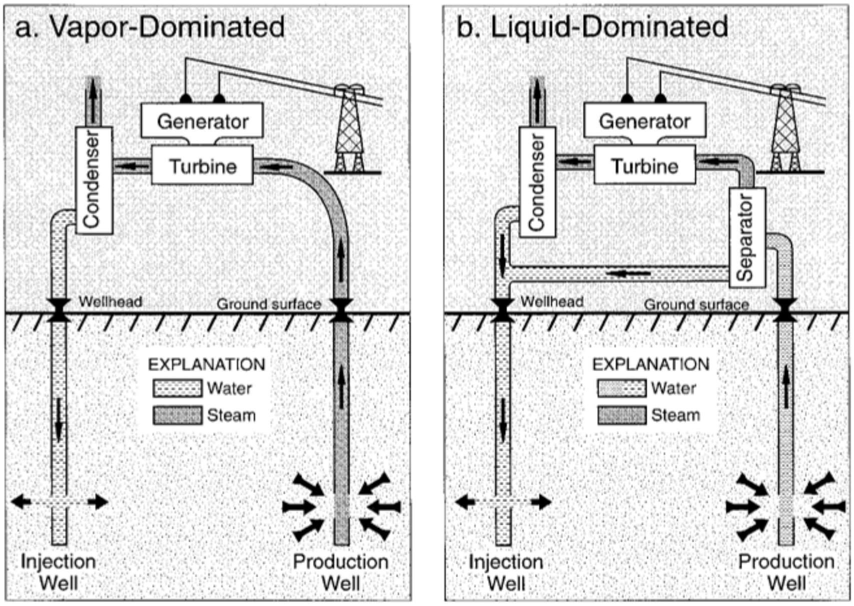

FIGURE 8 Diagrams showing power generation schemes for (a) vapor- and (b) liquid-dominated geothermal reservoirs.

face water or treated with chemicals to prevent or retard mineral encrustation and corrosion of wells, pipelines, and turbines. These methods are occasionally futile, requiring intermittent mechanical reaming of pipes and wells and replacement of turbine parts.

Reservoirs with temperatures below 200°C are often exploited with binary cycle power plants that use heat exchangers and organic working fluids to extract heat. For example, binary plants at Long Valley Caldera and Steamboat Hills (USA) use isobutane as the working fluid to extract heat from reservoirs at 170 to 175°C. One advantage of binary plants is that the production fluid is circulated under pressure without flashing, which prevents gas release and precipitation/corrosion problems. Although binary plants generate less power per unit mass of consumed fluid because of lower enthalpy, they are becoming more common for power production as technology improves. Binary cycles are often added to older flash plants to capture additional energy from waste fluids.

Power plant size depends on many variables including the need for immediate cash flow. Well-head generators can be placed on single wells to immediately produce as little as 500 kWe, but these installations are very inefficient. Large plants in well-established fields produce as much as 130 MWe, although 55 MWe plants are more typical.

D. Decline

Geothermal resources are not limitless, although they are often classified as "renewable" resources. With time, power output drops at most fields as reservoir pressures decline due to withdrawal of fluid. For example, average flow rates of wells supplying steam to NCPA Plant 1 in the southeast sector of The Geysers dropped anywhere from 7 to 24% annually during 1982 to 1990. During this period, average wellhead pressures dropped more than 50%. Additional steam was provided to the plants by drilling make-up wells within the producing block, but eventually this strategy was ineffective to maintain the total installed capacity of the plant. A new strategy injects treated waste waters from nearby towns to help increase reservoir pressure.

Long-term (>30 yr) sustainable power production requires a balance between fluid production rates and natural recharge of the reservoir. Injection of fluids from power plants and other sources, usually around the margins of the field, helps maintain this balance. However, many geothermal fields have multiple operators or other economic characteristics that create financial incentives conflicting with sustainable production.

E. Nonelectrical Uses

Few high-temperature systems are developed for nonelectrical uses. A noteworthy exception is Kawerau geothermal field (NZ), in which ≤280°C fluid generates electricity, strips bark from logs, runs mechanical equipment, provides silica, and dries paper at a large mill. Reservoirs with temperatures less than 130°C are usually not practical for electrical generation, even at high flow rates. The most common direct-use applications for intermediate- to low-temperature geothermal fluids are spas and health resorts, space heating, greenhousing, and fish/reptile farming. Fluids above 60°C can be used in many industrial applications (preheating, spraying, steaming, pasteurizing, deicing, and sterilizing). More specialized applications include fruit/vegetable drying, refrigeration, fermentation and distillation of alcohol, mushroom growing, advanced oil recovery, and heap-leach mining.

F. Monitoring

Reservoir characteristics, besides those relating directly to power utilization, are also monitored during production. These may include seismic monitoring, measurements of emissions to the atmosphere or groundwater, temporal changes in fluid chemistry and heat content of production fluids, and any changes in the behavior of thermal features, faults, landforms, streams, and nearby volcanoes. The data are used for legal, economic, environmental, safety, and scientific purposes.

VII. ENVIRONMENTAL AND SAFETY ISSUES

Geothermal power plants release much less CO_2 to the atmosphere than fossil-fuel burning plants (≤7% of the total released by an equivalent gas-fired plant). Although geothermal energy is environmentally a relatively benign resource, there are many impacts that occur during development. Any large-scale construction and drilling operation will produce visual impacts on the landscape, create noise and wastes, and affect local economies.

Many countries have strict environmental regulations regarding some impacts, whereas others do not. The following list of common issues (with example sites mentioned) is usually addressed during the development stages at geothermal fields.

1. *H_2S pollution of atmosphere.* H_2S is a noxious gas that is immediately dangerous to life and health (IDLH) at levels above 142 mgm^{-3} of air. During the early development years at The Geysers (pre-1975), there were many complaints about the odor from H_2S that was released by power plants. Since then, H_2S abatement systems have virtually eliminated this problem. About 1.5 t/day S is now scrubbed from a typical 55 MWe power plant at The Geysers and is usually sold for agricultural purposes. However, some developing countries have casual regulations on H_2S pollution and no installed abatement systems. As a result, air quality at some power plants is obnoxious if not hazardous.
2. *Brine pollution of groundwater.* Spent brine from liquid-dominated systems commonly contains excessive quantities of As, B, Cl, SiO_2, and other compounds with potential risks to humans, livestock, and crops. Many brines are considered toxic wastes in most developed countries and must be treated or disposed of to render them harmless. Because of obvious economic advantages, most producing fields inject the brine to help maintain reservoir fluid volume and pressure. However, there are fields where spent brine has been dumped into nearby streams or the ocean (Tiwi, Philippines; Ahuachapán). In some countries, brines produced during flow tests of new wells are dumped on the ground or into local streams, contaminating shallow groundwater systems. Usually, considerable dilution with cool near-surface waters brings the concentrations of contaminants down to acceptable levels.
3. *Hydrothermal explosions.* Many geothermal fields contain shallow vapor-rich caps that will occasionally exceed lithostatic pressure and periodically explode. In some geothermal systems, production of reservoir fluids has caused subsurface pressures to decrease, thereby inducing boiling and increasing fumarolic activity. Commonly, hydrothermal explosion craters form where fumaroles and acid springs already exist, attesting that these explosions are sometimes induced by natural processes. Ancient hydrothermal explosion craters often pock-mark portions of geothermal systems (Rotokawa, NZ). These areas may make poor drill pads and construction sites due to potentially acid conditions and unstable ground. However, it is not unusual for local inhabitants in underdeveloped countries to build houses around such areas because the natural heat flow reduces heating costs and the hot springs are used for cooking. On rare occasions hydrothermal explosions near geothermal fields have killed people and collapsed buildings during unexpected showers of hot mud, steam, and rock (Ahuachapán).
4. *Landslides.* Many geothermal fields are located in volcanic and tectonic terrains having high relief and rainfall. Because thermal fluids react with the host rocks to produce clays, silica residues, and other alteration products, much of the ground on the slopes above some geothermal systems is unstable. Ancient and modern landslides are common features of many systems (The Geysers). Landslides are often attractive building sites because they produce flat areas. However, landslides in geothermal fields have destroyed roads and infrastructure, have cracked geothermal well casings due to creep, have decapitated wells causing "blow-outs," and have buried inhabitants during sudden collapse (Zunil, Guatemala).
5. *Reservoir interference, depletion, subsidence, and induced seismicity.* Long-term production of geothermal fluids can affect some production wells by drawing cooler water in from the margins of the system (Cerro Prieto). Thermal features such as hot springs, fumaroles, and geysers may cool down or cease as reservoir pressures and overlying water levels decrease and as cold groundwaters mix with reservoir fluids (Rotorua and Ohaaki, NZ). Extensive removal of reservoir fluids may initiate ground subsidence (Wairakei and Ohaki). Usually the subsidence is differential and causes damage to roads and rare damage to wells and buildings. Major subsidence can eventually produce microseismicity and local faulting. Fluid injection often induces seismic activity within and near the margins of the reservoir.
6. *Earthquakes and volcanic hazards.* Most high-temperature geothermal systems are found in tectonically active regions where historic earthquakes and fault displacements have occurred (Dixie Valley). Buildings must be constructed to withstand reasonable levels of ground shaking in worst-case scenarios. Some geothermal fields are located on the flanks of historically active volcanoes (Kilauea, USA). Eruptive style and eruption frequency of nearby volcanoes must be evaluated before power plants and infrastructure are constructed in hazardous locations.

VIII. SUMMARY

Geothermal systems occur wherever reservoirs of hot water and steam exist at comparatively shallow depths.

High-temperature systems most commonly exist near volcanic and tectonically active regions of the Earth. Although magma bodies may contain immense quantities of heat, convection of groundwater brings heat toward the surface much more effectively than conduction of heat through rock. Geothermal fluids are different from magmatic fluids because of their lower temperature, lower content of acid volatiles, equilibration in various near-surface rocks, and high content of meteoric water or other groundwater/seawater. Lifetimes of some geothermal systems exceed 1 million years and some systems are presently forming ore deposits. The geologic, hydrogeochemical, and geophysical characteristics of convecting geothermal fluids, their reservoirs, and their heat sources form the basis of geothermal exploration methods and development models. Commercial geothermal fields produce electricity by piping extracted hot fluids from wells to turbine-driven generators. Nonelectrical applications continue to increase, but spas, space heating, greenhousing, and aquaculture remain the prime uses. Like many other energy resources, geothermal systems are depletable and have a unique set of environmental and safety characteristics. Proactive measures to mitigate potential environmental problems are beneficial to the long-term health and financial well-being of commercial developments. Worldwide geothermal energy utilization increases yearly because it is an attractive alternative to burning imported and domestic fossil fuel resources.

ACKNOWLEDGMENTS

Table I data provided by J. Lund, Oregon Institute of Technology. Reviewers were D. Bergfeld (Los Alamos National Laboratory), R. O. Fournier (Geothermal Consultant), J. Lowenstern and M. Sorey (U.S. Geological Survey), and D. Sussman (Union Geothermal Co.). Partial funding for Goff and Janik came from the U.S. Dept. of Energy, Office of Geothermal Technologies.

SEE ALSO THE FOLLOWING ARTICLES

Calderas • Exploitation of Geothermal Resources • Magma Chambers • Migration of Melt • Surface Manifestations of Geothermal Systems

FURTHER READING

Barbier, E., Frye, G., Iglesias, E., and Pálmason, G. (1995). "Proceedings of the World Geothermal Congress, 1995," Vols. 1 to 5. International Geothermal Association, Inc., Auckland, New Zealand.

Clemente, W. C., and Villadolid-Abrigo, F. L. (1993). The Bulalo geothermal field, Philippines: Reservoir characterization and response to production. *Geothermics* **22,** 381–394.

D'Amore, F., ed. (1991). "Application of Geochemistry in Geothermal Reservoir Development: Series of Technical Guides on the Use of Geothermal Energy." UNITAR/UNDP Centre on Small Energy Resources, Rome.

DiPippo, R. (1980). "Geothermal Energy as a Source of Electric Power," U.S. Government Printing Office, Washington, DC.

Duffield, W. A., Sass, J. H., and Sorey, M. L. (1994). "Tapping the Earth's Natural Heat," U.S. Geological Survey Circ. 1125.

Enedy, S., Grande, M., and Smith, J. L. B. (1990). A case history of steamfield development, reservoir evaluation, and power generation in the southeast Geysers. *Geothermal Resources Council Bull.* **19,** 232–248.

Giggenbach, W. F. (1992). Isotopic shifts in waters from geothermal and volcanic systems along convergent plate boundaries and their origin. *Earth Planet. Sci. Lett.* **113,** 495–510.

Goff, F., and Gardner, J. N. (1994). Evolution of a mineralized geothermal system, Valles caldera, New Mexico. *Econ. Geology* **89,** 1803–1832.

Grant, M. A. (1996). "Geothermal Resource Management," Geothermal Energy New Zealand, Ltd., Auckland, New Zealand.

Henley, R. W., and Ellis, A. J. (1983). Geothermal systems ancient and modern: A geochemical review. *Earth-Sci. Rev.* **19,** 1–50.

Hunt, T. M., and Scott, B. J. (1998). Recovery of natural thermal features after field testing: NZ examples. *Geothermal Resources Council Trans.* **22,** 49–54.

Janik, C. J., Truesdell, A. H., Goff, F., Shevenell, L., Stallard, M. L., Trujillo, P. E., and Counce, D. (1991). A geochemical model of the Platanares geothermal system, Honduras. *J. Volcanol. Geotherm. Res.* **45,** 125–146.

Lovekin, J. W. (1998). Sustainable geothermal power: The life cycle of a geothermal field. *Geothermal Resources Council Trans.* **22,** 515–519.

Rybach, L., and Muffler, L. J. P., eds. (1981). "Geothermal Systems: Principles and Case Histories." Wiley, New York.

White, D. E., Muffler, L. J. P., and Truesdell, A. H. (1971). Vapor-dominated hydrothermal systems compared with hot-water systems. *Econ. Geology* **66,** 75–97.

SURFACE MANIFESTATIONS OF GEOTHERMAL SYSTEMS WITH VOLCANIC HEAT SOURCES

MANFRED P. HOCHSTEIN
PATRICK R. L. BROWNE
Geothermal Institute, The University of Auckland

I. Introduction
II. Manifestations of Volcanic Hydrothermal and Affiliated Systems
III. Manifestations of High Temperature Systems
IV. Manifestations of Intermediate and Low Temperature Systems
V. Classification of Manifestations
VI. Surface Alteration and Deposits
VII. Perspectives

GLOSSARY

advection Subsurface movement of groundwater in permeable rocks under the influence of a lateral pressure gradient (from high terrain to a broad valley, for example).

alteration (or hydrothermal alteration) Change in the mineralogical composition of a rock, brought about by the action of hydrothermal fluids. The term includes direct deposition of secondary minerals as veins or vug fill.

buoyancy A vertical, upwardly directed force caused by the density difference between a hydrostatic column of hot fluid within a geothermal reservoir and an equal column of colder fluid outside it. The resulting fluid movement is called "free convection" or "natural convection."

conduction, convection Modes of heat transfer. Conduction involves transmission of heat in a rock without mass transfer; heat transfer in a permeable rock by convection results from mass (fluid) transfer.

fluids A summary term that describes the phases of the medium convectively transferring heat, i.e., liquid, gas, and their combinations. Liquids may originate from infiltrated ground water ("meteoric" water) or from magma ("magmatic" water). The subsurface gas phase of water is "vapor," but at the surface it is "steam," containing condensate droplets. Gases in hydrothermal systems are usually less reactive (vapor, CO_2, and H_2S) than those in volcanic systems (vapor, HCl, SO_2, HF, for example).

geothermal system A general term that describes natural heat transfer within a confined volume of the Earth's crust where heat is transported from a "heat source" to a "heat sink," usually the free surface.

hydrothermal system A type of geothermal system where heat transfers from a heat source (often a cooling pluton) to the surface by "free convection," involving "meteoric" fluids with or without traces of magmatic fluids. Liquids discharged at or near the surface are replenished

Copyright © 2000 by Academic Press
All rights of reproduction in any form reserved.

by "meteoric" water derived from the outside ("recharge") that is drawn in by the rising fluids. A hydrothermal system consists of (1) a heat source, (2) a reservoir with thermal fluids, (3) a surrounding "recharge region," and (4) a (heat) discharge area at the surface with "manifestations."

manifestations A term that describes (1) features at ground surface where fluids discharge, mainly as single-phase fluids (e.g., hot springs, hot lakes and pools, fumaroles); (2) features resulting from fluid/rock interactions and hydrothermal mineral deposition, also at ground surface. The term, in its widest sense, refers to both active and inactive thermal features.

volcanic system A type of geothermal system where heat and mass transfers from an igneous body (usually a magma chamber) to the surface involving convection of magmatic fluids and sporadic discharge of magma (subsurface melts); meteoric fluids are not involved in the heat transfer process or are minor.

volcanic–hydrothermal systems A combination of a "hydrothermal" and a "volcanic" system, where ascending magmatic (primary) fluids commonly mix with meteoric (secondary) fluids (rarely sea water); also called a "magmatic–hydrothermal system."

I. INTRODUCTION

In hydrothermal and volcanic systems heat and mass transfer in the upper crust from a deep source to a discharge region at the surface. The heat moves by both convection and conduction. In hydrothermal systems the convecting heat transfer medium is dominantly infiltrated surface water (i.e., of meteoric origin). The fluids that transfer most heat, albeit intermittently, in volcanic systems are magma and magmatic gases. However, ascending magmatic fluids may mix with mantling or descending meteoric fluids; convection of such a mixture is characteristic of volcanic–hydrothermal systems, which thus constitute a blending of volcanic and hydrothermal systems (Fig. 1). Active volcanic systems produce characteristic high-temperature ($T \gg 150°C$) surface discharge features described elsewhere in this Encyclopedia. In this chapter, the surface manifestations of volcanic–hydrothermal and hydrothermal systems are discussed.

Surface manifestations are the only directly observable expressions of geothermal systems. These manifestations vary widely in their appearance, often reflecting the type of geothermal reservoir from which their discharged fluids derive. Controlling parameters include reservoir temperature, type of reservoir fluid, type of reservoir rocks, and the nature of the heat source. Indeed, the nature of the heat sources is of major importance. These can be grouped as follows:

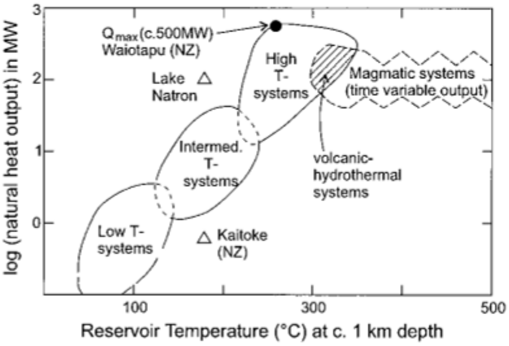

FIGURE 1 Subdivision of convective hydrothermal systems with their natural heat outputs and inferred reservoir temperatures (~1 km depth) as discriminants.

1. Magmas within the crust (local or extensive)
2. Intracrustal nonmagmatic
3. Conductive heat flow within the upper crust

This grouping can be subdivided further by considering the plate-tectonic settings of each, since most of the anomalous heat transfer is via geothermal systems concentrated along active plate boundaries (active margins).

Geothermal systems can also be divided by using their reservoir temperatures at about 1 km depth (arbitrarily chosen) as a discriminating parameter. Here we distinguish among the following systems:

1. High (>225°C) temperature (high-T)
2. Intermediate (125–225°C) temperature
3. Low (<125°C) temperature (low-T) systems

Hence, we use, for example, the phrase "manifestations associated with high-temperature systems" as a specific term. However, not all geothermal systems, especially those that are quasi-stagnant, have surface manifestations.

The amount of heat (unit: joule) transferred by a fluid can be assessed by measuring its mass flow rate at the surface and its enthalpy (heat content). These parameters define the heat discharge rate of surface manifestations, Q_s, in joules/second (J/s) or watts (W); a widely used unit is the megawatt (1 MW = 10^6 W). Q_s is an important parameter that can be used to classify geothermal systems since the extent of convection reflects the magnitude of their heat outputs. The natural output of typical low-temperature systems is commonly of the order of 0.1 to 3 MW, and that of high-temperature systems between 30 and 300 MW. The types, numbers, and sizes of surface manifestations present at each reflect this.

The rate of heat discharge from volcanic systems, Q_v, can also be estimated from the mass of material erupted over a long but finite period, allowing for degassing. High-temperature hydrothermal systems hosted within volcanic regimes along many active plate margins (volcanic arcs, for example) have heat outputs (Q_s) of about the same magnitude as Q_v.

Types of surface manifestation, listed in *italics*, are introduced in the following sections with reference to their occurrence over prominent types of geothermal systems. The links between various systems, using their inferred reservoir temperatures (c. 1 km depth) and their natural heat outputs as discriminants, are depicted in Fig. 1. Characteristic geothermal deposits and alteration are also introduced concurrently and underlined. The **locality** of individual manifestations is listed in bold font at its first mention. In the last two sections, all manifestations are grouped according to the modes of surface heat transfer, their characteristic surface alteration, and surficial deposits.

II. MANIFESTATIONS OF VOLCANIC–HYDROTHERMAL AND AFFILIATED SYSTEMS

Ascending magmatic fluids in active volcanic systems commonly mix with mantling meteoric fluids. Such volcanic–hydrothermal systems have only been recognized recently as a separate type of geothermal system from the characteristic isotopic signatures of their fluids. It is possible that most volcanic systems have mantling hydrothermal fluids; for example, even the hot (>500°C) gases discharged from the **White Island** volcano (NZ) contain fluids with both magmatic and secondary (nonmagmatic) components. A subdivision of volcanic–geothermal systems is warranted where the magmatic fluid component is no longer dominant by volume, e.g., in waning volcanic systems, which are here termed "quasi volcanic–hydrothermal systems."

A. Manifestations of Volcanic–Hydrothermal Systems

Volcanic–hydrothermal systems are mainly confined to stratovolcanoes or young calderas and exhibit characteristic surface manifestations that are spatially zoned with respect to their volcanic center, namely *solfataras*, *fumaroles*, *hot acid lakes*, *acid hot springs* (discharging sulfate- and sulfate-chloride waters), and rare *acid streams*. At lower elevations, minor *thermal springs* may discharge neutral pH, chloride, or sometimes bicarbonate–chloride waters. The typical zonation of these discharge features is shown in Fig. 2.

The term *solfatara* derives from a local name, probably from the **Phlegrean Fields** (S. Italy), an active volcanic–hydrothermal system (Forum Vulcani) within a caldera that was described by Pliny the Elder. Solfataras here deposit large amounts of sulfur around their vents and discharge steam, CO_2 and H_2S (rarely SO_2). Sometimes sulfur mounds develop, for example, at **Biliran** (Philippines), **Tatun** (Taiwan), and **Kawah Ijen** (Java). An accumulation of molten sulfur can occur at shallow depths. Active solfatara fields with a massive accumulation of sulfur have been mined at Tatun and Kawah Ijen.

In addition to sulfur, these manifestations also include deposits of sulfate minerals such as alunite, natroalunite, jarosite, gypsum, and a range of usually ephemeral hydrous sulfates. Kaolin group minerals such as dickite occur, and diaspore and pyrophyllite are also present in places. As the acid condensates become progressively neutralized by interacting with the host rocks, they may form smectites. However, the alteration process is dominantly destructive; amorphous silica that deposits as silica residue in this environment is dominantly derived from the surrounding rocks and remains at the surface as other constituents are leached.

The term *fumarole* has been used to describe vents that discharge vapor that turns into steam. It was used initially to describe and to classify features discharging volcanic gases, for example, by St. Claire Deville in the 1850s. It is not a specific term and has to be qualified with respect to discharge temperature, gas velocity, and gas composition. Fumaroles associated with volcanic–hydrothermal systems may discharge vapor at high speed (>150 m/s). The steam usually contains minor amounts of aggressive magmatic gases (such as HF, HCl, and SO_2). If the magmatic component (with SO_2) is dominant, fumarole temperatures may be >130°C (Kawah Ijen) but are usually <130°C where the hydrothermal component (with H_2S) is dominant (Biliran).

Vents discharging steam over high-temperature systems without traces of magmatic gases were also described as "fumaroles"; the Italian naturalist Tozzetti applied this term in 1751 to the high-temperature fields of Tuscany, but he assumed that all the steam discharged was of magmatic origin. Isotope studies made in the 1950s showed that steam and hot water discharged by almost all high-temperature systems derives from mete-

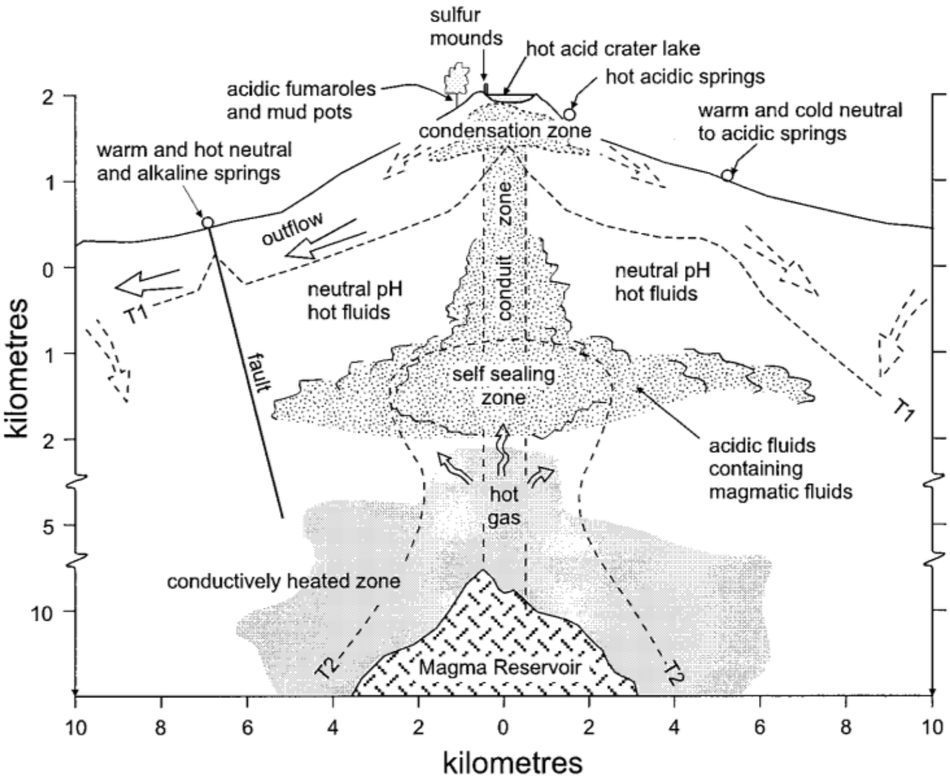
sulfur mounds
hot acid crater lake
hot acidic springs
acidic fumaroles and mud pots
condensation zone
warm and cold neutral to acidic springs
warm and hot neutral and alkaline springs
outflow
conduit zone
neutral pH hot fluids
neutral pH hot fluids
T1
T1
fault
self sealing zone
acidic fluids containing magmatic fluids
hot gas
conductively heated zone
Magma Reservoir
T2
T2
kilometres
2
1
0
1
2
5
10
10
8
6
4
2
0
2
4
6
8
10
kilometres

FIGURE 2 Conceptual model of a volcanic hydrothermal system with associated characteristic surface manifestations. The model is based on the Suretimeat system (Vanuatu) but shows features typical of other volcanic–hydrothermal systems (broken lines with T1 and T2 represent inferred isotherms for 150°C and ~350°C, respectively). (Modified from Hochstein and Sudarman, 1993.)

oric water, so the term "fumarole" appeared then to be a misnomer. However, more recent isotope studies have shown that a magmatic water component occurs in many high-temperature hydrothermal systems. The term now survives, therefore, to encompass all natural steam discharge features over hydrothermal systems.

Vapor and most magmatic gases condense at shallow depths (or dissolve in perched or descending meteoric waters), producing acid waters that may discharge in hot, *acid crater lakes* (Kawah Ijen) and as *hot acid springs* where vapor fluxes are high. The near-surface condensates can be channelled to discharge as *acid streams;* these are typical of volcanic–hydrothermal systems and occur, for example, on the outer flanks of **Sorik Marapi** (Sumatra). The pH of these waters is usually <2, and rock leaching is common. Discharge rates of up to 200 kg/s have been reported for a single acid stream at Sorik Marapi, but lower discharge rates (a few kg/s) are much more typical.

Acid condensates move downslope in the subsurface and mix with shallow groundwater, often within perched aquifers, to become slowly neutralized by progressive fluid/rock interactions. Warm acid springs further downslope, therefore, have higher pH values, as demonstrated by the discharge from subsurface outflows of initially acidic condensates on the flanks of **Tangkubanprahu** (Java) and **Nevado del Ruiz** (Colombia). Rapid neutralization occurs where the acid condensates pass through limestones (**Sibayak,** Sumatra).

Most volcanic–hydrothermal systems appear to be surrounded by a reservoir containing neutral pH waters (the reservoir can have a "toroid" structure, as indicated in Fig. 2). Such a structure, drilled at the **Biliran** (Philippines) and the **Sulphur Springs** (St. Lucia) prospects, have "acid cores" of small diameter (probably <1 km). A much larger diameter core (>7 km) is likely for Nevado del Ruiz, where a mantling buffer of two-phase fluids (hot water plus vapor) probably separates it from neutral pH chloride waters in the outer reservoir. The low permeability of the rocks hosting the reservoir explains the commonly low discharge rates of *chloride springs* on the lower flanks.

B. Surface Manifestations of Quasi Volcanic–Hydrothermal Systems

These develop when the flux of magmatic gases decreases and a volcanic–hydrothermal system becomes a fully convecting high-temperature system. They also occur beneath older composite (andesitic and dacitic) volcanic complexes, calderas, and silicic (rhyolitic) domes. The heat they discharge derives mainly from deeply penetrating groundwater that taps a cooling pluton. *Acid condensates* are less common than in true volcanic–hydrothermal systems, but *acid altered ground* occurs. *Solfataras* produce only minor amounts of sulfur and *fumaroles* do not discharge corrosive volcanic gases, although the ratios of noncondensable volatiles (for example, CO_2, He, Ar) are close to those in volcanic fumaroles. Minor, shallow *lateral outflows* of neutralized chloride–sulfate waters may discharge on the outer flanks.

Kaolin, cristobalite, hematite, and silica residue are common alteration products, but sulfate minerals are also common, including alunite and jarosite. However, diaspore and pyrophyllite are absent except where there has been considerable erosion (e.g., at **Matsukawa,** Honshu). Lead-rich barite (hokutolite) is precipitating from the highly acidic **Tamagawa Springs** (also in Honshu).

Relics of an earlier volcanic–hydrothermal phase, however, can persist as drillholes sometimes intersect saline, strongly acid, or neutral pH fluids. The **Alto Peak** system (Philippines), which contains a core of rocks saturated with vapor, is an example. There are many others of this type whose history can be inferred from the occurrences of deep acid alteration: for example, **Mahanagdong** (Philippines), **Dieng** (Java), **Kirishima** (Kyushu), and **Kakkonda** (Honshu). With prolonged convection in the main reservoir, steam-condensate and magmatic fluids become neutralized and diluted. Matured, quasi volcanic–hydrothermal systems can thus become indistinguishable from high-temperature systems beneath eroded volcanic centers.

III. MANIFESTATIONS OF HIGH-TEMPERATURE SYSTEMS

The characteristic active and nonactive surface manifestations of high-temperature systems are discussed with respect to the topography of surrounding volcanic rocks and their inferred heat sources. This allows recognition of three groups:

1. Manifestations of hydrothermal systems hosted by high standing volcanic centers (with an inferred local cooling pluton as their heat source)
2. Manifestations of hydrothermal systems in rather flat terrain transferring heat from inferred extensive hot crust or plutons
3. Manifestations associated with high-temperature systems over extensive hot crustal rocks in a plate collision regime

A. Manifestations of Hydrothermal Systems Associated with High Standing Volcanic Centers

Many well-known high-temperature systems have this setting. Depending on the overall permeability of the reservoir rocks and their surroundings and the extent of recharge (infiltration of groundwater), three distinct types of reservoirs can be recognized. Here we use the terms “low,” “moderate,” and “high” permeability for rocks with average permeabilities, k, of the orders of <1 to 3, 3 to 10, and >10 millidarcy (1 millidarcy $= 1 \times 10^{-15}$ m^2), respectively. In each case almost all the heat reaching the surface is carried by deeply circulating meteoric waters that sweep heat from a source (usually a cooling pluton) and ascend under free convection.

If the k value of the reservoir rocks is high but that of rocks in the recharge area is moderate, then this results in the formation of a *liquid dominated system* (liquid saturation of the reservoir rocks, S_l, is between 1 and 0.7). If the k values of both the reservoir rocks and those in the recharge area are moderate, than a two-phase mixture can develop in parts of the reservoir (*natural two-phase system*) with $0.7 < S_l < 0.4$. Where k in the surrounding area is low (i.e., there is little recharge) but the k value of the reservoir rocks is high, then the dominant fluid in the reservoir will be vapor ($0.4 < S_l < 0$), i.e., a *vapor dominated system.*

In all three cases, however, most hydrothermal minerals that form by replacement in the reservoir do so from interaction between the host rocks and a liquid phase. Further, rocks at the **Kawah Kamojang** and the **Darajat** fields (both in Java) contain vein calcsilicate minerals such as epidote, wairakite, and prehnite that clearly deposited directly from liquid even though boreholes in both fields discharge steam. This is because the permeability of the host rocks determines whether a field will

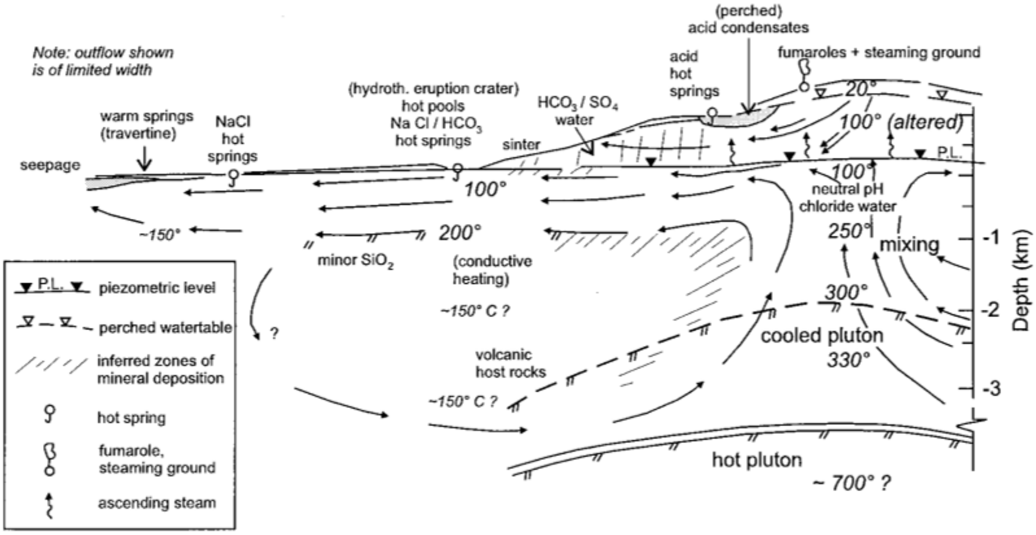
Note: outflow shown is of limited width
(perched) acid condensates
acid hot springs
fumaroles + steaming ground
(hydroth. eruption crater) hot pools Na Cl / HCO3 hot springs
HCO3 / SO4 water
warm springs (travertine)
NaCl hot springs
seepage
sinter
20°
100° (altered)
P.L.
100°
neutral pH chloride water
100°
~150°
200°
minor SiO2
(conductive heating)
250°
mixing
~150° C ?
300°
cooled pluton
330°
volcanic host rocks
~150° C ?
hot pluton
~ 700° ?
-1
-2
-3
Depth (km)
piezometric level
perched watertable
inferred zones of mineral deposition
hot spring
fumarole, steaming ground
ascending steam
?

FIGURE 3 Conceptual model of a liquid dominated, high-temperature system beneath a partially eroded, high standing volcanic complex exhibiting lateral zonation (downstream) of surface manifestations. A large amount of heat is discharged by concealed outflows that are partly sealed through mineral deposition. The model is based, in part, on the Palinpinon system (Philippines); the heat source is a cooling pluton. (Modified from Hochstein, 1990.)

supply steam only or a two-phase mixture of steam and water to producing boreholes.

1. *Manifestations of Liquid Dominated Systems*

A schematic diagram of a liquid dominated system beneath an eroded volcanic complex (Fig. 3) shows that all manifestations over the central part of the reservoir derive from ascending steam that is discharged by *fumaroles* and from minor *steaming* (*hot*) *ground.* Condensed steam, with oxidised H_2S gas, feeds minor *hot acid springs.* Steam and CO_2 can discharge together through *hot mud pools*, or separated CO_2 (rarely with H_2S) can discharge at the surface producing characteristic *gas discharge features* that have local names: for example, *kaipohan* in the Philippines, *putizza* in Italy. Downslope, the ascending CO_2 dissolves in perched groundwaters to produce *warm springs* that discharge bicarbonate (HCO_3) waters.

Many liquid dominated systems with the hydrological setting shown in Fig. 3 have *concealed* (subsurface) *outflows* of neutral pH chloride waters originating from the upper part of the reservoir. Silica deposition can partly seal the top of the outflows to descending surface water. Where these outflows discharge in valleys or at lower elevations, *hot springs* and *hot pools* occur (often boiling and occupying *hydrothermal eruption* or *dissolution craters*). Some manifestations here discharge a mixture of hot water and steam (*spouting spring* or *geyser*). Further downstream, mixed chloride–bicarbonate waters may discharge as *warm springs* and *seepages*, some with travertine (mainly $CaCO_3$) deposits. This lateral zonation of discharge features is a characteristic of these systems and was first described for the **Hakone** system (Japan).

Liquid dominated systems with the manifestations just described occur at **Palinpinon** and **Tongonan** (Philippines). At Tongonan, another characteristic discharge feature occurs near the toe of an outflow, a *hot ebullient pool*, whose ebullition is caused by ascending CO_2 gas. Manifestations over major outflows from a liquid dominated system occur also at **Berlin** (El Salvador) and **Momotombo** (Nicaragua). Elsewhere, the locations of reservoirs below steep and sometimes inaccessible terrain are not well known, and the existence of a liquid dominated system can only be inferred from discharge features along an outflow. This occurs, for example, at **El Tatio** (Chile), the "type system" for this hydrological setting. Other prospects, known only from manifestations at the toe of subsurface outflows, are **Cisolok** and **Cisukarame** (Java), whose outflows, based on geophysical evidence, extend for more than 10 km. The prospects at **Sipoholon** (Sumatra) and **Songwe** (Tanzania) are only known from their travertine depositing springs. Spouting springs (*spouters*) occur over an outflow of the **Ulebulu** system (Sumatra) and at El Tatio. A seasonal geyser occurs at the toe of a small concealed outflow from the **Rajabasa** system (Sumatra).

2. *Manifestations of Natural Two-Phase Systems*

The fact that water in many liquid dominated systems beneath high standing volcanic complexes boils, thus creating a two-phase zone (Tongonan, for example), does not mean these are themselves two-phase systems; these can only be recognized where wells intersect a deep, coherent two-phase zone.

The **Olkaria** prospect (Kenya) was such a two-phase system prior to its exploitation. Extensive areas of *steaming ground* with minor *fumarolic activity* occur there. Practically all heat from this huge reservoir transfers to the surface by ascending steam that condenses at shallow depths, maintaining dominantly conductive heat transfer to the surface with only feeble *fumaroles.* There are no significant liquid discharges except for some *minor warm springs* that discharge small amounts of condensate (Fig. 4). Extensive steaming ground is also the dominant type of manifestation at the nearby **Eburru** prospect and over many other high-temperature systems associated with young volcanic centers in the Kenya Rift Valley. None discharge appreciable amounts of hot water. In part, this is due to the semiarid conditions and the regionally deep water table. Fossil sinter occurs in this setting (shown in Fig. 4), at **Namarumu** (N. Kenya), for example, indicating that when infiltration rates were higher in the past some reservoirs were liquid dominated. Further north, in the Ethiopian Rift, another natural two-phase system, **Aluto**, discharges not only heat from steaming ground and fumaroles, but also neutral pH chloride water from *hot springs* and *seepages* that are located above an outflow at the foot of the young volcanic dome that hosts the reservoir.

3. *Manifestations of Vapor-Dominated Systems*

A characteristic spectrum of manifestations occurs over these rare systems, for example, on the broad volcanic massifs at **Kawah Kamojang** and **Darajat** (Java). Heat transfer is dominantly by steam ascending from the top of a thick concealed layer with condensates (*condensate*

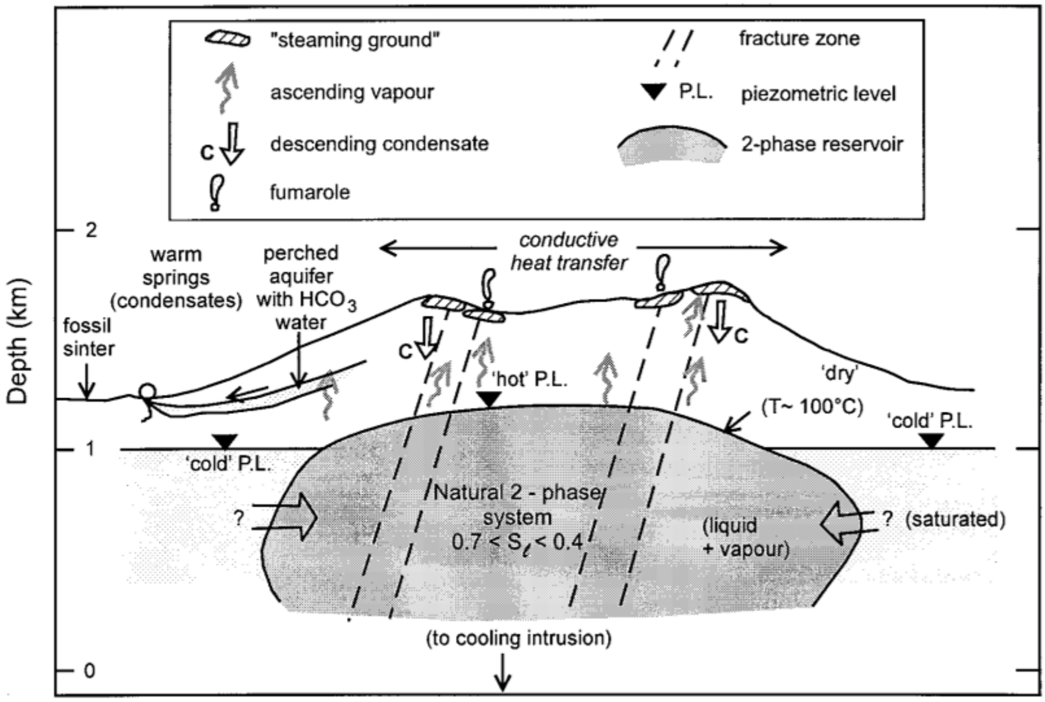
"steaming ground"
ascending vapour
C descending condensate
fumarole
fracture zone
P.L. piezometric level
2-phase reservoir
Depth (km)
2
1
0
warm springs (condensates)
perched aquifer with HCO3 water
fossil sinter
conductive heat transfer
C
C
'hot' P.L.
'dry'
(T~ 100°C)
'cold' P.L.
'cold' P.L.
Natural 2 - phase system 0.7 < Sℓ < 0.4
(liquid + vapour)
?
? (saturated)
(to cooling intrusion)

FIGURE 4 Simplified model of a high-temperature steaming ground system with a natural two-phase (coexisting liquid and vapor) reservoir beneath a broad volcanic center in a semiarid environment showing the restricted variety of surface manifestations in this setting. The model has some affinity to the Olkaria system (Kenya) and many other similar systems in the East African Rift Valley.

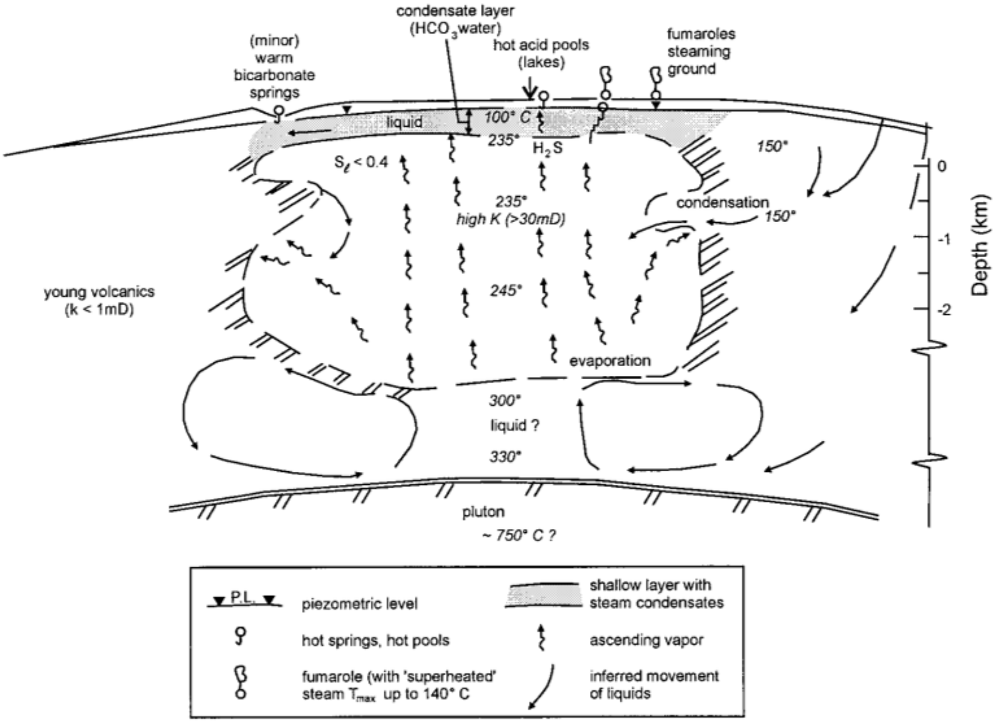
condensate layer (HCO$_3$water)
(minor) warm bicarbonate springs
hot acid pools (lakes)
fumaroles steaming ground
liquid
100° C
235°
H$_2$S
150°
S$_\ell$ < 0.4
235°
high K (>30mD)
condensation
150°
young volcanics (k < 1mD)
245°
evaporation
300°
liquid ?
330°
pluton
~ 750° C ?
Depth (km)
0
-1
-2
P.L.
piezometric level
shallow layer with steam condensates
hot springs, hot pools
ascending vapor
fumarole (with 'superheated' steam T$_{max}$ up to 140° C
inferred movement of liquids

FIGURE 5 Conceptual model of a vapor dominated system beneath a broad, high standing volcanic complex. The reservoir has a condensate layer on its top. Heat transferred within the reservoir is discharged at the surface by steam and hot condensates (bicarbonate waters). The model has some similarity to the Kamojang system (Java); the heat source is a cooling pluton. (Modified from Hochstein, 1990.)

layer) of almost neutral pH bicarbonate waters (Fig. 5) that, together with intense alteration, may act as a confining cover. *Steaming ground* and *fumaroles* are common; in addition, minor acid condensates form "muddy" *hot pools* and small *acid lakes* with very low mass discharge. The low permeability of the rocks surrounding these reservoirs prevents any significant mass outflow, although shallow, minor bicarbonate–sulfate springs occur about 15 km outside Darajat. There are no neutral pH chloride springs on the lower flanks, and their absence is probably the most characteristic feature of these systems. The same types of surface manifestations also occur over **Ketetahi** (NZ), hosted by a young andesite volcano (Mt. Tongariro), although no drillholes have yet tested this tentative classification.

Surficial and shallow hydrothermal alteration is extensive above vapor dominated systems but does not, in itself, reveal whether or not the underlying reservoirs are occupied by vapor or a two-phase fluid: kaolin clays dominate (kaolinite, halloysite, and more rarely dickite), but sulfur and sulfates are also common (alunite, natroalunite, gypsum, and a variety of hydrous phases, many ephemeral). Hematite and hydrous iron oxides are also typically present, as is silica residue, although fine-grained, black pyrite may persist near some thermal features. The alteration is usually pervasive and the overall process is dominantly destructive of the host rocks rather than depositional. The **Matsukawa** field (Honshu, Japan) has extensive alteration (7 × 1.5 km) comprising pyrophyllite and diaspore, alunite, kaolinite, and smectite zonally distributed around the main structural feature of the field. This alteration records former thermal activity as the present-day thermal manifestations consist of only a few areas of warm ground.

B. Manifestations of High-Temperature Systems in Moderate Terrain

The heat sources for these systems appear to be extensive, hot crustal rocks whose thermal energy is maintained by the following:

1. Partial melting within the ductile upper crust (setting for the NZ systems hosted by young rhyolitic rocks and also for some at Yellowstone, Wyoming)

2. Deep, laterally aligned crustal and dyke intrusions in rift environments beneath systems hosted in basalts (e.g., systems over spreading centers such as Iceland) or sedimentary rocks (Baja California)
3. Deep cooling plutons (relics of an older subduction cycle?) now distant from an active subduction zone

In all these settings there are systems with one of the three reservoir types mentioned in the previous paragraph. An additional reservoir type with the second setting listed is the *nonconvecting brine system*.

1. *Manifestations of High-Temperature Systems in Moderately Steep Terrain Underlain by Extensive Hot Crustal Rocks*

The terrain surrounding these systems is not steep, and young volcanic cones are usually peripheral to the geothermal reservoirs. Because of their high recharge rate and the terrain, the hot fluids can ascend close to or reach the surface. Any *zonation of discharge features*, if it occurs, is not controlled by lateral pressure gradients created by differences in relief. Manifestations of discharging steam (*fumaroles* and *steaming ground*), condensates and noncondensable gases (minor *acid springs* and *mudpools*) can, therefore, occur close to others that discharge neutral pH chloride waters (*clear hot pools*, *hot springs*). This thermal regime favors *hydrothermal eruptions*, if the liquid is very close to boiling in the shallow subsurface. The setting also favors the discharge of two-phase boiling fluids as *large geysers*. *Outflows* are rare because the horizontal pressure gradient is very small (flat terrain). Systems with the largest natural heat discharges (up to 500 MW at Waiotapu, NZ; see Fig. 1) occur in this setting with many prospects discharging >300 MW. An idealized section through a liquid dominated reservoir with its spectrum of manifestations is shown in Fig. 6.

The silica sinter that deposits from discharging waters shows a wide variety of forms. *Spouters* (spouting springs) or geysers deposit nodular silica called geyserite. Terracing is a common feature, with individual steps having heights ranging from a few millimeters to 2 meters (as at the **Rotomahana** system near Rotorua, New Zealand, destroyed by a volcanic eruption in 1886). The steps typically have lips to them and are usually closest together on the steepest slopes. The flow paths of the cooling waters change constantly through deposition of

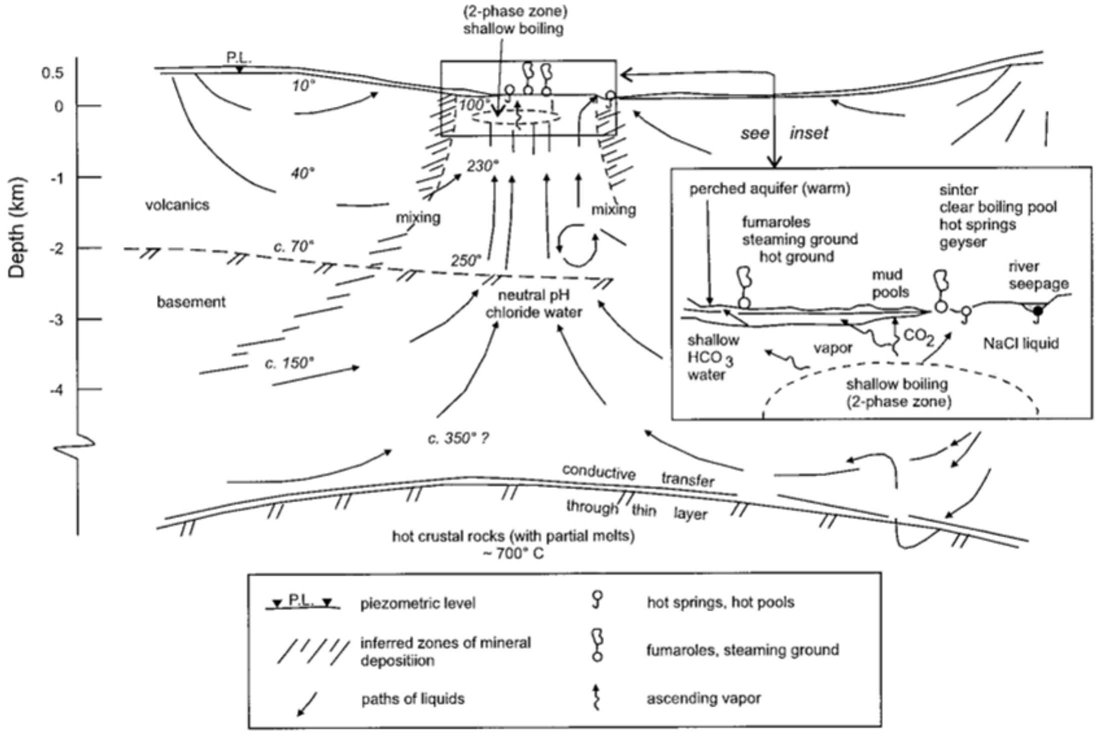
(2-phase zone)
shallow boiling
P.L.
0.5
0
-1
-2
-3
-4
Depth (km)
10°
100°
40°
230°
see inset
volcanics
mixing
mixing
c. 70°
250°
basement
neutral pH
chloride water
c. 150°
c. 350° ?
conductive transfer
through thin layer
hot crustal rocks (with partial melts)
~ 700° C
perched aquifer (warm)
fumaroles
steaming ground
hot ground
sinter
clear boiling pool
hot springs
geyser
mud pools
river seepage
shallow
HCO_3
water
vapor
CO_2
NaCl liquid
shallow boiling
(2-phase zone)
P.L.
piezometric level
inferred zones of mineral depositiion
paths of liquids
hot springs, hot pools
fumaroles, steaming ground
ascending vapor

FIGURE 6 Conceptual model of a liquid dominated system standing in rather flat terrain; the heat source is an extensive layer of hot crustal rocks that contains some partial melts and host intrusions. The model has some similarity to the Wairakei system (NZ). (Modified from Hochstein, 1990.)

silica. Other silica varieties include banding, palisade structures, and wave forms. The last have the form of barchan sand dunes, but their crests grow toward the flow direction of thermal water. Silica sinter is usually hard and white, but it also may be porous, pale yellow, and friable. Microbiological activity plays a major part in silica deposition in some areas and bacteria and plants may be preserved as fossils.

Sinter covers several acres at **Norris Geyser Basin** (Yellowstone) and **Waiotapu** (New Zealand). When first deposited, silica sinter is opaline, but it transforms with time, first to cristobalite and finally to quartz, progressively losing water as it does so. Metal rich deposits precipitate with the silica from some springs: for example, ore grade gold and silver plus appreciable arsenic, antimony, and thallium, as are now precipitating at the Champagne Pool, Waiotapu. Sinter with locally 3 wt% tungsten is depositing at **Waimangu** (New Zealand).

The heat output (Q_s) of all (~20) high-temperature hydrothermal systems in the Taupo Volcanic Zone (TVZ), over an active arc segment about 200 km long, is probably three times greater than the extrapolated cumulative heat discharged (Q_v) from all its volcanic centers. The **Wairakei** system was liquid dominated prior to its exploitation and its manifestations included all those listed earlier. Impressive manifestations also occur over other liquid dominated systems nearby, such as at Waiotapu, which exhibits an apparent *reversed hydrological zonation* whereby the deep reservoir fluid discharges from a slightly higher *large hot pool* (an old hydrothermal eruption crater) that is surrounded by acid springs at lower elevations. Acid leaching of thick pumice has produced a number of steep sided or overhanging walled *dissolution pits*, some with acid condensates in them. A rare manifestation which occurs over the **Rotokawa** system is a *cold acid lake* into which a vigorous flux of H_2S dissolves. The **Whakarewarewa** system is well known for the occurrence of *large geysers*, *clear hot (near boiling) pools*, and widespread sinter deposits. Natural two-phase systems also occur (e.g., **Broadlands-Ohaaki**) but have few or no major discharge features. The rate of natural heat discharge (Q_s) from Broadlands (before exploitation) was only ~75–100 MW compared with that from the other three prospects just cited (each with Q_s values between 300 and 500 MW).

A large number (up to eight) of probably liquid dominated high-temperature systems occur in the **Yellowstone National Park** (Wyoming, USA). The heat source here is a mantle plume extending into the base of the crust, which it has heated and partially melted. The total thermal output from all the systems at Yellowstone is therefore large, its magnitude being probably half that of the Taupo Zone systems. Many geothermal systems in Yellowstone show the characteristic thermal manifestations that occur over the liquid dominated systems, including *large geysers*, *clear boiling pools*, and extensive sinter deposits at the **Norris Geyser Basin,** for example.

Deposits of calcium carbonate occur in the outflow areas of high-temperature systems but are also associated with lower temperature systems. The carbonates deposit as a consequence of loss of CO_2 from the discharging water in which it was formerly dissolved. Calcite is the dominant carbonate, but where loss of CO_2 is very fast, aragonite occurs instead. The reason for this is not known. The calcium carbonate forms deposits that resemble those of silica sinter, e.g., bedded or layered, terraced or forming ridges and even columns up to 3 m high. Extensive and beautiful deposits of calcium carbonate occur at **Mammoth** (Yellowstone), but travertine very commonly surrounds many small springs or pools.

2. Manifestations of High-Temperature Systems in Crustal Spreading Environments

Many geothermal systems are hosted by young basaltic rocks in active rifts, such as Iceland. These high-temperature systems derive their heat from a set of dykes or sills. Generally, their manifestations are less vigorous than those listed in the previous paragraph. *Acid alteration* and sinter deposits are not extensive; the salinity of thermal water in prospects away from the ocean is low, generally <1 g/kg of total dissolved solids (TDS). A few liquid dominated systems have *geysers*, as at **Haukadalur,** including Great Geyser itself which gave its name to all similar intermittently discharging features; the term comes from the Viking verb "gjose" (to gush). Liquid and two-phase geothermal reservoirs occur together at **Krafla** and **Namafjall,** as indicated by the initial enthalpy of fluids discharged from wells there. Near the coast, infiltration of sea water is shown by the high mineral concentration (up to 20 g/kg) in hot water from the **Svartsengi** and the **Reykjanes** high-T reservoirs (both liquid dominated). Several wells at **Krafla** discharged fluid with a magmatic signature as a result of an intrusion and eruption that occured there in 1975.

The term "geothermal brine" has been used for liquids with high total dissolved solids (TDS). This term applies, in general, to liquids with TDS >20 g/kg (i.e., more saline than seawater); hot brines with TDS > 100 g/kg are called "hypersaline" brines.

Elongate, deep (>6 km) intrusions likely heat a number of the geothermal systems in Baja California (Mexico) and the Imperial Valley (California); these are liquid dominated and mainly high-temperature systems. The fluviatile sediments host reservoirs that contain a brine or "hypersaline" brine that arguably derives its high salinity by dissolving surrounding evaporites. Because of their high density, the brines have little surface discharge, so the dominant mode of heat transfer is by conduction. An example is **Cerro Prieto** (Mexico) where, prior to exploitation, some heat reached the surface via small *patches of hot, steaming ground* and conductive losses were about 30 MW. Other brine systems in the Imperial Valley (USA), such as **Brawley,** have no surface manifestations whatsoever. Minor *steaming ground* and *small mud pots* occur over the "hypersaline," stagnant high-temperature reservoir of the **Salton Sea** (also Imperial Valley). This is similar to the "hypersaline" system with a similar geological setting, the **Cesano** prospect, in Central Italy.

Hypersaline brines derived from the lateral infiltration of seawater occur in the **Lake Assal** system (Djibouti), hosted by basalts, over an incipient rift with extensive evaporites at its surface. At **Dallol** (Danakil Depression, N. Ethiopia) meteoric water enters a salt dome by advection and dissolves salt almost to the limit of NaCl solubility. The hypersaline brine is heated by conduction from a cooling intrusion. This produces hot, *hypersaline brine pools* ($T = 110°C$); the TDS of the brine can be up to 420 g/kg, high in Na, K, Mg, and Cl. Here an overflow of hot brine causes the formation of salt mounds.

3. Manifestations of High-Temperature Reservoirs Hosted by Sedimentary Rocks

Another group of high-temperature systems occur in sedimentary to low grade metamorphic rocks in a setting with deep cooling plutons (perhaps the product of an older subduction cycle). A hot water–CO_2 gas dominated reservoir occurs, for example, at **Ngawha** (NZ), which is several hundred kilometers distant from the presently active subduction zone, but lies above a subduction zone that was active more than 10 Myr ago. Quaternary basalts occur nearby but are not part of the high-temperature reservoir, which comprises Mesozoic greywackes covered by about 600 m of almost impermeable (to water) sediments. Vigorous *upflow of* CO_2 with mercury occurs throughout the entire area and through several cold lakes, but most heat (~50 MW) transfers to the surface by conduction.

The two largest systems known have similar settings and are both vapor-dominated, namely **Larderello** (Italy) and **The Geysers** (California). There is circumstantial evidence that steam, which ascended to the surface prior to the exploitation of both reservoirs, came from an extensive condensate carapace similar to that shown in Fig. 5. At Larderello, large amounts of boron were mobilized by vapor from marine sediments and deposited at the surface in borax ponds, the *laguni* that were once mined. *Fumaroles* discharging B-rich steam have been described as *soffioni*. The magnitude of natural heat transfer and that by steam was unfortunately not assessed at either place before exploitation began.

C. Manifestations of Systems over extensive Hot Crustal Rocks in a Plate Collision Environment

The heat sources for all the high-temperature systems mentioned so far involve mobilization of upper mantle melts and fluids. A characteristic trace component which reveals the involvement of subcrustal melts is the ^{3}He isotope. Its role can be assessed from the ^{3}He/^{4}He ratios, R, of gases, normalized with respect to its atmospheric ratio. Geothermal gases from all high-temperature systems described so far have R values that are 1 to 2 orders of magnitude greater than typical values (<0.15) of gases discharged by low-temperature systems far distant from active margins, e.g., over a "cold" continental crust (with no volcanic history).

However, a number of high-temperature systems, hosted by metamorphic or sedimentary rocks, occur in Tibet and Kashmir that discharge steam and gases with anomalously low ^{3}He/^{4}He ratios ($R < 0.15$). These systems transfer heat derived from young granites, probably generated by shear-heating from plate collision. At one, **Yangbajing** (Tibet), temperatures >250°C have been measured in drillholes. Hot geothermal fluids here ascend beneath the flanks of a high mountain range (Inner Himalayas) and discharge as a *concealed outflow* within a wide valley. The *zonation of manifestations* is again controlled by the relief of the terrain. Traces of *acid condensates* and extensive acid steam alteration (alunite, residual silica) occur over the flanks near the inferred upflow. There is no significant discharge of liquid over the outflow, whose top is sealed by extensive deposits of silica and carbonates. Only at the toe of the outflow is there a spectrum of manifestations that discharge neutral pH chloride waters, namely; *boiling pools, hot springs, spouting (two-phase) boiling springs,* and some *steaming ground.* A number of *large hydrothermal eruption craters* occur further down the valley, where there are also massive deposits of travertine. A similar, although less obvious, zonation of manifestations occurs at the nearby **Yangyi** prospect, another system with temperatures >200°C in 500-m deep wells. From descriptions of their discharge features and chemical geothermometry, it is inferred that at least another dozen such high-temperature systems occur in Tibet. These appear to be associated with 30 to 50 km wide, elongate bands of hot, upper crustal rocks ("heat bands") produced by shear heating resulting from lateral movements of large crustal blocks. Also impressive are the intermediate-temperature systems within the same *heat bands* that occur at more than 100 places (see later discussion).

IV. MANIFESTATIONS OF INTERMEDIATE- AND LOW-TEMPERATURE SYSTEMS

Intermediate- and low-temperature systems occur in many different geological and hydrological settings, both along and outside active plate margins. It is often difficult to distinguish them from high-temperature systems, since standard chemical and isotopic geothermometers, based on slow equilibration processes (i.e., Na/K and most gas geothermometers), give temperatures reflecting conditions much deeper than, say, 1 km depth. However, faster equilibrating fluid/rock interactions allow application of the silica (assuming equilibration with chalcedony) and the Mg/K geothermometers. These, and the lack of significant shifts in the ^{18}O isotope values, can be used to predict likely temperatures in the upper few kilometers of such reservoirs. Because of their lower temperatures and less buoyant fluids, their natural heat outputs are also lower. They thus have fewer surface manifestations. All intermediate temperature prospects have *liquid dominated reservoirs* that can extend to great depths (>5 km). *Fumaroles* and *steaming ground* are absent, although *boiling springs* occur in some; however, the maximum fluid discharge temperatures are usually below boiling.

Although a few intermediate-temperature systems are located in active and inactive volcanic arcs, where they are heated by convecting plumes of hot water, the majority derive their energy from deeply penetrating meteoric water that "sweeps" heat from the hot but brittle upper crust into a discharge area ("sink"), often via fractures ("fracture zone" systems). According to their geological and hydrological settings, most intermediate-temperature systems can be grouped as follows:

1. Systems over active and inactive volcanic arcs, i.e., hosted by volcanic rocks
2. "Heat-sweep" systems in active rifts and at plate collision boundaries
3. Fracture zone systems hosted by sedimentary or metamorphic rocks

A. Intermediate-Temperature Systems over Volcanic Arcs

A few intermediate-temperature systems have this setting but they are everywhere outnumbered by the high-temperature systems (~1 : 10 in New Zealand and Sumatra). Some intermediate-temperature systems are probably decaying high-temperature systems over a waning heat source. A few dead systems host epithermal mineral deposits, but most of these were likely once high-temperature systems. A well-studied dead reservoir is at **Ohakuri** (NZ), which was probably a high-temperature system about 100 kyr ago. Still active intermediate-temperature systems occur at **Horohoro** and **Atiamuri** (NZ). Their surface manifestations are not impressive. Minor silica sinter and a boiling spring occurs at Atiamuri, where drilling shows that the temperature at a depth of about 1 km is only 175°C. At Horohoro, there is *minor hot spring activity* and *cold altered ground*. The chemical composition of these thermal waters points to their being appreciably diluted with ground waters.

Hot crustal rocks beneath an extinct arc segment can take several million years to cool conductively. In such a setting, a few intermediate-temperature systems may survive, for example, at **Te Aroha** (Coromandel, NZ), which is hosted by andesites along an arc segment that became extinct ~5 million years ago. Here little heat (~1 MW; see Fig. 1) is transferred by a *few hot springs* and CO_2-rich fluids that deposit aragonite. Over the same extinct arc segment occurs the **Kaitoke** hot springs (Great Barrier Island, NZ), which are similar to those at Te Aroha.

B. "Heat-Sweep" Systems

The reservoirs of "heat-sweep" systems may be of volcanic or sedimentary rocks. Fracture zone systems can develop in a part of the crust with anomalously high heat flow but not associated with volcanism, and in continental rifts. Intermediate-temperature systems have not been described in detail, but some, however, have been explored by drillholes in the hope that they were high-temperature systems. The number of examples that follow is therefore small and restricted to a few of the better known prospects.

1. Heat-Sweep Systems in Active Rifts

The East African Rift Valley is underlain along its entire length by hot crustal rocks heated mainly by intrusions. Rain infiltrating over its higher standing rift shoulders favors the development of large heat-sweep systems which discharge hot fluids along the axis of the arid rift valley (see Fig. 7). The large hydraulic head sets up its own convection pattern, that is, a pattern of "forced convection." If hot fluids ascend through evaporites they discharge hot saline water in springs at 40 to 80°C, for example, along the margins of **Lake Natron** (Tanzania), **Lake Magadi** (Kenya), **Lake Afrera,** and **Lake Asale** (both in northern Ethiopia). Evaporation produces large surface deposits of crystalline carbonates of sodium (trona) at the first two lakes. The compositions of brines of shallow origin is not governed by temperature-dependent equilibria; however, silica and isotope data indicate that the deep fluid temperatures are most likely <170°C. The area affected by such heat sweeps is large (>100 km^2), which explains the high heat outputs (of the order of 100 MW) of the first two examples cited; the anomalous position of the Lake Natron heat output is shown in Fig. 1. They are the largest intermediate-temperature systems known.

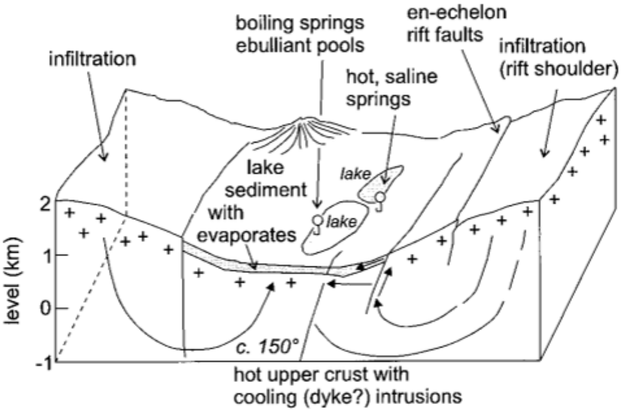

FIGURE 7 Conceptual model of a heat-sweep system (forced convection) producing intermediate-T reservoirs within an active continental rift. The model is based on lake systems such as those in northern Tanzania, Kenya, and Ethiopia.

Elsewhere along the East African Rift, where evaporites are thin or absent, less saline hot water discharges into lakes and sinks. **Lake Bogoria** (Kenya) has a heat output from several *boiling springs* and *ebullient pools* of the order of 100 MW. Cation geothermometers clearly point to the mean reservoir temperature of this sweep system as being <180°C. The surface discharge features could be mistakenly interpreted as being manifestations of a high-temperature system. Manifestations of intermediate-temperature sweep systems occur also in northern Kenya and the Southern Lakes District of Ethiopia.

Several systems in the Basin and Range Province of the United States are probably heat-sweep systems (**Soda Lake, Beowawe,** and **Stillwater** in Nevada, for example). Their manifestations are mostly minor.

2. Heat-Sweep Systems in a Plate Collision Setting

In Tibet, Kashmir, and west Yunnan, there are several intermediate-temperature systems, as indicated by the chemical geothermometry of their discharge fluids. The topography, high infiltration (some from snow melt), and large hydraulic heads over recharge areas favor the development of a heat-sweep hydrology over crustal strips heated by shear deformation ("heat bands"). A good example is the **Naqu** prospect in Central Tibet characterized by *hot springs* (T max = 60°C), which deposit travertine from waters that the K/Mg geothermometer indicates to be ~130°C at depth. **Laduogang** (near Yangbajing) is another intermediate-temperature system explored by drilling. Ebulliant pools discharging bicarbonate waters here locally deposit carbonate nodules (pseudo-geyserite). In the foothills of the Himalayas, similar systems occur (**Manikaran** in northern India, for example). Subsurface temperatures as hot as 150°C are indicated by the K/Mg geothermometer for most systems in Tibet depositing travertine. This is also a characteristic product of many extinct systems there.

C. Fracture Zone Systems

Deep-reaching heat-sweep systems can also develop in terrain with rather flat topography if fluids ascend via a deep, highly permeable (>100 millidarcy) fracture zone in a brittle crust of high heat flux (>70 mW/m^2). Such high fluxes often occur where thick gran-

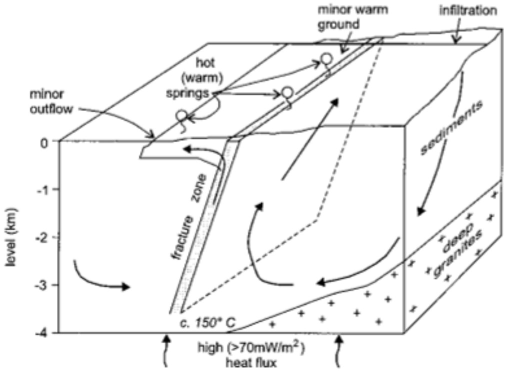

FIGURE 8 Conceptual model of a heat sweep system (free convection) discharging hot fluids through a deep reaching fracture zone (fracture zone system). The heat source gives a higher than normal terrestrial heat flow; this setting can occur far away from active margins and volcanism. The model is based on the Fuzhou system in South China.

ites provide radiogenic heat (see Fig. 8). Fracture zones near the surface may be "narrow" (<100 m) or "wide" (>200 m). A good example of the former is the **Fuzhou** prospect in southern China; the **San Kamphaeng** prospect in northern Thailand is an example of a wide fracture system. Another dozen or so fracture zone-sweep systems occur in northern Thailand (e.g., **Fang**) and a few within the coastal strip of southern China (e.g., **Zhangzhou**).

The dominant manifestations of all these systems are hot springs, and occasional hot pools, both with minor encrustations of sinter and travertine; alteration of the surrounding rocks is rare. Conduction contributes to the heat transfer, which commonly lies between 3 and 10 MW. Prospects with indicated high Na/K equilibrium temperatures (some greater than 225°C) can also be misinterpreted as being "high-temperature systems," although their low heat outputs and isotopic signatures (no significant ^{18}O shift) show them to have intermediate-temperature reservoirs.

D. Manifestations of Low-Temperature Systems

A large number of convective low-temperature systems occur in geological settings that favor the development of structurally controlled, smaller heat sweep systems. Most discharge warm (i.e., <40°C) water from a network of fractures that constitute their reservoir. Stratigraphically controlled systems in sedimentary rocks, discharging over an anticline, for example, are rare. Since temperatures in their upper reservoirs are low (i.e., <125°C), buoyancy forces, and hence the heat output of these systems, are also low (typically between 0.1 and 3 MW). Rock/fluid interactions occur at a much slower rate and mineral–fluid equilibrium is seldom attained; ^{18}O shifts do not occur. The "true" low-temperature systems are rare in volcanic arc settings, whereas they are common where topography and tectonics allow small heat-sweep systems to develop, for example, along the margin of large rift valley lakes, such as **Lake Malawi** (East Africa). Low-temperature systems can form even in brittle crust with an average terrestrial heat flux (~60 mW/m^2), corresponding to temperature gradients of only ~25 to 30°C/km, although they are more common where fluxes are higher. In the Basin and Range Province and Colorado Plateau in the western United States, there are at least 900 low-temperature systems, which thus outnumber the intermediate and high-temperature systems by ~20 : 3 and 20 : 1, respectively. In the Himalayan area there are ~500 low-temperature systems that discharge fluids hotter than 40°C; they outnumber the intermediate and high-temperature systems by ~20 : 6 and ~20 : 1, respectively.

Despite the worldwide occurrence of low-temperature systems, their surface manifestations differ little, consisting usually of *warm* ($T < 40°C$) and sometimes *hot springs* ($T > 40°C$) without any surface alteration or deposits other than travertine. The compositions of the discharge fluids reflect the sweep depth and mixing contribution from saline pore fluids in the sedimentary host rocks. Numerical modeling shows that these systems are longer-lived than all others. The development of free convection in a fracture network of a low-temperature system, for example, can take a million years, whereas full convection within permeable high-temperature reservoirs may develop in only 10,000 years. Because of their low temperatures, mineral deposition is so slow that it does not block the fluid-flow channels, and they are likely to be long-lived systems.

Manifestations of a few low-temperature systems differ, but include warm, often tepid springs that deposit travertine, for example at **Acque Albule** near Rome (Lacus Albulus), which was the main quarry for ancient Rome, and distant from active volcanoes. In western Turkey, **Bursa** and **Pamukkale** have a similar setting. However, CO_2 gas also discharges close to low-temperature systems depositing travertine, and these could be described as "moffete." Because of the high solubility of CO_2 in cold water, carbon dioxide rising from the mantle, as recognized by its typically high $^3He/^4He$ ratio, can dissolve at the bottom of cold lakes, such as at **Lake**

Nyos (Cameroon) and the **Laacher See** (Germany), which thus act as "gas" traps.

V. CLASSIFICATION OF MANIFESTATIONS (MODE OF HEAT TRANSFER)

Based upon the various types of manifestations in their settings, some provisional classifications and groupings are attempted. Since the same types of manifestations associated with heat discharge occur over a large number of convective systems, this classification is only tentative. We can distinguish between manifestations associated with the following modes of heat discharge: (1) diffusive; (2) direct and continuous; (3) intermittent; (4) catastrophic; and (5) concealed. The various manifestations associated with these modes have been ranked in Table I according to their role in surface heat transfer.

1. *Diffusive Heat Discharge*

Diffusive heat transfer by thermal conduction results in *warm ground;* it is not obvious at the surface and can only be recognized by temperature surveys in shallow (say, 1-m deep) holes. It may be the dominant mode of heat transfer of some intermediate- and low-temperature systems. At Fuzhou (South China) almost half of the total heat transfer of ~10 MW is by warm ground. It is also the dominant mode where high-temperature systems are covered by almost impermeable sediments. More than 80% (~40 MW) of the heat transferred from the Ngawha (NZ) system is by conduction through warm ground. Since near-surface conductive heat transfer does not raise the surface temperature, warm ground cannot be detected by infrared sensing; however, under suitable conditions warm ground with stunted vegetation produces *reflective infrared anomalies* (due to small differences in leaf chlorophyll condition). Such plants constitute, therefore, in the widest sense, a surface manifestation, albeit a surrogate one.

Diffusive heat transfer by thermal conduction is also dominant in *steaming ground*, where vapor rises to shallow depths but does not discharge because of an almost impermeable surface layer, produced by intense alteration (e.g., clays are widespread in this setting). Vapor condenses and the condensates drain away. This produces steep thermal gradients, above 100°C/m in the top 15 cm, thus raising the surface temperature well above ambient. Conductive heating of moist air produces a thin diffuse layer of steam that explains the name (although it is strictly a misnomer, since no steam is visible if the air is dry). Steaming ground can always be recognized from the air by infrared anomalies. This manifestation occurs over many high-temperature systems. Steaming ground is the most important signature of heat transfer over high-temperature systems (with two-phase zones) in the arid parts of the African Rift Valley and contributes at least, together with minor steam vents, about 50% (~200 MW) of the amount of heat discharged from the Olkaria system (Kenya).

Evaporation from the surface of *hot pools* also constitutes a diffusive heat discharge. These pools can be subdivided as *calm*, *boiling*, or *ebulliant* (*effervescent*). They are widespread and occur mainly over liquid dominated, high-temperature reservoirs in flat terrain (where they usually occupy hydrothermal eruption or dissolution craters), but also over outflows from reservoirs beneath steep terrain, over vapor-dominated reservoirs (often over quenched fumaroles), and occasionally over intermediate-temperature fracture zone systems. The amount of heat transferred is proportional to the pool area, its temperature, and other parameters that enhance evaporation. Hot pools may be fed by ascending hot water, by steam-heated groundwater, or by steam. In the first case the water has almost neutral pH; in the last case it is acid. Ebullition and effervescence are usually the result of discharge of CO_2. The largest hot pool at Waiotapu (NZ), for example, discharges ~20 MW. Hot pools discharging neutral pH chloride water from high-temperature reservoirs are characterized by a rim of thick silica sinter. A type of hot pool is the *mud pool*, whose mud is kept liquid by the condensation of steam and rainwater and the upwelling is caused by the discharge of gas from below. A *mud volcano* is a feature at the margin of a mud pool produced where gas discharges from a vent and builds a cone of mud as high as 2 m. The mud usually comprises cristobalite and kaolin clays, but smectites may also occur.

2. *Direct and Continuous Heat Discharge*

The most common manifestations over all types of geothermal systems are *warm* or *hot springs. Boiling springs* are present over many high-temperature systems but rarely over intermediate-temperature ones. Artesian discharge of hot water produces *spouting hot springs* (spouters), which sometimes occur in a valley that drains a liquid dominated system. A spouter may also discharge a mixture of steam and boiling water, thus acting like a continuous geyser (Steady Geyser at Yellowstone Park, for example). *Acid hot springs* are typical discharge fea-

TABLE I Ranking of Surface Manifestations (Discharge Features) According to Their Role in Transferring Heat in Geothermal Systems

	A1	A2	B3	B4	B5	C3	C4	C5	C6	D7	D8	D9	D10
Warm Ground	x	x	x	x	x	xx	x	x	x	x	x	x	xx
'Steaming' Ground	xx	x	xx	xx	xx	xx	xx	xx	x	-	(x)	-	-
Hot Pools	-	x ac*,n*	-	-	xx ac*	xx n*	xx n*	xx ac*	xx n*	(x) n*	(x) n*	(x) n*	-
Hot Lakes	xx ac*	x ac*	-	-	x ac*	xx n*	-	-	x n*	-	xx n*	-	-
Mud Pools	-	-	x	(x)	x	x	x	x	x	-	-	-	-
Acid Hot Springs	xx	xx	x	(x)	x	(x)	-	x	(x)	-	-	-	-
Neutr. Hot Springs	-	(x)	x	(x)	-	xx	x	(x)	xx	xx	xx	xx	xx
Fumaroles	xx	xx	x	x	xx	xx	x	xx	(x)	-	-	-	-
Geysers	-	-	(x)	-	-	x	-	-	(x)	-	-	-	-
Hydroth. Eruptions	-	-	(x)	(x)	(x)	xx	x	x	xx	-	(x)	-	-
Concealed Outflows, Seepage	(x)	(x)	xx	xx	-	x	x	-	xx	-	x	(x)	(x)

Symbols for Ranking:

-	Not known
(x)	Occasionally present
x	Usually present (minor heat transfer)
xx	Usually present (major heat transfer)
xx	In some prospects manifestation may transfer > 50% of all heat discharged.

Other Symbols:

ac*	dominantly 'acidic' pH of liquids in pool or lake
n*	dominantly 'neutral' pH of liquids in pool or lake

Types of Geothermal Systems:

A1	Volcanic - Hydrothermal
A2	Quasi Volcanic - Hydrothermal

Systems associated with high standing Volcanic Centres:

B3	High T, Liquid dominant
B4	High T, Natural 2-Phase
B5	High T, Vapor dominant

Systems associated with flatter terrain:

C3	High T, Liquid dominant
C4	High T, Natural 2-Phase
C5	High T, Vapor dominant
C6	High T, Plate Collision
D7	Interm. T, Volcanic Arc Setting
D8	Interm. T, Heat Sweep Setting
D9	Fracture Zone Types
D10	Low T

tures associated with volcanic–hydrothermal systems, but also occur over high-temperature systems beneath high standing volcanic centers. Heat discharge rates of most single hot springs rarely exceed a few megawatts, although this is higher where springs occur in clusters or are aligned over a fracture. Large discharge rates from a single spring are unusual. However, if thermal fluids collect in a large confined aquifer and then funnel beneath a stream, large discharges may occur. The **Hippo Pool** hot spring in Ethiopia occurs in such a setting and constitutes the largest single discharge of thermal water (~1000 kg/s, transferring ~105 MW) in the East African Rift.

"Wet" steam, that is, steam at the saturation temperature containing condensation droplets, is discharged by most *fumoroles* over almost all types of high-temperature systems and volcanic–hydrothermal systems. "Dry" steam, hotter than saturation temperature, is discharged by a few fumaroles at high flow rates. The terms *wet* and *dry fumarole* have been used to describe these features. Fumaroles that discharge at speeds >20 m/s are noisy; vents with a quiet discharge (i.e., <20 m/s) have been called *steam vents.* Temperatures up to 145°C were measured in a dry fumarole at Darajat (Java) whose vapor derives from the top of the reservoir. Heat discharge rates of fumaroles are usually low despite the impressive appearance of their large steam cloud; the largest fumarole in the Ketetahi fumarole field (NZ) discharges only ~5 MW. Steam vents that deposit significant amounts of sulfur are called *solfataras;* those with high boric acid are *soffioni*.

Noncondensable gases, such as CO_2 and H_2S, sometimes discharge without any steam component; they transfer little heat since gas temperatures are usually low. Minor, cool CO_2 discharges, called *moffete*, occur both over volcanic–hydrothermal systems and nonvolcanic (usually travertine depositing) low-temperature systems. Vents and ground discharging a mixture of CO_2 and H_2S gases are called *kaipohan* in the Philippines, where they occur over high-temperature systems with an "acid core" (Palinpinon, for example). Peripheral CO_2 discharges at many other systems may have large gas fluxes (Sibayak in Sumatra, for example), or the gas can diffuse through the ground (lack of vegetation and dead birds in depressions are signs of such diffuse discharges).

3. *Intermittent Heat Discharge*

Geysers are spectacular manifestations discharging intermittently a mixture of boiling water, gas, and steam; they are, therefore, apart from some spouters, the only natural two-phase discharge feature of hydrothermal systems. Geysers occur over liquid dominated high-temperature systems, usually in rather flat terrain, and rarely at the toe of outflows. The average heat output, even of the largest geysers, is moderate, rarely exceeding 5 MW. They are the best-known of all thermal manifestations, and more has been written about them than about all other manifestations, although they are very rare. Geysers require fractured rocks filled with hot water at boiling temperature at shallow depth. Filling and flashing then causes a sudden discharge from a shallow cavity. This occurs regularly, but that from a complex fracture/cavity network may result in irregular discharges. Since they discharge deep water that is oversaturated with silica, geysers are always associated with wide sinter aprons. The discharge characteristics of geysers are very sensitive to pressure changes in the supply water. Effervescence of dissolved CO_2 can also trigger intermittent geyser-like discharges.

Thermal discharge features may show seasonal variations, especially in countries with a pronounced rainy season that raises the groundwater level. A famous seasonal discharge feature is the geyser at Rajabasa (Sumatra), which only discharges during the rainy season. Springs with intermittent discharge of hot water occurring in a geyserlike cycle in Iceland have been referred to as *pulsating springs.* A similar feature is the lake in Inferno Crater at Waimangu (New Zealand), which usually overflows every 5 weeks.

4. *Catastrophic Discharges*

In a setting that favours geyser activity and also over some vapor-dominated systems, there may be *hydrothermal eruptions.* These eruptions are triggered by an instability in a hydrostatic liquid column very close to boiling temperature. A slight pressure drop, for example, is sufficient to initiate an eruption. Once the upper portion of the vent has been uplifted by steam expansion, the resulting drop in pressure within the liquid column beneath induces further flashing discharges at progressively greater depth. The ejected debris forms a characteristic ring of hydrothermal eruption breccia. Hot water often later fills the crater, thus forming a large hot pool, as occurs at Waiotapu (NZ), which is surrounded by its eruption breccia. Some hot lakes can widen by marginal, smaller hydrothermal eruptions, which occurred, for example, in an acid lake over the vapor-dominated Kawah Kamojang field (Java).

Hydrothermal eruptions have also been triggered by engineering activity such as at Yangbajing (Tibet), where the pressure of drilling fluid was not sufficient to balance the pressure of shallow (<50 m) reservoir fluids. Naturally induced hydrothermal eruption craters surround the drill site.

5. *Heat Discharge Associated with Seepage*

Seepage is an ill-defined term, used to describe any type of subsurface discharge of thermal fluids, at both shallow and deep levels. Shallow seepage occurs if hot water from a geothermal reservoir discharges by concealed springs at the bottom of a river, a lake, or into shallow groundwater. If a river seepage is fed by an outflow from a nearby high-temperature system, almost no surface manifestations associated with it may be visible. This is the situation at **Mokai** (NZ), where ~300 MW of heat is discharged by hot chloride water into a large river at the toe of an 8-km long concealed outflow. Seepage into rivers and streams can be recognized from the different mass fluxes of nonreactive constituents, such as Cl and B, measured up- and downstream of the place where such an inflow is likely.

VI. SURFACE ALTERATION AND DEPOSITS

The thermal activity that is the surficial surface expression of a geothermal system is usually much smaller in its extent than is the surficial hydrothermal alteration. For this reason the hydrothermal minerals and their distribution provide useful clues about a geothermal system. For example, the surface alteration at **Matsukawa** in northern Honshu (Japan) was the single most important exploration guide for deducing the extent and potential of this important field.

The intensity of surface alteration at a particular site reflects a variety of parameters, including the shallow hydrology of the field, its near surface plumbing, the reactivity of the host rocks and the fluids, and the duration of fluid/rock interactions or mineral deposition. The extent of surficial hydrothermal alteration ranges from zero, for fields such as **Brawley** and **Heber** (Imperial Valley, California), to several hectares, as in the Yellowstone fields and at Waiotapu (NZ).

More than 100 minerals are known to occur in active geothermal fields. Some are rare (e.g., gold) and unexpected (e.g., lepidolite), but there are about 20 that are common and widespread in a large number of thermal fields hosted by a wide variety of rock types. Typical assemblages of surface alteration minerals associated with different types of geothermal systems are listed in Table II.

The identities of the hydrothermal minerals that form at a specific location depend upon a variety of factors, but the main ones are temperature and the composition of the reacting fluid, especially its pH and the amount of gases it has dissolved in it. In addition, the duration of fluid/rock interactions is reflected in the intensity of alteration, together with hydrological factors such as rock permeability.

Alteration produced by steam, or strictly steam condensate and gases, is dominantly destructive of the host rocks, but that associated with thermal waters of near neutral pH is mainly constructive. Thus, silica residue occurs as a product of steam alteration and silica sinter occurs where alkali waters discharge. The former derives its silica from the surficial rocks as most other cations are removed, but the silica in sinter is transported to the surface from the reservoir itself by the ascending alkali chloride waters.

Despite the corrosive behavior of steam condensate and acid gases, they produce a wide variety of hydrothermal minerals, including sulfur and many sulfates, of which alunite, gypsum and jarosite are usually the most common. Kaolin clays are also typical of this type of alteration and are usually either kaolinite, halloysite or, more rarely, dickite. Fine-grained hematite and hydrous iron oxides are also common products of oxidation, and

TABLE II Typical Assemblages of Surface Alteration Minerals Associated with Different Types of Geothermal Systems

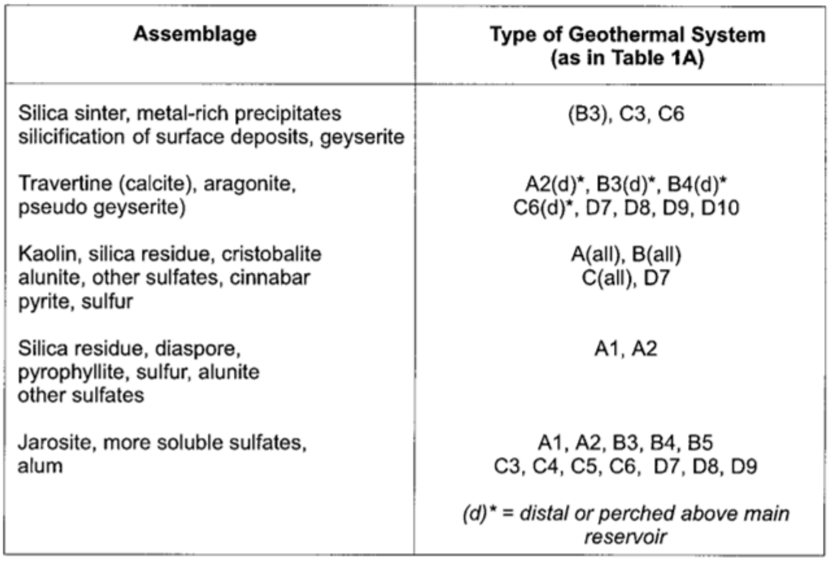

Assemblage	Type of Geothermal System (as in Table 1A)
Silica sinter, metal-rich precipitates silicification of surface deposits, geyserite	(B3), C3, C6
Travertine (calcite), aragonite, pseudo geyserite)	A2(d)*, B3(d)*, B4(d)* C6(d)*, D7, D8, D9, D10
Kaolin, silica residue, cristobalite alunite, other sulfates, cinnabar pyrite, sulfur	A(all), B(all) C(all), D7
Silica residue, diaspore, pyrophyllite, sulfur, alunite other sulfates	A1, A2
Jarosite, more soluble sulfates, alum	A1, A2, B3, B4, B5 C3, C4, C5, C6, D7, D8, D9
	(d) = distal or perched above main reservoir*

cristobalite is fairly widespread. This type of alteration is common above vapor dominated reservoirs, but also is present in those that have reservoirs with water only or else two phases. They are thus not diagnostic of reservoir type. Silica sinter and travertine have a variety of morphologies, many of which are similar, e.g., banding, terraces, geyserite (and pseudo-geyserite), overhangs, palisade structures, and postdepositionally formed features such as pressure ridges and fragmentation textures. Both also commonly record extensive microbiological activity, and many contain plant material. However, travertine (calcite or aragonite) and silica sinter have a quite different genesis and significance. Silica sinter deposits as thermal waters that are oversaturated with respect to quartz, chalcedony, or cristobalite cool at the free surface, whereas travertine forms as the depositing waters lose CO_2 formerly dissolved in them.

The presence of silica sinter is thus usually a reliable indication that the depositing fluids are derived from a reservoir hotter than about 180°C, but travertine has little geothermometric significance and the waters from which it deposits could have traveled several kilometers laterally.

VII. PERSPECTIVES

A. Heat Transfer and Classification

The magnitude of heat discharged by the thermal manifestations of hydrothermal systems has not been studied in detail, but some estimates are available. Comparison of these estimates with inferred, average, long-term heat discharge rates based on accumulated volume discharge rates of lava and tephra (say, 50 km^3 per 10 kyr) from highly active volcanoes indicates that many high-temperature hydrothermal systems can deliver as much energy, at a steady rate, as large volcanoes through their intermittent discharges, namely of the order of 100×10^{18} joule per 10 kyr (e.g., accumulated and extrapolated natural output of the Wairakei hydrothermal system versus that of the nearby Taupo caldera in New Zealand). Some of the energy throughput of hydrothermal systems replenishes their reservoirs, which may store between 10 and 30×10^{18} joule in the upper few kilometers, that is, about equal to the energy stored in the largest hydrocarbon reservoirs.

For appropriate and applicable temperature ranges, the dynamic viscosity of magma ($T > 1000$°C) is more than six orders of magnitude greater than that of hot water and vapor ($T > 250$°C); the heat energy transferred per unit mass by various magma types can be half that of mixtures of hot water and vapor. It appears, therefore, that in the longer term, hydrothermal systems are more effective in transferring heat energy than are volcanic systems, although details of the settings that favor the development of hydrothermal systems are not well understood.

Identification and ranking of high-temperature systems needs more attention. Ranking, in turn, requires assessment of the natural heat output and the likely reservoir temperatures in the same way as eruption characteristics have been used to assess and to classify volcanic systems. In this respect, geothermal research lags volcanological research, where several catalogues listing the worldwide distribution of volcanoes have been published. These catalogues list a volcano as "active" if it erupted at least once during historic times or during the last 2000 yr. The listed "active" volcanoes usually comprise both centers that discharge or have discharged magmatic fluids and volcanic–hydrothermal systems. The catalogues also list a number of high-temperature systems that have had historic hydrothermal eruptions as being "active" volcanoes, where such eruptions have been misclassified as "phreato-magmatic eruptions." In addition, hydrothermal systems that discharge only steam (i.e., steaming ground) are sometimes misidentified as "active" volcanoes. When the spatial distribution of volcanic versus hydrothermal systems is assessed, these problems have to be considered.

Although no comprehensive lists of high-temperature hydrothermal systems exist, most of them have been identified over active plate margins, often showing a clear alignment of both active volcanoes and high-temperature geothermal systems. There are probably 12 such centers in Sumatra that can be classified as "active volcanoes"; there are also at least 30 high-temperature systems, each discharging between 30 and 300 MW. Thus, the high-temperature hydrothermal systems of Sumatra outnumber the active volcanic systems by 2.5 : 1.

B. Thermal Alteration and Mineral Deposition

Ore-grade concentrations of some minerals occur at the surface of several active hydrothermal systems where they have deposited from ascending thermal waters. For example, the Champagne Pool at Waiotapu (NZ) is now depositing a precipitate rich in gold (up to 80 mg/kg) and silver (up to 200 mg/kg). At the Waimangu field nearby, silica sinter is precipitating that locally contains 3% elemental tungsten. The surface and near-surface parts (down to about 300 m) of many fields are thus analogues of typical low sulfidation epithermal ore deposits. The hydrological processes, such as boiling and fluid mixing, that occur in active hydrothermal systems leave mineralogical signatures (such as vein adularia and bladed calcite) that persist after the activity has ceased. For example, silica sinter of similar appearance to that at Waiotapu, but of Carboniferous age, occurs at the Wobegong epithermal mineral prospect in Queensland. The famous Devonian Rhynie cherts of northeast Scotland show unequivocal evidence that they deposited from hot chloride waters that once discharged at the surface.

In the deeper subsurface (>300 m, i.e., where boiling temperatures are >230°C in saturated reservoir rocks), the hydrological conditions in active hydrothermal systems more closely match those that once prevailed in some mesothermal ore deposits hosted by volcanic rocks. Here base metal sulfides sometimes deposit in concentrations locally up to ore grade, usually as a result of boiling, cooling, or fluid mixing. These sulfides most likely deposit where temperature gradients within the reservoir are steepest (near reservoir boundaries, for example). Little is known about the thermal regimes that occur below 3 km depth in active geothermal fields. Near the magma–host rock interface the conditions and processes that occur are likely to be the same as those that occurred when some of the large porphyry copper deposits formed in the western United States, such as Bisbee (Arizona) and Bingham (Utah).

Thermal and hydrological conditions can change during the lifetime of a hydrothermal system, as is evident from cores (with cross-cutting veins and mineral overprints) recovered from deep drillholes. The lifespans of geothermal systems are still poorly known, although this is an important research problem. At present we know that some hydrothermal systems, such as Ohaaki-Broadlands (NZ), have lasted for at least 300,000 yr and the Kawerau Field (NZ) has been active, in some form or other, for at least 280,000 yr. Icelandic geothermal systems do not usually live longer than 250,000 yr, but systems transferring heat from huge plutons, such as that beneath the greater Larderello Region (Italy), can have geothermal surface activity for >3 million years.

C. Outlook

In the past the lessons learned from studying active geothermal systems and the processes that occur within them have been applied to interpreting and understanding hydrothermal ore deposits. However, the opposite direction in research outlook could be equally revealing. Thus, rocks exposed through mining or erosion, which once reacted with thermal fluids deep in the bowels of an active geothermal system record, through their mineralogy and textures, evidence about the fluid characteristics and the thermal evolution of the system. There are many valuable insights waiting to be learned from studies of these rocks.

Geothermal systems are dynamic phenomena. Their surface manifestations are often beautiful and fascinating and have attracted admiration or fear since ancient times. They are, however, visible expressions of heat energy that has been transferred from great depth to the surface and so they are analogous to volcanoes. In the same way that the products of individual volcanoes differ widely, depending on their structural settings and the composition of their magmas, so do geothermal systems have a great variety of characteristics. Each system seems to be unique, although we have here tried to group them into broad but distinguishable categories.

The energy that geothermal systems hold has barely been tapped. Only about 9000 MW of electrical energy is now produced worldwide from geothermal fluids with ~90,000 MW thermal energy. Almost the same amount is utilized in myriad other ways (domestic and industrial heating, air conditioning, production of industrial bulk heat). Improvement in technology and plain need will lead to their being exploited more fully in future. However, geothermal systems are also, literally, wonderful natural laboratories worthy of study for their own sakes.

SEE ALSO THE FOLLOWING ARTICLES

Deep Ocean Hydrothermal Vents • Exploitation of Geothermal Resources • Geothermal Systems • Magma Ascent at Shallow Levels

FURTHER READING

Allen, A. T., and Day, A. L. (1935). Hot springs of the Yellowstone National Park. Carnegie Inst. Publication 466, Washington, DC.

Browne, P. R. L. (1978). Hydrothermal alteration in active geothermal fields. *Ann. Rev. Earth Planet. Sci.* **6,** 229–250.

Elder, J. (1981). "Geothermal Systems." Academic Press, London.

Ellis, A. J., and Mahon, W. A. J. (1977). "Chemistry and Geothermal Systems." Academic Press, New York.

Giggenbach, W. F. (1997). The origin and evolution of fluids in magmatic-hydrothermal systems. *In* "Geochemistry of Hydrothermal Ore Deposits," 3rd ed., (H. L. Barnes, ed.), John Wiley & Sons, New York.

Hochstein, M. P. (1990). Classification and assessment of geothermal resources. *In* "Small Geothermal Resources: A Guide to Development and Utilization" (M. H. Dickson and M. Fanelli, eds.). UNITAR/UNDP Centre for Small Energy Resources, Rome.

Hochstein, M. P., and Sudarman, S. (1993). Geothermal resources of Sumatra. *Geothermics* **22,** 181–200.

Rinehart, J. S. (1980). "Geysers and Geothermal Energy." Springer Verlag, New York.

Rybach, L. (1980). Geothermal systems, conductive heatflow, geothermal anomalies. *In* "Geothermal Systems" (L. Rybach and L. J. P. Muffler, eds.). John Wiley & Sons, Chichester.

Simkin, T., and Siebert, L. (1994). "Volcanoes of the World," 2nd ed. Geoscience Press, Tucson, and Smithsonian Institution, Washington, DC.

Waring, G. A. (1965). Thermal springs of the United States and other countries of the world—a summary. U. S. Geol. Survey Prof. Paper 492, U. S. Govt. Printing Office, Washington, DC.

White, D. E. (1955). Thermal springs and epithermal ore deposits. *Economic Geology* (50th Anniv. Volume), pp. 99–154.

This Page Intentionally Left Blank

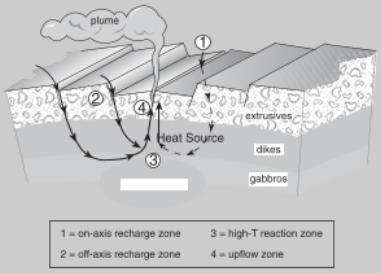

DEEP OCEAN HYDROTHERMAL VENTS

DAVID A. BUTTERFIELD
University of Washington

I. Definition and Significance of Submarine Hydrothermal Vents
II. Overview
III. Chemistry in the Three Zones of a Hydrothermal System
IV. Role of Phase Separation
V. Hydrothermal Chemistry of Seamounts and Non-MORB Environments
VI. Effect of Volcanic Activity on Hydrothermal Systems

GLOSSARY

black smoker A hot (generally > 330°C) hydrothermal vent that produces fine, dark mineral precipitates upon mixing with cold, ambient seawater. As the temperature and metal content of the vent fluid source decreases, the "smoke" grades from black to gray to white.

chimney A steep-sided hydrothermal mineral formation on the seafloor, formed by precipitation of primarily metal sulfides and sulfates when hot hydrothermal fluids mix with seawater.

dike A bladelike, tabular injection of magma that cuts through country rock.

fluid inclusion A fluid trapped within a rock. Small droplets of hydrothermal fluid may become trapped within secondary minerals, thus recording information about the kind of fluids present during mineral formation.

hydrosphere The layer of water existing within and between the lithosphere and atmosphere.

hydrothermal plume Hydrothermal effluent diluted with seawater after venting. Analogous to a smoke plume rising through the atmosphere from a smokestack, hydrothermal effluent rises from seafloor vents, entraining cold seawater until it reaches a level of neutral buoyancy, then spreads laterally. The thermal and chemical signal of hydrothermal plumes can be used to measure the output of a hydrothermal system, to help locate vents on the seafloor, and to assess the chemistry of the vented fluids.

lithosphere The rigid, rocky, outer crust of Earth or any planet.

major elements The most abundant chemical elements in a material. In seawater, for example, those elements present at millimolar levels (Na, Cl, K, Mg, Ca, SO_4).

magnesium metasomatism Uptake of Mg from seawater into secondary minerals.

MORB Midocean ridge basalt; the dominant rock type along midocean ridge spreading centers, derived from partial melting of the mantle and containing on average 50% by weight SiO_2.

ophiolite Ocean crust that has been tectonically placed on a continent. Ophiolites often host hydrothermal metal sulfide minerals.

phase separation Generally, the formation of immiscible vapor and liquid phases by heating or decompressing a fluid. For a pure liquid, phase separation is synonymous

Copyright © 2000 by Academic Press
All rights of reproduction in any form reserved.

with boiling, or the formation of vapor bubbles from a bulk liquid. In multicomponent aqueous fluids such as seawater, phase separation may also occur as condensation of dense brine from a bulk, vaporlike fluid.

stockwork A network, within a host rock, of cracks and veins filled by minerals precipitated from hydrothermal fluids.

upflow zone Region in the crust through which buoyant fluids rise in a network of cracks.

water/rock ratio A measure of the intensity or extent of water–rock reaction, that is, how much rock has reacted with a given quantity of water. Low water/rock ratios indicate intense reaction, analogous to making strong coffee. To calculate water/rock ratio requires a specific chemical or isotopic exchange reaction.

I. DEFINITION AND SIGNIFICANCE OF SUBMARINE HYDROTHERMAL VENTS

Submarine hydrothermal vents are the exit points on the sea floor for thermally driven convection of seawater within the ocean crust and are the result of interaction between seawater and submarine volcanoes. Vents are located in volcanic environments where seawater penetrates into permeable ocean crust, is heated by volcanic heat sources, reacts with ocean crustal rocks, and rises back to the seafloor. Hydrothermal circulation is a fundamental part of the production of new oceanic crust and transports a significant amount of the heat that escapes from the interior of the Earth. The associated chemical exchange between the hydrosphere and lithosphere has important impacts on the chemical balance of the oceans, the alteration of oceanic crust, and the reincorporation of altered oceanic lithosphere into the mantle at subduction zones.

Hydrothermal fluids transport high concentrations of metals through the ocean crust and deposit them as sulfide, sulfate, oxide, and silicate mineral deposits in stockwork feeder zones, in seafloor chimneys and mounds, and in metalliferous sediments. Through tectonic motion at convergent plate boundaries, some ancient submarine mineral deposits have been emplaced on continents and are mined for copper, zinc, and other metals. Hydrothermal fluids also transport gases produced by water–rock interaction or exsolved from magmas. The chemical energy available when hot, reduced hydrothermal fluids react with cold, oxygenated seawater can be harnessed by microbes at and below the seafloor. Similar volcanically powered life forms may exist on other planetary bodies where a hydrosphere interacts with volcanoes.

II. OVERVIEW

A. History

As the theory of plate tectonics and seafloor spreading was developed in the 1960s, it became clear that global-scale volcanism on the ocean floor has been a fundamental and dominating aspect of the Earth's geology, though eruptions remain hidden under thousands of meters of water. The theory of hydrothermal circulation of seawater through the ocean crust, which developed alongside the plate tectonic theory, had power to explain many different oceanographic observations, including (1) anomalous accumulation of metals in sediments and concentrated mineral deposits along midocean ridges; (2) excess of the primordial, mantle-derived isotope ^{3}He in seawater above midocean ridge depths; and (3) measured heat flow much lower than predicted by theoretical conductive cooling models for ocean crust less than ~65 million years old. Although hydrographic work revealed the presence of 60°C brines in the Atlantis II Deep in the Red Sea in the mid-1960s, the first seafloor vents directly observed and sampled took the form of warm (17°C) water discharging through dense animal communities at the Galapagos spreading center in 1977. This was followed in 1979 by the discovery of 350°C water discharging from metal sulfide chimneys at 21°N on the East Pacific Rise, a dramatic confirmation of the prediction of hot springs along submarine volcanic centers. The incredible density of previously undescribed fauna at hydrothermal vents was a scientific revelation. In the succeeding years, a great deal of exploration and sampling has been done along seafloor spreading centers, revealing tremendous variety in the form of hydrothermal venting and how it changes through time and space. This chapter will review some of what is known about seafloor hydrothermal venting, with emphasis on the chemistry of midocean ridge (MOR) hydrothermal fluids, the evolution of venting through time, and the effects of volcanic activity on hydrothermal systems.

B. Setting of Submarine Hydrothermal Systems

More than 35 active submarine hydrothermal vent fields have been located and sampled for vent fluids, minerals, and fauna. Table I and Fig. 1 include most of the known hydrothermal sites in deep water that have been thoroughly sampled. Table II contains some fluid chemistry data for a range of different deep ocean hydrothermal environments. More than 100 instances of hydrothermal mineral occurrences have been documented at seafloor volcanic sites, and comprehensive lists of these are found in references in Further Reading. Most active hydrothermal sites have been located by oceanographic water column studies of hydrothermal plumes, followed by seafloor submersible studies to conduct detailed sampling. Both diffuse low-temperature and focused high-temperature vents (Fig. 2) have been found across the range of tectonic environments from the slow-spreading Mid-Atlantic Ridge to the fastest-spreading portions of the East Pacific Rise, as well as in intraplate hot-spot, island arc, and backarc basin environments. In some cases, as at Guaymas Basin, Escanaba Trough, or Middle Valley (Table I), submarine volcanoes erupt beneath or within a thick layer of terrigenous sediment, giving rise to sediment-hosted sulfide mineral deposits and unique hydrothermal fluid chemistry (Table II). Wherever there is submarine volcanism, there is also hydrothermal activity due to the active role that circulating seawater plays in cooling and cracking newly emplaced magma. This chapter deals with midocean ridge and other deep-ocean hydrothermal systems; it does not include the many shallow hydrothermal systems around volcanic islands.

Although MOR volcanism is generally restricted to the <1 km-wide zone around the ridge axis, global heat flow studies have clearly shown that about 80% of the hydrothermal heat loss occurs in older (1 to ~65 Myr) crust away from the ridge. It is hypothesized that warm water circulation on volcanically inactive MOR flanks results in larger water and geochemical fluxes, but, as of this writing, Baby Bare Seamount on the eastern flank on the Juan de Fuca ridge on 3.5 Myr crust is the only clear example of a ridge flank warm-water vent. Ridge flank vents are difficult to locate because of the minuscule thermal signal they create in the water column, and because they may have little visual impact in the vast areas of older ocean floor. The exact nature and chemical composition of ridge flank fluids escaping to the ocean are poorly known. As search strategies improve, more ridge flank hydrothermal vents are likely to be found.

The location and form of seafloor vents is a complex function of heat source location, crustal permeability, and physical and chemical feedbacks. Only a few generalizations will be made here. On MOR segments that are volcanically robust, vents are often located within the narrow axial graben or aligned along eruptive fissures (Fig. 2a). In more tectonic regimes, where a well-developed graben exists, vents are often associated with normal faults on the graben walls (Fig. 2b). Long-lived, mature vent fields with large sulfide structures are often associated with faults and fault intersections. For example, persistent high-temperature venting is found near the caldera-bounding fault in Axial Volcano on the Juan de Fuca ridge. Within the well-mapped Main Endeavour vent field, dozens of hot smoker vents describe a curved line extending over 100 m and joining several large sulfide structures. In these and many other areas, it is likely that active fault zones maintain high permeability between a hot reaction zone and the seafloor.

C. Structure of Hydrothermal Systems

All hydrothermal systems have three essential features: (1) water, (2) a heat source, and (3) a permeable medium through which the water flows. In the case of submarine hydrothermal systems (Fig. 3), water is derived from seawater which saturates the brittle upper layer of oceanic crust. The heat is ultimately derived from radioactive decay and other sources within the earth, which is transferred to magmatic systems, predominantly along volcanically active, midocean-ridge spreading centers in the oceanic crust. Magma chambers are discontinuous beneath the midocean-ridge axis and vary in depth from several kilometers below the seafloor up to 1 km or less in areas of very high magma supply. Heat may be conducted through the roof of a magma chamber (Fig. 4a) to circulating seawater in the overlying crust, or heat may be actively mined from a magma chamber (Fig. 4b) as it solidifies and cracks. In the case of an active seafloor eruption (Fig. 4c), heat is transferred from the erupting lava, from the feeder dike, and deeper in the system from the magma source region. The structure and dynamics of hydrothermal systems are determined by the physics of water flowing through a permeable medium driven by density gradients induced by volcanic heating. Perturbations due to ocean and earth tides, chemical exchange and mineral precipitation, microbial activity, and feedback between the physical and chemical processes occurring in hydrothermal systems add many layers of complexity to the essential equation involving water, heat, and a permeable medium. There are still many gaps in our knowledge of the structure of hydrothermal systems and what controls their evolution through time.

Hydrothermal systems can be viewed as having three parts: a *recharge zone* where seawater percolates down

TABLE I Confirmed Active Submarine Hydrothermal Vent Sites

Map ref #	*Site name*	*Max. T (°C)*	*Depth (m)*	*Comment*	*Reference*
Mid-Atlantic					
1	Kolbeinsey ridge (67°N)	185	100	MOR hotspot	*a*
2	Steinaholl (63°6′N)	?	300	MOR hotspot	*b*
3	Lucky Strike (37°17′N)	333	1670	Ridge-axis seamount	*c*
4	Menez-Gwen (37°50′N)	320	840	MOR near Azores	*d*
5	Rainbow (36°14′N, 33°54′W)	362	2300	MOR	*e*
6	Broken Spur (29°10′N)	364	3090	Axial volcanic ridge	*c*
7	TAG (26°8′N, 44°44′W)	366	3650	E wall axial valley	*c*
8	MARK (23°20′N)	366	3840	Neovolcanic ridge	*c*
9	Logatchev (14°45′N)	>300?	2950	Uplifted block	*f*
Eastern Pacific					
10	Explorer ridge (49°45′N)	306	1900	Large sulfide mound	*g*
		Juan de Fuca			
11	Middle Valley (48°27′N)	276	2425	Sedimented MOR	*c*
12	Endeavour—Salty Dog (47°59′N)	324	2140		*h*
12	Endeavour—High Rise (47°58′N)	342	2170	Horst	*c*
12	Endeavour—Main Field (47°57′N)	380	2200	Near E axial wall	*c*
12	Endeavour—Mothra (47°56′N)	294	2270		*h*
13	CoAxial—Source (46°10′N)	294	2060	Near 1993 eruption	*i*
14	Axial Volcano—ASHES (45°56′N)	348	1540	1998 eruption	*c, j*
14	North Cleft—Monolith (44°59′N)	330	2300	Mid-1980s eruption	*c*
15	South Cleft (44°40′N)	342	2300		*c*
16	Baby Bare Seamount, Eastern flank	30	2600	3.5 Ma old crust	*k*
		Gorda Ridge			
17	Escanaba Trough (41°00′N)	217	3200	Sedimented MOR	*c*
		Guaymas Basin			
18	Guaymas (27°2′N)	315	2000	Sedimented basin	*c*
		Northern East Pacific Rise			
19	21°N (20°50′N)	355	2600	First black smoker site	*c*
20	13°N (12°49′ to 12°51′N)	380	2600		*c*
21	11°N (10°57′ to 11°15′N)	347	2600		*c*
22	9°50′N	388	2600		*c*
22	9°47′N	403	2600	1991 eruption	*c*
22	9°39′N	345	2600		*c*
22	9°33′N	308	2600		*c*
22	9°17′N	388	2620		*c*
		Galapagos Rift			
23	Galapagos (0°N, 86°W)	13	2450	First observed vents	*c*

continues

Continued

Map ref #	*Site name*	*Max. T (°C)*	*Depth (m)*	*Comment*	*Reference*
Southern East Pacific Rise					
24	14°S	374	2630	Fissure/collapse area	*l*
25	17°26′S	340	2600	Recent volcanism	*m*
25	18°10′S	305	2670	50-m deep graben	*m*
25	18°26′S	374	2635	90-m deep axial graben	*m, l*
	21°30′S	402	2835	>50-m deep graben	*f, n*
34	31°51′S	370	2330	Sampled Jan. 1999	*n*
Hawaiian Hot Spot					
26	Loihi Seamount	30	980	1996 earthquake swarm	*o*
Western Pacific					
Okinawa Trough					
27	Izena Cauldron (27°16′N, 127°05′E)	320	1400	CO_2 hydrates	*p*
27	Iheya Ridge (27°33′N, 126°58′E)	220	1400		*p*
Mariana Trough					
28	Mariana Trough (18°33′N)	287	3650	Local andesites	*q*
Manus Basin					
29	Vienna Woods (3°10′S, 150°17′E)	302	2500		*r*
29	DESMOS (3°42′S, 151°52′E)	120	1925	Magmatic SO_2	*r*
Woodlark Basin					
30	Franklin Seamount (9°54′S, 151°50′E)	30	2275	Au-rich deposits	*s*
North Fiji Basin					
31	White Lady (16°58′S, 173°55′E)	285	2000	Anhydrite chimney	*t*
Lau Basin					
32	Valu Fa Ridge (22°S, 176°W)	400	1900	Highest Pb, Zn in fluid	*u*
Society Islands Hotspot					
33	Teahitia Seamount (17.5°S, 148.5°W)	30	1460	Low-temperature system	*v*
Red Sea					
35	Atlantis II Deep (21°20′N, 38°05′E)	66	2000	Dense brine pool	*w*

Map reference numbers refer to location on Fig. 1. All sites have had fluids sampled except Steinholl and Logatchev.

[a] Olafsson, J., *et al.* (1990). Geochemical observations from a boiling hydrothermal site on the Kolbeinsey ridge. *EOS Trans. AGU* **71,** 1650.

[b] Fricke, H., *et al.* (1989). Hydrothermal vent communities at the shallow subpolar Mid-Atlantic Ridge. *Marine Biology* **102,** 425–429.

[c] Data and primary references found in Von Damm, K. (1995). Controls on the chemistry and temporal variability of seafloor hydrothermal fluids. *In* "Seafloor Hydrothermal Systems: Physical, Chemical, Biological, and Geological Interactions," Geophysical Monograph 91 (S. E. Humphris, R. A. Zierenberg, L. S. Mullineaux, and R. E. Thomson, eds.). American Geophysical Union, Washington, DC.

[d] Donval, J. P., *et al.* (1994). Compared chemistry of hydrothermal fluids collected with the Nautile at Lucky Strike (37°17′N) and the new Menez-Gwen (37°50′N) sites on the Mid-Atlantic Ridge (DIVA 1 cruise, May 1994). *EOS Trans. AGU* **75,** 309.

[e] Fouquet, Y., *et al.* (1997). Discovery and first submersible investigations on the Rainbow hydrothermal field on the MAR, 36°14′N. *EOS Trans. AGU* **78,** F832.

[f] Krasnov, S. G., *et al.* (1995). Geological setting of high-temperature hydrothermal activity and massive sulphide formation on fast- and slow-spreading ridges. *In* "Hydrothermal Vents and Processes" (L. M. Parson, C. L. Walker, and D. R. Dixon, eds.). Special Publication No. 87, The Geological Society, London.

continues

[g] Tunnicliffe, V., *et al.* (1986). Hydrothermal vents of Explorer Ridge, northeast Pacific. *Deep-Sea Res.* **33,** 401–412.

[h] Delaney *et al.* (1997). The Endeavour hydrothermal system I: Cellular circulation above an active cracking front yields large sulfide structures, "fresh" vent water, and hyperthermophilic archaea. *RIDGE Events* **8**(2), 11–19.

[i] Butterfield *et al.* (1997). Seafloor eruptions and evolution of hydrothermal fluid chemistry. *Phil. Trans. Roy. Soc. London A* **355,** 369–386.

[j] Butterfield *et al.* (1995). Spatial and temporal variability in hydrothermal vent fluid composition along the Juan de Fuca Ridge. *EOS Trans. AGU* **76,** F420.

[k] Mottl, M. J., *et al.* (1998). Warm springs discovered on 3.5 Ma oceanic crust, eastern flank of the Juan de Fuca Ridge. *Geology* **26,** 51–54.

[l] Butterfield, D. A., Roe, K. K., Ishibashi, J.-I., and Lupton, J. E. (1997). Time series chemistry of hydrothermal fluids from the Southern East Pacific Rise, 14–18°S. *EOS Trans. AGU* **78,** F706.

[m] Charlou, J.-L., *et al.* (1996). Mineral and gas chemistry of hydrothermal fluids on an ultrafast spreading ridge: East Pacific Rise, 17° to 19°S (Naudur cruise, 1993) phase separation processes controlled by volcanic and tectonic activity. *J. Geophys. Res.* **101,** 15,899–15,919.

[n] Butterfield, D. A. (1999). Unpublished results.

[o] Karl, D., *et al.* (1988). Loihi seamount, Hawaii: a mid-plate volcano with a distinctive hydrothermal system. *Nature* **335,** 532–535.

[p] Sakai, H., *et al.* (1990). Venting of carbon dioxide-rich fluid and hydrate formation in the mid-Okinawa Trough back arc basin. *Science* **248,** 1093–1096.

[q] Campbell, A. C., *et al.* (1987). Chemistry of hydrothermal fluids from the Mariana Trough back arc basin in comparison to mid-ocean ridge fluids. *EOS Trans. Am. Geophys. Un.* **68,** 1531.

[r] Gamo, T., *et al.* (1997). Acidic and sulfate-rich hydrothermal fluids from the Manus back-arc basin, Papua New Guinea. *Geology* **25,** 139–142.

[s] Binns, R. A., *et al.* (1993). Hydrothermal oxide and gold-rich sulfate deposits of Franklin Seamount, Western Woodlark Basin, Papua New Guinea. *Econ. Geol.* **88,** 2122–2153.

[t] Grimaud, D., *et al.* (1991). Chemistry of hydrothermal fluids from the 17°S active site on the North Fiji Basin Ridge (SW Pacific). *Chem. Geol.* **93,** 209–218.

[u] Fouquet, Y., *et al.* (1991). Hydrothermal activity in the Lau back-arc basin: Sulfides and water chemistry. *Geology* **19,** 303–306.

[v] Michard, A., *et al.* (1993). Submarine thermal springs associated with young volcanoes: The Teahitia vents, Society Island, Pacific Ocean. *Geochim. Cosmochim. Acta* **57,** 4977–4986.

[w] Craig, H. (1969). Geochemistry and origin of the Red Sea brines. *In* "Hot Brines and Recent Heavy Metal Deposits in the Red Sea" (E. T. Degens and R. A. Ross, eds.). Springer-Verlag, Berlin.

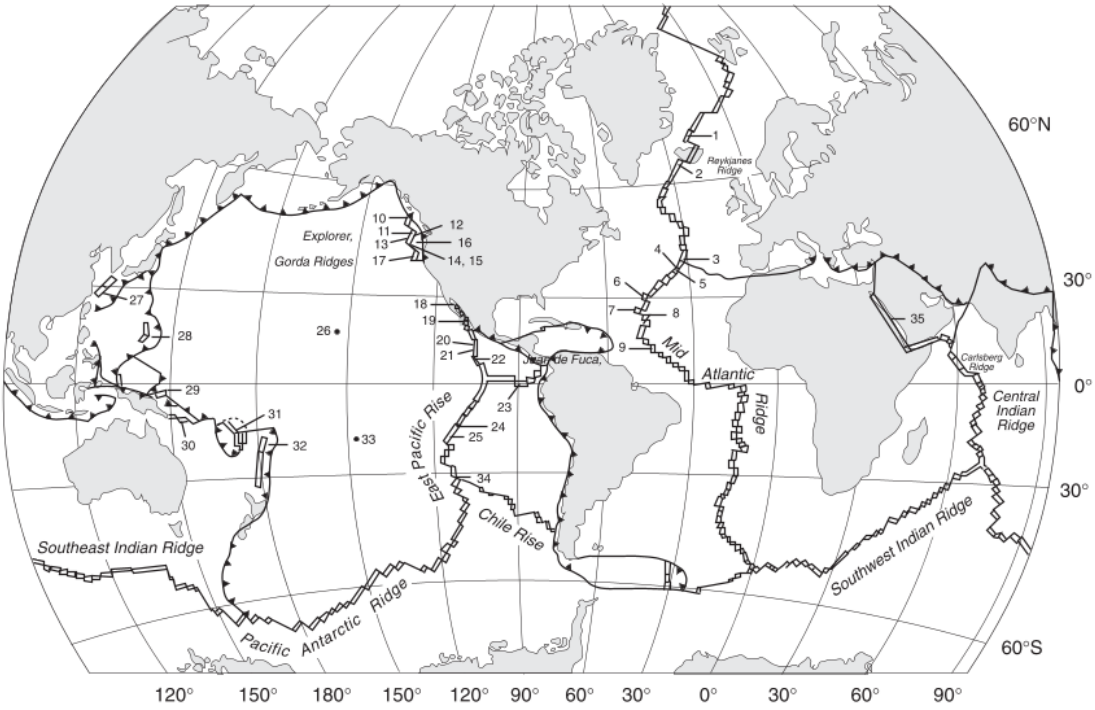
60°N
30°
0°
30°
60°S
120°
150°
180°
150°
120°
90°
60°
30°
0°
30°
60°
90°
1
2
Reykjanes Ridge
3
4
5
6
7
8
9
Mid
Atlantic
Ridge
10
11
12
13
16
17
14, 15
Explorer,
Gorda Ridges
18
19
20
21
22
Juan de Fuca,
23
24
25
26
27
28
29
30
31
32
33
34
35
Carlsberg Ridge
Central Indian Ridge
East Pacific Rise
Chile Rise
Southeast Indian Ridge
Pacific Antarctic Ridge
Southwest Indian Ridge

FIGURE 1 Map of global spreading centers and subduction zones. Numbers correspond to the descriptions in Table I and indicate hydrothermally active sites where fluids have been collected. There are many additional sites of known submarine mineral deposits of volcanic origin. Large portions of the midocean ridge system remain unexplored, including most of the high-latitude ridges and the mid-Atlantic ridge south of the equator.

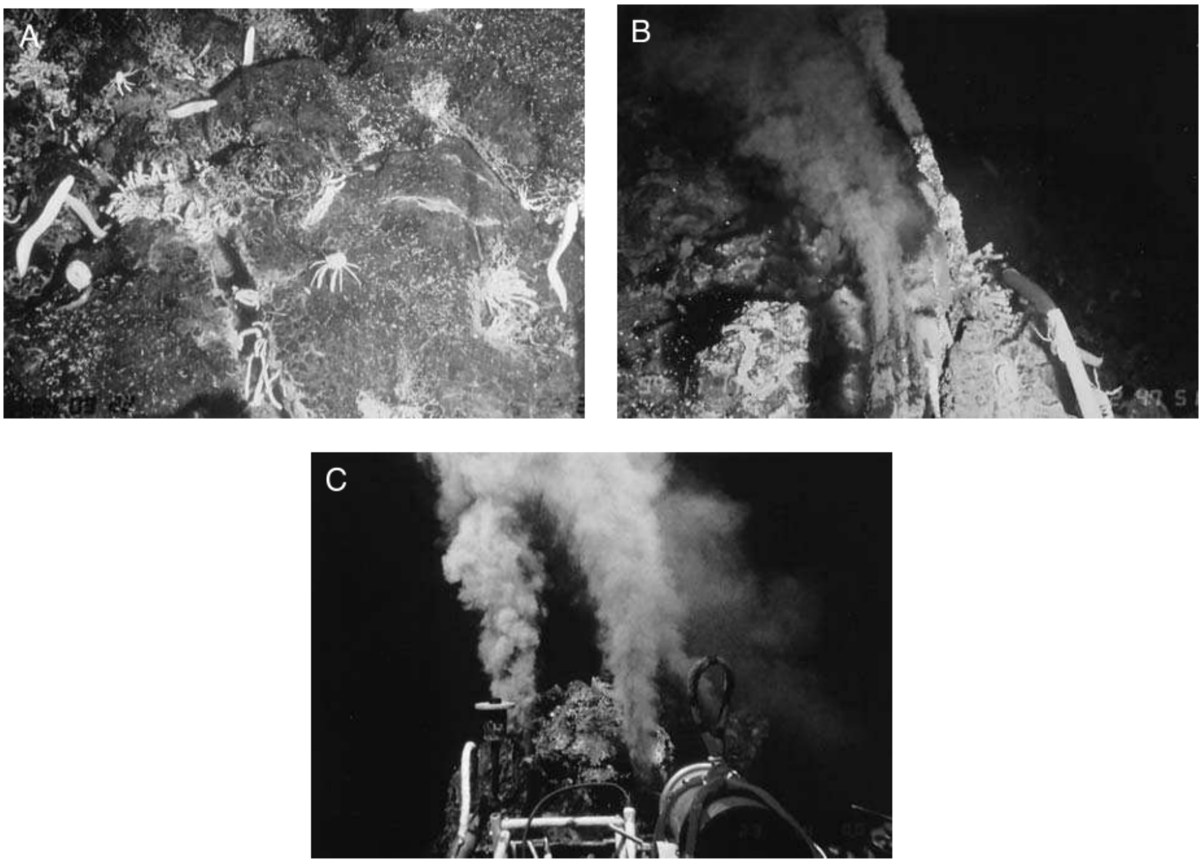

FIGURE 2 Photographs of submarine hydrothermal vents. (A) Diffuse vent environment photographed in 1994 from the submersible *Shinkai 6500* on the southern East Pacific Rise at 17°25′S, with Zoarcid fish, Bythograeid crabs, amphipods, tube worms (possibly Tevnia), serpulid worms, and other fauna. Warm water is venting from the small fissure in the lower center of the photo, and also around the edges of basalt lobes in upper half. The fissure is associated with hydrothermal activity over a distance of >500 m. (B) 370°C black smoker vent at 18°26′S on the EPR. Crabs cling to the tube of a Riftia tubeworm in lower right. The spindly black smoker in upper center may well be the mineral-encrusted remains of a large tubeworm that has been incorporated into the growing sulfide edifice. It is not unusual for vent fauna to become part of seafloor mineral deposits. This is one of a series of vents growing in lines perpendicular to a normal fault within a 90 m-deep axial graben. (C) Top of the 300°C, 4-m high "Monolith" sulfide chimney on the Juan de Fuca ridge near 44°59′N. Science gear in the *Alvin* basket in foreground includes the handle and intake to the manifold fluid sampler at left and the SUAVE *in situ* chemical analyzer at right.

through the crust and is slowly heated and chemically modified by low-temperature reactions; a high-temperature *reaction zone* near the heat source where fluid equilibrates with hot rock; and an *upflow zone* where heated, buoyant fluids ascend rapidly to the seafloor. The location of the heat source and the permeability structure of the crust are extremely important factors in any hydrothermal system.

Very little can be said with certainty about the recharge zone. It is not known whether recharge (Fig. 3) is predominantly along near-vertical faults and fissures along the ridge axis, through inclined, ridge-parallel faults near the ridge axis, from cross-cutting faults perpendicular to the ridge axis, or through a crack network distributed over a very broad region. It is likely that different combinations of these recharge pathways are involved in particular hydrothermal systems depending on their tectonic and volcanic history.

Convecting fluids reach their maximum temperatures in the high-temperature reaction zone. In midocean ridge systems, the reaction zone is generally believed to be over a magmatic heat source near the base of the sheeted dike complex (a set of ridge-parallel volcanic dikes through which magma is delivered from the

TABLE II Selected Vent Fluid Compositions from Different Environments

Area	Host environment	Date sampled	Depth (m)	Temp. (°C)	pH @25°C	Cl (mmol/kg)	Li (μmol/kg)	Na (mmol/kg)	K (mmol/kg)
Ambient deep seawater			2100	2.5	7.9	541	26	464	9.9
[a]EPR, 21°N, OBS vent	MORB	1979, 1981	2600	350	3.4	489	891	432	23.2
[a]EPR, 13°N, vent 2	MORB	1984	2600	354	3.1	712	592	551	27.5
[b]EPR, 9.8°N, F-vent	MORB	1991	2582	388	2.8	46.5	18	38.4	1.16
[b]EPR, 9.8°N, F-vent	MORB	1994	2582	351	2.6	846	1620	683	41.5
[c]SEPR, 18.5°S	MORB	1993	2620	310	3	155	50	137	2.8
[c]SEPR, 17.5°S	MORB	1993	2575	340	3	190	183	125	6.7
[a]JFR, Axial Volc., Inferno vent	MORB	1988	1540	330	3.5	624	636	499	26.8
[a]JFR, Axial Volc., V.M. vent	MORB	1988	1540	299	4.4	176	184	148	6.98
[a]JFR, Main Endeavour, Grotto	MORB	1988	2200	360	4.25	425	379	331	24.42
[a]JFR, S. Cleft, Vent 1	MORB	1984	2300	285	3.2	896	1108	661	37.3
[a]JFR, N. Cleft, Pipe Organ	MORB	1990	2300	262	2.8	1245	2350	926	58.7
[d]MAR, TAG, black smoker	MORB	1990	3700	365	3.35	636	850	557	17.1
[d]MAR, TAG, white smoker	MORB	1990	3700	300	3		850		17.1
[a]Gorda, Escanaba trough	sediment	1988	3270	217	5.4	668	1286	560	40.4
[e]JFR, Middle Valley, Dead Dog	sediment	1990	2430	265	5.5	578	500	398	18.7
[f]Lau BAB, Vai-Lilli-1	andesite	1989	1720	280	2	712	580	552	64
[f]Lau BAB, Vai-Lilli-3	andesite	1989	1720	334	2	790	623	590	79
[g]Mid-Okinawa trough, JADE	rhyolite/dacite	1989	1350	320	4.7		2500		73
[h]N. Fiji Basin, White Lady	MORB	1989/91	1980	285	4.7	255	200	210	10.5

[a] Von Damm, K. L. (1995), as in Table I.

[b] Von Damm, K. L., *et al.* (1995), as in bibliography.

[c] Charlou, J.-L., *et al.* (1996), as in Table I.

[d] Edmond, J. M. *et al.* (1995). Time series studies of vent fluids from the TAG and MARK sites (1986, 1990) Mid-Atlantic ridge: a new solution chemistry model and a mechanism for Cu/Zn zonation in massive sulphide orebodies. *In* "Hydrothermal Vents and Processes" (Parson, Walker, and Dixon, eds.). The Geological Society, London.

[e] Butterfield, D. A., *et al.* (1994). Geochemistry of hydrothermal vent fluids from Middle Valley, Juan de Fuca Ridge. *Proceedings ODP, Sci. Res.* **139,** 395–410.

[f] Fouquet, Y., *et al.* (1991), as in Table I.

[g] Sakai, H., *et al.* (1990), as in Table I, and Sakai, H., *et al.* (1990). Unique chemistry of the hydrothermal solution in the Mid-Okinawa Trough backarc basin. *Geophys. Res. Lett.* **17,** 2133–2136.

[h] Ishibashi, J.-I., *et al.* (1994). Fluctuation of chemical compositions of the phase-separated hydrothermal fluid from the North Fiji Basin Ridge. *Marine Geol.* **116,** 215–226.

magma source to the upper extrusive layer; Fig. 3). Once fluids penetrate close enough to the heat source, they reach temperatures of at least 300–450°C at 250–500 bar pressure, and reaction rates greatly increase. Based on (1) thermodynamic calculations applied to some hydrothermal fluid compositions and (2) relatively stable compositions in some time series studies of vent fluids, it is believed that MOR hydrothermal fluids may reach a steady-state composition or approach equilibrium with a greenschist alteration mineral assemblage. Hydrothermally altered seawater at 350–450°C and 250–500 bar pressure is quite buoyant and will rise quickly from the reaction zone near the heat source into the upflow zone.

The upflow zone is in many ways an extension of the reaction zone up to the sea floor, because hot, buoyant fluids may continue to react with wall rocks and secondary minerals as they rapidly rise to seafloor vents. However, although the reaction zone is characterized by heating to maximum temperature and extensive water–rock exchange, the upflow zone is characterized by cooling and mineral precipitation. The rising fluids cool in the upflow zone by adiabatic decompression, conductive heat loss, and mixing with cooler fluids surrounding the upflow conduits. The residence time of hydrothermal fluid in the reaction zone (at temperatures >150°C) is poorly constrained and is estimated to be of the order of 2 yr or less based on radium isotopes measured in hot fluids. Based on the observed exit velocities of hot

Ca (mmol/kg)	SiO_2 (mmol/kg)	Mn (mmol/kg)	Fe (mmol/kg)	Fe/Mn	Cu (μmol/kg)	Zn (μmol/kg)	Pb (nmol/kg)	H_2S (mmol/kg)	CO_2 (mmol/kg)	CH_4 (μmol/kg)	NH^3 (mmol/kg)
10.2	0.18				<.01	<.01	<.1	0	2.5	0	0
15.6	17.6	0.96	1.664	1.7	35	106	308	7.3	5.7	94	0.01
53.7	19.4	2.932	10.37	3.5		5	27	8.2	18.4	54	
1.8	5.93	0.174	1.49	8.6				41	15.5		
45.6	20	3.28	12.1	3.7				8.71	11.4		
6.6	14	0.45	3.4	7.6	13	80		27	21.2	70	
5.2	10.6	0.25	0.59	2.4	10	90		8.6	13.1	7.5	
46.8	15.1	1.081	1.006	0.9	12	113	302	7	50		
10.2	13.5	0.162	0.009	0.06	0.7	2.3	101	12	285		
32.6	15.77	0.286	0.915	3.2	25	37	210	5.3	12.6	2100	0.6
84.7	22.8	2.611	10.349	4.0	<2	300	650	3	4.2	110	
109	24	4.25	16.4	3.9	0.9	406	1085	1.99			0.002
30.8	20.75	0.68	5.59	8.2	140	46		3	3.4	147	
27	19.1	0.75	3.83	5.1	3	350		0.5			
33.4	6.9	0.021	0.01	0.5				1.5			5.6
81	10.1	0.063	0.014	0.22	0.6	1.6	100	3	4.5		2.8
35.5	13.8	6.2	1.16	0.19	16	1400	7000		<7.8	<5	
41.3	14.5	7.1	2.5	0.35	34	3000	3900				
22								12.4	200	2400	5.2
6.5	14	0.012	0.013	1.1				2	14.5	30.4	

vents and on recent time series measurements, the residence time of fluids in the upflow zone must be of the order of days. In a well-established hydrothermal plumbing system, the upflow zone should be thoroughly altered and the conduits lined with secondary minerals, so that passage of the hot fluid should have relatively little effect on the fluid composition. The primary imprint of high-temperature water–rock reaction is established at the base of the upflow zone.

III. CHEMISTRY IN THE THREE ZONES OF A HYDROTHERMAL SYSTEM

The three zones of hydrothermal systems on the mid-ocean ridge can each be characterized by a set of dominant chemical reactions. In the recharge zone, the exact nature of fluids remains unknown because they have not been sampled. The general picture of recharge zone fluids is based on thermodynamic calculations, studies of oceanic rocks altered at low temperature, and experimental water–rock reaction studies at low temperature. Seawater in contact with basalt at low temperatures (0–100°C) gradually becomes more reduced, losing first oxygen, then nitrate and sulfate. Magnesium, which makes up about 10% of the cations in seawater on a molar basis, is removed from seawater into secondary minerals. This process of magnesium metasomatism generates acid that promotes further attack on the basalt, releasing calcium, iron, and other cations into the hydrothermal fluid. At temperatures below about 50°C, boron and alkali metal ions (K, Li, Rb, and Cs) are taken up from the fluid into the rock, but as temperatures increase, the reactions reverse and the rocks become a source of these elements to the hydrothermal solutions. The net effect of recharge zone reactions on the fluid depends primarily on the residence time and the rate of temperature increase.

Direct sampling of crustal fluids in a MOR recharge zone is a difficult proposition and has not been done. However, fluid samples have been recovered recently on the sediment-covered east flank of the Juan de Fuca ridge from natural warm springs on "Baby Bare," a basaltic outcrop, and from a man-made Ocean Drilling Program (ODP) hole penetrating a 60–70°C fluid reservoir in the basaltic crust beneath 250 m of sediment. These off-axis fluids are important for two reasons: (1) They provide a direct measure of fluid compositions

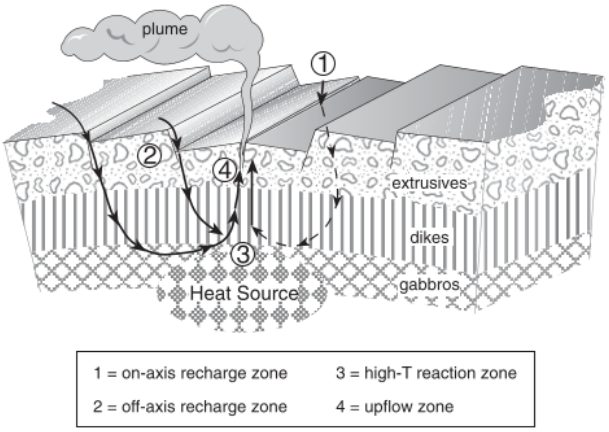

FIGURE 3 Cutaway view of essential structure of midocean ridge hydrothermal systems. This idealized structure is derived from drilling and seismic studies of the ocean crust and from studies of ophiolites. The uppermost layer of extrusive volcanics is the most permeable and has a thickness from several hundred meters to over a kilometer. The extrusive layer transitions into sheeted dikes, which are the feeder system between the magma source and upper extrusives. Below the sheeted dikes are gabbros, which have crystallized out of the magma source percolating up from the mantle. Arrows denote flow of hydrothermal seawater, with the dashed arrows denoting flow along the ridge axis behind the cutaway plane of the figure.

from off-axis hydrothermal venting, where approximately 80% of the total hydrothermal heat flux to the deep ocean occurs, and (2) they are an analogue for recharge zone fluids on the MOR axis because they are the result of prolonged, low-temperature reaction of seawater with basaltic crust.

The fluids venting at Baby Bare seamount and the fluids recovered from nearby ODP Hole 1026B reveal a great deal about conditions in relatively warm basaltic ocean crust and generally confirm the theoretical and experimental predictions. More than 90% of the seawater Mg has been removed from solution, confirming that Mg uptake by hydrothermal circulation on ridge flanks is important and has a major impact on the balance of Mg in the oceans. Alkalis are depleted, as inferred from altered basalts. The fluid redox state is still dominated by seawater: Significant seawater sulfate is present, and hydrogen sulfide concentrations are very low (less than 0.5 micromol/kg). Metal concentrations are generally limited by oxide or oxyhydroxide solubility rather than by sulfide mineral solubility. Total CO_2 and alkalinity are lower than in seawater, indicating that precipitation of calcium carbonate has taken place. The general character of the off-axis fluids, an analogue for recharge zone fluids, is in agreement with thermodynamic predictions and inferences from studies of altered basalts.

As fluids move through the transition from the recharge zone to the reaction zone, they pass through an important temperature horizon of ~150°C, above which anhydrite ($CaSO_4$) becomes saturated and precipitates from solution. As sulfate is the second most abundant anion in seawater, this has a major impact on the fluid chemistry and can produce substantial volumes of anhydrite in pore spaces. The sulfur isotope signature of hydrogen sulfide in hot vent fluids requires contributions both from basaltic sulfur and from reduced seawater sulfate, and there is evidence that anhydrite may be present in some high-temperature reaction zones.

By the time fluids reach the high-temperature reac-

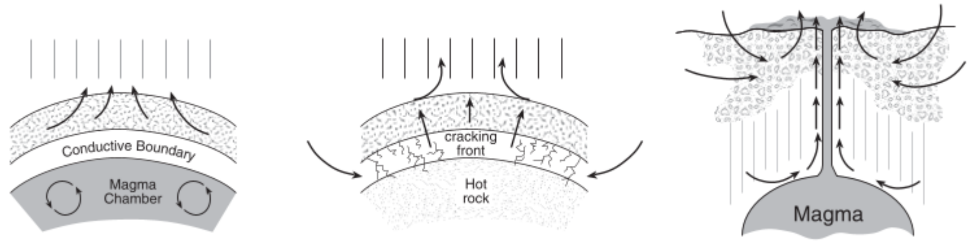

A. Magma Chamber - conductive boundary B. Frozen Magma - cracking front C. Active Eruption - freezing dike

FIGURE 4 Hydrothermal heat transfer and reaction zones. Arrows denote flow of hydrothermal fluids. (A) Fluids circulate below the base of the sheeted dike section, extracting heat through a relatively thin conductive boundary layer over a convecting magma chamber. In this case the reaction zone remains relatively stationary as long as there is a strong supply of magma. (B) Circulating fluids mine heat from a solidified magma body by advancing downward along a cracking front, continuously exposing fresh rock in the reaction zone. (C) Flow of fluids around a dike and over and through erupted lavas during an active seafloor eruption. Putting the heat source at the seafloor and within highly permeable volcanics may result in rapid extraction of heat and formation of "event plumes" in the overlying water column.

tion zone, most of their Mg has been taken up into secondary minerals, and what remains is quickly removed as Mg metasomatism accelerates with increasing temperature. As temperatures approach 400°C, the solubility of many species that are trace elements in seawater greatly increases. Many transition metals are extracted from basalt and increase in concentration over their seawater concentration by 3 to 7 orders of magnitude. Dissolved silica reaches concentrations at or near quartz saturation (~15 to 25 mmol/kg depending on temperature, pressure, and salinity). Hydrogen sulfide reaches millimolar levels as metal sulfides are leached from the host rock and as seawater sulfate is reduced (Fig. 5). Other volatile compounds (e.g., CO_2 and He) are extracted from the host rock, acquired from magmatic degassing or generated from water/rock reactions (e.g., H_2). The isotopic ratios of hydrogen and oxygen in water and of many of the dissolved elements in solution are changed by isotopic exchange with the ocean crust. Hydrothermal fluids emerge from the reaction zone highly altered from the original seawater composition.

In MORB-hosted hydrothermal systems, it is thought that the overall reactions governing fluid–mineral equilibrium are the alteration of primary olivine and plagioclase to form secondary plagioclase, chlorite, epidote, and quartz (i.e., a greenschist assemblage). Although greatly simplified, the process can be represented in part by these reactions:

$$\overset{\text{Olivine}}{2\mathrm{Mg_2SiO_4}} + \overset{\text{Plagioclase}}{\mathrm{CaAl_2Si_2O_8}} + 4\mathrm{H_2O} + \mathrm{Mg^{2+}} = \overset{\text{Clinochlore}}{\mathrm{Mg_5Al_2Si_3O_{10}(OH)_8}} + \overset{\text{Quartz}}{\mathrm{SiO_2}} + \mathrm{Ca^{2+}} \quad (1)$$

$$\mathrm{Na^+} + \overset{\text{Anorthite}}{2\mathrm{CaAl_2Si_2O_8}} + 2\mathrm{SiO_2} + \mathrm{H_2O} = \overset{\text{Albite}}{\mathrm{NaAlSi_3O_8}} + \overset{\text{Clinozoisite}}{\mathrm{Ca_2Al_3Si_3O_{12}(OH)}} + \mathrm{H^+} \quad (2)$$

It is thought that hydrothermal fluids approach equilibrium with a greenschist mineral assemblage in the reaction zone, and that the redox state of hot fluids is buffered near the pyrite–pyrrhotite–magnetite triple point. If the mineral assemblage and the major element composition (Cl, Na, Ca, K) of the fluid are specified, then the concentrations of other metals and hydrogen sulfide in the hydrothermal solution are determined by the major variables of the system: temperature, pressure, pH, and redox potential. A change in any one of these variables changes the position of equilibrium and can result in redistribution of chemical species in solution (i.e., shifts in acid dissociation or ionic complexation) or in precipitation or dissolution of minerals. As hot, buoyant fluids rise from the reaction zone, the extent of cooling they undergo depends upon the pathway to the seafloor (i.e., how well insulated is the pathway, and how much mixing with cold "groundwater" takes place). The result of cooling a solution saturated with respect to metal sulfide solubility is an oversaturated solution that will precipitate if the reaction kinetics are fast enough. Metal sulfide precipitation releases acid, so if

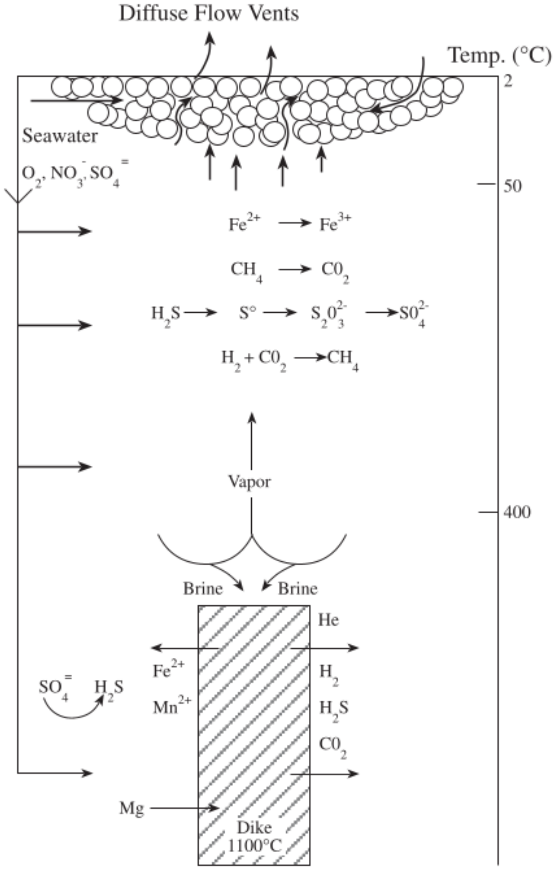
Diffuse Flow Vents
Temp. (°C)
2
Seawater
O_2, NO_3^-, $SO_4^=$
50
$Fe^{2+} \rightarrow Fe^{3+}$
$CH_4 \rightarrow C0_2$
$H_2S \rightarrow S° \rightarrow S_2O_3^{2-} \rightarrow SO_4^{2-}$
$H_2 + C0_2 \rightarrow CH_4$
Vapor
400
Brine
Brine
He
Fe^{2+}
Mn^{2+}
H_2
H_2S
$C0_2$
$SO_4^=$
H_2S
Mg
Dike
1100°C

FIGURE 5 Chemical and microbial processes in hydrothermal reaction and upflow zones. Hydrothermal fluid circulating around a magmatic heat source picks up volatiles and metals through outgassing and water–rock interaction. Phase separation partitions volatiles and some metals into the vapor phase, and metal-rich brines accumulate around the heat source. A thermal and redox gradient is produced as hot, reduced fluids mix with cold seawater in the upflow zone. Some important energy-yielding redox reactions are shown in the sequence in which they might occur as mixing proceeds (methanogenesis, oxidation of sulfur compounds, oxidation of methane and iron). Diffuse vent fluids on the seafloor bear the imprint of these chemical and microbially mediated reactions occuring in hotter zones below. [From Butterfield *et al.*, 1997.]

substantial cooling and precipitation take place, the resulting fluid will become more acidic, which in turn can cause dissolution of other minerals further along the flow path. For example, cooling a 400° C fluid to below 350° C results in precipitation of much of the copper as chalcopyrite and lowers the pH, and if the resulting fluid is in contact with sphalerite or other zinc sulfides, they may dissolve and greatly increase the zinc concentration in the fluid. This process of zone refining is reflected in mineral deposits and in the global data for vent fluids (Fig. 6, Table II).

The permeability structure of the upflow zone will have a major influence on the chemistry of the vented fluids, and on the potential for microbial growth and mineral precipitation below the seafloor. If hot fluids are effectively flowing up through a system of sealed pipes lined with sulfide minerals, then mineral precipitation will be limited to the relatively minor effects of adiabatic expansion and conductive cooling. Real hydrothermal systems are much more complex than this. For example, it is estimated that as little as 10% of the heat flux on the MOR axis occurs as focused, hot vents. The remaining 90% of axial heat loss is through diffuse venting, which is in large part a result of high-temperature fluids mixing with cold crustal seawater below the seafloor. This requires a high degree of mixing and cooling below the seafloor, which leads to substantial precipitation of metal sulfides and sulfates (anhydrite, barite, etc.).

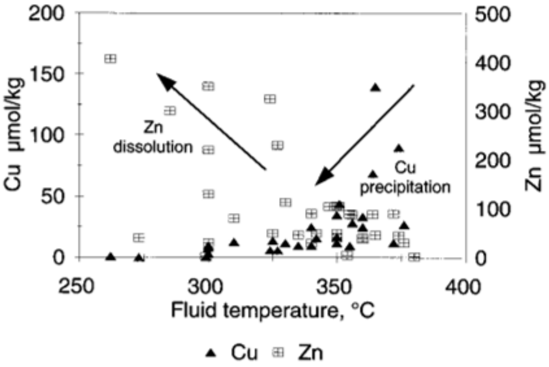

FIGURE 6 Concentration of copper (triangles) and zinc (rectangles) in hydrothermal fluids from various MOR sites as a function of vent fluid temperture. Copper and zinc have nearly the same concentration in the MORB source rock, but copper requires higher temperatures for transport in aqueous fluids. Copper concentrations fall as temperature decreases because of the temperature control on solubility. The cooling-induced precipitation produces acidity that can redissolve zinc sulfide minerals, resulting in higher zinc concentrations at lower temperatures. High Cu/Zn ratios in the hottest fluids are probably the result of dissolution of chalcopyrite linings in fluid conduits.

The existence of microbes and their metabolic activity in hydrothermal systems is a function of the major environmental parameters (temperature, pressure, salinity) and chemical processes in the three hydrothermal zones. Microbial metabolism in the low-temperature recharge (or off-axis) zone must be based on degradation of detrital organic matter and slow reactions between crustal rocks and seawater as the reducing power of the rocks consumes the oxidants in seawater. Aerobic iron oxidizers, followed by sulfate-, iron-, and manganese-reducing microbes (among others), are likely to be found in the recharge zone. The high-temperature reaction zone is most probably abiotic, as no known organisms can grow at temperatures of 300–450°C (and certainly not at magmatic temperatures). The upflow zone is the focus of intense thermal and chemical energy. Mixing of hot and cold fluids below the seafloor creates a thermal and chemical gradient that provides tremendous energy flow through highly porous rock, a prime habitat for microbial growth. When the electron donors in hot, reduced hydrothermal fluid (H_2S, H_2, CH_4, Fe^{2+}, etc.) meet the electron acceptors in cold seawater (O_2, SO_4^{2-}, NO_3^-, etc.), many energy-yielding reactions occur that can be catalyzed by microbes. Many different species of microbes, both Archaea and Eubacteria, have been isolated from hydrothermal vent environments, but they represent only a small fraction of the organisms that are likely to exist there. Microbes clearly play a role in catalyzing reactions, and in so doing they effect geochemical transformations that might otherwise be kinetically impeded. For example, the reaction

$$4H_2 + CO_2 = CH_4 + 2H_2O \qquad (3)$$

proceeds very slowly even at 300–400°C in the absence of a suitable catalyst, but methanogenic microbes carry out this reaction at temperatures up to 110°C in the sub-seafloor mixing zone. Low-temperature vents sampled in several MOR sites have millimolar levels of methane, presumably due to the activity of methanogens. Seafloor sampling continues to unveil novel microbes from vent environments, and it appears likely that microbes are involved in catalyzing many geochemical transformations in portions of hydrothermal systems that are below the upper temperature limit for life.

IV. ROLE OF PHASE SEPARATION

The chemical composition and the transfer of heat by hydrothermal vent fluids cannot be understood unless one considers the important process of fluid phase separation. Hydrothermal fluids circulating through the ocean crust reach temperatures high enough (370–450°C) to separate into vapor and liquid phases at the hydrostatic pressures (200–400 bar) encountered beneath midocean ridges (Fig. 7). If fluids encounter the two-phase curve at temperatures less than the critical point (point A in Fig. 7), then normal boiling occurs and produces a low-salinity vapor phase from a bulk seawater-like liquid. As the critical point is approached, the properties of vapor and liquid phases become more and more similar and are identical at the critical point. If fluids encounter the two-phase curve at temperatures higher than the critical point (point B in Fig. 7), then a dense high-salinity brine condenses out of a bulk fluid of near seawater salinity. The vapors and brines produced by phase separation span a range of salinity from near zero for subcritical vapors to several times seawater in supercritical brines.

Phase separation produces a vapor and brine that are chemically very different from each other and from their parent fluid. Every chemical species in the fluid at the time of phase separation is distributed between vapor and liquid phases according to its physical and chemical properties. Dissolved species that are primarily ionic (e.g., Na^+, Cl^-) have a very strong affinity for the liquid phase, and there is little change in the ratios of these species (e.g., Na/Cl, K/Na) in the liquid phase as a result of phase separation. Neutral species, including neutrally charged acids or bases (e.g., silicic acid, boric acid, ammonia), neutral ionic complexes (e.g., aqueous $NaCl^0$), and gaseous species (e.g., carbon dioxide, methane, helium), have a stronger affinity for the vapor phase. The distribution of neutral species between liquid and vapor can be calculated from Henry's law:

$$K_H^p = \frac{f_g}{m_g}, \tag{4}$$

where K_H is the Henry's law constant at pressure p, f is the fugacity of the volatile component g, and m is the molality of the volatile component in the liquid phase.

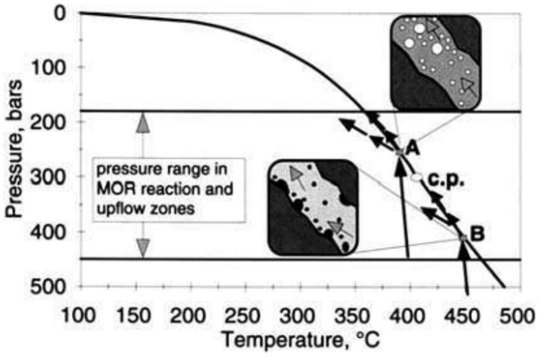

FIGURE 7 Two-phase boundary for seawater. The oval marked c.p. is the critical point for seawater. Solid black arrows denote adiabatic fluid flow. Arrows with stippled heads denote fluid flow with heat loss. Inset figures attached to A and B illustrate flow of two-phase fluids through a hydrothermal conduit. If fluids ascending from a deep reaction zone cross the two-phase curve at label B, temperature and pressure higher than the critical point, the result is condensation of dense brine (dark drops in inset B) from a vaporlike liquid. If the fluid crosses the two-phase curve at label A, below the critical temperature, the result is formation of vapor bubbles (light circles in inset A).

The net result when phase separation occurs and the liquid and vapor phases become physically segregated, is the creation of low-chlorinity, vapor-dominated fluids enriched in gases, and residual liquids depleted in gases. (Chlorinity is essentially a measure of the chloride concentration in a fluid and is used in preference to salinity for fluids where chloride is the only major anion in solution.) Subcritical boiling produces residual liquids that are only marginally above seawater chlorinity. Supercritical phase separation is required to produce high-chlorinity, brine-dominated fluids depleted in gases. If phase separation did not occur in submarine hydrothermal systems, then all vent fluids would have chloride concentrations within about 10% of the seawater concentration, because chloride has no major source within the oceanic crust, and chloride-bearing minerals are not a major hydrothermal alteration phase. In fact, the chlorinity of vent fluids ranges from less than 10% of that of seawater to more than twice that of seawater (Fig. 8a). All of the major cations are strongly correlated with chloride (Fig. 8b) because they all partition heavily into the liquid or brine phase. Gases are more enriched in the vapor-dominated phase (Fig. 8c). Thus, phase separation has a first-order effect on the chemistry of hydrothermal fluids, and this must be taken into account before other second-order effects (such as depth of reaction zone or minor differences in rock composition) can be discerned.

The range of fluid chlorinities at seafloor vents is much smaller than the range of chlorinities that can be produced by phase separation in hydrothermal systems. The maximum chlorinity observed in any MOR vent fluids sampled to date is slightly more than twice the chlorinity of seawater (Fig. 8a). A brine produced by condensation from seawater-derived fluid at 450°C would have a salinity five times greater than that of seawater. Brines produced by exsolution of an aqueous phase from a magma at temperatures in excess of 700°C have salinities more than 10 times that of seawater. The

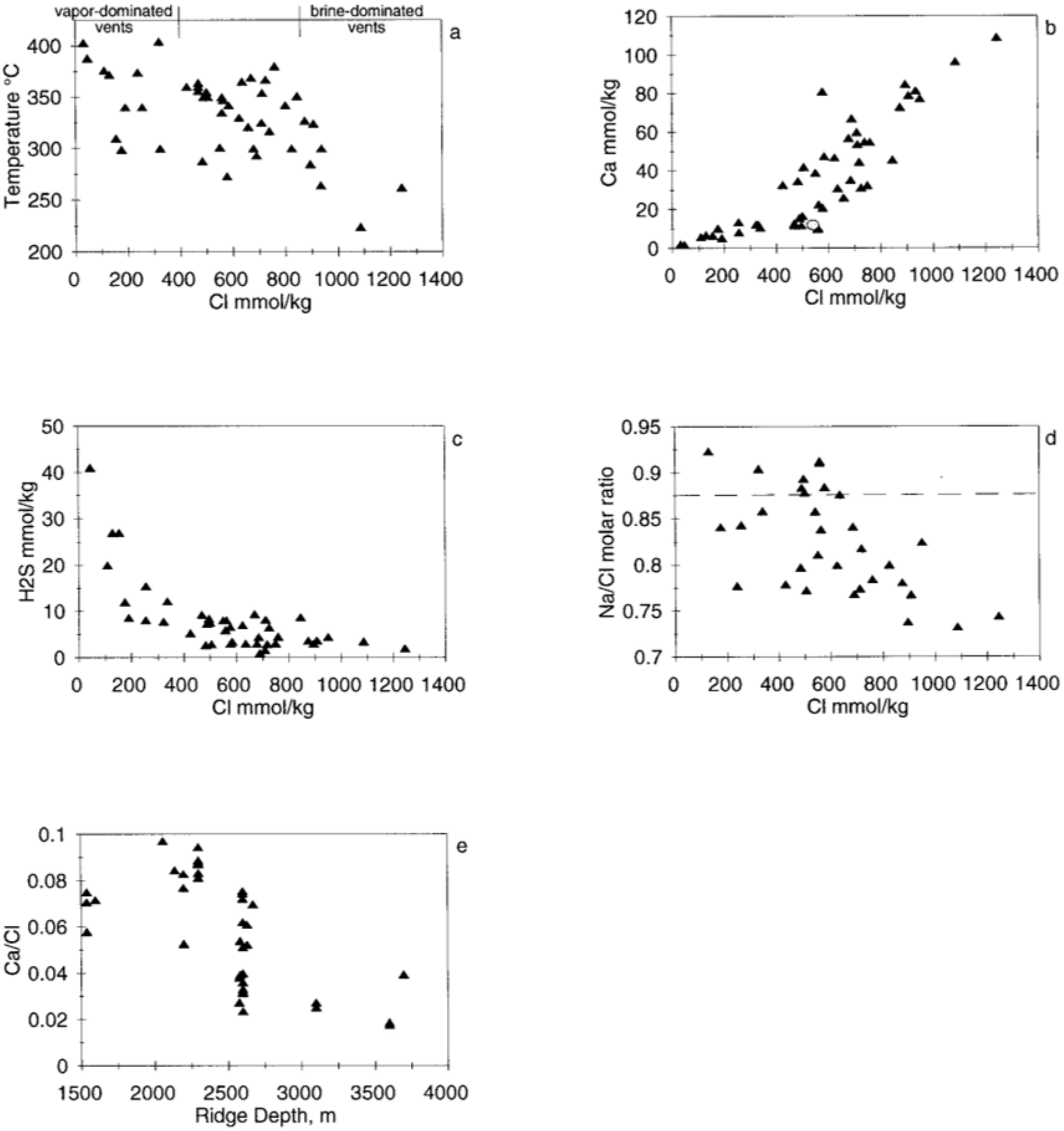

FIGURE 8 Vent fluid properties reflecting sub-seafloor processes. (a) Concentration of chloride in vent fluids as a function of measured vent fluid temperature. Vapor dominated fluids are found only in the hottest systems where active phase separation (boiling) takes place. (b) Calcium vs chloride concentration in fluids from MOR vents. All major cations have a strong positive correlation with chloride because of partitioning during phase separation. (c) Hydrogen sulfide concentration vs chloride in fluids from MOR vents. Volatile components in MOR fluids are highest in low-chloride vent fluids. (d) Na/Cl ratio vs chloride concentration in MOR vent fluids. Na uptake by minerals is most pronounced in brine-dominated fluids, probably because of longer residence times and the effect of chloride complexing on the activity of Na^+ and Ca^{2+}. (e) Ca/Cl ratio in MOR vent fluids vs seafloor depth. The trend of decreasing Ca/Cl ratio with ridge depth may be due to the effect of increasing reaction zone pressure on fluid–mineral reactions involving calcium.

full range of fluid salinities and temperatures is recorded in fluid inclusions trapped over a range of depths within the ocean crust, with the highest salinities and temperatures found in the deepest plutonic rocks. Although high-salinity brines definitely occur within the oceanic crust, they either are too dense to ascend to the seafloor or are highly diluted by circulating seawater-derived hydrothermal fluids prior to venting at the seafloor.

If a fluid has approached equilibrium with a mineral assemblage before phase separation occurs, then the resulting brine and vapor phases produced will almost certainly be moved away from that equilibrium. If there is sufficient time, the fluids produced by phase separation will reequilibrate through water–rock reactions. Vapor-dominated fluids are more buoyant than their parent fluid or the conjugate brines, so we expect them to have a shorter residence time, and less time to react with the surrounding rock. If that is the case, then their cation ratios should not depart significantly from the ratios of near-seawater chlorinity fluids that have not undergone phase separation and segregation. Denser, high-chlorinity brines, however, may reside longer in the crust and have sufficient time to approach a new equilibrium. For this reason, their cation ratios may depart from those of fluids with chlorinity near or below that of seawater.

It is possible to see second-order effects in the existing global hydrothermal fluid chemistry data. A simple way to see through the effects of phase separation on fluid chemistry is to compare the ratios of selected elements to chloride. For major ions, these ratios are not changed substantially by vapor–brine partitioning, so differences are due to other processes. For example, the Na/Cl ratio of vent fluids varies around the seawater value, and high-chlorinity fluids have the lowest Na/Cl ratios (Fig. 8d), as well as the highest Ca/Cl ratios. The conclusion is that reactions that remove sodium from solution (e.g., albitization) have progressed farther in the brines, which may be due to the higher chloride concentration favoring exchange of Na for Ca in the rock, combined with a longer residence (reaction) time. Another second-order effect suggested by the global MOR vent fluid data is the correlation of Ca/Cl ratio with ridge depth (Fig. 8e). Although there is considerable range in Ca/Cl at any depth, there is a clear trend to lower Ca/Cl at deeper sites. Because the thermodynamic driving force is toward increasing Ca fixation at higher pressure and temperature, the global trend in vent fluid Ca/Cl may be due to deeper reaction zones at deeper ridges, although the details of the rock composition at each site may also play a role. An example of how variations in MORB composition can have a subtle effect on the major element composition of vent fluids is seen at the Endeavour segment of the Juan de Fuca Ridge. The K content of Endeavour basalts is nearly three times higher than that of average MORB from the rest of the Juan de Fuca ridge, and likewise the K/Cl ratio of fluids from Endeavour (0.057 ± 0.003) is significantly higher than for the rest of the Juan de Fuca ridge (0.047 ± 0.003) and other MORB-hosted sites. As databases for hydrothermal fluid chemistry and host rock petrology are compared and analyzed, it is expected that more relationships between the two will become apparent. This, in turn, will allow the effects of other geological parameters (e.g., spreading rate, ridge depth) to be better understood so that models of global hydrothermal fluxes over time can be developed.

V. HYDROTHERMAL CHEMISTRY OF SEAMOUNTS AND NON-MORB ENVIRONMENTS

Seamounts located on divergent plate boundaries or at intraplate hotspots are characterized by high magma supply to shallow crustal depths. The most striking effect on the fluid chemistry in this environment is due to magmatic degassing of carbon dioxide. The CO_2 content of stable MOR hydrothermal fluids ranges from near-seawater levels (~2 mmol/kg) up to about 25 mmol/kg. The CO_2 content (Table II) exceeds 250 mmol/kg at Axial Volcano on the Juan de Fuca ridge and the intraplate Loihi seamount, both basaltic volcanoes. The helium content of these fluids is also a factor of 10 higher than that of typical MOR fluids. The decompression associated with transporting basaltic magma higher up into the crust at seamounts clearly results in significant transfer of gases from the magma to hydrothermal fluids. In vapor-dominated fluids at Axial Volcano, where active boiling occurs in the upflow zone, the concentration of carbon dioxide exceeds the concentration of chloride, making it the most abundant species in the fluid. Although Axial Volcano fluids have exceptionally high volatile content and a wide range of chlorinity, the ratios of major elements to chloride are typical of other MORB-hosted vents of similar temperature. Input of high levels of carbon dioxide from magmatic degassing in this case has little effect on the primary fluid characteristics; high-temperature reactions similar to other MOR environments govern the bulk fluid major element composition. At Loihi seamount and at Teahitia seamount, however, the fluid temperatures are much lower, and the high levels of magmatic carbon dioxide and sulfur dioxide appear to provide acidity that drives the dissolution of basalt glass at low temperatures within the volcanic edifice. The result is warm fluid of relatively low pH with high levels of iron and other metals.

A small percentage of the global seafloor volcanic spreading centers are covered with sediment due to their position near continental runoff sources (e.g., Middle Valley, Escanaba Trough, Guaymas Basin—Fig. 1, Table I). The presence of sediment cover has a striking impact on the chemistry of hydrothermal fluids. Relative to sediment-starved MOR vent fluids (Table II), they are generally depleted in ore-forming metals and enriched in boron, ammonia, bromide, iodide, alkalis, and organic-derived hydrocarbons, and have higher pH and alkalinity. However, the effects of sediment cover vary considerably because there is such a large range in sediment composition in different environments (percentage and type of carbonate, organic, and terrigenous components) and in the location of the heat source (below or within the sediments) and the structure of the recharge and upflow zones.

MORB composition occupies a narrow band in the spectrum of submarine volcanic rock types. Although most of the ocean basins are of MORB compositon, and most of the hydrothermal systems sampled to date are MORB-hosted, a range of more silicic rocks (basaltic andesites, andesites, rhyodacites) are common in island arc and backarc environments (e.g., Manus basin, Lau basin, North Fiji basin, Okinawa trough), and ultramafic rocks are exposed on portions of slow spreading ridges (e.g., Rainbow hydrothermal site on the MAR). Differences in rock type can lead to large differences in hydrothermal fluid composition. Because the bulk composition and primary minerals of the source rock are different, the reaction sequence and the position of equilibrium that governs the master chemical variables, pH and redox state, are changed. For example, when seawater reacts with more silicic rocks, the fluids are more enriched in K and other alkalis and less enriched in Ca than in MORB-hosted fluids. Under some conditions, uptake of Mg by minerals can be reversed, so the working assumption of near-zero Mg in high-temperature end-member hydrothermal fluid that is universally applied in MORB-hosted systems is no longer valid. Reaction of hydrothermal seawater with ultramafic rocks produces much higher levels of methane than does reaction with MORB. The incompatible and trace element concentrations vary considerably from ultramafic to acidic rocks, which can be directly reflected in the fluid trace element chemistry, especially for highly soluble trace alkalis. Consideration of hydrothermal fluxes and how they affect the chemistry of the oceans must include the full range of submarine environments.

Because of the subduction of hydrated ocean crust beneath volcanic arcs and the potential involvement of a wider range of magma sources, the volatile content (H_2O, CO_2, and SO_2) of magmas near convergent plate boundaries can be much higher than in MORBs. In the JADE hydrothermal field at ~1500 m depth in the Okinawa trough, the flux of CO_2 is so great that CO_2 gas hydrates form and bubble up out of the volcaniclastic sediments. In the DESMOS caldera in the Manus backarc basin, input of magmatic SO_2 to the hydrothermal system followed by disproportionation results in vent fluids with both high H_2S and sulfate concentrations higher than in seawater. There is a very wide range in both the fluid chemistry and types of mineralization in non-MORB hydrothermal systems.

VI. EFFECT OF VOLCANIC ACTIVITY ON HYDROTHERMAL SYSTEMS

Submarine volcanic eruptions illustrate clearly that geological, chemical, and microbiological processes are intimately linked in hydrothermal systems. Intense physical, thermal, and chemical energy is focused near the seafloor during an eruption, significantly perturbing the preexisting flow of energy through the ocean crust. Recent research has begun to unveil the hydrothermal response to a seafloor volcanic event.

Basaltic eruptions on the midocean ridge can range from small pillow lava mounds to extensive sheet flows, depending on the eruption rate and volume. It is thought that dikes generated from axis-parallel, elongated magma chambers feed seafloor eruptions. MOR eruptions have been detected remotely from seismic t-waves traveling through the ocean sound channel, and *Alvin* submersible dives encountered the immediate aftermath of an eruption at 9° N on the East Pacific Rise in 1991, but an eruption in progress has yet to be observed and studied in real time. What is known in general about the hydrothermal response to seafloor eruptions is based on a composite of posteruption observations on the seafloor and in the overlying water column on time scales from days to years.

A submarine dike injection and eruption places a large quantity of heat suddenly in the upper, most permeable, volcanic layer of the ocean crust (Figs. 4c and 6). The immediate response is rapid heat loss at the seafloor directly from erupted lavas to bottom seawater, and below the seafloor from the molten dike to the rock and water saturating the porous upper crust. Whether the local crust is hydrothermally active or not prior to the eruption, the dike-induced convection will flush out the "groundwater" and eject it into the deep sea to form a hydrothermal plume. Although the exact mechanism is not known, it is clear that seafloor eruptions are associated with hydrothermal "event plumes": very large quantities of heat (equivalent to a year or more of black smoker output) transported in a matter of days high up into the water column (of the order 1000 m vertical rise compared to 100–300 m for typical 350°C smoker effluent).

The properties of event plumes are different from "normal" or "steady" plumes resulting from black smoker output. The event plumes for which data is available have in common a helium-to-heat ratio near the low end of the range for smoker fluids, while the contemporaneous deeper "steady" plumes in the same locations have high helium-to-heat ratios that decay over time back toward lower values. A simple physical mechanism can account for the pattern of helium-to-heat ratios. If event plumes form during the period immediately after eruption, they are driven by heat conducted out of the dike and erupted lavas into the surrounding seawater, and because conduction of heat through rock is orders of magnitude faster than diffusion of helium, the event plumes will have low helium-to-heat ratios. As the heat transfer rates decline and event plume formation dies out, the cooling dike and lavas crack and the helium is extracted by circulating fluids, generating high helium-to-heat ratios (because the large heat loss preceded the helium extraction). As both helium and heat are exhausted from the dike, the ratio returns to the steady-state value.

There are direct seafloor observations of hydrothermal systems at eruptive sites after event plume formation is over. The observations have included extensive diffuse venting along what is believed to be the eruptive fissure or the seafloor trace of a dike injection. The initial posteruptive vent fluids are volatile-rich and vapor-dominated as the heat flux is high enough to drive active phase separation. Over a period of months to years, the heat flux declines, widespread diffuse venting contracts to more limited areas, and the chlorinity of vented fluids increases as brine dominated fluids replace vapor dominated fluids (Fig. 9). The observations require that brines accumulate below the seafloor during the high heat flux period of active phase separation and are later flushed from the system. Volcanic eruptions cause a transient perturbation in hydrothermal systems, characterized by a cycle from low-chloride fluids during high heat flux periods to high-chloride fluids during low heat flux periods. The reaction zone moves downward from very near the seafloor during the eruption toward the base of the dike as the dike is cooled. The water/rock ratio is high during vigorous circulation through the highly permeable volcanic layer, and decreases toward normal black smoker values (~1) as the reaction zone moves into the sheeted dike layer where permeability is lower.

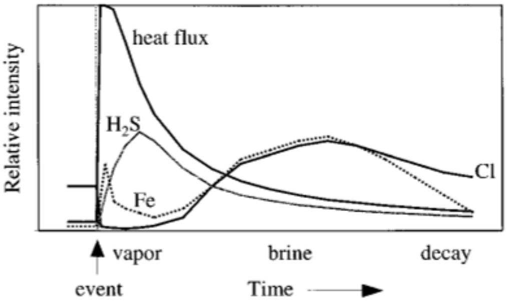

FIGURE 9 Evolution of hydrothermal heat flux and selected fluid properties (Cl, Fe, and H_2S concentrations relative to initial levels) following a seafloor volcanic eruption. Initial chloride concentration is the same as in seawater. Systems evolve from vapor dominated, high heat flux stage, through a transition to brine dominated discharge, and eventually decay back toward zero heat flux and seawater composition. Both the magnitude of the heat flux and the length of the time scale depend on the size of the volcanic event. The transition from vapor to brine may take several months to a few years. [From Butterfield *et al.,* 1997.]

Just as subaerial volcanic eruptions can have devastating effects on plant and animal life, seafloor eruptions cause major disruptions in the submarine ecosystem. Observations show that lava flows have paved over existing communities of hydrothermal vent fauna. The boundary between life and death for vent animals is remarkably sharp; live tube worms have been observed within centimeters of newly erupted pillow basalts at Axial Volcano on the Juan de Fuca ridge, attesting to the very rapid quenching of seafloor lavas by ambient seawater. Time series observations indicate that recolonization of newly created hydrothermal habitat following seafloor eruptions begins within the first year.

A dramatic and rapid microbial response to the sudden increase in energy flow associated with volcanic events has been repeatedly observed. In the first weeks or months following an eruption, microbial production below the seafloor appears to bloom, resulting in the emission of fluids loaded with white, flocculent particulate material. There is some laboratory and field evidence that this material is rich in elemental sulfur generated from sulfide-oxidizing microbes. This phenomenon has only been observed in areas affected by recent volcanic activity.

The pattern of evolving heat flow and fluid chemistry that is set up as a transient effect of individual volcanic eruptions may also be reflected in the evolution of entire vent fields or ridge segments as they experience changes in magma supply rate and tectonic stretching that control the rate of heat output over time. When volcanic and tectonic processes allow highly efficient mining of heat from the deep reaction zone, the brine generated from supercritical phase separation at depth will remain in the crust while vapor-enriched fluids transport large quantities of heat and volatiles out of the system. When the conditions evolve to lower the heat output, the brine that has accumulated begins to be flushed from the system. Along the Endeavour segment of the Juan de Fuca ridge, there are four vent fields spread over 10 km along axis. The central Main Endeavour field is the hottest (360–380°C) and most vigorous and is vapor dominated, while the two distal vent fields have much lower heat output and brinelike fluids. Further south on the Cleft segment, brine-enriched fluids have vented for more than a decade, illustrating the longevity of hydrothermal cycles and the remarkable storage capacity of the ocean crust. To truly understand the dynamics of hydrothermal systems in submarine volcanic centers will require continued exploration, real-time observations and sampling during seafloor eruptions, sub-seafloor sampling capability, accurate measurement of the heat flux from vent fields and ridge segments, and active imaging of the three-dimensional thermal and permeability structure of the ocean crust.

ACKNOWLEDGMENT

This article draws on the work of scientists too numerous to include in a short bibliography, but the seven book compilations cited below contain an excellent cross-section of work on hydrothermal systems. Thanks to Mark Hannington, Ian Jonasson, and an anonymous reviewer for their helpful and constructive comments on the first draft. Thanks also to Aries Galindo and Jim Anderson for graphics support. This publication was supported by the University of Washington Joint Institute for the Study of the Atmosphere and Ocean (JISAO) under NOAA Cooperative Agreement No. NA67RJ0155, contribution number 683, and by the NOAA VENTS Program, PMEL contribution number 2042.

SEE ALSO THE FOLLOWING ARTICLES

Basaltic Volcanoes and Volcanic Systems • Composition of Magmas • The Ecology of Volcanoes: Recovery and Reassembly of Living Communities • Mantle of the Earth • Plate Tectonics and Volcanism • Seamounts and Island Building • Submarine Lavas and Hyaloclastite

FURTHER READING

Baker, E. T., and Lupton, J. E. (1990). Changes in submarine hydrothermal ^{3}He/heat ratios as an indicator of magmatic/tectonic activity. *Nature* **346,** 556–558.

Baker, E. T., Massoth, G. J., and Feely, R. A. (1987). Cataclysmic hydrothermal venting on the Juan de Fuca Ridge. *Nature* **329,** 149–151.

Butterfield, D. A., Jonasson, I. R., Massoth, G. J., Feely, R. A., Roe, K. K., Embley, R. E., Holden, J. F., McDuff, R. E., Lilley, M. D., and Delaney, J. R. (1997). Seafloor eruptions and evolution of hydrothermal fluid chemistry. *Phil. Trans. Roy. Soc. London A* **355,** 369–386.

Delaney, J. R., Kelley, D. S., Lilley, M. D., Butterfield, D. A., Baross, J. A., Wilcock, W. S. D., Embley, R. W., and Summit, M. (1998). The quantum event of oceanic crustal accretion: impact of diking at mid-ocean ridges. *Science* **281,** 222–230.

Desbruyeres, D., and Segonzac, M. (1997). "Handbook of Deep-Sea Hydrothermal Vent Fauna." Editions IFREMER, Brest, France.

Edmond, J. M., Measures, C. I., McDuff, R. E., Chan, L. H., Collier, R., Grant, B., Gordon, L. I., and Corliss, J. B. (1979). Ridge-crest hydrothermal activity and the balances of the major and minor elements in the ocean: The Galapagos data. *Earth Planet. Sci. Lett.* **46,** 1–18.

Embley, R. W., Jonasson, I. R., Perfit, M. R., Franklin, J. M., Tivey, M. A., Malahoff, A., Smith, M. F., and Francis, T. J. G. (1988). Submersible investigation of an extinct hydrothermal system on the Galapagos Ridge: Sulfide mounds, stockwork zone, and differentiated lavas. *In* "Seafloor Hydrothermal Mineralization," special issue of *The Canadian Mineralogist* **26,** 429–888.

Haymon, R. M., Fornari, D. J., Von Damm, K. L., Lilley, M. D., Perfit, M. R., Edmond, J. M., Shanks, W. C. III, Lutz, R. A., Grebmeier, J. M., Carbotte, S., Wright, D., McLaughlin, E., Smith, M., Beedle, N., and Olson, E. (1993). Volcanic eruption of the mid-ocean ridge along the East Pacific Rise crest at 9° 45–52′N: Direct submersible observations of seafloor phenomena associated with an eruption event in April, 1991. *Earth Planet. Sci. Lett.* **119,** 85–101.

Karl, D. M. (1995). Ecology of free-living, hydrothermal vent microbial communities. *In* "The Microbiology of Deep-Sea Hydrothermal Vents" (D. M. Karl, ed.). CRC Press, Boca Raton, FL.

Lister, C. R. B. (1983). The basic physics of water penetration into hot rock. *In* "Hydrothermal Processes at Seafloor Spreading Centers" (P. A. Rona, K. Bostrom, L. Laubier, and K. L. Smith, Jr., eds.). Plenum Press, New York.

Mottl, M. J., Wheat, G., Baker, E., Becker, N., Davis, E., Feely, R., Grehan, A., Kadko, D., Lilley, M., Massoth, G., Moyer, C., and Sansone, F. (1998). Warm springs discovered on 3.5 Ma oceanic crust, eastern flank of the Juan de Fuca Ridge. *Geology* **26,** 51–54.

Norton, D. L. (1984). Theory of hydrothermal systems. *Ann. Rev. Earth Planet. Sci.* **12,** 155–177.

Reed, M. H. (1997). Hydrothermal alteration and its relationship to ore fluid composition. *In* "The Geochemistry of Hydrothermal Ore Deposits" (H. L. Barnes, ed.), 3rd ed. John Wiley and Sons, New York.

RISE Project Group (1980). East Pacific Rise: Hot springs and geophysical experiments. *Science* **207,** 1421–1433.

Rona, P. A., and Scott, S. D. (1993). A Special Issue on Seafloor Hydrothermal Mineralization: New Perspectives. *Economic Geology* **88,** 1933–1976.

Seyfried, W. E., Jr., and Ding, K. (1995). Phase equilibria in subseafloor hydrothermal systems: A review of the role of redox, temperature, pH and dissolved Cl on the chemistry of hot spring fluids at mid-ocean ridges. *In* "Seafloor Hydrothermal Systems: Physical, Chemical, Biological, and Geological Interactions" (S. E. Humphris, R. A. Zierenberg, L. S. Mullineaux, and R. E. Thomson, eds.). American Geophysical Union, Washington, DC.

Staudigel, H., Hart, S. R., and Richardson, S. H. (1981). Alteration of the oceanic crust: Processes and timing. *Earth Planet. Sci. Lett.* **52,** 311–327.

Van Dover, C. L. (1995). Ecology of Mid-Atlantic Ridge hydrothermal vents. *In* "Hydrothermal Vents and Processes" (L. M. Parson, C. L. Walker, and D. R. Dixon, eds.), Special Publication No. 87, The Geological Society, London.

Von Damm, K. L., Oosting, S. E., Kozlowski, R., Buttermore, L. G., Colodner, D. C., Edmonds, H. N., Edmond, J. M., and Grebmeier, J. M. (1995). Evolution of East Pacific Rise hydrothermal vent fluids following a volcanic eruption. *Nature* **375,** 47–50.

Wilcock, W. S. D., and Delaney, J. R. (1996). Mid-ocean ridge sulfide deposits: Evidence for heat extraction from magma chambers or cracking fronts? *Earth Planet. Sci. Lett.* **145,** 49–64.

Wolery, T. J., and Sleep, N. H. (1976). Hydrothermal circulation and geochemical flux at mid-ocean ridges. *J. Geol.* **84,** 249–275.

This Page Intentionally Left Blank

VOLCANIC LAKES

PIERRE DELMELLE
Université de Montréal

ALAIN BERNARD
Université Libre de Bruxelles, Belgium

I. Introduction
II. Processes in Volcanic Lakes
III. Hazards of Volcanic Lakes, Their Monitoring and Mitigation
IV. Future Directions

GLOSSARY

caldera Volcanic crater formed by collapse during an eruption.

fumarole Vent from which volcanic gases are emitted.

geothermal system Any regionally localized geological setting where portions of the Earth's internal heat flow are transported close enough to the Earth's surface by circulating steam or hot water to be readily harnessed for use.

hydrothermal eruption Explosion that follows transformation of groundwater into steam. No incandescent or juvenile material is erupted. Synonym for phreatic eruption.

hydrothermal system A groundwater system that has a source (or area) of recharge, a source (or area) of discharge, and a heat source. Hydrothermal systems associated with volcanoes are termed volcanic hydrothermal systems. When a magma supplies the heat source and volatiles, the hydrothermal system qualifies as a magmatic hydrothermal system.

hydrovolcanic eruption Eruption that results from the interaction between magma and groundwater or surface water. Synonym for phreatomagmatic eruption.

isotope Atoms with the same number of electrons and protons, but a different number of neutrons and therefore different masses. Most chemical elements occur in nature as two or more isotopes. The relative abundances of isotopes of a given chemical element are not constant in all natural materials. Hydrogen, carbon, oxygen and sulfur, which are prominent elements in volcanic fluids, all have stable isotopes. As opposed to radionuclides, stable isotopes do not undergo spontaneous decomposition.

maar Small volcano characterized by a crater that is wide (several hundreds meters to several kilometers in diameter) relative to its height and whose floor commonly lies below the general level of surrounding topography. Maar volcanoes can form during hydrovolcanic eruptions or very energetic gas eruptions.

meteoric water Waters of any age that originate from precipitation: rain, snow, ice, river, lake, and most low-temperature groundwaters. They are derived from ocean water through the atmospheric circulation process.

I. INTRODUCTION

The Catalog of Active Volcanoes of the World (CAVW) reports that about 16% of the 714 Holocene (~10,000 years old) or younger terrestrial volcanoes contain a lake (Table I), but the exact number varies with time because of their ephemeral nature. Volcanic lakes occur all over

Copyright © 2000 by Academic Press
All rights of reproduction in any form reserved.

TABLE 1 Volcanic Lakes Hosted by Holocene or Younger Volcanoes[a]

Volcano name	*Lake name*	*Location*	*Crater type*	*Status*
Europe to Caucasus				
West Eifel volcanic field		Germany	Maars	
Chaine des Puys	Pavin	France	Cinder cone	
Albano Monte	Albano	Italy	Caldera	
Larderello	Lago Vecchienna	Italy	Crater	Neutral
Vulsini	Lago Bolsena	Italy	Caldera	Neutral
Ischia	Lago Vico	Italy	Caldera	Neutral
Nemrut Dagi		Turkey	Caldera	
Africa				
Oku volcanic field	Lake Nyos	Cameroon	Maar	Alkaline/acidic
Mid-East and Indian Ocean				
Karthala	Chahale crater	Great Comoro	Crater	
Heard	Mawson Peak	Heard	Caldera	
New Zealand to Fiji				
Rotorua	Rotokawa	New Zealand	Crater, hydr.	
Okataina	Frying Pan Lake	New Zealand	Crater, hydr	
	Lake Rotomahana		Crater	
Taupo	Lake Taupo	New Zealand	Caldera	
Ruapehu	Crater Lake	New Zealand	Active	Acidic
Raoul Island	Blue Lake	Kermadec	Caldera	Neutral
	Green Lake			Acidic?
	Tui Lake		Caldera	
Niuafo'ou	Big Lake (Vai Lahi)	Tonga	Caldera	Alkaline
	Small Lake (Vai Sii)		Caldera	
Melanesia and Australia				
Long Island	Lake Wisdom	New Guinea	Caldera	
Sakar		New Guinea	Crater	
Benda	Lake Dakataua	New Britain	Caldera	
Galloseulo	Lake Hargy	New Britain	Caldera	
Waiowa		New Guinea	Crater	
Iamelele	Sulfur Lake	New Guinea	Crater, hydr.	
	Salt Lake		Crater, hydr.	
Billy Mitchell	Crater Lake	New Guinea, Boungainville	Crater	
Gaua		Vanuatu	Caldera	
Aoba	Lake Vui	Vanuatu	Active	Acidic
Indonesia and Andaman I.				
Sorikmarapi		Indonesia, Sumatra	Crater	Acidic
		Indonesia, Sumatra	Crater	
Tandikat		Indonesia, Sumatra	Crater	
Kerinci		Indonesia, Sumatra	Crater	
Lumutdaun, Bukit		Indonesia, Sumatra	Crater	Acidic?
Kaba	Lama Crater	Indonesia, Sumatra	Crater	
	Baru Crater		Crater	
	SW explosion pit		Crater	
	Vogelsang crater		Crater	
Dempo		Indonesia, Sumatra	Crater	Acidic?
Ranau		Indonesia, Sumatra	Caldera	
Patoha		Indonesia, Java	Active	Acidic
Galunggung		Indonesia, Java	Crater	Neutral
Talagabodas		Indonesia, Java	Active	Acidic
Dieng volcanic complex	Sikidang	Indonesia, Java	Crater	
Kelut		Indonesia, Java	Crater	Neutral

continues

Continued

Volcano name	Lake name	Location	Crater type	Status
Ijen		Indonesia, Java	Active	Acidic
Batur		Indonesia, Bali	Caldera	Neutral
Rinjani		Indonesia, Lombok	Caldera	
Sano, Wai		Indonesia, Flores	Caldera	Acidic?
Kelimutu	Tiwu Nua Muri Koohi Fah	Indonesia, Flores	Active	Acidic
	Tiwu Ata Mbapu	Indonesia, Flores	Active	Acidic
	Tiwu Ata Polo	Indonesia, Flores	Active	Acidic
Egon		Indonesia, Flores	Active	Acidic
Sirung		Indonesia, Pantar	Active	Acidic
Sempu		Indonesia, Sulawesi	Caldera	Acidic
Mahawu		Indonesia, Sulawesi	Crater	Acidic?
Klabat		Indonesia, Sulawesi	Crater	
Karangetang		Sangihe Island	Active	Acidic
Awu		Sangihe Island	Active	Acidic
Gamkonora		Indonesia, Halmahera	Crater	
Todoko-ranu		Indonesia, Halmahera	Caldera	Acidic?
Philippines and SE Asia				
Cabalian		Philippines, Leyte	Crater	
Taal	Main Crater Lake	Philippines, Luzon	Active	Acidic
	Lake Taal		Caldera	Alkaline
Pinatubo		Philippines, Luzon	Active	Acidic
Japan, Taiwan, and Marianas				
Kirishima	Shinmoe-dake	Japan, Kyushu	Crater	Acidic?
Aso	Naka-dake	Japan, Kyushu	Active	Acidic
Kusatsu-Shirane	Yugama Lake	Japan, Honshu	Active	Acidic
	Karagama Lake		Crater	
	Mizugama Lake		Crater	
Zao	Okama Lake	Japan, Honshu	Active	Acidic
Narugo	Katunama	Japan, Honshu	Active	Acidic
Chokai		Japan, Honshu	Caldera	
Iwate	Onawasiroko Lake	Japan, Honshu	Crater	
	Okama Lake		Crater	
Osore-Yama		Japan, Honshu	Caldera	Neutral
Akita-Yakeyama	Yunuma	Japan, Honshu	Crater	Acidic?
Kuttara	Oyunuma	Japan, Hokkaido	Crater, hydr.	
Mashu		Japan, Hokkaido	Caldera	Neutral
Anatahan		Mariana Islands	Caldera	
Kuriles, Kamchatka, and Asia				
Golovnin		Kuriles, Kunashir	Crater, hydr.	Neutral
	Goryavhyee		Active	Acidic
Zavaritzky		Kuriles, Simushir	Caldera	Acidic?
Ketoi	Pallas Peak	Kuriles, Kurile	Crater	Acidic?
Kuntomintar		Kuriles, Shiashkotan	Caldera	Neutral?
Tao-Rusyr		Kuriles, Onekotan	Caldera	Acidic?
Ebeko		Kuriles, Paramushir	Active	Acidic
			Crater	Acidic?
Pauzhetka	Kurile Lake	Kamchatka	Caldera	
Ksudach	Stubel	Kamchatka	Caldera	Neutral
	Klyuchoe	Kamchatka	Caldera	Neutral
Mutnovsky		Kamchatka	Crater	Acidic?
Gorely		Kamchatka	Active	Acidic
Karimsky		Kamchatka	Active	Acidic
Maly Semiachik		Kamchatka	Active	Acidic

continues

Continued

Volcano name	*Lake name*	*Location*	*Crater type*	*Status*
Uzon	Bannoe	Kamchatka	Crater, hydr.	Acidic
	Lake Dal'nee		Crater, hydr.	
Baitoushan	Tien-Chi Lake	China/Korea	Caldera	Neutral
Alaska				
Emmons Lake		Alaska	Caldera	
Aniakchak	Surprise Lake	Alaska	Caldera	
Katmai	Katmai Lake	Alaska	Caldera	Acidic?
Spurr	Crater Peak	Alaska	Crater	Acidic
Western USA				
Newberry volcano	East Lake	USA	Caldera	
	Paulina Lake			
Medicine Lake	Medicine Lake	USA	Caldera	
Crater Lake	Crater Lake	USA	Caldera	Neutral
Mono Lake volcanic field	Mono Lake	USA	Caldera	
Yellowstone	Yellowstone Lake	USA	Caldera	
Mexico and Central America				
Colima volcanic complex		Mexico	Crater	
El Chichón		Mexico	Crater	Acidic
Atitlan		Guatemala	Caldera	
Tecuamburro	Lake Ixpaco	Guatemala	Crater	Acidic
Santa Ana		El Salvador	Crater	Acidic
	Lago Coatepeque		Caldera	
Cosiguina		Nicaragua	Crater	Neutral?
Apoyeque	Laguna Jiloa	Nicaragua	Maar	Neutral
	Laguna Apoyeque		Maar	Neutral
Masaya	Laguna de Masaya	Nicaragua	Caldera	Neutral
Apoyo		Nicaragua	Caldera	Neutral
Rincon de la Vieja		Costa Rica	Crater	Acidic
Poás	Laguna Caliente	Costa Rica	Crater	Acidic
	Botos Cone		Crater	Neutral
Irazú		Costa Rica	Crater	Acidic
South America				
Azufral	Laguna Verde	Colombia	Crater	Acidic
Cuicocha	Lago Cuicachi	Ecuador	Caldera	Alkaline
Quilotoa		Ecuador	Caldera	Alkaline
Fernandina		Galapagos	Caldera	Alkaline
Licancabur		Chile	Crater	
Copahue		Chile/Argentina	Crater	Acidic
Carran-Los Venados	Lake Nilahue	Chile	Crater	
West Indies				
Soufrière St. Vincent		West Indies, St. Vincent	Crater	Neutral?
Iceland & Arctic Ocean				
Grimsvotn		Iceland	Caldera	Neutral
Askja		Iceland	Caldera	Neutral
Atlantic Ocean				
Sete Citades	Blue Lake	Azores, San Miguel	Caldera	Alkaline
	Green Lake			
Agua de Pau		Azores, San Miguel	Caldera	Alkaline
Furnas		Azores, San Miguel	Caldera	Neutral

[a] hydr.: hydrothermal area; acidic: ($pH < 5$); neutral: ($5 \leq pH \leq 7$); alkaline: ($pH > 7$).

the world, with a higher percentage in volcanic arcs. These lakes may look like other natural reservoirs that accumulate meteoric water from precipitation, runoff, and inflowing streams. Yet, many volcanic lakes are hot and contain large amounts of dissolved solids in their waters. In fact, a few of these lakes consist of concentrated mixtures of sulfuric and hydrochloric acids that represent the most acidic and mineralized natural waters on Earth. Some also host long-lived molten sulfur bodies, a spectacular phenomenon shared only with Io, a moon of Jupiter. Lastly, a few volcanic lakes can store large amounts of potentially lethal gas in their bottom waters.

Such distinctive characteristics reflect the influence of volcanic inputs on the lake physical and chemical conditions. These inputs consist of hot gas and liquids that ultimately result from the interactions between groundwater and fluids released by a magma body at depth. To some extent, volcanic lakes can be viewed as the uppermost manifestation of a hydrothermal reservoir between the surface and an underlying magma. As such, they constitute unique windows for better understanding the processes that dictate how ascending magmatic fluids are transported toward the surface and react with their surrounding environment within the volcanic edifice. By studying volcanic lakes, scientists have acquired a general knowledge of the physical and chemical signatures of eruptible magma and of the thermal and/or chemical changes that may precede an eruption. Some researchers aim to use volcanic lakes to provide insight into the magnitude of terrestrial degassing; others consider volcanic lakes as the shallow part of ore-depositing magmatic/hydrothermal systems. Volcanologists also study volcanic lakes because of their highly hazardous nature. Once released, the large volumes of water that they hold may generate devastating debris flows (lahars) and floods. Since 1500 A.D., debris flows from crater lakes have killed many people (Table II). Another danger is related to the sudden escape of carbon dioxide (CO_2) from gas-rich lakes. Such an event occurred twice in Cameroon in the mid-1980s, killing nearly 1800 people.

Historically, visual accounts of volcanic lakes go back to the Spanish conquest era. Dutch, Japanese, and Russian geologists reported the first water analyses of a few crater lakes early in this century. After the Second World War, comprehensive research on volcanic lakes was begun. Rapid progress was accomplished where the proximity of a volcano observatory allows for repeated sampling of the lake. The lake of Mt. Ruapehu volcano (New Zealand), Yugama Lake at Kusatsu-Shirane volcano (Japan), and Laguna Caliente at Poás volcano (Costa Rica) are the best examples for which long-term

TABLE II Hazards at Volcanic Lakes since 1500 A.D. Associated with More Than 100 Fatalities

Volcano lake	*Country*	*Year*	*Hazard type*	*Deaths*	*Damage to constructions*
Agua	Guatemala	1541	Debris flows	?	Former capital destroyed
Kelut	Indonesia	1586	Debris flows	10,000?	
Raung	Indonesia	1638	Debris flows	>1,000	
Awu	Indonesia	1711	Debris flows	3,200	
Raung	Indonesia	1730	Debris flows	>100?	
Cotopaxi	Ecuador	1741	Debris flows	1,000	
Galunggung	Indonesia	1822	Debris flows	4,000	114 villages destroyed
Kaba	Indonesia	1833	Debris flows	126	Villages destroyed
Awu	Indonesia	1856	Debris flows	3,000	
Aoba	Vanuatu	1870	Debris flows	>100?	
Awu	Indonesia	1892	Debris flows	1,530	
Taal	Philippines	1911	Base surges/tsunami	>1,335	
Kelut	Indonesia	1919	Debris flows	5,110	9000 houses destroyed
Ruapehu	New Zealand	1953	Debris flows	154	Road and railway bridges
Taal	Philippines	1965	Base surges/tsunami	>200	
Kelut	Indonesia	1966	Debris flows	282	12,000 hectares of land destroyed
Nyos	Cameroon	1986	Gas burst	1,746	Almost no damage

studies are available. The presence of a lake in a crater during or immediately after an eruption also has drawn the attention of volcanologists, for example at Soufrière volcano, St. Vincent, in 1971–1972 and El Chichón in 1982. In 1984 and 1986, the unforeseen gas bursts of Lake Monoun and Lake Nyos in Cameroon put volcanic lakes into the spotlight among the scientific community.

In this chapter, we explain the principal processes occurring in volcanic lakes and show how these can be linked with the monitoring and mitigation of their hazards. We also devote a short section to the mineralization associated with some volcanic lakes. Lakes on top of active craters have received most attention from volcanologists. However, we shall see that lakes in dormant craters also feature striking characteristics, among which gas accumulation is of particular importance.

II. PROCESSES IN VOLCANIC LAKES

Volcanic lakes on Earth do not display the same physical, chemical, and biological conditions. Physical and chemical differences reflect the complex interplay of volcanic and nonvolcanic phenomena. The volcanic phenomena relate to the nature and amount of volcanic–hydrothermal fluids entering the lake as well as to the crater morphology and permeability, whereas the nonvolcanic phenomena depend primarily on atmospheric conditions (e.g., precipitation). Volcanologists collect and analyze a wide variety of geophysical and geochemical data to understand how volcanic lakes work. These data are also used to constraint box models that quantify heat, water, and chemical fluxes into and out of volcanic lakes.

A. Physical, Chemical, and Biological Variability

1. Volcanic Setting

Volcanic lakes occur chiefly along continental margins (e.g., Central America) or island arcs (e.g., Indonesia), but some also sit astride the Mid-Atlantic Ridge (e.g., Iceland). They lie in craters formed by hydrothermal, hydrovolcanic, or magmatic eruptions and more rarely occupy valleys blocked by lava or debris flows. Lakes in hydrothermal depressions are usually small (e.g., Oyunuma), those in maar craters ordinarily are bigger and deeper (e.g., Nyos), and those on top of degassing active craters typically have intermediate dimensions. The most voluminous systems fill vast calderas. Volcanic lakes occasionally form unusual settings. For example, three adjacent lakes occupy the summit craters of Keli Mutu volcano in Indonesia. At Taal, a renowned volcano in the Philippines, a large caldera lake hosts a volcanic island that also contains a comparatively smaller crater lake. Buried under the 250-m thick ice shelf of Vatnajökull glacier is the warm lake of Grimsvötn, the most active volcano in Iceland.

2. Water Composition

Volcanic lakes display a wide range of water compositions. The data reported in Table III illustrate this diversity. There are systems with neutral pH (~7), dilute (total dissolved solids or TDS $<$ 100 mg/kg) waters (e.g., Crater Lake at Mt. Mazama, United States) or, conversely, with highly acidic (pH $<$ 1) and strongly mineralized (TDS $>$ 100,000 mg/kg) waters (e.g., Kawah Ijen, Indonesia). In between, many volcanic lakes such as Kelut in Indonesia, Oyunuma in Japan, and Lake Nyos in Cameroon have intermediate acidity (pH ~2–6) and lower TDS ($<$ 2000 mg/kg). In addition to these differences in acidity and mineralization, volcanic lakes also can differ from each other by the type of dissolved chemical constituent(s) that they contain. For example, the lake of Kelut is sodium- and chloride-rich, that of Oyunuma is chloride- and sulfate-rich, and that of Nyos is carbon dioxide-rich (Table III). Lastly, volcanic lakes can be chemically well mixed to their bases (e.g., Kawah Ijen) or stratified (e.g., Nyos).

Unlike other terrestrial water reservoirs, the chemical composition of a volcanic lake may be altered with no apparent relation to seasonal variations. This may happen when the host volcano changes its activity suddenly. A good illustration of this was observed at Karimsky volcano, Russia. Following the 1995 eruption from a nearby cone, the initially dilute neutral caldera lake rapidly acquired acidic pH (~3) and high TDS (~800 mg/kg) values. In other cases, the chemical evolution of a volcanic lake is more progressive. Posteruption monitoring of El Chichón's crater lake indicates gradual decrease in acidity and dissolved solids concentrations, suggesting inputs of more dilute volcanic fluids or reduction of their fluxes.

3. Thermal Regime

Approximately 40 lakes are reportedly hot with temperatures above that of the ambient air. The majority of these lakes are perched atop degassing summit craters, whereas some fill hydrothermal depressions in geothermal areas. Interestingly, only a few systems sustain tem-

TABLE III Chemical Compositions of Some Volcanic Lakes[a]

Name	*Kawah Ijen*	*Poás*	*Poás*	*Kelut*	*Galunggung*	*Crater Lake*	*Batur*	*Oyunuma*	*Bannoe*	*Nyos*	*Nyos*
Depth of sampling	*0 m*	*0 m*	*0 m*	*0 m*	*0 m*	*200 m*	*0 m*	*0 m*	*0 m*	*0 m*	*205 m*
Setting[b]	*a*	*a*	*a*	*a*	*a*	*b*	*b*	*c*	*c*	*d*	*d*
Date	*08/96*	*10-11/87*	*06/89*	*12/93*	*12/93*	*08/94*	*09/89*	*10/95*	*10/95*	*03/96*	*03/96*
surface area ($\times 10^3$ m^2)	390	~42	~20	240	—	53,000	1.6	20	16	1580	
maximum depth (m)	170	~32	~5	33	—	589	—	26	23	209	
volume ($\times 10^6$ m^3)	32	~0.5	~0.03	1.8	—	17,300	—	—	—	150	
temperature (°C)	36	61	87	41	23	9	23	51	42	26	
pH	0.3	0.0	−0.4	5.9	7.0	7.0	8.9	2.7	5.7	7.1	5.1
TDS[c]	106,950	82,340	249,500	3430	605	100	1240	1030	300	65	1470
Na	1,160	520	2,720	720	18	11	360	100	20	2.8	66
K	1,470	250	1,730	92	4	1.7	30	12	6	1.4	7.0
Mg	630	550	2,040	55	34	2.2	70	<1	5	3.3	90
Ca	970	2,340	650	100	110	6.6	30	60	20	3.8	55
B	53	20	83	—	—	<0.5	—	22	0.7	<0.1	<0.1
Al	5,410	2,700	13,700	<0.1	<0.1	—	—	19	<0.5	—	—
SiO_2	160	170	440	240	30	20	30	156	105	16	81
Fe	2,060	1,300	5,770	<0.1	<0.1	n.r.	<1	4.4	<0.5	<0.1	120
Mn	40	36	130	1.7	<1	n.r.	—	0.5	<0.5	<0.1	1.7
SO_4	71,300	48,200	167,000	660	400	8	490	440	130	<1	<1
F	1,050	1,560	8,960	7	<1	0.1	<1	—	—	—	—
Cl	22,630	24,700	46,300	1290	6	9.8	230	221	10	<2	<1
HCO_3	—	—	—	260	—	41	—	—	—	38	1040
δD	0.8	−14	−33	−26	—	−79	−10	—	—	−10.8[d]	−11.9[d]
$\delta^{18}O$	8.7	12.3	7.3	−1.8	—	−9.8	−1.4	—	—	−2.6[d]	−3.0[d]
$\delta^{34}S(SO_4)$	22.3	14.4	12.3	15.1	—	—	—	2.2	11.0	—	—

[a] Concentrations are given in mg/kg; isotopic compositions are in delta (δ) units per mil (‰).

[b] a, active crater; b, dormant caldera; c, hydrothermal area; d, dormant crater.

[c] TDS: total dissolved solids.

[d] Values in 10/93.

peratures above ~45–50°C for prolonged periods of time (e.g., Kawah Ijen). Hot lakes are thermally homogeneous, whereas cool lakes may be stratified (e.g., Oyunuma, Nyos).

4. *Color*

Volcanic lakes display a variety of colors. Crater Lake in Oregon is a splendid blue water body, Kawah Ijen is turquoise-green, Maly Semiachik, Russia, is whitish-blue, and Oyunuma is black (Fig. 1). Surface coloring of a lake may also fluctuate temporarily, as shown at Keli Mutu, where one of the lakes sometime switches from dark green to blood red at the onset of the wet season. Hue changes at Ruapehu and Poás appear to be associated with increasing subsurface volcanic activity.

5. *Biotic Diversity*

Algae, diatoms, fungi, and bacteria are the only organisms that may survive under moderately to highly acidic conditions. Diatoms may partly control silica geochem-

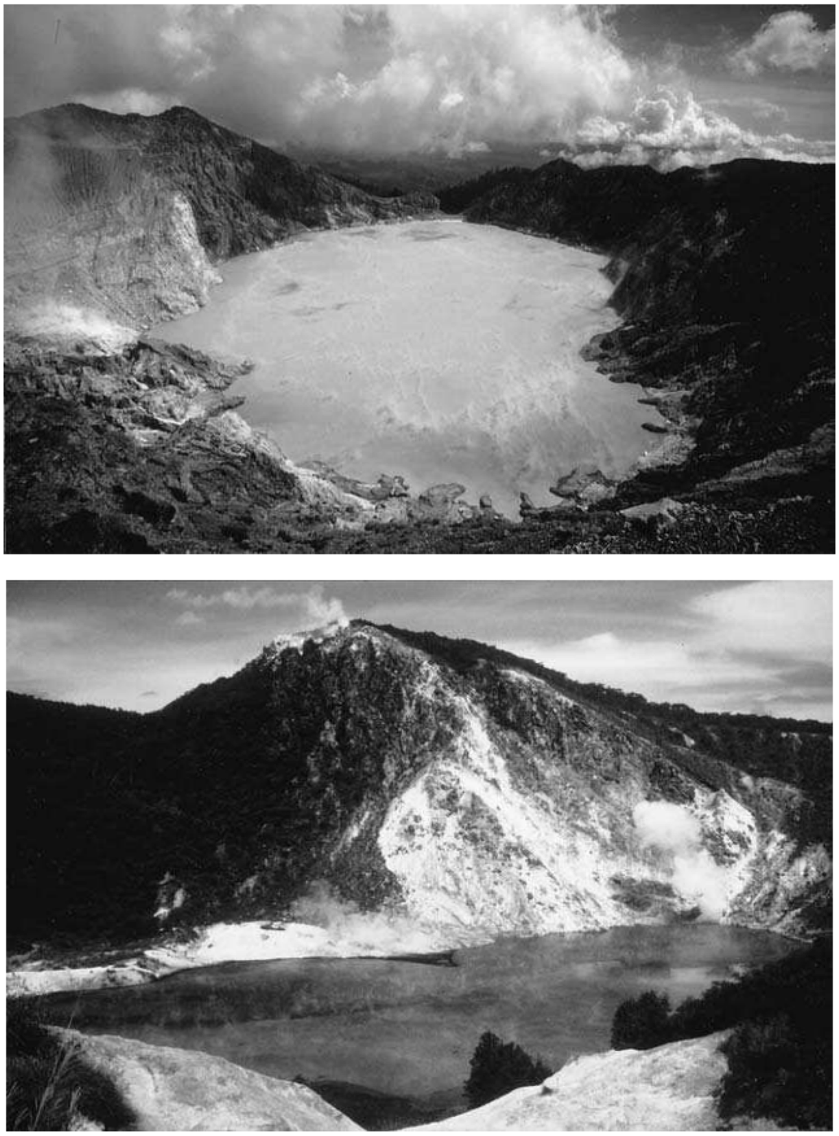

FIGURE 1 (*Top*) Photograph of Kawah Ijen volcanic lake (Indonesia, June 1995). Note variations in lake shading, steaming from the lake surface, and the light streaks of sulfur slicks toward the center of the lake. (From Oppenheimer, 1997, Taylor & Francis.) (*Bottom*) Photograph of Oyunuma lake (Japan, September 1995). Note the black color of the lake and the dark streaks of sulfur slicks covering its surface.

istry in acidic volcanic lakes with pH as low as ~1.5 (e.g., Katanuma, Japan). Recently, Japanese scientists confirmed that sulfur-oxidizing bacteria (*Thiobacillus thiooxidans*) participate in the sulfur cycle in Yugama Lake and Maly Semiachik, two strongly acidic crater lakes (pH < 1.5). The discovery of organic markers such as branched alkanoic acids in Yugama Lake suggests that other unidentified bacteria also may grow in these harsh environments.

B. Volcanic Lakes on Top of Active Craters

1. *Calorimeters and Condensers for Volcanic Heat and Fluids*

Assuming that persistent volcanic lakes represent the surface expression of a hydrothermal system that transports heat, water, and chemical constituents upward from a cooling and degassing magma body situated at depth, one can estimate these fluxes by heat and mass balance analysis. To do this, volcanologists use a "box model" to equate volume and temperature changes in a crater lake with fluxes of water and heat into and out of the lake. Inputs of water to the lake consists of volcanic–hydrothermal fluids (i.e., steam plus ascending brines) and meteoric water (i.e., precipitation, runoff, streamflow, and groundwater seepage). Outputs are due to evaporation, lake water seepage, and overflow. Heat is derived from the enthalpy of the hot fluids entering the lake and from solar and atmospheric radiation; it is lost by evaporative and radiative fluxes from the lake surface, by seepage and overflow, and by heating precipitation and runoff into the lake. Evaporation is the most important energy sink, and its magnitude depends primarily on the wind velocity and on the difference between the lake surface temperature and that of the ambient air temperature. Figure 2 illustrates the influxes and outfluxes used in the box model, and Table IV summarizes results obtained by applying this method to different volcanic lakes.

The box model has been used to infer the main dynamic processes that dictate the existence and physical properties of volcanic lakes. The authors concluded that the ratio between volcanic heat input and heat dissipation of a lake determines the persistence and the temperature of a lake in a crater. Since most heat loss occurs at the lake surface through evaporation, small lakes have only a small capacity for heat dissipation and their temperature rises quickly with small heat inputs; large lakes are better buffered against variations in heat input. The flux of meteoric water into a lake is also an important parameter in the lake's heat and mass budget, and this depends on the surface area. On a local scale, each lake size will have a limiting gas input for a given rainfall and an upper temperature limit at which it starts to lose mass. Calculations suggest that steady-state lakes have temperatures less than 45°C. Field observations confirm this deduction.

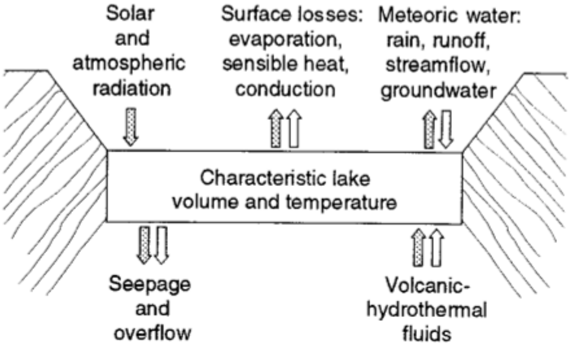
Solar and atmospheric radiation
Surface losses: evaporation, sensible heat, conduction
Meteoric water: rain, runoff, streamflow, groundwater
Characteristic lake volume and temperature
Seepage and overflow
Volcanic-hydrothermal fluids

FIGURE 2 Cartoon showing fluxes of water (white arrows) and heat (shaded arrows) into and out of a volcanic lake as used in the "box model."

Knowledge of magmatic heat and volatile fluxes serves in monitoring programs, as well as to help assess the volcanic contributions to the atmospheric budget of carbon, sulfur, chlorine, and fluorine. Using time-series data on the level (i.e., lake volume) and temperature of lakes along with the box model, we have been able to deduce release rates of magmatic heat and volatiles (in particular sulfur) during passive degassing of magmas underlying volcanic lakes. The incentive is that these calculations provide long-term estimates, whereas most other estimates for volcanoes that degas freely into the atmosphere rely on short-term measurements that are extrapolated to longer time scales. Degassing volcanoes that host hot lakes typically deliver heat outputs ranging from ~20 to 1000 megawatts (10^6 W) and sulfur fluxes ranging from ~50 to 400 tons per day, comparable to estimates for other volcanoes that do not contain a lake. Researchers have noticed that some crater lakes may retain significant amounts of native sulfur, as part of the volcanic sulfur input is precipitated in the lake or just below.

By analogy with shallow geothermal systems, and using results from the box model, volcanologists have proposed a model for transferring heat and water from a degassing magma to a lake above it (Fig. 3). Below the lake, a two-phase vapor–liquid zone is formed as high temperature magmatic gases condense into groundwater. Heat pipes or vapor–liquid counterflows may play an important role during heat transfer in the two-phase zone. Beyond this zone is a comparatively cool liquid envelope. The hot gas–water mixture is injected into the lake as a buoyant jet that powers wholesale convection of the water column, thus allowing for both thermal and chemical homogeneity. Seepage of the lake water through the crater floor and recirculation within the subsurface gas condensation zone probably complicate this picture and can be important components of the lake's hydrologic budget.

2. *Chemical and Isotopic Characteristics*

Escape of steam and other gases from a shallow magma can provide the raw material for the chemistry of volcanic lakes on top of degassing craters. Absorption of ascending magmatic vapors containing the acidic gases sulfur dioxide (SO_2), hydrochloric acid (HCl), and minor hydrofluoric acid (HF) into the hydrothermal vapor–liquid zone beneath the crater produces low-pH solutions that subsequently discharge into the lake. SO_2 reacts with water (H_2O) to form sulfuric acid (H_2SO_4) plus native sulfur (S°),

$$3SO_2 + 3H_2O \Leftrightarrow 2H_2SO_4 + H_2O + S^\circ, \qquad (1)$$

or H_2SO_4 plus hydrogen sulfide (H_2S),

$$4SO_2 + 4H_2O \Leftrightarrow 3H_2SO_4 + H_2S. \qquad (2)$$

Both reactions refer to the disproportionation of SO_2 and can be simultaneous. The acidity of the waters originates principally from proton (H^+) release due to the dissociation of HCl and H_2SO_4 at temperatures below ~300°C. The resulting sulfate- and chloride-rich waters acquire low pHs and are capable of completely dissolving silicate rock. Although this reaction consumes protons (therefore reducing water acidity), it may be a non-buffered, simple rock-dissolution process, because condensation of magmatic acidic gases continuously replenishes the system with H^+. As a result, the low-pH hydrothermal fluids that reach the lake also become enriched in chemical components (e.g., silica, aluminium, iron, magnesium, sodium) leached from the rock. In the lake, dilution by meteoric inputs and evaporation somewhat alter the composition of these hydrothermal fluids. However, the lake may retain very low pH values that prevent precipitation of secondary minerals. Only silica (cristobalite or opal) and occasionally gypsum tend to precipitate in these volcanic lakes. Kawah Ijen and Poás are good examples of lakes containing waters formed by these processes (Table III).

TABLE IV Volcanic Influx, Evaporation Outflux, and Rain Influx as Calculated with the Box Model for Some Volcanic Lakes.[a]

Lake	Surface area (10^4 m^2)	T (°C)	Evaporation output water flux (m^3/day)	Rain input water flux (m^3/day)	Volcanic input Water flux (m^3/day)	Volcanic input Heat flux (10^6 W)
Ruapehu	21	0–60	8920	1082	7838	385
Kerintji	5	30–35	2057	451	1607	79
Dempo	11	30–35	3870	970	2900	142
Kelut	24	30–35	3655	1460	2195	107
Kawah Ijen	41	27–42	7284	2180	4977	244
Tiwu Nua Muri	13	28–33	1732	621	1110	54
Okama Lake	10	30–35	4512	1521	3619	177
Katunama	12	30–35	3426	892	2534	124
Goryavhyee	4	36–55	2770	707	2064	100
Ebeko	3	30–62	1658	247	1411	69
Rincon de la Vieja	5	38	3136	980	2155	105
Quilotoa	310	13–23	7315	5878	1437	72
Copahue	7	30–35	4150	609	3540	173

[a] Modified from Pasternack and Varekamp (1997).

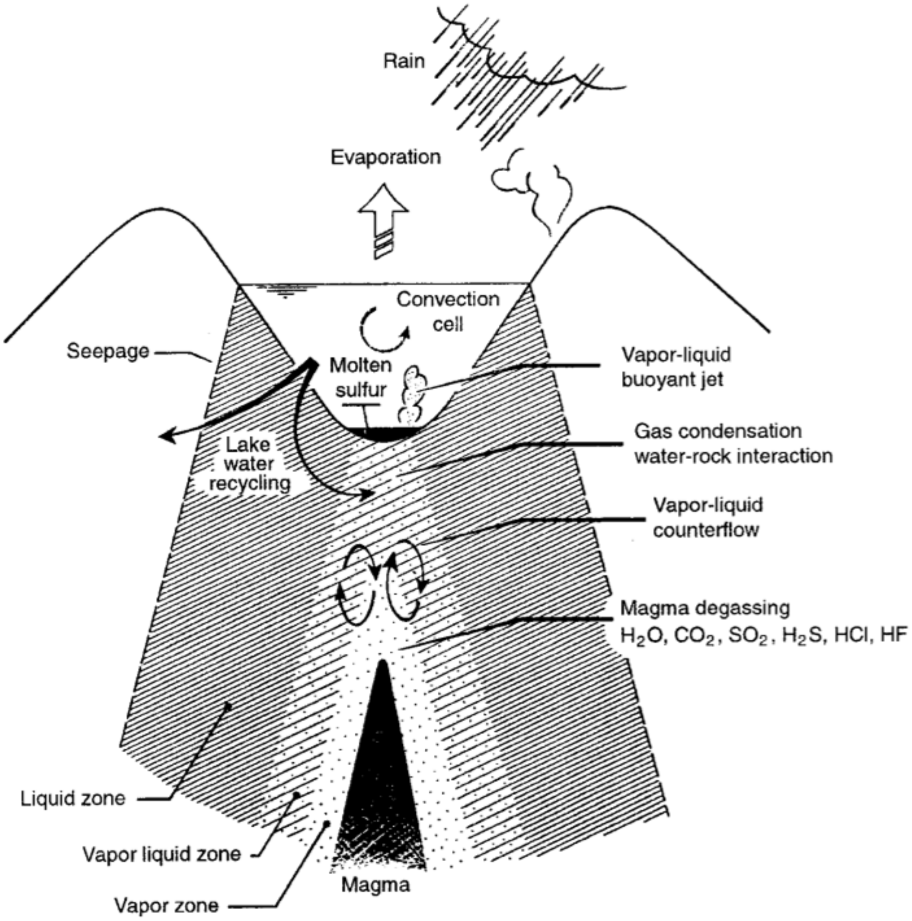
Rain
Evaporation
Convection cell
Seepage
Molten sulfur
Vapor-liquid buoyant jet
Lake water recycling
Gas condensation water-rock interaction
Vapor-liquid counterflow
Magma degassing
H_2O, CO_2, SO_2, H_2S, HCl, HF
Liquid zone
Vapor liquid zone
Magma
Vapor zone

FIGURE 3 Illustration showing processes that may occur in and below hot acidic volcanic lakes on top of active degassing craters.

The occurrence of carbon dioxide (CO_2) in hot acidic crater lakes remains puzzling. Like other magmatic volatiles, this gas should be released into the subsurface acidic two-phase hydrothermal zone connected to the lake. Owing to its very low solubility in hot, low-pH solutions, CO_2 gas bubbles should rise through the lake–hydrothermal system and escape at the lake surface. However, we generally do not see CO_2 bubbling at the surface of hot acidic lakes. This could indicate that CO_2 leaves the hot, acidic hydrothermal vapor–liquid zone at depth and dissolves into the comparatively less acidic, cooler liquid envelope that surrounds it. This process would eventually lead to the formation of the carbonate-rich springs typically found at lower elevations on the volcano's flanks.

In contrast to the highly acidic and mineralized lakes found in degassing craters, there are also lakes that exhibit dilute to intermediate water compositions although hosted by active volcanoes that recently erupted fresh magma. This situation occurs at Kelut volcano, where the lake has near-neutral pH values (~5.5–6.5) and moderate dissolved solids concentrations (TDS ~ 3400 mg/kg) (Table III). Yet, heat and mass budget calculations as well as geochemical data clearly show that Kelut's hot crater lake is fed mostly by magmatic-hydrothermal inputs. The case of Galunggung in Indonesia, the last violent explosion of which occurred only in 1982, is similar; local inhabitants catch fish in the cool lake that fills the summit crater. The waters are neutral (pH ~ 7) but show an anomaly in dissolved sulfate (Table III). These examples reveal that the structure of the magmatic–hydrothermal system below the lake is likely to play an important role in controlling the ability of hot, acidic fluids to reach the summit crater lake. In this respect, the host edifice's hydrology and permeability may be key characteristics.

Together with chemical data, stable isotopes are used by geochemists to assess the volcanic and nonvolcanic contributions to a crater lake. Volcanic lake waters that receive inputs of hot magma–hydrothermal fluids from below may be significantly enriched in "heavy" isotopes such as deuterium (D) and oxygen-18 (^{18}O) with respect to local meteoric water. This results from the combined effects of hydrothermal condensation of hot magmatic steam, with characteristic high D and ^{18}O contents, and continuous evaporation from the lake surface; evaporation fractionates the heavy isotopes into the liquid phase. In addition, enrichment in ^{18}O may also partly be due to high-temperature water–rock interactions in the magmatic hydrothermal system beneath the lake.

In a similar fashion, the sulfur isotopic ratios in a volcanic lake may be indicative of the origin and formation process of its sulfur compounds (i.e., SO_4, H_2S and/or S°). For example, a large fractionation of the heavy sulfur isotope (^{34}S) into H_2SO_4 typically accompanies the SO_2 disproportionation reaction [Eqs. (1) and (2)]. Accordingly, the isotopic difference (Δ in ‰) between H_2SO_4 and $H_2S/S°$ measured for several acidic sulfate–chloride lakes in degassing craters tends to be larger ($\Delta_{H2SO4-S°}$ up to 26‰) than that found in systems lacking this sulfate formation process ($\Delta_{H2SO4-S°} < 15‰$). Assuming isotopic equilibrium is reached between dissolved SO_4 and S°, these values suggest that the SO_2 disproportionation reaction occurs at hydrothermal temperatures between ~200 and 350°C.

Generally, sulfate dissolved in hot acid lake waters also has a high ^{18}O concentration. Some workers have suggested that this results from equilibration with lake water at relatively high temperature (~100–170°C) in the hydrothermal vent feeding the lake. However, partial or complete equilibration with other fluids of unknown isotopic compositions that exist in the subsurface magmatic–hydrothermal system may also lead to the ^{18}O compositions observed in the lake sulfate.

C. Volcanic Lakes in Dormant Craters

1. *Freshwater-like Reservoirs in Large Calderas*

There are many large dormant calderas on Earth that are partly or wholly filled by voluminous lakes whose compositions are close to meteoric (e.g., Crater Lake and Batur, Indonesia, Table III). Yet, these waters may still exhibit a dilute volcanic hydrothermal signature. For example, Crater Lake in the 6800-year-old caldera of Mt. Mazama shows near-neutral to slightly alkaline pH and dissolved solids contents quite typical for fresh water reservoirs (TDS ~ 80–100 mg/kg). However, the lake is well mixed to total depth (589 m) and its concentrations of dissolved chloride, sulfate, boron, lithium, and silica are higher than expected, suggesting existence of an active hydrothermal system associated with some remnant of a magma body at depths greater than 7.5 km. Indeed, warm bicarbonate-, sodium-, and sulfate-rich springs are discharged on the crater floor. The estimated volcanic heat input is in the range ~15–30 10^6 W.

2. *Volcanic Lakes in Geothermal Areas*

Low-relief hydrothermal fields associated with active, or inactive but still hot, volcanic systems classically feature various surface manifestations, including steaming grounds, boiling springs, and low-temperature fumaroles. Small crater lakes are also common. These can receive volcanic inputs from below, but unlike lakes on top of active craters, they condense only a fraction of the total heat and chemical fluxes associated with the subsurface hydrothermal activity. The thermal energy output of Noboribetsu geothermal area in Japan is ~40 MW; a quarter is apparently directed to the hot lake ($T \sim 50°C$) in Oyunuma crater. Typically, volcanic inputs consist of hot water and low-temperature ($T < 100°C$) steam discharges that are vented as small buoyant jets into the lake or as diffuse emissions through the lake sediment pile.

Not surprisingly, the water compositions of volcanic lakes in hydrothermal areas are similar to those of nearby sodium-chloride boiling and steam-heated acid sulfate spring discharges. The NaCl waters are derived from prolonged water–rock interactions and dilution of magmatic fluids at depth followed by near-surface boiling. Acid sulfate waters originate from the oxidation of H_2S-rich steam phase separated from the rising sodium chloride as it mixes with cool oxygenated groundwater. These sulfate waters, with minor, if any, amounts of chloride are moderately acidic ($2.5 \leq pH < 5$) and can leach the rock from its chemical constituents. Acid sulfate waters usually have high total dissolved solids concentrations. Oyunuma lake displays a mixed thermal water composition, whereas Bannoe lake, Russia, is dominated by a steam-heated sulfate composition (Table III). From an isotopic viewpoint, the D and ^{18}O contents of sodium-chloride waters show the influence of extensive water–rock interaction, whereas the isotopic compositions of steam-heated sulfate waters reflect a meteoric origin. In the same way as active volcanic lakes behave, evaporation at the hot lake surface may concentrate the "heavy" isotopes in the lake waters. Dissolved sulfate in hydrothermal lakes have a distinct sulfur isotopic composition; they retain the low ^{34}S-content of H_2S from which they derive. This results from the fact that oxidation of H_2S by oxygen at shallow levels does not involve significant fractionation of the “light” and “heavy” sulfur isotopes between the sulfur species.

3. Gas-Rich Volcanic Lakes

Monoun and Nyos, two lakes in maar craters along the Cameroon Volcanic Line, suddenly expelled massive amounts of CO_2 in 1984 and 1986, respectively. Following these events, geochemical surveys revealed that both lakes are unusual environments, because their bottom waters store “free” CO_2 gas dissolved by the pressure. Together with their basin topography, the Nyos and Monoun water columns thus have a chemically and thermally stratified structure and the capacity to accumulate tremendous amounts of CO_2 gas. It is believed that CO_2-rich soda thermal springs ($T < 30°C$) discharge as diffuse emissions into these lakes. Geochemical evidence suggests that the Cameroon Volcanic Line is a zone of enhanced mantle degassing. Apparently, the mantle may ultimately be the source of CO_2 at Nyos, judging from the isotopic composition of its carbon and from that of helium in the waters. Recent calculations indicate that Lake Nyos contains about 0.5×10^6 tons of CO_2 in its waters. From 1987 to March 1995, the estimated CO_2 flux to the lake decreased from 11,000 to 6600 tons per year. By comparison, the long-term CO_2 release rate deduced for Grimsvötn is ~3.5 to 7 times higher, but the gas does not accumulate in this lake.

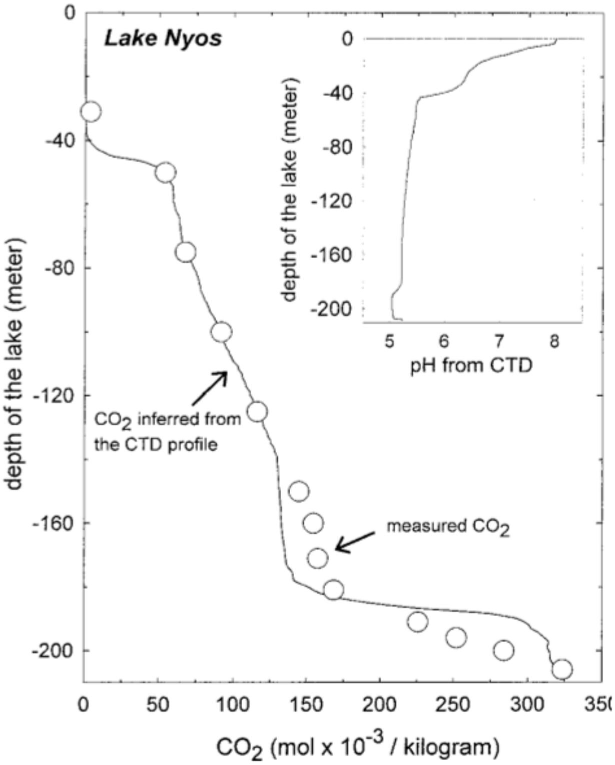

FIGURE 4 “Free” carbon dioxide (CO_2) gas concentrations in the water column of Lake Nyos measured *in situ* in November 1993 and calculated from conductivity–temperature–depth (CTD) profile obtained in April 1996. Inset: pH values in the water calculated from the CTD profile.

Lake Nyos has a maximum depth of 209 m, and vertical profiles of dissolved solids indicate that “free” CO_2 gas is overwhelmingly the most abundant chemical species in the lake. Carbonic acid (H_2CO_3) is also present in the lake waters. Concentration builds up with increasing depth because of the pressure-dependent solubility of CO_2 (Fig. 4). From a depth of 48 m, a gradual and temperature gradient is observed that corresponds to the position of the surface mixing layer with meteoric water (chemocline). Below this, as the total CO_2 concentration increases, the pH decreases as a result of the dissociation of H_2CO_3. At Nyos, the pH of the waters change from 8.0 at the surface to a minimum of 5.1 at the bottom (Table III). Iron is highly soluble under the slightly acidic conditions found below the chemocline, making the lake strongly enriched in this element. The presence of iron in its reduced redox state (ferrous iron) indicates that the water is anoxic below the surface mixing layer. Together with the high CO_2 gas concentration of the bottom waters, this leads to precipitation and deposition of small amounts of siderite ($FeCO_3$), a rather rare mineral in a freshwater lake environment. After the 1986 catastrophe, the surface of Lake Nyos turned red-brown, because of the formation of iron hydroxide as the ferrous bottom waters were carried up to oxidizing shallow levels.

The occurrence of density-stratified gas-charged lakes is not very common. An example, on a much larger scale, is Lake Kivu, East African Rift, where the predominant gas is also CO_2, but accompanied by large quantities of methane (CH_4). Of the 37 systems inspected along the Cameroon Volcanic Line, only Lake Nyos and Lake Monoun exhibit the CO_2 anomaly. Existence of a CO_2-recharge similar in size to that of Lake Nyos has been reported for Lake Mashu, a 1000-year old caldera lake on Hokkaido, Japan. Fortunately, there is insufficient time for CO_2 gas to accumulate in the bottom waters, since the seasonal overturns of the lake expel the gas into the atmosphere twice a year. Anomalies of CH_4 and CO_2 gases have been detected in the bottom waters from Lake Piccolo on Mt. Vuture, Italy. The origin of these gases is likely organic, but an inorganic contribution for CH_4 cannot be ruled out.

D. Mineralization in Volcanic Lakes

1. *Liquid Sulfur on Earth*

Early in this century, Japanese observers inferred the presence of molten sulfur on the lake bed of Yugama Lake. They based their interpretation on the morphology of S° spherules that are continuously conveyed to the surface of the lake. Later, scientists recognized the presence of similar S° material floating on the surface of other hot volcanic lakes in both active craters and geothermal areas. Although less frequent, the ejection of sulfur tephra during mild eruptions through a lake (e.g., Poás in 1989, Kawah Ijen in 1993, and Copahue, Argentina, in 1995) is also suggestive of the presence of subaqueous molten S°. Such bodies of liquid S° have been probed successfully at Ruapehu, Maly Semiachik, Kusatsu-Shirane, Poás, and Bannoe lakes, revealing temperatures between ~120 and 170°C. Apparently, the heat flow through the crater floor can be sufficiently high to melt S° trapped within sediments lying on the lake bed. The color of quenched liquid S° samples collected from different lakes varies from yellow to black and may be controlled by the type and amount of impurities present in S°.

We do not have a precise idea of the size of these subaqueous molten S° bodies. There is strong evidence that substantial deposits of S° form in certain lake environments. Such deposits can be sizeable, for example, 2.6×10^6 tons of S° accumulated over 1420 years at Rotokawa, New Zealand. The sediments of Poás crater lake may host 0.5×10^6 tons of S°, whereas El Chichón crater had stored 4×10^3 tons of S° in the space of less than 1 year after a lake had formed. In volcanic lakes, S° can be produced directly through the disproportionation reaction of SO_2 [reaction (1)], produced during oxidation of H_2S derived from reaction (2), or transported to shallow levels by steam boiled off from a hydrothermal system.

2. *Acidic Crater Lakes as Potential Ore Forming Environments?*

From the mineralogy and stable isotopic compositions of the alteration assemblage associated with certain base metal deposits found at shallow levels and containing a high proportion of sulfide minerals (the "high-sulfidation" deposits), economic geologists have deduced that circulation of low pH, oxidizing, sulfur-rich fluids occurred at early stages of ore deposition in this class of ore deposits. Seepage of acidic mineralized brines formed by condensation of hot magma–hydrothermal mixtures in crater lakes may be one mechanism by which this type of alteration signature is produced at depth. Tops of some ore deposits contain breccias and sedimentary structures that are interpreted to be the roots of acidic crater lakes.

Geochemical modeling indicates that subsurface circulation of strongly acidic waters within a magmatic hydrothermal system underlying a crater lake only dissolves the rock to produce the silica-rich core that invariably constitutes the most altered parts of high-sulfidation ore deposits. However, seepage of acidic lake waters away from the central zone of acid gas condensation may also permit precipitation of an alteration mineral assemblage similar to that observed in association with the high sulfidation deposits. Indeed, infiltration through permeable stratigraphic units and/or flank fractures of the host edifice allows for prolonged water–rock interactions and mixing with groundwater. Both processes will gradually decrease the acidity of the circulating lake fluids, leading to saturation of secondary minerals such as alunite, clays, and pyrite and eventually to that of sulfides such as covellite and enargite.

III. HAZARDS OF VOLCANIC LAKES, THEIR MONITORING AND MITIGATION

The compilation "Volcanoes of the World" lists 55 volcanoes with a record of at least one eruption through a lake. Water and hot magma make an explosive combination, and a summit crater lake on an active volcano places these two components in dangerous proximity. Lake water adds to the danger by contributing, in an eruption or in a crater rim failure, to debris flows and floods that can devastate the volcano's flanks and beyond. This kind of activity has caused a great number of deaths (Table II). Toxic water releases, sector collapses, and gas bursts constitute additional hazards associated with volcanic lakes. Yet, very few lakes are monitored on a regular basis. Changes in a lake's appearance and thermal and/or chemical output are the diagnostic symptoms that are watched for. Manual collection of data is the most widely used technique, but volcanic lake surveillance by means of automated instrumentation and satellite remote sensing is being developed. At Kelut, extensive efforts to drain the lake have successfully reduced the danger posed by overflow of the lake, causing lahars. A new challenge for volcanologists and engineers is to artificially degas the CO_2-rich Nyos and Monoun lakes in order to prevent another sudden CO_2 release.

A. Hazards

1. *Hydrovolcanic Eruptions, Base Surges, and Tsunamis*

Hydrovolcanic eruptions result from the mixing of water and hot rock. Active edifices hosting a lake present a high potential for this type of interaction, leading to hydrovolcanic eruptions that are more destructive than equivalent size eruptions that lack a lake. This phenomenon was first documented at Taal during a series of eruptions that involved the caldera lake in 1965–1966. Base surges swept over the landscape like hot hurricanes, tearing trees from the ground and destroying houses, then flowed across Lake Taal and engulfed fleeing boats before hitting the shores. As huge masses of water were suddenly displaced, a tsunami formed in the large lake. Damage extended up to 6 kilometers from the vent, and more than 200 people died. It was later recognized that more violent base surges accompanied by tsunamis also occurred during the 1911 eruption through the lake-hosted Main Crater.

2. *Debris Flows (Lahars) and Floods*

The Indonesian word "lahar" refers to a debris flow that contains mostly fragments of volcanic origin mixed with water. Crater lakes on active volcanoes with steep slopes can release water to form lahars that, in the case of acidic lakes, can be caustic. The volcanic lakes are often situated in densely populated areas, and some of the worst lahars in history are associated with crater lakes (Table III). Indonesia has suffered dreadfully from crater lake–related lahars, the most devastating of which have occurred at Kelut. In 1919, an eruption expelled the lake and generated lahars that traveled as far as 37 km, destroying 100 villages over a 130-km^2 area and killing 5000 persons. Lahars from the 1586 eruption reportedly took the lives of 10,000 people. Sudden drainage of a volcanic lake due to crater collapse or crater rim failure/breaching, without precursor activity, is another source of debris flows and floods. This happened in 1953 at Ruapehu when a breach in the crater walls caused the lake waters to gush out, forming a debris flow that swept away the Tangwai bridge just before the arrival of an express train. The carriages plunged into the valley, and 151 people perished. Catastrophic draining of a crater lake at Agua volcano, Guatemala, created lahars that totally destroyed the former capital of Ciudad Vieja in 1541.

3. *Toxic Water Releases and Flank Collapses*

Highly acidic and mineralized waters in summit crater lakes sometime seep into flank watersheds, profoundly affecting the water quality. At Kawah Ijen, the Banyupahit River continuously receives toxic discharges from the acidic crater lake. Seven kilometers from its source, the river waters display pH values < 1 and TDS contents $> 20{,}000$ mg/kg. Over most of its length, the river is totally devoid of life. When it reaches a vast irrigation system about 30 km from the summit, it carries ~1500 tons of sulfate, 28 tons of fluoride, 500 tons of chloride, 100 tons of aluminum, and 0.03 ton of copper daily. When the lake overflows and sometimes during the rainy season, the villagers are forced to divert the toxic flow from the rice fields directly into the sea, causing the near-shore fauna to perish. Contamination of the river watershed by the lake water also occurs at Poás and Copahue.

In addition to contaminating local water supplies, the low-pH crater lake waters that seep and circulate within the host edifice alter and dissolve the rock, in some instances significantly. For example, over a 100-year period the bulk dissolution rates at Poás and Kawah Ijen volcanoes have removed $\sim 6 \times 10^5$ and 1.4×10^6 m^3 of rock, respectively. Although the edifice volumes (~100 km^3) are much larger than these values, the process may result in an increase in the permeability of flank aquifers over the lifetime of the hydrothermal system (hundreds to thousands of years). In turn, this may weaken the volcano along preferential fluid pathways (i.e., fractures and faults) and eventually promote sector collapse of these volcanoes.

4. *Gas Bursts*

Some crater lakes can rapidly release free CO_2 amassed in their bottom waters. The tragedies of Monoun and Nyos are the only two historical examples of this type of crater lake hazard. The exact triggering mechanism for releasing the CO_2 remains controversial. Complete overturn of the lakes induced by sinking of cool and denser water from heavy rainfall is not regarded as a viable mechanism, because a well-developed stratified structure persisted immediately after the catastrophe. Gas exsolution may have been initiated quietly at shallow levels, although the possibility remains that the process began from the lake bottom. A plausible hypothesis is that sudden upward displacement of the chemocline initiated the saturation of CO_2 gas and formation of bubbles by reducing the pressure exerted on the water column. Once upwelling started, the process escalated as more CO_2 was released from solution during ascent of deep waters. In this model, we still do not know what raised the chemocline. A small landslide on the inner crater walls may have been the trigger, but other external energy sources could plausibly trigger the eruption. Unfortunately, volcanologists cannot substantiate their hypotheses using geological records alone, since the Monoun and Nyos events did not leave such evidence.

B. Monitoring

1. *Visual Observations of Lake Color, Bubbling, and Sulfur Slicks*

The color of a water body results from absorption and scattering of solar radiation by inorganic and organic materials that are dissolved and/or suspended in the waters. Thus, the color of a volcanic lake is affected by chemical precipitation rates, particle sizes and the vigor of convective circulation in the lake. The volcano observatory staff who monitor Ruapehu volcano look for a shift in the lake's color from blue-green, when the water temperature drops to 10–20°C and visible signs of convection are not evident, to pale gray, an indication that bottom sediments are being remobilized by increasing water movements associated with enhanced vent activity. Eruptions through the lakes of Kawah Ijen and Kelut also were reportedly preceded and followed by color changes that apparently involved remobilization of the bottom sediments. Several times, the lake of Poás went from grayish green to bright yellow green following the start of hydrovolcanic eruptions through the lake. Here, the color change was attributed to an increased flux of sulfur dioxide, which causes oxidation of dissolved iron.

2. *Lake Temperature, Lake Level, and Thermal Energy Budget*

Several eruptions at lake-hosted volcanoes have been preceded by large temperature changes. For example, the Main Crater Lake of Taal recorded a 10°C increase 2 to 3 months prior to the September 1965 eruption. Similarly, the lake temperature at Kelut increased from 30°C in September 1989 to 38°C several days before the 10 February 1990 eruption. About 10 months before the main 1995 eruption of Ruapehu, the lake temperature reached a 13-year high of 55°C. However, identifying a forthcoming eruption solely on the basis of lake temperature variations is not straightforward. The 30-year record from Ruapehu reveals that a significant decrease of near-surface temperatures over several hours can be associated with rain and snow storms at the summit, whereas the opposite trend may reflect instability of convective heat transfer within the lake rather than changes in magmatic activity.

Because of difficult, dangerous, or limited access to the lake shore, direct recording of temperature on a continuous basis can be disrupted. In the late 1970s, temperature telemetry buoys were deployed at Mt. Ruapehu with transmission by high-frequency radio. Recently, satellite communications have allowed transmission of instrumental data from Ruapehu, Kelut, and Taal lakes. The drawback of this automated method to monitor active volcanic lakes is that instrumentation suffers from the harsh conditions encountered in these environments, causing equipment failure and loss of data.

Results of heat and water budget analysis for which time-series data on lake temperature and lake level are available suggest heat discharge patterns that generally coincide with the onset of a new stage of volcanic activity. At Ruapehu, pre-eruptive periods are characterized by low heat input to the lake ($<150\ 10^6$ W compared with a normal average of $\sim 400\ 10^6$ W). At Poás and Yugama crater lakes, departures from a steady heat inflow coincided with increase in the lake activity and sometimes with the number of volcanic earthquakes. In both cases, these perturbations were attributed to the formation of fractures in the envelope surrounding a cooling magma body, allowing release of magmatic volatiles to the overlying hydrothermal system. Upward migration of magma also may have occurred at Poás.

The potential of remote sensing for monitoring volcanic lakes by means of images recorded by satellite was recently explored using visible and infrared data provided by the Landsat Thematic Mapper (TM) platform. A reasonable agreement between remote sensing estimates and ground measurements of temperature and surface area were obtained. Problems arise from atmospheric influences on water reflectance and from the generally small surface area of lakes compared with satellite spatial resolution. In addition, gases rising from hot lakes may complicate the reflectance spectra. Nevertheless, temperature and surface area data can be used to model lake heat outputs in the same fashion as *in situ* data. The Advanced Spaceborne Thermal Emission (ASTER) and Enhanced Thematic Mapper (ETM+), both of which were due for launch in 1998, will offer improved capabilities for the remote surveillance of volcanic lakes.

3. *Geochemical Methods*

The pH of lakes in degassing craters chiefly depends on the injection rate and composition of the condensing acidic magmatic–hydrothermal fluids. pH is easy to monitor directly or remotely on a real-time or near-real-time basis. Decreasing pH correlated with increasing Cl concentrations at Yugama Lake in 1990–1993. A marked increase in acidity was also reported in the Main Crater Lake of Taal before the 1968–1969 eruptions. By contrast with these hot acidic systems, pH variations at Lake Nyos and Lake Monoun vary with the CO_2 content, because pH is inversely correlated with total CO_2. Coupled with conductivity–temperature–depth (CTD) profiles, retrieval of pH data allows the estimation of CO_2 concentrations in the water column (Fig. 4). This method is essential to monitor the rate of its accumulation in bottom waters.

Since the 1980s, a Japanese team has been developing a real-time capability for monitoring changes in polythionate concentrations in crater lakes. Polythionates ($S_xO_6^{2-}$, $x = 4$–6) are transient sulfur compounds produced by reaction of SO_2 with H_2S in acidic solutions. In acidic crater lakes, their concentrations typically reach a few hundred parts per million. The method relies on the dependence of polythionate stability on the SO_2/H_2S ratio in lake waters. Changes in this ratio may indeed indicate fluctuations in the activity of the magma–hydrothermal system at depth. The method was applied to Yugama Lake, Poás, and Ruapehu with success. Sharp declines in polythionate concentrations and corresponding increases in dissolved sulfate correlated in all cases with renewed hydrovolcanic/seismic activity in these lakes (Fig. 5). These observations strongly support the idea that variations in lake chemistry and heat output can be closely related.

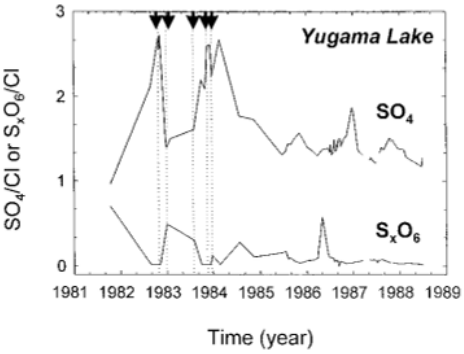

FIGURE 5 Changes in the chloride (Cl)-normalized dissolved polythionate (S_xO_6) and sulfate (SO_4) contents measured between 1981 and 1988 in Yugama Lake on Kusatsu-Shirane volcano, Japan. Black arrows indicate eruptions occurring in the lake. [Modified from *J. Volcanol. Geotherm. Res.* **40,** Takano, B., and Watanuki, K., Monitoring of volcanic eruptions at Yugama Crater Lake by aqueous sulfur oxyanions, 71–87 (1990) with permission from Elsevier Science.]

The evolution of the Mg/Cl ratio in the waters has been used by New Zealand scientists since the mid-1970s to monitor the crater lake of Ruapehu. As shown in Fig. 6, the five main eruptions that occurred between 1965 and 1995 in the lake (1966, 1968, 1969, 1971, and 1977) were all preceded by six months or more of constant Mg/Cl ratios, followed by an abrupt increase and a long-term decline thereafter. Assuming that Cl is derived solely from the condensation of high temperature volcanic gases into the magmatic-hydrothermal system and that Mg is leached from the rock during water–rock interaction, the increase in the Mg/Cl ratio reflects injection of fresh magma into the vent feeding the lake

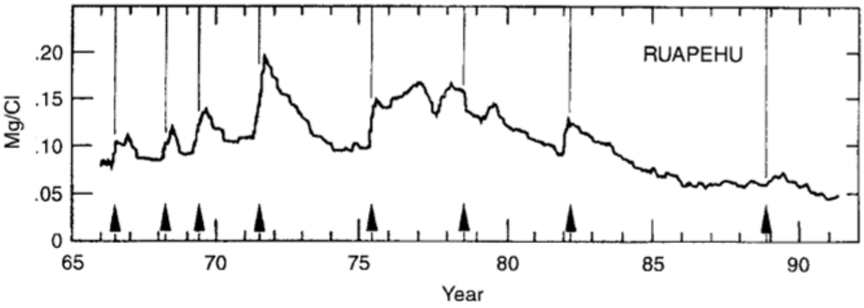

FIGURE 6 Changes in the Mg/Cl ratio measured between 1965 and 1991 in the crater lake of Ruapehu volcano, New Zealand. Arrows indicate time of eruptions into the lake. Data compiled from Christenson and Wood (1983) and references therein.

and its decrease indicates subsequent strong HCl degassing. Apparently, the Mg/Cl ratio can also record smaller perturbations occurring at depth. For example, the variations observed in 1976, 1982, and 1988 seem to be associated with hydrothermal explosions that cleared the subaqueous vent of fluids with compositions differing from those of the lake.

The Mg/Cl method and other chloride-based ion ratios are, unfortunately, not without ambiguities. A survey carried out at Poás from 1984 to 1990 revealed that HCl vapor starts to evaporate at lake temperatures above 50°C, therefore also changing the Mg/Cl ratio in the waters. At Taal, the source of Cl in the crater lake is not only the magma, but also hydrothermal fluids contaminated by seawater. Fluctuations in the Mg concentration in a lake may also relate to dissolution or precipitation of Mg-bearing minerals (e.g., chlorite and biotite) in the underlying magmatic–hydrothermal system. This process is strongly dependent on temperature. We also note that the Mg/Cl method cannot provide real-time information on the state of the lake, since water samples collected on site must be analyzed and interpreted in the lab.

4. Underwater Acoustic Surveys

Geophysicists have suggested that underwater noise measurements across a broad frequency band can be useful to observe changes in the crater floor region. High-sensitivity hydrophones have been deployed in the lake of Kelut during intereruptive and eruptive phases. During the seismic crisis preceding the 1989–1990 activity, the hydrophones recorded powerful signals of bubbles that originated from subaqueous fumarolic activity. As the crisis progressed, the bubble noise increased and persisted until the eruption destroyed the instrumentation. Ruapehu was the site of a second series of measurements. Between 1993 and 1994, the acoustic and seismic records at Ruapehu revealed the increase of heat transfer to the lake several days before an increase in the lake temperature could be detected. Several weeks of high-energy acoustic signals preceded the 29 June 1995 eruption that destroyed the equipment.

C. Mitigation

1. Drainage Tunnels at Kelut Volcano

Kelut has erupted 29 times since 1311, with repose intervals between eruptions ranging from 1 to 75 years. The major volcanic hazard for people living near the volcano is lahars that come from the crater lake. Aware of the permanent threat posed by the presence of 4×10^7 m^3 of water stored in the summit crater, the Dutch administration built a dam on the Badak river in 1905 to divert the debris flows from reaching the town of Blitar. Unfortunately, the voluminous lahars from the 1919 eruption swept away the dam.

Upset by this tragic event, which killed 5000 people, the Volcanological Survey of Indonesia decided to drain the crater lake by means of tunnels. This constituted one of the first and most ambitious examples of an engineering project aimed at reducing volcanic hazards. The work started 4 months after the 1919 eruption when the lake had not yet reformed, with the objective to drill a 955-m-long tunnel through the crater wall. This plan could not be completed quickly because of the harsh conditions encountered at the excavation front. By 1923, when the lake had filled with 2.2×10^7 m^3 of water, sudden flooding of the tunnel ended the tunnelling efforts. A new strategy was then adopted to lower the lake level progressively by excavating seven superimposed tunnels while draining the lake waters with a siphon pipe. This work was completed in 1926, and the lake volume was successfully lowered to less than 2×10^6 m^3. Later eruptions in 1951, 1966, and 1990 produced only minor lahars whose damage was much more limited. At present, the tunnels of Kelut still control the volume of the 33-m deep crater lake, although their maintenance demands constant attention.

2. Artificial Degassing of Lake Nyos

Lake Nyos and Lake Monoun have been increasing their CO_2 contents since the last catastrophes in the 1980s, and future CO_2 bursts cannot be discounted. However, these gas disasters are unique because they can be effectively controlled through continuous monitoring and degassing. Scientists and engineers have recently proposed an elegant solution based on the creation of an artificial self-sustained gas eruption to degas the CO_2-rich waters. The principle consists in tapping the bottom waters by means of pipes. As the waters rise up the pipe, the pressure progressively drops, causing saturation and exsolution of CO_2 gas bubbles. As a result, the density of the gas–water mixture is decreased and the internal buoyancy becomes sufficient to expel the fluid at the surface. Once the process has started, it becomes self-sustaining, requiring no external energy and lasting for several months or years until no gas is left at depth.

A French team has already carried out test experiments on Monoun and Nyos lakes. In March 1995, a 200-m-long pipe was installed vertically in the middle of Lake Nyos and delivered a 20-m-high fountain of water and CO_2 that lasted several hours until the experiment was stopped deliberately. The team concluded that the gas-lift process is feasible and estimated that 10 years would be necessary to degas the 5×10^5 tons of CO_2 stored in Lake Nyos if 12 pipes of 12 cm diameter are used. Similarly, 5 years of pumping through three pipes would completely remove the dissolved gas from Monoun. Scientists have recently submitted a project (Lake Nyos Monoun Degassing Project) aimed at operational degassing of the lakes. In this, they acknowledge that close monitoring of the physical and chemical conditions during the experiment is essential, although numerical simulations suggest that the process is safe.

IV. FUTURE DIRECTIONS

Data on the past activity and current status of crater lakes, particularly those on active volcanoes, are too few and, in some cases, unreliable. It is critical to understand how and why the physical and chemical parameters in a crater lake respond to changes in volcanic inputs. The few examples of crater lake energy budget analysis and geochemical monitoring illustrate the complexity and uniqueness of each crater lake system. Ideally, we need to infer and validate a model of heat and mass transport from a magma intrusion to the crater lake bottom, taking gas–rock, gas–water, and water–rock interactions into account. Experience shows that optimum monitoring is achieved by a combination of methods, rather than reliance on one method alone. Toward this end, recent research on stable isotopes to determine lake dynamics by considering heat and mass flow constraints is promising. Similarly, we need to integrate detailed hydrologic considerations into crater lake studies, as these probably play an important role in determining the dynamic state of a lake. Prediction of the evolution of a crater lake system is also important and should give insights into ore forming environments. More biological studies of hot acidic crater lakes may provide insights into life in extreme environments. In the particular case of Nyos and Monoun lakes, the volcanological community faces a formidable challenge to safely degas the lake waters.

SEE ALSO THE FOLLOWING ARTICLES

Calderas • Deep Ocean Hydrothermal Vents • Lahar and Jökulhlaup Hazards • Surface Manifestations of Geothermal Systems • Volcanic Gases • Volcanism on Io • Volatiles in Magmas

FURTHER READING

Brantley, S. L., Agustsdottir, A., and Rowe, G. L. (1993). Crater lakes reveal heat and volatile fluxes. *Geol. Soc. Amer. Today* **3,** 176–178.

Christenson, B. W., and Wood, C. P. (1993). Evolution of a vent-hosted hydrothermal system beneath Ruapehu Crater Lake, New Zealand. *Bull. Volcanol.* **55,** 547–565.

Bacon, C. R., and Nathenson, M. (1996). Geothermal resources in the Crater Lake area, Oregon. *U.S. Geological Survey Open-File Rep.* **96-663,** 34.

Kusakabe, M., ed. (1994). Geochemistry of Crater Lakes, *Geochem. J.* **28,** special issue.

Kusakabe, M. (1996). Hazardous crater lakes. *In* "Monitoring and Mitigation of Volcanic Hazards" (R. Scarpa and R. I. Tilling, eds.). Springer-Verlag, Berlin.

Le Guern, F., and Tazieff, H., eds. (1989). "Lake Nyos," *J. Volcanol. Geotherm. Res.* **39,** special issue.

Oppenheimer, C. (1997). Remote sensing of the color and temperature of volcanic lakes. *Int. J. Rem. Sen.* **18,** 5–37.

Oppenheimer, C., and Stevenson, D. 1989. Liquid sulfur lakes at Poás volcano. *Nature* **342,** 790–793.

Pasternack, G. B., and Varekamp, J. C. (1997). Volcanic lake systematics 1. Physical constraints. *Bull. Volcanol.* **58,** 528–538.

Takano, B., and Watanuki, K. (1990). Monitoring of volcanic eruptions at Yugama crater lake by aqeuous sulfur oxyganions. *J. Volcanol. Geotherm. Res.* **40,** 71–87.

Varekamp, J. C., and Rowe, G. L., eds. (1999). "Crater Lakes and Hyperacidic Fluids in the Terrestrial Environment," *J. Volcanol. Geotherm. Res.*, special issue.

This Page Intentionally Left Blank

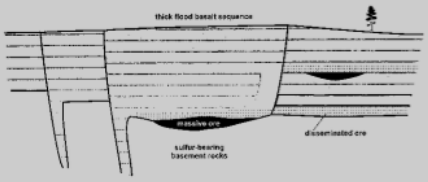

MINERAL DEPOSITS ASSOCIATED WITH VOLCANISM

NOEL C. WHITE
BHP Minerals

RICHARD J. HERRINGTON
The Natural History Museum, London

I. Processes That Produce Mineral Deposits in Volcanic Environments
II. Porphyry Copper, Molybdenum, and Gold Deposits
III. Epithermal Gold, Silver, and Base Metal Deposits
IV. Volcanic-Hosted Massive Sulfide Deposits
V. Deposits Associated with Continental Flood Basalts
VI. Nickel Sulfide Deposits Associated with Komatiitic Lavas
VII. Diamond Deposits
VIII. The State of Knowledge and Future Research

GLOSSARY

cumulate An igneous rock formed by the accumulation of crystals that settle out from a magma by the action of gravity. The most common cumulate rocks are ultramafic in composition, formed by the accumulation of olivine crystals

dunite A type of peridotite in which the mafic mineral is almost entirely olivine, with accessory chromite almost always present.

eclogite Rock of basaltic composition containing minerals that indicate that it has been subjected to very high pressures deep in the crust.

geothermal system A present-day natural system in which hot water, typically heated by magmas, circulates. Surface expressions may be silica sinters, boiling pools, and geysers.

harzburgite A type of peridotite composed chiefly of olivine and orthopyroxene.

hydrothermal system Any natural system involving the circulation of hot water. The water and the heat can be derived from any source. Presently active hydrothermal systems that we can see near the earth's surface are called geothermal systems.

kimberlite A porphyritic alkalic peridotite containing abundant phenocrysts of olivine (commonly altered to serpentine or carbonate minerals) and phlogopite in a fine-grained groundmass of calcite, olivine, and phlogopite with accessory minerals. Kimberlite is the main host rock for diamonds.

lamproite A group name for dark-colored intrusive or extrusive rocks rich in potassium and magnesium. Lamproites can contain diamonds.

lherzolite A type of peridotite composed chiefly of olivine, orthopyroxene, and clinopyroxene, in which olivine is generally most abundant; a two-pyroxene peridotite.

ocelli A textural feature of some igneous rocks, in which central crystals are surrounded radially or tangentially by small crystals of another mineral, forming rounded eyelike branching forms.

ore Naturally occurring material from which economically valuable minerals can be extracted at a reasonable profit. The term is generally but not always used to refer to

Copyright © 2000 by Academic Press
All rights of reproduction in any form reserved.

rocks containing metals, and is often modified by the name of the metal extracted, e.g., "copper ore."

peridotite A general term for a coarse-grained plutonic rock composed chiefly of olivine with or without other mafic minerals such as pyroxenes, amphiboles, or micas and containing little or no feldspar. Peridotite is commonly altered to serpentinite.

pluton A general term for an igneous intrusion, typically a large body composed of medium to coarse grain-size minerals.

porphyry An igneous rock of any composition showing a texture in which phenocrysts occur in a fine-grained groundmass.

picrite A dark-colored rock containing abundant olivine along with pyroxene, biotite, possibly amphibole, and less than 10% plagioclase.

xenocryst A crystal that resembles a phenocryst in an igneous rock but is foreign to the body of rock in which it occurs.

IN ACTIVE VOLCANIC areas most of what we see at the surface has been erupted recently, so it hides earlier deposits. However, below the surface processes are occurring that can produce major ore deposits. When we examine older volcanic environments where erosion has exposed the subsurface, we see several important types of ore deposits. Even though these deposits occur in or close to volcanic rocks, it is not always obvious how the ores relate to the volcanism.

I. PROCESSES THAT PRODUCE MINERAL DEPOSITS IN VOLCANIC ENVIRONMENTS

There are three main processes that produce ores associated with volcanic rocks:

1. Formation from minerals that crystallize from the magma itself
2. Formation from volatile fluids (mostly hot water) that are in the magma and are driven out as it solidifies
3. Formation from fluids that do not come from the magma, but that are driven by heat from magmatic intrusions

Volcanism is a way for the Earth to lose heat, as large amounts of heat are carried to the surface of the Earth and dissipated during volcanic activity. Magmas that reach the surface may represent only about 20–30% of the magma that was generated and brought to crustal levels, with the rest forming intrusive rocks that solidify below the surface. So in considering ores in the volcanic environment, the intrusions below the volcanoes are often more important than the volcanoes themselves.

Intrusive rocks lose their heat in several different ways:

1. By transferring heat to the porewater present in the rocks that host the intrusion. Heating of this water causes it to become less dense and rise, drawing in other water to take its place, which in turn becomes heated. In this way the magma drives a heat pump that takes heat from the magma at depth and carries it to near-surface levels where it becomes dispersed. In the process of fluid convection, the heated fluids can dissolve metals from the country rocks, depositing them near the Earth's surface and possibly forming ore deposits.

2. By expelling the volatiles that they contain. Magmas contain varying amounts of water and sulfur-bearing compounds, and as they solidify the concentration of these builds up in the part that has not yet crystallized. If water becomes saturated, a magmatic hydrothermal fluid forms that, when expelled from the intrusion, can carry away both heat and dissolved metals and may lead to the formation of ores.

3. By conduction through the rocks they have intruded, though this is a slow and relatively inefficient process.

In some cases the relationship between mineral deposits and volcanism is very direct, with both forming at the same time. In other cases more deeply formed ores are more related to the magma chamber that feeds the volcanism. In still other cases the magmas below may only provide heat to drive the hydrothermal processes that produce ores. In these last two cases, the volcanic rocks may simply provide a site for deposition of ores. Although the relationship between ores and volcanism is complex (and we do not fully understand it in many cases), the Earth's volcanic environments are host to a wide variety of different ore deposit types.

A. Tectonic Setting, Volcanic Rocks, and Ore Deposits

There are three main settings for the generation of volcanic rocks that are of the greatest importance for ore deposits (Fig. 1):

1. Mantle plumes or hotspots
2. Midocean ridges
3. Subduction zones

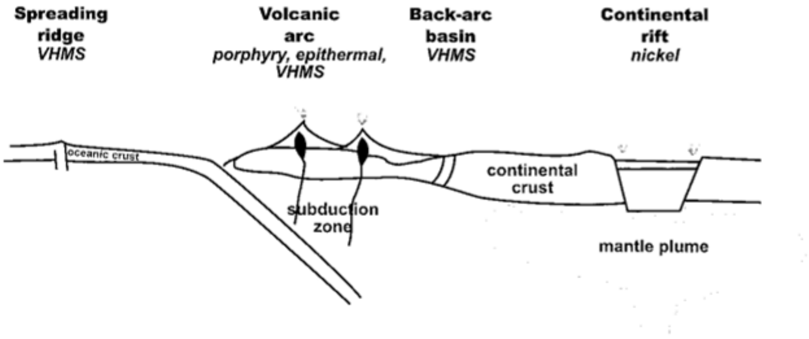

FIGURE 1 Tectonic settings of volcanic-associated ore deposits. Note the three different settings for volcanic-hosted massive sulfide deposits (VHMS).

All three environments can produce huge volumes of magmatic rocks: however, their volumes and the importance of the ore deposits they host are very different.

1. Mantle Plume or Hot Spot Settings

Mantle plumes (or hot spots) can occur beneath oceans or continents and are associated with immense outpourings of tholeiitic and alkalic volcanic rocks. Volcanic rocks generated by this process in oceanic regions (such as Hawaii) are typically barren of major metal deposits. However, where mantle plumes occur below continents, flood basalt provinces can result. Flood basalts occur where mantle plumes well up beneath continents and cause arching of the crust, which results in rifting and massive outpourings of basalts. This process has occurred many times throughout the Earth's history. Although the very well-preserved flood basalt provinces are relatively young, there are remnants of flood basalts of many ages on all continents. Some are host to important nickel–copper and platinum-group metal deposits (see later discussion).

In ancient environments similar processes to those responsible for the flood basalt sequences are believed to have produced another style of nickel sulfide deposit, associated with distinctive magnesium-rich volcanic rocks called komatiites. They host a class of nickel sulfide deposits that are generally referred to as Kambalda-type after the best-known locality in Western Australia. Komatiites are mainly restricted to Archaean sequences (>2.5 billion years old), although some early Proterozoic (2.5–2.0 billion years old) analogues host deposits in Canada.

2. Midocean Ridge Settings

At midocean ridges the crust is spreading, allowing magmas to have access to the surface where they form submarine volcanoes and subvolcanic intrusions consisting of sheeted basaltic dykes and gabbros. The igneous rocks interact with seawater that penetrates and convects through fractured, heated crust to dissolve, transport, and deposit metals. Volcanic rocks generated at midocean ridges are exposed at the Earth's surface where slices of the oceanic crust (ophiolites) become thrust up (obducted) onto continental margins, and so are preserved in older sequences. Many ophiolites contain volcanic-hosted massive sulfide (VHMS) deposits (see later discussion). The settings of these deposits are identical to many of the active "black smoker" systems of hot springs discharging at spreading ridges that have been studied by deep-sea diving over the past 25 years.

3. Volcanic Arcs and Subduction-Related Settings

VHMS deposits not only form in association with midocean ridges, but are also associated with volcanic arcs. Volcanic arcs are common throughout the geological record and are best represented today by the volcanic Ring of Fire that surrounds the Pacific Ocean, generated by subduction. Volcanoes form where the plates that cover the Earth's surface come together and one slides under the other. As one plate slides down, parts of it melt to form magmas that penetrate the plate above and erupt in a volcanic arc. As subduction continues it is common for stretching and thinning to occur in the crust behind the arc, forming a backarc basin. In volcanic arcs the VHMS deposits can form within the arc, and in backarc basins. We can see VHMS deposits forming today in both these settings.

The most obvious examples of volcanism on land are related to volcanic arcs (e.g., Mt. St. Helens, Mt. Pinatubo, Mt. Etna). During the early stages of their development volcanic arcs typically contain little or no mineralization of economic value. As they mature, a wide range of hydrothermal systems and thus ore deposit styles can develop. Porphyry copper deposits, copper–gold skarns, high-sulfidation epithermal gold deposits, and low-sulfidation epithermal deposits all form in this setting (see later discussion).

II. Porphyry Copper, Molybdenum, and Gold Deposits

A. Significance

The porphyry deposits are the world's greatest accumulations of copper and molybdenum and are among the largest gold deposits. They take their name from their characteristic association with shallow depth intrusive rocks with porphyritic textures. Many deposits occur within small intrusions originating from larger plutons at depth that have intruded into volcanic sequences; in some cases these intrusions underlie volcanoes (Fig. 2). The ore can occur in the intrusion, and in the surrounding volcanic rocks. In some cases the intrusion was emplaced in nonvolcanic rocks that formed a basement to the overlying volcanic rocks, and the ores can also occur in these basement rocks.

Important examples include the following:

Escondida	Chile	1800 Mt at 1.6% Cu
Chuquicamata	Chile	9500 Mt at 0.6% Cu, including 800 Mt at 1.85% Cu
Bingham Canyon	USA	2000 Mt at 0.9% Cu, 0.35 g/t Au
Grasberg	Indonesia	3150 Mt at 0.88% Cu, 0.75 g/t Au
Sar Cheshmeh	Iran	1300 Mt at 0.67% Cu, 0.27 g/t Au, 0.03% Mo, including 450 Mt at 1.13% Cu
Ok Tedi	Papua New Guinea	550 Mt at 0.69% Cu, 0.63 g/t Au, including 25 Mt at 2.08 g/t Au
Panguna	Papua New Guinea	950 Mt at 0.48% Cu, 0.56 g/t Au
Climax	USA	907 Mt at 0.240% Mo

Mt = million tonnes

B. Distribution and Age

The porphyry copper deposits are widely distributed around the world. The distribution is not regular, and major deposits are particularly abundant in Chile and the southwest United States. Other important belts of deposits follow ancient volcanic arcs that are no longer active, such as the one that runs along the Tethys Belt from Slovakia, through Hungary, Romania, Yugoslavia, Bulgaria, Greece, Turkey, Iran, and into Pakistan. Other arcs occur in Central Asia, with important deposits in Kazakhstan, China, and Mongolia. In many parts of the world, deposits are known from preserved fragments of ancient volcanic belts.

Most economically important porphyry copper deposits are of Late Tertiary to Cretaceous age (10–130 million years old), although both younger and older deposits are known and new deposits are believed to be forming today beneath some active volcanic areas. This age distribution is probably due to erosion and preservation. The deposits form at depths of 2–4 km below volcanoes. In most cases the very young deposits have not yet eroded enough to be exposed whereas deposits formed in Tertiary to Cretaceous time have eroded sufficiently to be exposed, but not to have been removed entirely. The further back in time we go, the less likely it is for the deposits to be preserved. Despite this, we know examples that have been preserved from very early Earth history, so it appears that these deposits have probably formed throughout geological time.

C. Classification of Types

Porphyry deposits are classified on the basis of their most economically significant metals, which are copper, molybdenum, and gold, though minor amounts of other metals such as silver and rhenium may occur.

Porphyry molybdenum deposits are distinct from the other combinations and are relatively uncommon. They are characteristically associated with very silica-rich magmas. Porphyry gold deposits are also relatively uncommon and are found associated with calcalkalic composition rocks of Andean volcanic arcs. Porphyry copper–molybdenum deposits occur with calcalkalic magmas associated with continental crust (Andean volcanic arcs). Porphyry copper–gold deposits occur in either of two ways: with calcalkalic magmas emplaced into thin crust (island arcs), or with alkalic magmas emplaced far from subduction zones (e.g., Grasberg, Indonesia).

D. General Characteristics

Porphyry deposits show characteristic features that make them easy to distinguish from other deposit styles.

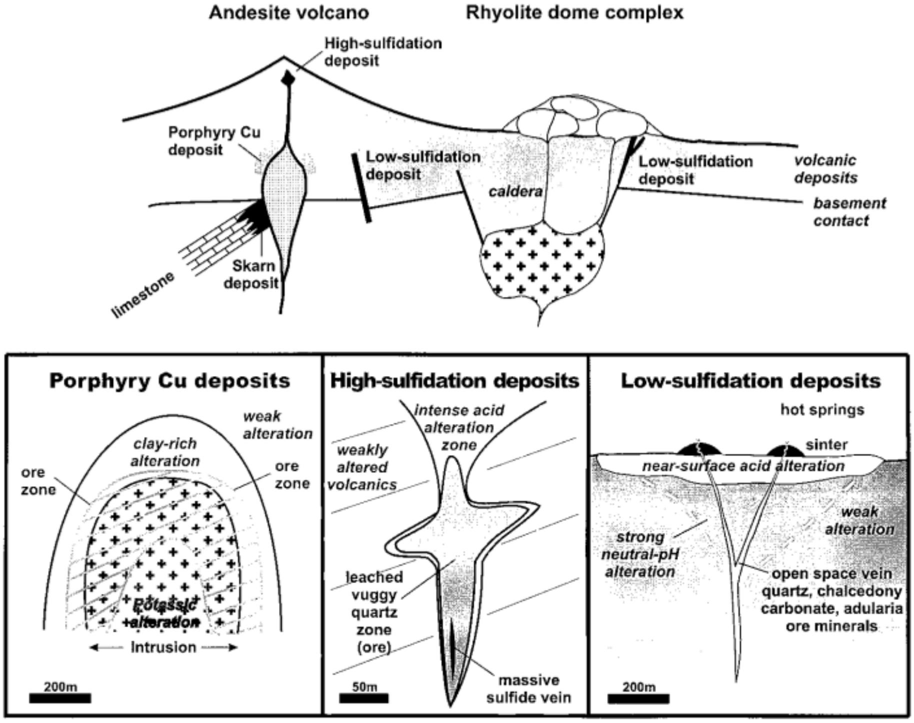
Andesite volcano
Rhyolite dome complex
High-sulfidation deposit
Porphyry Cu deposit
Low-sulfidation deposit
caldera
Low-sulfidation deposit
volcanic deposits
basement contact
Skarn deposit
limestone
Porphyry Cu deposits
weak alteration
clay-rich alteration
ore zone
ore zone
Potassic alteration
Intrusion
200m
High-sulfidation deposits
intense acid alteration zone
weakly altered volcanics
leached vuggy quartz zone (ore)
massive sulfide vein
50m
Low-sulfidation deposits
hot springs
sinter
near-surface acid alteration
weak alteration
strong neutral-pH alteration
open space vein quartz, chalcedony carbonate, adularia ore minerals
200m

FIGURE 2 Setting of ore deposits in volcanic arcs (top). The small figures below show details of the most important deposit styles. (Left) Detail of a porphyry copper deposit. The intrusion is overprinted by zones of alteration; potassic (central), then clay-rich, and weak alteration of surrounding rocks. The ore zone overprints the alteration, typically focusing in the potassic zone or, more commonly, forming a shell around the contact between the potassic and clay-rich zones. (Middle) Detail of a high-sulfidation deposit. The vuggy quartz ore zone expands upward with irregular shape determined by permeability of the host volcanic rocks. It narrows at the top with a zone of clay-rich acid alteration. (Right) Detail of a low-sulfidation deposit. The ore is typically in structurally controlled veins, surrounded by neutral pH alteration.

The ore in porphy copper deposits contains copper minerals, usually chalcopyrite, but in some cases with bornite, covellite, or enargite. Typically the ore includes large amounts of pyrite, and in some cases magnetite. Native gold and molybdenite may accompany the copper minerals, and in some cases may be the most economically important minerals. The ore minerals are widely distributed throughout very large volumes of the host rocks, typically at low grade. However, the huge volumes of mineralized rock make these deposits especially suitable for low-cost bulk mining methods.

Ore minerals in the deposits typically occupy very complex sets of small veinlets or are on minor fractures. The distribution of minerals in deposits is zoned, so the level of the deposit that is exposed is important (Fig. 2a). For example, in some deposits the copper is distributed like an inverted cup over and around the margins of the porphyry intrusion. In deeply eroded deposits, the core of the deposit may be barren; in other cases the core may enriched in gold compared to the margins. Magnetite is common in the core of deposits, whereas pyrite is especially common on the margins, and in some cases a shell of barren pyrite-rich rock surrounds the copper mineralization. If the intrusion has been emplaced into reactive rocks, such as limestone, skarn mineralization may occur at the contact between the intrusion and the limestone. Skarn commonly consists of copper and gold mineralization, often with abundant magnetite, within a calcsilicate rock produced by high-temperature reaction between the intrusion and the limestone.

Most porphyry deposits are low grade, so any process that enhances their grade can be of great economic importance. Weathering processes can enrich deposits near the surface by concentrating the ore metals (possibly as more easily extractable minerals) and by making the rock softer and so easier to mine. In some cases (e.g., in Chile) this occurs on a spectacular scale, greatly enriching the value of the deposit.

Some porphyry copper deposits have ore zones that are over a kilometer in diameter. Ore deposits of this size form from huge hydrothermal systems. The reaction between the rocks and the hydrothermal fluids results in zoned alteration patterns. The margins of the system show signs of reaction with hot water that has changed the mineralogy of the rocks, but has not significantly changed their composition. The intensity of the alteration increases toward the center of the system where the hot fluids have intensely altered the original rocks, substantially changing their composition, mineralogy, and texture. This alteration zoning is an important guide in exploration for new deposits.

E. Origin of Deposits

Porphyry deposits result from a combination of processes that occur in the Earth's mantle and at shallow crustal levels. The mantle processes determine whether the magma contains significant amounts of the metals required to form ore deposits. The shallow processes determine whether the metals are released from the magma and if they are deposited in a small enough volume of rock to form ore.

The first stage in the genesis of a porphyry deposit occurs in the Earth's mantle with the generation of magma of suitable composition. To form copper and gold deposits, low reduced sulfur content in the source region favors the metals being incorporated into the magma; this can be best achieved if conditions are oxidizing, which means that whatever sulfur is present is dominantly oxidized. This is consistent with the observation that porphyry copper and gold deposits are related to oxidized magmatic systems. The water content of the magma is also important, as it plays a crucial role later in the generation of the deposits.

Once a magma of suitable composition has been generated, it rises into the crust. At this point the amount of water present in the magma becomes important. If there is too much water present, the magma will explode as it approaches the surface, producing pyroclastic volcanic eruptions. If there is insufficient water, the ore-forming process is inhibited as an aqueous fluid cannot exsolve from the magma.

Geologists believe that the intrusions associated with porphyry deposits probably rise to within 2–4 km of the Earth's surface, then stop and begin to cool. An outer surface chills, allowing the still-molten inner parts to evolve. As the intrusion continues to crystallize, the pressure in the molten center builds up. Eventually this pressure cannot be contained; the crystallized rind fractures, causing the remaining magma to quench rapidly and exsolve a metal-bearing hydrothermal fluid. This fluid streams out along available fractures and deposits sulfides. This process involves complex chemical changes in the released magmatic volatiles due to the pressure release and intense wall–rock reactions. Mixing caused by interaction with dilute groundwater that surrounded the intrusion becomes important over time as the intrusion cools and dissipates its heat.

III. Epithermal Gold, Silver, and Base Metal Deposits

A. Significance

The age distribution of gold deposits is very irregular. Two of the most important gold-forming events were in Archaean time. The third great period of gold deposition is very much younger, mostly during Tertiary to Recent time (less than 66 million years). Most of these deposits occur within volcanic rocks or are related to the magmatism that produced the volcanic rocks.

There are many different styles of gold deposits found in the young period of gold mineralization, including gold porphyries, skarns, and diatreme-hosted deposits. In some of these deposits, gold is not the main metal produced, but is a by-product to the production of other metals (especially copper). Of the deposits in which gold is the main economic metal, the largest and most productive class in this period of geological time is the epithermal deposits. These deposits are themselves quite diverse, but they share characteristics that indicate that they formed at shallow crustal levels (typically from the water table to about 1000 meters below at the time of formation). There are two important classes of epithermal deposits, here called high-sulfidation and low-sulfidation (Fig. 2).

Important examples include the following:

High-Sulfidation

El Indio	Chile	>12 Mt at 8 g/t Au, 50 g/t Ag, 3% Cu
La Coipa	Chile	52.1 Mt at 1.58 g/t Au, 50 g/t Ag
Summitville	USA	24.3 Mt at 1.46 g/t Au
Lepanto	Philippines	38 Mt at 3.53 g/t Au
Chinkuashih	Taiwan	20 Mt at 4.6 g/t Au, 10 g/t Ag
Pueblo Viejo	Dominican Republic	150 Mt at 7 g/t Au

Low-Sulfidation		
Martha Hill	New Zealand	83.3 Mt at 3.2 g/t Au, 33 g/t Ag
McLaughlin	USA	17.5 Mt at 5.2 g/t Au
Hishikari	Japan	3.2 Mt at 63 g/t Au
Kushikino	Japan	8 Mt at 6.5 g/t Au, 62 g/t Ag
Gunung Pongkor	Indonesia	6 Mt at 17 g/t Au, 162 g/t Ag

B. Distribution and Age

Epithermal and related deposits are widespread around the world. They occur principally in the circum-Pacific Rim of Fire, and also in volcanic are settings in other parts of the world where processes were active that were similar to those now occurring around the Pacific Ocean.

Areas famous for their epithermal deposits include Chile and Peru, Mexico and the southwest United States; Japan, Philippines, Indonesia, and New Zealand. Other significant deposits occur in Serbia and Romania, and ancient examples are known in Sweden, Saudi Arabia, and Australia.

Epithermal deposits typically occur within subaerial volcanic rocks, though they may extend below the volcanic cover into underlying basement rocks. In some very rare cases there may have been a shallow water cover when the deposits formed.

The majority of economically important epithermal deposits are of Tertiary age, and some are undoubtedly forming today beneath areas of geothermal activity. This age distribution is probably due to variations in the intensity of volcanic activity and to the depth of erosion. Erosion has so far exposed few of the very young deposits. Erosion of Tertiary sequences has generally gone on for long enough to expose the deposits, but not enough to remove them entirely. The further back in time we go, the less likely it is that deposits have been preserved. We know rare examples of Precambrian age, so it appears that these deposits have probably formed throughout geological time and have been preserved wherever their host geology has been preserved.

C. Classification of Types

We can subdivide epithermal deposits in various ways. First, there is a major difference between two contrasting classes, here called low-sulfidation and high-sulfidation (referring to, respectively, the low and high oxidation state of the sulfur in the hydrothermal systems). These two classes are significantly different in many ways, especially the character of deposits, the associated alteration zoning, and the textures of ores (Figs. 2b and 2c). The mineralogy of ores shows some overlap, but there are also distinct differences.

D. General Characteristics

The most important characteristics of low-sulfidation deposits are their typically open-space vein-fill character, their diverse range of distinctive textures, their mineralogy (especially adularia and carbonates), and the characteristic alteration zoning (Fig. 2c). For high-sulfidation deposits the most important features are their typically massive, disseminated character, their mineralogy (especially enargite and alunite), and their quite different characteristic alteration zoning (Fig. 2b).

There is no difference in the overall setting for the two styles, as both occur in subaerial volcanic settings of intermediate to felsic composition. Calcalkalic magmatic suites are favorable for either style; alkalic magmatic suites are also favorable for low-sulfidation deposits. High-sulfidation deposits tend to occur close to the centers of host volcanoes, whereas low-sulfidation deposits can occur in any volcanic setting. Both styles are localized by structures, but any suitable permeable structure may be used by hydrothermal fluids.

E. Origin of Deposits

Despite decades of study, there are many aspects of the origin of epithermal deposits that we do not understand. The systems are diverse, and it may be that apparently similar deposits form by different mechanisms.

Many *high-sulfidation deposits* have a close association with porphyry copper deposits, so the processes that form the two are probably closely related. Vapors separate from the brines that form porphyry copper deposits and ascend to shallow depths where they condense into groundwater. The magmatic volatiles such as hydrochloric acid and sulfur dioxide that are contained in the vapor produce an extremely acidic fluid, resulting in the intense rock alteration that characterizes high-sulfidation deposits. The ore minerals that deposit in this leached and permeable alteration zone may arrive by one of two mechanisms; we are not sure which actually happens. The metals may be introduced by high-temperature gases, or alternatively they may be transported by saline magmatic fluids that travel up the same conduits that focused the gases. Deposition of the metals results from mixing with dilute groundwater and boiling of fluids.

The origin of *low-sulfidation* deposits has been debated for many years and is still far from settled. Studies of the origins of the water in the hydrothermal systems clearly show that most of the water was meteoric, but does not preclude a small proportion of magmatic fluid. In a few deposits there is isotopic evidence for a significant magmatic component that appears closely related to the introduction of metals. The main problems are where the metals come from and how they were transported.

Studies of active geothermal systems in different volcanic areas around the world have shown that vast volumes of meteoric water are circulating, driven by heat from deep magmatic intrusions. As this hot water approaches the surface it is focused into structures where the water boils. This is associated with major changes in the fluid chemistry, such as removal of dissolved gases (including hydrogen sulfide that transports the gold), a decrease in temperature, and an increase in pH, and as a result the dissolved metals are deposited. This process produces the low-sulfidation deposits.

Some researchers argue that the metals were introduced into the geothermal systems by injection of concentrated magmatic fluids at depth. Others argue that the circulating meteoric water was capable of leaching the metals from the huge volumes of rock they traversed. It is likely that in different cases both processes occurred.

IV. VOLCANIC-HOSTED MASSIVE SULFIDE DEPOSITS

A. Significance

These deposits have been variously called volcanogenic massive sulfide deposits, volcanic massive sulfide deposits (VMS), or volcanic-hosted massive sulfide deposits (VHMS). Here we will call them VHMS deposits.

VHMS deposits are an important source for copper and zinc as well as lead, silver, and gold. They are the world's third most important source of copper. They have great historical importance, as the word copper comes from the island of Cyprus where mining of VHMS deposits dates from the earliest use of metals by prehistoric people. They also have the distinction of being one of the few deposit styles that researchers can directly study while it is forming today.

Important examples include the following:

Kidd Creek	Canada	300 Mt at 9.5% Zn, 1.5% Cu, 0.4% Pb, 130 g/t Ag
Bathurst	Canada	110 Mt at 7.3% Zn, 2.4% Pb, 1% Cu, 65 g/t Ag
Rio Tinto	Spain	500 Mt at 2.5% Zn, 0.8% Pb, 0.7% Cu, 0.8 g/t Au, 30 g/t Ag
Rosebery	Australia	19.4 Mt at 16.2% Zn, 5% Pb, 0.74% Cu, 2.9 g/t Au, 155 g/t Ag

B. Distribution and Age

The oldest known deposits of this type are over 3.7 billion years old, and the youngest are forming today. Two styles of VHMS deposits are distinguished, one dominated by copper and zinc, the other by zinc, lead, and copper. Both styles occur throughout the geological record.

Many of the world's Archaean greenstone belt sequences contain copper–zinc VHMS deposits. The Canadian Shield hosts the most important deposits, although many other Archaean provinces also contain deposits. The Proterozoic Churchill province of Canada contains deposits in greenstone belts analogous to the Archaean examples, and similar Proterozoic deposits occur in the USA, Sweden, and Finland. In Paleozoic sequences, there are important copper–zinc VHMS deposits in the Urals of Russia, Newfoundland, and Scandinavia. Mesozoic ophiolites are host to deposits in Cyprus and Oman, and obducted Jurassic ophiolite slabs host deposits in the western United States and South America. Tertiary deposits of this type occur in ophiolites in the Philippines and New Caledonia.

The zinc–lead–copper style is poorly represented in Archaean rocks apart from some small deposits in Western Australia. The largest deposit of this style occurs in the Paleozoic of Canada. Other Paleozoic belts include the deposits of eastern Australia and the Iberian pyrite belt in Spain and Portugal. The most famous deposits in this group are of Miocene age and occur in the Hokuroko district of Japan. These deposits have led to the name Kuroko-type deposits, a synonym for this style of deposits.

C. Classification of Types

VHMS deposits are typically subdivided in two ways. The first (discussed earlier) considers the proportions of the dominant metals. On this basis we can define two major groups, namely the copper–zinc and zinc–lead–copper deposits. The zinc–lead–copper deposits have felsic rocks (including micaceous sediments) in their underlying sequences, whereas the copper–zinc group has dominantly mafic volcanic rocks beneath them.

The second classification considers the tectonic setting in which the deposits are interpreted to have formed. On this basis we recognize two types of VHMS deposits. The more important formed in subduction settings (volcanic arcs) and are commonly referred to as Kuroko-type. They can be either copper–zinc or zinc–lead–copper deposits. The second type formed at spreading centers and is commonly called Cyprus-type: They are typically copper–zinc deposits.

Morphologically, two broad settings of VHMS deposits can be recognized: (1) proximal, which are thick lens-shaped deposits formed in or around a seafloor hydrothermal vent, and (2) distal, which are sheetlike deposits, possibly formed in depressions peripheral to the hydrothermal vent (Fig. 3).

D. General Characteristics

Most VHMS deposits show very similar features. The seafloor hydrothermal vent system is represented by an underlying stockwork, overlain by the massive sulfide lens that developed on the seafloor as sulfides precipitated from the venting hydrothermal fluid. Individual deposits vary widely in size and shape, and most mines consist of several closely spaced lenses.

In the copper–zinc deposits, the massive sulfide lenses are dominated by pyrite with pyrrhotite, chalcopyrite, and sphalerite normally forming the other major sulfide minerals. Magnetite is a common accessory mineral, and quartz, chlorite, barite, gypsum and carbonates are the main gangue minerals. Grain size of the minerals and the textures of ores vary widely, depending on the depositional processes and the effects of subsequent recrystallization. Metal ratios in the orebodies commonly are strongly zoned with copper enriched at the base of the deposit, and zinc (and lead) at the top. An extensive thin cherty sedimentary unit containing variable amounts of pyrite or hematite may mark the regional ore-equivalent stratigraphy. This unit, commonly referred to as an exhalite, is believed to form as a chemical sediment mixed with tuffaceous material.

The zinc–lead–copper orebodies represented by the Kuroko deposits also show a mineralogical zonation. The basal part of the orebody comprises a siliceous stockwork containing pyrite and chalcopyrite, interpreted to be the hydrothermal feeder zone. Above this is massive pyrite and chalcopyrite, overlain by layered sphalerite, galena, and chalcopyrite with pyrite and barite. Flanking the massive sulfide body there may be a zone rich in gypsum and anhydrite, which may pass to a zone dominantly composed of barite. Capping the orebody there is typically an exhalative ferruginous chert layer.

Hydrothermal alteration in the rocks that underlie (and sometimes overlie) the copper–zinc deposits is extensive. It takes the form of either discrete pipelike features or broader semiconformable zones. The zinc–lead–copper deposits also show zoned alteration beneath the ore lenses, typically forming a diffuse pipelike zone.

The tectonic setting of ancient deposits is difficult to determine; however, in Phanerozoic sequences, VHMS deposits can be shown to have formed in association

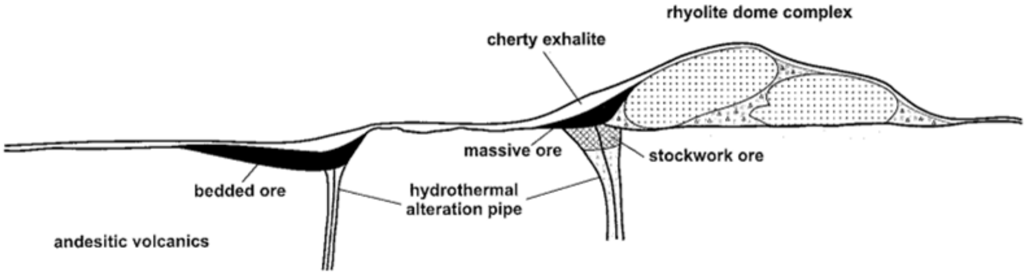

FIGURE 3 Setting of formation of submarine volcanic-hosted massive sulfide deposits. Proximal ores sit directly above the hydrothermal alteration pipe, which represents the pathway along which the ore fluids were introduced to the seafloor. Distal ores occur laterally away from the vent site.

both with spreading ridges and with volcanic arcs. In volcanic arcs the deposits can form within the arc and in backarc basins. The volcanic rocks that are the immediate hosts for VHMS deposits are typically of two types. Bimodal tholeiitic basalt–rhyolite sequences are important copper–zinc hosts in Archaean greenstone sequences, and tholeiitic basalts are copper–zinc hosts in Phanerozoic spreading ridge settings. Differentiated calcalkaline volcanic sequences are important hosts for zinc–lead–copper deposits.

Many ophiolitic sequences in the geological record have associated Cyprus-type VHMS deposits. These deposits are generally hosted in basaltic pillow lava sequences that are typically several kilometers thick. Active black smoker systems developing at spreading ridges (Mid-Atlantic Ridge, Juan de Fuca Ridge, East Pacific Rise) are forming similar VHMS deposits in a similar geological setting. Actively forming seafloor massive sulfide deposits are also being studied in modern backarc basins with active volcanism (e.g., Okinawa trough); these are modern analogues of the Kuroko deposits.

A very common feature of ore settings is the occurrence of clusters of deposits around felsic eruptive centers. Rhyolitic domes are very commonly associated with VHMS deposits of any age, and of both copper–zinc and zinc–lead–copper type, though the significance of the association is not well understood.

In districts containing VHMS deposits it is very common to find that most (not necessarily all) deposits occur at a single stratigraphic position. This position is commonly related to a pause or change in the character of volcanism or to the end of volcanic activity. In many ore fields it is marked by the occurrence of a regionally extensive exhalite, and most deposits occur immediately under this thin unit. It seems that whatever triggers the formation of VHMS ores commonly does so over an entire district and is likely to produce many individual centers of mineralisation. This provides a useful guide for exploration.

E. Origin of Deposits

As early as the middle 19th century, French researchers recognized that VHMS deposits formed from seafloor hydrothermal exhalations, and Japanese workers in the early 1920s proposed exhalative origins for the Kuroko deposits. In the 1970s researchers discovered submarine hydrothermal vents depositing base metal sulfides, dramatically confirming what geologists had believed for over a century. Since then, many more sites of submarine base metal deposition have been found and are being studied to learn about the processes that form these deposits.

Studies of the modern active sites, and of ancient ore deposits, have shown that VHMS deposits form from hydrothermal fluids venting onto the seafloor, precipitating sulfides around the vent. These vent sites are colonized by unique communities of organisms based on the reduced sulfur in the hydrothermal fluid. Some of the ancient VHMS deposits have preserved assemblages of vent fossils, demonstrating the similarity of the environment in both ancient and modern VHMS deposits. Isotopic studies show that the dominant source of the hydrothermal fluids is seawater. Nevertheless, there is still controversy surrounding the source of the ore fluid and the transported metals, and three contrasting models have been proposed.

In one model, downward percolating seawater penetrates the crust, becomes heated by subvolcanic intrusions, leaches metals, and returns to form VHMS deposits on the seafloor. In this model, downward-migrating seawater interacts with massive volumes of underlying rock to produce a metal-bearing fluid. One problem with this model is that the volume of leached rock necessary seems impossibly large to produce some of the huge deposits that exist. However, the observation that the metal content of deposits more closely reflects underlying rock types, rather than the chemistry of closely associated magmatic rocks, supports this model.

A second model proposes that the ore fluids originate from a porous horizon where fluids (in chemical equilibrium with host rocks) were trapped during burial. The brine heated during burial was able to scavenge metals and then be catastrophically released by tectonic activity, with the brine expelled onto the seabed. The third model proposes that the fluids have a magmatic origin. It is proposed for the Kuroko district of Japan because of the close association of the sulfide deposits with rhyolite domes. The presence of very saline (therefore unlike seawater) ore-fluids in some systems supports this model, but the lack of a clear relationship between magma composition and ores does not.

Whatever the ultimate source of the metals and the fluids that introduced them, the character of the depositional environment is clear. Deep water is essential to prevent hydrothermal fluids boiling and precipitating sulfides before they exhale on the seabed. This requires a minimum seawater depth of the order of 500 to 700 m. Deposition in deep water also enhances the chances of preservation, as the deep marine environment favors rapid burial and preservation of these deposits.

V. DEPOSITS ASSOCIATED WITH CONTINENTAL FLOOD BASALTS

A. Significance

The world's nickel resources occur as two main types: deposits developed by lateritic weathering of ultramafic rocks (nickel laterite deposits), and nickel sulfide deposits. Although nickel laterites contain huge amounts of nickel, for economic reasons the most important production to date has come from the sulfide deposits, though this may change with the introduction of new extraction technology. There are three main types of nickel sulfide deposits: those associated with layered ultramafic intrusions (principally Sudbury in Canada); those associated with Archaean-age ultramafic volcanic rocks (considered later); and those associated with continental flood basalts.

The nickel sulfide deposits associated with continental flood basalts include some of the largest nickel deposits known. The best known examples are Noril'sk in Russia, Jinchuan in China, and Voisey's Bay in Canada. The great importance of these deposits results from their high grade and relatively low-cost extraction of nickel. In addition they commonly contain significant amounts of other valuable metals, particularly copper and platinum group metals. The immense economic significance of these deposits is indicated by these figures for the three main examples:

Noril'sk, Russia	900 million tonnes	Average grade 2.70% nickel
Jinchuan, China	515 million tonnes	Average grade 1.06% nickel
Voisey's Bay, Canada	>80 million tonnes	Average grade 1.93% nickel

B. Distribution and Age

Flood basalts are generated by mantle plumes (hot spots) that well up beneath continents and cause arching of the crust, as described earlier. Despite their wide distribution on the Earth, not all flood basalt provinces have nickel sulfide deposits associated with them. Special conditions (discussed later) appear necessary to produce the nickel sulfides, and then to trap and retain them in ore deposits.

C. General Characteristics

These deposits consist of huge masses composed dominantly (>80% by volume) of sulfide minerals, plus large amounts of disseminated sulfides. The relative proportions of the two styles of mineralization vary widely, with massive mineralization dominant at Noril'sk, but minor at Jinchuan. The principal minerals are pyrrhotite, pentlandite, and chalcopyrite, though there are minor amounts of many other minerals.

The igneous provinces that host these deposits are typically very large, commonly over 1000 km in diameter. They are mostly made up of tholeiitic rocks, though alkaline volcanic rocks may also be present. An important feature of the volcanic sequence is the presence of picrites and other olivine-rich rocks, indicating high-temperature partial melting.

D. Origin of Deposits

There is no doubt about the source of the metals in these deposits, as the host rocks contain significant amounts of the metals that form the ores. The key question is how the metals can be carried in the magma, then deposited as sulfides, and the sulfides accumulated. Part of that question is the source of the sulfur.

The largest, best-preserved, and best-studied deposits of this style occur at Noril'sk, in Russia, and most of our understanding of these deposits has developed there. It appears that at Noril'sk a major mantle hot spot developed during late Permian to early Triassic times, and it generated an upwelling plume of mantle material. The overlying crust cracked open along deeply penetrating faults, allowing high-temperature magma to form in response to the pressure drop and ascend to the surface along the faults. The huge flood basalt province known as the Siberian Traps that formed as a result has a volume of over 1.5 million cubic kilometers.

Studies of the chemistry of the Noril'sk volcanic and intrusive rocks show that the earliest-erupted volcanic rocks have lost metals that partition into sulfide minerals (nickel, copper, and platinum group metals). By contrast, the late-erupted lavas show much less depletion. Some of the volcanic rocks show strong evidence for having reacted with sedimentary rocks, as they are severely contaminated with crustal material. The ores are associated with late-stage magmas that were injected as sills and sheets into the base of the volcanic pile and into the basement sedimentary rocks (Fig. 4). Some of the massive nickel and copper ores appear to have injected as melts late in the history of the pile.

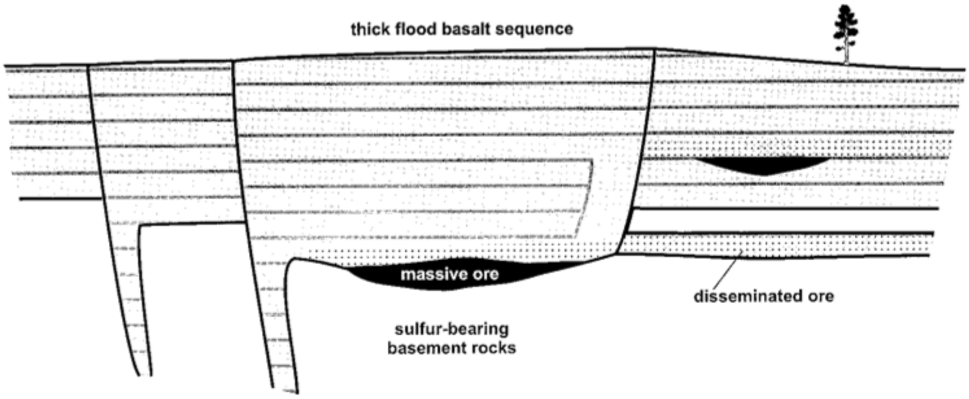

FIGURE 4 Setting of formation of nickel sulfide deposits associated with continental flood basalts. Ores are localized where the dense sulfide droplets can accumulate at the base of a conduit through which magma was flowing to erupt at higher levels.

Our present understanding of the genesis of the sulfide ores at Noril'sk is that interaction of the early magmas with sedimentary rocks caused the melt to become saturated with sulfur. Sulfide droplets formed as a result and, despite their high density, were swept along with the erupting magma. Where the eruptive conduit flattened and had embayments, the sulfides were able to settle out and accumulate, but were regularly swept by successive pulses of magma. This allowed more sulfides to accumulate, but also exposed the early-formed sulfides to more of the metal-rich melt. They progressively scavenged metals from the successive eruptions, so becoming more and more enriched in ore metals.

A key element in our current understanding of these deposits is the need for well-established magma flow paths, so that very large volumes of magma flow along the same conduits. In this way sulfides in these conduits can be exposed to huge volumes of magma in successive pulses. It is also important that the geometry of the conduit allow the dense sulfide droplets that settle to be trapped, rather than drain back down into the lower crust or mantle.

The huge scale of sulfide entrapment in these deposits is illustrated at Talnakh (Noril'sk). There the massive ore zone covers an area 1 km by 3 km, with a thickness of greater than 20 m. Its grade averages 3.72% nickel and 3.78% copper with high platinum and palladium values. At Voisey's Bay the Ovoid is a pod of massive sulfide 600 m long by 350 m wide, with a thickness up to a maximum of 110 m.

At both Voisey's Bay and Jinchuan the nickel orebodies are preserved within Precambrian-age intrusive rocks. The general scenario involved in forming the ores is strikingly similar to that at Noril'sk, so a similar origin seems very probable. The mass and grade of the sulfides present demands that a far greater volume of magma than is now preserved in the associated intrusions had to be involved, so it seems inescapable that the extra magma required must have erupted to form flood basalts that have since been eroded away.

VI. NICKEL SULFIDE DEPOSITS ASSOCIATED WITH KOMATIITIC LAVAS

A. Significance

Komatiites form a suite of igneous rocks, the most characteristic representatives of which are ultramafic (i.e., low silica, high magnesia) volcanic rocks. They host the Kambalda-type nickel deposits that are responsible for over 10% of historic nickel production from sulfide deposits, and substantial reserves remain. Although individual deposits are typically small, their grade is high, which can make them economically significant. The Kambalda camp consists of many individual deposits and contains an aggregate 25 million tonnes of ore averaging 3.5% nickel.

B. Distribution and Age

Komatiites are mainly restricted to greenstone belts, which consist of volcanic and sedimentary rocks of Precambrian age. Although komatiites are very rare after the Precambrian, there are some much younger ones found in Colombia, and very similar high magnesia lavas (boninites) of late Cretaceous age occur in Colombia and Costa Rica. The komatiite-hosted nickel sulfide deposits are mostly mid to late Archaean in age, with the best known examples from the greenstone belts of Western Australia, notably Kambalda, but good examples occur in Zimbabwe and Canada, and deposits are also recorded in Brazil and Russia. Some younger rocks (early Proterozoic age) host similar deposits in Canada. Older (early Archean) sequences in southern Africa and the Pilbara region of Western Australia contain only a few minor deposits, and younger (post–early Proterozoic) sequences do not contain deposits of this style. This limited range in age seems to be related to a stage in the evolution of the Earth.

C. General Characteristics

Deposits of this type show distinctive characteristics, both in their ores and in their host rocks. The nickel sulfide orebodies consist of variable amounts of massive and matrix or disseminated ores hosted by ultramafic komatiites. They have been subdivided into stratiform and stratabound types.

Stratiform deposits typically occur as tabular or ribbon-shaped bodies, situated at the base of the host units (Fig. 5). They have dimensions from a few hundred meters to 5 km in length, but mostly the stratigraphic thickness of the sulfide zone is less than 10 m, with distinct lower and upper contacts. Massive and matrix sulfides are present at the base of the host unit, and there is usually an abrupt boundary between the massive and matrix sulfide. Disseminated sulfides overlie the matrix sulfides. In some cases the orebodies show marked elongation parallel to the regional volcanic or tectonic grain; these orebodies are believed to have formed at the base of relatively thin flows.

Stratabound mineralization is not confined to the base of ultramafic units, but can be distributed through the lower to central portion of the host unit. The shape and size of these deposits are more difficult to quantify because of their diffuse, gradational character; the margins are defined by economic grades. Broadly, they have oblate to elongate lens shapes, depending on the shape and size of the host unit. Dimensions are generally much larger than equivalent stratiform deposits, particularly stratigraphic thickness, which may be up to several hundred meters. Stratabound deposits consist of disseminated or blebby mineralization, with rare local accumulations of matrix sulfide. These orebodies are believed to have formed in very thick lava flows or large feeder dykes.

Primary magmatic sulfide minerals characterize most komatiite-hosted nickel deposits, with dominant pyrrhotite and pentlandite. Chalcopyrite, pyrite, and chromite are the other principal minerals present. Copper, cobalt, and the platinum-group elements are minor components of the mineralization.

The nickel sulfide ore deposits are always found in komatiitic host rocks that are part of mafic–ultramafic volcanic sequences. These commonly occur in the lower to central parts of the greenstone stratigraphy, with the komatiites overlying apparently unrelated thick tholeiitic basalt sequences. The normal hosts for komatiite-associated nickel deposits are ultramafic olivine cumulates, metamorphosed to serpentinite or talc-carbonate rock. Ultramafic lavas differentiate strongly during eruption, largely because of fractionation and accumulation of olivine at the base of flows. The magnesia content ranges from 50% in the olivine adcumulates at the base to 15% or less in the upper parts of flows; ores only occur with the most magnesia-rich parts.

The thickness and composition of the host flows vary widely. Thick cumulate sections are closely associated with ores and may represent near-vent sequences, or

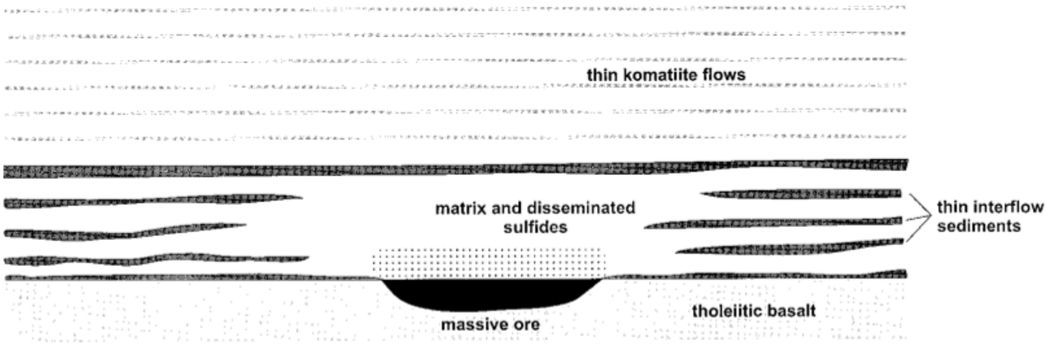

FIGURE 5 Setting of nickel sulfide deposits associated with komatiite lavas. Above ore the character of the host volcanic sequence is markedly different from other areas, which is an important guide in exploration for these deposits.

else deep lava channels. These thick sections have their upper contacts marked by flow top breccias and chill zones passing down to a zone with distinctive spinifex-textured skeletal olivine crystals. This then passes down to crystal-rich cumulate sections of dunite or peridotite (commonly more than 100 m thick), at the base of which the ores occur.

Sections of flows overlying or laterally equivalent to sections containing ores are distinctly different from the ore-bearing sections, having numerous thinner flows and an absence of thick olivine-rich cumulates. These sections of thin komatiites or komatiitic basalts are typically completely barren of nickel sulfides. This suggests that the conditions of formation for mineralized and unmineralized flow units were markedly different. The restriction of sulfide concentrations to the base of distinctive, anomalously thick olivine accumulations is an important guide in exploration, and the clear textural zoning across individual flow units allows detailed mapping, which assists in recognition of favorable sites for mineralization. On a regional scale clustering of deposits is common.

D. Origin of Deposits

Models for the formation of the sulfide deposits have varied widely, but researchers now favor magmatic processes for formation of these deposits. Both nickel and sulfur in the deposits appear to have a primary mantle source. The silicate and platinum group element geochemistry of komatiite lavas indicates that the parent magmas had a high sulfur capacity and were undersaturated in sulfur at depth in the mantle. It seems that the sulfur saturation occurred upon ascent, but only near the surface, allowing accumulation of sulfides in the lava flows.

Sulfur saturation could have resulted from cooling of the magma, from mixing of magmas, or from contamination of the magma with chemically distinct wallrocks. The addition of silica or sulfur, or reducing agents (such as carbon), can significantly lower the solubility of sulfur in a mafic magma, which leads to the separation of an immiscible sulfide melt.

In the past decade some major advances in the study of komatiites have been achieved through consideration of the physical properties of the melts and the consequent fluid dynamic and volcanological implications. Komatiite magmas must have ascended through the crust rather rapidly. The low viscosity and high temperature of a komatiite melt would result in turbulent flow, both during ascent and after eruption. Turbulence would have allowed rapid transfer of heat from the magma to adjacent rocks, which could melt and be incorporated in the magma. Melting of and incorporation of underlying rocks is the favored mechanism for inducing sulfur saturation and sulfide accumulation in komatiite lavas. Careful mapping by geologists at Kambalda showed that the sulfide-hosting komatiites embayed the underlying rocks. Also in the Kambalda area, rare felsic ocelli found at the upper margins of ore-hosting flows are believed to be remnants of molten sediments in the process of being assimilated into the melt, and subtle geochemical evidence of assimilation of sediments is also recognized. This fits with the observation that siliceous, sulfidic, and carbonaceous sediments are common between flows regionally, but are absent in the immediate area of the orebodies.

VII. DIAMOND DEPOSITS

A. Significance

Annual sales of uncut diamonds are about $5 billion per year (many times higher when converted to jewelry), making them one of the world's most valued commodities. They have a unique relationship to volcanism: Without volcanism there would be no diamond deposits, yet there is no direct genetic relationship between diamonds and the volcanic rocks that host them.

B. Distribution and Age

Diamonds occur widely around the world; however, most occurrences are very minor and result from the great durability of diamonds. They probably eroded from their original source and deposited in sedimentary rocks, then eroded from those and recycled again, perhaps many times, in the process becoming widely dispersed. These widespread occurrences are mineralogical curiosities and generally do not produce deposits of economic significance.

The major diamond-producing regions of the world are in southern Africa (South Africa, Botswana, Angola), Russia (Siberia), and Western Australia. Other important diamond-producing areas are Brazil, China, and West Africa, and a major new field has recently commenced production in Canada. Because every diamond is unique, it is not possible to describe deposits simply in terms of tonnage and grade. Some deposits produce few carats, but their average value is very high, whereas other deposits produce many carats but their average value is low. This makes it very difficult to assess the economics of mining a diamond deposit.

Economic diamond deposits occur with volcanic centers of unusual, very alkaline volcanic and subvolcanic intrusive rocks, called kimberlites and lamproites. Important economic deposits can also form by erosion of these primary deposits and accumulation of the diamonds in river and coastal marine placer deposits.

Kimberlites and lamproites are widespread though volumetrically very minor volcanic rocks, and in most cases they do not contain diamonds. Diamond-bearing kimberlites and lamproites only occur around the margins of, or within, stable cratonic blocks that have not undergone major deformation or metamorphism. Productive kimberlites (there is presently only one lamproite-hosted diamond deposit being mined) vary widely in age from Precambrian to Mesozoic. It is probable that the process that brings diamonds to the surface has gone on throughout geological time (and is continuing). Whether an economic deposit occurs depends on a number of factors, including the depth of erosion that has occurred since eruption of the volcanic host.

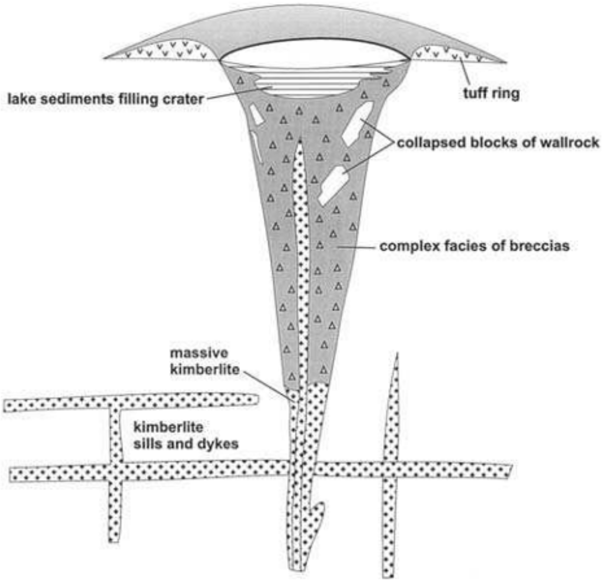
lake sediments filling crater
tuff ring
collapsed blocks of wallrock
complex facies of breccias
massive kimberlite
kimberlite sills and dykes

FIGURE 6 Cross-section through a kimberlite diatreme or pipe. Rapid expansion of the kimberlite magma near the surface produces the pipe. Within it there are different breccia facies composed of varying proportions of intrusive kimberlite, kimberlitic tuff, and wallrock fragments. Near the surface a crater lake may have formed and filled with fine lake sediments, redeposited tuff, and eroded wallrocks.

C. General Characteristics

Both kimberlites and lamproites are formed from very volatile-rich magmas that are generated at great depth in the earth (about 200 km for lamproites, 200–300 km for kimberlites). Kimberlites are more gas-charged (with carbon dioxide) than lamproites, so they have a more distinctive mode of occurrence. In both cases they occur as dykes, sills, and minor plugs formed at depths of several kilometers; however, these are generally small and so cannot provide the tonnage required for an economic deposit.

Kimberlite magma expands rapidly as it approaches the surface of the Earth because of its high gas content, producing a deep conical explosion crater or diatreme (Fig. 6). Depending on the magma supply and depth of exposure, these so-called pipes typically range from 50 to 500 m in diameter. Characteristic facies occur at different levels. The diatreme facies consists of fragmented wall rocks and material brought up from deep below. The maar facies contains bedded material that fell back into the crater after eruption. The crater facies includes finely bedded ash and crater-lake sediments, locally containing fossils. The pyroclastic facies forms as a tuff ring around the vent. All facies can contain diamonds, though the grade usually varies widely.

The shape of kimberlite pipes is typically steeply conical, rather like a carrot. Lamproites, by contrast, form conical to irregular bodies that commonly do not continue to great depth.

D. Origin of Deposits

There is no genetic relationship between diamonds and their host volcanic rocks. Diamonds are xenocrysts ripped off the walls of the vent as the magma rose. The reason for the characteristic association between diamonds and kimberlite and lamproite magmas is very simple: These two magma types are generated very deep, so they have to rise through the diamond-bearing levels of the Earth and so may bring diamonds up with them. Other magmas are generated at depths that are above where diamonds occur, and so they are not capable of bringing them up.

Studies of small mineral grains sometimes found inside diamond crystals led to recognition of three types of diamonds, two derived from the Earth's mantle, and one from the crust. The deepest diamonds occur with garnet lherzolite within the asthenospheric mantle. From shallower depths there are diamonds that occur with garnet lherzolite or garnet harzburgite within the lithospheric mantle. Diamonds of crustal origin may occur between the level of these two types of mantle diamonds. They occur in eclogite, which formed by high-pressure metamorphism of a subducted slab of oceanic crust. Under conditions of moderate temperature but extremely high pressure, any carbon remaining in the subducted slab must convert to diamond, and the broken-off slabs may accumulate below cratonic blocks along the lithosphere–asthenosphere boundary.

The upper limit of diamond stability depends on pressure and temperature. The higher the temperature, the higher the pressure required for diamond to remain stable, hence the deeper the boundary between regions of diamond stability and graphite stability. Only in the cool, deep ancient roots of continents that have not been deformed or metamorphosed are there sufficient diamonds at shallow enough depths to be brought up by magmatism. Most magmas are generated at relatively shallow depths in regions of graphite stability, and so are not capable of bringing diamonds to the surface. Only kimberlites and lamproites are generated below the level of diamond stability, which is why the largely accidental relationship between diamonds and kimberlites and lamproites is so important.

VIII. THE STATE OF KNOWLEDGE AND FUTURE RESEARCH

Ore deposits have received a great amount of research attention because of their economic importance. However, in most cases we are forced to interpret their origin from the faint traces of evidence left long after the processes have ceased. The major exceptions to that are for VHMS deposits, which can be seen forming today on the seafloor, and epithermal deposits, which formed beneath geothermal systems similar to ones now active.

A major consequence of this is that many of our beliefs are based on limited evidence, and so new evidence can force major changes: There is still a great deal for us to learn. Of recent years there are two major controversies that keep recurring in research into ore deposits: (1) From where are the metals derived, and (2) what determines whether a major deposit forms, or just a minor occurrence?

The source of metals is relatively clear for the magmatic nickel deposits, which are only found with nickel-rich magmatic rocks, but in all cases of hydrothermal ore deposits, the source for the metals is far from clear. In porphyry deposits the weight of evidence favors a source in the associated magmas, but some systems suggest involvement of other sources. In the case of VHMS and epithermal deposits the source of metals is uncertain. There are two schools of researchers, one that favors magmatic sources, and another that believes that a magmatic source is not essential, based on knowledge of the related fluids and the processes believed to have formed the deposits. The debate arises from the fact that we have no reliable means of tracing metal sources except for lead, so we need to rely on inference from the geochemistry of other elements that can be modeled (such as isotopes of hydrogen and oxygen).

Even as our insights into the processes that form deposits improve, we are still left with the problem of what determines whether a great deposit forms, or just an ordinary one. For all deposits there are processes that occur far from the deposit in the source region, along the transport path, and in the region of deposition. What is the relative importance of these? Are there recognizable systematic controls that determine that a giant deposit forms, or is it the accidental consequence of essentially random processes? We simply do not have answers for these fundamental questions, which could have immense economic importance if we could predict where the major metal resources of the Earth will occur. Because of the immense scope for discovery of new insights into ore deposits, and the potential for them to be of great economic importance, the future for ore deposit research should be assured.

SEE ALSO THE FOLLOWING ARTICLES

Composition of Magmas • Geothermal Systems • Physical Properties of Magmas • Volcanic Materials in Commerce and Industry • Volcanic Soils

FURTHER READING

Evans, A. M. (1993). "Ore Geology and Industrial Minerals: An Introduction," 3rd ed. Blackwell, London, 390 pp.

Kirkham, R. V., Sinclair, W. D., Thorpe, R. I., and Duke, J. M., eds. (1993). "Mineral Deposit Modelling," Geological Association of Canada Special Paper 40, 798 pp.

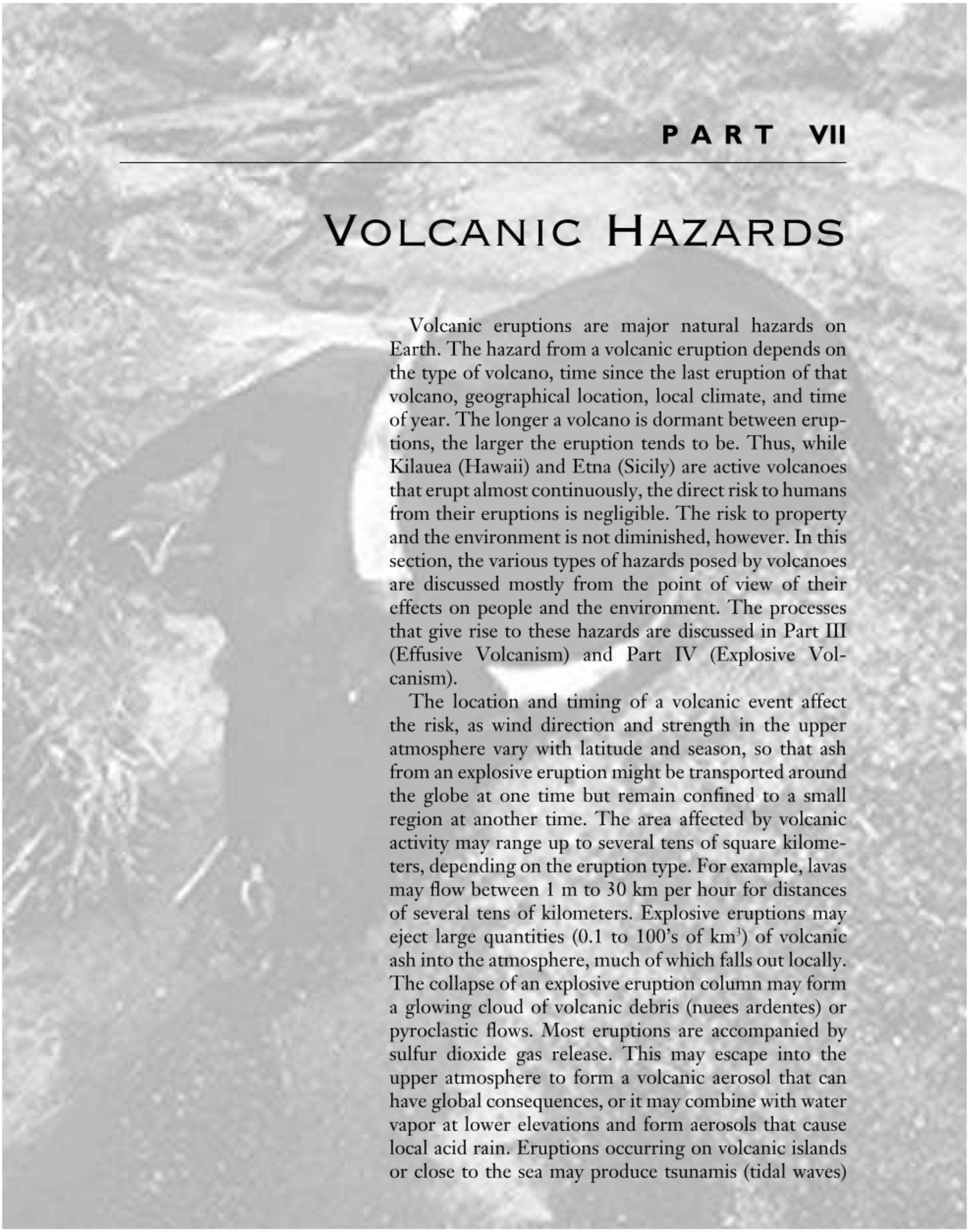

PART VII

VOLCANIC HAZARDS

Volcanic eruptions are major natural hazards on Earth. The hazard from a volcanic eruption depends on the type of volcano, time since the last eruption of that volcano, geographical location, local climate, and time of year. The longer a volcano is dormant between eruptions, the larger the eruption tends to be. Thus, while Kilauea (Hawaii) and Etna (Sicily) are active volcanoes that erupt almost continuously, the direct risk to humans from their eruptions is negligible. The risk to property and the environment is not diminished, however. In this section, the various types of hazards posed by volcanoes are discussed mostly from the point of view of their effects on people and the environment. The processes that give rise to these hazards are discussed in Part III (Effusive Volcanism) and Part IV (Explosive Volcanism).

The location and timing of a volcanic event affect the risk, as wind direction and strength in the upper atmosphere vary with latitude and season, so that ash from an explosive eruption might be transported around the globe at one time but remain confined to a small region at another time. The area affected by volcanic activity may range up to several tens of square kilometers, depending on the eruption type. For example, lavas may flow between 1 m to 30 km per hour for distances of several tens of kilometers. Explosive eruptions may eject large quantities (0.1 to 100's of km^3) of volcanic ash into the atmosphere, much of which falls out locally. The collapse of an explosive eruption column may form a glowing cloud of volcanic debris (nuees ardentes) or pyroclastic flows. Most eruptions are accompanied by sulfur dioxide gas release. This may escape into the upper atmosphere to form a volcanic aerosol that can have global consequences, or it may combine with water vapor at lower elevations and form aerosols that cause local acid rain. Eruptions occurring on volcanic islands or close to the sea may produce tsunamis (tidal waves) with devastating effects reaching tens or even hundreds of kilometers.

Passenger airliners that encounter volcanic ash clouds are subject to complete engine failure, which can have catastrophic effects. The first chapter of this section, Volcanic Ash Hazards to Aviation, documents several cases of eruption-induced aviation incidents and explains why this hazard is becoming increasingly important.

The release of gases to the atmosphere is one of the hazards associated with volcanic eruptions. The several million tons of gases released during large eruptions can be of global significance. Etna volcano (Sicily) emits about 13 Mt of CO_2 per year, equivalent to a 1000-MW coal-fired power station in terms of greenhouse gas production. Etna also produces some 1.4 Mt of SO_2 per year. The 1991 eruption of Pinatubo (Philippines) ejected 15 Mt of SO_2, causing surface temperatures to fall globally by about 0.1° C. The aerosol formed from this gas contributes to global cooling by absorbing incoming solar radiation. The next chapter, Volcanic Aerosol and Global Atmospheric Effects, documents unusual climatic features caused by volcanic eruptions as far back as the 17th century B.C.

The following chapter, Hazards from Pyroclastic Flows and Surges, illustrates the power of pyroclastic flows and surges to devastate whole communities. The speed and great extent of pyroclastic flows make them by far the greatest and most lethal volcanic hazard. Lava flows represent a much more sedate volcanic eruption process, but the effects, as the chapter Lava Flow Hazards demonstrates, are still significant.

Volcanic eruptions can trigger secondary events if significant quantities of groundwater, snow, or ice are involved. Risk may then extend beyond the immediate region of the eruption. A relatively minor eruption of Nevado del Ruiz (Colombia, 1985) resulted in the loss of 23,000 lives as the glacier on the top of the volcano melted. Water flowed down the river valleys, removing the loose material from the banks, and the muddy torrent rushed downslope at 30 km per hour to cover the village of Armero to a depth of 3 m. A similar muddy torrent (lahar) resulted in the death of about 900 people after the eruption of Mount Pinatubo in 1992. The Hazard from Lahars and Jökulhlaups illustrates how these devastating events can continue to occur even without further volcanic activity, sometimes for decades after the eruption has ceased.

The next chapter, Hazards of Volcanic Gases, illustrates the effects that various volcanic gases have on people, but perhaps more importantly when these gases fall as acid aerosols on crops, vegetation, and communities downwind. Persistent gas release may cause asphyxiation by inhalation locally and asthma more regionally. Acid rain may also produce skin disorders. All these phenomena are devastating to wildlife and farmland for the duration of the eruption and sometimes far longer.

Most of the world's volcanoes are below the sea, and many are located in coastal areas. Explosion or collapse of a volcano can therefore often cause a large body of water to move suddenly, creating a tsunami. The chapter Volcanic Tsunamis presents several mechanisms that are thought to produce tsunamis and shows that in the last 250 years some 25% of volcano related fatalities have been attributed to tsunamis.

Volcanic earthquakes have different characteristics from the deep and tectonic seismic events that occur along great faults. They are considerably less devastating and may continue at a detectable level for weeks or months prior to eruption. As the chapter Volcanic Seismicity demonstrates, they are the most important window to the processes going on inside a volcano before eruption, and their study has considerable scientific value and application to risk mitigation.

As human populations continue to grow and expand, many people live close to active or potentially active volcanoes. The chapter Impacts of Eruptions on Human Health presents a graphic account of the nature of injuries and the cause of death from various types of eruptions. On a more global scale, the next chapter discusses the origin and fate of carbon and sulfur from volcanic sources and the implications for climate. Following this, the chapter Ecology of Volcanoes considers the various effects of volcanic activity on plant and animal communities. It is striking how resilient life is in the face of volcanic activity. Eruptions do not completely eradicate life and many species survive; even newly formed volcanic islands soon become home to a wide range of opportunists.

A look back through the geological record reveals considerable evidence for huge eruptions. If we scale up the observed effects of recent eruptions, the global consequences of large eruptions are awesome. The concluding chapter of this section, Volcanism and Biotic Extinctions, provides compelling evidence for a correlation between mass extinctions and the largest basalt lava flows on Earth. Whether these flood basalts, mass extinctions, and asteroid impacts are related in some way is a matter of ongoing debate.

Thus, volcanic hazards have always impinged on life and the environment, and an understanding of their past and present effects is vital for effective monitoring, prediction, and mitigation.

Hazel Rymer
The Open University

VOLCANIC ASH HAZARDS TO AVIATION

T. P. MILLER
U.S. Geological Survey, Alaska Volcano Observatory

T. J. CASADEVALL
U.S. Geological Survey

I. Hazard
II. Extent
III. Mitigation
IV. Discussion

GLOSSARY

AVHRR	Advanced very-high-resolution radiometry.
AVO	Alaska Volcano Observatory.
FAA	Federal Aviation Administration (USA).
GMS	Geostationary meteorological satellite.
GOES	Geostationary operational environmental satellite.
IAVW	International Airways Volcano Watch.
ICAO	International Civil Aviation Organization.
IATA	International Air Transport Association.
KVERT	Kamchatkan Volcanic Eruption Response Team.
MWO	Meteorological Watch Offices.
NWS	National Weather Service (USA).
NOPAC	North Pacific composite air routes.
TOMS	Total ozone mapping spectrometer.
VAAC	Volcanic Ash Advisory Center.
WMO	World Meteorological Organization.

JET AIRCRAFT ENCOUNTERS with airborne volcanic ash between 1980 and 1998 caused more than U.S. $250 million in damages to engines, avionics, and airframes not only in areas proximal to erupting volcanoes but at distances of up to 3000 km away. Loss of life was narrowly and fortuitously averted following sudden multiple engine loss to individual aircraft during major eruptions in Indonesia, Alaska, and the Philippines. The hazard is compounded by the development of large (wide-body) jet aircraft whose engines operate at such high temperatures as to make them even more susceptible to damage by volcanic ash. Increasing commercial air traffic worldwide, and the post-cold war opening of heavily traveled air routes close to active volcanoes, add to the problem (Figure 1). Volcanologists, the airline industry, and government officials have only recently recognized the seriousness of this newly emerging hazard.

I. HAZARD

Volcanic ash clouds are not detectable by aircraft radar and often not easily visible; complete avoidance of volca-

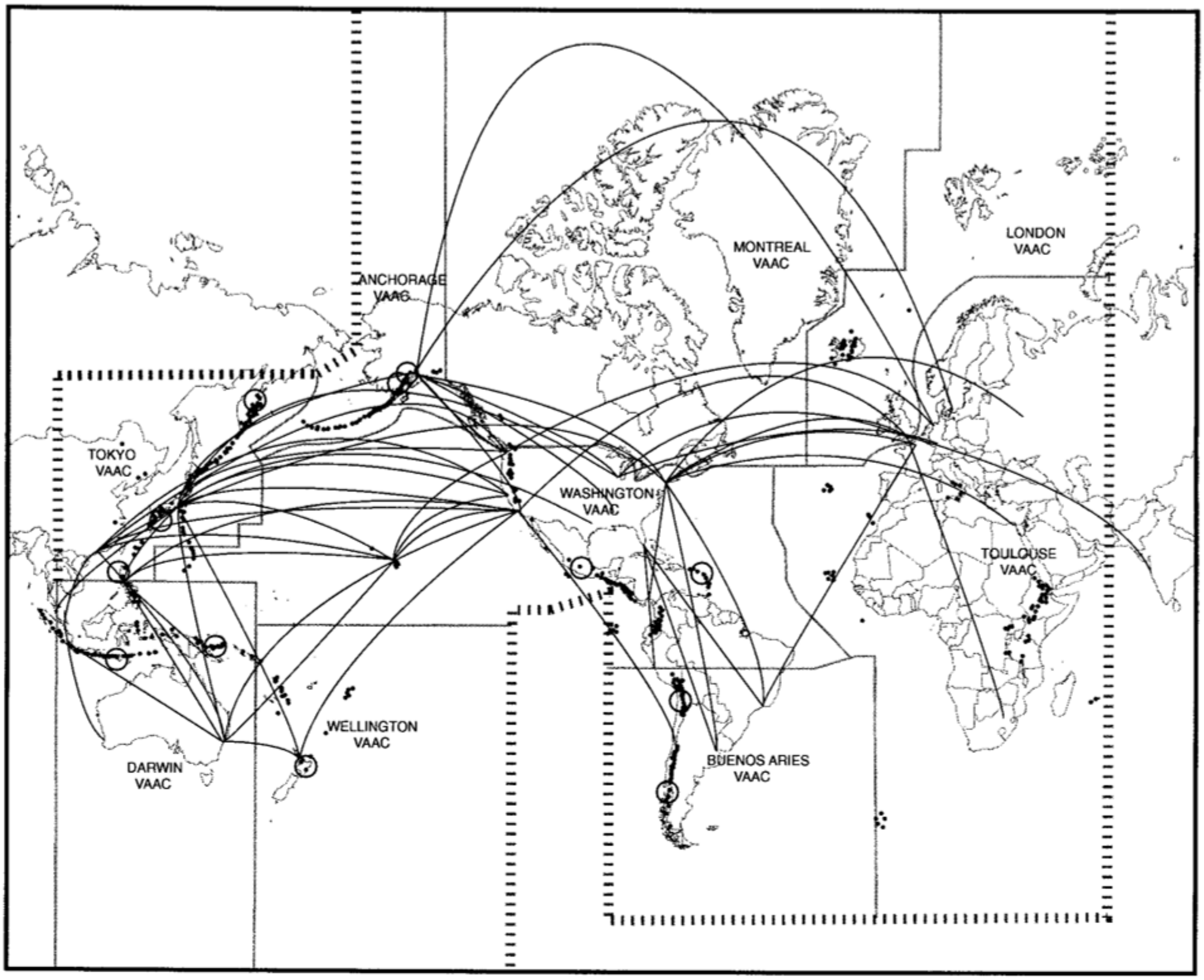

FIGURE 1 A world map of active volcanoes, principal air routes (modified from Casadevall and Thompson, 1995), and the areas of responsibility of individual Volcanic Ash Advisory Centers (VAACs). VAACs are located in Montreal (Canada); Anchorage, Alaska (USA); Washington, DC (USA); Buenos Aires (Argentina); London (England); Toulouse (France); Darwin (Australia); Wellington (New Zealand); and Tokyo (Japan). Open circles indicate volcanoes that produced ash clouds that damaged aircraft or disrupted air traffic between 1990 and 1999. Note that areas outside hachured boundaries in northern Russia, the central Atlantic Ocean, and the Indian Ocean are not presently covered by a VAAC.

nic ash clouds is considered the only procedure that guarantees flight safety from airborne volcanic ash. Increasing international cooperation between volcanologists, meteorologists, airline dispatchers and pilots, and government aviation groups, a hitherto unlikely combination of disciplines, produced a series of actions to lessen this hazard.

Volcanic ash is composed of fine-grained rock and mineral fragments and glass shards, commonly with acid droplets coating the ash-grain surfaces. The properties of the ash depend mostly on the relative proportions of their main constituents. Ash results from fragmentation of foamy magma (following decompression) and of country rock (during rapid expansion of steam) and from explosive mixing of magma with water. Shard shapes and sizes depend upon the shape and size of gas bubbles in the magma immediately before eruption and fragmentation of the magma. Particle sizes range from several meters across for large proximal blocks to micron and submicron sizes for fine ash and aerosol droplets within distal eruption plumes. Particle size in ash clouds away from the volcano is usually less than 0.5 mm.

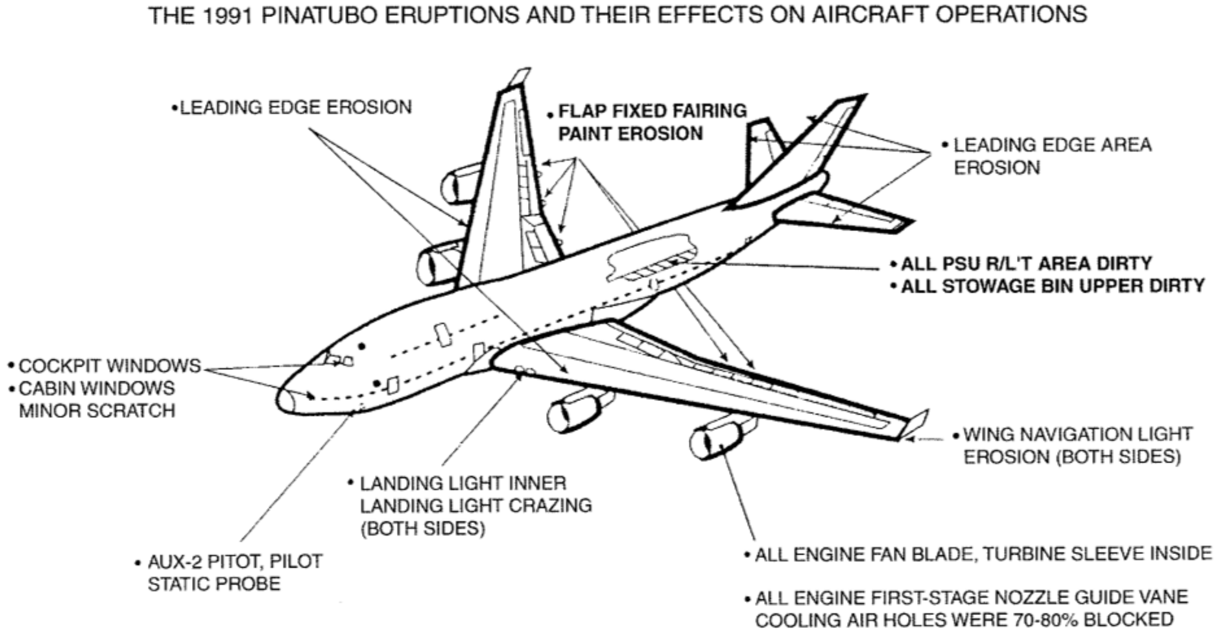
THE 1991 PINATUBO ERUPTIONS AND THEIR EFFECTS ON AIRCRAFT OPERATIONS
•LEADING EDGE EROSION
• FLAP FIXED FAIRING PAINT EROSION
• LEADING EDGE AREA EROSION
• ALL PSU R/L'T AREA DIRTY
• ALL STOWAGE BIN UPPER DIRTY
• COCKPIT WINDOWS
• CABIN WINDOWS MINOR SCRATCH
• WING NAVIGATION LIGHT EROSION (BOTH SIDES)
• LANDING LIGHT INNER LANDING LIGHT CRAZING (BOTH SIDES)
• AUX-2 PITOT, PILOT STATIC PROBE
• ALL ENGINE FAN BLADE, TURBINE SLEEVE INSIDE
• ALL ENGINE FIRST-STAGE NOZZLE GUIDE VANE COOLING AIR HOLES WERE 70-80% BLOCKED

FIGURE 2 Damage to exterior surface of a 747-400 jumbo jet following an encounter with the June 15, 1991, ash cloud from Mount Pinatubo volcano in the Philippines [from Casadevall *et al.*, 1996]. Damage of this type is typical of encounters between jet aircraft and airborne volcanic ash.

Although volcanic ash is produced to at least some degree in most eruptions, it is generally silicic magmatic eruptions as opposed to effusive basaltic, hydromagmatic, or phreatic eruptions that constitute the chief hazard to aviation.

A. Damage and Impact

When a jetliner flying in excess of 840 km/hour enters a cloud of finely fragmented rock particles and acid gases, the principal damage will be abrasion of the exterior forward-facing surfaces and accumulation of ash into surface openings, including engines (Figure 2). The hardness and angularity of the ash fragments often cause complete frosting of windshield surfaces and further damage to the onboard avionics and fuselage surfaces. Ingestion of ash into the engines causes abrasion damage, especially to compressor fan blades.

Numerous examples of engine failure, complete loss of visibility, and loss of critical navigational and operational instruments have occurred in volcanic ash and aircraft encounters around the world (Table I). The primary problem centers around the composition (and hence the melting point), hardness, and abrasive character of ash's constituents. Volcanic glass in the ash has melting temperatures that lie within the operating temperatures (in excess of 700°C) of modern large jet engines. Hence ingestion of volcanic ash in a jet engine can result in melting and accumulation of resolidified

TABLE I Volcanic Eruptions in the 1990s That Caused Damage or Significantly Affected Aircraft Operations around the World

Volcano	*Location*	*Eruption*
Redoubt	Alaska, USA	1989–1990
Unzen	Japan	1991
Mount Pinatubo	Philippines	1991
Hudson	Chile	1991
Mount Spurr	Alaska, USA	1992
Lascar	Chile	1993
Rabaul	New Britain	1994
Klyuchevskoy	Kamchatka, Russia	1994
Rinjani	Indonesia	1994–1995
Ruapehu	New Zealand	1995
Soufriere Hills	Montserrat	1996–1998
Popocatepetl	Mexico	1996–1998

ash on turbine nozzle guide vanes in the engine (Figure 3), causing compressor stall and, in the worst cases, complete loss of engine thrust. Studies of ash deposits that caused engines to stop operating reveal that volcanic ash melts and accumulates more commonly when engines are operated at maximum power during takeoff or climb than at cruise altitudes. Recognition of this condition resulted in these manufacturer operational recommendations for pilot response when an ash cloud is inadvertently entered: a pilot should not attempt to climb out of a cloud but should reduce power and quickly exit the cloud by turning 180°. This and other similar

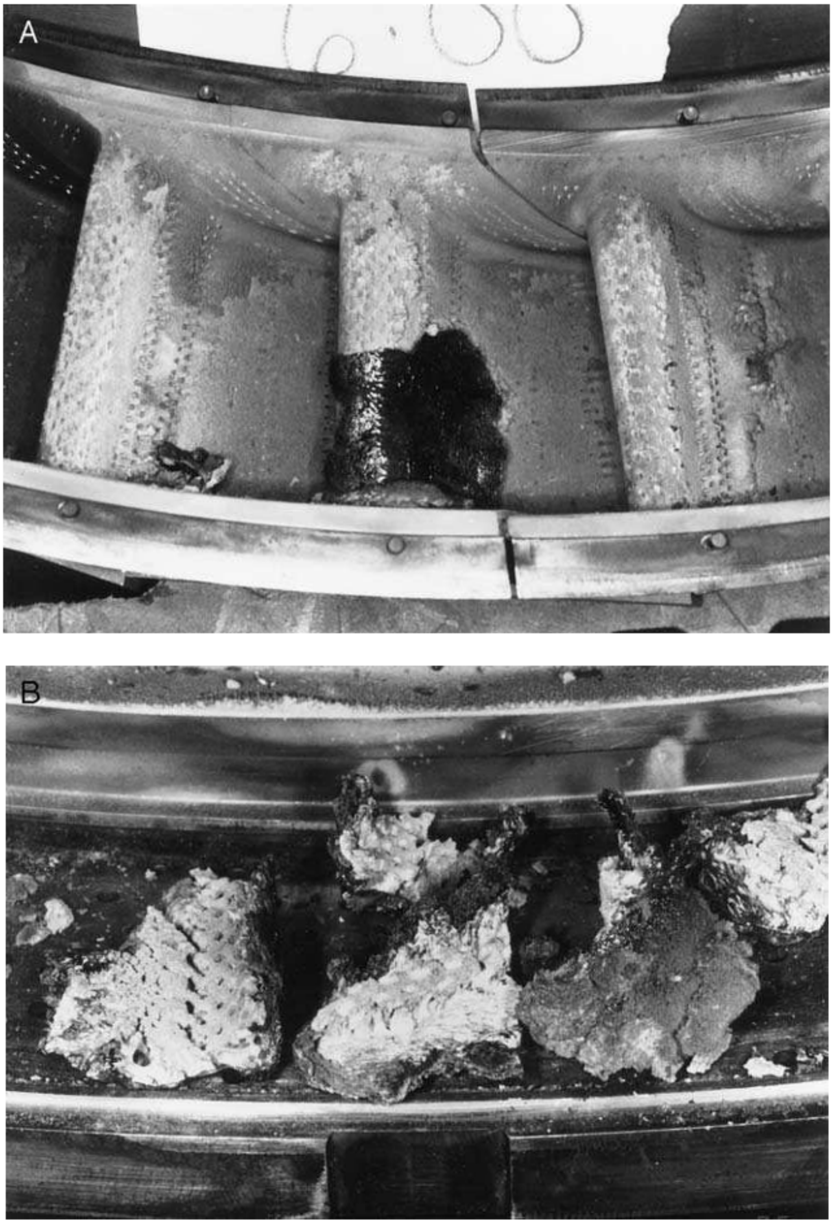

FIGURE 3 Examples of remelted volcanic ash in jet engines following the encounter of a 747-400 with airborne volcanic ash from the Redoubt eruption of December 15, 1989 (Przedpelski and Casadevall, 1994). (A) Dark glassy deposits of remelted volcanic ash on leading edge of high-pressure-turbine nozzle guide vane. (B) Leading-edge deposits dislodged during disassembly of high-pressure-turbine nozzle guide vanes.

recommendations have been included in official Operations Manual Bulletins. A number of airline companies worldwide began including ash-avoidance training for their pilots in the 1990s.

Eruptions which release very large amounts of sulfur dioxide, such as El Chichon (1982) and Mount Pinatubo (1991) in the Philippines, have caused longer-term damage through crazing of acrylic windows. A year after the Mount Pinatubo eruption in June of 1992, a jumbo jet suffered engine power loss that was traced to an accumulation of sulfate deposits in the engines. Isotopic studies suggested that the sulfate was derived from SO_2 and sulfuric acid aerosols that originated from the Mount Pinatubo eruption.

Volcanic ash can have an important economic impact on aviation without causing direct damage to aircraft or facilities. The mere possibility of jet aircraft flying into a volcanic ash cloud and its potential risk to life and property or the possibility of "trapping" an aircraft at an ash-bound airport for up to several days is enough to cause widespread cancellations, rerouting of aircraft, and decreasing payload by adding fuel.

Besides affecting in-flight operations, volcanic ash presents other threats to aviation as it eventually settles to the ground and affects airport runways, taxiways and aprons, buildings, ground services, electrical utilities, communication facilities, and aircraft parked on the ground. The characteristics of volcanic ash that are dangerous to aircraft in flight (high glass content, hardness, and abrasiveness) cause problems on the ground. Recently deposited fine ash is easily entrained in the air by wind or vehicle movement (e.g., taxiing aircraft), and can rapidly contaminate parked aircraft and the ancillary operations necessary to support them at the airport.

Generally airports have been unprepared for handling of even minor amounts of volcanic ash and each incident has been a learning experience for the individual airport. However, while volcanic ashfall at an airport may be considered a relatively rare event, the increase in commercial aviation in the Pacific region means that the closing of an airport for any length of time causes major air traffic disruptions and has serious economic ramifications. Between 1980 and 1998, over 35 airports in 11 countries (USA, Japan, New Zealand, Mexico, Guatemala, Colombia, Argentina, Indonesia, Papua New Guinea, Philippines, and the Falkland Islands) have been closed or had operations severely impacted because of ashfalls that were as light as 3 mm.

Airport managers have gradually developed mitigation procedures that include rapid communication; handling of deposited ash (moving it as few times as possible) using plows, water, and emulsions; shutting down of nonessential equipment, and restriction of on-the-ground aircraft movement. In spite of these procedures developed by trial and error, aircraft caught on the ground during an ashfall have been trapped for days in some cases until the ash has stabilized and the aircraft decontaminated. A Boeing 767, for example, was stranded at Manila airport for 6 days during the Mount Pinatubo eruption due to ash contamination. This situation points out the importance of advance warning of an impending ash cloud so as to move aircraft out of the impacted area.

B. Chronology and Case Histories

Volcanic ash is harmful to the mechanical parts of any engine, be it reciprocating or jet, and numerous accounts of damage to aircraft from volcanic ash have been reported since the first airplane flight in 1903. Prior to about 1975, events were minor and typically consisted of abrasion of windshields and leading wing edges. The ingestion of sharp abrasive particles into reciprocating engines was certainly harmful but neither the frequency of incidents nor the damage done was sufficiently high to merit much concern in the aviation community. Economic losses were small and encounters of piston-engine aircraft with volcanic ash were regarded more as interesting oddities than hazards of significant import. Probably the most serious incident occurred during World War II when 88 U.S. B-25 Mitchell bombers parked on airfields near Mount Vesuvius had to be scrapped after their fabric control surfaces were burned off and all clear plexiglas was crazed following ashfall from the volcano in March 1944.

The advent of widespread use of jet aircraft, particularly large so-called "wide-body" types such as Boeing 747s, DC-10s, and MD-11s, with their high-operating-temperature engines, exposed the extent of the hazard presented to modern aviation by airborne volcanic ash. By the late 1970s, several jet aircraft had flown into volcanic ash clouds in Japan and Alaska but the damage sustained was still minor and primarily to surface edges. The 1980 eruption of Mount St. Helens in Washington marked a threshold in the recognition of the seriousness of the hazard posed by airborne volcanic ash. During this eruption, a four-engine (turboprop) C-130 lost two engines while climbing through an ash cloud at 3400 m above sea level and suffered damage to the remaining two engines; total damage amounted to about U.S. $500,000. In addition, numerous other aircraft suffered minor surface damage.

Between 1980 and 1999, more than 100 jet airliners were known to have sustained at least some damage after having flown through volcanic ash clouds. Although at least eight different types of aircraft were involved in these incidents, the most severe damage occurred to wide-body (747, DC-10, MD-11, etc.), or jumbo, jets. Wide-body aircraft began to enter commercial service in large numbers in the early 1980s and the number and severity of volcanic ash encounters slowly began to grow. In at least eight instances, one or more engines were lost; in three incidents, all four engines were lost. Examining five of the more consequential incidents between 1982 and 1994 in chronological order illustrates both the increasing severity of the problem and the efforts to mitigate it.

In June 1982, a British Airway Boeing 747 with 240 passengers on board unexpectedly penetrated an ash cloud 150 km west-southwest of Galunggung volcano in Indonesia at 11,300 m ASL (above sea level) and lost power in all four engines. The aircraft lost 7500 m of altitude in 16 minutes before restarting the engines and making a safe emergency landing in Jakarta. Soon after, in mid-July 1982, a Singapore Airlines Boeing 747 with 230 passengers at 9000 m ASL lost three engines in an ash cloud from the same volcano. The aircraft was able to get one engine restarted after losing 2400 m of altitude and make an emergency landing. Both incidents occurred at night; in each incident, serious damage was done to the engines and major loss of life was only narrowly averted. Both aircraft suffered extensive damage to engines and exterior surfaces; in each instance, a glassy ceramic layer was found deposited on the surfaces of the turbine section along with ablation damage to other engine parts.

An even worse ash encounter (and probably the most serious to date) occurred after a 7-year hiatus. On December 15, 1989, at 11:46 A.M. local time, a KLM Boeing 747 in Alaska flying at 8500 m ASL with 231 passengers on board flew into a volcanic ash cloud from an eruptive event at Redoubt volcano located 150 km away (Figure 4). The aircraft lost all four engines and dropped 4450 m in 4 minutes to an altitude of 4050 m ASL in a mountainous region whose peaks ranged from 2130 to 3350 m ASL. The aircraft's engines were thus restarted only within 1–2 minutes of impact, and the aircraft was able to land safely in Anchorage. Damage to the aircraft's engines, avionics, and airframe was estimated at over U.S. $80 million and it was several months before it flew again.

The explosive eruptions of Mount Pinatubo in June 1991 ejected voluminous clouds of volcanic ash and acid gases into the stratosphere to altitudes >30 km and provided the setting for the next significant encounter of volcanic ash and aircraft. An ash cloud from the June 15 eruption spread laterally into some of the world's busiest air traffic corridors. At least 20 commercial jet aircraft were involved in the incidents related to volcanic ash from the eruptions of Mount Pinatubo volcano. Three of these occurred within 200 km of the volcano when the cloud was less than 3 hours old, while 12 others took place over Southwest Asia 720 to 1740 km west of the volcano when the ash cloud was 12 to 24 hours old. No loss of life occurred but damage estimates to aircraft may have exceeded U.S. $100 million.

By 1991, recognition of the gravity of the hazard resulted in the First International Symposium on Volcanic Ash and Aviation Safety, held in Seattle, Washington, USA. It was sponsored by the Airline Pilots Association, the Air Transport Association of America, the FAA (Federal Aviation Administration), the National Oceanic and Atmospheric Administration, and the U.S. Geological Survey. Following closely after the late-1989 incident related to the Redoubt eruption in Alaska and the 1991 Mount Pinatubo eruption, the meeting was packed with attendees from around the world, many of whom had just recently become aware of this "new" hazard following damaging encounters or disruptions. The awareness of the extent of this hazard following this seminal meeting was reflected in the response to the two major incidents which are described next.

Crater Peak vent on the south side of Mount Spurr volcano 125 km west of Anchorage, Alaska, erupted on June 27, August 18, and on the evening of September 16–17, 1992. Each eruption produced an ash column that rose to 13–15 km above sea level; the ash clouds were carried downwind across eastern Alaska, western Canada, and the northcentral United States. Ashfall from the August 18 eruption deposited 1–3 mm of ash at the Anchorage airport (one of the busiest airports in the United States), causing closure and diminished operations for several days. Ash removal and associated costs were estimated at over U.S. $680,000, and revenue loss because of flight cancellations was estimated at $276,000. No aircraft were damaged by ash clouds from this eruption, principally because a streamlined process of eruption warnings and monitoring, tracking of volcanic ash clouds, education of pilots and dispatchers, and communication had been developed in the region following the Redoubt eruption only 2 years earlier.

A dramatic example of the rapid transport of volcanic ash across air routes occurred when Klyuchevskoy volcano, one of the most active volcanoes in Kamchatka,

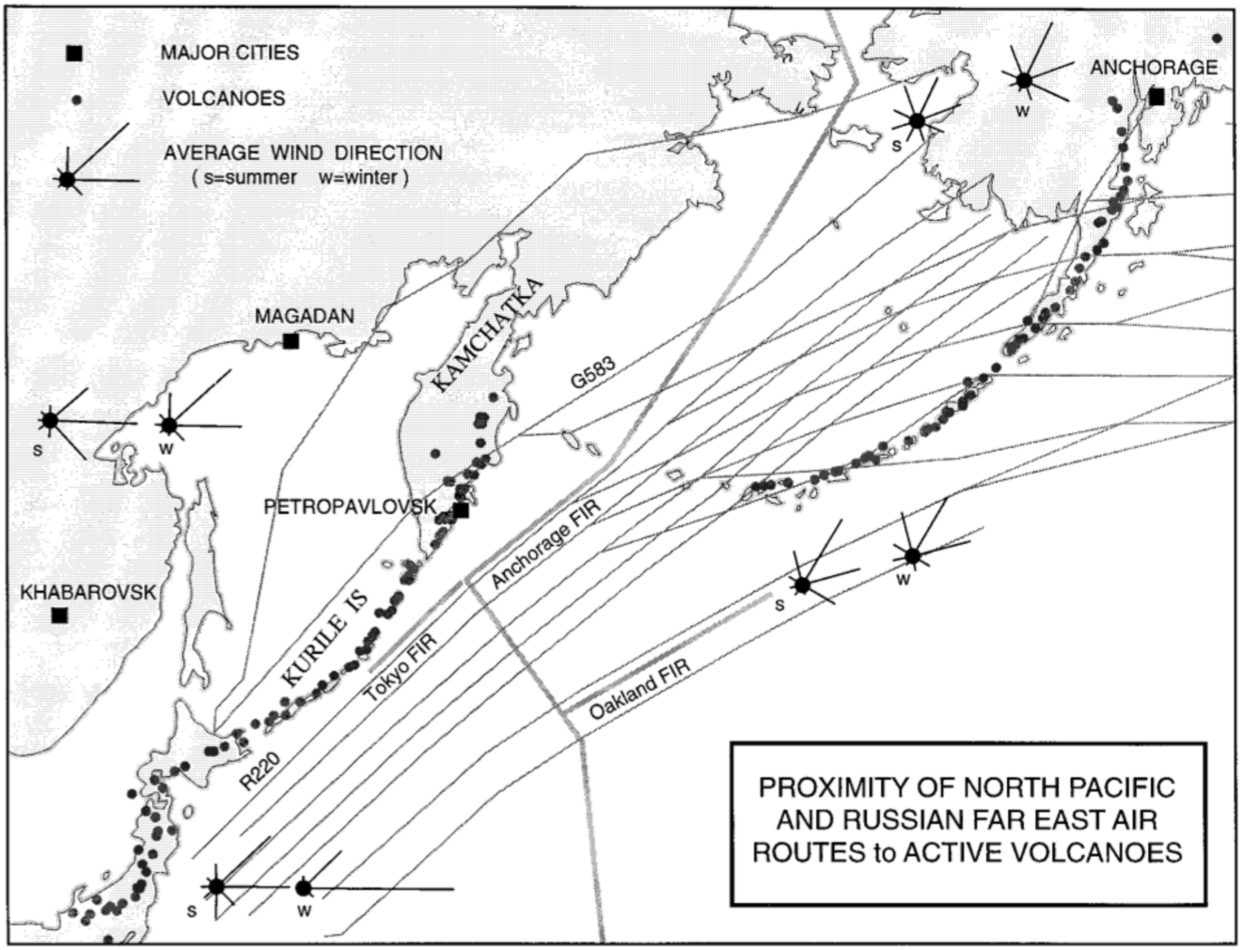
MAJOR CITIES
VOLCANOES
AVERAGE WIND DIRECTION
(s=summer w=winter)
ANCHORAGE
MAGADAN
KAMCHATKA
G583
PETROPAVLOVSK
KHABAROVSK
KURILE IS
Anchorage FIR
Tokyo FIR
Oakland FIR
R220
s
w
PROXIMITY OF NORTH PACIFIC AND RUSSIAN FAR EAST AIR ROUTES to ACTIVE VOLCANOES

FIGURE 4 North Pacific (NOPAC) air routes and the 100 active volcanoes in Alaska, Kamchatka, and the Kurile Islands; wind-rose diagrams show that most of these air routes are downwind or cross the belt of active volcanoes. In 1998, more than 20,000 passengers and millions of pounds of cargo were being transported daily over these routes, including more than 90% of the all-cargo flights between Asia and North America.

Russia, erupted in 1994. On October 1, the volcano erupted explosively, sending volcanic ash to an estimated height of 12–15 km (Figure 5). A strong jet stream rapidly carried the ash to the southeast across the NOPAC (North Pacific) composite air routes, where it was visible on satellite images (Figure 6). Pilots reported extensive visible volcanic ash clouds as much as 80 km wide and up to 1000 km from the volcano at altitudes ranging from 9 to 11.5 km ASL. The major explosive phase of the eruption lasted about 36 hours and was intense for about 10 hours. Because of excellent communication between Russian and American volcanologists, meteorologists, and air traffic controllers, aircraft were quickly rerouted for the next 48 hours and no damaging incidents occurred.

II. Extent

On numerous occasions volcanic eruptions have wreaked havoc with mankind, causing catastrophic loss of life and damage to property. Indeed, R. J. Blong has identified 564,612 deaths associated with volcanic eruptions between 1600 and 1986. The horrific loss of

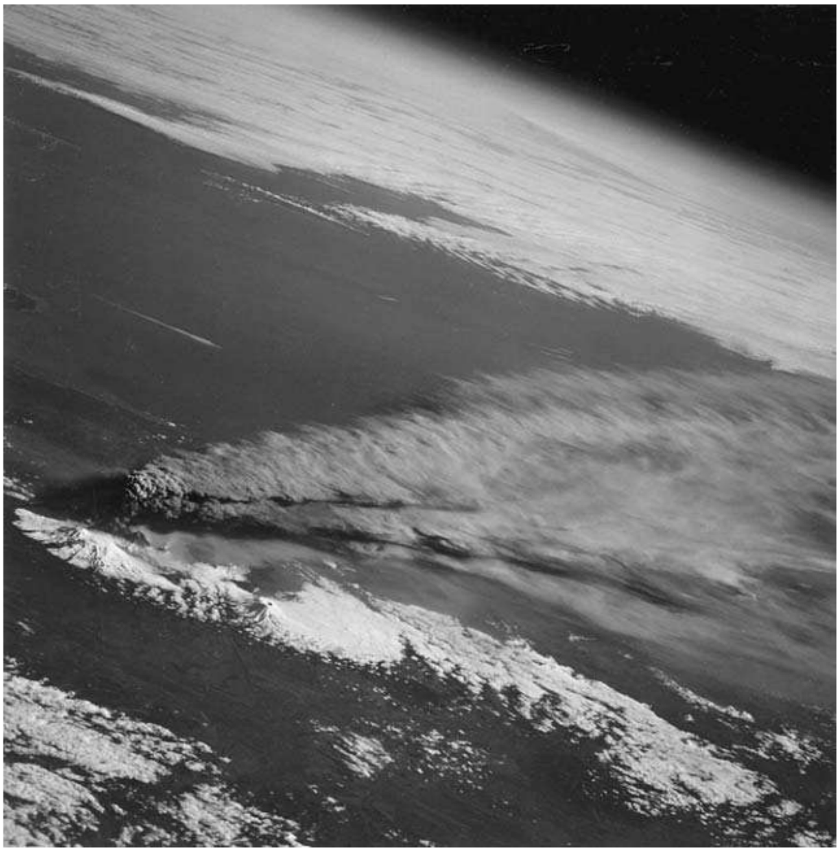

FIGURE 5 Shuttle photo of 4723-m-high Klyuchevskoy volcano, Kamchatka, Russia, erupting on October 1, 1994. View is looking northeast; the top of the ash cloud is estimated at about 15 km ASL. Bezymianny volcano, another frequently active volcano, is visible under the ash cloud to the right of Klyuchevskoy. A thin white-vapor plume can be seen trailing from the summit and the volcano is separated from Klyuchevskoy by the Holocene Kamen volcano.

thousands of lives following eruptions at Mount Pelée, Krakatau, Tambora, Unzen (in 1792), and Nevado del Ruiz in the past 2 centuries is etched in volcanologists' minds. Before 1900, most deaths were by starvation, but pyroclastic flows and lahars account for most fatalities in the 20th century, and volcanogenic tsunamis remain a worrisome hazard. The prominence of pyroclastic-flow- and lahar-related deaths has focused attention on proximal hazards of volcanic eruptions. When hundreds of thousands of people live within a few tens of kilometers of active explosive volcanoes, volcanologists and public safety officials understandably devote much of their efforts to the local hazard.

The hazard to modern aviation from airborne volcanic ash, however, is a newly recognized and emerging hazard that is both proximal and distal in character, and that presents problems in response and mitigation. Significant incidents of aircraft damage or disruption of air traffic by volcanic ash clouds emanating from 12 volcanoes have been reported every year in the decade between 1990 and 1999 (Table I). Since the number of volcanic eruptions is assumed to have been constant throughout this period, the frequency of incidents attests to the global increase of air traffic, particularly wide-body jet aircraft.

Most of the volcanoes that have produced hazardous ash clouds in the past decade are located along the Pacific Basin Rim (Table I) but the hazard should not be regarded as confined to that region. The 1996–1998 eruptions at Soufriere Hills did not cause significant damage to aircraft but did disrupt air traffic in the Caribbean and adjacent Atlantic Ocean. The eruptions of Hudson and Lascar volcanoes in 1991 and 1993, respectively, produced ash clouds that were carried east over the Atlantic Ocean where they interfered with air traffic and damaged aircraft as far away as the Falklands. A 1998

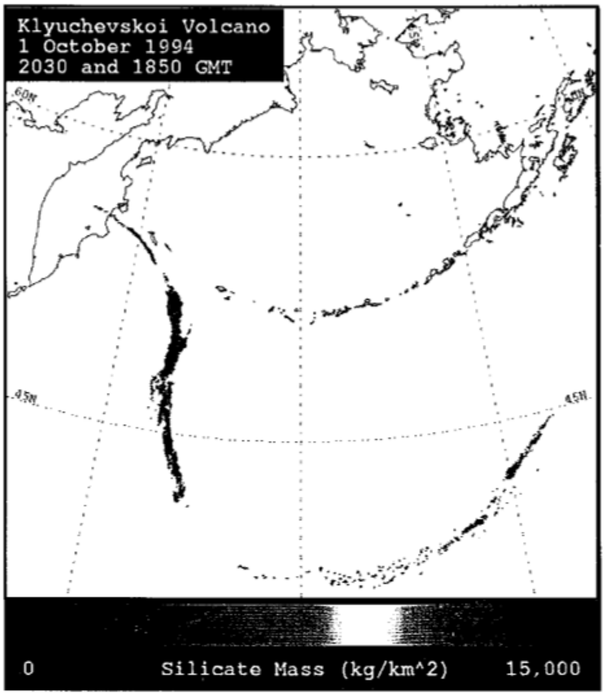

FIGURE 6 Satellite-derived volcanic ash mass retrieval of the ash cloud from the October 1, 1994, eruption of Klyuchevskoy volcano which traveled across NOPAC composite air routes, severely disrupting commercial air traffic for 48 hours.

eruption of Grimsvotn volcano in Iceland carried a notable potential for disrupting traffic across the North Atlantic, as will be discussed later.

Consideration must be given both to the nature of flight operations, that is, whether aircraft are in extended flight operation (cruising at >9 km for long distances) or in terminal flight operation (landing or taking off), and to the type and duration of eruptive activity that might be occurring. The proximity of many of the world's active volcanoes to major cities with their airports and to commercial air routes is well illustrated in Figure 1. Those airports and terminal flight operations close to volcanoes erupting ash and coarser ejecta obviously run a higher risk of aircraft damage than do those farther away because of higher rates of sedimentation from airborne ash clouds. Rinjani volcano in Indonesia erupted several times between June 1994 and March 1995 and caused much disruption of air traffic throughout this heavily populated region. Although ash clouds were generally below 6 km ASL, they interfered with terminal traffic approaches and takeoffs at the numerous nearby airports in the region, causing extensive rerouting.

A similar situation at Sakurajima volcano, located only 22 km from Kagoshima City, Japan, has been at least partially mitigated by real-time seismic monitoring at the airport itself. Sakurajima has been in sporadic eruption since 1957 with over 4000 short-lived volcanic eruptions causing numerous damaging ash and aircraft encounters. Extensive mitigation procedures introduced in 1991 included the installation at the airport of a seismometer and infrasonic microphone to detect air shocks caused by explosive events, which allowed aircraft to be quickly notified and plan their approach or takeoff accordingly, thus allowing continued use of a busy airport.

The nature of the eruptive activity must be kept in mind. Eruptions that are chiefly effusive (e.g., the long-lived Kilauea eruption in Hawaii that began in 1983) obviously pose little likelihood (but not zero) of producing much ash although acidic gases can be a hazard to low-flying aircraft or aircraft on approach or takeoff from nearby airports.

The size of eruptions (and the amount of emitted ash) that constitutes a hazard varies, as does the areal extent of the cloud. Aircraft have been damaged or operations disrupted from eruptions ranging from short-lived vulcanian episodes of a few tens of millions of cubic meters (Mount Spurr, Alaska, 1992) to long-lived caldera-forming eruptions (Mount Pinatubo, 1991) of several cubic kilometers of ejecta. Also, an "eruption" may consist of single to multiple explosive events spread over minutes to months. The 1989–1990 eruption of Redoubt volcano in Alaska, for example, had over 20 explosive episodes, each of which affected aviation over a 4- to 5-month period, yet had an overall VEI (volcanic explosivity index) of 2–3. The 1992 eruption of neighboring Mount Spurr volcano, with a similar VEI, had only 3 explosive events over a 3-month period. For this reason, it is impossible to merely look at a listing of VEIs for volcanoes or groups of volcanoes to estimate probabilities of ash eruptions hazardous to aviation. Once a slug of ash of any size is ejected to altitudes of >9 km and carried into air routes, it is a hazard. The duration and/or size of the eruption or of the ash slug itself will, of course, effect the extent of the hazard. Additional related items include how long an aircraft might actually be exposed to volcanic ash—for example, whether the ash cloud crosses the aircraft's flight route orthogonally or obliquely will be a significant factor.

As was stated, the hazard posed by volcanic ash to aircraft is not only proximal but distal as well—that is, it is not confined to the country or region containing the eruptive volcano but can persist for 2000 km or more based on reported damage figures. An example of the far-flung effects of airborne volcanic ash on air traffic is shown in Figure 7. The long-distance transport of an ash cloud emitted from the Crater Peak vent of Mount Spurr, Alaska, on September 17, 1992, beginning ~0940 Z, is illustrated from AVHRR satellite imagery over a 3-day period. The cloud followed a U-shaped track across western Canada and the northern tier states (USA) into eastern Canada. Approximately 48 hours after the eruption, the ash cloud was spotted near Cleveland, Ohio, extending over a length of 1320 km at an altitude of 5.5 to 10 km. The presence of this ash cloud, some 5000 km downwind of the erupting volcano, caused major disruption of commercial air traffic in the eastern United States for about 12 hours. This disruption highlights the fact that the concentration of ash in an eruption cloud that constitutes a potential hazard to

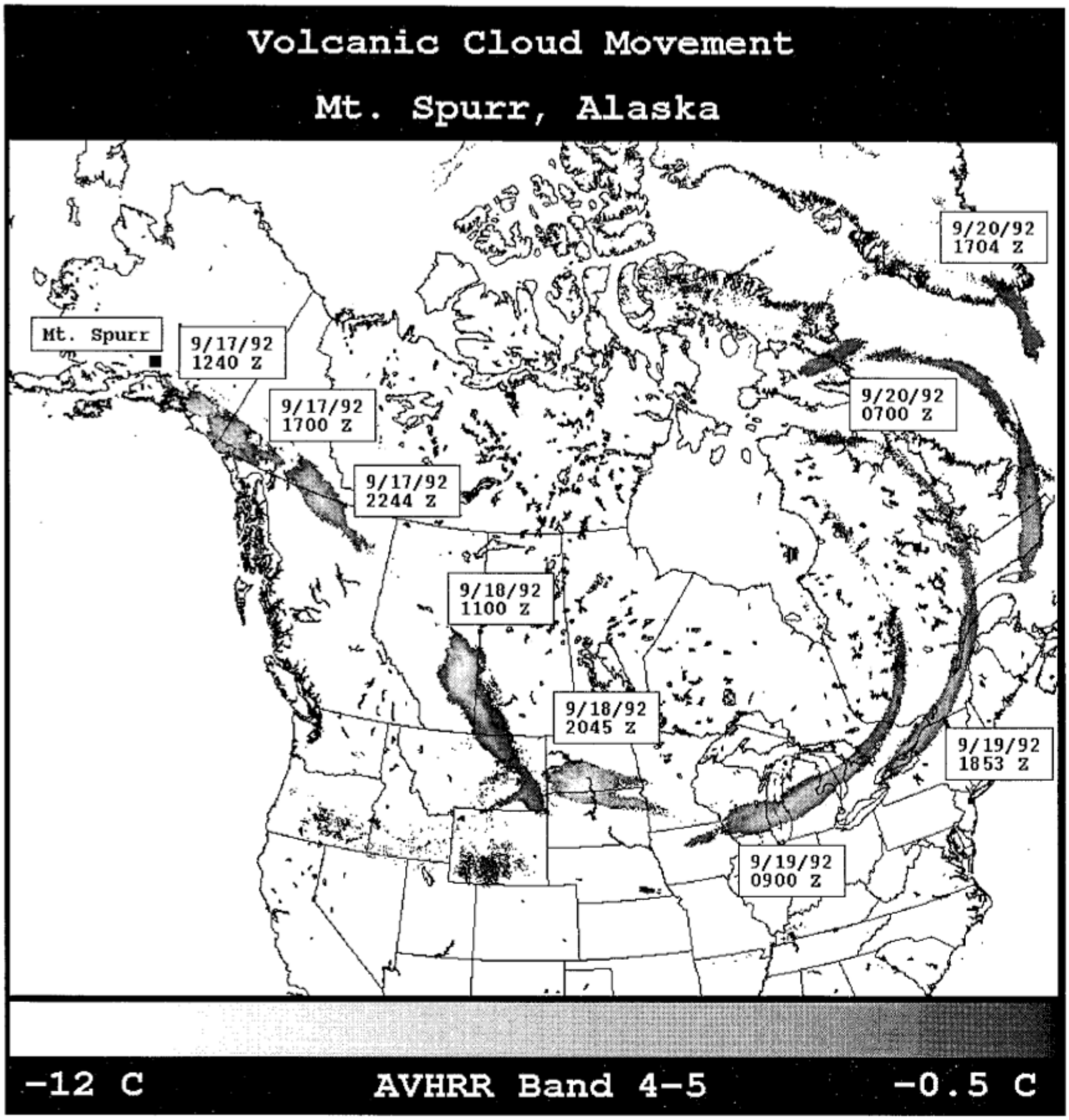
Volcanic Cloud Movement
Mt. Spurr, Alaska
Mt. Spurr
9/17/92 1240 Z
9/17/92 1700 Z
9/17/92 2244 Z
9/18/92 1100 Z
9/18/92 2045 Z
9/19/92 0900 Z
9/19/92 1853 Z
9/20/92 0700 Z
9/20/92 1704 Z
-12 C
AVHRR Band 4-5
-0.5 C

FIGURE 7 Composite satellite image illustrating the movement of the ash cloud from the September 16–17, 1992, eruption of Mount Spurr volcano, Alaska, across Canada and the northern tier states of the United States. On September 19th (more than 2 days after the eruption and 5000 km downwind), the ash cloud disrupted air traffic near Cleveland, Ohio, as pilots refused to fly through the visible ash cloud.

aircraft is unknown, as is the distance beyond which an ash cloud is no longer a hazard.

Some areas of the Earth's airspace are at greater risk from volcanic ash clouds than others simply because of the juxtaposition of volcanoes and air routes (Figures 1 and 4). Critical regions include the North Pacific, Southeast Asia (including Japan), Central and northern South America, Mexico, the Caribbean, and Iceland (the North Atlantic). The nature of the hazard differs significantly between the regions, however, being of importance chiefly to extended flight operations in the remote NOPAC and North Atlantic regions and to both terminal and extended flight operations in heavily populated Southeast Asia and the Americas.

The North Pacific region is instructive in considering the extent of the hazard (Figure 4). Air routes in this region are heavily traveled: over 200 flights per day in 1999 carried 20,000 passengers and more than 12 millions pounds of cargo between Asia and the USA and Europe. These air routes cross or lie downwind of 100 historically active volcanoes in Alaska, Kamchatka, and the Kurile Islands (Figure 4) that average 5–6 eruptions a year. It has been estimated that on 4–5 days a year, on average, volcanic ash will actually be in the NOPAC routes at altitudes of 9 km or more (above which most modern jet airliners fly), causing a major threat to thousands of passengers and tons of cargo. This estimate is empirical and based on a combination of the past 20-year record and a 200-year historical record. On an additional 10–12 days per year, volcanic ash clouds are estimated to be close enough to flight routes to be a matter of concern to aviation.

This analysis for the NOPAC composite routes can perhaps be extended further to a worldwide perspective. The North Pacific region has 100 active volcanoes, or about 20% of the world's 534 historically active volcanoes. If the (very) broad assumption is made that the same empirical likelihood of hazardous ash encounters with aircraft that exists for the North Pacific holds for other volcanic belts, then perhaps on a worldwide basis, volcanic ash could be expected to be in air routes at altitudes greater than 9 km 20–25 days per year on the average, and would be a matter of concern an additional 50–60 days per year. Having volcanic ash in the air routes at high altitudes does not mean that encounters with aircraft will necessarily occur given the speed of the aircraft, the length of time the cloud is in the air route, and its area. However, some support for the general validity of these figures comes from the reported 100 damaging encounters to aircraft from volcanic ash over a 15-year period, which yields an average of 5 encounters per year. These figures almost certainly represent underreporting of the actual number of damaging incidents but they give credence to the rough estimate of about 20 days per year that volcanic ash is in air routes worldwide.

Similar volcanic ash hazards to extended flight operations in the NOPAC region affect flight operations in the other aforementioned critical regions. These latter regions, however, are much more populated than the remote NOPAC region and are the locations of concentrated terminal flight operations in and out of busy local and regional airports. These landing and takeoff operations add the problems of dense ash clouds, heavy ashfall, and short warning times to the hazards described above for extended flight operations.

III. MITIGATION

No onboard cockpit instruments currently exist that can detect volcanic ash clouds. Ash clouds can usually be detected visually during daylight hours from the cockpit of an aircraft at altitudes of more than 9 km, but identification is much more difficult if meteorological conditions are poor, and it is essentially impossible at night. Yet if an eruption and associated ash cloud is unreported, the first knowledge of a hazard can come from an aircraft flying into the cloud, as happened in the Galunggung incidents in 1982. The time between the start of an eruption and the first notification is thus a period of great risk to the aircraft and so early detection of the eruption and ash cloud is essential to flight safety. Pilot groups have gone so far as to propose that notification messages announcing a potentially hazardous eruption should be in the cockpit of an in-flight airliner within 5 minutes after detection. So how are volcanologists, meteorologists, flight controllers, and modelers addressing this problem?

A. Monitoring

Reports of volcanic activity typically originate from volcano observatories, pilot reports, satellite observations, and ground observers. The need to integrate and evaluate reports received from these varied sources is typically the responsibility of the volcano observatories and similar establishments who rely on instrumental monitoring networks and knowledge of past eruptive activity at the volcano in question. Increasingly, the widespread availability of volcanic information on the Internet has become a valuable source of readily accessible near-real-time information for aviation user groups.

Volcano observatories use a number of techniques in monitoring volcanoes of interest to aviation. Real-time seismic monitoring of potentially active volcanoes, for example, has proven highly successful in providing warnings of impending or actual eruptions by detecting changes in the rates and character of volcanic earthquakes. These warnings have been largely based on empirical observations of volcanic seismicity. Strong increases in the rates of the activity, appearance of distinctive long-period events and continuous tremor, and shallowing of earthquake hypocenters are signs that have been attributed to rising magma or increases in magmatic pressure. Seismic networks around erupting volcanoes can usually detect explosions associated with major ash eruptions in real time (assuming appropriate telemetry exists). During the eruptions of Redoubt (1989–1990) and Mount Spurr (1992) volcanoes in southcentral Alaska, notification of more than 20 explosive eruptive episodes was made to aviation user groups (among others) within 3–8 minutes of the actual event.

Although seismic monitoring of active volcanoes has been shown to be effective, less than 20% of the world's active volcanoes have adequate seismic networks around them. Recognition of the frequency at which airborne volcanic ash occurs in the North Pacific region, however, has led to increased funding from the U.S. government over the past 10 years for monitoring and mitigation of the hazard. For example, in 1999 real-time seismic monitoring was available for 20 of 41 active volcanoes in Alaska, allowing identification of eruptive events and, in some instances, prediction. Other volcanic areas of the world are slowly experiencing similar increases but large gaps exist in coverage, particularly in remote and economically depressed parts of the world.

Satellites are an important source of information on volcanic activity and have the advantage of providing global coverage (depending on the sensors on board) at reasonable cost. Satellite imagery has been useful in detecting significant changes at remote volcanoes where other monitoring techniques are not feasible, and it complements seismic monitoring techniques by providing information on the height of an eruption cloud and on the presence of volcanic ash when an eruption is detected. Remote sensing data from the AVHRR, GOES, GMS, and TOMS (see Glossary) satellite-borne sensors are now used routinely across the North Pacific and elsewhere to monitor volcanic activity by initially detecting (in some cases) thermal anomalies and then identifying and tracking potentially hazardous volcanic ash clouds. Imagery is utilized to detect a variety of volcanic phenomena at a number of different wavelengths, including ultraviolet (volcanic ash and sulfur dioxide), visible (volcanic aerosols), short wavelength infrared (thermal anomalies), and thermal infrared (volcanic ash). Satellite monitoring of the entire North Pacific is now done routinely twice a day by the Alaska Volcano Observatory (AVO), and more frequently during times of volcanic unrest. Imagery from these sensors gives snapshots at intervals ranging from 15 minutes to once or twice a day, depending on the sensor and location of the volcano. Particular use has been made of thermal image data from two channels of the AVHRR, GOES, and GMS sensors to detect and to distinguish volcanic ash plumes from meteorological clouds using the split window brightness temperature difference between spectral bands 4 (10.3–11.3 μm) and 5 (11.5–12.5 μm). The routine use of high-spatial-resolution imagery by volcano observatories has been limited due to the high cost of obtaining commercial imagery, but this should change in 1999 with the successful launches of noncommercial satellites such as Landsat-7 (operated by the U.S. Geological Survey) and Terra (the first NASA EOS satellite).

A 5-cm C-band ground-based radar system in the Cook Inlet region of Alaska proved helpful in estimating cloud height during the 1992 Crater Peak (Mount Spurr) eruptions in Alaska. This system has now been replaced by a network of seven NEXRAD (Next Generation Weather Radar) doppler radars operated by the NWS (National Weather Service) primarily for other aviation purposes, but their increased power and sensitivity will allow monitoring of ash clouds at ranges of <200 km.

Forecasts of ash cloud movements are provided by the use of one or more volcanic ash tracking models. A number of transport and dispersion models exist; in the North Pacific, the VAFTAD (Volcanic Ash Forecast Transport and Dispersion) and PUFF models are used most commonly.

Visual observations by pilots themselves are obviously a valuable aid in the detecting and monitoring of eruptions and their ash clouds. Pilot cooperation is essential to the successful avoidance of airborne ash, and a special Volcanic Activity Reporting (VAR) Form has been devised to be carried in the cockpit for this use. This form allows for the description and location of the ash cloud and the erupting volcano, and numerous other characteristics along with directions as to where to send the information.

Other standard monitoring techniques such as ground deformation, gas analyses, geologic field studies, and aerial observations have correspondingly been increased. The ultimate goal of these efforts in terms of aviation is to provide notification of eruptions to user groups within minutes of their occurrence, detect thermal anomalies, track volcanic ash clouds across air routes in this remote region, and furnish information on size, character, and likely duration of an eruption.

B. Communication

Knowledge of an erupting volcano is of little use in mitigating hazards unless it is immediately conveyed to the proper authorities and users. At Mount Pinatubo, information regarding the restless state of the volcano was available to the aviation industry and government officials for up to 2 months before the June eruptions, yet over 16 aircraft were damaged during the eruptions. A posteruption analysis suggested that information and warnings about the hazard either did not reach the proper aviation authorities or that pilots, dispatchers, and air traffic controllers were not sufficiently educated about the hazard to take preventative action.

The key to communicating information about volcanic eruptions in a timely and readily understandable form is to involve all interest groups, including volcanologists, meteorologists, atmospheric modelers, pilots, and air traffic controllers, in the development of information, and to streamline the distribution of this information between essential parties. To avoid volcanic ash clouds, pilots and dispatchers need to be informed that a volcano has erupted, the time of eruption, whether ash has been produced, and the altitude of the plume. When this information is integrated with wind speed and direction, the trajectory of the cloud is forecast, an area of concern is identified, and a warning is issued alerting pilots to the hazards.

The first step in this coordinated response is the reporting of an eruptive event that could impact aviation. A simple but useful aid in communicating that a potential hazard exists to aviation was developed by the Alaska Volcano Observatory during the eruption of Redoubt volcano in 1990. This was a level-of-concern "color code" (Figure 8) to communicate rapidly and clearly to the nonscientific community the likelihood of an eruption at a restless volcano. The color code procedure for summarizing the status of a volcano has proven extremely effective in alerting the aviation community to potential ash hazards across the North Pacific, and the ICAO has recommended its use on a worldwide basis.

In the North Pacific (Figure 4), the Alaska Volcano Observatory monitors volcanoes in Alaska and works closely with the Kamchatka Volcanic Eruption Response Team (KVERT) to monitor and report on volcanic activity throughout the region. An interagency operating plan for volcanic ash episodes has been developed to provide a coordinated structure to mitigate volcanic ash hazards. This plan outlines the response procedures for the AVO, the NWS, the FAA, the U.S. Air Force, the Alaskan Division of Emergency Services, and the adjacent U.S. airspace Flight Information Regions (FIRs). It includes responsibility for communicating information on volcanic ash transported by upper-level winds from erupting volcanoes outside the U.S. FIRs into Alaskan airspace. Although the initial report of an eruption may originate from the AVO, from pilots or other observers, or from satellite imagery, information is immediately shared.

The response to frequent eruptions in the region, plus drills, formal written agreements, and conferences, has yielded a rapid flow of information to user groups (ultimately the airlines) through the Anchorage Volcanic Ash Advisory Center (VAAC) and AVO. At the AVO, for example, upon determination that an eruption potentially hazardous to aviation is occurring, or about to occur, a short telephone call-down list is utilized to inform the NWS and the FAA of the situation. The phone message follows a rigid format as follows: THIS IS AN ERUPTION NOTIFICATION FROM THE ALASKA VOLCANO OBSERVATORY. SEISMIC (or other) DATA INDICATE THAT A (small, moderate, large) ERUPTION OF ______ VOLCANO, LAT ______, LONG ______, BEGAN AT ______ UTC ON (date). THE LEVEL OF CONCERN COLOR CODE IS (orange, red). An immediate follow-up update message is sent out by e-mail and fax to an extended list of government, airline industry, and media users with more detailed information on the eruption and a prognosis of future activity. Phone messages concerning significant changes in the eruption are repeated as necessary during the course of the activity. Updates are sent out on a situation-warranted basis as often as several times a day.

The other participating agencies, the NWS and the FAA, immediately comunicate information on potentially hazardous eruptions and ash clouds to airliners and dispatchers. The NWS sends out a Volcanic Ash Significant Meteorological Advisory (SIGMET) as its primary notification and the FAA issues a Notice to Airmen (NOTAM). Although much remains to be done, these multidisciplinary efforts to date have been successful in the mitigation of hazards to aircraft operations from numerous volcanic eruptions in the North Pacific and serve as a model to be used elsewhere in the world.

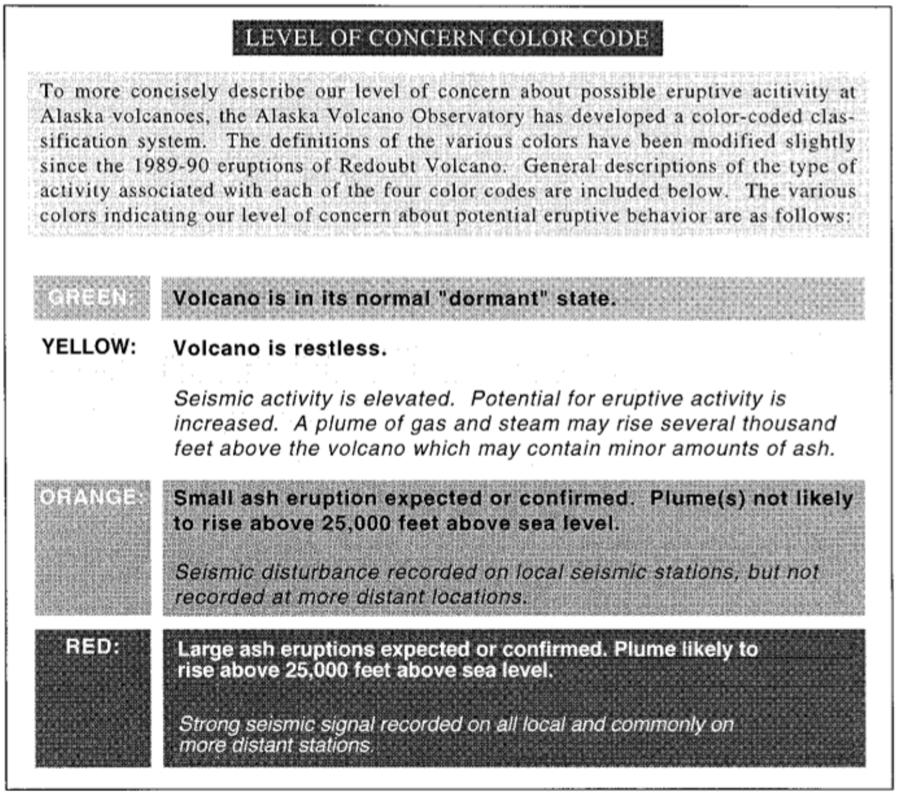

LEVEL OF CONCERN COLOR CODE

To more concisely describe our level of concern about possible eruptive acitivity at Alaska volcanoes, the Alaska Volcano Observatory has developed a color-coded classification system. The definitions of the various colors have been modified slightly since the 1989-90 eruptions of Redoubt Volcano. General descriptions of the type of activity associated with each of the four color codes are included below. The various colors indicating our level of concern about potential eruptive behavior are as follows:

GREEN:	**Volcano is in its normal "dormant" state.**
YELLOW:	**Volcano is restless.** *Seismic activity is elevated. Potential for eruptive activity is increased. A plume of gas and steam may rise several thousand feet above the volcano which may contain minor amounts of ash.*
ORANGE:	**Small ash eruption expected or confirmed. Plume(s) not likely to rise above 25,000 feet above sea level.** *Seismic disturbance recorded on local seismic stations, but not recorded at more distant locations.*
RED:	**Large ash eruptions expected or confirmed. Plume likely to rise above 25,000 feet above sea level.** *Strong seismic signal recorded on all local and commonly on more distant stations.*

Alaska Volcano Observatory's level of concern color code. This code and eruption updates are distributed to government agencies, the media, airlines, and the public.

FIGURE 8 A level-of-concern color code developed by the Alaska Volcano Observatory to rapidly and clearly communicate the likelihood of an eruption at potentially dangerous volcanoes. This format for summarizing the status of a volcano has proven extremely effective in alerting the aviation community to potential ash hazards in the North Pacific region.

C. Volcanic Ash Advisory Centers

Ash clouds often drift far from their source volcanoes, crossing over national boundaries and between FIRs, so regional air traffic facilities and carriers must be informed about potential volcanic threats not just in their local flight region but in adjacent regions as well. The hazards posed by volcanic clouds thus have a scope that requires both local and global approaches to ensure a solution.

Recognition of this feature of the hazard led the World Meteorological Organization (WMO) to establish the International Airways Volcano Watch (IAVW). The purpose of the IAVW is to address the threat to aviation safety and the economic loss from aircraft encounters with volcanic ash clouds. As a key part of the IAVW, nine regional Volcanic Ash Advisory Centers have been established around the world (Figure 1) under International Civil Aviation Organization (ICAO) auspices to advise Meteorological Watch Offices (MWOs) on the issuance of volcanic ash warnings to aircraft. The VAACs have been specifically tasked with the detection, tracking, and forecasting of the movement of volcanic ash clouds within their respective areas of responsibility. In addition, they cooperate in "passing off" a drifting ash cloud from VAAC to VAAC as it moves around the globe. Fulfillment of this task requires international cooperation among the meteorological, volcanological, and aviation communities to provide the VAACs with current information. To further foster the VAAC efforts, the WMO and the ICAO cosponsor international workshops to provide a forum for interaction between providers and users of volcanic ash advisories and warnings.

IV. DISCUSSION

A new volcanic hazard with a significant attendant risk has developed that quite simply did not exist in any notable way before 1980. In the last 2 decades of the 20th century, more than 100 jet aircraft have flown into drifting clouds of volcanic ash in air routes and near airports around the world. This has resulted in hundreds of millions of dollars in damages, placed thousands of passengers at risk, and disrupted air commerce. This marks a time when the number of jet transports in the world's civilian air fleet has expanded to approximately 13,000 aircraft as of 1999.

This hazard extends to life and property, and is a dynamic phenomenon that can occur in regions far from erupting volcanoes. An explosive eruption from a remote volcano with only a sparse local population would formerly have been chiefly of scientific interest. Now, however, such a volcano can suddenly threaten large segments of unsuspecting airborne travelers and commerce. The response to this hazard has resulted in international cooperation among the meteorological, volcanological, and aviation communities.

Anticipated increases in aviation traffic globally and changes in equipment type and operational procedures will increase the probability of aircraft and volcanic ash encounters. In the North Pacific and Russian Far East region alone, air traffic is projected to increase by a factor of 3 from about 200 flights per day to 600 flights by the year 2017, with a corresponding increase in passenger load from 20,000 to 60,000 people per day. These figures are impressive given the thousands of passengers involved and the monetary value of the aircraft and cargo. Modern trends in commercial aviation point to similar vigorous growth across the globe. If the number of volcanic eruptions remains constant over sufficiently long periods of time but the number of encounters increases (i.e., the number of flights increases without mitigation procedures), then the risk of a catastrophic accident will increase dramatically.

Other airline operational factors raise the potential for route disruption because of volcanic eruptions. Increasingly, airlines are using large twin-engine jet aircraft for transoceanic flights because of favorable operating costs. However, many countries have placed restrictions on operation of twin-engine aircraft that require the aircraft to be within 3 hours of flight time from an alternate airport at all times. One of the heaviest flight paths in the world is across the North Atlantic, and airports in Iceland are used to meet the availability restriction. If airports are not available because of volcanic ash, regardless of whether it is airborne or deposited at the airport, air traffic can be shut down. An additional complicating factor is that the ever larger engines, because of higher operating temperatures, are more susceptible to damage from ash.

Clearly, the volcanology community needs to work closely with the airline community and with government aviation groups to address these problems. A successful start in mitigation of airborne volcanic ash hazards by a multidisciplinary group provides encouragement that the hazard can be mitigated. However, given the expected growth in global air traffic, much remains to be done if the successes to date are to continue. Tracking of ash clouds by satellite imagery has improved, but future generations of GOES satellites will lose the ability of split window detection of ash. The ability to detect volcanic ash needs to be considered along with other meteorological requirements when designing future satellite sensors. The availability of adequate orbital platforms and the transfer of satellite data between VAACs and to other user groups continues to present problems. Standard dispersion models must be agreed upon using more realistic eruption parameters, particularly in the critical first few hours of an eruption.

Advances in satellite remote sensing technology will further aid in the detection and tracking of volcanic ash clouds (observable parameters) but will not provide immediate information on the probable character, size, type, and likely duration of the eruption (interpretive parameters). Prognostic information needs to come from thorough pre-eruption studies of the volcanic history and petrology of the erupting volcano. Increased monitoring by real-time continuously recording seismic, ground deformation, and gas sampling networks will increase the demonstrated ability to predict at least some explosive events.

The necessity for the immediate communication of eruption information to the cockpit of a jet aircraft traveling at over 800 km/hour has always been paramount: location of the volcano, start time of eruption, duration, plume height, and wind direction have been and will remain critically important elements. However, as information on these observable parameters has become available, aviation stakeholders have demanded more information from volcanologists and atmospheric modelers. How long might an eruption be expected to last? Will it wax and wane in intensity? What will its volume be? These are factors that effect the payload versus fuel equation and the safety of the aircraft. They are questions that are among those asked at any eruption by any concerned group, but now they must also be addressed from an aviation perspective.

The establishment and utilization of contact volcanology groups that are knowledgeable about hazards to aviation for a particular eruption is very important. At many erupting volcanoes, volcanologists are understandably deeply involved in mitigating hazards proximal to the erupting volcano. Concern for aircraft up to hundreds of kilometers downwind from the volcano and over other countries, while often acknowledged, gets lost in the immediate local response. The existence of a knowledgeable contact group that can be contacted by dispatchers, pilots, and air traffic officials can help rectify this situation.

It is unlikely that jet engines, air frames, and avionics will ever be built that can safely withstand flying though a volcanic ash cloud without a serious risk to life and property. It is also unlikely that in the foreseeable future jet aircraft in extended flight will be operating at altitudes totally above the reach of volcanic ash clouds. These factors suggest that the problems posed by airborne volcanic ash to aircraft will concern volcanologists for a long time to come.

SEE ALSO THE FOLLOWING ARTICLES

Hazards of Volcanic Gases • Magmatic Fragmentation • Seismic Monitoring • Synthesis of Volcano Monitoring • Volcanic Hazards and Risk Management

FURTHER READING

Blong, R. J. (1984). "Volcanic Hazards." Academic Press, Sydney, Australia.

Blong, R. J. (1996). Page 675–700 *in* "Monitoring and Mitigation of Volcanic Hazards" (R. Scarpa and R. I. Tilling, eds.). Springer-Verlag, Berlin/Heidelberg.

Casadevall, T. J. (1993). "Volcanic Ash and Airports." U.S. Geological Survey Open-File Report 93–518.

Casadevall, T. J. (1994). The 1989-90 eruption of Redoubt volcano, Alaska: Impacts on aircraft operations. *J. Volcanol. Geotherm. Res.* (Special issue) V **62**(1–4), 301–316.

Casadevall, T. J., ed. (1994). "Volcanic Ash and Aviation Safety: Proceedings of the First International Symposium on Volcanic Ash and Aviation Safety." U.S. Geological Survey Bull. 2047.

Casadevall, T. J., and Krohn, M. D. (1995). Page 205–220 *in* "The 1992 Eruptions of Crater Peak Vent, Mount Spurr Volcano, Alaska" (T. Keith, ed.). U.S. Geol. Survey Bull. 2139.

Casadevall, T. J., and Thompson, T. B. (1995). "World Map of Volcanoes and Principal Aeronautical Features." U.S. Geological Survey Geophysical Investigations Map GP-1011.

Casadevall, T. J., Delos Reyes, P. J., and Schneider, D. J. (1996). Page 1071–1088 *in* "Fire and Mud, Eruptions and Lahars of Mount Pinatubo, Philippines" (E. G. Newhall and R. S. Punongbayan, eds.). Univ. of Washington Press, Seattle/London.

Heffter, J. L., and Stunder, B. J. B. (1993). Volcanic ash forecast transport and dispersion (VAFTAD) model. *Weather Forecasting* **8,** 534–541.

Przedpelski, Z. J., and Casadevall, T. J. (1994). Page 129–136 *in* "Volcanic Ash and Aircraft Safety" (T. J. Casadevall, ed.). U.S. Geological Survey Bull. 2047.

Scarpa, R., and Tilling, R. I. eds. (1996). "Monitoring and Mitigation of Volcanic Hazards." Springer-Verlag, Berlin/Heidelberg.

Searcy, C. K., Dean, K., and Stringer, B. (1998). PUFF: A volcanic ash tracking and prediction model. *J. Volcanol. Geotherm. Res.* **40,** 1–16.

Sparks, R. S. J., Bursik, M. I., Carey, S. N., Gilbert, J. S., Glaze, L. S., Sigurdsson, H., and Woods, A. W. (1997). "Volcanic Plumes." Wiley, New York.

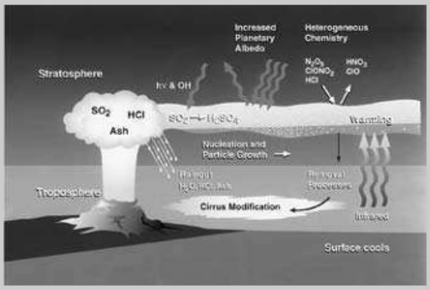

VOLCANIC AEROSOL AND GLOBAL ATMOSPHERIC EFFECTS

MICHAEL J. MILLS
University of Colorado

I. Introduction
II. The Atmosphere
III. Stratospheric Aerosol
IV. Volcanic Aerosol
V. Aerosol Microphysics
VI. Character of Volcanic Input
VII. Volcanic Effects on Stratospheric Dynamics
VIII. Radiative and Climate Effects
IX. Effects on Stratospheric Chemistry
X. Lessons for the Future

GLOSSARY

aerosol A suspension of fine liquid or solid particles in air. Natural aerosols include fog, smoke, and stratospheric sulfate.

albedo The fraction of incident radiation reflected by a surface. The Earth's planetary albedo is the fraction of the Sun's incoming radiation that reflects off the Earth and back into space.

coagulation The process of two particles fusing to become one larger particle.

condensation The process by which gas (vapor) changes into liquid. Stratospheric aerosol particles grow by condensation of water, sulfuric acid, and nitric acid.

denitrification The removal of active nitrogen species from the stratosphere by sedimentation of polar stratospheric clouds containing large amounts of nitric acid.

direct effects of aerosol Attenuation of atmospheric radiation by absorption and scattering on atmospheric particles.

evaporation The process by which liquid changes into gas (vapor). Evaporation prevents the presence of aerosol in the relatively warm upper stratosphere.

greenhouse gases Gases such as carbon dioxide, water vapor, and methane that allow incoming sunlight to pass through but absorb infrared rays radiated back from the Earth's surface, heating the atmosphere.

heterogeneous chemistry Reactions occurring between reactants of different phases. In the atmosphere, these are reactions of gases with species in solid or liquid aerosol, forms.

indirect effects of aerosol Processes such as cloud modification by which aerosols affect the Earth's radiation budget without interacting with radiation.

microphysics The processes affecting the size, number, and distribution of aerosol particles. Microphysical processes include nucleation, condensation, evaporation, coagulation, and sedimentation.

mixing ratio The abundance of a chemical species as a fraction of the total volume (number), or mass of ambient air. Mixing ratios of gas-phase constituents are often expressed as parts per million by volume (ppmv), parts per billion by volume (ppbv), or parts per trillion by volume (pptv). Mixing ratios of condensed-phase constituents, such as liquid sulfate, are often expressed as mass fractions, such as parts per billion by mass (ppbm).

nucleation The process by which gas- or liquid-phase species form new liquid or solid particles. Nucleation may

Copyright © 2000 by Academic Press
All rights of reproduction in any form reserved.

occur by heterogeneous means, if an involatile substrate (e.g., soot particles or meteoric dust) is present on which molecules aggregate. Homogeneous nucleation occurs in the atmosphere when molecules cluster together spontaneously in the absence of preexisting nuclei. Binary nucleation is the formation of nuclei from two different chemical species. The source of liquid stratospheric sulfate aerosol is believed to be binary homogeneous nucleation of water vapor and sulfuric acid vapor.

optical depth A measure of the cumulative attenuation of electromagnetic radiation in transit through a medium, such as the Earth's atmosphere. At an optical depth of one, the irradiance of radiation is diminished to 1/2.7 of that entering the atmosphere.

sedimentation The process by which aerosol falls through the atmosphere due to gravity.

sulfate The SO_4^{2-} radical molecule found in solution with liquid water; the dissolved form of sulfuric acid (H_2SO_4).

HUMANS HAVE LONG experienced the global atmospheric effects of volcanic eruptions. Benjamin Franklin may have been the first to report the link between volcanism and unusual atmospheric phenomena in 1784, when a strange "dry fog" and unseasonably cold weather struck Europe. Franklin speculated that the fog was the cause of the cold summer, and that it originated as smoke from either meteorites or volcanic eruptions he knew to have occurred in Iceland over the course of the previous year. The eruption of Krakatoa in 1883, however, produced the first widespread reports of strange atmospheric effects linked to volcanoes. The arrival of global communications ensured that the intense sunsets seen for several years subsequent were attributed to the news of the massive eruption. In retrospect, historical records back through antiquity reveal numerous examples of atmospheric anomalies that correlate with major volcanic eruptions, often in an entirely different part of the world.

I. Introduction

One of the greatest volcanic disasters to have occurred in human history was the eruption of Santorini, also known as Thera, which occurred circa 1620 B.C. The eruption transformed a 3000-feet-high mountain rising from the Aegean Sea into an island ring surrounding an enormous crater filled with 2000 feet of seawater. Such was the power and notoriety of the Santorini eruption that some have linked it with the parting of the Red Sea described in the Bible and the demise of the 1400-year-old Minoan civilization on nearby Crete, itself sometimes linked to the fabled lost continent of Atlantis. While serious doubt surrounds such speculation, historical records reveal that the atmospheric effects of the eruption were felt around the globe.

Much of astronomer Kevin Pang's research focuses on examining historical records of the atmospheric disturbances due to volcanic eruptions. While there are no written European records describing the 17th Century B.C., Pang has searched provincial records from China to discover accounts of severe climatic hardships experienced there at around the same time as the Santorini eruption. These include "yellow fog," a "distressed" and "dimmed" sun, floods, followed by a 7-year drought, crop failure, famine, and the appearance of "three suns … together." The latter is often seen in a cold atmosphere, due to refraction of the Sun's image by ice crystals. Pang dates the period of these events as 1600 B.C. plus or minus 30 years, correlating well with ice core and tree ring samples showing the volcanic influences of Santorini.

In 44 B.C., Romans marked the appearance of a bright red comet, a planet Venus "stained with dark rust," and a Moon "stained with blood" as signs of divine displeasure with the murder of Julius Caesar on the ides of March that year. Caesar's biographer Plutarch described the Sun that year as "pale and without radiance … and the fruits, imperfect and half ripe, withered away and shriveled up on account of the coldness of the atmosphere." The Romans knew of the eruption of Mount Etna in Sicily, which threw a vast cloud of ash, dust, and sulfur into the atmosphere, but did not attribute these atmospheric and climate changes to the event. Tiny particles freshly nucleated from the nearby eruption would have scattered blue light, making celestial bodies appear red as the volcanic cloud passed over Rome. In China, the year 43 B.C. marks the first of six consecutive failed harvests in a period of summer frosts and widespread famine. Tree rings from the bristlecone pines of the western United States show frost damage in the year 42 B.C. Ice cores from the glaciers of Greenland show evidence of volcanic fallout in the atmosphere at some time between 80 and 20 B.C.

In 1453, after over a century of chipping away at the Byzantine Empire, the Ottoman Turks finally won possession of its coveted capital, Constantinople. In the triply walled city's final days, ancient myths about its demise after a sign from the Moon seemed to come true. On May 22, 7 weeks into the Turks' siege, the full

Moon was eclipsed for 4 hours, and was pitch dark, similar to a 1992 eclipse which followed the eruption of Mount Pinatubo. A few days later a hailstorm of unprecedented strength pelted the city, followed by an unheard-of and unseasonably dense fog. When the fog lifted, lights could be seen flickering like fires on the horizon, where there should be no lights, as well as around the dome of Constantinople's great cathedral. Chinese records from that period indicate that tens of thousands of people and animals froze to death in 1453, the Yellow Sea froze more than 20 km out from the shore, and a southern region of China with a climate like that of Florida experienced 40 days of continuous snow. German and Swedish records show extensive crop damage for up to 9 years following 1453. Tree rings from around the world show frost damage for several years starting in 1453.

Pang, who uncovered many of these records, believes the culprit to have been the eruption of Kuwae, a volcanic island in the South Pacific. For over 500 years, the eruption was known only in the oral tradition of the local tribes in what is now the Republic of Vanatu. Archaeological research into these legends and radiocarbon dating of vegetation burned in the blast indicate that the eruption occurred between 1420 and 1475. Antarctic ice cores show strong volcanic influence for several years following 1453, while cores from Greenland show a weaker signal in that year. Geologists put the size of the eruption as the second largest known to have occurred in recorded human history.

The most explosive eruption of the last 10,000 years was that of Mount Tambora on the Indonesian Island of Sumbawa in 1815. Of the island's 12,000 inhabitants, 26 survived. In all, the eruption and accompanying earthquake killed some 90,000 people. The area within 200 miles of the volcano experienced 3 days of total darkness.

Half a world away, 1816 became know as "the year without a summer," or "eighteen hundred and froze to death." Average temperatures fell 1 to 2.5°C below normal throughout New England and western Europe, and the global average is estimated to have fallen by 0.4 to 0.7°C. New England experienced snows or frosts in every month of that year. The cold summer of 1816 drove farmers from New England to warmer climes to the south and west. It is estimated that Vermont's population was diminished by 8% of what it would have otherwise been. Agricultural staples failed, and in New York and France, wheat reached its highest price in the 19th century. The winter of 1816 proved a hardship to endure. Europe, just beginning its recovery from the devastation of the Napoleonic Wars, suffered famines and riots. In late 1816, a typhus epidemic, which has been linked to famine, began to spread from Ireland to the rest of the British Isles; 1816 also saw bad harvests in India, leading to famine and the spread of cholera.

Few experiencing the climatic abnormalities of 1816 had heard of the eruption of Tambora. The speed of communications at the time meant the news would have taken at least 6 months to reach New England. There appear to have been no attributions of the frosty summer to the volcano.

The first intensive scientific studies of the atmospheric effects of volcanoes followed the 1883 eruption of Krakatoa. In this article we review current scientific knowledge of the atmospheric effects of volcanoes based on studies of numerous eruptions in the period since Krakatoa. While the climatic effects of volcanic eruptions recorded in human history have been sometimes extremely severe, these eruptions pale in comparison to those we know that the Earth produced over its history. The eruption of Toba, 75,000 years ago, for example, ejected 20 to 50 times the volume of material ejected by Tambora in 1815.

II. THE ATMOSPHERE

In order to understand the ways in which volcanic input influences the atmosphere, we first review the structure and dynamics of the atmosphere. The atmosphere is divided into a number of regions based on its thermal structure. The troposphere is the region closest to the surface. From the surface, temperature decreases with altitude to a minimum at the top of the troposphere, known as the tropopause. The temperature and altitude of the tropopause vary from about 190 K and 18 km at the equator to 220 K and 8 km in polar regions. In the region above the tropopause, known as the stratosphere, the ozone layer heats the atmosphere by absorption of high-energy ultraviolet rays from the sun. Temperature increases with altitude to a maximum at the top of the stratosphere, known as the stratopause, near 50 km. In the layer above the stratosphere, known as the mesosphere, temperature decreases again to a minimum at the mesopause. Together the troposphere, stratosphere, and mesosphere make up the homosphere, a region in which the composition and molecular weight of air varies little throughout. While the mixing ratios of trace constituents may vary greatly, the homosphere is dominated by N_2 and O_2, which make up about 80 and 20%, respectively, of the total number density of gas molecules.

The troposphere, the region of the atmosphere we inhabit, is a turbulent and dirty region. Absorption of solar radiation at the surface heats air, which may then rise through colder, denser air above. We experience such instability as weather. Particles of limitless composition and type, many arising from surface sources such as soil and organic gases, pollute this region heavily. Tropospheric particles, however, are destined to be removed from the atmosphere in a period of several weeks by frequent precipitation. Rainout provides the dominant sink for volcanic sulfur injected into the troposphere. Most volcanic eruptions have little chance to impact the global atmosphere, because their plumes do not penetrate the tropopause. Some types of volcanoes, such as those in the Hawaiian Islands, do not have significant explosive eruptions. It is only those volcanoes with very explosive eruptions that are of concern to climate and stratospheric chemistry.

Because warm air is less dense than cold air, the increasing temperature profile of the stratosphere ensures it is a much more stable region of the atmosphere than the troposphere. Air from the troposphere enters the stratosphere in the tropics, where convective storm systems create strong updrafts capable of breaking through the cold tropical tropopause. In the process, much of the water vapor freezes out of the rising air, leaving the stratosphere much drier than the troposphere. Particles in the stratosphere are therefore not rained out, and may remain in the stratosphere until removed with ambient air parcels. At midlatitudes, tongues of stratospheric air are folded into the troposphere. This removes about three-quarters of the air that enters the stratosphere. Air removed at midlatitudes experiences an average stratospheric residence time of approximately 2 years. The remaining quarter of stratospheric air is removed by descending air at the poles, when a ring of rapidly moving wind is established in winter. Observations of chemical tracers indicate that stratospheric air is about 3 to 5 years old by the time it reaches high latitudes.

III. STRATOSPHERIC AEROSOL

Triangulation measurements of twilight effects following the eruption of Krakatoa led to the formal proposal of the existence of a layer of particles in the stratosphere. Proof of the existence of this layer was left until 1961 and the pioneering work of Christian Junge and coworkers. Junge's team sampled aerosol directly from high-altitude balloons and measured concentrations of particles in two size ranges. These measurements showed concentrations of larger particles (0.1 to 1 μm), which contain the bulk of sulfate mass, peaking at 20 km, or 8 km above the tropopause. Vaporization measurements later determined the particles to be liquid solutions of sulfuric acid (H_2SO_4) in water, or sulfate (SO_4^{2-}).

Junge's measurements followed a period of unusually low volcanic activity. The observation of a peak in aerosol mass in the stratosphere under such conditions suggested a nonvolcanic source is responsible for maintaining stratospheric sulfate aerosol. In 1976, Paul Crutzen suggested carbonyl sulfide (OCS) as the major source of this "background" layer. OCS originates from biological, volcanic, and some anthropogenic sources, such as coal combustion. In the troposphere, it is relatively inert, having a chemical lifetime of about 30 years. Thus it accumulates uniformly throughout the troposphere to a mixing ratio of about 500 parts per trillion by volume (pptv), making OCS the most abundant sulfur-bearing compound in the atmosphere. In the stratosphere, ultraviolet light and reaction with atomic oxygen destroy OCS, producing SO_2, which then oxidizes to sulfuric acid. While OCS clearly provides an important source of stratospheric sulfate, it dissociates too high to account for much of the aerosol observed in volcanically quiescent periods. SO_2 of tropospheric origin, arising from industrial pollution and reduced sulfur compounds produced biologically, appears to have a major influence on aerosol in the lower stratosphere.

IV. VOLCANIC AEROSOL

In the period since Junge's first measurements, the vast bulk of total sulfate mass in the stratosphere has originated from volcanic eruptions. With the exception of the volcanically quiescent periods in the early 1960s, the late 1970s, the late 1980s, and the period since 1996, most of our measurements of stratospheric aerosol include signals of volcanic influence. The greatest of these have resulted from volcanic plumes that rise well into the stratosphere in the tropics. Plumes which do not break through the troposphere, or which occur at high latitudes, have fewer global consequences.

Figure 1 shows many of the atmospheric perturbations induced by volcanic eruptions that we will be dis-

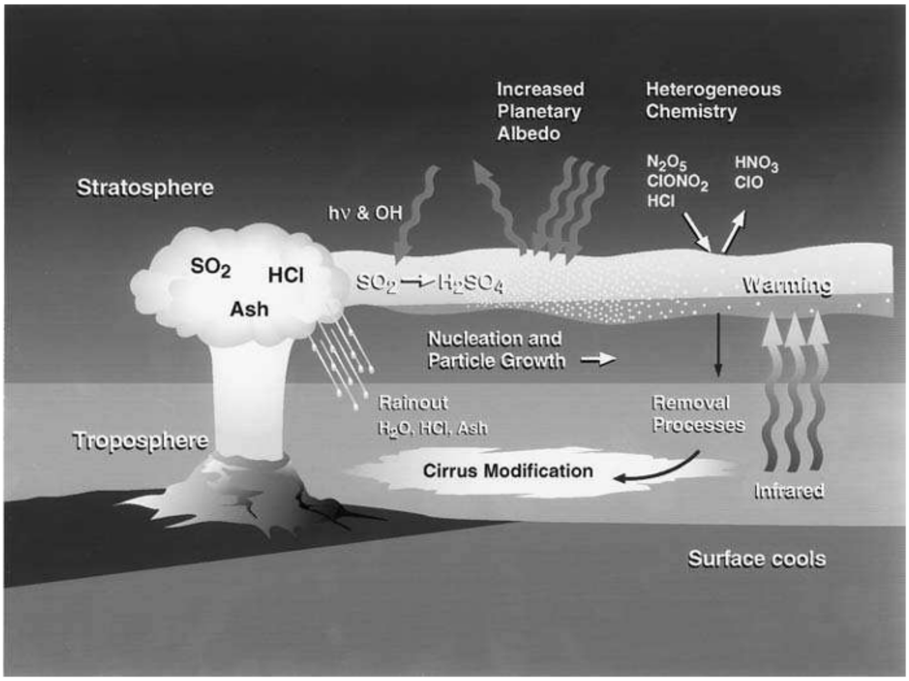

FIGURE 1 Volcanic eruptions that penetrate the tropopause can significantly perturb the Earth–atmosphere system via a number of processes shown here. Volcanic clouds may include ash, water vapor, sulfur dioxide (SO_2), and hydrochloric acid (HCl). Water vapor and soluble gaseous components, such as HCl, condense as temperatures drop in the upper troposphere and fall out of the cloud before it enters the stratosphere. Ash that survives the journey may remain in the stratosphere for several months before sedimenting out due to its relatively large size. SO_2 oxidizes within about a month to produce sulfuric acid, which together with ambient water vapor is responsible for nucleation and growth of stratospheric sulfate aerosol. Depending on the latitude and altitude of the initial injection, stratospheric aerosol may remain at elevated levels for several years following an eruption. Volcanic aerosol may cool the Earth's surface by reflecting additional solar radiation back to space, and may warm the stratosphere by absorbing infrared radiation escaping from the surface and troposphere. Chemical reactions between gaseous and aerosol components activate anthropogenic chlorine, amplifying stratospheric ozone depletion at midlatitudes and polar regions. Sedimentation and atmospheric circulation eventually remove aerosol to the troposphere, where it may be taken up in clouds or rain. When taken up by clouds, the aerosol may again increase planetary albedo by decreasing the average size of droplets in cirrus clouds, modifying their optical properties. [Reprinted by permission from *Nature* (McCormick *et al.,* 1995), copyright 1995 Macmillan Magazines Ltd.]

cussing in some detail in this article. Volcanic eruptions introduce large quantities of ash and magmatic gases into the atmosphere. The major gases released are water vapor (>80% by volume) and carbon dioxide (~10%), with smaller, more variable contributions of SO_2, H_2S, CO, H_2, N_2, HCl, and HBr.

Of these gases, sulfur dioxide (SO_2) creates the only major stratospheric perturbation. Many explosive volcanic eruptions, such as that of Mount St. Helens in 1980, have little SO_2 in their plumes, and consequently produce minor climatic or chemical effects. Equally explosive events such as that of El Chichón in 1983 contained much more SO_2 and do impact climate.

H_2S may add some sulfur to the stratosphere, but it quickly oxidizes to SO_2, and is generally much less abundant than SO_2 in volcanic plumes that penetrate the tropopause. The stratospheric masses of many species, such as CO_2, CO, N_2, and H_2, are much larger than that which could be released by volcanic eruptions. The background stratospheric mass of water vapor (~10^{15} g) is comparable to that released by only the most massive eruptions, such as Tambora in 1815. Water vapor and the highly soluble species HCl and HBr are rained out of the volcanic plume as it rises, exapands, and cools. Volcanic ash provides effective nuclei on which water and soluble species condense, forming large water droplets or ice particles which fall out of the atmosphere. The cold trap at the tropopause effectively prevents HCl or HBr from entering the stratosphere.

Sulfur dioxide is less soluble than HCl, and reaches the stratosphere in considerable quantities, which vary considerably between volcanic events. In the stratosphere, SO_2 oxidizes by reaction with the hydroxyl radical (OH) to produce products which quickly yield sulfuric acid. Satellite observations of the SO_2 cloud produced by the eruption of Mount Pinatubo in 1991 indicate that this oxidation occurs on a timescale of about 1 month. Pinatubo, the largest eruption of this century, put about 20 million tons of SO_2 into the stratosphere.

V. AEROSOL MICROPHYSICS

Processes affecting the size and atmospheric distribution of aerosol particles fall under the field of microphysics. These processes include nucleation, condensation, evaporation, coagulation, and sedimentation. Aerosol microphysics determines the influence of volcanic perturbations on the stratosphere.

Very small aerosol particles are produced in the tropical upper troposphere by a process known as binary homogeneous nucleation. This process is distinguished from heterogeneous nucleation in that particles do not form on existing solid nuclei, but directly from the gas phase. Under atmospheric conditions, binary clusters composed of both sulfuric acid and water molecules are required to create stable nuclei. For a given concentration of water and sulfuric acid, nucleation will proceed faster at colder temperatures. The formation of significant concentrations of new particles in the atmosphere requires the extreme cold of the tropical tropopause. The gently rising motions in the tropics loft these small particles from the tropopause region into the stratosphere, where they grow to become stratospheric aerosol. New particles are also nucleated in the polar stratosphere in winter and spring, also under extreme cold conditions. Following large volcanic eruptions, nucleation of new particles also occurs in the stratosphere. However, much of the new sulfate injected into the stratosphere condenses on particles that were previously present or formed during the earliest weeks following the eruption.

Condensation of sulfuric acid molecules on existing particles provides an important growth mechanism for stratospheric aerosol. Even under volcanic conditions, concentrations of sulfuric acid in the stratosphere are small enough that it takes several months for condensation to equilibrate the vapor and aerosol phases. As temperatures increase with altitude in the stratosphere, the equilibrium vapor pressure increases dramatically. At about 30–40 km (varying with latitude, season, and volcanic state) all aerosol boils away as the equilibrium vapor pressure exceeds the available sulfuric acid. Volcanic injections increase available sulfuric acid and the altitude of the top of the aerosol layer.

Stratospheric air contains 3 to 5 parts per *million* by volume (ppmv) of water vapor, compared to 0.5 to 10 parts per *billion* (ppbv) of sulfuric acid. The exchange of water between vapor and aerosol occurs about 10^8 times faster than that of sulfuric acid, and water equilibrates within a few seconds. As sulfuric acid condenses or evaporates, water vapor quickly adjusts to maintain a constant fractional composition, determined by temperature. A particle descending in the stratosphere usually will cool and "swell" with water. In the extremely cold winter polar lower stratosphere, aerosol begins to take up significant amounts of nitric acid as well, becoming a ternary solution.

When aerosol particles run into one another, they coagulate, producing one larger particle from two smaller ones. Coagulation occurs predominantly due to the Brownian motion of the particles, at timescales proportional to the number density of particles (number per cm^3). It is effective at reducing the number of small particles in the lower stratosphere, but does not significantly increase the size or number of larger particles. As air parcels containing freshly nucleated particles rise from the tropical tropopause, particle mixing ratios (number of particles per milligram of air) are observed to decrease due to coagulation, up to about 22 km. (In the absence of a source or loss process, atmospheric motions do not change the mixing ratio of a gas or aerosol contained in an air parcel. Hence chemists refer to atmospheric abundances in mixing ratio, rather than concentration, to exclude changes induced by changing air density as air parcels move.) At higher altitudes, particle concentrations (which decrease with air density) are too small for coagulation to be important, and particle mixing ratios remain constant.

As particles grow larger than about a micrometer, they begin to fall rapidly. Sedimentation plays an important role in redistributing mass at the top of the aerosol layer. As particles fall to lower altitudes, however, rising pressures slow their fall. In the nonvolcanic aerosol layer, sedimentation does not play a significant role in removing particles from the stratosphere because the particles are so small. Volcanic input, however, can cause particles to grow larger than 0.5 μm and sediment from the lower stratosphere before they are removed with ambient air parcels.

VI. CHARACTER OF VOLCANIC INPUT

Microphysical calculations and observations show that volcanic SO_2 generally results in larger particles, rather than greater concentrations, because coagulation limits the particle concentrations. As Table I shows, stratospheric aerosol mass may increase by one or two orders of magnitude following a significant eruption. Aerosol properties such as surface area and optical depth (which determines the probability that an arbitrary photon will encounter a particle in its path through the atmosphere) show similar increases. Figure 2 shows global satellite observations of aerosol optical depth before and after the June 1991 eruption of Mount Pinatubo. Aerosol in the initial equatorial band was 100 times optically thicker than the pre-eruption background throughout the second half of 1991. Two and a half years after the eruption, aerosol had spread to higher latitudes, at about 10 times the background optical depth.

The global distribution of aerosol from volcanoes depends primarily on the latitude at which the eruption occurs. The atmospheric influence of eruptions outside the tropics is almost entirely contained within the middle and polar latitudes of the hemisphere of origin. Volcanic sulfur and ash are rained out of the troposphere within days or weeks of the eruption, much faster than interhemispheric exchange of air occurs in the troposphere. In the stratosphere, the circulation carries aerosol poleward and downward from the tropics. A branch of stratospheric circulation also carries air up into the mesosphere at the summer pole. Mesospheric circulation then brings air back across the equator to the winter hemisphere, where it descends back into the stratosphere. The mesosphere, however, contains about 1% of the mass of air in the stratosphere, limiting the influence of this method of interhemispheric exchange.

TABLE I

Eruption	Date	Estimated stratospheric aerosol loading (Tg of SO_4)
Tambora (Indonesia)	April 1815	>100
Krakatoa (Indonesia)	August 1883	~ 50
Katmai (Alaska)	June 1912	20
Agung (Indonesia)	March 1963	16–30
Fuego (Guatemala)	October 1974	3–6
Stratospheric background?	1979	<1
El Chichón (Mexico)	April 1982	12
Pinatubo (Philippines)	June 1991	30
Cerro Hudson (Chile)	August 1991	3

Aerosol from tropical eruptions has the potential to spread globally in the stratosphere, as was the case with Mount Pinatubo (15°N). However, aerosols from many tropical eruptions, such as El Chichón (17°N) in 1982, have remained largely in their hemisphere of origin. In the next section, we examine how volcanic aerosol can affect the dynamics that determines its own distribution.

Observations of volcanic aerosol have taught us much about the meridional transport of air in the stratosphere. The eruptions of El Chichón in 1982, Nevado del Ruiz in 1985, and Pinatubo in 1991 each produced enhanced reservoirs of aerosol in the tropical stratosphere that persisted for several years. The transport of air out of the tropics to higher latitudes depends on the direction of zonal winds over the equator, which vary with altitude and time. Winds over the equator change direction between easterly and westerly with a periodicity that varies about a 28-month average. This variation, known as the quasi-biennial oscillation (QBO), dominates the circulation of the lower stratosphere. In periods when easterly winds lie over the equator, wind shear inhibits transport out of the tropics to the winter hemisphere, where westerly winds circulate through the extratropics. Poleward mixing occurs more rapidly during westerly phases of the QBO, when wind shear is weaker.

For example, easterly winds prevailed at altitudes above 23 km in the tropics for 6 months following the Mount Pinatubo eruption. The initial dispersion of aerosol in the stratosphere toward the higher latitudes therefore occurred at altitudes below 23 km. This aerosol produced the first spectacular sunsets seen in northern midlatitudes due to the eruption. Above 23 km, a tropical reservoir formed, with sharp boundaries near 20°N and 20°S. Progression of the QBO allowed much of this tropical reservoir to disperse in 1992, after which stratospheric aerosol mass decreased for several years with a lifetime of about 1 year.

VII. VOLCANIC EFFECTS ON STRATOSPHERIC DYNAMICS

The input of volcanic aerosol may affect atmospheric dynamics, and thereby determine its own distribution throughout the stratosphere. By absorbing infrared en-

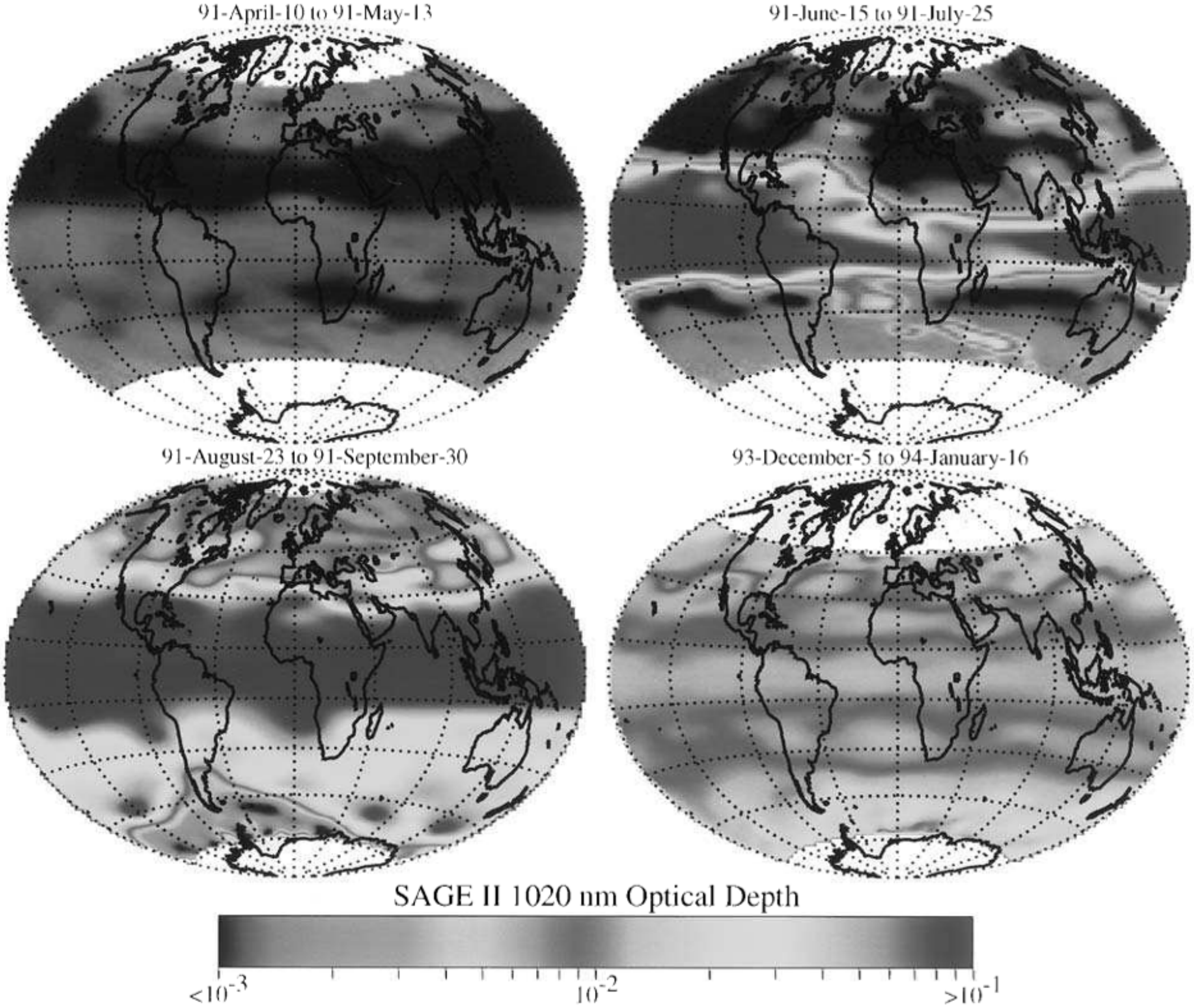
91-April-10 to 91-May-13
91-June-15 to 91-July-25
91-August-23 to 91-September-30
93-December-5 to 94-January-16
SAGE II 1020 nm Optical Depth
<10^-3
10^-2
>10^-1

FIGURE 2 The stratospheric aerosol and gas experiment (SAGE) II was one of several satellite-borne instruments to monitor the distribution of stratospheric aerosol following the June 1991 eruption of Mount Pinatubo. Initially confined to the tropics, Pinatubo aerosol increased the 1-μm optical depth by two orders of magnitude. Over 6 months, the aerosol spread to higher latitudes, as evident in the one order of magnitude increase in optical depth globally. The stratospheric aerosol layer continued to be dominated by steadily decreasing volcanic aerosol for 3 years. [Reprinted by permission from *Nature* (McCormick *et al.,* 1995), copyright 1995 Macmillan Magazines Ltd.]

ergy rising from the Earth's surface as well as sunlight at near-infrared wavelengths, aerosol can heat the atmosphere and alter both vertical and meridional winds. The extent of this affect appears to depend on the mass of volcanic input.

For example, while aerosol from the 1982 eruption of El Chichón (17°N) and other subtropical eruptions remained largely in its hemisphere of origin, that from the 1991 eruption of Mount Pinatubo (15°N) spread within several weeks to a latitude band covering nearly all of the tropics. Numerical simulations of atmospheric transport point to local heating, rather than planetary-scale transport patterns, as the cause of the unusual southward movement of Pinatubo aerosol.

In the lower tropical stratosphere, temperatures increased by about 3.5°C within 4 months of the Pinatubo eruption, putting them more than three standard deviations above the mean. The warm air rose more vigorously than usual, lifting aerosol to altitudes above 35 km within 5 months of the eruption. The increased vertical motion had strong consequences for the Earth's ozone layer.

Ozone and atomic oxygen make up the "odd oxygen" family of atmospheric species. The two species interchange rapidly with one another by numerous chemical reactions. Reactions that produce or destroy total odd oxygen, however, are much slower. The lifetime of odd oxygen varies sharply with altitude in the stratosphere. While odd oxygen is produced and destroyed within several hours at 60 km, it survives for weeks at 35 km, and for several years at 20 km. Because transport in the stratosphere generally takes weeks to months to move air over planetary distance scales, we say that odd oxygen (hence, ozone) concentrations are dynamically controlled in the lower stratosphere, and chemically controlled in the upper stratosphere.

Changing the atmospheric dynamics in a region where ozone is dynamically controlled will result in a changed distribution of ozone. When volcanic aerosol heats and lofts tropical air, ozone has less chance to accumulate in the tropical lower stratosphere before being pushed up and out to higher latitudes. In the first several months following the eruption of Pinatubo, total column ozone over the equator was observed to decrease by 6–8%. This effect is substantially greater than ozone depletion in the tropics caused by anthropogenic compounds. Tropical ozone loss is of some concern because the Sun can be directly over head at these latitudes and is less attenuated by the atmosphere than at higher latitudes. However, this natural dynamical perturbation lasted less than a year in the case of Pinatubo, making it less worrisome than long-term ozone depletion observed at midlatitudes.

VIII. RADIATIVE AND CLIMATE EFFECTS

History has shown us that volcanic eruptions are associated with colder-than-normal temperatures at the Earth's surface. However, it turns out that volcanic aerosol affects the Earth's radiation budget in a variety of ways, some of which involve heating.

In the Earth's radiation budget, incoming radiation from the Sun must be balanced by outgoing radiation. The Sun's rays cover a broad spectrum of wavelengths, which penetrate the atmosphere to varying depths. Much of the high-energy radiation is absorbed by atmospheric species high in the atmosphere. Ozone efficiently absorbs ultraviolet rays in the stratosphere, allowing life intolerant of its effects to exist below. Much of the remaining radiation is absorbed at the surface. Radiation absorbed by matter heats it, causing the matter itself to radiate to maintain balance. The Sun heats the Earth to temperatures that cause it to radiate in the infrared, wavelengths shorter than visible light. On its way out to space, some of this infrared radiation is itself absorbed by greenhouse gases and particles in the atmosphere, increasing atmospheric temperatures substantially.

Some of the sun's incoming radiation is not absorbed, but reflects off the Earth's surface, or scatters off of particles in the atmosphere, and returns to space (Figure 1). Increases in the planetary albedo decrease the amount of radiation absorbed, decreasing the Earth's temperature. The scattering efficiency of a single particle varies as a complex function of particle radius and wavelength. Generally, for a given mass of aerosol, a large number of small particles provide greater optical depth than a small number of large particles. The albedo of an aerosol layer also depends on its optical depth. The radiative response to volcanic input therefore depends on the increased optical depth due to increased aerosol mass and the change of optical depth with scattering efficiency due to increased aerosol radius.

The satellite-borne Earth Radiation Budget Experiment (ERBE) made the first unambiguous, direct measurements of large-scale volcanic forcing following the June 1991 eruption of Mount Pinatubo. These measurements determined the albedo between 30°N and 30°S in August 1991 to be more than five standard deviations above the 5-year mean for that region in August, with similar increases in July and September 1991. The increased optical depth (Figure 2) which accompanied more than an order of magnitude increase in aerosol mass was the predominant factor, termed the "direct effect" of volcanic aerosol. Pinatubo's eruption had the greatest relative effect on albedo over regions of the Earth usually free of clouds.

ERBE also measured increased albedo in regions frequented by high-albedo deep convective clouds. This albedo increase may have been due to an indirect effect of volcanic aerosol. Aerosol may indirectly change the optical properties of clouds. In this case, an eruption dramatically increases the number of particles in the atmosphere available to act as nuclei for cloud particles. The same amount of water distributed over a larger number of particles means the average particle will be smaller. Smaller cloud particles scatter visible radiation more efficiently, increasing albedo.

A. Stratospheric Warming

As we noted in our discussion of volcanic effects on atmospheric dynamics, aerosol absorbs the Earth's infrared radiation, thereby heating the tropical stratosphere.

(Because the Earth is colder at high latitudes, it provides less infrared radiation to heat the stratospheric aerosol layer there.) Significant temperature anomalies in the lower tropical stratosphere were observed within two seasons of the eruptions of Agung (Bali, 8°S) in March 1963, El Chichón, and Pinatubo. Adjusting for the temperature cycle associated with the QBO, researchers have shown that each of these eruptions raised lower stratospheric temperatures by nearly 2°C in the tropics, with lesser or no effects at higher latitudes. These anomalies are three to four standard deviations above the mean of the 13 QBO cycles between 1958 and 1996 that do not include these eruptions. The warming events lasted up to 2 years following these eruptions, and extended at least as high as 30 km in the case of El Chichón. Although Pinatubo is believed to have injected considerably more SO_2 into the stratosphere than the other two eruptions studied, Agung was found to have raised stratospheric temperatures by approximately the same degree. Possibly this near equality is due to the wider distribution of the Pinatubo debris, which diluted its input. The Agung and El Chichón clouds were primarily concentrated in one hemisphere.

By the end of 1993, stratospheric temperatures had moved from higher than average to new lows. This cooling is likely the result of an observed decrease in stratospheric ozone following the eruption of Pinatubo. Ozone heats the stratosphere, and is responsible for the increasing temperature profile there. In the section on stratospheric chemistry, we discuss how volcanic aerosol amplifies the depletion of ozone by anthropogenic chlorine.

B. Tropospheric Cooling

Whether the net effect of aerosol absorption and reflection is to cool or to heat the Earth depends on particle size. For the warming effect to overcome the cooling effect, particles must be larger than about 2 μm in radius. The Pinatubo eruption is estimated to have caused the mass-averaged aerosol radius to increase from 0.3 μm to about 1 μm, resulting in a net cooling of the Earth. Particles of radius greater than 2 μm fall at rates of more than 30 km per year in the lower stratosphere, ensuring their removal within months. Thus, sedimentation limits the size of stratospheric aerosol, making it unlikely that volcanic aerosol could be large enough to warm the Earth for significant periods.

Recent major volcanic eruptions have clearly produced significant cooling anomalies in the troposphere for 1 to 3 years. The magnitude of volcanic effects can be masked by natural variations in temperature and the global warming trend seen in the last several decades. Just as stratospheric temperatures are driven by the quasi-biennial oscillation in high-altitude tropical winds, so the average annual temperatures we experience in the troposphere are strongly correlated to the El Niño-Southern Oscillation (ENSO) in sea surface temperatures in the eastern equatorial Pacific. Removal of the ENSO-driven variability clarifies the influence of major volcanic eruptions.

Examination of global average temperature data from 1958 to 1992 shows the two greatest departures from the mean temperature for this period occurred in 1964 and 1992, the years immediately following the eruptions of Agung and Pinatubo. Both of these eruptions cooled the troposphere by about 0.4°C, compared to the average temperature for the phase of ENSO in these years. That the ENSO-adjusted temperature anomalies are similar is surprising, given that Agung is believed to have injected significantly less SO_2 into the stratosphere than Pinatubo. However, Agung's cloud was primarily limited to the southern hemisphere. Also, Pinatubo erupted in an atmosphere containing more greenhouse gases, and followed 6 years of above-average temperatures. As perhaps the largest eruption of the 20th century, Pinatubo more then offset the climate forcing of all greenhouse gases added to the atmosphere since preindustrial times, at least for a short time. While a background of rising temperatures made 1992 was the 8th warmest year since 1951, Pinatubo made it the 2nd coolest since 1987.

There exists significant evidence for global tropospheric cooling following many other major volcanic eruptions, with the greatest data and study associated with those of recent decades. The 1982 eruption of El Chichón also produced a cooling which lasted 2 or 3 years, and which becomes evident only when the warming influence of the very strong 1982–1983 El Niño is taken into consideration. The great eruptions of the 19th century, Krakatoa and Tambora, present greater uncertainties in global surface temperatures and in the influence of ENSO. Estimates from northern hemisphere temperature data suggest that Krakatoa may have cooled the atmosphere by about 0.3°C and Tambora by 0.4 to 0.7°C.

Larger eruptions do not necessarily produce greater or more protracted temperature anomalies. Microphysical calculations show that greater input of volcanic SO_2 results in larger particles, rather than greater numbers. In addition to falling out of the stratosphere faster, larger particles have a smaller optical depth per unit mass than smaller particles. These properties moderate the radiative and climate influences of volcanoes, and may limit them as the size of a volcanic eruption increases.

IX. EFFECTS ON STRATOSPHERIC CHEMISTRY

As we have discussed, volcanic clouds can contain large volumes of HCl and some HBr, which rain out before they enter the stratosphere. Observations following the eruption of Pinatubo confirmed that HCl did not increase significantly from pre-eruption levels. Stratospheric chlorine is derived from anthropogenic chlorofluorocarbons (CFCs) and methyl chloroform (which has natural sources), rather than volcanic eruptions. Stratospheric bromine comes from anthropogenic halocarbons and methyl bromide, not volcanoes. Volcanic aerosol, however, does alter stratospheric chemistry in such a way that it activates chlorine and bromine for ozone depletion. It does so by means of reactions on surfaces, whose importance to atmospheric chemistry was not appreciated until the report of a rather alarming development in 1985.

A. The Antarctic Ozone Hole

Since the mid-1970s, scientists have understood that CFCs, used for a variety of purposes since the 1930s, could break down in the stratosphere, releasing chlorine which was predicted to deplete ozone in the upper stratosphere by a few percent by the middle of the 21st century. In 1985, the British Antarctic Survey astounded the world by reporting the development of a seasonal ozone hole over Antarctica in the lower stratosphere each spring. The observed depletion was much lower in altitude and far greater in magnitude than the predicted depletion. In fact, in the region where ozone normally reaches peak concentrations, springtime observations now showed ozone to be almost completely depleted. In the lower stratosphere, chlorine and bromine are partitioned in favor of inactive chemical forms that should not participate in catalytic destruction of ozone. The explanation for the development of the Antarctic ozone hole each spring focused attention on chemical reactions which occur on atmospheric particles.

While much of stratospheric chemistry focuses on reactions that occur in the gas phase, heterogeneous chemistry also occurs between atmospheric gases and liquid or solid aerosols. The rates of most heterogeneous reactions increase strongly as these aerosols become more dilute, at low temperatures. Thus heterogeneous reactions often go faster at colder temperatures. The Antarctic stratosphere is cold enough to encourage heterogeneous reactions, which directly repartition chlorine and bromine from inactive reservoirs (HCl, $ClONO_2$, HBr, and $BrONO_2$) to active forms (Cl_2 and BrCl). Cl_2 and BrCl break down into highly reactive Cl and Br, which participate in numerous catalytic cycles that destroy ozone. Direct observations of ClO, a product and participant in such cycles, have confirmed that anthropogenic chlorine and bromine are responsible for the ozone hole.

As winter approaches and temperatures decrease in the polar stratosphere, sulfate aerosol becomes very dilute, taking up not only water but also significant quantities of nitric acid (HNO_3). This process results in severe losses of gas-phase reactive nitrogen species, such as NO_2 and N_2O_5, which produce nitric acid. The resulting $H_2O/HNO_3/H_2SO_4$ liquid ternary solution aerosols constitute a type of polar stratospheric clouds (PSCs). Some of these may freeze or otherwise solidify to form PSCs composed of solid particles. As PSC aerosol grows large, it can fall out of the stratosphere, bringing the condensed nitric acid with it. This results in irreversible denitrification of the polar stratospheric vortex. Denitrification greatly reduces the formation of the inactive reservoirs of $ClONO_2$ and $BrONO_2$ from active chlorine and bromine species.

Heterogeneous reactions proceed at rates proportional to the surface area of aerosol present in the polar stratosphere. At the low temperatures of polar winter, these reactions occur quite rapidly on liquid or solid aerosol. Ozone loss does not begin until the spring, however, with the return of the sunlight necessary for ozone photochemistry.

Model studies have shown that variations in observed stratospheric aerosol due to volcanic eruptions over the 1975–1994 history have modulated the severity of the Antarctic ozone hole. Following the eruptions of El Chichón and Pinatubo, springtime Antarctic ozone declined relative to pre-eruption levels by about 15 to 20%, respectively, before recovering somewhat as aerosol declined for several years. Model chemistry shows that interannual variations in the magnitude of the ozone hole result from volcanic perturbations to stratospheric aerosol, while longer-term declines are related to increasing stratospheric chlorine over the period examined. Thus, while stratospheric chlorine and bromine are expected to decline over the 21st centrury due to international treaties regulating CFCs and halocarbons, their ozone-depleting effects may be greatly magnified over this period by volcanic eruptions. As we shall see, this concern is not limited to the relatively unpopulated polar regions.

B. Midlatitude Ozone Depletion

Many of the reactions responsible for directly converting chlorine and bromine reservoir species into active forms do not occur at significant rates in the warmer middle latitudes. Heterogeneous hydrolysis of bromine nitrate is an exception, and remains fast. In addition, heterogeneous hydrolysis of nitrogen pentoxide (N_2O_5), which forms nitric acid, occurs on sulfate aerosol independent of temperature. This reaction has important implications for the partitioning of chlorine and bromine in the lower stratosphere. N_2O_5 forms in the atmosphere only at night, and interchanges with short-lived NO_2 on a timescale of several days. At midlatitudes, nitric acid has an atmospheric lifetime of several weeks. Heterogeneous hydration of N_2O_5 therefore moves nitrogen from a moderately active species to a long-lived reservoir, reducing nitrogen available to form NO_2. Decreased NO_2 concentrations decrease formation of the $ClONO_2$ and $BrONO_2$ reservoirs from active chlorine and bromine. Thus heterogeneous chemistry pushes the partitioning of chlorine and bromine toward active, ozone-depleting forms.

As with the Antarctic ozone hole, northern middle latitudes experienced interannual ozone variations between 1979 and 1994, which model calculations have linked to volcanic influences on stratospheric aerosol. Following the eruptions of El Chichón and Pinatubo, respectively, observed ozone at 45–55°N fell by 2 and 4% before recovering somewhat. The model showed that, in addition to causing these losses lasting 2–3 years, volcanic aerosol, evident as increases in surface area relative to 1979, suppressed ozone throughout the entire period studied. The primary mechanism by which aerosol modulates midlatitude ozone loss in the model is suppression of NO_2 and related species. However, observed variations in ozone were 50% greater than those modeled, leaving room for the involvement of additional chemistry, not currently understood, in aerosol modulation.

C. Global Ozone Loss from Mount Pinatubo

The effects of the Mount Pinatubo eruption on global ozone are powerfully illustrated in Figure 3. This figure contrasts the global mean ozone measured in the period from 1992 through 1994 to the full range of observations from 1979 to 1990. Six months after the eruption, column ozone had fallen to the low range of the normal annual cycle. By mid-1992, the global mean was well below previous minima, and on a downward trend that continued well into 1993. As previously mentioned, ozone loss observed over the equator in the months following the eruption resulted primarily from dynamical uplifting, not heterogeneous chemistry. This tropical ozone loss did not last beyond mid-1992, while global losses persisted a year and a half longer. Midlatitude ozone loss was most severe in the northern hemisphere. Over the United States, record low ozone values were set between January and April of 1993. Globally, ozone levels began to recover in the second half of 1993, although, as Figure 3 shows, they persisted at record lows throughout 1994. Observations of highly perturbed concentrations of NO_2 and nitric acid, correlated with enhanced aerosol, confirm the importance of heterogeneous chemistry in this prolonged ozone loss.

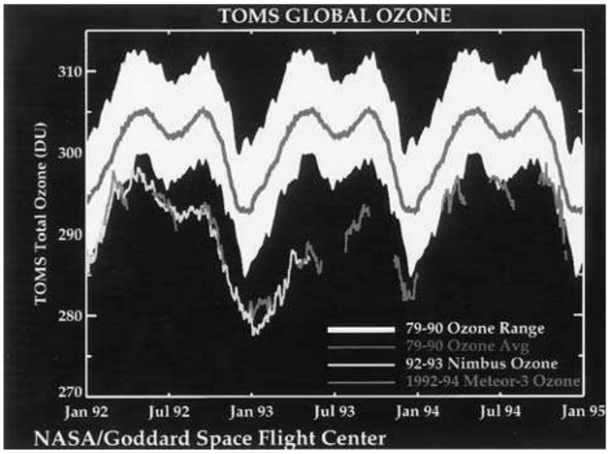

FIGURE 3 Global mean ozone in Dobson units (DU) from the total ozone mapping spectrometer (TOMS) carried aboard the NIMBUS 7 and METEOR 3 satellites. Measurements from the 1992–1994 post-Pinatubo period (in thinnest and medium lines) are compared to the range of measurements from 1979 to 1990 (in white, repeated for three annual cycles). The thick line shows the average total ozone for this period. Global ozone remained at record lows throughout the 1992–1994 period due to increased heterogeneous activation of anthropogenic chlorine on aerosol. In the tropics, ozone loss resulted mainly from dynamical uplifting that resulted from aerosol heating. Tropical ozone loss, measured by TOMS, did not last beyond mid-1992. [Reprinted by permission from *Nature* (McCormick *et al.,* 1995), copyright 1995 Macmillan Magazines Ltd.]

X. LESSONS FOR THE FUTURE

The timing of the eruption of Mount Pinatubo provided a demonstration of the combined atmospheric effects of volcanic aerosol and anthropogenic perturbations. For ozone, the presence of volcanic aerosol accelerates the destructive effects of anthropogenic halogens. At the same time, the radiative effects of volcanic aerosol can act to offset global warming from anthropogenic greenhouse gases.

The volcanic risk to global ozone will remain high as long as stratospheric halogens remain significantly elevated from preindustrial levels. Current international treaties banning chlorinated and brominated source gases should reduce stratospheric halogen concentrations to natural levels toward the end of the 21st century. In the absence of anthropogenic halogens, volcanic eruptions are not expected to chemically reduce ozone, although their dynamical effects may result in short-term, localized losses such as that seen in the tropics following the Pinatubo eruption.

While the atmospheric cooling that follows volcanic eruptions may seem a relief from projected increases in global temperature, the social disruptions they have been known to have caused throughout human history serve as a grim warning of the dangers of even small changes in global mean temperature. If famine and disease resulted from just a few years of abnormally cold temperatures, the consequences of longer-term climate changes could be dire.

By tracking the changes caused by volcanic perturbations to the natural laboratory of the Earth's atmosphere, scientists have been able to study the dynamical and chemical processes around us that affect our lives. What they have learned may help predict future consequences of global change due to both natural and anthropogenic distrubances. The study of the atmospheric effects of volcanoes better prepares us for not only future volcanic eruptions, but also aerosol generated by everything from stratospheric aricraft to impacting comets and nuclear war. Our better understanding can tell us which patterns of human behavior are destructive to the well-being of life on Earth, and allow us the choice of changing such patterns before it is too late.

SEE ALSO THE FOLLOWING ARTICLES

Geothermal Systems • Volcanic Contributions to the Carbon and Sulfur Geochemical Cycles and Global Change

FURTHER READING

Angell, J. K. (1990). Variation in global tropospheric temperature after adjustment for the El Nino influence. *Geophys. Res. Lett.* **17**(8), 1093–1096.

Hamill, P., Jensen, E. J., Russell, P. B., and Bauman, J. J. (1997). The life cycle of stratospheric aerosol properties. *Bull. Am. Meteorol. Soc.* **78**(7), 1–16.

McCormick, M. P., Thomason, L. W., and Trepte, C. R. (1995). Atmospheric effects of the Mt. Pinatubo eruption. *Nature* **373,** 399–404.

Pang, K. D. (1991). The legacies of eruption: Matching traces of ancient volcanism with chronicles of cold and famine. *Sciences* **31**(1), 30–33.

Portmann, R. W., Solomon, S., Garcia, R. R., Thomason, L. W., Poole, L. R., and McCormick, M. P. (1996). Role of aerosol variations in anthropogenic ozone depletion in the polar regions. *J. Geophys. Res.* **101**(D17), 22991–23006.

Rampino, M. R., Stephen, S., and Stothers, R. B. (1988). Volcanic winters. *Annu. Rev. Earth Planet. Sci.* **16**(41), 1–516.

Solomon, S. (1990). Progress towards a quantitative understanding of Antarctic ozone depletion. *Nature* **347,** 347–354.

Solomon, S., Portmann, R. W., Garcia, R. R., Thomason, L. W., Poole, L. R., and McCormick, M. P. (1996). The role of aerosol trends and variability in anthropogenic ozone depletion at northern mid-latitudes. *J. Geophys. Res.* **101,** 6713–6727.

Stommel, H., and Stommel, E. (1983). "Volcano Weather: The Story of 1816, the Year without a Summer." Seven Seas Press, Newport.

Toon, O. B., and Pollack, J. B. (1982). *In* "The Stratospheric Aerosol Layer" (R. C. Whitten, ed.). Springer-Verlag, New York.

This Page Intentionally Left Blank

HAZARDS FROM PYROCLASTIC FLOWS AND SURGES

SETSUYA NAKADA
University of Tokyo

I. Introduction
II. Physical Properties of Pyroclastic Flows and Surges
III. Volcanic Disasters Involving Pyroclastic Flows and Surges
IV. Stories of the 3 June 1991 Event at Unzen
V. Mitigation of Pyroclastic Flow and Surge Hazards

GLOSSARY

base surge This is usually formed when an eruption starts in a lake or coastal environment and is due to the explosive interaction of hot magma with water. Water-surface-hugging ash clouds move outward from the base of an eruption column. In the 1965 eruption at Taal volcano, Philippines, base surges traveled more than 4 km over the water surface of the lake in which the eruption center was located and impacted on lakeside villages, killing 189 people.

DRE Dense rock equivalent, this refers to the volume or mass that erupted material would have if it were dense (unvesiculated) rather than vesiculated.

hazard map A map used to illustrate geographic regions in terms of expected hazard.

lateral blast Is caused by the sudden decompression of highly pressurized magma by a volcano's flank or lava dome failure. At Mount St. Helens, on 8 May 1980, a northward-directed lateral blast of rock, ash, and hot gases occurred some seconds after a debris avalanche was triggered by flank failure of the volcano. It began with an initial velocity probably exceeding supersonic speeds and rapidly overtook the avalanche and traveled up to 25 km, devastating an area of about 600 km^2 in a fan-shaped sector north of the volcano.

plinian eruption An eruption with a powerful, convecting column reaching up to 45 km high.

pyroclastic flow A flow of volcanic material ranging from vesiculated, low-density pumice to unvesiculated, dense lava and clasts which tends to follow topographic lows (i.e., valleys) as it moves.

pyroclastic surge A turbulent, low-density, high-velocity part of a pyroclastic flow. It is not so constrained by topography as a pyroclastic flow.

vulcanian eruption An explosive event of less than 1 km^3, but with an eruption column often reaching 10–20 km high.

MANY OF THE largest historical volcanic disasters have involved pyroclastic flows or surges (29,000 killed at Mount Pelée, Martinique, in 1902; 12,000 at Tambora, Indonesia, in 1815; and 6000 at Santa Maria, Guatemala, in 1902). Even relatively small-scale events can have devastating human consequences. Pyroclastic flows contain massive mixtures of hot lava blocks, ash, pumice, and volcanic gas descending the slopes of volcanoes at very high speeds. Pyroclastic and base surges are constituents of pyroclastic flows, which

Copyright © 2000 by Academic Press
All rights of reproduction in any form reserved.

are characteristically diluted, lacking a high concentration of particles and containing a lot of gases. Surges can be generated directly by column collapse and by separation from the moving, relatively dense main body of the pyroclastic flow. Surges rarely have sufficient force to destroy buildings in their path and are short-lived compared with pyroclastic flows because of their lower momentum and density. Surges often run over topographic barriers, however, and have therefore also been called "hot hurricanes" or "blasts."

I. INTRODUCTION

Pyroclastic flows can derive from gravitational collapse of Plinian eruption columns. In this case, the flows descend radially down the volcano's slopes. At Pinatubo, Philippines, on 15 June 1991, for example, more than 4 km^3 of ash and pumice moved radially down from the summit crater as several flows within a few hours. Column collapse and vulcanian explosions at Soufriere Hills volcano, Montserrat, in August 1997, also produced pyroclastic flows in multiple directions which traveled as far as 5 km from the vent.

Pyroclastic flows can also originate directly from the vent rather like a pot of rice boiling over. The 1980 explosive eruptions at Mount St. Helens produced pyroclastic flows of this type.

Lateral explosions directly from a summit dome or lava flow may produce small but explosive pyroclastic flows like those at Mount Pelée volcano, Martinique, in 1902, where the associated pyroclastic surges killed about 29,000 people, mainly in the city of St. Pierre. Finally, pyroclastic flows may also originate from gravitational collapse of lava domes or lava flows. These types of pyroclastic flows were frequently observed during the 1991–1995 eruption at Unzen, Japan (Figure 1), and in the 1995–1998 eruption at Soufriere Hills, Montserrat, West Indies. In both eruptions, several tens of people lost their lives as a direct consequence of being overwhelmed by pyroclastic flows and surges.

II. PHYSICAL PROPERTIES OF PYROCLASTIC FLOWS AND SURGES

A. Mobility

Driven by gravity, pyroclastic flows seek topographically low areas of the volcano and tend to be channeled into valleys. Large-scale pyroclastic flows associated with

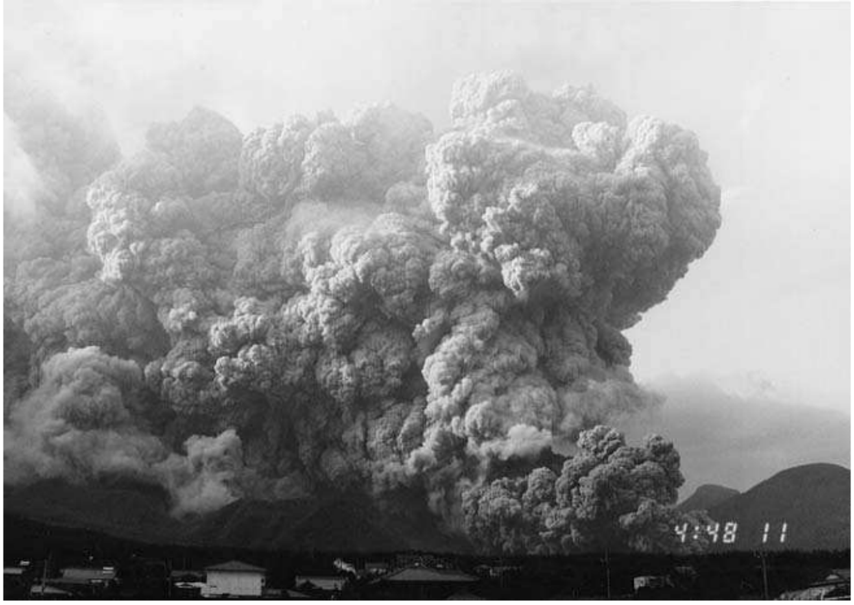

FIGURE 1 Ash cloud associated with the pyroclastic flows that descended the Oshigadani Valley at Unzen. The cloud grew vigorously from the valley mouth. (Taken by Kenji Ohkawa on 15 September 1991.)

caldera-forming ash flows can move distances of more than 100 km. The travel distance depends largely on the mass of pyroclastics thrown out from the source and the height at which pyroclastic flows start to descend (or collapse). The ratio of the height (*H*) dropped over the travel distance (*L*) is as small as 0.2–0.29 for large-scale pyroclastic flows and higher than 0.33–0.39 for small block-and-ash flows. This indicates that larger flows are more mobile than small flows. High-mobility pyroclastic flows may be fluidized by volcanic gases released from the interior of lava blocks and particles or by expansion of heated air trapped in the moving front. These gases may reduce friction between grains and the ground. It is not clear, however, that pyroclastic flows except for diluted pyroclastic surges have a significantly different emplacement mechanism from other flows such as debris avalanches. This is because the relationship between volume erupted and the *H*/*L* ratios, which is negative, is almost identical for pyroclastic flows and debris avalanches. Therefore, we can predict the travel distance from the starting point of pyroclastic flows, assuming a constant apparent friction (*H*/*L*) for the flow. The value of apparent friction can be estimated from field observations of pyroclastic flow deposits only when they did not result from column collapse. Measurements of *H* and *L* tend to produce underestimates of the actual values for column-collapse-type large and prehistoric pyroclastic flows, leading to low *H*/*L* ratios. It is very difficult to estimate the height of column collapse, even if the eruption can be observed.

Prehistoric large-scale pyroclastic flows sometimes traveled over the sea for distances of several tens of kilometers. This implies that at least the upper parts of the pyroclastic flow were less dense than water. Most pyroclastic flows are considered to consist of a clast-rich bottom portion (basal avalanche) and an overlying low-density cloud. Surges are relatively short-lived and the area impacted by them is limited around the source (vent or moving front of basal avalanche) to generally less than a few kilometers (Figure 2). However, although

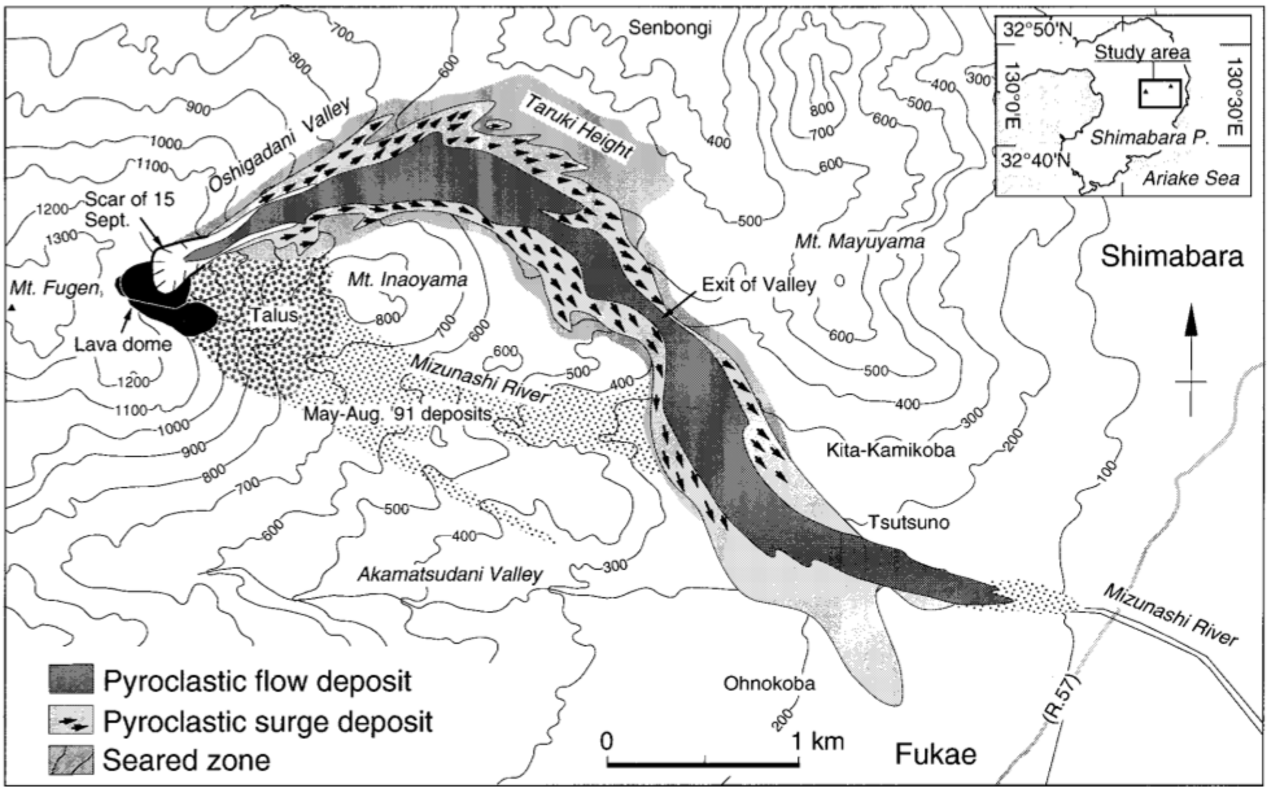
Senbongi
32°50'N
Study area
130°0'E
130°30'E
Shimabara P.
32°40'N
Ariake Sea
Oshigadani Valley
Taruki Height
Scar of 15 Sept.
Mt. Fugen
Lava dome
Talus
Mt. Inaoyama
Mt. Mayuyama
Exit of Valley
Shimabara
Mizunashi River
May-Aug. '91 deposits
Kita-Kamikoba
Tsutsuno
Akamatsudani Valley
Ohnokoba
Mizunashi River
(R.57)
Fukae
0
1 km
Pyroclastic flow deposit
Pyroclastic surge deposit
Seared zone
700
800
900
1000
1100
1200
1300
600
500
400
300
200
100

FIGURE 2 Map showing deposit distribution of the 15 September 1991 pyroclastic flow at Unzen and detachment of the pyroclastic (ash cloud) surges from the main stream (basal avalanche) of pyroclastic flows. Devastation by the surge in Kita-Kamikoba was such that a car was thrown about 120 m by the surge. In contrast, houses and an elementary school in the Ohnokoba District engulfed by the detached surges were burned but otherwise undamaged by the surges.

lateral blasts are also a short-lived diluted turbulent current, they may travel large distances (for example, at Mount St. Helens, the initial velocity was supersonic).

B. Speed

Pyroclastic flow and surge travel speeds are generally greater than 10 m s^{-1} and sometimes reach more than 100 m s^{-1}. Speeds of recent pyroclastic flows have been measured using video footage and precise observations based on seismic signals. The 1980 Mount St. Helens lateral blast traveled up to 150 m s^{-1}, with an internal velocity of 235 m s^{-1}. Pyroclastic flows of 7 August 1986 at Mount St. Helens had a maximum speed of 30 m s^{-1}, and at Soufriere Hills volcano, Montserrat, small flows had an average speed of 3–10 m s^{-1}, while flows which traveled further were in the range 15–30 m s^{-1}.

C. Temperature

Temperatures of pyroclastic flows may be estimated indirectly if carbonized wood or melted or deformed household materials can be found after a flow has passed. In the 1902 pyroclastic flows at Mount Pelée, glass materials were melted but gold coins were not; temperatures in the range of 100–1100°C have been suggested. However, melting can take place due to fires ignited by hot pyroclastic flows. The estimate of these temperatures is therefore ambiguous, as it is not clear whether they represent the condition of the ash cloud, ash particles drifting inside, or the deposit. Direct measurements of the temperature, pressure, and speed of pyroclastic flows can be made by placing devices in the expected path of a flow. On Montserrat, temperatures ranging from 99 to 250°C have been determined in this way. On Unzen volcano in 1992, maximum temperatures of over 660°C were found. The temperature of the ash cloud was as high as 350°C, and the pressure of the surge did not exceed 0.5 bar (a pressure of 0.1 bar corresponds to a moving pressure with strong wind of 125 m s^{-1}). The velocity of ash particles ranged from several tens of meters per second to 160 m s^{-1}. The moving front of pyroclastic flows at Unzen had a velocity of 6–50 m s^{-1}; however, since the surge moves turbulently, particle velocities are not necessarily the same as those of the whole flow.

III. VOLCANIC DISASTERS INVOLVING PYROCLASTIC FLOWS AND SURGES

A. Mount Pelée, Martinique

One of the most tragic volcanic disasters in the world took place at Mount Pelée, Martinique, West Indies, in May 1902. The city of St. Pierre, with a population of 28,000, was located only 7 km southwest of the volcano's summit. One month before the tragic event, phreatic eruptions began spewing ash and sulfurous gas. A large mudflow descended along the Riviere Blanche on 5 May, and during 7–8 May swept the mountain flanks, burying 23 people working at a sugar mill and 400 people in a coastal village. It is thought that explosions displaced the water of a summit lake into the head of the river. Then ash fell on the city of St. Pierre and birds fell dead onto the streets, suffocated by gases. Although many people wanted to leave the city, they were urged to stay in the city by the government because of an important forthcoming election.

A series of violent explosions took place on the morning of 8 May. A great black cloud of ash rose above the mountain top, and simultaneously another cloud shot southward from the crater. Pyroclastic flows descended along the Riviere Blanche and reached the coast, while pyroclastic surges spread south of the river (Figure 3) and engulfed the city within several minutes. Nearly every one of the 28,000 inhabitants was killed. The surge struck the city with tremendous force, such that 1-m-thick stone walls were knocked over and large trees toppled. Trees that remained standing were stripped of leaves and branches, and on many the bark was stripped away on the side toward the volcano. A few people survived the surges. One of them was a prisoner shut up in a well-sealed cell, and one was in a house located on the periphery of the surge cloud. Both were severely burned. The explosive eruptions were renewed on 20 May and 30 August 1902, and produced 1000 additional victims in two villages about 5 km southeast and 6 km northeast of the mountain.

B. Pinatubo, Philippines

Mount Pinatubo in the Philippines became active suddenly in 1991. This volcano had been quiet for more than 500 years and more than 30,000 people lived in small villages on the volcano's flanks, with a much larger population in surrounding cities. Felt earthquakes began

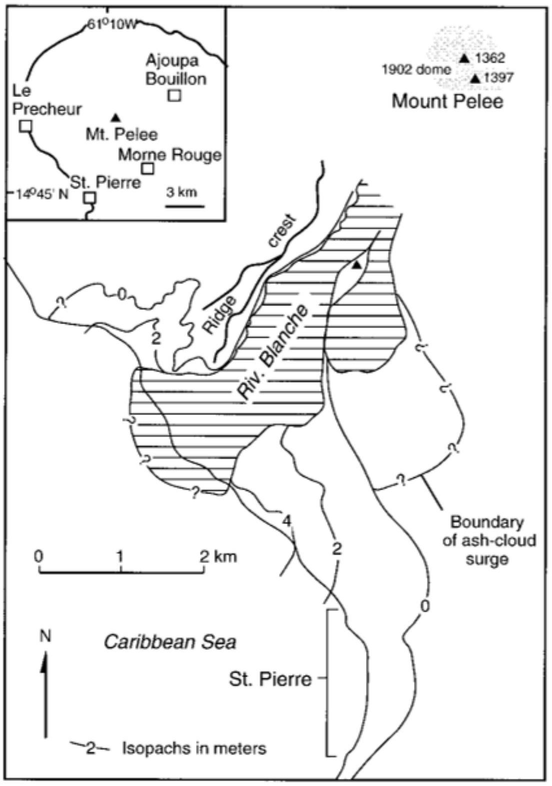

FIGURE 3 Distribution of block-and-ash flow deposits and the associated ash cloud surge deposits from the 8 and 20 May 1902 eruption of Mount Pelée, Martinique. The thickness of the surge deposits in most parts of St. Pierre was less than 1 m. [Simplified from Fisher and Heiken, 1982.]

3 months before the 15 June 1991 explosive eruption, and a phreatic eruption started a month before that. Release of seismic energy continued at a constant rate, while SO_2 emissions increased. A lava dome appeared within the summit crater on 7 June and continued to grow. A series of vertical eruptions and long-period earthquakes occurred between the morning of 12 June and the early afternoon of 14 June. In addition a number of pyroclastic surge-producing eruptions occurred, and seismic activity evolved toward the climactic explosion on 15 June. The climactic explosion continued for about 9 hours after 1:42 P. M. This eruption caused the summit of the volcano to collapse and resulted in the formation of a caldera 2.5 km across.

This Plinian eruption sent ash into the stratosphere and pumice fell over an area of 2000 km^2 with $>$10-cm-thick deposits. At the same time, voluminous pyroclastic flows were emplaced that extended 12–16 km from the vent down all sectors of the volcano and impacted an area of approximately 400 km^2, stripping vegetation and dramatically modifying the preexisting topography. Massive deposits filled valleys to depths of up to 200 m, and the estimated volume of the whole pyroclastic flow deposits was 4.2–4.5 km^3.

After identification of precursory phenomena, volcanologists hurried to study volcanic rocks around the volcano and drew up a risk map of the area. By 14 June, officials had ordered the evacuation of more than 80,000 people from their land and homes. The next morning, Mount Pinatubo produced a large eruption. However, less than 300 lost their lives as roofs collapsed under the weight of heavy wet ash.

C. Soufriere Hills, Montserrat

A lava-dome-forming eruption started in the Soufriere Hills volcano, Montserrat, West Indies, in December 1995, and continued until March 1998. As at Pinatubo, historic eruptions were not documented for this volcano, although the volcano contained old summit lava domes and pyroclastic flow deposits extensively distributed on the flanks. Partial collapse of the growing lava dome frequently generated pyroclastic flows together with vulcanian explosions during 1996–1998. At first, the dome grew inside the old English's crater and repeatedly collapsed to the east where the crater wall was lowest. The resultant pyroclastic flows descended eastward along the Tar River Valley and entered into the Caribbean Sea, making a delta of pyroclastics. As the lava dome size increased, it grew beyond the old crater rim and started to collapse northward in May 1997. The travel distance of pyroclastic flows extended in the northern flank day by day (Figure 4). A pyroclastic flow started from the lava dome at 12:55 P.M., 25 June 1997. In the following 20 minutes, a series of three devastating flows swept the northern flanks of the volcano, moving along Mosquito Ghaut and following the Paradise River close to the sea. The flows and associated surge clouds damaged or destroyed 100–150 houses, with villages being severely affected. Nineteen people died and another 9 were missing, presumed dead. An estimated 5 $\times 10^6$ m^3 of lava dome collapsed during the event, and the resulting flow and surge deposits covered 4 km^2.

A sequence of 13 vulcanian explosions occurred in early August 1997 with ash columns up to 15 km high. Column collapse resulted in the generation of radial pumiceous pyroclastic flows (Figure 5). Pyroclastic flows destroyed the capital city, Plymouth, located 4 km west of the summit, where all inhabitants had been evacuated.

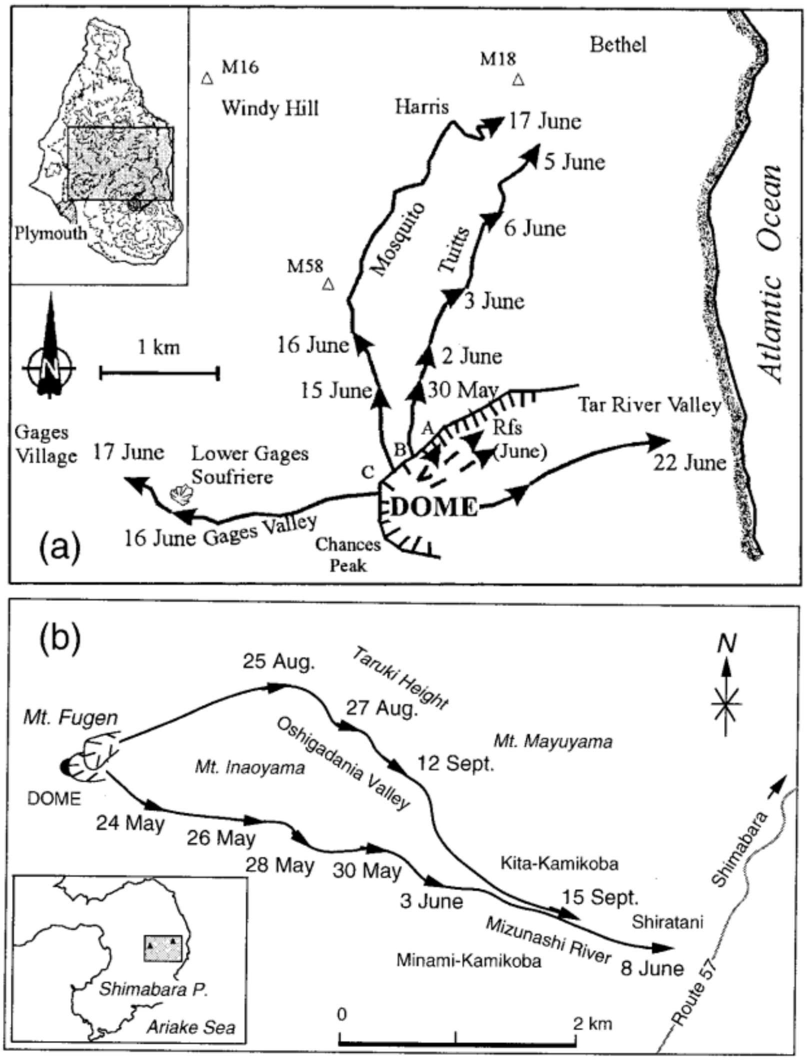
(a)
M16
Windy Hill
M18
Bethel
Harris
17 June
5 June
Mosquito
Tuitts
6 June
M58
3 June
Atlantic Ocean
Plymouth
1 km
N
16 June
2 June
15 June
30 May
Tar River Valley
A
Rfs
(June)
B
22 June
Gages Village
17 June
Lower Gages Soufriere
C
DOME
16 June Gages Valley
Chances Peak
(b)
25 Aug.
Taruki Height
N
27 Aug.
Mt. Fugen
Oshigadania Valley
Mt. Mayuyama
Mt. Inaoyama
12 Sept.
DOME
24 May
26 May
28 May
30 May
Kita-Kamikoba
Shimabara
3 June
15 Sept.
Shiratani
Mizunashi River
8 June
Minami-Kamikoba
Route 57
Shimabara P.
Ariake Sea
0
2 km

FIGURE 4 Time variations in travel distance of dome-collapse-type pyroclastic flows. (a) During May–June 1997 at Soufriere Hills volcano, Montserrat. [After (1997) *Bull. Global Volcanism Network* **22**(6), 2.] (b) During May–June and August–September 1991 at Unzen volcano, Japan.

On Boxing Day, 26 December 1997, the largest sector collapse (landslide), including the dome and crater walls, took place. The total volume of collapsed materials reach 6.4×10^7 m^3 DRE (dense rock equivalent). As a result, extensive volumes of debris avalanches and pyroclastic flows (and surges) swept the whole area of the southwestern flanks and reached the southern coast. Deposits rushing into the Caribbean Sea caused a small tsunami, 1 m high. Fortunately, there were no casualties.

Periods of elevated productivity of pyroclastic flows and sustained dome collapse events are linked to pulses of high magma extrusion rates.

D. Unzen, Japan

Unzen began erupting in November 1990, and a lava dome grew between May 1991 and February 1995. Partial collapse of the dome generated frequent pyroclastic flows, and a total of 9500 pyroclastic-flow events were counted from seismographs. The active center of this eruption was 7 km from the center of Shimabara City. On the afternoon of 3 June 1991, pyroclastic flows reached the Kita-Kamikoba area, and the associated ash cloud surge swept 43 people away in the evacuated zone (Figure 6). The victims included volcanologists and

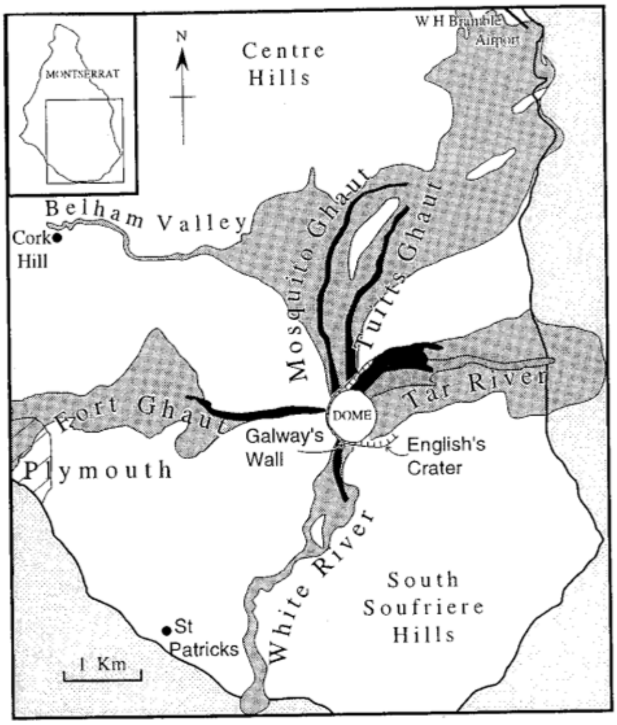

FIGURE 5 Map showing the distribution and extent of pyroclastic flows deposits during 1996–1997 eruption at Soufriere Hills volcano, Montserrat, West Indies. [Cole *et al.*, 1998.] The distributions expanded from the solid areas to the gray areas in each river.

journalists waiting to take images of descending pyroclastic flows.

The largest pyroclastic flow in this eruption occurred on the evening of 15 September 1991. This event consisted of a relatively large failure of the lava dome and underlying older rocks (total volume 4×10^6 m^3). As a result, four pyroclastic flows cascaded down the Oshigadani Valley, the largest one reaching the Mizunashi River after passing through a narrow gorge in the valley (Figure 2). The main pyroclastic flow followed the topographically lowest areas. In contrast, the surge moved separately and went directly from the exit of the Oshigadani Valley for 0.9 km into the Ohnokoba District (Figure 2). The surge climbed 10 m up the southern bank of the Akamatsudani River. In Kita-Kamikoba, most trees were swept away by the surge and a car was thrown 120 m. Contrasting with the devastation in Kita-Kamikoba, trees in the Ohnokoba District impacted only by the surges were not toppled, although most houses engulfed by the surge were burned. This indicates that the surge had lost much of its force by the time it reached Ohnokoba, although it kept its high temperature.

When the lava effusion rate was high, frequent pyroclastic flow events were observed. The major pyroclastic flow events, including the 15 September 1991 flows, occurred during periods with high lava effusion rates.

IV. STORIES OF THE 3 JUNE 1991 EVENT AT UNZEN

When a man and his wife opened their front door a few minutes after the surge arrived at their house, a mass of hot ash rushed inside. They closed the door immediately, but breathed in some ash-laden air. Fortunately, this did not affect them significantly. A minute later, they decided to go outside and opened the door, and no more ash-laden air entered the house. Houses nearby were burning fiercely as the couple fled. Their house later also caught fire.

Another person opened his door soon after the surge hit his house. A hot mass of black smoke (ash) avalanched into the house. He suffered burns on his arms where he had no sleeves. Then glass in upstairs windows was broken and a mass of ash invaded the house. The hot ash caused burns to his stomach. Houses nearby were burning as he fled. He left the house without shoes, and felt intense heat as he stepped on the ash deposits. His house was still burning the next morning.

A man took refuge in a car as he was engulfed by the surge. He saw that small pebbles hit the windscreen, crackling and glowing in the darkness and he felt intense heat in the darkness. He suffered some burns on his neck and back and it was later found that the surges had melted the vinyl cover of the car seat.

French photographers Katia and Maurice Krafft and the American volcanologist Harry Glicken were engulfed by a pyroclastic surge during the 3 June 1991 event. A series of pyroclastic flows started at 16:08 (JST). They stood together with more than 10 Japanese journalists, facing the summit at a place called Teiten ("fixed point") within the evacuated zone (Figure 6). Although the summit area was covered with rain clouds, they were waiting for pyroclastic flows that were large and vigorous enough to film and photograph. The travel distance of pyroclastic flows extended day by day (Figure 4). Teiten was only 40 m higher than the river bottom, and the river curved to the south at that point. Teiten was engulfed by

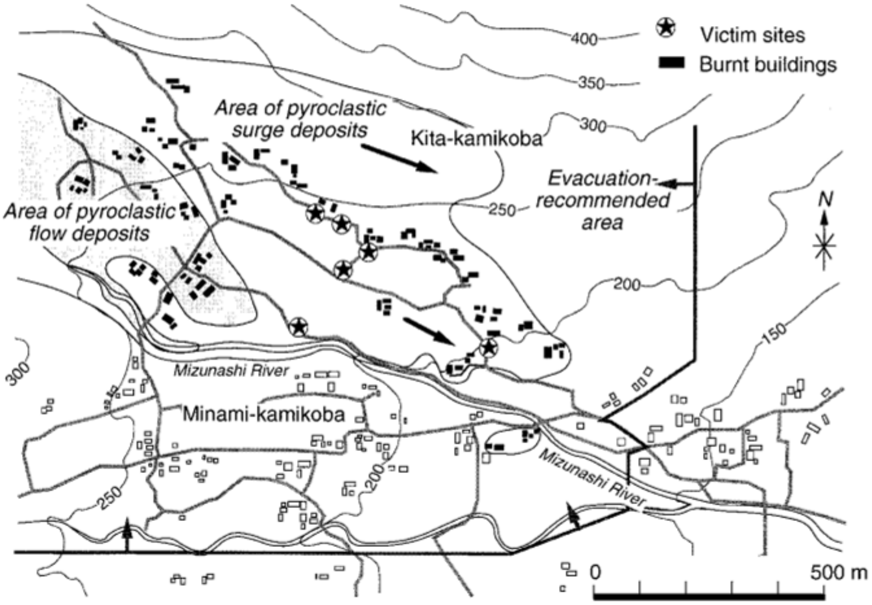
Victim sites
Burnt buildings
400
350
300
250
200
150
Area of pyroclastic surge deposits
Kita-kamikoba
Evacuation-recommended area
N
Area of pyroclastic flow deposits
Mizunashi River
Minami-kamikoba
300
250
200
Mizunashi River
0
500 m

FIGURE 6 Map showing disaster area of a pyroclastic flow event at Unzen on 3 June 1991. Ash cloud surges associated with pyroclastic flows that stopped moving within the upper stream of the Mizunashi River swept higher parts in Kita-Kamikoba District (Teiten), where three volcanologists and journalists were engulfed in an instant. Arrows within the surge deposit area represent the direction of movement, which can be estimated from fallen trees. [Modified from the data by Shimabara Earthquake and Volcano Observatory, Kyushu University, and Prof. Kazuya Ohta.]

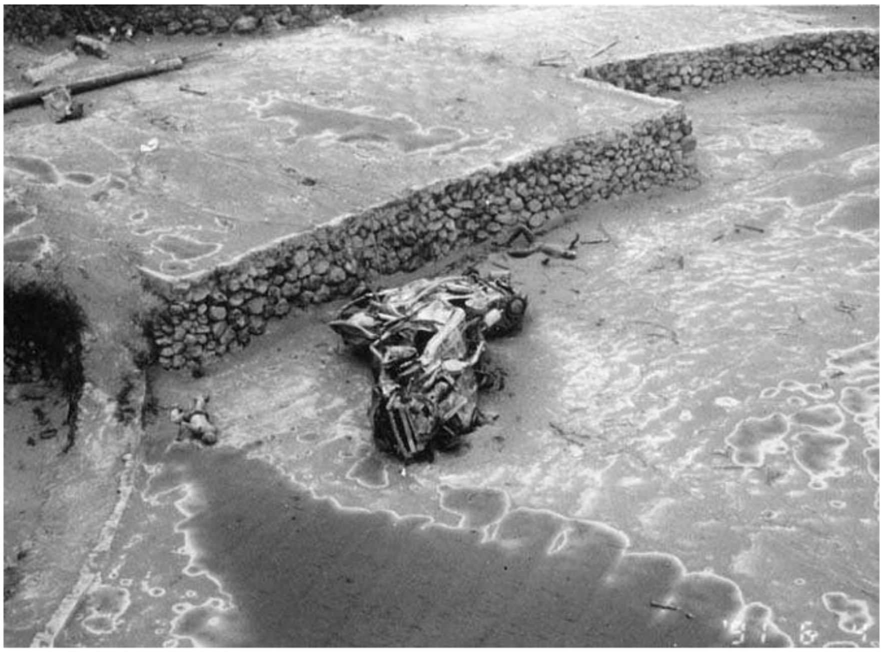

FIGURE 7 Crumpled cars and victims of ash cloud surge at Unzen volcano on 3 June 1991. They were thrown about 80 m from their original position. [Courtesy of Genji Maruta.]

a surge but not by the main stream of pyroclastic flows at 16:10. Trees and electric poles were toppled down and all wooden houses were knocked down. Cars together with dead bodies were also thrown as far as 80 m from Teiten, and landed in a tobacco field (Figure 7). A taxi was caught on a road, but inside, the completely carbonized bodies of journalists and a driver were found. They presumably rushed inside the car to take a refuge from the oncoming surge.

Dentists from the Dental Association of Minami Takaki District (Shimabara) examined the cause of death of the casualties. The bodies were described as showing rigor mortis and looking like sooty mannequins. Most of the clothes and hair were burned away. Hands were set close to the face, suggesting that victims lay with their faces on the ground trying to escape the effects of the hot ash. They probably lost their lives due to dyspnea in hot ash. The tongues were hypertrophic and stuck out of the mouths. Ash and pebbles filled their mouths. Both mucous membranes and gums were decomposed.

Causes of death in pyroclastic flows and surges are believed to be mainly asphyxiation and thermal distress, except for victims who are first burned by the deposits. A further example comes from the A.D. 79 eruption of Vesuvius. Pompeii, an ancient city on the southeastern

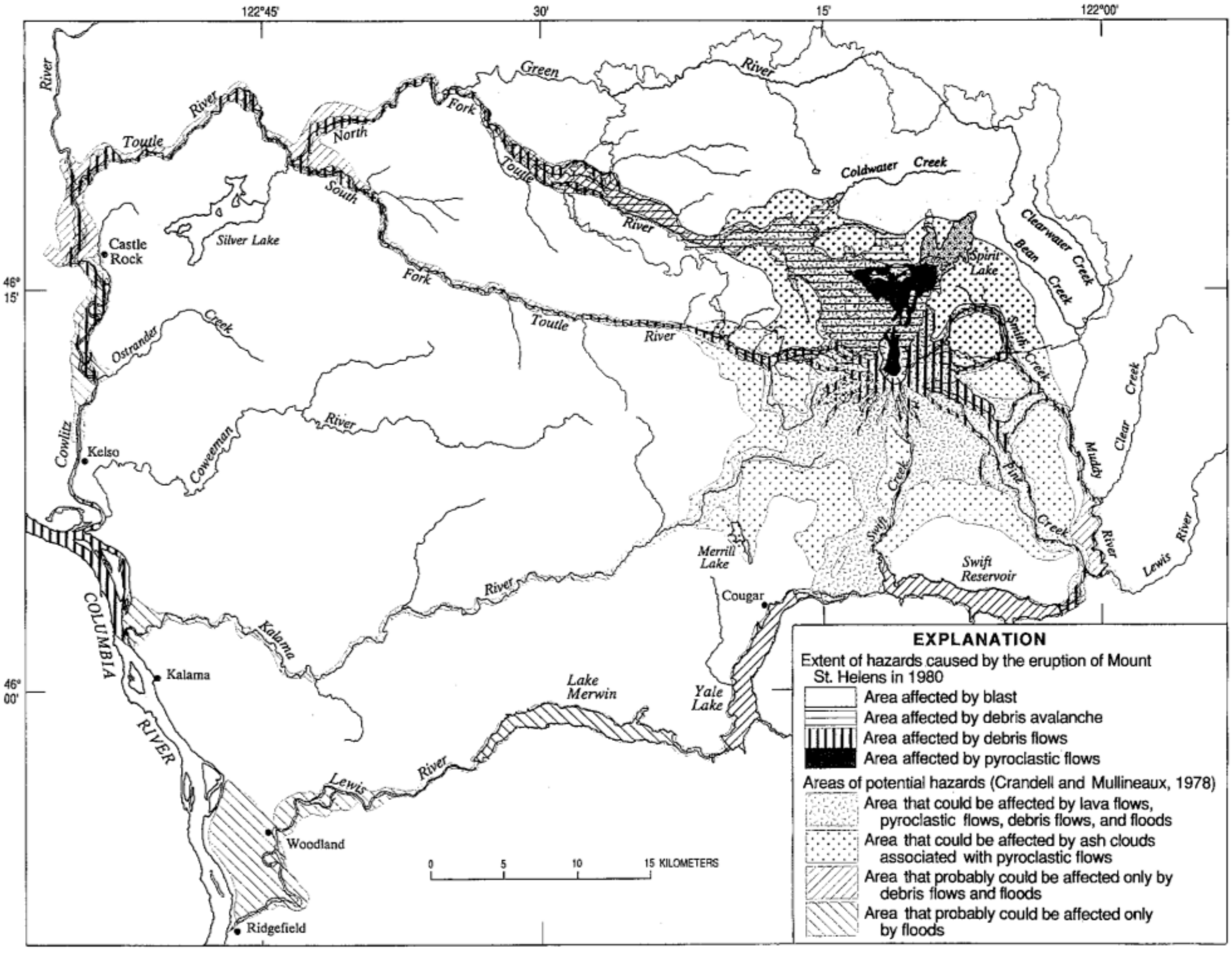
122°45'
30'
15'
122°00'
46° 15'
46° 00'
River
Toutle
River
North
Green
Fork
River
Toutle
South
Fork
Coldwater Creek
Clearwater Creek
Bean Creek
Spirit Lake
Castle Rock
Silver Lake
Toutle
River
Ostrander Creek
Smith Creek
Cowlitz
Kelso
Coweeman
River
Clear Creek
Muddy River
Pine Creek
Swift Creek
Lewis River
Merrill Lake
Swift Reservoir
Cougar
River
Kalama
COLUMBIA RIVER
Kalama
Lake Merwin
Yale Lake
Lewis River
Woodland
Ridgefield
0 5 10 15 KILOMETERS
EXPLANATION
Extent of hazards caused by the eruption of Mount St. Helens in 1980
Area affected by blast
Area affected by debris avalanche
Area affected by debris flows
Area affected by pyroclastic flows
Areas of potential hazards (Crandell and Mullineaux, 1978)
Area that could be affected by lava flows, pyroclastic flows, debris flows, and floods
Area that could be affected by ash clouds associated with pyroclastic flows
Area that probably could be affected only by debris flows and floods
Area that probably could be affected only by floods

FIGURE 8 The actual extent of damage during the 18 May 1990 eruption of Mount St. Helens, Washington, USA, compared with that anticipated in the hazard zone map published 2 years earlier. Except for the lateral blast, the actual hazards by pyroclastic flows, debris avalanches, and flows occurred within the expected areas of potential hazards. [Reproduction from (1992) "Living with Volcanoes." U.S. Geological Survey's Volcano Hazards Program, U.S. Geological Survey Circular 1073.]

foot of Vesuvius, was impacted by pyroclastic surges, and deeply buried by pyroclastic flow deposits. Uneaten food laid out on tables was found in houses after the deposits were excavated. This shows that normal life continued in the town until the last moment. Many human fossils have been found as holes in the deposits (natural molds in ash). Plaster casts made from these molds clearly show hands covering the mouths, implying that the victims had difficulty in breathing.

V. MITIGATION OF PYROCLASTIC FLOW AND SURGE HAZARDS

It is most likely that an eruption similar to previous eruptions will occur in the future. A comprehensive understanding of eruption phenomena and frequency is therefore needed for hazard mitigation. Areas impacted by pyroclastic flows previously are likely to be affected again in future eruptions. Hazard maps show the probability of pyroclastic flows, surges, and other hazards for different areas and provide guidelines for long-range land-use planning around volcanoes and for evacuation from pyroclastic flows and surges. Distribution of maps (where they exist) to local people and public education are essential for hazard mitigation.

When an explosive eruption occurred on a spring Sunday morning at Mount St. Helens, the tourist season had just started. After the beginning of volcanic activity there, regulation of entry into the volcano area was set according to the hazard map which had been drawn 2 years previously (Figure 8). Pyroclastic flows and surges swept the areas shown on the map. Less than 60 people became victims of a laterally directed blast, which resulted from a sudden collapse of the volcano, on 18 May. Lessons at Mount St. Helens and Unzen teach us that diluted pyroclastic surges or blasts are less influenced by the topography and may easily climb up topographic obstacles, though dense pyroclastic flows tend to descend along valleys.

Once an eruption with the potential for pyroclastic flows and surges starts, we can take steps to mitigate hazards from them using knowledge from recent eruptions at other volcanoes. Specifically, dome-collapse-induced pyroclastic flows can occur as successive events in a period ranging from days to weeks. During this period, the magnitude of pyroclastic flows increases generally with time (Figure 4). Since dome eruptions commonly last a few years or longer, the pyroclastic flow hazards become modified. As a lava dome increases in volume and height with time, pyroclastic flows tend to travel larger distances due to the increase in *H*, increasing the risk of larger-scale dome collapse. As the valleys around a dome become filled, later pyroclastic flows are likely to descend further and to spread out more.

The degree of volcanic explosions primarily depends on the extrusion rate of lava from the vent and may be very variable. For example, at Soufriere Hills volcano, although small dome collapse pyroclastic flow events were dominant, column collapse pyroclastic flows often occurred following a long period of quiescent lava effusion.

Large-scale explosive eruptions (>10 km^3 in volume) like those producing caldera-forming eruptions are historically rare. Despite their low frequency, the associated pyroclastic flows tend to travel distances of several tens of kilometers in any direction from the crater. Identification of volcanoes with a high risk of such large-scale eruptions is required through field observations of old deposits and age determination studies. Evaluation of future eruptions is required through patient and continuous volcanological monitoring. When there is a high possibility of large explosions, people living around the volcano should be ordered to evacuate the area. This course of action has economic and political difficulties as well as volcanological uncertainties.

SEE ALSO THE FOLLOWING ARTICLES

Lava Domes and Coulees • Lava Flow Hazards • Lava Flows and Flow Fields • Plinian and Subplinian Eruptions • Pyroclast Transport and Deposition • Pyroclastic Surges and Blasts • Volcanic Hazards and Risk Management • Volcano Warnings • Vulcanian Eruptions

FURTHER READING

Blong, R. J. (1984). “Volcanic Hazards. A Sourcebook on the Effects of Eruptions.” Academic Press Australia, Sydney.

Cole, P. D., Calder, E. S., Druitt, T. H., Hoblitt, R., Robertson, R., Sparks, R. S. J., and Young, S. R. (1998). Pyroclastic flows generated by gravitational instability of the 1996-97 lava dome of Soufriere Hills volcano, Montserrat. *Geophys. Res. Lett.* **25**(3), 425–428.

Fisher, R. V., and Heiken, G. (1982). Mt. Pelée, Martinique:

May 8 and 20, 1902, pyroclastic flows and surges. *J. Volcanol. Geotherm. Res.* **13,** 339–371.

Suzuki-Kamata, K., Kamata, H., Taniguchi, H., and Nakada, S. (1992). Installation of penetrator-type thermometers and blastmeters for detecting pyroclastic surges during eruptions of Unzen volcano, Kyushu, Japan. *J. Natural Disaster Sci.* **14**(2), 1–8.

Tilling, R. I. (1989). Page 1–8 *in* "Volcanic Hazard" (R. I. Tilling, ed.), "Short Course in Geology" (Vol. 1). American Geophysical Union, Washington, DC.

This Page Intentionally Left Blank

LAVA FLOW HAZARDS

DONALD W. PETERSON
ROBERT I. TILLING
U.S. Geological Survey

I. General Nature of Lava-Flow Hazards
II. General Character and Behavior of Lava Flows
III. Hazards from Mafic Lava Flows
IV. Hazards from Intermediate and Silicic Lava Flows
V. Mitigation of Risks from Lava-Flow Hazards

GLOSSARY

aspect ratio The ratio of the mean thickness of a lava flow (or flow field) to the diameter of a circle with an area equal to the area covered by the flow.

effusive eruption A nonexplosive volcanic eruption in which coherent fluid molten rock is extruded from the vent to form lava flows.

explosive eruption A volcanic eruption powered by the abrupt release of dissolved gas which propels broken and torn solid and molten matter of all sizes upward and outward through the air that fall to form fragmental (pyroclastic) deposits.

hazard The existence of a condition under which a potentially dangerous volcanic process might occur.

intermediate lava Lava with a silica content (by weight) between about 55 and 62%.

lava dome A steep-sided rounded accumulation of lava extruded from a volcano to form a dome-shaped or bulbous mass of congealed lava above and around the vent.

lava flow An outpouring of molten rock from a vent or fissure spreading along the ground; also the body of solidified rock resulting from the outpouring.

lava-flow field The rock body made up of a succession of individual lava flows.

littoral An adjective used to describe features that lie, or processes that occur, along the shoreline of an ocean, sea, or lake.

mafic lava Lava with a silica content (by weight) less than about 55%.

risk The probability of a loss of life, property, or productive capacity within an area subject to volcanic hazard.

silica Silicon dioxide (SiO_2).

silicic lava Lava with a silica content (by weight) more than about 62%; a close synonym, sometimes used, is felsic lava.

AT THE OUTSET it should be emphasized that, in theory at least, lava flows would pose no hazards or risks to society if people simply avoided regions with potential for active volcanism. Obviously, however, such a simplistic option is unrealistic, inasmuch as about three-quarters of the Earth's surface—above and below sea level—is composed of rocks of igneous (mostly volcanic) origin. It has been estimated that about 10% of the world's population lives near active and potentially active volcanoes and, therefore, cannot ignore the possibility of eruptions and associated hazards. With continued increase in population growth and attendant economic development, the challenge to reduce volcano risk in the 21st century becomes even more critical.

I. GENERAL NATURE OF LAVA-FLOW HAZARDS

Lava flows are inherently dangerous. Scenes of flows of molten rock advancing down the slopes of volcanoes occasionally enliven TV news broadcasts; these flows can consume trees and crops, and sometimes they bury or surround, push over, and burn houses and parts of villages and towns. Such events dramatically illustrate the destructive potential of lava flows, which are the products of effusive eruptions. A few examples of devastating lava flows in recent decades include those of Kilauea (Fig. 1) and Mauna Loa, Hawaii; Etna, Italy; Parícutin, Mexico; and Heimaey, Iceland. Most lava flows advance slowly enough to allow people to get out of harm's way, but everything left behind can be damaged or destroyed, and the land covered by lava is generally rendered uninhabitable and (or) unproductive for years, decades, or centuries.

In addition to the readily recognized hazards posed by lava flows, other less-obvious hazardous processes often accompany and (or) follow the emplacement of lava flows that may have even more serious social consequences than the immediate damage caused by lava inundation. Some of these processes and results include landslides caused by the increasing weight of new lava on unstable slopes, people being displaced owing to losses of homes, farms, and livelihood, and disease and starvation resulting from damage to vital stocks of supplies and from disruption of communication and transportation networks.

The focus of this article is to describe and explain the character of the hazardous processes associated with lava flows and to discuss the methods that have been utilized and proposed for mitigating their risks.

A. Hazard and Risk

In everyday usage, the terms *hazard* and *risk* are commonly treated as interchangeable. However, in some disciplines, including studies of volcanoes, it has been useful to distinguish between these two terms and define each of them more narrowly. In volcanology, hazard can be thought of as the existence of a condition under which a potentially dangerous process might occur. Risk, in contrast, is the degree of probability of a loss of life, property, or productive capacity if the hazardous process does occur. The relation between the terms can be expressed in the equation, risk = (value) × (vulnerabil-

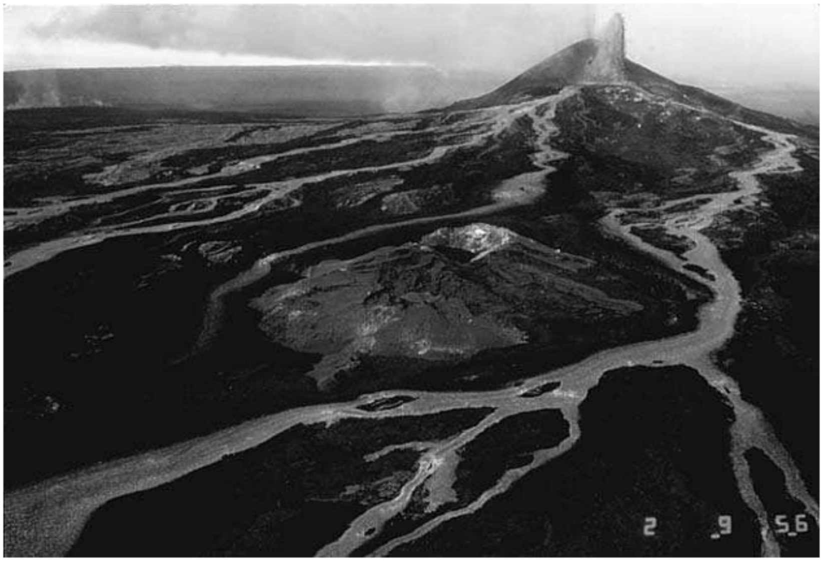

FIGURE 1 Aerial view of fluid lava flows advancing great distances from the Pu'u 'O'o vent on the east rift zone of Kilauea volcano, Island of Hawaii, in 1983. Some of these flows traveled more than 12 km to reach the south coast of the island and destroyed many dwellings. (Photograph, J. D. Griggs, USGS.)

ity) × (hazard). Value is a measure of the number of people, amount of property, and productive capacity in the potentially affected area, and vulnerability is a measure of the proportion of this value that might be lost if a hazardous process should occur. In this more strict sense, hazard is just one of the elements that constitute risk.

For example, a particular volcano in an unpopulated area would present a certain degree of hazard, but its risk to people and property on the ground would be relatively small. As people move into the area near the volcano and establish farms, towns, and cities, the hazard would remain unchanged, but the risk would be proportionately increased. Further, different methods are used for determining the two factors. The hazard posed by a potentially active volcano can be investigated by systematic observation and monitoring and by studying the history of the volcano and analyzing its past behavior. When the hazard is assessed in this way and applied to the societal and economic framework of the surroundings, the degree of risk can be evaluated.

The hazard of a dormant volcano is determined by its past behavior as revealed by its geological record, which explains the character and products of its past activity. However, hazard can also be expressed in a more immediate sense by describing the threat posed to land in the path of lava flows while an eruption is in progress. While the term is properly used in both senses, in this article we emphasize the first sense because several of the articles on effusive volcanism emphasize hazards in the second sense.

II. GENERAL CHARACTER AND BEHAVIOR OF LAVA FLOWS

Lava flows are outpourings of molten rock from vents or fissures that spread across the ground. The vast majority of lava flows are composed of silicate rocks whose compositions range from basalt to andesite and dacite to rhyolite, as well as basanite, latite, trachyte, phonolite, and others. The volumes of individual flows vary widely; historically they have ranged from small ponds to widespread bodies approaching a cubic kilometer. Flow fields are formed by a succession of individual flows, erupted through time, which cumulatively build a larger and thicker topographic feature. Flow fields can aggregate several cubic kilometers; the largest historical flow field of Lakagígar, Iceland, was about 12 km^3.

The prehistoric worldwide geologic record includes several immense lava-flow fields that have volumes of hundreds and even thousands of cubic kilometers; two good examples are the massive plateau basalts of Tertiary age that form the Columbia River Plateau of the northwestern United States (Fig. 2) and the Deccan Plateau of western India. These flow fields were emplaced by

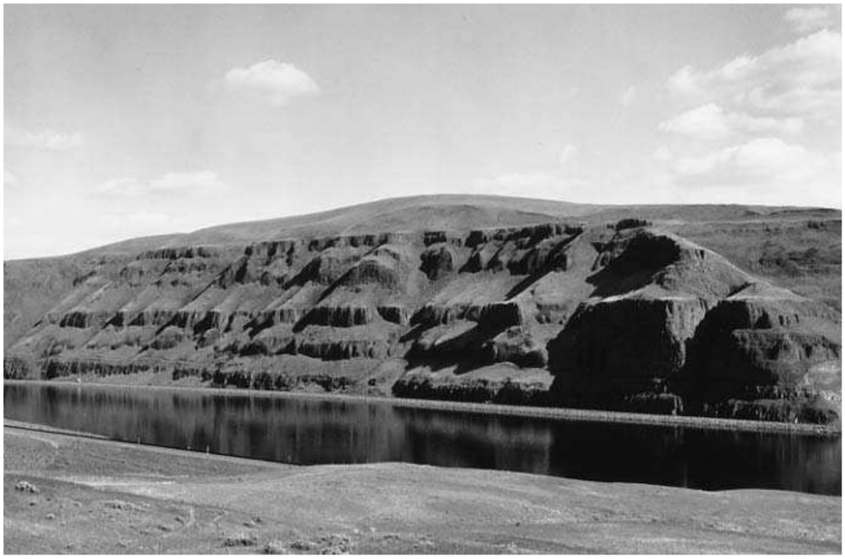

FIGURE 2 Columbia River Plateau, Washington State (USA), showing a high cliff exposing a series of thick lava flows (plateau basalts). A car on the highway at the base of the cliff (lower left) gives scale. (Photograph, D. A. Swanson, USGS)

huge, mobile flows that would have obliterated everything in their paths. Because of the vast time span since the eruptions of the most recent plateau basalts, the probability of renewed eruptions of this type is regarded as too low to be practical or useful, and their hazards are not considered in the present discussion.

Historical flow fields may reach tens of kilometers long, a few kilometers wide, and hundreds of meters thick, although most are smaller and more typically range from hundreds of meters to a few kilometers long, tens to hundreds of meters wide, and a few to tens of meters thick. Lengths of individual flows generally range from a few tens of meters to a few kilometers, and, depending on their properties and ground-surface controls, thicknesses may vary from a few centimeters to tens of meters. Historical lava effusions have lasted from just a few minutes to several decades, although commonly their durations range from days to a few years.

The consequences of the largest known historical effusive eruption, that of Lakagígar (Laki Fissure), Iceland, 1783–1784, illustrate well the kinds of hazards associated with a large effusive emplacement of a lava-flow field. Although the lava flows covered more than 500 km^2 during an 8-month period, the human casualties ($\approx$9000) were not caused from engulfment by lava but instead by starvation and disease resulting from the loss of crops and livestock. The Lakagígar eruption ranks among the world's six deadliest eruptions since 1600 A.D. (Fig. 3).

To describe the relationship between the thickness and the area covered by a lava flow or flow field, the term *aspect ratio* has recently come into common use. The term, regrettably, has not been used consistently throughout the literature, so the definition used here needs to be explained. In accord with most of the recent literature, aspect ratio is here used as the ratio of the mean thickness of a flow to the diameter of a circle having an area equal to the area of the flow (or flow field). By this definition, a flow with low viscosity would tend to have a low aspect ratio because it would have a small thickness in comparison to its area. A flow of viscous lava would have a higher aspect ratio because its thickness would be larger in comparison to its area. The majority of mafic lava flows have low aspect ratios, and most, but not all, silicic lava flows have relatively higher aspect ratios.

The specific behavior of a lava flow is controlled by a number of factors, the most important of which include the rate of discharge of lava from the vent, the duration of the effusion, the slope of the ground and other details of topography, and the viscosity of the lava, which in turn is governed by its chemical composition, crystal and gas content, and temperature. Diverse combinations

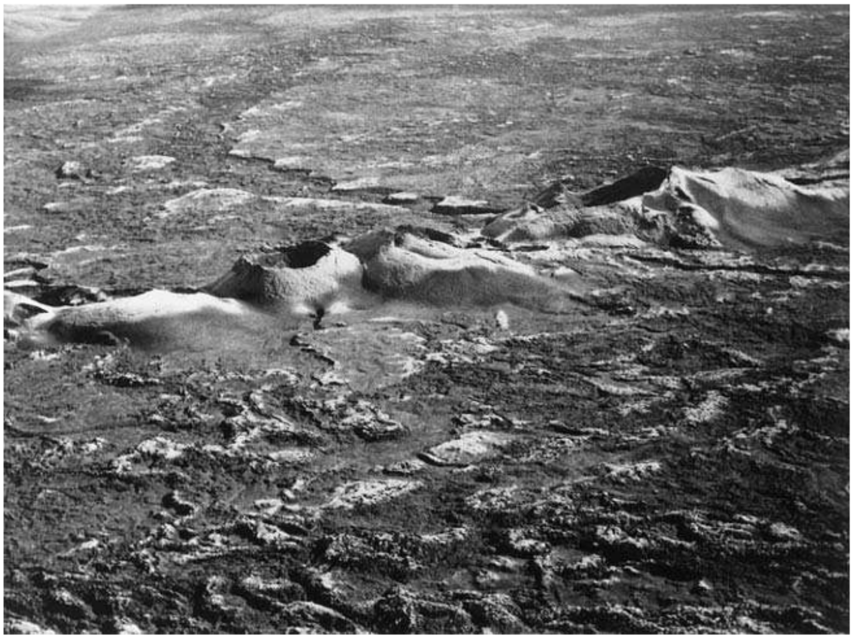

FIGURE 3 Aerial view of cinder cones along fissure vent of the Lakagígar (Laki), Iceland, eruption of 1783, the largest known effusive outpouring of lava in recorded history. (Photograph by R. W. Decker.)

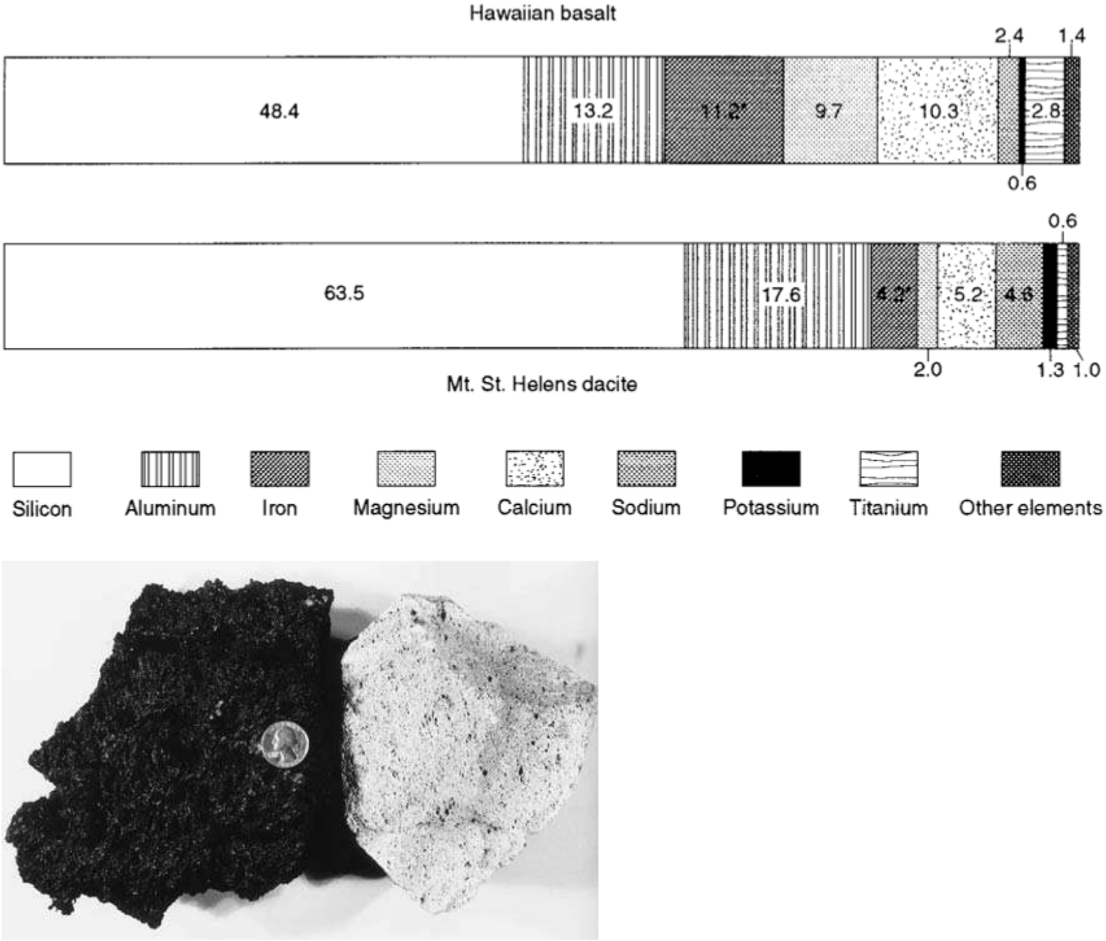

FIGURE 4 Differences in color and average chemical composition between Hawaiian basalt (dark) and Mount St. Helens dacite (light). The number given for each chemical element gives the amount (in weight percent) of that element (expressed as oxide) contained in the lava.

of all these factors influence such matters as the speed of advance of the flow, both forward and laterally, the thickness of the flow and size of the area covered (which in turn determine the aspect ratio), and the physical nature of the lava during flow (such as pahoehoe, aa, or block lava). All of these parameters are involved in helping to understand and explain the nature of the lava-flow hazards.

Chemical composition is a major determinant in the behavior of lava during its eruption and flow. Magmas of mafic composition (those with silica content less than about 55%) tend to have lower viscosity at typical eruption temperatures than magmas of intermediate and silicic compositions. Thus mafic lavas, which chiefly include basalts of various types and some basaltic andesites, tend to have low viscosity, flow readily, and spread out easily and rapidly from their vents to form flows with low aspect ratios. With progressive increase of silica content of lava from basalt to andesite, decite, and rhyolite, lava viscosity increases (Fig. 4); in general the more silicic lava does not spread as fast or as far from the vent, but instead builds shorter, thicker lobes or blankets with higher aspect ratios than those of mafic lava. The silicic end members of this progression may form lava domes, built by multiple extrusions of viscous lava that pile up as steep-sided edifices with even higher aspect ratios. In recent years, however, a few exceptions to the thick, stubby shape of silicic lava flows have been recognized. Extensive silicic lava flows have been identified in several regions of the world that have relatively low aspect ratios, approaching those of plateau basalts. Well-studied examples include widespread (as much as

3000 km^2) rhyolite flows in southwestern Idaho and in Trans-Pecos Texas. Like the plateau basalts, these voluminous flows are chiefly of Tertiary age or older, so the hazard posed by their possible recurrence is negligibly small, although recurrence is geologically possible.

Another characteristic of increasingly viscous lava is that the gas dissolved in the magma cannot escape easily, so the exsolving gases build up to high internal pressures that are more likely to be released abruptly instead of gradually. The sudden release of pent-up pressure results in an explosion which produces broken fragments (pyroclastic deposits) instead of lava flows. Explosive behavior constitutes a completely different, and more dangerous, type of hazard, not covered in this article. Eruptions of intermediate and silicic magmas commonly include a progressively higher proportion of explosive events, along with a lower proportion of effusions, as silica content increases. While many eruptions of mafic magmas may include explosive events, they are proportionately less common.

The differences in form and behavior between mafic, low-viscosity flows and intermediate and silicic, higher viscosity flows provide a convenient basis for organizing the discussion to follow. Nonetheless, it must be emphasized that the distinctions made between types of lava-flow behavior are gradational throughout the entire compositional range of lavas, owing to the gradational nature of all of the factors that influence flow behavior. (Additional information about the characteristics, properties, behavior, and variations in the different kinds of lava and their resulting bodies is provided in the articles on Effusive Volcanism.)

III. HAZARDS FROM MAFIC LAVA FLOWS

The principal hazards of effusive mafic eruptions are, of course, the lava flows themselves, which can damage or destroy whatever lies in their paths. However, other, generally less destructive hazards are also associated with mafic lava flows, the most common of which involve the fall of fragments from lava fountains, explosive interactions sometimes triggered when hot lava enters the ocean, and explosions when lava flows advance into vegetated areas. For a well-illustrated summary of the volcanic hazards associated with mafic lava flows, as typified by the basaltic eruptions of Hawaiian volcanoes, the interested reader is referred to the website of the U.S. Geological Survey's (USGS's) Hawaiian Volcano Observatory, currently located at: (http://wwwhvo.wr.usgs.gov/hazards/).

A. Primary Hazards

A typical eruption of mafic lava is commonly preceded by a period of increasing seismicity concentrated near the site, almost always accompanied by cracking and (or) swelling of the ground and increased emission of volcanic gases. If these associated activities intensify, they commonly lead to the eruption of lava, which may range from quiet welling out from the vent, to low to moderate fountains of lava, to spectacular fountains that can shoot upward to heights as great as several hundreds of meters. The lava moving along the ground away from the vent(s) constitutes the lava flow; its behavior and characteristics are determined by the combination of all the factors governing lava behavior. During vigorous fountaining, lava is disrupted into discrete irregularly shaped masses (variously described as blobs, shreds, drops, etc.), and those that remain fluid coalesce upon falling to form, or add to, a lava flow issuing directly from a vent. Airborne lava masses that solidify during their flight and fall within the flow are incorporated into it, and those that fall beyond the margins of the flow form spatter or cinder deposits. The falling pieces of lava constitute a separate hazard from that of the flow itself; they are among the several kinds of hazards associated with, but distinct from, the hazards directly caused by the flows.

If the eruption issues from a vent in an area of nearly flat topography, or from a line of fountains (popularly termed a "curtain of fire"), the lava may spread across the land as a sheet flow. The lava in a moving sheet soon tends to coalesce into discrete channels of flowing lava, while the lava remaining within the sheet proper (i.e., exclusive of the channels) gradually cools, slows, and solidifies. Whether originating from a single vent or a sheet flow, much mafic lava is ultimately transported by discrete lobes and by channels, and the characteristics and behavior of the flows are determined by the discharge rate, total volume, topography, and temperature and lava composition, which, in turn, determine the viscosity. Mafic lava is commonly erupted and transported as either pahoehoe or aa, and rarely as block lava. Under particular conditions determined chiefly by viscosity, rate of shear strain, and yield strength, during flow pahoehoe may change to aa, but not the reverse (Fig. 5). Large flows with high discharge rates show a

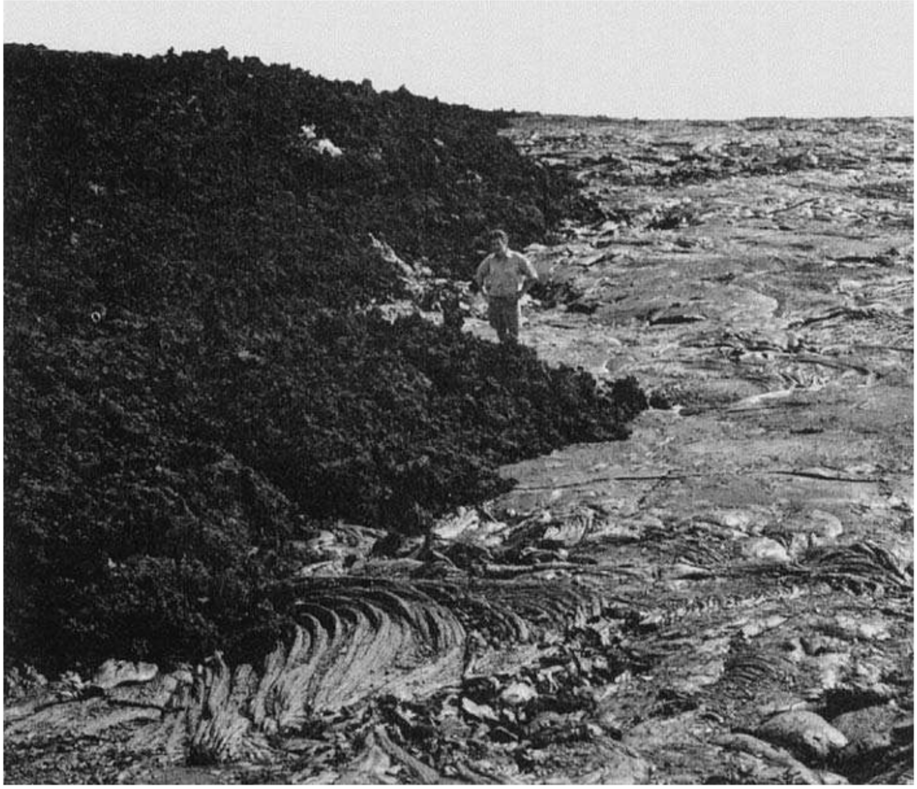

FIGURE 5 Dark, rough-surfaced aa lava flows (left) that have advanced across older smoother-surfaced, shiny pahoehoe lava flows (right); volcanologist (center) gives scale. Both the aa and the pahoehoe lava shown were erupted in 1973 during the Mauna Ulu eruption on the east rift zone of Kilauea volcano, Hawaii. (Photograph by Barbara Decker.)

strong tendency to form aa as they cool and become more viscous during the advance of the flow, but aa can also form in smaller and slower flows under appropriate conditions.

Pahoehoe flows in well-established channels with stable, moderate discharge tend to have crusts develop across their surface, and as the crusts grow laterally and in thickness, they merge to form the roofs of lava tubes. Lava flowing beneath the crust in tubes is better thermally insulated than lava flowing in the open, and thus it better retains its heat and fluidity. As the tubes extend themselves downslope, the lava travels progressively greater distances before emerging from the tube to eventually cool and solidify. Even moderate-sized flows fed by lava tubes can extend to distances many kilometers from their source. Some of the most systematic observations of the behavior of mafic lava flows, both open-channel and tube-fed, have been made at Kilauea and Mauna Loa volcanoes in Hawaii and at Mount Etna in Sicily, and the principles deduced from these studies seem to apply generally to most mafic effusions throughout the world.

Advancing lava flows, whether large or small, and whether aa or pahoehoe, pose obvious hazards to the land in their paths, principally involving the possibility of surrounding and overrunning both natural and man-made features and structures (Fig. 6). Depending on their character and size, these features may be burned, buried, crushed, and rendered agriculturally unproductive, with consequences ranging from partial damage to total loss. In turn, the valuation of economic development on this land, its agricultural worth, and the size of the population it supports determine the degree of risk in the path of the lava flow.

Although most lava flows travel slowly enough for people to move out of harm's way, a tragic exception occurred at Nyiragongo volcano, Zaire, in 1977. A long-lived lava lake at the summit of the volcano drained abruptly when fissures on the flank opened and highly fluid fast-moving lava emerged and rapidly advanced

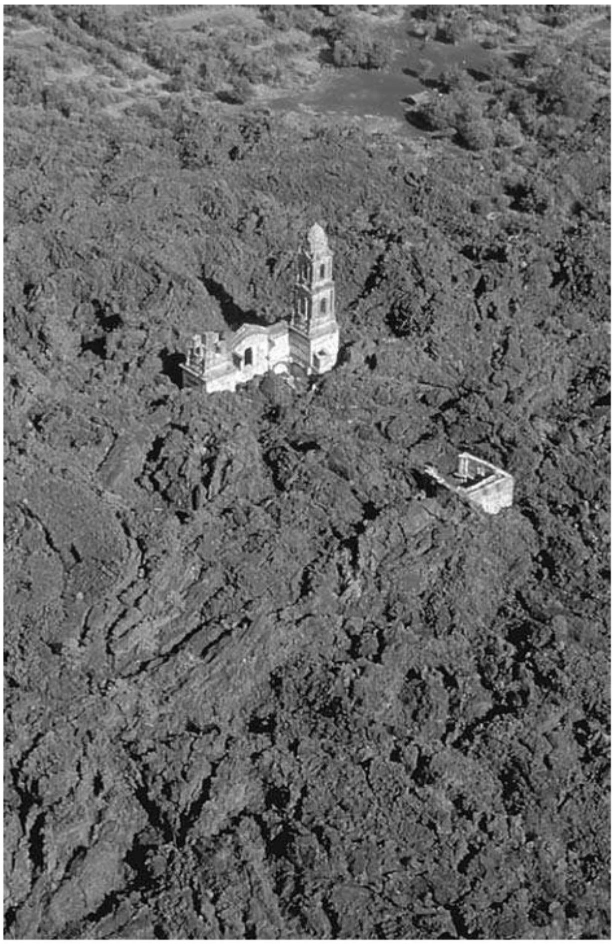

FIGURE 6 Aerial view of San Juan Parangaricutiro church surrounded by 1944 lava of the 1943–1952 eruption of Parícutin volcano, Michoacán, Mexico. [Photograph in 1981 by Katia Krafft, provided courtesy of Agence Hoa-Qui, Paris, France.]

downslope. The entire lake drained in less than an hour, and speeds of some parts of the flows were estimated as high as 100 km per hour. The lava had an exceptionally low silica content (about 42%), which, along with high temperature, accounted for its very high fluidity. Several villages on the flanks of the volcano were engulfed before the inhabitants could flee, and resulting deaths were variously reported from 60 to 300 people. Other examples of fast-moving voluminous lava flows have been observed at some eruptions of Mauna Loa, Hawaii, at which speeds reached a few tens of kilometers per hour. More customary rates of advance of Hawaiian flows on moderate slopes are only a few kilometers per hour, whereas flows spreading over relatively flat terrain advance much more slowly.

B. Other Hazards

Several types of hazards beyond those caused directly by lava flows commonly accompany effusive eruptions. The most ubiquitous are from the volcanic gases that are dissolved in the magma and escape from it at various rates as the ascending magma encounters progressively lower confining pressures as it approaches the surface. Expansion of the escaping volcanic gas propels the expulsion of liquid and solid material during any eruption; the rate of gas release is the predominant factor in determining the style of the eruption, which varies from violent explosions to quiet effusions. Upon escaping the magma, however, the volcanic gases may pose several types of additional hazards. Their effects are most intense near the vents and active lava flows, particularly on the downwind side, but they become less severe at increasing distances from active areas. Volcanic gases include some components that are toxic and (or) corrosive; in dilute concentrations they generally cause unpleasant odors and other sensory irritations, but even when dilute they can affect the health of people, corrode and cause other damage to structures and machinery, and adversely affect the growth of plants and agricultural productivity (Fig. 7). At higher concentrations volcanic gases can cause serious health problems and even be lethal. Another serious hazard from gases is confined to areas that include enclosed depressions. Several of the gaseous components are heavier than air (e.g., carbon dioxide), and during times of gentle or no wind, drifting heavy gases can collect within the depressions in dangerous concentrations. Unwary people and animals entering such depressions can suffer asphyxiation.

Flows that are accompanied by vigorous lava fountaining cause the additional hazard of hot, falling material. This hazard, distinct from those caused directly by lava flows, is generally restricted to areas within a few hundred meters downwind of the vent. Stronger explosive activity is unusual during many eruptions of mafic lava, such as most of those at Hawaiian volcanoes, but at many other mafic volcanoes, such as Mount Etna, Sicily, volcanoes in Iceland, and during the 9-year-long eruption of Parícutin, Mexico (1943–1952), large explosions often have accompanied or were interspersed with lava effusions. While the hazards of explosions are not covered here, it must be remembered that mafic lava flows are often punctuated by explosive activity.

Another type of explosion is fairly common when mafic lava flows advance into vegetated areas. When plants are engulfed by the lava without being completely burned, organic gases distilled from the buried plants can travel through the pores and cracks in the ground

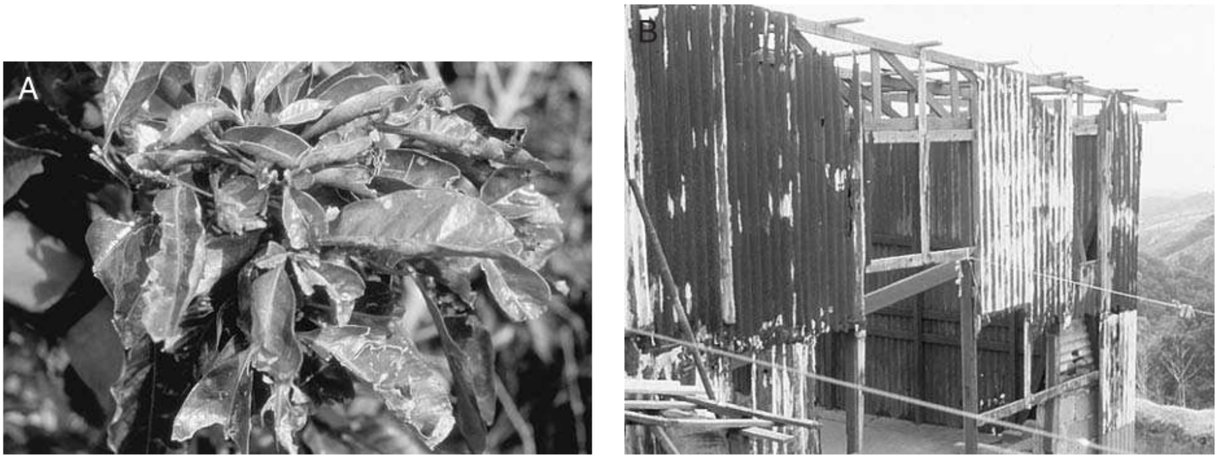

FIGURE 7 Damage sustained by a coffee plantation more than 15 km downwind from vents at the summit of Pòas volcano, Costa Rica. Frequent rainfall in the region mixes with volcanic gas to form *acid rain.* (A) Severe damage to leaves of a coffee plant by acid rain. (B) Extensive corrosion of corrugated metal by acid rain on a plantation building. [Photographs by R. I. Tilling, USGS.]

beneath. When this gas blends with atmospheric oxygen, a highly volatile mixture is created, and if heat from the lava ignites it, an explosion results. Such explosions can occur directly beneath the lava flow, and molten spatter is thrust upward and outward, sometimes falling beyond the flow margins. If the volatile gas mixture, while still underground, migrates outward beyond the margin of the lava flow, a confined explosion may rapidly travel within the ground both below the flow and beyond it, and it sometimes reaches as much as tens of meters outside the flow margin before the explosion breaks through to the surface. Such explosions are random, unpredictable, and sometimes quite violent, hurling dirt, rocks, shrubs, and even trees high into the air. Because of this hazard, the areas along the edges of new lava flows advancing through heavy vegetation should be regarded as extremely dangerous. This type of explosion has been common in Hawaii during long-lived activity on the east rift zone of Kilauea both during the Mauna Ulu eruptions of the 1970s and the Pu'u 'O'o eruptions of the 1980s and 1990s.

Still another type of explosion may occur during eruptions when mafic lava flows enter the ocean or other bodies of water. For these explosions to take place, some sort of special configuration must exist among the flowing molten lava, a confining channel or tube, and proximity to the shoreline. Perhaps the most common configuration is when the mouth of a lava tube lies right at the shoreline and discharges lava directly into the water. When the surging surf submerges the mouth of the tube, a large amount of water enters the tube into the confined space and is abruptly converted to steam by the intense heat of the flowing lava. A steam explosion results that hurls shreds of molten lava and broken solidified lava in various directions, both out the mouth of the tube and through any nearby openings in the tube roof. Another configuration is when lava in an open channel drains into the entry of a littoral lava tube near the shoreline in the surf zone. Such tubes enable lava to pass undisturbed beneath the vigorous surf to emerge later as a submarine lava flow. However, when an occasional extra strong wave floods the entry to the tube, water is carried into the tube and is transformed instantly to steam, which explodes out of the tube entrance and propels shreds of molten lava and fragments of broken solidified lava high into the air. When such explosions are repeated frequently over a sustained period of lava entry into the sea, the ejecta accumulate to form a littoral cone. Such cones are common along the shorelines of Kilauea and Mauna Loa volcanoes in Hawaii, as well as on other volcanic islands and coastal volcanic areas. The possibility of littoral explosions is a distinct hazard to persons attempting to make close-up observations of the dynamics of molten lava flowing into the sea.

A different variety of hazard results when flowing lava encounters snow and (or) ice on volcanoes at high latitudes or on high mountains. Lava flows with high discharge rates can quickly thaw large amounts of snow and ice, leading to floods, lahars, and debris flows. A unique variety of this process occurs at intervals in Iceland, where frequently active volcanoes lie beneath large glaciers. Lava from an eruption melts overlying ice, and meltwater collects beneath and may be temporarily dammed by the ice. If the eruption is large or continues

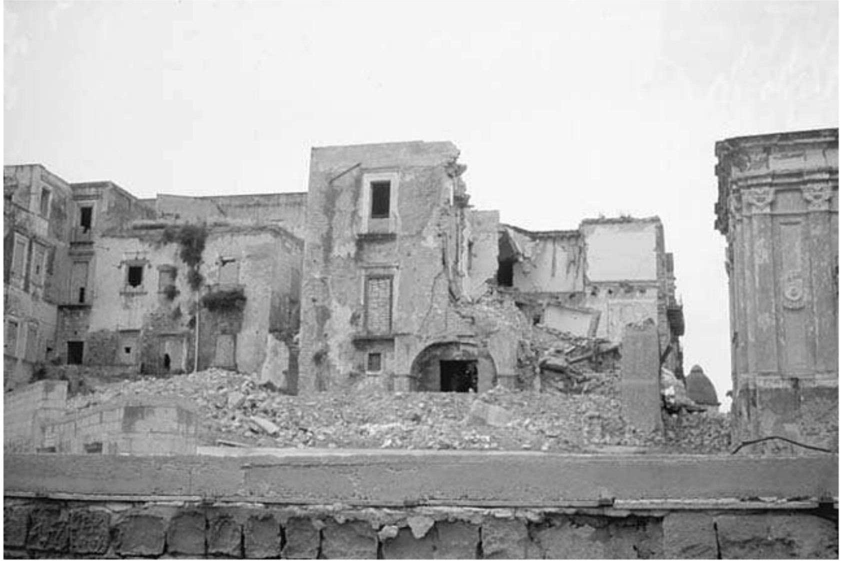

FIGURE 8 Destruction of older brick structures in Pozzuoli (Bay of Naples), Italy, caused by earthquakes during the volcanic unrest at Campi Flegrei caldera during 1982–1984; although involving increased seismicity and 1.8 m of ground uplift, the unrest did not culminate in eruption. (Photograph by David Chester.)

for a sustained period, the water may break through the dam and descend the drainage as a massive and devastating flood, termed in English a "glacier burst," and commonly known by its Icelandic term, *jökulhlaup.*

Still other hazards sometimes precede, accompany, and (or) follow effusions of mafic lava, and, indeed, they are commonly associated with all types of volcanic eruptions. These hazards include shifting ground, opening of cracks, and sudden ground subsidence. Although most volcanic earthquakes are relatively mild, shaking caused by them, especially during swarms precursory to new eruptions, can be damaging (Fig. 8). A potential hazard develops when deposits of new lava accumulate on or above sloping ground with appreciable gradients. The increasing load being added to the deposit may exceed the limit of stability, and the entire block of ground may give way as a landslide. Such collapse events also may occur along shorelines when new flows advance into the ocean. The offshore gradient is generally steeper than that inboard from the shore, and large blocks of "new" land, built over formerly offshore areas, may suddenly fail and collapse into the sea. A shoreline landslide in April 1993, involving part of a growing lava bench, resulted in the first fatality caused by the volcanic activity of Kilauea in seven decades when a visitor was swept into the sea (Fig. 9). Earthquakes may trigger landslides of fresh, unstable lava long after an eruption has finished. Landslides related to slope instability have caused damage and casualties in Hawaii, on Mount Etna, and at many other volcanoes throughout the world.

IV. HAZARDS FROM INTERMEDIATE AND SILICIC LAVA FLOWS

Lava flows of intermediate and silicic composition have higher viscosity than mafic lavas, and so, as mentioned earlier, they generally flow more sluggishly, travel shorter distances, spread less widely, and tend to build higher edifices in comparison with area covered (higher aspect ratios). They have a greater tendency to erupt explosively, and even during effusive activity, eruptions are frequently punctuated by explosive activity.

The higher viscosity of the lava results in other differences in the character of intermediate and silicic flows. For example, block lava is the common surface form of many of these flows, in contrast to the pahoehoe and aa surfaces characteristic of mafic flows. Some highly viscous lava of rhyolitic and dacitic composition piles up above and around its vent to form steep-sided lava domes; andesitic domes are less common. If a silicic magma is erupted with high total volume, or with rapid effusion rates, or in long sustained eruptions, the resulting lava may spread downslope away from a dome

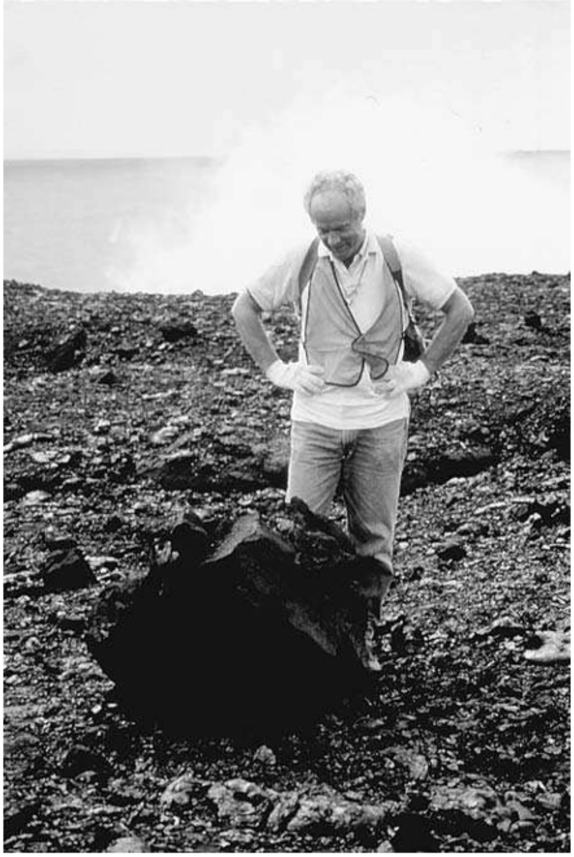

FIGURE 9 Large lava block hurled 30 m inland by explosions caused by the interaction of still-hot lava with seawater during a collapse of a lava bench in January 1988 on the south coast of Hawaii. This bench was one of many that have formed—then subsequently collapsed or was covered by new lava—during the eruption on Kilauea volcano's east rift zone that began in 1983 and has continued essentially nonstop to the present. (Photograph by Christina Heliker, USGS.)

or other vent to form thick, stubby lava flows, which are commonly termed coulees; examples include those of the rhyolitic Mono Craters and of the Medicine Lake Highlands in, respectively, eastern and northern California. But in spite of the differences in behavior between silicic and mafic lava flows, some of their hazards are the same, for advancing flows can obliterate cropland and can bury, burn, and crush everything that lies in their paths. But the additional hazards of silicic volcanism, inherent with its greater potential for explosive activity, require that additional precautions be taken by those who venture near the flows. The hazards associated with andesitic and other intermediate effusions, however, are somewhat less severe, being gradational between those of silicic and mafic lava flows.

Although severe or total damage can be the result when flows and domes of silicic and intermediate lava overwhelm what lies in their path, and although injuries and loss of life can be high during explosive episodes of silicic volcanism, the lava flows themselves rarely are the direct cause of casualties. The viscous lava of these flows typically advances much more slowly than mafic lavas and, with rare exceptions, generally does not spread widely, so people and animals can easily get away from the flow itself. Furthermore, people are probably warned away by the explosions that commonly herald the new activity before the lava flows even begin, so people are rarely if ever caught by advancing lava. The principal hazards to life associated with intermediate and silicic flows are from the primary explosions and other phenomena that precede and accompany the viscous flows.

The flanks of lava domes and the sides and advancing fronts of highly viscous lava flows are typically steep and unstable, and the block lava breaks to form loose piles of broken lava (talus) that constantly falls and results in hazardous conditions all around the margins of flows and domes. The blocks form talus aprons that accumulate at the base of the slopes; in advancing flows these are overrun and incorporated as basal breccias. A hazard much more severe and widespread than falling talus is the possibility of landslides and debris avalanches spalling from the unstable slopes. Depending on the volume of material and the topographic gradient, landslides and avalanches may travel rapidly for considerable distances; for example, avalanches spawned from the lava dome in the crater of Soufriere Hills volcano on Montserrat traveled for several kilometers at rates of tens of kilometers per hour at temperatures exceeding 700°C. This illustrates that this hazard extends to areas well beyond the immediate vicinity of a dome or flow.

If gas pressure, confined by the solidified crust within the dome or flow, has not yet equilibrated with the atmosphere, the abrupt release of pent-up gas pressure by a landslide or avalanche may trigger an explosion, which can range from jets of gas blasting forth from the newly exposed surface to the escaping gas hurling both solidified and fluid lava upward and outward from the flow. Some of these events spawn pyroclastic flows that can travel many kilometers from the source. All these events are dangerous, especially the pyroclastic flows, and small events of each type occurred during the growth of the dacitic dome at Mount St. Helens between 1980 and 1986. In addition, during the decade of the 1990s, larger pyroclastic and debris flows of this origin caused multiple casualties downslope from the growing lava domes at Unzen, Japan, and Merapi, Indonesia.

Phreatic explosions blasting from a dome or flow result in a similar kind of hazard but are rooted in a different cause than those resulting from volcanic gas explosions. When rainwater or groundwater seeps through fractures in the outer solidified crust and meets the high-temperature zone around the still-molten core of the dome of flow, it generally boils off and escapes through cracks and pores in the overlying carapace of solidified lava as clouds of vapor. However, in some circumstances, the water may become trapped, and as it turns to steam the pressure increases within the confined space until steam explodes through the crust, carrying pulverized ash and fragments with it. Such explosions were common during the growth of the lava dome in the crater at Mount St. Helens, which required constant vigilance by the volcanologists who were monitoring the growth of the dome. An additional series of phreatic explosions occurred from the dome in the early 1990s, several years after the cessation of the major period of intermittent growth that ended in 1986.

Along with these special hazards accompanying silicic and intermediate lava flows, all of the hazards associated with mafic flows, such as ground movement, cracking, and collapse, and shaking from earthquakes, also accompany silicic and intermediate lava flows and are prevalent in their vicinity. Additionally, toxic gases pose a pervasive potential hazard, especially when they accumulate in topographic depressions.

V. MITIGATION OF RISKS FROM LAVA-FLOW HAZARDS

More than 1500 volcanoes have erupted during the last 10,000 years, and more than 500 of these have erupted during the span of recorded human history. The volcanoes with recorded historical eruptions must be regarded as most likely to erupt again and are those for which mitigation efforts are most needed. However, even in the industrialized countries, scientific and economic resources are not sufficient to study all high-risk volcanoes. Thus, priority must be given to those in populated and developed areas that are known to erupt frequently and to those that erupt less frequently but have had major eruptions in historical time. Several times in recent decades, however, strong unrest has begun at volcanoes that have had no record of historical activity but which culminated in catastrophic explosive eruptions; examples include Lamington (1951), El Chichón (1982), and Pinatubo (1991). No advance mitigation had been instituted at Lamington or El Chichón, but emergency mitigation efforts of several kinds were quickly organized at Pinatubo, which led to saving thousands of lives and to reducing economic loss.

Although these explosive eruptions involved hazards much more serious than those anticipated for lava flows, mitigation efforts for hazards from lava flows depend on many of the same techniques and practices as those used in attempts to mitigate volcano risk in general. Details of the techniques, however, differ from one volcano to another and must be adapted as needed to the individual characteristics of each volcano. Efforts to reduce volcano risk can be grouped into four broad categories: (1) identify, (2) monitor, (3) control, and (4) inform. Categories 1, 2, and 4 are applicable for volcanic hazards of all types, but category 3 is only sometimes attempted in favorable situations for flowage processes of different kinds, including lava flows.

A. Category 1: Identify the Types of Hazard at the Volcano

An essential prerequisite for mitigation of volcanic risk at any volcano is to determine its history of eruptive activity and associated hazardous processes. This can only be accomplished by studying the geology of both the volcanic edifice and the region around the volcano. These studies, especially geologic mapping and dating of the volcanic deposits, are aimed chiefly at determining the rock types that have been erupted and their distribution and relations between one another in time and space. Such data are used to interpret the kinds of eruptions that have occurred at the volcano and their frequency, size, and impacts. Experience has shown that past activity of a volcano is generally a reliable indicator of the kinds of activity that can be expected in the future, so the results of the geological studies can provide an indication of what and where the hazards are likely to be. This information can guide plans for appropriate use of land in potentially hazardous areas, can indicate recurrence intervals between past eruptions, can provide estimates for timing of future eruptions, and can serve as a guide for organizing the other elements of risk reduction. If the population has grown and economic development has expanded since earlier eruptions, hazard zone maps can form the basis for estimating the risk to these newly developed areas. The geological studies, while essential to a complete mitigation program, should not be expected to reveal every type of activity that might occur in the future. For example, the geological studies of Mount St. Helens, completed several years prior to 1980, served as an excellent guide to most of the types of potential activity and hazards, and even indicated the time frame in which renewed activity might take place, but they did not foresee the immense landslide that carried away much of the north flank of the volcano nor the magnitude of the resulting powerful laterally directed density currents that were the chief agents of destruction. Even so, the precautions that the geological studies had prompted were a key factor in reducing the casualty toll.

B. Category 2: Monitor and Observe the Current Status of the Volcano

The objective is to determine current volcanic behavior and to detect and interpret significant changes that might signal impending activity. Regular observations and systematic monitoring, utilizing techniques tested and proven worldwide, operated continuously through periods of both quiescence and unrest, will provide a background database that enables meaningful changes to be recognized and interpreted promptly. Some of the most common and useful monitoring techniques include seismic monitoring to detect movement of magma or hydrothermal pressurization, along with geodetic monitoring to detect ground displacements, detecting the types and amounts of gas emissions, and regular field observations of important sites on the volcano. When resources permit, other monitoring tools can be added, such as gravity and electromagnetic monitoring, ground- and satellite-based infrared sensing, space geodesy (e.g., global positioning system, interferometric synthetic aperture radar), and utilization of digital telemetry and computer-controlled data management systems. Improvements in electronics and computer technology and miniaturization have led to the development of rugged, lightweight equipment with real-time and telemetry capabilities that have been used to develop a mobile monitoring system that has many of the capabilities of a complete volcano observatory. Such a system can be quickly established at volcanoes which lack adequate monitoring capabilities during volcano emergencies to provide vital data during crises. This type of system has been deployed several times in recent years by the USGS at restless volcanoes in Latin America and elsewhere. During increasing restlessness at Pinatubo volcano (Luzon, Philippines) in 1991, the system was used collaboratively by the Philippine Institute of Volcanology and Seismology and the USGS, enabling data to be gathered, in near real time, that played a key role in convincing officials that evacuation of vulnerable areas was necessary, which saved tens of thousands of lives when the restlessness culminated in a catastrophic eruption on June 15.

C. Category 3: Control of Lava Flows by Diversion or by Slowing Their Advance

When geologic studies or historical events have shown evidence of repeated flows from a volcano (such as lava flows, debris flows, lahars, and volcano-generated floods), it may be feasible in some circumstances to consider attempts to hamper or divert future flows by erecting barriers, by clearing channels to provide alternative paths, and (or) by disrupting their source of supply. Under special and favorable conditions, such attempts can be launched after flows are in progress. In this chapter, the focus is limited to attempts to control lava flows. Very large flows with high discharge rates cannot be controlled by any methods now known, but, by flow-modeling studies, estimates can be made of their likely ultimate distance and area to be covered. Several methods have been attempted to control smaller and slower lava flows at different volcanoes, and these have had varying degrees of success.

An early example was an effort in 1669 when a flow from Etna was advancing toward the city of Catania. Residents of the city tried a diversion tactic by attacking the crust on the side of the flow with picks and shovels, but they were later prevented from doing so by people from a neighboring village that would have lain in the path of the diverted flow. Later the flow advanced to breach the city wall of Catania and destroyed part of the city.

Three centuries later, a large-scale effort was again made to divert lava at Etna, during the 1991–1993 eruption, to protect the village of Zafferana Etnea. The construction of several earthen barriers during January–April 1992 achieved temporary, limited success in delaying the advance of the flow front before the barriers were successively overtopped. However, the barriers gained time to attempt—by means of explosives—to breach the natural lava channel (at a point about 8 km from the village) and divert the lava into an artificial channel (Fig. 10). The explosive “intervention” in May 1992, when the flow front was only 850 m from Zafferana, successfully diverted about two-thirds of the lava flow into the artificial channel. Shortly thereafter, the effusion rate about halved, and ultimately the eruption

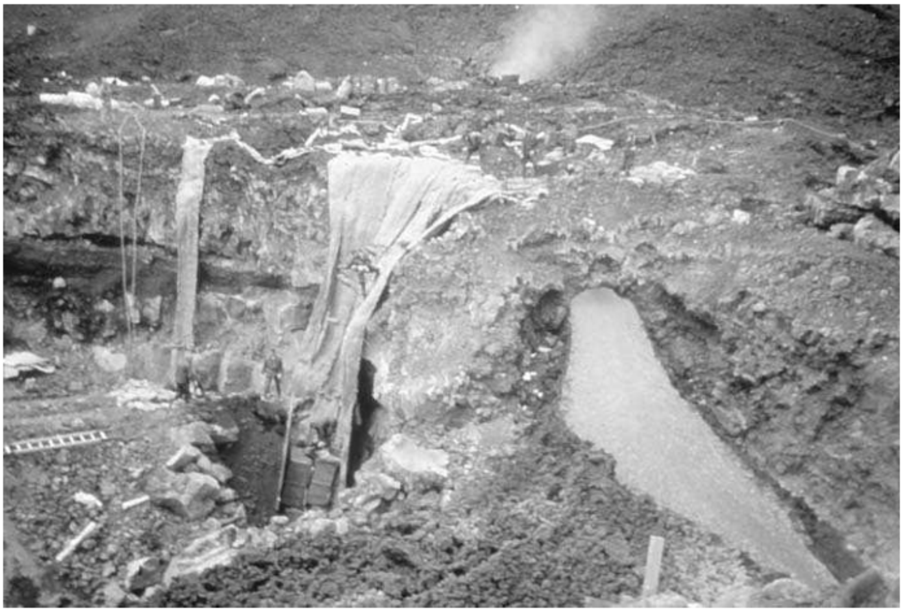

FIGURE 10 Scene showing the engineering preparations to attempt diversion of the natural lava channel (lower right) into an artificial channel (foreground) during the 1991–1992 eruption of Mount Etna, Italy. On 27 May 1992, the detonation of explosives carefully placed in the thin natural separation wall (center) did divert about two-thirds of the lava into the artificial channel (see text); two people (center) give scale of the operations. (Photograph by Franco Barberi.)

ceased on March 31, 1993, with the front of the diverted lava flow stopping about 6 km from Zafferana. The 1992 lava diversion at Etna, while involving substantial expenditure of resources, is generally regarded as being successful in saving the village from lava inundation. Even so, the lava diversion tactics became controversial as serious questions were raised regarding their cost–benefit effectiveness.

Various efforts have been made in Hawaii to change the course of lava flows or to block their paths. In 1935 and 1942, attempts were made to divert the source of supply from Mauna Loa flows advancing toward the city of Hilo by bombing critical segments of the flow by aircraft. Each of these attempts showed promise of success, but both of the eruptions stopped by natural processes before the results could be fully evaluated. Diversion barriers were hastily constructed during eruptions in 1955 and 1960 in attempts to protect villages and other structures from flows issuing from the lower east rift zone of Kilauea. Most of the barriers were eventually overrun, but they succeeded in gaining time. For example, an eastward-moving flow, delayed by a barrier, resumed its advance and was just reaching the base of the lighthouse at the eastern tip of the island when the eruption stopped and the lighthouse was spared. Diversion tactics, however, have been controversial, for complex legal problems can arise when property, which otherwise would have escaped, is overrun by the diverted lava. Further, in Hawaii, many residents are deeply offended when attempts are made to subvert the intentions of Pele, the Hawaiian goddess of volcanoes; they believe, instead, that her mischief should either be accepted with no resistance or be appeased by offerings and ceremonies.

On the island of Heimaey, south of Iceland, an eruption producing massive, slow-moving flows of aa and blocky lava in 1973 destroyed part of the town of Vestmannaeyjar and was threatening to flood the harbor, which was and still remains Iceland's most important fishing port. Initial small-scale trials to cool and hamper progress of the flow by water sprayed from fire hoses showed promise, so the effort was quickly expanded, and finally dozens of high-capacity pumps, mounted on barges in the harbor, pumped as much as a cubic meter of seawater per second through a system of movable plastic pipes, and water was conveyed to strategic areas of the advancing flows and sprayed onto the lava. These efforts succeeded in reducing damage to the town, and, even more importantly, deflected parts of the flow toward the broad mouth of the harbor and into the sea, narrowing the harbor entrance. Fortuitously, the eruption stopped after 5 months, which halted further damage, and at the end of the eruption the newly added land provided the harbor with greatly improved protection from storm waves.

D. Category 4: Inform and Educate Public Officials, Community Leaders, the News Media, and the General Public

A vital element of effective risk reduction is for the population at large to gain an adequate understanding of the current status of neighboring volcanoes, the types of behavior and nature of the hazards characteristic of these volcanoes, and the kinds of work being done by the volcanologists. Scientists should work closely with officials so that each will gain understanding and appreciation of the type of work and responsibilities of the other and of the functions that each must carry out during times of crisis. Good relations with members of the news media should also be fostered, so that news stories about the volcano will be as reliable and informative as possible and will avoid sensationalistic exaggeration. The population at large can be informed by illustrated talks to clubs, service organizations, civic groups, and schools. A well-informed populace is more likely to be willing to promote support for the geological studies, monitoring activities, and efforts at control because they understand the reasons behind the needs for such efforts. Good relations need to be cultivated among all elements of the local population so that officials will understand the need for planning for emergency-management procedures, so the public will be willing to accept them, and so that the scientists will have already established credibility and support for times when it is necessary to declare emergencies.

Mitigation capabilities are still far from being able to stop or control the actual source of lava flows, that is, the volcanic eruptions themselves. However, by making diligent and wise use of resources now available, and the combined procedures summarized above, it should be possible to reduce the loss of life and the damaging effects of many eruptions. By learning to avoid expanding developments into the most vulnerable areas, by planning economic growth in ways that will reduce the risk from volcanoes, by making plans for effective emergency management, and by developing and maintaining monitoring networks aimed at learning the characteristic background behavior of volcanoes and recognizing unrest when it begins, much can be accomplished toward protecting life and property from avoidable losses from volcanic eruptions.

SEE ALSO THE FOLLOWING ARTICLES

Flood Basalt Provinces • Hazards from Pyroclastic Flows and Surges • Hazards of Volcanic Gases • Lava Domes and Coulees • Lava Flows and Flow Fields • Risk Education and Intervention • Volcanic Hazards and Risk Management • Volcano Warnings

FURTHER READING

Blong, R. J. (1984). "Volcanic Hazards: A Sourcebook on the Effects of Eruptions." Academic Press, Sydney.

Chester, D. K. (1993). "Volcanoes and Society." Edward Arnold, London.

Decker, R. W., and Decker, B. (1989). "Volcanoes" (rev. ed.). Freeman, New York.

Fink, J. H., ed. (1989). "Lava Flows and Domes: Emplacement Mechanisms and Hazard Implications," IAVCEI Proceedings in Volcanology, Vol. 2. Springer-Verlag, Berlin.

Fisher, R. V., Heiken, G., and Hulen, J. B. (1997). "Volcanoes: Crucibles of Change." Princeton Univ. Press, Princeton, NJ.

Kilburn, C. R. J., and Luongo, G., eds. (1993). "Active Lavas: Monitoring and Modelling." UCL Press, London.

Scarpa, R., and Tilling, R. I., eds. (1996). "Monitoring and Mitigation of Volcano Hazards." Springer-Verlag, Berlin.

Tilling, R. I. (1989). Volcanic hazards and their mitigation: Progress and problems. *Rev. Geophys.* **27,** 237–269.

This Page Intentionally Left Blank

THE HAZARD FROM LAHARS AND JÖKULHLAUPS

KELVIN S. RODOLFO
University of Illinois at Chicago

I. Introduction
II. Lahar Characteristics and Hazard Implications
III. Crater Lake Expulsions: The Lahars of Gunong Kelut
IV. Eruption Snowmelt: The 1985 "Worst-Case" Armero Disaster
V. Mount Pinatubo: The Long Aftermath of Rain Lahars
VI. Mitigating the Lahar Hazard

GLOSSARY

debris flow Viscous, flowing slurry of rock fragments containing 10 to 25 wt% water. Unlike normal streamflows, in which water carries sediment, in debris flows the solid material carries water, which lubricates the flow. Debris flows commonly move as fairly coherent "plugs" with laminar flow, but they also may display pronounced turbulence and standing waves. Debris flows are not restricted to volcanoes; they occur in any environment with abundant soil or rock debris that experiences intense rains or sudden floods.

hyperconcentrated streamflow Turbulent flow of water mixed with enough sediment (60–75 wt%) to possess some yield strength. Such flows look little different from normal sediment-laden stream floods, but flow faster and with greater energy, and commonly display large standing waves that may break like surf in the upstream direction. They display a spectacular tendency to erode stream banks laterally.

jökulhlaup An Icelandic term that refers without distinction to both water floods and lahars that are generated when a volcano erupts under a glacier.

lahar An Indonesian term meaning a stream of water mixed with more rock than normal streams carry that roars as it flows rapidly down a volcano, and commonly reaches the surrounding plains. Most scientists reserve the term for the *process* and not to the deposit it leaves, but this distinction is ignored in much popular usage. Lahars closely associated with eruptions sometimes are called "primary lahars" to distinguish them from the "secondary lahars" that are not induced by eruptions. Some pre-1980s scientific literature uses "lahar" and "volcanic debris flow" synonymously, or refers to laharic debris flows as "true lahars." This usage incorrectly ignores the more fluid lahars (the hyperconcentrated transitions from normal, turbid streamflow to debris flow), and the fact that a single lahar can consist of multiple, alternating hyperconcentrated and debris flow phases. Many lahars are composed chiefly of sand and coarser materials, and thus should not be called "mudflows." The rock content of a lahar deposit is usually, but not exclusively, volcanic, because a lahar can flow through nonvolcanic terrain from which it can erode and incorporate enough rock to increase its load several times.

mudflow A flowing mixture of water and sediment composed dominantly of mud. They occur in both volcanic

Copyright © 2000 by Academic Press
All rights of reproduction in any form reserved.

and nonvolcanic terrains. Mudflows can entrain and buoy along boulders and equivalently sized artifacts like vehicles. The term is popularly and even scientifically used as a synonym for lahar—incorrectly for many lahars that are coarser than mud, and therefore flow much differently and leave different deposits. To avoid confusion that may worsen the lahar hazard, the term should be used exclusively for flows that genuinely are composed mostly of mud. Genuine laharic mudflows, if their fine components are powders of glass and feldspar instead of phyllosilicate minerals, also do not behave like mudflows in well-weathered terrains.

muds Admixtures of silt (particle diameters of 2–62 μm) and clay (grains finer than 2 μm), regardless of mineralogy. The most common clays in muds are weathering products, phyllosilicates ("leaf silicates") with platy or fibrous crystal structures that can assimilate and release water molecules and carry electrostatic charges, and thus strongly influence the properties and behavior of the mud. All tephra grains finer than 2 μm are technically clay, but ground glass and feldspar, such as compose the fine content of fresh volcanic debris and lahars, do not have phyllosilicate properties, and even when abundant do not affect the properties of slurries in the same way.

A SLURRY OF water and volcanic debris that roars loudly as it flows down a volcano is what Indonesians call a *lahar*, and it rivals the pyroclastic flow for the distinction of being the most deadly and destructive volcanic phenomenon. In terms of deaths from individual 20th century disasters, the lahars generated by the 1985 eruption of the Colombian volcano Nevado del Ruiz that buried more than 23,000 people in the town of Armero are outranked only by the pyroclastic flows that destroyed the town of St. Pierre and killed 29,000 people during the 1902 eruption of Mount Pelée on the Caribbean island of Martinique.

I. Introduction

In terms of the cumulative fatalities they have caused, lahars are more devastating than pyroclastic flows for several reasons. They flow farther down volcanic slopes to the more heavily populated plains. Requiring only the sudden admixture of large amounts of water with abundant, loose or easily eroded debris on a volcano slope, they can be formed in a remarkable variety of ways (Table I). Thus they occur more frequently, at many more volcanoes, and over longer periods of time than pyroclastic flows.

Unlike any other volcanic hazard, lahars do not require an eruption to occur. They can be triggered by bad weather or by edifice failure long after an eruption—a timing that can worsen the hazard, because the people in harm's way have become less alert. For example, during a hurricane in October 1998, an avalanche and lahars on Casita volcano in Nicaragua killed an estimated 1600 people. Only one of five volcanoes in a complex that is dominated by the frequently active San Cristobal volcano, Casita itself has no historic record of eruption. Similarly, during the 4 centuries that records have been kept at Mount Mayon in the Philippines, the most lethal of all events, including eruptions, was a lahar that killed 1500 people in 1875. It was generated by typhoon rains 3 years after an eruption, and thus is excluded from most catalogs of volcanic disasters. Many other lahars that occur during volcanic quiescence in remote wilderness, lethal or not, go unobserved and unreported because, unlike an eruption, a lahar descending a single valley is not visible from afar.

The laharic aftermath of the 1902 eruption of Santa Maria volcano in Guatemala lasted at least 22 years. A comparable period of lahar activity is well underway following the 1991 eruption of Mount Pinatubo in the Philippines. In that developing country, poor people cannot avoid the hazard, and must learn to live with it.

Death and devastation from a natural hazard very often have been compounded by societal inadequacies. By unfortunate coincidence, the Earth's tropical belt holds more than its share of rainstorms; explosive, debris-generating volcanoes; and developing countries with exploding populations. Lahars can be triggered by the strongest normal monsoon rains, which can be intensified and sustained greatly by passing typhoons or hurricanes. The warm, moist climate immediately attacks and weathers fresh lahar deposits into fertility, and so farmers resettle volcano aprons in increasing numbers, forced by poverty, population pressure, and custom to accept natural risks in exchange for livelihood.

The theoretical and physical bases for laharic flow are treated in detail elsewhere in this volume; here, lahar characteristics are reviewed insofar as they impinge directly on the lahar hazard. Then, to illustrate the variety and behaviors of lahars, and how the hazards they pose may be mitigated, we examine those that have occurred at three volcanoes: Gunong Kelut in Indonesia, where lahars were first described; the Colombian volcano Nevado del Ruiz; and Mount Pinatubo in the Philippines, where lahars began to flow during the 1991

TABLE I Notable Examples of Lahars and Their Triggering Mechanisms

Mechanism	*Volcano, occurrences*	*Fatalities*	*Remarks*
Penecontemporaneous with eruption			
Crater lake expulsion	Galunggung, Indonesia, 1822	3,600	10^8 m^3 of deposits
	Kelut, Indonesia, 1919	5,110	130 km^2 covered
	Ruapehu, New Zealand, 1975		
Crater lake breakout (wall failure)	Pelée, Martinique, 1902	25	
Subglacial eruption (jökulhlaups)	Öraefajökull, 1727	3	
	Katla, Iceland, 1918		Peak discharge 3–4 × 10^5 m^3/s
	Gjálp, Iceland, 1996		
Snowmelt	St. Helens, USA, 1980[a]	6[a]	
	Nevado del Ruiz, Colombia, 1985	23,000	
	Ruapehu, New Zealand, 1975		
Pyroclastic flows entering streams	Asama, Japan, 1783	550	
	Santa Maria, Guatemala, 1929		Lahars traveled 100 km
	St. Helens, USA, 1980[a]	6[a]	
Landslide	White Island, New Zealand, 1914	11	
Avalanches into lakes and streams	St. Helens, USA, 1980[a]	6[a]	
Rain during eruption	Agung, Indonesia, 1963	200	
During volcanic quiescence			
Avalanche	White Island, New Zealand, 1914		
Crater lake failure	Ruapehu, New Zealand, 1953	151	Peak discharge 850 m^3/s; 1.9 × 10^6 m^3
Crater lake failure (man-made?)	Parker, Philippines, 1995	100–500	
Heavy posteruptive rain	Irazu, Costa Rica, post-1964		Peak discharge 497 m^3/s
	Mayon, Philippines, post-1984		
	Pinatubo, Philippines, post-1991		
	Semeru, Indonesia, 1981		
Lake breakouts	Santa Maria, Guatemala, post-1902		
	Pinatubo, Philippines, post-1991		
Earthquake-induced avalanche on extinct volcano	Ontake, Japan, 1984		

[a] Multiple triggering mechanisms.

eruption and likely will continue to be generated into the 21st century.

II. LAHAR CHARACTERISTICS AND HAZARD IMPLICATIONS

A. Jökulhlaups

In Antarctica, arctic North America, and Iceland, eruptions of volcanoes under glacial ice generate large amounts of meltwater that are suddenly released as great "glacier bursts" called *jökulhlaups* in Iceland, where they have been best studied. Jökulhlaups include water floods as well as the dilute and viscous lahars that, by definition, carry more sediment than normal floods do.

Meltwater from subglacial eruptions collects in calderas, forming lakes that can be entirely covered by ice, as at Katla volcano in Iceland, or partly visible at the surface, as at Grimsvötn volcano. In either case, when meltwater has accumulated deeply enough to float the ice off its base, it can suddenly escape in large volumes—7 km^3 during the 1937 Grimsvötn eruption. Discharge rates are enormous, estimated at 300,000 to

400,000 m^3 per second during the 1918 Katla eruption—on the order of 20 times the discharge of the Mississippi River. Huge blocks of ice, fresh volcanic debris including hyaloclastites or shattered volcanic glass, and large boulders incorporated by the floods along the way can be carried large distances, forming, for example, the extensive "sand plains" of southern Iceland.

A subglacial fissure eruption in October 1996 at a new site between the subglacial Grimsvötn and Bárdarbunga calderas under the Vatnajökull icecap (Figure 1) gives a sense of the duration and magnitude of a large jökulhlaup. Gjálp, the new volcano, erupted for 13 days, melting 3 km^3 of ice, at peak rates of 0.4 to 0.6 km^3 per day. An additional ice volume of 1.2 km^3 was melted during the first 3 posteruption months. Much of the water, with temperatures of 15 to 20°C, drained south into the Grimsvötn caldera, from which a jökulhlaup with a volume of 3.5 km^3 was discharged on November 4–7, at peak discharges of 45,000 m^3 per second, carrying large volumes of sediment and blocks of ice up to 15 m in diameter and weighing up to 2000 tons.

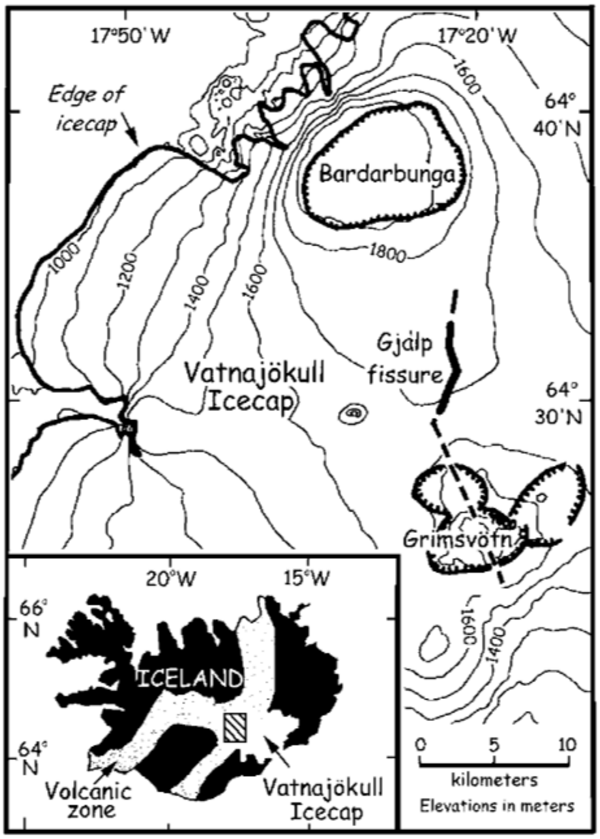

FIGURE 1 Map of the northwest part of the Vatnajökuli icecap, showing the Grimwsvötn and Bárdarbunga calderas and the Gjálp fissure volcano between them. [Modified from Gudmundsson, M. T. *et al.* (1998). Ice-volcano interaction of the 1996 Gjálp subglacial eruption, Vatnajökul, Iceland. *Nature* **389,** 954–957.]

Given the intense scientific and media scrutiny before the Gjálp event, it is no surprise that no casualties were incurred. Curiously, historical records of casualties from jökulhlaups are very rare, possibly due to low population densities. The only fatalities mentioned in the literature are of two women and a boy swept off a roof by the Öraefajökull jökulhlaup in 1727, which also killed 600 sheep and 150 horses. Only one woman was recovered; the mud had been hot enough to parboil her corpse.

B. Dilute Lahars (Hyperconcentrated Streamflows)

The more dilute lahars are called hyperconcentrated streamflows because their sediment loads are greater than those of the most turbid normal streams. Apart from displaying prominent standing waves, dilute lahars look deceptively little different from normal, dirty floodwaters (Figure 2). But more than half of the slurry—anywhere from 60 to 75% by weight—is solid material, and velocities of 20 km per hour are not uncommon. People or even trucks and buses trying to cross dilute lahars have often been carried downstream.

Even while flowing vigorously, a hyperconcentrated lahar can deposit sediment, raising its bed several centimeters in an hour. Thus the lahar may force itself to shift sideways and vigorously erode its bank. Lateral erosion rates of 6 m per minute have been documented at Pinatubo volcano. If the flow persists, a stream bank can retreat as much as a kilometer in a few hours, and if houses are in the way, they fall in and are washed away (Figure 3). The least intense lahar events consist entirely of hyperconcentrated streamflows.

C. Channelized Debris Flows

In the larger and most powerful lahars, hyperconcentrated flows are merely the dilute advance warning of approaching debris flows, the most spectacularly sediment-laden and destructive variety of lahar. In a debris flow, the water is no more than about 25 wt%, and as low as 10%—barely enough to mobilize the debris. Being viscous, debris flows tend to move in a fairly straight-line or laminar fashion, or even as coherent "rigid plugs"

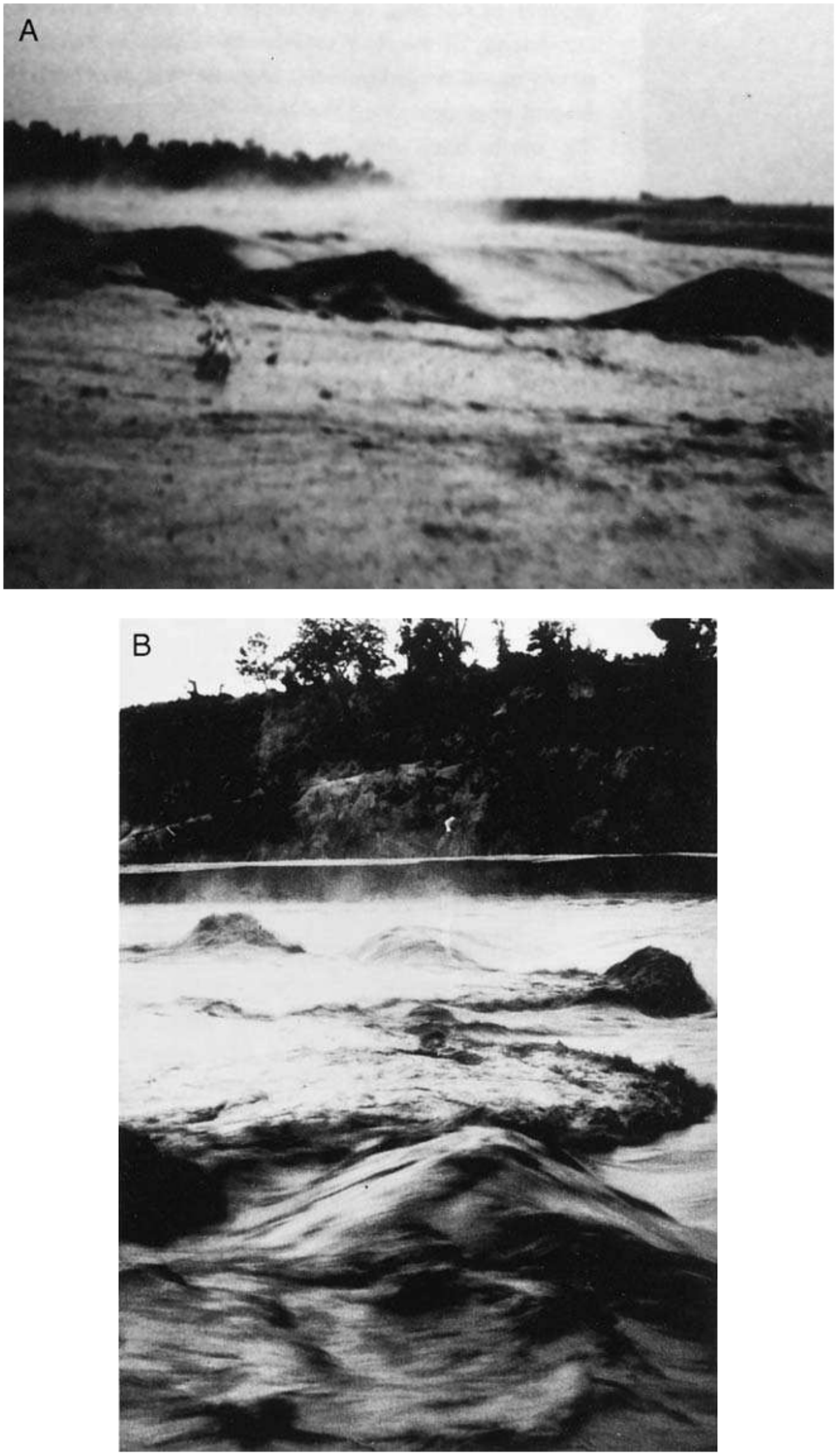

FIGURE 2 Hyperconcentrated lahars along the Santo Tomas River, southwestern sector of Mount Pinatubo. (A) Standing waves 6 m long and 1.5 m high. (B) Waves breaking in the upstream (right) direction during transition from hyperconcentrated to debris flow. [Reproduced with permission from Rodolfo *et al.* (1996). Page 1002 *in* "Fire and Mud: Eruptions and Lahars of Mount Pinatubo, Philippines" (C. G. Newhall and R. S. Punongbayan, eds.). Univ. Washington Press, Seattle.]

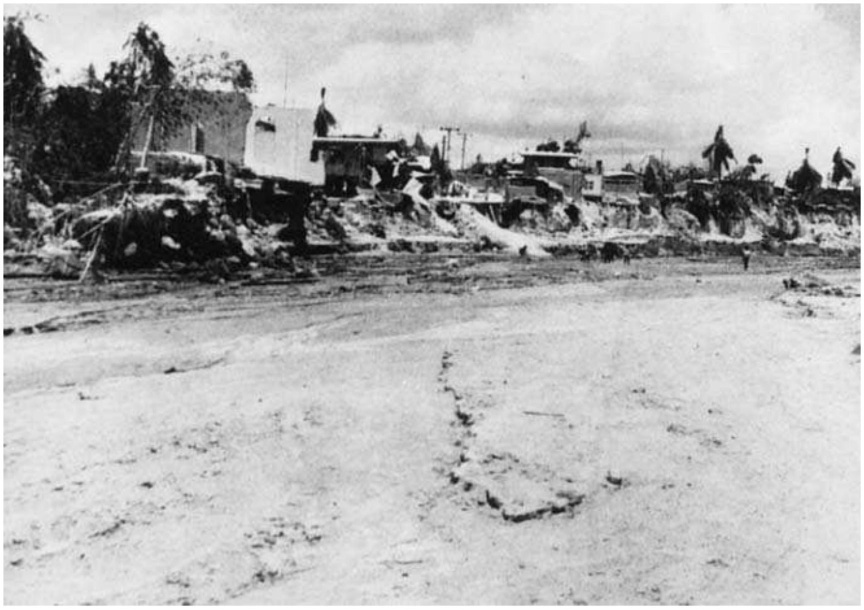

FIGURE 3 Damage to houses caused on June 15, 1991, by lateral bank erosion along the Abacan River, eastern sector of Mount Pinatubo. Also see Figure 7. [Reproduced with permission from Major, J. J., *et al.* (1996). Page 909 *in* "Fire and Mud: Eruptions and Lahars of Mount Pinatubo, Philippines" (C. G. Newhall and R. S. Punongbayan, eds.). Univ. Washington Press, Seattle.]

(Figure 4A). Unlike floodwaters, however, they have the curious property of being less viscous at higher speeds, and can display remarkable turbulence (Figure 4B). Flow velocities of 15 to 30 km per hour (4–8 m/s) are common on the slopes of typical composite volcanoes. At Nevado del Ruiz in 1985, laharic debris flows confined in long, steep, narrow valleys attained velocities of over 60 km per hour (17 m/s). Lahar speeds of 140 km per hour were reported at Mount St. Helens in the United States in 1980, and 180 km per hour at the Japanese volcano Tokachi in 1926.

Owing to their high densities, thicknesses, and velocities, debris flows exert powerful shear stresses on their channels and especially on their bases. Thus, they feed on their own success—"bulking up" or swelling to a remarkable degree as they travel by eroding and incorporating an even more remarkable amount of rock along the way. If, for example, the average specific gravity of the rock is twice that of water, a debris flow starting out with 25% of its weight as water can bulk up to twice its original volume by eroding enough rock from its channel to triple its weight of solid load. The potential to bulk up is limited only by the need for the minimum 10% water necessary to lubricate the flow. Lahars that flowed down Irazu volcano in Costa Rica after its 1964 eruption reportedly swelled sixfold in volume.

The hazard implication of bulking is that reports of lahar size and consistency from an upstream observer may greatly underrepresent the lahar that reaches the plains below. For example, at Pinatubo in 1995, when typhoon floodwaters began arriving at an upstream observation post, lahar watchers on the Pasig-Potrero River radioed the authorities below. Being used to floods, the people were reassured and went about their business. However, as the floods continued descending along 22 km of channel, they bulked up enormously and with shocking speed into debris flows that entirely buried Barangay Cabalantian, a village with 2000 houses, in debris up to 9 m thick (Figure 5), killing hundreds of people.

It is difficult to determine the maximum depth of scour attained during the peak debris flow stages of a lahar, because as it wanes, hyperconcentrated streamflows usually fill up the channel again to an unknown degree that depends on the size of the lahar and on other factors that vary from site to site. A lahar-containment structure with an appropriately deep foundation cannot be built until the maximum possible scour depth at that site can be estimated, because debris flows also migrate laterally and could undermine footings that are too shallow. One lahar at Mount Pinatubo in 1997 first deposited about 12 m of debris, and then eroded through it and continued scouring downward an additional 25 m. At this site, then, an effective dike would be much too

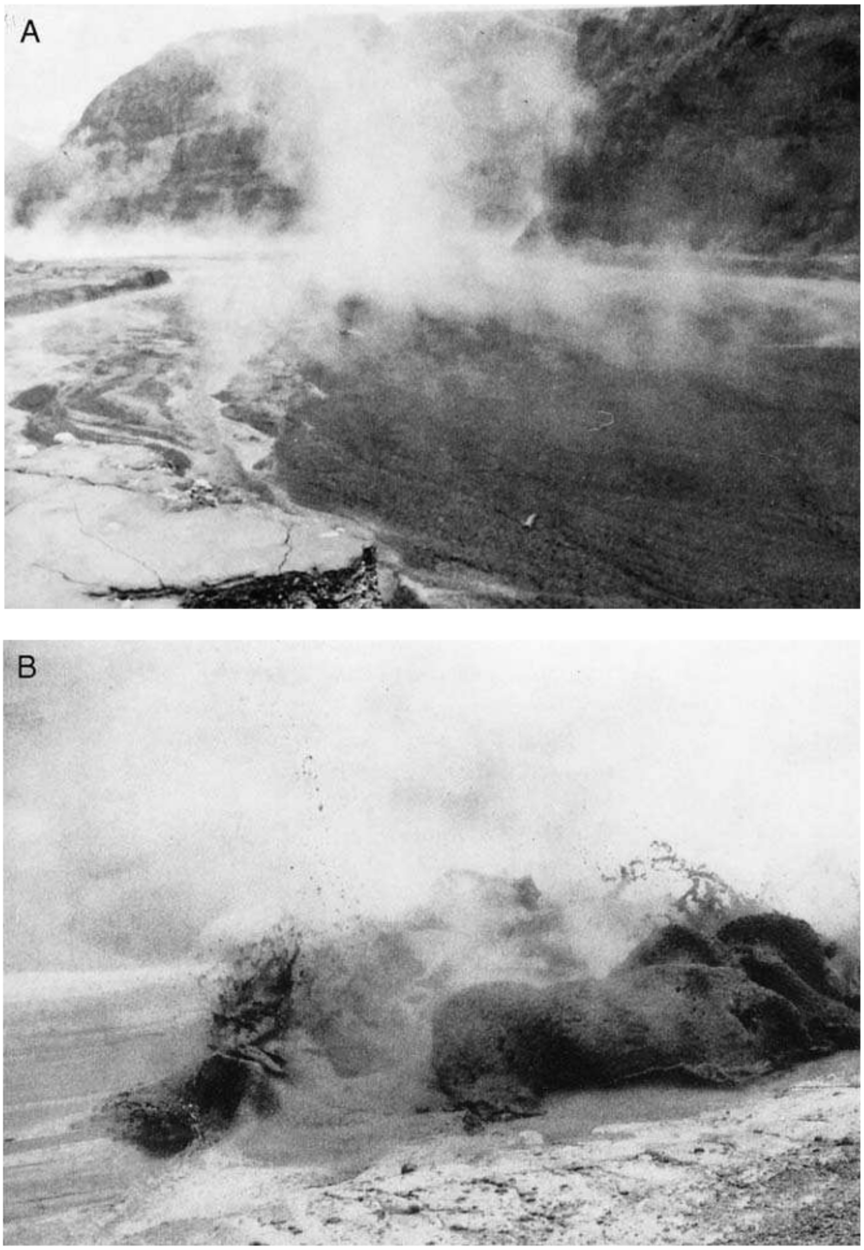

FIGURE 4 Steaming debris flows at adjacent sites along the Sacobia River, northeastern sector of Mount Pinatubo, Philippines, in August 1991, 2 months after the paroxysmal eruption. The fluid temperatures were 50–60°C, and sediment contents were 85% by weight and 70% by volume. The flows were 15 m wide and about 2 m deep. Velocities were 17 to 21 km per hour (4.8–5.9 m/s). (A) The flow here, toward the camera, appears to be a "rigid plud" in its center. (B) Here, downstream from (A), the channel was locally steeper and more constricted. Flowing from left to right, the tubulent debris flow formed standing waves about 1 to 2 m high that broke violently in the upstream direction. [From Pierson *et al.* (1996). Page 942 *in* "Fire and Mud: Eruption and Lahars of Mount Pinatubo, Philippines" (C. G. Newhall and R. S. Punongbayan, eds.). Univ. Washington Press, Seattle.]

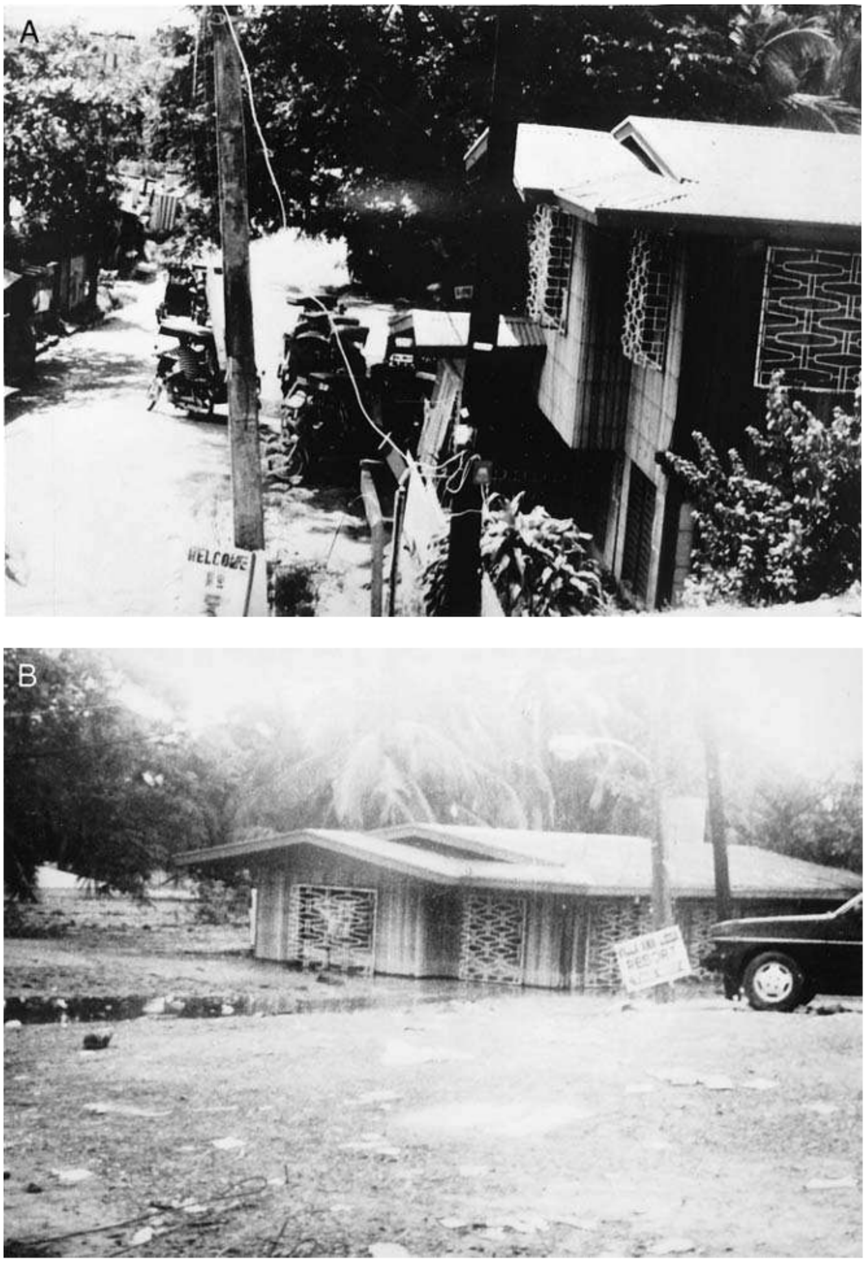

FIGURE 5 A house in the village of Cabalantian, 30 km from the caldera of Pinatubo volcano (A) before and (B) after the lahar disaster of October 1, 1995. Previously untouched by lahars, the entire village was buried in the deposits of lahars that flowed for 4 to 6 hours. [Photographs collected and taken by the Philippine Institute of Volcanology and Seismology. Modified with permission.]

expensive to construct because it would have to be seated too deeply.

Debris flow densities can be twice that of water, and buoyancy effects cause flow behaviors that are spectacularly different from stream floods. Even the strongest of mountain torrents preferentially transport finer sediment and leave the boulders behind. In many debris flows, however, the boulders immersed in the slurry have lost much of their effective weight, and jostle each other so strongly that they may be bounced and lifted toward the surface and center of the lahar. There, the flow is smoothest and velocities are greatest, and bobbing boulders weighing up to 200 tonnes can be rafted 10 km or more to the front of the lahar (Figure 6). A moving, rapidly evolving dam consisting of boulders that have reached the front maintains the thickness of the flow behind it that is pushing it along.

A lahar can fling boulders and logs against a bridge or dam, exerting impact forces of 10 to 1000 tonnes per square meter—forces that few structures can withstand. In addition, most engineering edifices are designed to withstand gravity, not the opposite buoyant forces exerted by the higher densities of debris flows that reduce their effective weights, lifting them and making them even more susceptible to the lateral battering. Furthermore, lahars triggered by protracted rains can flow for several days as alternating dilute flows and debris flows, each in turn testing a structure with its own destructive behaviors (Figure 7).

D. Lahar Noise

To Indonesians who have experienced lahars, the very term evokes the roaring of clashing and tumbling boulders, "like a thousand stampeding water buffalo." Mount Pinatubo tephra contains few boulders, and so when it is mobilized into flowing lahars the frequencies of the noise are higher, "like a giant's sandpaper." The sound, if not drowned out by eruption or storm noise, is commonly loud enough to precede the arrival of the lahar by as much as half an hour—a precious interval during which people can escape to safety on high ground.

E. Debris Flow Temperatures

Being volcanic debris admixed with water, lahars cannot have bulk temperatures above that of boiling water, although individual boulders or cobbles may have internal temperatures of several hundred degrees. If the tephra are pumiceous and thus are poor thermal conductors, as at Mount Pinatubo, they may insulate the deposits on volcano flanks and keep temperatures only a few meters below the surface at several hundred degrees for many years after an eruption. During that period, the flood from a strong rainstorm or the sudden breaching of a crater lake wall can incise quickly into the hot debris, generating large steam explosions and hot lahars.

Although common, scalding is not the main cause of injury and death from either eruption or posteruptive lahars. Most trauma and fatalities are effected by suffocation, resulting from rapid burial, because rates of deposition are typically meters per hour or minute or, exceptionally, per second.

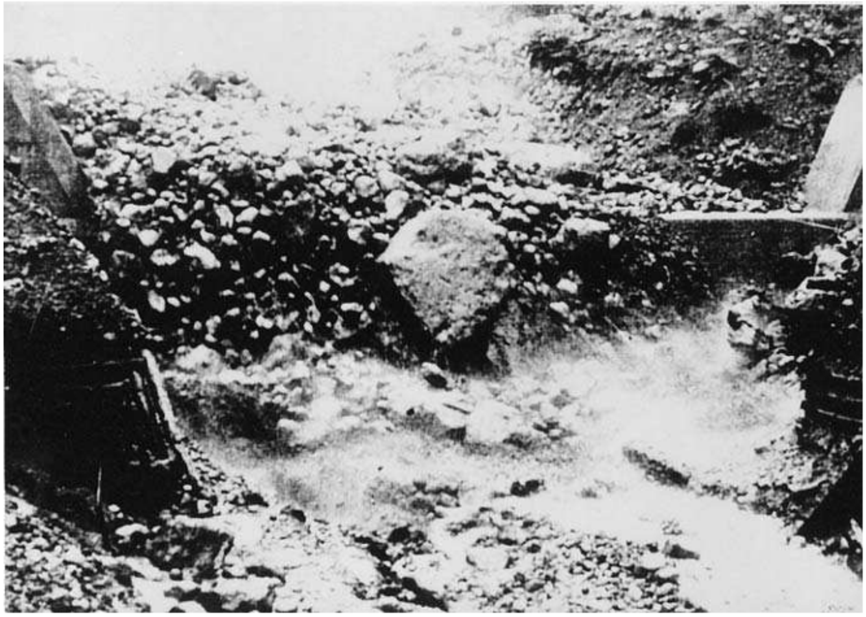

FIGURE 6 Boulder front of a laharic debris flow overtopping a sediment-retention structure. The largest boulder is 2 m in diameter. [Reproduced with permission from the Ministry of Construction, Japan.]

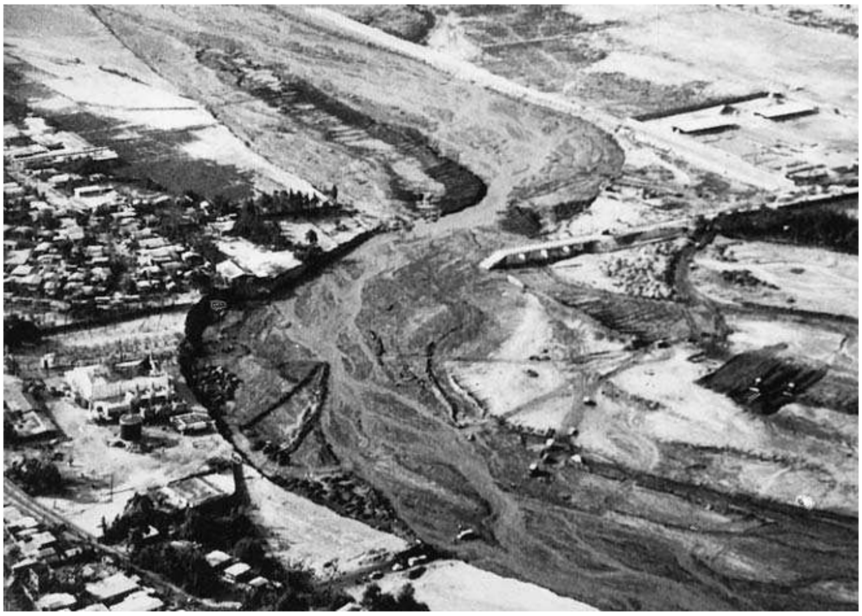

FIGURE 7 Bridge across the Abacan River in Angeles City destroyed by debris flows during the 1991 eruption of Mount Pinatubo. The channel bank to the left has been severely eroded by hyperconcentrated streams. [Reproduced with permission from Major *et al.,* 1996, p. 910.]

Hot debris can continually release heat into a debris flow, generating water vapor that may decrease its viscosity, lubricate it, and increase its speed. In that sense, lahar temperature may enhance the hazard.

F. Overbank Debris Flows

The slope down which a debris flow moves is a primary factor in determining its speed, and so it must eventually slow down and stop. Emerging from a mountain canyon and spreading out over gentler slopes, or bulking up so much that it overflows its banks, a debris flow is rarely more than several meters thick, and so any low hill or slope can serve as safe refuge. As a debris flow spreads, basal area and frictional resistance increase, slowing it down. Debris flows are more viscous at lower speeds; this causes them to slow down even more quickly. As a consequence, spreading lahars are not powerful enough to topple even fragile structures such as thatched huts, and merely flow around and into them, and bury their bases (Figure 8). People trapped in the path of an overbank lahar can escape by climbing to the roofs of the tallest buildings or trees in their vicinity.

Owing to the rapid rates at which lahars can lay down their sediments, fresh deposits may remain loose and water-saturated for days to weeks. Debris flows possess strength even while they flow, and leave lobate deposits with abrupt edges. If the sediment masses contain little silt and clay, the water can drain out of their higher portions fairly quickly. Draped over a high-standing road, new deposits can harden enough to take the weight of vehicles in only a few hours. The deposits drain less rapidly if they contain substantial clay. If they are deposited in topographic lows, especially river channels, they can remain saturated and have the consistency of quicksand for weeks or months. People and vehicles bogged down in such deposits can be extricated only with difficulty, and entrapped animals often starve to death.

III. CRATER LAKE EXPULSIONS: THE LAHARS OF GUNONG KELUT

Lahars have been generated on many volcanoes that contain crater lakes, including 16 in Indonesia alone. Of these, Mount Kelut on the island of Java (Figure 9) is the most famous, for its crater expulsion in 1919 holds the record for the number of people killed by lahars generated in that manner. Kelut also offers one of the more spectacular examples of lahar mitigation by engi-

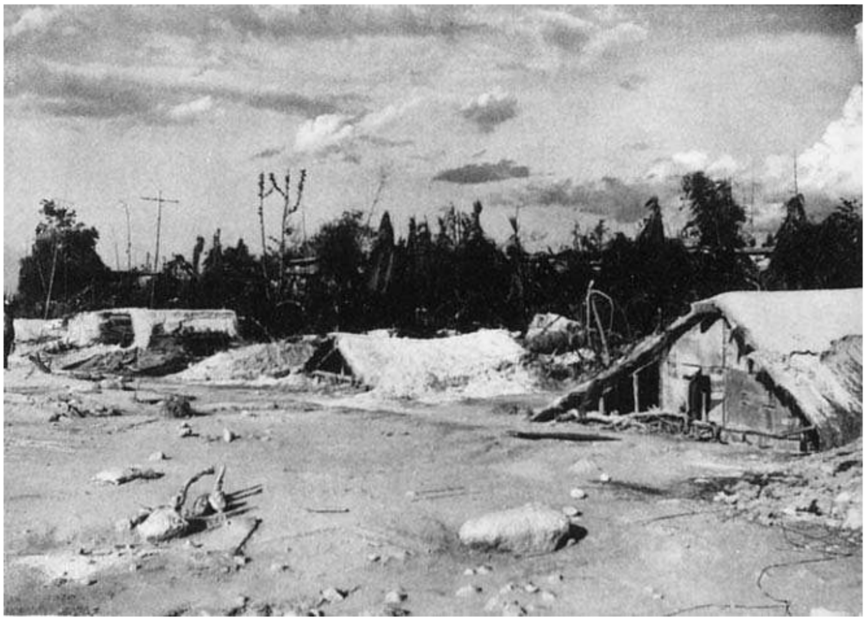

FIGURE 8 Thatched huts buried by lahars during the 1991 eruption of Mount Pinatubo. [Reproduced with permission from Major *et al.,* 1996, p. 909.]

neering. (J. B. Scrivenor's 1929 description of that event also introduced the term *lahar* to the scientific literature.)

The summit crater of Kelut contains a lake elevated about 1700 m (more than a mile) above sea level. As is characteristic of composite volcanoes in the tropics where fresh tephra weathers quickly into fertility, the area surrounding the volcano is intensively cultivated and densely populated by more than 500 people per square kilometer. Kelut erupted without warning in 1919, suddenly disgorging 40 million m^3 of lake water. Escaping from the lowest portions of the crater rim, the water rushed down three sides of the volcano. The floods were so strong and turbulent that they quickly picked up large amounts of rock debris along the way, bulking up into lahars. Carrying huge numbers of boulders and trees, the three lahar tongues raced down the flanks of the volcano at speeds up to 64 km per hour. In less than an hour, the longest flow had extended 38 km from the summit. Spreading out over an area of 131 km^2, the lahars buried many villages, killing more than 5000 people. Especially hard hit was the southwestern sector of the volcano, where coalescing flows overwhelmed the adjacent drainages of the Temas and Ngoglik rivers.

The Dutch colonial government recognized that the volumes and distances reached by Kelut's eruption lahars depend on the volume of crater lake water released. In 1923 engineers began to tap the crater lake with a series of drainage tunnels in order to reduce its volume in stages from 38.5 to 1.8 million m^3 (Figure 10). Continuous crumbling of the inner crater wall raised the bottom of the crater, further reducing the lake volume. In 1951, when a minor eruption occurred, the lake contained only about 1 million m^3 of water, and so no major lahars were generated. The eruption, however, deepened the crater floor and restored the original capacity of the lake.

Mount Kelut erupted again on April 24, 1966, again with little warning. Only about 20 million m^3 of water was expelled—about half the volume of the 1919 event—and thus the lahars were much smaller. As anticipated, they followed the same general paths of the 1919 flows. Fortunately, even though the inhabitants had little warning, most had experienced lahars in the past, and were alerted by their roaring approach. Overtopping the river banks about 500 m above sea level, the lahars fanned out, burying 45 km^2 of farmland and several villages. Most of the people had fled to designated safe areas, but 282 people were killed, mostly the aged, women, and children.

A new tunnel to drain the crater lake, completed in 1967, has kept the lake at low levels. Three successive eruptions have since shown that destructive eruption lahars are not generated if the volume of the crater lake is kept below 1 million m^3.

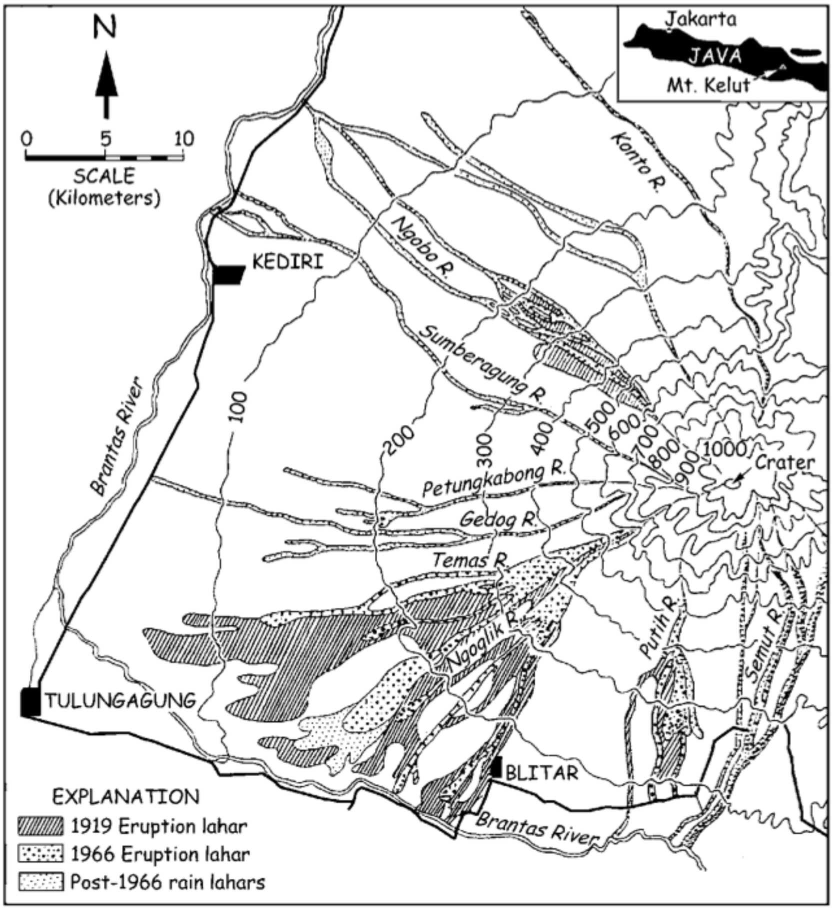
N
0
5
10
SCALE
(Kilometers)
Jakarta
JAVA
Mt. Kelut
Konto R.
Ngobo R.
KEDIRI
Sumberagung R.
Brantas River
100
200
300
400
500
600
700
800
900
1000
Crater
Petungkabong R.
Gedog R.
Temas R.
Ngoglik R.
Putih R.
Semut R.
TULUNGAGUNG
BLITAR
Brantas River
EXPLANATION
1919 Eruption lahar
1966 Eruption lahar
Post-1966 rain lahars

FIGURE 9 Map of Mount Kelut. [Modified from an unpublished monograph of the Japan International Cooperation Agency.]

A. Containing Rain Lahars at Kelut

Lahars in the years of quiescence following the 1951 eruption raised the bed of the Brantas River by 2 m or more, causing flooding of the lower reaches of the river and its tributaries during rainy seasons. Pyroclastic flows of the 1966 eruption filled the summit valleys, and the downstream valleys were choked with the deposits of eruption lahars. Much of this loose material was remobilized and transported downslope during subsequent rainy seasons, dramatically increasing the load of the Brantas River (Figure 9). Massive lahar deposits in the lower reaches caused the river to overflow its banks and to create new courses, and so new areas were successively buried, and seasonal flooding increased in the industrial city of Kederi.

To minimize the volume of loose volcanic material entering the river, a series of check dams and sand pockets with a total storage capacity of 40 million m^3 were constructed. To contain the rain lahars, the depositional area was bounded by dikes, but by 1994 the continuous deposition had raised the river bed 1.5 m above the surrounding paddy fields. Such a situation itself constitutes a hazard, because major lahars can be produced if the dikes are breached and the escaping waters remobilize the previously trapped debris.

IV. ERUPTION SNOWMELT: THE 1985 "WORST-CASE" ARMERO DISASTER

Nevado del Ruiz is a volcano in the Central Cordillera of Colombia (Figure 11). *Nevado* means "snowy"; although the volcano is situated near the equator (lat. 4°54′ N), it stands more than 5 km above sea level, and thus has a permanent cap of snow and ice. On November 13,

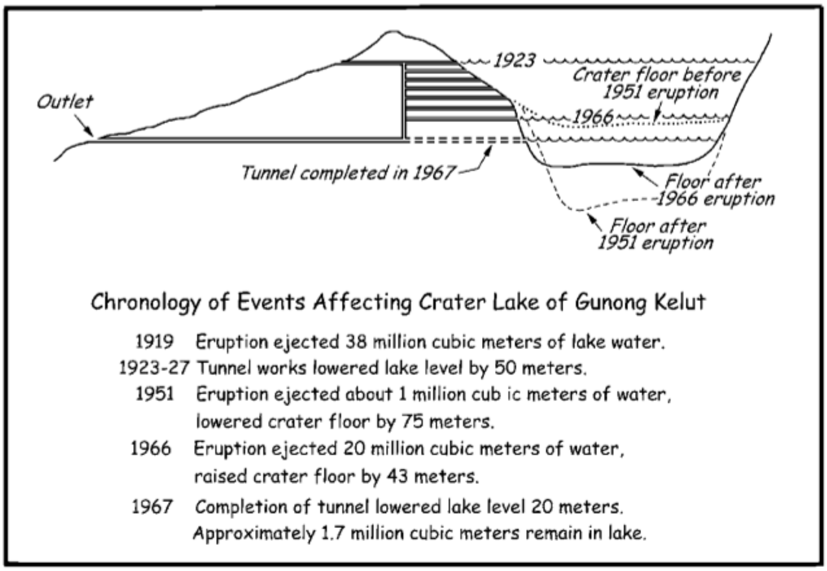
1923
Crater floor before 1951 eruption
Outlet
1966
Tunnel completed in 1967
Floor after 1966 eruption
Floor after 1951 eruption

Chronology of Events Affecting Crater Lake of Gunong Kelut

1919 Eruption ejected 38 million cubic meters of lake water.
1923-27 Tunnel works lowered lake level by 50 meters.
1951 Eruption ejected about 1 million cub ic meters of water, lowered crater floor by 75 meters.
1966 Eruption ejected 20 million cubic meters of water, raised crater floor by 43 meters.
1967 Completion of tunnel lowered lake level 20 meters. Approximately 1.7 million cubic meters remain in lake.

FIGURE 10 Cross-sectional sketch of Mount Kelut showing drainage-tunnel system and modifications of crater lake level and floor due to tunnel drainage and eruptions. [Modified from an unpublished monograph of the Japan International Cooperation Agency.]

1985, shortly after 9 P.M., hot tephra from a relatively small series of pyroclastic flows and surges swept across the snowpack, generating an estimated 20 million m^3 of meltwater. Mixed with tephra into dilute slurries, the discharge descended along three major valley systems that drain the volcano. Coursing down the narrow valleys, the flows eroded great quantities of rock from their channels, and bulked up into huge lahars, with peak discharges of 48,000 m^3 per second and maximum velocities of over 60 km per hour (17 m/s). Only 4 hours after the eruption, the flows had descended 5100 m, wreaking havoc as far as 104 km away from the summit crater and burying more than 2100 km^2 of volcano apron and adjacent plains in 90 million m^3 of slurry.

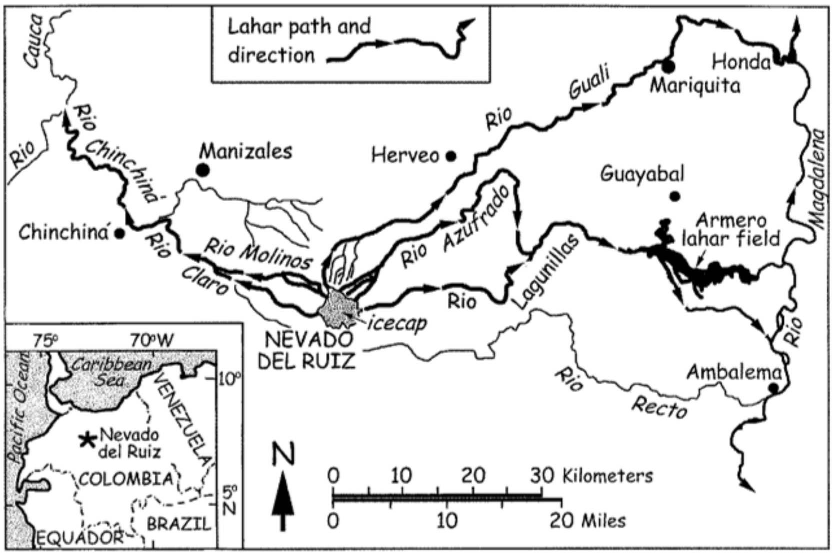
Lahar path and direction
Cauca
Rio
Rio Chinchiná
Manizales
Herveo
Rio
Guali
Mariquita
Honda
Guayabal
Magdalena
Chinchiná
Rio Claro
Rio Molinos
Rio Azufrado
Lagunillas
Armero lahar field
Rio
icecap
NEVADO DEL RUIZ
Rio
Rio Recto
Ambalema
75°
70°W
Caribbean Sea
Pacific Ocean
VENEZUELA
10°
Nevado del Ruiz
COLOMBIA
5° N
BRAZIL
EQUADOR
N
0 10 20 30 Kilometers
0 10 20 Miles

FIGURE 11 Map of Nevado del Ruiz volcano showing routes followed by the lahars of the 1985 eruption of Nevado del Ruiz volcano.

The Rio Azufrado, the principal lahar conduit, enters the Rio Lagunillas about 20 km upstream of the town of Armero, which lay 74 km from the summit crater along the more circuitous Azufrado route. The first and strongest Azufrado lahar emerged from the Lagunillas Valley and arrived at Armero at about 11:35 P.M. with a frontal velocity of about 43 km per hour (12 m/s). Lasting 10 to 20 minutes, it inundated the town in slurry 2 to 5 m thick (Figure 12). At 11:50 P.M., before the first lahar could recede, a second pulse with about half the velocity arrived and lasted approximately a half hour. Six to eight smaller pulses ensued in the next hour. Finally, a smaller lahar from the upper Lagunillas arrived shortly after 1 A.M. and, lasting about 15 minutes, ended the catastrophe. Armero had been virtually wiped out, and more than 23,000 of its citizens had been killed.

The Armero event is the "worst-case" lahar event of record in terms of many parameters: the sheer volume of slurry, distances of transport, peak velocities, size of the devastated areas, and number of fatalities. Its occurrence at night worsened the disaster by making warning and evacuation difficult. An even greater contributing factor was that, although the hazard had been thoroughly studied, life-saving information had not been disseminated among the threatened populace. The legacy of Armero is the important lesson that understanding a hazardous phenomenon is not enough to avert its threat—scientific information has little life-saving value if it is not shared in timely fashion with those in harm's way.

A. Sociopolitical Enhancement of Catastrophe

The first social circumstance that paved the way to the disaster was the total lack of land-use planning in the location and growth of Armero. The town was built on deposits left by lahars that killed 600 people in 1595 and 1000 in 1845—events that were both larger than the lahars of 1985.

Authorities had an entire year of warning that Nevado del Ruiz was restless, after mountain climbers reported heavy steaming at the summit in November 1984. By February 1985, Colombian geologists had visited the volcano several times. Scientific teams from several countries began working on the volcano in March. A preliminary hazard map that proved to be tragically accurate had already been published in newspapers before the eruption, and its final version had been scheduled to be released on the day after the eruption. Ironically, one of the problems was that there were too many scientific teams to coordinate well, and too much inconclusive argument among them. Scientists later also complained that it was hard to work because of the numerous

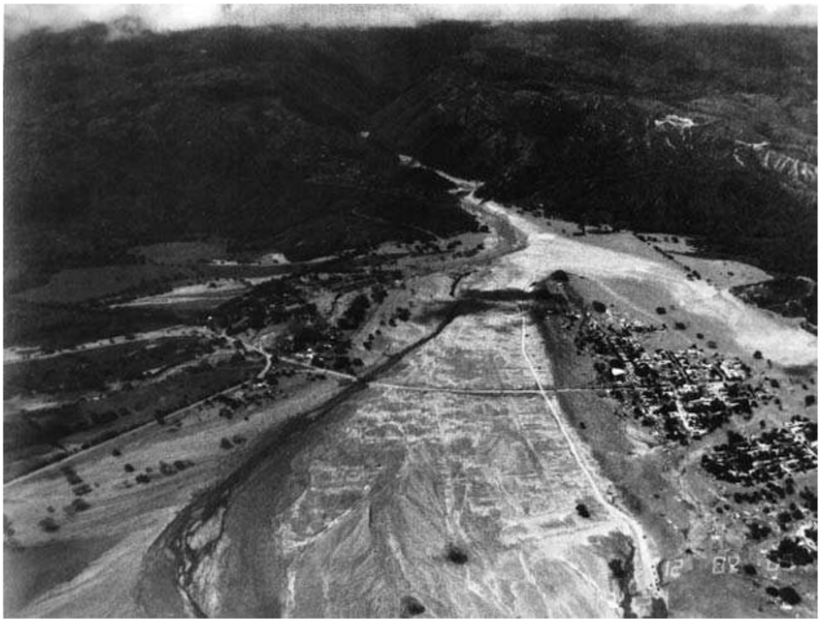

FIGURE 12 Aerial view of Armero after the 13 November 1984 lahar. [From Pierson *et al.,* (1990) with permission from Elsevier Science.]

"briefings" they had to provide to various government officials who, unfortunately, did not pass the information on to the threatened population.

Shortly before the Armero catastrophe, leftist rebels took over the Palace of Justice in Bogotá and held the Supreme Court justices hostage. On November 6, a week before the eruption, the President of Colombia ordered the army to attack the Palace, and a hundred people, including 10 of the judges, were killed. Officials responsible for managing the Nevado del Ruiz emergency were distracted from their duties by the continuing political crisis.

But the worst problem of all was the lack of communication. To avoid disaster, scientists and decision makers must communicate often and well, and the information must be passed on to the people at risk. Neither happened at Nevado del Ruiz. Shortly after 3 P.M. on the day of the tragedy, a minor phreatic eruption lasting about 15 minutes caused a small landslide into the upper Rio Azufrado. Mixing with the river water, this mass movement was liquified into a lahar that destroyed a bridge 4.5 km downstream from the crater. This should have been a clear signal for increased vigilance. But in the evening, as tephra from explosions began falling in Armero, the town mayor spoke on the radio, telling the people that nothing had been reported from Nevado, and instructing them not to worry and to stay in their houses. The radio transmission ended abruptly as the lahar arrived.

V. MOUNT PINATUBO: THE LONG AFTERMATH OF RAIN LAHARS

The 1985 lahar of Nevado del Ruiz is the single-event worst-case lahar in recorded history, but, together, the lahars that ensued in the years after the 1991 eruption of Mount Pinatubo constitute the most voluminous, the most devastatingly widespread, and one of the longest-lasting laharic episodes of record. Its occurrence in an area inhabited by people with no previous experience of volcanoes and lahars has brought about socioeconomic and political responses that have aggravated the continuing calamity.

The 1991 eruption deposited about 5.5 km^3 of pyroclastic flow debris on the volcano (Figure 13). Since the last, prehistoric eruption 5 centuries earlier, torrential runoff on Pinatubo had cut deep canyons into the mountain. After the eruption, large areas of the gullied terrain were smoothed into sloping surfaces by the new pyroclastic deposits that completely filled pre-eruption valleys, some as deep as 200 m.

Lahars began to flow shortly before the paroxysm because, by unfortunate coincidence, a minor typhoon passed within a hundred kilometers of the volcano and caused locally heavy rains that destroyed bridges and roads on all sides of the volcano. The channels draining Pinatubo were still unclogged, and so the lahars did not overflow the river banks. Except for the bridges, the lahars caused little damage to land and property and few casualties.

The eruption killed over 900 people, most from malnutrition and disease in refugee camps. About 200 people died when roofs collapsed under the weight of rain-soaked tephra, and a smaller but indeterminate number who did not evacuate from the volcano slopes were killed by pyroclastic flows. Lahars generated by the monsoonal rains that followed on the heels of the eruption claimed an estimated hundred lives. Some wide river valleys received sediment 15 m or more thick (Figure 14). More than 350 km^2 of farmlands on river plains were buried or eroded away by lahars in 1991. But the devastated area and the number of casualties were increased greatly in the following years during the seasons of monsoonal and typhoon rains. The affected area eventually may be double or triple that of 1991.

A. Lake Breakouts

Some of the largest and most lethal lahars are produced by outbreaks from temporary or permanent lakes that form when a lahar channel is blocked by a landslide or by a steam explosion. Other lakes, for example, Mapanuepe Lake at Pinatubo, can form where a lahar channel is joined by a tributary that drains an area on the volcano, or even outside it. Lahars can deposit so rapidly at the junction that the tributary is dammed, and a lake forms behind it (Figure 15). After the landslide, or when the damming lahars stop flowing, water can continue to rise in the lake, eventually overtopping and breaching the natural dam. The large volumes of water released then erode the channel and bulk up into new lahars. Although cold, such so-called lake-breakout lahars can be as large and destructive as hot lahars. They can be even more dangerous if the lake is breached during good weather, several days after the lahars have stopped coming down from the volcano, and the threatened populations have relaxed their guard. Communities below the lake should monitor the temperature of arriving flow. Cold water means that the lake is draining, and hot lahars mean the

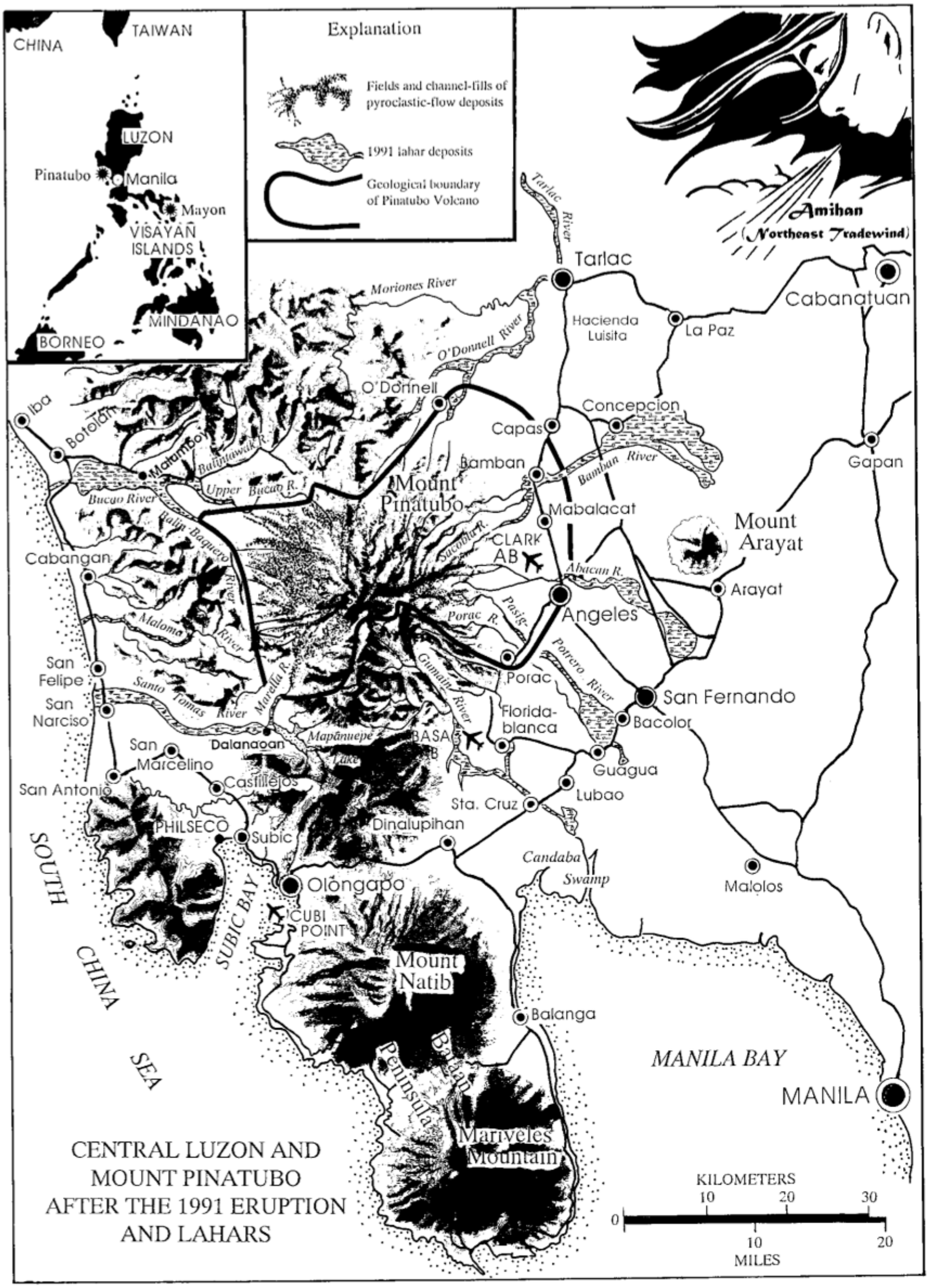
CHINA
TAIWAN
LUZON
Pinatubo
Manila
Mayon
VISAYAN ISLANDS
MINDANAO
BORNEO
Explanation
Fields and channel-fills of pyroclastic-flow deposits
1991 lahar deposits
Geological boundary of Pinatubo Volcano
Amihan
(Northeast Tradewind)
Tarlac River
Tarlac
Cabanatuan
Hacienda Luisita
La Paz
Moriones River
O'Donnell River
O'Donnell
Concepcion
Capas
Iba
Botolan
Malomboy
Balintawak R.
Upper Bucao R.
Bucao River
Bamban
Bamban River
Mount Pinatubo
Mabalacat
Gapan
Mount Arayat
Baliin-Baquero
Sacobia R.
CLARK AB
Cabangan
Abacan R.
Arayat
Angeles
Porac R.
Pasig-
Maloma River
Marella R.
Porac
Potrero River
San Felipe
San Narciso
Santo Tomas River
Gumain River
San Fernando
Bacolor
Florida-blanca
Dalanaoan
Mapanuepe Lake
BASA AB
San Marcelino
Guagua
San Antonio
Castillejos
Lubao
Sta. Cruz
PHILSECO
Subic
Dinalupihan
Candaba Swamp
Olongapo
Malolos
SUBIC BAY
CUBI POINT
SOUTH CHINA SEA
Mount Natib
Balanga
Bataan Peninsula
MANILA BAY
MANILA
Mariveles Mountain
CENTRAL LUZON AND MOUNT PINATUBO AFTER THE 1991 ERUPTION AND LAHARS
KILOMETERS
0
10
20
30
10
20
MILES

FIGURE 13 Map of Mount Pinatubo and its lahar avenues in 1991. [From Rodolfo, 1995.]

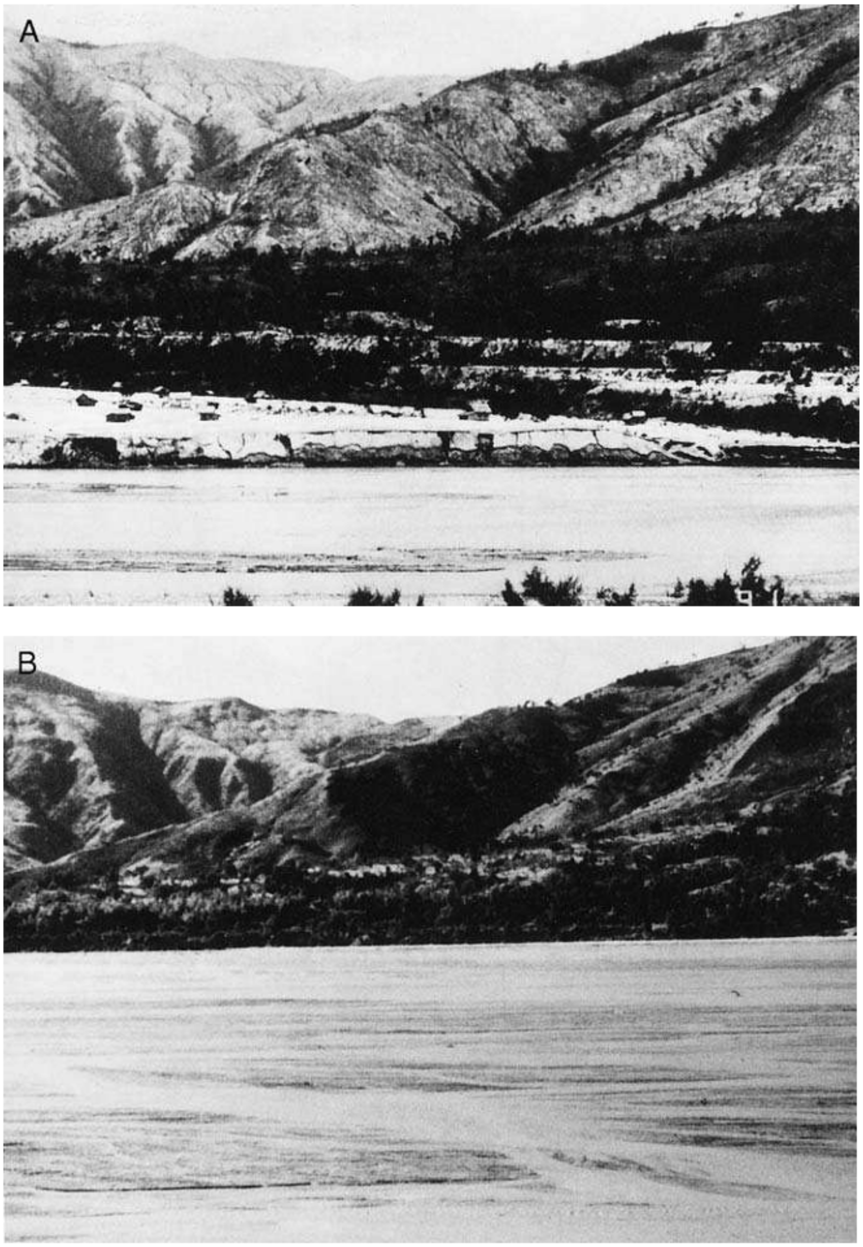

FIGURE 14 A portion of the terraced south bank of the Bucao River. (A) June 1991, before lahars began to flow. For scale, the largest hut on the lowest terrace is about 3 m tall. (B) The same area in January 1992, after the deposition of about 15 m of lahar sediment.

lake has been blocked and may be accumulating toward a breakout.

B. Mitigation Engineering

Soon after the 1991 Pinatubo eruption, the government decided that abandoning doomed towns and resettling their populations would be more expensive than building structures to protect the towns. This judgment was made in circumstances of crisis and emergency, and before proper feasibility studies could be conducted to determine the power and behaviors of lahars, the necessary designs to contain them, and what such structures would cost. Confronted by the threat of huge and imminent lahars, the government and communities alike

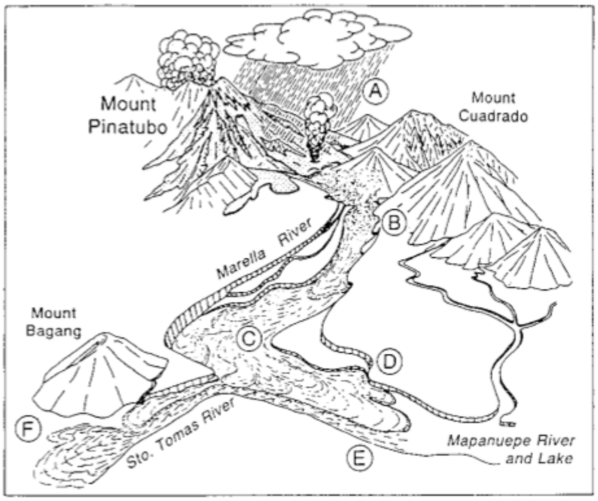

FIGURE 15 Diagram of the generation of lake-breakout lahars at the Santo Tomas River southwest of Pinatubo. (A) Heavy rain on the pyroclastic field generate steam explosions and hot lahars. (B) Lahars cascade down the Marella River. (C) Marella lahars spread and deposit along the wide channel reach and choke the constriction at the Mapanuepe junction. (D) At the confluence, Marella lahars invade upstream along the Mapanuepe River, damming it. (E) After Marella lahars cease, rising Mapanuepe Lake waters breach the dam. (F) Breakout waters remobilize deposits of previous lahars along the Santo Tomas River and erode its banks as they descend toward the sea.

stampeded into building costly structures that did not work, and even enhanced the danger by encouraging an unjustified sense of security. Every year, the government has built structures without proper planning, employing floodwater techniques in attempts to contain and deflect lahars, and the structures have failed.

Perhaps the biggest mistake persistently made was to use lahar deposits for the bulk of dikes. The only advantages this material offered were its abundant availability and that quarrying it out of lahar channels helped to restore their capacity. But lahar material is almost exclusively pumice—porous, low-density sand and gravel—that provides minimal mass and inertia against impact. Its laharic history already attests to its ease of remobilization. In large part this is because it lacks silt and clay to bind it together. Moreover, without these fines to clog the pores between the grains of sand and gravel, it is very porous and permeable. Expensive structures, even some armored in concrete, have failed not only from lahars, but also from the mere passive pressure of impounded water that, seeping rapidly through and under them, erodes large, natural pipes that riddle and undermine them.

Intelligent, surgical engineering with explosives was applied successfully to mitigate breakout lahars from Mapanuepe Lake. An engineering scheme devised by a Filipino volcanologist to cut an artificial outlet to the lake and keep its level stable has eliminated dangerous buildups and breakouts. The lake itself has also served as a natural trap for large volumes of laharic sediment.

C. Predicting the End of the Pinatubo Lahar Crisis

Rehabilitation of the area surrounding Pinatubo urgently requires sound predictions of the rates at which lahars will occur, and the duration of the laharic aftermath. Data gathered from 1991 to 1994 indicate that the volumes of debris on the volcano flanks that were

TABLE II Predicting the Continuing Sediment Yield of Pinatubo Lahars

Year	*Actual*	*Best fit*	*Low*	*High*
1991	805	801	725	925
1992	555	596	539	688
1993	505	444	401	512
1994	310	330	299	381
1995		246	222	283
1996		183	165	211
1997		136	123	157
1998		101	91	117
1999		75	68	87
2000		56	51	65
2001		42	38	48
2002		31	28	36
2003		23	21	27
2004		17	16	20
2005		13	12	15
2006		9	9	11
2007		7	6	8
2008		5	5	6
2009		4	4	5
2010		3	3	3
Total	2175	3122	2864	3604

Note. See Figure 16. From Umbal, J. V. (1997). Five years of lahars at Pinatubo Volcano: Declining but still potentially lethal hazards. *Geological Soc. Philippines Bull.* **52,** 1–19.

mobilized into lahars roughly followed an exponential decay rate. Extrapolated into the future, this predictive model projects another decade of significant lahar activity (Table II and Figure 16). However, the model has several serious drawbacks. First, it cannot be used to predict lahar activity along any individual channel, because all are unpredictably subject to major reorganization. In February 1992 a large secondary explosion blocked the Abacan River and rerouted its lahars into the Sacobia River, worsening the lahars there, but greatly diminishing the threat to Angeles City. After the 1991 eruption, the Pasig-Potrero River had few lahars for 2 years, but in 1993 virtually all flow on the eastern half of the volcano was rerouted into it by another secondary explosion. The years 1994 and 1995 were catastrophic ones along this river.

The second drawback to the exponential decay model is that it presumes a fairly constant supply of lahar-triggering rain, and so a pronounced dry spell such as the years from 1996 to 1998, enhanced by a major El Niño episode, temporarily stopped the clock on the decay curve. The model also does not take into consideration the very real possibility of a "50-year" or "100-year" rainstorm, which would certainly produce catastrophic lahars greatly exceeding any "high" estimate of sediment yield based on normal rainfall.

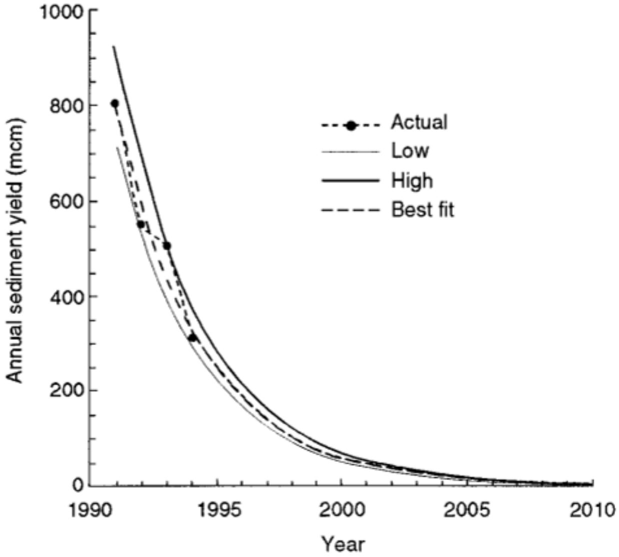

FIGURE 16 Three predictive curves for continuing sediment yield of Pinatubo lahars, based on the data of Table II. [Modified from Umbal, J. V. (1997). Five years of lahars at Pinatubo volcano: Declining but still potentially lethal hazards. *J. Geol. Soc. Philippines* **52,** 1–19.]

Perhaps the most serious drawback is that the model does not take into consideration the fact that lahar deposits can be remobilized in large volumes. In 1994, a large breakout from a lahar-dammed lake sent floods down the Pasig-Potrero River, carving a prominent new channel by remobilizing much sediment that had been deposited since 1991 (Figure 17). The resulting lahars inundated the municipality of Bacolor in lahar deposits several meters thick (Figure 18). The following year, water floods from a typhoon followed the new channel, greatly enlarging it, cutting it deeply into centuries-old, hardened lahar deposits left by earlier eruptions. Huge debris flows carrying many boulder-sized pieces of the ancient materials buried the previously untouched Bacolor village of Cabalantian (Figures 5 and 19). In short, none of the hundreds of millions of cubic meters of lahar deposited on Bacolor in 1994 and 1995 came from the fresh debris perched on the volcano. Scientists continue to grapple with the problem of properly estimating how much fresh and ancient material will be remobilized before lahars finally stop flowing.

VI. MITIGATING THE LAHAR HAZARD

A. Recognizing Old Lahar Deposits

The first step in minimizing death and damage by lahars is to recognize the danger and its extent. Eruptions and lahars can occur at intervals of thousands of years, and so any inhabited area within the possible reach of lahars needs to be examined closely for evidence of past flows. Debris flow deposits consist of very poorly sorted rock fragments that range in size from clay to boulders. They are difficult to distinguish from the deposits of pyroclastic flows, but tend to have a wider range of the coarser sizes. Larger fragments in the deposits of both pyroclastic flows and hot lahars, unlike those of cold lahars, may share a common magnetic alignment adopted when they cooled down enough to regain their magnetism.

Layers left by debris flows characteristically are chaotically mixed, but their bases may be finer grained than the middle and upper portions, in which boulders may be found. More dilute lahars leave layers that are finer-grained and crudely bedded. Commonly, finer material in small vertical zones in lahar deposits show where water escaped upward after deposition.

Inasmuch as lahars were not well recognized and understood before the 20th century, many areas have only recently been discovered to be lahar terrain. The area

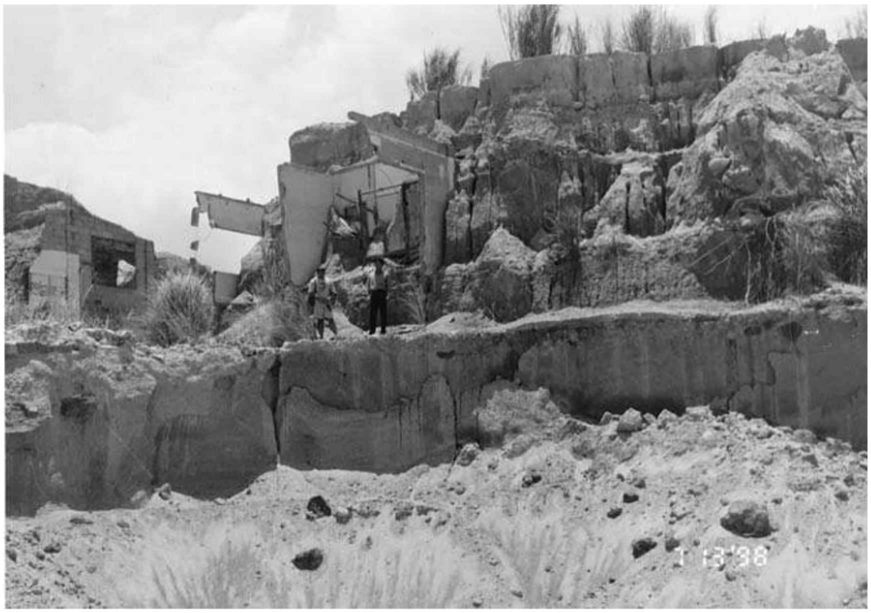

FIGURE 17 House in Porac town, buried by lahars in 1991, exhumed and exposed in the wall of a new canyon that was incised when these deposits, as well as pre-eruption materials, were remobilized by the lahars of 1994 and 1995 that buried Bacolor and Barangay Cabalantian.

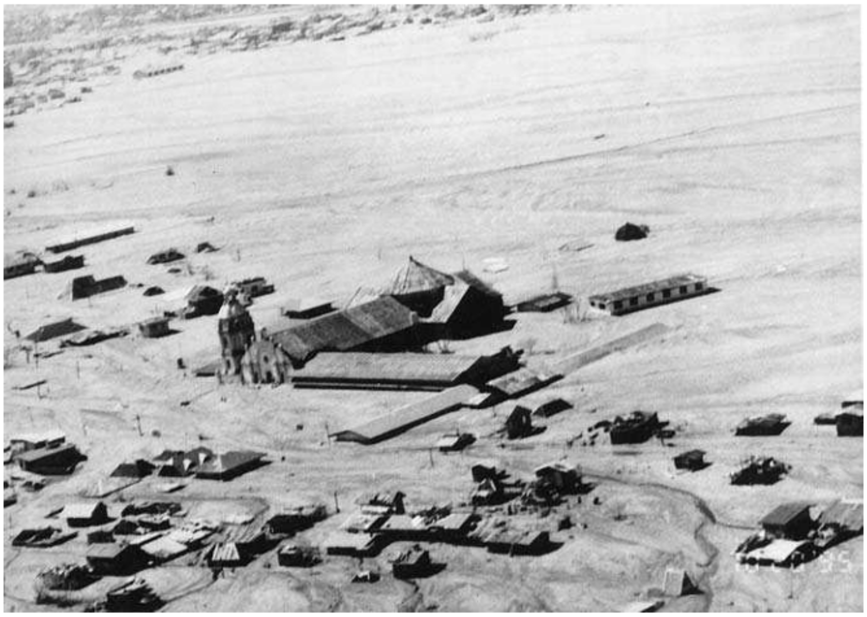

FIGURE 18 Aerial view of the town of Bacolor after the disastrous lahars of 1994 and 1995. Note the large San Guillermo Church in the center of the picture. Its basal portion was buried to a depth of 6.5 m (21 ft.).

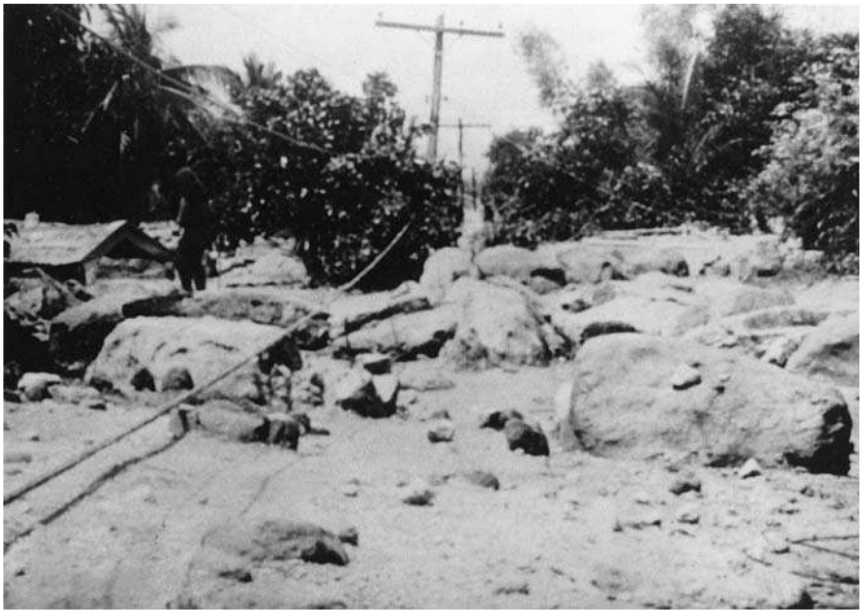

FIGURE 19 Debris flows in Cabalantian village after the 1995 disaster. The high-tension cable touching the ground is a measure of the thickness of the deposits, which was 9 m in some places. The boulders are coherent pieces of lahar deposits from ancient eruptions and illustrate that an unknown but substantial percentage of the later Pinatubo lahars are derived not only from debris of the 1991 eruption, but from older material as well.

around Mount Rainier in the northwestern United States has received enormous prehistoric lahars (Figure 20). A single series of flows called the Osceola Mudflow occurred 5700 years ago when a huge portion of the northwestern sector of the volcano collapsed. Incorporating glacial ice and stream waters of the White, Green, and Puyallup rivers, the debris became lahars that traveled 100 km and covered more than 500 km^2.

Hundreds of thousands of people live in five towns built on the Osceola deposits. Even larger prehistoric lahars spread their debris farther away from Mount Rainier, over the areas where millions of Seattle and Tacoma citizens now live. If such an event occurring today were to flow at typical lahar speeds, it could reach Tacoma in only an hour. Given the enormous financial investment that the communities in this area represent, and the fact that the most recent of the large lahar events took place millennia ago, it simply is not feasible for the towns and cities to be evacuated and resettled elsewhere. Little can be done to mitigate such a disaster, other than closely monitoring the volcano and local seismicity, familiarizing the threatened populaces with the hazard, and encouraging individual families and neighborhoods to make contingency plans.

B. Delineating Lahar Paths

Lahars flow in obedience to gravity, and so any drainage channel on a volcano can funnel lahars downslope, given the necessary water and debris ingredients. Using topographic maps, it is a fairly simple matter to trace the avenues that lahars may follow. If lahars have occurred several times in the past along a channel, they will have left a conical fan of deposits spreading outward from an apex at the valley mouth.

On volcanoes that have a continuing lahar threat, such as those that experience seasonal rain lahars, active lahar channels need to be mapped in microtopographic detail between events. This is because each lahar modifies its conduit and the topography of its depositional area, thereby helping to determine the path the next lahar will take.

C. Monitoring

At volcanoes where lahars have been triggered only during eruptions, monitoring for lahars is inseparable

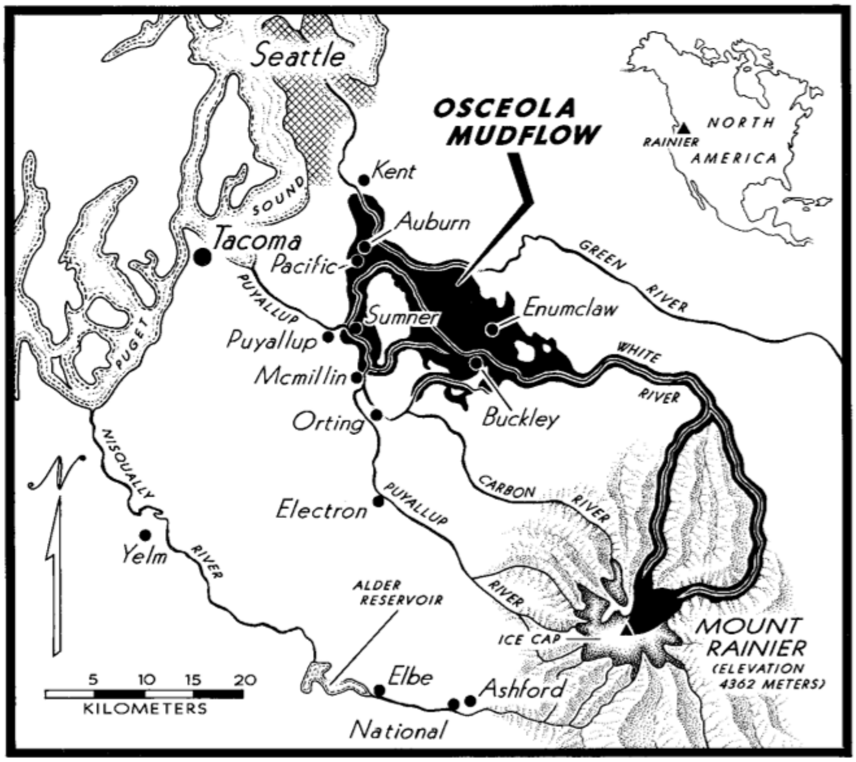
Seattle
OSCEOLA MUDFLOW
RAINIER
NORTH AMERICA
SOUND
Kent
Auburn
Tacoma
Pacific
GREEN RIVER
PUYALLUP
Sumner
Enumclaw
Puyallup
PUGET
WHITE RIVER
Mcmillin
Orting
Buckley
N
NISQUALLY
CARBON RIVER
Electron
PUYALLUP RIVER
Yelm
RIVER
ALDER RESERVOIR
ICE CAP
MOUNT RAINIER
(ELEVATION 4362 METERS)
5 10 15 20
KILOMETERS
Elbe
Ashford
National

FIGURE 20 Areas north and west of Mount Rainier, including the sites of the cities of Seattle and Tacoma, are underlain by the deposits of enormous prehistoric lahars. [From Fisher *et al.,* 1997, p. 131, reprinted by permission of Princeton University Press.]

from that for eruption, using standard seismographic, ground-tilt, and other equipment. At a volcano that experiences recurring rain lahars, the regional weather must be watched closely as it develops. Evolving storms can be tracked using satellite imagery for days or even weeks before their arrival. When rain actually begins to fall, its intensity and duration can be monitored in real time with unmanned, telemetered rain gauges on the volcano, and if the combinations of intensities and durations that trigger lahars are known for a particular site, warnings of imminent danger can be issued when these thresholds are approached. Observers can be stationed as high as possible along known lahar channels to warn the communities below when lahars actually start to flow. At Gunong Kelut, alarms are given by striking tong-tong, large wooden drums. Bells, flares, and cannons can also be used, but none of these are of much use in the noise of a howling gale or heavy downpour. Two-way radios are inexpensive and have been successfully used to transmit lahar warnings at Pinatubo.

In Japan, wires are stretched across lahar channels high up volcanoes to trigger warning devices when broken by lahars. To avoid false alarms from animals or falling trees, the devices are designed to be activated only after several wires are broken in the proper downstream succession. At Pinatubo, volcanologists from Mount St. Helens have developed and installed seismic equipment that detects and transmits the low-frequency vibrations of lahars shaking the ground. These work well, but, as can be expected in an impoverished area, the unmanned rain gauges and flow sensors at Pinatubo have been decimated by theft. In developing countries, manned observation stations may be cheaper and more effective.

D. Structural Measures

Engineering technology to contain debris flows in nonvolcanic terrain has been adapted with varying degrees of success to trap or divert lahars. Not surprisingly, Japanese engineers have been at the forefront of such efforts, their country being both volcanic and technologically advanced. Check dams across lahar channels, called "sabo," are meant to trap lahar sediment. Their use, singly or in series, is feasible only if lahar volumes are not too great. They may actually make a single catastrophic event out of a succession of small flows when they are filled and breached. "Training dikes" and deflection dams have been built at Kelut, Pinatubo, and elsewhere to divert lahars away from towns and cities. Such an approach is more appropriate for water floods, which eventually subside, leaving only a minor amount of silt in their wakes. A single debris flow can leave meters of impounded sediment, thereby transforming a dike into a dam that is subjected not only to the pressure of the accumulated sediment, but to undermining seepage driven gravitationally through and under the dike by the difference in elevation across it. To maintain its efficacy, and prevent it from becoming a man-made hazard, any such structure needs to be cleaned out whenever it has acquired substantial fill. Such cleaning may not be feasible in areas that receive lahar sediment very rapidly.

Like any major engineering undertaking, a structure meant to deflect and contain lahars must be designed with careful attention to the strength and behavior of lahars, and to topographic factors such as channel slope and width, and abutment height. The rock types and joints or other structures within the abutment and foundation need to be known. Dimensional elements of the structure, such as crestal thickness, gradients of front and back slopes, wing slopes and penetration, and footing depths, need to be appropriate to withstand the powers of debris flows. The rock used to fill the structure must be of high density to withstand the high density of lahars and the resulting buoyant forces they exert, and its porosity and permeability must be too low to allow damage by seepage and piping.

Theoretically, artificially widening a channel might retard a debris flow by decreasing its depth, thereby stranding large boulders and increasing basal friction to decrease flow velocity. The feasibility of such a measure depends on the rates with which the debris descends and can be removed. At the Pasig-Potrero channel of Mount Pinatubo, the work of removing a thousand truckloads of lahar deposits every day for 3 months can be undone by 1 hour of lahar flow.

E. Temporary Refuges

People anywhere in the world are loath to abandon their homes in any circumstance, and this is especially true for rural areas in developing countries. Coupled with warning systems that give at least a half to 1 hour of warning, the construction of temporary refuges on high ground, and easy access paths to them, is one of the simplest and least expensive ways to save lives from lahars. At some Indonesian volcanoes where lahars are fairly common events, high ground is too distant from some villages, and so artificial hillocks are built. The hillocks have flat tops that can be used as marketplaces and soccer fields. Such artificial havens should have bases deep and strong enough to withstand the lateral scour of lahars. If the area experiences protracted rains, and if fresh lahar deposits may isolate the hill for some time, it should have shelters to prevent illness and death due to prolonged exposure.

SEE ALSO THE FOLLOWING ARTICLES

Debris Avalanches • Lahars • Risk Education and Intervention • Subglacial Eruptions • Volcanic Hazards and Risk Management • Volcanic Lakes • Volcano Warnings

FURTHER READING

Blong, R. J. (1986). "Volcanic Hazards: A Sourcebook on the Effects of Eruptions." Academic Press, Sydney.

Fisher, R. V., Heiken, G., and Hulen, J. B. (1997). "Volcanoes: Crucibles of Change." Princeton Univ. Press, Princeton, NJ.

Major, J. J., and Newhall, C. G. (1989). Snow and ice perturbation during historical volcanic eruptions and the formation of lahars and floods. *Bull. Volcanol.* **52,** 1–27.

Pierson, T. C., Janda, R. J., Thouret, J.-C., and Borrero, C. A. (1990). Perturbation and melting of snow and ice by the 13 November 1985 eruption of Nevado del Ruiz, Colombia, and consequent mobilization, flow and deposition of lahars. *J. Volc. Geotherm. Res.* **41,** 17–66.

Pierson, T. C., Janda, R. J., Umbal, J. V., and Daag, A. S. (1992). "Immediate and Long-Term Hazards from Lahars and Excess Sedimentation in Rivers Draining Mt. Pinatubo, Philippines." U.S. Geological Survey Water-Resources Investigations Report 92-4039.

Rodolfo, K. S. (1995). "Pinatubo and the Politics of Lahar: Eruption and Aftermath, 1991." Univ. of the Philippines Press, Quezon City.

Scrivenor, J. B. (1929). The mudstreams ('lahars') of Gunong Keleot in Java. *Geol. Mag.* **66,** 433–434.

Voight, B. (1988). Countdown to catastrophe. *Earth Mineral Sci.* **57,** 17–30.

This Page Intentionally Left Blank

HAZARDS OF VOLCANIC GASES

GLYN WILLIAMS-JONES
HAZEL RYMER
The Open University

I. Toxicity of Volcanic Gas Species
II. Hazards to the Population and Environment: Case Studies
III. Gas Hazard Mitigation
IV. Summary

GLOSSARY

aerosol A colloidal dispersion of liquid particles in a gas, for example, SO_2, which will react with the OH radical in the atmosphere to form tiny droplets of sulfuric acid (H_2SO_4).

COSPEC An ultraviolet correlation spectrometer used to detect the concentration and emission rate of SO_2 from degassing volcanoes.

δ_{gas} The vapor density of a gas relative to air (density = 1), measured in g/liter.

gas solubility The maximum amount of a gas which can be dissolved in a given amount of water at 20°C. Measured in g/liter.

Giggenbach bottle An evacuated alkaline-solution-filled bottle (e.g., sodium hydroxide, NaOH) generally connected to a titanium or silica tube which is inserted into a fumarole. The gases bubble through the solution, condense, and are absorbed by the solution, which can then be analyzed.

hazard In a volcanic context, hazard refers to the phenomena produced by an eruption and is directly related to *risk*, where (*risk*) = (*hazard*) × (*vulnerability*), with *vulnerability* referring to the consequences for population and infrastructure.

PEL The recommended permissible exposure limit to a given chemical compound above which health risks may occur. The exposure limit is generally averaged over an 8-hour day, 40-hour week. It is measured in parts of compound (e.g., CO_2) per million parts of air (ppm).

GASES ARE THE invisible yet often continuous products of volcanic activity. Even volcanoes in a state of quiescence, not actually erupting lava or showing signs of unrest through seismic activity, are able to degas continuously. Eruptions can produce lethal quantities of toxic gases, but long-term exposure to a lower dose also can pose a significant hazard. Although volcanic gases are only directly responsible for ~3% of volcano-related deaths (1900–1986), they are nevertheless hazardous and responsible for deaths every year, including volcanologists such as Werner Giggenbach. They have an important effect on the regional and global environment and may contribute greenhouse gases to the atmosphere. Indirectly, through the destruction of crops, volcanic gas emissions have resulted in starvation and disease (40% of volcano-related deaths between 1600 and 1982).

Copyright © 2000 by Academic Press
All rights of reproduction in any form reserved.

The composition of volcanic gases depends on the type of volcano and its eruptive state. However, the most common volcanic gases in order of abundance are water (H_2O, 30–90 mol%) carbon dioxide (CO_2, 5–40 mol%), sulfur dioxide (SO_2, 5–50 mol%), hydrogen (H_2, <2mol%), hydrogen sulfide (H_2S, <2mol%), and carbon monoxide (CO, <0.5mol%). Some of these, when emitted from active vents (Figure 1), react in the atmosphere or volcanic plume to form aerosols, the most important being hydrochloric acid (HCl), hydrofluoric acid (HF), and sulfuric acid (H_2SO_4).

I. TOXICITY OF VOLCANIC GAS SPECIES

It is difficult to determine accurately the contribution of gases to volcano-related deaths since much of the data reflect deaths during eruptive periods, whereas the majority of gas-related deaths have occurred during noneruptive periods. The long-term health effects of volcanic gases are poorly understood; they may be responsible for or accelerate epidemic diseases because of their irritant and depressing effects, which reduce the resistance of ocular, respiratory, and digestive systems to microbial attack. From a health perspective, the most important volcanic gases and aerosols are CO_2, SO_2, Rn, H_2S, HCl, HF, and H_2SO_4 (Table I). Exposure to these has been the cause of the majority of volcanic-gas-related fatalities.

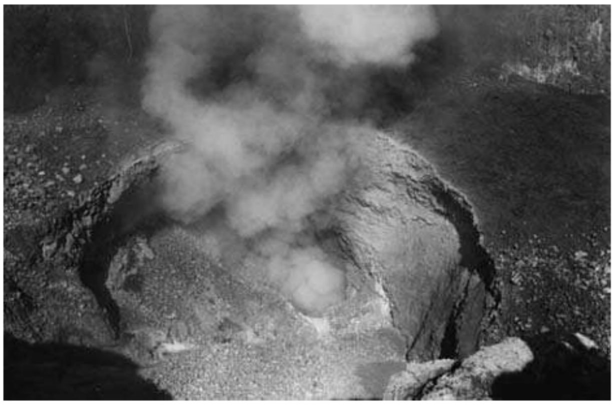

FIGURE 1 Degassing vent at Santiago crater at Masaya volcano, Nicaragua.

II. HAZARDS TO THE POPULATION AND ENVIRONMENT: CASE STUDIES

The relative degree of hazard from volcanic gases is also dependent upon the type of gas emitted. Some gases are poisonous while others are dangerous only if present in such high concentrations that they block oxygen respiration. The dispersion of a given gas species is also directly related to the hazard. Ejection of gases at high elevations (e.g., Mount Etna) will have less direct impact on population than low-level gas plumes (e.g., Masaya). Relatively short-lived eruptions may eject significant amounts of gases into the stratosphere with short-term global consequences. Persistently active volcanoes, however, degas continuously and may present a long-term hazard. In some instances, even dormant volcanoes can pose a threat to human health and the local environment.

A. CO_2 Hazards

The most lethal CO_2-related events have been those in which CO_2, which is colorless, odorless, and denser than air, flowed downhill as a density current, collecting in low-lying areas and asphyxiating all life in its path. The first recorded incident of this occurred in the Dieng Volcanic Complex (or Dieng Plateau), Indonesia, a complex of volcanic centers forming a large depression approximately 14 km long and 6 km wide. On the morning of February 20, 1979, the inhabitants of the village of Batur felt three seismic shocks at 2:00 A.M., 3:30 A.M., and 4:00 A.M., and then observed a phreatic eruption at 5:15 A.M. which ejected a dark gray cloud from the Sinila crater (a small water-filled vent, 3 km northeast of the village). This eruption, which formed a 90-m wide and 100-m deep crater, was accompanied by the ejection of blocks, mud, steam, and gas, and by a hot lahar that flowed 3.5 km downslope. At 6:45 A.M., a second minor eruption occurred 300 m west of Sinila that resulted in the formation of a new crater, Sigludung. Many of the villagers from Koputjukan fled west toward Batur and were killed by a gravity current of gas (probably CO_2 and H_2S) which was emitted from multiple small vents and fissures to the south and west of the two craters. Others, having witnessed the deaths along the Koputjukan–Batur road, retreated to a nearby elementary school where they were also killed. In total, the gas killed at least 149 people and injured over 1000 people.

The crater lakes of Monoun and Nyos, located along the Cameroon Volcanic Line, a great fracture consisting of a chain of alkalic volcanoes, are the only two recorded examples of rapid free-CO_2 release from lakes. The CO_2 is believed to have originated from cold springs degassing below the lakes, which being thermally stratified, allowed for the gas accumulation. Although still controversial, it is generally believed that these two events may have been triggered by landslides which caused the deep gas-rich layer to rise to a point in the lakes where the hydrostatic pressure was insufficient to keep the CO_2 in solution. Being denser than air, the CO_2 gas which was released formed a large density current that flowed over the crater rim and downslope.

On August 15, 1984, at approximately 11:30 P.M. local time, a lethal cloud of CO_2 burst from the crater in Lake Monoun and flowed down the valley several hundred meters where it settled along the Panke River depression. The emission was heralded by an explosion heard by the people in Njindoun village (1 km north of the lake), and by seismic shocks felt 6 km to the north in the village of Mbankouop. At approximately 3 A.M., the majority of the victims (39 in total) had left the village of Njindoun and were heading south toward the Foumbot market. The location of the bodies indicated that the victims encountered and succumbed to the dense gas cloud near the bridges over the Panke River. When police arrived at the scene (~6:30 A.M.), a whitish smoky cloud still covered the area, drifting with the wind off Lake Monoun. They were only able to enter the area when the cloud was finally dissipated at approximately 10:30 A.M.. It was then that they noted that the bodies of the victims were covered with reddish first-degree burns and blisters and that mucus and blood had frothed from their noses and mouths. The surrounding vegetation was bleached yellowish and withered, yet the victims' clothes were unaffected. The carcasses of domestic and wild animals were also found nearby.

Between 9 and 10 P.M. (local time) on August 21, 1986, almost 2 years after the Lake Monoun event, a cloud of concentrated CO_2 was emitted from the lowest point of the Nyos crater lake and spread into the surrounding valleys, affecting an area approximately 20 km long and 15 km wide. The gas emission appears to have been preceded by the rise of a gas column at 4 P.M. and a weak explosion at 8 P.M., and then by two or three violent explosions between 9 and 10 P.M. No seismic events were recorded. There was little or no damage to vegetation or housing although taller vegetation was flattened in some areas between the lake and Lower Nyos. As with the Lake Monoun event, the carcasses of many domestic and wild animals were found in the affected area (Figure 2). The exact number of casualties is unknown, but according to government sources, at least 1700 people died while approximately 5000 people in the affected area escaped exposure or survived its effects.

Another type of CO_2-related hazard is that seen at Mammoth Mountain, California, a large dacitic volcano located on the southwestern rim of the 760,000-year-old Long Valley caldera. Beginning in 1990, extremely high levels of CO_2 soil degassing (20–90% CO_2) on the flanks of Mammoth Mountain have resulted in tree kill areas which cover $>500{,}000\ m^2$. The CO_2, which probably kills the trees during the winter by inhibition of root function and oxygen deprivation, most likely originates from the degassing of an intruded magma and gas release from magmatically heated carbonate metasedimentary rocks beneath the caldera. The CO_2 flux from Mammoth Mountain was estimated at 1200 metric tonnes/day (t/d) in 1995 and 500 (t/d) in 1998, occurring principally in the tree kill areas. This diffuse degassing may also be producing catastrophic acidification of the soil and mobilization of toxic Al^{3+} into local aquatic ecosystems.

Although CO_2 generally dissipates when it leaves the ground, its relatively high density causes it to collect in hollows, wells, and confined places where it creates a serious asphyxia hazard. During the winter months, the relatively impermeable snow prevents CO_2 from escaping, dramatically increasing the hazard; a number of cases of near-asphyxia were reported by people entering small snow-covered cabins.

Global CO_2 emission from subaerial volcanoes has been calculated, using CO_2/SO_2 ratios and SO_2 flux estimates, to be approximately 6500 metric kilotonnes of CO_2 per year, with over half of that coming from passively degassing volcanoes. Although only 0.2% of anthropogenic emissions, volcanoes nevertheless contribute large amounts of CO_2 to the atmosphere. In earlier geologic times, catastrophic volcanic events such as the eruption of the Deccan Traps may have added significant amounts of CO_2 to the atmosphere and therefore may be partially responsible for increased global warming.

B. SO_2 Hazards

When sulfur dioxide is released to the atmosphere, it oxidizes with the OH radical in air to form sulfurous acid (SO_3), which then reacts with water to produce sulfuric acid particles. At Masaya volcano, a basaltic complex of nested calderas and craters located in northwestern Nicaragua, the long-term degassing activity from the currently active crater, Santiago, has had a significant impact on the surrounding vegetation; high

TABLE 1 Toxicology of Volcanic Gases and Aerosols

	Carbon dioxide (CO_2)
Characteristics	Colorless, odorless gas. Irritation of eyes, nose, and throat only at high concentrations. Vapor density relative to air (δ_{gas}) = 1.52 g/liter. Gas solubility in water at 20°C = 0.04 g/liter. Permissible exposure limit (PEL) averaged over 8 hours = 5000 ppm in air; 9000 mg/m^3 of air.
Effects of overexposure	
Short-term	A simple asphyxiant, symptoms appear only when such high concentrations are reached that there is insufficient oxygen to support life. Inhalation may cause rapid breathing, increased heart rate (at >7.5%), headaches, sweating, dizziness, shortness of breath, muscular weakness, mental depression, drowsiness, and ringing in the ears. Concentrations at >11% result in unconsciousness in a minute or less. Convulsions may occur at concentrations of >25%. Rapid recovery occurs on removal from exposure.
Long-term	Prolonged exposure to concentrations of >10% may result in unconsciousness.
	Sulfur dioxide (SO_2)
Characteristics	Colorless gas or liquid (<−10°C) with characteristic pungent odor. Perceptible odor at 0.3–1.0 ppm and easily noticeable at 3 ppm. δ_{gas} = 2.26 g/liter. Gas solubility = 10 g/liter. PEL = 5 ppm in air; 13 mg/m^3 of air.
Effects of overexposure	
Short-term	Inflammation and irritation of the eyes and respiratory tract resulting in burning of the eyes, coughing, and difficulty in breathing. Approximately 90% of inhaled SO_2 is absorbed in the upper respiratory tract where it forms sulfurous acid, which then oxidizes to form sulfuric acid. Concentrations of 6–12 ppm cause immediate irritation of nose and throat. Exposure to >20 ppm causes irritation of the eyes, while concentrations of 10,000 ppm irritate moist skin within minutes.
Long-term	Prolonged exposure to low concentrations may be dangerous for persons with preexisting cardiopulmonary diseases.
	Hydrogen sulfide (H_2S)
Characteristics	Colorless, flammable gas with offensive odor (rotten eggs). Characteristic odor perceptible at 0.77 ppm and easily noticeable at 4.6 ppm. δ_{gas} = 1.19 g/liter. Gas solubility = 2.9 g/liter. PEL (averaged over 10 min) = 20 ppm in air; 28 mg/m^3 of air.
Effects of overexposure	
Short-term	Inhalation of 20–150 ppm may cause eye irritation while slightly higher concentrations cause irritation of upper respiratory tract. In low concentrations, exposure may result in headache, fatigue, dizziness, excitement, staggering gait, and diarrhea, followed sometimes by bronchitis and bronchopneumonia. In small amounts the gas acts as a depressant, and is a stimulant in larger amounts. Very large amounts result in paralysis of the respiratory center and death; exposure to 1000–2000 ppm may cause coma after a single breath.
Long-term	Prolonged exposure to concentrations as low as 50 ppm may cause pharyngitis and bronchitis while concentrations > 250 ppm may result in pulmonary edema.
	Radon (Rn)
Characteristics	Colorless, odorless, tasteless, radioactive gas, formed from the radioactive decay of uranium. δ_{gas} = 9.73 g/liter. Gas solubility = 51 g/liter. PEL = 200 Bq/m^3.
Effects of overexposure	
Short-term	There is no information on the acute noncancer effects of radionuclides in humans; however, animal studies have reported inflammation in the nasal passages and kidney damage from acute inhalation exposure to uranium.
Long-term	Chronic exposure by inhalation has been linked to respiratory disorders, such as lung disease and lung cancer, in humans. Smokers exposed to radon are at ~10–20 times greater risk for lung cancer than nonsmokers.

continues

Continued

	Hydrochloric acid (HCl)
Characteristics	Colorless gas or colorless fuming liquid with an irritating pungent odor. Detectable odor by most people between 1 and 5 ppm. $\delta_{gas} = 1.27$ g/liter. Gas solubility = 62 g/liter. PEL = 5 ppm in air; 7 mg/m^3 of air.
Effects of overexposure	
Short-term	Irritation of the mucus membranes of the eyes and respiratory tract with burning, choking, and coughing. At concentrations $>$ 35 ppm, there is irritation of the throat after only short exposure. Severe breathing difficulties may occur along with skin inflammation or burns. Concentrations $>$ 100 ppm will result in pulmonary edema, and often laryngeal spasm.
Long-term	Repeated or prolonged exposure may lead to erosion of the teeth and skin rash.
	Hydrofluoric acid (HF)
Characteristics	Clear, colorless, fuming corrosive liquid or gas with strong irritating odor. Irritation of nose and eyes at $<$5 ppm. $\delta_{gas} = 0.7$ g/liter. Gas solubility = miscible in all proportions. PEL = 3 ppm in air; 2 mg/m^3 of air.
Effects of overexposure	
Short-term	Extreme irritation and corrosion of the skin and mucus membranes. Contact with the eyes will cause deep-seated burns, and if the chemical is not removed immediately, permanent visual impairment or blindness may result. Skin exposure produces severe burns which are slow to heal. Subcutaneous tissues may be affected, becoming blanched and bloodless, which may result in gangrene. A severe irritant to the nose, throat, and lungs, inhalation of the vapor may cause ulcers of the upper respiratory tract; concentrations at 50–250 ppm are dangerous even for brief exposures.
Long-term	Repeated or prolonged exposure to lower concentrations may cause changes in the bones as well as chronic irritation of the nose, throat, and lungs.
	Sulfuric acid (H_2SO_4)1
Characteristics	Colorless to dark brown, oily, odorless liquid. Irritation of nose and eyes at low concentrations. $\delta_{gas} = 3.4$ g/liter. Gas solubility = miscible in all proportions. PEL = 20 ppm in air; 1 mg/m^3 of air.
Effects of overexposure	
Short-term	Irritation of eyes, nose, and throat. Severe burns with rapid destruction of tissue and erosion of teeth may occur. Inhalation may also lead to difficulty in breathing and inflammation of upper respiratory tract.
Long-term	Repeated or prolonged exposure to the vapor may cause erosion of the teeth, and chronic irritation of the eyes, nose, throat, and lungs.

concentrations of SO_2 disturb stomatal respiration and cause necrosis. Sulfur dioxide fluxes from the crater have been measured at as much as 2500 (t/d) (Figure 3). The presence of this gas, as well HCl and HF, has led to extensive fumigation and destruction of most of the vegetation to the west of the volcano. Concrete and metal fences, telephone wires, and other metal equipment are also severely damaged in the effected areas (Figure 4). Since the 19th century, the significant economic impact from the degassing has led local coffee farmers to even demand the capping or destruction (by aerial bombardment) of the degassing vent; none of these attempts proved successful. Mixing of rain from Hurricane Mitch (late 1998) with the volcanic gas plume produced concentrated acid rain which local farmers blamed for the damage to young palm trees and even the complete destruction of a soya field during a single afternoon.

On June 6, 1912, Novarupta, a dacitic volcano located on the Alaska Peninsula, explosively erupted ~15 km^3 of magma and triggered the collapse of Mount Katmai volcano. The Katmai-Novarupta eruption released substantial amounts of gas which created acid rains that appear to have greatly impacted the local environment. As with Masaya, acid rain was reported to have dissolved metal work of buildings 400 km northeast at Seaward, while polished brass was tarnished 1100 km away at Cape Spencer. A month after the eruption, housewives in Vancouver, Canada (2400 km south), reported that clothes left out to dry had "turned to shreds" upon being ironed.

The conversion of volcanic sulfur dioxide into aerosol particles is often responsible for formation of an acid smog or "vog" (e.g., Kilauea volcano, Hawaii). This acid vog is slowly neutralized by NH_3 in the atmosphere to form a haze which may block solar ultraviolet rays from

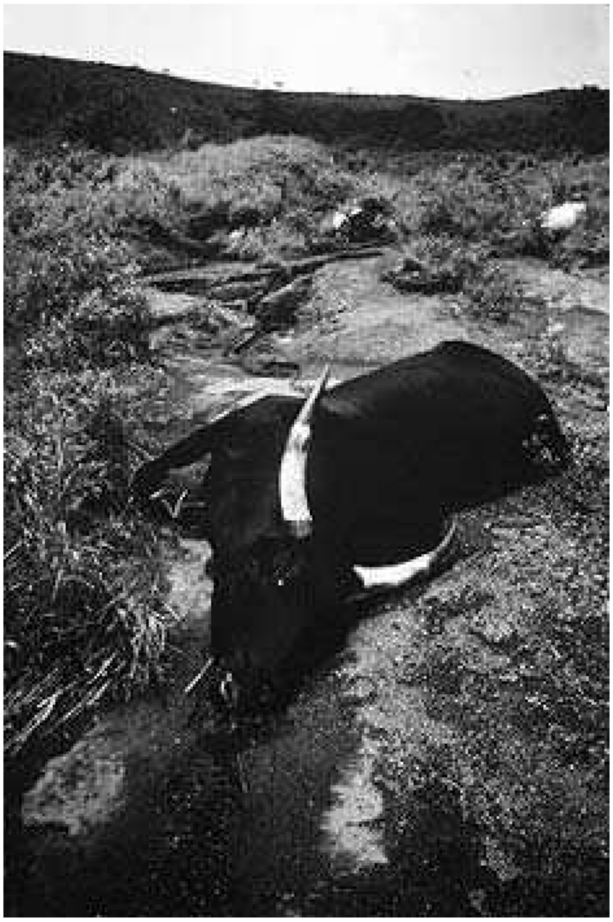

FIGURE 2 One of the domestic animals asphyxiated by the dense CO_2 cloud emitted from Lake Nyos, Cameroon. [Photo by Jack Lockwood.]

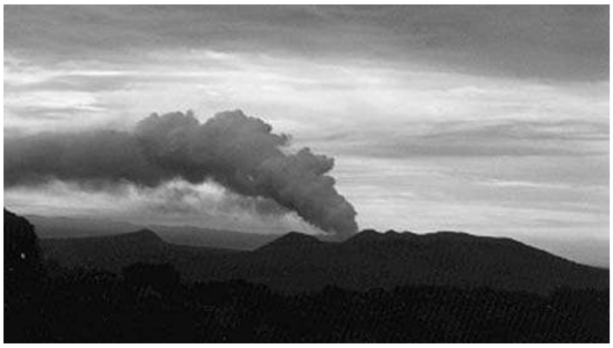

FIGURE 3 A continuous gas plume rises from Masaya volcano, Nicaragua. The volcano currently emits approximately 2000 metric tonnes per day of SO_2, resulting in considerable damage downwind.

reaching the lower atmosphere, which in turn may lead to a global cooling effect (e.g., Mount Pinatubo, Philippines). The volcanic haze may also act as cloud condensation nuclei and perhaps even as sites for the catalytic destruction of ozone, with obvious global implications.

C. H_2S Hazards

Hydrogen sulfide is an extremely toxic gas which has been responsible for numerous fatalities, and in the case of Japan it is believed to be the most common cause of volcanic gas accidents (at least 10 incidents since the early 20th century). This has led many volcano observatories in Japan to install H_2S detectors and automated warning systems.

One such incident occurred in 1971 on the flanks of Kusatsu-Shirana volcano, Honshu, when six downhill skiers died almost instantly after passing through a depression filled with H_2S. Being denser than air, the gas may accumulate in snow-covered depressions or caves which are breached from time to time, releasing lethal concentrations to the surface. Another more recent accident occurred on Adatara volcano, Honshu, a basaltic to andesitic volcano which forms part of the volcanic front of northeastern Japan. On September 15, 1997, 4 hikers, from a party of 14, were killed after inhaling volcanic gases on the floor of the Numano-taira crater. The group had become disoriented because of fog and left the trail, which had signs warning of volcanic gas hazards in the area. Three of the hikers fell into the crater where they succumbed to noxious gases that had

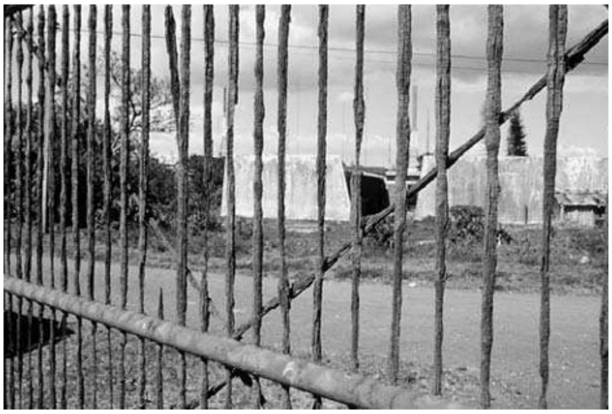

FIGURE 4 A metal gate damaged by prolonged exposure to acid gases emanating from Masaya volcano, Nicaragua [photo by Pierre Delmelle].

accumulated on the crater floor due to calm wind conditions. The fourth hiker killed also succumbed to the gases while attempting a rescue. Scientists from the Kusatsu-Shirane Volcano Observatory reported that the fumarolic gas from the southwest rim of the crater was composed of 0.5% SO_2, 33–37% CO_2, and 60–65% H_2S.

D. HCl Hazards

Although there are few cases of hydrochloric acid being solely and directly responsible for volcano-related fatalities, it is nevertheless an important component because of its effects on the environment. HCl is highly soluble in water and is therefore easily removed by rain from a volcanic plume, resulting in low-pH acid rains (e.g., Kilauea, Masaya). Significant amounts of HCl may also have been injected into the stratosphere during the cataclysmic eruption of El Chichon in 1982 with potentially serious environmental implications. In Hawaii, clouds of lava haze or "laze" are formed from the boiling and vaporization of seawater when lava flows enter the sea. These large white laze plumes contain a mixture of HCl (up to 10–15 ppm) and seawater and produce acid rains (pH 1.5–2) which pose a hazard to the local population.

E. HF Hazards

Hydrogen fluoride is an aerosol which is indirectly responsible for the most lethal gas-related volcanic event. The Laki fissure, a northeast-trending 27-km-long row of cones and craters, was the source of the Grímsvötn caldera eruption which lasted from June 8, 1783, to May 26, 1785. The second largest historic basaltic fissure eruption since the ~935 A.D. Eldgja eruption, it was preceded by tremors and earthquakes starting on May 15. The eruption involved at least 18–20 km^3 of basaltic magma, of which 15 km^3 was erupted as lava and tephra covering 565 km^2. Fire fountains are thought to have risen as high as 1400 m and were accompanied by convecting eruption columns which rose to a maximum altitude of 15 km, resulting in an atmospheric loading of 122 MT of SO_2, ~7.0 MT of HCl, and 15.0 MT of HF over an 8-month period. A low-altitude gas haze caused grasses contaminated by fluorine to be stunted, leading to the loss of over 50% of Iceland's grazing livestock. This consequently led to the "Haze Famine" which, in combination with various diseases and two severe winters, caused the death of 10,521 people, 22% of Iceland's population. The injection of ash, gases, and aerosols into the lower stratosphere also affected parts of western Europe, north Africa, and western Asia, and resulted in cooling of the northern hemisphere by 1–2°C.

A similar hazard, also in Iceland, occurred with the Plinian eruptions of Hekla volcano. HF gas can be adsorbed on tephra and transported hundreds of kilometers from the active vent. Populated areas around the volcano have been heavily impacted due to significant tephra fall, but also by the lethal fluorosis of livestock. As with the Laki fires, grazing livestock were affected after eating fluorine-contaminated grasses, even outside the areas of major tephra deposition.

III. GAS HAZARD MITIGATION

Volcanic gases may be monitored and studied using a variety of techniques ranging from direct sampling of fumaroles (e.g., Giggenbach bottles) to remote sensing techniques (e.g., COSPEC). Ideally, gas monitoring is carried out sufficiently frequently by volcano observatories in order to develop an idea of the baseline or background activity for each volcano. Following the example of those working on industrial-related gas emissions, volcanologists have begun to develop and apply models of gas dispersion and deposition downwind from the

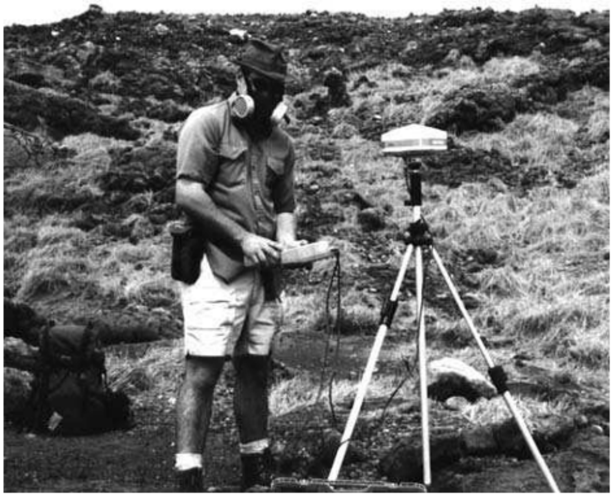

FIGURE 5 Example of a typical gas mask worn by the authors during work in the gas cloud at Masaya volcano.

volcanic source (e.g., Vulcano, Masaya). Based on this information, alert levels and hazard maps can then be developed and used for risk management. However, it is often the case that areas at risk lack the necessary funding and infrastructure to support such studies.

In only a few instances, such as the artificial degassing being carried out at Lake Nyos, is it possible to reduce or eliminate the gas hazard physically. In most cases, monitoring of the volcano and limitation of access by the public to affected areas are the only means of reducing the risk. On an immediate level, the impact of volcanic gases can be reduced by limiting exposure time, not overexerting oneself, and resting frequently. One should try to keep to the windward side of the gas source and wear full or half-face gas masks (respirators) with appropriate absorbers/filters (Figure 5). In the case where masks are unavailable, a wet cloth held over the face can greatly reduce the amount of water-soluble gases entering the lungs.

In some cases, evacuation is necessary, but for extended long-term activity such as at Masaya volcano, it is clearly not feasible. Education of the population at risk is therefore critical, and some excellent public information is now available on video. Produced by the International Association of Volcanology and Chemistry of the Earth's Interior (IAVCEI), "Understanding Volcanic Hazards" and "Reducing Volcanic Hazards" are available in Spanish or English from Northwest Interpretative Association, 3029 Spirit Lake Highway, Castle Rock, WA 9861360-27402101, USA.

IV. SUMMARY

Volcanic gases, although a relatively minor hazard in comparison with other volcanic phenomena, can have an important long-term impact on people and the environment. Gases and resulting acid rains may sometimes be detected over 1000 km from the volcanic source, but are generally directly responsible for relatively few deaths. Their effects on buildings are rarely totally destructive except in the case of long-term exposure (e.g., Masaya). Sulfur dioxide emissions from the 1783 Laki fires were responsible in part for global temperature decreases while CO_2 from subaerial volcanoes may contribute to global warming. Although some attempts have been made to physically reduce gas hazards (e.g., artificial degassing), gas monitoring and education of the public are likely the most effective means of reducing the hazard from volcanic gases.

SEE ALSO THE FOLLOWING ARTICLES

Impacts of Eruptions on Human Health • Volcanic Aerosol and Global Atmospheric Effects • Volcanic Gases • Volcanic Lakes

FURTHER READING

Blong, R. J. (1984). "Volcanic Hazards." Academic Press, Orlando, FL.

Farrar, C. D., Sorey, M. L., Evans, W. C., Howle, J. F., Kerr, B. D., Kennedy, B. M., King, C.-Y., and Southon, J. R. (1995). Forest-killing diffuse CO_2 emission at Mammoth Mountain as a sign of magmatic unrest. *Nature* **376,** 675–678.

Le Guern, G., Tazieff, H., and Faivre-Pierret, R. (1982). An example of health hazard: People killed by gas during a phreatic eruption, Dieng Plateau (Java, Indonesia), February 20th 1979. *Bull. Volcanol.* **45,** 153–156.

Le Guern, G., and Tazieff, H., eds. (1989). "Lake Nyos." *J. Volcanol. Geotherm. Res.* **39,** (special issue).

Scarpa, R., and Tilling, R. I., eds. (1996). "Monitoring and Mitigation of Volcano Hazards." Springer-Verlag, Berlin.

Sigurdsson, H., Devine, J. D., Tchoua, F. M., Presser, T. S., Pringle, M. K. W., and Evans, W. C. (1987). Origin of the lethal gas burst from Lake Monoun, Cameroon. *J. Volcanol. Geotherm. Res.* **31,** 1–16.

Thordarson, Th., and Self, S. (1993). The Laki (Skaftár fires) and Grímsvötn eruptions in 1783–1785. *Bull. Volcanol.* **55,** 233–263.

Thordarson, Th., Self, S., Óskarsson, N., and Hulsebosch, T. (1996). Sulfur, chlorine, and fluorine degassing and atmospheric loading by the 1783–1784 AD Laki (Skaftár fires) eruption in Iceland. *Bull. Volcanol.* **58,** 205–225.

VOLCANIC TSUNAMIS

JAMES E. BEGÉT
Alaska Volcano Observatory and University of Alaska

I. Introduction
II. Examples of Different Volcanic Processes Which Can Produce Tsunamis
III. Future Research in Volcanic Tsunamis and Evaluation of Tsunami Hazards

---

GLOSSARY

bore A high wall-like wave of water caused by the meeting of two bodies of water. Displacement of water by volcanic processes can produce bores, although they are more usually generated by tidal action in narrow channels.

hydromagmatic Hydromagmatic eruptions involve interactions between magma and water, and can result in the production and explosive expansion of steam. Hydromagmatic eruptions in oceans and lakes often produce tsunamis.

impulse wave A wave generated by energy and momentum transfer from a rapidly moving debris avalanche, lahar, or pyroclastic flow to water.

run up The maximum vertical height which a wave attains as it floods the shore. The run-up height may be somewhat greater than the actual height of the wave as it is affected by both the potential energy (height) and the kinetic energy (velocity) of the shoaling tsunami wave. Run-up heights may also be increased if wave energy is focused or channeled at the shore.

seiche An oscillating wave in an enclosed or semienclosed basin (i.e., a lake, bay, or harbor) with a period of minutes to hours. Seiches in volcanic areas are typically initiated by earthquakes and may continue for some time after the triggering event.

tsunami Japanese term which can be directly translated as "long wave in a harbor." The term was originally applied to seismic sea waves, but its usage has been expanded to include waves of volcanic origin generated in the ocean or in lakes.

volcanic explosivity index (VEI) A measure of the magnitude and energy of volcanic eruptions based on several basic parameters, including eruption duration and style, volume of eruptive products, and the eruption column height.

A VOLCANIC TSUNAMI is a high wave or surge of water produced by a variety of eruptive and noneruptive processes at volcanoes. Tsunami waves are generated when some of the tremendous amounts of energy produced during volcanic eruptions are transferred to ocean water or nearby large lakes. At least nine different mechanisms have been documented by which volcanoes produce tsunamis, including volcanic earthquakes, eruptions of undersea volcanoes, travel of pyroclastic flows into the sea, caldera collapse, debris avalanches and landslides, large lahars entering the sea, phreatomagmatic explosions, coupling between water

Copyright © 2000 by Academic Press
All rights of reproduction in any form reserved.

and turbulent air waves traveling from an explosive eruption, and collapse of lava benches during effusive lava eruptions.

Volcanic tsunamis can transmit the energy of volcanic eruptions to great distances from the volcano, producing much more devastation than would occur from the direct effects of the volcanic eruption alone. Volcanic tsunami waves are comparable in height to those produced by the largest known earthquakes, and waves 1–30 m high have inundated low-lying coastal areas at distances of tens or even hundreds of kilometers from source volcanoes. Most volcanic tsunami waves have been produced by extremely energetic explosive volcanic eruptions in or near water, or by flow of voluminous pyroclastic flows or debris avalanches into the sea. The most devastating volcanic tsunami known was produced by the eruption of Krakatoa in 1883, which resulted in more than 36,000 casualties, some at distances of up to 800 km from the eruption. The volcanic tsunamis at Krakatoa produced more fatalities than any other historic volcanic eruption. Altogether, about 25% of all fatalities directly attributable to volcanic eruptions during the last 250 years have been caused by tsunamis.

The height of volcanic tsunami waves is strongly influenced by the morphology of the coastline on which they impinge. In some cases, waves can more than double in height where the wave energy is focused and amplified into bays and coves. The velocity of volcanic tsunamis is directly proportional to water depth, reaching typical speeds of between 10–100 km/hour in shallow, coastal areas, and up to 800 km/hour when crossing deeper waters.

I. INTRODUCTION

Tsunamis (also called tidal waves) are sometimes thought to be produced only by large seismic events. However, about 5% of all historic tsunamis, including some of the most destructive tsunami waves ever seen on Earth, were produced at volcanoes by eruptions or other volcanic processes. More than 90 tsunamis of volcanic origin have been produced in the world's oceans during the last 250 years. Destructive waves have also been produced by eruptions which occured within caldera lakes and other lakes, or at volcanoes adjacent to lakes.

Numerous mechanisms exist by which volcanoes can generate tsunamis. In general, volcanic tsunamis are produced when part of the tremendous energy released during volcanic eruptions is directly or indirectly transmitted to the sea. One of the simplest mechanisms involves the generation of impulse waves by the displacement of water when debris avalanches and pyroclastic flows enter the sea or a lake and rapidly displace huge volumes of seawater. Water is also displaced and waves generated during explosive eruptions which occur in underwater environments, as may occur during eruption of undersea volcanoes, eruptions through crater lakes, and phreatomagmatic eruptions from shallowly submerged, near-shore vents. Processes which can transfer volcanic energy to water, including volcanic earthquakes and wave coupling with explosive atmospheric waves, have occasionally produced tsunamis during large eruptions. More rarely, small tsunamis have been produced when large lahars enter the sea, or when avalanches of recent tephra or collapse of lava benches displace water.

While relatively rare, volcanic tsunamis are of great concern because they typically occur with little warning and can devastate populated coastal areas at considerable distances from the volcano. Some of the most significant volcanic disasters in human history were caused by volcanic tsunamis (Table I). Indeed, about a quarter of all volcano-related deaths in historic time are attributable to the direct effects of volcanic tsunamis. Over 36,000 fatalities resulted from volcanic tsunamis produced during the 1883 eruption of Krakatoa alone, marking the single most catastrophic volcanic event in recent history.

Volcanic tsunamis have probably affected the development of human societies around the world. One of the earliest known carvings from archaeological sites in North America illustrates an erupting volcano (Figure 1). This carving, dating to about 500 years ago, was excavated at a paleo-Aleut archaeological site on Kodiak Island in Alaska, and appears to show a volcanic eruption associated with a tsunami wave (Figure 1). This carving is about the same age as an eruption at Augustine volcano on Augustine Island which sent a large debris avalanche into the waters of Cook Inlet. In Europe, a large tsunami is thought to have been produced circa 1628 B.C. by the Bronze Age eruption of Santorini volcano on the Greek island of Thera in the Mediterranean. The explosive eruption destroyed the original volcanic island, buried a thriving Bronze Age Minoan-style city, Akrotiri, and left a partly submerged caldera, perhaps accounting for the origin of the legend of Atlantis. A tsunami as much as 30 m high produced by the eruption is thought to have destroyed coastal areas near the Cretan Bronze Age city of Knosses, contributing to the collapse of

TABLE I Characteristics of Selected Volcanic Tsunamis

Location	*Age*	*Volcano type*	*Cause of tsunami*	*Wave height*	*Travel distance*	*Impact of tsunami*
Santorini Mediterranean Sea	1638 B.C. (?)	Island	Explosive eruption, caldera formation Pyroclastic flows into sea	10–50 m[a]	150–500 km ?[a]	Destruction of Minoan civilization on Crete[a]
Unzen, Japan Ariake Sea	1782 A.D.	Coastal	Debris avalanche into sea	10–55 m	20–50 km	More than 10,000 fatalities
Tamboro, Indonesia Java Sea	1815 A.D.	Island	Pyroclastic flows into sea	>10 m	>100 km	More than 10,000 fatalities
Krakatoa, Indonesia Sundra Straits	1838 A.D.	Island	Explosive eruption, caldera formation Pyroclastic flows into sea	5–35 m	800 km	More than 36,000 fatalities
Augustine, Alaska Cook Inlet	1883 A.D.	Island	Debris avalanche into sea	7–9 m	>100 km	Damage to coastal villages, no known fatalities
Ritter Island, New Guinea Bismarck Sea	1888 A.D.	Island	Debris avalanche into sea	4–12 m	450 km	Numerous fatalities
Paluweh Island, Indonesia Java Sea	1928 A.D.	Island	Debris avalanche into sea	5–10 m	>100 km	More than 150 fatalities
Iliwerung, Indonesia Java Sea	1979 A.D.	Coastal	Debris avalanche into sea	9 m	>100 km	More than 500 fatalities
Mt. St. Helens, Washington Spirit Lake	1980 A.D.	Mainland	Debris avalanche into lake	260 m	4 km	No known fatalities
Lake Nyos, Cameroon	1986 A.D.	Mainland	Exhalative emission of CO_2	25–75 m	5 km[b]	No known fatalities from tsunami
Kick 'em Jenny Caribbean Sea	Numerous	Submarine	Submarine eruptions	1–5 m	1–10 km	No known fatalities
Karymskoye, Kamchatka Karymskoye Lake	1996 A.D.	Caldera lake	Phreatomagmatic eruptions	30 m	5 km[b]	No known fatalities

[a] The size, travel distance, and impact of a tsunami wave from the eruption of Santorini are inferred from the magnitude of the eruption and the elevation of tsunami deposits.
[b] Tsunami waves at Karymskoye caldera caused flooding for many kilometers downstream from the caldera.

the advanced Minoan civilization which dominated the Mediterranean at the time.

II. Examples of Different Volcanic Processes Which Can Produce Tsunamis

A. Submarine Eruptions (Kick 'em Jenny, Caribbean Sea)

Although there are many more submarine than terrestrial volcanoes, there are very few instances in which tsunamis can be confidently attributed to individual submarine eruptions. The best known and studied examples involve the Kick 'em Jenny submarine volcano in the Caribbean Sea. While not all of the processes by which volcanoes produce tsunamis are well understood, direct observations have clearly linked submarine volcanic eruptions and small tsunamis at Kick 'em Jenny.

The tsunami waves at Kick 'em Jenny submarine volcano are apparently generated by multiple mechanisms. Direct transfer of seismic and explosive energy produced during hydromagmatic eruptions to the ocean appears to produce most tsunamis. Less frequently, large steam bubbles form above the vent and generate waves either by submarine cavitation and collapse or by rapid ascent to the surface. Also, masses of ocean water can be heated near the vent and rise convectively to the surface, pro-

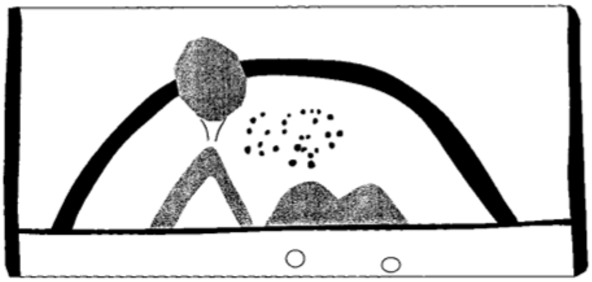

FIGURE 1 Reproduction of a carving on a circa 500-year-old wooden box excavated from an archaeological site on Kodiak Island, Alaska, showing an erupting volcano and a large wave. This carving is virtually identical in age to a large eruption of Augustine volcano that sent a debris avalanche into the waters of Cook Inlet (see Figure 2). This paleo-Aleut carving is the oldest known illustration of a volcanic eruption and volcanic tsunami in the western hemisphere.

ducing waves. On one occasion a scientific submersible vessel became trapped in a rapidly rising hot water mass, and only narrowly escaped.

In recent years, eruptions of Kick 'em Jenny have occurred approximately every 5–10 years. These eruptions were typically quite small (VEI = 0–1), and eruption columns rarely rose through the water to the atmosphere. Waves as much as several meters high have been produced and constitute a significant and well-known hazard to local shipping and yacht traffic among the Windward Islands of the southeastern Caribbean Sea.

The size of hydromagmatic eruptions at Kick 'em Jenny is limited because the summit of the volcano lies at a depth approximately 150 m below sea level, where hydrostatic pressures inhibit the occurrence of large hydromagmatic explosions. The energy of these explosions may also be minimized because of high water-to-magma ratios during the submarine eruptions. The volcano currently rises about 500 m above the surrounding seafloor and has been increasing in height by ~4 m/year. If Kick 'em Jenny volcano continues to erupt and grow in height, its submarine explosive eruptions are likely to become more energetic as it approaches the ocean surface and hydrostatic pressures decrease, and the local tsunami hazard may increase.

The documentation of submarine eruptions and a concomitant tsunami hazard at Kick 'em Jenny raises questions about the number, distribution, and eruptive style of other submarine volcanoes around the world, as well as the possibility of associated tsunami hazards. The number and distribution of active submarine volcanoes are poorly known, but are probably at least comparable to the total number of terrestrial volcanoes. In the Kurile arc south of Kamchatka, detailed surveys by Russian scientists identified at least 90 fresh-appearing submarine volcanic cones in the sea besides the many island volcanoes rising above the sea. There are likely hundreds of other submarine volcanoes along oceanic arcs, spreading ridges, and hot spots, including Loihi volcano east of Hawaii and vents such as the Surtsey volcanoes along the mid-Atlantic Ridge near Iceland.

Is it possible that an eruption of a submarine volcano may someday result in a major catastrophic event, even though no major historic tsunamis are known to have been produced by submarine volcanoes? The largest known wave from a submarine eruption capsized boats in 1781 off Sakurajima near the island of Kyushu, Japan. Unfortunately, at the present time there is no reliable way to predict the location or likelihood of such events, and no submarine volcano is continuously monitored by a volcano observatory.

B. Tsunamis Produced by Eruptions through Lakes (1996 Eruption of Akademia Nauk Caldera, Kamchatka)

As originally defined, the Japanese term "tsunami" applied only to great waves produced in the ocean. However, eruptions can also produce high waves in lakes, and these are now also referred to as volcanic tsunamis. Volcanic eruptions often occur through large caldera lakes, and occasionally eruptions are initiated through preexisting nonvolcanic lakes. Such eruptions may be characterized by violent hydromagmatic explosions, especially where the lake is shallow but large in size. In some cases high tsunami waves have been produced. For instance, during a day-long sequence of hydromagmatic eruptions in January 1996 through the 60-m-deep and 8-km^2-area Karymskoye Lake in the Akaemia Nauk caldera at the foot of Karymsky volcano in Kamchatka, waves with a maximum height of more than 30 m were generated. These waves stripped vegetation and sediment from beaches and cliffs around the shore of the lake, and also overtopped the lake outlet and flooded down the Kamchatka River for many kilometers. Smaller waves were produced on at least five separate occasions by phreatomagmatic eruptions and base surges during eruptions in 1965 through the Taal Caldera Lake in the Philippines.

An unusual tsunami was produced during the gas eruption at Lake Nyos in Cameroon in 1986. The sudden release of about 3 million m^3 of carbon dioxide from the lake waters produced a wave from 25 to 75 m high.

Occasionally eruptions occur through lakes that have not previously been volcanic vents. In the 1886 Tarawera eruption in New Zealand, a 17-km-long fissure eruption cut across older volcanic vents and adjacent nonvolcanic areas, producing phreatic explosions which enlarged and excavated what is now Lake Rotomahana. The eruption was immediately preceded by a small wave about 30 cm high on nearby Lake Tarawera. This seiche was apparently produced by earthquakes just prior to the main eruption, as Lake Tarawera was not in contact with either the faulting or the fissure eruption.

Although volcanic tsunamis in lake basins are much more restricted in their potential travel distance than those in the ocean, lake basins may be densely populated. Some caldera lakes are surrounded by agricultural developments, population centers, and recreation facilities. If tsunamis of similar size to those at Karymskoye Caldera Lake were produced by eruptions through the Taal Caldera Lake in the Philippines, the Towada and Toya Caldera lakes in Japan, the Taupo or Rotorua calderas in New Zealand, Yellowstone Lake in Yellowstone Caldera, or many other caldera lakes around the world, significant damage and casualties would result.

C. Landslides and Debris Avalanches (Unzen, Japan, in 1782; Mount St. Helens, Washington, in 1980; and Mount St. Augustine, Alaska, in 1883)

Volcanic debris avalanches generate impulse waves as they enter the sea by displacing huge volumes of water. The precise nature of the interactions and processes which generate waves during giant landslides is not well understood, as they have never been directly observed or measured. Physical models of these processes are also difficult to develop, as little information is available on the multiple factors which can influence the eventual size of waves. These include beach aspect, coastal morphology and water depth, the size and shape of the lake or bay where the avalanche occurs, and the thickness, density, mass, and velocity of the debris avalanche itself. The nature of the interaction between the front of the landslide debris and the propagating wave front in the ocean is also poorly understood. For instance, avalanches which are thicker than the water which they enter must act as a wall sweeping the water before them, while avalanches which dive into deeper water must displace the water in a much different way. The travel distance of the avalanche mass as it moves into the water, and the magnitude of possible explosive interactions between hot rock debris in the debris avalanche, any associated blast or surge, and the seawater, may also influence the size of the resultant wave.

If the mass of the avalanche is very large relative to the size of the body of water, then masses of water can be totally displaced in a "splash" or surge of water, producing an exceptionally high, although volumetrically small, impulse wave. For instance, during the Mount St. Helens eruption in 1980, one arm of the debris avalanche completely crossed the Spirit Lake basin and produced a wave that reached 260 m up the hills surrounding the lake. The wave swept back downhill across the surface of the debris avalanche, crossed the lake basin, and sloshed up slope toward the volcano, and continued to oscillate for some time in the lake basin.

A similar but smaller well-documented debris avalanche and tsunami occurred in 1883 at Mount St. Augustine in Cook Inlet, southcentral Alaska. The debris avalanche travelled ~5 km into the waters of Cook Inlet on the north side of Augustine Island (Figure 2). Recent computer modeling suggests that the wave generated by the debris avalanche at Augustine volcano was as

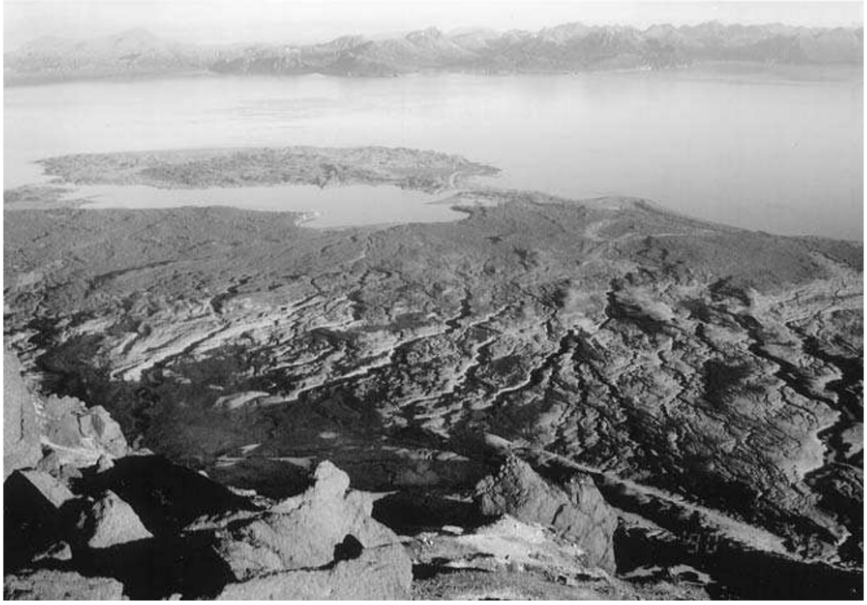

FIGURE 2 The 500-year-old West Island debris avalanche deposit, viewed from the summit of Augustine volcano, buried the former coastline of Augustine Island and traveled 5 km farther into the waters of Cook Inlet. Debris avalanches of this size typically generate tsunami waves that run up to 5–30 m above sea level at distances of 80–100 km.

much as 30 m high when generated at the leading edge of the debris avalanche and attenuated to heights of 7–9 m as the wave traveled toward the Kenai Peninsula and the mainland of Alaska. The computer models are in very good agreement with contemporary records of the tsunami waves. About an hour after the avalanche occurred, several tsunami waves 7–9 m high struck the small, native village of Port Graham at the southwest end of the Kenai Peninsula some 80 km southeast of Augustine Island. The waves inundated houses built along the beach and carried away fishing boats. Cook Inlet has the second largest tidal range of any inlet on Earth, with tidal cycles of 8 m. The debris avalanche and tsunami occurred at dead low tide, minimizing the impact on the small settlements which existed around Cook Inlet at that time. While only a few villages and scattered settlements were present around Cook Inlet in 1883, tens of thousands of people live around the shores of Cook Inlet today.

Geologic studies at Augustine volcano indicate the 1883 debris avalanche was just the latest of at least 12 debris avalanches which have occurred during the last 2000 years. This unusual pattern of activity in part reflects a very high and sustained eruption rate of 2–3 km^3 per thousand years. The pattern of frequent eruptions and high eruption rate has continued to the present, as the horseshoe-shaped crater left by the 1883 debris avalanche has been filled in and the volcano summit has regrown to the elevation it had as a result of five subsequent dome-building eruptions. If the volcano continues the same pattern of activity it has exhibited over the last 2000 years it is highly likely to collapse again into Cook Inlet and produce a tsunami wave. Indeed, a scientific prediction has been made that Augustine volcano will probably collapse and generate a tsunami again sometime during the 21st century, making this the only volcano on Earth where a volcanic tsunami is predicted to occur in the near future.

In some cases large rockfall avalanches can occur from volcanic edifices with little or no accompanying eruptive or seismic activity. Catastrophic events which happen without any warning are particularly dangerous to nearby human populations. A rockfall avalanche, possibly triggered by an earthquake, occurred without warning from Mount Maruyama dome on the Shimabara Peninsula in Japan in 1792, about a month after lava eruptions had ended on nearby Unzen volcano. The debris avalanche went through the historic town of Shimabara and traveled several kilometers into the Ariake Sea, generating a tsunami. The wave swept away numerous farmhouses and villages at elevations more than 30 m above the sea and produced an estimated 14,000 casualties.

D. Explosive Eruptions (Krakatoa, Indonesia, 1883)

The largest and most devastating volcanic tsunami of the last 250 years was produced by the August 26, 1883, eruption of Krakatoa volcano. This extremely energetic explosive eruption produced multiple tsunami waves as much as 37 m high, among the greatest tsunami waves seen in recent historic time. The waves raised large ships to 10 m above sea level and carried them as far as 3 km inland. These waves deluged more than 250 villages in western Java and eastern Sumatra, killing more than 36,000 people. Fatalities due to waves occurred as far as 800 km from the volcano (Figure 3). Small tsunami waves were recorded throughout the Pacific Ocean, and small sea level oscillations were measured at sites thousands of kilometers away in the Indian Ocean, France, and England.

The precise mechanisms associated with the generation of specific waves during the Krakatoa eruption remain controversial, as at least five different processes may have been involved. Firstly, the magmatic and phreatomagmatic explosions that destroyed the summit edifice were among the greatest volcanic explosions ever documented, being audible up to 4600 km away and recorded on barographs around the world. These energetic explosions may have directly generated waves. Secondly, coupling between the sound waves and the ocean surface may also have generated tsunamis and seiches. The small waves recorded at very remote sites such as England and France almost certainly were formed by coupling between the sea and atmospheric shock waves, while larger waves may have been produced closer to the eruption. Thirdly, after the explosion, several cubic kilometers of seawater from the Sundra Strait rushed into the caldera crater, filling it and perhaps producing a giant bore which propagated away from the crater as a tsunami. Fourthly, debris avalanches were generated during caldera collapse at Krakatoa, and may have produced tsunamis as they were emplaced into the sea around the caldera. And finally, recent field investigations, including submarine fieldwork done by scuba diving, have identified an extensive ignimbrite sheet preserved beneath the sea surrounding the caldera. Rapid emplacement of voluminous, hot pyroclastic flows into the ocean floor radially around the caldera evidently

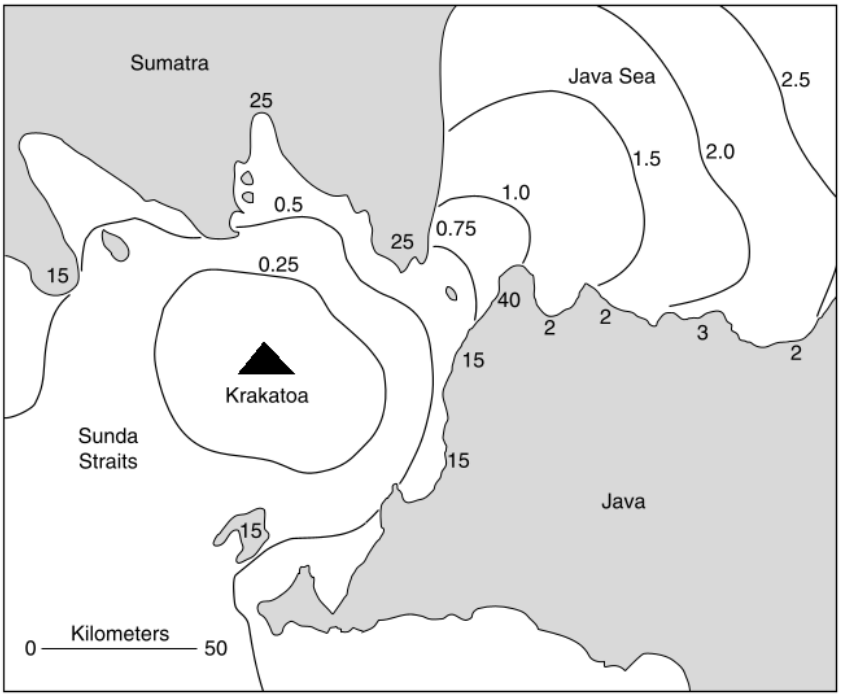

FIGURE 3 Travel times (hours) and wave heights (meters, bold) of the devastating Krakatoa tsunami as it propagated along the coastline away from the volcano. More than 36,000 people were killed by the tsunami wave as it inundated low-lying coastal areas. Note the significant differences in maximum wave height at similar distances from the volcano due to local variations in coastal aspect and morphology and their effect on wave run up.

displaced huge volumes of water and gave rise to tsunami waves.

III. FUTURE RESEARCH IN VOLCANIC TSUNAMIS AND EVALUATION OF TSUNAMI HAZARDS

Volcanic tsunamis, like many volcanic hazards, occur rarely but can be highly dangerous and destructive. In order to evaluate future tsunami hazards realistically at active volcanoes, it is desirable to learn much more about the frequency and magnitude of past tsunamis. In addition, the behavior of potentially hazardous volcanoes around the world that generate tsunamis, and the processes of tsunami generation, travel, and wave run up, must be better understood.

Information on volcanic tsunamis comes mainly from historic events within the last 250 years, but it is desirable to examine the geologic record for the last several millennia or longer to learn more about the frequency and magnitude of volcanic tsunami events. Unfortunately, tsunamis typically leave thin and discontinuous geologic deposits which are extremely difficult to find and unambiguously characterize. It can be difficult to find deposits from tsunamis only weeks after their occurrence, and is likely to be much more difficult after centuries or millennia have passed. All evaluations of volcanic tsunami hazard must therefore integrate both investigations of ancient volcanic tsunami deposits and studies of the volcanic eruption history of island volcanoes and volcanoes lying near coastal areas to connect records of volcanic activity with the much more fragmentary geologic record of past tsunamis.

Much more also needs to be learned about the multiple processes that can trigger tsunamis. While it appears that some volcanic processes are more likely to trigger large tsunamis than others (Table II), the actual physics of the interactions between water and all types of volcanic phenomena is poorly understood. Similarly, the behavior of large waves is a complicated mathematical problem. In particular, the amount of run up which can

TABLE II Processes of Volcanic Tsunami Generation

Cause of tsunami	*Percentage of total*	*Location*	*Tsunami magnitude*
1. Volcanic earthquakes	20	I, C, L	S
2. Pyroclastic flows entering water	20	I, C, L	L
3. Submarine eruptions	20	—	S (L?)[a]
4. Debris avalanches (hot and cold)	15	I, C	L
5. Caldera collapse	10	I	L
6. Phreatomagmatic explosive eruptions	5	I, C, L	L
7. Air waves	5	I, C	S (L?)[b]
8. Lahars entering water	5	I, C, L	S
9. Lava flow entering water	<1	I, C, L	S

Notes. Table modified from Latter (1982) and Smith and Shepherd (1993). Location symbols are I, island volcanoes; C, coastal volcanoes; L, caldera lakes or volcanoes near lakes. Tsunami magnitude is S, small (waves > 10 m uncommon); L, large (waves 5–10 m common, may exceed 30 m in large events).

[a] Tsunami waves from historic undersea eruptions have been small, but it is possible that larger waves may be produced in some cases.

[b] Some distant seiches and tsunamis produced in 1883 at Krakatoa have been attributed to air wave coupling with the ocean surface, but it is uncertain if the largest proximal waves were formed in this way. No other large tsunamis can be definitely linked with air waves.

occur at specific locations along a coast is very difficult to estimate, as the height of tsunami waves usually increases as they near the shore in response to shoaling and refraction in bays and along curved coastlines. The wave height at the beach (run-up height) may be 3–10 times greater than wave amplitudes in the open sea.

The processes which trigger volcanic tsunamis are also poorly understood. Volcanic earthquakes are among the most prolific causes of volcanic tsunamis (Table II) but usually generate only relatively small seiches. Volcanoseismic events are predominantly caused by magma movement and its effects on conduits and surrounding rocks within volcanoes. Such processes are very unlikely to result in fault displacements in undersea areas that directly displace water and generate tsunamis. Also, although thousands of volcanic earthquakes typically accompany an eruption, the maximum known volcanoseismic events are circa Richter magnitude 7, and such large events are relatively rare. Earthquakes of this size generally produce tsunamis that have less than a 1-m run-up height, while seismic events of lesser magnitude are associated with even smaller tsunamis, so that seismic events large enough to trigger tsunamis are, fortunately, uncommon.

As discussed above, the potential hazards from submarine volcanoes are extremely poorly understood. During the last 250 years about 20% of all volcanic tsunamis have apparently been produced by eruptions of submarine volcanoes (Table II). Much more work is needed to identify possibly hazardous submarine volcanoes, as well as to learn more about the processes which generate tsunamis during undersea eruptions. The debris avalanche from the Maruyama dome at Unzen in 1792 raises the possibility that some volcanoes can collapse, essentially without warning, and generate destructive tsunamis. The magnitude of such hazards is important to evaluate for several reasons, including: (1) most arc volcanoes around the world are located on islands or near mainland coasts, producing numerous potential debris avalanche sites; (2) active volcanoes tend to grow through time, producing increasingly higher and steeper edifices; (3) polygenetic cones typically consist of interstratified lava and pyroclastic rocks with variable hydraulic and geotechnical properties, and zones of weakness are probably present within most volcanic cones; (4) geothermal activity and high heat flow within volcanoes can alter rock to clay and further facilitate the development of zones of weakness within volcanic cones; and finally (5) most volcanic arcs are strongly affected by great subduction zone earthquakes, so the possibility that incipient debris avalanches can be triggered by giant seismic events without volcano eruptions must be evaluated. The 1792 debris avalanche and tsunami at Maruyama dome near Unzen volcano raises questions about the proclivity to failure and collapse of volcanic edifices and the likelihood of tsunami generation by debris avalanche, even when volcanoes are not in eruption.

Based on the pattern of volcano tsunami generation during recent times, it appears that large, destructive volcano tsunamis with more than 5-m waves are most likely to be generated by eruptions which produce voluminous pyroclastic flows or debris avalanches, or which are highly explosive and produce calderas at the sites of former volcanic islands (Table II). Explosive submarine eruptions or submarine avalanches may also have the potential to produce large tsunamis, although there are no well-documented historic examples of this type of event. Phreatomagmatic eruptions in lakes have also produced high tsunamis, although the potential for damage has been limited by the generally small size of lake basins. The other volcanic processes known to produce tsunamis have, in historic time, shown less ability to generate large, regionally destructive waves, and research is needed to confirm whether these types of volcanic events and eruptions actually present less tsunami hazard.

SEE ALSO THE FOLLOWING ARTICLES

Calderas • Debris Avalanches • Hazards from Pyroclastic Flows and Surges • Surtseyan and Related Phreatomagmatic Eruptions • Volcanic Lakes

FURTHER READING

Antonopolos, J. (1992). The great Minoan eruption of Thera volcano and ensuing tsunami in the Greek Archipelago. *Natural Hazards* **5,** 153–168.

Begét, J., and Kienle, J. (1992). Cyclic formation of debris avalanches at Mount St. Augustine volcano. *Nature* **356,** 701–704.

Belousov, A., Voight, B., Belosouva, M., and Murveyev (1999). Tsunamis by sub-aquatic volcanic explosions: Unique data from 1996 eruption in Karymskoye Lake, Kamchatka, Russia. *J. Appl. Geophys.*, in press.

Kienle, J., Kowalik, Z., and Murty, T. S. (1987). Tsunamis generated by eruption from Mt. St. Augustine volcano, Alaska. *Science* **236,** 1442–1447.

Latter, J. N. (1982). Tsunamis of volcanic origin: Summary of causes with particular reference to Krakatoa, 1883. *Bull. Volcanol.* **44,** 467–490.

Lockridge, P. A. (1990). Nonseismic phenomena in the generation and augmentation of tsunamis. *Natural Hazards* **3,** 403–412.

Sigurdsson, H. (1989). Submarine investigations in the crater of Kick 'em Jenny volcano. *Bull. Scientific Event Alert Network* **4,** 45–49.

Smith, M. S., and Shepherd, J. B. (1993). Preliminary investigations of the tsunami hazard of Kick 'em Jenny submarine volcano. *Natural Hazards* **7**(3), 257–278.

This Page Intentionally Left Blank

VOLCANIC SEISMICITY

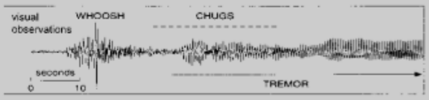

STEPHEN R. MCNUTT
Alaska Volcano Observatory and University of Alaska Fairbanks

I. Introduction
II. Types of Volcanic Earthquakes and Terminology
III. General Features of Earthquakes at Volcanoes
IV. Case Histories
V. Conclusions

GLOSSARY

A-type earthquake Events with clear P waves and S waves occurring under volcanoes at depths of 1–10 km [synonyms are volcanotectonic (VT) or high-frequency (HF) earthquake].

B-type earthquake Events with weak P waves and no S waves, a low-frequency content, and occurring under volcanoes at depths < 1 km (see also long-period and low-frequency earthquakes).

explosion earthquake Events with seismic waves in the ground (including P waves and S waves) and often air waves, which travel through the air and are transmitted back into the ground in the vicinity of the seismometer.

long-period event Discrete events with very regular, low-frequency (1–5 Hz) waveforms that resonate for many cycles.

low-frequency event General term for discrete events with either enriched low frequencies or deficient high frequencies compared with typical earthquakes (includes long-period and B-type earthquakes).

magnitude A measure of the size of an earthquake, determined by measuring the highest-amplitude waves and correcting for distance and type of instrument. The scale is logarithmic, so each increase of one unit corresponds to an amplitude increase of a factor of 10.

P wave Primary wave, an elastic wave with primarily compressional or longitudinal particle motion that travels faster than other waves and is thus the first to appear on seismograms.

S wave Secondary wave, a shear elastic wave with transverse particle motion, and usually the most prominent wave on a seismogram; travels more slowly than P waves and thus arrives later on seismograms; cannot pass through liquids.

swarm A group of many earthquakes of similar size occurring closely clustered in space and time with no dominant main shock.

volcanic tremor Continuous seismic signal with regular or irregular sine wave appearance and low frequencies (0.5–5 Hz). Harmonic tremor has a very uniform appearance, whereas spasmodic tremor is pulsating and consists of higher frequencies with a more irregular appearance.

VOLCANO SEISMOLOGY IS the study of earthquakes of volcanic origin as well as of velocity structure, attenuation, and other physical properties of earth materials that affect the passage of seismic waves at volcanoes. Volcanic earthquakes may be defined as

Copyright © 2000 by Academic Press
All rights of reproduction in any form reserved.

earthquakes which occur at or near volcanoes, generally within 10 km, or are related to volcanic processes. Volcanoes are places where heat and mobile fluids are concentrated, so the number of earthquakes per unit time is high compared with normal crust. Volcanic earthquakes take place at shallower depths (1–9 km) than tectonic earthquakes on typical faults (deeper than 15 km in the crust; as deep as 600 km in subduction zones). Volcanic events also differ in their patterns of occurrence: they often occur in swarms, groups of many small events with similar sizes and locations. This is in contrast with the typical mainshock–aftershock sequences on most faults for tectonic earthquakes. Volcanoes produce different types of earthquakes which represent different processes. Among these are high-frequency events, low-frequency events, explosions, and volcanic tremor. These occur in increasing numbers prior to or during eruptions. The seismicity also increases during intrusions—like eruptions, but where the magma fails to reach the surface—and thus the processes that cause various types of volcanic earthquakes are similar even though the eruptive outcomes differ. The source mechanisms of some volcanic earthquakes are not yet understood.

I. INTRODUCTION

Volcanoes are the sources of a great variety of seismic signals which behave differently than events on earthquake faults. Nearly every recorded volcanic eruption has been preceded by an increase in earthquake activity beneath or near the volcano, and accompanied and followed by varying levels of seismicity. For this reason, seismology has become one of the most useful tools for eruption forecasting and monitoring. At the present time, approximately 200 of the world's volcanoes are seismically monitored, although the number and quality of stations at each varies considerably. This represents about one out of three of the 538 volcanoes that have erupted in historic times. Over the last several decades, 55 to 70 individual volcanoes have erupted each year. Because erupting volcanoes draw attention both publicly and scientifically, over half of these are seismically monitored.

This article reviews some of the developments in volcano seismology over the last 25 years that have led to an improved understanding of volcanoes and the volcanic processes that cause earthquakes and other seismicity. The article also describes a number of patterns and relationships in volcano seismology that form the physical basis of contemporary monitoring and forecasting, although these topics are covered in greater detail elsewhere.

A. Some Famous Early Eruptions

Throughout history the relation between earthquakes and volcanoes has been close, although there has been confusion about causal relations between the two. This is because of the parellel belts of volcanoes and earthquakes found at subduction zones, where 95% of the Earth's subaereal volcanoes are located. It is common in the historic record, and recently as well, to find an increase in reports of regional earthquakes around the times of eruptions. The reports of the eruption of Vesuvius in 79 A.D. tell of numerous local earthquakes preceding the eruptive activity. People living near Mount Nuovo, Italy, in 1538 and Mount Usu, Japan, in 1663 fled from the areas before the eruptions because of many felt earthquakes. Early observatories at Vesuvius starting in 1856, Usu in 1910, and Hawaii in 1912 recorded different types of earthquakes and began systematic study of eruption precursors. Three weeks of felt earthquakes heralded the formation of the new volcano Paricutin in Mexico in 1943. These and many other examples illustrate that volcanoes are active seismic features.

B. Brief Review of Earthquake Seismology

In order to appreciate the unique features of earthquakes at volcanoes, it is first necessary to review some features of typical earthquakes. Most earthquakes, which volcanologists often refer to as "tectonic earthquakes" to distinguish them from the volcanic varieties, are caused by shear fracture. That is, rock masses on either side of a planar fracture slip past each other in a shearing motion, generating heat, deformation, and elastic waves. It may surprise most readers to learn that only about 1% of the energy of an earthquake is in the form of elastic waves, which is the part that is felt or recorded by instruments as ground shaking. Most of the energy is liberated as heat and deformation. While rock is fractured at all scales, in many places fractures are organized into large planar features known as faults. Faults can be the sites of large earthquakes, those that involve a large surface area of the fault, as well as many smaller ones that rupture only a small surface area. In general there are many more small earthquakes than large ones; in fact the distribution of earthquake numbers versus magnitude follows a power law, known to seismologists as the frequency–magnitude distribution. The slope of the relation,

$$\log_{10} N = a - bM,$$

where N is cumulative number and M is magnitude, and a and b are constants, is known as the b-value, and usually takes on the value of 0.9 to 1.0 for tectonic earthquakes. This means that for every $M = 3$ earthquake there are 10 $M = 2$ earthquakes, 100 $M = 1$ earthquakes, and so on.

There are several different measures of earthquake size. The most widely known is magnitude, which is the amplitude of the recorded elastic waves on a particular instrument (the Wood–Anderson torsion seismometer) corrected for distance. A more physical measure of earthquakes is seismic moment, which is the product of fault area, slip, and the rigidity or strength of the rock. The ranges of these parameters and how they relate to each other are called scaling relations, and they permit the calculations of Table I, which shows typical dimensions and other parameters for earthquakes of different magnitudes.

Once an earthquake occurs at the source (such as a fault), the elastic waves travel away along different paths and eventually reach the seismometers. Characteristics that contribute to a seismogram (the way the earthquake appears on a paper record or other media) may occur at the source, along the path, and at the recording site, thus a major task for seismologists is to determine, for each seismogram, the relative contributions of source, path, and site effects. Once these are known a basis exists to demonstrate that a particular earthquake is low-frequency, harmonic, etc., and physical models are then constructed to evaluate the likely causes of peculiar (and normal) waveforms.

TABLE I Typical Earthquake Parameters (Circular Fault, 30-Bar Stress Drop)

Magnitude	*Radius*	*Slip*	*Moment*[a] *(dyne-cm)*	*Duration*[b] *(s)*
−2	0.85 m	0.06 mm	4×10^{13}	0.00053
0	8.5 m	0.6 mm	4×10^{16}	0.0053
2	85 m	6 mm	4×10^{19}	0.053
4	0.85 km	6 cm	4×10^{22}	0.53
6	8.5 km	60 cm	4×10^{25}	5.3
8	85 km	6 m	4×10^{28}	53

[a] Rigidity $= 3 \times 10^{11}$ dyne/cm^2.
[b] Assumed $\beta = 3.18$ km/s.

Seismology is also concerned with the distribution of velocities within the Earth. Seismic velocites are much higher than normal everyday velocities and are usually measured in kilometers per second, about the speed of satellites in outer space. For example, a car traveling on a highway at 60 mph is only going about 27 m per second, whereas air waves (sound waves) travel at 331 m per second and typical P waves at volcanoes travel at about 3 to 5 km per second or faster. Seismic waves travel more slowly in molten rock than they do in solid rock, so seismic tomography, similar to medical tomography, uses variations in the speed of elastic waves to recover information about where the magma is located.

With this brief overview as a reference frame, we now turn our attention to some of the features of volcanic earthquakes.

II. TYPES OF VOLCANIC EARTHQUAKES AND TERMINOLOGY

Active volcanoes are the sources of a great variety of seismic signals. Traditionally, volcanic earthquakes have been classified based on seismogram appearance into four different types: high-frequency (HF) or A-type, low-frequency (LF) or B-type, explosion quakes, and volcanic tremor. This classification scheme works very well at a large number of volcanoes, but see below for additional discussion on terminology. Other local signals, such as those caused by glaciers or landslides, are also recorded at volcanoes. Although the original classification included restricted depth ranges for various events, these have often been relaxed because of improvements in location accuracy and better understanding of source and propagation effects. Examples of volcanic events from several volcanoes are shown in Figure 1.

A. High-Frequency Events

Most high-frequency events are thought to be caused by shear failure or slip on faults, and differ from their tectonic counterparts only in their patterns of occurrence. At volcanoes, earthquakes typically occur in swarms rather than mainshock–aftershock sequences. A swarm may be defined as a group of many earthquakes of about the same size and location with no dominant

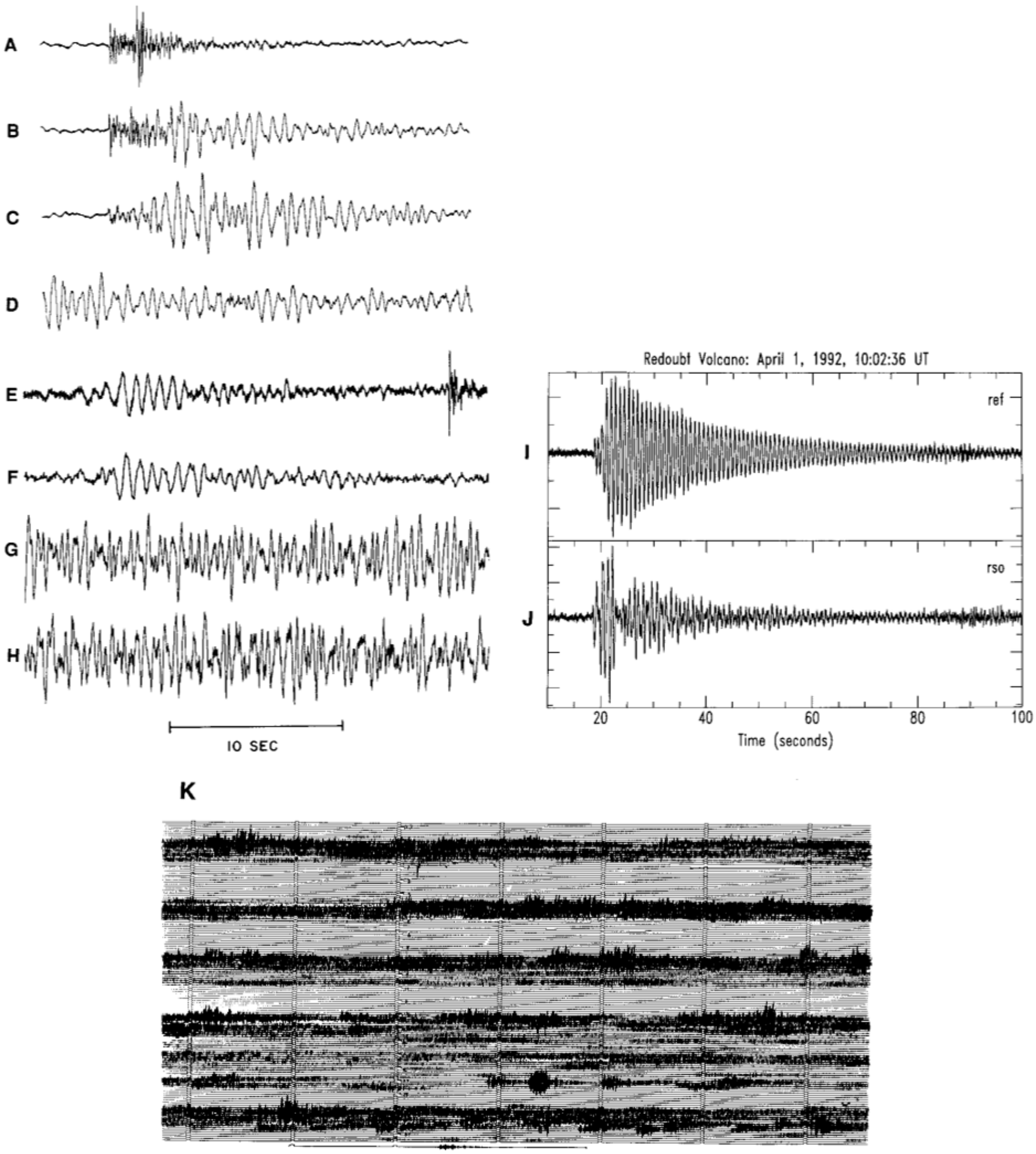

FIGURE 1 Typical waveforms of volcanic earthquakes: (A) High-frequency or volcanotectonic earthquake, 6.8 km depth, Redoubt volcano, Alaska, station RED, 8 km from the vent. (B) Hybrid or mixed-frequency event, −0.6 km depth (0.6 km above sea level), Redoubt volcano, station RED. (C) Low-frequency or long-period event, −0.4 km depth, Redoubt volcano, station RED. (D) Volcanic tremor, Redoubt volcano, station RED. (E) Explosion quake, Pavlof volcano, Alaska, station PVV, 8.5 km from the vent (note prominent air-wave arrival). (F) Low-frequency of B-type event, Pavlof volcano, station PVV. (G) Volcanic tremor before eruption, Mount Spurr, Alaska, station CRP, 4.8 km from the vent. (H) Volcanic tremor during eruption, Mount Spurr, station CRP. (I) Tornillo, long-coda event, or long-period event, Redoubt volcano, station REF, 3 km east of the vent. (J) Same event as (I) as recorded at station RSO, 3 km south of the vent. (K) Banded tremor from Manam volcano, Papua New Guinea, station TBL, 4 km from the vent (bands correspond to strong phases of subcontinuous Strombolian activity; tick marks are at 1-minute intervals; and recording speed is six lines (revolutions) per hour). Amplitudes for A–J are normalized. [After McNutt, 1996.]

shock. In practical terms, the difference in magnitude between the largest and second largest event of a swarm is 0.5 magnitude units or less, as opposed to 1.0 magnitude units or more for most mainshock–aftershock sequences. High-frequency events have clear P and S waves, and dominant frequencies are 5–15 Hz. Higher frequencies may be generated at the source, but are not recorded because of instrumental limitations or high local attenuation. A typical small high-frequency event is shown in Figure 1A.

B. Low-Frequency Events

Most low-frequency events are thought to be caused by fluid pressurization processes such as bubble formation and collapse, and also by shear failure, tensile failure, or nonlinear flow processes which occur at very shallow depths for which attenuation and path effects play an important role. These events often have emergent P waves, lack S waves, and have dominant frequencies between 1 and 5 Hz, with 2–3 Hz most common. Examples of low-frequency events are shown in Figures 1C, 1F, 1I, and 1J.

Prior to eruption, magma must move from depth to the Earth's surface through conduits, dikes, sills, reservoirs, or various combinations of these. Thus, models of low-frequency volcanic earthquakes select a geometry, such as a rectangular crack or a cylindrical pipe, and then attempt to reproduce seismograms by appropriate choice of length, width, and velocity of the material within it, which can be either magma or water. (Seismicity similar to that at volcanoes is found at geysers and geothermal areas.) A source of mechanical energy is needed; this can be a small earthquake adjacent to a conduit, a flow transient or pressure fluctuation within a conduit, gas bubbles expanding or contracting, a shock wave from choked flow, or other causes. Some workers consider the source to be the mechanical energy alone, while others treat the source as the ensemble of the mechanical energy and the resonant response of the magma or water in conduits or dikes.

Some earthquakes share attributes of both high- and low-frequency events. These are called hybrid events. For example, the event shown in Figure 1B displays the high-frequency onset of a high-frequency event, but the later part of the signal (the coda) is similar to low-frequency events. It is thought that such events may represent a mixture of processes, such as an earthquake occurring adjacent to a fluid-filled cavity and setting it into oscillation. Others suggest that hybrids are shallower than low-frequency events and thus preserve most of the high-frequency energy which is attenuated for deeper events.

C. Explosion Earthquakes

Explosion quakes accompany explosive eruptions, and many are characterized by the presence of an air-shock phase on the seismograms. There is a partitioning of energy at the source: part of the energy travels through the ground as seismic waves and part travels through the air as acoustic or air waves. The air wave then couples back into the ground and is detected by the seismometer. The air wave also shows up clearly on microphones or barographs. An example of an explosion earthquake is shown in Figure 1E.

D. Volcanic Tremor

Volcanic tremor is a continuous signal with a duration of minutes to days or longer. The dominant frequencies of tremor are 1–5 Hz (2–3 Hz is most common), similar to low-frequency events, and many investigators have concluded that tremor is a series of low-frequency events occurring at intervals of a few seconds. Harmonic tremor and spasmodic tremor are two special cases of more general volcanic tremor. Harmonic tremor is a low-frequency, often single-frequency sine wave with smoothly varying amplitude, or sometimes it consists of a fundamental frequency with many overtones. Spasmodic tremor is a higher-frequency, pulsating, irregular signal. Examples of volcanic tremor are shown in Figures 1D, 1G, 1H, and 1K.

It has previously been stated that earthquakes obey a power law, known in seismology as the frequency–magnitude relation. There are more small earthquakes than large ones, and the relative numbers of events form a power law distribution. Volcanic tremor, however, obeys a different type of relation, which is an exponential law (Figure 2). For tremor, which is a continuous signal, we cannot count the number of events, so we compute the duration at different amplitudes. Synthetic experiments have shown that this is equivalent to counting events because large and small earthquakes have different durations (large ones shake longer). The exponential law has implications for the source of volcanic tremor. For earthquakes, both the fault area and the slip increase as magnitude increases, but for tremor, either the source size (such as conduit length) or the magnitude of pres-

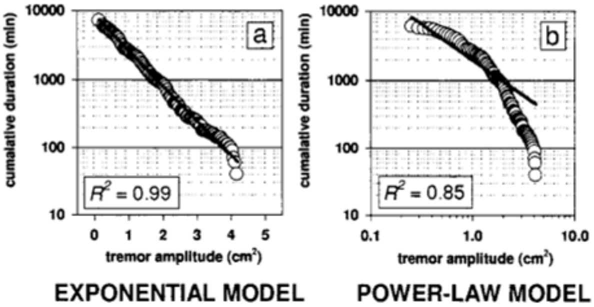

FIGURE 2 Volcanic tremor data from Mount Spurr, Alaska, comparing an (a) exponential and a (b) power law model. Note that the vertical axis is logarithmic in both cases, but the horizontal axis is linear for the exponential model and logarithmic for the power law model. The circles show the duration of tremor observed at various amplitudes; strong tremor occurs less often than weaker tremor. The lines are weighted least-squares mathematical fits of the data to the two models shown. The data fitted better using the exponential model, as shown by the higher value of the correlation coefficient R^2. [After Benoit, 1998.]

sure fluctuations (analogous to slip) must remain constant to produce the observed exponential scaling. The available evidence suggests that the source (conduit) size remains constant.

E. Very-Long-Period Events

Over the past decade new types of seismometers known as a broadband seismometers have been deployed at volcanoes. These have the ability to detect a wider frequency band, particularly at the low end (down to $f = 0.016$ Hz, or a period of 60 s). Not surprisingly, a new class of events called very-long-period (VLP) events have been observed at some volcanoes. Observations to date show events with periods of 3 to 20 s originating from shallow depths of 1.5 km or less under several active volcanoes including Kilauea, Stromboli, Aso, Sakurajima, and Satsuma-Iwojima. The VLP events at these volcanoes have been associated with either eruptions or vigorous fumarolic activity, and the observed events have fairly small amplitudes.

Normally it takes a large structure, such as a long fault, to produce waves with these long periods. However, many of the VLP events at volcanoes appear to come from small source zones despite the long wavelengths. Some current models suggest that these events may be produced as magma moves through a flapper valve (such as a restriction in a dike or sill) in distinct pulses. Additionally, theoretical calculations show that it is possible for a crack or tube filled with fluid to produce long-wavelength (and long-period) waves if the acoustic velocity in the fluid is slow compared to the rigid walls. The interaction between the fluid and walls produces low phase velocities along the interface. Such waves are called crack waves or tube waves.

During its climactic eruption on June 15, 1991, Mount Pinatubo, Philippines, produced strong seismic waves with periods of 228 to 270 s. These are thought to be caused by a type of oscillation in the atmosphere in which thermal energy from the vent travels up and then reflects off the top of the ash column (in this case in the stratosphere). These waves also coupled into the ground and appeared on seismic stations thousands of kilometers away, lasting for over 2 hours.

Broadband sensors have been deployed at a number of volcanoes that produced no VLP signals, even though several of these were erupting. They include Mount Spurr, Montserrat, Arenal, Akutan, and Augustine volcanoes. Further, the scientific community has yet to record any precursors to truly large eruptions on broadband instruments. In spite of this, the VLP signals made visible by the new broadband instruments are an exciting part of volcano seismology, and it is anticipated that many new advances will be made in this area over the next few years.

F. Surficial Events

Seismometers located on volcanoes may record a variety of local signals caused by shallow processes. These include nonvolcanic processes such as glacial events, shore ice movement, and landslides, as well as volcanic processes such as outburst floods and lahars, pyroclastic flows, and rockfalls from crumbling lava domes. Some of the seismograms are similar, so they must be recognized and properly treated by analysts.

- *Glacial events.* Volcanoes at high latitudes and tall volcanoes are frequently covered by glaciers, which produce seismic events along the ice–rock boundary, and within the ice when cracks and crevasses form. Because the seismic wave velocity in ice is lower than that in rock, the seismic waves may become partially trapped in the ice and set up oscillations of the ice itself. Seismograms from such events resemble those for LF volcanic events. Glacial events are more common in the summer months when the glaciers are moving faster.
- *Shore ice.* Ice forms from seawater when the air temperature falls below 10°F. Large blocks of such ice gather

on the shores of Augustine Island, Cook Inlet, Alaska, and move around as the tides ebb and flood. When the blocks collide or break, they produce seismic events because the blocks are coupled to the ground. The events are shallow (surface) so the seismic waves are mostly low-frequency surface waves traveling in thin sediment layers. The individual ice events resemble LF volcanic events, and the events occur in swarms of a few hours duration because of the tides. Both of these features are similar to to seismicity preceding eruptions, so good thermometers are needed to measure air temperature in such situations!

- *Landslides.* Avalanches and landslides of various sizes occur on volcanoes. Those associated with partial melting of ice and snow mainly occur in the spring and summer. The main avalanche or landslide generates a seismic signal of several minutes duration, depending on the size and runout. The amplitude varies with the amount of material, with larger avalanches generating stronger seismic signals. Some landslides on volcanoes (and elsewhere) are preceded by small discrete seismic events whose rate of occurrence increases up to the time of the main event. This is similar to a common pattern of earthquakes before some eruptions, so again, additional information is needed to distinguish between volcanic and nonvolcanic causes on the seismograms.
- *Rockfalls.* Rockfalls are a special type of landslide in which one or a few pieces of bedrock become detached and free fall. They are especially common at the edges of volcanic domes and at volcanoes with very steep slopes or cliffs. In the summer of 1995 workers at Mount Spurr, Alaska, observed rocks more than 1 m in diameter falling several hundred meters and impacting on the crater floor. The corresponding seismograms showed strong local signals lasting more than 1 minute.
- *Pyroclastic flows.* Pyroclastic flows are products of explosive eruptions and consist of particles of hot molten rock and gases which move rapidly over the ground surface. Large-scale collapses of volcanic domes can also produce pyroclastic flows. These latter events are characterized by complex seismograms which have been modeled as a sequence of forces. First, rock is removed from the dome (the dome moves up slightly in response); second, the falling rock collides with the slope below (an impact); and third, the rock breaks apart and the fragments continue to move down the slope as an irregular flow. These seismograms last several minutes, may contain high frequencies, and the larger flows are associated with larger amplitude signals.

Pyroclastic flows have also been associated with another seismic feature. At Pinatubo volcano, Philippines, pyroclastic flows traveled down a prominent valley between two seismic stations, one of which transmitted its signal to the other. As the ash clouds rose into the air the telemetry path was interrupted for several tens of minutes, after which the signal returned. Thus, the temporary absence of the telemetry could be used to infer that pyroclastic flows were occurring.

- *Outburst floods and lahars.* The surface melting of ice and snow, or heavy rains, may cause floods and lahars (volcanic mudflows). Similarly, a volcanic eruption under a glacier will melt the ice, and the flooding that subsequently occurs is called a jokulhlaup. All these floods or lahars cause long-duration seismic signals that resemble volcanic tremor, except that the signal is stronger near the flow channel, as opposed to tremor, which is stronger nearest the volcanic vent. The floodwater travels downstream, so the source is moving. Also, the recorded frequencies may be high if the seismometer is near the flow channel, even though this may be far from the vent.

Different groups of investigators and various observatories have used a number of different local terminologies. This is not a problem, however, because the goal of terminology at the local level is to communicate rapidly in an observatory setting. (This is similar to the local names of sandwiches, which can be "hoagie," "grinder," or "submarine sandwich" in different parts of the United States.) However, no consensus has yet emerged about an appropriate global terminology. The lack of a global terminology makes it difficult to evaluate critically the observations from different volcanoes, and creates confusion in the literature. Table II compares several of the more common local terminologies.

Different mechanisms acting at the seismic source are responsible for many of the features of the different events, and path and site effects, which are extreme at many volcanoes, may greatly modify the signals. Three principal seismic sources are shear failure, also called "double-couple" mechanisms; tensile failure, or "non-double-couple" mechanisms; and passive and active fluid involvement in producing low-frequency events and volcanic tremor. Nonlinear flow has also been modeled as a source for volcanic tremor. Some authors have investigated differences between volcanic and tectonic earthquakes by comparing factors such as magnitude using different waves, and seismic moment versus fault length. Such comparisons reveal that many volcanic earthquakes are enriched in low frequencies and occur on smaller structures (faults) than tectonic earthquakes of the same magnitude.

Intermittent or "banded" tremor occurs in regular, periodic bursts separated by periods of quiescence of

TABLE II Selected Volcano Seismology Terminology

This article	*Minakami (1960)*	*Latter (1979)*	*AVO*[a]	*Other names*	*Example (Figure 1)*
High-frequency (HF)	A-type	Tectonic, volcanotectonic	Volcanotectonic (VT)	Short-period earthquake	A
Low-frequency (LF)	B-type	Volcanic	Long-period (LP)		C,F
				Long-coda event tornillo[b]	I,J
Mixed-frequency	—	Medium-frequency	Hybrid	Medium-frequency	B
Explosion quake	Explosion quake	Volcanic explosion	Explosion	—	E
Volcanic tremor	Volcanic tremor	Volcanic tremor	Volcanic tremor	Harmonic tremor, Spasmodic tremor	D,G,H,K

[a] Alaska Volcano Observatory.
[b] Tornillo is the Spanish word for "screw." The codas of these events resemble a wood screw in profile.

uniform duration. The resulting pattern looks like stripes or bands on seismograms recorded on rotating drum recorders (Figure 1K). Many other patterns are observed and various terms are used as adjectives to describe them, but this does not necessarily mean that different source processes are required.

III. GENERAL FEATURES OF EARTHQUAKES AT VOLCANOES

The goals of volcano seismology include monitoring the present status of a volcano, forecasting eruptions, estimating size of eruptions in progress, locating magma chambers, and understanding the physical processes that are occurring. The following topics elucidate many of the features that are common to earthquakes at volcanoes.

A. Seismicity Rates and Background

Volcanoes nearly always have a high background level of seismicity caused by heat; movement of groundwater, volatiles, or magma; glaciers (if present), landslides, and rockfalls; and reactions to stresses from regional tectonics, tides, or other forcing functions. Thus, a baseline of measurements of at least a few years duration is necessary to characterize and understand the background seismicity. The background may consist of several different types of events, which are related to different processes. Typical background rates of seismicity are a few to a few tens of events per day, depending on the locations and magnifications of the seismic stations. In contrast, the rates of seismicity before and during eruptions are typically several tens to several hundreds or more events per day, and include larger-magnitude events. Examples of rates and magnitudes of seismicity prior to selected eruptions are shown in Table III.

Many successful eruption forecasts have been made because of an increase in seismicity above previously recorded background levels. This is based on the idea that the level of seismicity reflects the level of volcanic activity, and suggests that there is a constant long-term probability of eruption, usually assumed to be a Poisson process. This means that eruptions behave as a random variable, and have no memory (mathematically) of previous eruptions. The average rate of eruptions is also assumed to be constant, and the probability increases when earthquake swarms occur. The main physical processes monitored, however, are those associated with magma intrusion. Thus, there will always be a false alarm rate because some intrusions remain at depth whereas others reach the surface and erupt.

B. Seismicity Associated with Large versus Small Eruptions

In general, large eruptions are relatively easier to detect than smaller ones. The amount of magma involved is large, and earthquakes tend to be numerous as well as

TABLE III Seismicity Rates for Selected Earthquake Swarms

Location and date	*Detected*[a]	$M > 1$	$M > 2$	$M > 3$	$M > 4$	M_{max}	*LP*[b]*/ tremor*	*Eruption*
Long Valley								
May 80					≈15/day	6 (4)	No	No
May 82				7/3 days		4.1	No	No
July 82				4/10 days		3.4	No	No
Nov. 82	≈100/day		≈9/day			2.8	No	No
Jan. 83	≈800/day			25/hour	≈10/day	5.3 (2)	No	No
June 89	≈40/day	≈25/day	2/day			3	No	No
Mar. 90	>300/day					3	No	No
Campi Flegri								
Oct. 83	>300/day					4	No	No
Mar. 84	≈500/day		5/day			4	No	No
Rabaul								
Aprl. 84	≈1700/day					4.8	No	No
Mt. St. Helens								
Mar. 80	≈600/day		>70/day	≈50/day	1–4/day	4	Yes	Yes
Matsushiro								
Nov. 65	≈2000/day			>200/day		5.0	No	No
Off-Ito								
July 89	≈400/hour			40/day		5.5	Yes	Yes
Redoubt								
Dec. 89	≈150/hour					<2	Yes	Yes
Fuego								
Jan. 77	2000/day	70/day	≈5/day			2.8	No	No
Augustine								
Feb. 86	>5000/day					2.5	No	Yes
Usu								
Aug. 77	200/hour			5/hour		3.8	Yes	Yes
Pavlof								
Apr. 86	800/day	400/day				2.1	Yes	Yes
Galapagos								
June 68				90/day	33/day	5.2	?	No
Kilauea								
Jan. 83	>1100/day	92/day	18/day	1/day		3.3	Yes	Yes
Mt. Hood								
July 80	20/hour		14/hour			2.8	No	No
Medicine Lake								
Sep. 88	80/hour			2/hour		4.2	No	No

[a] Minimum magnitude not specified but generally $M < 1$.

[b] LP, long-period earthquake.

distributed over a large volume. Other precursors such as deformation and steaming are usually observed in conjunction with earthquake swarms. Recent examples include Mount St. Helens, Washington, 1980; Pinatubo, Philippines, 1991; and Spurr, Alaska, 1992. Small eruptions and many phreatic (water driven) eruptions, in contrast, involve much smaller amounts of magma, and have subtle precursors or sometimes no precursors. They are, hence, generally harder to forecast. Recent examples include Galeras, Colombia, January–June

1993; Arenal, Costa Rica, August 1993; and White Island, New Zealand, February 1992.

Occasionally "unexpected" eruptions occur; often these take place during the later phases in a sequence of eruptions. Even though these may be large, they may have subtle or undetectable seismic precursors. This is a consequence of the vent remaining "open" or mechanically weak following an initial stage of activity, preventing buildup of stresses which would cause earthquakes. A recent example is the second eruption of Mount Spurr in August 1992, which occurred without immediate detectable precursors.

C. Locations of Volcanic Earthquakes

Generally volcanic earthquakes occur beneath the point of eruption. This helps reduce the monitoring problem to that of estimating the time of eruption since the place is considered known. However, several cases have occurred in which the locations of earthquake swarms did not coincide with the eruptive vent, because different mechanisms were acting. During the Matsushiro, Japan, earthquake swarm of 1965–1967, which began beneath Mount Minakami, an extinct volcano, epicenters were aligned northeast-southwest, but a fissure oriented northwest-southeast appeared at the ground surface. Water flowed from this fissure but no magmatic eruption occurred. During the Miyake-jima, Japan, basaltic eruption of 1962, the epicenters were located northwest of the summit crater but the eruption occurred from a flank fissure on the northeast side. More recently, the initial earthquake swarms prior to the dacitic eruption of Pinatubo occurred about 5 km northwest of the volcano. Twelve days before the climactic eruption these earthquakes declined and vigorous shallower swarms began beneath the eventual eruption site. For volcanic systems with large dimensions, earthquakes may be widely separated: for Katmai, Alaska, 1912, there was a 10-km separation between the collapse structure (Mount Katmai) and the Novarupta vent; at Rabaul, Papua New Guinea, 1994, two vents, Tavurvur and Vulcan, erupted simultaneously 10 km apart. These cases demonstrate that earthquakes occur where stresses are concentrated, not necessarily where the magma is located.

It is expected that earthquake locations would migrate from depth toward the Earth's surface as magma rises from depths prior to eruption. There are, however, surprisingly few well-documented cases of such a trend. This overall pattern was first shown for Kilauea volcano, Hawaii, in 1960; more recent examples include Augustine, Alaska, 1986; Unzen, Japan, 1991; Pinatubo, 1991; and additional 1960–1983 eruptions of Kilauea. One spectacular case of lateral migration of hypocenters was observed at Krafla in September 1977; when the earthquakes passed a geothermal borehole, fresh pumice actually erupted from the hole!

D. Large Regional Earthquakes Near Volcanoes

Large regional earthquakes occasionally trigger eruptions. Well-known examples include the eruption of Puyehue 48 hours after the $M = 9.3$ Chile earthquake of 1960, and a small summit eruption of Kilauea shortly after the $M = 7.1$ Kalapana earthquake of 1975. Exact mechanisms for this triggering are poorly understood, yet probably reflect local stress changes near the volcano induced by the nearby large earthquake (analogous to squeezing a tube of toothpaste). Recently, it has been demonstrated convincingly that the June 1992 $M = 7.3$ Landers, California, earthquake remotely triggered earthquake swarms at 17 volcanic areas in the western United States at distances of 165 to 1250 km. Although no eruptions occurred, these swarms demonstrated that small transient stress changes can trigger significant changes in seismicity in volcanic areas. One possible mechanism for this is known as rectified diffusion, in which oscillatory strains, such as those caused by passage of seismic waves, make existing bubbles expand and contract. Because the surface area is proportional to the radius squared, the bubble's average size is larger than normal during the oscillations, and gases diffuse into the bubble, causing a pressure increase. Other mechanisms are currently under investigation.

E. Caldera Earthquakes

Large earthquakes often occur at large structures, such as calderas. For example, $M \geq 6$ earthquakes have occurred at or near calderas in Long Valley, California; Yellowstone, Wyoming and Idaho; and Aso, Japan. $M = 5.1$ earthquakes have occurred at Rabaul caldera, Papua New Guinea, in 1982 and 1984. While small eruptions have occurred frequently at the central vent of Aso, no eruptions have occurred at Long Valley or Yellowstone. Rabaul finally erupted on September 19, 1994, following 13 years of caldera-wide seismicity and 37 hours of intense local seismicity. It is normal for large calderas to show frequent signs of unrest, the vast majority of which

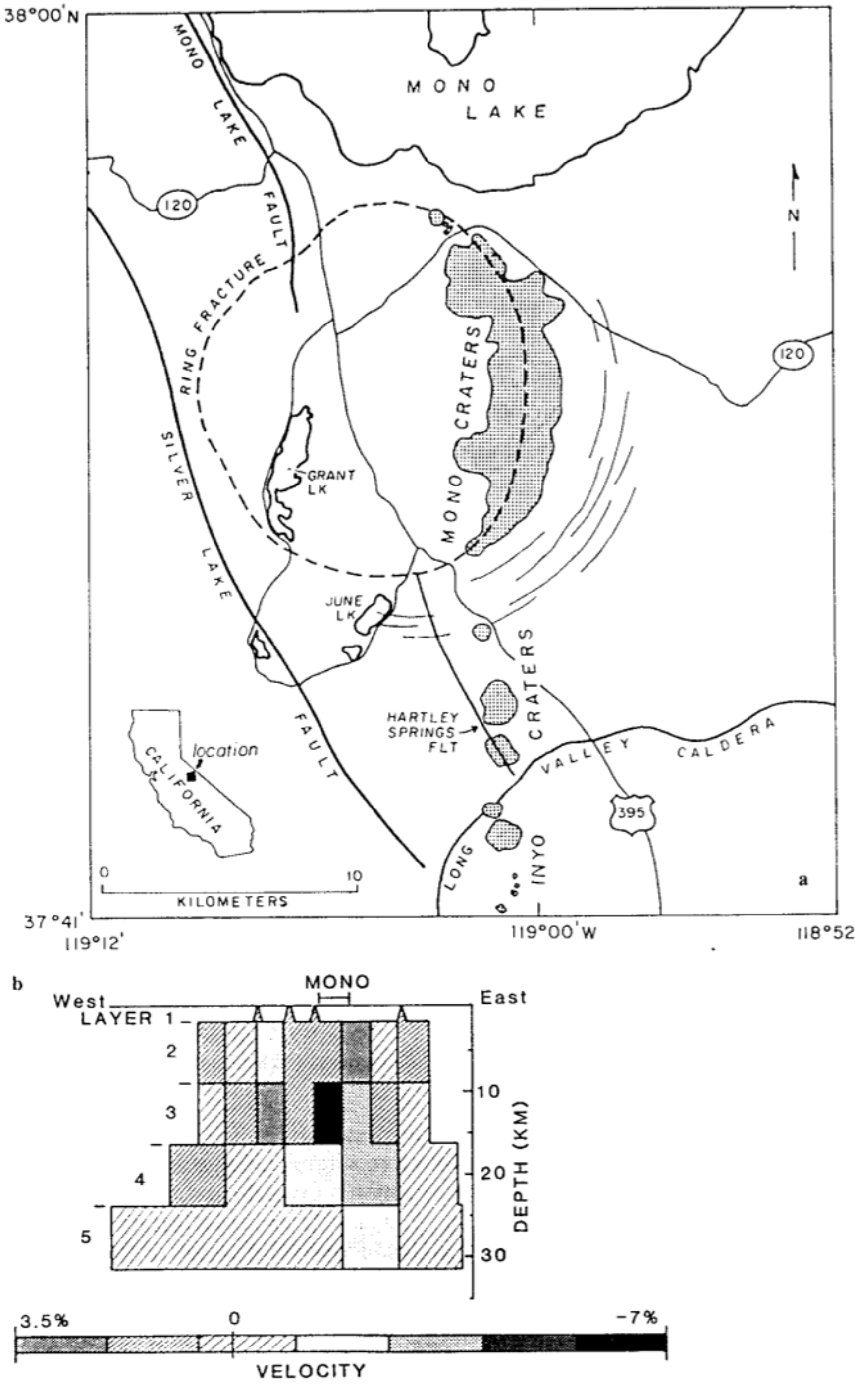
38°00'N
MONO LAKE FAULT
MONO LAKE
N
120
RING FRACTURE
MONO CRATERS
120
SILVER LAKE FAULT
GRANT LK
JUNE LK
CRATERS
HARTLEY SPRINGS FLT
LONG VALLEY CALDERA
395
INYO
location
CALIFORNIA
0
10
KILOMETERS
a
37°41'
119°12'
119°00'W
118°52'
b
MONO
West
East
LAYER 1
2
3
4
5
10
20
30
DEPTH (KM)
3.5%
0
-7%
VELOCITY

FIGURE 3 Tomography of Mono Craters, California, using P waves from distant earthquakes. (a) Map of tectonic and geographic features of the area of Mono Craters, just northeast of Long Valley caldera. Shaded areas are Holocene volcanic flows and domes. (b) An east–west cross section showing tomographic results. The velocities vary from 3.5% higher to 7% lower than the reference values. The strongest anomaly, a 7% lowering of the velocity (black rectangle), occurs 9 to 16 km beneath the Mono Craters. [After Iyer, 1992.]

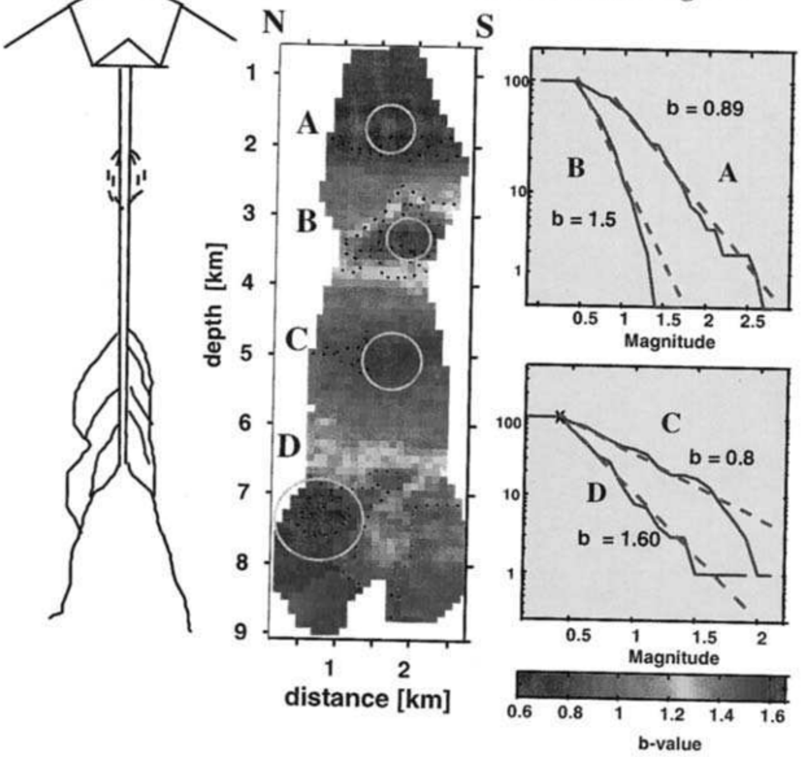

Mt. St. Helens, Washington

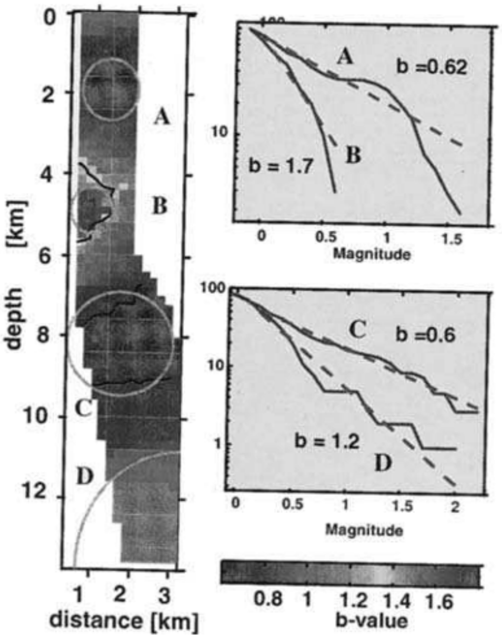

Mt. Spurr, Alaska

are not precursors to eruptions. This adds to the uncertainty in dealing with earthquake swarms at calderas: false alarms are more likely, but large eruptions are also possible.

F. Seismicity at Volcanoes with Long Repose Times

Large eruptions often follow long repose periods, and the earthquake swarms may include relatively large events. Recent examples include Arenal volcano, Costa Rica, in 1968 (repose 440 years, $M = 4.5$), Mount St. Helens, 1980 (repose 123 years $M = 5.0$), and Pinatubo, 1991 (repose 600 years, $M = 4.3$). This feature, however, is problematic at large structures such as calderas which routinely produce large earthquakes. While calderas are more likely to have large earthquakes not followed by eruptions, the possibility of a large eruption suggests caution when interpreting an earthquake sequence such as that at Long Valley caldera in May 1980 (four $M = 6$ earthquakes; see case histories below). This and some of the later seismicity at Long Valley may have been related to intrusions of magma.

G. Synchronous Volcanic and Tectonic Activity

A 40-km-wide belt of volcanoes and frequent shallow crustal earthquakes is located above the subduction zone in Central America. While the general structural features are similar to most other subduction zones, the Central American tectonic seismicity is more abundant and appears to be more closely linked to volcanism. Both eruptions and damaging earthquakes have occurred in isolation, but occasionally the two have been coincident. For example, at Boqueron volcano, El Salvador, an $M = 6.2$ earthquake alone occurred in May 1965, while in June 1917 and September 1659 eruptions and destructive ($M \approx 6$) earthquakes occurred simultaneously. These may be cases of one phenomenon modifying or triggering the other, or an external agent may be the cause of both.

H. Seismicity at Basaltic versus Dacitic Volcanoes

Differences between seismic activity at basaltic versus andesitic and dacitic volcanoes may be subtle. Extremely short-duration swarms of small events are more common at basaltic volcanoes. For example, the January 1991 eruption of Hekla volcano, Iceland, occurred after an earthquake swarm lasting only 0.5 hour, with the largest event about $M = 3$. Most of the handful of known eruptions that occurred essentially without detectable precursors took place at basaltic volcanoes (e.g., Hekla, 1981; Mount Etna, Italy, flank, March 1985). However, once initial eruption has occurred and the vent is open, subsequent eruptions may occur with virtually no additional seismicity at andesitic or dacitic volcanoes (e.g., Mount Spurr, August 18, 1992). Energetic earthquake swarms after eruptions are common at basaltic centers. Spatially, basaltic centers more often produce flank eruptions, whereas andesitic and dacitic volcanoes tend to erupt repeatedly from the same central vent.

I. Seismic Features of Magma Chambers

Magma is thought to be stored in some type of chamber or reservoir underground, and seismology is useful for determining the parameters of such chambers. Magma chambers at stratovolcanoes are generally equant in shape, and on the order of 1 to 20 km^3 in volume. Those at calderas are larger. Their depths are mapped at about 5 to 20 km or deeper based on tomography, S-wave screening, and posteruption seismicity. Seismic tomography, similar to medical tomography, requires seismic waves to travel through the target region. Thus, a good distribution of earthquakes and seismic stations is needed; both local and distant earthquakes have been used as sources for such studies. The technique exploits the fact that P waves speed up in competent rock and

FIGURE 4 Images showing the distribution of *b*-values beneath Mount St. Helens and Mount Spurr. Each grid element shows the *b*-value for the nearest 100 earthquakes (original color version has low *b*-values as blue, normal values as green and yellow, and high values as red). Four samples labeled A–D are plotted to the right of each cross section. These show the actual data used to compute each *b*-value. Note the anomalies at 3–4 km for each volcano and 7–9 km for Mount St. Helens and 10–13 km for Mount Spurr. The deeper anomalies are near magma chambers and the shallower ones are at depths of vesiculation of gases. The black line drawing represents a schematic view of the Mount St. Helens plumbing system. [Original color version in Wiemer and McNutt, 1997.]

TABLE IV Parameters of Volcanic Activity: Seismic Case Histories

Volcano name	*Date*	*VEI*[a]	*Swarm duration (days)*	*Time since previous eruption (years)*	*Precursor event type*[b]	*Precursor maximum magnitude*	*Strongest tremor (DR)*[c]
Arenal	7/68 to present	4	3	∼450	H, T	4.5	Not known
	4/94	1–2	n.a.[d]	n.a.	L, T	n.a.	20
Long Valley caldera	10/78 to present	n.a.	Variable	∼600	H, L	6.2	n.a.
Mount St. Helens	5/18/80	5	59	123	H, L, T	5.0	260
Spurr	6/27/92, 8/19/92, and 9/17/92	3	311	39	H, T	1.8	30

[a] Volcanic Explositivity Index.
[b] H, high-frequency earthquakes; L, low-frequency earthquakes; and T, volcanic tremor.
[c] DR, reduced displacement, which is root-mean-square (rms) amplitude multiplied by distance. Units are cm^2.
[d] n.a., not applicable.

slow down in unconsolidated materials or magma. An example of a tomographic image of a magma chamber under Mono Craters, California, is shown as Figure 3. S-wave screening exploits the fact that S waves cannot pass through liquids. Thus, the target region will be illuminated by the presence of P waves but lack S waves for those waves that pass through magma. Posteruption seismicity is often concentrated at depths of 5 to 20 km. Here, the removal of magma upward during eruption causes stress changes at depth that induce earthquakes. The idea is that the magma chamber walls collapse inward, and earthquakes are concentrated where these processes are most pronounced.

A new technique that requires well-distrubuted seismicity (as opposed to concentrated at one spot) looks for systematic spatial variation in the *b*-value, discussed

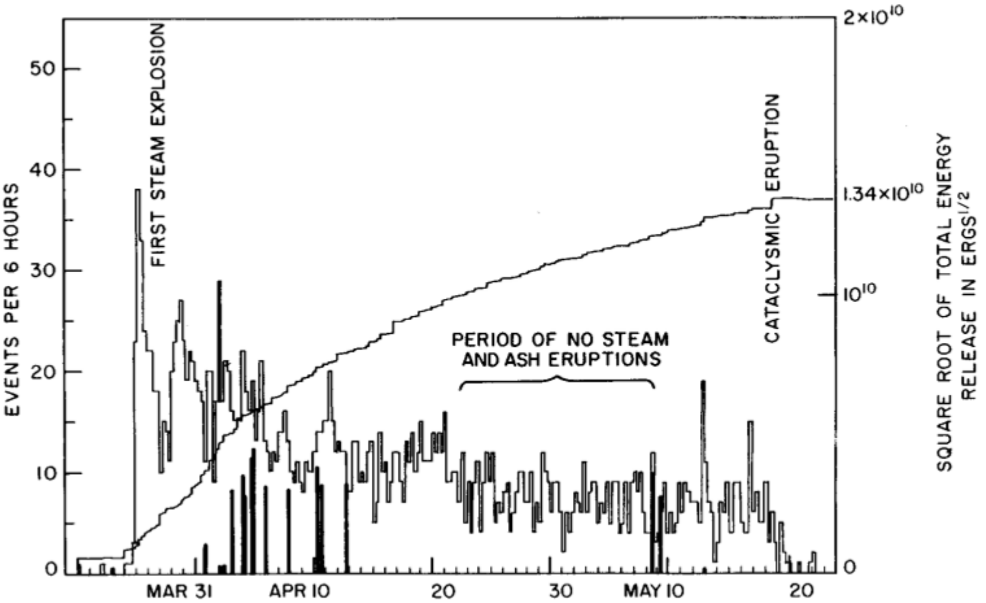

FIGURE 5 Counts of Mount St. Helens earthquakes larger than $M = 2.5$ per 6 hours, volcanic tremor (vertical lines, length proportional to tremor duration), and square root of cumulative energy release (a way to convert from magnitude to energy) from March 20 to May 24, 1980. [After Endo *et al.,* 1981, and Malone *et al.,* 1981.]

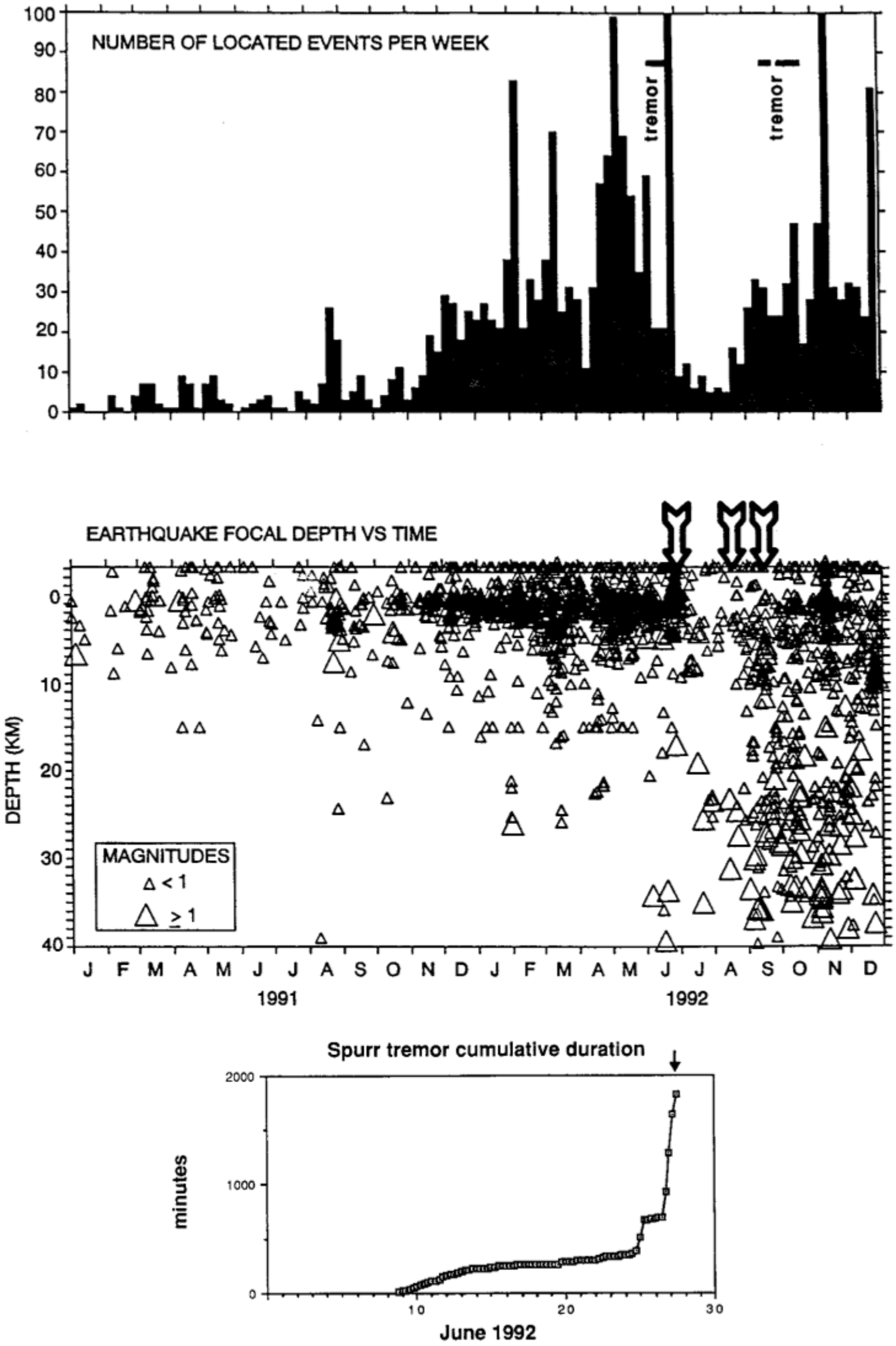

FIGURE 6 Seismicity in 1991 and 1992 associated with the eruptions of Mount Spurr. (Top) Number of events per week. Episodes of volcanic tremor are shown as horizontal bars. (Middle) Earthquake depth versus time. Each symbol represents one earthquake, and symbol size is related to earthquake magnitude, either $M < 1$ (small symbol) or $M \geq 1$ (large symbol). The three eruptions are shown as arrows. (Bottom) Mount Spurr volcanic tremor cumulative duration versus time. Data are computed for 6-hour intervals. The eruption occurred on June 27 (arrow). [After Alaska Volcano Observatory, 1993, and McNutt *et al.,* 1995.]

earlier. It has been shown in the laboratory that heat, high pore pressure, low applied stresses, or heterogeneous materials all produce high *b*-values. These are also the conditions that would be expected in the vicinity of magma bodies. Although this technique cannot uniquely identify which process is dominant, strong anomalies have been found at depths of 3–4 km and 7–9 km beneath six volcanoes studied. Examples of *b*-value anomalies thought to represent magma chambers beneath Mount St. Helens and Mount Spurr are shown in Figure 4.

IV. CASE HISTORIES

We consider the earthquake activity at four volcanoes to illustrate the variety of seismic activity. The four include small and large eruptions, a noneruption, and systems dominated by basalt, andesite, and dacite magmas. The volcanoes chosen had high-quality seismic data. Parameters of the four cases are summarized in Table IV. The bibliography at the end of this article gives at least one recent reference for each of the case histories.

A. Mount St. Helens, May 1980: A Large Dacite Eruption

Mount St. Helens, Washington, USA, produced a large explosive dacite eruption including a lateral blast on May 18, 1980, following 59 days of increased seismicity. On March 20, 1980, a $M = 4$ earthquake occurred, followed by many smaller events. Activity increased, reaching 8 $M \geq 4$ events in a single hour on March 25. Phreatic eruptions began on March 27. The earthquake sequence eventually included over 10,000 earthquakes, including high- and low-frequency events and volcanic tremor (Figure 5). Most events were located at depths of 3 to 7 km beneath the north flank of the volcano, the site of the eventual eruption. There were no immediate precursors in the hours before the climactic eruption. However, the shaking from a $M = 5.1$ earthquake initiated the eruption by causing a sector collapse which uncapped the volcano. Strong volcanic tremor accompanied the main eruption (Table IV). Deep (5 to 20 km) earthquakes began shortly after the eruption and lasted for several days. Later smaller eruptions were generally preceded by swarms of small earthquakes lasting several hours to several days, and were accompanied by volcanic tremor.

B. Mount Spurr, June–September 1992: A Typical Andesite Eruption

The Crater Peak vent of Mount Spurr, Alaska, erupted on June 27, 1992, following a 10-month swarm of high-frequency events. The largest event of this swarm was $M = 1.8$. Bursts of volcanic tremor began 3 weeks before the first eruption, and continuous tremor began 19 hours before (Figure 6). The final precursor to the first eruption was a 4-hour swarm of shallow HF events directly beneath the active vent. The vulcanian eruption lasted 4 hours and produced 44 million m^3 of andesite tephra. The second, larger eruption on August 18 occurred essentially without precursors. The third eruption, on September 17, occurred following several weeks of increased deeper (15 to 40 km) seismicity and 3 hours of small shallow events and weak tremor. This last eruption was followed by a vigorous swarm of earthquakes be-

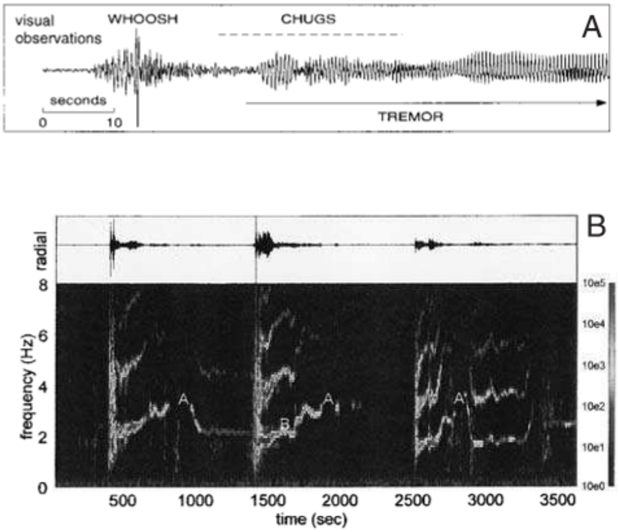

FIGURE 7 (A) An example seismogram of a small eruption (whoosh) at Arenal volcano, followed by rhythmic degassing (chugs), followed by harmonic tremor. The eruption ejected ash to 500 m above the crater and the chugs were audible at 2.8 km for 25 s. (B) Seismogram and spectrogram from April 1994 showing three small eruptions. The dark colors show lowest signal levels and the light the strongest. The spectra are dominated by narrow peaks spaced regularly in frequency, each of which changes frequency systematically with time. Spectrogram vertical scale is 0 to 8 Hz, and horizontal scale is 3600 s (1 hour). [After Benoit and McNutt, 1997; original version in color.]

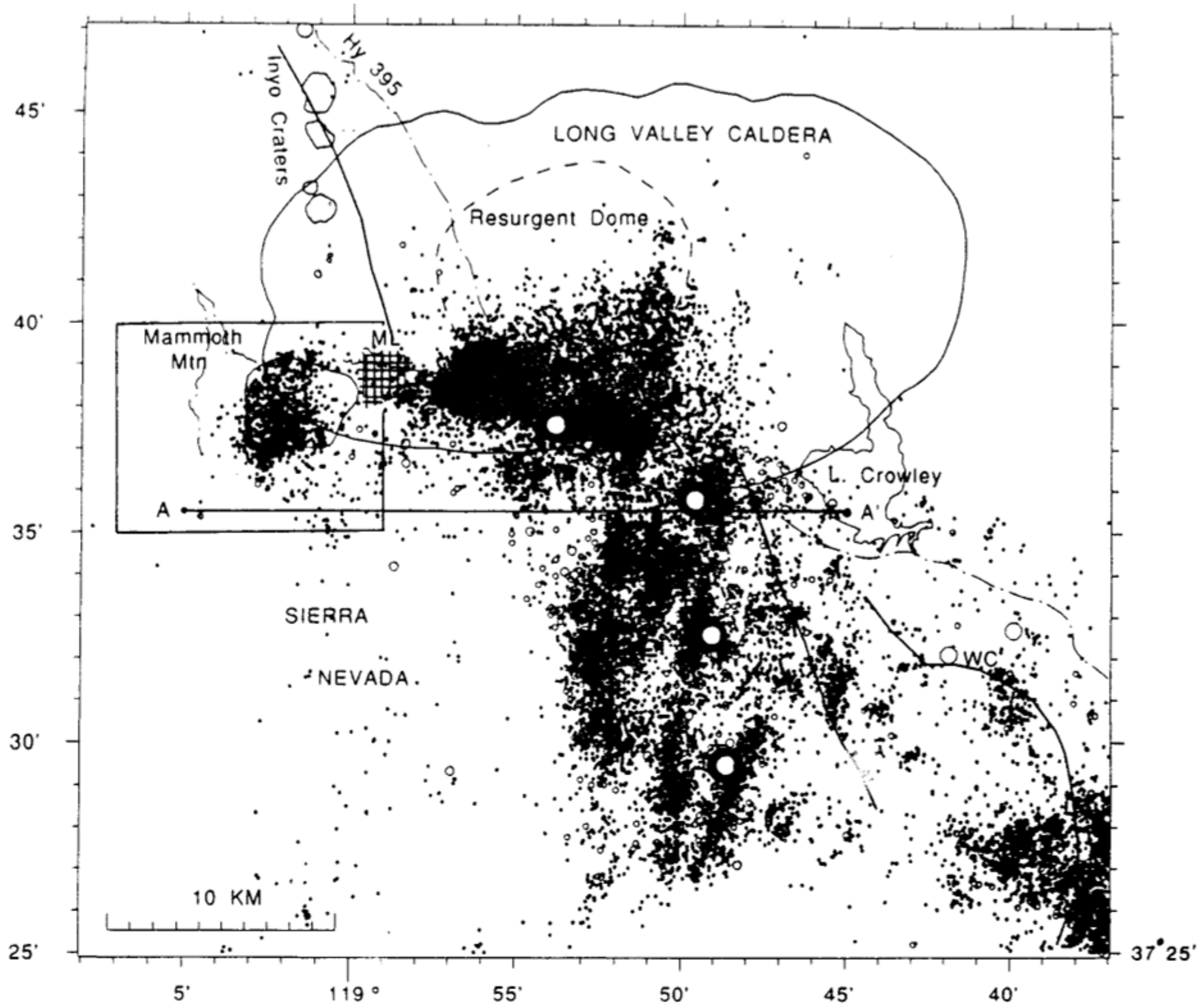

FIGURE 8 Map of Long Valley caldera and Sierra Nevada mountains to the south showing epicenters of $M > 1.2$ earthquakes occurring from January 1978 to June 1995. Each symbol represents one earthquake, and symbol size is proportional to magnitude. The heavy circles are the four $M \sim 6$ earthquakes that occurred in May 1980. ML is the town of Mammoth Lakes; WC is the epicenter of the $M = 5.4$ Wheeler Crest earthquake of October 1978; Hy 395 is Highway 395; and L. Crowley is Lake Crowley. The caldera outline is shown as a solid line and the uplifted resurgent dome by a dashed line. [After Hill, 1996.]

tween 5 and 10 km in depth (Figure 6). A shallow swarm of several hundred events occurred on November 9 and 10 without eruption.

C. Arenal Volcano, July 1968 and Continuing: Strombolian Activity

Arenal volcano, Costa Rica, erupted explosively in July 1968 after several days of felt earthquakes (no local seismometers were operating at the time). Four new vents were formed along a fissure. At first activity was strongest at the lower craters, but shortly afterward activity shifted to a vent near the summit and an approximately steady-state eruption of andesite has occurred ever since. The eruption of a block andesite lava flow is punctuated several times per hour by small explosive eruptions of several types. A typical sequence is an explosion, followed by a whoosh (which sounds like a jet plane), followed by chugs (which sound like a steam locomotive). The seismic expression of these is an explosion quake, followed by irregular tremor, and then regular tremor (Fig. 7) with variable amplitude which gradually fades to background levels (similar data and frequencies are found in acoustic data). The tremor consists of several integer harmonics or overtones, and these change frequency systematically over the course of several minutes (Figure 7). This suggests that the upper few hundred meters of the conduit is changing its bubble concentration, and hence its velocity and frequency. Every few years activity escalates and larger explosions occur, producing pyroclastic flows.

D. Long Valley, May 1980 and Continuing: A Restless Caldera

The Long Valley caldera region of eastern California has been a prolific producer of earthquakes from 1980 to 1998. The sequence began on May 25, 1980, when three $M = 6$ earthquakes occurred, along with thousands of smaller events, followed two days later by a fourth $M = 6$ event (Figure 8). Extensive ground deformation had also occurred, with uplift of 0.5 m near the center of the caldera. Later, it was found that measurable deformation actually preceded increases in earthquake activity by about 2 months, suggesting that earthquakes were a symptom of the deformation (or whatever caused it, such as underground movement of magma) rather than the cause. Repeated swarms of earthquakes occurred in the southern part of the caldera, and the strongest of these, in January 1983, included two $M = 5.3$ events. Altogether 27 earthquakes with $M > 5$ have occurred in and near the caldera over the last 18 years, a very high rate. No eruption has occurred; however, large quantities of CO_2 gas have been measured near Mammoth Mountain and have caused tree kills. It is also thought that several of the earthquake swarms accompanied intrusions of magma to shallow depths of about 5 km. Long Valley has become an archetype of a "restless caldera."

V. CONCLUSIONS

This article has discussed many general features of earthquake activity at volcanoes, and it has been shown that the activity varies widely. This is true because the volcanoes and their eruptions vary, and also because the stresses differ, and volcanoes have different geometries as well as combinations of rock, magma, water, and gases within them. Although seismic data are plentiful, the complexities of the volcanic environment often make interpretations difficult. Different processes can generate similar seismograms, and similar processes can generate different seismograms, although detailed diagnostics can often distinguish between them. This keeps volcano seismology challenging, but also suggests that seismology alone can be a somewhat limited tool.

There is a close link between earthquakes and volcanoes. This is true at a large scale in the parallel belts of volcanoes and earthquakes at subduction zones. It is also true at the smaller scale of individual volcanoes, where rates of local seismicity often mimic eruptive activity. Although seismology is often viewed as a separate subject, we may also view seismology as a component of volcanology. Similarly, volcanology may be viewed simply as a component of the larger study of tectonics.

In spite of this, volcano seismology has helped to answer some fundamental questions: (1) Where is the magma? Tomography and *b*-value anomalies have identified large (kilometer scale) magmatic or near-magmatic structures, while low-frequency events and volcanic tremor are associated with small-scale movement of magma or water. (2) What is "normal" earthquake activity at volcanoes? The case studies and general features sections showed that activity varies widely, but with a number of systematic trends. Successful separation of source, site, and path effects of seismograms helps to elucidate the causes of specific activity. (3) What will happen next? Understanding of physical processes and study of case histories are the two main tools used to evaluate this question, which is treated more fully elsewhere. It is also possible, and indeed likely, that new high-quality data may lead to fresh insights about the new as well as older examples of earthquake activity at volcanoes.

SEE ALSO THE FOLLOWING ARTICLES

Calderas • Hawaiian and Strombolian Eruptions • Lahars • Magma Chambers • Migration of Melt • Plate Tectonics and Volcanism • Seismic Monitoring • Synthesis of Volcano Monitoring

FURTHER READING

Alaska Volcano Observatory (1993). Mt. Spurr's 1992 eruptions. *Eos Trans. Am. Geophys. Union* **74**, 217, 221–222.

Benoit, J. P., and McNutt, S. R. (1997). New constraints on source processes of volcanic tremor at Arenal volcano, Costa Rica, using broadband seismic data. *Geophys. Res. Lett.* **24,** 449–452.

Benoit, J. P. (1998). "Pattern and Process in Volcano Seismology." Ph.D. Dissertation, Univ. of Alaska Fairbanks, Fairbanks, Alaska, 165 p.

Chouet, B. A. (1996). Long-period volcano seismicity: Its source and use in eruption forecasting. *Nature* **380,** 309–316.

Endo, E. T., Malone, S. D., Noson, L. L., and Weaver, C. S. (1981). Locations, magnitudes, and statistics of the March 20–May 18 earthquake sequence. *U.S. Geol. Survey Prof. Paper* **1250,** 93–107.

Ferrucci, F. (1995). *In* "Monitoring Active Volcanoes: Strategies, Procedure, and Techniques" (W. J. McGuire, C. R. J. Kilburn, and J. B. Murray, eds.). Univ. College London Press, London.

Hill, D. P. (1996). Earthquakes and carbon dioxide beneath Mammoth Mountain, California. *Seismol. Res. Lett.* **67,** 8–15.

Iyer, H. (1992). Page 299–338 in "Volcanic Seismology" (P. Gasparini, R. Scarpa, and K. Aki, eds.). Springer-Verlag, Berlin/Heidelberg.

Julian, B. R. (1994). Volcanic tremor: Nonlinear excitation by fluid flow. *J. Geophys. Res.* **99.**

Kanamori, H., and Mori, J. (1992). Harmonic excitation of mantle Rayleigh waves by the 1991 eruption of Mount Pinatubo, Philippines. *Geophys. Res. Lett.* **19,** 721–724.

Kaneshima, S., Kawakatsu, H., Matsubayashi, H., Sudo, Y., Tsutsui, T., Ohminato, T., Ito, H., Uhira, K., Yamasoto, H., Oikawa, J., Takeo, M., and Iidaka, T. (1996). Mechanism of phreatic eruptions at Aso volcano inferred from near-field broadband seismic observations. *Science* **273,** 642–645.

Keith, T. E. C., ed. (1995). The 1992 Eruptions of Crater Peak Vent, Mount Spurr Volcano, Alaska. *U.S. Geological Survey Bull.* **2139**.

McNutt, S. R. (1992). Page 417–425 *in* "Encyclopedia of Earth System Science," Vol. 4. Academic Press, San Diego.

McNutt, S. R. (1996). Page 99–146 *in* "Monitoring and Mitigation of Volcano Hazards" (R. Scarpa and R. Tilling, eds.). Springer-Verlag, Berlin/Heidelberg.

McNutt, S. R., Tytgat, G., and Power, J. A. (1995). Preliminary analyses of volcanic tremor associated with the 1992 eruptions of Crater Peak, Mt. Spurr, Alaska, *U.S. Geol. Survey Bull.* **2139,** 161–177.

Malone, S. D., Endo, E. T., Weaver, C. S., and Ramey, J. W. (1981). Seismic monitoring for eruption prediction. *U.S. Geol. Survey Prof. Paper* **1250,** 803–813. [Mount St. Helens.]

Newhall, C. G., and Punongbayan, R. S., eds. (1996). "Fire and Mud: Eruptions and Lahars of Mount Pinatubo, Philippines." Univ. of Washington Press, Seattle.

Ohminato, T., Chouet, B. A., Dawson, P., and Kedar, S. (1998). Waveform inversion of very long period impulsive signals associated with magmatic injection beneath Kilauea volcano, Hawaii, *J. Geophys. Res.* **103,** 23839–23862.

Wiemer, S., and McNutt, S. R. (1997). Variations in the frequency-magnitude distribution with depth in two volcanic areas: Mount St. Helens, Washington, and Mt. Spurr, Alaska. *Geophys. Res. Lett.* **24,** 189–192.

This Page Intentionally Left Blank

IMPACTS OF ERUPTIONS ON HUMAN HEALTH

PETER J. BAXTER
University of Cambridge Clinical School and Addenbrooke's Hospital

I. Introduction
II. Early Studies on Human Impacts of Eruptions
III. Injury Agents
IV. Deaths in Volcanic Eruptions
V. Causes of Death and Injury
VI. Conclusion

GLOSSARY

acid rain Pure water in equilibrium with atmospheric carbon dioxide has a pH of 5.6, but with pollution by strong acids the rain pH ranges from 2 to 4.

asphyxia Death from lack of oxygen.

acute respiratory distress syndrome A severe reaction of the lungs to injury, manifested by fluid filling the air spaces.

crystalline silica The three crystalline forms of silicon dioxide, namely quartz, cristobalite, and tridymite.

gas gangrene A soft-tissue infection caused by contamination of wounds by gas-producing organisms (*Clostridium welchii*) that thrive in the absence of oxygen.

necrotizing fasciitis A soft-tissue infection characterized by rapidly spreading inflammation and destruction of connective tissue (muscle fascia) and subcutaneous fat.

silicosis Chronic silicosis is a fibrous (scarring) reaction of the lungs caused by inhalation of crystalline silica.

tetanus A soft-tissue infection caused by contamination of wounds by the bacterium *Clostridium tetani*. The bacteria produce a toxin that affects the nervous system, resulting in involuntary muscle spasms.

traumatic asphyxia Fixation of the chest by external pressure so the victim is unable to breathe.

tympanic membrane The eardrum, or the thin membrane between the outer and middle ear, which is in contact with the air and transmits sound energy to the auditory apparatus.

KNOWLEDGE OF THE causes of death and injury in explosive eruptions has grown alongside the recent advances made by volcanologists in field studies of eruptive phenomena. A whole range of injury agents are involved in major eruptions and these are described for pyroclastic flows and surges, lahars, explosions, tephra falls, and gas emissions. The Earth's biological and geological activities have been linked throughout its long history. Burgeoning human populations have formed high-density settlements in volcanic areas, some of which were barely populated less than 100 years ago. Recent eruptions have revealed how explosive eruptions inflict death and injury, and provide insights into the mitigation measures needed for the management of volcanic crises. This chapter summarizes these observations, many of which have been made in and since the eruption of Mount St. Helens in 1980.

Copyright © 2000 by Academic Press
All rights of reproduction in any form reserved.

I. INTRODUCTION

The solar system was formed 4.5 billion years ago, and life as microscopic single-celled organisms was born on Earth in an atmosphere of volcanic gases 1 billion years later. Plate tectonics and evolutionary theory have opened our eyes to the uniqueness of our planet and the interdependency of geological and biological processes in sustaining the living Earth. Many scientists now believe that mass extinction episodes in the Earth's remote history coincided with periods of intense volcanic activity, while in more recent times good evidence is found for major eruptions being able to affect global climate, which in today's world, with its large human population, could disrupt agriculture and lead to economic disruption and even famine.

Homo sapiens made its appearance in only the last 500,000 years, with much of the brain development of our species having occurred over a quarter of a million years, or the time scale for the building of the existing edifices of major composite volcanoes such as Vesuvius and Mount Etna. Early human populations settled in volcanic areas for many reasons, with the fertility of soils being an important factor, and they learned through religious rituals to coexist with their fiery mountains. Archaeologists have shown how major eruptions over the last few thousand years have had important destructive influences on early civilizations—Santorini in 1600 B.C. (east Mediterranean) and Popocatapetl in 800 B.C. to A.D. 822 (Mesoamerica). But the rapid growth of the world population over the last hundred years has increased the risks to life from volcanic activity as settlements continue to expand into areas at risk, especially those open to the direct impacts of explosive volcanoes. By ignoring the natural forces that have shaped our planet the human species is exposing itself, in its technological hubris, to the risk of more frequent and greater disasters.

II. EARLY STUDIES ON HUMAN IMPACTS OF ERUPTIONS

Curiosity over the fate of victims in volcanic eruptions has always been at the heart of popular interest in the excavations at Pompeii and Herculaneum ever since they began in the 18th century. The younger Pliny's account of the A.D. 79 eruption of Vesuvius is the first recorded description of an eruption and it includes the first written report describing the death of a victim, his uncle, Pliny the Elder, who was probably caught on the edge of a pyroclastic surge. In 1863, Italian archaeologists devised a method of preserving the positions of Pompeiians in the moment of death; it involved forming a cast by pouring plaster of paris into the cavity that had once contained the victim's body. These eerie replicas led archaeologists to speculate on causes of death and it was widely believed that victims had died by being buried by mud or a heavy fall of ashes. In 1902, two eruptions occurred within 1 day of one another in the Caribbean and would alert scientists to a newly reported and highly destructive volcanic phenomenon. A May 8 eruptive blast from Mount Pelée on Martinique devastated the city of Saint Pierre, killing 28,000 people and leaving only two survivors in the city itself. In Saint Vincent over 1500 people died in another eruption of a "glowing cloud" from La Soufriere containing intensely hot ash and gases. But it was not until the eruption of Mount St. Helens in 1980 that volcanologists were able to extensively study firsthand the eruption of what by then were known as a pyroclastic flow and pyroclastic surge. About 60 people were killed, and for the first time it was possible to perform autopsies on surge victims to establish the mode of death. In the years that followed volcanologists investigated and reinterpreted the eruptive deposits around Vesuvius to show that Herculaneum and Pompeii had been overwhelmed by these phenomena, as well as from the fallout of pumice and ash.

Mount St. Helens also renewed scientific interest in lahars, but it was the lahar tragedy at Nevado del Ruiz in 1984 (see below) that demonstrated the scale of the threat posed by these phenomena and the importance of devising adequate emergency planning and warning measures. This disaster was a spur to the declaration of the 1990s as the UN International Decade for Disaster Reduction (IDNDR).

III. INJURY AGENTS

We can categorize injury agents in general as various forms of energy, all of which may inflict harm in volcanic eruptions. These agents (and examples) are mechanical (lahars and rock/debris avalanches, ballistic ejecta, and tephra falls), thermal (pyroclastic flows and surges), chemical (gases and aerosols), electrical (lightning), and ionizing radiation (radon gas), or the result of too little energy as in the case of asphyxiation (carbon dioxide, pyroclastic flows, lahars). The explosivity of an eruption is driven by the immense energy stored in the heat of the magma that becomes converted into kinetic energy in the event. But volcanoes can also present hazards in repose periods. People living on the flanks of volcanoes can be subjected to soil gas emissions that can flow into houses, or they may be in areas subject to fumigation by gases discharged in the plume from the crater or active fumaroles. Much more deadly are the hazards of lahars, for they can form without warning even in the absence of eruptive activity since many parts of volcanoes can be unstable because the rock has been weakened by hydrothermal activity and exposure to corrosive gases. The U.S. Geological Survey has extensively studied this hazard around Mount Rainier in Washington State, USA.

IV. DEATHS IN VOLCANIC ERUPTIONS

A recent study of records of eruptions since A.D. 1783 found that 220,000 deaths were reported. Most of the fatalities resulted from posteruption famine and epidemic disease (30%), pyroclastic flows and surges (27%), lahars (17%), and volcanogenic tsunamis (17%). These data should be regarded cautiously, as accurate mortality figures are not even obtainable today in natural disasters in developing countries. A span of just over 200 years is not representative of the whole range of eruption types and minimizes the real potential threat from a massive eruption, especially today when concentrations of populations around some volcanoes are much greater than even several decades ago. Estimates suggest that about 500 million people, or 10% of the world's population, are living in areas of active volcanism. In the Vesuvius area alone over 100,000 people could be killed in the first minutes of a major eruption in the absence of warning and evacuation measures. Thus a range of vulnerability factors and mitigation measures need to be considered when estimating mortality risks, and it is quite deceptive to use total deaths in the past as a reflection of the importance of volcanoes in the league of natural hazards. The dominance of winds, floods, and earthquakes in terms of numbers of deaths this century, with only a relatively small number attributable to volcanic eruptions, ignores the fact that volcanoes are capable of unleashing the most destructive forces on earth. It is indeed fortunate for our world that the recurrence rate of major eruptions in populated areas is substantially lower than that of other natural hazards.

Deaths in lava flows are rare. The flows of most effusive eruptions move slowly enough for people to avoid them, but vents may open unexpectedly at a low level on a volcano and rapidly threaten settlements. In the 1928 eruption of Mount Etna, the town of Mascali was destroyed in just over 1 day, the lava moving silently at about 2 m/minute over a 400-m front. Although eruptions of high effusion, low-viscosity flows of lava are rare, two have occurred on Hawaii and one in Zaire during historical times, with velocities of 40–100 km/hour. Possibly 600 people died in the Zaire event in 1977, when the lava lake at Mount Niragongo rapidly emptied. Onlookers may face the dangers of small explosions when flows come into contact with seawater and of the ignition of hydrocarbon gases formed by the pyrolysis of organic matter beneath the moving lava and escaping through porous old rock to and beyond the flow margin.

V. CAUSES OF DEATH AND INJURY

By studying eruptive phenomena and their impacts on people, we can learn to understand the types of injuries or health effects that can be caused by eruptions, as well as the special problems that may arise in the pre- and posteruptive phases that themselves can last for prolonged periods. Of course, such information is invaluable for health professionals, especially emergency workers, facing a volcanic crisis, who may be responsible for planning the management of casualties. But of much greater importance in terms of preventing loss of life is the application of this information to all aspects of volcanic emergency management, especially community preparedness and evacuation planning. Health sector involvement in volcanic risk management is therefore crucial to any risk assessment process, which with hazard assessment is a key step in setting priorities in emergency planning and long-term mitigation measures. The most common hazards to arise in explosive eruptions are now described, together with their consequences for human safety and health.

A. Pyroclastic Flows and Surges

The definitions of pyroclastic flows and surges are controversial, but here surges are regarded for convenience as similar to pyroclastic flows in being mixtures of gas and ash, but being much more dilute (and therefore much less dense) and hence leaving behind fine ash deposits. The lateral eruption of Mount St. Helens on May 18, 1980, is regarded by most volcanologists as a surge, and certainly in its more distal parts conformed to this basic definition. Over a hundred people were enveloped by the surge cloud which sped out from the volcano at an average velocity of 160 m/s, slowing to about 28 m/s by the time it reached 25 km away. Fifty-two people who were at or near the edge of its run-out survived, mostly with minimal injuries, while 58 people who were closer to the crater died, many being buried by volcanic debris. The area impacted by the surge was wedge-shaped, extending 28 km from the crater, and was clearly demarcated by the flattening of the pine trees in the direction of the surge flow. The surge temperature was 200–300°C, except at its periphery, where it was hot enough only to singe hair and kill or singe the foliage of trees. Most victims caught in the main part of the surge, but who escaped burial, died from exposure to intense heat or, most commonly asphyxiation from breathing overwhelming amounts of ash into their lungs. One man was killed by a falling tree and another by a rock which flew through his car windshield. Two men who were employed logging trees at the time of the event subsequently died in the hospital from lung injury due to inhaling fine, hot ash (acute respiratory distress syndrome).

This remarkable eruption demonstrated the enormous destructive power of surges and highlighted the main human hazards they present. The flattening of the trees might suggest that an immense explosion was involved but, as in a snow avalanche or a strong wind, the destructive impact was due to the dynamic pressure of the surge, which is the product of its density and the square of its velocity. The human body cannot survive being in temperatures over 200°C for more than a few moments, especially in the fast moving current of a surge. Trying to breathe in the dense cloud of hot ash in the absence of oxygen would lead to unconsciousness in a few breaths, as well as causing severe burns to the respiratory tract. In hotter surges than at Mount St. Helens, the clothes and hair would immediately ignite, but then go out in the absence of oxygen, only to rekindle again when the flow had passed and the body came into contact with fresh air. On the other hand, survival is possible in the more distal parts of a surge if there is adequate shelter to protect against the surge flow and its high temperature, as well as the missiles (rocks, building debris) entrained in the moving cloud of material. As the Mount St. Helens disaster showed, survival under such conditions is possible because the duration of the main impact is not more than a minute or two as the hot cloud convects and creates turbulence in its flow, thereby entraining air and cooling, as well as losing momentum.

More recent findings from victims caught in surge clouds at eruptions of Unzen, Japan (1991), Merapi, Indonesia (1994), and Soufriere Hills, Montserrat (1997), have added further weight to these conclusions from Mount St. Helens (Table I). The implications for future disaster planning apply mainly to human settlements around active volcanoes, such as Vesuvius. Failure for any reason to evacuate in time before a surge strikes would obviously result in many deaths, but there would also be areas in which large numbers of people could survive, especially if adequately protected by houses. Many would be injured, and fires could cause further deaths. The last time a city was struck by a surge was

TABLE I Casualties Due to Pyroclastic Flows in 20th Century Explosive Eruptions

Eruption	*No. of deaths*	*Dead : injured ratio*	*Survivors after treatment*
Pelée, 1902	28,000	230 : 1	163 treated, 123 survived
La Soufrière, 1902	1,565	11 : 1	194 treated, 120 survived
Taal, 1911	1,335	10 : 1	Not known
Lamington, 1958	2,942	44 : 1	70 treated, 67 survived
St. Helens, 1908	58	16 : 1	130 airlifted; 9 required treatment, 7 of whom survived
Unzen, 1991	43	5 : 1	17 treated, 4 with minor burns survived
Merapi, 1994	63	3 : 1	86 treated, 11 dead on arrival at hospital
Soufriere Hills, Montserrat, 1997	19	4 : 1	7 treated, all survived

in the destruction of Saint Pierre in 1902, but this was a lateral blast—a rarer and even more destructive type of event than the surge or flow that occurs in most explosive eruptions. The enormous forces involved were seen in a lateral blast that occurred on Montserrat on December 26, 1997. In the main area of impact all trees and structures were leveled to the ground with every piece of debris blown into the sea!

B. Lahars

Just as the cataclysmic eruption of Mount St. Helens revealed much about the impact of pyroclastic flows, the eruption of Nevado del Ruiz, Colombia, in 1984 also confirmed the most destructive features of lahars. The eruption melted glacial ice on the summit and the mobilized water-entrained debris scoured out valley bottoms to produce a huge mudflow that ran under gravity toward the towns of Chinchina and Armero. As much as 85% of the town of Armero was left covered in 3–4 m of mud. Official figures put the death toll in the town at 21,015 out of a total population of 29,170. Altogether, there were 22,942 deaths and 4470 injured survivors in this event. In the rescue operation over the following 3 to 4 days, 1244 survivors, mainly from Armero, were admitted to hospitals (138 subsequently died). The main lahar struck Armero at around 11:30 P.M. and was preceded by a river of water that flowed along the streets and was fast and deep enough in places to overturn cars and sweep away people. The height of the lahar as it left the Langunillas River and headed toward Armero was 30 m above the riverbed. It traveled at an estimated velocity of 12 m/s and lasted for 10–20 minutes, during which time most of the town was devastated as buildings collapsed and broke up. Survivors clung to moving pieces of debris or were miraculously swept along on top of the mud. Overall, the inundation of mud lasted about 2 hours, with two slower moving major pulses and several smaller pulses over this period.

The head of the lahar would have been in turbulent motion and contain cobbles and boulders. Most people would have been killed immediately by the severe trauma caused by the collapse of buildings, flying debris, and burial by the slurry mass. As well as the risk of being engulfed, bodies would have been driven against stationary objects, or contorted and crushed by entrained debris such as trees and collapsed parts of buildings, resulting in mutilation and fractures of limbs and skull bones. Stones and other sharp objects would cut into the skin, causing deep lacerations. Mud was inhaled as it forced its way into the eyes, mouth, ears, and open wounds. The pressure of the mud against the chest would have inhibited breathing in those buried to the neck and caused some deaths by traumatic asphyxia.

This type of flow arising after a volcanic eruption is described as being noncohesive, and in Armero became mostly granular or sandy in consistency, which would explain the presence of so many survivors trapped in the mud. Video film shows how the soft consistency made access to the injured so difficult, with many having to be airlifted from the mud by helicopter. The commonest lesions in the hospitalized patients were lacerations, penetrating wounds, and infections. Many of the wounds were infected on admission. Most of the deaths in hospitals were due to infections including gas gangrene, tetanus, and a form of necrotizing fasciitis, which occurred almost exclusively in victims rescued after being in the mud for 3 days. This dreaded complication was due to normally nonpathogenic soil organisms replicating in wounds in the absence of oxygen, and is resistant to medical treatment.

The eruption of Mount Pinatubo in 1991 left huge quantities of tephra on the flanks of the volcano, and repeated noncohesive flows are formed in the wet season every year when heavy rains readily mobilize the ash deposits. Six years later, the death toll had exceeded 500 and over 40,000 families remained evacuated from the at-risk lowland areas.

The Ruiz disaster has many implications for disaster planners. Emergency workers need to be aware of the special problems of trying to rescue people from lahars, including the danger to rescuers being themselves engulfed in further pulses of material which might come down 1 or 2 hours after the initial wave. Evacuation is the only safe precaution in the face of a continuing threat from an active volcano, but community preparedness should include last-resort advice to move quickly to higher ground if a lahar is on its way. A warning system located on a volcano might give an hour or more's warning of a moving debris flow. Such advice, however, is going to be of little value for the elderly, the sick, patients in hospitals, etc., who are obviously not going to be able to flee, or be moved, in time.

C. Explosions

Ballistic ejecta and blast/sound waves come under this heading. Minor explosions on volcanoes can be steam driven, or phreatic, with rocks being hurled without warning from fumaroles or craters. Very powerful blasts may occur in explosive eruptions. Small explosions may occur without warning at lava domes or plugged vents, which can be lethal to volcanologists taking gas samples, as happened at the crater of Galeras, Colombia, in 1994, when six scientists met their deaths.

Most explosive eruptions do not produce shock or blast waves since the release of energy is too slow. The sound of an eruption may not be heard at all close by and instead may undergo atmospheric reflection and concentration to be heard loud enough to rattle windows 100–300 km away, as occurred at Mount St. Helens in 1980. In some eruptions, initial shock velocities exceeding the speed of sound arise when ejecta are released at subsonic velocities and a shock wave can be produced. In some Vulcanian eruptions rocks may be hurled from vents with ejection velocities as high as the speed of sound, and in explosive eruptions at Ngauruhoe and Arenal, maximum ejecta velocities have been estimated as high as 660 m/s. The shock waves from these eruptions are unlikely to directly cause injuries unless an individual is close to the erupting center, when they are most likely to be killed in the eruption itself by being struck or obliterated by erupted material.

Loud sound waves can have enough energy to rattle and even break windows, as when a plane flying overhead breaks the sound barrier, but there should be no serious harm to hearing. Eruptions on Stromboli can rattle windows as far as 6 km away from the crater. The ear is the most sensitive organ to shock wave damage, but the blast required to rupture eardrums or cause more serious internal injuries to other organs will also cause major structural damage to buildings as well. Blast waves of this magnitude at some distance from the eruptive center are only rarely reported in eruptions. A possible example of this was at Mount Asama in 1958, which produced terrific detonations and airshocks which were heard at the foot of the volcano in an area 8–18 km away from the crater and caused damage to windows of houses as far out as 15 km. Seven persons were injured by flying glass. At Galeras, historic eruptions were reported to have generated shock waves that knocked down people as far as 13 km from the crater. In summary, injuries to the tympanic membrane of the ear (eardrum), or the hearing apparatus, from loud noise or blast waves in eruptions are rare, as are deaths and injuries caused by the effect of blast waves on major organs. Blast waves with overpressures of 7 kPa may break windows, and the threshold for rupture of the normal eardrum is 35 kPa.

In contrast, ballistic ejecta thrown out in explosions present a more common hazard. To be truly ballistic the diameter of clasts of typical density has to be at least 15–20 cm for them to have the momentum to be driven against air resistance in an explosion. Rocks (clasts) of this size, unless they are made of light pumice, are easily capable of causing lethal skull injuries, lacerations, and internal chest and abdominal injuries on impact at their terminal falling velocities. Nevertheless, reports of people being killed from such fallout are rare. Mount Sakurajima, Japan, has been erupting every few days for years, and schoolchildren on Sakurajima Island wear hard hats to walk to school; concrete shelters have also been built in fields and public places. A potentially more serious risk to life is the danger of fire from ballistics since large clasts can readily penetrate galvanized steel or wooden board roofs and shatter in small, hot pieces inside. The maximum recorded range for ballistic hazards is about 5 km from the crater.

D. Tephra Fall

Although it has been recognized that the weight of ash from the fallout in volcanic eruptions can bring down roofs and cause serious damage as well as injury, it was not until the eruption of Mount Pinatubo in 1991 that the potential scale of this hazard became fully appreciated. Most of the 300 deaths in this eruption occurred outside the 30- to 40-km radius of evacuation as a result of roofs collapsing under the weight of ash. The ash on the roofs had been made even denser by the addition of rain from Typhoon Yunya on the afternoon of June 15, when the climatic eruption occurred. At the city of Olangapo, about 35 km from the summit, widespread damage to roofs occurred as a result of a deposited depth of ash of 15 cm, which when wet gave a loading of some 2.0 kN/m^2 (approximately 200 kg/m^2). Typical designed loads for pitched roofs would rarely approach this level. Longer-span roofing fared worse than domestic roofs. Although the causes of death were not studied at Pinatubo, the collapse of roof members may cause direct impact injury to the skull and the body, and the inflowing ash may partially bury and suffocate those inside unless they are able to rapidly extricate themselves. Future eruptions with ashfalls into cities will present a similar hazard, especially as heavy rainfall is known to be triggered by Plinian eruptions. Unfortunately, the best way to mitigate the risk is not clear at present, as shoveling ash off tall house roofs, for example, is not an easy option for householders during a heavy ashfall.

Much concern is usually voiced over the respiratory effects of ash. Ashfalls from explosive eruptions, either falling directly from eruption columns (e.g., Mount St. Helens, 1980) or from coignimbrite clouds generated by pyroclastic flows (e.g., Montserrat, 1996–1998), can contain a large component of particles less than 10 μm in diameter, the size of most concern in health studies of air pollution (PM_{10}). Inhaling ash 5–10 μm in diameter in sufficient amounts will irritate the lungs and provoke symptoms in asthma sufferers. In the weeks after the Mount St. Helens eruption in 1980, increased numbers of asthma sufferers attended hospital for treatment, and patients with chronic respiratory conditions in general were significantly affected, but no deaths were recorded as a result. Rainfall has a dramatic effect in clearing the air and reducing levels of suspended fine ash in the air. PM_{10} is routinely monitored in cities in developed countries because of pollution from vehicle emissions. The UK air quality standard for PM_{10} is 50 $\mu g/m^3$ over a 24-hour averaging period, but concentrations of PM_{10} during and after a heavy ashfall can be in the mg/m^3 range until it rains!

An important new respiratory hazard was encountered in the eruptions of Soufriere Hills volcano on Montserrat in 1995–1998. The fine, respirable ash that fell in populated areas as a result of the pyroclastic flow activity contained elevated amounts of cristobalite, a form of crystalline silica that can cause silicosis, a disabling and potentially fatal lung disease typically found in miners and quarry workers exposed to high concentrations of siliceous dust. It was shown that the cristobalite formed in the hot lava dome and was invariably present in the ash clouds generated whenever portions of the dome collapsed.

High levels of respirable ash in the ambient air are not in themselves a reason for medically advising the evacuation of a population from an area of heavy ashfall unless the conditions are persistently arid and dry. People should stay indoors or wear lightweight industrial masks during very dusty periods, but children and even adults with bad asthma and other lung disorders could need to be advised to leave temporarily as a precaution. Repeated or persistent exposure to ash in the air containing harmful levels of cristobalite, or quartz, would be an indication for evacuation from, or not returning to, an area, if exposure was likely to continue over years (as with repeated eruptions), rather than months. In all instances a full risk assessment, based on monitoring airborne ash levels in the populated areas, must be undertaken before the appropriate advice can be given.

E. Gases

The principal volcanic gases are water vapor, carbon dioxide, sulfur dioxide, hydrogen chloride, hydrogen fluoride, and hydrogen sulfide, with minor amounts of radon, helium, hydrogen, and carbon monoxide. Exposure to these gases in active craters or discharging fumaroles can present a hazard to volcanologists monitoring volcanoes unless adequate respiratory equipment is worn. Sudden loss of consciousness and death is a hazard from hydrogen sulfide if its concentration in the air goes above 1000 ppm, especially as its presence is not readily detectable by smell at dangerous concentrations. Fortunately, the usually more abundant and highly irritant acid gases ward off scientists from receiving too much exposure to this lethal gas, and no cases of asphyxiation are known to have been reported among them.

People living close to degassing volcanoes can suffer from air pollution if local topography and weather result in the grounding of plume emissions. Sulfur dioxide is the main gas of interest as it can provoke asthma attacks in asthma patients at the low concentrations that can be found at long distances from the source of emission. The classic example is Masaya in Nicaragua, where an extensive area as far as 30 km from the crater is denuded of normal vegetation as a result of the prevailing winds blowing the plume into a populated area during years of repeated degassing. About 50,000 people live in an area where WHO air quality standards for sulfur dioxide countries have been regularly exceeded in years of strong degassing. Acid rain also has an important impact on soils and vegetation at Masaya. Around volcanoes the principal agent in the formation of acid rain is hydrogen chloride, which is very soluble and immediately taken up by rainwater falling through the plume (this is in contrast to acid rain formation in industrialized countries where it is mainly due to sulfur dioxide which is slowly oxidized to eventually form the more soluble sulfuric acid; nitrogen oxides and nitric acid may also contribute). In Hawaii the abundant white clouds which are formed when the outpouring lava from Kilauea runs into the sea comprises water vapor, hydrogen chloride gas, and hydrochloric acid, which can be blown downwind toward residential areas where acid rain can fall. The visible lava-induced haze in the air is known locally as LAZE. Sulfur dioxide emissions from the eruptive site of Pu'u O'o have also been of concern at times during the period of activity that began in 1983, the haze of gas, sulfuric acid, and ammonium sulfate aerosols being labeled as VOG (volcanic smog).

Poas volcano in Costa Rica went through a period of increased emissions starting around 1986 and lasting until 1995. The crater lake began to dry out in the dry season and refill with rainwater at other times of the year. The already acidic lake became even more so when its level fell and gas emissions through the lake carried with them highly concentrated acid aerosols that damaged vegetation and provoked respiratory complaints in the local villages exposed to the prevailing winds. The crater lakes of active volcanoes can therefore make the air pollution hazard worse. As well as its impact on humans, volcanic air pollution can impair the health of farm animals since they may spend most of their lives outdoors, and may cause marked deterioration in the outer fabric of buildings.

Gas bursts of carbon dioxide from the ground or from lakes have been agents of disaster in volcanic areas. In 1979 at the Dieng Plateau in Java, 139 people died fleeing from a phreatic eruption when a gas cloud flowed out from a crater above their route of escape. The release had probably been triggered from the ground hydrothermal system by earthquake activity associated with the eruption. In 1986, an estimated quarter of a million tons of carbon dioxide were suddenly released from Lake Nyos, Cameroon, in West Africa, on a still night in August as local villagers were going to bed. About 1700 people and countless numbers of birds and animals died as the denser than air gas flowed down the adjacent valleys. A similar overturning of the lake waters had occurred at Lake Monoun, only 100 km south of Lake Nyos, in 1984 when 35 people died. The source of gas at Lake Nyos is believed to be a soda water spring at the bottom of the 200-m-deep lake. This recharges the lower, well-stratified water layers where the gas is held under high pressure until some unknown trigger provokes an overturning of the lake, releasing the gas rather like opening a champagne bottle.

Soil gas emissions are another way in which carbon dioxide from the underlying magma can present a ever-present hazard in volcanic areas. Studies at Vulcano (Italy), Furnas (Azores, Portugal), and Mammoth Mountain (California, USA) have shown that enough gas may be released into structures to present an asphyxia hazard to occupants by accumulating in confined spaces or parts of buildings below ground level. Carbon dioxide will induce distressed breathing and eventual loss of consciousness at levels of 5–10% in the air, but it is odorless, and at concentrations above 10–15% can cause immediate loss of consciousness after a few breaths and before the individual becomes aware of any danger. Carbon dioxide is a carrier of radon gas from the magma, and at Furnas levels of radon daughters can also accumulate in the indoor air in sufficient concentrations to be hazardous to health. Radon acts as a cause of lung cancer in conjunction with tobacco smoke. The ground emissions of carbon dioxide may increase without warning during periods of magma unrest or unfelt seismic activity, and so the hazard should be regularly monitored. In pre- and posteruptive phases of Vesuvius there are reports of people having been overcome by carbon dioxide in cellars or caves on the volcano's flanks.

Undoubtedly, more attention needs to be given to the hazard of carbon dioxide in areas of volcanic and hydrothermal activity. Where volcanic gas emissions are considered to be a health and safety hazard the concentrations should be carefully monitored as part of a risk assessment. The hazard of gases in eruptions has tended to be ignored by volcanologists since gas bursts such as that at Dieng have so far proved to be rare events. However, gas releases may have occurred in past eruptions and in some unexplained incidents but gone unrecognized.

VI. CONCLUSION

Understanding the human impacts of eruptions requires interdisciplinary studies of the behavior of volcanoes in periods of repose as well as during and after eruptive events. The lessons learned are essential for devising mitigation measures to reduce losses of life in future explosive eruptions. For such events of great destructiveness but low probability, mitigation measures need to be interdisciplinary-based and placed in the context of sustainable development, rather than seen among a host of what are usually the more immediate and pressing health priorities for decision makers. Computer numerical simulation models may become important tools for predicting injury impacts in the future. With the continuing rise of global urbanization it will be the management of volcanic crises in cities and other densely populated areas that will present the major challenges for scientists and disaster workers in the next millennium.

SEE ALSO THE FOLLOWING ARTICLES

Debris Avalanches • Hazards from Volcanic Gases • Lahar and Jökulhlaup Hazards • Lava Flow Hazards • Pyroclastic Surges and Blasts • Risk Education and Intervention • Volcanic Tsunamis

FURTHER READING

Baxter, P. J. (1997). *In* "The Public Health Consequences of Disasters" (E. K. Noji, ed.). Oxford Univ. Press, New York.

Blong, R. J. (1984). "Volcanic Hazards." Academic Press, Sydney.

Fisher, R. V., Heiken, G., and Hulen, J. B. (1997). "Volcanoes: Crucibles of Change." Princeton Univ. Press, Princeton.

Lamb, S., and Sington, D. (1998). "Earth Story." Princeton Univ. Press, Princeton.

This Page Intentionally Left Blank

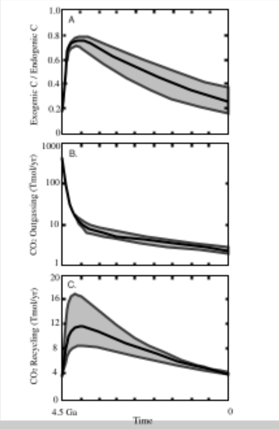

VOLCANIC CONTRIBUTIONS TO THE CARBON AND SULFUR GEOCHEMICAL CYCLES AND GLOBAL CHANGE

MICHAEL A. ARTHUR
Pennsylvania State University

I. Introduction
II. Making Global Estimates of Volcanic Volatile C and S Fluxes
III. Present Volcanic Carbon Fluxes
IV. Present Volcanic Sulfur Fluxes
V. Impact of Volcanism on the Geochemical Cycles of Carbon and Sulfur
VI. Possible Variations in Volcanic Emissions and Their Effects in the Past
VII. Conclusions and Future Research

GLOSSARY

CDT The reference standard for expressing sulfur isotope values in delta ($\delta^{34}S$) notation. This standard is troilite from the Canon Diablo Meteorite and has been assigned a value of 0 by definition. In the delta notation (see PDB below), the relative isotopic differences are expressed in permil (o/oo) or parts per thousand.

isotope An element may have several isotopes which differ in mass but have the same number of protons in the nucleus as the element itself. For example, carbon (^{12}C) has six protons and six neutrons in the nucleus, giving it an atomic mass of 12. The other stable isotope of carbon (^{13}C) has six protons and seven neutrons for an atomic mass of 13. The difference in mass between the two isotopes of carbon leads to slightly different behavoir during chemical reactions, thereby leading to changes in the ratio of one isotope to another. Usually, the relative abundance of isotopes of the same element differs greatly. For example, ^{13}C is about 1.1% and ^{12}C is 98.9% of the total carbon on Earth.

juvenile gas A volatile phase that was formed or present during the initial accretion of the Earth and degassed to the Earth's surface through time.

MORB Midocean ridge basalt.

pCO_2 The partial pressure of carbon dioxide gas in the atmosphere (taken in this paper as 365 ppmv).

PDB The reference standard for expressing carbon isotope values in delta ($\delta^{13}C$) notation. This standard is Peedee Belemnite and is assigned a value of 0 permil by definition: $\delta^{13}C = [(^{13}C/^{12}C_{samp}/^{13}C/^{12}C_{PDB})-1] \times 10^3$.

THE PROCESSES THAT lead to outgassing of the Earth include: (1) midocean ridge volcanism; (2) hot spot or intraplate (plume) volcanism; (3) island arc or convergent plate margin volcanism; (4) subduction and collision zone metamorphism; and (5) volatile loss during burial diagenesis of sediments. Outgassing

Copyright © 2000 by Academic Press
All rights of reproduction in any form reserved.

processes 1–4 are strongly influenced by mass transport in the plate tectonic cycle, coupled to the upwelling of partially molten mantle material beneath midocean ridges, plate subduction, and associated arc volcanism over subduction zones. In fact, many geochemical cycle models have assumed that the total rate of outgassing of carbon dioxide scales linearly with seafloor spreading rate and/or subduction rate. This article is concerned primarily with presenting estimates of the present fluxes of volatile carbon (mainly carbon dioxide) and sulfur (mainly sulfur dioxide) from subaerial and submarine volcanism, and an assessment of their fluxes and impacts on the carbon and sulfur geochemical cycles now and in the past.

I. INTRODUCTION

The flux of primary (juvenile) volatile gases to the surface (outgassing) from the Earth's interior has, over time, supplied much of the inventory of carbon, sulfur, water, and other elements in the crust, ocean, and atmosphere. It has been suggested that this outgassing accompanied volcanism and that the volatiles were added gradually over geologic time to Earth-surface reservoirs. Subsequently, it has been argued that rapid outgassing may have occurred in the early stages of Earth accretion, when intense bombardment during bolide impacts may have maintained a hot interior, vigorous mantle convection, and a "steam" atmosphere. Some workers have suggested that a substantial proportion of the Earth's volatiles could have been derived from the impactors themselves. Nonetheless, following the early accretionary phase of the Earth, the flux of heat from the Earth's interior decreased progressively, resulting in surface cooling, condensation, and rain-out of the early steam atmosphere and formation of an early ocean. Most models for degassing history assume that the outgassing rate has been proportional to the heat flux from the Earth's interior. The Earth does continue to outgas primary volatiles, as evident from measurable fluxes of ^{3}He, a primordial volatile element, occuring today. For example, on the basis of primordial rare gas (^{20}Ne and ^{26}Ar) distributions in the atmosphere at present it is estimated that these rare gases are presently outgassed at about 10–15% of their average rate through geologic time.

It is thought that the contribution of juvenile carbon to the outgassing of carbon dioxide at present is minor, and that continued recycling and degassing of carbon dioxide is necessary as a part of the plate tectonic crust/mantle. For example, the total inventory of carbon in the crust-ocean-atmosphere at present is about 8×10^{9} Tmol (Tmol = 10^{12} mol). If we stipulate that this carbon accumulated as the result of some average rate of juvenile CO_2 degassing over the past 4×10^{9} years, we would obtain an estimate of 2 Tmol year^{-1}. If today's juvenile CO_2 outgassing rate is only between 10 and 20% of this average flux, as might be suggested by the rare gas data mentioned above, the present rate of juvenile CO_2 outgassing could be 0.2–0.4 Tmol year^{-1}. As will be shown below, this is only a very small proportion of the total carbon flux required to balance the preindustrial global carbon cycle and less than about 20% of the estimated contribution of CO_2 by subaerial volcanism today.

II. MAKING GLOBAL ESTIMATES OF VOLCANIC VOLATILE C AND S FLUXES

Estimates of volcanic emissions are based on measurements for relatively few volcanoes. For carbon dioxide emission rates this is particularly critical because the measurements must usually be made directly from the volcanic eruption plume by using instruments aboard light aircraft.

At issue in extrapolation to global degassing rates are the emissions accompanying eruptive activity of subaerial volcanoes as compared to longer-term "passive" degassing and the number of volcanoes or events that must be sampled in order to extrapolate the results to a global average emission rate. A further consideration is what area of a given volcano is included in measurements of degassing rates—for example, summit crater versus flank degassing. Another possible normalization factor useful in making these estimates is the volcanic explosivity index (VEI). Clearly, it is not a simple procedure to quantify emissions, particularly for carbon species, which cannot be measured in any straightforward way. Volcanic sulfur emissions are somewhat easier to quantify because of the variety of remote sensing techniques that may be applied. These methods include instruments such as COSPEC (correlation spectrometer) which can be deployed at the active crater or flown in a plane, or even driven under a gas plume in a car. The atmospheric loading of sulfur dioxide can be measured by satellite-based methods (e.g., a total ozone mapping spectrometer, or TOMS). In some cases, direct measurements of sulfur outgassing are made, and carbon dioxide emissions are estimated by measuring or assuming an average sulfur/carbon mass ratio in the volcanic gases.

The problems confronting those who extrapolate emissions from one or more volcanoes to global emission rates are best illustrated for the case of carbon degassing estimates for Mount Etna (Italy). This volcano, which is not associated with a subduction zone, is by far the major CO_2-emitting volcano on Earth at present. Degassing occurs both during episodic eruptive events mainly from summit craters and as diffuse emissions from the flank of the 25-km diameter volcano. The carbon isotope composition ($\delta^{13}C$) of CO_2 from the volcano's flank is similar to that of summit CO_2 and indicates a magmatic source. The total Mount Etna carbon dioxide flux has been estimated at 1 Tmol C year^{-1}1, with about 0.6 Tmol year^{-1} from summit crater degassing and the remainder from diffuse flank emissions. The CO_2 degassing rate from this one volcano represents between 30 and 60% of global volcanic CO_2 emissions (see below). How do we treat this single volcano which is clearly unusual today?

Such problems have received considerable attention in the literature. For example, some workers have shown that there is merit in treating volcanic volatile emissions as power-law distributions rather than Gaussian distributions. Rates of many geologic processes appear to obey power laws. A power-law distribution indicates what measurements are necessary to satisfactorily predict global degassing rates; in other words, the community does not have to measure every volcano to assure that a given flux is known adequately. The adequacy of emission estimates depends on the power-law exponent. Raw CO_2 emission data suggest that the power-law exponent is much less than 1 and that large volcanoes dominate degassing; analysis of emissions from the 20 largest volcanoes would, therefore, provide a good estimate of degassing rates associated with volcanism. If this reasoning holds up, we may be able to effectively estimate global degassing rates for many gaseous species with the proper distribution of measures. Such considerations have also been applied to volcanic SO_2 emissions.

III. PRESENT VOLCANIC CARBON FLUXES

A number of recent estimates for volcanic emissions of CO_2 for subaerial and marine volcanism are given in Table I. These estimates must be used with caution because they are based on relatively few direct measurements of emission rates and depend on a variety of techniques and assumptions outlined briefly in the preceding section. The range of CO_2 emission estimates for subaerial volcanism (mainly subduction-zone-related volcanoes but including continental rift and subaerial extensions of midocean ridge and/or hot spot volcanoes) is narrower than that for submarine volcanism at midocean ridges. Subaerial volcanoes are estimated to emit a minimum of 1.47 Tmol year^{-1} to a maximum of 3 Tmol year^{-1} at present.

However, the CO_2 outgassing accompanying submarine volcanism at midocean ridges is not well quantified (range of estimates is 0.23–16.4 Tmol year^{-1}). It seems likely that present CO_2 emissions from this source lie between 2 and 8 Tmol year^{-1}. Many estimates of degassing rates use fluxes of noble gases to estimate degassing rates of other gases. Models for melt-vapor partitioning of noble gases can account for most observed noble gas ratios in midocean ridge basalt (MORB), hot spot volcanoes, the atmosphere, and various elements of the mantle. However, the noble gas technique for degassing estimates may lead to inaccurate estimates because of

TABLE I Estimates of Annual Subaerial Volcanic Carbon Dioxide Emissions at Present

Volcanic CO_2 flux (Tmol year^{-1})	*Method*	*Source*
0.33	Arc volcanic flux	Le Cloarec and Marty (1991)
1.8	Extrapolation (to 60 volcanoes) of measured flux (7 volcanoes)	Gerlach (1991)
1.47	Passive and active crater degassing, extrapolation from measurements using S/C ratios in gases	Williams *et al.* (1992)
1.5	C/^{3}He in arc volcanoes with extrapolation	Varekamp *et al.* (1992)
1.8	Plume volcanism (magmatic CO_2 content and eruption rate)	Varekamp *et al.* (1992)
2.0–3.0	Power-law distribution of nine volcano flux measurements	Brantley and Koepenick (1995)

the wide variety of gas solubilities, which would lead to different degassing histories for each gas considered. Nonetheless, the C/^{3}He ratio of gases emitted from the midocean ridge may provide a reasonable indication of the C/^{3}He ratio in degassed mantle because the experimentally determined solubilities for CO_2 and ^{3}He are similar. If we adopt a reasonable C/^{3}He outgassing ratio at the midocean ridge (MOR) of $2 \pm 0.5 \times 10^9$ (range 1–8) and a ^{3}He outgassing flux of 1140 ± 150 mol year^{-1} we obtain an estimated CO_2 degassing flux for MORs of 2.3 ± 0.6 Tmol year^{-1}. A similar CO_2 degassing flux of 2.5 Tmol year^{-1} has been obtained based on a simple estimate using a 20 km^3 year^{-1} MORB emplacement rate with a CO_2 concentration of 1900 ppm. However, in more recent carbon cycle models the MOR CO_2 flux is estimated at only 1.5 Tmol year^{-1}. The estimates in Tables I and II suggest that the emissions from arc volcanoes, plume volcanoes, and the midocean ridges are roughly equivalent at about 1.5 Tmol year^{-1} each.

IV. Present Volcanic Sulfur Fluxes

Some recent estimates of volcanic sulfur emissions, primarily as SO_2, are given in Table III. These estimates are primarily for subaerial volcanic sources. The sulfur emission rates to the atmosphere for subaerial volcanism range from 0.2 to 0.8 Tmol S year^{-1}. Most of the estimates are on the lower side of this range. The most recent estimate for subaerial volcanic S outgassing is based on the most comprehensive data set of volcanoes (72) and measurements and suggests a time-integrated annual sulfur flux of 0.33 Tmol year^{-1}.

TABLE II Estimates of Annual Carbon Dioxide Degassing Along the Midocean Ridge at Present

Volcanic CO_2 flux (Tmol year^{-1})	*Method*	*Source*
1.32–16.4	C/^{3}He and ^{3}He flux	Javoy *et al.* (1982)
2.0–7.5	C/^{3}He and ^{3}He flux	Des Marais (1985)
1.5–4.9	MOR basalt degassing only	Arthur *et al.* (1985)
2.1	C/^{3}He and ^{3}He flux	Marty and Jambon (1987)
0.23–0.86	Gas samples at subaerial MOR	Gerlach (1989)
1.5	C/^{3}He	Gerlach (1991)

The estimated S flux associated with submarine volcanism is more uncertain by far than that for subaerial volcanoes. The midocean ridge hydrothermal circulation is primarily a sink for sulfur, at least initially, with seawater sulfate precipitating mainly as anhydrite in the oceanic crust. At 380°C, sulfate is more or less completely removed from seawater and a flux from seawater to oceanic crust has been estimated as high as 3.8 Tmol S year^{-1}. This is certainly an upper limit (see below). There is a flux of sulfur to seawater from oceanic crust, in the form of H_2S, at hydrothermal vents. The sulfur isotopic composition of this reduced sulfur is consistent with the hypothesis that it is *magmatic* sulfur leached from basalt by the high-temperature hydrothermal fluids. This flux is probably less than about 0.1 Tmol year^{-1} (Table III), consistent with the estimated loss of S during low-temperature alteration of the upper oceanic crust (0.08 Tmol S year^{-1}). We will nominally refer to this as the volatile sulfur flux from the mantle to seawater. No direct degassing during actual submarine basalt eruptions has been observed or measured, although this flux could be important, as it is in subaerial basalt eruptions. The rather large flux of sulfur from seawater to oceanic crust in the form of anhydrite requires an equally large sulfur flux from some other source, as yet poorly understood or quantified (see discussion of sulfur cycle below).

V. Impact of Volcanism on the Geochemical Cycles of Carbon and Sulfur

A. The Preindustrial Carbon Geochemical Cycle

The estimated present rate of outgassing of carbon dioxide from all sources—volcanism, metamorphism, and geothermal activity—is generally thought of as the amount required to balance the carbon fluxes required in weathering and carbonate precipitation (Figure 1). This value is at least 6 Tmol year^{-1} and has been estimated to be as high as 6.6 Tmol year^{-1}. If we take the reasonable "median" estimates of present-day CO_2 degassing associated with subaerial (ca. 1.5 Tmol year^{-1}) and submarine (ca. 2.5 Tmol year^{-1}) volcanism, we find that the flux is about two-thirds of that needed to balance

TABLE III Selected Estimates of Global Sulfur Degassing Rates from Subaerial and Submarine Volcanic Sources

Volcanic S flux (T mol y^{-1})	*Method*	*Source*
0.1	COSPEC extrapolation from Central American volcanoes to 100 volcanoes	Stoiber and Jensen (1973)
0.8	Viscous vs. fluid lava estimates	LeGuern (1982)
0.37	1961–79 55 volcanoes/y by class	Berresheim and Jaeschke (1983)
0.2	$^{210}Po/SO_2$ ratios in volcanoes	Lambert *et al.* (1988)
0.29	Extrapolation from C degassing using CO_2/SO_2 ratio	Williams *et al.* (1992)
0.18	Power law extrapolation from CO_2 degassing and C/S ratio (9 volcanoes)	Brantley and Koepenick (1995)
0.33	1972–97 extrapoolation, time-averaged SO_2 measurements + other	Andres and Kasgnoc (1997)

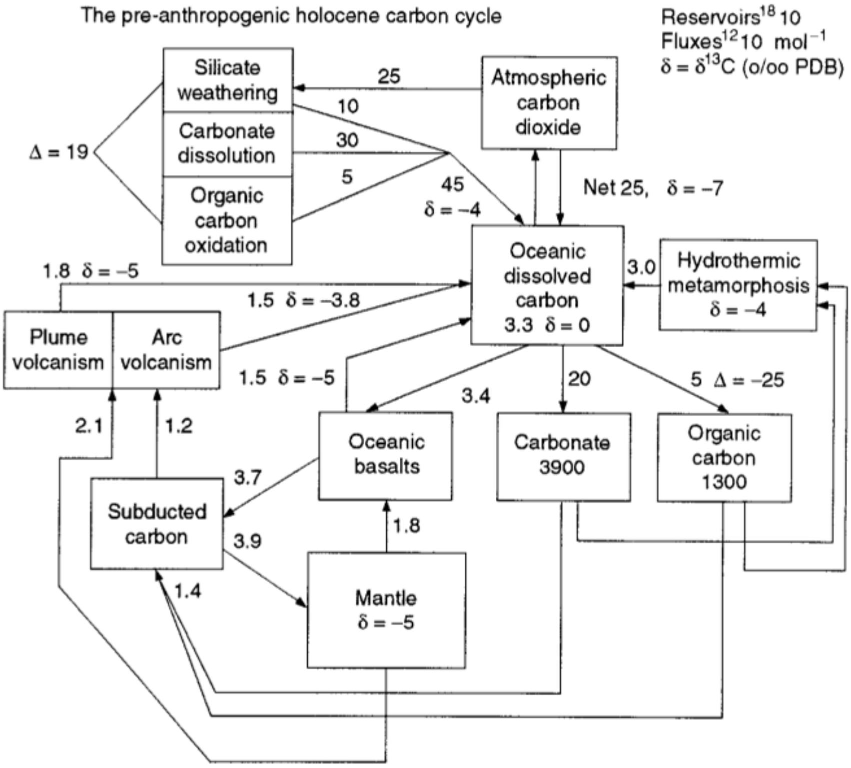
The pre-anthropogenic holocene carbon cycle
Reservoirs^{18}10
Fluxes^{12}10 mol^{-1}
δ = δ^{13}C (o/oo PDB)
Silicate weathering
Carbonate dissolution
Organic carbon oxidation
Δ = 19
25
10
30
5
45
δ = −4
Atmospheric carbon dioxide
Net 25, δ = −7
Oceanic dissolved carbon
3.3 δ = 0
3.0
Hydrothermic metamorphosis
δ = −4
1.8 δ = −5
1.5 δ = −3.8
1.5 δ = −5
Plume volcanism
Arc volcanism
3.4
20
5 Δ = −25
2.1
1.2
Oceanic basalts
Carbonate
3900
Organic carbon
1300
3.7
Subducted carbon
3.9
1.8
1.4
Mantle
δ = −5

FIGURE 1 Reservoirs (10^{18} mol C), fluxes (Tmol year^{-1}), and carbon isotopic values ($\delta^{13}C$ in permil, PDB) in a balanced carbon cycle as estimated for the preindustrial Holocene. Most reservoirs and fluxes after Kump and Arthur (1997) and Berner (1994); volcanic CO_2 fluxes adopted from Tables I and II (see text).

the carbon cycle. However, it has also been suggested that alteration of oceanic crust represents an additional carbon sink of 2–3.7 Tmol year^{-1}. If the upper estimate is valid, the basalt alteration source would demand all of the estimated midocean ridge carbon flux and more, and would increase the total CO_2 outgassing flux required to balance the carbon cycle to about 10 Tmol year^{-1}. In other words, the metamorphic-hydrothermal flux would have to be 6 Tmol year^{-1}, assuming a total volcanic flux of 4 Tmol year^{-1} given above.

Metamorphism and hydrothermal activity associated with collisional orogenys could supply substantial fluxes of CO_2 to the atmosphere. These sources presently are being more explicity considered in carbon mass balance models. For example, it has been estimated that hydrothermal activity associated with Eocene metamorphism of the North American cordillera alone could have resulted in degassing of a substantial 3 Tmol C year^{-1}. Today, it appears that the present major areas of metamorphic-hydrothermal degassing are focused in extensional regions, and the estimated global flux of CO_2 by this mechanism is roughly equivalent to estimates of that derived from volcanic degassing. Therefore, it seems reasonable that the estimated total volcanic CO_2 flux is about 50% of that required to balance the preindustrial global carbon cycle as presently understood. Thus, variations in past rates of volcanic outgassing are probably important to the carbon cycle and to considerations of global climate variation.

B. The Preindustrial Sulfur Geochemical Cycle

The volcanic volatile sulfur flux, mainly as SO_2 evolving from silicic magmas (and not including venting of hydrothermal sulfide at the MOR), is generally not explicitly included in global sulfur cycle models. However, the volcanic sulfur flux *is* important. The sulfur isotopic composition of this source is somewhat depleted (ca. +1–3 permil, CDT) relative to average weathering-related sulfate (+6–7 permil, CDT) transported by rivers. Also, the estimated volcanic sulfur flux amounts to between 20 and 40% of the preanthropogenic riverine sulfur (Figure 2), excluding the contribution of recycled sea salt sulfate and other forms of rapidly recycled sulfur such as DMS (dimethyl sulfide). In other words, subaerial volcanism may continually add *new* sulfur to the exogenic system, and/or that sulfur may balance the loss through subduction (see below). The present-day sulfur cycle is imbalanced because of the very large pollutant sulfur source to rivers and atmosphere and, ultimately, to the oceans. However, the preindustrial long-term sulfur cycle can be balanced as shown in Figure 3. This version of the sulfur cycle uses the estimates of pyrite and evaporite sulfur contributions to the river dissolved sulfate flux and the subaerial volcanic sulfur flux adopted for this contribution (Table III). Mass and isotopic steady state then requires a pyrite to oxidized sulfur burial ratio of 9 : 1, with a relative sulfur isotopic difference between these burial outputs of 33.3 permil (so-called $\Delta^{34}S_{\text{pyr-evap}}$). This assumed value of $\Delta^{34}S_{\text{pyr-evap}}$ lies within the range of published estimates.

A major uncertainty in the sulfur cycle lies in how seawater–basalt interactions are treated. As discussed briefly above, the cycling of seawater through oceanic crust probably results in wholesale extraction of seawater sulfate from seawater into the crust as anhydrite at temperatures of 150–200°C. This contention is supported by laboratory experiments and theory, the absence of sulfate in high-temperature hydrothermal vent fluids, and anhydrite veins observed in the upper oceanic crust recovered in Deep Sea Drilling Project drillholes. This apparently limits the amount of sulfate that penetrates into the higher temperature regions of the hydrothermal system, and there is apparently little direct reduction of seawater sulfate to sulfide at higher temperatures. Thus, the sulfide that does emanate from high-temperature vents is hypothesized to be primarily of magmatic origin. Further support for this concept of seawater sulfate cycling is that the anhydrite in veins has sulfur isotopic values very similar to those of seawater sulfate. Unfortunately, the sulfur isotopic composition of sulfide emanating from high-temperature vents is consistent with either a magmatic source, possibly contaminated by seawater sulfate drawn in and reduced during seafloor venting, or with reduction of seawater sulfate within the hydrothermal system at 300° C.

Nonetheless, the mass flux of sulfate (0.8 Tmol S year^{-1}) estimated to enter the near-ridge crest hydrothermal system (estimated using axial, high-temperature venting of 2.9×10^{13} kg seawater year^{-1} at a sulfate concentration of 28×10^{-3} mol kg^{-1}) is much larger than the flux of sulfide out of oceanic crust estimated for axial vents (about 0.1 Tmol S year^{-1}). Thus, we must appeal to redissolution, with increasing age, of much of the anhydrite precipitated from seawater in oceanic crust (Figure 2). Then, this sulfate must diffuse or be advected into seawater with little or no difference in sulfur isotopic composition in order to maintain mass and isotopic balance in the sulfur cycle. On the basis of this consideration, it is not clear whether the presumed magmatic contribution, ultimately from the mantle, is a net contribution to the global sulfur cycle or must be considered as part of the compensation for longer-term seawater

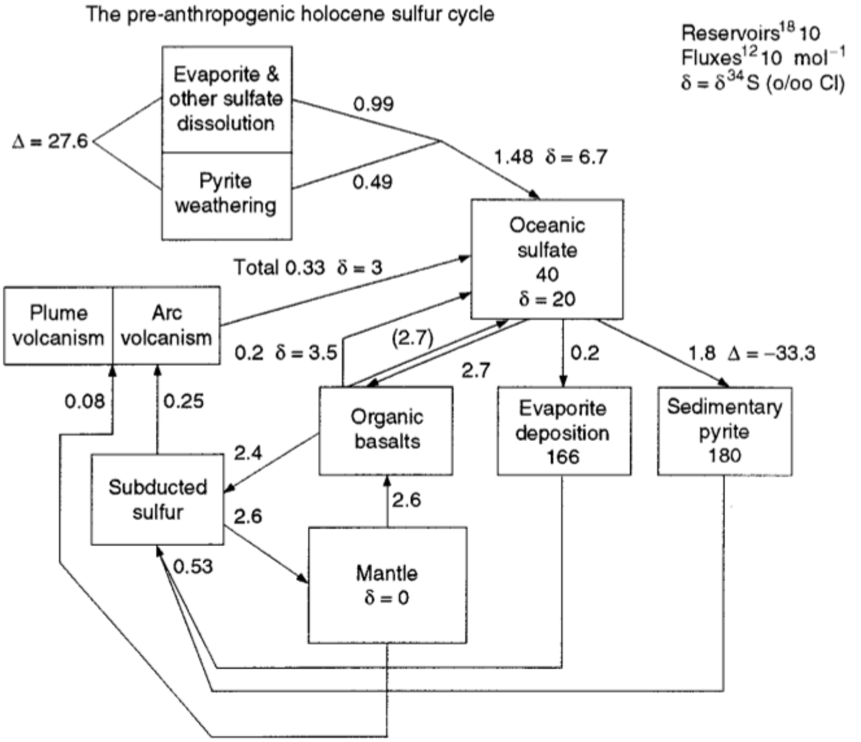
The pre-anthropogenic holocene sulfur cycle
Reservoirs^{18} 10
Fluxes^{12} 10 mol^{-1}
δ = δ^{34}S (o/oo Cl)
Evaporite & other sulfate dissolution
Pyrite weathering
Δ = 27.6
0.99
0.49
1.48 δ = 6.7
Oceanic sulfate 40 δ = 20
Total 0.33 δ = 3
Plume volcanism
Arc volcanism
0.2 δ = 3.5
(2.7)
2.7
0.2
1.8 Δ = −33.3
0.08
0.25
Organic basalts
Evaporite deposition 166
Sedimentary pyrite 180
2.4
Subducted sulfur
2.6
2.6
0.53
Mantle δ = 0

FIGURE 2 A balanced (mass and isotopic) preindustrial Holocene sulfur cycle, with reservoirs (10^{18} mol S) and fluxes (Tmol year^{-1}). Note that the fluxes of sulfur that represent short-term cycling mainly from ocean-land-ocean, such as DMS production and atmospherically cycled sea salt, are not included. The flux of sulfur representing weathering accepts the value estimated for "natural" (less, DMS, volcanic, and recycled sea salt contributions) sources to rivers (Berner and Berner, 1996). The sulfur isotopic composition (δ^{34}S) of riverine sulfate is taken as 6.68 o/oo (CDT), assuming that one-third derives from pyrite oxidation and two-thirds from evaporites and other sources of sulfate (e.g., Berner and Berner, 1996). The mass and isotopic compositions of oceanic sulfate, sedimentary evaporite, and pyrite reservoirs are from Holser *et al.* (1989). Sizes of other reservoirs and fluxes are summarized in this article.

sulfate storage in the oceanic crust. Of course, if most of the hydrothermal sulfide is precipitated in chimneys and other metal-sulfide-bearing sediments near the ridge axis and not later oxidized, the hydrothermal sulfur flux would not be a consideration in the longer-term sulfur cycle; it would continue to be associated with oceanic crust. Thus, most models treat the midocean ridge-related system as having no net influence on the global sulfur cycle. A net flux of 0.1 Tmol S year^{-1} from the "mantle" to seawater at the MOR is adopted for this article.

If the estimates of exogenic sulfur sources and sinks tabulated in Figure 2 are valid then volcanic sulfur sources might be considered part of the mass flux required to balance extraction of seawater sulfate at midocean ridges. This could be the case if either a significant remainder of the anhydrite stored in subducted upper oceanic crust or subducted sedimentary sulfide minerals contribute to volatile sulfur fluxes from volcanic arcs. If, however, we assume that the submarine sulfur cycle is in balance in the long term, we must accept that the average annual preindustrial fluxes of sulfur to pyrite and evaporite reservoirs are as shown in Figure 2. If not, the preindustrial sulfur cycle is not balanced, in terms of either mass or isotopic composition.

VI. Possible Variations in Volcanic Emissions and Their Effects in the Past

At the suggested present-day rate, the entire crust–atmosphere–ocean C inventory could have accumulated in about 3×10^9 years. Some workers favor continuous slow degassing of CO_2 throughout Earth's history without recycling back to the mantle. However, it is likely

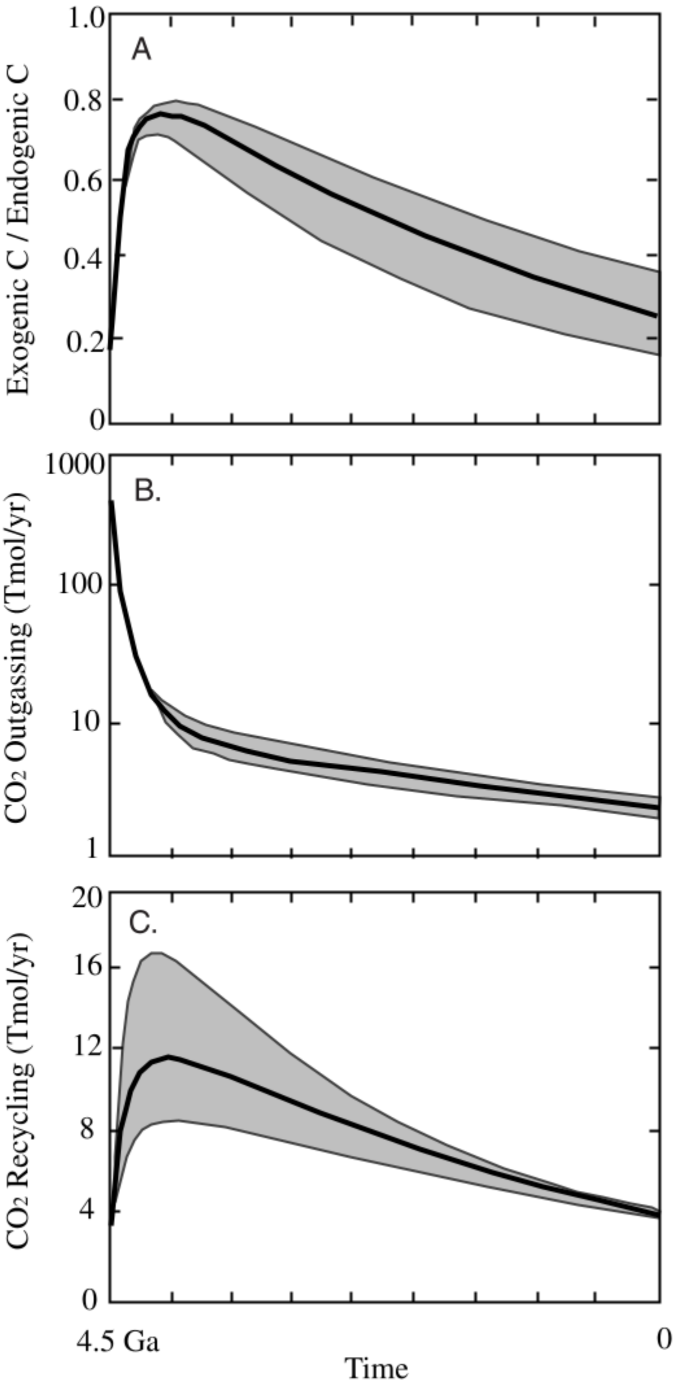

FIGURE 3 Results of simulations of the carbon degassing history of the Earth modified after Zhang and Zindler (1993). (A) Ratio of carbon in exogenic reservoirs (crust-ocean-atmosphere) to that in degassed (upper) mantle. (B) rate of CO_2 degassing from the upper mantle for the past 4 Ga. (C) The CO_2 recycling rate representing carbon subducted back to the mantle. Shaded area represents model uncertainties.

that recycling by subduction has occurred because the mantle contains significant CO_2 that could be degassed (estimated at ca. 1.8×10^{10} Tmol), representing about 72% of the total carbon in the crust-ocean-atmosphere plus upper (degassed) mantle. This is in sharp contrast to the suggested severe depletion of noble gases in the degassed mantle.

The recycling of CO_2 back to the mantle during subduction is reasonable in light of the amount of carbonate in veins in altered oceanic crust, which is estimated as perhaps 3.7 Tmol year^{-1} entering subduction zones today. This subducted carbon flux may have been higher in the past because of much higher subduction rates, assuming that carbonation during MORB alteration occurred at all times in the past. The advent of pelagic carbonate sedimentation about 200 m.y. ago could have increased the total carbon being subducted, and thereby compensate, or even overcompensate, for the diminishing rates of subduction toward the present.

Figure 3 provides the results of one of several numerical model simulations which portray CO_2 outgassing and recycling rates for the Earth through time. The curves presented are for a model simulation driven by assumed rates of outgassing for noble gases, which depend on an assumed model for the thermal evolution of the Earth. The numerical simulation assumes a constant average carbon content in subducted crust and sediment, but requires that the recycling rate constant be sufficient to produce a degassed mantle at present with 72% of its original carbon content as required by available carbon inventory estimates discussed above. The final rate of carbon outgassing equals that estimated for outgassing at the midocean ridge today. Note that this simulation produces an initial crust–ocean–atmosphere carbon inventory for the Archean that is considerably higher (by a factor of about 2.5) than today's inventory. Required recycling rates of C into the mantle by subduction are higher than the degassing rate over the past 3.5×10^9 years. The results of this particular simulation suggest that the amount of carbon in the crust–ocean–atmosphere reservoir has progressively decreased since the early Archean and is still decreasing today!

The results of this numerical simulation may also generally account for the evolution of pCO_2 over the past 4 Ga envisioned by other workers. The suggested very high CO_2 outgassing rates would have produced a high Archean pCO_2 (perhaps 1–10 bars) that would have offset the much lower solar flux to the Earth at that time and produced rather warm surface temperatures. Evidence for glaciations at about 2.5–2.3 Ga and again at about 0.8–0.6 Ga probably required substantially lowered pCO_2 consistent with much reduced CO_2 outgassing and high rates of carbon recycling to the mantle in the model (Figure 3) for that interval of time.

This model has appeal as a general model for the Earth because it has reasonable implications for cycling of other elements as well. Nonetheless, if, as portrayed in the simulation, the carbon recycling rate has exceeded the outgassing rate for several billion years by a factor of 2 or so, we are left with a dilemma. There must be other sources of CO_2 that provide for the flux required by weathering. In this consideration we assume for the moment that there is no net CO_2 source or sink associated with the organic carbon subcycle, that is, that in the long term (10^7–10^8 years) organic carbon burial is offset by organic carbon oxidation.

In various versions of models for the carbonate–silicate geochemical cycle, total CO_2 flux to the atmosphere from magmatic-metamorphic sources is scaled to the seafloor-spreading rate inferred from long-term variations in sea level. Doing so results in CO_2 outgassing rates about 1.65 times higher 100 million years ago than at present. This is essentially the result obtained when using estimates of the seafloor creation rate for the Cretaceous, which suggest oceanic crustal production at rates as high as 1.8 times the present rate. These models treated CO_2 degassing as a long-term rate increase, and the impact on global mass balances included other CO_2 sources such as metamorphic and geothermal processes.

Using a simple carbon cycle box model (Figure 1), we can illustrate the possible effects of a sudden and prolonged (0.5 m.y.) 1.5× increase in volcanic CO_2 outgassing on pCO_2 and $\delta^{13}C$ of oceanic total dissolved inorganic carbonate and consequent changes in $\delta^{13}C$ of marine organic carbon. If such variations occur, they have the potential to leave an imprint on the geologic record, but calculations show that the effects are subtle and complex (Figure 4) and likely to be masked by changes in burial outputs or other factors. Figure 4 indicates that the greatest change in carbon cycle indicators might be expected in the carbon isotopic composition of organic matter produced by marine phytoplankton because the fractionation of carbon isotopes by such organisms is sensitive to pCO_2 changes. The increase in pCO_2 (Figure 4A) that results from the simulated volcanic CO_2 outgassing produces greater relative carbon isotope fractionation by the phytoplankton—an approximately 2 permil decrease in $\delta^{13}C_{org}$ (Figure 4B). Because the burial of this ^{13}C-depleted organic matter drives changes in $\delta^{13}C_{carb}$, the increase in relative carbon isotope fractionation damps the response of the oceanic dissolved carbon reservoir to the addition of ^{13}C-depleted volcanic CO_2 (which has a $\delta^{13}C$ similar to riverine dis-

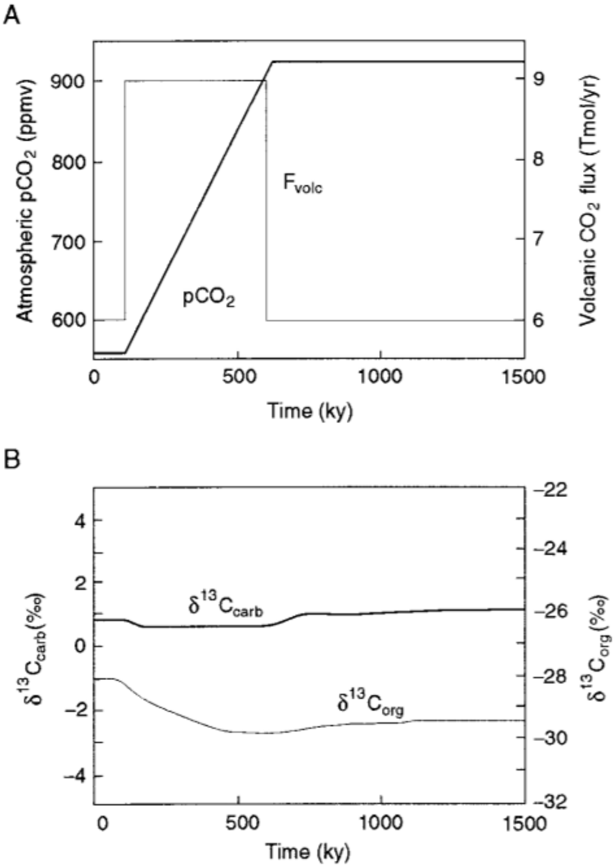

FIGURE 4 Carbon box model results using values for fluxes and reservoirs shown in Figure 1. The plots illustrate the effects of a 1.5 × increase in volcanic CO_2 outgassing for 0.5 m.y. (modified after Kump and Arthur, 1999). (A) F_{volc} is history of volcanic CO_2 flux stipulated in the model and pCO_2 is the computed atmospheric CO_2 concentration. (B) $\delta^{13}C_{carb}$ represents oceanic dissolved inorganic carbon reservoir and $\delta^{13}C_{org}$ is the carbon isotopic composition of marine phytoplankton organic carbon.

solved carbon; Figure 1). Thus, we might detect the effects of such relatively short-term volcanic events in the geologic record by the differential response of $\delta^{13}C_{org}$ and $\delta^{13}C_{carb}$.

However, the question is whether such significant changes in rate of outgassing really do occur. For example, LIPs (large igneous provinces) represent significant increases in eruptive activity, largely through extrusion of flood basalts, either subaerially or as a submarine process. One such event, the latest Cretaceous, earliest Tertiary Deccan Traps of India, has been examined in several studies for potential effects of resulting enhanced rates of CO_2 and SO_2 emissions. Using the volume of basalt erupted of 3×10^5 km^3 and assuming that 80% of this was erupted in just 1×10^6 years, one can calculate a cumulative CO_2 yield of 0.68 to 4.6×10^4 Tmol C. This corresponds to an average rate of 0.007 to 0.05 Tmol C $year^{-1}$, corresponding to an average basalt eruption rate of 0.3 km^3 $year^{-1}$. For this calculation a CO_2/SO_2 ratio (0.5–2.6) was assumed for volatile degassing measured or estimated for basaltic eruptions of Laki and Surtsey and the SO_2 emission rate per km^3 of basalt erupted (about 0.04 Tmol S/km^3) in the 1738 eruption of Laki. Using these data, even at eruption rates of 3 × the average estimated for the Deccan Traps, the annual carbon and sulfur fluxes to the atmosphere would only represent an increase of about 3–6% over present subaerial volcanic carbon emissions, and 5–20% over present subaerial volcanic sulfur emissions. Other workers have used a degassing rate of 0.06 Tmol km^{-3} extruded for the Deccan Trap basalts and arrived at a total outgassing of CO_2 of $0.6–2.0 \times 10^5$ Tmol, using larger basalt volume estimates. Nonetheless, a carbon cycle model predicted a very small (<40 ppmv) increase in pCO_2 during the Deccan eruption event, assuming that the eruptions ensued over at least 0.5 m.y.

The impact of changes in rates of volcanism or individual volcanic events, such as LIP episodes, on total rates of CO_2 outgassing appears to be relatively minor. Inasmuch as sulfur emission rates are, on average, a factor of about 0.4 to 0.7 times that of CO_2 emissions in subaerial volcanoes, and as little as a factor of 0.15 of CO_2 emanated from MORB settings (on the basis of vesicle gas compositions), the general effects of LIP episodes on sulfur cycling should be relatively minor. Figure 5 illustrates the effects of doubling volcanic sulfur degassing rates for 1×10^6 years. This simulation uses

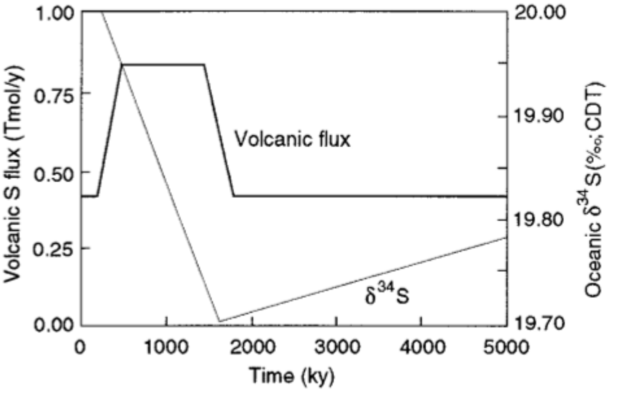

FIGURE 5 The response of oceanic sulfate sulfur isotopic composition to a doubling of volcanic S flux of 1 m.y. (shown as a curve), using values of fluxes and reservoirs in Figure 2.

the flux and reservoir sizes for the sulfur cycle shown in Figure 2 and assumes that, with the exception of the volcanic S flux, there is no other change. Because the oceanic residence time of sulfur is long (10^7 years) relative to the interval of the perturbation, the doubling of volcanic sulfur degassing causes only minor changes in the sulfur isotopic composition (Figure 5) and concentration (not shown) of oceanic sulfate. Thus, with these assumptions, only the effects of more sustained and massive changes in volcanic sulfur input would be observable in the ocean geochemical record.

VII. CONCLUSIONS AND FUTURE RESEARCH

Mass and stable isotopic fluxes of volatiles from volcanic activity must be taken into account when attempting to balance the modern carbon and sulfur geochemical cycles. At present, volcanic-associated outgassing must be about 50% of the total flux of carbon dioxide to the atmosphere. However, the proportion of the carbon dioxide volatile flux assigned to each of the arc-volcanic, midocean ridge, and metamorphic sources remains uncertain. Past variations in long-term outgassing rates assume some scaling between volatile production and crustal production rate at midocean ridges and/or subduction rates. Such longer-term variations could have produced an increased $p\mathrm{CO}_2$. Although it has been proposed that increases in the rate of carbon dioxide outgassing may have been associated with rapid formation of LIPs, which in turn could have caused short-term (e.g., $<10^6$ years) perturbations of $p\mathrm{CO}_2$ and climate, the impact of these events remains questionable.

The volcanic volatile sulfur flux, mainly as SO_2 evolving from silicic magmas (and not including venting of hydrothermal sulfide at midocean ridges), amounts to between 20 and 30% of the preanthropogenic riverine sulfur flux, excluding the contribution of recycled sea salt sulfate and other forms of rapidly recycled sulfur. The impact of volcanic sulfur outgassing at midocean ridges and associated with submarine volcanism in general is difficult to assess because of uncertainties in the values assigned to hydrothermal sources and sinks. The subaerial volcanic sulfur flux is generally not explicitly included in global sulfur cycle models, but is important in that the sulfur isotopic composition of this source is depleted (ca. +2 permil, CDT) relative to average weathering-related sulfate (+7 permil, CDT) transported by rivers. Short-term (e.g., $< 10^6$ years) variations in volcanic sulfur flux have little impact on the global sulfur cycle. However, long-term changes in volcanic sulfur emanations potentially could have produced some of the observed changes in the sulfur isotopic composition of the oceans through time.

SEE ALSO THE FOLLOWING ARTICLES

Deep Ocean Hydrothermal Vents • Volatiles in Magmas • Volcanic Aerosol and Global Atmospheric Effects • Volcanic Gases

FURTHER READING

Allegre, C. J., Staudacher, T., and Sarda, P. (1986–1987). Rare gas systematics: Formation of the atmosphere, evolution and structure of the Earth's mantle. *Earth Planet. Sci. Lett.* **81,** 127–150.

Andres, R. J., and Kasgnoc, A. D. (1998). A time-averaged inventory of subaerial volcanic sulfur emissions. *J. Geophys. Res.* **103,** 25251–25261.

Arthur, M., *et al.* (1985). Page 504–529 *in* "The Carbon Cycle and Atmospheric CO_2: Natural Variations Archean to Present." (E. T. Sundquist and W. S. Broecker, eds.), Geophys. Monograph 32. Am. Geophys. Union, Washington, DC.

Berner, R. A., Lasaga, A. C., and Garrels, R. M. (1983). The carbonate-silicate geochemical cycle and its effect on atmospheric carbon dioxide over the past 100 million years. *Am. J. Sci.* **283,** 611–683.

Brantley, S. L., and Koepenick, K. W. (1995). Measured carbon dioxide emissions from Oldoinyo Lengai and the skewed distribution of passive volcanic fluxes. *Geology* **23,** 933–936.

Des Marais, D. (1985). Page 602–611 *in* "The Carbon Cycle and Atmospheric CO_2: Natural Variations Archean to Present" (E. T. Sundquist and W. S. Broecker, eds.), Geophys. Monograph 32. Am. Geophys. Union, Washington, DC.

Gerlach, T. M. (1989). Degassing of carbon dioxide from basaltic magma at spreading centers. II. Mid-oceanic ridge basalts. *J. Volcanol. Geotherm. Res.* **39,** 221–232.

Gerlach, T. M. (1991). Present-day CO_2 emissions from volcanoes. *EOS* **72,** 249–255.

Gerlach, T. M., Delgado, H., McGee, K. A., Doukas, M. P., Venegas, J. J., and Cardenas, L. (1997). Application of the LICOR CO_2 analyzer to volcanic plumes: A case study, Volcan Popocatepetl, Mexico, June 7 and 10, 1995. *J. Geophys. Res. B* **102,** 8005–8019.

Javoy, M., Pineau, F., and Allegre, C. J. (1982). Carbon geodynamic cycle. *Nature* **300,** 171–173.

Kasting, J. F. (1993). Earth's early atmosphere. *Science* **259,** 920–926.

Kump, L. R., and Arthur, M. A. (1997). Page 399–426 *in* "Tectonics Uplift and Climate Change" (W. Ruddiman, ed.). Plenum Press, New York.

Lasaga, A., Berner, R. A., and Garrels, R. (1985). Page 397–411 *in* "The Carbon Cycle" (E. T. Sundquist and W. S. Broecker, eds.), Geophys. Monograph 32. Am. Geophys. Union, Washington, DC.

Le Cloarec, M.-F., and Marty, B. (1991). Volatile fluxes from volcanoes. *Terra Nova* **3,** 17–27.

Le Guern, F. (1982). Les d'Èbits de CO_2 et de SO_2 volcaniques dans l'atmosphere. *Bull. Volcanol.* **45,** 197–202.

Lupton, J. E. (1983). Terrestrial inert gases: Isotopic tracer studies and clues to primordial components in the mantle. *Annu. Rev. Earth Planet. Sci.* **11,** 374–414.

Marty, B., and Jambon, A. (1987). C/^{3}He in volatile fluxes from the solid Earth: Implications for carbon geodynamics. *Earth Planet. Sci. Lett.* **83,** 16–26.

Varekamp, J. C., *et al.* (1992). Carbon sources in arc volcanism; with implications for the carbon cycle. *Terra Nova* **4,** 363–373.

Williams, S. N., Schaefer, S. J., Calvache, M. L., and Lopez, D. (1992). Global carbon dioxide emission to the atmosphere by volcanoes. *Geochim. Cosmochim. Acta* **56,** 1765–1770.

THE ECOLOGY OF VOLCANOES: RECOVERY AND REASSEMBLY OF LIVING COMMUNITIES

IAN W. B. THORNTON
La Trobe University

I. The Effects of Volcanic Activity on Living Communities
II. Primary Colonizers of New Volcanic Habitats
III. Biotic Reassembly
IV. The Assembly of New Biotas on Emergent Volcanic Islands
V. Some Colonization Comparisons
VI. Establishment and Community Assembly
VII. Theoretical Considerations
VIII. Summary

GLOSSARY

aerial plankton The usually small plants, plant parts (e.g., seeds, spores), and animals with little or no powers of locomotion that drift passively in the air.

arthropod Segmented animal with an exoskeleton and jointed legs.

biota The full complement of species of living things (fauna, flora, and, strictly, micro-organisms) of a region.

carnivore, carnivorous Feeding on animals.

collembolans Small wingless insects known as springtails which have a forked springing organ on the abdomen; most live on or near the soil surface and feed on decomposing organic material.

community A well-defined assemblage of interacting species, almost always including both animals and plants.

crepuscular Active at or around dawn or dusk.

cyanobacteria Photosynthetic bacteria formerly known as blue-green algae.

debris avalanche Debris flow resulting from the partial collapse of the volcano's edifice.

ecosystem The system formed by the interacting living organisms of an area and the nonliving environment with which they in turn interact.

effusive eruption An eruption in which lava is poured out of a vent or fissure.

extirpation Destruction, wiping out.

frugivore, frugivorous A feeder on fruit, feeding on fruit.

guild A group of species having similar feeding habits and thus similar roles in the community; for example, taking animal prey in midair or feeding exclusively on grasses.

heliophilous Adapted to grow in full sunlight.

herbivore A plant eater.

invertebrate An animal without a backbone; the term includes arthropods (q.v.), worms, and mollusks, among others.

kipuka A Hawaiian term, now in general use, for a habitat "island" of land not covered by ash or lava, in an ash- or lava-covered landscape.

legume Plant of the pea family, Leguminosae.

macrobiota The biota of an area, excluding micro-organisms.

Copyright © 2000 by Academic Press
All rights of reproduction in any form reserved.

magma Molten rock produced by the partial melting of material in the layer of the Earth below the outer crust. Becomes lava when extruded.

microsite The space occupied by a single plant.

monitor A large lizard-like reptile of the family Varanidae. In this article, the five-banded monitor, *Varanus salvator*, often over a meter in length.

neuropterans Insects of the order Neuroptera, including lacewings and ant lions.

nitrogen-fixing The incorporation of atmospheric nitrogen into living tissues and its chemical conversion into a form that can be used by the organism.

omnivore, omnivorous A mixed feeder whose diet includes plant and animal food.

photosynthesis The process whereby green plants use light energy trapped by the green pigment chlorophyll to build up carbohydrate from carbon dioxide and water, releasing oxygen.

primary colonist A species that becomes established in an environment devoid of life; the first species in a primary succession (q.v.).

primary producer A species that synthesizes organic matter from inorganic materials; green plants are primary producers.

primary succession Succession (q.v.) on an area previously devoid of life.

pumice Highly vesiculated, low-density, glassy rock formed when large volumes of gas expand within magma (q.v.).

pyroclastic flow Very hot, glowing mass of solid fragments ejected by a volcano, cushioned on escaping gases and moving at high speed.

scavenger An animal that feeds on the dead remains or waste material of animals and plants.

scoria Loose rubble of pieces of pumice.

strombolian/vulcanian Eruption style or phase in which intermittent eruptions send plumes of steam, gas, and ash several kilometers high and cause a rain of fine ash downwind.

succession (biological) The sequence of natural stages (in structure and species representation) of a developing ecosystem such that one community gradually replaces another.

successional mosaic The pattern resulting when an area has a number of smaller patches at different stages of succession (q.v.).

symbiotic Pertaining to a close, usually obligatory, association of two species living together.

tephra Solid fragmented matter ejected by a volcano, often extremely rapidly; includes ash, lapilli ("little stones"), and larger bombs, and blocks.

tertiary consumers Consumers (usually animals) of species that eat species that consume primary producers (q.v.).

vascular plants Plants with well-defined tracts of fluid-filled supporting cells within their tissues; seed plants and ferns are the largest groups.

zoochorous Dispersed by animals, either internally, in their guts, or by adhering externally.

OBVIOUSLY VOLCANIC ACTIVITY can damage and may even destroy natural living communities, and yet from even a cursory examination of volcanoes it is equally clear that sooner or later life returns to devastated areas. From studying oceanic volcanic islands we know that, given time, rich and complex land communities may develop on substrates that must have been devoid of life, certainly of land life, when they first broke the sea's surface. Here I review some of the destructive and constructive processes involved in the interaction between volcanoes and living communities.

I. The Effects of Volcanic Activity on Living Communities

The damage caused to living organisms by volcanic activity clearly depends on the type of eruption. Damage may result from the effects of volcanic gases, explosive blast, debris avalanche, pyroclastic flows, mudflows (lahars), lava flows, or tephra (including ash) fall. The extent of the damage varies with the physical and chemical properties of the eruptive products, time of year, amount of snow and ice cover, behavior of the organism, type of vegetation, and even time of day of the eruption. Because so many factors are involved, generalizations about eruptive effects are unwise, and extrapolations from one environment or one eruption to others are likely to be unreliable.

A. Types of Volcanic Damage

Perhaps the most well-known case of the effect of toxic gases on a biota is the 7-month-long effusive eruption of Lakagigar in Iceland in 1783. Emissions of SO_2, SO_3, CO_2, and HF destroyed birch woods 200 km away from the vent and were mainly responsible for so stunting the grass crop that about 70% of the livestock and 20% of Iceland's human population perished.

The effects of blast and of debris avalanche were clearly seen at Mount St. Helens (northwestern USA). Trees were felled and the vegetation razed to the ground by the blast, which reached supersonic speeds as it expanded, creating a substrate on which only primary colonists could become established. An area of almost complete devastation—the "blast zone"—could be clearly identified, and its bare mineral surfaces were the slowest to recover; 5 years after the eruption this zone appeared much as it did in the immediate aftermath. The 45-m-deep, 2-km-wide debris avalanche moved at about 75 m/s and extended for 25 km, breaking off and transporting plants and covering mature forest in a new raw substrate composed of particles the size of sand grains. The few survivors were the result of regrowth from roots and suckers of plants transported by the avalanche.

Pyroclastic flows (previously known as *nuées ardentes* or "glowing clouds") are infamously dangerous. Such a flow is a turbulent, ground-hugging, expanding cloud of gas-charged incandescent particles that are fluidized (i.e., moving freely among themselves, flowing like a liquid). It moves silently and rapidly (up to 100 km/hour) on a cushion of its own continously exsolved gases. These flows are lethal to animals and death comes rapidly; they are the most dangerous to humans of all volcanic effects. Pyroclastic flows are a feature of Peléan eruptive phases, named after the 1902 eruption of Mount Pelée, on the island of Martinique in the West Indies, where a pyroclastic flow rolled silently and rapidly down the volcano's slopes to engulf and incinerate the town of St. Pierre and its 30,000 inhabitants. In the same year, 144 km to the south, pyroclastic flows from the eruption of La Soufrière devastated about a third of the island of St. Vincent's surface, and killed about 1350 people of the (fortunately) sparse population. The depth of ash and pumice varied from a few centimeters on steep slopes to 27 m in some valleys. In 1911 on Taal volcano on Luzon in the Philippines, such flows totally destroyed the vegetation over most of Volcano, an island in Taal's crater lake, although the ash deposits were neither very deep (up to 2 m) nor very hot. The zone devastated by 1968 pyroclastic flows on Mayon volcano, also on Luzon, Philippines, was surrounded by a "seared zone" from a few meters to over 2 km wide, within which all animals were killed outright, presumably from burns or by inhaling the fluidized incandescent cloud. On the inner parts of the zone all vegetation was charred and many trees stripped of foliage on the side facing the crater; at the zone's outer edges plant leaves were shriveled and browned.

Mudflows (lahars) can also be devastating. They are sometimes formed when dust clouds rising from pyroclastic flows trigger torrential rainstorms within minutes of the passage of the flow, as on Mayon in 1968. Burial in mud halts photosynthesis and exchange of gases in plants, and surviving animal herbivores are deprived of access to food.

Clearly, lava flowing over an area will obliterate and kill all organisms on the surface that are unable to move out of its path, but the damage, although extreme, may be sharply circumscribed. Anak Krakatau is an active volcano that emerged from Krakatau's submarine caldera in Sunda Strait, Indonesia, in 1930 and was self-sterilized in 1952. Trees only a meter from the edge of its 1993 lava flow, which obliterated trees in its path, survived without evident ill effects.

From his review of large Icelandic eruptions, Thorarinsson concluded that the extent of damage from ashfall depends on the fall's thickness, timing, and chemical and physical properties. A depth of 10 cm of freshly fallen tephra (ash) caused farms to be abandoned for a year, ash 15–20 cm deep led to abandonment for from 1 to 5 years, and where the thickness was 20–50 cm, settlements were abandoned for decades. In the 1902 eruption of Santa Maria in Guatemala, coffee plants that received less than a meter of tephra recovered within a year, although grazing areas were seriously damaged where it was over 15 cm thick. In contrast, during the 1912 Katmai eruption in Alaska most trees in an area covered by 50 cm or more of tephra were killed, and a 30-cm-thick layer at Kodiak, 160 km from the volcano, caused extreme crop damage.

Ash can be removed quickly by erosion, of course, and rain erosion can be quite rapid on volcanic slopes. For example, after the 1964 Irazu eruption in Costa Rica, at least a third of newly fallen tephra was lost from the upper slopes within a year, and more than half the tephra deposited around La Soufrière in 1902 had been eroded to the ocean within 6 months.

Susceptibility to damage by tephra and gases also varies widely between species. On Mount St. Helens, in grassland communities that had received ash deposits more than 1 cm thick, plant damage through overloading and necrosis (tissue and cell death) was greatest among species with a prostrate habit or with broad, sheathing leaves; annual and perennial grasses, for example, were unaffected. Living communities in subalpine meadows that were covered by less than 20 cm of tephra in spring appeared to have returned to normal by the end of summer. Regrowth penetrated the ash layer, and insects, birds, and terrestrial vertebrates recolonized as the plant cover was re-established. In Alaska, small mammals such as squirrels, mice, and marmots were killed by tephra falls less than 10 cm deep. Massive ash deposits, several meters thick, can maintain temperatures of from 600 to 800°C for weeks and months, and the survival chances of macrobiota under such conditions are practically zero.

Ash fallout can have a significant and special effect on insects. The Mount St. Helens tephra, for example, consisted of a fine powder of volcanic glass fragments which acted as a natural insecticide. They abraded the insects' thin, outer layer (epicuticle) of external skeleton, which is waxy and waterproof, thus causing fatal dehydration. Insects exposed to the tephra in the laboratory lost water and died within 30 hours. In the field, Colorado potato beetles died within 24 hours of exposure unless they happened to have been washed clean by overhead irrigation systems, and an economically significant outbreak of grasshoppers was controlled by tephra fallout, obviating the need for insecticide treatment. In contrast to these effects, however, on Sertung, an island some 2–3 km away from the vent of Anak Krakatau, daily fallout of basaltic ash in 1996 had no obvious effect on grasshoppers, carpenter bees, or dragonflies. Physical texture of the particles is of prime importance for ash to have insecticidal effects.

The chemical nature of tephra fallout also may be an important determinant of its lethality. Sometimes chemical poisoning occurs. Fluorine, for example, becomes concentrated on the surface of ash grains, and fluorine poisoning of livestock is a fairly common hazard in Iceland.

Size of the tephra particles also affects the extent of damage, and is important in relation to fluorine poisoning. Whereas coarse-grained wind-blown tephra, such as that of the 1875 Askja eruption in Iceland, can destroy plants by tearing, finer-grained ash, deposited further afield, may carry fluorine concentrations 20 times higher (at 20,000 ppm) than those of the coarser ash falling close to the source. In contrast, at Mount St. Helens, fodder containing up to 10% by weight of ash was not toxic to livestock, milk production and growth rate of cattle were unaffected, and day-old chicks given tephra as 30% by weight of food suffered no additional mortality. Over most of the fallout area plants and animals seem to have resumed normal activities fairly quickly.

The timing of the ashfall may be crucially important. A thin, fine-grained layer deposited during the plant growing season may have a greater effect than a thicker layer falling at other times. As illustrated at Mount St. Helens, tephra falling onto a winter covering of snow or ice under which the living community is often dormant will have far less damaging effects than would the same fallout in the summer, when the community is active and lacks this protection.

B. Local Survival

The distinction between total eradication and the local survival of a few individuals, although seemingly trivial, is important to the biologist considering the process of revival of a natural community. Spread from survival foci, what Edwards termed "survival and revival," is very different from colonization of a "clean slate" by immigrants from outside the devastated area, and the species assembly process as well as the nature of the resultant community may be quite different in the two cases. In the recovery of vegetation, survival of preexisting plants is generally more important than the establishment of new immigrants.

On a number of volcanoes rapid erosion of ash by heavy rainfall has facilitated recovery. There are many reports of herbaceous plants (i. e., having a nonwoody green stem) surviving burial to depths of over 30 cm, and the large grass *Saccharum spontaneum* survived burial to 1.5 m in New Guinea. After the Katmai eruption most plant species withstood burial for a year or more. Herbaceous plants may take up to 4 years to penetrate the deposit, and a growth from of "runners" or adventitious roots is related to survival ability. The growth of woody plants may sometimes actually increase after burial in tephra, in spite of the low concentration of available nutrients. On Hawaii, Paricutin (Mexico), Katmai, and Taal, trees have recovered from a 2-m-thick tephra fall.

As on Mount St. Helens, but much more slowly, on the Galapagos Islands' Fernandina volcano erosion of an 8-m-thick layer of tephra facilitated the reestablishment of plant communities, and these survivors were important as pioneers. On Mount St. Helens a grylloblattid insect (grylloblattids are a small group of cricket-like wingless terrestrial insects confined to cold damp situations) and 15 species of nonballooning spiders (in which juveniles are not dispersed aerially, suspended on trailing silken threads) were recorded as surviving by sheltering in rock debris in an area where tephra fallout was 10 cm deep, and whereas only a single ant species was collected at depths of about 50 cm, 9 species were found at depths averaging a third of this. Those buried trees that had their roots exposed by rapid rain erosion resprouted, stabilizing the ash slopes. But on this volcano the question of survival was complicated in some cases by the possibility of local reinvasion from contiguous unaffected areas. For example, lupins, which appeared early on the cooled pyroclastic flows, may have grown either from viable seed that survived the eruption in sheltered sites or from wind-borne seed dispersed into the area after the eruption (perhaps less likely, for their seeds are rather large and heavy). A carabid (ground beetle) with reduced eyes and wings that lives underground was captured at a pyroclastic site in 1983 and may have been a survivor, but even in this case immigration by wind was thought to be a more likely explanation.

After the eruption of Krakatau in 1883 there was no question of immigration from contiguous unaffected reservoirs; the recovery was either from survivors or from colonists arriving from over the sea. Nevertheless the question was the topic of considerable international debate for some years. The speed and nature of recovery of communities on Krakatau's remnant and its two closely neighboring islands strongly indicated that the macrobiota had been eradicated and recovery was from new colonists. The two Dutch biologists who studied the reassembly of Krakatau's biota, Docters van Leeuwen and Dammerman, both argued that the first organisms to appear were not those likely to have survived by persisting underground, for example, but those with good dispersal powers. The question of bacterial survival under deep hot ash deposits is unresolved and must be regarded as a possibility, and some species of soil nematodes are also capable of surviving very high temperatures. In contrast to the Krakataus, the first plants to appear on Sebesi, an island about 15 km from Krakatau which received a much shallower deposit of ash in 1883, were largely species with underground storage organs or vegetative structures; they were survivors, not new colonists. Dammerman pointed out that on Krakatau any animal survivors would not have found sufficient food in the devastated landscape and would soon have perished. This point is illustrated by observations of ants on Komagatake volcano, Japan. Two species of *Formica* were active a days after ash fell in the 1929 eruption but lasted for only another 11 days.

A plant or animal may be spared the effects of lava flows or lahars by being in the lee of natural obstacles, by being on high ground when the flow will move around it, leaving a *kipuka* (Figure 1), or of course, in the case of animals, by moving out of the way. Crannies and overhangs may also provide shelter from tephra fallout and obstacles may protect organisms in their lee even from the effects of pyroclastic flows. In 1883, Ketimbang village in Sumatra was devastated by pyroclastic flows traveling 40 km across the sea surface from Krakatau, whereas just a kilometer or so away, in the lee of the intervening island of Sebesi, there was no such damage.

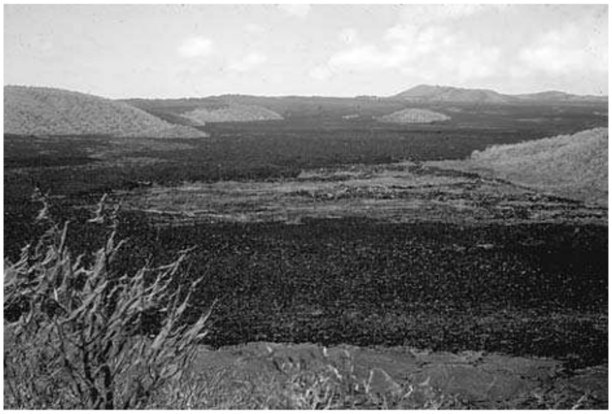

FIGURE 1 Kipukas, "islands" of vegetation not covered by lava, in Marchena Island's crater, Galapagos Islands, 1967.

Seed "banks" can survive in the soil under ash deposits, and plants have been grown from seeds covered for more than 60 years by 106 to 175 cm of Anak Krakatau ash. Had such seeds been exposed by erosion, germination would have been possible *in situ.* Whether seeds could remain viable under the very much deeper (30 m or more) and therefore more persistently hot layers resulting from cataclysmic eruptions such as those of Thera (Cyclades, Mediterranean), Krakatau, or Long Island (off New Guinea) is doubtful.

On Mount St. Helens at the end of the first growing season no vascular plants were found in regions that had been subjected to pyroclastic flows. In the blast zone, however, ferns, grasses, horsetails, rosette biennials, and other plants with underground stem tips survived extensively, but the only woody species surviving were those resprouting from basal buried portions of stems. Almost all survivors in upland habitats after the first year were perennials which had sprouted from underground plant parts present in the pre-eruption soil and penetrated the ash cover, or which were protected from the effects of the blast and associated ash deposits by packed snow. Snow also protects small organisms from desiccation and heat, and moistens and compacts tephra, making it less likely to abrade arthropod cuticle. A few plants of about 20 species survived the debris avalanche by regrowth from roots and suckers transported by the landslide, and lupins were shown to be capable of regrowth from root fragments 10 cm long.

Animals' lifestyles may also protect them. The Mount St. Helens eruption had no long-term impact on birds; they quickly returned to devastated areas except where trees had been killed. Many of the small mammals that survived the event are burrowing species, and in May

1980 they had the additional protection of snow cover. Even within a single guild, lifestyle may be of vital importance. Leaf-feeding caterpillars inevitably ingest ash lying on the surfaces of their food leaves, and those feeding on hairy leaves that retain ash suffered significantly greater mortality than those feeding on vegetation, such as grasses, from which ash tends to be shed. Time of day was also a factor on Mount St. Helens. Had the volcano erupted 6 hours earlier than 08:30, many animals would have been out of their burrows, exposed on the surface.

Aquatic insect larvae withstand the effects of accumulated ash on their exoskeleton well, the ash deposits quickly dissipating in water. Within 5 years of the Mount St. Helens eruption several fish and amphibian species that had become locally extinct had returned, and invertebrate faunas of even drastically disturbed streams had returned to 80% of their orginal diversity within 10 years. Amphibians proved to be surprisingly resilient, returning even to the pyroclastic zone, with some populations recovering quickly.

Recovery clearly varies between damage zones on the same volcano. On Mount St. Helens, 7 years after the eruption, 6 of the presumed 32 resident small mammal species had returned to the zones of pyroclastic and debris flow, 15 had reoccupied the areas of tree blowdown, and 22 were found in the area of tephra fall.

San Benedicto is an island of the Revillagigedos group, about 700 km from the Pacific coast of Mexico. Bayard Brattstrom reported that in 1952 it carried an oceanic biota; mammals, reptiles, amphibians, and freshwater fish were completely lacking and there was only one species of land bird (a rock wren). There were several species of seabirds and the island was almost completely covered in 11 species of grasses and low herbs. The only invertebrate that happened to have been recorded on the island was a land crab.

In August 1952, a highly explosive eruption on the island created Barcena volcano. Within a day the cone was 335 m high and activity continued until February 1953, when the whole island was covered in ash and pumice almost a meter deep, and no plants were visible. Some 20,000 seabirds perished. Six plant species survived by resprouting from surviving root stocks or germinating from buried seeds that were exposed by subsequent erosion. Three of these species became extinct but three others colonized the island. The rock wren survived only until December 1952, but after a slow start the seabirds recovered well, and there are now seven species. The land crab also survived.

Recovery need not be uniform over the whole volcano of course. On Anak Krakatau a successional mosaic was apparent by 1992. The developing communities on the three coastal ash forelands were not at the same stage of biological succession. The North Foreland, which from 1979 to 1989 was largely grassland (Figure 2), was rapidly changing to *Casuarina* woodland and lagged by about 17 years behind the East Foreland, where *Casuarina* woodland was already beginning the transition to mixed forest (Figures 3 to 5). The Northeast Foreshore was intermediate between the two. This mosaic appears to have resulted from differentially damaging eruptions in 1972 and 1973 and involved not only plants but also

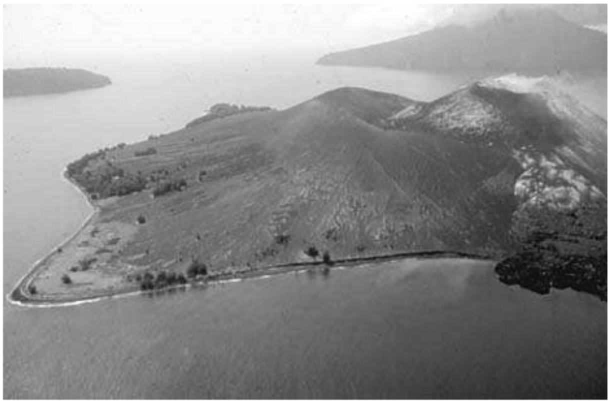

FIGURE 2 Anak Krakatau, 1985, from the north. The North Foreland, in the foreground, was largely grassland at this time, when the Northeast Foreshore and East Foreland (foreground of Figure 5) were *Casuarina* woodland. Rakata, Krakatau's remnant, is to the south of Anak Krakatau, and the southern tip of Panjang is seen to the east.

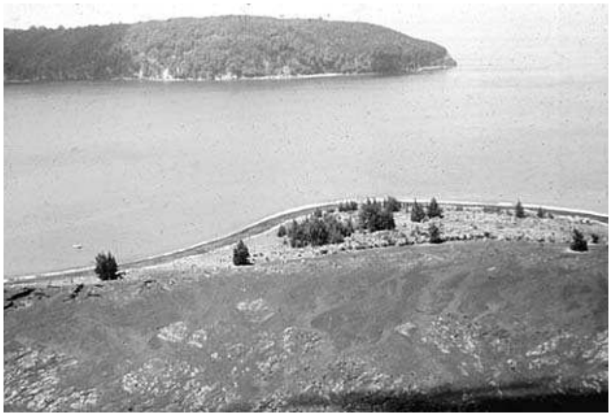

FIGURE 3 East Foreland of Anak Krakatau, with Panjang Island in the distance, in 1971. Cover of grass *Imperata cylindrica* and patches of the taller grass *Saccharum spontaneum,* with some *Casuarina equisetifolia* tress. (Photograph by Kyoji Yoda.)

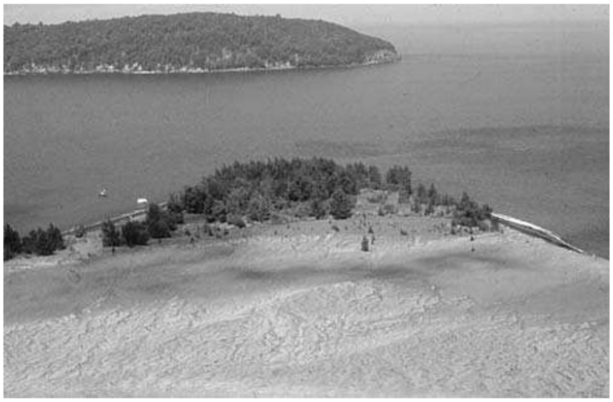

FIGURE 4 East Foreland of Anak Krakatau, with Panjang Island in the distance, in 1979. Note change of grassland to *Casuarina* woodland. (Photograph by Nigel Barker.)

birds, spiders, butterflies, tropical fruit flies, and invertebrate communities feeding on microepiphytes (algae, fungi, and lichens living on the bark and leaves) of the *Casuarina* trees.

On Anak Krakatau the species of resident land birds, mammals, reptiles, and butterflies that persisted after a 3-year episode of almost continuous strombolian/vulcanian activity in the 1990s were predominantly those that had been early colonists three times on the Krakataus after destructive eruptions. The fact that early colonizers tend also to be those that persist after disturbance may mean that they tolerate volcanic disturbance better than later colonists, or simply that they recolonize more rapidly after local extinction.

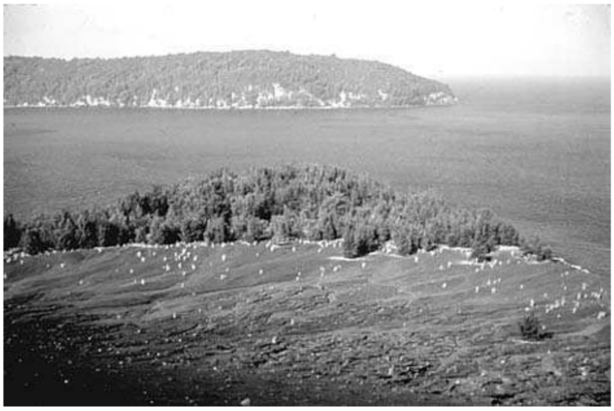

FIGURE 5 East Foreland of Anak Krakatau, with Panjang Island in the distance, in 1983. Note change of grassland to *Casuarina* woodland. By 1990 this woodland incorporated a number of other forest trees. (Photograph by Nigel Barker.)

II. PRIMARY COLONIZERS OF NEW VOLCANIC HABITATS

One of the central questions of ecology is the origin of communities. This comprises a number of subsidiary questions, one of which is how the primary plant and animal colonists become established on abiotic (nonliving) substrates. After an extirpating eruption, biologists have a rare opportunity to monitor the natural reassembly of a biota from the beginning. Systematic observations on the new, sterile habitats formed by lava flows and tephra deposits provide the framework for an attempt to answer the first of these questions: how pioneers become established in such forbidding environments.

A. Starter Nitrogen

Volcanic substrates are unweathered, without organic content to begin with, and often with poor availability of water and phosphorus. Nitrogen must come from a source other than the substrate itself. This may be (as at Paricutin) the ammonium chloride of fumaroles, but is more usually the atmosphere, via a number of possible intermediaries: rain water (if plant cover reduces wasteful runoff); photosynthetic bacteria known as cyanobacteria (and formerly as blue-green algae) that "fix" or incorporate atmospheric nitrogen into their living substance, converting it chemically into a form that they can use; plants (mostly legumes) that have symbiotic nitrogen-fixing bacteria in their root nodules; or water- or wind-borne organic material.

The first colonization of the barren surfaces by macroscopic organisms is often by animals arriving by air. Terrestrial arthropods, particularly ballooning spiders and small weakly flying or wingless insects, can be lifed into the air under certain atmospheric conditions and carried for considerable distances. Fallout of this arthropod component of the "aerial plankton" can be considerable and diverse: for example, in the Canaries, on deposits on the snowfields of Teneriffe's 3718-m-high volcano Pico Tiede, the Ashmoles found individuals of 37 families, 17 of them Diptera (flies), at densities reaching 18 individuals/m^2.

Such fallout is not restricted to volcanoes of course; it probably occurs on all mountains, but is most noticeable on those (including extinct volcanoes) which have barren upland areas, above the plant zone or covered with snow, ice, lava, or ash. On new volcanoes, however, the fallout often takes on a special significance, providing an input of organic resources, including nitrogen, from outside the barren area, which can serve as a basis for an important pioneer food chain. On the ash-covered lava flows of Anak Krakatau, in 10 days water traps set for arthropod fallout collected more than 70 species of arthropods representing 10 orders. Diptera and Hymenoptera (which comprises the ants, bees, and wasps) made up more than half the catch, and beetles were represented by 10 families. Aerial fallout onto the island was shown to be considerable; 20 individual arthropods were collected per square meter of trap surface per day and it was estimated that over the 10 days at least half a million arrived on the 2.34 km^2 of the island's surface. Many of these may have originated on the adjacent islands some 2 km away, but many others probably had traveled at least 44 km from the mainlands of Java and Sumatra.

On Mount St. Helens, aggregations of arthropod, spore, and seed fallout were thought to contribute to the fertility of the pyroclastic flow and tephra substrates and to facilitate the early development of micro-organisms and plants by providing nitrogen (and nutrients). John Edwards estimated conservatively that from 2 to 10 mg dry weight of fallout/m^2/day represented nonresident arthropod bodies, and in the summer the total organic (arthropod and plant) fallout was 5–15 mg dry weight/m^2/day. The nitrogen content of this deposit decreased by 25% within the first 17 days, then stayed fairly constant for the following 2 years. This longer-lasting nitrogen was presumably locked in the chitin and sclerotized protein of the arthropod cuticle, which remained more or less intact over the period. In contrast, phosphorus declined by 73% in the first 17 days, and by a total of 83% over the whole period. It was estimated that for the years 1983–1985 the mean net seasonal (150 days) input of nitrogen was 81.8 mg/m^2, and for phosphorus 5.5 mg/m^2.

Sprent noted that although, at its maximum, nitrogen fixation by bacteria could supply all the nitrogen necessary for the growth of some angiosperms, plants that have root nodules containing nitrogen-fixing bacteria are rare in early stages of primary succession. He thought that this was probably not because of difficulty in acquiring their symbiotic bacteria, but rather that their seeds, necessarily rich in starter nitrogen, are too heavy for rapid or long-distance dispersal. And in fact cyanobacteria, including forms that fix nitrogen, were the first colonists of Rakata (the remnant of Krakatau's explosive 1883 eruption), Surtsey (North Atlantic), La Soufrière, Paricutin, and Vesuvius since its 1944 eruption. In most cases these were probably wind dispersed, although on Surtsey they were found particularly in the splash zone. On La Soufrière (1456 m), where persistent cloud maintains hydration, they provided a substrate for nitrogen-fixing lichens, and their gelatinous substrate facilitated the colonization of ferns on Rakata, of mosses on Surtsey, and of lichens, mosses, and ferns on Paricutin. Both mosses and lichens obtain nitrogen from the activities of nitrogen-fixing cyanobacteria. Lichens appeared on 1944 Vesuvius lava after 10 years, but seed plants not until 14 years after the eruption, and most surfaces were still at the lichen stage in 1989. Even on Mount St. Helens, where legumes (lupins) were pioneers, their role was localized; their seed dispersal was poor and they did not spread. Here, nonsymbiotic mechanisms—rain and organic fallout—were the initial means of nitrogen supply and this atmospheric deposition rate was estimated as more than twice the rate for nitrogen fixation.

On Rakata wind-dispersed seed plants followed the fern phase. One of the important pioneers of ash on the Krakataus, the sea- and then wind-dispersed tree *Casuarina equisetifolia*, has root nodules that harbor nitrogen-fixing bacteria. Like the *Casuarina*, most of the 34 or so legumes (30 of them known to possess root nodules) which make up almost half the pioneer sea-dispersed group of plants in the Krakatau flora are strand or near coastal species. Although several (again like *Casuarina*) have spread inland, none occurs above about 100 m altitude. Schlesinger's research group estimated that the accumulation of organic nitrogen in the soil profiles of Rakata implies a minimum nitrogen input from twice to three times the atmospheric deposition rate reported in a forest of central Java. This of course suggests that much of the nitrogen in the Rakata soils must derive from biological fixation.

B. Pioneers Tapping Extrinsic Energy Sources

Energy usually enters a system as sunlight, passing through the photosynthetic pathways of green plants to animal herbivores and then carnivores, parasites, and scavengers. The general textbook sequence of colonization is plants, herbivores, and carnivores. In this context spiders have been regarded as exceptional carnivores; they arrive early because most have good dispersal as ballooning juveniles, and can survive on food carried to the area, like themselves, in the air. But they may not be so exceptional.

There is now a considerable body of evidence to show that in many instances the first organisms to colonize areas devastated by volcanic activity may not be primary producers. In the case of several volcanic areas the first colonists are carnivore-scavengers that are members of guilds which exploit organic input arriving either by sea as flotsam or as wind-borne organic fallout onto the new volcanic substrates. These guilds of secondary consumers may themselves form the base of a volcanic food web. The tapping of energy flowing through ecosystems outside the area, through the conduits of these guilds and (on volcanic islands) through land-based feeders on fish, sea snakes, crabs, and turtle eggs, short circuits the usual plant–herbivore–carnivore energy pathway and enables the establishment of some animals without the need for the prior establishment of plants.

1. *Exploitation of Organic Flotsam*

On volcanic islands, both vertebrates and invertebrates may exploit organic matter that arrives by floating on the water surface. A pair of ravens, *Corvus corax*, has been seen on Surtsey regularly from the second year after its emergence. These carrion-feeding omnivores exploit resources such as washed-up carcasses, in many cases those of marine organisms, that derive from outside the island. A pair of this species also nested at one of the Ashmoles' coastal sampling sites on Lanzarote in the Canaries, and Brattstrom noted that the same species was an occasional visitor to San Benedicto Island after the 1952–1953 eruption of Barcena (see above). A pair of large-billed crows (*Corvus macrorhynchus*) were early pioneer animals on Anak Krakatau.

Seabirds, the only vertebrates on Surtsey other than the raven, and the first to reside there, also derive their sustenance from the surrounding ocean, bringing their catch onto land to feed, and sometimes feeding on carcasses washed ashore.

Very few of the arthropod species that arrived early on Surtsey by air (see below) became established, but within 6 months of the island's emergence in 1963 a strand community dependent on washed-up flotsam such as bird carcasses, algae, or logs had become established. Flies were one such group, but without carrion they became extinct. By 1975 only three terrestrial invertebrates were thought to have become established, a fly, a midge, and a collembolan, all of them inhabiting washed-up carcasses.

In contrast, within 6 months of Anak Krakatau's emergence from the sea in 1930 a pioneer community consisting of representatives of three families of beetles, large numbers of collembolans (springtails), and chloropid flies was exploiting sea-borne organic debris. Shore birds and kingfishers, which feed on crabs, fish eagles, which feed on sea snakes as well as fish, and the large monitor, *Varanus salvator*, whose food includes organic flotsam, carcasses, crabs, and eggs of the green turtle, have together also acted as food web links through which marine resources entered the land system.

On Motmot, an emergent volcanic island in the large freshwater caldera lake of Long Island, off New Guinea, a primary succession began in the 1960s with a strand fauna again depending directly or indirectly on the input of organic material from outside the island. Ants and bugs among vegetation around Motmot's pond and rove beetles and springtails beneath a hardened algal crust at the pond margins had all arrived within about 4 years.

2. *Exploiters of Organic Airborne Fallout*

Not all volcanic substrates are surrounded by water of course. Another conduit of extrinsic energy (i. e., energy deriving from outside the island system) was discovered when the barren ash/lava areas of a number of volcanoes were carefully investigated. The organic airborne fallout which was noted above as being a source of nitrogen provides a resource base for a guild of consumers (carnivores and scavengers), enabling them to become established on the otherwise barren ash and lava fields, free from the competition that would occur in more complex habitats.

Traps set on Anak Krakatau's barren ash, but not those set near vegetated areas, captured representatives of a guild of scavenger-predators including wolf spiders, earwigs, ants, a mantis, and numbers of a crepuscular flightless cricket. Feeding in turn on these on the ground was a guild of tertiary consumers which included two migrant birds, the common sandpiper and grey wagtail. Aerial predators—two or three species of dragonfly, two swiftlet species, a swift, and a swallow—took some of the fallout before it settled. They, in turn, were preyed upon by the oriental hobby and perhaps also by the peregrine falcon when this replaced the hobby.

This aeolian-based community is the ecological analogue of communities found on other volcanic areas such as Mount Etna, the Canary Islands, and Mount St. Helens, and, in particular, on lava fields on the island of Hawaii. In the alpine zone near the 4205-m summit of Mauna Kea on Hawaii, Frank Howarth had found an unusual, long-legged, flightless lygaeid bug, *Nysius wekiuicola*, and on the heights of Haleakala (3055 m) on the island of Maui a strange flightless moth, *Thyrocopa apatela*. On both islands lycosids (wolf spiders) were also present. Hawaiian species of *Nysius* are seed-feeders, but the Mauna Kea species is unusual in being a scavenger and predator, presumably having evolved the scavenging/carnivorous habit as an adaptation to the barren habitat. The larvae of the Haleakala moth make silken web traps under stones and feed on wind-borne debris, mostly fragments of the dead leaves of *Dubautia menziesi*, an endemic alpine shrub. On bare lava fields of the Kilauea volcano on Hawaii (but, as on Anak Krakatau, not in adjacent vegetated areas) the fallout-exploiting community comprised a wolf spider, an earwig, a mantis, and, dominating this guild, a nocturnal flightless cricket of the same subfamily as that occurring on Anak Krakatau. The parallel between this community and that later found on Anak Krakatau is remarkable.

On the Canaries, an earwig, two species of Thysanura ("silverfish" relatives), and a cricket are important scavenging/predaceous pioneers both on the surface and in subsurface cavities. Some members of this guild exploit fallout on the surface by night and take refuge during the day in deep cracks and subterranean spaces. In the course of succession this lavicolous (i. e., inhabiting lava) community is replaced by more specialized communities above and below ground. A guild of tertiary consumers, feeding on the fallout exploiters, includes pipits and lizards.

On Anak Krakatau, Hawaii, and the Canaries, the scavenging/predaceous guild is present on new lava flows or areas of recent ashfall, where there is little or no primary productivity. It is absent or poorly represented in areas where productivity is provided by macroscopic terrestrial plants.

Organic fallout derived from outside the area was also shown to be an important source of nutrients in the recolonization of Mount St. Helens (see above), and here the resident pioneer predator and scavenger guilds included ground beetles, darkling beetles, spiders, and neuropterans. The first successful colonists of the blast zone were three ground beetle species of a genus that is generally restricted to disturbed, barren habitats, and whose species are specialist, necessarily transient, pioneer colonists. Within the first two summers 43 species of spiders had ballooned in from lowland areas. However, only 19 species of arthropods showed evidence of breeding within the first 3 years, including 11 predaceous ground beetles and representatives of three families of scavenging beetles. In the first 5 years more than 30 ground beetle and 125 spider species (mostly lycosids) had arrived in the blast zone, making up about a quarter of the fallout fauna and contributing about 100 individuals per square meter per year. On the surface of pyroclastic flow deposits, populations of 6 spider species were established by 1986. Other colonizing insects included neuropterans, and in later years hemipteran bugs [lygaeids and saldids ("shore bugs")], orthopterans (gryllacridids, a cricket-like family), and members of the Grylloblattodea (an order of small, soft-bodied, apterous, cryptozoic insects evidently confined to cold, damp situations) made their appearance. For all of these the fallout was shown to be an important source of nutrients; for example, ground beetles were frequently seen with aphids or nematoceran flies in their mouthparts, particularly at night. Crows (*Corvus* species) were also significant consumers of fallout during the day.

Such aeolian (wind-dependent) communities appear to be characteristic of, and may have evolved in, areas with a long history of sustained volcanic activity. Howarth suggested that the entire aeolian community is a special subset of a more extensive guild of arthropods living below the surface of lava flows and dependent on input of organic material to the network of caves and interstices. For example, most species of the Hawaiian endemic cricket genus *Caconemobius* are rock dwellers on cliffs, lava flows, and lava caves, and Howarth believed *Caconemobius fori*, the exploiter of organic airborne fallout, to be closely related to a cave-dwelling species.

On Surtsey, an island of about the same height and size as Anak Krakatau but more isolated and in a much harsher environment, colonization by airborne pioneer animals has been slow. Spiders of the family Linyphiidae, which includes the "tent spiders," were seen alighting on the lava, and flies were the most diverse group of the island's early fauna. However, 7 years after the island's emergence there were still only three species of beetles.

On Motmot, wolf spiders were seen in inland high dry areas in 1969, "when, in spite of a careful search, no other life was found there," and Ball and Glucksman believed that a major part of the spiders' diet may have been fallout of aerial plankton sucked in following updraughts caused by differential heating of the island's surface and the surrounding lake. Damsel flies, dragonflies, and Pacific swallows may have exploited the aerial plankton before it reached the ground; all were present at the first survey, in 1969, and the swallow nested on Motmot in 1971.

C. Colonists of Primary Volcanic Substrates

Erosion of the purely mineral, infertile substrates that are the first provided by volcanic activity is rapid and unimpeded, and water retention very poor. Primary colonists of such dry, unsheltered, unconsolidated substrates must not only have good dispersal powers but also the ability to survive and grow in this forbidding habitat, among the most inhospitable of Earth's environments.

Although bacteria, algae, lichens, mosses, and ferns are often the first pioneers, in many cases it is seed plants that are the primary colonizers. They are often long-lived, perennials, or slowly growing woody shrubs or trees with light seeds that are wind dispersed. For example, on Vesuvius after the 1944 eruption, the first colonizers in the primary succession on coarse scoria were woody species; annuals were unimportant. Also on Anak Krakatau, Mount St. Helens, Motmot, Hawaii, Galapagos, and Usu and Sakurajima in Japan, seed plants were among the pioneer colonists. The success of all primary colonists depends on their growth form and growth rate being appropriate to the substrate's supply of water and minerals. In contrast, secondary pioneers, which in many volcanic situations follow the primary colonists, generally have high growth rate.

1. *Colonists of Lava Flows*

As noted above, on many newly formed barren volcanic areas biological aerial fallout is the most important resource for animals. New lava flows are of course completely devoid of even the rudiments of soil, and their surfaces are fully exposed to the elements and subjected to temperature extremes. Yet where there is enough moisture, micro-organisms, mosses, and lichens colonize them. Temperature, humidity, nature of the substrate, and nature and size of the reservoir of potential colonists all determine the primary succession, which thus varies according to different primary situations.

On Lanzarote in the Canaries, lava flows were colonized primarily by lichens and mosses provided they were not far from kipukas and not within 2 km of the sea. In contrast to Surtsey, for example, on the dry Lanzarote lava significant populations of heterotrophic bacteria (that take in nutrients from external sources rather than photosynthesizing them) were recorded and the Ashmoles' group believed that input of marine bacteria is important in order to maintain the lava ecosystem close to the sea.

New lava flows on the Icelandic mainland, particularly those at high altitude, are colonized first by lichens, as those on the Canaries, yet although Surtsey was searched carefully for lichens each summer since its 1963 emergence, the first lichen was found on its lava only in 1970. Three years later there were 12 species, 4 of which were thought to have been dispersed by wind, and 1 by seabirds. On Rakata (where the volcanic substrate was ash) lichens were also unimportant but the buildup of bryophyte species was much slower than on Surtsey's lava and ash, which after 9 years supported 68 moss and 4 liverwort species. Although 2 moss species were present on Rakata in 1886, 3 years after the eruption, no more had been found by 1906. By 1922 there were 18, but the bryophyte flora did not achieve the diversity of Surtsey's remarkable 9-year-old flora until some time between 1933 and 1979 (50–96 years after the eruption); 32 moss and 37 liverwort species were recorded in 1983.

On the Galapagos, as well as lichens, primary pioneers are cereoid cactuses of the genus *Brachycereus* (Figure 6; see also color insert), and on the Hawaiian Islands lichens predominate where it is relatively dry, but ferns and flowering plants can get in first in very wet areas. Indeed, the tree *Metrosideros* is capable of becoming established on new Hawaiian lava flows and forming a forest.

2. *Colonists of Tephra Deposits*

Mazzoleni and Ricciardi noted that after the 1944 eruption of Vesuvius, colonization of scoria was much faster than that of lava. This observation was supported by Galapagos work; Hendrix and Smith found that Fernandina lava flows mostly remained barren for more than 100 years, whereas tephra on Fernandina's rim was revegetated after less than 10 years. In general, tephra deposits are colonized much more quickly than lava flows.

Del Moral and Bliss stressed that the nature and localization of microsites (a microsite is the place at which an individual plant grows) may affect colonization success in the harsh environments immediately after catastrophic eruptions. On Fernandina, for example, major sites of colonization were water runoff channels and

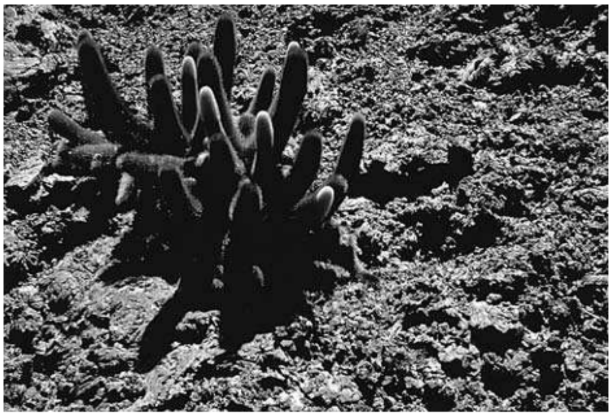

FIGURE 6 A colony of *Brachycereus nesioticus* on a lava flow on Santiago Island, Galapagos. (See also color insert.)

collapsed land iguana burrows. The effect of microsite patterns, however, is complex. On Mount St. Helens the presence of a colonizing plant species in the early stage of primary succession depends in a complex way on interaction between the seed-trapping ability of the microsite, the density and composition of the seed rain, and the ability of the species to become established under the conditions obtaining there. Plant establishment and growth were monitored in two seasons both in seeds planted at different naturally occurring microsites and in seeds naturally dispersed into different artificially constructed microsites. The microsites at which most seeds arrived naturally were not those at which there was peak establishment and seedling growth. Moreover, microsites with the highest establishment rate of seedlings when artificially seeded did not have the seedlings with greatest growth. Further, microsite colonization patterns changed from year to year, as climatic differences presumably affected the amelioration of microsites and the amount of seed "rain" coming to them.

On Anak Krakatau's tephra deposits, grasses, including *Ischaemum muticum*, *Imperata cylindrica*, and *Saccharum spontaneum* (a wild relative of sugarcane) (Figure 7; see also color insert), are also found inland of the beach, and on new substrates the tree *Casuarina equisetifolia* is a pioneer species. The sea-dispersed primary colonizers of the Krakataus' black sand beaches, the creepers *Ipomoea pes-caprae* and *Canavalia rosea* (a legume), were both found covering bare ash some distance from the sea on Anak Krakatau. They were also primary colonists of Volcano Island in the crater of Taal volcano, where they were found some distance from the shore. Brattstrom noted that colonization of San Benedicto Island would be slow because of lack of rainfall and slow soil formation, but the *Ipomoea* species was the first immigrant to become re-established on Barcena volcano there.

III. BIOTIC REASSEMBLY

Most cases of the recovery of biotas following natural extirpation occurred too long ago for the predevastation biota and stages of recovery to be known. One of the many problems besetting studies of these cases is that destruction may have been incomplete, as on Taal and Barcena, and its extent often only imprecisely known, as on Thera, so that the base from which recovery proceeded can only be guessed. Sometimes insight can be gained by assuming that the pre-eruption biota was similar to the existing biota of similar but unaffected islands in the same area, if such "control" islands exist. A comparison between these biotas and the reassembled biota of the affected island may provide a fairly rough and ready estimate of the extent of recovery. One such case is Long Island, 50 km north of New Guinea.

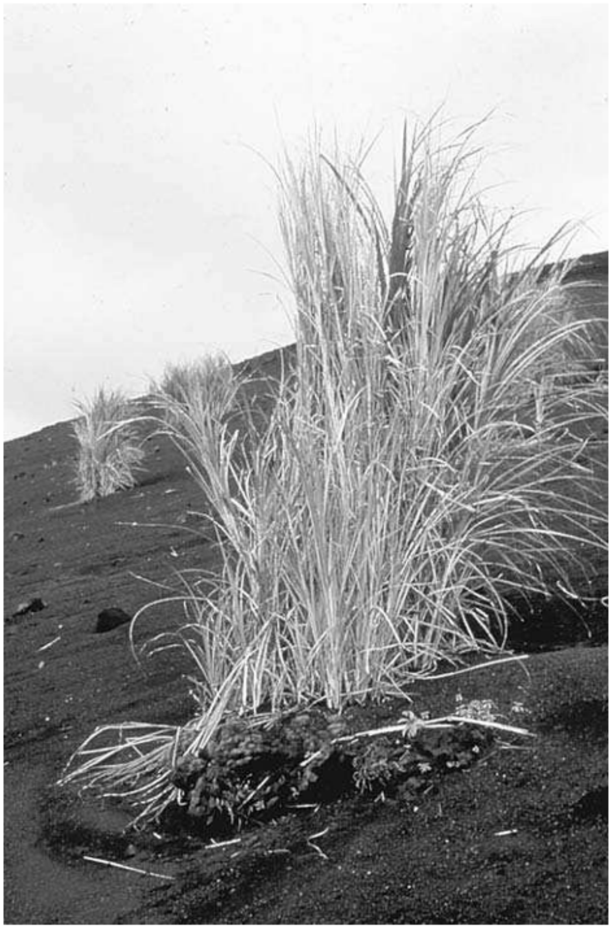

FIGURE 7 A clump of so-called wild sugarcane (*Saccharum spontaneum*) growing on the ash slopes of Anak Krakatau, 1992. [Photograph by David Walsh.] (See also color inserts.)

A. Long Island

Some time around the middle of the 17th century an explosive eruption occurred on Long which was later estimated to have been several times larger than that of Mount St. Helens and about the size of that of Krakatau. The layer of hot ash deposited on its forested surface was 30 m or more thick, resulting in completely carbonized trees and destroying most or all life.

Long's present rainforest flora has not been studied in the context of recolonization but Jared Diamond described the lowland vegetation 3 decades ago as an arrested subclimax which probably has not yet returned to its former composition, and the description is still appropriate. Diamond noted that the trees are either sea-dispersed (e.g., *Terminalia catappa* and *Barringtonia asiatica*, both also present on the Krakataus) or bird- or bat-dispersed (e.g., species of *Ficus*, *Canarium*, and *Eugenia*). Around the rim of the 13-km-diameter caldera the forest is fairly open, and although a few very large old banyan figs and other trees might date from immediately after the eruption, most trees are clearly much younger. Recovery may have been constrained by the porous substrate and lack of streams, as Diamond suggested, as well as intermittent ashfall (not all subsequent eruptions may have been recorded). In the clouds above 700 m on the two higher mountains the forest evidently recovered more quickly and is already structurally mature. The island now has c. 50 species of land birds, from 9 to 12 reptiles [a crocodile, monitor, snake (the Pacific tree boa), two geckos, and several skinks], six bats (one insectivorous bat, two fruit bats, and three long-tongued nectar bats), and the Pacific rat. The cuscus (a loris-like arboreal marsupial) is common and probably introduced by humans.

In 1888 another event occurred on the island of Ritter, about 100 km east of Long. About 2 km^3 of the island disappeared in a massive collapse which left only about 5% of the island's bulk and a submerged caldera 2.5 km in diameter. Large tsunamis triggered by this event wiped out coastal villages within a radius of 112 km, causing many casualties and eradicating the fauna of several coral islets in the vicinity. It is very likely that all life on Ritter was destroyed. The island remnant's eastern slopes are now covered in scrub and grass.

Diamond studied the Long and Ritter cases, comparing their bird faunas and those of coral islets from which birds had been exterminated with those of islands whose bird faunas had been unaffected by the eruptions or tsunamis. On the devastated coral islets bird species numbers quickly returned to equilibrium. By the 1970s the avifaunas on Ritter and the lowlands of Long had also reached equilibria but species numbers were less than those of unaffected islands of their size, in spite of the fact that the latter are low and so may be expected to carry a smaller fauna. After almost 3 centuries Long had recovered three-quarters of its expected number of species but it gained few if any between 1933 and 1972. Diamond attributed the relative poverty of the new avifaunas on Long and Ritter to the fact that their lowland forest habitats were still at an immature developmental stage. However, although Long's montane forest had recovered more quickly, bird species numbers were low there also, and Diamond concluded that montane bird species generally had poorer dispersal powers than lowland species. Ball has suggested to me an alternative explanation: Long's forests may have returned to a climax and the biotic poverty may reflect the fact that, apart from the two isolated peaks, the island is relatively dry.

B. The 1883 Krakatau Islands

From ships' reports we know that before the 1883 eruption the Krakatau Islands were clothed in forest, although only about half a dozen plant species are identifiable from various reports and sketches. Two-thirds of the island of Krakatau disappeared in the explosive eruption, and its remnant, Rakata, and the two adjacent islands, Sertung and Panjang, were covered in hot ash to depths of more than 30 m (Figure 8).

The first living thing to be found on the islands, 9 months after the eruption, was a spider. Sea-dispersed plants were among the first to colonize, forming an association of creeping beach plants and a coastal forest of small trees and shrubs just inland of the shore. Pioneers of the inland areas were wind-borne plants able to survive in full sun (heliophilous) and with little water. The plant colonists of the first 3 years comprised only such water- and wind-borne pioneers, most of which were hermaphrodites (with male and female organs in the same flower) (Table III).

On the inland slopes of Rakata (Krakatau's remnant),

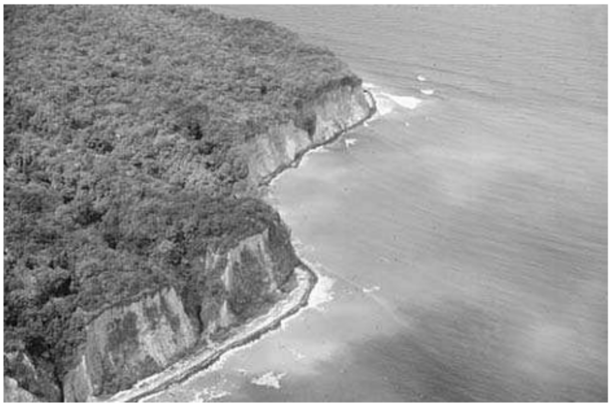

FIGURE 8 The west coast of Sertung, Krakatau Islands. The cliffs are composed of tuff from the 1883 eruption of Krakatau, which enlarged Sertung considerably. (Photograph by David Walsh.)

the microclimatic and soil conditions were modified by the heliophilous fern cover which followed the cyanobacteria. The fern cover was succeeded by wind-dispersed flowering plants such as grasses and orchids, capable of growing in open sun. In contrast, in the later development of forest, dispersal by birds and bats was a major factor; only one important forest tree on the islands is wind-dispersed.

The early coastal pioneers included some fruit-bearing, small-seeded small trees and shrubs, which are diplochorous, that is, have two means of dispersal—the sea surface and fruit-eating bats and birds—and could have made their first landfall by sea. Flying frugivores may have been first attracted to the islands by the presence of these pioneer fruiting trees, and it is not surprising that facultative frugivores (generalist fruit-eating birds that are capable of surviving on seeds and/or insects, without fruit) predominated on the fairly open, unforested islands in the early years after the eruption. It was these early facultative frugivores that were responsible for extending the range of the pioneer fruit-bearing trees inland.

Some of the early-arriving facultative fruit eaters, like the black-naped oriole, were certainly capable of bringing seeds of fruit-bearing trees, such as several heliophilous pioneer fig tree species, from the rich sources of the Javan or Sumatran mainlands some 44 km distant. Four such fig species were established and fruiting within 14 years of 1883. Once figs were established in numbers, their fairly constant supply of fruit would permit obligate frugivores (which feed only on fruit) to colonize, including larger fruit bats and some of the doves and pigeons that are extremely effective seed dispersers. These wide-ranging animals were largely responsible for bringing important forest canopy trees (almost all the Krakataus' canopy trees are bird- or bat-dispersed) from the rich sources on Java and Sumatra, and thus instigating an important ecological change on the islands (forest formation and canopy closure) which affected all future colonization. Small dog-faced fruit bats probably assisted the spread of fruit-bearing trees throughout the archipelago and Louise Shilton has recently shown that they could have brought some of the fig species to the islands.

In the calmer, cooler, shaded, more humid, mesic environment of the forest, many of the heliophilous pioneer species persisted, but with the changed role of gap fillers. Now a second wave of wind-dispersed plants, shade-loving forest dwellers, mainly ferns and orchids, were able to become established. Also, with the change to forest conditions several animal species, such as grass-feeding skipper butterflies, sphecid wasps, and ground-living beetles that prefer dry to moist surface conditions, and open-country birds and reptiles, became extinct, and forest animals began to colonize.

Sea-dispersed species colonized all the Krakatau islands and reached an equilibrium number of species fairly quickly (Table III). Zoochorous species made up 14% of plants arriving between 1887 and 1897 (6 being present in 1896), 35% of those arriving between 1898 and 1908 (23 were established by 1905), and, considering only nonhuman dispersal, 40% of those arriving later. Although the animal-dispersed group of plants were in general the last to colonize, they are the group that has increased most markedly in the past 6 or 7 decades.

The Krakataus' biota is disharmonic, that is, some groups are underrepresented or absent compared to the mainland biota, and others are overrepresented. Some absences clearly are the result of the sea barrier of 13–44 km. Birds with weak powers of flight are lacking, as are terrestrial mammals other than rats, and thus so too are many trees that have seeds dispersed by terrestrial forest mammals. Plant species with fairly heavy, wind-scattered seeds are also poorly represented. In other cases the barrier is ecological—the plant succession on the islands may be either too young or too mature to provide optimal habitat for a given species. For example, the lack of old mature trees with hollows suitable as nesting sites precludes the establishment of hornbills. Or a particularly crucial plant species may be missing; thus the lack of bamboos means that bamboo bats, for example, which have very restricted roosting preferences, would have difficulty in becoming established. These barrier effects of course mean that some groups, such as pteridophytes, which have very effective spore-based dispersal, are unusually well represented.

Animals like the monitor and reticulated python probably arrived on the recovering archipelago by swimming or floating on the sea surface, while others like the paradise tree snake, blind snake, two gecko species, and a skink are more likely to have rafted on natural vegetation, and such rafts do make landfalls on the islands quite frequently (Figure 9). Termites are weak fliers and the fact that all seven species on the islands are wood or tree nesters, although over a third of the mainland's termite fauna nest in or on soil, supports the view that the Krakatau termites arrived by rafting (Table I).

Although the islands are uninhabited, four gecko species, a skink, two rat species, and a number of insects and grasses are thought to have arrived adventitiously through the sporadic visits of fishermen, scientists, and tourists.

Flight is an obvious mode of arrival for many winged insects and for birds and bats, and yet not all those

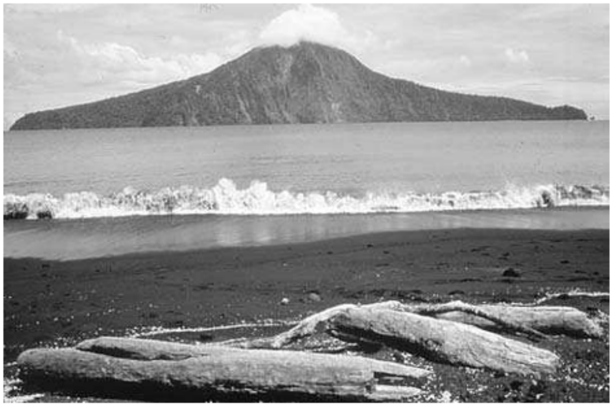

FIGURE 9 Washed-up logs on Anak Krakatau's black sand beach, 1984. Such logs may act as rafts for a number of animal species. Rakata, Krakatau's remnant, is in the background. (Photograph by David Walsh.)

capable of the journey have reached the islands, and not all those that regularly arrive have colonized. Behavioral limitations sometimes preclude colonization. Thus many birds are philopatric, that is, they do not normally fly far from their home range or territory and are thus unlikely to reach the islands, and most social bees and wasps cannot maintain their swarms over long distances and few such species have colonized. There are also ecological constraints. Lack of substantial bodies of freshwater precluded the establishment of five families of aquatic birds present in the source area of Java, and of any of the dozen or so dragonfly species that regularly visit the Krakataus.

Successful animal colonists are, in general, species with wide distributions and broad ecological tolerance. For example, some 75% of the archipelago's present land birds are inhabitants of urban or garden areas and other disturbed habitats in southeast Asia, and the bat fauna comprises widespread species that do not have specialized roosting requirements and can tolerate disturbed habitat fairly well. Many of the insect colonists, such as bark lice, butterflies, and chloropid flies, are exploiters of ephemeral, temporary habitats or those associated with disturbed forest.

In several cases colonization is dependent on the prior establishment of other species; in a simple example, tree-nesting birds colonize after the establishment of trees. Although some animals, such as the monitor, are able to colonize very early by exploiting energy derived from outside the islands (in the form of shore crabs or turtle eggs), others require the prior establishment of their food source. Insect herbivores can survive only if their food plants are present and many have narrow food ranges, some being restricted to a single plant species. Some highly vagile butterfly species that are known to have reached the islands have not colonized; their food-plant families are absent. Similarly, parasites must have appropriate hosts. The poor early representation of braconid parasites, for example, was probably because of the poor representation of their insect hosts, which in turn may have been the result of the late appearance of the appropriate phase in the plant succession. The koel, a nest parasite of other birds, did not colonize until after its hosts, the large-billed crow and black-naped oriole, were established. More generally, predators tended to become established late in the process, when appropriate prey was available. The carnivorous gecko, *Gekko gecko* and the lizard- and bat-eating Malay false vampire bat, as well as the serpent eagle, changeable hawk-eagle, Oriental hobby, peregrine falcon, and barn owl, were all relatively late colonists (Figure 10; see also color insert).

TABLE I Distribution of Termite Species by Lifestyle on Java and Sumatra and on the Krakataus

	H	*S*	*Trees S*	*Soil*	*?*	*Total*
Species on Java/Sumatra	6	6	7	5	0	24
Species on the Krakataus	5	2	1	0	1	9

Note. In comparison with the mainlands, the Krakatau termite fauna is characterized by the paucity of softwood termites [i.e., those which feed on soft wet wood and nest in the same environment (S) or in the dead part of the trunks of living trees (trees S)], the absence of soil nesters (soil), and the preponderance of hardwood termites (H), which feed and nest in hard, dry wood. [Following Yamane, Seiki, Abe, T., and Yukawa, J. (1992). Recolonization of the Krakataus by Hymenoptera and Isoptera. *GeoJournal* **28**(2), 213–218.]

IV. THE ASSEMBLY OF NEW BIOTAS ON EMERGENT VOLCANIC ISLANDS

Although the above cases of reassembly of biotas involve islands, one cannot always be absolutely sure that the reappearing biota is the result of immigration and not survival. For example, it is not known whether any plants or animals survived Long's eruption, and although there is very little likelihood of survivors of the 1883 Krakatau eruption the possibility cannot be entirely ruled out. There is one situation, however, in which there can be no doubt that newly assembling communities of land

FIGURE 10 A juvenile Galapagos hawk on an aa lava flow, Fernandina Island, Galapagos. Avian raptors are often late colonists of volcanic islands. (See also color insert.)

organisms comprise only new colonists. This is where a volcano has emerged from the sea or from freshwater as a pristine substrate, devoid of land life; there could have been no survivors for there was no previous biota. Such cases are few and some have attracted the attention of biologists. The best known biologically are Surtsey, Motmot, and Anak Krakatau. Because these are cases of assembly of island communities *de novo*, with no possibility of recovery from surviving foci, and in all cases there has been little impact from humans, they provide rare information on dispersal as well as on the assembly of biotic components.

A. Surtsey

The island of Surtsey emerged in November 1963 from the submarine North Atlantic ridge some 20 km southwest of Heimaey, largest of the Westman Islands and itself about 15 km south of Iceland. Surtsey's phreatic, explosive phase of activity lasted until April 1964, when the vent became sealed from the sea and lava flows began. This second, effusive phase ended in May 1965 but activity was resumed in 1966, producing less extensive flows. Since 1987 there has been no eruption and the island has been shrinking through erosion; it now covers 2.7 km^2 and is 152 m high. It is our very good fortune that biological colonization has been monitored meticulously from the start by a group of mostly Icelandic biologists led by Sturla Fridriksson, in one of the most important long-term ecological studies of the century.

Fridriksson and his team showed that objects could float to Surtsey from Heimaey in 2.5 days under favorable conditions of wind and currents, and that seeds of three coastal and three alpine plants of mainland Iceland remain viable after varying periods of immersion in seawater. Two of the coastal species tested had been found on Surtsey in beach drift only 6 months after the island's emergence; one, the sea rocket, *Cakile edentula*, was the first plant to grow on Surtsey, in 1965; the other, mayweed, *Matricaria maritima*, became established in 1972.

Between 1964 and 1972 seeds and other diaspores (plant parts that are dispersed and have the potential to produce new plants) of 38 species of vascular plants were found on Surtsey's shores; all grow in Iceland and 31 occur on Heimaey, but the 21 that grow on the Westman islands nearest to Surtsey were the most abundant. Only 6 months after Surtsey's emergence leaves and stems of lyme grass (*Leymas arenarius*) and a rush were found in beach drift, and seeds of the sea rocket, lyme grass, and *Angelica archangelica* were collected. Whole green plants of mayweed and *Sedum rosea* were found on the shore, and a mayweed plant was potted and kept alive for some time. In May 1969 mermaid's purses (the empty, chitinous egg capsules of the ray *Raja batis*) drifted ashore, and on their rough outer surfaces were seeds of 4 grass species which are common in mainland Iceland and occur on Heimaey; only 1 of them, lyme grass, is found growing on the smaller Westman islands close to Surtsey. Overall, Fridriksson believed that 3 vascular plant species probably could have arrived on Surtsey by sea from a small islet 5 km away, 2 from islets 10 km distant, and 7 from Heimaey, including the two important pioneers, lyme grass and sea sandwort, *Honkenya peploides*.

Waterborne dispersal was important in Surtsey's animal colonization also. There is good circumstantial evidence that a mite, a weevil, three species of shore flies, and a parasitic wasp of one of the flies all rafted, probably from Heimay. Grass tussocks washed ashore in 1972 and 1974 together harbored some 700 living invertebrates, largely mites and springtails. The nature of the grit and the proportions of pollen in the 1974 tussock suggested that it came from bird cliffs on the Westman Islands.

The spores of ferns, mosses, and lichens were carried from Heimaey or Iceland's mainland in the air, and the mosses were very important ecologically (see above). All the insects found on Surtsey by 1970 were winged and included a moth, *Autographa gamma*, which migrates from Europe and is not native to Iceland. Some 77 species of flies are thought to have arrived by flight assisted by wind, and in 1966 a linyphiid spider arrived, evidently by ballooning. Springtails are wingless but some salt-intolerant species were found in moss quite far inland, suggesting the possibility of aerial dispersal also for these small flightless arthropods.

Ravens almost certainly brought in seeds of the thrift, or sea pink, *Armeria maritima*, which was found flowering in 1986 at a place where they had attempted to nest. But it is seabirds which have been of greatest importance in the colonization of Surtsey. Their excreta, dead chicks, and eggs provide minerals and organic matter, fertilizing the soil in the area of their colonies. The fulmar and black guillemot have bred regularly since 1970 and the number of vascular plant species on the island rose sharply between 1971 and 1972. By 1993, six seabird species were nesting each year and there were 30 species of plants. Almost half the plant species were restricted to bird roosting and breeding sites, and 10 to seabird colonies. Since herring gulls started to form a colony in 1985 there has been a great increase in the number of plant species; the gull carried plant material from islands of the Westman group to its nesting ground on Surtsey and fertilized the area heavily. There are now 22 plant species in the gull area, 18 of which have arrived since colonies were established. Colonization and spread of the low-growing perennial ground creeper *Sagina procumbens* have been rapid since 1985 and it is now the main pioneer of laval areas both within and outside the gull colony. Three small crowberry bushes (*Empetrum nigrum*) were found in 1993 on lava in the gull nesting ground; gulls, probably herring gulls, may have taken berries on Heimaey or, more likely, on the mainland of Iceland, 30 km away.

Within 12 years of Surtsey's emergence 60 species of migratory birds had been recorded and some were almost certainly involved in plant dispersal. In studies in 1967 and 1968 the only arriving migrants found to be carrying seeds in their gut were snow buntings of a subspecies that migrates from the British Isles to Greenland via Iceland. The seeds were of eight species, mostly common in Iceland and the British Isles, but some absent from or rare in Iceland. In a fine detective study Fridriksson's group found that the minerals in the birds' gizzards were of a type that must have been acquired outside Iceland along with the seeds, most likely in the highlands of Scotland. Thus seeds of several species of vascular plants were brought in the gizzards of snow buntings from either the mainland of Iceland or the British Isles, probably the latter. Seeds of two species had retained their viability.

Borgthor Magnússon and his colleagues have listed a total of 44 species of vascular plants that have been recorded from Surtsey, with 35 persisting to the summer of 1995. Most of the 20 plant colonists in the first two decades were species of coastal, sandy habitats, probably dispersed by sea or birds. Fridriksson noted that although viable seeds were collected on Surtsey's shores during the first summer (1964), higher plants were not found growing until the second summer. The sea rocket, an annual, was found in 6 of the years from 1965 to 1973, and the nearest colony of sea rockets is on Heimaey. In the summer of 1966 seedlings of lyme grass were found at the high-tide mark but were destroyed by waves after a few weeks. In 1967 the sea sandwort and the lungwort, *Mertensia maritima*, were found, together with lyme grass and sea rocket. In 1969 a fifth higher plant species, scurvy grass, *Cochlearia officinalis*, had arrived, the location (bird droppings near rainwater barrels) showing that birds had been involved. In 1970 the common chickweed, *Stellaria media*, was found among pieces of egg shells, feathers, and bird droppings, and in 1971 the bladder fern, *Cystopteris fragilis*, was found in a lava cave.

As might be expected, colonization by vascular plants has been slow. Away from the bird colonies, infertile areas of lava and tephra had been colonized by 1973 by only 10 species of perennial herbs with extensive roots, such as lyme grass, lungwort, and sea sandwort, the most widely dispersed and successful plant colonist. Even by 1992 there were only 30 species, about one successful colonist per year, and the first woody plant, the crowberry, was not found until 1993. Three more new immigrants, a rush, a willow, and a *Galium* species, were recorded in 1995 in the gull colony, although establishment has not yet been reported.

Six months after Surtsey's emergence a fly was collected on the shore and in the next summer more flies and midges, two species of moth, and a mite were found. In 1966, when regular collecting began, 22 species of insects and four arachnids were recorded. The number of species increased annually, until by 1970, 158 species had arrived, almost a fifth of the Icelandic fauna. Although Heimaey was the likely source of most arrivals, some must have originated on the mainland of Iceland 35 km distant, and others, active fliers like some moths, from Europe. Only 2 or 3 species, however, had become established, and all these were carrion feeders. By 1981, 41 species of arthropods other than springtails were present, comprising an aphid (on the sea sandwort plants), a *Plutella* moth, a ground beetle and two staphylinids (rove beetles), five linyphiid spiders, two mites, an enchytraeid oligochaete, worm, and 28 species of fly representing 15 families.

B. Motmot

Between 1953 and 1955 intermittent volcanic activity of a type that is now known as Surtseyan was reported at a point in Long Island's large caldera freshwater lake, about 5 km from the nearest shore. By 1968 an islet of tephra, Motmot, was formed (Figure 11). Lava flows in 1973 and 1974 ensured its future existence, and the islet is now about 300 m long and 50 m high. It was investigated at intervals from 1969 to 1985 by Eldon Ball and his colleagues, and in 1988 the botanists Osborne and Murphy made a short visit.

The first plants were mosses and the sedge *Cyperus polystachios*, both found in 1968. After 2 more years 13 plant species were present, including mosses, the fern *Pityrogramma calomelanos* (one of the Krakatau pioneers), two sedge species, a composite, two (perhaps three) figs, and five other flowering plants. By 1972 there were 14 vascular plant species. Three more ferns were present (including a species of *Nephrolepis*), and six more seed plants, including a third sedge, two grasses, and a fourth fig species.

Scavenging omnivorous earwigs and carnivorous wolf spiders were among the earliest animal arrivals on Motmot. They were probably not foraging on the beach for they gradually moved inland until by 1972 they could be found over almost the whole island.

The 1973–1974 series of eruptions devastated the new flora, setting it back to a total of only three individuals, of the sedge *Cyperus cyperinus*. Invertebrates survived, however, the earwigs and wolf spiders still being abundant after the eruptions. In 1980 plant numbers were rising again and insect and spider diversity was high. In 1988, 20 species of vascular plants were recorded by Osborne and Murphy, at least 5 of which were represented in the previous flora. Wind (for ferns, grasses, and composites) and birds (figs and *Polygonum attenuatum*) were thought to be the chief modes of dispersal of the new flora, and dispersal through human activity was thought to be very unlikely.

Along with a few invertebrates, many plant propagules arrive on Motmot via the surface of the lake. However, the combination of volcanically heated beaches, chang-

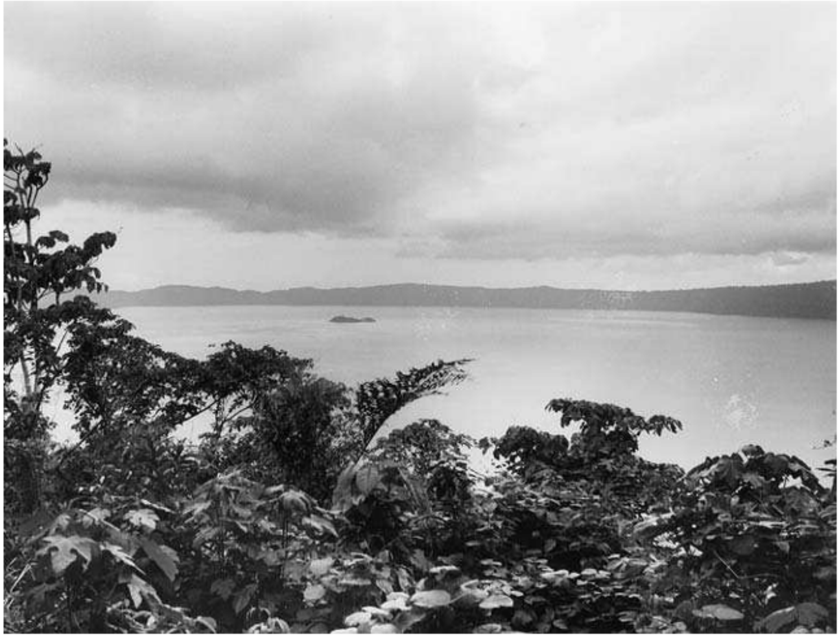

FIGURE 11 Lake Wisdom, the freshwater lake in the crater of Long Island, in 1980; the islet of Motmot can be seen in the middle distance. (Photograph by Eldon Ball.)

ing water levels, and strong wave action ensures that surface transport is not a major contributor to Motmot's flora. On a floating log drifting past Motmot with soil in its roots were earwigs (not the species found on Motmot) and two ant and two spider species. Sedge seeds may have been brought by the black duck (see below) but they may also have been carried on the lake surface; sedges were also early pioneers on the Krakataus.

Wind dispersal was important. Almost half the plant species known by 1988 were probably dispersed in the air. Mosses and nine fern species, as well as four composites and two ecologically important grasses, *Saccharum ?robustum* and *Imperata cylindrica*, were almost certainly wind-dispersed. There is some indication that aerial fallout of arthropods onto the island was providing sufficient sustenance for early populations of wolf spiders and earwigs (see above).

Of the 24 species of plants recorded in the 4 years after 1968, the seeds of 14 could have been brought by birds, 6 (including four figs) internally, 6 as minute seeds thought to adhere to mud on birds' feet, and 2 by becoming attached to feathers. The 20 species of the second primary succession (after the 1974 eruptions) included 8 species that could have been bird-dispersed, 4 internally and 4 in mud.

From the composition and distribution of the flora, Ball's group concluded that many plants arrived as seeds carried by the black duck, *Anas superciliosa*, which nested on the island from 1969. However, although the ducks' gut contents included many seeds of five plant species, including a sedge, no seeds could be found in the feces, so seeds adhering to the birds externally, on feathers and in mud, were the likely propagules. But Osborne and Murphy pointed out that pigeons and fruit doves are likely to be more efficient dispersers of plants like figs. Long Island has 11 species of frugivorous birds and a species of large fruit bat; doves and pigeons abound and include two species of fruit dove and two imperial pigeons which are excellent plant dispersers. Volant frugivores have not yet been reported on Motmot, however.

Two raptor species were seen on Motmot, the peregrine falcon (perhaps seeking pigeons?) and white-bellied fish eagle. Ball and Glucksman speculated that plant seeds could have been brought within the gut of birds taken by falcons and carried to the island to be consumed there. Since they made this suggestion, the Lannar falcon has been shown to be a secondhand disperser of plant seeds in this way in South Africa, and observations on Anak Krakatau indicate that peregrines may perform a similar role there.

C. Anak Krakatau

In 1930 a tephra island, to be known as Anak Krakatau ("Krakatau's Child"), emerged from the submarine caldera resulting from Krakatau's 1883 eruption. The island persisted, grew, and was consolidated by lava flows in the 1960s. It was colonized by plants and animals, probably largely from the neighboring older islands, a kilometer or two away, themselves in process of recovery from the 1883 eruption of Krakatau. A young biota was gradually assembled, which, however, was eradicated by eruptions in 1952–1953. The colonizing process then recommenced, but damaging eruptions at fairly regular intervals have set it back repeatedly. Lava was first emitted in the 1960s and flows now cover over half the island, which is about 2 km in diameter and some 500 m high.

Since a nested pair of natural experiments in colonization was now in progress at the same site (colonization of the Krakataus from the mainland and colonization of Anak Krakatau from the older Krakataus), the experiments having started several decades apart, a number of comparative studies became possible. Anak Krakatau's continuing volcanic activity, which had no counterpart on Rakata (or on Surtsey), has complicated comparisons but has also provided replicate sequences of succession from zero or near-zero baselines.

The dispersal of sea-borne plant propagules to Anak Krakatau was studied over two monsoon seasons by Tukirin Partomihardjo. Stranded propagules of 66 plant species representing 38 families were found on the island's beaches. Disseminules of 30 species could have been derived from plants growing on the three older Krakatau island, mostly from the "core group" of coastal species present on them all, but the other 36 species must have originated from outside the archipelago, largely from Sumatra to the north. Twenty-eight of the species were already established on Anak Krakatau.

From such sea-borne propagules as these a coastal "forest" developed fairly quickly. Just inland were grasslands, the dominant grass being *Saccharum spontaneum.* In just over a decade these were succeeded by a *Casuarina equisetifolia* woodland (Figures 3–5). *Casuarina* is intolerant of shade, and on a stable substrate intrusions of some of the animal-dispersed heliophilous shrubs and trees such as small figs initiated change toward mixed forest. Further inland clumps of *Saccharum* dotted the bare ash and *Pityrogramma* and *Nephrolepis* ferns grew in the shade of laval outcrops (Figure 12; see also color insert). The present flora of about 150 species is largely the result of a classic succession frequently interrupted by eruptions.

The prevegetation colonization by animals has been discussed above. The postvegetation faunal develop-

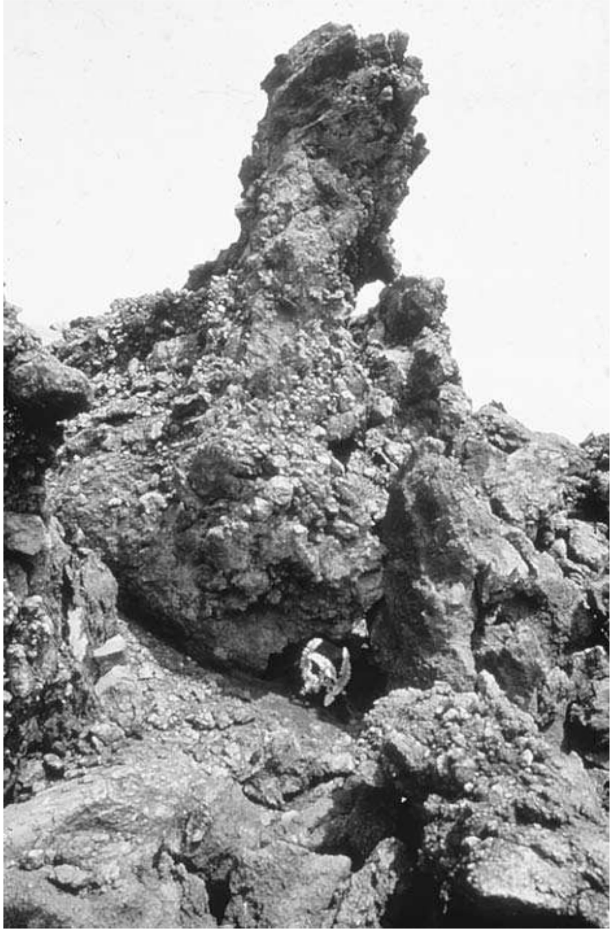

FIGURE 12 A "pioneer" fern, a species of *Nephrolepis,* grows in the shade of a laval outcrop on Anak Krakatau. (Photograph by David Walsh.) (See also color inserts.)

ment was also of interest because at the time Anak Krakatau provided one of only two areas of fairly open habitat on the archipelago. The first birds to become established were the ground-nesting savannah nightjar and white-breasted waterhen, which would have fed upon grasshoppers, moths, skippers, and other grassland insects, as well as the collared kingfisher, which also nests without trees (in termite nests and on gully sides) and takes a variety of foods including shore crabs. The large omnivorous monitor lizard also was an early colonist. As *Casuarina* woodland developed, generalist insect/fruit eaters such as bulbuls and large-billed crows colonized, as well as arboreal insectivores and the paradise tree snake. There was a surge of colonization of avian frugivores after the island's first figs fruited in 1985, and some of the earlier colonists declined in numbers or became extinct. A number of fruit bats and frugivorous dove and pigeon species colonized together with about six fig species in the early 1990s as the diversification of the small forest area accelerated. Raptors finally became established in the form of the small-bird specialist the Oriental hobby, which was succeeded after doves and pigeons arrived by the peregrine falcon. The barn owl colonized and fed on the rats which arrived in the 1980s.

The colonization of this island has provided a number of insights into early successional processes but renewed volcanic activity in the 1990s has set back the process (and its monitoring) for some years.

V. SOME COLONIZATION COMPARISONS

The various priseres of plant colonization that have occurred on Anak Krakatau following its periodic outbursts may be compared with one another, with that seen on Rakata after 1883, and, for contrast, with that on Surtsey.

The comparison between colonization of Anak Krakatau and the older Krakatau islands is one between processes occurring at different times at almost the same place. But it was far from the same place biologically. Unlike the Krakataus after 1883, Anak Krakatau emerged into the midst of an archipelago with a biota itself selected for good colonizing ability and including potential seed dispersers—nine frugivorous bird species and two species of *Cynopterus,* small dog-faced fruit bats. Moreover, with distances from sources of only 2 km or so, these small bats and some of the smaller facultative avian frugivores could in this case easily mediate initial dispersal to the island.

Thus, in contrast to the colonization of the older Krakataus, on Anak Krakatau the animal-dispersed component of the early developing flora was substantial. On the three Krakatau islands after the 1883 eruption there was no animal-dispersed plant among the colonists within the first 3 years, but in 1896 six species were present. Zoochorous plants made up 35% (23 species in 1905) of plants arriving (i.e., first recorded) between 1898 and 1908, and, considering only nonhuman dispersal, 40% of those arriving later. In contrast, on Anak Krakatau the animal-dispersed component was 17% in the first 4 years, increasing to 38% of plants arriving in the second decade.

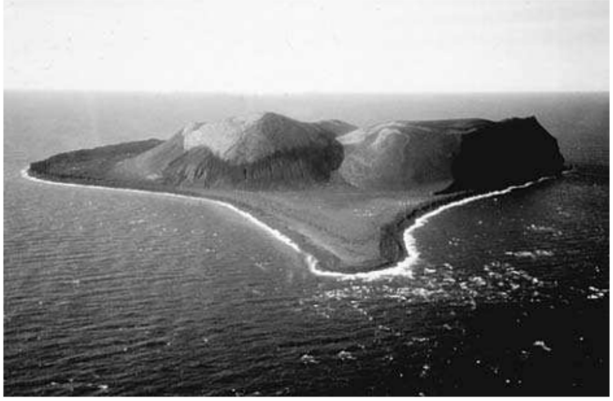

FIGURE 13 The emergent island Surtsey (from the north, 1991). Surtsey and Anak Krakatau are about the same size (Surtsey is about 1500 m from east to west and is some 150 m high; Anak Krakatau is 2000 m from north to south and 190 m high) and their biotas about the same age (Surtsey from 1963, Anak Krakatau from 1957), but they differ markedly in isolation, climate, and the richness of their potential source biotas (Iceland and Java/Sumatra, respectively). (Photograph by Borgthor Magnusson.)

Surtsey is Anak Krakatau's cold-temperate analogue. The islands are about the same in their size and height (Figures 13 and 14), age, and physical isolation. Both have extensive lava shields that have ensured their permanence, and ash-covered areas that include highly mobile lowland promontories subjected to rapid marine erosion and deposition. Anak Krakatau's biota dates from self-devastating eruptions in 1952–1953, and there have been checks to biotic development at least three times for substantial periods. Surtsey's biota dates from its emergence in 1963, and there has been no eruption since 1967. Both have island neighbors carrying biotas that are subsets of their mainlands' biotas—the Westman Islands, the closest of which is 5 km from Surtsey, and the older pre-1883 companion islands of the Krakatau group, 2–4 km from Anak Krakatau.

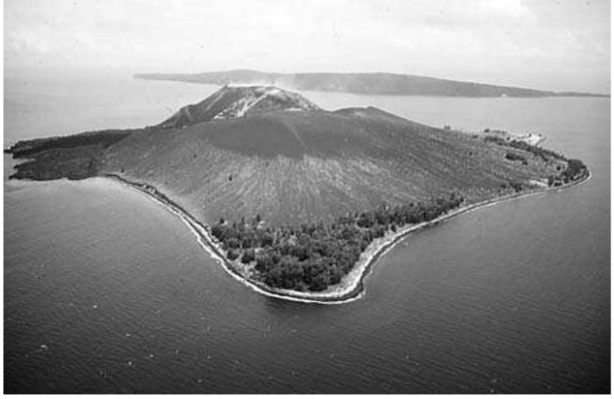

FIGURE 14 The emergent island Anak Krakatau (from the east, 1985). Surtsey and Anak Krakatau are about the same size and their biotas about the same age, but they differ markedly in isolation, climate, and the richness of their potential source biotas (Iceland and Java/Sumatra, respectively). (Photograph by David Walsh.)

The two islands differ markedly in biological isolation. The colonization of Surtsey has been slow, yet Fridriksson showed that, if water is available, plants can grow just as well on Surtsey's tephra as on other young volcanic tephra. He concluded that Surtsey's slow colonization is not due to the nature of its substrate. Surtsey's source pool of species is an impoverished one and its climate is harsh, factors which impose constraints on both the dispersal and the establishment of living propagules. For example, it was not until 1992, 32 years after its emergence, that Surtsey had the resources to support continuously resident land birds; Fridriksson informed me that in that year the snow bunting became the first land vertebrate to breed on the island. By comparison, at the same age Anak Krakatau supported over 25 species of resident land birds, paradoxically including not a single seed-eating species. Birds nevertheless played a relatively more important role in the colonizing of Surtsey by vascular plants than did both birds and bats on the Krakataus over equivalent time periods. The important birds on Surtsey are seabirds, which are not frugivorous or seed-eating, and which carry plant propagules externally. They are, of course, colonial and more numerous than the land birds of the Krakataus. Surtsey thus has a greater proportion of zoochorous plant colonists than do the Krakataus (Table II), and on Surtsey seabirds have also provided an important conduit, lacking on the Krakataus, for energy from the surrounding sea.

A significant proportion of the invertebrates colonizing Surtsey were sea-borne, and, as on Anak Krakatau, included collembolans and other insects exploiting washed-up carcasses.

The early importance of mosses on Surtsey had no parallel on the Krakataus, where they were unimportant in the early succession on ash. On Rakata (but probably not on Anak Krakatau) ferns took on an important role. Airborne invertebrates arrive on both Surtsey and Anak Krakatau in substantial numbers, and in both cases Diptera form a major component of the airborne invertebrate fauna. An animal community exploiting this airborne fallout is present on Anak Krakatau (Figure 15) but evidently not on Surtsey, although it is probably present on Motmot.

TABLE II Dispersal Spectra of Vascular Plant Assemblages[a]

	Birds/ bats	*Water*	*Wind*	*Humans*	*n*
Surtsey, 1990 (+27)	64	27	9	0	30
Motmot, 1988 (+12)	42	4	51	0	37
Rakata, 1908 (+25)	20	43	37	0	106
A.K., 1979 (+27)	17	59	22	2	64*

[a] Dispersal spectra (percentages of species arriving by various dispersal means) of vascular plant assemblages reaching the volcanic islands of Surtsey, Motmot, Rakata, and Anak Krakatau (A.K.) at various times (years in parentheses) since the "clean slate" was created either on the island's emergence or from a devastating eruption. *n*, total number of species; *, total species in two successive priseres. [Data from Fridriksson, S. (1992). Development of the ecosystem on Surtsey with reference to Anak Krakatau. *GeoJournal* **28**(2), 287–291; Osborne, P. L., and Murphy, R. (1989). Botanical colonisation of Motmot Island, Lake Wisdom, Madang Province. *Sci. New Guinea* **15**(2), 57–63; Whittaker, R. J., Bush, M. B., Partomihardjo, T., Asquith, N. M., and Richards, K. (1992). Ecological aspects of plant colonisation of the Krakatau Islands. *GeoJournal* **28,** 201–211; and Partomihardjo, T., Mirmanto, E., and Whittaker, R. J. (1992). Anak Krakatau's vegetation and flora circa 1991, with observations on a decade of development and change. *GeoJournal* **28,** 233–248. Dispersal spectra of Motmot flora estimated from Osborne and Murphy (1989, see above); Brown, W. H., Merril, E. D., and Yates, H. S. (1917). The revegetation of Volcano Island, Luzon, Philippine Islands, since the eruption of Taal volcano in 1911. *Philipp. J. Sci.* **12**(4), 177–248; Ridley, H. N. (1930). *"The Dispersal of Plants throughout the World."* L. Reeve, UK; and Dr. Tukirin Partomihardjo (personal communication).

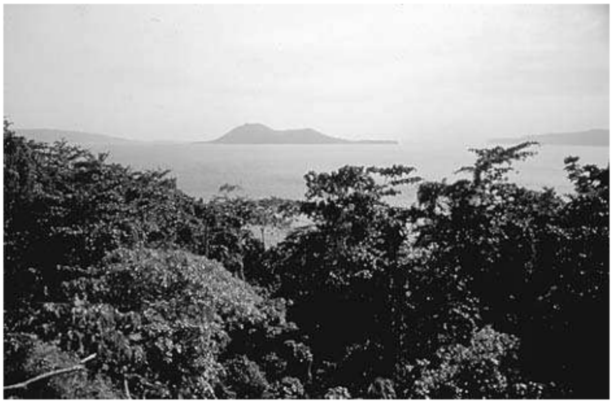

FIGURE 15 Anak Krakatau seen from Rakata, 1992. (Compare with Ball's photograph of Motmot in Figure 11.)

Motmot differs from the two other emergent islands in being much smaller, only about a hundredth of their area, and having additional components of isolation. It is isolated from the sea by rings of land and freshwater, so that dispersal by sea, of great importance in the colonization of the two marine islands, particularly in the early stages of biotic assembly, can play no part at all in Motmot's colonization. Over-water dispersal has been unimportant in its colonization (Table II). Lake Wisdom is itself very isolated from possible sources of lake biota and its peripheral edges, like those of Motmot, fall off steeply. Thus few shore plant species are available for dispersal to Motmot's shores. Moreover, as noted above, Motmot's shore is very hot (the water temperature may reach 95°C in places), its wave action strong, and its water level changeable, so few of the propagules that do reach Motmot become established. Motmot's biota is thus impoverished.

After only 3 years after 1968 Motmot had two resident land birds—the black duck and Pacific swallow—but it was not until 1980 that a third resident species was recorded. The very high importance of birds as a mode of transport of disseminules to Motmot compared to Rakata almost certainly results from the short distances from the source that are involved. Moreover, for this reason and because of Motmot's small size, temporary visits by birds and bats may have played, and may continue to play, a quite important role.

VI. ESTABLISHMENT AND COMMUNITY ASSEMBLY

In only a few cases do we know anything about the chances of successful establishment of immigrating organisms, and the early stages of integration of species into communities has been followed only rarely.

A. Establishment Rates

The Icelandic biologists precisely grid-plotted the positions of individual plants on Surtsey, so that arrivals that failed to become established could be recorded even when they persisted for only 1 year. A total of four species failed to colonize after one arrival, but nine have failed more than once, and one has arrived as many as five times and has not yet colonized.

Anak Krakatau's simple early community enabled animal immigrants and sea-borne plant arrivals to be recognized and their fates noted. Over two seasons 66 plant species were found as stranded propagules on Anak Krakatau's beaches by Partomihardjo, yet less than half these (28) had already become established on the island.

In a span of 8 years of sporadic observation on Anak Krakatau for short periods, there are records of 54 animal species (25 of them vertebrates) arriving on the island, 14 of which were new to the archipelago. More than 20 of the 54 did not become established. I estimate that hundreds of individuals may have arrived over this period, many being of species new to the island and many representing failed colonization attempts.

The barriers to the establishment of waterborne propagules on Motmot have been noted above.

The crucial test of successful establishment is acceptance into an ecological community. Only rarely can the beginnings of such associations be observed.

B. Assembly of the First Communities

The main factor affecting vegetation on the scoria of Vesuvius was found to be soil particle size, followed by soil stability. An early pioneer, *Rumex scutatus*, became dominant on the coarse mobile scoria and pumices of the 1944 eruption although it was rare in the surrounding region. On steeper slopes it was seen to facilitate the establishment of other plant species, apparently acting as a nurse plant for broom, *Bromopsis (= Bromus) erecta*, for example, which was found growing within its clumps.

It is perhaps not surprising that the beginnings of ecosystem development have been detected on Surtsey, where there are few species, colonization has been slow, and monitoring has been meticulous and regular since the island's birth.

In 1978 Fridriksson noticed that the sea sandwort, *Honkenya peploides*, a low-growing, sand-binding pioneer, and the tall lyme grass, *Leymus (= Elymus) arenarius*, appeared to be forming a simple sand dune association. Where this association is found on mainland Iceland it is succeeded by grasses (much as on the Krakataus, where the two pioneer beach creepers are sometimes succeeded by two or three grass species, although dunes are not found on the Krakataus). On Surtsey, dune height increased from 20 cm in 1980 to 1 m 10 years later. Young lyme grass plants were growing in the center of some of the sea sandwort patches, where they were better sheltered than on open ground and received a more even supply of moisture. A young lyme grass plant was found in each of 20 patches of sea sandwort in 1983, yet no new lyme grass seedlings were found in the open ground around the patches. The number of such patches had increased to 100 in 1984 and to 166 by 1986. The patch of pioneer sea sandwort thus acts as a kind of nursery, providing favorable conditions for the establishment of a lyme grass plant within it. The parallel with *Rumex* and *Bromopsis* on Vesuvius is clear.

On Surtsey, fledglings of the great black-backed gull used the *Honkenya-Leymus* dunes for shelter in 1975 and 1976, and a pair of adults used as many as 20 sea sandwort plants as nesting material, together with the red fescue grass *Festuca rubra* and the sedge *Carex maritima*. In 1981 the association had six component species: an aphid was abundant on the sea sandworts and a collembolan (springtail) was common in the rotting, fungus-covered branches of the larger clumps.

Another "embryonic" plant association on Surtsey involved three grass species (two of *Poa* and one of *Puccinellia*) and the low-growing, creeping perennial *Sagina procumbens*. Since 1986 a colony of *Sagina procumbens* had been developing on ropy pahoehoe lava on the south of the island, where the *Sagina* and grasses were well fertilized by a herring gull colony. Fridriksson reported that the soil in this seabird breeding area had become quite fertile, with 60 mg nitrogen, 7 mg potassium, and 2.9 mg phosphorus per 100 ml of dry matter. The same association is found in mainland Iceland on cliffs and in seabird colonies, as well as around farmhouses.

Surtsey's rich moss vegetation provided a habitat for several soil animals in 1976 but this fauna seems to have been destroyed by drought in 1978 and has only partially recovered.

Birds' nests also provide a habitat for land arthropods on Surtsey. One greater black-backed gull nest contained two staphylinid (rove) beetle species, a springtail, and a mite, and the decaying materials beneath the nest were exploited by larvae of four species of flies, feeders on dung and dead organic matter. Two species of spiders, in their turn feeding on the insects, completed this community.

Thus after almost 30 years a simple and probably rather unstable ecosystem had developed on Surtsey, comprising a few species of vascular plants, seabirds, and fungi, and several species of land invertebrates. Two embryonic associations of plants and animals, one associated with slowly growing sand dunes, and another with birds' nests, had been formed. Another, involving mosses, appears to have been badly damaged but is now showing signs of repair.

VII. THEORETICAL CONSIDERATIONS

Experiments with laboratory "microcosms," mathematical modeling studies, and the observation of natural systems all indicate that the end result of the course of development of any individual system is highly contingent on several factors. First, and most obviously, it depends upon which biotic components arrive at the new area from outside. The relative importance of various modes of immigration varies with the environmental factors that obtain from case to case, as does the rate of assembly of the biota. Miles and Walton, discussing primary succession on a mineral substrate, pointed out that since there is no seed bank, no "memory" of a previous flora (for there was none), the assembly of species depends only on their chances of dispersal. They noted that the nature and direction of early plant succession on Mount St. Helens reflect only the order of species arrival by predominantly aerial dispersal and suggested that repeatability of successions in different places at the same time or at different times in the same place is likely to be low.

On the Krakataus, however, some determinism is evident in the early stages of biotic assembly; instances at different times in the same place (on Anak Krakatau) and in different places in the same local area (on the older Krakatau islands and Anak Krakatau) show fairly high similarity. This difference from Mount St. Helens may derive from the island situation and the high predictability of sea-borne pioneers.

The composition of the assembling biota also depends on which of the arriving species become established, and this in turn may depend in part on the site of the propagule's landfall. Whereas airborne propagules may land in a variety of microsites, many of which may be unsuitable, sea-borne immigrants have a landfall on the upper shore, which is usually a highly suitable habitat for the propagule, for it was in such a situation that its parent plant grew, to shed it into the sea. On the Krakataus a large, important group of widely distributed sea-borne plant species forms a consistent, determinate core of pioneer colonists that is repeated in several cases.

The chances of establishment of a new species also may be affected by an important biotic factor—the species that are already present, so that sequence of arrival is important. Even with the same pool of colonizing species, final outcomes—the composition of resulting biotas—will differ unless the sequence and even also the length of the interval between arrivals (colonizing interval) are identical. There are both stochastic and deterministic influences on these factors.

Seamus Ward and I have considered the relative roles of chance and determinism in this biotic aspect of species assembly in isolated habitats, both from a theoretical point of view and with regard to the Krakatau cases. A simple model predicts that the degree of stochasticity will depend in part on the relative dispersal abilities of potentially interacting colonizing species. Variation in priority will be high where two such species have similar, low, arrival rates, and variation in the interval between colonizations will depend on the dispersal ability of the second species to arrive. We concluded that early colonization should be relatively deterministic, as the assembly of Krakatau's early, pioneer sea-borne flora appears to be. Later in the colonization process both priority and the colonizing interval will be more variable. We identified possible instances of the increasing importance of chance in the later colonization of the Krakataus by large animal-dispersed forest trees and lianas. On the Krakataus the increasing importance of chance in these later stages of floral assembly is demonstrated by the fact that after a century of colonization, closely adjacent Krakatau islands, separated by only a few kilome-

TABLE III Changing Dispersal-Mode Spectra of Cumulative Vascular Plant Floras Present on Rakata (Krakataus) at Successive Survey Periods (Some Surveys Grouped)

Dispersal	*1886*	*1897*	*1908*	*1920–1924*	*1929–1934*	*1979–1989*
Sea	9	22	46	55	57	68
Wind	15	28	39	99	116	192
Animal	0	2	21	47	62	119
Human	0	0	0	18	18	18
Total	24	52	106	219	253	397

Note. Based on Table 3b of Whittaker *et al.* (1992).

ters, developed forests dominated by quite different species.

VIII. SUMMARY

The effect of volcanic eruptions on living communities depends on a number of factors, most importantly on the type of eruption, and at the extreme the macrobiota may be entirely extirpated. Where there is survival from refugial foci, this is usually more important than the immigration of new biotic elements in the recovery process. There are two aspects to the assembly of a new biota through the colonization of immigrants—the arrival and establishment of incoming species. In general, the plant–herbivore–carnivore sequence is followed, but there is a growing evidence that on primary substrates a guild of animals that exploit airborne organic input may precede plant colonization. Although generally colonization by bacteria and cryptogamic plants (e.g., lichens, mosses, and ferns) precedes that of seed plants, there are many instances in which seed plants were the primary colonists.

Successful establishment in some cases appears to involve incorporation into simple communities of a few interacting species. These communities are then integrated into the larger, more complex developing ecosystem. Both chance and deterministic factors are involved in colonization and the development of a new biota, and their relative importance may vary from case to case and over time within a single case of biotic renewal.

ACKNOWLEDGMENTS

I have been greatly assisted by discussions with the following, most of whom commented on early drafts of this paper, and on whose works I have drawn freely: Eldon Ball, who encouraged me to try to further his own significant work on Motmot; Bayard Brattstrom, who provided unpublished data from his pioneer studies on Barcena; John Edwards, who sent me the manuscript of his own excellent review on a very similar topic but focusing particularly on his own special study area, Mount St. Helens; Sturla Fridriksson, who introduced me to Surtsey and kept me up-to-date with his team's fundamentally important long-term studies there; Tukirin Partomihardjo and Rob Whittaker, whose detailed knowledge of the Krakataus' flora and masterly overview of their phytogeography must underpin all biological work on those islands; and my Australian colleague Seamus Ward, who has sharpened my appreciation of the theoretical approach to developmental ecology.

SEE ALSO THE FOLLOWING ARTICLES

Hazards from Pyroclastic Flows and Surges • Hazards of Volcanic Gases • Impacts of Eruptions on Human Health • Lahar and Jökulhlaup Hazards • Lava Flow Hazards • Surtseyan and Related Phreatomagmatic Eruptions • Volcanic Soils • Volcanism and Biotic Extinctions

FURTHER READING

Ball, E. E., and Glucksman, J. (1975). Biological colonisation of Motmot, a recently created tropical island. *Proc. R. Soc. London B* **190,** 421–442.

Brattstrom, B. H. (1963). Barcena Volcano, 1952. Page 499–524 *in* "*Pacific Basin Biogeography*" (J. L. Gressitt, ed.). Bishop Museum Press, Honolulu.

Edwards, J. S. (1999). In "*Volcanoes and the Environment*" (J. Marti and G. J. Ernst, eds.). Cambridge Univ. Press, Cambridge, UK.

Fridriksson, S. (1975). "*Surtsey: Evolution of Life on a Volcanic Island.*" Butterworths, London.

Thornton, I. W. B. (1996). "*Krakatau. The Destruction and Reassembly of an Island Ecosystem.*" Harvard Univ. Press, Cambridge, MA.

Whittaker, R. J., Bush, M. B., Partomihardjo, T., Asquith, N. M., and Richards, K. (1992). Ecological aspects of plant colonisation of the Krakatau Islands. *GeoJournal* **28,** 201–211.

This Page Intentionally Left Blank

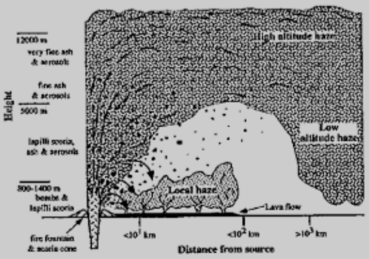

VOLCANISM AND BIOTIC EXTINCTIONS

Michael R. Rampino
New York University and NASA

Stephen Self
University of Hawaii at Manoa

I. Correlation between Continental Flood Basalts and Biotic Extinctions
II. Environmental Effects of Flood Basalt Eruptions
III. Flood Basalts and Impacts: Possible Connections
IV. Explosive Volcanism and Effects on Life

GLOSSARY

flood basalt Large outpourings of basaltic lava composed of individual flows with volumes up to thousands of km^3. The lava flows, erupted over a total time interval usually less than 1 million years, produce lava plateaus typically more than 1 million km^3 in volume and covering more than 1 million km^2.

greenhouse warming Climatic warming caused by gases in the atmosphere, such as CO_2, SO_2, and methane, that absorb outgoing infrared radiation and warm the planet.

Jurassic Period of geologic time ranging from about 201 to 144 million years ago.

K/T boundary The stratigraphic boundary between rocks of Cretaceous age and rocks of Tertiary age, now dated at 65 million years ago. The boundary stratum is marked by evidence of a comet or asteroid impact, which is widely believed to have caused the extinction of some 75% of marine species and most nonmarine organisms at the end of the Cretaceous period.

mass extinction Simultaneous or near-simultaneous disappearance of a large number of extant species. Five major mass extinctions, in which more than 75% of marine life and many nonmarine species died out, are recognized at the end of the Ordovician period (439 Ma); the Late Devonian period (365 Ma); the end of the Permian period (250 Ma); the end of the Triassic period (201 Ma); and the end of the Cretaceous period (65 Ma). About 20 "minor mass extinctions" have also occurred in the last 545 million years.

Oligocene Epoch of geologic time from 35 to 23 million years ago.

Permian Period of geologic time ranging from about 290 to 250 million years ago. Last period of the Paleozoic era. The Permian ended with the greatest mass extinction in the geologic record.

sulfuric acid aerosols Small droplets of sulfuric acid formed in the atmosphere from oxidation of sulfur-rich gases. These aerosols can form a haze in the upper atmosphere after volcanic eruptions, which can reduce incoming sunlight and cool the planet.

Triassic Period of geologic time ranging from 250 to 201 million years ago. The first period of the Mesozoic era.

volcanic winter Term used for the severe global and regional cooling that can be caused by large amounts of volcanic aerosols in the atmosphere after very large eruptions.

EXTINCTION EVENTS are increasingly seen as important factors in the history of life on Earth, and recent studies suggest catastrophic causes for at

Copyright © 2000 by Academic Press
All rights of reproduction in any form reserved.

least some biotic mass extinctions. Two catastrophic processes that have been invoked are impacts of asteroids or comets and series of large volcanic eruptions. On one hand, the end-Cretaceous (65 Ma) mass extinction (the Cretaceous/Tertiary or K/T boundary) has been convincingly correlated with the impact of a 10-km-diameter comet or asteroid, and evidence of impact has been found close to the times of several other extinction events. On the other hand, the coincidence of the eruption of the Siberian flood basalt lava flow province and the even more severe end-Permian extinctions (250 Ma), and the near-coincidence of the Deccan flood basalt province (India) and the K/T extinctions, fostered speculations that flood basalt eruptions have contributed to a number of mass extinctions. Several workers compared the dates of extinction events of various magnitudes with dates of flood basalt episodes and found some significant correlations, supporting a possible cause-and-effect connection. Thus, it could be that extreme events of both extraterrestrial and terrestrial origin are responsible for many of the punctuation marks of the fossil record.

A major question regarding any possible relationship between flood basalt lava eruptions and extinction events involves the nature and severity of the environmental effects of the eruptions and their potential impact on life. Although the correlation between some flood basalt episodes and extinctions may implicate volcanism in the extinctions, it is also possible that other factors lead to the apparent association. Flood basalt episodes have been related to the inception of mantle plume activity, and thus may represent one facet of a host of geological factors (e.g., changes in seafloor spreading rates, rifting events, increased tectonism and volcanism, and sea-level variations) that tend to be correlated, and may be associated with unusual climatic and environmental fluctuations that could lead to significant faunal changes. It has also been suggested that a coincidence of both a large impact and a flood basalt eruption might be necessary in causing severe mass extinctions, and some workers have even proposed that large impacts might in some way trigger or enhance the volcanism.

I. CORRELATION BETWEEN CONTINENTAL FLOOD BASALTS AND BIOTIC EXTINCTIONS

Continental flood basalt eruptions are the largest subaerial eruptions of basaltic composition, with known volumes of individual lava flows > 2000 km^3. A series of these huge eruptions piles up a thick stack of basalt lava flows, creating vast provinces extending to more than a million km^2 and containing more than 2 million km^3 of basaltic lava. The estimated inception dates of the continental flood basalts compiled from recent sources (based on the latest high-quality ^{40}Ar/^{39}Ar and U/Pb age determinations) are shown in Table I. Radiometric, paleomagnetic, and stratigraphic data all indicate that in most instances the greatest number of individual eruptions and the largest volume of lava occurred within a million years or less (Figure 1).

We can compare the ages in Table I with estimated ages of stratigraphic boundaries that involved significant

TABLE I Flood Basalt Provinces of the Last 250 Ma

Province	*Age (Ma)*	*Volume (10^6 km^3)*	*Paleolatitude*	*Duration (m.y.)*
Columbia River	16 ± 1	0.25	45°N	≤1 (for 90%)
Ethiopian	31 ± 1	≤1.0	10°N	≤1
North Atlantic	57 ± 1	>1.0	65°N	≤1
Deccan	66 ± 1	>2.0	20°S	≤1
Madagascar	88 ± 1	?	45°S	≤6?
Rajmahal	116 ± 1	?	50°S	≤2
Serra Geral/Etendeka	132 ± 1	>1.0	40°S	≤1 or ~ 5?
Antarctica	176 ± 1 or 183 ± 1	>0.5	50–60°S	≤1?
Karoo	183 ± 1	>2.0	45°S	0.5–1
Newark	201 ± 1	>1.0	30°N	~0.6
Siberian	249 ± 1	>2.0	45°N?	≤1

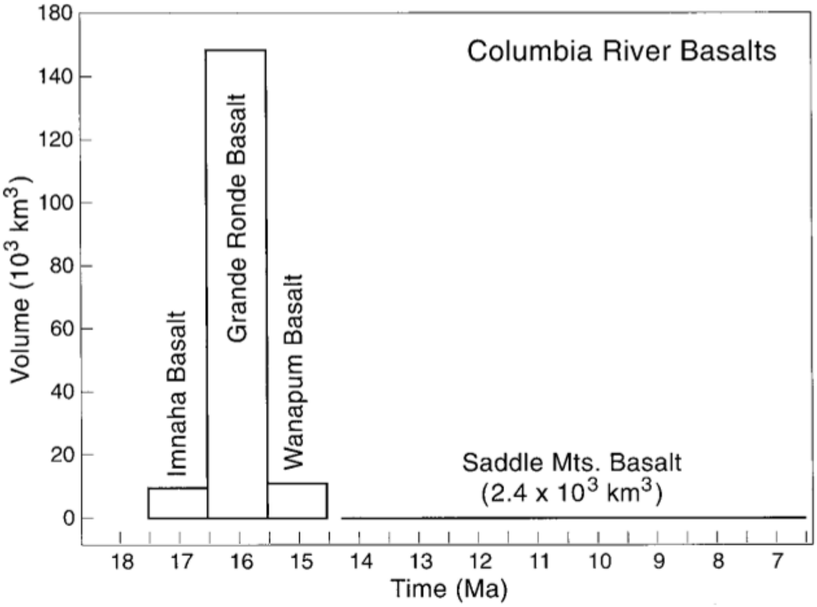

FIGURE 1 Estimate of erupted volume of Columbia River Basalts over the duration of the eruptive activity. Note that most of the magma was discharged during less than 1 million years, centered at about 16 Ma. Other flood basalt eruptions have a similar narrow age distribution.

faunal changes, dated according to the most recent geologic timescale (Table II and Figure 2).

In at least three cases, the Deccan, Newark, and Siberian flood basalts, a more direct measure of correlation with mass extinction boundaries is possible. For example, the Deccan Traps Flood Basalts of India contain >50 recognized flows in 1200-m sections in the best exposed region around Mahabaleshwar. The Deccan lavas were previously believed to have been erupted over a long period of time ranging from ~80 to ~30 Ma,

TABLE II Flood Basalt Episodes and Faunal Events

Flood basalt episode	*Age (Ma)*	*Stratigraphic boundary*	*Age (Ma)*
Columbia River	16 ± 1	Early/Mid-Miocene	16.4
Ethiopian	31 ± 1	Early/Late Oligocene	30
North Atlantic	57 ± 1	Paleocene/Eocene	54.8
		(Thanetian/Selandian)	(57.9)
Deccan	66 ± 1	Cretaceous/Tertiary	65.0 ± 0.1
Madagascar	88 ± 1	Cenomanian/Turonian	93.5 ± 0.2
		(Turonian/Coniacian)	(89 ± 0.5)
Rajmahal	116 ± 1	Aptian/Albian	112.2 ± 1.1
Serra Geral/Etendeka	132 ± 1	Jurassic/Cretaceous	142 ± 2.6
		(Hauterivian/Valanginian)	(132 ± 1.9)
Antarctica	176 ± 1 or 183 ± 1	(Aalenian/Bajocian)	(176.5 ± 4)
Karoo	183 ± 1	Early/Middle Jurassic	180.1 ± 4
Newark	201 ± 1	Triassic/Jurassic	205.7 ± 4
Siberian	249 ± 1	Permian/Triassic	248.2 ± 4.8

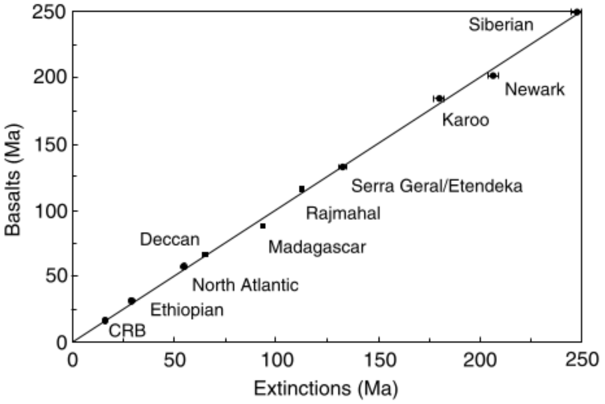

FIGURE 2 Possible correlation of flood basalts and extinctions/faunal changes. This graph uses 16.4, 30, 54.8, 65, 93.5, 112.2, 132, 180, 206, and 248.2 Ma ages for faunal changes (see Table II).

based on the large range of K/Ar age determinations. Redating of the basalts using refined $^{40}Ar/^{39}Ar$ techniques, however, indicates that the vast bulk of the thick stack of flows was erupted over a period of only about 500 ky, bracketing the time of the Cretaceous/Tertiary boundary. Most recently, the K/T boundary impact fallout layer has been reported to lie in sediments interbedded within the Deccan lavas, supporting the radiometric dating and paleomagnetic results that indicate that the eruptions began prior to the K/T boundary.

In the case of the Newark Basalts of eastern North America, the pollen changes that mark the Triassic/Jurassic boundary have been located just below ($\leq$40 ky) the first lava flows. For the Siberian Basalts, the paleontological evidence has been interpreted as placing the time of the Permian/Triassic mass extinction within the lowest lava suite. The probability that three major episodic volcanic events that typically last $\leq$1 m.y. should occur within 1 m.y. (to be conservative) of major mass extinction boundaries during the last 250 Ma (of which there are ~12) is about $\sim 10^{-4}$. For a few other basalts precise dating and paleomagnetic work suggest correlations with boundaries involving lesser faunal and floral changes. For example, the Ethiopian Basalts, recently dated at 31 ± 1 Ma, may correlate with the faunal changes that mark the Lower/Upper Oligocene boundary, dated at close to 30 Ma. The Karoo Basalts, recently dated at 183 ± 1 Ma, might correlate with the boundary between the Early and Middle Jurassic, at 180.1 ± 4 Ma, which is also marked by a faunal turnover event.

II. ENVIRONMENTAL EFFECTS OF FLOOD BASALT ERUPTIONS

Several kinds of environmental effects of flood basalt eruptions have been suggested, including climatic cooling from sulfuric acid aerosols, greenhouse warming from CO_2 and SO_2 gases, and acid rain. Indirect environmental effects include changes in ocean chemistry, circulation, and oxygenation, especially from basaltic volcanism associated with large submarine oceanic plateaus that may represent flood basalt volcanism in an oceanic environment. Before we proceed to evaluate these effects, however, we briefly examine the nature of flood basalt volcanism and estimate the amounts climatically active gases these volcanic events can release into the atmosphere.

A. The Style of Flood Basalt Eruptions

The style of eruption of flood basalt lavas is an important determinant in the atmospheric and climatic effects of these events. In fissure-fed basaltic lava flow eruptions, the volumetric eruption rate is a critical parameter in determining the height of fire fountains over active vents, the convective rise of the volcanic gas plumes in the atmosphere, and hence the climatic impact of an eruption.

Flood basalt eruptions were originally envisioned as flowing as turbulent sheets 10 to 100 m thick that covered large areas in a matter of days. By contrast, it is now believed that flood basalts are erupted mainly as fissure-fed pahoehoe flows that inflate to their great thicknesses during the time that they reach their great extent. This suggests relatively slow emplacement of the flows over longer periods of time, most likely years to decades. Yet, average eruption rates must still have been higher than in any historic eruption except perhaps the extremes of some Icelandic lava outpourings. For example, the time required to emplace a large (1000–2000 km^3) lava flow at the peak output rate (about 1.4×10^7 kg/s) of the largest historical lava flow eruption, the 1783 Laki (Iceland) event, would be $\geq$10 years.

B. Climate Cooling

Climatic cooling at the Earth's surface attributed to volcanic eruptions is primarily a result of the formation and spread of stratospheric H_2SO_4 aerosols. These small droplets are formed from sulfur volatiles (largely SO_2) injected into the stratosphere by convective plumes rising above volcanic vents and fissures. The sulfuric acid aerosols have a residence time in the stratosphere of several years, where they backscatter incoming sunlight. Fine volcanic ash also lofted into the stratosphere largely settles out of the atmosphere in less than 3 months.

Basaltic eruptions are commonly effusive in character, last much longer, and are much less explosive than silicic eruptions of comparable volume. They are commonly considered to be much less effective in lofting volatiles to significant altitudes, where stratospheric aerosols could be produced. Observations and model calculations suggest, however, that the high eruption rates during the (~15 km^3) 1783 Laki basaltic fissure eruption in Iceland produced high fire fountaining (~600 to 1450 m), so that convective plume rise above the fountains could have attained altitudes up to 13 km above sea level (Figure 3). In support of this estimate, observations of the widespread sulfurous haze over Europe in 1783, and a marked sulfuric acidity peak in Greenland ice in 1784, suggest that the eruption plume reached the tropopause over Iceland (~9 km), and intruded into the base of the stratosphere. For the much larger volume lava flows typical of flood basalt episodes, the models of convective plume rise also indicate that sulfur-rich eruption plumes could reach the lower stratosphere.

Moreover, basaltic magmas are usually very rich in dissolved sulfur (commonly with concentrations of >1500 ppm sulfur), and therefore the release of sulfur-rich gases from a large basaltic eruption can be much higher than that from an explosive silicic eruption of equal volume. For example, studies of the Laki lava flow and ash indicate that the magma originally contained ~1700 ppm of sulfur, and the eruption could have released ~125 MT of SO_2 (65% during the first 2 months of intense activity) from the vent and lava flows (1 MT = 10^{12} g). This could have created about 160 MT of high-altitude H_2SO_4 aerosols, and about 50 MT of local aerosols in the Icelandic troposphere.

The atmospheric effects of the Laki eruption were severe and quite widespread, supporting the creation of at least some stratospheric aerosols. Haziness and dimming of sunlight were noticeable in 1783–1784 in Europe (Figure 4), and the so-called "dry fog" was reported in North America and as far east as China. Climatic cooling followed, and the winter of 1783–1784 was the coldest winter recorded in the eastern United States in a 225-year record.

The observed sulfur content of basaltic magmas and evidence of degassing of the lava flows suggest that the sulfur release from a large flood basalt eruption of ≥1000 km^3 volume [such as the Roza Flow of the Columbia River Basalts (14.7 Ma)] can be about 10,000

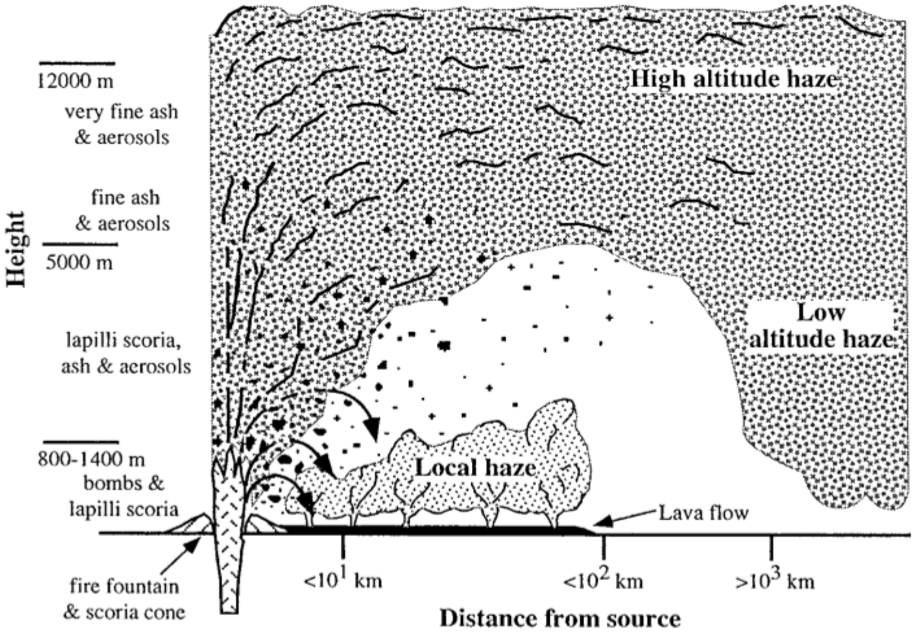

FIGURE 3 Eruption column height and levels of atmospheric injection of ash and aerosols from the 1783–1784 Laki (Iceland) eruption. Information obtained from calculations and observations. [After Thordarson and Self, unpublished.]

MT of SO_2, along with significant amounts of HF and HCl. At maximum eruption rates for Laki, the Roza eruptions would have produced lava fountains $\geq$ 1.5 km in height, and created a convective column rising $\geq$15 km above the vents. If the Roza eruption went on for 10 years, the annual aerosol burden in the atmosphere could have been greater than 1000 MT per year, with a portion going into the lower stratosphere. This would be enough to produce a large increase in the opacity of the regional and perhaps hemispheric atmosphere.

The conversion of such a large amount of SO_2 to H_2SO_4 would have probably greatly depleted stratospheric H_2O and OH, which at present consists of about 1000 MT globally, but a large amount of water could have been injected into the stratosphere by the eruption plumes. Some have suggested that self-limiting physical and chemical effects in very dense aerosol clouds might mitigate severe volcanic perturbations. It may be, however, that some features of dense clouds prolong the lifetime of aerosols in the upper atmosphere, as evidenced by the extended 6-year ice core acidity peak possibly related to the Toba (Indonesia) explosive eruption of 74,000 years ago. More accurate modeling of dense stratospheric aerosol clouds, and their effects on atmospheric dynamics and chemistry, is needed.

Volcanic aerosols at all altitudes should cool the Earth's surface, with maximum cooling effects from low-level tropospheric aerosols. In most volcanic eruptions, however, tropospheric aerosols have a very short lifetime of about a week before they are washed out of the lower atmosphere. A flood basalt eruption could release such large amounts ($\sim$1000 MT) of sulfuric acid aerosols, however, that a regional tropospheric aerosol cloud might be maintained despite washout. Climate cooling might also lead to suppression of atmospheric convection, so that rainout might be less effective at removing the aerosols.

Historic stratospheric aerosol clouds such as from the eruptions of El Chichón in 1982 and Pinatubo in 1991 have typically shown an atmospheric lifetime of a few years, so that the ocean–atmosphere climate system did not have a chance to come to equilibrium with the short-lived volcanic perturbation. Thus, these historic eruptions that created on the order of tens of MT of stratospheric aerosols are associated with surface coolings of only a few 10ths of a degree Celsius in the 1 or 2 years following the eruption (although a prompt cooling in the month after the eruption, probably related to volcanic ash in the atmosphere, has also been noted). Studies using a global climate model (GCM) suggest that if maintained for 50 years, a stratospheric loading of only about 10 MT of aerosols would lead to a 5°C global cooling. Therefore, if flood basalt eruptions were continuous at the average activity level for decades, significant cooling of climate is possible through involvement of the oceans.

Basaltic eruptions can also have episodes of more explosive activity. Laki, for example, produced ash estimated to have been about 3% of the total erupted volume. Some continental flood basalt eruptions are known to have been accompanied by more explosive volcanism. The North Atlantic Basalts were apparently coincident with a series of 200 or more basaltic ashes, equivalent to a magma volume of several thousand cubic kilometers. These explosive basaltic eruptions probably involved hydrovolcanic processes, and the widespread ash in the atmosphere could have led to some cooling.

C. Greenhouse Warming: Carbon Dioxide and Sulfur Dioxide

Greenhouse warming caused by large emissions of carbon dioxide from flood basalt volcanism has also been suggested as a cause of climatic change leading to mass extinctions. For example, based on published estimates of the CO_2 weight fraction of basaltic magmas, the fraction of CO_2 degassed, and the volume and timing of the Deccan eruptions, it has been estimated that from $\sim$6 to 20×10^{16} mol of carbon dioxide could have been released over a period of several hundred thousand years. Results of models designed to estimate the effects of this increased CO_2 on climate and ocean chemistry suggest, however, that the total increase in atmospheric pCO_2 would have been less than 200 ppm, leading to a predicted global warming of less than 2°C over the period of eruption of the lavas. It is unlikely that such a small and gradual warming would have been an important factor in mass extinctions of life.

Another possible source of greenhouse warming from flood basalt eruptions is SO_2 gas emissions. The Laki eruption showed that prolonged basaltic fissure eruptions can create large, persistent downwind plumes of SO_2 gas and H_2SO_4 aerosols in the lower atmosphere. During the summer of 1783 in Europe, while the sulfurous dry fog hung in the air, the weather was stifling. Historical reports of acrid odor, difficult breathing, dry deposition of sulfate, and vegetation damage indicate especially high SO_2 concentrations in the lower atmosphere from mid-June to early August (Figure 4). The July 1783 temperatures in Western Europe were up to $\sim$3°C warmer than the long-term average, and contemporary reports describe the weather as hazy, hot, and

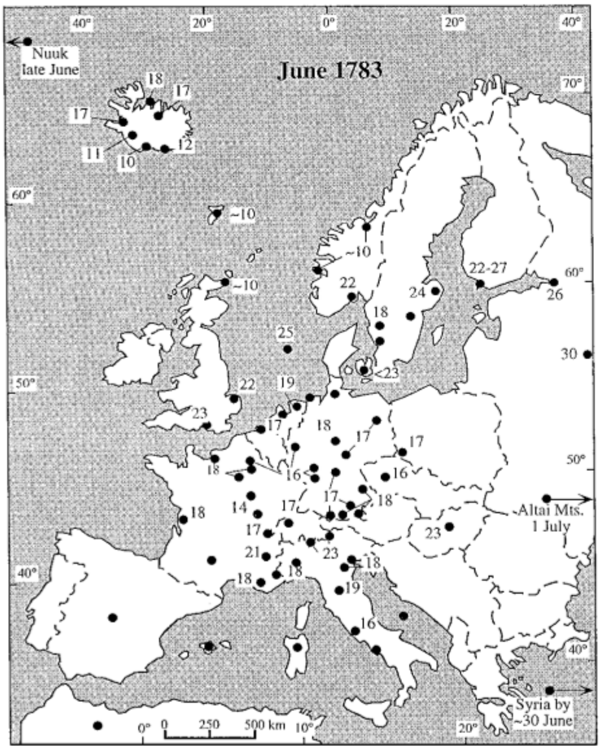

FIGURE 4 The inferred dispersal of the Laki haze (dry fog) of 1783, from contemporary reports. Dots indicate locations of observations; numbers give dates of observation in June 1783. [After Thordarson and Self, unpublished.]

very dry, but with frequent thunderstorms and hailstorms of unusual intensity.

The average concentration of SO_2 in the atmosphere over Western Europe in July 1783 could have been up to several ppm (background values are $\sim$1 ppb), and calculations suggest that the greenhouse effect of the SO_2-rich volcanic haze could have led to significant regional short-term warming. The even greater emissions of SO_2 from flood basalt volcanism could have led to more severe regional warming events that might have affected flora and fauna over wide areas.

D. Acid Rain

Acid rain from flood basalt eruptions is another possible environmental effect. For the historic Laki eruption, the local haze over Iceland contained high concentrations of sulfuric acid, causing skin lesions in animals and humans. Grass growth was stunted, trees were killed, and 50% of livestock perished from fluorine poisoning. The resulting "haze famine" led to the death of >20% of the Icelandic population, and acid rain effects were also reported from Northern Europe.

Calculations for flood basalts suggest that H_2SO_4, HF, and HCl release from a typical eruption of $\sim$1000 km^3 could have been about 10^{14} mol. If spread worldwide, this acid would give $\sim$0.2 mol/m^2, and if deposited over a year, then the daily acid fallout would be $\sim 5 \times 10^{-4}$ mol/m^2. If the eruption lasted $\sim$10 years, however, the daily deposition would be only $\sim 5 \times 10^{-5}$ mol of acid.

For comparison, total current anthropogenic sulfur release is about 10^{14} g per year, or about 10^{12} mol H_2SO_4 equivalent. Total global annual rainfall at present is $\sim 5 \times 10^{17}$ liters. As a rough estimate, if 1×10^{14} mol H_2SO_4 (equals $\sim 2 \times 10^{14}$ mol of H^+) is added to this precipitation, the result is $\sim 4 \times 10^{-4}$ mol/liter of H^+, equivalent to a pH of $\sim$3.7. The acidity of rainfall nearer to the flood basalt eruption would be higher (lower pH), and rainfall at distant sites would be less acidic (higher pH). Although it seems clear that local or regional effects of acid rain from flood basalt eruptions could have been considerable, global effects are much less likely.

E. Other Environmental Perturbations

Several other less well-constrained extinction mechanisms for flood basalt volcanism have been suggested. In the case of the Siberian Flood Basalts and the Permian/Triassic extinctions, it has been suggested that the volcanism caused the release of vast quantities of methane from hydrates that had accumulated on adjacent high-latitude shelf areas, leading to greenhouse warming. In other scenarios, the addition of volcanic CO_2 into the atmosphere was proposed to contribute to global warming and overturn of anoxic ocean bottom waters, and perhaps create physiological problems for land animals. As discussed above, however, it is very unlikely that the flood basalt volcanism could have produced enough CO_2 by itself to lead to these conditions.

It has also been suggested that large-scale ocean-plateau volcanism, such as that which created the Ontong Java Plateau and the Caribbean volcanic province in the Cretaceous period, could have altered ocean chemistry through the oxidation of material in hydrothermal effluents and stimulation of primary productivity in the surface oceans by release of hydrothermally derived iron. Such a submarine volcanic scenario has been proposed as a cause of global ocean anoxia at times of Cretaceous extinction (e.g., the Cenomanian-Turonian mass extinction at 93 Ma).

III. FLOOD BASALTS AND IMPACTS: POSSIBLE CONNECTIONS

Several authors have explored the possibility that flood basalt volcanism might be triggered or enhanced by the occurrence of large comet or asteroid impacts. Rough calculations implied that large impacts (impactors of ≥10 km diameter) could excavate initial transient cavities deep enough to result in decompression melting in the upper mantle, with ensuing volcanism along deep fractures that penetrated the lithosphere. To date, however, there is no firm evidence that impacts can directly induce terrestrial volcanism, and convincing evidence for local large impacts has not been reported at the sites of flood basalt eruptions. Thus, a direct connection seems unlikely.

Is an indirect connection possible? Energy considerations suggest that the impact of a large (several kilometer-diameter, $\sim 10^{18}$ g) asteroid or comet traveling 20 to 60 km s^{-1} releases $\sim 10^{23}$ to 10^{24} J. Even with a low seismic efficiency of about 10^{-4}, the total seismic energy would be $\sim 10^{19}$ to 10^{20} J, and such an impact is estimated to produce an earthquake with a Richter magnitude ≥ 10. Furthermore, the impact energy is delivered over a very short time period, and thus the rate of energy input into the terrestrial system is orders of magnitude greater than the rate of energy release from terrestrial tectonic processes. Lithospheric stresses created by updoming from a rising mantle plume might be released during such a global seismic event, leading to the kind of rapid decompression melting thought to be required to produce flood basalts.

More recently, calculations indicate that focusing of seismic waves from large impacts can also produce relatively large stresses at their antipodes (and perhaps other caustics) on the Earth, possibly causing lithospheric fracturing and deposition of heat in the upper mantle, that might help to induce or increase ongoing volcanism. Some evidence for this idea comes from finite-element modeling and studies of volcanic centers (e.g., Alba Patera) antipodal to large impact basins on Mars. The Deccan Province was erupted as India sat above the Reunion hot spot, which today lies at about 21°S, 55°E. Reconstructions, however, place the large (>150-km diameter) end-Cretaceous Chicxulub impact structure in Yucatán at ~20°N, 70°W, in the Late Cretaceous, 55° in longitude from the antipodal position from the Reunion hot spot. For the Deccan, at least, the evidence suggests that the eruptions began prior to the large Chicxulub impact, and thus it looks as though that impact could not have triggered the initiation of volcanism.

The wealth of physical evidence for an extraterrestrial impact or impacts at the K/T boundary, and the close timing of many of the extinctions with the worldwide impact ejecta layer, suggests that the primary cause of the K/T mass extinctions was the collision of an asteroid or comet with the Earth. If, indeed, some species of life died out prior to the large impact event, then the Deccan eruptions might be implicated. Some critics of the impact interpretation, however, have attempted to attribute all of the important components of the K/T boundary layer to volcanism. Suggestions that the anomalous iridium at the boundary was a product of Deccan volcanism are ruled out by the generally low iridium values in the Deccan lavas, in soils and weathering profiles between flows, and in K/T boundary sections on the Indian subcontinent. Furthermore, despite arguments to the contrary, experimental and observational evidence clearly shows that shocked quartz and stishovite cannot be produced at the pressures characteristic of volcanic eruptions, and the K/T tektite glass has features incompatible with a volcanic origin. If volcanism did contribute to the end-Cretaceous extinctions, it did not produce these forms of evidence.

IV. EXPLOSIVE VOLCANISM AND EFFECTS ON LIFE

Explosive volcanic eruptions can definitely produce global aerosol clouds in the stratosphere, and historic explosive events, such as Tambora in 1815 and more recently Pinatubo in 1991, have had significant short-term climatic effects. Thus, it is also worthwhile to consider the environmental effects of the largest known explosive eruptions.

A. The Toba Eruption and Volcanic Winter

The largest (~2800 km^3 of magma) explosive eruption of the last few hundred thousand years was the ~74,000 year B.P. Toba eruption (Indonesia). Toba occurred during a relatively rapid interglacial-glacial cooling and sea-level drop, which may have played a role in triggering the eruption. Stratospheric dust and aerosols (~1000 MT) could have accelerated the cooling by causing a "volcanic winter" with global temperature decreases of 3 to 5°C, and ~10°C during the growing season at mid-to-high latitudes for a year or more, with possible longer term climatic effects. Ice core studies indicate that the Toba aerosols remained in the stratosphere for the unusually long time of ~6 years.

Botanical studies suggest that very cold-sensitive tropical vegetation would be affected disastrously by abrupt low-latitude cooling. Furthermore, computer model simulations show that reduction of early growing-season temperatures by ~10°C can kill ≥50% of temperate to sub-Arctic evergreen forests, and severely damage the surviving trees. Temperate deciduous trees, and other less cold-hardy vegetation, are expected to fare even worse. These results suggest a global ecological crisis, with reductions in standing crops of plants and animals. Evidence for such abrupt environmental changes in the aftermath of Toba might be detectable in high-resolution records (e.g., lakes and bogs) and ice cores.

Although no major extinctions are seen at the time of Toba's blast, human genetic studies indicate that prior to ~50,000 years ago the human population suffered a severe bottleneck (perhaps only 4000 to 10,000 individuals for ~20,000 years), followed by rapid population increases, technological innovations, and spread of humans "out of Africa." The predicted environmental and ecological effects of the Toba eruption lend support to a possible connection between that volcanic event and the human population bottleneck, and other faunal/floral changes are predicted.

SEE ALSO THE FOLLOWING ARTICLES

The Ecology of Volcanoes: Recovery and Reassembly of Living Communities • Flood Basalt Provinces • Hazards of Volcanic Gases • Volcanic Contributions to the Carbon and Sulfur Geochemical Cycles and Global Change • Volcanism on Mars

FURTHER READING

Courtillot, V., Jaeger, J.-J., Yang, Z., Feraud, G., and Hofmann, C. (1996). The influence of continental flood basalts on mass extinctions: Where do we stand? *Geological Soc. Am. Special Paper* **307,** 513–525.

Mahoney, J. J., and Coffin, M. F., eds. (1997). Large igneous provinces: Continental, oceanic and planetary flood volcanism. *Geophys. Monograph* **100**.

Rampino, M. R., and Self, S. (1994). Climate-volcanic feedback and the Toba eruption of ~74,000 years ago. *Quat. Res.* **40,** 69–80.

Rampino, M. R., Self, S., and Stothers, R. B. (1988). Volcanic winters. *Annu. Rev. Earth Planet. Sci.* **16,** 73–99.

Self, S., Kesthelyi, L., and Thordarson, Th. (1998). The importance of pahoehoe. *Annu. Rev. Earth Planet. Sci.* **26,** 81–110.

Thordarson, Th., and Self, S. (1996). Sulfur, chlorine and fluorine degassing and atmospheric loading by the Roza eruption, Columbia River Basalt Group, Washington, USA. *J. Volcanol. Geotherm. Res.* **74,** 49–73.

This Page Intentionally Left Blank

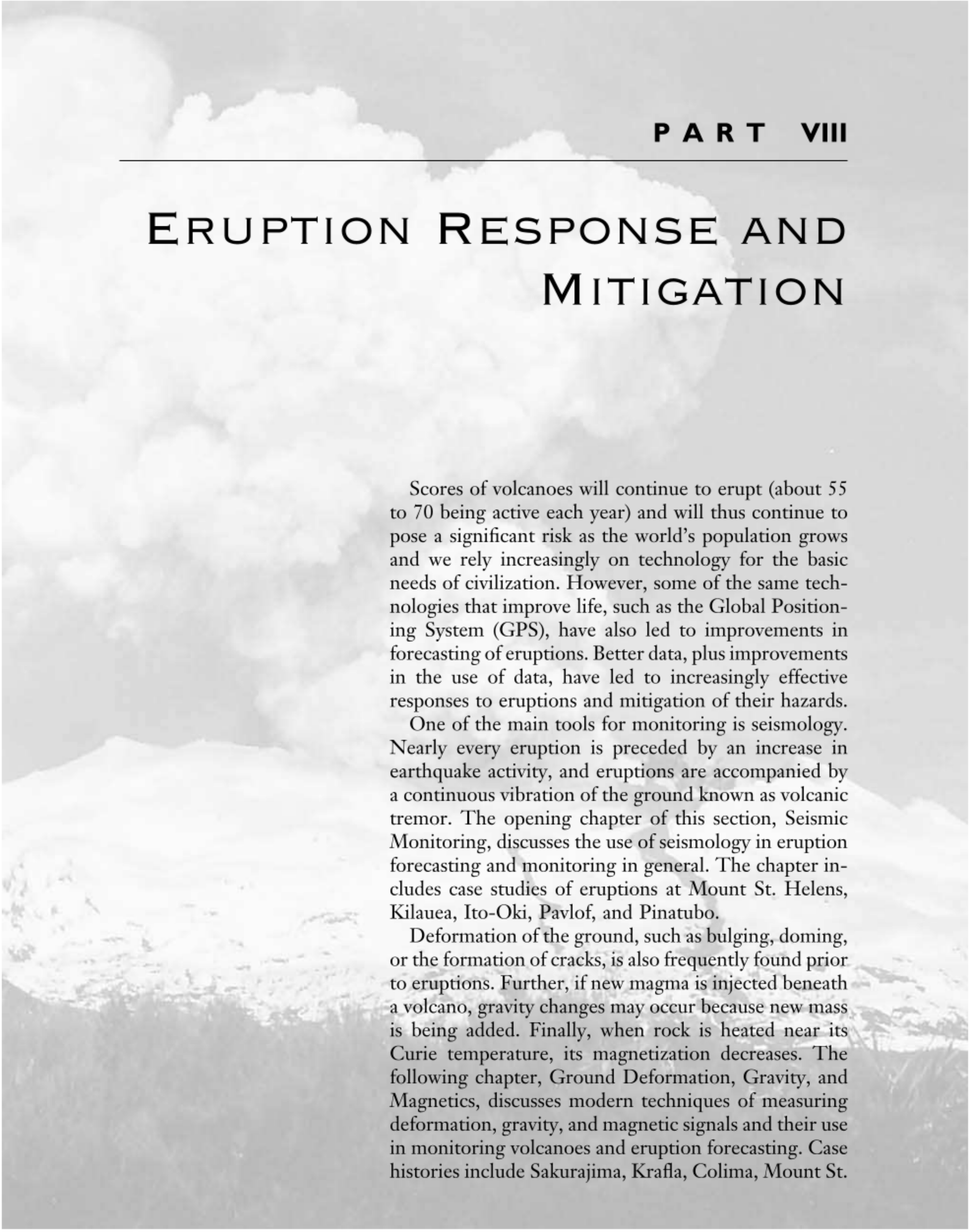

PART VIII

ERUPTION RESPONSE AND MITIGATION

Scores of volcanoes will continue to erupt (about 55 to 70 being active each year) and will thus continue to pose a significant risk as the world's population grows and we rely increasingly on technology for the basic needs of civilization. However, some of the same technologies that improve life, such as the Global Positioning System (GPS), have also led to improvements in forecasting of eruptions. Better data, plus improvements in the use of data, have led to increasingly effective responses to eruptions and mitigation of their hazards.

One of the main tools for monitoring is seismology. Nearly every eruption is preceded by an increase in earthquake activity, and eruptions are accompanied by a continuous vibration of the ground known as volcanic tremor. The opening chapter of this section, Seismic Monitoring, discusses the use of seismology in eruption forecasting and monitoring in general. The chapter includes case studies of eruptions at Mount St. Helens, Kilauea, Ito-Oki, Pavlof, and Pinatubo.

Deformation of the ground, such as bulging, doming, or the formation of cracks, is also frequently found prior to eruptions. Further, if new magma is injected beneath a volcano, gravity changes may occur because new mass is being added. Finally, when rock is heated near its Curie temperature, its magnetization decreases. The following chapter, Ground Deformation, Gravity, and Magnetics, discusses modern techniques of measuring deformation, gravity, and magnetic signals and their use in monitoring volcanoes and eruption forecasting. Case histories include Sakurajima, Krafla, Colima, Mount St.

Helens, Campi Flegrei, Poas, Etna, White Island, and Aso volcanoes.

In addition to earthquakes and deformation, volcanoes typically show signs of increased heat or changes in degassing prior to eruptions. These may be measured from the Earth's surface or from satellites if the signal is strong enough. During eruptions, plumes of ash and gases rise and may then travel great distances downwind. The next chapter, Gas, Plume, and Thermal Monitoring, examines the monitoring of gases, heat, and plumes and illustrates these with examples from Mount St. Helens, Pinatubo, Showa-Shinzan, Usu, Vulcano, Long Valley caldera, Galeras, Masaya, Etna, Popocatepetl, El Chichon, Spurr, Erebus, Lascar, and others.

Each type of data may be handled and interpreted individually, but experience has shown that much more can be learned when various data sets are combined. Indeed, closely monitored eruptions with many data sets provide much of the basis for progress in volcanology. The chapter Synthesis of Volcano Monitoring describes how various types of data contribute to an evolving understanding of the activity of volcanoes. The sequence of geological, geochemical, and geophysical events is different for different types of eruptions. These ideas are illustrated using detailed case studies from Mount Etna and from Soufriere Hills (Montserrat).

Once scientists agree about the meaning of the data (and even if they disagree), a series of communications need to occur between scientists and those responsible for emergency response. The actions that need to be taken, appropriate for the current or expected hazards, need to be identified and assigned to the right people. The content and distribution of warning messages, maps, videos, alert levels, etc., are the focuses of the chapter Volcano Warnings. Concepts are illustrated using examples from two volcanoes that have erupted, Mount St. Helens and Pinatubo, and one that has not, Long Valley caldera.

Although most eruptions are small, any eruption can pose a risk if people or structures are close to the volcano. Large eruptions, in contrast, affect nearby populations with certainty and have many effects at great distances. In each case, the perception of the events, and the response of society, will dictate whether an eruption is benign or whether a disaster will occur. The next chapter, Volcanic Crises Management, discusses elements of volcanic crises management, drawing on experiences at El Chichon, La Soufriere (Guadeloupe), Popocatepetl, Nevado del Ruiz, and others.

Past eruptions have left deposits that can be studied to learn about the type and distribution of specific volcanic hazards. Further, contemporary eruptions at similar volcanoes may be studied to learn about the general effects of hazards. Once these are identified, coherent strategies may be developed to help mitigate risk. Some of these are direct, such as building dams to protect areas from mudflows. Some are longer term and less direct, such as land use zoning. Others are indirect and strategic, such as setting appropriate rates for insurance. These and other related topics are discussed in the chapter Volcanic Hazards and Risk Management.

When an eruption occurs or is about to occur, the need for information suddenly becomes acute. Much of the needed information can be prepared ahead of time; indeed, the in-between periods last much longer than the eruptive periods. Effective strategies for education and intervention are the subjects of the final chapter of this section, Risk Education and Intervention. Although few studies have been done on the subject, the authors of this article assess the effects of a brief school-based intervention program that they conduct at three schools following the 1995 eruptions of Mount Ruapehu, New Zealand.

Although volcanoes will continue to erupt, knowledge of their behavior and effects, and adequate monitoring programs, can greatly reduce the risks from future eruptions. People can coexist with volcanoes provided they do so intelligently.

Stephen R. McNutt
University of Alaska Fairbanks

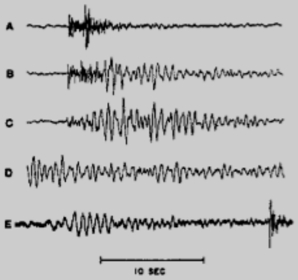

SEISMIC MONITORING

STEPHEN R. MCNUTT
Alaska Volcano Observatory and University of Alaska Fairbanks

I. Introduction—History and Organization
II. Seismic Instruments and Networks
III. Terminology and Types of Volcanic Earthquakes
IV. Forecasting Eruptions
V. Characterizing Eruptions in Progress
VI. Case Histories
VII. Conclusions

GLOSSARY

anomaly An observation that differs from normal or expected values.

deterministic A statement of the likelihood of an event based on a physical model and measurements.

forecast A general description of future events, including rough estimates of time, location, and likely activity.

precursor A geological event that occurs prior to an eruption and is related to the preparation processes of the forthcoming eruption.

prediction A specific description of future events, including time, size, type, location, and formal errors for each.

probabilistic A statement of the relative likelihood of an event based on study of a population of similar events that have occurred in the past.

reduced displacement The root-mean-square (rms) amplitude of volcanic tremor multiplied by the distance from the station to the source. This has the effect of correcting data to a common reference point.

seismic network A group of seismic stations that are deployed in a region for the purpose of detecting and locating earthquakes.

seismic station A set of instruments including a seismometer (buried in the ground), cables, batteries, solar panels, amplifiers, radios, and antennae located in an enclosure nearby.

spectrogram A plot of frequency in hertz (Hz) of seismic signals as a function of time. Typically the strength of the signal is shown as a color or shading.

swarm A group of many earthquakes of similar size occurring closely clustered in space and time with no dominant main shock.

telemetry The set of instruments and communications that send a data signal from their source to a distant data acquisition system. May include radio, microwave, telephone, and satellite components.

SEISMOLOGY IS AN important and effective tool for monitoring volcanoes and forecasting eruptions. In the past 2 decades there have been over 25 successful forecasts. Well-monitored volcanoes have six or more local seismic stations within 15 km and several regional stations (>15 km) which are able to detect volcanic earthquakes of $M \geq 0$ under the volcano.

Copyright © 2000 by Academic Press
All rights of reproduction in any form reserved.

The recording of several years of background seismicity is important to establish a baseline for evaluation of possible precursors. Four main types of events are recorded: high-frequency earthquakes, low-frequency earthquakes, explosion earthquakes, and volcanic tremor. Surface events such as rockfalls, avalanches, and mudflows are also recorded. Volcanic earthquakes prior to eruptions generally occur in swarms; have maximum sizes of $M < 5$; include many events with similar waveforms; have high b values; increase in numbers before eruptions; and occur beneath or near the site of eruptions. Many swarms follow a regular sequence consisting of the following components: background, swarms of high-frequency events, relative quiescence after the peak rate, low-frequency events, volcanic tremor, eruption, and deep earthquakes following eruption. This sequence reflects systematic changes in locations of earthquakes and in the dominant physical processes.

I. INTRODUCTION—HISTORY AND ORGANIZATION

Seismic monitoring is the systematic checking of the status of seismic activity at a volcano. Monitoring attempts to associate key diagnostics, such as rates, types of earthquakes, and changing locations, with physical processes involved in the movement of magma. This can be done probabilistically by comparing current activity at the volcano of interest with comparable past activity at similar volcanoes. It can also be done deterministically when a particular process can be associated with seismic signals with a high degree of confidence. Seismic monitoring can help determine if a volcano: (1) is in a background or restful state; (2) is restless; (3) shows precursory activity; (4) has begun to erupt; (5) is actively erupting; (6) is ending an eruption; or (7) is returning to a background state. Seismic monitoring is fairly effective alone, but is better utilized as one component of an integrated monitoring effort.

TABLE I Selected Early Volcano Observatories and Observations with Seismometers

Volcano	*Country*	*Date*	*Type of instrument*
Vesuvius	Italy	1856	Mechanical
Usu	Japan	1910	Electromechanical
Kilauea	USA	1912	Electromechanical
Sakurajima	Japan	1914	Electromechanical
Aso	Japan	1930	Electromechanical
Merapi	Indonesia	1924	Electromechanical

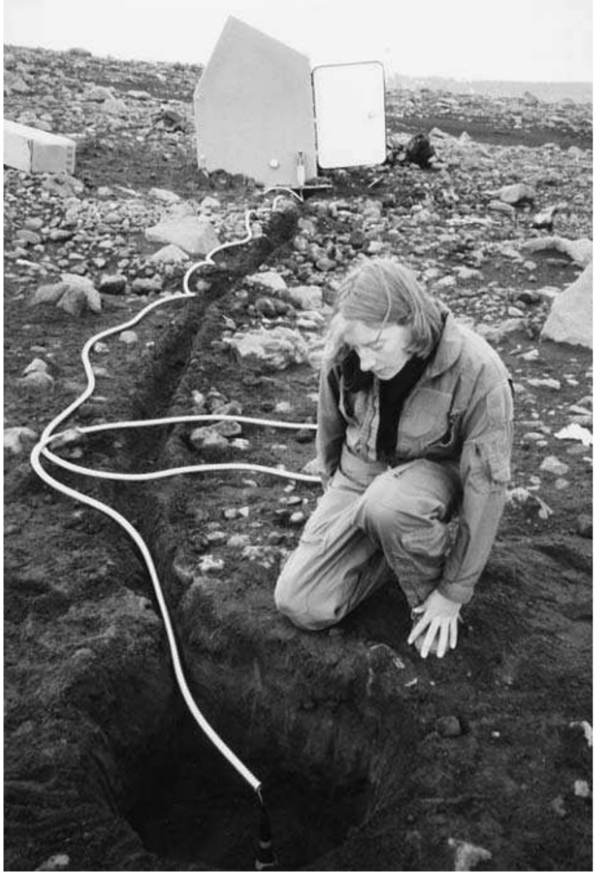

FIGURE 1 Seismic station PN7 at Pavlof volcano, Alaska. The seismologist is checking to make sure the seismometer is level in the bottom of the hole in which it will be buried. A cable carries the signal to a custom-designed hut which houses the batteries, antenna, and electronics. Solar panels are mounted on the top left of the hut, which faces south. (Photo by S. McNutt.)

Nearly every recorded volcanic eruption has been preceded by changes in seismic activity beneath or near the volcano. For this reason, seismology has become one of the most useful tools for eruption forecasting. Early observatories (Table I) included seismometers that were at first crude mechanical devices, but were later upgraded to more modern electromechanical types (see Figure 1). At the present time, approximately 200 of the world's volcanoes are seismically monitored (about one-third of the 538 volcanoes that have erupted in historic times). Volcanoes that are actively erupting draw attention both publicly and scientifically, and over half of these are seismically monitored. A good example of this is Montserrat, West Indies, which is active at the time of this writing. There have been a number of generally successful forecasts during the last 2 decades (Table II), although the exact criteria for claiming success and the levels of precision have been variable.

A key development in monitoring during the last 20 years has been the proliferation of modern computers, which has led to dramatic improvements in speed and precision in locating earthquakes as well as in determining properties of seismic waves, often in "near real time." For example, many digital data acquisition systems record at 100 samples per second, so arrival times can be measured to the nearest 0.01 as opposed to 0.1 for old paper records and 0.05s for film recorders. This precision, together with close station spacing, has the effect of improving location accuracy, and the best located earthquakes have formal errors as low as 50–100 m horizontally and 100–300 m vertically.

TABLE II Some Successful Forecasts of Explosive Volcanic Eruptions, 1980–1999

Volcano and location	*Year of forecast*
Mount St. Helens, Washington	1980–1986
Galunggung, Indonesia	1982
Merapi, Indonesia	1984
Izu Oshima, Japan	1986
Banda Api, Indonesia	1988
Kie Besi, Indonesia	1988
Tokachi-dake, Japan	1988
Galeras, Colombia	1989
Izu-Tobu, Japan	1989
Redoubt volcano, Alaska	1989–1990
Kelut, Indonesia	1990
Unzen, Japan	1990–1991
Mount Pinatubo, Philippines	1991
Colima, Mexico	1991
Lonkon, Indonesia	1991
Mount Spurr, Alaska	1992
Mayon, Philippines	1993
Mount Klyuchevskoi, Kamchatka	1994
Rabaul Caldera, Papua New Guinea	1994
Popocatepetl, Mexico	1994
Montserrat, West Indies	1995–1997
Pavlof, Alaska	1996
Shishaldin, Alaska	1999

Note. Compiled by J. Power, C. Newhall, T. Casadevall, and S. McNutt.

Electronic data bases have greatly facilitated the storage and manipulation of large data sets, which in turn have facilitated the use of data-intensive forms of analysis. An example is seismic tomography, which uses data from thousands of earthquakes to produce 3D images of earth structures. Automation of many tasks has improved the ability to analyze many types of data in near real time, which leads to better methods of both forecasting and characterizing eruptions in progress. For example, near-real-time (several minutes after the fact) reduced displacement measurements and spectrograms measure time-domain amplitudes and frequency-domain amplitudes automatically. Both of these produce time series (see below) which are routinely interpreted in terms of changing volcanic processes. The plots now can be produced automatically and posted to the World Wide Web, so anyone with a computer and modem can view them.

II. SEISMIC INSTRUMENTS AND NETWORKS

Most seismometers used to monitor volcanoes are located on the flanks at distances within 15 km (Figure 2). About a third of the monitored volcanoes have at least one station within 1 km of the active vent. Modern networks generally consist of six or more stations. Station spacing of a few kilometers enables better detection of small earthquakes and generally small location errors (<0.5 km). Data are usually telemetered to a common site and recorded on drum recorders as well as on digital computers.

Many tasks are now automated on computers and run in near real time, which means the data are available for viewing a few minutes after the fact. For example, when an earthquake occurs, there is an abrupt increase in the signal level at several stations at nearly the same time. This feature is exploited by algorithms that look for an increase in the short-term average (STA) of 0.5–1.0 seconds above a long-term average (LTA) of 30 seconds to 1 minute at a certain LTA/STA threshold, such as a factor of four. When the algorithm is triggered, a file is opened and 1 minute or so of data are written for all stations of a given network. This type of strategy is efficient because only the data that matter—from the earthquake—are kept, in compact form.

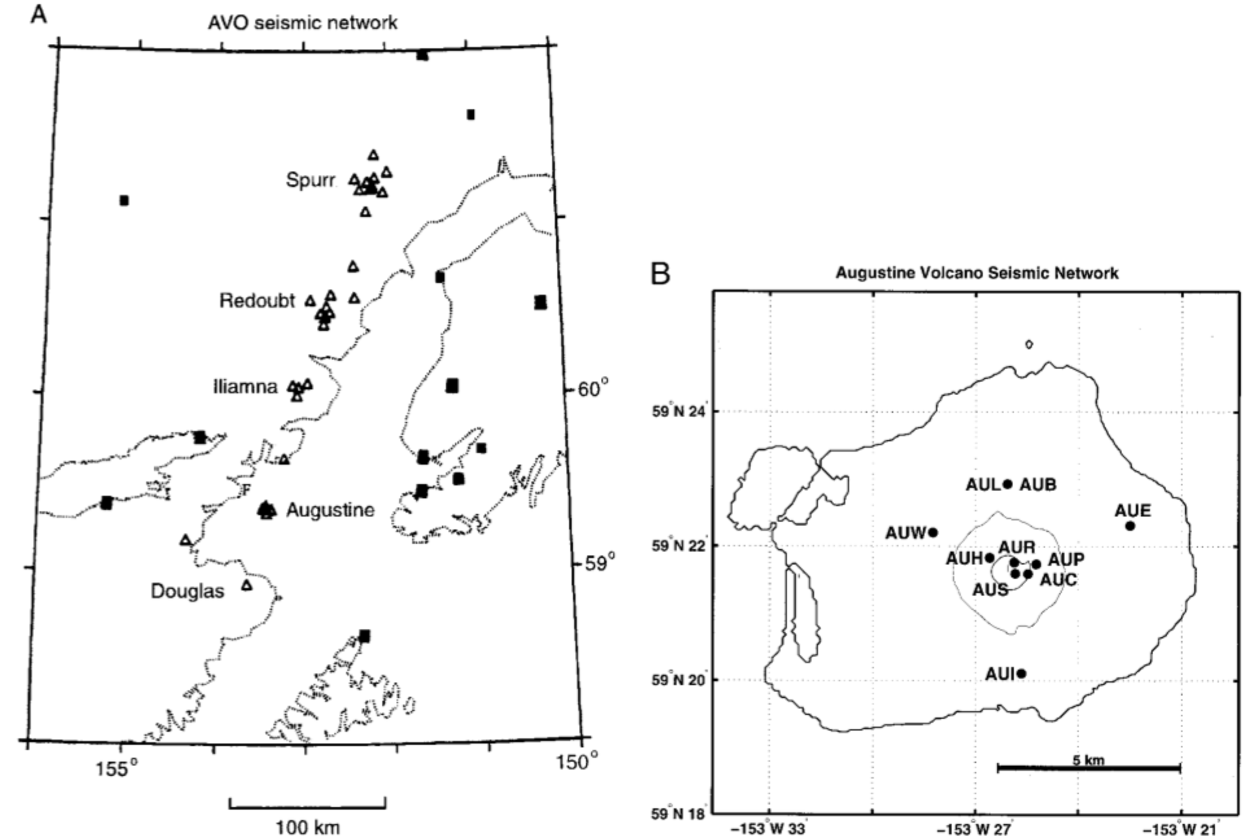

FIGURE 2 (A) Map of local (open triangles) and regional (solid squares) seismic stations in the Cook Inlet region of Alaska. Clusters of stations are located near each of the five active volcanoes. (B) Map of local seismic stations near Mount St. Augustine. Most well-monitored volcanoes have similar networks of six to eight stations.

To retain small events and emergent signals like tremor, several observatories continuously record digital data. A number of volcanoes are monitored indirectly because a nearby (>15 km) seismic station is part of a larger regional seismic network. Maps showing distributions of seismic stations near several volcanoes in Alaska are shown in Figure 2. Topography, telemetry, and ease of access often determine the exact location of stations.

Most seismometers at volcanoes are short-period (1 s) vertical instruments which record useful data between about 0.7 and 30 Hz. They consist of a magnetic mass suspended on a spring, surrounded by a coil of wire. When the mass moves in response to ground motion, a current is generated in the coil. Modern three-component, digitally telemetered, high-dynamic-range, broadband seismometers record over a much wider band of frequencies (0.02 to 50 Hz). These instruments also have a mass and spring, but the coil that senses the motion is connected to a feedback circuit which sends a current through another coil exactly to oppose the motion. Thus the mass is held fixed, and the feedback current is proportional to the ground motion. Such broadband seismometers also have a much higher dynamic range, up to 145 dB, as opposed to about 40 dB for analog telemetry. Temporary deployments of these broadband instruments have become common recently, and permanent deployments of 1 to 10 instruments at well-monitored volcanoes are becoming more widespread. Microphones are often added to seismic stations to add an additional independent data channel. They are used to record air waves from explosions and other features of the radiated sound field; they also measure atmospheric pressure fluctuations from wind and storms.

Volcano observatories vary widely in location and sophistication. The simplest observatories may be a small observation hut, with a single seismograph recorded on paper on a revolving drum. Many larger observatories are located near volcanoes at distances of several tens to several hundreds of kilometers, and seismic data from local and regional stations are telemetered to them by cable, radio, and telephone. Some observatories are colocated with universities or other research organizations. These may be hundreds of kilometers from the volcanoes of interest, yet the vast array of modern communications available today make such facilities common and economical. They are, further, safe from large eruptions which may affect closer facilities. There are approximately 90 members of the World Organization of Volcano Observatories (WOVO) as of this writing, most with some kind of seismic monitoring capability.

The distance from an earthquake to a seismic station and the magnification of the station are the main factors that determine the magnitude detection threshold, that is, the smallest signals that can be recorded. Typical magnifications at volcanoes are 5000 to 50,000, and the corresponding magnitudes of detection are about $M = 0$ to $M = 1$ for the 1- to 15-km distances involved. It is desirable to record the smallest earthquakes possible, but because volcanoes often have high noise levels, this is usually achieved by putting stations close to the vent rather than operating more distant stations at higher magnifications.

The largest events in swarms preceding most eruptions typically have magnitudes of $M = 2$ to $M = 3$. However, many larger events have occurred at volcanoes, especially calderas (Table III), and some of these

TABLE III Selected Large Earthquakes Near Volcanoes

Volcano	*Year*	M_{max}	*Comment*
Arenal	1968	4.5	Pre-eruption
Asama	1916	6.3 M_S	No eruption
Aso	1975	6.0	No eruption
Bandai	1888	5	Triggered eruption
Bezimianny	1956	5.0	Pre-eruption
Fernandina	1968	5.7 M_S	Caldera collapse
Gorely	1985	≤ 6	Posteruption (8 months)
Ito-oki	1989	5.5	Pre-eruption
Jan Mayen	1954	5.8	No eruption
Kalapana	1975	7.1 M_S	Shallow thrust
Katmai	1912	7.0	Posteruption
Long Valley	1980	6.2 M_L	4 earthquakes with $M \geq 6$, no eruption
Miyake-jima	1962	5.9	Strong swarm
Miyake-jima	1982	6.4 M_{JMA}	Swarm 20 km deep
Miyake-jima	1983	6.2 M_S	During eruption
Mt. St. Helens	1980	5.2 M_S	Triggered eruption
Mt. Usu	1910	5.5	Pre-eruption
Mt. Usu	1943–1944	5.0	Pre-eruption
Mt. Usu	1977	3.7	Pre-eruption
Mt. Usu	1977–1980	4.3	Emplacement of cryptodome
Pinatubo	1991	5.7	Co-eruption
Sabancaya	1991	5.6 M_S	10 km NE of summit
Sakurajima	1914	7.0 M_S	10.5 hours posteruption, depth 13 km
Sheveluch	1964	5.5	Pre-eruption
Showa-Shinzan	1944–1945	3.8	Dome emplacement
Unzen	1792	5–5.5	Accompanied collapse

Note. M_{max}, maximum magnitude; M_S, surface wave magnitude; M_L, local (Richter) magnitude; and M_{JMA}, Japan Meteorological Agency magnitude.

are large enough to be hazardous in their own right. Magnitude 4 to 5 earthquakes are common at volcanoes with large deformations in the form of doming, bulging, and sector collapses; events associated with the latter may reach $M = 5.5$. To date no definitive correlations have been found between the size of preceding earthquakes and the volume or explosivity of the resulting eruption.

A seismometer in the vicinity of a volcano will typically record seismic signals from four sources: the volcano, local earthquakes (<15 km), regional earthquakes (>15 km), and teleseisms (generally >600 km). Part of the job of the seismologist is to recognize and discriminate among these. It is especially helpful to record data from several stations at regional distances of 50–200 km to aid in the identification process. Two examples illustrate why these are helpful. At Nevado del Ruiz volcano, Colombia, in November 1985 and later, many earthquakes from the Bucaramonga nest, a persistent deep source of earthquakes beneath Colombia, appeared on seismograms from stations near the volcano. The Bucaramonga event seismograms resembled many of the volcanic events, and their occurrence created confusion. At Spurr volcano, Alaska, in 1992, the seismic signal for two eruptions began gradually but the third began sharply and its onset looked like that of a regional earthquake. However, the pattern of arrival times and relative amplitudes at local versus regional stations quickly revealed that the event was an eruption at the volcano.

In general, there are many more small earthquakes than large ones. This is a consequence of the fact that the size distribution of earthquakes obeys a power law, which in seismology is of the form $\log_{10}N = a - bM$, (where N is the cumulative number of events, M is magnitude, and a and b are constants) and is known as the Gutenberg–Richter relation. The slope, or b value, determines the relative number of large versus small events. While for tectonic earthquakes the b value has typical values of 0.9 to 1.0 worldwide, more extreme values have been observed at volcanoes. High-frequency events have values ranging generally between 0.6 and 1.3, but low-frequency events have b values of up to 3.0. This means, for low-frequency events, that small earthquakes dominate, and also implies that the source size is restricted. Determination of the b value for volcanic earthquakes is an important diagnostic tool for identifying changes in seismicity.

At volcanoes, most earthquakes occur at depths of 10 km or less. Deeper events are common but the number of events is considerably smaller. A trend recently observed at several volcanoes is that deeper earthquakes (10–40 km) occur after major phases of eruption. It is thought that these events are occurring in response to stress changes caused by the removal of magma at depth. The cumulative energy of deep quakes may be proportional to the volume of magma erupted.

It is important to keep track of the amplitude of the ground shaking, so calibration information for each seismic station is stored and used to help determine earthquake magnitudes and the reduced displacement of continuous signals such as volcanic tremor. These "normalized" measures allow comparison between different volcanoes. Similarly, several observatories compute spectrograms—plots of the frequency of ground shaking versus time—to help identify low-frequency events and to help distinguish between earthquakes, noise, and other types of signals.

Some volcanic signals have gradual onsets or very long durations (hours to days or more). For these events, traditional location methods, which depend on measuring arrival times for P and S waves, cannot be used. New techniques use data from dense networks or "arrays." Here, the stations are very close, a few tens to hundreds of meters apart, so it is possible to see the same wave coherently on all the stations (the wave need not be a first or prominent arrival). Because the physics of waves are well known, it is possible to determine what type of wave is present, which direction it is coming from, and how fast it is moving. All these provide information about the sources. Thus, dense arrays can be used like antennae to discern certain features of specific types of seismic waves even when the signals are weak or noise is present. Array methods look at different features of seismograms and thus extend the information available for analyses.

III. TERMINOLOGY AND TYPES OF VOLCANIC EARTHQUAKES

Active volcanoes are the sources of a great variety of seismic signals. Traditionally, volcanic earthquakes have been classified based on seismogram appearance into four different types: high-frequency or A-type, low-frequency or B-type, explosion quakes, and volcanic tremor. This classification scheme works very well at a large number of volcanoes. For monitoring, it is important to quickly recognize different types of events and the exact terminology is less important. Other local signals, such as those caused by glaciers or landslides, are also recorded at volcanoes, and need to be distinguished

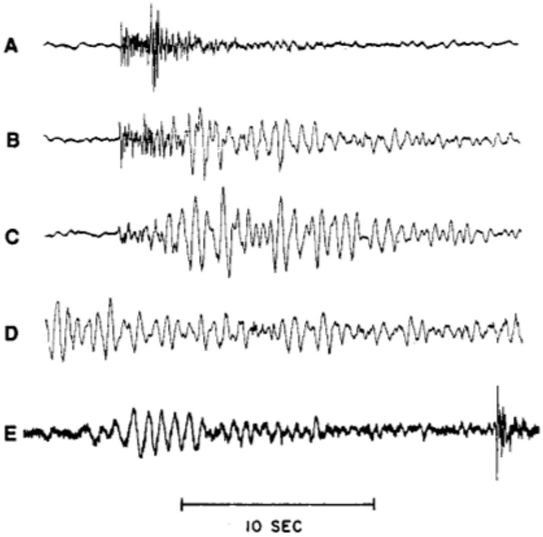

FIGURE 3 Typical waveforms of volcanic earthquakes. (A) High-frequency or volcanotectonic earthquake, 6.8 km depth, Redoubt volcano, station RED, 8 km from the vent. (B) Hybrid or mixed-frequency event, −0.6 km depth (0.6 km above sea level), Redoubt volcano, station RED. (C) Low-frequency or long-period event, −0.4 km depth, Redoubt volcano, station RED. (D) Volcanic tremor, Redoubt volcano, station RED. (E) Explosion quake, Pavlof volcano, station PVV, 8.5 km from the vent (note prominent air-wave arrival). [After (A–D) Power, J., *et al.* (1994). *J. Volcanol. Geotherm. Res.* **62,** 69–94; and (E) McNutt (1986).]

from the volcanic events. Although the original classification included restricted depth ranges for various earthquakes, these have often been relaxed because of improvements in location accuracy and better understanding of source and propagation effects. Examples of volcanic events are shown in Figure 3.

A. High-Frequency Events

Most high-frequency events are thought to be caused by shear failure or slip on faults, and differ from their tectonic counterparts only in that they occur predominantly in swarms at volcanoes. High-frequency events have clear P and S waves, and dominant frequencies are 5–15 Hz. A typical small high-frequency event is shown in Figure 3A.

B. Low-Frequency Events

Most low-frequency events are thought to be caused by fluid pressurization processes such as bubble formation and collapse, and also by shear failure, tensile failure, or nonlinear flow processes which occur at very shallow depths for which attenuation and path effects play an important role. These events often have emergent P waves, lack S waves, and have dominant frequencies between 1 and 5 Hz, with 2–3 Hz most common. An example of a low-frequency event is shown in Figure 3C.

C. Hybrid Earthquakes

Some earthquakes share attributes of both high- and low-frequency events. These are called hybrid events, and may represent a mixture of processes. For example, the event shown in Figure 3B displays the high-frequency onset of a high-frequency event, but the later part of the signal (the coda) is similar to low-frequency events.

D. Explosion Earthquakes

Explosion quakes accompany explosive eruptions, and many are characterized by the presence of an air-shock phase on the seismograms. There is a partitioning of energy at the source; part of the energy travels through the ground as seismic waves, and part travels through the air as acoustic or air waves. The air wave then couples back into the ground near the seismometer. The air wave also shows up clearly on microphones or barographs. An example of an explosion quake is shown in Figure 3E.

E. Volcanic Tremor

Volcanic tremor is a continuous signal with a duration of minutes to days or longer. The dominant frequencies of tremor are 1–5 Hz (2–3 Hz is most common), similar to low-frequency events, and many investigators have concluded that tremor is a series of low-frequency events occurring at intervals of a few seconds. Harmonic tremor and spasmodic tremor are two special cases of more general volcanic tremor. Harmonic tremor is a low-frequency, often monotonic sine wave with smoothly varying amplitude, and spasmodic tremor is a higher-frequency, pulsating, irregular signal. An example of volcanic tremor is shown in Figure 3D.

F. Very-Long-Period Events

Over the past decade broadband seismometers have been deployed at volcanoes. These have the ability to detect a wider frequency band, particularly at the low end (down to $f = 0.016$ Hz, or a period of 60 s). A new class of events called very-long-period (VLP) or very-low-frequency (VLF) events have been observed at some volcanoes. Observations to date show events with periods of 3 to 20 s originating from shallow depths of 1.5 km or less under several active volcanoes including Kilauea, Stromboli, Aso, Sakurajima, and Satsuma-Iwojima. The VLP events at these volcanoes have been associated with either eruptions or vigorous fumarolic activity, and the observed events have fairly small amplitudes.

G. Superficial Events

Seismometers located on volcanoes may record a variety of local signals caused by shallow processes. These include nonvolcanic processes such as glacial events, shore ice movement, and landslides, as well as volcano-related processes such as outburst floods and lahars, pyroclastic flows, and rockfalls from crumbling lava domes.

- *Glacial events.* High-latitude and/or tall volcanoes are frequently covered by glaciers. Glaciers produce seismic events along the ice–rock boundary, and within the ice when cracks and crevasses form. Seismograms from such events resemble those for low-frequency (LF) volcanic events.
- *Shore ice events.* Ice forms from seawater when the air temperature falls below 10°F. Large blocks of such ice gather on the shores of Augustine Island, Cook Inlet, Alaska, and move around as the tides ebb and flood. When the blocks collide or break, they produce seismic events because the blocks are coupled to the ground. The individual ice events resemble LF volcanic events, and the events occur in swarms of a few hours duration because of the tides.
- *Landslides.* Avalanches and landslides of various sizes occur on volcanoes. Those associated with partial melting of ice and snow mainly occur in the spring and summer. The main avalanche or landslide generates a seismic signal of several minutes duration, depending on the size and runout. The amplitude varies with the amount of material, with larger avalanches generating stronger seismic signals.
- *Rockfalls.* Rockfalls are a special type of landslide in which one or a few pieces of bedrock become detached and free fall. They are especially common at the edges of volcanic domes and at volcanoes with very steep slopes or cliffs. In the summer of 1995 workers at Mount Spurr, Alaska, observed rocks more than 1 m in diameter falling several hundred meters and impacting on the crater floor. The corresponding seismograms showed strong local signals lasting more than 1 minute.
- *Pyroclastic flows.* Pyroclastic flows are products of explosive eruptions and consist of particles of hot molten rock and gases which move rapidly over the ground surface. Collapses of volcanic domes can also produce pyroclastic flows. These latter events were characterized by complex seismograms which have been modeled as a sequence of forces. First, rock is removed from the dome (the dome moves up slightly in response); second, the falling rock collides with the slope below (an impact); and third, the rock breaks apart and the fragments continue to move down the slope as an irregular flow. These seismograms last several minutes and may contain high frequencies, and the larger flows are associated with larger amplitude signals.
- *Outburst floods and lahars.* The surface melting of ice and snow, or heavy rains, may cause floods and lahars (volcanic mudflows). Similarly, a volcanic eruption under a glacier will melt the ice, and the flooding that subsequently occurs is called a jokullhaup. All these floods or lahars cause long-duration seismic signals that resemble volcanic tremor, except that the signal is stronger near the flow channel, as opposed to tremor, which is stronger nearer the volcanic vent.

Seismic monitoring requires regular checks of data at times of interest, and preparation of plots and maps to display data so that anomalies may be indentified and interpreted. For example, counts are often made of the number of earthquakes of each type per hour or day. These are especially helpful to identify small events which increase in numbers before eruptions. Maps and cross sections are made of all locatable earthquakes at periodic intervals such as a day or week. Locatable events must be large enough to show up on three or more stations, so these are fewer in number than countable events. Spectra may be computed for background signal and earthquakes to look for the onset of low-frequency events or tremor. Signal amplitudes are determined to distinguish storm noise from possible tremor, and to track tremor once it starts.

All the seismic data are combined with other data on a regular basis, and attempts are made to develop a working hypothesis of what is physically occurring to cause the observed signals. Such hypotheses or conceptual models are continually revised as conditions change.

These are the link between the raw data and the science. In the remainder of this article it is assumed that the seismic events have been properly identified and classified.

IV. FORECASTING ERUPTIONS

The main goals of seismic monitoring of volcanoes are to know the present status of a volcano, to forecast eruptions, to estimate the size of eruptions in progress, and to understand the physical processes that are occurring. Seismic monitoring can help determine if a volcano: (1) is in a background or restful state; (2) is restless; (3) shows precursory activity; (4) has begun to erupt; (5) is actively erupting; (6) is ending an eruption; or (7) is returning to a background state. The primary focus of this article is forecasting eruptions. For this, goals are estimating the date and time, the place, the size and type, and the likely duration of eruptions. A variety of observations have a bearing on these problems.

A. Seismicity Rates and Background

Volcanoes nearly always have a high background level of seismicity. Thus, a baseline of measurements of at least a few years duration is usually necessary to characterize and understand background seismicity. The background may consist of several different types of events, which are related to different processes. Typical background rates of seismicity are a few to a few tens of events per day, depending on the locations and magnifications of the seismic stations. In contrast, the rates of seismicity before and during eruptions are typically several tens to several hundreds or more events per day, and include larger-magnitude events. Many successful eruption forecasts have been made based on an increase in seismicity above previously recorded background levels. However, the main physical processes that cause seismicity are those associated with magma intrusion. Thus, there will always be a false alarm rate because some intrusions remain at depth whereas others reach the surface and erupt.

In terms of trying to assess the *type* of eruption prior to its onset, previous eruptive activity is a better guide than any seismic feature yet identified. This is true for all of the case studies discussed in Section VI except for Ito-oki in 1989, which formed a new vent. For the formation of new volcanoes, such as Paricutin, Mexico (1943), Surtsey, Iceland (1963), or Novarupta, Alaska (1912), geology of the surrounding area is a better guide than earthquake activity to determine the type of impending eruption.

B. Statistics of Volcanic Seismicity

Statistical information on many volcanoes, swarms, and eruptions provides a broad perspective to evaluate potential precursors (Table IV). It is helpful to have such information available during a seismic crisis to have an idea of the possible range of activity. However, a comparison of seismic activity at Kilauea and Krafla demonstrates a potential pitfall. Both of these volcanoes produce basalt, and fissure eruptions are common at each. For Kilauea, of 73 swarms studied, 31% accompanied eruptions, 42% accompanied intrusions, and 27% were associated with inflation episodes. Except for harmonic

TABLE IV Parameters of Volcanic Eruption Seismic Precursor Case Histories

Volcano name	*Date*	*VEI*[a]	*Swarm duration (days)*	*Time since previous eruption (years)*	*Precursor event type*[b]	*Precursor maximum magnitude*
Mount St. Helens	5/18/80	5	59	123	H, L, T	5.0
Kilauea	1/3/83	3	99	0.25	H, L, T	4.2
Ito-oki	7/13/89	2	53	—	H, L, T	5.5
Pavlof	9/16/96	3	5	8	L, T	0.5
Pinatubo	6/15/91	6	70+	600	H, L, T	4.3

[a] Volcanic explosivity index.

[b] H, high-frequency or volcanotectonic earthquakes; L, low-frequency or long-period earthquakes; and T, volcanic tremor.

tremor generated near an erupting vent, intrusions and eruptions were seismically indistinguishable. This suggests that the only difference between an intrusion and an eruption is the magma level compared to ground level. At Krafla, similar numbers were obtained for 20 swarms which included volcanic tremor and occurred in association with deflation episodes; 9 swarms accompanied eruptions and 11 occurred during intrusions. However, the first 5 were intrusions and the last 6 were eruptions; thus the statistics changed substantially as a function of time. Here the magma level was presumably lower for the intrusions and higher for the eruptions.

C. Volcanic Tremor

Volcanic tremor (Figure 3D), which has several possible mechanisms, is an especially common short-term precursor to eruptions. Tremor was the most common short-term precursor in a recent study of 132 historical cases of phreatic eruptions. This suggests a close link between tremor and hydrothermal processes (tremor known to be related to hydrothermal processes is weaker than that associated with magmatic activity, although frequencies are similar). Tremor was the most consistent short-term indicator of impending eruptions in a study of 200 calderas worldwide. This study did not distinguish between different tremor mechanisms. While most tremor episodes accompany eruptive activity, about 20% precede eruptions on a time frame of 10 days. This value of 20%, however, did not distinguish between different tremor mechanisms. Nevertheless, in spite of different mechanisms, clearly volcanic tremor is a common and important precursor to many eruptions.

D. Generic Volcanic Earthquake Swarm Model

Common observations suggest a general model of earthquake activity at volcanoes. The model, which is termed a generic volcanic earthquake swarm model, is shown as a time series in Figure 4. Seismicity rates, types of events, and dominant processes are indicated in the commonly observed temporal sequence. Variations in the involvement of groundwater, as well as variations of parameters such as magma composition, temperature, rate of flow, and volatile content, can explain many of the observed differences from this model of seismic activity at different volcanoes.

In the generic model, high-frequency earthquakes reflect shear fracture of the country rock in the vicinity of volcanoes in response to increasing magmatic pressure. Since magma movement at depth may occur over large

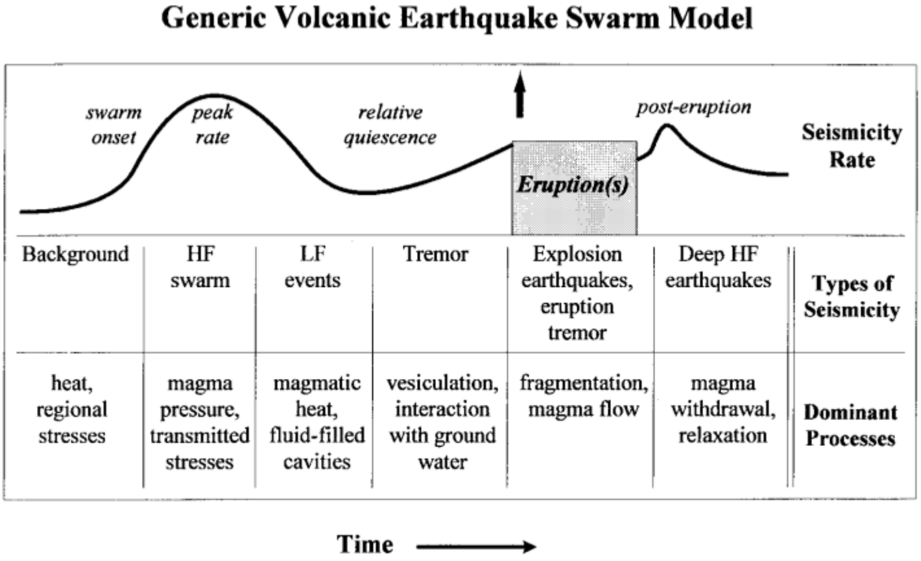
Generic Volcanic Earthquake Swarm Model
swarm onset
peak rate
relative quiescence
post-eruption
Eruption(s)
Seismicity Rate
Background
HF swarm
LF events
Tremor
Explosion earthquakes, eruption tremor
Deep HF earthquakes
Types of Seismicity
heat, regional stresses
magma pressure, transmitted stresses
magmatic heat, fluid-filled cavities
vesiculation, interaction with ground water
fragmentation, magma flow
magma withdrawal, relaxation
Dominant Processes
Time

FIGURE 4 Schematic diagram of the time history of a generic volcanic earthquake swarm model. Seismicity rates are shown along with the main types of events observed at each stage. Some ideas about dominant processes are presented at the bottom of the figure. [After McNutt, S. (1996). Page 99–146 *in* "Monitoring and Mitigation of Volcanic Hazards" (Scarpa/Tilling, eds.). Springer-Verlag, Berlin/Heidelberg.]

distances and long periods of time, the durations of high-frequency swarms are long. At shallow depths of 1 to 3 km, several significant changes occur. First, gases begin to exsolve from the magma, changing its mechanical behavior and, hence, its ability to transmit or reflect seismic waves. For example, exsolution of volatiles will increase the viscosity and lower the acoustic velocity. A seismic event generated by resonance of a magma-filled cavity would thus be richer in lower frequencies. Second, the magma may encounter groundwater, modifying the shallow hydrothermal system and removing some of the available magmatic heat by conduction and advection. Most low-frequency events and tremor originate at shallow depths, and several models for their origin involve fluids, either water, magma, exsolved volatiles, or all three. Tremor caused by boiling of water is generally weaker than tremor involving magma movement. Third, open cracks are found above 3 km depth in the earth, permitting venting of excess pressure. This may explain the relative quiescence after the peak rate of a swarm as well as the inverse relation between high-frequency events and tremor.

The upper 1 to 3 km are small distances compared with depths to magma chambers (5–20 km) or crustal thicknesses (about 35 km). Thus, if vertical magma ascent rates are constant, then durations of low-frequency event swarms and tremor sequences will be shorter than those of high-frequency events simply because the distances are smaller. Deep earthquake swarms following eruptions probably reflect stress changes associated with partial evacuation of magma chambers deeper than 5 km.

Relative seismic quiescence following an initial seismicity peak occurred in 25% of a worldwide sample of 192 swarms. While quiescence 25% of the time may seem too low a percentage to be included in a generic model, it is included because of its importance in terms of eruption forecasting and identifying physical processes. Factors that may cause quiescence include strain hardening; high temperatures near the brittle–ductile transition; increased water content (e.g., groundwater) lowering effective stress; or a reduction in strain rate. It is common for low-frequency events and tremor to occur after seismicity rate peaks, during times of relative quiescence. This may be explained by gradual shoaling of the source, particularly magma interacting with groundwater or exsolution of volatiles.

Each volcano is unique in its seismic behavior, but the observations suggest that variations in a few parameters such as those discussed above may account for the main differences. Minor variations in each of several parameters may greatly affect one observed parameter, such as swarm durations. The durations of earthquake swarms are characterized by a log-normal distribution with a mean of 5 days (Figure 5). No definitive correlations exist between the duration of a swarm and the size or type of eruptive activity. This is not surprising given the ranges of sizes, rates, compositions, and types of structures observed.

Recently, parameters of 700 volcanic earthquake swarms have been compiled into an electronic data base called the Global Volcanic Earthquake Swarm Database (GVESD). The data base has one table of basic information on each volcano, such as type of lava, height, and location; one table on eruptions, including volume, time of occurrence, and type; and a table of swarm parameters such as duration, number of earthquakes, depths, and magnitudes. Using electronic search commands, it is possible to find all known cases of earthquake swarms that fit a particular profile. For example, we can search for the cases that last 3 weeks, have 60 events per day, and a largest event of $M = 3.3$. The "answer" is a list of similar swarms which can then be analyzed to determine whether eruptions occurred, how long they lasted, etc. These answers are probabilistic in that they look for a likelihood of something happening based on past occurrences. Such information is complementary to simultaneous efforts to determine and to constrain what is happening physically at a volcano.

E. Other Methods

Several recent works have addressed analytical techniques and instrumental or computational methods of reducing volcano seismic data. One method of analysis is based on the materials science approach of estimating failure criteria. An observable parameter, such as strain or seismicity, is fit to the equation

$$\dot{\Omega}^{-\alpha}\,\ddot{\Omega} - A = 0, \tag{1}$$

where A and α are constants, Ω is the observed quantity, and the dot refers to differentiation with respect to time. This method has been shown to be successful in several volcano applications in retrospect, but not beforehand. These included the March 1982 eruption of Mount St. Helens, the April 1960 eruption of Bezymianny, and the 1987 summit eruption of Izu-Oshima. The method predicts the time of the eruption onset.

The RSAM (Real-Time Seismic Amplitude Measurement) and SSAM (Seismic Spectral Amplitude Measurement) systems are rapid analysis tools that have been developed by the U.S. Geological Survey. They are similar to the D_R and spectrogram techniques described

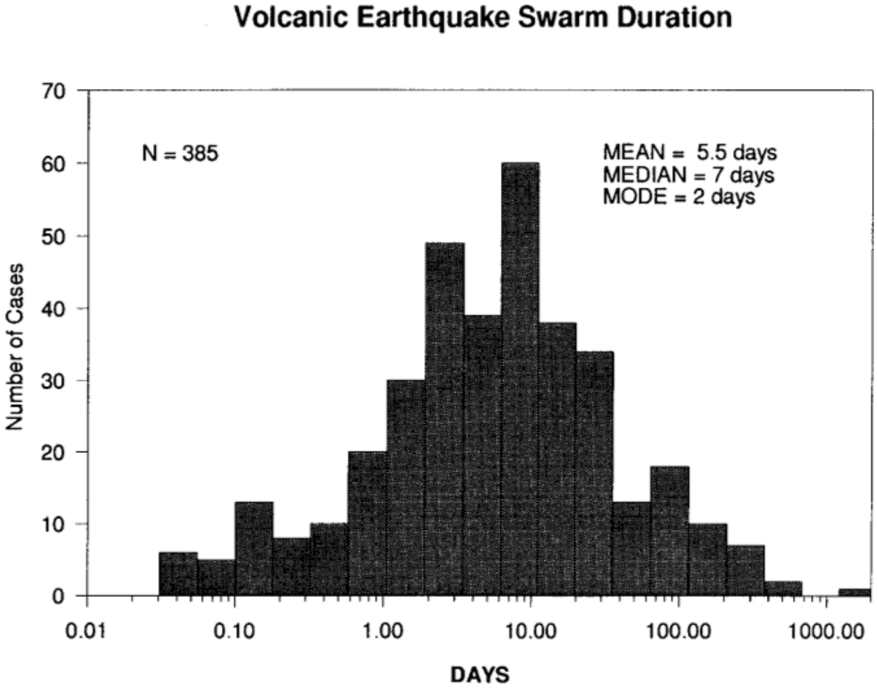

FIGURE 5 Histogram of volcanic earthquake swarm durations. The horizontal axis is logarithmic, and the numbers shown represent the middle value of each bin. The data form a log-normal distribution with a mean and median of 5.5 and 7 days, respectively. [After Benoit, J., and McNutt, S. (1996). *Annali Geophys.* **33,** 221–229.]

below. The RSAM system provides consecutive 1- or 10-minute averages of absolute seismic amplitude or energy for each seismic station, regardless of event type. RSAM data are generally plotted as time series for each individual station. The SSAM system determines the average spectral amplitude for 16 user-defined frequency bands. Calculations are performed once per minute for each individual seismic station. SSAM data are generally displayed using time–frequency–amplitude plots where the intensity of the signal corresponds to an 11-step gray or color scale. Both of these monitoring tools are useful for quantitatively determining the gross features of seismicity automatically and quickly during crises when detailed manual analyses are not possible. RSAM and SSAM are especially useful digital recording techniques when signals are continuous or when signal amplitudes on visual drum recorders begin to overlap, or exceed the physical dynamic range of analog recording, so that reliable amplitudes cannot be easily obtained.

RSAM data from four volcanoes have been analyzed using an automated curve-fitting scheme. The same exponential equation was objectively selected to best fit pre-eruption normalized RSAM data from dome-building eruptions at Mount St. Helens and Mount Pinatubo, suggesting that a common process is acting regardless of the details of the seismicity. Selected portions of premonitory seismicity at Redoubt, Mount Spurr, and Pinatubo also showed exponential increases with different durations. The best-fit equation is of the form

$$\mathrm{NORMALIZED\_RSAM\_COUNT}(t) = a + b\exp(-t/c), \tag{2}$$

where NORMALIZED_RSAM_COUNT(t) is the normalized RSAM value at time t, and a, b, and c are parameters determined by the curve-fitting program. This approach aims at identification of an aggregate process which does not depend on specific types of earthquakes or their relative times of occurrence.

V. CHARACTERIZING ERUPTIONS IN PROGRESS

Forecasting eruptions has received dominant focus as a goal of volcano monitoring, especially when the volcano

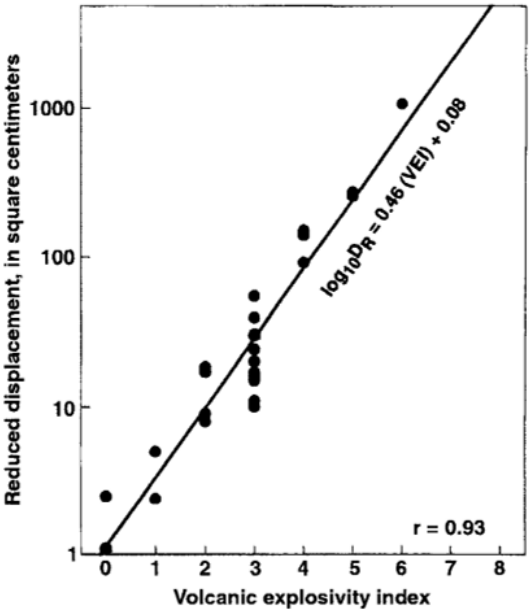

FIGURE 6 Volcanic tremor reduced displacement versus the volcanic explosivity index (VEI) of Newhall and Self (1982). *J. Geophys. Res.,* **87,** 1231–1238. The plotted line is a regression fit to the data. [After McNutt, 1994.]

is located near population centers. However, characterization of eruptions in progress, including estimates of tephra volume, height of ash column, and end time of eruption, is also of importance for hazard mitigation, particularly regarding aviation. Progress has been made recently to estimate the volcanic explosivity index (VEI) based on tremor reduced displacement (D_R) measured during eruptions (Figure 6). The computed relation is

$$\log_{10}(D_R) = 0.46(\mathrm{VEI}) + 0.08. \tag{3}$$

Reduced displacement is a method of normalizing volcanic tremor to a common scale. For body waves (e.g., P waves and S waves) the formula is

$$D_R = \frac{A \cdot r}{2\sqrt{2}M}. \tag{4}$$

For surface waves (e.g., Rayleigh waves, Love waves, and PL waves) the formula is

$$D_R = \frac{A\sqrt{\lambda r}}{2\sqrt{2}M}, \tag{5}$$

where A is amplitude in centimeters peak-to-peak; r is distance from source to seismic station in centimeters; M is seismograph magnification at the tremor frequency;

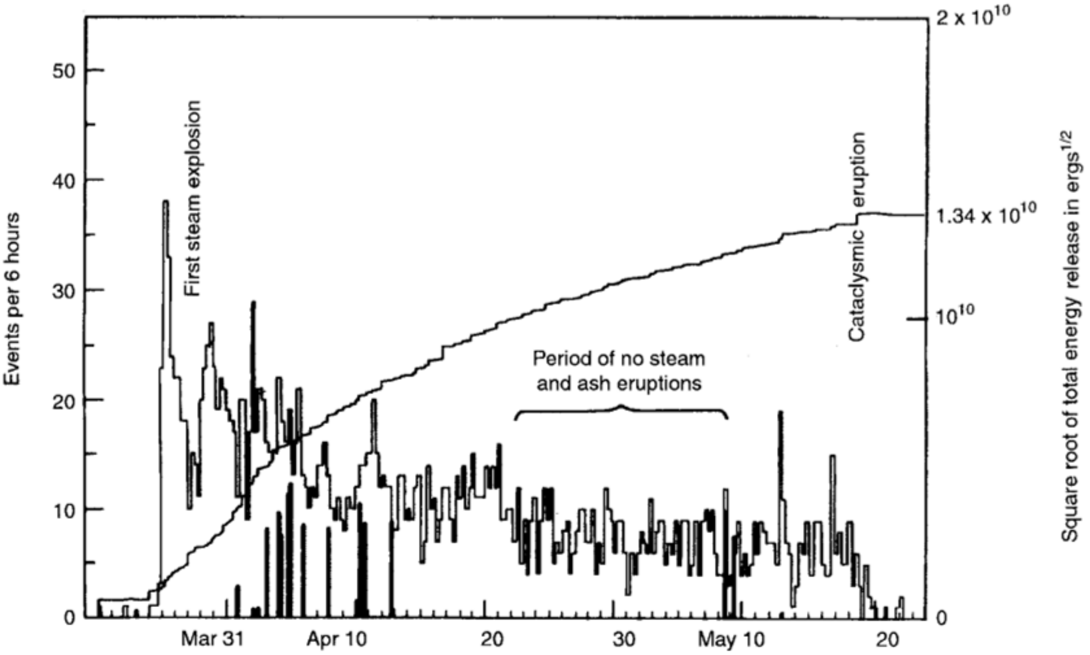

FIGURE 7 Counts of Mount St. Helens earthquakes larger than magnitude 2.5 per 6 hours (histogram), volcanic tremor (vertical solid lines, length proportional to tremor duration), and square root of cumulative energy release (irregular curve) from March 20 to May 24, 1980, Universal Time. [After McNutt, S., and Beavan, J. (1984). *J. Geophys. Res.* **89,** 3075–3086.]

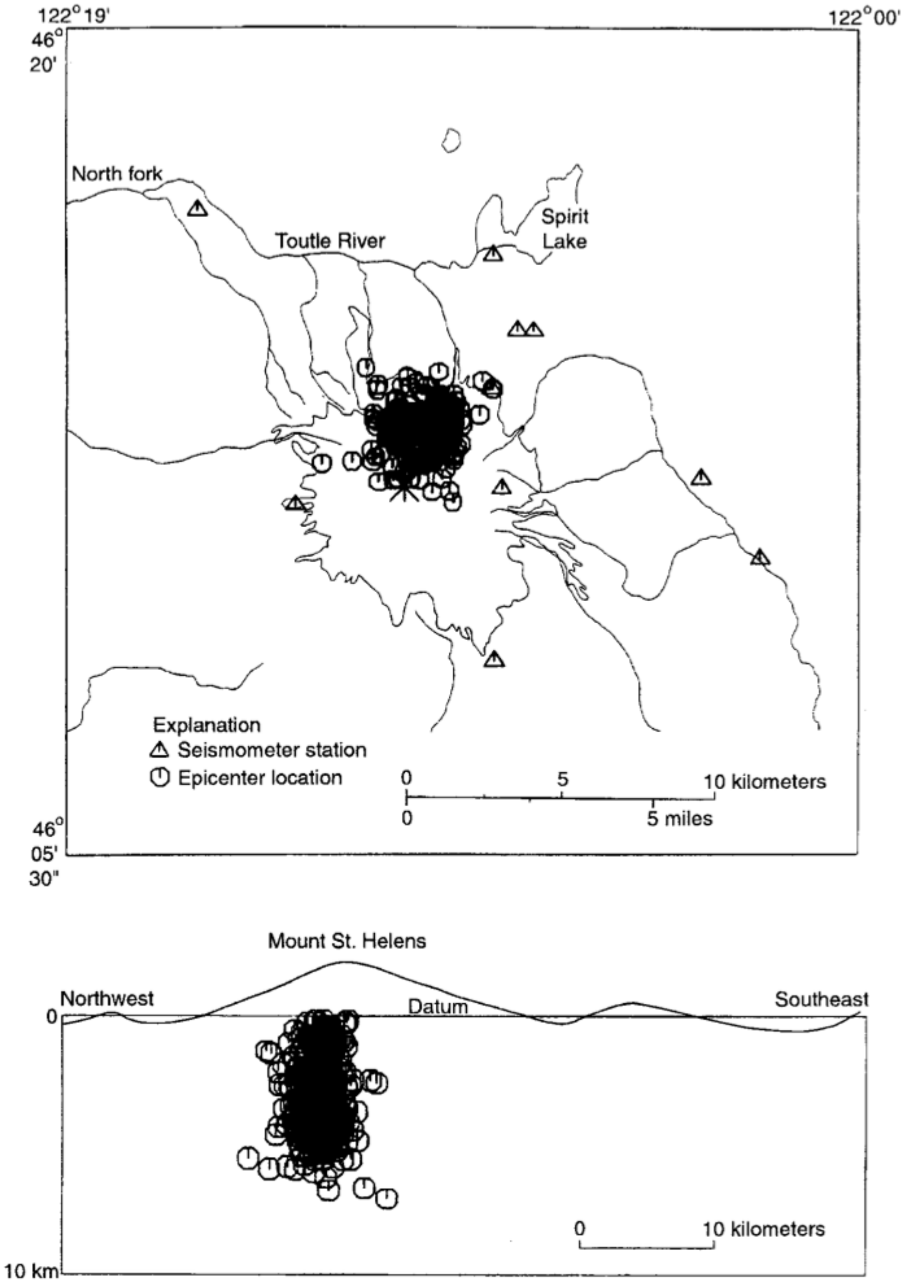
122°19'
122°00'
46° 20'
North fork
Toutle River
Spirit Lake
Explanation
⚠ Seismometer station
Ⓣ Epicenter location
0 5 10 kilometers
0 5 miles
46° 05' 30"
Mount St. Helens
Northwest
Datum
Southeast
0
10 km
0 10 kilometers

FIGURE 8 Epicenter map and cross section of seismicity from March 27 to May 18, 1980, at Mount St. Helens volcano. Contour on map is 4000 ft.; datum for cross section is average elevation of seismic stations, approximately 3000 ft. [After Endo *et al.*, 1981.]

and λ is tremor wavelength in centimeters. $2\sqrt{2}$ is the root-mean-square (rms) amplitude correction.

Such information is helpful for estimating plume heights and tephra volumes. The ends of eruptions can be estimated as coinciding with the end of strong tremor associated with eruptions. In many cases tremor declines more or less exponentially on a timescale of minutes to tens of minutes and returns to background levels. In some cases, eruptions of ash end but weak tremor continues for days in association with hydrothermal activity.

The ends of eruption sequences, which may last months to years, are more difficult to determine than the ends of individual eruption pulses, which last a few hours to days. Generally volcanic tremor ceases altogether and the number of earthquakes per unit time decreases regularly. Volcanic earthquake swarms decline with a similar power law decay to aftershocks, except that the timescale is often longer.

VI. CASE HISTORIES

A. Mount St. Helens, May 1980

Mount St. Helens, Washington, USA, produced a large explosive dacite eruption, including a lateral blast, on May 18, 1980, following 59 days of increased seismicity. On March 20, 1980, an $M = 4$ earthquake occurred, followed by many smaller events. Activity increased, reaching eight $M \geq 4$ events in a single hour on March 25. Phreatic eruptions began on March 27. The earthquake sequence eventually included over 10,000 earthquakes, including high- and low-frequency events and volcanic tremor (Figures 7 and 9). Most events were located at depths of 3–7 km beneath the north flank of the volcano, the site of the eventual eruption (Figure 8). There were no immediate precursors in the hours before the climactic eruption. However, the shaking from a $M = 5.1$ earthquake initiated the eruption by causing a sector collapse which uncapped the volcano. Deep (5–20 km) earthquakes began shortly after the eruption and lasted for several days. Later smaller eruptions were generally preceded by swarms of small earthquakes lasting several hours to several days.

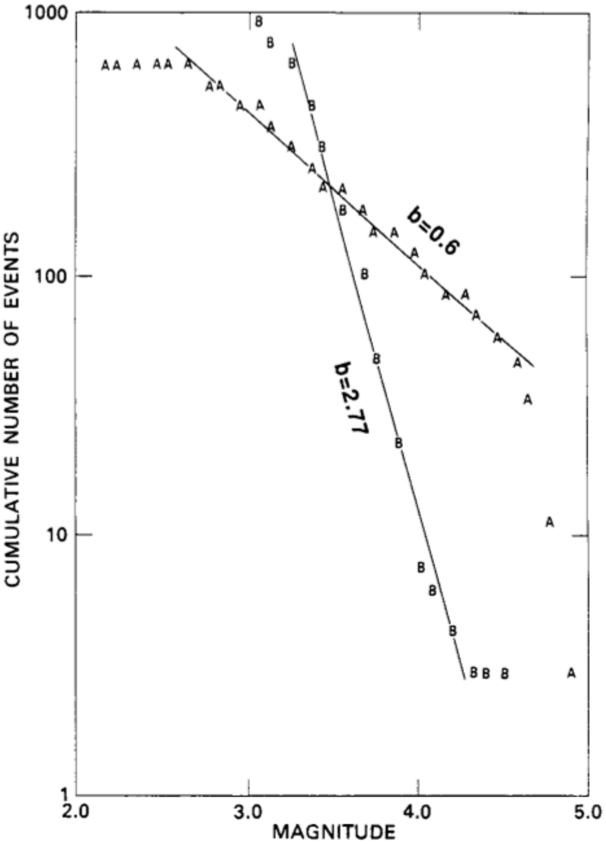

FIGURE 9 Frequency–magnitude relations for high-frequency (A) and low-frequency (B) earthquakes at Mount St. Helens. Regression lines fit to selected portions of the data produce the *b* values indicated. [After Endo *et al.*, 1981.]

B. Kilauea, January 1983

Kilauea volcano, Hawaii, is a shield volcano with a summit caldera and rift zones to the southwest and east. Earthquakes are numerous and are associated with all three of these features, as well as with a deeper nearly horizontal fault on the south flank of the volcano (Figure 10). New magma typically rises from depth near the summit, causing earthquake swarms and inflation, and then either erupts near the summit or moves laterally into the east rift zone, accompanied by summit deflation. A fissure eruption began on the east rift zone on January 3, 1983, near Napau Crater, extending 8 km downrift toward Puu Kamoamoa. Prior to this, earthquake swarms had occurred on September 26 and December 9, 1982, near the summit, followed by an intense swarm on the upper east rift from December 30, 1982, to January 6, 1983 (Figure 11). Most of the earthquakes were shallow, between depths of 2 and 4 km, and the largest was $M = 4.2$. Volcanic tremor first occurred weakly, and then was strong at frequencies of 5 to 10 Hz at the time of fissure opening. Later, tremor was predominantly 2.5 Hz with bursts of stronger activity paralleling the behavior of intermittent high lava fountains. After the initial fissure eruptions, the volcanic activity localized south of Puu Kamoamoa (Figure 10) and formed a new cone called Puu Oo. In July 1986, activity shifted to a lava lake 3 km downrift. The eruption is continuing as of this writing, and is Kilauea's longest historical eruption.

C. Ito-oki, July 1989

A submarine eruption occurred offshore of the Izu Peninsula, Japan, on July 13, 1989, following 53 days of in-

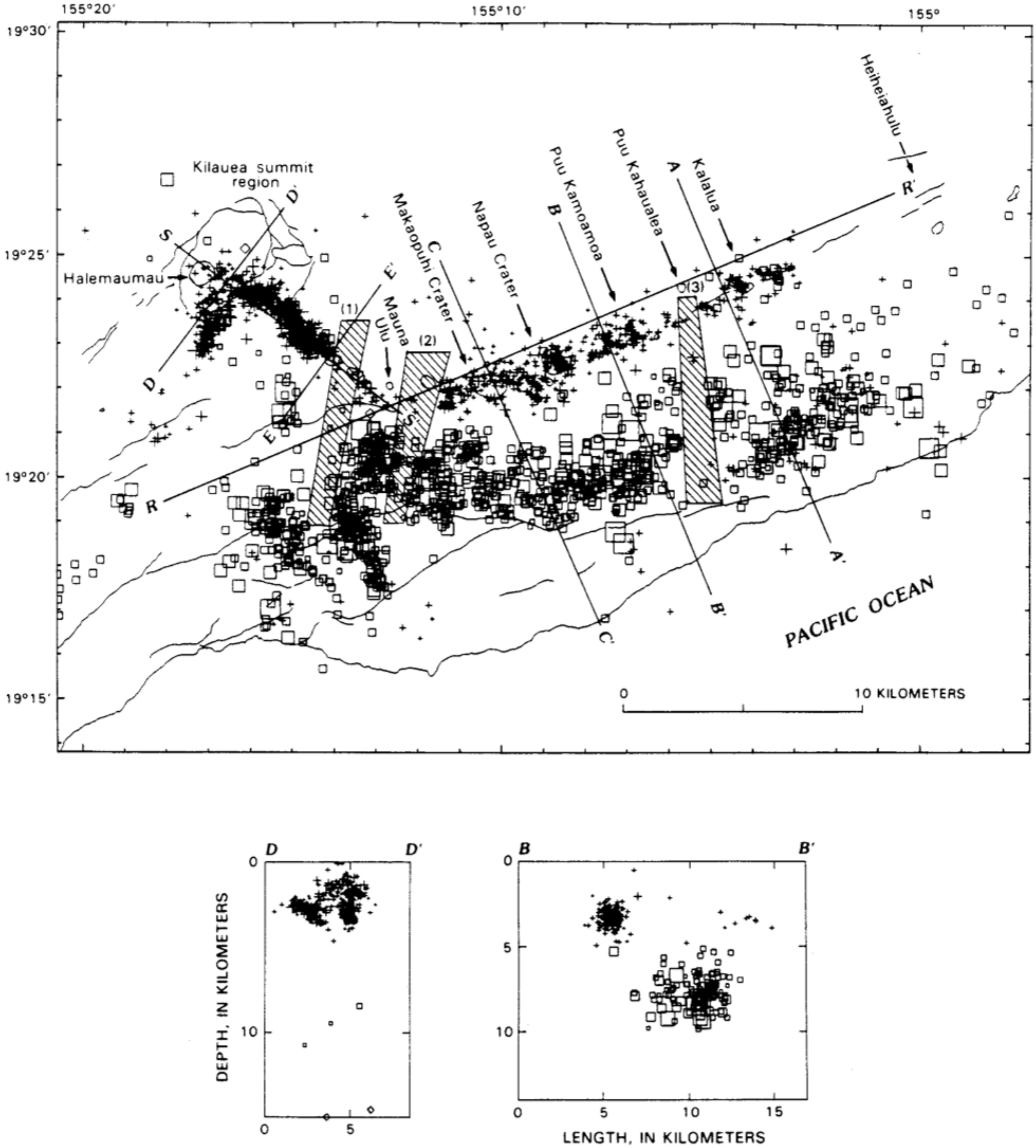
155°20′
155°10′
155°
19°30′
19°25′
19°20′
19°15′
Kilauea summit region
Halemaumau
Heiheiahulu
Kalalua
Puu Kahaualea
Puu Kamoamoa
Napau Crater
Makaopuhi Crater
Mauna Ulu
(1)
(2)
(3)
A
A′
B
B′
C
C′
D
D′
E
E′
S
S′
R
R′
PACIFIC OCEAN
0
10 KILOMETERS
D
D′
B
B′
DEPTH, IN KILOMETERS
0
5
10
15
LENGTH, IN KILOMETERS

FIGURE 10 (Top) Map of Kilauea volcano and the east rift system showing earthquakes less than 15 km deep for the period September 1982 to January 1983. Shallow earthquakes (<5 km) are shown as crosses, and deeper earthquakes (>5 km) as squares; symbol size is proportional to magnitude. Note the concentrated shallow seismicity near Kilauea's summit and the more diffuse seismicity along the east rift zone. The deeper events occur mostly on a nearly horizontal fault. The January 3 eruption began near Puu Kamoamoa. Zones free of earthquakes are shown with cross hatching. Lines labeled A–A′, B–B′, etc., show cross sections. (Bottom) Two cross sections (see map) showing the depth distribution of earthquakes near the summit and near the eruption site. [After Koyanagi *et al.*, 1988.]

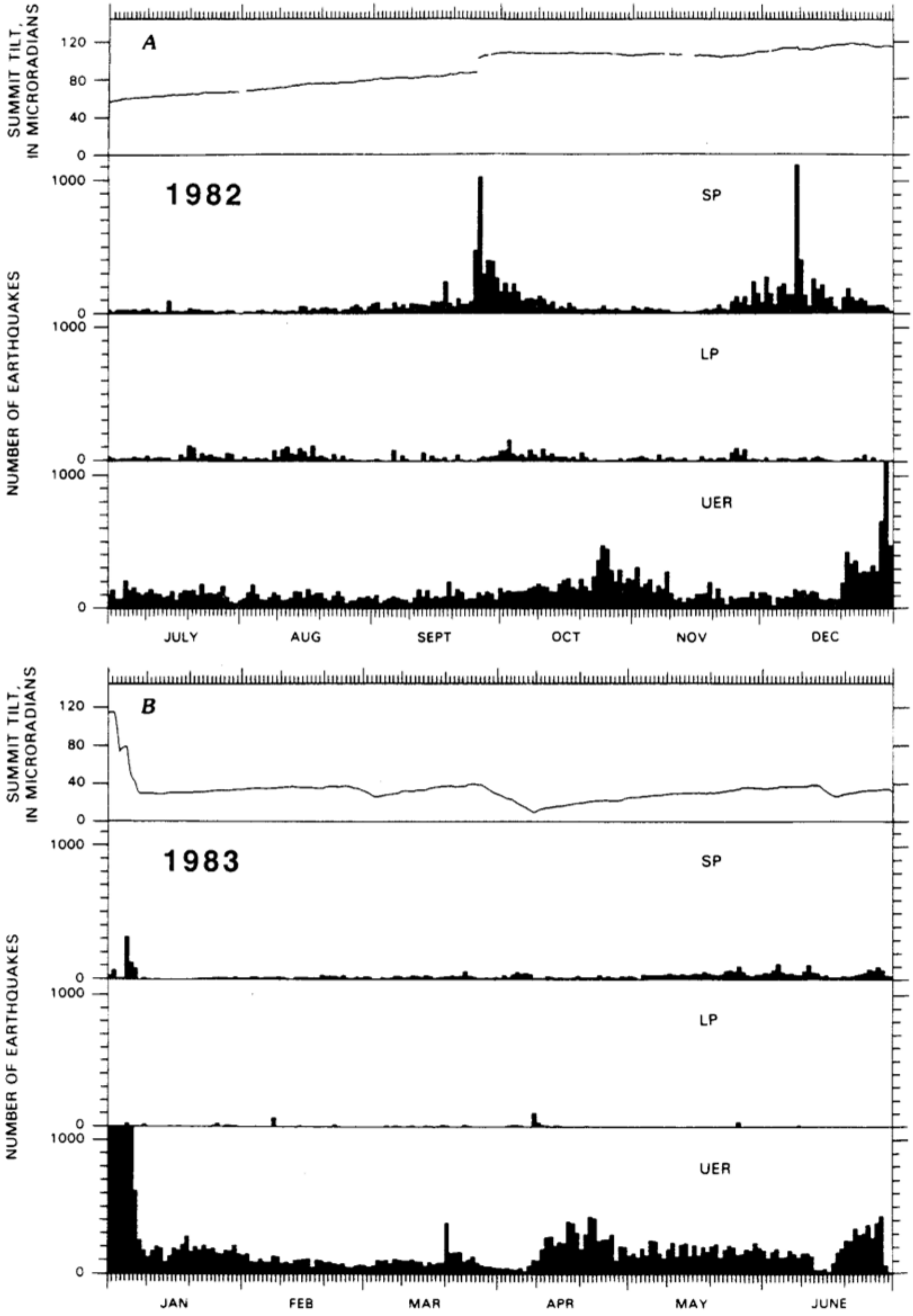

FIGURE 11 Summit tilt and daily number of earthquakes at Kilauea summit and upper east rift (UER) for the periods (A) July to December 1982 and (B) January to June 1983. Summit earthquakes are divided into short-period (SP) and long-period (LP) types based on their waveforms. Note the summit swarms in September and December, and the strong UER swarm just before the eruption of January 3, 1983. Summit deflation typically accompanies the migration of magma into the east rift system. [After Koyanagi *et al.*, 1988.]

creased seismicity. An earthquake swarm occurred May 22–26, and then subsided. On July 2 earthquake activity resumed. Earthquake counts increased first, followed by the largest event of the sequence, a $M = 5.5$ event on July 9. After this event, the number of earthquakes decreased, and then low-frequency events appeared, followed 2 days later by the occurrence of volcanic tremor (Figure 12). After 1 day of relative quiescence the eruption began, accompanied by visible boiling at the sea surface. This eruption was accompanied by unusually strong tremor. Seismicity occurred sporadically in the days following the eruption. The seismicity associated with the eruption was embedded in the high seismicity characteristic of the surrounding area (Figure 13).

D. Pavlof, September–December 1996

Pavlof is the most active volcano in North America and has had over 40 eruptions since 1760. It is monitored by a network of six seismic stations within 11 km, and three others from 33–40 km. An eruption report was received on the morning of September 16, 1996, from residents of Cold Bay, 37 miles to the Southwest. This was a surprise to scientists because no significant precursors had been seen on seismic records, which were partially obscured by a storm in the area. Later analyses showed that the small-scale seismicity had actually increased on September 11, which was only revealed after digitally filtering the data (Figure 14) to remove storm noise. The eruption lasted continuously from September 16 to December 4, declined, and then had two stronger bursts on December 10–12 and December 27–29 (Figure 15). The challenge during this eruption was not to forecast the onset, which was missed, but to quickly determine escalations of activity that represented more explosive phases of the eruption. These occurred five times (Figure 15). The data were analyzed automatically in near real time (a few minutes) to determine reduced displacement and this was used to establish an alarm threshold of 6 cm^2. Further, spectrograms were determined and were used to help identify explosions and escalations in tremor (Figure 16).

E. Pinatubo, June 1991

Pinatubo volcano, Philippines, produced a dacitic caldera-forming eruption on June 15, 1991, which was the

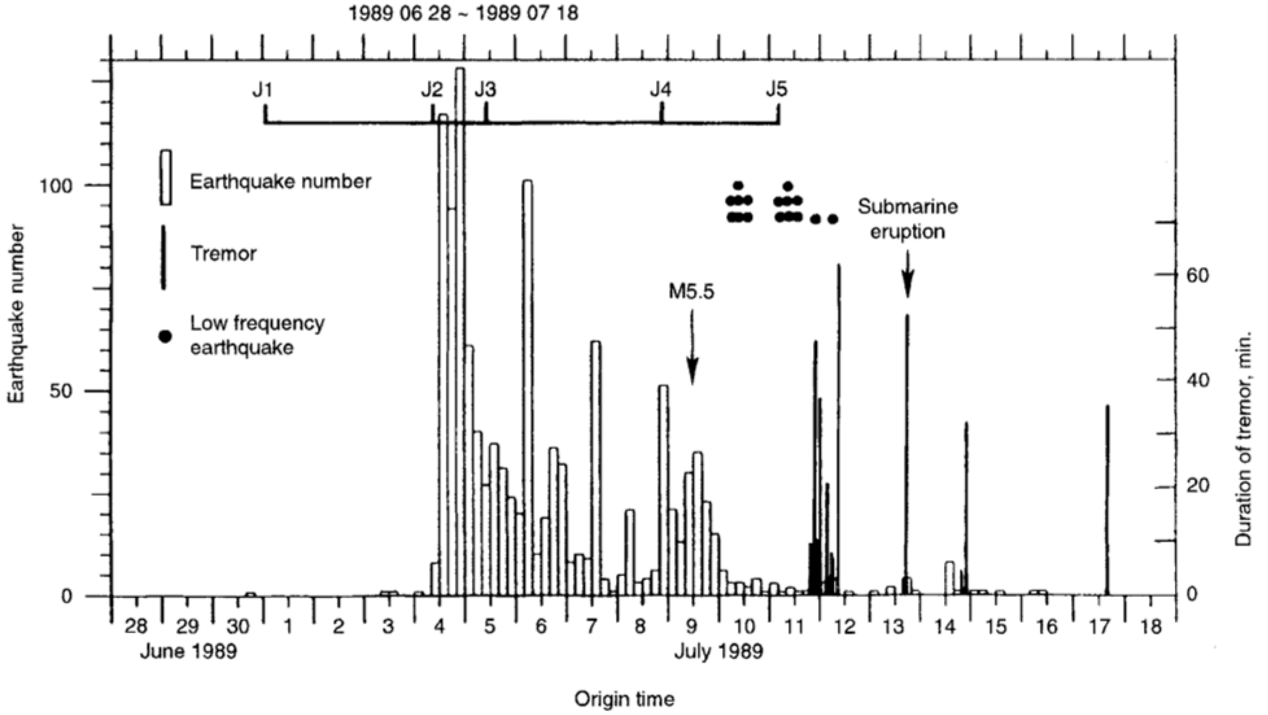

FIGURE 12 Crustal seismicity associated with the 1989 Ito-oki submarine eruption. Number of earthquakes per 4 hours, duration of tremor events, periods of crustal movement (J1–J5), and occurrence of low-frequency earthquakes are indicated. [After Ukawa, 1993.]

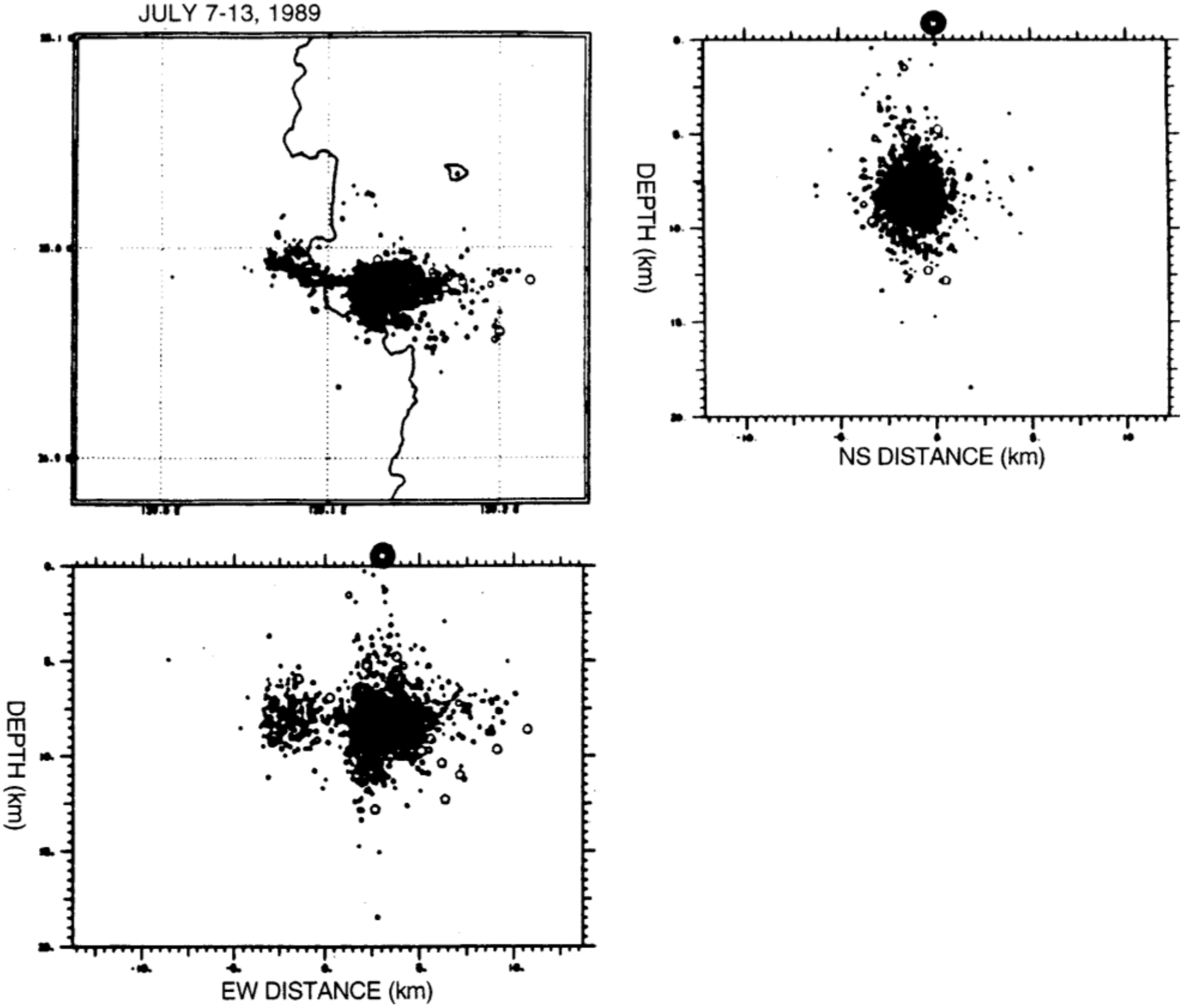

FIGURE 13 Map and cross sections of hypocenters in the vicinity of the July 1989 Ito-oki eruption. The submarine eruption produced the topographic feature known as Teishi Knoll (large round symbol). [After Matsumura *et al.* (1991). *J. Phys. Earth* **39,** 93–106.]

largest explosive eruption worldwide in 79 years. The eruption produced about 10 km^3 of tephra, generated an eruption column to a height of 33 km, and affected global climate for several years. Seismicity increased 2 months or more before the eruption and was generally shallower from June 1 to 12 (Figures 17 and 18). The exact start date is not known because seismometers were not installed until after phreatic explosions on April 2, 1991. Epicenters were located about 5 km northwest of the volcano until June 3, when activity shifted to beneath the northwest flank near the summit (Figure 18). Tremor began on June 3 and a small dome was emplaced June 7. Two episodes of stronger tremor occurred several hours before the first dacite Plinian explosion, which occurred June 12. This was followed by a strong swarm of low-frequency events and tremor. The climactic caldera-forming eruption occurred on June 15 (Figure 19). Following this, the volcano entered a phase of periodic smaller eruptions lasting about 3 weeks. Large deeper earthquakes, up to $M_s = 5.7$ and to 25 km depth, occurred over an area out to 20 km from the summit starting at the time of the climactic eruption.

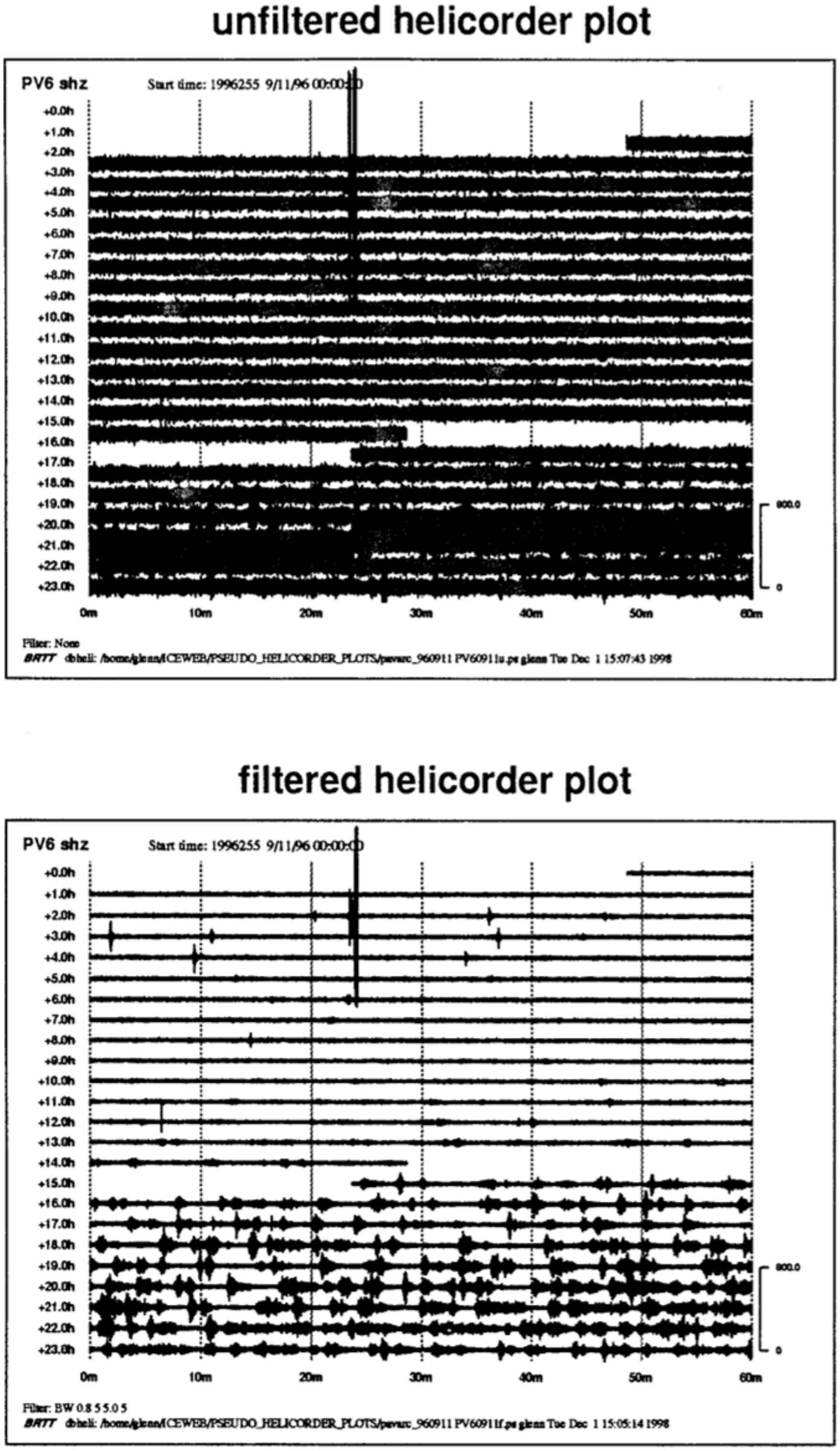

FIGURE 14 Unfiltered and filtered digital seismograms from station PV6 at Pavlof volcano, September 11, 1996. Each record is for 1 day, one line per hour. The unfiltered seismogram shows only noise with variable amplitude. The lower seismogram was filtered to remove noise below 0.8 Hz and above 5 Hz. It shows the rapid onset of a swarm of small earthquakes that occurred a few days before the eruption. (Courtesy G. Thompson.)

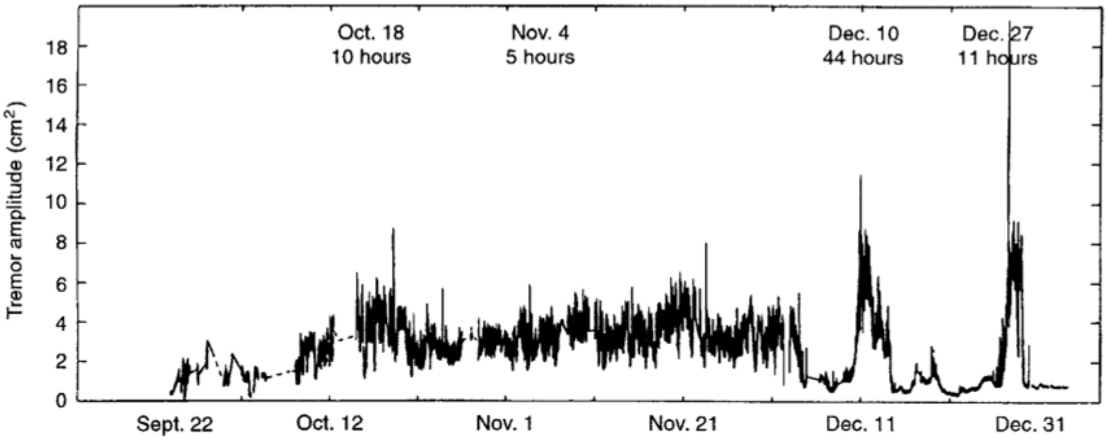

FIGURE 15 Plot showing the normalized amplitude (reduced displacement) of volcanic tremor during the 3.5 months of the 1996 Pavlof eruptions. Stronger tremor accompanied more explosive phases of the eruption on October 18, November 4 and 23, and December 10 and 27, 1996.

VII. CONCLUSIONS

Several of the observations and conclusions presented in this chapter deserve additional emphasis. First, it is very important to have a sample of background seismicity of several years duration to serve as a benchmark for comparison of possible precursors. This requires establishing a seismic network or at least a single station before a volcano shows signs of reawakening. Second, a variety of recording methods are necessary to emphasize different features of the data. These may include drum recorders, event-triggered computers, continuous digital recording, spectrograms, and reduced displacement plots (or RSAM and SSAM). Third, three-component and broadband seismometers are necessary to properly analyze many signals. These provide improved monitoring at the time, and much needed data for later analysis to understand the physical processes. Broadband, high-dynamic-range seismometers are particularly important because existing instruments always saturate for large eruptions, and because energy at long periods ($\gg$1 s) is simply not seen on standard short-period seismometers. Thus our current understanding does not incorporate either the full spectrum or high-amplitude near-source effects. Fourth, monitoring strategies need to be flexible and should not rely exclusively on a single process or type of signal. In spite of better understanding and greatly improved data quality and precision, volcanoes are still capable of new and unexpected activity. Finally, false alarms are inevitable. These may be reduced as patterns and processes become better understood, but the fundamental processes that are monitored using seismology are common to both intrusions and eruptions. Progress toward probabilistic methods may help overcome this obstacle.

Volcano seismology has matured in the last 2 decades, helped by the advent of computers and detailed study of many eruptions of different types and sizes. And yet, despite the extraordinary increase in amount and precision of knowledge, there is no guaranteed method for forecasting eruptions. Rather, volcanoes remain complex structures for which a great variety of behaviors are possible. Several general patterns of seismic activity and physical models have been discussed here, yet these may be overlooked during crises. This happens for two main reasons. First, during crises there simply is not time to perform many detailed analytical or research tasks. For this reason, most monitoring tasks are designed to be simple and reliable, and hence less prone to error. Many can be automated. Second, scientists tend to be conservative in their decision making, and crises are poor times to test new hypotheses. Rather, the best observations which are built on the most secure, previously published foundation will guide response. This trend sometimes delays response, but prevents unacceptably high false alarm rates.

Although seismology is a powerful tool in terms of eruption monitoring, it is nowhere near as powerful alone as it is when combined with other techniques. These include visual observations, geodesy, gas sampling, satellite images, and others. Nevertheless, seis-

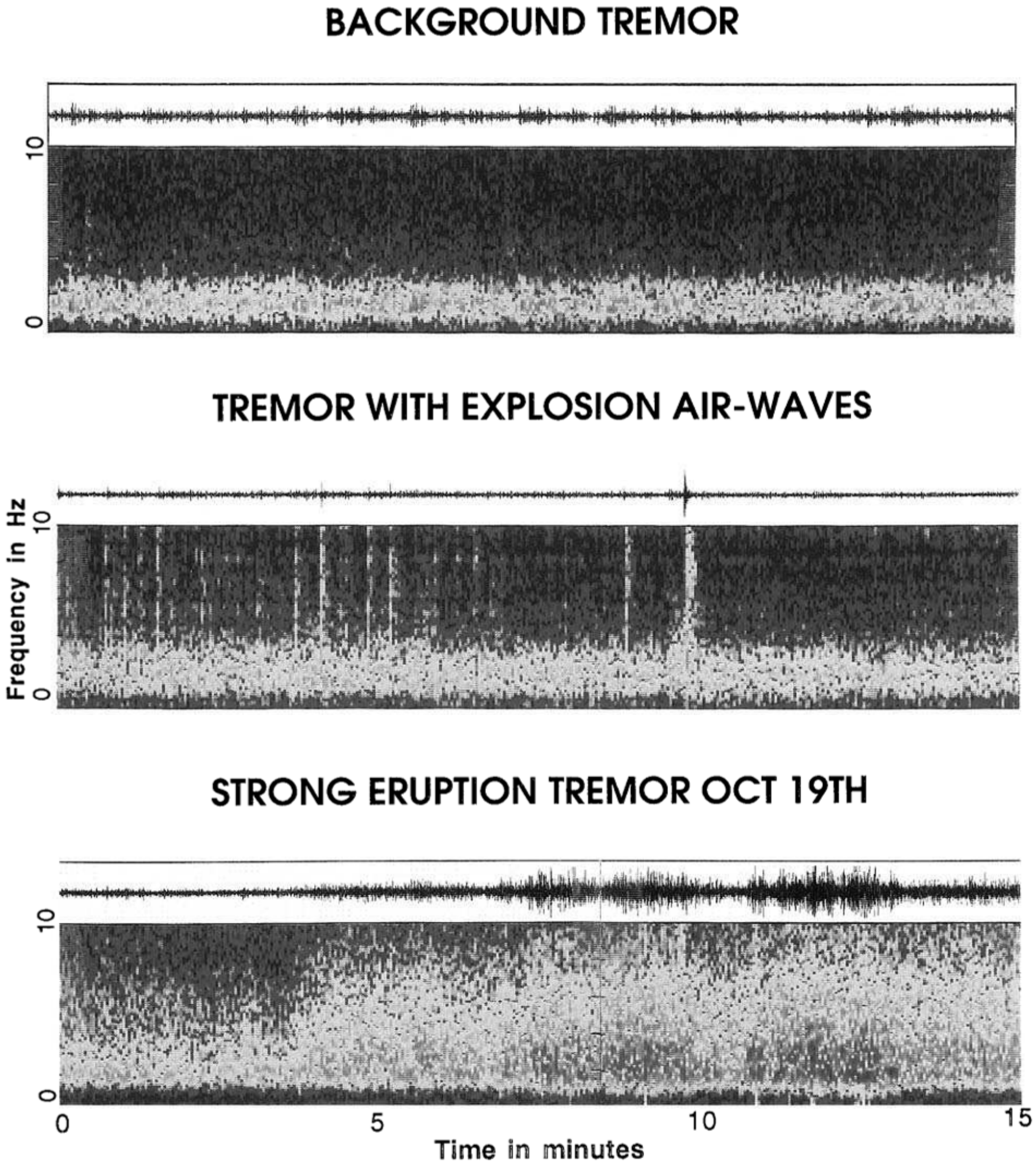

BACKGROUND TREMOR

TREMOR WITH EXPLOSION AIR-WAVES

STRONG ERUPTION TREMOR OCT 19TH

FIGURE 16 Spectrograms from the 1996 Pavlof eruptions. Each data sample shows a 15-minute seismogram and the corresponding spectrogram beneath it. Vertical axis is from 0 to 10 Hz, and strength of signal is proportional to shading, with darkest weak, lightest intermediate, and medium strong. Seismograms and spectrograms for: (top) background tremor, station PVV, November 29; (middle) tremor with explosion air waves, station PN7, mid-October; and (bottom) strong eruption tremor, station PN7, October 19. (Courtesy J. Benoit.)

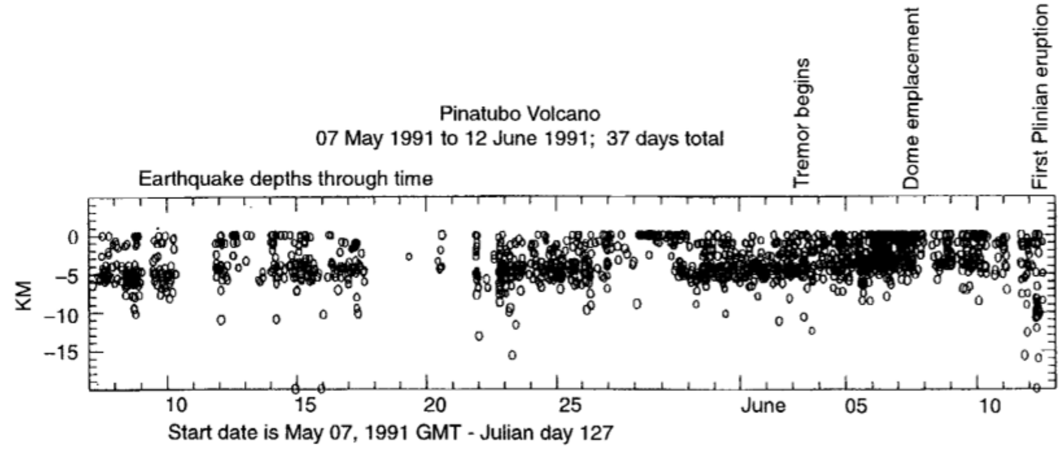

FIGURE 17 Earthquake depths as a function of time for Pinatubo volcano, May 7 to June 12, 1991. Data gaps occurred on May 10–11, 17–19, and 21–22. Depth control was poor on May 28–29. (Courtesy J. Power.)

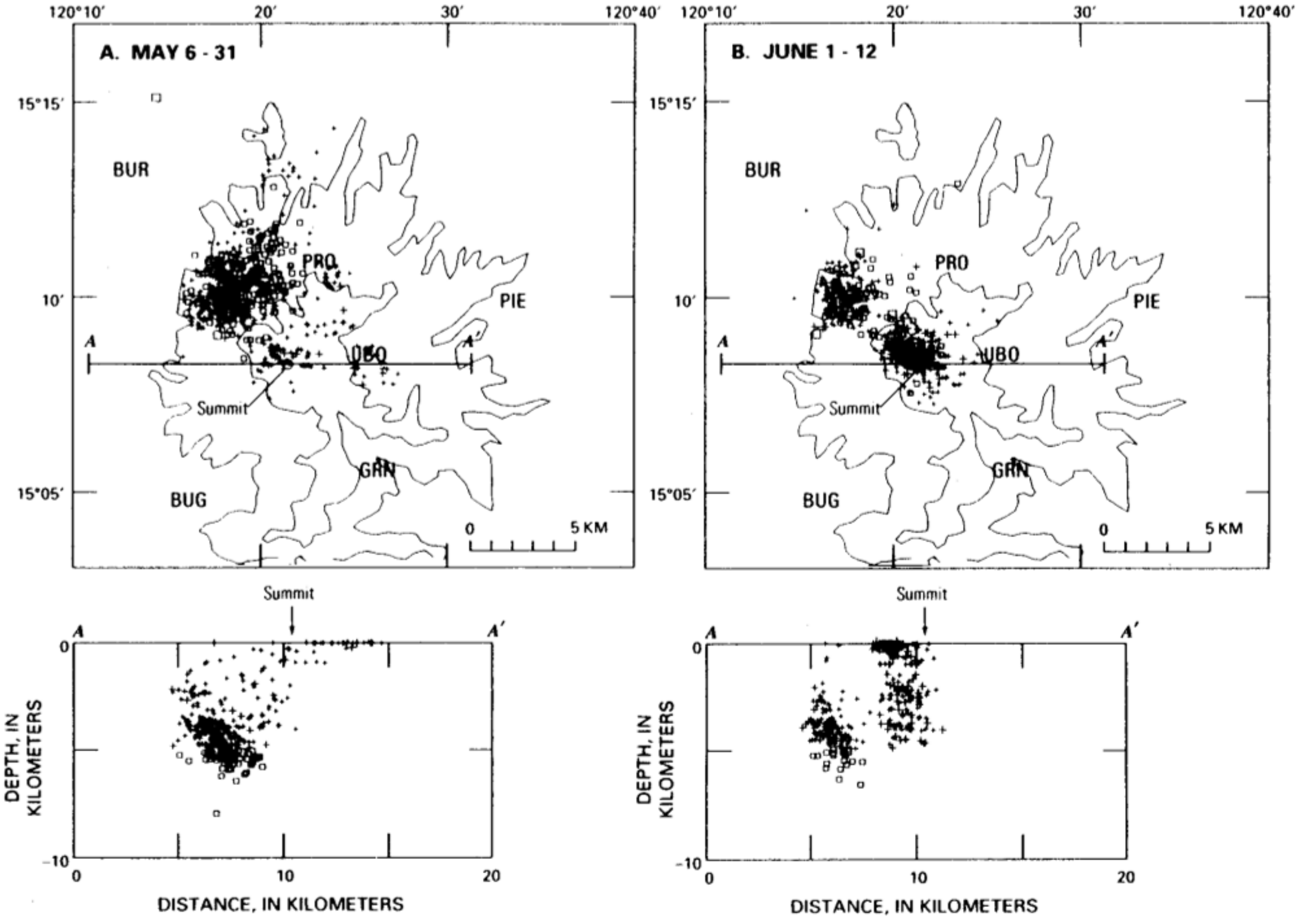
120°10′
20′
30′
120°40′
A. MAY 6 - 31
B. JUNE 1 - 12
15°15′
10′
15°05′
BUR
PRO
PIE
UBO
GRN
BUG
Summit
A
A′
0
5 KM
DEPTH, IN KILOMETERS
0
−10
10
20
DISTANCE, IN KILOMETERS

FIGURE 18 (A) Seismicity during the period May 6–31, 1991, showing concentration of hypocenters northwest of Pinatubo. (B) Seismicity during the period June 1–12, 1991, showing shift of hypocenters to shallow depths beneath the north flank of Pinatubo. [After Pinatubo Volcano Observatory Team (1991). *Eos Trans. Am. Geophys. Union* **72,** 545, 552–553, 555.]

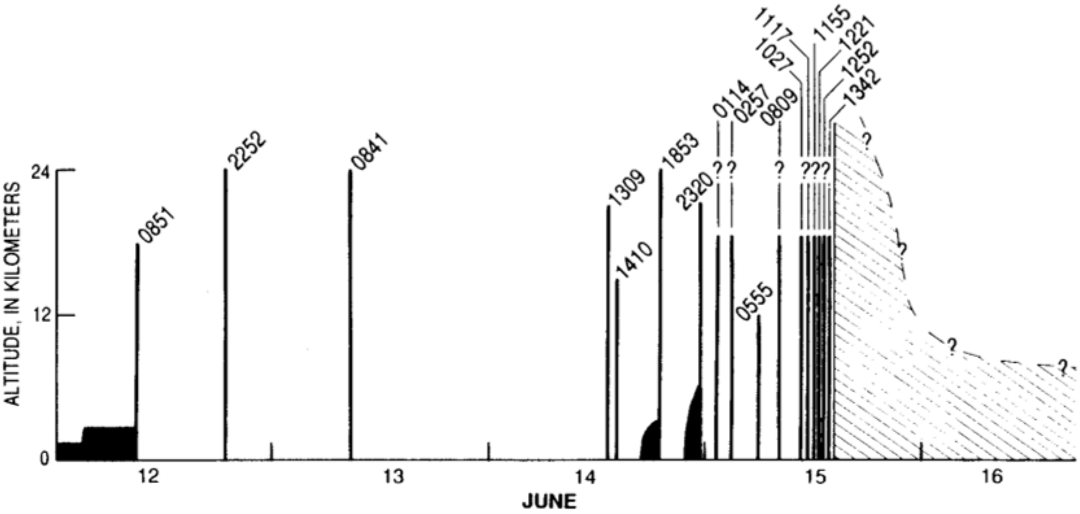

FIGURE 19 Chronology of explosive eruptions of June 12–15, 1991, at Mount Pinatubo determined from visual observations, weather-radar observations, seismic data, and a recording barograph. Vertical bars correspond to individual explosions. Four-digit number is local time of eruption onset. Emission indicated by diagonal pattern is schematic. [After Wolfe (1992). *Earthquakes Volcanoes* **23,** 5–37.]

mology is the backbone of most volcano observatories, and a strong seismic monitoring program generally results in effective hazard mitigation. Future efforts will undertake to provide a more physical basis for eruption forecasting, and to continually search new and existing high-quality data sets for better diagnostics. Such data, and well-trained and experienced scientists, will help reduce the potential for disasters at dangerous volcanoes.

SEE ALSO THE FOLLOWING ARTICLES

Gas, Plume, and Thermal Monitoring • Synthesis of Volcano Monitoring • Volcanic Ash Hazards to Aviation • Volcanic Seismicity • Volcano Warnings

FURTHER READING

Barberi, F., Bertagnini, A., Landi, P., and Principe C., (1992). A review on phreatic eruptions and their precursors. *J. Volcanol and Geatherm. Res.* **52,** 231–246.

Endo, E. T., Malone, S. D., Noson, L. L., and Weaver, C. S. (1981). Locations, magnitudes, and statistics of the March 20–May 18 earthquake sequence. *U.S. Geol. Survey Prof. Paper* **1250,** 93–107.

Endo, E. T., and Murray, T. (1991). Real-time seismic amplitude measurement (RSAM): A volcano monitoring and prediction tool. *Bull. Volc.* **53,** 533–545.

Hill, D. P., *et al.* (1993). Seismicity remotely triggered by the magnitude 7.3 Landers, California, earthquake. *Science* **260,** 1617–1623.

Klein, F. W., Koyanagi, R. Y., Nakata, J. S., and Tanigawa, W. R. (1987). The seismicity of Kilauea's magma system. *USGS Prof. Paper* **1350,** 1019–1185.

Koyanagi, R., Tanigawa, W. R., and Nakata, J. S. (1988). The Puu Oo eruption of Kilauea Volcano, Hawaii: Episodes 1–20, 1983–84. *USGS Survey Prof. Paper* **1463,** 183–235.

McNutt, S. R. (1986). Observations and analysis of b-type earthquakes, explosions, and volcanic tremor at Pavlof volcano, Alaska. *Bull. Seis. Soc. Am.* **76,** 153–175.

McNutt, S. R. (1994). Volcanic tremor amplitude correlated with volcano explosivity and its potential use in determining ash hazards to aviation. *USGS Bull.* **2047,** 377–385.

Newhall, C. G., and Dzurisin, D. (1988). Historical unrest at large calderas of the world. *USGS Bull.* **1855.**

Newhall, C. G., and Punongbayan, R. eds. (1996). "Fire and Mud: Eruptions and Lahars of Mount Pinatubo, Philippines." Univ. of Washington Press, Seattle.

Okada, Hm. (1983). Page 43–61 *in* "Arc Volcanism: Physics and Tectonics" (Shimozuru and Yokoyama, eds.).

Shimozuru, D. (1972). Page 19–45 *in* "The Surveillance and Prediction of Volcanic Activity." UNESCO Earth Sci. Monograph 8, Paris.

Swanson, D. A., Casadevall, T. J., Dzurisin, D., Malone, S. D., Newhall, C. G., and Weaver, C. S. (1983). Predicting eruptions at Mount St. Helens, June 1980 through December 1982. *Science* **221,** 1369–1376.

Ukawa, M. (1993). Excitation mechanism of large amplitude volcanic tremor associated with the 1989 Ito-oki submarine eruption, central Japan. *J. Volcarol. Geotherm. Res.* **55,** 33–50.

Voight, B. (1988). A method for prediction of volcanic eruptions. *Nature* **332,** 125–130.

WOVO (World Organization of Volcano Observatories) (1994). "Directory of Volcano Observatories 1993–1994." WOVO/IAVCEI/UNESCO, Paris.

This Page Intentionally Left Blank

GROUND DEFORMATION, GRAVITY, AND MAGNETICS

JOHN B. MURRAY
HAZEL RYMER
The Open University, U.K.

CORINNE A. LOCKE
University of Auckland, New Zealand

I. Principles of Ground Deformation Monitoring
II. Techniques Used in the Field
III. Case Histories of Deformation
IV. Principles of Gravity Monitoring
V. Techniques Used in the Field
VI. Case Histories of Gravity Changes
VII. Principles of Magnetic Monitoring
VIII. Techniques Used in the Field
IX. Case Histories of Magnetic Observations
X. Concluding Remarks

GLOSSARY

earth tides The change in gravity at the surface of the Earth caused by the relative movement of the Sun and Moon.

GPS A surveying technique that uses signals from a series of artificial satellites to determine position on the Earth's surface.

gravimeter Sensitive geophysical instrument used for measuring the relative acceleration due to gravity.

microgravity Technique using gravimeters at the limit of precision to measure gravity differences of the order 10^{-6}–10^{-8} ms^{-2}.

microgravity network Array of stations used in a microgravity survey.

piezomagnetic Magnetic properties of rock produced by stress.

proton precession magnetometer A geophysical instrument which exploits the property of protons (usually water or hydrocarbon is used as a proton source) whereby their magnetic moment vector aligns itself parallel to an applied field. When the applied field is switched off, the magnetic moments precess (like a spinning top) about the remaining (Earth's) magnetic field. The frequency of the precession is proportional to the strength (magnitude) of the field, which provides a measure of the prevailing Earth's magnetic field strength.

SAR interferometry Synthetic aperture radar (SAR) interferometry is a powerful remote sensing technique for measuring the distance to the Earth's surface. It requires that the surface is imaged by the radar at least twice from almost the same position in space. The property measured is the phase of the reflected radar signal. The differences in phase between the two images produce interferometric fringes that will represent both the topography of the surface and any changes in position of the surface during the period between the acquisition of the two images. Thus it is possible with this technique to measure both the gross topography of volcanoes at a

Copyright © 2000 by Academic Press
All rights of reproduction in any form reserved.

scale of 10 m and the dynamic changes of surface at the centimeter scale.

PRECURSORS TO VOLCANIC eruptions include changes in the physical properties (e.g., density, temperature) of rocks beneath the surface. If these properties are measured and monitored, they can give some indication as to the likely magnitude and nature of the following eruption. Local changes in subsurface density may be produced by magma movements (intrusion/withdrawal) and by variations in the degree of magma vesiculation. These changes can be detected by measuring variations in the acceleration due to gravity. Variations on the order of 10s to 100s of μGal are typical, where 1 $\mu\text{Gal} = 10^{-8}\ \text{ms}^{-2}$. These magmatic processes may also induce changes in the total magnetic field strength. Magnetometers regularly deployed on volcanoes measure field strength to 0.1 nanoTesla and fluctuations of a few nanoTesla to a few thousand nanoTesla are typical. Ground deformation also accompanies volcanic processes such as subsurface magma movements. Deformation may be horizontal (opening cracks) and vertical and ranges from millimeters to meters in scale. Measurements are made using surveying levels, electronic theodolites, and more recently the satellite-based methods of GPS and SAR interferometry. Measurements of gravity, magnetic fields, and ground deformation can also be made during and between eruptions, providing information on the processes going on inside a volcano when it is not erupting.

I. PRINCIPLES OF GROUND DEFORMATION MONITORING

For many volcanoes, ground deformation is among the most useful indicators of the general state of the volcano and any impending eruption. The work of the Japanese scientist Mogi, published in 1958, marks the beginning of modern deformation studies on volcanoes. His model describes the effect at the surface of an increase in pressure of a small, spherical source in an infinite elastic half-space, simulating the effect of increasing magma pressure within a buried magma chamber before an eruption. Despite the fact that volcanoes are not strictly elastic in behavior, nor are their surfaces flat and horizontal, many volcanoes show behavior surprisingly close to Mogi's model, particularly on a scale of several kilometers. Mogi applied his model successfully to Sakurajima volcano, Japan, and Kilauea volcano, Hawaii.

Recent developments of Mogi's model have included the effects of volcano topography in three dimensions and other nonspherical, non-axisymmetric-shaped magma chambers.

Until recently, deformation was measured at permanent markers by surveying methods such as leveling (which gives relative vertical height), distance measurement and theodolite angular measurement (which give horizontal measurements of position), and dry tilt (which gives ground tilt only). In the past few years, GPS has overtaken theodolite and distance measuring as the fastest and most precise way of measuring horizontal position.

Once a network of fixed stations has been established and measured on a volcano, the detection of displacements due to ground deformation will depend upon a later remeasurement of the same stations. The deformation is then usually expressed relative to one of the stations in the network (the reference station), normally the station furthest from the volcanically active areas, and preferably off the volcano altogether. However, using GPS, it is now possible to refer movement to stations hundreds of kilometers away which may thus introduce irrelevant tectonic movement of the reference stations. As a general rule, reference stations should be close to the area studied without being actually involved in the movement under investigation.

It takes a finite amount of time to occupy all the stations on a volcano using these surveying methods—typically from a couple of days to a month, depending upon the methods used, the size of the measuring network, the manpower available, and the weather. It is therefore not usually practicable to measure the network more than once a month; financial and logistic considerations often mean that once or twice a year is nearer the norm for many volcanoes.

Surveying methods complement electronic tiltmeters on volcanoes very effectively, in that they provide a high spatial resolution, which combined with the high time resolution of tiltmeters can provide an overall picture of events taking place within the volcano. They are particularly suited to studies of internal structure, and also to long-term monitoring of ground deformation. As a predictive tool, they have been effective in predicting position, as well as giving an indication of the likelihood of future eruptions.

Electronic tiltmeters use a different approach. They measure ground tilt continuously, but at one place only, so that although the progress of changing tilt can be recorded from minute to minute, there is no information on what is happening between tilt stations; nor is it necessarily true that the tilt site is representative of the whole volcano. However, for volcanoes with fluid magma of low viscosity, such as the Hawaiian or Icelandic volcanoes, tiltmeter records can provide immediate information on events within the interior of the volcano. Episodes of magma injection, for example, can be followed in detail as they unfold, and increasing ground tilt can be used to help predict the time of an impending eruption.

Newly developed satellite techniques such as GPS and SAR interferometry have the potential of bridging the gap between tiltmeters and surveying methods. SAR interferometry, like ground surveying, is capable of providing a map of altitude changes, and can do so every time the satellite passes over. At present, this technique has been attempted using satellites which have been able to overfly the same region of the Earth every month or so, but there is no reason why future satellites could not increase this coverage to as often as necessary for key volcanoes, thus approaching tiltmeters in temporal coverage, with the advantage that information can be derived at any point on the volcano. Permanent GPS stations have now been installed on some volcanoes and volcanic areas which provide continuous information on how the edifice is deforming with time. If enough of these are installed, then they can replicate ground deformation surveying, but with the advantage that, like tiltmeters, they can do so continuously, thus providing the ideal monitoring system, the only drawback being the high cost of GPS receivers.

II. TECHNIQUES USED IN THE FIELD

A. Precision Leveling

Leveling is the most accurate method of deriving changes in relative heights on a volcano. It was first used in this way in Japan, to investigate the 1910 eruption of Usu volcano and the 1914 eruption of Sakurajima volcano, but did not come into use as a regular monitoring tool until 1965 at Kilauea volcano, Hawaii. In its simplest form, leveling involves the use of a vertical graduated measuring staff and an instrument called a level, consisting of a telescope with a central crosshair set up to read exactly horizontally. Figure 1 illustrates the method of precision leveling between two fixed markers on a volcano. Using this technique, accuracies of 0.8 mm over 1 km are obtainable.

B. Conventional Ground Surveying

Both trigonometric leveling and trilateration (determining angles between sets of markers), sometimes combined, were in use to measure horizontal and three-dimensional changes in position of networks of benchmarks at volcanoes prior to about 1995. Distances were measured by EDM (electronic distance measurement), and heights determined from vertical angles read with a theodolite. However, the proliferation of GPS satellites and advances in GPS techniques have made these methods of deformation measurement largely obsolete, ex-

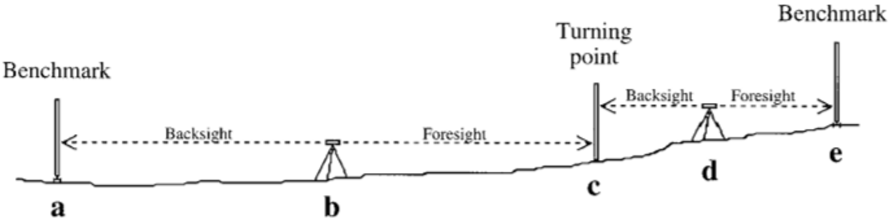

FIGURE 1 Diagram of leveling procedure. The staff is set up over the reference benchmark a, and the level at b. The value on the staff at the horizontal crosshair seen through the level is read and noted down; this first value is the backsight. The staff is then moved forward to a temporary position c, known as a turning point, where it is placed on the ground, not on any fixed station, and the staff value read and recorded again. This forward observation is called the foresight. The instrument is then moved to position d, and the staff at c (now the backsight) is read again. Finally, the staff is set up over the second benchmark e, and the foresight read. The difference in height of e relative to a is the sum of all the foresight values minus the sum of all backsight values. In this example, only one staff turning point is required at position c, but in practice any number of turning points can be used between the two permanent benchmarks. The speed of leveling depends upon the steepness of the slope, steeper slopes requiring shorter sights, as well as the distance between the two points to be measured.

cept where the higher costs of equipment have as yet precluded this, or where dangerous activity prevents occupation of a remote station. Among traditional surveying methods, only precise leveling now remains more accurate than GPS as a volcano monitoring technique.

C. GPS

GPS is now the most accurate way of measuring horizontal position over large distances. Signals from a series of satellites (at present about 30) are processed by a receiver on the ground which determines the distance to each satellite and derives its position on the Earth's surface. Because of continuous signal scrambling for military reasons, absolute positions are only accurate to tens or hundreds of meters, but by using two dual-frequency receivers in the same region, the scrambling is virtually the same and so relative positions between the two can be obtained to accuracies of a few millimeters over tens of kilometers, depending on satellite configurations at the time of measurement. Vertical positions are never so accurate as horizontal positions because the satellites are only on one side (above the instrument) and so the configuration is perforce poorer.

A great advantage of GPS (Figure 2) is that it can be carried out in any weather, including rain, snow, fog, and high winds, which would preclude conventional surveying altogether. Like ordinary trigonometric surveying, when measuring a network of points a strong triangulation net should be constructed with good redundancies, so that error ellipses can be calculated. Displacement can then be distinguished from the various sources of error. For the highest accuracies, lines and stations should be observed for longer than 24 hours at a time, but logistical constraints on inaccessible volcanoes may preclude this. A more practical procedure may be to ensure that stations are reoccupied on different days and times of day, when the satellite positions are completely different.

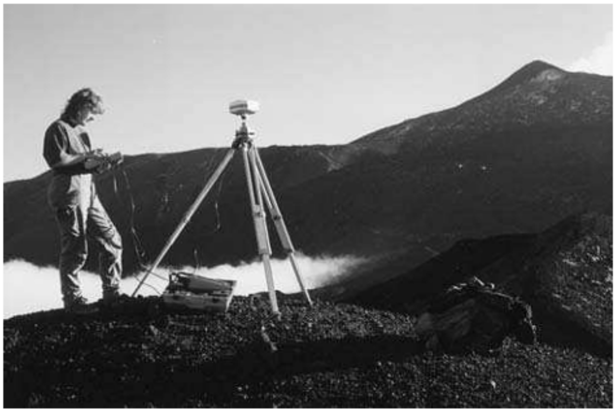

FIGURE 2 Wild dual-frequency GPS receiver in use near the summit of Mount Etna volcano, Sicily. The sensor is set up vertically above a ground marker, and the data stored in the handheld controller. Another receiver is left running at a base station at the start of the day's work. With occupation times between 15 minutes and 3 hours (depending on satellite configuration and distance between the receivers), the relative position and height of the two receivers can be determined with a precision of a few millimeters.

D. SAR Interferometry

Synthetic aperture radar (SAR) interferometry by satellite, a technique being developed at present, can provide information on ground deformation at any point on the volcano without the need to deploy any instrumentation on the ground at all. Two satellite radar images taken on different orbits but from almost the same point in space are compared. The differences in phase between the two images produces interferometric fringes that will represent both the topography of the surface and any changes in position of the surface during the period between the acquisition of the two images, that is, any deformation that has taken place in the interval. One of its disadvantages is that the displacements are measured in the satellite vector only, normally approaching the vertical but not necessarily so. The results can be affected by atmospheric changes (humidity, pressure, etc.), and vegetation and snow cover preclude measurement at present, though algorithms may eventually be developed to overcome these problems. Early attempts to use the technique on volcanoes of high topographic relief were also dogged by errors associated with subtracting the topography. Highest accuracies achievable depend upon the wavelength used; heretofore this has been just under 3 cm.

The end product of SAR interferometry is an interferogram: essentially a map of the volcano showing interference fringes which correspond to contours of displacement in the satellite direction between two radar images. The technique promises to be particularly important for remote or rarely monitored volcanoes where no other means of deformation monitoring is possible.

E. Dry Tilt

Dry tilt is the colloquial name given to a method of measuring changes in tilt of the ground which employs the same optical instruments as leveling. The technique came to be known as "dry tilt" by way of contrast with the end state of those making water-tube tiltmeter measurements.

In its simplest form, a dry tilt station consists of at least three benchmarks arranged in a roughly equilateral triangle with sides of about 50 m. The level is set up in the center, and the staff placed on each of the three benchmarks in turn with their relative altitudes measured to a high precision. Next time the station is measured, any tilt of the ground in the intervening period will show up as a slight change in relative altitudes of the three benchmarks.

Dry tilt stations must always be regarded as a poor second to leveling, as they provide no information on altitude changes at widely separated parts of the volcano, and the same limitations apply as for tiltmeters. However, the advantage of dry tilt stations is that they are cheap and quick to measure, and can be occupied several times a day during periods of crisis. For poorly funded or infrequently visited volcanoes, they are a simple means of providing rudimentary information on deformation, for example, where heavy forest cover precludes SAR interferometry.

F. Tiltmeters

Various kinds of tiltmeter have been deployed on volcanoes, the first being a horizontal pendulum seismometer that proved to be an effective tiltmeter installed at Kilauea volcano, Hawaii, in 1912. Borehole tiltmeters can now be bought off-the-shelf, and have been installed at many volcanoes to provide a continuous record of deformation. The choice of site is important, as most tiltmeters are affected to some degree by temperature and rainfall. Installation in a temperature-stable underground vault is the best location for most types of tiltmeter, though lava tubes have also been used as a naturally available alternative. Most sensitive tiltmeters also suffer a "running-in" period when a constant tilting occurs, sometimes for several months, before the signal settles down.

These problems are largely overcome when hydrostatic level tiltmeters are used which have a much longer baseline and so escape the anomalies consequent upon measuring tilt essentially at one spot. Tiltmeters sensitive enough to record Earth tides can be installed without the need for temperature-stable vaults.

Problems with tiltmeters as a means of measuring deformation are that they do not measure relative altitude change nor horizontal deformation. Instead they provide a measure of ground tilt only at individual sites. If, for example, tilt at such sites around the volcano is always away from the summit, it is assumed that the summit is rising. However, such a deduction has to be based on the assumption that the intervening ground between the tiltmeters is behaving in the same way, and this may not be the case, particularly in highly faulted terrains.

III. CASE HISTORIES OF DEFORMATION

Ground deformation on volcanoes may be due to several causes. These include: (1) inflation/deflation of a buried magma storage zone, (2) injection of a dike or sill which may or may not be an eruption conduit, (3) subsidence due to lava loading, gravitational settling, or spreading of the whole volcano, and (4) slope movement caused by slope creep prior to failure or by magma pressure variations on steep slopes. Combinations of these causes frequently occur to produce a complex pattern of deformation.

A. Sakurajima Volcano (Japan, 1914)

After a large eruption in 1914, leveling benchmarks around Sakurajima volcano, which had been installed and leveled in 1895 as part of a country-wide survey, were resurveyed in June 1914. The results showed a broad, roughly circular subsidence of more than a meter and at least 60 km wide, not centered on the volcano itself, but roughly concentric with the center of Kagoshima Bay, an old caldera. These results were analyzed by Mogi, who found that when plotted against the distance from the center of subsidence, the data fitted very closely to the deformation expected from elastic deformation caused by a buried source, from which he was able to develop his model.

The Mogi model predicts that

$$\Delta d = \frac{3a^3Pd}{4\mu(f^2 + d^2)^{3/2}}$$

$$\Delta h = \frac{3a^3Pf}{4\mu(f^2 + d^2)^{3/2}},$$

where

a = radius of the source sphere
P = change in hydrostatic pressure in the sphere
f = depth to the center of the sphere
μ = Lamé's constant
d = radial distance on the surface from point above source
Δd = radial horizontal displacement of a point at the surface
Δh = vertical displacement of a point at the surface

Mogi found that the Sakuraijima data were consistent with a depth to source (f) of 10 ± 1 km (Figure 3).

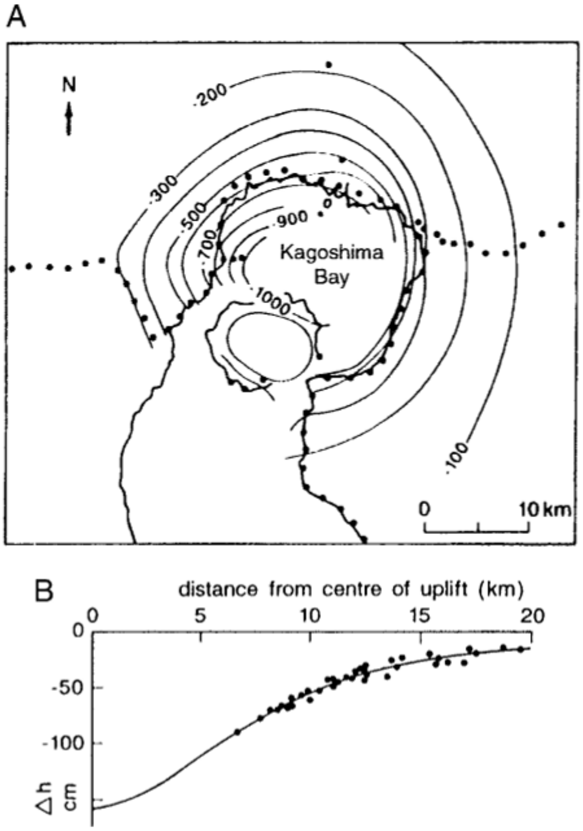

FIGURE 3 (A) Map and diagram of a deflation episode at Sakurajima volcano, Japan, measured between 1895 and June 1914, just after the voluminous eruption of that year. The map above is overlaid with contours of deformation at 100-mm intervals, interpolated between values of vertical displacement measured at benchmarks around the volcano. A benchmark distant from the volcano has been used as a zero reference. Below vertical displacement is plotted against distance from the volcano in Kilometers. The black dots show displacement at individual benchmarks, while the curves show the theoretical displacement expected from a buried pressure source according to Mogi's (1958) model. The center of deflation lies not at the volcano itself, but in the center of Kagoshima Bay, the adjacent caldera. The curve in (B) is for a pressure source at a 10-km depth.

B. Krafla Volcano (Iceland, 1978)

The Krafla fissure swarm in northern Iceland began erupting in December 1975 after 230 years of dormancy. There were nine eruptions in the following 9 years. The accompanying deformation patterns showed repeated inflation and deflation sequences, essentially of the Mogi type, centered on the 9-km-wide Krafla caldera. It appears that a magma chamber was being supplied with magma over this 9-year period, and that the consequent steady inflation of the chamber was punctuated by about 20 rapid deflation events. During these deflation events, vertical fissures crossing the area widened and filled with magma from the reservoir, forming dikes which extended rapidly to distances up to 50 km from the caldera center. Eleven of these dikes did not reach the surface, but remained as intrusions.

Characteristic ground deformation can be expected on the ground surface above a vertical or near-vertical dike undergoing dilation during emplacement. In general, points on either side of the dike will displace away from the dike, normal to its long axis, as it inflates. The vertical displacement increases rapidly with distance from the dike, reaches a peak value, and then decreases slowly toward an asymptote of zero displacement (Figure 4a). In the case of vertical dikes, this displacement is symmetrical about the center of the dike. For near-vertical dikes, displacements are greater on the side in the direction of dip and the point which experiences zero displacement is above the uppermost tip of the dike rather than its center. Horizontal ground strain is the first derivative of this displacement with respect to distance. Its peak tensile value occurs above the tip of the dike, and then decreases rapidly, through zero at the peaks of the displacement, to a relatively low compressive strain which then asymptotes back to zero (Figure 4b). The exact shape of the displacement against distance curve depends upon the depth, height, and angle of dip of the dike.

Models so far derived have been two-dimensional, that is, they apply to a dike of infinite length and constant cross section, located at a constant distance from a plane surface in a semi-infinite homogeneous isotropic elastic medium. By contrast, a real dike is of finite length and has a varying cross section, and its path may be curved. Its depth may vary beneath an irregular topography and the material surrounding it will be a mixture of magmatic products. All of these factors will influence the displace-

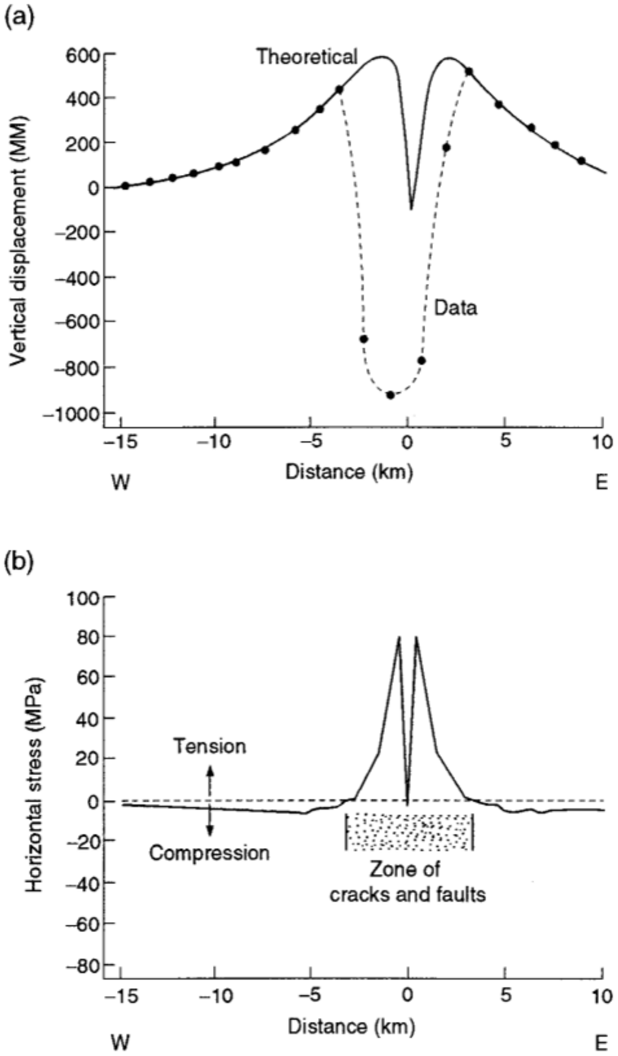

FIGURE 4 (a) Plot of vertical displacement against distance from a dike emplaced during a rifting event north of Krafla volcano, Iceland, on 7 January 1978. Data points closely follow the theoretical curve (solid line) for a vertical dike whose center lies at a 3-km depth, and whose height is 5.5 km. The fit is good apart from close to the dike itself, where tensional stress is calculated to be very high [see (b)]. (b) Calculated horizontal stress in MPa plotted against distance from the dike modeled in (a).

ment of a point on the surface as the dike inflates or deflates, and cause it to deviate from the theoretical curve. However, measurements of real dike-emplacement events like those at Krafla show that the observed displacements can be remarkably close to the simplified models, suggesting that these deviations are not too important in practice (Figure 4a).

Analysis of the measured vertical displacements associated with one of the intrusive events at Krafla (that of 7 January 1978) indicated that the intrusion was consistent with a vertical dike 5.5-km in height, whose center lay at a depth of 3 km. The measured values in Figure 4a depart from the theoretical curve only near the dike itself, where the theoretical horizontal stresses are tensile, and many faults and cracks were visible at the surface, indicating that in this zone, the ground was not behaving elastically, so would not be expected to conform to the model.

This kind of analysis can be used to build up a record of positions of injected dikes within a volcano which can aid in studies of subsurface structure and future eruption prediction.

C. Colima (1982–1997)

The loading, compaction, or gravitational distortion of the volcanic pile by recent volcanic products may cause subsidence of more than a meter per year in extreme cases at some volcanoes. In the case of Colima volcano, Mexico, subsidence of the entire volcano has dominated the deformation pattern at least since 1982 when the first ground deformation network was installed.

Colima has been in more or less continuous dome-building eruption for decades, yet despite this dome growth, deformation measurements have shown continuous subsidence roughly centered on the summit. Leveling stations 1 to 3 km distant from the summit have subsided nearly 1 cm per kilometer per year radially on average. Recent measurements between 1994 and 1997 show a greater subsidence of 2 cm per kilometer per year near the summit and 5 cm per kilometer per year at the edge of the dome (Figure 5). Subsidence continued even through the period of rapid dome extrusion and lava flows in 1991. It probably results from compaction and elastic/plastic deformation of the edifice, which is a steep-sided cone reaching to 3880 m.

D. Mount St. Helens (1980)

As a volcano builds up by the steady accumulation of lavas and pyroclastics, its slopes become progressively steeper, and there comes a time when it becomes an unstable structure. If eruptions continue, this instability may ultimately resolve itself in slope failure, where a large section of the volcanic edifice may peel off and slide downslope in a sector collapse. The most famous example of this kind of event was the Mount St. Helens eruption of 18 May 1980, where nearly 3 km^3 of the northern slopes of the volcano collapsed and slid off the volcano, taking the pressure off the magma beneath and

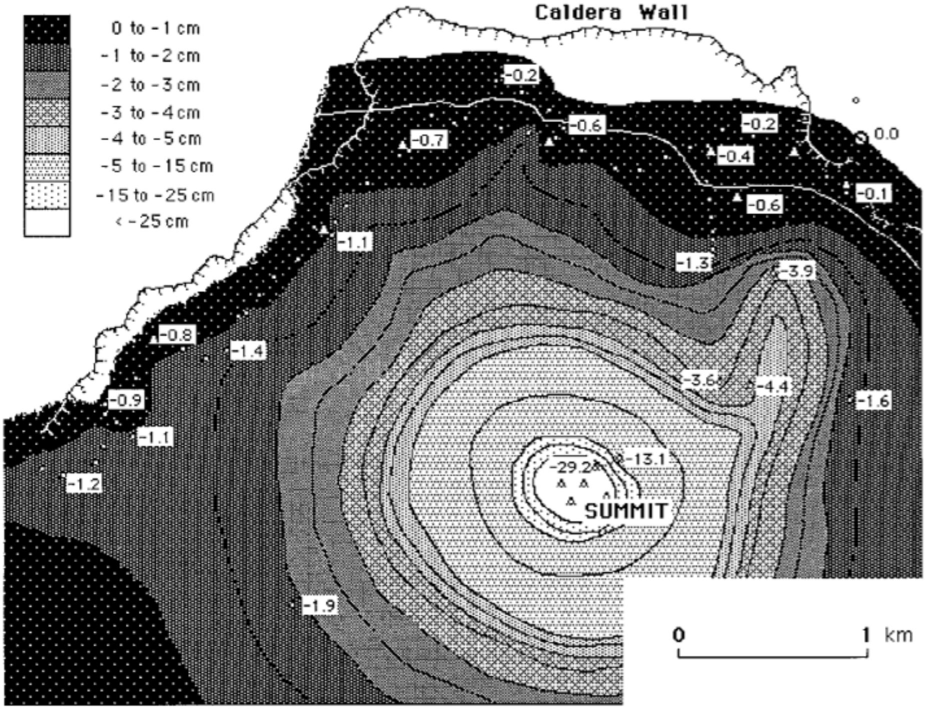

FIGURE 5 Subsidence concentric to the summit of Colima volcano, Mexico, measured between 1994 and 1997. The relation to the topography, and the continuous nature of the subsidence since 1982, suggests that compaction and downwarping due to loading of the volcano is responsible for most of this movement.

provoking a large pyroclastic eruption. A similar event occurred at Bezymianny volcano, Kamchatka, in 1956. At Bandai San volcano, Japan, in 1888, a large slope failure occurred without a concurrent pyroclastic eruption, probably because the volcano was inactive and no magma had been present near the surface.

Before such catastrophic events occur, slope creep and other precursory movements may take place on the unstable slope and may be capable of indicating both where and when failure will take place. The best monitored eruption of this type was that of Mount St. Helens in 1980.

Slope movements prior to the event were enormous—so great that they were first detected not by sensitive instruments but from air photographs, where the enormous changes were plainly visible. Air photographs had been taken the previous year, on 15 August 1979, and were taken again on 7 and 12 April 1980 and 1 and 12 May 1980.

Between each of these dates, there was subsidence close to the summit, and broad inflation about 1 km downslope on the northern flank. The amount of subsidence had totaled more than 70 m by May 12, the subsiding area forming an expanding trough or graben on the north side of the summit aligned approximately east–west. This graben was 1.5 km long and grew from 360 m wide on April 7 to about 600 m wide on May 12. The inflation further down eventually raised some areas more than 150 m above the pre-eruption topography (Figure 6), forming a prominent bulge which became increasingly obvious down the northern flank. This bulge measured nearly 2 km in diameter, with a zone of maximum uplift that moved northward as time progressed.

Dry tilt stations were also set up and measured frequently during the crisis, and in some cases showed large short-term fluctuations in tilt, measured at up to 50 μrad per hour on April 10th.

At the same time, distance measurements to reflectors installed at several points on the upper slopes of the mountain showed that stations on the bulge were moving north at a fairly constant rate of up to 2.5 m per day. Many reflectors were in fact moving in an almost horizontal direction or even slightly downhill, though the fact that this carried them north into regions well above the pre-eruption slope made them appear as inflated areas on the topographic difference maps.

Sector collapses and the associated pyroclastic flows

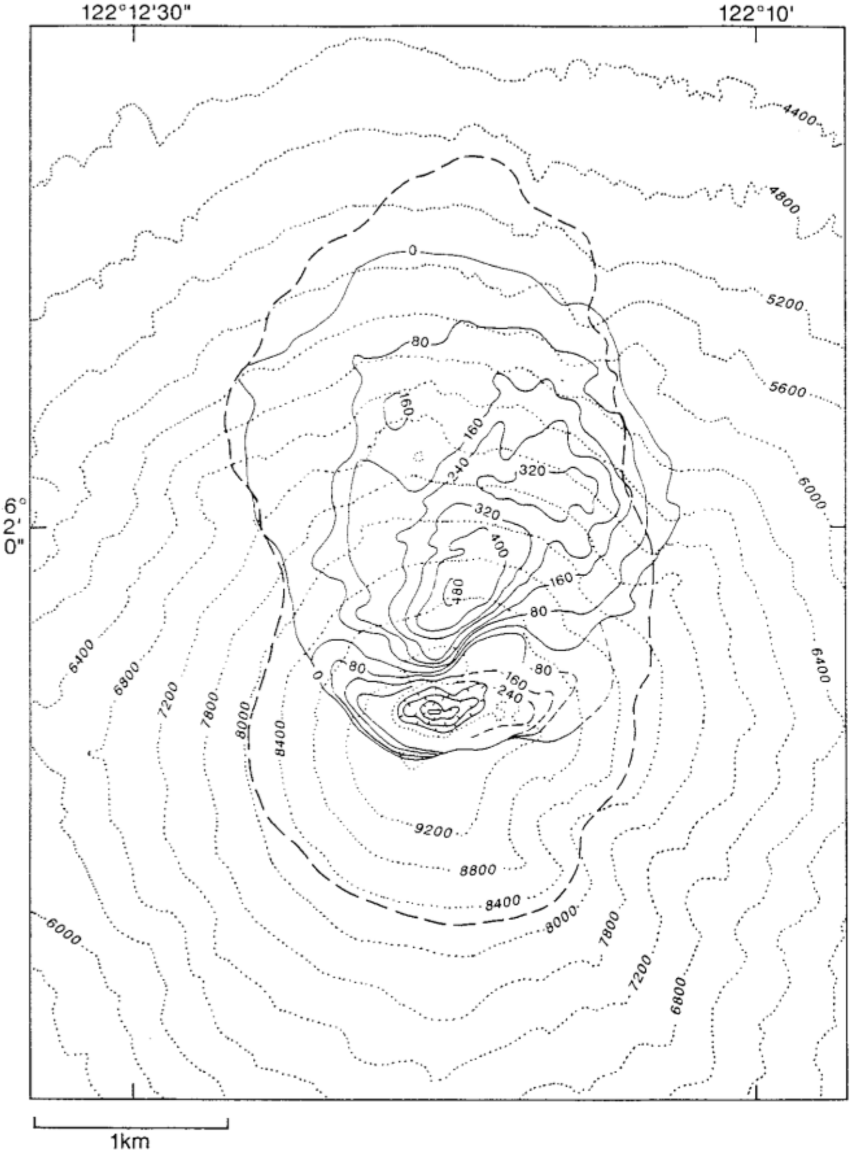
122°12'30"
122°10'
6° 2' 0"
4400
4800
5200
5600
6000
6400
6800
7200
7800
8000
8400
9200
8800
8400
8000
7800
7200
6800
6000
6400
0
80
160
160
240
320
320
400
480
160
80
0
80
80
160
240
1km

FIGURE 6 Map showing topography (dotted lines) and elevation changes in feet (solid lines) between 15 August 1979 and 12 May 1980 at Mount St. Helens volcano, USA, before the catastrophic slope failure and pyroclastic eruption of May 18. The bold dashed line shows the position of the crater rim that formed in the May 18th eruption.

that may accompany them are among the most potentially dangerous and destructive types of volcanic activity as they occur suddenly and progress very rapidly, and are capable of wiping out towns as far as 100 km distant from the volcano in some cases. The Mount St. Helens eruption of 18 May 1980 is the only example of sector collapse on a volcano where monitoring has been carried out both before and after the event, and as such contains important information to bear in mind when facing possible future sector collapses on other volcanoes. As far as deformation goes, it seems that the enormous rates of ground movement began only 8 weeks before the eruption, and continued at a fairly constant rate until the moment of eruption. This indicates a different behavior from slope creep observed before some types of slope failure, where a progressively increasing rate of deformation is observed, which can be used to predict the time of failure.

IV. PRINCIPLES OF GRAVITY MONITORING

The acceleration due to gravity at the Earth's surface is approximately 9.8 ms^{-2}. Gravity varies by 7000 μGal (7×10^{-5} ms^{-2}) between mountains on the equator (where the Earth's radius is greatest) and sea level at the poles. Modern gravimeters can measure gravity differences (either between different places or at one place through time) to about 1 in 10^8; in other words, variations as small as 0.00000001 ms^{-2} can be detected. Such variations occur naturally over the face of the Earth due to lateral heterogeneities in the density structure. Thus buried dikes, feeder pipes, and even magma chambers can be identified by making a map of the variations in gravity, provided there is a density contrast between the subsurface structures of interest and the surrounding rock. Local variations in gravity occur due to contrasts in subsurface mass distribution and in elevation (gravity decreases vertically at roughly 308 μGal m^{-1} = 3×10^{-6} ms^{-2}; this is called the free-air gradient).

The most common type of gravimeter used on volcanoes basically comprises a mass on a spring (Figure 7). A complex array of gears provides a very accurate measure of the force that needs to be applied (mechanically or electronically) to the mass to return the spring to its original length within the prevailing gravity field. Calibration of the instrument allows differences in the measured force (either between stations on a network or with time at one place) to be expressed in terms of gravity differences. Gravity measurements are usually made at ground level, although instruments have been developed to operate on the seabed, from a ship, and on an airplane.

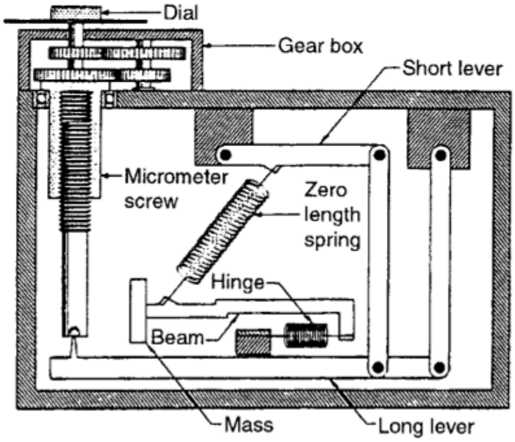

FIGURE 7 Basic operating mechanism of a LaCoste and Romberg gravimeter.

V. TECHNIQUES USED IN THE FIELD

A. Earth Tides

The Earth tides are variations in gravity caused by the relative movement of the Sun and Moon. On large water masses, these bodies produce the familiar ocean and river tides. On land, the solid mass of the Earth also deforms in response to the varying gravity pull of the Sun and Moon.

For any point on the Earth's surface, Earth tides vary by up to 400 μGal peak to peak with a maximum rate of change of about 60 μGal $hour^{-1}$ (1.8×10^{-10} ms^{-2}). For any time, the Earth tides can be computed (Figure 8); any deviations from the tide, called residual gravity changes, are due to instrumental effects or external processes such as ground deformation and volcanic activity. It is usual to have a continuously operating GPS receiver adjacent to a tidal gravimeter so that the effects of elevation changes can be constantly monitored. A volcano tide, which would be a volcanically induced residual, is expected to be present if large subsurface volumes of magma are free to move.

This is a relatively new technique for monitoring volcanoes and there are only limited examples of its use. The potential is enormous though, once unwanted "noise" such as changing groundwater levels and the effect of tremor on the instrumentation have been removed. A gravimeter operating in a remote location (telemetering data to an observatory) can provide valuable information on subsurface processes without any risk to human operators.

There are two ways in which the Earth tides on a volcano can be analyzed usefully. The first is to record the tides and then to determine the "delta factor" or the amount by which the predicted tide needs to be multiplied to produce the observed tide. The amplification is needed because the tidal prediction calculations assume a solid Earth. The elasticity of the real Earth means that it responds to the tides differently from a solid spheroid. Variations through time of the delta factor preceding eruptive activity, for example, can then be interpreted in terms of changes in the elastic properties of the volcano. Another way of investigating the Earth tides is to subtract the observed tide from the computed tide and to study the residual tide. For this

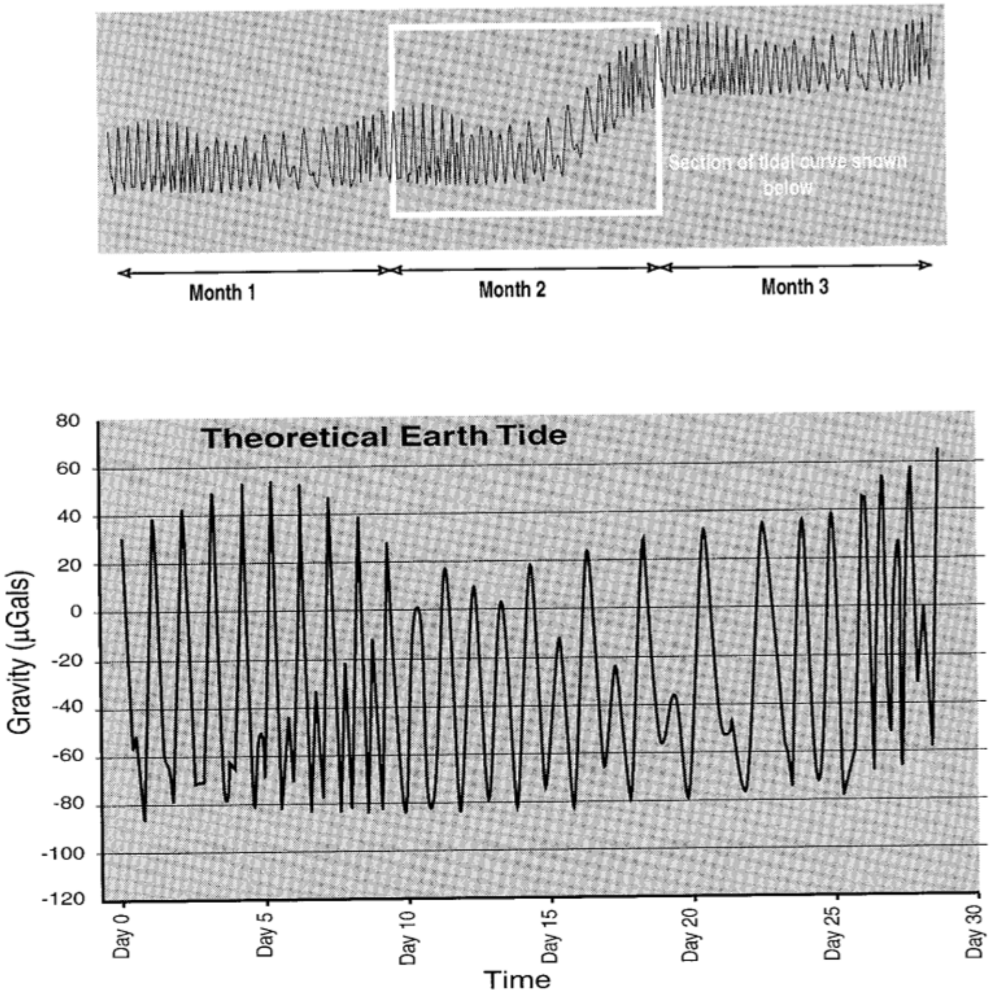

FIGURE 8 The top graph shows a sample of continuous gravity measurements at a hypothetical volcano over a 3-month period. The Earth tide signal dominates until the end of month 2, when a volcanic event causes a steep gravity increase. The theoretical Earth tide for month 2, such as might be measured at a reference station at the foot of the volcano, is shown beneath.

second approach, a delta factor is assumed, although changes in this factor through time may become apparent.

B. Microgravity

Microgravity monitoring involves the measurement of small changes in the value of gravity at a network of stations. Microgravity is becoming increasingly recognized as a valuable tool for mapping out the subsurface mass redistributions that are associated with volcanic activity. As for all types of gravity work, it is essential for the unambiguous interpretation of the data that any changes in elevation are measured at the same time as the gravity measurements are made. Gravity values are tidally corrected (the effects of the computed Earth tides are removed) and then the data are usually expressed relative to the value of gravity at a base or reference station which is preferably outside the area of volcanic activity and interest. The network is then remeasured some weeks, months, or years later, or after some volcanic event has occurred. The tidally corrected gravity difference at each station relative to the base station must then be corrected for any elevation changes that have taken place. Any residual gravity changes are due to subsurface density changes.

C. Absolute Gravity

The most common method for determining the absolute value of gravity in volcanoes involves measuring the rate of fall of a mass. A laser interferometer is used to track the vertical rise of a corner cube reflector propelled vertically upward and its subsequent fall. The instrumentation is expensive, very heavy, and only transportable by vehicle. It is also complex to use, taking a day or so for one value to be measured, and the technique is therefore not often used. However, the advantage of absolute gravity values is that, unlike relative gravity values, there is no dependence on reference to a base station that may or may not be stable. Earth tides, elevation, and even atmospheric pressure will influence the value of gravity determined; these effects must be removed before an absolute value is obtained.

The absolute value of gravity has been measured at the oldest volcano observatory in the world, at Vesuvius, Italy. The first measurement was made in 1986 and the second in 1994. The first value obtained was 980,133,453 ± 4 μGal, and 8 years later the value was 980,133,396 ± 3 μGal. This approximately 60-μGal gravity increase is consistent with the results of microgravity surveying in the area, which showed a similar increase relative to a reference station away from the volcano. Similar results on Etna and elsewhere have shown small changes, but to data there have only been two or three measurements made at each volcano.

VI. CASE HISTORIES OF GRAVITY CHANGES

Microgravity surveys have been made at active volcanoes since the 1950s, but tidal gravity, with its requirements of continuous power, accurate time keeping, and large volumes of data output, has only been a realistic option for volcano monitoring since the mid-1990s. Absolute gravity is still too cumbersome and expensive to use regularly at volcanoes.

A. Microgravity at Calderas: Campi Flegrei (1969–1984)

The typical compositions of eruptive products at a volcano provide a basis for classification of the nature of precursory microgravity changes. Large silicic calderas, where long-term unrest is common and devastating eruptions occur infrequently, are characterized by periods of inflation and deflation with residual gravity changes indicating subsurface mass increases (Figure 9). Gravity changes differing from those predicted from the elevation changes have been interpreted in terms of magma movements and hydrothermal fluid migration. Observed elevation changes have been large at these calderas (ca. 1 m) and the gravity data fall close to, but not always on, the free-air gradient.

In the center of Campi Flegrei caldera, the ruins of an ancient Roman market (Serapeo; see Figure 10) bear witness to long-term caldera unrest. Mollusk borings in the stone columns indicate earlier periods below sea level and recent measurements indicate that during two crisis periods (1969–1972 and 1982–1984), uplift of some 3.3 m occurred. During uplift, gravity at Serapeo decreased less than predicted by the free-air gradient, suggesting a subsurface mass increase. Inflation and gravity increases were seen over a large area and were thought to be caused by a magmatic intrusion of around 2×10^{11} kg at some 3 km of depth. Slower deflation continued until 1990. Similar observations (though with a mass increase of only 10^{10} kg) at Rabaul caldera in Papua New Guinea preceded an explosive eruption by about 10 years.

B. Microgravity at Andesitic Volcanoes: Poas Volcano (1985–1989)

The explosive nature of many andesitic eruptions and the possibility of risk mitigation make this category of volcanoes the most important to monitor effectively in the short to medium term. These volcanoes are intermittently active and tend to have rather complex edifice structures with several craters. The intrusion of magma into poorly consolidated material and even the buildup of magmatic gas pressure are sometimes detectable because these processes can occur close to the surface and the density contrasts are large.

A characteristic of andesitic volcanoes is that the gravity–height change data tend to plot close to the Δg axis of Figure 9 (the height changes are usually rather small). One of the longest time series of microgravity data for a volcano is from Poas in Costa Rica. A network of stations in and around the active crater revealed increases and decreases in gravity associated with phreatic eruptions and the gradual disappearance and final re-establishment of the crater lake (Figure 11). Increases at

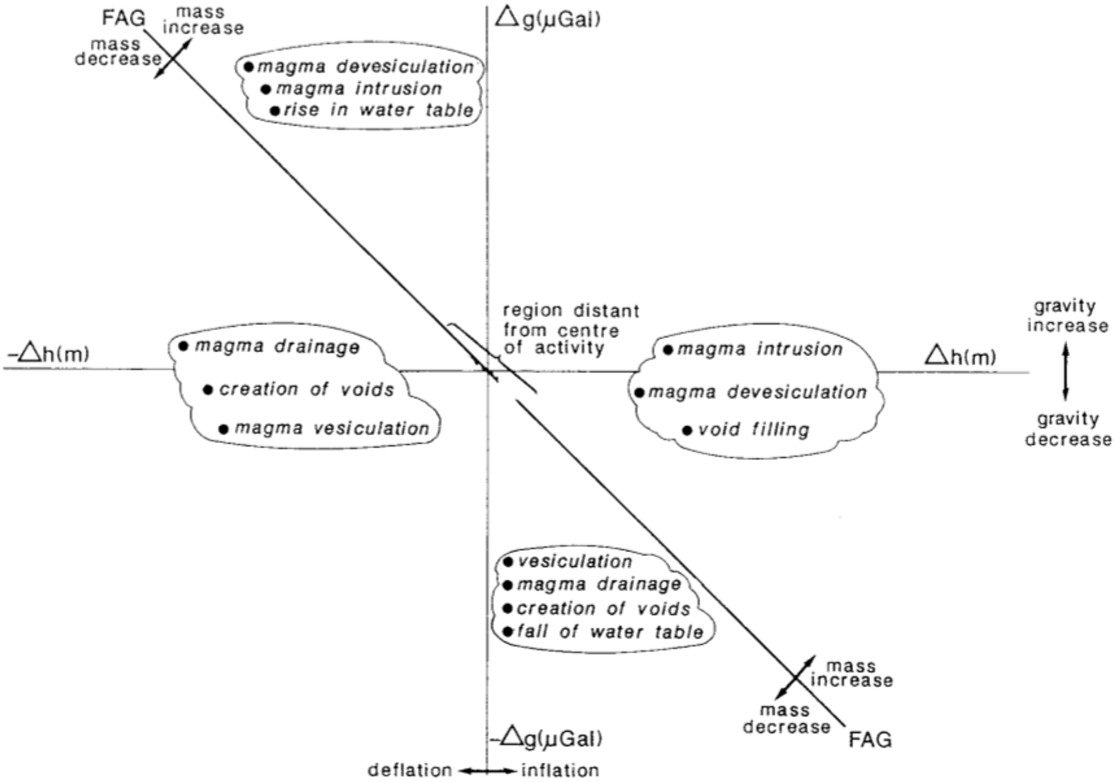
FAG
mass increase
mass decrease
Δg(μGal)
• magma devesiculation
• magma intrusion
• rise in water table
region distant from centre of activity
-Δh(m)
• magma drainage
• creation of voids
• magma vesiculation
• magma intrusion
• magma devesiculation
• void filling
Δh(m)
gravity increase
gravity decrease
• vesiculation
• magma drainage
• creation of voids
• fall of water table
mass increase
mass decrease
FAG
-Δg(μGal)
deflation
inflation

FIGURE 9 Graph of height changes (horizontal axis) against gravity changes (vertical axis). Measured gravity and elevation changes may be plotted on this graph and the interpretations read off. The diagonal line is the free-air gradient (FAG) at $-308\ \mu\text{Gal m}^{-1}$. Data plotted above this line on the right-hand side (positive Δh, i.e., inflation) represent net gravity increases and therefore subsurface mass increases which, on volcanoes, are most likely caused by magma intrusion, magma devesiculation, and void filling. Data falling in other regions of the graph have correspondingly different interpretations as marked.

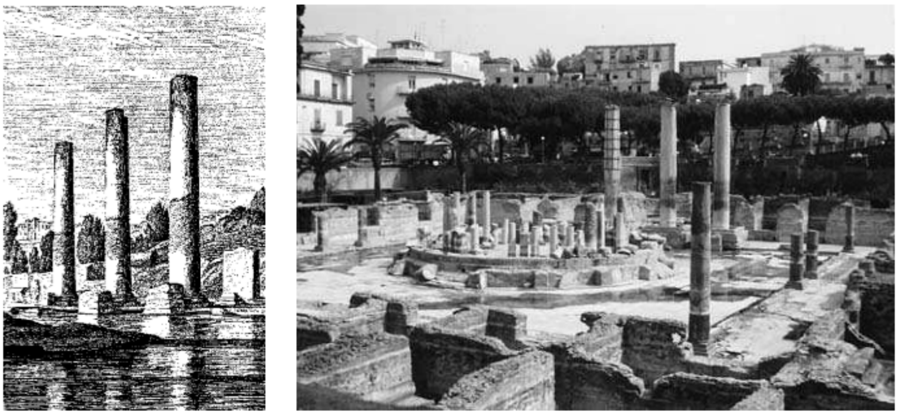

FIGURE 10 The ruins of the market of Serapeo at the center of Campi Flegrei caldera (Naples, Italy) provide a classic example of long-term caldera unrest. When built in ancient Roman times, the market must have been above sea level, yet by 1834 (left) it had sunk below sea level, and the mollusk borings more than a meter up the columns indicate lengthy periods even further below sea level prior to this. However, recent surveying measurements show that the region rose by 3.3 m between 1969 and 1984, raising the whole market well above sea level again by 1991 (right).

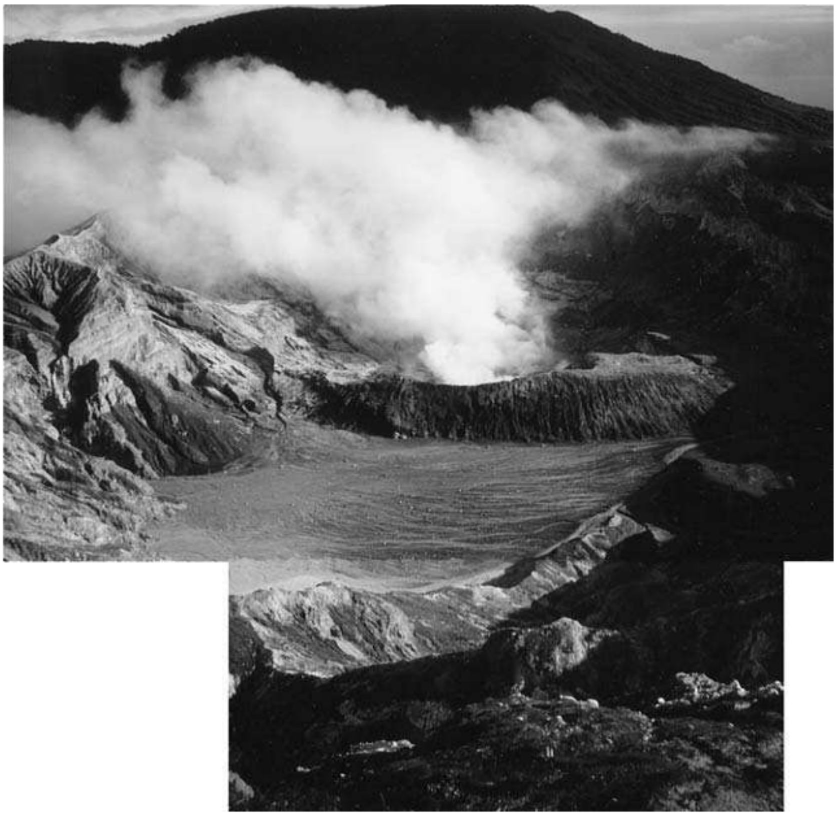

FIGURE 11 Summit crater of Poas volcano, Costa Rica, in 1994. The photo shows the crater rim with the crater bottom some 200 m below. Behind the ridge in the center is the hot, acidic lake that disappeared between 1989 and 1997. By 1998 it had overfilled to such an extent that it was beginning to flood the main crater floor.

stations in the southern part of the crater bottom began in 1985, preceding the phreatic activity and loss of the lake by 4 years (Figure 12). By integrating the magnitude of the residual gravity changes over the area of their extent, the subsurface mass increase can be deduced: 10^8 kg of new mass appeared beneath the crater between 1985 and 1989. This new mass may have been a magmatic intrusion, deposition of sulfur, the redistribution of the hydrothermal system, or some combination of these.

C. Microgravity at Basaltic Volcanoes: Mount Etna (1990–1993)

The hazard to human life and property at these volcanoes is smaller, but comprehensive surveillance program have been carried out at the more active ones such as Kilauea on the island of Hawaii and Etna on Sicily. An important characteristic of these volcanoes that influences the observed microgravity changes is their tendency to develop flanking rift systems. Magma may be intruded passively into dikes and can feed flank eruptions exploiting these rifts. Thus very large mass changes can occur without elevation changes (data plot near the Δh axis on Figure 9), but large elevation changes can also occur (during rifting events, for example) and then gravity data fall close to the free-air gradient. Separate deflation events on Kilauea had gradients between -171 and -607 μGal m^{-1}, thought to indicate magma migration away from the rift zone leaving voids, and then later passive intrusion into these void spaces.

Microgravity increases as large as 400 μGal were found between June 1990 and June 1991 at a network of stations near the summit of Etna volcano, Sicily (Figure 13). There was no eruptive activity at this time, and the ground deformation was less than a few centimeters, the microgravity increases were therefore caused by subsurface mass changes. A model for the gravity increases (Figure 14) shows the change in the shallow plumbing system at this time. The level of magma within the summit feeder pipe (modeled with a radius of 25 m)

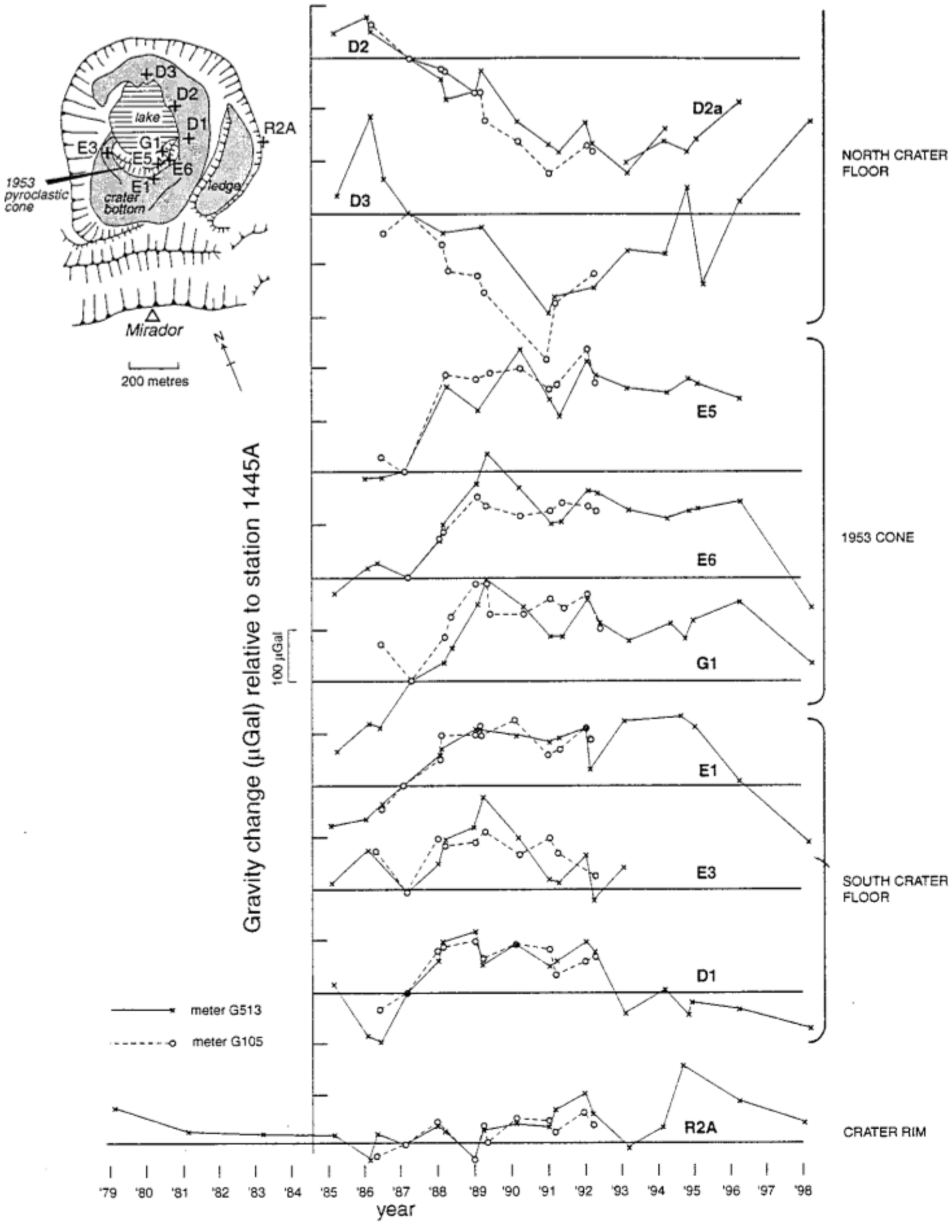

FIGURE 12 Microgravity changes at stations in and around the active crater at Poas between 1979 and 1998. Geyser activity began at the lake in 1987–1978 and the lake disappeared in 1989. It was reestablished in 1997.

rose at some time between the two sets of observations and a dike was apparently intruded in a south-southeasterly direction trending away from the summit. The point at which this modeled dike intersects the topography is the site of the vent for the December 1991–April 1993 eruption. In this case it would appear that the gravity increases indicated rising magma which later fed a large eruption.

VII. PRINCIPLES OF MAGNETIC MONITORING

A total magnetic field map can be drawn using data from a network of stations either near the ground surface or from an airplane or helicopter. Variations through time

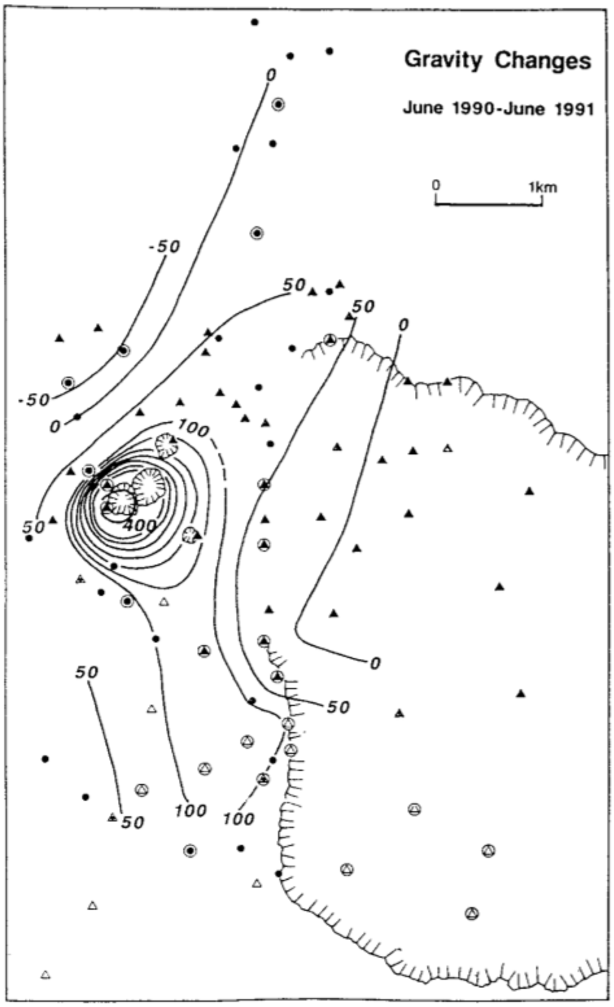

FIGURE 13 Map of microgravity increases at Etna volcano measured between June 1990 and June 1991. The largest increases are close to the summit craters and reflect an increase in magma level within the feeder system. Gravity increases were also seen in an elongated south-southeasterly trending region close to fractures which opened up at the end of an eruption in 1989. This was probably caused by the intrusion of a dike.

may also be monitored using a stationary continuously recording magnetometer or by repeating measurements at a network of stations, if stations can be precisely relocated.

Magnetic monitoring of volcanoes is relatively underdeveloped compared with ground deformation and microgravity monitoring. Magnetic changes associated with volcanic activity have been successfully observed, some of which were precursory to eruption and hence identify the potential of magnetic monitoring methods. However, magnetic effects are generally more complex and difficult to interpret than gravity or deformation data.

The magnetic field at the surface of the Earth ranges in intensity from approximately 25,000–70,000 nT, depending mainly on latitude. About 99% of this field is generated by circulation in the Earth's partially molten outer core, with minor contributions from the magnetic effect of near-surface rocks themselves and external sources such as the ionosphere.

There are two main types of rock magnetism; remanent magnetism and induced magnetism, both of which depend on the occurrence of magnetic or magnetizable minerals in the rock. Remanent magnetization, the essentially permanent magnetization in rocks, is acquired at the time of either rock formation or a subsequent crystallization event. Induced magnetization is a temporary magnetization generated in rocks by the present-day ambient magnetic field of the Earth. Rock magnetism only occurs at temperatures below the Curie point (ca. 550°C).

The intensity of magnetization in a rock depends largely on the abundance of magnetite in the rock. Since most volcanic rocks commonly contain magnetite they are often strongly magnetized, enough to divert a compass needle in some cases, and hence the unreliability of the compass as a navigational tool in volcanic areas. The intensity of magnetization in more basic rocks (e.g., basalt) is in general stronger than that in less basic rocks (e.g., andesite). Surveys of the spatial distribution of magnetic effects of volcanic rocks can be used to generate models of structures within volcanoes or to determine the depth and volume of lava flows. In magnetic monitoring of active volcanoes, measurements of the magnetic field are repeated, either continuously or intermittently, at the same location over a period of time in order to detect changes in the magnetization of the subsurface rocks.

"Volcano-magnetic" effects are caused by a number of mechanisms, the most important being thermal demagnetization or remagnetization, and piezomagnetic effects. Thermal demagnetization occurs as the rock heats through its Curie temperature. The effect is reversible, and remagnetization occurs when the rock cools again. Piezomagnetic effects are magnetic changes due to changes in stress regime such as magma intrusion or depressurization, which are generally irreversible. Other possible mechanisms for volcano-magnetic effects include (1) chemical changes to magnetic minerals, for example, alteration by hydrothermal activity, (2) mass redistribution such as intrusion or major landslides, or (3) electrokinetic effects due to fluid flow in the rocks.

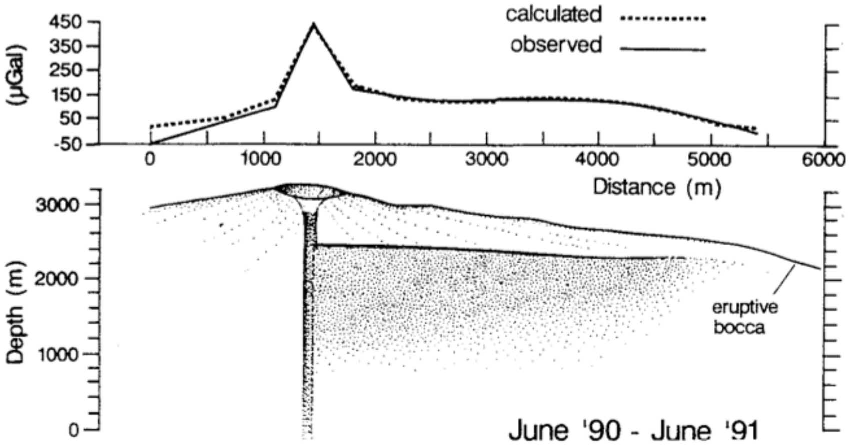

FIGURE 14 Model of the subsurface magma movements thought to have caused the microgravity changes seen in Figure 13. The south-southeasterly trending dike is only 4 m wide, but the summit feeder pipe is 25 m in radius, which accounts for its larger gravitational effect.

VIII. TECHNIQUES USED IN THE FIELD

The intensity of the total magnetic field only is generally measured, though it is possible to measure its constituent parts (e.g., horizontal and vertical components); however, this requires precisely leveled instruments which can be difficult to maintain in areas undergoing significant ground deformation. Instruments used are either proton precession magnetometers (accurate to 0.1 nT) or cesium/rubidium vapor magnetometers (accurate to 0.01 nT). Measurements must be corrected for secular variations (i.e., changes with time) in the Earth's magnetic field itself, which is achieved by monitoring magnetic field changes at a base station outside the region influenced by the volcano. Each site on the volcano may respond differently to these ambient field changes but this can be calculated mathematically and subtracted from the observed data.

IX. CASE HISTORIES OF MAGNETIC OBSERVATIONS

Most commonly, magnetometers are set up at a site on a volcano and left to record "continuously" (i.e., measurements are recorded every 1–10 minutes). If these data are telemetered to an observatory and the system is powered by solar cells, the site need only be visited for maintenance. Other continuously measuring devices may be battery powered or the data may be recorded on site, in which case they need to be serviced more often, which can be logistically demanding in difficult terrain. Alternatively, measurements may be repeated intermittently (e.g., every few days or weeks) at monumented sites using a portable magnetometer (Figure 15). In this case it is essential that the magnetometer be relocated in precisely the same position (horizontally and vertically) for each measurement. In some studies, combinations of both continuous and intermittent sites have been used.

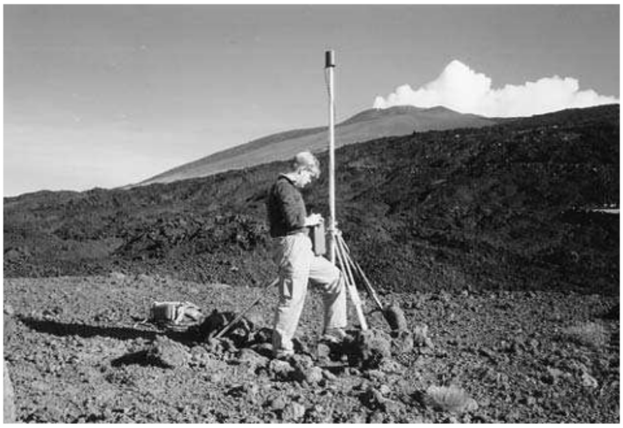

FIGURE 15 Portable proton precession magnetometer in use on the south flank of Mount Etna, Sicily. Precise centering over a permanent marker is essential where repeat measurements of a network are to be made.

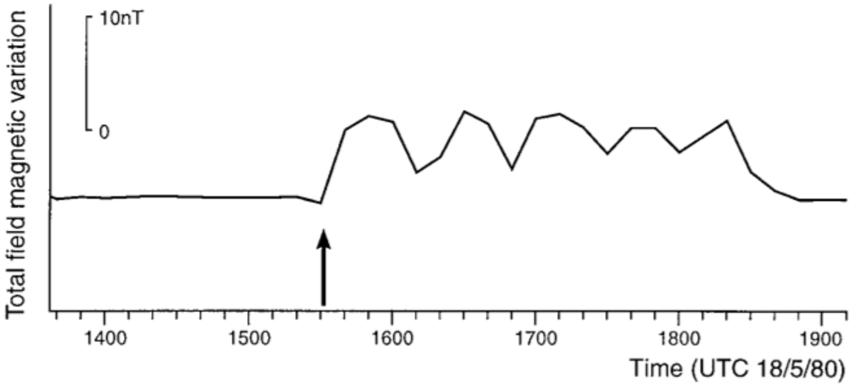

FIGURE 16 Variations in total magnetic field recorded at a site on the west of Mount St. Helens volcano before and after the catastrophic eruption of 1980 May 18 at 0832 PDT (1532 UTC). Time of eruption denoted by arrow.

A. Mount St. Helens Volcano (USA, 1980)

Magnetic changes were observed on the west side of the edifice of Mount St. Helens volcano at the times of the three major eruptions on May 18, May 25, and June 12, 1980. No magnetic changes were observed immediately before the catastrophic May 18 eruption (Figure 16); this is consistent with the triggering of the eruption by a sudden depressurization of the magma by a landslide. The increase of 9 ± 2 nT occurring during the 12 hours following the May 18 eruption has been interpreted as a piezomagnetic effect resulting from the release of stress during the eruption. Since the net magnetic change is permanent, electrokinetic and thermal demagnetization mechanisms cannot have played a major role, and also the magnetic effects are in the opposite sense than could be attributed to the accompanying mass redistribution. This interpretation has been endorsed by mathematical models which show that a magnetic change with the same amplitude and sense would be generated by a pressure release of ~100 MPa in a cylindrical or spherical magma chamber ~1 km in diameter at a depth of ~5 km. There was some indication of magnetic disturbances for several hours before the May 25 (Figure 17) and June 12 events, and even greater effects were recorded after these eruptions. These post-eruption changes are considered to reflect the effect of eruptive shockwave events on the ionosphere and were also recorded at least 1000 km away from the mountain.

B. White Island (New Zealand, 1974)

Magnetic measurements have been made at White Island in surveys repeated at approximately 4-month intervals since 1968. Localized changes of up to 400 nT were measured within the crater between 1976 and 1982; both increases and decreases were observed during this time. Increases occur after eruption sequences and indicate cooling, while decreases are associated with eruptions and result from heating of the rocks at depths of 500–1000 m. For example, the magnetic changes observed between February and August 1974 (Figure 18) were interpreted as resulting from localized heating below Donald Mound. This was confirmed by the opening of a vigorous fumarole in that vicinity in September 1974. Modeling has shown that variations of 200–300°C

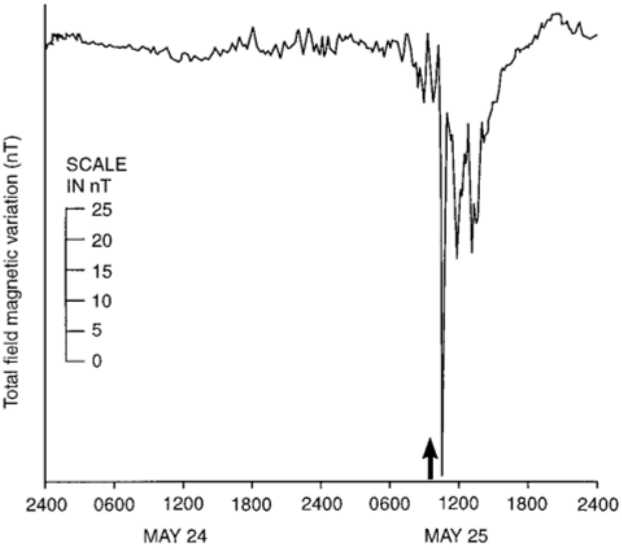

FIGURE 17 Variations in total magnetic field recorded at a site on the west side of Mount St. Helens before and after the eruption on May 25. Time of eruption denoted by arrow.

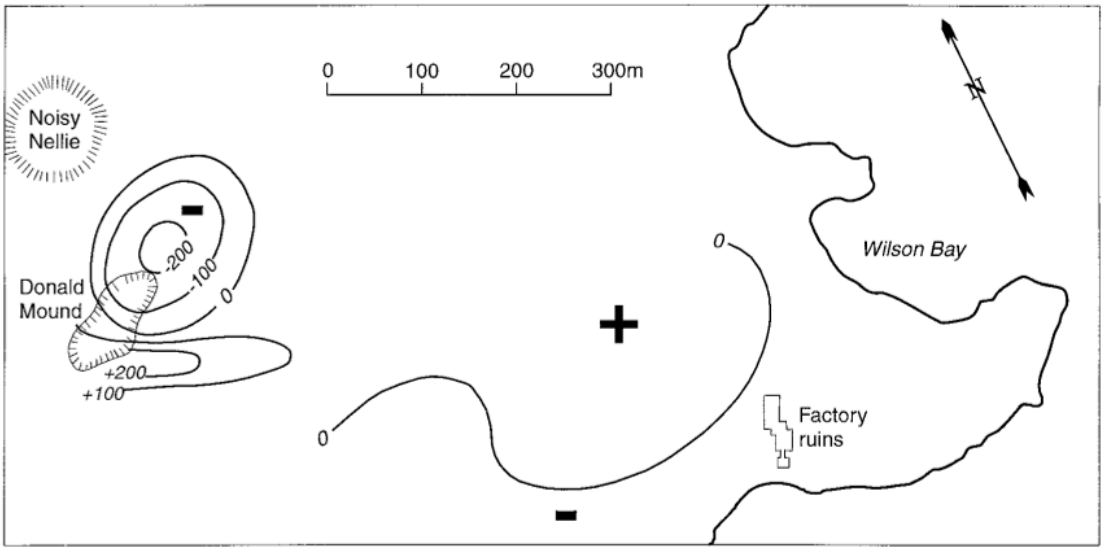

FIGURE 18 Map of the total field magnetic changes within the crater of White Island volcano between February and August 1974. Contour interval is 100 nT.

are required to account for the observed field changes. The rapid occurrence of these changes indicates convective (rather than conductive) transport mechanisms to be active in this case, such as the movement of hot gases or the ingress of cold rainwater.

C. Aso Volcano (Japan, 1989–1990)

Increases and decreases in the magnetic field during an eruption sequence, recorded near the active crater in 1989–1990, occurred in five stages (Figure 19), each of a few months duration. These stages correlate with specific volcanic events and the occurrence of seismic tremor, and have been explained in terms of thermal magnetization (stages 1, 3, and 5) and demagnetization. Magnetic field decreases resulting from thermal demagnetization occurred when the system was heated because either the vent was plugged (stage 4) or the volcanic activity was enhanced (stage 2). Magnetic field increases followed either the opening of a vent (stage 1) or large explosions which made the vent more permeable (stage

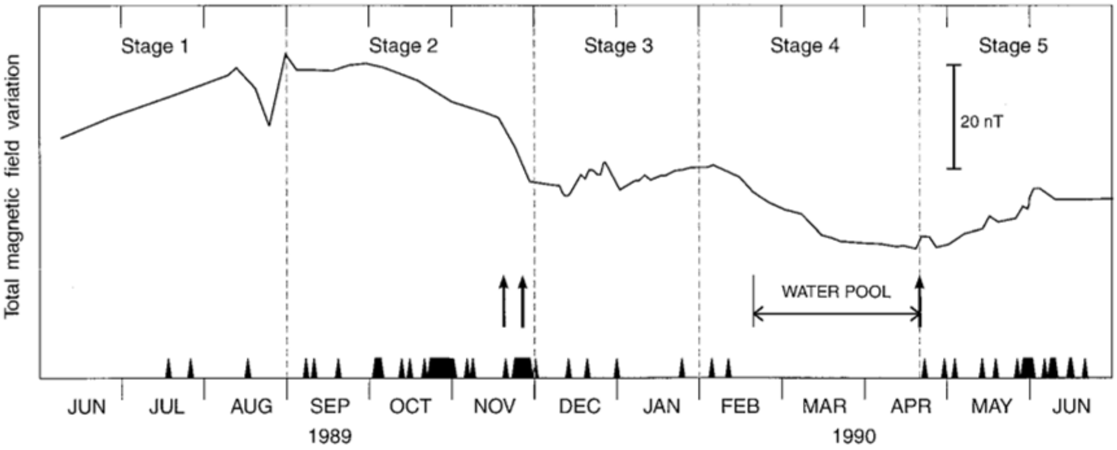

FIGURE 19 Variations in total magnetic field at Aso volcano together with details of eruptive activity. Vertical arrows indicate explosions, and black triangles show occurrence of eruptions. A pool of water formed within the crater in spring 1990.

5), thereby cooling the system. These magnetic changes have been modeled as originating in rocks at a 200-m depth at the vapor–fluid boundary. The vapor pressure is determined by the permeability of the vent cap and the heat supply from magma at depth. This vapor–fluid boundary therefore moves in response to vapor pressure, expanding or contracting the demagnetized zone and causing the magnetic changes observed at the surface.

X. CONCLUDING REMARKS

Ground deformation has long been used as a tool for monitoring and predicting volcanic activity. By combining the method with gravity and magnetic potential field techniques, it becomes a more powerful and rigorous indicator of subsurface processes. Each technique alone can produce results which are misleading or ambiguous, but by integrating data sets, many of the ambiguities are resolved. Not all volcanoes lend themselves equally well to each monitoring technique. Nevertheless, measurable changes in the physical properties of shallow subsurface structures beneath volcanoes ranging from young basaltic cones to andesitic stratocones to silicic calderas have been observed before, during, and after magma movement or eruption.

The cost of regular visits to a volcano to make routine measurements and the hazard to human life are such that there is an understandable drive to develop reliable, automated instrumentation with a telemetering capacity to send data in real time or at discrete intervals. SAR interferometry is clearly going to become a valuable ground deformation early warning tool once software for image processing is easily accessible to volcanologists. However, the fact that deformation can only be observed in the satellite vector means that this technique is unlikely to replace ground survey measurements. Of these, dual-frequency GPS is the most promising technique. With continuously recording GPS combined with remotely operating gravimeter and magnetometer stations, the temporal coverage of data is going to improve dramatically, although the spatial coverage will never be as good using a few continuously recording instruments as it is with a large network of stations. However, by careful choice of station location (close enough to the activity to measure significant changes and far enough away to avoid direct damage and continuous disturbance) a compromise can be reached whereby virtual real-time data can be obtained at little or no risk to human life. Alternatively, if costs come down in the future it may be possible to deploy much larger numbers and denser arrays of continuously recording instruments, which, if data are telemetered to a remote operations center, would constitute an ideal surveillance system.

SEE ALSO THE FOLLOWING ARTICLES

Gas, Plume, and Thermal Monitoring • Seismic Monitoring • Volcanic Hazards and Risk Management • Volcano Warnings

FURTHER READING

Mogi, K. (1958). Relations between the eruptions of various volcanoes and the deformations of the ground surfaces between them. *Bull. Earthquake Res. Inst.* (*Univ. Tokyo*) **36,** 99–134.

Murray, J. B., Pullen, A. D., and Saunders, S. (1995). Pages 113–150 *in* "Monitoring Active Volcanoes" (W. J. McGuire, C. R. J. Kilburn and J. Murray, eds.). UCL Press, London.

Rymer, H. (1996). Pages 169–198 *in* "Monitoring and Mitigation of Volcanic Hazards" (R. Scarpa and R. I. Tilling, eds.). Springer, Berlin/Heidelberg.

Zlotnicki, J. (1995) Pages 275–301 *in* "Monitoring Active Volcanoes" (W. J. McGuire, C. R. J. Kilburn, and J. Murray, eds.). UCL Press, London.

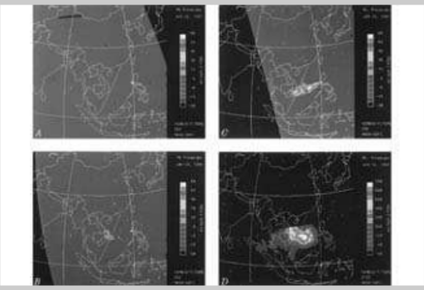

Gas, Plume, and Thermal Monitoring

John Stix
McGill University

Hélène Gaonac'h
Université du Québec à Montréal

I. Gas Measurements and Monitoring
II. Ash Measurements and Monitoring
III. Thermal Measurements and Monitoring
IV. Future Directions

Glossary

COSPEC A ground-based, remote sensing, ultraviolet correlation spectrometer which measures the flux of sulfur dioxide gas from volcanoes.

crystal fragments Pieces of crystals which precipitated in magma prior to eruption.

emissivity The ratio of the radiant flux emitted by a body to that of a perfect emitter ("blackbody") at the same kinetic temperature.

FTIR Fourier transform infrared spectrometer, a ground-based, remote sensing infrared instrument which measures concentrations of various gases from volcanoes.

fumarole A crack or fissure through which volcanic gas is emitted.

glass shards Small fragments of quenched magma.

lithic fragments Pieces of the preexisting volcano which are incorporated and ejected during an eruption.

magmatic-hydrothermal system The plumbing system of a volcano within which a magma body is surrounded by an envelope of water derived from shallow levels.

pumice A low-density, bubble-rich material consisting mainly of natural glass; it is a quenched sample of magma erupted explosively.

remote sensing The detection of a body's properties from a distance.

spatial resolution The ability of a remote sensor system to discriminate points or objects.

thermal infrared Part of the electromagnetic spectrum where a blackbody at room temperature (300 K) predominantly radiates. The thermal infrared region is usually defined between 3 and 1 μm.

TOMS Total ozone mapping spectrometer, a space-based, remote sensing, ultraviolet spectrometer which measures sulfur dioxide erupted by volcanoes into the stratosphere.

ACTIVE VOLCANOES DURING an eruption or between eruptions exhibit various signs reflecting their current activity, including degassing and thermal anomalies. Because of the high temporal and spatial variability of volcanic phenomena volcanoes need to be regularly monitored to better understand the dynamics of each volcano. Thirty years ago, volcanologists focused their efforts on qualitative field observations of volcanic phenomena. In the past 25 years, there has been an explosion of research on volcano dynamics. This includes the development of modeling, laboratory experiments, advances in technology, and a better understanding of theoretical principles concerning physical and chemical volcanology.

Copyright © 2000 by Academic Press
All rights of reproduction in any form reserved.

Gas measurements and thermal monitoring are research fields which have developed rapidly during this time, with data acquired at the ground, from the air, and from space with various instruments. This article describes the available measurement methods, data, and scientific objectives presently being pursued. It concludes with a view of the next scientific steps needed to advance the knowledge of eruption dynamics and to make accurate forecasts of volcanic activity.

As datasets grow in size and complexity, it becomes a formidable challenge to better integrate and quantitatively interpret the information so that new technologies will have their full impact on providing clues for volcanic modeling. Some new approaches concerning the dependence of the data on their scale or resolution of observation and acquisition are also discussed.

I. GAS MEASUREMENTS AND MONITORING

A. Principles

Volcanologists have long recognized that volatiles are an essential component in volcanic systems. Since volatiles play an important role, their behavior can be examined to provide a better understanding of volcanic activity. Volatiles escape from magma bodies through fumaroles and hot springs, which are often located on a volcano's flanks. Thus, studies of volcanic gas can furnish important insights on the sources of magmas, how magmas move upward to the surface, the influence of hydrothermal systems, and the types of eruptions—for example, explosive vs. effusive—that are observed. The amount of gas dissolved in a magma determines, in large part, whether an eruption will be violent or not. Armed with this information, our ability to forecast future activity is improved. Studies of volcanic gases provide important information not only for the behavior of magma before an eruption, but also when and why a volcano erupts.

Despite the utility of gas information, such studies traditionally have been neglected in favor of geophysical investigations such as seismic and deformation monitoring. There are several reasons. The access to high-temperature fumarolic discharges in an active crater is often difficult and hazardous, and the sampling and subsequent analysis of the gases require considerable skill. Compared to seismic information which is collected on a continual basis at a site which is remote from the active crater, direct sampling of gas normally is done on a sporadic basis, with intervals of weeks, months, or even years between samples. Until recently, we have had a poor theoretical understanding of how multicomponent gases behave in high-temperature environments such as volcanoes. Compared to experimental studies which examine only one or two individual gas species, the study of volcanic gas is complicated because it is a mix of many different major, minor, and trace gases.

Since the last 30 years, these limitations are being overcome for four principal reasons. First, volcanologists have begun to apply remote sensing techniques to measuring gas. These measurements have facilitated the sampling of the gas, since a scientist can make measurements at a distance from the crater on a semicontinual basis. Furthermore, a number of different gas species are now being studied by remote sensing. Second, advances in technology are beginning to permit semipermanent installation of gas sensors in craters, allowing around-the-clock monitoring. Third, the use of stable isotopes has helped define the origin and transport of gases. Fourth, our understanding of volcanic gas thermodynamics has been greatly improved in the last 15 years. Much of this progress can be ascribed to the work of Werner Giggenbach of the Institute of Geological and Nuclear Sciences in New Zealand.

Equipped with direct sampling of crater gas, remote sensing measurements, and theoretical understanding, we can begin to understand the behavior of volcanic systems through the study of gases. As importantly, we can start to see the local effects of volcanic gas upon the surrounding terrestrial and aquatic environments, namely health effects upon people, livestock, agriculture, soils, and forests. Lastly, the information is essential for understanding regional and global effects of volcanic gas upon our atmosphere and climate.

B. Direct Measurements of Volcanic Gases

1. High-Temperature Fumarolic Discharges from Active Craters

The spectacular emanations of gas that are seen in the craters of active volcanoes are visible manifestations of the presence of magma at depth beneath the crater. However, gas observed escaping at the surface is not derived solely from the magma. Rather, the gas is a mixture from different sources that have interacted during the lifetime of the volcano. A certain percentage of the gas is derived from magma, which will be initially rich in components such as sulfur and carbon dioxide (CO_2). Since these gases have comparatively low solubilities in magma, they are progressively lost during degassing, while more soluble gases such as water (H_2O) and hydrochloric acid (HCl) are retained. Indeed, water is the most abundant volatile component in magmas and therefore will constitute most of the gas that escapes at the fumaroles. This magmatic water, as well as the other gas components, is mixed with surface waters that infiltrate the volcano's permeable structure and contribute to the gas discharge at the surface. As these surface waters are added, the magmatic gas is diluted, increasing the water content to an even greater extent. Certain types of hydrothermal systems are created by the interaction of acidic magmatic gases (e.g., SO_2, HCl) with surface waters and with rock. These hydrothermal reactions can provide a source of gases such as CO_2 and hydrogen sulfide (H_2S). A component of the gas mixture may be added at deeper levels (e.g., chloride, boron) as a result of the subduction of tectonic plates, which transports and/or liberates volatiles. In a marine setting, there may be a direct or indirect addition of seawater, which enriches the chloride concentration of the gas.

To sample high-temperature gas, a volcanologist seeks out the hottest fumaroles which are most representative of magmatic gas compositions. These fumaroles are visited and sampled on a periodic basis over weeks, months, or years, depending on the activity of the volcano and the ease of access. If a volcano is erupting frequently, there will likely be a large gap in the data! Typically, the volcanologist first measures the temperature of a fumarole with a thermocouple, and then inserts a titanium or quartz glass tube into the fumarole. Once the gas is flowing through the tube, it is connected to an evacuated cylindrical bottle partly filled with concentrated sodium hydroxide (NaOH) solution (Figure 1). The NaOH solution absorbs acid gases such as CO_2, SO_2, and HCl by neutralization reactions, for example, $NaOH + HCl = H_2O + NaCl$. Other gases which do not react with NaOH (e.g., hydrogen, helium, carbon monoxide) are collected in the evacuated headspace of the bottle. These bottles are informally called "Giggenbach bottles" by volcanologists after Werner Giggenbach, who first developed the technique in the 1970s. In addition to this gas sample, the hot gas is rapidly cooled in a condenser placed in an ice bath. This "condensate" provides a quenched liquid sample of the gas which is analyzed for various elements and isotopes.

Gas data which are collected over a period of time can provide important information concerning the activity of a volcano. First, it is possible to follow the declining magmatic influence as activity wanes. Second, changes in permeability and pressure within a volcano can be interpreted using gas data. Below we present several examples of these two types of activity.

Certain volcanoes go through long periods of quiescence and comparatively short periods of activity (e.g., Mount St. Helens, Washington State, USA; Mount Pinatubo, Philippines). Normally the activity is the result of magma being emplaced at shallow levels in the

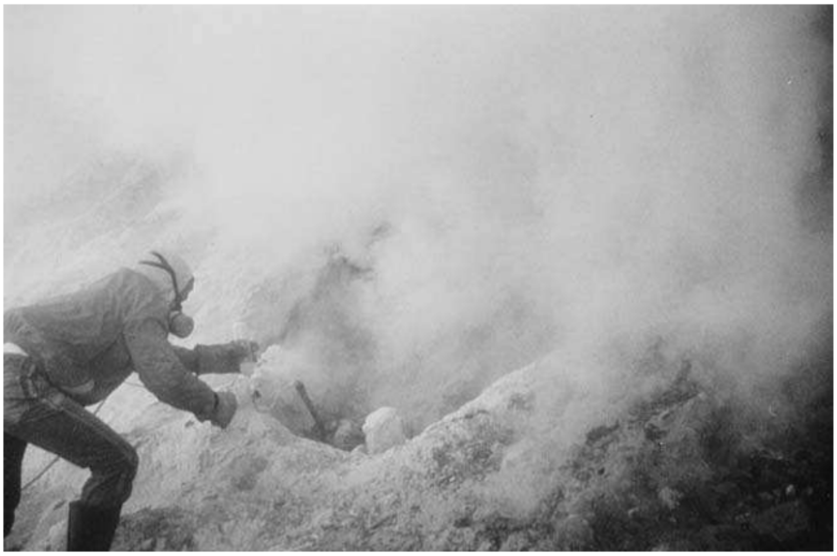

FIGURE 1 Sampling of volcanic gases from a fumarole at Galeras volcano, Colombia. A titanium tube has been inserted into the fumarole. The tube is connected to an evacuated gas sampling bottle by using heat resistant plastic tubing. The gas flows through this system to the bottle, where it is trapped by the alkaline solution or in the headspace. (Photo courtesy of Eric Fontaine.)

crust. When this occurs, the volcano reactivates, accompanied by vigorous degassing. At this stage of activity, the magma is comparatively gas-rich. If the magma continues to degas without new injections from below, gases such as CO_2 and SO_2 decline in concentration. At the same time, surface waters infiltrate progressively into the system. Figures 2a and 2b show changes in H_2O and CO_2 for crater fumaroles at Mount St. Helens during 1980–1981. In its initial stages during 1980, the levels of CO_2 in the gas were comparatively high. With continued degassing, CO_2 was lost and the gas was enriched in water. Similar trends are observed for the Showa-Shinzan lava dome at Usu volcano, Japan. The dome was emplaced during the 1940s and degassed thereafter. This can be seen from Figures 2c and 2d, which show significant declines in carbon and sulfur in the 1950s and 1960s as the system became water-dominated. During this time, the carbon/sulfur ratio declined (Figure

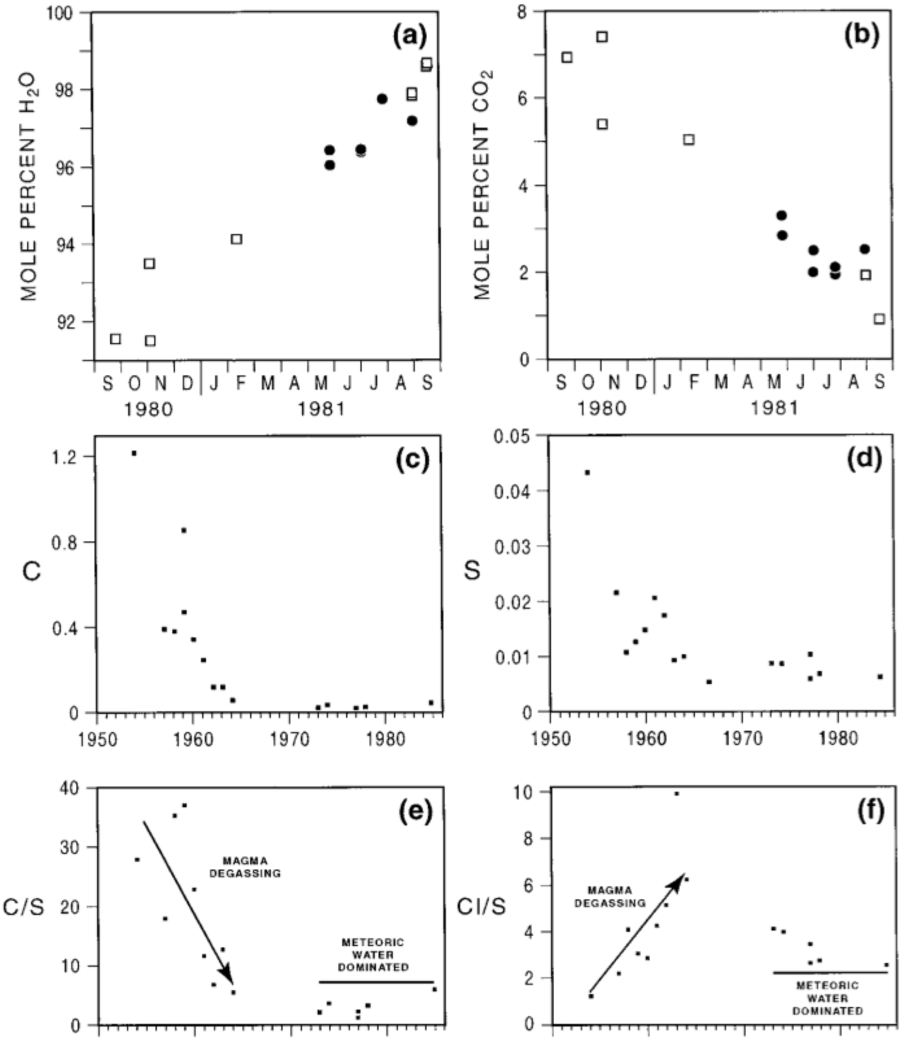

FIGURE 2 (a) H_2O concentrations and (b) CO_2 concentrations in gas from crater fumaroles, Mt. St. Helens, 1980–1981. Open squares represent complete gas analyses, solid circles represent noncondensable gas analyses. (Reprinted with permission from Casadevall *et al.,* 1983. Copyright 1983 American Association for the Advancement of Science.) (c) Carbon contents and (d) sulfur contents in gas from a high-temperature fumarole on the Showa-Shinzan lava dome, Japan. Note the progressive declines with time over the period 1954–1985. (e) C/S ratio and (f) Cl/S ratio in gas from Showa-Shinzan. Magma degassing causes C/S to decrease and Cl/S to increase. (Reprinted from Symonds, R. B., Mizutani, Y., and Briggs, P. H., 1996. Long-term geochemical surveillance of fumaroles at Showa-Shinzan dome, Usu volcano, Japan. *J. Volcanol. Geotherm. Res.* **73,** 177–211. Copyright 1996, with permission from Elsevier Science.)

2e), since CO_2 is less soluble than SO_2 in magma. Conversely, the chlorine/sulfur ratio increased (Figure 2f), since HCl is more soluble than SO_2. These examples show how volcanic activity can be traced using gas analyses. If fresh new magma were to be added to the volcano's shallow magma reservoir, the gas should exhibit corresponding increases of CO_2, SO_2, and C/S, and a decline of Cl/S.

The plumbing system of a volcano also can change during its activity. For example, fractures may develop as a result of earthquakes or eruptions, thereby facilitating the liberation of gas from the magma. By contrast, the system also may close at times from filling and plugging of fractures and cracks. High-temperature gases and fluids transport significant quantities of elements in solution. With cooling, these dissolved materials may precipitate and help fill open spaces such as fractures. The simple rise of a plug of magma within a volcanic conduit also can be sufficient means to partially close a volcanic system. There is thus an interesting interplay between processes which serve to keep a magmatic-hydrothermal system relatively open and other processes which can partially or completely seal the system. As a result, the plumbing systems of active volcanoes have permeabilities which vary both spatially and temporally during the course of activity. If permeabilities change, so can the internal pressures within the volcano. If pressures reach a certain critical threshold, an eruption may be imminent. One way to monitor these changes in permeability and internal pressure is by using gas analyses. When a system is permeable and "open," the flow of magmatic gas is high, and concentrations of magmatic gas components such as SO_2 and HCl are elevated. When the system is partially sealed and "closed," magmatic gas flux declines; instead, a hydrothermal gas component becomes more important, with proportionately larger amounts of CO_2 and H_2S released.

As discussed above, the relative amounts of reactive and abundant gas species (e.g., CO_2, SO_2, H_2S, and HCl) can be interpreted to better understand the activity of a volcano and to determine whether the chances for an eruption may be increasing. Many other components in gases are present in small quantities; among these are nonreactive gases such as helium (He), argon (Ar), and nitrogen (N_2), and trace amounts of metals such as lead, zinc, and gold. The trace metals are important for ore deposit formation but are generally not used to interpret volcanic activity. The concentrations and isotopic composition of nonreactive gases, however, may vary significantly in time and space on a volcano, and they can provide the volcanologist with valuable information on the sources of the gases. For example, the concentration and isotopic composition of helium in a gas provide insight into new inputs of magma into a chamber beneath the volcano. This type of information is essential for monitoring purposes.

2. *Soil Gas*

Volcanoes release gas not only from the central crater through openings such as fumaroles, but also on their flanks by diffuse degassing of species such as CO_2, helium, and radon (Rn). Whereas the high-temperature gases in craters tend to be highly acidic and reactive (e.g., SO_2, HCl), species such as CO_2, He, and Rn do not react with country rocks. These gases can be emitted at lower temperatures through subsurface fractures and faults. The distributions and quantities of these gases provide information on the overall permeability of a volcanic edifice, the potential for lateral degassing from areas other than the active crater, and the ability of a volcano to diffusely release large quantities of CO_2 and other gases.

Diffuse degassing is typically monitored by measuring gas concentrations in soil gas or dissolved gas from springs. For soil gas analyses, a probe is inserted into the soil to approximately a meter in depth, a gas sample is pumped into an infrared gas detector or into a syringe and the gas is then transferred to an evacuated container (Figure 3a). Alternatively, gas detectors are installed in the soil for a period of time. At springs, water samples are taken at the source and placed in bottles which are sealed to prevent gas loss.

Before interpreting spatial or temporal trends of diffuse gases on a volcano in terms of volcanic, seismic, or tectonic activity, it is important to identify other mechanisms which may influence the gas distributions. For example, climatic effects such as rain, humidity, and barometric pressure can significantly influence the amounts of diffuse degassing.

Volcanoes can exhibit diffuse degassing anomalies at various scales. Volcanologists have recognized that elevated soil gas concentrations are associated with faults and fractures. Figure 3b shows a soil gas traverse across a faulted zone on the flanks of Vulcano, an active cone on the island of the same name in the Aeolian Islands of Italy. CO_2 and He concentrations are both high and variable across the faulted zone, which appears to be 300–400 m wide. Maximum CO_2 concentrations exceed 50%, compared to background levels close to zero. Helium reaches a maximum of 7.5 parts per million (ppm), compared to an atmospheric background of approximately 5.0–5.5 ppm.

Mammoth Mountain is located on the southwestern

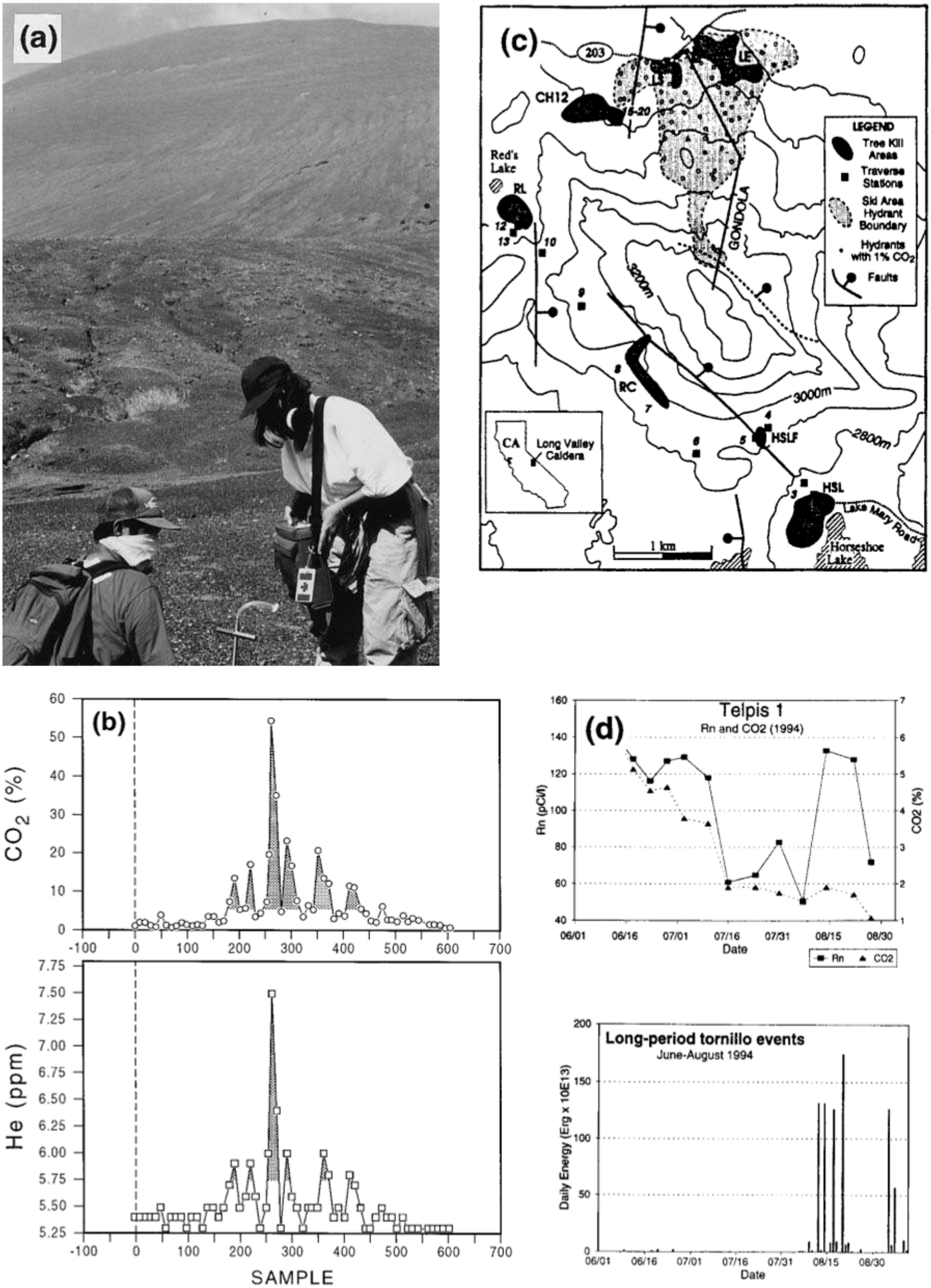
(a)
(c)
203
CH12
L3
LE
6-20
Red's Lake
RL
12
13
10
9
3200m
GONDOLA
8
RC
7
3000m
2800m
4
5
6
HSLF
3
HSL
Lake Mary Road
Horseshoe Lake
CA
Long Valley Caldera
1 km
LEGEND
Tree Kill Areas
Traverse Stations
Ski Area Hydrant Boundary
Hydrants with 1% CO2
Faults
(b)
CO2 (%)
He (ppm)
SAMPLE
-100
0
100
200
300
400
500
600
700
(d)
Telpis 1
Rn and CO2 (1994)
Rn (pCi/l)
CO2 (%)
Date
Rn
CO2
06/01
06/16
07/01
07/16
07/31
08/15
08/30
Long-period tornillo events
June-August 1994
Daily Energy (Erg x 10E13)

margin of Long Valley caldera in eastern California, east of Yosemite National Park. In 1990, a broad region of tree kill began to develop on Mammoth Mountain after elevated seismicity was observed in 1989 (Figure 3c). The tree kill resulted from the diffusive release of CO_2; the source of the CO_2 appears to be magmatic, at least in part. Figure 3c suggests that the areas of tree kill and elevated CO_2 concentrations in the soil gas are associated with faults. Thus, the CO_2 released since 1990 may have been the result of fault reactivation associated with the 1989 seismicity and/or intrusion of magma beneath Mammoth Mountain.

In certain instances, soil gases can be correlated with volcanic or seismic activity. Figure 3d shows variations of CO_2 and Rn at Galeras volcano, Colombia, during the period June–September 1994. The occurrences of constant- and low-frequency seismic events ("tornillos"), which are related to the internal pressure of the volcano, also are shown for this period. Both Rn and CO_2 show general declines with time; however, Rn concentrations increase abruptly when tornillos first appear. By contrast, CO_2 continues to decline. The overall declines appear to be climatically controlled, specifically a drying out of the ground. However, Rn also exhibits an anomalous response to seismic activity within the volcano, while CO_2 does not.

C. Remote Sensing Measurements of Volcanic Gases

As we have discussed above, direct measurements of gas from volcanoes are not simple, due to logistical difficulties, limited access to active craters, and the danger and risk that are sometimes involved. Since the late 1960s volcanologists have been increasingly experimenting with methods to measure volcanic gas using remote sensing. This approach is attractive, since the measurements are made at a distance from the volcano, and the instrument and observer are not actually in the gas plume. Thus, the approach is inherently safer and logistically easier. Furthermore, remote sensing offers a means to make a greater number of measurements than can generally be done when sampling volcanic gas directly. Lastly, remote sensing measurements of a gas plume are more representative than direct measurements of individual fumaroles, although the number of gas species determined remotely is less than that for a gas sample collected at a fumarole. In this section we examine remote sensing techniques, both ground-based and from satellite platforms, which are being used by volcanologists. These include ground- and aircraft-based COSPEC correlation spectroscopy to measure SO_2 emissions and total ozone mapper spectrometer (TOMS) satellite measurements of SO_2. We also discuss some of the promising new methods that are currently being developed to remotely sense volcanic gas. At the millenium we appear to be in a period of transition between first-generation remote sensing and a second generation which will offer us new insights into how volcanoes degas and their effects on the Earth's atmosphere.

1. Sulfur Dioxide Emissions Measured by COSPEC

The COSPEC is an instrument developed in the 1960s by Barringer Research, a company in Toronto, Canada, to measure emissions of SO_2 from industrial stacks for pollution monitoring, as public and government consciousness was raised. Volcanologists quickly realized the potential of the COSPEC, since volcanoes are essentially natural smokestacks. The COSPEC was first used at volcanoes in Japan, but most of the credit for developing and championing use of the COSPEC at active volcanoes goes to Richard Stoiber of Dartmouth College, who demonstrated the power and versatility of the

FIGURE 3 (a) Measuring CO_2 in soil gas by infrared absorption, Masaya volcano, Nicaragua. The soil gas is pumped through a probe inserted into the ground. The volcanologists are wearing gas masks to protect against acid gases from the active crater several kilometers distant. (b) High levels of CO_2 and helium in soil gases observed across a faulted zone at the base of Vulcano, Vulcano Island, Italy. The gray areas are considered anomalies. The spacing between points is 10 m. (From Baubron, J.-C., Allard, P., Sabroux, J.-C., Tedesco, D., and Toutain, J.-P., 1991. Soil gas emanations as precursory indicators of volcanic eruptions. *J. Geol. Soc. London* **148,** 571–576. Reprinted by permission of the Geological Society Publishing House.) (c) Map of tree kills from CO_2 in soil gas on Mammoth Mountain, Long Valley caldera, California. Note the association between areas of tree kill and mapped faults. (From Rahn, T. A., Fessenden, J. E., and Wahlen, M., 1996. Flux chamber measurements of anomalous CO_2 emission from the flanks of Mammoth Mountain, California. *Geophys. Res. Lett.* **23,** 1861–1864.) (d) Relationship between radon and CO_2 in soil gases and seismic energy, Galeras volcano, Colombia. Radon increases with seismicity, while CO_2 does not show a response. (Reprinted from Heiligmann, M., Stix, J., Williams-Jones, G., Sherwood Lollar, B., and Garzón V., G., 1997. Distal degassing of radon and carbon dioxide on Galeras volcano, Colombia. *J. Volcanol. Geotherm. Res.* **77,** 267–283. Copyright 1997, with permission from Elsevier Science.)

instrument at volcanoes worldwide. He and his students not only showed how the COSPEC could provide important information on volcano degassing, they also made a fundamental contribution to climate studies by estimating the amount of SO_2 that is released by volcanoes on a global basis. These calculations were based largely on their COSPEC results at many individual volcanoes.

The COSPEC functions in the ultraviolet part of the electromagnetic spectrum, with the sky used as the source of ultraviolet energy. Light enters the instrument and travels through a series of mirrors, lenses, and slits to reach a detector and photomultiplier, where the light is converted into electric pulses and amplified. If gas is present in the path of the instrument, the COSPEC detects the amount of ultraviolet radiation that is absorbed by the SO_2. Since the COSPEC is measuring the concentration of gas through a thin cylindric slice of the atmosphere, the concentration of SO_2 in this slice is expressed as parts per million-meters (ppm-m), rather than simply as ppm for an instrument which directly measures gas within a plume.

Typically, the COSPEC is mounted in a vehicle, with the telescope, mirror, and lens assembly oriented vertically upward (Figure 4a). The vehicle then makes traverses beneath the gas plume, with the traverses oriented perpendicularly to the direction of the plume. If there is no road access, the COSPEC can be placed in an aircraft which is flown under the plume. The COSPEC also can measure from a stationary position. Since the volcanologist's goal is to measure the amount of SO_2 released from the volcano over a period of time, it is essential to measure the width and speed of the plume as it is dispersed downwind from the actively degassing crater or craters. Unfortunately, the speed of the plume frequently is difficult to estimate, and scientists often rely upon the wind speed as a proxy.

As use of the COSPEC became more widespread through Stoiber's influence, volcanologists recognized that explosively erupting volcanoes emit large quantities of SO_2. Nevertheless, it was frequently difficult to make such measurements, since volcanic ash from the eruption could interfere with the COSPEC measurements. Despite these problems, COSPEC measurements have shown that erupting volcanoes are capable of emitting thousands to millions of metric tons (tonnes) of SO_2 each day. During its cataclysmic eruption on 18 May 1980, Mount St. Helens injected between 480,000 and 2,200,000 tonnes of SO_2 into the atmosphere. Afterward, COSPEC measurements revealed that the SO_2 emissions declined progressively during 1980 and 1981 (Figure 4b). The decline in SO_2 from the volcano was

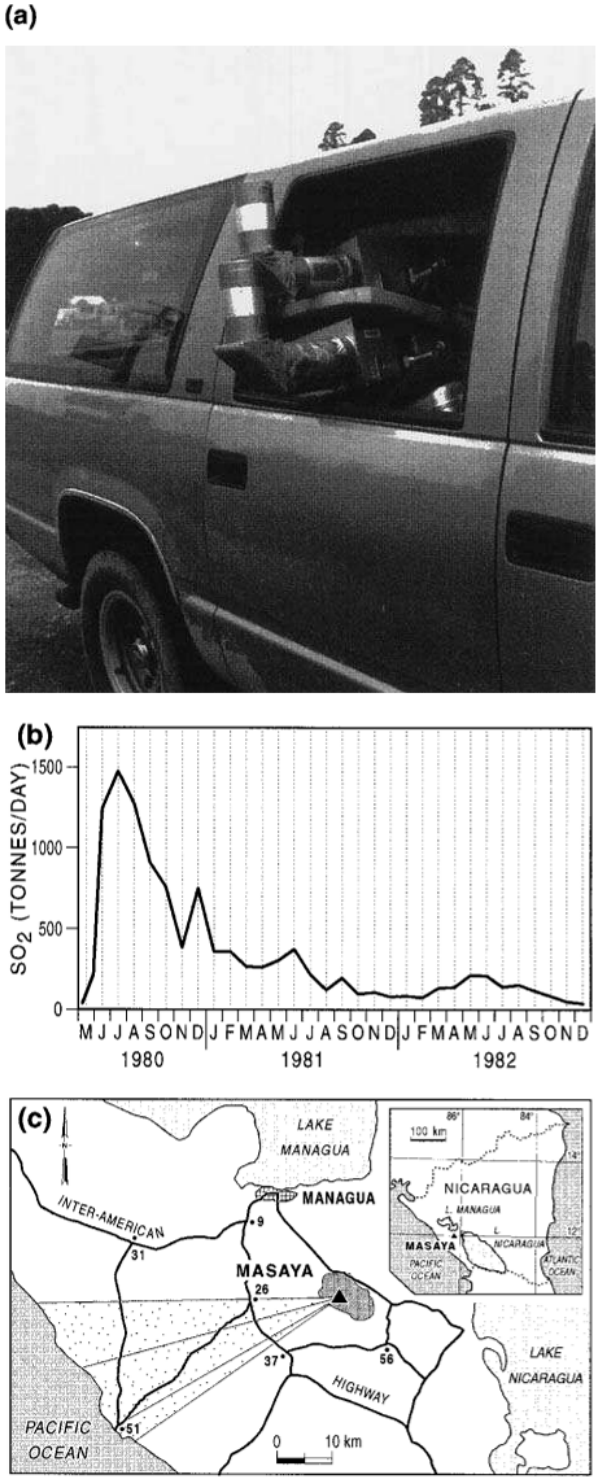

coincident with increasing H_2O and decreasing CO_2 fumarolic gas concentrations during this time (see Figures 2a and 2b above). The two datasets indicate that the magma beneath the volcano was becoming increasingly depleted in gas during this period.

In addition to erupting volcanoes, there are others which are active but do not erupt, or they erupt infrequently. Instead, their activity is manifested by nearly continuous degassing, and the COSPEC is used to monitor this style of degassing. Masaya volcano in Nicaragua is a good example. Its recent activity has been characterized by periods of degassing lasting years, with little or no ash or lava erupted. The acid gas is blown westward by tradewinds, and a large region is adversely affected (Figure 4c). Much of the vegetation and crops such as coffee plants are killed, and people and livestock living in the affected zone suffer respiratory problems.

At first, scientists did not appreciate the levels of gas emitted from passively degassing volcanoes such as Masaya. As COSPEC measurements became more routine, it was realized that certain volcanoes emit very large quantities of SO_2 indeed, sometimes rivaling the amounts from erupting volcanoes. In addition to Masaya, which releases up to several thousand tonnes of SO_2 each day, Mount Etna in Italy and Popocatepetl in Mexico are significant producers. Etna emits between 5000 and 20,000 tonnes/day depending on its activity. Popocatépetl was observed to passively release close to 50,000–60,000 tonnes SO_2/day on occasion in 1997! These are staggeringly large quantities, and scientists do not fully understand how volcanoes can release such large amounts without eruptive activity. This problem is a challenge for future volcanologists.

Since SO_2 is but one component of the overall gas budget emitted by both erupting and passively degassing volcanoes, it is clear that significant quantities of H_2O, CO_2, HCl, and other gases also are injected into the atmosphere by these volcanoes. Once we independently know gas ratios (e.g., the sulfur/chlorine ratio determined from fumarole gas analyses or other remote sensing techniques) and the SO_2 flux measured by COSPEC, we can calculate volcanic emissions of other gases to the atmosphere.

By extrapolating their COSPEC measurements at different types of volcanoes worldwide, Stoiber and his colleagues were able to estimate that volcanoes emit an average of 19 million tonnes of SO_2 annually. By comparison, industrial sources emit about 70–80 million tonnes each year. Although industrial emissions are larger than volcanic emissions, volcanoes clearly inject important quantities of SO_2 into our atmosphere. In fact, volcanoes are the only natural source of SO_2. This is a good example of Earth's degassing. Without the COSPEC, we would be unable to make such calculations and estimates.

FIGURE 4 (a) Two COSPEC instruments installed in a vehicle to measure SO_2 fluxes from Popocatépetl volcano, Mexico. The vehicle is driven underneath the plume with the COSPEC telescope oriented vertically upward. (Photograph courtesy of Glyn Williams-Jones.) (b) Average SO_2 fluxes in metric tons per day from Mount St. Helens, 1980–1982. Note the progressive decline with time. (Reprinted with permission from Casadevall *et al.,* 1983. Copyright 1983 American Association for the Advancement of Science.) (c) Dispersion of gas westward from Masaya volcano in Nicaragua, as determined by repeated COSPEC measurements. (From Stoiber, R. E., Williams, S. N., and Huebert, B. J., 1986. Sulfur and halogen gases as Masaya caldera complex, Nicaragua: Total flux and variations with time. *J. Geophys. Res.* **91,** 12215–12231.)

2. *Sulfur Dioxide Emissions Measured by TOMS*

The first total ozone mapping spectrometer was launched aboard the Nimbus 7 satellite spacecraft in 1978. Since that time, it and other similar instruments have been making measurements of stratospheric ozone, using the near-ultraviolet region of the spectrum. During the El Chichón eruption, Mexico, in 1982, it was observed that ozone levels were anomalously high, until it was realized by Arlin Krueger and his colleagues at NASA that TOMS was detecting volcanic SO_2, in addition to ozone. In effect, SO_2 produces strong absorption at the shortest TOMS wavelengths (300–320 nm, similar to COSPEC). Thus, TOMS immediately became an invaluable means to measure large injections of SO_2 into the stratosphere by volcanic eruptions. Since 1979, TOMS has measured SO_2 from over 50 eruptions worldwide. The largest emissions so far observed were about 20 million tonnes of SO_2 from the 1991 eruption of Mount Pinatubo, 7 million tonnes from El Chichón in 1982, 4 million tons from Nyamuragira, Zaire, in 1981, 1.5 million tonnes from Cerro Hudson, Chile, in 1991, and 1.2 million tonnes from Sierra Negra, Galápagos, Ecuador, in 1979.

Figure 5 shows SO_2 measured by TOMS during the June 1991 Mount Pinatubo eruptions. The 12–13 June 1991 SO_2 outputs were relatively small compared to the climactic eruptions on 15 June. Figure 6 shows SO_2 emissions measured by both TOMS and COSPEC during the August–September 1982 eruptions of Galunggung. Frequently, the two sets of measurements do not

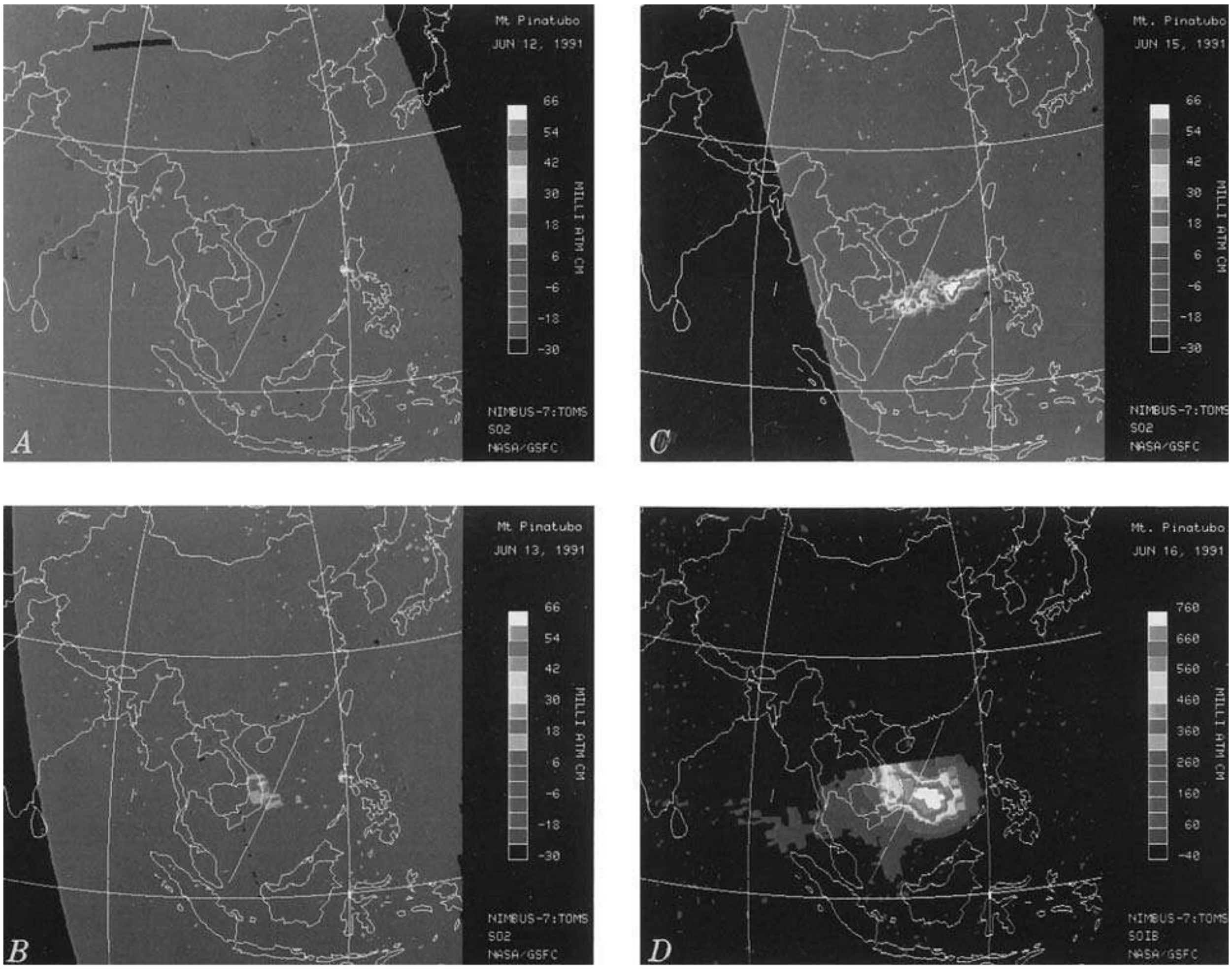
Mt Pinatubo
JUN 12, 1991
66
54
42
30
18
6
-6
-18
-30
MILLI ATM CM
NIMBUS-7:TOMS
SO2
NASA/GSFC
A
Mt. Pinatubo
JUN 15, 1991
66
54
42
30
18
6
-6
-18
-30
MILLI ATM CM
NIMBUS-7:TOMS
SO2
NASA/GSFC
C
Mt Pinatubo
JUN 13, 1991
66
54
42
30
18
6
-6
-18
-30
MILLI ATM CM
NIMBUS-7:TOMS
SO2
NASA/GSFC
B
Mt. Pinatubo
JUN 16, 1991
760
660
560
460
360
260
160
60
-40
MILLI ATM CM
NIMBUS-7:TOMS
SO2B
NASA/GSFC
D

FIGURE 5 (a)–(d) Emissions of SO_2 during the climactic eruptions of Mount Pinatubo volcano. Philippines, 12–16 June 1991, as measured by TOMS. The highest SO_2 concentrations are shown in white, and the lowest in black. In (b) two masses of SO_2 can be seen, one located near the volcano from the 13 June eruption, and the other 1300 km to the west from the 12 June eruption. The figure in (d) shows the very high SO_2 concentrations produced by the largest eruption on 15 June. For (d) note the change in concentration scale for the right-hand column of SO_2 concentrations. The spatial scale is defined by the two curved latitude lines (0° and 30°N), which are separated by approximately 3300 km. (From Krueger *et al.,* 1994. Figure kindly provided by the U.S. Geological Survey.)

correspond, probably because TOMS recorded high SO_2 values from explosive eruptions, while COSPEC measured lower SO_2 levels between the eruptions.

The TOMS does have some disadvantages. Its 50 × 50-km spatial resolution is relatively coarse, and it cannot easily make measurements at night, at low sun angles, or at high latitudes. It is designed to make measurements of stratospheric SO_2 injected by relatively large eruptions; therefore, it cannot measure low levels of SO_2 in the troposphere. If ash and sulfate aerosols are present in the eruption column, SO_2 can be overestimated.

A second generation of TOMS instruments was launched on the Earth Probe and ADEOS satellites in 1996. These instruments were designed to better measure volcanic SO_2 by increasing the spatial resolution and selecting wavelengths optimum for SO_2. Unfortunately, the ADEOS satellite failed in 1997.

3. Other Remote Sensing Measurements

While COSPEC and TOMS have provided us with valuable information on SO_2 emissions from volcanoes, we know comparatively little about emissions of other

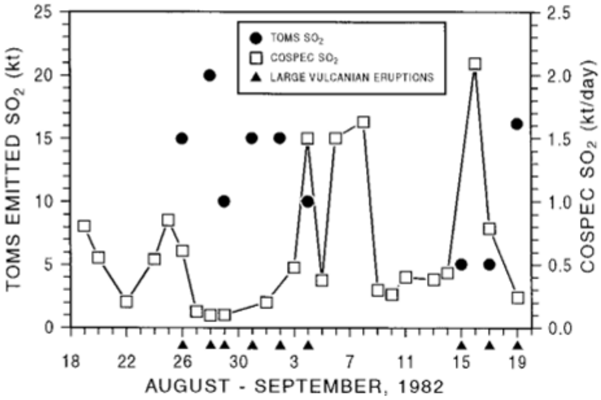

FIGURE 6 SO_2 fluxes from Galunggung volcano, Indonesia, during the months of August and September 1982, as measured by TOMS and COSPEC instruments. The SO_2 scale for TOMS is an order of magnitude higher than that for COSPEC. The triangles indicate the occurrence of vulcanian eruptions, which generally coincide with the TOMS measurements. (Reprinted from Bluth, G. J. S., Casadevall, T. J., Schnetzler, C. C., Doiron, S. D., Walter, L. S., Krueger, A. J., and Badruddin, M., 1994. Evaluation of sulfur dioxide emissions from explosive volcanism: The 1982–1983 eruptions of Galunggung, Java, Indonesia. *J. Volcanol. Geotherm. Res.* **63,** 243–256. Copyright 1994, with permission from Elsevier Science.)

gas species such as CO_2, H_2S, HCl, and HF. We know even less concerning gas species which are present in volcanic gas in trace amounts. Unfortunately, the ultraviolet part of the spectrum is not particularly useful when trying to measure these gases. Instead, the infrared region holds much more potential, and this is where current efforts are being directed to measure gases other than SO_2. As we have discussed earlier in this chapter, the use of gas ratios may hold very useful information in terms of volcano behavior, particularly when the gas solubilities in magma are different. Thus, remote sensing measurements of gas ratios are an important line of inquiry. If two gases are ratioed, the variability of the plume speed (which is needed for flux measurements) is eliminated, and thus gas ratio measurements are inherently more precise and accurate than flux measurements of individual gas species.

Infrared measurements of gas must contend with potential interferences from nonvolcanic gases which are present in the atmosphere. Chief among these is water vapor, and CO_2 and methane (CH_4) are also potential interferants. Three principal lines of research currently are being pursued: Fourier transform infrared spectroscopy (FTIR); gas correlation radiometry; and thermal infrared multispectral mapping.

An FTIR instrument is typically deployed in a stationary position on the ground and pointed at a hot source, for example, an infrared lamp, the crater, or the Sun. Volcanic gas which is present between the instrument and the source is then measured (Figure 7a). The FTIR method is powerful because it enables a volcanologist to rapidly measure different gases at various wavelengths simultaneously. By knowing the absorption wavelength of a particular gas and correcting for interferences, it is possible to calculate gas concentrations in ppm-m. From these data, gas ratios can be calculated. Figure 7b shows a plot of SO_2 vs. HCl concentrations as measured by FTIR. It can be seen that the SO_2/HCl ratio of the gas is higher at Mount Etna than at Vulcano.

Another infrared technique being explored is that of gas correlation radiometry. The basic principal is similar to that of FTIR, except that the radiometer is set to look at specific spectral regions, rather than a broad spectrum of absorbances, each with their own characteristic wavelength. During measurements, a gas cell and a clear cell, which are mounted on a rapidly spinning disk called a chopper, are compared for their relative signals. This approach is being used to measure volcanic CO_2, which is difficult because the atmosphere contains about 365 ppm CO_2. Thus there is an important background interference which is present. Gas correlation also is being used to measure trace gases such as carbon monoxide (CO) and carbonyl sulfide (COS).

In the past several years, the thermal infrared multispectral scanner (TIMS) has been employed to map SO_2 plumes from aircraft. This work has been conducted at Mount Etna and Kilauea volcanoes. Essentially, the TIMS is a small-scale version of TOMS but operates in the infrared region rather than the ultraviolet. TIMS has the important ability to make two-dimensional maps of SO_2 distributions within volcanic plumes. This is difficult or impossible to do by COSPEC, FTIR, or gas correlation. Thus, TIMS can map spatial and temporal variability of SO_2 within a volcanic plume, and such maps will help us better understand the heterogeneous distribution of gas within the plume. A satellite-based version of TIMS, called ASTER, is planned for launch in 1999. ASTER has the potential to map volcanic plumes from space on a worldwide basis.

II. ASH MEASUREMENTS AND MONITORING

A. Principles

Volcanic ash is released by explosive eruptions. While causing much misery for people downwind from a vol-

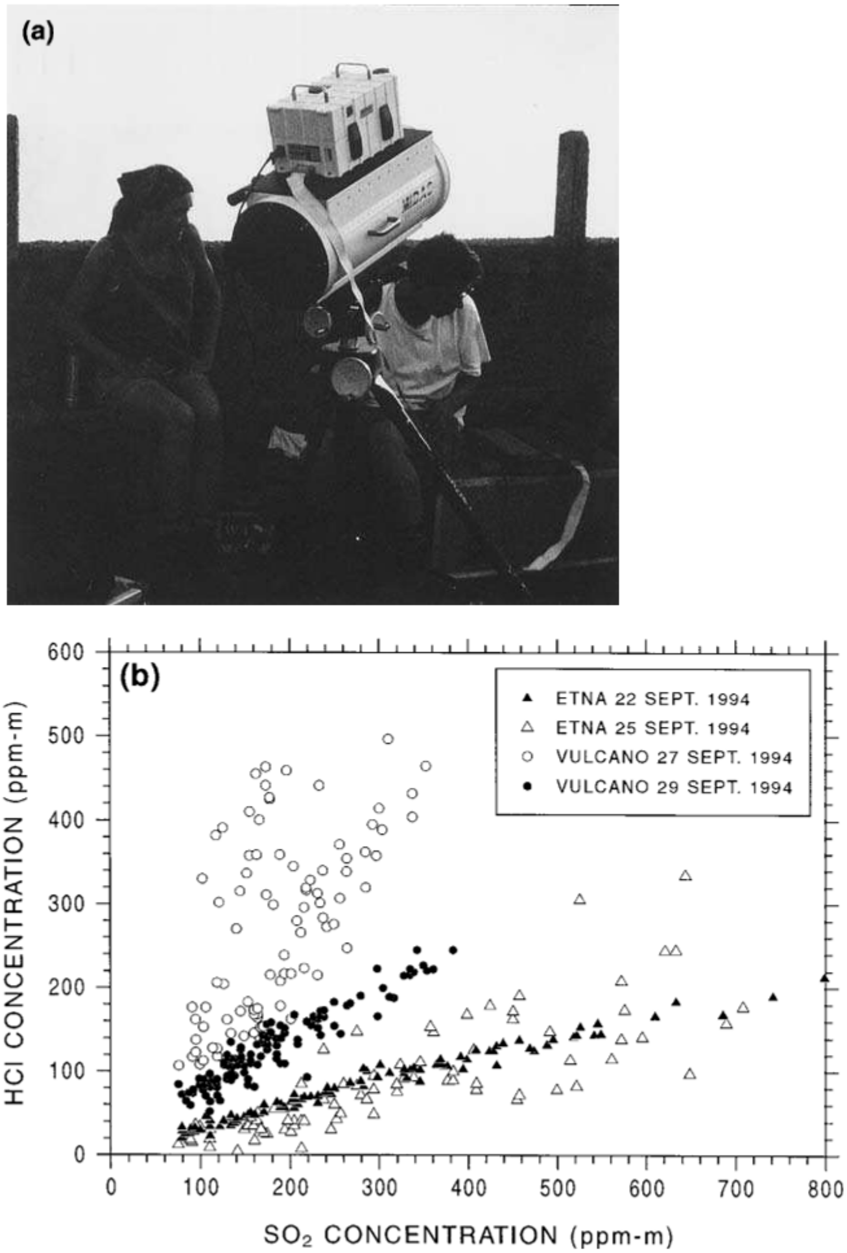

FIGURE 7 (a) Deployment of a Fourier transform infrared spectrometer at Masaya volcano, Nicaragua. The spectrometer is using the Sun as a source of infrared energy. (b) Plot of SO_2 vs. HCl concentrations at Vulcano and Mount Etna volcanoes, Italy, as measured by FTIR. The SO_2/HCl ratios are higher at Mount Etna. (From Francis *et al.,* 1995.)

cano, the ash can be studied in a number of ways that provide important insights into the nature of the eruption. Indeed, the ash provides a record of the magmatic and plume conditions during the eruption. If one is able to sample the ash at different points in time during the eruption, it is possible to examine changes that are occurring within the volcano and in the eruption column. Essentially, the ash layers provide a way to reconstruct different events at the volcano during the eruption.

With these points in mind, a volcanologist takes careful note of the stratigraphic position of an ash layer at a particular geographical locality. For example, an observer stationed at one site carefully records the accumulation rate of the ash by noting the cumulative thickness at given time intervals. Changes in texture and grain size of the ash also are recorded. The observer will take periodic samples of the ash, noting the time and the sample's stratigraphic position.

After the ashfall has ended, the observer will visit many different sites around the volcano, making detailed measurements of the ash accumulation by recording information such as thickness, changes in textures and grain sizes, and maximum fragment sizes. With this information, it is possible not only to reconstruct the dispersal pattern of the ash but also to estimate volumes of erupted material and eruption dynamics.

B. Composition of Volcanic Ash

Volcanic ash consists of three main components: (1) fragments of minerals, (2) glass shards and pumice grains, and (3) accidental lithic fragments (Figures 8a–8c). Mineral fragments are crystals which originally precipitated from the magmatic liquid before the eruption. The variety of crystals provides information on the composition of the magma. In addition, the chemistry of the minerals can be used to determine the temperature, pressure, and depth conditions of the magma prior to the eruption. In this way, ash samples at different stratigraphic positions from a deposit can tell us if the composition, temperature, or depth of the magma changed during the course of an eruption. Mineral grains also can contain small inclusions of trapped magma, typically 0.05–0.2 mm in diameter, which have solidified to glass (Figure 8d). This glass can be analyzed by specialized microanalytical techniques to estimate the amount of gas that was dissolved in the magma before the eruption.

Glass shards and pumice grains are solidified samples of the magma. Essentially, the liquid magma froze during the eruption due to rapid cooling. Since an explosive eruption is violent, the frozen magma is broken into small pieces of bubbly pumice and even smaller glass shards. The density and percentage of bubbles in the pumice can be measured to estimate indirectly the amount of gas originally present. For example, a bubble-rich, low-density pumice implies high gas contents. The chemical composition of the pumice and glass fragments also is determined to see if the chemistry of the magma changed during the course of an eruption, or if mixing of different magmas occurred. For example, the chemistry of ashes from the 1992 eruptions of Mount Spurr, Alaska, represented three different magma compositions.

Lastly, the composition of accidental lithic fragments helps us understand the types of rocks surrounding the volcanic conduit and plumbing system. If the geology of the region has been studied previously, then it may be possible to estimate if an eruption deepens with time, based on the nature of the lithic fragments at different stratigraphic levels of the ash bed.

C. Morphology of Juvenile Glass Shards

The presence of juvenile material such as pumice grains or glass shards in ash is an indication that fresh magma is present beneath a volcano (Figure 8b). This is a very important determination, because explosive magmatic eruptions can be very large and destructive events. If glass shards are detected in ash from a volcano that has suddenly reactivated, this observation has significant implications for hazard assessments. Specifically, the glass indicates the presence of magma beneath the volcano, and the potential for larger, more explosive and destructive eruptions clearly exists. By contrast, some volcanoes that reactivate contain little or no glassy material, the ash being dominantly accidental lithic material that has been scraped from the conduit walls (Figure 8c). The lack of glassy juvenile material does not necessarily imply that fresh magma is not present, but it does suggest that the possibility of a magmatic eruption is somewhat lessened. For the volcanologist who is trying to use the content of the ash as a guide to future activity, perhaps the most difficult situation is when there are only traces of glassy material present. Do the very small amounts of glass indicate fresh magma, or is the glass a remnant of a previous eruption involving magma? Fresh glass has a comparatively low refractive index, while older glass shards can have higher or variable refractive indexes, resulting from water that has been incorporated into the glass structure at low temperatures.

The morphology of glass shards can help identify the nature of the eruption. Shards that are bubble-rich with cuspate shapes are indicative of a gas-rich magmatic eruption. Other shards can be platy and planar, lacking bubble walls. These shards are suggestive of either a gas-poor eruption or one where magma has interacted with groundwaters, fragmenting the magma before significant bubble growth could occur. These eruptions are termed phreatomagmatic. During an eruption, the shard morphologies in ash samples may vary, and these

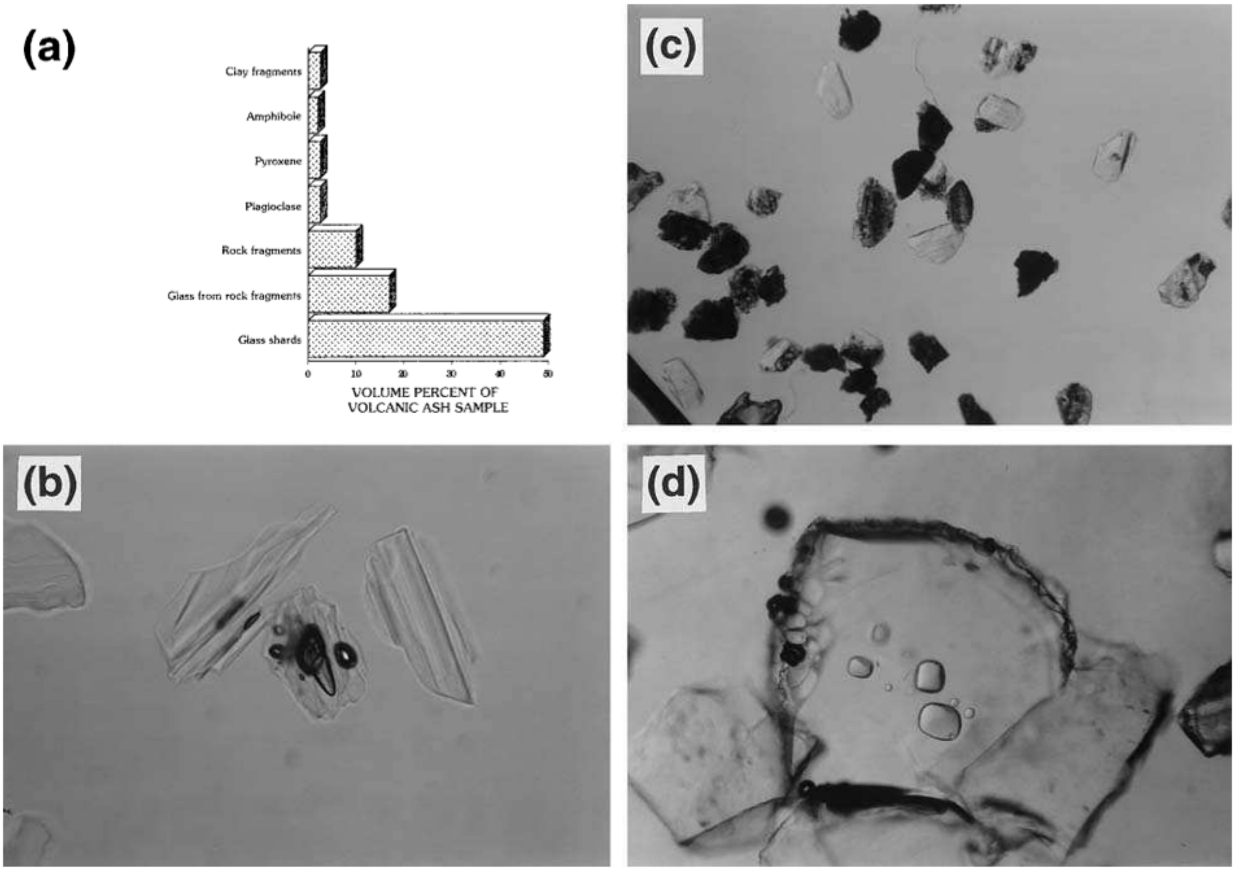

FIGURE 8 Different types of volcanic ash. (a) Composition of volcanic ash from the March 1986 eruption of Augustine volcano, Alaska, showing glass shards, rock fragments, and pieces of minerals. (From Heiken, G., 1994. Volcanic ash: What it is and how it forms. *U.S. Geol. Surv. Bull.* **2047,** 39–45. Figure kindly provided by the U.S. Geological Survey.) (b) Shards of magmatic glass produced by the eruption of the Lower Bandelier Tuff, New Mexico. Length of longest shard is 0.3 mm. Width of photo is 0.8 mm. (c) Photomicrograph of ash from the 14 January 1993 eruption of Galeras volcano, Colombia, showing presence of mineral fragments (transparent colors) and rock fragments (dark colors). Width of photo is 2 mm. (d) Photomicrograph of inclusions of glass trapped in a quartz crystal from the Bandelier Tuff, New Mexico. Largest inclusion is about 0.12 mm in diameter. Width of photo is 2 mm.

variations can be correlated to other changes that are observed.

D. Soluble Components on Volcanic Ash

When volcanic ash is suspended in an eruption column, a certain proportion of the gas phase is condensed onto the surfaces of the ash particles. When these particles fall to the ground, they remove a component of the gas phase. This component can indirectly provide valuable information on the magmatic gas. By collecting and then leaching freshly fallen ash that has not been rained on, a volcanologist can measure the amount of gas (SO_2, HCl, HF) removed by the ash. When the ash is leached, the gases are in the form of anionic complexes such as sulfate (SO_4^{2-}), chloride (Cl^-), and fluoride (F^-) in the solution. From this information, ratios such as S/Cl can be calculated to obtain an indirect estimate of the magmatic component which is present in the gas. For example, S/Cl leachate ratios greater than 0.5 indicate that the ash has an important magmatic component, while lower ratios imply a smaller magmatic influence. While these values are only rough guidelines which are somewhat arbitrary, experience has shown the information can be useful, particularly if integrated with other indicators such as the percentage of glass shards. Before the cataclysmic 18 May 1980 eruption of Mount St. Helens, S/Cl ratios of ash leachates were less than 1, indicating a variable magmatic component in the gas phase. During the 18 May eruption, the ratios were as high as 1.3, showing that the magmatic component had increased significantly.

E. Tracking Volcanic Ash Clouds by Satellite Remote Sensing

Volcanic eruption plumes may be transported significant distances. The largest eruptions form stratospheric plumes which circle the Earth many times. In regions surrounding a volcano, ash is frequently deposited over a wide area. Further afield, the plume continues to move, containing gas, aerosols, and very fine-grained ash particles. The dispersion of volcanic plumes thus can be a global phenomenon, and remote sensing techniques such as Earth-orbiting satellites can be used to track the evolution of plumes as they are transported in the atmosphere. Practically speaking, the monitoring of eruption plumes is very important for people on the ground who may be affected, and for aircraft flying overhead, since volcanic ash can foul jet engines.

Near the volcano, a type of radar called C-band radar (also referred to as Doppler or NEXRAD radar systems) can be used to map eruption columns and to detect ash which is between 1 mm and several centimeters in size. Unlike radar in aircraft which is unable to detect the presence of ash, C-band radar can sense the presence of ash up to 100–200 km from the volcano. It also can be used in all types of weather, and clouds do not pose a problem. The radar can detect the height of an eruption column; with this information, eruption rates can be estimated as

$$H = 236.6Q^{1/4},$$

where H is the height of the column in meters and Q is the eruption rate in kilograms per second. Sometimes the top of the column may be underestimated, since the radar does not detect ash particles much smaller than 1 mm. C-band radar also can be used to study the fallout of ash particles, particularly the loss of large particles, and size distributions of ash can be obtained from different patterns of radar reflectivity. The radar is useful in environments close to the volcano where ash particles are comparatively big. It is less effective at greater distances after the large particles have fallen out of the column.

Further from a volcano where C-band radar is no longer effective, weather satellites can track the movement and velocity of eruption plumes. For example, the geostationary GOES-7 satellite is able to observe a significant part of the western hemisphere on a nearly continual basis. However, discriminating between eruption plumes and meteorologic clouds can be difficult. The advanced very high-resolution radiometer (AVHRR), aboard the polar-orbiting NOAA-11 and NOAA-12 satellites, has proven very useful not only for tracking eruption plumes, but also for distinguishing between volcanic plumes and clouds. The AVHRR contains two thermal infrared bands at 10.3–11.3 microns (μm) (Band 4) and 11.5–12.5 μm (Band 5). For the individual bands, volcanic plumes and meteorologic clouds frequently appear similar on the satellite images. When Band 5 is subtracted from Band 4 during image processing, the volcanic plumes can be more easily resolved from clouds. Transparent volcanic plumes are most easily distinguished, while opaque plumes laden with large ash particles, water droplets, or ice are more difficult to tell apart from clouds. An example of Band 4 and Band 4–5 data is shown in Figures 9a and 9b for the eruption plume generated by the 18 August 1992 eruption of Mount Spurr, Alaska.

Using the AVHRR data, eruption plumes can be viewed every few hours. In addition to tracking the plume, it is potentially feasible to measure the top of a cloud, its temperature, and the amount of thermal energy released. Figure 9c shows an AVHRR image of plume dispersal across North America on successive days after the 16–17 September 1992 eruption of Mount Spurr.

III. THERMAL MEASUREMENTS AND MONITORING

A. Principles

The thermal aspect of surface and subsurface volcanic activity is crucial in monitoring and interpreting the dynamics of intereruptive cooling and degassing, as well as surface heating due to magmatic activity. The thermal measurements characterize the volcanic heat output of these active regions. While the measurements give direct information on the subsurface state via various types of thermal anomalies (e.g., small spatial anomalies with high intensity, and large thermal anomalies with low intensity), they also provide direct or indirect information on the internal volcanic dynamics: injection of

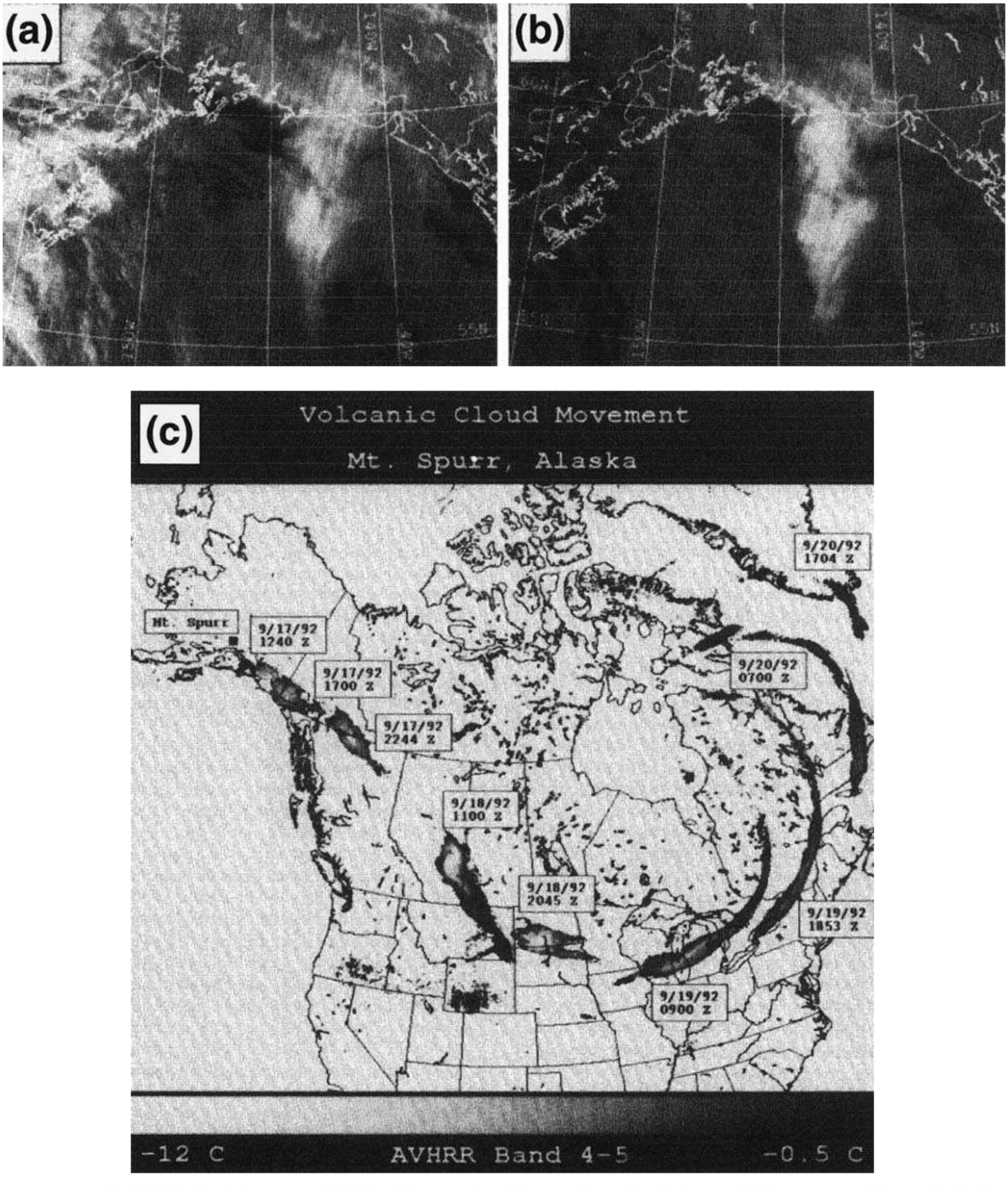
(a)
(b)
140W
60N
150W
55N
(c)
Volcanic Cloud Movement
Mt. Spurr, Alaska
Mt. Spurr
9/17/92 1240 Z
9/17/92 1700 Z
9/17/92 2244 Z
9/18/92 1100 Z
9/18/92 2045 Z
9/19/92 0900 Z
9/19/92 1853 Z
9/20/92 0700 Z
9/20/92 1704 Z
-12 C
AVHRR Band 4-5
-0.5 C

FIGURE 9 (a) AVHRR Band 4 image and (b) Band 4 minus Band 5 image from the 18 August 1992 eruption of Crater Peak, Mount Spurr, Alaska. The volcanic plume is better defined in (b) due to the subtraction procedure. (c) Composite Band 4 minus Band 5 AVHRR image showing long-distance transport of the volcanic plume from the 16–17 September 1992 eruption of Crater Peak. (From Schneider *et al.,* 1995. Figure kindly provided by the U.S. Geological Survey.)

magma from depth via lava coming to the surface, gas escaping through fractures, and active lava flow emplacement. Such information is important for the interpretation and modeling of volcano dynamics. The thermal monitoring of the surface can give precursory warning of future eruptions. Finally, the monitoring of eruption plumes has become another important challenge in recent years for improved safety of air travel in many regions of the world.

For these reasons, volcanologists are interested in surveying thermal fields outlined by unusual temperature distributions at the surface of a volcano. This can be done by thermal or radiant flux measurements from the ground and from space. Thermal measurements directly in the ground give absolute temperatures at a single point but cannot cover large regions. However, the growing access to remotely sensed data during the last 30 years has been a powerful means to monitor volcanic activity globally.

B. The Origin of Thermal Anomalies

The internal geothermal heat produced by the ascent of magma toward the surface of a volcano will dissipate predominantly via underground convection, surface transfer, and/or radiative transfer into the atmosphere. Indeed, the transfer of volcanic heat by conduction (e.g., of the magma through adjacent rock walls) is itself very inefficient. Such an input of volcanic heat at the surface will increase the geothermal flux (80 mW m^{-2} on average). The heat budget at the surface of the volcano can be expressed as

$$\phi_{\mathrm{sol}} + \phi_{\mathrm{geo}} = -W_s - W_{cr},$$

where ϕ_{geo} represents the geothermal flux at the surface, and ϕ_{sol} represents diurnal and annual solar heating variations. W_s is the radiative heat output and W_{cr} the convective heat transfer from the ground to the air. Positive and negative signs indicate a gain and a loss, respectively, from the surface. ϕ_{sol} is usually the most significant component which will increase the temperature of a surface.

However, volcanic areas exhibit a large increase of the geothermal flux, thus we may observe thermal anomalies which have a localized increase in the surface temperature. Since it is important to compare warm and cold thermal values in the same region which have similar atmospheric, meteorological, and emissivity conditions, fluxes are better described by their relative intensities between areas of volcanic activity compared to neighboring inactive regions. The heat loss by wind convection may be estimated with the knowledge of meteorological variables including local wind speed and air temperature. The relative radiative heat loss, in W m^{-2} sr^{-1}, may be measured from various remotely sensed platforms, the choice of spectral bands of the electromagnetic spectrum being made in accordance with the temperatures of interest and the Planck law. In general, the higher the surface temperature, the lower the wavelength of its maximum radiative energy (Figure 10). For example, surfaces with temperatures of 100°C or less will only be observed from Landsat satellites in thermal infrared (TIR, 8–14 μm) bands, while surfaces with temperatures of 600°C and greater can be detected in the short wavelength infrared (SWIR, 1–3 μm) and near infrared (NIR, 0.7–1 μm), and even sometimes in the visible (VIS, 0.4–0.7 μm).

The physics of radiation between the ground and the sensor is in fact more complicated, because part of the emitted radiation is absorbed, scattered, or emitted by the atmosphere. Furthermore, when data are acquired during the day, reflected solar radiation is also captured by the detector. However, data acquired at night may be corrected with the help of standard atmospheric models to deduce a quantitative thermal image of the observed surface. The emissivity of the surface, which is a property of the surface or an object, also controls the radiant energy fluxes. Emissivity for a blackbody is unity and for most natural materials is less than 1 (a function of its texture, composition, age, erosion state, etc.). As a consequence, if a natural surface and blackbody surface have identical temperature, then the blackbody surface

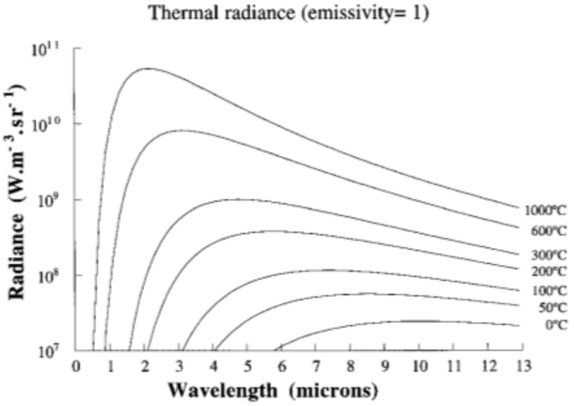

FIGURE 10 Graph showing thermal radiance and temperature sensitivities versus the wavelength. The TIR band (8–14 μm) is sensitive to emitted thermal radiance from surfaces with temperatures in the range of those characteristic of sea and land (300 K). With an increase in the surface temperature, the peak of maximum radiations is displaced to shorter wavelengths.

will emit more than the natural body. Hence, depending on the scientific objectives, images can be processed to provide maps of the emissivities of an area or maps of the temperature distributions.

Spatial, temporal, and spectral clues provide additional information to discriminate between different thermal volcanic features. For example, circular anomalies are generally associated with crater lakes and domes, while elongated anomalies may suggest lava tubes or lava flows. Knowledge of the topography of a volcano also gives valuable information to better interpret the thermal anomalies, since both fields are intimately related; for example, flows will erupt either from craters or flank fractures. The temporal evolution of a volcanic event provides additional constraints on the interpretation of thermal anomalies; a series of images showing the evolution of an active lava flow and its cooling stages will be easier to interpret than a single image taken as a snapshot. Of course, such a series also will be very valuable for the modeling of the dynamics of lava flows.

Fluids such as gases and water escape through the volcano via open conduits such as fumaroles, lava lakes, or fractures. The temperature of these volcanic pathways will depend partly on the origin of the gases. A magmatic origin will be associated with high-temperature gases (>300°C), while water vapor of atmospheric origin (water from rain penetrating into the ground) will give lower temperature volcanic surface areas. Hence, to take a convenient example, the measurement of the temperature of a fumarole will be indicative of the origin of the gas. In many cases, however, an increase in the intensity of a thermal anomaly will not be a straightforward precursor of an eruption. In some circumstances, the preeruptive period is instead distinguished by decreased thermal anomalies due to the sealing of fracture networks as was observed on Lascar volcano (Chile) in 1992 where the dome activity was inversely related to its surface temperature. Hence, whenever possible, thermal measurements and observations need to be interpreted with caution in conjunction with other types of measurements. In particular, it is important to be able to discriminate between eruptive (e.g., active lava flow) and noneruptive volcanic phenomena (e.g., high-temperature fumaroles).

C. Acquisition of the Thermal or Radiance Data

1. *Ground-Based Measurements*

Direct measurements of thermal activity require the use of a thermocouple or of thermometers in a network to estimate the ground temperature at various depths by local contact measurements (Figure 11). Other ground-based methods consist of making the measurements from a remote point of observation using a radiometer, giving an integrated temperature over a narrow target typically of one arc degree or less in one or more wavelength bands. Caution must be taken when interpreting the thermal data since they represent isolated measurements over an entire active volcano. In the case of remote instruments, they may give nonrepresentative temperature estimates due to resolution problems and solar reflection.

New technologies allow the use of handheld thermal infrared video-imaging instruments. Figure 12 shows an example of such a video camera which provided thermal anomalies on Masaya and Telica volcanoes (Nicaragua) in 1997. Imaging digital radiometers have not yet been extensively used on the ground despite their great potential in monitoring the entire spatial distribution of the observed area, instead of a single averaged thermal value. The principal reason is the heavy weight of the instrument, making it difficult to use in the field. However, with new focal plane array technology, digital video cameras will soon become very portable to use in both the SWIR and the TIR spectral windows.

2. *Airborne Sensors*

Airborne missions provide regional synoptic viewing of a temperature distribution of a volcanic region at large scales from tens of kilometers down to a few meters. They have been equipped with thermal sensors since at least the late 1960s. For example, activity on Hawaii has been monitored at several different periods in the 1980s and 1990s with thermal infrared sensors on a NASA aircraft flying at various altitudes between 1 and 10 km above the ground. The sensors provide images acquired simultaneously in different spectral bands from the visible to the thermal infrared regions. Daytime and nighttime flights are performed, with the nighttime thermal images giving the best thermal contrast between active volcanic regions and their neighboring inactive areas. Other volcanic regions have been surveyed by aircraft campaigns in remote areas such as Kamchatka. Infrared video cameras can be used from helicopters to survey the temporal evolution of volcanic activity.

3. *Spaceborne Sensors*

Satellite images provide global viewing of the planet (e.g., 185 × 185 km for a Landsat satellite image) on a continuous basis with a periodicity depending on the type of satellite. This offers great potential for monitor-

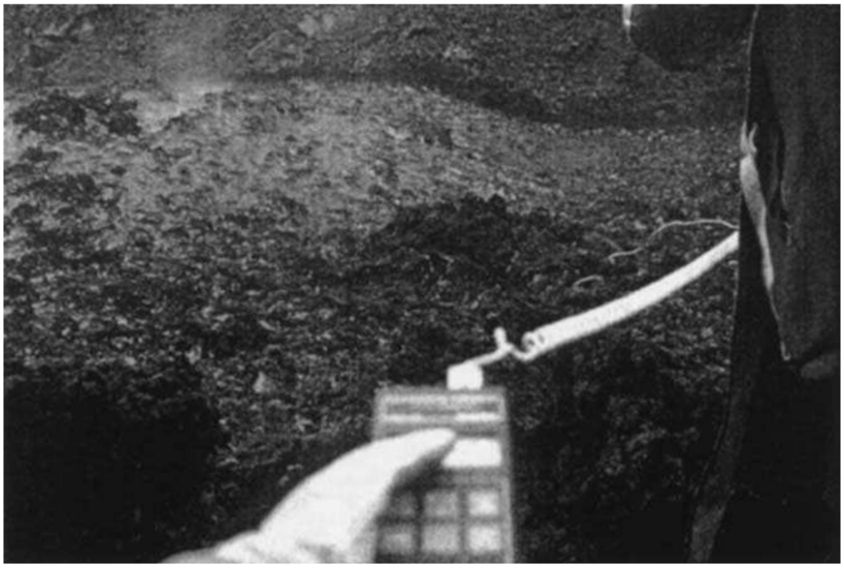

FIGURE 11 Temperature measurements in an active lava flow on Mount Etna obtained with a thermocouple during the 1991–1993 eruption. Temperatures varying between 800 and 1080°C were found locally.

ing active volcanoes. However, depending on the type of study, we usually have to choose between images acquired with high spatial resolution and low temporal resolution (e.g., panchromatic SPOT images with a spatial resolution of 10 m and a temporal coverage of 16 days) or images with low spatial resolution and high-frequency temporal coverage. For example, the AVHRR sensor on the NOAA satellite series gives images with a maximum spatial resolution of 1 km and a temporal frequency of 12 hours. Moreover, in many volcanic regions, acquisition of data will be reduced by meteorological or volcanic conditions which may prevent analysis and interpretation of these images. Examples include clouds and volcanic plumes obscuring the clarity of the region of interest.

D. Space–Time Resolution of the Data

A crucial question when analyzing and interpreting remotely sensed data is that of the spatial resolution. The best qualitative and quantitative interpretation is obtained when combining data from different sources, in different spectral ranges, and at various spatial resolutions. A related question is how to account for the subscale thermal components associated with subscale volcanic structures (e.g., a lava dome 300 m wide compared with the AVHRR 1-km resolution). These questions are important since volcanic phenomena are highly variable in space and time; the temperature of an active region (e.g., a lava flow or a fumarolic vent) may vary significantly within a few centimeters of the ground, as well as over the course of a few hours or minutes. To precisely interpret and analyze such variability surveyed from various distances, the dependence of the remotely sensed data on the spatial and temporal resolution has to be known. Attempts have been made to divide the estimated temperature obtained at a satellite into subscale temperatures. Another approach is to consider the observed thermal field as highly variable and to estimate its dependence on the scale of observation. This is the basis for a new statistical approach of multifractals and multiscaling being developed to analyze and model highly variable geophysical fields such as thermal regions of volcanoes.

E. High-Amplitude Anomalies

Thermal anomalies are considered to be of high intensity when they include temperatures above 300°C at the centimeter scale. Lava flows, lava lakes, lava domes, and some fumarole fields fall into this category. Examples of active lava flows which have been studied include Hawaii, Mount Etna (Italy), and Lonquimay (Chile), in some cases during an eruption when the flows were advancing down the flanks of the volcano. In the case of Lonquimay, the interpretation of Landsat TM (The-

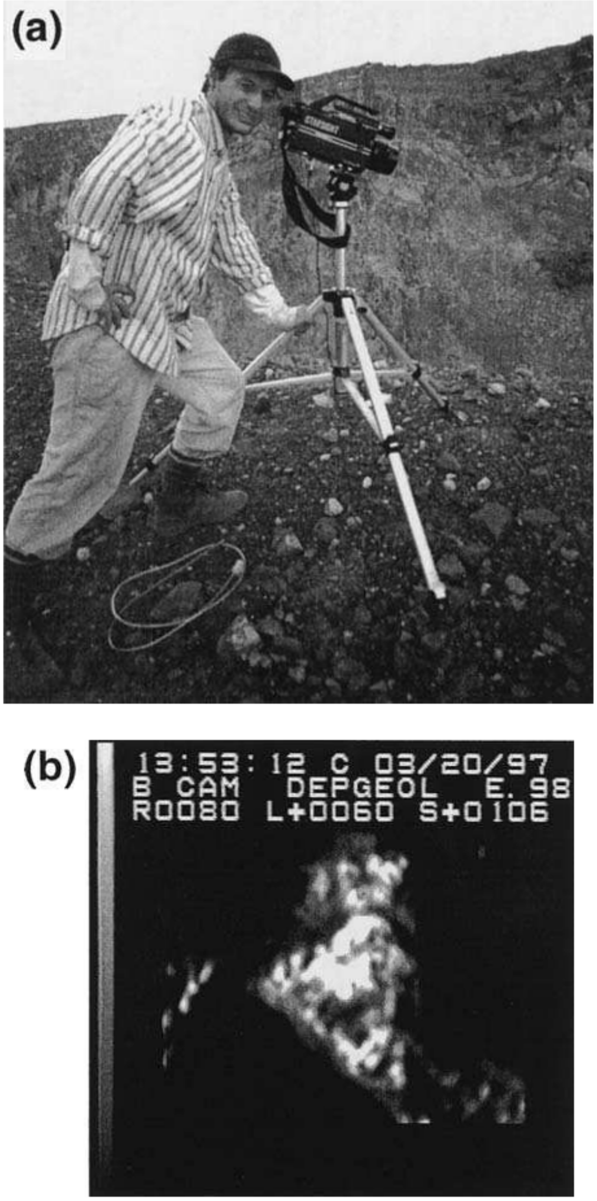

FIGURE 12 (a) Insight Vision portable video camera used to take thermal images on Telica volcano (Nicaragua) during March 1997. (b) Thermal image of the crater wall of Telica acquired with the camera. Escape of gases through fissures in the wall can be observed in this thermal image using the distribution of temperatures. The maximum temperature is about 140°C.

matic Mapper) satellite data suggested that the temperature of the crust forming the outer part of the flowing lava was in the range of 170–250°C for the top of the flow, with a very small fraction of incandescent lava at higher temperatures around 1100°C. Characterizing the surface temperature distribution across active lava flows helps validate thermal models. For example, the viscosity of the lava depends strongly on its temperature, and a small decline in the temperature may therefore lead to a large increase in the viscosity. A thermal anomaly observed on Vulcano with the Landsat TM thermal infrared band in 1986 showed a maximum temperature of the fumarolic field of 10°C above the surrounding background temperature, while temperatures of 319°C were measured on the ground during the same period. This is not surprising, since these thermal measurements have been acquired at a different resolution: 120 × 120 m for the Landsat sensor and on the order of centimeters for the ground temperature. Various approaches recently have been used, such as the dual-band method or the multiscaling framework (see above), to account for such discrepancies in the thermal intensities versus the resolution.

Although lava lakes are uncommon, their thermal signatures also have been measured. For example, the Mount Erebus (Antarctica) and Erta 'Ale (Ethiopia) lava lakes have been observed using various satellites. Satellite thermal images of crater lakes are particularly useful in regions where field measurements are difficult or impossible to obtain on a regular basis. In the second case, complementary satellite and field data have provided an opportunity to follow the evolution of the two Erta 'Ale crater lakes since 1960.

The volcanic history of Lascar volcano (Chile), which has been well studied, is a good case study of a lava dome. While the general activity of the dome is easily monitored remotely, exhibiting a circular thermal anomaly of high intensity, the more detailed intracrater activity is more difficult to follow because of the low resolution of the images. However, it is interesting to note that the thermal intensity of the dome anomaly is observed to decrease prior to small eruptions, in relation to a pressure buildup associated with subsidence of the dome.

Another high-amplitude anomaly which has been successfully studied remotely is fumaroles. In high-temperature fumaroles, gases are generated from magmatic activity with varying concentrations of SO_2, HCl, CO_2, and H_2O, whereas low-temperature fumaroles are dominated by water vapor. High-temperature fumarole fields have been identified at Poás (Costa Rica), Colima (Mexico), Lascar, Vulcano, and Momotombo (Nicaragua), to name a few. On Lascar, the high-intensity fumaroles along the margin of the lava dome were identified as very small spots of irregular shapes. However, because of the large abundance of volcanic gases and aerosols present above the fumarole vents, thermal measurements from remote platforms have been less useful. Hence, the emitted or reflected radiations are highly absorbed or scattered by the gases and vapors which are present above a fumarolic field, and most of this radiative signal will not be received by the detector.

F. Low-Amplitude Anomalies

Weak thermal anomalies may be observed when a magma body is approaching the surface (e.g., lava tubes, magmatic intrusions), leading to low-intensity anomalies. Cooling lava flows, as well as escape of gases through fumaroles or crater lakes, also may form thermal anomalies of low intensity. In such cases, the only useful wavelength band is the TIR region. Examples of small thermal anomalies are the lava flows observed on Mount Etna 1 month after the 1986 eruption, or 11 months after the emplacement of the 1986 lava flow on Stromboli Island (Italy) (Figure 13). In this case, a Landsat TIR image exhibited an elongated anomaly corresponding to a 10-m-thick lava flow that had flowed down the volcano 11 months previously. This thermal anomaly was estimated from space to be 150 m wide with a relative amplitude of 6°C compared to inactive areas on the island. Two other thermal anomalies were discovered on the same image, one associated with strombolian activity present in two crater vents at the summit of the volcano and the other due to topography. This last anomaly shows the importance of knowing the relation between the thermal radiance field and the topographic field.

Most impressive is the monitoring of active lava tubes, such as at Kilauea, where the active lava is flowing in underground tubes from the crater to the coast. While the lava tubes are not noticeable in the visible part of the spectrum (e.g., with our eyes), they can be surveyed using thermal images from aircraft, helicopters, or satellites (Figure 14).

More often the low-temperature anomalies are due

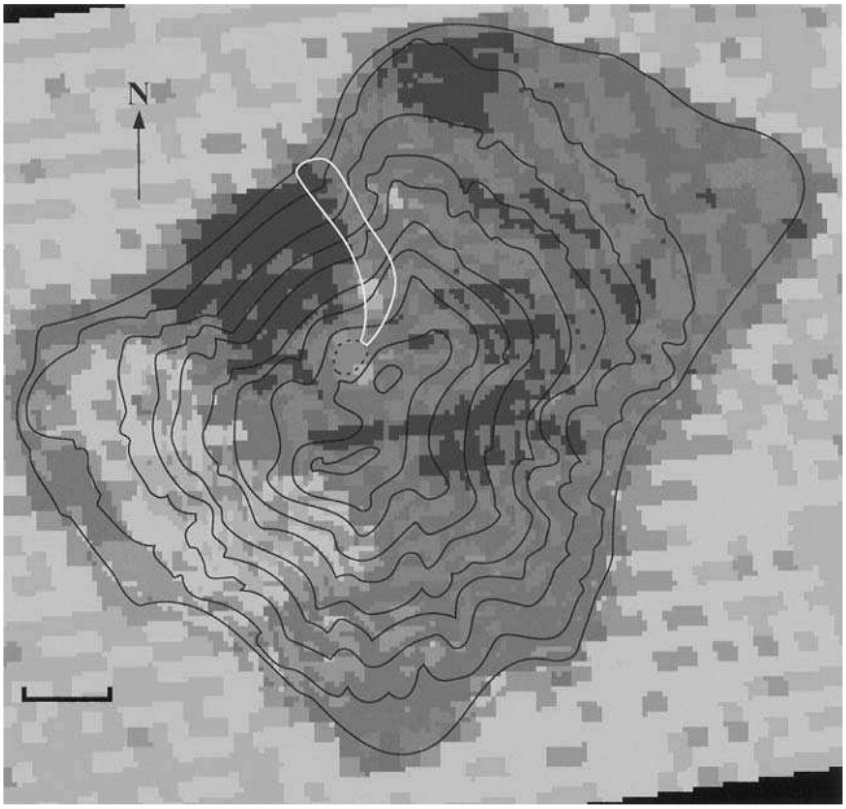

FIGURE 13 Nighttime Landsat TM Band 6 image of Stromboli with 100-m contours from 1986. An anomaly is outlined in white, representing a lava flow emplaced 11 months before the acquisition of the data. The highest temperatures are shown in light tones (≈30°C at 120 × 120-m resolution), while the lowest intensities are shown in dark tones (≈18°C). The scale bar is 530 m, and the spatial resolution is 120 by 120 m. (Adapted from Gaonac'h *et al.,* 1994.)

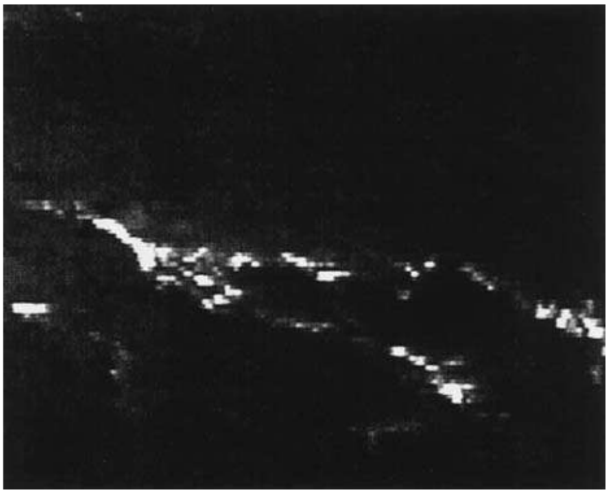

FIGURE 14 Digital thermal image of active lava flowing in tubes within a lava flow field at Kilauea volcano during December 1995. This image was acquired with an Inframetrics 760 video camera in the 8- to 12-μm region from a helicopter.

to fumarolic areas which may represent a larger area than lava flows or lava tubes. Well-known examples are the fumarolic areas on Vulcano or Pozzuoli (Italy), which have been monitored for several decades. Figure 12b shows an example of a low-amplitude fumarolic field present at the bottom of the crater of Telica volcano in 1997. This image, taken with a portable video camera, provides an instantaneous distribution of the thermal anomalies observed in the field. However, temperature measurements made from the ground may be very different from estimates made from space. This is especially obvious for fumarolic fields which may exhibit a temperature variation of 200°C over several centimeters. Interpretation of the temperatures should be made with caution, especially when interpreting local variations.

The last case of low-temperature anomalies are crater lakes where the acidic water may have a variable surface temperature related to injection of magmatic gases. Examples include the crater lakes of Taal volcano (Philippines) and Poás (Costa Rica).

IV. FUTURE DIRECTIONS

Where will we be in 5, 10, or even 50 years' time regarding these approaches to monitoring volcanoes? We see three main avenues of development. First, technology will surely improve in terms of detection capabilities, size, and cost effectiveness. Probably it will be possible to place *in situ* gas monitoring devices in craters for extended periods of time, allowing us to have a continuous record of gas emissions. For this to happen, the devices will need to (1) withstand the incredibly harsh environments of active craters, and (2) selectively analyze individual gases without significant interferences from other gas species. These are the main problems that confront us today. Given these problems, infrared remote sensing devices will improve to become smaller, more portable, and capable of detecting a multitude of gases. We can envision the day when infrared instruments are installed permanently on certain volcanoes to record gas data continuously. Such *in situ* and remote sensing techniques will permit volcanologists to record gas data in much the way real-time seismic data are recorded today.

Second, new generations of remote sensing instruments will be placed into orbit around the earth. These instruments will study volcanoes on a global basis. They will examine the detailed structure of volcanic plumes and track volcanic gases which are emitted. The measurements will provide three-dimensional maps of gas and thermal plumes and will allow scientists to study the interactions and effects of volcanic eruptions and emissions on the troposphere and stratosphere. Temperature measurements will continue to be made on active volcanoes, especially from remote sensing platforms. Yet, several problems will limit the interpretation of the data, such as the spatial resolution of the sensors, daytime instead of nighttime acquisition, and the distinction between different high-temperature anomalies. Other problems include the acquisition of temperatures from the ground, for example, isolated measurements, inaccessibility of the active volcanic area, and the practical impossibilities of high-resolution *in situ* mapping. Other questions arise when interpreting the thermal behavior of the surface of a volcano in relation to the activity of the volcano prior, during, and after an eruption. In the future, we expect thermal monitoring of active volcanoes to benefit from acquisition of data using sensors with higher spectral and spatial resolutions, and better models to interpret the evolution of the volcanic activity. The result will be temperature and thermal flux maps which will enhance our understanding of volcano dynamics. For example, sensors such as MODIS or ASTER, to be launched on the U.S. Earth Observation Satellite EOS-AM platform in 1999, will acquire data of the same volcanic region in various spectral bands, which may then be handled together to be either processed through the dual-band technique or through more elaborate methods of analyzing and interpreting thermal anomalies such as the multifractal/multiscaling approach.

Lastly and perhaps most important, the new data which are provided will help scientists to better understand the overall behavior of an active volcanic system. As we develop our notions of gas solubilities, gas and heat transport in magma, and phenomena such as volcanic seismicity, we will be able to integrate this knowledge with the new data to comprehend the physical basis of how and why volcanoes reactivate and erupt. An important challenge is how to appropriately combine the various datasets in order to make significant advances in monitoring and developing robust models for volcanoes.

SEE ALSO THE FOLLOWING ARTICLES

Hazards of Volcanic Gases • Seismic Monitoring • Synthesis of Volcano Monitoring • Volatiles in Magmas • Volcanic Ash Hazards to Aviation • Volcanic Contributions to the Carbon and Sulfur and Carbon Geochemical Cycles • Volcanic Gases

FURTHER READING

Casadevall, T., Rose, W., Gerlach, T., Greenland, L. P., Ewert, J., Wunderman, R., and Symonds, R. (1983). Gas emissions and the eruptions of Mt. St. Helens through 1982. *Science* **221,** 1383–1385.

Farrar, C. D., Sorey, M. L., Evans, W. C., Howle, J. F., Kerr, B. D., Kennedy, B. M., King, C.-Y., and Southon, J. R. (1995). Forest-killing diffuse CO_2 emission at Mammoth Mountain as a sign of magmatic unrest. *Nature* **376,** 675–678.

Francis, P., Maciejewski, A., Oppenheimer, C., Chaffin, C., and Caltabiano, T. (1995). SO_2:HCl ratios in the plumes from Mt. Etna and Vulcano determined by Fourier transform spectroscopy. *Geophys. Res. Lett.* **22,** 1717–1720.

Francis, P. W., Wadge, G., and Mouginis-Mark, P. J. (1996). Pages 257–298 *in* "Monitoring and Mitigation of Volcano Hazards" (R. Scarpa and R. I. Tilling, eds.). Springer-Verlag, Berlin.

Gaonac'h, H., Vandemeulebrouck, J., Stix, J., and Halbwachs, M. (1994). Thermal infrared satellite measurements of volcanic activity at Stromboli and Vulcano. *J. Geophys. Res.* **99,** 9477–9485.

Giggenbach, W. F. (1994). Pages 221–256 *in* "Monitoring and Mitigation of Volcano Hazards" (R. Scarpa and R. I. Tilling, eds.). Springer-Verlag, Berlin.

Giggenbach, W. F., García P., N., Londoño C., A., Rodriguez V., L., Rojas G., N., and Calvache V., M. L. (1990). The chemistry of fumarolic vapor and thermal-spring discharges from the Nevado del Ruiz volcanic-magmatic-hydrothermal system, Colombia. *J. Volcanol. Geotherm. Res.* **42,** 13–39.

Heiken, G., and Wohletz, K. (1985). "Volcanic Ash." Univ. of California Press, Berkeley, CA.

Krueger, A. J., Doiron, S. R., Bluth, G. S. J., Walter, L. S., and Schnetzler, C. C. (1994). Volcanic hazard detection with the total ozone mapping spectrometer (TOMS). *U.S. Geol. Surv. Bull.* **2047,** 367–372.

Laferrière, A., and Gaonac'h, H. (1999). Multifractal properties of visible reflectance fields from basaltic volcanoes. *J. Geophys. Res.* **104,** 5115–5126.

Rothery, D. A., Oppenheimer, C., and Bonneville, A. (1995). Pages 184–216 *in* "Monitoring Active Volcanoes" (J. Guest, C. R. J. Kilburn, and J. B. Murray, eds.). UCL Press, London.

Schneider, D. J., Rose, W. I., and Kelley, L. (1995). Tracking of 1992 eruption clouds from Crater Peak vent of Mount Spurr volcano, Alaska, using AVHRR. *U.S. Geol. Surv. Bull.* **2139,** 27–36.

Stoiber, R. E., Malinconico, L. L., and Williams, S. N. (1983). Pages 425–444 *in* "Forecasting Volcanic Events" (H. Tazieff and J.-C. Sabroux, eds.). Elsevier, Amsterdam.

This Page Intentionally Left Blank

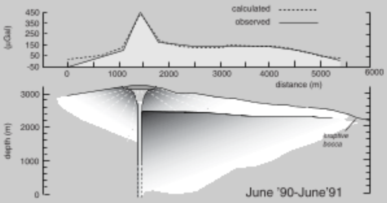

Synthesis of Volcano Monitoring

Stephen R. McNutt
Alaska Volcano Observatory and University of Alaska Fairbanks

Hazel Rymer
Open University

John Stix
McGill University

I. Introduction
II. Instruments and Networks
III. Monitoring before Eruptions
IV. Monitoring during Eruptions
V. Monitoring after Eruptions
VI. Case Histories
VII. Discussion
VIII. Volcano Monitoring in the Future

THIS ARTICLE SYNTHESIZES the monitoring of active volcanoes using a wide range of techniques and instrumentation. It covers definitions, concepts of instrument design and use, and patterns and processes that occur before, during, and after eruptions. Ideas are illustrated using published case histories of Mount Etna, Italy, and Soufriere Hills, Montserrat. Both advantages and limitations of monitoring are discussed.

I. Introduction

Volcano monitoring serves two key functions: it provides basic scientific data to develop our understanding of the structure and dynamics of volcanoes, and it is crucial for hazard assessment, eruption forecasting, and risk mitigation at times of volcanic unrest. Monitoring provides the means to address questions of vital interest to communities affected by impending eruptions, such as, when and where will the volcano erupt? Which areas are safe or dangerous? When will eruptions cease? Optimal interpretation of data from monitoring, especially for the purpose of forecasting, depends critically on an adequate scientific understanding of volcano structure and processes, both in general and for each specific volcano. Thus, volcano monitoring at its most effective is a synergy between basic science and hazard assessment.

Historically, volcanic activity has been considered to be primarily of local interest because, with the exception of relatively infrequent large explosive events, most eruptions seriously affect small areas of only a few km^2. As populations expand, however, more people are at risk from the direct or indirect impact of volcanic eruptions. In addition to the immediate hazards posed by eruptive products to life, property, and food production, volcanic activity of any kind may have a significant effect on the economy. During minor eruptions tourism may increase and boost the local economy. The loss, however, of agricultural farmland, farmhouses, communication and service infrastructure (roads, ports, water supplies, elec-

Copyright © 2000 by Academic Press
All rights of reproduction in any form reserved.

tric cables, etc.), and permanent changes in the local groundwater and drainage system can have severe economic consequences. A volcanic disaster on one side of the world can now have a significant economic impact on countries on the other. It is therefore of interest to all nations that volcanoes are monitored so that eruptions can be forecast and mitigating action taken. Successful mitigation of the local effects of an eruption (such as lava flow diversion and community evacuation) requires a detailed understanding of the eruption process, for which monitoring data are a vital component. More widespread effects can be mitigated to some degree with early warning, for example, allowing aircraft rerouting. Similarly, an appreciation of the climatic effects both locally and globally requires data from surveillance before, during, and after eruptive activity.

Volcano monitoring comprises the systematic checking of various types of geological, geochemical, and geophysical data at a volcano. Each type of data (such as measurements of temperature, gravity, or earthquakes) provides information about physical processes which may be related to movement of molten rock or other eruption precursory phenomena. All the available data should be synthesized in a coherent way so that interpretations may be arrived at that are consistent with all the observations. This interpretation then serves as a guide to anticipate what may happen next, and provides an opportunity to take appropriate mitigation measures.

Monitoring is complicated by the fact that data come in at different times and in different formats. Some data can be viewed "raw," but other data must be processed first, causing additional delays. For example, a seismic drum record may show that an earthquake has occurred, but additional processing is necessary to determine magnitude and location.

Monitoring results may be ambiguous. For example, thermal anomalies may occur if lava is erupted, but can also result from fires and from solar heating of the ground. Similarly, ground deformation may be caused by the injection of magma prior to eruption, but also by water table movements.

Until relatively recently, the only way to monitor a volcano was to watch it, and the amount of warning that could be given would depend on the communication between the lookout and the local population. For example, although Pliny the Elder was in a good position to assess the eruption of Vesuvius in 79 A.D., he was unable to provide any assistance to the fleeing people of Herculaneum and himself perished at Stabiae. Some people may have escaped by boat, but for most, there was insufficient time to evacuate. Modern techniques of volcano surveillance involve the use of a wide range of physical and chemical measurements, some of which require lengthy laboratory work to analyze and some of which provide instant results. Each technique has advantages and drawbacks of some kind, but the more methods that can be used at one time, the better the chances of detecting precursory variations and therefore of being able to provide a warning. The most appropriate techniques to use depend on the type and scale of the hazard envisaged.

Thirty years ago volcanologists concentrated their efforts on field observations including seismic tremor, magnetic intensity, and thermal and gas output. About 20 years ago, advances in methods and technology allowed better modeling and lab experiments. In the last decade, completely new technologies involving satellites, GPS, SAR interferometry, and digital data, and the easy transmission of data from remote locations to computers in observatories and laboratories for automatic analyses and interpretation, have provided dramatically better data resolution at some volcanoes. Thus the potential exists to use better and more complete data to monitor volcanoes, but with higher initial costs and more equipment to maintain.

Monitoring a volcano has some similarities with monitoring the health of a patient. Some tests, such as checking a pulse, are simple and direct. Others, such as blood tests, take time to perform and to analyze, but provide fuller results. Like volcanoes, people can show similar symptoms that may be related to a wide variety of illnesses or conditions. For example, a simple skin rash may be caused by a minor and temporary allergic reaction, or it may herald a terminal disease. New fumaroles may open up at a volcano simply because the previous path for passive degassing has become blocked by precipitation of minerals, or because a new batch of gas-rich magma has been intruded to shallow depth. The first situation may not be too serious, but the second certainly is. Monitoring techniques were formerly based on the most easily measured phenomena; other effects were either not recorded or were treated as noise. Future progress will be enhanced by taking account of these more subtle or complex effects and by the more comprehensive acquisition and real-time analysis of continuous data sets over extended periods.

II. INSTRUMENTS AND NETWORKS

The instruments used to monitor volcanoes vary widely in type, sophistication, cost, and effectiveness. Some instruments are permanent; once installed they continue to collect data for long periods of time (e.g., a seismic network). Other instruments are usually deployed in temporary networks (e.g., gravimeters) whereas others are driven or flown in the vicinity of volcanoes to make measurements (e.g., COSPEC). It is important to realize that only a small number of the world's active and potentially active volcanoes are being monitored today. There is not a single volcano at which all these types of instruments are simultaneously in use over an extended period of time. However, several volcanoes have had at least some measurements of each type, and these are the ones about which the most is known.

A. Seismic Monitoring

A century of seismological data testifies that seismic unrest in the form of earthquakes and tremor almost always precedes and/or accompanies volcanic unrest at all types of volcanoes. Seismic activity is considered to be the best indicator, and often a reliable short- to midterm (days to weeks) forecaster, of the level and evolution of volcanic activity. Seismic monitoring is one of the most common surveillance tools used by geophysicists and the equipment is fairly cheap and simple to install, although data collection and transmission become difficult in remote areas. Once the background seismicity has been characterized for a particular volcano, changes in the level or intensity, or appearance of different types of events, may herald the onset of activity. However, the resolution of the technique is not always very good, and sources (such as the movement of volcanic gases or cracking of rocks as fresh magma is intruded) are difficult to distinguish unless there are several seismic receivers spread out near the active crater. Successful forecasts of eruption have been made using seismology, and countless lives were recently saved after evacuation around Pinatubo and Mayon volcanoes (Philippines) following seismic precursors to renewed activity. However, although Galeras volcano (near Pasto, Columbia) was monitored for seismic precursors, none were observed for several hours prior to the fatal eruption in January 1993.

Seismic sources at volcanoes are highly complex and involve the interaction of gases, melts, and solids. The role of the melt and gas may be either (i) active, giving rise to pressurized intrusions of magma into preexisting or newly formed zones of weakness, or to sustained vibration of the melt and host rocks, or (ii) passive, where brittle failures and the consequent stress readjustments modify the distribution of melts in the crust. Since volcanic media comprise dense systems of pores, fractures, and faults at all scales, sudden modification of the local stress field may induce seismic failure independent of melt propagation. These factors contribute to the substantial degree of ambiguity in volcano eruption forecasting on the basis of seismology alone.

B. Ground Deformation

Ground deformation is another relatively cheap and common technique for volcano monitoring. Repeated measurements of relative vertical height and/or horizontal distance are made, and changes often precede a change in activity. Traditionally measurements have been made with levels and EDM (electronic distance measurement) theodolities, but GPS (global positioning system) measurements using a constellation of more than 20 satellites are being used increasingly. GPS monitoring provides a measure of changes in the distance to a satellite from any number of ground-based receivers by moving the receivers from place to place during a survey; thus, a large ground deformation network can be covered. The advantage of this method over the conventional ground deformation techniques is that it is quicker and less labor intensive, and is not dependent on clear weather. Another new satellite-based technique that has revolutionized ground deformation monitoring is synthetic aperture radar (SAR) interferometry, which involves taking radar "pictures" of large areas (such as a whole volcano) and comparing the image taken with images obtained on previous passes of the satellite (approximately monthly observations are currently possible). Differences between the images reflect ground deformation and the method is sensitive to movements of a few centimeters. However, these measurements cannot be made in areas with abundant vegetation, steep slopes, or snow cover.

It is usually assumed that a volcanic edifice behaves elastically, and that as pressure builds up within or beneath it, the volcano expands in a predictable way to accommodate the increased stress. However, brittle fracture rather than elastic deformation also occurs at volcanoes and the effect is that ground deformation is abrupt, often contemporaneous with eruption, rather than gradual and precursory. Thus, like seismic monitoring, this method is unreliable on its own for the forecasting of volcanic activity. Further, even though instruments are in place, some eruptions have no measurable deformation associated with them.

C. Gas Monitoring

Volcanic gas analysis and temperature measurements are also commonly made. Precursory variations have been observed prior to some eruptions, but often the changes occur with the beginning of the eruption. The measurements are rather difficult to make within active volcanoes, as they necessitate someone climbing right down into the vent. Even modern high-sensitivity equipment must be located close to the source for accurate observations to be made. Satellite measurements of infrared radiation (temperature) can be made, although the source (a vent in a volcanic crater) is often too small for quantitative observations. Similarly remote measurements of SO_2 gas flux can be made, and while these methods are useful for monitoring the progress of an ongoing eruption, they are limited in application for eruption forecasting. Sharp increases or decreases in SO_2 may be precursors, but the measurements cannot be made continuously so information may be missed.

D. Gravity and Magnetic Monitoring

The strength of a potential field varies with distance from the source, but never falls away to zero. Thus observation of gravity and magnetic fields can be made at relatively safe distances from the source, and provided they are made over a wide enough area, can reveal significant precursory variations. Magnetic precursors to eruption have yet to be observed, partly because the field is very complicated in volcanic regions. Gravity measurements are ambiguous without simultaneous elevation (ground deformation) observations, but the combination has been found to be an extremely powerful tool for volcano monitoring. The combined technique, which has become known as microgravity monitoring, has been found to be capable of detecting precursory changes within a volcano that other techniques have not resolved.

III. MONITORING BEFORE ERUPTIONS

There is a period of time between the end of dormancy and the onset of eruptive activity, that may last days, weeks, years, or even decades, during which processes go on inside and beneath a volcano in "preparation" for eruption. These processes can be detected by making measurements at the surface and are termed "precursors."

Before magma or gases are erupted at the surface, they must either be transported from a deep storage region to a shallow region for temporary storage, or simply intruded into pipes and dikes feeding to the surface without storage (hence the difference in "preparation" time described above). Often the first observed signal is a change in deformation. If the magma movement is deep, the signal is small and spread out over a wide area. If it is shallow, then the deformation signal is stronger and is concentrated in a smaller area. The same processes that cause deformation also frequently cause small fractures to occur below ground level which are detectable as earthquakes. The earthquakes may occur in swarms at areas of stress concentrations—such as nearby faults—and in the immediate vicinity of magma where pressure changes are occurring (earthquakes do not occur in magma itself because magma is a liquid and has no shear strength). Magma movement may also disturb the local water table, and changes in flow and temperature of groundwater may be detected using a variety of electromagnetic techniques.

When magma is ascending the gases dissolved in it change their relative concentrations because different gases have different solubilities. Carbon dioxide (CO_2) has very low solubility so it is the first to exsolve. Areas of CO_2 release have killed trees and other vegetation at several sites on Mammoth Mountain, California. Other gases such as chlorine (Cl) and sulphur (S) exsolve at shallower depths, and measurements of the Cl/S ratio can help determine whether fresh magma is present at shallow depths. The total amount of SO_2 also typically increases and may reach several hundred or even several thousand tons per day when magma reaches very shallow depths. Gases may begin to escape from newly opened vents at this time, and changes in the gravity and magnetic fields may also occur as the subsurface density and magnetic properties respond to the intrusion. Ground deformation may accompany all these phenomena.

Another common precursor is evidence of increased heat. Typically the temperature at fumaroles increases, and the average ground temperature may increase as well; this is especially easy to spot on snow-covered volcanoes because the snow melts.

The precursors to an eruption will depend on the type of volcano. Basaltic volcanoes tend to erupt freely flowing lavas, and the precursors might be a swelling of the volcano associated with the intrusion of magma into the edifice and the corresponding mass increase (observed as a gravity increase). Andesitic volcanoes erupt explosively and so the precursors might be a build up in volcanic gas pressure beneath the surface or the intrusion of magma within the edifice. These would be seen as net microgravity decreases and increases, respectively, possibly associated with ground deformation. Calderas erupt large volumes explosively, and although a large caldera eruption has not been observed, it is thought that such an eruption may be triggered by the intrusion of hot basaltic magma into a reservoir of more silicic magma. The silicic magma would become superheated and the dissolved gases would rapidly expand and escape to the surface. The bubbles would entrain hot magma that itself would be degassing rapidly. Magma intrusion should be detectable as a gravity increase, while increased gas content would appear as a gravity decrease.

At a volcano that has not been historically active, or one where ground surveillance is not available, the first information that an eruption is imminent may come from "remotely sensed" or satellite thermal infrared data. The area near the vent may appear as a "hot spot," an area that is significantly warmer than its surroundings. Hot spots often grow larger with time as more heat affects the Earth's surface. The appearance of a new lava lake in a crater can be seen using these techniques, for example, although strictly speaking, an eruption has already begun by this stage. When magma is very close to the Earth's surface, incandescence may be seen in cracks, areas of steaming ground appear, lakes (of water) dry up, cracks and bulges may be evident, and volcanic tremor occurs on seismometers.

Many or all of the monitoring techniques available could, in theory, detect the processes that occur before an eruption. The problem is that monitoring networks are costly to install and maintain and it is very rare to operate a network "just in case." Therefore, unless a network has been previously installed and happens to be capable of providing data during the buildup phase prior to eruption, precursors are likely to be missed simply because the relevant observations are not made.

IV. MONITORING DURING ERUPTIONS

Interestingly, and perhaps surprisingly, the most important yet ambiguous monitoring data are those collected during an eruption. The processes that occur during an ongoing eruption involve the movement of magma and gases from a shallow storage or feeder region to the surface. During an eruption, the feeder system remains open and variations in geophysical phenomena that can be measured (seismicity, potential fields, temperatures, etc.) are limited as the process, albeit rather violent in some cases, is continuous and the changes in physical properties which are exploited by monitoring techniques are not occurring. However, there may be some changes during an eruption, such as in the ratio of gases species, the gas flux, etc., that can be detected. These observations provide valuable information about the next stage in the eruption (whether it will be more or less explosive, involve a large volume of magma extrusion, etc.). Variations in the degree of magma vesiculation may occur during an eruption and these can be monitored using microgravity methods. Disturbances of the water table or hydrothermal system can be detected using seismic and electromagnetic methods.

We next approach what happens during eruptions by considering several different types of eruptions.

A. Explosions

An explosion is a very short-lived (a few seconds) but energetic event. When a strong explosion occurs at a volcano, seismic waves are generated in the ground, acoustic waves in the atmosphere, and a plume starts to rise. Seismic waves travel at several km/s so the seismic ground waves are often the first signal recorded on monitoring instruments. Air waves travel more slowly, about 330 m/s, so these take several tens of seconds to reach instruments on the flanks of a volcano, either microphones, barographs, or seismometers (the air wave couples back into the ground). Gas is suddenly expelled during the explosion. Plumes rise at rates of 50–100 m/s, so these may be observed locally and seen on satellites as they rise and spread laterally with the wind. Depending partly on atmospheric conditions, lightning may form within an ash plume, as early as tens of seconds for Surtsey volcano but more typically 5 to 20 minutes after charge separation has occurred. Deformation may include static strain steps as well as permanent changes in the shape of the vent, such as the excavation of a large crater. Gravity changes will accompany ground deformation (as the ground goes up, the value of gravity decreases). Any long-period seismicity associated with the explosion will be seen as noise on a gravity meter located within a few kilometers of the vent. There are not likely to be significant magnetic variations directly associated with explosive activity.

B. Sustained Explosive Eruptions

A sustained explosive eruption may occur on a timescale of a few minutes to a few hours. Such events are very energetic, and produce primarily ash and tephra. The onset of such an event produces seismic waves and acoustic waves as above, and a plume rises as well. However, when sustained, the seismic disturbance is continuous and long lasting (volcanic tremor) and the strength of the signal is proportional to the intensity of the eruption. This typically changes as a function of time within the sustained eruption. Gravity changes are likely to be associated with ground deformation and seismicity but magnetic changes are not expected. Acoustic waves are continuous or episodic, and typically occur in bursts during strong pulses of explosions. In some cases acoustic waves can be heard 200 km or more away from the volcano. Lightning occurs in the eruption column a few minutes after eruption onset, and continues to occur for as long as the eruption lasts. Some lightning extends from the ash cloud to the ground, and some extends between charged regions within the ash cloud (intracloud lightning). If the plume is injected into the stratosphere, the amount of SO_2 can be estimated by TOMS satellite measurements. Plumes may travel hundreds of kilometers downwind, connected to the vent, and when the eruption stops, the plume continues to travel as a discrete mass carried by the winds. Some plumes have remained hazardous several days after the eruptions that produced them have ended. Large plumes that reach the stratosphere have been known to circle the Earth.

C. Effusive Eruptions

Effusive eruptions produce lava flows instead of tephra. They are thus not explosive. The seismic signal produced by effusive eruptions is volcanic tremor, which may have a very gradual onset. The strength of the tremor varies with the rate of flow of lava. Since no explosions occur, no air waves are produced, although a hissing sound may be heard at close range. The ash plumes from effusive eruptions are typically small, rising to 1 or 2 km, so lightning is rare. (Ash plumes from effusive eruptions may account for less than 1% of the total erupted volume.) Deformation is of several types. New lava flows cover and change the shape of the land surface. Effusive eruptions often start at fissures, and the flow later localizes to one or more cylindrical vents. Each of these has a characteristic pattern of deformation which occurs before and during the eruption. Gravity is affected by the deformation, and the presence of new material on the surface will increase gravity. The filling and emptying of subsurface dikes and feeders also affects the gravity (causing increases and decreases respectively). Magnetic intensity will increase over a lava flow or dike as it cools, but decrease over a dike or feeder as it drains.

V. MONITORING AFTER ERUPTIONS

A. General Cases

It is not easy to predict the beginning of an eruption, but it is even more difficult to predict the end of an eruption. Partly this is a problem of definition. A volcano never looks quite the same after an eruption as it did before and so it cannot return to exactly the state it was previously in. Therefore the definition of the end of an eruption may be rather subjective. It is clear when lava is no longer coming out of a vent, but there may be gases still being emitted, and lava flows take weeks or more to cool down to ambient temperatures. In some cases, the end of an eruption means simply the end of a particular phase of activity, or a type of activity. For example, a volcano may move from a continuous lava flow coming from a distinct vent to sporadic, strombolian activity from another vent. By some definitions, the volcano is still erupting; by others it is quiescent. It rather depends on the normal state of activity of the volcano and the experience or prejudices of the observer. Here we define an eruption as the flux (mass flow per unit time) of lava through a vent, including steam and gases. This is an operational definition to help put boundaries on the subject at hand; other definitions appear throughout this encyclopedia.

Most explosive eruptions, those that produce ash and tephra, generate volcanic tremor as the eruption is under way. In particular, the strength of the tremor is proportional to the intensity of the eruption as measured by ash column height or flux. Thus when an eruption wanes and approaches its end, the tremor decreases and reaches background values. Tremor generally accompanies each phase of eruption, and may occur between phases and after the last eruption as well. Earthquake swarms often occur throughout eruptive sequences, with some clusters of events associated with eruptive phases and some as indications of changing stresses in the vicinity. As eruptions near their ends, the swarms typically decay in rate with a power law, very similar to aftershock sequences following large earthquakes. Thus the two chief seismic indicators, earthquake swarms and tremor, both decay from high levels to background levels as eruptions are ending.

Lightning often occurs in ash columns of explosive eruptions, beginning a few minutes after the onset of the eruption. Lightning also ends as the eruption ends because the supply of new material cases; the new material is needed to produce charged particles and separate them. When this stops happening the lightning stops.

At the end of an eruptive period when intruded magma is cooling and solidifying *in situ*, the ground may begin to subside slightly due to thermal contraction. At the same time, as magma cools it will acquire a magnetic signature measurable at the surface and the density may increase, raising the values of the magnetic and gravity fields at the surface.

Degassing decreases also, although frequently it decays slowly and sporadically. Gas may continue to be released months or even years after an eruption.

Tephra eruptions deposit large amounts of unconsolidated material on steep slopes. If water is abundant, either rain or glacial, then lahars may be easily formed and may continue to occur for months or years after eruptions end. Low-magnification seismometers placed near flow channels may serve as effective lahar sensors. Several sensors are needed along channels at intervals of a few kilometers to be able to tell if a lahar is moving and to estimate its speed.

Although the eruption of lava and ash onto the ground may end, some of the finest ash, gases, and aerosols may remain suspended in the air for quite some time. If the suspended particles reach the stratosphere, they may be carried by strong winds all the way around the globe. One component of monitoring, satellite remote sensing, is concerned with precisely such ash clouds. In addition to climatic effects such as global cooling, the fine particles cause additional abrasion to airliner leading edges and produce "crazing" of windows, resulting in more frequent replacement. Thus the economic effects of eruptions—one component of the hazard—can last for years.

B. Restless but No Eruption

A large-magnitude caldera-forming eruption has not taken place since volcano monitoring techniques have been developed. However, although a caldera eruption is less likely to occur than a smaller, explosive eruption such as occurred at Pinatubo, its effect would be so devastating that calderas in regions of dense population are monitored closely. There were crises during the 1980s at two such calderas, Rabaul (Papua New Guinea) and Campi Flegrei (Naples, Italy). In both cases, the ground rose up by over a meter and gravity decreased (as would be expected for an elevation increase), but not by as much as it should if the gravity change could be attributed solely to the height change. Thus in both cases, an overall increase in subsurface mass occurred (approximately 10^{11} kg), but in neither case did an eruption follow. Thousands of microearthquakes occurred beneath and adjacent to each caldera, but virtually no volcanic tremor was detected. Thus while it seems that magma was added to the reservoir of silicic magma beneath the calderas, there was apparently not enough to cause the catastrophic superheating expected to precede an explosive eruption. Although the amount of ground uplift was large enough to be alarming, the calculated increased volume of magma was small (a few percent), and so the risk in fact was small, although in both cases people were evacuated temporarily. Rabaul eventually erupted in 1994, but this was nearly 10 years after the seismic and deformation crisis. This implies that appreciable amounts of time may pass between the time when the magma reservoir is replenished and the time when the volcano finally erupts.

VI. CASE HISTORIES

A. Mount Etna

1. Introduction

Mount Etna is important to the economy of Eastern Sicily, with agriculture and summer and winter tourism providing employment for thousands of people. Although there are no permanent homes within 10 km of the summit, year-round human activities on the upper slopes are proliferating and the risks from even a small eruption are consequently magnified. The earliest form of monitoring at Etna, as for other volcanoes, was direct observation. A huge array of monitoring techniques have been tested on Etna; methods that have proved successful in monitoring and sometimes in predicting eruptions include observations of seismicity, ground deformation, and microgravity. These, together with electromagnetic, magnetic, gas geochemistry, and various remote sensing techniques, have also provided key information on the volcanic plumbing system and the eruption process.

Techniques applied during the 1989 and 1991–1993 Etna eruptions are taken as examples of volcano monitoring today. The high level of activity at Etna and its easy accessibility have led to most available techniques for volcano monitoring, and some involving mitigation, being tested there. In 1989, 4 months of strombolian activity at the summit craters was followed in September by an effusive eruption from the southeast (SE) crater and the opening of two fractures. A noneruptive south-southeast (SSE) trending fracture extended more than

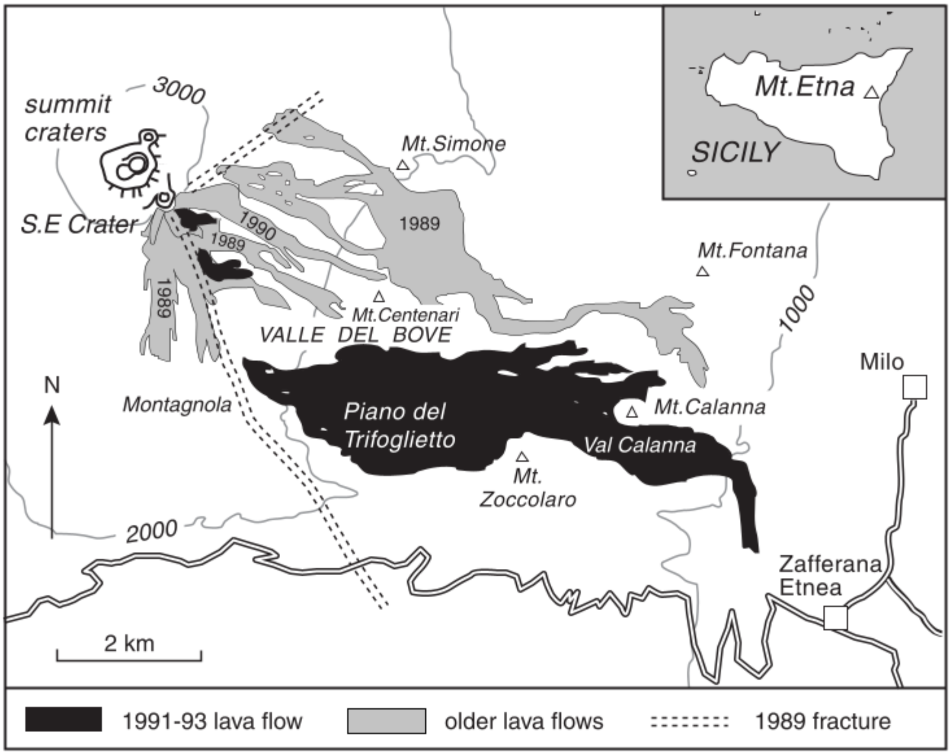

FIGURE 1 Index map of the summit region of Mount Etna, Italy. The 1991–1993 lava flow is shown in black and older lava flows in gray. Prominent fracture systems are indicated by pairs of dashed lines. Elevation contours are in meters.

7 km from the summit (Figure 1), passed close to the headwall of the Valle del Bove, and crossed the road between the Sapienza and Zafferana Etnea. The northeast (NE) trending fracture extended about 2 km from the summit crater area and lava was erupted along much of its length. No further activity occurred until a small explosive eruption from the SE crater in January 1990.

Activity on Etna was then unusually quiet until 14 December 1991 with the start of the most voluminous eruption since the end of the 1669 eruption. The activity was largely confined to a single bocca within the western wall of the Valle del Bove [2200 m ASL (above sea level)] erupting 231 × 10^6 m^3 of lava at an average rate of 5.7 m^3 s^{-1}. The flow was more than 8 km long and threatened the town of Zafferana Etnea when it was successfully diverted. The eruption ended on March 31 1993, after 471 days.

2. *Seismology*

The first instruments set up to record earthquakes at Etna were deployed in the early 1900s; however, the first network of seismometers was not established on Etna until 1973. This network, comprising two to six stations recording the short-period vertical component of seismic waves, was used to investigate eruption-related earthquakes and volcanic tremor. These studies showed that shallow (1–5 km) seismic activity usually preceded flank fissure eruptions by a few days. In contrast precursory seismic activity is not usually associated with summit eruptions, although they are often accompanied by tremor. Increased levels of tremor energy are consistent with an increased probability that an eruption may occur within weeks, days, or even hours. Modern seismometers detect ground vibration in three dimensions over a range typically of 0.1 to 10 Hz. "High-frequency" events (several hertz) are usually associated with deep (several kilometers) fracture events, while "low-frequency" events and tremor are thought to be caused by forced resonance of fluids in shallow (few kilometers) volcanic conduits.

A new seismic array was being developed and expanded on Etna by the Istituto Internazionale di Vulcanologia, Catania, prior to the 1989 activity, and data from up to 22 seismometers were available for analysis and comparison. Seismicity at Etna remained at background levels until July 1989 when a 10-km-deep (below sea level, or BSL) magnitude 2.9 event beneath the southeastern Valle del Bove, and later a seismic swarm, heralded the onset of renewed activity. A second swarm in August 1989 originated only 5 km BSL. No noticeable seismicity occurred subsequently until the beginning of eruptive activity in the SE crater in September 1989 when a further swarm and large individual events, some of magnitude >3.0 to the northwest of the summit craters, occurred. These events may have been linked to the opening of the NE trending fracture that erupted a small amount of magma (Figure 1), while several hundred shallow seismic events over a 2-day period (1–2 October) accompanied the opening of the noneruptive SSE trending fracture (Figure 2). Although the causative mechanism of the seismicity is unclear, a temporal relationship exists between the occurrence of the swarm and the propagation of the fracture beyond the scarp of the Valle del Bove. No definitive evidence for shallow magma beneath this fracture was found (see below). Volcanic tremor throughout the 1989 eruption correlated strongly with eruptive activity; in particular a sharp increase in tremor amplitude always accompanied the change in activity from weak strombolian, to strong strombolian, to lava fountaining, to lava flows.

There was no further noteworthy seismic activity observed from the end of the 1989 eruption until 1 month prior to a small explosive eruption from the NE crater in January 1990. The brief explosive activity in 1990 was associated with a significantly higher amplitude tremor than the 1989 eruptions.

Seismic activity on Etna ceased until January 1991. Earthquake swarms were located along the NNW-SSE trending structure, along which magma later rose to erupt in December 1991. Focal-plane solutions and the hypocentral pattern for these data have led to the suggestion that activation of the intrusion at depth occurred about 2 months before the eruption. The foci of the events became shallow (1–4 km BSL) only 1 week before the eruption began.

3. Ground Deformation

Like other flank events, this eruption appears to have been fed by a near-vertical dike, but in this case there were two dikes radiating from the SE crater. In the first, the magma traveled NE and intersected the surface, erupting lava. In the second, the magma traveled SSE but did not reach the surface though it did cause fracturing. There is evidence for dike intrusion up to 3 km from the summit along the SSE fracture, but the pattern of ground deformation at the distal end of the fracture was characteristic of an elastoplastic medium, and therefore was not linked with magma intrusion.

Precise leveling and triangulation measurements were made before, during, and after the 1991–1993 event. Data from over 300 stations in the summit region of Etna revealed a narrow trough of more than 1 m of subsidence running SSE from the summit, connecting the SE crater with the eruption site, flanked by two zones of inflation up to 37 cm to the east and 7 cm to the west (Figure 3a). This is consistent with a syneruption dike intrusion at a depth of 450 m to its top and 1100 m to its base.

GPS is now widely used; by placing two or more GPS receivers either permanently or for the duration of a survey at locations of interest, the user can obtain *x*, *y*,

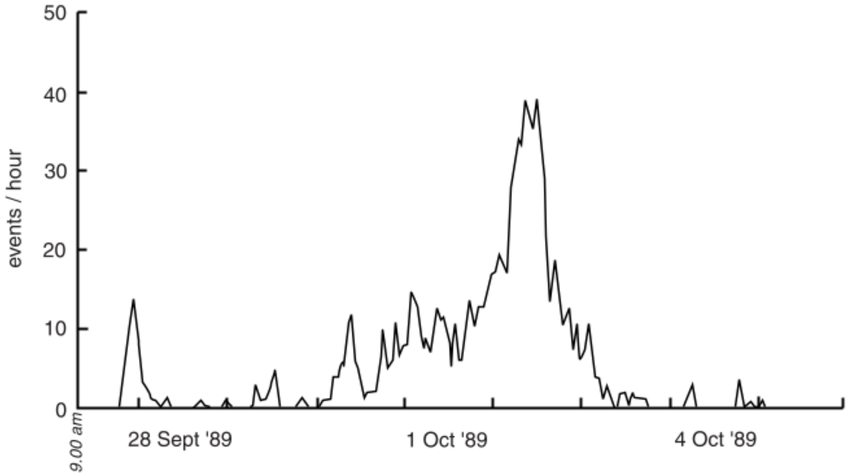

FIGURE 2 Number of seismic events per hour at Mount Etna for late September to early October 1989.

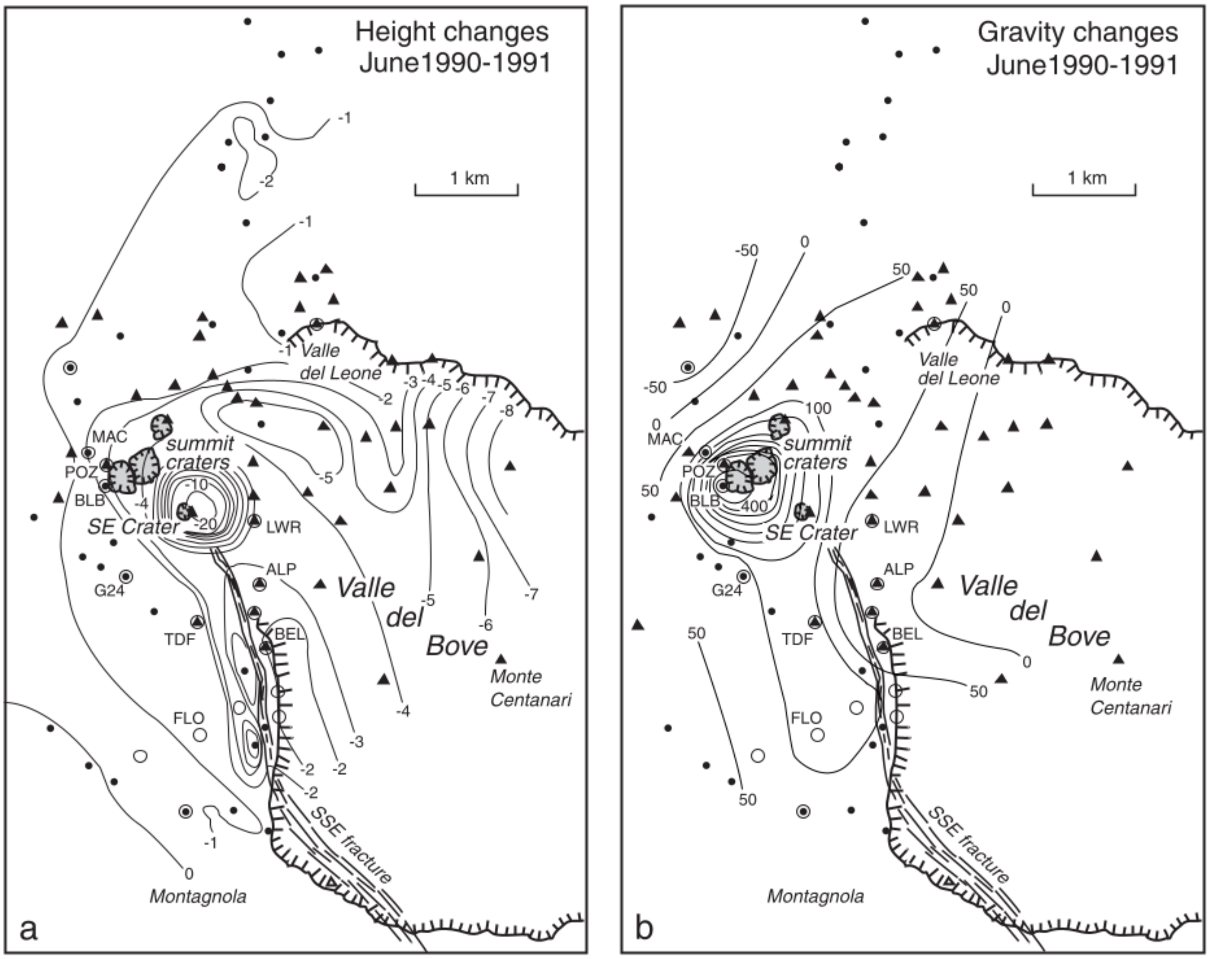
Height changes
June1990-1991
1 km
-1
-2
-1
-1
Valle
del Leone
-2
-3
-4
-5
-6
-7
-8
summit
craters
MAC
POZ
BLB
-4
-10
-20
SE Crater
LWR
-5
ALP
Valle
del
Bove
G24
TDF
BEL
-5
-6
-7
Monte
Centanari
FLO
-4
-3
-2
-2
-2
-1
0
SSE fracture
Montagnola
a
Gravity changes
June1990-1991
1 km
-50
0
50
50
0
-50
0
MAC
100
summit
craters
Valle
del Leone
POZ
50
BLB
400
SE Crater
LWR
ALP
G24
Valle
del
Bove
50
TDF
BEL
0
50
Monte
Centanari
FLO
50
SSE fracture
Montagnola
b

FIGURE 3 Height and gravity changes at Mount Etna from two surveys in June 1990 and June 1991. (a) height changes in cm; (b) gravity changes in milligals. For both, note the stronger gradient (closer contour lines) near the summit craters.

and *z* coordinates for each location with centimeter or even subcentimeter precision horizontally and vertically. Feasibility studies on the possibility of using permanently fixed receivers capable of automatically tracking satellites and recording and transmitting data for automatic processing and storage began on Etna in 1988. Data collected during the 1991–1993 eruption on a network of stations over the summit of the volcano extending down the flanks as far as Catania indicate that contraction of the whole edifice occurred during the first months of 1992. This has been modeled in terms of depressurization within a source (magma storage region) 1.5–3.5 km BSL. The volume of magma erupted during the same period exceeds the volume loss within the modeled region, suggesting this relatively superficial storage region may be linked to a deeper feeder system.

GPS technology has improved dramatically since 1993, and permanent stations have now been established at several key locations on and around the volcanic edifice. In addition, twice yearly campaigns now aim to occupy stations in the summit and flank areas; results have shown consistent radial expansion since 1992, consistent with relaxation of the edifice.

4. *Microgravity*

Etna was one of the first volcanoes to be studied using microgravity; the technique typically involves repeated high-precision surveys in which the relative value of gravity at a number of stations is determined. Repeat microgravity surveys are used to investigate subsurface mass changes. Since their effect is sensitive to variations in the distance from mass anomalies, microgravity data must be corrected for height changes and hence these surveys must always be accompanied by a ground deformation survey.

A microgravity increase (ca. 20 μGal) attributed to a shallow (few hundred meters depth) source was observed across the southernmost end of the SSE trending noneruptive fracture a few days after formation in October 1989. However, neither these data nor data from a network of microgravity stations around the volcano flank at an elevation of 1500–2000 m provided evidence in support of a magma intrusion associated with the fracture process.

The period June 1989–November 1989 was characterized by a gravity increase in the summit region (up to 100 μGal) and was followed by a decrease of similar magnitude between November 1989 and June 1990. These data imply subsurface mass increases of 10^9–10^{10} kg followed by decreases, and are consistent with the eruption of 10^9 kg of pyroclastic material in January 1990. Between June 1990 and June 1991, although there was no surface eruptive activity, there were significant gravity changes (Figure 3b) in the summit area; the changes are too large by an order of magnitude to be caused by the minor deflation observed over the same period. The data have been interpreted in terms of a passive (aseismic) intrusion of magma into the prestressed region beneath the 1989 SSE trending fracture. The intrusion must have occurred some time between June 1990 and June 1991, several months after the formation of the surface fractures and several months before the onset of the 1991–1993 eruption. The intrusion appeared to be in the location of the dike that fed the later eruption (Figure 4). Relative microgravity values remained constant in the vicinity of the fracture zone after the end of the 1991–1993 eruption, but decreased and subsequently increased again by 1994 in the summit crater region. This suggests that intruded magma solidified within the fracture zone, and the magma level within the summit feeder fell and then rose again, which is consistent with the increased summit activity observed since 1994.

5. *Tidal Gravity*

Microgravity data are corrected for the effects of Earth tides (up to ca. 200 μGal peak-to-peak, diurnal) before interpretation. A predicted Earth tide can be calculated for any location which represents the vertical component of gravitational acceleration on a solid, uniform Earth but does not account for variations due to topography, rheological heterogeneities, and ocean loading. Use of the predicted tide is satisfactory for many applications of microgravity (it is good to better than 8 μGal). Currently there are continuously recording tidal gravimeters operating at Serra la Nave (for control) and at the Torre del Filosofo (TDF) near the summit. Clearly, although the spatial resolution of tidal gravity data is very limited compared with that provided by a microgravity survey, the temporal resolution is considerably improved (typically one observation per minute rather than several per year), which allows the rates of processes (such as dike intrusion, magma emplacement/drainage, etc.) to be determined.

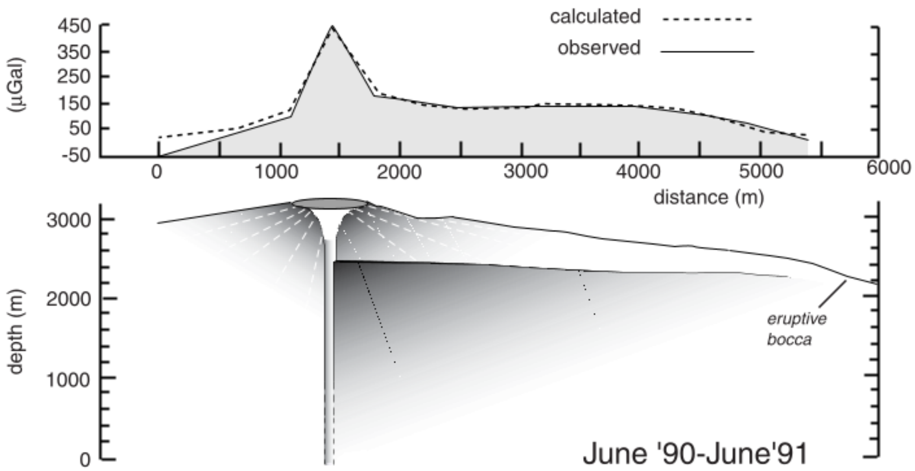

FIGURE 4 (top) Theoretical (dashed line) and observed (solid line) gravity profiles at Mount Etna. The theoretical curve is determined from a model of the distribution of light and dense rocks. (bottom) Model of a dike emplacement at Mount Etna. The dike is shown as the dark gray shaded structure extending to the right from the main conduit.

6. *Self-potential (SP)*

Several electromagnetic techniques have been used to investigate variations in electrical conductivity due to subsurface volcanic structures. SP measurements, for example, made across the lower part of the SSE trending fracture after the end of the 1989 eruption, with an electrode separation of 110 m over a profile length of 1.32 km, showed two large positive anomalies up to about 100 mV in magnitude and several hundred meters in wavelength. These were interpreted in terms of shallow (near-surface) fluid movements in response to magma intrusion. These data therefore suggest that magma was intruded at depth beneath the SSE trending fracture during the 1989 active period although there was no eruption south of the summit. The SP anomaly was attributed to the heating of water in saturated rocks by volcanic gases from the intrusion. Regular SP observations (approximately monthly) between October 1989 and April 1993 showed that the anomaly gradually decreased, which was considered to be consistent with such a heating process.

7. *Gas Geochemistry*

Magmatic intrusions can influence the concentration of soil gases. For a period of several days after the formation of the SSE trending fracture, H_2, CO_2, CO, and ^{222}Rn variations were monitored at the distal end of the fracture in an attempt to determine whether or not a magmatic intrusion was responsible. Continuous CO_2 flux monitoring revealed a dramatic increase from ~500 to 2000 ppm about 1 week after the appearance of the fracture, but the flux returned to normal values after 1 day. Although the ^{222}Rn activity was 5 times higher in the fractured region than in the adjacent unfractured areas, it was not possible to prove a link between the data and degassing of a magmatic body because observations were in the range previously measured in Etnean soil gases.

The 1991 eruption was preceded by a relative decrease in CO_2 flux across the distal part of the SSE trending 1989 fracture, suggesting that as magma rises, degassing preferentially occurs through the main conduits in the summit area. Some rapid fluctuations of soil gas fluxes across the SSE trending 1989 fracture also occurred during the 1991–1993 eruption. These results suggest that soil gas monitoring along the flanks of Etna can be useful for detecting early phases of volcanic unrest, while monitoring of degassing from the summit or fractures can provide early indications of near-surface magmatic intrusion.

8. *SO_2 Flux*

The most widely used non-satellite-based instrument for remote sensing of volcanic plume compositions is the correlation spectrometer (COSPEC). The relative absorption of solar UV light by a volcanic plume is analyzed along with plume width and wind speed to give an estimate of the flux of SO_2 molecules. Relatively low SO_2 flux has been identified previously as a precursor to eruptions on Etna.

A slow increase in SO_2 flux was observed from August 1989, with a transition from a low, 1000 metric tons per day (T day^{-1}) to medium values (7000T day^{-1}) by mid-September. During the second half of September and coinciding with the opening of the eruptive NE trending fissure in the Valle del Leone, SO_2 flux increased to an average of 15,000 T day^{-1} and peaked at 23,000 T day^{-1}. The flux decreased after this time and was at a low of 850 T day^{-1} just 5 weeks before the 1991 eruption began. During the 1991–1993 Etna eruption, COSPEC measurements were taken regularly—sometimes as much as twice weekly. Comparison of data from the summit craters and the SSE trending 1989 fracture during the first few months of the eruption showed an anticorrelation which may indicate that while the magma is degassing significantly from the summit craters, the magma from the fissure is relatively volatile poor and vice versa (Figure 5). It was not often possible to compare the flux from the summit and fissure sites as the plumes were usually quickly mixed by the wind. The average SO_2 flux during the eruption was 5800 T day^{-1}, but in April 1992 it dropped to 980 T day^{-1}—this may have presaged the introduction of new magma to recharge the volcano feeder system.

9. *Remote Sensing*

Fumarole and ground temperature increases have been found to precede volcanic eruptions. Changes in the radiant energy flux, or even the ground temperature of a volcano, can be measured remotely via satellite or airplane and can, in certain circumstances, provide eruption precursor information. Remote sensing is a fast growing field of volcano monitoring as more data and software become readily available. Data from the thematic mapper (TM) carried by the Landsat satellites and the advanced very-high-resolution radiometer (AVHRR) carried by NOAA satellites have been used to test the viability of the technique at Etna.

Airborne TIMS (thermal infrared multispectral scanner) data were collected in the summit and SE flank regions immediately after the cessation of eruptive activity in 1989. The temperature distribution in lava flows

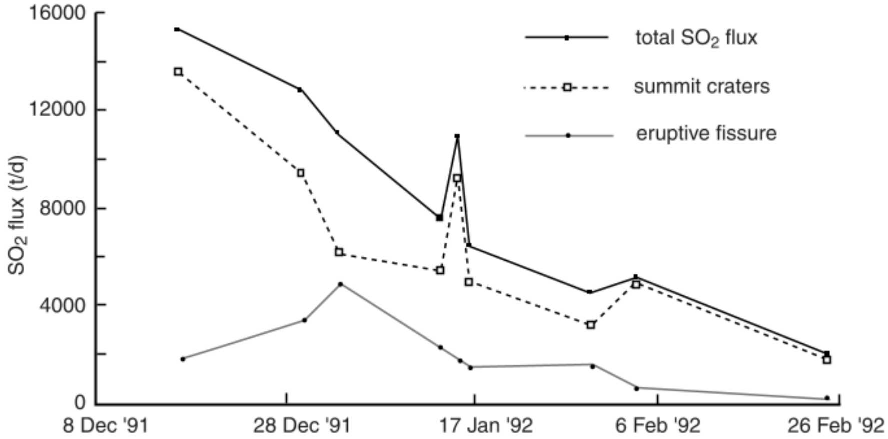

FIGURE 5 Sulfur dioxide (SO_2) flux in tons per day at Mount Etna from 8 December 1991 to 26 February 1992. Measurements were made at the summit craters and near the eruptive fissure. The two were added together to give the total.

identified using this technique agreed well with "ground truth" observations made on the ground, but no thermal anomaly was detected along the SSE trending fracture. This supports the conclusion based on other data that the opening of at least the lower end of this fracture was not driven by the shallow intrusion of a dike. The possibility of real-time volcano monitoring using remote sensing came closer during analysis of the 1991–1993 lava flow field using AVHRR data. Ground truth data and lava flow maps were used to confirm remote sensing estimates of lava flow volume, active lava area, thermal flux, and effusion rates. Although this technique does not have an application for eruption prediction, it could provide frequent information on the progress of an inaccessible lava flow, the sites of secondary breakouts, and assessment of the associated hazards.

10. SAR Interferometry

Synthetic aperture radar satellites illuminate the Earth's surface with microwave radiation and can be used for mapping topography to high precision. Provided that a reliable digital elevation model (DEM) is available, images obtained on ascending and descending orbits of the host satellite can be obtained. Interferograms are obtained by combining two such images and removing the effects of topography. Images for Etna during the waning stages of the 1991–1993 eruption indicated possible volcano-wide deflation. There are concerns, however, about the validity of this model as almost simultaneous ground surveys with GPS did not show the deflation, and there seems to be a strong correlation between apparent elevation change and topography.

B. Soufriere Hills Volcano, Montserrat

1. Introduction

The reactivation of Soufriere Hills volcano, Montserrat, on 18 July 1995 took many people by surprise, including those who lived on the island. Yet there were signs beforehand that the volcano was preparing itself for eruption. Montserrat is part of the Lesser Antilles island arc, formed by the westward subduction of the North American tectonic plate beneath the Carribbean plate. Soufriere Hills is the active volcano on Montserrat, located on the southern part of the island. The volcano consists of a horseshoe-shaped crater which is open to the east. The crater was partly filled with remnants of a lava dome which probably had been emplaced around 1600 A.D. The youngest volcanic rocks are hornblende-bearing andesites.

Periods of seismic activity were recorded in 1933–1937 and 1966–1967; the seismicity was located underneath or near Soufriere Hills volcano. The seismic activity may have indicated shallow movements of magma beneath the volcano, and the activity could be regarded as "abortive eruptions." Increased levels of seismicity were again recorded beginning in 1992, with a significant increase in deep earthquakes in November 1994. The three episodes demonstrate the cyclic nature of the seismic swarms which appear to occur approximately every 30 years. The seismicity may represent intrusion of mafic magma into a holding reservoir at depths of 5–10 km.

No direct precursory activity was noted in the days immediately preceding the beginning of activity on 18 July 1995, although it should be noted that the monitoring equipment only comprised a seismic network. It is possible therefore that certain precursory signals were not recorded or observed.

2. *Early Activity, July 1995 to January 1996*

Initial activity consisted of phreatic explosions and cold base surges. No solid material such as glass shards was observed in the ash to indicate the presence of new magma. Yet SO_2 flux measurements by COSPEC correlation spectrometer showed values of 300 T day^{-1} on average initially, with SO_2 increasing to 800 T day^{-1} in early August 1995 immediately before a seismic swarm. The high levels of SO_2 are clearly indicative of magma residing at shallow levels beneath the volcano, with the seismic swarm implying magma intrusion or ascent. The early activity at Soufriere Hills nicely illustrates the problem of whether a reactivation of a volcano is "magmatic" or "nonmagmatic." The lack of fresh glassy material in the ash does not indicate the presence of magma, while the high SO_2 levels clearly do.

This style of activity continued for approximately 4 months, accompanied by volcanotectonic earthquakes. In late September 1995 a small lava dome was extruded in the crater; the extrusion was immediately preceded by shallow hybrid seismicity. The hybrid seismic events are characterized by a high-frequency beginning and a long-period coda. A lava dome began to be extruded continuously in mid-November 1995, preceded by deformation in the crater area. During this time, the rate of dome extrusion was less than 2 m^3/s, which was low compared to subsequent activity (Figure 6). This slow growth also was reflected by hornblende crystals which had reaction rims, indicative of slow magma ascent at shallow levels where hornblende was unstable and had time to react.

3. *Accelerating Dome Growth, January to July 1996*

The extrusion rate of the dome accelerated to about 2 m^3/s in January 1996 (Figure 6). The first pyroclastic flows from collapse of the dome occurred in late March 1996 and were directed eastward due to the horseshoe-shaped nature of the crater.

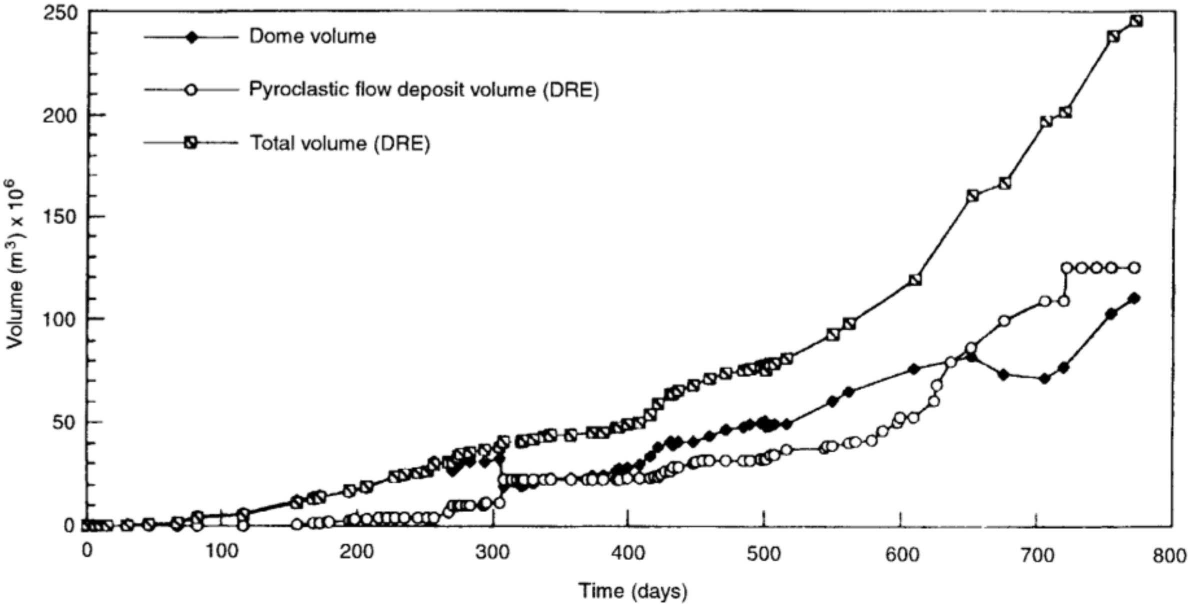

FIGURE 6 Diagram showing cumulative volumes of material erupted from Soufriere Hills volcano since 15 November 1995. Pyroclastic flow deposit and total volumes expressed as dense rock equivalents, dome volume is not. Note the generally accelerating rates with time. [From Sparks, R. S. J., Young, S. R., Barclay, J., Calder, E. S., Cole, P., Darroux, B., Davies, M. A., Druitt, T. H., Harford, C., Herd, R., James, M., Lejeune, A. M., Loughlin, S., Norton, G., Skerrit, G., Stasiuk, M. V., Stevens, N. S., Toothill, J., Wadge, G. and Watts, R. (1998). Magma production and growth of the lava dome of the Soufriere Hills volcano, Montserrat, West Indies: November 1995 to December 1997. *Geophys. Res. Lett.,* **25,** 3421–3424]

The extrusion rate accelerated further in July 1996 to greater than 4 m^3/s (Figure 6). This was a critically important time period for a number of reasons. First, as a result of the increased effusion rate, collapse of the dome occurred both more frequently and on a larger scale, generating larger pyroclastic flows in the process. Second, the magma appeared to rise at a faster rate, as shown by the lack of reaction rims on hornblendes. Third, the magma contained larger quantities of gas, as shown by higher SO_2 fluxes (at times >500 T day^{-1}) and dome rocks with higher vesicularities than previously. The enhanced activity in late July 1996 was characterized by many hybrid seismic events, accompanied by increased levels of long-period seismicity. Cyclic tremor also appeared, termed "banded" by the visual observation of bands of tremor on seismic paper records. The banded tremor was sometimes accompanied by increased degassing or steaming from the dome.

Taken together, the monitoring data suggest that magma rose at an accelerated rate, thereby impeding degassing of the magma during its ascent. As a result, magma which emerged at the surface was more gas-rich. An alternative but related interpretation is that magma in the reservoir became richer in gas at this point. The higher gas contents propelled magma to the surface at an accelerated rate. This second hypothesis implies that the magma reservoir was open to replenishment by gas-rich magma from deeper levels. The two hypotheses may both have validity.

4. High Dome Growth Rates, July 1996 through 1997

The first magmatic explosive eruption began on 17 September 1997, prompted by large collapses of the dome beforehand. The eruption was preceded by increased levels of hybrid and long-period seismicity, which reached their highest levels 5–6 days before the eruption. The seismic data suggest that the interior of the dome was pressurized and richer in gas. When the interior was exposed by the collapses, the explosive eruption ensued. A blast, surges, and pyroclastic flows containing pumice were generated by the explosion. The lack of rims on hornblendes in the pumice suggests that the magma rose quickly to higher levels, being able to retain a significant fraction of its original gas content. The presence of pumice in the pyroclastic flows is direct evidence for high gas contents in the magma prior to the eruption.

High levels of dome growth, magma production, seismicity, and SO_2 flux continued through the end of 1996 and into 1997 (Figure 6). Magma was intruded near the southwest crater wall in late 1996, thereby deforming and destabilizing it. By March 1997, material from the dome overtopped the weakened southwest wall, producing pyroclastic flows to the south for the first time. By June 1997 similar events occurred on the northern and eastern crater walls, also generating pyroclastic flows. The capitol of Plymouth was directly threatened by these events. On 25 June 1997 a large collapse occurred on the northeastern part of the dome, sending pyroclastic flows and accompanying surges in these directions which killed 19 people. Cycles of hybrid seismicity and deformation were observed to occur during this time (Figure 7). The cycles had periods on the order of tens of hours. During an individual cycle, it was observed that the highest level of hybrid seismicity corresponded with the peak of inflation. Immediately afterward, rockfalls and pyroclastic flows were generated, sometimes accompanied by minor vulcanian eruptions. The cyclic behavior was used to forecast likely times when pyroclastic flows would occur. The data suggest a model of repeated pressurization of the dome by rapidly ascending magma and gas release at shallow depths.

In August 1997 a series of vulcanian explosive eruptions occurred which produced pyroclastic flows on all flanks of the volcano. The eruptions were preceded by several days of elevated long-period seismicity. The eruptions were associated with cycles of seismicity and deformation similar to those observed in late June, and the individual hybrid seismic events sometimes merged into continuous tremor. The eruptions occurred immediately after the peaks in hybrid seismicity and inflation, lending credence to the overpressure hypothesis. Vulcanian eruptions also occurred in September 1997, but without hybrid seismic swarms. By 1998, the dome growth had slowed somewhat, although it continued to be active.

5. Summary

Perhaps the two most notable aspects of the Montserrat eruption have been the accelerated dome growth in 1996–1997 and the episodic nature of this growth. The acceleration clearly implies a reservoir of magma which is open to inputs of magma from deeper levels. The episodic growth is interesting and enigmatic, perhaps partially a function of the very viscous andesite magma which may impede continuous magma ascent and dome growth. It is clear that in July 1996 the volcano underwent an important change and enhancement in its activity, possibly as a result of magma intrusion at deep levels. All major collapses of the dome have been preceded by enhanced levels of hybrid seismicity, implying increased internal pressures beforehand. The eruption of 17 September 1996 was preceded by a major collapse event

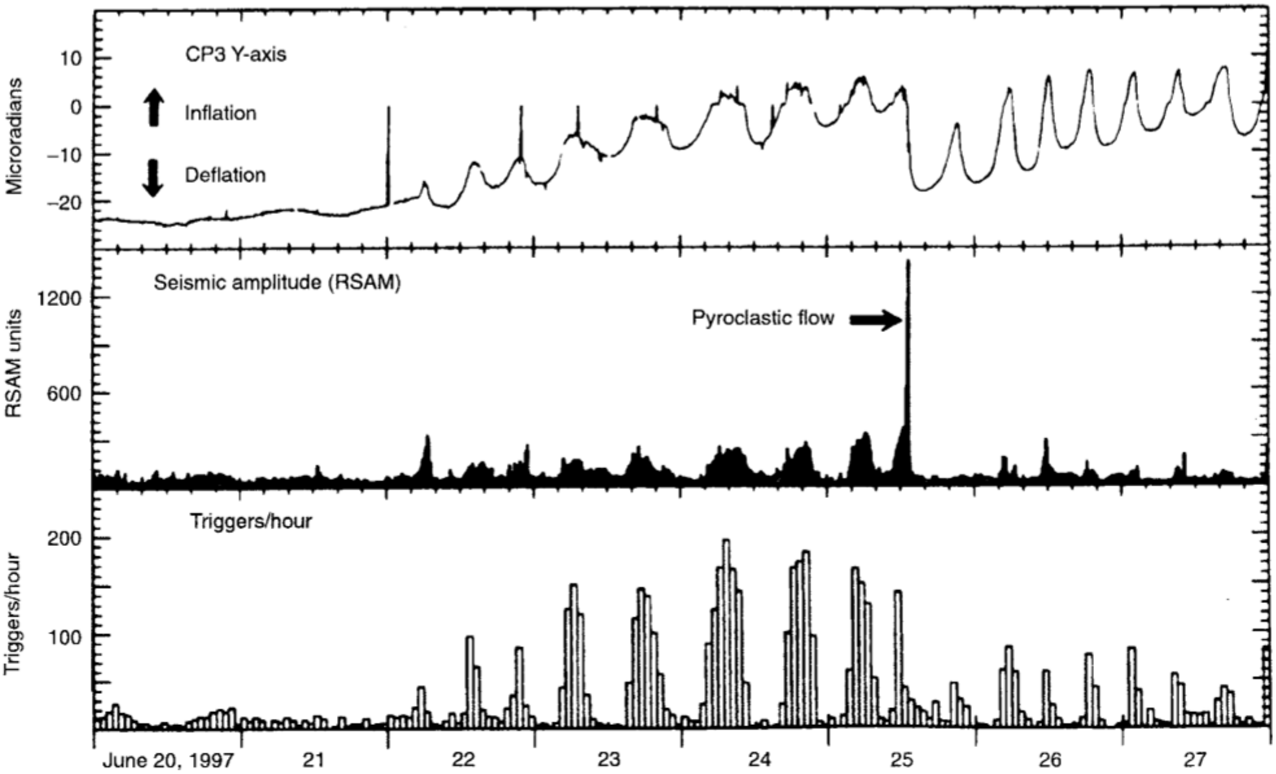

FIGURE 7 Diagram showing cyclic behavior of hybrid seismicity and deformation, 20–27 June 1997, at Soufriere Hills volcano. Note the overall increase in inflation and seismicity before 25 June. The lethal pyroclastic flow on 25 June occurred immediately after the peaks in seismicity and inflation. [From Voight, B., Hoblitt, R. P., Clarke, A. B., Lockhart, A. B., Miller, A. D., Lynch, L. and McMahon, J. (1998). Remarkable cyclic ground deformation monitored in real time on Montserrat and its use in eruption forecasting. *Geophys. Res. Lett.,* **35,** 3405–3408]

which exposed comparatively deep regions of the dome at the surface. Perhaps there is a depth threshold within the dome beyond which explosive eruptions are triggered. The model of internal dome pressure is also supported by the 1997 cycles of hybrid seismicity and deformation.

VII. DISCUSSION

A. Techniques Alone versus in Combination

Most of the monitoring techniques discussed in this article can give ambiguous data or, in worst cases, can give misleading data or even fail to give needed data. For example, earthquake swarms may happen during eruptions or when no eruption is occurring. If a large regional earthquake happens to occur, it will swamp the seismometer for several minutes so that any volcanic signals cannot be seen. Further, instruments are subject to noise and physical damage. Radio and electronic interference can degrade many types of telemetered data, and eruptions themselves, or related phenomena like lightning, can damage or destroy instruments. Therefore it is generally best not to rely on only one instrument or one type of data, but rather to consider data from several different types of instruments simultaneously. This can increase the complexity of a volcano observatory but provides more complete information upon which to base decisions.

As an example, volcanic tremor is a common and fairly reliable precursor to many eruptions. However, there are many incidences of tremor without eruption. If satellite thermal data are available at the same time, then images may be checked for the presence of hot spots or plumes. Coincidence of tremor, hot spots, and plumes would be reasonably compelling evidence that an eruption was occurring, especially if the presence of ash in the plume could be determined. As another example, gravity data alone may indicate that a change has occurred, but gravity data along with precise geodetic data permit the identification of whether water, air, or magma has been intruded (assuming a gravity increase).

The second or later data not only provide additional measurements, but they also provide confirmation that the activity is real or significant. A number of documents such as response plans for volcanic crises require more than one type of data to trigger various alert levels. Typical needed data include earthquakes or tremor, deformation of the ground such as bulges or cracks, and evidence of juvenile gases or heat. These have all occurred together during many well-documented eruptions, so the presence of all of them has a strong likelihood of being real precursors which must be taken seriously.

B. Reliability, False Alarm Rate, and Safety Margin

Many types of data occur over various size ranges, and the small signals are "safe" whereas the larger ones indicate significant hazard. Thus a threshold must be determined which will serve as a guide to judge the appropriate level of concern. Examples would be earthquakes of a certain magnitude or deformation of a certain amount. Once a threshold is agreed upon, however, several issues arise. It is possible to make the threshold too sensitive: this means the dangerous signals will definitely be registered, but with a very high false alarm rate. Alternatively, the threshold may be set too high: this will keep the false alarm rate low, but may miss the onset of dangerous activity. A few minutes extra warning time may not seem like a lot, but could be significant for a commercial jetliner traveling at 8 miles per minute. The ideal threshold minimizes the false alarm rate while providing the earliest warning. Thus it gives the highest reliability and safety margin. Appropriate threshold estimates may be made in advance of eruptions, but then need to be fine tuned as the activity evolves, because physical changes may occur at the volcano.

C. Intrusions versus Eruptions

One of the main large-scale problems of monitoring volcanoes is that many of the signals regarded as precursors, such as earthquakes and deformation, occur before both eruptions and intrusions. The reason the signals look the same is that the processes are the same at depth, differing only in whether or not the magma reaches the Earth's surface. Thus not every geophysical event is regarded as a precursor; they often simply drive an additional inquiry or checking of other data.

Calderas are notorious for having high levels of unrest, so there are lots of potential precursors. For example, Long Valley caldera in eastern California has experienced more than 25 earthquakes of $M = 5$ or larger, uplift of 60 cm, degassing of CO_2, long-period earthquakes, local deformation, and increased heating, all in the last 19 years. No eruption has occurred, but it is thought that several intrusions of magma to depths of about 5 km have occurred. Thus, it is clear that intrusions do not always result in eruptions; the challenge is to decide if an intrusion will progress to an eruption or not.

VIII. VOLCANO MONITORING IN THE FUTURE

While monitoring solely for the purpose of risk mitigation may reduce loss of life or property to a degree, its effectiveness can be greatly improved through the concurrent development of scientific methods and enhanced understanding of volcanic processes. Given the average interval between eruptions at many volcanoes, volcano monitoring tends not to be a high spending priority of governments, yet major volcanic eruptions can be national (and international) social and economic disasters.

Future developments in volcanic monitoring will depend on many factors including technological advances, improvements in analytical and interpretation methods, the ability to successfully integrate multiple data sets, and having detailed knowledge of volcanic structure and processes. The continued development of robust, inexpensive, and effective technologies for monitoring volcanoes is a vital and sometimes urgent requirement for volcano-affected countries. Advances in electronics in recent decades have helped progress toward cheap expendable sensors, thus reducing the inherent financial risk of losing expensive monitoring equipment and greatly benefiting the monitoring of volcanoes in developing countries. The World Wide Web has added a new standard for communication and it is now routine at some volcano observatories to run analyses tasks automatically and to post the results on web pages. These can then be checked on demand by anyone with a computer and modem. The web protocols have made it no longer necessary for each observatory to develop its own unique way of handling data.

The importance of a good knowledge of the geological and volcanic history and the nature of background activity at each particular volcano cannot be overemphasized; if what is "normal" is not known then the "abnormal" cannot readily be recognized. Again we appeal to a medical analogy: we know that a person's normal temperature is 98.6°F, so this provides the basis for identifying a fever. Most of the world's potentially active volcanoes, however, are not currently monitored. Furthermore, since no reliable laws of forecasting can be determined from the data collected by volcanologists to date, multiple integrated monitoring methods are needed at each volcano.

Monitoring techniques were, of course, originally based on the most easily measured phenomena; other phenomena were either not measured, or filtered from the signal as noise. The recording and analyses of these more subtle or complex effects using a variety of methods are the future of volcano monitoring. For example, it is now recognized that three-component and broadband seismometers provide vital information on shallow magmatic processes and should be incorporated into any volcano-seismological network. In the case of microgravity monitoring, the effects of the Earth tides are subtracted from the data before analysis and modeling. Advances in technology and analytical methods, however, will allow modeling of the response of both the volcanic edifice and the plumbing system to tidal effects, from which further insight could be gained into eruption precursors and processes at depth.

Traditionally, most types of data (e.g., for gravity or ground deformation) have been recorded periodically at a number of stations. Data collection in such cases is labor intensive, time consuming, and hence expensive and only provides "snapshots" of the real picture. Ideally, continuously recorded data at numerous stations should be telemetered to an observatory at which initial analysis could take place automatically, in real time, as has been achieved at some seismic networks. Recent advances in telemetry make such systems more viable, and once established would be less labor intensive and, in times of eruption, safer.

GPS and SAR have the potential to revolutionize ground deformation studies given the large areas that can be covered simultaneously. Since these methods give information of broad-scale changes they would be particularly effective in determining the significant edifice-wide inflation that might be expected to precede a dramatic change in eruptive style. COSPEC data are likely to become more reliable and consistent as more instrumentation becomes available and data collection becomes automated. Other promising techniques for remotely investigating volcanic gases, for example, GASPEC, which measures CO_2 flux, and Fourier transform infrared (FTIR) spectroscopy, which measures the ratio of various gas species, are currently being developed. For example, variations in the $SO_2:HCL$ and $HCl:SO_2:SiF_4$ ratios have been measured using FTIR. Multispectral infrared instruments to be carried by the first Earth Observing System satellite, due for launch in 1999, will greatly expand the capabilities and accessibility of spaceborne remote sensing for both thermal and gas studies.

Potential developments in analysis and interpretation include improvements to automatic detection and processing (ADP) of seismic data such that the large volume of data generated by an intense seismic swarm can be processed and that real events can be more reliably distinguished from noise. The effectiveness of ADP depends on the density and geometry of the array compared with the extent and depth of the active zones; data from the 1989 and 1991–1993 events on Etna suggest an array density of one seismometer per km^2 is required to resolve events associated with shallow magmatic intrusion. The Integrated Mobile Volcano Monitoring System developed by the USGS for use in volcanic crises was used to very good effect in the 1991 Pinatubo eruption; however, portable seismometers do not constitute an adequate alternative to permanent recording stations. While they provide satisfactory monitoring during volcanic events, they have no role in background surveillance or in recording the onset of seismic activity. Advances in interpretation will require more detailed knowledge of the structural complexities and heterogeneities typical of volcanoes in order to develop adequate models. Recent advances in nonlinear, high-resolution three-dimensional seismic tomography, for example, may allow the detailed interpretation of broadband seismic data. Such broadband data with a period greater than a few seconds are considered to be associated with mass transport and are currently the subject of much research into their causative mechanisms.

Although seismology will remain the most important monitoring tool for the foreseeable future, the integration of seismic data with results from other methods, for example, geodesy, gravity, electrical, and gas and temperature flux, will be far more powerful. "Smart" systems using artificial neural networks (ANNs) are now being developed to integrate the vast quantities of data resulting from technological developments to produce the simplest best-fitting models consistent with as much of the data as possible. Such systems, however, are only as good as the input data, and hence the need for detailed structural models and background information. Important questions in contemporary volcanology include, what are the processes that trigger eruptions? Can the timing and location of an eruption be predicted? Is it possible to determine in advance the nature of an eruption and its likely duration? These issues present pressing problems both to basic science and to affected societies; they are being studied at several active volcanoes using a combination of geophysical and geochemical techniques.

The priority now in volcanic monitoring is the acquisition of more data and the development of rapid and reliable methods to collate, analyze, and interpret them. We do have some basic understanding of the mechanisms and processes operating within some volcanoes but we now need to expand this knowledge by integrating the experience gained from decades of independent researches. As well as technological and scientific advances, effective communication and interaction between volcanologists, civil authorities, and the affected populace are required to improve the mitigation of volcanic disasters.

SEE ALSO THE FOLLOWING ARTICLES

Gas, Plume, and Thermal Monitoring • Ground Deformation, Gravity, and Magnetics • Seismic Monitoring • Volcanic Gases • Volcanoes and Tourism • Volcano Warnings

---

FURTHER READING

Aramaki, S., Barberi, F., Casadevall, T., and McNutt, S. (1994). Report of the IAVCEI Sub-committee for Reviewing the Safety of Volcanologists, Bull. Volcanol., v. 56, no. 2, p. 151–154.

Chester, D. K., Duncan, A. M., Guest, J. E., and Kilburn, C. R. J. (1985). "Mount Etna: The Anatomy of a Volcano." Stanford Univ. Press, Stanford, CA., 404 p.

Eruption of the Soufriere Hills Volcano, Montserrat, Part 2, Special section, 1998. *Geophys. Res. Lett.*, **25,** 3651–3700.

Ewart, J. W., and Swanson, D. A. (Eds.) (1992). Monitoring volcanoes: Techniques and strategies used by the staff of the Cascades Volcano Observatory, 1980–1990. *U.S. Geol. Survey Bull. 1966*, 223 p.

McGuire, B., Kilburn, C. R. J., and Murray, J. (Eds.) (1995). "Monitoring Active Volcanoes." UCL Press, London, 421 p.

McNutt, S. R. (1996). Seismic monitoring of volcanoes: A review of the state-of-the-art and recent trends. *In* (R. Scarpa and R. Tilling, eds.) "Monitoring and Mitigation of Volcano Hazards" Chapter 3. Springer-Verlag, Berlin, 99–146.

Rymer, H. (1996). Microgravity monitoring. *In* (R. Scarpa and R. Tilling, eds.) "Monitoring and Mitigation of Volcano Hazards" Chapter 5. Springer-Verlag, Berlin, p. 169–197.

Scarpa, R., and Tilling, R. I. (Eds.) (1996). "Monitoring and Mitigation of Volcano Hazards." Springer-Verlag, Berlin Heidelberg, 841 p.

Sparks, R. S. J., Young, S. R., Barclay, J., Calder, E. S., Cole, P., Darroux, B., Davies, M. A., Druitt, T. H., Harford, C., Herd, R., James, M., Lejeune, A. M., Loughlin, S., Norton, G., Skerrit, G., Stasiuk, M. V., Stevens, N. S., Toothill, J., Wadge, G., and Watts, R. (1998). Magma production and growth of the lava dome of the Soufriere Hills volcano, Montserrat, West Indies: November 1995 to December 1997. *Geophys. Res. Lett.*, **25,** 3421–3424.

Voight, B., Hoblitt, R. P., Clarke, A. B., Lockhart, A. B., Miller, A. D., Lynch, L., and McMahon, J. (1998). Remarkable cyclic ground deformation monitored in real time on Montserrat and its use in eruption forecasting. *Geophys. Res. Lett.*, **25,** 3405–3408.

This Page Intentionally Left Blank

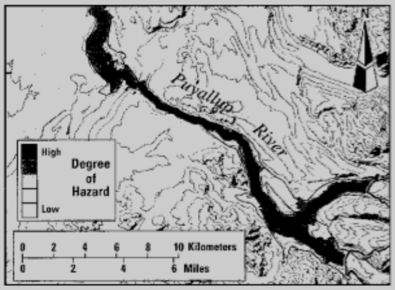

VOLCANO WARNINGS

Christopher G. Newhall
U.S. Geological Survey and University of Washington

I. The Basis and Content of Volcano Warnings
II. The Form of Volcano Warnings
III. Dissemination of Volcano Warnings
IV. Case Histories

GLOSSARY

acceptable risk Risk that an individual or community is willing to accept, or that a public official is prepared to allow persons in his or her charge to accept. Acceptable risk is a function of the benefits of risk mitigation (safety and avoided losses) and its costs (losses of jobs and business, community disruption, the costs of transportation, housing, and food for evacuees, and costs of any structures to divert hazards). Tolerance for risk varies considerably, mainly because the benefits and costs of mitigating risks vary greatly from individual to individual and community to community.

intermediate-range Pertaining to the coming months and, occasionally, years. Intermediate-range forecasts are typically issued when a volcano is restless (or even erupting) but an eruption (or sharp change in an ongoing eruption) is not thought to be imminent.

long-range Pertaining to the coming years, decades, or longer. For most long-range hazard forecasts, also called "hazard assessments," the volcano in question is dormant and any seismic, ground deformation, or fumarolic activity is at background levels.

short-range Pertaining to coming hours, days, and weeks. Short-range or "immediate" forecasts or warnings are issued when unrest (or an eruption) is escalating sharply, or a hazardous eruption has just begun.

volcanic hazards Potentially damaging eruptive and post-eruptive phenomena such as pyroclastic flows, wind-borne ash, lava flows, volcanic gases, lahars, and large landslides. In probabilistic assessments, "hazards" are the probabilities of such phenomena.

volcanic risks The adverse effects of volcanic hazards, and the product of (*volcanic hazard* × *vulnerability* to those hazards × *value* of what is at risk). In probabilistic assessments, "risk" means the probability or likely magnitude of loss, calculated by the same formula.

MOST VOLCANIC ERUPTIONS leave deposits that allow reconstruction of eruptive histories and generalized projection of future activity. On shorter timescales, most eruptions develop over periods of hours to decades, announcing progress at every step. Most pre-eruption unrest and eruptions are driven by exsolution and expansion of a volatile phase, and associ-

Copyright © 2000 by Academic Press
All rights of reproduction in any form reserved.

ated failure of confining rock, both of which can be detected by geochemical and geophysical monitoring.

Officials and citizens can take precautionary actions on the same timescales. Thus, warnings of future eruptions or the further course of ongoing eruptions can avert many potential losses from volcanic hazards, including most loss of life and some economic and social losses.

To succeed, a warning must be:

1. *Accurate.* Accurate about the "what, when, and where" of volcanic hazards.
2. *Understandable.* In plain, nontechnical language, supplemented, if possible, by video or other images.
3. *Timely.* Early enough for recipients to take needed precautions.
4. *Widely disseminated.* Reaching all who need to hear it, for either individual or official decisions about mitigation.
5. *Credible.* From a trusted source or based on ample data and clear logic, and presented with enough certainty that it can be used for mitigation decisions.
6. *Catalytic.* With clear suggestions about what recipients can do to avoid the threat, and convincing reasons why these actions are preferable to inaction.

I. THE BASIS AND CONTENT OF VOLCANO WARNINGS

A. Pre-eruption Warnings

Three types of pre-eruption warnings are long-range forecasts and hazard maps; intermediate-range forecasts; and short-range forecasts. Each requires different data as input and different strategies for dissemination.

1. *Long-range forecasts and hazard maps.* For most volcanoes, the first warnings will be an assessment of the long-range likelihood of eruptions and a map of the areas that are subject to various eruptive impacts, for example, to lava flows, pyroclastic flows, eruption-induced mudflows, or ashfall >10 cm thick (Figure 1). Such assessments typically rely on the geologic or recorded history of eruptions at the volcano in question, estimation of the recurrence frequencies of various sizes and severity of eruptions, and the areas that have been affected by each type and scale of eruption. Some long-range forecasts are without memory of the previous eruption and assume a Poisson distribution of eruption years and magnitudes. Other forecasts "remember" the year and magnitude of the previous eruption, especially if the volcano in question exhibits a pattern of regularly spaced (time-predictable) eruptions, or eruptions whose magnitudes are proportional to the length of the preceding repose (volume-predictable). Long-range forecasts also consider any tendency for eruptions to occur in clusters or to show cycles of eruptive behavior. Long-range forecasts and hazard maps are needed for land-use planning and for development of emergency plans.

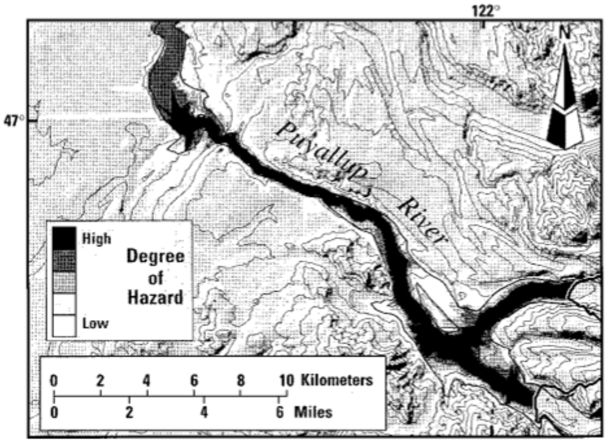

FIGURE 1 GIS-based hazard map, in this case for lahar hazard in the Puyallup River, northwest of Mount Rainier. Pre-existing lahar hazard boundaries (heavy lines along the valley walls) bracket deposits of prehistoric lahars. Grayscale "degree of hazard" is based on empirical equations that predict lahar inundation as a function of local topography (DEM) and lahar volume. The two match each other closely in this reach of the river. Gray area outboard of the white zone is not subject to lahar hazard. Modified from Iverson et al. (1998) by L. Faust.

2. *Intermediate-range forecasts.* Whenever unrest begins that might lead to an eruption within weeks to months, volcanologists may issue a warning such as, "The volcano is restless and might erupt within weeks to months, and needs to be watched closely." At such an early stage of unrest, it is usually impossible to forecast the exact day or week of an eruption, or even whether an eruption will occur at all. Such forecasts help scientists and public officials to increase surveillance of the volcano, to review their emergency plans, and to renew public education about volcanic hazards.

3. *Short-range forecasts.* When a restless volcano gives a strong signal that it will erupt within hours to days, urgent short-range warnings are issued. Such warnings will be as specific as possible, including probable vent(s), areas subject to each hazard, and the estimated date, time, and likely ranges of type and magnitude of the impending eruption. A progression of increasingly spe-

cific and urgent warnings is sometimes issued as the signals and details of an impending eruption become clearer, and as uncertainties decrease. Short-range, "immediate" forecasts are often used to trigger evacuations, 24-hour watches, and other intensive mitigation measures.

B. Syneruption Warnings

Though a forecast made during an eruption might seem too late, two important types of forecasts are needed after an eruption has begun: immediate forecasts of travel directions, arrival times, and intensity of various hazards, and intermediate-range forecasts of the further course and duration of an eruption.

1. *Forecasts of travel directions, arrival times, and intensity of various hazards.* All volcanic hazards require time to reach point(s) at risk. Real-time detection and tracking of slower-moving hazards allows messages to be sent to those at risk, while there is still time to flee, find shelter, or take other mitigation measures. For example, likely areas and times of volcanic ashfall from an explosive eruption can be forecast from wind data and from radar tracking of the ash cloud. The thickness and grain-size distribution of that fall can be projected from wind data and from the intensity and duration of the eruption. Eruption intensity, in turn, can be judged from the energy of volcanic tremor and from estimation of eruption column height.

2. *Intermediate-range forecasts of the further course and duration of an eruption.* Unlike earthquakes, hurricanes, and most other natural hazards, volcanic eruptions may continue for weeks, months, or even years. During this period, the eruptions may change in character or intensity. Some forecasts of the evolution of an eruption will rely on the course of past eruptions of this volcano; other forecasts may rely more on interpretation of current unrest (for example, of seismicity that is accompanying the eruption). Ideally, forecasts will combine both past history and interpretations of current unrest.

C. Posteruption Warnings

All eruptions, and especially explosive ones, disturb watersheds around the volcano. Vegetation is killed or buried, and infiltration of rainfall into the soil is sharply reduced when fine ash covers the surface. Rainfall can trigger flash floods, lahars, and massive sedimentation in and around the rivers of surrounding lowlands. Short-, intermediate-, and long-range warnings can be issued.

1. *Short-range warnings of lahars.* Dangerous lahars can continue for years after a large explosive eruption. If the lahars are triggered by intense rainfall, warnings can state that rainfall has exceeded a threshold known to trigger lahars. Warnings can also state that a lahar of measured stage ("magnitude") and velocity has been observed at an upstream point and will soon reach downstream points. Generally, these warnings will be specific for a particular river or set of rivers, and will complement a long-range lahar hazard map such as described in the next paragraph.

2. *Intermediate- and long-range estimates of sediment yield, channel shifts, and related flood hazard.* Annual rates of sediment yield and the number of years over which sediment is flushed from fresh pyroclastic deposits into the surrounding lowlands will vary with the nature and magnitude of watershed disturbance, climate, and topography. Although understanding of exactly how each of these factors controls the rates and locus of sedimentation is still evolving, some useful approximations can be made shortly after an eruption and refined as the sedimentation event and watershed recovery proceed. Because the volcanic sediment chokes existing channels, flooding occurs frequently and lahars can spread across alluvial fans. Lahar and flood hazard maps consider topography and expected sediment delivery to identify areas of likely inundation.

D. Warnings of Risk (All Timeframes)

Warnings of hazards can be converted to warnings of risk by telling people what effects to expect on health, homes, other structures, crops, and the myriad of complex systems (for example, telecommunications, transportation, water, and power) of modern society. Some volcano warnings correctly anticipate the natural events but fail to explain how these events will affect people and their surroundings; as a result, official and citizens' responses to warnings are delayed or inappropriate.

II. THE FORM OF VOLCANO WARNINGS

In order to be useful, a warning of volcanic hazard must not only contain accurate information, but it must also be in a form that gets the attention and is easily understood by those who must make mitigation decisions, either personal or official. Some forms for volcano warnings follow.

A. Factual Statements

Factual statements describe past and present activity of a volcano and make no extrapolation to the future. Factual statements are useful before any forecast can be made.

B. Forecasts of a Specified Outcome within a Specified Time Window

To provide the basic "what and when" of volcanic hazards, one of the most common types of warnings describes either a single event or a scenario and indicates a "window" of time within which that event or scenario is expected. A warning of this form might refer to the volcano as a whole, for example, stating that a moderate-size explosive eruption is expected within the next week. Alternatively, it might apply to a specific place, for example, stating that a lahar is expected to arrive at town X within Y hours. Sometimes, especially for eruption forecasts, a qualification like, "If current trends continue, then … ," is added, because the behavior of a volcano can always change. The time windows for eruptive events may "open" at the time the forecast is issued, or at some later date; the length of the window will be proportional to uncertainty about when the events will begin. In principle, as an eruption approaches, successive forecasts can define shorter windows, such as "within a month," then "within a week," and finally "within a day" (Figure 2). In practice, opportunities to be precise

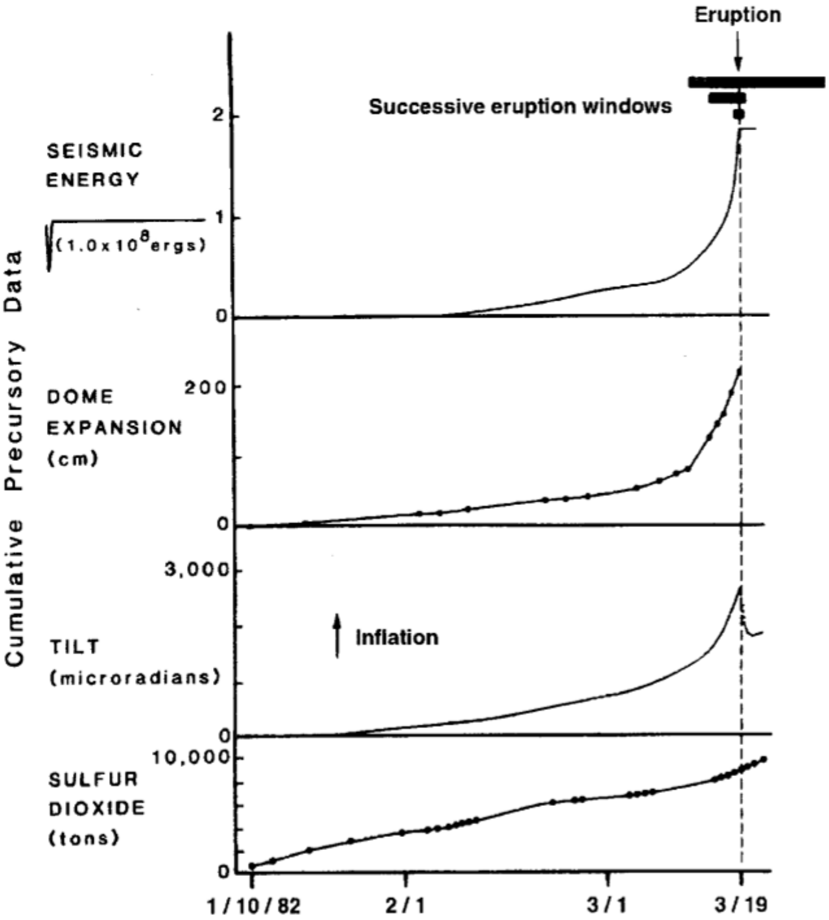

FIGURE 2 Escalating unrest and forecast windows for a small explosive eruption that occurred at Mount St. Helens on March 19, 1982. Solid bars show the "time windows" of three successive forecasts, each getting shorter as unrest escalated and the eruption drew nearer. [From Brantley and Topinka (1984).]

to the nearest day are still rare. When events such as downslope flow of a lahar or lava or downwind transport of volcanic ash are in progress, and current position and velocity are known, arrival times of such phenomena at specified locations can be projected.

C. Probabilities of Several Possible Outcomes

A common situation of volcanic crises is that scientists know that an eruption is likely, but do not know what type or size of eruption will occur. The eruptive history of that volcano might include a wide range of possibilities, or monitoring data for the current unrest might be ambiguous. In such cases, an alternative to forecasts of specific phenomena within specific time windows is a probability tree of all possible outcomes, ranging from no eruption to the worst-case eruption. A time frame must be specified, perhaps days or perhaps decades, depending on immediacy of the threat. In the 1970s, probability trees were used to assess volcanic hazard near proposed nuclear power plant sites. More recently, probability trees have proven useful in volcanic crises because they (a) recognize natural variability and stochastic elements of volcanic phenomena, and uncertainties of interpretation; (b) educate those at risk about the full range of possible events, without oversimplification; and (c) show users the most likely scenarios, together with a semiquantitative basis for comparison with more familiar, nonvolcanic risks. Probabilities also help to avoid confusion between unquantified adjectives such as "low, medium, or high." The latter can mean different things to different people. Unfortunately, probabilities can also be confusing to those who are unaccustomed to their use. An interesting and promising experiment is in progress on Montserrat, in which expert elicitation estimates the probabilities of various scenarios and associated uncertainties.

D. Alert Levels

Often, it is useful for volcanologists to simplify their interpretations of unrest into a numerical, letter, or color code of alert levels. Regardless of whether numbers, letters, or colors are used, the basic concept is to define a small number of states of the volcano, from background rest to the highest level of unrest (usually, vigorous eruption). Most schemes have six or fewer categories. A scheme could be strictly factual—for example, stating only the physical state of the volcano without an explicit forecast. Categories might be defined by rates of seismic energy release, ground deformation, and gas release, or by the nature of an eruption in progress. Looking forward, a scheme can indicate what is expected within a specified time window. One of the most useful aspects of alert levels, in addition to their simplicity, is that users understand that alert levels will be raised or lowered whenever the activity of the volcano warrants. To maintain their credibility, scientists must be equally willing to raise or lower alerts.

In some countries, civil defense plans are keyed directly to alert levels. For example, a plan might tell officials to evacuate a particular zone around a volcano if the alert level is raised to a specified level. This is a clear and appropriate use of alert levels, provided that (a) scientific decisions about alert levels are not dictated by political concerns about mitigation measures, and (b) the alert levels are simply a guide, not a rigid requirement, for mitigation decisions. Unfortunately, in the decade or so that alert levels have been in popular use, examples have arisen of public officials trying to influence scientists' judgments about the activity of the volcano, and of unnecessarily rigid reactions to alert levels. Scientific and political judgments are better kept separated, and decisions about mitigation measures should remain political decisions that include factors such as community sentiment, economic risk, and acceptable risk.

D. Hazard and Risk Maps

Maps are a convenient way to show the areal distribution of hazard and risk. One zone on a map might show areas subject to pyroclastic flows, another might show areas subject to lahars, and so on. Some maps also show areas that have statistically high likelihoods of tephra fall. However, examples of statistically unlikely falls at Mount St. Helens, Pinatubo, and several other volcanoes caution that the hazards of tephra fall are better shown by a sample plume and wind rose diagrams for each season. Increasing use of numerical models, digital elevation models, and geographic information systems (GIS) are enabling production of the next generation of hazard maps, in which various data layers can be compared to likely areas and travel distances of various hazards (Figure 1).

From maps, easy, visual comparisons can be made between hazards or risks in various sectors, or at various distances around a volcano, or at various elevations above a valley floor. Some maps show different levels of hazard or risk expressed in adjectives such as low, medium, or high. If desired, the same hazards and risks can be expressed in terms of probabilities—with the advantages and disadvantages of probabilities noted above.

Although maps are everyday tools for volcanologists, they are too abstract and difficult for many users of volcano warnings. If users are embarrassed to admit map-reading difficulty, and if scientists are oblivious to it, information is not communicated and misunderstandings become likely. Three-dimensional perspective drawings are less abstract and easier to understand, and can be used to show virtually the same information. GIS technology allows 3D drawings to be made from any perspective.

Traditionally, hazard maps have been used to show long-range hazard assessments but, with improvements in computer technology, it has become technically easier to prepare updates for intermediate- and short-range warnings. One of the first uses of short-range warnings in map form is the projected trajectory of wind-borne ash from an explosive eruption. These maps can be transmitted to the cockpits of aircraft so that pilots can avoid the high risk from encounters with ash clouds. Another potential use is for short-range revisions of lahar hazard, if community responses could be fast enough to take advantage of such revisions.

Just as alert levels can be raised or lowered according to the unrest of the volcano, the boundaries of zones of hazard and risk can also be moved away from or closer to the volcano as the level of unrest or understanding of the hazard changes. Expandable or shrinkable zone boundaries make sense in principle, but require a substantial level of public education to avoid confusion.

If risks are quantified and used to define evacuation zones, public officials and their constituents should discuss acceptable risk. To seek zero risk is unrealistic because it automatically requires total evacuation of the entire region of a volcano. Sensible mitigation decisions will seek to minimize risk and, at the same time, to minimize unnecessary disruption of communities. Some trade-offs between the two are inescapable and public acknowledgment of this fact will make dialogue and decisions easier.

E. Video and Other Educational Materials

Tragic experience at Nevado del Ruiz (Colombia) in 1985 demanded that volcanologists find more effective ways to teach about volcanic hazards. Video is one such way. The International Association of Volcanology and Chemistry of the Earth's Interior (IAVCEI), through the late Maurice Krafft and the USGS's Steve Brantley, prepared two videos for this purpose. "Understanding Volcanic Hazards" shows graphic footage of each major volcanic hazard, how fast and far it travels, and what it does to people and structures; a companion video, "Reducing Volcanic Risk," is a primer for public officials and citizens on how volcanic risks can be mitigated. As of this writing, a third IAVCEI video that would show engineering options for volcanic hazard mitigation is under discussion.

A variety of other educational materials have also been prepared in various countries—leaflets, colorful posters, comic books, and Web sites are all in use. No definitive study has yet been made of the effectiveness of these various materials, but we know anecdotally that all of them have been effective for different segments of populations at risk. The first IAVCEI video was especially effective before the eruption of Mount Pinatubo in 1991—a place where no eruption had occurred in people's memory. Web sites have been effective for "wired," computer-equipped segments of populations around Ruapehu (New Zealand, 1995), Popocatépetl (Mexico, ongoing), Soufriere Hills (Montserrat, ongoing), and Long Valley caldera (USA, ongoing).

Hazard and risk maps, and videos, will become increasingly available on the Internet, and opportunities will soon arise for public officials and citizens to pose interactive "what if" queries to Web- or compact-disk-based hazard estimation programs.

Volcano education needs to discuss the uncertainty of forecasts and the problem of false alarms. The difficulty has its roots in a more general problem of science education, in which students are often taught scientific facts but not taught about hypotheses and uncertainties. Scientists are therefore expected to know simple truths, such as whether or when a volcano will erupt, and many citizens do not understand that there are inevitable uncertainties in forecasts of complex systems. A corollary of uncertainties is that there will be false alarms. The frequency of false alarms will depend upon how well the volcanic system is understood, the specificity or vagueness of forecasts, and societal and scientists' own tolerance for risk. For obvious reasons, improved understanding of the volcano will result in fewer false alarms. So, too, will keeping forecasts relatively general, though there is no sense in making forecasts so general that they lose their utility. High tolerance for risk gives scientists some extra time to study the volcano and to be relatively sure about their forecasts, and thus to lower the chances of false alarm; conversely, low tolerance for risk pushes scientists to issue forecasts before their data are conclusive, thereby raising the chance for false alarms.

III. DISSEMINATION OF VOLCANO WARNINGS

Volcano warnings need adequate dissemination before they will be useful. Sometimes, scientists need only to convey their warning to a civil defense office and that office will pass the warning onward. More often, scientists need to remain involved in the process, partly to answer any questions that arise, and partly to learn what information and formats are most useful for users. In a few instances, scientists are left to handle dissemination entirely by themselves; this is far from ideal, because it erodes much needed time for field work and analysis, and because many scientists find it difficult to step outside their specialized technical world to communicate effectively with nonscientists. Some of the means for conveying volcano warnings follow.

A. Briefings, Community Meetings, and One-on-One Meetings

The best way for scientists to convey the general nature of volcanic hazards is in person at briefings of government and nongovernmental organization (NGO) officials, community meetings, and the like. It is important for scientists to build recognition and credibility among those who will receive warnings. Careful attention to developing credibility and personal rapport with officials and those at risk—before or early in a crisis—will make later dissemination of warnings easier and more effective. Personal contacts also tell scientists what the recipients of their warnings need to know. Meetings that are organized by a crisis center are also a good way of ensuring that all participants receive the same message and have a chance to hear each other's questions and answers. Information presented at such meetings becomes the background for subsequent, urgent warnings. Field and lab tours are also helpful, so that officials see the data gathering and analyses that form the basis of scientific warnings.

B. Concise, Formal Notification

Formal procedures generally use telephone "call-down" lists, faxes, specially tagged e-mail, and notices via dedicated warning networks such as those operated by civil defense, law enforcement, and aviation safety authorities. Messages over these channels are typically short, concisely worded, and serve as the legal documentation of warnings. Both providers and recipients of formal warnings commit to 24-hour-per-day, 7-day-per-week operation. Dissemination is generally completed within tens of minutes and prioritized so that the most urgent contacts are made within minutes of a warning being issued. Partial automation of warning dissemination speeds the process. Additional details can be offered by regular e-mail or on Web sites soon after an initial notification. Short, urgent messages sent by these channels presume that recipients already understand the general nature of the hazard, from prior education and briefings.

C. Public Information through News Media

The most effective way to reach a large population is through the news media—mainly through radio, television, and newspapers. Internet news services are a fledgling but growing source of volcano information. Effective warnings through news media require good communication between scientists and reporters and careful reporting. Most reporters and news organizations recognize their public responsibility for hazards warnings and try to discharge that responsibility faithfully, though short deadlines and space limits for reporters, competitive pressures for "scoops," and scientists' impatience with confused reporters can sometimes degrade the result. Many volcano observatories have found it useful to employ a person with both scientific and journalistic skills to be an effective bridge between the scientists and the news media. Larger media organizations have skilled science reporters; smaller news organizations without science reporters can greatly improve their coverage by assigning one or two people to report the volcano story throughout its duration.

D. New Channels for Warning Dissemination

A variety of new technologies have opened up new possibilities for volcano and other hazard warnings. One, the

World Wide Web, is a wonderful information tool, but requires the user to actively seek out the information. Other new communication technologies include distinctive telephone rings and recorded messages to all subscribers, and special signals that preempt radio and television broadcasts, and can even turn on radios or televisions automatically for warnings.

IV. CASE HISTORIES

Brief synopses of warnings at three volcanoes illustrate both successes and problems with volcano warnings.

A. Mount St. Helens, Washington, USA

Long-range warnings of Mount St. Helens' frequent, explosive eruptions were published by the U.S. Geological Survey (USGS) in a scientific journal in 1975 and issued officially in 1978 together with a booklet of details by D. R. Crandell and D. R. Mullineaux. These warnings outlined the types of future eruptions that might be expected, and noted that the volcano erupted once every few hundred years, and had last erupted from 1800 to 1857. On this basis, the 1978 report concluded that "the current quiet interval will not last as long as a thousand years; instead, an eruption is more likely to occur within the next hundred years, and perhaps even before the end of this century." Except for a brief flurry when an official misunderstood the long-range warning to indicate an imminent eruption, this warning attracted little attention and was soon forgotten by most recipients.

Just a few years later, the volcano awakened. Recipients of the booklet that accompanied the official warning discovered a valuable handbook. In late-March 1980, earthquakes beneath the volcano were reported as following "a classic pre-eruption pattern." Small phreatic eruptions began on March 27 and continued intermittently for the next 2 months. When rapid bulging of the north flank of the volcano was discovered in April, that, too, was reported. Initially, public statements said that any eruption was likely to be like those within St. Helens' past. As the earthquakes and bulging of the north flank continued, warnings were more explicit that an eruption was likely, and that a landslide was also likely and could trigger an eruption. Regrettably, it never became possible to forecast an exact date for the climactic eruption—even in retrospect. Scientists were hoping to see diagnostic last-minute escalations of microseismicity and creep of the bulge, but neither occurred.

The main events of May 18, 1980, were a massive landslide and a laterally directed blast, followed by a plinian, vertically -directed eruption. No landslide of this scale had been positively identified in St. Helens' geologic history, although two were subsequently recognized. A laterally directed blast had been recognized before the 1978 long-range warning, though it was apparently of much smaller magnitude than that which occurred on May 18 and was not emphasized in 1980 warnings. Both the landslide and the blast that occurred on May 18 were substantially larger than anticipated.

In contrast, the plinian eruption that occurred after the landslide and blast was similar to eruptions described in the 1978 hazard booklet and countless preclimactic 1980 briefings for public officials and the news media. Tephra blew to the east-northeast and blanketed large areas of eastern Washington, as anticipated in the booklet and in 1980 warnings. Mudflows, too, followed paths anticipated in the hazards booklet, even though that of the North Fork, Toutle River, had an unexpected origin by dewatering of a debris avalanche deposit. Effects on downstream towns were more or less as expected.

On balance, the long-range forecast was as good as geologic exposures at that time would have permitted; the significance of the bulge and possibility of a lateral blast were underestimated; and the short-term forecast of an actual date of failure was simply not possible. In retrospect, closer study of reports from Galunggung, Raung, Bandai, and Bezymianny might have focused more discussion on the possibility of a large landslide and lateral blast.

After the climactic eruption of May 18, 1980, five smaller explosive eruptions occurred through the summer months and, after those, 16 episodes of dome growth occurred until October 1986. All of these smaller eruptions were anticipated and warnings were issued. The most precise and prescient of these warnings were a set of four in March 1982 (Figure 2). The first warning, a factual, nonpredictive statement issued on March 5, described an increase in seismicity and "slow" ground deformation. On March 12, scientists predicted that if seismicity and ground deformation continued to increase, an eruption was likely within the next 3 weeks. This second statement also noted differences from earlier episodes that implied the potential for pyroclastic flows and rapid melting of snow and ice. The third warning was issued on March 15 for "an eruption, most likely of the dome-building type . . . within 1 to 5 days." The possibility of explosive activity was mentioned in press interviews, but omitted in the formal statement because of intense media response to the March 12 prediction. Finally, at 0900 h on March 19, scientists predicted that "an eruption would begin soon, probably within 24 hours." A moderate-sized explosive eruption occurred at 1927 h on March 19, generating a mudflow that traveled >35 km down the North Fork, Toutle River, and buried a number of pieces of heavy earth-moving equipment that had been left in the river bed by a skeptical contractor.

For the postclimactic period of eruptions at Mount St. Helens, three broad types of warnings were issued: "predictions," "forecasts," and "factual statements." "Predictions" were relatively precise, confident, short-range warnings of the time, place, and type of expected eruptions, based on interpretation of monitored changes. "Forecasts" were less-precise, longer-range projections of activity based on historical and geologic records of previous eruptive episodes, or still-ambiguous unrest, and on comparisons with eruptions elsewhere in the world. "Factual statements" were issued at an early stage of unrest or at any other time when trends were not yet well enough defined to issue a prediction or forecast. In this article, "predictions" and "forecasts" are treated as a single spectrum and called "forecasts."

In late 1980, when it became apparent that hazards at Mount St. Helens were diminishing faster than public apprehension and that adjectives of "low" and "high" hazard now had greatly different meanings to geologists and officials, an effort was made to quantify hazards and risks to individual life around the volcano. Though crude, and with order-of-magnitude uncertainties, these estimates helped officials to see that, between eruptions, risks in most areas around the volcano were by then low enough to be acceptable.

B. Mount Pinatubo, Luzon, Philippines

Mount Pinatubo was first recognized as a potentially active volcano in the late 1970s and early 1980s during safety studies for a nuclear power plant and exploration for geothermal resources. It was officially designated as "active" in 1988, but with little publicity and to little effect. In early August 1990, two weeks after a $M=7.8$ earthquake along the Philippine Fault 100 km to the northeast of Pinatubo, highland residents noted a new, steaming ground crack on the upper northwest flank of Pinatubo. Earthquakes were also felt, but the seismic network was insufficient to say whether these were of local origin or distant aftershocks. A cursory field investigation noted a new landslide and attributed it to the regional earthquake, with no further significance.

Earthquakes began to be felt again around March 15, 1991, and, on April 2, phreatic explosions opened a set of craters along a fissure across the northeast flank of Pinatubo. In response, the Philippine Institute of Volcanology and Seismology (PHIVOLCS) began monitoring seismicity, steaming, and stream chemistry, and recommended evacuation of villages within a 10-km radius of Pinatubo's summit. U.S. Geological Survey scientists were invited to help and arrived in late April. On May 13, the team adopted a five-level alert scheme (Table I).

As the alert levels were raised, zones of recommended evacuation were also expanded. On June 7, when level 4 was declared, the radius for evacuation was expanded to 20 km, and on June 14, as large explosive eruptions and strong seismicity continued, the recommended radius of evacuation was expanded to 30 km. Most of Clark Air Base (spanning a distance of 15 to 25 km from the summit) had been evacuated on June 10, and many villages between 10 and 20 km distance were also evacuated before and after the evacuation of Clark. Before nightfall on June 14, about 85,000 persons, including >14,500 from Clark Air Base, had moved to safe, distant areas.

A probability tree for pyroclastic flow hazard on the east side of Pinatubo was prepared on May 17 and updated on June 10 for select civil defense and military leaders (Figure 3). They found the tree helpful, though, in retrospect, the probability estimates were too low. The tree was not used for the larger group of warning recipients, mainly for lack of the time that would have been required to fully develop and explain a comprehensive Pinatubo tree.

Official and public skepticism remained a serious problem at Pinatubo until large explosive eruptions began on June 12. Some of the hardest skeptics remained unconvinced until the climactic eruption on June 15. No single action overcame that skepticism, but solid data, public warnings, blunt talk in private meetings with officials, and the powerful first IAVCEI video all helped.

Pre-eruption warnings at Pinatubo saved many lives and much mobile property, including military aircraft. The decisions to evacuate were high-stakes decisions and could not be taken lightly. Both scientists and officials were apprehensive about the possibility of false alarm. It is a credit to the scientists involved that the warnings were correct, and a credit to the officials that they were ultimately willing to order the necessary evacuations. Credit also goes to several Catholic nuns who worked as effective liaisons between scientists and the highland people who lived on Pinatubo.

TABLE 1 Alert Levels for Mount Pinatubo, May–June 1991[a]

Alert level	*Criteria*	*Interpretation*
No alert	*Background*; quiet	No eruption in foreseeable future
Level 1	*Low level* seismicity; other unrest	Magmatic, tetonic, or hydrothermal disturbance; no eruption imminent
Level 2 (May 13)	*Moderate level* of seismicity, other unrest, with positive evidence for involvement of magma	Probable magmatic intrusion; could eventually lead to an eruption
Level 3 (June 5)	*Relatively high and increasing unrest* including numerous b-type earthquakes, accelerating ground deformation, increased vigor of fumaroles, gas emissions	If trend of increasing unrest continues, eruption possible within 2 weeks
Level 4 (June 7)	*Intense unrest,* including harmonic tremor and (or) many "long-period" (low-frequency) earthquakes	Eruption possible within 24 hours
Level 5 (June 9)	*Eruption in progress*	Eruption in progress
	(Note that large-scale explosive eruptions began June 12; climactic eruption occurred on June 15)	

Stand-down procedures

In order to protect against "lull before the storm" phenomena, alert levels will be maintained for the following periods after activity decreases to the next lower level:

from Alert Level 4 to 3—Wait 1 week
from Alert Level 3 to 2—Wait 72 hours

[a] Alert levels are defined subjectively, based on changing rates of unrest and interpretation of processes and "time-to-eruption." (From Newhall and Punongbayan, 1996.)

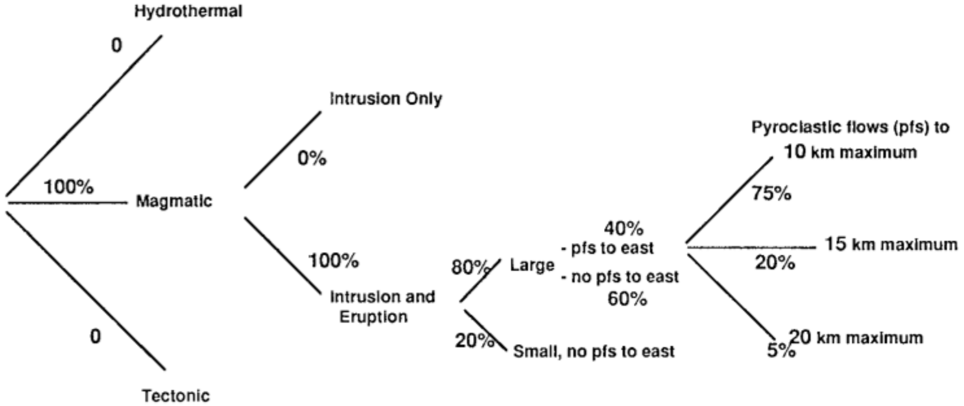

FIGURE 3 Logic tree to assess the probability of pyroclastic flows reaching Clark Air Base and adjoining cities of Angeles and Mabalacat. The first version of this tree was prepared and presented to civil defense and military leaders on May 17, 1991, during what was then still low-level, steady-state unrest. The update of June 10 (shown) was used for internal discussions only because the necessary evacuations had already been ordered. The probability that a pyroclastic flow would reach into these populated areas (≥15 km from the summit) within one year was judged to be about 1% on May 17, and about 8% on June 10. If the tree had been updated after the explosive eruptions of June 12–14, 1991, this estimate would have risen significantly.

After the climactic eruption of June 15, 1991, and a period of smaller ash eruptions, the main hazard at Pinatubo became rain-induced lahars and flooding. Enormous volumes of loose pyroclastic debris were washed from the volcano's slopes into densely populated, low-gradient lowlands. River channels were immediately choked with sediment and lahars began to spread. Rainfall and streams in the lowlands were unable to drain because the river channels were full of sediment, so flooding was also widespread. Two kinds of lahar warnings were used. The first was a map of areas that would be subject to lahars and flooding, and a companion intermediate-range estimate of the volumes of sediment that would be brought into the lowlands each year. The second was the immediate warning of heavy rainfall and lahars, as detected by telemetered rain gauges and acoustic flow sensors (inexpensive, high-frequency seismometers installed near flow channels). Regrettably, though, vandalism and official skepticism kept this network of instruments from ever being used to its full potential. Manned police watch stations were also established at the heads of alluvial fans, and these tended to supplant, rather than complement, the instrument-based warnings.

C. Long Valley Caldera, California, USA

A period of protracted unrest began at Long Valley in 1978 and continues to this writing (March 1999) with neither eruption nor obvious escalation or diminution. USGS, state, and university scientists installed additional instruments immediately after four $M = 6$ earthquakes in May 1980, just 1 week after the major eruption of Mount St. Helens. Initially, it looked as if the unrest might have been of wholly tectonic origin, related to basin and range extension. Now it appears that magma intrusion also occurred, including an intrusion in 1989 beneath Mammoth Mountain. A new aspect of the unrest began in 1990—increased outgassing of magmatic CO_2 that has killed trees in several patches around Mammoth Mountain. There is, as yet, no basis on which to forecast either an eruption or an end to the unrest.

In this difficult situation in which the causes of unrest are not entirely understood, USGS and State of California scientists have had to advise officials and residents of the affluent resort town of Mammoth Lakes, California, about areas and levels of danger. Messages of volcanic hazard are never welcome in resort towns, and Mammoth Lakes was no exception; in recent years, though, patient and sensible liaison between scientists and officials has developed greater mutual respect and more serious contingency planning. After initial hostility from some local business owners and residents, and a USGS retreat from its early warning system, a new set of alert codes has been established. Higher alert levels are invoked if unrest exceeds preselected thresholds. The current color codes (Table II) are simplified from an earlier set of letter codes, but the principle remains the same. Unlike subjective schemes at other volcanoes, the Long Valley color codes are determined by preset thresholds of seismicity, ground deformation, and other change. Between green and orange, the chief scientist can override the preset criteria to set the alert code at whatever level team scientists believe to be correct.

Specific actions within the USGS monitoring team are keyed to alert levels, as are some mitigation actions by local and state officials.

To complement the alert levels, a hazard map shows areas that would be affected in the event of eruptions like those which occurred ≈500–600 years ago in the area. The town of Mammoth Lakes is vulnerable, so its residents are staking their hopes on the short-term alert levels.

One of the difficult problems at Long Valley caldera is the huge range of sizes of past eruptions. The most recent eruption occurred about 250 years ago from an island in nearby Mono Lake. This eruption was small and, even today, would have little impact. Moderate-size, Holocene explosive eruptions of the Mono–Inyo chain are the basis for emergency planning. The largest known eruption from Long Valley—the caldera-forming Bishop Tuff eruption of ~700,000 years B.P., sent pyroclastic flows and surges over much of the area, and ash from that eruption fell from coast to coast across North America. Despite its huge potential effects, the long-range probability of another Bishop Tuff eruption is judged to be so small (10^{-5} or 10^{-6} per year) that no serious plans are being made for such an event.

Another difficult aspect of the unrest at Long Valley has been its long duration. After a time, usually quite short, citizens may stop listening to warnings. Strident warnings, especially if they are false alarms, can easily reduce citizen responsiveness when an eruption truly is imminent. Most warnings at Long Valley have been intentionally low-key to avoid this problem. Unlike the crises at Mount St. Helens and Mount Pinatubo, which climaxed within about 2 months of their start, unrest at Long Valley has continued for nearly 2 decades and shows no indication that it has climaxed or will end soon. Ironically, as unrest continues and false alarms are avoided, some skeptics have become believers and the

TABLE II Color-Coded Alert Level Scheme Used at Long Valley (Modified July 16, 1997)[a]

Geologic behavior	*Condition*	*USGS response*
Typical behavior since 1980 includes: *Background.* As many as 10 to 20 small earthquakes with magnitudes (M) less than 3 ($M < 3$) per day and uplift of the resurgent dome at an average rate of about 1 inch per year.[b] *Weak unrest* (likely to occur several times a year). For example, increased number and (or) strength of small earthquakes or a single felt ($M > 3$) earthquake. *Minor unrest* (likely to occur a few times a year). For example, a swarm with several $M > 3$ earthquakes. *Moderate unrest* (likely to occur about once a year). For example, a $M > 4$ earthquake or more than 300 total earthquakes in a day.	Green (no immediate risk)	*Routine monitoring,* plus information calls to USGS personnel and town, county, state (California OES, State Geologist), and local federal agencies (USFS, BLM) regarding locally felt earthquakes and notable changes in other monitored parameters such as ground deformation, fumarole activity, and gas emissions.
Intense unrest (may occur about once per decade). For example, a swarm with at least one $M = 5$ earthquake and (or) evidence of magma movement at depth as indicated by an increased rate in ground deformation.	Yellow (watch)	*Intensified monitoring.* Set emergency field headquarters at Long Valley caldera. Initial WATCH message sent by USGS to California OES, which promptly informs local authorities. (Includes above information calls.)
Eruption likely within hours or days (may occur every few hundred year). Strong evidence of magma movement at shallow depth.	Orange (warning)	*Geologic hazard warning* issued by USGS to governors of California and Nevada and others who inform the public. (Includes WATCH response.)
Eruption underway (may occur every few hundred years).	Red alert	*Sustained on-site monitoring and communication.* Maintain intensive monitoring and keep civil authorities informed on progress of eruption and future likely development.

[a] Alert levels are defined objectively, but "time-to-eruption" is interpretive. (From U.S. Geological Survey, 1999.)

[b] Details of criteria for each parameter are given in U.S. Geol. Survey Open-File Rept. 91-270. After unrest decreases, watch and warning downgraded after 14 more days, and alert after 1 more day.

town is now better prepared for an eruption than it was earlier in the crisis.

SEE ALSO THE FOLLOWING ARTICLES

Earth's Volcanoes and Eruptions: An Overview • Ground Deformation, Gravity, and Magnetics • Lahars • Risk Education and Intervention • Volcanic Crises Management • Volcanic Episodes and Rates of Volcanism • Volcanic Hazards and Risk Management

FURTHER READING

Blong, R. J. (1984). "Volcanic Hazards." Academic Press, Sydney.

Brantley, S. R., and Topinka, L. (1984). Volcanic studies at the U.S. Geological Survey's David A. Johnston Cascades Volcano Observatory, Vancouver, Washington. *Earthquakes Volcanoes* **16,** 1–122.

Crandell, D. R., Booth, B., Kusumadinata, K., Shimozuru, D., Walker, G. P. L., and Westercamp, D. (1984). "Sourcebook for Volcanic-Hazards Zonation." UNESCO, Paris.

Crandell, D. R., and Mullineaux, D. R. (1978). "Potential Hazards from Future Eruptions of Mount St. Helens Volcano, Washington." U.S. Geological Survey Bull. 1383-C.

Hoblitt, R. P., Miller, C. D., and Scott, W. E. (1987). "Volcanic Hazards with Regard to Siting of Nuclear-Power Plants in the Pacific Northwest." U.S. Geological Survey Administrative Report for U.S. Nuclear Regulatory Commission.

Iverson, R. M., Schilling, S. P., and Vallance, J. W. (1998). Objective delineation of lahar-inundation hazard zones. *Geol. Soc. Am. Bull.* **110,** 972–984.

Lipman, P. W., and Mullineaux, D. R., eds. (1981). "The 1980 Eruptions of Mount St. Helens, Washington." U.S. Geological Survey Prof. Paper 1250.

Miller, C. D. (1985). Holocene eruptions at the Inyo volcanic chain, California. Implications for possible eruptions in Long Valley caldera. *Geology* **13,** 14–17.

Montserrat Volcano Observatory. (1997). Assessment of the status of the Soufriere Hills Volcano, Montserrat and its hazards. Report at http://www.geo.mtu.edu/volcanoes/west.indies/soufriere/govt/miscdocs/assess121897html#AD.

Newhall, C. G., and Punongbayan, R. S., eds. (1996). "Fire and Mud: Eruptions and Lahars of Pinatubo Volcano, Philippines." PHIVOLCS, Quezon City, and Univ. of Washington Press, Seattle.

Scarpa, R., and Tilling, R. I., eds. (1996). "Monitoring and Mitigation of Volcanic Hazards." Springer-Verlag, Berlin.

Swanson, D. A., Casadevall, T. J., Dzurisin, D., Malone, S. D., Newhall, C. G., and Weaver, C. S. (1983). Predicting eruptions at Mount St. Helens, June 1980 through December 1982. *Science* **221,** 1369–1376.

UNDRO-UNESCO. (1985). "Volcanic Emergency Management." UNDRO, Geneva.

U.S. Geological Survey. (1999). Long Valley caldera. Found at http://quake.wr.usgs.gov/VOLCANO/LongValley/index.html (updated frequently).

This Page Intentionally Left Blank

VOLCANIC CRISES MANAGEMENT

SERVANDO DE LA CRUZ-REYNA
Centro Nacional de Prevención de Desastres SEGOB, and Instituto de Geofísica UNAM, Istituto de Ingeniería UNAM

ROBERTO MELI P.
Centro Nacional de Prevención de Desastres SEGOB

ROBERTO QUAAS W.
Centro Nacional de Prevención de Desastres SEGOB and Instituto de Ingeniería UNAM

I. Introduction
II. Pre-event Management
III. Critical Phase Management
IV. Summary

GLOSSARY

alert A condition of heightened watchfulness or preparation for action. A warning method or system to make people aware of impending danger.

alert code A set of rules or a system used for transmitting alert messages requiring brevity and clarity. The symbolic arrangement of instructions in a warning system.

consensus General agreement in the diagnostics and the prognosis of the majority of scientists involved in the study of an episode of volcanic activity. Consensus of the involved scientists is essential for the decision making of authorities.

crisis An unstable situation of increased danger or difficulty. A crucial stage in the course of volcanic unrest, when the threat of an eruption, or the possibility of an eruption, exceeds some reference level.

critical phase A crisis situation or point in time when a critical decision must be made. Time in which decisions regarding the protection of population must be taken in light of developing volcanic activity.

disaster Calamity. An event produced by a natural phenomenon resulting in great loss and a state of extreme ruin and misfortune, capable of breaking the fabric of society.

pre-event Period of time when there is significant evidence that a natural phenomenon that may cause a disaster could occur.

preparedness A state of readiness or preparation for use or action in the case of volcanic activity or any other threat. It involves a clear understanding by the population and authorities of the natural phenomena and their destructive effects.

return code A set of rules or a system used for transmitting brief and clear messages about the reduction of a threat resulting from the decline of the volcanic activity.

vulnerability The susceptibility of physical and human systems to be affected by hazardous natural phenomena. It can be expressed as a probability of damage, or as the proportion of the total exposed assets expected to be affected by a given manifestation.

Copyright © 2000 by Academic Press
All rights of reproduction in any form reserved.

POTENTIALLY DESTRUCTIVE phenomena such as volcanic eruptions occur independently of any human action. Disasters may occur when a social group fails to respond to a threatening situation resulting from volcanic activity or any other natural manifestation. Society may thus react to a threat and reduce the possibility of disaster. Volcanic crises management means developing a degree of social organization and a set of response measures aimed toward the mitigation of the effects of an eruption.

I. INTRODUCTION

Volcanic disasters, as well as other natural catastrophes, were once considered as Acts of God, reflecting the inevitability not only of the eruption, but also of the related damage and destruction. Nowadays, society has as one of its main goals the reduction of risk to life and property, and expects scientists to provide knowledge and technologies aimed at increasing protection against natural hazards. Consequently, governments are expected to implement preventive measures for the reduction of risk and plans for the management of emergencies in order to minimize the effects of the natural events.

Volcanic crisis management may be defined as the set of actions involving the vulnerable sectors of the society, the scientists in charge of assessing the volcanic hazard, and the government through its civil defense or civil protection bodies. These actions are directed toward the prevention and reduction of disaster when volcanic activity develops, or when there is sufficient evidence that an eruption may occur.

Volcanic disaster reduction and crisis management involve very complex and uncertain situations, on both the scientific and the management sides; although eruptions with catastrophic consequences still occur, the cases of successful management of large eruptions with a minimum number of victims are increasing in number. However, according to UNESCO figures, the average number of fatalities per year has been larger this century than it was in past centuries, indicating that population vulnerability has grown at a rate higher than disaster-reduction capabilities. Increasing population in hazardous areas, attracted by the fertility of the volcanic soils and by the availability of generally cheap land, has been one of the main causes of disaster in recent times, for there is no evidence that the frequency and intensity of volcanic eruptions have increased. Effective prevention measures and crisis management should thus be further improved and extended.

Although at first sight a disaster appears to derive from an unexpected intensity of a given phenomenon (which may be an outcome of a lack of preparedness), disasters, or at least serious crisis managing problems, often result from the inadequate behavior of different social sectors, even in populations that rely on some degree of preparedness. Preparedness and response plans must then be continuously revised in light of worldwide experiences. Particularly, all possible situations before and during a volcanic crisis must be carefully considered and at least some procedures for managing a possible crisis should be designed for any volcano that may have some potential of erupting.

A natural phenomenon, such as a volcanic eruption, may generate a number of manifestations—over different time scales—that can affect different sectors of society in a variety of ways, and with different degrees of intensity. Should a volcanic crisis develop, its management involves factors of very different natures, some depending on the degree of previous preparedness. The number of variables involved makes it difficult even to define the problem for which the management plan is to be designed. Dealing with it may prove to be rather difficult, particularly when a large population is at risk.

Ideally, the logical solution to the problem of volcanic hazards would be constructing realistic scenarios based on the study of previous episodes of activity and on elaborate computer simulations, and implementing relocation programs to reduce the threatened population to zero—or at least to a minimum—before any eruptive activity develops. In real life, we are not aware of any place in the world in which this kind of solution can be effectively implemented. The land attachment of people, the difficulty (most times impossibility) of finding alternative places, and many other cultural, economic, and social factors force scientists and officials to look for solutions that permit large populations to live together with a potentially active volcano. Some level of risk acceptance depending on the degree of disaster prevention should thus be defined and specific emergency management plans should be developed to be put into action when that level is exceeded.

A general methodology for management of eruptive crises is not available nor possible due to the great variety of situations deriving from differences in physical settings and, mainly, in social, cultural, economic, and political conditions. However, some basic components of the management plan can be identified, together with some steps necessary for its successful implementation. These steps result from the careful analysis of recent volcanic crises and the reasons for the success or failure of their management.

Volcanic crisis management may be considered as an evolutionary process involving two phases, with the following major components:

1. Pre-event (or precritical) phase (preparedness measures):
   - Risk assessment, hazard and risk mapping, and postulation of expected scenarios
   - Volcano monitoring
   - Emergency planning
2. Critical phase (operational measures):
   - Alert, communication, and information procedures
   - Response—implementation of emergency measures
   - Defining the end of the critical phase

During the evolution of a volcanic crisis these components have different degrees of relevance. The quality of a crisis management plan, measured by its success in mitigating damage (from the eruption or from the countermeasures), depends on the extent to which different sectors of society involved react to the countermeasures in expected ways inferred from adequately constructed scenarios.

II. PRE-EVENT MANAGEMENT

A. Preparedness

Preparedness may be defined as a state of readiness in the case of volcanic activity. It involves a clear understanding by the population and authorities of the related phenomena and their destructive effects. It also involves the design of preventive measures based on that understanding and response plans in case major eruptive activity develops.

If the population and authorities decide to adopt a policy of living together with the volcano, a proper level of risk acceptance must be defined. To do so, some basic components are needed:

- A long-term risk assessment, which may be depicted as a risk map that portrays likely eruptive scenarios, and procedures to disseminate that information
- A short-term risk evaluation device, namely a monitoring system and a procedure for continuous dissemination of the surveillance assessments
- An operative plan based on the risk assessments
- A decision-making process and an operative plan to respond to a nonacceptable level of risk

The first step of the preparedness plans for disaster reduction must be done well before any expected eruptive crisis in the preventive phase. This is the assessment of risk, understood as a combined measure of hazard and vulnerability.

B. Hazards Assessment

After identifying the volcanoes that have a potential to produce eruptions, a thorough knowledge of the characteristics of each volcano and of its past activity allows postulation of eruptive scenarios with their associated probability of occurrence based on statistical evidence. This involves thorough geological mapping and dating of older eruptive deposits. Computer simulations can help to include some new possible situations that may occur.

The ultimate product of these studies is a hazard map depicting the areas that could be reached by each type of eruptive manifestation. This map should include the probability that a given area may be affected in a given way. The large amount of information contained in this system makes it difficult to handle as a conventional printed map. Geographic information systems (GIS) allow a more efficient manipulation of the information. However, the conventional printed map cannot be discarded, for it is still the best way to transmit the hazard information to large sectors of the authorities and population. It is also very useful to divide each hazard area into sectors and consider the possibility of setting different levels of alert in different sectors for particular scenarios (Figure 1). A separate probability tree is a very useful tool for describing the probability of different scenarios and a very helpful support for decision making. It relates each eruptive scenario with an assigned probability, and also describes the possible evolution and concatenation of scenarios. Assigned probabilities must be updated as the crisis evolves.

C. Vulnerability Assessment and Reduction

Because natural phenomena and their associated hazards can hardly be modified, risk mitigation is mainly related to the reduction of the hazard exposure and of the vulnerability of the exposed systems. Vulnerability is de-

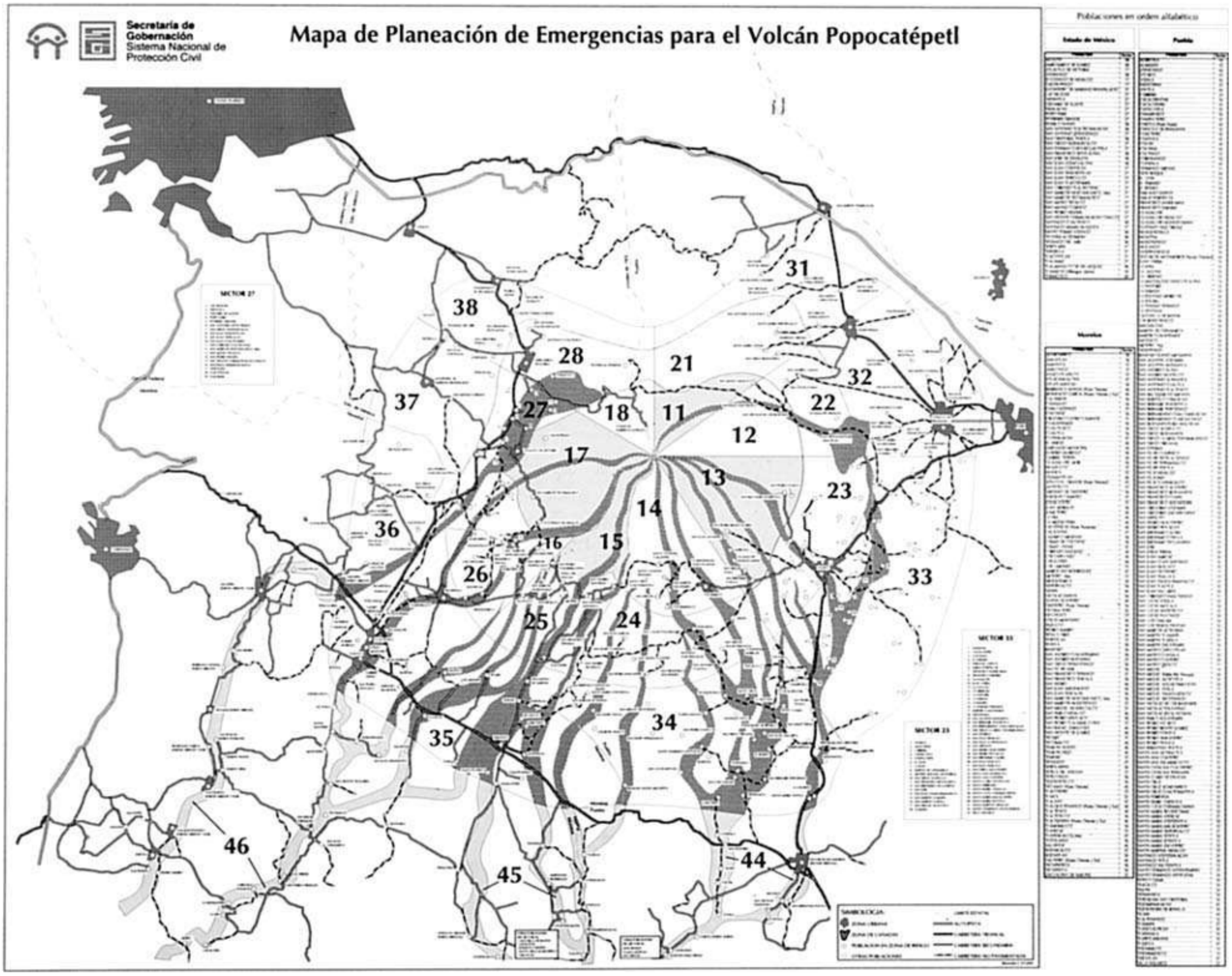
Secretaría de Gobernación
Sistema Nacional de Protección Civil
Mapa de Planeación de Emergencias para el Volcán Popocatépetl
Poblaciones en orden alfabético
SECTOR 27
SECTOR 33
SECTOR 35
31
38
28
21
32
37
27
18
11
22
12
17
13
23
14
36
16
15
26
33
25
24
34
35
46
44
45
SIMBOLOGIA

FIGURE 1 A hazard-emergency planning map for Popocatépetl volcano. The shaded regions depict the areas around the volcano that may be directly affected by eruptions of different intensity and different probabilities of occurrence. These areas have been divided in numbered sectors. The first digit indicates the level or risk of the sectors, and the second its azimuthal position. Regions beginning with a 4 are threatened by lahars. The towns in each sector are listed on the right.

fined as the susceptibility of physical and human systems to being affected by a natural hazard. Formally, it can be stated in terms of a probability of damage, or as a percentage of the total exposed assets expected to be affected by a given manifestation.

Assessing vulnerability and expected damage for each possible eruptive scenario is essential for the design and implementation of preparedness and emergency-management plans. A thorough gathering of the physical and demographic information on the region at risk is fundamental to assess vulnerability and to design the most effective measures of risk reduction. This information should be added to the GIS database.

Specifically, among the most effective measures for volcanic vulnerability reduction are those directly affecting the public. These measures should aim to achieve a proper response from the population in the threatened area, mainly through building a collective consciousness about the existing hazard, the implementation of a policy of land development (discouraging new settlements and encouraging emigration into safer areas), and the careful design of plans for a timely evacuation. Frequent rehearsals of the emergency operations for different scenarios are necessary for the proper functioning of the plan.

Dissemination of properly explained information about the phenomenon, its reach and effects, and the prevention plans should thus be one of the top priorities in any preparedness plan. Specifically, the hazard map and the main measures of self-protection and response to a volcanic emergency must be widely distributed.

Some difficulties in this dissemination process may be anticipated. For instance, in highly developed, industrialized countries, the possibility of land devaluation may sometimes pose a problem in the handling of this information. In developing countries, finding economic resources for these measures is always a problem. Sometimes political problems, particularly when the volcano is located at or near a border region, may arise. In these cases, constructing a responsibility matrix, resulting from an agreement among the involved parties, and disseminating it are important parts of preparedness.

Another important step for vulnerability reduction is the implementation of the so-called structural measures, related mainly to engineering works aimed at protecting structures and their inhabitants. Although not much can be done in this respect for the safekeeping of structures from the most severe eruptive manifestations, such as pyroclastic and lava flows, protection from the fall of tephra can be achieved with proper roof structure and coating at reasonable costs.

Some of the most destructive volcanic manifestations are mudflows or lahars. The energy and range of lahars may be reduced through barriers to retain or deviate solid materials in the mudflows. These constructions are rather complex and expensive. However, they have been extensively implemented in several countries; for example, in Japan a general technology (SABO Engineering) has been developed for this purpose.

D. Monitoring: Minimum Instrumentation Needed in the Pre-event Phase

A monitoring system aims at gathering the maximum relevant information about the volcanic activity in order to detect premonitory signals of an impending hazardous event. For that purpose, it is important that the monitoring system be in place well in advance of the eruptive crisis in order to establish a baseline of activity to which anomalies can be related.

Experiences in eruptive crises obtained in the past decades have demonstrated that appropriate monitoring and surveillance systems are essential parts of volcanic crisis management. These systems consist of the instrumentation of the volcano with specialized measuring equipment adequate for timely detection of any geophysical or geochemical changes of the volcano for correct decision making and management of a possible emergency.

Once an active and potentially hazardous volcano has been identified in a certain region, a minimum monitoring system should be implemented to allow the detection of the first symptoms of reactivation. However, setting up, maintaining, and updating a volcano monitoring system represents a significant expense. Also expensive is maintaining a continuous operation in the long term, which requires a stable institution and trained personnel. To ensure its proper operation, volcano monitoring must be included in a nation's development planning as part of comprehensive disaster prevention programs. In view of other high-priority needs, the conditions for permanent monitoring are often difficult to achieve in developing countries without technical and economic international cooperation.

The minimum monitoring system for a given volcano depends on the hazard and risk levels, its eruptive history, the availability of economic and technical resources, the location and access difficulties of the volcano, and other aspects. It is generally accepted that the reactivation of a volcano usually involves a progressive appearance of certain unrest signals or precursors. A minimum instrumentation should aim at timely detection of these early symptoms of reactivation and allow setting of a baseline against which any unusual activity can be compared. Precursor signals are sometimes strong enough to be perceived by people living close to the volcano, for example, noises, vibrations, gas emissions or fumaroles, water level changes in wells and springs, deformations, and opening of fractures. In other cases, these signals are very small and can only be detected by sensitive instruments. Among the most important symptoms of unrest that can be measured with a basic monitoring system are changes of the seismicity, volcano deformations, and chemical changes in springs or fumaroles.

A basic monitoring system should consist of one, or preferably several, seismic and deformation sensors located close to the crater of the volcano. A good choice is starting with something simple and inexpensive and gradually upgrading the monitoring system as experience is gained and more and better data are required for specific scientific purposes. Discussion of several measurement techniques is beyond the scope of this article and is found in other chapters. A complete description of instruments and techniques used by the USGS to monitor volcanoes, with emphasis on seismic and geodesic measurements, may be found in the work of Ewert and Swanson (1992). In general terms, the type of instrumentation that is convenient for monitoring purposes is not necessarily the same as that which would be needed for research on basic volcanic behavior.

During the process of selection and installation of a basic monitoring system, several factors should carefully be considered: reliability of the equipment, protection, site selection (geology and noise levels), access, maintenance, etc. Also, one has to take into account that these systems might need to be operative during long periods of time (most likely years), sometimes in harsh environments, before the volcano of interest shows any sign of reactivation. This permanent surveillance, monitoring, and instrument maintenance can become tedious. Especially the absence of volcanic activity could induce lack of motivation, lead to budget cuts for operation and maintenance, or even complete abandonment of the system with the possible consequence of failing to detect any critical precursor activity which might lead to a short-term eruption. It must be emphasized that once an eruption is in progress, it is usually too late or impossible to implement the desired monitoring system. There are many examples in the literature of volcanic disasters that could have been prevented if minimum monitoring systems had been operating. One such example was El Chichón volcano, located in the southeast part of Mexico. It erupted in 1982 causing a death toll estimated to be around 2000, though only 122 bodies were found (Figure 2). Had proper monitoring systems been instrumented on this volcano in the early stages before the eruption, precursor activity could have been detected and adequate countermeasures implemented to save the lives of many people. However, it is important to point out that, by the definitions accepted at that time, El Chichón was considered a low-risk volcano. Priority criteria for setting monitoring instruments on different volcanoes should thus be carefully reviewed at regular intervals.

E. Scientific Advice

The organization of a scientific group in charge of hazard assessment and responsible for providing specific recommendations to the authorities must be included in any preparedness plan. It is common that volcanologists, especially when they are specialized in different aspects of the volcanic activity, such as geology, seismology, and geochemistry, have rather distinct views about the actual risk and give different opinions to authorities and media. Great confusion could arise from such a situation, causing a general disbelief about the capability of scientists to make a sound assessment of the risk or a reliable forecast of an eruption, eventually leading to a poor response to warning and evacuation orders. An organization that guarantees scientific consensus is thus essential.

A framework in the disaster prevention scheme must be established in advance of any volcanic emergency.

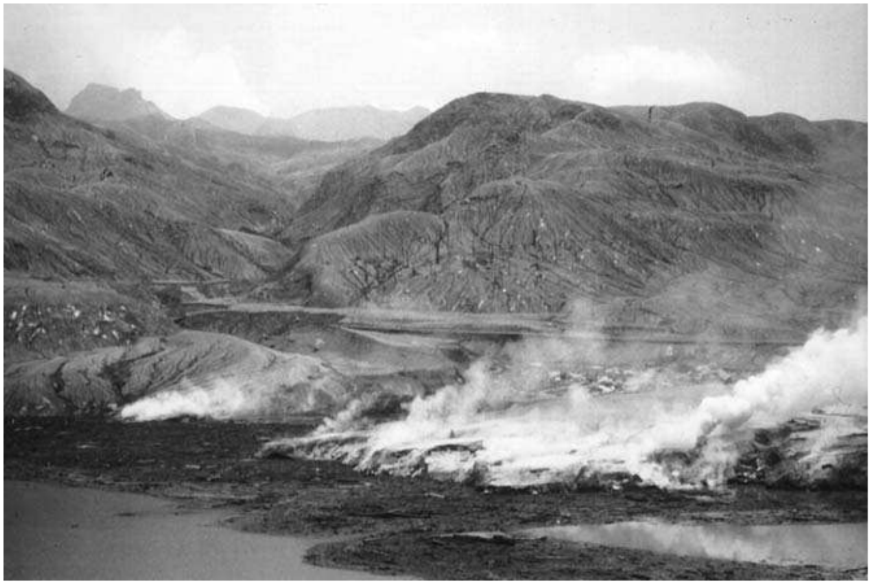

FIGURE 2 Pyroclastic flow deposits at the foot of El Chichón volcano, near the town of Francisco León. The flows produced during the eruptions of April 3 and 4, 1982, descended along the valley and devastated several towns. The flow deposits also dammed the river shown in the photograph, and the accumulated water and debris produced lahars 6 weeks later.

This may help to preclude the possibility of scientific groups divided by competition for the attention of the media and authorities, which can be particularly harmful. An example of such a situation is the case of La Soufrière volcano on the eastern Caribbean island of Guadeloupe in 1976, where the differences of opinions among groups of scientists, greatly emphasized by the media, caused confusion, misunderstandings, and incorrect decisions leading to a situation in which about 72,000 people were evacuated for several months at a very high cost without a clear definition of the actual level of risk. No eruption followed a set of improperly evaluated volcanic manifestations.

In many cases, there is an official agency responsible for monitoring and risk evaluation. It is necessary that all external specialists channel their findings and opinions through such an official body. A suggested procedure is to create a scientific advisory committee where all recognized specialists, local and visiting, can present the results of their studies and discuss their opinions with the purpose of reaching a consensus about the evaluation of risk, forecasts, and recommendations to be given to authorities. It is also convenient that the speaker for the committee be a representative of the official body and should make efforts to reflect the most important positions of the specialists, without generating an impression of uncertainty and confusion.

F. Alert and Communication Procedures

Another essential part of volcanic risk preparedness is the definition and implementation of an alert code. The basic function of an alert code is to transfer the consensus of the scientific advisors to the responsible authorities, so they have the essential means for decision making. Then, the authorities should have efficient ways to communicate the scientists' consensus and their own decisions to the vulnerable population so it reacts to the authorities' actions and recommendations in a knowledgeable way. Usually, the consensus and the authorities' decisions are communicated to the population through an alert code based on colors or numbers, generally with three to six levels. A small number of levels could make it difficult to define the proper hazard level of a given volcano. Nonetheless, a small number of levels leaves less options to the population, reducing the chances of inaction derived from an ambiguous perception of the risk.

Recent experiences show the convenience of using a combined code in which a six-level scale is used to communicate the hazard between the scientific advising body and the civil protection or civil defense authorities. The vulnerable population is advised through a three-level color scale. In this way the first multilevel scale of the code reflects the state of the volcano, whereas the second scale reflects the level of alertness of the population. As an example of this type of combined code, the so-called traffic light alert, used at Popocatépetl volcano, is shown in Table I. The actual process of communication of the alert levels by itself represents a difficult problem, similar to the dissemination of a hazards map, which must be addressed in the precritical phase. Public campaigns of information, not only on the volcanic phenomena but also on the alert code and the preventive actions, should be started in regions neighboring potentially active volcanoes in quiet periods. An improved confidence in the management may be obtained through direct contact of scientists and government officials with local authorities of communities in the hazard area and persons who have influence on public opinion.

Summarizing, the alert, communication, and warning procedures can be done in different ways, according to specific social, economic, and cultural conditions. Perhaps the common denominator for the transmission of the actual risk condition would be a systematic redundancy of information leading to the reduction of misunderstandings to a minimum. This can be achieved by establishing a communication routine consisting of periodic bulletins briefly explaining, with simple words, the state of the volcano—as determined by a scientific committee—and the level of alert of the population. This develops among the population an awareness of the relation between the level of hazard of the volcano and their level of alertness. Bulletins containing the same information may be issued in different formats and should be handed to authorities and media, and can also be posted at sites easily available to the general public, such as Internet sites and telephone mailboxes.

III. CRITICAL PHASE MANAGEMENT

A. Changing to a Critical Phase

In general terms, the procedure for declaring a critical phase begins when the monitoring system detects any unusual activity on a volcano and a reasonable suspicion is shared by the members of the scientific advisory committee that it could be a precursory manifestation of a possible eruption.

TABLE 1 The “Traffic Light” Alert Code Used at Popocatépetl Volcano[a]

Alert level for the communication between the scientific committee and the civil protection system	*Possible associated phenomena (may change according to the type and evolution of activity)*	*Actions recommended to be taken by civil protection authorities*	*Alert level for the public and general recommended actions*
Green phase 1	• The volcano is dormant	• Develop preparation plans; inform the public about the volcanic phenomena; install a scientific committee; install a basic monitoring system; develop risk mapping; develop emergency plans	Green (normality) • Stay informed • Locate yourself in the hazard map • Memorize signals of Evacuation routes Meeting places Shelters • Attend training courses • Participate in exercises and drills • Promote relocation of settlements in high-risk areas
Green phase 2	• Moderate increase in background seismicity, fumarolic activity, minor changes in the composition or temperature of fumaroles or springs	• Increase monitoring; promote sporadic meetings of the scientific committee; revise communication procedures between scientists and authorities; revise emergency plans; give more information to the public on volcanic risk	
Yellow phase 1	• Significant increase in the above parameters • Low-magnitude earthquakes • Some deformation • Clear increase in fumarolic activity • Nonexplosive lava emissions at low rates • Low-level ash emissions	• Promote frequent meetings of the scientific committee; increase consultations between scientists and authorities • Test availability of personnel and equipment involved in evacuations • Test logistic capabilities • Limit access to the volcano, according to recommendations of the scientific committee	Yellow (alert) • Stay continuously informed • Visit the safety areas, meeting places, and shelters • Observe instructions from authorities • Stay alert and prepared for a possible evacuation
Yellow phase 2	• Significant increase of the above parameters • Moderate phreatic or magmatic explosions If some eruptive activity is already in progress, evidence of increased magmatic activity: • Increased volcanotectonic seismicity ($M \sim 2$–3), tremors • Significant deformations • Significant chemical changes in gas, water, or rock samples	• Warn local, regional, and federal civil protection authorities • Set watch shifts • Define a larger radius of limited access to the volcano area • Warn airborne traffic systems	
Yellow phase 3	• Acceleration of the rate of seismic energy release • Larger volcanotectonic earthquakes ($M \sim 3$–4), tremor signals of increased amplitude and duration or lower frequency • Important or rapidly changing deformations • Extensive chemical anomalies • Increased rate of lava production • Increased rate of explosive activity • Eruptive columns exceeding 5 km above the volcano summit	• Make public announcements of the volcano evolution and the adopted measures • Prepare emergency personnel and shelters • Implement specific measures in the more vulnerable regions • Alert air traffic controllers • Extend radius of limited access to the volcano	
Red	• Solid evidence of large increase in the magma rate production • Increased volcanotectonic activity ($M > 4.5$) • Tremors detected in remote seismic stations • Very large deformations • Development of major explosive eruptive activity ($VEI \sim 3$–4) • Eruptive columns exceeding 10 km above the volcano summit	• Selective evacuations in threatened sectors, according to recommendations of the scientific committee • Encourage self-evacuation • Start preventive measures in other sectors • Start preventive measures against ashfall in metropolitan areas around the volcano • Start preventive actions to protect energy, water, and communication lines in the risk area • Alert air traffic controllers	Red (alarm) • Attend and follow instructions of authorities • Go to security areas, meeting places, or shelters • If you can leave the risk by your own means, do it! • Stay permanently informed about the situation
	• Solid evidence of large amounts of magma accumulating in the volcanic cone • Major volcanotectonic earthquakes (magnitude 5 or more) • Very large deformations, or development of major explosive eruption ($VEI = 5$ or more) • Eruptive columns more than 15 km above the volcano summit	• Selective evacuations of threatened sectors, according to recommendations of the scientific committee • Start preventive actions against heavy ashfall in metropolitan areas around the volcano; start extraordinary measures to protect energy, water, and communication lines • Alert air traffic controllers	

The decision-making process that defines a critical phase involves, first, the way scientists in charge of monitoring and evaluating volcanic activity recommend to the authorities some major emergency measures, such as an evacuation. Then, the recommendation evolves into a decision of declaring an emergency condition, and corresponding actions are taken by the concerned authorities. Clear responsibility assignment and a timely response are essential to the proper functioning of this stage. Matters become more complicated when authorities of different ranks and jurisdictions become involved, at municipal, state, or federal levels.

Therefore, the rules for responsibilities in the decision-making process must be established well in advance of crises, and must be clearly specified in the alert code and in the operative response plans.

Should a situation of slow buildup of the volcanic activity persist, a more complete and permanent monitoring network should be immediately implemented to acquire the necessary information needed, first, to better understand the physical processes and, second, to manage an eventual emergency.

B. Critical Phase Monitoring and Alarm

An optimal volcanic surveillance is best obtained by using a combination of measuring schemes. The most common and widely used types of high-profile monitoring systems will be described briefly.

- *Visual surveillance*. This consists of a continuous observation and recording of the volcano by means of video and photographic cameras, as well as frequent visual reconnaissance missions from the ground and air (including satellite pictures) from which any conspicuous anomaly can be detected. Lava, debris and mudflows, ash emissions, fumaroles, dome growth, landslides, deformation, ice and snow changes, and weather conditions, among others, are phenomena which can be observed and qualitatively assessed. As an example, a real-time picture, posted on an Internet web page, has been used by the monitoring system of the Popocatépetl volcano in Mexico (Figure 3).
- *Seismic monitoring*. Seismic stations provide fundamental information about the internal structure of the volcano, its state of activity, and the way it changes. Recording of seismicity can be done locally, using autonomous portable instruments at lower-risk locations, or remotely, through radiotelemetry links into a central recording station. From a crisis management point of view, several signals from standard low-cost instruments are preferred to one sophisticated but expensive broadband seismograph.
- *Geodetic monitoring*. Deformation is the other physical parameter that provides fundamental information about the internal state of the volcano and supplies additional insight on the expected dimension of the developing process. Usually, its measurement is done using conventional geodetic methods (leveling, trilateration, EDM, dry tiltmeters, GPS, etc.). Only a few deformation data, like electronic tiltmeter readings, can be continuously telemetered to a central monitoring center.
- *Geochemical monitoring*. This implies frequent chemical analyses of gases, water from springs and crater lakes, volcanic ash and rocks, and, in general, all volcanic materials that may provide information about the evolving state of the volcano. Remote sensing by means of satellite images and ground or airborne spectrography (COSPEC, LICOR, etc.) are remote methods for measuring concentration of gases, like SO_2 and CO_2, emitted by a volcano.
- *Hydrometeorologic monitoring*. Monitoring weather conditions (temperature, barometric pressure, wind speed and direction, rainfall, etc.) on a volcano is very important for the forecasting and detection of ash plumes and mudflows produced by rain or melting of glaciers and snowcaps. Doppler radar is being used in different sites to detect heavy rainfall, as well as dense ash emissions rich in coarse clasts. Additionally, flow and lahar detection systems, installed along different drainage paths of the volcano, are devices which should definitely be considered if there is any indication that potentially destructive flows might be triggered by the volcanic activity, as occurred at the Nevado del Ruiz volcano. Fast-response barometers for detecting and measuring pressure waves from volcanic explosions are also quite useful.

---

[a] The left column includes six levels or phases reflecting the state of the volcano. The second column associates those levels to observed phenomena. Since the relevance of different volcanic manifestations changes as the activity evolves, these associations are kept flexible. The third column describes some general recommendations to the authorities. Detailed instructions should be included in an operative plan. The column at the far right describes the level of public alertness in terms of a simple color scale. It is assumed that a minimum number of options left to the population reduces the ambiguity in the perception of the risk, and thus the chances of misunderstanding the importance of a threat.

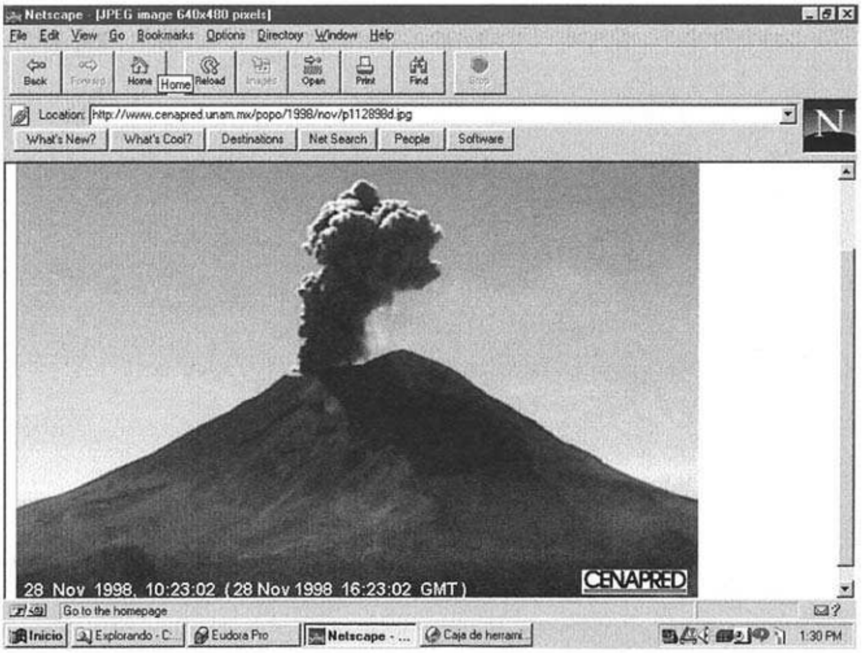
Netscape - [JPEG image 640x480 pixels]
File Edit View Go Bookmarks Options Directory Window Help
Back
Forward
Home
Home
Reload
Images
Open
Print
Find
Stop
What's New?
What's Cool?
Destinations
Net Search
People
Software
28 Nov 1998, 10:23:02 (28 Nov 1998 16:23:02 GMT)
CENAPRED
Go to the homepage
Inicio
Explorando - C...
Eudora Pro
Netscape - ...
Caja de herrami...
1:30 PM

Location: http://www.cenapred.unam.mx/popo/1998/nov/p112898d.jpg

FIGURE 3 A real-time picture (and a photo album of past events, which is not shown) posted on an Internet web page has proved to be useful tools for communicating the evolution of the volcano activity to the public. Similar web sites may be found for other volcanoes of the world.

- *Other measuring and monitoring systems.* Detection and study of gravity and geomagnetic anomalies, temperature of the volcanic edifice, domes and plumes, concentrations of soil gases such as radon and other tracers, and groundwater levels provide additional and important information on the state of a volcano. Some of these usually involve a higher number of support staff and sophisticated and costly measuring equipment, and therefore cannot always be widely implemented.
- *Data processing and internal alarm systems.* A well-equipped and centralized data collecting and processing facility is essential for a volcanologic observatory, defined as the main source of information for the scientific advisory committee during a critical stage. Four aspects are important in a center: display systems, data processing, alarms, and communications.

1. *Display.* To be able to quickly assess the state of activity, a convenient and efficient display system of the continuously acquired signals should be implemented. Computer screens, drum and chart recorders, TV and radar monitors, etc., need to be arranged in such a way to provide a proper display. Real-time data such as seismic energy or tilt should be represented as plots, histograms, or any other analog display which allows a user to easily recognize a change of a variable and perceive its trend. Because seismicity is one of the main monitored parameters of a volcano, most observatories use drum recorders as primary devices to display and record on paper the seismic signals. Any sign of activity can be detected at a glance, and signals of the same event can be readily compared on different stations and correlated with other monitored parameters. If, in addition, a visual image of the volcano is displayed on a monitor close to the drums, an optimum combination of visual tools to detect and judge the internal condition of the volcano and its external effects is obtained (Figure 4).

2. *Data processing.* Among others, basic data processing routines commonly used in a crisis condition are seismic-energy release rates, event detection and location, and spectral analyses. These data, together with other measurements like tilt, temperature, SO_2 values, etc., should be integrated in databases for quick display and analysis. Data are optimally handled and managed using local computer networks linked to the Internet. Thus inspection, supervision, and monitoring can be accomplished locally and remotely, and information efficiently disseminated and exchanged with other scientists and observatories.

3. *Monitoring alarms.* Computer systems that process volcanic information can easily be adapted with auto-

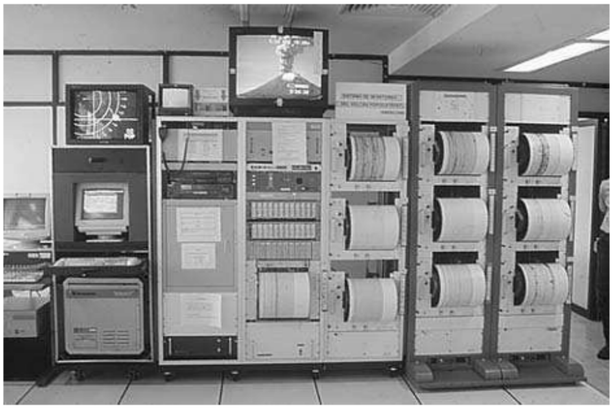

FIGURE 4 Display of the monitoring system of Popocatépetl volcano. The analog seismic drum recorders on the right record signals received from stations located near the crater. In the central part, the radio-receiver bank allows quick checking of the transmission status of the signals. Above it, a television set displays the real-time image of the volcano, which is continuously recorded on tape. On the left a Doppler radar, installed by the U.S. Geological Survey, allows detection of larger ash emissions. Seismic data are digitized and analyzed by a set of computers. Visual and radar images are also digitized and put on the Internet.

matic alarm and dial-up systems providing audible signals and warnings when one or more of the monitored parameters exceed a preset threshold. Alarms can be triggered by seismic activity, deformation signals, detection of mud, water, or pyroclastic flows, ash emissions, etc. Such alarm systems are key elements, especially for personnel on duty in an observatory, to warn workers of a sudden volcanic unrest and allow them to respond according to pre-established procedures, triggering in turn other alarm signals and devices to alert other scientists, authorities, emergency agencies, or the threatened population. To discriminate seismic activity originating at the volcano from other nonvolcanic sources, like regional earthquakes, which could falsely trigger an alarm, one or several signals from remote seismic stations should be considered to inhibit the alarm upon detection of a regional earthquake. An ideal automatic seismic-alarm system should also be able to recognize seismic patterns or signals. In practice, even though sophisticated devices and early warning techniques are available, a fully automatic fault-proof alarm system cannot be used without human judgment, and in most cases cannot be used to automatically start an emergency plan or evacuation procedure. It should be used only to assist and alert personnel of a possible critical situation.

4. *Communication.* Proper and sufficient communication services like telephone lines, faxes, access to the Internet and e-mail, modems, and voice-band radios should be available to effectively manage an observatory. Particularly during an emergency, insufficient communication channels to contact authorities, officials, and members of a scientific committee, as well as to issue reports and provide information to the media and the general public, are usually critical aspects often underestimated when setting up an observatory or emergency management center.

C. Response to Monitoring Alarms

When a monitoring alarm goes off at any time, the problem arises of how to respond to this alarm and decide what action to take within the volcano observatory. It is likely that monitoring alarms may result from false triggers induced by momentary states of unrest of the volcano, and consequently would not imply starting a pre-established emergency plan involving authorities and the general population. Judging whether a signal is just a minor event of no serious consequence or a critical precursor indicating the onset of a more important manifestation is a crucial problem, and a few basic guidelines can be proposed in terms of some assumptions.

First, it is assumed that an adequate monitoring system exists, with sufficient instrumental diversity and reliability to be able to detect and correlate different signals and patterns detected on a volcano. Secondly, it is assumed that a moderate to large eruption would produce significant changes of different parameters. If an internal volcanic process is developing, it is unlikely that deformation, seismicity, and visual effects, like ash and gas emission, might change independently, or a mudflow be produced without heavy rainfall or any seismic indication of an instability or melting of a glacier. Therefore, a major change in the state of equilibrium of an active volcano will in most cases be detected by different monitoring devices. Third, it is assumed that a limited number of trained scientists, namely the members of the scientific advisory committee, are dedicating most of their time to volcanic-hazard assessment, and that other staff, in different fields and with differing levels of training, are available to maintain an around-the-clock volcano surveillance.

Experience has shown that keeping two watch levels may help to deal with possible situations of monitoring alarms, particularly when the volcanic unrest has extended for some time. A pool of watchers may be programmed to keep an around-the-clock "operative" watch. The usually larger general staff pool takes the direct watch, keeping a continuous presence in the monitoring room with shifts of 6–8 hours. Two or more scientists take the "permanent" watch, making themselves available around-the-clock in shifts of a week or so. Should the operative watch detect any unusual manifestation, it calls the "permanent" watch, who has the responsibility of making a preliminary assessment of the situation. If judged necessary, this person may call other members of the scientific committee and decide whether a meeting is necessary or whether immediate actions should be recommended to the authorities. How to organize such a group and implement a specific action plan depends on many local circumstances and policies.

D. Communication and Information about the Critical Condition

Once a critical condition is identified, the consensus of the scientists or scientific committee in charge must be transmitted to the authorities in a clear and unambiguous way. Even when a consensus has been attained in that respect, the opinions of individual scientists may have important divergences. A delicate balance must be held between the right of individual specialists to make public their own views by direct access to the media and the need of giving to the population a unified position. It is particularly important that the position be expressed in a language that can be understood by the great majority of the population with a minimum content of technicalities. The risk to life and wealth is such a critical issue to the threatened people that messages can be easily misinterpreted, rumors can spread immediately, and contending opinions dispersed, leading to confusion and disbelief.

The high credibility of the scientific group in charge of the risk evaluation and recommendations is essential for a quick response to warning and for the success of the emergency plan. The failure of the warning about the great mudflow produced by a relatively moderate eruption of Nevado del Ruiz in 1985 has been mainly attributed to the disbelief or lack of understanding of people and authorities about a recommendation by the scientific group to evacuate areas that could be affected by a large lahar (Figure 5). The communication of the critical condition was not made clear and strong enough, and the perception of the risk by the population at risk differed from that of the scientific community.

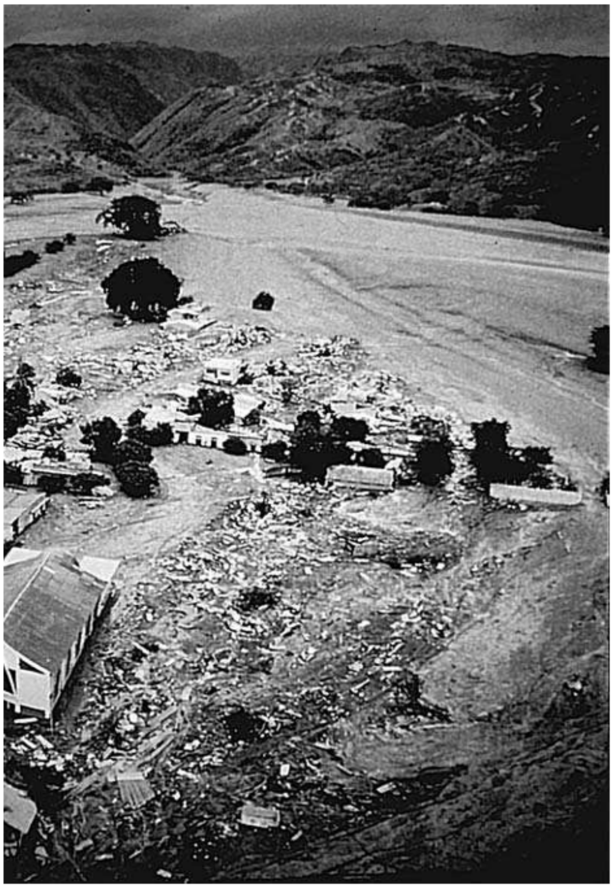

FIGURE 5 Over 21,000 people were killed when mudflows devastated the city of Armero (Colombia) in November 1985. The disaster occurred despite the existence of basic volcanic emergency management elements and resulted from misunderstanding and indecision. (Photo courtesy of Omar D. Cardona.)

To prevent information mishaps, a single voice must act as speaker for the scientific group. Ideally, the highest ranking officials of the civil protection or civil defense body should attend the decisive meetings of the scientific advisors to hear directly the assessment and recommendations about the crisis. Otherwise, the person assigned as speaker for the scientists to the authorities must corroborate that the scientists' consensus has been fully understood by the officials.

Whether the speaker for the scientific committee should advise directly the population at risk or should the alert to the population be issued by the civil protection authorities after a recommendation of the scientific group depends on the design of the responsibility matrix and the local legal framework. Since major decisions involving displacements of people involve aspects other than volcanological, a careful balance must be achieved to define this responsibility, considering the social aspects, better understood by the authorities, and the delays involved in longer chains of information.

A particularly sensitive issue in this regard is the position of international specialists determining risks of eruption in a developing country. Their opinions are sometimes given more credit by the media, the authorities, and the public than those of the local scientists in charge of the problem, and can again give rise to confusion and lack of credibility. A code of ethics should be established and promoted among the international volcanological community regarding procedures for giving opinions about the risk and forecast of eruptions to the public. Such procedures should consider that the opinions and facts on which they are based should be first submitted to the local body in charge of the risk evaluation or to the scientific advisory committee before being given to the public or the local authorities. One of the International Association of Volcanology and Chemistry of the Earth's Interior commissions has prepared a document on the professional conduct of scientists during volcanic crises in which some of these subjects are addressed.

Media play an increasingly important role in this problem, for there is a tendency to overemphasize any discrepancy among scientists, or between scientists and authorities. The roles of the speakers for the scientific group and for the authorities become crucial in transmitting the best estimate of the hazard condition and the existing countermeasures. When transmitting this information, the speakers should take into account that the attitude of local media is generally different from those having a national or international reach. News intended for people external to the problem tends to highlight the most negative aspects of the situation and to exaggerate the extent of risk, thus causing serious consequences for people involved in the crisis. For instance, in the crisis of Popocatépetl (1994–present) there has been a clear trend by national and international media to overemphasize the risk to Mexico City, which is located farther than 65 km from the volcano, thus giving more emphasis to the most catastrophic scenarios, with a low probability of occurrence, than the more probable ones affecting the vicinity of the volcano (Figure 6).

An effective way to keep a stream of reliable information to the media is establishing a more intense routine of daily (or more frequent) bulletins with different formats but containing the same information. In this way, unexpected calls or interviews from media, which sometimes have to be attended by staff of the permanent watch that may not be experienced in dealing with media, can always be addressed to the official report, keeping in this way a single source of information. The bulletins should contain information about the scientific committee's assessment of the state of the volcano and the level of alertness of the population. Additionally, keeping a frequently updated Internet web page and

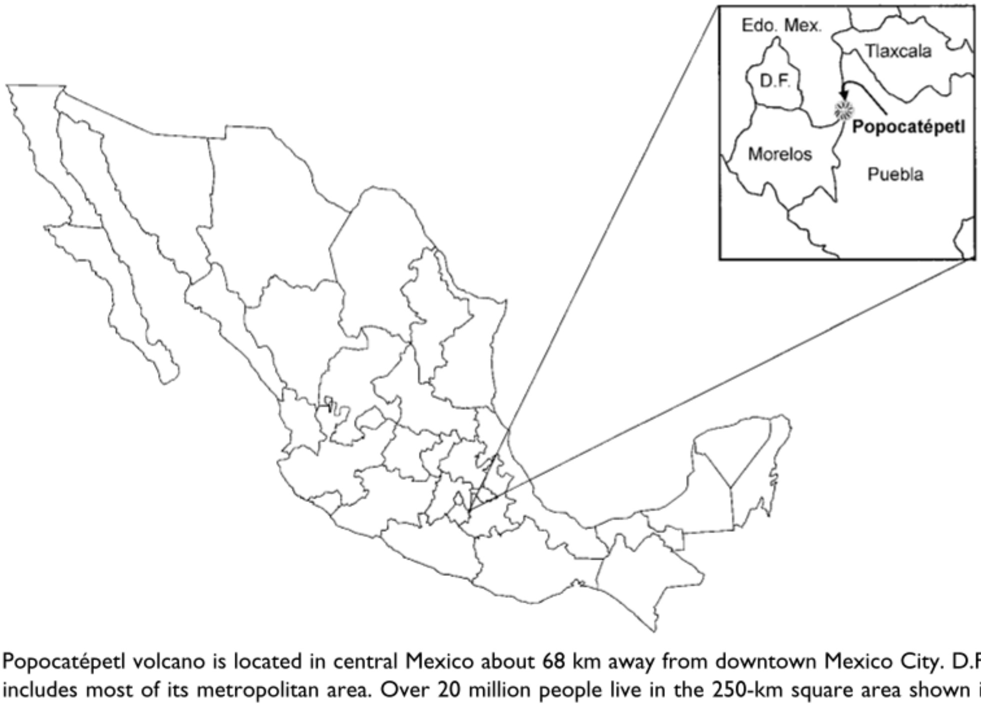

FIGURE 6 Popocatépetl volcano is located in central Mexico about 68 km away from downtown Mexico City. D.F. is the Federal District, which includes most of its metropolitan area. Over 20 million people live in the 250-km square area shown in the insert.

telephone voice mail source with the same information as the bulletins has proven to be very efficient in dealing with the large demand for information.

E. Decision Making and Operative Plans

The decision-making criteria for establishing an emergency condition depend on different factors. A fundamental one is the degree of risk acceptance defined by the operative emergency plan. This level should be the result of a consensus between the scientific group and the civil protection authorities. In general terms, given the above conditions, the level of risk acceptance would be directly related to the quality of the monitoring, the efficiency of the warnings, and the logistic capabilities of authorities and the population.

It is expected that an elaborate monitoring system may detect early volcanic manifestations that could be interpreted as precursors to hazardous eruptive activity. In general terms, it also may be expected that the earlier this interpretation is made, the higher the probability of having a false alarm. On the other hand, an inefficient warning procedure or insufficient logistic capabilities may result in a long delay in the implementation of response actions. Looking for a compromise among these factors is a task that should be addressed from the earliest stages of the detection of increased activity, and must be updated according to the evolution of the activity.

Another factor is the geographic, economic, and urbanization situation around the volcano, which imposes different conditions on the decision making and emergency management. For instance, about 2.7 million people live within a radius of 15 km around Vesuvius (a similar number would be at risk in the case of volcanic reactivation of the Campi Flegrei), 1 million within 40 km from Popocatépetl, and about 530,000 within 20 km of Sakurajima. Mobilization or a general evacuation of such a large number of people requires a very complex operation. In addition, these cases face particular problems. For instance, while the population at Pozzuoli or near Vesuvius is mainly urban and high-income, and it can rely to a great extent on alert communication channels and its own resources for an evacuation, the high population density adds special difficulties of automobile traffic flow in an emergency. In contrast, the population around Popocatépetl is mainly rural and low-income, scattered in hundreds of small villages, with great differences in culture and even language, thus making the dissemination of information and alert communications particularly difficult, and requiring great support for the evacuation. The emergency plans cannot be transferred from one volcano to the other, and the decision-making criteria should take into account the social and economic conditions, as well as the extent of the population.

Once a critical condition has been declared by the scientific group and communicated to the authorities, the decision of declaring an emergency condition to the population must be addressed by the authorities in terms of the emergency plan, defining all tasks involved in each operative phase, such as priorities of evacuation (what places should be evacuated first), rescue, and relief. It must be clearly defined who is in charge of each task, how to mobilize the necessary resources for the plan's implementation, and how to coordinate with other groups. The main parts of the plan are those related to warnings, transportation, shelter, and health and food services. In this case, a map with the hazard areas divided in sectors (Figure 1) may be helpful in allocating levels of risk to each sector and assigning specific tasks and responsibilities.

The way the volcanic activity develops and reaches a critical stage has a great influence on the management of the situation. If the activity shows a clear trend toward a major event, with convincing evidence of impending hazard, it is easier for scientists to obtain the support of the authorities, and thus the support of the population and task forces for the implementation of the emergency plan. The 1991 Pinatubo and the 1994 Rabaul crises are good examples of situations in which the clear consensus of scientists and authorities led to successful management of the emergency.

In some cases, the increased activity fluctuates for a time that may extend for several years, with contradictory signs of a possible evolution toward a major eruption. In a situation like this, there is enough time to organize, test, and improve the emergency management plan, but on the other hand, it is difficult to maintain the consciousness and preparedness of the population and the authorities. There is an increased possibility of false alarms and of growing differences of opinion among scientists which may result in loss of credibility by the population. Several cases of slow development of activity and of misleading signals of an imminent eruption exist, as happened at La Soufrière in Guadeloupe. Popocatépetl volcano had a sharp increase in activity in late 1994 and since then has shown large fluctuations, several times reaching stages that were close to an evacuation order, causing great unrest among the population. The persistency of a state of intermediate alert has also caused some loss of interest in the warning signals among the population.

F. Return to a Subcritical Phase

A decision as difficult to make as declaring the start of a volcanic emergency condition is declaring the end of the emergency condition. Once a major eruption has started, it may be followed by periods of quietness that may not represent the end of the eruption. There is an increased difficulty in assessing the state of the volcano, for the remaining activity may obscure precursors to new eruptive episodes. Additionally, some social pressure may build up from the population and authorities to return to a normal state, particularly if the eruptive event was not very intense, few or no external manifestations can be viewed by the public, or people have remained in shelters for a long time. This pressure may be high enough to exceed the authorities' actions and recommendations about remaining in safe areas. On the other hand, the decision of allowing the return of evacuated people can only be made in the context of the type of eruption and its evolution. This may result in conflicting situations in the way in which the information on the existing hazard is transmitted to the affected population.

To deal with this, in some cases, it is possible to define a "return" alert code in which the actions recommended to the authorities and population are equally simple as those in the "direct" alert code, but different, and strongly dependent on whether the mobilized population is urban or rural. Although such a "return" code may be designed in the pre-event phase, or during the onset of the critical phase, it is difficult to establish a program and disseminate it to the population in those stages. A more practical solution would be to work out a version of the code for the authorities in which some actions of partial or gradual return may be defined, under additional security conditions.

This "return" code has to take into account the current degree of acceptable risk. If some level of hazard (understood as the probability that a hazardous eruption may occur in this phase) has been defined, the only way to stay within the level of acceptable risk is by reducing vulnerability through the reduction of exposure. For instance, if a rural area was evacuated, and the eruptive activity decreases, but there is no evidence that it has ended, a "return" alert code may define a condition under which it is possible to allow part of the population to return and work during the daytime in specific relatively low hazard areas. This would help to reduce the degree of economic effects of the region, a factor that must also be taken into account in the definition of acceptable risk.

In these kinds of actions, all scenarios must be carefully considered, and if there is any evidence that hazardous events may occur without any precursory activity (as for instance, in dome collapse), the return should be delayed.

IV. SUMMARY

Managing a volcanic crisis requires a preparation involving the elaboration of an organized set of actions for use in the case that volcanic activity develops. This pre-eruption phase includes scientific work aimed at the identification of hazardous volcanoes, the elaboration of risk scenarios, and the installation and operation of monitoring devices. The scientists involved in these tasks should become the core of a scientific committee acting as an advisor to the authorities in charge of the safety of the population. It also includes social work involving communication procedures that guarantee a clear understanding by the population and authorities of the natural phenomena and their destructive effects, and developing an operative plan in which the responsibilities of scientists, authorities, and the population are defined and the actions to be taken for different scenarios are clearly specified.

Should an eruption develop, or clear evidence of precursory activity detected, a warning of the critical condition must be declared and communicated through an appropriate alert code. Alarm methods have to be developed to make sure that the information through the communication chain, monitoring–scientists–authorities–population, is clear and unambiguous. In reply to the alarms, response plans should be implemented and the programmed measures taken according to the responsibility matrix defined in the operative plan. When the volcanic activity stops or declines, a return to a subcritical phase has to be designed according to the evolution of the eruption.

SEE ALSO THE FOLLOWING ARTICLES

Earth's Volcanoes and Eruptions: An Overview • Risk Education and Intervention • Synthesis of Volcano Monitoring • Volcanic Hazards and Risk Management • Volcano Warnings

FURTHER READING

Arañia, V. and Ortiz, R. (1993). Page 277–385 *In* "La Volcanología Actual" (J. Martí and V. Araña, eds.). CSIC, Madrid.

Barberi, F. and Carapezza, M. L. (1996). page 771–786 *in* "Monitoring and Mitigation of Volcano Hazards" (R. Scarpa and R. I. Tilling, eds.). Springer-Verlag, Berlin/Heidelberg.

Blong, R. J. (1984). "Volcanic Hazards: A Sourcebook on the Effects of Eruptions." Academic Press, Orlando.

Cardona, O. (1997). Management of the volcanic crisis of Galeras volcano: Social, economic and institutional aspects. *J. Volcanol. Geotherm. Res.* **77,** 313–324.

CENAPRED/SINAPROC-SEGOB/UNAM (1995). "Volcán Popocatépetl. Estudios Realizados durante la Crisis de 1994–1995." CENAPRED, Mexico.

Cepeda, H., Michael, J., Murcia, A., Parra, E., Salinas, R., and Vergara, H. (1985). "Mapa de riesgos volcánicos potenciales del Nevado del Ruiz." INGEOMINAS, Medellin, Colombia.

Crandell, D. R., Booth, B., Kusumadinata, K., Shimozuru, D., Walker, G. P. L., and Westercamp, D. (1984). "Sourcebook for Volcanic-Hazard Zonation." UNESCO, Paris.

Ewert, J. W. and Swanson D. A., eds. (1992). "Monitoring Volcanoes: Techniques and Strategies Used by the Staff of the Cascades Volcano Observatory, 1980–90." U.S. Geol. Surv. Bull. 1966.

Fiske, R. S. (1984). Page 110–121 *in* "Explosive Volcanism" (National Research Council, Geophysics Study Committee, eds.). National Academy Press, Washington, DC.

Fournier d'Albe, E. M. (1979). Objective of volcanic monitoring and prediction. *J. Geol. Soc. London* **136,** 321–326.

IAVCEI Subcommittee for Crisis Protocols (1999). Professional conduct of scientists during volcanic crises. *Bull. Volcanol.* **60,** 323–334.

Miller, C. D., Mullineaux, D. R., and Crandell, D. R. (1981). Page 789–802 *in* "The 1980 Eruptions of Mount St. Helens, Washington" (P. W. Lipman and D. R. Mullineaux, eds.). U.S. Geol. Surv. Prof. Paper 1250.

Peterson, D. W. (1996). Page 701–718 *in* "Monitoring and Mitigation of Volcano Hazards" (R. Scarpa and R. I. Tilling, eds.). Springer-Verlag, Berlin/Heidelberg.

Punogbayan, R. S., Newhall, C. G., Bautista, M. L., García, D., Harlow, D. H., Hoblitt, R. P., Sabit, J. P., and Solidum, R. U. (1996). Page 67–85 *in* "Fire and Mud: Eruptions and Lahars of Mount Pinatubo, Philippines" (C. G. Newhall and R. S. Punongbayan, eds.). Univ. Washington Press, Seattle.

Shimozuru, D. (1996). Page 787–806. *in* "Monitoring and Mitigation of Volcano Hazards" (R. Scarpa and R. I. Tilling, eds.). Springer-Verlag, Berlin/Heidelberg.

Tilling, R. I. (1989). Volcanic hazards and their mitigation: Progress and problems. *Rev. Geophys.* **27**(2), 237–269.

UNDRO/UNESCO (1985). "Volcanic Emergency Management." UNDRO/UNESCO.

Voight, B. (1996). Page 719–769 *in* "Monitoring and Mitigation of Volcano Hazards" (R. Scarpa and R. I. Tilling, eds.). Springer-Verlag, Berlin/Heidelberg.

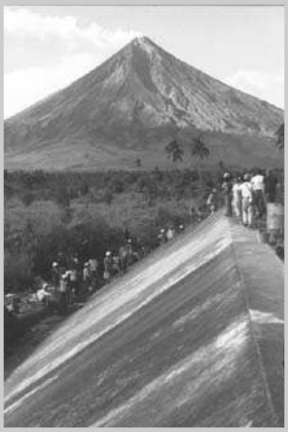

VOLCANIC HAZARDS AND RISK MANAGEMENT

Russell Blong
Macquarie University

I. Introduction
II. Risk Identification
III. Risk Analysis
IV. Risk Reduction
V. Risk Transfer
VI. Conclusions

GLOSSARY

acceptable risk A risk for which, for the purposes of life or work, we are prepared to accept as it is with no regard to its management. Society does not generally consider expenditure in further reducing such risks justifiable.

ALARP Acronym for a principle that specifies that risks should be As Low As Reasonably Practicable.

disaster relief Disaster relief has two broad aims: (1) to save life, ameliorate suffering, and salvage what remains from the immediate crisis—in broader terms, to return afflicted communities to the predisaster status quo—and (2) to increase disaster resilience by improving warning systems, strengthening infrastructure, etc.

hazard The annualized probability of the specific volcanic hazard—tephra fall, pyroclastic flows, lahars, etc.—occurring in the area under consideration.

insurance A common method, at least in developed countries, by which the losses produced by a volcanic eruption or other natural hazard can be distributed across a group much broader than the group suffering direct losses.

risk Risk = Hazard × Vulnerability.

risk management A chain of activities progressing through the sequence of risk identification → risk analysis → risk reduction → risk transfer, and aimed at minimizing the risk of loss of life and/or damage resulting from volcanic hazards.

tolerable risk A risk that society is willing to live with so as to secure certain net benefits in the confidence that it is being properly controlled, kept under review, and further reduced as and when possible.

vulnerability The average degree of loss, expressed on a scale of 0.0 to 1.0, to elements exposed to a hazard.

VOLCANIC HAZARDS AND their consequences are best viewed in a risk management framework where identification → analysis → reduction → transfer are the important elements in the risk chain. Careful identification and analysis of volcanic risks is required before risk reduction strategies are implemented. Proactive risk management will involve volcanologists in strategic planning and in interpreting the characteristics of volcanic hazards for emergency managers and others vitally concerned with reducing the potential consequences of eruptions.

Copyright © 2000 by Academic Press
All rights of reproduction in any form reserved.

I. INTRODUCTION

The fundamental equation of risk reduction is

$$\text{Hazard} \times \text{Vulnerability} = \text{Risk}.$$

Hazard refers to the annualized probability of the specific volcanic hazard—tephra fall, pyroclastic flows, lahars, etc.—occurring in the area under consideration. Vulnerability can be described as the average degree of loss, expressed on a scale ranging from 0.0 to 1.0, to elements exposed to the hazard—for example, humans, buildings, agriculture, and other economic activity. More commonly, no attempt is made to attach units to this equation and it merely provides a simple shorthand emphasizing the two components to risk—hazard and vulnerability.

Three types of adjustment can be made to reduce the risk associated with the occurrence of natural hazards:

1. The hazard itself can often be modified, though this is only rarely possible in the case of volcanic hazards
2. Vulnerability to the impact of the hazard can be modified—for example, modifications to houses that improve resilience under ash loads, the protection of crops under plastic sheeting, the diversion of lahars, land-use planning, or broadcasts of volcano weather forecasts allowing local inhabitants to plan daily activities
3. The loss associated with damage produced by an eruption can be "distributed" to a wider community through disaster relief and/or insurance

Despite the range of adjustments that can be made, doing nothing is still the most common form of adjustment to natural hazards risk.

Management strategies that involve modifications to vulnerability or insurance can be described as proactive, those focusing on disaster relief as reactive, and those where nothing is done as inactive. Despite the International Decade for Natural Disaster Reduction, most of the efforts of the United Nations and those of national and local emergency managers are still reactive or inactive.

Ideally, risk management efforts are proactive and designed to minimize risk before the impacts of volcanic hazards are experienced. The purpose of volcanic hazards risk management can be stated as:

1. To minimize the risk of loss of life from structure collapse or damage in the event of an eruption
2. To facilitate appropriate warning and evacuation systems
3. To protect food-producing areas and other areas of significant economic activity
4. To improve the expected performance of structures and lifelines
5. To improve the functional capability of structures and lifelines that are essential to posteruption recovery during and after an eruption, and to minimize the risk of damage to hazardous facilities

Ideally, risk management for volcanic hazards will involve a wide range of stakeholders including volcanologists; local and national governments; utility companies and transport and communication providers; representatives of business, construction, education, health, tourism, finance, insurance, and the agricultural sectors; professional organizations and researchers; volunteer and community organizations; the media; and international organizations. Part, possibly a large part, of risk management involves focusing the divergent agenda, priorities, and energies of these groups.

The attitudes of all stakeholders to risk and to risk management will be influenced, perhaps markedly, by their risk perceptions. Cultural theories of risk recognize five broad categories of people as risk takers:

1. The individualist takes an optimistic view of history; building codes have been improved, so risk is decreased.
2. The egalitarian invokes the precautionary principle and presses for urgent action. Buildings are better, but exposure is increasing (more people and buildings and contents) so we need better land-use planning.
3. The hierarchist: everyone knows his/her place. Things are about right as they are, but more research and a slight change of course might be advisable. Building codes are good, but they could be better; more regulation required.
4. The fatalist: hopes for the best, fears the worst. Whatever risk reduction is done, building codes will not be good enough and the volcano will get you anyway.
5. The hermit: what volcano?

Certainly, the risk profiles of individuals, stakeholders or not, are more complex than these five caricatures suggest. Nonetheless, the risk management strategies adopted by groups of stakeholders may owe as much to cultural attitudes to risk as they do to scientific attitudes to risk. Risks to individuals arising from voluntary activities, for example, are often acceptable at levels up to 1000 times higher than those imposed involuntarily.

"Acceptable risk" has been defined as "a risk for which, for the purposes of life or work, we are prepared to accept as it is with no regard to its management. Society does not generally consider expenditure in further reducing such risks justifiable" (IUGS, 1997, 12). Acceptable risk is distinct from "tolerable risk," defined as "a risk that society is willing to live with so as to secure certain net benefits in the confidence that it is being properly controlled, kept under review and further reduced as and when possible" (1997, 12).

In the late 1980s, Don Peterson suggested volcanologists have "an ethical obligation to convey effectively their knowledge to benefit all of society" (1988, 4161). Increasingly, volcanologists and other emergency managers can expect to find themselves concerned with issues such as "the standard of care of a reasonable practitioner," often embodied in the law of negligence. While risk reduction may be the major focus, it forms one link in the risk management chain that begins with risk identification and proceeds through risk analysis to risk reduction, and then (where possible) to risk transfer.

II. RISK IDENTIFICATION

Volcanic hazards risk identification has two major components—recognition of the range of volcanic hazards that an area is exposed to, and identifying the elements of the environment that are vulnerable.

Table I identifies a range of volcanic hazards, itemizing those physical characteristics that may be significant from a risk viewpoint. Identifying the range of volcanic hazards that might be relevant at any one volcano, or site near a volcano, may not be a simple task. Maps, particularly hazard maps, where the nature of previous eruptions, oral histories, and results from tephrostratigraphic studies are taken into account together with expert judgments and the conclusions from eruption scenarios can be very useful. The intervals between successive eruptions can be so long that written histories are inadequate. Indeed, the eruptions of Lamington in Papua New Guinea in 1951, Heimaey in Iceland in 1973, and Pinatubo in the Philippines in 1991 indicate that repose periods of hundreds, even thousands, of years are not uncommon. Thus, considerable judgment is required in identifying *all* potential volcanic hazards.

The list of hazard characteristics in Table I, relevant to volcanic hazard risk management, is problematic. Although apparently comprehensive, volcanologists have made rather limited efforts to characterize volcanic hazards or to publish detailed posteruption reviews that might be used to refine the list. Further efforts are required to ensure that this list is comprehensive.

The second aspect of risk identification involves vulnerability to a particular hazard or hazards. Major elements at risk might include people, houses, commercial and industrial buildings, disaster-relevant facilities, other infrastructure (roads, rail, bridges, airports, telecommunications, utilities, etc.), crops, and other economic activity. Vulnerability varies significantly from element to element. Nearly all elements show almost total vulnerability to pyroclastic flows. On the other hand, humans can often be evacuated from the path of an advancing lava flow, crops may be vulnerable to relatively light tephra falls only at specific growth stages, and a water storage and reticulation network may be vulnerable only at the single point where a pipeline is supported by a bridge across a lahar-prone stream.

Numerous factors contribute to the vulnerability of elements. For example, factors contributing to building vulnerability may include:

1. Locations in marginal and potentially hazardous areas, such as floodplains, where lahars, pyroclastic flows, lava flows, and/or CO_2 inundation may occur
2. Densely populated areas with older residential buildings that may be poorly maintained, illegally altered or extended, built to standards now considered inadequate, or substantially overcrowded
3. Poor design and/or construction quality
4. Locations adjacent to industrial complexes where potentially hazardous releases can occur

Any risk matrix or audit that takes account of spatial variability in hazard occurrence around a volcano and the comprehensive identification of hazards and the elements at risk is unlikely to be simple, unless the objective of the risk management is quite limited.

III. RISK ANALYSIS

Risk analysis focuses on the magnitude and frequency of the consequences of volcanic hazards, as well as on the volcanic hazards themselves. Such analyses may begin with a reasonably quantitative understanding of eruption magnitude and frequency, based on a long historical and tephrostratigaphic record with good estimates of the Volcanic Explosivity Index (VEI) for each eruption. For example, data on historic lava flows from Mauna Loa have been used to produce a hazard zone map based on areal coverage, distance from active vents,

TABLE 1 Volcanic Hazard Characteristics Pertinent to Risk

Lava flows
—Temperatures above ignition points of many materials
—Velocities from a few tens of m/hour to 60 km/hour
—Bury or crush objects in their path
—Follow topographic depressions; can be tens of kilometers long
—Noxious haze from sustained eruptions

Ballistic ejecta
—10+ km radius of vent
—High impact energies
—Densities < 3 t/m^3
—Fresh bombs above ignition temperatures of many materials

Tephra falls
—Downwind transport velocity < 10 to <100 km/hour
—Exponential decrease in thickness downwind
—Can extend 1000+ km downwind
—Material < 64 mm diameter at thermal equilibrium
—Can produce impenetrable darkness
—Compacts to half initial thickness in a few days
—Surface crusting encourages runoff
—Abrasive, conductive, and magnetic

Pyroclastic flows
—Concentrated gas–solid dispersion
—Flow velocities up to 160 m/s
—Emplacement temperatures < 100 to >900°C
—Small flows travel 5–10 km down topographic lows
—Large flows travel 50–100 km
—Large flows climb topographic obstructions

Pyroclastic surges
—Low concentration but high kinetic energy
—Radius of deposition 10–15 km
—Climb topographic obstructions
—Emplacement velocities $>$ tens of m/s

Lahars
—Generated with rainfalls < 10 mm/hour
—Bulk fluid densities 2–2.4 t/m^3, sediment content 75–90 wt%
—Peak flow rates $> 10{,}000$ m^3/s; velocities > 10 m/s not uncommon
—Increase turbidity and chemical contamination in water bodies
—Rapid aggradation, incision, or lateral migration
—Travel distances up to tens of kilometers
—Hazard may continue for months or years after eruption

Jökulhlaups
—Can occur with little or no warning
—Discharges may be $>100{,}000$ m^3/s

continues

Continued

Rock/debris avalanches
—Sector collapse, minimum volume 10–20 million m^3
—Travel distances 20–30+ km
—Deposits cover 100+ km^2
—Emplacement velocities up to 100 m/s
—Create topography, pond lakes
—Can produce tsunamis in coastal areas

Earthquakes
—Maximum Modified Mercalli intensity of 8 or less
—Damage limited to small areas
—Damage dependent on subgrade conditions

Ground deformation
—Damage limited to 15–20 km radius
—Subsidence may affect hundreds of km^2

Tsunamis
—Open ocean travel rate > 800 km/hour
—Exceptionally, waves to 30+ m
—Inundation velocities 1–8 m/s

Air shocks
—Up to 15-fold amplification of atmospheric pressure

Lightning
—Cloud-to-ground lightning from ash cloud
—Strikes related to quantity of tephra

Gases and aerosols
—Water vapor a major component
—SO_2 next most important
—SO_2, H_2S, HF, HCl (corrosive/reactive)
—CO_2 in areas of low ground or poor drainage
—pH of associated rainwater may be 4.0–4.5

ground surface slope, and sheltering topography. Similarly, at Mount Shasta, California, the proportion of concentric zones at 10, 20, and 30 km from the summit affected at least once in the last 10,000 years was used to estimate the future average frequency of pyroclastic flows and lahars. Consideration should also be given to whether eruptions “characteristic” of a particular volcano in terms of magnitude and style can be identified.

Studies combining hazard analysis with a thorough consideration of vulnerable elements (i.e., risk analysis) are relatively rare. At a general level, volcanic hazard maps have been combined with land-use capability maps to produce land-use suitability maps. For Miyake-jima volcano in Japan, such maps emphasize that areas with a high potential for crater formation and/or lava flows are suitable for only low-density, low-value uses.

Given the current state of information about hazard and vulnerability, much of the analysis is likely to depend on expert opinion. Order of magnitude estimates may be sufficient for some risk analyses. For example, Table II estimates of the frequency of a range of volcanic hazards produced in VEI 4 eruptions in Papua New Guinea, lists estimates of the areas affected by each hazard in VEI 4 eruptions, and a building damage index based on the proportion of replacement cost. It is assumed that buildings are uniformly distributed across each of the hazard zones. The subjective estimates in this table are based on expert opinion.

The Relative Risk Index is the product of the frequency, the area affected, and the Building Damage Index, divided by the lowest nonzero value (that for gases and aerosols) and rounded. The order of importance column is a simple generalization of the Relative Risk Index, with 1 being the most important.

There might be considerable uncertainty and debate about some of the empirical values in the table, but the results in the final column are reasonably robust. For example, changing values in the first three columns by 10% changes little in the last column. The table indicates where risk management should be focused for the case in point. The "quick" analysis shows the overwhelming dominance of tephra fall as a risk to buildings, despite the gross underestimate of the area affected. Obviously, these estimates are unlikely to be appropriate for volcanoes outside Papua New Guinea, or for eruptions with a differing VEI.

Similar tables could be constructed with specific relevance to an individual volcano and/or a specific building type, economic activity, human population, etc. In each case, the relative risk indexes, and possibly the order of importance estimates, would be different. Considerable refinement of this simple risk analysis is required, taking into account the spatial distribution of the items at risk in relation to the areas mapped as hazard-prone. In most cases it would be appropriate if the table or matrix reflected the views of a range of experts with differing backgrounds.

A number of limitations to the consistency or reliability of risk analysis deserve attention (after IUGS, 1997, 6):

1. Subjective judgments may result in values of assessed risks with considerable inherent uncertainty
2. The variety of approaches that can be adopted to assess risk can result in significant variance in outcomes if the same problem is considered separately by different experts (or even by different groups of experts)
3. Revisiting an analysis can lead to significant change

TABLE II Relative Risk Indexes: Papua New Guinea Volcanoes at VEI = 4

Hazard	*Frequency (%)*	*Area affected (km²)*	*Building damage index (%)*	*Relative risk index*	*Order of importance*
Lava flows	15	<2	100	10	3
Ballistic ejecta	20	20	30	50	2
Tephra falls	30	500[a]	20	1000	1
Pyroclastic flows	10	20	100	100	2
Pyroclastic surges	<5	20	100	50	2
Lahars	25	20	80	150	2
Jökulhlaups	0	0	80	—	4
Rock avalanches	<1	200	100	100	2
Earthquakes	<5	20	20	10	3
Ground deformation	<1	20	60	5	3
Tsunami	2	20[b]	60	10	3
Air shocks	2	100	<5	5	3
Lightning	30	10	20	20	2
Gases and aerosols	5	10	<5	1	3

[a] Deliberate underestimate of area affected.
[b] Coastal strip, 1 km wide.

due to increased data, applying a different method, or changing circumstances

4. Inability to recognize a significant hazard and the consequential underestimation of the risk
5. The results of an analysis are seldom verifiable, though peer review can be useful
6. The available methodologies are not widely accepted and thus there is sometimes aversion to their application
7. It is difficult to accurately assess risk for low-probability events

Uncertainties in risk analyses need to be noted. Uncertainty is commonly understated, with analysts being a lot prouder of their subjective answers than they should be.

IV. RISK REDUCTION

The primary aim of risk analysis is to identify those volcanic hazards and the associated consequences that most require risk reduction efforts. It is unlikely that many risks are regarded as acceptable, with further risk reduction efforts unjustified. However, tolerable risks need to be reviewed with reduction efforts applied where possible.

Tolerable risk criteria for volcanic hazards have not been established but some general principles can be applied (after IUGS, 1997, 9):

1. The incremental risk from a volcanic hazard to an individual or element should not be significant compared to other risks to which a person or element is exposed in everyday life
2. The incremental risk from a volcanic hazard should, wherever reasonably practicable, be reduced; that is, the As Low As Reasonably Practicable (ALARP) principle should apply
3. If the possible loss of life from an eruption of specified magnitude is high, the probability that that eruption might actually occur should be low as society has a particular intolerance to incidents that cause many simultaneous casualties
4. People will tolerate higher risks than they regard as acceptable when they are unable to control or reduce the risk because of financial or other limitations
5. Tolerable risks may vary from country to country, and within countries, depending on historic exposure to eruption hazards and a variety of cultural factors

Risk reduction can be achieved through hazard reduction or by changing the vulnerability of elements at risk. Examples of both sorts are given here.

A. Lava Flows

The speed of advance of a lava flow is primarily a function of slope, viscosity, and effusion rate. The rheological properties of lava are such that, if the thrust exerted by the lava issuing from an eruptive vent is significantly reduced, the most advanced lava fronts come to a halt. This suggests two modes of intervention that could be applied—slowing the advance and diverting the flow.

Water has been sprayed on advancing lava fronts at several eruptions. The most publicized of these was at Heimaey (Iceland) in 1973 where up to 32,400 t (metric tons) of seawater per hour were pumped onto the lava surface. Opinions diverge as to whether these efforts were instrumental in saving the harbor or of only limited success. In any case, abundant water appears to slow the advance of (thin) lava flows, buying valuable time for the evacuation of property or even the removal of frame buildings.

Numerous attempts have been made to divert lava flows using aerial bombing, particularly on Hawaii. In 1975–1976, 900-kg bombs failed due to imprecise bomb placement. The new generation of weapon guidance systems could overcome this difficulty.

Earth barriers have been built to force lava flows to accumulate and expand laterally. Even low-density barriers made from incoherent material such as scoriae, lapilli, and ash seem to work, effectively resisting the thrust of the flow. At Etna in 1992 a 21-m-high barrier constructed of incoherent material resisted lava flow advance for 4 weeks before it was overtopped. This and three smaller barriers allowed considerable time to be devoted to lava flow diversion.

Figure 1 illustrates the important elements of a successful lava flow diversion at Etna, involving the digging of an artificial channel with a steep drainage and blasting the wall of the active lava channel. Complete diversion of the 30 m^3/s lava flow was achieved. With the experience gained in 1992, it is estimated that in similar circumstances a diversion could be accomplished in 10 days.

Successful lava flow diversion implies that areas that may be relatively risk-free are likely to be inundated. One community's risk reduction efforts may well increase risks at another! Since the first attempts at lava flow diversion at Etna in 1669, it has been apparent that risk reduction is not free of legal, social, or spiritual constraints.

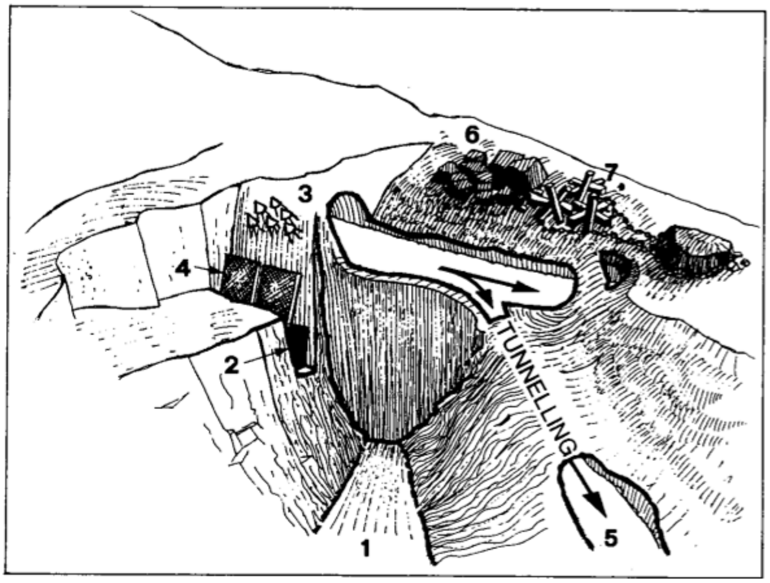

FIGURE 1 A successful lava flow diversion at Etna in May 1992. (1) An artificial channel 10 m wide and 15 m deep; (2) metal containers with 7000 kg of explosive placed into a trench against the thinned solid separation wall; (3) shaped charges placed against a massive lava bank; (4) steel plates interposed between the explosive and the trench filling; (5) earlier artificial channel where lava poured out spontaneously; (6) lava boulders piled on the left bank of the tunnel skylight; and (7) hedgehogs chained together and anchored with steel cables. [After Barberi *et al.,* 1993. Copyright © Elsevier Science Publishers. Reprinted by permission Elsevier Science Publishers.]

B. Lahars

Lahars can produce alternating periods of rapid incision and aggradation and extensive areas of lateral erosion. Additional areas may be inundated by water ponded as a result of channel changes. Deposition on alluvial fan areas can inundate tens of square kilometers. Although more than 50% of the available sediment is likely to be transported in the first 5 years or so, the lahar hazard can persist long after an eruption has ceased. For example, lahars continued around Pinatubo in 1999, 9 years after the eruption.

As lahars can be produced by even a few millimeters of rainfall, opportunities for hazard reduction may be rare. However, drainage of crater lakes provides one such opportunity. At Kelut (Indonesia), a series of tunels were completed in 1926 to reduce the volume of the crater lake after the disastrous eruption of 1919 when more than 5000 people were killed in lahars and 9000 houses were destroyed. Recently, the drainage system has been reinstated, restricting the lake volume to 2.5×10^6 m^3 (cf. 40×10^6 m^3 before the 1919 eruption). Similarly, the water level at Spirit Lake, near Mount St. Helens, has been regulated by a series of pipes and tunnels to control both water level and discharge.

Revegetation of slopes mantled with fresh tephra can also be effective in reducing the frequency and magnitude of lahar development. Ironically, vegetation often reestablishes first where tephra has already been stripped, exposing the pre-eruption topsoil. Aerial reseeding programs have been used in some cases. However, fresh tephra surfaces often develop an impermeable crust that encourages runoff (and lahar formation) and inhibits seedling growth. Tephra layers less than 15–20 cm thick can be plowed so that fresh tephra and topsoil are mixed, but encouraging water and seedling penetration of thicker layers is difficult.

Vulnerability to lahars can be reduced by using lahar flow warning systems, retention basins, engineered channels, and land-use planning. Warning systems based on acoustic flow monitoring systems, wire sensors, water level gauges, cameras, or seismographs are practicable where warning times are adequate to allow those at risk to reach refuge on high ground or in protected structures. Warning systems only reduce the vulnerability of humans and readily removable objects. Such systems also imply that an education system is in place to ensure that warnings produce appropriate human responses.

Retention basins, sand pockets, or Sabo dams have been used around many volcanoes including Galunggung (Indonesia), Kelut (Indonesia), Mount St. Helens (USA), Usu, Unzen, and Sakura-jima (Japan). Some basins have been designed to hold as much as 200 million m^3 of sediment; others enclose areas as great as 10 km^2. Many basins are cleaned out periodically, or at least are designed so that they can be. Retention basins are not suitable for the gentle slopes of large alluvial fans such as those around Pinatubo, because channels can migrate rapidly.

Engineered channels have been used in numerous situations. In the simplest cases, levees or dikes of unconsolidated earthen material are thrown up in (often) futile attempts to confine or divert lahars to existing channels. At Mayon (Philippines), lahars have sometimes ended up on the wrong side of the dikes designed to contain them. The failure of many poorly conceived structures of this type occurred around Pinatubo in the aftermath of the 1991 eruption. Nonetheless, even temporary structures may buy time, providing they are recognized as short-term countermeasures. Boulder-lined levees may be more effective, but as lahars can have bulk densities of more than $2t/m^3$, even large boulders can be readily entrained. The use of gabions is appropriate in some situations, though the wire baskets may not survive long where exposed directly to sediment-charged flows. Concrete levees are probably more effective (Figure 2; see also color insert).

Long-term countermeasures such as expensive concrete-lined and hydraulically efficient lahar channels have been constructed at Usu, Unzen, and Sakura-jima volcanoes in Japan (Figure 3). Frequently, sediment retention basins are incorporated into the design, with steel and concrete structures built to impede the passage downstream of successively smaller boulders and trees. The basic principle is to reduce the energy of the flow, trap the larger material, and reduce the volume. These systems are expensive to build and maintain, and suitable only for relatively small steep drainage basins where the long-term protection of assets with very high values is desirable. Living in harmony with the risk is likely to be the most "effective" countermeasure in many situations.

Reducing vulnerability by land-use planning or zonation is the most obvious and effective risk reduction methodology in many circumstances. Areas likely to be affected by lahars can usually be mapped using tephrostratigraphic techniques and geomorphic knowledge. Successful land-use planning depends on a clear understanding of the risk related to a specific eruption magnitude and character. Sadly, land-use planning is impracticable around many volcanoes, particulary in less-developed countries with high population densities concentrated on the fertile but lahar-prone volcanic soils. The extent of devastation by lahars around Pinatubo emphasizes the additional risks associated with large eruptions.

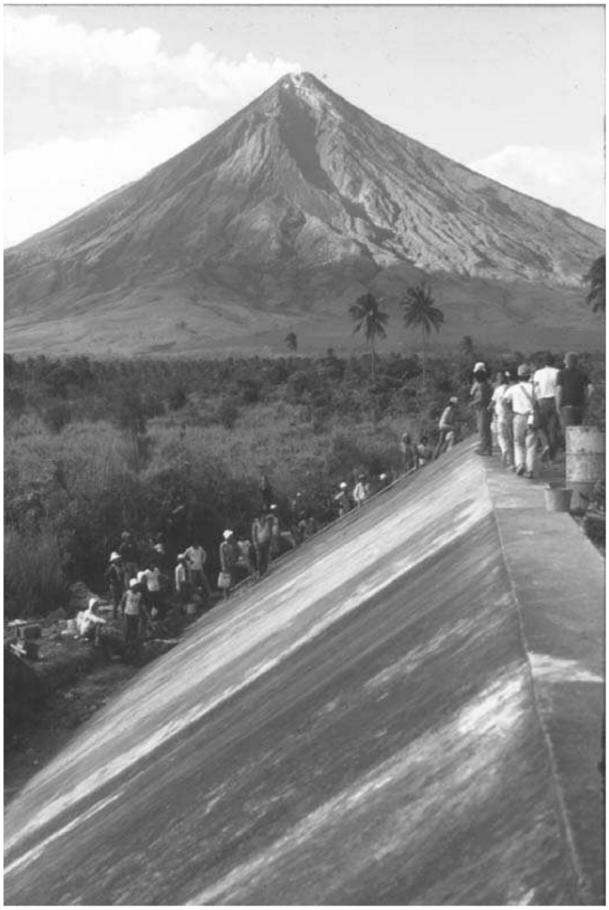

FIGURE 2 A concrete levee designed to retain lahars from Mayon volcano, Philippines. (Photo, R. Blong.) (See also color insert.)

C. Tephra Fall

Reduction of the tephra fall hazard is virtually impossible, but reduction of the consequences of tephra fall forms one of the prime risk management objectives (cf. Table II). While a wealth of information was gained from the Mount St. Helens (1980) eruption about ways in which ashfalls could be removed and the undesirable effects on specific structures, utilities, and agriculture minimized, on a global scale remarkably little has been translated into sound attempts to reduce risk *before* an eruption occurs.

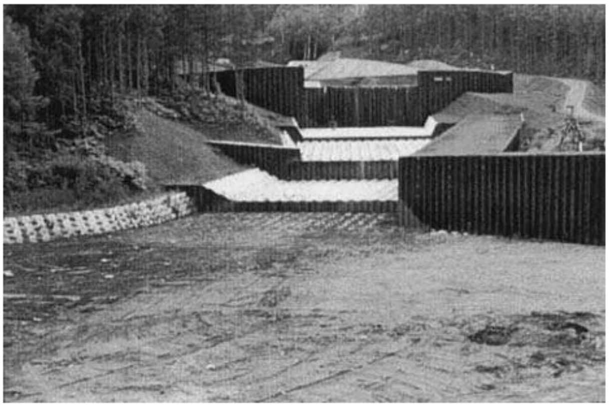

FIGURE 3 Sabo construction using piled steel, tetrapods, and reinforced concrete to form settling basins on the slopes of Usu volcano, Hokkaido, Japan. (Photo, R. Blong.)

Rather cursory investigations in Castillejos (Philippines), where about 200 mm of wet tephra fell during the Pinatubo eruption (1991), suggest that this was sufficient to cause partial or complete collapse of about one-third of roofs. A similar proportion received no damage or slight damage. Long spans (>5 m), timber frames (as opposed to reinforced concrete frames), and steeper roof pitches were identified as factors contributing to greater damage. A similarly incomplete survey after the Rabaul (Papua New Guinea) eruption (1994) suggested that 80–90% of roofs sustained loads imposed by <200 mm of wet tephra with little apparent damage, >50% of roofs survived ash depths of 300 mm, and >50% of roofs failed under loads of 500–600 mm. Thicker falls resulted in the collapse of most roofs, though steeply pitched roofs survived preferentially, contradicting the evidence from around Pinatubo. Even where roofs survived under loads of 500 mm, interior walls bowed and significant damage was produced to floors, electrical systems, and contents by the ingress of minor amounts or tephra through damaged portions of roofs.

In the Azores, roof materials have been tested to ascertain likely resistance to potential tephra loads. The use of upright props along trusses or purlins to spread tephra loads was recommended, along with the taping of plastic sheeting over windows and other openings and the provision of strengthened refuges within buildings (usually bathrooms are preferred for this purpose), in order to reduce risk to the inhabitants. Subsequent work in Montserrat has provided new estimates of the ranges of impact resistance of a variety of building materials from which survival rates for buildings with different roofing materials and structures can be determined. Similarly, the proportions of roofs likely to collapse under tephra loads in different parts of the island have been estimated together with the locations of the sites where search and rescue will be most required.

Around Sakura-jima in southern Japan, where the volcano has been in eruption for more than 40 years, improved roofing tiles have been designed, allowing less ash to accumulate and less rain to be drawn in between tiles. Other innovations include a tunnel ventilation system which improves ventilation during ash falls. In areas at risk from ballistic ejecta, reinforced concrete or steel shelters have been erected for personal protection (Figure 4), and a model ash-resistant house has been designed.

In the Kokopo area, near Rabaul, an attempt has been made to develop a building code for commercial and public buildings. This code takes into account the fall of 100 mm of tephra with a return period of 1/500 years, equivalent to a 9.5% probability of occurrence in the 50-year life of the building. As Kokopo is located south of the caldera in an area where, it is believed, trade winds would only rarely deliver tephra, the design ash load is relatively low. Examples of the main provision of the proposed code are:

- Use steeper roof pitches (>45°), short spans in roof structure, short cantilever overhangs and eaves, simple roof designs, and roof-sheeting profiles with fluorocarbon polymer coatings noted for corrosion resistance and low frictional resistance
- Include snap-off awnings and gutters independent of main building frame

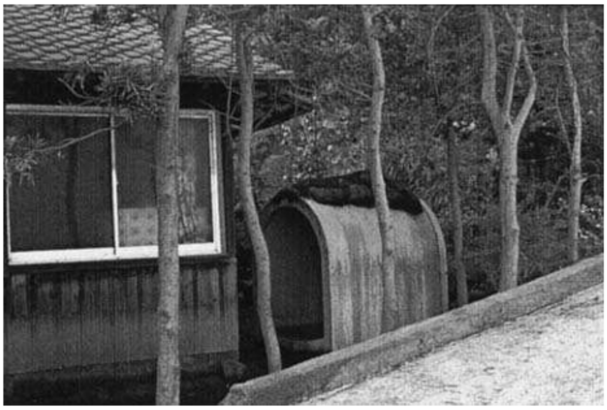

FIGURE 4 A reinforced concrete shelter designed to resist the impact of ballistic ejecta, Sakurajima volcano, Kyushu, Japan. (Photo, R. Blong.)

- Utilize underground electrical supply (seal switchboards, etc.)
- Provide floor area elevated 300 mm above ground surface to prevent ingress of mudfills (squeezing of muddy ash under hydrostatic head through openings under doors during and immediately after ashfalls)

The Kokopo "code" appears to be the first attempt to include formally in the design of significant buildings the potential impacts of tephra fall. Refinement, so that it could be used in a variety of situations, would be a useful step in risk management for volcanic hazards.

D. Other

Limited opportunities exist for risk reduction in relation to other volcanic hazards. Pyroclastic flow paths can be estimated and avoided, at least for relatively small flows. Containing or diverting pyroclastic flows is problematic given the forces involved. Nonetheless, the construction of training dikes with interior tunnel shelters and nets and fences for directing hot ash clouds to control pyroclastic flows produced by dome collapse at Unzen (Japan) have been proposed. Much of the construction would be carried out using remotely directed construction equipment to reduce the risk to human operators. For rock/debris avalanches, one or more of the height/length formulas can be used to estimate potential runout distances; possibly these areas can then be sterilized from high-risk land uses. Similarly, land-use planning and structural engineering measures can be used to reduce risks in tsunami-prone areas.

The hundreds of deaths in the degassing of Lakes Nyos and Monoun in Cameroon (1980s) led to detailed investigations and experiments. These indicated that the hazard could be reduced by degassing the bottom water of the lakes within a reasonable time using 140-mm diameter pipes. Although the solution is reasonably clear, and the problem moderately urgent, constraints, including the availability of finance and the difficulties of transporting heavy equipment to remote locations, mean that no hazard reduction has taken place to date.

Human vulnerability to most volcanic hazards could be reduced by prudent land-use planning. However, political and social realities dictate that land-use zoning that restricts occupation of areas where humans and structures are particularly vulnerable is only likely to occur where hazards are frequent. High-consequence, low-frequency volcanic events are unlikely to be included in the zoning process in most countries. Nonetheless, in developed countries considerable attention has been paid to high-consequence, low-probability dam failure under probable maximum precipitation conditions. The potential consequences of such events have annual probabilities of $<10^{-4}$. High-magnitude, low-frequency volcanic events with similar annual probabilities, and a similar severity of consequences, deserve at least similar risk reduction strategies.

Table III provides a selected list of risk reduction strategies that can be, or have been, employed in relation to a variety of structures, utilities, machinery, and crops. Most of the strategies relate to reducing the effects of tephra falls, reflecting the fact that this hazard affects by far the largest area. Most strategies have been developed for protecting equipment, cleaning equipment, removing ash, and operating on reduced supply and/or increased demand. Most strategies have been developed reactively (after the event), but most can be proactive—as expected in quality risk management. In almost all cases, proactive risk management will involve volcanologists in strategic planning and in interpreting the characteristics of volcanic hazards (Table I) for emergency managers and others vitally concerned with reducing the potential consequences of eruptions.

V. RISK TRANSFER

In the risk management chain (risk identification → risk analysis → risk reduction → risk tranfer), at some stage in the risk reduction process it will be recognized that there are a number of intractable risks. These are the risks that can be transferred to others—to other individuals, organizations, communities, institutions, entities, and/or governments. Often, the transfer involves only a portion of the risk; for example, rarely would either disaster relief or insurance involve a total transfer of the cost of damage. Disaster relief and insurance are the two broad ways in which risk is transferred.

A. Disaster Relief

Disaster relief has two broad aims: (1) to save life, ameliorate suffering, and salvage what can be salvaged from the immediate crisis—in broader terms, to return afflicted communities to the predisaster status quo—and

TABLE III Selected Risk Reduction Strategies

Risk reduction strategy	*Volcanic hazard*
Evacuate building contents	Lava flow, ground deformation
Improved fire resistance and reinforcement of disaster-relevant structures such as schools and civic halls	Projectiles, tephra falls
Place shutters, corrugated sheeting, and/or plastic sheets over windows and other openings; improve window frames and air-conditioning	Tephra falls
Remove tree branches above overhead power and communication lines	Tephra falls
Institute preventative management program for vehicles, machinery, filters, bearings, compressors, pumps, chains, switches, computers, and other electromagnetic equipment	Tephra falls
Revise emergency maintenance plan for power reticulation failures	Tephra falls
Remove dry ash from transformer insulators, bushings, etc., by air blowing, pressure washing, or brushing	Tephra falls
Plough switchyard gravel, bringing ash-free gravel to surface, to reduce step-and-touch potentials	Tephra falls
Allow household taxation deductions for ash removal	Tephra falls
Provide roofs for public school swimming pools and similar public areas	Tephra falls
Develop road clearance and traffic management strategies	Tephra falls
Develop water-use policies to cope with supply failures and increased demand	Tephra falls
Isolate storm water collection from sewage system	Tephra falls
Develop additional maintenance and monitoring for all sewage treatment equipment	Tephra falls
Clean roofs to prevent excessive tephra loads on buildings	Tephra falls, corrosion
Disconnect downpipes from roof water collection systems and seal tanks	Tephra falls, acid rains
Protect electromechanical systems from dust and corrosion; reduce maintenance intervals	Tephra falls, gases and aerosols
Review maintenance of clean areas in telecommunications centers; seal rooms with sensitive equipment	Tephra falls, floods
Install crossing gates on roads across lahar channels	Lahars
Reconsider bridge clearances; raise where necessary	Lahars
Revegetate unconsolidated tephra	Secondary lahars
Protect water supply intake structures in streams and initiate enhanced water quality management procedures	Lahars, tephra fall, and acid rain
Optimize lowered water levels behind water storage and electricity generation dams	Lahars, landslides
Cut off gas supply in areas where impacts expected	Lahars, pyroclastic flows, lava flows, ground deformation
Create refuges in air-tight below-ground cellars	Small pyroclastic flows
Increase resilience of disaster—relevant buildings	All
Improve and harden communication systems and information networks	All
Conduct evacuation and emergency management drills	All

(2) to increase disaster resilience by improving warning systems, infrastructure, etc. (in effect, risk reduction).

Disaster relief includes a wide range of activities from short-term search and rescue to long-term trauma counseling and resettlement. Typical relief activities include search and rescue; medical assistance; feeding, clothing, and sheltering evacuees, often for months or years; provision of clean-up equipment, material goods for house repairs, and tools of trade; short- and long-term financial assistance; and resettlement in safer areas around the volcano or even to other parts of the country.

The number of players in disaster relief can be enormous. One estimate suggests that 246 organizations were involved in relief efforts around Mount St. Helens in 1980. Typically, charities, community organizations, local government, and national government play a role.

International organizations including foreign governments, nongovernmental organizations (NGOs), and United Nations agencies may also participate. Both the media and politicians can play significant multifaceted roles in the disaster aftermath.

Traditionally, disaster relief has been concerned broadly with the immediate disaster aftermath, perhaps extending over a period of several years as the emphasis changes from saving lives to recovery and reconstruction. All of these activities effectively transfer risk, whereby part of the cost of the disaster is borne by groups not immediately affected—the community, taxpayers, international charities, and foreign governments (and taxpayers).

In the last two decades, increasing efforts have been made by disaster relief organizations to increase the resilience of vulnerable communities to risk. This process has been hastened by the UN-declared International Decade for Natural Disaster Reduction (1990–1999). On a global scale it seems difficult to argue that these efforts have been successful, but there are numerous local examples of enhanced warning systems, improved resilience of houses to hurricanes and/or earthquakes, coordinated relief efforts, and emergency management.

B. Insurance

Insurance is one of the most common methods, at least in developed countries, by which the losses produced by a volcanic eruption can be alleviated or distributed across a group much broader than the group suffering direct losses. Insurance allows rapid reinstatement of property as well as an infusion of funds into communities at a time when economic activity may have slowed. As insurers commonly reinsure against catastrophic losses, in order to spread the risk, the costs of insurance claims from a single eruption could be distributed around the world.

Volcanic eruptions have never produced billion dollar insurance claims, though 29 other natural disasters around the world between 1970 and 1996 have. Although the total economic losses resulting from the 1980 eruption of Mount St. Helens reached about U.S. \$1 billion, only about 3% of these were insured losses. Similarly, around Pinatubo insured losses amounted to only about 4% of total losses. Numerous cities around the world—Kagoshima, Naples, Catania, Auckland, Quito, Managua, San Salvador, Mexico City, Bandung, Yokyakarta, Manila, Legazpi City, and Guatemala City, for example—are close enough to volcanoes to suffer catastrophic losses. With the exception of Auckland, none of these cities has a high insurance density and insured losses would be low relative to total losses.

However, numerous other cities with high insurance densities—Tokyo, Yokohama, Vancouver, Seattle, and Portland, for example—have the potential to receive minor ashfalls that might produce limited direct damage but considerable business interruption. In a world where globalization of industry, just-in-time manufacturing, and electronic commerce are of increasing importance, an eruption on one side of the world that damages a component factory can trigger business interruption insurance claims from an assembly plant on another continent.

Individual corporations can also transfer risks by "Insuring" against potential losses from volcanic eruptions using hedges against currency and commodity values. The extent to which hedging against future eruptions actually occurs is unknown, but is likely to be small. Unlike the potential losses associated with earthquakes and hurricanes, the catastrophe potential of volcanic eruptions remains largely unrecognized by insurers or financial markets.

Insurance is clearly proactive in that coverage must be arranged before the impact of the event. Where insurance offers premium rates that reflect actual risks, there can be a strong incentive for risk reduction, rather than risk transfer. Of course, where the risk is regarded as excessive, insurers withdraw from the market, "redline" the most exposed policies, or raise premiums to levels that customers find unacceptable. In Rabaul, 10 years before the eventual eruption, the seismic crisis of 1984 produced just these results—in effect, some insurers transferred the risk back to property owners, to the community, and to government.

VI. CONCLUSIONS

1. Risk management for volcanic hazards involves partnerships between volcanologists and a wide variety of community stakeholders. Risk management involves an appreciation of cultural attitudes to risk as much as it does the quantification of risk. The sequence of activities—risk identification →risk analysis→ risk reduction→ risk transfer—provides a logical framework for risk management.

2. Commonly, after earthquakes, teams of earthquake engineers analyze building and lifeline perfor-

mance, adding to the global body of knowledge and influencing seismic codes worldwide. In contrast, posteruption volcanological investigations have only rarely considered vulnerability reduction. Provisions to reduce the impact of tephra fall have rarely been incorporated into building codes.

3. There are numerous opportunities for the reduction of risk posed by volcanic hazards. These are likely to be particularly effective in the event of small to moderate eruptions.

4. Risk reduction can be reactive, for example, the posteruption development of engineering structures that divert or pond lahars or lava flows. Disaster relief alleviates suffering and reasserts the status quo. Proactive risk reduction and transfer, on the other hand, utilize the whole risk management chain to promote activities that minimize the risk of life loss, facilitate appropriate warning and evacuation systems, and improve the resilience of structures, lifelines, and economic activities.

SEE ALSO THE FOLLOWING ARTICLES

Hazards from Pyroclastic Flows and Surges • Impacts of Eruptions on Human Health • Lahar and Jökulhlaup Hazards • Lava Flow Hazards • Risk Education and Intervention • Volcanic Crises Management • Volcano Warnings

FURTHER READING

Adams, J. (1995). "Risk." UCL Press, London.

Barberi, F., Carapezza, M. L., Valenza, M., and Villari, L. (1993). The control of lava flow during the 1991-1992 eruption of Mt Etna. *J. Volcanol. Geotherm. Res.* **56,** 1–34.

Blong, R. J. (1984). "Volcanic Hazards—A Sourcebook on the Effects of Eruptions." Academic Press, Sydney.

ICE (1995). "Megacities—Reducing Vulnerability to Natural Disasters." The Institution of Civil Engineers, Thomas Telford, London.

IUGS, Working Group on Landslides (1997). Page 3–12 *in* "Landslide Risk Assessment: Proceedings of the International Workshop on Landslide Risk Assessment, Honolulu, February 1997, A. A. Balkema, Rotterdam" (D. Cruden and R. Fell, eds.).

Molak, V., ed. (1996). "Fundamentals of Risk Analysis and Risk Management." CRC, Lewis, FL.

Peterson, D. W. (1988). Volcanic hazards and public response. *J. Geophys. Res.* **93,** 4161–4170.

Rodolfo, K. S. (1995). "Pinatubo and the Politics of Lahar—Eruption and Aftermath, 1991." Univ. of the Philippines Press, Manila.

Scarpa, R., and Tilling, R. I., eds. (1996). "Monitoring and Mitigation of Volcano Hazards." Springer-Verlag, Berlin.

Sparks, R. S. J., Bursik, M. I., Carey, S. N., Gilbert, J. S., Glaze, L. S., Sigurdsson, H., and Woods, A. W. (1997). "Volcanic Plumes." Wiley, Chichester.

This Page Intentionally Left Blank

SCENIC FLIGHTS

RISK EDUCATION AND INTERVENTION

DAVID JOHNSTON
Institute of Geological & Nuclear Sciences

KEVIN RONAN
Massey University

I. Noncrisis Public Education Programs
II. Crisis Response
III. Summary

GLOSSARY

"cry wolf syndrome" An informal term for the phenomena where the public fail to respond to a warning after repeated false alarms.

distress A state of anguish brought about by some situation or event over which an individual has little or no control.

imaginal Exposure to a setting associated with distress in the imagination.

intervention Pre- or postevent action undertaken by responding agencies or groups to reduce the physical and psychological impacts of an event.

in vivo Direct exposure to an actual setting associated with distress.

multiple gating A model of intervention designed to capitalize on available resources when addressing the needs of large numbers of people both before and following an eruption.

PTSD Post-traumatic stress disorder. An anxiety-based psychiatric disorder that follows exposure to an extremely stressful event.

warnings A message usually given to a specific community or communities when a direct response to a threat is required.

VOLCANOLOGISTS REFER TO a "volcanic crisis" as the realm of events concerned with the awakening of a volcano, the building up to an eruption, the eruption itself, and the aftermath as the affected region recovers. Accordingly, the management of volcanic hazards can be divided into four distinct time frames. Noneruptive or quiescent times are the most common and afford the best opportunity to develop mitigation strategies and prepare society for an eruption. The crisis period is divided into three periods: pre-eruption, eruption, and posteruption (or recovery). During the crisis period, risk education and effective interventions are critical in reducing the adverse effects of volcanism on society.

I. NONCRISIS PUBLIC EDUCATION PROGRAMS

A. Background

Dissemination of information about potential volcanic hazards is important in encouraging an appropriate pub-

Copyright © 2000 by Academic Press
All rights of reproduction in any form reserved.

lic response and in reducing social impacts. Research over the past 2 decades has shown that the majority of the public do not engage in the self-protective measures recommended by civil defense authorities during non-crisis times. This finding may question the value of public education activities but there is good evidence that hazard knowledge and understanding lead to appropriate responses during a crisis (evacuation, warning compliance, etc). However, several studies have found that multiple messages, delivered by multiple agencies, through multiple channels, but carrying a consistent theme, can lead to an interactive personal search for more information. From this "personal information searching" emerges a personal definition of risk which in turn leads to protective behavior. A survey in New Zealand following the 1995 Ruapehu eruptions found that although some agencies are perceived as more credible than others as the source of volcanic-hazard information, no one agency has a monopoly on perceived credibility (i.e., different people recognize different agencies as the best source of information for volcanic-hazard information and warnings), and this finding supports the need for interorganizational cooperation in hazard education. Similar results have been found in the United States and Japan.

Schools play a vital role in natural hazard education, with volcanic hazards included in the science and geography curricula (Figure 1). Research into the content of educational material suggests that the following ingredients are important: personalized information, facts about the likelihood and severity of the hazard, and practical precautionary measures. It has also been found that children involved in an education program discuss what they learned in such a program with parents or caregivers.

Volcanic eruptions are generally less common than other types of hazardous phenomena, such as floods or extreme weather; therefore, in most cases children (and adults) seldom gain personal experience of such events. The mass media provides a large amount of natural disaster news annually. Disasters that do occur provide an ideal opportunity for children (and adults) to gain an improved understanding of the event. But a note of caution: media reports often contribute to biased perceptions that exist among the public. The media frequently give uneven coverage focusing on high-impact, low-frequency events. There is commonly a bias toward reporting on the victims and not those who survived or who were only lightly impacted within the disaster area. The lack of valuable follow-up reporting when disaster-impacted communities successfully cope with their predicament is noteworthy. Thus, responding agencies need to plan for media involvement in order to promote messages that are aimed at assisting

TAUPO VOLCANIC ZONE
29 20:3

FIGURE 1 School children visiting the Taupo Volcano Observatory, New Zealand. The public information center is popular with school groups and adult visitors. It proved extremely valuable during the 1995–1996 Ruapehu eruption as a venue for press conferences and providing updated information on the eruptions to the visiting public. [Photo copyright Institute of Geological and Nuclear Sciences Ltd.]

preventive efforts versus, for example, simply raising alarm.

B. Designing and Monitoring an Education Program

Education programs about volcanic hazards (Figure 2) should be carefully designed in order to achieve the desired outcomes, and monitoring can be put in place to assess their success. The planning process should address the following:

- Identification of existing education resources related to volcanic hazards and all current methods of disseminating public information on volcanic hazards
- Consideration of the appropriateness of current resources and methods of dissemination

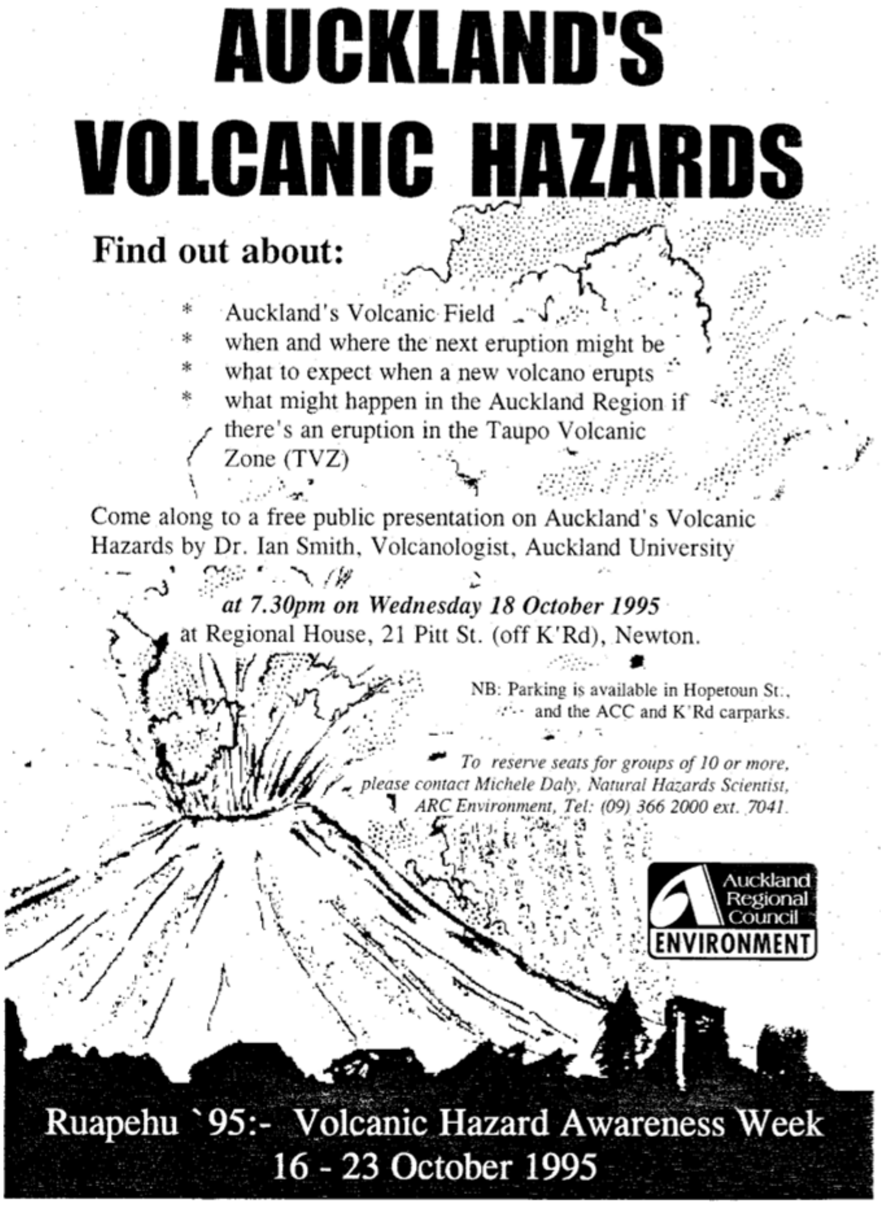

AUCKLAND'S VOLCANIC HAZARDS

Find out about:

* Auckland's Volcanic Field
* when and where the next eruption might be
* what to expect when a new volcano erupts
* what might happen in the Auckland Region if there's an eruption in the Taupo Volcanic Zone (TVZ)

Come along to a free public presentation on Auckland's Volcanic Hazards by Dr. Ian Smith, Volcanologist, Auckland University

at 7.30pm on Wednesday 18 October 1995
at Regional House, 21 Pitt St. (off K'Rd), Newton.

NB: Parking is available in Hopetoun St., and the ACC and K'Rd carparks.

To reserve seats for groups of 10 or more, please contact Michele Daly, Natural Hazards Scientist, ARC Environment, Tel: (09) 366 2000 ext. 7041.

Auckland Regional Council
ENVIRONMENT

Ruapehu `95:- Volcanic Hazard Awareness Week
16 - 23 October 1995

FIGURE 2 An advertisement for a public talk on volcanic hazards from the Auckland Volcanic Field. The talk was part of a national volcanic hazard awareness week organized to promote awareness of volcanic hazards in New Zealand.

- Development of new resources and methods of dissemination where required
- Identification of resources to staff and operation of media/public information functions

C. Examples of Hazard Education Initiatives

1. *Mount Rainier Volcano, USA*

In an effort to inform local inhabitants and officials of the volcanic and landslide hazards posed by Mount Rainier volcano (Washington, USA), the U.S. Geological Survey (USGS) has developed a multiyear educational program specifically for public officials, educators, the media, and the general public (Figure 3). The goal is to motivate each audience to (1) participate in the education effort, (2) develop personal emergency preparedness plans, and (3) develop emergency response plans for their communities. The USGS is using a range of methods to achieve their goals, including permanent and temporary exhibits, annual workshops for educators, public talks, release of a video about volcanic hazards at Mount Rainier, and the release of printed material on the hazards. A mailing list keeps concerned citizens informed of new developments.

2. *Egmont Volcano, New Zealand*

The Taranaki Regional Council in New Zealand has taken the lead role in raising awareness of volcanic hazards in communities around the Egmont volcano. A 2-year public education and awareness program was initiated in 1995 to promote public awareness of (a) the hazard and (b) the need to prepare for a volcanic event. The Egmont Volcanic Contingency Plan was the basis for the program, and this plan stressed the importance of four evacuation zones defined by the severity of the volcanic risk (Figure 4). Volcano-education kits were developed and distributed to every school in the region along with 36,000 volcanic brochures and 40,000 book-

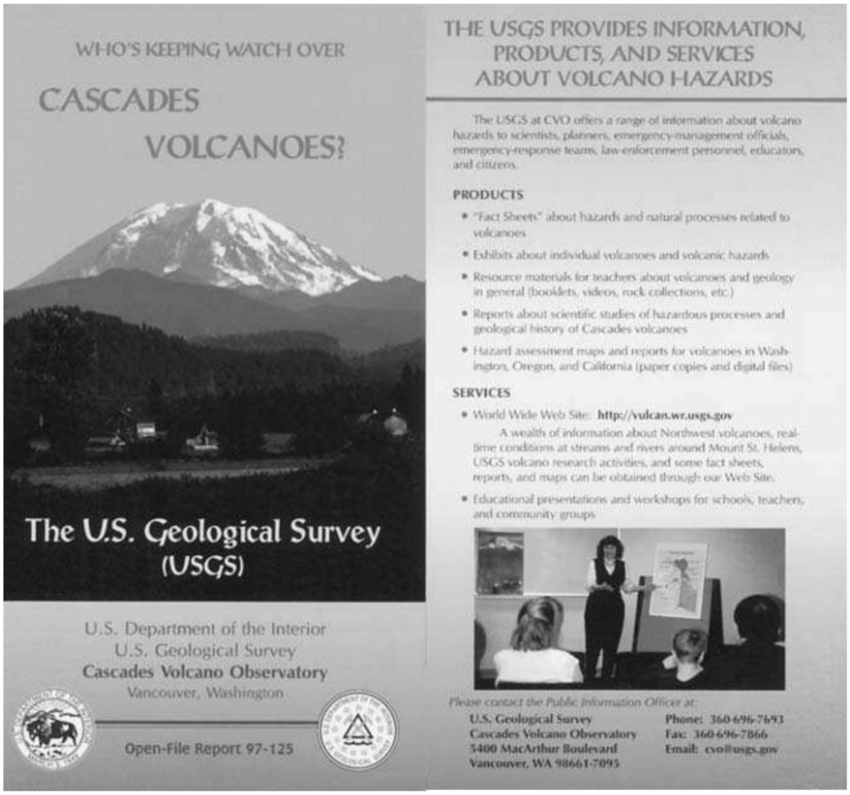

WHO'S KEEPING WATCH OVER

CASCADES

VOLCANOES?

The U.S. Geological Survey

(USGS)

U.S. Department of the Interior

U.S. Geological Survey

Cascades Volcano Observatory

Vancouver, Washington

Open-File Report 97-125

THE USGS PROVIDES INFORMATION, PRODUCTS, AND SERVICES ABOUT VOLCANO HAZARDS

The USGS at CVO offers a range of information about volcano hazards to scientists, planners, emergency-management officials, emergency-response teams, law-enforcement personnel, educators, and citizens.

PRODUCTS

- "Fact Sheets" about hazards and natural processes related to volcanoes
- Exhibits about individual volcanoes and volcanic hazards
- Resource materials for teachers about volcanoes and geology in general (booklets, videos, rock collections, etc.)
- Reports about scientific studies of hazardous processes and geological history of Cascades volcanoes
- Hazard assessment maps and reports for volcanoes in Washington, Oregon, and California (paper copies and digital files)

SERVICES

- World Wide Web Site: **http://vulcan.wr.usgs.gov**

  A wealth of information about Northwest volcanoes, real-time conditions at streams and rivers around Mount St. Helens, USGS volcano research activities, and some fact sheets, reports, and maps can be obtained through our Web Site.
- Educational presentations and workshops for schools, teachers, and community groups

Please contact the Public Information Officer at:

U.S. Geological Survey
Cascades Volcano Observatory
5400 MacArthur Boulevard
Vancouver, WA 98661-7095

Phone: 360-696-7693
Fax: 360-696-7866
Email: cvo@usgs.gov

FIGURE 3 A brochure produced by the U.S. Geological Survey as part of their volcanic hazards education program.

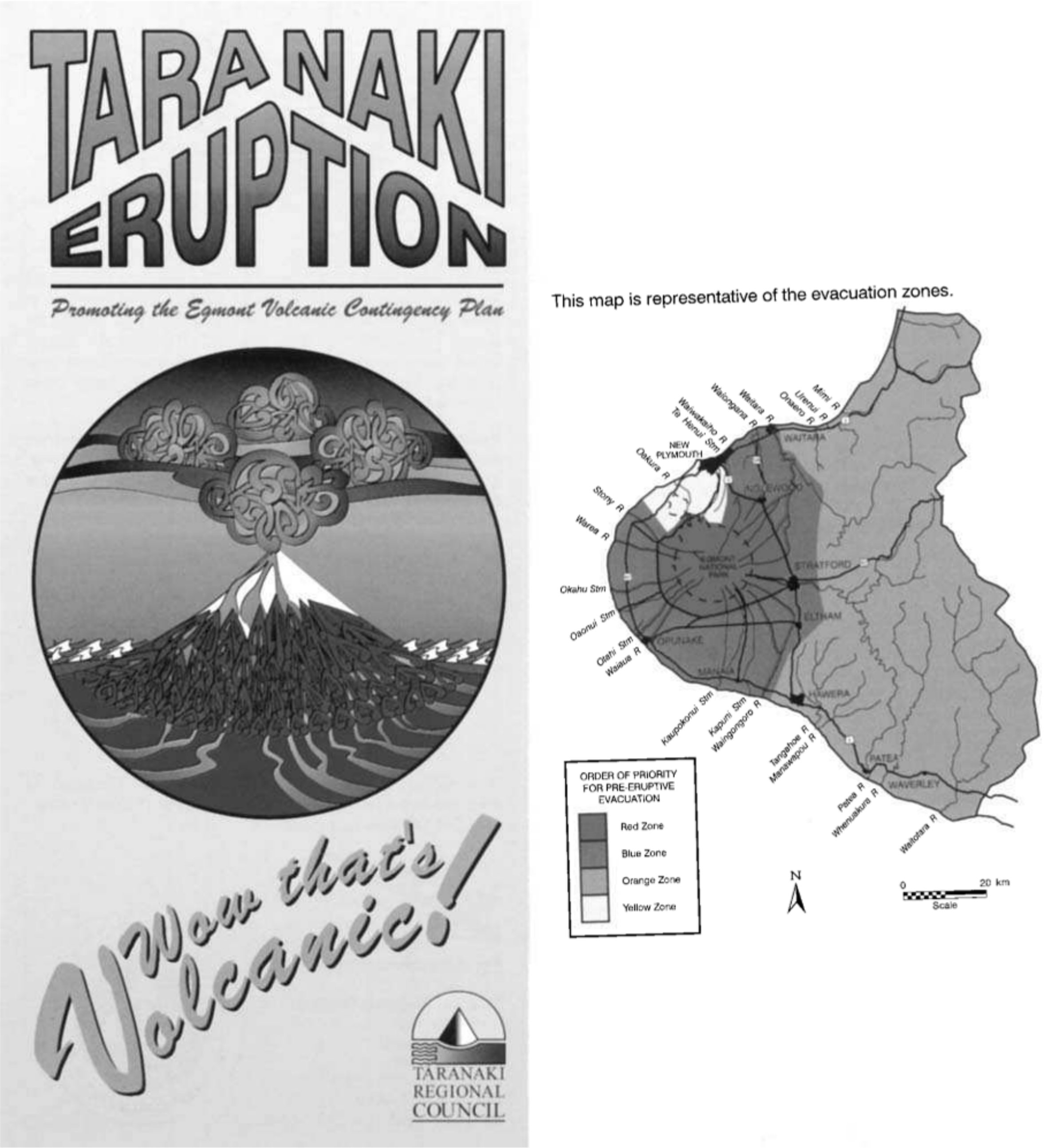
TARANAKI ERUPTION
Promoting the Egmont Volcanic Contingency Plan
Wow that's Volcanic!
TARANAKI REGIONAL COUNCIL
This map is representative of the evacuation zones.
Mimi R
Urenui R
Onaero R
Waitara R
Waiongana R
Waiwakaiho R
Te Henui Stm
NEW PLYMOUTH
Oakura R
Stony R
Warea R
Okahu Stm
Oaonui Stm
Otahi Stm
Waiaua R
Kaupokonui Stm
Kapuni Stm
Waingongoro R
Tangahoe R
Manawapou R
Patea R
Whenuakura R
Waitotara R
WAITARA
INGLEWOOD
EGMONT NATIONAL PARK
STRATFORD
ELTHAM
OPUNAKE
MANAIA
HAWERA
PATEA
WAVERLEY
ORDER OF PRIORITY FOR PRE-ERUPTIVE EVACUATION
Red Zone
Blue Zone
Orange Zone
Yellow Zone
N
0
20 km
Scale

FIGURE 4 A brochure produced by the Taranaki Regional Council, New Zealand, as part of their volcanic hazards education program. The map shows the four predefined evacuation zones.

marks. Fifty copies of the video "Understanding Volcanic Hazards" were distributed to all public libraries for use by local communities, along with presentations to community groups by members of the civil defense staff. The Taranaki Eruption program survey completed in August 1997 indicates that the level of awareness about volcanic hazards increased from 37 to 56% in the Taranaki region. The educational material is still available in the community and will be reviewed every 2 years.

II. CRISIS RESPONSE

A. Public Information

During a volcanic crisis, demand for information is intense and this demand will place a strain on all responding agencies. Experience during past eruptions has shown that a crisis period is not the best time to prepare educational material for the public. However, public information prepared in advance can be printed during the crisis (if required) and disseminated rapidly. Communications networks can be severely disrupted during and after an eruption, and therefore information about what to expect and what to do during an eruption must be distributed early. When an emergency is in progress, civil defense officials have to distinguish between sending messages which direct an emergency response and sending those providing public information about the emergency. It is important that responding agencies put information into the news instead of waiting for the media to discover their own "news" (i.e., the need for a media response plan or plan component).

During a crisis, systems often break down, data are misinterpreted, and conditions rapidly change, rendering previously released information "out-of-date." Incorrect or misleading information should be corrected by follow-up information, accompanied by explanations as to the origins of apparently "unreliable" information. When the current information is full of uncertainty (a common situation prior to an eruption and during an eruption) it is important to avoid making or disseminating unrealistic forecasts. This will lessen concerns about the "cry wolf syndrome," a concern common among many public officials. Rumor control is a critical function for agencies responsible for giving out public information, and these agencies should be proactive in identifying and correcting incorrect or misleading information. However, some caution is needed because immediate and harsh official denouncement of popular views may be counterproductive and treated with suspicion as the public often prefer to hear a range of opinions before drawing their own conclusions on a subject.

The social and economic impacts of adverse events are determined not only by direct physical consequences but by the interaction of psychological, social, cultural, and institutional processes that can amplify and attenuate the public response. This is commonly referred to as "social amplification of risk" and this was clearly evident during the 1995–1996 Ruapehu (New Zealand) eruptions. Much of this "social amplification" was fueled by the media coverage which brought dramatic images of the eruption to people throughout New Zealand and the world.

B. Warnings

Warning messages are usually given to a specific community or communities when a direct response to a threat is required. The response to warnings by individuals has been found to relate to (i) individual risk perception (understanding, belief, and personalization); (ii) the nature of the warning information (specificity, consistency, certainty, accuracy, clarity, media, frequency, etc.); and (iii) the personal characteristics of the recipient (demographics, knowledge, experience of the hazard, social network, and so on). A consistent and clear conclusion of social science research is that the warning message itself is one of the most important factors that influences the effectiveness of the warning system. Unfortunately one or more of the important attributes required of warning messages (specificity, consistency, certainty, accuracy, clarity) is usually deficient or missing during a volcanic crisis. Commonly specificity and certainty about the time and nature of the eruption are missing. Responding authorities must recognize this.

Five topics are important when constructing a warning message: (1) the hazard and/or risk, (2) guidance, (3) location, (4) time, and (5) source. The warning message must contain information about the impending hazard with sufficiently simple detail that the public can understand the characteristics of the hazard that they need to protect themselves from. The message should include guidance about what they should do to maximize their safety. The warning message must describe the exact location that is at risk and address the "when" aspect of the required response.

The final important dimension is the source of the information. Warnings are more likely to be believed if they come from "credible" sources. The public's perception of credibility of information sources is a subjective judgment and has been shown to be related to notions of expertise and trustworthiness. Three general bases on which credibility can be judged are: (1) the "credentials" of the person or agency issuing the warning; (2) the relationship of the organizations to other "credible" organizations; and (3) the past history of job performance. Trust and credibility are valuable assets—difficult to obtain and once lost, difficult to regain. Prior to a volcanic crisis, agencies which may have to issue warnings or at least have a role in their dissemination can take a proactive step toward enhancing their credibility. Agencies working in a coordinated and collaborative way with other agencies can improve their own credibility. Having a senior or publicly recognized person issuing or associated with the issuing of a warning notice and issuing warnings in association with other "lead" agencies will enhance credibility.

C. Examples of Crisis Responses

1. *Mount Pinatubo, 1991: Learning Lessons*

Thousands of lives were saved during the eruption of Mount Pinatubo in the Phillipine Islands following a cooperative effort between the Phillipine Institute of Volcanology and Seismology (PHIVOLCS) and the USGS. The primary reason for successful evacuation of inhabitants was the cooperative effort between volcanologists and government officials. Through the use of a straightforward and readily comprehensible alert level scheme (ranging from 1 = low-level unrest to 5 = eruption in progress; see Table I) and the presentation of a nonjargonistic video to public officials on the dangers of volcanoes (pyroclastic flows, lahars, etc.), both public officials and citizens became aware of the potential need for evacuation. As the alert level was progressively raised, so too was the radius of evacuation around Mount Pinatubo. By the time the eruptions of June 15, 1991, had begun, 58,000 people were evacuated. A major point to be taken from the Mount Pinatubo eruption and response is the role that volcanologists play in helping initiate a sequence of crisis response activities. That is, government officials may, as described in the next example, be reluctant to act for a variety of reasons. However, if scientists can describe volcanic processes and hazards in simply understood language and combine that with a message of the need for action in certain circumstances, this can set in motion the necessary events to save people's lives.

2. *Nevado del Ruiz, 1985: A Failure*

The eruption of Nevado del Ruiz volcano in Colombia on November 13, 1985, was about one-tenth the size of the 1980 Mount St. Helen's eruption. However, over 20,000 people died as a result of volcanic mudflows (lahars) whereas less than 100 died in the Mount St. Helens eruption as a consequence of a directed volcanic blast. Though the town of Armero, 72 km from the

TABLE I Alert Levels for Mount Pinatubo, May 13, 1991[a]

Alert level	*Criteria*	*Interpretation*
No alert	Background; quiet	No eruption in foreseeable future
1	Low-level seismicity; other unrest	Magmatic, tectonic, or hydrothermal disturbance; no eruption imminent
2	Moderate level of seismicity, other unrest, with positive evidence for involvement of magma	Probable magmatic intrusion; could eventually lead to an eruption
3	Relatively high and increasing unrest including numerous b-type earthquakes, accelerating ground deformation, increased vigor of fumeroles, gas emissions	If trend of increasing unrest continues, eruption possible within 2 weeks
4	Intense unrest, including harmonic tremor and (or) many "long-period" (low-frequency) earthquakes	Eruption possible within 24 hours
5	Eruption in progress	Eruption in progress

Stand-down procedures:

In order to protect against "Lull before the storm" phenomena, alert levels will be maintained for the following periods after activity decreases to the next lower level:

from Alert level 4 to 3—Wait 1 week
from Alert level 3 to 2—Wait 72 hours

[a] Slightly different schemes have been developed for other volcanoes worldwide. Some volcano observatories use a numbering system whereas others use a color scale.

Source: Newhall, C. G., and Punongbayan, R. S., eds. (1996). Page 90 *in* "Fire and Mud: Eruptions and Lahars of Mount Pinatubo, Philippines." Philippine Institute of Volcanology and Seismology and Univ. of Washington Press.

volcano, was identified by geological studies as being at risk from lahar inundation—it was directly in the flow path of lahars resulting from pyroclastic flows melting the snow on Nevado del Ruiz—an assortment of human errors contributed to a lack of warning.

After the eruption began, and even though the Armero police were notified, there was no or very little response. This was probably linked to the fact that the eruption happened 2 days before an emergency management plan was to have been reviewed. Thus, despite the scientific knowledge, various human factors precipitated this disaster. At the time of the eruption police may not have known how to translate the warning into public protective activity. In addition, there was a lack of risk education and information about volcanic hazards available to the public. These included no pre-event public education programs and the lack of a warning system and evacuation plan established, tested, and in place. From a human factors perspective, the element of fear in government officials was great—the most common human reaction to uncertainty about the environment is fear and anxiety. The prediction of volcanic eruptions brings with it uncertainty and the fear of false alarms. We know from psychological research that the most common behavior associated with fear and uncertainty is avoidance of action. Thus, an issue worth bearing in mind is the necessity of appropriately trained personnel being in charge of pre-event planning, education programs, warning systems, and risk mitigation—not only those who have the intimate knowledge of what needs to be done but also those who have the courage to counter fear, avoidance, and inactivity and be willing to initiate warning systems and evacuation plans when necessary despite protests from official quarters.

D. Postevent Interventions

1. Rationale

Postevent education and intervention need to focus on both physical needs and social factors. Of course, there is a close relationship between these factors following a major disaster. Generally, people affected by a major disaster not only have physical needs to be met, including physical safety, they also have to cope with the distress, fear, and grief that can be associated with such events. Often, people will lose a sense of control and feel very uncertain about the future. As we have discussed, what usually accompanies uncertainty and a lack of control is a decreased ability to enact adaptive behaviors. In the first instance, these behaviors need to focus on physical survival; however, people who are very distressed or in shock often lack the necessary psychological resources to initiate recovery-based activities. Thus, while issues related to safety and physical needs take necessary precedence as seen in the case examples of Nevado del Ruiz and Pinatubo, social factors are obviously implicated in risk and recovery-related communication. Responding agencies have an obligation to build in information speaking to these factors. For example, part of planning for warning systems includes having in place guidelines for informing people when eruption and warning levels are declining, and what people should be doing to keep themselves and their families safe and to meet their physical needs. An issue of critical importance related to both physical needs and social factors is the absolute necessity of pre-event planning and coordination across all responding agencies. As we pointed out earlier in discussing pre-event education programs, the critical issue of consistent messages being sent out by multiple agencies through multiple channels is just as relevant following an event as it is in helping the public be prepared. When various agencies are not coordinated and are putting out inconsistent or even conflicting information, uncertainty will result. As we have pointed out, the most common emotion associated with uncertainty is anxiety and fear; the most common behavior is avoidance. Consistent themes presented by various agencies can help people not only reduce uncertainty, but also help them to gain an increased sense of control about what constitutes appropriate mitigation and recovery-based behaviors. Thus, the process of planning and coordination across agencies combined with the actual consistent content of messages will set the stage for helping people reduce uncertainty, feel more in control, and begin to take action.

Owing to the fact that enacting response and recovery-related behaviors following a disastrous event may be competing with distress and grief, all postevent education approaches need to be mindful of psychological factors. An initial way to include such factors was just discussed (i.e., planning and coordination across agencies and consistent messages to help people reduce uncertainty and reestablish a sense of control). Another way that we have found is to pursue collaborations between physical and social scientists. As we articulated earlier, given that the credibility of a communication source is an issue in this field, our own approach in New Zealand has increasingly emphasized such collaborations. For example, as we will expand upon in the case example section later, following the Ruapehu eruptions, misinformation about physical aspects of the eruptions (e.g., safety and effects of ash in water supplies) led to distress in some children and adolescents (and some parents). Information provided by a volcanologist (senior author)—in consultation with a child clinical psychologist (second author)—helped reduce fears and distress and increase coping ability.

In terms of social and emotional factors, a necessary first step in any intervention is an awareness of the normative effects of hazards and disasters on communities and individuals. While a fairly sizable data base has focused on such factors, systematic research looking at the effectiveness of postevent interventions is sparse. One reason for this is that the topic of postdisaster research is in its infancy. The formal concept of posttraumatic stress disorder (PTSD) did not gain formal recognition in the psychology profession until the 1980s. Though some research has looked at the effectiveness of different approaches following other traumatic events (e.g., assault), very little has looked at these approaches following a natural disaster. However, this has not prevented numerous education and intervention approaches being developed for disaster victims. They range from those emphasizing predisaster readiness as discussed earlier to a range of approaches emphasizing postdisaster coping. Postevent approaches range from community-based early intervention (i.e., soon after the event) to longer term approaches for those who do not cope effectively.

We focus here on general issues identified as important following distressing events as a guide to developing specific programs following volcanic eruptions. The first includes a technique called "multiple gating," followed by a discussion of elements included in education and intervention approaches.

2. *Multiple Gating*

Multiple gating is a model of intervention designed to capitalize on available resources when addressing the needs of large numbers of people both before and following an eruption. This approach is designed to use a parsimonious assessment methodology to help identify those at risk for increased distress. For example, self-report measures are available that can be filled out in a matter of minutes. For those identified at this initial "gate," brief education programs can focus on providing relevant information (see next sections for the content of this information) in large group, community-based settings (e.g., at local schools). For those who do not respond to such efforts, later gates can become increasingly comprehensive in terms of both assessments used and intervention offered (e.g., small groups, family-based, individually focused). When large numbers of people are impacted and when a dearth of resources are available for individual attention to each person's needs, this approach can be ideal.

The first step in this model is primary prevention. As we discussed earlier, predisaster readiness has been identified as effective in helping people more readily adapt to the effects of a disaster. While some eruptions can be anticipated to a degree, others occur with less warning. In these cases, crisis response and other forms of early intervention are vital. Crisis response can assist people to cope with safety issues and physical needs while also serving as a first line of intervention to help with negative emotional arousal. Early intervention is designed to help victims establish a sense of control that can prevent future problems. These interventions can be planned and implemented first to assist at a community-wide level. For example, community-and school-based education programs can provide efficient information dissemination that includes specifics on safety, physical needs, what constitutes normal reactions to a disaster, coping skills, and information about how to access agencies and support. A brief education program presented by a volcanologist and child clinical psychologist reduced symptoms of PTSD and increased coping ability in 7- to 13-year-old schoolchildren following the 1995 Mount Ruapehu eruptions. These children continued to show reduced distress at follow-up 7 months after the initial disaster. We illustrate this program shortly.

For those who continue to have problems despite such initial efforts, the next gate would emphasize group- or individually focused interventions to provide additional help. The major point to be taken from this section is that the use of a gating methodology allows for efficient use of available resources. We now discuss features of education and intervention programs that we believe are important.

3. *Support and Information*

While support is often a given following a natural hazard, some focus on this factor is necessary owing to its importance. Victims of disasters need support. One vital part of support discussed above includes helping victims become aware of important information as soon as possible after the disaster. As discussed, victims can begin to regain control as they receive information that addresses safety factors, physical needs, normal psychological effects of natural hazards, and simple coping skills (e.g., simple problem-solving skills, how and where to access information and agency-based support, the rationale behind using social support networks). There may be loss associated with an eruption. Within supportive environments, victims can be provided with information that helps them understand issues related to the normal grieving process.

4. Specific Ingredients: Focus on Exposure and Related Techniques

Despite differences across a variety of intervention approaches, most emphasize looking back at the event and dealing with the distressing thoughts and associated feelings.

The rationale behind the technique of exposure is that the distress associated with an event will diminish as a function of a habituation process (i.e., "extinction") associated with the willingness to look back at stimuli associated with that distressing event. An issue that underlies this technique is the time interval allowed for exposure to traumatic stimuli. Overly brief exposure intervals are not recommended. In fact, too brief an interval may actually increase distress. Generally, exposure intervals need to be sufficiently long enough that the persons begins to experience reduced arousal and distress. Variation in application does, however, exist in terms of the level of arousal (low versus high) as well as the type of actual exposure (imaginal versus *in vivo*). For example, the variant "systematic desensitization" uses a hierarchy of fears ranked from least to most distressing and imaginal exposure. By contrast, *in vivo* flooding involves direct exposure to the actual setting associated with distress. The idea here is to induce a high level of anxiety that begins to reduce with prolonged exposure intervals. For example, intervention following volcanic eruptions most often cannot involve direct exposure to eruptive activity. However, exposure can nevertheless take place. For example, video excerpts of the 1995 Mount Ruapehu eruptions were used in an intervention with children and adolescents (see later case example).

Interventions that use exposure generally include other techniques. For example, relaxation (e.g., breathing relaxation, deep muscle relaxation) during exposure is designed as a competing response to excess arousal. Exposure-based approaches may also include the technique of modeling (i.e., watching another cope effectively) and practice (e.g., role play) of coping skills. Self-reward (the ability to "pat oneself on the back") is a skill designed to reinforce consistent attempts at mastery and coping. Homework is designed to help the victim practice skills learned in naturalistic settings.

In addition to these techniques, intervention often includes other components aimed at cognitive and affective processes (e.g., reducing uncertainty). For example, in working with anxious children, including those who have experienced traumatic events, we use a FEAR acronym to help children remember problem-solving steps and increase their sense of control: identifying unwanted arousal as a signal to using relaxation techniques (*f*eeling upset?), identifying fear-related thinking (*e*xpecting bad things to happen?), devising and carrying out coping plans (*a*ttitudes and actions that can help), and engaging in self-reward and coping with less than complete success (*r*esults and rewards). Once learned, this approach is then used to help the child cope during the second half, or exposure phase, of the intervention. Other techniques—modeling and role play, praise, concrete reinforcement, homework tasks, and assisting parents—are used to help the child (and family) use these skills. This kind of approach appears to have promise for children following volcanic eruptions. Similar problem-solving models have proved useful with adults and families.

E. Case Study: Ruapehu Early Intervention

In this section, we provide one example of an early intervention with children—that is, what would constitute the initial steps in a multiple gating intervention model. At the end of the case example, we provide ideas on multiple gating with adults (and families).

A study by the authors has assessed the effects of a brief, school-based intervention with children following the 1995 eruptions of Mount Ruapehu, New Zealand (Figure 5). One hundred twelve children, ages 7 to 13, from three separate schools all within an 11-km radius of the base of Mount Ruapehu participated in two preintervention assessments 1 and 3 months following the initial eruptions. The children were assessed on self-reported levels of (a) PTSD symptoms as well as (b) the ability to cope with stimuli related to the eruptions (e.g., thoughts about the eruptions). Of the children involved, 62% were identified as having mild or greater self-reported PTSD-related distress 1 month following the eruptions. It is also a common finding in working with distressed children that some who were deleteriously impacted very likely were not willing to admit distress on self-reports. Consequently, it is likely that there was another small subsample of distressed children not identified through our self-report methodology.

The intervention itself was administered 2 months after this first assessment. Children from each school were randomly assigned to one of two 1-hour intervention conditions: (1) video-based exposure combined with

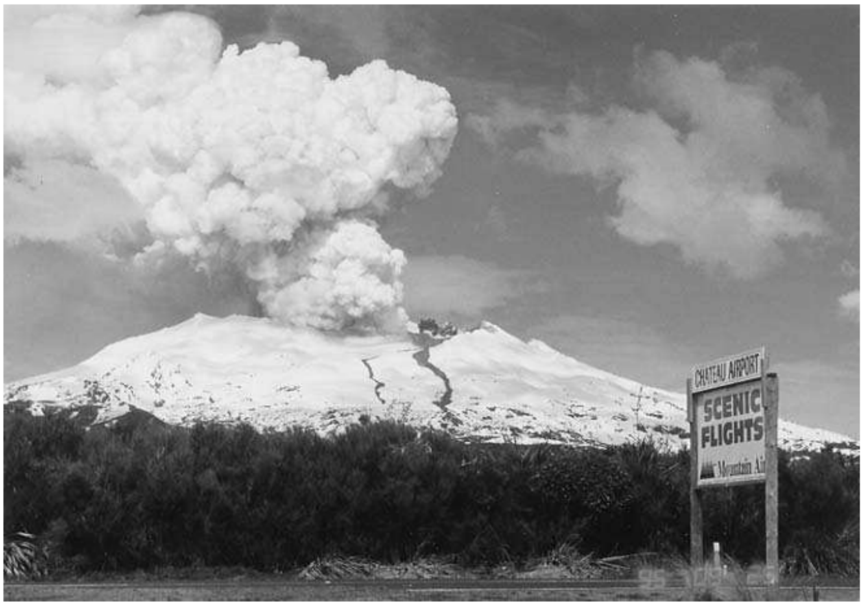

FIGURE 5 Eruptive activity from Ruapehu on Monday, 25 September 1995. The 1995 eruptions lasted for 3 months and caused closure of three ski fields and had a major economic impact on surrounding communities. Further eruptions in 1996 amplified the effects from the previous year's eruptions. [Photo copyright Institute of Geological and Nuclear Sciences Ltd.]

expert information or (2) video-based exposure, expert information, and additional cognitive-behaviorally based intervention. The first condition included a 20-minute video of the initial eruptions and a presentation by a volcanologist on physical science. This presentation included issues related to general safety (e.g., ash was a nuisance rather than life threatening) following consultation between the volcanologist (first author) and a child clinical psychologist (second author). In this condition, the child clinical psychologist also presented information intended to help children understand that fears following such an event were normal (i.e., presented information related to normal psychological effects). The second condition included these components as well as additional techniques designed to help children actively cope with distressing reactions. The techniques—active problem solving, seeking social support, and modification of negative self-talk—were discussed and modeled by the child clinical psychologist.

The findings of the intervention indicated that both conditions were found to help distressed children significantly reduce PTSD-related distress. The cognitive-behavioral condition was found to be slightly superior to the exposure-only condition with regard to helping children significantly increase self-reported coping ability. At a follow-up assessment done 4 months after the intervention, positive changes were maintained for coping ability. Continuing, significant improvement was indicated for PTSD-related distress. Additionally, comparisons between treated children and a nontreated group at this gate found superior effects for the combination of time and intervention versus the effects of time alone on both coping ability and PTSD-related distress. In fact, the treated group's mean PTSD-related distress score was in the nondistressed range whereas the nontreated group's mean symptom score continued to be in the distressed range.

One issue worth highlighting here was the value of collaboration between a volcanologist and a clinical psychologist. Combining expertise areas may have potential implications in a wide range of applications, with this area being a fruitful one for more collaboration and research. Another issue is the fact that children who are not in communities vulnerable to products from an eruption may nevertheless experience distress. There were indications in our research that children 11 km from the base of Mount Ruapehu on the leeward side were as impacted initially as those children who lived at the base of the mountain on the windward side.

In our research, this precedence appears to have been emphasized more in the two communities at the base of the mountain than in the community 11 km from the base. Prior to our intervention, we found that a child's ability to cope improved over the 2-month interval between our preintervention assessments in the two communities at the base whereas it was seen to deteriorate slightly in the children living 11 km away. The point here is that adults need to be sensitive to the fact that natural disasters like volcanoes can be upsetting for children in a wide range of locations both near and far from an actual impact area. Thus, simply because adults may not be experiencing any ill effects, this should not be taken as a gauge for children's reactions.

Another issue worth highlighting is how to deal with those who have continued distress despite early, group-based interventions. In following a multiple gating methodology, follow-up interventions would include those that were increasingly more comprehensive. For example, after large group interventions, smaller group interventions might represent the next step, particularly if larger numbers of people continue to show elevated levels of distress. Following that gate, for those who do not respond to small group applications, more intensive individual therapy may be recommended. For adults and families, this gating procedure would be similar to that used with children and adolescents though necessarily adjusted to meet particular needs of the target population. For example, for adults, larger group interventions might be held in a community-based setting and include developmentally appropriate versions of exposure, expert information, and cognitive-behavioral strategies combined with information on how to assist their children and other family members (e.g., normalizing fears for their children while demonstrating confidence and means by which a disaster can be coped with).

III. SUMMARY

Noneruptive or quiescent times are the most common and afford the best opportunity to develop mitigation strategies and prepare society for an eruption. Public education programs should aim to improve a community's understanding of the nature of volcanic hazards. During a crisis period, risk education and effective interventions are critical in reducing the adverse effects of volcanism on society. It is contingent upon governments, emergency services, and other relevant organizations being able to understand the significance of information they receive and respond appropriately. Agencies issuing warnings must distinguish the function of sending out messages which direct an emergency response, such as an evacuation, from that providing information about the emergency. Developing links with the media before a volcanic crisis will help response agencies better coordinate information during an event. During and after an eruption, hazard-relevant education programs can help reduce fears associated with uncertainty and increase the ability of affected populations to cope with the event.

SEE ALSO THE FOLLOWING ARTICLES

Impacts of Eruptions on Human Health • Volcanic Hazards and Risk Management • Volcano Warnings

FURTHER READING

Fisher, R. V., Heiken, G., and Hulen, J. B. (1997). "Volcanoes: Crucibles of Change." Princeton Univ. Press, Princeton.

Klingman, A. (1993). *In* "Children and Disasters" (C. F. Saylor, ed.). Plenum Press, New York.

Long, N. R., Ronan, K. R., and Perreira-Laird, J. (1998). *In* "Comprehensive Clinical Psychology: Applications in Diverse Populations" (N. N. Singh, ed.). Pergamon Press, New York.

Mileti, D. S., and Sorensen, J. H. (1990). "Communication of Emergency Public Warnings: A Social Science Perspective and State-of-the-Art Assessment." Oak Ridge Laboratory ORNL-6609.

Perry, R. W., and Hirose, H. (1991). "Volcano Management in the United States and Japan." JAI Press, Greenwich, CT.

Perry, R. W., and Lindell, M. K. (1990). "Living with Mount St. Helens: Human Adjustment to Volcano Hazards." Washington Univ. Press, Pullman, WA.

Ronan, K. R. (1997). The effects of a "benign" disaster: Symptoms of post-traumatic stress in children following a series of volcanic eruptions. Aust. J. Disaster Trauma Studies. (Also at http://www.massey.ac.nz/~trauma/.)

Ronan, K. R., and Deane, F. P. (in press). *In* "Cognitive Behaviour Therapy for Children and Families: Cambridge Monograph Series in Child and Adolescent Psychiatry" (P. Graham, ed.). Cambridge Univ. Press, Cambridge.

Rothbaum, B. O., and Foa, E. B. (1993). *In* "Posttraumatic Stress Disorder: A Behavioral Approach to Assessment and Treatment" (P. A. Saigh, ed.). MacMillan, New York.

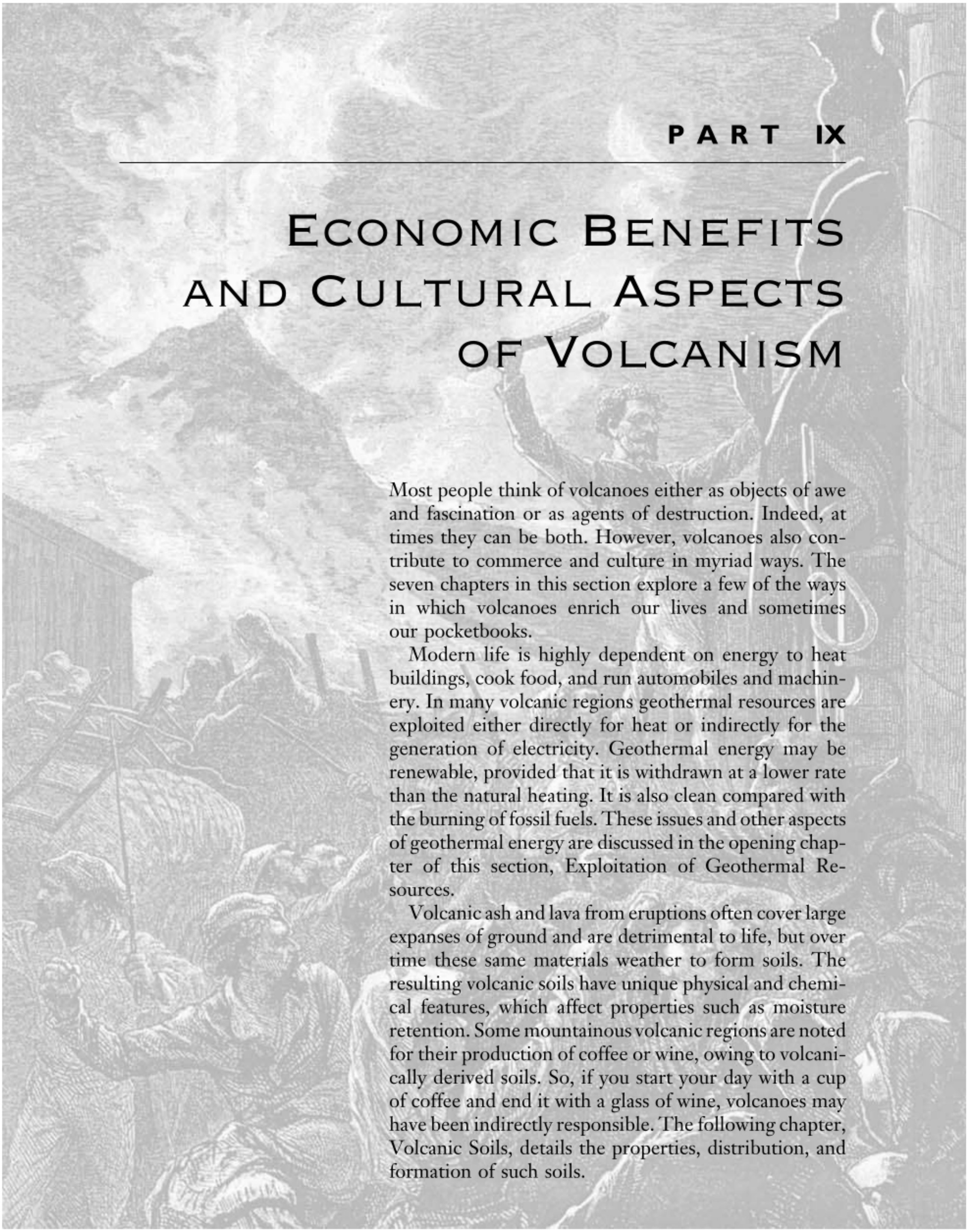

PART IX

ECONOMIC BENEFITS AND CULTURAL ASPECTS OF VOLCANISM

Most people think of volcanoes either as objects of awe and fascination or as agents of destruction. Indeed, at times they can be both. However, volcanoes also contribute to commerce and culture in myriad ways. The seven chapters in this section explore a few of the ways in which volcanoes enrich our lives and sometimes our pocketbooks.

Modern life is highly dependent on energy to heat buildings, cook food, and run automobiles and machinery. In many volcanic regions geothermal resources are exploited either directly for heat or indirectly for the generation of electricity. Geothermal energy may be renewable, provided that it is withdrawn at a lower rate than the natural heating. It is also clean compared with the burning of fossil fuels. These issues and other aspects of geothermal energy are discussed in the opening chapter of this section, Exploitation of Geothermal Resources.

Volcanic ash and lava from eruptions often cover large expanses of ground and are detrimental to life, but over time these same materials weather to form soils. The resulting volcanic soils have unique physical and chemical features, which affect properties such as moisture retention. Some mountainous volcanic regions are noted for their production of coffee or wine, owing to volcanically derived soils. So, if you start your day with a cup of coffee and end it with a glass of wine, volcanoes may have been indirectly responsible. The following chapter, Volcanic Soils, details the properties, distribution, and formation of such soils.

Volcanic rocks are the most plentiful rocks in many areas and are often used as building materials for structures and road beds and in some types of cinder blocks, landscaping, and walls. The altered volcanic clay, bentonite, is commonly used in diverse products from drilling mud to cosmetics. The next chapter, Volcanic Materials in Commerce and Industry, describes many products derived from volcanoes.

Hot springs and fumaroles are often found in close association with volcanoes. This combination has led to the development of many spas and resorts at volcanoes. The attractive mountainous terrain of volcanic areas is also suitable for hiking, camping, and climbing as well as for viewing the various surface manifestations of volcanic activities. These and related topics are discussed in the following chapter, Volcanoes and Tourism.

Ironically, volcanic deposits are wonderful preservers of ancient buildings and artifacts, even though at the time of eruption they were undoubtedly viewed as destructive. Much of what we know of some ancient civilations was instantly preserved by the devastating force of volcanic eruptions. Examples include the well-known Roman cities of Pompeii and Herculaneum and the Bronze Age Akrotiri in the Aegean. Other less well known sites near Ilopango in El Salvador, Arenal in Costa Rica, Sunset Crater in Arizona, Mount Rainier in Washington, Mount St. Helens in Washington, and sites in the Yukon Territory have yielded clues showing the widespread effects of eruptions on the life of early peoples. The chapter Archaeology and Volcanism explores how archaeological sleuths have harvested information about early cultures and describes the origins of geomythology.

Volcanoes are often used as metaphors for power or unpredictability. Volcanoes are also frequently viewed as windows to the interior of the earth. These ideas show up repeatedly in popular culture and often make their way into books, movies, cartoons, and other forms of expression. Two famous examples that began as books and were later made into films are the novel *The Last Days of Pompeii* by George Bulwer-Lytton (1834) and the science fiction work *Journey to the Center of the Earth* by Jules Verne (1864). This section of the encyclopedia, and the entire text, concludes with the chapter Volcanoes in Literature and Film. This chapter provides brief descriptions and synopses of many volcano books and movies.

Readers may be surprised by the far-reaching benefits of volcanoes outlined in this section and their broad impact on our lives. Although we tend to think about volcanoes primarily while they are erupting, their products and images are found in many places in both ancient and modern life. A world without volcanoes would be a duller, less economically viable, and certainly less interesting place.

Stephen R. McNutt
University of Alaska Fairbanks

EXPLOITATION OF GEOTHERMAL RESOURCES

STEFÁN ARNÓRSSON
University of Iceland

I. Introduction
II. The Potential Use of Earth's Heat as an Energy Resource
III. Drilling for Geothermal Water and Steam
IV. Strategy in Geothermal Exploration, Development, and Production
V. Monitoring of Geothermal Reservoirs
VI. Is Geothermal Energy a Renewable Resource?
VII. Environmental Aspects

GLOSSARY

geothermal exploration well A well drilled for the purpose of locating a potentially exploitable geothermal reservoir.

geothermal field (area) An area with finite surface boundaries, often defined by the distribution of hot springs and/or fumaroles, overlying a potential geothermal energy resource.

geothermal fluid Hot water and/or steam hosted in a geothermal system. Geothermal fluids contain both dissolved gases and solids. Occasionally geothermal fluids are highly mineralized containing as much as 30% dissolved salts, such as at Salton Sea, California. Such salty fluids are typically high in many metals and probably represent ore-forming fluids.

geothermal reservoir A body of hot rock containing geothermal fluid that is economically exploitable.

geothermal system A body of hot rock and hot fluid in a particular rock-hydrological situation.

injection well A well used for disposing of waste geothermal fluid from production wells/power plants.

production well A well that produces steam/hot water that can be economically exploited.

permeability The property of a rock which allows the passage of fluids without impairment of its structure of displacement of its parts. A rock is said to be permeable, if it permits an appreciable quantity of fluid to pass through it in a given time, and impermeable, if the passage is negligible.

porosity The proportion of pore space occupied by the rock as a whole.

I. INTRODUCTION

The ultimate source of all energy exploited by mankind is the Sun, except for nuclear energy and geothermal energy. The heat within the Earth, which constitutes geothermal energy, comes from the decay of radioactive

Copyright © 2000 by Academic Press
All rights of reproduction in any form reserved.

elements, particularly uranium, thorium, and potassium, and the Earth's gravity field.

The amount of heat stored within the Earth is enormous. However, use of this energy has only proved to be economical where geological, hydrological, and geophysical conditions are favorable for the formation of geothermal systems. Basically, a geothermal system represents groundwater that circulates to a depth of a few kilometers where the water gains heat by contact with hot rock. Hot water is less dense than cold and, therefore, tends to ascend by buoyancy. Groundwater convection (circulation of groundwater) may be driven by hydrostatic head or by the density difference between colder water in the downflow limb of the convection cell and hotter water in the upflow limb. For the same groundwater level, within and adjacent to a geothermal field, the pressure at any depth will be higher in the descending cold water than in the ascending hot water. Provided this difference and rock permeability are sufficiently high, groundwater convection will be sustained.

Geothermal systems typically form in active volcanic regions where geothermal gradients and rock permeabilities are high. However, economic geothermal reservoirs have also been discovered in sedimentary strata, including oil-bearing strata, and in fractured volcanic rocks outside areas of recent volcanism. The exploitation of geothermal resources has had a relatively insignificant environmental effect. With respect to atmospheric pollution, it is superior to the use of fossil fuel.

Extraction of heat from impermeable rock has been attempted in a few areas. It involves the drilling of injection and production wells, hydrofracturing of the rock to create permeability, pumping of cold water into the injection well, and extraction of this water from the production well. As the water flows through the artificial fractures between the two holes, it gains heat from the rock. So far, extraction of heat from impermeable rock (hot dry rock) has not proved to be economical, although it is technically achievable.

Modern usage of geothermal energy started at Larderello in Italy. On July 4, 1904, the first electric power exploiting natural steam discharges was generated in the area. In 1912, the first turbine generator unit powered by underground steam was installed at Larderello. By 1944, the installed electric generating capacity at Larderello was 127 MW. In the 1920s geothermal power investigtions were carried out in California and Japan, but there were no significant power developments there at that time. Many countries have been actively involved in developing their geothermal resources since the 1960s, both for various types of direct use and electric power generation (Fig. 1). During this period, the exploitation of geothermal resources has been increasing rapidly. As an example, the installed capacity for electric power generation increased by 40% in the period 1990–1998.

The present world use of geothermal energy is summarized in Table I. As may be deduced from this table, in some countries (e.g., Indonesia, Italy, Mexico, Philippines, and the United States), exploitation of geothermal resources has emphasized their use for electric power generation. Many other countries (e.g., China, Hungary, Iceland, Japan, and the United States) use geothermal water directly on a large scale, particularly for space heating.

Geothermal energy accounts for only a small fraction of the world's energy consumption. In that sense it is not an important energy resource. However, in some countries, particularly many third world countries, geothermal reservoirs constitute an important energy resource in terms of their total energy consumption. Iceland is unique for the extent and economic importance of its use of geothermal energy. Geothermal resources account for a little more than 50% of the country's annual energy consumption. In the United States, geothermal resources account for about 0.4% of the annual energy usage. For the world, it is a little less than 0.3%.

Geothermal fluids have been utilized on a small scale as a source of various chemicals. At Larderello, boron was extracted from the steam before electric power generation started. In Japan, cesium was extracted from hot spring waters, and mercury was extracted from hot spring deposits at Sulphur Bank in California. Extraction of various base metals from the geothermal brine in the Salton Sea area in California has been considered. In New Zealand, a technique was developed to extract silica from the waste brine of the Wairakei geothermal power plant by coprecipitating it with lime to form a useful calcium-silicate for the building industry. This technique was not economical.

II. THE POTENTIAL USE OF EARTH'S HEAT AS AN ENERGY RESOURCE

The principal features that determine the potential use and economics of geothermal resources include the geothermal reservoir temperature, rock permeability, volume of the reservoir, and amount and chemical composition of its fluid. Of these, temperature is the most important. The location of the resource is also of much importance, at least, when using hot water or steam

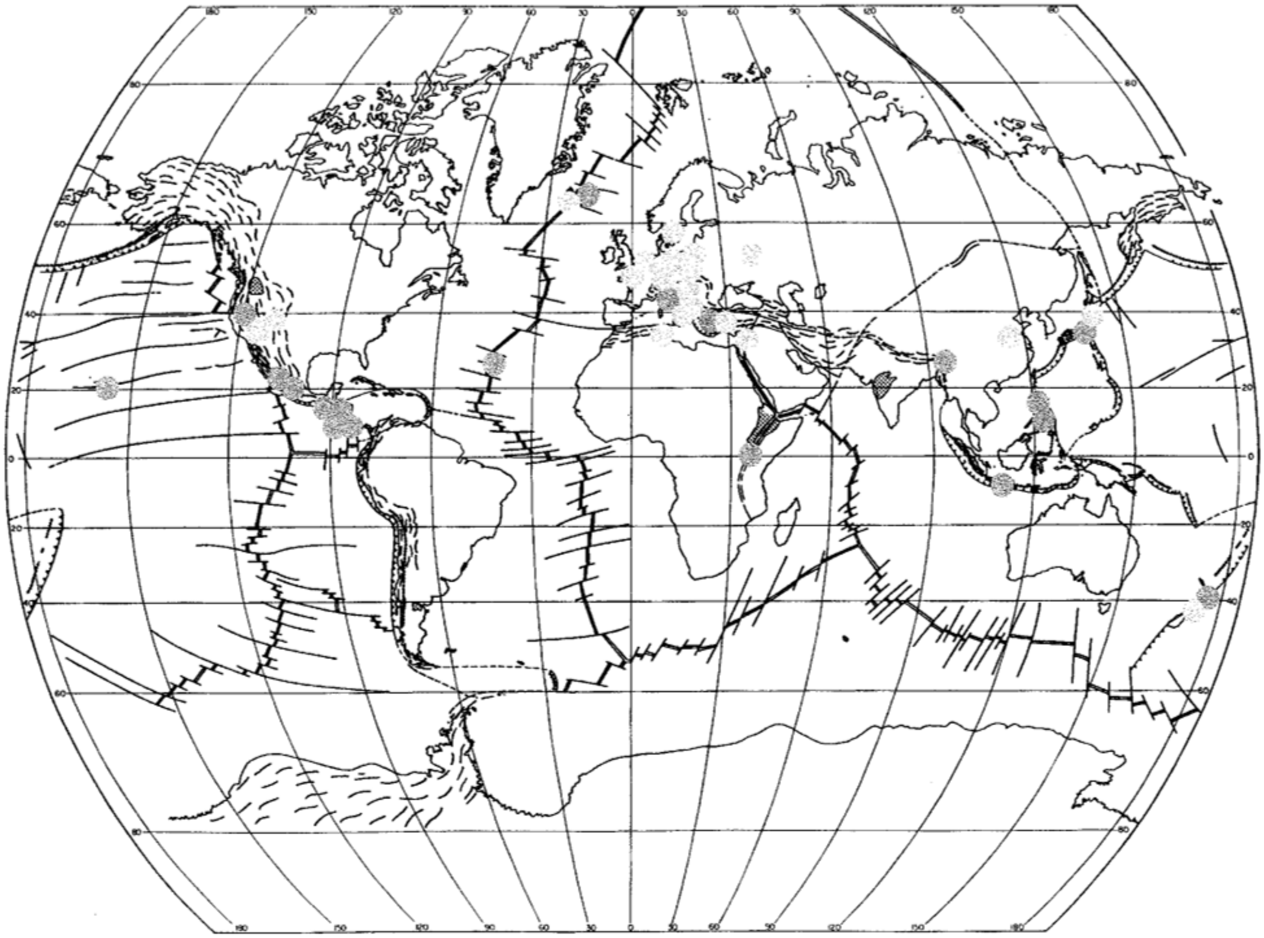

FIGURE 1 World map showing countries where geothermal energy is harnessed. Dark shading; power production. Light shading; direct use.

directly. For cost and technical reasons, transport of heat over long distances is not possible. In this respect the value of geothermal energy is inferior to fossil fuel and nuclear energy.

Baldur Líndal, an Icelandic chemical engineer, assessed the potential use of geothermal water and steam in relation to their temperature (Fig. 2). From this figure it is clear that thermal water with temperatures as low as 20–30°C constitutes a useful energy resource.

Some geothermal fields (e.g., Larderello in Italy and the geysers in California) are vapor-dominated, but most drilled fields are liquid-dominated. In liquid-dominated fields, water forms a continuous fluid phase in fractures, but vapour is the continuous phase in vapor-dominated fields.

The boiling point of water is pressure and salinity dependent, the temperature of boiling rising with increasing pressure. In the geothermal industry, the boiling point of water is frequently related to depth (Fig. 3). The depth is calculated on the assumption that the pressure exerted at each depth is that of a water column, which is at the boiling point at all depths. Rising water in a geothermal reservoir, or in a producing well, boils in response to pressure drop. At the same time, the water cools, and some of it is transformed into steam. The amount of steam that forms depends on the initial temperature of the reservoir water and the magnitude of the pressure drop. For example, 41% of 300°C water is converted into steam by allowing the pressure to drop to atmospheric. At the same time, the water-steam mixture cools to 100°C. Thus, steam is produced not only from vapor-dominated fields but also from liquid-dominated ones.

When water boils in the aquifer of producing wells as a result of pressure drop, the temperature of the flowing fluid becomes lower than that of the enclosing rock. As a

TABLE I Use of Geothermal Energy in the World by Country in 1997

	Electric production		*Direct use*	
Country	*Power (MW)*[a]	*Annual use (GWh)*[b]	*Power (MW)*[a]	*Annual use (GWh)*[b]
Algeria			1	5
Argentina	0.7			
Australia	0.4	3.5		
Austria		0.8	21.1	84
Belgium			3.9	19
Bosnia-Herzegovenia			33	230
Bulgaria			95	346
Canada	32		3	13
China	120	175	1,914	4,717
Costa Rica		447		
Croatia			11	50
Czech Republic			2	15.4
Denmark	105		3.2	15
El Salvador	4	486		
France		24	309	1,359
Georgia			245	2,145
Germany			307	806
Greece	5		22.6	37.3
Guatemala				
Hungary	140		750	3,286
Iceland	590	375	1,443	5,878
Indonesia		4,385		
Ireland			0.7	1
Israel	768		42	332
Italy	530	3,762	314	1,026
Japan	45	3,530	1,159	7,500
Kenya		390		
Macedonia	743		75	151
Mexico	345	5,682	28	74
New Zealand	70	2,900	264	1,837
Nicaragua	1,848	250		
Philippines		8,000		
Poland	11		44	144
Portugal	2	52	0.8	6.5
Romania	11	?	137	528
Russia		25	210	673
Serbia			86	670
Slovakia			75	375
Slovenia			34	217
Sweden			47	351
Switzerland			190	420
Thailand	0.3	2	2	8
Tunisia			70	350
Turkey	20	71	160	1,232
Ukraine			12	92
United States	2,850	14,660	1,905	3,971
Europe	936	4,309	4,368	20,505
America	3,883	21,529	1,908	3,984
Asia	3,031	16,092	3,075	12,225
Oceania	345	2,901	264	1,837
Africa	45	390	71	355
Total	8,240	45,220	9,686	38,906

[a] Megawatts. The numbers are valid for 1998 and are based on information from the International Geothermal Association (http://www.demon.co.uk/geosci/igahome.html).

[b] Gigawatt-hours. From Fridleifsson and Stefánsson (1998).

result, heat tends to flow from the rock to the fluid, which enhances steam formation in excess of that caused by the pressure drop. Due to their different flowing properties, the water and steam may segregate in the aquifer, the steam flowing preferentially to the well. Both processes cause the steam-to-water ratio in the well discharge to be higher than that caused by pressure drop alone. It is, in fact, not uncommon that wells drilled into liquid-dominated reservoirs yield steam only. Such wells occur, for example, in the liquid-dominated fields of Olkaria in Kenya and Krafla in Iceland.

Geothermal steam is used in much the same way to generate electric power as is steam formed in boilers using fossil fuel or nuclear energy as the energy resource. There is, however, one major difference. In the case of fossil fuel or nuclear energy, the steam inlet pressure for the turbines can be chosen as desired. For geothermal steam, the characteristics of the reservoir determine, at least to an extent, what the optimum turbine inlet pressure should be. Long-term well tests are required to determine the optimum inlet pressure.

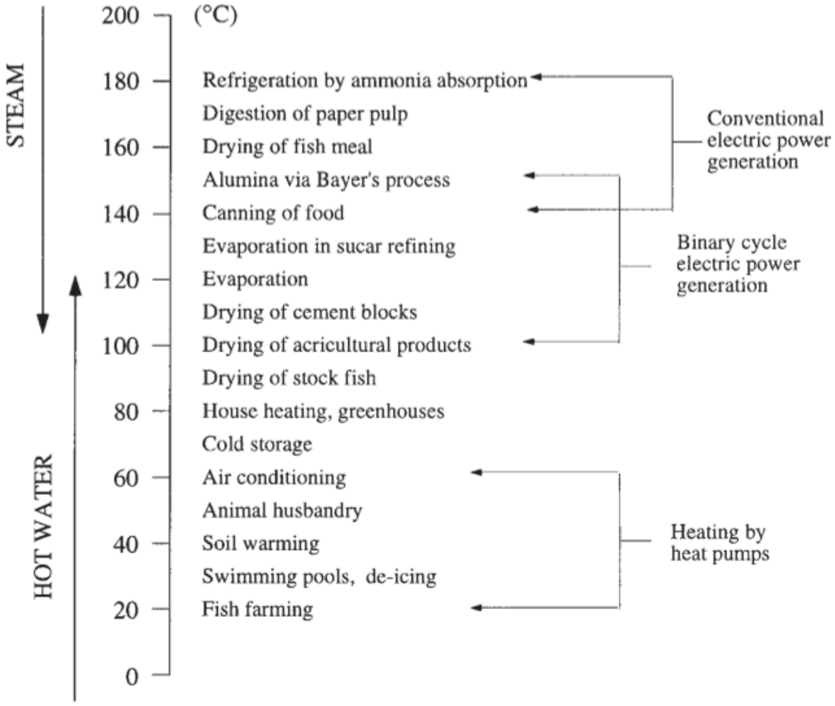
The Líndal Diagram
STEAM
HOT WATER
200
180
160
140
120
100
80
60
40
20
0
(°C)
Refrigeration by ammonia absorption
Digestion of paper pulp
Drying of fish meal
Alumina via Bayer's process
Canning of food
Evaporation in sucar refining
Evaporation
Drying of cement blocks
Drying of acricultural products
Drying of stock fish
House heating, greenhouses
Cold storage
Air conditioning
Animal husbandry
Soil warming
Swimming pools, de-icing
Fish farming
Conventional electric power generation
Binary cycle electric power generation
Heating by heat pumps

FIGURE 2 The Líndal diagram.

The efficiency of conventional use of geothermal steam for electric power generation is poor. Only some 10% of the heat discharged from drillholes is converted into electric energy, the exact number depending on the reservoir temperature and the well-discharge enthalpy. As an example, consider a reservoir at 200°C with a wellhead steam separation pressure of 6 bars abs. (this is equal to a temperature of 159°C for steam-saturated water). Boiling by pressure drop from 200 to 159°C will cause 8.7% of the reservoir water to be converted into steam. Only this 8.7% will be utilized to generate power; the remaining 91.3% of the discharged mass goes to waste. For a reservoir temperature of 300°C and the same turbine inlet pressure, 67.6% of the discharged fluid would go to waste. About 2 kg/s of steam are required to generate 1 MW of electricity.

Direct use of geothermal heat is much more efficient. For space heating, heat can easily be extracted from water by cooling it down to 35°C. Taking the initial temperature to be 80°C and defining useful heat as that in excess of 20°C gives an efficiency factor of 0.75 (75%).

The poor utilization of geothermal energy by conventional electric power production has led to improved exploitation technology and more versatile use of the resource. Two methods have largely been practiced. One involves the so-called binary cycle, and the other, combined utilization (Fig. 4). The binary cycle improves

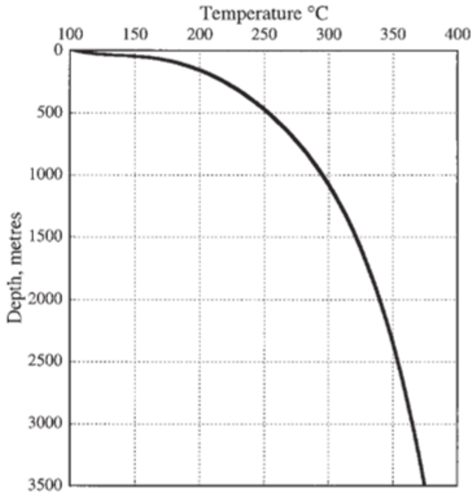

FIGURE 3 The boiling point curve of pure water with depth.

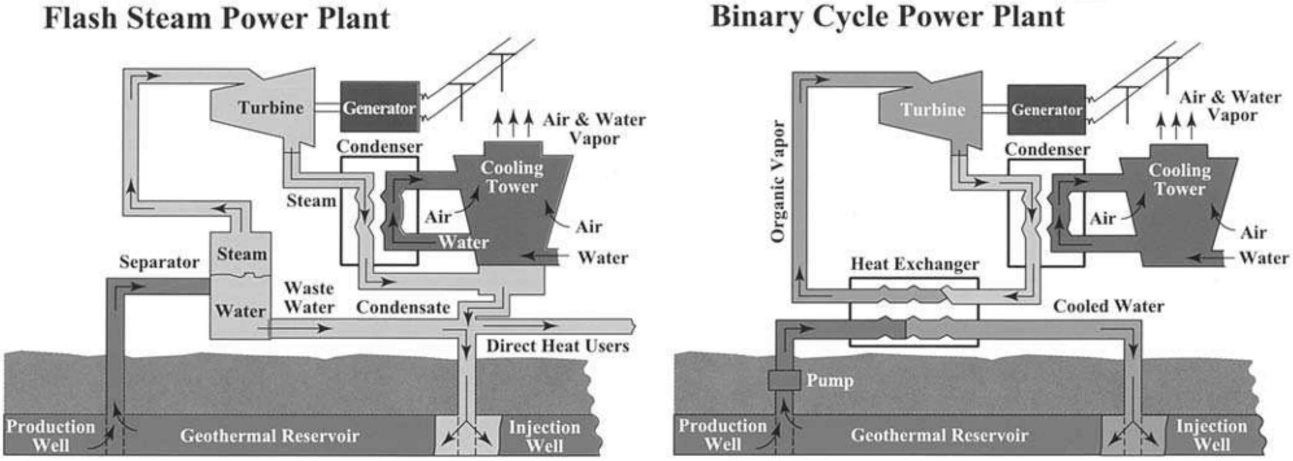
Flash Steam Power Plant
Turbine
Generator
Air & Water Vapor
Condenser
Cooling Tower
Steam
Air
Water
Air
Water
Separator
Steam
Water
Waste Water
Condensate
Direct Heat Users
Production Well
Geothermal Reservoir
Injection Well
Binary Cycle Power Plant
Organic Vapor
Turbine
Generator
Air & Water Vapor
Condenser
Cooling Tower
Air
Air
Water
Heat Exchanger
Cooled Water
Pump
Production Well
Geothermal Reservoir
Injection Well

FIGURE 4 A schematic layout of conventional flash steam and binary cycle geothermal power plants.

use of the resource for electric power generation. It involves heating a low-boiling point fluid in a closed loop of a heat exchanger. That fluid is then used to drive a low-pressure turbine. Combined utilization commonly involves electric power generation as well as direct use. Back pressure turbines are generally used in this case. Low-pressure steam emerging from the turbine is conveyed through a heat exchanger to heat up fresh water that is in turn used directly for space heating or other purposes. In this way, the geothermal resource can be more effectively utilized.

The possibilities of combined utilization schemes depend on the local market. Two examples of such schemes include the Svartsengi and Nesjavellir power plants (Fig. 5), both in Iceland. In these operations, high-pressure steam is utilized to generate electric power, and the hot water is conveyed through heat exchangers to heat up fresh water that is in turn used for space heating. It is not possible to use the geothermal water directly because of its chemical composition. As combined schemes improve the efficiency of the exploitation of the resource, they effectively extend the life of any geothermal reservoir. They also reduce the environmental impact of the exploitation. Because of all this, combined utilization should become more widely applied in the future.

Some problems are associated with efficient use of high-temperature geothermal fluids. This usage requires much cooling of the fluid which can induce scaling (formation of chemical deposits) in wells and surface equipment, particularly of amorphous silica. Such scaling can hinder smooth operation of a geothermal installation.

III. DRILLING FOR GEOTHERMAL WATER AND STEAM

Only a very minor part of exploited geothermal water comes from natural springs. All geothermal steam and practically all geothermal water are recovered from subterranean geothermal reservoirs by wells. Geothermal wells are commonly 1000–2500 m deep. The deepest ones at present reach about 4 km. Many wells drilled for direct use of hot water may, however, be much shallower, in some cases only about 100 m.

The purpose of geothermal drilling is to (1) locate a potential geothermal reservoir, (2) characterize this reservoir, and (3) ultimately recover steam and/or water from it cost-effectively.

Geothermal drilling technology is mainly obtained from the oil industry. However, some modifications are required, mostly because geothermal systems are largely hosted in fractured volcanic rocks, whereas drilling for oil and gas is primarily into sediments and sedimentary rocks. Rotary drilling is used for geothermal wells. The rotary drillbit is connected to the engine of a drill rig via a string of hollow drillrods. Rotation of the rods causes the bit to rotate at the bottom of the hole. The lowest part of the drillrods, called collars, is massive and heavy and gives the required load on the drillbit to squeeze its teeth into the rock at the bottom of the hole, whereas the rest of the drillrods are suspended in the mast of the rig. As the teeth push into the rock at the bottom of the hole, they break loose chips of rock.

A drilling fluid, typically water, is pumped down the drillrods and out through the holes in the drillbit. The fluid ascends through the annulus between the rods and the walls of the hole bringing with it to the surface the rock chips. Occasionally detergent foam is used if the water level in the geothermal reservoir is very low and, in the case of vapor-dominated fields, air has been used. During drilling, it is feasible not to build up much higher pressure in the well than in the surrounding formation. This may cause movement of the drilling fluid with the rock chips it carries, into adjacent horizons, deteriorating their permeability. Loss of drilling fluid is also undesirable for drilling technological reasons. It may cause the drill chips to cumulate in the hole causing the drillrods to beome stuck.

A complicated casing programe is required for geothermal wells, especially when temperatures are high (Fig. 6). After drilling through soil and any loose sediments, a surface casing is lowered into the well and cemented in place by pouring concrete into the annulus

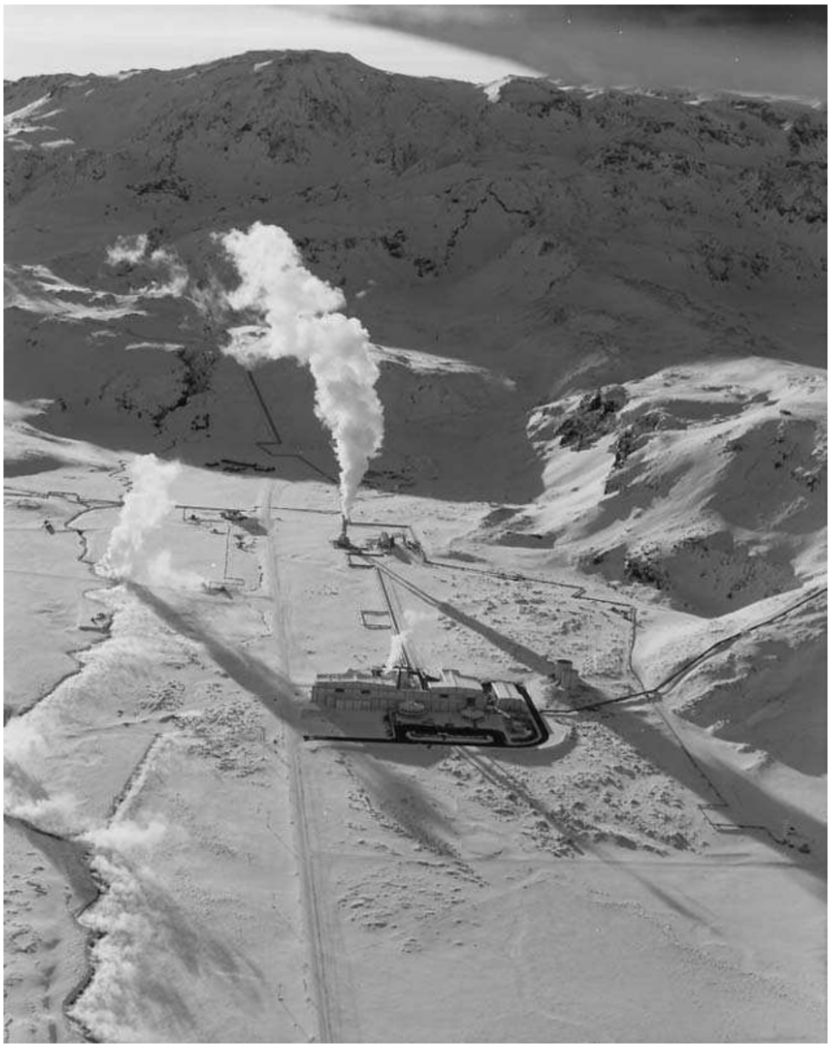

FIGURE 5 Photo taken in midwinter of the Nesjavellir power plant, Iceland. High pressure steam is used to generate 60 MW of electric power. Water and steam is passed through heat exchangers to heat up 1100 liter of fresh water to 85°C (equivalent to 200 MW thermal) which is piped for 27 km to Reykjavík and used for space heating. The pipe to Reykjavík runs up the hill on the right-hand side of the photograph. Steam separator station is behind the power station next to chimneys discharging excess steam from the wells into the atmosphere. Photo Emil Thor Sigurdsson.

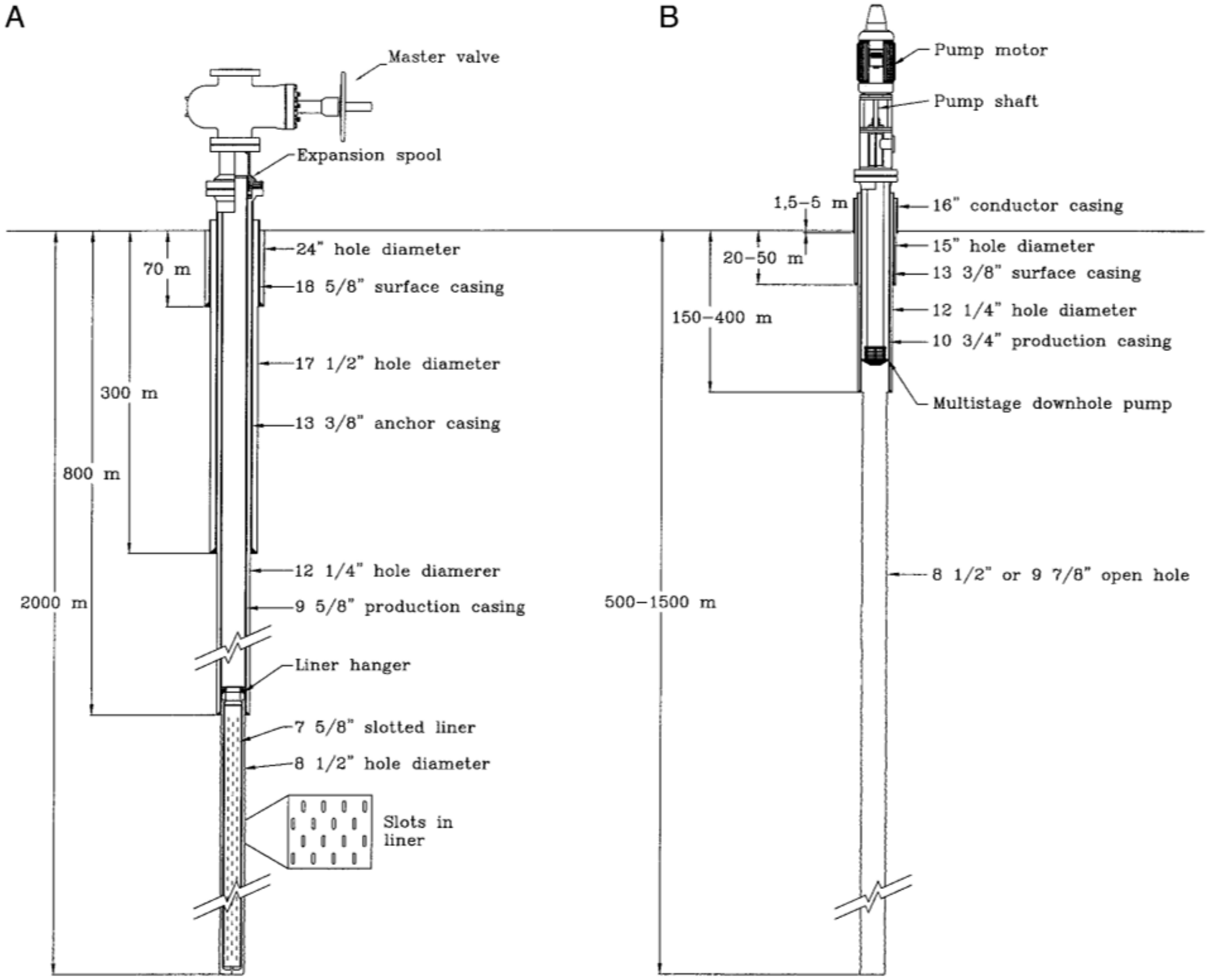
A
Master valve
Expansion spool
70 m
24" hole diameter
18 5/8" surface casing
17 1/2" hole diameter
300 m
13 3/8" anchor casing
800 m
12 1/4" hole diamerer
2000 m
9 5/8" production casing
Liner hanger
7 5/8" slotted liner
8 1/2" hole diameter
Slots in liner
B
Pump motor
Pump shaft
1,5–5 m
16" conductor casing
20–50 m
15" hole diameter
13 3/8" surface casing
150–400 m
12 1/4" hole diameter
10 3/4" production casing
Multistage downhole pump
8 1/2" or 9 7/8" open hole
500–1500 m

FIGURE 6 Schematic layout of wells drilled into (A) high- and (B) low-temperature geothermal fields.

from above. The purpose of this casing is to prevent collapse of the loose top layer into the hole when deepened. After the surface casing has been cemented, drilling for anchor casing starts. It is termed anchor because the wellhead equipment is welded to this casing. If the final well depth is projected to be about 2000 m, this casing is frequently set at about 300 m. The anchor casing is cemented in place by pumping cement sludge down through the drillrods so that it ascends through the annulus between the casing and the wall of the hole. It is important to cement this casing well. The next casing is the production casing. For a 2000-m deep well, it is often set at about 800 m depth and cemented similarly to the anchor casing. Like the anchor casing, the production casing reaches the surface. Finally, the well is drilled to the target depth. A liner, or perforated casing, is set below the production casing to prevent the walls of the well from collapsing during production. The total length of casing, including the liner, in a 2000-m deep well is about 2400 m. The casing programe requires the diameter of the drilled well to be largest at the top and successively narrower for each casing. The surface casing is typically 14 in. in diameter and the liner is 8 in. A typical geothermal well drilled into a high-temperature volcanic system costs about U.S. \$1.5 million and takes 1.5–3 months to complete. As much as half of the drilling cost goes into the casing material.

The casing program depends not only on intended drilling depth but also on stratigraphy and the spatial distribution of temperature in the reservoir. Anchor and production casings may be set at deeper levels than in the example given in order to case off either loose strata or relatively cold aquifers or both.

Casing programs for low-temperature fields are simpler than for high-temperature ones (Fig. 6). Both the production casing and the liner are, as a rule, omitted. The depths of the surface and anchor casings are determined by stratigraphy and reservoir temperature distribution. Further, the depth at which the anchor casing is set depends on the anticipated maximum drawdown of water level, at least if submerged pumps will be used. For safety reasons, such pumps must not be lowered below the lower end of the casing. Rock debris falling from the uncased walls of the well onto the pump could make it impossible to pull it out for maintenance.

IV. STRATEGY IN GEOTHERMAL EXPLORATION, DEVELOPMENT, AND PRODUCTION

A. General

The presence of geothermal reservoirs is generally manifested by hot springs and/or fumaroles at the surface and, in some cases, by hydrothermal alteration and sinter deposits. Exploration has, however, revealed hidden reservoirs with no surface manifestations. There is sometimes little relationship between the distribution and intensity of surface geothermal activity in an area and the lateral extent and productivity of the underlying geothermal reservoir.

As with exploitation of Earth's mineral resources, uncertainty is always involved with the success and economy of exploration and development of geothermal resources. At the onset of geothermal exploration, it is uncertain if it will result in economically, technically, and environmentally feasible exploitation of the resource. The cause of the uncertainty lies in the limited information available about the characteristics and size of the anticipated resource. Geothermal exploration and development, therefore, invariably requires risk capital. Sometimes the exploration and development work yields negative results in the sense that the characteristics of the resource are not favorable for economic exploitation.

Due to the uncertainty in geothermal exploration and development, it has become common practice to divide exploration and development into phases (Fig. 7). For each phase, costs are minimized and information is maximized. At the end of each phase, a decision is whether to continue or terminate the project. The phases are:

1. Surface exploration to obtain indirect information about the extent of the geothermal reservoir, subsurface temperatures, and other features such as permeability control for fluid flow
2. Exploration drilling to obtain the first direct information on reservoir temperature, pressure, permeability, and the like
3. Appraisal drilling (also called production drilling) to evaluate the characteristics of a prospective well field
4. Feasibility study and preliminary power plant design, the purpose of which is to analyze the economy of the project and to decide on erecting the plant
5. Final design, financing, additional production drilling, preparation of tender documents, bidding, and construction

B. Surface Exploration

Surface exploration is used to locate both favorable geothermal areas for development and sites within them for drilling. It includes geological studies and geochemical and geophysical surveys.

Geological studies focus on mapping the distribution of geological formations and the distribution and types of thermal manifestations. An attempt is always made to relate the distribution of the thermal manifestations with local structures, such as faults. Frequently, the overall distribution of the geothermal activity can also be linked with some regional geological structures such as calderas, in which case favorable drilling targets might be confined to that caldera. Calderas, which form in response to rapid emptying of a magma chamber during a major volcanic eruption, define approximately the areal extent of the underlying magma chamber, which in turn constitutes the heat source for the overlying geothermal system.

The principal purpose of geochemical surveys is to predict temperatures in the underlying geothermal system based on the chemical compositions of hot spring waters and fumarole steam. They also provide information on the origin of the geothermal fluid and subsurface flow directions. Studies in many drilled geothermal fields have shown that the chemical and isotopic compositions of well discharges are controlled by equilibrium

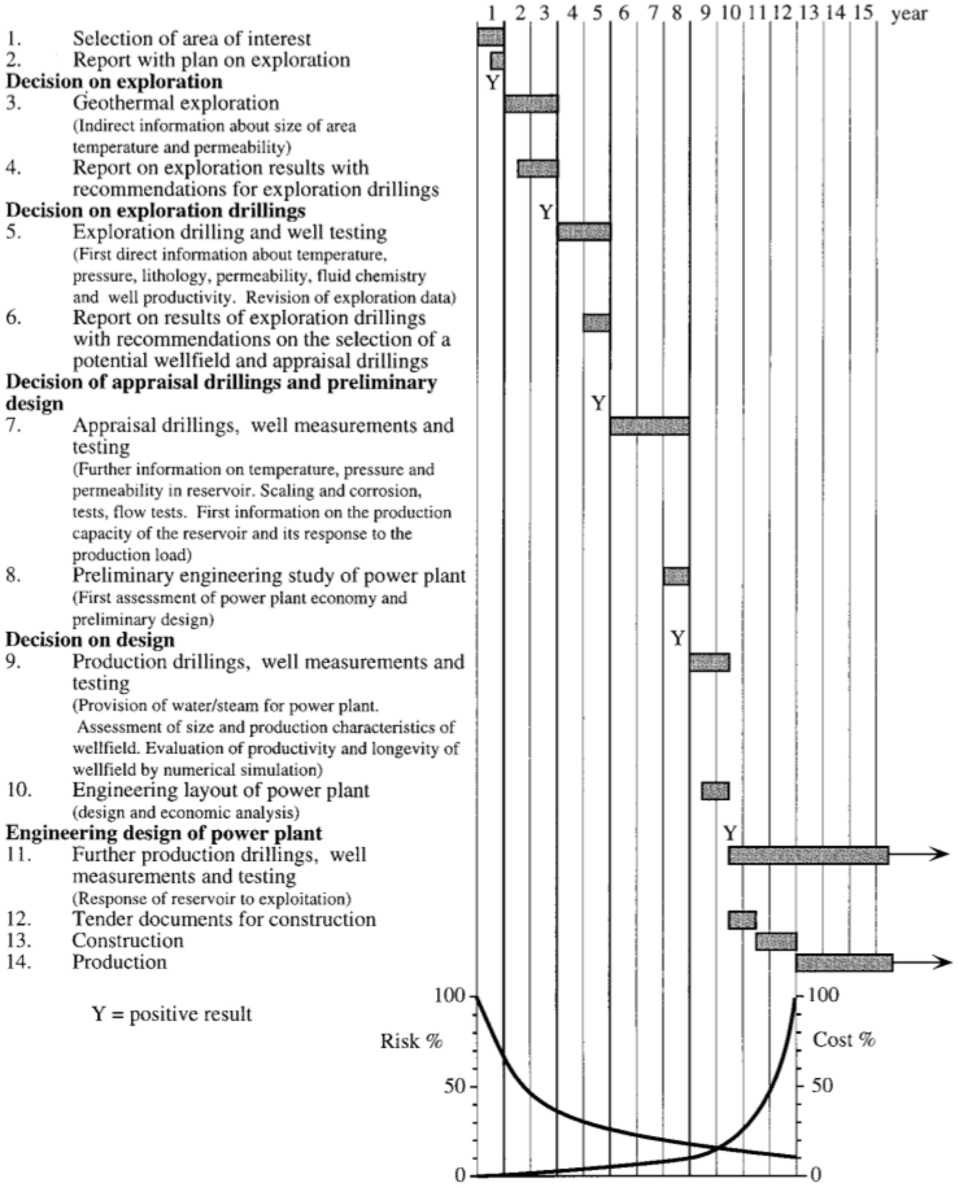

FIGURE 7 Strategy in geothermal exploration and development.

reactions with minerals in the reservoir rock. Equilibria between solution and minerals are generally temperature dependent in such a way that concentrations, or concentration ratios, of aqueous components change with temperature. In upflow zones of geothermal systems, the rising fluid often cools, by conductive heat loss, boiling, or both. However, reequilibration may be limited, partly because of the short residence time in the upflow and partly because reaction rates decrease with decreasing temperatures. As a result, the chemical and isotopic compositions of the fluid discharged at the surface can, and often do, reflect temperature conditions in the geothermal system below the zone of cooling in the upflow. Several mathematical equations have been developed to describe the relationships between specific aqueous concentrations, or concentration ratios, and temperature.

Geophysical surveys have been classified into two groups: one that provides information on geological structures, and another that supplies temperature data.

The most widely used geophysical exploration tool maps electrical resistivity of bedrock. The resistivity of bedrock to induced electric current is inversely related to temperature, hydrothermal alteration, rock porosity, and water salinity. Intense rock alteration is typically associated with geothermal systems, and geothermal waters contain more dissolved salts than nonthermal groundwaters. Therefore, geothermal systems characteristically show up as resistivity lows. Resistivity surveying has proved useful to map the lateral extent of geothermal reservoirs, which is important because one of the features that affects the generating capacity of a particular geothermal reservoir is its size. Magnetic and gravity surveys are sometimes useful in locating faults and intrusive bodies which tend to have higher density than volcanic strata.

Drilling of shallow gradient holes (few tens to a few hundreds of meters deep) has also been used in geothermal exploration. Ascending hot water produces anomalously steep thermal gradient near the surface, and the drilling of the gradient holes aims at locating such anomalies.

The results of exploration surveys are synthesized as a conceptual model of the reservoir, which shows predicted subsurface temperatures, structural control of groundwater flow, the lateral extent of the area and possibly some other geological features such as caldera structure. If the outcome of the exploration survey is favorable, the report describing the results will include proposed sites for exploration drillholes.

C. Exploration Drilling

Exploration drilling provides the first direct information on the geothermal reservoir. It is much more expensive than the surface exploration. The most important data obtained from exploration drilling include temperature, permeability, fluid chemical composition, and well-discharge rates. Successful results from exploration drilling lead to the selection of a potential production well field within a particular geothermal area.

In a geothermal field that is tens of square kilometers in size, it is common to drill about four exploration holes initially. These holes are drilled at prospective production well fields according to the results of the surface exploration surveys.

The main purpose of any exploration drilling is to locate a promising production well field. However, some exploration wells might be drilled near the anticipated margins of the geothermal area to verify its boundaries, especially when exploring a small field, in which case its size and capacity are of concern for the intended utilization. New information from the exploration drilling and later drilling and well-testing require updating the conceptual reservoir model.

D. Appraisal Drilling

Having located a promising production field within a geothermal area through exploration drilling, the next phase often involves the drilling of step-out wells to appraise the production characteristics of the site and the size of the prospective production field. Step-out wells are drilled at a radius of about 1 km away from the successful exploration hole.

Further drilling around a successful exploration well, called appraisal drilling, aims at quantifying the characteristics of the geothermal reservoir. Appraisal drilling provides the necessary information for design and economic analysis of the project and last but not least recovery of water/steam for the intended utilization. For this reason, appraisal drilling is often termed production drilling. Having delineated a production well field, additional production wells are drilled between the appraisal wells to recover steam/water for the intended exploitation.

E. Feasibility and Design of Power Plant

There are no rules as to how much steam (water) should be proved before a decision is made to construct a power plant. In a new area, the amount of steam to be proved may be as much as 80% of the total required. However, if a new production field is being developed within a geothermal area that has been under exploitation for some time, the number may be considerably lower (50%) because understanding of the characteristics of the area is probably high based on information and experience gained from previous development.

It is common practice to discharge all wells drilled in a particular well field simultaneously for several months to test interference and measure decline in output with time. Through numerical simulation the flow-test results are used to predict the generating capacity and the longevity of the production well field.

In detail the strategy of geothermal exploration and development depends on the size of the plant to be constructed. The scheme described earlier was drawn up with a 50- to 100-MW electric plant in mind, which is a common size for such plants.

The generating capacity per unit area of a geothermal field depends on many factors such as temperature, permeability, and porosity. A useful working rule, when information is limited, is to assume a capacity of 15 MW electric/km^2. Thus, a well field of 4 km^2 would be required for a 60-MW plant, plus some reserve for the drilling of additional wells to replace the anticipated decline in output from the initial production wells.

Geothermal wells are never bonanzas like oil and gas wells. Oil wells produce a commodity measured in dollars, whereas geothermal wells produce a commodity measured only in cents. For this reason, geothermal exploration and development demands a high ratio of successful wells for any geothermal project. To generate electric power in a particular area from geothermal steam that would be very attractive economically, the average yield of every drilled geothermal well needs to be about 10 kg/s of steam (equivalent to 5 MW electric) over a period of 10 years or proportionally longer if the yield is lower. The average yield per drilled steam well in the world is 4–5 MW. The best wells drilled so far have capacities of about 25 MW electric. The poorest average yield of wells drilled into exploited geothermal reservoirs is a little less than 2 MW.

V. MONITORING OF GEOTHERMAL RESERVOIRS

During the early days of geothermal exploitation, it was generally considered sufficient to prove the required flow rate of steam to water for the intended use by drilling and short-term testing (6–12 months, maybe less) of the wells, and extrapolation of the results into the future. Experience has, however, shown that pressure declines in exploited geothermal reservoirs, which results in decreased yield of wells and sometimes incursion of cold groundwater into the reservoir. This problem has necessitated monitoring of the response of geothermal reservoirs to the production load. Therefore, as earlier considered, geoscientific work is not complete at the onset of production.

Overexploitation of geothermal reservoirs is not uncommon. It leads to rapid drawdown of reservoir pressure and a corresponding decline in well output and power generation. For example, this has been the case at the Geysers in California, which is a vapor-dominated field. One of the reasons for the rapid pressure drawdown at the Geysers is the low porosity of the reservoir rock and correspondingly low quantity of reservoir fluid. To counteract the pressure decline, water has been injected into the reservoir at the Geysers.

Today, monitoring of the response of a geothermal reservoir to the production load has become the general practice worldwide. Data on the long-term response of a geothermal reservoir to production are necessary for specifying how the reservoir should be best exploited both economically and environmentally. Data to be collected are both physical and chemical. Essentially they involve regular measurement of flow rates and discharge enthalpy of wells and regular sampling and analysis of the well fluid. Pressures are also frequently monitored at depth in nonproducing wells. The chemical data are useful in assessing any changes in scaling tendencies and whether the discharged steam forms only by pressure drop or whether heat flow from rock also contributes to the steam formation.

Monitoring data are also valuable for both the timing and siting of new wells that need to be drilled to make up for the decline in flow from initial production wells. The data are further used to update the reservoir production model and to improve predictions about the longevity of the reservoir.

VI. IS GEOTHERMAL ENERGY A RENEWABLE RESOURCE?

Geothermal energy is commonly considered to be a renewable resource. Technically this is not correct. First, each geothermal system has a given lifetime, which typically lies between 10^5 and 10^6 years. Second, heat extraction from a drilled geothermal reservoir generally outpaces the reservoir's ability to replenish the extracted heat. It is, therefore, reasonable to regard geothermal reservoirs as mines of heat. The quantity of heat stored in a given volume of rock is positively related to temperature, porosity, and the steam-to-water ratio. Water has about five times higher heat capacity than rock, which explains why porosity influences the amount of heat storage. For a rock porosity of 17%, close to half of the heat is in the water, whereas the other half is in the rock. Furthermore, there is a lot more heat stored in a specific volume of water than in the same volume of steam. Consequently, other things being equal, the quantity of heat stored in boiling geothermal reservoirs decreases with increasing steam-to-water ratios.

The heat stored in the rock cannot be extracted and exploited in a sustained way in subboiling systems unless cooler water is drawn into the reservoir. In boiling systems, on the other hand, this is not the case. Extensive boiling caused by pressure drop in producing aquifers leads to cooling of the geothermal fluid, thus favoring flow of heat from the rock to that fluid. Theoretically, heat can be extracted from the reservoir rock until its temperature approaches that of the fluid entering wells. The fluid inflow temperature will be somewhat higher than the wellhead temperature depending on the pressure drop of the fluid in the well. The wellhead temperature is related to the wellhead pressure and is equal to that of steam-saturated liquid water. During operation, the pressure on each wellhead is set to satisfy the design turbine-inlet pressure.

Deep drilling in Iceland indicates that nonvolcanic geothermal systems are transient rather than steady-state features. Such systems are typically associated with recent subvertical tectonic fractures in which groundwater circulates to a depth of a few kilometers. An example is provided by the Laugarnes geothermal field within the city of Reykjavík. At deep levels, the temperature in the Laugarnes geothermal reservoir is lower than outside it. At shallow levels, on the other hand, temperatures within the reservoir are higher than in the surrounding rocks (Fig. 8). One explanation for this temperature distribution is that relatively cold groundwater flows to deep levels where it gains heat by contact with hot rock. At the same time, the rock cools. Due to buoyancy, the hot water rises and heats the rock at shallow levels. This density-driven circulation of the groundwater will cease when the convecting water has cooled the rock at deep levels to a certain degree. At this time, the geothermal system becomes extinct. The quantity of heat transported to shallow levels at Laugarnes by the convecting groundwater is much larger than the terrestrial conduction heat. Therefore, a nonvolcanic geothermal system, like Laugarnes, is clearly transient in nature and is appropriately viewed as a mine of heat rather than a renewable energy resource. The same applies to volcanic geothermal systems except those that receive continuous or episodic supplies of new magma into the roots of the system, either into chambers or as small intrusions.

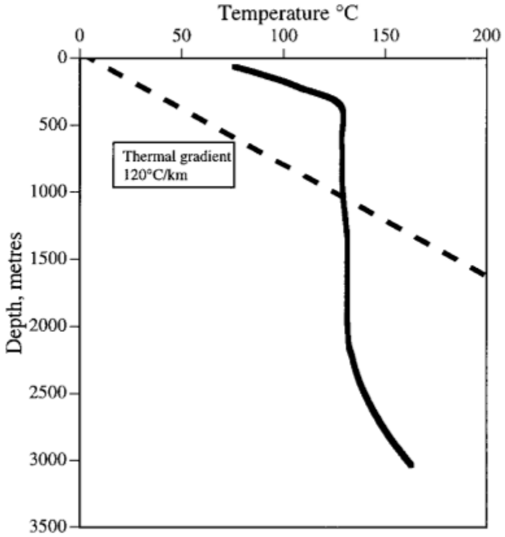

FIGURE 8 Temperature profile in a deep well in the Laugarnes geothermal field within the city of Reykjavík, Iceland.

Because geothermal reservoirs are viewed as mines of heat, they should be efficiently exploited, considering not only the economics of depreciation and return of investment capital but also environmental aspects and conservation of natural resources for future generations.

VII. Environmental Aspects

A. Atmospheric Pollution

Geothermal energy is a relatively clean resource in comparison with fossil fuel. Geothermal steam always contains carbon dioxide together with some other gases. However, the emisson of carbon dioxide into the atmosphere associated with exploitation of geothermal steam for electric power generation is much less than that from burning coal, oil, or gas. It is frequently around 10% of the carbon dioxide emission from fossil fuel-fired electric power plants and much less, if the gas is injected with the waste fluid back into the reservoir through special wells drilled for this purpose. Exploitation of water from low-temperature geothermal reservoirs for direct use is often not associated with any emission of carbon dioxide into the atmosphere. The water is low in this gas and has no tendency to degas when exposed to the atmosphere because its carbon dioxide partial pressure is less than atmospheric. In Iceland, hot water usage from low-temperature geothermal reservoirs low in carbon dioxide amounts annually to over 5000 GWh, which is equivalent to 570 MW thermal for 100% load factor. This use is very substantial considering that the country's population is only 270,000. In Hungary and China, which both use geothermal water extensively for space heating (Table 1), the situation is not as favorable because the water contains substantial amounts of carbon dioxide.

B. Other Pollution

Although geothermal energy is a relatively clean resource, its exploitation has considerable environmental impact. The pollution associated with harnessing geothermal resources is: (1) visual, (2) thermal, and (3) chemical. Additional effects are local land erosion and soil disturbance as well as noise pollution.

Thermal fields often occur in areas of scenic beauty, which are highly valued and of economic importance for tourism. Power plants, steam supply systems, and roads to individual wells can degrade the scenery, particularly in areas of rugged terrain. However, in some areas, like the Geysers in California, both power plants and pipelines have been tastefully camouflaged. The power plants are inconspicuous, and the pipelines are painted in colors that blend with the normal background. In other areas of the world, care has not been taken to reduce visual pollution as far as possible.

It is necessary to build a road to every drill site for transportation of the drill rig and for maintenance after the well has been completed. For the same reason, roads are also required along pipelines. This leads to much disturbance of the land surface, particularly on steep slopes. The combination of heavy rains and steep slopes of incompetent rock in such areas can also cause landslides and high soil erosion rates.

Direct use of hot water generally has much less effect on the environment than exploitation of steam for power generation. This is partly because low-temperature or nonvolcanic geothermal fields tend to occur in areas of lower relief than high-temperature or volcanic geothermal fields. Hot water pipelines require less maintenance and can, therefore, be subsurface. Also, the hot water is generally pumped from the wells, and the quantity pumped is in harmony with the usage so no water is wasted. For example, in the hot water fields exploited by the Reykjavík Heating Service in Iceland, there is practically no visual pollution except for small shelters that cover each wellhead.

The withdrawal of large quantities of water from a geothermal reservoir may lead to substantial ground subsidence depending on the strength of the rock. Subsidence can cause tilting and stressing of pipelines and surface structures, change stream beds, and lead to flooding. At Wairakei in New Zealand, maximum ground subsidence presently exceeds 10 m. It is also a problem in the Broadlands field, near Wairakei.

Geothermal steam always contains some hydrogen sulfide. This noxious gas is lethal if in sufficient quantity, and it may have adverse effects on crops and aquatic life. Hydrogen sulphide, and other gases, escape into the environment from condenser gas ejectors discharge, with warm air and surplus condensate from cooling towers, and in solution in waste water. Escape of hydrogen sulfide into the atmosphere may cause some acid rain as a result of its oxidation into sulfuric acid. It is now common to scrub this gas from the geothermal steam and oxidize it to sulfate by passing the steam through an alkaline solution containing hydrogen peroxide.

Geothermal waters have, as a rule, much higher salt content than nonthermal groundwaters. Many elements can occur in concentrations higher than acceptable for domestic use and for irrigation and stock watering. This is particularly the case for boron, arsenic, hydrogen sulfide, and overall salt concentration. Furthermore, the concentrations of some trace metals, especially in saline waters, may be unacceptably high. These include elements such as mercury, lead, manganese, and zinc, among others. On the Greek islands of Milos and Nisyroz, drillholes tap waters from over 300°C geothermal reservoirs, which have about three times seawater salinity. Development of the respective reservoirs has been postponed for the time being because of concern for possible groundwater and seawater pollution by the geothermal fluid.

C. Directional Drilling

Directional drilling has received increased attention in recent years to reduce the environmental impact of geothermal exploitation. Such drilling involves drilling of several wells from the same platform. First, every well is drilled vertically, but below the production casing each is deviated from the vertical, the deviation increasing with depth. By directional drilling, roads and drill rig platforms are reduced in number. The success of directional drilling depends on the level of producing aquifers. If permeable aquifers are abundant in the reservoir just below the production casing, the directionally drilled wells will be closely spaced at the level of these aquifers, and interference between them is likely. The success of directional drilling is best when productive aquifers occur at deep levels in the reservoir.

D. Injection of Waste Fluids

During the early years of geothermal utilization, the waste fluid was generally disposed of by the least-expensive method available. This most often involved surface disposal into the nearest stream or into ponds constructed for this purpose. To minimize the environmental impact of geothermal exploitation, injection of the waste fluid into wells has been adopted in many fields during the last 10–20 years.

Injection may require the drilling of special wells, either within the geothermal reservoir or outside it. Alternatively, production wells that turn out to be nonproductive or very poor may be used for injection. At any rate, if injection is intended, this has to be taken into account during phase 3 (Fig. 7) in the development procedure for a geothermal resource.

Injection of used geothermal fluids was seriously discussed for the first time at the UN Conference on Geothermal Energy held in Pisa, Italy, in 1970. There are two basic reasons for the interest in injecting used geothermal fluid (water and condensed stam). One is that injection helps maintain reservoir pressure and in this way reduces decline in flow from wells with time, thus increasing the operational life of the well field. The second reason is to reduce the environmental impact caused by surface disposal of water with high concentrations of undesirable elements.

The waste fluid may be injected into shallow or deep wells. Ideally injection into the reservoir is preferred. Caution is advised on such injection, however, because of the risk of thermal breakthrough (i.e., the relatively cool injected water may flow rapidly into the aquifer of producing wells and cause their performance to deteriorate). Because permeability within a reservoir is generally so variable and anisotropic, it is not possible to predict with confidence how an injection well will perform, with respect to either its capacity or which way the injected fluid will flow once in the reservoir.

Another problem associated with injection is deposition of minerals from the fluid. The mineral generally of primary concern is amorphous silica, but also at times calcite and anhydrite. Deposition is mostly affected by boiling of the geothermal water and changes in temperature. If deposition occurs, it may block the injection well and/or damage formation permeability in the vicinity of the well. It is now possible to predict with reasonable confidence the conditions under which deposition tends to occur and, thus, specify desired injection conditions.

SEE ALSO THE FOLLOWING ARTICLES

Gas, Plume, and Thermal Monitoring • Geothermal Systems • Surface Manifestations of Geothermal Systems • Volcanic Contributions to the Carbon and Sulfur Geochemical Cycles and Global Change

---

FURTHER READING

Armstead, H. C. H. (1978). "Geothermal Energy." John Wiley & Sons, New York.

Arnórsson, S. (1995a). Geothermal systems in Iceland: Structure and conceptual models. I. High-temperature areas. *Geothermics*, **24,** 561–602.

Arnórsson, S. (1995b). Geothermal systems in Iceland: Structure and conceptual models. II. Low-temperature areas. *Geothermics*, **24,** 603–629.

D'Amore, F. (1991). "Application of Geochemistry in Geothermal Reservoir Development." UNITAR/UNDP Centre on Small Energy Resources, Rome, Italy.

Ellis, A. J., and Mahon, W. A. J. (1997). "Chemistry and Geothermal Systems." Academic Press, New York.

Fridleifsson, I. B. (1996). Present status and potential role of geothermal energy in the world. World Renewable Energy Congress IV, Denver, Colorado, June 15–21.

Fridleifsson, I. B., and Freestone, D. H. (1994). Geothermal energy research and development. *Geothermics*, **24,** 175–214.

Fridleifsson, I. B., and Stefánsson, V. (1998). Geothermal visions. 5th Geothermal Conference of Geothermische Vereinigung eV, Straubing, Germany, May 1998. Tagungsband 5, Geothermische Fachtagung, pp. 578–587.

Grant, M. A., Donaldson, I. A., and Bixley, P. F. (1982). "Geothermal Reservoir Engineering." Academic Press, New York.

Henley, R. W., Truesdell, A. H., Barton, Jr. P. B., and Whitney, J. A. (1984). Fluid-mineral equilibria in hydrothermal systems. *In* "Review in Economic Geology," (J. M. Robertson, ed.). Society of Economic Geologists.

International Geothermal Association. (1995). Proceedings of the World Geothermal Congress, 1995, Florence, Italy, May 18–31. Volumes 1–5.

Rinehart, S. (1980). "Geysers and Geothermal Energy." Springer-Verlag, New York.

Rybach, L., and Muffler, L. J. P., eds. (1981). "Geothermal Systems: Principles and Case Histories." Wiley, Chichester.

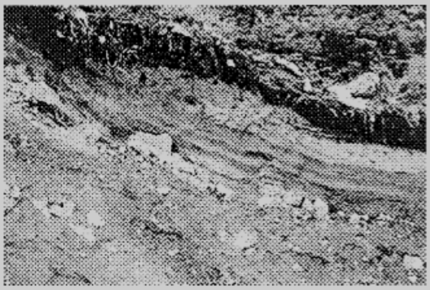

VOLCANIC SOILS

CHIEN-LU PING
University of Alaska, Fairbanks

I. Definition
II. Geographic Distribution
III. Classification of Volcanic Soils
IV. Formation of Andisols
V. Soil-Forming Processes in Andisols
VI. Properties of Volcanic Ash Soils
VII. Volcanic Soils and Agriculture
VIII. Summary and Future Needs

GLOSSARY

A horizon A dark mineral soil horizon that formed at the surface or below an organic horizon and has humus accumulation.

B horizon A mineral soil horizon that formed below an A or organic horizon and shows evidence of chemical weathering or alteration.

C horizon A mineral horizon underlying the B horizon that shows very little alteration from its parent rock materials.

E horizon A mineral soil horizon formed below the organic horizon but above the B horizon. The main feature is the loss of silicate clay, iron, aluminum, or some combination of these leaving a concentration of sand and silt.

Alfisols One of the 12 soil orders in the U.S. soil classification system. These are soils with subsurface silicate clay accumulation by illuviation. They form in cool and humid regions but sometimes in semiarid regions.

allophane A poorly crystallized aluminosilicate mineral usually formed from weathered volcanic ash, commonly referred to as an amorphous mineral.

Andisols One of the 12 soil orders in the U.S. soil classification system. These soils form in volcanic deposits that show evidence of weathering.

Andosols One of the soil great groups in the World Reference Base (WRB) used to classify volcanic ash-derived soils.

Aridisols One of the 12 soil orders in the U.S. soil classification system. These soils form in dry conditions such that there is redistribution of soluble materials, but there is not enough water to leach salts out of the soil profile.

clay There are two definitions: (1) A particle size grade, mineral particle with diameter <0.002 mm; (2) clay sized secondary minerals, mainly layered silicates.

Entisols One of the 12 soil orders in the U.S. soil classification system. These are the recently formed soils with little if any profile development.

Gelisols One of the 12 soil orders in the U.S. soil classification system. These soils commonly have permafrost within 1 m.

glass Short for volcanic glass. Glass is a supercooled silicate comonly used for window glass. Volcanic ash has chemical and physical properties similar to glass.

Histosols One of the 12 soil orders in the U.S. soil classification system. These soils form in organic matter.

Copyright © 2000 by Academic Press
All rights of reproduction in any form reserved.

humus The portion of soil organic matter that largely consists of an amorphous and colloidial mixture of complex organic substances no longer identifiable as plant tissue.

Inceptisols One of the 12 soil orders in the U.S. soil classification system. These soils have few diagnostic features, except a pale brown horizon or mottled or gleyed B horizons.

liquid limit Soil water content at which the soil starts to form puddles.

Mollisols One of the 12 soil orders in the U.S. soil classification system. These soils have high accumulations of calcium-rich organic matter, largely from the root systems of grasses in the A horizon.

noncrystalline Clay minerals that lack a three-dimensional crystal structure, yet the arrangement of atoms is not entirely random. Atoms behave as spheres with definite radii and have their own coordination tendency.

ochric epipedon A surface horizon of mineral soil that is too light in color, too high in chromium, too low in organic carbon, or too thin to be any other diagnostic soil horizon and that is hard and massive when dry.

Oxisols One of the 12 soil orders in the U.S. soil classification system. These are the most highly weathered soils with B horizons which are very high in clay-size particles dominated by hydrous oxides of iron and aluminum. Most silica has been leached out.

paracrystalline In crystals, atoms are packed in a three-dimensional pattern and are called crystalline (long-range order), whereas in amorphous (without form) materials, they are not arranged in such a regular manner. Instead, they form a two-dimensional crystallite.

plastic limit Soil water content at which soils material becomes plastic, or capable of flowing.

permanant charge The negative charges on clay surfaces due to isomorphous substitution in the tedrahedral and octahedral layers of aluminosilicate clays.

sand Soil mineral particles with diameters ranging from 0.05 to 2.0 mm.

silt Soil mineral particles with diameters ranging from 0.002 to 0.05 mm.

Spodosols One of the 12 soil orders in the U.S. soil classification system. These soils are characterized by an albic (E) horizon overlying a spodic (B) horizon that had illuviated organic matter alone or in complex association with aluminum and iron.

Ultisols One of the 12 soil orders in the U.S. soil classification system. These soils are leached Alfisols. They lost most of their calcium and magnesium on the exchange sites of clays, thus they are more acidic.

Vertisols One of the 12 soils orders in the U.S. soil classification system. These soils form in parent materials rich in expanding clays such as smectite. They swell when wet and shrink when dry, thus creating deep cracks during the dry season and hummocky microtopography.

variable charge It is also called pH-dependent charge, which is due to the broken O bonds and edge hydroxyls. The charge changes with pH; net negative charge develops when soil solution pH is higher then zero point charge and net positive charge develops when solution pH is lower then zero point charge.

SOIL IS A natural body composed of solids (minerals made up of sand, silt, and clay size particles and organic matter), liquids, and gases that form on the land surface, occupy space, and are characterized by one or both of the following: horizons, or layers, that are distinguishable from the initial material as a result of additions, losses, transfers, and transformations of energy and matter or the ability to support rooted plants in a natural environment (Fig. 1). Most soils derived from volcanic ash and pumice show distinctive properties that are not found in soils derived from other parent materials under the same vegetation and climate. Volcanic soils have several important properties in common The amorphous clays have a low permanent charge and a high pH-dependent charge, and phosphorus fixation and water retention are high relative to most other soils with comparable textures. Carbon contents are high relative to other mineral soils due to low bulk densities. Volcanic ash soils pose unique engineering problems due to the fragile nature of ash and pumice and also, because it is not uncommon for the liquid limit to be reached before the plastic limit. This chapter details the geographic distribution of volcanic soils and their unique chemical, mineralogical, morphological, and physical properties; the soil formation processes; and the importance in agriculture.

I. DEFINITIONS

Volcanic ash soils are often synonymous with the Andisols order which is the 11th soil order in Soil Taxonomy—the official U.S. soil classification system. The name *Ando soils* was introduced by U.S. soil scientists in 1947 during reconnaissance soils surveys in Japan. The name was connotative of soils formed in volcanic ash which had thick, dark surface horizons and were acid in reaction. In Japan, they are called Ando soils, whereas the name Andosol is used for

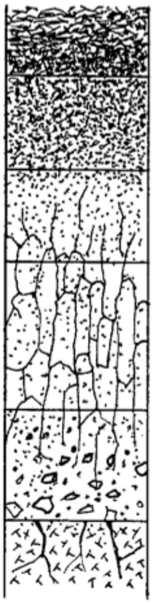

O Horizons: Organic horizons in which the main feature is the accumulation of plant residue with various degree of decomposition

A Horizons: Mineral horizons that form at the surface or below an O horizon and are characterized by an accumulation of humified organic matter intimately mixed with the mineral fraction

E Horizons: Mineral horizons in which the main feature is loss of silicate clay, Al, Fe, or combination of these, leaving a concentration of sand and silt particles of resistant minerals

B Horizons: Horizons that formed below an O, A, or E horizon and are dominated by obliteration of all or much of the original rock structure and by illuvial concentration of silicate clay, Al, Fe, humus, carbonates, gypsum or silica, alone or in combination

C Horizons: Horizons or layers, excluding hard rock, that are little affected by soil forming processes and lack properties of the above horizons

R layers: Hard rock or bedrock

FIGURE 1 Hypothetical mineral soil profile showing the major horizons that may be present in a well-drained soil in temperate humid region. Any particular profile may have some of these horizons, and the relative depths vary.

volcanic soils in the World Reference Base (WRB) soil classification system.

Although often interchangeable with volcanic soils, the definition for Andisol is more rigorous. The central concept of Andisols is a soil that develops in volcanic ash, pumice, cinders, and other volcanic ejecta and/or volcaniclastic materials, with an exchange complex that is dominated by X-ray amorphous compounds of aluminum (Al), silicon (Si), and humus or by a matrix dominated by glass, having one or more diagnostic horizons other than an ochric epipedon. Bulk densities are low in most horizons, although the absolute values vary with the degree of weathering, the humidity of the soil climate, and in a few cases the degree of cementation by silica or other cements. Some Andisols are not derived from volcanic ash or volcanic ejecta but are formed in silicious or tuffaceous materials. On the other hand, volcanic soils includes all soils derived in materials of volcanic origin with or without the previously mentioned unique properties.

These soils exist in a wide range of climate conditions from cold to hot and from dry to humid. Even though Andisols form from parent materials that have appreciable amounts of glass, other soil orders such as Spodosols, Mollisols, Ultisols, Alfisols, and Oxisols may form from volcanic materials if conditions are suitable. Entisols form in recent ash or older ash with very little weathering due to very dry conditions. Thus, in this article *volcanic soil* refers to soils derived from volcanic ash that includes soil orders in addition to the Andisol order.

II. GEOGRAPHIC DISTRIBUTION

Volcanic ash soils cover more than 1.5 million km^2 or about 1% of the Earth's land surface (Fig. 2). By far the most striking pattern in the distribution of volcanic ash soils follows the Circum-Pacific Ring of Fire, the concentration of active tectonic zones and volcanoes along the western coast of both North and South America, across the Aleutian Islands down the Kamchatka Peninsula and Kurile Islands of Russia, through Japan, the Philippine Islands and Indonesia, across Papua New Guinea, and Pacific islands to New Zealand. Another large area of volcanic ash soils exists along the Rift Valley in Africa through Yemen, Ethiopia, Kenya, Rwanda, and Burundi. Other areas of volcanic soils associated with active volcanism exist in the Cameroons, West Indies, southern Italy, the Canary Islands, and Iceland. In China, volcanic soils formed in Quaternary ash deposits are found in the northeastern and southern provinces, Inner Mongolia, Xinjiang, Hainan, and Taiwan.

In Alaska, volcanic ash deposits are widespread and

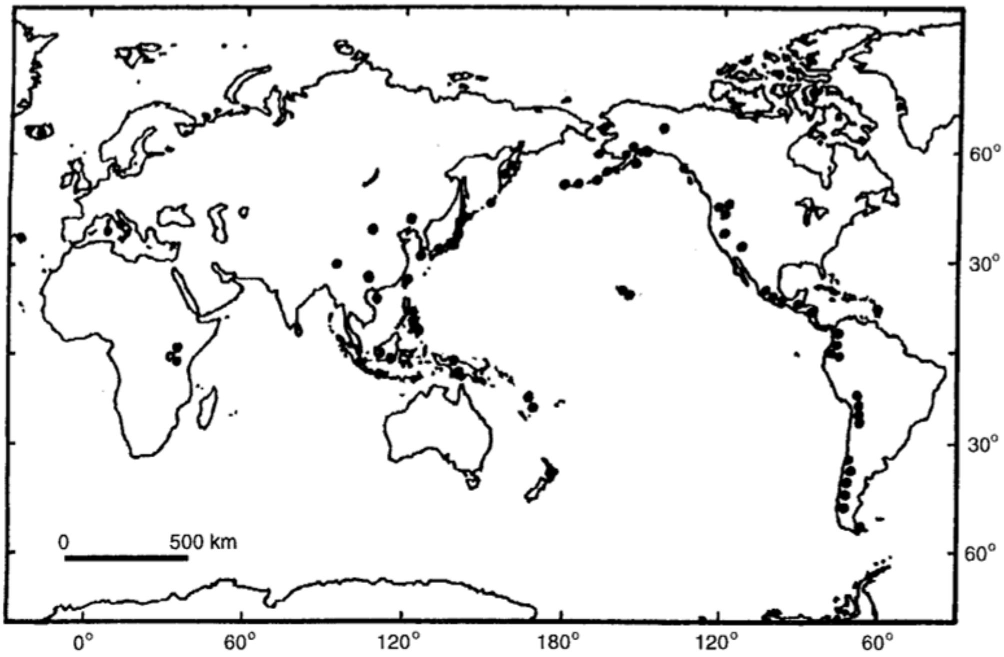

FIGURE 2 Distribution of volcanic soils in the world (indicated by black dots).

abundant in Quaternary sediments throughout the southern region; however, they are less abundant in the central region and are only found to a limited extent in the northeast region. In the Aleutian Islands, there are approximately 80 active volcanoes that produced about 120,000 km^2 of soils formed in volcanic ash and other pyroclastic materials. Volcanic ash soils also exist in Washington, Oregon, California, and Idaho, all of which are affected by the 17 active volcanoes in the Cascades Range. Volcanic soils form in Tertiary volcanic ash deposits in Arizona. Volcanic ash deposits are also found in permafrost regions of southern Yukon Territory, southern portions of British Columbia, and Alberta of Canada.

At present about 1500 volcanoes remain from the periods of intense activity of the Holocene, Pleistocene, and late Tertiary periods. These volcanoes have extruded thousands of cubic kilometers of lava and related volcanic material, and it is from this material that Andisols form.

III. CLASSIFICATION OF VOLCANIC SOILS

Soil classification is designed to group our knowledge on different soils for land-based technology transfer. Soil Taxonomy is the U.S. soil classification system, which is based on soil properties. There are 12 soil orders in Soil Taxonomy. The hierarchy of the U.S. soil classification system is order, suborder, great group, subgroup, and series. In this chapter only the suborders of Andisol will be introduced for discussion in the following sections. Details for each category can be found in the Keys to Soil Taxonomy.

The majority of volcanic soils are derived from volcanic ash and are classified in the Andisols order. Andisols are those soils that contain $<25\%$ organic carbon and have >35 cm within the top 60 cm of the mineral soil surface that meet the Andic soil properties, which differentiate them from the freshly deposited or unweathered ash or pumice. These properties are defined based on the presence of weathered products such as amorphous material and humus–metal complexes, bulk density <0.90 g/cm^3, and high phosphate retention ($>85\%$), or the presence of volcanic glass if the weathered products are low but measurable.

The seven suborders of Andisols are based on soil climate and drainage conditions. Aquands are Andisols with saturated and reducing conditions within the upper 25 cm. Cryands are those formed in areas with a mean annual soil temperature less than 8°C. Torrands are those with an aridic (dry) moisture regime. Xerands are those with a xeric moisture regime (moist and cool winter, warm and dry summer). Vitrands are those with high volcanic glass and thus lower water retention than other suborders. Ustands are those with a ustic (subtropic) moisture regime. And Udands are those with a humid climate. In the next category, there are 29 great groups that are based on soil profile characteristics. The great groups are further divided into 196 subgroups based on deviations from the typical ones. The subgroups are differentiated into several thousands soil series based on soil horizon arrangement. In general, Andisols are formed in parent materials of volcanic origin, but this is not a requirement for an Andisols, as there are some Andisols formed in nonvolcanic materials. An example of the hierarchy is illustrated here:

Andisols	Order
Cry**and**s	Suborder
Fulvicry**and**s	Great group
Typic Fulvicry**and**s	Subgroup

Fulvicryands are those Cryands that have more than 6% organic carbon but that have a light color.

However, not all volcanic ash soils fall into the Andisol order. For those in which the ash layers are too thin, they are classified into Andic subgroups of the other 10 orders except Histosols. Those in which the ash layer is deeper than 35 cm but that are too young or have little or no weathered product are classified as Entisols. When Andisols undergo further weathering, the amorphous minerals may transform into 1 : 1 and 2 : 1 layer silicates. Then bulk density increases, variable charges and P fixation decreases, and the soils become Inceptisols. Aridisol may form in volcanic deposits that may be old and thick but the dry climate limits the weathring to salt accumulation. Mollisols generally form in older and basic volcanic deposits under temperate and humid climatic conditions. The allophane and imogolite have transformed to halloysites and other 2 : 1 layer silicates; thus the variable charge decreases, bulk density increases, and layered clays are saturated with basic ions, mainly calcium (Ca) and magnesium (Mg). In Japan, some volcanic Mollisols developed in tephras older than 12,000 years. Under cool and humid environments, Andisols transform into Spodosols in a relative short time (i.e., several thousand years) due to strong leaching and the high susceptibility of volcanic glass to weathering. Alfisols and Ultisols form under subtropical environments, when the poorly crystalline minerals in Andisols transform to crystalline layer silicates such as kaolinite and vermiculite. Ultisols are more leached than Alfisols, thus they are more acidic. In the subtropic environment, Vertisols are formed when volcanic ash weathers to expanding 2 : 1 layer silicates, such as smectite. Oxisols form under the hot and humid conditions where volcanic deposits have undergone strong weathering and have lost most of the silica through leaching, and with residual accumulation of hydrous iron and aluminum oxides. Gelisols may form from volcanic ash and pumice if the ash layer is underlain by or partially within permafrost.

IV. FORMATION OF ANDISOLS

A. Parent Material

The parent material of volcanic ash soils includes ash, pumice, cinders, and other volcanic ejecta. These soils are formed in volcanic materials from ultrafine dusts to a mixture of large boulders and volcanic bombs which are ejected by explosive volcanic eruptions. Many volcanic ash soils are multisequa (repeated A-B-horizon sequences) resulting from a series of eruptions laying down ash and then pumice or cinders. This interbedding results in unique soils that can be easily studied by dating the various layers present. The soil properties are affected by the chemical and mineralogical properties, texture, and deposition features of the volcanic ash. Volcanic ash can be divided into the light-colored and dark-colored groups. Felsic tephra is acidic and light-colored. The main rock types include rhyolite and dacite with a total SiO_2 content >62%. Mafic tephra contain dark-colored material with the major rock type being basalt with a 45–54% SiO_2 content. Rock types of the intermediate group are andesite and basaltic andesite with SiO_2 contents ranging from 54 to 62%. The mafic rock types contain more of the minerals plagioclase and pyroxene. Opaque minerals are present in all three groups. The rate of chemical weathering is much faster in soils derived from dark-colored glass-rich tephras (basaltic tephras) than from light-colored glass-rich dacite tephra. In Alaska, light-colored tephras exist in southcentral Alaska and dark-colored tephra exist in the Aleutian Islands and southeastern Alaska. Thus the volcanic ash soils in southcentral Alaska are more acidic than those from the Aleutian Islands, and those in the Aleutians are more fully developed.

B. Climate

Climate plays an important part in Andisol formation, and it is the key to differentiating the Andisol order into suborders with the exception of Aquands and Vitrands. The Torrands (Latin *torridus,* hot and dry) are Andisols formed in hot and dry climates and are least weathered, thus there is calcite accumulation in the soil profile.

The Ustands (Latin *ustus*, burnt; implying dryness) are Andisols formed in semiarid climates and experience some degree of leaching. The silica is leached from the upper to lower profile and, in some cases, forms a hardpan. The Xerands (Greek *xeros*, dry) are Andisols formed in Mediterranean climates with dry, hot summers and cool, moist winters. Organic matter started to accumulate in the Xerands. The Udands (Latin *udus*, humid) formed under humid or very humid climates. These soils are highly leached, thus very acidic, and have a high organic matter content. Cryands (Greek *kryos*, coldness) are Andisols that form in climates with cool summers and mean annual soil temperatures that are less than 8°C. Most Cryands are found in Alaska, the Kamchatka Peninsula, and the high mountains of East Africa, Iceland, the Cascades Range, and the Andes Mountains. The suborder, Vitrands are Andisols with soil materials dominated by only weakly weathered volcanic glass. Aquands are Andisols with an aquic (wet) condition.

The "classic" Andisol of Japan and other areas along the Ring of Fire forms in humid environments which also tend to be fairly cool. These are deep, organic-rich soils. This suggests the optimum climate for rapid formation is one of cool temperatures and high rainfall. Even within the tropics, the better expressed Andisols are found at higher elevations with cooler temperatures. In the warm areas, the transformation to Ultisols and Oxisols is even more rapid.

C. Topography

Andisols tend to be in mountainous to hilly areas because that is where volcanoes are found, but fine ash can be carried over long distances and deposited on a variety of landscapes. Also water can rework ash such that extensive flat areas of Andisols are found in intermountain valleys. Large lava flows may likewise result in fairly flat areas for the formation of Andisols. Aquands are Andisols that form in topographic positions with restricted drainage. They tend to be dark-colored because of the accumulation of organic matter due to the anaerobic conditions. Because of the mode of ash deposition there is no single dominant topographic area where Andisols are expected.

D. Vegetation

The natural vegetation associated with Andisols varies but has a major influence on the type of Andisol formed. Many areas in the Pacific Northwest and Alaska are under forests. Udands generally are formed under forest vegetation, but in south central Alaska and Japan, some Udands form under dense grass. Cryands generally form under conifer forest, but the Cryands in the Aleutians form under tundra vegetation. Vitrands and Xerands have a mixed vegetation of grass and forest, such as those found in northern California, central Washington, and Oregon. Torrands have shrubby or grass vegetation. In general the soils are moderately acid so that any vegetation associated with acidic materials will predominate.

E. Time

As with all soils, time is a major factor in the formation of Andisols. Andisols generally are found on young parent materials in humid climates. By their very nature, the older and more stable the landscape, the more weathering will have taken place, and either Ultisols or Oxisols will be found. The drier and/or cooler the environment, the longer it takes for an Andisol to form. For example, there are volcanic materials in extremely dry areas that have not weathered at all and are still Entisols. An A horizon can form on newly deposited ash in several hundred years, whereas an A-B sequence can take several thousand years. In Japan, most Andisols are 4000–7000 years old. In southeastern Alaska, a highly developed Cryand has a C-14 date of 12,000 years old. Yet, in a Haplocryand from northeast Kodiak Island, Alaska, an incipient profile including a dark A horizon, weak E horizon, and an iron-stained B horizon have already formed in the 1912 Mount Katmai ash (Fig. 3).

V. SOIL-FORMING PROCESSES IN ANDISOLS

Soil formation is the combined effects of five soil forming factors: parent material, climate, topography, vegetation, and time. The genetic concept of an Andisol is that of a soil that forms in a humid environment from volcanic ash. There needs to be a minimum amount of weathering to produce Andic Soil Properties as defined in the Keys to Soil Taxonomy. Because most Andisols are formed in humid environments, weathering is quite rapid in volcanic ash. In surface (A) horizons, most of the active aluminum and iron released from volcanic

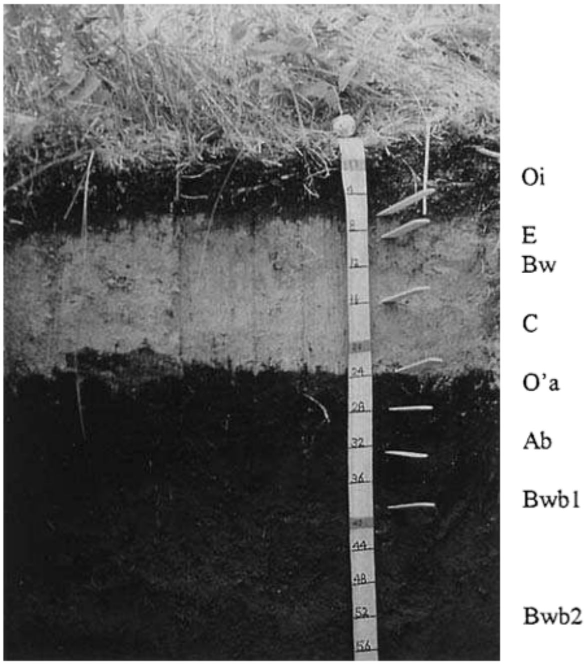

FIGURE 3 A volcanic soil formed in the 1912 Mount Katmai ash over a buried, well-developed Andisol in northeast Kodiak Island, Alaska. The photo was taken in 1986, and a dark O horizon, a thin E horizon, and an incipient B horizon have already formed in the younger ash under the cool and humid environment. The dark color of the upper buried horizon is due to high humus content. (Explanation of subscripts in the B horizons: w, weathering; b, buried and in O horizons; i, least decomposed; a, highly decomposed).

ash forms complexes with humus. In the subsurface (B) horizons, aluminum and silicon oxides precipitate together to form allophane and imogolite. Allophane and imogolite are the early weathering products of volcanic glass and can be extracted with acid-oxalate. If there is more extensive weathering, halloysite and other crystalline minerals may be formed.

Because Andisols form under many different environments, there is an extensive range in properties. Properties common to most volcanic soils including Andisols are: low bulk densities, high levels of carbon to depth, and a high level of phosphorus fixation; it is these properties that are used to define Andic soil material. The overall processes are ones which lead to the formation of stable complexes of aluminium, iron (Fe), silicon and organic matter. If the weathering process continues, other types of soils are formed when more crystalline minerals develop (e.g., Ultisols, Oxisols, Inceptisols, and Alfisols).

VI. PROPERTIES OF VOLCANIC ASH SOILS

A. Morphological Properties

Most volcanic ash soils have striking morphological features. They usually have multiple sequences of horizons (Fig. 3) as a result of intermittent volcanic fallout. In the field, it is easy to identify the dark surface horizons (A) overlying a reddish brown or dark yellowish brown subsurface horizons (B). The A-B sequence generally represents one deposition (eruption) event and multiple sequences are common, which reflect the intermittent nature of volcanic ash deposits. Such stratification is an important tool for dating volcanic activities and geological events. Often a thin gray or whitish layer of recent ash fall may be found at or near the surface. Because of the nature of the ash fall, the horizons are generally flat, and the transition from one horizon to another is distinct. In the field, when excavated, volcanic ash soils give a feeling of "puffiness" due to the low density. On grassland, the soils generally have a granular structure in the A horizons due to the disturbances of roots and soil fauna. The structures in the B horizons are generally subangular blocky. Udands that formed in high rainfall areas have a high clay content and are subjected to wet/dry cycles that result in columnar structures. Soils that are high in allophane are sticky in moist field conditions. Andisols generally have deep rooting zones due to the low bulk density.

B. Mineralogical Properties

The mineralogical properties of volcanic ash soils are what give rise to the unique chemical and physical properties of these soils. The primary minerals in tephra are commonly divided into light (specific gravity <2.96) and heavy (specific gravity >2.96) minerals. The light minerals include volcanic glass, phenocrysts, feldspar, and silica minerals (mainly quartz). The heavy minerals include dark-colored volcanic glass and all the iron- and magnesium-rich minerals including pyroxines, ferromagnetic minerals, amphiboles, biotite, and olivine. The major secondary minerals in volcanic ash soils are allophane, allophane-like materials, imogolite, zeolite, noncrystalline and crystalline silicate clays.

Volcanic ash consists mainly of volcanic glass, which contains noncrystalline silica and aluminum with minor inclusions of ferromagnesium minerals. On weathering, the glass releases aluminum and iron into solution, which forms a stable complex with humus resulting from plant material decomposition in surface soil horizons. These Al, Fe–humus complexes are immobilized and accumulate at the surface to form a dark A horizon. The Al– or Fe–humus complexes are dominant components of the collodial fraction of the A horizon. With the dissolved Al being tied up with humus, the soil solution accumulates an excess amount of dissolved silica (Si). A secondary Si mineral forms in this Si-saturated solution, called laminar silica, which is commonly circular or elliptical in shape and extremely thin with diameters ranging from 0.2 to 0.5 μm. Opaline silica is found in the surface horizons of soils from the Aleutian Islands and the Kenai Peninsula. It is easily identified with an electron microscope (Fig. 4). In humid environment, it takes few hundred years for opaline silica to form.

As depth increases in the B horizons, the supply of organic matter or humus becomes limited. The dissolved Al and Si from all kinds of volcanic ash can form noncrystalline and paracrystalline substances, mainly allophane and imogolite. In the early 1940s, allophane was considered synonymous with amorphous clay because it is nearly X-ray amorphous, although under an electron microscope, it appears as hollow spheres 3.5–5.0 nm in diameter. Chemically, allophane has a formula of 1.0–2.0 $SiO_2 \cdot Al_2O_3 \cdot 2.5–3.0 \cdot H_2O$. Imogolite was first described in 1962 by Japanese researchers in a soil derived from glassy volcanic ash known as imogo. Imogolite is paracrystalline, gives a characteristic X-ray diffraction pattern, and infrared and differential thermal curves. In the 1970s, the introduction of high-resolution electron microscope in clay minerals research provide us an insight view of the internal structures and morphology of allophane and imogolite. Under an electron microscope, it appears as smooth, curved threads or tubes with inter-

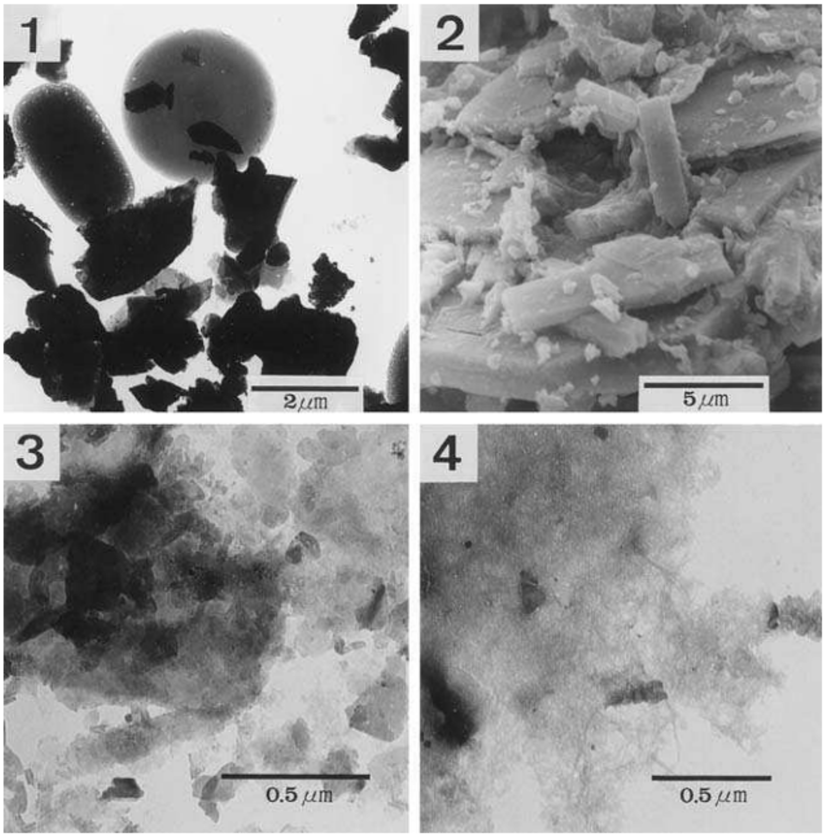

FIGURE 4 Electron micrographs of clay minerals in from some Haplocryands from Aleutian Islands, Alaska: (1) Laminar opaline silica (OS) and volcanic glass (VG) in the A horizon. (2) Zeolite (clinoptilolite) (CL) in a buried B horizon. (3) Humus (dark color) and volcanic glass (light color) in the A horizon of another profile. (4) Allophane in the buried B horizon. [Adapted from Ping *et al.,* 1988; copyright Soil Science Society of America, with permission.]

nal and external diameters of 1.0 and 2.0 nm, respectively. Chemically it has a formula of $SiO_2 \cdot Al_2O_3 \cdot 2H_2O$. The Al : Si atomic ratio of allophane and imogolite are 1.0–2.0 and 2.0, respectively. Imogolite formed from transformation of allophane through removal of silica. Both allophane and imogolite are found in B horizons 5000–10,000 years old. Generally, it takes more than 1000 years for allophane to form and more than 2000 years for imogolite to form in a humid environment. The allophane content in a soil increases with depth, usually in the B horizon and buried horizons. It increases with the age of the volcanic deposit and the amount of annual precipitation. Allophane and imogolite can be dissolved in acid-oxalate solution, and the dissolved Si can be used to quantitatively measure their contents in soils. In south central Alaska, allophane in the B horizons ranges from 2 to 12%, in the Aleutians it ranges from 4 to 14%, and on Baranof Island it ranges from 10 to >20%.

Ferrihydrite is another amorphous mineral found in volcanic ash soils formed in areas of high rainfall (e.g., southeastern Alaska) or in soils with restricted drainage. It is a widespread and characteristic component of young iron-oxide accumulations precipitated from iron-rich soil solutions. It has a bulk form of $5Fe_2O_3 \cdot 9H_2O$. Ferrihydrite can be quantified by the difference between dithionite citrate-extractable and oxalate-extractable Fe. In the B horizons, allophane, with or without ferrihydrite, dominates the colloids with Al– and Fe–humus complexes being minor components. The lower B and C horizons are also rich in allophane and ferrihydrite but contain few Al– and Fe–humus complexes. In addition to ferrihydrite, iron-hydroxides also exist in other noncrystalline or poorly crystalline forms. Most Al released from weathered volcanic materials is in complex with humus. But the mineral gibbsite is found in B horizons formed in old or buried volcanic ash or pumice.

Halloysite is a fast-forming member of the kaolinite (clay) subgroup primarily in porous volcanic glass deposits. Thus it has poor crystallinity. The spheroidal or tubular morphology is characteristic of halloysite, and platy halloysite is rare. Most halloysites are formed in weathered volcanic deposit or igneous rocks under semiarid to humid environments. In New Zealand some halloysites formed from fine-grained rhyolitic tephra in places with annual rainfall of 1200 mm. In Japan and the Aleutian Islands of Alaska, halloysites were found in old and buried ash or pumice deposits, which indicates that their formation is governed by the availability of silica from percolating soil solutions. Halloydites were found in B horizons more than 7000 years old.

Layer silicate minerals of structure 1 : 1, 2 : 1, and 2 : 1 : 1 and their Al interlayers are also common in Andisols. They are either the pedochemical products resulting from transformation of amorphous minerals (allophane) or the weathering product of of mafic minerals (e.g., pyroxenes, amphiboles, and micas in parent ash). Zeolite minerals are found in some Andisols from the Aleutian Islands (Fig. 4). The existence of zeolite indicates that the parent material of the soil contains hydrothermally formed material.

The dominant components in the silt and sand fraction of Andisols are volcanic glass and other primary minerals. Normally, volcanic glass particles are like shattered glass, with sharp angles and edges; thus they are very abrasive. However, in soils, the glass particles are usually coated with allophane, Al- and Fe-oxides, and their humus complexes. These coatings on volcanic glass or other mineral particles can be easily removed with a oxalate solution, thus the freed mineral particles can be used for mineralogical analysis.

C. Chemical Properties

The chemical properties of volcanic soils are dominated by humus and certain unique minerals. Some general chemical characteristics of these soils show that they have pHs ranging from 5 to 7 (weak acid range). This is in contrast to Spodosols which have similar minerals present but generally have pHs less than 5. The Al–humus complexes and the short-range-order colloids have Al-dominated exchange sites. In humid environments, the basic cations (Ca and Mg) are leached out. Therefore, most volcanic ash soils have high exchangeable Al and thus high Al saturation, generally over 40%. Base saturation is low (generally less than 10% in Alaskan soils). The Al on the Al–humus complex is the major source of acidity. Soils with high Al–humus can have a pH lower than 5.0. Volcanic ash soils, especially Andisols and Andic subgroups in other soil orders, have high phosphorus (P) retention capacity due to the high content of active Al and Fe compounds. Thus P retention was adopted as one of the criteria of Andisol classification.

Weathered volcanic soils have two distinct colloidal compositions dominating the chemical properties of the soil. The humus-rich allophanic Andisols generally have a mixture of variable-charge colloids (allophane and humus), whereas the humus-rich nonallophanic Andisols generally have a mixture of variable and permanent-charge colloids (layered silicates and humus). The permanent charges are from isomorphic exchange in layered aluminosilicates, whereas the variable charge is created in allophanic minerals and humus when the pH increases. Anion exchange capacity exits in allophanic Andisol but not in nonallophanic Andisol. These soils also have very large surface areas as high as 600 $m^2 g^{-1}$ and give rise to very large number of exchange sites. Thus for an allophanic A horizons, the effective cation exchange capacity is more than twice that of an nonallophanic soils with same amount of organic matter.

D. Physical Properties

Soil physical properties are dominated by clay fractions and humus which are the exchange complexes of a soil system responsible for nutrient retention and exchange, water retention, shrink–swell potential, aggregate and structure formation, and many other properties. In well-developed volcanic ash soils such as Andisols and the Andic Spodosols, the exchange complexes are dominated by Al– and Fe–humus complexes, ferrihydrite, allophane/imogolite, and a small fraction of crystalline clay minerals. These colloidal components give these soils their unique properties.

1. Low Bulk Density

Soils derived from volcanic ash usually have a bulk density of <0.9 g cm^{-3}. Organic matter, amorphous material, porous glass, and pumice all contribute to the low bulk density. Thus, the well-developed volcanic soils have higher organic carbon and allophane contents resulting in bulk density as low as 0.5–0.9 g cm^{-3}. Most Andisols are a good growth medium for plants because they are very permeable due to their low bulk density and high porosity.

2. Thixotropy and High Water Retention

Most well-developed volcanic ash soils in moist field conditions have a smeary feeling when rubbed between one's fingers. The soil appears barely moist, but after prolonged rubbing, the soil becomes greasy and wet. Once the pressure is relieved, the excess water is reabsorbed into the soil. Such a unique property is called thixotropy, which develops the unusually high water retention of allophanic soils. Allophane has a large specific surface area of approximately 1000 $m^2 g^{-1}$, which is responsible for such a high water retention. Weathered volcanic ash soils may retain 40–90% water in humid regions and more than 100% in the highly weathered soils which exist in high rainfall (>2000 mm) regions such as southeastern Alaska, the Cascades Range of the Pacific Northwest, and New Zealand. Thixotropy and low bulk density contribute to the low bearing capacity and poor traction of volcanic ash soils.

3. Irreversible Drying and Plasticity

Allophane is generally electrically neutral with its natural pH value close to 5.2. Thus, once dried, the allophane particles will go through dehydration and form closely packed aggregates of silt or sand size. These aggregates do not disperse on rewetting. Thus, a crust may form on ground surfaces without vegetative cover during hot, dry summers. The irreversible drying also results in unreliable particle size determinations if the samples are air-dried or even oven-dried before rewetting and dispersion. Thus, the traditional method of particle size distribution tends to underestimate the clay content of soils containing amorphous minerals. Newly formed volcanic ash soils do not have this problem because they do not contain allophanic minerals.

Plasticity is one of the physical properties distinguishing soils containing allophane from those containing crystalline clay minerals. Generally, moderately to well developed volcanic ash soils in their field-moist state have high liquid and high plastic limits. Field-moist samples from south central Alaska have a liquid limits ranging from 60 to over 100%, whereas those from south eastern Alaska have liquid limits ranging from 100 to 250%. In the field conditions, some highly weathered volcanic soils may reach their liquid limits before the plastic limits. Soils containing allophane and imogolite exhibit irreversible drying, thus after a loamy soil is air-dried, it forms strong aggregates, shows very little plasticity, and behaves like sandy soils.

VII. VOLCANIC SOILS AND AGRICULTURE

Although volcanic ash soils cover slightly less than 1% of the total Earth's land surface, their importance to civilization is great as they support more than 10% of the total world population. The Rift Valley in East Africa nourished the earliest known human race. The fertile volcanic soils of Central and South America have long supported the Mayan and Inca civilizations by providing them with fiber and food and grazing ranges. Today, the volcanic ash soils support the most important cash crop for this region: coffee. In addition, these soils also produce large quantities of tropical fruits and hardwood forests and, in recent years, support the beef industry. In Japan, Indonesia, and the Philippines, both native crop and rice fields were cultivated in volcanic ash soils for more than 10 centuries. In the South Pacific, from Hawaii to New Zealand, as well as in the Philippines and Indonesia, volcanic ash soils support various crops including sugar cane and tropical fruits and provide productive grazing ground for animals.

For centuries, vineyards have flourished in volcanic ash soils in southern Italy and nourished the Mediterranean culture. In southern Alaska and along the coastal regions of the Pacific Northwest of the United States, volcanic ash soils support the most productive conifer forests, providing an important economic base for the region. In the semiarid regions of California, Oregon, and Washington, some of the most productive vineyards and orchards of apples, peaches, cherries and apricots grow in volcanic ash soils. In this region, most volcanic ash soils are formed in Pleistocene and Holocene volcanic deposits, whereas in Napa Valley, most of the volcanic soils formed in Tertiary pyroclastic deposits.

The vineyards and orchards favor the Mediterranean climate of these regions, rather than volcanic soils alone. However, the volcanic soils developed under this climate share similar properties; they are less weathered and retain most of the bases which are essential for the crops. Thus most of those soils are Vitrands, Xerands, Andic Inceptisols, and Mollisols, and some Aridsols with irrigation.

Acidic Andisols exist extensively in subhumid and humid regions. The high Al saturation limits crop selection to acid-tolerant crops unless lime is applied. Thus, phosphorus fertilizer efficiency and Al-toxicity are major concerns in Andisols and associated Spodosols.

VIII. SUMMARY AND FUTURE NEEDS

Soils formed in volcanic ash have unique morphological, chemical, and physical properties. The importance of volcanic ash soils is demonstrated by the fact that they account for only 1% of the Earth's land surface, yet they support more than 10% of the world's population. These soils have nourished many ancient civilizations. The moderately and well-developed volcanic ash soils are fertile and provide the economic basis for some regions. Yet, changing land-use patterns over past decades due to economic growth have resulted in land and soil quality deterioration. Sustained agriculture practices become more critical to maintain the social and economic structure. Volcanic soils formed in humid environments are highly leached and have developed strong acidity and aluminum toxicity; these soils deserve special management practices. More research is needed in soil fertility, especially phosphorus fertilizer efficiency, and acid-tolerant crops deserve more attention. The bountiful gift of these soils given by Nature cannot be taken for granted. The recent calamity resulting from volcanic eruption in Central America is a reminder of the hazard associated with the soils and the region. The prosperity of the people in the volcanically active regions can be guaranteed only with adequate tectonic monitoring and efficient infrastructure.

SEE ALSO THE FOLLOWING ARTICLES

Composition of Magmas • The Ecology of Volcanoes: Recovery and Reassembly of Living Communities • Physical Properties of Magmas • Volcaniclastic Sedimentation Around Island Arcs • Volcanic Materials in Commerce and Industry

FURTHER READING

Bay-Peterson, J., Eswaran, H., and Juang, T. C. (1989). Classification and management of rice growing soils. Proceedings of the Fifth International Soil Management Workshop. Dec. 11–23, 1988, Taichung, Taiwan. Food and Fertilizer Technoilogy Center for the Asian and Pacific region, Taipei, Republic of China.

Maeda, T., Takenaka, H., and Warkentin, B. P. (1977). Physical properties of allophane soils. *Adv. Agron.*, **29,** 229–264.

Panel on Volcanic Ash Soils In Latin America. (1969). "Volcanic Ash Soils in Latin America." Training and Research Center of the IAAIS, Turrialba, Costa Rica.

Parfitt, R. L., and Henmi, T. (1982). Comparison of an oxalate extraction method and an infrared spectroscopic method for determining allophane in soil clays. *Soil Sci. Plant Nutr.*, **28,** 183–190.

Ping, C. L., Shoji, S., and Ito, T. (1988). The properties and classification of three volcanic ash derived pedons from Aleutian Islands and Alaska Peninsula. *Soil Sci. Soc. Am. J.*, **52,** 455–462.

Ping, C. L., Shoji, S., Ito, T., Takahashi, T., and Moore,

J. P. (1989). Characteristics and classification of volcanic ash-derived soils in Alaska. *Soil Sci.* **148,** 8–28.

Shoji, S. (1986). Mineralogical characteristics. *In* “Ando Soils in Japan,” (K. Wada, ed.) pp. 21–40. Kyushu University Press. Fukuoka, Japan.

Shoji, S., and Fujiwara, Y. (1984). Active aluminum and iron in the humus horizons of Andisols from northeastern Japan: Their forms, properties, and significance in clay weathering. *Soil Sci.*, **137,** 216–226.

Shoji, S., and Masui, J. (1971). Opaline silica of recent ash soils in Japan. *J. Soil Sci.*, **22,** 101–108.

Shoji, S., Nanzyo, M., and Dahlgren, R. A. (1993). “Volcanic Ash Soils: Genesis, Properties, and Utilization,” Development in Soil Science 21. Elsevier, Amsterdam, The Netherlands.

Smith, G. D. (1987). The Andisol Proposal: A preliminary proposal for reclassification of the Andepts and some Andic subgroups. *In* “International Committee on Andisols: Final Report,” SMSS Technical Monograph No 20 (M. L. Leamy, D. I. Kinloch, and R. L. Parfitt, Eds.), pp. 1–165.

Soil Survey Staff. (1998). “Keys to Soil Taxonomy,” 8th ed. USDA–Natural Resources Conservation Service, Washington, DC.

Wada, K. (1977). Chapter 21. Allophane and imogolite. *In* “Minerals in Soil Environments,” (J. B. Dixon and S. B. Weed, eds.), 2nd ed., pp. 1051–1088. Soil Science Society of America, Madison, WI.

Wada, K. (1986). “Ando Soils in Japan.” Kyushu University Press, Fukuoka, Japan.

VOLCANIC MATERIALS IN COMMERCE AND INDUSTRY

JONATHAN DEHN
STEPHEN R. MCNUTT
Alaska Volcano Observatory and University of Alaska Fairbanks

I. Introduction
II. Types of Materials
III. Prehistoric Uses
IV. Modern Uses
V. Additives
VI. Aggregates
VII. Construction
VIII. Decorative Uses
IX. Conclusions

GLOSSARY

absorbent A material that takes up, assimilates, or incorporates liquids through pores or interstices.

aggregate Mineral material composed of a mixture of different sizes that is separable by mechanical means. Aggregate is passed through sieves and other sorters to grade its size. Graded aggregates are mixed with cement or bituminous material to form mortar or concrete.

basalt A fine-grained, sometimes glassy igneous rock. Basalts have low SiO_2 contents of 45–50%. They are usually found in lava flows which may be of variable size. They are frequently erupted from fissures and less often from central vents.

bentonite A special assemblage of clay minerals often formed from weathering of volcanic ash. Typically, it is composed of nonrefractory clays rich in montmorillinite and is off-white in color. When the principal ion in the clay is sodium, bentonite is highly absorbent and subject to large volume changes.

cinder block A type of brick made from compressed aggregate material, often volcanic.

drilling mud A mud mixture of clays and water with a high density, viscosity, and strength. Acts as a lubricant, coolant, and sealant and floats drill cuttings up and out of the hole.

montmorillinite A clay mineral common as a weathering product of volcanic material.

obsidian A black, wholly glassy rock which displays conchoidal fracture. Most obsidians are of rhyolitic composition. Because glass is thermodynamically unstable, most obsidians undergo a process of devitrification and form crystal structures.

perlite A glassy and devitrified rock of rhyolitic composition which contains many curved or spherical cracks caused during cooling and contraction. These may be so well developed that the rock easily breaks into irregular pieces. Contained spherical pieces of unaltered obsidian are known as "Apache's tears." Perlite is used as an absorbent and insulator.

pumice A highly vesicular pyroclastic rock produced during explosive eruptions. It tends to accumulate as rounded lumps and also as abraded fragments called shards. Den-

Copyright © 2000 by Academic Press
All rights of reproduction in any form reserved.

sities are typically less than 1.0 g/cm^3, so pumice often floats on water.

refractory A material which does not significantly deform or change chemically at high temperatures. Bricks of such material in various shapes are used to line furnaces.

tephra All fragmental volcanic ejecta which are produced during explosive volcanism, including ash, cinders, lapilli, scoriae, pumice, bombs, etc.

trap rock An older term for compact, fine-grained igneous rocks such as lava flows, which have been broken into roughly uniform fragments. Often used for road beds, running tracks, and the like.

tuff A general name for consolidated ash or tephra, usually with largest clasts less than 2 cm. The material is erupted and is still hot when it hits the ground, resulting in consolidation and partial welding. Tuffs may be crystal rich (crystal tuffs), lithic rich (lithic tuffs), glass rich (vitric tuffs), or lapilli rich (lapilli tuffs).

THE PRODUCTS OF volcanic eruptions have provided useful raw materials for man throughout history. In many regions of the world volcanic rock is ubiquitous, and the inhabitants of these regions have developed ingenious uses for this natural resource. Ranging from early weapons and implements to building materials, volcanic rocks have been sought out because of their physical properties for use in manufacturing processes, or as insulators, absorbents, or abrasives. Volcanic materials play an important role in our lives, regardless of whether we live near volcanoes or not, although most of us do not realize their wide variety of applications.

I. INTRODUCTION

The use of volcanic materials most certainly sprang from necessity, but it was quickly learned that many volcanic materials are ideal for a variety of uses. They have a unique set of physical properties, and their natural occurrence makes them relatively inexpensive and thus ideal for construction and manufacturing. For example, pumice has a relatively high strength, yet in some cases a low enough density to float on water, and provides excellent insulation and absorption characteristics. Most explosive eruptions produce pumice and spread it over a large area. Volcanic rocks are present almost everywhere in the world and annually 6–8 km^3 of new volcanic material is erupted, nearly 2 km^3 subaerially, and about 80% of this is particulate material from pyroclastic flows, debris avalanches, and ash falls. This is enough to cover 1600 football or soccer fields a kilometer deep in ash.

Before the industrial age, volcanic rocks were used for a wide range of purposes and provided a tradable commodity and a basis for local economies. Volcanic soils are fertile, and to this day many countries use volcanic ash as a soil supplement in agriculture (see "Volcanic Soils"). The use of volcanic materials has increased as additional applications have been found, strengthening the practical and economic relationship between mankind and volcanoes. Few data exist on the amount of volcanic material used or the "size" of the affected industries. To help get an idea of the number of volcano-related products available, Fig. 1 shows a histogram of the number of pages in the *Thomas Register of American Manufacturers: Products and Services Section* devoted to several volcano-related topics. We then added several familiar everyday examples to provide a basis for comparison. We found that one page or less was devoted to sulfur, monuments and memorials, pumice, bentonite, and additives; however, each of these volcano-related products had more entries than surfboards. Abrasives, on the other hand, is a substantially larger industry than air conditioners. Absorbents, polishers, and refractories, of which volcanic materials are components, offer a moderate number of products, slightly smaller than refrigerators. All the examples given have fewer manufacturers than batteries. Although crude, these estimates give a sense of the significant positive impact volcanic materials have on our everyday lives.

II. TYPES OF MATERIALS

Volcanic products can be divided into several categories based on their use and chemical composition. These materials are summarized in Table I. The density and strength of each type of material depends on its chemistry and eruptive style, and in turn determines the ideal use for each product.

As a result of the eruption process, explosive volcanic products tend to be in the form of aggregates and have lower densities. In addition, they are often vesicular, giving them excellent insulating qualities. Many industrial processes, for example the manufacture of perlite, are designed to enhance these characteristics.

Volcanic materials often have very high strengths relative to their density, particularly for massive deposits,

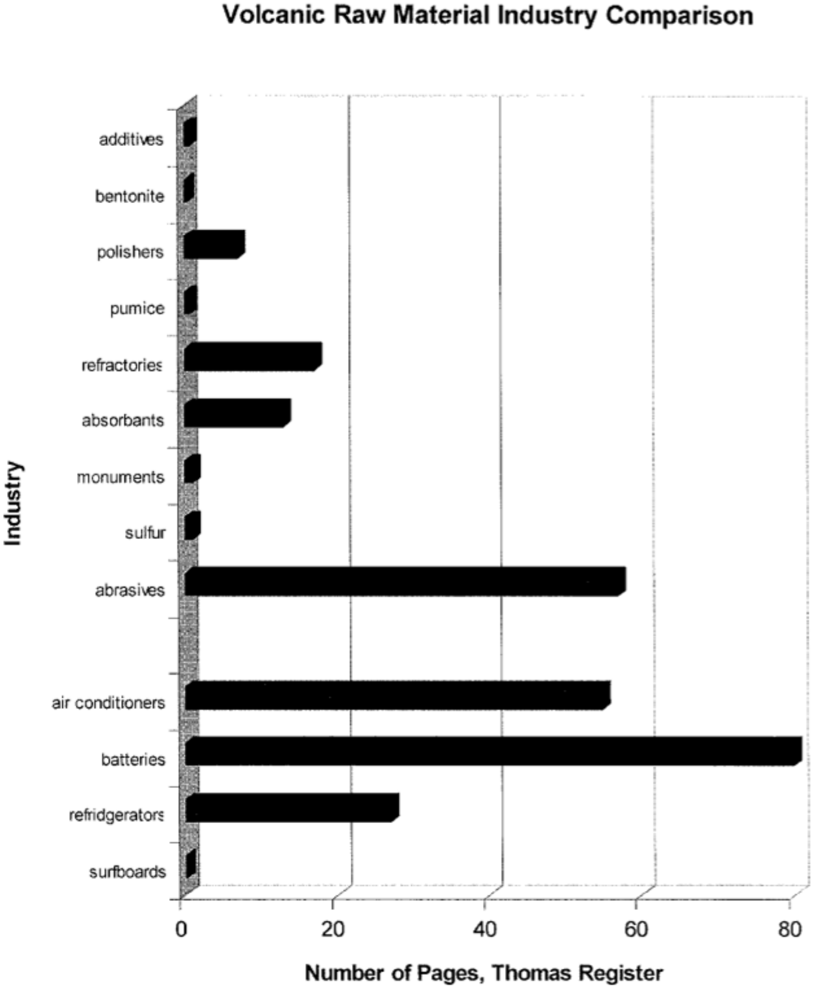

FIGURE 1 A histogram showing the number of pages of the *Thomas Register of American Manufacturers: Products and Services Section* devoted to various volcano-related topics. Several familiar everyday examples of other products are shown in the lower part of the chart to provide a basis for comparison.

such as lava flows or welded ignimbrites. This makes them cost-effective building materials. In the case of aggregate material, the irregular angular shapes allow particles to stick together, yielding very high angles of internal friction. This makes these aggregates ideal for use in constructing road beds or in laying railroad tracks. Because volcanic glass fragments are made of silica, a very hard substance, and the shards are often in the form of bubble-wall junctions, or small sharp tetrahedra, ash fall deposits are a good source of abrasives.

Volcanic rocks are not readily soluble in water nor do they take on water and increase in volume (with the exception of volcanic clays, see following discussion). This makes them more resistant to weathering than limestone or sandstone. Volcanic glass is resistant to corrosion and forms the ground mass of most volcanic rocks. Most volcanic rocks have very small coefficients of thermal expansion (on the order of 1×10^{-7} cm deformation/cm distance/°C or less), and thus will not change in size or shape even under very large changes in temperature. This makes them very good refractories.

Concrete fabricated from volcanic cinders is a better insulator by a factor of 3 to 4 than normal concrete (thermal conductivities of 0.35 –1.5 kcal/m hour deg). This is because of the high vesicularity of the cinders used in its manufacture. The small vesicles resist the transfer of heat, making it more difficult for thermal energy to move through the block.

Igneous rocks (e.g., granite) are also used in construction and have similar strengths compared to volcanic

TABLE I Physical Properties of Useful Volcanic Materials: Color, Typical Grain Size in a Volcanic Occurrence, Density, Strength (Compressive), Thermal Conductivity, Heat Capacity, and Common Uses[a]

Volcanic product	*Color*	*Typical grain–size*	*Density (g/cm^3)*	*Strength (kbar)*	*Thermal conductivity (kcal/m hr deg)*	*Common uses*
Raw products						
Basaltic scoria	Black to red	Coarse aggregate < 3 cm	1.2–2.5	0.6–1.6	<1.0	Road construction, use in cinder blocks, moderate insulator
Basaltic lava	Black/gray	Massive	2.4–3.1	<2	2.0–3.0	Construction, decorative purposes, moderate insulator
Rhyolite ash	Light gray/brown	Fine aggregate < 2 mm	1.5–2	<0.1	<1.0	Abrasives, creation of perlite, a good refractory, insulator
Pumice	Light gray/brown	Aggregate 0.2–10 cm	0.5–1.5	<0.5	<0.75	Absorbent, abrasives, good insulator
Silicic ignimbrite	Light to dark brown	Massive	2.1–2.8	<1	2.0–3.0	Decorative uses, construction, poor to moderate insulator
Rhyolite lava	Brown to gray black	Massive	2.1–2.8	<25	2.0–3.0	Decorative uses, construction, poor to moderate insulator
Obsidian	Clear black	Small lenses or tears (cm)	2.0–2.5	<11	2.7–3.5	Decorative uses, cutting implements, poor insulator
Native sulfur	Yellow	Microcrystalline	1.95–2.1	<0.1	0.13	Chemical additive, component needed to “vulcanize” rubber
Bentonite clays	Light brown	<0.005 mm	1.8–2.6	<0.1	Varies widely	Additive to drilling muds, good insulator and sealant
Man-made products						
Perlite	White to light gray	Coarse aggregate < 3 cm	0.3–1.2	<0.1	<1.0	Absorbent, insulator, lightweight concrete
Cinder concrete	Gray	Blocks (man-made)	2.0	<0.5	3.0–4.5	Construction, insulation

[a] Where appropriate, a range of values has been given. The values given are typical for the materials shown but there can be considerable variance. For example, basaltic scoria has been observed up to meters in size, though these are typically not used for raw materials. The thermal character of the materials is greatly dependent on physical factors, such as vesicularity, or for aggregates their grain size and spatial relationship to one another.

materials, but have higher thermal conductivity and thus do not insulate as well. Because these rocks were typically created at some depth, and thus pressure, the crystals are tightly pressed to one another, giving very good heat conduction across these boundaries. These materials often have larger crystals, making them useful for aesthetically pleasing facades. This chapter will not go into depth on the use of igneous materials, although in many ways they parallel similar volcanic products.

III. PREHISTORIC USES

Volcanic glass has been used for early cutting implements, as have microcrystalline volcanic rocks, such as fine-grained basalts or andesites. Arrowheads, scrapers, and knives made from volcanic products are common finds at prehistoric sites near volcanic regions (Fig. 2). How our ancestors used volcanic rocks is nearly as varied as how we use them today. Pumice can be used as a float in fishing, and as an excellent abrasive, like sandpaper, to fashion other tools. Nonvesicular volcanic rocks are also ideal for crushing and have been used to grind wheat, by hand and in more carefully fashioned millstones. Blocks of tuff are good refractories, reflecting and holding in heat, thus ideal for the construction of oven walls, chimneys, and kilns. The clays produced by the weathering of volcanic ash are ideally suited for making pottery (Fig. 3). A culture which had a good source of volcanic rocks nearby was not just threatened by possible eruption but also had a strong economic base. In Mexico, the early empire of Teotihuacan (pre ninth century) was founded on the manufacture and export of obsidian blades.

Volcanic rocks have also made good building materials, not only for stand-alone structures but for caves and tunnels as well. Large ignimbrites have been excavated by the local inhabitants in Japan, Italy, and Turkey for living space, storage, and emergency shelter. During the second world war, the Japanese military dug over 300 miles of tunnels in ignimbrites in Rabaul, Papua New Guinea (Fig. 4). These were used for shelter, to hide weapons and to provide bomb-proof storage for ammunition.

Because of the sharp color contrasts of volcanic rocks (e.g., basalt to sandstone or limestone), volcanic rocks have also been used for decorative purposes. Monuments, temples, and churches throughout Asia and Europe have used volcanic rock for sculpture and decoration.

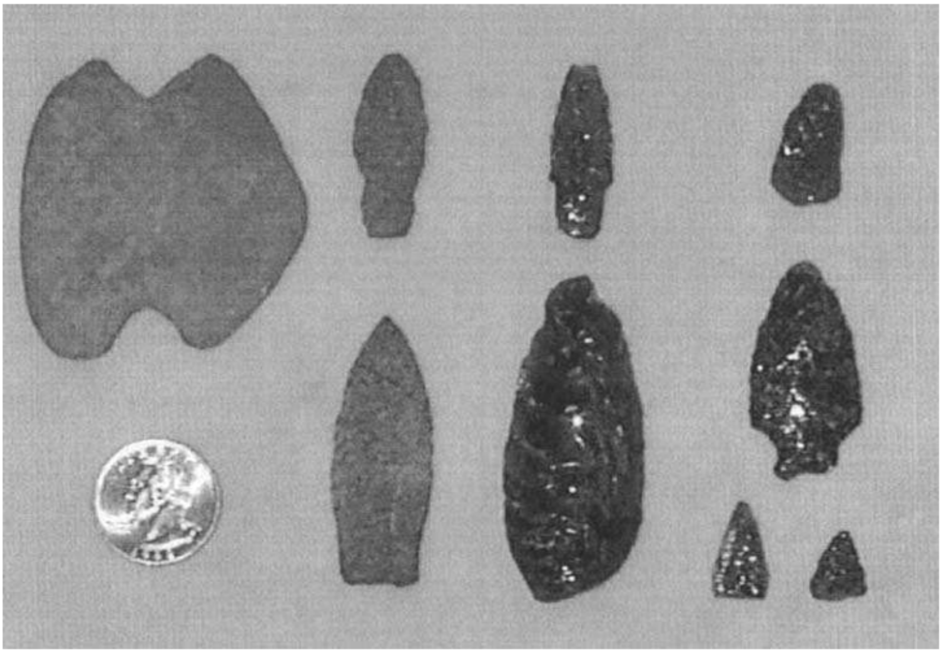

FIGURE 2 Implements have often been created using volcanic materials. The arrowheads are made of obsidian and the hammer of basalt. Such weapons maintained a keen edge after several uses and are easily as sharp as modern implements. These artifacts are from St. Lawrence Island, courtesy of the University of Alaska Fairbanks Museum.

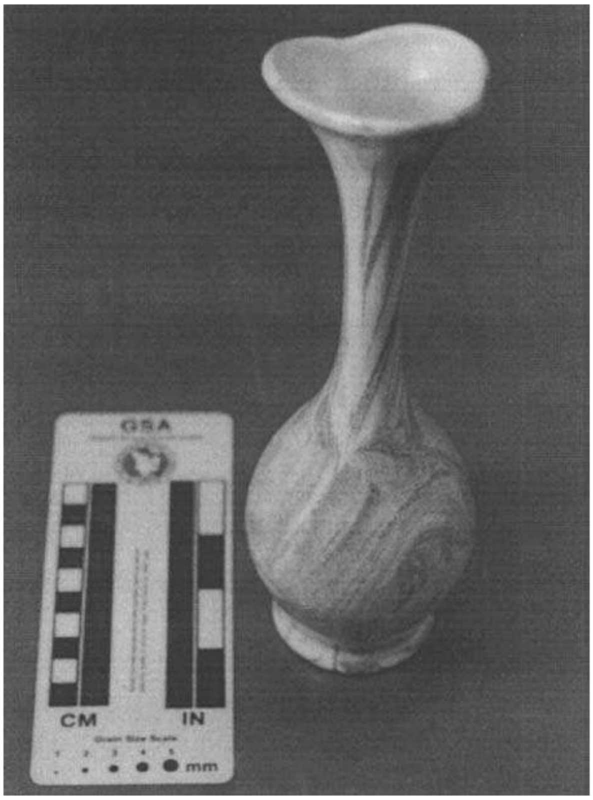

FIGURE 3 A vase decorated with volcanic ash from the 1980 eruption of Mount St. Helens. The ash, which occurs in different colors ranging from tan to gray to black to red, is used to add color and texture to pottery. Here the potter's clay is white, and brown ash is added to the exterior to make the swirl pattern.

IV. MODERN USES

Since the time when these early tools were used, because of the growth in world population and modern industry, more sophisticated uses for volcanic materials have been developed. These uses range from the mining of volcanogenic minerals to manufacturing aids, lubricants, and abrasives to construction materials. Volcanic products have also been used for artistic purposes (e.g., in gardens or as monuments). Often the applications are local, although certain types of volcanic minerals and rocks have become important exports for many countries.

V. ADDITIVES

Additives covers an extremely wide range of products, and we review several of the main volcanic contributors here. Volcanic ash and clays are common additives to many industrial materials. Whereas pumice and ash are excellent abrasives, volcanic clays can be used as lubricants and additives.

A. Bentonite

Bentonite is an off-white montmorillinite clay formed from altered volcanic ash. It has a sheet-silicate structure and is especially notable for the way in which it absorbs and loses water and for its base exchange properties.

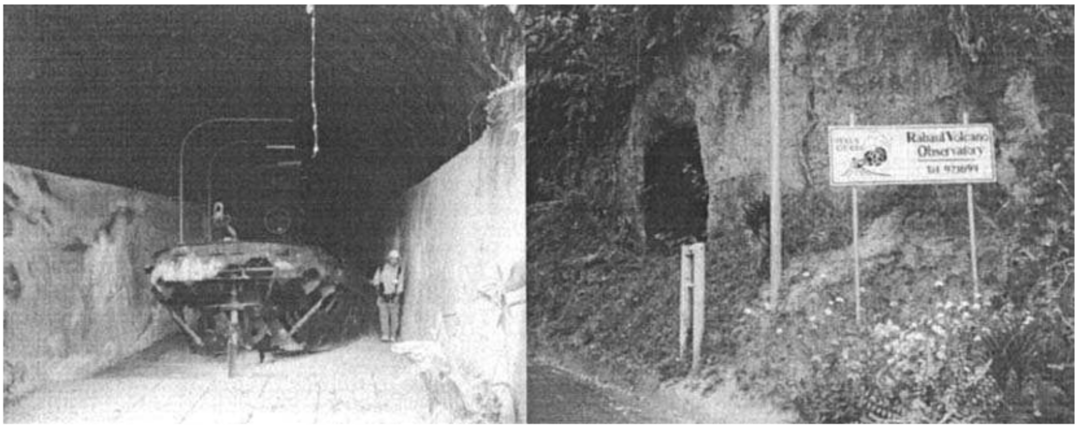

FIGURE 4 Right: Entrance to a tunnel cut into volcanic tuff from Rabaul caldera, Papua New Guinea. Hundreds of miles of tunnels were dug by the Japanese military during World War II. Left: Inside view of one of the larger tunnels. This one was used to store boats and barges to protect them from Allied bombing raids. The boats were moved using winches, sometimes with trolleys and rail tracks. This tunnel is about 100 m from the water's edge.

Sodic bentonite can absorb up to 10 times its own weight in water and can swell to 18 times its dry volume. Thus, it can be applied where its colloidal properties can be exploited. Bentonite has a wide variety of uses including foundry, animal feed, drilling mud, absorbent, industrial, and specialty uses.

About 70% of the world's known supply of western or sodium-type bentonite occurs in the state of Wyoming (notably in the Mowry Formation), with additional significant deposits elsewhere in the western United States. Volcanoes of the Yellowstone area of Wyoming were active for long periods in the early Cretaceous (ca. 100 million years) and deposited ash layers of a few centimeters up to 15 m thick into nearby shallow seas. The ash weathered with time, forming the bentonite.

Early uses of bentonite in the 1800s included lubricant for wagon wheels, sealant for log cabin roofs, and soap. Modern uses are highly variable. In foundry or metal casting, bentonite is mixed with sand to make the molds. The bentonite forms a pliable bond with the sand grains, so the mixture holds its shape well. Molten metal is then poured into the impression to make the casting. When complete, the bentonite and sand mold can then be broken away from the casting and reused. Bentonite is used as a binder for food pellets for animals and poultry and as a carrier for food supplements. Bentonite also absorbs excess moisture and oils, helping to prevent malodor, lumping, and caking of the pellets. Some recent research has shown that the base exchange properties of bentonite allow it to help remove certain toxins and ammonia. It also reduces feed flow through the intestines so that nutrient uptake is improved, indirectly aiding such factors as milk production, wool growth, and the quality and production of eggs.

Bentonite is widely used as drilling mud. It is mixed with water to form a slurry that is pumped through the drill string and out through the drillbit. The drilling mud helps to cool and lubricate the drillbit, and due to its high viscosity and yield strength, it extracts drill cuttings, carrying them to the surface, and helps to seal the drillhole and to prevent wall cave-ins. Bentonite is used to fill and seal abandoned drillholes. Similarly, bentonite has been used for sealing other waterways such as ponds, irrigation ditches, reservoirs, and industrial lagoons and has sometimes been used as a grout.

Because of its ability to absorb water and odors, bentonite has become a major component of the new "clumping" types of cat litters. (Nonclumping or regular cat litter is made from Georgia clay and other similar nonmontmorillinite clays.) The bentonite clumps are easy to handle, and the rest of the unused material remains intact, so the litter lasts longer between changes. With 54 million domestic cats in the United States alone, this could be a significant impact! Materials very similar to cat litter, both clumping and nonclumping, are used in industry to clean up liquid spills.

Bentonite has been used as a binder for taconite, a low-grade iron ore. The taconite is ground finely, mixed with bentonite to make pellets or balls, and then briefly sintered in kilns to give the pellets a hard surface. The pellets can then be easily handled and shipped to steel mills.

Bentonite additives have been used to emulsify oils in asphalt and detergents; to improve strengths of ceramics and bricks; to retain microparticles in papermaking; to clarify water, wine, and juice; to treat wastewater, de-ink paper, and control airborne stack emissions; and to gel cosmetics and pharmaceuticals. It has also been used as an ingredient in cleansers, polishes, and sprays of various types. For obvious reasons, bentonite has been called the product of 1000 uses. The uses are dependent on its absorption characteristics, which are in turn dependent on the chemical composition of the clay.

B. Pumice

Pumice is a porous, bubble-rich volcanic glass with low density. It is easily handled because of its low density and, when broken into finer particles, is widely used as an abrasive. The presence of the many bubbles means that the small pieces produced upon breaking are sharp and irregular. The particles are typically graded by size and backed with paper or other materials to produce sandpaper, grinding wheels, and other tools. Some pumice also had a highly specialized abrasive use until recently. Pumice that floats on water may be used in large washing machines to gently abrade cloth such as "stone-washed jeans." Eventually the pumice became waterlogged and sank, but it could be dried and used again.

Pumice is included in small amounts in certain soaps (e.g. "Lava" hand soap among others, Fig. 5) to provide a mildly abrasive action to aid in cleaning. Thus it adds a mechanical component to the cleaner that enhances the soap's chemical action.

VI. AGGREGATES

Aggregates are broken pieces of rocks which range in size from fine sand to several centimeters in diameter. Volcanic aggregates, cinders, or scoria have been used for road construction, and the production of building

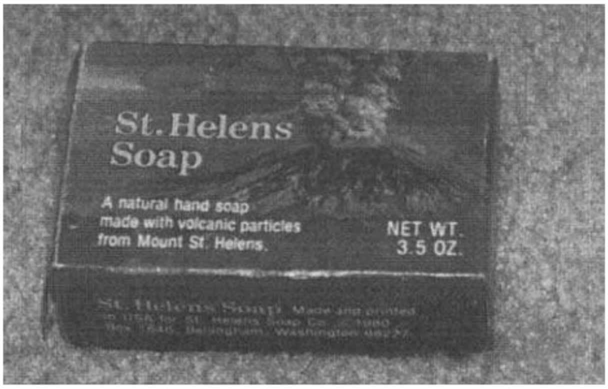

FIGURE 5 Soap made using volcanic ash. Most of the soap is made from standard materials, but small amounts of fine-grained volcanic ash were added to provide a mild abrasive action in addition to the chemical action. This particular soap was sold in tourist shops soon after the famous Mount St. Helens eruption of May 18, 1980.

materials (e.g., concrete and cinder blocks). In addition, they have widespread use as ballast, and as a component in plaster and related materials. In general, the use of aggregates falls into three categories; loose aggregates, refractories, and absorbents.

Both perlite and pumice are used as aggregates, especially in applications in which low weight is desired, such as lightweight precast masonry or concrete floors. The main cost of aggregate is its transportation, so pumice is widely used wherever it is the closest available source of aggregate. Many countries, however, export pumice, taking advantage of its low density to minimize shipping costs. Both perlite and pumice are also used in certain types of insulation and acoustic tiles.

A. Perlite

Perlite is a highly hydrated volcanic glass. The hydration occurs along conchoidal fractures which pervasively criss-cross the material, so that perlite breaks up easily into small pieces. Many of these have round surfaces and a waxy luster of typically light gray color, although greenish, brown, blue, and red also occur. The pieces resemble pearls, hence the name perlite.

Perlite is used generally as a lightweight aggregate but also has some specialty uses. It is a substitute for sand in lightweight wall plaster and is also used in ceramic products, fillers, and filters. In agriculture, perlite is mixed with peat from 25 to 75% and used to grow many types of plants. Because of its high fracture density and high surface area, perlite is ideal for simultaneously holding water and air pockets. This dual ability of aeration and water retention is necessary for plant roots to function properly. Even when wet, a perlite–peat mixture weighs about four times less than wet sand, so the perlite is easier to handle and much less expensive to ship. Economic deposits of perlite are found in California, Nevada, and New Mexico in the United States as well as in Russia and Greece.

B. Cinder

Mining of cinder cones for loose aggregate is common in central Europe, the southeastern United States, and Japan. In the United States alone, ca. 1.5 tons of aggregate per person per year are used. Cinders are primarily used in the fabrication of concrete and cinder blocks. This was also one of earliest industrial uses of volcanic aggregates, developed by the Romans, who had convenient sources of many types of volcanic products from the nearby volcanoes (e.g., Colli Albani near Rome and Vesuvius near Naples).

Today, aggregates are still an important resource. It is inconceivable to think of modern construction without the use of concrete or pressed cinder blocks.

In the construction of roads, a flexible bed of high strength, with good insulating properties is important to build a long-lasting roadway. Volcanic cinders are ideal for this purpose. The irregular surface allows particles to stick together, providing high angles of internal friction (up to 45°). The insulating properties ensure that the ground beneath the roadway is protected from extreme temperatures, and the associated deformation. In Alaska road beds like these are sometimes used to minimize the effect of annual frost heave and permafrost on roads. In addition to the thermal insulation, cinders provide a sound insulation as well, and individual vesicles can act as tiny cushions, absorbing vibrations.

Cinder can also hold water in open vesicles, or in the pore space between aggregates. It is often used to hold water around plants. In addition, cinder sorted to specific sizes becomes an effective barrier for tunneling pests, such as termites. The material is too well anchored to be moved, and large enough that a termite cannot grasp or carry each particle. The cinders are too strong to be broken, are resistant to weathering, yet are small enough and so closely packed that the termite cannot fit between individual particles.

C. Refractories

Refractories are materials that are not deformed or damaged by high temperatures, thus they are used to make firebricks, crucibles, insulation, furnace linings, and furnaces themselves for metallurgy and glass making. Pumice and clays are sometimes ingredients of refractories, and bentonite is used as a binder during production. Ignimbrites or welded tuffs can be cut into bricks and are used directly as refractories.

VII. CONSTRUCTION

Volcanic stone has been used worldwide due to its stability, strength, coloring, availability, and resistance to weathering. Its uses vary from simple garden walls to baroque cathedrals to modern skyscrapers.

A. Massive Stones

Massive volcanic stone provides a good building material because lavas and ignimbrites have high strengths and good insulating qualities. Such stone has been used throughout Europe and Britain for monuments and churches. One of the best examples of this is the Cologne Cathedral (Fig. 6), which is composed of 12 different types of stone, over 300,000 tons, more than half of which are volcanic, derived from the nearby Eifel Volcanic Field in central Germany. As with aggregate, a significant cost of this building material is its transport, and thus local sources are often preferred over imported materials. Lavas tend to dominate the use of massive volcanic rocks in construction, though less resistant rocks have also been used. In the past, ignimbrites were much easier to cut and shape but are more susceptible to weathering. As the science of masonry has progressed, harder and more resistant stone could be just as easily shaped or fabricated. In the case of the Cologne Cathedral, many of the older stones were made of more malleable softer rock and are now being replaced with harder, more massive stone (e.g., basalt).

Volcanic material is also ideal for use in monuments, markers, or gravestones. This is the most common use of volcanic rock throughout Asia. In Japan, one of the most volcanically active countries in the world, lanterns, sign posts, carved idols and icons are typically made from one of the many volcanic stones of the region (Fig. 7). Often the dark colors of volcanic rock provide a somber presentation, appropriate for many religious ceremonies.

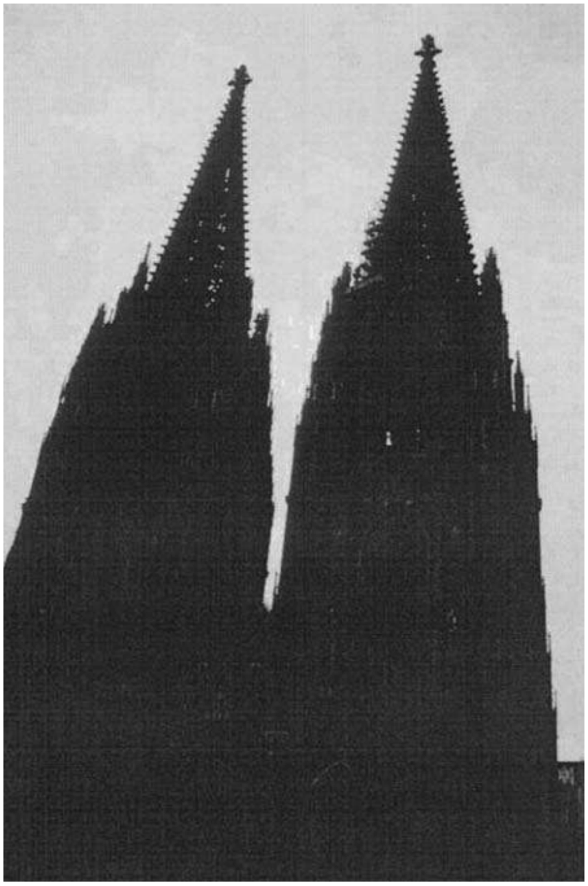

FIGURE 6 The imposing dark spires of the Cologne Cathedral. Over 100,000 tons of volcanic rock was used along with other materials in its construction, which lasted over 700 years. Most of the material was derived from the nearby Eifel Volcanic Field. Volcanic stone was often used during the Middle Ages, not only because it was local and easily acquired but also because it was resilient, and the dark colors were very imposing.

Larger-scale construction projects in Japan are seldom made of stone because these buildings tend to fracture and collapse in this earthquake-prone region. Strict regulations are imposed to ensure that the supporting frame of a building is made of a more flexible material (e.g., wood or steel). Today, even with improved con-

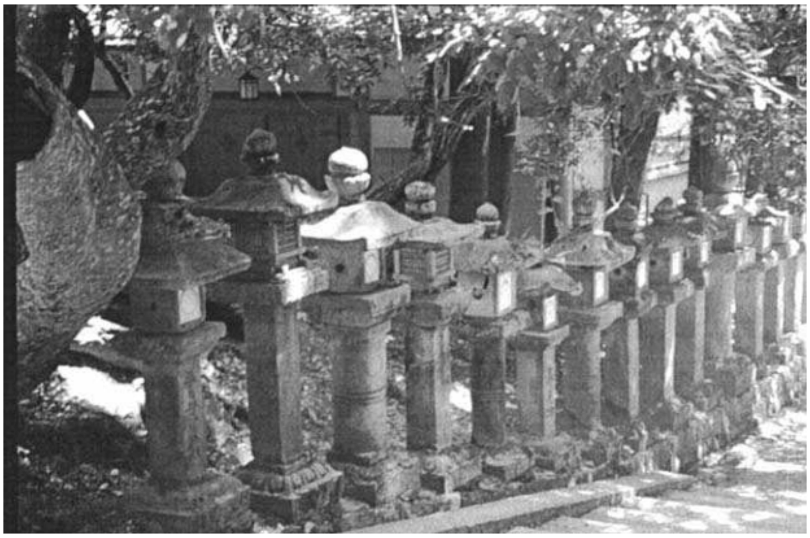

FIGURE 7 Lanterns at a temple in Kyoto, Japan. These were created using local andesite. Volcanic rocks are often used in monuments and idols.

struction techniques, the use of massive volcanic stone is limited to tiles, steps, sidewalks, and facades.

B. Concrete and Cinder Blocks

Concrete is one of the oldest uses of volcanic products and was originally developed by the Romans as a non-water-soluble alternative to the gypsum-based mortar used by the Egyptians. Primarily developed to tile and seal the aquaducts, this strong new material was used in many of the classic Roman structures, a number of which are still standing today. The precise technique used by the Romans is still a mystery, and modern concrete has not yet achieved the durability shown by these early structures. Although concrete can be made from any aggregate material, volcanic aggregate provides enhanced strength and insulation, making it a preferred material.

Today pumice and cinders are used in creating concrete prefabricated parts for buildings. In addition to its strength and insulation characteristics, pumice concrete can withstand flexure better than its counterparts. Although it has limited flexibility, it has a small coefficient of thermal expansion, and when reinforced, it can withstand significant thermal shock, as in the case of a fire. For example, when heated to 1000°C, a temperature where a metal door or window frames would melt, and then suddenly quenched with cold water, pumice concrete shows little or no damage whereas concrete made of nonvolcanic material rapidly and severely fractures. This difference is the result of the very small coefficient of thermal expansion of volcanic material. Buildings made of pumice concrete or cinder blocks are less likely to collapse when on fire than buildings made with limestone concrete or even steel.

This material also has the advantage of weighing less than normal aggregates or massive blocks. When shear strength is not the dominant factor in the design of a building, a lightweight concrete is a good low-cost alternative.

C. Tunneling

Soft volcanic rocks, such as ignimbrites have often been used for tunneling, for storage, and for housing. Examples of this can be found in Japan, Ischia, Herculaneum, and New Guinea (Fig. 4). In Japan, the soft volcaniclastics, which were formed submarine and are now subaerial, are tunneled for roads, although there is often a danger of collapse because these rocks are porous and have low strengths, only a little stronger than loose aggregate material. In the winter, water trapped in the rock freezes and expands and can cause fatal tunnel collapses like the one in the Fall of 1995 on Japan's northern island Hokkaido.

D. Mining

Sulfur is the ninth most abundant element in the universe and one of the four most basic chemical commodities. The chief sources of free sulfur are volcanoes, fumaroles, and certain sedimentary deposits. Sulfur occurs naturally in several forms, of which rhombic sulfur is the most common at volcanoes (often as flowers of sulfur).

Important compounds of sulfur include hydrogen sulfide (H_2S), which has the familiar rotten egg smell, and is used extensively in chemical plants and laboratories as an analytical agent. Sulfur dioxide (SO_2) is a precursor of sulfuric acid; it is also used as a bleach and as an industrial reducing agent. In small amounts, sulfur dioxide is used as a food preservative and to aid the ripening of fruits. Sulfur dichloride (S_2Cl_2) is used in the manufacture of chemical products such as lubricants and mustard gas. Sulfur hexafluoride (SF_6) is used as an insulator in many electrical devices. Sulfurous acid (H_2SO_3) forms the salt sodium sulfite (Na_2SO_3) which is used in the manufacture of paper pulp, in photography, and in removing oxygen from boiler feedwater. Sulfuric acid (H_2SO_4) is used in the manufacture of explosives, detergents, dyes, drugs, pigments, fertilizers, and many inorganic compounds. Synthetic organic sulfur compounds are components of pharmaceuticals, insecticides, and solvents and are also used to help vulcanize rubber and to produce rayon.

The first recorded therapeutic use of sulfur was by Philippus Aureolus Theophrastus, Bombast of Hohenheim, in the late 15th century, not only as a bath additive but also in various compounds taken internally to relieve minor ailments.

VIII. DECORATIVE USES

Volcanic rocks are often aesthetically pleasing and can take many forms. Minerals in the rocks can often reach sizes useful for decorative purposes and can even be used as precious or semiprecious stones. Volcanic products can supply the materials used to create works of art, such as decorative pottery (Fig. 3).

Polished banded rhyolites, or basalts, are commonly used as veneer for countertops, walkways, or stair steps and facades for buildings. In some cases, volcanic rocks are exported for this purpose from famous localities, such as the Clermont-Ferrand region of France.

Volcanic rocks often yield semiprecious stones. Olivines are common in basalts, as are pyroxenes. Even more exotic minerals can be found in lavas (e.g., hauene, a rare pyroxene mineral, in the trachytes of central Germany and topaz in rhyolites of the southwestern United States and Mexico).

Over time, volcanic ash weathers into fine clays which are preferred for delicate pottery in Japan. The fresh glass can be used as glaze due to its low melting temperature. Decorative uses of volcanic rocks can be more coarse; different colored cinders are often used in gardens or in more elaborate arrangements such as in Japanese rock gardens. Fresh lava is pliable, and local vendors in Italy gather the fresh lava and create souvenirs for tourists (Fig. 8). This is the most direct use of lava known to us.

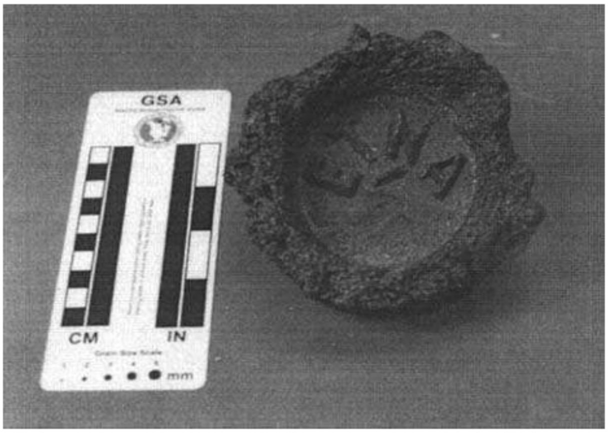

FIGURE 8 An ash tray made from lava at Mount Etna. In perhaps the most direct use of red hot lava, the still molten rock is scooped up and placed into a mold and squeezed immediately. The ash trays are then set aside to cool and are ready for sale a few hours later.

IX. CONCLUSIONS

Volcanic raw materials have been used by man throughout history. The oldest uses relied on the fact that volcanic rocks were plentiful locally and were easy to fashion into tools, such as the shaping of obsidian arrowheads. Modern uses include those for which volcanic rocks are a local source of aggregate, such as road beds, but also a variety of new specialty uses. For example, most uses of bentonite were developed in the last 100 years, and perlite has been exploited only since the 1950s. Volcanic rocks have some unusual properties, particularly density and thermal conductivity, so it is likely that new uses will continue to be found. These materials may have uses in combination with reinforced platinum, carbon fibers, or other new products to make unique composite materials for construction.

Volcanic eruptions occur at more or less steady rates on a global scale, thus there will always be replenishment of volcanic raw materials from new eruptions. Therefore, in addition to the excitement, awe, and scientific value of eruptions, in a very substantial way volcanoes will continue to contribute raw materials to sustain the industrial needs of modern life.

SEE ALSO THE FOLLOWING ARTICLES

Earth's Volcanoes and Eruptions: An Overview • Ignimbrites and Block-and-Ash Flow Deposits • Mineral Deposits Associated with Volcanism • Volcanic Soils

FURTHER READING

Bordaz. J. (1971). *Tools of the Old and New Stone Age.* David & Charles Newton Abbot, Devon.

Carmichael, R. S., ed. 1989. *Practical Handbook of Physical Properties of Rocks and Minerals.* CRC Press, Boca Raton, FL.

Chestermann, C. W. (1956). *Pumice, Pumicite and Volcanic Cinders in California.* State of California Press, San Francisco.

Fischer, R. V., Heiken, G., and Hulen, J. B. (1997). *Volcanoes: Crucibles of Change.* Princeton University Press, Princeton.

Thomas Publishing Company (1994). *The Thomas Register of American Manufacturers: Products and Services Section*, 84th ed., Thomas Publishing Co., New York.

VOLCANOES AND TOURISM

HARALDUR SIGURDSSON
University of Rhode Island

ROSALY LOPES-GAUTIER
Jet Propulsion Laboratory

I. Introduction
II. History of Tourism
III. Volcanoes and National Parks
IV. What Volcanoes Have to Offer to Tourists
V. Conclusions and the Future

I. INTRODUCTION

Volcanic regions have increasingly become major destinations for tourism. People visit volcanoes for a variety of reasons, the major one probably being the fascination of being close to nature's power. When we discuss volcanoes as benefactors, we usually focus on their energy and mineral resources. However, another major economic resource that stems from volcanoes is tourism; it is in fact the largest resource in some volcanic areas and certainly one with the greatest economic potential worldwide.

Active volcanoes have long attracted visitors. In the 17th and 18th centuries, the northern European aristocracy visited Vesuvius and Etna as part of the Grand Tour. Today, people from all social classes visit volcanic regions for their scenery and for their educational, ecological, and adventurous aspects. Some of the world's most visited volcanoes highlight the reasons why people choose them for tourism. The thrill of seeing a live volcanic eruption draws millions of people every year to Kilauea in Hawaii, Stromboli in Italy, and Arenal in Costa Rica. History and archeology, and the fascination always present in "lost cities," attract visitors to Vesuvius and Santorini. The educational aspects of volcanoes in terms of their role in nature and society are a major attraction of volcanoes in national parks, such as Mount St. Helens and Yellowstone. Interest in ecology brings millions to see Costa Rica's volcanoes in the rainforest, the Galapagos volcanic islands, and the Virunga Mountains in eastern Zaire. Some volcanoes are popular mainly for their magnificent scenery. Crater Lake is a prime example; others include the Lake Myvatn area in Iceland and the Canaries and Azores Islands. People also visit volcanoes simply because they are mountains to climb or ski. Rainier, Kilimanjaro, and Cotopaxi are among the world's favorite volcanoes to climb, and the slopes of Mauna Kea and Etna have become well-known ski areas. Volcanic hot springs and spas cash in on their supposedly medicinal aspects. In the 18th century, Sir William Hamilton used to ride from Naples to La Solfatara for baths, today the mudbaths in nearby Ischia and Vulcano in the Aeolian Islands fulfill the needs of those seeking cures and restoration.

The development of volcano tourism has mirrored that of general western tourism, which evolved from a minority activity of the Elite in the 18th century to the mass participation industry of today. This change has

Copyright © 2000 by Academic Press
All rights of reproduction in any form reserved.

been one of the most significant social phenomena of the past 200 years and of the postwar era in particular. Travel is now considered a basic human right—it makes the quality of life better—and the right to travel has become part of political freedom. A global tourism boom is one of the major characteristics of the economy of the last decade of the 20th century, and it is likely to continue into the next millennium. Spending on travel now accounts for 10% of the world's annual economic growth and is expected to increase in the next two decades. Today, the number of trips for tourism is estimated to be 6 billion per year, and the number of tourists is growing faster than the populations of many of the countries they visit or come from. International tourism arrivals, just one barometer of this phenomenon, have risen from just 25 million in 1950 to 287 million in 1979 and to 595 million in 1996. In 2020, this number is expected to be 1.6 billion. The increase has been made possible because of economic and social factors, as well as technological advances in modes of transportation. Long-haul flights on large-capacity airplanes are a major factor in the increase of far-away tourism. In recent years, the Internet has proved to be a tremendous boost to tourism, as more and more people browse home pages of foreign tourism authorities, electronic encyclopedias, and other information resources before they book their travel, often electronically.

One of the main manifestations of the increase in the number of tourists worldwide is their impact on local societies and cultures. Although tourism has considerably helped the economies of many countries, to the point of becoming the major industry in several, it has also been destructive, both to culture and environment. Despite—or perhaps because of—the fact that eco-tourism is now one of the fastest growing sectors of the travel industry, mass international tourism has been very damaging to natural settings, including some of the world's most beautiful volcanic regions. Fortunately, many nations are waking up to this fact in time to save their land and heritage.

Another manifestation of mass tourism has been an increase in the diversity of places visited, and the types of activity pursued by tourists. The last two decades of the 20th century have seen a trend toward adventure travel, eco-tourism, and far away destinations. The focus of global tourism destinations has recently shifted from Europe toward East Asia and the Pacific region. Although Vesuvius and Etna continue to draw visitors from all over the world, lesser known volcanoes everywhere are becoming increasingly popular.

II. HISTORY OF TOURISM

The history of tourism is not well known, but the Romans, for example, besides extensive and well-documented military tourism, used island locations such as Ischia and Capri for leisure and recreation purposes. Some pilgrimages and crusades may also be considered a form of tourism, such as described in Chaucer's *The Canterbury Tales.* It was in Europe, particularly in Great Britain, that the tourist industry was invented, refined, and developed as the Grand Tour—a socially acceptable way of sowing wild oats, of letting off steam for the young, well educated, and wealthy. The Grand Tour had its origins among the British aristocracy in the 16th century but increased dramatically in the 1760s. It became so popular that in 1749 Thomas Nugent published *Grand Tour*, the first guidebook to European travel.

Italy was the heart of the Grand Tour. As Samuel Johnson stated, "A man who has not been in Italy, is always conscious of an inferiority, from his not having seen what it is expected a man should see." A "must" in Italy was Naples, with excursions to the archaeological excavations of Pompeii and Herculaneum, begun in 1755 and 1738, respectively. The more adventurous also climbed Vesuvius to see the fireworks up close. Many aristocrats, including the German poet-geologist Goethe, enjoyed the local hospitality of the near-legendary Sir William Hamilton, the British Ambassador in Naples (Fig. 1).

The Grand Tour was originally a selective, primarily aristocratic prerogative, providing a classical educational journey from Britain to France, Italy, Switzerland, Germany, and the Low Countries. The original conception of the Grand Tour and its related journeying to fashionable resorts and spas during the 18th century was very much an extension of the normal pattern of aristocratic living. This is reflected in the employment structure that existed at that time to support this form of travel. Essentially, the rich and well-bred traveled with all or part of their normal retinue of servants. The fundamental principle of social distance between tourists and those providing service was established through early tourist travel of this nature and then widely adopted in the mass expansion of international travel.

The origins of modern mass tourism can be traced to rather more recent European development. The popularization of travel came, not surprisingly, with industrialization and the growth of increasingly leisured middle classes. It also benefited greatly from enhanced

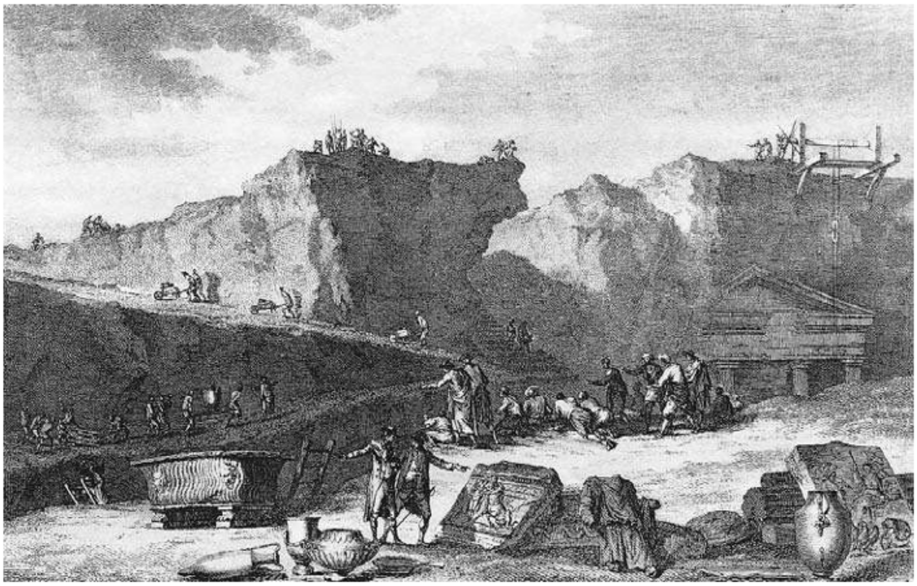

FIGURE 1 Eighteenth century print of the excavation of the Roman city of Herculaneum, buried in volcanic ash by the A.D. 79 Vesuvius eruption. The excavations and the volcano were an important stop on the Grand Tour of the northern European aristocracy—marking the first step in volcano tourism (author's collection).

transportation, particularly the growth of the railways. Indeed, changes in the nature of travel, transportation, and, most importantly, those participating in travel meant that the average length of the Grand Tour fell from 40 months in the mid-17th century to just 4 months in 1830, the dawn of the railway era. By that time, some 150,000 Britons a year were visiting Europe. The great leap forward in European tourism was made by Thomas Cook, who started tours for the masses in England in 1841 and on the Continent in 1855, marking the beginning of public tourism (Whitey 1997). Cook was certainly aware of the attraction of volcanoes for tourists. The first Cook party to Pompeii and Vesuvius volcano arrived in 1864 and aroused the wrath of the British resident bourgeoisie, who resented this intrusion of strangers (Fig. 2).

Cook's strangest acquisition was the Vesuvius Railway. The railway took tourists up the volcano, but it presented serious competition to the local Italian men who had earned a living by carrying people to the top in sedan chairs and who saw the railway as a threat to their livelihood. Cook had to be firm with saboteurs when he took over the operation of the railway, but he made it safe enough for even King Edward VII to travel on (Fig. 3). The local men had demanded that every passenger carried on the railway should pay tax in compensation, and the original owners of the railway had agreed to this. Cook refused to give way to what he considered extortionate blackmail. The Vesuvius porters then damaged the railway, throwing the carriages down the volcano and setting fire to the station. Cook then kept his customers away from the volcano until he succeeded in convincing the local brigands that if they allowed the railway to operate peacefully, they would profit in other ways from the tourists who traveled on it. The funicular railway was destroyed three times by lavas, and it was not rebuilt after the damage suffered from the eruption of 1944. In its place a chairlift was constructed to carry tourists up to the crater rim, but it is now no longer operating. Visitors today have no alternative but to walk to the crater rim.

At the turn of the last century, the consummate volcano tourist was the Englishman Tempest Anderson, an accomplished photographer and amateur volcanologist, who chose this activity of leisure because it "had the advantge of offering exercise in the open air, and in districts often remote and picturesque." For two decades he spent his holidays in exploring volcanic regions, including Vesuvius, Etna, Lipari Isles, Auvergne, Eifel, Canaries, and Iceland, as well as numerous volcanoes of the Cascades and Yellowstone. In May 1902, when the Soufriere of St. Vincent and Mont Pelee erupted in the Lesser Antilles, Anderson was quickly on the spot with his camera. He gave illustrated lectures about his jour-

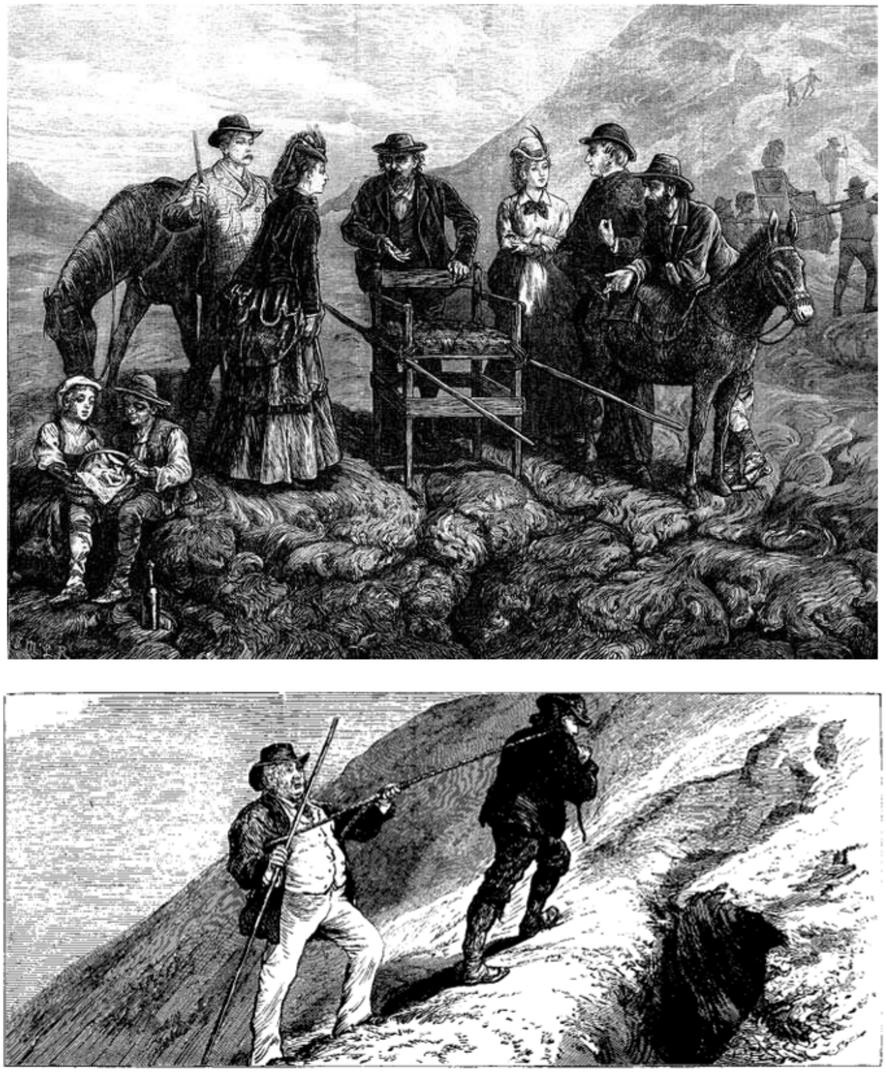

FIGURE 2 Nineteenth century tourists visiting Vesuvius had three choices. Either they could walk, be carried to the crater rim in a chair (top), or be dragged up on a rope by the Neapolitan porters (bottom). Woodcuts from *The Illustrated London News*, 1872.

neys at the British Association and the Royal Society; he also published his work, including an influential and widely admired volume with 105 full-page photographs of volcanic features (Anderson 1903).

III. VOLCANOES AND NATIONAL PARKS

Many volcanic regions throughout the world have now been set aside or protected by their designation as national parks. Shortly after the spectacular geologic and natural wonders of the Yellowstone caldera had been described in the report of the Hayden expedition, the U.S. Congress passed a bill in 1872 that designated over 3000 square miles of land to establish the Yellowstone National Park, the first park of its type in the nation—and in the world (Fig. 4).

The unique qualities of the Cascades volcanic range were also recognized by Congress and four national parks were established. The first to be created was Crater Lake National Park, established in 1902, to preserve the spectacular caldera, its unique lake, and the surrounding environment. Crater Lake was discovered quite by acci-

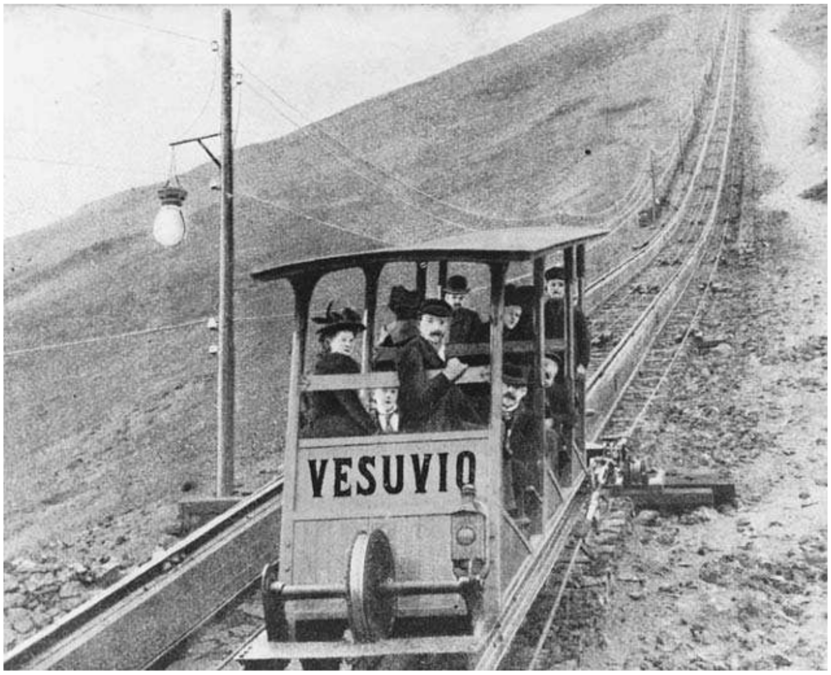

FIGURE 3 In 1880 the Thomas Cook company opened the Funiculare railway to the top of the Vesuvius cone. It was an event that transformed tourism to Vesuvius and put many of the volcano's guides out of work. But many felt that this application of industrial advance had "robbed the mountain of its poetry." The funicular was destroyed three times by lava flows; it was not rebuilt after the 1944 eruption.

dent by a prospector, John Wesley Hillman, in 1835. The creation of Crater Lake National Park happened largely due to the efforts of Judge William Gladstone Steel, who had read about the mysterious lake when he was a boy and vowed that he would find it one day. He finally did, in 1885, after 13 years of searching. Upon looking at the magnificent landscape for the first time, he decided that it must be protected and preserved. Judge Steel was appointed the Park's Superintendent in 1913, and it was he who first put fish into the lake—by hiking nearly 50 miles carrying minnows from the Rogue River.

Other national parks were established in the Cascades, including Lassen National Park in 1916, while the Mount Lassen volcano was still erupting. It includes vast hydrothermal areas and a dozen other smaller volcanoes such as Chaos Crags and Cinder Cone. The creation of Mount St. Helens National Monument was also prompted by an eruption, the cataclysmic event of 1980 that vastly changed the landscape. The desire to preserve a unique volcanic landscape was also behind the creation of Sunset Crater National Monument in Arizona. In 1928, a Hollywood film company planned to dynamite part of the crater to simulate an eruption. Angry protests from local groups put a stop to this outrageous plan and eventually led President Hoover to declare Sunset Crater a national monument in 1930.

Although the United States still leads the world in the range and quality of national parks in volcanic areas, many other countries are following its example. Developed countries, in general, are careful to protect their more spectacular volcanic regions, and the last two decades have seen a significant increase in the number of national parks. Many developing countries have followed their example, despite their considerably more limited resources. In the Americas, Costa Rica is a leading example, with 25% of the country's land—including several of its volcanoes—now protected as national parks and forest reserves. Ecuador also preserves many of its fantastic volcanic regions as national parks, including the Galapagos Islands and Cotopaxi. Chile and Argentina have also established national parks to protect its Andean volcanoes such as Villarica, and Colombia's notorious Nevado del Ruiz is within Los Nevados National Park. Many volcanoes in Africa are now also protected as national parks, particularly those in the Great Rift Valley. Indonesia has a long tradition of wildlife reserves and preservation areas; the first reserve, in Sumatra, was

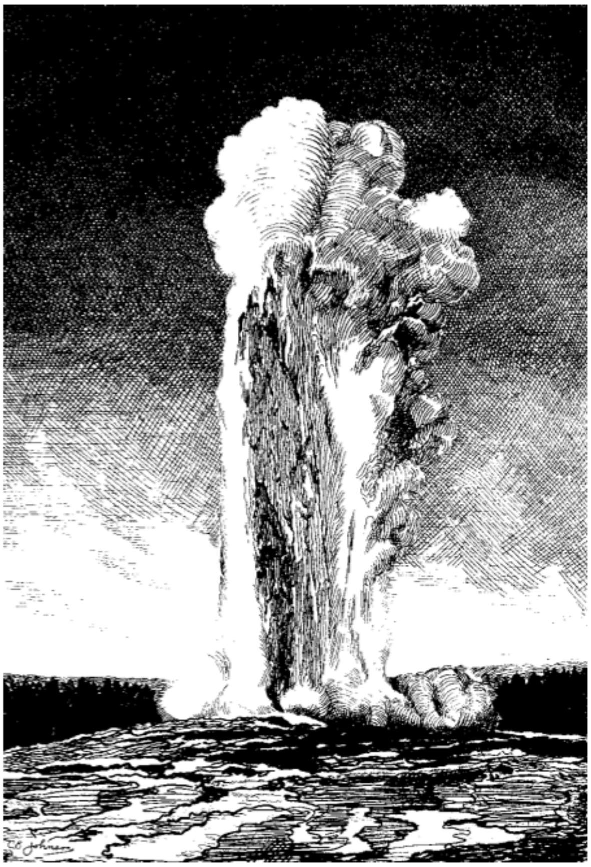

FIGURE 4 A 19th century etching of Old Faithful erupting, the centerpiece of Yellowstone National Park, and a major lure for tourists (author's collection).

set up in A.D. 684 by the King of Srivijaya. More recently, in 1982, Bali hosted the third International Parks conference, during which the Indonesian government announced the creation of ten new national parks.

National parks fulfill one of the most important roles in volcano tourism—education. Learning about the world has always been one of the major factors driving tourism. Volcanoes are a fascinating topic to people of all ages and volcano national parks are ideal places to learn about how volcanoes work, particularly if there are well-laid out trails and displays in museums on site. Hawaii Volcano National Park, established in 1916, is undoubtedly one of the world's most educational national parks. The park preserves a large fraction of Mauna Loa and most of Kilauea, two of the world's most active volcanoes. Thanks largely to the existence of the park, Kilauea has become the world's most visited and most photographed volcano. The Thomas A. Jagger Museum within the park has been open since 1987 and attracts 3000 to 5000 visitors per day. Although small, it is a very informative museum, with displays that include a volcanologist's partly melted boots and a portable seismograph that visitors delight in jumping next to, producing their own earthquakes. The park's major contribution to education, however, is in the numerous well-laid out trails and stop-over viewpoints for those who prefer to drive. A large number of plaques with explanations about what the visitor is seeing are dotted at points of interest along the trails and roads. The spectacular scenery and frequent eruptions contribute to the public's enthusiasm about these volcanoes. Most other volcano national parks in the United States are highly educational, but parks in other countries, particularly in poorer areas, often lack the resources to educate visitors. However, the fact that a national park exists at all in many of these countries, protecting and preserving volcanic and other regions for the future, is truly commendable.

IV. WHAT VOLCANOES HAVE TO OFFER TO TOURISTS

A. Scenery

Some volcanoes are so visually spectacular that this alone makes them major tourism destinations. Perhaps the best known example is Crater Lake, which is thought to have one of the most beautiful blue colors of nature. Surrounded by forests and volcanic peaks, the lake lies inside the caldera of Mount Mazama. A cataclysmic eruption about 7700 years ago destroyed the top of the mountain and eventually water from rain and snow filled the caldera, forming the 6-mile wide lake. The lake's depth (1932 feet) makes it the deepest lake in the United States. Inside the lake is the small Wizard Island. The purity of the water and the great depth of the caldera are responsible for the startling indigo blue. Because it is a closed system, it is devoid of vegetation and until fish were introduced some 60 years ago, it was also free of aquatic life.

Haleakala in Hawaii is another leading example of spectacular volcanic scenery. The vast summit crater (49 km^2) is a breathtaking sight that many visitors compare to the Grand Canyon. Haleakala crater is indeed an impressive geologic wonder, with walls that plunge down up to a kilometer and enclose a barren but colorful landscape. The crater floor is covered with ash deposits in hues of gray, red, brown, and russet, broken up here and there by steep cinder cones and dark lava flows. The crater, like the Grand Canyon, was enlarged by erosion.

The most spectacular sight offered by this volcano is sunrise. Haleakala means House of the Sun in Hawaiian and legends say that the island used to receive only a few hours of sunlight a day until the demi-god Maui snared the sun's rays with a lasso made of vines. To be released, La, the Sun, had to promise to travel very slowly across the sky. Many visitors today make the trip to the summit in darkness to watch the spectacular sunrise, when it seems that La is indeed keeping his word. Mark Twain described the sunrise over Haleakala as "the sublimest spectacle I ever witnessed, and I think the memory of it will remain with me always".

Other volcanic regions that attract tourists mainly because of their spectacular scenery include the Canary Islands, the Azores, the Lake Myvatn area in Iceland, and Soufriere volcano in St. Vincent.

B. The Spectacle of Volcanic Activity

Volcanic eruptions are one of nature's most awesome spectacles. An active volcano can create a major economic boom for a region, or else it can destroy the local economy and infrastructure. From a tourism point of view, the best types of volcanic activity are long-lived Hawaiian or Strombolian eruptions. These types of eruptions allow tourists to see the activity at reasonably close range in relative safety. If the eruption lasts for months or years, the local economy can truly prosper from the sustained number of visitors. However, other factors—notably accessibility—are important for turning an active volcano into a major tourist destination. Stromboli, continuously active for over 2000 years, can be considered the world's top destination for those who want to see a live volcano, but its remote location makes it far less popular than many other volcanic regions around the world. Travel to Stromboli island is only possible by boat, and because rough winter weather can disrupt services, the bulk of the tourism is restricted to the summer months. Yasur in Vanuatu is another example of a volcano that sustains long-lived Strombolian activity, but it does not attract large number of visitors because of its remoteness.

Two of the most popular active volcanoes in the world today are Kilauea and Arenal. Kilauea has attracted tourists since the early 20th century, when a lava lake filled Halemaumau crater. A hotel, Volcano House, was built in 1846 on the edge of Kilauea caldera, with full view of Halemaumau, and counted Mark Twain and Robert Louis Stevenson among its distinguished guests. Although Halemaumau is no longer active, Kilauea has continued to erupt often and spectacularly. The present Pu'u O'o-Kupaianaha eruption, which started in 1983, is the longest on record in Hawaii. The sustained activity has been a boom for local tourism and has spawned businesses ranging from new hotels to helicopter tours. Even when the eruption stops, Kilauea should continue to be one of the world's most popular volcanoes, because of its accessibility—one can drive right up to the edge of the caldera and to many other attractions—and because of the well-laid out trails within the national park.

Costa Rica's Arenal was not known to be an active volcano until its present eruption started in 1968. Before that, a few visitors came to climb to the main crater, which was home to thousands of finches. The current eruption has contributed to making Arenal and its surrounding area into one of the most popular destinations in the country. The volcano and its environs have recently become part of a national park. The Laguna Arenal, an artificial lake, has become a major recreation area, and new hotels and lodges with views of the volcano continue to be built. Although considerably more dangerous than Kilauea, Arenal's eruption can be watched in safety from a number of vantage points around the volcano, including the well-known Arenal Observatory Lodge. Many visitors stay up all night watching the red lava flows slowly come down the volcano's steep flanks. Only a few dare to make the dangerous climb to the summit, and at present only one guide is willing to make the journey.

Volcanic eruptions invariably change the tourism potential of a region. Although the mild current activity of Kilauea and Arenal attract visitors, violent eruptions can completely destroy the tourism infrastructure of a region. Often, however, the aftermath of a violent eruption will bring visitors back. Perhaps the best recent example is Mount St. Helens. Before the 1980 eruption, visitors were attracted to Spirit Lake and its magnificent setting. When the lake and its surrounding forests were destroyed, and the once alpine-looking landscape became bare and gray, it seemed that tourism in the area would not recover. Many people, however, wanted to come to see the eruption's effects and the new lunar-like landscape became a major attraction. In fact, the eruption has brought a steady stream of visitors and has made the area considerably more popular than it was before 1980. A landmark event was the creation of the Mount St. Helens National Monument in 1982. In 1993, the Coldwater Ridge was opened and during that year alone received about 1 million visitors. It offers exhibits and lectures about the volcano, its eruption, and the gradual return of life to the devastated areas. Coldwater Ridge is still popular, but now it is only one of the four visitors' centers devoted to St. Helens. The boom in tourism is evident from facilities such as a local IMAX theater that shows movies about volcanoes and from the helicopter tours that are now available to visitors. The climb to the crater rim, from where one can see the impressive dome growing inside the gaping crater, has become one of the most popular in the Cascades.

C. Hot Springs and Spas

Volcanic hot springs have long been thought to have health benefits. Long after the days of Sir William Hamilton's visits to La Solfatara, visitors still come to southern Italy to seek cures in the natural hot springs of Ischia and Vulcano. Ischia's spas are popular with day-trippers from Naples, while Vulcano, further away in the Aeolian Islands, is crowded every summer with about 10,000 visitors. Many of them visit the famous Laghetto di Fungi (the mudbaths) and afterwards take a dip in the ocean at the nearby Acqua Calda (hot water) beach. Hot springs bubble through the sand, making the seawater above feel like a natural jacuzzi.

Many other volcanic areas offer tourists the experience of volcanic hot springs and, sometimes, luxurious spas to take full advantage of the natural phenomenon. Hot springs in Japan are fully utilized by both locals and visitors for traditional communal bathing. Tourism from hot springs is the main source of income for the small city of Beppu, located on the Inland Sea. Beppu attracts some 12 million visitors every year from both Japan and abroad, thanks to its 4000 hot springs that were created by the A.D. 867 eruption of the now-dormant Mount Tsurumi.

In Iceland, an entire tourist and spa industry has built up around the hot springs in the town of Hveragerdi and a similar development is occurring at the Blue Lagoon, where the hot waters are reputed to have various therapeutic properties.

A particularly interesting area of volcanic hot springs is Tabacon near Arenal volcano in Costa Rica. The waters of the Tabacon River are heated by the active Arenal and, in the past few years, a lavish resort has been and has become very popular with visitors. The resort offers more than just hot springs: visitors can view Arenal's activity while wallowing in the pools and have the dubious pleasure of knowing that they are actually inside one of the most hazardous zones around the volcano devastated in the 1976 eruption.

D. Climbing and Skiing on Volcanoes

High volcanoes are an irresistible lure for many climbers. Unlike the craggy peaks of the Himalayas or the Rockies, however, they normally only present two major difficulties—the altitude and the weather—apart from the occasional eruption. There are virtually hundreds of high, ice-covered volcanic peaks that present a challenge to the climber and will become increasingly more popular as targets for adventurous tourists in the future. Only a few of the more popular ones are discussed here.

Mountaineering on volcanoes began with the spectacular expedition of the English medical doctor Edward Whymper to Ecuador in 1880, where he climbed ten volcanic peaks, including the 6900 m high Chimborazo and the 6500 m Cotopaxi (Whymper 1987). He and his companions climbed Chimborazo from the southwest ridge, setting up several camps, but suffered from mountain sickness. As they approached the summit on the final assault, they became bogged down in exceedingly soft and thick snow, but managed to complete the ascent and return to camp in the dark after a 16-hour heroic effort. Whymper and his companions found, on the other hand, that the ascent of majestic Cotopaxi "was a walk," but when they crawled out to the very edge of the crater, they looked down into a deep and raging inferno of molten lava, steam, and volcanic gases (Fig. 5).

In Mexico there are several major ice-covered volcanoes that are popular targets for climbers. The lowest of these is Nevado de Colima in the west (4450 m), with a nearly continuously active crater of Volcan de Colima on its south flank. The highest volcano in Mexico is the 5700 m high El Pico de Orizaba (Citlaltepetl), at the eastern end of the range of volcanoes. In intermediate position are the famous volcanic peaks of Popocatepetl (5452 m) and Iztaccihuatl (5286 m), also known simply as Popo and Ixta. These volcanoes present a great attraction, as they allow climbers to experience high altitude with relatively modest expense, time, and equipment needs (other than ice ax, crampons, and rope) and with minimal technical difficulties. As pointed out by Secor (1981), the principal difficulties associated with these climbs may not be the ascent or descent, but rather the approach to the volcano. The remote roads are often in very poor condition and unmarked.

El Pico de Orizaba is Mexico's most majestic and highest volcano (5700 m). Located within about 100 km of the Gulf of Mexico coast, it is due west of the city of Veracruz. The usual approach to this volcano is from the village of Tlachichuca on the northwest side and then by four-wheel drive over a rough dirt road to the Piedra Grande rustic mountain hut at 4230 m on the

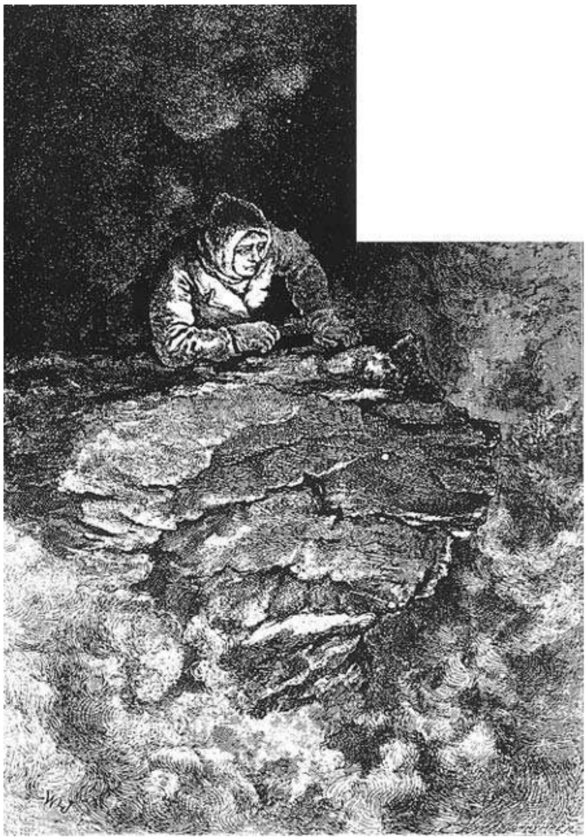

FIGURE 5 Edward Whymper was the first mountaineer to scale volcanoes, including Cotopaxi and Chimborazo in the Andes of Ecuador. When he crawled to the very edge of the Cotopaxi crater in 1880, he looked down into a deep and raging inferno (Whymper 1987).

north flank. From here, the standard climbing route up the mountain is the Glaciar de Jamapa, typically a 6- to 9-hours ascent. However, some climbers set up a camp at the 4900 m level, before pushing on to the summit. From the edge of the Glaciar de Jamapa, the climb requires roping up, and the use of crampons and ice axes to the summit. The magnificent views include the Gulf of Mexico to the east and the volcanoes Popo and Ixta to the west. Climbing and hiking around Pico has the great advantage that the mountain is not surrounded by urban sprawl but is relatively remote. Many of the villages on its flanks can only be reached by footpaths.

The Popo-Ixta National Park contains two of the most famous volcanoes of Mexico. As it is within only 80 km of Mexico City, it is a very popular and busy area, but there is ample space here for climbers to strike out on spectacular trails and ascents (Secor 1981). Interest in Popocatepetl (5452 m) has of course been heightened greatly since the beginning of its current volcanic crisis, but access to the upper flanks has of necessity been restricted while the conditions remain hazardous. Meanwhile, Iztaccihuatl (5286 m) is accessible to all. The normal starting place for visitors to both volcanoes is the town of Amecameca to the west of the volcanoes, and from here good roads lead to Tlamacas mountain lodges on the north slope of Popo, and La Joya on the south slope of Ixta. The most popular route up Popo is Las Cruces, which has been done successfully even by burros and dogs —an ascent of five to eight hours. Above the Las Cruces hut (4480 m), ice axes and crampons are generally required for ascending the 30° slope to the crater rim above. The summit crater is the main attraction, with spectacular near-vertical walls, steaming fumaroles and nearly-suffocating sulfur fumes. Ixta, the seventh highest peak in North America, is generally approached from La Joya trailhead at 4000 m, on the south side of the volcano. The standard route is La Arista del Sol, with Popo to one's back and Pico to the east. It is a two-day climb for most people, and huts are available en route for spending the night. The ascent is about seven hours from the huts.

Nevado de Toluca (4704 m) is Mexico's fourth highest mountain, but is unique in that one can drive right into the crater of this extinct volcano, only about 30 km south of the city of Toluca. The ice-bound crater rim rises another 500 m above the crater lake, and ice axes, crampons, ropes and other suitable climbing gear is required for the final ascent.

The summit of the extinct Nevado de Colima can normally be approached by a dirt road north from the village of Atenquique, that leads to a microwave station at the 4000-m elevation; from here, the snow-clad summit at 4450 m is a mere scramble. Its smaller but very active neighbor Volcan de Colima is reached by a dirt road heading west from Atenquique, and this track will carry the climber most of the way to the slopes of the active crater, depending on weather. However, it is an active volcano, with frequent eruptions, and ascent up the loose pumice-covered slopes to the crater rim should not be attempted because of danger from explosions that can occur without warning.

One of the world's best known volcanoes among climbers is Kilimanjaro in Tanzania. Although located only 3° from the equator, this dormant volcano is capped by a glacier. It consists of three major peaks—Shira, Mawenzi and the most recently active Kibo (5895 m), the tallest point on the African continent. There are hundreds of small cinder cones on its slopes. Kilimanjaro is regarded as a 5-day climb.

The second most often climbed snowpeak in the world—after Fuji—is the 3450 m high Mount Hood volcano in Oregon. It attracts thousands of skiers, climbers, and hikers every year, and they usually congregate in the famed Timberline Lodge. This huge and picturesque log cabin was constructed at the 1800-m level entirely of natural materials, as a public works project in the early part of the 20th century. The volcano can be viewed from many vantage points (e.g., Cloud Cap Saddle), but only experienced climbers should proceed to the summit.

Mount Adams is the second highest peak in the Pacific Northwest (3750 m), but it remains relatively unknown to tourists and little visited. The volcano has a relatively flat and broad summit plateau, and a large, ice-filled crater that is open to the west. Access is relatively difficult, and most climbers start hiking from Cold Springs on the south side of the volcano and then ascend the Suksdorf Ridge to the summit. This climb requires crampons and ice axes.

The earliest known ascent of Mount St. Helens volcano was in 1853 by Thomas J. Dryer, first editor of *The Oregonian*. This climb took place only about a decade after the 1842–1844 volcanic episode and before activity resumed on the north flank in 1857. Access to the volcano improved greatly after a wagon road was built to Spirit Lake in 1901, and climbing Mount St. Helens became a popular pastime in the Northwest. Outdoor clubs from Seattle (The Mountaineers) and Portland (The Mazamas) made regular excursions and climbs of the volcano throughout the 20th century—up to the cataclysmic 1980 eruption. This event reduced the mountain's height from 2950 to 2550 m. Access was restricted for a number of years, due to potential volcanic hazard to climbers. With the establishment of the Mount St. Helens National Monument, the volcano was re-opened to summit climbers in 1987, although they must obtain climbing permits from the U.S. Forest Service and use the south side route up to the crater rim.

The highest among the Cascades, the gleaming and ice-capped Mount Rainier towers at 4450 m above Puget Sound. This national park area is blessed with virgin forest and an unusual abundance of summer wildflowers that carpet its slopes. Because of the carving work of its glaciers, the volcano now has a complex shape. The Rainier National Park is readily accessible from all sides, and it is visited by hundreds of thousands of people every year. Climbing this volcano requires skill, experienced guides, and proper equipment. The fickle and rapidly changing weather is the climber's worst enemy, and sudden fierce storms are common around the summit.

Shasta volcano is attractive to mystics, skiers, and climbers. Skiers will normally drive to the Shasta Ski Bowl, but at this location, neither the summit of Shasta nor Shastina are visible. Those wishing to climb to the summit will normally proceed to the Sierra Clubs Horse Camp on the volcano's southwest side, at an elevation of 2150 m. The trail leads up through Avalanche Gulch, to a 60m high bank of pumice named the Red Banks, and thence to the 4350 m high summit. Crampons and ropes are required for this climb.

E. Ecology, Eco-tours, Nature, and Adventure Travel

Ideally, those tourists who explore the Earth do so without trampling down and defacing its fragile nature and practice eco-tourism. Inevitably, eco-tourists are attracted to and avidly seek out the most vulnerable regions, which are off the beaten track and have remained untouched by the regular tourist hordes. Thus the development of eco-tourism may defeat its very goals. In reality, eco-tourism has become a marketing tool, in order to attract visitors to new and hitherto undeveloped regions. Volcanoes are often set in remote, unspoiled locations that become major attractions for this emerging market. In such cases, tourists come mostly to see the flora and fauna, whereas the volcano often takes the role of a secondary attraction. The Galapagos islands, Costa Rica's volcanoes in the rain and cloud forests, and the volcanoes of the Virunga Mountains in Eastern Zaire are all popular with tourists largely because of their ecological appeal.

Many volcanic regions are the targets of modern eco-tourists, and Costa Rica is a prime example of a country where the concept of eco-tourism was proven. Rather than profit from the destruction of rainforests, Costa Ricans chose to use them as a magnet for the emerging eco-tourism market. About 25% of the land is now protected as national parks and forest reserves, some of which are private, bought with charitable donations from all over the world. Many tourists come to see the country's remarkable flora and fauna, which include over 1000 types of orchids and 850 species of birds, but the volcanoes are increasingly gaining in popularity. Volcan Arenal, active since 1968, has become one of Costa Rica's major attractions, and it is now used in the official logo of the country's Tourism Authority.

Although the major attraction of Arenal is its spectacular activity, and of Poas is its crater lake, most visitors take the nature trails which cut through the rainforests around the volcanoes. Toucans, hummingbirds, howler monkeys, and coatis are common sights, and the flora along the trails include native orchids, ferns, and exotic plants such as bromeliads and Gunnera insignis, which the locals call poor man's umbrella because its leaves can be as large as two meters. Costa Rica's more remote volcanoes, notably Turrialba, are becoming more popular with tourists looking for unspoiled locations rich in wildlife.

The Galapagos islands have long been known for their unusual wildlife, which continue to be their main attraction for visitors. Tourism in the Galapagos has become a major source of income for Ecuador and helps to support the islands' conservation and research programs. Although the Galapagos have been protected since the unsettled areas of the islands were declared a national park in 1959, their popularity as a tourist destination has made restrictions necessary. The national park has designated vast areas to be off-limits to anyone except scientific researchers with a good cause. All tours to the islands are led by guides specially trained to follow a system of keeping interference with nature to the minimum possible. The number of visitors to the Galapagos increased from fewer than 10,000 in the 1960s to about 18,000 in the 1970s and is still on the rise.

Among the exotic creatures in the islands are spiky land and marine iguanas, four-eyed fish, flightless cormorants and albatross, and, most of all, the giant land tortoises that gave the islands their name (*Galapago* is Spanish for tortoise). All the Galapagos islands are volcanic in origin and geologically young. Eight of the volcanoes have erupted since the mid-18th century. Among these, Fernandina on the island of the same name, and Volcan Wolf, Sierra Negra, and Cerro Azul in Isabella island erupt frequently. Tourists climb some of the active volcanoes, in particular Alcedo and Cerro Negro in Isabella island, but Fernandina island is off-limits to all but researchers.

The remote volcanoes of Africa's Rift Valley, particularly those of the Virunga range in eastern Zaire, are emerging as a major eco-tourism destination. Most of the Virunga volcanoes are extinct, and their appeal is ecological—they are the natural habitat of the mountain gorillas, which live at altitudes of about 3500 m. The gorillas are naturally shy and elusive, and were discovered by westerners only at the beginning of the 20th century. Captain Oscar von Beringe, the first European to see these forest-dwelling apes, had no hesitation in shooting two of them and, presumably because of this, the apes were named *Gorilla gorilla beringei.* Years later, the animals gained worldwide appeal thanks largely to the movie *Gorillas in the Mist*, based on the story of Diane Fossey. The movie also helped to put the Virunga mountains in the itinerary of many adventure and eco-tourism tours, even though spotting the gorillas is not easy. The high altitudes, difficult terrain, thick vegetation, and natural shyness of these animals can make the experience frustrating. Most tour groups, led by experience trackers, eventually manage to meet the gorillas, or at least hear their terrifyingly loud yells. The main destination for the gorilla-spotting tours are Karisimbi, which last erupted in the Holocene, and Mount Mikeno, now considered extinct. Other regions of Africa's Rift Valley that are notable for their ecological role include the Ethiopian highlands, habitat of the rare Simien fox, and the soda lakes, such as the much-photographed Lake Nakuru in Kenya, where vast numbers of flamingos come to feed. Close to Mount Lengai volcano is Lake Natron, where Great Flamingos breed, even though the water's high concentration of soda makes it lethal for most other creatures. Mount Kenya volcano, the second highest peak in Africa, is known for its African-Alpine environment, where unique giant lobelias flourish and are pollinated by the colorful scarlet-tufted malachite sunbird. Other volcanoes in the Rift Valley are beginning to attract ecologically oriented tourism, as Africa itself becomes a more popular destination.

Other volcanoes that are emerging as destinations for eco-tourism include Iceland, particularly the Lake Myvatn area, on the outskirts of the Krafla caldera. The lake, which was created when lava flows formed a natural dam in a large river, is the habitat for the largest number of species of ducks in the world, and offers a unique natural environment. This area combines more volcanological and ecological features per square kilometer than any other in the world, with numerous hot springs, fumaroles, eruptive fissures, cinder cones, pseudocraters, maars, calderas, domes, and virtually all imaginable volcanic landforms (Fig. 6).

F. Black and Green Sand Beaches

Volcanoes by the sea often offer exotic black sand beaches, though most tourists seeking beaches do not value pulverized volcanic materials as highly as finely powdered coral. The travel magazine *Conde Nast Traveler* described black sand as feeling "like a bed of hot coals—and irregularly shaped grains aren't particularly comfy." The magazine editors chose Ficogrande on the island of Stromboli as the world's best black sand beach. The beach is certainly popular, as most of the 2000 or so tourists that Stromboli hosts each summer spend time on the black sand. Other well-known and long-visited

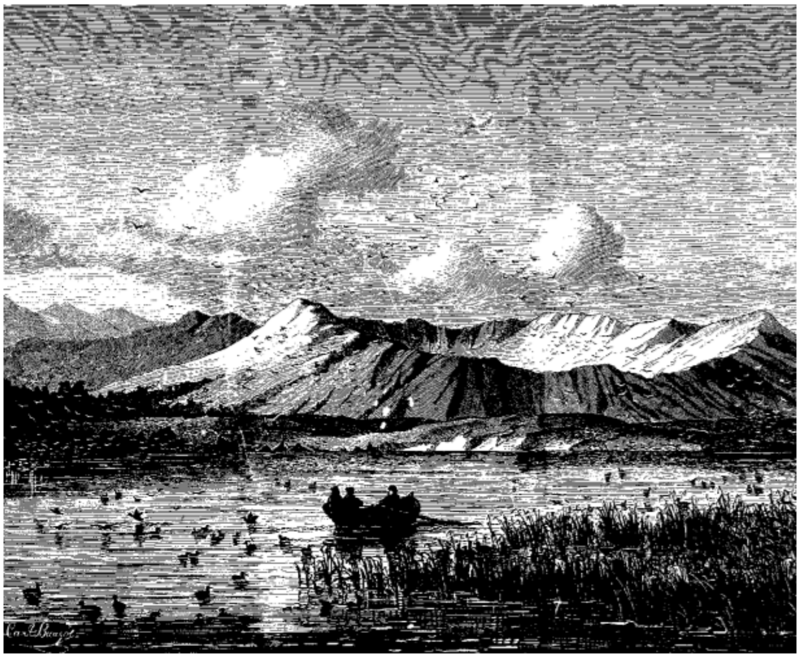

FIGURE 6 An engraving of the Lake Myvatn area in Iceland, a paradise for tourists interested in both ecology and volcanology. In the background is Hverfjall, a recent maar explosion crater. The lake also has a unique duck population (author's collection).

black sand beaches are found on Santorini—Kamari and Perissa beaches are both made up of black sand and attract many thousands of tourists every year. Other volcanic islands with well-known black sand beaches include St. Vincent (Black Point Beach) and Grenada (Antoine Beach). However, most tourists who have a choice will head for these islands' white sand beaches instead.

Beaches near active volcanoes can prove to be ephemeral. This point was well demonstrated by the famous Kaimu Black Sand Beach on the southeastern shore of Kilauea. This much-photographed spot, a favorite of local surfers, was destroyed by the Puíu Oío eruption, as was the nearby Kalapana Beach. The same eruption, however, created several replacements, including the half-kilometer long Kamoamoa that was formed between January and April 1988.

A more exotic type of volcanic beach is the green sand beach. These are considerably rarer, although the finely ground olivine feels no better than black sand—according to *Conde Nast Traveler*, the sand is "like finely ground Coke bottles." However, tourists are attracted to the prime example of a green sand beach—Papakolea in Hawaii's Big Island—because of its exotic looks. Located near South Point, the green sand is made up of olivine crystals weathered out of a cinder cone. The original cone was formed about 7700 years ago by the Awawa Kahao eruption of Mauna Loa. Wave action eroded away about half the cone, leaving it open to the sea. Getting to this beach requires some work, as visitors either have to use a 4-wheel drive road or walk about 3 km from South Point. The road ends at an overlook, where most visitors stop. Climbing down onto the narrow beach is not recommended, not only for preservation reasons—this is an extremely rare type of beach—but also because the sea is rough and dangerous.

G. Archaeology and Volcanoes

The relationship between anthropology, archaeology and volcanoes reaches way back to the origin of the human race in the Great Rift Valley of Africa. All along the rift, from the Olduvai Gorge in Tanzania in the south, to Hadar in the Afar Triangle in the north, the remains of human ancestors and the earliest humans are intimately associated with volcanism and generally preserved in volcanic deposits. However, it is the excavation of entire cities, buried under volcanic ash in ancient times, that has captured the attention of the tourist and created a steady stream of visitors to Akrotiri, Pompeii, and Herculaneum.

The amazing discovery of Herculaneum and Pompeii on the slopes of Vesuvius in 1738 and 1748, respectively, created a new "must" destination on the Grand Tour of aristocratic northern Europeans. However, great secrecy surrounded the excavations initially, and only certain visitors, mainly through the assistance of Sir William Hamilton, were able to gain admission. Thus the excavations of the lost Roman cities did not become accessible to the general tourist until the late 19th century. Ever since, the tourist has remained amazed at the wonderful preservation of even the smallest and most fragile objects that were embedded in the volcanic ash of Vesuvius in A.D. 79 (Sigurdsson *et al.* 1985). The most sensational discovery was that of the Roman library in the Villa dei Papyri in Herculaneum, containing hundreds of papyrus rolls of ancient Greek texts.

There is no mirror of the past that offers us a more vivid reflection than Pompeii and Herculaneum. Here the visitor walks virtually into history and witnesses innumerable signs of long-arrested activity, with life and death on intimate terms. But they were by no means ordinary cities. The presence of so many fine sculptures, paintings, and mosaics is astonishing to the visitor, as is the grand scale of many of the homes and public buildings. The discovery of these art objects of classical antiquity had an immediate impact on taste and design in 18th-century Europe and, among others, inspired the pottery designs of Josiah Wedgewood in England. The visit of the German scholar Johann Joachim Winckelmann to the Herculaneum excavations in 1758 may be regarded as the birth of archaeology, and it certainly marks the beginning of the study of the history of ancient art. The early excavations of the Roman cities were conducted, under the direction of King Ferdinand IV, as a treasure hunt, with total emphasis on recovering valuable art objects from the ruins and no regard given to their context or history or the preservation of the buildings in which they were found. Winckelmann was shocked by these barbaric methods and published highly critical open letters in an attempt to save the cities from further destruction by the royal treasure hunters. His effort in Italy gradually placed excavations on a scientific basis and shaped the course of all later archaeological work. Practices were initiated, where objects were carefully recovered, identified, and cataloged; their location and position were documented; and the objects eventually exhibited for the benefit of later generations. As the first classical archaeologist, Winckelman also brought intellectual discipline to excavations such as those in Pompeii and Herculaneum by analyzing the context of an object and assigning it to its proper place, not just within the temporal range in which it is found, but in the cultural, artistic, economic and climatic conditions of the time. After his time, archaeologists did not just dig and collect, but they wrote of their findings.

The Pompeii of the Bronze Age is the city of Akrotiri, a major tourist attraction on the southern part of the Greek Santorini island in the Aegean Sea. When it was destroyed in ca. 1500 B.C. by the great eruption of Thera (Santorini) volcano, Akrotiri was a flourishing Minoan city. Like Vesuvius, Thera volcano is both a creator and a destroyer. It buried a treasure that has been brought back into the daylight for us to see, a wealth of information on the cultural and material civilization of the Bronze Age in the Aegean world of the Minoans.

In 1967 the Greek archaeologist Spyridon Marinatos began an excavation at a site called Akrotiri. It was just a hunch, based on some visible traces at the surface, such as pottery shards, and the fact that the soil here was very soft, even collapsing under the weight of a passing donkey. The excavations over the next few years revealed a magnificent city beneath a thick cover of pumice (Doumas 1983). Over 10,000 m^3 of the town have been excavated and are accessible to the tourist. Here the visitor can take in the atmosphere in a Minoan town, with carefully restored houses, pottery and magnificent frescoes, whose preservation to our day was made possible by their instantaneous burial in the pumice fallout and the pyroclastic surges during the Minoan eruption. Many of the finer works of art have been removed and are now exhibited in the Archaeological Museum in the town of Phira on Santorini and in the Archaeological Museum in Athens.

Marinatos and other scholars were aware of the sudden and mysterious destruction of the Minoan civilization on Crete in the Bronze Age, and in the 1930s Marinatos formulated a theory of a volcanic destruction of Minoan Crete, which he attributed to the Thera eruption. The causal relationship between this catastrophic eruption and the sudden demise of the Minoans in the Aegean region has been a topic of debate amongst archaeologists and volcanologists ever since.

A major natural disaster in Central America occurred in the third century A.D. The eruption of Ilopango volcano in what is now El Salvador disrupted agriculture and settlements in the southeast Maya area for a considerable time. Tephra from the eruption covered more than 10,000 km^2 with a deposit over 50 cm thick. It is estimated that tens of thousands of people were forced to migrate out of the region, and human occupation was only possible after several hundred years of weathering of the tephra deposit had taken place (Sheets 1983). In the sixth century, another major eruption buried farms and small villages in the region of Ceren, which have been excavated to reveal house styles of the Maya, and agricultural and settlement patterns typical of Central America at this time. Just as Vesuvius has preserved for us the daily life of the Romans in Herculaneum and Pompeii, the on-going excavations in the volcanic regions of Central America are now revealing many fascinating details of the life of the Mayans. Tourists who are traditionally drawn to the magnificent stone temples of the Mayans will now be able to explore the new archaeological sites that are being unearthed from underneath thick blankets of tephra.

In North America, the best known volcanic archaeological site is at Sunset Crater in Arizona. When the area was inhabited by the Sinagua Indians, a series of eruptions began about A.D. 1064, creating a large cinder cone, lava flows, and several smaller cones. Tephra from the eruptions buried a number of circular and subsquare pit houses of the local tribe, as well as larger ceremonial pit houses. Artifacts found at these sites are now available for view by tourists visiting the Sunset Crater and Wupatki National Monument. The Wupatki (meaning tall house in Hopi) settlement was formed as a direct consequence of the eruption of Sunset Crater, as the Sinagua natives were forced to leave their farmlands near Sunset Crater. They settled on the Wupatki basin, where they were joined by two other tribes. The settlement thrived, partly because the thin ash layer deposited by the eruption contributed to the soil's fertility. For unknown reasons, the settlement was abandoned around A.D. 1225. Today, the Wupatki ruins are the best place for visitors to learn about the effects of the eruption of Sunset Crater on the local population.

H. Volcanoes and Religion

An ancient Chinese account of Japan states: "In the Empire of Wo there is a mountain called O-Su which unaccountably belches out fire as high as the heavens. This is truly a strange thing, and people go there to offer sacrifices." Virtually all cultures living with volcanoes have considered them as sacred abodes of gods, demons, or beneficent deities. Here we mention only four of the volcanoes that continue to inspire religious response.

Many Indonesians still believe that sacred volcanoes are the abodes of gods. Even today, during an annual ceremony, pieces of the hair and nails of the Sultan of Yogyarkarta (whose title is "Life-Giving Mountain") are placed on the crater rim of the dreaded Merapi volcano in central Java, as offerings to retain the Sultan's spiritual power over a dragon that resides deep inside the mountain. The holy Mount Bromo, which lies inside the Tengger caldera of east Java, is the most worshipped volcano in Indonesia. The Tenggerese people who live on its slopes still retain a mixture of Hindu-Buddhist beliefs and are very sensitive to the changing moods of the volcano. Annually, on Buddha's birthday, the 14th day of the last Tenggerese month, they climb to the summit of Bromo's smoking cone to pray and to give offerings of money, vegetables, flowers, live chickens, goats, and, in the past, even humans. These sacrifices are probably stimulated by the story of Kiai Koesomo and his wife Njai. In return for Brahma's gift to them of fertility, they promised the god one of their sons. They soon forgot their duty and eventually Brahma demanded they return their 14th child, a son named Madin, who was swallowed up by the crater. As Madin departed, he asked the people to pray and make annual sacrifices in his memory. They continue to do so, praying for health and a rich harvest. Visitors to Bromo must arrive at dawn, usually by riding tiny Tenggerese ponies along the caldera rim and up the steep path to the base of the Bromo cone. Concrete steps now lead up to the crater rim.

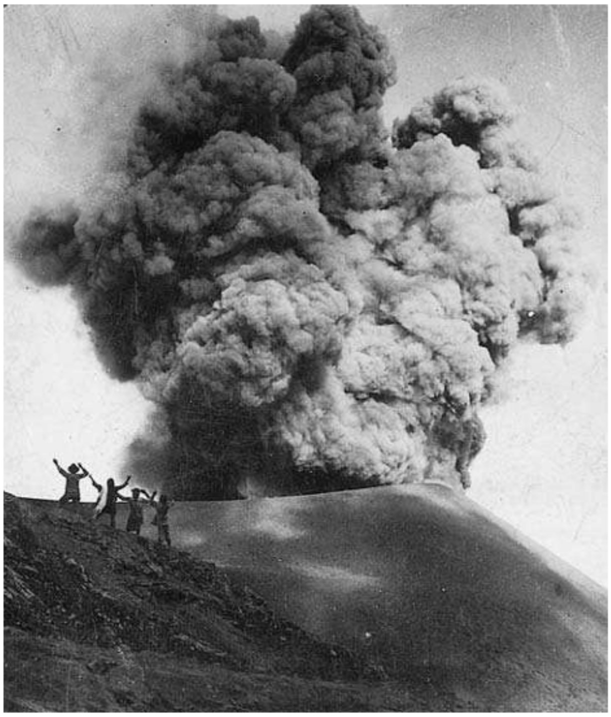

FIGURE 7 Many Indonesians consider the Bromo crater in east Java as the abode of the gods and make frequent sacrifices here. A late 19th century photograph (author's collection).

The sacred Mount Fuji is Japan's most famous volcano. It is Japan's highest mountain (3776 m), perfectly symmetrical, and about 50 km in diameter at its base. Rising isolated from a plain, it totally dominates the landscape and can be seen from 13 of Japan's provinces. It approximates a symmetrical cone in shape, but it is the sweeping and graceful catenary curve of its slopes which has made it a token of all the scenic beauty of Japan and an object of veneration and even obsession. Fuji is in every way an uplifting sight. The ascent of the volcano is a pilgrimage that every Japanese wishes to make at least once in a lifetime. Mount Fuji is also known as Huchi, a word that may be derived from Fuchi, the Ainu goddess of fire. It is rightfully considered by many as the most beautiful mountain in the world. Fuji has erupted at least 14 times since the beginning of written records in the Heian era in the eighth century A.D. Its last eruption was in A.D. 1707 during the Hoei era, when explosive activity spread ash and pumice over vast areas of Japan, including the city of Tokyo. Already in the eighth century, Fuji was revered with superstitious awe, as shown for example in Manyoshu, one of the earliest poems of the Japanese language:

No words may tell of it
No name know I that is fit for it
But a wondrous deity it surely is!
It is the peace giver, it is the god, it is the treasure.
On the peak of Fuji, in the land of the Suruga
I never weary of gazing.

Already in the earliest scrolls of Japanese painting from the 12th and 13th centuries, the isolated grandeur of Fuji is shown, drawn with reverence. In folk culture, it was one of the three lucky things to dream of—Fuji, falcon, and eggplant (a dream symbol of good fortune). As a symbol of good luck, it also figured prominently on surimono, the Japanese New Year's greeting cards, as well as a popular motif for decorating just about everything made in Japan.

Japanese legends of Fuji describe the formation of the mountain as an instantaneous event. Geologically, this is almost appropriate, as the volcano has a very high extrusion rate, and has been built up remarkably rapidly. One legend has it that many years ago, a poor woodman named Visu lived on the Suruga plain. One night he heard a great rumbling in the Earth, which terrified the woodsman so much that he gathered his children and ran out of the hut. Where there had been an empty plain, he now beheld a lofty mountain, which spewed forth fire and clouds of smoke. The next morning, when the peak was bathed in sunlight, it gleamed like opal, and Visu gave it the name the Eternal Mountain. In another legend, a Japanese giant decided one day to fill up the Pacific Ocean, and spent the night carrying huge bags of earth to the sea. When morning came, he was disappointed to see the lack of progress made, and decided to abandon the project, dumping the last bagful of earth on the plain in a heap, which now is Fuji.

Another majestic volcano that has attracted religious worship is Mount Shasta in the Cascades range. Shasta stands more than 14,100 feet above sea level and is a truly impressive volcano. The native Indians once held that the volcano was the abode of the spirit chief Skell, who had descended from heaven to its summit, where his presence was marked by fire and smoke (Harris 1988). More recently, Shasta has attracted a variety of nontraditional religions, cults, and sects that have their headquarters in the small village of Mt. Shasta at the western base of the volcano. The diverse groups, who all believe that the volcano is a holy place and a magic mountain, include the Radiant School of the Seekers and Servers, the I AM Foundation, the Rosicrucians, the Association Sananda and Sanat Kemara, and the Knights of the White Rose. Shasta volcano is also alleged to be the home of the Lemurians, the refugees from the lost kingdom of Mu, now allegedly submerged beneath the Pacific Ocean. Few have claimed to see the Lemurians, who are said to inhabit tunnels within the volcano. Other lost tribes are also said inhabit the mountain, including the Atlanteans and the Secret Commonwealth (Fig. 8).

It is not clear what has brought Shasta such a wealth of mythology, but it is almost certainly due to the strong presence that this mountain projects, in its physical power and beauty, making it a credible gateway to mystical realms.

Kilauea is another volcano that has deep religious significance to the local people. Before Westerners came to Hawaii, natives worshipped Pele, the temperamental volcano goddess who made her home in Kilauea's fiery pit, Halemaumau. It is surprising how much the early Hawaiians understood about volcanic activity, as we can grasp from their stories about Pele. For example, Pele was thought to have made her first home in the northern islands of the Hawaiian chain, where the oldest volcanoes are. The stories of Pele's wanderings make it clear that the Hawaiians understood that the islands get progressively younger down the chain, toward the Big Island and Kilauea in particular.

The worship of Pele suffered a setback when Christianity was introduced by missionaries. The most serious blow to the old religion was dealt by the high chieftess Kapiolani in 1824. Kapiolani, who had become a Chris-

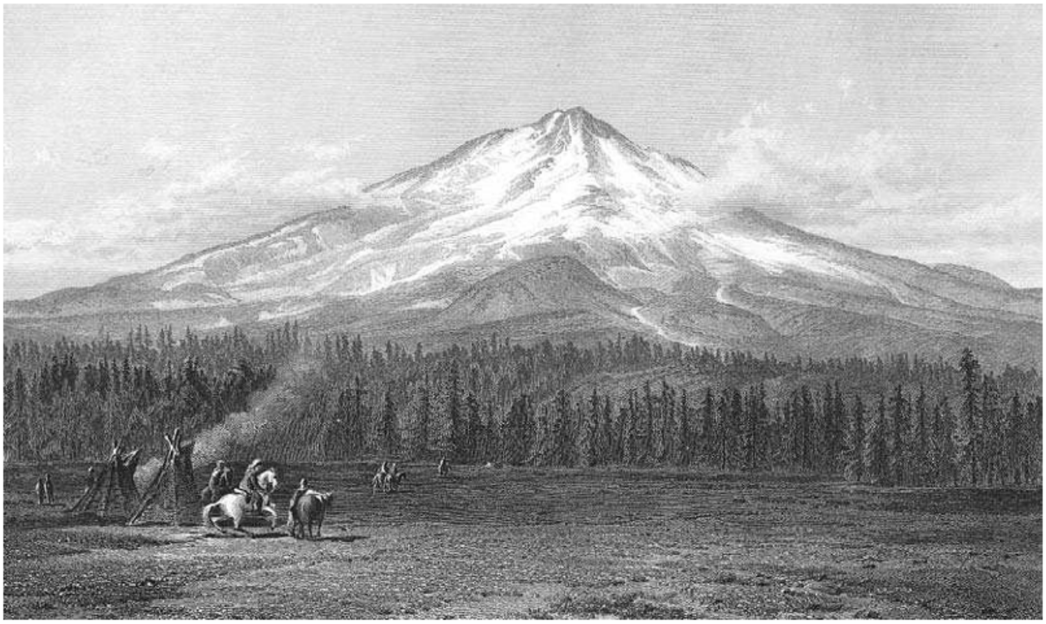

FIGURE 8 Mount Shasta in the Cascades volcanic range still has a unique attraction for various modern religious sects. An 1873 engraving (author's collection).

tian, knew that the worship of Pele was the most firmly entrenched in the hearths of Hawaiians and so the best way to earn converts to Christianity was to show that Pele did not exist. Kapiolani defied Pele by going down into the fiery pit of Halemaumau, throwing stones into the crater and eating ohelo berries that are consecrated to the goddess. When Kapiolani returned to the crater rim unharmed, the foundation of the old religion had been irreversibly shaken. However, the worship of Pele was never forgotten, and, in these days of religious tolerance, it has gained some popularity. Although few tourists come to Kilauea for religious reasons, local people still hold Pele and her volcano in great reverence and often throw offerings of flowers, money, and food into Halemaumau. Pele's High Priestess is well known to the volcanologists who work in the island, and she is respectfully allowed to offer prayers to the goddess when eruptions start.

V. CONCLUSIONS AND THE FUTURE

The most popular volcanoes in terms of tourism are probably in the United States, as the national parks attract many millions of visitors every year. Yellowstone, Kilauea, Haleakala, Crater Lake, and Mount St. Helens are top attractions. In the Mediterranean, Vesuvius has retained its popularity, particularly because of the appeal of Pompeii and Herculaneum, but Santorini is increasingly attracting tourists. In the Caribbean, St. Vincent, St. Lucia, Guadeloupe, and Martinique are popular, although they are not among the most visited islands. In the Atlantic, the Canary Islands and the Azores are often the chosen destinations of British and other Europeans on vacation. New Zealand is very popular with Australians, but also European tourists, particularly British. In Asia, the Japanese volcanoes continue to attract the greatest number of tourists.

As interest in adventure and ecologically oriented travel increases, a number of other volcanoes are gaining considerably in popularity. Iceland is an example, particularly for European travelers. Americans are increasingly choosing Costa Rica and Alaska. Destinations such as Antarctica, the Andes, and Africa are becoming more affordable for the average tourist from all over the world.

Many of the world's most interesting volcanoes are not often visited because of the unstable political situation and the high crime rates of the countries they are in. Prime examples are the very active volcanoes of Guatemala and Nicaragua. Changes in the political system can completely transform a region's tourism industry.

A major recent example is Kamchatka. This region, and all its spectacular volcanoes, were completely off-limits to visits during the Soviet regime. Although few tourists yet travel to Kamchatka, this is very likely to change in the next decade.

Volcanic eruptions can attract tourists but also temporarily destroy the infrastructure needed to accommodate them. The recent volcanic activity in Montserrat has caused considerable disruption of local services, including the destruction of the capital and of the airport, and massive a exodus of the island's residents. Tourism used to be the island's main source of income, but the "Ireland of the Caribbean" can no longer accommodate visitors and, except for volcanologists, few people now want to visit the island. However, in a few years, it is very likely that the tourism industry will pick up again. Pinatubo, and the Philippines in general, are rising from the ashes of the 1991 eruption. When Pinatubo erupted in the Philippines in June 1991, the country was on the verge of a financial and economic disaster. The eruption forced the closing of American military facilities at both Subic Bay Naval Station and Clark Air Base, two important economic factors for the country. In recent years, however, an economic miracle has been happening in the Philippines, under a stable government. Visitor arrivals have doubled in 4 years, Clark Air Force Base is now an international airport, and a complex of luxury waterfront villas has been constructed at Subic Bay to house the tourists. The next big tourist draw that is planned for the Philippines are the crater lakes of Pinatubo. As happened at Mount St. Helens, a major eruption may be, in the long term, a boom for the local tourist industry.

SEE ALSO THE FOLLOWING ARTICLES

Archaeology and Volcanism • Hawaiian and Strombolian Eruptions • The History of Volcanology • Volcanic Lakes • Volcanoes in Art • Volcanoes in Literature and Film

FURTHER READING

Anderson, T. (1903). *Volcanic Studies in Many Lands.* C. Scribner's, New York.

Anon. (1995). Sand, a user's guide. *Conde Nast Traveler Magazine,* July, p. 56.

Doumas, C. G. (1983). *Thera: Pompeii of the Ancient Aegean.* Thames and Hudson, London.

Harris, S. L. (1988). *Fire Mountains of the West.* Mountain Press, Missoula, MT.

Sheets, P. D., ed. (1983). *Archeology and Volcanism in Central America.* University of Texas Press, Austin.

Secor, R. J. (1981). *Mexico's Volcanoes; A Climbing Guide.* The Mountaineers, Seattle.

Sigurdsson, H., Carey, S., Cornell, W., and Pescatore, T. (1985). The eruption of Vesuvius in AD 79. *National Geographic Research,* **1,** 332–387.

Swinglehurst, E. (1974). *The Romantic Journey: The Story of Thomas Cook and Victorian Travel.* Pica, London.

Whitey, L. (1997). *Grand Tours and Cook's Tours.* William Morrow.

Whymper, E. (1987). *Travels amongst the Great Andes of the Equator.* Gibbs M. Smith, Salt Lake City.

This Page Intentionally Left Blank

ARCHAEOLOGY AND VOLCANISM

STEPHEN L. HARRIS
California State University, Sacramento

I. Volcanoes as Preservers of Archaeological Sites
II. Herculaneum and Pompeii: Cities of the Early Roman Empire
III. Akrotiri: An Aegean Bronze Age City
IV. Catal Huyuk: The Earliest Representation of a Volcanic Eruption
V. Mesoamerican Archaeological Sites
VI. North American Archaeological Sites
VII. Geomythology: Volcanoes in Prehistoric Oral Traditions
VIII. Summary

GLOSSARY

archaeology The scientific study of the physical remains of ancient human cultures and the art of interpreting their significance.

Bronze Age Period of human cultural development in Europe and the Near East characterized by the use of bronze tools and weapons that began between 4000 and 3000 years ago and ended with the Iron Age (about 1200 B.C.).

etiology From a Greek term meaning cause, origin, or source; in the study of ancient myth, it refers to oral traditions that attempt to explain the origins of natural or social phenomena.

geomythology The study of ancient oral traditions that preserve memories of prehistoric geologic events, such as earthquakes or volcanic eruptions.

lahar An Indonesian term for a debris flow or mudflow originating on a volcano.

Minoan culture An ancient civilization centered on Crete and characterized by the building of large palace complexes, such as that at Knossos; it dominated the Aegean region from about 2000 to 1450 B.C.

mudflow A water-saturated mass of rock debris that moves downslope as a liquid under the pull of gravity; it can travel many tens of miles beyond its source.

Neolithic The New Stone Age; in Europe and the Mediterranean basin, it refers to prehistoric cultures using stone implements and characterized by settled agrarian pursuits.

phreatic Refers to a steam eruption that produces no fresh magma. A common precursor of eruptive activity, it is caused when groundwater, heated by a magmatic source, flashes into steam.

Plinian eruption Named for Pliny the Younger, a violently explosive eruption that ejects a large volume of tephra high into the stratosphere.

pyroclastic A Greek term meaning fire-broken; it refers to fragmental rock ejected during an eruption.

pyroclastic flow A dense, hot, dry mixture of gas and incandescent rock fragments that travels rapidly along the ground surface, typically at speeds of hundreds of feet per second.

pyroclastic surge A turbulent cloud of gas and fine rock

Copyright © 2000 by Academic Press
All rights of reproduction in any form reserved.

particles that flows over and above the ground surface at extremely high velocities. More dilute than pyroclastic flows, surges are not topographically constrained but sweep over ridges, hills, and other topographic obstacles.

tephra Rock fragments blown into the air above an erupting volcano; tephra ranges in size from fine ash to blocks many tens of feet in diameter.

DESPITE THEIR REPUTATION as agents of destruction, explosive volcanoes have provided a major aid to archaeologists' study of ancient human remains. Large-volume eruptions of tephra can not only quickly and thoroughly bury entire settlements and other artifacts, effectively sealing them for posterity, but also typically lay down widespread layers of ash that, when dated, serve as valuable time markers. When the date of an extensive tephra layer is known, it enables researchers to establish the relative ages of objects found within, above, or below the deposit.

I. VOLCANOES AS PRESERVERS OF ARCHAEOLOGICAL SITES

A. The Science of Archaeology and Its Relation to Volcanism

Almost from its inception, archaeology has been intimately associated with volcanism. In many important ways, archaeology evolved as a scientific discipline in the laboratory provided by Herculaneum and Pompeii, Roman cities located on Italy's Bay of Naples that were buried in A.D. 79 by a catastrophic eruption of Mount Vesuvius. Rediscovered in the early 18th century, the two sites were first viewed as mere repositories of artistic plunder to furnish the private estates of European collectors. By the mid-19th century, however, under the leadership of such pioneering archaeologists as Giuseppe Fiorelli, excavators at Pompeii eventually established the systematic criteria for uncovering, cataloging, and conserving antiquities that characterize archaeology today.

An interdisciplinary science that utilizes the contributions of anthropology, geology, paleontology, ethnology, chemistry, and physics, modern archaeology involves studying and interpreting the material remains of ancient human cultures. Its objectives combine scientific and humanistic goals, including the identification and analysis of artifacts to illuminate the long-forgotten cultural processes that created them. As a multidisciplinary enterprise, archaeology includes attempts to reconstruct the full spectrum of elements composing a vanished society, including such components as its economy, commerce, political organization, religious beliefs, and mythology.

Paradoxically, volcanoes, which are popularly regarded as mere destroyers, are perhaps nature's most effective preservers of ancient human structures and settlements. No other natural phenomenon can so quickly and thoroughly bury large areas, including evidence of human occupation, protecting artifacts from subsequent damage. Exposed sites gradually covered by slower geologic processes, such as sporadic flooding or sedimentation, are typically subject to severe erosion and destructive human activities, including war, vandalism, and the deliberate demolition of older edifices. By contrast, towns such as Pompeii, Herculaneum, and Akrotiri, a Bronze Age settlement on the island of Thera (Santorini), were rapidly engulfed in pyroclastic ejecta and survive relatively intact. Besides being spared the depredations inescapable in surface exposure, the buildings, artwork, and other artifacts buried by voluminous tephra falls or pyroclastic flows remain in their original context, their spacial and functional relationships largely undisturbed.

Volcanism's agency in preserving the human record extends to the earliest stages of human evolution. About 3.5 million years ago, at Laetoli in Tanzania, an adult hominid and one or two smaller companions, perhaps a female and/or child, walked upright across a newly deposited layer of ash. After a brief rainstorm splattered across the area, a second ash eruption covered the hominid footprints, effectively sealing one of the oldest surviving evidence of bipedalism until its discovery by 20th century investigators.

II. HERCULANEUM AND POMPEII: CITIES OF THE EARLY ROMAN EMPIRE

A. Historical Significance

Pompeii, in A.D. 79 a thriving commercial center of about 20,000 inhabitants, and Herculaneum (Figs. 1 and 2) a largely residential town of about 5000, are uniquely important. Frozen in time, they offer a superbly detailed picture of life in the early Roman Empire, encompassing

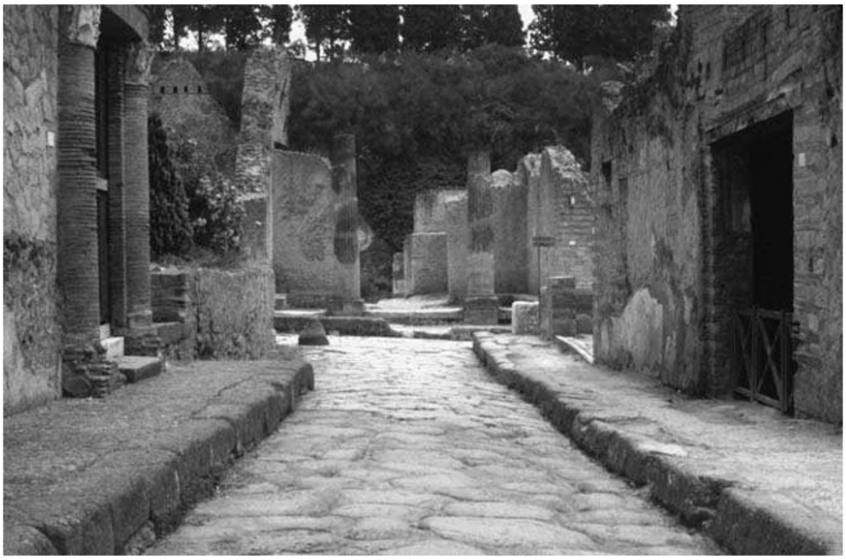

FIGURE 1 Whereas most buildings in Pompeii are roofless, crushed by the accumulation of tephra from Vesuvius, many of Herculaneum's structures, such as these small shops, retain their upper stories. An affluent resort town on the Bay of Naples, Herculaneum is perhaps the best-preserved urban site of the early Roman Empire. (Photo courtesy of Dr. James Straukamp.)

temples, theaters, shops, private houses, gardens, fountains, public baths, swimming pools, and a miraculously preserved library. Interred so swiftly that most residents had no time to save their possessions, the ruins contained a rich variety of rare items, including gold jewelry, silver dishes, the most complete known set of Roman surgical instruments, and even wax tablets inscribed with bank records. Recovery of Greco-Roman statuary, paintings, and furniture influenced 18th and early 19th century art and architecture throughout Europe and America, where Thomas Jefferson modeled Monticello on classical styles.

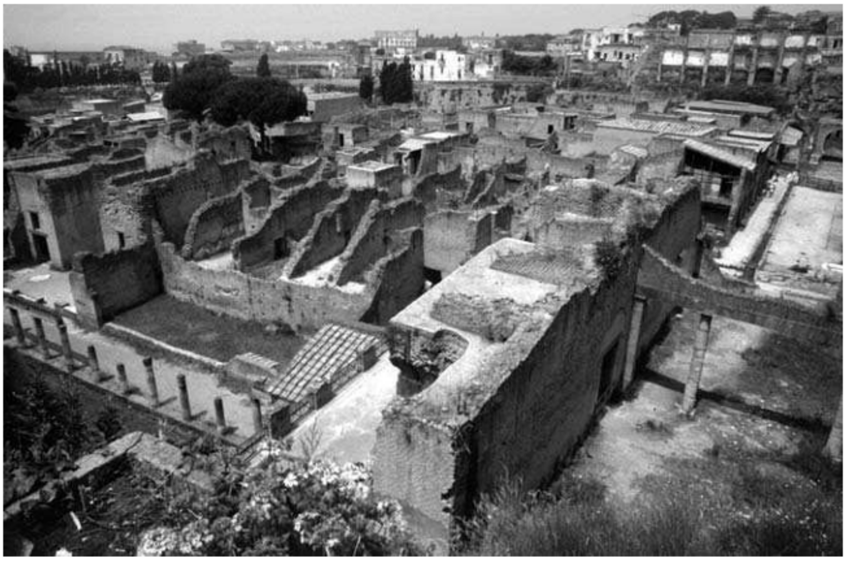

FIGURE 2 Engulfed by pyroclastic flows during the A.D. 79 eruption of Mount Vesuvius, the Roman town of Herculaneum has been only partially excavated. Property owners of the modern town of Resina, built atop the site, effectively prevent further excavation. (Photo courtesy of Dr. James Straukamp.)

B. Recent Discoveries at Herculaneum

Besides their historical role as a testing ground for new archaeological techniques and concepts of preservation, Pompeii and Herculaneum continue to yield invaluable information about the Roman world, including the physical attributes of the cities' former inhabitants. Until the early 1980s, when about 130 largely intact skeletons were exhumed along Herculaneum's former waterfront, it was assumed that most of Herculaneum's population had managed to escape the city alive. The discovery of so many well-preserved remains is particularly important because the Romans, who typically cremated their dead, otherwise have left little evidence of their bodily characteristics. Caught in the fierce heat and swirling ash of a pyroclastic surge, the victims had apparently been asphyxiated while attempting to flee by boat. (An overturned 30-foot wooden vessel was found nearby.) The skeletal remains at Herculaneum are considered invaluable because they encompass individuals of all ages and classes, ranging from a bejeweled Roman matron to a teenaged slave girl to a middle-aged soldier, sword in hand, whom the surge had thrown to the ground facedown. Hundreds more skeletons may still await discovery.

C. Sequence of Eruptive Events in A.D. 79

The effects of Vesuvius's outburst on the nearby human population are now better understood than those of any other ancient volcanic disaster. Not only did a remarkably observant Roman nobleman, Pliny the Younger, write two letters to the historian Tacitus in which he carefully described Vesuvius's behavior, but modern volcanologists led by Haraldur Sigurdsson have been able to correlate Pliny's account with particular strata deposited by the eruption. The eruptive sequence, and its effects on the human population, is now well understood. After some preliminary activity, which dusted one slope of the volcano with a light tephra fall, the main eruption began about 1 P.M., August 24 with an explosive discharge of pumiceous ash, forming an ash column that, in Pliny's words, resembled a towering pine tree with spreading upper branches. For the next 11 hours, Vesuvius ejected a vertical eruption cloud (called Plinian after the Roman author who first described the phenomenon) that rose approximately 12 miles into the stratosphere. Carried south-southeastward by the prevailing winds, the ash canopy enshrouded Pompeii, extinguishing sunlight and raining lapilli (the Latin term for small stones) over the city, where pumice accumulated at the rate of 6 inches per hour. Lying four miles upwind from Vesuvius, Herculaneum received only a trace of ash during this phase of the eruption.

Shortly after midnight, however, the character of the eruption abruptly changed. As Vesuvius tapped deeper levels of its magma chamber, the gas-rich volatile mixture that had sustained the Plinian cloud became increasingly depleted, causing the ash column to collapse. Expanding horizontally, the turbulent ash cloud separated into a fast-moving pyroclastic surge that swept through Herculaneum, killing all who remained there, and a somewhat slower-moving pyroclastic flow that enveloped the town, initiating its burial. As the eruption column continued to fluctuate, a second surge and pyroclastic flow were generated an hour later. A third, at 5:30 A.M. on August 25, finished the work of entombing Herculaneum under a hot ash deposit tens of feet thick.

The third pyroclastic flow, which had interred Herculaneum, was deflected from Pompeii by the city's massive walls. The fourth, however, exhibited lethal energy, racing 6 miles from Vesuvius's crater and blasting through the city like an incandescent sandstorm. Rushing across the 7-foot thickness of pumice that had previously fallen, the flow toppled exposed walls, sheared off roofs and upper stories of buildings, and asphyxiated the remaining inhabitants.

Trapped in the fourth pyroclastic flow, thousands of fleeing Pompeiians were instantly entombed. When their bodies decayed, they left behind hollow spaces in the ash. Recognizing that these cavities were, in effect, molds of human figures, 19th century archaeologists filled them with liquid plaster, allowed it to solidify, and then removed the surrounding ash. The plaster casts thus formed are astonishingly lifelike, some showing in detail the agonized facial expressions of the volcano's victims.

In 1961, archaeologists unearthed a particularly poignant group in a location called the Fugitives Garden, where casts were made of seven adults and six children. Like many of the 57 people killed in the 1980 pyroclastic surge from Mount St. Helens, the fugitives appeared to have died of suffocation from inhaling the pervasive ash. Estimates of the fatalities in Pompeii—some archaeologists state that about 2000 perished—were based on the number of skeletons found in the lower pumice deposits and the body-shaped cavities formed in the upper pyroclastic flow deposits. With the realization that the pyroclastic surges and flows probably killed simultaneously many of the people who were

TABLE 1 Some Representative Archaeological Sites Related to Volcanism

Site name and location	*Volcano*	*Date*	*Significance*
Pompeii & Herculaneum, Italy	Vesuvius	79 A.D.	Entire Roman cities preserved
Akrotiri, on Santorini, Greece	Thera	late 17th century B.C.	Minoan-age city; rare murals
Catal Huyuk, central Turkey	Karapinar cinder cone field (?)	6200 B.C.	Earliest known painting of a volcanic eruption
Maya settlements, El Salvador, Central America	Ilopango	Third century A.D.	Massive disruption of Maya population centers
Northwest Costa Rica, Central America	Arenal	c. 1550 B.C. to A.D. 1080	Average of 4 eruptions per century fails to disrupt population
Arizona, U.S.A.	Sunset Crater	c. 1060 A.D.	Causes redistribution of native agricultural sites in vicinity
Washington State, U.S.A.	Rainier	c. 3600 B.C.	Mudflow buries campsite and tools
Washington State, U.S.A.	St. Helens	c. 1500 B.C.	Abandonment of native habitats in southwest Cascade Range
Yukon Territory, Canada	White River Volcano, Alaska	20 A.D. and 720 A.D.	Triggered mass migrations of Athapaskan peoples, northwestern Canada
Aleutian Islands, Alaska	Aleutian Range volcanoes	18th Century A.D.	Probable submarine activity and tsunamis displaces coastal Aleut tribes

fleeing along the roads outside Pompeii's city gates, historians now believe that many more thousands perished in the disaster.

At 8:30 A.M. on August 25, Pliny witnessed the generation of the sixth and largest pyroclastic surge, "a fearful black cloud … rent by forked and quivering bursts of flame" that swept across the Bay of Naples toward Misenum, located 20 miles west of Vesuvius. Fleeing the city with hoards of panicked refugees, Pliny noted that "many besought the aid of the gods, but still more imagined there were no gods left, and that the universe was plunged into eternal darkness for evermore."

D. Rediscovery and Excavation

Although some survivors later burrowed into the deposits covering Pompeii, retrieving valuable objects and even building materials, the buried cities eventually became almost entirely forgotten until 1709, when laborers digging a well happened upon Herculaneum's theater. Despite being rediscovered first, most of Herculaneum still lies underground, embedded in pyroclastic flow deposits that hardened to the consistency of cement. Besides the enormous difficulty of removing the solidified ash enshrouding the site, landowners in the modern town of Resina, which sprawls atop the deposits covering Herculaneum, refuse to permit archaeologists to expand the excavations.

Beginning in 1738, excavators bored a network of tunnels through part of the town, haphazardly looting statuary and other portable art and carelessly wrecking any structure considered uninteresting. One of the most promising 18th century finds was an elaborate residence known as the Villa of the Papyri, which sheltered a library of 1800 carbonized scrolls. Hopes that this collection would yield literary masterpieces, such as a lost tragedy by Sophocles, were dashed when most of it turned out to be the work of a minor Epicurean philosopher, Philodemus. The villa's presumed owner, L. Calpurnius Piso, the father-in-law of Julius Caesar, was Philodemus's patron.

Today most of the 18th century tunnels burrowing through underground Herculaneum are closed, and visitors can no longer walk across the theater's ancient stage. Even though most of Pompeii has been opened to light and air, Herculaneum remains largely buried, its mysteries still hidden. The few buildings now exposed, such as the elaborate suburban baths, represent only a fraction of structures waiting to be discovered, along with an unknown number of sculptures, paintings, and scrolls.

III. AKROTIRI: AN AEGEAN BRONZE AGE CITY

A. Relation to Minoan Civilization

A particularly spectacular example of volcanic preservation occurs on the Aegean island of Thera (also called Santorini), about 60 miles north of Crete, where a late Bronze Age city, named for the nearby modern village of Akrotiri, was engulfed during a cataclysmic eruption of the Thera Volcano in the late 17th century B.C. Dubbed the Pompeii of the Aegean, Akrotiri was similarly buried by voluminous tephra falls and pyroclastic flows. By far the best preserved settlement of its era (corresponding to Late Minoan III-A on Crete), Akrotiri was a prosperous sea port, enriched by maritime trade with Crete and other parts of the eastern Mediterranean region. The luxury and opulence of its multistory dwellings (some rose three or even four stories high) is indicated by their technological sophistication (indoor running water and flush toilets) and artistic splendor (some of the most extensive and beautiful wall paintings to have survived from the ancient world).

Although the site of Akrotiri was continuously inhabited since the Neolithic period and hence represented a native Cycladic culture, pre-eruption Akrotiri was profoundly influenced by Minoan civilization. Named by modern archaeologists after Minos, a mythical king of Knossos on Crete, Minoan culture dominated the Aegean region between about 2000 and 1450 B.C. The Akrotiri wall paintings reveal a typically Minoan delight in physical nature and the human form. Most of the human figures, including richly dressed and bejeweled female figures and nude youths carrying fish, probably depict participation in religious processions or other rituals. Other paintings focus on portraying highly stylized flowering plants, soaring birds, or animals, both wild and domestic, including the famous blue monkeys adorning the aptly named House of the Frescoes. Perhaps most important for archaeologists are the lavish wall murals showing a Bronze Age naval fleet and urban waterfront scenes, one of which may represent Akrotiri and its people.

Because the artists made no attempt to keep the plaster they painted on wet and continued to paint over patches that had already dried, the frescoes are unevenly preserved. Generally intact where the paint had permeated wet plaster, the wall paintings quickly flake away from the dry areas, challenging the techniques of Greece's most skilled archaeologist-restorers. Even so, Akrotiri's frescoes survive in larger fragments than the roughly contemporary murals from other Aegean sites, including Cretan Knossos. Besides their exceptional state of preservation, the paintings are unusual in that they generally remain in their original positions, allowing archaeologists to reconstruct the original decoration of entire rooms and to speculate on the probable relationship between scenes painted on different parts of the same room.

B. Architectural Sophistication

At the time of its destruction, Akrotiri was probably one of the Aegean's major ports, with a population of several thousand. Although only a small fraction of the town, which may have covered several tens of acres, has thus far been excavated, it appears that prehistoric Akrotiri closely resembled the general layout of modern villages on the island. Designed for a society functioning without vehicles, its streets were narrow, wide enough only for two loaded donkeys or other pack animals to pass one another. Some archaeologists suggest that the town's zigzag streets and small, irregularly shaped open spaces, such as the aptly named Triangle Square, may have been deliberately planned to block gusty winds and to prevent heavy rains from transforming thoroughfares into stream beds.

Judging from the small portion of the town now exposed—a mere ten houses have been exhumed and most of these have not been fully explored—it seems that the community was highly organized, with special attention given to sanitation. The streets, apparently well maintained, were generally paved with large, relatively flat stones; beneath this flagstone surface ran a carefully constructed sewage system consisting of stone-lined ditches covered with stone slabs. These underground sewers received effluents from neighboring houses via clay pipes incorporated in house walls. The closely packed, multistory domestic edifices and the entire absence of accommodations for livestock or other animals indicates that Akrotiri's inhabitants were thorough-going urbanites.

Individual houses were built of native stone and clay, the masonry walls strengthened against seismic hazards by both horizontal and vertical timber reinforcements. Although no standard house plan exists at Akrotiri, most builders observed some accepted conventions, including the placement of a window next to the main doorway, a practice that may account for the Greek word for "window" (*parathyron,* which literally means beside the door). The same passion for interior light and color that characterize the Minoan palace architects on Crete appears in Akrotiri's private houses. Virtually every room contains a window, with relatively large ones punctuating upper storeys, and every house uncovered to date boasts vivid wall paintings. It is possible that the presently excavated dwellings represent the home of the town's more affluent residents, but the abundance of these distinctive amenities indicate that at least a significant part of the population enjoyed both a luxurious domestic environment and a strong aesthetic sense.

With some structures rising three stories or higher, staircases are common and are built of both stone and wood. Most stairways rested on piles of rubble enclosed in a solid wood framework set between parallel walls, with stone treads laid atop the rubble. Whereas families had their living quarters on the upper levels, the ground floor was typically devoted to storage of foodstuffs and other supplies. Most houses also had workshops equipped with such stone tools as hammers and anvils, as well as private mills, complete with grindstones and containers to catch the ground flour.

Although no wooden furniture or building materials have survived, the decay of these objects left cavities in the surrounding ash deposit, into which archaeologists poured liquid plaster, resulting in plaster molds of such household items as beds, tables, and even an elaborately carved three-legged stand that may have been used for religious purposes. Besides a plethora of decorated pottery and huge storage jars, some examples of beautifully crafted metalwork have also been found, ranging from bronze awls and daggers to large bronze cooking utensils.

C. The Thera Eruption

The scarcity of valuable jewelry or metal goods, as well as the total absence of human remains, indicates that Akrotiri's people had ample warning of the disaster that overtook their city. As at Pompeii, the combined efforts of volcanologists and archaeologists have enabled researchers to interpret the stratigraphic record, reconstructing the order of events that doomed Akrotiri. According to recent studies, precursory earthquakes severely damaged buildings throughout the town, perhaps years or even decades before the eruption occurred. The city's high degree of social organization is suggested by major communal program following the temblor to clear debris from the streets, tear down ruined buildings, and repair weakened structures. Extensive reconstruction was still underway when further seismic activity apparently prompted the inhabitants to abandon Akrotiri permanently, taking with them their most valuable possessions. The volcano's interruption of this restoration process is effectively symbolized by the presence of two vessels of dried plaster and a third containing dried paint in a second-story bedroom of the West House, where painters were busily redecorating until forced to lay aside their work.

The climactic eruptive sequence began with phreatic blasts that produced a thin layer of ash, followed by a paroxysmal outburst that ejected between 5 and 7.5 cubic miles of magma, creating approximately 12.5 to 19 cubic miles of pyroclastic material. It was previously assumed that this Plinian event triggered the collapse of Thera's former summit, creating the large caldera, subsequently flooded 1000 feet deep by the invading sea, that occupies most of the island today. Geologists have recently concluded, however, that a caldera already existed on Thera at the time of the "Minoan" eruption, although it was probably enlarged by further subsidence of the volcanic edifice. The island's present crescent shape, deriving from a prehistoric collapse long before the Minoan era, inspired its ancient name *Stronghyle*, which means round.

The Thera catastrophe is notable for reputedly spawning two celebrated theories—one ancient and one modern—about the sudden disappearance of a technologically advanced prehistoric civilization. According to one hypothesis, the eruption that buried Akrotiri and other prosperous towns on Thera was the inspiration for Plato's famous myth of Atlantis. In his dialogues, the *Critias* and *Timaeus*, Plato has the Athenian statesman Solon relate a tale he heard from Egyptian priests in the sixth century B.C. concerning a tyrannical island kingdom, supposedly located beyond the Pillars of Hercules (the Straits of Gibralter), that disappeared in a sudden catastrophe. The Atlantis tradition, in this view, was based on the classical Greeks' dim memories of the disaster that overtook Thera and other Minoan sites. Plato's locating the vanished civilization out in the Atlantic was merely an imaginative but inaccurate attempt to place the ancient culture beyond the realm of the known world.

D. Thera and the Decline of Minoan Political Dominance

A second, contemporary theory links Thera's outburst with the demise of Minonan civilization. In 1939, the Greek archaeologist Spyridon Marinatos suggested that the Thera event was powerful enough to change the course of Mediterranean history, weakening Minoan political dominance of the Aegean and permitting the warlike Mycenaeans of the Greek mainland to invade and conquer Crete. Tsunamis generated by Thera's collapse, Marinatos suggested, may have overwhelmed Minoan ports, demolishing any fleets harbored there and decimating their maritime empire. Recently revised dating of the Thera eruption, placing it about 1645 B.C. (according to ice core samples) or 1628 B.C. (from tree-ring evidence), however, makes it unlikely to have triggered the final decline of Minoan power, which did not occur until about 1450 B.C. In the absence of a substantial ash layer on Crete or unequivocal evidence of flood damage to its ports, most historians now conclude that Thera's explosions were not responsible for the eclipse of Minoan hegemony in the Aegean. Efforts to connect the eruption with the biblical plagues on Egypt, described in the Book of Exodus, or with the Israelites' miraculous deliverance at the Red Sea, when a pursuing Egyptian army was allegedly overwhelmed by a "wall of water" and drowned, are equally unsubstantiated. The exodus from Egypt, which most scholars place in the 13th century B.C., occurred almost four centuries after the Thera disaster.

IV. CATAL HUYUK: THE EARLIEST REPRESENTATION OF A VOLCANIC ERUPTION

Although archaeologists have not yet discovered a fresco depicting the Theran volcano, the ruins of Catal Huyuk in central Anatolia (modern Turkey) contain a remarkable Neolithic portrayal of an active volcano, the earliest known visual record of a volcanic eruption. Dating to about 6200 B.C., the Catal Huyuk mural (Fig. 3) shows a cinder cone, looming steeply above a town nestled at its base, ejecting tephra from the summit vent. More than six millennia older than the fresco at Pompeii that portrays Bacchus (the Roman wine god) presiding over vineyards near Vesuvius, this painting bears witness that human interest in documenting volcanic phenomena began at an extremely early date.

V. MESOAMERICAN ARCHAEOLOGICAL SITES

A. Probable Effects of the Ilopango Eruption on Maya Cultural Development

Volcanic activity has also preserved a number of important archaeological sites in the New World. During the third century A.D., a caldera-forming eruption of the Volcan Ilopango devastated the highlands of El Salvador, Central America, covering a broad area under pyroclastic flows and a much larger region under thick layers of tephra. Whereas land lying within a radius of about 60 miles of the vent was rendered completely uninhabitable, areas lying father away suffered varying degrees of environmental damage, leaving a large population of survivors with no means of subsistence. Recent studies by Payson Sheets and others suggest that the eruption, occurring at the close of the Protoclassic Maya period (A.D. 200–300), had unusually long-term social and economic effects on the evolution

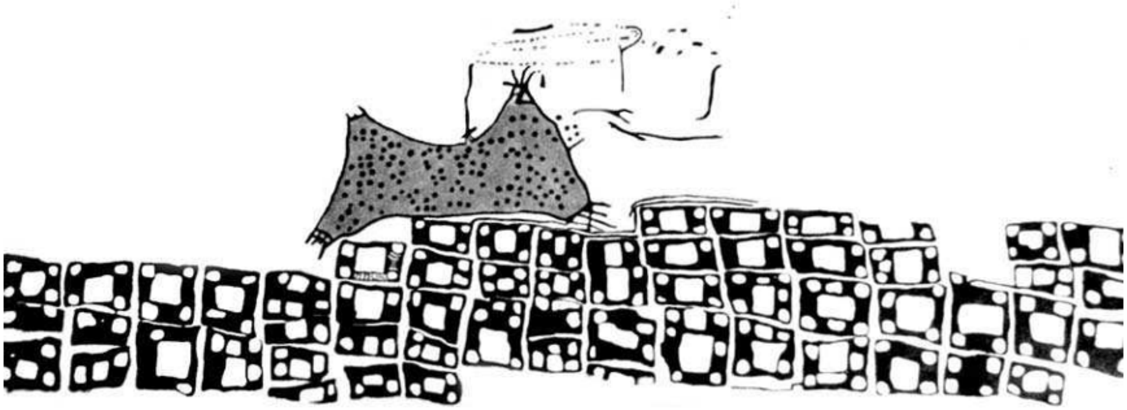

FIGURE 3 Dating from about 6200 B.C., this wall painting from a shrine at Catal Huyuk (central Anatolia, Turkey) is the oldest extant picture of an active volcano, perhaps one of the cinder cones in the Karapinar volcanic field that lies about 30 miles east of Catal Huyuk. Although the volcano is shown exhibiting only mild Strombolian activity, the artist's placement of a Neolithic town in such close proximity to its base suggests some anxiety about its eruptive behavior. (Courtesy of James Mellaart, *Catul Huyuk: A Neolithic Town in Anatolia,* 1967, McGraw-Hill.)

of Maya culture. Besides totally destroying farmlands and villages in the most severely impacted zone around the volcano and disrupting agricultural production over a vast region, the eruption may also have been responsible for a massive redistribution of the Maya population, causing an estimated 320,000 survivors to migrate northward from Salvador to Belize and northern Guatemala. The influx of migrants, displaced by the Ilopango event, may have been a catalyst that helped accelerate the already in-progress development of Classic Maya civilization. Flooding lowland towns and villages north of Ilopango, these tens of thousands of refugees may have stimulated rapid social and political responses by the Maya leadership to accommodate the suddenly increased populations. After the eruption forced abandonment of the major highland trade route, rulers at Tikal gained control of regional commerce.

Excavations at sites scattered over central and western El Salvador which were affected by the Ilopango cataclysm reveal a wealth of Preclassic Maya artifacts. Located about 40 miles from Ilopango, pre-eruption Chalchuapa was a major residential, economic, and ritual center in the southeast Maya highlands, featuring numerous 50 foot high pyramids arranged around open plazas and elaborately sculptured monuments, some of which bore calendric dates. Numerous ceramic vessels, some with polychrome painting, were found under Ilopango's ubiquitous layer of light-colored ash, known locally as the *tierra blanca*. Digs at rural sites have uncovered farms, fields (many apparently irrigated), and villages The ruins of a farmhouse at the village of Joya de Ceren, buried under 16 feet of ash, disclosed much about the Maya villagers' diet and way of life, indicating that they ate corn, wild and domesticated beans, and squash, liberally spiced with an array of chilies. Enjoying a variety of shellfish, they cooked their food in cottonseed oil and wove cotton cloth that they may have traded for obsidian, a desirable raw material for tools in the New as well as the Old World.

B. Mount Arenal and the Prehistoric Culture of Costa Rica

In contrast to the long-term effects of the Ilopango disaster, repeated eruptions of the Mount Arenal in the rainforests of northwest Costa Rica do not seem to have had a significantly disruptive impact on the native population. Sheets' investigations around Arenal, one of Central America's most active volcanoes, indicates that village life, established about 2000 B.C., was remarkably stable. Despite at least nine explosive outbursts during the prehistoric period, villagers were resilient and maintained permanent settlements near the volcano. Whereas the Ilopango paroxysm was large enough to generate massive changes in Mayan society and mark a definable boundary between distinctive phases of Mayan cultural development, the frequent Arenal eruptions—averaging four per century—did not effect a comparable alternation in the culture of prehistoric Costa Rica. Aerial photographic surveys and digital remote sensing devices have detected numerous linear anomalies in the region, many of which have been identified as prehistoric footpaths, representing a long-established system of transportation and communication through the rainforests that persisted in spite of Arenal's many explosive eruptions.

VI. NORTH AMERICAN ARCHAEOLOGICAL SITES

A. Eruptions at Sunset Crater, Arizona

In the southwestern United States, native peoples pursued a sedentary existence and farmed land near the present site of Flagstaff, Arizona, since at least A.D. 600. Then, during the 1060s, Strombolian eruptions formed Sunset Crater, blanketing the landscape with tephra and emitting a series of lava flows that buried previously arable fields. Until recently, anthropologists believed that tephra ejected during the eruptions greatly enhanced the soil's fertility, causing large number of Native Americans from other territories to flock to the posteruption Sunset area. Reexamination of the archaeological evidence, however, indicates that the presumed population increase is illusory; instead of other cultural groups migrating to cultivate the ash-enriched fields, the indigenous peoples merely transferred their settlements to new locations near the cinder cone, readjusting their practices to cope with the volcanic changes wrought in the physical environment. Unusually heavy rains that characterized the three decades following the ash eruption probably accounted for the Sunset area's posteruption increase in crop productivity, not deposition of the ash itself.

B. Native American Site Near Mount Rainier, Washington

Most of the world's archaeological sites conserved by volcanic activity are those rapidly buried by tephra or pyroclastic flows. By contrast, lava flows typically crush, pulverize, and/or burn man-made structures in the process of covering them. Similarly, most volcanic debris flows and lahars, which resemble churning wet concrete as they stream downslope, also destroy more than they preserve. A rare exception is a Native American settlement in the Cascade Range foothills of western Washington, near the present towns of Enumclaw and Buckley (Fig. 4). Discovered in 1972, the prehistoric campsite contained numerous stone projectile points, scrapers, and other tools, as well as charcoal that helped to fix the date of its burial. The encampment, located on what was then a hilltop above a valley floor, was engulfed almost instantly by an enormous lahar, the Osceola Mudflow, generated when an explosive eruption caused the former summit of Mount Rainier to collapse (Fig. 5). Almost a cubic mile of rock, much of it hydrothermally altered, avalanched down the volcano's northeast flank and was transformed into a thick lahar as it traveled more than 65 miles down the White River Valley, beyond the Cascade mountain front, where it easily swept over the hilltop camp, and ultimately into an arm of Puget Sound. Although the Osceola Mudflow had transformed the area beyond recognition and many centuries elapsed before native peoples reoccupied it, a new settlement was eventually established directly above the buried site. Two thousand years older than Akrotiri, this collection of native artifacts is one of the oldest evidences of human culture in the Puget Sound region.

C. Effects of the Mount St. Helens "Y" Tephra

As the most frequently and violently explosive volcano in the 48 contiguous states, Mount St. Helens in southwest

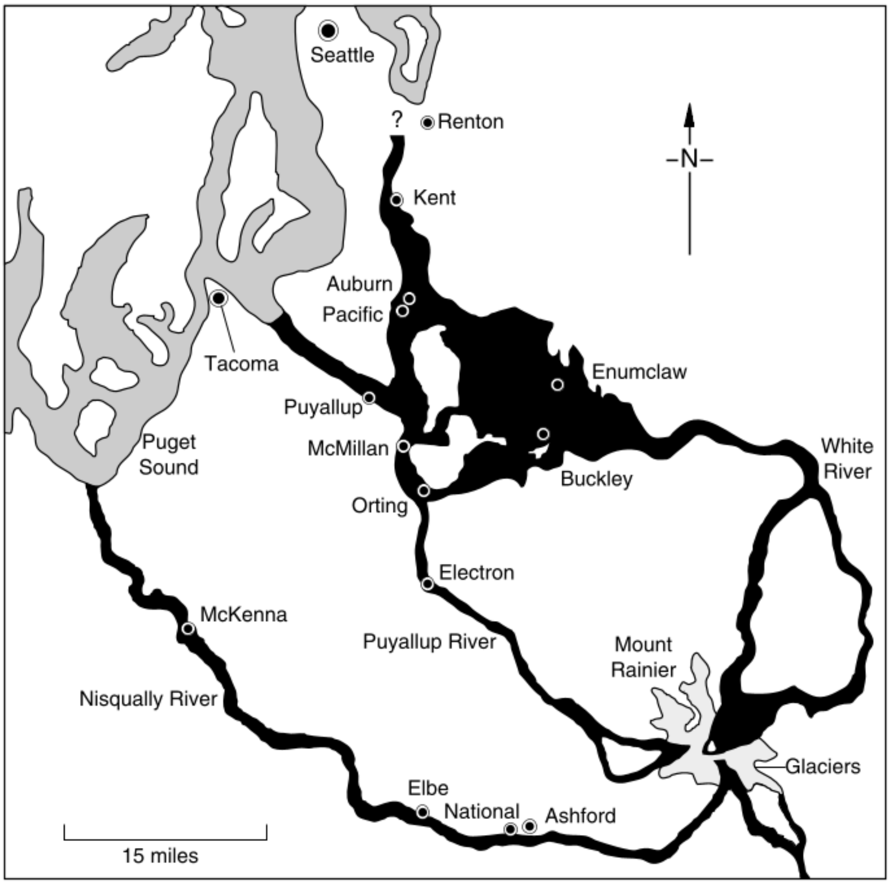

FIGURE 4 Map showing hazard zones for mudflows (lahars), lava flows, and pyroclastic flows from Mount Rainier, Washington State. About 5600 years ago, the volcano's former summit collapsed, generating the Osceola Mudflow that buried an Indian encampment near the present town of Buckley, preserving the oldest known human artifacts in the Puget Sound region. More recent mudflows followed the channels of the Puyallup and Nisqually Rivers, inundating areas where tens of thousands of people now live. (From U.S. Geological Survey Open-File Report 98-428).

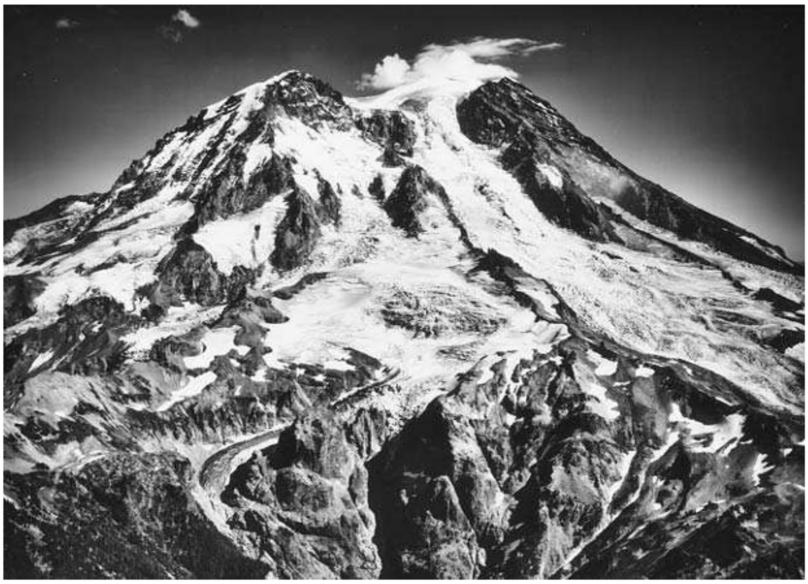

FIGURE 5 Mantled by a cubic mile of glacial ice, Mount Rainier (14,411 feet) towers above the densely populated Puget Lowland of western Washington State. Considered the most potentially dangerous volcano in the 48 contiguous states, Rainier has repeatedly produced massive debris flows, some of which have inundated areas where hundreds of thousands of people now live. (Photo by Austin Post, U.S. Geological Survey.)

Washington apparently affected the settlement patterns of some Native Americans. About 3600 years ago, St. Helens began a series of intermittent outbursts that produced the "Y" (yellow) tephra sequence, pumiceous deposits mantling much of the Pacific Northwest. Although the degree of environmental degradation to the affected areas is not known, comparisons with similarly voluminous eruptions at other volcanoes indicate that a heavy fall of coarse lapilli typically defoliates trees, smothers vegetation, pollutes water sources, and depletes both animal populations and the human predators who depend on them. Recent studies by the U.S. Forest Service and others indicate a hiatus in settlements throughout the southwest Cascade Range between about 3600 and 1600 years ago. During approximately the same period, there was a coincidental increase of native populations in the Columbia Plateau to the east, a shift perhaps attributable to St. Helens' repeated ejections of tephra.

D. Effects of the White River Ash on Native Inhabitants of the Yukon

The White River Volcano, located in southeastern Alaska near the headwaters of the White River, produced two cataclysmic eruptions, about A.D. 20 and A.D. 720, that covered most of the southwestern Yukon Territory with voluminous ashfalls. Anthropological studies indicate that the later and larger of the two outbursts, which deposited the east lobe of the White River Ash, caused profound disruption of the native population, possibly initiating a series of migrations that culminated in the formation of the Pacific Athapaskans in British Columbia and of the Apache and Navajo of the southwestern United States. Athapaskan lore, transmitted orally for more than 1200 years, refers to fiery explosions and a collapsing mountain that caused the people's ancestors to abandon their original homeland and, in small bands, eventually drift westward or southward to their present locations.

One of the world's most active volcanic regions, the Aleutian Range of Alaska hosts at least 45 historically active volcanoes. Studies of peoples inhabiting the Aleutian Islands during the 18th century A.D. indicate that eruptions, including submarine activity, have repeatedly influenced the movements of native inhabitants. Dependent exclusively upon marine fauna for their existence, the Aleuts have apparently been forced to abandon settlements destroyed by tsunamis generated during earthquake-induced underwater landslides or submarine eruptions. In some cases, it appears that the Aleuts have deserted settlements because underwater activity killed the sea life that constitutes their sole food supply.

VII. GEOMYTHOLOGY: VOLCANOES IN PREHISTORIC ORAL TRADITIONS

A. Greco-Roman Myths

Dealing with the social customs and belief systems of ancient cultures, as well as their tangible remains, archaeology encompasses the relatively new discipline of geomythology, the study of oral traditions that perpetuate memories of prehistoric geologic events, such as earthquakes, floods, and volcanic eruptions. Geomythology provides not only some of humanity's oldest surviving verbal responses to volcanic activity but also some basic terminology for describing volcanic phenomena. The term "volcano" derives from the name of Vulcano, an Aeolian island in which Vulcan, the Roman god of fire and metalcraft, was believed to have set up his blazing smithy. When busy working, Vulcan employed a giant bellows that roared and sent huge sparks rising skyward. Vulcan's earlier Greek counterpart, Hephaestus, similarly a god of fire and the forge, was said to have landed on the volcanic island of Lemnos when Zeus, king of the Olympian gods, threw him from heaven, presumably accounting for the long-lived thermal activity there.

As the tale of Vulcan's noisy workshop implies, the myths of classical Greece and Rome reflect the volcanic nature of the eastern Mediterranean. In his *Theogony*, an epic poem about the origin of the Greek gods, Hesiod (c. 750 B.C.) describes a cosmic battle between Zeus and his giant enemies, the Titans, that depicts the conflict as it were a violently explosive eruption, perhaps a mythic echo of the Thera paroxysm. Hesiod also narrates Zeus's defeat of another fiery opponent, the dragon Typhoeus, using similar volcanic imagery. According to the dramatist Aeschylus in his *Prometheus Bound*, Zeus finally imprisons Typhoeus, an embodiment of primal chaos, under the bulk of Mount Etna, Europe's largest and most active volcano. Aeschylus's etiological account thus explains Etna's outbursts as Typhoeus's struggles to escape his subterranean prison, his fiery breath melting rock to produced outpourings of lava that endanger human settlements.

B. A North American Myth: The Formation of Crater Lake, Oregon

The largest Holocene eruption in North America, that which decapitated Mount Mazama about 7500 years ago to form the caldera holding Crater Lake in the Cascade Range of southern Oregon, deposited ash over a half million square miles and, without a doubt, had an impact on the lives of countless prehistoric Native Americans. Although researchers have not yet been able to correlate the physical effects of Mazama's eruption on the flora and fauna of eastern Oregon, native survivors of the volcanic holocaust apparently were so deeply impressed by it that they created an exceptionally long-lived oral tradition about the event. However improbable it seems, oral accounts of the eruption must have been transmitted through approximately 250 generations!

In 1865, Lalek, an aged member of the Klamath tribe, told William M. Colvig, then a young soldier stationed at Fort Klamath, Oregon, the story of a battle between Llao, an underworld deity who inhabited Mount Mazama, and Skell, a sky god who dwelt atop Mount Shasta, 125 miles to the south. Although it ascribes volcanic phenomena to the tempestuous rivalry between two supernatural figures, Lalek's tale includes geologic facts then unknown to white settlers, including the extreme devastation wrought by Llao's flaming mountain and its subsequent collapse to create the basin now occupied by a lake almost 2000 feet deep. The fact that Mazama once towered high above neighboring peaks and that its former summit subsided rather than blew apart was not generally recognized by geologists for many decades after Lalek's time.

C. The "Bridge of the Gods" and Cascade Volcanism

About 200 miles north of Crater Lake, native tribes living along the Columbia River Gorge of the Pacific Northwest transmitted to early missionaries other ancient myths involving seismic and volcanic events. Perhaps the best known of these concerns the "Bridge of the Gods," a natural formation that reputedly once spanned the Columbia River near the present site of Cascade Locks, Oregon. Although it is probably now impossible to disentangle later embellishment and Caucasian interpretation from the original tradition, a Klickitat account reflects some of the region's actual geologic history. According to Klickitat storytellers, long before white people appeared on the scene, native tribes were able to cross the Columbia via a land "bridge" that was *tomanowos*, a creation sacred to the gods. But when the tribes became greedy and quarrelsome, *Tyee Sahale* (commonly translated the Great Spirit) took steps that eventually led to the bridge's destruction. First, he caused all the fires in their lodges to go out. Only the fire maintained by Loowit, an aged lady who avoided the violence that divided her people, remained burning, so that all her neighbors had to come to her to reignite their campfires. When *Tyee Sahale* asked Loowit to name a reward for her generosity, she instantly demanded youth and beauty. Transformed into a lovely young woman, Loowit inadvertently rekindled the fires of war, attracting two intensively competitive brothers, Pahto, who ruled over territory north of the Columbia, and Wyeast, who led the Willamette people south of the river.

When Pahto and Wyeast contended furiously for Loowit's favor, hurling red-hot boulders at each other, *Tyee Sahale* separated them by destroying the *tomanowas* bridge linking their two territories, its fragments creating the cataracts for which the neighboring Cascade Range was later named. The Great Spirit also changed the three principals of this love triangle into volcanic mountains: Pahto became the broad-shouldered giant that white settlers called Mount Adams; Wyeast became Mount Hood; and Loowit, Mount St. Helens. Although St. Helens's two alpine suitors repeatedly thundered their passion, the temperamental St. Helens (whom some tribes named *Tahonelatclah*, fire-mountain) remained active longest, her 1980 outburst continuing the lovers' saga into the late 20th century.

An etiological myth explaining the eruptive behavior of three sentinel peaks guarding the lower Columbia, the Bridge of the Gods tradition also evokes memories of an enormous avalanche (the Bonneville Landslide) that completely dammed the river between about A.D. 1100 and 1250, forming a causeway that allowed the Indians to cross the river dry-shod. (Because the local tribes had no word for "bridge," the notion that this formation was a soaring natural arch is a Caucasian invention.) It is possible that some of the large basaltic blocks forming the landslide dam remained in place long after the river cut a new channel through its southern toe. If so, the famed Bridge of the Gods was in fact a chaotic pile of lava slabs (a native leader described the formation to a French missionary as "a long range of towering and projecting rocks") before it collapsed, possibly in the Cascade Subduction Zone earthquake of January of A.D. 1700.

VIII. SUMMARY

In many important ways, volcanoes have proven a boon to the science of archaeology. Widespread deposits of ash create valuable time-markers, helping to date artifacts associated with a distinctive ash layer. Unusually large eruptions of tephra that have been dated by radiocarbon or other methods, such as those produced by the Thera volcano (traces of which have been found from eastern Crete and the Aegean sea floor to central Turkey) and Oregon's ancient Mount Mazama (which mantled almost the entire Pacific Northwest and southwestern Canada), can provide even greater precision in dating objects found directly covered by the tephra. Because even exceptionally large explosive eruptions typically last for only a few hours or days, in a single moment of time, they are able to bury nearby cities and other settlements with great rapidity, preserving, as at Pompeii, Herculaneum, and Akrotiri, the whole gamut of a culture's material artifacts. Volcanic outbursts also inspire survivors to create richly imaginative traditions about the supernatural forces that precipitate such terrifying manifestations of power, generating some of the world's most intriguing myths.

SEE ALSO THE FOLLOWING ARTICLES

Hazards from Pyroclastic Flows and Surges • The History of Volcanology • Plinian and Subplinian Eruptions • Pyroclastic Surges and Blasts • Volcanic Soils • Volcanoes and Tourism • Volcanoes in Literature and Film

FURTHER READING

Black, L. T. (1981). Volcanoes as a factor in human ecology: The Aleut case. *Ethnohistory*, **28,** 313–335.

Deiss, J. J. (1985). "Herculaneum: Italy's Buried Treasure," rev. ed. Harper & Row, New York.

Doumas, C. (1983). "Thera, Pompeii of the Ancient Aegean: Excavations at Akrotiri, 1967–79." Thames and Hudson, New York.

Doumas, C. G., Hardy, D. A., Sakellarakis, J. A., and Warren, P. M., eds. (1990). "Thera and the Aegean World," Vols. 1-2, Papers presented at the Second International Scientific Congress, Santorini, Greece, August, 1978. Vol. 3, Proceedings of the Third International Congress, Santorini, Greece, September, 1989.

Etienne, R. (1992). "Pompeii: The Day a City Died." Harry N. Abrams, New York.

Fagin, B. M., ed. (1990). "The Oxford Dictionary of Archaeology." Oxford University Press, New York.

Fisher, R. V., Heiken, G., and Hulen, J. B. (1997). "Volcanoes, Crucibles of Change." Princeton University Press, Princeton, NJ.

Hedlund, G. C. (1976). Mudflow disaster. *Northwest Anthropological Research Notes* **10,** 77–89.

Malde, H. E. (1964). The Ecological Significance of Some Unfamiliar Geologic Processes. *In* "The Reconstruction of Past Environments. Proceedings of the Fort Burgwin Research Center on Paleoecology 1962" (assembled by James A. Hester and James Schoenwetter). Fort Burgwin Research Center. Fort Burgwin, NM.

Marinatos, N. (1984). "Art and Religion in Thera: Reconstructing a Bronze Age Society." Athens (no publisher given).

Moodie, D. W., and Catchpole, A. J. W. (1992). Northern Athapaskan oral traditions and the White River volcano. *Ethnohistory*, **39,** 148–171.

Pellegrino, C. (1991). "Unearthing Atlantis, An Archaeological Odyssey." Random House, New York.

Sheets, P. D., and Grayson, D. K., eds. (1979). "Volcanic Activity an Human Ecology." Academic Press, New York.

Sigurdsson, H. Carey, S., Cornell, W., and Pescatore, T. (1985). The eruption of Vesuvius in A.D. 79, *National Geographic Research*, **I,** 332–387.

Vitaliano, D. B. (1976). "Legends of the Earth: Their Geologic Origins." The Citadel Press, Secaucus, NJ.

VOLCANOES IN ART

HARALDUR SIGURDSSON
University of Rhode Island

I. Introduction
II. The Beginnings of Landscape Painting
III. Vesuvius 1631 Eruption
IV. Empedocles Leaps into Etna
V. The Neapolitan School
VI. Neoclassicism
VII. Turner's Fire
VIII. Hokusai and the Spell of Fuji
IX. American Exploration of Unknown Volcanoes
X. Hawaiian Eruptions
XI. Dr. Atl—Volcanologist and Artist
XII. The Modern Volcano Landscape
XIII. Artistic Illustration

GLOSSARY

classicism The type of art that was characteristic of Greek and early Roman culture. It was revived in Florence in the 15th century, when it was often regarded as the highest point that art could reach.

edo painting The style of painting typical in Japan up to the mid-19th century, before the arrival of a strong western influence in art.

genre A type of painting showing realistically scenes from everyday life; a category or style of art.

iconography The study of the symbolic meaning of objects, persons, or events depicted in art.

impressionism A type of realism in art, with the aim of showing the immediate impression of the scene on the artist, mainly in terms of the representation of light.

neoclassicism An art form that was the result of the revival of interest in Classical forms and values in the 18th century, largely due to the discoveries of ancient Greek and Roman classical art works during the 18th century excavations in Pompeii and Herculaneum.

picturesque In the late 18th century, European people began to travel specifically to enjoy the scenery, seeking out spectacular natural scenery, ruined castles, and unusual sights. Picturesque tourism coincided with the rise of landscape painting and a romantic celebration of the landscape in art. It is an art form that is first and foremost an expression of our worship of Nature.

romanticism An attitude in art and literature that stems from the 19th century philosopher Rousseau, where moral passion counted for more than intellectual analysis, and where principal values were sincerity, authenticity, and moral exaltation.

sublime Nature overwhelming the onlooker and filling him with awe for its unpredictable force. The epitomy of the sublime in art is the terrifying spectacle of a volcanic eruption.

Copyright © 2000 by Academic Press
All rights of reproduction in any form reserved.

Ukiyoe Traditional Japanese woodblock color prints, generally portraying the ever-changing world of the city or village. This form of print popularized the landscape in Japanese art in the 18th century.

I. INTRODUCTION

Volcanoes create the most beautiful landscapes in the world. No one who has viewed the symmetry of Fuji volcano in Japan will forget its esthetic profile, defined by a perfect catenary curve. Volcanic mountains are associated with a great geologic process which has resulted in the construction of a fascinating variety of landforms, but the spectacle of volcanoes goes far beyond their pleasing landscape form. Their eruptions are exciting and thrilling because they are dangerous and exceed all natural catastrophes known to man in their explosive release of energy; they are without doubt the most spectacular natural phenomenon witnessed by humans. In terms of the cultural context of the 19th century, volcanic eruptions are sublime, invoking an expression of terror, awe, fasciantion, and savage beauty. They are also amongst the most stunning of visual phenomena, as they display an overabundance of fire, light, energy, and terror on the grandest scale. It is therefore not surprising that volcanic eruptions have been a subject for landscape artists in the western world from the 16th century to our time. Similarly, because of their purity of form and mythological significance, volcanoes have also featured prominently in Oriental art, particularly in the treatment of Japanese landscape pioneered by Hokusai in the early 19th century. This chapter discusses the artists' vision of volcanic eruptions in painting from the earliest examples to our time. The topic is vast in scope, and only a few examples of the principal and better known works can be given here. Table I lists over 90 artists who have painted volcanic eruptions or related phenomena.

II. THE BEGINNINGS OF LANDSCAPE PAINTING

Artists began to paint volcanoes and other landscape forms in the Renaissance, the period of artistic creativity which began in the 15th century and brought us genius such as Copernicus and Leonardo da Vinci. In Renaissance culture, art and science were closely associated and were in fact almost interchangeable types of mental activity, as both were stimulated by a new vision of the Earth, humans, and the world as a whole. Through its representation of objects in their true proportions, for example, Renaissance art opened the door for a new methodology in the empirical sciences, whereby scholars could accurately demonstrate their findings in drawing or illustration. The impact of art on anatomy and on the biological sciences is well known. Similarly, in geology, the storing of information and observations through the new dimension in art led to advances in the study of fossils and minerals by simply enabling communication through graphic representation of natural objects.

The study of landscape advanced much more slowly. There are glimpses of natural scenery in some Medieval manuscripts, and, in the Renaissance, admirable landscapes were portrayed by some artists, such as Leonardo da Vinci's graphic panoramic drawing of the Arno Valley in Italy, but on the whole the study of landscape did not captivate artists and scholars until late in the 17th century. By that time, the surveying of the land and the development of geography had opened the realm of landscape to the human mind and made the study of the Earth's wrinkled surface a worthy and manageable topic for art and science. During the age of Romanticism, which began in the late 18th century, admiration for the wilder natural phenomena, such as mountains, storms, and waterfalls, is abundantly expressed in landscape art. Another phenomenon common in Romantic landscapes are volcanic eruptions, which also inspired exhilirating terror and most dramatically expressed the sublimity of nature.

After their common origins in the Renaissance, science and art have steadily and inexorably diverged from one another on their separate cultural paths. This regrettable trend has developed to the point of schism in our modern society, where these two cultural pursuits are in practice often mutually exclusive, in contrast to their unity in the Renaissance age. The gradual parting of the ways was of course an inevitable consequence of the cultural specializations which our structured society imposes on its members, and in our age, the division has reached a level where most artists and scientists are largely illiterate in each other's fields. It is, for example, ironic and symptomatic that Roger Brown's painting of the Mount St. Helens 1980 eruption is styled after an industrial oil refinery fire, displaying surprising ignorance of a volcanic process, and harking back to the Medieval concept that volcanic eruptions were the con-

TABLE 1 Artists and the Volcanoes They Painted

Artist	*Volcano*
Cesare Ripa (ca. 1550), Italian	Etna
Pieter Bruegel (1528–1569), Dutch	Vesuvius 1558, 1561, Monte Nuovo
Annibale Carracci (ca. 1594), Italian	Etna
Filippo D'Angeli (1587–1640), Italian	Vesuvius 1631
Didier Barra (1590–c.1650), French	Vesuvius
Guercino (Giovanni Francesco Barbieri (1591–1666)	Vesuvius
Claude Lorrain (1600–1682), French	Vesuvius (1631)
Micco Spadaro (Domenico Gargiulo; 1609–1675), Italian	Vesuvius (1631)
Scipione Compagno (?–c.1670), Italian	Vesuvius (1631)
Salvator Rosa (1615–1673), Italian	Etna (Empedocles)
Thomas Wijck (1616–1677), Dutch	Vesuvius
Johannes Lingelbach (1622–1674), German	Vesuvius 1669
Jan Wyck (17th century), Dutch	Vesuvius 1689
Antonio Joli (1700–1770), Italian	Vesuvius
Claude-Joseph Vernet (1714–1789), French	Vesuvius 1748
Carlo Bonavia (18th century), Italian	Vesuvius (1757)
Katsukawa Shunsho (1726–1793), Japanese	Fuji
Pierre-Jacques Volaire (1729–1802), French	Solfatara, Vesuvius (1777)
Joseph Wright of Derby (1734–1779), English	Vesuvius 1774
Tomasso Ruiz (18th century), Italian	Vesuvius (1737)
Jacob Philipp Hackert (1737–1807), German	Vesuvius 1774, 1779
Michael Wutky (1739–1822), Austrian	Vesuvius
Pietro Antoniani (1740–1781), Italian	Vesuvius 1767
Pietro Fabris (?–1784), Italian	Vesuvius 1776, Solfatara, volcanic rocks
Jacob More (1740–1793), English	Vesuvius 79 A.D.
Angelica Kauffmann (1741–1807), Swiss	Vesuvius 79 A.D.
Jean-Louis Desprez (1743–1804), French	Vesuvius 1779
Alessandro D'Anna (1749–1810), Italian	Vesuvius 1794, Etna (1766)
Xavier Della Gatta (?–1827), Italian	Vesuvius 1794
Jean-Baptiste Genillion (1750–1829), French	Vesuvius
Giovan Battisa Lusieri (1755–1821), Italian	Vesuvius 1787, 1794
Saverio Della Gatta (1755–1827), Italian	Vesuvius
Odoardo Fischetti (late 18th century), Italian	Vesuvius (1805)
Camillo De Vito (c.1760–c.1830), Italian	Vesuvius (1794, 1820, 1822, 1828)
John Webber (1751–1793), English	Krakatau
Pierre-Henri de Valenciennes (1750–1819), French	Vesuvius (A.D. 79)
Katsushika Hokusai (1760–1849), Japanese	Fuji
Joseph Franque (1774–1833), French	Vesuvius (A.D. 79)
Joseph Mallord William Turner (1775–1851), English	Vesuvius, Soufriere of St. Vincent
John Vanderlyn (1775–1852), American	Vesuvius (A.D. 79)
Martin Johnson Heade (19th century), American	Omotepe, Nicaragua, 1867
William Hodges, American	Mauna Loa
Jacob Munch (1815), Norwegian	Vesuvius

continues

Continued

Artist	*Volcano*
Francois-Joseph Heim (1787–1865), French	Vesuvius allegorical
Johann Christian Dahl (1788–1857), Norwegian	Vesuvius 1820–1823
John Martin (1789–1854), English	Vesuvius (A.D. 79)
Keisai Eisen (1790–1848), Japanese	Fuji
Sebastian Pether (1790–1844), English	Destruction of Pompeii A.D. 79
Jean-Baptiste Louis Gros (1793–1870), French	Popocatepetl
Utagawa Hiroshige (1797–1858), Japanese	Fuji, Sakurajima
Carl Rottmann (1797–1850), German	Etna, Santorini
Karl P. Briullov (1799–1852), Russian	Vesuvius (Pompeii A.D. 79)
Titian Ramsay Peale (1799–1885), American	Kilauea
James Baker Pyne (1800–1870), English	Vesuvius 1856
Thomas Cole (1801–1848), American	Etna, Vesuvius
Johann Moritz Rugendas (1802–1858), German	Colima
Robert S. Duncanson (1802–1872), Afro-American	Vesuvius and Pompeii
Paul Kane (1810–1871), Canadian	Mount St. Helens
Raden Saleh (1816–1880), Indonesian	Merapi 1865, Vesuvius 1839
James Hamilton (1819–1878) American	Vesuvius (Pompeii A.D. 79)
Frederic Edwin Church (1826–1900), American	Cotopaxi, Sangay, Chimborazo
Louis Remy Mignot (1831–1870), American	Cotopaxi
Archibald D. Willis, New Zealand	Tarawera (1886)
Albert Bierstadt (1830–1902), American	Vesuvius 1868
Degas, Edgar (1834–1917), French	Vesuvius 1890
Charles Furneaux (1835–1913), American	Kilauea, Mauna Loa 1881
Jose Maria Velasco (1840–1912), Mexican	Popocatepetl, Iztaccihuatl, Orizaba
Auguste Renoir (1841–1919), French	Vesuvius
Masayoshi Tokonami (1842–1897), Japanese	Sakurajima 1895
D. Antonio Munoz Degrain (1843–1924), Spanish	Vesuvius
Jules Tavernier (1844–1889), French	Kilauea 1887
D. Howard Hitchcock (1863–1943), American	Kilauea, Mauna Loa 1896
Charles H. Woodbury (1864–1940), American	Montagne Pelee
Seiki Kuroda (1866–1924), Japanese	Sakurajima 1914
Dr. Atl (Geraldo Murillo; 1875–1964), Mexican	Paricutin, Popocateptl
Asgrimur Jonsson (1876–1958), Icelandic	Laki, Grimsvotn
Hiroshi Yoshida (1876–1950), Japanese	Fuji
Kawase Hasui (1883–1957), Japanese	Fuji
Johannes Kjarval (1885–1972), Icelandic	Volcanic landscapes
Diego Rivera (1886–1957), Mexican	Paricutin 1943
Saturnino Herran (20th century), Mexican	Legend of volcanoes
Ruyzaburo Umehara (1888–1986), Japanese	Asama, Sakurajima 1935
David Alfaro Siqueros (20th century), Mexican	Volcanic eruption
Gudmundur Einarsson (20th century), Icelandic	Grimsvotn 1934
Ichien Somiya (1893–), Japanese	Sakurajima 1957
Alfredo Zalce (1908–), Mexican	Paricutin 1956
Misao Yokoyama (1920–1973), Japanese	Sakurajima 1956

continues

Continued

Artist	*Volcano*
Walter Womacka (1925–), German	Vesuvius
Matazo Kayama (1927–), Japanese	Sakurajima 1961
Andy Warhol, (1928–1987), American	Vesuvius
Emilia Cersosimo (1944–), Costa Rican	Arenal, Poas, Irazu
David Haste (contemp.), English	Etna
Robert Hawkins (contemp.), American	Surreal volcanoes
Gudni Hermannsson (contemp.), Icelandic	Surtsey 1963, Heimaey 1973
Bill Martin (contemp.), American	Imaginary volcanic landscapes
Sandra Del Valle (contemp.), Mexican	Myths of Popocatepetl and Iztaccihuatl
Roger Brown (contemp.), American	Mount St. Helens 1980
Bill Sullivan (contemp.), American	Cotopaxi
Wahru (contemp.), Indonesian	Galunggung 1982
Vaino Kola (contemp.), Finnish	Icelandic volcano landscapes
Beth Neville (contemp.), American	Volcanoes as metaphors of change
Dennis Bayuzick (contemp.), American	Volcano symbolism and surrealism
Mario Schifano (contemp.), Italian	Vesuvius
Tony Foster (1946–), English	Mount St. Helens, Soufriere Hills

sequence of the combustion of fossil fuels in the Earth. In contrast, many of the 17th century paintings of Vesuvius display details of eruption, pyroclastic surges and lava flows which indicate a high degree of understanding of the volcanological process, based on direct observation by an eyewitness.

The earliest visual representation of volcanic eruption dates to one of the oldest village cultures on Earth, which thrived on the Anatolian plateau in southeastern Turkey more than 8000 years ago. Excavation of this site, known as Çatal Hüyük, revealed a Stone Age town, with a long and rich cultural and artistic history, that flourished between 6500 and 5700 B.C. Numerous shrines found at the site attest to the development of religion and display a wealth of decoration, reliefs, and wall paintings. In their work the early artisans of Çatal Hüyük used rich colors and had a full range of pigments at their disposal, derived from a variety of minerals. They also manufactured fine artifacts of highly polished obsidian. A wall painting of an erupting volcano was found in one of the older shrines at a level carbon-14 dated to 6200 B.C. In the foreground is a group of domino-like rectangular houses, which represents the town, and in the background rises a twin-peaked volcano, ochre in color, and spotted with black dots, with an eruption spewing from the higher cone (see Fig. 3 in "Archaeology and Volcanism"). The eruption is portrayed as curved lines or spray above the crater, and the dots on the cone and outside its outline may represent falling volcanic "bombs" or large pieces of semiliquid lava. The lines emerging from the base of the volcano may represent lava flows. Today the plain surrounding Çatal Hüyük is indeed dominated by the twin volcanic peaks of Hasan Dag and Karaca Dag, and it is very likely that this ancient painting represents an eruption of Hasan Dag. It has been proposed that the painting had religious meaning, but several factors may have motivated the artist: perhaps it was a response to the threat from the erupting volcano, a work to appease the powers of the underworld? Was it inspired by gratitude to the volcano, the source of valued obsidian? A large number of obsidian spearheads and other implements have been found in the excavations, and it has been suggested that the town derived much of its wealth from the obsidian trade. Or was the painting simply inspired by fear in witnessing Earth's greatest display of power?

Most of the known examples of early Roman landscapes have been unearthed at Pompeii and Herculaneum, the cities buried by eruptions of Mount Vesuvius. These landscapes show a variety of views, natural forms, cultivated lands, wooded groves, streams and harbors, populated by shepherds, farmers, nymphs and other mythological figures. Several Roman wall paintings of Vesuvius have survived in houses excavated from the A.D. 79 volcanic deposits in Herculaneum and Pompeii. A painting from the lararium of the House of the Cente-

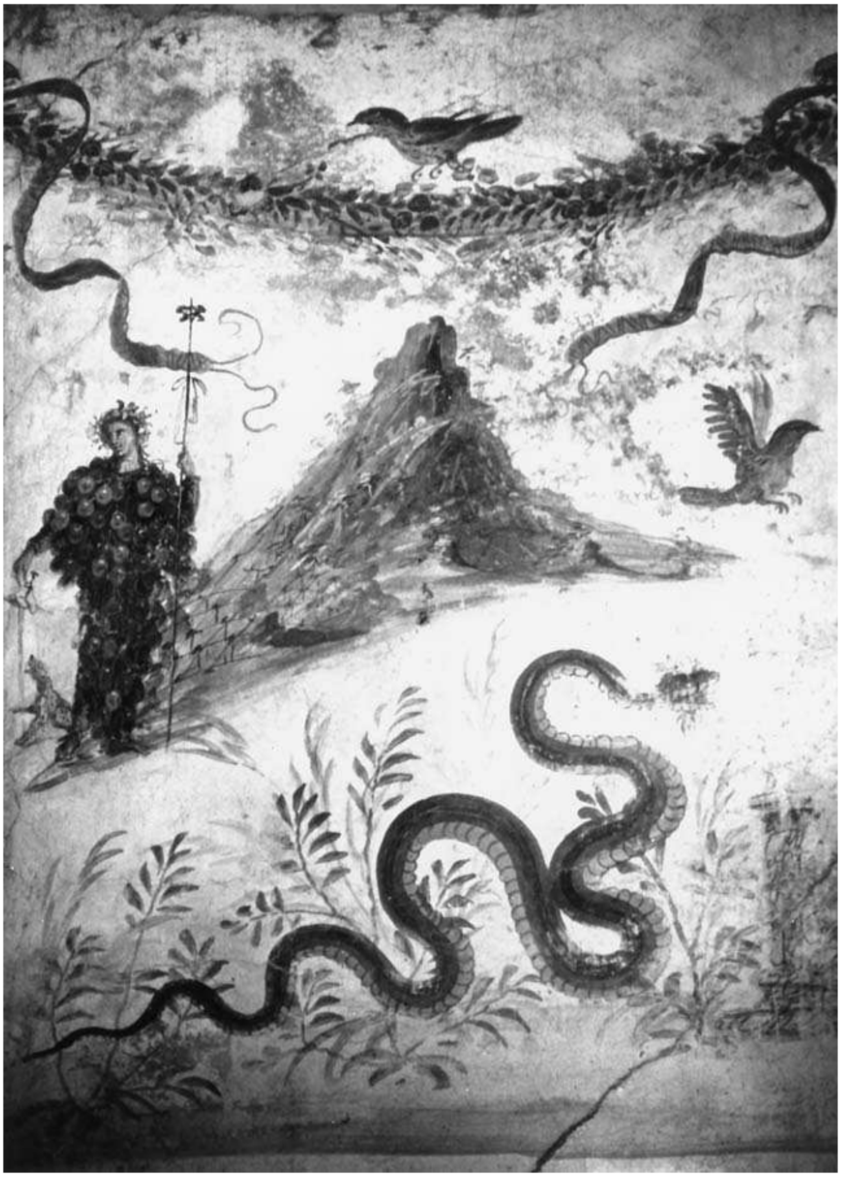

FIGURE 1 This is one of the oldest surviving paintings of a volcano, and it was preserved for posterity due to the volcanic burial of a city. Before the eruption of A.D. 79, Vesuvius was covered with forests, vineyards, and other vegetation up to the summit crater, as shown in this Roman wall painting, found in the House of the Centenary in Pompeii. The figure draped in bunches of grapes is the god Dionysus (Bacchus), and the snake represents the household gods. Archaeological Museum of Naples.

nary in Pompeii shows the steep volcanic cone as it appeared before the A.D. 79 eruption (Fig. 1). The mountain is covered in vinyards and other vegetation to the top. In the foreground stands Dionysus (Bacchus) clad in a mantle of grapes. Thus the few images which can be identified as Vesuvius show it as a benign mountain, its slopes covered with an abundance of the vines which thrive in the rich volcanic soil. Of course, these were painted before A.D. 79, but even after this time there is no evidence of a painter attempting to portray the awesome spectacle of the eruption. A violent eruption or any other catastrophe would be quite unsuitable as a wall decoration! Pliny Younger's vivid and stirring description of Vesuvius erupting would have to wait some 1700 years before its expressive, visual qualities could be appreciated.

During the Middle Ages, the only images associated with volcanoes are vivid, but symbolic pictures of flaming Hell, devils, and burning rocks found in illuminated manuscripts and frescoes. After 1400, with the Renaissance revival of classical culture, a new world view emerged as people began to examine the natural world around them and to consider mankind's place within it, but the first portrayals of a real volcano are not seen until around 1550. In Cesare Ripa's *Iconologia*, a handbook of symbolic personifications used by painters, "Sicily" is described as represented by a seated woman holding attributes that identify her as this particular island. Behind her is a representation of Etna volcano shown simply as a truncated, irregular pyramid topped by flames. This symbolic images does not attempt to show the actual appearance of Etna in particular or any volcanic eruption as observed in nature. A 1541 woodcut of Etna erupting in the *Cosmographia Universa* of Sebastian Münster indeed shows the volcano as icon (Fig. 2). The volcano, with the appearance of a block of wood, emits flames, with rounded boulders flying through the air, threatening the near-by town of Catania.

One of the earliest attempts at showing a more realistic view of Etna erupting was made in 1594 by the two Bolognese painters Annibale and Agostino Carracci, who decorated the Farnese Palace in Rome with fresco scenes representing moral actions taken from classical literature. In one scene, we see an erupting Etna in the background. In the foreground two young men flee from the flames and smoke, carrying their mother and father on their backs to safety. This story of the legendary Catanian brothers was intended as a moral allegory, for unlike the Catanians who attempted to save material possessions and perished, the brothers showed filial devotion by rescuing their aged parents. The primary subject of the painting is the moral action of the brothers, and the volcano is relegated to the background providing a reason for this heroic deed but stimulating little interest in itself. This portrayal of an eruption is unusual at this time, for neither Etna nor Vesuvius appear in a landscape for another 40 or 50 years.

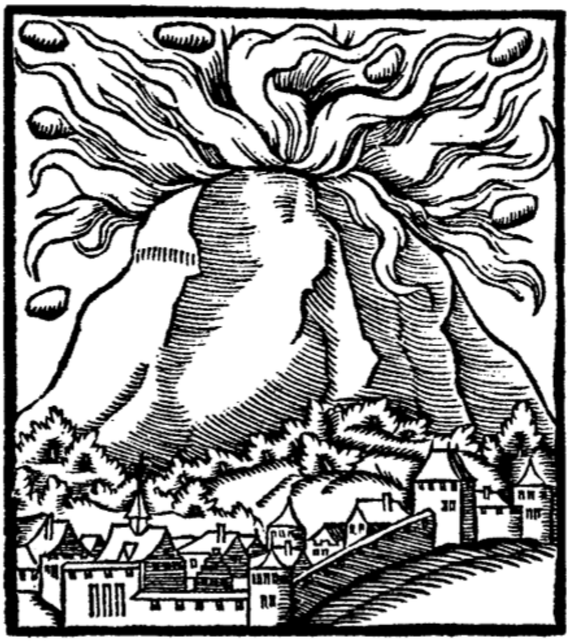

FIGURE 2 An eruption of Etna volcano, shown in a woodcut from the *Cosmographia Universa* of Sebastian Münster, from 1541 (author's collection).

Volcanic eruptions have been witnessed and described by mankind for thousands of years in many parts of the world, but it is mainly within the past 300 years, since the Renaissance, that the subject has appeared in the visual arts. In fact, most paintings of volcanic activity have been produced only since the latter half of the 18th century when the birth of scientific investigation and systematic observation of the workings of nature stimulated an interest in unusual and marvelous phenomena, which most people would never actually see in their own lives. Before artists could represent volcanic eruptions and the human reaction to them, they had to create a visual vocabulary for such depictions. It was therefore necessary to invent an iconography of volcanoes, which until the 18th century had rarely been seen in painting. Volcanoes were not part of the standard schema for landscape painting, which had developed during the Renaissance. Most European artists would have been totally unfamiliar with the appearance of an eruption. Furthermore, volcanoes had no place in the range of conventional subjects of the arts: Biblical scenes, mythological themes and genre, that is, views of common folk at work or play.

The European exploration of distant lands, such as the East Indies in the 16th century, revealed many new volcanoes, whose topography and eruptions were at times documented in art. Such is the case with the early 17th century eruption of Gunnung Api in the Banda Islands in Indonesia (Fig. 3).

III. VESUVIUS 1631 ERUPTION

In 1631 Vesuvius erupted with a violence it had not demonstrated since ancient times. This catastrophe

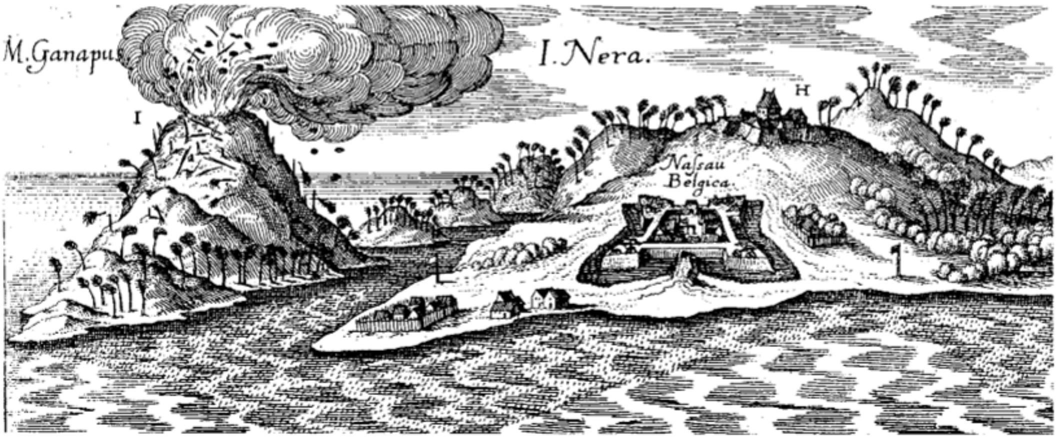

FIGURE 3 Engraving from 1631 of an eruption of Gunnung Api volcano in the Banda Islands in the South Moluccas. An early 17th century example of the representation of a volcanic eruption (author's collection).

killed over 4000 people and devastated the population of Naples, as has been recorded in several vivid eyewitness accounts. The event is described not only as frightening but also spectacular to see. By this time, Italian artists had developed a full range of techniques for portraying landscape images with convincing naturalism, and there are several pictorial records of this eruption. As a result of this eruption, a new interest and direction in the depiction of volcanic eruptions arises in the 17th century. Rather than purely documentary or religious, the volcano itself becomes the focus as a powerful, aweinspring phenomenon. A sketch by Filippo D'Angeli shows a view of the 1631 eruption from the harbor, with people fleeing, and a lightly rendered view of Vesuvius with line suggesting flames and lava (Fig. 4). The main focus of the drawing, however, is Saint Gennaro (St.

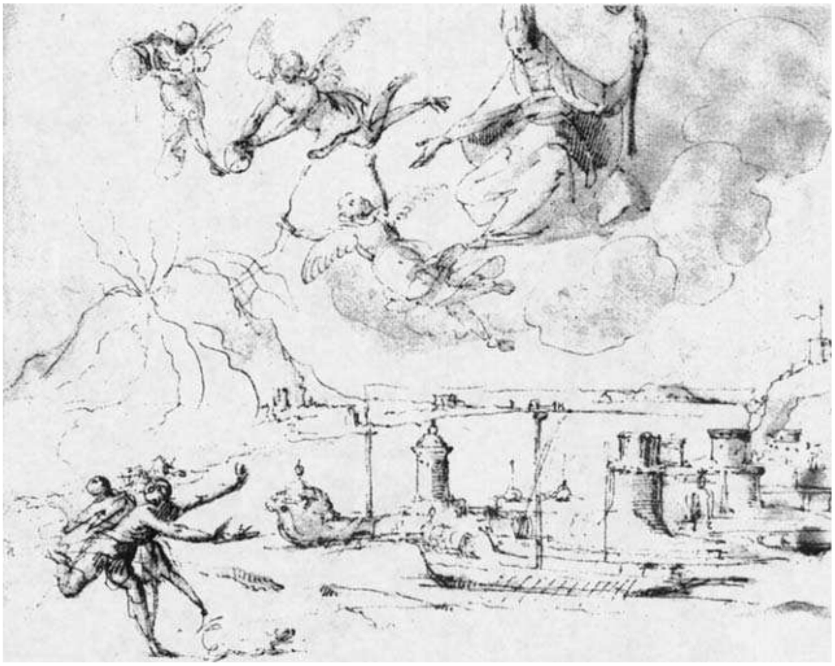

FIGURE 4 As seen by the contemporary Neapolitan artist Filippo D' Angelo, the 1631 Vesuvius eruption brought out Saint Gennaro, the patron saint of Naples, and his helpers, serving as a fire brigade, but the eruption also caused panic among the citizens. Janos Scholz collection, Pierpont Morgan Library, New York.

Januarius), the patron saint of Naples, in the heavens. Januarius gestures toward Vesuvius while three angels pour down water in an attempt to quench the flames. In essence, this is still a symbolic representation expressing the hope of averting the eruption, rather than recording its spectacle. The image of the saint is unremittingly tied to the volcano, and the saint's duty, in the eyes of the populace, is to avert volcanic catastrophe. If the saint fails in his duty, the people may take strong measures, which include attacking the images of the saint himself. During the unusually violent Vesuvius eruption of 1872, the people of Campania felt totally abandoned by the patron saint, and attacked the statue of Saint Gennaro in anger (Fig. 5). A detailed and finished contemporary view of the 1631 disaster can be seen in a painting by Micco Spadaro, who also witnessed this eruption. A city square is shown from above to display the crowds in a procession, to invoke the protection of St. Januarius whose relics are carried by the clergy. The saint and angels can again be seen hovering in the clouds,

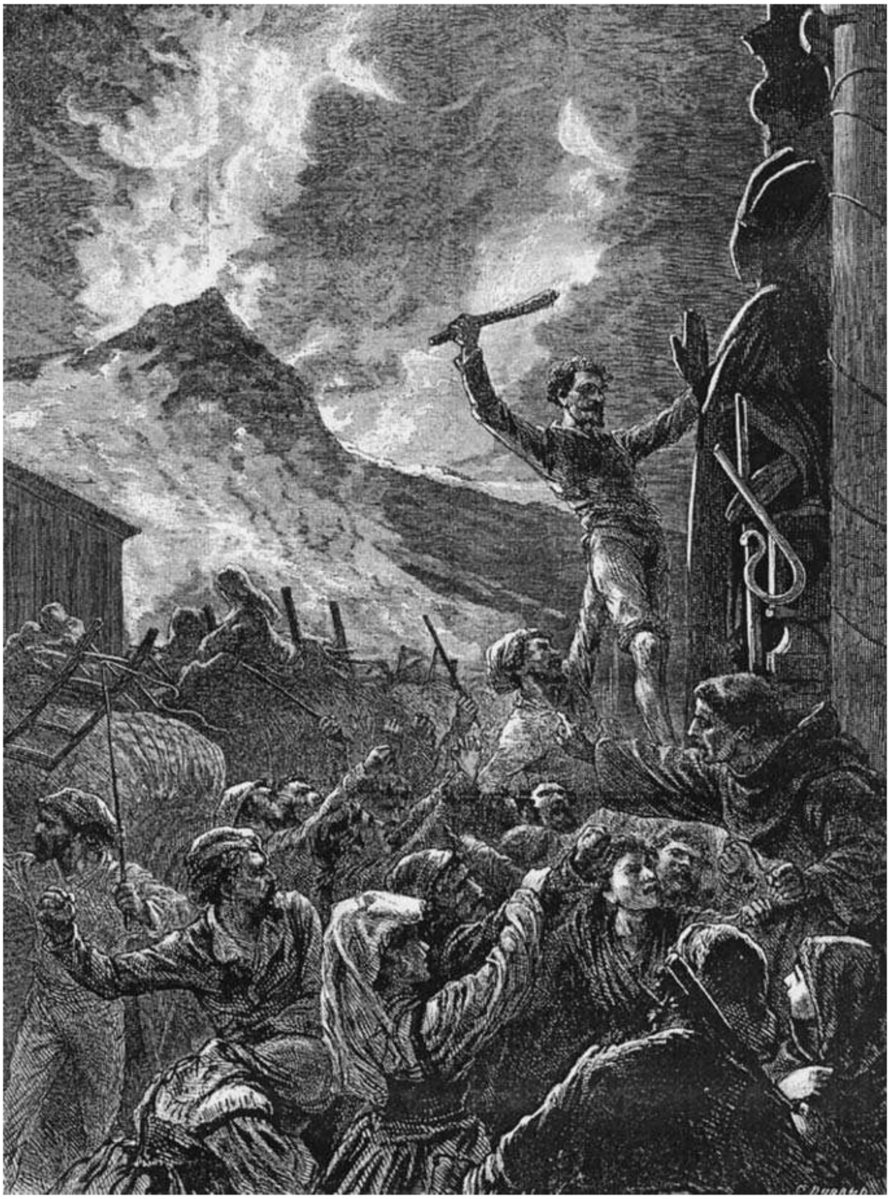

FIGURE 5 The Neapolitan population attacking the statue of Saint Gennaro, patron saint of Naples, when their appeals to the saint failed to stop the April 1872 Vesuvius eruption (*Harper's Weekly,* June 1872).

while in the distance Vesuvius belches forth flows of ash. Another contemporary artist, Scipione Compagno also painted two views of the eruption, which focus more on Vesuvius itself. What is particularly interesting in these paintings is the phenomenon of ground-hugging surge clouds, that sweep down the slopes of Vesuvius—a process that these artists clearly witnessed. If the early 20th century volcanologists had only bothered to look at these paintings, they would have appreciated that the deadly phase of the eruption was associated with surges and pyroclastic flows and not with mud flows.

IV. EMPEDOCLES LEAPS INTO ETNA

A remarkable volcanic painting by the Neapolitan painter Salvator Rosa also dates from this time. It portrays the Greek philosopher Empedocles hurling himself into the flaming crater of Etna in order to commit suicide (Fig. 6). According to ancient legends he had done this so that the followers of his philosophy would believe he had disappeared from Earth and thus gained godlike immortality. The truth became known when the philosopher's followers found one of his sandals at the crater's edge. Rosa's Empedocles hurtles headlong into the turbulent, steaming crater, his fluttering robes and outflung arms echoing the shapes of the rocks and clouds. He seems to merge with the volcano, a small man lost in the immensity of nature's turbulence. Painting toward the end of his life, in 1666, Rosa, who was something of a poet and philosopher as well as painter, intended the volcano as a metaphor for uncontrolled creative inspiration which can overwhelm the artist. Although he took the idea from a poem by Horace, this is the first time the image appears in painting. The volcano has taken on new meaning, and its violent spectacle, unpredictability, and deadly might are exploited for their aesthetic qualities. The idea that an eruption, even while destroying life, could contain beauty worthy of artful speech or painting was developed by Rosa and others in the 17th century, and it helped to create a taste for the marvelous, unusual, and awesome in nature. The style that captured these qualities was termed the sublime, that which was great and inspired feelings of awe, fear, and amazement in the spectator.

In a treatise on the art of painting published in 1715 by Jonathan Richardson, the superiority of visual expression over verbal description was exemplified by an eruption of Etna. The poets since classical times had described eruptions, but how much more effective a picture could be when the whole scene opened up at once! The taste for the sublime became most popular in England after the 1757 publication *A Philosophical Enquiry into the Origin of Our Ideas of the Sublime and the Beautiful* by Edmund Burke. He defined the "beautiful" as something that is well-proportioned, graceful, smooth, clear, quiet, and harmonious, a prospect which elicits an emotional response of calm, security, and joy. In striking contrast Burke's "sublime" contains darkness, noise, overwhelming magnitude, stenches, and sudden danger that evokes emotions of terror, fear, and pain. This notion suggests an earthquake, terrible storm, or a volcanic eruption as an ideal sublime image and experience filled with the sights and sounds of uncontrolled forces, immensity, darkened skies, stinking fumes, harsh lights,

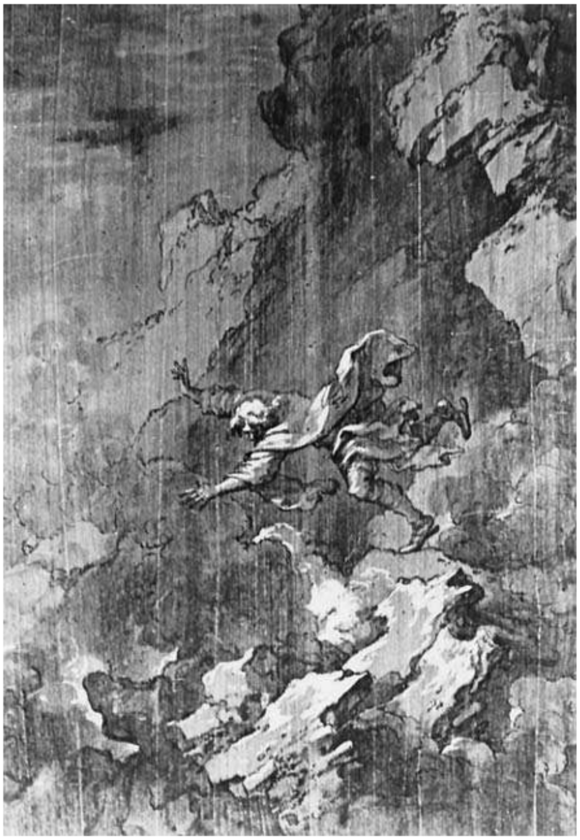

FIGURE 6 Empedocles leaping into the crater of Etna. The Greek philosopher Empedocles lived in Sicily and studied the activity of Etna. He had novel ideas about volcanic activity, but legend has it that he took his life by secretly jumping into the crater of Etna, in order to convince his pupils that he had ascended to heaven. Brown ink and chalk drawing by Salvator Rosa, ca. 1666 (Galleria Palatina, Palazzo Pitti, Florence).

burning, and perhaps death. The sublime is not seen as the opposite of the beautiful, but as an alternative aesthetic taste. This taste soon became widespread among the cultured, art-loving classes, an audience now attuned to seeing the terrifying as pleasing—and for them a volcanic eruption was the ultimate sublime experience.

V. THE NEAPOLITAN SCHOOL

From the middle of the 18th century, the subject of Vesuvius in eruption became increasingly popular in painting, gouache, and prints. These were frequently produced as souvenirs for the English, German, and French gentlemen and ladies who came to Italy on the Grand Tour, a highlight of which was a visit to Naples and Vesuvius. Luckily for the travellers, Vesuvius became very active once again and was in frequent eruption from the 1730s through the end of the century. It was a great tourist attraction for those who could safely view the fiery lava and clouds of smoke from a distance, a scene they would later recall back home in London or Paris—where they could share their sublime experience with friends through these colorful works of art.

Claude-Joseph Vernet arrived in Naples in 1734, where he had a profound and pioneering influence on the painting of Vesuvius, establishing a formula for the representation of its eruptions. In his numerous works, the fiery glow of molten lava is shown silhouetted against the night or ash-darkened sky, with the steely blue cool light of the moon in strong contrast. In the foreground, relatively tiny human figures gesticulate toward the eruption in a mixture of wonder, terror, and admiration. Many contemporary artists adapted this scheme of volcano painting, such as the English Joseph Wright of Derby, the German Jacob Phillip Hackert, the Austrian Michael Wutky, and later the Norwegian Johann Christian Dahl. Vernet's most prominent pupil, Pierre Jacques Volaire, stayed in Naples for 20 years and established himself as Vesuvius' visual biographer. His painting of the *Eruption of Vesuvius in 1771* epitomizes this genre. He plays the burning red against the ice cold blue, a fiery lava fountain illuminates red clouds of steam and a river of molten lava contrasts with the silvery moonlight and the tranquil Bay of Naples on the other side. In earlier times Vesuvius, the powerful, earth-shaking giant, might have been represented as a Cyclops at the forge, a fiery, muscular figure, but now the mountain itself takes on the characteristics of sublime beauty. The dark side of Nature had become worthy of portrayal, and these artists arranged their compositions and choice of colors to convey both the actual appearance as they observed it and the dramatic artistic effects. No longer does St. Januarius hover protectively over Naples; now the figures are excited spectators who study and enjoy the phenomenon.

Natural catastrophes and landscape were among the subjects which were considered potentially sublime in late 18th century painting in Europe. In no subject matter, however, did the catastrophic possibilities become as manifest as in the painting of volcanic eruptions, as was demonstrated by the paintings by Joseph Wright of Derby of the eruptions of Vesuvius. Wright had climbed the volcano in 1774 and witnessed its eruption, and his pictures of this subject are startling for their vividness of colors and tumultous movement of the volcanic emissions. His views of the volcano were both at the very edge of the crater, from within the crater, or from a great distance, such as in *Vesuvius from Posillipo*, creating scenes that were almost too intense to be natural. One of the paintings of Vesuvius from this time, and most pleasing to modern taste, is a gouache study of 1774 by Wright of Derby. The reddened mountain and billowing gray smoke are made in a sketchy, soft manner with emphasis on the color and shapes. Here there are no small fleeing figures or scientific observers but simply the volcano in splendid isolation.

The German artist Jacob Philipp Hackert was also attracted to Italy by the strength of the 17th century Roman landscape tradition. He became the court painter for King Ferdinand IV in Naples, where he had ample opportunity to paint Vesuvius in action. Many of his views of Vesuvius erupting are remarkable because of the close-up of the volcano in action and are closer to a geological study than most other paintings of the mountain, in particular his painting of *The Eruption of Vesuvius in 1774* (Fig. 7). This emphasis on scientific process may have been influenced by Hackert's close association with the pioneer volcanologist William Hamilton, also a resident of Naples.

VI. NEOCLASSICISM

When Herculaneum was discovered out of the ashes of Vesuvius in 1709, and Pompeii in 1748, European artists became fascinated by the great eruption of A.D. 79 and by the cities which had been buried in layers of ash, as well as the newly revealed classical culture. The recovered buildings and artifacts quickly promoted a taste for classical styles in furniture, clothing, and art, and the evidence of the inhabitants's swift deaths, and the immensity of destruction further stimulated fascination with the sublime. Paintings which depicted scenes of this ancient catastrophe were now made, along with the landscapes of Vesuvius as it looked in modern times.

In 1785 the Swiss painter Angelica Kauffman made a painting based on the events of 24 August A.D. 79 as described by Pliny Younger (Fig. 2 in "Introduction"). The young Pliny and his mother are shown in the courtyard of their villa at Misenum where a friend urges them to flee before it is too late. In the distance, framed within the archway of a gate is Vesuvius, an outline on the horizon shooting forth lava, pumice, and ash. The sky is dark and the waves on the usually calm sea are agitated. The only suggestions of sublime emotion here are the expression and gestures of the two frightened women on the steps down to the sea. The painting has the cool, detached crispness and clarity typical of Neoclassicism. The artist has recreated a historical moment in which the human figures dominate, rather than the volcano.

A more emotional version on the subject of the A.D. 79 eruption of Vesuvius can be seen in a spectacular painting by Pierre Henri de Valenciennes in 1813. Now in the Romantic era, the sublime becomes even more powerful through emotional and imaginative imagery to emphasize the horror of the moment in the appearance of the sky, brilliant color, and small-scale figures. Valenciennes also used Pliny's letters as a source, in a scene where his uncle Pliny Elder is carried by two slaves as he succumbs to choking clouds of fumes issuing from the volcano. This subject had been painted as early as 1780 by Jacob More in *Mount Vesuvius in Eruption: The Last Days of Pompeii*, but the subject became increasingly popular through the 19th century in many versions that stressed the physical agony, fear, and other sublime emotions in romanticized paintings. This was especially true after the 1834 publication of Bulwer-Lytton's tremendously popular novel *The Last Days of Pompeii.* Vesuvius in eruption was interpreted as divine retribution for wicked mankind; corrupt civilization was contrasted with the purity of nature.

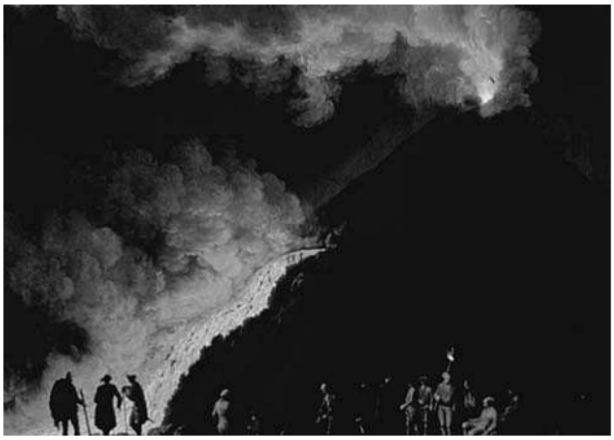

FIGURE 7 *The Eruption of Vesuvius in 1774* by the German artist Jacob Philipp Hackert (1737–1807), the court painter for King Ferdinand IV in Naples. The painting is an unusual close-up view of an erupting volcano, with pioneer volcanologists clambering right up to the vent on the volcano's flank to get a closer look. The Hessen State Collection, Germany. (Also see color insert.)

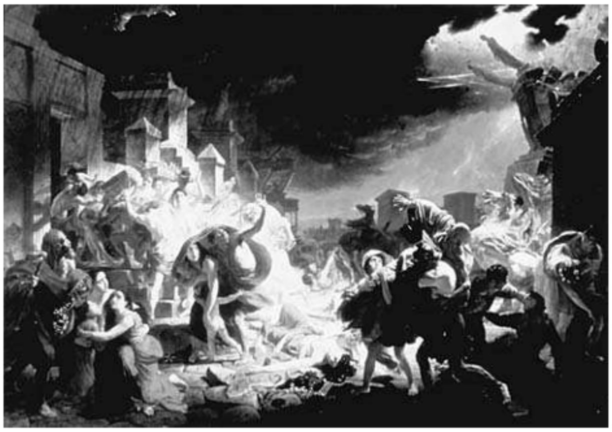

FIGURE 8 In 1832 the Russian artist Karl Briullov painted *The Last Day of Pompeii,* a representation of the catastrophic 79 A.D. eruption and its effects on Pompeii. It is the quintessential example of Neoclassicism, with Greek and early Roman architectural and physical forms juxtaposed to the terror of the volcanic eruption. The State Russian Museum, St. Petersburg. (Also see color insert.)

In 1833 the Russian artist Karl Briullov painted a huge composition titled *Last Day of Pompeii*, which was inspired by the opera by Pacini: *Ultimo giorno di Pompeia*, performed in Naples 1827. Briullov had visited the excavations of Pompeii, and the sight of the city buried by layers from the great A.D. 79 eruption astounded the artist. He became captivated by the idea of sudden interruption of life by this great natural catastrophe. Briullov made many sketches of the composition and then began a study of historical documents of the excavations of Pompeii as well as Pliny Younger's description of the A.D. 79 eruption, in order to create authenticity and to follow the Romantic principle of historical truth (Fig. 8).

VII. TURNER'S FIRE

By far the most notable artist to paint volcanic eruptions was Joseph Mallord William Turner (1775–1851).

Turner was the greatest British painter of his age and probably the greatest painter England has ever produced. He was both by training and inclination a true landscape painter in the tradition of the picturesque sublime, and his choice of subject matter included apocalyptic and catastrophic topics. He had a brilliant gift to translate onto canvas the most fleeting effects of light, such as a passing storm, sunrise, or dissolving mist. In 1817 Turner painted *Vesuvius in Eruption*, creating a work that has a sense of volcanic energy and the spectacle of light that is unique to this artist. However, Turner's basic treatment of the eruption follows the 18th century formula: a white to red-hot fire fountain out of the central cone, reflected on the Bay of Naples, a cool blue-gray sky with a crescent moon in the background, contrasting with the conflagration around the volcano. Lightining and the arched trails of glowing volcanic bombs are shown by generous use of a scraping-out technique.

Turner's earliest painting (1815) of a volcanic eruption is *The Eruption of the Souffrier Mountains, St. Vincent.* In April 1812 the Soufriere volcano on St. Vincent in the Caribbean erupted explosively. The eruption resulted in ash fall on the island of Barbados to the east and produced deadly hot ash flows down the flanks of the volcano. The eruption blasted out a new crater in Soufriere's summit and killed many of the Carib Indians living on the volcano's slopes. News of the eruption spread with the British colonialists to England, and these reports stimulated Turner to put his impression of this volcanic eruption on canvas. Turner wrote these lines in the catalogue published at the first Royal Academy showing in 1815:

> *Then in stupendous horror grew*
> *The red volcano to the view.*
> *And shook in thunders of its own,*
> *While the blaz'd hill in lightning shone,*
> *Scattering their arrows round.*
> *As down its sides of liquid flame*
> *The devastating cataract came,*
> *With melting rocks, and crackling woods,*
> *And mingled roar of boiling floods,*
> *And roll'd along the ground.*

In 1815 another volcanic eruption occurred in far-off Indonesia which may have influenced Turner's art in a fundamental way. The volcano Tambora erupted in 1815, lifting into the atmosphere more ash and volcanic gases than any other eruption in history. The atmospheric effects of the eruption included spectacular twilights of yellow and red skies in the years following the event. Turner undoubtedly experienced this marvelous coloration of the skies caused by the aerosols or fine particles injected into the atmosphere after the eruption. Is it possible that Turner's fiery skies, for which he is so justly famous, were in this way inspired by the effects of a distant volcanic eruption of which he was unaware and would never hear of in his lifetime?

VIII. HOKUSAI AND THE SPELL OF FUJI

At the time when Turner was executing his rich paintings of Vesuvius, there was at work in Japan an artist gifted with extraordinary powers of draftmanship and design, who devoted much of his career to the imagery of Fuji volcano near Tokyo. Like Turner, Hokusai was the most eccentric of men and dedicated to his art with the passion and singlemindedness of a saint to his religion. Hokusai, like Minsetsu, Hiroshige, and other Japanese artists, was drawn to Fuji volcano, not because of its spectacular eruptions, but because of the veneration and idolatry for the volcano by the Japanese people. From 1823 to 1829 Hokusai created *Thirty-Six Views of Fuji*, often regarded as among his finest landscapes. The series of landscape colorprints includes the incomparable *Fuji in Clear Weather.* Here the calm selection of lines and graduation in colors bears the imprint of the woodblock printer's art (Fig. 9). In 1834–1835, he published another set of prints entitled *One Hundred Views of Fuji.* The earlier 36 landscapes are dwarfed by the eternal and monumental cone of Fuji, which hints at the transitoriness of human life. Is it the gentle curve of the cone, with its near-perfect geometric form, sweeping the eye to the sky, which has led to Japanese idolatry of this volcano? Or was it based on fear because of the history of Fuji's deadly eruptions? The phenomenon is outside our western experience, and thus we miss some of the special significance that Houkusai's views of Fuji have for his countrymen. Already in the eighth century, Fuji was revered with superstitious awe, as shown for example in Manyoshu, one of the earliest poems of the Japanese language:

> *No words may tell of it*
> *No name know I that is fit for it*
> *But a wondrous deity it surely is!*
> *It is the peace giver, it is the god, it is the treasure.*
> *On the peak of Fuji, in the land of the Suruga*
> *I never weary of gazing.*

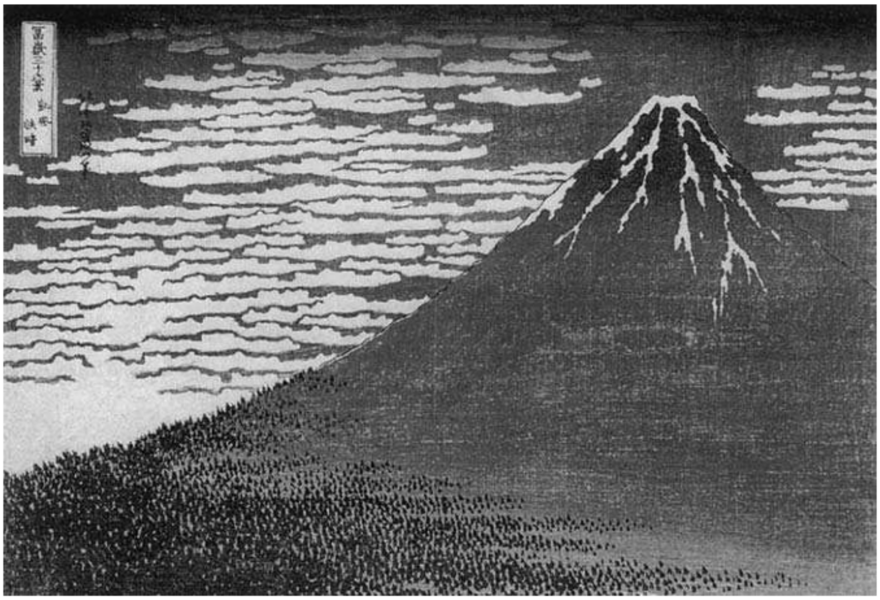

FIGURE 9 *Fuji in Clear Weather.* Color woodcut by the Japanese artist Katsushika Hokusai (1760–1849). From the series *Thirty-Six Views of Fuji,* ca. 1830.

In the later 100 views, the curious and unexpected glimpses of Fuji, reflected in the sake-cup held by a tippler or seen through a bamboo thicket, transmute the ordinary into the memorable.

To my knowledge, Hokusai only executed one picture featuring a volcanic eruption, which is *The Upthrow of Mount Hoei* in his great book of woodblock prints *One Hundred Views of Fuji* published in 1834. In the winter of 1707, the great volcano exploded in one of the largest eruptions of the historical period. In this flank eruption, Fuji created a new cone or "hump" on the slope of the volcano that was named Hoei. In the woodcut *The Upthrow of Mount Hoei* Hokusai lets his imagination run free in what is an image of the effects of the eruption on the people and an utter demolition of their world (Fig. 10). The plate shows the terror the eruption and its associated earthquake created among the villagers living near the volcano. Rocks and stones are hurled from the new crater and showered down in destructive abundance over the village. Men, women, and children are tossed about the air, together with the debris of their ruined homes. Some villagers try to escape, dragging after them their fainted wives. The terrible eruption has created panic, destruction, and despair among the helpless folks. Fuji itself is not to be seen in this picture of chaos, but its effects are devastating. In the woodcut *Sono ni* in the same volume, Hokusai shows us the quiet volcano after the eruption (Fig. 11). The great eruption of 1707 did not occur from the central crater but rather from a lateral vent on the southeast slope of the volcano, forming Hoeizan, an unsightly lump on the otherwise perfect profile of Fuji.

Hokusai's colorprints achieved a compromise between representation of actuality on one hand and creation of an abstract design in color and line. His style of brushwork was consistent with the highest ideals of Japanese calligraphy. Hokusai's prints lie between two opposing styles—the Japanese ancient Edo school, suggesting a landscape of the imagination, and the school of Western landscape artists, approaching as near as the oil or water color mediums will allow to a realistic representation of a certain place. His work had significant influence upon Western art in the direction of a new formalism and simplification (e.g., in the French Impressionists). Hokusai's work was, however, most influential in Western book illustration and design.

A large number of other Japanese artists, who had mastered the color woodblock, were captivated by Fuji, including Keisai Eisen (1790–1848), Utagawa Hiroshige (1797–1858), Hiroshi Yoshida (1876–1950), and many others listed in Table I. In addition to Fuji, another volcano has received much attention among Japanese artists, particularly in the 20th century. This is Sakurajima in Kagoshima Prefecture in south Japan. Early studies of this volcano are shown in the oil paintings of Masayoshi Tokonami (1842–1897), who was a pioneer in making the transition from Edo style painting to a more modern form of Western painting. Seiki Kuroda (1866–1924) also painted a number of works showing the 1914 eruption, which he witnessed. The dramatic Sakurajima landscapes of Ryuzabnuro Umehara (1888–1986) are Impressionistic works, but he studied under Renoir in France and was acquainted with Picasso. He successfully fused the traditions of Japanese and European painting, and his Sakurajima works brought Japanese art into another phase. Ichien Somiya (1893–) painted a close-up of the Sakurajima crater during the 1956 eruption. Perhaps the most striking works of Sakurajima is the 1961 painting *Island of Fire* by Matazo Kayama (1927–), where a modern approach to Japanese painting is combined with a traditional sense of design that turns the volcanic landscape into a fantastically designed fabric screen.

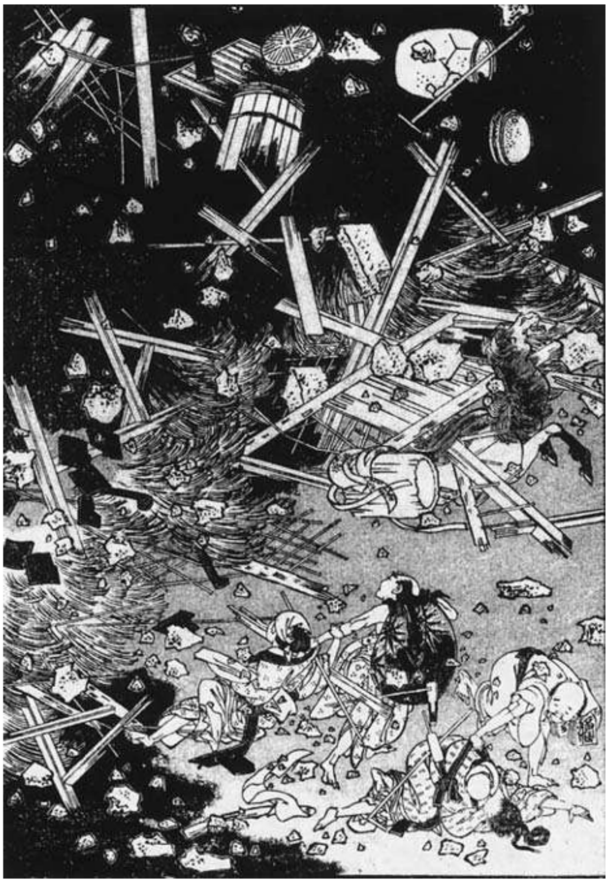

FIGURE 10 *The Upthorw of Hoei.* Woodcut by the Japanese artist Katsushika Hokusai (1760–1849), showing the effects of the 1707 eruption of Fuji on the local people. From the series *One Hundred Views of Fuji,* ca. 1830.

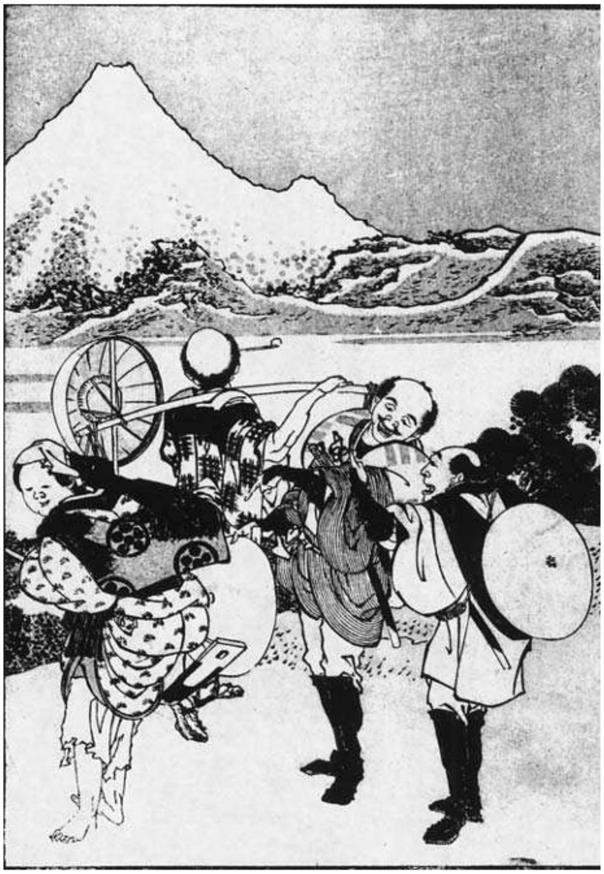

FIGURE 11 In the woodcut *Sono ni* Hokusai shows the changed profile of Fuji after the 1707 eruption, which took place from a lateral vent on the southeast flank of the volcano and created the cone of Hoei.

IX. AMERICAN EXPLORATION OF UNKNOWN VOLCANOES

With the opening of the American continent in the 19th century came the discovery of new worlds, which included volcanic mountains greater and more terrifying than any of the European experience. In the 1840s, a young Canadian artist, Paul Kane, was employed by the Hudson Bay Company to aid in the documentation of the Pacific Northwest. During his travels, he stumbled upon Mount St. Helens volcano, which he represented in a series of paintings, mostly in vigorous eruption. In the painting *Mount St. Helens Erupting,* Kane shows a fiery strombolian-like fountain rising out of a crater on the north flank and a dark eruption cloud billows away from the eruption column, watched by awestruck Indians in a canoe. The eruption site appears to be the Goat Rocks dome, a parasitic vent on the north flank, which was about 2000 feet lower than the summit of Mount St. Helens. Today there is no trace remaining of Goat Rocks: the entire north flank of the volcano was completely obliterated during the explosive eruption on May 18, 1980. Although Kane's view appears to be accurately observed and was intended as a scientific record, it is composed using the conventional formulae for the depiction of volcanoes that had developed during the 18th century in conjunction with Vesuvius. He shows the darkened sky, the silhouetted volcano, the fiery reflection on the water, and the small foreground figures who react with expressive gestures.

The most prominent American artist in the early 19th century belonged to the Hudson River School, which still contained residual elements of European influence. Thomas Cole (1801–1848) was the father of the Hudson River School of painting and one of the leading figures in the development of a national tradition of American art. His work was a mixture of devotion to natural scenery on one hand and illustration of moral truths on the other. Gradually, however his natural landscape themes gave way to the moral and allegorical themes and strong religious influences.

Several American landscape painters of the 19th century chose volcanic eruptions as subjects for painting, and Thomas Cole painted *View of Mt. Aetna* in 1844. The development of tourism as an aspect of leisure and education may have had a profound and stimulating effect on appreciation of landscape painting in America in the early 19th century. The appreciation of the wilderness grew with the developing middle class and urban elite, and people sought pleasure through tourism and developed a demand for views of the familiar and picturesque landscape. Cole, as one of the greatest landscapists in North America, was perfectly suited to meet this new demand, when fine art was becoming popular in the emerging American culture at large. Cole was the first American artist to tackle the wilder and untamed features of the scenery of American mountains. By 1825, his Romantic pictures of the Hudson Highlands and the Catskill Mountains had received attention, particularly because of their sublime representation of American mountain tops and inaccessible peaks.

Cole was a close friend of the geologist Amos Eaton, and Cole was also acquainted with the pioneer American geologist Benjamin Silliman. It is likely that Cole's interest in volcanoes may have been influenced by these friendships. Cole spent several years in Italy, including an extended stay at the foot of Vesuvius volcano in 1832. He ascended Mount Etna volcano in Sicily in 1842, but the ascent of the volcano took a strong hold of Cole's imagination and formed the subject of four pictures. The famous painting of Mount Etna from Taormina took 5 days to paint. It was then sold for $500 to the Hartford Lyceum, which was "pretty good for five days work," as Cole stated in a letter to his wife. The painting produces the effect of a huge and lofty mountain, whose summit is white in perpetual snow, while its slopes below are basking in perpetual summer. In this distant view from the northeast, a gentle steam plume rises from the main crater, and the northeast crater is also visible on the upper slopes. The height and steepness of the top cone are exaggerated in this painting to attain the sublime effect.

In the early 19th century, biblical ideas of a volcanic judgment day appear frequently in American poetry and art. In 1828, Cole painted the *Expulsion from the Garden of Eden*, where he introduced the more terrible objects of Nature including a volcano in violent eruption. Here Adam and Eve leave the sunlit paradise, to enter desolation and darkness, with all the elements raging against them—including a volcanic eruption towering overhead. Cole had not yet seen a volcano at this stage but borrowed the image from the conventional view of an eruption of the time.

The work of many early 19th century American artists reflects a viewpoint and a social evolution that has been referred to as Manifest Destiny—the Euro-American dream of discovering, exploring, and conquering an unspoilt and undeveloped terrain, toward creating an authentic American civilization. The works of Cole and his brilliant disciple Frederic Church reflected this spirit. Frederick Edwin Church (1826–1900) was a central figure in 19th century American landscape painting and prominent in the group of artists associated with the Hudson River School. But he was first and foremost an adventurer–explorer artist. As a former pupil of Thomas Cole, Church received the mantle of American landscape painting from the master who had carried it for an entire generation.

Church replaced the subjectivity of his romantic teacher with an objectivety perceived by a mind steeped in geology. He was particularly influenced by the writings of the great German geographer Alexander von Humboldt whose descriptions of South American volcanoes drew Church on his first expedition to Cotopaxi in 1853. Church was, however, primarily a product of the golden era of prosperity and cultural nationalism just before the Civil War, the years of Manifest Destiny, which fostered a New World authentic movement of painting and heroic art. Taken to its extreme, the faith of Manifest Destiny was the faith that natural history had dictated Anglo-Saxon domination of the great American continent and regeneration of the whole world. Thus Church's art was premised on the Grand Design that the Creation existed for man.

Church's famous volcano painting *Cotopaxi* (1862) was painted early in the Civil War and dramatizes the struggle between the forces of darkness, represented by the belching volcano, and the forces of light. This work resulted from Church's travels to South America in 1857, when he was at the base of Cotopaxi volcano in Ecuador. In his painting *Cotopaxi,* he invokes the moment of creation itself. It is painted with the fidelity of a naturalist, yet the style suggests Earth's terrible power and Mankind's insignificance. His monumental South American scenes started with the *Heart of the Andes* in 1859. They attempt to combine into a single colossal scene the geological, meteorological, and botanical history of the continent, and his volcanic paintings metaphorically suggest a new world in the making. On his second journey to South America in 1857, Church made a trip to Sangay volcano in Ecuador. Traveling in the pathless wilderness of the high Andes mountains, Church ascended a ridge to obtain a view of the volcano, which rewarded him with a series of explosions:

> *Above a serated, black, rugged group of peaks which form the crater, the columns arose, one creamy white against an opening of exquisitely blue sky, delicate white, cirrus formed, flakes of vapor hung about the great cumulus column and melted away into the azure. The other, black and sombre, piled up in huge, rounded forms cut sharply against the dazzling white of the column of vapor and piling up higher and higher, gradually was diffused into a yellowish tented smoke through which would burst enormous heads of black smoke which kept expanding, the whole gigantic mass gradually settling down over the observer in a way that was appalling.*

This experience resulted in his painting *Distant View of Sanguy Ecuador.*

The great public following and admiration for the landscape works of Church and other American artists went into rapid decline in the late 19th century for reasons that can be attributed to an advance in science. By the 1880s, the Scientific Revolution sparked by Darwin's world-shaking theory of evolution had triumphed in the intellectual world. The concept of the Grand Design was shattered, and man's place in nature shifted from the heroic to the unheroic. Church was one of the victims of this revolution, and by the 1990s his work was all but forgotten.

Albert Bierstadt (1830–1902) was one of the artists who discovered the grandeur of the American West and was the principal rival of Frederic Church. He became well known for his paintings of the spectacular mountainous vistas of the Rocky Mountains. Bierstadt's interest in volcanoes was kindled when he visited Naples in 1857 and climbed Vesuvius, resulting in the painting *Mount Vesuvius and the Bay of Naples.* His second treatment of the subject was painted in 1868, showing the volcano in full eruption, as seen from the upper slopes of Vesuvius, northwest of the crater, in a gaudy, almost fluorescent view.

X. HAWAIIAN ERUPTIONS

The painting of Hawaiian volcanoes begins with the visit of Robert Dampier to Hawaii in 1825. Another important interpreter of Hawaii's volcanoes was Titian Ramsay Peale, son of the noted American painter Charles Willson Peale, who painted the famous portrait of George Washington. The younger Peale traveled widely and was selected to participate as an illustrator in the U.S. Exploring Expedition of the South Seas (1838–1842) under the command of Lieutenant Charles Wilkes. On the fleet of six ships were a large number of naturalists and scientists, who collected a wealth of specimens which were returned to Washington, DC, and formed the nucleus of the National Museum of the United States in the Smithsonian Institution. One of the scientists on board was the American geologist James Dwight Dana. In September 1840, the expedition reached Hawaiian waters and remained near the volcanic islands until April 1841. A major eruption of Kilauea volcano had partly filled in the caldera with lava in 1839, which solidified to form the Black Ledge. During their climb on the flanks of Mauna Loa volcano, Peale sketched a view of the distant Kilauea, which he later used for the painting *Volcano Kaluea Pele.* The painting shows Peale's companions hiking across lava formations in the foreground, and in the background is the shield of Kilauea, fuming from the summit region and from the site of a recent eruption on the lower flank. When Peale reached the summit of Kilauea volcano, the Black Ledge was still about 200 m below the caldera rim and there was an inner pit, about 100 m deep below the Black Ledge, with several erupting lava pools on the floor. From this vantage point, he painted West crater "Kaluea Pele" from "Black Ledge," showing the outer caldera wall, inner Black Ledge, and the main firepit (Halemaumau).

Charles Furneaux (1835–1913) became the first of Hawaii's resident volcano painters. He arrived in Hawaii in 1880 with the volcano enthusiast William T. Brigham. At the time, an eruption of Mauna Loa produced a major lava flow, which advanced toward the town of Hilo. Furneaux took advantage of this opportunity to the fullest, and painted over 40 views of the advancing lava and other landscapes in connection with the eruption.

Jules Tavernier arrived in Hawaii in 1884 and can be credited with starting the Hawaiian "volcano school" of painting. He was born in Paris, and traveled widely in Europe and North America as an illustrator and writer. Upon arriving in Hawaii, Tavernier immediately went to view Kilauea, and from that day forward, the volcano became his chief subject, painting about 100 views of it during his stay in Hawaii. At this time, the caldera of Kilauea was flooded by a lava lake, and Tavernier devoted much effort to capturing this spectacle on canvas. Many of these paintings are based, however, on the Italian iconography of Vesuvius painting developed by Vernet in the 18th century, with the caldera shown at night, the glowing lava lake sluggishly rolling and flashing steam, surrounded by massive walls of lava cliffs, and the cold silvery moon emerging from the clouds in the background. One of Jules Tavernier's art students was the Hawaiian-born David Howard Hitchcock, whose output of Hawaiian volcano landscapes was enormous.

XI. DR. ATL—VOLCANOLOGIST AND ARTIST

In the early 20th century, the visual arts turned away from attempts at rendering the visible world and turned instead toward the representation of abstract forms. This may have been brought about in part by the invention of photography. Thus interest in landscape painting declined, and along with it, volcanoes vanished as part of the painted natural scene. One notable exception is the Mexican artist Dr. Atl, who showed the same devotion to Paricutin volcano that Volaire had shown to Vesuvius in the 18th century. In February 1943, a fissure opened in a farmer's cornfield in the state of Michoacan in western Mexico. A volcanic eruption out of the fissure threw up scoria and lava, which during the following 9 years built up the 410 m high volcanic zone known as Paricutin. In his vibrant, expressionistic paintings, Atl has recorded the actual birth of Paricutin producing a unique pictorial biography of the volcano. Atl was a representative of Impressionism in Mexican art, but his simplified forms and details and brilliant coloring made his art highly personal and new.

Dr. Atl was one of the outstanding figures in Mexican cultural and political life in the first half of the 20th century. He was one of the original creators of Mexican landscape painting and a leading figure in the revolution in Mexican art. Thus he fought for the identity of national and racial consciousness in his nation's art, against the Spanish colonial past. The modern vision of Mexican landscape created by Dr. Atl is a reflection of the enthusiastic temperament, travels, and explorations of this man of culture and wide artistic experience. He spent whole seasons on the snow-covered peaks of the Mexican volcanoes, which he painted many times.

He made major contributions in art, literature, philosophy, poetry, history, revolutionary politics, and the science of volcanology. Jose Gerardo Francisco Murillo was born in Guadalajara, Mexico, in 1875. When he came of age, he renounced the Spanish name and took an Indian pseudonum, changing his name to *Atl*, meaning *water* in the Aztec language, to declare his separation from the dreary influences of the second-hand European culture into which he was born. He knew instinctively that the arts in Mexico were counterfeit, and he set out to rediscover or create a contemporary native art—striving for a renaissance of Mexican and pagan culture. At the age of 21, he was already noted in Mexico as an outstanding artist and writer. He traveled widely during a 7-year stay in Europe, Egypt, and China, but upon his return to Mexico in 1907, he took up mountaineering, which led to his lifelong affair with the volcanoes of his country. In Mexico City, he set about to revolutionize the Academy of San Carlos, where he lectured about the art of the Impressionists, but he also encouraged his students—including the young Diego Rivera—to paint out of doors and appreciate the drama of the Mexican landscape.

In 1912, he traveled to Italy, where he studied volcanology for a time under the expert guidance of Immanuel Friedlander and Frank A. Perret at the University of Naples—the leading volcanologists of the time. From this period, he began to combine his two primary interests in a unique manner—painting and volcanoes. Prior to the work of Dr. Atl, the only Mexican artist to paint the volcanoes was Jose Maria Velasco, who painted more than 200 Mexican landscapes, noted for their poetic realism and sensibility. He explored Popocatepetl before Dr. Atl's time and published texts and lithographs and engravings of the revered mountain. Several Mexican volcanoes had been painted earlier by European vistors, such as the French artist Jean-Baptiste Louis Gros whose 1883 work shows in a vivid manner the sulfur encrustation of the interior of the crater of Popocatepetl, and numerous dramatic paintings of Colima volcano were exectued by the German artist Johann Moritz Rugendas (1834).

Dr. Atl required a new medium to capture the striking colors of the Mexican volcanoes. He therefore invented the Atl-colors, which were, like pastel, for use on surfaces like wood, paper, plaster, fabric, and board. The colors were composed of wax, dry resins, oil color, and gasoline, manufactured in small bars like the sticks of sealing wax. The color itself is apparently unalterable, although the sticks can be melted like wax or dissolved in gasoline for spreading with a brush or palette knife.

The Mexican revolution at the beginning of the 20th century not only transformed the political and social fabric but also created a new tremendous flowering of artistic and intellectual creative energy that changed the course of Mexican culture. Intense nationalism reacted to the largely European-oriented culture of the regime of the dictator Porfirio Diaz. In 1910, Dr. Atl organized an exhibition of nationalistic paintings in honor of the centenary of Mexican independence, which has often been regarded as the beginning of the revolution in Mexican art. A few months later, the political revolution broke out, and Dr. Atl became a leader of the revolutionary intelligensia, persuading other artists to devote their energies to journalism and political propaganda in the cause of the revolution. Among his assistants were the young David Alfaro Siqueiros and José Clemente Orozco, who later became Mexico's best known painters. Prior to the Mexican revolution, many artists and writers had felt intellectually oppressed, forced to admire the foreign and to scorn the native and the ordinary. With the revolution, they were able to share these feelings and become fully absorbed in the revolutionary movement—and for many, the volcano was a potent symbol. This sentiment is illustrated in the novel *Los de Abajo* (Those from Below) by Mariano Azuela, when one of the characters states: "You ask me why I am still a rebel? Villa, Obregon, Carranza? What's the difference? I love the revolution like a volcano in eruption; I love the volcano because it is a volcano, the revolution because it's the revolution! What do I care about the stones left above or below after the cataclysm? What are they to me?"

Following the revolution, Dr. Atl spent much time exploring and painting the Mexican volcanoes. His interest in volcanic activity was further aroused when Popocatepetl erupted in 1919. He had earlier written of his beloved volcano:

> *For millions of years it slept in the silence of death, for millions of years the wind lashed it, for millions of years the forces of nature have tried to destroy it. They closed its mouth, gnawed at its vertebra, they shook its formidable mass and tore its lips which in other times vibrated from thundering eloquence. But one day in its venerable old age, its entrails stirred and from the decayed lips of the Colossus, fire shot forth again. Oh marvellous teaching of nature! Nothing is old and nothing has died: in the end of the Destruction of Life.*

In 1939 he published a monograph on this volcano, *Volcanes de Mexico: La actividad del Popocatepetl.* In it he put forward the curious view that the eruption of 1919 had "acquired an importance of the first order in the history of geology, because it was the result of purely artificial action." Sulfur deposits around fumaroles in the bottom of the volcano's crater had been mined since the 16th century. When the volcanoeros or sulfur miners blasted the fumarole deposits with dynamite, it was apparently Dr. Atl's belief that the dynamite blasting by the volcanoeros had triggered the 1919 eruption. Popular tradition in Mexico claimed that the by-now legendary Dr. Atl lived in a cave in the side of Popocatepetl volcano, where he sustained himself by eating locusts and honey. Legend also has it that he was erupted out of the volcano into this world:

Subio al Popocatepetl,
Bajo del Ixtaccihuatl,
Y es hombre de gran valer
el inquieto Doctor Atl.

Dr. Atl also used to good effect the curvilinear perspective in his landscapes and flew in an airplane over his beloved volcanoes to paint them from a new vantage point; a method he called aeropainting. The finest examples of Dr. Atl's aeropainting give a panoramic view of Mexico's most famous volcano, Popocatepetl. Atl uses this extraterrestrial view repeatedly when painting his favorite volcanoes. In a 1960 painting, Popocatepetl pokes its majestic snow-clad crater above the clouds, framed by the curving horizon and the starlit Milky Way. For all its 20th century realism, Atl retains the romanticized vision with which earlier ages viewed volcanoes. He enhances this mood by juxtaposing the volcanoes to our contemporary sublime, the vastness and mystery of the stars and space. The volcano as part of the Earth has become one of the last natural phenomena that we can still awe. In Atl's paintings, there are no small, frightened figures, no evidence of human devastation, no moralizing overtones, just the volcano itself.

During the 1920s and 1930s, Atl dropped out of the postrevolutionary government of Mexico and began to wander the world, chiefly in the study of volcanoes. When the volcano Paricutin was born in a corn field in 1943, the aging Dr. Atl disappeared from Mexico City and moved to a shack at the foot of the growing volcano and began to paint. He produced 130 drawings, 11 paintings, and a large book on the activity, documenting all stages of its evolution. Births of new volcanoes is a common experience in the history of the Mexican people. In 470 B.C., the birth of Xitle volcano destroyed the Mexican city of Cuicuilco. Again in 1759 the volcano Jorullo was born in the State of Michoacan.

In 1950, Dr. Atl published his observations of the eruption in a unique volume, including a large number of paintings and sketches of the activity, which document the growth of the volcano, in *Como nace y crece un volcano: El Paricutin.* The illustrations in brilliant color capture and preserve the spectacle of the eruption and the artist's excitement in the presence of this awesome display of nature's force. The text includes a detailed chronological description of the eruption and his conclusions regarding the fundamental mechanisms of volcanic activity. He rejects the ideas that volcanic heat is derived from reactions between iron and sulfur or from the combustion of petroleum or indeed the modern concept of heat generation by the decay of radioactive elements. Instead, he proposes that the volcanic energy is residual heat left over from the primitive globe, and only a small amount of additional heat from chemical reactions or from radioactive decay are needed to trigger an eruption. As a fundamental driving force for volcanism, Dr. Atl embraced Alfred Wegener's theory of continental drift: "It is possible to conclude, as a consequence, that this abundance of volcanic structures is due to innumerable fractures caused by continental drift." Atl was not alone in painting Paricutin; his most illustrious student, the famous Mexican painter Diego Rivera, was also fascinated by the activity and created *Volcano Erupting* in 1943.

In *Crater en Llamas*, we see a full view of the volcano in the height of activity, with fiery fountains of red scoria mixed with black ash clouds billowing out of the crater, while a lava flow creeps along the ground toward the observer (Fig. 12). In *Paricutin Violeta al Am* (1946), the activity produces mostly ash-fall to one side of the volcano with the entire landscape draped by a uniform layer of gray ash. In *Falda Incendiada del Paricutin* (1948), the lava flow creeps forward, oozing red hot molten lava at its base. The waning phase of the eruption is shown in *Paricutin en Eruption* with a wispy black plume of ash rising from the crater. These paintings dominate the materials, colors, and movements of the volcano, but the artist uses the expressive qualities of the paint to render the scene as experienced by human eyes rather than with the objective clarity of the camera.

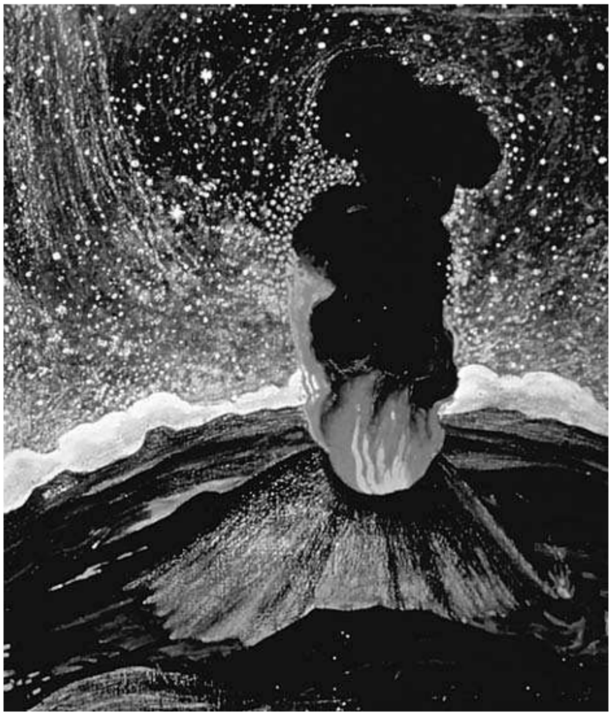

FIGURE 12 The painting *Crater en Llamas* (Crater on Fire) by the Mexican artist and volcanologist Dr. Atl shows the Paricutin volcano in 1943 in the height of activity.

In *Paricutin en Noche Estrellada*, we see the eruption from a vantage point characteristic of Atl's works. As if gliding by Earth in a spaceship, hundreds of kilometers above the planet's surface, we have a full view of the erupting volcano against the strongly curved horizon of the planet in the background.

XII. THE MODERN VOLCANO LANDSCAPE

Until Mount St. Helens reminded us of Nature's fury, strength, and indifference in 1980, our modern fears had been those we created ourselves—wars and the horror of nuclear devastation. What most Americans had forgotten was both the power and beauty of natural cataclysm, the coming together of earth and sky, brilliant color contrasted with uniform gray, the sight of all those trees laid flat in parallel lines, and the emotional impact of lives disrupted or gone. Artists like Dr. Atl had followed earlier painters in giving form to these observations so that we can appreciate and understand volcanoes as both real phenomena and as symbols of our own states of mind and emotions. Toward the end of the 20th century, a new interest is emerging among artists in capturing on canvas the spectacle of volcanic eruption.

In the 1980 painting *First Continental Eruption* by Chicago artist Roger Brown, the residents of two high-rise apartment buildings gaze out their windows at the erupting volcano and its billowing clouds of ash (Fig. 13). The painting cleverly expresses the surprise of the American nation over this volcanic eruption in their own backyard, and the effrontery of Mount St. Helens volcano to intrude into their lives in the spring of 1980. After all, volcanic eruptions belonged to Hawaii and Italy and were definitely not part of the safe continental scene! In this painting, the stylized volcano is erupting a black plume which rises sinuously like smoke toward the sky. The nasty-looking eruption plume spreads horizontally on top, with black to gray mammary-like clouds of ash and steam marching across the sky and fading in the distance. At the tip of the volcano is a red hot flame which feeds the black smoke plume rather like the flame which continuously burns off waste products at an oil refinery. The artist has reached back to the Middle Ages in his interpretation of volcanic activity, when eruptions were thought to be the burning of combustible rocks in the earth. Roger Brown's paintings have been grouped with the art movement of the 1980s referred to by some as Survival Art. The politics of survival in his paintings address the idea of a definitive upheaval from which none will escape, such as in this volcanic eruption. The gloom is, however, tempered by a jazzy, parodic idiom with a vaudeville touch. In *Mania* (1984), the American artist Robert Hawkins conveys a dark, whimsical view of reality. Hawkins often selects the most menacing gifts of nature and blows them up to a frightening scale. In his aerial view of a volcano, the active crater has an inner pool of glowing, steaming lava, while several rows of volcanoes spew out ashes in the background.

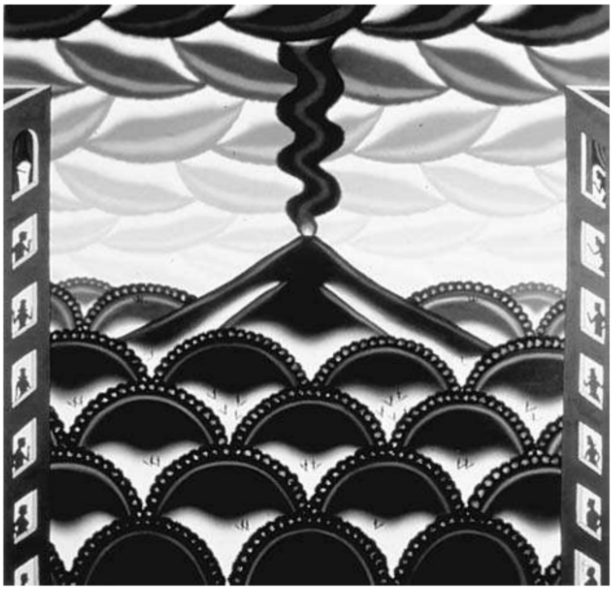

FIGURE 13 The 1980 painting of the *First Continental Eruption* by American artist Roger Brown was inspired by the Mount St. Helens eruption.

The contemporary American artist Bill Sullivan has the temerity to take on the panoramic tradition of 19th century American art. Like his 19th century predecessors Church and Heade, some of Sullivan's pictures have been inspired by the volcanoes of the Ecuadorian Andes, particularly Cotopaxi. In painting volcanoes, he plays with the theatrical qualities of the subject, heightening it with extravagant color combinations and a sense of elegance that keeps his work from turning into kitsch. In the *Last Refuge*, the painting is of Cotopaxi, the highest active volcano on Earth, and the Lord of Terror of the Incas. The volcano is framed between snow-covered rocks, across a vast gray plain. Cotopaxi is almost completely covered with snow, and a full moon breaks through the clouds, punctuating the majestic stillness.

In 1985, the Museo di Capodimonte in Naples in Italy mounted an exhibition of the work of American artist Andy Warhol, commissioned especially on the theme of *Sterminator Vesevo* or Vesuvius the exterminator. The hallmark of Andy Warhol's Pop Art was to take a mass-media image out of context, be it a soup can label or a photo of Marilyn Monroe, and to formulate a new meaning for it. An erupting Vesuvius is such a well-known artistic icon that it too approaches a mass-media image. In 1980, Warhol spent some time in Naples and returned in 1985 to work on the image of Vesuvius and transferred it to his realm of fantasy. For Warhol, a Vesuvius "eruption is an overwhelming image, an extraordinary happening and even a great piece of sculpture." His product from the stay in Naples was a great one: 16 hand-painted canvases and 26 silk-screen images of Vesuvius erupting, each one developing a highly distinctive color scheme. The basic image of an eruption is nearly identical, however, with the symmetrical cone of Vesuvius rising out of the ruins of Monte Somma, whose ragged outline is apparent on the left (Fig. 14). Warhol could not witness a Vesuvius eruption—the last one was in 1944—but he has created a very powerful and fiery Plinian eruption, probably based on his impressions

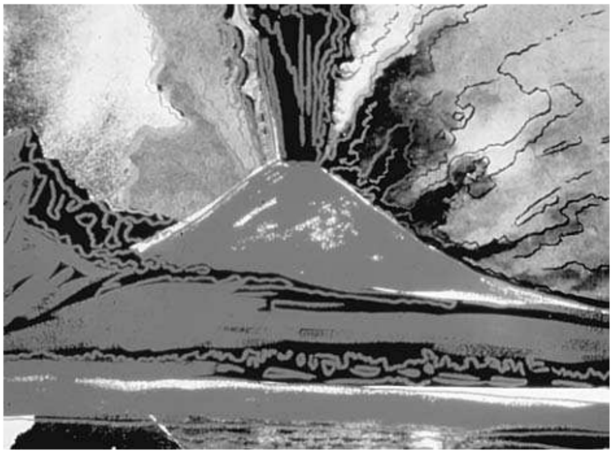

FIGURE 14 *Vesuvius 1985* by the American artist Andy Warhol. Silk screen on cardboard (author's collection).

from the widely distributed photographs of the great 1980 eruption of Mount St. Helens in the state of Washington, or from the common images of erupting Vesuvius by Pierre Jaques Volaire and his contemporaries in the late 18th century.

XIII. ARTISTIC ILLUSTRATION

Pictorial representation of volcanoes, eruptions, and other geologic phenomena is found in the domain of the artists and illustrators of books and media as well as among the works of geologists. A spectacular example of an early volcanic illustration is the Japanese color woodcut of the July 1783 eruption of Asama in Japan, which resulted in a large loss of life and was associated with the Ten-mei famine (Fig. 15). Earth science has a visual language, which relates to the communication of ideas and information between geologists by visual materials, especially maps, diagrams, and landscapes. Geologists are not only concerned, however, with the visual representation of topography but also with the penetration of the topography to form a three-dimensional picture of the structure of Earth. The main medium for geologic illustration in the 18th century was the copper engraving, which provided an excellent means of reproducing several hundred copies of the kinds of illustrations presented in early texts on the subject of Earth. The process was, however, very expensive, and only rarely was it used to its full effect. However, the copper engraving was a complex process, consisting of several steps, that could result in a finished product significantly different than that conceived by the naturalist who commissioned the illustration. Between the naturalist and the reader stood not only the artist but also the engraver and printer. Few scholars who explored volcanoes were in the position of William Hamilton (1776–79), who had at his disposal a fine artist Pietro Fabris. At the request of Hamilton, Fabris lavishly illustrated his volcano monograph *Campi Phlegrei* and showed the volcanic features of Vesuvius and other craters in southern Italy in superb hand-colored engravings (Fig. 16). He is also the only artist who has turned humble rock specimens of obsidian, lava, and sulfur into pure works of art.

In the early part of the 19th century, the invention of lithography had a far-reaching impact on geologic illustration, as it cut out the engraver as a middle man between artist and printer and enabled greater precision, a finer shading, and more subtle expression of detail. Lithography began to be exploited widely for scientific purposes in the 1820s, and it had the great advantage of being much cheaper than copper engraving, and thus allowed authors to illustrate their publications relatively lavishly. In the 18th century, an artistic tradition of realism had developed in the presentation of geologic landscape. In a way, this may be related to the development of Neoclassical movement in art, which encouraged a realistic and clear landscape style, although the Neoclassical artist would be generally scorned for painting an identifiable scene and, therefore, preferred to invent one that suited that overall composition. Similarly, the depiction of wild mountain landscapes was a common theme adopted by the artists of the Romantic movement, but they generally exaggerated the vertical

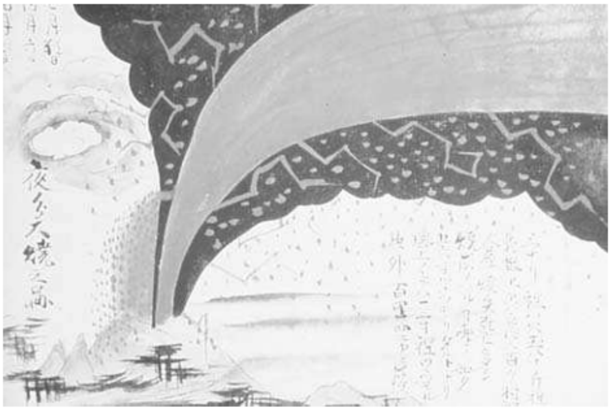

FIGURE 15 A contemporary Japanese color woodcut showing the great July 1783 Asama eruption, which took many lives, both as a result of pyroclastic flows as well as a famine. (Also see color insert.)

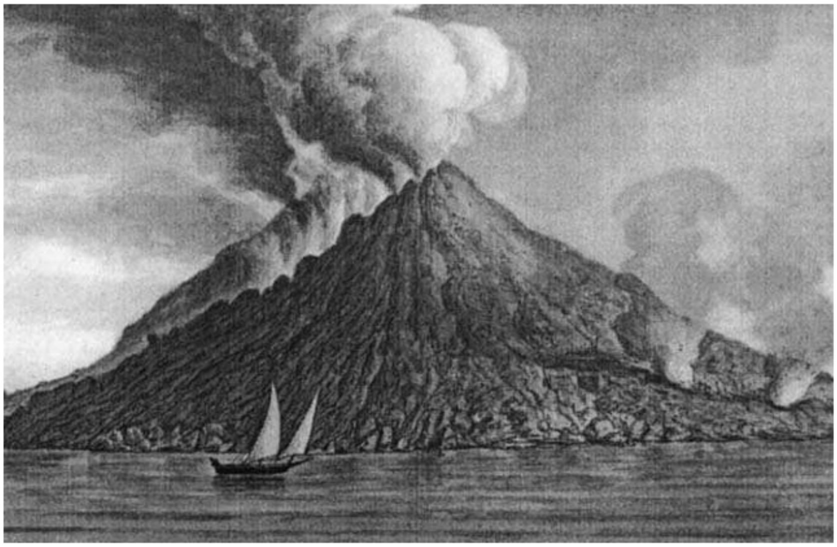

FIGURE 16 In 1768 the Neapolitan artist Pietro Fabris illustrated the great Italian volcano monograph *Campi Flegraei* for William Hamilton. Among the illustrations is this colored engraving of Stromboli erupting. (Also see color insert.)

scale greatly in order to heighten the Romantic impact of the work, with little regard for realism or accurate representation of the actual landscape. Therefore, the accurate representation of topography or landscape was looked upon with undisguised scorn by the principal spokesmen of 18th century art; consequently, most of the illustrators of geologic and other natural history subjects were from a socially humbler level of documentary topographical drawing and painting. The topographic art or accurate prepresentation of landscape was referred to by Henry Fuseli as "that last branch of uninteresting subjects, that kind of landscape which is entirely occupied with the tame delineation of a given spot." Similarly, Thomas Gainsborough declined to paint "*real Views* from Nature in this country." Thus topography was held in very low esteem by academic artists, and Twyman, for example, argued that "the whole concept of the picturesque is at variance with the needs of topography." Fortunately, this was not the view of all artists, and we are thankful to them for bringing us several wonderful and informative views of the volcanic eruptions of the past.

SEE ALSO THE FOLLOWING ARTICLES

Archaeology and Volcanism • Plinian and Subplinian Eruptions • Volcanoes and Tourism • Volcanoes in Literature and Film

FURTHER READING

Atl, Dr., (1950). "Como nace y crece un volcan?: El Paricutin, Mexico." Editorial Stylo, Mexico City.

Boime, A. (1991). "The Magisterial Gaze. Manifest Destiny and American Landscape Painting c. 1830–1865." Smithsonian Press. Washington, DC.

Crausaz, W. (1985). "Dr. Atl: Pioneer Mexican volcanologist," Geological Society of America Centennial Special Vol. 1, pp. 251–256. Boulder, CO.

Forbes, D. W., and Kunichika, T. K. (1983). "Hilo: A Century of Paintings and Drawings." Lyman House, Hawaii.

Helm, M. (1968). "Modern Mexican Painters." Books for Libraries Press, Freeport, NY.

Huntington, D. C. (1966). "The Landscapes of Frederic Church." G. Braziller, New York.

Luhr, J. F., and Simkin, T. (1993). "Paricutin, the Volcano Born in a Mexican Cornfield." Geoscience Press, AZ.

Luna Arroyo, A. (1992). *Dr. Atl.* Hachette, Mexico.

Manthorne, K. (1985). "Creation and Renewal: Views of Cotopaxi by Frederic Church." National Museum of American Art and Smithsonian Institution Press, Washington, DC.

Mellaart, J. (1967). "Catal Huyuk: A Neolithic Town in Anatolia." McGraw-Hill, New York.

Myers, B. S. (1956). "Mexican Painting in Our Time." Oxford University Press, New York.

Nicolson, M. H. (1959). "Mountain Gloom and Mountain Glory." Cornell University Press, Ithaca, NY.

Parry, E.C. (1981). Acts of god, acts of man: Geological ideas and the imaginary landscapes of Thomas Cole. *In* "Two Hundred Years of Geology in America" (C. J. Schneer, ed.), pp. 53–71. University Presses of New England.

Rudwick, M. J. S. (1976). The emergence of a visual language for geological science, 1760–1840. *History of Science*, **14,** 149–195.

Wallach, A. (1981). Thomas Cole and the aristocracy. *Arts Magazine*, **56,** 94–106. "Vesuvius by Warhol, Exhibition Catalogue" (1985). Museo di Capodimonte, Electa, Napoli.

VOLCANOES IN LITERATURE AND FILM

HARALDUR SIGURDSSON
University of Rhode Island

ROSALY LOPES-GAUTIER
Jet Propulsion Laboratory

I. Introduction
II. Pre-20th Century Novels
III. 20th Century Novels
IV. Juvenile Fiction and Comics
V. Volcano Films

I. INTRODUCTION

Volcanoes are terrifying, sublime, and awesome, and their eruptions represent the ultimate exterminator. It is therefore natural that they have been frequently used in literature and film, both as a metaphor and as a plot device. In one of the better if lesser known novels, *Gentlemen in England*, the potency implied by erupting volcanoes allows the Victorian volcanologist to win over the younger woman he is courting. In the most famous volcano film, Rossellini's *Stromboli*, the erupting volcano is used as an image of the despair felt by the young bride, unwelcome and trapped in a foreign society on a tiny island.

This chapter reviews several of the principal works of fiction and film that feature volcanoes and their eruptions. Many of the novels and films are based on or strongly influenced by historical eruptions, whereas others are in the genre of science fiction or fantasy, such as the pioneering work of Jules Verne in *The Journey to the Center of the Earth*. The various works differ dramatically in how accurately they portray volcanoes and volcanic eruptions. Some novels and films attempt to portray volcanoes in a credible, realistic way. For example, *Juan of Paricutin* was written by a geologist and can be considered a mostly historical account of the eruption. Authors of some other novels have taken considerable care to describe volcanoes in a realistic light. Some authors, such as Jules Verne, present scientific views that are no longer accepted, but their novels reflect the prevailing thinking of their times. Other authors use the power and fury of volcanoes purely for dramatic effect, and their works can only be considered fantasy.

Most films that prominently feature volcanoes unfortunately fall into the fantasy category or, as they are known in the industry, "disaster movies." Yet even these differ in their attempts to present reality; for example, the 1997 film *Dante's Peak* portrayed well the difficult decision of whether or not to evacuate a threatened town—a dilemma that is often faced by volcanologists and public officials, but little known to the general public.

The volcanoes that have most often inspired works of fiction are those that either erupt frequently, such as Kilauea in Hawaii, or those whose eruptions brought tragedy to the people living near them, such as Vesuvius in A.D. 79, Krakatau in 1883, and Mt. Pelee in Martinique in 1902. All these events are major catastrophes that

Copyright © 2000 by Academic Press
All rights of reproduction in any form reserved.

still capture the imagination of the public and are rich, exciting themes for stories about the interaction between volcanoes and the people who live around them.

The authors acknowledge that the literary works discussed here are predominantly from Western sources and in English, and that the volcano-related literature from the volcanic regions in Russia, Japan, the Philippines, Indonesia, and other parts of Asia, as well as Africa, are as yet largely unexplored.

II. PRE-20TH CENTURY NOVELS

Probably the earliest Western novel that features volcanic activity is *Montalbert*, a Gothic novel by Charlotte Smith (1795). The heroine Rosalie undertakes a journey from England to Italy, where she witnesses the activity of Etna volcano and is captivated by its sublime beauty and force: We are never surprised at the sight of a small Fire that burns clear, and blazes out on our own private Hearth, but view with Amaze the celestial Fires, tho' they are often obscured by Vapours and Eclipses. Nor do we reckon any thing in nature more wonderful than the boiling Furnaces of Etna, which cast up Stones and sometimes whole Rocks from their labouring Abyss, and pour out whole Rivers of liquid and unmingled Flame.

A. The Last Days of Pompeii

The first major novel that features a volcano as a central theme is *The Last Days of Pompeii* by the English writer George Bulwer-Lytton (1803–1873). The novel, dealing with the catastrophic eruption of Vesuvius in A.D. 79, was first published in 1834 and became an immediate and spectacular success, with numerous editions published up to our day. It is a work that is based upon substantial research by Bulwer-Lytton in Pompeii and Herculaneum and elsewhere around the volcano. The novel is particularly important because the author attempts to describe the volcanic processes on the basis of the eyewitness report of Pliny Younger, it is thus the earliest recreation of a volcanic eruption.

Bulwer-Lytton's novel coincides with the rise of awareness for volcanoes among the European intellectuals. It is virtually certain that he was aware of the volcanological research of his British contemporaries, such as the experiments of Sir Humphry Davy (who gave frequent popular lectures on volcanoes in London) and the pioneering field work of George Poulett-Scrope on the volcanoes of Central France, as well as the writing of Charles Lyell.

The author with his wife arrived in Naples in 1832 to spend a winter abroad and to write. He explored the ruins of Pompeii and Herculaneum with the guidance of the archaeologist Sir William Gell, whose major work *Pompeiana* (1852) described in great detail the topography, edifices, and ornaments of Pompeii.

Bulwer-Lytton got the idea for the subject matter of the Pompeii novel—and the title—from the painting *The Last Days of Pompeii* that he had seen in the Brera Gallery in Milan. This was the huge 1831 work of the Russian Karl Bryullow. In Italy, Bulwer-Lytton pored over literature sources about Vesuvius volcano, the eruption of A.D. 79 and the Roman cities, reading Vitruvius, Strabo, Livy, Tacitus, Seneca, and Dio Cassius, as well as the letters of Pliny Younger. He returned to England in 1833, after having written most of the novel in Naples.

While exploring Pompeii, Bulwer-Lytton heard a suggestion that during the blackness in the city at the time of the eruption, a blind person would have a better chance of escape than one who had full sight. This remark led to the creation of Bulwer-Lytton's blind flower girl Nydia, the main heroine of the story, who leads her friends to safety in the total darkness beneath the eruption cloud (Fig. 1).

The novel has been justly criticized for turgid oratory and lush style, pseudo-poetical excesses, pretentious striving for wit and profundity, melodrama, ham philosophy, and moralizing. These are said to be features of style that match well Bulwer-Lytton's personality: ostentation, pomposity, and hauteur. Still, *The Last Days of Pompeii* triumphed over all its deficiencies, and made an immediate and spectacular conquest of the readership, becoming by far the most popular of all Bulwer-Lytton's works. His accuracy to history was justly praised, as was his description of Pompeiian life and architecture. In this sense, the novel is one of the great recreations of the past. Perhaps the novel's most notable achievement is in the mounting suspense of its plot, beginning as a dark cloud hangs over the summit of Vesuvius. It reaches a climax in the last scenes of the earthquake and the eruption, with terrified crowds, crashing buildings, darkness, the falling of hot rocks and ash over the city, destruction, and chaos.

The threat of Vesuvius is gradually brought into the story and is used effectively to create suspense. Early on in the novel, the young lovers Ione and the Greek Glaucus are discussing the enigmatic Egyptian Arbaces:

> *"His calm, his coldness," said Ione, evasively pursuing the subject, "are perhaps but the exhaustion of past*

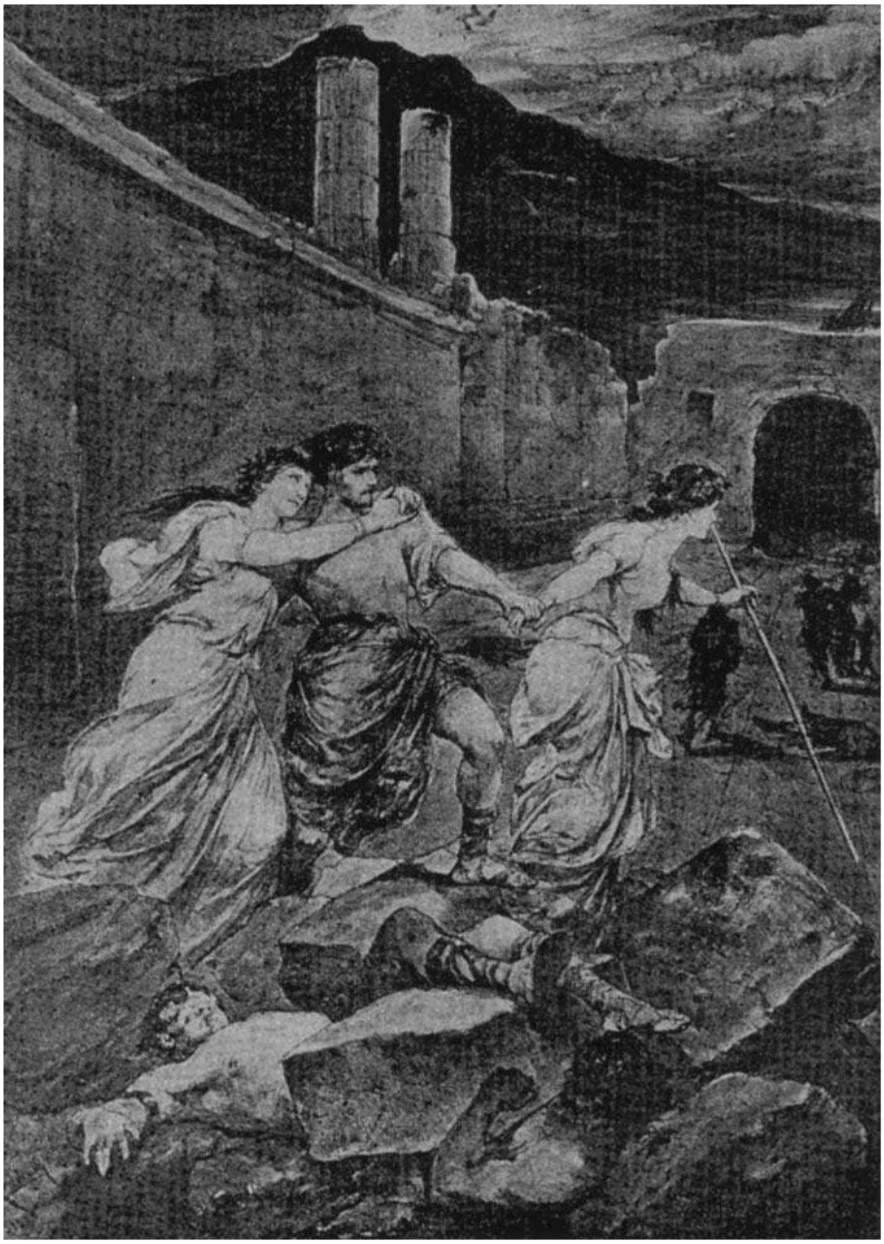

FIGURE 1 The blind Nydia leading Glaucus and Ione to safety out of Pompeii during the eruption of Vesuvius in A.D. 79 (from the historic novel *The Last Days of Pompeii* by Bulwer-Lytton, 1850 edition).

> *sufferings; as yonder mountain" (and she pointed to Vesuvius), "which we see dark and tranquil in the distance, once nursed the fires forever quenched." They both gazed at the mountain as Ione said these words; the rest of the sky was bathed in rosy and tender hues, but over that gray summit, rising amidst the woods and vineyards that then climbed half-way up the ascent, there hung a black and ominous cloud, the single frown of the landscape. A sudden and unaccountable gloom came over each as they thus gazed....*

Bulwer-Lytton even makes an attempt at a volcanic hazard assessment when he describes the population sprawl up the slopes of the volcano:

> *Villas and villages stretched on every side up the ascent of Vesuvius, not nearly then so steep or so lofty as at*

> *present. For as Rome itself is built on an exhausted volcano, so in similar security the inhabitants of the South tenanted the green and vine-clad places around a volcano whose fires they believed at rest forever. From the gate stretched the long street of tombs, various in size and architecture, by which, on that side, the city is yet approached. Above all, rose the cloud-capped summit of the Dread Mountain, with the shadows, now dark, now light, betraying mossy caverns and ashy rocks, which testified the past conflagrations, and might have prophesied—but man is blind—that which was to come!*

The fact that the residents of Pompeii may have noticed some atypical behavior of the volcano is brought into the lovers' conversation. "Could that mountain have any connection with the last night's earthquake? They say that, ages ago, almost in the earliest era of tradition, it gave forth fires as Etna still. Perhaps the flames yet lurk and dart beneath'." Bad omens continue: "From the summit of Vesuvius, darkly visible at the distance, there shot a pale, meteoric, livid light—it trembled an instant and was gone." An earthquake from Vesuvius later saves the hero Glaucus, as he is about to be killed by the villain Arbaces the Egyptian, who also lusts for Ione: "... at that awful instant, the floor shook under them with a rapid and convulsive throe,—a mightier spirit than that of the Egyptian was abroad!"

The suspense continues as, on the last day of Pompeii, Arbaces is visited by an old hag, a witch, who comes to warn him of the evil that hangs over the city. Living in a cavern under the volcano, she has been able to witness a great change in the nether world, with hissing and roaring and an intensely luminous glowing red stream within the cavern. The witch plans to cross over to safety in the city of Herculaneum, and urges Arbaces to do likewise.

Glaucus is saved once again by the volcano on the city's last day. Arbaces has framed Glaucus for murder, and the Greek hero is sentenced to go before the lions in the Amphitheater that fateful day, armed only with a dagger. In a suspenseful scene, the grating is lifted and the lion jumps into the arena. But miraculously it shows no interest in attacking Glaucus, which the crowd takes as a proof of his innocence. Glaucus is saved by a witness, who pins the crime on the Egyptian. "Arbaces to the lion!" screams the crowd, and rushes in to throw him into the arena. Arbaces has noted, however, that the volcano has become active:

> *"Behold!" he shouted with a voice of thunder, which stilled the roar of the crowd; "behold how the gods protect the guiltless! The fires of the avenging Orcus burst forth against the false witness of my accusers!" The eyes of the crowd followed the gesture of the Egyptian, and beheld, with ineffable dismay, a vast vapor shooting from the summit of Vesuvius, in the form of a gigantic pine-tree: the trunk, blackness,—the branches, fire!—a fire that shifted and wavered in its hues with every moment, now fiercely luminous, now a dull and dying red, that again blazed terrifically forth with intolerable glare!" ... an instant more and the mountain-cloud seemed to roll toward them, dark and rapid, like a torrent; at the same time it cast forth from its bosom a shower of ashes mixed with vast fragments of burning stone! It was sudden and more ghastly Night rushing upon the realm at Noon!"*

In describing the next stage of the eruption, Bulwer-Lytton takes the common view that mud flows overwhelmed the cities around Vesuvius: "Amidst the other horrors, the mighty mountain now cast up columns of boiling water. Bent and kneaded with the half-burning ashes, the streams fell like seething mud over the streets in frequent intervals."

Bulwer-Lytton describes the climax of the eruption by citing Pliny's Letters in footnotes, in what is perhaps the earliest (1834) volcanological interpretation of the eyewitness account:

> *The cloud, which had scattered so deep a murkiness over the day, had now settled into a solid and impenetrable mass. It resembled less even the thickest gloom of night in the open air than the close and blind darkness of some narrow room.... Sometimes the cloud appeared to break from its solid mass, and, by the lightning, to assume quaint and vast mimicries of human or monster shapes, striding across the gloom.... The ashes in many places were already knee-deep; and the boiling showers which came from the steaming breath of the volcano forced their way into the houses, bearing with them a strong and suffocating vapor. In some places, immense fragments of rock, hurled upon the house roofs, bore down along the streets masses of confused ruin, which yet more and more, with every hour, obstructed the way....*

Glaucus and Ione escape the horror of the eruption with help from their friend and guide, the blind Nydia, who alone can find the way in the total darkness below the eruption cloud. They reach the shore and find safety on a boat at sea: "Meanwhile the showers of dust and ashes, still borne aloft, fell into the wave, borne by winds, those showers descended upon the remotest climes, startling even the swarthy African; and whirled along the antique soil of Syria and of Egypt." Here Bulwer-Lytton cites, in a footnote, the writings of Dio Cassius as evidence for the ash fallout in Africa and the Levant. At the very end of the novel, Nydia, unable to attain the love of Glaucus, slips out of the boat and into the sea while the lovers sleep, and drowns below the waves.

In a footnote, Bulwer-Lytton discusses the various theories that have been advanced for the mode of destruction of Pompeii. He adopts the one " . . . which, upon inspecting the strata, appears the only one admissible by common sense; namely, a destruction by showers of ashes, and boiling water, mingled with frequent eruptions of large stones, and aided by partial convulsions of the earth. Herculaneum, on the contrary, appears to have received not only the showers of ashes, but also inundations from molten lava." Where did he get his relatively advanced volcanic ideas? Was he a friend of his geological contemporaries, the pioneer volcanologist George Poulett-Scrope and the geologist Charles Lyell? Although he is close to the mark on Pompeii, his assertion that lava flows inundated Herculaneum, on the contrary, is of course wrong and is probably based on the misidentification of the outcrops of consolidated pyroclastic flow deposits in that city as lava flows.

B. The Crater

The American author James Fenimore Cooper, famous for his Leatherstocking Tales, published a novel *The Crater*, or *Vulcan's Peak*, in 1847. The story begins in the style of Robinson Crusoe, with a shipwreck on a desert island. The hero is Mark Woolston, who becomes a sailor for the East India trade in 1793. Between voyages, he marries his childhood sweetheart and then sails again for the Pacific Ocean, now as first officer on the *Rancocus*. The vessel is shipwrecked, and the only two survivors land on a reef-fringed volcanic island, which Cooper describes in considerable geologic detail. Mark and his companion Bob take advantage of the volcanic formations in many ways, using hollows in the lava as water catchment cisterns, the good soil inside the crater as a natural garden in fertile volcanic ash, and the sheltered crater as their home. Bob is driven off to sea in a small boat during a storm and feared lost, but Mark continues to eke out a living in solitude on the volcanic island for many months.

One day Mark wakes up to terrifying tremors and a violent volcanic eruption, with suffocating gases. Smoke and ashes fill the air. A large part of the surrounding reef and his island has been thrust up above the surrounding sea, by a sudden elevation of the Earth's crust. The volcanic outburst came from a new crater offshore. A new mountain—Vulcan's Peak—has risen overnight to at least 1000 feet above the ocean. Mark climbs the new mountain and sees other islands in the distance and, much to his joy, a boat approaching, with Bob, a native from a distant island, and a group of new settlers. Bob had returned to America and had told the news of their shipwreck. Then he returned to the Pacific in the company of Mark's wife and several other settlers—the Craterinos. Soon a virtual Utopia is established on the new volcanic island and they begin to multiply, ruled by the author's concept of the ideal government (Scudder 1947). Years later, Vulcan's Peak sinks back into the ocean, and their Utopia is destroyed in a catastrophe, leading to disintegration and physical destruction of the Craterinos.

The Crater is a story of survival by courage and ingenuity, with precise description and explanation of many geological phenomena. The central scientific idea of *The Crater* is the Craters of Elevation theory of the German geologist Leopold von Buch (1774–1853). He was probably the most illustrious student of the arch-Neptunist Leopold Werner and one of the most traveled of all field geologists. Von Buch proposed a volcanic origin of oceanic islands from his studies in the Canary Islands in 1815. There he devoted much energy to the study of the form of volcanic mountains and developed his Craters of Elevation theory, which stated that volcanic mountains were thrust up by upheaval of the Earth's crust. Volcanoes, he noted, were generally conical in form, and their strata dipped in all directions away from the central crater at the summit.

Curiously, he did not recognize that this was due to the pouring out of lava and ash from the summit but attributed their form to uplift, accounting for the craters through the bursting and collapse of a bubble-like mass at the summit. In order to support his theory, he proposed cavernous openings beneath the volcanoes, separated by walls or arches, and hypothesized that these caverns were periodically subject to influx of great quantities of gases and lava. Although von Buch abandoned the Neptunist theory, he never abandoned the Craters of Elevation theory. The theory was shattered, however, by a volcanic eruption in the Mediterranean in 1831, creating a new island variously called Graham Island, Isola Julia, Ferdinanda, Sciacca, Corrao among others, depending on the nationality of the namegiver. Charles Lyell was quick to point out that the dip of strata on Graham Island was due to deposition, not upheaval. The island has since disappeared beneath the waves—not by subsidence but rather by erosion.

Cooper's contemporary Herman Melville also featured geology in several of his novels, notably in *Mardi* (1849), *Moby Dick* (1851), and *The Encantadas* (1854), a tale of the Galapagos Islands. Melville was most likely influenced by the popular and widely read writings of the British geologist Charles Lyell, particularly his *Elements of Geology* (1841). In *Mardi*, the philosopher Babbalanja offers his theory of volcanism and the evolution of his island:

> *The coral wall which circumscribes the isles but continues upward the deep buried crater of the primal chaos. In the first times the crucible was charged with vapours nebulous, boiling over fires volcanic. Age by age, the fluid thickened; dropping, at long intervals, heavy sediment to the bottom; which layer on layer concreted, and at length, in crusts, rose towards the surface. Then, the vast volcano burst; rent the whole mass; upthrew the ancient rocks; which now in diverse mountain tops tell tales of what existed ere mardi was completely fashioned.*

Foster (1945) has proposed that Melville, with the elevation of strata by "volcanic throes," was here parodying the Plutonian theory, particularly the ideas of Buffon and Hutton.

C. Journey to the Center of the Earth

The French writer Jules Verne (1828–1905) is the undisputed founder of the genre of science fiction. *Journey to the Center of the Earth* (1864) was the third in his series *Les Voyages Extraordinaires*, where he spins a tale of high adventure around a credible scientific hypothesis—in this case a geological theory about the physical conditions in the interior of the Earth. Verne was clearly very familiar with the conflicting ideas about the origin of heat in the Earth, which basically reflected the debate between the Neptunists and the Volcanists of the later 18th century. One hypothesis centered on primordial heat in the Earth and predicted a gradual increase in temperature with depth, all the way down to the Earth's core. The competing hypothesis was that heat in the Earth was superficial and caused by combustion at or near the surface, involving heat-giving reactions of the alkali metals on contact with air and water—a hypothesis championed by Sir Humphry Davy. Verne's German hero, Otto Liedenbrock, is firmly in the Davy camp and insists that there is no proof that heat increases greatly with depth. He is basically a Neptunist at heart—the typical position of German scholars of his time—but he is always on the lookout for evidence that can support his theory.

The professor is therefore ecstatic when he and his nephew Axel discover a soiled slip of ancient parchment with runic lettering, in a volume of the 12th century chronicle of Heimskringla by the Icelandic scholar Snorri Sturluson. After much effort, they manage to decipher the message: "Descend, bold traveler, into the crater of Snaefellsjokull, which the shadow of Scartaris touches before the kalends of July, and you will attain the center of the Earth; which I have done, Arne Saknussemm." The professor and his nephew prepare for their journey and take the first ship to Iceland, in order to reach the volcano's summit before the kalends of July. Upon arriving in Reykjavik, they waste no time in hiring Hans, an Icelandic guide, who is intimately familiar with the terrain and will assist them in carrying their instruments into the bowels of the Earth, including thermometers, aneroid barometer, chronometer, compasses, and Ruhmkorff's apparatus (based on a Bunsen pile and the bichromate of potash) to give an abundant supply of crucial electric light.

As they approach the glacier-capped volcano, Axel becomes increasingly worried about the prospects of descending into a crater that could erupt at any moment. The professor reassures him and insists that there is no cause for concern, pointing to the widespread fumaroles and jets of hot springs around the volcano: "You see all these volumes of steam, Axel: well, they demonstrate that we have nothing to fear from the fury of a volcanic eruption." His logic is that:

> *At the approach of an eruption these jets would redouble their activity, but disappear altogether during the period of the eruption. For the elastic fluids, being no longer under pressure, go off by way of the crater instead of escaping by their usual passages through the fissures in the soil. Therefore, if these vapours remain in their usual condition, if they display no augmentation of force, and if you add to this the observation that the wind and rain are not ceasing and being replaced by a still and heavy atmosphere, then you may affirm that no eruption is preparing.*

The next day, they climb the volcano and find three chimneys, which are the principal vents of the eruptions of Snaefellsjokull, but the travelers know that only one of these leads down to the center of the Earth. The pointed shadow of the peak Scartaris falls on the middle opening, and they lower themselves into the bottomless pit. The Professor makes geological observations, and after a near-vertical descent of thousands of feet he declares, "The further I go the more confidence I feel. The order of these volcanic formations affords the strongest confirmation to the theory of Davy. We are now among the primitive rocks, upon which the chemical operations took place which are produced by the contact of elementary bases with water. I repudiate the notion of central heat altogether. We shall see further proof of that very soon."

The travelers are pleased to find that, even at a depth of 1100 feet, the temperature has scarcely increased. They make good progress downward in an inclined lava tube during the next few days, through a succession of fossil-bearing geologic periods. After 20 days, they reach a depth of 16 leagues, at the base of the crust, but the temperature has increased only slightly. Among the wonders conceived by Verne is a subterranean sea in a vast cavern, which the professor promptly names the Liedenbrock Sea. On the shore is a forest of gigantic mushrooms, lycopodium, and other trees from the Carboniferous period. The travelers fashion a raft and set sail across the sea until they are caught in a violent torrent or waterfall that carries their raft instantly to great depths. The torrent reverses direction, and now they are carried upward at even greater speed, and the heat becomes unbearable. The walls of the shaft are burning hot, and the professor concludes that they are being carried up the throat of an erupting volcano! The water column below their raft is replaced by red-hot lava lifting them rapidly up the conduit. Suddenly they are ejected violently from the crater, and, badly shaken but not injured, find themselves lying on the crater rim of an erupting volcano—Stromboli, thousands of miles from Iceland.

III. 20TH CENTURY NOVELS

A large number of 20th century novels feature a volcano, either as a central theme or as a symbol. Perhaps the most famous modern novel that features a volcano in the title is Malcolm Lowry's *Under the Volcano* (1947), which has been referred to as having the best account of a "drunk" in fiction. This modern classic is regarded as one of the major novels of our time, but its relevance to volcanic activity is little or none, except for the memorable title—and perhaps the use of the volcano as a metaphor for the mental and physical hell that the British consul, the novel's main character, descends into. Similarly, don't look for wisdom about eruptions in the massive novel *The Volcano God* by Philip Freund (1959). It is an epic profile of our age and, again, has no relation to volcanism except for the enigmatic title.

Modern novels about volcanoes can be roughly divided into literature and adventure genres, with works in the latter being by far the most numerous. Perhaps the most popular adventure writer of our time, Patrick O'Brian, puts a volcanic eruption to good use in *The Wine-Dark Sea*. When naval Captain Aubrey is chasing a privateer in the South Pacific Ocean, amazing natural phenomena occur, as the sky turns wine-red, a tidal wave swamps his ship, and violent explosions emerge from the deep. When daylight breaks, they witness the eruption of a new volcanic island, that has devastated their prey with ash fall and bombardment of volcanic ejecta.

The novels in the literary genre often take real volcanoes and their eruptions as a backdrop for the plot but not as the main theme. The 1902 eruption of Montagne Pelee is featured in several of these novels, which is not surprizing, considering the strong human appeal of the story. In addition to novels, a few literary accounts of volcanic eruptions have been written. Two very good historical accounts of the catastrophic Pelee eruption are *The Tragedy of Pelee* by George Kennan (1902) and *The Day the World Ended* by Gordon Thomas and Max Witts (1969). Similarly, *Krakatoa* by Rupert Furneaux (1964) is an excellent historical account of the great 1883 eruption. However, in the category of historical accounts of volcanic eruptions, *The Night of Purnama* by Anna Mathews (1965) is unique. Shortly after the author and her husband took up residence in the village of Iseh on the south flank of Mount Agung in Bali, the volcano burst into a furious series of eruptions, producing numerous and deadly pyroclastic flows. Her book is a tense and thrilling account of the impact of the lethal eruption on the Balinese village community, providing much insight on the relationship between the Balinese and their gods—the most powerful of which reside in Agung.

In the theater, a recent work based on the 1902 eruption of Montagne Pelee is the play *The Prisoner of St. Pierre* by Pat Gabridge, which describes the real-life ordeal of the prisoner Ciparis, a black man sentenced to death. When the eruption took place, Ciparis was being held in a dungeon below the city, which protected him from the worst effects of the scalding hot pyroclastic surge. He became the most famous survivor of the catastrophe, and the play describes the hallucinations he experiences while waiting for rescue. Ciparis later made a living by touring in the United States as a member of the Barnum and Bailey Circus. It is perhaps surprizing that his fantastic story has not yet been featured as the central theme of a novel or a film.

A. The Violins of Saint-Jacques

Patrick Leigh Femor traveled in the Caribbean after World War II and as a result published *The Violins of*

Saint-Jacques in 1953. This beautiful and haunting novel was immediately hailed as a rare and exotic seep of color across the drab monochrome of the postwar years. It is set on a Caribbean island of romantic passion, tropical luxury, and European decadence, and the story captures the delicacy of high society entanglements and the unforeseen drama of the volcanic forces beyond human control.

The narrator first encounters the Caribbean volcanic island in a painting during his visit to the artist Berthe. It is a picture of a colorful town, above which "a tropical forest rises in a cone, hiding to its crater the steep and concave flanks of a volcano from whose blunt apex curled a languid blue-gray banner of smoke." It is inscribed by the artist and the year 1902. Bethe tells him she had spent 6 years as a governess to the Sheridans, a patrician family on the island of Saint-Jacques, in the shadow of the ever-smoldering Salpetriere volcano.

Every year on the last day of carnival, a great ball was traditionally held in the Count Sheridan household in Saint-Jacques. On this occasion, in the days when preparations were under way for the ball, the Salpetriere had been burning for a week or so with unaccustomed vigor: "Now it hung in the dark like a bright red torch, prompting the island wiseacres, mindful of the terrible eruptions that had coincided over a century ago with the fall of the Bastille, to shake their heads." The ball is attended by the governor of the island and turns out to be a tremendous success, but it was interrupted by an unexpected event.

> *In the middle of a dance, a deep ominous rumble was heard above the notes of the orchestra. A bright flash like lightning drowned the many candle flames for a second with its brighter intensity and a rush of wind filled the curtains in their confining coils of hibiscus and blew them into the ballroom in wavering cylinders. The dancers stopped and looked through the long windows at the top of the Salpetriere where a sparkling fountain of fire had suddenly sprung to a great height in the air; a brilliant red gold needle, whose mounting summit bore all the gazing eyes upwards and then down again as it broadened and lost its shape and subsided. A wide stream of lava burnt its way down from the crater's rim. It looked as if the volcano itself were conspiring with the Count to add lustre to his rout.*

Shortly afterwards, one of the guests remarks: 'Look, it's snowing.' The observation was so unexpected and irrelevant that everybody burst out laughing. And snow was indeed falling. It was that light descent of feather-soft ash that often followed any usual activity of the Salpetriere.

Bethe discovers that the Count's beautiful daughter, Josephine, has run off with an undesirable suitor, and she suspects they have headed for the harbor, in order to get on the next boat to Paris. She gets a skiff to bring her to the schooner anchored outside the harbor but is disappointed—Josephine is nowhere to be found. While still on the ship, Bethe is startled by

> *an incandescent ball of light . . . then two seconds later came a deafening clap of thunder as though the world had been blown in two. The night had vanished. Everything was suddenly brighter than noonday and from the crater of the Salpetriere a broad pillar of red and white flame, thickly streaked with black, was shooting into the sky like the fire from a cannon's mouth. It climbed higher every second until it had reached a fierce zenith miles up in the air, and the roar that accompanied its journey was interrupted by hoarse thunder claps that almost broke the eardrum. A great wave of heat, as though an oven door had been opened, swept over the watchers on the schooner, and the sea, reflecting the conflagration. Fiery fragments from the centre of the earth were flying through the sky and missiles like jagged lumps of fire, coming apart in their flight as liquidy as sealing wax, fell dripping to the water.*

Bethe sees that in the streets on shore, all is in panic and turmoil, with people leaping onto the water and swarming aboard the boats. A crowd of dancers in flight crowded the terraces around Count Sheridan's house. After a brief pause, the eruption resumed with a blinding flash,

> *followed by something which seemed for a moment, by contrast, pitch darkness. For a black cloud had burst out of the volcano's flank far below the crater. The fires inside the mountain had blown a new rift which spread upwards towards the steaming chaudieres. This jagged, growing tear revealed the inside of the mountain for a blazing fraction of a second before it was obscured by the rapidly swelling volume of a cloud that came rolling and billowing down towards the town, setting fire to everything in its track. At last the entire cloud was growing from the island's side in a great unfolding rose. It slowly faded again into fire-rimmed blackness and all was opaque and impenetrable. Gently it settled over the town and enfolded the houses and the spires.*

What follows is a scene based entirely on the May 8, 1902, eruption of Montagne Pelee, when ships in the harbor were set aflame by fiery hot surges passing over the ocean, while ships further out in the bay were singed, but limped away to safety. Safe on the schooner outside the harbor, Bethe watches in horror as the citizens are halted in their flight and swept down to the ground by the descending gas cloud that invaded the city when the mountainside opened up. The cloud rolls into the harbor and over the bay, as ships caught on fire. She is terrified that the deadly cloud will reach the schooner, but "The cloud's soft progress over the water halted and its edges began to creep backwards again as though the ghostly mass were drawing in its skirts."

The captain orders all sails set and steers the schooner due west, out of harms way. They look back and see that the island is literally coming apart, with the erupting fissure opening in a fiery yawn. Hills near the coast collapse, sending up a huge tidal wave that wildly tosses the schooner on the sea. Saint-Jacques is sinking into the ocean as the schooner speeds away. Soon only the summit of la Salpetriere remains above the waves, with huge billows of steam around. Then only the crater rim remains visible, with an immense plume of fire, but at last that too subsides into the sea, "and the water flowed in and snuffed it almost in silence."

Bethe goes ashore in the island of Dominica. Soon she finds out that there is not a single other survivor from Saint-Jacques. Ships sailing over the point find not a trace of the island. However, in the following years, the fishermen of Dominica and Guadeloupe claim that they have observed a sign of the vanished town. When they sail over the submerged city at carnival time, they can hear the faint sound of violins coming up through the water. As though a ball were in full swing at the bottom of the sea. They call it "the violins of Saint-Jacques."

B. The Sleeper of the Moonlit Ranges

In the novel *The Sleeper of the Moonlit Ranges* by Edison Marshall (1925), the native Alaskan Breed Bert from Pavlof village becomes a guide for rich and spoiled Americans in the Alaskan volcanic and rugged wilderness. It is a story that is strongly influenced by the Katmai eruption of 1912 and makes frequent references to the rapidly changing face of the Earth as a result of volcanic activity. Bert and beautiful Grace fall in love, and their journey eventually turns into a deadly love triangle, involving Grace's jealous fiancee Paul. But Pavlof Mountain begins to erupt, at first with a ruddy fountain of lava from the summit crater. The native Alaskans begin a dance to pacify the god of evil in the volcano, and Paul joins them in a frenzied dance. In a trancelike condition, Paul demands that the natives sacrifice both Grace and Bert to the fire god, but they escape—at least for a while—by running straight up the flank of the volcano. But now they are caught in a vast volcanic outburst, as Pavlof explodes and they loose consciousness in the cataclysm. When they come to, Bert discovers that one side of the volcano has been blown out, the village has been destroyed, and lakes of molten lava are forming in the crater and flowing toward them. The lovers escape miraculously and begin a new life as pioneers of the Alaskan frontier.

Human sacrifices to the volcano gods have been a highly popular topic in a number of other novels, including *The Phantom City* by William Westall (1870), where a young maiden is sacrificed to the fire god in an erupting volcano in the Mayan region of Mexico.

C. Paricutin

Paricutin is a truly historical volcano novel, written by Bernice I. Goodspeed (1945) and published immediately after the birth and growth of Paricutin volcano in Mexico. The central theme of the novel is the mental struggle among the native Tarascan Indians in response to the devastating eruption. It is a struggle over whether to follow the Christian ways and pray or to pay homage to their ancient fire gods and make human sacrifices to appease their wrath. It is thus a story about a people caught at the crossroads of two cultures as they react a natural disaster.

Some of the elders of Paricutin village still secretly worship the fire god Ome Teotl. Thus when Mazatl witnesses an erupting fissure opening up in his field, he

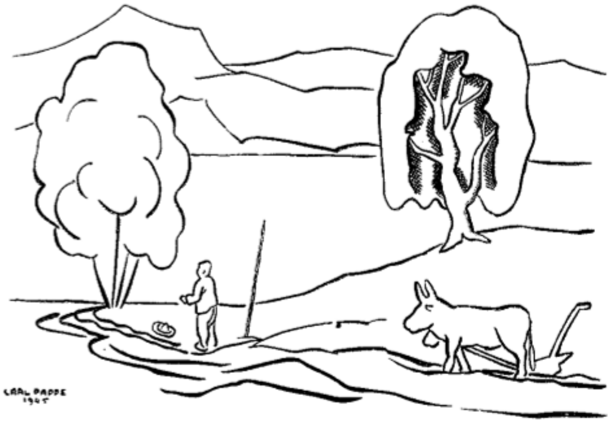

FIGURE 2 When Mazatl plows his field, a fissure opens up in the ground, marking the beginning of a violent eruption and the birth of Paricutin volcano in Mexico. The illustration is from the historic novel *Paricutin* by Bernice I. Goodspeed.

is convinced that someone must have offended Ome Teotl and that more tributes to the god are required (Fig. 2). The priest of their village, however, tries to persuade his people that the eruption is an act of nature, and not due to the actions of the christian god or of Ome Teotl. But the elders recall the creation of Jorullo volcano nearby, that had severely affected their ancestors. When all prayers had failed at Jorullo, the elders gathered in the temple, and decided that only a human sacrifice would pacify the god of fire. A youth was chosen, and he climbed up the cone to the very brink of the erupting crater, where great tongues of the flames reached out and swept him down into the fiery abyss of Ome Teotl. After a final explosion, the Jorullo crater subsided, and it appeared that their sacrifice had brought them peace.

As the eruption of Paricutin intensifies, the elders become increasingly worried, convinced that the prayers to the Christian god are of little or no value in calming their fire god. Mazatl and his two friends become convinced that only a human sacrifice will save their community from destruction, and select their teenage children, the virgin Zolintzin and young Tochtil, to sacrifice to the flames. They decide, however, that the sacrifice must be made to Popocatepetl—father of all volcanoes—the principal residence of Ome Teotl. The children are convinced that the sacrifice is a necessity and set out on the long journey to Popocateptl with one of the elders. As they near the crater, the elder is killed in a fall into a canyon, and the frightened youngsters are taken under the protection of an old forester and a Padre in a nearby village. They are torn in a great conflict between the promise they have made to the elders to sacrifice themselves in the volcano crater, and what they hear from the forester and the Padre. Their new guardians gradually convince them that such a sacrifice is not essential for the well-being of their village. The teenagers settle down in the village at the foot of Popocateptl, marry, and have a child.

Meanwhile, the eruption of Paricutin continues and lavas engulf more fields and villages. Mazatl is now convinced that the sacrifice of his children has been in vain, the ancient god has let him down, and he is heart-broken. The youngsters return to Paricutin one year later, where they are welcomed by all, except Mazatl, the father of Zolintzin, who is furious over the breach of promise of the sacrifice. He then runs up the side of Paricutin's erupting cone to sacrifice himself to Ome Teotl.

D. Volcano

As a land where volcanoes are a dominant part of the landscape and often threaten lives and property, Japan is the source of a number of volcano novels. An excellent example is Shusaku Endo's *Volcano* (1959). In this carefully elaborated Japanese thriller, the aging volcanologist Jinpei Suds and the Catholic priest Dehorned become obsessed by the Akadake volcano. For both, the question whether the volcano is still active or not becomes the overriding concern in their lives. Suds has spent 15 years studying Akadake and is convinced that it is dying. This opinion is very good news to a tycoon who is building a lavish hotel resort on the volcano's slopes. Dehorned is equally certain that the volcano will erupt again, pouring streams of lava down over the religious Christian sanctuary being built at its foot. To Dehorned, the volcano is a symbol of evil and a judgment on the people who cannot understand the significance of sin and redemption: "Akadake is absolutely going to explode. Because evil is a volcano that will never be extinct." To Suds the volcano must remain dormant, or else it will wreck the scientific thesis on which he has spent much of his life and on which the book he is about to publish, *The History of the Eruptions of Akadake*, is based. The book is the result of 15 years of research, with the financial support of the business tycoon.

The novel's volcano has had numerous historical eruptions, the latest at the end of the 19th century, but since Suda's arrival at the observatory, only a plume of thin smoke rises from the crater. Professor Koryama of Kyoto University has declared that this is sign of dormancy; the volcano was stricken with old age: "What a mount of heartache it is. A volcano resembles human life. In youth it gives reign to the passions, and burns with fire. It spurts out lava. But when it grows old, it assumes the burden of past evil deeds, and it turns as quiet as a grave."

Shortly after the ailing Suds is admitted to the hospital, Akadake suddenly explodes:

> *It came at high noon, when the people were at lunch. At first they seemed to hear a dull rumble as of distant thunder. Then a sudden ear-splitting detonation. Houses shook, windows rattled. People panicked and ran into the streets, where they beheld a black column of smoke rising into the sky beyond the bay. The top of the column expanded into a shape like the round head on a sprig of cauliflower. They watched the head uncoil.*

The observatory monitoring the volcano stresses that there was no cause for alarm and no imminent danger, even though the eruption was totally unexpected. Investigators report that no tremors of any kind, that might be portents of volcanic activity, have been recorded before the event. They also report that the eruption has not produced any new magma, merely a discharge of gases trapped in the crater mouth. After a few days, life is back to normal, and it seems as if people have completely forgotten about the event—Akadake appears to have resumed its old forlorn appearance.

Suds had earlier observed that, historically, the volcano has had a peculiar behavior. Successive eruptions always originate at a higher elevation on the flanks than the previous one: It is "an upward moving volcano." He is relieved when he finds out that the new explosion has taken place from the very top—it is just the last gasp of a dying volcano. This is challenged by a young Tokyo University professor who discovers that the gas emissions include enormous amounts of halogen elements. He predicts the coming of a big eruption at the 900-m level on the volcano's eastern flank, which would devastate the planned hotel complex. Suds feels humiliated, and his pride is hurt by this novelty hypothesis concocted without evidence by a greenhorn scholar. He reassures the tycoon that all is well; "Everybody wants to publish novel ideas." "Look it's safe, I tell you. Akadake is impotent with old age." When Suds regains some of his strength, he accompanies the tycoon on an excursion to inspect the volcano. They are both pleased to find that the hotel site appears normal and safe—until Suds notices a dead field mouse and withered vegetation. He remains quiet about his find and terminates the investigation, fearing what he might find. A few days later, when he visits the observatory, he discovers to his dismay that ominous tremors have occurred during the night, suggesting an imminent explosion. He returns to the flanks of the volcano, where he finds unmistakable warning signs, such as increased temperature of the ground. Still keeping his findings secret, he returns in silence and in deteriorating health, dying a few days later. His son carries a crock with his ashes to the slopes of the volcano for burial. Shortly afterward, Father Dehorned also dies, but a single plume of smoke continues to rise from Akadake. Will it erupt tomorrow, or is it truly dormant? The reader is left to wonder at the novel's end.

This is a geologist's novel in many ways. It is full of field observations, historical volcanological data, and lucid descriptions of landscape and Earth Processes. The author Shusaku Endo had great affection for Kyushu Island, the setting for his novel. Thus the city in the novel is based on Kagoshima, and Akadake volcano is inspired by Sakurajima, one of Japan's most active volcanoes. Sakurajima began as a volcanic island in Kagoshima Bay but joined the mainland in the 1914 eruption. The frequent eruptions have often caused ash fall on the city of Kagoshima, only 8 km from the crater. It is reported that the author's curiosity about the volcano was so great that he had himself lowered from a helicopter into the Sakurajima crater.

E. The Volcano Ogre

The Volcano Ogre by Lin Carter (1976) is a good example of a bad science fiction/fantasy novel. The action takes place on the slopes of the fictitious Mount Rangatoa volcano on a Polynesian island. In its innards, the volcano harbors a grotesque, humanlike monster, covered with glowing hot lava, who occasionally lumbers out of the crater to threaten the local inhabitants. After the lava devil kills again, the islanders send a plea of assistance to the all-powerful Prince Zarkon and his crime-fighting Omega Crew. The hideous volcano monster, wading through red-hot molten lava as if it were tepid sea water, turns out to be an American geologist, wrapped in protective plastic boron-fiber insulation against the heat of the lava. There is no knowledge of volcanoes to be gained from this novel, although the idea of a geologist as an evil volcano monster is no doubt appealing to some people.

F. Genesis Rock

In this fantasy novel, Edwin Corley (1980) spins a lively tale about a volcanic eruption in the heart of New York's Central Park. It is indeed a far-fetched concept but an entertaining story that drops the names of several contemporary volcanologists and makes abundant references to famous eruptions and geological processes. Janet McCoy, a beautiful and brilliant volcanologist who works for the U.S. government, is recalled to New York from Iceland, where she has been studying methods to harness geothermal energy. The reason for Janet's recall is that she has been picked by NASA for a mission to explore the geothermal energy resources of the planet Mars. Passing through Central Park, she is amazed to come across a chunk of anorthosite lying by the path—a Genesis Rock. In her opinion, it is a very rare rock type that is only found at the surface when hurled out of the Earth by cataclysmic upheavals, such as volcanic explosions. She also finds out that Central Park is riddled with dikes.

A homeless man, who has made shelter in a cave in Central Park, notices hot steam venting out of a fissure in the rock and makes use of it to cook squirrels for lunch. Events unfold as mysterious bubbles of sulfur-rich gases emerge from the lake, and a construction team blasting a subway tunnel through the park encounters steam veins in the solid rock. When a violent steam explosion scalds a worker to death and injures several others, the news spreads rapidly that something very unusual is afoot below Central Park.

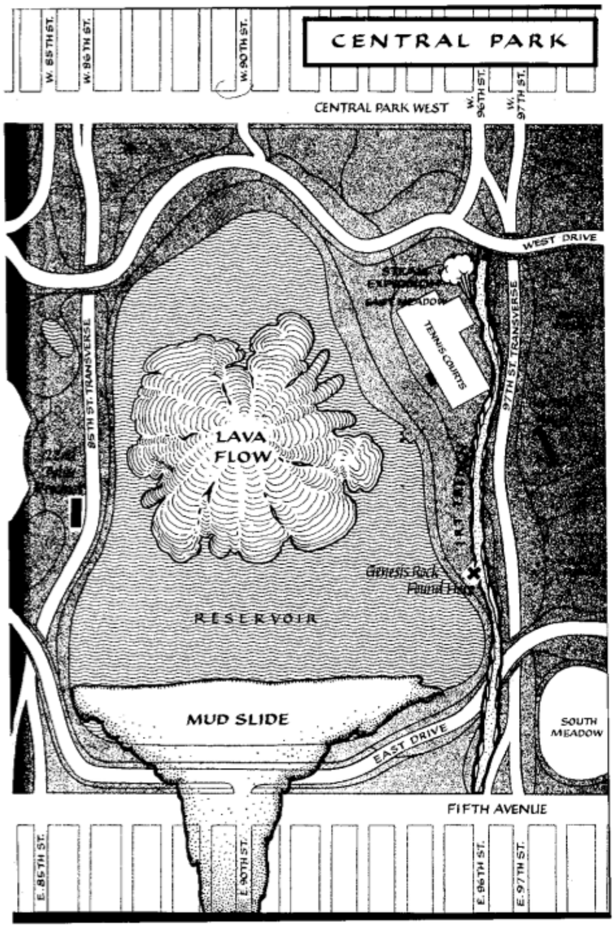

FIGURE 3 In the novel *Genesis Rock,* a new volcano bursts forth in Central Park, New York.

Janet assembles a team of Earth scientists to study this strange phenomenon, and they are startled to find that infrared aerial photos show a "hot" line that strikes from the Baltimore Trench, goes across the continental shelf and terminates near Staten Island. Is this thermal anomaly associated with a magmatic intrusion at depth? Or is it just a stringer from the Gulf Stream? Meanwhile, the fissure erupts again, forming a geyser that shoots up steam to a great height. Janet McCoy informs the mayor that the birth of a new volcano may very well be taking place in Central Park, and that the entire New York region may soon be covered with 4 feet of ash from a Krakatau-size explosion; alternatively, it may result in an Icelandic-type eruption, with widespread lava flows covering the park and large parts of the city. Meanwhile, her geophysicist colleagues are exploring ways to head off a volcanic eruption, possibly with the detonation of a nuclear bomb. They discuss an alternative scenario of diverting lava flows by pumping water on them, as was done successfully on Heimaey in Iceland in 1973.

The subway tunnel construction crew decides to pump large volumes of water down the fissure to cool things off at depth before they resume drilling—but with disastrous results. "With an incredible belch, the solid rock heaved and began to reject the liquid diet." Several steam explosions occur, ejecting boiling water and superheated steam all over the park and into the city. A thick mudflow rushes down the East Drive and into the East River, resulting in many casualties and destruction of buildings, including the mayor and his residence. Huge fountains of steam and water rise to thousands of feet above the boiling reservoir. When most of the water is dissipated, the top of a glowing lava mass begins to emerge (Fig. 3).

Janet predicts that worse is to come and demands that the city be evacuated before more deaths occur. The president agrees, and, at Janet's suggestion, the Joint Chiefs of Staff plan to bomb the hot vein of magma that runs across the continental shelf to New York with a nuclear device, in order to relieve the pressure below the city. Meanwhile, the reservoir has nearly filled with lava and it is about to burst out of the park. A submarine delivers the nuclear bomb to a spot above the magmatic sill in the ocean floor, and shortly after it is detonated, the magma extrusion rate in the new Central Park volcano slows down to a trickle. Janet McCoy has saved New York City.

The author of this novel came up with an extremely unlikely scenario, but he did some homework, making use of ideas behind the lava diversion in Heimaey in 1973, as well as early bombing of lava flows on Kilauea.

G. Gentlemen in England

A. N. Wilson (1985) has written a novel of repressed Victorian life and manners, set in London in 1880. *Gentlemen in England* is not a novel about volcanoes, but it features a volcanologist as one of the main characters. The plot centers around young Charlotte, who is courted by the much older Professor Horace Nettleship, an enormously respected volcanologist. She is impressed by the potency that is implied by his fieldwork on volcanoes, and they marry. Soon however, the marriage is in trouble, largely because her husband confines all his passion to the three volumes he is writing about his research. As the plot develops, husband and wife have not spoken privately for 15 years, but keep up the ap-

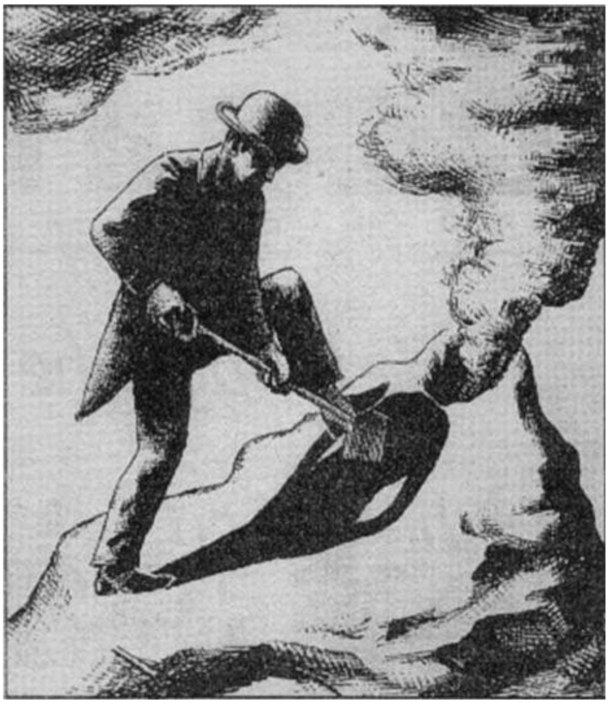

FIGURE 4 In the novel *Gentlemen in England* (1985) by A. N. Wilson, the volcanologist becomes alienated from his wife and society as his preoccupation with his geologic monographs deepens.

pearance of a happy marriage in public—a caricature of Victorian society. The author makes the perfect statement—indeed the epitaph—of the typical volcanologist: "Volcanoes his expertise, he found out about the world by peering at little pieces of it through a microscope, by hammering little chunks of it, and keeping specimens of it in boxes." The volcanologist's alienation from society is also perfectly captured (Fig. 4). The professor is too absorbed in his work: "He has been working on a great book about volcanoes ever since my daughter married him.... All their little holidays as far as I can recollect have been spent in places of particularly volcanic interest." Soon the professor realizes that his wife does not care for him in the least:

> *He toiled at his treatise on volcanoes. In his youth he had explored the earth's surfaces and seen eruptions in Iceland and Mexico. It was the experience of twenty or thirty years which he poured into his three-volume monograph, so there was no temptation of idleness when his study door closed behind him. But the silence had made him into a stranger—not merely to his wife and servant, but also to his children.*

H. Texaco

Martinican writer Patrick Chamoiseau won the prestigious Prix Goncourt, France's most celebrated literary award, for *Texaco* (1992), a novel about his French Caribbean island home, written in the French Creole oral storyteller tradition. Like *The Violins of Saint-Jacques*, the deadly 1902 eruption of Montagne Pelee is a subplot within the novel, but here it is seen from the perspective of a former slave. *Texaco* is a mythic history of the rise of the Creole nation in Martinique from its African and French roots. The title refers to a gas station at the outskirts of Fort-de-France, around which a shantytown developed.

Esternome Laborieux is born into slavery on a plantation near the city of Saint-Pierre, at the foot of Montagne Pelee. The slaves knew that "... the lumpish mountain overlooking Saint-Pierre was in reality a raging bull." When slavery is abolished, Esternome abandons the plantation and takes up carpentry in Saint-Pierre. Here he meets beautiful Ninon, "with eyes glittering like childhood's water, eyebrows curving thickly like strange umbrellas, a mouth for smiling, lips more bluish than the skin, and large voracious teeth." Together, they leave the city and squat on abandoned land in the hills, living the life of subsistence farmers. After a few years, the idyll is shattered when Ninon runs off to Saint-Pierre with a musician. Esternome lives on in sadness, and in this daze he did not "see how from time to time the horizon became roaring and how ash from the mountain suddenly floured the land, more and more often, for a longer and longer time." One morning a huge bang blogodoom shook him into consciousness. He came out of his thousand-year stupor with a ball of hope. His first word upon his return to life was:

> *Ninon. Ninon, which he repeated in the general tumult. Manic fleeing shook the Quarter. A fragrance of sulfur, of scorched red-wood, singed life, thickened the air. Each and every one around was screaming, Soufriere has exploded! This rumbling had undone the world. On the horizon, a night that defied the sun was rolling down. Esternome went down to City. He wanted to seek, see, save Ninon.*
>
> *On the edge of a hill, my Esternome discovered a lump of coal instead of Saint-Pierre. Despite his barbecued heart, it stunned him.... Soon he couldn't take another step forward. His eyes were burning. Even his gray hair burned him. The grass, the trees had withered.... And he moved on and on and on. So that he was the first to enter Saint-Pierre.*
>
> *He walked on like that, not seeing anything any*

> *more, so much had he seen. A tide of ash. A deposit of still heat. The stone's red glow. Intact beings stuck to wall corners, going up in strings of smoke. Some were shriveled up like dried grass dolls.*

He went from cadaver to cadaver and examined every blackish thing, but of course he never found Ninon.

The tragedy of Montagne Pelee, so vividly descried here, is a recurring theme in novels about the Caribbean. Chamoiseau's later novel, *Solibo Magnificent* (1998), also refers to the eruption, with discussion of Mount Pelee, the ash of Le Precheur, and other geological scenes on Martinique.

I. The Volcano Lover

In 1992 there appeared a romanticized biography or a historical novel about the life of Sir William Hamilton, by the celebrated American writer Susan Sontag. In this novel, the life of the central character is intertwined intimately with the past and present volcanic activity of Vesuvius. The plot is a well-known tale: Hamilton, an elderly diplomat and nobleman, is the British ambassador to the Kingdom of Naples, where he becomes fascinated by the activity of nearby Vesuvius. His interest in the volcano gradually evolves from amateurish enthusiasm to a fully fledged research project, that culminates in a series of important and lavishly illustrated scientific publications by this first volcanologist. He is tireless in studying the object of his fascination, traversing its lava flows, repeatedly climbing to the fire-spitting summit crater, and facing danger for the sake of more information about the workings of the inner Earth. He collects rock samples and ships them back to England for chemical analysis. When his wife dies, the lonely and aging nobleman begins a relationship with Emma, a young and strikingly beautiful former mistress of his nephew, and soon the unlikely pair weds. The celebrated couple participate in the rediscovery of the cities of Pompeii and Herculaneum, unearthed from the ashes of the A.D. 79 eruption of Vesuvius; the ambassador acquires a fine collection of antiquities, and the wife develops a new performance art form, with her "attitudes" or posing inspired by the recovered Roman paintings. When the great British naval hero Lord Nelson appears in Naples, he is nursed back to health by Emma, and here begins a somewhat scandalous long-term relationship that the ambassador manages to ignore.

The Volcano Lover is a formidable romantic biography that is based on meticulous research. All volcanologists are familiar with Hamilton's pioneering work on Vesuvius and on the entire volcanic region of Campi Phlegraei in Italy, and it is fascinating to read an account where this historic figure of volcanology is brought back to life in vivid detail.

J. Swimming in the Volcano

In *Swimming in the Volcano*, a love story and sophisticated political novel by Bob Shacochis (1993), the American economist Mitchell Wilson becomes unwittingly involved in a struggle between two factions of the government of a small Caribbean island, against the backdrop of volcanic activity. The novel's smoldering volcano is Mount Soufriere on the Caribbean island of St. Catherine, and it is of course based on La Soufriere volcano on St. Vincent. The volcano is correctly described as dormant since 1902, with a hot brown lake surrounding a steaming magmatic island in the crater.

In the novel, forest ranger Godfred Ballantyne of the Ministry of Agriculture is dispatched weekly up to the crater to monitor any change in activity. The topographic descriptions of the volcano are excellent, and many details about the monitoring of the Soufriere in the 1970s are brought to life:

> *… and then, as though a lid had been pried and removed, the immense bore of the volcano's crater, shattering any sense of human proportion. To Wilson, the scale seemed borrowed from another world—a fantasy land of fire giants, a geography more dreamlike and therefore more threatening than it actually appeared or was. The light spilled into a huge bowl, and they could see across the span of the vent almost a mile to the sheer walls of the opposite side. There was no slope, only a raw precipice of rock that dropped straight for hundreds of feet to the surface of the doomed lake. The interior island appeared incongruous, inappropriate, and trashy, as if somehow and old coal barge had been abandoned here in the eye of disaster, the cargo still smoldering in the hold. …*
>
> *Ballantyne checked the water level. Despite a constant replenishment by storms, the level had been receding at the rate of two inches per week for several months, which Ballantyne took for a sign that the core was heating up.*

Because of Mitchell's liberal, leftist leanings and a nonconformist lifestyle, he is viewed with suspicion by the authorities and politicians on both sides. Some suspect that he may have connections with a group of guerrillas that are operating from camps on the remote flanks of La Soufriere. When Mitchell leads a group of friends on an ill-fated climb of the volcano, they are intercepted by a group of policemen. During the questioning, Mitchell's girlfriend is shot by an unknown assailant—a guerrilla or a government agent? The victim, a Peace Core worker, dies shortly afterward. Mitchell is jailed without trial, but then he is released after the next election.

Although this is not primarily a novel about a volcano or an eruption, the author did his homework on Soufriere, and his descriptions of the volcano and its monitoring are excellent.

IV. JUVENILE FICTION AND COMICS

Volcanoes are a favorite topic with children and many authors of children and teen-age fiction bring in volcanoes and their eruptions as a subtopic, but rarely are volcanoes featured as a central theme. Probably the best known children's novel to feature volcanoes is *The Little Prince*, written and illustrated by Antoine de Saint-Exupery. First published in 1943, it quickly became one of the world's favorite books. Although written as a story for children, it contains an urgent humanitarian message for people of all ages. Volcanoes are brought into the story as the prince describes his home, the asteroid B-612, to his newly found terrestrial friend. There are two active volcanoes on the asteroid, and the prince finds them convenient for heating up his breakfast in the morning (Fig. 5). He is careful to clean the volcanoes out regularly.

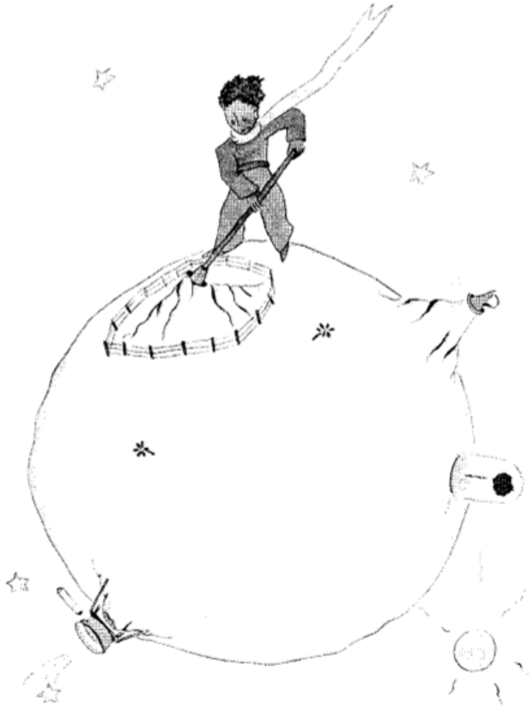

FIGURE 5 In *The Little Prince* (Antoine de Saint-Exupery, 1943) the prince is careful to clean out his volcanoes regularly, so that they burn slowly and steadily, without violent eruptions.

> *He also had one volcano that was extinct. But, as he said, 'One never knows!' So he cleaned out the extinct volcano too. If they are well cleaned out, volcanoes burn slowly and steadily, without any eruptions. Volcanic eruptions are like fires in a chimney. On our Earth we are obviously much too small to clean out our volcanoes. That is why they bring no end of trouble upon us.*

The illustration of the Prince, straddling his tiny planet and cleaning out a volcano with a long poker, is an unforgettable image for children and adults alike.

A. The Twenty-One Balloons

The Twenty-One Balloons, a humorous story by William Pene du Bois (1947), tells of a fabulous voyage around the world in a balloon, undertaken by Professor Sherman from San Francisco in August 15, 1883. The date is important, because his only stop on the journey is on the island of Krakatau. The cataclysmic eruption of Krakatau actually occurred on August 26, 1883. In the story, the professor makes an emergency landing on a small volcanic island, after his balloon is punctured by seagulls. He soon finds out that this is Krakatau, and that it is inhabited by a handful of highly sophisticated American settlers, wealthy beyond belief because they have discovered a fabulous diamond mine under the volcano. The island is ruled by the Gourmet Government, whose motto is "Not new things, but new ways." The only major drawback of the island are the frequent earthquakes and rumblings of the volcano. To avoid earthquake damage, the Krakatoans build their houses on foundations of solid diamond boulders.

The professor settles into a life on the island and joins the Krakatoans in short trips in their own balloon. One trip takes them directly over the crater, where the professor notes that a lake of molten lava seethes in the bottom, emitting clouds of sulfur. The islanders are acutely aware of the danger of living on Krakatau: "This whole island is like a turkey stuffed with nitroglycerin."

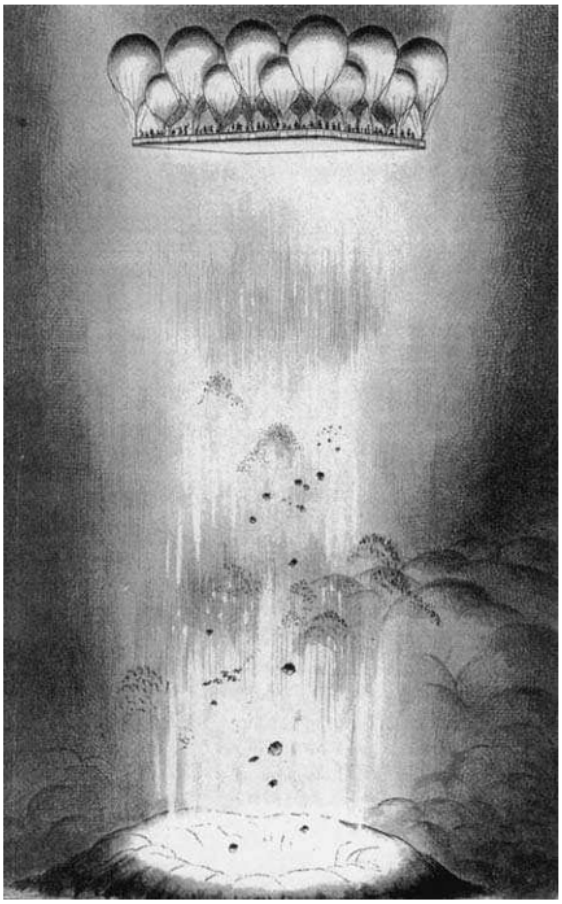

FIGURE 6 In *The Twenty-one Balloons,* by William Pene du Bois (1947), the Krakatoans escape their island in a balloon when the volcano erupts.

As an escape mode for a fast getaway in case of a violent eruption, they have constructed a flying platform to carry the 20 families to safety, lifted by 21 balloons (Fig. 6).

On August 26, during the professor's lecture, a violent earthquake strikes the island, cracking walls and breaking windows. The order is given to all to dash to the balloon platform for evacuation. They take off, but unfortunately the wind carries them directly toward the volcano and over the crater. Here they "were greeted by a roaring swift upward blast of hot air which catapulted the balloon far up into the sky." Trapped above the fiery red crater, they bob up and down on top of the eruption column for the entire night, in hot sulfurous fumes. Fortunately, they eventually drift off the eruption column, toward Java, just before the entire island of Krakatau blows up in a tremendous explosion. A thick blanket of ash settles on the balloon, and the Krakatoans are deadly afraid that diamonds from the mine will fall and puncture their balloons. They drift away, over the Indian Ocean, the Mediterranean, and Europe. Finally the professor makes a controlled crash of the balloon into the North Atlantic Ocean. This is an unusual novel because it uses a major volcanic eruption as the central theme for a lighthearted story, with delightful illustrations of the volcanic activity.

B. Juan of Paricutin

The children's novel *Juan of Paricutin* (1953) is unusual in that it was written by a geologist—Marion Isabelle Whitney, who witnessed the eruption and spent considerable time with the local people. Her book can thus be properly regarded as a historical novel. It is a tender and sympathetic story of the hardships that a family in the village of Paricutin experiences as a result of the eruption.

When Juan and his grandparents visit a nearby village, a strong earthquake strikes, swaying the church tower and toppling another tower into the plaza. Rumblings from the Earth and quakes are common during the next few weeks. One day Juan and his family accompany his uncle Dionisio to help him prepare a field. While they get ready, Paricutin village is struck by the strongest earthquake yet. When they arrive in the field, they hear loud rumbling and tremors underground and see a pit opening in the cornfield right before their eyes! A part of the field appears to sink into the Earth, as trails of white smoke curl out of the fissure. A column of black dust rises from the center of the pit, and stones are ejected, as the deep rumble changes to a loud roar. They rush back to the village, where others have seen the activity from afar. An incessant roar comes from uncle Dionisio's cornfield during the night, and a fountain of brilliant red stones plays above the fissure, higher and higher. When morning comes, Dionisio and Juan return to the cornfield and find a terrible sight. A huge cone of rock and black ash had formed around the pit, and the cornfield was ruined. Back in the village, black ash spreads over everything, killing crops and making life nearly unbearable. The volcano grows in height and is up to 450 feet high after 12 days, and it is 1000 feet high after 2 months, still showering the countryside with rocks and dusty ash. Leaves wither on the trees and corn and all other plants die. Their livestock also die in the fields.

Tourists of all nations are now flocking into Paricutin to see the new volcano. Juan's father sets up a stand to sell soft drinks to the thirsty visitors, and the family manages to eke out an existence on this trade. The roof of their house falls in due to the thick ashfall, and eventually they are forced outdoors to set up tents. Most other villagers flee the area. One day a violent explosion blows the top off the cone, and a new vent opens up on its side, sending out a river of red-hot lava. After the initial fright, Juan begins to marvel at the fascinating spectacle and even at the beauty of sparkling crystals in the cooling lava. Gradually the river of hot lava begins to cover some of the houses of Paricutin village. But the American tourists keep coming, and the demand for bottled drinks is high. Juan's father gets the bright idea of selling the tourists donkey rides to the volcano, which enables his family to survive in the face of the disaster.

One day when young Juan is guiding American visitors, he witnesses a great outbreak of lava which threatens to engulf the rest of the village. Soon the village is totally covered by thick lava, and not even the church is spared—only the church tower stands, sticking out of the black flow. One of Juan's customers, Bill, is a knowledgable American volcanologist who teaches Juan many things about the workings of the volcano and the nature of the rocks they produce. In turn, Juan tells Bill about the sequence of events during the first day of activity—the birth of a new volcano.

There are some excellent passages in the book that are highly educational for young readers interested in volcanoes. Juan cries over the loss of his village, but he can also see another side of his situation: "I don't like that old volcano. He makes me very unhappy. But he is beautiful."

C. The Comics

The beauty and excitement of volcanic eruptions make them excellent material for comics. Two notable examples are *The Volcano With Hiccups*, one of the Flintstones stories, and *Donald Duck in Volcano Valley*. *The Volcano With Hiccups* (Horace J. Elias, 1982) is Mount Firepot, about 10 miles outside of Bedrock. It has not erupted for a long time but huffs and puffs a little once in a while. A couple of visitors, masquerading as the Flintstones' "lost cousins" show up in Bedrock for a few days, and, coincidentally, the very day they leave town, the banks are robbed. Fred Flintstone suspects that the robbers have sought refuge and a hiding place for the loot in the crater of Mount Firepot. When he and the police approach the volcano, it huffs and puffs, and spews out rocks, brushes, and 50 suitcases of money!

In *Donald Duck in Volcano Valley* (1973), Donald and his three nephews acquire a government-surplus airplane for 3. Major Mañana, a stranger from the Latin American republic of Volcanovia, offers Donald 300,000 pezozes for the plane. The major takes them for a test flight to Volcanovia, where they narrowly avoid crashing into several erupting and fire-spitting volcanoes. When attempting to land, however, they end up crashing on the summit of one of the active volcanoes. The situation turns serious when that volcano, Old Ferocio, gets ready to explode. Donald and his nephews get the bright idea to fill the crater with corn in order to stop an eruption. This results, however, in an explosion that spreads a thick layer of popcorn over the entire country of Volcanovia.

V. VOLCANO FILMS

A. Early Films and Movie "Classics"

It is appropriate that the first volcano film was *The Last Days of Pompeii* (1897), a British silent film inspired by Bulwer-Lytton's novel. Another black-and-white film of the same title but with a different plot was made in 1935, starring Basil Rathbone. This version is notable for its special effects, which are considered remarkable for its time. Italian filmmakers have also worked on this theme, first in the silent film *Gli Ultimi Giorni di Pompeii* (1913) and again in 1960, when writer Sergio Leone and director Mario Bonnard made an Italian-Spanish film with this title, featuring Steve Reeves and Fernando Rey. The theme's appeal is lasting; in 1984 Bulwer's novel was the basis of a television miniseries, starring Ernest Borgnine and Laurence Olivier.

The most important film that relates to a volcano is the American-Italian production *Stromboli* (1950). The film is remembered in part for its artistic merit and in part because of the American establishment's fervently puritanical reaction to the love affair between the actress, Ingrid Bergman, and the film's Italian director and producer, Roberto Rossellini (Fig. 7).

Rosselini wrote the script for Stromboli. In 1948, he wrote a personal letter to Ingrid Bergman, then a major Hollywood movie star, about the plot he had conceived: A young and beautiful Latvian woman, victim of the horrors of war, seeks freedom by marrying an Italian soldier. Her simple husband takes her to his home on the volcanic island of Stromboli. Rossellini explains in his letter to Bergman that the Lipari islands consist of seven volcanoes in the Tyrrhenian Sea, with Stromboli

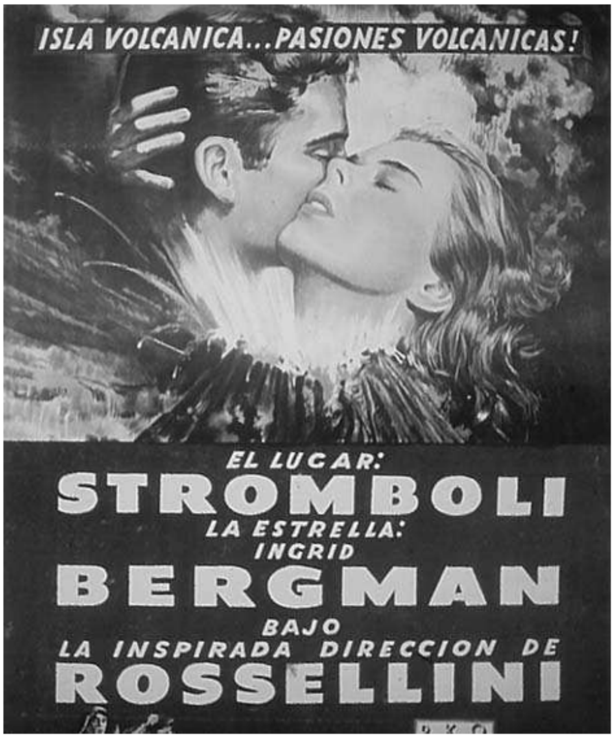
ISLA VOLCANICA...PASIONES VOLCANICAS!
EL LUGAR:
STROMBOLI
LA ESTRELLA:
INGRID
BERGMAN
BAJO
LA INSPIRADA DIRECCION DE
ROSSELLINI

FIGURE 7 A poster advertising *Stromboli,* the movie about a beautiful foreign woman who settles with her fisherman husband on his remote, isolated, and active volcanic island.

continuously active. The islands "earned sad fame during fascism, because it is there that the enemies of the Fascist Government were confined." On this island, Rossellini wishes Bergman to act out "the life of the Latvian girl, so tall, so fair, in this island of fire and ashes, amidst fishermen, small and swarthy, amongst the women with the glowing eyes, pale and deformed by childbirth, with no means to communicate with these people of Phoenician habits, who speak a rough dialect." The girl "is stranded in this savage island, all shaken up by the vomiting volcano, and where the earth is so dark and the sea looks like mud saturated with sulfur."

In April 1949 Bergman, Rossellini, and their film crew boarded a fishing schooner from Sicily to Stromboli. They sailed past Volcano Island, where Anna Magnani, Rossellini's former mistress, was starring with Rossano Brazzi in the film *Volcano* (1953).

> *They crossed the open sea for two more hours before the high cone of Stromboli, smeared with white smoke, rose against the horizon. As the San Lorenzo drew closer, they could stare two thousand feet upward to the black gullet of the live volcano. A semicircle of crimson lava curled like a bloody lip around the smoking cone, and a vast chute of recently spewed pitch-black rock spilled downwards at a steep angle to plunge directly into the bright seas below.*

The crew settled in the small village clinging to the side of the volcano and began shooting a movie. It was not without incident, however. One crew member was overcome by the volcanic fumes and died of a heart attack (Miss Bergman paid the 60,000 lira funeral expenses and set up a 600,000 lira fund for his family).

In her autobiography, Bergman said of Stromboli: "And the volcano … the volcano! The first time I had to try to climb it, we slogged for four hours upward. After I climbed for two hours, I just sat down, gasped and said, 'I'm sorry, I can't make it.' But after a rest I did make it, and at the top I could have just lain down and died." During the filming on the island, a full-scale and highly publicized love affair blossomed between the married star and Rossellini. Puritan America was not yet ready for this display of free love, however, and the establishment attacked the famous actress publicly. On March 14, 1950, the Honorable Edwin C. Johnson of Colorado stood up in the U.S. Senate to introduce a new censorship bill, and began: "Mr. President, now that the stupid film about a pregnant woman and a volcano has exploited America with the usual finesse, to the mutual delight of RKO and the debased Rossellini, are we merely to yawn wearily, greatly relieved that this hideous thing is finished and then forget it? I hope not. A way must be found to protect the people in the future against that sort of gyp…".

Stromboli may be the only volcano film that can be considered a classic in movie history. However, a recent film that has attained high praise is *Joe Versus the Volcano* (1990), described as a "story of love, lava, and burning desire." In this light-hearted story by John Patrick Shanley, Joe (played by Tom Hanks) is diagnosed with a destructive brain disease—a brain cloud—and given 6 months to live. A business tycoon makes Joe a peculiar offer: he can have an unlimited expense account, if he agrees to jump into the smoldering volcano of Big Woo on the South Pacific island of Wapuni Woo. The local Waponis believe that there is an angry fire god in the volcano that will destroy their island home in a violent eruption unless they toss a human into the smoldering crater, a sacrifice that must be carried out every 100 years. In return for a volunteer, the Waponis offer the American tycoon exclusive rights to mine bubureau, a mineral that is only found on Waponi Woo and is essential for the manufacture of superconductors.

Joe agrees to the "bargain," not realizing that he has been fooled into believing he will die. He sails off on a private luxury yacht across the Pacific Ocean, with the tycoon's beautiful daughter, Patricia (played by Meg Ryan), as an escort. On the way, the two develop a friendship, are shipwrecked, drift for days atop Joe's expensive luggage, and eventually are washed up on the beaches of Waponi Woo. Patricia declares her love to Joe and pleads with him not to jump into the crater. However, the volcano is showing increasing unrest, and Joe insists on keeping his part of the bargain. Patricia decides to die with him but, as they jump into the crater, a violent eruption ejects them off the island and into the ocean—not only miraculously alive, but again able to use Joe's expensive luggage as a raft. As the lovers float away, they see the island explode and subside into the ocean—and they live happily ever after. *Joe* has become something of a "cult" movie, probably because of its zany plot and dialogue. The theme of a volcano in the South Pacific and of natives who believe in human sacrifice to appease their volcano god has appeared in several other films.

An unusual type of volcano film is Akira Kurosawa's *Dreams*. In 1990 Japan's most celebrated film director, Akira Kurosawa, made a film consisting of a number of short stories, based on the director's dreams. The film was produced by Steven Spielberg, with special effects by George Lucas. Two of the short stories involve volcanoes. *Mount Fuji in Red* is a nightmare about the future, where the meltdown of a nuclear plant causes Fuji to erupt. Six nuclear reactors explode in succession as fireballs rise from the volcano, and a panicked crowd swamps the roads. The "hero" watches Mount Fuji turn incandescent, while multicolored smoke drifts down its slopes. The colored smoke symbolizes different types of radioactive gas. People all around commit suicide by throwing themselves off a cliff. This is followed by a dialogue between the hero, a woman, and an older man about the lies about nuclear plants and their safety. The older man turns out to be one of the plant's engineers, excuses himself politely, and also jumps off the cliff. The hero stands alone, trying to protect the woman and her baby from the radioactive fumes, in vain, as they become surrounded by the colored gas.

In *Demons* the same hero meets tortured souls on the flanks of a volcano. These are men who have survived the nuclear holocaust and are condemned to everlasting pain—they have become grotesque-looking "demons"—and they try to eke out an existance as they regret their past greed and the stupidity that wrecked the planet. There is no direct mention of volcanoes in this short story, but the landscape is clearly volcanic. Monstruous, degenerate plants are growing out of the ash. Moaning demons roll around in the dirt inside a crater.

B. Science Fiction and Disaster Movies

Jules Verne's classic science fiction novel, *Journey to the Center of the Earth*, was made into a major Hollywood production in 1959, starring Pat Boone, James Mason, and Arlene Dahl. The novel was the subject of two other films, in 1976 and in 1989, and of a television movie in 1993. None of the versions has been rated particularly highly by critics, although the special effects of the 1959 film were considered impressive for its time. Another volcano film that can be considered a science fiction thriller is *Crack in the World* (1965). The plot centers around a terminally ill villain, played by Dana Andrews, who is tapping geothermal energy from the Earth's interior by detonating a thermonuclear device at great depth. The explosion causes a crack to form that spreads through the Earth's crust and threatens to split the planet in two if not stopped in time. The film's slogan was, appropriately, "Thank God it's only a movie!"

Most other volcano films fall squarely into the disaster movie category. *Volcano* (1942) is a Superman animation movie, where a lethal eruption is predicted on the island of Monokoa. *The Daily Planet* reporters Clark Kent and Lois Lane rush to the scene, and immediately Lois is threatened by hot lava. In *The Devil at 4 O'Clock* (1961), a priest, played by Spencer Tracy, and three convicts land on a South Sea island where a volcanic eruption threatens the inhabitants. The priest and the convicts, one of whom is played by Frank Sinatra, rescue the situation. The epitome of a volcano disaster movie is *Krakatoa East of Java* (1969). The all-star cast, including Maximillian Schell, Rossano Brazzi, and Diane Baker, battle the elements at sea and on land during the Krakatau eruption of 1883. For some reason, the producers could not figure out on which side of Java the volcano sits. The 1980 production *When Time Run Out*, also known as "Earth's Final Fury" is another mediocre disaster movie featuring famous stars, including Paul Newman, Jacqueline Bissett, and William Holden. The theme is a tired one, also seen in *Jaws* and ultimately based on Ibson's *Enemy of the People*: A volcano in a tropical island becomes active, and evil resort developers insist there is no danger. The resort's architect, played by Newman, leads a small party across the island to safety and the resort is eventually destroyed by the volcanic eruption.

The most recent major volcano movies are the 1997 productions *Dante's Peak* and *Volcano*. The two films differ substantially in terms of plot and in how they portray a volcanic crisis. In *Dante's Peak*, a volcano in the Cascades threatens to wake up. The movie producers used three volcanologists from the U.S. Geological Survey as consultants, and the result is a disaster movie that is more true to life than most, although it still uses abundant artistic license. The plot centers around a dashing but brooding volcanologist (Harry Dalton, played by Pierce Brosnan), who believes the volcano is about to blow up; his boss from the Geological Survey, who sees no concrete evidence for an impending disaster; and the town's mayor, an embattled single mother whose kids eventually need to be rescued by the hero. One of the movies' major accomplishments is the portrayal of the difficult decision of whether or not to evacuate a town when the signs of an impending eruption are dubious. Harry's boss points out that evacuation of the town will lead to economic disaster for the residents—even if there is no eruption.

Dante's Peak eventually erupts and the usual disaster movie ingredients are brought in. The volcano gives out the widest possible range of products, from Hawaiian-type lavas to an acid lake to a pyroclastic flow. The pyroclastic flow simulation near the end of the movie is very impressive, and several real-life volcanologists have pointed out that it is highly educational. Relatively few people are aware that this type of flow exists and how totally deadly it is.

Dante's Peak provoked something of a flurry in the volcanological community, probably because it can be considered the least inaccurate of all volcano disaster movies. It was generally well received by scientists and even reviewed in the scientific periodical *Nature* (Fink 1997). The Harry Dalton character is credible as a volcanologist and will probably be remembered by professionals for his line, "I move around a lot, wherever there is a volcano with an attitude"

The second volcano disaster movie of 1997 was *Volcano* ("the Coast is toast"), a film written by Jerome Armstrong, directed by Mick Jackson (1997). The story seems to be loosely based on the plot from the *Genesis Rock* novel, but transferred from New York to Los Angeles. Like *Genesis Rock*, the principal character is a female volcanologist, and an eruption in the city leads to the growth of a volcano on the streets and brings about a terrifying catastrophe. The main characters, Mike Roark (Tommy Lee Jones) of the Office of Emergency Management and geologist Amy Barnes (Anne Heche), team up to save the city. The plot unfolds as seven men perish in a hot cloud of yellowish sulfur-bearing gas in the manholes below the street. The La Brea tar pits begin to steam and bubble like a pot on the stove. Mike Roark, investigating the deaths in the manhole, just manages to escape before a hot yellow gas cloud explodes through the tunnel system. "We'd better call a geologist," he says. Here enters Dr. Amy Barnes, driving a Humvee that is a science lab on wheels. She concludes that magma is moving below the city, but the Office of Emergency Management is highly skeptical—until manhole covers start rocketing into the sky, borne on top of columns of white steam, and a huge ball of a fiery explosion from the La Brea tar pits sends white ash fall over the city. A violent volcanic eruption has begun in the heart of Los Angeles. Magma breaks up to the surface, and a thick river of lava flows along the streets, setting fires, choking off traffic, and hindering evacuation. The volcano (later named Mount Wiltshire) quickly grows to 200 feet in height, threatening large parts of the city. Emergency workers build up barricades of cars and earth to try to contain the lava, which begins to form a huge pool. Suddenly Amy has an idea: bring in all available fire trucks, tankers, and helicopters to dump water on the lava pool. It works! A brittle crust begins to form on the lava. The lava diversion idea is used again—this time by the explosive demolition of a large new building. The city is saved as the lava flows harmlessly into the Pacific Ocean.

The lava diversion concept is probably the only credible idea in this movie. Explosives have been used to breach and divert lava on Mount Etna, and the cooling of lava using water hoses was successful in Heimaey, Iceland. Real-life volcanologists were quick to point out that the only real-eruption footage used in the movie was in the final scene, when lava pours into the sea.

The two 1997 movies were welcomed, by the professional community because, despite their artistic license, they succeeded in bringing the potential threats of volcanoes to the attention of the public and, perhaps more importantly, because scientists were portrayed as heroes in both movies. *Dante's Peak* can even be considered generally educational. These and many of the earlier movies contain special effects that are difficult to create—an article in the *New York Times* (1997) discusses how "flowing lava is one of the most difficult illusions to pull off in special effects." Even though the work in creating these effects has to be commended, it is disappointing that the large resources and tremendous creativity available in the movie industry have been limited to making disaster-type films about volcanoes. The fantastic real-life stories of human endurance, courage, and tragedy during volcanic eruptions have not yet been seen in the movies.

SEE ALSO THE FOLLOWING ARTICLES

Archaeology and Volcanism • Hazards from Pyroclastic Flows and Surges • The History of Volcanology • Mantle of the Earth • Risk Education and Intervention • Volcanoes and Tourism • Volcanoes in Art

FURTHER READING

Bergman, I., and Burgess, A. (1980). "Ingrid Bergman, My Story." Delacorte Press, New York.

Bulwer-Lytton, E. (1850). "The Last Days of Pompeii." Routledge and Sons, New York. Carter, L. (1976). "The Volcano Ogre." Popular Library, New York.

Chamoiseau, P. (1997). "Texaco." Random House, New York.

Chard, C. (1990). Rising and Sinking on the Alps and Mount Etna. The Topography of the Sublime in Eighteenth-Century England. *Journal of Philosophy and the Visual Arts*, 61–69.

Cooper, J. F. (1962). "The Crater, or Vulcan's Peak." Belknap Press, Cambridge.

Corley, E. (1980). "The Genesis Rock." Doubleday, New York.

Dean, D. R., (1981). The influence of geology on American literature and thought. *In* "Two Hundred Years of Geology in America" Schneer, pp. 289–303. University Press of New England.

du Bois, W. P. (1947). "The Twenty-One Balloons." Viking Press, New York.

Endo, S. (1980). "Volcano." Taplinger, New York.

Fermor, P. L. (1985). "The Violins of Saint-Jacques." Oxford University Press, New York.

Fink, J. (1997). Cinemagmatic mayhem. *Nature*, **386,** 33.

Foster, E. M. (1945). Melville and geology. *American Literature*, **27,** 50–65.

Goodspeed, B. I. (1945). "Paricutin." The American Book and Printing Co., Mexico.

Kennan, G. (1902). "The Tragedy of Pelee." Outlook Co., New York.

Marshall, E. (1925). "The Sleeper of the Moonlit Ranges." Cosmopolitan, New York.

Mathews, A. (1965). "The Night of Purnama." Jonathan Cape, London.

New York Times, 28 April 1997, page C8.

O'Brian, P. (1993). "The Wine-Dark Sea." Norton, New York.

Scudder, H. H. (1947). Cooper's The Crater. *American Literature*, **19,** 109–126.

Sontag, S. (1992). "The Volcano Lover." Farrar Strauss, New York.

Spiller, R. E. (1955). "Literary History of the United States." New York, Macmillan.

Verne, J. (1966). "A Journey to the Center of the Earth." Heritage Press, New York.

Westall, W. "The Phantom City." Cassell, New York.

Whitney, M. I. (1953). "Juan of Paricutin." Steck Co., Austin, Texas.

Wilson, A. N. (1985). "Gentlemen in England." Hamish Hamilton, London.

This Page Intentionally Left Blank

APPENDIX 1: COMMON UNITS AND CONVERSION FACTORS

1. MATHEMATICAL PREFIXES OF UNITS:

Prefix	*Symbol*	*Multiple*
tera-	T	10^{12}
giga-	G	10^{9}
mega-	M	10^{6}
kilo-	k	10^{3}
hecto-	h	10^{2}
deka-	da	10
deci	d	10^{-1}
centi-	c	10^{-2}
milli-	m	10^{-3}
micro-	μ	10^{-6}
nano-	n	10^{-9}
pico-	p	10^{-12}
femto-	f	10^{-15}
atto-	a	10^{-18}

2. MEASUREMENT UNITS AND CONVERSION FACTORS:

Unit	*Conversion factor*
Length Units:	
Ångstrom	$1\ \text{Å} = 0.1\ \text{nm} = 10^{-8}\ \text{cm} = 10^{-10}\ \text{m}$
nanometer	$1\ \text{nm} = 10\ \text{Å} = 10^{-7}\ \text{cm} = 10^{-9}\ \text{m}$
micron (micrometer)	$1\ \mu\text{m} = 10^{-6}\ \text{m} = 0.00003937\ \text{in}$
millimeter	$1\ \text{mm} = 1000\ \mu\text{m} = 0.1\ \text{cm} = 0.03937\ \text{in}$
centimeter	$1\ \text{cm} = 10{,}000\ \mu\text{m} = 10\ \text{mm} = 0.3937\ \text{in}$
meter	$1\ \text{m} = 100\ \text{cm} = 39.37\ \text{in} = 3.2808\ \text{ft} = 1.0936\ \text{yd}$
kilometer	$1\ \text{km} = 3280.8399\ \text{ft} = 1000\ \text{m} = 10^{5}\ \text{cm} = 0.6214\ \text{mi}$
inch	$1\ \text{in} = 2.54\ \text{cm} = 0.0833\ \text{ft}$
foot	$1\ \text{ft} = 30.48\ \text{cm} = 12\ \text{in} = 0.3048\ \text{m}$

continues

Continued

Unit	*Conversion factor*
yard	1 yd = 91.44 cm = 36 in = 3 ft = 0.9144 m
statute mile	1 mi = 5280 ft = 1760 yd = 1609.344 m = 1.6093 km
nautical mile	1 n.m. = 1852 m = 1.852 km = 1.1508 mi
Area Units:	
square centimeter	1 cm^2 = 100 mm^2 = 0.155 in^2
square meter	1 m^2 = 10,000 cm^2 = 10.7639 ft^2 = 1.1960 yd^2
hectare	1 ha = 10^8 cm^2 = 10,000 m^2 = 2.4711 a = 0.01 km^2 = 0.003861 mi^2
square kilometer	1 km^2 = 10^6 m^2 = 100 ha = 0.3861 mi^2
square inch	1 in^2 = 6.4516 cm^2
square foot	1 ft^2 = 929.0304 cm^2 = 144 in^2 = 0.0929 m^2
square yard	1 yd^2 = 1,296 in^2 = 9 ft^2 = 0.8361 m^2
acre	1 ac = 43,560 ft^2 = 4840 yd^2 = 4046.8564 m^2 = 0.4047 ha
square mile	1 mi^2 = 640 ac = 2.5900 km^2
Volume Units:	
cubic centimeter	1 cm^3 = 0.0610 in^3
cubic meter	1 m^3 = 35.3147 ft^3 = 1.3080 yd^3 = 1,000 l = 264.1721 gal
cubic kilometer	1 km^3 = 10^{15} cm^3 = 10^9 m^3 = 0.2399 mi^3
cubic inch	1 in^3 = 16.3871 cm^3
cubic foot	1 ft^3 = 1,728 in^3 = 0.02832 m^3
cubic yard	1 yd^3 = 27 ft^3 = 0.7646 m^3
liter	1 l = 10 dl = 1,000 cm^3 = 61.0237 in^3 = 1.0567 qt = 0.2642 gal
deciliter	1 dl = 0.1 l = 100 cm^3 = 6.1023 in^3
pint	1 pt = 28.875 in^3 = 0.4732 l
quart	1 qt = 57.75 in^3 = 2 pt = 0.473 l
U.S. gallon	1 gal = 231 in^3 = 8 pt = 4 qt = 3.7854 l
Weight Units:	
kilogram	1 kg = 1,000 g = 2.20461 lb
gram	1 g = 0.03527 ounces avoirdupois
metric ton	1 t = 10^6 g = 2204.6226 lb = 1,000 kg
teragram	1 Tg = 10^{12} g = 10^6 t
gigaton	1 Gt = 10^{15} g = 10^9 t
Energy Units:	
electron-volt	1 eV = 1.6022×10^{-19} J
erg	1 erg = 10^{-7} J = 0.23885×10^{-7} cal = 1
g	cm^2/sec^2
joule	1 J = 10^7 erg
calorie	1 cal = 4.1868 J
kilogram-meter	1 kg-m = 2.344 cal
kilocalorie	1 kcal = 1,000 cal = 3.9683 BTU

continues

Continued

Unit	*Conversion factor*
Force Units:	
dyne	1 dyn = 10^{-5} N = 1 g cm/sec^2
newton	1 N = 1 kgm/s^2 = 10^5 dyn
Frequency Units:	
hertz	1 Hz = 1 cps
Power Units:	
watt	1 W = 1 J/s = 0.05687 BTU/min = 0.01433 kcal/min = 0.001341 hp = 10^7 erg/sec
horsepower	1 hp = 745.6999 W
kilowatt	1 kW = 1,000 W = 1.341 hp
megawatt	1 MW = 10^3 kW = 10^6 W = 1341.0221 hp
Pressure Units:	
nanobar	1 nbar = 10^{-9} bar
centimeter of mercury	1 cm Hg = 0.01316 atm
pound per square inch	1 psi = 0.06805 atm = 0.07031 kg/cm^2
kg per square cm	1 kg/cm^2 = 0.9678 atm
bar	1 bar = 10^5 N/m^2 = 0.9869 atm = 10^6 dyn/cm^2 = 10^6 g/cm/sec^2 = 10^5 Pa
kbar	1000 bars = 100 MPa
atmosphere	1 atm = 1.01325 × 10^5 N/m^2 = 76 cm Hg = 29.9213 in Hg = 14.6959 psi = 1.0332 kg/cm^2 = 1.01325 bar = 1.013 × 10^5 Pa
MPa	1 megapascal = 10^6 Pa = 10 bar
GPa	1 gigapascal = 10^9 Pa = 10 kilobar = 10^3 bar = ca. 30 km depth in Earth's mantle
Torr	1 Torr = 1 mm Hg = 1.3332 × 10^{-3} bar
Time Units:	
Year	1 yr = 1 a = 3.15567 × 10^7 sec = 5.2560 × 10^5 min = 8,760 hrs
Ma	one million years before present, in terms of absolute geologic time
Ga	billion years = 10^9 years, in terms of absolute geologic time
m.y.	million years, in terms of duration; a relative term
Temperature Units:	
Degree Celsius	°C = (°F − 32) × 5/9) = K − 273.15
Kelvin	K = °C + 273.15 = (°F − 32) × 5/9) + 273.15
Degree Fahrenheit	°F = °C × (9/5) + 32
Gravimetric Factors:	
Fe_2O_3 × 0.89985 = FeO	
FeO × 1.1113 = Fe_2O_3	
FeO × 0.77731 = Fe	
Fe_2O_3 × 0.69944 = Fe	
K_2O × 0.83015 = K	

continues

Continued

Unit	*Conversion factor*
Viscosity Units:	
poise	1 poise (after Poiseuille) = 1 g/cm/sec − 10^{-1} Pa.s − 100 centipoise (cp) = 0.1 Pa.s
Pa.s	1 pascal second
Perfect Gas Constant:	R = 8.31441 J K mol
Density:	1 g/cm^3 = 1000 kg/m^3
Velocity:	1 m/s = 3.6 km/h = 2.2369 mi/h = 0.003017 Mach number

APPENDIX 2: CATALOG OF HISTORICALLY ACTIVE VOLCANOES ON EARTH

TOM SIMKIN AND LEE SIEBERT
Smithsonian Institution

This appendix consists of two parts. The first is an alphabetical listing of all historically active volcanoes. Each name is followed by the volcano's catalog number, to facilitate its rapid location in the catalog forming the second and main part.

The catalog is a condensed and updated version of the 129-page "Directory" table in *Volcanoes of the World*, 1994 (see "Earth's Volcanoes and Eruptions: An Overview"; this volume), to which the reader is referred for more information. It is restricted to historical activity (to the start of 1999), and does not include month/day dates, exact vent locations, eruptive characteristics, or precise durations. Sequence is regional, following the numbering system established decades ago by IAVCEI and modified in *Volcanoes of the World:* after a 4-digit subregion number, sequential individual numbers proceed along generally linear volcanic belts. Gaps in the numbering shown here indicate non-historical, Holocene volcanoes numbered in *Volcanoes of the World* but not included in this catalog. Regional sequencing starts in Europe, then moves south and east to New Zealand, generally clockwise around the Pacific, then down the Atlantic from Iceland to Antarctica. A geographic sequence allows the perspective of viewing a wide region's volcano data at once, but readers interested in finding a single, unfamiliar volcano may do so through the alphabetic name index. Noteworthy volcanoes meeting criteria of eruption size, frequency, or fatalities are highlighted in **boldfaced** type (and these are the volcanoes named on the world map making up the inside back cover).

Coordinates (in *italics*) are given in decimal degrees, and elevations in meters above/below sea level. Volcano edifice type follows *Volcanoes of the World* (and "Earth's Volcanoes and Eruptions: An Overview") and subsidiary morphologic features are not included. Unusually large eruptions, as measured by the Volcanic Explosivity Index, or VEI (see "Sizes of Volcanic Eruptions"; this volume), are highlighted by typography (see header) allowing swift location of these larger events. However, the historical record generally becomes less reliable as one goes further into the past, and many early eruptions are missing from the known record (see "Earth's Volcanoes and Eruptions: An Overview").

Uncertainty is unavoidable in the historical record, and the following conventions are used to display this aspect of eruptive histories. A question mark (**?**) before a year indicates that the eruption itself is uncertain, while a commercial "at" sign (**@**) before a year indicates that the location of the eruption is uncertain (it may have been a neighboring volcano). A question mark after a year indicates that the date is uncertain, but if the size of that uncertainty is known it is expressed by a letter code immediately after the year (**a** = ±1 year, **j** = ±10 years, **p** = ±20 years, **t** = ±50, etc). When an eruption is known to have begun sometime prior to a particular year, the "less than" symbol (**<**) appears after that date. If an eruption was continuing when last observed, but the actual stop date is unknown, then the "greater than" symbol (**>**) follows the observation date. Volcanoes for which the only historical eruptions are questionable are included in the catalog but appear on the map as the smallest red symbol. Long-running eruptions are shown by a range of years, and when two separate eruptions occur in a single year, that year is listed twice.

The historical volcanic record, in contrast to the instrumentally determined seismic record, is based on human observation. Readers may well know of eruptions that we have missed, so we urge you to contact us with any additions or corrections to the catalog that follows. Such feedback helps us build the more accurate record that will benefit us all.

VOLCANO INDEX: name with regionally sequenced volcano number

ACATENANGO	1402-08=
ADATARA	0803-17=
ADWA	0201-17=
AGRIGAN	0804-16=
AGUA DE PAU	1802-09=
AGUNG	0604-02=
AHYI	0804-141
AKADEMIA NAUK	1000-123
AKAGI	0803-13=
AKAN	0805-07=
AKITA-KOMAGA-TAKE	0803-23=
AKITA-YAKE-YAMA	0803-26=
AKUTAN	1101-32-
ALAID	0900-39=
ALAMAGAN	0804-18=
ALAYTA	0201-112
ALCEDO, VOLCAN	1503-04=
ALMOLONGA	1402-04=
AMAK	1101-39-
AMBANG	0606-02=
AMBRYM	0507-04=
AMUKTA	1101-19-
ANDAHUA VALLEY	1504-002
ANIAKCHAK	1102-09-
ANTISANA	1502-03=
ANTOFALLA, VOLCAN	1505-123
ANTUCO	1507-08=
AOBA	0507-03=
AOGA-SHIMA	0804-06=
API SIAU [KARANGETANG]	0607-02=.
ARACAR	1505-107
ARDOUKOBA	0201-126
ARENAL	1405-033
ARHAB, HARRA OF	0301-09-
ARJUNO-WELIRANG	0603-29=
ASAMA	0803-11=
ASKJA	1703-06=
ASO	0802-11=
ASUNCION	0804-15=
ATITLAN	1402-06=
ATKA	1101-16-
ATSONUPURI	0900-05=
AUGUSTINE	1103-01-
AVACHINSKY	1000-10=
AWU	0607-04=
AYELU	0201-16=
AXIAL SEAMOUNT	1301-011
AZUL, CERRO	1503-06=
AZUL, C [QUIZAPU]	1507-06=.
AZUMA	0803-18=
BABUYAN CLARO	0704-03=
BAGANA	0505-02=
BAITOUSHAN	1005-07-
BAKER	1201-01=
BALAGAN-TAS	1001-03-
BALBI	0505-01=
BALUAN	0500-02-
BAM	0501-01=
BAMUS	0502-11=
BANAHAW	0703-05=
BANDA API	0605-09=
BANDAI	0803-16=
BANUA WUHU	0607-03=
BARANSKY	0900-08=
BARCENA	1401-02=
BARDARBUNGA	1703-03=
BARREN ISLAND	0600-01=
BARRIER, THE	0202-03=
BARU	1406-01-
BARVA	1405-05=
BATUR	0604-01=
BAYONNAISE ROCKS	0804-07=
BERUTARUBE	0900-04=
BESAR, GUNUNG	0601-25=
BEZYMIANNY	1000-25=
BILIRAN	0702-08=
BINULUAN	0703-088
BIR BORHUT	0301-18-
BOGOSLOF	1101-30-
BRENNISTEINSFJOLL	1701-04=
BRIMSTONE ISLAND	0402-02=
BRISTOL ISLAND	1900-08=
BROMO [TENGGER]	0603-31=.
BUCKLE ISLAND	1900-01=
BULUSAN	0703-01=
BURNEY, MONTE	1508-07=
CAGUA	0703-09=
CALAYO	0701-07=
CALBUCO	1508-02=
CALLAQUI	1507-091
CAMEROON, MT.	0204-01=
CAMIGUIN D BABUYANES	0704-01=.
CAMPI FLEGREI	0101-01=
CAMPI FLEGREI SICILIA	0101-07=.
CANDLEMAS ISLAND	1900-10=
CANLAON	0702-02=
CARLISLE	1101-23-
CARRAN-LOS VENADOS	1507-14=.
CEBORUCO, VOLCAN	1401-03=
CENTRAL ISLAND	0202-01=
CEREME	0603-17=
CHACANA	1502-022
CHANGBAISHAN	1005-07-
CHICHON, EL	1401-12=
CHIGINAGAK	1102-11-
CHIKURACHKI	0900-36=
CHILLAN, NEVADOS	1507-07=
CHIRINKOTAN	0900-26=
CHIRIP	0900-09=
CHIRPOI	0900-15=
CHOKAI	0803-22=
CLEVELAND	1101-24-
COLIMA	1401-04=.
COLO [UNA UNA]	0606-01=
CONCEPCION	1404-12=
CONCHAGUITA	1403-12=
COPAHUE	1507-09=
CORCOVADO	1508-05=
CORDON CAULLE	1507-141
COSIGUINA	1404-01=
COTOPAXI	1502-05=
CUMBAL	1501-10=
CURACOA	0403-101
CURTIS ISLAND	0402-01=
DALLOL	0201-041
DAMA ALI	0201-141
DARWIN, VOLCAN	1503-03=
DATONG	1005-01-
DECEPTION ISLAND	1900-03=
DEMPO	0601-23=
DESCABEZADO GRANDE	1507-05=.
DHAMAR, HARRAS OF	0301-12-
DIENG VOLC COMPLEX	0603-20=.
DON JOAO DE CASTRO	1802-07=.
DONA JUANA	1501-07=
DUBBI	0201-10=
DUKONO	0608-01=
E-SAN	0805-011
EAST EPI	0507-06=
EASTERN GEMINI SEAMNT	0508-001
EBEKO	0900-38=
EBULOBO	0604-10=
EGON	0604-16=
EKARMA	0900-27=
EMPEROR OF CHINA	0605-01=
ERCIYES DAGI	0103-01=
EREBUS	1900-02=
ERTA ALE	0201-08=
ES SAFA	0300-05-
ESJUFJOLL	1704-02=
ESMERALDA BANK	0804-21=
ETNA	0101-06=
EYJAFJOLL	1702-02=
FALCON ISLAND	0403-05=
FARALLON DE PAJAROS	0804-14=.
FAYAL	1802-01=
FENTALE	0201-19=
FERNANDINA	1503-01=
FISHER	1101-35-
FOGO	1804-01=
FONUALEI	0403-10=
FOURNAISE, PITON DE LA	0303-02=.
FUEGO	1402-09=
FUJI	0803-03=
FUKUJIN	0804-133
FUKUTOKU-OKANOBA	0804-13=.
FURNAS	1802-10=
FUSS PEAK	0900-34=
GALAPAGOS RIFT	1303-02-
GALERAS	1501-08=
GALUNGGUNG	0603-14=
GAMALAMA	0608-06=
GAMKONORA	0608-04=
GARELOI	1101-07-
GAUA	0507-02=
GEDE	0603-06=
GILIBANTA	0604-051
GLACIER PEAK	1201-02-
GOLOVNIN	0900-01=
GORELY	1000-07=
GORIASCHAIA SOPKA	0900-17B
GRAHAM I [C FLEG SICILIA]	0101-07=.
GREAT SITKIN	1101-12-
GRIMSVOTN	1703-01=
GROZNY GROUP	0900-07=-
GUADELOUPE, SOUF	1600-06=.
GUAGUA PICHINCHA	1502-02=
GUALLATIRI	1505-02=
GUGUAN	0804-19=
GUNTUR	0603-13=
GUNUNGAPI WETAR	0605-03=
HACHIJO-JIMA	0804-05=
HAKU-SAN	0803-05=
HALEAKALA	1302-06-
HALLA	1006-04-
HARIMKOTAN	0900-30=
HAROHARO [OKATAINA]	0401-05=.
HEARD	0304-01=
HEIMAEY [VESTMANN IS]	1702-01=
HEKLA	1702-07=
HIBOK-HIBOK	0701-08=
HIERRO	1803-02-
HIUCHI	0803-131
HODSON	1900-11=
HOME REEF	0403-08=
HOOD	1202-01-
HUALALAI	1302-04-
HUAYNAPUTINA	1504-03=
HUDSON MOUNTAINS	1900-028
HUDSON, CERRO	1508-057
HUEQUI	1508-03=
HUILA	1501-05=
HUNTER ISLAND	0508-02=
IBU	0608-03=
IBUSUKI VOLC FIELD	0802-07=.
IJEN	0603-35=
ILIAMNA	1103-02-
ILIBOLENG	0604-22=
ILIWERUNG	0604-25=
ILOPANGO	1403-06=
ILYINSKY	1000-03=
INIELIKA	0604-09=
IRAYA	0704-06-
IRAZU	1405-06=
IRIGA	0703-041
IRIOMOTE-JIMA	0802-01=
IRRUPUTUNCU	1505-04=
ISANOTSKI	1101-37-
ISCHIA	0101-03=
ISKUT-UNUK RIVER	1200-09-
ISLUGA	1505-03=
IWAKI	0803-27=
IWATE	0803-24=
IWO-JIMA	0804-12=
IYA	0604-11=
IZALCO	1403-03=
IZU-TOBU	0803-01=
JORULLO [MICHOACAN]	1401-06=
KABA	0601-22=
KADOVAR	0501-002
KAGAMIL	1101-26-
KAIMON [IBUSUKI FIELD]	0802-07=.
KAITOKU SEAMOUNT	0804-10=
KANAGA	1101-11-
KANPU	0803-261
KARANGETANG	0607-02=.
KARAPINAR FIELD	0103-001
KARKAR	0501-03=
KARPINSKY GROUP	0900-35=
KARS PLATEAU	0103-05-
KARTHALA	0303-01=
KARYMSKY	1000-13=
KASATOCHI	1101-13-
KASUGA SEAMOUNT	0804-134
KATLA	1702-03=
KATMAI	1102-17-
KAVACHI	0505-06=
KAWAHKARAHA	0603-16=
KELIMUTU	0604-14=
KELUT	0603-28=
KERINCI	0601-17=
KETOI	0900-20=
KHAYBAR, HARRAT	0301-06=
KIARABERES-GAGAK	0603-03=
KICK-'EM-JENNY	1600-16=
KIEYO	0202-17=
KIKAI	0802-06=
KILAUEA	1302-01-
KIRISHIMA	0802-09=
KISKA	1101-02-
KITA-IWO-JIMA	0804-11=
KIZIMEN	1000-23=
KLIUCHEVSKOI	1000-26=
KOLBEINSEY RIDGE	1705-01=
KOLOKOL GROUP	0900-12=
KOMAGA-TAKE	0805-02=
KONE	0201-20-
KOROVIN [ATKA]	1101-16-
KORYAKSKY	1000-09=
KOSHELEV	1000-02=
KOZU-SHIMA	0804-03=
KRAFLA	1703-08=
KRAKATAU	0602-00=
KRISUVIK	1701-03=
KRONOTSKY	1000-20=
KSUDACH	1000-05=
KUCHINOERABU-JIMA	0802-05=
KUJU GROUP	0802-12=
KUNLUN VOLC GROUP	1004-03-
KUPREANOF	1102-06-
KURIKOMA	0803-21=
KUSATSU-SHIRANE	0803-12=
KUWAE	0507-07=
KVERKFJOLL	1703-05=
LA PALMA	1803-01-
LAKI [GRIMSVOTN]	1701-06=
LAMINGTON	0503-01=
LAMONGAN	0603-32=
LANGILA	0502-01=
LANZAROTE	1803-06-
LARDERELLO	0101-001
LASCAR	1505-10=
LASSEN VOLC CENTER	1203-08-.
LATE	0403-09=
LAUTARO	1508-06=
LENGAI, OL DOINYO	0202-12=
LEREBOLENG	0604-20=
LEWOTOBI	0604-18=
LEWOTOLO	0604-23=
LIAMUIGA	1600-03=
LIPARI	0101-041
LITTLE SITKIN	1101-05-
LLAIMA	1507-11=
LLULLAILLACO	1505-11=
LOIHI SEAMOUNT	1302-00-
LOKI-FOGRUFJOLL	1703-02=
LOKON-EMPUNG	0606-10=
LOLOBAU	0502-13=
LONG ISLAND	0501-05=
LONQUIMAY	1507-10=
LOPEVI	0507-05=
LUNAYYIR, HARRAT	0301-04-
MACDONALD	1303-07-
MAGEIK	1102-15-
MAHAGNOA	0702-07=
MAHAWU	0606-11=
MAIPO	1507-021
MAKUSHIN	1101-31-
MALINAO	0703-04=
MALY SEMIACHIK	1000-14=
MANAM	0501-02=
MANDA-INAKIR	0201-122
MARAPI	0601-14=
MARCHENA	1503-08=
MARION ISLAND	0304-08-
MARTIN	1102-14-
MASAYA	1404-10=
MATTHEW ISLAND	0508-01=
MAUNA LOA	1302-02=
MAYON	0703-03=
MCDONALD ISLANDS	0304-011
MEDICINE LAKE	1203-02-
MEDVEZHIA	0900-10=
MEHETIA	1303-06-

VOLCANO INDEX: name with regionally sequenced volcano number (*continued*)

MENDELEEV .... 0900-02=
MERAPI .... 0603-25=
MERBABU .... 0603-24=
MERE LAVA 0507-021
MERU .... 0202-16=
METHANA .... 0102-02=
METIS SHOAL .... 0403-07=
MICHAEL .... 1900-09=
MICHOACAN FIELD .... 1401-06=.
MICOTRIN .... 1600-10=
MINAMI-HIYOSHI 0804-131
MINCHINMAVIDA .... 1508-04=
MIRAVALLES .... 1405-03=
MISTI, EL .... 1504-01=
MIYAKE-JIMA .... 0804-04=
MOCHO-CHOSHUENCO .... 1507-13=
MOMBACHO .... 1404-11=
MOMOTOMBO .... 1404-09=
MONACO BANK .... 1802-11=
MONO LAKE FIELD .... 1203-11-.
MONOWAI SEAMOUNT 0402-05-
MONTSERRAT [SOUF HILL] 1600-05=.
MOUA PIHAA 1303-05-
MUTNOVSKY .... 1000-06=
MYOJIN-SHO [BAYONAISE] 0804-07=.
NAKANO-SHIMA .... 0802-04=
NARUGO .... 0803-20=
NASU .... 0803-15=
NEGRA, SIERRA .... 1503-05=
NEGRO DE MAYASQUER .... 1501-11=
NEGRO, CERRO .... 1404-07=
NEMO PEAK .... 0900-32=
NEMRUT DAGI .... 0103-02=
NIEUWERKERK .... 0605-02=
NII-JIMA .... 0804-02=
NIIGATA-YAKE-YAMA .... 0803-09=
NIKKO 0804-132
NIKKO-SHIRANE .... 0803-14=
NILA .... 0605-06=
NIPESOTSU-UPEPESANKE 0805-061
NISHINO-SHIMA 0804-092
NISYROS .... 0102-05=
NIUAFO'OU .... 0403-11=
NOVARUPTA 1102-18-
NYAMURAGIRA .... 0203-02=
NYIRAGONGO .... 0203-03=
NYOS, LAKE [OKU FIELD] 0204-003.
OFU-OLOSEGA .... 0404-01=
OKATAINA .... 0401-05=
OKAMA [ZAO] .... 0803-19=.
OKINAWA-TORI-SHIMA .... 0802-02=.
OKMOK 1101-29-
OKU VOLC FIELD 0204-003
OLCA-PARUMA .... 1505-05=
OLLAGUE .... 1505-06=
OMACHI SEAMOUNT 0804-091
ON-TAKE .... 0803-04=
ORAEFAJOKULL .... 1704-01=
ORIZABA, PICO DE .... 1401-10=
OSHIMA .... 0804-01=
OSHIMA-OSHIMA .... 0805-01=
OSORE-YAMA .... 0803-29=
OSORNO .... 1508-01=
PACAYA .... 1402-11=
PAGAN .... 0804-17=
PAGO .... 0502-08=
PALUWEH .... 0604-15=
PANTELLERIA 0101-071
PAPANDAYAN .... 0603-10=
PARICUTIN [MICHOACAN] 1401-06=
PARKER 0701-001
PAULET 1900-041
PAVLOF 1102-03-
PAVLOF SISTER 1102-04-
PELEE .... 1600-12=
PENANGGUNGAN 0603-291
PENGUIN ISLAND 1900-031
PEUET SAGUE .... 0601-03=
PICO .... 1802-02=
PICHINCHA, GUAGUA .... 1502-02=.
PILAS, LAS .... 1404-08=
PINACATE PEAKS 1401-001
PINATUBO 0703-083
PINTA .... 1503-07=
PLANCHON-PETEROA .... 1507-04=
POAS .... 1405-04=
POGROMNI [~WESTDAHL] 1101-34-.
POPOCATEPETL .... 1401-09=
PREVO PEAK .... 0900-19=
PROTECTOR SHOAL 1900-14-
PULAR 1505-105
PUNTIGUIDO-CORDON 1507-16-
PURACE .... 1501-06=
PUTANA .... 1505-09=
QUALIBOU .... 1600-14=
QUETRUPILLAN 1507-121
QUILOTOA .... 1502-06=
QUIZAPU [CERRO AZUL] .... 1507-06=.
RABAUL .... 0502-14=
RAGANG .... 0701-06=
RAHAT, HARRAT .... 0301-07=
RAIKOKE .... 0900-25=
RAINIER 1201-03-
RANAKAH, GUNUNG 0604-071
RANAU 0601-251
RAOUL ISLAND .... 0402-03=
RASSHUA .... 0900-22=
RAUNG .... 0603-34=
REDOUBT 1103-03-
REVENTADOR .... 1502-01=
REYKJANES .... 1701-02=
REYKJANESHRYGGUR .... 1701-01=
RINCON DE LA VIEJA .... 1405-02=.
RITTER ISLAND .... 0501-07=
ROBINSON CRUSOE .... 1506-02=
ROCARD 1303-04-
RUANG .... 0607-01=
RUAPEHU .... 0401-10=
RUBY 0804-201
RUBY MOUNTAIN 1200-03-
RUIZ .... 1501-02=
RUMBLE III 0401-13-
SABA .... 1600-01=
SABANCAYA 1504-003
SAKURA-JIMA .... 0802-08=
SALAK .... 0603-05=
SAN CRISTOBAL .... 1404-02=
SAN JORGE .... 1802-03=
SAN JOSE .... 1507-02=
SAN MARTIN, VOLCAN .... 1401-11=.
SAN MIGUEL .... 1403-10=
SAN PEDRO .... 1505-07=
SAN SALVADOR .... 1403-05=
SANGANGUEY 1401-023
SANGAY .... 1502-09=
SANGEANG API .... 0604-05=
SANTA ANA .... 1403-02=
SANTA ISABEL 0204-02-
SANTA MARIA .... 1402-03=
SANTIAGO .... 1503-09=
SANTIAGUITO [S MARIA] .... 1402-03=.
SANTORINI .... 0102-04=
SARYCHEV PEAK .... 0900-24=
SAVAI'I .... 0404-04=
SAVO .... 0505-07=
SAWAD, HARRA ES- 0301-16-
SEAL NUNATAKS .... 1900-05=.
SEGUAM 1101-18-
SEMERU .... 0603-30=
SEMISOPOCHNOI 1101-06-
SEMPU .... 0606-04=
SERUA .... 0605-07=
SETE CIDADES .... 1802-08=
SEULAWAH AGAM .... 0601-02=
SHASTA 1203-01-
SHIKOTSU .... 0805-04=
SHIN-IWO-JIMA .... 0804-13=
SHIRETOKO-IWO-ZAN .... 0805-09=
SHISHALDIN 1101-36-
SHIVELUCH .... 1000-27=
SIBAYAK .... 0601-07=
SINABUNG .... 0601-08=
SINARKA .... 0900-29=
SIRUNG .... 0604-27=
SLAMET .... 0603-18=
SMITH ROCK .... 0804-08=
SOCORRO 1401-021
SOPUTAN .... 0606-03=
SORIKMARAPI .... 0601-12=
SOUFRIERE GUADELOUPE 1600-06=.
SOUFRIERE ST. VINCENT 1600-15=.
SOUF HILL[MONTSERRAT] 1600-05=.
SOUTH ISLAND .... 0202-02=
SOUTH SISTER 1202-08-
SPURR 1103-04-
SREDNII 0900-211
ST. ANDREW STRAIT .... 0500-01=
ST. HELENS 1201-05-
ST. PAUL .... 0304-03=
ST. VINCENT, SOUFRIERE 1600-15=.
STROMBOLI .... 0101-04=
SUCHITAN VOLC FIELD .... 1402-17-.
SUMACO .... 1502-04=
SUMBING .... 0601-18=
SUMBING .... 0603-22=
SUNDORO .... 0603-21=
SUOH .... 0601-27=
SUPPLY REEF 0804-142
SURTSEY [VESTMANN IS] .... 1702-01=
SUWANOSE-JIMA .... 0802-03=
TAAL .... 0703-07=
TACANA .... 1401-13=
TACORA .... 1505-01=
TAFTAN 0302-05-
TAJUMULCO .... 1402-02=
TALAKMAU .... 0601-13=
TALANG .... 0601-16=
TANAGA 1101-08-
TANDIKAT .... 0601-15=
TANGKUBANPARAHU .... 0603-09=
TAO-RUSYR CALDERA .... 0900-31=
TARA, BATU .... 0604-26=
TARUMAI [SHIKOTSU] .... 0805-04=.
TATE-YAMA .... 0803-08=
TEAHITIA 1303-03-
TECAPA .... 1403-08=
TELEKI'S VOLC [BARRIER] 0202-03=.
TELICA .... 1404-04=
TELONG, BUR NI .... 0601-05=
TENERIFE 1803-03-
TENGCHONG 0705-11-
TENGGER CALDERA .... 0603-31=
TEON .... 0605-05=
TERCEIRA .... 1802-05=
TEYR, DJEBEL .... 0201-01=
THERA [SANTORINI] .... 0102-04=.
THOMPSON ISLAND 1806-03-
TIANSHAN VOLC GROUP 1004-02-.
TIATIA .... 0900-03=
TINAKULA .... 0506-01=
TINGUIRIRICA .... 1507-03=
TJORNES FRACTURE .... 1703-10=
TOFUA .... 0403-06=
TOKACHI .... 0805-05=
TOLBACHIK .... 1000-24=
TOLIMA .... 1501-03=
TONGARIRO .... 0401-08=
TONGKOKO .... 0606-13=
TORFAJOKULL .... 1702-05=
TORI-SHIMA .... 0804-09=
TOWADA 0803-271
TRAITOR'S HEAD .... 0507-09=
TRES VIRGENES .... 1401-01=
TRIDENT 1102-16-
TRISTAN DA CUNHA .... 1806-01=
TROMEN 1507-071
TSURUMI .... 0802-13=
TULLU MOJE 0201-25-
TULUMAN [ST A STRAIT] 0500-01=.
TUNGURAHUA .... 1502-08=
TUPUNGATITO .... 1507-01=
TURFAN 1004-01-
TURRIALBA .... 1405-07=
TUTUPACA .... 1504-04=
UBINAS .... 1504-02=
UGASHIK-PEULIK 1102-13A
UKINREK MAARS 1102-13B
ULAWUN .... 0502-12=
UNA UNA [COLO] .... 0606-01=
UNZEN .... 0802-10=
USHISHUR .... 0900-21=
USHKOVSKY 1000-261
USU .... 0805-03=
VEER 1000-102
VENIAMINOF 1102-07-
VESTMANNAEYJAR .... 1702-01=
VESUVIUS .... 0101-02=
VETERAN 0705-07-
VICTORY .... 0503-03=
VIEDMA, VOLCAN 1508-061
VILLARRICA .... 1507-12=
VISOKE 0203-05-
VSEVIDOF 1101-27-
VULCANO .... 0101-05=
VULSINI 0101-003
WAIMANGU [OKATAINA] .... 0401-05=
WAIOWA .... 0503-04=
WESTDAHL 1101-34-
WHITE ISLAND .... 0401-04=
WOLF, VOLCAN .... 1503-02=
WRANGELL 1105-02-
WUDALIANCHI 1005-04-
WURLALI .... 0605-04=
XIANJINDAO 1006-01-
YAKE-DAKE .... 0803-07=
YANTELES, CERRO 1508-051
YAR, JABAL 0301-08-
YASUR .... 0507-10=
YUCAMANE 1504-05-
YUNASKA 1101-21-
ZAO .... 0803-19=
ZAVARITZKI CALDERA .... 0900-18=.
ZAVODOVSKI .... 1900-13=
ZENGYU .... 0801-05=
ZHELTOVSKY .... 1000-04=
ZHUPANOVSKY .... 1000-12=
ZUBAYR, JEBEL .... 0201-02=

NUMBER	VOLCANO NAME	LAT	LONG	ELEV	TYPE	ERUPTION YEARS (VEI≤3 **VEI=4** **VEI=5** ***VEI=6-7***)
Italy (N to S)						
0101-001	LARDERELLO	*43.25N*	*10.87E*	*500*	Explosion craters	1282<
0101-003	VULSINI	*42.60N*	*11.93E*	*800*	Caldera	-0104
0101-01=	CAMPI FLEGREI	*40.82N*	*14.13E*	*458*	Caldera	1538, 1198
0101-02=	**VESUVIUS**	*40.82N*	*14.42E*	*1281*	Complex volcano	1913-44, **1875-1906**, 1874, 1870-72, 1864-68, 1855-61, 1854-55, 1841-50, 1835-39, 1824-34, 1796-1822, 1783-94, 1770-79, 1764-67, 1744-61, 1732-37, 1724-30, 1712-23, 1708, 1706-07, 1701-04, 1697-98, 1696, 1685-94, 1682, 1654-80, 1637-52, **1631-32**, 1500, ?1347, ?1270, ?1150, 1139, 1073e, ?1049, 1037, 1007, ?0999, ?0991, 0968, 0787, 0685, 0536, **0512**, 0505, **0472**, 0379-95, ?0222-35, 0203, 0172, **0079**
0101-03=	ISCHIA	*40.73N*	*13.89E*	*789*	Complex volcano	1302, 0295j, 0145?, 0080a, 0069, -0006p, -0091, -0250t, ?-0350?, -0470?, -0500?
0101-04=	**STROMBOLI**	*38.78N*	*15.21E*	*926*	Stratovolcano	1994-99>, 1985-86, 1975, 1971, 1967, 1966, 1959, 1956, 1954-55, 1954, 1952, 1951, 1950, 1949, 1944, 1943-44, 1941, 1938-39, 1938, 1938, 1937, 1937, 1936, 1935, 1935, 1934, 1934, 1930, 1930, 1921, 1919, 1916, 1915, 1912, 1907, 1906, 1906, 1905, 1903, 1903, 1900, 1900, 1898, 1897, 1896, 1895, 1893, 1893, 1892, 1891, 1888-89, 1885, 1882, 1881, 1879, 1879, 1874, 1865, 1856, 1855, 1850, 1833, 1822, 1778, 1770, 1768, 1558< to 1999>, -0450<
0101-041	LIPARI	*38.48N*	*14.95E*	*602*	Stratovolcano	0729
0101-05=	VULCANO	*38.40N*	*14.96E*	*500*	Stratovolcano	?1892, 1888-90, 1886, 1873-79, ?1831, ?1822-23, ?1812, ?1786, 1780, ?1775, 1771, 1731-39, 1727, 1688, 1651, 1631, 1626, 1618, 1550, 1444, 1250t, 0925q, 0729, 0526?, 0144, 0050t, -0010j, -0024e, -0091, -0126, **-0183**, -0215, -0300, -0360j, -0475?
0101-06=	**ETNA**	*37.73N*	*15.00E*	*3350*	Shield volcano	1994-99, 1993, 1993, 1991-93, 1990-92, 1989-90, 1989, 1988-89, 1987, 1986-87, 1985, 1985, 1984-86, 1984, 1983, 1981, 1981, 1981, 1980, 1980, 1979-92, 1979, 1978, 1978, 1978, 1975, 1974-78, 1974, 1971-79, 1971, 1968, 1966-71, 1959-64, 1959, 1958, 1957-58, 1957, 1955-56, ?1953, 1951-52, 1950-51, 1949-50, 1947, 1947, 1946, 1945, 1942-44, 1942, 1940-42, 1935-39, 1934, 1931-33, 1930, 1929, 1928, 1928, 1926, 1924-25, 1923-24, 1923, 1919-23, 1918, 1918, 1917, 1913-17, 1912, 1911, 1911, 1910-11, 1910, 1908-09, 1908, 1899-1907, 1899, 1893-98, 1892, 1892, 1891, 1886, 1884-85, 1883, 1879, 1878-83, 1874, 1874, 1869, 1868, 1865, 1864, 1863, 1857, 1852-53, 1843, 1842, 1838-39, 1833, 1832, 1828-32, 1827, 1822, 1819, ?1816, 1811-12, 1810, 1809, 1803-09, 1802, 1797-1801, 1792-93, 1792, 1791, **1787**, 1781, 1780, 1776, ?1770, 1767, 1766, 1764-65, 1763, 1763, 1758-59, 1755, 1752-58, 1747-49, 1744-45, 1735-36, 1732-33, 1723-24, 1702, 1693-94, ?1693, 1689, 1688, 1682, 1669, 1654-56?, 1651-53, 1646-47, 1643, 1634-38, ?1633, 1614-24, 1610, 1607, 1603-10, 1595?, 1579-80?, 1566, ?1554, 1541, 1540, 1537, 1536, 1494?, 1447, 1446, 1444, 1408, 1381?, 1350, 1333, 1329, 1329, 1284-85, 1250, 1222, 1194, ?1169, 1164, 1160, 1157, 1063a, ?1044, ?1004, ?0911, ?0859, ?0814, 0812?, ?0644, 0417?, 0252?, 0080?, 0039a, 0010j, ?-0010?, -0032, -0036, -0044, -0049, ?-0056, ?-0061, **-0122**, -0126, -0135, -0141, -0350?, -0396?, -0425-24?, -0479-76?, ?-0565, -0695b, ?-0735, **-1500t**
0101-07=	CAMPI FLEGREI SICILIA	*37.10N*	*12.70E*	*-8*	Submarine volcano	1911, 1867, 1863, 1846, 1831, ?1701, 1632, -0253k
0101-071	PANTELLERIA	*36.77N*	*12.02E*	*836*	Shield volcano	1891, ?1891
Greece (W to E)						
0102-02=	METHANA	*37.61N*	*23.33E*	*760*	Lava domes	?1922, -0258o
0102-04=	**SANTORINI**	*36.40N*	*25.39E*	*564*	Shield volcanoes	1950, 1939-41, 1925-28, 1866-70, 1707-11, **1650**, 1570-73, 0726, 0046-47, -0197
0102-05=	NISYROS	*36.58N*	*27.18E*	*698*	Stratovolcano	1888, 1873, 1871, ?1422
Turkey (W to E)						
0103-001	KARAPINAR FIELD	*37.67N*	*33.65E*	*1302*	Cinder cones	@-6200>
0103-01=	ERCIYES DAGI	*38.52N*	*35.48E*	*3916*	Stratovolcano	?0253<
0103-02=	NEMRUT DAGI	*38.65N*	*42.02E*	*3050*	Stratovolcano	1441
0103-05-	KARS PLATEAU	*40.75N*	*42.90E*	*3000*	Volcanic field	?1959, ?1450t
Ethiopia & Red Sea (N to S)						
0201-01=	TEYR, DJEBEL	*15.70N*	*41.74E*	*244*	Stratovolcano	1883, 1863, 1833, 1750t
0201-02=	ZUBAYR, JEBEL	*15.08N*	*42.17E*	*191*	Shield volcano	?1846, 1824
0201-041	DALLOL	*14.24N*	*40.30E*	*-48*	Explosion crater	1926
0201-08=	**ERTA ALE**	*13.60N*	*40.67E*	*613*	Shield volcano	1967<-99>, 1960, 1940, 1906, ?1904, ?1903, ?1873
0201-10=	**DUBBI**	*13.58N*	*41.80E*	*1625*	Stratovolcano	?1900?, ?1863, 1861, 1400
0201-112	ALAYTA	*12.88N*	*40.57E*	*1501*	Shield volcano	1915, 1907
0201-122	MANDA-INAKIR	*12.38N*	*42.20E*	*600*	Fissure vents	1928
0201-126	ARDOUKOBA	*11.58N*	*42.47E*	*298*	Fissure vents	1978
0201-141	DAMA ALI	*11.28N*	*41.63E*	*1068*	Shield volcano	@1631
0201-16=	AYELU	*10.08N*	*40.70E*	*2145*	Stratovolcano	?1928
0201-17=	ADWA	*10.07N*	*40.84E*	*1733*	Stratovolcano	?1928, ?1828
0201-19=	FENTALE	*8.97N*	*39.93E*	*2007*	Stratovolcano	1820?, 1250t
0201-20-	KONE	*8.80N*	*39.69E*	*1619*	Calderas	1820j
0201-25-	TULLU MOJE	*8.15N*	*39.13E*	*2349*	Pumice cone	1900?
Kenya & Tanzania (N to S)						
0202-01=	CENTRAL ISLAND	*3.50N*	*36.04E*	*550*	Stratovolcano	?1974
0202-02=	SOUTH ISLAND	*2.63N*	*36.60E*	*700*	Stratovolcano	1888
0202-03=	BARRIER, THE	*2.32N*	*36.57E*	*1032*	Shield volcano	1921, ?1920c, 1917, ?1906, 1897, 1895, 1888, 1871c
0202-12=	**LENGAI, OL DOINYO**	*2.75S*	*35.90E*	*2890*	Stratovolcano	1994-98, 1983-93, ?1969, 1967, 1960-66, 1958, 1955, 1954, 1940-41, 1926, 1921, 1916-17, 1914-15, 1882-83, 1880
0202-16=	MERU	*3.25S*	*36.75E*	*4565*	Stratovolcano	1910, 1886?, 1878a

NUMBER	VOLCANO NAME	LAT	LONG	ELEV	TYPE	ERUPTION YEARS (VEI≤3 **VEI=4** **VEI=5** *VEI=6-7*)
0202-17=	KIEYO	*9.23S*	*33.78E*	*2175*	Stratovolcano	1800?
Congo						
0203-02=	**NYAMURAGIRA**	*1.40S*	*29.20E*	*3058*	Shield volcano	1998, 1996, 1994, 1991-93, 1989, 1987-88, 1986, 1984, 1981-82, 1980, 1976-77, 1971, 1967, 1958, 1957, 1956, 1954, 1951-52, 1951, 1948, 1938-40, 1921-38, 1920, 1912-13, 1909, 1908, 1907, 1907, ?1906, 1905, 1904, 1902, 1901, 1899, 1896, 1894, 1882, 1865
0203-03=	**NYIRAGONGO**	*1.52S*	*29.25E*	*3469*	Stratovolcano	1994-96, 1982, 1977, 1927-77, 1920-21, 1918, 1911, ?1908, 1906, 1905, 1902, 1901, 1900, 1899, 1898, 1894, @1891<, 1884
0203-05-	VISOKE	*1.47S*	*29.49E*	*3711*	Stratovolcano	1957, @1891
Cameroon & Bioko						
0204-003	OKU FIELD **[LAKE NYOS]**	*6.25N*	*10.50E*	*3011*	Maars	?1986
0204-01=	CAMEROON, MT.	*4.20N*	*9.17E*	*4095*	Stratovolcano	1982, 1959, 1954, 1925, 1922, 1909, 1871, 1868, 1866, 1865, 1852, 1838, 1825j, 1807h, 1650t, -0450t
0204-02-	SANTA ISABEL	*3.58N*	*8.75E*	*3007*	Shield volcano	1923, 1903, 1898?, 1222
Syria & Arabia (NW to SE)						
0300-05-	ES SAFA	*33.08N*	*37.15E*	...	Volcanic field	1850j
0301-04-	LUNAYYIR, HARRAT	*25.17N*	*37.75E*	*1370*	Volcanic field	1000<
0301-06=	KHAYBAR, HARRAT	*25.00N*	*39.92E*	*2093*	Volcanic field	0650t
0301-07=	RAHAT, HARRAT	*23.08N*	*39.78E*	*1744*	Volcanic field	?1292, 1256, 0641
0301-08-	YAR, JABAL	*17.05N*	*42.83E*	*305*	Volcanic field	1810j
0301-09-	ARHAB, HARRA OF	*15.63N*	*44.08E*	*3100*	Volcanic field	0500v
0301-12-	DHAMAR, HARRAS OF	*14.57N*	*44.67E*	*3500*	Volcanic field	1937
0301-16-	SAWAD, HARRA ES-	*13.58N*	*46.12E*	*1737*	Volcanic field	1253
0301-18-	BIR BORHUT	*15.55N*	*50.63E*	...	Volcanic field	?0950?
Indian Ocean						
0303-01=	KARTHALA	*11.75S*	*43.38E*	*2361*	Shield volcano	1991, 1977, 1972, 1965, 1956, 1952, 1948, 1928b, 1918, 1910, 1904, 1883-84, 1880, 1876, 1872, 1865, ?1862, 1860, 1859, 1858, 1857, 1855, 1850?, 1848, 1833, 1830, 1828, 1821, 1814, 1808, 1050w
0303-02=	**FOURNAISE, PITON**	*21.22S*	*55.71E*	*2631*	Shield volcano	1998, 1992, 1991, 1990, 1985-88, 1983-84, 1981, 1979, 1977, 1977, 1976, 1975-76, 1973, 1973, 1972, 1966, 1964-65, 1964, 1963, 1961, 1960, 1959, 1958, 1957, 1955-57, 1954, 1953, 1952, 1951, ?1951, 1950, 1950, ?1949, 1948, 1947?, 1946, 1945, 1944, 1943, 1942, 1941?, 1938-39, 1938, 1937, 1936, 1935?, 1933-34, 1932, 1931, 1930, 1929, 1926-27, 1925-26, 1924, 1924, 1921, 1920, 1917, 1915, 1913, 1910, 1909, ?1908, 1907, 1905, 1904, 1903?, 1902, 1901, 1901, 1900, 1899, 1898, 1898, 1897, 1894, 1890-91, 1889, 1884, ?1882, 1878, 1876, 1875, 1874, 1874, ?1872, 1871, ?1870, 1869?, 1868, 1865, 1863-64, 1861, 1860, 1859, 1858-59, 1852, 1851, 1850, 1849, 1848, 1847, 1846, 1845, 1844, 1844, 1843, 1842, 1832, 1830, 1824, 1824, 1821, 1820, 1817, 1816, 1815, 1815, 1814, 1813, 1812, 1810, 1809, 1807, 1802, 1801-02, 1800, 1797?, 1795, 1794, 1792, 1791, 1789, 1787, 1786, 1784-85, 1776, 1775, 1774, 1772, 1772, 1771, 1768, 1766, 1760, 1759, 1753, 1751, 1734, 1734, 1733?, 1721, 1709, 1708, 1703<-05, 1672, 1671, 1669, 1649, 1640
0304-01=	HEARD	*53.10S*	*73.51E*	*2745*	Stratovolcano	1993, ?1992, 1992, 1985-87, 1954, 1953, 1950-52, 1910, ?1881
0304-011	MCDONALD IS	*53.03S*	*72.60E*	*186*	Complex Volcano.	1996-97
0304-03=	ST. PAUL	*38.72S*	*77.53E*	*268*	Stratovolcano	1793
0304-08-	MARION ISLAND	*46.90S*	*37.75E*	*1230*	Shield volcanoes	1980
0305-01=	UNNAMED	*11.75N*	*80.75E*	*?*	Submarine volcano	?1757
New Zealand						
0401-04=	**WHITE ISLAND**	*37.52S*	*177.18E*	*321*	Stratovolcanoes	1998-99, 1998, 1995, 1986-94, 1983-84, 1976-81, 1974, 1971, 1971, 1970, 1969, 1968-69, 1966-67, 1962, 1959, 1958, 1957, 1955, 1947, 1933, 1930, 1928, 1926, 1924, 1922, 1909, ?1908, ?1886, 1886, ?1885, 1885, ?1856h, 1836b, 1826
0401-05=	OKATAINA	*38.12S*	*176.50E*	*1111*	Lava domes	1973, 1951, 1926, 1924, 1918-20, 1917, 1915, 1915, 1914, 1913, 1912, 1910, 1908, 1906, 1905, 1905, 1900-04, 1896, **1886** **(Tarawera)**
0401-08=	TONGARIRO	*39.13S*	*175.64E*	*1978*	Stratovolcanoes	1977, 1976, 1975, 1972-74, 1972, 1969, 1968, 1962, 1959, 1958, 1956, 1954-55, 1952-53, 1951, 1950, 1949, 1948, 1948, 1940, 1939, 1937, 1934-35, 1934, 1931, 1928, 1928, ?1927, 1926, 1926, 1925, 1924, 1924, 1924, 1917, 1914, 1913, 1913, 1910-11, 1910, 1909, 1907, 1907, 1906, 1905, 1904, 1898, 1897, 1896, 1892, 1892, 1892, ?1890, 1886, 1885a-87, 1883, 1881, 1878, ?1875, 1870, 1869, 1869, 1864-65, 1863-64, 1862, 1859, 1857, 1855, 1844-45, 1841, 1839 (**Ngauruhoe**)
0401-10=	**RUAPEHU**	*39.28S*	*175.57E*	*2797*	Stratovolcano	1997, 1996, ?1996, 1995, ?1994, 1992, ?1991, 1990, 1990, 1989, 1988-89, 1988, 1987, 1986, 1985, 1981-82, 1980, 1979-80, 1979, 1977-79, 1976, 1976, 1975, 1975, 1973-74, 1972-73, 1971, 1970, 1969, 1968, 1967, 1966, 1959, 1956, 1952, 1951, 1950, 1948, 1946-47, 1946, 1945, 1944, 1942, 1940, 1936, 1934-35, 1934, 1925, 1921, 1918, 1906, 1903, 1895, 1889, 1861
0401-13-	RUMBLE III	*35.74S*	*178.47E*	*-140*	Submarine volcano	1986, 1973, 1970, 1963-66, 1958-62
Kermadec Is (S to N)						
0402-01=	CURTIS ISLAND	*30.54S*	*178.56W*	*-137*	Submarine volcano	?1936
0402-02=	BRIMSTONE ISLAND	*30.23S*	*178.92W*	*-2000*	Submarine volcano	?1825
0402-03=	RAOUL ISLAND	*29.27S*	*177.92W*	*516*	Stratovolcano	1964-65, 1870, 1814
0402-04=	UNNAMED	*29.18S*	*177.87W*	*-560*	Submarine volcano	?1987, 1886
0402-05-	MONOWAI SEAMOUNT	*25.88S*	*177.18W*	*-100*	Submarine volcano	1997-98, 1997, 1996, 1995, 1990-91, 1988, 1986, 1982, 1980, 1977, 1977-79, ?1944
Tonga (S to N)						
0403-01=	UNNAMED	*21.38S*	*175.65W*	*-500*	Submarine volcano	1932, 1907

NUMBER	VOLCANO NAME	LAT	LONG	ELEV	TYPE	ERUPTION YEARS (VEI≤3 **VEI=4** **VEI=5** ***VEI=6-7***)
Tonga (cont)						
0403-03=	UNNAMED	20.85S	175.53W	-13	Submarine volcano	1923, 1911
0403-04=	UNNAMED	20.57S	175.38W	?	Submarine volcano	1988, 1937, 1912
0403-05=	FALCON ISLAND	20.32S	175.42W	-145	Submarine volcano	@1970, 1936, 1933, 1928, 1927, 1921, 1894, 1885-86, 1877, ?1865, ?1781
0403-06=	TOFUA	19.75S	175.07W	512	Caldera	1958, 1906, 1906, 1885, 1854, 1792, 1774
0403-07=	METIS SHOAL	19.18S	174.87W	-4	Submarine volcano	1995, 1979, 1967-68, 1894, 1886, 1878, 1858, 1852, 1851
0403-08=	HOME REEF	18.99S	174.77W	-2	Submarine volcano	1984, ?1857, 1852
0403-09=	LATE	18.80S	174.65W	518	Stratovolcano	1854, 1790
0403-10=	FONUALEI	18.02S	174.32W	200	Stratovolcano	?1974, 1957, 1951, 1939, 1906, **1847**, 1846, 1791
0403-101	CURACOA	15.62S	173.67W	-33	Submarine volcano	1979, 1973
0403-11=	NIUAFO'OU	15.60S	175.63W	260	Shield volcano	1985, ?1959, ?1947, 1946, 1943, 1935-36, 1929, 1912, 1887, **1886**, 1867, 1853, 1814
Samoa (E to W)						
0404-00-	UNNAMED	14.23S	169.07W	-650	Submarine volcano	?1973
0404-01=	OFU-OLOSEGA	14.17S	169.61W	639	Shield volcanoes	1866
0404-04=	**SAVAI'I**	13.61S	172.52W	1858	Shield volcano	1905-11, 1902, 1725s
Offshore New Guinea & Admiralty Is						
0500-01=	ST. ANDREW STRAIT	2.38S	147.35E	270	Complex volcano	1953-57, 1883
0500-02-	BALUAN	2.57S	147.28E	254	Stratovolcano	?1931
0500-03-	UNNAMED	3.03S	147.78E	-1300	Submarine volcano	1972
0501-002	KADOVAR	3.62S	144.62E	365	Stratovolcano	?1700
0501-01=	BAM	3.60S	144.85E	685	Stratovolcano	1960, 1959, 1958, 1958, 1957, 1954-57, 1947, 1944, ?1936-39, 1924, ?1920b, 1913, 1909, 1908, 1907, ?1897-98, ?1888, ?1885, ?1883, 1877, 1874, 1872d
0501-02=	MANAM	4.10S	145.06E	1807	Stratovolcano	1974-99>, 1965-66, 1963-64, 1963, 1962, 1961, 1959-60, 1959, 1956-58, 1954, 1953, 1946-47, 1936-39, 1932-34, 1926-28, 1925, ?1924, ?1923, 1922, 1920-21, **1919**, 1917, 1909-14?, ?1907, 1904, 1904, ?1901-02, 1899a, 1887-95, 1885, ?1884, 1877, 1830, 1700, 1643, 1616
0501-03=	KARKAR	4.64S	145.96E	1839	Stratovolcano	?1980, 1979, 1974-75, 1974, ?1962?, 1895, 1885, ?1830, 1643
0501-04=	UNNAMED	4.31S	146.25E	-2000	Submarine volcano	?1951, ?1944
0501-05=	**LONG ISLAND**	5.35S	147.12E	1280	Complex volcano	1993, 1976, 1973-74, 1968, ?1961, 1955, 1953-54, 1943, 1938, 1933
0501-07=	**RITTER ISLAND**	5.52S	148.12E	140	Stratovolcano	1974, 1972, 1888, @1887, ?1885, ?1878, ?1848, 1793, 1700
New Britain (W to E)						
0502-001	UNNAMED	5.20S	148.57E	?	Submarine volcano	?1983
0502-01=	**LANGILA**	5.52S	148.42E	1330	Complex volcano	1973-99>, 1971-72, 1970, 1969, 1967-68, 1964-66, 1962-63, 1960-61, 1958, 1956, 1955, 1955, 1954, ?1942e, 1907, 1900, 1890, 1884, 1878
0502-08=	PAGO	5.58S	150.52E	742	Caldera	1933, 1920b, 1911-18
0502-11=	BAMUS	5.20S	151.23E	2248	Stratovolcano	1886h
0502-12=	**ULAWUN**	5.05S	151.33E	2334	Stratovolcano	1994, 1993, 1989, 1985, 1984-85, 1984, 1983-84, 1980, 1978, 1973, 1970, 1967, 1963, 1960-62, 1958, ?1951, 1941, ?1937, 1927, 1919, 1918, 1915, 1898, 1878, 1700
0502-13=	LOLOBAU	4.92S	151.15E	858	Caldera	**1911-12**?, ?1908, **1904-05**
0502-131	UNNAMED	4.75S	150.85E	?	Submarine volcano	?1970, ?1951
0502-14=	**RABAUL**	4.27S	152.20E	688	Pyroclastic shield	1995-99>, **1994-95**, 1943, 1941-42, 1940, **1937**, 1878, 1850?, 1791, 1767
New Guinea (SE)						
0503-01=	**LAMINGTON**	8.95S	148.15E	1680	Stratovolcano	**1951**-56
0503-03=	**VICTORY**	9.20S	149.07E	1925	Stratovolcano	1890?-1935e, ?1810j
0503-04=	WAIOWA	9.57S	149.07E	640	Pyroclastic cone	1943-44
Bougainville						
0505-01=	BALBI	5.83S	154.98E	2715	Stratovolcano	?1825q
0505-02=	**BAGANA**	6.14S	155.19E	1750	Lava cone	1972-99>, 1970-71, 1968, 1966-67, 1964-65, 1962-63, 1961, 1959?-60, 1956, 1953, **1952**, 1948-51, 1945-47, 1943, 1939, 1938, 1937, ?1909, 1908, 1899, 1897, 1894-95, 1883, 1865c-83, 1842
Solomon Is (W to E)						
0505-06=	**KAVACHI**	9.02S	157.95E	-20	Submarine volcano	1991, 1986, 1985-86, 1982, ?1981, 1980-81, 1978, 1977, 1977, 1976, 1975, 1974, 1972, 1969-70, 1966, 1965, 1963-64, 1962, 1961, 1958, 1957, 1952-53, 1951, 1950, 1942?, 1939
0505-07=	SAVO	9.13S	159.82E	510	Stratovolcano	1835e-47?, 1568
0506-01=	TINAKULA	10.38S	165.80E	851	Stratovolcano	1984-85, 1971, 1965-66, ?1955, 1951, 1909, 1886, 1871, 1869, 1857, 1855, 1840?, 1797, 1768, 1595, 1965-66, 1865?, 1860?
Vanuatu (N to S)						
0507-02=	GAUA	14.27S	167.50E	797	Stratovolcano	1982, 1981, 1980, 1977, 1976, 1973-74, 1971, 1969, 1968, 1967, 1966, 1965, 1963, ?1962
0507-021	MERE LAVA	14.45S	168.05E	1028	Stratovolcano	?1606
0507-03=	AOBA	15.40S	167.83E	1496	Shield Volcano	1995

NUMBER	VOLCANO NAME	LAT	LONG	ELEV	TYPE	ERUPTION YEARS (VEI≤3 **VEI=4** VEI=5 *VEI=6-7*)
Vanuatu & S (cont)						
0507-04=	**AMBRYM**	16.25S	168.12E	1334	Stratovolcano	1998-99, 1997, 1996, 1994, 1990-91, 1989, 1988, 1986, 1984-86, 1983, 1981, 1980, 1979, 1979, 1977, 1977, 1973-76, 1972, 1971, 1967-70, 1964-66, 1963, 1961-63, 1960, 1959, 1958, 1957, 1955, 1954, 1953, 1952, **1950-51**, 1942, 1938, 1937, 1935-36, 1929, 1915, 1913-14, 1912, 1910, ?1909, 1908, 1898, 1894-95, 1888, 1886, 1884, 1883, 1871, ?1870, 1863-64, 1820?, 1774
0507-05=	**LOPEVI**	16.50S	168.34E	1413	Stratovolcano	1982, 1980, 1979, 1978-79, 1976, 1975, 1974, 1970-72, 1967-69, 1963-65, 1962, 1960, 1939, 1939, 1933, 1922, 1908, ?1898, 1893, ?1892, 1884, 1874, 1864, 1863
0507-06=	EAST EPI	16.68S	168.37E	-34	Caldera	?1988, 1979e, ?1974, ?1973, ?1972, ?1971, 1960, 1958, 1953, ?1953, 1920
0507-07=	KUWAE	16.82S	168.53E	-2	Caldera	?1980, ?1979, ?1977, 1974, ?1973, ?1972, 1971, ?1970, 1959, 1958, 1953, 1952, 1949, 1949, 1948, 1923-25, 1897-1901
0507-09=	TRAITOR'S HEAD	18.75S	169.23E	837	Stratovolcano	?1959, 1881
0507-10=	**YASUR**	19.52S	169.42E	361	Stratovolcano	1774<-1999>
0508-001	EASTERN GEMINI	20.98S	170.28E	-80	Submarine volcano	1996
0508-01=	MATTHEW ISLAND	22.33S	171.32E	177	Stratovolcano	?1976, ?1966, 1956b, 1954, 1949<, ?1828
0508-02=	HUNTER ISLAND	22.40S	172.05E	297	Stratovolcano	1903, 1895, ?1892, 1841, 1835, ?1797
0508-03-	UNNAMED	25.78S	168.63E	-2400	Submarine volcano	1963-64
Sumatra & Andaman Is (NW to SE)						
0600-01=	BARREN ISLAND	12.29N	93.87E	305	Stratovolcano	1994-95, 1991, ?1852, 1803-04, 1795, 1789, 1787
0601-02=	SEULAWAH AGAM	5.42N	95.60E	1726	Stratovolcano	?1839, ?1510j
0601-03=	PEUET SAGUE	4.92N	96.33E	2780	Complex volcano	1998, 1918-21
0601-05=	TELONG, BUR NI	4.77N	96.80E	2624	Stratovolcano	1937, 1924, 1919, 1856, 1839, 1837
0601-07=	SIBAYAK	3.20N	98.47E	2212	Stratovolcano	1881
0601-08=	SINABUNG	3.17N	98.39E	2460	Stratovolcano	?1881
0601-12=	**SORIKMARAPI**	0.68N	99.53E	2145	Stratovolcano	?1996, 1986, 1970, 1917, 1893, 1892, 1879, 1829?
0601-13=	TALAKMAU	0.07N	99.98E	2912	Complex volcano	?1937
0601-14=	**MARAPI**	0.38S	100.47E	2891	Complex volcano	1987-94>, 1984, 1983, 1982, 1982, 1980, 1975-79, 1973, 1970-71, ?1968, 1967, 1966, 1958, 1958, 1954-57, 1950-52, 1949, 1949, 1943e, 1932, 1930, 1929, 1927, 1925, 1919, 1918, 1918, 1917, 1916, 1915, 1914, 1913, 1911, 1910, 1907-08, 1905, 1904, 1889, 1888, 1886, 1885, 1883, 1883, 1876-77, 1876, 1871, 1871, 1863, 1861, 1855-56, 1854, 1845, 1833-34, 1822, 1807, 1770
0601-15=	TANDIKAT	0.43S	100.31E	2438	Stratovolcano	1924, 1914, 1889
0601-16=	TALANG	0.97S	100.67E	2896	Stratovolcano	?1986, 1968, 1968, 1967, 1963, 1876?, 1845, 1843, 1833
0601-17=	KERINCI	1.69S	101.27E	3805	Stratovolcano	1998, 1998, 1996, ?1971, 1969-70, 1968, 1967, 1966, 1964, 1963, 1960, 1952, 1938, 1937, 1936, 1936, 1923, 1921, 1908-09?, 1887, 1878, 1874?, 1842, 1838
0601-18=	SUMBING	2.42S	101.73E	2508	Stratovolcano	1921, 1909
0601-22=	**KABA**	3.52S	102.62E	1952	Stratovolcano	1956, 1952, 1950-51, 1939-41, ?1918, 1907, 1873-92, 1868-69, 1853, 1834, 1833
0601-23=	DEMPO	4.03S	103.13E	3173	Stratovolcano	1994, 1974, 1973, 1964, 1940, 1939-40, 1939, 1936, 1934, 1926, 1923, 1921, 1908, 1905, 1900, 1900, 1895, 1884, 1881, 1881, 1880, 1879, 1853, 1839?, 1817
0601-25=	BESAR, GUNUNG	4.43S	103.67E	1899	Stratovolcano ?	1940
0601-251	RANAU	4.83S	103.92E	1881	Caldera	?1903, ?1887-88
0601-27=	SUOH	5.25S	104.27E	1000	Maars; Lava dome	**1933**
0602-00=	**KRAKATAU**	6.10S	105.42E	813	Caldera	1997, 1996, 1994-95, 1992-93, 1988, 1981, 1980, 1979, 1978, 1975, 1972-73, ?1969, 1965?, 1959-63, 1958-59, 1955, 1953, 1953, 1952, 1950, 1949, 1946-47, 1946, 1945, 1944, 1943, 1942, 1941, 1938-40, 1937, 1936, 1935, 1932-34, 1931-32, 1927-30, **1883** 1680-81, 1550t, 1350t, 1150t, 1050t, 0950t, 0850t, 0416, 0250t
Java (W to E)						
0603-03=	KIARABERES-GAGAK	6.73S	106.65E	1511	Stratovolcano	1939, 1938, 1936, 1935, 1929, 1923
0603-05=	SALAK	6.72S	106.73E	2211	Stratovolcano	1938, 1935, 1919, 1902-03, 1780, ?1699
0603-06=	GEDE	6.78S	106.98E	2958	Stratovolcano	1957, 1956, ?1955, 1948-49, 1947-48, 1909, 1899, 1891, ?1889, 1887, 1886, 1870, 1866, 1853, 1852, 1848, 1847, 1845, 1843, 1840, 1832, 1761, 1747-48
0603-09=	TANGKUBANPARAHU	6.77S	107.60E	2084	Stratovolcano	?1985, 1983, 1969, 1967, 1965, 1965, 1961, 1957, 1952, 1929, 1926, 1910, 1896, 1846, 1842, 1829, 1826
0603-10=	**PAPANDAYAN**	7.32S	107.73E	2665	Stratovolcano	1942, 1923-25, 1772
0603-13=	**GUNTUR**	7.13S	107.83E	2249	Complex volcano	?1887, ?1885, 1847, 1843, 1843, 1841, 1840, 1836, 1834-35, 1833, 1832, 1832, 1829, 1828, 1827, 1825, 1818, 1816, 1815, 1809, 1807, 1803, 1800, 1780, 1777, 1690
0603-14=	**GALUNGGUNG**	7.25S	108.05E	2168	Stratovolcano	1984, **1982**-83, 1918, 1894, **1822**
0603-16=	KAWAHKARAHA	7.17S	108.08E	1155	Fumarole field	?1861
0603-17=	CEREME	6.89S	108.40E	3078	Stratovolcano	1951, 1937-38, 1805, 1775, 1772, 1698
0603-18=	**SLAMET**	7.24S	109.20E	3432	Stratovolcano	1989, 1988, ?1974, 1973, 1969, 1967, 1966, 1960-61, 1958, 1958, 1957, 1955, 1953, 1951-52, 1951, 1948, 1944, 1943-44, ?1943, 1940, 1939, 1939, 1937, ?1934, 1933, 1932, 1930, 1929, 1928, 1927, 1926, 1923, 1904, 1890, 1885, 1875, 1875, 1860, 1849, 1835, 1825, 1772
0603-20=	**DIENG** VOLC COMPLEX	7.20S	109.92E	2565	Complex volcano	1993, 1986, 1981, 1979, 1964, 1956, 1954, 1953, ?1952, 1944, 1943, 1939, 1928, 1883-84, 1847, 1826, 1825, 1786, ?1776, 1375u
0603-21=	SUNDORO	7.30S	109.99E	3151	Stratovolcano	1971, 1906, 1903, 1902, 1887, 1883, 1882, 1818, 1806?

NUMBER	VOLCANO NAME	LAT	LONG	ELEV	TYPE	ERUPTION YEARS (VEI≤3 **VEI=4** **VEI=5** ***VEI=6-7***)
Java (cont)						
0603-22=	SUMBING	*7.38S*	*110.05E*	*3371*	Stratovolcano	1730?
0603-24=	MERBABU	*7.45S*	*110.43E*	*3145*	Stratovolcano	1797, ?1570, 1560
0603-25=	**MERAPI**	*7.54S*	*110.44E*	*2911*	Stratovolcano	1992-98, 1972-90, 1971, 1967-69, 1961, 1953-58, 1948-49, 1944-45, 1942-43, 1939-40, 1933-35, 1930-31, 1924, 1923, 1922, 1920-21, 1918, 1915, 1909-13, 1908, 1906-07, 1905, 1902-04, 1902, 1897, 1894, 1893, 1891, 1889, 1888, ?1885, 1883-84, 1878-79, 1872-73, **1872**, 1869, 1865-67, 1862-64, ?1854, 1849, 1849, ?1848, 1846-47, 1846, 1840, 1837-38, 1832-35, 1828, 1822-23, 1820-22, 1812-13, 1810, 1807, 1797, 1786, 1768, 1755, 1752, 1745, 1678, 1677, 1672, 1663, 1658, 1587, 1584, 1560, 1554, 1548
0603-28=	**KELUT**	*7.93S*	*112.30E*	*1731*	Stratovolcano	**1990**, 1967, 1967, **1966**, 1951, 1920, **1919**, 1901, 1864, 1851, 1848, 1835, **1826**, 1825, 1811, 1785, 1776, 1771, 1752, 1716, **1641**, **1586**, 1548, 1481, 1462, 1451, 1450, 1411, 1395, 1385, 1376, 1334, 1311, 1000
0603-29=	ARJUNO-WELIRANG	*7.72S*	*112.58E*	*3339*	Stratovolcano	?1991, 1952
0603-291	PENANGGUNGAN	*7.62S*	*112.63E*	*1653*	Stratovolcano	?0200?
0603-30=	**SEMERU**	*8.10S*	*112.92E*	*3676*	Stratovolcano	1967-99>, 1950-64, 1946-47, 1946, 1945, 1941-42, 1913, 1912, 1911, 1910-11, 1909-10, 1908, 1907, 1907, 1905, 1904, 1903, 1901, 1900, 1899, 1899, 1899, 1898, 1897, 1896, 1895, 1893-94, 1893, 1892, 1889-91, 1888, 1887, 1887, 1886, 1884-85, 1879, 1878, 1877, 1877, 1872, 1867, 1865, 1860, 1857, 1856, 1851, 1848, 1848, 1845, 1844, 1842, 1838, 1836, 1832, 1830, 1829, 1818
0603-31=	**TENGGER** CALDERA	*7.94S*	*112.95E*	*2329*	Stratovolcano	1995, 1984, ?1983, 1983, 1980, 1972, 1956, 1955, 1950, 1948, 1940, 1939, 1935, 1930, 1929, 1928, 1928, 1922, 1921, 1915-16, 1910, 1909, 1907-08, 1907, 1906-07, 1896, 1893, 1890, ?1888, 1886-87, 1886, 1885-86, 1885, 1877, 1867-68, 1866, 1865, 1865, 1860, 1859, 1858, 1858, 1857, @1856, 1844, 1843, 1842, 1835, 1830, 1830, 1829, 1825, 1822-23, 1820, 1815, 1804, ?1775, ?1767
0603-32=	LAMONGAN	*8.00S*	*113.34E*	*1651*	Stratovolcano	?1953, 1898, 1896, 1893, 1891, 1890-91, 1890, 1889, 1888, 1887-88, 1887, 1885-86, 1884, 1883, 1877, 1874, 1872, 1870-71, 1870, 1869, 1869, 1864, 1861, 1859, 1856, 1849, 1847, 1847, 1843-44, 1841-42, 1838, 1838, 1830, 1829, 1826, 1824, 1821-22, 1818, 1817, 1808, 1806, 1799
0603-34=	**RAUNG**	*8.12S*	*114.04E*	*3332*	Stratovolcano	1997, ?1995, 1993, 1991, 1990, 1987-89, 1985, 1982, 1978-79, 1977, 1976, 1975, 1974, 1973, 1971, 1956, 1955, 1953, 1944-45, 1943, 1941, 1940, 1938-39, 1937, 1936, 1933, 1929, 1928, 1927-28, 1924, ?1924, 1921, 1917, 1916, 1915, 1913, 1903-04, 1902, 1897, 1896, 1890, 1885, 1881, 1864, 1860, 1859, 1849, 1838, **1817**, 1815, 1812-14?, 1804d, 1793f, 1730, **1638**, 1597, **1593**, ?1586
0603-35=	IJEN	*8.05S*	*114.24E*	*2386*	Stratovolcanoes	1994, 1993, 1952, 1936, 1917, 1817, 1796
Lesser Sunda Is (W to E)						
0604-01=	**BATUR**	*8.24S*	*115.37E*	*1717*	Caldera	1994, ?1976, 1974, 1973, 1972, 1971, 1970, 1968, 1966, 1965, 1963-64, 1926, 1925, 1924, 1923, 1922, 1921, 1905, 1904, 1897, 1888, 1854, 1849, 1821, 1804
0604-02=	**AGUNG**	*8.34S*	*115.50E*	*3142*	Stratovolcano	1963-64, 1843, ?1821, 1808
0604-03=	RINJANI	*8.42S*	*116.47E*	*3726*	Stratovolcano	1994, 1966, 1965, 1953, 1949-50, 1944-45, ?1941, 1915, 1909, 1906, 1901, 1900, 1884, 1847
0604-04=	**TAMBORA**	*8.25S*	*118.00E*	*2850*	Stratovolcano	1967p, 1880r, 1819, ***1812-15***
0604-05=	SANGEANG API	*8.18S*	*119.05E*	*1949*	Complex volcano	1985-88, 1966, 1964-65, 1958, 1957, 1956, 1955, 1954, 1954, 1953, 1927, 1912, 1911, 1860, 1821, 1715, 1512
0604-051	GILIBANTA	*8.52S*	*119.35E*	*?*	Submarine volcano	?1957
0604-071	RANAKAH, GUNUNG	*8.62S*	*120.52E*	*2100*	Lava domes	1991, 1987-89
0604-09=	INIELIKA	*8.73S*	*120.98E*	*1559*	Complex volcano	1905
0604-10=	EBULOBO	*8.80S*	*121.18E*	*2124*	Stratovolcano	1969, 1941, 1938, 1924, 1910, 1888, 1830
0604-11=	IYA	*8.88S*	*121.63E*	*637*	Stratovolcano	?1971, 1969, 1953, ?1888, 1882, 1871, 1868, 1867, 1844, 1671?
0604-14=	KELIMUTU	*8.75S*	*121.83E*	*1640*	Complex volcano	1968, 1938, 1865e
0604-15=	**PALUWEH**	*8.32S*	*121.70E*	*875*	Stratovolcano	1985, 1984, 1980-81, 1973, 1972-73, 1963-66, 1928, 1650t
0604-16=	EGON	*8.67S*	*122.45E*	*1703*	Stratovolcano	1907, ?1888-92
0604-18=	LEWOTOBI	*8.53S*	*122.77E*	*1703*	Stratovolcanoes	1991, 1990, 1971, 1970, 1968-69, 1939-40, 1935, 1932-33, 1921, 1914, 1909-10, 1907, 1889, 1869, 1868, 1868, 1865, 1861, ?1859, 1675q
0604-20=	LEREBOLENG	*8.35S*	*122.84E*	*1117*	Complex volcano	1881, 1876, 1873
0604-22=	ILIBOLENG	*8.34S*	*123.25E*	*1659*	Stratovolcano	1993, 1991, 1991, 1987, 1986, 1983-84, 1982, 1973-74, 1951, 1950, 1949, 1949, 1948, 1944, 1927, 1925, 1909, 1904, 1888, 1885
0604-23=	LEWOTOLO	*8.27S*	*123.50E*	*1423*	Stratovolcano	1951, 1920, 1899, 1864, 1852, 1849, 1819, 1660
0604-25=	**ILIWERUNG**	*8.54S*	*123.59E*	*1018*	Complex volcano	1993, 1983, ?1976, 1973-74, 1952, 1951, 1950, 1949, 1948, ?1941, 1928, 1910, 1870
0604-26=	TARA, BATU	*7.79S*	*123.57E*	*748*	Stratovolcano	1847-52
0604-27=	SIRUNG	*8.51S*	*124.14E*	*862*	Complex volcano	1970, 1965, 1965, 1964, 1960, 1953, 1947, 1934, ?1927, ?1899, ?1852
Banda Sea						
0605-01=	EMPEROR OF CHINA	*6.62S*	*124.22E*	*-2850*	Submarine volcano	?1927, ?1893<
0605-02=	NIEUWERKERK	*6.60S*	*124.67E*	*-2285*	Submarine volcano	?1927, ?1925, ?1893<
0605-03=	GUNUNGAPI WETAR	*6.64S*	*126.65E*	*282*	Stratovolcano	1699, 1512
0605-04=	WURLALI	*7.12S*	*128.67E*	*868*	Stratovolcano	1892
0605-05=	TEON	*6.92S*	*129.12E*	*655*	Stratovolcano	1904, 1693, 1663, **1660**, 1659
0605-06=	NILA	*6.73S*	*129.50E*	*781*	Stratovolcano	1968, 1964, 1932, 1903

NUMBER	VOLCANO NAME	LAT	LONG	ELEV	TYPE	ERUPTION YEARS (VEI≤3 **VEI=4** **VEI=5** *VEI=6-7*)
0605-07=	SERUA	*6.30S*	*130.00E*	*641*	Stratovolcano	1921, 1919, 1859, 1858, 1846, ?1845, 1844, 1694, **1693**, ?1692, 1687, 1683
0605-09=	BANDA API	*4.52S*	*129.87E*	*640*	Caldera	1988, ?1902, 1901, 1890, ?1855, ?1835, 1825?-31, 1824, 1820, 1816, 1778, 1775, 1773, 1765-66, 1762, 1749, 1722, 1712, 1690-96, 1683, 1635, 1632, 1615, 1609, 1598-1602, 1586
Sulawesi (NE)						
0606-01=	COLO [UNA UNA]	*0.17S*	*121.60E*	*507*	Stratovolcano	**1983**, 1938j, 1898-1900?
0606-02=	AMBANG	*0.75N*	*124.42E*	*1795*	Complex volcano	1845e
0606-03=	**SOPUTAN**	*1.10N*	*124.72E*	*1784*	Stratovolcano	1991-93, 1991, 1989, 1985, 1984, 1982, 1973, 1971, 1970, 1968, 1966-67, 1953, 1947, 1923-24, 1917, 1915, 1913, 1911-12, 1910, 1908-09, 1907, 1906, 1901, 1890, 1845, 1833?, 1819, 1785
0606-04=	SEMPU	*1.14N*	*124.73E*	*1549*	Caldera	?1819
0606-10=	**LOKON-EMPUNG**	*1.35N*	*124.79E*	*1580*	Stratovolcano	1991-92, 1988, 1986-87, ?1984, 1975-80, 1973-74, 1971, 1969-70, 1966, 1965, 1963-64, 1962, 1961, 1958-59, 1951-53, 1949, 1942, 1930, 1893-94, 1829, 1775q, 1375q
0606-11=	MAHAWU	*1.35N*	*124.85E*	*1324*	Stratovolcano	1977, 1958, 1952, 1904, 1846, 1789, 1788<
0606-13=	**TONGKOKO**	*1.52N*	*125.20E*	*1149*	Stratovolcano	1880, 1843-46, 1821, 1801, 1694, 1683, **1680**
Sangihi Is (S to N)						
0607-01=	**RUANG**	*2.28N*	*125.42E*	*725*	Stratovolcano	?1996, 1949, 1914-15, 1904-05, 1889, 1874, 1871, 1870, 1856, 1840, 1836?, 1808
0607-02=	**KARANGETANG**	*2.78N*	*125.48E*	*1784*	Stratovolcano	1998, 1996-97, 1995, 1991-93, 1989, 1983-88, 1982, 1980, 1979, 1978, 1976-77, 1972-76, 1970-71, 1967, 1965-67, 1962-63, 1961, 1961, 1953, 1952, 1949, 1948, 1947, 1947, 1941, 1940, 1940, 1935, 1930, 1930, 1926, 1924, 1922, 1921, 1905, 1900, 1899, 1892, 1887, 1886, 1883, 1864, 1825, 1712, 1675
0607-03=	BANUA WUHU	*3.13N*	*125.49E*	*-5*	Submarine volcano	?1968, 1918-19, 1904, 1904, 1895, 1889-99, 1835
0607-04=	**AWU**	*3.67N*	*125.50E*	*1320*	Stratovolcano	1992, ?1968, **1966**, 1930-31, 1922, 1921, 1913, 1893, 1892, 1885, 1883, 1875, 1856, **1812**, 1711, 1646e, 1640-41 (see Parker 0701-011 below)
0607-05=	UNNAMED	*3.97N*	*124.17E*	*-5000*	Submarine volcano	?1955, ?1922
Halmahera (N to S)						
0608-01=	**DUKONO**	*1.70N*	*127.87E*	*1087*	Complex volcano	1933-99>, 1901, 1868?, 1719w, 1550
0608-03=	IBU	*1.48N*	*127.63E*	*1325*	Stratovolcano	1998-99, 1911
0608-04=	**GAMKONORA**	*1.37N*	*127.52E*	*1635*	Stratovolcano	1987, 1981, 1952, 1951, 1950, 1949, 1926, 1917, 1911, 1885e, **1673**, 1564
0608-06=	**GAMALAMA**	*0.80N*	*127.32E*	*1715*	Stratovolcanoes	1994, 1993, ?1991, 1990, 1988, 1983, 1980, 1962-63, 1938, 1933, 1932, 1923, 1918, 1911, 1907, ?1900, 1898, 1897, ?1896, 1895, 1884, ?1884, 1871, 1868-69, 1868, 1864-65, 1864, ?1864, ?1863, 1862, ?1860, ?1858-59, 1849-50, 1847, 1847, 1846, ?1845, ?1844, 1843, 1842, ?1841, 1840, 1839, 1838, 1835, 1833, 1831, ?1821, 1814, 1812, 1811, 1775, 1773-74, 1773, 1771-72, 1770, 1763, 1739, 1737, 1687, 1686, 1676, 1659, 1653, 1648, ?1643, 1635, 1608, 1605, 1561, 1538
0608-07=	**MAKIAN**	*0.32N*	*127.40E*	*1357*	Stratovolcano	1988, 1890, 1864, 1863, **1861-62**, ?1860, ?1854, **1760-61**, **1646**, 1550<
Philippines - S & Central						
0700-01=	BUD DAJO	*5.95N*	*121.07E*	*440*	Pyroclastic cones	1897, 1641
0701-011	**PARKER**	*6.12N*	*124.89E*	*1824*	Stratovolcano	**1640-41**
0701-06=	RAGANG	*7.67N*	*124.50E*	*2815*	Stratovolcano	1915, 1873, 1871, 1865, 1858, 1856, 1840, 1834, 1765
0701-07=	CALAYO	*7.87N*	*125.06E*	*646*	Tuff cone	1886
0701-08=	**HIBOK-HIBOK**	*9.20N*	*124.67E*	*1332*	Stratovolcano	1948-53, 1871-75, 1862, 1827
0702-02=	CANLAON	*10.41N*	*123.13E*	*2435*	Stratovolcano	1996, 1993, 1992, 1992, 1989, 1988, 1987, 1986, 1985, 1985, 1978, 1969, 1932-33, 1927, 1905-06, 1904, 1902, 1894, 1893, 1866
0702-07=	MAHAGNOA	*10.87N*	*124.85E*	*800*	Stratovolcano	?1895
0702-08=	BILIRAN	*11.52N*	*124.53E*	*1187*	Compound volcano	1939
Philippines - Luzon & N						
0703-01=	BULUSAN	*12.77N*	*124.05E*	*1565*	Stratovolcano	1994-95, 1988, 1983, 1981, 1979-80, 1978, 1933, 1928, 1918-22, 1916, 1894, 1892, 1889, 1886, ?1852
0703-03=	**MAYON**	*13.25N*	*123.68E*	*2462*	Stratovolcano	1993, 1984, 1978, 1968, 1947, 1943, 1941, 1939, 1938, 1928, ?1902, **1897**, 1896, 1895, 1893, 1891-92, 1890, 1888, 1886-87, 1885, 1881-82, 1876, 1876, 1873, 1872, 1871-72, 1868, ?1863, 1862, 1861, 1860, 1859, 1858, 1857, 1855, 1853, 1851, 1846, 1845, 1839, 1834-35, 1827-28, **1814**, ?1811, 1800, 1766, 1616
0703-04=	MALINAO	*13.42N*	*123.59E*	*1548*	Stratovolcano	1980
0703-041	IRIGA	*13.45N*	*123.45E*	*1196*	Stratovolcano	1628?
0703-05=	BANAHAW	*14.07N*	*121.48E*	*2177*	Complex volcano	?1730
0703-07=	**TAAL**	*14.00N*	*120.99E*	*400*	Stratovolcano	1977, 1976, 1970, 1969, 1968, 1967, 1966, **1965**, **1911**, 1904, 1903, ?1885, 1878, 1874, 1873, 1842, 1825, 1808, 1790, **1754**, 1749, 1731, 1729, 1716, 1715, 1709, 1707, 1645, 1641, 1635, 1634, 1608c, 1591, 1572
0703-083	**PINATUBO**	*15.13N*	*120.35E*	*1450*	Stratovolcano	1992, ***1991***
0703-088	BINULUAN	*17.30N*	*121.09E*	*2329*	Compound volcano	?1952
0703-09=	CAGUA	*18.22N*	*122.12E*	*1133*	Stratovolcano	?1860
0704-01=	CAMIGUIN DE BABUY	*18.83N*	*121.86E*	*712*	Stratovolcano	1857<, 1978, 1969, 1952-53?, ?1900, 1856-60, 1773
0704-03=	BABUYAN CLARO	*19.52N*	*121.94E*	*1180*	Stratovolcanoes	1924, 1919, 1918, 1917, ?1913, 1907, 1860, 1831, 1652?
0704-05=	UNNAMED	*20.33N*	*121.75E*	*-24*	Submarine volcano	1854, 1850, 1773

NUMBER	VOLCANO NAME	LAT	LONG	ELEV	TYPE	ERUPTION YEARS (VEI≤3 **VEI=4** **VEI=5** ***VEI=6-7***)
0704-06-	IRAYA	*20.46N*	*122.01E*	*1009*	Stratovolcano	1464
Indochina						
0705-06-	CENDRES, ISLE DES	*10.16N*	*109.01E*	*-20*	Submarine volcano	1923
0705-07-	VETERAN	*9.83N*	*109.05E*	*?*	Submarine volcano	?1928, ?1880?
0705-11-	TENGCHONG	*25.32N*	*98.47E*	*2865*	Pyroclastic cones	1609
Taiwan - offshore						
0801-01=	UNNAMED	*20.93N*	*134.75E*	*-6000*	Submarine volcano	?1850
0801-011	UNNAMED	*19.17N*	*132.25E*	*-10*	Submarine volcano	?1955
0801-02=	UNNAMED	*21.83N*	*121.18E*	*-115*	Submarine volcano	1854
0801-03=	UNNAMED	*24.00N*	*121.83E*	*?*	Submarine volcano	1853-54
0801-04=	UNNAMED	*25.42N*	*122.33E*	*-100*	Submarine volcano	1867
0801-05=	ZENGYU	*26.18N*	*122.45E*	*-418*	Submarine volcano	1916-27?
Ryukyu Is (S to N)						
0802-01=	IRIOMOTE-JIMA	*24.55N*	*124.00E*	*-200*	Submarine volcano	**1924**
0802-02=	OKINAWA-TORI-SHIMA	*27.85N*	*128.25E*	*217*	Complex volcano	1968, 1967, 1959, 1903, 1868, 1855, 1829, 1796, 1664
0802-03=	**SUWANOSE-JIMA**	*29.53N*	*129.72E*	*799*	Stratovolcano	1949-99>, 1940, 1938, 1934, 1925, 1921-22, ?1915, ?1914, **1889**, 1885, 1884, **1877**, **1813**
0802-04=	NAKANO-SHIMA	*29.85N*	*129.87E*	*979*	Stratovolcanoes	?1949, 1914
0802-05=	KUCHINOERABU-JIMA	*30.43N*	*130.22E*	*649*	Stratovolcanoes	1980, 1976, 1974, 1973, 1972, 1968-69, 1966, 1945, **1933-34**, ?1932, 1931, 1914, ?1906-07, 1841, 1840<
0802-06=	KIKAI	*30.78N*	*130.28E*	*717*	Caldera	1998, 1988, 1934-35, ?1914
Kyushu (S to N)						
0802-07=	IBUSUKI VOLC FIELD	*31.22N*	*130.57E*	*922*	Calderas	?1615, **0885**, ?0882, **0874**, ?0866, ?0860
0802-08=	**SAKURA-JIMA**	*31.58N*	*130.67E*	*1117*	Stratovolcano	1955-99>, ?1954, 1950, 1948, 1946, 1942, 1941, 1940, 1939, 1938, 1935, **1914-15**, ?1899, 1860, 1799, 1797, 1794, 1792, 1791, 1790, 1785, 1783, 1782, 1779-81, 1756, 1749, 1742, 1706, 1678, ?1670, 1642, 1478, **1471-76**, 1468, 0778, 0766, **0764**, 0716-18, ?0712, 0708
0802-09=	KIRISHIMA	*31.93N*	*130.87E*	*1700*	Shield volcano	1992, 1979, 1971, 1959, ?1946, 1923, 1914, 1913-14, 1903, 1899-1900, 1898, 1898, 1897, 1896, 1895-96, 1894, 1891, 1891, 1889, 1888, 1887, 1880, 1832, 1822, 1771-72, 1769, 1768, 1719, 1717, 1716-17, 1716, 1706, 1690, 1678, 1677, ?1667, 1662-64, 1659-61, 1637-38, 1628, 1620, 1615-18, 1613-14, 1598-1600, ?1596, 1595, 1588, 1587, 1585, 1576-78, 1574, 1566, 1566, 1554, 1524, 1381, 1235, 1184, ?1175, 1167, 1113, 1112, 0945, 0858, 0857, 0843-48, 0837-39?, **0788**, 0742
0802-10=	**UNZEN**	*32.75N*	*130.30E*	*1359*	Complex volcano	1996, 1990-95, ?1798, 1792, ?1690-92, 1663, 1663, ?0860
0802-11=	**ASO**	*32.88N*	*131.10E*	*1592*	Caldera	1994-95, 1992-93, 1989-91, 1988, 1988, 1984-85, 1983, 1981, 1980, 1979-80, 1977-78, 1975-76, 1973-75, 1970-72, 1967-69, 1964-66, 1964, 1963-64, 1963, 1960-62, 1960, 1959, 1957-58, 1957, 1956, 1956, 1956, 1955, 1954, 1953, 1953, ?1952, 1951, 1950-51, 1949, 1948, 1947, 1946, 1946, 1945, 1943-44, 1943, ?1942, 1940-41, 1938-39, 1937, 1937, 1936, 1936, 1935, 1934, 1932-33, ?1931, 1930, 1928-29, 1926-28, 1925, 1923, 1920, 1919, 1918, 1916, 1914, 1911-12, 1910, 1909, 1908, 1907, 1906, 1898-99, 1897, 1894, 1884, 1874, 1872-73, 1856, 1854, 1838, 1837, 1835, 1830-32, 1830, 1829, 1828, 1827-28, 1827, 1826, 1816, 1815, 1814, 1806, 1804, 1781-88, 1772-80, 1765, ?1753-54, 1709, ?1708, 1691, 1683, 1675, 1671, 1668-69, 1668, 1649, 1637, 1631, 1620, 1613, 1612, 1611, 1598-99, 1592, 1587, 1584, 1583, 1582, 1576, 1564, ?1563, 1562, 1558-59, 1542, 1533, 1522, 1506, 1505, 1485, 1473-74, 1438, 1434, ?1390, ?1388, 1387, 1377, 1376, 1375-76, 1369, 1346, 1343, 1340, 1335, 1331-33, 1331, 1324, 1305, 1286, 1281, 1274, 1273, 1272, 1272, 1271, 1269, 1265, 1240, 1239, 1229, ?0986, 0867, 0864, ?0796, 0553
0802-12=	KUJU GROUP	*33.08N*	*131.25E*	*1788*	Stratovolcanoes	1995-96, 1675, 1662?
0802-13=	TSURUMI	*33.28N*	*131.43E*	*1374*	Lava domes	0867, 0771
Honshu (S to N)						
0803-01=	IZU-TOBU	*34.92N*	*139.12E*	*1406*	Pyroclastic cones	1989, ?1930
0803-03=	**FUJI**	*35.35N*	*138.73E*	*3776*	Stratovolcano	?1709, **1707-08**, 1700, ?1627, 1560, 1511, ?1427, 1083, 1033, ?1017, 0999, ?0993, ?0952, 0937, 0932, 0870, 0864-65, 0830, 0826, 0802, **0800**, 0781
0803-04=	ON-TAKE	*35.90N*	*137.48E*	*3063*	Complex volcano	1979-80
0803-05=	HAKU-SAN	*36.15N*	*136.78E*	*2702*	Stratovolcano	1659, 1658, 1640, 1582, 1579, 1554-56, 1548, 1547, 1177, 1042, ?0900?, ?0859, ?0853, 0706
0803-07=	**YAKE-DAKE**	*36.22N*	*137.58E*	*2455*	Stratovolcano	1995, 1962-63, 1939, 1935, 1932, 1931, 1930, 1929, 1927, 1927, 1924-26, 1923, 1922, 1921, 1920, 1919, 1918, 1917, 1916, 1915, 1913, 1912, 1911, 1910, 1907-09, 1585, @0686
0803-08=	TATE-YAMA	*36.57N*	*137.60E*	*2621*	Stratovolcano	?1858, 1839
0803-09=	NIIGATA-YAKE-YAMA	*36.92N*	*138.03E*	*2400*	Lava dome	1989, 1987, 1983, 1974, 1963, 1962, 1949, 1854, 1852, 1773, 1361, ?0989, **0887**
0803-11=	**ASAMA**	*36.40N*	*138.53E*	*2560*	Complex volcano	1990, 1983, 1982, 1982, 1973, 1965, 1961, 1958-59, 1953-55, 1952, 1952, 1950-51, 1949, 1947, 1946, 1944-45, 1938-42, 1935-37, 1934, 1934, 1933, 1931-32, 1930, 1929, 1929, 1927-28, 1924, 1922, 1920-21, 1919, ?1918, 1917, 1916, 1915, 1914, 1909-14, 1908, 1908, 1907, 1907, 1906, ?1905, 1904, 1903, 1902, 1902, 1900-01, 1899, 1899, 1894, 1889, 1879, ?1878, 1875, 1869, 1815, 1803, 1803, **1783**, ?1779, 1777, 1776, @1769, 1762, 1755, 1754, 1733, 1732, 1731, 1729, 1729, 1728, 1723, 1723, 1722, 1721, 1720, @1719, 1718, 1717, 1711, 1710, 1708-09, 1706, 1704, 1703, 1669, 1661, 1661, 1660, 1659, 1658, 1657, 1656, 1655, 1653, 1652, 1651, ?1650, 1649, 1648, 1648, 1647, 1645, 1644, 1609, 1605, 1604, 1600, 1598, 1597, 1596, 1596, ?1595, 1591, 1590, 1532, 1528, 1527, 1518, ?1427, 1281, **1108**, 0887, 0685
0803-12=	KUSATSU-SHIRANE	*36.62N*	*138.55E*	*2176*	Stratovolcanoes	?1989, 1983, 1982, 1976, 1958, 1942, 1939, ?1938, 1937, 1934, ?1933, 1932, 1927, 1925, 1905, ?1903, 1902, 1900, 1897, 1882, 1805
0803-13=	AKAGI	*36.53N*	*139.18E*	*1828*	Stratovolcano	?1938, 1251

NUMBER	VOLCANO NAME	LAT	LONG	ELEV	TYPE	ERUPTION YEARS (VEI≤3 **VEI=4** **VEI=5** *VEI=6-7*)
Honshu (cont)						
0803-131	HIUCHI	36.95N	139.28E	2346	Stratovolcano	1544
0803-14=	NIKKO-SHIRANE	36.80N	139.38E	2578	Shield volcano	1889, 1873, 1872, ?1871, 1649, 1625
0803-15=	**NASU**	37.12N	139.97E	1917	Stratovolcanoes	?1963, 1963, 1960, 1953, 1881, 1846, 1410, 1408, 1404, 1397
0803-16=	**BANDAI**	37.60N	140.08E	1819	Stratovolcano	1888, 1808?, 1787<, ?1767n, ?1719<, ?1611, 0806
0803-17=	ADATARA	37.62N	140.28E	1718	Stratovolcanoes	1996, 1900, 1899, ?1813
0803-18=	AZUMA	37.73N	140.25E	2024	Stratovolcanoes	1977, ?1966, 1952, 1950, 1914, ?1896, 1895, 1894, 1893, ?1844, 1800?, ?1711?, ?1331
0803-19=	ZAO	38.15N	140.45E	1841	Complex volcano	1940, ?1939, ?1927, 1905, ?1897, 1896, 1896, 1895, 1895, 1894, ?1890, 1873, 1867, 1833, 1831, 1830, 1821, 1809, 1806, 1804, 1796, 1794, 1694, 1670, 1669, 1668, 1641, 1630, 1623-24, 1620, ?1350?, ?1331-33, 1230, 1227, 1183, 0884, ?0773
0803-20=	NARUGO	38.73N	140.73E	462	Lava domes	0837
0803-21=	KURIKOMA	38.95N	140.78E	1628	Stratovolcano	1950, 1946, 1944, ?1783, 1744, 1726j
0803-22=	CHOKAI	39.08N	140.03E	2237	Stratovolcanoes	1974, 1834, 1821, 1800-04, 1764, 1740-41, 1738, 1735, 1659-63a, ?1560, ?1477, ?0999, 0948, 0939, 0915, ?0884, 0871, 0861, 0857, 0856, 0839, 0829e, 0817g, 0804-06, ?0717, 0711c, ?0610o, 0577-78, 0573
0803-23=	AKITA-KOMAGA-TAKE	39.75N	140.80E	1637	Stratovolcanoes	1970-71, 1932, ?1902, 1890-91, ?0807
0803-24=	IWATE	39.85N	141.00E	2041	Complex volcano	1919, 1731-32, 1719, 1689, 1687, 1686
0803-26=	AKITA-YAKE-YAMA	39.97N	140.77E	1366	Complex volcano	1997, 1957, 1951, 1949, 1948, 1929, 1890, 1887, 1867, ?1678, ?0807
0803-261	KANPU	39.93N	139.88E	355	Stratovolcano	?1810
0803-27=	IWAKI	40.65N	140.30E	1625	Stratovolcano	1863, 1856, 1848, 1845, 1844, 1833, 1807, 1800, 1794, 1793, 1790, ?1783, 1782-83, ?1782, ?1769, ?1709, ?1694, ?1672, 1618, 1605, 1604, 1600, 1600, 1597, 1597
0803-271	**TOWADA**	40.47N	140.92E	1159	Stratovolcano	**0915**
0803-29=	OSORE-YAMA	41.32N	141.08E	879	Stratovolcano	1787<
Izu & Volcano Is (N to S)						
0804-01=	**OSHIMA**	34.73N	139.38E	758	Stratovolcano	1990, 1987-88, 1986, 1974, 1971, 1970, 1970, 1969, 1968, 1968, 1967, 1965-66, 1962-65, ?1961, 1959-60, 1959, 1958, 1957, 1956, ?1956, 1953-54, 1950-51, 1940, 1939, 1939, 1938, 1937, 1935, 1934, ?1934, 1933, 1928, 1922-23, ?1920, 1919, 1915, 1914, 1912-13, 1910, 1876-77, 1870, ?1868, 1846, 1837-38, 1827, 1822-24, 1803, 1792, 1789, 1783-86, 1777-79, 1695, 1684-90, 1636-38, 1612-13, 1600-01, 1588, **1552**, 1527, **1442**, 1421, 1416, 1415, 1338, **1267**, **1112**, **0936**, 0886, ?0854, **0751**, 0684?, ?0681, ?0680, 0654, 0630, 0605
0804-02=	NII-JIMA	34.37N	139.27E	432	Lava domes	**0886**, 0840
0804-03=	KOZU-SHIMA	34.22N	139.15E	574	Lava domes	**0838**, 0832
0804-04=	MIYAKE-JIMA	34.08N	139.53E	815	Stratovolcano	1983, 1962, 1940, 1874, 1835, 1811, 1763-69, 1712-14, 1709, 1643, 1595, 1535, 1469, 1154, 1085
0804-05=	HACHIJO-JIMA	33.13N	139.77E	854	Stratovolcanoes	?1707, 1606, 1605, 1518-23, 1487
0804-06=	**AOGA-SHIMA**	32.45N	139.77E	423	Stratovolcano	1780-85, 1670-80, 1652
0804-07=	**BAYONNAISE ROCKS**	31.92N	139.92E	-10	Submarine volcano	?1988, ?1987, ?1986, ?1983, ?1980, ?1979, ?1971, 1970, 1960, 1959, 1958, 1957, 1955, 1954, 1952-53, 1946, 1934, 1915, 1906, 1896
0804-08=	SMITH ROCK	31.32N	140.05E	-136	Submarine volcano	1916, ?1873, @1871, 1870, 1870, @1869, 1672?
0804-09=	**TORI-SHIMA**	30.48N	140.32E	403	Stratovolcano	1965, 1975, 1939, 1902, 1871
0804-091	OMACHI SEAMOUNT	29.22N	140.80E	-1700	Submarine volcano	?1975
0804-092	NISHINO-SHIMA	27.24N	140.87E	52	Caldera	?1985, ?1982, ?1980, ?1978, ?1975, 1973-74
0804-093	UNNAMED	26.13N	144.48E	-3200	Submarine volcano	?1974
0804-10=	KAITOKU SEAMOUNT	26.12N	141.10E	-10	Submarine volcano	1984, 1543
0804-11=	KITA-IWO-JIMA	25.43N	141.23E	792	Stratovolcano	?1953, 1930-45, 1880-89, 1780
0804-12=	IWO-JIMA	24.75N	141.33E	161	Caldera	1982, 1982, 1980, 1978, 1976, ?1974, ?1969, 1967, 1957, 1943a, 1930?, 1922
0804-13=	**SHIN-IWO-JIMA**	24.28N	141.52E	-14	Submarine volcano	?1995-97, ?1993, 1992, ?1991, ?1987-91, 1987, 1986, ?1976-85, 1974-75?, 1973-74, ?1972, ?1968, ?1968, ?1967, ?1963, ?1962, ?1960, ?1959, ?1958, ?1956, ?1955, ?1954, ?1953, ?1952, ?1950, 1914, 1904-05
0804-131	MINAMI-HIYOSHI	23.50N	141.90E	-30	Submarine volcano	?1996, ?1992, ?1978, ?1976-77, ?1976, 1975
0804-132	NIKKO	23.07N	142.30E	-391	Submarine volcano	?1979
0804-133	FUKUJIN	21.92N	143.44E	-217	Submarine volcano	?1982, ?1982, ?1981, ?1979-80, ?1978, ?1977-78, ?1976-77, 1973-74, 1968, ?1959, ?1958, ?1952, 1951
0804-134	KASUGA SEAMOUNT	21.77N	143.72E	-558	Submarine volcano	?1975
Mariana Is (N to S)						
0804-135	UNNAMED	21.00N	142.90E	?	Submarine volcano	?1975
0804-136	UNNAMED	20.30N	143.20E	?	Submarine volcano	?1975
0804-14=	FARALLON DE PAJAROS	20.53N	144.90E	360	Stratovolcano	1967, 1952-53, 1951, 1947, 1943, 1941, 1939, 1936, 1934, 1932, 1928, 1925, 1912, 1900?-01, 1874?-76, 1864
0804-141	AHYI	20.43N	145.03E	-70	Submarine volcano	?1979
0804-142	SUPPLY REEF	20.13N	145.10E	-8	Submarine volcano	1989, 1969, ?1985
0804-15=	ASUNCION	19.67N	145.40E	857	Stratovolcano	?1924, 1906, ?1775j, ?1690j
0804-16=	AGRIGAN	18.77N	145.67E	965	Stratovolcano	1917

NUMBER	VOLCANO NAME	LAT	LONG	ELEV	TYPE	ERUPTION YEARS (VEI≤3 **VEI=4** **VEI=5** *VEI=6-7*)
Mariana Is (cont)						
0804-17=	PAGAN	*18.13N*	*145.80E*	*570*	Stratovolcanoes	1993, 1992, 1988, ?1988, 1987, **1981-85**, ?1929-30, 1925, 1923, 1917, 1909, 1873?, 1864, 1825e, 1669
0804-18=	ALAMAGAN	*17.60N*	*145.83E*	*744*	Stratovolcano	?1887, ?1864
0804-19=	GUGUAN	*17.32N*	*145.85E*	*287*	Stratovolcano	1883a
0804-201	RUBY	*15.62N*	*145.57E*	*-230*	Submarine volcano	1995, 1966
0804-21=	ESMERALDA BANK	*15.00N*	*145.25E*	*-43*	Submarine volcano	?1987, ?1982, ?1975, ?1970a, ?1964, ?1944
Hokkaido (SW to NE)						
0805-01=	**OSHIMA-OSHIMA**	*41.50N*	*139.37E*	*737*	Stratovolcano	1790, ?1786, 1759, **1741-42**
0805-011	E-SAN	*41.80N*	*141.17E*	*618*	Stratovolcano	1874, 1846
0805-02=	**KOMAGA-TAKE**	*42.07N*	*140.68E*	*1140*	Stratovolcano	1998, 1996, 1942, 1937, ?1935, **1929**, ?1928, 1924, 1923, 1922, 1919, 1905, 1888, **1856**, 1784, 1765, ?1710, **1694**, **1640**
0805-03=	**USU**	*42.53N*	*140.83E*	*731*	Stratovolcano	1977-82, 1944-45, 1910, **1853**, **1822**, **1769**, **1663**, 1638, 1626, ?1611
0805-04=	**SHIKOTSU**	*42.70N*	*141.33E*	*1320*	Caldera	1981, 1978-79, 1978, 1954-55, 1954, 1953, 1951, 1951, 1944, 1936, 1936, 1933, 1931, 1928-29, 1928, 1926, 1923, 1921, 1920, 1919, 1918, 1917, 1909, 1894, 1894, 1887, 1886, 1885, 1883, 1874, ?1871, 1867, 1804-17, **1739**, **1667**
0805-05=	**TOKACHI**	*43.42N*	*142.68E*	*2077*	Stratovolcanoes	1988-89, 1985, 1962, 1961, 1959, 1958, 1957, 1956, 1954, 1952, 1931, 1928, 1928, 1925-27, 1889, 1887, 1857
0805-061	NIPESOTSU-UPEPESANK	*43.45N*	*143.03E*	*2013*	Lava domes	1898
0805-07=	AKAN	*43.38N*	*144.02E*	*1499*	Caldera	1988, 1966, 1965, 1964, 1962, 1960, 1959, 1958, 1957, 1956, 1955, 1954, ?1951-52, ?1927, 1808?, 1800<
0805-09=	SHIRETOKO-IWO-ZAN	*44.13N*	*145.17E*	*1563*	Stratovolcano	1936, 1890, 1889, ?1880, 1876, ?1857?
Kurile Is (SW to NE)						
0900-01=	GOLOVNIN	*43.85N*	*145.53E*	*541*	Caldera	1848
0900-02=	MENDELEEV	*43.98N*	*145.70E*	*887*	Stratovolcano	?1900, 1880
0900-03=	TIATIA	*44.35N*	*146.27E*	*1819*	Stratovolcano	?1982, 1981, 1978, **1973**, 1812
0900-04=	BERUTARUBE	*44.47N*	*146.93E*	*1220*	Stratovolcano	?1812
0900-05=	ATSONUPURI	*44.80N*	*147.13E*	*1205*	Stratovolcano	1932, 1812
0900-061	UNNAMED	*45.03N*	*147.20E*	*-930*	Submarine volcano	?1967
0900-07=	GROZNY GROUP	*45.02N*	*147.87E*	*1211*	Complex volcanoes	1989, 1973, 1973, 1970, 1968
0900-08=	BARANSKY	*45.10N*	*148.02E*	*1132*	Stratovolcano	1951
0900-09=	CHIRIP	*45.38N*	*147.92E*	*1589*	Stratovolcanoes	1860?, 1843
0900-10=	MEDVEZHIA	*45.38N*	*148.83E*	*1124*	Somma volcano	1958, ?1946, 1883, 1778
0900-12=	KOLOKOL GROUP	*46.04N*	*150.05E*	*1328*	Somma volcanoes	1973, 1970, 1952, 1946, 1940f, 1924, 1894, 1845-46, 1780j
0900-13-	UNNAMED	*46.10N*	*150.50E*	*-100*	Submarine volcano	?1978
0900-15=	CHIRPOI	*46.52N*	*150.87E*	*742*	Caldera	1982, 1960, 1879, 1857, 1854, 1811, 1790p, **1712**
0900-16-	UNNAMED	*46.47N*	*151.28E*	*-502*	Submarine volcano	1972
0900-17B	GORIASCHAIA SOPKA	*46.83N*	*151.75E*	*891*	Stratovolcano	?1944, 1914, 1883, 1881, 1849, 1842
0900-18=	ZAVARITZKI CALDERA	*46.92N*	*151.95E*	*624*	Caldera	1957, 1923h
0900-19=	PREVO PEAK	*47.02N*	*152.12E*	*1360*	Stratovolcano	1825q, 1765e
0900-20=	KETOI	*47.35N*	*152.47E*	*1172*	Stratovolcano	1960, 1924, 1843-46
0900-21=	USHISHUR	*47.52N*	*152.80E*	*401*	Caldera	1884, 1769>, 1710j
0900-211	SREDNII	*47.60N*	*152.92E*	*-36*	Submarine volcano	?1880?
0900-22=	RASSHUA	*47.77N*	*153.02E*	*956*	Stratovolcano	1957, 1846
0900-23=	UNNAMED	*48.08N*	*153.33E*	*-150*	Submarine volcano	1924
0900-24=	SARYCHEV PEAK	*48.09N*	*153.20E*	*1496*	Stratovolcano	1989, 1986, 1976, 1965, 1960, 1954, **1946**, ?1932?, 1930, 1928, 1927, 1923, 1879, 1805, 1765e
0900-25=	RAIKOKE	*48.29N*	*153.25E*	*551*	Stratovolcano	**1924**, **1778**, 1765e
0900-26=	CHIRINKOTAN	*48.98N*	*153.48E*	*724*	Stratovolcano	1986, 1979-80, 1955?, 1900j, 1884f, ?1760?
0900-27=	EKARMA	*48.95N*	*153.93E*	*1170*	Stratovolcano	1980, 1767-69
0900-29=	SINARKA	*48.87N*	*154.17E*	*934*	Stratovolcano	**1872-78**, 1855, 1846, 1725q
0900-30=	HARIMKOTAN	*49.12N*	*154.50E*	*1145*	Stratovolcano	1933, 1931, 1883, 1848, 1846, 1713
0900-31=	TAO-RUSYR CALDERA	*49.35N*	*154.70E*	*1325*	Stratovolcano	1952
0900-32=	NEMO PEAK	*49.57N*	*154.80E*	*1018*	Caldera	1938, ?1932?, 1906, 1710j
0900-34=	FUSS PEAK	*50.27N*	*155.25E*	*1772*	Stratovolcano	1854
0900-35=	KARPINSKY GROUP	*50.13N*	*155.37E*	*1345*	Cones; Maar	1952
0900-36=	**CHIKURACHKI**	*50.32N*	*155.45E*	*1816*	Stratovolcanoes	**1986**, 1973, 1967, 1964, 1961, 1958, 1957, ?1933, **1853-59**
0900-38=	EBEKO	*50.68N*	*156.02E*	*1156*	Somma volcano	1991, 1989-90, 1987-88, 1971, 1969, 1967, 1965-66, 1963, 1934-35, 1859, 1793
0900-39=	ALAID	*50.85N*	*155.55E*	*2339*	Stratovolcano	?1997, 1996, 1986, 1982, 1981, **1981**, ?1973, 1972, 1933-4, 1894, 1860, 1854, **1790-3**

NUMBER	VOLCANO NAME	LAT	LONG	ELEV	TYPE	ERUPTION YEARS (VEI≤3 **VEI=4** **VEI=5** *VEI=6-7*)
Kamchatka (S to N)						
1000-02=	KOSHELEV	*51.35N*	*156.75E*	*1812*	Stratovolcano	1690j
1000-03=	ILYINSKY	*51.49N*	*157.20E*	*1578*	Stratovolcano	1901
1000-04=	ZHELTOVSKY	*51.57N*	*157.32E*	*1953*	Stratovolcano	1972, 1923, ?1823e
1000-05=	**KSUDACH**	*51.80N*	*157.53E*	*1079*	Shield volcano	**1907**
1000-06=	MUTNOVSKY	*52.45N*	*158.19E*	*2322*	Complex volcano	1960-61, 1945, 1939, 1938, 1929, 1928, 1927, 1917, 1916, 1916, 1904, 1898, 1853-54, 1853, 1852, 1848, 1750t, 1650t
1000-07=	GORELY	*52.55N*	*158.03E*	*1829*	Caldera	1984-86, 1980-81, 1961, 1947, ?1932, 1931, 1930-31, 1929-30, 1869, ?1855, 1832, 1828, ?1821
1000-09=	KORYAKSKY	*53.32N*	*158.68E*	*3456*	Stratovolcano	1956-57, 1926, 1895-96
1000-10=	AVACHINSKY	*53.25N*	*158.83E*	*2741*	Stratovolcano	1991, **1945**, 1938, 1938, ?1927, 1926, ?1910, 1909, 1901, 1894-95, 1881, 1878, 1855, ?1837, 1828, 1827, ?1789, 1779, 1772, 1737
1000-102	VEER	*53.63N*	*158.42E*	*350*	Cinder cones	1856
1000-12=	ZHUPANOVSKY	*53.59N*	*159.14E*	*2958*	Compound volcano	1959, 1956-57, 1940, 1929, 1925, 1882, 1776
1000-123	AKADEMIA NAUK	*53.98N*	*159.45E*	*1180*	Stratovolcanoes	1996
1000-13=	**KARYMSKY**	*54.05N*	*159.43E*	*1486*	Stratovolcano	1996-99>, 1970-82, 1967, 1965-67, 1960-64, 1956-57, 1955, 1953, 1952, 1947, 1946, 1946, 1945, 1943, 1940, 1938, 1934-35, 1933, 1932, 1929, 1925, 1923, 1921, 1915, 1912, 1911, 1908, 1854, 1852, 1830, 1771
1000-14=	MALY SEMIACHIK	*54.13N*	*159.67E*	*1560*	Caldera	1952, 1945-46, 1852, 1851, 1804
1000-20=	KRONOTSKY	*54.75N*	*160.52E*	*3528*	Stratovolcano	1923, 1922
1000-23=	KIZIMEN	*55.13N*	*160.32E*	*2485*	Stratovolcano	1927-28
1000-24=	**TOLBACHIK**	*55.83N*	*160.33E*	*3682*	Shield volcano	**1975-76**, ?1971-74, 1970, 1970, 1968-69, 1967, 1967, 1966, 1965, 1964, 1962-63, 1961-62, 1959-60, 1958, 1956-57, 1955, 1955, 1954, 1947, 1940-41, 1940, 1939, 1936-37, 1931-32, 1904, 1793, 1790, 1789, 1788, 1769, 1740, 1739, ?1699a
1000-25=	**BEZYMIANNY**	*55.97N*	*160.58E*	*2882*	Stratovolcano	1998, 1997, 1996-97, 1994-95, 1993-94, 1992, 1991, 1990, 1989, 1986-88, 1986, 1985, 1984, 1981-83, 1980, 1980, 1979, 1979, 1978, 1977, 1976, 1971-74, 1965-70, 1964, 1964, 1963, 1962, 1961, 1961, 1961, 1960, 1959, 1958-59, 1958, 1958, 1957, **1955-57**
1000-26=	**KLIUCHEVSKOI**	*56.05N*	*160.63E*	*4835*	Stratovolcano	1998, 1996-97, 1994-95, 1993, 1992, 1991, 1986-90, 1986, 1985-86, 1984-85, 1982-83, 1982, 1981, ?1981, 1977-80, 1974, 1971-73, 1971, 1970, 1969, 1968, 1967, 1965-66, 1963-64, 1960-63, 1959, 1958, 1957, 1956, 1954, 1953, 1951, 1949, 1948, 1946, 1945, **1944-45**, 1937-39, 1935-36, 1932, **1931**, 1931, 1929, 1926, 1925, 1923, 1922, 1915, 1913, 1911, 1910, 1909, 1907, 1904, 1898, 1896-97, 1890, 1883, 1882, 1879, 1878, 1877, 1865, 1853-54, 1852, 1852, 1848, 1840, **1829**, 1819-22?, 1813, 1812, 1807, 1791, 1791, 1789-90, 1788, 1788, 1787, 1785, 1772, 1770, 1767, 1762, 1740, 1737, 1727-31, 1720-21, 1697-98
1000-261	USHKOVSKY	*56.10N*	*160.47E*	*3943*	Compound volcano	1890
1000-27=	**SHIVELUCH**	*56.65N*	*161.36E*	*3283*	Stratovolcano	1998, 1997, 1993-94, 1991, 1990, 1989, 1988, 1986-88, 1985, 1984, 1980-81, **1964**, 1944-50, 1930, 1928-29, 1905, 1897-98, 1879-83, **1854**
Mainland Asia						
1001-03-	BALAGAN-TAS	*66.43N*	*143.73E*	993	Cinder cone	1775e
1004-01-	TURFAN	*42.90N*	*89.25E*	...	Cone	1120w
1004-02-	TIANSHAN GROUP	*42.50N*	*86.50E*	...	Volcanic field	0650t, 0050t
1004-03-	KUNLUN VOLC GROUP	*35.52N*	*80.20E*	*5808*	Pyroclastic cones	1951
1005-01-	DATONG	*40.00N*	*113.28E*	*1882*	Cinder cones	0450t
1005-04-	**WUDALIANCHI**	*48.72N*	*126.12E*	*597*	Volcanic field	1719-21
1005-07-	BAITOUSHAN	*41.98N*	*128.08E*	*2744*	Stratovolcano	1702, 1668, 1597, 1413
1006-01-	XIANJINDAO	*41.33N*	*128.00E*	...	Unknown	1597
1006-04-	HALLA	*33.37N*	*126.53E*	*1950*	Shield volcano	1007, 1002
Aleutian Is (W to E)						
1101-02-	KISKA	*52.10N*	*177.60E*	*1220*	Stratovolcano	1990, ?1987, 1969, 1964, 1962, ?1927, ?1907
1101-05-	LITTLE SITKIN	*51.95N*	*178.53E*	*1188*	Stratovolcano	1828-30?, 1776
1101-06-	SEMISOPOCHNOI	*51.95N*	*179.62E*	*1221*	Stratovolcano	1987, 1873, ?1830, ?1792, ?1790, ?1772
1101-07-	GARELOI	*51.78N*	*178.80W*	*1573*	Stratovolcano	?1996, 1989, 1987, 1982, 1980, 1952, 1950-951, 1929-30, ?1927, 1922, 1873, ?1828-29, 1792, 1791, 1790, ?1760
1101-08-	TANAGA	*51.88N*	*178.13W*	*1806*	Stratovolcanoes	1914, 1829, ?1791, 1763-70
1101-11-	KANAGA	*51.92N*	*177.17W*	*1307*	Stratovolcano	1994, 1942, 1933, 1906, 1904, ?1829, ?1827, ?1791, ?1790, 1783-87?, 1768, 1763
1101-12-	GREAT SITKIN	*52.08N*	*176.13W*	*1740*	Stratovolcano	?1987, 1974, 1950, 1949-50, ?1946, 1945, 1933, ?1904, ?1829, ?1828, 1792, ?1784, ?1760
1101-13-	KASATOCHI	*52.18N*	*175.50W*	*314*	Stratovolcano	?1899?, ?1828, ?1827, 1760
1101-16-	ATKA	*52.38N*	*174.15W*	*1533*	Stratovolcanoes	1998, 1996, ?1995, 1987, ?1986, ?1976, 1973, ?1953-54, ?1951, 1907, ?1844, ?1829-30, 1812
1101-18-	SEGUAM	*52.32N*	*172.52W*	*1054*	Stratovolcanoes	1993, 1992, 1977, ?1927, 1902, 1892, 1891, ?1827, 1786-90
1101-19-	AMUKTA	*52.50N*	*171.25W*	*1066*	Stratovolcano	1997, 1996, 1987, 1963, 1878, ?1876, 1786-91, ?1770
1101-21-	YUNASKA	*52.63N*	*170.63W*	*550*	Shield volcano	1937, ?1929, ?1873, 1830, 1824, ?1817
1101-23-	CARLISLE	*52.90N*	*170.05W*	*1620*	Stratovolcano	?1987, ?1838, 1828, 1774

NUMBER	VOLCANO NAME	LAT	LONG	ELEV	TYPE	ERUPTION YEARS (VEI≤3 **VEI=4** VEI=5 *VEI=6-7*)
Aleutian Is (cont)						
1101-24-	CLEVELAND	*52.82N*	*169.95W*	*1730*	Stratovolcano	1994, ?1989, 1987, 1986, ?1985, 1984, ?1975, ?1953, ?1951, 1944, 1938, 1932, ?1929, 1897, 1893
1101-26-	KAGAMIL	*52.97N*	*169.72W*	*893*	Stratovolcano	1929
1101-27-	VSEVIDOF	*53.13N*	*168.68W*	*2149*	Stratovolcano	?1957, ?1880, 1878, 1830, 1817, ?1790, ?1784
1101-29-	OKMOK	*53.42N*	*168.13W*	*1073*	Stratovolcano	1997, 1986-88, 1983, 1981, 1960-61, 1958, 1945, 1943, 1938, ?1936, 1931, 1899, 1878, 1824-30, 1817-20, 1805
1101-30-	BOGOSLOF	*53.93N*	*168.03W*	*-101*	Submarine volcano	1992, ?1951, 1931, 1926-1928, ?1913, 1909-10, ?1908, 1906-07, 1883-95b, 1806-23, 1796-1804
1101-31-	MAKUSHIN	*53.90N*	*166.93W*	*2036*	Stratovolcano	1995, 1987, 1980, ?1952, 1951, 1938, 1926, ?1912, 1907, 1883, ?1867, 1865, ?1844a, 1826-38?, ?1818, 1802, ?1792, ?1790, 1768-69
1101-32-	**AKUTAN**	*54.13N*	*165.97W*	*1303*	Stratovolcano	1992, 1992, 1991, 1990, 1990, 1989, 1988, 1987, 1986, 1982-83, 1980, 1978, 1976-77, 1974, 1972-73, 1962, 1953, 1951, 1948, 1946-47, 1931, 1929, 1927-28, 1912, 1911, 1908, 1907, 1896, 1892, 1887, 1883, 1867, 1865, 1852, 1848, ?1845, ?1838, ?1828, ?1790
1101-34-	WESTDAHL	*54.52N*	*164.65W*	*1654*	Stratovolcano	1991-92, ?1979, 1978, 1964, 1827-30, 1820, 1796, **1795**
1101-35-	FISHER	*54.67N*	*164.35W*	*1094*	Stratovolcano	1830, 1826-27, 1795<
1101-36-	**SHISHALDIN**	*54.75N*	*163.97W*	*2857*	Stratovolcano	1997, 1995, 1993, 1986-87, ?1981, 1979, 1978, 1976, 1975, 1967, 1963, 1955, 1953, 1951, 1948, 1946-47, 1932, 1929, 1928, 1927, 1925, 1922, ?1912, 1901, ?1899, 1898, ?1897, 1883, ?1880-81, ?1865, 1842, 1838, 1830, 1827-29, 1826, 1825, 1824, ?1790, ?1775-78
1101-37-	ISANOTSKI	*54.75N*	*163.73W*	*2446*	Stratovolcano	?1845, @1831, 1830, @**1825**, @1795
1101-39-	AMAK	*55.42N*	*163.15W*	*513*	Stratovolcano	1796, 1700-10
Alaska - Peninsula, SW, & E						
1102-03-	**PAVLOF**	*55.42N*	*161.90W*	*2519*	Stratovolcano	1996-97, 1974, 1990, 1986-88, 1983, 1983, ?1982, 1981, 1981, 1980, 1980, 1975-77, 1974-75, 1973, 1966, 1960?-63, 1958, 1953, 1951-52, 1950-51, 1936-48, 1929-31, 1924, 1922-23, 1917, 1914, 1906-11, 1901, 1894, 1892, 1886, 1880, @1866, ?1852, 1846, 1845, ?1838, 1825, 1817, 1790
1102-04-	PAVLOF SISTER	*55.45N*	*161.87W*	*2142*	Stratovolcano	**1762-86**
1102-06-	KUPREANOF	*56.02N*	*159.80W*	*1895*	Stratovolcano	1987
1102-07-	VENIAMINOF	*56.17N*	*159.38W*	*2507*	Stratovolcano	?1995, 1993-94, 1987, 1984, 1983-84, 1956, 1944, 1939, 1939, 1930, 1892, 1874, ?1852, 1838-39, ?1830-38
1102-09-	ANIAKCHAK	*56.88N*	*158.17W*	*1341*	Caldera	?1951, ?1942, 1931
1102-11-	CHIGINAGAK	*57.13N*	*157.00W*	*2075*	Stratovolcano	1998, 1971, ?1929, ?1852
1102-13A	UGASHIK-PEULIK	*57.75N*	*156.37W*	*1474*	Stratovolcano	?1852, 1814
1102-13B	UKINREK MAARS	*57.83N*	*156.52W*	*91*	Maars; Lava dome	1977
1102-14-	MARTIN	*58.17N*	*155.35W*	*1860*	Stratovolcano	@1953, @1951
1102-15-	MAGEIK	*58.20N*	*155.25W*	*2165*	Stratovolcano	?1946, 1936, ?1929, 1927
1102-16-	TRIDENT	*58.23N*	*155.08W*	*1864*	Stratovolcano	1974-75, 1968, 1967-68, 1966?, 1964, 1963, 1963, 1962, 1961, 1957-60, @1956, 1953-54, @1950, 1949, 1913
1102-17-	KATMAI	*58.27N*	*154.98W*	*2047*	Stratovolcano	1912
1102-18-	**NOVARUPTA**	*58.27N*	*155.16W*	*841*	Caldera	*1912*
1103-01-	AUGUSTINE	*59.37N*	*153.42W*	*1252*	Lava domes	**1986**, **1976-77**, 1971, 1963-64, 1935, ?1908, **1883-84**?, 1812
1103-02-	ILIAMNA	*60.03N*	*153.08W*	*3053*	Stratovolcano	1953, ?1952, ?1947, ?1933, 1876, 1867, ?1843, ?1793, ?1786, 1778-79, ?1768
1103-03-	REDOUBT	*60.48N*	*152.75W*	*3108*	Stratovolcano	1989-90, 1967-68, 1966-67, 1966, ?1965, ?1933, 1902, ?1819, ?1778
1103-04-	SPURR	*61.30N*	*152.25W*	*3374*	Stratovolcano	**1992, 1953**
Alaska - E, & Canada - W						
1105-02-	WRANGELL	*62.00N*	*144.02W*	*4317*	Shield volcano	?1907, 1902, 1899, 1884-85, 1819
1200-03-	RUBY MOUNTAIN	*59.68N*	*133.32W*	*1523*	Cinder cones	1898
1200-09-	ISKUT-UNUK RIVER	*56.58N*	*130.55W*	*1880*	Cinder cones	?1904
Washington, Oregon, California						
1201-01=	BAKER	*48.78N*	*121.82W*	*3285*	Stratovolcano	?1884, 1880, 1870, ?1869, ?1867, ?1865, 1863, ?1860, 1859-60, 1858, ?1856, 1854, 1852-53, ?1850, ?1846, 1843, 1820?, 1792
1201-02-	GLACIER PEAK	*48.11N*	*121.11W*	*3213*	Stratovolcano	?1300y
1201-03-	RAINIER	*46.87N*	*121.75W*	*4392*	Stratovolcano	?1894, ?1882, ?1879, ?1870, ?1858, ?1854, ?1843
1201-05-	**ST. HELENS**	*46.20N*	*122.18W*	*2549*	Stratovolcano	1990-91, 1989-90, **1980**-86, ?1921, ?1903, ?1898, 1857, 1854, 1853, 1850, ?1849, 1848, 1847, 1842-45, 1835, 1831
1202-01-	HOOD	*45.37N*	*121.69W*	*3426*	Stratovolcano	?1907, ?1869, 1865-66, 1859, ?1854, ?1853
1202-08-	SOUTH SISTER	*44.10N*	*121.77W*	*3157*	Complex volcano	?1853
1203-01-	SHASTA	*41.42N*	*122.20W*	*4317*	Stratovolcano	1786
1203-02-	MEDICINE LAKE	*41.58N*	*121.57W*	*2412*	Shield volcano	?1910
1203-08-	LASSEN VOLC CENTER	*40.49N*	*121.50W*	*3187*	Stratovolcano	1914-17, ?1650?
1203-11-	MONO LAKE FIELD	*38.00N*	*119.03W*	*2121*	Cinder cones	?1890
NE Pacific Ocean						
1301-01-	UNNAMED	*46.52N*	*129.58W*	*-2400*	Submarine volcano	1993
1301-011	AXIAL SEAMOUNT	*45.95N*	*130.00W*	*-1500*	Submarine volcano	1998

NUMBER	VOLCANO NAME	LAT	LONG	ELEV	TYPE	ERUPTION YEARS (VEI≤3 **VEI=4** **VEI=5** ***VEI=6-7***)
NE Pacific Ocean (cont)						
1301-02-	UNNAMED	*45.03N*	*130.20W*	*-2300*	Submarine volcano	1986
1301-021	UNNAMED	*42.67N*	*126.78W*	*-3300*	Submarine volcano	1996
1301-03-	UNNAMED	*31.75N*	*124.25W*	*-2533*	Submarine volcano	?1972
Hawaii (SE to NW)						
1302-00-	LOIHI SEAMOUNT	*18.92N*	*155.27W*	*-980*	Submarine volcano	1998, 1996, ?1986, ?1984-85, ?1975, ?1971-72
1302-01-	**KILAUEA**	*19.42N*	*155.29W*	*1222*	Shield volcano	1983-99>, 1982, 1982, 1980, 1979, 1977, 1975, 1974, 1974, 1974, 1973, 1973, 1971, 1971, 1969-74, 1969, 1968, 1968, 1967-68, 1965, 1965, 1963, 1963, 1962, 1961, 1961, 1961, 1961, 1960, 1959, 1955, 1954, 1952, 1934, 1931-32, 1930, 1929, 1929, 1927, 1924, 1924, 1923, 1922, 1921, 1919-20, 1919, 1918, 1906-24, 1905-06, 1903-04, 1902-03, 1902, 1897, 1896, 1896, 1884, 1868, 1840, 1832, 1823-94, 1823, 1820?, 1790?, 1790, 1750?
1302-02=	MAUNA LOA	*19.47N*	*155.60W*	*4170*	Shield volcano	1984, 1975, 1950, 1949, 1942, 1940, 1935-36, 1933, 1926, 1919, 1916, 1914-15, 1907, 1903, 1899, 1896, 1892, 1887, 1880-81, 1880, 1879, 1877, 1876, 1875, 1875, 1873-74, 1873, 1872, 1871, ?1870, 1868, 1865-66, 1859, 1855-56, 1852, 1851, 1849, 1843, 1832, 1750?
1302-04-	HUALALAI	*19.69N*	*155.87W*	*2523*	Shield volcano	1800-01
1302-06-	HALEAKALA	*20.70N*	*156.25W*	*3055*	Shield volcano	1790d
1302-08-	UNNAMED	*21.75N*	*158.75W*	*-3000*	Submarine volcano	?1956
1302-09-	UNNAMED	*23.58N*	*163.83W*	*-4000*	Submarine volcano	1955
Equatorial & Cent S Pacific						
1303-01-	UNNAMED	*9.82N*	*104.30W*	*-2500*	Submarine volcano	1991
1303-02-	GALAPAGOS RIFT	*0.79N*	*86.15W*	*-2500*	Submarine volcano	?1972
1303-03-	TEAHITIA	*17.57S*	*148.85W*	*-1600*	Submarine volcano	?1985, ?1983-84, ?1983, ?1982
1303-04-	ROCARD	*17.64S*	*148.60W*	*-2100*	Submarine volcano	?1972, ?1971, ?1966
1303-05-	MOUA PIHAA	*18.32S*	*148.67W*	*-180*	Submarine volcano	?1970, ?1969
1303-06-	MEHETIA	*17.87S*	*148.07W*	*435*	Stratovolcano	?1981
1303-07-	MACDONALD	*28.98S*	*140.25W*	*-50*	Submarine volcano	1986, 1983-84, 1983, 1982, 1980-81, 1980, 1979, 1977, 1967, 1987-89, @1936, @1928
1304-02-	UNNAMED	*53.90S*	*140.30W*	*-1000*	Submarine volcano	?1991
1304-03-	UNNAMED	*55.97S*	*143.17W*	*?*	Submarine volcano	?1990
Mexico - NW						
1401-001	PINACATE PEAKS	*31.77N*	*113.49W*	*1200*	Cinder cones	1934-35, 1928
1401-008	UNNAMED	*28.00N*	*115.00W*	*?*	Submarine volcano	?1953
1401-01=	TRES VIRGENES	*27.47N*	*112.59W*	*1940*	Stratovolcano	?1857, 1746
Mexican Is						
1401-02=	BARCENA	*19.30N*	*110.82W*	*332*	Cinder cones	1952-53
1401-021	SOCORRO	*18.78N*	*110.95W*	*1050*	Shield volcano	1993, 1951, 1905, ?1896, ?1848
Mexico - central belt (W to E)						
1401-023	SANGANGUEY	*21.45N*	*104.73W*	*2353*	Stratovolcano	?1742
1401-03=	**CEBORUCO**, VOLCAN	*21.12N*	*104.50W*	*2164*	Stratovolcano	1870-75, 1567, 1542
1401-04=	**COLIMA**	*19.51N*	*103.62W*	*4100*	Stratovolcano	1998-99, 1994, 1991, 1988-90, 1987, 1985-86, ?1983, 1977-82, 1975-76, ?1973, 1965-70, 1963-64, 1960-62, 1957-59, ?1941, **1913-31**, 1908-09, 1904-06, 1903, 1893-1902, 1891-92, 1890, **1889-90**, 1885-86, 1882-84, 1881, 1879-80, 1875-78, 1874, 1872-73, 1870-71, 1869, 1866-68, 1819, **1818**, 1806-09, 1804, 1795, 1771, 1770, 1749, 1743, 1690, **1622**, 1611-13, **1606**, 1590, **1585**, 1576, 1560
1401-06=	MICHOACAN FIELD	*19.48N*	*102.25W*	*3170*	Cinder cones	**1943-52 (Paricutin)**, **1759-74** (Jorullo)
1401-09=	POPOCATEPETL	*19.02N*	*98.62W*	*5465*	Stratovolcanoes	1996-99>, 1994-95, 1947, 1942-43, 1933, 1923-24, 1920-22, 1852, 1827-34, 1802-04, 1720, 1697, 1663-67, 1642, 1592-94, 1590, 1580, 1571, 1548, 1542, 1539-40, 1530, 1528, 1519-23?, 1518, ?1512, ?1509, 1504, 1488, 1363, 1354, 1345-47
1401-10=	ORIZABA, PICO DE	*19.03N*	*97.26W*	*5610*	Stratovolcano	1687, 1630, 1613, 1569, 1566, 1545-65?, 1537
1401-11=	SAN MARTIN, VOLCAN	*18.57N*	*95.16W*	*1650*	Shield volcano	?1932, ?1838, ?1797-1805, 1794-96, **1793**, 1664
Mexico - S						
1401-12=	**CHICHON, EL**	*17.36N*	*93.22W*	*1060*	Lava domes	**1982**
1401-13=	TACANA	*15.13N*	*92.11W*	*4110*	Stratovolcano	1986, 1949-50, 1878, ?1855
Guatemala (NW to SE)						
1402-02=	TAJUMULCO	*15.03N*	*91.90W*	*4220*	Stratovolcano	?1863, ?1821
1402-03=	**SANTA MARIA**	*14.75N*	*91.55W*	*3772*	Stratovolcano	1922-99>, 1903-13, ***1902***
1402-04=	ALMOLONGA	*14.82N*	*91.48W*	*3197*	Stratovolcano	1818, 1765
1402-06=	ATITLAN	*14.58N*	*91.18W*	*3535*	Stratovolcano	?1856, 1853, ?1852, 1843, 1837, 1833, 1827-28, 1827, 1826, @1717-21, 1663, 1579?-81, 1505?, 1469
1402-08=	ACATENANGO	*14.50N*	*90.87W*	*3976*	Stratovolcano	1972, 1926-27, 1924-25
1402-09=	FUEGO	*14.47N*	*90.88W*	*3763*	Stratovolcano	1987, 1977-79, 1977, 1975, **1974**, 1973, 1971, 1967, 1966, 1966, 1963, 1962, 1957, 1955, 1953, 1949, 1947, 1944, **1932**, 1896, **1880**, ?1867, ?1861, 1860, 1857, **1857**, 1856, 1856, 1855, ?1852, ?1850, 1829, 1826, 1799, ?1773, ?1765, ?1751, **1737**, 1732, 1730, **1717**, 1710, ?1709, 1706, 1705, 1702, 1699, ?1689, 1686, @1685, ?1679, 1629-32, 1623, 1620, 1617, 1614, 1587, 1586, 1585, **1581-82**, ?1577, ?1576, ?1575, ?1571, ?1565, ?1559, ?1557, 1551-52, 1542, @1541, 1531, ?1526, 1524

NUMBER	VOLCANO NAME	LAT	LONG	ELEV	TYPE	ERUPTION YEARS (VEI≤3 **VEI=4** **VEI=5** *VEI=6-7*)
Guatemala (cont)						
1402-11=	**PACAYA**	*14.38N*	*90.60W*	*2552*	Complex volcano	1990-99>, 1965-89, 1961, 1885, 1846, ?1830, 1805, 1775, ?1760, ?1717, 1699, 1693, 1690, 1687, 1678, ?1677, 1674, 1671, 1668-69, 1664, 1655, 1651, 1623?, 1565
1402-17-	SUCHITAN VOLC FIELD	*14.40N*	*89.78W*	*2042*	Stratovolcanoes	?1469
El Salvador (W to E)						
1403-02=	SANTA ANA	*13.85N*	*89.63W*	*2365*	Stratovolcano	1920, 1904, 1884, ?1882, 1880, 1879, ?1878, 1874, 1734, 1722, ?1621, 1576, 1570?, 1524, 1521, ?1520
1403-03=	**IZALCO**	*13.81N*	*89.63W*	*1950*	Stratovolcano	1966, 1948-57, 1939-48, 1937?-38?, 1933-34, 1931, 1930, 1927-28?, 1925-27, 1924, 1920-21, 1912-16, 1903-05, 1902, 1899-1900, 1891-98, 1890, 1887-89, 1885, 1884, 1883, 1882, 1881, 1879-80, 1878, ?1874-75, 1872-73, ?1870, 1869, 1868, 1867, 1866, 1864-65, 1863, 1859-60, 1858-59, 1857, 1856, 1854, 1850, 1844, 1842, 1838-40, 1836, 1825, 1817, 1805-07, 1802-03, 1798, 1793, 1783, 1772?, 1770
1403-05=	**SAN SALVADOR**	*13.73N*	*89.28W*	*1893*	Stratovolcano	1917, ?1806, 1671, 1658, 1572b
1403-06=	ILOPANGO	*13.67N*	*89.05W*	*450*	Caldera	1879-80
1403-08=	TECAPA	*13.49N*	*88.50W*	*1592*	Stratovolcano	?1878
1403-10=	**SAN MIGUEL**	*13.43N*	*88.27W*	*2130*	Stratovolcano	1995, 1985-86, 1976-77, 1970, 1967, 1966, 1966, 1964, 1954, 1939, ?1936?, 1931, 1930, 1929, 1920-25, 1919-20, 1890-91, 1884, 1882, 1867-68, 1862, 1857, 1855, ?1854, 1844-48, 1819, ?1811, ?1798?, 1787, 1769, 1762, 1699, 1510e
1403-12=	CONCHAGUITA	*13.22N*	*87.76W*	*550*	Stratovolcano	1892
Nicaragua (NW to SE)						
1404-01=	**COSIGUINA**	*12.98N*	*87.57W*	*859*	Stratovolcano	1859, 1852, **1835**, 1809, 1709?, ?1609
1404-02=	SAN CRISTOBAL	*12.70N*	*87.00W*	*1745*	Stratovolcano	1997, ?1987, ?1985, 1977, 1976, 1976, 1971, 1685, 1684, 1680, ?1613, 1528a
1404-04=	**TELICA**	*12.60N*	*86.84W*	*1010*	Stratovolcanoes	1994, 1987, 1981-82, 1981, 1976-78, 1975-76, 1969-71, 1966, 1965, 1962, 1951, 1948-49, 1946, 1943-44, ?1941, 1940, 1939, 1939, 1937-38, 1934, 1929, 1928, 1927, ?1918, 1907, 1791, 1765, ?1743, 1685, 1613, 1529, 1527?
1404-07=	**NEGRO, CERRO**	*12.50N*	*86.70W*	*675*	Cinder cones	1995, 1992, 1971, 1969, 1968, 1964, 1963, 1962, 1961, 1960, 1957, 1954, 1950-51, 1949, 1948, 1947, 1929, 1923, 1919, 1914, 1899, 1867, 1850
1404-08=	PILAS, LAS	*12.49N*	*86.68W*	*1050*	Complex volcano	1954, 1952, @1528
1404-09=	MOMOTOMBO	*12.42N*	*86.54W*	*1258*	Stratovolcano	1905, 1902, 1886-87?, 1882, 1878, 1870, 1858-66, 1854, 1852, 1849, 1764, 1736, ?1609, **1605-06**, 1578, 1524
1404-10=	**MASAYA**	*11.98N*	*86.16W*	*635*	Caldera	1996, 1993-94, 1989, 1987, 1965-85>, 1946-47?, 1919-24, 1913, 1906, 1904, 1902-03, 1858-59, ?1858, 1856-57, 1853, 1852, 1772, 1670, ?1613, ?1586, 1570, 1551, 1524-44?
1404-11=	**MOMBACHO**	*11.82N*	*85.96W*	*1345*	Stratovolcano	?1570
1404-12=	**CONCEPCION**	*11.53N*	*85.62W*	*1610*	Stratovolcano	1985-86, 1984-85, 1983, 1982, 1978, 1977, 1973-74, 1963, 1962, 1961, 1957, 1951-55, 1948-50, 1944-45, 1935, 1929, 1928, 1921-26, 1918-19, 1907-10, 1902, 1891, 1884-86, 1883, ?1800t
Costa Rica & S						
1405-02=	RINCON DE LA VIEJA	*10.83N*	*85.32W*	*1916*	Complex volcano	1998, 1995, 1992, ?1992, 1991, 1991, 1987, 1986, 1985-86, 1984, 1983, 1970, 1969, 1969, 1966-67, 1922, ?1917, 1912, ?1902, 1861-63, 1860, 1853-54, ?1851, @1849, @1844, 1765, ?1529
1405-03=	MIRAVALLES	*10.74N*	*85.15W*	*2028*	Stratovolcano	1946
1405-033	**ARENAL**	*10.46N*	*84.70W*	*1657*	Stratovolcano	1968-99>
1405-04=	**POAS**	*10.20N*	*84.23W*	*2708*	Stratovolcano	1996, 1994, 1992-93, 1992, 1991, 1991, 1987-90, 1981, 1980, 1980, 1979-80, 1978, 1977-78, 1977, 1976, 1974-75, 1972-73, 1970, 1969, 1967, 1964-65, 1963, 1958-61, 1952-57, 1948-51, 1946, 1941-46, 1929, 1925, 1914-15, 1914, 1910, 1910, 1907, 1898-1906, 1895, 1888-91, 1880, ?1879, 1860, ?1838, 1834, 1828
1405-05=	BARVA	*10.13N*	*84.10W*	*2906*	Complex volcano	?1867
1405-06=	IRAZU	*9.97N*	*83.85W*	*3432*	Stratovolcano	1994, 1963-65, 1939-40, 1933, 1930, 1928, 1924, 1917-21, 1914, 1910, 1909, 1899, 1894, 1889, 1883, ?1882, 1875e, 1847, 1844, 1842, ?1826, 1823, 1822, 1821, 1775?, 1726, 1723
1405-07=	TURRIALBA	*10.03N*	*83.77W*	*3340*	Stratovolcano	1866, 1864-65, ?1861, 1855, 1853, ?1847, ?1723
1406-01-	BARU	*8.80N*	*82.55W*	*3477*	Complex volcano	1550?
Colombia (N to S)						
1501-02=	**RUIZ**	*4.89N*	*75.32W*	*5321*	Stratovolcano	?1994, 1985-91, 1984-85, 1916, 1845, ?1833, 1831, 1829, 1828, ?1826, 1805, 1623, **1595**, 1570, ?1541
1501-03=	TOLIMA	*4.67N*	*75.33W*	*5200*	Stratovolcano	1943, 1826, 1825, 1822
1501-05=	HUILA	*2.92N*	*76.05W*	*5365*	Stratovolcano	1555e
1501-06=	PURACE	*2.32N*	*76.40W*	*4650*	Stratovolcanoes	1977, 1957, 1956<, 1949, 1947, 1946, 1927, 1926, 1925, 1924, 1906, 1902?, 1899, 1885, 1881, 1878, 1870, 1869, 1860i, 1847-52, 1840, 1835, 1827, 1816
1501-07=	DONA JUANA	*1.47N*	*76.92W*	*4150*	Stratovolcano	**1897-1906**
1501-08=	**GALERAS**	*1.22N*	*77.37W*	*4276*	Complex volcano	1993, 1990-92, 1989, 1974-83>, ?1973, 1950, ?1947, 1936, ?1933, 1932, ?1930, 1924-27, 1923, 1891, 1889, 1865-70, 1836, 1828-34, 1823, 1796-1801, 1754-56, 1670-1736, 1616, **1580**, 1535
1501-10=	CUMBAL	*0.98N*	*77.88W*	*4764*	Stratovolcano	1926, 1877
1501-11=	NEGRO DE MAYASQUE	*0.82N*	*77.96W*	*4445*	Stratovolcano	@1936
Ecuador – mainland (N to S)						
1502-01=	REVENTADOR	*0.07S*	*77.65W*	*3562*	Stratovolcano	1976, 1973-74, 1972, 1960, 1958, 1955, 1944, 1936, 1929, 1926, 1912, 1898-1906, 1894, 1871, 1856, 1844, 1843<, 1843, @1802, 1797, @1748<, 1691, 1590, 1541
1502-02=	GUAGUA PICHINCHA	*0.17S*	*78.59W*	*4784*	Stratovolcano	1998-99, 1997, 1993, 1990, 1985, 1981-82, 1881, 1869, 1869, 1868, 1868, 1831, 1830, **1660**, 1582-98, ?1580, ?1577, 1575, 1566, ?1560, ?1539, ?1538, ?1535, ?1534, ?1533

NUMBER	VOLCANO NAME	LAT	LONG	ELEV	TYPE	ERUPTION YEARS (VEI≤3 **VEI=4** **VEI=5** *VEI=6-7*)
Ecuador (cont)						
1502-022	**CHACANA**	*0.37S*	*78.25W*	*4643*	Caldera	1773, 1760
1502-03=	ANTISANA	*0.48S*	*78.14W*	*5753*	Stratovolcano	1801-02, ?1728, @1590?
1502-04=	SUMACO	*0.53S*	*77.62W*	*3990*	Stratovolcano	?1933, 1895r, ?1650t
1502-05=	**COTOPAXI**	*0.67S*	*78.43W*	*5911*	Stratovolcano	?1942, 1940, 1939, 1931, 1926, 1922, 1908-14, 1907, 1906, 1905, 1903-04, 1895, 1886, 1885, 1883, 1883, 1882, 1880, 1879, 1878, **1877**, 1870-76, 1869, 1868, 1867, 1866, 1863, 1860-62, 1859, 1858, 1857, 1856, 1856, 1855, 1854, 1854, 1853, 1852, 1851, 1850, 1845, 1844, 1803, **1768**, 1766, 1750, 1747-49, 1746, **1744**, 1743, 1743, 1742, 1742, 1740-41, 1738, 1698, **1534**, ?1533, ?1532
1502-06=	QUILOTOA	*0.85S*	*78.90W*	*3914*	Caldera	?1797, ?1759, ?1740, ?1725
1502-08=	TUNGURAHUA	*1.46S*	*78.44W*	*5023*	Stratovolcano	1944, **1916-25**, ?1900, **1886-88**a, ?1885, 1857, ?1781, ?1777, 1776, 1773, ?1757, ?1646, ?1644, 1641, ?1640, ?1557, @1534
1502-09=	**SANGAY**	*2.03S*	*78.33W*	*5230*	Stratovolcano	1934-99>, 1728-1916<, 1628
Galapagos Is						
1503-01=	FERNANDINA	*0.37S*	*91.55W*	*1495*	Shield volcano	1995, 1991, 1988, 1984, 1981, 1978, 1977, 1973, 1972, **1968**, 1968, 1961, 1958, 1937, 1927, 1926, 1888, 1846, 1825, 1819, @1817<, 1814, 1813
1503-02=	WOLF, VOLCAN	*0.02N*	*91.35W*	*1710*	Shield volcano	1982, ?1973, 1963, 1948, 1938, 1935, 1933, 1925-26, 1800, 1797
1503-03=	DARWIN, VOLCAN	*0.18S*	*91.28W*	*1330*	Shield volcano	@1813
1503-04=	ALCEDO, VOLCAN	*0.43S*	*91.12W*	*1130*	Shield volcano	1953g
1503-05=	NEGRA, SIERRA	*0.83S*	*91.17W*	*1490*	Shield volcano	1979-80, 1963, @1957, @1954, 1953-54, 1948-49, 1911, @1860, @1844, @1817, @1813
1503-06=	AZUL, CERRO	*0.90S*	*91.42W*	*1690*	Shield volcano	1998, 1979, ?1968, 1959, 1951, 1949?, 1948, 1943, 1940, 1932
1503-07=	PINTA	*0.58N*	*90.75W*	*780*	Shield volcano	1928
1503-08=	MARCHENA	*0.33N*	*90.47W*	*343*	Shield volcano	1991
1503-09=	SANTIAGO	*0.22S*	*90.77W*	*920*	Shield volcano	1904-06, 1897
Peru (NW to SE)						
1504-002	ANDAHUA VALLEY	*15.42S*	*72.33W*	*4713*	Cinder cones	?1913
1504-003	SABANCAYA	*15.78S*	*71.85W*	*5967*	Stratovolcanoes	1998, 1997, 1990-94, 1988, 1986, 1784, 1750
1504-01=	MISTI, EL	*16.29S*	*71.40W*	*5822*	Stratovolcano	?1870, ?1869, ?1831, ?1830, ?1826, 1787, 1784, 1677, ?1599, ?1542, 1454n
1504-02=	UBINAS	*16.35S*	*70.90W*	*5672*	Stratovolcano	1969, 1956, 1951, 1937, 1907, 1906, 1869, 1867, 1865, 1862, 1830, ?1826, 1784, 1677, 1662, 1600, 1550t
1504-03=	**HUAYNAPUTINA**	*16.60S*	*70.85W*	*4850*	Stratovolcano ?	1667, ***1600***
1504-04=	TUTUPACA	*17.02S*	*70.35W*	*5815*	Stratovolcano	1902, 1862, 1802, 1780
1504-05-	YUCAMANE	*17.18S*	*70.20W*	*5550*	Stratovolcano	1787
Chile - N, Bolivia, Argentina						
1505-01=	TACORA	*17.72S*	*69.77W*	*5980*	Stratovolcano	?1937, ?1930
1505-02=	GUALLATIRI	*18.42S*	*69.17W*	*6071*	Stratovolcano	?1985, 1960, 1959, 1913, ?1908, 1825q
1505-03=	ISLUGA	*19.15S*	*68.83W*	*5050*	Stratovolcano	?1960, 1913, 1885, 1878, 1877, 1869, 1868, 1863
1505-04=	IRRUPUTUNCU	*20.73S*	*68.55W*	*5163*	Stratovolcano	1995, ?1989
1505-05=	OLCA-PARUMA	*20.93S*	*68.48W*	*5407*	Stratovolcanoes	1865-67
1505-06=	OLLAGUE	*21.30S*	*68.18W*	*5868*	Stratovolcano	?1903
1505-07=	SAN PEDRO	*21.88S*	*68.40W*	*6145*	Stratovolcanoes	?1960, 1938, ?1923, ?1917, ?1916, 1911, 1901, 1891?, 1877?, ?1870
1505-09=	PUTANA	*22.57S*	*67.87W*	*5890*	Stratovolcano	1972, 1810j
1505-10=	**LASCAR**	*23.37S*	*67.73W*	*5592*	Stratovolcanoes	1994-95, 1994, 1993-94, **1993**, 1991-92, 1990, 1990, 1987-89, 1986, ?1985, 1974, 1972, 1969, 1959-68, 1954, 1951-52, 1940, 1933, 1902, 1898, 1883-85, 1875, 1858, 1854, ?1853, 1848
1505-105	PULAR	*24.18S*	*68.05W*	*6233*	Stratovolcanoes	?1990
1505-107	ARACAR	*24.27S*	*67.77W*	*6082*	Stratovolcano	1993
1505-11=	LLULLAILLACO	*24.72S*	*68.53W*	*6739*	Stratovolcano	1877, 1868, 1854
1505-123	ANTOFALLA, VOLCAN	*25.53S*	*68.00W*	*6100*	Stratovolcano	?1911, ?1901
Chilean Is						
1506-02=	ROBINSON CRUSOE	*33.65S*	*78.85W*	*922*	Shield volcanoes	1835, ?1743
1506-04=	UNNAMED	*33.62S*	*76.83W*	*-642*	Submarine volcano	?1839
Chile - cent, Argentina						
1507-01=	TUPUNGATITO	*33.40S*	*69.80W*	*6000*	Stratovolcano	1986, 1980, 1968, 1964, 1961, 1960, 1959, 1959, 1958, 1946-47, 1925, 1907, 1901, 1897, 1889-90, ?1881, 1861, ?1835, @1829
1507-02=	SAN JOSE	*33.78S*	*69.89W*	*5856*	Stratovolcano	1960, 1959, 1895-97, 1889-90, 1881, 1822-38
1507-021	MAIPO	*34.16S*	*69.83W*	*5264*	Caldera	1912, 1905, 1826, ?1822
1507-03=	TINGUIRIRICA	*34.81S*	*70.35W*	*4280*	Stratovolcano	?1994, 1917
1507-04=	PLANCHON-PETEROA	*35.24S*	*70.57W*	4107	Calderas	1998, 1991, 1967, 1962, 1960, 1959, 1938, 1937, 1889-94?, 1878, ?1872, ?1869, 1860, ?1842, 1837, 1835, **1762**, 1660
1507-05=	DESCABEZADO GRANDE	*35.58S*	*70.75W*	*3953*	Stratovolcano	1932-33
1507-06=	AZUL, C [**QUIZAPU**]	*35.65S*	*70.76W*	*3788*	Stratovolcano	1967, 1949, 1933-38, **1916-32**, 1914, ?1913, 1912, 1907, 1906, ?1903, 1846-53?

NUMBER	VOLCANO NAME	LAT	LONG	ELEV	TYPE	ERUPTION YEARS (VEI≤3 **VEI=4** **VEI=5** *VEI=6-7*)
Chile - cent, Argentina (cont)						
1507-07=	**CHILLAN, NEVADOS DE**	*36.86S*	*71.37W*	*3212*	Stratovolcano	1973-87>, 1972, 1965, 1946-47, 1945, 1934, 1929, 1923, 1906, 1898, 1891, 1883, 1877, 1872, 1864-65, 1861-62, @1752, 1750-51, 1650t
1507-071	TROMEN	*37.14S*	*70.03W*	*3978*	Stratovolcano	?1822
1507-08=	ANTUCO	*37.40S*	*71.34W*	*2979*	Stratovolcano	1869, 1863, 1862, 1861, 1852-53, 1848, 1845, 1839, 1828, 1820, 1806, 1752, 1750j
1507-09=	COPAHUE	*37.85S*	*71.17W*	*2965*	Stratovolcano	1992, 1961, 1937, 1867?, ?1759?, 1750?
1507-091	CALLAQUI	*37.92S*	*71.45W*	*3164*	Stratovolcano	1980, ?1937, ?1864, 1751
1507-10=	LONQUIMAY	*38.37S*	*71.58W*	*2865*	Stratovolcano	1988-90, ?1940, 1933, 1887-90, 1853
1507-11=	**LLAIMA**	*38.69S*	*71.72W*	*3125*	Stratovolcano	1998, 1998, 1997, 1995, 1994, 1992, 1990, 1984, 1979, 1971-72, 1964, ?1960, 1955-57, 1949, 1946, 1945, 1944, 1942, 1941, 1938, 1937, 1932-33, 1932, 1930, 1929, 1927, 1922, 1917, 1914, 1912, 1907-08, 1903, 1895-96, 1893-94, 1892, 1889, 1887, 1883, 1877, 1875-76, ?1874, 1872, 1869, 1866, 1864, 1862, 1852-53, 1822, 1759, 1751-52, **1640**
1507-12=	**VILLARRICA**	*39.42S*	*71.93W*	*2847*	Stratovolcano	1998-99, 1996-97, 1995, 1994, 1992, 1991, 1984-85, 1983, 1980, 1977, 1971-72, 1964, 1963, ?1960-61, 1958-59, ?1950, 1948-49, 1938, 1935, 1933, 1929, 1921, 1920-29, ?1919, 1915-18?, ?1910, 1909, 1908, 1907, 1906, 1904, 1897-98?, 1893-94?, 1883, 1879, 1877, 1875-76, 1874, 1869, ?1867-68, 1864, 1859-60, 1853, ?1852, 1837, 1832, 1822, 1815-18, 1806, 1801, 1799, 1796, 1792, 1790, 1787, 1780, 1777, 1759, 1751, 1745, 1742, 1737, 1730, 1716, 1688, ?1657, ?1647, 1640, 1594, 1562, 1558
1507-121	QUETRUPILLAN	*39.50S*	*71.70W*	*2360*	Caldera	1872
1507-13=	MOCHO-CHOSHUENCO	*39.92S*	*72.02W*	*2422*	Stratovolcano	1937, 1864
1507-14=	CARRAN-LOS VENADOS	*40.35S*	*72.07W*	*1114*	Pyroclastic cones	1979, **1955**, 1907
1507-141	CORDON CAULLE	*40.52S*	*72.20W*	*1798*	Fissure vents	1960, 1934, 1929, 1921-22, ?1905, 1893?
1507-16-	PUNTIGUIDO-CORDON	*40.96S*	*72.26W*	*2493*	Stratovolcano	?1930, 1850
Chile - S, Argentina						
1508-01=	OSORNO	*41.10S*	*72.49W*	*2652*	Stratovolcano	1869, 1855, 1851, 1837, 1834-35, 1790-91, 1765m, 1719, ?1644, ?1640, ?1575
1508-02=	CALBUCO	*41.32S*	*72.61W*	*2003*	Stratovolcano	1961, 1929, 1917, 1911-12, 1909, 1907, 1906, 1895, **1893-94**
1508-03=	HUEQUI	*42.37S*	*72.57W*	*1318*	Stratovolcano	1920?, 1906-07, 1896, 1893, 1890
1508-04=	MINCHINMAVIDA	*42.78S*	*72.43W*	*2404*	Stratovolcano	1835, 1834, 1742
1508-05=	CORCOVADO	*43.18S*	*72.80W*	*2300*	Stratovolcano	1835, 1834
1508-051	YANTELES, CERRO	*43.42S*	*72.83W*	*2050*	Stratovolcano	1835
1508-057	**HUDSON, CERRO**	*45.90S*	*72.97W*	*1905*	Stratovolcano	**1991**, 1971, 1891
1508-06=	LAUTARO	*49.02S*	*73.55W*	*3380*	Stratovolcano ?	@1961, 1960, 1945, @1879, ?1878
1508-061	VIEDMA, VOLCAN	*49.35S*	*73.28W*	*1300*	Subglacial volc	1988
1508-07=	BURNEY, MONTE	*52.33S*	*73.40W*	*1758*	Stratovolcano	1910
W Indies (N to S)						
1600-01=	SABA	*17.63N*	*63.23W*	*887*	Stratovolcano	1636<
1600-03=	LIAMUIGA	*17.37N*	*62.80W*	*1156*	Stratovolcano	?1843, ?1692
1600-05=	SOUF. MONTSERRAT	*16.72N*	*62.18W*	*915*	Stratovolcano	1995-99>
1600-06=	SOUF. GUADELOUPE	*16.05N*	*61.67W*	*1467*	Stratovolcano	1976-77, 1956, 1903, 1837-38, 1809-12, 1798-99, 1797, 1696, 1690?
1600-10=	MICOTRIN	*15.33N*	*61.33W*	*1387*	Lava domes	1880
1600-12=	**PELEE**	*14.82N*	*61.17W*	*1397*	Stratovolcano	1929-32, **1902**-05, 1851-52, 1792, 1635<
1600-14=	QUALIBOU	*13.83N*	*61.05W*	*777*	Caldera	1766
1600-15=	**SOUF. ST. VINCENT**	*13.33N*	*61.18W*	*1220*	Stratovolcano	1979, 1971-72, **1902**-03, ?1880, 1814, **1812**, 1784, 1718
1600-16=	KICK-'EM-JENNY	*12.30N*	*61.63W*	*-160*	Submarine volcano	1990, 1988, 1977, 1972, 1966, 1965, 1953, 1943, 1974, 1939
Iceland - SW						
1701-01=	REYKJANESHRYGGUR	*63.67N*	*23.33W*	*-80*	Submarine volcano	1970?, 1966, 1926, ?1884, 1879, 1830-31, 1783, 1583, 1422, 1240, 1238, 1231, 1223, 1211, 1179<
1701-02=	REYKJANES	*63.88N*	*22.50W*	*230*	Crater rows	1226-27?, 1211
1701-03=	KRISUVIK	*63.93N*	*22.10W*	*379*	Crater rows	1188, 1151
1701-04=	BRENNISTEINSFJOLL	*63.92N*	*21.83W*	*626*	Crater rows	1341a, 1188?, 1000?
1702-01=	VESTMANNAEYJAR	*63.43N*	*20.28W*	*-279*	Submarine volcano	1973 (Heimaey), 1963-67 (Surtsey), 1896, 1637-38
1702-02=	EYJAFJOLL	*63.63N*	*19.62W*	*1666*	Stratovolcano	1821-23
1702-03=	KATLA	*63.63N*	*19.05W*	*1512*	Subglacial volcano	?1955, **1918**, 1860, 1823, **1755-56**, **1721**, **1660-61**, **1625**, 1612, 1580, **1416**, **1357**c, **1311**, 1262, 1245, 1177b, 0950?
1702-05=	TORFAJOKULL	*63.92N*	*19.17W*	*1259*	Stratovolcano	1477
1702-07=	**HEKLA**	*63.98N*	*19.70W*	*1491*	Stratovolcano	1991, 1981, 1980, 1970, 1947-48, 1913, 1878, 1845-46, 1766-68, 1725, 1693, 1636-37, 1597, 1554, 1510, 1389-90, 1341, 1300-01, 1222, 1206, 1158, 1104
Iceland - E & NE						
1703-01=	**GRIMSVOTN**	*64.42N*	*17.33W*	*1725*	Caldera	1998, 1996, ?1984, 1983, ?1972, 1954, ?1948, 1945, ?1941, ?1939, 1938, 1934, @1934, 1933, 1922, **1902-04**, @1897, 1891-92, 1887-89, **1883** (Laki), 1873, 1867, ?1861, 1854, 1838, 1823, 1816, ?1794, 1783-85, 1774, @1768, 1753, 1725, 1716, 1706, 1684-85, @1681, 1659, 1638, 1629, 1619, @1603, 1598, 1500?, 1354?, 1341, 1332, 1060?, 0905?

NUMBER	VOLCANO NAME	LAT	LONG	ELEV	TYPE	ERUPTION YEARS (VEI≤3 **VEI=4** **VEI=5** *VEI=6-7*)
Iceland - E & NE (cont)						
1703-02=	LOKI-FOGRUFJOLL	64.48N	17.80W	1570	Subglacial volcano	?1991, ?1986, 1910
1703-03=	**BARDARBUNGA**	64.63N	17.53W	2000	Stratovolcano	@1902-03, @1872?, 1862-64, ?1807, @1797, @1769, 1766, @1729, 1726, 1717, 1716, 1712, 1707, 1706, @1702, **1477**, 1410?, 1159?, 1080?, 0940?
1703-05=	KVERKFJOLL	64.65N	16.72W	1920	Stratovolcano	1968, 1959, 1929, 1729, 1729, 1655
1703-06=	**ASKJA**	65.03N	16.75W	1516	Stratovolcano	1961, 1938, 1926, 1924?, 1923, 1922, 1921, 1919, **1875**, 1797?
1703-08=	KRAFLA	65.73N	16.78W	650	Caldera; Fissure	1984, 1981, 1981, 1980, 1977, 1975, 1746, 1729, 1728, 1728, 1727, 1724
1703-10=	TJORNES FRACTURE	66.30N	17.10W	?	Submarine volcano	1867-68
1704-01=	**ORAEFAJOKULL**	64.00N	16.65W	2119	Stratovolcano	**1727-28**, **1362**
1704-02=	ESJUFJOLL	64.27N	16.65W	1760	Stratovolcano	1927
1705-01=	KOLBEINSEY RIDGE	66.67N	18.50W	?	Submarine volcano	@1755, 1372
Arctic Ocean						
1706-01=	JAN MAYEN	71.08N	8.17W	2277	Stratovolcano	1985, 1973, 1970-72?, 1851r, 1818, 1732, ?1558<
1707-01-	UNNAMED	88.27N	65.60W	-1500	Submarine	1957, 1725q, 1475q
Atlantic Ocean - N						
1801-02=	UNNAMED	49.00N	34.50W	-1650	Submarine volcano	1884
1801-03=	UNNAMED	39.95N	25.83W	-2835	Submarine volcano	?1856
1801-04=	UNNAMED	38.75N	38.08W	-4200	Submarine volcano	1865
Azores (W to E)						
1802-01=	FAYAL	38.60N	28.73W	1043	Stratovolcano	1957-58, 1672-73
1802-02=	PICO	38.47N	28.40W	2351	Stratovolcano	?1963, 1720, 1718, 1562-64?
1802-03=	**SAN JORGE**	38.65N	28.08W	1053	Fissure vent	?1964, 1907, 1902, 1808, 1800, 1757, 1580
1802-05=	TERCEIRA	38.73N	27.32W	1023	Stratovolcanoes	1998-99, 1867, 1761
1802-07=	DON JOAO DE CASTRO	38.23N	26.63W	-14	Submarine volcano	1720
1802-08=	SETE CIDADES	37.87N	25.78W	856	Stratovolcano	@1880, @1861, 1811, 1811, 1713, 1682, 1638, 1444?
1802-081	UNNAMED	37.78N	25.67W	350	Pyroclastic cones	1652
1802-09=	AGUA DE PAU	37.77N	25.47W	947	Stratovolcano	1564, **1563**
1802-10=	**FURNAS**	37.77N	25.32W	805	Stratovolcano	**1630**
1802-11=	MONACO BANK	37.60N	25.88W	-197	Submarine volcano	1911, 1907
Canary Is (W to E)						
1803-01-	LA PALMA	28.58N	17.83W	2426	Stratovolcano	1971, 1949, 1712, 1677-78, 1646, 1585, 1435e
1803-02-	HIERRO	27.73N	18.03W	1500	Shield volcano	1793, ?1692, ?1677
1803-03-	TENERIFE	28.27N	16.64W	3715	Stratovolcano	1909, 1798, 1706, 1704-05, 1492, ?1444, 1430, 1396c, ?1341
1803-06-	**LANZAROTE**	29.03N	13.63W	670	Fissure vents	1824, 1730-36
Atlantic - cent & S						
1804-01=	FOGO	14.95N	24.35W	2829	Stratovolcano	1995, 1951, 1909, 1857, 1852, 1847, 1816, 1799, 1785, 1769, 1500-1761?, ?1824
1805-02=	UNNAMED	4.20N	21.45W	-2900	Submarine volcano	?1878
1805-03=	UNNAMED	0.58S	15.83W	-1528	Submarine volcano	1836, ?1816, ?1761
1805-04=	UNNAMED	3.50S	24.50W	-5300	Submarine volcano	?1852
1806-01=	TRISTAN DA CUNHA	37.09S	12.28W	2060	Stratovolcano	1961-62
1806-03-	THOMPSON ISLAND	53.93S	5.50E	?	Submarine volcano	?1895
Antarctica						
1900-01=	BUCKLE ISLAND	66.80S	163.25E	1239	Stratovolcano	1899, 1839
1900-02=	**EREBUS**	77.53S	167.17E	3794	Stratovolcano	1972-99>, 1972, 1963, ?1957-58, 1955, 1947, 1915, 1915, 1912, 1911, 1911, 1908, 1903, ?1900, 1841
1900-028	HUDSON MOUNTAINS	74.33S	99.42W	749	Stratovolcanoes	?1985
1900-03=	DECEPTION ISLAND	62.97S	60.65W	576	Caldera	?1987, ?1972, 1970, 1969, 1967, 1912e, 1842, ?1839<, 1827b, 1800<
1900-031	PENGUIN ISLAND	62.10S	57.93W	180	Stratovolcano	1850?
1900-041	PAULET	63.58S	55.77W	353	Cinder cone	?1850
1900-05=	SEAL NUNATAKS	65.03S	60.05W	368	Pyroclastic cones	?1980, 1893
1900-051	UNNAMED	56.25S	72.17W	?	Submarine volcano	?1876
S Sandwich Is (S to N)						
1900-08=	BRISTOL ISLAND	59.03S	26.58W	1100	Stratovolcano	1956, 1950, 1936-37, 1935, 1823
1900-09=	MICHAEL	57.78S	26.45W	990	Stratovolcano	?1823, 1819
1900-10=	CANDLEMAS ISLAND	57.08S	26.72W	550	Stratovolcano	?1953, ?1911, 1823
1900-11=	HODSON	56.70S	27.15W	1005	Stratovolcano	?1930, ?1830
1900-13=	ZAVODOVSKI	56.30S	27.57W	551	Stratovolcano	?1908, ?1830, ?1823, 1819
1900-14-	PROTECTOR SHOAL	55.92S	28.08W	-27	Submarine volcano	1962

This Page Intentionally Left Blank

ACKNOWLEDGMENTS

The following people have generously provided their time, often at short notice, to review the various chapters of the *Encyclopedia of Volcanoes* and in other ways assisted the Editors in making this volume scientifically accurate and complete. The Editors gratefully acknowledge their assistance:

Barbara Alexander, University of Alaska, Fairbanks

Lorne Ayres, University of Manitoba

James E. Beget, University of Alaska, Fairbanks

John P. Benoit, Chevron Overseas Exploration Company

Steven Blake, The Open University

Wendy Bohrson, University of California, Los Angeles

Glenn Borchardt, California Division of Mines and Geology

Alan Boudreau, Duke University

Gordon R. Bower, University of Alaska, Fairbanks

James G. Brophy, Indiana University

Daniele Carbone, International Institute of Volcanology, Italy

Steven Carey, University of Rhode Island

Katherine Cashman, University of Oregon

William Chadwick, Oregon State University

Jean Chiu, University of Alaska, Fairbanks

Douglas H. Christensen, University of Alaska, Fairbanks

Millard Coffin, University of Texas

James Cole, University of Canterbury

Paul Cole, University of Luton

Richard M. Conrey, Washington State University

Brian Cousens, Carleton University

Randall T. Cygan, Sandia National Laboratories

Kenneth Dean, University of Alaska, Fairbanks

Pierre Delmelle, Université de Montréal

Jacqueline Dixon, University of Miami

Wendell Duffield, Northern Arizona University

Angus Duncan, University of Luton

Benjamin R. Edwards, Grand Valley State University

Sarah A. Fagents, Arizona State University

Judy Fierstein, U.S. Geological Survey

Tobias Fischer, Arizona State University

Hilary J. Fletcher, University of Alaska, Fairbanks

Robert O. Fournier, Dalhousie University
Peter Francis, The Open University
Armin Freundt, GEOMAR Research Center for Marine Geosciences
Sturla Fridriksson, University of Iceland
Hélène Gaonačh, Université de Québec, Montréal
Cynthia Gardner, U.S. Geological Survey
James Gardner, University of Alaska
Paul Geissler, University of Arizona
Jennie Gilbert, University of Lancaster
Jeffrey Gillis, Washington University, St. Louis
Lori Glaze, Proxemy Research, Inc.
David Graham, Oregon State University
John Green, University of Minnesota
Eric Grosfils, Brown University
James T. Gutmann, Wesleyan University
Mark D. Hannington, Geological Survey of Canada
Andrew J. L. Harris, University of Hawaii
Brian P. Hausback, California State University, Sacramento
Jeff Hedenquist, Geological Survey of Japan
O. Don Hermes, University of Rhode Island
Catherine Hickson, Geological Survey of Canada
Chris Higgins, California Division of Mines and Geology
Marc M. Hirschmann, California Institute of Technology
Barbara Hobden, University of Waikato
Leroy Hulsey, University of Alaska, Fairbanks
Marie Johnson, U.S. Military Academy
Arthur D. Jolly, University of Alaska, Fairbanks
Ian Jonasson, Geological Survey of Canada
Jeff Kargel, U.S. Geological Survey
Mary Keskinen, University of Alaska, Fairbanks
Rebecca Lange, University of Michigan
Jessica Faust Larsen, University of Alaska, Fairbanks
David Lescinsky, Arizona State University
Michael Lewis, University of Alaska, Fairbanks
Rosaly Lopes-Gautier, Jet Propulsion Laboratory
Jake Lowenstern, U.S. Geological Survey
James F. Luhr, Smithsonian Institution
Ray Macdonald, University of Lancaster
Heidy Mader, Univeristy of Bristol
Vernon Manville, Institute of Geological and Nuclear Sciences
Tony Maria, University of Rhode Island
Alfred McEwen, U.S. Geological Survey
Robert G. McGimsey, U.S. Geological Survey
William McGuire, University College, London
Rachel Mills, Cambridge University
Gordon Moore, University of California
Richard B. Moore, U.S. Geological Survey
Seth C. Moran, U.S. Geological Survey
Roman Motyka, Alaska Division of Geological and Geophysical Surveys
Wulf Mueller, Université de Québec
John B. Murray, The Open University
Ian Nairn, Rotorua
Vince Neall, Massey University
Juergen Neuberg, University of Leeds
Christopher J. Nye, Alaska Division of Geological and Geophysical Surveys
Clive Oppenheimer, University of Cambridge
Michael Ort, Northern Arizona University
Jeff Plescia, Jet Propulsion Laboratory
Richard Price, University of Waikato
David Pyle, University of Cambridge
Irene Ridge, The Open University
Gary Rowe, U.S. Geological Survey
Malcolm Rutherford, Brown University
Richard Smith, University of Waikato
David Sneider, U.S. Geological Survey
Eric Sonnenthal, Indiana University
Steven Sparks, University of Bristol
John Spencer, Arizona Geological Survey
Debra S. Stakes, University of California, Santa Cruz
Peter L. Stelling, University of Alaska, Fairbanks
Nicola F. Stevens, The Open University
David Sussman, UNOCAL Geothermal
Glenn Thompson, University of Alaska, Fairbanks
Thorvaldur Thordarson, CSIRO
Gareth J. P. Thornton, The Open University

GILLIAN THORNTON, British Geological Survey
PHIL THURSTON, Ontario Geological Survey
RICHARD TROEGER, North Pacific Volcano Learning Center
GREG VALENTINE, Los Alamos National Laboratory
JAMES VALLANCE, McGill University
BEN VAN WYK DE VRIES, University of Clermont-Ferrand
JOHAN VAREKAMP, Wesleyan University
GEOFF WADGE, University of Reading
CHRIS WAYTHOMAS, U.S. Geological Survey
JAMES WHITE, University of Otago
COLIN WILSON, Institute of Geological and Nuclear Sciences
ELLEN K. WILSON, University of Alaska, Fairbanks
LIONEL WILSON, University of Lancaster
WILLIAM WORKMAN, University of Alaska, Anchorage
MAX WYSS, University of Alaska, Fairbanks
JAMES ZIMBELMAN, Smithsonian Institution

This Page Intentionally Left Blank

INDEX

A

Aa lava flow
  breaching, 297
  channeling and tubing, 297
  definition, 285, 291
  diagnostic features, 295
  energy supply in formation, 299
  evolution, 295–297
  forecasting of behavior
    maximum potential length, 301–302
    time until front solidification, 302–303
    topographical control, 303
  interior solidification, 300
  reversibility of formation, 299
Absorbent, definition, 1271
Abyssal hill, definition, 383–384
Accessory mineral, definition, 115
Accretionary lapilli, *see* Lapilli
Achnelith, definition, 683
Acid rain
  biotic extinction role, 1089
  definition, 1035
  volcanic agents, 1041
Active volcano
  definition, 254
  number, 254
Acute respiratory distress syndrome, definition, 1035
Adakite, definition, 104
Adiabatic process
  decompression melting, 52, 56, 135–136, 138
  definition, 55, 133
Advanced very high-resolution radiometer (AVHRR)
  ash cloud tracking, 1157
  Mount Etna monitoring, 1178–1179
Advection
  chaotic, 527
  definition, 527, 835
Aerial plankton
  colonization of new volcanic habitats, 1063
  definition, 1057
Aerosol, *see also specific aerosols*
  climate effects, *see also* Climate
    radiation deflection, 939
    stratospheric warming, 939–940
    tropospheric cooling, 940–941
  definition, 2, 931, 997
  direct effects, 931
  global distribution, 937
  indirect effects, 931
  microphysics, 936
  optical depth, 932, 937
  ozone depletion
    Antarctic ozone hole, 941–942
    midlatitude depletions, 942
    overview, 938–939
    Pinatubo eruption effects, 942
  stratosphere, 934, 937–939
  sulfuric acid aerosols in climate cooling, 1086–1088
  volcanic components, 934–936
Agglutination
  definition, 321
  lava fountains, 324–327
  pyroclastic fall deposits, 566
  spatter, 321
  yield stress in preservation of piles, 325–326, 329
Aggregate
  cinder, 1278–1279
  definition, 1271, 1277
  perlite, 1278
  refractory materials, 1279
A horizon, definition, 1259
Aircraft, *see* Aviation hazards
Akrotiri
  architectural sophistication, 1306–1307
  Minoan civilization

Akrotiri (*continued*)
    decline following eruption, 1307–1308
    overview, 1301, 1306
  Thera eruption reconstruction, 1307
  tourism, 1295
ALARP, *see* As low as reasonably practicable
Albedo, definition, 697, 785, 931
Alert code, *see* Alert level
Alert level, volcano warnings, 1189, 1194, 1196, 1199, 1205
Alfisol, definition, 1259
Allophane, definition, 1259
Amazonian epoch, Mars, 771, 773, 781–782
Amphibole, definition, 133
Amphitheater, *see* Debris avalanche
Anak Krakatau, *see* Krakatau
Andesite
  definition, 219, 463
  formation, 121
  magma transport, 229–231
  volatiles, abundance, 161–162
Andisol, *see also* Soil, volcanic
  classification, 1262–1263
  definition, 1259–1261
Andosol
  definition, 1259
  physical properties, 1268
Annular flow
  definition, 237, 447
  magma ascent at shallow levels, 231
Anomaly, definition, 1095
Anorthosite, definition, 697
Antarctic ozone hole, *see* Ozone
Arachnoids
  definition, 727, 753
  Venus, 762
Arc, *see also* Island arc
  backarc basins, 105–106, 362
  continental margin arcs, 103
  definition, 89, 102–103, 271–272
  episodicity of volcanism, 277–279
  extensional versus compressional arcs, 104–105
  magma production estimation, 276–277
  mineral deposition processes, 899–900
  ocean crust creation, 362
  segmentation, 103
Archeology, *see also* Akrotiri; Vesuvius
  Catal Huyuk mural, 1308, 1319
  definition, 1301
  Ilopango eruption and Maya cultural development, 1308–1309
  Mount Arenal, 1309
  Mount Ranier, 1309–1310
  Mount St. Helens, Y tephra in archeology, 1310–1311
  site preservation by volcanoes, 1302
  Sunset Crater, 1296, 1309
  tourism draw to volcanoes, 1294–1296
  White River ash effects, 1311
Arenal
  archeology, 1309
  seismic activity in eruption of 1968, 1031–1032
  tourism, 1289
Aridisol, definition, 1259
Aristotle, views on volcanoes, 19–20
Armalcolite, definition, 697, 700
Armored lapilli, *see* Lapilli
Arthropod
  colonization of new volcanic habitats, 1063–1066
  definition, 1057
Artists, volcanoes and related phenomena, 1316–1319
Asama, paintings, 1336
Ash, *see also* Aerosol; Tephra
  aggregation, 513, 520–521
  aircraft hazards, *see* Aviation hazards
  characteristics, 916–917
  components, 1155
  definition, 321, 697
  monitoring
    juvenile glass shard morphology, 1155–1156
    principles, 1153–1155
    satellite remote sensing, 1157
    soluble components, 1156–1157
Ash-flow deposit, *see also* Block-and-ash-flow deposit
  definition, 581
  tuff, *see* Ignimbrite
As low as reasonably practicable (ALARP), definition, 1215
Aspect ratio, definition, 957, 960
Asphyxia, traumatic asphyxia, 1035
Assimilation, magma
  definition, 133
  oceanic magma, 142
  subduction zone magmas, 146–147
Asthenosphere
  characteristics, 90
  definition, 89, 133, 345
Atl, paintings, 1332–1334
Atoll
  definition, 383
  formation, 395
AVHRR, *see* Advanced very high-resolution radiometer
Aviation hazards
  ash damage characteristics, 917–919
  case examples, 920–921
  economic impact, 915, 920
  history, 919–920
  incidence, 922–923, 929
  mitigation
    advisory centers, 928, 930
    communication, 927, 929
    monitoring, 925–927, 929
  overview, 528, 544, 915–917
  risk areas, 925
  severity factors, 923
  size of ash clouds, 923–925
  trends, 920, 929
  types of hazards, 919
Axial graben, definition, 89
Aztecs, volcano mythology, 18–19

B

Backarc basin, *see* Arc
Basalt, *see also* Basaltic magma; Basaltic volcanic field; Flood basalt; Midocean ridge basalt
  backarc basins, 106
  composition and formation
    continental basalts, 122–123, 125
    elements, 117, 119
    island arc basalts, 121–122
    ocean floor basalts, 115, 119–120
    ocean island basalts, 120–121, 123–125
    trace elements, 123–125
  definition, 41, 219, 345, 697, 1271
  discovery of volcanic origin, 25
  melting, 46
  moon, *see* Moon
  radiogenic isotope analysis, 128–129
Basaltic magma
  definition, 171
  definition, 321
  pressure gradients for flow, 228–229
  subglacial eruption, *see* Subglacial eruption
  volatiles, abundance in magma
    backarc basin basalts, 161
    continental margin basalts, 160–161
    flood basalts, 161
    island arc basalts, 160–161

    - midocean ridge basalts, 158–159
    - ocean island basalts, 159–160
- Basaltic volcanic field
  - faults, occurence of vents, 340–341
  - origins, 342
  - overview of features, 331, 333
  - petrogenesis, 341–342
  - physical characteristics of selected fields, 332–333
  - probability estimation for future eruptions, 337–338
  - rationale for study, 332
  - spatial patterns in vent distribution, 336–337
  - temporal recurrence rates, 333–336
  - vent alignment, 339–340
- Base surge, *see also* Pyroclastic surge
  - definition, 945
  - volcanic lake hazard, 890
- Batholith
  - definition, 191
  - plutons, 192
- Beach, volcano tourism, 1293–1294
- Bentonite
  - commercial uses, 1277, 1281
  - definition, 1271
  - deposits, 1277
  - properties, 1276–1277
- B horizon, definition, 1259
- Bimodal volcanism, definition, 111
- Biota
  - definition, 1057
  - volcanic hazards, *see specific hazards*
- Birds, colonization of new volcanic habitats, 1065–1066, 1069–1071, 1073, 1075, 1078–1079
- Black smoker, definition, 857, 873
- Blast, *see* Pyroclastic surge
- Block
  - debris avalanche, 617, 620
  - definition, 463
  - vulcanian eruptions, 471
- Block-and-ash-flow deposit
  - composition, 592–593
  - distribution, 592
  - facies associations, 592
- Blocky lava flow
  - breaching, 297
  - channeling and tubing, 297
  - definition, 291
  - diagnostic features, 295
  - energy supply in formation, 299
  - evolution, 295–297
  - forecasting of behavior, 304
  - reversibility of formation, 299
- Bomb, definition, 321, 463
- Bombardment, definition, 697
- Bore, definition, 1005
- Bowen, Norman, petrology contributions, 34
- Breadcrust texture, definition, 403
- Breccia, *see* Hyoclastite; Ignimbrite; Pillow lava
- Bridge of the Gods, geomythology, 1312–1313
- Brinkman number
  - definition, 219
  - viscous dissipation effects on magma flow, 225
- Brittle failure, melt localization and flow focusing, 84–85
- Bromo, religious significance, 1296
- Bronze age, definition, 1301
- Bubble
  - definition, 421
  - growth, 323–324, 424–425
  - magma storage regions, 422–423
  - nucleation, 423–424
  - volatile loss, 426
- Bubbly flow
  - definition, 237
  - magma ascent at shallow levels, 241
- Bulking
  - apparent bulking factor estimation, 613–614
  - definition, 601
  - lahar transformation, 609–610
- Bunsen, Robert
  - decompression melting contributions, 30
  - petrology contributions, 33–34
- Buoyancy, definition, 835

C

- Calcalkaline differentiation trend, subduction zone magmas, 145
- Caldera
  - classification, 653, 658
  - climate impact, 659, 661
  - definition, 219, 643, 697, 771
  - earthquakes, 1024, 1027, 1032
  - eruptive processes, 644
  - examples
    - extraterrestrial, 644
    - Fernandina, 646
    - Katmai, 646
    - Kilauea, 646–647
    - Krakatau, 646, 661
    - Pinatubo, 646, 661
    - Santorini, 645
    - table, 645’
    - Taupo, 647
  - freshwater lakes, 887–888
  - hazard potential, 658–659, 661
  - history of study, 644–645
  - hydrothermal activity and mineralization, 653
  - Io, 713
  - Mars, 775
  - microgravity monitoring, 1133–1134
  - monitoring, 1173
  - postcollapse magmatism and resurgence, 652–653
  - precollapse volcanism, 647
  - size, 643
  - structure and morphology
    - bounding faults, 649–650
    - collapse collar, 649
    - floor, 650–651
    - inner topographic wall, 649
    - intracaldera fill, 650
    - overview, 647
    - subcaldera magma chamber, 651–652
    - topographic rim, 649
  - subsidence processes
    - chaotic subsidence, 656
    - downsag subsidence, 654–655
    - funnel calderas, 656–657
    - ignimbrite shields, 657
    - overview, 653–654, 658
    - piecemeal disruption, 655–656
    - plate subsidence, 654
    - trapdoor subsidence, 655
    - volcano-tectonic depressions, 657–658
  - Venus, 757–758
- Campi Flegrei, gravity monitoring, 1133–1134
- Canali, *see also* Lava channel
  - definition, 727
  - Venus, 759–760
- Capture front, definition, 191, 194
- Carbon cycle
  - modeling for volcanic emission variation, 1052–1054
  - preindustrial geochemical cycle, 1048–1049
  - total carbon on Earth, 1046
- Carbon dioxide
  - annual emission estimates, 1047–1048
  - degassing and isotopes, 168–169
  - diffuse flank degassing, 813–814
  - emission concentration changes over time, 1146–1147

Carbon dioxide (*continued*)
  fumarole emission monitoring, 1146–1147, 1149
  greenhouse warming, 1088
  hazards, 998–999
  historic outgassing rates, 1053
  isotopic analysis, 807, 1047
  large ingneous province outgassing, 1054
  measurement of outgassing, 1046–1047
  outgassing rate, 1046
  pressure-dependent solubility in magma, 169
  recycling, 1052
  silicate melts, effects
    density, 166
    viscosity, 167
  solubility in silicate melts, 151–152
  toxicity, 998, 1000, 1042
  volcanic lakes
    artificial degassing, 894
    content, 887–889
    release hazard, 891
Carbon sulfide, stratospheric layer, 934
Carnivore, definition, 1057
Catal Huyuk, archeology, 1308, 1319
Catastrophist, definition, 271–272
C-band radar, ash cloud tracking, 1157
Central volcano
  definition, 283, 771
  features, 288–289
Chaotic subsidence, 656
Chasma, definition, 727
Chimney, definition, 857
Chlorine, *see also* Magnesium/chlorine ratio
  ash components, 1156–1157
  hydrothermal systems, 869, 871
  solubility in silicate melts, 153–154
  subduction, 169
Chlorofluorocarbons, ozone depletion, 941
Chondritic rock, definition, 41
C horizon, definition, 1259
Church, Frederic, volcano paintings, 1330–1331
Cinder
  blocks, 1271, 1280
  commercial uses, 1278–1279
  cone, 697
  properties, 1278
Classicism, definition, 1315
Clastogenic lava, definition, 321
Clathrate, definition, 785
Clausius-Clapeyron equation, decompression melting, 29–30, 60
Clay, definition, 1259
Climate, volcano effects
  Andisol formation role, 1263–1264
  atmospheric moisture and plume dispersal, 541
  caldera impact, 659, 661
  Etna eruption of 44 B.C. effects, 932
  flood basalt provinces, 358–359
  Kuwae eruption of 1453 effects, 932–933
  mass extinctions, 348
  Santorini eruption of 1620 B.C. effects, 932
  sulfuric acid aerosols in cooling, 1086–1088
  Tambora eruption of 1815, 10–12, 933, 1090–1091
Clinopyroxene (CPX)
  definition, 133
  pressure in formation, 139
Coagulation, definition, 931
Coalescence, definition, 321–322
Cocks tail jet, *see* Tephra jet
Coextrusion
  definition, 219
  magma flow, 230–231, 234
Cole, Thomas, volcano paintings, 1330
Colima, ground deformation monitoring, 1128
Collapse pit, definition, 697
Collembolan, definition, 1057
Colles, definition, 727
Comics, volcano depiction in literature, 1355
Community, definition, 1057
Compaction
  definition, 69
  magma chamber differentiation, 200
  melt migration, 70
Compaction length
  calculation, 79
  composition dependence, 72
  definition, 69
  melt migration, 71
Compatible element
  basaltic magmas, 123–125
  definition, 115
Component, chemical formulas, 55, 58
Componentry
  definition, 555
  deposit evaluation, 566
Composite volcano
  definition, 663–664, 771
  distribution, 664–666
  fatal eruptions, 667
  growth spurts, 675–676
  lifetime, 675–676
  Mars, 775
  morphology
    aggradation, 668–670
    cone volume, 668
    degradation, 670–672
    evolution, 667–668
    factors in control, 668
    overview, 666–667
    types, 667–668
    vent migration, 672–674
  volcanogenic products
    classification, 676–677
    cone-building association, 678–680
    flow direction and redistribution, 677
    main vent association, 677–678
    ring plain association, 680
    satellite vent association, 680–681
Compound volcano, definition, 663
Condensation, definition, 931
Conduction
  definition, 835
  mantle melting, 66
Conductive heat flow, equation, 819
Conduit, definition, 219
Cone, definition, 697
Consensus, definition, 1199
Construction
  cinder blocks, 1280
  concrete, 1280
  tunneling through volcanic rock, 1280
  volcanic stone, 1279–1280
Contact, definition, 219
Continental rifting, mechanisms, 109–110
Continuous uprush
  definition, 403, 495
  subglacial eruption, 412
  surtseyan eruption, 499–500
Convection
  definition, 1, 835
  driving forces, 51
  heat loss on Earth, 51

- history of discovery, 31–33
- mantle heat transfer, 49–51, 90
- pluton studies of sedimentation, 202

Convergent plate boundary, *see* Plate tectonics
Convergent plate volcano, definition, 803
Conversion factors, common measurement units, 1361–1364
Cooling star, historic view of volcanoes, 24
Copper, *see* Porphyry
Corona
- definition, 727, 753
- Venus, 761–762

Correlation spectrometry (COSPEC)
- definition, 1143
- history of volcano monitoring, 1149–1150
- principle, 1150
- sulfur dioxide monitoring, 809, 812, 997, 1046, 1149–1151

COSPEC, *see* Correlation spectrometry
Cotopaxi, paintings, 1335
Coulee, definition, 307–308
Coulomb friction, resisting stress modeling of lahars, 615
Cowpat bomb, definition, 403
CPX, *see* Clinopyroxene
Crater, definition, 643
The Crater, volcano depiction in literature, 1343–1344
Crater Lake
- geomythology, 1312
- national park establishment, 1286–1288

Crepuscular, definition, 1057
Crisis, definition, 1199, 1229
Crisis management, *see also* Warning
- centralized data processing
  - alarm monitoring, 1208–1209
  - communication, 1209
  - display, 1208
  - processing of data, 1208
- critical phase management
  - alarm response, 1209–1210
  - communications, 1209–1212, 1234
  - declaration of critical phase, 1206–1207, 1212
  - monitoring and alarms, 1207–1209
  - operative planning, 1212
  - return to subcritical phase, 1213
- overview, 1200–1201
- postevent interventions
  - exposure intervention, 1238
  - multiple gating, 1237
  - rationale, 1236–1237
  - Ruapehu eruption of 1995 interventions, 1238–1240
  - support and information, 1237–1238
- pre-event management
  - alert codes, 1189, 1194, 1196, 1199, 1205
  - communications, 1205
  - hazards assessment, 1201
  - monitoring, 1203–1204
  - preparedness, 1201
  - scientific advice, 1204–1205
  - vulnerability assessment and reduction, 1201–1203

Critical crystallinity, definition, 191, 195
Critical phase, definition, 1199
Crosswind, plume dispersal, 539–540
Crust
- definition, 89, 133
- definition, 291
- entrainment, 300–301
- evolution, 130–131
- formation in lava flow, 299
- lithosphere comparison, 90

Cryovolcanism, *see also specific satellites*
- conditions for cryovolcanism, 787
- cryoclastic eruption, 785
- definition, 785–787
- eruptive processes, 789–791
- explorations, 786, 799–800
- magma composition
  - densities, 789
  - determination techniques, 787
  - melting point effects, 788–789
  - variation with distance from sun, 787–788
  - viscosities, 789
  - water, 787–788
- overview, 785–786

Cryptodome
- definition, 307
- features, 311

Crystal fragment, definition, 1143
Crystalline silica, definition, 1035
Crystal structure, mineral changes with depth, 47–48
Cry wolf syndrome, definition, 1229
Cumulate, definition, 897
Cyanobacteria, definition, 1057

D

Dacite, abundance of volatiles, 162–163
Dante's peak, volcano depiction in film, 1339, 1359
Darcy's law, melt flow, 70, 72
Dark mantle deposit, definition, 697
Darwin, Charles, petrology contributions, 33, 192
Davy, Humphry, views of volcanoes, 23
Debris avalanche
- amphitheater, 617, 620, 625
- blocks, 617, 620
- definition, 601, 617, 663, 1057
- discovery, 618, 625
- examples
  - Bandai type, 625
  - Bezymianny type, 624–625
  - Unzen type, 625
- flow and emplacement models, 623–624
- formation
  - eruption processes, 622–623, 625
  - sector collapse, 617–618
- frequency, 621–622
- geomorphology, 618, 620
- hazards, Mount St. Helens, 1059
- hummocks, 617
- jigsaw cracks, 617, 620
- magnitude, 621
- matrix, 617, 621
- transformation from lahars, 621
- tsunami generation, 1009–1010

Debris flow, *see also* Lahar
- characteristics, 976, 978, 980–982
- definition, 601, 627, 973
- deposits, 610–614
- downstream processes, 605–610
- formation, 603, 605
- physical modeling, 614–615
- temperature, 981–982

Debulking
- apparent debulking factor estimation, 613–614
- definition, 601

Decollement, definition, 283
Decompression melting
- adiabatic process, 52, 56, 135–136, 138
- batch melting, 55, 62, 138
- definition, 15, 271
- equilibrium porous flow, 138
- fractional melting, 55, 62, 138

Decompression melting (*continued*)
  history of discovery, 28–31
  overview, 3, 67–68, 135–136
  polybaric near-fractional melting, 138–140
  thermodynamic modeling
    beginning of melting, 59–60
    multicomponent system modeling, 61–63
    one-component system modeling, 58–61
    overview, 56–59
    progress of melting, 60–61
Decoration, volcanic rocks, 1275, 1281
Deformation
  effects on melt distribution, 76, 79
  enhancement with increasing melt fraction, 80
  melt localization and flow focusing
    anisotropic permeability development, 82–83
    brittle failure, 84–85
    strength and viscosity contrast role, 82
Degassing, *see also* Exsolution; Gas; Volatiles
  artificial degassing of volcanic lakes, 894
  definition, 237
  diffuse flank degassing
    carbon dioxide, 813–814
    helium, 814
    hot and cold springs, 814
    hydrogen, 814
    mechanisms, 814–815
    overview, 813
    radon, 814
  Earth
    degassing rate, 168
    outgassing mechanisms, 1045–1046
  hawaiian and strombolian eruptions, 453–454
  lava dome mechanisms, 316–317
  magma ascent, 208–210
  modeling for magma ascent at shallow levels, 244–245
  nonexplosive degassing, 507
  open versus closed systems, 815
  plume formation, 528
  system types, 322–323
Demons, volcano depiction in film, 1357
Denitrification, definition, 931
Dense rock equivalent (DRE)
  definition, 945
  deposit mass and volume estimation, 264–265
Density
  cryomagma, 789
  equations of state, 175, 177
  magma/gas mixture calculation, 240
  melt density evaluation, 175–176
  molar volumes of silicates, 177–178
  molten carbonate, 176
  pressure dependence, 176–178
  supercritical water, 176
  volatile effects on silicate melts, 166
Deposits, *see also specific deposits*
  mass and volume estimation, 264–265
Descartes, Ren&eacute;, views of volcanoes, 24, 27
Destructiveness index, definition, 263, 268–269
Deterministic, definition, 1095
Diamond deposits
  characteristics, 911
  distribution and age, 10–911
  origin, 911–912
  significance, 910
  volcanic activity in formation, 11
Diatreme, definition, 683
Differentiation, planets and satellites, 709
Diffusion
  chemical diffusion, 186–188
  diffusivity values
    basaltic melts, 187
    rhyolitic melts, 188
  self-diffusion, 186–187
  temperature dependence, 186–187
  tracer diffusion, 186–187
  turbulent diffusion of plumes, 527, 543
Dihedral angle
  definition, 69
  measurement, 75–76
  melt network geometry in partially molten rocks, 74–75
Dike
  critical initial width in formation, 221
  definition, 191, 219, 857
  dimensions, 222
  encapsulation, 230–231
  features, 192
  feeder dikes for seamounts, 383, 391
  flow modeling
    computer modeling
      basaltic magma, 224–225
      overview, 222, 224
      rising gas bubble effects, 226–227
      viscosity effects, 227–228
      viscous dissipation effects, 225–226
    dynamic viscosity, 222–223
    heat loss and flow rates, 221, 223–224
    laminar flow models, 221, 234
  fracture propagation by vapor and magma, 220
  injection in hydrothermal systems, 872–873
  Inyo volcanic chain connection, 232–234
  lava domes as tectonic stress orientation indicators, 317–318
  pressure gradients for flow
    basaltic magma, 228–229
    coextrusion and transport of viscous magma, 229–231, 234
Dilatancy, definition, 191, 195
Dione, *see* Saturn moons
Directionalism, definition, 271–272
Disaster, definition, 1199
Disaster relief
  aims, 1215, 1224–1225
  sources, 1225–1226
  types, 1225
  vulnerability reduction, 1226
Dispersal index
  definition, 513, 555
  phreatoplinian eruptions, 524
  pyroclastic fall deposits, 558–559
Dispersed flow, definition, 237
Distress, definition, 1229
Divergent plate boundary, *see* Plate tectonics
Divergent plate volcano, definition, 803
Dome, *see* Lava dome
Doppler radar, *see* C-band radar
Downsag subsidence, calderas, 654–655
DRE, *see* Dense rock equivalent
Dreams, volcano depiction in film, 1357
D″ region
  characteristics, 43–44
  definition, 41
Drilling mud, definition, 1271
Dry tilt, ground deformation monitoring, 1125

Dunite
  channel formation, 85
  definition, 897

E

Eardrum rupture, volcano explosions, 1040
Earth
  degassing rate, 168
  solar position and life sustenance, 2–3
Earthquake, *see also* Tremor
  accuracy of localization, 1097
  Arenal volcano eruption of 1968, 1031–1032
  A-type, 1015, 1017, 1019, 1100–1101
  background and seismicity rates, 1022–1023, 1100, 1103, 1115
  basaltic versus dacitic volcanoes, 1027
  B-type, 1015, 1019, 1100–1101
  caldera earthquakes, 1024, 1027, 1032
  declining activity following eruption, 1109
  definition, 1015–1016
  energy release, 1016
  explosion earthquake, 1015, 1019, 1100–1101
  faults, 1016–1017
  frequency–magnitude distribution, 1017, 1100
  generic volcanic earthquake swarm model, 1104–1105
  geothermal system hazard in power utilization, 833
  Global Volcanic Earthquake swarm database, 1105
  historic eruptions, 1016
  hybrid earthquakes, 1101
  large regional earthquakes, 1024
  large versus small eruptions, 1022–1024
  locations of occurrence, 1024
  long repose time volcanoes, 1027
  magma chambers, seismic features, 1027–1028, 1030, 1032
  magnitude, 1015, 1017
  monitoring
    data analysis in networks, 1097–1098, 1102, 1115
    decay, 1172
    forecasting eruptions, 1095, 1097, 1103–1106, 1115, 1118
    goals, 1096
    history, 1096
    instrumentation, 1098
    Ito-oki eruption of 1989, 1109, 1112
    Kilauea eruption of 1983, 1109
    Mount Etna, 1174–1175
    Mount St. Helens eruption of 1980, 1030, 1109
    Mount Spurr eruption of 1992, 1030–1031
    overview, 1169
    Pavlof eruption of 1996, 1112
    Pinatubo eruption of 1991, 1112–1113
    seismometer placement, 1097–1099
    Soufriere Hills volcano monitoring, 1179
    statistical analysis of seismicity, 1103–1104
  plume height estimation, 1108
  primary wave, 1015, 1027–1028, 1100
  real-time seismic amplitude measurement, 1105–1106
  secondary wave screening, 1015, 1028, 1100
  seismic spectral amplitude measurement, 1105–1106
  size distribution, 1100
  surficial events
    glacial events, 1020, 1100, 1102
    lahars, 1021, 1102
    landslides, 1021, 1100, 1102
    pyroclastic flow, 1021, 1102
    rockfalls, 1021, 1102
    shore ice, 1020–1021, 1102
  swarms, 1015, 1095–1096, 1099–1100, 1103–1104, 1109, 1172
  synchronous volcanic and tectonic activity, 1027
  tephra volume estimation, 1108
  terminology for types, 1021–1022
  very long-period events, 1015, 1020, 1102
  zone linearity with volcanoes, 32
Earth tide
  definition, 1121
  gravity monitoring, 1131
Eccentricity, orbit, 785
Eclogite
  definition, 1, 15, 345, 897
  plume component, 359
Ecosystem, definition, 1057
Edifice
  definition, 663
  height in composite volcanoes, 668–669
EDM, *see* Electronic distance measurement
Edo painting
  definition, 1315
  Fuji, 1327–1328
Education, volcano risks
  crisis response, *see* Crisis management; Warning
  initiatives
    Egmont volcano, 1232–1233
    Mount Ranier, 12322
  program design and monitoring, 1231–1232
  school children, 1230
  value, 1229–1230
  video and other materials, 1190–1191
Effusive eruption
  definition, 957, 1057
  monitoring, 1172
Egmont volcano, education initiatives, 1232–1233
E horizon, definition, 1259
El Chichon, field observation, 482, 484–485
Electronic distance measurement (EDM), ground deformation monitoring, 1123
Element, classification for magma composition, 116–118
El Pico de Orizaba, tourism, 1290–1291
Elutriation, definition, 527
Emissivity, definition, 1143
Encapsulation
  dike wall lubrication by magmas, 230–231
  Inyo volcanic chain connection, 232–234
Enceladus, *see* Saturn moons
Endemic organism
  definition, 383
  seamount fauna, 401
Endogenic explosion, definition, 307, 309
Entisol, definition, 1259
Entrainment, definition, 527
Eolian deposit, distinguishing from pyroclastic surge deposits, 578–579
Epiclastic, definition, 627

Episodicity, volcanic activity
  arcs, 277–279
  basaltic volcanic field, 333–336
  calculation, 335
  composite volcano eruptions, 676
  flood basalt provinces, 350
  large igneous provinces, 274–275
  midocean ridge, 272–273
  probability estimation for future eruptions, 337–338
Equilibrium, definition, 55–56
Erosion, *see also* Ring plain
  composite volcanoes, 670–671
  lahars, 605–606
  seamounts, 393
  syneruptive erosion in phreatoplinian eruption, 522–523
Eruption, *see also* Explosive eruption; Mass eruption rate; Subglacial eruption; Volcanic explosivity index
  culmination, 256
  definition, 255–256
  destructiveness index, 263, 268–269
  duration, 256
  energy release, 267–268
  gas, *see* Volatiles
  intensity, 263–267
  interval and individual magnitude, 259–261
  largest in recent history, 260–261
  magnitude and global frequency, 258–259, 263–267
  patterns through recorded history, 256–258
Esker, definition, 403
Etiology, definition, 1301
Etna, *see* Mount Etna
Europa, *see* Jupiter moons
Evaporation, definition, 931
Exogenic explosion, definition, 307, 309
Exothermic reaction
  definition, 15
  historic view of volcanoes, 23–24
Explosive earthquake, *see* Earthquake
Explosive eruption, *see also* Hawaiian eruption; Lava fountain; Phreatoplinian eruption; Plinian eruption; Strombolian eruption; Subplinian eruption; Surtseyan eruption; Volcanic explosivity index; Vulcanian eruption
  classification by fall deposits, 481
  definition, 321, 957
  dry versus wet, 422
  monitoring, 1171–1172
  ocean sediments, 630, 632
  submarine lava, 362
  volatiles, 229, 256, 322–323
Exsolution, *see also* Bubble; Fragmentation
  definition, 219
  vulcanian eruptions, 473–474
Exsolved gas
  definition, 149
  rates on Earth, 168
  sulfur dioxide, 164–165
Extinction, *see* Mass extinction
Extirpation, definition, 1057

F

Farrum, definition, 727
Fault
  earthquakes, 1016–1017
  transform fault volcanism, 102
  vent association in basaltic volcanic fields, 340–341
  volcanism at divergent plate boundaries, 100
FCI, *see* Fuel–coolant interaction
Felsic rock, definition, 115
Fernandina, caldera, 646
Fields, *see* Basaltic volcanic field; Lava flow field
Field volcanology, history, 25, 331–332, 342
Film, volcano depiction, 1355–1358
Fire fountain
  definition, 683, 697
  plume generation, 530–531
Fissure
  definition, 321
  eruption, 383
Flood basalt
  continental flood basalt, 115
  continental rifting, 109–110
  definition, 89, 271, 1083
  flow field features, 287–288
  magma flux, 94
  mass extinction correlation with eruptions
    climate cooling, 1086–1088
    continental flood basalts, 1084–1086
    extraterrestrial impact correlation, 1090
    lava flow rate, 1086
  mineral deposits
    characteristics, 907
    distribution and age, 907
    origin, 907–908
    significance, 907
  volcano characteristics, 255
Flood basalt province
  categorization, 349–350
  chemical types and isotopic parameters, 352–355
  climate effects, 358–359
  crustal contamination, 355
  episodicity, 350
  formation, 347–348
  genetic modeling, 357–358
  global distribution, 345–346
  hot spot sources, 347–348, 354–355, 357
  oceanic flood basalts, 356
  overview of features, 345, 347
  physical parameters
    dimensions, 349–350
    flow volume, 350–351
  reservoirs, 351–352
  sources, 355–357
  tectonic implications, 356–358
Flow field, *see* Fluctus; Lava flow field
Flow front, definition, 697
Flow phase, definition, 602
Flow stage. definition, 602
Fluctus
  definition, 727
  Venus, 758–759
Fluid, definition, 835
Fluid inclusion, definition, 857
Fluorine
  effects on silicate melt density, 166
  solubility in silicate melts, 154
Fluted dome
  definition, 727
  Venus, 756
Fly-by, spacecraft, 709
Forecast, *see also* Crisis management; Monitoring; Warning
  definition, 1095
  eruption forecasting with seismicity, 1097, 1103–1106, 1115, 1118
  intermediate-range, 1185–1186
  long-range, 1185–1186
  short-range, 1185–1187
  syneruption warnings, 1187
  time window forecasts, 1188–1189
Fossae
  definition, 771

  Mars, 778
Fossil, volcanic preservation, 16
Fountain collapse, definition, 709
Fourier transform infrared spectrometry (FTIR)
  definition, 1143
  gas monitoring, 1153
Fractional crystallization
  definition, 133
  effects on magma composition, 120–121
  oceanic magma, 141–142
  subduction zones, 144–146
Fragmentation, *see also* Phreatomagmatic fragmentation
  bubbles
    growth, 323–324, 424–425
    magma storage regions, 422–423
    nucleation, 423–424
    volatile loss, 426
  definition, 237, 241, 421
  magma ascent modeling, 425
  mechanisms
    product analysis, 427, 429
    rapid acceleration of liquid, 426–427, 429
    rapid decompression model, 427, 429
  models, 422
  plinian eruptions, 479–480
  wave, 426
Fragmentation index, definition, 513, 555
Frittering, definition, 495
Frugivore
  colonization of new volcanic habitats, 1070, 1075–1076
  definition, 1057
FTIR, *see* Fourier transform infrared spectrometry
Fuel–coolant interaction (FCI)
  definition, 431, 683
  phreatomagmatic fragmentation homology, 433–434, 437–439
  vulcanian eruption model, 474
Fugacity
  definition, 149
  oxygen, 152
  sulfur species, 156
Fuji
  paintings, 1327–1328
  religious significance, 1297
Fumarole, *see also* Geothermal system
  definition, 1143
  gas monitoring, 1144–1147
  thermal signature, 1162–1164
Funnel caldera, *see* Caldera

G

Gabbro, definition, 41
Galeras
  gas analysis, 812–813
  vulcanian eruption, 466–469
Galilean satellites, *see* Io; Jupiter moons
Ganymede, *see* Jupiter moons
Garnet, composition, 124
Gas, *see also* Degassing; Volatiles; *specific gases*
  chemical composition, overview, 804–805, 998
  examples of analysis
    Galeras, 812–813
    Kudriavy, 809–810
    Mount Etna, 1178
    Mount St. Helens, 810
    Usu, 810–811
    Vulcano, 812
    White Island, 811
  hazards
    carbon dioxide, 998–999
    causes of death and injury, 1041–1042
    hydrochloric acid, 1003
    hydrogen fluoride, 1003
    hydrogen sulfide, 1002–1003
    Lakagígar eruption of 1783, 1058–1059
    mitigation, 1003–1004
    mortality, 997
    sulfur dioxide, 999, 1001–1002
  hydrothermal system reactions, 808–809
  information available from study, 804
  isotopic analysis, 806–807
  monitoring
    correlation spectrometry, 1149–1151
    Fourier transform infrared spectrometry, 1153
    fumarolic discharges, 1144–1147
    overview, 1169–1170
    principles, 1144
    soil gas, 1147–1149
    total ozone mapping spectrometry, 1151–1153
    trace elements, 1147
  pressure and temperature effects on composition, 805–806
  ratio analysis, 808–811
  redox potential effects on composition, 806
  solubility, 997
  toxicity, 998, 1000–1001
Gas gangrene
  definition, 1035
  lahar association, 1039
Gas–piston activity, definition, 447
Genesis Rock, volcano depiction in literature, 1349–1350
Genre, definition, 1315
Gentlemen in England, volcano depiction in literature, 1339, 1350–1351
Geographic distribution
  flood basalt provinces, 345–346
  geothermal systems, 817–818
  hyaloclastite, 371–374
  large igneous provinces, 274
  seamounts
    intraplate seamounts, 387, 389
    island arcs, 390
    midocean ridge seamounts
      fast spreading ridges, 389–390, 401
      overview, 389
      slow spreading ridges, 390, 401
    Pacific plate seamounts, 390–391
  volcanic lakes, 877–880
  volcanic soils, 1261–1262
  volcanoes, overview, 252, 254
  Volcanoes of the World, condensed and updated table, 1366–1383
Geomythology
  Bridge of the Gods, 1312–1313
  Crater Lake, 1312
  definition, 1301
  Greco-Roman myths, 1312
Geotherm, definition, 115
Geothermal system
  applications, nonelectrical, 817, 832
  chemical geothermometers, 828
  definition, 835, 897, 1243
  elements, 817
  energy utilization, *see* Power production, geothermal systems
  field, 1243
  fluid, 1243
  fumaroles, 837–839, 845–846, 850–851

- Geothermal system (*continued*)
  - gas chemistry, 824–825
  - geysers, 843–844, 851
  - global distribution, 817–818
  - heat discharge rate, 836–837, 853
  - heat flow
    - Earth, 819–820
    - magmatic intrusions, 820–821
  - heat sources, 836
  - hot spring tourism, 1290
  - lifetimes, 834
  - mineral mining, 829–830
  - mining, 1244
  - modeling
    - liquid-dominated systems, 824
    - tectonic model, 822–823
    - vapor-dominated systems, 823–824
    - young igneous model, 821–822
  - permeability of rock, 1243
  - reservoir, 1243
  - solfataras, 837–839, 851
  - space heating utilization, 1247
  - surface alteration and deposits, 852–854
  - surface manifestations
    - fracture zone systems, 847–848
    - heat-sweep systems, 846–847
    - high-temperature systems associated with high standing volcanic centers
      - classification of systems, 839
      - liquid-dominated systems, 840–841
      - two-phase systems, 841
      - vapor-dominated systems, 841–842
    - high-temperature systems associated with moderate terrain
      - crustal spreading environments, 844–845
      - heat sources, 842–843
      - moderately steep terrain underlain by extensive hot crustal rocks, 843–844
      - sedimentary rock systems, 845
    - hot crustal rock systems in plate collision environments, 845–846
    - intermediate-temperature systems over volcanic arcs, 846
    - low-temperature systems, 848–849
    - quasi volcanic–hydrothermal systems, 839
    - volcanic–hydrothermal systems, 837–838
  - types
    - classification of manifestations by mode of heat transfer
      - catastrophic discharge, 851
      - diffusive heat discharge, 849
      - direct and continuous heat discharge, 849–851
      - intermittent heat discharge, 851
      - seepage, 851
    - geopressured systems, 819
    - hot dry rock systems, 819
    - magma tap systems, 819
    - tectonic systems, 819, 822–823
    - temperature classification scheme, 836
    - young igneous systems, 818–819, 821–822
  - water
    - chemistry, 825, 827–828
    - origins and system age, 828–829
- Giggenbach bottle
  - definition, 997
  - gas sampling, 1145
- Glacier, *see also* Subglacial eruption
  - burst, *see* Jökuhlhlaup
  - seismic events, 1020, 1100
- Glass
  - definition, 149
  - definition, 697, 1259
  - prehistoric uses, 1275
  - volatiles, analysis in magma, 155, 157
- Glass shard
  - definition, 1143
  - morphology of juvenile shards, 1155–1156
- Global distribution, *see* Geographic distribution
- Global Positioning System (GPS)
  - advantages in monitoring, 1184
  - definition, 1121
  - ground deformation monitoring, 1122–1124, 1141
- Global Volcanism Network (GVN), formation, 249
- Gold, *see* Gold deposits; Porphyry
- Gold deposits
  - characteristics, 903
  - distribution and age, 903
  - origin, 903–904
  - significance, 902–903
  - types, 903
- GPS, *see* Global Positioning System
- Graben, formation, 100
- Graham Island, seamount emergence, 394
- Grain size half-distance
  - definition, 555
  - fining of fall depositis, 559
- Grand Tour, *see* Tourism
- Granite
  - composition, 117, 125–128
  - formation, 126
  - radiogenic isotope analysis, 130
  - water in magma evolution, 127
- Granular temperature, definition, 601
- Grass
  - colonization of new volcanic habitats, 1072, 1079, 1081
  - volcanic survival, 1060–1063
- Gravity monitoring
  - absolute gravity, 1132–1133
  - Campi Flegrei monitoring, 1133–1134
  - Earth tides, 1131, 1177
  - Etna monitoring, 1134–1135, 1176–1177
  - gravimeters, 1121, 1130–1131
  - microgravity, 1121, 1131–1135
  - overview, 1170
  - Poas monitoring, 1134
  - principles, 1129
- Greek mythology, volcanoes, 19
- Greenhouse gas, definition, 931
- Greenhouse warming
  - definition, 1083
  - gases, 1088–1089
- Grignon, Pierre Clement, views of volcanoes, 25
- Ground deformation monitoring
  - Colima monitoring, 1128
  - combination with other techniques, 1140–1141
  - conventional ground surveying, 1123–1124
  - dry tilt technique, 1125
  - electronic distance measurement, 1123
  - Global Positioning System, 1122–1124, 1141
  - Krafla eruption of 1978, 1126–1128
  - Mogi model, 1126
  - Mount Etna, 1175–1176
  - Mount St. Helens eruption of 1980, 1128–1129
  - overview, 1169
  - precision leveling, 1123
  - principles, 1122–1123
  - Sakurajima eruption of 1914, 1126
  - synthetic aperture radar interferometry, 1122–1124, 1141
  - tiltmeters, 1126

Guild, definition, 1057
Guyot
  definition, 395
  formation, 395
GVN, *see* Global Volcanism Network

H

Hagen–Poiseuille law, magma ascent calculation, 213
Haleakala, tourism, 1288–1289
Half-life, definition, 803
Hall, James, views of volcanoes, 26–27
Harker, Alfred, contributions to decompression melting, 30
Harzburgite, definition, 897
Hawaian eruption, *see also* Scoria cone
  bubble growth and magma fragmentation, 323–324
  definition, 321, 447
  degassing, 453–454
  deposition features, 452
  magma reservoirs and conduits, 455–456
  models, 458–460
  overview, 447–448
  paintings, 1331–1332
  products, 451–452
  style of eruption, 448–451
  transition to Strombolian eruption, 448, 460
  tremor sources, 456–458
  two-phase flow, 454–455
Hazard, *see also specific hazards*
  assessment in crisis management, 1201
  characteristics pertinent to risk, 1217–1218
  definition, 957–959, 997, 1185, 1215
  education, *see* Education, volcano risks
  injury agents, 1036–1037
  maps, 945, 1186, 1189–1190
  vulnerability, 1199, 1201–1203, 1215
Heat loss, mechanisms for intrusive rocks, 898
Heliophilous
  definition, 1057
  plant colonization of new volcanic habitats, 1069
Helium
  diffuse flank degassing, 814
  isotopic analysis, 807
  ratio with other gases, 807–808
Hell, volcanic legends, 18–19
Hemispheric flow, definition, 527
Henry's law, distribution of neutral species between liquid and vapor, 869
Herbivore, definition, 1057
Hesperian epoch, Mars, 771, 773, 781–782
HFSE, *see* High field strength element
High field strength element (HFSE), definition, 115
Holmes, Arthur, contributions to convection, 31–32
Homosphere, definition, 933
Hooke, Robert, views of volcanoes, 22
Hot spot, *see also* Mantle plume
  definition, 271, 345
  definition, 383
  flood basalt provinces, 347–348, 355, 357
  Io, 709, 719–721
  large igneous provinces, 274–275
  magma origins, 7
  seamounts, *see* Seamount
  seismic movement, 53
Hot spot volcano
  characteristics, 255
  definition, 89, 93, 803
Hot spring, *see* Geothermal system
Human sacrifice, volcanoes, 18–19
Humus, definition, 1259
Hutton, James, views of volcanoes, 25–26
Hyaloclastite
  ancient examples, 374–377
  definition, 361, 371, 383
  eruption depth dependence, 380
  formation, 371
  geographic distribution, 371–374
  pelagic sediment in production, 374
  present seafloor examples, 371–374
  rhyolitic hyaloclastites, 378
Hydrochloric acid
  Fourier transform infrared spectrometry, 1153
  hazards, 1003
  toxicity, 998, 1001
Hydroclastic, definition, 627
Hydroclastic rock
  definition, 361, 371
  formation, 371
Hydrogen, diffuse flank degassing, 814
Hydrogen fluoride, hazards, 1003
Hydrogen sufide
  equilibrium in formation, 805–806, 886
  geothermal systems in power utilization, 833
  hazards, 1002–1003
  toxicity, 998, 1000
Hydromagmatic eruption, definition, 1005
Hydrosphere, definition, 857
Hydrothermal activity, midocean ridge volcanos, 5
Hydrothermal alteration, definition, 835
Hydrothermal plume, definition, 857
Hydrothermal system, *see also* Submarine hydrothermal vent
  chemical reactions
    chemical gradients, 866
    fluid sampling, 865–866
    magnesium metasomatism, 857, 867
    microbes, 868
    midocean ridge basalt systems, 867–868, 871–872
    reaction zone, 867
    recharge zone, 865
    seamounts, 871–872
  components, 859
  cyclic sealing at Galeras, 812–813
  definition, 803, 835–836, 897
  gases, 808
  phase separation, 868–869, 871, 874
  reaction zone, 863–864
  recharge zone, 859, 863
  site locations, 858–862
  upflow zone, 863–865
  volcanic activity effects, 872–874
  volcanic–hydrothermal system, 836
Hydrovolcanic eruption, *see also* Scoria cone
  biological effects, 873–874
  definition, 683
  deposit features, 686–687
  particle features, 685
Hyoclastite breccia, definition, 403
Hypabyssal intrusive complex
  ancient complexes, 378, 380
  definition, 361
  intrasediment extrusion, 378
Hyperconcentrated flow, *see also* Lahar
  definition, 601, 973
  deposits, 610–614
  downstream processes, 605–610

Hyperconcentrated flow (*continued*)
  formation, 603, 605
  physical modeling, 614–615
Hypocenter
  definition, 207
  migration and magma ascent, 213–214

I

Icelandite, definition, 771
Iconography, definition, 1315
Igneous rock
  definition, 697
  porphyry, *see* Porphyry
Ignimbrite
  alteration and cementation, 596
  areal distribution, 583
  caldera shields, 657
  carrying distance of clasts, 585
  compaction and reworking, 595–596
  composition and componentry, 584
  definition, 271, 643
  eruption column collapse in formation, 596–597
  facies variations
    lithic breccias, 590
    local variations, 588–589
    regional variations, 587–588
  grain size, texture, and structure
    distribution of sizes, 584–585
    flow units for texture
      layer 1, 586
      layer 2, 586–587
      layer 3, 587
  source vents, 595
  valley-ponded ignimbrite, 588
  veneer deposit, 588
  welded ignimbrites
    cooling units, 591
    large-scale features, 591
    lithophysae, 591
    rheomorphism, 590–592
    small-scale features, 590–591
    temperature, 590
Iherzolite, definition, 897
Ilmenite, definition, 697
Ilopango, eruption effects on Maya cultural development, 1308–1309
Imaginal distress, definition, 1229
Immiscible liquids
  definition, 149
  magma, 157
Impact, extraterrestrial
  calculation of heat generation, 65
  crater properties, 65
  dark hallow crater, 697
  flood basalt correlation with mass extinction, 1090, 1090
  heating of Earth interior, 51, 134
Impressionism, definition, 1315
Impulse wave, definition, 1005
Inceptisol, definition, 1259–1260
Inclination, orbit, 785
Incompatible element
  basaltic magmas, 123–125
  definition, 115
Incompatible trace element, definition, 89
Infrared interferometer spectrometer (IRIS), Voyager, 709, 711, 718–720
Insurance, volcano risks, 1215, 1226
Intensity, eruptions
  calculation, 263–264
  definition, 477
  distribution of values in historic eruptions, 265–266
  magnitude relationship, 267
  plume height correlation, 266
Intermediate lava, definition, 957
Internal combustion, historic view of volcanoes, 20–21
Intervention, definition, 1229
Intracontinental volcano, characteristics, 255
Intraplate seamounts, *see* Seamount
Intrusion, definition, 643
Invertebrate, *see also* Arthropod
  colonization of new volcanic habitats, 1074–1075
  definition, 1057
Io, volcano activity
  active centers, 714–715
  atmosphere composition, 724–725
  discovery, 710–711
  explorations, 710–712, 725–726
  global distribution, 723
  heat flow, 712
  hot spot temperatures and magma composition, 719–721
  moon features, 710
  mountain origins, 717
  overview, 7
  plumes, 723–724
  surface
    changes over time, 717
    colors, 717–718
    composition, 718–719
    expressions of volcanism, 712–713, 715, 717
  temporal variability, 721–723
  torus, 725
IRIS, *see* Infrared interferometer spectrometer
Iron, hydrothermic release impact on biota, 1089
Isentropic process
  definition, 55
  mantle melting, 60
Island arc, *see also* Arc
  basalt composition and formation, 121–122
  basaltic magma volatile abundance, 160–161
  definition, 103, 627
  seamounts, *see* Seamount
  sediments
    drilling observations, 633, 641
    early intra-arc rift, 635–636
    evolution of depositional environments, 629
    facies evolution
      basin maturity, 640–641
      early basin spreading, 640
      initial arc rifting, 638, 640
      old age, 641
    forearc, 633–635
    mature marginal basin, 637–638
    overview, 627–628
    sources
      backarc, 632
      subaerial arc, 629–630, 632
      submarine arc, 632
    young marginal basin, 636–637
  structural elements for deposition, 628–629
Isobaric entropy, melting reaction, 61
Isopatch, definition, 555
Isopleth, definition, 555
Isostasy
  definition, 89, 803, 1045
  volcanic gas analysis, 806–807
  volcanic lake analysis, 887–888
Ito-oki eruption of 1989, seismic activity, 1109, 1112

J

Joe Versus the Volcano, volcano depiction in film, 1356–1357
Jökuhlhlaup
  characteristics, 975–976
  definition, 403, 973
  hazards, *see* Lahar

  Vatnajökull ice cap eruption, 406
Jorden, Edward, views of volcanoes, 22
Journey to the Center of the Earth, volcano depiction in literature, 1339, 1344–1345
Juan of Paricutin, volcano depiction in literature, 1339, 1354–1355
Jupiter moons, *see also* Io
  cryovolcanism
    Europa, 796–799
    Ganymede, 796
  explorations, 796, 800
  physical properties, 786
Jurassic period, definition, 1083
Juvenile clast
  definition, 383, 463
  fragmentation product, 427
  pyroclastic fall deposit
    morphology, 567
    vesicularity, 567–568
  vulcanian eruptions, 470
Juvenile gas, definition, 1045

K

Katmai, caldera, 646
Kelut lake
  containment, 984–985
  expulsion, 982–983
Kelvin–Helmholtz instability
  definition, 431
  phreatomagmatic fragmentation, 440–441
Kick 'em Jenny, tsunami, 1007–1008
Kilauea
  caldera, 646–647
  eruption of 1924, 503–504
  paintings, 1331–1332
  religious significance, 1297
  seismic activity in eruption of 1983, 1109
  tourism, 1289
Kilimanjaro, tourism, 1291
Kimberlite
  definition, 41, 45, 207, 897
  pressure, 46
  xenolith transport, magma ascent rate estimation, 214–215
King, Clarence, contributions to decompression melting, 30
Kipuka
  definition, 1057
  local survival, 1061
Kozeny-Carman equation, permeability modeling, 73–74
Krafla eruption of 1978, ground deformation monitoring, 1126–1128
Krakatau
  Anak Krakatau, biota assembly, 1075–1077, 1079–1080
  caldera, 646, 661
  eruption of 1883
    biotic reassembly, 1069–1071
    tsunami, 1006, 1010–1011
KREEP
  basalt accumulation, 699, 705
  definition, 697
  lunar basalts, 699, 705
K/T boundary
  definition, 1083
  mass extinction, 1084, 1086, 1090
Kudriavy, gas analysis, 809–810
Kuwae eruption of 1453, climate effects, 932–933

L

Lahar, *see also* Debris flow; Hyperconcentrated flow; Jökuhlhlaup
  definition, 602–603, 973, 1301
  deposits
    apparent bulking factor estimation, 613–614
    characteristics
      debris-flow deposits, 610–612
      hyperconcentrated-flow deposits, 612–613
      overview, 610
    distinguishing from other deposits, 614
  downstream processes
    bulking in transformation, 606, 609–610
    deposition, 609
    dilution and transformation, 607–608
    erosion, 605–606
    particle segregation, 606–607
  examples, 602
  formation
    collapse induction, 603, 605
    rains, floods, or melts, 603
    requirements, 603
  hazards, 602
    causes of death and injury, 1039
    channelized debris flows, 976, 978, 980–981
    heat, 981–982
    hyperconcentrated streamflows, 976
    jökuhlhlaups, 975–976
    Kelut lake
      containment, 984–985
      expulsion, 982–983
    mitigation
      monitoring, 993–994
      old deposit recognition, 991, 993
      path delineation, 993
      structural measures, 994–995
      temporary refuge, 995
    Nevado del Ruiz eruption of 1985
      Armero destruction and lack of mitigation, 986–987
      snowmelt eruption, 984–985
    overbank debris flows, 982
    Pinatubo eruption of 1991
      lake breakouts, 987, 989
      mitigation engineering, 989–990
      mortality, 987
      prediction of crisis end, 990–991
  historic examples, 974–975
  noise, 974, 981
  ocean discharge, 630
  physical modeling, 614–615
  risk reduction, 1221–1222
  seismic features, 1021, 1102, 1173
  volcanic lake hazards, 890–891
  warnings, 1187
Lakagígar eruption of 1783
  gas hazards, 1058–1059
  lava flow, 960
Lake, volcanic
  active crater lakes
    acidity, 886–887
    box modeling of dynamic processes, 882, 884–885
    carbon dioxide bubbling, 887
    degassing volcano effects, 885
    heat and water transfer, 882, 884–886
    isotope analysis, 887
    sulfur equilibria, 886
  biotic diversity, 882
  chemical composition, 882–883, 886–887
  color, 882
  dormant crater lakes

Lake, volcanic (*continued*)
    calderas, 887–888
    gas-rich lakes, 888–889
    geothermal area lakes, 888
  geographic distribution, 877–880
  hazards
    base surge, 890
    fatalities, 877, 881, 890
    gas release, 891
    hydrovolcanic eruption, 890
    Kelut lake
      containment, 984–985
      expulsion, 982–983
    lahars, 890–891
    toxic water release, 891
    tsunami, 890
  lava lake, *see* Lava
  mineralization
    liquid sulfur, 889
    ore formation, 890
  mitigation
    artificial degassing, 894, 1224
    drainage, 893–894
  monitoring
    acoustic survey, 893
    magnesium/chlorine ratio, 892–893
    pH, 892
    polythionates, 892
    temperature and lake level, 891–892
    visual observation, 891
  rationale for study, 877
  thermal regime, 882
  tsunamis, 890, 1008–1009
  volcanic settings, 881–882
Laminar flow
  definition, 237
  modeling, 221, 234, 243–244
Lamprolite, definition, 897
Landscape painting, history, 1316, 1319–1321
Landslide, seismic features, 1021, 1100, 1102
Lapilli
  accretionary, 495, 501, 513, 520–521, 683
  armored, 495, 683
  definition, 321
  phreatomagmatic eruptions, 501
  phreatoplinian eruptions, 517–518, 520–521
  pipes, 586
  pseudo-ballistic, 495, 502
Large igneous province (LIP)
  carbon dioxide outgassing, 1054
  definition, 271, 274
  episodicity of volcanism, 274–275
  geographic distribution, 274
Large ion lithophile element (LILE)
  basaltic magmas, 125
  definition, 115
The Last Days of Pompeii, volcano depiction in literature, 1340–1343
Latent heat
  condensation, 527
  crystallization, 133
  melting, 133
Lateral blast
  definition, 945
  pyroclastic flow origination, 946
Lava, *see also* Lobate lava; Pillow lava; Submarine lava
  definition, 219, 291, 697
  moon, *see* Moon
  rationale for study, 291–292
Lava channel, *see also* Canali
  definition, 697
  moon, 705
Lava dome
  collapse, 308–310
  cryptodome, 307, 311
  definition, 292, 307, 463, 697, 957
  degassing mechanisms, 316–317
  endogenic growth, 307
  exogenic growth, 307
  explosive versus effusive behavior, transitions, 316
  features, 307–308
  flow bands, 316
  geophysical and geodetic studies, 317
  joints, 316
  mortality, 308
  rationale for study, 308–309
  Soufriere Hills volcano, growth monitoring
    acceleration, 1180–1181
    high growth rate, 1181–1182
  surface features
    blocks, 312–313
    compressional ridges, 314–315
    crease structures, 312, 315
    explosion pits, 314
    vesicular lava textures, 313–314
  tectonic stress orientation indicators, 317–318
  thermal signature, 1162
  tools for study, 309
  types, 310–311
Lava flow *see also* Aa lava flow; Blocky lava flow; Pahoehoe lava flow; Turbulent lava flow
  aspect ratio, 960
  channeling and tubing, 292–293, 297
  colonization of new volcanic habitats, 1067
  composition and behavior, 961–962
  crustal growth, 293–294
  definition, 291–292, 957
  evolution of types, 298–299
  field features, 957, 959–960
  hazards
    avoidance, 957–958
    examples of eruptions, 958
    explosions, 964–965, 967
    fast-moving flows, 963–964
    gas release, 964
    intermediate and silicic flows, 966–968
    lahars, 965–966
    Lakagígar eruption of 1783, 960
    landslides, 966
    mafic lava, 962–966
    mitigation
      control by diversion or slowing, 969–971
      history, 968–970
      identification of hazard, 968–969
      informing of hazards, 971
      monitoring volcano status, 969
  interior features, 294–295
  lengthening dynamics, 299–300
  margin shapes, 301
  physical properties by composition, 294
  planetary development role, 304–305
  risk reduction, 1220
  structures, 292–293
  typical features, 292–293
Lava fountain, *see also* Explosive eruption
  agglutination, 324–327
  bubble growth and magma fragmentation, 323–324
  collapse, 709
  definition, 321, 447
  generation mechanisms at Izu-Oshima, 327
  structure
    fountains, 324
    products, 326–327
  two-phase flow, 454–455

  volatiles, role in production, 322–323
  welding, 324–326
Lava lake, thermal signature, 1162
Lava pond
  definition, 447
  Hawaiian and Strombolian eruptions, 451
Lava shield volcano
  definition, 283
  features, 284–285
  lava flow types, 285
  lava lakes, 285–286
  types, 284–285
Lava tube
  definition, 697
  thermal signature, 1163–1164
Legume, definition, 1057
Lightning, eruption correlation, 1172
LILE, *see* Large ion lithophile element
Limu fragment
  definition, 361
  hyaloclastites, 372
LIP, *see* Large igneous province
Liquid limit, definition, 1260
Liquidus
  definition, 41, 55, 133
  mantle melting, 60, 65
  values for natural melts, 176
Literature, volcano depiction
  juvenile fiction and comics, 1353–1355
  overview, 1339–1340
  pre-20th century novels, 1340–1345
  20th century novels, 1345–1353
Lithic fragment, definition, 1143
Lithosphere
  definition, 41, 89, 133, 345, 857
  effects on volcanism, 111–112
  flood basalt eruptions, 358
  plume effects, 109
  structure, 90
Lithostatic pressure
  definition, 219
  depth distribution, 228
  magmatic flow driving, 228–229
Littoral, definition, 957
Lobate lava
  definition, 361
  physical characteristics, 367–368
  pillow lava similarities, 367–369
Long Island, biotic reassembly, 1068–1069
Long Valley, warning and crisis management, 1195–1196
Low-velocity zone
  definition, 41, 43
  temperature, 43

M

Maar
  characteristics, 684
  morphology, 689
  surge deposits, 686–687
  tectonic settings, 691
  xenoliths, 692
Macrobiota, definition, 1057
Mafic, definition, 698
Mafic lava
  definition, 957
  hazards, 962–966
  ultramafic lava on Io, 720
Mafic rock, definition, 115
Magma
  assimilation, *see* Assimilation, magma
  composition
    basaltic magmas, 119–125
    element classification, 116–118
    silicic magmas, 125–128
    variation
      overview, 173
      representation, 136–137
  convergent plate boundaries, 103–104
  cryomagma, *see* Cryovolcanism
  crystallization, 193
  definition, 41, 116, 133, 149, 171, 173, 219, 345, 361, 643, 698, 1058
  degassing, *see* Degassing
  divergent plate boundaries, 99–100
  dynamic properties, 507–508
  flow, *see* Dike; Magma ascent
  fracturing, melt localization and flow focusing, 84–85
  global rate of production, 135
  history of study, 34–35
  intraplate volcanism, 107–109
  intrinsic properties, 506–507
  length scales, 174
  mixing, 134, 142, 146–147
  ocean, 698
  origins
    midocean ridges, 138–140
    subduction zones, 142–144
  plate tectonic effects
    composition, 110–111
    generation, 93–94
  primary magma, 89, 134, 137–138
  quenching, 361
  rheology, 171
  thermodynamic properties
    density and equation of state, 175–178
    enthalpy, 178–179
    entropy, 178
    heat capacity, 179
    model development, 188
    overview, 174–175
  time scales, 174
  transport properties
    diffusion, 186–188
    magma viscosity, 183–185
    melt viscosity, 181–183
    overview, 172–173, 179, 181
    thermal conductivity, 185
  variables influencing volcanic processes
    overview, 8
    viscosity, 9
    water content, 9
  viscosity, *see* Viscosity
  volatiles, *see* Volatiles
Magma ascent
  crystallization, 507
  degassing, 208–210
  factors affecting rate
    crystallization, 208, 210–211
    overview, 207–208
    volatiles and degassing, 208–210, 238–240
  flow dynamics at shallow levels
    annular flow, 231
    bubbly flow, 241
    bulk flow conditions, 241–242
    slug flow, 241
    viscosity effects, 240
  flow regimes, 237
  mass discharge rate at shallow levels
    calculation, 242
    conduit geometry effects, 243
    degassing model, 244–245
    driving pressure, 242–243
    laminar flow modeling, 243–244
    postfragmentation events, 245
  modeling, 425
  phenocryst-melt reactions, 211–213
  pressure changes, 238
  rate estimation
    calculation from mass eruption rate, 213
    hypocenter migration, 213–214
    overview, 208, 216–217
    U-Th isotopic series disequilibrium, 216

Magma ascent (*continued*)
    xenoliths
        magma reactions, 215
        transport, 214–215
    source and reservoir determination, 208–209
    Venus, 766–767
Magma chamber
    calderas, 651–652
    definition, 643
    differentiation processes
        chemical fractionation effects, 200
        compaction, 200
        mush flow fractionation, 198–199
        overview, 197–198
        reprocessing, 199
        silicic segregation, 198
    heat content, 820–821
    heat flow, 821
    mush column
        features, 203–204
        geophysical detection, 204–205
        igneous diversity and bimodality, 205
    outer core of Earth, 192
    pluton formation and chamber evolution, 202–203
    pluton studies of processes, 200–202
    seismic features, 1027–1028, 1030, 1032
    volumes, 193
Magma discharge rate (MDR), plinian and subplinian eruptions, 480, 484–486, 488–493
Magma fragmentation, *see* Fragmentation
Magmastatic, definition, 219
Magmatic center
    definition, 728
    radial fracture center, 728
Magnesium/chlorine ratio, volcanic lake monitoring, 892–893
Magnesium metasomatism, definition, 857, 867
Magnetic monitoring
    Aso monitoring, 1139–1140
    measurement techniques, 1137–1138
    Mount Etna self-potential in magnetic monitoring, 1177–1178
    Mount St. Helens eruption of 1980, 1138–1139
    overview, 1170
    principles, 1135–1137
    sources of magnetism, 1136–1137
    White Island eruption of 1974, 1139
Magnitude, earthquakes, 1015, 1017
Magnitude, eruptions
    calculation, 263–264
    definition, 1, 477
    distribution of values in historic eruptions, 265–266
    intensity relationship, 267
Major element, definition, 857
Mallet, Robert, contributions to plate tectonics, 32
Manifestation
    definition, 836
    geothermal systems, *see* Geothermal system
Mantle
    adiabats, 66–67
    core boundary, 53
    cosmochemistry, 48–49
    definition, 134, 345, 698
    heat
        sources, 51–52
        transfer, 49–51
    melting, *see* Melting, mantle
    mineralogy, 44–49
    structure, 42–44
    temperature, 49–51
    viscosity, 50–51
Mantle plume
    core–mantle boundary, 53
    definition, 89, 108, 271, 345
    flood basalt province sources, 355–356, 358
    intraplate volcanism, 107–109
    lithosphere effects, 109
    mantle decompression, 93
    melt production rates, 275–276
    mineral deposition processes, 899
    ocean island basalt origin, 120–121
    origin, 53
Margin basin
    definition, 627
    island arc deposits
        mature marginal basin, 637–638
        young marginal basin, 636–637
Maria, definition, 698
Mars, volcanic activity
    calderas, 775
    comparison with Earth activity, 772
    composition analysis, 780–781
    distribution, 772–774
    epochs, 773, 781–782
    explorations, 772–774, 780–782
    large central volcanoes, 774–776
    patera, 775–778
    plains, 779–780
    small constructs, 778–779
    SNC meteorites, 771, 781
    tholus, 776
Mass eruption rate (MER)
    definition, 1
    eruption column correlation, 8–9
    estimation with C-band radar, 1157
    intensity scale, 263–264
    magma ascent rate calculation, 213
    magnitude correlation, 8
Mass extinction
    acid rain, 1089
    climate cooling, 1086–1088
    correlation with flood basalt eruptions
        climate cooling, 1086–1088
        continental flood basalts, 1084–1086
        extraterrestrial impact correlation, 1090
        lava flow rate, 1086
    definition, 1083
    greenhouse warming, 1088–1089
MCR, *see* Mechanical conversion ratio
MDR, *see* Magma discharge rate
Mechanical conversion ratio (MCR)
    efficiency, 442
    water-to-melt mass ratio correlation, 436
Megamullion, formation, 100
Melt fraction, strength correlation, 80–81
Melt inclusion
    definition, 149
    volatiles, analysis in magma, 155
Melting, mantle, *see also* Decompression melting; Magma
    causes, 52, 66
    composition and solidus dependence, 56, 63–65
    crystal–melt reactions in control, 138–140
    frictional heating and viscous dissipation, 66
    heat generation, 31, 51–52, 66
    pressure dependence, 56, 135
    radioactivity
    temperature dependence, 56, 65–66, 135
    thermodynamic theory, 56–63
Melt migration
    matrix mechanical property dependence, 78–81
    melt localization and flow focusing, 81–86

  permeability dependence, 72–78
  porous flow model, 69–71
  viscosity dependence, 71–72
Melt reaction coefficient, definition, 134
Melt viscosity, *see* Viscosity
MER, *see* Mass eruption rate
Metaluminous rock, definition, 115
Metasomatism, definition, 172
Metis Shoal, seamount emergence, 394
Mg#
  calculation, 136–137
  midocean ridge basalt, 141
Microgravity
  definition, 1121
  gravity monitoring, 1131–1135
  network, 1121
Microphysics
  aerosols, 936
  definition, 931
Microsite, definition, 1058
Midocean ridge
  axial morphologies, 95–96
  episodicity of volcanism, 272–273
  fast-spreading ridges, 97–98, 100
  formation, 94
  heat transfer, 50
  hydrothermal circulation, 5
  hydrothermal systems, *see* Hydrothermal system
  intermediate-spreading ridges, 98–99
  intrusion versus extrusion of rock, 95
  magma production, 135, 138–140
  mineral deposition processes, 899
  neovolcanic zone, 95
  off-axis volcanism, 100–102
  plate growth rate, 272–273
  seamounts, *see* Seamount
  slow-spreading ridges, 96–97
  structure, 94–95
  subduction, 106–107, 272–273
  volcanic activity, 4–5
  volcano characteristics, 255
Midocean ridge basalt
  composition, 81, 99, 121, 123–125, 141
  definition, 345, 803, 857
  isotopic analysis of helium, 807
  oceanic flood basalts, 356
Migration, *see* Melt migration
Minoan civilization, *see* Akrotiri
Miranda, *see* Uranus moons
Mixing ratio, definition, 931
Moho, definition, 41
Mollisol, definition, 1260
Molybdenum, *see* Porphyry
Monitor, lizard colonization of new volcanic habitats, 1058, 1070
Monitoring, *see also specific volcanoes*
  artificial neural networks in data analysis, 1184
  automatic detection and processing of data, 1184
  comparison with medicine, 1168, 1183
  continuous recording of data, 1183–1184
  crisis management
    critical phase, 1207–1209
    pre-event, 1203–1204
  effusive eruptions, 1172
  explosive eruptions, 1171–1172
  gas monitoring, *see* Gas
  goals, 1096, 1167–1168
  gravity, *see* Gravity monitoring
  ground deformation, *see* Ground deformation monitoring
  Internet communications, 1183
  intrusions versus eruptions, 1183
  magnetic monitoring, *see* Magnetic monitoring
  posteruption monitoring, 1172–1173
  preruption monitoring, 1170–1171
  seismic monitoring, *see* Earthquake
  synthesis of data from various sources, 1168, 1182
  threshold setting, 1182–1183
Monogenetic volcano
  definition, 283, 331
  flow field features, 286–287
Mons, definition, 771
Montmorillinite, definition, 1271
Montserrat, *see* Soufriere Hills volcano
Moon
  evolution of mare volcanism
    early phase, 706
    late phase, 707–708
    main phase, 706–707
  lava flows, 701–703
  mare basalts
    composition, 700–701
    discovery, 698–699
    origin, 699–700
  nonmare volcanism, 705
  pyroclasts, 703–704
  search for volcanic activity, 7, 698
  sinous rilles, 704–705
Mortality
  causes of death and injury
    explosions, 1039–1040
    gases, 1041–1042
    lahars, 1039
    pyroclastic flow, 1037–1039
    pyroclastic surge, 1037–1039
    tephra fall, 1040–1041
  volcano-related mortality between 1600 and 1986, 921–922, 1037
  volcanoes versus other natural disasters, 9–10
Motmot, biota assembly, 1074–1075, 1078
Mount Etna
  climate effects, 932
  eruption of 44 B.C.
  fractures, 1173–1174
  gas monitoring, 1178
  gravity monitoring, 1134–1135, 1176–1177
  ground deformation monitoring, 1175–1176
  human activity, 1173
  monitoring
    Earth tides, 1177
    gases, 1178
    gravity, 1176–1177
    ground deformation, 1175–1176
    radar, 1178–1179
    seismology, 1174–1175
    self-potential in magnetic monitoring, 1177–1178
  paintings, 1321, 1324–1325, 1330
Mount Hood, tourism, 1292
Mount Pelée eruption of 1902, pyroclastic flow and surge, 948
Mount Pinatubo, *see* Pinatubo
Mount Ranier
  archeology, 1309–1310
  education initiatives, 12322
  tourism, 1292
Mount Spurr eruption of 1992, seismic activity, 1030–1031
Mount St. Helens
  biosystem effects, 1061–1062
  eruption of 1980
    field observation, 482–484
    gas analysis, 810
    ground deformation monitoring, 1128–1129
    seismic activity, 1030, 1109
    warning and crisis management, 1192–1193
  lava dome studies, 317
  magma ascent, 211, 213

Mount St. Helens (*continued*)
  paintings, 1329–1330, 1335
  tourism, 1289–1290, 1292
  Y tephra in archeology, 1310–1311
Movies, *see* Film
Mud
  definition, 974
  lump, 513
  rain, 513
Muddy streamflow, definition, 602–603
Mudflow
  definition, 973–974, 1301
  hazards, *see* Lahar
Multiple gating, definition, 1229
Mush column
  features, 203–204
  geophysical detection, 204–205
  igneous diversity and bimodality, 205
Mush zone
  definition, 191, 194
  flow fractionation, 198–199
Myojinsho
  eruption of 1952–1953, 500–501
  seamount emergence, 394–395
Mythology, *see* Geomythology

N

National park, establishment and tourism, 1286–1288
Neck
  definition, 191
  features, 192
Necrotizing fasciitis
  definition, 1035
  lahar association, 1039
Neoclassicism
  definition, 1315
  Pompeii paintings, 1325–1326
Neolithic, definition, 1301
Neovolcanic zone, definition, 89, 95
Nephelenite, definition, 345
Neptune moon, *see* Triton
Neptunist
  beliefs, 24–25
  definition, 15
Neuropteran, definition, 1058
Neutral buoyancy level
  definition, 527
  plume umbrella region formation, 532
Nevado del Ruiz eruption of 1985
  lahar hazards
    Armero destruction and lack of mitigation, 986–987
    snowmelt eruption, 984–985
  warning and crisis management, 1235–1236
News media
  communication of warnings, 1191, 1211–1212
  education of public, 1230–1231
Newton, Isaac, views of volcanoes, 22–23
Newtonian fluid
  definition, 207
  magma modeling, 213
Ngauruhoe, vulcanian eruption, 464–466
Nickel sulfide deposits, komatiitic lava
  characteristics, 909–910
  distribution and age, 908–909
  origin, 910
  significance, 908
Nitrogen
  fixation, 1058, 1064
  ratio with other volcanic gases, 807–808
  sources in new volcanic habitats, 1063–1064
Noachian epoch, Mars, 771, 773, 781–782
Noncrystalline mineral, definition, 1260
Nucleation, definition, 931–932

O

Obsidian
  definition, 15, 1271
  prehistoric uses, 1275
Ocelli, definition, 897
Ochric epipedon, definition, 1260
Off-axis volcanism
  midocean ridge, 100
  seamount formation, 101–102
  transform fault volcanism, 102
Oligocene epoch, definition, 1083
Olivine
  definition, 134, 698
  green sand beaches, 1294
  liquidus volume, 137
  melt exchange, 136–137
  pressure in formation, 139
Omnivore, definition, 1058
Ophiolite
  definition, 41, 44, 134, 857
  features, 44–45
Optical depth, definition, 932, 937
OPX, *see* Orthopyroxene
Orbital period, definition, 785
Orbital resonance, definition, 785
Ore
  definition, 897–898
  formation processes
    arcs and subduction zones, 899–900
    heat loss by intrusive rocks, 898
    mantle plumes, 899
    midocean ridges, 899
Orthopyroxene (OPX)
  definition, 134
  pressure in formation, 139
Oxisol, definition, 1260
Oxygen, aerosol effects on atmospheric chemistry, 938–939
Ozone depletion, *see also* Total ozone mapping spectrometer
  Antarctic ozone hole, 941–942
  midlatitude depletions, 942
  overview, 938–939
  Pinatubo eruption effects, 942

P

Pahoehoe lava flow
  definition, 285, 291
  diagnostic features, 295
  energy supply in formation, 299
  evolution, 298
  examples, 298
  forecasting of behavior, 304
  reversibility of formation, 299
Palagonite
  definition, 15, 403
  discovery, 37
Paracrystalline, definition, 1260
Paricutin
  paintings, 1334
  Paricutin, depiction in literature, 1347–1348
Particle cohesion
  definition, 545
  pyroclast deposit control, 549
Particle trajectory
  definition, 545
  pyroclast deposit control, 548–549
Passage zone, definition, 403, 411
Patera
  definition, 709, 728, 771
  Mars, 775–778
  Venus, 757–758

Pavlof eruption of 1996, seismic activity, 1112
PDC, *see* Pyroclastic density current
Pegmatite, definition, 116
PEL, *see* Permissible exposure limit
Pelagic sediment, hyaloclastite production, 374
Pele, religious significance, 1297–1298
Pele's tears, Hawaiian and Strombolian eruptions, 451
Peperite
  definition, 361, 383
  formation, 362
Peralkaline rock
  definition, 116
  granite, 126
Peraluminous rock
  definition, 116
  granite, 126
Peridotite
  composition, 45–47
  composition, 119
  cosmochemistry, 48–49
  definition, 1, 15, 41, 134, 898
  magma source hypothesis, 34–35
  melting, 46
  reaction coefficient variation with pressure, 139
Perlite
  commercial uses, 1278, 1281
  definition, 1271
  properties, 1278
Permanent charge, clay, 1260
Permeability
  anisotropic permeability development in deformation, 82–83
  calculation, 70
  definition, 69, 1243
  measurement, 77–78, 87
  melt migration dependence, 78–81
  melt network geometry in partially molten rocks, 74–77
  models, 73–74, 87
Permian period, definition, 1083
Permissible exposure limit (PEL), definition, 997
Petrogenesis, definition, 89, 116
Petrology, history, 33–34
Phase
  definition, 55
  mantle melting, 60
Phase separation
  definition, 857–858
  hydrothermal systems, 868–869, 871, 874
Phenocryst
  definition, 219
  fates in solidification front, 195–196
  melt reactions in magma ascent, 211–213
  phenocryst-free intrusions, 196–197
Photodissociation, definition, 1
Photolysis, definition, 785
Photosynthesis, definition, 1058
Phreatic, definition, 1301
Phreatomagmatic eruption, *see* Explosive eruption
Phreatomagmatic fragmentation
  depth, 444
  dry versus wet, 444
  eruption styles, 432–433
  evolution classification, 442
  field observation, 443–444
  fuel–coolant interaction homology, 433–434, 437–439
  global occurrence, 432–433
  grain shapes and mechanisms, 435–436, 439–441
  mechanical conversion ratio, 436, 442
  mild activity, *see* Surtseyan eruption
  overview, 507–508
  plinian eruptions, 486, 488
  rock sample experiments, 437–439
  shock wave, 442
  stages
    ejection, 442
    premixing, 441
    pressure growth, 441–442
  subplinian eruptions, 489–490
  temperature/pressure control, 442–443
  tephra characteristics, 433
  thermite experiments with water, 435–437
  types, 439–441
  viscosity control, 443
  water effects, 508–509
Phreatomagmatism, definition, 431
Phreatoplinian eruption
  accretionary lapilli, 520–521
  ash aggregation, 520–521
  definition, 524
  deposits
    processes of deposition, 521–522
    syneruptive erosion, 522–523
    types, 513, 517–519, 523
  examples
    Askja phase C eruption of 1875, 514
    Mount St. Helens, 519–520
    Taupo eruptions of 181 A.D., 515–516
    Vesuvius eruption of 79 A.D., 519, 523
  external water role, 513–514
  fragmentation
    eruption mechanisms, 520
    fragmentation index, 516–517
  graduation to other eruptive styles, 524
  numerical models, 521
  plume, 532–533
  pyroclastic density currents, 518, 520–521
  wet eruption versus wet deposition, 523
Picrite, definition, 345, 898
Picritic basalt, definition, 89
Picturesque. definition, 1315
Piecemeal disruption, caldera subsidence, 655–656
Piezomagnetic, definition, 1121
Pillow lava
  composition, 367
  crystallization, 364–365
  definition, 361, 383–384, 403
  discovery, 37
  para-pillow lava, 368–369
  physical characteristics, 364
  pillow breccia, 361, 366–367, 376–377
  pillow volcanoes, 361, 366
  shelves, 365
  spall fragmentation, 361, 367
  spreading rate, 365–366
  subglacial eruption, 410, 416
  surface features, 364
Pinatubo
  caldera, 646, 661
  lahars in eruption of 1991
    lake breakouts, 987, 989
    mitigation engineering, 989–990
    mortality, 987
    prediction of crisis end, 990–991
  pyroclastic flow and surge, 948–949
  seismic activity, 1112–1113
  tourism, 1299
  warning and crisis management, 1193–1195, 1235
Pit crater, definition, 384
Plagioclase
  definition, 134
  liquidus volume, 137
Planeze, definition, 663
Plastic limit
  definition, 1260

Plastic limit (*continued*)
  volcanic soils, 1268
Plate subsidence, calderas, 654
Plate tectonics
  convergent plate boundaries
    architecture, 102–103
    backarc basins, 105–106
    extensional versus compressional arcs, 104–105
    magmas and volcanoes, 103–104, 135
    ridge subduction, 106–107
  cooling role, 90
  cycle initiation, 4
  discovery, 32–33
  divergent plate boundaries
    faulting, 100
    magmas, 99–100
    midocean ridge volcanism, 94–99
    off-axis volcanism, 100–102
  flood basalt province implications, 356–358
  flow pattern in convecting mantle, 49–50, 90
  intraplate volcanism
    flood basalts and continental rifting, 109–110
    plumes and distribution, 107–109
  magma
    composition influence, 110–111
    generation influence, 93–94
  plate boundary
    relationship to volcanism, 91, 93
    relative volumes of magma fluxes, 94
    types, 91
  slab pull, 4
  volcano role, 3–4
Plateau basalt, *see* Flood basalt
Playfair, John, contributions to decompression melting, 28
Plinian eruption
  characteristic features, 478
  definition, 945, 1301
  deposits, 480–481, 485
  field observation
    El Chichon, 482, 484–485
    Mount St. Helens, 482–484
  fragmentation of magma, 479–480
  graduation between plinian and subplinian activity, 493
  history of classification, 477–478
  plumes, 478–479
  Vesuvius eruption of 79 A.D. reconstruction
    caldera collapse and phreatomagmatic activity, 488
    column, 486, 488
    constraints in product analysis, 491–493
    historic account, 477–478, 485–486, 531, 1036
    initial phreatomagmatic phase, 486
    product analysis, 488
Plug
  definition, 191
  features, 192
Plume
  aircraft hazards, *see* Aviation hazards
  discrete plume from single vent
    modeling of thermals, 533–534
    shallow water eruptions, 534
  dispersal, atmospheric effects
    crosswinds, 539–540
    downwind evolution, 541–543
    latitudinal control of vertical temperature profile, 540–541
    moisture, 541
  duration of formation, 527–528
  generation mechanisms
    degassing, 528
    elutriation from pyroclastic flows and surges, 528, 530
    external water interactions, 528
    fire fountaining, 530–531
  height estimation from seismic activity, 1108
  hydrothermal plume, *see* Hydrothermal plume
  Io plumes, 723–724
  maintained plumes from extended sources
    basaltic fissure eruptions, 537–539
    co-ignimbrite plumes, 527, 534, 536–537
    formation, 534, 536–537
    modeling, 537
    structure, 536
    types, 537
  mantle, *see* Mantle plume
  pyroclast transport, 546
  sustained plume from single vent
    maximum height, 532
    source, 531
    trunk, 531
    umbrella region, 532, 542
    vertical velocity, 531
    water effects, 532–533
Pluto moons
  cryovolcanism, *see* Cryovolcanism
  explorations, 800
  physical properties, 786
Pluton
  definition, 191–192, 898
  features, 192–193
  formation and chamber evolution, 202–203
  magma chamber process studies
    convection in sedimentation, 202
    layered plutons, 200–202
    thermal convection, 202
Plutonist
  beliefs, 25
  definition, 15
  experiments, 25–27
Poas, gravity monitoring, 1134
Polygenetic volcano, definition, 283
Porosity, definition, 1243
Porous flow model, melt migration, 69–71
Porphyry
  copper, molybdenum, and gold deposits
    age, 900
    characteristics, 900–902
    distribution, 900
    origin, 902
    significance, 900
    types, 900
  definition, 898
Post-traumatic stress disorder
  definition, 1229
  interventions, 1237–1239
Power input, volcano requirements, 284
Power output, distribution of values in historic eruptions, 265
Power production, geothermal systems
  available power estimation, 831, 1253–1254
  combined utilization schemes, 1248
  decline of output, 832, 1254–1255
  development, 830–831
  drilling
    casing programs, 1249–1251
    directional drilling, 1256–1257
    exploration and appraisal, 830, 1253
    purposes, 1248
    technique, 1248–1249
  efficiency, 1247–1248
  environmental and safety issues

    atmospheric pollution, 1255–1256
    ground subsidence, 1256
    overview, 832–833
    scenery impact, 1256
    waste fluid injection, 1257
    water pollution, 1256
  examples, 817–818, 1244, 1246
  exploration
    drilling, 830, 1253
    feasibility and design of plant, 1253–1254
    phases, 1251
    surface exploration, 1251–1253
    wells, 1243
  injection well, 1243, 1257
  monitoring of systems, 832, 1254
  popularity, 1244
  potential, 11, 13, 854, 1243–1244
  production well, 1243
  schemes for power generation, 831–832
  selection of system for power utilization, 1244–1246
Precursor, definition, 1095
Prediction, definition, 1095
Preparedness
  crisis management, 1201
  definition, 1199
Primary colonist, definition, 1058
Primary producer. definition, 1058
Primary succession
  colonization of new volcanic habitats, 1080
  definition, 1058
Probabilistic, definition, 1095
Productivity
  definition, 55
  mantle melting, 60–61
Proterozoic eon, definition, 1
Proton precision magnetometer, definition, 1121
Pseudocrater, definition, 771
Pumice
  commercial uses, 1277
  definition, 421, 1058, 1143, 1271–1272
  fragmentation product, 427
  prehistoric uses, 1275
  properties, 1277
Pyroclast
  boundaries between fields
    fall:flow, 551–552
    fall:surge, 550–551
    surge:flow, 552
  commercial uses, 1272–1274, 1276
  composite volcano products
    classification, 676–677
    cone-building association, 678–680
    flow direction and redistribution, 677
    main vent association, 677–678
    ring plain association, 680
    satellite vent association, 680–681
  constraints in eruption reconstruction from deposits, 491–493
  definition, 1, 321, 421, 447, 698, 709
  deposition system
    controls
      fluctuations of particle concentration, 549, 553
      particle cohesion, 549, 552–553
      particle concentration, 549
      particle trajectory, 548–549
    definition, 545
    overview, 548
  fall deposits, *see* Pyroclastic fall
  flow deposits, 550
  fragmentation product analysis, 427, 429
  moon, 703–704
  plinian eruptions, 480–481, 485
  surge deposits, *see* Pyroclastic surge
  transport systems
    overview, 545–546
    plume, *see* Plume
    pyroclastic density current, *see* Pyroclastic density current
Pyroclastic, definition, 627, 1301
Pyroclastic density current (PDC), *see also* Block-and-ash-flow deposit; Ignimbrite; Pyroclastic flow; Pyroclastic surge
  blocking, 571, 576
  classification of types, 546
  concentrated currents, 547–548
  definition, 545, 581, 583
  dilute currents, 546–547
  modeling of flow, 597–598
  phreatoplinian eruptions, 518, 520–521
  plinian and subplinian eruptions, 478, 481, 485–486, 488–489, 491, 493
  rationale for study, 599
  runout
    dense mass flows, 597–598
    dilute suspension currents, 598
Pyroclastic fall
  absolute grain size and sorting, 563–565
  agglutination, 566
  boundaries with other deposition fields, 550–552
  classification of deposits, 569
  definition, 545, 555
  dispersal index, 558–559
  eruption sources, 556
  external water flashing, 569
  features of deposits, 549–550
  fining of depositis, 559–560
  juvenile clasts
    morphology, 567
    vesicularity, 567–568
  stratification and grading in deposits, 561–563
  thinning of deposits
    controlling factors, 556–558
    rate, 556
  volume determination for deposits, 560–561
  wallrock lithic content, 568–569
  welding, 566
  whole-deposit grain size, 561
Pyroclastic flow, *see also* Block-and-ash-flow deposit; Ignimbrite
  definition, 545, 583, 643, 945, 1058, 1301
  deposits
    alteration and cementation, 596
    boundaries with other deposition fields, 551–552
    compaction and reworking, 595–596
    features, 550, 581–582
  features, 547–548
  hazards and disasters
    causes of death and injury, 1037–1039
    mitigation, 954
    Mount Pelée eruption of 1902, 948, 1059
    Mount Pinatubo eruption of 1991, 948–949
    Soufrierer Hills, 949–950
    Unzen eruption of 1991, 950–951, 953
    Vesuvius eruption of 79 A.D., 953–954
  lava dome collapse, 309
  mobility and size, 946–948
  origins, 946

- Pyroclastic flow (*continued*)
  - risk reduction, 1224
  - sea entry
    - flow–water interaction, 593, 630
    - Krakatau eruption of 1883, 593–595
  - seismic features, 1021, 1102
  - speed, 948
  - temperature, 948
- Pyroclastic surge
  - atomic bomb homology, 573
  - base surge, 571, 573
  - characteristics, 546–547, 572
  - compressible flow effects, 580
  - critical particle loading, 579–580
  - definition, 545, 571, 945, 1301–1302
  - deposits
    - bedforms, 571, 573–574, 580
    - bedset, 571
    - boundaries with other deposition fields, 550–552, 578
    - distinguishing from eolian and water-lain deposits, 578–579
    - facies variations
      - condensed water-induced variations, 577–578
      - proximal to distal variations, 575–576
      - topography-induced variations and blocking, 576–577
      - vertical variations, 577
    - features, 550, 572–573, 581
    - granulometry, 574–575
  - generation mechanisms, 572
  - hazards and disasters
    - causes of death and injury, 1037–1039
    - mitigation, 954
    - Mount Pelée eruption of 1902, 948
    - Mount Pinatubo eruption of 1991, 948–949
    - Soufrierer Hills, 949–950
    - Unzen eruption of 1991, 950–951, 953
    - Vesuvius eruption of 79 A.D., 953–954
  - hydrovolcanic eruptions, 573
  - mobility and size, 946–948
  - origins, 946
  - physical processes, 570
  - risk assessment, 580
  - speed, 948
  - temperature, 948
- Pyrolite
  - composition, 46
  - definition, 41
- Pyroxene, definition, 698

Q

- QBO, *see* Quasi-biennial oscillation
- Quasi-biennial oscillation (QBO), equatorial winds, 937

R

- Radioactive decay, heat generation, 31, 51–52, 66, 819
- Radiogenic isotope
  - applications, 128
  - argon, 167–168
  - basaltic magma analysis, 128–129
  - definition, 116
  - granite analysis, 130
  - helium, 167
  - types, 128
- Radiolysis, definition, 785
- Radiometric dating, definition, 698
- Radionuclide, definition, 1
- Radon
  - diffuse flank degassing, 814
  - fumarole emission monitoring, 1147, 1149
  - toxicity, 998, 1000, 1042
- Rare earth element
  - basaltic magmas, 125
  - definition, 116
- Rayleigh number
  - definition, 191
  - determination, 202
- Rayleigh–Taylor instability
  - definition, 431
  - phreatomagmatic fragmentation, 440–441
- Reaction channels, formation, 85–86
- Reaction rim
  - definition, 207
  - hornblende reaction rim, 211–212
- Real-time seismic amplitude measurement (RSAM), volcano forecasting, 1105–1106
- Recurrence rate, *see* Episodicity, volcanism
- Redox potential, definition, 803
- Reduced displacement, definition, 1095
- Refractory, definition, 41, 1272
- Relative Risk Index, formulation, 1219
- Remote sensing
  - definition, 1143
  - gases, 1149–1153
  - prospects, 1164–1165
- Resurfacing, definition, 785
- Reticulite
  - definition, 447
  - fragmentation product, 427
  - Hawaiian and Strombolian eruptions, 452
  - porosity, 323
- Return code, definition, 1199
- Reversible reaction
  - adiabatic processes, 56
  - definition, 55
- Reynolds number
  - bulk flow modeling, 242
  - definition, 219–220, 237, 242
- Rheology, definition, 220, 307
- Rhyolite
  - composition, 117, 125–128
  - definition, 220
  - formation, 126
  - hyaloclastites, 378
  - magma properties, 172
  - magma transport, 229–231
  - reprocessing of magma, 199
  - volatiles, abundance, 162–163
  - water in magma evolution, 127
- Rigid crust, definition, 191, 194
- Rille, definition, 698
- Ring plain
  - definition, 663
  - pyroclast association, 680
  - volcano erosion, 672
- Risk
  - acceptable risk, 1185, 1215–1217
  - analysis, 1217–1220
  - categorization of risk takers, 1216
  - definition, 957–959, 997, 1185, 1215–1216
  - education, *see* Education, volcano risks
  - identification, 1217
  - management, overview, 1215–1216, 1226
  - reduction
    - lahar, 1221–1222
    - lake degassing, 1224
    - lava flow, 1220
    - overview, 1220, 1224–1225, 1227
    - pyroclastic flow, 1224
    - tephra fall, 1222–1224
  - Relative Risk Index formulation, 1219

  tolerable risk, 1215, 1217
  transfer
    disaster relief, 1224–1226
    insurance, 1226
  warnings, 1187, 1189–1190
Ritter Island, biotic reassembly, 1069
Rockfalls, seismic features, 1021, 1102
Romans, ancient views of volcanoes, 20–21, 1312
Romanticism
  definition, 1315
  volcano paintings, 1336–1337
RSAM, *see* Real-time seismic amplitude measurement
Ruapehu eruption of 1995, postevent interventions, 1238–1240
Run up, definition, 1005

S

Sakurajima eruption of 1914
  ground deformation monitoring, 1126
  vulcanian eruption, 466
San Sebastiano, rebuilding, 291–292
Sand, definition, 1260
Santorini
  archeology, *see* Akrotiri
  caldera, 645
  eruption of 1620 B.C., climate effects, 932
SAR interferometry, *see* Synthetic aperture radar (SAR) interferometry
Satellite vent, *see* Vent
Saturation, melts, 149, 152, 164
Saturn moons
  Cassini exploration, 800
  cryovolcanism
    Dione, 796
    Enceladus, 794–795
    Tethys, 796
    Titan, 795–796
  physical properties, 786
Scavenger, definition, 1058
Scientific Event Alert Network (SEAN), 249
Scoria
  abundance, 683
  characteristics, 684
  definition, 321, 421, 447, 684, 1058
  deposit features, 685–686
  examples
    Capelinhos, 692–693
    Miyake-jima eruption, 693
    Paricutin, 693–694
  morphology and internal structure, 688–689
  particle features, 684–685
  tectonic settings
    groups and complexes, 689
    islands, 690
    rift areas and subduction zones, 690–692
Scrope, George Poullettt, contributions to volcanology, 29, 36
Seamount
  abundance, 384–385
  asperity, 384, 400–401
  biota assembly
    Anak Krakatau, 1075–1077, 1079–1080
    Motmot, 1074–1075, 1078
    Surtsey, 1072–1074, 1077
  chemical composition
    intraplate seamounts, 397
    island arc seamounts, 397–398
    midocean ridge seamounts, 397
  definition, 362, 384
  emplacement and fragmentation processes, factors affecting, 391
  endemic fauna, 401
  geographic distribution
    intraplate seamounts, 387, 389
    island arcs, 390
    midocean ridge seamounts
      fast spreading ridges, 389–390, 401
      overview, 389
      slow spreading ridges, 390, 401
    Pacific plate seamounts, 390–391
  growth stages
    deep-water stage, 391
    drilling results, 393–394
    emergent stage, 393
    erosional stage, 393
    intermediate water/shoaling stage, 392–393
    overview, 391
  historical observations of emergence, 394–395
  hydrothermal activity
    hot spot seamounts on active spreading centers, 398
    intraplate hot spot seamounts, 398–399
    island arc seamounts, 399
  hydrothermal chemistry, 871–872
  lithosphere load, 399
  oceanic crust formation, 399–400
  off-axis volcanism in formation, 101–102
  plate techtonic implications, 399
  size and morphology
    craters, 386
    factors affecting, 386
    intraplate and midocean ridge seamounts, 386
    island arc seamounts, 386–387
    mapping, 386
    nonvolcanic seamounts, 387
  types, 384
  upper mantle composition, 400
SEAN, *see* Scientific Event Alert Network
Sector collapse
  debris avalanche production, 617–618
  definition, 617
Sedimentation, definition, 932
Seiche, definition, 1005
Seismic monitoring, *see* Earthquake
Seismic network
  data analysis, 1097–1098
  definition, 1095
Seismic spectral amplitude measurement (SSAM), volcano forecasting, 1105–1106
Seismic station, definition, 1095
Shape, volcanoes, 250–252
Shasta
  religious significance, 1297
  tourism, 1292
Shear stress, resistance in lahar modeling, 614–615
Sheet flow
  characteristics, 369–370
  definition, 361
Shield field
  definition, 728
  Venus, 768
Shield volcano, definition, 698, 771
Shock wave
  definition, 463
  fragmentation induction, 507
  vulcanian eruptions, 466–467, 471
Sideromelane
  definition, 15, 384, 495
  discovery, 37
Silicate, definition, 41
Silicic lava, definition, 957
Silicosis, definition, 1035
Sill
  definition, 191
  features, 192
Silt, definition, 1260
Silver deposits
  characteristics, 903

Silver deposits (*continued*)
  distribution and age, 903
  origin, 903–904
  significance, 902–903
  types, 903
Sinous rille
  definition, 698
  moon, 704–705
Slab
  definition, 90
  rollback, 105
The Sleeper of the Moonlight Ranges, volcano depiction in literature, 1347
Slug flow
  definition, 226, 237, 447
  magma ascent at shallow levels, 241
SNC meteorites, compositional analysis of Mars, 771, 781
Soil, volcanic
  agriculture and civilization impact, 1268–1269, 1272
  charge, 1267
  classification, 1262–1263
  climate role in formation, 1263–1264
  general features, 1260–1261, 1265
  geographic distribution, 1261–1262
  mineralogy, 1265–1267
  morphology, 1265
  parent materials, 1263
  physical properties, 1268
  time of formation, 1264
  topography, 1264
  vegetation, 1264
Solfatara, *see* Geothermal system
Solid Earth theory, historical view, 27–28
Solidification front
  chemical fractionation effects, 200
  crystal fractionation, 197
  definition, 191
  divisions, 194
  features, 194–195
  formation, 193
  instability and silicic segregation, 198
  phenocryst fates, 195–196
Solids concentration
  definition, 545
  pyroclast deposition effects, 549, 553
Solid-state greenhouse, definition, 785
Solid-state imaging (SSI), Galileo imaging of Io, 709, 712, 719
Solidus
  composition and melting dependence, 56, 63–65
  composition dependence, 56
  definition, 41, 55, 116, 134
  mantle adiabat intersections, 67
  slope from Clausius-Clapeyron equation, 60
Soufriere Hills
  monitoring
    dome growth
      acceleration, 1180–1181
      high growth rate, 1181–1182
    early activity, 1179–1180
    seismology, 1179
  pyroclastic flow and surge, 949–950
Spall dome
  definition, 495
  surtseyan eruption, 496
Spall fragment, definition, 361, 367
Spatial resolution, definition, 1143
Spatter, *see also* Agglutination
  definition, 362
  welded spatter, 370
Spatter bomb
  definition, 447
  Hawaiian and Strombolian eruptions, 451
Spectrogram, seismic signals, 1095
Spinel
  definition, 134
  pressure in formation, 139
Spodosol, definition, 1260
Sputtering, definition, 785
SSAM, *see* Seismic spectral amplitude measurement
SSI, *see* Solid-state imaging
Stock
  definition, 191
  features, 192
Stockwork, definition, 858
Stratosphere
  aerosol effects
    dynamics, 937–939
    polar clouds, 941
    warming, 939–940
  aerosol, 934
  definition, 527
  sulfur dioxide perturbation, 935–936
  sulfuric acid aerosols in climate cooling, 1086–1088
Stratovolcano
  definition, 283, 664
  features, 286
Strength, partially molten rock, 80–81
Stromatolite
  definition, 1
  plate tectonic cycle initiation, 4
Stromboli, volcano depiction in film, 1339, 1355–1356
Strombolian eruption, *see also* Scoria cone
  bubble growth and magma fragmentation, 323
  definition, 321, 447, 683
  degassing, 453–454
  deposition features, 452
  magma reservoirs and conduits, 455–456
  models, 458–460
  overview, 447–448
  products, 451–452
  style of eruption, 448–451
  transition to Hawaiian eruption, 448, 460
  tremor sources, 456–458
  two-phase flow, 454–455
Subduction
  continental accretion, 6
  convergent plate boundariy zones, 103–104
  crust and mantle recycling, 5
  definition, 1, 804
  isotope tracing, 6–7
  mechanism, 6, 52
  midocean ridges, 272–273
  ridge subduction, 106–107
  volatiles, recycling, 168–169
  water functions, 5–6, 52
Subduction zone
  definition, 90, 271
  fractional crystallization, 144–146
  mineral deposition processes, 899–900
  volcano characteristics, 207, 254–255
Subglacial eruption
  basaltic eruptions
    thick glaciers, 409, 411–414
    thin glaciers, 409–411
  criteria for determination in geologic record, 406–408
  felsic eruptions, 414–415
  fluid dynamics, 417
  glacier properties affecting, 408–409
  meltwater generation, 406, 416–417
  paleoenvironmental information from volcanoes, 415–417
  sea level impact, 417
  Vatnajökull ice cap, 404, 406
  volcano formation, 404

Sublime, definition, 1315
Subliquidus, definition, 220
Submarine hydrothermal vent, *see also* Hydrothermal system
  biological significance, 858, 868
  definition, 858
  fluid compositions, 859, 864
  history of study, 858
  site locations, 858–862
Submarine lava, *see also* Hyaloclastite; Lobate lava; Pillow lava; Sheet flow
  arc volcanoes, 632
  eruption style control, 362
  flow types and features, 363
  laboratory simulation, 363
  modern versus ancient examples, 363
  silicic flows, 370
  welded spatter, 370
Subplinian eruption
  characteristic features, 478
  deposits, 480–481, 485
  fragmentation of magma, 479–480
  graduation between plinian and subplinian activity, 493
  history of classification, 477–478
  plumes, 478–479
  Vesuvius eruption reconstructions
    AP2 eruption, 490
    constraints in product analysis, 491–493
    1631 A.D. eruption
      opening phase, 489
      phreatomagmatic phase, 489–490
      vulcanian phase, 489
Succession, biological, 1058
Successional mosaic, definition, 1058
Sulfates, ash components, 1156–1157
Sulfide deposit, *see* Volcanic-hosted massive sulfide deposit
Sulfur
  allotropes on Io, 709, 718
  historic applications, 16, 18
  liquid sulfur in volcanic lakes, 889
  mining of volcanic products, 1280–1281
  solubility in silicate melts, 152–153
Sulfur cycle
  preindustrial geochemical cycle, 1049–1050, 1052
  recycling, 1054–1055
Sulfur dioxide
  annual emission estimates, 1048
  asthma induction, 1041
  conversion to sulfuric acid, 1087–1088
  correlation spectrometry, 809, 812, 997, 1046, 1149–1151
  emission concentration changes over time, 1147, 1150–1151
  Fourier transform infrared spectrometry, 1153
  greenhouse warming, 1088–1089
  hazards, 999, 1001–1002
  hydrothermal system reactions, 808–809
  isotopic analysis, 807
  measurement of outgassing, 1046–1047
  Mount Etna monitoring, 1178
  silicic magma release, 164–165
  stratosphere perturbation, 935–936
  thermal infrared multispectral scanner monitoring, 1153
  total ozone mapping spectrometry, 1151–1152, 1172
  toxicity, 998, 1000
Sulfuric acid
  aerosols in climate cooling, 1086–1088
  toxicity, 998, 1001
Summit pit, definition, 698
Sunset Crater, archeology, 1296, 1309
Superheated liquid, definition, 431
Surtsey, biota assembly, 1072–1074, 1077
Surtseyan eruption
  classifications of mild phreatomagmatic activity, 510
  continuous plumes, 510
  definition, 496, 683
  discrete explosions, 510
  emergence from sea, 497, 499–500
  plume, 534
  related phreatomagmatic eruptions
    heterogeneity of eruptive processes and products, 505–506
    Kilauea eruption of 1924, 503–504
    Myojinsho eruption of 1952–1953, 500–501
    Taal eruption of 1965, 501–502
    Teishi knoll eruption of 1989, 504–505
    Ukinrek eruption of 1977, 502–503
    White Island eruption of 1976–1982, 502
  subaqueous explosion, 496–497
  vents
    geometry, 509–510
    wall properties, 509
  water and phreatomagmatic fragmentation, 508–509
Suspension zone, definition, 191, 194
Swarm, *see* Earthquake
Swimming in the Volcano, volcano depiction in literature, 1352–1353
Syenite, definition, 345
Symbiosis, definition, 1058
Synthetic aperture radar (SAR) interferometry
  advantages, 1184
  definition, 728, 1121–1122
  ground deformation monitoring, 1122–1124, 1141
  Mount Etna monitoring, 1179
  Venus studies, 730–731

T

Taal, eruption of 1965, 501–502
Tachylite
  definition, 495
  surtseyan eruption, 496–497
Tambora eruption of 1815
  climate effects, 10–12, 933, 1090–1091
  impact on civilization, 10–11
Taupo, caldera, 647
Teishi, knoll eruption of 1989, 504–505
Telemetry, seismic stations, 1095
Temperature monitoring, *see* Thermal monitoring
Tephra, *see also* Ash
  colonization of new volcanic habitats, 1067–1068
  definition, 421, 1058, 1272, 1302
  erosion rate, 1059
  falling damage, 421
  phreatomagmatic eruption, 433
  volume estimation from seismic activity, 1108
  vulcanian eruption characteristics, 469, 471, 473
Tephra fall
  biosystem effects of fallout
    animals, 1059–1060
    insects, 1060
    local survival
      animals, 1061–1062
      plants, 1060–1061

Tephra fall (*continued*)
    particle size effects, 1060
    timing effects, 1060, 1062
  death and injury, 1040–1041
  risk reduction, 1222–1224
Tephra jet
  definition, 495
  finger jet
    definition, 403
    subglacial eruption, 412
  surtseyan eruption, 496–497, 499–500
Tephra layer, definition, 271
Terra, definition, 698
Tertiary consumer, definition, 1058
Tessera, definition, 728
Tetanus
  definition, 1035
  lahar association, 1039
Tethys, *see* Saturn moons
Texaco, volcano depiction in literature, 1351–1352
Thera, *see* Santorini
Thermal conductivity
  estimation, 185
  radiative conductivity, 185
  values for solids and melts, 185–186
Thermal
  definition, 527
  modeling, 533–534
Thermal diffusivity, definition, 220
Thermal infrared, definition, 1143
Thermal monitoring
  airborne sensors, 1160
  anomalies
    high-amplitude anomalies, 1161–1163
    low-amplitude anomalies, 1163–1164
    origins, 1159–1160
  ground-based measurements, 1160
  principles, 1157, 1159
  spaceborne sensors, 1160–1161
  space–time resolution of data, 1161
Thickness half-distance
  definition, 555
  fining of fall depositis, 560
Tholeiite, definition, 345
Tholeiitic trend, subduction zone magmas, 146
Tholus
  definition, 728, 772
  Mars, 776
Thomas Register of Products and Services, volcano-related commerce, 1272–1273
Tidal wave, *see* Tsunami
Tillite
  definition, 403
  formation, 410
Tiltmeter, ground deformation monitoring, 1126
Tindar
  definition, 403
  formation, 411
Titan, *see* Saturn moons
Toba, *see* Tambora eruption of 1815
TOMS, *see* Total ozone mapping spectrometer
Topographic inversion, definition, 663
Tornillo, vulcanian eruption warning, 468–469
Total ozone mapping spectrometer (TOMS)
  definition, 1143
  sulfur dioxide monitoring, 1151–1152, 1172
Tourism
  development, 1299–1300
  Grand Tour, 1284–1285
  history of volcano tourism, 1283–1286
  national parks, 1286–1288
  offerings of volcanoes
    archeological interest, 1294–1296
    beaches, 1293–1294
    climbing and skiing, 1290–1292
    ecotourism, 1292–1293
    hot springs and spas, 1290
    religious interest, 1296–1298
    scenery, 1288–1289
    spectacle of volcanic activity, 1289–1290
  overview of sites, 1283
  trends, 1284
Trachyte, definition, 403
Trap rock, definition, 1272
Trapdoor subsidence, calderas, 655
Tremor, *see also* Earthquake
  definition, 447, 1015, 1019
  features, 1019–1020, 1101
  Hawaiian and Strombolian eruptions, 456–458
  mechanisms, 1104
  volcanic explosivity index relationship to reduced displacement, 1107
  vulcanian eruptions, 465, 467, 471
Triassic period, definition, 1083
Triton, *see also* Cryovolcanism
  cryovolcanism, 791–793
  explorations, 791–792
  heating, 793
  orbit, 791
  origin, 793
  physical properties, 786
Tropopause
  definition, 527, 933
  plume dispersal, 540–541
Troposphere
  aerosol-induced cooling, 940–941
  definition, 527, 933
  particles, 934
Tsunami
  definition, 1005
  historic characteristics, 1006–1007
  Krakatoa eruption of 1883, 1006, 1010–1011
  mechanisms of volcanic production
    debris avalanches, 1009–1010
    explosive eruption, 1010–1011
    lake tsunamis, 890, 1008–1009
    overview, 1005–1006, 1011–1013
    submarine eruptions, 1006–1007, 1012
Tuff, *see also* Ash-flow deposit; Vesicular tuff
  definition, 1272
Tuff cone
  characteristics, 684
  morphology, 689
  surge deposits, 686–687
  tectonic settings, 691–692
Tuff ring
  characteristics, 684
  morphology, 689
  surge deposits, 686–687
  tectonic settings, 691
  xenoliths, 692
Turbidite, definition, 404, 627
Turbidity current, definition, 627
Turbulence. definition, 602
Turbulent flow
  definition, 237
  features, 304
Turner, Joseph Mallord William, volcano paintings, 1326–1327
Tuya, definition, 404
The Twenty-One Balloons, volcano depiction in literature, 1353–1354
Tympanic membrane, *see* Eardrum rupture

U

Ukinrek, eruption of 1977, 502–503
Ukiyoe, definition, 1316

Ultisol. definition, 1260
Ultra-low velocity zone (ULVZ), definition, 41–42
Ultramafic, definition, 41
ULVZ, *see* Ultra-low velocity zone
Uniformitarian, definition, 271–272
Units, conversion factors, 1361–1364
Unzen eruption of 1991, pyroclastic flow and surge, 950–951, 953
Upflow zone, definition, 858, 963
Uranus moons
  cryovolcanism, 793–794
  physical properties, 786
Usu, gas analysis, 810–811

V

Vapor density, definition, 997
Vapor film
  collapse in phreatomagmatic fragmentation, 434, 440
  definition, 431
  oscillation and turbulence production, 440
Variable charge, clay, 1260
Vascular plant
  colonization of new volcanic habitats, 1073
  definition, 1058
  local survival, 1061
Vatnajökull ice cap, subglacial eruption, 404, 406
VEI, *see* Volcanic explosivity index
Vent, *see also* Plume; Submarine hydrothermal vent
  basaltic volcanic fields
    alignment, 339–340
    faults, occurence of vents, 340–341
    patial patterns in distribution, 336–337
  composite volcanoes
    migration, 672–674
    pyroclast association
      main vent, 677–678
      satellite vent, 680–681
  definition, 663, 698
  ignimbrite source vents, 595
  satellite vent, 663
  subsidiary vents, 674
  Surtseyan eruptions
    geometry, 509–510
    wall properties, 509
Venus, volcanic activity
  abundance, 728
  active centers, table, 732–751
  calderas, 757–758
  distribution, 731, 752–753
  explorations, 729–731, 752–753
  factors influencing eruptions and landforms
    magma ascent, 766–767
    magma composition, 765
    surface temperature and pressure, 765–766
  fluted domes, 756
  intermediate volcanoes, 727–728, 754–756
  large volcanoes, 728, 753–754, 768
  lava
    channels, 759–760
    flow fields, 758–759
    plains, 758
    unusual flows, 759
  magma ascent, 766–767
  magmatic structures
    arachnoid, 762
    corona, 761–762
    overview, 760–761
    radial fracture centers, 764–765
  origins, 728–729
  planetary characteristics, 729–730
  rationale for study, 729
  small volcanoes, 728, 756–757
  steep-sided domes, 728, 755–756
  tectonics, 768–769
Vertisol, definition, 1260
Vesicle, definition, 421, 698
Vesicularity
  definition, 421
  pyroclastic fall deposit juvenile clasts, 567–568
Vesicular rock
  definition, 307
  lava textures, 313–314
Vesicular tuff, definition, 683
Vesiculated tuff
  definition, 495
  surtseyan eruption, 500
Vesiculation
  bubble nucleation, 423, 430
  definition, 421
  magma acceleration, 429–430
Vesuvius
  AP2 eruption reconstruction, 490
  eruption of 79 A.D
    pyroclastic flow and surge, 953–954
    reconstruction
      caldera collapse and phreatomagmatic activity, 488
      column, 486, 488
      constraints in product analysis, 491–493
      historic account, 477–478, 485–486, 531, 1036
      initial phreatomagmatic phase, 486
      product analysis, 488
  eruption of 1631 A.D. reconstruction
    opening phase, 489
    phreatomagmatic phase, 489–490
    vulcanian phase, 489
  Herculaneum archeology, 1302–1304
  history of tourism, 1284–1285
  paintings
    artistic illustration, 1336
    eruption of 1631, 1321–1324
    eruptions of 1770's, 1325
    modern paintings, 1335–1336
    neoclassicism, 1325–1326
    pre-eruption of 79 A.D., 1319–1320
    Turner paintings, 1326–1327
  Pompeii archeology
    historic accounts of eruption, 477–478, 485–486, 531, 1036, 1304–1305
    overview, 1295, 1302–1303
    rediscovery and excavation, 1305
  reconstruction constraints in product analysis, 491–493
VHMS, *see* Volcanic-hosted massive sulfide deposit
The Violins of Saint-Jacques, volcano depiction in literature, 1345–1347
Viscosity
  composition dependence, 71–72
  cryomagma, 789
  definition, 69, 149–150, 220, 698
  dike flow effects, 225–226
  factors affecting, 506–507
  lunar lava, 701
  magma viscosity
    capillary number, 184
    shear rate effects, 185
    volume fraction effects, 183–184
  melt migration dependence, 71–72, 79–80
  melt viscosity
    prediction with Adams-Gibbs-Di Marzio theory, 182–183
    pressure dependence, 182
    temperature dependence, 181–183

Viscosity (*continued*)
  molten carbonate, 176
  relative viscosity, 172
  supercritical water, 176
  volatile effects on silicate melts, 166–167
Visible maria
  definition, 698
Volatiles, *see also* Bubble; Degassing; Gas; *specific volatiles*
  basaltic magma abundances
    backarc basin basalts, 161
    continental margin basalts, 160–161
    flood basalts, 161
    island arc basalts, 160–161
    midocean ridge basalts, 158–159
    ocean island basalts, 159–160
  bubble growth and magma fragmentation, 323–324
  definition, 1, 42, 90, 150, 220, 237, 322, 709, 803
  degassing, *see* Degassing
  dike flow, rising gas bubble effects, 226–227
  effects on silicate melt properties
    density, 166
    viscosity, 166–167
  explosive eruptions, 229, 256, 322–323
  importance in volcanic eruptions, 165
  loss from conduits, 426
  magmatic content measuring
    fluid inclusion analysis, 156–157
    phase equilibrium experiments, 154–155
    quenched glass analysis, 155
    saturation with volatile-rich minerals and immiscible liquids, 157
    thermodynamic calculation based on mineral compositions, 155–156
  noble gases, 167–168
  partial pressures in solubility, 152
  recycling by subduction, 168–169
  silicate glass abundance measurements, 157, 322
  silicic magma abundances
    andesite, 161–162
    dacite, 162–163
    gradients, 163–164
    rhyolite, 162–163
    saturation, 164
    sulfur dioxide emission, 164–165
  silicic magma evolution role, 127–128
  solubility, 149–154, 238–239, 322–323, 808
  storage in basaltic magmas, 157–158
Volcanic aerosol, *see* Aerosol
Volcanic arc, *see* Arc
Volcanic explosivity index (VEI)
  definition, 263, 477, 1005
  distribution of eruptions, 258–259
  features by index value, 264
  interval and individual magnitude, 259–261
  relationship to tremor reduced displacement, 1107
Volcanic-hosted massive sulfide deposit (VHMS)
  characteristics, 905–906
  distribution and age, 904
  origin, 906, 912
  significance, 904
  types, 905
Volcanic lake, *see* Lake, volcanic
Volcaniclastic, definition, 627
Volcaniclastic apron, definition, 627
Volcanic winter, *see also* Climate
  definition, 1083
  Tambora eruption of 1815, 933, 1090–1091
Volcano, volcano depiction in film, 1356–1358
Volcano, volcano depiction in literature, 1348–1349
Volcanoes of the World
  categorization of volcanoes, 1365
  condensed and updated table, 1366–1383
Volcanology
  definition, 2, 16
  history, 16–37
The Volcano Lover, volcano depiction in literature, 1352
The Volcano Ogre, volcano depiction in literature, 1349
Vulcanian eruption
  ballistic injection, 469
  definition, 945
  deposit characteristics, 469–471
  destructive potential, 464
  field examples
    Galeras, 466–469
    Ngauruhoe, 464–466
    Sakurajima, 466
    Vulcano, 464
  fuel–coolant interaction model, 474
  history of classification, 463–464
  overview of features, 463, 474
  plumes and dynamics, 471–473, 533–534
  shock waves, 466–467, 471
  source models, 473–474
  tremors, 465, 467, 471
  velocity and pressure estimates, 469
Vulcano
  gas analysis, 812
  vulcanian eruption, 464
Vulnerability
  definition, 1199, 1201–1203, 1215
  modification, 1216

W

Warning
  alert levels, 1189, 1194, 1196, 1199, 1205
  case studies
    Long Valley, 1195–1196
    Mount St. Helens, 1192–1193
    Nevado del Ruiz eruption of 1985, 1235–1236
    Pinatubo, 1193–1195, 1235
  characteristics of successful warnings, 1186
  contents, 1234
  credibility, 1234–1235
  definition, 1229
  dissemination
    concise statements, 1191
    Internet, 1191–1192
    meetings, 1191
    news media, 1191, 1211–1212
  educational materials, 1190–1191
  factual statements, 1188
  hazard maps, 945, 1186, 1189–1190
  posteruption, 1187
  pre-eruption warning, *see* Crisis management; Forecast
  probabilities of several possible outcomes, 1189
  response of public, 1234
  risk warnings, 1187
  syneruption, 1187
  time window forecasts, 1188–1189
Water
  connate water, 803
  emission concentration changes over time, 1146–1147
  geothermal system
    chemistry, 825, 827–828
    origins and system age, 828–829

history of theories in volcanic processes, 35–37
importance in volcanic eruptions, 165
isotopic determination of subduction versus primary magma water, 806–807
magma melting role, 52
meteoric water, 803, 808
phreatomagmatic fragmentation role, 508–509
plume
  behavior effects of external water, 532–534
  formation, external interactions, 528
pressure-dependent solubility in magma, 169
pyroclastic fall interactions, 569
saturation, 152
silicate melt properties, effects
  density, 166
  viscosity, 166–167
silicic magma evolution role, 127, 154–155
solubility in magma
  overview, 135, 150–151, 238–239
  silicate melts, 151–152
subduction, 169
volcanic process effects, 9
Water/rock ratio, definition, 858
Weather, *see* Climate, volcano effects
Welding, *see also* Ignimbrite
  definition, 321
  lava fountains, 324–326
  pyroclastic fall deposits, 566
Werner, Abraham Gottlob, views of volcanoes, 24–25
White Island
  eruption of 1976–1982, 502
  gas analysis, 811
Wind in the Earth, ancient views of volcanoes, 19–20

X

Xenocryst, definition, 898
Xenolith
  definition, 15, 42, 45, 207, 220, 698
  magma ascent rate estimation
    magma reactions, 215
    transport, 214–215

Y

Yardang, definition, 772
Yield stress
  definition, 321
  preservation of agglutinate piles, 325–326, 329

Z

Zoochorous
  definition, 1058
  species colonization of new volcanic habitats, 1070